2nd Croatian Conference on Earthquake Engineering

22-24 March 2023

Zagreb, Croatia

Conference Proceedings

Title

2nd Croatian Conference on Earthquake Engineering – 2CroCEE

March 22 to 24, 2023· Zagreb, Croatia

Editors

Josip Atalić

Marta Šavor Novak

Petra Gidak

Ivo Haladin

Marina Frančić Smrkić

Maja Baniček

Iva Dasović

Marija Demšić

Mario Uroš

Tomislav Kišiček

Proceedings of the 2nd Croatian Conference on Earthquake Engineering

Zagreb, Croatia - March 22 to 24, 2023

2nd Croatian Conference on Earthquake Engineering

ORGANIZING COMMITTEE

Josip Atalić, University of Zagreb
Mario Bačić, University of Zagreb
Ana Baričević, University of Zagreb
Ivan Ćurković, University of Zagreb
Domagoj Damjanović, University of Zagreb
Iva Dasović, University of Zagreb
Marija Demšić, University of Zagreb
Ivan Duvnjak, University of Zagreb
Marina Frančić Smrkić, University of Zagreb
Petra Gidak, University of Zagreb
Davor Grandić, University of Rijeka
Ivica Guljaš, Josip Juraj Strossmayer University of Osijek
Ivo Haladin, University of Zagreb
Tomislav Kišiček, University of Zagreb

Senad Medić, University of Sarajevo
Eva Ocvirk, University of Zagreb
Zvonko Sigmund, University of Zagreb
Ana Skender, University of Zagreb
Mislav Stepinac, University of Zagreb
Marta Šavor Novak, University of Zagreb
Boris Trogrlić, University of Split
Mario Uroš, University of Zagreb
Anđelko Vlašić, University of Zagreb
Maja Baniček, University of Zagreb
Romano Jevtić Rundek, University of Zagreb
Ante Pilipović, University of Zagreb
Igor Tomić, École Polytechnique Fédérale de Lausanne

ACADEMIC SCIENTIFIC COMMITTEE

Dražen Aničić, Croatian Academy of Engineering
Josip Atalić, University of Zagreb
Mario Bačić, University of Zagreb
Bojan Baletić, University of Zagreb
Maja Baniček, University of Zagreb
Ana Baričević, University of Zagreb
Katrin Beyer, École Polytechnique Fédérale de Lausanne
Svetlana Brzev, University of British Columbia
Anita Cerić, University of Zagreb
Andrew Charleson, Victoria University of Wellington
Nicola Chieffo, University of Minho
Helen Crowley, EUCENTRE
Nina Čeh, University of Rijeka
Ivan Ćurković, University if Zagreb
Domagoj Damjanović, University of Zagreb
Iva Dasović, University of Zagreb
Marija Demšić, University of Zagreb
Matjaž Dolšek, University of Ljubljana
Ivan Duvnjak, University of Zagreb
Peter Fajfar, University of Ljubljana
Marina Frančić Smrkić, University of Zagreb
Radomir Folić, University of Novi Sad
Marco Francesco Funari, University of Surrey
Petra Gidak, University of Zagreb

Agostino Goretti, Civil Protection Department of Italy
Davor Grandić, University of Rijeka
Marin Grubišić, Josip Juraj Strossmayer University of Osijek
Maurizio Guadagnini, University of Sheffiled
Ivica Guljaš, Josip Juraj Strossmayer University of Osijek
Marijana Hadzima-Nyarko, Josip Juraj Strossmayer University of Osijek
Iman Hajirasouliha, University of Sheffield
Sanja Hak, Basler & Hofmann, Zürich
Ivo Haladin, University of Zagreb
Marijan Herak, University of Zagreb
Sanja Jerković, City of Zagreb
Antonia Jaguljnjak Lazarević, University of Zagreb
Tanja Kalman Šipoš, Josip Juraj Strossmayer University of Osijek
Tomislav Kišiček, University of Zagreb
Lampos Koutas, University of Thessaly
Meho Saša Kovačević, University of Zagreb
Damir Lazarević, University of Zagreb
Paulo B. Lourenco, University of Minho
Ivan Lukačević, University of Zagreb
Ana Mandić Ivanković, University of Zagreb
Marko Marinković, University of Belgrade
Senad Medić, University of Sarajevo
Mladen Meštrović, University of Zagreb
Ljubomir Miščević, University of Zagreb

Paolo Morandi, University of Pavia, EUCENTRE

Marija Mustać Brčić, University of Zagreb

Miroslav Nastev, Geoscience for Public Safety Geological Survey of Canada

Eva Ocvirk, University of Zagreb

Jelena Pejović, University of Montenegro

Davorin Penava, University of J.J. Strossmayer in Osijek

Ljupko Perić, ETH Zürich

Kyriazis Pitilakis, Aristotle University

Savvas Saloustros, École Polytechnique Fédérale de Lausanne

Marijana Serdar, University of Zagreb

Veronika Shendova, University of SS Cyril and Methodious in Skopje

Neritan Shkodrani, Polytechnic University of Tirana

Zvonko Sigmund, University of Zagreb

Vitor Silva, GEM, EUCENTRE, University of Aveiro

Davor Skejić, University of Zagreb

Ana Skender, University of Zagreb

Hrvoje Smoljanović, University of Split

Sri Sritharan, Iowa State University

Davor Stanko, University of Zagreb

Mislav Stepinac, University of Zagreb

Marta Šavor Novak, University of Zagreb

Ingrid Tomac, University of California (San Diego)

Igor Tomić, École Polytechnique Fédérale de Lausanne

Thanasis Triantafillou, University of Patras

Boris Trogrlić, University of Split

Mario Uroš, University of Zagreb

Anđelko Vlašić, University of Zagreb

Mihaela Zamolo, Croatian Society for Earthquake Engineering

Mariano Angelo Zanini, University of Padova

PREFACE

The organization of the Conference, in the period after two devastating earthquakes in Croatia, in the period of community recovery when it is crucial to take care of the citizens affected by the earthquake, in the period of reconstruction of a number of the most important buildings in the capital of the country (including the building of the Conference organizers), in the period when the whole country is reaching the limits of its capacities – is extremely challenging and requires special emotion and sacrifice from experts in the field of earthquake engineering because they are aware that knowledge and continuous raising of its level are crucial for recovery of the community and the for laying foundations for the future (of our children).

Nowadays, education in schools and research on faculties are not in the foreground (they are not popular), but the earthquakes in Croatia have shown that in difficult times, the eyes are focused on knowledge as an indispensable support (e.g., earthquakes, Covid-19, ...). Will the time overshadow the importance of knowledge again? Of course it will, and our children will play "their games" again, but on the other hand it is up to us to continuously fight, to play our "game" for the benefit of all (and those who ignore the problems), hoping that we will pass this passion to next generations.

The first Croatian Conference on Earthquake Engineering (1CroCEE), held on the first anniversary of the 2020 Zagreb earthquake, was a "gamechanger" in Croatia in terms of raising the level of knowledge, connecting experts (promoting international cooperation) and maintaining a high level of risk awareness following the earthquakes that struck central Croatia twice in one year. It emerged in response to the need for reconstruction and as a conclusion to the many post-earthquake activities led by scientific community: damage assessment process, preparation of manuals for urgent retrofitting measures (120 pages) and comprehensive guidelines for the retrofitting of masonry buildings (600 pages), preparation of guidelines for the recovery/reconstruction process, comprehensive education on the monthly basis (every 22nd of the month), estimates of losses and reconstruction costs (initial government and RDNA reports), preparing data for application for the EU Solidarity Fund, steering of public policy and many others. All these activities would not have been possible, truly effective and long lasting without the unity/togetherness of numerous colleagues from Croatia and abroad, and collaboration with many practicing engineers, seismologists, architects, and government officials. The conference was a great success, gathering more than 700 researchers, practicing engineers and architects, government representatives (including Prime Minister), students and others from 26 countries (very large "playground").

The 2nd Croatian Conference on Earthquake Engineering (2CroCEE), organised on the third anniversary of the 2020 Zagreb Earthquake, aims to enforce a continuous and decisive "playing with earthquakes" in a small and vulnerable country like Croatia. With this conference, we want to establish a new tradition where earthquakes are not forgotten (even if they do not occur very often) and where knowledge is passed on to new generations. We hope to bring us together again, to share knowledge, expertise, ideas and experiences, which is crucial for the reconstruction process of the earthquake-struck areas, a hot topic in Croatia. Therefore, we are organizing a series of technical visits to the earthquake-affected areas and reconstruction sites in Zagreb and Petrinja to experience the "power of the enemy" and share experiences and lessons learned for enhanced resilience of communities, which is of utmost importance for stable future development, as well as for preservation of our rich cultural heritage.

We may conclude with joy and pride that we have once again brought together large number of leading scientists in the field of earthquake engineering and almost all experts from Croatia. We firmly believe that the newly acquired knowledge will significantly help to achieve a further step towards earthquake-resilient future in Croatia.

Finally, the organizers of the Conference express thanks to all companies and institutions that supported this Conference. Special thanks go to the International Association for Earthquake Engineering, the European Association for Earthquake Engineering and the Croatian Association for Earthquake Engineering, for their assistance and support in organizing this conference. The Editors would like to thank all authors for their excellent contributions to these proceedings and the members of the Organizing Committee and Academic Scientific Committee, as well as the numerous experts who participated in the review process. The gratitude is also extended to all participants for attending the conference 2CroCEE. The lectures organised at the conference are based on interesting technical solutions and latest findings in the field of earthquake engineering from projects that have already been implemented, those that are in the design phase, or projects that are currently being implemented in all parts of the world. In addition to representatives from the research community, the conference will also feature presentations from the industry representatives, which constitutes the best possible synergy of theoretical and practical achievements. We believe that these 2CroCEE proceedings will prove to be highly interesting and useful to all experts exhibiting a scientific and professional interest in earthquake engineering.

Thank you for joining us at 2CroCEE to *reshake* Croatia with knowledge and establish a new tradition aimed at reconstructing the past in Croatia for resilient future.

Josip Atalić
Marta Šavor Novak
Petra Gidak
Ivo Haladin
Marina Frančić Smrkić
Maja Baniček
Iva Dasović
Marija Demšić
Mario Uroš
Tomislav Kišiček

Zagreb, March 2023

CONFERENCE SUPPORT

SUPPORTING ORGANIZATIONS

The European Association for Earthquake Engineering

www.eaee.org

The International Association for Earthquake Engineering

www.iaee.or.jp

The Croatian Association for Earthquake Engineering

Croatian Center for Earthquake Engineering

Branch office of the Faculty of Civil Engineering University of Zagreb

www.hcpi.hr

UNDER AUSPICE OF

	MINISTRY OF SCIENCE AND EDUCATION	**Ministry of Science and Education** Donje Svetice 38 10000 Zagreb, Croatia www.mzo.gov.hr
	MINISTRY OF PHYSICAL PLANNING, CONSTRUCTION AND STATE ASSETS	**Ministry of Physical Planning, Construction and State Assets** Ulica Republike Austrije 20 10000 Zagreb, Croatia www.mpgi.gov.hr
	MINISTRY OF THE INTERIOR	**Ministry of the Interior** Ulica grada Vukovara 33 10000 Zagreb, Croatia www.mup.gov.hr
	MINISTRY OF CULTURE AND MEDIA	**Ministry of Culture and Media** Runjaninova 2 10000 Zagreb, Croatia www.min-kulture.gov.hr
	CROATIAN CHAMBER OF ECONOMY	**Croatian Chamber of Economy** Rooseveltov trg 2 10000 Zagreb, Croatia www.hgk.hr
	CROATIAN ENGINEERING ASSOCIATION	**Croatian Engineering Association** Berislavićeva 6 10000 Zagreb, Croatia www.his-hr.hr
	ACADEMIA SCIENTIARUM ET ARTIUM CROATICA	**Croatian Academy of Sciences and Arts** Foundation Zrinski trg 11 10000 Zagreb, Croatia www.zaklada-hazu.hr

GENERAL SPONSOR

Croatian Chamber of Civil Engineers

Ulica grada Vukovara 271
10000 Zagreb, Croatia

www.hkig.hr

PLATINUM SPONSORS

Spegra

Ante Petravića 23, 21000 Split, Croatia

www.spegra.hr

RÖFIX Ltd. Croatia

Donja Pušća, Ulica Lusci br. 3
10294, Pojatno, Hrvatska

www.roefix.com

Fibre Net S.p.A.

Via Jacopo Stellini, 3 – Z.I.U.

33050 Pavia di Udine (Ud) ITALY

www.fibrenet.it

GOLDEN SPONSORS

MC-Building Chemicals d.o.o.

Kovinska 4a, 10090 Zagreb

www.mc-bauchemie.hr

Wienerberger d.o.o.

Donje Pokuplje 2, 47000 Karlovac

www.wienerberger.hr

SILVER SPONSORS

Samoborka d.d.

Zagrebačka 32/A, Samobor

www.samoborka.hr

TIS

Emirgazi Mahallesi No:35/M Kahramankazan, Ankara, Turkey

www.tis.com.tr/en/home/

Leviat

www.leviat.com

Mapei Croatia d.o.o.

Purgarija 14, Kerestinec
10431 Sveta Nedelja, Hrvatska

www.mapei.com/hr

FIP MEC S.r.l.

Via Scapacchiò, 41
35030 Selvazzano Dentro PD, Italy

https://www.fipmec.it

BRONZE SPONSOR

TOPOMATIKA d.o.o.

Industrijska ulica 3, Novaki
10431 Sveta Nedelja

www.topomatika.hr

Progetto Sisma SRL

via Marzabotto 4, 41042 Fiorano Modenese, Italy

www.progettosisma.it

Freyssinet Adria Sl, d.o.o.

Žnidarčičeva 37, 5290 Šempeter pri Gorici, Slovenia

www.freyssinet-adria.si

TABLE OF CONTENTS

ENGINEERING SEISMOLOGY

GEOTECHNICAL EARTHQUAKE ENGINEERING

EXPERIMENTAL TECHNIQUES FOR CHARACTERIZATION OF MATERIALS AND STRUCTURES

SEISMIC PERFORMANCE OF STRUCTURES

REPAIR AND STRENGTHENING OF STRUCTURES

POST-EARTHQUAKE RECONSTRUCTION PROCESS

LESSONS LEARNT FROM EARTHQUAKE DISASTERS

PREPAREDNESS AND EMERGENCY MANAGEMENT

SEISMIC LOSS AND RISK ANALYSIS

PHD SPECIAL SESSION

Keynote Lecture

PREDICTING THE SEISMIC RESPONSE OF HISTORICAL MASONRY BUILDINGS – WHICH MODELLING ASSUMPTIONS MATTER?

Katrin Beyer

École Polytechnique Fédérale de Lausanne, Switzerland, katrin.beyer@epfl.ch

Abstract

Historical unreinforced masonry buildings are among the most vulnerable buildings when subjected to seismic loading. The high vulnerability results from the quasi-brittle response of the masonry material itself but also from the limited diaphragm effect of the slabs, which are typically timber slabs, and weak connections between slabs and walls. This presentation looks at common structural details of historical unreinforced masonry buildings and on how these details can be represented in finite element models suitable for engineering practice. Furthermore, it investigates the sensitivity of the analysis results to the modelling assumptions. To do so, we model masonry buildings that have been tested under dynamic loading and compare modelling assumptions to observed results. The presentation concludes with lessons learnt from these comparisons and an outlook on the impact of computer vision solutions on generating models of historical buildings.

Biography

Katrin Beyer is Associate Professor at the École Polytechnique Fédérale de Lausanne (EPFL) in Switzerland and head of the Earthquake Engineering and Structural Dynamics Laboratory (http://eesd.epfl.ch). After completing her undergraduate studies at the Federal Institute of Technology in Zurich (ETHZ), she worked for two years for the consulting firm ARUP in London, UK, on projects related to structural dynamics, impact and seismic analysis. She received her PhD from the University of Pavia, Italy. Her research interests include the seismic behaviour of reinforced concrete walls and of unreinforced masonry structures and large-scale structural testing. She is member of the executive committee of the European Association for Earthquake Engineering and was responsible for the revision of the masonry section of the European seismic design code (Eurocode 8 Part 1). She is an advocate of open science, publishing next to manuscripts also relevant experimental data and models (https://eesd.epfl.ch/data_sets/, https://zenodo.org/communities/eesd_at_epfl/about/, https://github.com/eesd-epfl). Since September 2020, she is associate dean of the School of Architecture, Civil and Environmental Engineering (ENAC) at EPFL.

Keynote Lecture

COUPLING OF HIGHRISE BUILDING EARTHQUAKE RETROFIT AND BUILDING INFORMATION MANAGEMENT (BIM) SYSTEM

Amr S. Elnashai [1] and Do-Soo Moon [2]

[1] *Civil and Environmental Engineering Department, University of Houston/University of Houston System, USA, elnashai@uh.edu*
[2] *University of Hawaii at Manoa, dsmoon@hawaii.edu*

Abstract

Highrise buildings that have structural irregularities are in general more susceptible to damage from earthquakes. Such damage is primarily due to the coupling of torsional and translational vibrational response whereby the building twists even though it is being excited in translational modes only. For optimal earthquake design and retrofit of such structures, several cycles of iterations of structural analysis followed by design change are often needed. To provide efficiency and accuracy of iterative assessment-adjustment cycles in the design process, this study proposes an integrated seismic design and assessment framework. The 'Revit Structure' platform from Autodesk, a prominent member of the Building Informational Modeling software family, and ZEUS-NL from Mid-America Earthquake Center, one of the most advanced earthquake simulation programs, are utilized for seismic design and analysis tools, respectively. An advanced bi-directional linkage interface is developed so that two distinct and complex computer codes can exchange essential structural or non-structural member data in both directions without any loss of information. This coupled approach also provides improved earthquake analysis and design guidelines which can address damaging torsional effects. The feasibility of the proposed framework and its components are successfully evaluated and verified through an application example. It is observed and verified that more reliable and better seismic design for irregular buildings can be achieved using the proposed framework.

Full paper is available in the Proceedings (https://doi.org/10.5592/CO/2CroCEE.2023.71).

Biography

Fellow of the UK Royal Academy of Engineering Amr Elnashai is Professor in Civil and Environmental Engineering at the University of Houston, USA. His immediate past position was Vice Chancellor and Vice President for Research and Technology Transfer at UH. Prior to his Houston, he was Dean of Engineering at the Pennsylvania State University, and the Harold and Inge Marcus Endowed Chair of Engineering. As dean, Amr was responsible for all aspects of operation and leadership of the College of Engineering. He also served as head of the Department of Civil and Environmental Engineering at the University of Illinois at Urbana-Champaign (June 2009 to December 2013) and the Bill and Elaine Hall endowed professor. He was Director of the NSF multi-institution interdisciplinary Engineering Research Center (ERC), MAE Center (2004-2009). He was also Director of the NSF Network for Earthquake Engineering Simulations (NEES) Laboratory at Illinois (2002-2009). Before moving to the USA, Amr was division head at Imperial College, London, and a chaired professor. His tenure at Imperial College lasted from 1986 to 2000 during which time he was the national technical contact on Eurocode 8 and member of the drafting panel. From 1984 to 1986, he worked as a senior engineering in Wimpey Offshore Engineering Limited, London, in the technology development department, and led a team of highly qualified designers and analysts focusing on the North Sea oil and gas industry. He is the founder and editor-in-chief of the Journal of Earthquake Engineering. His research interests are multi-resolution distributed analytical simulations, network analysis under stress and disruption, large-scale fire ignition and spread modeling, hybrid testing and field investigations of the response of complex networks and structures to earthquakes. His early research was on design and stability of offshore oil and gas production platforms. He has advised 47 PhD students and over 100 MS thesis students. He published 148 refereed journal papers, 3 books, 11 book chapters, and a large number of research and field investigation reports.

Keynote Lecture

DAMAGE, LOSSES, RECONSTRUCTION POLICIES, AND RETROFIT INTERVENTIONS ON RESIDENTIAL BUILDINGS IN HISTORICAL CENTERS AFTER RECENT ITALIAN EARTHQUAKES

Marco Di Ludovico

Department of Structures for Engineering and Architecture University of Naples Federico II
Via Claudio, 21 - 80125 Naples - Italy, diludovi@unina.it

Abstract

The reconstruction process of residential buildings damaged by L'Aquila 2009 earthquake initially involved buildings outside historical centres and then, starting from August 2012, residential buildings in historical centres. The reconstruction model related to buildings in historical centres was developed by two special offices, involved in the reconstruction process of L'Aquila municipality and other municipalities, respectively. Both special offices introduced new procedures to manage the reconstruction based on a parametric model to define the maximum public grant to repair and strengthen the damaged buildings in historical centres. The new model was necessary to deal with the reconstruction of historical centres mainly characterized by old masonry building aggregates with a cultural and architectural heritage value. The data collected in the management process of reconstruction outside and inside historical centers, allowed obtaining precious and unique information on buildings and aggregates characteristics, damage and usability ratings as well as repair and retrofitting cost data obtained by funding requests. Furthermore, these data are the basis to carry out a comparison between the repair and retrofit cost data and peculiarities of residential buildings outside and inside historical centers.

Extended abstract is available in the Proceedings (https://doi.org/10.5592/CO/2CroCEE.2023.1).

Biography

Prof. Marco Di Ludovico is Associate Professor of Structural Engineering at the University of Naples Federico II. His research activities deal with theoretical and experimental aspects on: non linear behavior of reinforced concrete and masonry structures; structural vulnerability, post-earthquake damage and repair costs; repair, strengthening and seismic retrofit of concrete and masonry structures with composites; response of reinforced concrete buildings under tsunami-induced loads; protection of historical monumental buildings. Following the earthquake of April 6th, 2009, is member of ReLUIS (Network of University Laboratories for Earthquake Engineering) working group, that: coordinated, in partnership with the Department of Civil Protection, the checks of conformity to standards for public and strategic buildings in L'Aquila and all the other municipalities of the crater. Within the 2022–2024 research agreement between the Civil Protection Department (DPC) and ReLUIS, he currently coordinates the work package "Post-Earthquake data analysis" and within the work package "Seismic Risk Maps—MARS", a task group related to "Loss predictions". He is author of more than 250 scientific papers on journals or proceedings of national and international conferences and two books on the reconstruction process of residential buildings outside and inside the historical centres after L'Aquila 2009 earthquake. He participates to National and International Scientific Bodies: Working Group "Learning from Earthquakes (LFE)" by Earthquake Engineering Research Institute (EERI); EAEE (European Association for Earthquake Engineering) WG1 Future Directions for Eurocode 8; fib (Federation International du Beton) TG 9.3 "FRP Reinforcement", TG 5.1 'FRP Reinforcement for Concrete Structures'; CNR (Italian National Research Council) working groups on the development of technical documents on the use of composite materials.

Keynote Lecture

EXPLORING THE COMPLEXITIES OF THE 6 FEBRUARY 2023 EARTHQUAKE SEQUENCES IN TÜRKIYE AND THEIR INSIGHTS FOR REGIONAL SEISMIC HAZARD MODELING

Laurentiu Danciu

Swiss Seismological Service (SED), ETH Zurich, Switzerland, laurentiu.danciu@sed.ethz.ch

Abstract

On February 6, 2023, a devastating series of earthquakes occurred along East Anatolian Fault System in southeastern Türkiye. A powerful mainshock earthquake with a moment magnitude of 7.8 was followed by a 7.5 earthquake, as well as numerous strong and numerous aftershocks, causing massive damage, fatalities and losses in Turkey and Syria. From the perspective of the seismic hazard modeling, these earthquakes are challenging due to their unique characteristics: large magnitude, multiple ruptures propagations, progressive aftershock sequences, extreme ground motions and ground displacement. Recognizing that one earthquake sequence is not intended for the validation of seismic hazard models, the goal of this contribution is to examine the anatomy of these earthquakes, the recording data, and their multifaceted impacts in comparison with the regional seismic hazard models, i.e., 2020 European Seismic Hazard Model (Danciu et al. 2021).

Biography

Dr. Laurentiu Danciu is a senior researcher at ETH Zurich's Swiss Seismological Service (SED). His research interests range from seismology and earthquake engineering to structural engineering, with a current emphasis on probabilistic seismic hazard and risk assessment. He is leading the development of numerous regional and national seismic hazard models, including the most recent update to the 2020 European Seismic Hazard Model, the 2013 European Seismic Hazard Models, the 2014 Earthquake Model of the Middle East , and the Swiss Hazard Model from 2015. He has an active role in the integration of the European Facilities of Earthquake Hazard and Risk (EFEHR) with the European Plate Observing System infrastructure and the Global Earthquake Model.

Keynote Lecture

IZIIS - 57 YEARS OF RESEARCH EXCELLENCE AND BUILDOUT OF EUROPEAN SEISMIC RESILIENCE

Vlatko Sesov

Ss. Cyril and Methodius University in Skopje, Institute of Earthquake Engineering and Engineering Seismology-IZIIS, N. Macedonia, vlatko@iziis.ukim.edu.mk

Abstract

58 years of existence! This year, these two digits mark the 58th anniversary of IZIIS. Lots of years, many great people, many outstanding careers, many excellent Master of Science, many distinguished doctors of science, a lot of magnificent scientific projects, many excellent missions have been interwoven in almost six decades of existence of IZIIS. It is not immodest to say that everything has been marked by excellence.

To write about IZIIS portfolio, we need to look through the past that teaches us to understand the present and, what is more important, how to build the future. The beginnings of IZIIS are inseparably linked to the Skopje 1963 earthquake. The tragedy that struck the city of Skopje meant the beginning of one of the most prestigious scientific institutions in European and world frames. On 27 May 1965, in the aftermath of the Skopje earthquake, the University Council of the University in Skopje made a decision on establishment of an Institute for General and Engineering Seismology. The Institute started to develop with limited human resources, but with national and, mainly, international support provided by experts. Despite the modest beginnings, the vision of the first generations of professors, engineers and scientific collaborators contributed, within a very short time, to the growth of IZIIS into a recognizable centre for earthquake engineering and engineering seismology even beyond the boundaries of the then existing country. Then, there followed years of dedicated work, building of own scientific staff, education of generations of masters and Doctor of Science, building of own capacities representing an excellent basis for successful functioning and further advancement of the Institute. It is this strenuously achieved legacy that represents a great responsibility for all of us that are currently part of IZIIS, to preserve it and enrich it for the future generations. This is an exceptional challenge that we can overcome, in the conditions of our existence, only through the joint and teamwork of the entire collective. In fact, this has been one of the secrets of success in these 58 years, team morale, team work of the Institute and the maximum commitment of all employees. The close connection between the scientific investigations and the applicative activities as well as the application of the most recent knowledge in the educational activities are specificities of IZIIS that have been cherished since its establishment and will continue to be upgraded with new contents and ideas.

The complex social conditions, the distorted system of values, globalization, the climate changes, create daily challenges that we must solve and overcome although they are not our professional priority. The objective of this paper is to present IZIIS to wider earthquake community by presentation of the most recent achievements within the main activities of the Institute, namely the scientific-research, the applicative and the educational activity.

Finally, I would like to express my deepest respect and gratitude to all generations of IZIIS employees who have contributed, throughout these 58 years, to what IZIIS is today – a symbol of science

Biography

Prof. Vlatko Sesov is Director of the Institute of Earthquake Engineering and Engineering Seismology – IZIIS, University Ss Cyril and Methodius in Skopje, and Professor of Earthquake Geotechnical Engineering. He has over 27 years of experience in the area of soil dynamics, liquefaction and its remediation, local site effects, seismic zonation, physical modelling and model testing. Prof. Sesov has vast international experience, he was doctoral and postdoctoral researcher at the University of Tokyo, Japan (2003 - 2005), visiting professor at the Ruhr University, Bochum, Germany (2008 - 2009), Fulbright Scholar at University of California, Davis (2013-14) and professor at ROSE School, University of Pavia (2020). He is former President of Macedonian Geotechnical Society, member of Technical Committee (TC203) at ISSMGE and National Contact Point for Widening Participation and ERA. Prof. Sesov was national coordinator of several European project: INFRA-NAT – Increased Resilience of Critical Infrastructure to Natural and Human-Induced Hazards (2018-2019), coordinator of CRISIS - Comprehensive RISk assessment of basic services and transport InfraStructure (2020-2022).

Keynote Lecture

POST-EARTHQUAKE RETROFIT OF THE ZAGREB CATHEDRAL

Petra Gidak and Damir Lazarević

Faculty of Civil Engineering, University of Zagreb, Croatia, damir@grad.hr

Abstract

Neo-Gothic Cathedral in Zagreb, the largest Croatian sacral building was severely damaged by the 5.4 magnitude earthquake on March 22, 2020. These days three years after seismic main event aftershocks are still causing displacement progression of stone blocks of the towers. For the static and dynamic analysis of the Cathedral the distinct element method is chosen. The continuum model (on which the finite element method is based) is hardly acceptable in the case of the Cathedral. Simply, in order to insist on equal displacements and rotation angles of the nodes, the model would be too compatible. Such an assumption, given the manner of construction and the current condition of the building, was violated immediately. Even for small levels of load and displacement, blocks slipping and rotation on the joints will (at least) occur.

The numerical model consists of deformable blocks and their contacts. The blocks are internally discretized by tetrahedra based on the finite difference method, and their behaviour is nonlinear with the possibility of hardening and softening. The connection between the discretized blocks is defined by a series of nonlinear springs. With the model based on elements and springs, discretized and connected blocks can deform and move (slip, separate, break, rotate, fall) practically without restrictions. The software 3DEC is used for the structural analysis of the Cathedral. Due to the complicated geometry, considerable effort was invested in the generation of the numerical model. Presentation will also discuss choice of input data for modelling materials and load-bearing elements, even with in-situ test results. The basic principle is to adjust the input parameters of the elements and springs so that the characteristic points on the response curve (forces with associated displacements) correspond to those from the statistical analysis of numerous well-documented experiments.

Biography

Petra Gidak is associate professor at the Faculty of Civil Engineering University of Zagreb. In her scientific work, she deals with the numerical modeling, shape optimization of load-bearing systems and form finding methods of tensile and compressive structures. As part of her doctoral research, she dealt with the stability assessment of form finding methods for tensile structures. The current focus of her research is the application of tension-compression analogy for defining the thrust line of cross vaults and the transmission of forces through the system of walls and buttresses, as well as the transmission of forces in the towers of sacred buildings using graphical and numerical methods. She participated in the definition of an important document for decision-making on post-earthquake reconstruction and application to international aid funds entitled Croatian December 2020 Earthquake - Rapid Damage and Needs Assessment. She is a member of a team of engineers from the Faculty of Civil Engineering University of Zagreb, that are engaged in the analysis of the current state of the Zagreb Cathedral.

Damir Lazarević is tenured full professor at the Department of Engineering Mechanics, Faculty of Civil Engineering, University of Zagreb, Croatia (UZ FCE). He graduated in 1993 and received his PhD in 2000 from the UZ FCE. He teaches four courses in the graduate programme and four courses in the postgraduate doctoral programme at the UZ FCE. He has supervised more than 120 graduate theses and 5 PhD theses. He was the Chairman of the Chair for Statics, Dynamics and Stability of Structures in the Department of Engineering Mechanics at the UZ FCE from 2010 to 2014, and the Head of the same Department from 2014 to 2016. His research interests include the broad field of engineering mechanics and numerical methods in structural analysis, as well as the earthquake engineering with the focus on the performance of heritage buildings, bridges and industrial facilities. He is the author of more than 70 scientific papers in journals or proceedings of national and international conferences, as well as a book on the principles and methods of analysis of structures. He participated in several research projects and led two of them - the national scientific project "Non-standard models of civil engineering structures" under the Ministry of Science, Education and Sports of the Republic of Croatia and the project "Novel Efficient Iterative Procedure for the Structural Analysis", funded by the Croatian Science Foundation. After the earthquakes in 2020 Croatia, he actively participated in the rapid inspections of damage and usability of the critical infrastructure, and other activities important for mitigation of the earthquake impacts. In collaboration with Croatian industry he participated in almost 100 structural designs and retrofit projects of the facilities in the cement industry, critical infrastructures buildings, large-span bridges and heritage buildings among others, where his scientific expertise was essential.

Invited Lecture

SEISMIC CHARACTERIZATION OF THE SHALLOW SUBSOIL BY AMBIENT VIBRATION MEASUREMENTS: A TOOL FOR SEISMIC MICROZONATION

Dario Albarello

Department of Physics, Earth and Environmental Sciences, University of Siena, Italy, dario.albarello@unisi.it

Abstract

Seismic microzonation at the scale of single municipalities is a basic element of land planning policies aiming at seismic risk reduction. Any technical tool supporting this kind of studies must be effective and cheap enough to allow the application to wide areas when economic resources available on purpose are scarce. Moreover, these tools should not require high level skills to be managed, since one cannot expect that Academy or Research Centers will be charged for field surveys relative to a large number of municipalities. While engineering geological mapping represents the qualitative basis for any microzonation study, seismic characterization (in terms of shear wave velocity profile) of the subsoil at the scale of tens to hundreds of meters is mandatory to forecast ground motion amplification effects induced by local stratigraphical configurations. Most common seismic prospecting tools (SH refraction, MASW, etc.) present severe limitations when depths larger than a few tens of meters are of concern for an effective characterization of the local seismic response. Moreover, in urban areas, anthropic noise and logistics may hamper their affective application. In these situations, seismic surveys based on ambient vibration monitoring by single station and array configurations may represent an effective solution. In Italy, these tools have been extensively used in a huge amount of seismic microzonazion studies relative to hundreds of municipalities. Main features of these techniques will be presented along with some case studies in Italy.The manuscript analyses, summarizes, and presents the crucial seismo-tectonic aspects and seismological data of both affected cities, then defines P-nodal planes for both strongest earthquake events affecting Skopje 2016 (M_L=5.3) and Zagreb 2020 (M_L=5.5). We analysed and compared macroseismic data, and strong motion records in respect to their amplitude and frequency characteristics and showed the building damage and usability statistics.

Biography

Physicist, he is Full Professor of Solid Earth Geophysics at the University of Siena where he teaches 'Applied Geophysics' and 'Seismic Hazard'. He is Research Associate of the National Research Council (CNR). He is presently member of the advisory board of the Prime Minister of the Italian Government for Seismic Risk (Great Risks Commission) and of the International Atomic Energy Agency of United Nations (IAEA) for seismic microzoning and testing seismic hazard estimates at Nuclear Power Plants. Hi is presently the PI of the National Research Project for mapping site effects at national scale. During his scientific career, he was involved in quantitative modelling of geodynamic processes with numerical and analytic methods, assessment of stress and strain fields at regional scale from geodetic and seismic data, of seismicity induced by large dams, deformation processes in geothermal areas, mud volcanoes dynamics and probabilistic seismic hazard assessment at regional scale. He has been also engaged in the study of pre- and co-seismic phenomena relative from RADON and deep piezometric data, and of statistical studies relative to short and medium term earthquake prediction. In the last years he has been mainly involved in the development and application of passive seismic methods for subsoil exploration and has been also responsible for field surveys in the field of archaeological and geotechnical exploration of the shallow subsoil. As a member of a number of Scientific Committees and International and National research groups, he developed and applied innovative techniques for seismic hazard assessment at national and local (seismic microzoning) scales. In particular, on behalf of the Dept. of Civil Protection of the Italian Government he was a member of the working group for the definition of the National Guidelines for Seismic Microzoning. From 2013 until 2015 he directed the National Research Project (DPC-INGV) devoted to short term earthquake prediction. From 2017 to 2022 he has been the President of the Centre of Seismic Microzoning. He also coordinated a number of seismic microzoning studies in Central and Northern Italy. He is the author of more than 260 extended papers (SCOPUS H-index=32).

Invited Lecture

CLASSIFICATION OF RESIDENTIAL BUILDING STOCK IN SERBIA

Svetlana Brzev [(1)], Jovana Borozan [(2)], Marko Marinković [(3)], Marijana Hadzima-Nyarko [(4)], Nikola Blagojević [(5)], Milica Petrović [(6)], Veljko Koković [(7)], Borko Bulajić [(8)], and Božidar Stojadinović [(9)]

[(1)] *Department of Civil Engineering, University of British Columbia, Canada, sbrzev@mail.ubc.ca*
[(2)] *Nanometrics Inc., Kanata, Ontario, Canada, jovanaborozan@nanometrics.ca*
[(3)] *Faculty of Civil Engineering, University of Belgrade, Serbia, mmarinkovic@grf.bg.ac.rs*
[(4)] *Faculty of Civil Engineering and Architecture, University of Osijek, Croatia, mhadzima@gfos.hr*
[(5)] *Department of Civil, Environmental and Geomatic Engineering, ETH Zurich, Switzerland, blagojevic@ibk.baug.ethz.ch*
[(6)] *Faculty of Architecture, University of Belgrade, Serbia, milica.petrovic@arh.bg.ac.rs*
[(7)] *Faculty of Civil Engineering, University of Belgrade, Serbia, veljko@imk.grf.bg.ac.rs*
[(8)] *Faculty of Technical Sciences, University of Novi Sad, Serbia, borkobulajic@uns.ac.rs*
[(9)] *Department of Civil, Environmental and Geomatic Engineering, ETH Zurich, Switzerland, stojadinovic@ibk.baug.ethz.ch*

Abstract

Developing a classification system (taxonomy) for buildings is a critical step for seismic risk assessment studies. Such a system can be used to characterize a building portfolio within urban/rural settlements or building stock for the entire country. Serbia is located in a region characterized by a moderate seismic hazard. In the last century, 10 earthquakes of magnitude 5.0 and higher occurred in Serbia, the strongest (M 6.0) in 1922. The strongest earthquake in the 21st century (Mw 5.5), with an epicenter close to Kraljevo, occurred in November 2010 and caused significant damage to residential buildings. In 2019, members of the Serbian Association for Earthquake Engineering (SUZI-SAEE) contributed to the SERA project and its goal to develop a seismic risk model for Europe. A taxonomy of residential buildings in Serbia was developed based on previous national and regional building stock studies. The proposed taxonomy includes the Lateral Load-Resisting System (LLRS) (e.g., wall, frame, dual wall-frame system) and material of the LLRS (e.g., masonry, concrete, wood) as the main attributes. The type of floor diaphragm (rigid or flexible) has been specified only for masonry typologies with unreinforced masonry walls, while building height and date of construction have been implicitly considered. According to the proposed taxonomy, there are 9 residential building typologies in Serbia; out of those, 5 typologies are related to masonry structures, 3 are related to RC structures, and one is related to wood structures. This paper describes the proposed taxonomy and outlines the characteristic features of different building typologies and their relevance for estimating seismic vulnerability and risk. A comparison of the proposed taxonomy for Serbia and published taxonomies for Croatia is also presented.

Full paper is available in the Proceedings (https://doi.org/10.5592/CO/2CroCEE.2023.100).

Biography

Prof. Dr Svetlana Brzev is Adjunct Professor in the Department of Civil Engineering at the University of British Columbia, Canada and is a member of the Smart Structures group https://smartstructures.civil.ubc.ca/research/. She has more than 35 years of consulting and academic experience from Canada, Serbia, and India related to structural and seismic design and rehabilitation of reinforced concrete and masonry structures. Her research focus has been on seismic behaviour, design and construction issues related to reinforced and confined masonry structures. As a practicing engineer in Canada, she has worked on applications of advanced technologies such as seismic isolation and dampers for seismic retrofitting of existing structures in Canada, India, and Chile. She received bachelor's and master's degrees in civil/structural engineering from the University of Belgrade and Ph.D. degree in earthquake engineering from the Department of Earthquake Engineering, University of Roorkee (currently IIT Roorkee), India. She serves on the Technical Committee responsible for developing design standard for masonry buildings in Canada (CSA S304) and is a member of the Eurocode 8 Technical Committee 250/SC8/WG1 for the development of design provisions for seismic design and retrofitting of masonry buildings. She was a part of the team that developed the Global Earthquake Model (GEM). She served as a Director and Vice-President of the EERI, a Director of the Masonry Society (TMS), and is currently a Director of the International Association of Earthquake Engineering (IAEE). She has served as the founding President of the Serbian Association for Earthquake Engineering (SUZI-SAEE) since 2018. Dr Brzev has published more than 200 papers and reports, and has co-authored three textbooks related to structural and seismic design of masonry and reinforced concrete structures in Canada. In 2015, she was named a Fellow of the Engineers Canada for her contribution to the engineering profession in Canada.

Invited Lecture

ADVANCEMENTS IN IMPLEMENTING SHORT-TERM COUNTERMEASURES AFTER THE RECENT EARTHQUAKES IN ITALY

Stefano Grimaz

University of Udine, Italy, stefano.grimaz@uniud.it

Abstract

Will be presented an overview on the experiences that allowed the Italian National fire Services to obtain relevant improvements in the short term countermeasures (shoring activities with the STOP procedures) and technical triage (for zoning the affected area and prioritizing the first technical interventions for safety purposes), obtained by the synergy between science and practice, both in the response and preparedness phases. These techniques and procedures have been adopted in post-earthquake international missions and are at the base of new specific modules of the European mechanism of civil protection.

Biography

Prof. Stefano Grimaz is the Chairholder of the UNESCO Chair on Intersectoral Safety for Disaster Risk Reduction and Resilience at the University of Udine (Italy). He is director of the Safety and Protection Intersectoral Laboratory (SPRINT-Lab) at the Polytechnic Department of Engineering and Architecture of University of Udine where he is professor of Engineering Seismology and of Safety and Civil Protection at the Master Degree Courses of Engineering. He is scientific director of the SERM Academy: the Safety and Emergency Response Management International training school based in Friuli Venezia Giulia (Italy) aimed at developing and experimenting techniques of safety assessment and emergency response and at improving the interoperability in transborder areas. He carries out research on risk assessment, safety and emergency management with a holistic and intersectoral approach for developing multi-hazard safety assessment and decision-making support tools for the different phases of the disaster management cycle. He is scientific consultant of national and international institutions and organizations working in the fields of safety, emergency management and resilience. For the Italian National Fire Services he conceived and developed the technical triage method and the standardized short-term countermeasures for the rapid safety assessment of buildings damaged by earthquakes and for prioritizing and implementing the urgent technical interventions in emergency. For his activities, he was awarded with the Order of Merit of the Italian Republic (4th Class Officer). He is author of more than 150 papers in the field of safety and risk management.

Invited Lecture

EXPERIMENTAL TEST OF UNREINFORCED MASONRY WALLS UNDER VARIOUS BOUNDARY CONDITIONS

Ivica Guljaš

University of J.J. Strossmayer in Osijek, Croatia, iguljas@gfos.hr

Abstract

Unreinforced masonry (URM) constructions exhibited poor seismic performance during the past earthquakes thus resulting in unacceptably huge loss of lives and properties. Therefore, the evaluation of their shear (and other) behaviour is absolutely essential. In that sense a series of static and dynamic earthquake simulation tests of unreinforced masonry walls under various boundary conditions were carried out at the Faculty of Civil Engineering and Architecture Osijek.

After a plane unreinforced masonry walls were tested and their shear behaviour evaluated, confined masonry, a construction system where the walls are built first, and the columns and beams are poured in afterwards to enclose (confine) the wall followed. Those experiments focused specifically on different tie column - masonry wall connection details in which the most effective connection scheme was evaluated and quantified.

The next step was to evaluate the contribution of masonry infill to the RC frames seismic behaviour. Here infill wall panels acted as compressive diagonal struts due to lack of good bonding with more complicated transmission of forces. One story RC infilled frames were built and subsequently infilled with high strength hollow clay brick blocks, without additional shear connection to the frame. The specimens were tested under constant vertical and cyclic lateral loads applied in a direction along the plane.

And finally, dynamic earthquake simulation shake table tests on masonry infilled RC frame test building were carried out. The following constraints in development of proper experimental structure were adopted: to have multiple stories in order to approach the fluctuations of axial force that a structural system which involves the interactions of a reinforced concrete frame with masonry infill walls would experience, to use near full-scale materials and dimensions, to include an intermediate column in the test structure, and to limit the building dimensions according the limits of available earthquake simulation systems.

Biography

Ivica Guljas is a full professor at the Department of Technical Mechanics, Faculty of Civil Engineering and Architecture Osijek, University Josip Juraj Strossmayer in Osijek, Croatia. He is a structural engineer, whose research is concerned with inelastic and performance based procedures in earthquake resistant design, as well as with structural codes and computerized design methods for RC and masonry structures. His technical skills and competencies involve testing of materials and structures, structural analysis and software applications in the field of structural static, dynamic and earthquake engineering. His teaching activities involve Structural Dynamics, Structural Stability and Testing of Structures at the Faculty of Civil Engineering and Architecture Osijek where he was a vice-dean for science and then for professional affairs and development for several years. He also teaches the course Seismic Design at the University of Pecs, Hungary. As an active participant of several research projects, he has written more than 50 scientific, professional and educational papers published in journals and proceedings of expert conventions dealing mainly with theoretical and practical aspects of static and dynamic analysis of structures. He was the principal investigator of the European project titled „Development of investigation and analysis techniques for the assessment and lifetime expectancy of historical structures", as well as of the project „Frame-masonry composites for modelling and standardization (FRAMA)" endorsed by the Croatian Science Foundation. Also, he participated as a team member in several joint research projects between Republic of Croatia and Republic of Slovenia and Republic of Northern Macedonia, all in the field of earthquake engineering. He is the president of the Croatian Association for Earthquake Engineering, a member of the Croatian Society of Mechanics, Croatian Association of Civil Engineers, European Committee for Standardization CEN/TC 250/SC 8/TG 3, Infilled frames and claddings and Technical Committees TC108 and TO548 at CSI.

Invited Lecture

PERFORMANCE-BASED OPTIMISATION OF ENERGY DISSIPATION DEVICES FOR SEISMIC APPLICATIONS

Iman Hajirasouliha

Department of Civil and Structural Engineering, The University of Sheffield, UK, i.hajirasouliha@sheffield.ac.uk

Abstract

Energy dissipation devices are increasingly used in modern construction for design of new buildings or improving the seismic performance of existing structures in earthquake prone regions. However, optimum design of such systems can be very challenging due to their non-linear complex behaviour under earthquake excitations. This study presents a novel low-cost approach for performance-based seismic design optimisation of multi-storey buildings equipped with energy dissipation systems. The method is based on the concept of Uniform Distribution of Damage (UDD), which aims to utilise the full capacity of structural elements by redistribution the unused material throughout the structure. To investigate the efficiency of the proposed method, two case study examples are considered. In the first example, a 10-storey RC frame with friction dampers and chevron bracing is selected. The aim is to reduce structural material and improve seismic performance, while satisfying multiple performance targets. A multi-stage UDD optimisation process is proposed, for the first time, to deal with discrete optimisation of brace elements and continues optimisation of friction forces simultaneously. First, a discrete optimisation method is adopted for optimal design of the brace elements to satisfy Immediate Occupancy (IO) performance level under a Design Basis Earthquake (DBE) event. Subsequently, the mechanical properties of the friction devices are optimised to satisfy Life Safety (LS) performance level under a Maximum Considered Earthquake (MCE) record. The results indicate that, unlike most conventional Heuristic optimisation methods such as Genetic Algorithm (GA), the proposed approach can lead to an optimum design solution in only a few steps. It is shown that compared to the code-based design solution with fixed bracings, the optimum frame requires around 70% less amount of bracing elements while also exhibits a considerably lower base shear forces. This is achieved by efficiently activating the friction mechanism to satisfy the prescribed performance levels under the representative design earthquakes. In the second example, the application of the proposed performance-based optimisation method is demonstrated by optimising a 7-storey moment resisting steel frame equipped with non-linear viscous dampers using drift-based, velocity-based, and energy-based UDD approaches. It is shown that regardless of the selected performance parameter, the optimum damping distribution identified by the proposed methodology leads to a design solution that exhibits considerably lower maximum plastic rotation, maximum inter-storey drift and global damage index compared to an equal-cost uniform damping distribution system generally used in common practise. The presented results, in general, indicate that the proposed low-cost optimisation method can provide an efficient tool for performance-based design of structures with energy dissipation devices in seismic regions.

Biography

Prof. Iman Hajirasouliha is Full Professor of Structural Engineering and Leader of Earthquake Engineering Group (EEG) at the University of Sheffield, UK. He has over 20 years of research and consultancy experience in the fields of earthquake engineering, performance-based optimisation, lightweight steel structures, vulnerability assessment, and novel strengthening techniques, leading to over 160 refereed journal papers and 100 conference publications in these areas. He has been Principal or Co-investigator of over €10M EU and UK funded projects. Professor Hajirasouliha is a member of several national and international technical committees and research networks, including the International Federation for Structural Concrete (fib) Task Groups 6.6 and 7.6, and the International Association for Bridge and Structural Engineering (IABSE) Task Group 1.1. He is currently Associate Editor of Practice Periodical on Structural Design and Construction (ASCE) and Frontiers in Built Environment (Earthquake Engineering Section) and also serves on the editorial board of several international journals in the field of structural engineering. Professor Hajirasouliha has been recognised as one of the world's top 2% scientists in his discipline since 2020 according to the database published by Stanford University and Elsevier.

Invited Lecture

RISK-BASED SEISMIC ASSESSMENT OF EXISTING BUILDINGS. APPROACH APPLIED IN SWITZERLAND

Pierino Lestuzzi

École Polytechnique Fédérale de Lausanne, Switzerland, pierino.lestuzzi@epfl.ch

Abstract

Due to the enormous costs related to the application of the recent standards in case of existing structures, an approach different from the one for new constructions should be used. Since 2004 an approach based on risk is applied in Switzerland. The minimal security level is defined in relation to the acceptable individual risk. Afterwards, an evaluation based on the principle of commensurability should be performed to decide on the efficiency of the measures. This evaluation is achieved based on the human life saving costs. This innovative procedure for the seismic evaluation is first explained and then illustrated with some real cases recently performed in Switzerland.

Biography

Dr Pierino Lestuzzi did his master in Civil Engineering from the Ecole Polytechnique Fédérale de Lausanne (EPFL) and its PhD from ETH-Zurich, Switzerland. He was lecturer and senior researcher at EPFL. He was also president of the norm commission SIA 261 (Swiss standard for actions) and committee member of the Swiss Society of Earthquake Engineering and Structural Dynamics (SGEB). His primary research interests include Earthquake Engineering, Seismic Risk Assessment and Structural Dynamics. Pierino Lestuzzi has published more than hundred journal and conference papers and 6 textbooks related to statics, structural dynamics and earthquake engineering. He is now active in the engineering practice by the specialized engineering company Exigo Expertises SA in Switzerland.

Invited Lecture and Workshop

EXTENDED REALITY TECHNOLOGIES AND METAVERSE TO ENHANCE EMERGENCY PREPAREDNESS

Massimo Migliorini

Fondazione LINKS, Italy, massimo.migliorini@linksfoundation.com

Summary of the workshop

During a catastrophic event, the ability of the assigned personnel to react to this event is due not only to pre-existing knowledge or skills, but also to the degree of familiarity with the scenario that is being faced. Especially in the event of high-impact but potentially unlikely events, an adequate response relies on personnel being able to perform their assigned tasks accurately and coordinate efficiently with other operators. The psychological effects of stress from having to deal with an unfamiliar situation for staff can have a significant impact on performance, thus leading to a degradation of intervention effectiveness and consequent loss of life.

Efficient training is a key point in emergency management preparedness. The quality, consistency and frequency of training are fundamental elements in the operator preparation. Conversely, if the importance of training is clearly recognised, there are factors which hinder its diffusion: the necessary time, costs and safety limits. These factors severely limit the possibility of adequately training "public safety" operators, and this is particularly evident in cases of large-scale mobilization where the preparation of the operators can heavily condition the quality of the intervention.

Furthermore, to be realistic and adequately represent the dynamics of an emergency situation, disaster and natural disaster training scenarios should incorporate a number of "critical" elements, such as:

• the presence of numerous victims and trapped civilians, often in panic situations;
• the presence of damage to structures, in progressive evolution, or to assets (eg works of art);
• the presence of fumes and toxic substances;
• the presence of visual and hearing disabilities for the operators;
• the possibility of being able to train even in contexts that are not normally accessible (e.g. areas of historical-cultural or environmental value) and present time-contingent difficulties (e.g. in winter firefighters may encounter difficulty in practicing with the fire hydrants as the water is subject to freezing);
• the certainty of not interfering with the normal functioning of the structures (eg closure of traffic for exercises in the tunnel);
• the certainty of adequate weather for the risk situations represented (eg wind, cloud cover, etc.).

Incorporating these elements into a realistic training scenario can be costly, dangerous, and in some cases even impossible.

A **virtual reality scenario** can instead approximate these elements, retaining all the advantages of a controlled simulation environment. In this way it is possible to train personnel to respond to particularly stressful real conditions, thus improving the ability to make decisions in critical conditions. The recent improvement of virtual reality technologies has made it possible to represent in an ever more realistic way the situations for which staff are to be trained, thus becoming an alternative form of training to the conventional one. Virtual reality simulated environments can therefore offer all the characteristics of conventional training techniques while reducing the costs and development times of real exercises. Training based on virtual reality technologies for simulating catastrophic events can be sized according to the specific use and organization that decides to adopt virtual reality for training. For example, virtual scenarios can be developed to provide the user with instant feedback on the inputs received (as in the case of organizing triage for the management of natural disasters); furthermore, a virtual

reality system can allow you to verify the effectiveness of an emergency plan, thus identifying gaps and aspects to improve.

Virtual training systems enable and facilitate collaborative training of geographically distributed personnel; for example, virtual simulation can provide a consistent and synchronized training platform in the event of natural disasters such as earthquakes and hurricanes that require a geographically distributed response.

Traditional teaching methods such as slide presentations can be easily incorporated into virtual simulation systems, thus making them accessible in a new form. While on the one hand the advantages that a virtual simulation system can transmit to the user in terms of visual stimuli are evident, it is also important to underline the advantage in terms of found stimuli that can be inserted into virtual environments.

Compared to traditional training, training systems based on virtual reality therefore have a number of advantages. Environmentally, it is easy to present realistic life scenarios that incorporate other users; moreover, it is possible to manage user inputs to provide feedback in real time. By populating the simulated environments with avatars (representation of users in the virtual world) it is possible to provide those who are being trained with immediate feedback. Behavioral modules can be assigned to the various avatars to manage the decisions made by the personnel undergoing training.

Virtual reality systems also allow the level of difficulty to be calibrated according to the degree of preparation of those to be trained. During the training it is possible to interact both with objects that make up the virtual environment and with other participants in the training; the interaction between participants (real and virtual) can take place through textual and/or vocal communication, also allowing to simulate different cultural and socio-economic scenarios. The virtual simulation can be locked (paused) allowing instructors to discuss with the trainee how best to deal with unexpected events. If necessary, the exercise can be repeated, introducing a series of variations controlled by the instructor. Environmental features can be easily incorporated: buildings, vegetation, humans and sounds are just some of the elements that can be incorporated. Virtual scenarios such as the creation of safety zones within urban areas with a high population density can be easily created, in spite of large-scale real exercises which would require times and costs that are often too high. These last aspects are among the major benefits of virtual training systems: real exercises can require costs that are out of reach for most administrations. Virtual reality offers a viable alternative by incorporating adequate realism at a fraction of the cost that real exercises would have. Furthermore, the flexibility of the virtual scenario allows to simulate different conditions, thus allowing to evaluate the possible results in the face of different simulation conditions.

Finally, the digital nature of virtual simulations can allow data to be archived for study and later evaluation. This can be a further added value in the case of emergency management, as it allows for a better understanding of behavioral phenomena and therefore to prepare improved training procedures. It is important to remember that virtual reality must be seen as a complementary tool to traditional training methods and not as a pure substitute.

Biography

Prof. Massimo Migliorini is the Program Manager Responsible for the Extended Reality Laboratory at LINKS Foundation. He has worked at LINKS Foundation (former SiTI - Higher Institute on Territorial Systems for Innovation) since 2005, focusing his activities on exploring the potential of digital technologies to support risk assessment and mitigation of sensitive assets, including cultural heritage. He participated and coordinated a relevant number of EU projects. As an example, in 2018 he coordinated the European Project RESCULT (https://rescult-project.eu/), funded by DG ECHO and participated by UNDRR (United Nation office for Disaster Risk Reduction), devoted to enhance the capability of Civil Protection to prevent and mitigate impacts of disasters on sites of Cultural Heritage through the realization of an integrated European Interoperable Database (EID); in 2016 he coordinated the WATERCRIMES project (www.watercrimes-project.eu), funded by DG HOME, aimed at qualifying the risk of crimes against water resources; in 2015, he coordinated LINKS activities within PRODIGE Project (http://www.pro-prodige.eu/), funded by INTERREG Program, aimed at creating VR simulation to support First Responders Training to deal with emergency situations. From 2018 he is member of the European Scientific and Technology Advisory Group, set up by the European Commission (DG-JRC) and the United Nations (UNDRR - United Nation office for Disaster Risk Reduction) to promote the application of Sendai Framework for Disaster Risk Reduction principles. From 2015 he has been appointed in LINKS as responsible of the Extended Reality Lab, an infrastructure exploring and valorising emerging digital technologies potential (in particular Virtual Reality, Augmented Reality, Mixed Reality and Metaverse) in different cross-fields including disaster prevention, cultural heritage, communication, education, healthcare.

Invited Lecture

AUTOMATION OF NON-DESTRUCTIVE EVALUATION SYSTEMS FOR THE STRUCTURAL DIAGNOSIS OF THE BUILT HERITAGE

Javier Ortega

Instituto de Tecnologías Físicas y de la Información (ITEFI) "Leonardo Torres Quevedo" of the Consejo Superior de Investigaciones Científicas (CSIC), Madrid, Spain, javier.ortega@csic.es

Abstract

When working on conservation projects of historical masonry structures, a key challenge is to ensure its structural safety having little to no information about the existing building. Uncertainties concern materials, geometry, construction details, loads and existing damage. The success of any structural retrofitting measure, which needs to fulfill the criteria of minimum intervention and compatibility with cultural heritage values, essentially depends on our ability to properly characterize the structure. We can improve our analysis and simulation tools to assess the structural behavior of masonry buildings. However, without a proper understanding of the structure condition, we cannot be certain that our models simulate the reality.

The characterization of masonry structures is a complex task that is further limited due to the need of following a non-invasive approach to protect the valuable fabric. The talk will discuss advances in the field of on-site inspection of architectural heritage by presenting new automated non-destructive systems recently developed. The talk will be structured along two recent European research projects that have resulted in the fabrication of acoustic tomography systems that were later applied for the inspection of stone masonry structures. Despite the need of further research to optimize the information extracted from the tomographic images, which are still difficult to interpret by non-experts, the novel systems address a common limitation of conventional inspection techniques, namely the limited amount of data that can be collected when the inspection is performed manually. Both systems reveal a significant correlation between the acoustic wave propagation through an element and its inner morphology, material properties and damage. Acoustic-based on-site inspection methods are fully non-invasive and, automating and scaling the procedure to inspect full buildings, can greatly enhance current inspection and monitoring methods of heritage structures.

Biography

Prof. Javier Ortega is an architect with a PhD in Civil Engineering and a Marie Skłodowska-Curie Individual Fellow at the Instituto de Tecnologías Físicas y de la Información (ITEFI) "Leonardo Torres Quevedo" of the Consejo Superior de Investigaciones Científicas (CSIC), in Madrid, Spain. He was awarded the MSCA-IF to develop novel non-destructive inspection tools for the mechanical characterization of historical masonry, through the 3D internal reconstruction of masonry assemblies based on acoustic wave propagation techniques. His research has focused on the structural diagnosis of the built heritage, detailed and large-scale seismic vulnerability assessment, and, more recently, on the development of new technologies (equipment and methods) for the non-destructive evaluation and tomographic imaging the interior of historical construction elements. Such systems are expected to provide accurate information about the interior of existing heritage structural elements (e.g., inner morphology or damage). He has participated in nine research projects in the field of conservation of heritage structures, leading three of them, the Heritage Within European research project, the INHAVIT Portuguese research project and the EU-funded project DocumeNDT. He is co-founder and associate of FENEC, a consulting engineering association providing non-destructive testing and specialized structural analysis services for the built heritage. He has over nine years of professional and academic experience in the field of conservation of historical and vernacular structures, with work on many monuments throughout the world including several UNESCO World Heritage sites.

Invited Lecture

ON-SITE OBSERVATIONS OF PERFORMANCE OF BUILDINGS AFTER THE 2023 TURKEY-SYRIA EARTHQUAKE DURING MUSAR OPERATIONS

Ante Pilipović and Karlo Jandrić

University of Zagreb, Faculty of Civil Engineering Croatia, ante.pilipovic@grad.unizg.hr, karlo.jandric@grad.unizg.hr

Abstract

The Turkey-Syria earthquakes of 6th February 2023 have caused devastating damage to several cities in 10 provinces of Turkey and also in Syria, and the population of the area has been greatly affected. Search and rescue efforts started immediately with many countries sending help to Turkey as requested by the Turkish government. Croatian MUSAR module was deployed to Turkey the same day, consisting of 41 people and 7 rescue dogs. Among them 2 structural engineers from the Croatian Centre for Earthquake Engineering – Intervention Unit (HCPI – IS), were deployed to help with building damage assessments and safety recommendations regarding entering damaged buildings and ruins during MUSAR operations. During the mission, us engineers had the opportunity to observe damaged and collapsed buildings in the city of Antakya, Hatay province, and various collapse mechanisms that occurred. We received invaluable support from the senior engineers from HCPI -IS during deployment phase through scientific and technical data describing past experiences during and after earthquakes in Turkey. On-site, we found all of the therein described consequences of earthquakes specific to Turkey. The building stock mostly consists of reinforced concrete moment-resisting frame buildings with 10-15 storeys and infill walls on most storeys except the first where they were removed along with some of the columns due to unprofessional adaptations and reconstructions, thus creating soft storeys. Problems were also observed with concrete quality, rebar quality and detailing, missing shear and infill walls and soil collapse. All of these observations have been photo-documented on-site and are presented here. Solid scientific and technical information that we had been equipped with during deployment was of the utmost importance in building assessments on-site during high intensity MUSAR operations where decisions need to be made quickly based on limited knowledge. In this way, the importance of ongoing scientific research in earthquake engineering including case-studies and building stock descriptions cannot be overstated enough and has very practical applications even in MUSAR operations.

Biography

Ante Pilipović is a PhD candidate at the Faculty of Civil Engineering, University of Zagreb. His scientific work is focused on seismic hazard and risk assessment and includes seismic fragility and vulnerability modelling of typical buildings in urban areas of Croatia, ground motion record selection techniques, optimal intensity measure selection criteria and soil effects in seismic response. He collaborates with seismologists on site-specific seismic hazard calculations. He is a part of Croatian Civil Protection MUSAR (Medium urban search and rescue) module as a structural engineer. He participated in damage assessment of buildings in Albania after the 2019 Durres earthquake as part of Croatian Civil Protection support team. He participated in rapid damage assessments of buildings after the Zagreb and Petrinja earthquakes in 2020. He participated in international and national Civil Protection MUSAR exercises as part of Croatian MUSAR module. He is trained for participation in an European Union Civil Protection Team (EUCPT) as an expert in structural engineering. He participated in international search and rescue operations after the 2023 Turkey-Syria earthquake as part of the Croatian MUSAR module.

Karlo Jandrić is an employee at the Faculty of Civil Engineering, University of Zagreb. He works on a project for seismic hazard and risk assessment of the city of Zagreb which is a part of a project called "Multisensor aerial survey of the Republic of Croatia" co-financed by the European Union. He is a part of Croatian Civil Protection MUSAR (Medium urban search and rescue) module as a structural engineer. He is a search and rescue dog handler with a dog currently in training. He participated in damage assessment of buildings in Albania after the 2019 Durres earthquake as part of Croatian Civil Protection support team. He participated in rapid damage assessments of buildings after the Zagreb earthquake in 2020. He participated in international and national Civil Protection MUSAR exercises as part of Croatian MUSAR module. He participated in international search and rescue operations after the 2023 Turkey-Syria earthquake as part of the Croatian MUSAR module.

Invited Lecture

ASSESSING LIQUEFACTION IN GRAVELLY SOILS BASED ON FIELD CASE HISTORIES

Kyle Rollins [1] and Jashod Roy [2]

[1] *Brigham Young University, rollinsk@byu.edu*
[2] *Kiewit Engineering, Jashod.Roy@gmail.com*

Abstract

Gravelly soils have liquefied at multiple sites in at least 27 earthquakes over the past 130 years. These gravels typically contain more than 25% sand which lowers the permeability and makes them susceptible to liquefaction. Developing a reliable, cost-effective liquefaction triggering procedure for gravelly soils has been a challenge for geotechnical engineers. Typical SPT- or CPT-based correlations can be affected by large-size gravel particles and can lead to erroneous results. To deal with these problems, we have developed liquefaction triggering curves for gravelly soils based on (1) shear wave velocity (Vs) and (2) a large diameter cone penetrometer. With a cone diameter of 74 mm, the Chinese Dynamic Cone Penetration Test (DPT) is superior to smaller penetrometers and can be economically performed with conventional drilling equipment. Using logistic regression analysis, the DPT has been directly correlated to liquefaction resistance at sites where gravels did and did not liquefy in past earthquakes. Probabilistic liquefaction resistance curves were developed based on 137 data points from 10 different earthquakes in seven countries. Using a similar data set, probabilistic liquefaction triggering curves were also developed based on Vs measurements in gravelly soils. The Vs-based liquefaction triggering curves for gravels shift to the right relative to similar curves based on sands. New magnitude scaling factor (MSF) curves have also been developed specifically for gravel liquefaction which were found to be reasonably consistent with previous curves for sand.

Full paper is available in the Proceedings (https://doi.org/10.5592/CO/2CroCEE.2023.141*).*

Biography

Prof. Kyle Rollins received his BS degree from Brigham Young University and his Ph.D. in Civil Engineering from the University of California at Berkeley. After working as a geotechnical consultant, he joined the Civil Engineering faculty at BYU in 1987 following after his father who was previously a geotechnical professor. His research has involved geotechnical earthquake engineering, deep foundation behavior, bridge abutments, collapsible soils, and soil improvement techniques. He has published over 190 technical papers and supervised over 130 graduate students. He was recognized as the engineering educator of the year by the Utah State Engineers Council and received a Governor's Award for Science and Technology in 2017. ASCE has recognized his work with the Huber research award, the Wellington prize, and the Wallace Hayward Baker Award. In 2009, he was the Cross-Canada Geotechnical lecturer for the Canadian Geotechnical Society and in 2013 he received the Jorj Osterberg Award for innovation in foundation testing from the Deep Foundation Institute.

Invited Lecture

SEISMIC ASSESSMENT OF A TYPICAL STONE BUILDING IN THE OLD TOWN OF DUBROVNIK AND RETROFITTING MEASURES

Mario Uroš, Marija Demšić, Maja Baniček, Petra Gidak, Marta Šavor Novak, Jakov Oreb, Josip Atalić and Ivan Duvnjak

University of Zagreb, Faculty of Civil Engineering Croatia, uros@grad.hr

Abstract

This paper presents the procedure for the seismic performance assessment of a typical residential stone masonry building in the old city center of Dubrovnik. All steps are systematically presented and described. Experimental investigations of the building's materials were carried out in situ and in the laboratory, and the ambient vibrations of the building were measured.

The city of Dubrovnik is located in a seismically very active area where strong earthquakes have already occurred in the past. The reference peak ground acceleration is 0.3g for earthquakes with a return period of 475 years, so the protection of cultural heritage is of key importance for the city. The case-study building is about 400 years old and is part of a valuable cultural heritage that has been protected by UNESCO since 1979.

Several numerical models were created and the most interesting is volume model in Abaqus software with complex constitutive material model. A nonlinear dynamic analysis was carried out, using time-histories that were carefully selected for the site.

Various cases of retrofitting were analyzed, and conclusions were given about the effectiveness of each of them. Based on this, recommendations and a critical review of methods and techniques for retrofitting buildings that are part of a protected historic heritage were given.

Biography

Mario Uroš is an associate professor at the Faculty of Civil Engineering, University of Zagreb. He received his PhD in 2013 at the Faculty of Civil Engineering in Zagreb. In his professional and scientific work, he deals with the field of numerical modeling, dynamics and stability of structures and earthquake engineering. He participates in numerous scientific projects as a participant or leader. He is the author of numerous relevant scientific and professional papers. In the area of seismic risk assessment and seismic design of buildings he participates in the preparation of various documents important for seismic risk assessment at the City of Zagreb and the Republic of Croatia. He participated in various European projects and exercises of the Civil Protection for damage assessment, and in 2019 he participated in the damaged assessment of the buildings in Albania as part of the team for technical-tactical support of the Civil Protection of the Republic of Croatia and the EU. He participated in the creation of the Updated Disaster Risk Assessment for the Republic of Croatia - Seismic Risk Assessment. He was one of the coordinators of the rapid damage assessments of buildings by civil engineers after the earthquakes in Zagreb in March 2020 and Petrinja in December 2020, and participated in the creation of a series of strategic documents such as "Rapid Damage and Needs Assessment" for Zagreb and Petrinja for The World Bank. He is a member of the subcommittee for design of seismic resistance of structures at the Croatian Standards Institute. He received several awards, including the Medal of the City of Zagreb and the "Kolos" award of the Croatian Chamber of Civil Engineers in 2020 for his contribution to post-earthquake activities.

EVALUATION OF THE LOCAL SITE EFFECTS OF THE UNESCO WORLD HERITAGE SITE OLD CITY OF DUBROVNIK (CROATIA)

Davor Stanko [1,3], Tvrtko Korbar [2], Jakov Stanislav Uglešić [3], Iva Lončar [2], Mario Gazdek [1], Snježana Markušić [3]*

[1] *Faculty of Geotechnical Engineering, University of Zagreb, Hallerova aleja 7, HR-42000 Varaždin, Croatia; davor.stanko@gfv.unizg.hr*

[2] *Croatian Geological Survey, Department of Geology, Sachsova 2, HR-10000 Zagreb, Croatia; tkorbar@hgi-cgs.hr(*

[3] *Department of Geophysics, Faculty of Science, University of Zagreb, Horvatovac 95, 10000 Zagreb, Croatia, markusic@gfz.hr, *SeisRICHerCRO project leader*

Keywords: Dubrovnik, Local site effects, Seismic microzonation, Seismic risk

1. Introduction and aim of the study

The most seismically active region in Adriatic part of Croatia is the SE coastal region that have numerous cultural heritage sites. Therefore, it is important to estimate seismic risk for cultural heritage sites and to develop procedures for seismic risk assessment. These are the goals of the research project Seismic Risk Assessment of Cultural Heritage Buildings in Croatia (SeisRICHerCRO, https://seisrichercro.wordpress.com/) funded by the Croatian Science Foundation.

Local site effects, a known problem in earthquake engineering, play significant role in earthquake damage distribution. The old town of Dubrovnik is particularly vulnerable in terms of local site effects because the old city is built on three geomorphological and geological entities: southern bedrock ridge, central filled and flattened part (former sea embayment), and northern bedrock ridge. Apart from the last devastating historical earthquake in Dubrovnik area in 1667 of M~7), instrumentally recorded strong earthquake on 15 April 1979 M6.8 with mainshock at the epicentral distance of 105 km from Dubrovnik caused strong damage effects in the wider Dubrovnik area (intensity of VII °MSK) with incalculable damage to cultural and historical objects the old town Dubrovnik (Fig.1).
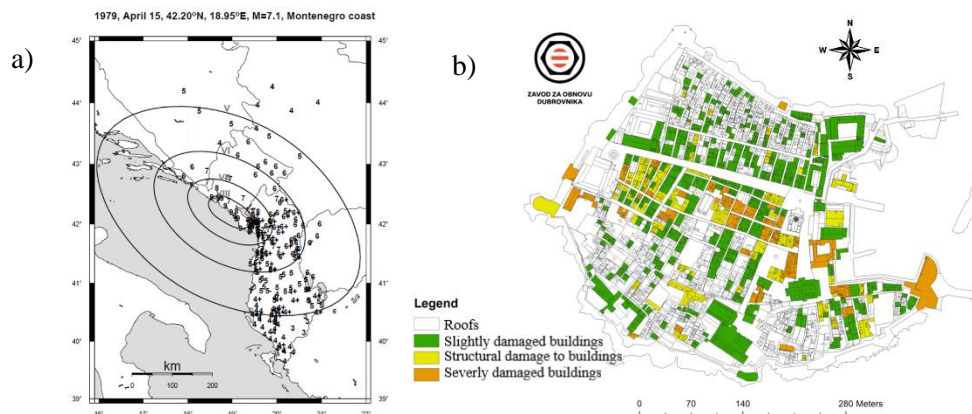
Figure 1. a) 15 April 1979 M6.8 earthquake damage [1] b) damage to the Old City of Dubrovnik [2]

The main aim of this study is mapping of local site effects variations in the old city of Dubrovnik using old investigation data as a starting point from 1980's, after 1979 Reconstruction of Dubrovnik. Data quality and spatial uncertainty brough by older equipment used in 1980's compared to using novel and sophisticated geophysical research methods followed by new geological investigations will significantly improve planning and reconstruction of Dubrovnik following new microzonation maps.

2. Main results and conclusions

Non-invasive microtremor Horizontal-to-Vertical-Spectral Ratio (HVSR) [3] and geophysical Multichannel Analysis of Surface Waves (MASW) [4] have been adopted as common seismic site characterization methods (especially in heritage sites instead of expensive and invasive drilling) for the purpose of this study (Fig.2) with examples of analysed HVSR and MASW results.
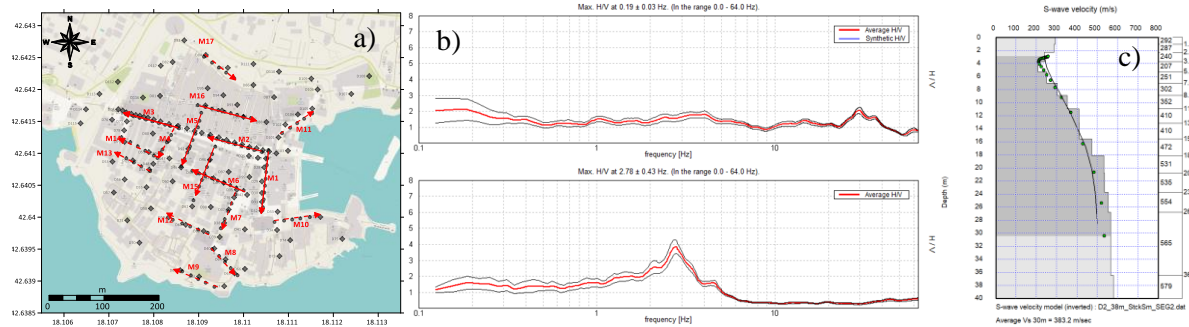
Figure 2. a) Map of microtremor measurements (grey markers) and MASW profiles (red lines), b) example of HVSR frequency curves (D27, D83), c) example of 1D MASW Vs profile (profile M2)

Based on individual results and using interpolation methods, mapping of the local site effects in the Old City of Dubrovnik in terms of site resonance frequencies, H/V amplitudes, Vs30 and carbonate bedrock depths can be derived following revision of the Eurocode 8 [5]. Definition of the seismicity and variations of the local site conditions are one of the inevitable phases of the complex process of repair and strengthening of existing structures in the old town Dubrovnik together with design seismic parameters and the seismic risk level of building inventory as a basis to define the necessary preventive measures against expected strong earthquakes in the future.

Acknowledgements

References

[1] Papazachos, B.C., Savvaidis, A.S., Papazachos, C.B., Papaioannou, C.A., Kiratzi, A.A., Muço, B., Kociuand, S., Sulstarova, E. (2001): Atlas of isoseismic maps for shallow earthquakes in Albania and surrounding area (1851–1990). University of Thessaloniki, Geophysical Laboratory, Publication No. 10, pp. 4–48

[2] URL: https://zod.hr/ (accessed 13.1.2023.)

[3] Nakamura, Y., (1989): A method for dynamic characteristics estimation of subsurface using microtremor on the ground surface. Quarterly Report of the Railway Technical Research Institute 30(1), 25-30.

[4] Park, C.B., Miller, R.D., Xia, J. (1999): Multichannel analysis of surface waves. Geophysics 64 (3):800–808. https://doi.org/10.1190/1.1444590

[5] Labbé, P., Paolucci, R. (2022): Developments Relating to Seismic Action in the Eurocode 8 of Next Generation. In: Vacareanu, R., Ionescu, C. (eds) Progresses in European Earthquake Engineering and Seismology. ECEES 2022. Springer Proceedings in Earth and Environmental Sciences. Springer, Cham. https://doi.org/10.1007/978-3-031-15104-0_2

FRIBAS: A PARAMETRIC DATABASE OF BUILDING AND SOIL FEATURES INCLUDING THE FUNDAMENTAL FREQUENCY OF RESONANCE

Chiara Scaini [1], Bojana Petrovic [2], Maria Rosaria Gallipoli [3], Giuseppe Calamita [4], Nicola Tragni [5], Carla Barnaba [6], Marco Vona [7], Stefano Parolai [8]

[1] *Researcher, Seismological Research Center, National Institute of Oceanography and Applied Geophysics - OGS, cscaini@ogs.it*
[2] *Research fellow, Seismological Research Center, National Institute of Oceanography and Applied Geophysics - OGS, Italy, bpetrovic@ogs.it*
[3] *Researcher, National Research Council - CNR, Institute of Methodologies for Environmental Analysis (IMAA), Tito Scalo (PZ), Italy, email: mariarosaria.gallipoli@imaa.cnr.it*
[4] *Researcher, National Research Council - CNR, Institute of Methodologies for Environmental Analysis (IMAA), Tito Scalo (PZ), Italy, email: giuseppe.calamitra@imaa.cnr.it*
[5] *Research fellow, National Research Council - CNR, Institute of Methodologies for Environmental Analysis (IMAA), Tito Scalo (PZ), Italy, email: nicola.tragni@imaa.cnr.it*
[6] *Researcher, Seismological Research Center, National Institute of Oceanography and Applied Geophysics - OGS, cbarnaba@ogs.it*
[7] *Professor, School of Engineering, University of Basilicata, Potenza, Italy, email: marco.vona@unibas.it*
[8] *Professor, Università degli Studi di Trieste, Italy and Seismological Research Center, National Institute of Oceanography and Applied Geophysics - OGS, Italy, stefano.parolai@units.it, sparolai@ogs.it*

The fundamental period of vibration of buildings is an important parameter for assessing their behavior during earthquakes. It can be estimated using analytical [1] and empirical [2,3] approaches. In engineering practice, it is often estimated using simplified period-height relationships (e.g. [4]). The empirical determination of the fundamental period of buildings is extremely important to validate existing simplified period-height relationships and to develop new ones. Several parameters, apart from building height, might also influence the fundamental period of built structures. Currently, however, there are no empirical period-height relationships that account for building characteristics other than height (e.g. foundation soil type). In addition, there are very few empirical studies that provide both the fundamental period of buildings together with their main characteristics.

The FRIBAS database contributes to filling this gap by providing information on the fundamental period of vibration and characteristics of more than 300 reinforced concrete and masonry buildings. The studied buildings are located in northeastern Italy and in three towns of southern Italy (Matera, Potenza and Villa D'Agri, Fig. 1). To the best of our knowledge, FRIBAS is the first database that collects various building characteristics, including structural and geometric features, such as the age of construction, the construction material, storey number and other data regarding the such as geometric features (e.g. shape) and construction details (e.g. roof type, floor types). These characteristics were inferred from external and sometimes internal building inspections, and combined with information provided by residents. In addition, FRIBAS includes the fundamental period of buildings and foundation soil, which were empirically estimated using single station ambient noise measurements. The database was assembled based on data collected separately in northeastern and southern Italy (Fig.1) for different building types (including both low to mid-rise historical and modern masonry and low to high-rise reinforced concrete buildings). The buildings were chosen also based on the possibility of accessing the interior and performing measurements. The data were harmonized into 37 fields that allow for a general classification of building and soil parameters.
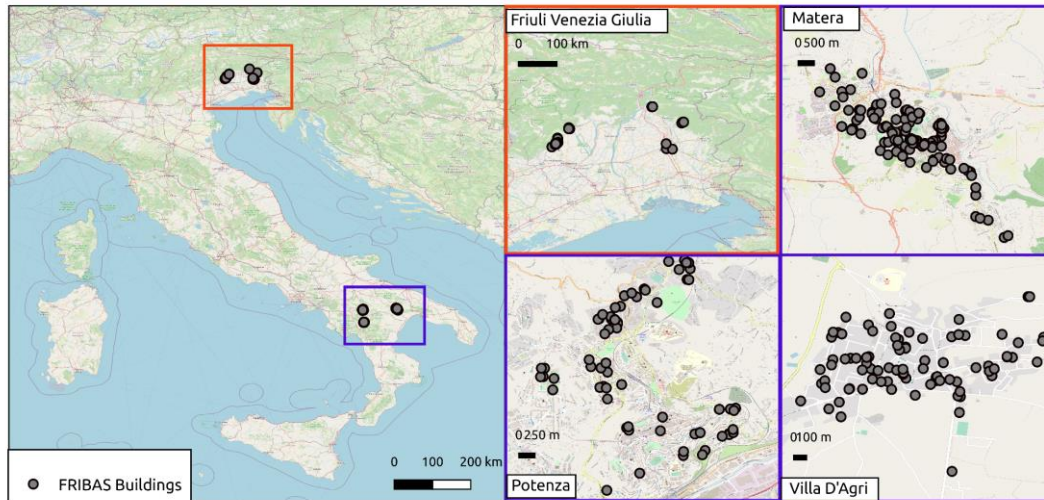
Figure 1: Map of the location of buildings where ambient vibration measurements were carried out.

FRIBAS was assembled with the specific goal of analyzing how different building parameters affect structural behavior (in particular, the fundamental vibration period). The database is available online in open access mode under the CC 4.0 license available at this link: https://doi.org/10.5281/zenodo.6505442. The first explorative analysis was focused on the period-height experimental relationship obtained from the entire dataset. Fig. 2 shows the period-height relationship obtained for this study in comparison with those developed by other authors and those prescribed by Eurocode 8. The plot shows that substantial differences between the empirical relationships and the Eurocode formula exist.
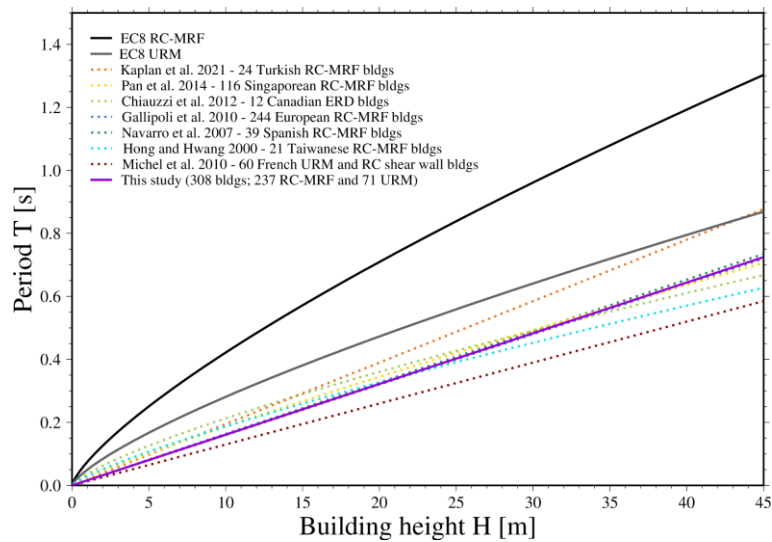
Figure 2: Period-height relationship derived from the FRIBAS database (violet solid line) in comparison with other relationships from literature and with the EC8 relationships proposed for RC and URM buildings.

FRIBAS also supports the definition of different period-height relationships based on construction material and soil types. Period-height relationships were developed for RC and URM buildings on rigid and soft soil, respectively [5]. Rigid and soft soils were defined using a simplified classification based on the geological map available for each town: outcropping bedrock and clean coarse gravels of northeastern Italy were classified as rigid soils, while all the other sediments were considered as soft soils. The results show that for the analyzed URM buildings the fundamental period differs by about 20% between buildings located on rigid respect to those on soft soil. The difference is smaller (11%), but still not negligible for RC buildings.

Results of the analysis highlight that soil type should be accounted for when developing simplified period-height relationships. In addition, they point out the need for characterizing the dynamic behavior of different building typologies, in particular to account for the variability of masonry building types. Empirical period-height relationships developed for specific building typologies and soil types can potentially improve damage assessment strategies and provide more realistic results. The fundamental period is, in fact, a crucial parameter for evaluating the expected impacts of seismic events For example, [6] apply a simplified approach to estimate the expected damage on selected building typologies. The method uses the fundamental period obtained from experimental period-height relationships for buildings of different construction materials and located on different soil types ([5],[7]). In addition, soil-building resonance phenomena can be identified based on experimental measurements of fundamental frequency on buildings and foundation soils (Gallipoli et al., 2020). Damage assessment methods can therefore benefit from datasets such as FRIBAS, which provides useful data for the development of new period-height relationships.

Acknowledgements

References

[1] Kwon, O.S., Kim, E.S. (2010). Evaluation of building period formulas for seismic design, *Earthquake Engineering and Structural Dynamics, 39(14):1569-1583*.

[2] Gallipoli, M.R., Mucciarelli, M., Šket-Motnikar, B., Zupančić, P., Gosar, A., Prevolnik, S., Herak, M., Stipecević, J., Herak, D., Milutinović, Z., Olumćeva, T. (2010). Empirical estimates of dynamic parameters on a large set of European buildings, *Bulletin of Earthquake Engineering 8:593–607*.

[3] Michel, C., Gueguen, P., Bard, P.Y. (2008). Dynamic parameters of structures extracted from ambient vibration measurements: an aid for the seismic vulnerability assessment of existing buildings in moderate seismic hazard regions, *Soil Dyn Earthq Eng 28:593–604*.

[4] Crowley, H., Pinho, R. (2006). Simplified equations for estimating the period of vibration of existing buildings, *First European Conference on Earthquake Engineering and Seismology (a joint event of the 13th ECEE & 30th General Assembly of the ESC), Geneva, Switzerland, 3-8 September 2006, Paper Number: 1122*.

[5] Gallipoli, M.R., Petrovic, B., Calamita, G., Tragni, N., Scaini, C., Barnaba, C., Vona, M., Parolai, S. (2022). FRIBAS database for better characterization of RC and URM buildings: Towards specific T-H relationships, *Bulletin of Earthquake Engineering, under review*.

[6] Petrovic, B., Scaini, C., Parolai, S. (2022). Applying the damage assessment for rapid response approach to the august 24 M6 event of the seismic sequence in central Italy (2016), *Front. Earth Sci., Sec. Geohazards and Georisks, Research Topic New Challenges for Seismic Risk Mitigation in Urban Areas, https://doi.org/10.3389/feart.2022.932110*

[7] Gallipoli, M.R., Calamita, G., Tragni, N., Pisapia, D., Lupo, M., Mucciarelli, M., Stabile, T.A., Perrone, A., Amato, L., Izzi, F., La Scaleia, G., Maio, D., Salvia, V. (2020). Evaluation of soil-building resonance effect in the urban area of the city of Matera (Italy), *Engineering Geology 272, 2020, https://doi.org/10.1016/j.enggeo.2020.105645*.

DAMAGE ASSESSMENT FOR RAPID RESPONSE: THE CENTRAL ITALY 2016 M6 EVENT

Bojana Petrovic [(1)], Chiara Scaini [(2)], Stefano Parolai [(3)]

[(1)] *Research fellow, Seismological Research Center, National Institute of Oceanography and Applied Geophysics - OGS, Italy, bpetrovic@ogs.it*

[(2)] *Researcher, Seismological Research Center, National Institute of Oceanography and Applied Geophysics - OGS, cscaini@ogs.it*

[(2)] *Professor, Università degli Studi di Trieste, Italy and Seismological Research Center, National Institute of Oceanography and Applied Geophysics - OGS, Italy, stefano.parolai@units.it, sparolai@ogs.it*

Keywords: seismic damage assessment, seismic building monitoring, rapid disaster response, damage thresholds, single-degree-of-freedom oscillator, simplified building models, Central Italy 2016 earthquake sequence, emergency management

In case of a seismic event, building damage is one of the main causes of fatalities [1]. For this reason, rapid estimation of expected structural damage in near-real time is of paramount importance to enhance and support rapid life-saving actions of emergency managers. In this framework, we have developed the Damage Assessment for Rapid Response (DARR) method [2,3], which allows us to estimate the expected damage in real time or near-real time using earthquake recordings and knowledge of the fundamental frequency and damping of the building. We simulate the linear dynamic behavior of buildings in a first-order approximation as single or multi-degree-of-freedom (SDOF and MDOF, respectively) oscillators depending on the complexity of the building under study. The relative displacement at the top of the building is estimated using the Z-transform [4] and compared with thresholds associated with damage states. Relative displacement thresholds are defined in the literature for different building typologies (e.g. low-rise historical masonry buildings) and allow evaluating the expected damage. DARR does not aim at the exact reconstruction of the dynamic behavior, but in evaluating if the relative displacement exceeds predefined damage thresholds. For this reason, we assume that linear SDOF/MDOF oscillators can successfully reproduce the peak relative displacement at the top of the building, and that the non-linear behavior does not need to be taken into account. The DARR method can be applied to individual buildings [3] or building typologies in target areas [2,5], using earthquake recordings from sensors installed in the basement of a building or on the ground nearby.

In this study, we apply DARR to four selected target areas (Amatrice, Norcia, Sulmona and Visso, Fig. 1) hit by the M6 event of August 24 of the 2016-2017 Central Italy seismic sequence [5]. The considered towns are located at different epicentral distances and are characterized by different predominant building typologies (e.g.low to mid-rise unreinforced masonry, low to high-rise reinforced concrete buildings) for which varying damage patterns were observed. The earthquake recordings of the M6 event are available from the Italian Accelerometric Archive (ITACA, [6]) and the Italian monitoring network OSS (Osservatorio Sismico delle Strutture, [7]) at different locations, including the four considered towns.

The DARR method assumes that the dynamic behavior of each building typology can be simulated by an SDOF oscillator. The fundamental frequencies are estimated using specific building-soil period-height relationships developed by [8]. The relationships are obtained from a database that collected the main characteristics of more than 300 buildings in northern and southern Italy, including empirically estimated fundamental frequencies. For all four considered tows, the foundation soil was classified as soft soil based on the literature (Amatrice: e.g. [9], Norcia: e.g. [10], Visso: e.g. [11] and Sulmona: e.g. [12]).
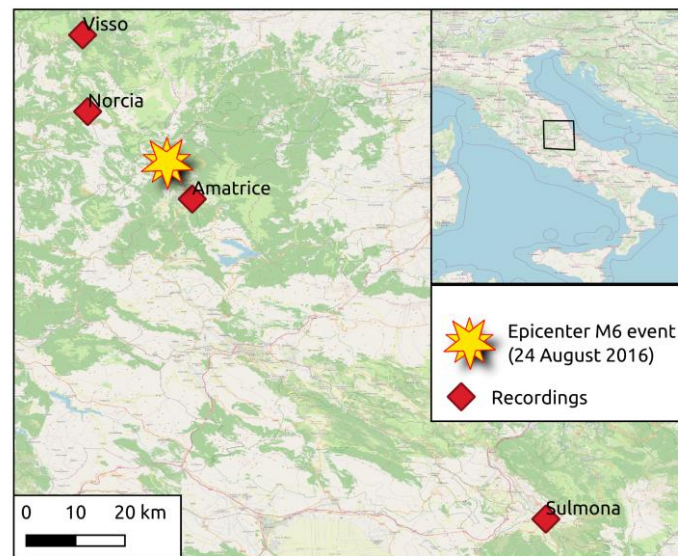
Figure 1. Locations of the considered towns, Amatrice, Norcia, Visso and Sumona, and the epicenter of the M6 event.

Expected damage is compared to and consistent with observed damage obtained from post-event surveys for most of the predominant building typologies (URM and RC frame buildings) in the four target areas considered. For example, expected damage was successfully estimated for mid-rise URM buildings in Amatrice, Norcia and Visso. However, for low-rise buildings in Amatrice, the DARR method did not estimate the observed damage. A possible explanation for this discrepancy is currently being discussed. Nevertheless, our results demonstrate the potential of DARR for rapid and cost-effective estimation of expected damage. An application of DARR in the aftermath of a destructive earthquake might therefore support rapid response and recovery strategies.

Acknowledgements

References

For journals:

[1] So, E., and Spence, R. (2013): Estimating shaking-induced casualties and building damage for global earthquake events: A proposed modelling approach. *Bull. Earthq. Eng.* **11**, 347–363. doi: 10.1007/s10518-012-9373-8

[2] Scaini, C., Petrovic, B., Tamaro, A., Moratto, L., and Parolai, S. (2021): Near-real-time damage estimation for buildings based on strong-motion recordings: An application to target areas in northeastern Italy. *Seismol. Res. Lett.* **92** (6), 3785–3800. doi: https://doi.org/10.1785/0220200430

[3] Petrovic, B., Scaini, C., and Parolai, S. (2022): Damage assessment for rapid response (DARR): Validation for different ground motion levels and building types. (submitted to SRL, under review).

[4] Lee, V. W. (1990): Efficient algorithm for computing displacement, velocity and acceleration responses of an oscillator to arbitrary ground motion. *Soil Dyn. Earthq. Eng.* **l9** (6), 288–300. doi: https://doi.org/10.1016/s0267-7261(05)80015-6

[5] Petrovic B, Scaini C and Parolai S (2022): Applying the damage assessment for rapid response approach to the august 24 M6 event of the seismic sequence in central Italy (2016). *Front. Earth Sci.* **10**:932110. doi: https://doi.org/10.3389/feart.2022.932110

[6] Russo, E., Felicetta, C., D'Amico, M. C., Sgobba, S., Lanzano, G., Mascandola, C., et al. (2022): Italian Accelerometric Archive v3.2 - Istituto Nazionale di Geofisica e Vulcanologia, Dipartimento della Protezione Civile Nazionale, Roma. doi: https://doi.org/10.13127/itaca.3.2

[7] Dolce, M., Nicoletti, M., De Sortis, A., Marchesini, S., Spina, D., and Talanas, F. (2017): Osservatorio sismico delle strutture: The Italian structural seismic monitoring network. *Bull. Earthq. Eng.* **15**, 621–641. doi: https://doi.org/10.1007/s10518-015-9738-x

[8] Gallipoli, M. R., Petrovic, B., Scaini, C., Calamita, G., Tragni, N., Barnaba, C., et al. (2022): FRIBAS database for better characterization of RC and URM buildings: Towards specific T-H relationships. (submitted to Bulletin of Earthquake Engineering, under review).

[9] Vignaroli, G., Mancini, M., Bucci, F., Cardinali, M., Cavinato, G. P., Moscatelli, M., et al. (2019): Geology of the central part of the Amatrice basin (central apennines, Italy). *J. Maps* **15**, 193–202. doi: https://doi.org/10.1080/17445647.2019.1570877

[10] Bindi, D., Luzi, L., Parolai, S., Di Giacomo, D., and Monachesi, G. (2011): Site effects observed in alluvial basins: The case of Norcia (central Italy). *Bull. Earthq. Eng.* **9**, 1941–1959. doi: https://doi.org/10.1007/s10518-011-9273-3

[11] Brunelli, A., de Silva, F., Piro, A., Parisi, F., Sica, S., Silvestri, F., et al. (2021): Numerical simulation of the seismic response and soil–structure interaction for a monitored masonry school building damaged by the 2016 Central Italy earthquake. *Bull Earthquake Eng.* **19**, 1181–1211. doi: https://doi.org/10.1007/s10518-020-00980-3

[12] Di Giulio, G., De Nardis, R., Boncio, P., Milana, G., Rosatelli, G., Stoppa, F., et al. (2015): Seismic response of a deep continental basin including velocity inversion: The Sulmona intramontane basin (central apennines, Italy). *Geophys. J. Int.* **204**, 418–439. doi: https://doi.org/10.1093/gji/ggv444

PETRINJA EARTHQUAKE AFTERSHOCKS – LOCATIONS, FOCAL MECHANISMS AND RELATED COULOMB STRESS CHANGE

Marijan Herak, Davorka Herak

Department of Geophysics, Faculty of Science, University of Zagreb, mherak@gfz.hr

Keywords: Petrinja earthquake, aftershocks, focal mechanism solutions, Coulomb stress change

The devastating Petrinja earthquake of 29 December 2020 ($M_w = 6.4$) was followed by a large number of aftershocks. In the first six months of the sequence we were able to hand-pick over a quarter of million earthquake phase onset times, corresponding to 13897 locatable events (Fig. 1, left). Most epicentres lie close to the NW–SE striking right-lateral causative fault, but considerable activity was recorded in the surrounding area up to about 50 km away. The hypocentres reach depths of over 20 km, with most of them located between the depths of 5 and 16 km. Very little activity was recorded around the patch of the largest coseismic displacement on the fault inferred from analyses of DInSar interferograms (Fig. 2).
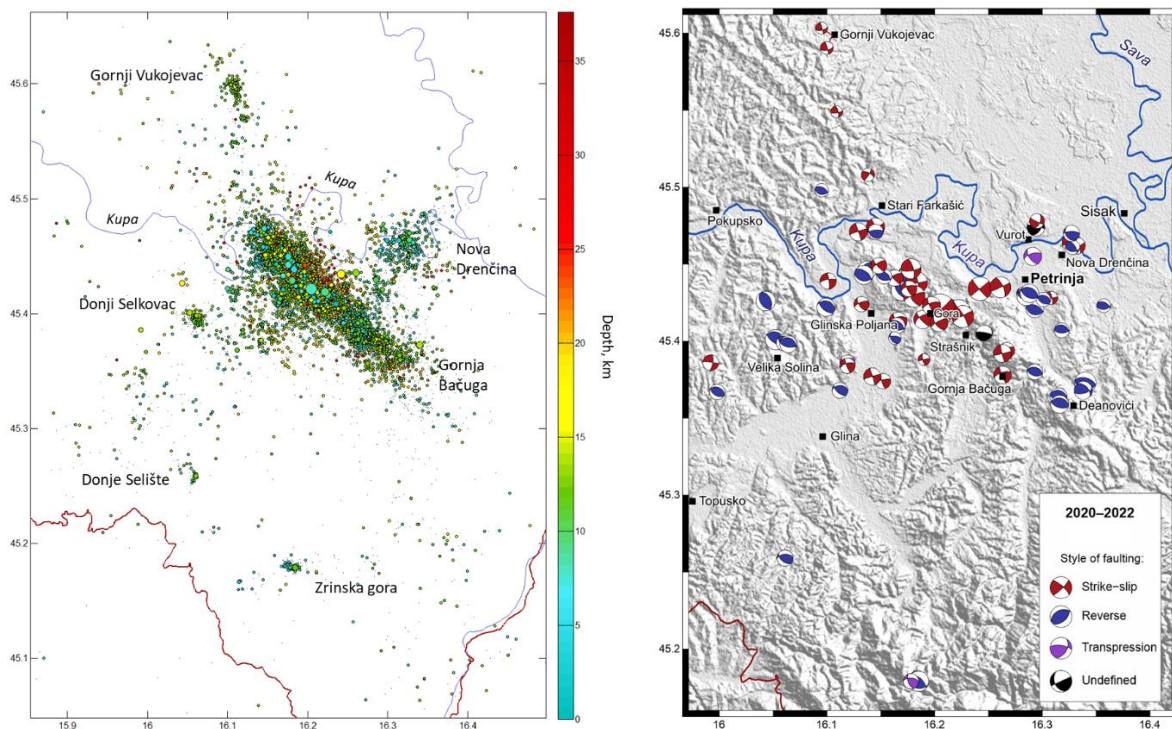
Figure 1. *Left:* Epicentres of all 13897 located events in the period 28 December 2020 – 28 June 2021. *Right:* Beach-ball diagrams of lower hemisphere equal area projections of focal mechanism solutions for 75 events from the Petrinja sequence.

The 75 focal mechanism solutions computed using the first motion polarities read from the seismograms of the local and regional seismic networks, indicate that about half of the aftershocks exceeding magnitude M = 3.0 occurred on strike-slip faults, while the large majority of the remaining ones were due to almost pure reverse dip-slip faulting (Fig. 1, right).
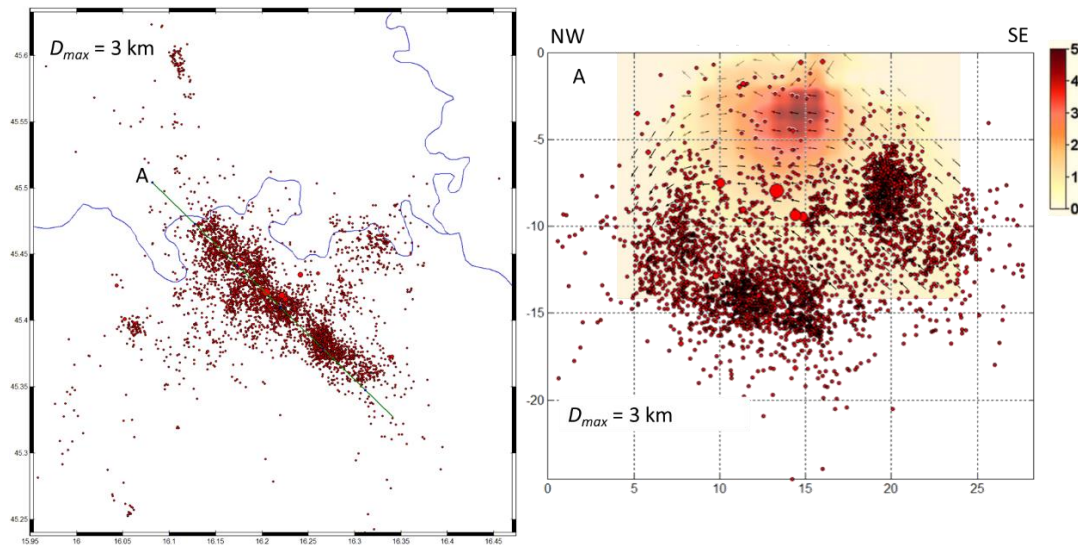
Figure 2. *Left:* Epicentres of the most reliably located events, with the green trace (A) of the cross-section through the hypocentral volume. *Right:* Vertical cross-section showing events in a 6 km wide corridor around the trace in the left sub-plot. The colour scale of the coseismic displacement on the fault after [1] is in meters.

Analyses of the Coulomb stress change on optimally oriented strike-slip and dip-slip faults following the mainshock rupture, reveals that a large majority of aftershocks occurred in the volumes characterised by the Coulomb static stress increase, whereas the areas where the effective stress decreased remained mostly quiet (Fig. 3). The distribution and preferred strike directions of strike-slip and reverse faulting inferred by the Coulomb stress transfer analyses are also in good agreement with individual focal mechanisms.
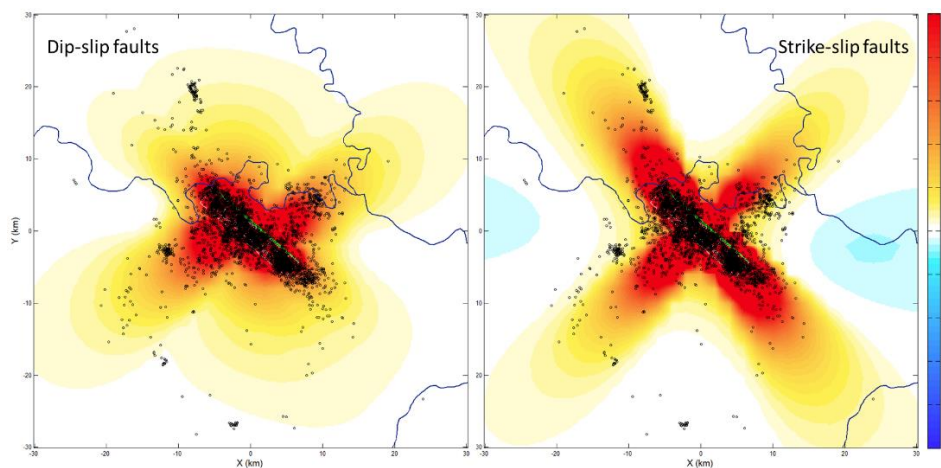
Figure 3. Maximum Coulomb stress change (in bars) considering depths 0–20 km for optimally oriented dip-slip faults (*left*) and strike-slip faults (*right*), assuming the source model presented in [1]. Warm colours indicate areas where optimally oriented existing faults were brought closer to rupture and where aftershocks are thus more likely than in the the white–blue regions. Small black circles are aftershock epicentres from Fig. 2.

Reference

[1] Kastelic, V., Atzori, S., Carafa, M.M.C., Govorčin, M., Herak, M., Herak, D., Matoš, B., Stipčević, J., Tomljenović, B. (2021): Petrinja Seismogenic Source and its 2020-2021 Earthquake Sequence (Central Croatia), *Book of Abstracts, EGU General Assembl*y, Vienna, Austria, p. EGU21-16579.

LATE HOLOCENE RELATIVE SEA-LEVEL CHANGE AND PALAEOEARTHQUAKES AT THE ELAFITI ISLANDS (SOUTHERN ADRIATIC, CROATIA)

Sanja Faivre [(1)], Tatjana Bakran-Petricioli [(2)], Marijan Herak [(3)], Jadranka Barešić [(4)], Davor Horvatić [(5)]

[(1)] *University of Zagreb, Faculty of Science, Department of Geography, Marulićev trg 19/II, 10 000 Zagreb, Croatia, sfaivre@geog.pmf.hr*
[(2)] *University of Zagreb, Faculty of Science, Department of Biology, Rooseveltov trg 6, 10 000 Zagreb, Croatia, tbakran@biol.pmf.hr*
[(3)] *University of Zagreb, Faculty of Science, Department of Geophysics, Horvatovac 95, 10 000, Zagreb, Croatia, marijan.herak@gfz.hr*
[(4)] *Ruđer Bošković Institute, Radiocarbon Laboratory, Bijenička 54, 10 000 Zagreb, Croatia, Jadranka.Baresic@irb.hr*
[(5)] *University of Zagreb, Faculty of Science, Department of Physics, Bijenička 32, 10 000 Zagreb, Croatia, davorh@phy.hr*

Keywords: Algal rim, Tidal notch, Lithophaga lithophaga boreholes, Coastal geomorphology, 1667 CE Dubrovnik earthquake, Palaeoearthquakes, Palaeoshoreline, Coseismic movements

In micro tidal settings, processes of bioerosion and bioconstruction can lead to the development of distinct morphological features that define the modern shoreline. When such features are discovered above or below the present-day mean sea level, they reveal relative sea-level (RSL) change. Among the best sea-level indicators on rocky coasts are fixed biological and geomorphological markers – algal rims, *Lithophaga lithophaga* borehole upper limits, and tidal notches [1, 2]. For instance, the coralline alga *Lithophyllum byssoides* can build algal rims that are considered one of the most precise RSL markers along rocky coasts [3, 4]. Consequently, studying RSL markers on Lopud, Koločep and Grebeni two elevated palaeoshorelines have been distinguished.

Their detailed survey allowed the distinction of seismotectonically uplifted sectors of the coast. The established high-resolution geochronology enables separation of coseismic uplift events from the periods of interseismic subsidence. Studying the local tectonic contribution to RSL change, we approach aspects of neotectonics and palaeoearthquakes offering new insights in a timetable (500 BC up to 1800 AD) where earthquake related data are either missing or incorporate high uncertainties, both regarding their epicentral localities and estimated magnitudes.

Our reconstruction provides evidence on two successive major earthquakes which affected approximately 5 km of coasts in the Pelješac-Dubrovnik fault zone, with an uplift amplitude between 40 and 80 ± 15 cm per event (Fig. 1). The earlier, older events, caused larger displacements (60-80 cm), while the later, younger events, revealed on average lower displacements (40-55 cm) corresponding to the 1520 AD quake and the 1667 Dubrovnik earthquake [5, 6].

Here we demonstrate the importance of *Lithophyllum* rims in the studies of RSL change as they make creation of high-resolution geochronology possible. This new approach refers to algal rims as a possible tool for constraining palaeoseismic events, allowing to supplement the database of instrumental records and historical observations through field-based evidence.

Furthermore, the study of algal rims, tidal notches and upper limits of *L. lithophaga* boreholes allow us to reconstruct the 2.6 ka evolution of Koločep and Grebeni islands and islets coasts, detect seismic events and demonstrate their effects, reconstruct the RSL changes at high resolution and finally distinguish the drivers of RSL change.
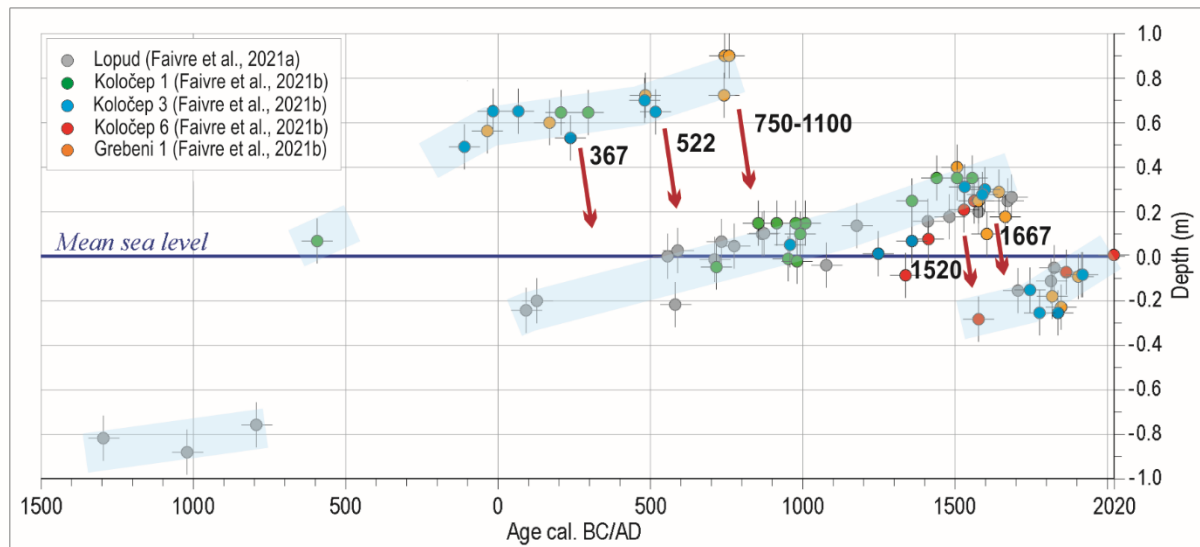
Figure 1. Relative sea-level changes at Lopud, Koločep and Grebeni island and islets based on the geochronology of algal rims. Error bars correspond to two standard deviations (2s). Blue band represents segmented linear trendlines. Red arrows mark periods of abrupt RSL fall i.e. potential seismic events [5, 6].

As the southern part of the eastern Adriatic coast is the area of highest seismic risk in Croatia, the new obtained data will thus be essential for assessment of recurrence rates of the largest earthquakes that the main faults in the area can produce, as well as for understanding of the Late Holocene geodynamics.

Acknowledgements

References

[1] Stewart, I.S., Morhange, C. (2009): Coastal geomorphology and sea-level change. In: Woodward, J. (Ed.), *The Physical Geography of the Mediterranean.* Oxford University Press, Oxford, pp. 385–414.

[2] Marriner, N., Morhange, C., Faivre, S., Flaux, C., Vacchi, M., Miko, S., Boetto, G., Radić Rossi, I. (2014): Post-Roman Sea-level changes on Pag Island (Adriatic Sea): dating Croatia's "enigmatic" coastal notch? *Geomorphology, 221*, 83–94.

[3] Laborel J., Delibrias G., Boudouresque C.F. (1983). Variations récentes du niveau marin à Port-Cros (Var, France), mises en évidence par l'étude de la corniche littorale à *Lithophyllum tortuosum*. *C.R. Acad. Sci., Fr*., 297 Sér. II: 157-160.

[4] Faivre, S., Bakran-Petricioli, T., Barešić, J., Horvatić, D., Macario, K. (2019): Relative sea-level change and climate change in the Northeastern Adriatic during last 1.5 ka (Istria, Croatia), *Quaternary Science Reviews*, **222**, https://doi.org/10.1016/j.quascirev.2021.107284

[5] Faivre, S., Bakran-Petricioli, T., Barešić, J., Horvatić, D. (2021a): Lithophyllum rims as biological markers for constraining palaeoseismic events and relative sea-level variations during the last 3.3 ka on Lopud Island, southern Adriatic, Croatia, *Global and Planetary Change* **202**, 103517. https://doi.org/10.1016/j.gloplacha.2021.103517

[6] Faivre, S., Bakran-Petricioli, T., Herak, M., Barešić, J., Borković, D. (2021b): Late Holocene interplay between coseismic uplift events and interseismic subsidence at Koločep island and Grebeni islets in the Dubrovnik archipelago (southern Adriatic, Croatia) *Quaternary Science Reviews*, **274**, 107284, https://doi.org/10.1016/j.quascirev.2021.107284

Invited Lecture

ASSESSING LIQUEFACTION IN GRAVELLY SOILS BASED ON FIELD CASE HISTORIES

Kyle Rollins [1] and Jashod Roy [2]

[1] *Professor, Brigham Young University, rollinsk@byu.edu*
[2] *Staff Engineer, Kiewit Engineering, Jashod.Roy@gmail.com*

Abstract

Gravelly soils have liquefied at multiple sites in at least 27 earthquakes over the past 130 years. These gravels typically contain more than 25% sand which lowers the permeability and makes them susceptible to liquefaction. Developing a reliable, cost-effective liquefaction triggering procedure for gravelly soils has been a challenge for geotechnical engineers. Typical SPT- or CPT-based correlations can be affected by large-size gravel particles and can lead to erroneous results. To deal with these problems, we have developed liquefaction triggering curves for gravelly soils based on (1) shear wave velocity (V_s) and (2) a large diameter cone penetrometer. With a cone diameter of 74 mm, the Chinese Dynamic Cone Penetration Test (DPT) is superior to smaller penetrometers and can be economically performed with conventional drilling equipment. Using logistic regression analysis, the DPT has been directly correlated to liquefaction resistance at sites where gravels did and did not liquefy in past earthquakes. Probabilistic liquefaction resistance curves were developed based on 137 data points from 10 different earthquakes in seven countries. Using a similar data set, probabilistic liquefaction triggering curves were also developed based on V_s measurements in gravelly soils. The V_s-based liquefaction triggering curves for gravels shift to the right relative to similar curves based on sands. New magnitude scaling factor (*MSF*) curves have also been developed specifically for gravel liquefaction which were found to be reasonably consistent with previous curves for sand.

Keywords: Gravels, Liquefaction, Case Histories, Shear Wave Velocity, Dynamic Cone Penetration Test, DPT

1. Introduction

Liquefaction of loose saturated granular soils results in significant damage to civil infrastructure such as buildings, bridges, roadways, pipelines, and ports in nearly every earthquake. Liquefaction and the resulting loss of shear strength can lead to landslides, lateral spreading, loss of vertical and lateral bearing support for foundations, and excessive foundation settlement and rotation. Direct and indirect economic losses resulting from liquefaction are substantial costs to society. A significant number of gravel liquefaction case histories have occurred during more than 20 earthquake events over the past 130 years, as shown in Table 1. Assessing the potential for liquefaction of gravelly soils in a reliable, cost-effective manner has always posed a great challenge for geotechnical engineers and researchers. Liquefaction assessment is particularly important for older dams that were constructed on gravelly soil foundations or with poorly compacted gravel shells before the potential for liquefaction in gravels was recognized. Likewise, many ports around the world were constructed of gravelly soils or rockfill which was believed to be immune to liquefaction. For these projects, assessing the potential for liquefaction and determining appropriate remedial measures are often multi-million-dollar decisions. These decisions involve both life-safety and regional economic issues. Over the past 15 years, gravel liquefaction has caused significant damage to ports in Greece, Chile, Ecuador, and New Zealand. Besides these large projects, gravel liquefaction must be routinely considered for a myriad of small to medium projects throughout the world.

Table 1 - Case histories involving liquefaction of gravelly soil

Earthquake	Year	M_w	Reference
Mino-Owari, Japan	1891	7.9	[1]
San Francisco, California	1906	8.2	[2]
Messina, Italy	1908	7.1	[3]
Fukui, Japan	1948	7.3	[4]
Alaska, USA	1964	9.2	[5,6]
Hatching, China	1975	7.3	[7]
Tangshan, China	1976	7.8	[8]
Friuli, Italy	1976	6.4	[9, 10, 11]
Miyagiken-Oki, Japan	1978	7.4	[1]
Borah Peak, Idaho, USA	1985	6.9	[12, 13, 14]
Armenia	1988	6.8	[15]
Limon, Costa Rica	1991	7.7	[16]
Roermond, Netherlands	1992	5.8	[17]
Hokkaido, Japan	1993	7.8	[18]
Kobe, Japan	1995	7.2	[19]
Chi-Chi, Taiwan	1999	7.8	[20]
Wenchuan, China	2008	7.9	[21]
Tohoku, Japan	2010	9.0	[22]
Cephalonia Is., Greece	2012	6.1	[23, 24]
Iquique, Chile	2014	8.2	[25, 26]
Muisne, Ecuador	2016	7.8	[27]
Kaikora, New Zealand	2016	7.8	[28]
Durres, Albania	2019	6.4	[29]
Petrinja, Croatia	2020	6.4	[30]

2. Penetration Testing Approaches

Typical laboratory investigation techniques have generally proven to be ineffective for characterizing gravelly soil due to the cost and difficulty of extracting undisturbed sample from gravelly deposits [21]. In addition, the large particle size of gravels can lead to artificially high penetration resistance values from traditional in situ tests such as the cone penetrometer (CPT) test and the Standard Penetration (SPT) test [31]. The 168 mm diameter Becker Penetration Test (BPT) [32, 33] reduces the potential for artificially high penetration values; however, this method is relatively expensive and is not available outside of North America. In addition, the method requires a correlation between the BPT blow count and the SPT blow count which leads to greater uncertainty relative to methods that are directly correlated with field liquefaction resistance.

As another approach for gravelly soils, Chinese engineers in the Chengdu region, faced with widespread gravel deposits, developed a Dynamic Cone Penetrometer (DPT) with a 74 mm diameter cone tip for site characterization. The methodology is a large-size implementation of the lightweight dynamic cone penetrometer that is used extensively for assessment of compaction of soils in pavement applications [34] and different cone geometries are also known as dynamic probing in Europe [35]. In the Chinese version of the DPT, the cone tip is driven continuously with a 120 kg hammer dropped from one meter and is capable of penetrating medium to dense gravel and cobbles. DPT soundings can be easily performed with conventional SPT drilling rigs or even simple tripod systems, making it viable worldwide. In contrast to the straight sides of the BPT, the cone tip tapers back to a 60 mm drill rod to reduce rod friction. At 74 mm, the DPT diameter is 50% larger than the SPT and 110% larger than a standard 10 cm^2 CPT; however, it is still 55% smaller than the BPT. Although the BPT provides the

largest diameter to particle size ratio of all tests, the DPT is superior to the SPT or CPT and could be a reasonable solution in many cases depending on the gravel size and percentage.

Based on field case histories of gravel liquefaction in the M_w 7.9 Wenchuan earthquake, Cao et al. [21] developed probabilistic liquefaction triggering curves for gravels based on the DPT blow count. However, these curves are based on relatively few data points from one earthquake and a geologic profile consisting of a loose alluvial fan gravel layers overlain by a clay surface layer typically 2- to 4-m thick [21]. Because of the limited number of data points and the possibility of false negatives (sites where liquefaction may have occurred but did not produce surface manifestation), the individual triggering curves (85 to 15%) are spread apart. In contrast, more mature probabilistic liquefaction triggering curves for sands based on CPT [36] have more closely grouped probability curves because of the larger size of the data set. In addition, the Cao et al. [21] triggering curves were developed for a single event of Mw 7.9 without incorporating any correction to the seismic demand by using the Magnitude Scaling Factor (*MSF*). Thus, applicability of these curves would become questionable for evaluating the liquefaction potential of gravelly soils for other seismic events of different Magnitude. Although existing *MSF* models developed for sand liquefaction [37] can be used, it is unclear whether they are appropriate for gravel liquefaction using the DPT. Therefore, it becomes crucial to add more case histories to the DPT database with different earthquake magnitudes and geologic settings and develop an improved DPT-based liquefaction triggering procedure and a gravel-based MSF curve.

3. Shear Wave Velocity Approaches

As an alternative to penetration resistance testing, in situ measurement of shear wave velocity (V_s) is a popular way of characterizing the liquefaction resistance of soil deposits. V_s is a basic mechanical property of soil materials, directly related to the small strain shear modulus (G_0), that is an essential parameter for performing soil-structure interaction analysis and liquefaction evaluation under earthquake loading. The use of V_s as a field index of liquefaction resistance is soundly based on the fact that both V_s and liquefaction resistance are similarly, but not proportionally, influenced by void ratio, effective confining stresses, stress history and geologic age [37]. In addition, V_s is considerably less sensitive to the problems of soil compression and reduced penetration resistance when fines are present, compared with SPT and CPT methods. Moreover, V_s requires only minor corrections for fines content (*FC*) at least for sands [38]. The primary advantage of the in-situ V_s approach is that testing can be performed at sites where borings are not possible, or the penetration test results may be unreliable. Hence, V_s measurement can be considered as a reliable and economical alternative to overcome the difficulties of penetration testing within gravelly strata.

The traditional methods of measuring V_s require a penetrometer or instrumented boreholes to measure the travel time of shear waves at various depths. A downhole test requires one borehole to measure the vertically propagating wave, while a cross-hole test requires at least two boreholes to directly measure the horizontally propagating wave [39]. These invasive test methods are usually quite expensive due to the cost of drilling, casing, and grouting boreholes. In the last two decades, some advanced non-invasive test methods (Spectral Analysis of Surface Waves (SASW) and Multichannel Analysis of Surface Wave (MASW) have been developed, which indirectly estimate the V_s through the surface wave dispersion characteristics of the ground [13, 38, 39]. These non-invasive test methods have significantly reduced the cost of in-situ V_s estimation and made soil exploration possible at sites where penetration is not possible or economically feasible.

Andrus and Stokoe [40] increased the population of V_s data by collecting a large database from locations around the world where both sandy and gravelly soils had liquefied in various seismic events. Based on this dataset, improved triggering curves were developed for sands and gravels for different *FC* percentages. The database of Andrus and Stokoe [40] only contained a limited number of data points where the V_{s1} was higher than 200 m/s even for gravelly soils. This is consistent with observations by Kokusho et al. [13] that loose gravels, even though well-graded, can exhibit shear wave velocities similar to those of loose sands. In contrast, the SPT-V_s correlation by Ohta and Goto [41] and the

correlation by Rollins et al. [42] suggest a higher range of V_{s1} (230 m/s) for liquefiable Holocene gravels. Such variation of shear wave velocity in gravelly soils can be due to variations in gravel content, grain size distribution, and the relative density of the soil matrix [13, 43, 44, 45].

Cao et al. [46] developed probabilistic liquefaction triggering curves for gravels using logistic regression techniques based on V_s data collected from the Chengdu plain in China where gravel liquefaction took place during the 2008 Wenchuan earthquake. These curves are based on 47 data points (19 liquefaction and 28 no liquefaction points) that refer to a single earthquake and a similar geological environment [46]. Because of the limited number of data points and the possibility of false negatives (sites where liquefaction may have occurred but did not produce surface manifestation), the individual triggering curves (15% to 85%) are relatively far apart. In contrast, V_s-based probabilistic liquefaction triggering curves for sands [38] have more closely grouped probability curves because of the larger size of the data set. Moreover, the Cao et al. [46] triggering curves were developed for a single event of M_w 7.9 without proposing any correction to the seismic demand for different earthquake magnitudes. Thus, the applicability of these curves becomes questionable for evaluating the liquefaction potential of gravelly soils for other seismic events of different magnitude. Although existing *MSF* models developed for sand liquefaction [37] can be used, it is unclear whether they are appropriate for gravel liquefaction assessment based on V_s. Therefore, additional effort is necessary to collect more V_s data from the gravel liquefaction sites to improve the existing V_s-based liquefaction triggering curves for gravelly soils.

4. Collection of Additional Field Case History Data

In the present study, a larger database consisting of 174 V_s data points and 137 DPT data points has been compiled by collecting additional data points from seven different countries around the world where gravel liquefaction did or did not take place in 17 major earthquake events and adding them to the existing data points from China reported by Cao et al. [21, 39]. Case histories with no liquefaction in Italy, Greece, and New Zealand were strategically identified, tested, and then added to the database to help constrain the position of the liquefaction triggering curves.

For each case history, the cyclic stress ratio (CSR) has been obtained by using the simplified equation

$$CSR = 0.65 \, (a_{max}/g) \, (\sigma_{vo}/ \, \sigma'_{vo}) \, r_d \tag{1}$$

originally developed by Seed and Idriss [47] where a_{max} is the peak ground acceleration, σ_{vo} is the initial vertical total stress, σ'_{vo} is the initial vertical effective stress, and the r_d value in Eq. 1 was updated to include the effect of both depth and earthquake magnitude using the equation

$$r_d \;=\; e^{[\alpha(z)+\beta(z)M_w]} \tag{2}$$

where:

$$\alpha(z) = -1.012 - 1.126 sin(^z/_{11.73} + 5.133) \tag{3}$$

$$\beta(z) = 0.106 + 0.118 sin(^z/_{11.28} + 5.142) \tag{4}$$

and z is the depth in meters, based on the work by Golezorkhi [48] and Idriss [49].

Peak ground accelerations *(PGA or a_{max})* for every location were taken from the literature or from USGS Shake Maps [50] where necessary as employed by Idriss and Boulanger [51] for their CPT database. Besides *CSR*, the moment magnitude (M_w) has been considered as another independent seismic variable for obtaining the liquefaction potential of gravelly soils. Values of M_w were found form available references regarding the appropriate earthquake. The data set contains a wide distribution of M_w ranging from 5.3 to 9.2 as well as *PGA* ranging from 0.17 to 0.6 g.

4.1 DPT Blow Count Corrections

The DPT blow count, N_{120}, represents the number of hammer blows to drive the penetrometer 30 cm deep with a 120 kg hammer dropped from a height of 1 m. Raw blow counts are typically reported at every 10 cm penetration, but are multiplied by three to get the equivalent N_{120} for 30 cm of penetration.

Based on 1200 hammer energy measurements, Cao et al. [52] found that the Chinese DPT provided an average of 89% of the theoretical free-fall energy. Since the energy delivered by a given hammer (E_{Hammer}) was different than the energy actually supplied by a Chinese DPT hammer ($E_{Chinese\ DPT}$), it was sometimes necessary to correct the measured blow count. In this study, the correction was made using the simple linear reduction suggested by Seed et al. [53] for SPT testing

$$N_{120} = N_{Hammer} \cdot (E_{Hammer}/E_{Chinese\ DPT}) \tag{5}$$

where N_{Hammer} is the number of blows per 0.3 m of penetration obtained with a hammer delivering an energy of E_{Hammer}. In addition, Cao et al. [21] recommend an overburden correction factor, C_n, to obtain the normalized N'_{120} value using the equation

$$N'_{120} = N_{120}\, C_n \tag{6}$$

where

$$C_n = (100/\sigma'_{vo})^{0.5} \leq 1.7 \tag{7}$$

and σ'_o is the initial vertical effective stress in kN/m². In the current study, a limiting value of 1.7 was added to be consistent with the C_n used to correct penetration resistance from other in-situ tests [37]. For each case history a critical layer was selected below the water table and with the lowest ratio of blow count divided by CSR over at least one meter. All the critical liquefaction layers were located at depths less than about 14 m which is consistent with other liquefaction case history databases and with blow counts typically less than about 20.

4.2 DPT Blow Count Corrections

The V_s values obtained by various in-situ methods were corrected for overburden pressure to obtain V_{s1} using the equation:

$$V_{s1} = V_s\, (P_a/\sigma'_{vo})^{0.25} \tag{8}$$

where σ'_{vo} is the initial vertical effective stress, and P_a is atmospheric pressure approximated by a value of 100 kPa as suggested by Sykora [54] and adopted by Youd et al. [37]. These normalized V_{s1} profiles based on the V_s testing were then plotted as a function of depth and a critical depth with the lowest average ratio of V_{s1}/CSR over a length of at least one meter. Once again, the critical layers based on V_{s1} were all shallower than 14 m.

5. Development of Probabilistic Triggering Curves

Based on the new expanded database, a new set of probabilistic liquefaction triggering curves has been developed by logistic regression analysis based on V_{s1} and also N'_{120}. The triggering equations developed in the present study include the earthquake magnitude as an independent variable.

5.1 Probabilistic DPT-Based Liquefaction Triggering Curves

The logistical regression analysis was carried out using M_w, N'_{120}, and ln(*CSR*) as independent variables and the following equation was developed to calculated the Cyclic Resistance Ratio (CRR)

$$CRR = exp\left[\frac{1.32M_w - 0.0008N'^{3}_{120} - \ln\left(\frac{1-P_L}{P_L}\right)}{5.2}\right] \tag{9}$$

where P_L is the probability of liquefaction expressed as a fraction. If a given probability and M_w of 7.5 is used in Eq. 9, a plot of *CRR* vs. N'_{120} can be produced for a given probability. Fig. 1 provides a plot of *CRR* vs. N'_{120} for M_w 7.5 for various P_L values. CSR and N'_{120} data points for each liquefaction and no liquefaction case history are also shown in Fig. 1 relative to the triggering curves proposed by Rollins et al. [55] .
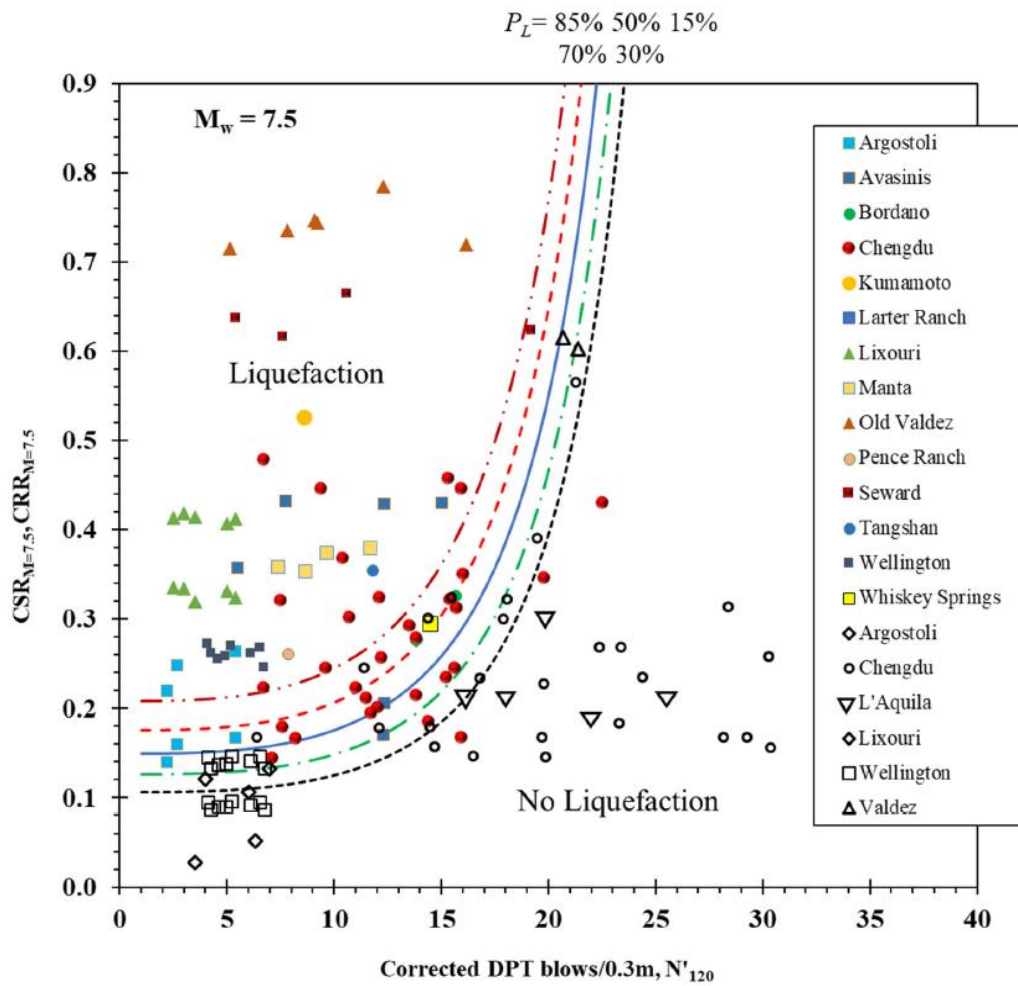
Figure 1. Plot of *CRR* vs. N'_{120} for a M_w 7.5 earthquake with various probabilities of liquefaction based on expanded DPT-based database proposed by Rollins et al. [55].

5.2 Probabilistic V_s-Based Liquefaction Triggering Curves

Logistical regression analysis was also carried out using M_w, V_{s1} and ln(CSR) as independent variables and the following equation was developed to calculated the Cyclic Resistance Ratio (CRR)

$$CRR = exp\left[\frac{1.438M_w - 3.8x10^{-7}V_{S1}^3 - \ln\left(\frac{1-P_L}{P_L}\right)}{4.026}\right]$$

(10)

where P_L is the probability of liquefaction expressed as a fraction. If a given probability and M_w of 7.5 is used in Eq. 9, a plot of *CRR* vs. V_{s1} can be produced for a given probability. Fig. 2 provides a plot of *CRR* vs. N'_{120} for M_w 7.5 for various P_L values proposed by Rollins et al. [56].
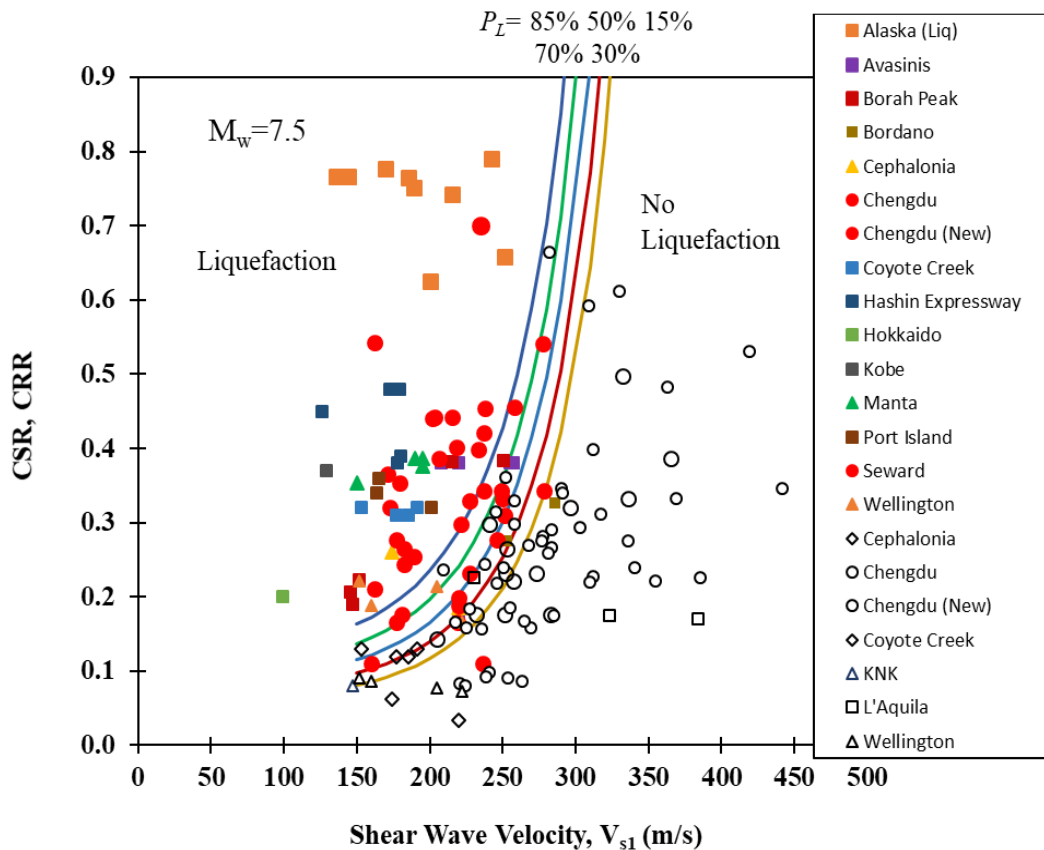
Figure 2. Plot of CRR vs. Vs1 for a Mw 7.5 earthquake with various probabilities of liquefaction based on expanded Vs -based database collected by Rollins et al. [56]

The new probabilistic triggering curves with liquefaction probabilities of 15% to 85% are plotted in Fig. 3(a) with solid lines along with similar curves developed by Cao et al. [46] with dashed lines to draw a distinct comparison between the two triggering procedures. For lower values of V_{s1} (around 150 m/s), the *CRR* for the new 50% probability of liquefaction curve is about 0.10 while it is only 0.04 for the Cao et al. [46] curves. This adjustment produces much better agreement with observed field performance. This higher *CRR* value at small velocities is also more typical of that predicted by the V_{s}-based triggering curves developed by Kayen et al. [38]. In fact, it can be seen from Fig. 3 that the points from the Port of Wellington where liquefaction did not take place during the Cook Strait and Lake Grassmere earthquakes (both M_w = 6.6) in 2013 and the "no liquefaction" points from Argostoli, KNK and Coyote Creek have had a significant effect in constraining the lower branch of the triggering curves to move upwards. Likewise, the triggering curves at the higher range of V_{s1} values have been tightened relative to the curves developed by Cao et al. [46] as a result of the additional "no liquefaction" data points from Chengdu, L'Aquila and Valdez. Additional data points would certainly be desirable to define the shape of the curve better in this range of V_{s1} values.

In the middle range of the curve, a few "no liquefaction" points from the Chengdu plain fall above the 70% triggering curve and some liquefaction points from the same region fall below the 30% triggering curve. These points may belong to the false negative or false positive categories leading to inconsistent evaluation of the actual incident. Due to the presence of these points, the set of triggering curves develop a slightly sloped shape above a V_{s1} value of 200 m/s such that a number of "no liquefaction" points fall marginally on the 30% triggering curve instead of falling distinctly below this line.

As shown in Fig. 3(a), for V_{s1} values above 200 m/s, the P_L = 50% curve for the new regression is very similar to that for the Cao et al. [46] regression. However, the addition of new liquefaction points has pulled the new P_L=85% curve to the right while the addition of no-liquefaction data points has pulled

the new P_L=15% curve to the left, relative to the Cao et al. [46] curves. Moving the new P_L=15% curve to the left is particularly significant because this curve is often recommended for deterministic evaluations [38]. However, the slope of the new set of curves from this study remains almost the same as for the Cao et al. [46] curves. Overall, the spread between the triggering curves for various probabilities of liquefaction is substantially reduced for the new triggering curves relative to the Cao et al. [46] curves. This result is consistent with the concept that the increased number of data points reduces the uncertainty that develops when an individual data point plots in an unexpected position. Furthermore, the addition of data points where liquefaction did not occur has helped constrain the triggering curves on the "no liquefaction side" in critical locations.

A comparison is provided between the newly developed triggering curves for gravel and the curves developed by Kayen et al. [38] for sand in Fig.3(b). To plot the triggering curves for Kayen et al. [38], an average effective vertical stress of 100 kPa, and fines content of 6% has been assumed to keep the values within a reasonable range. Although the probabilistic liquefaction triggering curves for gravel developed in this study are similar to those for sands [38] at lower $V_{s,1}$ values typical of looser gravels, the curves diverge as $V_{s,1}$ increases. For example, V_{s1} equals 275 m/s for the proposed $P_L = 50\%$ curve for gravel in this study at a CRR of 0.5 in comparison with a V_{s1} of only 225 m/s for the $P_L = 50\%$ curve for sand proposed by Kayen et al. [38]. This indicates that the probabilistic triggering curves for gravels from this study shift to the right relative to similar curves developed for sands as V_{s1} increases. This result indicates that gravels can still liquefy at V_{s1} values that would be high enough to preclude liquefaction in a sand. This does not mean that gravels are more or less likely to liquefy than sand, it simply means that for a comparable level of shaking, a higher V_{s1} is necessary to obtain the same probability of liquefaction for a sandy gravel than a sand. This result is consistent with liquefaction case histories in gravels reported by several investigators [24, 39, 44, 55, 57] where V_s-based triggering curves for sands would have incorrectly predicted no liquefaction, as well as laboratory testing (e.g. [58, 59]).
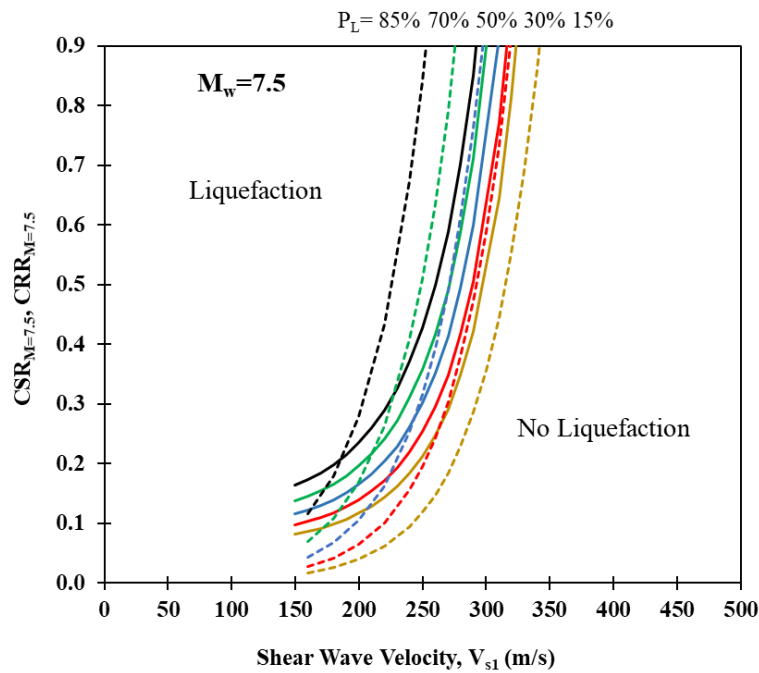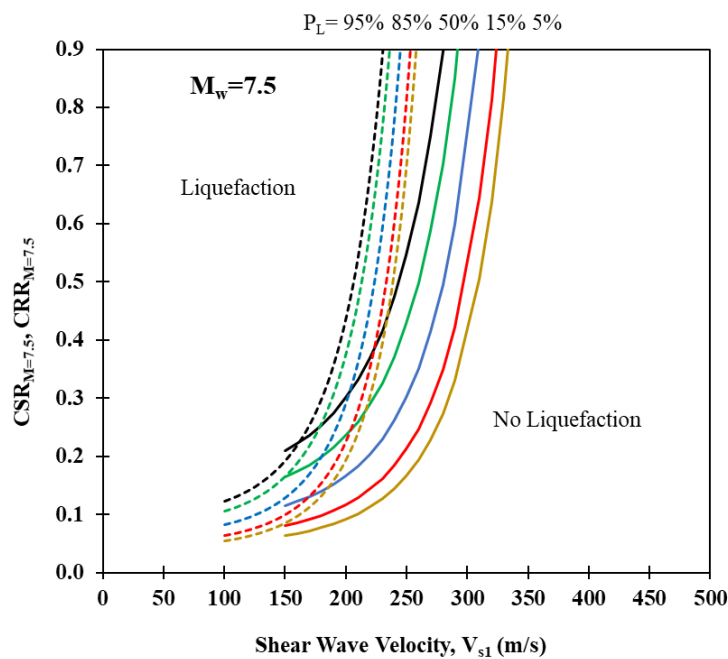
Figure 3. Revised liquefaction triggering curves from this study (solid lines) (a) relative to triggering curves originally proposed by Cao et al. [46] (dashed lines) and (b) relative to triggering curves proposed by Kayen et al. [38] for sands (dashed lines).

6. Development of Magnitude Scaling Factors

Most liquefaction triggering curves adjust the *CSR* for the earthquake magnitudes using a Magnitude Scaling Factor (MSF) to obtain an equivalent *CSR* for a Mw of 7.5 using the equation,

$$CSR_{M=7.5} = CSR/MSF \qquad (11)$$

As a part of the present study, we have developed a new *MSF* models specifically for gravelly soils that may help improve liquefaction evaluation at some gravel sites, although more data from other earthquakes would be desirable. To obtain the *MSF*, *CSR* values were first obtained from Eq. 9 for M_w 5.5 through 9 with an increment of 0.5 keeping N'_{120} and P_L constant. Then the *CSR*s for different magnitudes were divided by the *CSR* at M_w=7.5 to obtain the magnitude scaling factor. The same process was then repeated by substituting different values of N'_{120} and P_L in Eq. 9 to obtain the variation of *MSF* with these variables. But notably, the *MSF* pattern did not show any variation with the DPT blow count (N'_{120}) and the probability of liquefaction (P_L). Based on this analysis the *MSF* for triggering analyses using the DPT blow counts can be computed as a function of magnitude with the best-fit exponential equation:

$$MSF = 7.258exp(-0.264M_w) \tag{12}$$
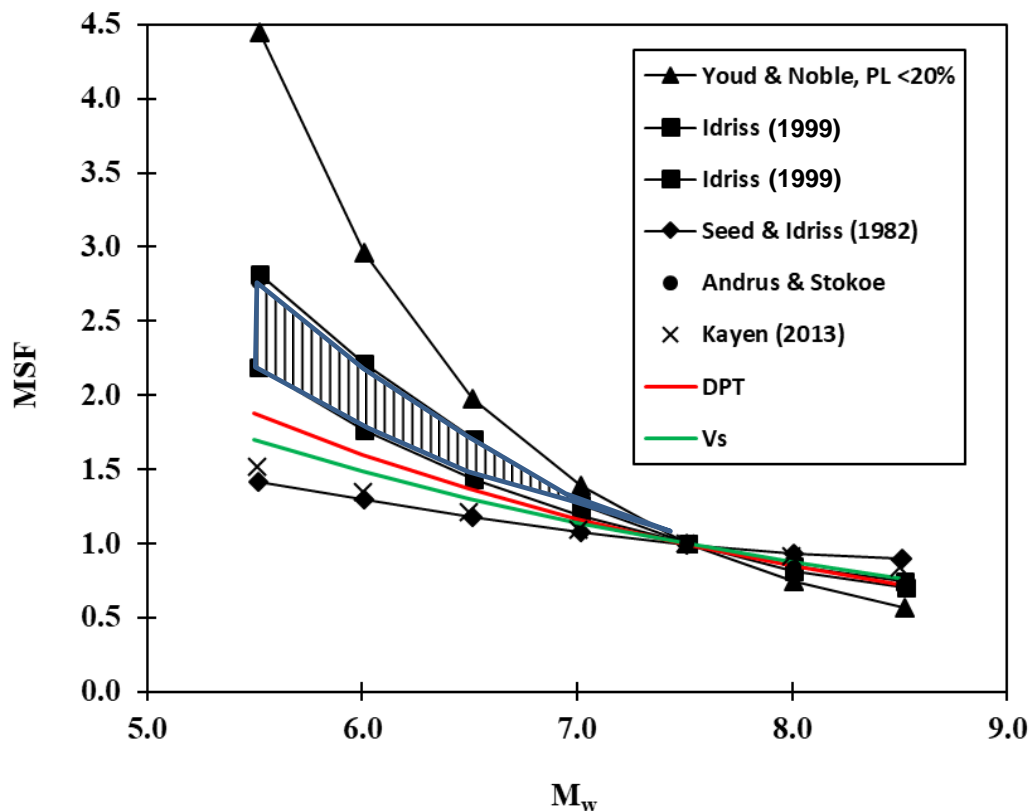
Figure 4. Comparison of *MSF* curves from logistical regression analysis of gravel liquefaction case histories based on *Vs* and DPT triggering curve with *MSF* curves proposed previously for sand [55, 56].

A similar approach was used to obtain the following best-fit exponential equation MSF equation for the Vs-based liquefaction triggering curve.

$$MSF = 10.667xp(-0.316M_w) \tag{13}$$

These *MSF* curves are plotted and compared with several other *MSF* vs. M_w curves in Fig. 4. It can be observed that the *MSF* curves developed for gravelly soil fall about mid-way between the *MSF* vs. M_w curves for sand suggested by Idriss as endorsed by the NCEER/NSF liquefaction workshop [37] at the high end and the Kayen et al. [38] curve at the low end. Hence, the proposed models for gravel appear to be reasonably consistent with existing *MSF* curves for sands.

Based on these *MSF* equations, the *CSRs* for all the case history data points have been converted to CSRs at M_w = 7.5 and plotted with the newly developed triggering curves as shown in Figs. 1 and 2. Generally, the data points fall on the correct sides of the P_L = 50% curves for the liquefaction and no liquefaction.

7. Summary and Conclusions

In this study, probabilistic liquefaction-triggering curves for gravelly soils based on the Dynamic Cone Penetration (DPT) test blow count (N'_{120}) and shear-wave velocity (Vs) were developed that can be used for liquefaction evaluation of gravelly soils for a wide range of earthquake magnitudes, tectonic settings, and geological environments. These curves are a significant step forward compared to those developed by Cao et al. [21, 39], asthe total number of data points increased significantly. The N'_{120} and Vs1 data were compiled from various sites around the world where liquefaction or no liquefaction case histories of gravelly soils were observed during several earthquake events in the past. The expanded data set consisted of 174 Vs data points and 137 DPT data points from 17 different earthquakes in 10 different countries in a variety of geological environments.

Based on the results of the field studies and data analysis performed in this study, the following conclusions were drawn:

1. The increased number of liquefaction and no-liquefaction data points in the expanded data set better constrain the probabilistic liquefaction-triggering curves. Relative to the Cao et al. [46] curves for V_s and the Cao et al. [21] curves for DPT, this shifted the $P_L = 85\%$ curve to the right and $P_L = 15\%$ curve to the left. The reduction in the range between the $P_L = 85\%$ and 15% curves indicate a considerable decrease in uncertainty, because false negative data points have less impact on the expanded data set. Shifting the $P_L = 15\%$ curve to the left is significant because this probability curve has been recommended for deterministic analyses (e.g. [38]).

2. At lower V_{s1} values ($\approx$150 m/s) and DPT blow counts less than 7, typical of looser gravels, the proposed triggering curves for gravel in this study start at a higher range of CSRs compared to the curves developed by Cao et al. [21, 46]. This modification was necessary to produce agreement with the no-liquefaction points from the field case histories and brought the CSR values in line with the V_{s1} value for sand as predicted by the Kayen et al. [38] probability curves.

3. Simplified *MSF* versus moment magnitude M_w equations were developed exclusively for gravel liquefaction. The *MSF* versus M_w curves plot about midway between similar curves proposed for sand. These results suggest that the effect of magnitude on liquefaction resistance is similar, but slightly different, for both sands and sandy gravels.

4. Although the probabilistic triggering curves for gravel are similar to those for sands [38] at low V_{s1} values typical of loose gravels ($\approx$150 m/s), they shift to the right as V_{s1} values increase. This indicates that gravels can still liquefy at values that would preclude liquefaction for sands. Therefore, using V_s-based triggering curves for sand when encountering gravels could incorrectly estimate gravel susceptible to liquefaction as being non-liquefiable.

Acknowledgements

References

[1] Tokimatsu, K., and Yoshimi, Y. 1983. "Empirical correlation of soil liquefaction based on SPT N-value and fines content."*Soils and Foundations*, 23(4), 56-74.

[2] Youd, T.L. and Hoose, S.N. 1978. "Historic ground failures in Northern California triggered by earthquakes." *U.S. Geological Survey Professional Paper 1993*, 180 p.

[3] Baratta, M., 1910. La Catastrofe Sismica Calabro-Messinese (28 dicembre 1908). Roma: Società Geografica Italiana.

[4] Ishihara, K. 1985. "Stability of natural deposits during earthquakes."*Proc., 11th Int. Conf. on Soil Mech. and Found. Eng.*, 1, 321-376.

[5] Coulter, H.W., and Migliaccio, R.R. 1966. "Effect of the Earthquake of March 22, 1964 at Valdez. Alaska."*U.S. Geological Survey Professional Paper 542-C.*

[6] McCulloch, D. S., & Bonilla, M. G. 1970. "Effects of the earthquake of March 27, 1964, on the Alaska Railroad". US Government Printing Office.

[7] Wang, W.S. 1984. "Earthquake damages to earth dams and levees in relation to soil liquefaction and weakness in soft clays." *In Proc. Intl. Conf. on Case Histories in Geotech. Eng.*, 1, 511-521.

[8] Wang, W.S. 1984. "Earthquake damages to earth dams and levees in relation to soil liquefaction and weakness in soft clays." *In Proc. Intl. Conf. on Case Histories in Geotech. Eng.*, 1, 511-521.

[9] Sirovich, L., 1996a. "Repetitive Liquefaction at gravelly site and liquefaction in overconsolidated sands." *Soils and Foundations*, (36)4, 23-34.

[10] Sirovich, L., 1996b. "In-situ testing of repeatedly liquefied gravels and liquefied overconsolidated sands."*Soils and Foundations*, (36)4, 35-44.

[11] Rollins, K.M., Amoroso, S., Milan, G., Minerelli, L., Vassallo, M., Di Giulio, G. 2020. "Gravel liquefaction assessment using the dynamic cone penetration test based on field performance from the 1976 Friuli earthquake." *J. Geotech. and Geoenviron. Eng.*, ASCE, https://DOI.org/10.1061/(ASCE)GT.1943-5606.0002252,

[12] Youd, T.L., Harp, E.L., Keefer, D.K., and Wilson, R.C. 1985. "The Borah Peak, Idaho Earthquake of October 29, l983-Liquefaction." *Earthquake Spectra*, 2, 71-90.

[13] Andrus, R.D. 1994. "In situ characterization of gravelly soils that liquefied in the 1983 Borah Peak earthquake." *Ph.D. Dissertation*, Civil Engineering Dept., Univ. of Texas at Austin, 579 pp.

[14] Harder, L.F., Jr., and Seed, H.B. 1986. "Determination of penetration resistance for coarse-grained soils using the Becker Hammer Drill." College of Engineering, University of California, Berkeley, Calif. Rep. No. UCB/EERC-86/06. May 1986.

[15] Yegian, M.K., Ghahraman, V.G., and Harutiunyan, R.N., 1994. "Liquefaction and embankment failure case histories, 1988 Armenia earthquake."*J. Geotech. Eng.*, 10.1061/(ASCE)0733-9410(1994)120:3(581).

[16] Franke, K.W. and Rollins, K.M. 2017. "Lateral spread displacement and bridge foundation case histories from the 1991 M7.6 Earthquake near Limón, Costa Rica." J. Geotechnical and Geoenvironmental Engineering, ASCE, Vol. 143, No. 6, 17 p.

[17] Maurenbrecher P.M., Den Outer, A., and Luger, H.J. 1995."Review of geotechnical investigations resulting from the Roermond April 13, 1992 earthquake.", *Proc. 3ʳᵈ Int. Conf. on Recent Advances in Geotech. Earthquake Eng. and Soil Dyn.*, 645-652.

[18] Kokusho, T., Tanaka, Y., Kudo, K., and Kawai, T., 1995. "Liquefaction case study of volcanic gravel layer during 1993 Hokkaido-Nansei-Oki earthquake."*Proc., 3rd Int. Conf. on Recent Advances in Geotech. Earthquake Eng. and Soil Dyn.*, 235-242.

[19] Kokusho, T., and Yoshida, Y., 1997. "SPT N-value and S-wave velocity for gravelly soils with different grain size distribution."*Soils and Foundations*, 37(4): 105-113.

[20] Chu, B.L., Hsu, S.C., Lai, S.E., and Chang, M.J. 2000. "Soil Liquefaction Potential Assessment of the Wu feng Area after the 921 Chi-Chi Earthquake." *Report of National Science Council* (in Chinese).

[21] Cao, Z., Youd, T., and Yuan, X. 2013. "Chinese Dynamic Penetration Test for liquefaction evaluation in gravelly soils."*J. Geotech. Eng.*, 10.1061/(ASCE)GT.1943-5606.0000857.

[22] Towhata (personal communication in 2016)

[23] Nikolaou, S., Zekkos, D., Assimaki, D., and Gilsanz, R. 2014. "GEER/EERI/ATC Earthquake Reconnaissance January 26th/February 2nd 2014 Cephalonia, Greece Events, Version 1."http://www.geerassociation.org/index.php/component/geer_reports/?view=geerreports&id=32

[24] Athanasopoulos-Zekkos, A., Zekkos, D., Rollins, K.M., Hubler, J., Higbee, J., Platis, A. 2019. "Earthquake performance and characterization of gravel-size earth fills in the ports of Cephalonia, Greece, following the 2014 Earthquakes." Earthquake Geotechnical Engineering for Protection and Development of Environment and Constructions, Procs. 7th Intl. Conf. on Earthquake Geotechnical Engineering, Taylor and Francis, p. 1212-1219.

[25] Rollins, K.M., Ledezma, C., and Montalva, G., Becerra, A., Candia, G., Jara, D., Franke, K., Saez, E. 2014. Geotechnical Aspects of April 1, 2014, M8.2 Iquique, Chile Earthquake." *GEER Association Report No. GEER-038*, 77 p.Version 1.2: October 22, 2014

[26] Morales, C, Ledezma, C., Saez, E., Boldrini, S., and Rollins, K.M., 2020. "Seismic failure of an old pier during the 2014 Mw8.2, Pisagua, Chile earthquake." Earthquake Spectra, EERI, https://journals.sagepub.com/doi/10.1177/8755293019891726

[27] Sebastian Lopez, J. Vera-Grunauer, X., Rollins, K., and Salvatierra, G. 2018. "Gravelly Soil Liquefaction after the 2016 Ecuador Earthquake." Procs. Geotechnical Earthquake Engineering and Soil Dynamics V, 13 p.

Seed, H. B., and Idriss, I. M. 1971. ''Simplified procedure for evaluatingsoil liquefaction potential.'' J. Geotech. Engrg. Div., ASCE, 97(9),1249–1273.

[28] Cubrinovski, M., Rhodes, A., Ntritsos, N., and Van Ballegooy, S. 2017. "System response of liquefiable deposits." *Proc., Performance Based Design III*, 18p.

[29] Pavlides, S., Muceku, Y., Chatzipetrow, A., Georgious, G., Lazos, I. 2020. "Preliminary report on the ground failures of the Albanian (Durres-Thumane) 26th of November Earthquake,

[30] Amoroso, S., Barbača, J., Belić, N., Kordić, B., Brčić, V., Budić, M., Civico, R., De Martini, P. M., Hećej, N., Kurečić, T., Minarelli, L., Novosel, T., Palenik, D., Pantosti, D., Pucci, S., Filjak, R., Ricci, T., Špelić, M., and Vukovski, M. 2021. Liquefaction field reconnaissance following the 29th December 2020 Mw 6.4 Petrinja earthquake (Croatia), EGU General Assembly 2021, online, 19–30 Apr 2021, EGU21-16584,

[31] DeJong, J.T., Ghafghazi, M., Sturm, A.P., Wilson, D.W., den Dulk, J., Armstrong, R.J., Perez, A., and Davis, C.A. 2017. "Instrumented Becker Penetration Test. I: Equipment, Operation, and Performance." *J. Geotech. Eng.*, doi.org/10.1061/(ASCE)GT.1943-5606.0001718.

[32] Harder, L.F., Jr., and Seed, H.B. 1986. "Determination of penetration resistance for coarse-grained soils using the Becker Hammer Drill." College of Engineering, University of California, Berkeley, Calif. Rep. No. UCB/EERC-86/06. May 1986.

[33] Harder, L.F. 1997. "Application of the Becker Penetration Test for evaluating the liquefaction potential of gravelly soils."*NCEER Workshop on Evaluation of Liquefaction Resistance*, held in Salt Lake City, Utah.

[34] ASTM. 2018. Standard test method for use of the dynamic cone penetrometer in shallow pavement applications. ASTM D6951/D6951M-18. West Conshohocken, PA: ASTM.

[35] British Standard 2012, Geotechnical investigation and testing — Field testing — Part 2: Dynamic probing BS EN ISO 22476-2:2005+A1:2011

[36] Boulanger, R.W. and Idriss, I.M. 2014. "CPT and SPT based liquefaction triggering procedures." Center of Geotechnical Modeling, Univ. of California-Davis, Report No. UCD/CGM-14/01.

[37] Youd, T.L., Idriss, I.M., Andrus, R.D., Arango, I., Castro, G., Christian, J.T., Dory, R., Finn, W.D.L., Harder, L.F., Hynes, M.E., Ishihara, K., Koester, J.P., Liao, S.S.C., Marcuson, W.F., Martin, G.R., Mitchell, J.K., Moriwaki, Y., Power, M.S., Robertson, P.K., Seed, R.B., and Stokoe, K.H. 2001. "Liquefaction resistance of soils: Summary Report from the 1996 NCEER and 1998 NCEER/NSF Workshops on evaluation of liquefaction resistance of soils."*J. Geotech. Eng.*, 10.1061/(ASCE)1090-0241(2001)127:10(817).

[38] Kayen, R., Moss, R.E.S., Thompson, E.M., Seed, R.B., Cetin, K.O., Der Kiureghian, A., Tanaka, Y., and Tokimatsu, K. (2013). "Shear-wave velocity-based probabilistic and deterministic assessment of seismic soil liquefaction potential." *J. Geotech. Eng.*, doi.org/10.1061/(ASCE)GT.1943-5606.0000743.

[39] Stokoe, K. H. II, Wright, S. G., Bay, J. A., and Roesset, J. M. 1994."Characterization of geotechnical sites by SASW method," ISSMFE, Technical Committee #10 for XIII ICSMFE, Geophysical Characterization of Sites, A. A. Balkema Publishers/Rotterdam & Brookfield, Netherlands,15–25.

[40] Andrus, R.D., and Stokoe, K.H., II 2000. "Liquefaction resistance of soils from shear-wave velocity." *J. Geotech. Eng.,* 10.1061/(ASCE)1090-0241(2000)126:11(1015).

[41] Ohta, Y. and Goto, N. 1978. "Physical background of the statistically obtained S-wave velocity equation in terms of soil indexes." *ButsuriTanko(Geophysical Exploration),* Tokyo, Japan, 31(1), 8-17 (In Japanese).

[42] Rollins, K.M., Evans, M., Diehl, N. and Daily, W. 1998b. "Shear modulus and damping relationships for gravels." *J. Geotech. and Geoeviron. Eng..*, ASCE, 124(5) p. 396-405.

[43] Weston, T. R. 1996. "Effects of grain size and particle distribution on the stiffness and damping of granular soils at small strains." MS thesis, University of Texas, Austin, Texas.

[44] Chang, W.J. 2016. "Evaluation of liquefaction resistance for gravelly sands using gravel content-corrected shear-wave velocity." *J. Geotech. Eng.*, 10.1061/(ASCE)GT.1943-5606.0001427.

[45] Chen, L. Yuan, X., Cao, Z. Sun, R. Wang, w., and Liu H. 2018. Earthquake Spectra, 34(3) p. 1091-1111

[46] Cao, Z., Youd, T.L., and Yuan, X. 2011. "Gravelly soils that liquefied during 2008 Wenchuan, China Earthquake, Ms=8.0." *Soil Dynamics and Earthquake Engineering*, 31(8), 1132-1143.

[47] Seed, H. B., and I. M. Idriss. 1971. "Simplified procedure for evaluatingcsoil liquefaction potential." J. Soil Mech. Found. Div. 97 (9): 1249–1273 https://doi.org/10.1061/JSFEAQ.0001662.

[48] Golesorkhi, R. 1989. "Factors influencing the computational determination of earthquake-induced shear stresses in sandy soils." PhD dissertation, University of California, Berkeley, California.

[49] Idriss, I.M. 1999. "An update to the Seed-Idriss simplified procedure for evaluating liquefaction potential." *Procs. TRB Workshop on New Approaches to Liquefaction*, Publication No. FHWA-RD-99-165, Federal Highway Administration.

[50] Worden, C. B., Wald, D. J., Allen, T. I., Lin, K., and Cua, G. 2010. "Integration of macroseismic and strong-motion earthquake data in ShakeMap for real-time and historic earthquake analysis." USGS website, http://earthquake.usgs.gov/earthquakes/shakemap/.

[51] Idriss, I. and Boulanger, R. W. 2008. "Soil liquefaction during earthquakes." Earthquake Engineering Research Institute.

[52] Cao, Z., Yuan, X., Youd, T.L., and Rollins, K.M. 2012. "Chinese Dynamic Penetration tests (DPT) at liquefaction sites following 2008 Wenchuan Earthquake." *Proc., 4th Int. Conf. on Geotechnical and Geophysical Site Characterization, Taylor & Francis Group, London*, 1499-1504.

[53] Seed, H.B., Tokimatsu, K., Harder, L.F., and Chung, R.M. 1985. "Influence of SPT procedures in soil liquefaction resistance evaluations." *J. Geotech. Eng.*, 10.1061/(ASCE)0733-9410(1985)111:12(1425).

[54] Sykora, D. W. 1987. ''Creation of a data base of seismic shear wave velocities for correlation analysis.'' *Geotech. Lab. Misc. Paper GL-87-26*, U.S. Army Engr. Waterways Experiment Station, Vicksburg, Miss.

[55] Rollins, K.M., Roy, J., Athanasopoulos-Zekkos, A., Zekkos, D., Amoroso, S., Cao, Z. (2021). "New dynamic cone penetration test-based procedure for liquefaction triggering assessment of gravelly soils." J. Geotechnical and Geoenvironmental Engrg. ASCE, 147(12), 13 p.

[56] Rollins, K.M., Roy, J., Athanasopoulos-Zekkos, A., Zekkos, D., Amoroso, S., Cao, Z., Millana, G., Vassallo, M., Di Giulio, G. (2022). "A New V_s-Based Liquefaction Triggering Procedure for Gravelly Soils." J. Geotechnical and Geoenvironmental Engrg., 148(6), 15 p. ASCE DOI: 10.1061/(ASCE)GT.1943-5606.0002784

[57] Rollins, K.M., Amoroso, S., Milan, G., Minerelli, L., Vassallo, M., Di Giulio, G. (2020). "Gravel liquefaction assessment using the dynamic cone penetration test based on field performance from the 1976 Friuli earthquake." J. Geotechnical & Geoenvironmental Engrg., ASCE, 146(6)

[58] Hubler, J., Athanasopoulos-Zekkos, A., and Zekkos, D. 2018 "Monotonic and cyclic simple shear response of gravel-sand Mixtures", *Soil Dynamics and Earthquake Engineering, Vol 115, pp. 291-304, Dec 2018,*

[59] Hubler, J., Athanasopoulos-Zekkos, A., and Zekkos, D. 2017. "Monotonic, cyclic and post-cyclic simple shear response of three uniform gravels in constant volume conditions", *J. Geotech. and Geoenviron Eng.* ASCE, Washington, DC, 143(9)

GEOTECHNICAL AND GEOPHYSICAL TESTS FOLLOWING THE 2020 EARTHQUAKE-INDUCED LIQUEFACTION PHENOMENA

Sara Amoroso[1], Kyle M. Rollins[2], Giuseppe Di Giulio[3], Lara Wacha[4], Kosta Urumović[5], Diana Faieta[6], Radovan Filjak[7], Daniela Fontana[8], Stefano Lugli[9], Maria Manuel[10], Giuliano Milana[11], Luca Minarelli[12], Marko Budić[13], Nikola Belić[14], Tomislav Kurečić[15], Luka Sorić[16], Marco Stefani[17], Gabriele Tarabusi[18], Maurizio Vassallo[19]

[1] *Associate Professor, University of Chieti-Pescara, Italy; Research Associate, Istituto Nazionale di Geofisica e Vulcanologia, Italy, sara.amoroso@unich.it*

[2] *Full Professor, Brigham Young University, Utah, USA, rollinsk@byu.edu*

[3] *Researcher, Istituto Nazionale di Geofisica e Vulcanologia, Italy, giuseppe.digiulio@ingv.it*

[4] *Researcher, Croatian Geological Survey, Croatia, lwacha@hgi-cgs.hr*

[5] *Researcher, Croatian Geological Survey, Croatia, kurumovic@hgi-cgs.hr*

[6] *Master Student, University of Chieti-Pescara, Italy, diana.faieta@studenti.unich.it*

[7] *Researcher, Croatian Geological Survey, Croatia, rfiljak@hgi-cgs.hr*

[8] *Full Professor, University of Modena and Reggio Emilia, Italy, daniela.fontana@unimore.it*

[9] *Associate Professor, University of Modena and Reggio Emilia, Italy, stefano.lugli@unimore.it*

[10] *Owner and Chief Geologist, Geo Geotecnica e Geognostica s.r.l., Italy, maria.manuel.geo@icloud.com*

[11] *Technologist, Istituto Nazionale di Geofisica e Vulcanologia, Italy, giuliano.milana@ingv.it*

[12] *Research Fellow, Istituto Nazionale di Geofisica e Vulcanologia, Italy, luca.minarelli@ingv.it*

[13] *Researcher, Croatian Geological Survey, Croatia, mbudic@hgi-cgs.hr*

[14] *PhD Student, Croatian Geological Survey, Croatia, nbelic@hgi-cgs.hr*

[15] *Researcher Croatian Geological Survey, Croatia, tkurecic@hgi-cgs.hr*

[16] *Owner and Chief Engineer, Geotehnički studio d.o.o., Croatia, Luka.Soric@geotehnicki-studio.hr*

[17] *Associate Professor, University of Ferrara, Italy, marco.stefani@unife.it*

[18] *Technologist, Istituto Nazionale di Geofisica e Vulcanologia, Italy, gabriele.tarabusi@ingv.it*

[19] *Researcher, Istituto Nazionale di Geofisica e Vulcanologia, Italy, maurizio.vassallo@ingv.it*

Abstract

Earthquakes and related coseismic effects at the surface, such as liquefaction and lateral spreading, can impact humans due to the resulting economic or social disruptions (e.g. slope and foundation failures, flotation of buried structures, etc.). In this respect, the 2020 Petrinja $M_w6.4$ earthquake (Croatia) provided many examples of liquefaction and lateral spreading, as identified by the post-earthquake field reconnaissance campaigns. The observed liquefaction cases occurred in the alluvial plains of the Kupa, Sava and Glina Rivers or along faults, with ejecta composed of sands and/or gravels of different grain size and mineralogy. The lateral spreading phenomena were observed along river embankments and roads. In this context interest in studying these different features arose, and an international research team from Italy, the United States and Croatia recently performed an intensive geological, geotechnical and geophysical campaign to assess the liquefaction susceptibility at selected sites located throughout the epicentral area (from Glina to Petrinja to Sisak). Innovative in-situ test equipment, such as the dynamic cone penetration test (DPT) for liquefied gravels and the Medusa flat dilatometer test (Medusa DMT) for liquefied sands, were employed in combination with standard in-situ tests, such as the standard penetration test (SPT), the piezocone test (CPTU), and shear wave velocity (Vs) measurements. These techniques were employed to verify their advantages relative to the existing liquefaction triggering charts and to characterize the soil properties of the buried liquefied layers and the non-liquefied crust. This paper presents preliminary results and comparisons at some of the investigated liquefaction sites.

Keywords: liquefaction, in-situ geotechnical and geophysical tests, dynamic cone penetration test, medusa flat dilatometer test, 2020 Petrinja $M_w6.4$ earthquake (Croatia).

1. Introduction

Earthquakes and related phenomena, such as liquefaction-triggered lateral spreading, can generate important economic or social disruptions. It is therefore necessary to adopt proactive measures to manage earthquake risk by ground strengthening to prevent slope and foundation failures, and flotation of buried structures, as stated in several building codes (e.g. [1]). In this respect, the collection of field data regarding liquefaction phenomena is critical to improving knowledge on ground failures and impacts to man-made structures.

The 2020 Petrinja M_w6.4 earthquake (Croatia) provided many examples of liquefaction and lateral spreading, as identified by the post-earthquake field reconnaissance campaigns and by remote surveys using drone photos [2, 3]. In this context, interest in studying such different features arose, and an international research team from Italy, the United States and Croatia began an intensive geological, geotechnical and geophysical campaign beginning in September 2022 which is still ongoing. This study is using innovative in-situ techniques and equipment to assess the liquefaction susceptibility at ten selected sites throughout the epicentral area (between Glina, Petrinja and Sisak; Fig. 1). The objectives were to verify their advantages relative to the existing liquefaction triggering charts and to characterize the properties of the liquefied deposits and the non-liquefied crust. This paper describes the field tests, and presents some preliminary results and comparisons at some of the investigated liquefaction sites.
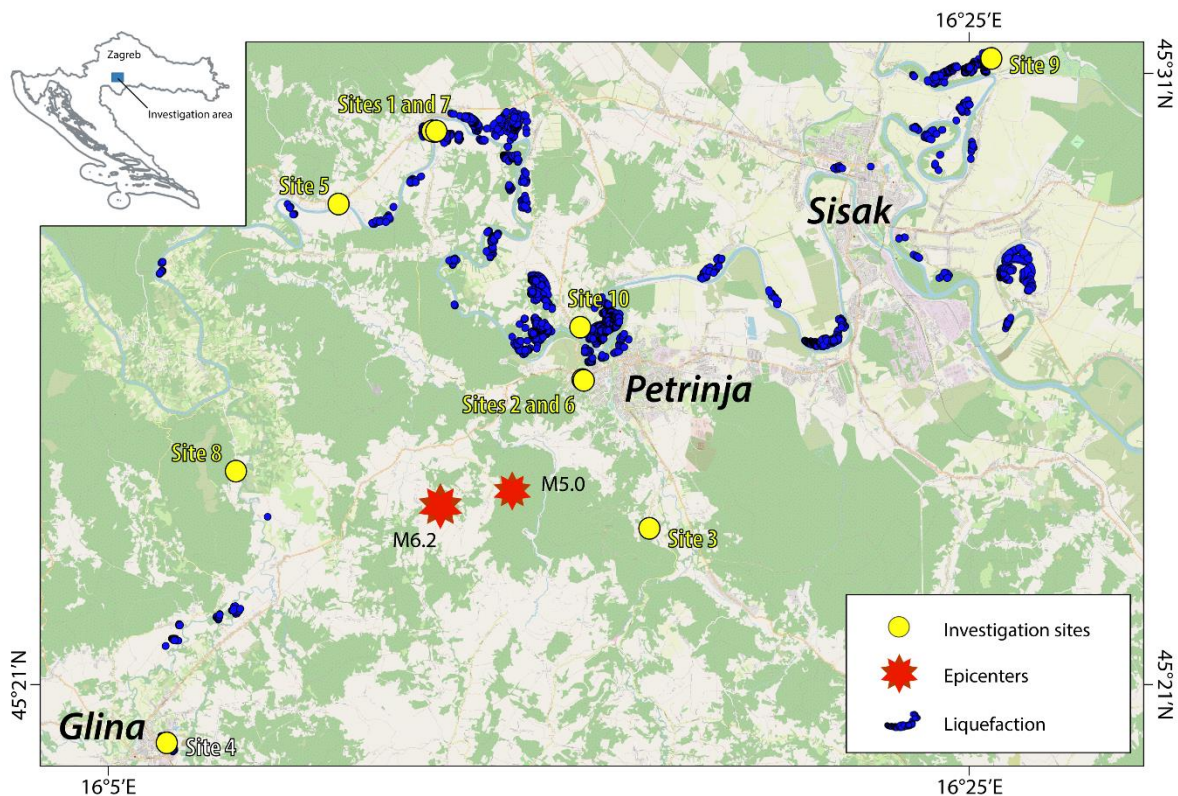
Figure 1. Location of the field investigation sites and epicenters of the 2020 M_w6.4 and M_w5.0 Petrinja earthquakes with OpenStreetMap as background [2]. The locations of the observed liquefaction manifestations were derived from drone images taken by HGI and available satellite images.

2. Geological setting

The earthquake-affected area [4] is located in the continental part of Croatia (Fig. 1), at the southwestern margin of the Sava Basin within the Pannonian Basin System. The wide Petrinja region is located between the Adria-derived units of the Dinarides to the southwest, and the Europe-derived

units (Tisza mega unit) of the Pannonian region to the northeast [2, 5]. During the Tertiary, the region was subjected to tectonic extension (Miocene), followed by a compressional phase (Pliocene-Quaternary), eventually generating a complex framework of NW-SE striking, inverted normal faults [6, 7]. The epicentral area of the 2020 earthquake is located in the Hrastovička mountain, composed of various basement rocks (Jurassic-Paleogene) such as metamorphites of the ophiolitic complex, volcanic rocks, spilites, marine limestone, turbiditic calcarenites, marls conglomerates, sandstones, shales and coals [8, 9]. The liquefaction phenomena occurred in the lowlands at elevations between 100 and 200 m (Fig. 1). The Neogene and Quaternary deposits form the sedimentary infill of the Pannonian Basin System [10]. Some of the coseismic effects were recorded within the Neogene bioclastic limestones and calcrudites, but most of them occurred in the alluvial plains of Glina, Kupa, and Sava Rivers. The affected sediments were deposited in different environments such as flood plain, meander oxbow, and active streams. The liquefaction affected lithologies widely vary from clays, to silts, sands, and gravels, although the silty sediments are prevailing. the overall thickness of the Quaternary succession is usually up to 5 m in alluvial plains, but it may reach estimated at a maximum of up to 30 m [8, 9].

3. The 2020 Petrinja earthquake

3.1 Seismic event

On 29th December 2020 at 11:19 (UTC), the town of Petrinja and its surroundings were hit by a destructive $M_w6.4$ earthquake [11]. The seismic sequence began in the morning of the previous day (05:28 UTC) with $M_w5.0$ earthquake centered about 5 km southwest of Petrinja [2]. According to [11] and the Croatian Earthquake Catalogue – CEC (updated and continuously supplemented version first described in [12]), the mainshock was with a shallow crustal depth of about 6 km, generating moderate to strong shaking in central Croatia, and was largely felt across Croatia and neighbouring countries. Earthquake shaking triggered surface ruptures along the fault trace, and extensive liquefaction and lateral spreading within approximately 20 km around the epicentre (Fig. 1) [2, 3]. Based on its surface projection and orientation, the ruptured zone was associated to the Petrinja-Pokupsko Fault (PPKF). Following the NW-SE orientation of the older faults, the PPKF most probably represents a re-activated deep-seated dextral strike-slip fault zone [2].

3.2 Liquefaction evidences

An European team of researchers (geologists and engineers), in tight collaboration with the Croatian Geological Survey, performed field reconnaissance campaigns with the aim of providing a detailed identification and characterization of the primary and secondary geological and geotechnical coseismic effects induced by the Croatian earthquakes [2]. To improve the understanding of the liquefaction phenomena [3], the Working Group integrated the data collected directly in the field with those from a remote survey by drone aerial photos acquired immediately following the earthquakes. This process allowed for the collection of the liquefaction record with the highest possible completeness both in terms of pattern and distribution of the phenomena. The data set includes several detailed case studies typified by the following characteristics: (a) liquefaction occurring on alluvial plain sites (Kupa, Sava and Glina rivers); (b) ejecta consisting of sand and/or gravel locally associated with shells and armoured mud balls; (c) lateral spreading phenomena along roads and river embankments; (d) sand ejecta of different grain size and composition, even at the same site; and (e) sand and/or gravel ejecta developed along fault traces.

Figure 2. Examples of liquefaction following the Petrinja earthquake (modified after [2]): a) lateral spreading along Kupa river embankment at Letovanic; b) crack with sand ejecta in the alluvial plain of the Sava river; and c) sand and gravel ejecta of different provenance with the presence of shells close to the Kupa river.

4. Site investigations

At the ten research sites, a thorough geological, geotechnical and geophysical site investigation was planned using innovative in-situ test equipment, as described in the following paragraphs. Most of the investigations were carried out in September 2022, although some of them are still ongoing due to weather conditions and flooding near the rivers. At each of the six gravel sites, dynamic cone penetration (DPT) tests were performed in combination with boreholes, piezocone test (CPTU), and shear wave velocity (V_S) measurements. At the lateral spreading site, boreholes with standard penetration tests (SPT) at approximately 0.5-meter intervals were performed. Finally, at the liquefied sandy sites with high fines content, the Medusa flat dilatometer test (Medusa DMT) was employed in combination with standard geotechnical in-situ tests, such as borehole with SPTs, CPTU and V_S measurements. Currently, laboratory analyses are being conducted on soil samples collected at all sites to provide information on mineralogy and geotechnical properties of the liquefied sandy and gravelly deposits and of the non-liquefied crusts.

4.1 Dynamic cone penetration test (DPT)

The dynamic cone penetration test (DPT) was developed in China in the early 1950s to measure penetration resistance of gravel for application in bearing capacity analyses. Based on their experience, standard test procedures and code provisions have been formulated [13, 14]. Because of widespread gravelly deposits beneath the Chengdu plain, the DPT is widely used in that region, particularly for the evaluation of liquefaction potential [15]. More recently, an updated liquefaction triggering curve has been proposed by [16] using a worldwide database.

DPT equipment is relatively simple, consisting of a 120-kg hammer, raised to a free fall height of 100 cm, then dropped onto an anvil attached to 60-mm diameter drill rods which in turn are attached to a solid steel cone tip with a diameter of 74 mm and a cone angle of 60º as shown in Fig. 3a. The larger cone makes it less affected by gravel particles, while the smaller rod diameter helps to reduce shaft friction on the rods behind the cone tip.

Prior to testing, the drill rods are marked at 10 cm intervals (see the detail in Fig. 3b, photo of the Petrinja DPT test) and the number of blows required to penetrate each 10 cm is recorded. The raw DPT blow count is defined as the number of hammer drops required to advance the cone tip 10 cm. A second penetration resistance measure, called N_{120}, is specified in Chinese code applications where N_{120} is the number of blows required to drive the cone tip 30 cm; however, N_{120} is calculated simply by multiplying raw blow counts by a factor of three which preserves the detail of the raw blow count record.
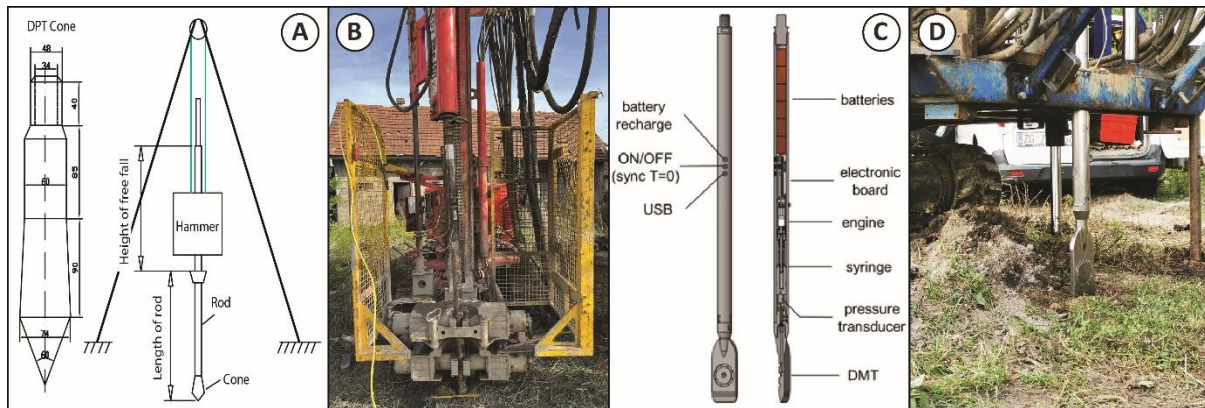
Figure 3. a) Component sketch of tripod and drop hammer setup for dynamic penetration tests (DPT) along with DPT cone tip (modified after [15]); b) photo of DPT testing at one of the Croatian site investigation with conventional drill rig; c) Medusa DMT layout [17]; d) photo of the Medusa DMT testing at one of the Croatian site investigation using a conventional light penetrometer combined with drill rig.

4.2 Medusa dilatometer test (Medusa DMT)

The Medusa DMT is the combination of a flat dilatometer with a hydraulic automation and measuring system for autonomously performing DMT tests [17]. Fig. 3 shows the main components of the instrument, together with a photo of a Medusa DMT test performed in September 2022 in Croatia. A rechargeable battery pack powers an electronic board, connected to a pressure transducer and to a custom-designed motorized syringe. The firmware coded in the electronics activates the motorized syringe for generating the pressure required to obtain the DMT readings. The maximum operating pressure is 25 MPa. A high accuracy pressure transducer is used to measure the pressure generated by the syringe and operating on the membrane. An electric wire provides the contact status of the membrane to the electronic board. The A, B, and C pressure readings are taken by the electronics firmware with the same criteria used for the traditional pneumatic DMT equipment. Details on calibration chamber and field validation of the Medusa DMT can be found in [17, 18, 19, 20].

4.3 Geophysical surveys (H/V and surface-wave analysis)

To better reconstruct the near-surface velocity profile an extensive geophysical survey was carried out using both two-dimensional (2D) arrays of seismic nodes and linear array of geophones. For the 2D array, a quite innovative technology in small-scale surveys based on seismic nodes was used [21, 22]. Seismic nodes are composed of compact digitizers with internal battery connected to 3C geophones (GSB-3C and GS-one manufactured by Geospace Technologies), and the absence of cable and their ease in the field installation allowed to quickly deploy a large number of nodes (from 20 to 46 depending on site). Seismic nodes were arranged at each selected site in a circular geometry (Table 1) with usually 3 circular rings with different radius (about 5, 12 and 25 m), and a node in the centre close to DPT or Medusa DMT surveys. Seismic nodes recorded at each site a few hours of ambient vibrations (seismic noise) with a sampling rate that was set equal to 250 Hz.

From seismic noise data collected by 3C nodes, it was possible to compute the horizontal-to-vertical noise spectral ratio (H/V curve), and derive the site resonance frequency (f0) from the peak in the H/V curve [23]. f0 is an important proxy for potential site amplification [24] used in site characterization analyses and microzonation mapping. It is related to the presence of a strong seismic impedance contrast in the subsoil profile, where f0 value is linked to the average thickness and shear-wave velocity of soft soil deposits overlaying a stiffer soil unit or bedrock interface [25].

For the linear array of geophones, a maximum of 72 vertical geophones (eigen-frequency 4.5 Hz) connected to a multi-channel acquisition system was used (Geode manufactured by Geometrics, connected in serial for a maximum number of 3 Geode) recording files with length of 1.5 s and sampling rate equal to 8000 Hz. The 72 geophones were equally spaced from 0.5 to 1 m, depending

on the site (Table 1). In contrast to the 2D array of nodes which collects seismic noise, the linear array records seismic signals produced by an active source composed of a 5 kg-sledge-hammerhitting a metal plate. The seismic source was located at the beginning, in the middle and at the end of the linear array of geophones in order to reproduce forward and reverse shot records.

To provide absolute positions for each seismic measurement, a real-time kinematic (RTK) positioning was used through a GNSS receiver (S900a new manufactured by Stonex). In this way, the position of each deployed node and the first and last geophones within the 1D line were measured with accuracy of a few cm. The absolute position was also measured for the geotechnical and borehole surveys previously discussed. In order to derive a surface-wave dispersion curve, active data collected by the linear geophones array and passive data from nodes will be analysed with the multichannel analysis of surface waves (MASW) technique [26, 27]. In particular, the analysis from 3-components data recorded by nodes will allow to retrieve the Rayleigh and Love dispersion curves.

The surface-wave dispersion curves obtained by 1D active array and 2D passive array will be combined to achieve information in a large frequency band. In general, active methods provide results at higher frequencies in comparison to passive techniques [28]. However, in the analysed experiment the dispersion curves are expected to extend toward high frequencies also in the passive case, due to the large number of seismic nodes deployed in a relatively small area (Table 1).

Table 1 – Geophysical surveys performed at the selected sites. For the position of the Site, refer to Fig. 1. For Sites 2 and 6, the geometry of array installation is reported in Fig. 6

ID site	Date of geophysical survey	2D arrays: number of seismic GSB nodes (and radius with maximum aperture)	1D array using 72 vertical geophones: spacing between adjacent geophone
Site 1	14 September 2022	32 (25 m)	1 m
Site 2	12 September 2022	46 (21 m); array A in Fig. 6	0.5 m
Site 3	13 September 2022	26	0.5 m
Site 4	15 September 2022	29 (22 m)	1 m
Site 5	14 September 2022	-	0.5 m
Site 6	15 September 2022	20 (10 m) array F in Fig. 6	-
Site 10	16 September 2022	25 (20 m)	-

5. Preliminary results

Considering that the field campaign is ongoing and most of the results are still under evaluation, this section presents only some preliminary results at two gravel liquefaction sites (Sites 2 and 6, Petrinja) and at a sand liquefaction site with high fines content (Site 8, Donje Jame).

The energy transfer measurements at Site 6 indicate that the DPT hammer was providing an average of 89% of the theoretical free-fall energy, which is practically identical to the Chinese standard without requirement for hammer energy correction. Plots of the soil profile, the DPT blow count (N_{120}), and the relative density are provided in Fig. 4. Preliminary analyses indicate that the friction on the drill rod behind the DPT cone artificially increased the N_{120} value in the clayey silt, while the CPT cone resistance remained essentially constant within similar materials. Therefore, the DPT blow counts below the clayey silt layer were corrected to account for this effect. Additional DPT testing is planned with an open borehole to the top of the gravel to confirm this correction. Using the corrected DPT blow counts in the sandy gravel to gravelly sand layers, correlations [29] indicate a relative density between 40 to 55%. These preliminary assessments indicate that the gravelly soil from about 4 to 6.25 m is the critical layer for liquefaction at this site. Ongoing mineralogical studies and liquefaction evaluations should help confirm this conclusion.
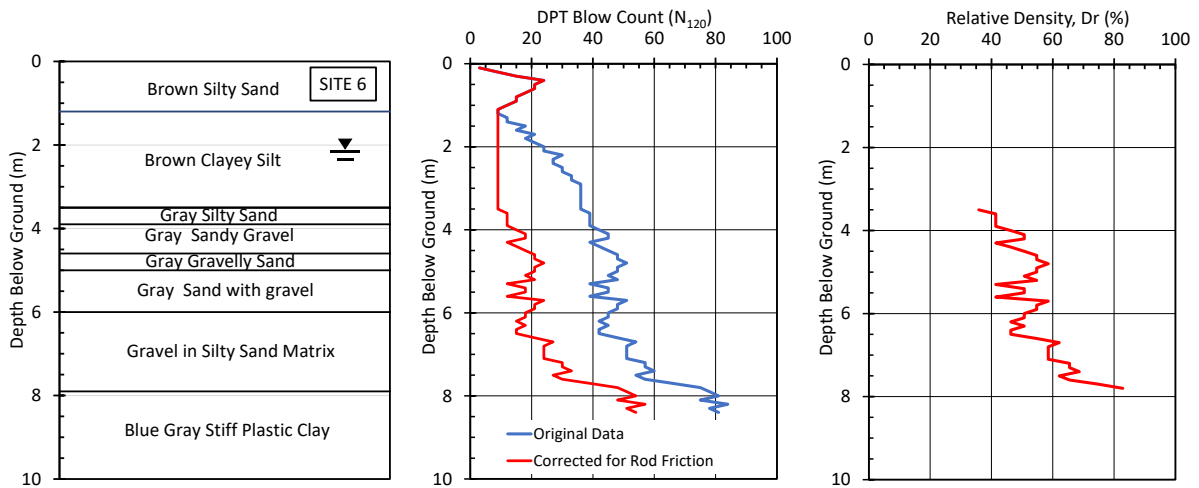
Figure 4. Preliminary DPT results for test site at Petrinja (Site 6).

At Site 8, a preliminary interpretation of the Medusa DMT was performed according to [30] correlations. Fig. 5 shows the DMT profiles in terms of: material index (I_D) and the soil behaviour type index (SBT_{DMT}) for the mechanical soil behaviour, constrained modulus (M) for the soil stiffness at "operative" strain level, undrained shear strength (s_u) and friction angle (ϕ') for the soil resistance, and horizontal stress index (K_D) for the stress history of the soil. The top 3.5 m are identified mostly as sands and silty sands, whereas silts, clayey and sandy silts are predominant at higher depths. This finding is in agreement with the borehole log and the CPTU data. According to the DMT and phreatimeter readings, the ground water table is located at 3 m depth, where the silty sandy layer is present. This body represents probably the one that liquefied during the Petrinja earthquake, as it was preliminary evaluated by examining the soil stratigraphy, the earthquake reconnaissance information and the K_D profile. However, liquefaction triggering analysis and laboratory tests on borehole samples and ejecta are required to confirm these preliminary outcomes.
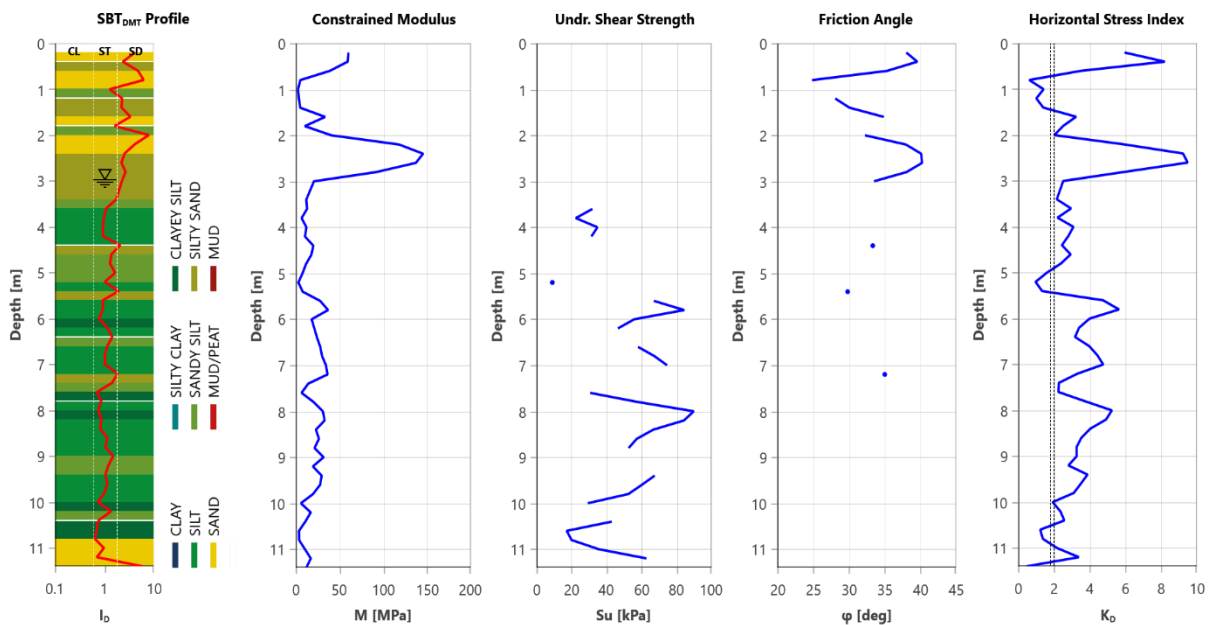
Figure 5. Preliminary Medusa SDMT results at the test site of Donje Jame (Site 8).

The objectives of the geophysical surveys were: (a) to infer the f0 value from the H/V curve (from 3C nodes); (b) to measure the surface-wave dispersion curve combining both passive and active array methods [31]; and (c) to infer the near-surface shear-wave velocity profile in the top few hundreds of meters by means of a joint inversion of the H/V and dispersion curves integrating results from geotechnical tests. Fig. 6 shows an example of the 2D array geometry applied in the field at two gravel sites in Petrinja (Sites 2 and 6), and the preliminary results in terms of H/V obtained at two arrays.
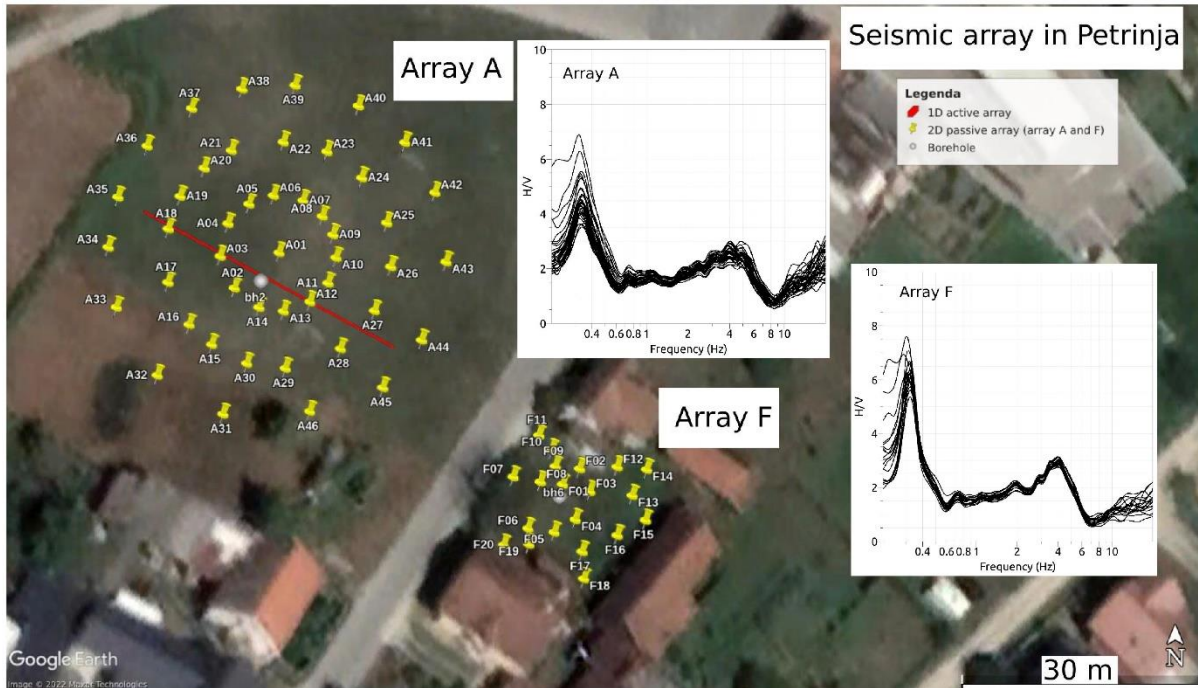
Figure 6. Seismic arrays in Petrinja. The yellow markers indicate the seismic nodes installed in 2D configuration (arrays A and F). The red line within array A shows the linear array of 72 geophones used for active experiment (the shot positions were situated at: -5 m and -2 m far from the first geophone, in the middle of the line, and at +2, +5, + 10 m far from the last geophone). The mean H/V curves computed at all seismic nodes of the two arrays are also shown.

6. Conclusions

The 2020 M_w6.4 Petrinja earthquake offered the possibility for an in depth study of the liquefaction-induced features in the epicentral area. In particular, the variety of coseismic evidences (gravel liquefaction, lateral spreading and sand liquefaction with high fines content) provided an opportunity to improve knowledge of issues for which the experience is still limited.

In this respect, an intensive geological, geotechnical and geophysical campaign was planned at ten selected sites along the Kupa, Glina and Sava Rivers to verify the use of existing liquefaction triggering charts and to evaluate the soil properties of the liquefied layers and the non-liquefied crust. Some preliminary findings are reported in this paper based on extensive geophysical survey and two innovative geotechnical in-situ tests, the dynamic cone penetration test (DPT) and the Medusa flat dilatometer test (Medusa DMT). These results already provide a valuable information regarding the soil deposits that liquefied during the earthquake. Additional liquefaction triggering analysis and laboratory tests on borehole samples and ejecta are required to confirm these preliminary outcomes. More definitive conclusions should be possible once the ongoing field campaign and subsequent analyses are completed.

Acknowledgements

References

[1] Kramer, S.L. (1996). Geotechnical earthquake engineering. *Prentice Hall*, Upper Saddle River, N.J, 1996.

[2] Baize, S., Amoroso, S., Belić, N., Benedetti, L., Boncio, P., Budić, M. Cinti, F.R., Henriquet, M., Jamšek Rupnik, P., Kordić, B., Markušić, S., Minarelli, L., Pantosti, D., Pucci, S., Špelić, M., Testa, A., Valkaniotis, S., Vukovski, M., Atanackov, J., Barbača, J., Bavec, M., Brajkovič, R., Brčić, V., Caciagli, M., Celarc, B., Civico, R., De Martini, P.M., Filjak, R., Iezzi F., Moulin, A., Kurečić, T., Métois, M., Nappi, R., Novak, A., Novak, M., Pace, B., Palenik, D. and Ricci T. (2022). Environmental effects and seismogenic source characterization of the December 2020 earthquake sequence near Petrinja, Croatia. *Geophysical Journal International* **230**(2): 1394–1418. https://doi.org/10.1093/gji/ggac123

[3] Amoroso, S., Barbača, J., Belić, N., Kordić, B., Brčić, V., Budić, M., Civico, R., De Martini, P.M., Hećej, N., Kurečić, T., Minarelli, L., Novosel, T., Palenik, D., Pantosti, D., Pucci, S., Filjak, R., Ricci, T., Špelić, M. and Vukovski, M. (2021). Liquefaction field reconnaissance following the 29th December 2020 Mw 6.4 Petrinja earthquake (Croatia). *Proc. EGU General Assembly 2021, online*; 19–30 Apr 2021, Abstract No. EGU21-16584. https://doi.org/10.5194/egusphere-egu21-16584

[4] Pollak, D., Gulam, V., Novosel, T., Avanić, R., Tomljenović, B., Hećej, N., Terzić, J., Stipčević, J., Bačić, M. and Kurečić, T. (2021). The preliminary inventory of coseismic ground failures related to December 2020 – January 2021 Petrinja earthquake series. *Geologia Croatica: Journal of the Croatian Geological Survey and the Croatian Geological Society* **74**(2): 189-208. https://doi.org/10.4154/gc.2021.08

[5] Schmid, S.M., Fügenschuh, B., Kounov, A., Maţenco, L., Nievergelt, P., Oberhänsli, R., Pleuger, J., Schefer, S., Schuster, R., Tomljenović, B., Ustaszewski, K. and van Hinsbergen, D.J.J. (2020). Tectonic units of the Alpine collision zone between Eastern Alps and western Turkey. *Gondwana Research* **78**: 308–374. https://doi.org/10.1016/j.gr.2019.07.005

[6] Tomljenović, B. and Csontos, L. (2001). Neogene–Quaternary structures in the border zone between Alps, Dinarides and Pannonian Basin (Hrvatsko zagorje and Karlovac Basins, Croatia). *International Journal of Earth Sciences* **90**: 560–578. https://doi.org/10.1007/s005310000176

[7] Ustaszewski, K., Kounov, A., Schmid, S.M., Schaltegger, U., Krenn, E., Frank, W. and Fügenschuh, B. (2010). Evolution of the Adria-Europe plate boundary in the northern Dinarides: From continent-continent collision to back-arc extension: Adria-Europe Plate Boundary, Dinarides. *Tectonics* **29**. https://doi.org/10.1029/2010TC002668

[8] Pikija, M. (1987). Basic Geological Map of SFRY 1:100.000, Sisak sheet. *Geol. Zavod*, Zagreb, Savezni geol. Zavod, Beograd [in Croatian].

[9] Šikić, K. (2014). Basic Geological Map of Republic Croatia 1:100.000, Bosanski Novi sheet. *Croatian Geological Survey*, Zagreb [in Croatian].

[10] Pavelić, D. and Kovačić, M. (2018). Sedimentology and stratigraphy of the Neogene rift-type North Croatian Basin (Pannonian Basin System, Croatia): A review. *Marine and Petroleum Geolology* **91**: 455–469. https://doi.org/10.1016/j.marpetgeo.2018.01.026

[11] Markušić, S., Stanko, D., Penava, D., Ivančić, I., Bjelotomić Oršulić, O., Korbar, T. and Sarhosis, V. (2021). Destructive M6.2 Petrinja Earthquake (Croatia) in 2020—Preliminary Multidisciplinary Research. *Remote Sensing* **13**: 1095. https://doi.org/10.3390/rs13061095

[12] Herak, M., Herak, D. and Markušić, S. (1996). Revision of the earthquake catalogue and seismicity of Croatia, 1908–1992. *Terra Nova* **8**: 86–94.

[13] Chinese Design Code (2001). Design code for building foundation of Chengdu region. *Administration of Quality and Technology supervision of Sichuan Province PRC* DB51/T5026-2001 [in Chinese].

[14] Chinese Specifications 1999. Specification of soil test. *Ministry of Water Resources of the People's Republic of China* SL237-1999 [in Chinese].

[15] Cao, Z. Youd, T.L. and Yuan, X. (2011). Gravelly soils that liquefied during 2008 Wenchuan, China Earthquake, Ms=8.0. *Soil Dynamics and Earthquake Engineering* **31**: 1132-1143.

[16] Rollins, K.M., Roy, J., Athanasopoulos-Zekkos, A., Zekkos,, D., Amoroso, S. and Cao, Z. (2021). A new dynamic cone penetration test–based procedure for liquefaction triggering assessment of gravelly soils. *Journal of Geotechnical and Geoenvironmental Engineering* **147**(12): 04021141. https://doi.org/10.1061/(ASCE)GT.1943-5606.0002686

[17] Marchetti, D. (2018). Dilatometer and Seismic Dilatometer Testing Off-shore: Available Experience and New Developments. *Geotechnical Testing Journal* **41**(5): 967–977. https://doi.org/10.1520/GTJ20170378

[18] Marchetti, D., Monaco, P., Amoroso, S. and Minarelli, L. (2019). In situ tests by Medusa DMT. *Proc. XVII European Conference on Soil Mechanics and Geotechnical Engineering*; Reykjavik, Iceland, 2019, 1–8. https://doi.org/10.32075/17ECSMGE-2019-0657

[19] Monaco, P., Marchetti, D., Totani, G., Totani, F. and Amoroso, S. (2022). Validation of Medusa DMT test procedures in Fucino clay. *Proc. 20th International Conference on Soil Mechanics and Geotechnical Engineering*; 1-5 May 2022, Sydney, Australia, 471-476.

[20] Monaco, P., Tonni, L., Amoroso, S., Martinez, M.F., Gottardi, G., Marchetti, D. and Minarelli L. (2021). Use of Medusa DMT in alluvial silty sediments of the Po river valley. *Proc. 6th International Conference on Geotechnical and Geophysical Site Characterization - ISC'6 Conference*; 26-29 September 2021, Budapest, Hungary.

[21] Dean, T., Tulett, J. and Barnwell, R. (2018). Nodal land seismic acquisition: The next generation. *First Break* **36**(1): 47-52.

[22] Dean, T. and Sweeney, D. (2019). The use of nodal seismic acquisition systems to acquire limited-scale surveys. *First Break* **37**(1): 55-60.

[23] Molnar, S., Cassidy, J.F., Castellaro, S., Cornou, C., Crow, H., Hunter, J.A., Matsushima, S., Sánchez-Sesma, F.J. and Yong, A. (2018). Application of microtremor horizontal-to-vertical spectral ratio (MHVSR) analysis for site characterization: State of the art. *Surveys in Geophysics* **39**(4): 613-631.

[24] Di Giulio, G., Cultrera, G., Cornou, C., Bard, P.Y. and Al Tfaily, B. (2021). Quality assessment for site characterization at seismic stations. *Bulletin of Earthquake Engineering* **19**(12): 4643-4691.

[25] Bonnefoy-Claudet, S., Cornou, C., Bard, P.Y., Cotton, F., Moczo, P., Kristek, J. and Fäh, D. (2006). H/V ratio: A tool for site effects evaluation. Results from 1-D noise simulations. *Geophysical Journal International* **167**(2): 827-837.

[26] Park, C. B., Miller, R. D., Xia, J. and Ivanov, J. (2007). Multichannel analysis of surface waves (MASW)-Active and passive methods. *The Leading Edge* **26**: 60-64

[27] Wathelet, M., Guillier, B., Roux, P., Cornou, C. and Ohrnberger, M. (2018). Rayleigh wave three-component beamforming: signed ellipticity assessment from high-resolution frequency-wavenumber processing of ambient vibration arrays. *Geophysical Journal International* **215**(1): 507-523.

[28] Foti, S., Lai, C.G., Rix, G.J. and Strobbia, C. (2015). Surface Wave Methods for Near-Surface Site Characterization, *CRC press*.

[29] Rollins, K.M., Amoroso, S., Milan, G., Minerelli, L., Vassallo, M. and Di Giulio, G. (2020). Gravel liquefaction assessment using the dynamic cone penetration test based on field performance from the 1976 Friuli earthquake. *Journal of Geotechnical and Geoenvironmental Engineering* **146**(6): 04020038 https://doi.org/10.1061/(ASCE)GT.1943-5606.0002252

[30] Marchetti, S., Monaco, P., Totani, G. and Calabrese, M. (2001). The Flat Dilatometer Test (DMT) in Soil Investigations – A Report by the ISSMGE Committee TC16. *Proc. International Conference on In situ Measurement of Soil Properties and Case Histories*; Bandung, Indonesia, 2001, 95–131. Official version approved by TC16 reprinted *Proc. 2nd International Conference on the Flat Dilatometer*; Washington D.C., USA, 2006, 7–48.

[31] Wathelet, M., Chatelain, J.L., Cornou, C., Giulio, G.D., Guillier, B., Ohrnberger, M. and Savvaidis, A. (2020). Geopsy: A user‑friendly open‑source tool set for ambient vibration processing. *Seismological Research Letters* **91**(3): 1878-1889.

GEOTECHNICAL RECONNAISSANCE OF COVER-COLLAPSE SINKHOLE AREA FOLLOWING PETRINJA 2020 EARTHQUAKE

Ingrid Tomac[1], Biljana Kovačević Zelić[2], Dunja Perić[3], Dubravko Domitrović[4], Nataša Štambuk Cvitanović[5], Helena Vučenović[6], Jelena Parlov[7], Josip Stipčević[8], Darko Matešić[9], Bojan Matoš[10] and Igor Vlahović[11]

[1] *Assistant professor, University of California, San Diego, US, itomac@eng.ucsd.edu*
[2] *Professor, University of Zagreb, Faculty of Mining, Geology and Petroleum engineering, Zagreb, Croatia, EU, biljana.kovacevic-zelic@rgn.unizg.hr*
[3] *Professor, Kansas State University, Kansas, US, peric@ksu.edu*
[4] *Associate professor, University of Zagreb, Faculty of Mining, Geology and Petroleum engineering, Zagreb, Croatia, EU, dubravko.domitrovic@rgn.unizg.hr*
[5] *Associate professor, University of Split, Faculty of Civil Engineering, Architecture and Geodesy, Split, Croatia, EU, nstambuk@gradst.hr*
[6] *Assistant professor, University of Zagreb, Faculty of Mining, Geology and Petroleum engineering, Zagreb, Croatia, EU, helena.vucenovic@rgn.unizg.hr*
[7] *Associate professor, University of Zagreb, Faculty of Mining, Geology and Petroleum engineering, Zagreb, Croatia, EU, jelena.parlov@rgn.unizg.hr*
[8] *Assistant professor, University of Zagreb, Faculty of Science, Zagreb, Croatia, EU, jstipcevic@gfz.hr*
[9] *Assistant, University of Zagreb, Faculty of Mining, Geology and Petroleum engineering, Zagreb, Croatia, EU, darko.matesic@rgn.unizg.hr*
[10] *Associate professor, University of Zagreb, Faculty of Mining, Geology and Petroleum engineering, Zagreb, Croatia, EU, bojan.matos@rgn.unizg.hr*
[11] *Professor, University of Zagreb, Faculty of Mining, Geology and Petroleum engineering, Zagreb, Croatia, EU, igor.vlahovic@rgn.unizg.hr*

Abstract

This paper shows an overview of extensive geotechnical and geological investigation of soils around cover-collapse sinkholes that appeared in a constrained area around Mečenčani and Borojevići villages following the 2020–2021 Petrinja earthquake sequence. A total of 122 new and 49 pre-existing historical sinkholes were recorded, mapped, and classified during the geological and geotechnical reconnaissance fieldwork. Many sinkholes collapsed within an area of only 1.13 km^2, a relatively rare phenomenon associated with earthquakes, thus motivating soil investigations to better understand associated failure mechanisms and underlying conditions. This paper shows an overview of triaxial test data in synergy with soil water retention curves of unsaturated soils detected in the area, along with results of standard physical soil tests. The soil in the area consists of a 4–15 m thick clayey cover with sporadic gravel lenses. Clays are mostly over-consolidated, with varying degrees of saturation ranging from very small to fully saturated. Underneath are intensely karstified Miocene carbonate rocks. Seasonal and climate-change-induced variations in the groundwater table interact with the artesian/subartesian karst aquifer, thus affecting the suction and the shear strength. In addition, soil water retention curves indicate that desaturation is possible for deeper groundwater table levels and can further affect effective stress, shear strength, and interparticle tensile forces. Collapsed sinkholes have predominately vertical walls, indicating brittle failure of a cohesive cover with varying degrees of saturation. Based on the specific geomechanical properties of soils, this paper offers several hypotheses of failure mechanisms based on the synergy of earthquake-induced dynamic loading and hydro-mechanical interactions of unsaturated soil layers and pore pressure dynamics between two interconnected aquifers.

Keywords: cover-collapse sinkholes, karstic aquifer, unsaturated soil dynamics, earthquake, progressive failure

1. Introduction

This paper shows an overview of geological, geotechnical, and geophysical investigations following the M$_w$ 6.4 Petrinja 2020–2021 earthquake sequence. The study shown herein is limited to the small

area surrounding two villages, Mečenčani and Borojevići located 20 km SE from the epicenter. Specific geological, seismological, geotechnical, and hydrological circumstances led to the collapse of numerous sinkholes between December 29, 2020 and the end of 2021 [1]. As a result, the reconnaissance team identified and mapped a total of 171 sinkholes, including 122 new and 49 historical sinkholes (Figs. 1 and 2). The occurrence of post-seismic sinkholes has been recorded sparsely and related to subsurface discontinuities [2, 3]. Historical sinkholes in the observed area are scattered and concentrated mostly in the central part around Pašino vrelo spring. New sinkholes are located within two small regions that have the combined area of 1.13 km². According to all available data, none of the new cover-collapse sinkholes formed during the main earthquake or strongest foreshocks and aftershocks. For example, a landowner noticed the soil collapsing at the location of the first documented sinkhole (S015) on the afternoon of December 29, about six hours after the main shock.
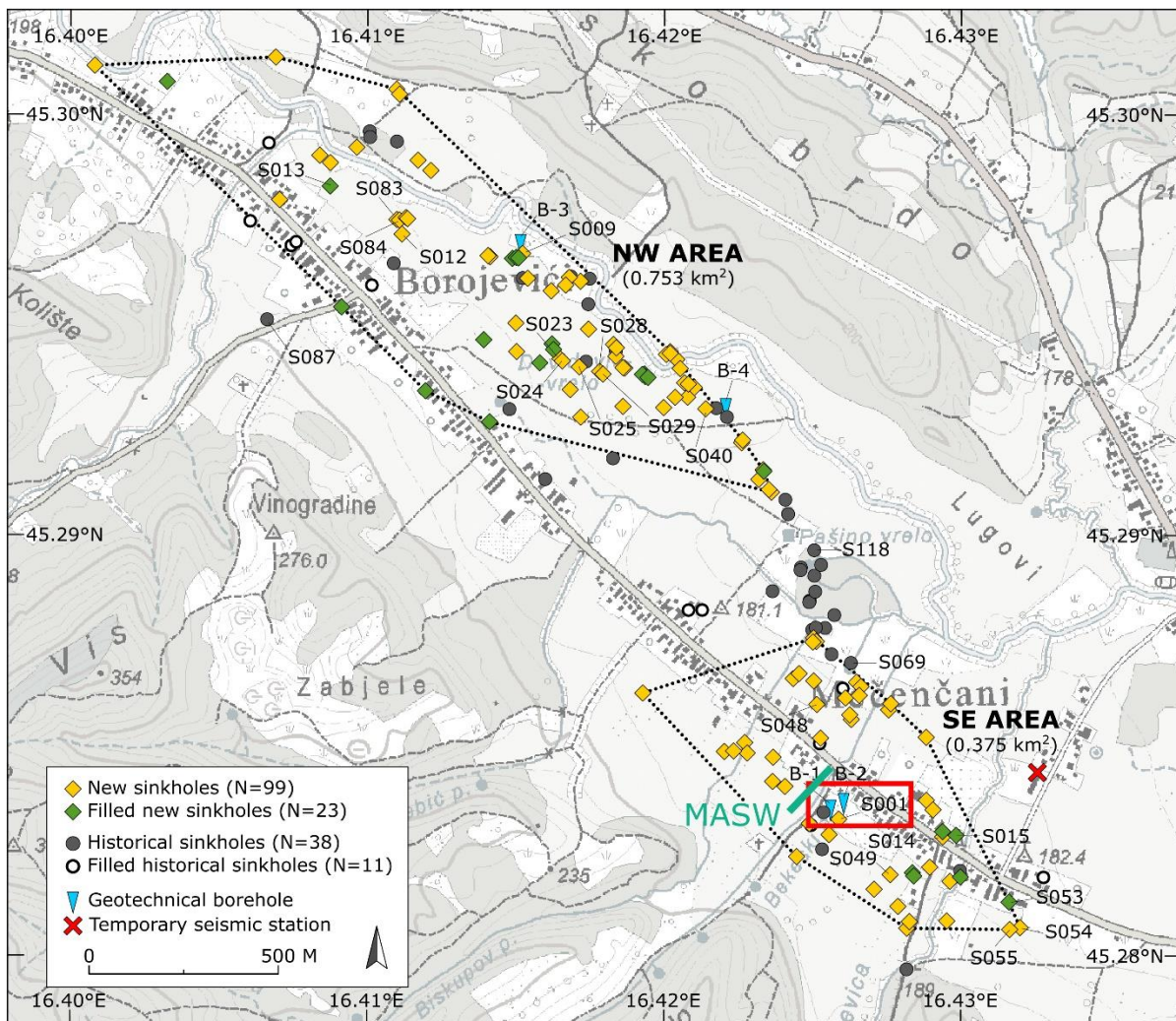
Figure 1. Graphical representation of sinkhole database (modified from [1]). A total of 49 historical sinkholes collapsed before the current seismic sequence (information on 11 previously filled were provided by the locals). Out of the 122 new sinkholes, six were remediated on the basis of geotechnical projects, and 17 were filled by the locals.
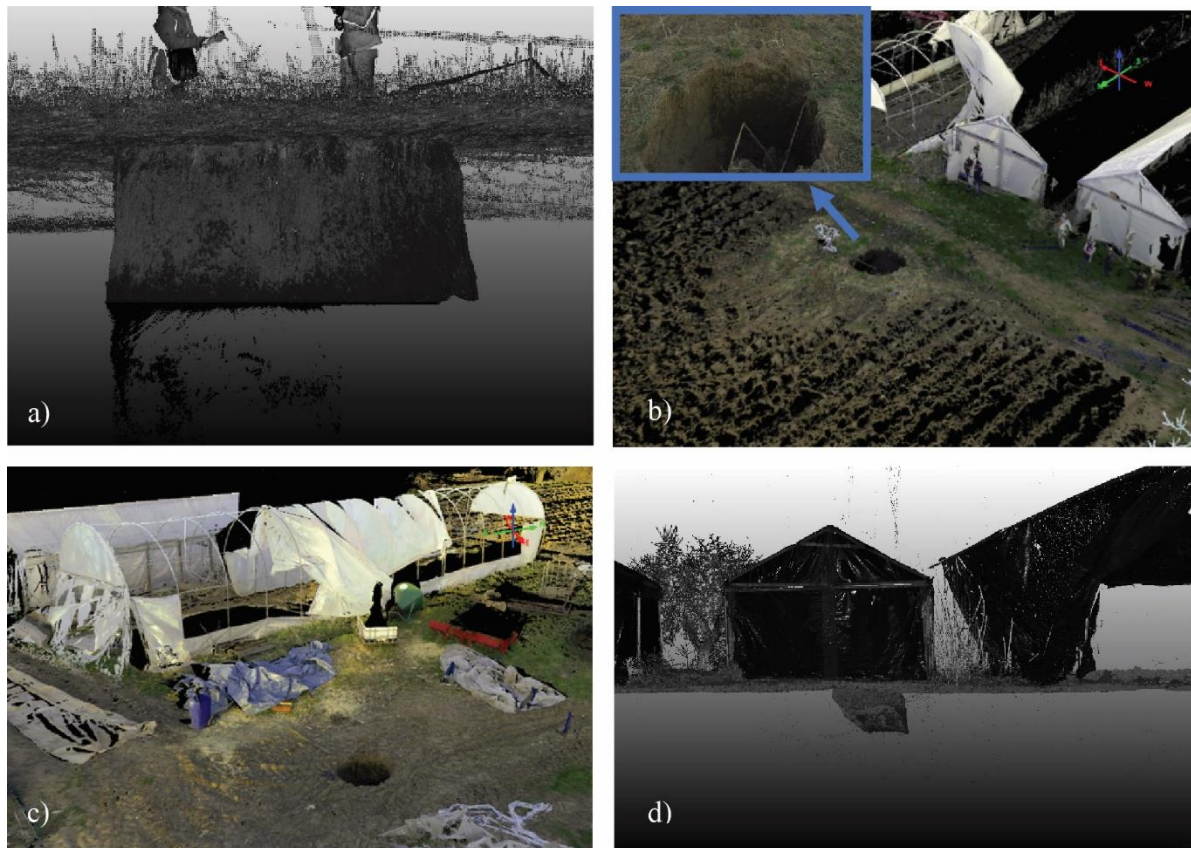
Figure 2. Point-cloud imagery of several representative sinkholes: a) side view of S025 sinkhole; b, d) panoramic view and side view of S054 sinkhole; c) panoramic view of S055 sinkhole.

2. Geological and Hydrogeological Setting and Seismicity

The area where sinkholes occurred is geologically specific, characterized by highly karstified limestones covered by relatively thick clayey soil. Middle Miocene highly porous Lithothamnion limestones and calcarenites are both very susceptible to karstification [4]. Karstified carbonates are directly overlain by a 4–15 m thick sequence of Holocene deluvial–proluvial deposits of clays with interlayers and lenses of gravel and sand [1, 4]. There are relatively few outcrops of karstic rocks in the area. Specifically, out of 1,079 km^2 area of the Bosanski Novi sheet of the Basic Geological Map [5], only a bit more than 60 km^2 is covered by Middle Miocene carbonates. The Sunja river valley in the studied area represents a flat terrain covered with Holocene deluvial–proluvial deposits of low permeability containing a certain amount of water and forming an aquitard. Most households in Mečenčani and Borojevići still use water from shallow dug wells, with an average depth of about 8 meters. The groundwater level fluctuation in the aquitard between dry and wet periods is about 2 m. The aquitard is underlain by a permeable confined karst aquifer, in which the water pressure during wet periods becomes subartesian to artesian [4]. Furthermore, the karst aquifer and overlying low-permeability aquitard are hydraulically connected, and pressure changes in one layer cause changes in hydraulic conditions within the other. During periods of high waters, specifically when the pressure rapidly rises in the karst aquifer, the piezometric level in the karst aquifer is higher than the groundwater level in the overlying aquitard, while during dry periods, the groundwater levels in both layers are equalized.

The Petrinja earthquake sequence started with two strong foreshocks on December 28, 2020, the first occurred at 05:28 UTC with M_L 5.1 and the second one at 6:49 UTC with M_L 4.7. The mainshock

occurred a day later (December 29, 2020, 11:19 UTC, M_L 6.2). The main earthquake caused widespread damage in Petrinja and the surrounding villages, and seven people lost their lives. According to the Croatian Seismological Survey data, the epicentral intensity was estimated to be VIII–IX EMS. At the onset of the Petrinja sequence, the closest seismic station was more than 30 km from the epicentral area, and six additional stations provided more accuracy. Nevertheless, in the first 60 days of the sequence, 4,430 events were located within 50 km of the mainshock. The bulk of the Petrinja sequence epicenters are elongated in the NW–SE direction across roughly 20 km in length and 2–4 km in width, within the Hrastovica Hill between the Kupa and Petrinjčica rivers. The mainshock is positioned in the central cluster part and has a hypocentral depth of about 8 km. The strongest foreshock of the December 28, 2020 (M_L 5.1) occurred within the main cluster, about 2 km easterly from the mainshock.

3. Geotechnical Investigation

Geotechnical and geophysical investigations at two sites in the Mečenčani and Borojevići area have been performed within the scope of the GEER reconnaissance efforts between March 15 and 26, 2021. Geotechnical investigation included drilling four boreholes by manually operated solid stem auger, field identification and classification of drilled core, Standard Penetration Test (SPT) and manually driven Dynamic Penetrometer Light (DPL), GW observations in boreholes, and collection of disturbed and undisturbed soil samples for further laboratory testing. Boreholes B-1 and B-2 were drilled on March 23, 2021 in Mečenčani village, close to the largest sinkhole in the area, S001 (Fig. 3). They were drilled in mostly clayey soil to a depth of 8.0 m and 7.6 m, respectively. Other two boreholes, B-3 and B-4 were drilled on March 26, 2021 in Borojevići village (near S009 and S040 sinkholes), close to the Sunja river (Fig. 1) to the depths of 4.0 and 2.5 m, respectively. Further advancement of boreholes below these depths was not possible due to presence of very stiff marly clay or increased content of gravel size particles.

Standard Penetration Test (SPT) was performed in all boreholes at approximately 1.0 m intervals by using a mechanical drive-weight unit with a standard donut-type hammer according to ASTM standard [6]. Split-barrel sampler was used with the exception of boreholes B-3 and B-4 below the depths of 3.0 m or 4.0 m, respectively, where it was replaced by a conical probe.

Two dynamic penetration tests were conducted near the S001 sinkhole (Fig. 3) with the manually driven dynamic penetrometer light (DPL). Dynamic penetrometer SD-10 (ZNWiG) compatible with the Eurocode 7: Geotechnical design – Part 2: Ground investigation and testing, was used [7]. For both probes, the test was terminated at a depth of 4.0 m, as the declared maximum penetration depth for the equipment was reached [4].
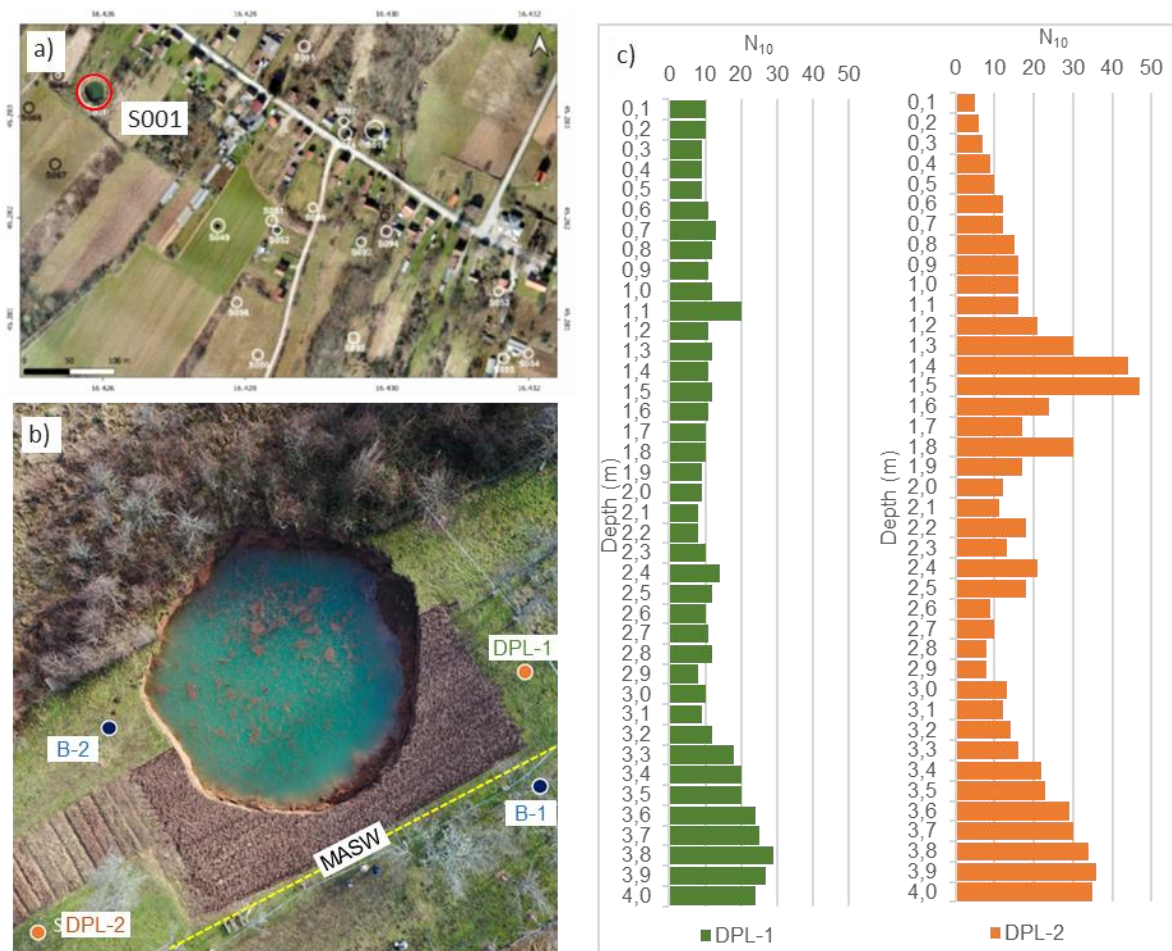
Figure 3. a) Areal image of cover-collapse sinkholes in Mečenčani village (red – S001 sinkhole) b) Locations of geotechnical and geophysical investigations around S001 sinkhole; c) DPL and corresponding test results.

Groundwater tables (GWTs) in boreholes B-1 and B-2 were initially detected at 4.7 and 4.0 m below the ground level, respectively. GWTs rose shortly after the drilling was completed, whereby the subsequent GWTs in both boreholes closely corresponded to the GWT inside the S001 sinkhole (Fig. 4).

Based on the field description and identification, as well as laboratory test results, soil samples were classified according to visual and manual procedures [8] and the Unified Soil Classification System (USCS) [9], thus enabling construction of a representative soil profile close to the largest S001 sinkhole (Fig. 4). Vertical cross sections through boreholes B-1 and B-2 indicate that approximately top 0.5 m consists of fill with organic content (denoted by F), followed by approximately 3.5 m of sandy lean and fat clay that is firm to stiff and contains sparse traces of limestone particles up to 20 mm in diameter in borehole B-1 and up to 50 mm in diameter in borehole B-2, and is classified as CL/CH. The third layer consists of stiff to very stiff lean clay and lean clay with sand that is classified as CL. At the bottom of boreholes, either gray lean (marly) clay (CL in borehole B-1) or a very moist clayey sand with gravel (SP-SC/SC in borehole B-2) was found.
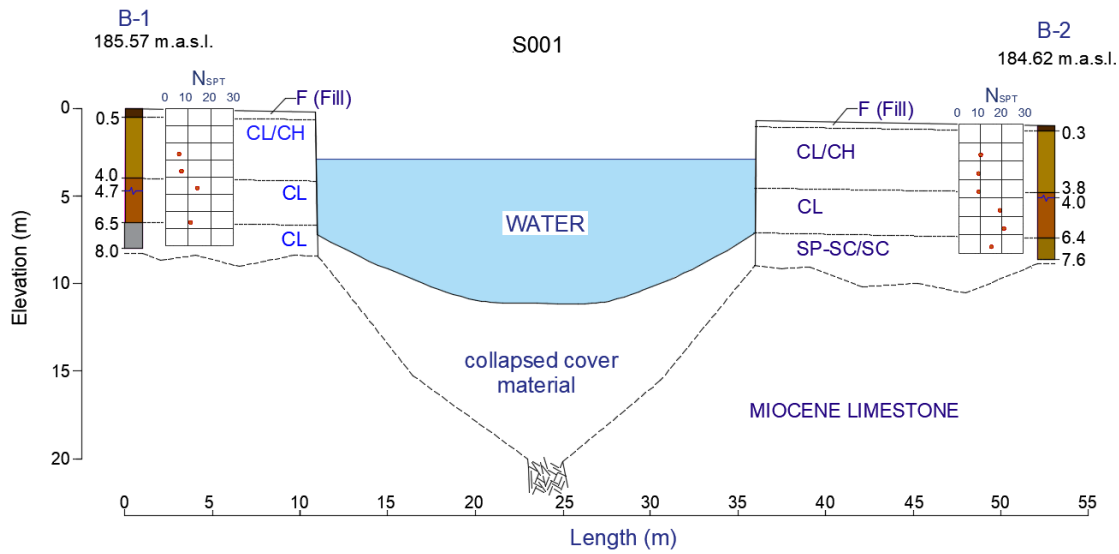
Figure 4. Vertical cross-section through S001 sinkhole, and borehole logs for B-1 and B-2 (modified from [1]).

Soil profiles reconstructed on the basis of boreholes B-3 and B-4 indicate top 0.2 to 0.3 m of fill with organic content (denoted by F). This is followed by about 1 m of lean clay (CL) that is underlain by 2.5 m of poorly-graded gravel (GP) in borehole B-3, and about 1 m of well-graded gravel (GW) in borehole B-4.

Multichannel Analysis of Surface Waves (MASW) has also been performed just along the edge of S001 (Fig. 3) in order to delineate the depth to bedrock, assess soil stiffness, and estimate average shear wave velocities [4]. Field data acquisition involved a 24-channel geophone array with 4.5 Hz vertical geophones spaced at 2 m intervals and a sledgehammer used as a shot source. Fig. 5 shows two-dimensional interpretation of the MASW profile near S001 shows that lower shear wave velocities of 180–220 m/s occur until 5–6 m depth, under which slightly higher velocities 300–400 m/s were recorded corresponding to depths between 6 and 10 m. Relatively uniform strata down to 25 m are shown in green and yellow colors, which has heterogeneous 400–500 m/s velocities, which could represent weathered and saturated Miocene carbonates. It can be concluded that the compact rock layer appears below 25 m, geologically characterized as compact Middle Miocene carbonates [4]. According to the MASW, depth of S001 of about 10–13 m is most likely also the depth of the carbonate-cover contact.
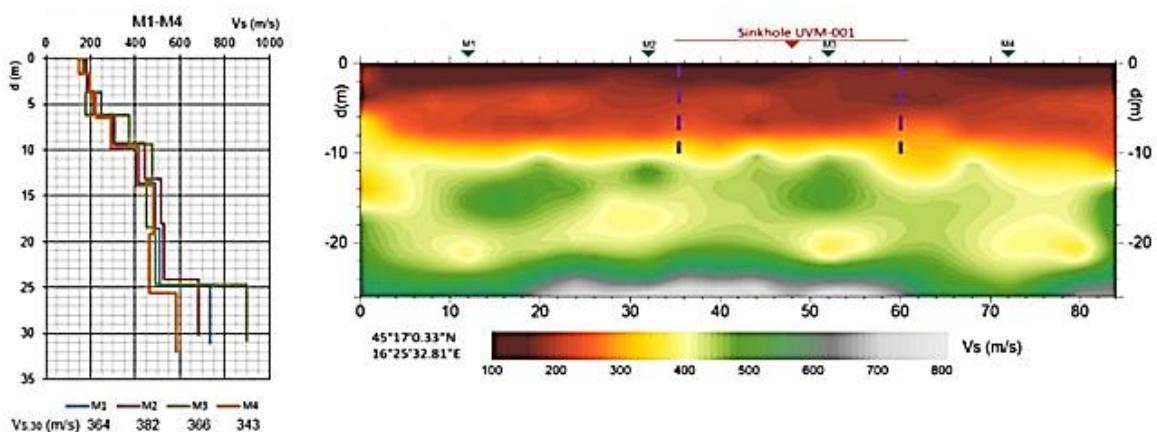
Figure 5. Results of MASW investigation in Mečenčani close to the largest sinkhole S001 (modified from [4]).
.

Laboratory testing was conducted at the Faculty of Mining, Geology and Petroleum Engineering of the University of Zagreb and Faculty of Civil Engineering, Architecture and Geodesy of the University of Split. Various geotechnical laboratory tests including specific gravity, moisture content, grain size distribution, Atterberg limits, oedometer test and conventional triaxial tests on saturated specimens, as well as measurement of Soil Water Retention Curve (SWRC) were performed on 31 soil samples.

Plasticity indices and liquid limits for various soil samples collected from boreholes B-1, B-2, B-3, and B-4 indicate that most of the soil samples are in the area of low-plasticity clays ($w_L<50\%$) with few exceptions that fall into the range of high-plasticity clays ($w_L>50\%$).

Oedometer tests were performed in accordance with the ASTM standard [10] on two samples (CL/CH) obtained from the boreholes B-1 and B-2 at the same depth of 3.0 to 3.3 m (layer 1 – CL/CH). Vertical effective preconsolidation stresses were determined based on Casagrande's procedure (σ'_c=230 kPa in B-1; σ'_c=310 kPa in B-2). The corresponding OCR values were computed based on two different GWT levels, one registered during drilling and the other one corresponding to the water level inside the sinkhole. OCR values are according to such a procedure estimated in the range of 3.9 to 4.4 for the B-1 borehole and in the range of 5.0 to 6.2 for the B-2 borehole.

Three series of consolidated isotropically undrained compression (CIUC) tests were also conducted in accordance with ASTM standard [11]. Each series comprised tests at three different cell pressures corresponding to 230, 260 and 300 kPa. Undisturbed samples from boreholes B-1 (depth 4.0–4.3 m, layer 2 – CL) and B-2 (depths 2.0–2.3 m and 3.0–3.3 m, layer 1 – CL/CH) were tested. Deviatoric and mean effective stresses (q and p') are shown in Fig. 6. Triaxial test results indicate that all samples were overconsolidated as it was already concluded based on the oedometer test results. Slopes of the critical state lines are very similar giving the critical state friction angles of 30.9°–31.1° for the layer 1 and 30.7° for the layer 2 (Fig. 6).

a)
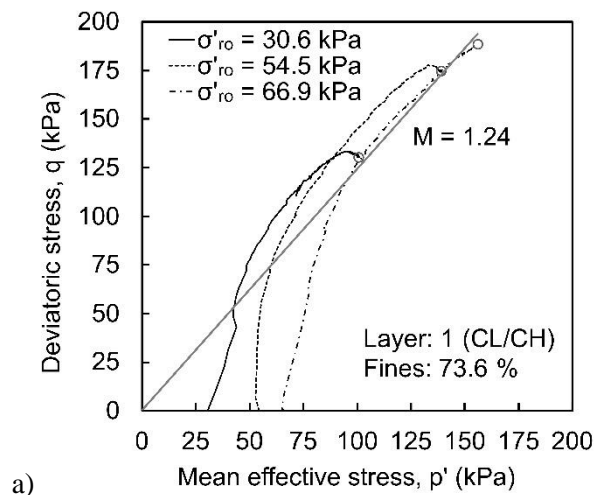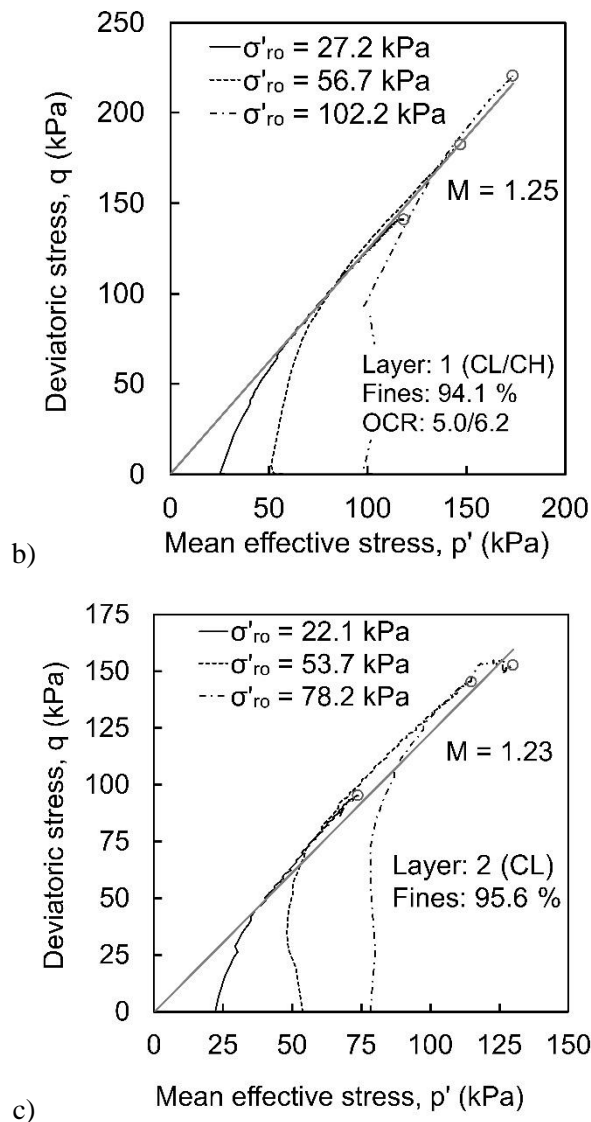
Figure 6. Triaxial (CIUC) test results a) borehole B-2 (2.0–2.3 m) – layer 1; b) borehole B-2 (3.0–3.3 m) – layer 1 and c) borehole B-1 (4.0–4.3 m) – layer 2 (modified from [1])

As it was also recognized that repeated cycles of saturation and desaturation may play a role in effective stress distribution within the clay cover layer, and thus affect shear and tensile strength and possibly contributing to a sinkhole collapse, soil water retention curves (SWRC) were also obtained. Laboratory tests were carried out in accordance with ASTM D6836-16 [12] by using the "chilled mirror hygrometer" or chilled mirror dew point method and WP4C potentiometer [13] suitable for making suction measurements in the range of 0.1 to 300 MPa. Undisturbed samples from boreholes B-1 (depth 2.00–2.15 m, layer 1 – CL/CH) and B-2 (depth 5.00–5.15 m, layer 2 – CL) were tested.

Closed form equation of SWCC proposed by van Genuchten [14] was used herein to fit the experimental data. Van Genuchten's equation in terms of effective degree of saturation (S_{eff}) is given by

$$S_{eff} = \frac{1}{[1+(a\psi)^n]^m} \tag{1}$$

$$S_{eff} = \frac{S(\psi)-S_r}{1-S_r} \tag{2}$$

where S_{eff} is the effective degree of saturation according to Equation (2), ψ is suction (kPa), a (kPa⁻¹), n, m are fitting parameters, $S(\psi)$ is degree of saturation corresponding to a given suction value while S_r is residual saturation.

The experimental data obtained from suction measurements in WP4C apparatus including drying and wetting paths are shown in Figs. 7 and 8. Van Genuchten curves [14], which were fitted to the experimental data with the parameters according to Table 1, are also shown.

Table 1 − Parameters of van Genuchten model for SWRC drying curve

Specimen	a (1/kPa)	m	n	S_r (%)
B-1 (2.00–2.15 m)	0.00950	0.390	1.250	7.483
B-2 (5.00–5.15 m)	0.00027	1.200	0.630	6.034
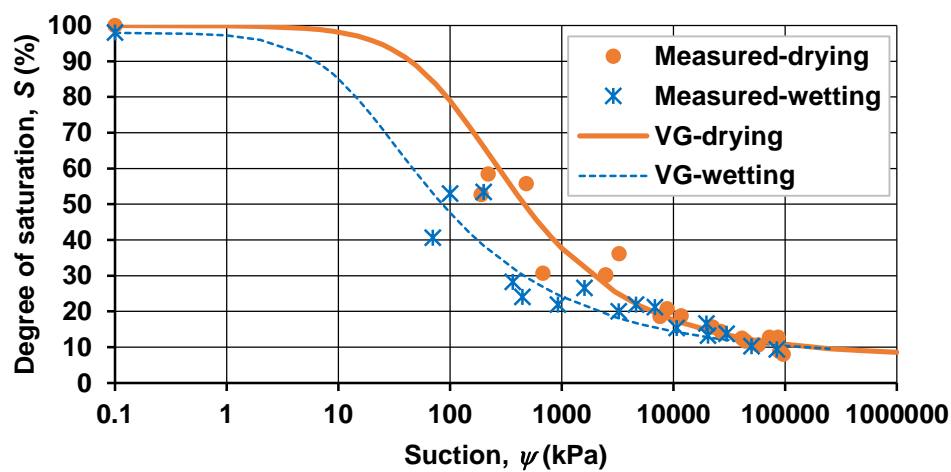
Figure 7. Experimental data and fitted van Genuchten (VG) curve for specimen B-1 (2.00–2.15 m).
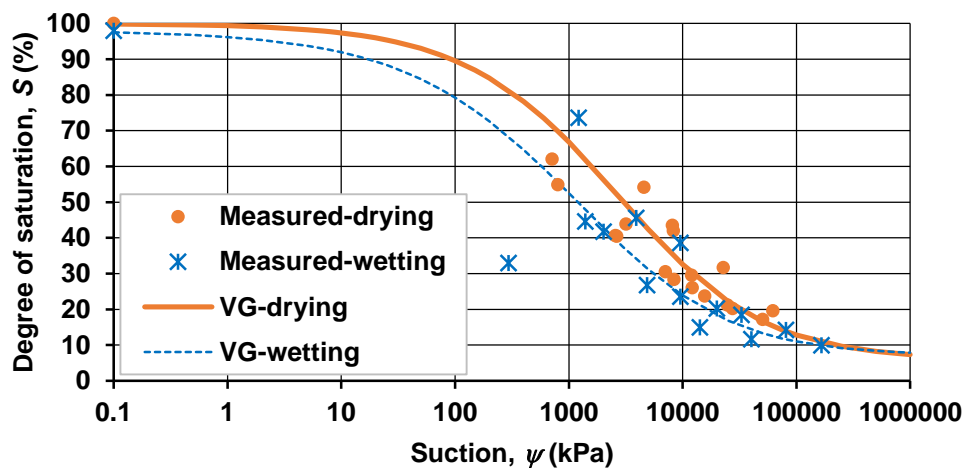
Figure 8. Experimental data and fitted van Genuchten (VG) curve for specimen B-2 (5.00–5.15 m).

The differences in SWRCs shown in figures 7 and 8 are consistent with differences in their grain size distributions. The sample from the borehole B-1 (layer 1, CL/CH) contains 53.6% fines, 43.8% sand-

65

sized particles and 2.6% gravel-size particles, and the sample from the borehole B-2 (layer 2, CL) contains 71.7% fines, 28.3% sand-sized particles and no gravel-size particles.

The presented results of the field and laboratory investigations provide essential geomechanical information necessary to understand the associated sinkhole failure at that specific location and to help in better preparation and performance of future investigations geared towards providing the clarification of failure mechanism in this type of geological settings.

4. Discussion and conclusions

This paper provides an overview of geotechnical, geological and geophysical investigation of soil in the area of Mečenčani and Borojevići villages, Croatia. The area was subjected to a M_L 6.2 earthquake on December 29, 2020, followed by numerous aftershocks. The motivation for better characterizing soil in this area is an extensive sinkhole collapse phenomena, that occurred post-seismically over the period of 12 months after the main shock. The sinkhole collapse area is relatively small and characterized with karst overlain by 4 m to 15 m thick deposit of clays with gravel lenses.

So far, no detailed analytical or computational modelling of the sinkhole collapse associated with Petrinja 2020 earthquake sequence has been conducted. Nevertheless, based on the results of in situ and laboratory geotechnical tests as well as geophysical tests a hypothesis can be formulated as to how sinkhole cover collapse might have occurred.

The pre-existing historical sinkholes indicate susceptibility of this region to a sinkhole formation. This is further corroborated by the presence of limestone in subsurface as well as karst topography visible in surrounding area. Thus, the initial process of a sinkhole formation by gradual expansion of large cavities on the contact between the soil and underlying karstified carbonates was ongoing at the time when the earthquake hit. Nevertheless, the cavity covers appear to have been relatively stable prior to the earthquake (cover-collapse sinkholes opened in the area of Mečenčani and Borojevići on average every few years in the decades before the 2020 Petrinja earthquake), but they started to collapse after the earthquake.

Clearly there are two factors that played important role in the process including the interplay between the groundwater located in the karst aquifer and the groundwater located in the overlaying clay aquitard, and the effect of the earthquake. Specifically, a decrease in suction and corresponding increase in pore water pressure decreases the effective stress in the clay layers, thus decreasing the shear and tensile strength of the clay and increasing the probability of the sinkhole collapse. Furthermore, the observed collapse pattern that is characterized by vertical walls would be expected in a brittle cohesive material such as the overconsolidated clay encountered at this site.

The role of the earthquake sequence is in that it may have simply accelerated the process of the sinkhole formation through the dynamic loading imposed to already partially formed underground arch like structures. That might have lead to further slimming of the arches, but according to available data there are no evidences of the instant, co-seismic collapse. Future computational and analytical modelling efforts are expected to shed more light on the sinkhole collapse scenario provided corresponding hydrogeological data are available.

Acknowledgements

References

[1] Tomac, I., Kovačević Zelić, B., Perić, D., Domitrović, D., Štambuk Cvitanović, N., Vučenović, H., Parlov, J., Stipčević, J., Matešić, D., Matoš, B., Vlahović, I. (2022): Geotechnical reconnaissance of an extensive cover-collapse sinkhole phenomena of 2020–2021 Petrinja earthquake sequence (Central Croatia). *Earthquake Spectra*, **0** (0), 1–34, doi:10.1177/87552930221115759

[2] Esaki, T., Kimura, T., Shikata, K. (1989): Subsidence and environmental impacts in Japanese coal mining, *30th US Symposium on Rock Mechanics as a Guide for Efficient Utilization of Natural Resources*, 19–22 June, West Virginia University, 511–518.

[3] Gutiérrez, F., Cooper, A.H. (2013): Surface morphology of gypsum karst. In: Shroder J (ed.) Treatise on Geomorphology. *Karst Geomorphology* (6), 425–437.

[4] Tomac, I., Vlahović, I., Parlov, J., Matoš, B., Matešić, D., Kosović, I., Pavičić, I., Frangen, T., Terzić, J., Pavelić, D., Pham, N. (2021): Cover-collapse sinkholes. In: Tomac I and Zlatović S (eds.): Geotechnical Reconnaissance and Engineering Effects of the December 29, 2020, M6.4 Petrinja, Croatia Earthquake and Associated Seismic Sequence – A report of the NSF-Sponsored Geotechnical Extreme Event Reconnaissance Association. 52–99.

http://www.geerassociation.org/index.php/component/geer_reports/?view=geerreports&layout=build&id=99.

[5] Šikić, K. (2014): Osnovna geološka karta Republike Hrvatske 1:100.000, List Bosanski Novi L33-105 (Basic Geological Map of the Republic of Croatia, 1:100,000 Scale, Bosanski Novi Sheet L33-105). Croatian Geological Survey, https://www.hgi-cgs.hr/osnovna-geoloska-karta-republike-hrvatske-1100-000/

[6] ASTM D1586-11 (2011): Standard Test Method for Standard Penetration Test (SPT) and Split-Barrel Sampling of Soils, ASTM International, West Conshohocken, PA, United States.

[7] EN 1997-2 (2007): Eurocode 7: Geotechnical design – Part 2: Ground investigation and testing, European Committee for Standardisation, Brusseles, Belgium, EU.

[8] ASTM D2488-17 (2017): Standard Practice for Description and Identification of Soils (Visual-Manual Procedures), ASTM International, West Conshohocken, PA, United States.

[9] ASTM D2487-17 (2017): Standard Practice for Classification of Soils for Engineering Purposes (Unified Soil Classification System), ASTM International, West Conshohocken, PA, United States.

[10] ASTM D2435-11 (2011): Standard Test Methods for One-Dimensional Consolidation Properties of Soils Using Incremental Loading, ASTM International, West Conshohocken, PA, United States.

[11] ASTM D4767-11 (2020): Standard Test Method for Consolidated Undrained Triaxial Compression Test for Cohesive Soils, ASTM International, West Conshohocken, PA, United States.

[12] ASTM D6836-16 (2016): Standard Test Methods for Determination of the Soil Water Characteristic Curve for Desorption Using Hanging Column, Pressure Extractor, Chilled Mirror Hygrometer, or Centrifuge, ASTM International, West Conshohocken, PA, United States.

[13] Meter (2023): WP4C Soil Water Potential Lab Instrument, https://www.metergroup.com/en/meter-environment/products/wp4c-soil-water-potential-lab-instrument (accessed January 11, 2023).

[14] van Genuchten, M.T. (1980): A Closed-form Equation for Predicting the Hydraulic Conductivity of Unsaturated Soils. *Soil Science Society of America Journal* **44** (5), 892–898.

GEOPHYSICAL RECONSTRUCTION OF BEDROCK DEPTH AT THE LARGE SINKHOLE IN THE 2020 PETRINJA EARTHQUAKE

Eric Ntambakwa [(1)], Ivan Salković [(2)], Ingrid Tomac [(3)],

[(1)]*Principal Engineer, DNV Energy USA Inc., eric.ntambakwa@dnv.com*
[(2)]*Senior Engineer, MOHO d.o.o., ivan.salkovic@moho.hr*
[(3)]*Assistant Professor, Structural Engineering Department, University of California San Diego, itomac@ucsd.edu*

Abstract

This paper shows the results of bedrock depth analysis around the largest cover-collapse sinkhole that occurred during the 2020-2021 Petrinja earthquake sequence. Horizontal to Vertical Spectral Ratio (HVSR) data was collected by the Geotechnical Extreme Events Reconnaissance (GEER) team after the Mw 6.4 December 2020 Petrinja earthquake in Croatia. In addition, the GEER team collected other data to assess the damage and geologic conditions, including two geotechnical boreholes with field and laboratory data and Multichannel Analysis of Surface Waves (MASW) profiles. Out of 61 HVSR readings performed during reconnaissance, 15 are around the largest sinkhole, S001, about 25 m wide and 12 m deep, with vertical walls and groundwater. The soil in the area consists of a clayey cover that is 4.0 m to 10.0 m thick, with sporadic gravel lenses. Clays are mostly over-consolidated, with varying degrees of saturation with intensely karstified carbonate rocks underneath. The HVSR data was analyzed using the HVSRweb platform and associated Python-based modules incorporating various statistical assessment models include single azimuth, multiple-azimuth, and geometric mean. The geometric mean results based on resampling frequencies between 3 Hz and 10 Hz indicate karst depths between 12.0 m and 18.0 m, which is generally consistent with the bedrock assumed from the sinkhole depth. Furthermore, an evaluation of the spatial variability of the resonance frequencies and the corresponding depth estimates assesses the presence and orientation of karstic features around S001. Based on the assessed data, HVSR measurements appear to be a helpful tool for evaluating variations in subsurface impedance contrasts and can be used to augment geotechnical data and other geophysical measurement techniques due to the relative ease of deployment and rapid data acquisition.

Keywords: Horizontal to Vertical Spectral Ratio (HVSR), sinkhole, post-seismic effect, karst geophysics

1. Introduction

On December 29, 2000, an earthquake with a moment magnitude of M_W 6.4 occurred in the Sisak–Moslavina county in Central Croatia at 12:19 PM local time (11:19 AM UTC; USGS 2020). According to the US Geological Survey, the earthquake hypocenter was at 45.422°N 16.255°E, at a depth of 10 km [1] within the central portion of the shallow Petrinja strike-slip fault in the marginal part of the Internal Dinarides, NE part of the Adria Microplate. Three foreshocks preceded the earthquake for one day, the strongest of which had a magnitude of M_W 5.2, followed by numerous aftershocks. In the first 60 days of the sequence, 4430 events were located within 50 km from the mainshock, including 85 aftershocks with a local magnitude $M_L \geq 3.1$ until February 22, 2021. Most aftershocks in the central cluster are distributed between 13 km and 17 km depth. Maximum depths below 25 km are observed only in the central cluster part, while the first 5 km of the crust hosted a small number of events through the entire cluster. Within the central cluster, the event distribution delineates a sub-vertical fault containing the mainshock. As a result, the earthquake caused widespread damage in Petrinja, Sisak, Glina, and the surrounding villages, and seven people lost their lives. According to the Croatian Seismological Survey data, the epicentral intensity was estimated to be VIII–IX EMS [1].

This paper focuses on analysing some aspects and features of a relatively rare post-seismic effect, a sinkhole collapse near Mečenčani and Borojevići villages 20 km SE of the mainshock epicentral area. Geotechnical Extreme Events Reconnaissance (GEER) team obtained data that support this study. GEER registered 91 new cover collapse sinkholes and 45 historical cover collapse sinkholes, opened

before the Petrinja earthquake [1]. All new sinkholes are within two small areas, 1.13 km^2 combined: 74 in the NW area close to the Borojevići village over approximately 0.753 km^2 and 48 in the SE area around Mečenčani village over approximately 0.375 km^2.

The uniqueness of the sinkhole region is that this is the only region where karstic geologic conditions were close to the epicenter. Highly karstified limestones are directly covered by relatively thick clayey soil. Middle Miocene carbonates (Badenian, M4) are composed of alternating highly porous Lithothamnion limestones and calcarenites, both very susceptible to karstification, as visible in the hills SW of the studied area [2, 3]. Karstified carbonates are overlain by a 4–15 m thick sequence of Holocene diluvial–proluvial deposits. Deposits are unsaturated to saturated clays with lenses of gravel and sand. Hydrological investigation reveals two distinct aquifers that are interconnected sporadically. The Sunja river valley in the studied area represents a flat terrain covered with Holocene diluvial–pluvial deposits of low permeability containing a certain amount of water and therefore forming an aquitard with the groundwater level fluctuations between dry and wet periods of about 2.0 m. The aquitard is underlain by a permeable confined karst aquifer, in which the water pressure during wet periods becomes sub-artesian to artesian [1].

This paper uses a combination of geophysical methods and horizontal to vertical spectral ratio (HVSR) to better understand the spatial horizon variations between clayey cover and underlying karstic rock around the largest sinkhole, S001. The geophysical investigation is supported by geotechnical soil investigation works and imaging [1]. The S001 sinkhole is the largest sinkhole that occurred in the area until the GEER field trip in middle March 2021. Fig. 1 shows the sinkhole lidar images and position. Fig. 2 shows geotechnical boreholes around the S001 sinkhole. Unsatureated and saturated low to high plasticity clays overlay karst. The extensive report of geotechnical research and investigation is presented in Tomac et al., 2022 [4]. Initial measurements of groundwater levels during drilling are shown in Fig. 2 and are between 4.0 m and 4.6 m depth. After a few hours, the groundwater level in boreholes were measured again and corresponded to the water level in the sinkhole [4].
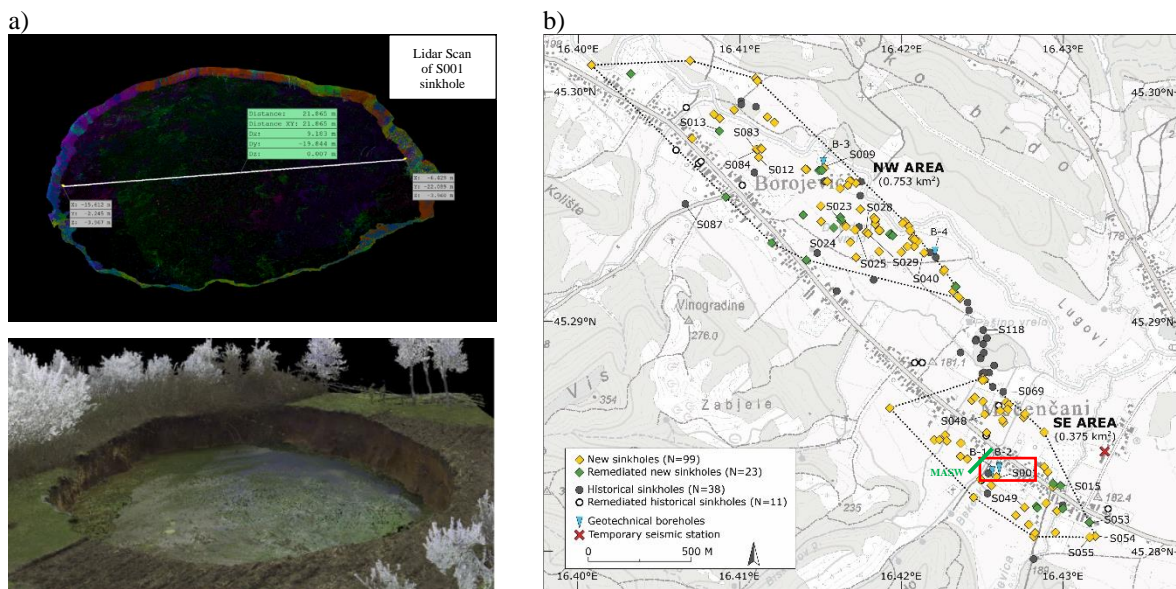
Figure 1. a) S001 (45.2833444N, 16.4259639E) imagery (modified from [1]); b) Sinkholes position on the map (modified from [3]).
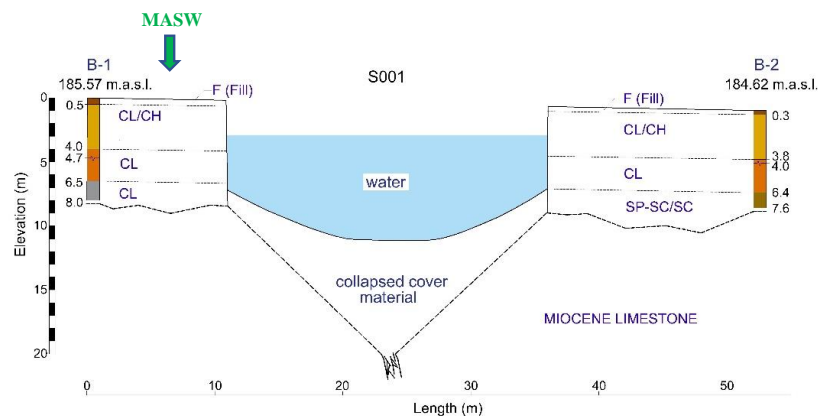
Figure 2. Sinkhole S001 (45.2833444N, 16.4259639E) geotechnical profile and MASW location (modified from [4]). Borehole depth is dependent on manual drilling equipment capabilities, where the bottom indicates the upper horizon of the weathered karst layer.

2. Methodology

HVSR in ambient noise measurements is commonly used to estimate site resonant frequency providing excellent estimates of resonant frequency for sites with strong impedance contrasts. Following the 2020 Petrinja Earthquake in Croatia, the GEER reconnaissance team [1] performed nanometrics measurements at 61 locations during their assessment to gain an understanding of the site resonant frequencies which are important in understanding seismic wave propagation. In addition, it was anticipated that the HVSR measurements could provide an additional tool for assessing depth to bedrock as well as for investigating karst features which are common in the sinkhole reconnaissance area in Mečenčani and Borojevići.

In this paper, an evaluation of the nanometrics data is performed to augment the results presented in the GEER report to incorporate sensitivity analyses to various factors including sampling frequency range and spatial and azimuthal variability. The presented analyses limits to the nanometrics measurements around the largest sinkhole S001. S001 developed a few days after the earthquake and was estimated to be about 25.0 m wide and 12.0 m deep by the GEER team end of March 2021. The impedance contrast depths are calculated from the following formula based on the estimated site resonant frequency for each azimuth [5]:

$$D = \frac{V_s}{4 \times f_o} \tag{1}$$

Analysis of the nanometrics data is performed using the web platform HVSRweb as well as associated Python-based modules that are part of the hvsrpy package, previously validated by Vantassel et al. [5], Vantassel [6], Cox et al. [7] and Cheng et al. [6]. Analyses are performed using the various statistical assessment models in hvsrpy including single azimuth, multiple-azimuth and geometric mean. Sensitivity analysis on azimuthal variability of the site resonant frequencies investigates a scatter in frequencies across azimuths from 0° to 180°, including the variability of the site resonant frequencies and the standard deviation at each azimuth. Additionally, the sampling frequency range is varied to assess whether the results would indicate the presence of strong impedance contrasts at shallower depths, consistent with potential depths of karst features. An evaluation of the spatial variability of the resonant frequencies around S001, and the corresponding depth estimates, also provide insight into potential presence and orientation of karst features around S001.

71

2.1   Initial Assessment

An initial assessment of the nanometrics data is performed for positions N-38, 44 through 48, 50 through 53, 55 through 59, and N-61 to evaluate overall HVSR frequencies and information on depths of strong impedance contrasts. The analysis is performed for data from nanometrics measurements around the area of S001, the measurement locations are show in Fig. 3.

Figure 3. Sinkhole S001 and nanometrics measurement locations (modified from [1])

The initial assessment evaluates the HVSR across the full range of ambient noise frequencies between about 0.1 Hz and 50.0 Hz. An example summary of the HVSR data is presented in Figure 4. The HVSR assessment is performed using HVSRweb and the following settings is shown in Table 1. The data indicates high random peaks at frequencies below 0.3 Hz that appeared to be transient noise and the lower resampling frequency is therefore adjusted to 0.3 Hz. The geometric mean results based on resampling frequencies between 3.0 Hz and 10.0 Hz indicate potential bedrock depths between 12.0 m and 18.0 m around S001, which is generally consistent with the bedrock depth assumed from the sinkhole depth [2]. For example, the data appear to be of good quality with some distinct peaks interpreted to correspond to shallow (2.0 m to 5.0 m) and deep (20.0 m to 40.0 m) impedance contrasts below ground surface. However, soil borings, as shown in Fig. 1, that were performed adjacent to the sinkhole S001 during the GEER team's site assessment meet refusal at depths between 7.6 m and 8.0 m [2, 4]. The refusal depths were interpreted as corresponding to bedrock depth although no bedrock samples could be obtained due to drilling equipment limitations. Fig. 5 shows a Multi-Channel Analysis of Surface Waves (MASW) survey performed along the eastern side of S001 indicated that there could be strong impedance contrasts at depths between 8.0 m (transition from v_s ~ 200 m/s to 300 m/s) and 12.0 m (transition from v_s ~ 400 m/s to 500 m/s) [2]. The transition to shear wave velocity of >500 m/s at 25.0 m depth corresponds to very stiff soil or soft rock conditions based on typical seismic site classification criteria. Since the initial assessment did not indicate strong impedance contrasts within the anticipated bedrock depth (8.0 m to 16.0 m) obtained from MASW and geotechnical boreholes, a narrower resampling frequency range is selected for the next round of assessments.

Table 1   HVSR Initial Data Processing Inputs

Window Length (sec)	60 and 120
Cosine Taper Width	0.1
Butterworth Filter	No
K-O Smoothing Coefficient	40
Resampling Frequency Min (Hz)	0.3
Resampling Frequency Max	50
Number of Frequency Points	200
Type	Logarithmic
Distribution of f_0	Lognormal
Frequency Domain Window Rejection	Yes
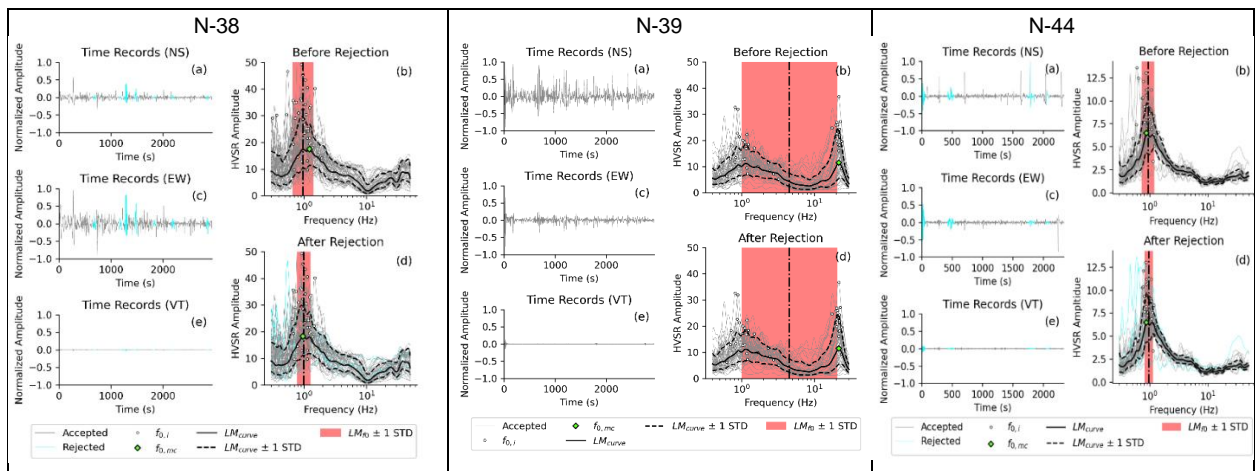
Figure 4. Example nanometrics results from initial assessment.
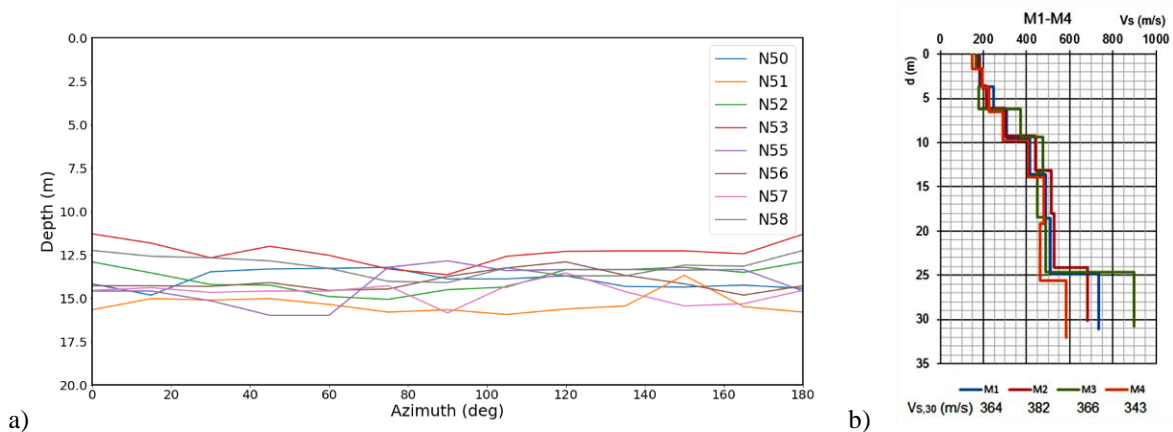
Figure 5. Weathered karst depth estimates s) azimuthal variability from the sinkhole S001 median frequencies and b) MASW profile across S001 (45.2833444N, 16.4259639E) from GEER reconnaissance [1].

2.2.   Resampling Frequency Variation

Since the initial assessment did not indicate strong impedance contrasts within the range of interest and suspected karst horizon, another round of data assessments is performed with a narrower resampling frequency range. The analysis settings were the same as those presented in Table 1 except that the

frequency ranges considered were 3.0 Hz to 10.0 Hz and 3.0 Hz to 50.0 Hz. The goal is to assess whether the data would indicate strong impedance contrasts at depths between about 6.0 m and 18.0 m to cover the range of anticipated bedrock depth below ground surface. This round of sensitivity checks is limited to sites N-55 and N-56 adjacent to sinkhole S001 to gain an indication of the impact on the overall results before applying similar frequency ranges to a wider range of nanometrics data. The results of the resampling frequency variation are summarized in Table 2, Fig. 6.

Table 2   N-55 and N-56 HVSR Re-sampling Frequency Variation Data Summary

Site	Min	Max	Component	$f_{o,mc}$ (Hz)	Apparent Bedrock Depth (m)
N-55	0.3	50	Geomean	1.5	36.7
	3	50	Geomean	27.4	2.0
	3	10	Geomean	4.63	11.9
N-56	0.3	50	Geomean	1.62	34.0
	3	50	Geomean	33.5	1.6
	3	10	Geomean	4.55	11.1
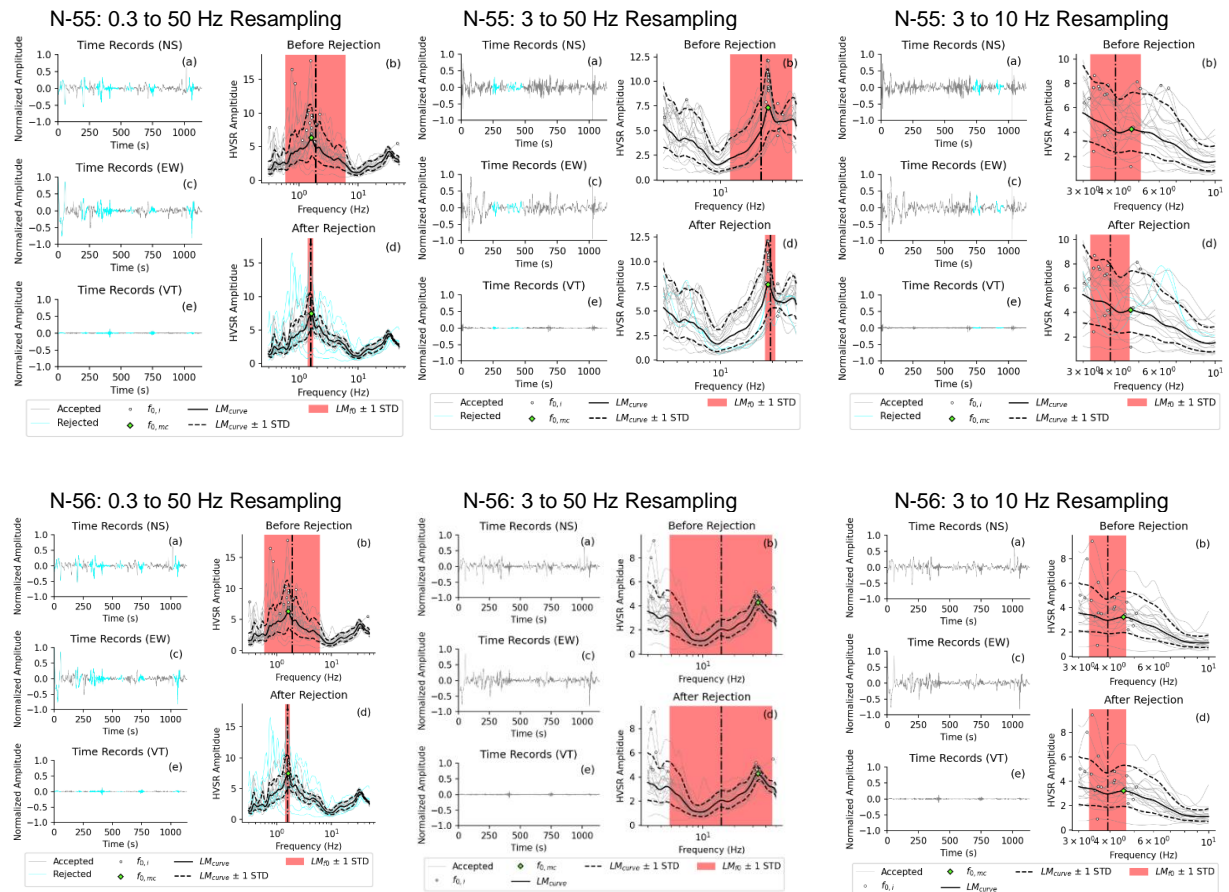
Figure 6. N-55 and N-56 HVSR re-sampling frequency variation summary plots.

2.3. Azimuthal Variation

Estimates of site resonant frequency from HVSR are subject to various sources of uncertainty due to the random nature of ambient noise in space and time, variations in subsurface conditions and sensor coupling conditions. To assess a potential impact of spatial variations on the site resonant frequencies from the nanometrics around S001 (N-50 through N-58), additional sensitivity analyses are performed on azimuthal variability of the results (N-54 data was not included due to data quality issues). The sensitivity analysis of azimuthal variability of the site resonant frequencies at 15° intervals indicates a scatter in frequencies across azimuths from 0° to 180° for most of the measurement locations. The variability is noted in both the site resonant frequencies as well as the standard deviation at each azimuth. The observed scatter may be due to lateral variability as azimuthal variability can be expected for subsurface conditions with significant lateral variability [5].

The results are also compared to the geometric mean results of resonant frequency across all azimuths. The assessment of azimuthal variability considered both the median resonant frequency and the peak frequency of the median curve. The impedance contrast depths corresponding to either the median or peak frequency appeared to be consistent with the MASW data collected by the GEER team at S001. Overall, the peak frequency values provide a better average fit to the MASW data. It should be noted that estimates of the impedance contrast depths were obtained from the quarter wavelength solution based on an average shear wave velocity of 220 m/s considered for the near surface deposits by the GEER team [1].

2.4. Spatial Variability

The next stage in the analyses is to assess variations in estimated depths of the strong impedance contrasts (apparent bedrock depth) across the measured locations. The assessment is performed for the nanometrics locations around S001 and locations N-44 through N-48, located in vicinity of S001.

The assessment of spatial variability is performed using the spatial interface Python module of hvsrpy. The algorithm uses Voronoi tessellations to obtain a statistical representation of site resonant frequency (or period) from spatially distributed HVSR measurements [6]. The assessment requires setting area boundaries and providing coordinates, the mean or peak resonant frequency and the natural log of the standard deviation of the site resonant frequency at each coordinate. The algorithm then applies Voronoi tessellation to yield unique spatial estimates of site resonant frequency.

The results of the spatial variability assessment are summarized in Fig. 7 showing site resonant frequency and bedrock depth estimates results for all the assessed locations and Fig. 8 showing data for locations around S001. The data appear to indicate several steep changes in bedrock depth in several directions around the sinkhole area which may indicate the presence of karst voids or potential fluid flow channels. The steep changes appear to be oriented in the southwest-northeast direction.
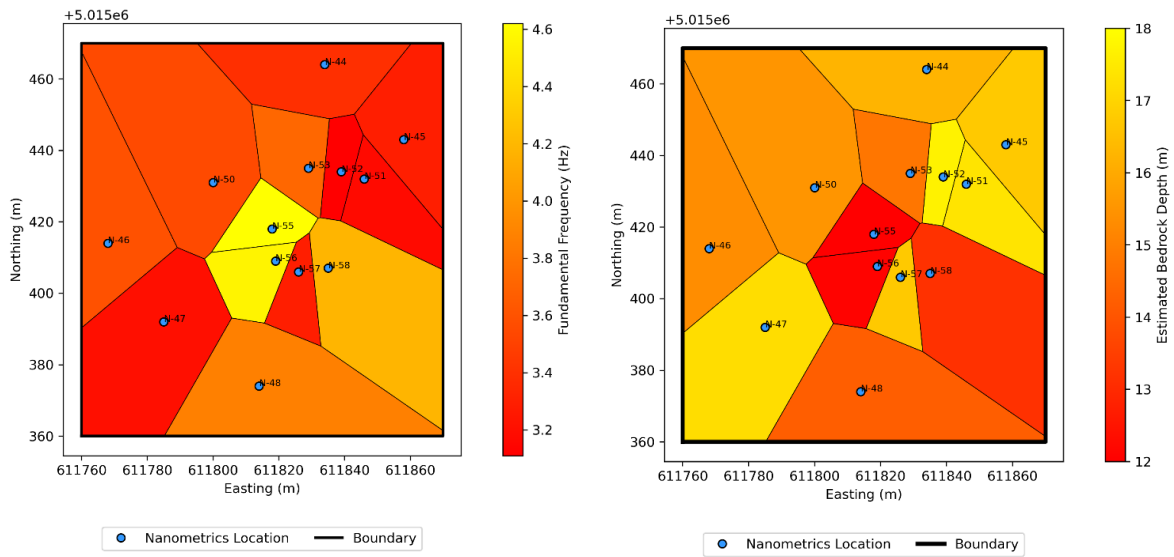
Figure 7. Spatial variation of site resonant frequency and bedrock depth estimates (N-44 to N-58).
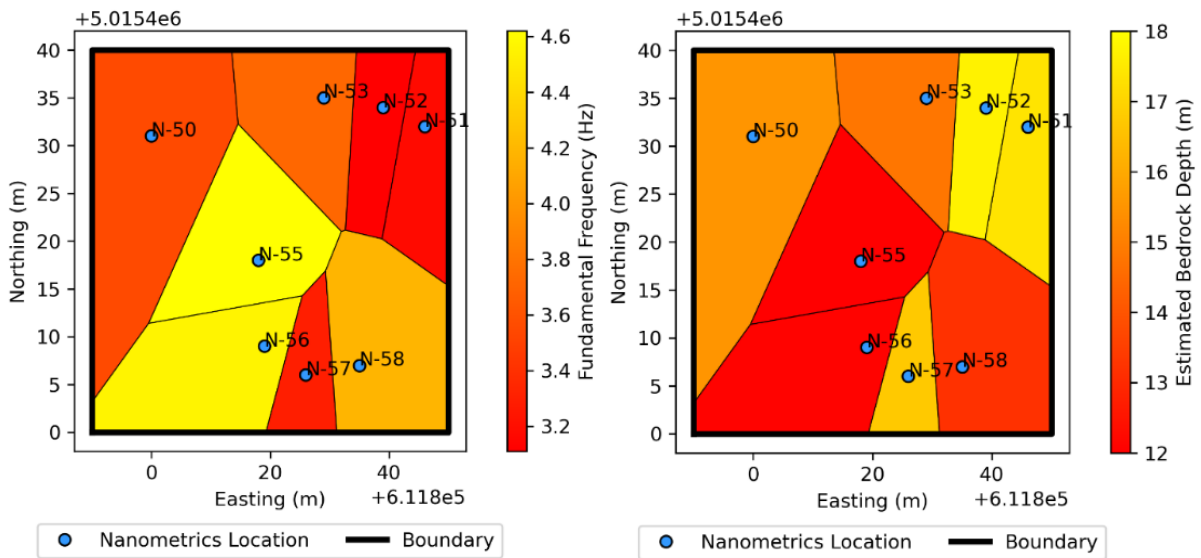
Figure 8. Spatial variation of site resonant frequency and bedrock depth estimates (around S001).

To better visualize the apparent steep changes in bedrock depth around the sinkhole, a three-dimensional plot of the data is developed as presented in Fig. 9 and Fig. 10. In Fig. 9, the cylinder represents sinkhole S001 only schematically, where the diameter corresponds to the reported diameter measured at the soil surface, and the in-situ sinkhole walls are vertical. The shape of the sinkhole under water has not been measured accurately, beyond detecting the collapsed material at the bottom, as shown in Fig. 2.
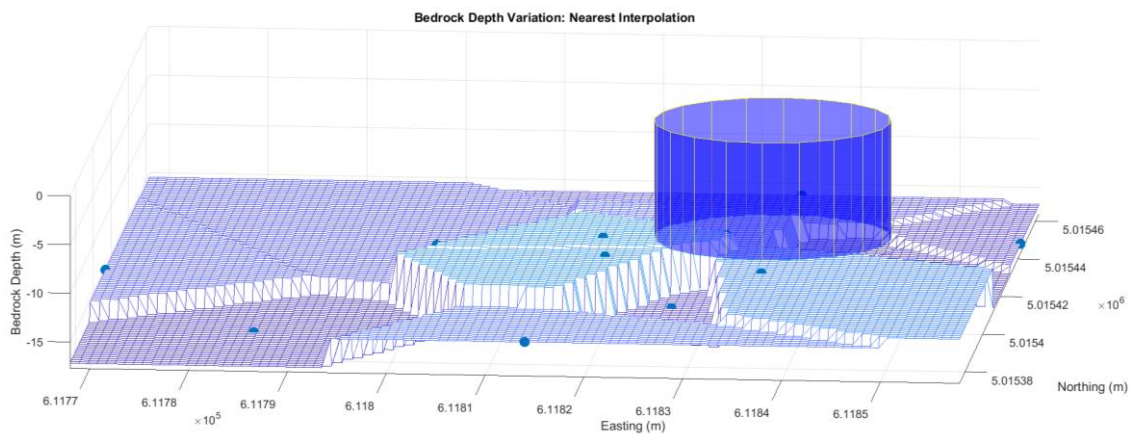
Figure 9. Bedrock depth estimates around sinkhole S001, looking north.
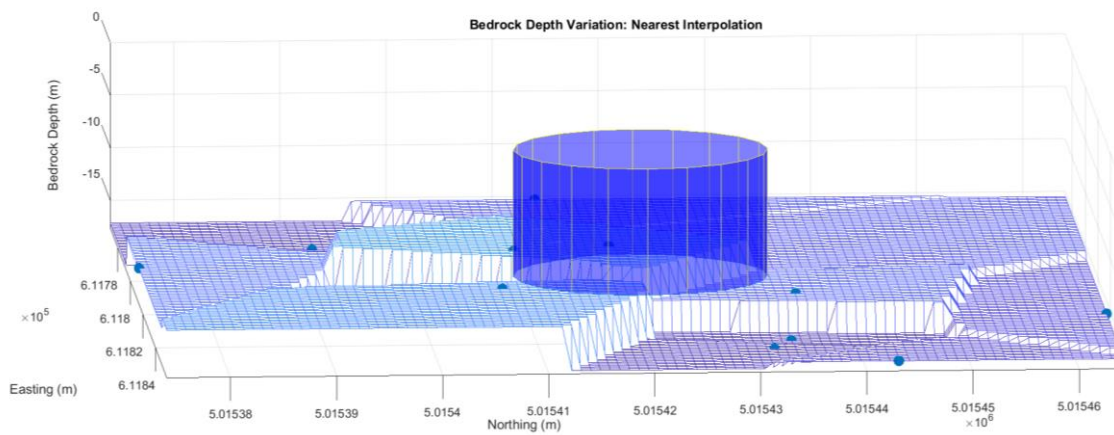
Figure 10. Bedrock depth estimates around sinkhole S001, looking west.

4. Conclusions

Evaluations of HVSR data collected by the GEER team following the December 2020 Petrinja earthquake in Croatia has been performed to gain an understanding of the site resonant frequencies in the area around Sinkhole S001. The primary goal was to assess whether the HVSR measurements can provide a reasonable estimate of depth to competent rock and the potential location of karst features which are common in the area where the measurements were obtained. Additionally, the presented results are novel from the perspective of complexity of interpretation and analysis of HVSR measurement in karst rock, which is typically weathered and contains numerous voids, dry and saturated fluid flow channels.

The assessments incorporated sensitivity analyses of HSVR results to various factors including sampling frequency range and azimuthal variability. Analysis of the nanometrics data was performed using the web platform HVSRweb [5] as well as associated Python-based modules that are part of the hvsrpy package. Sensitivity analysis on azimuthal variability of the site resonant frequencies indicated a scatter in frequencies across azimuths from 0° to 180° for most of the sites. The variability was noted in both the site resonant frequencies as well as the standard deviation at each azimuth. Additionally, the sampling frequency range was varied to assess whether the results would indicate the presence of strong impedance contrasts at shallower depths consistent with potential depths of karst features. The median

site resonant frequencies considering azimuthal variability based on resampling frequencies between 3 and 10 Hz indicated potential bedrock depths between 12.0 m and 18.0 m around S001, which is generally consistent with the bedrock depth assumed from the depth of the sinkhole. An evaluation of the spatial variability of the resonant frequencies around S001, and the corresponding depth estimates, also provided insight into potential presence and orientation of karst features around S001. A three-dimensional assessment of the estimated bedrock depth indicates several steep changes in upper karst horizon in several directions around the sinkhole area which may indicate the presence of voids or karst. The steep changes appear to be oriented in the southwest-northeast direction and may offer an indication of the location of voids which may have facilitated development of Sinkhole S001 following the earthquake. Based on the assessed data, HVSR data from nanometrics measurements appears to be a useful tool for assessing variations in subsurface impedance contracts and can be used to augment geotechnical data and other geophysical measurement techniques due to the relative ease of deployment and rapid data acquisition.

Acknowledgements

References

[1] USGS (2020). M 6.4 – 3 km WSW of Petrinja, Croatia. Available at: https://earthquake.usgs.gov/earthquakes/eventpage/us6000d3zh/executive (Accessed: December 29, 2020).

[2] Tomac I, Vlahović I, Parlov J, Matoš B, Matešić D, Kosović I, Pavičić I, Frangen T, Terzić J, Pavelić D and Pham N (2021): Cover-collapse sinkholes. In: Tomac, I. and Zlatović S. (eds.): Geotechnical Reconnaissance and Engineering Effects of the December 29, 2020, M6.4 Petrinja, Croatia Earthquake and Associated Seismic Sequence – A report of the NSF-Sponsored Geotechnical Extreme Event Reconnaissance Association. 52–99.

http://www.geerassociation.org/index.php/component/geer_reports/?view=geerreports&layout=build&id=99.

[3] Šikić K. (2014): Osnovna geološka karta Republike Hrvatske 1:100.000, List Bosanski Novi L33-105 (Basic Geological Map of the Republic of Croatia, 1:100,000 Scale, Bosanski Novi Sheet L33-105). – Croatian Geological Survey, https://www.hgi-cgs.hr/osnovna-geoloska-karta-republike-hrvatske-1100-000/

[4] Tomac I., Kovačević Zelić B, Perić D., Domitrović D, Štambuk Cvitanović N., Vučenović H, Parlov J., Stipčević J., Matešić D., Matoš B, and Vlahović I. (2022): Geotechnical reconnaissance of an extensive cover-collapse sinkhole phenomenon of 2020 – 2021 Petrinja earthquake sequence (Central Croatia). Earthquake Spectra. Online First.

[5] Vantassel, J.P., Cox, B.R., Brannon, D.M. (2021), HVSRweb: An Open-Source, Web-Based Application for Horizontal-to-Vertical Spectral Ratio Processing, International Foundations Congress and Equipment Expo.

[6] Vantassel, J.P. (2020) jpvantassel/hvsrpy: latest (Concept), http://doi.org/10.5281/zenodo.3666956

[7] Cox, B. R., Cheng, T., Vantassel, J. P., Manuel, L. (2020). A statistical representation and frequency-domain window-rejection algorithm for single-station HVSR measurements. *Geophysical Journal International*, 221(3), 2170–2183. https://doi.org/10.1093/gji/ggaa119

[8] Cheng, T., Cox, B. R., Vantassel, J. P., and Manuel, L. (2020). "A statistical approach to account for azimuthal variability in single-station HVSR measurements." Geophysical Journal International, 223(2), 1040–1053. https://doi.org/10.1093/gji/ggaa342

LIQUEFACTION SUSCEPTIBILITY BASED ON AN ARTIFICIAL NEURAL NETWORK

Matija Lozić[1], Sonja Zlatović[2], Ivan Mihaljević[3], Igor Gukov[4], Boris Uremović[5] , Marija Čačić[6]

[1] *Designer, Elektroprojekt d.d., matija.lozic@elektroprojekt.hr*
[2] *Professor, Zagreb University of Applied Sciences, sonja.zlatovic@tvz.hr*
[3] *Head of Consultancy Department, Geokon d.d., ivan.mihaljevic@geokon.hr*
[4] *Professor, Zagreb University of Applied Sciences, igor.gukov@tvz.hr*
[5] *Senior lecturer, Zagreb University of Applied Sciences, boris.uremovic@tvz.hr*
[6] *Student, Zagreb University of Applied Sciences, marija.cacic@tvz.hr*

Abstract

The traces of liquefaction were recognized in the area of Zagreb in the Sava valley in previous earthquakes and liquefaction can be expected in future earthquakes as well similar to the many cases which occurred in the Petrinja earthquake. Therefore, it is useful to have a tool allowing quick identification of susceptibility to liquefaction in larger areas.

CPTU testing covers many aspects of soil behaviour and enables the estimation of parameters needed in liquefaction susceptibility analysis. During the 2010-2011 series of earthquakes in Christchurch and Canterbury, New Zealand, a very rich dataset was collected that links soil data obtained by the CPTU, earthquake data, and on-site liquefaction manifestations – or lack of it. An artificial neural network was developed from these data. In addition to the description of location and time, the data contains CPTU measurements, earthquake magnitude, medial peak ground acceleration, its standard deviation, groundwater depth and classification of the manifestation of liquefaction on the ground surface.

The data collected after the Petrinja earthquake – obtained from CPTU tests and from analysis of the manifestations of liquefaction and the available data on the earthquake – are used in the developed artificial neural network.

Keywords: liquefaction, artificial neural networks, CPTU, Christchurch and Canterbury earthquakes

1. Liquefaction in Zagreb and Petrinja

It was found that during the 1880 Zagreb earthquake liquefaction occurred at several locations in the Sava valley [1], which means that liquefaction could be expected in future earthquakes in Zagreb again.

Figure 1. Examples of liquefaction in Petrinja earthquake: a) ejecta in the field in Hrastelnica, b) cracks in the levee in Sisak along the Sava river (Galdovo), c) subsidence of the road in Petrinja (Drenčinina)

The Petrinja earthquake in year 2020 [2] showed a vast array of various manifestations of liquefaction illustrating thus and reminding the citizens and engineers of Croatia that this phenomenon is to be taken in account seriously. An overview of geotechnical damages caused by Petrinja earthquake is given in the report led by Tomac and Zlatović for GEER [3]. The three characteristic damages caused by liquefaction are shown in Figure 1: a) liquefaction occurred in many fields in the area, and it was rather vast in the area of Hrastelnica; b) some of the levees protecting the area from the waters of the Kupa and Sava rivers got mostly longitudinal cracks due to liquefaction and lateral spreading as is seen here on the section in Galdovo; c) liquefaction in the villages caused cracking in several houses in the area, as well as subsidence of roads like one in this photograph and many of the wells in the area were filled with sandy soil.

2. Predictions of liquefaction

Since the Alaska M9.2 earthquake and Niigata M7.5 earthquake, both in the year 1964, when tremendous damages were caused by liquefaction, there has been a great deal of effort input to the liquefaction research. It is quite clear that both the properties of the soil on the location - including the presence of groundwater, and the properties of the earthquake and its impact on the location, influence the onset of liquefaction [4]. The understanding of this phenomenon has been developing in the last 60 years, as well as the models used to make the necessary evaluations [5].

One of the investigation methods covering the most of soil characteristics is CPTU. Therefore, various soil properties are derived from the CPTU measurements, to be used in estimations of the hazards and in design. [6, 7, 8, 9, 10]. However, it is worth noting that each of these estimations carries its own uncertainties. Therefore, it seems it would be valuable to relate the liquefaction susceptibility directly to CPTU measurements.

3. Cone Penetration Testing

In the Cone Penetration Test (CPT), a cone on the end of a series of rods is pushed into the ground at a constant rate, and continuous measurements are made of the resistance to penetration of the cone and of a surface sleeve – separately – as shown in Figure 2. Additionally, very often recently, at the same time, pore water pressure is measured during the penetration (CPTU). [8] These tests give a very good overview of the subsoil, especially if they are combined with some borings and appropriate laboratory testing, and some geophysical investigation, to obtain a more complete picture. Robertson developed the interesting Sol Behaviour Type index which is derived from the CPT data, which is describing soil behaviour and defines partially the Soil Behaviour Type as shown in Figure 2 [8].

	Soil Behavior Type	I_c
1	Sensitive fine grained	N/A
2	Organic soils – clay	>3,6
3	Clays: clay to silty clay	2.95-3.6
4	Silt mixtures: clayey silt & silty clay	2.6-2.95
5	Sand mixtures: silty sand to sandy silt	2.02-2.6
6	Sands: clean sands to silty sands	1.31-2.05
7	Dense sand to gravelly sand	<1.31
8	Very stiff sand to clayey sand*	N/A
9	Very stiff fine-grained*	N/A
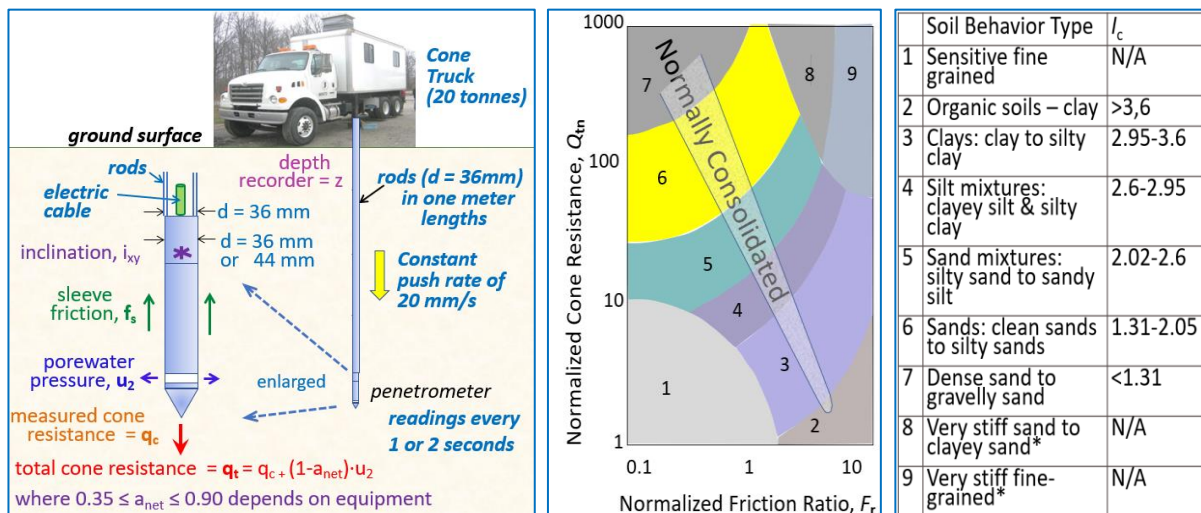
Figure 2. a) An overview of a Cone Penetration Test after ASTM D 5778 [11]. b) SBTn chart, where number corresponds to the Soil Behavior Type defined in c) I_c is the Soil Behavior Type index [8]

4. Canterbury earthquakes and New Zealand Geotechnical Database

M7.1 earthquake with an epicentre 70 km East from Christchurch, the largest city in the South Island of New Zealand and the seat of the Canterbury Region, caused widespread liquefaction. It was followed by a series of aftershocks (21 earthquakes with magnitude 5 or more, less than 20km from the city centre), and liquefaction was often repeated in the same place over and over again [12, 13]. A vast amount of data, including seismologic, hydrologic, geospatial, and geotechnical measurements (mostly CPT) was collected and related to the liquefaction manifestation during and after these earthquakes, and offered to the researchers in the whole world [14, 15], the newest base being New Zealand Geotechnical Database [16]. Figure 3 presents the organization of data in this Database. The liquefaction manifestation has been shown in 7 classes listed in Figure 4.
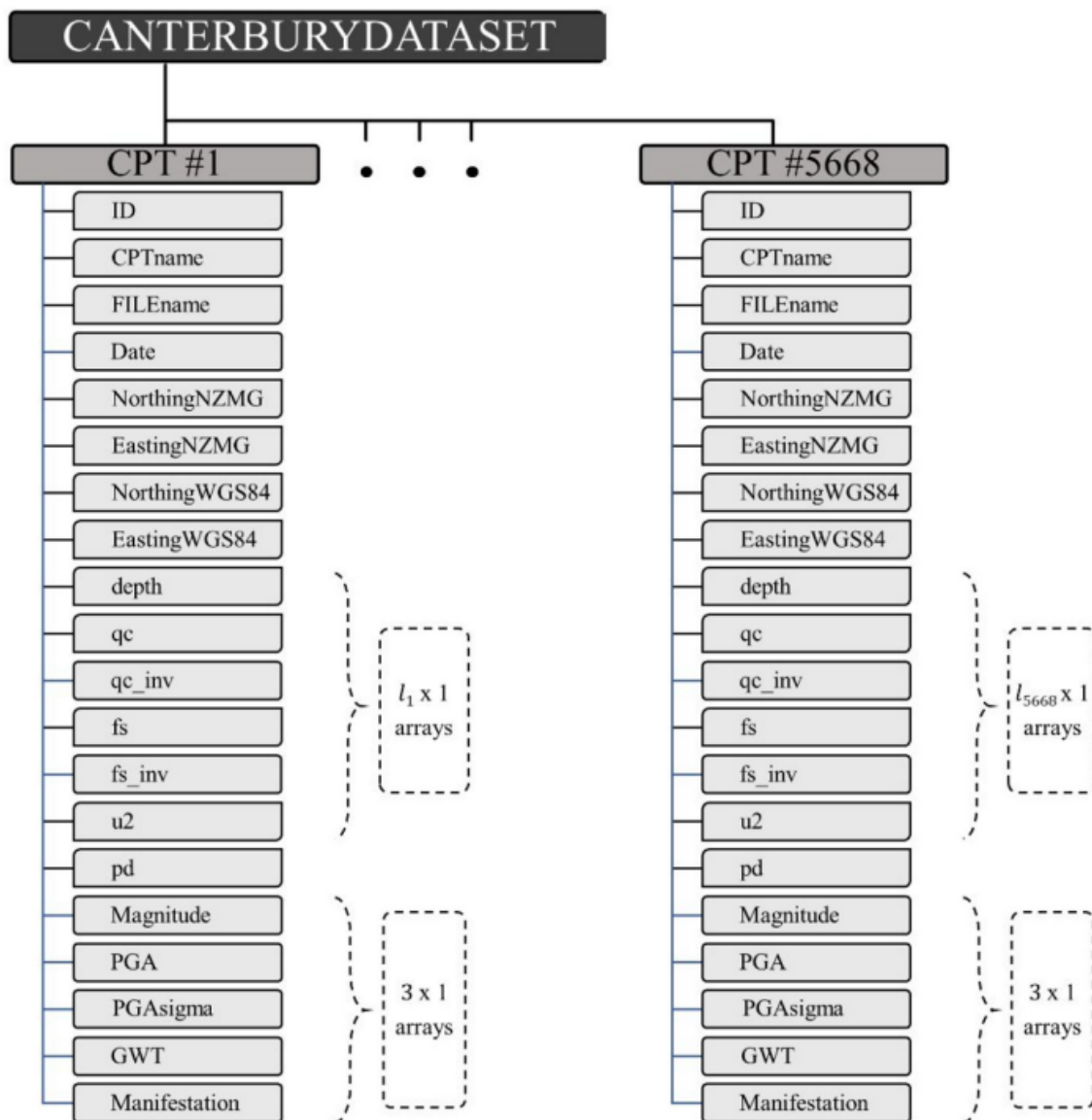
Figure 3. Depiction of the Canterbury case-history dataset structure array. [17].

Figure 4 presents a timeline of executed CPT measurements relative to the dates of the strongest earthquakes in Canterbury, from which the data of magnitude and peak ground acceleration (for the locations of the CPT measurements) were collected. Groundwater table depth at CPT locations was calculated from the data observed in numerous monitoring wells at the time of the mentioned earthquakes. Manifestations were collected from aerial footage and site reconnaissance.
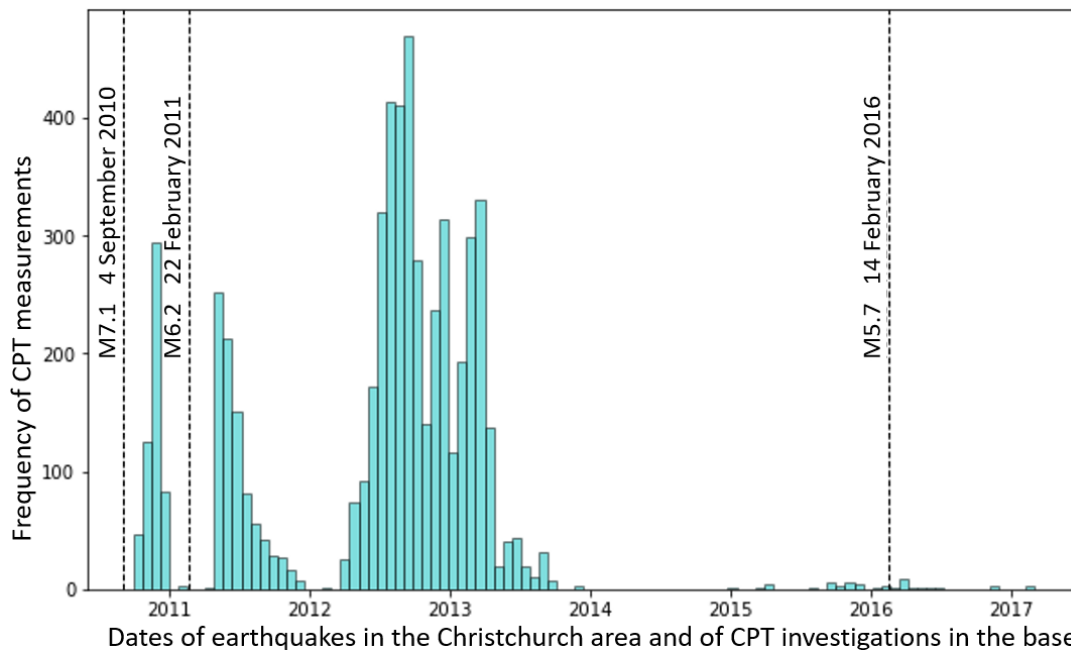
Figure 4. Frequency of CPT measurements through time and in relation to the dates of the strongest earthquakes in the Christchurch area

5. Artificial Neural Networks

Artificial Neural Networks are computational models which find solutions for input data after the so-called training in which a chosen set of examples is analysed. A network consists of thousands of simple processing nodes that are organized into layers and densely interconnected. To each of its incoming connections, a node assigns a number known as weight, with which it multiplies the input data coming from that node and then add a number known as bias. Adding those products together passes through activation function and yields a single number which is passed to the next layer. During training, the training examples are fed to the input layer, the data are multiplied and added, and sent to further layers, until the output layer. The weights and thresholds are continually adjusted until training data yield wished outputs in process known as backpropagation.

If the investigated phenomenon is too complicated, and each of the parameters carries a lot of uncertainty, it may be more feasible to use an Artificial Neural Network, developed on a well-chosen set of data, in other words: always considering if the training examples would fit the analysed problem.

This is why such an artificial neural network was developed to use raw data describing the location and the effect of earthquake and connect them directly to the liquefaction manifestation.

6. Developed Artificial Neural Network and Application to Petrinja Earthquake

The Artificial Neural Network for liquefaction prediction was developed using Python [18,19] by Matija Lozić during his last semester of the Polytechnic Professional Graduate Study at the Zagreb University of Applied Sciences [20].

For the training and validation, the New Zeland Geotechnical Database [16] was used.

First, the data were analized, and Figure 4 shows some data on the soil investigated [20].

The Artificial Neural Network was developed as a Multi-Layer Perceptron for classification. In total 5 models of Artificial Neural Network were developed; each model was fitted for specific data subset.

The individual parameters used are listed in Table 1, together with their boundaries, and listed by data subsets in Table 2.
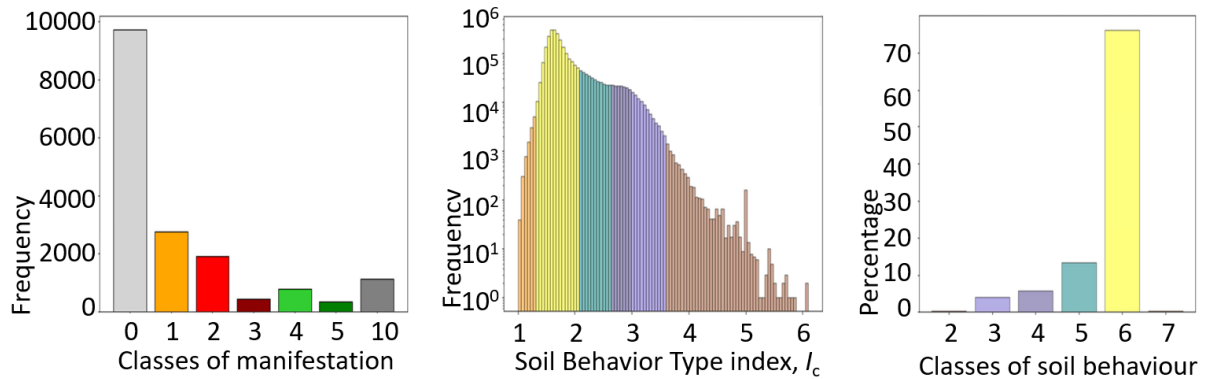
Figure 4. Data used for the network development. a) Frequency of examples by the classes of manifestation: 0 for no liquefaction; 1-3 for three levels of liquefaction intensity: minor, moderate and severe; 4 and 5 for lateral spreading and severe lateral spreading; 10 for cases with not enough of data. b) Frequency of measurements by the Soil Behaviour Type index, I_c after Robertson [8]. Colours show the class of soil behaviour as used in c) and in Figure 2b). c) Percentage of the measurements by the classes of soil behaviour after Robertson [8] as stated in Figure 2c). [20].

First data subset contains data of peak ground acceleration, cone tip resistance and cone sleeve friction. Second data subset contains earthquake magnitude, peak ground acceleration, maximal CPTu depth, depths of CPTu readings, depth of ground water table, cone tip resistance, cone sleeve friction, and measured pore pressure. Third data subset contains dana of normalized cone tip resistance and earthquake-induced cyclic stress ratio. Fourth data subset contains Robertson's Soil Behavior Type index and earthquake-induced cyclic stress ratio. Fifth data subset contains depths of CPTu readings, normalized cone tip resistance, normalized sleeve friction ratio and earthquake-induced cyclic stress ratio. All are further normalized according to simple min-max scaling, after removing some data outliers. Data boundaries are represented in Table 1. Further on, subset data were balanced according to equilibrium of binary classes of liquefaction manifestation.

Table 1 – Data boundaries for individual parameters

Parameter	Min	Max
Peak ground acceleration, a_{max} $[g]$	0.051	0.674
Cone tip resistance, q_c $[kPa]$	3.28	29994.02
Cone sleeve friction, f_s $[kPa]$	0.001	397
Earthquake magnitude, M	5.7	7.1
Depth of individual CPT measurement, $d_{CPT.max}$ $[m]$	5.08	34.94
Depths of CPT readings, d_{CPT} $[m]$	0	34.94
Ground water table depth, GWT $[m]$	0	6.78
Pore pressure measured behind cone u_2 $[kPa]$	-230	799.2
Normalized cone tip resistance, Q [1]	0.033	299.94
Earthquake induced cycling stress ratio, CSR [1]	0.529	1.009
Soil behavior type index, I_c [1]	1.008	6.094
Normalized friction ratio, F [%]	0	836.0

Table 2 – Parameters of data subsets

Data subset	Parameters
1	a_{max}, q_c, f_s
2	$a_{max}, M, d_{CPT.max}, d_{CPT}, GWT, q_c, f_s, u2$
3	Q, CSR
4	I_c, CSR
5	d_{CPT}, Q, F, CSR

For each data subset, after data normalizing and classes balancing, Artificial Neural Network model was defined with optimized model hyperparameters. Optimized hyperparameters for each Artificial Neural Network model were chosen from iterative process observing model performances as shown in Table 3. Detailed descriptions of each of the parameters are given in [18,19].

Table 3 – Hyperparameters for each model

Hyperparameter	MODEL 1	MODEL 2	MODEL 3	MODEL 4	MODEL 5
Input layer	2001	4004	2000	2000	4000
Hidden layer arhitecture	(100)	(100, 100)	(100, 100)	(100,100)	(100,100)
Backpropagation solver	'adam'	'adam'	'adam'	'adam'	'adam'
Activation function	'logistic'	'logistic'	'logistic'	'logistic'	'logistic'
Regularization coefficient	0.1	0.01	0.0001	0.0001	0.001
Initial learning rate	0.001	0.001	0.001	0.001	0.001
Maximal number of iterations	200	200	200	200	200
Shuffle	True	True	True	True	True
Tolerance	0.0001	0.0001	0.0001	0.0001	0.0001
Early stopping	True	True	True	True	True
Validation fraction in early stopping case	0.1	0.1	0.1	0.1	0.1
Initial weights value	0	0	0	0	0
Model accuracy on training data	0.863	0.869	0.756	0.776	0.740
Model accuracy on test data	0.836	0.834	0.745	0.750	0.725

After choosing hyperparameters for each model, models were trained on corresponding data subsets.

Trained models were used on collected data from locations affected by the Petrinja earthquake at locations Brest Pokupski, Galdovo, Krnjica and Palanjek, in total 61 measurements, already preproccesed by normalization and using data boundaries shown in Table 1. Collected CPTu data were analyzed and they were slightly different, difference being represented by Soil type behaviour index shown in Figure 5, where the frequency of the Soil Behaviour Index is shown for the 2 cm sections of CPT measurements. .
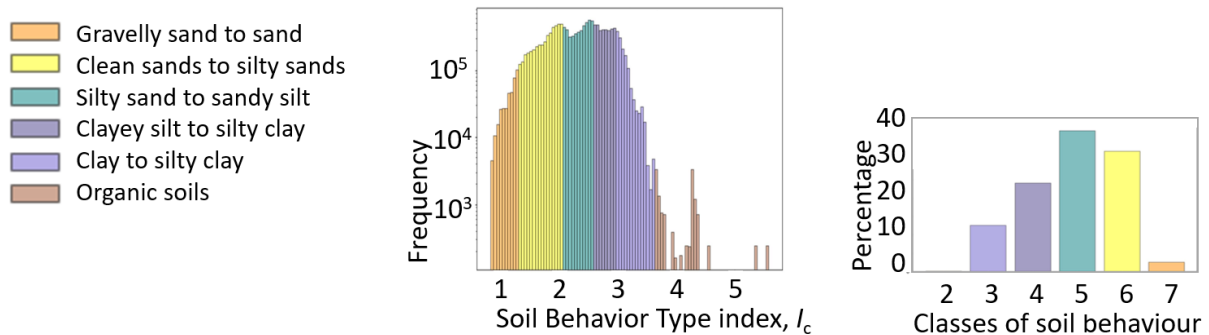
Figure 5. Data from the Petrinja area. a) Frequency of measurements by the Soil Behaviour Type index, I_c. b) Percentage of the measurements by the classes of soil behaviour. [20].

An overview of the main steps of the proces are shown in Figure 6. Pretprocessing was done on the Canterbury case-history dataset to obtain inputs for the 5 models of Artificial Neural Networks, and then on the data from Petrinja area, the developed models were used to predict liquefaction manifestation, i.e. its probability.
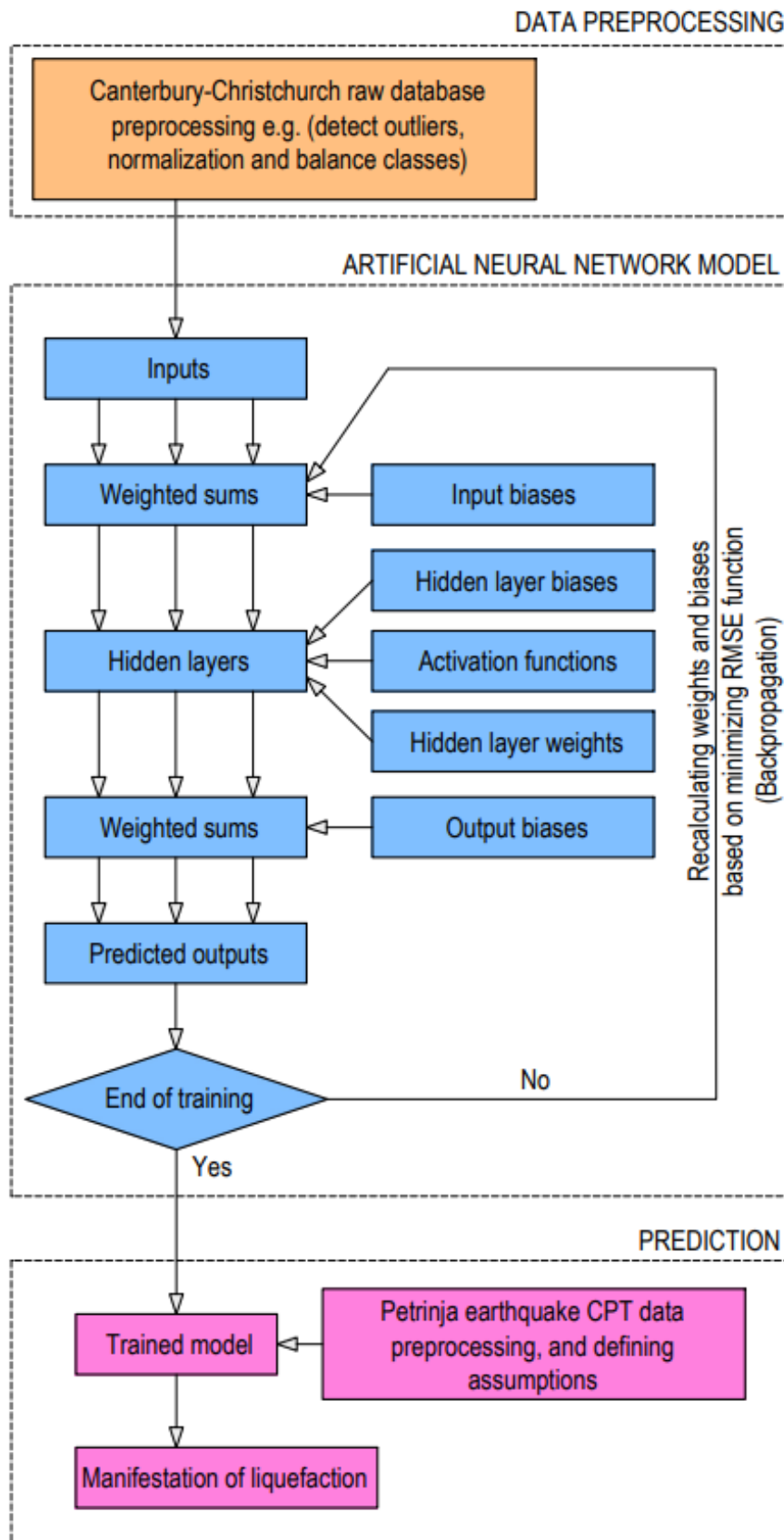
Figure 6. The three main steps of the development and application of the Artificial Neural Network

Results of implementing defined models are shown in Table 4. for one location in Brest Pokupski – the corresponding CPTu results are given in Figure 6. All five models predicted liquefaction, as it was noted on the site, but with different probabilities.
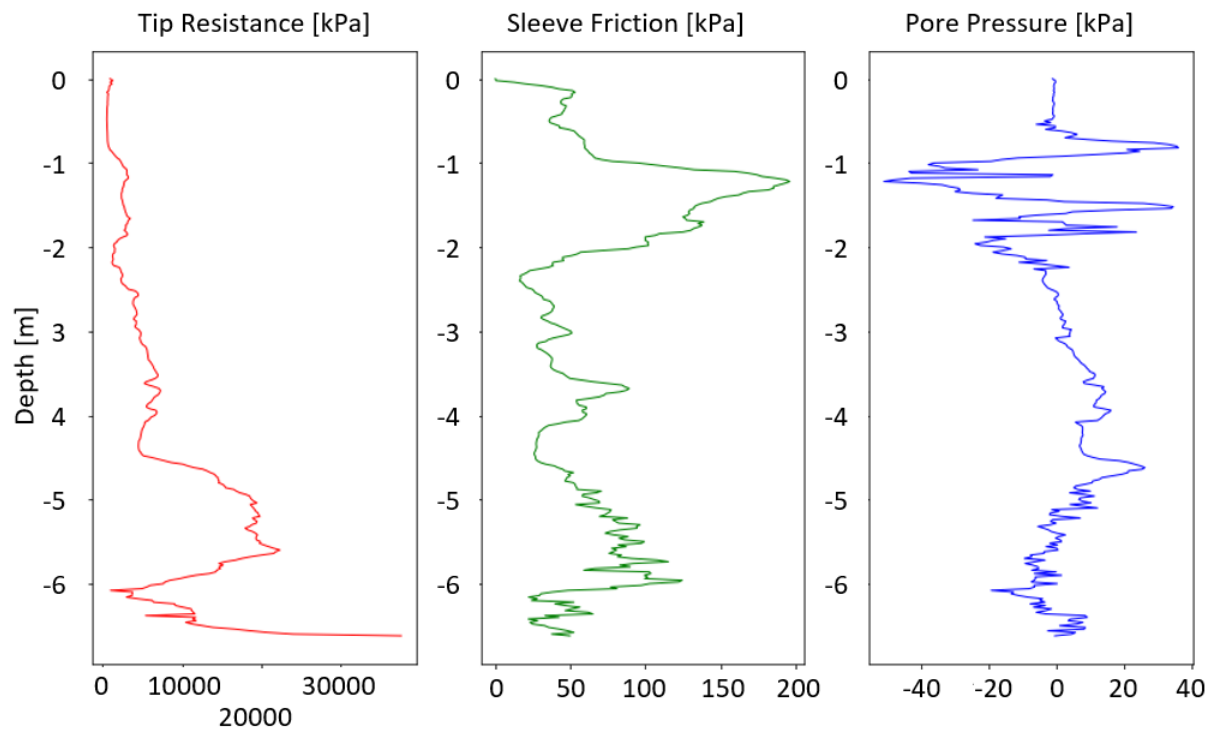
Figure 6. CPTu results for the chosen location in Brest Pokupski.

Table 4 – Results for C-13 in Brest Pokupski

CPTu	M	a_{max}	GWT	MODEL 1 Manifestation of liquefaction	MODEL 1 Probability	MODEL 2 Manifestation of liquefaction	MODEL 2 Probability	MODEL 3 Manifestation of liquefaction	MODEL 3 Probability	MODEL 4 Manifestation of liquefaction	MODEL 4 Probability	MODEL 5 Manifestation of liquefaction	MODEL 5 Probability
Brest Pokupski C-13	6.4	0.2	1	Yes	0.76	Yes	0.98	Yes	0.63	Yes	0.67	Yes	0.96

These results show that on the tested soil location, the liquefaction could be expected according to all five models. Model 2 and model 5 show the most likely soil liquefaction susceptibility. Results correspond to site liquefaction manifestation in form of sand ejecta. Output from this neural network generally shows liquefaction susceptibility at the location of the CPT measurements, and does not specify the depth of the liquefaction.

7. Discussion

The earthquakes which caused liquefaction in Christchurch and its vicinity were of magnitudes 7.0 to around 5. The subsoil of Canterbury contains thick layers prone to liquefaction.

The Petrinja earthquake with M6.2 and some aftershocks caused liquefaction in some layers not more than a meter or so, several meters deep.

The variety in results of different models suggests that it is good – in the training of the network, to use the training examples which correspond to the geological, geotechnical, seismological and hydrological conditions of the location in question. In such a way, it may be believed, the variety of influences will be accounted for.

Figure 7. One of many evidences of liquefaction in Brest Pokupski (Photo already published [2]).

8. Conclusions

The CPT measurements give valuable insight into the soil behaviour. The artificial neural network developed on the basis of the very rich New Zeland Geotechnical Database could be adjusted for the conditions on the investigated location to obtain the probability of liquefaction in various conditions.

References

[1] Veinović, Ž., Kovačević Zelić, B., Kvasnička, P., & Domitrović, D. (2008). Assessment of liquefaction potential of the Sava river plain near Zagreb. *Ulitsky, V.M., Kovalev, V.I. (ur.) Proceedings of the International Geotechnical Conference " Development of Urban Areas and Geotechnical Engineering"*

[2] Miranda, E.; Brzev, S.; Bijelic, N.; Arbanas, Ž.; Bartolac, M.; Jagodnik, V.; Lazarević, D.; Mihalić Arbanas, S.; Zlatović, S.; Acosta V..; Archbold, J.; Bantis, J.; Blagojevic, N.; Borozan, J.; Božulić, I.; Cruz, C.; Dávalos, H.; Fischer, E.; Gunay, S.; Hadzima-Nyarko, M.; Heresi, P.; Lignos, D.; Lin, T.; Marinkovic, M.; Messina, A.; Miranda, S.; Poulos, A.; Scagliotti, G.; Tomac, I.; Tomic, I.; Ziotopoulou, K.; Žugić, Ž.; Robertson, I. (2021) *PRJ-2959 | StEER-EERI: PETRINJA, CROATIA DECEMBER 29, 2020, Mw 6.4 EARTHQUAKE.* https://www.designsafe-ci.org/data/browser/public/designsafe.storage.published/PRJ-2959

[3] Tomac, I. (Co-Team Lead); Zlatovic, S. (Co-Team Lead) ; Athanasopoulos-Zekkos, A.; Bleiziffer, J.; Domitrovic, D.; Frangen, F.; Gjetvaj, V.; Govorcin, M.; Grilliot, M.; Gukov, I.; Herak, M.; Hrženjak, P.; Hutchinson, T; Hudyma, N.; Jagodnik, V.; Kalfatic, V.; Kinikles, D.; Kosovic, I.; Kovacevic-Zelic, B.; Lyda, A.; Matoš, B.; Maric, B.; Matešic, D.; Matos, B.; Mihaljevic, M.; Mijic, Z.; Miletic, M.; Monteiro de Silva, M.; Montgomery, J.; Oršulic, E.; Parlov, J.; Pavelic, D.; Pavicic, I.; Peric, D.; Pham, N.; Puz, G.; Burecic Šafran, M.; Salkovic, A.; Salkovic, I.; Šiša, P.; Sitar, N.; Terzic, J.; Vlahovic, I.; Vlahovic, Z.; Vucetic, M.; Vucenovic, J.; Wang, J.; Ziotopoulou, K.; Žderic, P.K. (2021) *2020 PETRINJA, CROATIA EARTHQUAKE.* https://geerassociation.org/index.php/component/geer_reports/?view=geerreports&layout=build&id=99

[4] Ishihara, K. (1993) Liquefaction and Flow Failure during Earthquake. *Géotechnique*, 43, 351-415

[5] Youd,. T.L.; Idriss. I.M.; Andrus, R.D.; Arango, I.;.Castro, G.; Christian, J.T.; Dobry, R.; Finn, W.D.L.; Harder, L.F. Jr.;Hynes, M.E.; Ishihara K.; Koester, J.P.; Liao, S.S.C.; Marcuson, W.F. III; Martin G.R.; Mitchell, J.K.; Moriwaki, Y.; Power, M.S.; Robertson, P.K.; Seed, R.B.; Stokoe, K.H. II. 2001. *Liquefaction Resistance of Soils: Summary Report from the 1996 NCEER and 1998 NCEER/NSF Workshops on Evaluation of Liquefaction Resistance of Soils.* Vol.l. Journal of Geotechnical and Geoenvironmental Engineering 127(10).

[6] Boulanger, R. W. & Idriss, I. M. (2014) *CPT and SPT based liquefaction triggering procedures, Report No. UCD/CGM-14/01,* s.l.: Center for Geotechnical Modeling, Department of Civil & Environmental Engineering, College of Engineering, University of California at Davis.

[7] Robertson, P. (2016) *Cone penetration test (CPT)-based soil behaviour type (SBT) classification system — an update*, Gregg Drilling & Testing Canada Ltd., Canada.

[8] Robertson, P.K; Cabal, K. (2022) *Guide to Cone Penetration Testing*, Gregg Drilling LLC, Signal Hill, CA, USA

[9] Kovacevic, M. S., Gavin, K., Reale, C. & Libric, L., 2018. The use of neural networks to develop CPT correlations for soils in northern Croatia. F. P. &. J. P. M. A. Hicks, editors. *Cone Penetration.*

[10] Kovacevic, M. S., Gavin, K., Reale, C. & Libric, L., 2019. *Developing correlations between the soil fines content and CPT results using neural networks.* s.l., Proceedings of the XVII ECSMGE-2019 Geotechnical Engineering foundation of the future ISBN 978-9935-9436-1-3.

[11] Mayne, P. (2016) *Geocharacterization by Seismic Piezocone in the Year 2016 and Beyond,* Nonveiller Lecture, http://www.hgd-cgs.hr/nonveiller-lectures/14-nonveiller-lecture-odrzat-ce-professor-paul-w-mayne-5-10-2016

[12] Cubrinovski, M., Henderson, D., Bradley, B.A. (2012) Liquefaction impacts in residential areas in the 2010-2011 Christchurch earthquakes. Tokyo, Japan: *One Year after 2011 Great East Japan Earthquake: International Symposium on Engineering Lessons Learned from the Giant Earthquake*, 3-4 Mar 2012.

[13] Cubrinovski, M., Taylor, M., Henderson, D., Winkley, A., Haskell, J., Bradley, B.A., Hughes, M., Wotherspoon, L., Bray, J., O'Rourke, T. (2014) Key factors in the liquefaction-induced damage to buildings and infrastructure in Christchurch: Preliminary findings. Auckland, New Zealand: 2014 *New Zealand Society for Earthquake Engineering Conference (NZSEE)*, 21-23 Mar 2014. 9pp.

[14] Brandenberg, S. J.; P. Zimmaro, J. P. Stewart, D. Y. Kwak, K. W. Franke, R. E. Moss, K. O. Cetin, G. Can, M. Ilgaç, J. Stamatakos, T. Weaver i S. Kramer (2020) Next-generation liquefaction database,*Earthquake Spectra*, Vol. 36, No. 2, pp. 939-959

[15] Zimmaro P., Brandenberg S.J., Stewart J.P., Kwak D.Y., Franke K.W., Moss R.E.S., Cetin K.O., Can G., Ilgac M., Stamatakos J., Juckett M., Mukherjee J., Murphy Z., Ybarra S., Weaver T., Bozorgnia Y., Kramer S.L. (2019) *Next-Generation Liquefaction Database.* Next-Generation Liquefaction Consortium. DOI: 10.21222/C2J040.

[16] New Zeland Geotechnical Database (2020) https://www.nzgd.org.nz/

[17] Geyin M, Maurer BW, Bradley BA, Green RA, van Ballegooy S. (2021) CPT-based liquefaction case histories compiled from three earthquakes in Canterbury, New Zealand. *Earthquake Spectra*. 37(4) 2920-2945. doi:10.1177/8755293021996367

[18] Pedregosa, F., Varoquaux, G., Gramfort, A., Michel, V., Thirion, B., Grisel, O., Blondel, M., Prettenhofer, P, Weiss, R., Dubourg, V., Vanderplas, J., Passos, A., Cournapeau, D., Brucher, M., Perrot, M., Duchesnay, E., Scikit-learn (2011) Machine Learning in Python, JMLR 12, pp. 2825-2830, available at https://jmlr.csail.mit.edu/papers/v12/pedregosa11a.html

[19] Géron, A. (2019) Hands-On Machine Learning with Scikit-Learn, Keras, and TensorFlow, O'Reilly Media, Inc.

[20] M. Lozić (2022) PRIMJENA UMJETNIH NEURONSKIH MREŽA NA PROCJENU LIKVEFABILNOSTI TLA KORIŠTENJEM STATIČKE SONDE CPT, Diploma work, Zagreb: Zagreb University of Applied Sciences

STRATEGIES FOR SEISMIC DESIGN OF SHALLOW FOUNDATIONS FOR STEEL BUILDING STRUCTURES

Sanda Koboevic [1], Angel Reyes-Fernandez [2], Usthanthan Murugananthan [3], Lydell Wiebe [4]

[1] *Associate professor, Department of Civil Engineering, Polytechnique Montreal, Montreal, QC, Canada, email: sanda.koboevic@polymtl.ca*

[2] *M.Sc. student, Department of Civil Engineering, Polytechnique Montreal, Montreal, QC, Canada, email: angel.reyes-fernandez@polymtl.ca*

[3] *Former M.Sc. student, Department of Civil Engineering, Polytechnique Montreal, Montreal, QC, Canada, email: ushanthan.murugananthan@gmail.com*

[4] *Associate Professor and Chair in Effective Design of Structures, Department of Civil Engineering, McMaster University, Hamilton, ON, Canada, email: wiebel@mcmaster.ca*

Abstract

Canadian provisions allow two alternatives for the seismic design of foundations: capacity-protected (CP) and not capacity-protected (NCP). CP foundations should develop the full resistance of seismic force resisting system (SFRS) and are favoured whenever possible. With such foundations the inelastic activity occurs predominantly in the superstructure, unexpectedly high seismic demands are better managed and the global system deformations are not increased significantly by foundation rotations. NCP foundations develop a partial capacity of the SFRS. Being weaker than the SFRS, such foundations uplift and rotate thus limiting the forces transmitted to the superstructure. Conversely, the foundation rotations increase displacements of the superstructure which must be considered in design.

Canadian design practice shows that foundations of steel frame buildings are often large causing a significant increase in construction cost, which may lead to selection of alternative structural solutions built in different materials. Knowing that the design requirements were developed mainly considering the seismic behaviour of concrete shear walls, characterized by the development of a single plastic hinge at the base, it appears necessary to validate their applicability to steel braced frames that exhibit a distributed yielding mechanism, associated with much larger overstrength and higher capacity design forces on foundations.

In this study, 3-storey steel buildings with X-type tension-compression bracing were designed for Vancouver, Canada, to examine different design strategies for foundation design. Two soil types were considered. The foundation design followed Canadian and US seismic design approaches. Non-linear time history analyses were then performed using the OpenSees program. The model included the inelastic frame behaviour and the nonlinear soil response. The forces imposed on foundations obtained from nonlinear time history analysis are compared with design predictions. The foundation displacements and stresses in the soil are also examined to assess the consequences of foundation flexibility on the global structural seismic response.

Keywords: Braced frames, Foundations, Soil-structure interaction, Design, Nonlinear time-history analysis.

1. Introduction

Even though seismic design requirements for shallow foundations have much advanced over time, foundation design for seismic loads is often given a lower priority by practicing engineers in comparison to that accorded to seismic design of superstructures. Foundation design considerations under seismic loads are complex in nature because of the variability of soil conditions and diverse building configurations and structural systems. Limiting the inelastic activity to the superstructure and avoiding foundation rocking and nonlinear soil response is justifiable in view of the difficulty to detect post-earthquake damage and the high cost of possible foundation repairs. On the other hand, the foundation rocking can in fact be beneficial by protecting the superstructure and reducing the need for intricate ductile detailing, provided that the demands on the soil are acceptable.

In Canada, foundations are generally treated as protected elements and designed to develop the full resistance of seismic force resisting system (SFRS). For unanchored foundations, the alternative design approach is also possible: the foundations can be sized to develop partial resistance of SFRS assuming that at a certain load level the foundation will "rock", and thereby limit the seismic demand on the superstructure. In the United States, practices in individual offices vary significantly as a function of experience and requirements from the client [1]. Because consideration of the SFRS overstrength is not mandatory for foundation seismic design, most often the foundations are designed for the same level of seismic loads as the ductile elements of the superstructure. This implies that some inelastic foundation response will occur at the level of design earthquake. Such approach is justified by the very limited observations of building failures caused by inadequate foundation behaviour during past earthquakes. In some instances, capacity design principles are applied to a certain extent with the objective to control some brittle failure modes related to shear and axial compression. On rare occasion, design offices would opt for a "strong foundation" approach which resembles to Canadian methodology for CP foundation design.

Canadian design requirements for the concrete foundations of buildings provided in the 2015 edition of the NBCC [2] and the corresponding concrete design standard (CSA A23.3-14) [3] have been significantly updated compared to previous editions. These developments were primarily driven by analytical studies conducted on reinforced concrete shear wall buildings, considering a variety of shear wall capacities, foundation capacities and soil types [4]. Even though the new provisions are comprehensive, well-structured and provide much clearer guidance to engineers, their application to concrete and steel buildings reveals some inconsistencies. The reasons behind these inconsistencies are twofold: on one hand, CSA A23.3 and CSA S16 [5] define differently the appropriate level of superstructure capacity that should be developed by foundations, and on the other hand, there is an inherent difference between the yielding mechanisms that develop in concrete walls (single plastic hinge at the base) and steel frames (distributed yielding mechanism). For these reasons, the overstrength tends to be more pronounced for steel frames, which in turn leads to very large foundation design forces and thus large foundation sizes. It has been observed in practice that, in some cases, the cost of concrete foundations may even surpass that of the bracing system, thereby calling into question the feasibility to use a steel frame to resist seismic loads. It is therefore of interest to re-evaluate foundation design provisions for steel braced frames, with the objectives of promoting safe and resilient seismic performance while avoiding unnecessary costs.

In this study, 3-storey steel buildings with X-type tension-compression bracing were designed for Vancouver, Canada, to examine different design strategies for foundation design. Two soil types were considered. The foundations design followed Canadian and US seismic design provisions. Non-linear time history analyses were then performed using the OpenSees program. The model included the inelastic frame behaviour and the nonlinear soil response. The forces imposed on foundations obtained from nonlinear time history analysis are compared with design predictions. The foundation displacements and stresses in the soil are also examined to assess the consequences of foundation flexibility on the global structural seismic response.

2. Building design

2.1 Design of the superstructure

The 3-storey building under study is in Vancouver, BC on Class C (very dense soil or soft rock; 360m/s $\leq$ vs $\leq$ 760m/s) and Class E (soft soil; vs $\leq$ 180m/s) sites. The plan view of the building and the design gravity loads are given in Fig. 1. In the N-S direction, examined in this study, lateral resistance is provided by four X-type tension-compression concentrically braced frames of moderate ductility (MD) type with R_d = 3 R_o= 1.6, where R_d and R_o represent force reduction coefficients related to system

ductility and overstrength, respectively. The braced bay width is 8m. The typical storey height is 4m, and the first storey height is 4.5m, giving a total building height of 13m.
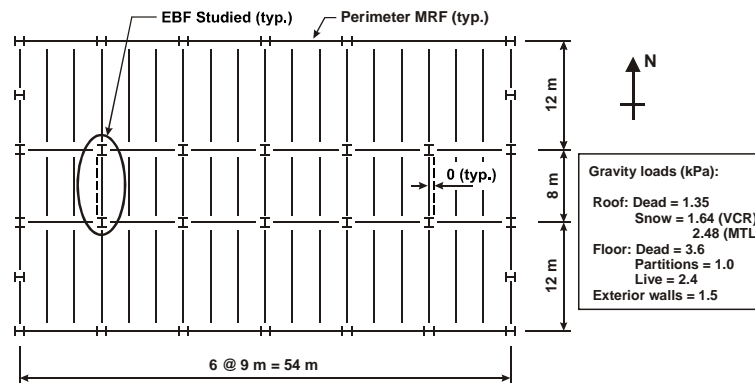
Figure 1. Plan view of the studied building and design gravity loads

The frames were designed following the requirements of NBCC 2015 and CSA S16-14. The seismic design base shear was determined from a response spectrum analysis assuming fixed-base conditions. The resulting seismic design base shears were 2753 kN and 4162 kN, for the VCR-C and VCR-E frames, respectively. Frame members were first sized to satisfy ductility requirements. Braces were selected from square cold-formed HSS sections while beams and columns were selected from W sections and designed to carry gravity loads and forces corresponding to the development of the brace probable resistances in tension and compression without exceeding forces induced by seismic loads calculated with $R_dR_o = 1.3$. As per CSA S16-14, in addition to vertical loads, a bending moment equal to 20 percent of the column plastic moment was considered to account for the bending moments that arise from non-uniform storey drift demands over the frame height. The frames were then verified for adequate stiffness and the strength under all relevant load combinations including gravity loads, notional loads, wind and seismic loads and drift requirements of NBCC. All initially selected sections proved satisfactory. More detailed information on the superstructure design can be found in [6].

2.2 Design of foundations

Foundations were first designed following the provisions of the Canadian concrete design standard CSA A23.3-14 for two design options: capacity-protected (CP) and not-capacity-protected (NCP). For comparison, an alternative design was also carried out using the US design approach, in which no capacity considerations were taken into account to determine foundation design forces. CSA A23.3-14 requires that the overturning moment resistance of CP foundations be sufficient to withstand the overturning moment introduced by gravity loading and the overturning capacity of SFRS. The latter is determined as a function of realistic estimate of system ductility. CSA A23.3 distinguishes between nominal and probable capacity for concrete systems by defining the specific resistance factors for concrete and steel reinforcement as well as the level of stress developed in tension reinforcement ($\phi_c = \phi_s = 1$, f_y for nominal; and $\phi_c = \phi_s = 1$, $1.25f_y$ for probable). CSA S16-14, on the other hand, explicitly addresses neither the capacity level of SFRS for seismic design of foundations, nor the nominal capacities of its components. Consequently, in this study, the design overturning capacities of the frames were determined using probable tensile and compressive brace resistances.

NCP foundations must satisfy the following design criteria: (i) they should withstand the overturning moment imposed by gravity loading and the larger of: (a) the overturning moment resulting from the factored loading that includes the seismic loads, calculated using $R_dR_o=2.0$, or (b) 75% of the nominal overturning capacity of the SFRS; (ii) the soil stress must not exceed the factored soil bearing resistance and (iii) the displacement of the superstructure determined for fixed-base conditions,

increased to account for the impact of foundation rotation, must not exceed the limit prescribed by NBCC 2015 for selected SFRS. The following criteria were considered for the US design approach: (i) the foundation must resist the overturning moment from the combined factored seismic and vertical loading and (ii) the soil stress must not exceed the factored soil bearing resistance. Note that the foundation design in US is done considering allowable bearing stresses in which case the service level of earthquake loading is used (one third of the full load), and the bearing stresses can be augmented by 30 percent for a combined effect of vertical and lateral loading. For consistency, this relaxation was not considered in the present study and the calculations were done with factored load and factored resistances.

Table 1– Summary of foundation dimensions and soil properties for studies frames

Footing dimensions (m)	VCR-C	VCR-E	Soil properties*	Site C	Site E
Capacity-protected foundations (CP)					
Length (L)	15	17.5	q_{ult} (kPa)	3000	400
Width (B)	4	6	q_f (kPa)	1500	200
Depth (d)	1.3	1.5	G (MPa)	100	20
Not capacity-protected foundations (NCP)					
Length (L)	14	15	* q_{ult}: ultimate bearing soil resistance		
Width (B)	4	6	q_f: factored bearing soil resistance		
Depth (d)	1.3	1.5	G: shear modulus		
US design approach					
Length (L)	10	12			
Width (B)	1.35	4			
Depth (d)	1.0	1.5			

A summary of soil properties used for the design is given in Table 1. Factored bearing resistances, q_f, for site class C and E soils were obtained from field data. Ultimate bearing resistance, q_{ult}, and shear modulus, G, were determined from the Canadian foundation manual [7]. Note that, even though q_{ult} varies as a function of the foundation dimensions, it was established by inspection that for the soil friction angles considered in this study, the impact on dimensions was negligible. For that reason, as seen in Table 1, the same values of factored bearing resistance were used for design of all foundations on the same class site. Table 1 also lists the footing dimensions of the two frames studied. For CP and NCP foundations, the overturning moment demand governed footings dimensions for Class C site. For the frames on Class E site the critical parameter for foundation design was the inter-storey frame drift, augmented to include anticipated foundation rotations. In order to avoid the increase in the frame overstrength the excessive drift of the superstructure for NCP foundations was controlled in this study by increasing the foundation dimensions to minimize its rotations. Foundation designed following the US approach was controlled by the bearing soil stress for Class E site while for the Class C site it was possible to optimize simultaneously the bearing resistance and the overturning capacity.

3. Nonlinear time history analysis: Modelling and ground motions

Nonlinear time history analysis (NLTHA) of the soil-foundation-structure system was done using the OpenSEES program [8]. Force-based nonlinear beam-column elements were used for braces whereas elastic beam-column elements were used for the beams and columns. The model can represent tension yielding and in-plane and out-of-plane flexural buckling of braces and thus permit to explicitly evaluate deformation and force demands imposed by braces to other frame members and foundations.

As recommended by Aguerro [9], each brace was divided into 16 elements, with 4 integration points per element and fiber discretization of the section to reproduce distributed plasticity. The Giuffré-Menegotto-Pinto (Steel 02) material with kinematic and isotropic hardening properties was assigned to the fibers. Initial out-of-straightness was considered. Zero-length elements with high axial and

negligible flexural stiffness were applied to model the beam-to-column connections. Column bases were assumed to be fixed. To include P-Δ effects in the analysis, a fictitious gravity column was added. 3% Rayleigh damping was specified [10].

A flexible boundary substructure approach [10] was applied to model the behaviour of the soil-foundation system, including rocking and permanent settlement of the foundation. Nonlinear soil-foundation response was represented using the Beam-on-Nonlinear-Winkler-Foundation concept [11]. The foundation was modelled as an elastic beam with a finite number of vertical (q-z type) nonlinear springs. Nonlinear springs were non-uniformly distributed to simulate the rocking behaviour. A variable spring stiffness was used in order to represent the higher reactions that can develop in the end-zones under the vertical loads. The footing end-length ratio (L_{end}/L) was set at 20%, and a spring spacing ratio (I_e/L) of 4% was selected considering a minimum of 25 springs along the footing length [12]. More detailed information about the frame and soil-foundation modelling is available in [6].

Ground motion records were selected on the basis of the magnitude-distance scenarios that contribute the most to the seismic hazard for the design cases studied [13]. Two distinct ground motion sets were constituted, one for each class site category. Each set was composed of 15 historical ground motions that were grouped in three subsets of five records for each typical tectonic source (crustal, in-slab and interface). All ground motions records were calibrated to match the NBCC design spectra following the procedure described in [14].

4. Results and discussion

The response of the soil-foundation-frame system was examined by tracking the overturning moment at the frame base, the foundation uplift and the settlement of the soil, maximal forces in the nonlinear soil springs and inter-storey drifts. The extent of inelastic activity in braces was also monitored and the principal mechanisms of energy dissipation were identified. The results are expressed as the mean value of the five largest peak response values found for individual ground motion records as recommended in [14].

Table 2– Summary of the results for the overturning moments on foundations

Building	Foundation type	$M_{f\ SSI}$ (kNm)	M_p (kNm)	M_d (kNm)	$M_{f\ SSI}/M_p$	$M_{f\ SSI}/M_d$	M_d/M_p
VCR-C	CP	22162	26552	26552	0,83	0,83	1
VCR-E		26806	31464	31464	0,85	0,85	1
VCR-C	NCP	20645	26552	20971	0.78	1.07	0.79
VCR-E		25519	31464	26544	0.81	1.01	0.84
VCR-C	US approach	15609	26552	10324	0.59	1.50	0.39
VCR-E		21500	31464	14069	0.68	1.53	0.45

In Table 2, the overturning moment demand on the foundation obtained from the analysis ($M_{f\ SSI}$) is compared to the foundation design overturning moment M_d to assess the values used in design. The ratio of M_d to M_p is also given. For CP foundations, the design overturning moment M_d is equal to the probable overturning resistance of the frame M_p. As seen in Table 2, the ratio of the overturning moment demand to design moment ($M_{f\ SSI}/M_d$) varies between 0.83 and 0.85. This result suggests that the design estimates are somewhat conservative and implies that the foundation has sufficient resistance to ensure energy dissipation primarily through inelastic frame response. Indeed, results obtained for brace axial forces and deformations confirm that a significant inelastic activity took place in these elements. On the other hand, the results obtained for foundation uplifts (VCR-C 11.6 mm, VCR-E 4.1mm) and permanent soil settlements (VCR-C 1.8 mm, VCR-E 12.4 mm) indicate that some limited inelastic

response of the foundation-soil system did occur, including primarily rocking for Class C site frame and a combination of predominant inelastic soil response and some rocking for Class E site frame. The maximum forces in the soil springs reached $0.1q_{ult}$ et $0.46q_{ult}$ for Class C and Class E sites, the values that can be easily accommodated by the soil.

For NCP foundation, ratios of $M_{f\,SSI}$ to M_d are close to one for both site classes, showing that the design foundation moments were well predicted. Inspection of inelastic brace response as well as recorded foundation uplifts (VCR-C 21.4 mm, VCR-E 18.3 mm) and permanent soil settlements (VCR-C 2.1 mm, VCR-E 23.8 mm) confirm that, for both sites, the energy was dissipated jointly in the frame and in the soil-foundation system, thereby limiting the inelastic frame demand. For Class C site frame, rocking behaviour dominated the soil-foundation response, while for Class E site frame the energy dissipation through rocking and inelastic soil deformations was comparable.

The foundations designed following the US methodology, which were the smallest two of the six foundations examined, underwent very important rocking and the inelastic response of the soil underneath was extensive. In fact, all energy dissipation happened in the foundation-soil system, eliminating completely the inelastic frame response. In Fig. 2 the normalized maximum brace compression and tensile forces for VCR-E frame are below one in all cases, confirming that no inelastic activity took place in the superstructure. Similar observation was made for the VCR-C frame, for which only two ground motion records induced small inelastic demand in the top storey braces. Note that sliding behaviour of foundation was not represented in the model because the previous studies conducted by the authors revealed that for CP and NCP foundation this failure mode was not critical. However, considering the size of the foundation, it is possible that for the VCR-C frame, and for the two records that induced some yielding in compression braces, the sliding would most probably have happened first thereby eliminating completely the inelastic response of the superstructure.
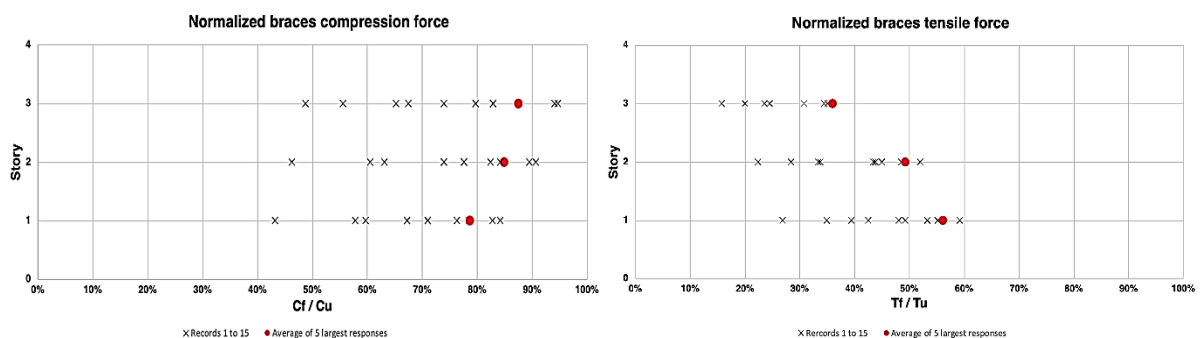
Figure 2. VCR-E frame: Normalized compressive and tensile forces in braces

Such behaviour was anticipated because of a relatively small size of the foundations that resulted from the US design approach; their volume (13.5 m³ and 72 m³) was approximately 5.5 and 2 times smaller compared to the volume of CP (78 m³ and 157.5 m³) and NCP (72.8 m³ and 135 m³) foundations for the VCR-C frame and VCR-E frame, respectively. To draw a picture of foundation-soil behaviour and to assess whether the imposed demand was acceptable or not, the permanent soil settlements and the maximum forces in the soil springs were examined. For the VCR-C frame the energy was principally dissipated through foundation rocking with maximum uplift reaching 38 mm, while the permanent soil settlements remained below 5 mm. However, the springs at the ends of foundation attained the ultimate bearing soil resistance q_{ult}, which level is of great concern even though there is uncertainty about the bearing soil resistance being fully mobilised in view of the small permanent settlement. For the VCR-E frame, the maximum uplift of 53 mm was recorded, while the maximum observed permanent soil settlement was extremely high (143 mm), exceeding by almost 6 times the limit of 25 mm considered in the literature as acceptable [15]. Even though the superstructure remained completely elastic in this case, the foundation was far too small to guarantee a satisfactory seismic response.

It is interesting to note that in all cases, the maximum inter-storey drifts remained well below the NBCC limit of 2.5%. The largest values were recorded for the frames with foundations designed following the US approach and were equal to 0.6% and 1.2% for the VCR-C and VCR-E frames respectively.

5. Conclusions

In this study, different strategies for seismic design of shallow foundations were examined on the example of a 3-storey steel building with tension-compression X-bracing of medium ductility (MD) type, located in Vancouver, BC, Canada. The study included two soil conditions: very dense soil or soft rock (Class C site) and soft soil (Class E site). Design of the frames was carried out in accordance with Canadian design requirements for steel structures. Foundations were designed in compliance with the Canadian requirements for both capacity-protected and not capacity-protected footing options. For comparison, the US design methodology was also applied whereby no overstrength of the superstructure was considered to determine the design loads for foundations.

The results showed that inclusion of soil-structure interaction reduced the overturning moment demand on the foundation in all cases. For CP foundations, design estimates were on the conservative side and the energy dissipation occurred mainly but not exclusively in the superstructure, contrary to what was foreseen in the design. For NCP foundations, the design estimates of the overturning moment demand on the foundation were accurate and the energy dissipation involved both inelastic frame response and nonlinear response of foundation-soil system. The latter involved rocking that was more prominent for Class C site and the inelastic soil response with permanent settlement that was more noticeable for Class E site. The US methodology resulted in the smallest foundations for sites considered and design moments were underestimated by about 35%. For both sites, the energy dissipation was observed in foundation-soil system and the superstructure remains elastic. For Class C site, most of the seismic energy was converted to kinematic energy developed by foundation rocking and very small permanent settlement were observed. However, the soil springs at foundation ends reached the ultimate bearing resistance, which is of great concern as the seismic performance of the superstructure can be jeopardized. For Class E site, excessive permanent settlement that were observed would fully compromise the integrity of the superstructure. The results of this study suggest that some overstrength needs to be considered in seismic design of shallow foundations for steel braced frames, but smaller than what is suggested in Canadian design procedures. Determining the most appropriate value is the subject of an ongoing study.

Acknowledgements

References

[1] Moehle, J. (2015): *Seismic design of reinforced concrete buildings*. McGrow-Hill education, 1st edition, USA.

[2] CSA. (2015): *National Building Code of Canada 2015* 13th ed. NRCC, Ottawa, ON, Canada.

[3] CSA. (2014): *CSA-A23.3-14: Design of Concrete Structures*. CSA, Mississauga, ON, Canada.

[4] Adebar, P., DeVall, R., Bazargani, P., and Anderson, D.L. (2014): Seismic Design of Foundations: The 2015 Canadian Building Code, *10th National Conference in Earthquake Engineering*, Earthquake Engineering Research Institute, Anchorage, AK, USA, 11 pages.

[5] CSA. (2014): *CAN/CSA-S16-14: Design of Steel Structures*. CSA, Toronto, ON, Canada

[6] Koboevic, S., Murugananthan, U. (2019): Impact of foundation rotations on seismic design of steel braced frames. 12th Canadian Conference on Earthquake Engineering, CAEE, Quebec City, QC, Canada, 8 pages.

[7] Canadian Geotechnical Society. (2013): *Canadian foundation engineering manual (in French). 4th ed*. Richmond, BC, Canada.

[8] McKenna, F., Fenves, G.L. (2004): *Open System for Earthquake Engineering Simulation (OpenSees)*. Pacific Earthquake Engineering Research Center, Berkeley, CA, USA.

[9] Aguero, A., Izvernari, C., Tremblay, R. (2006) : Modelling of the seismic response of concentrically braced steel frames using the OpenSees analysis environment. *International Journal of Advanced Steel Construction, 2*(3), 242-274, doi: https://doi.org/10.18057/IJASC.2006.2.3.5

[10] Deierlein, G., Reinhorn, A., Willford, M. (2010): *NEHRP Seismic Design Technical Brief No. 4-Nonlinear Structural Analysis for Seismic Design: A Guide for Practicing Engineers*. NIST, San Francisco, CA, USA.

[11] Gajan, S., Hutchinson, T. C., Kutter, B. L., Raychowdhury, P., Ugalde, J.A., Stewart, J. P. (2008): *Numerical Models for the Analysis and Performance-Based Design of Shallow Foundations Subjected to Seismic Loading*. Technical Report PEER 2007/04. PEER, Berkeley, CA, USA.

[12] Gajan, S., Raychowdhury, P., Hutchinson, T. C., Kutter, B. L. and Stewart, J. P. (2010). Application and validation of practical tools for nonlinear soil-foundation interaction analysis. *Earthquake Spectra, 26*(1), 111-129, doi: https://doi.org/10.1193/1.3263242

[13] Tremblay, R., Atkinson, G., Bouaanani, N., Daneshvar, P., Léger, P., Koboevic, S. (2015): *Selection and scaling of ground motion time histories for seismic analysis using NBCC 2015*. 11th Canadian Conference on Earthquake Engineering, Victoria, BC, Canada.

[14] Atkinson, G. M. (2009). "Earthquake time histories compatible with the 2005 National building code of Canada uniform hazard spectrum". *Canadian Journal of Civil Engineering, 36*(6), 991-1000, doi: https://doi.org/10.1139/L09-044

[15] Lindeburg, M. R. (2015): Civil engineering reference manual for the PE exam: www. ppi2pass. com.

EFFECTS OF CORE STRUCTURE IN MULTIPHASE SIMULATION OF AN EARTH DAM

Kemal Edip [(1)], Vlatko Sheshov [(2)], Julijana Bojadjieva [(3)], Toni Kitanovski [(4)], Dejan Ivanovski [(5)] and Irena Gjorgjeska [(6)]

[(1)] *Assoc. Prof, Ss.Cyril and Methodius University in Skopje, Institute of Earthquake Engineering and Engineering Seismology, Skopje, N.Macedonia, kemal@iziis.ukim.edu.mk*
[(2)] *Prof., Ss.Cyril and Methodius University in Skopje, Institute of Earthquake Engineering and Engineering Seismology, Skopje, N.Macedonia, vlatko@iziis.ukim.edu.mk*
[(3)] *Assoc. Prof.,, Ss.Cyril and Methodius University in Skopje, Institute of Earthquake Engineering and Engineering Seismology, Skopje, N.Macedonia, jule@iziis.ukim.edu.mk*
[(4)] *Assist., Ss.Cyril and Methodius University in Skopje, Institute of Earthquake Engineering and Engineering Seismology, Skopje, N.Macedonia, tonik@iziis.ukim.edu.mk*
[(5)] *Assist., Ss.Cyril and Methodius University in Skopje, Institute of Earthquake Engineering and Engineering Seismology, Skopje, N.Macedonia, ivanovski@iziis.ukim.edu.mk*
[(6)] *Assist., Ss.Cyril and Methodius University in Skopje, Institute of Earthquake Engineering and Engineering Seismology, Skopje, N.Macedonia, gj_irena@iziis.ukim.edu.mk*

Abstract

One of the most popular themes in earthquake geotechnical engineering is the simulation considering the phase interaction among different phases inside the soil medium. The present article aims at providing numerical simulations of an earth fill dam composed of multiphase material models. Moreover, the assessment of liquefaction potential is investigated considering the presence of core structure inside the dam body which obviously has great implications for the results. The formulation of the coupled approach is presented as a mixture of three constituents – soil grains, water and air in the pores.

Mixture theory is considered including the concept of volume fractions in defining of the coupled approach. An earth dam has a trapezoidal cross section with the presence of core structure inside the dam body. The flow of water is different and simulations are more time consuming for which results from literature are used in verification process. The simulation considers a nonlinear behavior with respect to the water retention curves and material model for the solid state. The hydrostatic distribution of water pressured at steady state conditions show obvious differences in saturation of the earth filled dam and are in accordance with the results from literature.

The dam is assumed to be situated above a hard rock formation. The soil material of the dam body is simulated as hypoplastic material model which is nonlinear even for the small deformations. The usage of hypoplastic model and the accumulation of strain in each cycle of the stress – strain relation makes the model advantageous. Results are compared accordingly, and conclusions provide directions for further usage of the multiphase model in simulation of this type of structures

Keywords: Earth Dam, numerical simulations, multiphase modelling

1. Introduction

Heterogeneous materials and their numerical simulations are of great interest for simulation as a multiphase medium [1-3]. In geotechnical engineering, multiphase modelling has great significance because realistic predictions of soil behaviour can be obtained both in cases of loading and unloading. In simulation of hydro mechanical behaviour of dam bodies, multiphase flow plays an important role in simulation due to the nonlinear nature of fluid flow in pores. In simulating porous mediums such as soil, behaviour is largely driven by the interaction of solid skeleton with water and/or air in the pores. Therefore, the coupled problems of fluid flow and deformation of the solid skeleton are considered in detail. In the description of soil media, different approaches are presented in the literature [4-7]. One of

the main advantages of using this particular numerical model is that the model can simulate different mechanical properties of porous geo-materials. In this work, the implementation of the numerical model is performed by using the software ANSYS [8].

2. Development of numerical model

In defining porous media, one of the great challenges is to mathematically represent the stages involved. In describing these porous media in the soil, factors such as water saturation and pore pressure have a strong influence on load distribution. In the description of the material, a macroscopic approach was used in which the behaviour of the soil is homogenized (smeared) through a representative volume element. The concept of the volume-share has been used to estimate the participation of each constituent in the formulation of equilibrium equations for each phase and to take into account the interaction between phases. Following the concept of volume fractions, the entire volume consists of a solid fraction *Vs* and a pore volume *Vp*. The pore volume fraction is composed of water and air phases *Vw* and *Va*, respectively as given in Figure 1.
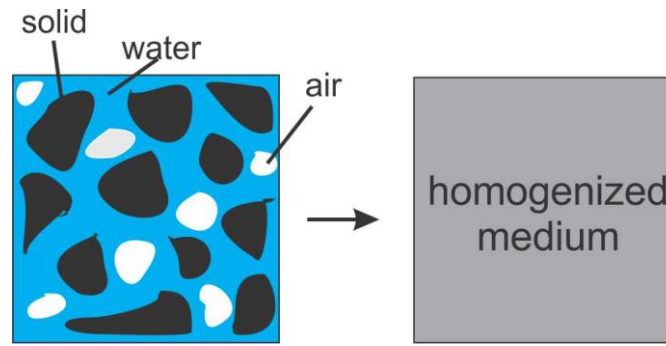
Figure 1. Homogenization of soil medium

In order to include the local composition of the mixture, local volume relations are introduced according to the concept of volume shares. The volume *V* of the total medium arises from the sum of the partial volumes of the constituent bodies.

$$V = \int_B dv = \sum_\alpha V^\alpha$$

(1)

The volume shares of solids in relation to the pore volume is given by void ratio n while the proportion of pores sizes are described by void ratio *e*.

$$n = \frac{\text{Pore volume}}{\text{Total volume}} = \frac{V_g + V_w}{V}$$

(2)

$$e = \frac{\text{Pore volume}}{\text{Solid volume}} = \frac{V_g + V_w}{V_S}$$

(3)

Assuming no mass exchange between phases the balance of mass can be written for each phase as:

$$\frac{d^\pi \rho^\pi}{dt} + \rho^\pi \nabla \cdot \upsilon_\pi = 0$$

(4)

On the other hand, the local form of momentum balance equation for the mixture under quasistatic conditions is given as follows:

$$\nabla \cdot \sigma + \rho g = 0$$

(5)

The capillarity and saturation relationships provide a link between the volume fractions of water and air. Their pressures describe the ability of the soil to store water. The relationship between capillarity and soil saturation depends not only on the properties of the fluid but also on the structure of the porous

medium. Probably the oldest relationship between capillarity and saturation and still widely used approach was first introduced by Brooks and Corey [9]. On the basis of test results, the capillarity saturation relationship is defined as:

$$S_e = \begin{cases} \left(\dfrac{p_e}{p_c}\right)^{\lambda} & \text{for} \quad p_c \geq p_e \\[2em] 1 & \text{for} \quad p_c < p_e \end{cases} \tag{6}$$

3. Numerical implementation

In this section, the focus is on the implementation of the finite element method of the proposed numerical model in the ANSYS software. Spatial discretization is done by interpolation polynomials (functions of forms). Usually, biquadratic and bilinear approaches are chosen for structural degrees of freedom. The solution of the differential equation is consistent with the physical nonlinearity in the time domain. The total implementation in ANSYS software can be shown as in Figure 2 below:
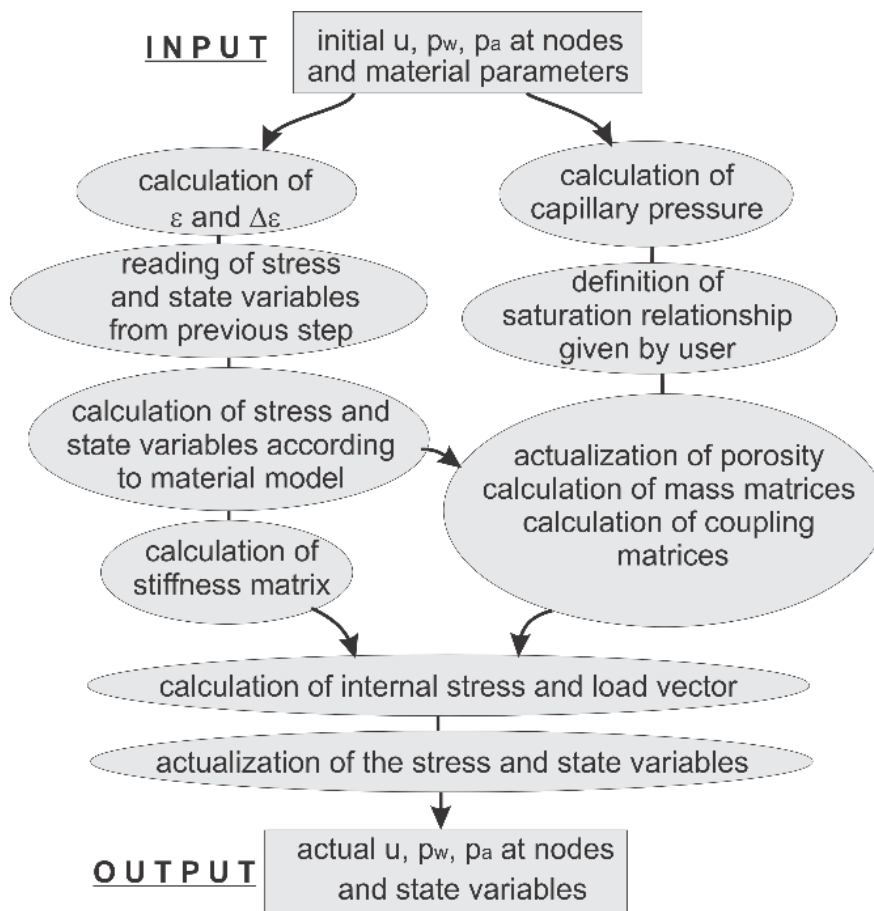
Figure 2. Implementation of the proposed model in ANSYS software

Following the work of first author [2] the finite element equations for the numerical model can be summarized as follows:

$$
\begin{pmatrix} \mathbf{M} & \mathbf{0} & \mathbf{0} \\ \mathbf{M_w} & \mathbf{0} & \mathbf{0} \\ \mathbf{M_g} & \mathbf{0} & \mathbf{0} \end{pmatrix} \begin{pmatrix} \ddot{\mathbf{u}} \\ \mathbf{0} \\ \mathbf{0} \end{pmatrix} + \begin{pmatrix} \mathbf{C} & \mathbf{0} & \mathbf{0} \\ \mathbf{C_{sw}}^T & \mathbf{P_{ww}} & \mathbf{C_{wa}} \\ \mathbf{C_{sa}}^T & \mathbf{C_{aw}} & \mathbf{P_{aa}} \end{pmatrix} \begin{pmatrix} \dot{\mathbf{u}} \\ \dot{\mathbf{p}}_w \\ \dot{\mathbf{p}}_a \end{pmatrix} + \begin{pmatrix} \mathbf{K} & -\mathbf{C_{sw}} & -\mathbf{C_{sa}} \\ \mathbf{0} & \mathbf{H_{ww}} & \mathbf{0} \\ \mathbf{0} & \mathbf{0} & \mathbf{H_{aa}} \end{pmatrix} \begin{pmatrix} \bar{\mathbf{u}} \\ \bar{\mathbf{p}}_w \\ \bar{\mathbf{p}}_a \end{pmatrix} = \begin{pmatrix} \mathbf{f_u} \\ \mathbf{f_w} \\ \mathbf{f_a} \end{pmatrix} \quad (7)
$$

The nodal degrees of freedom for displacement, water and air pressure are taken into consideration as u, p_w and p_a. Their first and second time derivative of solid phase complete the system of equations. The different matrices of the system of equations describe different properties of the numerical model. The indices provide information about the nature and function of the matrix, which can be interpreted as follows. The coupling matrices *Csw*, *Csa* describe the interaction of the solid phase with water and air phases. The mutual influence of the fluids with each are represented by *Cwa*. The compressibility of the various phases and their effects on the entire media is considered by compressibility matrix *Pww*. The permeability matrix *Hww* on the other hand, concerns the flow behavior.

4. SIMULATION OF DAM BODY SUBJECTED TO SEISMIC LOADING

This particular example shows the implementation of the proposed numerical model in partially saturated soil medium through a numerical simulation of the dam body given in the work of several authors [1, 7]. The dam body is a compacted earth dam with 52m length and 12 m height. The comparison and verification of the steady state is done in the work of authors [1]. The dam body has a core structure in order to hinder the increase of pore water pressure in case of earthquake excitations. The dam body configuration is shown in Figure 3 below.
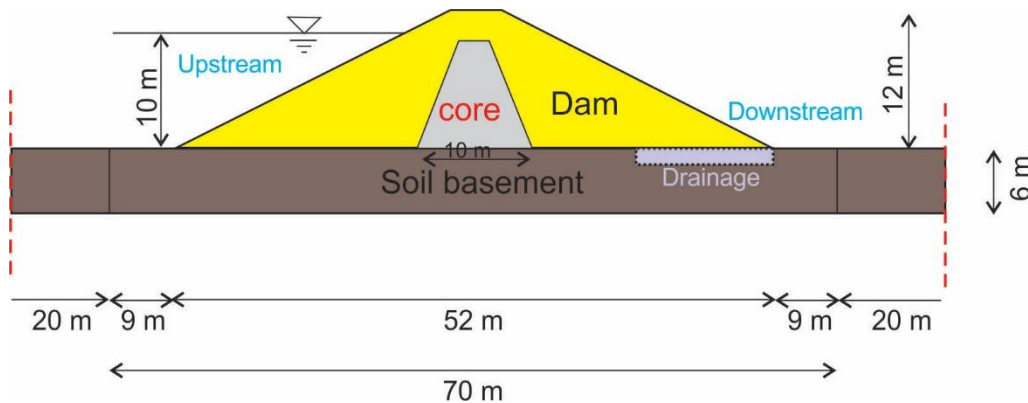
Figure 3. Dam body model with core inside

The dam body is assumed to be situated above a hard rock formation. Therefore, the base of the dam is assumed to be impermeable and fixed, i.e. the deformability is constrained apart from the drainage which has a length of 12m. The initial effective stress of the dam is obtained after the seepage analysis and static equilibrium has been reached. As can be seen in Figure 4 the presence of core inside the dam body does not allow the water to flow and thus the pore water pressure is mainly in the upfront part of the dam body.
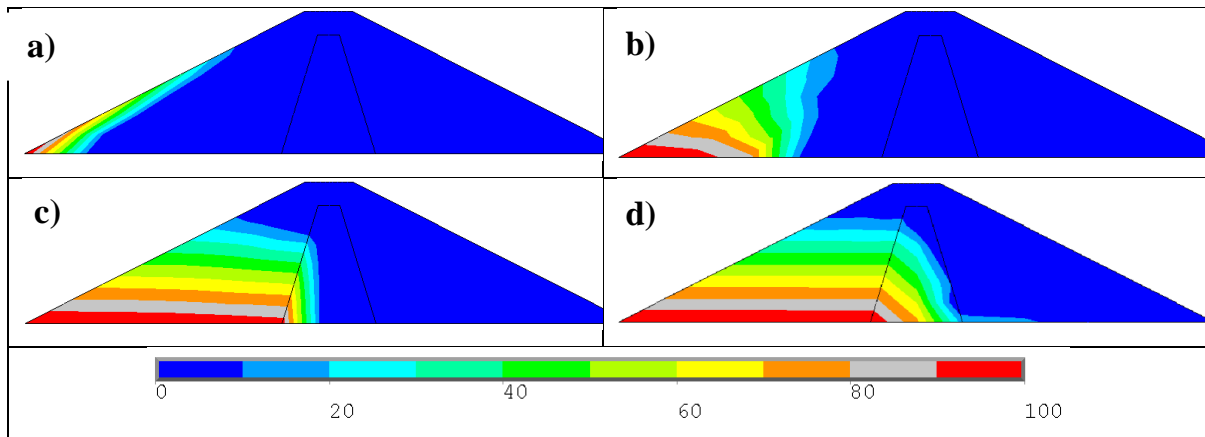
Figure 4. Pore pressure distribution inside the Dam body

On the other hand, the comparison of saturation shows that the presence of core structure inside the dam body has great effects on overall saturation. The saturation distribution inside the dam body is given in Figure 5 below.
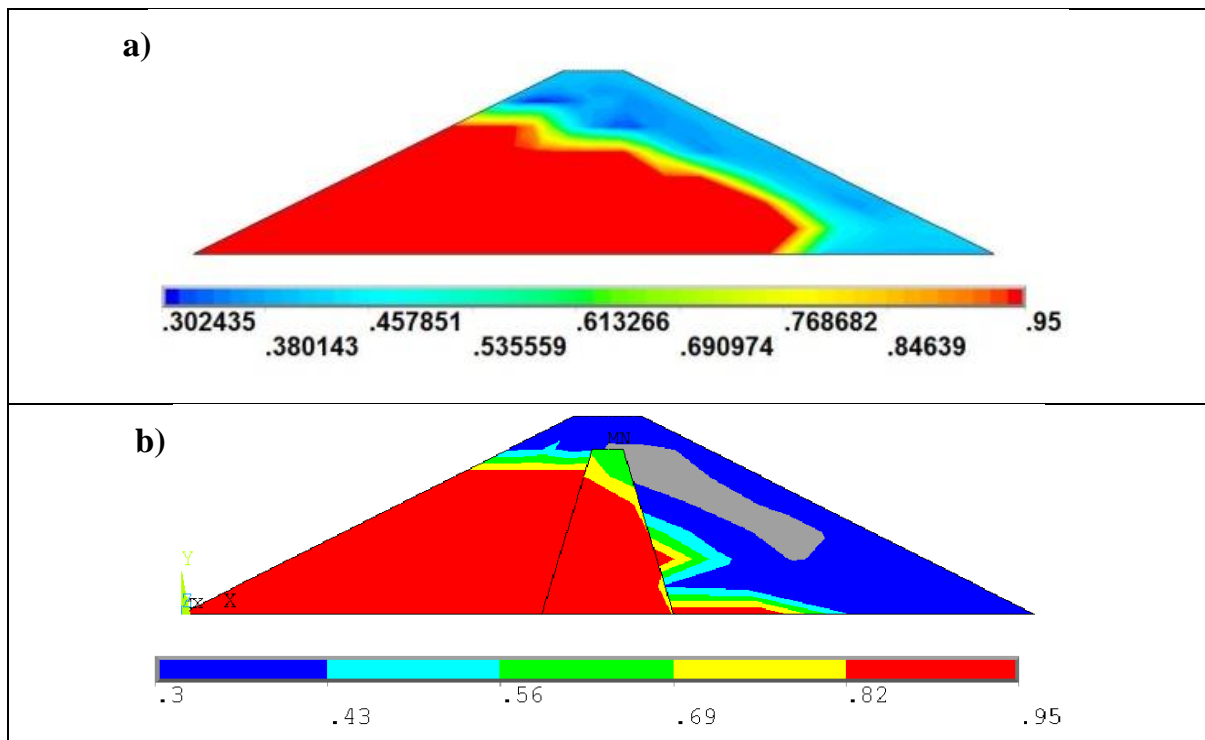
Figure 5. Comparison of saturation distribution

As can be seen from Figure 5, the core structure inside the dam body apart from hindering of saturation, can absorb water with slow permeability since the composition of the core is assumed to be clay.

101

5. Earthquake simulations of the dam body

In order to take account of earthquake triggering, three acceleration histories namely, El Centro N-S, USA, 1940, with magnitude M=6.7; Robic N-S, recorded during the Furlania (Italy) earthquake of 15.09.1976 with magnitude M=6.1., Bitola N-S, recorded on 01.09.1994 with magnitude M=5.2-5.4 have been used in order to analyze the behavior of the dam body under earthquake excitations. The input earthquake time histories are scaled to 0.25g and are given in the Figure6 below:
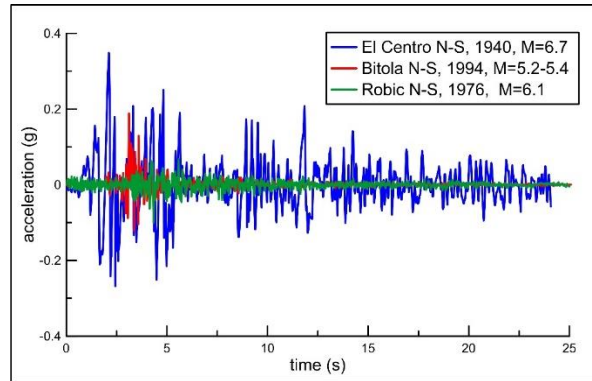
Figure 6. Selected acceleration histories from earthquakes

The earthquake time histories are used as input accelerations at the base of the dam body for analyses in order to estimate the dynamic response of the dam body under strong earthquakes. In this paper the numerical results of pore water pressures are simulated and discussed. The advantage of this model is that the used hypoplastic model takes into account the accumulation of strain in each cycle of the stress – strain relation [10]. In selection of the material model for solid phase the hypoplasticity material model of Von Wolffersdorff [11] has been used. The material parameters used in the simulations for the dam body are as follows: density of solid phase ρ_s=2.7ton/m^3 , density of water phase ρ_w=1.0ton/m^3, permeability k=1.0*10^{-7}m/s, compression modulus of solid phase Ks=10^{9}kPa, compression modulus of water phase Kw=2*10^{4}kPa, dynamic viscosity of water μw=1.31*10^{6}kNs/m^2, critical internal angle φc=30°, granulate hardness hs=1600MPa, exponent n=0.39, minimum void ratio e_{d0}=0.62, critical void ratio e_{c0}=0.94, maximum void ratio e_{i0}=1.08,numerical parameters α=0.2 and β=1, R=0.0001, m_r=2.5, m_t=9.0, β_r=0.25, χ=9. In simulation of earthquake time histories the duration used for simulation is considered only 25seconds during which the peak of accelerations of all earthquake time histories are found. In Figure. 7 the pore water pressure development during earthquake time histories are simulated. The presence of core structure inside the dam body is given with the notion of (core) and comparisons are done consequently.
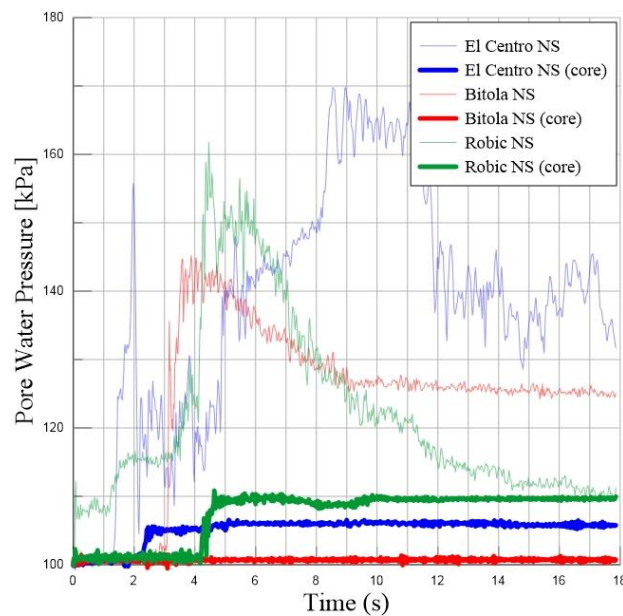
Figure 7. Development of pore water pressure at the top of the dam body

The obtained values in Figure7 are from the upfront part of the dam body in which pore water pressures in cases of dam body and dam body with core structure are compared. As can be seen from Figure 7 the pore pressures in case of earth dam without core structure show increase in values as earthquake time history is applied. On the other hand, the same earthquakes in case of earth dam with core structure does not allow the increase in the pore pressures. However, in the case of Robic NS earthquake time history, the pore pressure tends to increase although the increase is very small in comparison with the pore water pressure in case of dam body without the core structure. In a nutshell, the dam body with the core structure inside, subjected to earthquake excitations triggers very small increase in pore pressures inside the dam body. The increase in the pore water pressures is in the upfront side and is considered to be small in order to initiate any destructive conditions.

6. Conclusions

It should be noted that the presence of core structure inside the dam body contributed to the decrease in pore water pressures which are expected in case of earthquake excitations. Parametric analysis was considered to examine the effects of different acceleration time's histories on the behavior of dam body. In all three earthquakes the increase in pore water pressures in comparison with the case when the core structure is not present, is significantly smaller. The presented coupled approach gains importance because of the detailed presentation of the pore pressures which take place in multiphase medium such as the soil media. The disadvantage of the presented model is the slowness of the computations due to the big size of the included matrices in the calculations.

References

[1] Edip, K., et al. Coupled Approach in Simulation of Earth Dam. in 16th European Conference on Earthquake Engineering 2018. Thessaloniki, Greece: The European Association for Earhtquake Engineering.

[2] Edip, K., et al., Development of coupled numerical model for simulation of multiphase soil. Computers and Geotechnics, 2018. 96: p. 118-131.

[3] Edip, K., Development of three phase model with finite and infinite elements for dynamic analysis of soil media. 2013, Ss. Cyril and Methodius: Institute of Earthquake Engineering and Engineering Seismology.

[4] Biot, M., Generalized theory of acoustic propagation in porous dissipative media. The Journal of the Acoustical Society of America, 1962. 34: p. 1254.

[5] De Boer, R., Development of porous media theories—a brief historical review. transport in porous media, 1992. 9(1-2): p. 155-164.

[6] Schrefler, B.A. and Z. Xiaoyong, A fully coupled model for water flow and airflow in deformable porous media. Water Resources Research, 1993. 29(1): p. 155-167.

[7] Oettl, G., R.F. Stark, and G. Hofstetter, Numerical simulation of geotechnical problems based on a multi-phase finite element approach. Computers and Geotechnics, 2004. 31(8): p. 643-664.

[8] ANSYS. Fem Software. 2006.

[9] Corey, A.T. and R.H. Brooks, The Brooks – Corey Relationship. 2002: United States University of California at Riverside.

[10] Niemunis, A. and I. Herle, Hypoplastic model for cohesionless soils with elastic strain range. Mechanics of Cohesive-frictional Materials, 1997. 2(4): p. 279-299.

[11] 1von Wolffersdorff, P.A., A hypoplastic relation for granular materials with a predefined limit state surface. Mechanics of Cohesive-frictional Materials, 1996. 1(3): p. 251-271.

EXPERIENCES IN MODELING AND ANALYSIS OF MINE SEAL STRUCTURES

Viktor Hristovski [(1)], Emil Jankulovski [(2)], John Burke[(3)]

[(1)] *Professor, Ss. Cyril and Methodius University in Skopje, Institute of Earthquake Engineering and Engineering Seismology UKIM-IZIIS Skopje, P.O. Box 101, 165 Todor Aleksandrov Str., 1000 Skopje, Republic of Macedonia, viktor@iziis.ukim.edu.mk*

[(2)] *BE, ME, MIE Aust, Director, INDUCTA Pty Ltd, PO Box A2293, Sydney South, NSW Australia 1235, emil@inducta.com.au*

[(3)] *BE CPEng NER Civil/Structural, MIE Australia, Director, Burke Engineering Services P/L, Thornton, Australia*

Abstract

Mine seals are structures used to serve as protection shields against short term instantaneous pressure loadings like blasts, which could occur in underground mine workings during serviceability period in combination with possible hydrostatic pressure from ground water. They can also resist accidental loads, like earthquakes, that may occur during the excavation period. In this paper, experiences in modelling and nonlinear finite element analysis of mine seal structures that have preceded the design phase are presented. Namely, for the period of 10 years, more than 20 study cases of mine seals have been modelled and analysed by the authors. Each separate study case consisted of a number of different model types, depending on various assumptions about prescribed boundary conditions, material used, seal structure adopted, prescribed loading, existence of bolts, existence of openings, etc. For all cases, there have been performed force-displacement progressive failure analyses (PFM), with detailed description of the failure mechanism and critical points on the obtained diagrams. The design force-displacement diagrams have been constructed by using an overstrength factor and a material partial safety coefficient. The design limit states criteria have been defined for each study case taken separately. All study cases are presented comparatively in a tabular form according to the material and geometrical properties, failure mechanisms and design limit state criteria. The numerical analyses have been performed by using the software package FELISA/3M. Willam-Warnke and Drucker-Prager elastic-plastic criteria have been used to account for the material nonlinearity. Models have been built using SOLID iso-parametric finite elements with 20 nodes for modelling of the seal body and LINK elements for modelling of the contact surfaces between the body and the surrounding rocks. This study is believed to have given a valuable insight into modelling and methods for analysis of mine seals structures, useful for practitioners in this field.

Keywords: Mine seals, finite element method, nonlinear analysis, failure analysis, backward Euler scheme

1. Introduction

The purpose of mine seal structures is to isolate abandoned mine tunnels from still active mining workings (see Fig. 1). Namely, mine seals should prevent spreading of possible explosions from the abandoned areas into the active workings. Also, they may be designed to prevent the leakage of potentially explosive or toxic gases, or their migration into the active zones. The bearing system of the seal structures and the material from which it is made can be quite different, depending on the in-situ conditions. The technology of construction and the very design of the seal structures is a special topic of research [1,2] that should follow appropriate technical norms, depending on the country in which they are constructed. In this work, we will not deal with the technology and design phases themselves, rather than with the numerical modelling and analysis of the mine seal structures using the finite element method (FEM). It should be noted that, presently, this topic is very much of interest. Namely, it is anticipated that a huge number of underground mines in the world will be closed in near future because of the global climate change problem. This will require these types of seals.

With the recent technical norms in the world the level of seal design requirements and criteria related to the strength of the constructed mine seals have been increased [1, 2]. These requirements can be best

satisfied if the seal design includes the following three phases: laboratory testing, in-situ testing, and FEM nonlinear analysis. Usually, the properties of the proposed construction material are determined by laboratory tests. In addition, the in-situ testing provides the remaining input parameters for numerical finite element modelling related to properties of the surrounding rock deposit, conditions at the contact zones between the rock deposit and the seal structure, possible hydrostatic pressure level, the level of the risk pertaining to explosions, etc. Finally, FEM nonlinear analysis can simulate the failure mechanism of the seal structure based on the input parameters from the tests. According to the National Institute for Occupational Safety and Health (NIOSH) [1], the following failure modes of the mine seal structures are possible and permitted: (1) bending and tensile failure through the seal structure, (2) shear failure through the seal foundation, (3) shear failure along the seal-foundation interface, and (4) shear failure through the seal. Finite element numerical modelling and nonlinear parametric analysis can serve for control of the resulting failure modes and proportioning the mine seal structures (usually the seal thickness is the unknown parameter). To achieve these goals, push-over progressive failure analysis (PFA) for obtaining the force-displacement curve has been the basic task in the research.

Figure 1. a) Drift seal built of concrete, b) Tunnel seal with doors

The paper is organised as follows: In the subsequent Chapter 2, the adopted numerical finite element models, the material elastic-plastic constitutive relationships and the implemented computational stress-update methods are discussed. Discussion about the design criteria adopted in the analyses, depending on the obtained progressive failure mechanisms (PFM) is given in Chapter 3. In Chapter 4, a detailed comparative review of the performed analyses is made, describing and classifying them according to prescribed boundary conditions, adopted seal bearing structure, material used, prescribed loading, existence of bolts, existence of openings, obtained failure mechanism, etc. Then, conclusions and a table of consulted references are given.

2. Numerical modelling of mine seal structures

2.1 Finite element discretization

To accomplish the required goals – determination of the failure mode type and the seal thickness, a proper nonlinear finite element incremental force-displacement (or push-over) analysis is necessary. Nonlinear finite element modelling and analysis is generally a complex and a responsible task, especially for structures like mine seals built of concrete-like or foam-like materials. In this chapter, the assumptions regarding the developed finite element models and the used material models for the analysed structures are discussed in more details.

To get an insight into the total spatial distribution of the stresses and deformations in the seal structure, three-dimensional models that include 3D solid iso-parametric mapped elements for the seal body have been used for all study cases. The used solid elements have 20 nodal points and 3x3x3=27 Gaussian points that have been used for numerical integration. Each nodal point has 3 translational degrees of freedom (DOFs). In the cases where the contact zones are modelled, 3D link elements with two nodal

points are used, each with 3 translation DOFs. If models contain steel bolts, then 3D truss elements are also used to model them. The finite element mesh for all cases has been generated by using a special pre-processor software for automatic generation of the prescribed 3D domain with solid iso-parametric elements, considering the openings, and also including the link and truss elements, if necessary.

2.2 Elastic-plastic material modelling

Having in mind the properties of the materials, plasticity-based material models have been adopted. For seals built of concrete-like materials (as plaster only, plaster plus cement, "flexus" material, etc.) the three-parameter Willam-Warnke model of concrete formulation [3-8] has been adopted. Also, for seals built of Silcrete Thin Skin Lining (TSL) two-component material, the Willam-Warnke three-parameter yield criterion has proved to be convenient. On the other hand, the so called Rocksil (foam-like) material has been modelled by using the Drucker-Prager yield criterion [5-8]. In the following, we will focus on the numerical solution for the mentioned two elastic-plastic models, especially on the use of the so-called backward-Euler return method for stress update integration.

If the yield surface f is presented as a function of invariants I_1, i.e., the first stress tensor invariant, J_2 and J_3, i.e., the second and the third stress deviator tensor invariants, then the flow vector $\boldsymbol{a}$ can be determined using the following relation [10]:

$$\boldsymbol{a} = \frac{\partial f}{\partial \boldsymbol{\sigma}} = C_1 \boldsymbol{a}_1 + C_2 \boldsymbol{a}_2 + C_3 \boldsymbol{a}_3 = C_1 \frac{\partial I_1}{\partial \boldsymbol{\sigma}} + C_2 \frac{\partial J_2}{\partial \boldsymbol{\sigma}} + C_3 \frac{\partial J_3}{\partial \boldsymbol{\sigma}} \tag{1}$$

where the coefficients C_i depend on the yield function f adopted. For known tensor of stresses in Cartesian coordinates adopted in the vector form:

$$\boldsymbol{\sigma}^T = \{\sigma_x \quad \sigma_y \quad \sigma_z \quad \tau_{xy} \quad \tau_{yz} \quad \tau_{zx}\} \tag{2}$$

the partial derivatives in Eq. (1) depend only on the stress state, and they can be easily derived. Eq. (1) is sufficient to enable the forward-Euler method for stress update integration to be applied to the different yield criteria. However, to implement the backward Euler return method, differentiating of the flow vector $\boldsymbol{a}$ with respect to stresses $\boldsymbol{\sigma}$ is necessary, in which case we obtain:

$$\frac{\partial \boldsymbol{a}}{\partial \boldsymbol{\sigma}} = C_2 \frac{\partial \boldsymbol{a}_2}{\partial \boldsymbol{\sigma}} + C_3 \frac{\partial \boldsymbol{a}_3}{\partial \boldsymbol{\sigma}} + C_{22} \boldsymbol{a}_2 \boldsymbol{a}_2^T + C_{23} \boldsymbol{a}_2 \boldsymbol{a}_3^T + C_{32} \boldsymbol{a}_3 \boldsymbol{a}_2^T + C_{33} \boldsymbol{a}_3 \boldsymbol{a}_3^T \tag{3}$$

where $\frac{\partial \boldsymbol{a}_2}{\partial \boldsymbol{\sigma}}$ and $\frac{\partial \boldsymbol{a}_3}{\partial \boldsymbol{\sigma}}$ can be easily found. For Drucker-Prager yield criterion, given in the following form:

$$f = D I_1 + J_2^{1/2} - \sigma_0 \tag{4}$$

where D and σ_0 are constants, the coefficients in Eqs. (1) and (3) will be as follows [9,10]:

$$C_1 = D, \quad C_2 = \frac{1}{2} J_2^{-1/2}, \quad C_3 = 0, \quad C_{22} = -\frac{1}{4} J_2^{-3/2}, \quad C_{23} = C_{32} = C_{33} = 0 \tag{5}$$

The obtaining of the coefficients C_i and C_{ij} for the yielding surface of Willam-Warnke three-parameter elastic-perfect plastic model is much more complicated. It has been conducted by the first author and the resulting coefficients have been implemented in the FELISA/3M computer software [11]. The yield surface of Willam-Warnke three parametric criterion has straight meridians and is expressed by means of average stresses σ_m, τ_m and the angle of similarity θ has the following form [3,5]:

$$f(\sigma_m, \tau_m, \theta) = \frac{1}{\rho} \frac{\sigma_m}{f_c'} + \frac{1}{r(\theta)} \frac{\tau_m}{f_c'} - 1 = 0 \tag{6}$$

where:

$$\sigma_m = \frac{I_1}{3}, \tau_m = \sqrt{\frac{2}{5} J_2} \tag{7}$$

and f_c' is uniaxial compressive strength of the material (concrete). In the yield surface (6), $r(\theta)$ is the radius of the elliptic trace of the failure surface for $0 \leq \theta \leq 60^0$, with angle of similarity θ defined in terms of invariants by the following expression [5,7]:

$$\cos 3\theta = \frac{3\sqrt{3}}{2} \frac{J_3}{J_2^{-3/2}} \tag{8}$$

The solution of the coefficients C_i and C_{ij} has been conducted in terms of three parameters ρ, r_t and r_c. The three parameters ρ, r_t and r_c can be identified by the three typical concrete tests: the uniaxial-tension test, the uniaxial compression test and the equal-biaxial-compression test. Using the normalized strength values:

$$\bar{f}_t' = \frac{f_t'}{f_c'} \text{ and } \bar{f}_{bc}' = \frac{f_{bc}'}{f_c'} \tag{9}$$

where f_t' is the uniaxial tension concrete strength, and f_{bc}' is equival-biaxial-compression concrete strength, the three parameters can be found by the following relations [3,5]:

$$\rho = \frac{\bar{f}_{bc}' \bar{f}_t'}{\bar{f}_{bc}' - \bar{f}_t'} \tag{10}$$

$$r_t = \left(\frac{6}{5}\right)^{1/2} \frac{\bar{f}_{bc}' \bar{f}_t'}{2\bar{f}_{bc}' + \bar{f}_t'} \tag{11}$$

$$r_c = \left(\frac{6}{5}\right)^{1/2} \frac{\bar{f}_{bc}' \bar{f}_t'}{3\bar{f}_{bc}' \bar{f}_t' + \bar{f}_{bc}' - \bar{f}_t'} \tag{12}$$

The differentiation of the yield function (6) with respect to stresses $\boldsymbol{\sigma}$, having in mind the relation (8) for similarity angle θ, leads to the final coefficients $C_{i,}$ as follows:

$$C_1 = \frac{1}{3\rho f_c'} \tag{13}$$

$$C_2 = \frac{\sqrt{2}}{2\sqrt{5}} J_2^{1/2} \frac{1}{r(\theta)f_c'} \left[1 - \frac{\cos 3\theta}{\sin 3\theta} \frac{dr}{d\theta} \frac{1}{r(\theta)}\right] \tag{14}$$

$$C_3 = \frac{\sqrt{6}}{\sqrt{5}} \frac{dr}{d\theta} \frac{1}{2\sin 3\theta r^2(\theta)f_c' J_2} \tag{15}$$

The differentiation of the flow vector (3) results in the following coefficients C_{ij} :

$$C_{22} = -\frac{1}{2}\lambda_1 J_2^{-3/2} A_1(\theta) - \frac{3}{2}\lambda_1 J_3 J_2^{-3} \frac{dA_1(\theta)}{d\theta} A_3(\theta) \tag{16}$$

$$C_{23} = -\frac{3}{2}\lambda_2 \frac{dA_2}{d\theta} A_3(\theta) J_3 J_2^{-7/2} - \lambda_2 A_2(\theta) J_2^{-2} \tag{17}$$

$$C_{32} = \lambda_1 \frac{dA_1(\theta)}{d\theta} A_3(\theta) J_2^{-2} \tag{18}$$

$$C_{33} = \lambda_2 \frac{dA_2}{d\theta} A_3(\theta) J_2^{-5/2} \tag{19}$$

where coefficients λ_1 and λ_2 are the following:

$$\lambda_1 = \frac{\sqrt{2}}{2\sqrt{5}} \frac{1}{f_c'} \tag{20}$$

$$\lambda_2 = \frac{\sqrt{6}}{\sqrt{5}} \frac{1}{2f_c'} \tag{21}$$

The functions $A_i(\theta)$ and their derivatives $\frac{dA_i(\theta)}{d\theta}$, i=1,2,3, are the following:

$$A_1(\theta) = \frac{1}{r(\theta)}\left[1 - \frac{\cos 3\theta}{\sin 3\theta}\frac{dr}{d\theta}\frac{1}{r(\theta)}\right] \tag{22}$$

$$A_2(\theta) = \frac{dr}{d\theta}\frac{1}{r^2(\theta)\sin 3\theta} \tag{23}$$

$$A_3(\theta) = \frac{\sqrt{3}}{2\sin 3\theta} \tag{24}$$

$$\frac{dA_1(\theta)}{d\theta} = -\frac{1}{r^2(\theta)}\frac{dr}{d\theta}\left[\left(1 - \frac{\cos 3\theta}{\sin 3\theta}\frac{dr}{d\theta}\frac{1}{r(\theta)}\right) - \frac{3}{\sin^2 3\theta} + \frac{\cos 3\theta}{\sin 3\theta}\frac{\frac{d^2r}{d\theta^2}}{\frac{dr}{d\theta}} - \frac{1}{r(\theta)}\frac{dr}{d\theta}\frac{\cos 3\theta}{\sin 3\theta}\right] \tag{25}$$

$$\frac{dA_2(\theta)}{d\theta} = \frac{d^2r}{d\theta^2}\frac{1}{r^2(\theta)\sin 3\theta} - \left(\frac{dr}{d\theta}\right)^2\frac{2}{r^3(\theta)\sin 3\theta} - \frac{dr}{d\theta}\frac{3\cos 3\theta}{r^2(\theta)\sin^2 3\theta} \tag{26}$$

Note that the radius vector $r(\theta)$ function can be found in [5]. Also, the expressions for partial derivatives $\frac{\partial I_1}{\partial \boldsymbol{\sigma}}, \frac{\partial J_2}{\partial \boldsymbol{\sigma}}$ and $\frac{\partial J_3}{\partial \boldsymbol{\sigma}}$ in Eq. (1) and Eq. (3) can be found in [10].

Together with the stress-update algorithm based on the backward-Euler return method, a procedure for calculation of the so-called consistent tangent modular matrix D_p, necessary for integration of the tangent stiffness matrix of the structure, has been developed. These two parallel computational phases have been implemented in the software package FELISA/3M [11], by which the analyses of mine seal structures were performed. It is important to note that the implementation of the backward-Euler return method resulted in much faster convergence and consistency of the results, compared to our previous experience with the forward-Euler return method.

3. Design criteria based on progressive failure analyses

The performed nonlinear finite element incremental push-over analyses have provided the force-displacement curves and the failure mechanisms for all the analysed cases. The failure modes have been used further for definition of the design criteria for determination of the seal thickness. In the construction of the force-displacement curves, the corresponding force at each incremental step has been defined as the sum of the distributed forces over the loaded surface, and the corresponding displacement has been defined as a displacement at some representative point (usually, it is the midpoint of the loaded surface). The incremental analyses have been performed using the force-controlled approach.

The main question during the analyses was how to define the "ultimate" point, or the point with maximum values of both force and displacement. Note that the practical needs directed us to construct only the ascending part of the force-displacement curve, rather than its descending part, which was the reason why the force-controlled approach was adopted in the analyses. Consequently, the final converged incremental step was supposed to be the "ultimate" point. However, the analyses were often completed prematurely due to the displacement divergence over the iteration process, before reaching the final incremental step, which was regarded as an indication of failure, although, the computations were most frequently finished normally with the convergence of the last prescribed incremental step. In the case of convergence of all incremental steps, the measure for the ultimate point was judged based on the level of the obtained progressive damage during the incremental analysis.

From the comparative review of the performed analyses given in the subsequent Chapter 4, we will see that mainly two structural systems have been adopted for the mine seals: (1) A rectangular plate resting on its four edges, loaded in-plane and out-of-plane, or (2) A complex 3D continuum structure with an adhesion-type contact between the body and the surrounding rock. The failure mechanism of the first

structural type has been identified usually as bending cracking (BC), while the failure mechanism of the second structural type has been identified as a shear-slip failure (SSF) at the contact. However, sometimes, as a result of variation of the geometry, a mixed failure mode (MFM) has been obtained, where principal compression stresses or principal shear stresses in the body have received maximum values. For all analyses, the progressive failure mechanism in terms of critical damage phases (points) and consequently, the adopted design criterion will be described in the chapter that follows.

4. Comparative review of performed analyses and discussion of results

4.1 Adopted materials and their properties

Analyses were performed using the FELISA/3M software package for finite element nonlinear analysis of structures [11]. The properties of the seal materials adopted in the analyses are presented in Table 1, where f_c is uniaxial compressive cylinder strength in MPa, f_t' is uniaxial tension strength in MPa, E is initial Young's modulus of elasticity in MPa, ν is Poisson's ratio, and ρ is density in [kN s^2/m^3]. The study case numbers are indicated in the second column of the table, while in the last column the yield criterion used in the elastic-plastic analysis is given, where "W-W 3" means Willam-Warnke yield surface with 3 parameters, and "D-P" means Drucker-Prager yield surface. For the case of Drucker-Prager criterion, cohesion c in [MPa] and internal friction angle φ in degrees are given in the table, instead of uniaxial tensile strength f_t'. The material properties were adopted according to the obtained results from the appropriate laboratory tests. Note that for the first two analyses of the study case number 14, where HYG 2 PACK material was used, the unknown parameter was the uniaxial compressive strength, rather than the seal thickness, so that the resulting strength from the analysis is presented in the table. The original HYG 2 PACK used for the third analysis had a compressive strength of 3,3 MPa (see HYG 2 PACK (2) in the table), in which case the seal thickness was the unknown parameter. As an illustration, a photo of Rocsil foam material (see study case 15-16) is shown in Fig. 2.

Table 1– Properties of seal materials (body) used in the analyses

Material	Study case no.	f_c	f_t'	E	ν	ρ	Yield surface
Plaster only	1	4,375	1,93	21000	0,2	2,4	W-W 3
Plaster/cement	1	9,625	2,5	21000	0,2	2,4	W-W 3
Flexus	2	50,0	5,0	17000	0,2	2,1	W-W 3
Shotcrete	2	55,0	3,8	17000	0,2	2,1	W-W 3
Concrete grout (1)	3-8	7,28	1,6	17000	0,2	2,1	W-W 3
Concrete grout (2)	9	7,28	1,09	17000	0,2	2,1	W-W 3
Concrete grout (3)	10	15,0	2,25	17000	0,2	2,1	W-W 3
Silcrete TSL (1)	11-12	35,0	10,0	750	0,49	1,1	W-W 3
Rocksil (1)	13, 17-18	50,0	c=0,0217, φ=30,2º	4,166	0,1	0,045	D-P
HYG 2 PACK (1)	14	(unknown) obtained 8,5 and 4,2	0,78	20000	0,2	1,1	W-W 3
HYG 2 PACK (2)	14	3,3	0,78	20000	0,2	1,1	W-W 3
Rocsil foam (2)	15-16	70,0	c=0,0217, φ=30,2º	5,625	0,19	0,063	D-P
Concrete grout (3)	19-20	80,0	3,72	39348	0,2	2,4	W-W 3
Silcrete TSL (2)	21	35,0	10,0	512,62	0,49	1,33	W-W 3

4.2 Failure mechanisms and design criteria

Classification related to the obtained failure mechanisms and the design criteria for some study cases is presented in Table 2. Note that for design purposes, force-displacement curves with a strength reduction factor of φ=0.75 and loading safety factor of FS=1.5 have been generally used for mostly of the

analyses. For some study case these values are different. In the table, bending cracking is denoted by "BC". The progressive failure mechanism is denoted by the order of occurrence of the critical damage phases (or points in the force-displacement curve). The critical point abbreviations and other abbreviations are explained in the Legend, placed on the bottom of the table. For example, for the study case no. 1, the progressive failure mechanism denoted by "TC-BC-SC-MC-CL" means that the first top cracks occurred, then the bottom cracks, the side cracks, etc. The design criterion in the table is explained by use of the value of the design pressure. For example, for the study case no. 1, the design criterion was $1.8(P_{CL}-P_{TC})$ where P_{CL} is the corresponding pressure for the collapse (ultimate) point, and P_{TC} is the corresponding pressure for the first top cracks.

Figure 2. Tunnel seal – Rocsil foam

To illustrate the modelling, analysis, and obtained progressive fracture mechanisms, we will present some results from selected study cases. In Fig. 3 the obtained progressive failure mechanism for study case no. 4 of a plate mine seal structure with an opening is presented. It can be observed that the first cracks occur on the bottom corners of the opening, then on the top of the plate and finally on the sides of the plate.

In Fig. 4 the same results are presented for study case no. 5 of a plate mine seal structure without openings. For this study case the top and bottom cracks appear first, then the side ones, and finally the middle cracks develop at the end of the failure mechanism.

Study case 5 of mine seal structure with bolts is presented in Fig. 5. Note that bolts are modelled by truss elements (denoted in green colour). The local deformations near bolts are evident in this case. The presented study cases in Figs. 1-3 have been modelled by elastic-plastic Willam-Warnke yield surface with three parameters.

In Fig. 6 the results for study case 16 is presented. Note that for this case loading safety coefficient has been adopted with value of 1.1. This study case represents a dam-like mine seal structure built of Rocksil foam material, modelled by elastic-plastic Drucker-Prager yield surface. The principal aim of the analysis was to simulate all characteristic phases of the progressive failure mechanism of the analysed system. To this end, the numerical model has been developed in such a way to grasp two failure modes: (1) sliding in the contact between the Rocksil material and the surrounding rocks; and (2) shearing in the body of the Rocksil seal material. The sliding failure mechanism in the contact has been controlled by the Mohr-Coloumb law using the friction coefficient and the bond strength as parameters, via 3D Nonlinear Link elements. The criterion for control of shear stresses in the body was based on the maximum shear stress. occurring at the analysed points. As presented in the Fig. 6, both damage mechanisms - shear failure in the body and shear-slip in the contact, developed simultaneously, however, finally, the structure collapsed in shear-slip failure mode in the contact between the seal body and the surrounding rock. In the figure, red dots denote points where principal shear stresses exceed allowable values.

Table 2– Failure mechanisms and design criteria for some study cases

Study case no.	Loading	Failure mechanism	Design criterion
1	SW + normal pressure 5-20 PSI	BC: TC-BC-SC-MC-CL	$1.8(P_{CL}-P_{TC})$
2	SW + normal pressure 2 PSI	BC: TC-BC-SC-MC-CL	P_{CL}
3	SW + normal pressure 4,40,100 PSI	BC: TC-BC-SC-MC-CL	P_{CL}
4	SW + normal pressure 2 PSI (plate with an opening)	BC: TC-BC-SC- CL	P_{CL}
5	SW + normal pressure 2-50 PSI (with and without bolts)	BC: TC-BC-SC-MC-CL	P_{CL}
6	SW + HP (with bolts) (with bolts in two rows, with steel door and seal crem)	/	/
7	/	/	/
8	SW + HP (two blocks with cold joints, bolts in two rows, SF=3.0, φ=0.6)	SS: BC-SC-MC-TC-SCRSH	P_{CL}
9	SW + normal pressure 343 PSI (bolts + rock-concrete adhesion)	BC: TC-BC-SC-BCRSH-TCRSH-MC-CL	$P_{MC}+0.2(P_{CL}- P_{MC})$
10	SW + normal pressure 23 PSI (with and without openings)	BC: CC-MC-TORCH-BCRSH-BOCRSH-CL (openings)	P_{CL}
11	SW + normal pressure 5 PSI (φ=0.7)	BC: MC-TCF-BCF-SF-BF-TF	/
12	SW + normal pressure 5 PSI (φ=0.7)	BC: MC-(TC+BC)-MCRSH-BCRSH-UMCR-SCRSH-CL	P_{CL}
13	SW + normal pressure 35 & 39 PSI	SS: MC-(TC+BC)-MCRSH-BCRSH-UMCR-SCRSH-CL	/
14	SW + normal pressure 20 PSI (FS=1.6)	BC: MC-CL	P_{CL}
15	SW + normal pressure 50 PSI (FS=1.1)	SS: YP-CL	P_{CL}
16	SW + normal pressure 50 PSI (FS=1.1)	SS: YP-CL	P_{CL}
17	SW + normal pressure 20 PSI (FS=1.0)	SS: YP-CL	P_{CL}
18	SW + normal pressure 70 kPa (FS=1.0)	SS: YP-CL	P_{CL}
19	SW + normal pressure 140 kPa (FS=1.5, 2.0)	No damage	/
20	SW + normal pressure 14 & 35 kPa (with bolts)	BC: MC-CL	P_{CL}
21	SW + normal pressure 2 & 5 PSI (φ=0.7)	BC: MC-MCRSH-UMCR-BCRSH-TCRSH-CL	P_{CL}

Legend: SW - self-weight, HP - hydrostatic pressure
BC – bending cracking failure, TC- first top cracks, BC – first bottom cracks, SC – first side cracks,
MC – first middle cracks, CL – collapse (or end of analysis), SS – shear-slip failure on the contact, BCRSH – first bottom crush, TCRSH – first top crush, CC – corner cracks, TOCRSH – top opening crush, BOCRSH – bottom opening crush, TCF – first top corner fracture (ε_u reached),
BCC – first bottom corner fracture (ε_u reached), SF – first side fracture (ε_u reached),
BF – first bottom fracture (ε_u reached), TF – top fracture (ε_u reached), MCRSH – middle crush,
UMCR – ultimate middle cracks ((ε_u reached)), SCRSH – side crush, YP – yield point,
P_{CL} – collapse pressure, P_{TC} – first top cracks pressure, P_{MC} – first middle cracks pressure

The consistency of the obtained results using the backward-Euler return method can be clearly seen by the obtained diagrams of principal stresses and principal strains. For example, in Fig. 7, a representative $\sigma_1 - \varepsilon_1$ diagrams in principal directions (tension) is shown, selected from the results of the analysis of a

plate with bolts (study case no. 6) from where the mathematical consistency of the principal stress σ_1 update is evident.
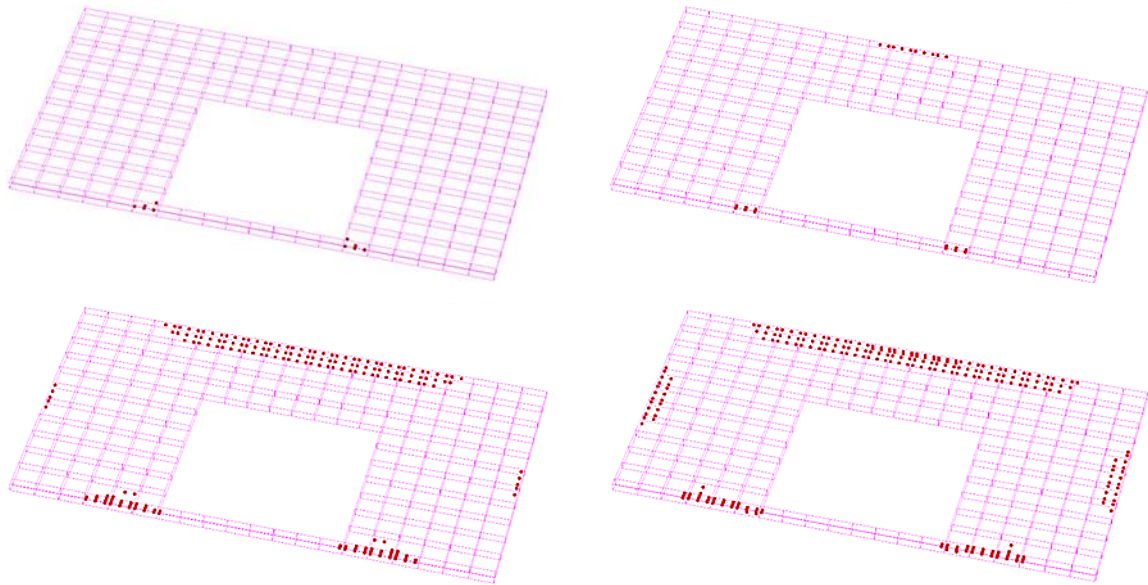
Figure 3. Study case 4, mine seal with opening: Critical steps of PFM (red dots denote cracks)
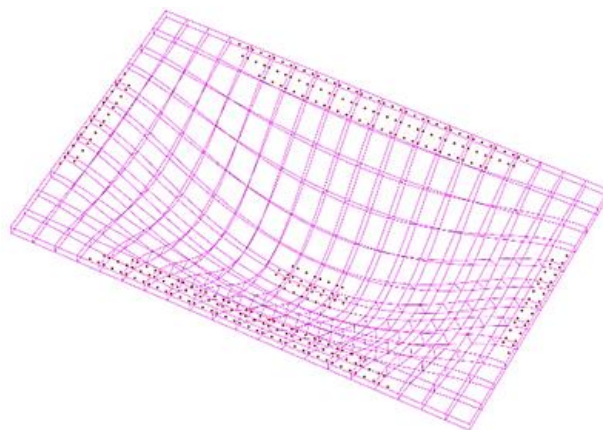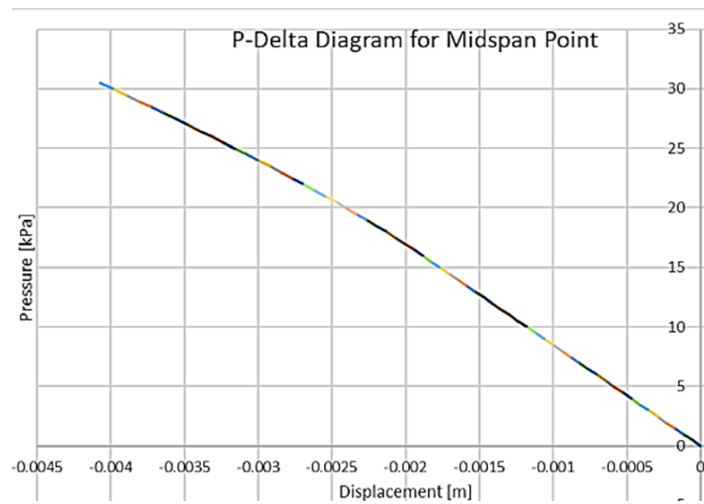
Figure 4. Study case no. 5, mine seal without openings: Obtained force-displacement curve and final step of PFM (red dots denote cracks)
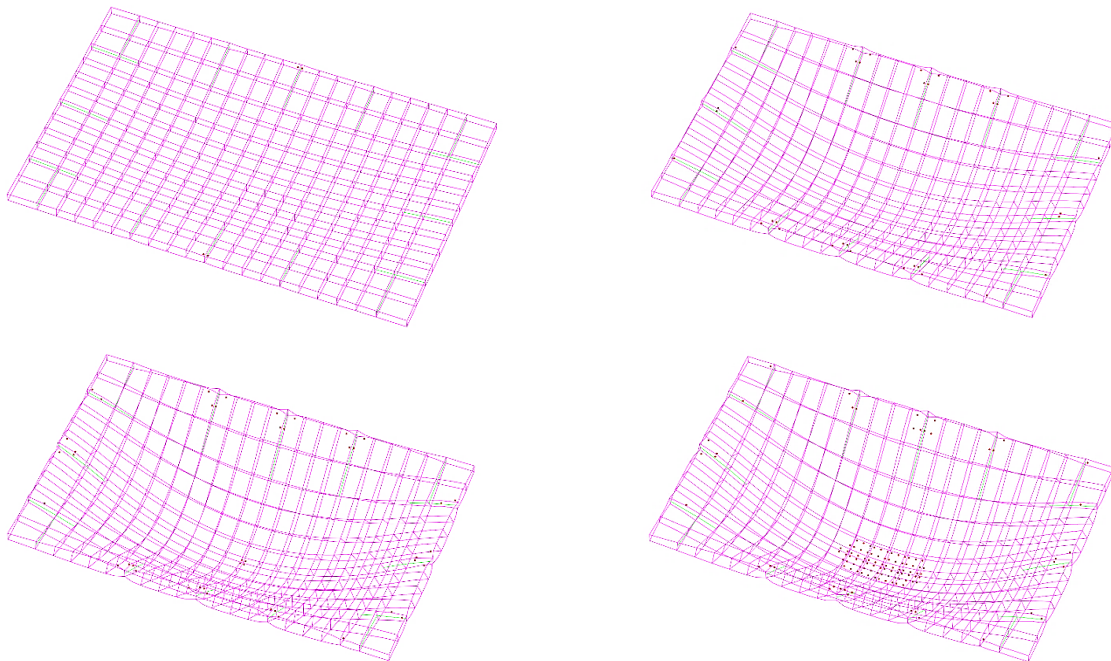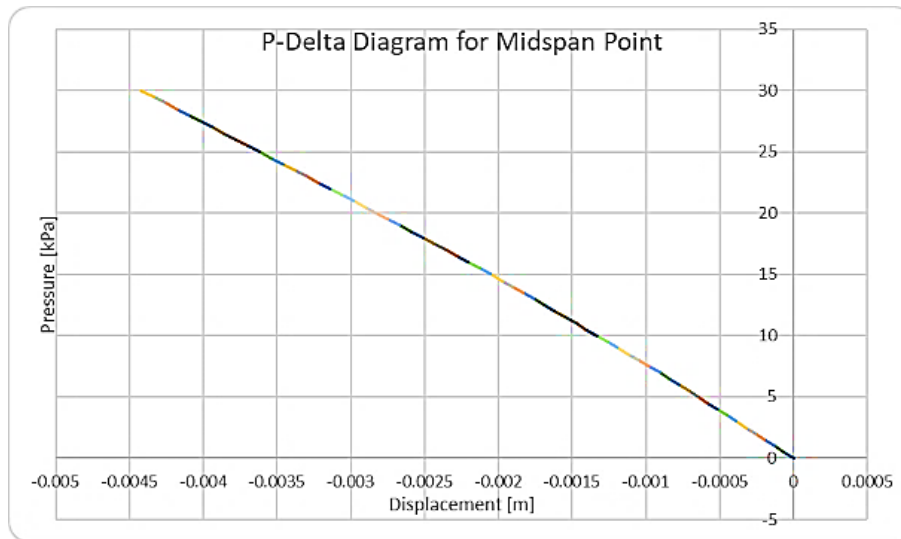
Figure 5. Study case no. 5 mine seal with bolts: Obtained force-displacement curve and critical steps of PFM (green lines denote bolts, while red dots denote cracks)

5. Conclusions

Mine seals are structures used to serve as protection shields against short term instantaneous pressure loadings like blasts, which could occur in mine cells during the excavation period. With the recent technical norms, the level of seal design safety requirements has been increased. In addition to other safety measures, these requirements can be satisfied if the seal design includes FEM nonlinear analysis. In the paper, the authors' experience in modelling and analysis of mine seal structures is briefly presented. From that point of view, the following conclusions can be made:

(1) According to results obtained from tests (that are not the subject of this paper), the new technological materials like Flexus, Rocksil, Silcrete etc, have been proved to have properties that can be well simulated by the Willam-Warnke and Drucker-Prager plastic criteria. Hence, the selected elastic-plastic material models implemented in the FELISA/3M software can realistically simulate the progressive failure mechanism of mine seal structures in practice.

(2) The implemented backward-Euler return method with the consistent tangent modular matrix has shown computational stability and fast convergence compared to the forward-Euler return method used in many contemporary software packages.
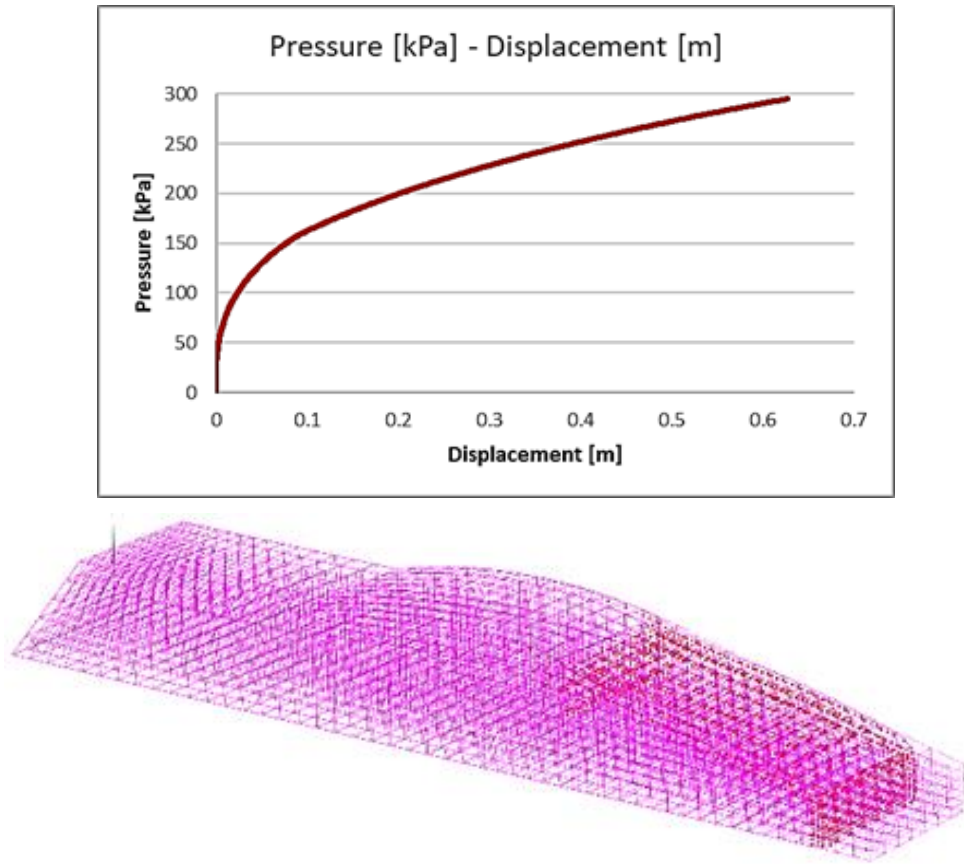
Figure 6. Study case no. 16: FEM Obtained force-displacement curve and final step of failure mechanism (red dots denote points where principal shear stresses exceed allowable values)
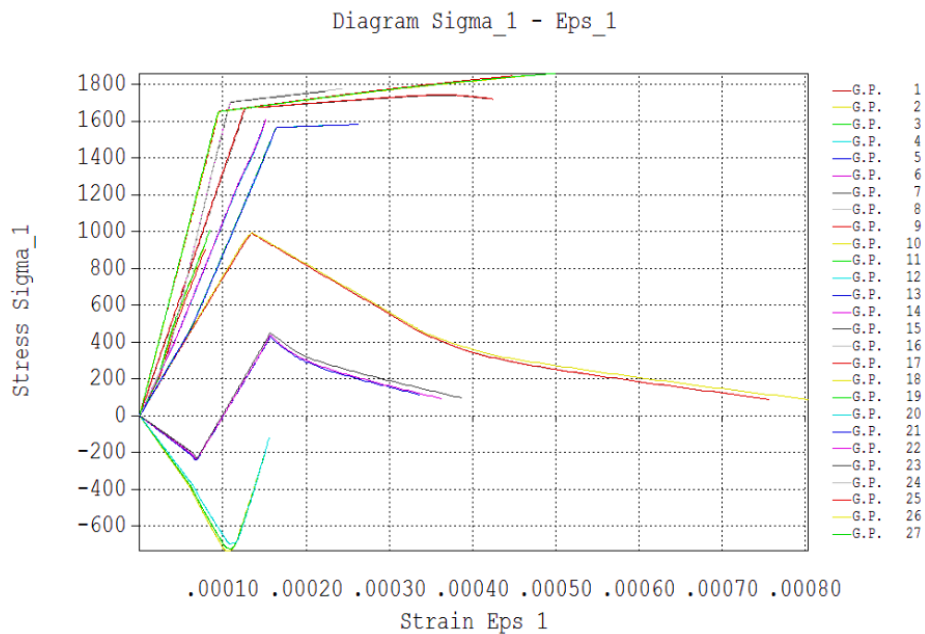
Figure 7. Obtained principal $\sigma_1 - \varepsilon_1$ diagrams for all 27 Gaussian points of a characteristic element, study case no. 6, plate structure with bolts

115

(3) Basically, two types of mine seal structures have been modelled: (1) Rectangular plates (with/without openings and with/without bolts), and (2) Dam-like mine seal structures built of Silcrete foam. The first type of structures usually failed in bending mode, while those of the second type usually failed in shear-slip mode. Structures of the first type were modelled by the Willam-Warnke yield criterion, while those of the second type were modelled by the Drucker-Prager yield criterion. The collapse of the structure (i.e., the end-of-analysis due to divergence indicating failure) was usually adopted as a design criterion for the plate mine seal structures. However, sometimes, different expressions were adopted, depending on the developed damage. On the other hand, the onset of the large shear-slip deformation (or the ultimate points when the analyses usually diverged and stopped) was adopted as a design criterion for dam-like mine seal structures.

(4) Two main tasks were performed in the analyses. The first task referred to the case of known material strength, so that the thickness of the seal had to be defined for the given loading level. The second task referred to an unknown material strength so that it had to be defined for the known loading level and thickness.

(5) Because the materials for mine seal structures are still developing, further investigation on their modelling is needed.

References

[1] Zipf, R.K. Jr., Mohamed, K.M., McMahon, G.W. (2009): Design and Analysis of a New Method to Test Mine Seals. *Proceedings of the 80th Shock and Vibration Symposium (DoD),* San Diego, California, October 25-29, 2009. Virginia: The Shock & Vibration Information Analysis Center,1-17.

[2] Kallu, R.R. (2009): *Design of reinforced concrete seals for underground coal mines*. Ph.D. Dissertation, College of Engineering and Mineral Resources, West Virginia University, Morgantown, West Virginia.

[3] Willam, K.J. and Warnke, E.P. (1974): Constitutive Model for the Triaxial Behaviour of Concrete. *Proceedings, IABSE Seminar on "Concrete structures subjected to triaxial stresses" 17-19 May 1974,* ISMES, Bergamo, Italy. http://dx.doi.org/10.5169/seals-17526 .

[4] ASCE (1982): *State-of-the-Art Report on Finite Element Analysis of Reinforced Concrete*. New York.

[5] Chen, W.F. (1982): *Plasticity in Reinforced Concrete*. McGraw-Hill Book Company.

[6] Chen, W.F., and Saleeb A.F. (1994): *Constitutive Equations for Engineering Materials", Volume 1: Elasticity and Modelling*. Elsevier. [7]   Chen, W.F., and Saleeb A.F. (1994): *Constitutive Equations for Engineering Materials", Volume 2: Plasticity and Modelling*. Elsevier.

[8] Owen, D.R.J., Hinton, E. (1980): *Finite Elements in Plasticity, Theory and Practice*. Pineridge Press Limited, Swansea, UK.

[9] Crisfield, M.A. (1991): *Non-linear Finite Element Analysis of Solids and Structures, Volume 1: Essentials.* John Wiley & Sons.

[10] Crisfield, M.A. (1997): *Non-linear Finite Element Analysis of Solids and Structures, Volume 2: Advanced Topics*. John Wiley & Sons.

[11] FELISA/3M (2022), *General purpose software package for analysis of structures*, UKIM-IZIIS, 1990-2022

EFFECT OF PRIOR CYCLIC LOADING ON TRIAXIAL MONOTONIC EXPERIMENTS

Toni Kitanovski [1], Vlatko Sheshov [2], Julijana Bojadjieva [3], Kemal Edip [4] and Dejan Ivanovski [5]

[1] *Research assistant, PhD Candidate, Ss. Cyril and Methodius University, Institute of earthquake engineering and engineering seismology-IZIIS, Skopje, Macedonia, tonik@iziis.ukim.edu.mk*

[2] *Professor, Ss. Cyril and Methodius University, Institute of earthquake engineering and engineering seismology-IZIIS, Skopje, Macedonia, vlatko@iziis.ukim.edu.mk*

[3] *Associate professor, Ss. Cyril and Methodius University, Institute of earthquake engineering and engineering seismology-IZIIS, Skopje, Macedonia, jule@iziis.ukim.edu.mk*

[4] *Associate professor, Ss. Cyril and Methodius University, Institute of earthquake engineering and engineering seismology-IZIIS, Skopje, Macedonia, kemal@iziis.ukim.edu.mk*

[5] *PhD Candidate, Ss. Cyril and Methodius University, Institute of earthquake engineering and engineering seismology-IZIIS, Skopje, Macedonia, ivanovski@iziis.ukim.edu.mk*

Abstract

Drained triaxial monotonic test is one of the most frequently used experiments in geotechnical engineering, mostly because its results are starting points for many research topics. This paper presents triaxial drained monotonic experiments on natural sand borrowed from the terraces of river Vardar, that passes through Skopje. This Skopje sand is highly uniform sand with only 2% fines, and a uniformity coefficient $C_u = 2$ with mean grain size of $d_{50} = 0.17$mm. It can be found at multiple places along the riverbank of Vardar River at different depths. Since this is an urban area, such sandy layers can be exposed to different sources of dynamic loads (traffic from roads, railways, factories, etc.) Knowing the fact that cyclic preloading has effects on the soil strength characteristics, these effects were investigated in the case of prior cyclic loading on consolidated drained triaxial compression monotonic test. The specimens were prepared using wet-tamping method at high range of different initial relative densities, then confined at three levels of initial effective stress $p_0 = 50$, 100 and 200kPa before shearing. The effect of the number of cycles and their amplitudes are also investigated not only on the curves of deviatoric stress q and volumetric strain ε_v versus axial strain ε_1 but additionally on the dependency curves that display the influence of the initial density I_{DO} and initial effective pressure p_0 on the peak friction angle φ_p, Young's modulus E_{50}, axial strain at peak ε_p and dilatancy angle ψ. The results indicate interesting outcomes concerning the physical behaviour of the investigated sand.

Keywords: Skopje sand, cyclic preloading, monotonic drained tests, initial density and pressure dependency

1. Introduction

Sand analysed in the paper can be found in multiple areas along the riverbank of Vardar river at different depths. Because the river passes through the urban city area these sandy layers are exposed to different sources of dynamic loading that can apply cyclic preloading on the sand. This calls for experimental data that will improve our understanding of the influence of cyclic preloading on the response to drained monotonic and cyclic loading for the investigated sand. For the purpose of the paper triaxial experiments were performed where specimens were prepared using a wet-tamping method [1] at different initial relative densities, then confined at three levels of initial effective stress p_0=50, 100, and 200kPa. Most of the monotonic drained tests without preloading are done in previous research [2,3], only now the database is enriched with additional experiments so that we can perceive the influence of cyclic preloading. This effect is presented throw the curves of deviatoric stress q and volumetric strain ε_v versus axial strain ε_1, but additionally on multiple dependency curves. Specimens are preloaded with 40 cycles with a shear strain amplitude of 0.01%. Cumulative strain from the preloading is at very low levels and doesn't change the specimen void ratio, which is probably the most important factor that needs to be fulfilled for a correct comparison to be made [4,5,6]. Additionally, the effect of the number of cycles and their amplitude is investigated. Tests with preloading of 20 cycles with the same amplitude

and tests with 40 cycles but the double amplitude of 0.02% are performed for a void ratio range of Dr=45-55% to conclude if there is a real need for additional experiments.

2. Testing material and triaxial equipment

As mentioned before, the testing material represents natural fluvial sand so-called "Skopje sand" that consists mainly of silica oxides (around 78%) with particles of subangular shape. Because we are working with natural sand small differences in each borrowed batch are expected, so initial investigations are necessary to determine its physical properties (Table 1). The sand is highly uniform and has only 2% fines with a mean grain size of $d_{50} = 0.17mm$ and a uniformity coefficient $C_u = 2$. The void ratios were determined using ASTM D4253-00 standards, $e_{min} = 0.51$ and $e_{max} = 0.90$, at mean pressure p = 0kPa.

Table 1 – Physical properties of Skopje sand

e_{max}	e_{min}	G_s	D_{10} (mm)	D_{50} (mm)	D_{60} (mm)	Cu	Cc	φ (o)	Fines (%)
0.95	0.51	2.615	0.095	0.26	0.19	1.8	0.8	33.5	2

The triaxial testing device used for the experiments presents a feedback-controlled cyclic triaxial system that can apply cyclic or dynamic loading to cylindrical soil specimens. This apparatus is a servo pneumatic system, with control on axial stress, confining pressure, and back pressure by incorporated Control and Data Acquisition System (CDAS). During the testing maximum of seven transducers in total are active. This includes measurements of the cell, back and pore pressure using pressure transducers, measurements of the applied axial load with submersible load cell and volume change of water entering or leaving the sample. Also, two axial transducers can acquire the deformations directly on the sample. All the data acquisition functions, critical control and timing are provided by the CDAS.

a) b)
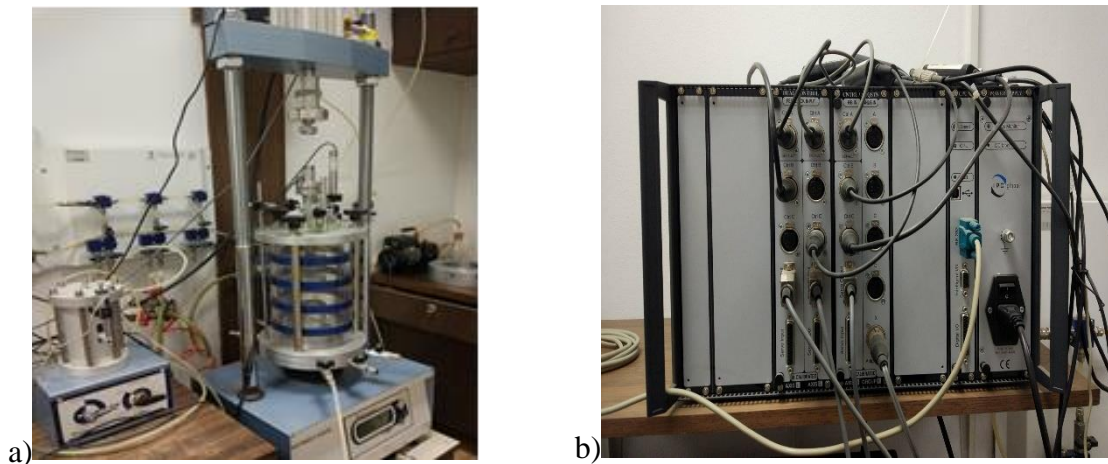
Figure 1. a) Triaxial and volume change equipment, b) Control and data acquisition system

As mentioned before all samples were reconstituted by wet-tamping in layers, using a three-piece steel cylinder lined with a rubber membrane. To speed up and achieve better saturation all samples were first saturated using CO_2 and only after with water up to B-value ≥0.95. The volume change was measured by pore-water volume change apparatus, while the specimens were axially strained at a rate of 0.2mm/min.

3. Results

Measured curves of deviatoric stress q and volumetric strain ε_v versus axial strain ε_1 from the drained monotonic triaxial tests are shown in the following figures and compared with the 40 cycles preloaded

experiments grouped in three levels of densities. The increase of the deviatoric stress with the increasing effective pressure and density can be observed, as well as the increase of dilatancy. In terms of the comparison, it can be noticed that the preloading effects the response constantly and has a higher effect on the test with higher effective stress and usually lowers the peak deviatoric stress that the specimen can sustain.
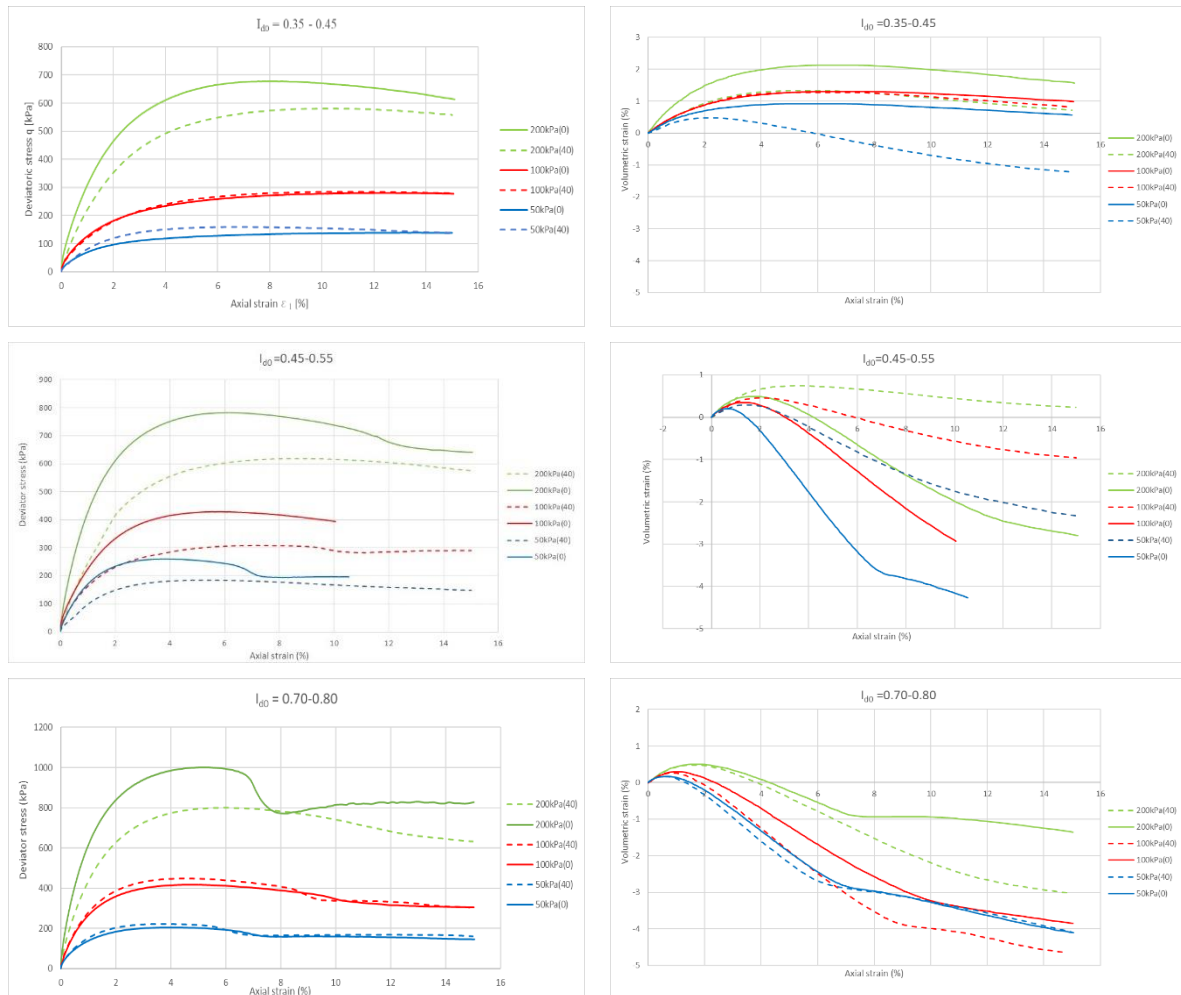
Figure 2. Comparison of deviatoric stress q and volumetric strain ε_v versus axial strain ε_1 as a result from drained monotonic triaxial tests

To investigate if there is an influence on the drained monotonic results from change in number of cycles applied in the preloading and their level of amplitude additional experiments were made. The number of cycles is lowered from 40 to 20 while in the second series of experiments the amplitude it is doubled from a shear strain of 0.01% to 0.02%. Again, the cumulative strain from the preloading is at a very low level that doesn't affect the initial void ratio of the specimens and the final results. All of the performed experiments were in the same range of initial densities I_{d0}=0.45-0.55 for three levels of effective stress, same as before, 50, 100 and 200kPa. From figure 3 can be noticed that the deviatoric stress q curve is not affected by the change in the number of cycles and their amplitude, at least not for the one that we are investigating. Further experiments will be made to find the limits where this is applicable and true.
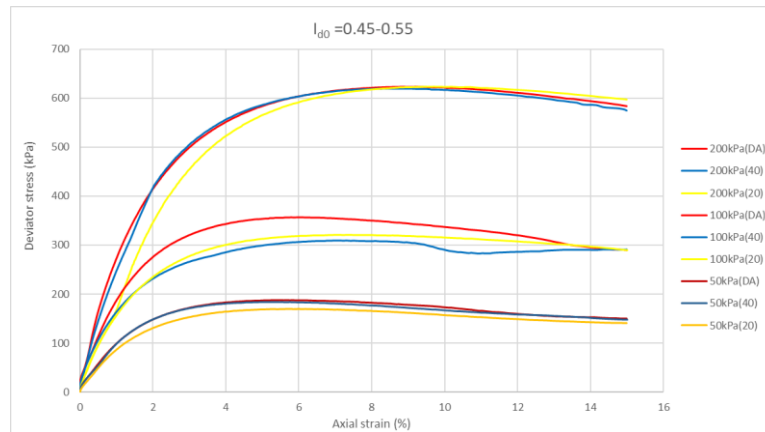
Figure 3. Effects of the number of preloading cycles and their amplitude to the deviatoric stress q versus axial strain ε_1 curve

Additionally, the effect of preloading is investigated on multiple dependency curves that mostly display the influence of the initial density I_{D0} and initial effective pressure p_0. Firstly we will look at the dependence of the friction angle. The critical friction angle φ_c that corresponds with the peak friction angle φ_p for zero initial density ($I_{do}=0$) has been determined from a loosely pluviated cone of sand, as an angle of repose, according to the procedure explained by Herle [7]. The measured critical friction angle together with all the peak friction angles derived from the drained monotonic triaxial tests are presented in Figure 4.
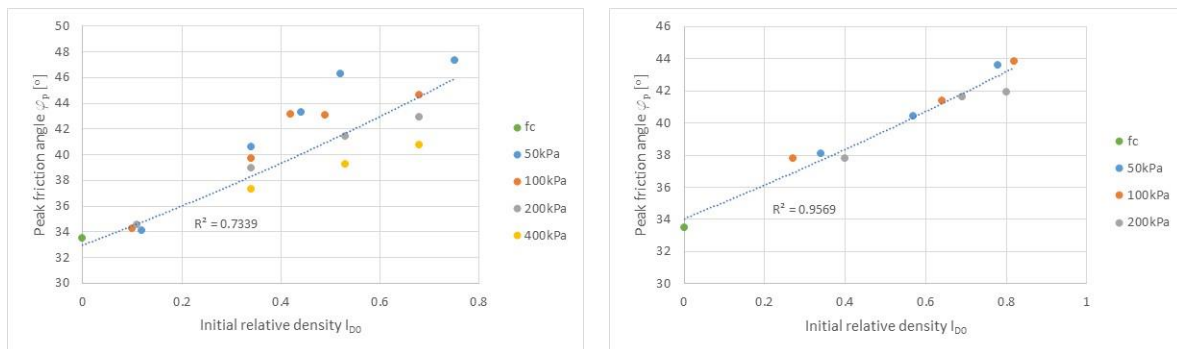
a) without preloading

b) with preloading

Figure 4. Peak friction angle φ_p versus initial relative density I_{DO}

The increase of the friction angle with the increase of the initial density can be observed on both trendlines, with or without applied preloading, together with a small decrease for higher initial effective pressures. A similar decrease in the friction angle as a consequence of the effective pressure is also noted in other researcher's work [8,9]. When all results are placed on a single graphic (Figure 5) it can be noticed that higher peak friction angles are obtained for tests without preloading.
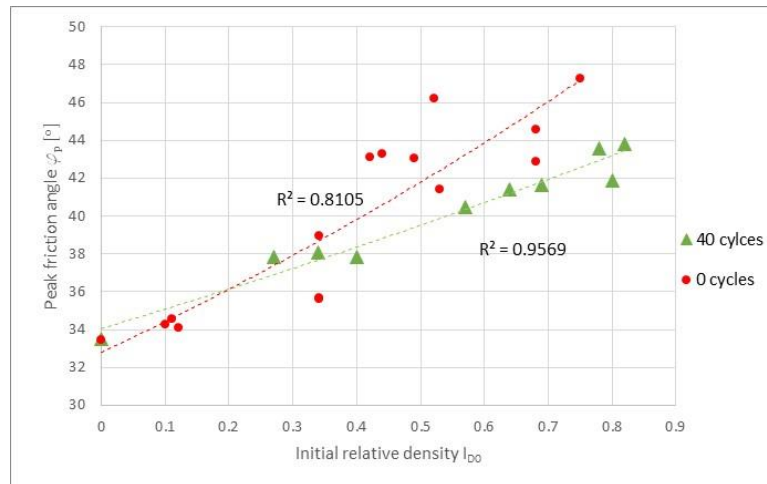
Figure 5. Summary graphic of peak friction angle φ_p versus initial relative density I_{DO}

The axial strains ε_p corresponding to the peak deviatoric stress from each experiment together with the initial relative densities are plotted in figure 6 for both types of experiments. Both plots reveal that in the case of higher initial densities the deviatoric peak occurs much sooner, also small pressure-dependence can be noted [10]. Both plots are combined in figure 7 where can be perceived that they follow almost the same trendline.
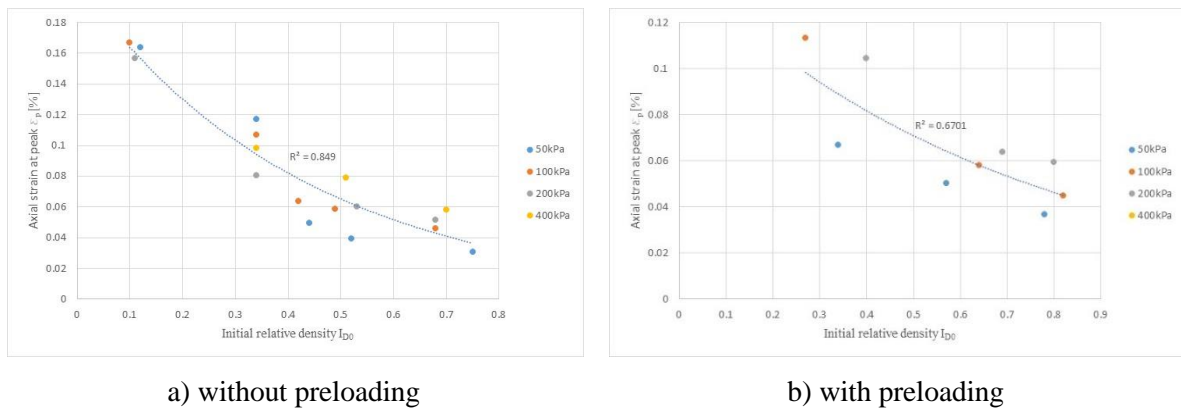
a) without preloading   b) with preloading

Figure 6. Axial strain at peak ε_p as a function of the initial relative density I_{DO}
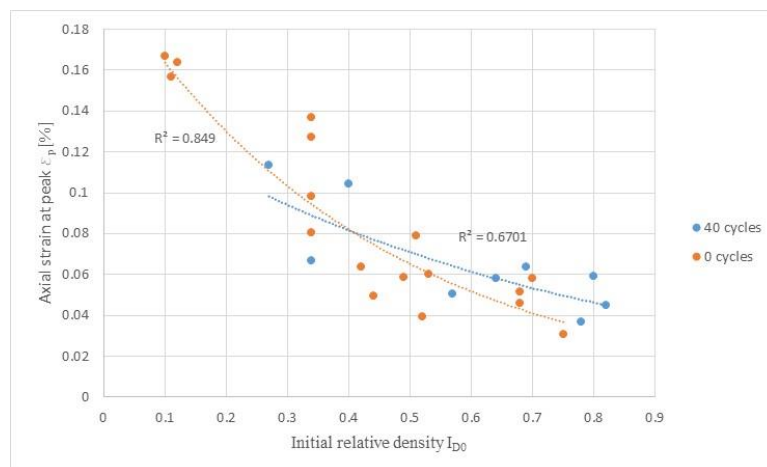
Figure 7. Summary graphic of axial strain at peak ε_p as a function of the initial relative density I_{DO}

Young's modulus E_{50} derived as a secant stiffness between q=0 and q= q_{max}/2 is presented as a function of the initial density I_{D0} in figure 8. In both cases the modulus increase with an increase of both initial density and effective pressure, with stronger pressure-dependence for a higher level of initial density. Preloaded experiments have significantly lower E_{50} values which is a common find in the literature [11] often cycle number and intensity dependant. The difference between the modulus is increased with the increase of both initial density and effective pressure.
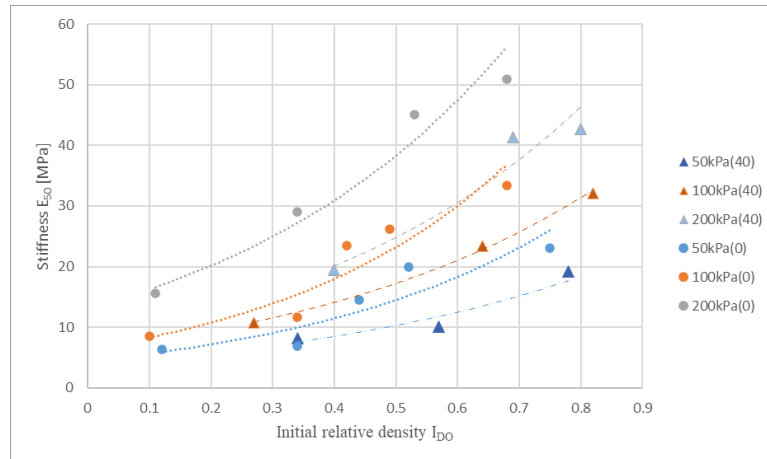
Figure 8. Summary graphic of Young's modulus E_{50} versus initial relative density I_{DO}

The last dependency curve that we will observe is the change of the dilatancy angle ψ as a function of the initial density I_{D0}. This angle can be recognized in the volumetric strain, ε_v, versus axial strain, ε_1, plots. In the case of triaxial conditions the two principal stresses are equal, $\sigma_2 = \sigma_3$, which implies that both mechanisms defined by the yield functions are simultaneously active [12]. Knowing the value of the increments of the volumetric strain $d\varepsilon_v$ and axial strain, $d\varepsilon_1$, the value of ψ in each step can be calculated using the equation (1):

$$\psi = \arcsin\left(\frac{\dfrac{d\varepsilon_v}{d\varepsilon_a}}{\dfrac{d\varepsilon_v}{d\varepsilon_a} - 2}\right);$$

(1)
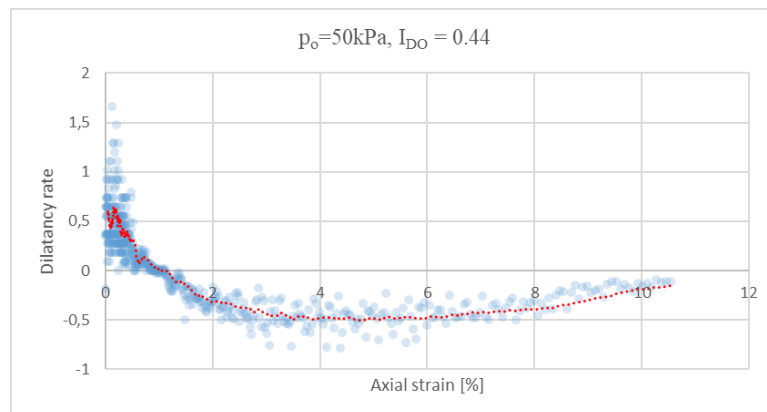
Figure 9. Dilatancy rate versus the axial strain from one experiment

Because there are jumps in the computed dilatancy rate from increment to increment acquired from the experiment to present a clearer trend, a smoothed curve, obtained by a moving average procedure is computed for each experiment (Figure 9). From the smoothed curve the maximum rate of dilatancy is attained which is coinciding with the deviatoric stress peak. Afterward using equation (1) the value of the dilatancy angle is computed and added to a graph versus the initial relative density (figure 10).
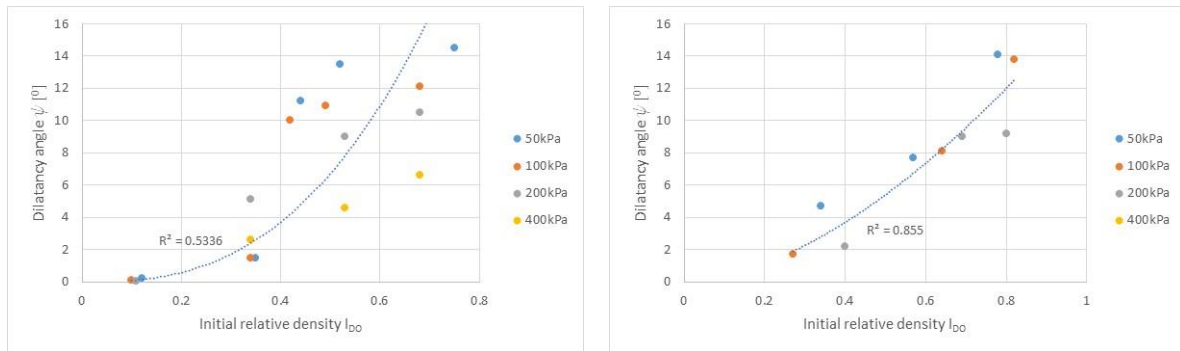
a) without preloading   b) with preloading

Figure 10. Dilatancy angle ψ as a function of initial relative density I_{DO}
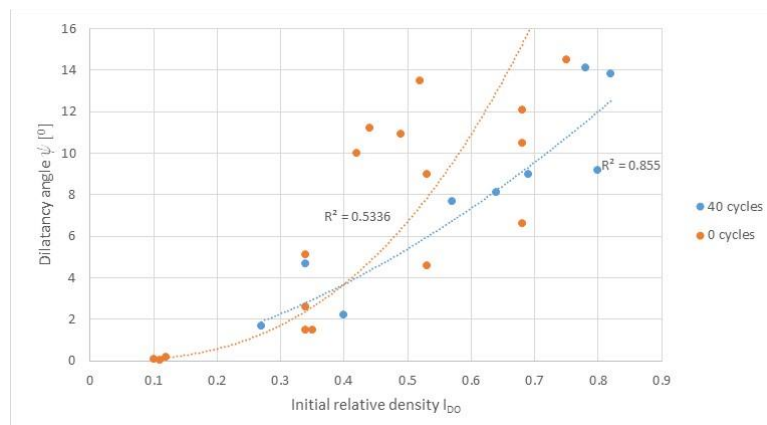
Figure 11. Summary graphic of dilatancy angle ψ as a function of initial relative density I_{DO}

The computed dilatancy angles are close to zero for low initial densities. The change of initial density and initial effective pressure in both cases have the same effect on the dilatancy angle as in the case of peak friction angle [13,14,15,16]. Preloaded samples demonstrate lower values of the dilatancy angles for similar initial densities, but more experiments are needed for the correlation to be proved.

5. Summary and conclusions

There are multiple studies published where Skopje sand is investigated to determine and establish its physical characteristic [2,3,17], but until this paper, there haven't been any experiments done using preloading. Since this type of sand can be found in the urban area of the city these types of experiments are necessary. Hopefully, this paper can act as a good foundation for further research on the subject.

From the curves of deviatoric stress q versus axial strain ε_a can be observed that cycling preloading often lowers the peak deviatoric stress that the specimen can sustain especially for tests done with higher initial effective stress, but no clear difference has been noticed when the number of preloading cycles and there amplitude is changed. The graph for Young's modulus E_{50} perfectly presents the effect of preloading where the difference between the modulus expands with an increase of both initial density

and effective pressure. A small influence of the preloading has also been noted in the values of peak friction angles and dilatancy angles, usually lower then than one obtained from experiments without preloading, but still additional experiments are needed to make a clear conclusion or correlation between them.

References

[1] F. Tatsuoka, Ochi K., Fujii S., Okamoto M.,"Cyclic undrained triaxial and torsional shear strength of sands for different sample preparation methods" Soils and foundations vol.26, no3, pp.23-41, 1986

[2] J. Bojadjieva, "Dynamic behavior of saturated cohesionless soils based on element and 1-G experiments" PhD Thesis University Ss. Cyril and Methodius-Skopje, Macedonia, 2015

[3] T. Kitanovski., et al. "Laboratory model tests on natural sand from Skopje region." ce/papers 2.2-3: 689-694, 2018

[4] Bouferra, R., Benseddiq, N., & Shahrour, I. (2007). Saturation and preloading effects on the cyclic behavior of sand. International journal of geomechanics, 7(5), 396-401.

[5] Chen, Q., Cui, D., Chen, Y., Tao, X., & Xiang, W. (2021). Effect of Prior Cyclic Loading on Triaxial Compression Strength of Sliding Zone Soil of the Huangtupo Landslide. Advances in Civil Engineering, 2021.

[6] Wichtmann, T., & Triantafyllidis, T. (2004). Influence of a cyclic and dynamic loading history on dynamic properties of dry sand, part I: cyclic and dynamic torsional prestraining. Soil Dynamics and Earthquake Engineering, 24(2), 127-147.

[7] I. Herle. "Hypoplastizitat und Granulometrie einfacher Korngeruste. Dissertation, Institut fur Bodenmechanik und Felsmechanik der Universitat Fridericiana in Karlsruhe, Heft Nr.142, 1997

[8] K.H. Andresen and K. Schjetne., "Database of friction angles of sand and consolidation characteristics of sand, silt, and clay", Journal of the Geotechnical Engineering and Geoenvironmental Engineering, ASCE, 139(7):1140-1155, 2013

[9] M.D. Bolton., "The strength and dilatancy of sands", Geotechnique, 36(1):65-78, 1986

[10] Y. Dafalias and M. Manzari.,"Simple plasticity sand model accounting for inherent fabric anisotropy", Journal of Engineering Mechanics, 130(11):1319-1333, 2004

[11] Bai, Lidong. "Preloading effects on dynamic sand behavior by resonant column tests." (2011).

[12] J. R. Maranha and E. Maranha das Neves. "The experimental determination of the angle of dilatancy in soils." (2009)

[13] P. Guo and X. Su.,"Shear strength, interparticle locking, and dilatancy of granular materials", Canadian Geotechnical Journal, 44(5):579-591, 2007

[14] S. Frydman, M. Talesnick, H. Nawatha and K. Schwartz.,"Stress-dilation of undisturbed sand samples in drained and undrained triaxial shear", Soils and Foundations, 47(1):27-32, 2007

[15] T. Schanz and P.A. Vermeer.,"Angles of friction and dilatancy of sand", Geotechnique, 46(1):145-151, 1996

[16] Y.P. Vaid and S. Sasitharan.,"The strength and dilatancy of sand", Canadian Geotechnical Journal, 29:522-526, 1992

[17] V.Sheshov., "Laboratory Experiments on Soil Dynamic Characteristics of NPP Site", 20th International Conference on Nuclear Engineering and the ASME 2012 Power Conference, 2012

SITE RESPONSE ANALYSIS BASED ON BOREHOLE ACCELERATION RECORDS FROM LOCATION TOWER, OHRID 3D SEISMIC NETWORK

Juijana Bojadjieva [(1)], Vlatko Sheshov [(2)], Aleksandra Bogdanovic [(3)], Kemal Edip [(4)]
Dejan Ivanovski [(5)], Irena Gjorgjeska [(6)], Toni Kitanovski [(7)], Dejan Filipovski [(8)]

[(1)] *Associate professor, Ss. Cyril and Methodius University, Institute of earthquake engineering and engineering seismology-IZIIS, Skopje, Macedonia, jule@iziis.ukim.edu.mk*

[(2)] *Professor, Ss. Cyril and Methodius University, Institute of earthquake engineering and engineering seismology-IZIIS, Skopje, Macedonia, vlatko@iziis.ukim.edu.mk*

[(3)] *Associate professor, Ss. Cyril and Methodius University, Institute of earthquake engineering and engineering seismology-IZIIS, Skopje, Macedonia, saska@iziis.ukim.edu.mk*

[(4)] *Associate professor, Ss. Cyril and Methodius University, Institute of earthquake engineering and engineering seismology-IZIIS, Skopje, Macedonia, kemal@iziis.ukim.edu.mk*

[(5)] *PhD Candidate, Ss. Cyril and Methodius University, Institute of earthquake engineering and engineering seismology-IZIIS, Skopje, Macedonia, ivanovski@iziis.ukim.edu.mk*

[(6)] *PhD Candidate, Ss. Cyril and Methodius University, Institute of earthquake engineering and engineering seismology-IZIIS, Skopje, Macedonia, gj_irena@iziis.ukim.edu.mk*

[(7)] *Research assistant, PhD Candidate, Ss. Cyril and Methodius University, Institute of earthquake engineering and engineering seismology-IZIIS, Skopje, Macedonia, tonik@iziis.ukim.edu.mk*

[(8)] *Research Assistant, Ss. Cyril and Methodius University, Institute of earthquake engineering and engineering seismology-IZIIS, Skopje, Macedonia, dejan@iziis.ukim.edu.mk*

Abstract

The Location Tower is one of the three sites from the 3D seismic network originally installed in the 80's which is recently re-established and enabled for real-time monitoring and recording acceleration data. The Location Tower is consisted of one surface and three downhole instruments up to 125 meters down the bedrock; a nine story building with two instruments installed on 6th and 9th storey & 4 instruments installed at the foundation level. In the period of 2021-2022 several small to moderate earthquakes have been recorded with the system. This study presents selected results and comparisons of equivalent linear analysis of the site using real recorded acceleration data. The soil profile is defined based on number of geophysical and geotechnical investigations at the location, both in-situ and laboratory tests. Obtained results are good starting point for further non-linear site response analysis at the location which can be validated with stronger recorded earthquakes in future.

Keywords: site response, amplification, borehole acceleration.

1. Introduction

Local site conditions can significantly influence the characteristics of earthquake ground motion, and hence the degree and extend of damage caused by an earthquake. The destruction of structures and ground motions recorded in Mexico City from 1985 Michoacan Earthquake and in the San Francisco Bay Area from the 1989 Loma Prieta Earthquake had promoted the need for investigation of the site effects. Furthermore, the effects of local soil conditions are of particular significance in seismic micro zonation, seismic design of important facilities, as well as in seismic safety assessment of existing structures and undertaking preventive measures for reduction of seismic risk of existing facilities and urban areas exposed to destructive ground motions.

The existing empirical methods and new techniques for seismic microzoning based on experience rom damage of the structures in the past earthquakes and consideration of local site conditions determined from the studies of microtremors and small earthquakes are hardly reliable methods for evaluation of the seismic design parameters. Verification is ultimately needed for the possibility of extrapolation of

small records to predict local soil behavior and site effects in the case of strong earthquake motions as well as to verify laboratory techniques for elaboration of dynamic soil properties under high strain levels. For that purpose registration from different location and different level of excitation sources is important to validate the available empirical and analytical analysis methods.

In order to study the local site effects on modification of strong ground motions and dynamic response of structural systems, a three-dimensional seismic network was established in the Ohrid Lake basin in the 80's [1] with the support of USGS (United States Geological Survey). This 3D strong motion array consisted of three free field sites with one surface and three downhole instruments each, 125 meters down the bedrock; a nine story building site with two instruments installed on the building, 4 instruments installed at the foundation level and one outcropping rock site with one instrument (location Tower). With the extensive recent activities, real time recording and health monitoring processes are enabled at the location [2]. This paper focuses on a site response analysis of the soil profile at the Location Tower in comparison to real acceleration records from different depths at the location.

2. Soil profile & location

2.1 Description of the site location

The Tower location is one of the four instrumented locations within the city of Ohrid. There is evidence on intensive seismic activity along the investigated location, namely the earthquakes with magnitudes greater than six (M>6) that happened in the distant past (1906, Ohrid, M_L=6.00; 1911, Ohrid, M_L=6.70). In 2016, an earthquake with a magnitude of 5 according to the European MCS scale was felt in Ohrid. The earthquake epicenter was 12 km northeast from Ohrid. It caused visible damage particularly to older structures and structures pertaining to cultural heritage, showing the gap between the scientific investigations and engineering practice. Previous studies performed for Ohrid by UKIM-IZIIS, [3] showed that, geological conditions in combination with a certain intensity of seismic exposure in some specific regions, could give rise to some geotechnically associated hazards that have an unfavorable effect upon engineering structures.
Based on the latest seismic hazard map of Macedonia prepared according to the Eurocodes (PGA), [4] the city of Ohrid is situated in a zone of moderate to high seismicity, with PGA of 0,3g at bedrock, for a return period of 475 years. The Ohrid city lies in the Ohrid lake watershed area and is characterized by the following geotechnical conditions:
1. Surface Quaternary and deep Pliocene sediments;
2. Surface Quaternary sediments consisting of fine gravel and sand as well as organic clays and sand down to depth of 20 m;
3. Heterogeneous nature characterized by unfavorable physical-mechanical characteristics. The underground water level is generally high.

2.2 Soil profile

To define the geotechnical characteristics of the site, data from previous investigations as well as data from additionally performed geophysical and geotechnical investigations and georadar measurements were used [5, 6]. The results from the geophysical investigations enabled the obtaining of seismic sections down to maximum depth of 150 m whereat local discontinuities and deformations in the terrain structure were defined. The models obtained by analysis of data from the investigations combined with application of seismic refraction, MASW and HVSR, distinguish 5 lithological media characterized by different physical-mechanical characteristics.

The following lithological media are distinguished:
- A surface layer – dusty, sandy and clayey, with seismic velocity values of Vs=150-200 m/s;
- Subsurface layer of clay, dust and sand with seismic velocity values of Vs=200-400 m/s;
- More compact Quaternary sediments with seismic velocity values in the range of Vs=400-600 m/s;

- Pliocene sediments with seismic velocity values in the range of Vs=650-800 m/s;
- Terrain bedrock, Paleozoic shales with seismic velocity values of Vs>1000 m/s.

From the performed analysis of data obtained from CPT (cone penetration tests) and SPT (standard penetration tests) as well as from the aspect of the lithological composition of the terrain and strength and deformability characteristics, it can be said that the soil on the investigated location is characterized by variable geomechanical characteristics. The investigation mainly shows a lithological structure with alternating occurrence of silty clays with fine gravel and clayey silt that are moderately plastic and with variable thickness of layers. The penetration resistance of silty parts ranges within the limits of $q_c=(0,5-1,2)$ MPa and the corrected number of SPT blows is $N_{60} = 4$, whereas those of the sandy and fine gravel parts are within the limits of $q_c=(6,0-10,0)$ MPa with $N_{60} = 14$. Based on the extensive soil investigation, the Vs soil profile was defined presented in Fig. 1.
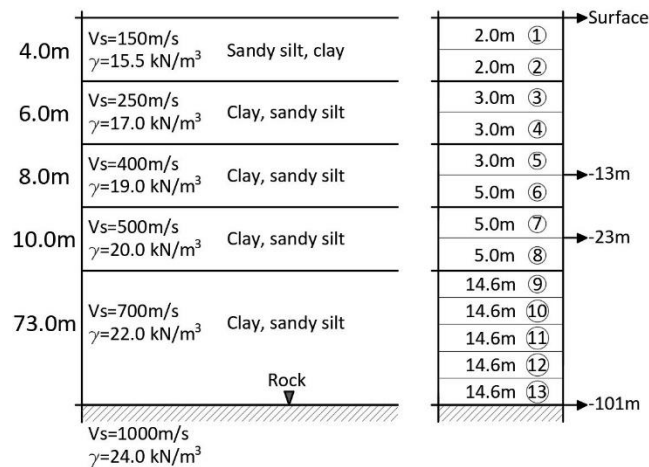
Figure 1. Shear wave velocity Vs [m/sec] profile for analysis of the local site effects.

3. Seismic instrumentation

3.1 Instrumentation at the site

The Location Tower from the 3D strong motion array is consisted of one surface and three downhole instruments each, 125 meters down the bedrock; a nine story building with two instruments installed on the building, 6th and 9th Storey and 4 instruments installed at the foundation level. The number and the depth of the instruments at the locations are presented in Fig. 2.
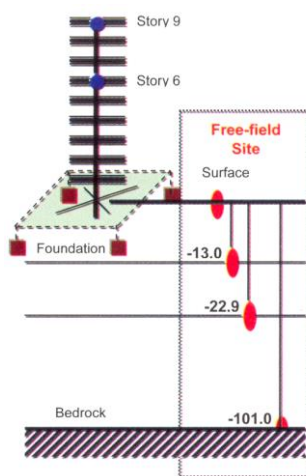
Instrumentation	Location – 1- Tower In situ laboratory
Site type	Instrumented building
Instruments on the building structure	2 (6th and 9th story)
Instruments at the level of the foundation structure	4
Instruments on soil surface	1
Instruments in soil profile	2 (13.0m, 22.9m)
Instruments at bedrock	1 (101m)
Total number of instruments	10

Figure 2. Instruments setup and depth at the Location Tower

3.2 Obtained records from small to moderate earthquakes

During planning and installation of the Ohrid Lake Seismic Network in the late 70's, the entire network was composed of the most advanced instruments produced by Kinemetrics Inc., Pasadena, California. However, the analogue recording system could not be maintained in the last decade and there was no possibility for recording real time earthquake events. The time period between 2020-2021 was the beginning of extensive revitalization of the network. Replacement of the recording system by an analogue-digital conversion device, which enables real time recording of earthquake events and thus structural and health monitoring at the Location Tower was realized. Since March 2021, several small to moderate earthquake events have proven the functionality of the installed instruments and have provided important data for further investigation at the location. Selected recorded earthquakes are analyzed in this paper which are given in Table 1. With the presented registrations simple 1-dimensional linear equivalent site response analysis was performed at the site which are presented in further chapter. It is worth noting that three directions are recorded with three channels, and for the analysis one horizontal acceleration per earthquake was used.

Table 1. Selected registered earthquakes with the monitoring system at the Location Tower

	DATE OF REGISTERED EARTHQUAKES	RICHTER MAGNITUDE	EPICENTER
EQ1	09 January 23:38 Pm (UTC) 2022	4.0	Bitola, Macedonia, 8 km southeast of Bistrica, Macedonia*
EQ2	11 January 17:01 Pm (UTC) 2022	3.5	Florina, West Macedonia, Greece*
EQ3	11 January 17:44 Pm (UTC) 2022	4.5	Florina, West Macedonia, Greece*
EQ4	12 January 03:01 Am (UTC) 2022	3.6	Florina, West Macedonia, Greece*
EQ5	22 April 21:07 (UTC) 2022	5.7	42 km SE of Mostar, Bosnia and Herzegovina

* these quakes were likely an aftershock of the 5.3 quake West Macedonia, Greece, Jan 9, 2022 11:43 pm (GMT +2)

4. Site response analysis

The local geotechnical media have a specific effect upon the characteristics of motion through the soil surface during earthquakes. Depending on the characteristics of the local geotechnical media and the characteristics of excitation at the level of seismic bedrock, these effects can be greater or lesser. The effect of the local soil conditions is expressed through variation of the amplitude-frequency characteristics of ground motion upon the surface in respect to the corresponding excitation at the level of the seismic bedrock. The analyses were performed by application of the method of vertical propagation of shear seismic waves through a linear viscoelastic system based on the solution of the Kanai wave equation. The procedure of definition of the nonlinear effects in soil resulting from seismic effects includes an approach that uses the equivalent linear characteristics of soil developed by Seed and Idriss, [7]. The analyses were performed by use of the SHAKE2000 software. The model presented on Fig. 1, was analyzed with the selected recorded acceleration records given in Table 1.

The effect of the local medium was evaluated based on the analysis of the dynamic response of the mathematical model. This analysis enabled definition of the peak accelerations along depth of the model as well as the response spectra of the models for the surface level. With the analyses of the local soil effects, there were obtained the mean periods of natural vibration of 0.63-0.65 s, for the real recorded acceleration level (without scaling) corresponding to low level of deformations. Fig. 3 and Table 2, show the variation of peak accelerations along depth of the models obtained by convolution of selected accelerograms, for real recorded input acceleration of a_{max} between 0.0027 and 0.0069g.
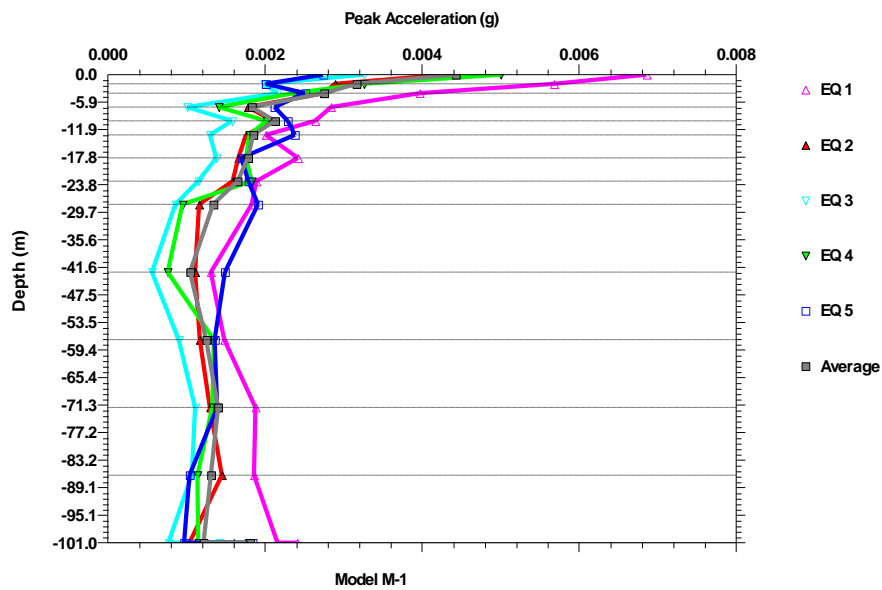
Figure 3. Peak accelerations along Depth for real recorded acceleration– response of the soil column.

Table 2. Calculated peak accelerations along depth, periods of the soil column and DAF_{mean}

DEPTH	MAXIMUM ACCELERATION					
	EQ 1: Florina 11.01.2022 **(M4.0)**	**EQ 2:** Bitola 09.01.2022 **(M4.0)**	**EQ 3:** Florina 12.01.2022 **(M3.6)**	**EQ 4:** Florina 11.01.2022 **(M3.5)**	**EQ 2:** B&H 22.04.2022 **(M5.7)**	**Average acc.** a_{max} **(g)**
0	**0.0069**	**0.0043**	**0.0033**	**0.0050**	**0.0027**	**0.0045**
-4.0	0.0040	0.0027	0.0021	0.0023	0.0025	0.0027
-10.0	0.00264	**0.0021**	0.0016	0.0020	0.0023	0.0021
-13.0	**0.0020**	**0.0018**	**0.0013**	**0.0018**	**0.0024**	**0.0019**
-18.0	0.0024	0.0017	0.0014	0.0017	0.0017	0.0018
-23.0	**0.0019**	**0.0016**	**0.0011**	**0.0018**	**0.0018**	**0.0016**
-57.20	0.0015	0.0012	0.0014	0.0013	0.0013	0.0013
-101.0	0.0024	0.0017	0.0015	0.0019	0.0018	0.0019
DAF (0/-101)	**2.88**	**2.53**	**2.20**	**2.63**	**1.56**	**2.36**
DAF (-4/-101)	**1.67**	**1.59**	**1.40**	**1.21**	**1.39**	**1.42**
PERIOD (S)	0.66	0.64	0.63	0.64	0.66	**Average period:** 0.65 s

Fig. 4 and 5 represent the average computed acceleration time history on the left and the real recorded acceleration time history from instruments on the right for the level of 101m and the surface level 0.0m. The graphs are compatible, and it can be concluded that the modelled soil profile represents the real amplification characteristics of the location.

129
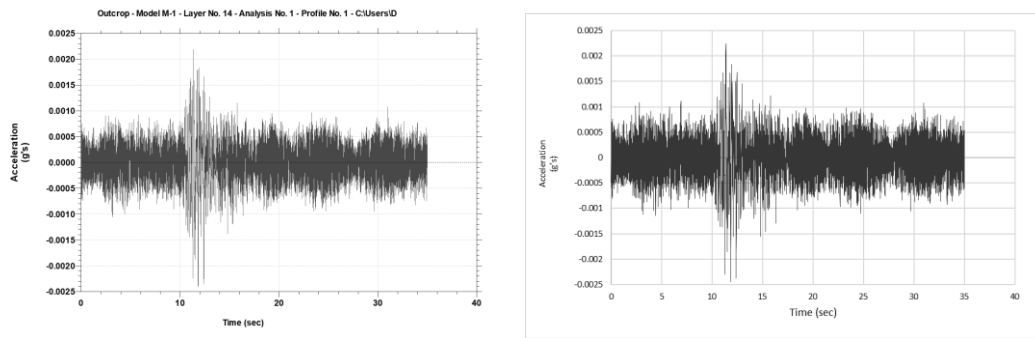
Figure 4. Computed acceleration time history (left) and the recorded acceleration time history (right) for the depth of -101.0 m
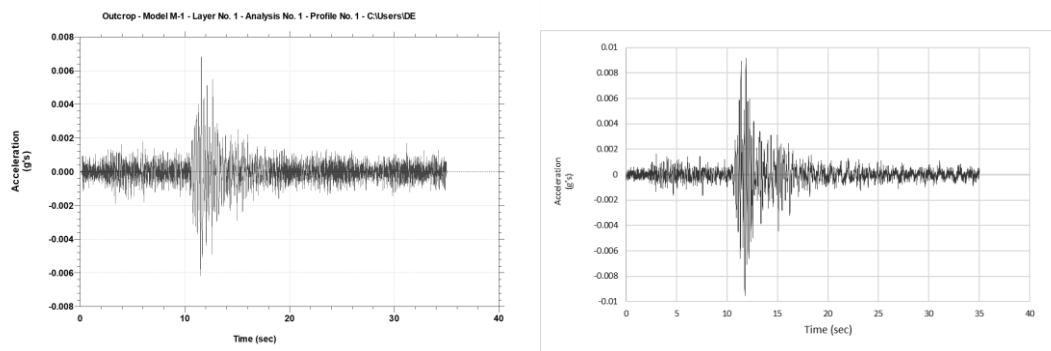
Figure 5. Computed acceleration time history (left) and the recorded acceleration time history (right) for the surface 0.0m.

Calculated acceleration records at the same depths where recorded acceleration records were available were compared and results presented in Table 3. The obtained dynamic amplification factor is presented in Table 4. Results show good correlation to the recorded values on the surface. Additionally, more detailed modelling of the materials model of the soil profile are needed to fit the records for the deeper soil layers at level of 23 meters.

Table 3. Difference in percentage of the recorded acceleration versus the calculated for each depth

| | RECORDED ACCELERATION [G] | | | | | | |
DEPTH	EQ 1: Florina 11.01.2022 (M4.0)	EQ 2: Bitola 09.01.2022 (M4.0)	EQ 3: Florina 12.01.2022 (M3.6)	EQ 4: Florina 11.01.2022 (M3.5)	EQ 2: B&H 22.04.2022 (M5.7)	Average acc. a_{max} [g]	Difference with calculation (%)
0	0.0095	0.0055	0.0024	0.0035	0.0036	0.0049	8.9
-13.0	0.0021	0.0021	0.0012	0.0022	0.0030	0.0021	10.5
-23.0	0.0039	0.0016	0.0011	0.0015	0.0027	0.0022	37.5
-101.0	0.0024	0.0017	0.0015	0.0019	0.0018	0.0019	/

Table 4. Dynamic amplification factor for each depth in respect to the seismic bedrock, calculated versus recorded

Depth [m]	DAF (calculated)	DAF (recorded acc.)
0.0	2.37	2.58
-13.0	1.0	1.1
-22.9	0.9	1.16
-101.0		

5. Discussion, conclusions and further work

Obtained results are good starting point for further non-linear site response analysis at the location which can be validated with stronger recorded earthquakes in future. The diagrams show that the surface layers considerably amplify the earthquake effect, which is the result of the low strength characteristics of the soil in these layers. The values of the DAF from the analyzed recorded acceleration match well with the DAF obtained from the site response analysis. Still, to get a more accurate insight, one of the next recommended research steps will be to analyze the local soil conditions by higher number of acceleration records from the site with different magnitudes, comparison of the obtained acceleration records with acceleration records from nearby seismic stations as well as more detailed modelling of the dynamic soil properties (shear modulus and damping) obtained from laboratory experiments on soil samples of the location.

References

[1] Petrovski J. et al.(1995). Characteristics of Earthquake Ground Motions Obtained on the Ohrid Lake Three Dimensional Strong Motion Array in the Republic of Macedonia.10th European Conference on Earthquake Engineering, Duma (ed.) © 1995 Balkema, Rotterdam, ISBN 90 5410 528 3.

[2] Bojadjieva et al., 2021. IZIIS In situ geo laboratory. Proceedings of 1ˢᵗ Croatian Conference on Earthquake Engineering, 1CroCEE Zagreb, Croatia - March 22ⁿᵈ to 24ⁿᵈ, 2021.

[3] Julijana Bojadjieva, Vlatko Sheshov, Kemal Edip, Jordanka Chaneva, Toni Kitanovski, Dejan Ivanovski (2019). "GIS Based Assessment of Liquefaction Potential for Selected Earthquake Scenario". Earthquake Geotechnical Engineering for Protection and Development of Environment and Constructions. Proceedings of the 7th International Conference on Earthquake Geotechnical Engineering. 7th ICEGE, Rome, Italy, 17-20th, June, 2019.

[4] Milutinovic Z., Shalic R., Tomic D. (2016). Seismic Hazard Map (PGA) for Macedonia, based on MKC EN 1998-1:2004 – Eurocode 8, Institute of Earthquake Engineering and Engineering Seismology, Ss. Cyril and Methodius University, Skopje, IZIIS Report 2016-26.

[5] J. Bojadjieva, V. Sheshov, K. Edip, A. Bogdanovic, I. Gjorgjeska, T. Kitanovski and D. Ivanovski. (2022) In situ geotechnical laboratory in urban environment. ICONHIC 2022, Athens, Greece.

[6] Three-dimensional Network of Instruments for Investigation of the Effect of Local Soil Conditions and Behaviour of Structures under the Effect of Earthquakes, Volume IX, IZIIS Report 85-154.

[7] Seed, H. B. (1970). Soil moduli and damping factors for dynamic response analyses. *Report*, EERC-70.

INFLUENCE OF THE SEISMIC ACTION ON THE STABILITY OF RETAINING CANTILEVER WALLS AND COMPARISON BETWEEN EX-YU REGULATIONS AND EUROCODES

Dejan Ivanovski[(1),] Kemal Edip[(2),] Julijana Bojadjieva[(3),] Vlatko Sheshov[(4),] Toni Kitanovski[(5),]

[(1)] *PhD Candidate, Ss. Cyril and Methodius University, Institute of earthquake engineering and engineering seismology-IZIIS, Skopje, Macedonia, ivanovski@iziis.ukim.edu.mk*

[(2)] *Associate professor, Ss. Cyril and Methodius University, Institute of earthquake engineering and engineering seismology-IZIIS, Skopje, Macedonia, kemal@iziis.ukim.edu.mk*

[(3)] *Associate professor, Ss. Cyril and Methodius University, Institute of earthquake engineering and engineering seismology-IZIIS, Skopje, Macedonia, jule@iziis.ukim.edu.mk*

[(4)] *Professor, Ss. Cyril and Methodius University, Institute of earthquake engineering and engineering seismology-IZIIS, Skopje, Macedonia, vlatko@iziis.ukim.edu.mk*

[(5)] *Research assistant, PhD Candidate, Ss. Cyril and Methodius University, Institute of earthquake engineering and engineering seismology-IZIIS, Skopje, Macedonia, tonik@iziis.ukim.edu.mk*

Abstract

Retaining structures in R. of North Macedonia until recently were only designed according to the concept of global safety factors, with the conventional methods of limit equilibrium. This method was widely used in ex-YU countries until Eurocodes have been published as regulations in the country formal legislation, where there are prescribed different design approaches, with specific partial coefficients for actions, materials, and/or resistances. For the seismic analysis of the walls, "Rulebook on technical norms for design and calculation of engineering structures in seismically active areas" (1987) was used. Currently, the use of both regulations is allowed, but after the expiration of this temporary period, Eurocodes will be the only standards for the design of buildings in our country. In this paper a comparison between the mentioned methods and regulations is made, in terms of the different approaches for the stability verification, as well as the required minimum width of the foundation for satisfying the stability criteria for 5 different heights of the walls, i.e. 3m, 4.5m, 6.0m, 7.5m and 9.0m. As our region is seismically active, special consideration is given to the parameters in seismic analysis procedure. It is shown that in order to satisfy the stability criteria, there is a need to increase the dimensions of the walls in relation to the dimensions obtained by the static analysis. The obtained results show significant differences between the regulations, especially when the seismic action is taken into account.

Keywords:Retaining, Structures, Cantilever, Wall, Eurocode

1. Introduction

With the acceptance of Eurocodes in R. of North Macedonia, as regulation codes for designing the structures, the need for their detailed elaboration has arisen, as well as understanding the differences and similarities with the previous practice and regulation (in the following text – "MKS").

Eurocodes are divided in 10 parts, depending on the area they relate to. The part that covers the retaining structures is Eurocode 7 - Part 1 (EN 1997:1), entitled "Geotechnical design - Part 1: General rules" [2]. Our country is a seismically active area, so retaining structures are also subject to aseismic design, which is specifically covered in Eurocode 8 entitled "Design of structures for seismic resistance - part 5 (EN 1998:5): Foundations, retaining structures and geotechnical aspects" [3].

As part of this paper, several analyses of a classic cantilever reinforced concrete wall (Fig. 1) with 5 different heights of 3m, 4.5m, 6m, 7.5m and 9m (above ground level), with assumed geomechanical parameters for the backfill and for the subsoil, shown in Table 1, have been performed. The analyses are done with the application of the current regulations - MKS and with the Eurocodes, considering that the approach to control the stability of retaining walls is completely different. The theoretical reviews of the regulations explain the calculation procedures and emphasize the biggest differences between the

Macedonian regulations, that is, the previous practice of designing retaining walls in relation to the new regulations - the Eurocodes. Also, special attention is given on the effect of seismic action on the retaining structures, in order to perceive and emphasize the differences in the required dimensions to satisfy the stability conditions. After the performed analyses, significantly large differences were obtained according to the different regulations used, as well as a significant increase in dimensions after the performed seismic pseudo-static analyses.
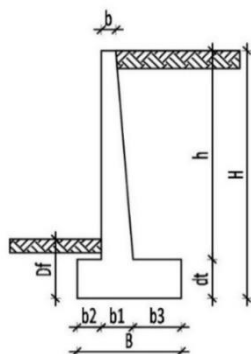
Fig. 1. Schematic view of the analysed wall

Table 1: Assumed geomechanical parameters for the backfill and subsoil

Soil type	γ [kN/m3]	φ [°]	c [kPa]
Gravel	21	30	0

2. Analysis of retaining walls according to MKS and Eurocode 7 – static conditions

Retaining walls are first analysed according to ex-YU, i.e. macedonian regulations - MKS, and then according to Eurocode - EC 7-1 [2]. The analyses are done using the software GEO-5, Cantilever wall module [4]. In order to make a relevant comparison, the walls are dimensioned with the minimum required dimensions that satisfy all conditions for stability, i.e. with maximum utilization of the section. Since the analysed wall is a cantilever, reinforced concrete section, stability is ensured through the deformation capacity of the wall, while the dimension that contributes the most to stability is the width of the foundation, so only this dimension was analyzed, while all other dimensions are adopted according to the recommendations for preliminary dimensions in the literature, as a ratio of the height of the wall, and are not changed for the different analyses. Also the total height is increased for some minimum embedment. The stability of the walls is controlled for the conditions against overturning, sliding, bearing capacity of the ground, as well as the eccentricity of the resultant force, which is limited to the middle third of the foundation, i.e. to B/6, in order not to cause tension in the foundation under static loads.

According to MKS, the analysis is based on the method with safety coefficients, i.e. the calculation is done by dividing the resistance by the actions on the structure. The ratio between them should be greater than a certain prescribed safety coefficient, which for static conditions is with a value of Fs ≥ 1.50, and for seismic conditions Fs ≥ 1.10. The bearing capacity of the soil, i.e. the permissible bearing capacity is generally obtained by reduction with a safety coefficient of Fs=3.0 in relation to the limit bearing capacity, which is calculated mostly according to the Terzaghi method for the specific type of foundation for adopted geomechanical parameters. However, the permissible stress is also adopted for realistically expected value in practice. The force from active earth pressure is calculated according to the Rankine or Coulomb method.

According to Eurocode 7-1, the analysis is based on the limit state method, where certain partial coefficients are prescribed for the actions (A), for the geomechanical parameters (M) and for the resistance of the structure (R). In EC 7-1, there are 3 possible design approaches for the design of geotechnical structures, labeled as DA-1 (C1 and C2), DA-2 and DA-3, from which each country has the right to choose its national design approach. access. In the Macedonian national annex "MKS_EN_1997_2012_NA_2020" [5], DA-2* approach is adopted, which is actually identical to the DA-2 approach, but instead of the actions, the partial coefficients are applied to the effects of the

actions, which generally gives identical final results. Also, this approach provides partial coefficients for the reduction of the global resistance of the construction, but does not reduce the soil strength parameters. In a general view, the same can be shown according to Eq. (1):

$$DA\ 2 = A1+M1+R2 \tag{1}$$

(A1): $\gamma_{G,unfav} = 1.35$; $\gamma_{G,fav} = 1.0$; $\gamma_{Q,unfav} = 1.5$; $\gamma_{Q,fav} = 0.0$
(M1): $\gamma_{\varphi'} = 1.0$; $\gamma_c = 1.0$; $\gamma_{cu} = 1.0$,
(R2): $\gamma_{Rh} = 1.1$; $\gamma_{Rv} = 1.4$, $\gamma_{Re} = 1.4$

Detailed explanation of the coefficients and how should be applied, can be found in the appropriate Annexes of the Eurocodes. The force from active earth pressure, same as by MKS, can be calculated according to the Rankine or Coulomb method, but can also be read directly from the graphs given in Annex C of EC 7-1. Moreover, in the national annex, the use of the Coulomb equation is recommended due to the inclusion of more general conditions and the greater conservatism of the Rankine theory. The bearing capacity of the soil is calculated according to the procedure given in Annex D in EC 7-1.

After the performed analyses, in Table 2 are shown the results for all walls, that is, the required foundation width to satisfy the stability conditions according to the two different regulations (MKS and EC-7). For the sake of analogy in the results, a percentage utilization for each condition is shown, rather than showing a safety coefficient. A utilization of 100% corresponds to the prescribed safety coefficient of 1.50 according to MKS. Additionally, Fig. 2 shows the analysed wall with a height of 6m, and the obtained width of the foundation with the different regulations.

Table 2: Required foundation width and utilization for static stability, for different wall heights and according to different regulations

Wall height - H [m]	Regulation	Required foundation width - B [m]:	Utilization [%]			
			Overturning	Sliding	Bearing	Eccentricity
3	MKS	1.45	73%	79%	56%	98%
	EC 7 DA-2	1.65	62%	76%	79%	99%
4.5	MKS	2.05	74%	89%	78%	99%
	EC 7 DA-2	2.4	66%	76%	95%	89%
6	MKS	2.65	74%	93%	100%	99%
	EC 7 DA-2	3.2	62%	76%	100%	79%
7.5	MKS	3.6	67%	85%	98%	84%
	EC 7 DA-2	4	66%	78%	100%	88%
9	MKS	4.4	66%	91%	99%	70%
	EC 7 DA-2	4.75	68%	82%	98%	87%

Fig. 2: *Obtained foundation width for the wall H=6.0m according to: a) MKS, b) EC 7-1*

Fig. 3, graphically shows the dependence between the height of the walls and the required width of the foundation to satisfy the stability according to the two analysed procedures - MKS and EC 7 (DA-2).

The resulting curves are plotted for the five analysed wall heights and can only be used orientationally due to the assumed input parameters.
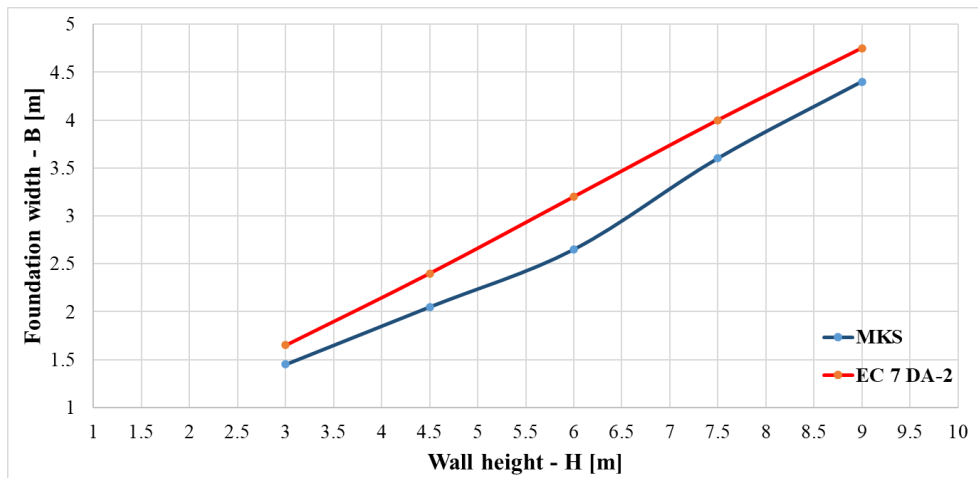
Fig. 3: Dependency: foundation height - width according to MKS and EC-7 (DA-2)

According to the presented results of the performed analyses, it can be concluded that the governing condition that dictates the dimensioning according to both approaches is the bearing capacity of the ground or the allowed eccentricity. It should be noted that the permissible bearing capacity of the soil according to MKS is assumed and it should be taken with a dose of caution, which is also the case for the bearing capacity according to EC 7-1, due to the assumption of all geomechanical parameters. Also, the sliding condition has a relatively high utilization, especially according to MKS, where for some of the walls the utilization is over 90%, so it can be concluded that even for a higher allowable stress on the ground, the dimensions will not change significantly, because the sliding will reach a critical value. On the other hand, overturning is the least utilized and is not relevant for dimensioning. According to the analyses performed for the different heights, it was found that according to EC 7-1 (DA-2), an increase in the width of the foundation of about 10-20% is needed in relation to the width calculated according to the MKS.

3. Analysis of retaining walls according to MKS and Eurocode 8 – seismic conditions

3.1. Seismic action according to MKS

The seismic analysis of the retaining structures in R. North Macedonia is prescribed in the "Rulebook for technical norms for design and calculation of engineering structures in seismic areas (1987)" [1]. This Rulebook prescribes the technical standards for designing in seismic zones VII, VIII and IX according to the MCS scale (Mercali – Cancani – Sieberg). The seismic calculation is carried out by the method of spectral analysis or dynamic analysis. According to this regulation, the seismic inertial force is calculated taking into account the self-weight of the structure - Eq. (2), as well as a calculation of additional active seismic pressure - Eq. (3):

$$S_{ik} = k_s * \beta_i * \eta_{ik} * \Psi * G_k \tag{2}$$

$$P_a = \frac{3 + 2 tan\beta}{4} * k_s * \Psi * \gamma_z * h^2 \tag{3}$$

S_{ik} – seismic inertial force from self-weight
P_a – total seismic ground pressure

The coefficient of seismic intensity k_s is calculated according to Eq. (4):

$$k_s = X_{max} / \mu_p \tag{4}$$

- X_{max} – maximum acceleration of the ground in g's - depends on the seismic zone (Table 3).
- μ_p – prescribed ductility factor of the structure

Table 3: Value of maximum acceleration X_{max} (g) in relation to the seismic zone

Seismic zone (MCS)	X_{max} (g)
VII	0.10
VIII	0.20
IX	0.40

In the accelerations shown in Table 3, although it is not explicitly stated, it is assumed that the amplification of the acceleration that can arise from the local soil conditions is also included, since there is no other coefficient that takes into account this influence. The coefficient μ_p=2.5, according to the Rulebookg, so the coefficient of seismic action k_s for seismic zone – IX is calculated in Eq. (5). The coefficients for which a detailed calculation is not shown in this paper, can be found in the Rulebook cited above. The seismic allowable stress on the ground is predicted with a value 50% greater than the allowable stress for static loads, which is the most common practice in our country.

$$k_s=0.40/2.5=0.16 \tag{5}$$

3.2. Seismic action according to Eurocode 8 – part 5

Eurocode 8, part 5 (EC 8-5) [3] complements Eurocode 7-1 (EC 7-1) [2] and describes the criteria and rules for the seismic resistance of the soil on which the foundation is built, as well as the rules for the design of various foundation structures, retaining structures and soil-structure interaction during an earthquake. For seismic analysis, it is stated that any proven method based on the methods of dynamics of structures and soils and supported by previous experience is acceptable. In this paper, the seismic analyses of the retaining walls is performed with the pseudo-static method, based on the theory of Mononobe (1929) [6] and Okabe (1926) [7]. The total horizontal force, which occurs as a sum of the static loads from the active earth pressure with added action from the seismic action is calculated according to Eq. (6).

$$E_d=0.5*\gamma*(1\pm K_v)*K*H^2+E_{ws}+E_{wd} \tag{6}$$

- γ - specific weight of the soil
- H – height of the wall
- E_{ws} - static water pressure
- E_{wd} - hydrodynamic pressure of water
- K - coefficient of earth pressure (static + dynamic)

If adequate drainage is designed and a non-cohesive, gravelly material is placed behind the wall, as well as the groundwater table is below the foundation level, then the water pressure forces can be ignored, so that $E_{ws} = E_{wd} = 0$. The active pressure coefficient (static + dynamic) is calculated according to Eq. (7) or (8):

$$\text{if } \beta \le \varphi'_d - \theta => \ K = \frac{\sin^2(\Psi+\varphi'_d-\theta)}{\cos\theta \sin^2\Psi \sin(\Psi-\theta-\delta_d)\left[1+\sqrt{\frac{\sin(\varphi'_d+\delta_d)\sin(\varphi'_d-\beta-\theta)}{\sin(\Psi-\theta-\delta_d)\sin(\Psi+\beta)}}\right]^2} \tag{7}$$

$$\text{or if } \beta > \varphi'_d - \theta => \ K = \frac{\sin^2(\Psi+\varphi-\theta)}{\cos\theta \sin^2\Psi \sin(\Psi-\theta-\delta_d)} \tag{8}$$

- $\varphi'_d=\tan^{-1}\left(\frac{\tan\varphi'}{\gamma_{\varphi'}}\right)$ – design angle of internal friction

- $\delta'_d=\tan^{-1}\left(\frac{\tan\delta}{\gamma_{\varphi'}}\right)$ – design angle of friction between soil and structure

- Ψ and β - slope angles on the back of the wall and on the ground behind the wall

- $\tan\theta = (\frac{k_h}{1 \pm k_v})$ – an angle that depends on the horizontal and vertical seismic coefficients (k_h and k_v) - if the groundwater level is below the wall, which is an assumption in this paper.

The coefficients for the horizontal and vertical seismic action (k_h and k_v) are shown in Eq. (9-11).

$$k_h = \alpha * * \frac{S}{r} \tag{9}$$

$$\alpha = \frac{a_{gR}}{g} * \gamma_I \tag{10}$$

$$k_v = \pm 0.5 \, k_h \text{ (if avg/ag > 0.6)} \tag{11}$$

- α - maximum acceleration for a certain category of the structure
- a_{gR} – reference ground acceleration for soil type "A"
- r – coefficient that depends on the permissible movement of the wall - Table 4
- S – soil factor that depends on the type of soil

Table 4: EC8-5 – Values of coefficient „r"

Type of retaining structure	r
Free gravity walls that can accept displacement up to dr=300*α*S	2
Free gravity walls that can accept displacement up to dr=200*α*S	1.5
Flexural RC walls, anchored or braced walls, RC walls founded on vertical piles, restrained basement walls and bridge abutments	1.0

The walls are supposed to be located in a zone with reference acceleration a_{gR} =0.25g, according to the seismic zoning map of R. North Macedonia for a return period of 475 years shown in the National Annex for EC 8 - "MKS_EN_1998-1/NA:2020" [8]. In order to make the analyses as much comparable as possible, the acceleration is selected for a region that generally corresponds to the seismic zone IX according to the current seismological map for a return period of 500 and also for 1000 years, which is used according to the above mentioned Rulebook. Type "B" soil is assumed, so the coefficient S=1.20. The coefficient r serves to reduce the input seismic force in relation to the allowed displacements for the different 3 types of structures, shown in Table 4. Although not explicitly shown in EC 8-5, this coefficient represents the ductility of the structure and is analogous to the coefficient q, i.e. the behavior factor for the calculation of seismic forces for high-rise structures. That is concluded because EC 8-5 does not provide another coefficient that takes into account this aspect of the behavior of retaining structures during an earthquake. In Table 4, the retaining structures are divided into 3 types, depending on the flexibility, that is, the displacement that is "acceptable" for the analysed structure, while for more flexible structures, a higher coefficient r is provided, i.e. a greater reduction of the seismic force. Some doubt occurs is the third row of the table, where "flexural RC walls" are located, for which r=1.0, that is, no seismic force reduction is allowed. Moreover, according to the division of retaining structures in EC 7-1, RC cantilever walls belong to gravity walls, which means that they can be placed in the upper 2 categories of this table. At the same time, these 2 categories differ only in the value of the "acceptable" displacement, which depends only on a certain coefficient (200 or 300), multiplied by the acceleration α and the soil coefficient S. In this way, for the analysed location we get acceptable displacement "dr" for the first category from the table of 300*0.25*1.20=90 mm, and for the second category dr=60 mm. The value is given in absolute value, without taking into account the height of the structure, which is the most important factor in determining or limiting the permissible, or acceptable displacement of a structure. What is more, no method is shown by which the displacement of the analysed structure can be calculated or evaluated. According to Fardis M., et al [9] "the designer should be aware that the magnitude of the seismic action calculated according to EN 1998-5, in the absence of specific studies, leads to a conservative design of the retaining structures. Therefore, the designer should make an individual assessment of the permanent displacements of the wall, in order to select a value for the coefficient r".

Regarding the design approaches, neither in EC 8-5, nor in the national annex, a design approach is specifically chosen according to which the seismic analysis should be performed. According to Fardis M., et al. [9], due to the fact that the pseudo-static method takes into account design values of the geomechanical parameters, for which partial coeffficients with a value greater than 1.0 are provided only in the design approaches DA-1 C2 and DA-3, it was concluded that these approaches are most compatible with EC 8-5, and will generate the most conservative seismic analysis results. These 2 approaches actually have identical partial coefficients in the absence of structure-generated actions, and give identical final results. Moreover, in EC 7-1, it is stated that in accidental situations, which include seismic loads, all values of partial coefficients for actions should be adopted with a value of 1.0, and all values of partial coefficients for resistances should be determined according to the "specific situation depending on the accidental action", without any further explanation, while the partial coefficients for the geomechanical parameters are not mentioned. Accordingly, using the DA-1 C1 and DA-2 approaches, which prescribe partial coefficients for actions, with reducing them to 1.0 according the statement above, would further reduce the seismicity forces, so that the differences between these approaches would be drastic compared DA-1 C2 and DA-3. This aspect is quite conservative, due to the fact that with these 2 approaches, the same values of partial coefficients are used as in static conditions, i.e. the structure is not allowed to have "lower" safety during an earthquake, as is the case in MKS (safety coefficient Fs≥1.10 for seismic conditions, in contrast to Fs ≥1.50 for static conditions). According to the mentioned aspects, a reduction coefficient of r=2.0 was adopted for the performed analyses, with which the coefficients k_h and k_v were calculated – Eq. (12) and Eq. (13):

$$k_h = \alpha * \frac{S}{r} = 0.25 * \frac{1.20}{2} = 0.15 \quad (12)$$

$$k_v = \pm 0.5 \, k_h = \pm 0.075 \quad (13)$$

The seismic bearing capacity of the ground is given in form of an empirical expression that needs to be satisfied, given in EC 8-5 - annex F.

After the performed analyses, a comparison was made of the dimensions obtained according to EC 8-5 and MKS - zone IX in terms of the required foundation width for all wall heights, summarized in Table 5, as well as in Fig. 5. It can be stated that according to EC 8-5 there is a rather large increase in the dimensions of the wall in relation to MKS, needed to satisfy the stability conditions, mostly the sliding, and also satisfying the expression for the seismic bearing capacity. The results lead to an unexpected and even illogical appearance of the width of the foundation compared to the wall height. The percentage increase is up to 40-60%. Fig. 4 shows the analysed wall with a height of 6m, and the obtained width of the foundation with the different codes.

Table 5: Required foundation width and utilization for seismic stability, for different wall heights and according to different regulations

Wall height - H [m]	Regulation	Foundation width - B [m]:	Utilization [%]		
			Overturning	Sliding	Bearing
3	MKS	1.9	79%	100%	69%
	EC-8-5	2.95	41%	97%	-0.016<0
4.5	MKS	2.65	79%	100%	93%
	EC-8-5	4.2	40%	100%	-0.010<0
6	MKS	3.7	71%	94%	98%
	EC-8-5	5.5	39%	100%	-0.021<0
7.5	MKS	4.7	72%	97%	99%
	EC-8-5	7	40%	100%	-0.006<0
9	MKS	6.05	65%	92%	99%
	EC-8-5	8.5	39%	100%	-0.041<0

Regarding the total force from seismic action, it was also found that according to EC 8-5 a larger force is obtained in relation to MKS, due to the partial coefficients of the materials (reduction of the soil strength parameters), although the coefficient k_h is obtained with a lower value in relation to the MKS. This means that the required reinforcement for the stem and the foundation will also be greater

compared to MKS, but such dimensioning has not been performed, because it is not a subject of analysis in this paper.
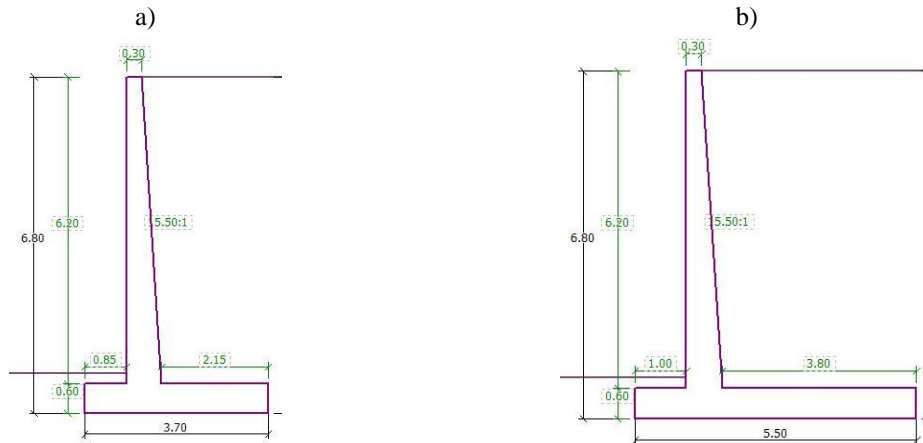
Fig. 4: *Obtained foundation width for a wall H=6.0m according to: a) MKS – Zone IX - MCS, b) EC 8-5, a=0.25g*
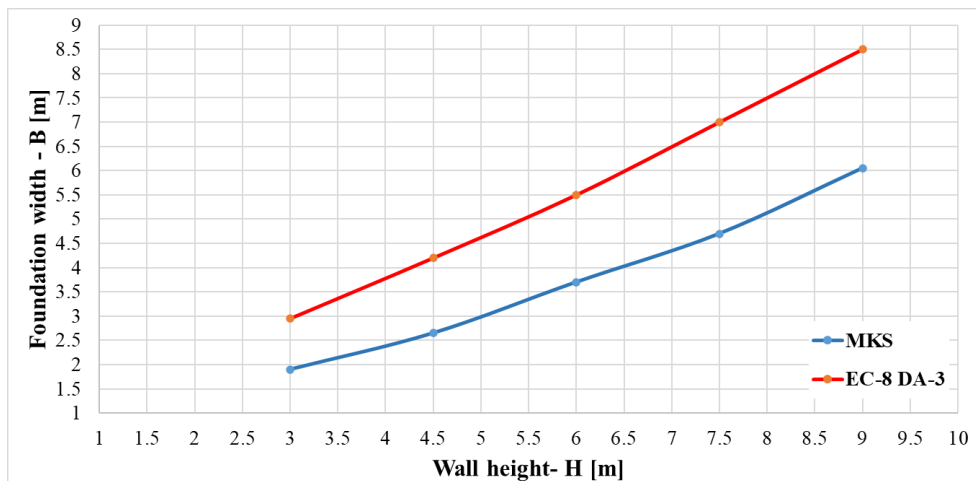
Fig. 5: Dependency: foundation height - width according to MKS and EC-8 (DA-3)

4. Comparative analysis between the static and seismic conditions

According to the results shown, an analysis of the seismic influence can be done for the required dimensions to satisfy the stability of the walls. In addition to the results shown, a seismic calculation was additionally performed for the seismic zone VIII according to MKS, with k_h=0.08, calculated according to Eq. (5), as well as for k_h=0.12 according to EC 8-5 - Eq. (9), as for a region that according to the new seismological map generally corresponds to the zone VIII according to the old seismological map, for the same type of soil (type B). The results are shown in Fig. 6 in form of percentage increase in the width of the foundation for seismic conditions, in relation to the static conditions. It can be concluded that according to MKS, a relatively small increase of up to 9% is needed for zone VIII, and for zone IX the increase is more pronounced, up to 30-40%. According to Eurocode (EC 8-5), approach DA-3, in relation to EC 7-1, DA-2, the increase for k_h=0.12 is about 55-60%, while for k_h=0.15, the increase is even up to 80%. It can be concluded that the seismic effect has a significant role in the dimensioning of the walls, and the seismic analysis should be mandatory for all new retaining structures, especially in seismically active areas.
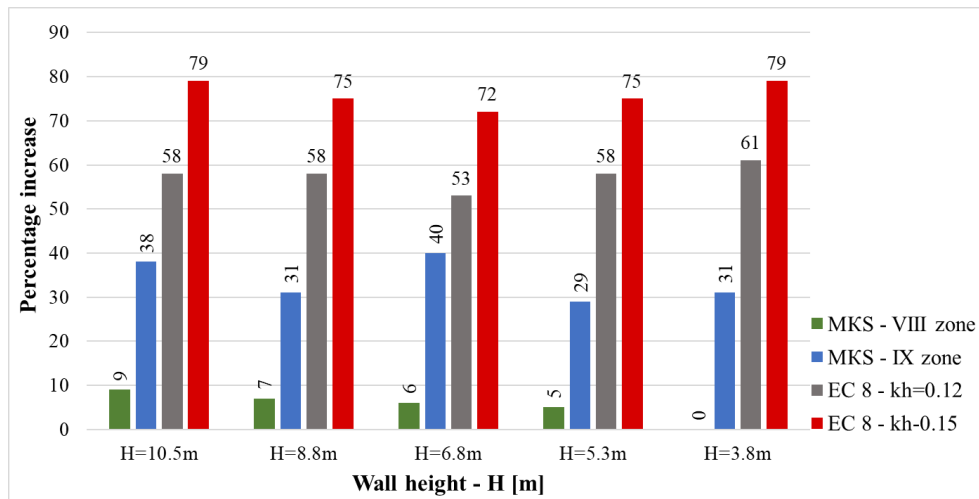
Fig. 3: Percentage increase in dimensions under seismic conditions compared to static conditions

5. Conclusion

According to the results of the performed analyses, the following can be concluded:

- The procedure for the analysis is conceptually different in the analysed regulations, i.e. in MKS it is based on global safety coefficients concept, while in Eurocodes it is based on limit state with application of partial coefficients.

- From the performed static analyses, it was found that according to EC 7-1, with the chosen design approach in the NA – DA2*, an increase in the width of the foundation of about 10-20% is required in relation to the width calculated according to MKS.

- The calculation of the seismic coefficients k_h is very similar between the two regulations, and although the given accelerations for same location are with a different value at first, using maps for different return period, the obtained values are very similar, that is, k_h=0.16 for seismic zone IX (MKS) and k_h=0.15 (EC 8-5). In fact, the theory for calculating the active seismic pressure is identical, which is Mononobe-Okabe theory. The main difference is the different concept for analysis, where with global safety coefficients (MKS) it is prescribed lower coefficient, i.e. it is allowed "less safety" under seismic actions. On the other hand, with EC 8-5 DA-3, there is no difference in the material partial coefficients between static and seismic calculations, so the structure is dimensioned with the same "safety" for both static and seismic condtions, which is the reason for the larger required dimensions, of up to 50-60%.

- The value of the coefficient r is not clearly enough explained in EC 8-5, which leads to uncertainty in adopting its value. It is also not specified which design approach should be used in seismic analysis, neither in the code, nor in the national annex.

- The seismic action has a great influence in the dimensioning, so that significantly larger dimensions are obtained to satisfy the stability of the walls in relation to the static conditions, so the seismic analysis of the retaining walls should be mandatory.

- The current situation of already constructed walls, as well as the design of new retaining structures with the safety coefficients method (ex-YU regulations), does not indicate a need to increase the cross-sections of the walls, because the cases of large and unallowed deformations or damages have not been registered or they are very rare, if the walls were designed and built following all the rules in the regulations.

References

[1] Rulebook for technical norms for design and calculation of engineering structures in seismic areas (1987)

[2] European Committee for Standardization (2004) Eurocode 7: Geotechnical design - Part 1: General rules. CEN, Brussels, EN 1997-1;

[3] European Committee for Standardization (2004) Eurocode 8: Design of Structures for Earthquake Resistance. Part 1: General Rules, Seismic Actions and Rules for Buildings. CEN, Brussels.

[4] GEO-5 software, Cantilever wall module, Spread Footing module.

[5] Standardization Institute of the Republic of North Macedonia (2020) Eurocode 7: Geotechnical design. Part 1: General rules – National annex. Reference number: MKC EN 1997-1:2012/HA:2020 (in Macedonian);

[6] Mononobe, N. and Matsuo, H. (1929). On the Determination of Earth Pressure during Earthquakes. Proceedings of the World Engineering Conference, 9, 176;

[7] Okabe S., (1926). General theory of earth pressure. Journal of the Japanese Society of Civil Engineers, Tokyo, Japan 12 (1);

[8] Standardization Institute of the Republic of North Macedonia (2020) Eurocode 8: Design of Structures for Earthquake Resistance. Part 5: Foundations, retaining structures and geotechnical aspects – National annex. Reference number: MKC EN 1998-1:2012/HA:2020

[9] Fardis, M. et al (2005). Designers' guides to the eurocodes, - Designers' guide to EN 1998-1 and EN 1998-5 Eurocode 8: Design of structures for earthquake resistance general rules, seismic actions, design rules for buildings and retaining structures.

[10] Official Gazette of Republic of North Macedonia, no. 211, 02/09/2020.

[11] Bond, A., & Harris, A. (2008). Decoding Eurocode 7. CRC Press

[12] Bowles E. J. (1996). Foundation analysis and design – fifth edition

SEISMIC SOIL-STRUCTURE INTERACTION EFFECTS ON A HIGH RISE RC BUILDING

Kemal Edip[1], Jordan Bojadjiev[2], Done Nikolovski[3], Julijana Bojadjieva[4]

[1]*j.bojadziev@ibu.edu.mk, [2]kemal@iziis.ukim.edu.mk, [3]done.nikolovski@ibu.edu.mk, [4]jule@iziis.ukim.edu.mk*

[2, 3] International Balkan University, Skopje

[1, 4] Institute of Earthquake Engineering and Engineering Seismology, Skopje

Abstract

Soil-structure interaction (SSI) is for sure one of the most neglected effects in seismic structural design practice. However, many researchers showed that it might notably affect seismic performance results. In fact, the state-of-the-art seismic codes are encouraging including SSI for structures with considerable p-Δ effects and mid to high-rise buildings. In the current research, seismic soil-structure interaction analysis is made for a selected mid-rise reinforced concrete building with several different SSI techniques (models). In order to quantify the effect of SSI on the overall response of the selected structure, the global seismic response within a frame of force-displacement relationship for different earthquake intensities, different SSI mathematical models and different soil categories is presented. Comparing the outcome of the performed analysis it was observed that the structural performance was affected significantly by the foundation system and contributes considerably to the overall structural performance of the selected structure in specific soil conditions. As the results indicate, more code-based recommendations are required for the improvement of the SSI structural seismic design, especially in soft soil cases, where the soil-structure interaction might significantly affect the seismic response of buildings.

Keywords: Soil-structure interaction (SSI), Reinforced concrete buildings, Seismic performance

1. Introduction

The constitutive modeling of soil media has been an important topic in the field of soil-structure interaction. In the past decades, many attempts have been performed to develop constitutive models for modeling of soil media. Two major classes are available in the literature: linear elastic models and nonlinear elastic model in which stress-strain relations deviate from linearity. It is of special attention to deal also with failure envelope where its description plays a crucial role in soil simulation. The aim of this study is to present the newly implemented material models in finite element software ANSYS for simulation of soil medium in soil-structure interaction problems. Although in numerical calculations constitutive models are the most difficult and tricky part of the problem, there are some elementary features of the soil behavior which should be taken into consideration in most cases. The constitutive models are usually classified with respect to their mathematical parameters. For a more detailed explanation the reader can refer to the following publications [1, 2]. Although the classification of the material models is useful for scientists it is still confusing for the wider professional public. In the end, the engineers are the users of the constitutive models for modeling properly the particular tasks. Therefore, model evaluation appears more useful for users of constitutive models in geotechnical engineering. Laboratory experiments of soil specimens are used for testing constitutive models and checking for some basic soil features such as nonlinearity, irreversibility, failure criteria, deformation history etc.

As given in the work of Herle [3] it is quite impossible to consider all features by using only single material model. In the work of Chi and Kuchwaha [4] a nonlinear finite element model has been

developed to study the soil failure by using the hyperbolic stress strain model. Experiments conducted by Rowe and Peaker [5] show that both deformation mode and magnitude affect the distribution of earth pressure. Building upon the pioneering works of Drucker-- and Prager [6] on soil plasticity the trend has been to develop more precise and correct elastoplastic models for simulation of real materials. In the work of Loret and Prevost [7] different parameters are considered in solutions for the Drucker-- Prager elasto plastic material models. On the other hand development of von Mises [8] elastic plastic equations has enabled considerable improvement in simulation of soil materials. Moreover, the dynamic non-linear characteristics of soil media are taken into account in the work of other authors [9-10].

2. Numerical modelling of soil

In the finite element context of integration of material models, the constitutive equations are carried out at integration points. The incremental analysis is done and the solution is assumed to be known at the start of the increments. Knowing the strain increment $\Delta\varepsilon$ it is possible to calculate the stress at the end of the increment. In general the integration of the elasto-plastic models presents a challenging numerical problem since the plastic strain is defined as a rate after the material behavior has changed at the yield point. In this work in numerical modeling the soil in the soil structure interaction problem is modeled as a non linear medium using the Drucker-Prager and Bilinear Isotropic (BISO) material models. In order to complete the investigation, an elastic model of soil is also simulated for completeness of the comparison. The frame structure is exposed to earthquake acceleration and the results compared accordingly. Then the non linear material models are compared with elastic soil medium and the results are discussed consequently. For more detailed explanation of the material models the reader is referred to [7, 11]. The calibration of the non linear material models for Bilinear and Drucker- Prager material laws is done according to the work of Kodama and Komiyo [12]. The Biliniear Isotropic material model (BISO) uses the von Mises yield criteria coupled with an isotropic work hardening assumption. The material behavior is described by a "bilinear" stress-strain curve starting at the origin with positive stress and strain values. The initial slope of the curve is taken as the elastic modulus of the material. At the specified yield stress the curve continues along the second slope defined by the tangent modulus. The tangent modulus cannot be less than zero nor greater than the elastic modulus [13]. The constitutive models are shown in the Fig.1 below:
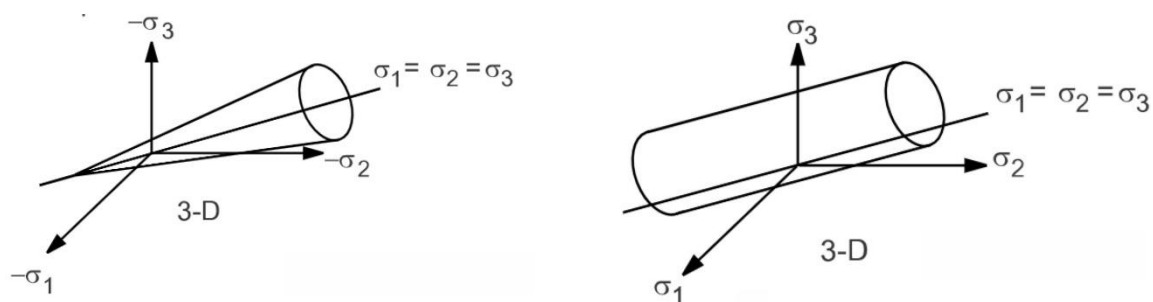
Figure 1. Graphical 3D representation of constitutive models, DP on the left and BISO on the right side

On the other hand the Drucker-Prager model uses the outer cone approximation to the Mohr-Coulomb law. The amount of dilatancy can be controlled with the dilatancy angle. If the dilatancy angle is equal to the friction angle, the flow rule is associative [13]. The soil medium is presented as a two dimensional model composed of four layers resting on bedrock. In Table 1 the soil layers properties are tabulated in a way that the bottom layers are characterized with better soil characteristics..

Table 1. Material parameters in finite element analysis

Soil medium	Layer number	Thickness (m)	Density (kg/m^3)	Elastic Modulus (kPa)	Friction angle (deg)	Uniaxial yield stress (kPa)
Elastic	1	3	1.1	2000		
	2	7	1.3	2200		
	3	6	1.5	2400		
	4	14	2	2600		
Drucker--Prager	1	3	1.1	2000	35	
	2	7	1.3	2200	35	
	3	6	1.5	2400	35	
	4	14	2	2600	35	
Von Mises	1	3	1.1	2000		0.1
	2	7	1.3	2200		0.1
	3	6	1.5	2400		0.1
	4	14	2	2600		0.1

The soil is discretized using eight nodded plane strain elements PLANE82. The dynamic analysis is performed by transient analysis using the step by step method. The proportional viscous damping matrix is taken to be proportional to mass and stiffness matrix (Rayleigh damping). The Rayleigh damping factors, alpha and beta are calculated such that the critical damping is 5% for first two modes. The bottom boundary of the soil model is fixed while side boundaries are simulated as viscous boundaries. The earthquake input is El Centro N-S, USA, 1940, with magnitude M=6.7 which is presented in Figure 2 below.
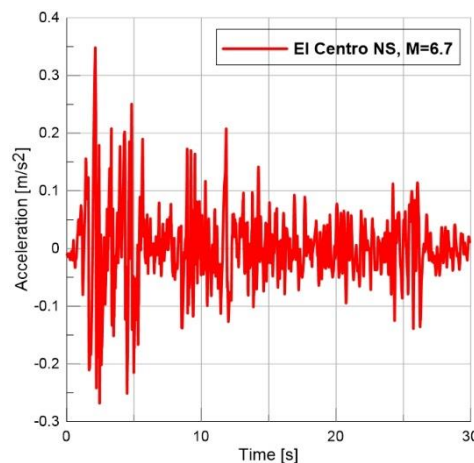
Figure 2 Selected acceleration history of El Centro N-S

3. SOIL STRUCTURE INTERACTION SYSTEM

In order to show the influence of the soil material modelling to the structural response a comparison of three different cases has been performed. First the soil medium is simulated as an elastic material model. Then the same soil medium is simulated as nonlinear by considering the Drucker-- Prager and BISO material models. In order to have a bigger range of results the frame is considered as one, three and five storey frames. The frame structural elements are idealized as two dimensional elastic beam elements BEAM3 having three degrees of freedom at each node, translations in the nodal x and y directions and rotation about the nodal z axis. The behaviour of the frame structure is supposed as elastic and is modelled using two parameters, the modulus of elasticity E=3.15x107 kPa and Poisson's ration n=0.2. The bay length of the frame is taken to be 4.0 m and storey height of 3.0 m. Section of beams is 40 x 50 cm while the column section is 50 x 50cm. A mass of 11 tons is assigned on each node to simulate the real structural behaviour (total 44 tons per floor). For all RC frames the beam and column sections, floor masses and number of bays are kept constant in all cases. The only parameter that is altered is the storey number.
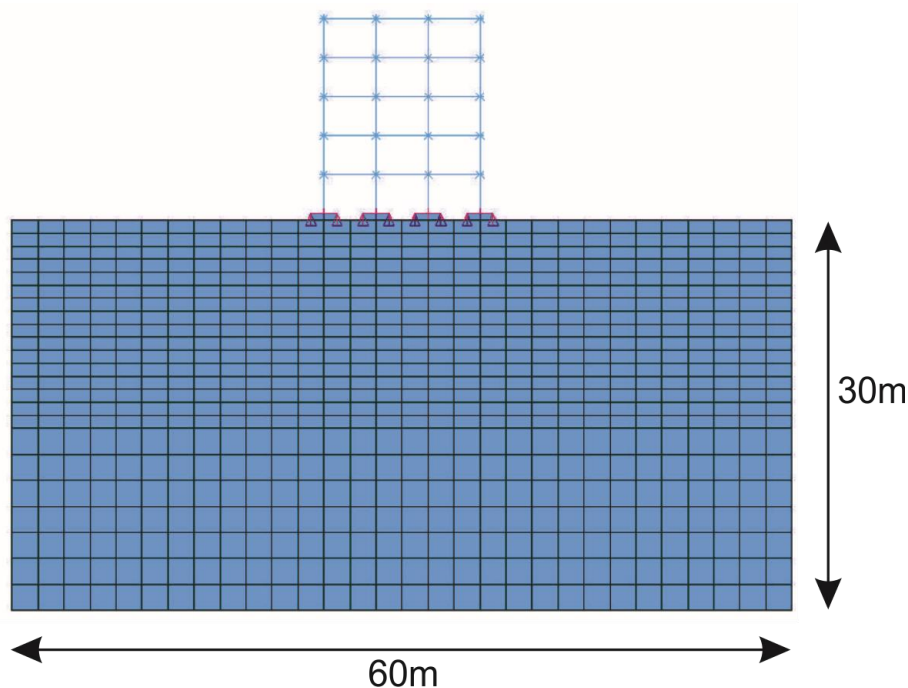
Figure 3. Coupled Soil structure system of a mid-rise building

Finite element modelling of the coupled soil-structure system is performed by the software ANSYS [13] as shown in Figure 3. The effect of soil-structure interaction is carried out with the acceleration time history of the El Centro earthquake with a scaled peak ground acceleration of 0.25g. The foundation where the structure is supported is taken to be 8 nodded plane element having two degrees of freedom in each node, translations in the nodal x and y directions. The moment transfer capability between the column and the footing is created by using a constraint equation where the rotation of the beam is transferred as force couples to the plane element. In Table 2 below the difference in the structural response is given.

Table 2. Structural values from the analysis of the frame structures

No. of Storey	Soil Medium	Max. acceleration at top of Str. (m/s²)	Max. displacement at top of Str. (mm)	Max. moment at top of Str. (kNm)

1	Elastic	2.54	9.44	28.5
	Drucker-Prager	2.77	9.33	25.6
	BISO	2.79	9.39	31.7
3	Elastic	2.60	4.89	2.02
	Drucker-Prager	2.60	4.08	4.03
	BISO	2.68	4.66	4.40
5	Elastic	2.55	5.67	2.75
	Drucker-Prager	2.60	5.57	5.49
	BISO	2.61	6.87	5.79

According to the acceleration values of the Table 2 the maximum displacement at the top of structure is considerably big when using linear elastic material model in a single and three storey frames. In the case of five storey frame the biggest displacement is obtained using the BISO model.

This illustrates that in soil medium analysis usage of material models for soil simulations should be considered carefully. On the other hand, in using Drucker-Prager material model the maximum structural moment at top of structure has smaller values when compared with elastic material model. This can be elaborated as nonlinearity taking place in the columns which prevent increase of structural moments. In moment comparison the usage of BISO model has similar values with the Drucker-Prager model although small deviation of the results is observed. In comparing of maximum acceleration values at the top of structures it can be concluded that the elastic material model has the smallest values while the usage of Drucker-Prager and BISO models vary accordingly. Thus it can be stated that in simulation of soil medium by nonlinear material models the calibration of the parameters with experimental results has to be performed previously.

4. Conclusions

It is to be stated that in the literature there are many examples where behavior of real geotechnical structures are compared. Eventhough, relatively little attention has been given to effects of material modeling on the results from analysis. The major advantage of the proposed model including simulation of both structure and soil is that the description of the soil model is both linear and non-linear which allows basic mechanical responses to be predicted accurately. Moreover, all parameters

used in the model have explicit physical meanings and can be calibrated through laboratory tests. On the other hand the main limitations of the model is that due to linear effects the predictability using linear material model can cause over prediction of the critical strength at high deformation values. The best algorithm of soil modeling is the one that combines computational efficiency with acceptable accuracy. Since analytical solution is not always available all elastoplastic models are implemented with some negligible error.

References

[1] Darve, F., Incrementally non-linear constitutive relationships. Geomaterials, Constitutive Equations and Modelling, 1990: p. 213-238.

[2] Cambou, B. and C. Di Prisco, Constitutive modelling of geomaterials2000: Hermes Science Publications.

[3] Herle, I., „On basic features of constitutive models for geomaterials". Journal of Theoretical and Applied Mechanics, 2008. 38(1-2): p. 61-80.

[4] Chi, L. and R. Kushwaha, A non-linear 3-D finite element analysis of soil failure with tillage tools. Journal of Terramechanics, 1990. 27(4): p. 343-366.

[5] Rowe, P. and K. Peaker, Passive earth pressure measurements. Geotechnique, 1965. 15(1): p. 57-78.

[6] Drucker--, D., W. Prager, and H. Greenberg, Extended limit design theorems for continuous media. Quart. Appl. Math, 1952. 9(4): p. 381-389.

[7] Loret, B. and J.H. Prevost, Accurate numerical solutions for Drucker---Prager elastic-plastic models. Computer Methods in Applied Mechanics and Engineering, 1986. 54(3): p. 259-277.

[8] Krieg, R. and D. Krieg, Accuracies of numerical solution methods for the elastic-perfectly plastic model. ASME, Transactions, Series J-Journal of Pressure Vessel Technology, 1977. 99: p. 510-515.

[9] Ghorbani, Javad, and David W. Airey. "Some aspects of numerical modelling of hydraulic hysteresis of unsaturated soils." Unsaturated soils: behavior, mechanics and conditions. Nova Science Publishers, 2019. 41-78.

[10] Zhang, Zhidong, Mickaël Thiery, and Véronique Baroghel-Bouny. "Numerical modelling of moisture transfers with hysteresis within cementitious materials: Verification and investigation of the effects of repeated wetting–drying boundary conditions." Cement and Concrete Research 68 (2015): 10-23.

[11] Nyssen, C., An efficient and accurate iterative method, allowing large incremental steps, to solve elasto-plastic problems. Computers & Structures, 1981. 13(1–3): p. 63-71.

[12] Kodama, N. and K. Komiya, Model Experiment and Numerical Modelling of Dynamic Soil-Structure Interaction, in Materials with Complex Behaviour, A. Öchsner, L.F.M. Silva, and H. Altenbach, Editors. 2010, Springer Berlin Heidelberg. p. 269-276.

[13] ANSYS. Fem Software. 2006.

EXPERIMENTAL INVESTIGATION OF SEISMIC BEHAVIOUR OF EXISTING MASONRY INFILLS

Riccardo R. Milanesi [1], Maithree Kurukulasuriya [2], Davide Bolognini [1], Luca Grottoli [1], Filippo Dacarro [1], Paolo Morandi [1]

[1] *European Centre for Training and Research in Earthquake Engineering,*
{riccardo.milanesi,davide.bolognini, luca.grottoli, filippo.dacarro, paolo.morandi}@eucentre.it
[2] *IUSS Pavia, University of Advanced Studies of Pavia, maithree.kurukulasuriya@iusspavia.it*

Abstract

The seismic vulnerability of masonry infills has been observed persistently during post seismic surveys, and their seismic behaviour has been investigated for decades due to its complexity involving different aspects that need to be addressed and the diversity of existing masonry infill typologies. Despite the copious experimental studies conducted, only a few of them had the opportunity to analyse different aspects of the same masonry typology due to the reduced number of specimens usually involved in a testing campaign. The out-of-plane response of masonry infills, and the reduction of the out-of-plane resistance of the infill panels due to the damage caused by in-plane deformations, are usually the most critical aspects regarding life safety. Furthermore, the out-of-plane experimental tests on masonry infills have almost always been conducted through pseudo-static tests with different loading techniques (4 point loading, central loading, constant pressure with airbags or other systems), meanwhile a complete experimental campaign on existing masonry infills through dynamic tests on a shaking table has not taken place yet.

Within this framework, an experimental campaign focusing on non-ductile infill specimens made of horizontally hollowed weak clay units representing one of the most common infill systems present in Italy, is currently ongoing at the Eucentre Foundation of Pavia. In the present paper, the results from the first phase of the ongoing study will be discussed. In the scope of this research program, in-plane cyclic tests and out-of-plane dynamic tests are conducted on full-scale infill panels built inside single storey single bay composite steel/reinforced concrete frames, along with tests of characterization of the masonry materials. The first phase of tests included five specimens, four of them built with all edges bonded to the frame and one specimen with free vertical edges. The four specimens with the same boundary conditions were used to characterize the pure in-plane behaviour, the pure out-of-plane behaviour, and the out-of-plane behaviour with previous in-plane damage. The specimen with the vertical edges free was subjected to pure out-of-plane excitation to explore the one-way bending/arching behaviour of infills.

Keywords: Masonry infills, Existing infills, Shaking table tests, In-plane, Out-of-plane, Seismic behaviour

1. Introduction

The poor performance and severe damage repeatedly observed in masonry infilled frame structures during earthquakes have posed significant threat to life safety and led to major economic losses [1, 2, 3]. In the last decades, extensive research has been carried out to explore and improve the seismic behaviour of masonry infills, which is inherently complex due to many interrelated aspects required to be considered. The seismic behaviour of infills has been studied in the literature mainly in terms of their in-plane response [4, 5, 6], out-of-plane response [7, 8, 9], and the interaction between in-plane and out-of-plane behaviour [10, 11, 12, 13], considering the influence of the infill typology and masonry properties, aspect ratio, boundary conditions, frame properties, local interaction between the panel and the frame, and the global response of the structure. Despite the attention that masonry infills have received over the last few decades, guidelines provided for masonry infills in current seismic codes are rather general [14, 15]. Infills are usually assessed as non-structural elements and their safety is verified

without giving special consideration to infill typology or structural configuration. Thus, expanding the current experimental database is crucial for more accurate seismic assessment of masonry infills.

The study reported in this paper was contrived to fully characterize the seismic behaviour of an infill typology which was commonly used between the 1960s-1980s in Mediterranean countries as enclosures and partitions in reinforced concrete frame structures which are typically not designed for seismic actions. The typology consists of horizontally perforated hollow clay masonry units of 8- 12 cm thickness, often in two layers of walls with a cavity in between. Such a type is recognized as "weak" infills due to its high percentage of perforation and slenderness introduced from the small thickness. In the present study, five single leaf infill panels have been constructed within steel/concrete composite single storey single bay frames; four specimens fully bonded to the frame in all edges and one specimen with two vertical gaps around 25 mm between the panel and the columns. The infills were 13 cm thick, including a 10 mm thick layer of plaster on one side. Out of the four specimens fully adhered to the frame, one was tested purely in-plane and another purely out-of-plane. The remaining two were first subjected to different levels of in-plane drifts and subsequently to out-of-plane excitation to study the influence of the level of previous in-plane damage on the out-of-plane capacity. The specimen with free vertical edges was tested in the out-of-plane direction, to investigate the out-of-plane arching mechanism in a single vertical bending wall. The in-plane tests were displacement-controlled pseudo-static cyclic tests at increasing target drifts and the out-of-plane tests were shake table dynamic tests with incremental peak floor accelerations applied until collapse. The results of the in-plane tests are reported in terms of force-displacement curves, drift capacity, damage propagation and performance levels. For out-of-plane tests, the recorded accelerations and displacements, the damage evolution and failure mechanisms observed during the tests, and the effect of boundary conditions and previous in-plane damage, are elaborated.

2. Experimental Programme

2.1 Description of specimens

The first phase of the experimental campaign consisted of tests on 5 infill specimens, herein after referred to as T1, T2, T3, T4 and T5. The structural frames in which the masonry infills were built were fabricated with steel C-sections filled with reinforced concrete, such that the infill boundaries are in contact with the reinforced concrete surface as shown in Fig. 1(a). The frame was designed to represent a single story single bay of an existing frame structure, and to remain undamaged during the tests, which enabled reuse of the frames in the subsequent phases of the experiment. The infills were built with horizontally perforated 12 cm thick 25 x 25 cm units (Fig. 1(b)), laid in running bond with 10 mm thick mortar joints. The head joints were poorly filled as seen in Fig. 1(c) to reflect the common Italian construction practices during 1960-1980. The infill panels were 3.5 m long and 2.75 m high with an aspect ratio of 1.27. Representing one leaf of a double wythe wall, the panel was plastered on one side with a thickness of 10 mm, and the resulting total thickness of the panel was 13 cm. The bond between the panel and the frame was achieved by applying a mortar joint. Four specimens (T1-T4) were fully adhered to the frame continuously along the boundaries. The specimen with the vertical gaps (T5) was bonded to the frame along the top and bottom horizontal edges to the frame beams. The vertical gaps were approximately 25 mm each and continuous along the entire height of the panel.
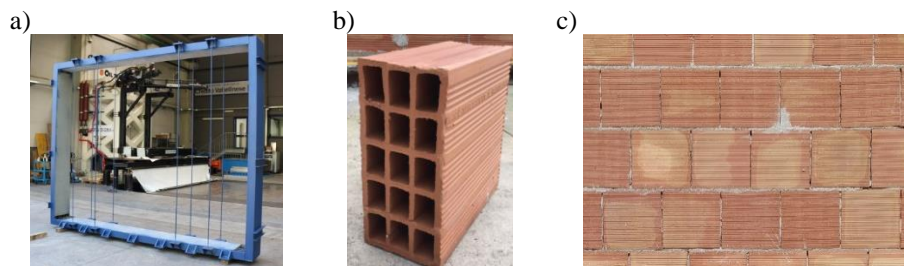
Figure 1. a) Steel concrete composite bare frame; b) Horizontally perforated units; c) poorly done head joints

2.2 Mechanical characterisation of units, mortar, and masonry

A comprehensive series of tests was carried out to determine the mechanical properties of units, mortar and the masonry. According to current standard provisions the resistance in compression of the units [16], the flexural and compressive resistance of the mortar [17], and the mechanical behaviour of the masonry in terms of vertical and horizontal resistance with and without plaster [18], diagonal compression test to determine the tensile resistance [19], pure shear tests [20] and flexural tests [21] have been conducted.

2.3 Test setup and instrumentation

The test setup and instrumentation were designed uniquely for the in-plane and out-of-plane tests. The in-plane tests were realized by applying pseudo static drift cycles in displacement control through a servo-hydraulic actuator supported by a strong steel frame. To restrain the out-of-plane movement of the frame at the top, four inclined steel braces (two in each side) have been used, connected to the top two corners of the frame and supported on the floor. The specimen was rigidly fixed to the floor through a steel beam foundation. The shake table has been used as a strong floor for the in-plane tests, which was kept stationary during the static tests with an active control. Such a disposition was necessary in order to conduct the entire test sequence on a specimen in one location, thus avoiding damage to the specimen due to transportation.

The out-of-plane excitations were applied to the specimen through the shake table, during which the actuator used for the in-plane tests was disconnected and the out-of-plane restraints remained attached. The schematic diagram and a picture of the full test setup is shown in Fig. 2(a) and (b).

a)　　　　　　　　　　　　　　　　　b)
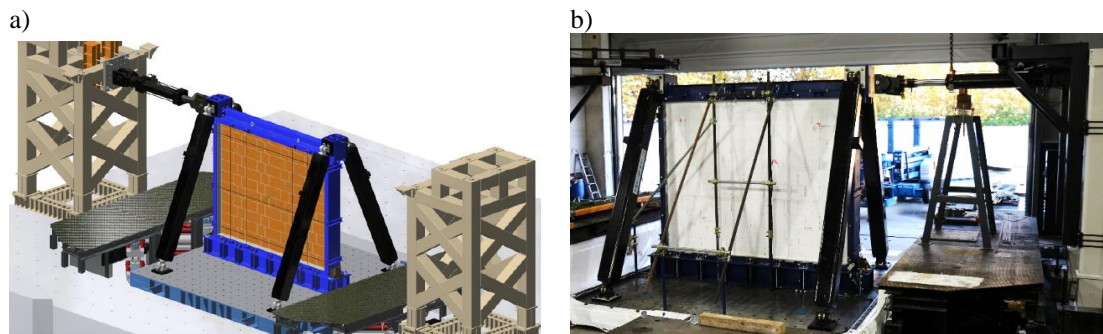
Figure 2. a) Schematic diagram of the test setup; b) actual configuration

The response of the entire specimen, i.e., the structural frame and the infill panel, was measured during the in-plane and out-of-plane tests. For the pseudo static cyclic in-plane tests, linear transducers were installed as shown in Fig. 3 to measure the applied displacements and the consequent drift. During dynamic tests, the out-of-plane accelerations were recorded through accelerometers placed along the length at mid height and along the height at centre as shown in Fig. 4(a). The out-of-plane displacements were monitored through an optical acquisition system with markers (Fig. 4(b)) and high-resolution infrared cameras.
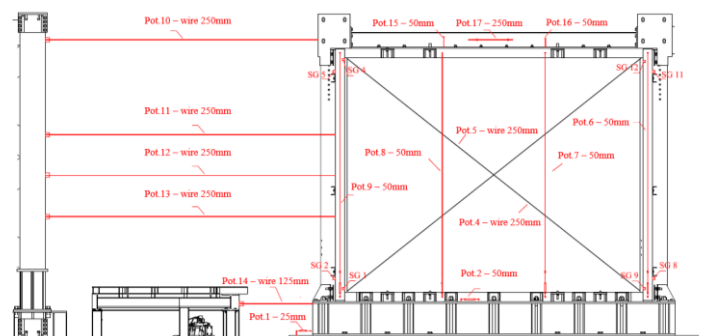
Figure 3. Instrumentation installed for the in-plane tests
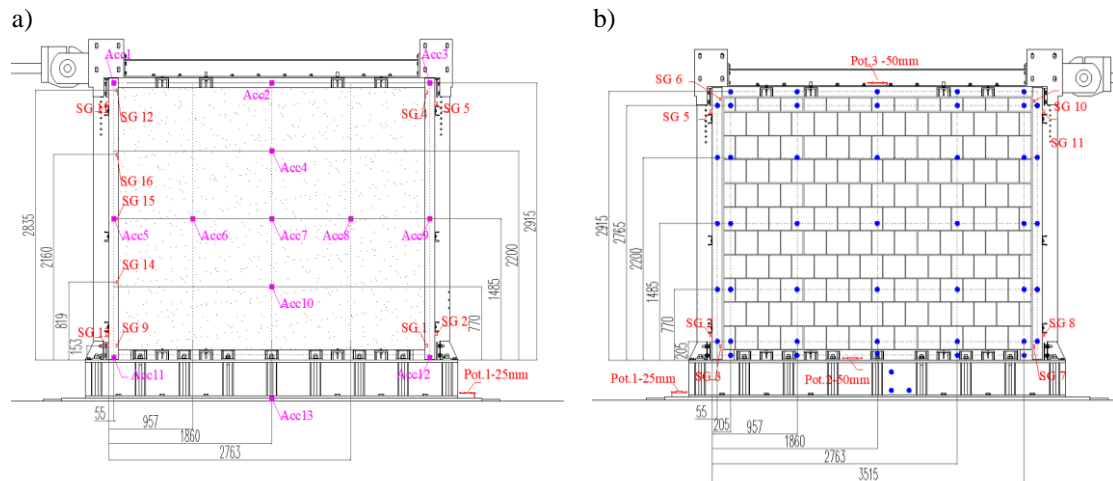
Figure 4 The layout of a) accelerograms; b) optical markers for the out-of-plane tests

2.4 Loading Protocol

The in-plane static cycles were applied with increasing target drift levels, and the cycles were repeated three times for each drift level. It should be noted that before the tests on the infilled specimens, all the bare frames were subjected to a maximum drift of 1.5%, which was the expected maximum drift for the infilled specimen. By subjecting the bare frames to the same drift level prior to tests on infills, it was aimed to bring all the bare frames to the same level of damage and thereby stiffness, ensuing a similar performance among them during the subsequent tests on infills. As will be elaborated later on with force-displacement curves obtained, it is important to emphasize that all the bare frames remained within the elastic region during the tests.

Then, the infills been constructed within the frame and the in-plane tests were performed on specimens T1, T2 and T3. Specimen T1 was loaded till its ultimate conditions were reached, incrementally increasing the target nominal drift up to 1.0%. The specimens T2 and T3 were stopped at nominal drift levels of 0.3% and 0.65% respectively, to be followed by out-of-plane tests to study the influence of the different levels of in-plane damage on the out-of-plane response.

Out-of-plane dynamic tests were performed on specimens T2, T3, T4 and T5 till the ultimate conditions were reached. The dynamic excitations were applied through the shake table in the out-of-plane direction only. The signals have been applied in the form of a target spectrum adapted from the Required Response Spectrum (RRS) method given in [22], with an incrementally increasing peak floor acceleration (PFA). The frequency range of the plateau of the target spectrum obtained with the RRS method was modified according to the methods proposed in [23], considering floor response spectra (FRS) from a series of nonlinear dynamic analyses performed on infilled frames with different heights (more details of the nonlinear dynamic analysis can be found in [24]). A summary of the loading protocols for in-plane and out-of-plane tests is presented in Table 1 and 2, respectively.

Table 1 – Summary of the in-plane tests

Nominal drift (%)	0.1	0.2	0.3	0.4	0.5	0.65	0.75	1.0
T1	x	x	x	x	x	-	x	x
T2	x	x	x	-	-	-	-	-
T3	x	x	x	x	x	x	-	-

Table 2 – Summary of the out-of-plane tests

Nominal drift (%)	0.10	0.20	0.30	0.40	0.50	0.60	0.70	0.75	0.80	1.00	1.25	1.50	1.80	2.00	2.25	2.50
T2	x	x	x	x	x	-	-	x	-	x	x	x	x	x	x	x
T3	x	x	x	x	x	-	-	x	-	x	x	x*	-	-	-	-
T4	x	x	x	-	x	-	-	x	-	x	x	x	x	-	-	-
T5	x	x	x	x	x	x	x	-	x	x	-	-	-	-	-	-

*Test repeated 3 times

3. Results

The experimental results will be presented in terms of the damage propagation in the infills in all tests, force-displacement response of in-plane tests, and the recorded displacements and accelerations in the out-of-plane tests.

3.1 In-plane response

The specimen T1 has been subjected to increasing in-plane cyclic drifts until ultimate conditions were reached. According to the level of damage experienced by the infill panel with increasing drift, damage limit states have been defined as operational, damage, life safety and ultimate. The horizontal boundaries were the first to crack at the starting nominal drift of 0.1%, although rather sporadically, followed by the fist main diagonal crack and continuation of the cracks along the boundaries at 0.2% nominal drift. At 0.3% it was deemed that the operational limit state has been reached, with two more diagonal cracks appearing along with a horizontal cracking zone above the 2nd course, accompanied by slight spalling of the plaster around some cracks. The damage state observed on each side of the specimen, i.e., bare and plastered, at 0.3% nominal drift is illustrated in Fig. 5(a) and (b). When the nominal drift was increased to 0.4%, large pieces of plaster was spalling around the horizontal crack and new diagonal cracks appeared as depicted in Fig. 5(c) and (d), the damage limit state was pertinent in this stage. Cracking of unit face shells, spreading and widening of the diagonal and horizontal cracks, and more spalling of plaster were observed at a nominal drift of 0.5%, which exacerbated at 0.75% with new cracks along bed joints, and pieces of units entirely detaching from the infill in the cracked zone. Therefore, life safety limit state was assumed at 0.75% nominal drift, and the damage state is illustrated in Fig. 5(e) and (f). The ultimate limit state was reached at 1.0% nominal drift, the infill having lost its robustness by losing most of the plaster and units around the main cracks. The level of damage was similar in specimens T2 and T3 for each level of nominal drift, the only difference was that the horizontal cracking zone was around the mid height of the wall, which is more conforming in a panel fully adhered to the frame. In specimen T1, it is likely that a local weakness shifted the damage to the lower courses.

The force-displacement cycles of specimen T1 are reported along with the backbone curves in Fig. 6(a). It should be noted that the backbone curve for the infill panel is derived by subtracting the response of the bare frame from the full response of the frame and the infill. As it was mentioned previously, the response of the bare frame remained elastic at all drift levels considered. A comparison of the backbone curves of the infill panels (only) for specimens T1, T2 and T3 is presented in Fig. 6(b).

a)

b)

c)

d)

e)

f)
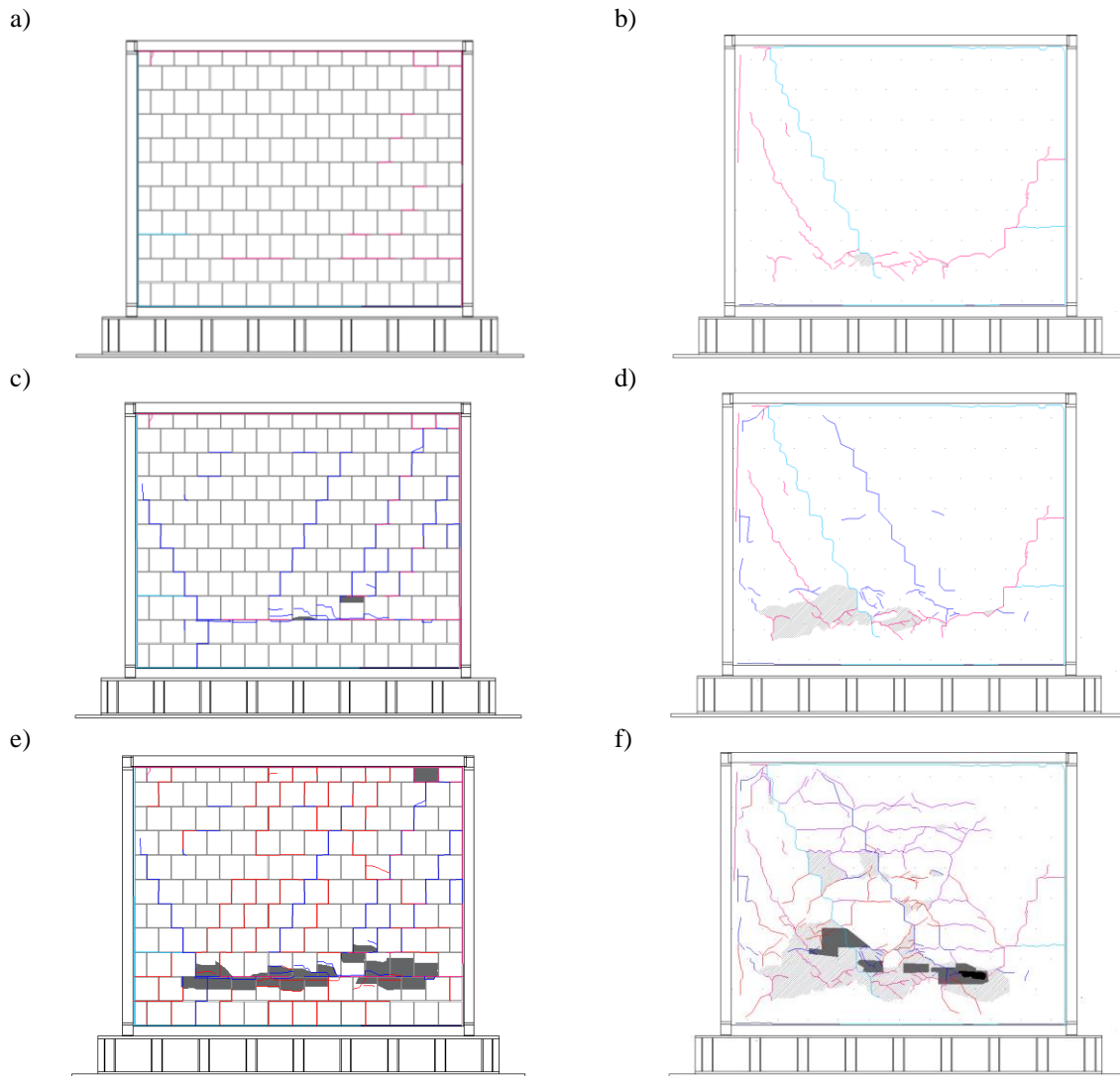
Figure 5. The damage state of the infill (a) bare face at 0.3% (b) plastered face at 0.3% (c) bare face at 0.4% (d) plaster face at 0.4% (e) bare face at 0.75% (f) plaster face at 0.75% drifts. (grey shade represent damage in the plaster, black shade stands for damage in the clay unit)

a)

b)
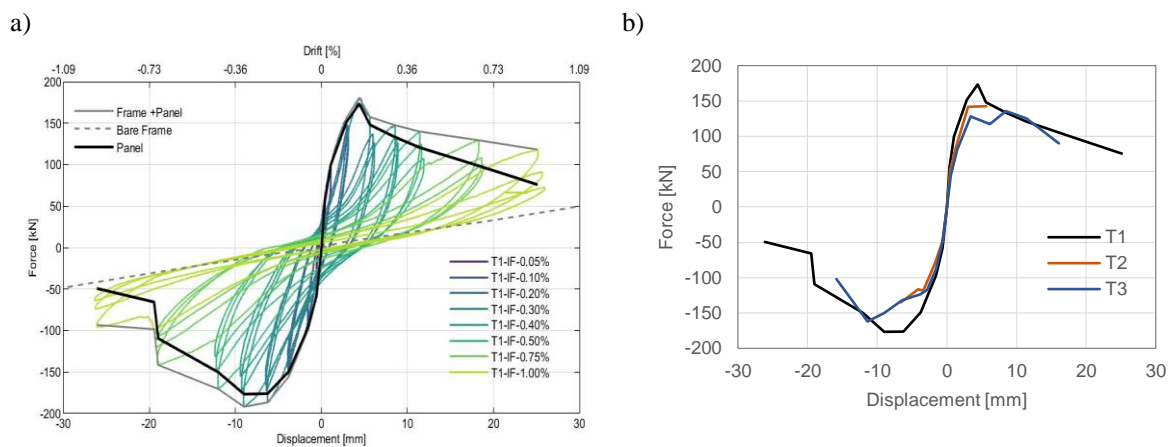
Figure 6. (a) The force-displacement cycles of specimen T1 (b) Force-displacement backbone curves derived for infill panels

3.2 Out-of-plane response

Specimens T2, T3, T4 and T5 have been subjected to out-of-plane acceleration signals with increasing amplitude till ultimate capacity was reached. Specimens T2 and T3, having previous in-plane damage (at drift levels 0.3% and 0.65%) suffered the most damage and then reached collapse at nominal PFA 2.5g and 1.5g (recorded PFA of 2.75g and 1.69g), respectively. The level of in-plane damage greatly influenced the out-of-plane capacity of the infills, with the maximum acceleration recorded at the centre of the panel reducing by 42% for the specimen T3 with respect to specimen T2. The existing damage caused by in-plane cycles propagated during the out-of-plane shaking, with widening of existing cracks, spalling and expulsion of plaster and units in the damage zone at mid height and at the top boundary. As example, the damage state succeeding the in-plane cycles and before the dynamic tests of T3, compared with the damage state attained before out-of-plane collapse is presented in Fig. 7.
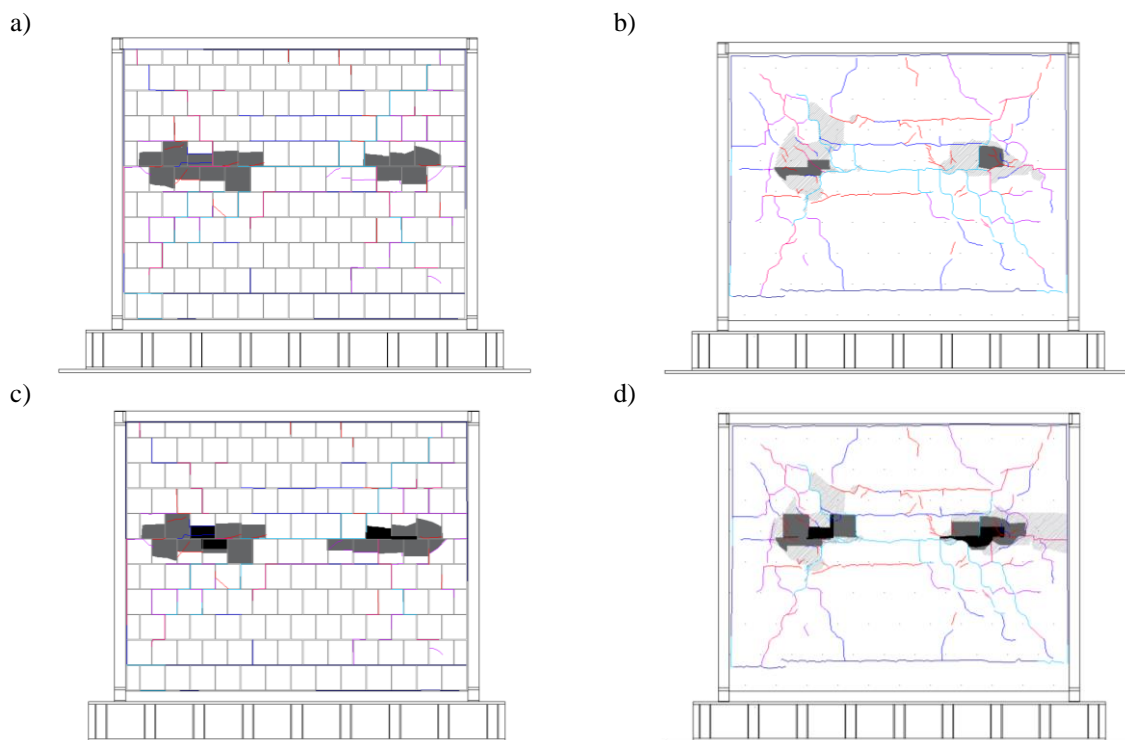
Figure 7. Damage state attained in specimen T3 after in-plane drift of 0.65% (a) bare face (b) plaster face and before collapse as seen on (c) bare face (d) plaster face

Without having any previous in-plane damage, specimen T4 was more robust and stronger, and did not exhibit any significant damage till 1.8g nominal PFA or reach collapse. The specimen presumably exhibited a double bending/arching mechanism, which is also perceived in the acceleration and displacement along the length at mid-height and along the height at centre profiles at maximum response with increasing PFAs (Fig. 8 and 9).

The behaviour of specimen T5 differed from the other specimens due to having free vertical edges. The specimen was subjected to only out-of-plane excitation without any previous in-plane damage, and the maximum acceleration on the panel was reached at the centre at a nominal PFA of 0.6g (recorded PFA 0.7g) without collapse. The behaviour of the panel during the tests resembled a single vertical bending/arching behaviour, also inferred from the damage pattern consisting of horizontal cracks along the top and bottom edges and along the bed joints above 6th and 7th courses (close to mid height), spanning the whole length of the wall. Towards the latter ground motions with higher intensities, the damage to the top boundary intensified, resulting in a gap between the top edge and the frame, however the arching mechanism could still be observed when the infill boundary came into contact with the beam surface. The described behaviour could also be exemplified by the acceleration and displacement

profiles measured along the height at mid length (Fig. 10(a) and (b)). The shape of the acceleration profile is a noteworthy result, indicating that the applied horizontal load on the panel is not uniform but more triangular. The triangular shape of acceleration profiles was observed in all specimens, in both directions (along length and height) for double bending specimens (T2, T3 and T4), and along the height in specimen T5.

a)   b)
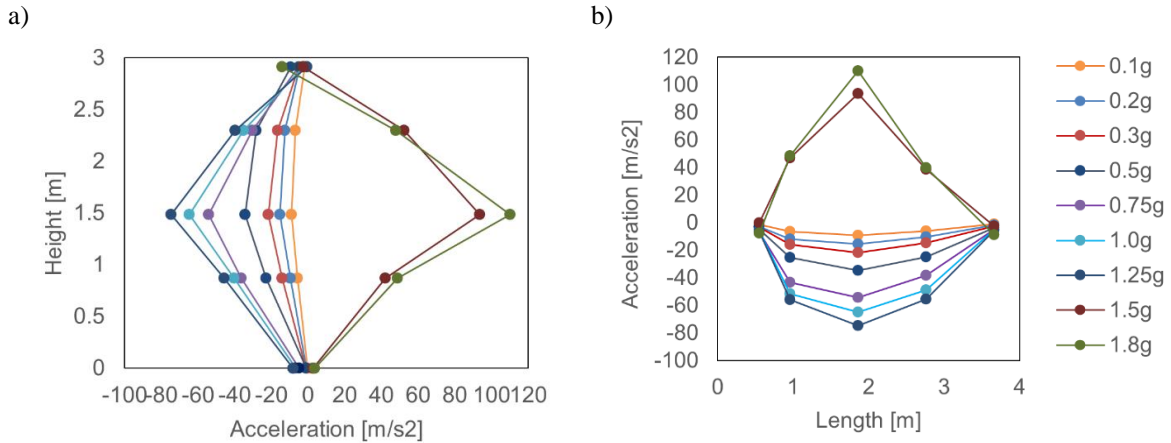
Figure 8. Acceleration profiles recorded on infill T4 (a) along height at centre (b) along length at mid-height

a)   b)
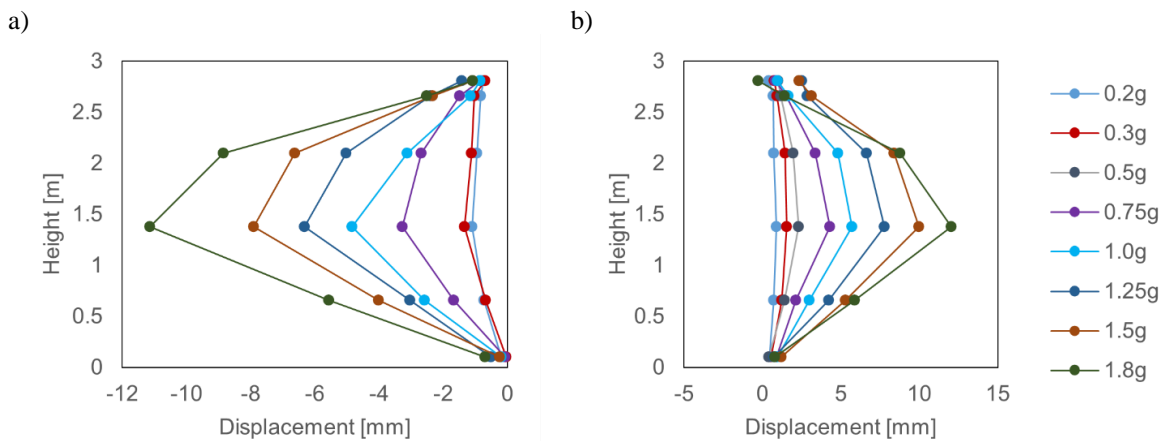
Figure 9. Displacement profiles recorded on infill T4 along height at centre (a) negative direction (b) positive direction

a)   b)
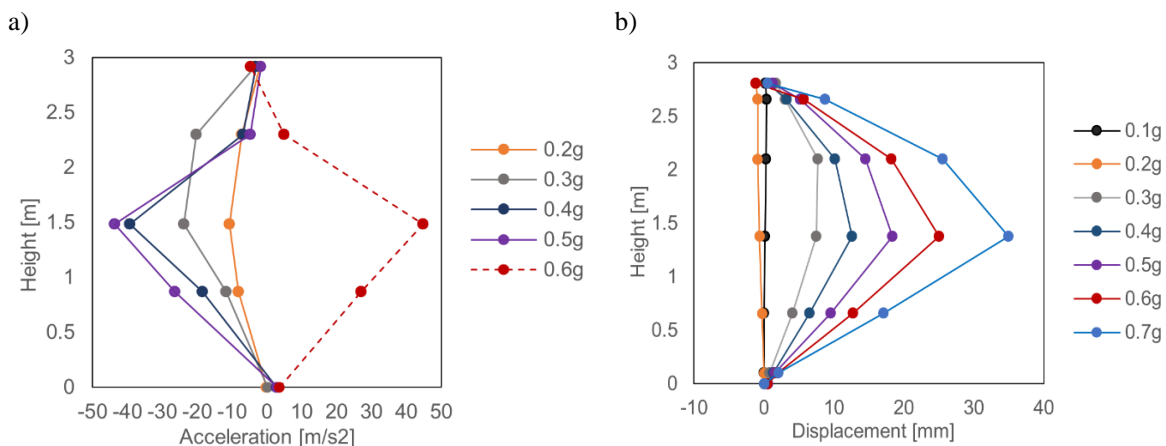
Figure 10 (a) T5 acceleration profile along the height (dashed line extrapolated profile from previous based on measured max acceleration at centre (b) Displacement profiles along height at maximum response in the positive direction

155

4. Discussion

The influence of the level of in-plane damage and the boundary conditions on the out-of-plane capacity of infills has been substantiated through the experimental results. Such effects could be further analysed through comparisons of the maximum accelerations recorded during the dynamic tests. In Fig. 11(a), the maximum recorded accelerations at the centre of the panel when the panel response was maximum (except for a few instances, the maximum response was always observed at the panel centre) with respect to the recorded PFA of the ground motion are presented, and the corresponding amplifications, i.e., the ratio of the maximum acceleration to the recorded PFA, are delineated in Fig. 11(b). The maximum accelerations in T4 are increasing almost linearly with the PFA, which can also be seen from the amplification, which fluctuates around a mean value of 5.85 not exceeding a variation of 5% from the mean. It should be kept in mind that the capacity has not been reached for T4, and at this stage no evident damage has been observed. On the other hand, specimens T2 and T3 reached collapse, and the drastic reduction of the capacity in the specimen with higher in-plane damage (T3) is prominent in terms of accelerations, reaching collapse much earlier at a lower PFA than the specimen with the lower damage (T2). Even though the amplification is also generally higher in the specimen T2 than T3, the variation is ambiguous with sudden drops and increases, while the variation is lower for specimen T3. It is also evident that the behaviour of specimen T5 with vertical bending is highly contrastive when compared to the fully supported specimens. Similarly, the maximum displacement at the centre of the panel is examined in Figure 12, and the results are consonant with the observations made hitherto. The reduction in stiffness is clearly observed decreasing from the undamaged specimen to the most damaged specimen, and the highest displacements are exhibited by the specimen with free vertical edges. Furthermore, from the damage patterns examined in the infills in the previous section, it could be inferred that the specimens fully connected to the surrounding frame exhibited a double bending/arching mechanism, and the specimen only connected to the top and bottom beams displayed single vertical bending/arching mechanism, when subjected to out-of-plane motions.

a) b)
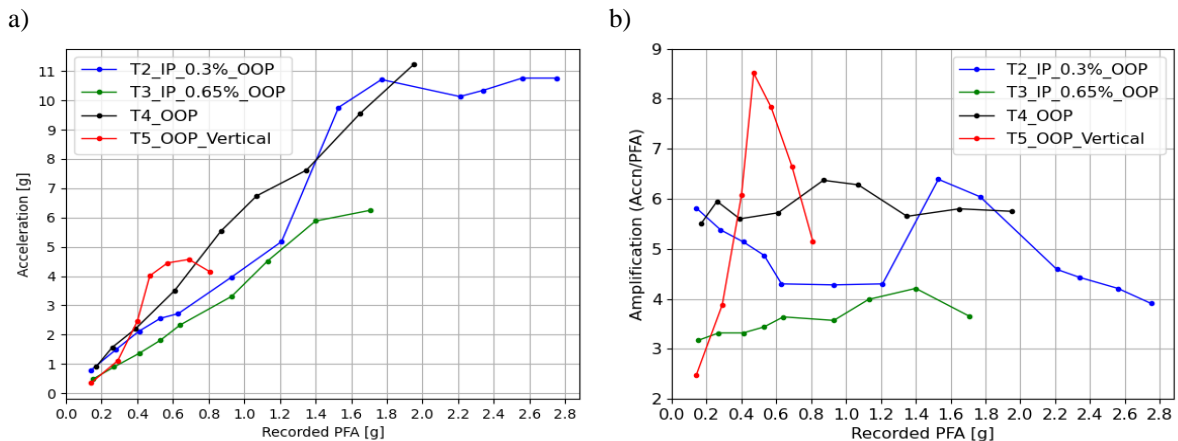
Figure 11. (a) Max acceleration at the centre vs recorded PFA (b) corresponding amplification at the centre with respect to recorded PFA
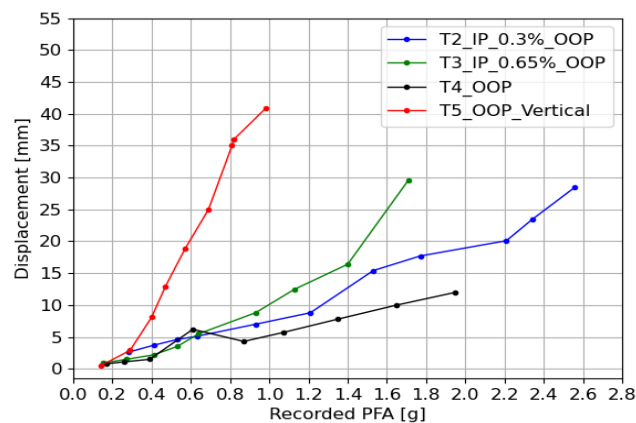
Figure 12. Max displacement at the centre vs recorded PFA

5. Conclusions

The seismic behaviour of an existing weak masonry infill typology has been investigated through an extensive experimental campaign, and the results from the first phase of the program have been presented and discussed. The first phase involved tests on five full scale masonry infill specimens surrounded by steel/concrete composite frames designed to simulate the behaviour of a r.c. existing structure. The in-plane behaviour, out-of-plane behaviour and the in-plane/out-of-plane interaction of infills fully adhered to the frame have been explored, and the out-of-plane behaviour of a vertically spanning specimen has been examined. The main observations from the test series are summarized as follows.

1.   An undamaged infill possesses a considerable out-of-plane capacity, which drastically reduced with the presence of previous damage due to in-plane loading.

2.   The boundary conditions of the panel significantly influence the out-of-plane response. The vertical spanning infill had a significantly lower stiffness compared to the fully supported infill exhibiting high displacements and had a lower out-of-plane capacity.

3.   The distribution of accelerations is not uniform over the panel but closer to being triangular. In double bending specimens the triangular distribution was two-way, and in the single bending specimen the distribution was observed along the vertical.

In the following phases of the experimental campaign, the seismic response of specimens with a thin gap at the top will be explored, as well as the influence of presence of openings on the seismic behaviour of infills.

Acknowledgements

References

[1] Braga, F., Manfredi, V., Masi, A., Salvatori, A., Vona, M. (2010) Performance of non-structural elements in RC buildings during the L'Aquila, 2009 earthquake, *Bulletin of Earthquake Engineering*, **9**(1), pp. 307–24.

[2] Hermanns, L., Fraile, A., Alarcón, E., Álvarez, R. (2012) Performance of masonry buildings during the 2011 Lorca earthquake, *Proceedings of 15th World Conference on Earthquake Engineering*, Lisbon, Portugal.

[3] Rossi, A., Morandi, P., Magenes, G., (2021) A novel approach for the evaluation of the economical losses to seismic actions on RC buildings with masonry infills, *Soil Dynamics and Earthquake Engineering*, **145**, pp. 106722, doi 10.1016/j.soildyn.2021.106722.

[4] Dawe, J. L., and Seah, C.K. (1989) Behaviour of masonry infilled steel frames, *Canadian Journal of Civil Engineering*. **16**(6), pp. 865-876. https://doi.org/10.1139/l89-129.

[5] Mehrabi, A. B., Benson Shing, P., Schuller, M. P., & Noland, J. L. (1996) Experimental Evaluation of Masonry-Infilled RC Frames, *Journal of Structural Engineering*, **122**(3), pp. 228–237.

[6] Morandi, P., Hak, S., Magenes, G., (2018) Performance-based interpretation of in-plane cyclic tests on RC frames with strong masonry infills, *Engineering Structures*. **156**(1), pp. 503–521. https://doi.org/10.1016/j.engstruct.2017.11.058.

[7] Abrams, D. P., Angel, R., Uzarski, J. (1996) Out-of-Plane Strength of Unreinforced Masonry Infill Panels, *Earthquake Spectra*, **12**(4), pp. 825–844.

[8] Furtado, A., Rodrigues, H., Arede, A., Varum, H. (2016) Experimental evaluation of out-of-plane capacity of masonry infill walls, *Engineering Structures*, **111**, pp. 48-63.

[9] Milanesi, R. R., Morandi, P., Hak, S., Magenes, G. (2021) Experiment-based out-of-plane resistance of strong masonry infills for codified applications, *Engineering Structures*, **242**, p. 112525.

[10] Angel, R., Abrams, D. P., Shapiro, D., Uzarski, J., Webster, M. (1994) *Behavior of reinforced concrete frames with masonry infills*, University of Illinois Engineering Experiment Station, College of Engineering, University of Illinois at Urbana-Champaign.

[11] da Porto, F., Guidi, G., Dalla Benetta, M., Verlato, N. (2013) Combined in-plane/out-of-plane experimental behaviour of reinforced and strengthened infill masonry walls, *Proc. 12th Canadian Masonry Symposium*, Vancouver, Canada

[12] Ricci, P., Di Domenico, M., Verderame, G. M. (2018) Experimental assessment of the in-plane/out-of-plane interaction in unreinforced masonry infill walls, *Engineering Structures*, **173**(1), pp. 960-978, doi 10.1016/j.engstruct.2018.07.033.

[13] Morandi, P., Hak, S., Milanesi, R. R., Magenes, G. (2022) In‐plane/out‐of‐plane interaction of strong masonry infills: From cyclic tests to out‐of‐plane verifications, *Earthquake Engineering Structural Dynamics*, **51**(3), pp. 648‐672.

[14] CEN (2004) *Eurocode 8 - Design of structures for earthquake resistance, Part 1: General rules, seismic actions and rules for buildings*, EN 1998-1, European Committee for Standardisation, Brussels, Belgium.

[15] NTC (2018) Istruzioni per L'applicazione Delle "*Nuove norme Tecniche per le Costruzioni" di Cui al Decreto Ministeriale 17 Gennaio 2018*, Ministero delle Infrastrutture e dei Trasporti, Circolare 20 Febbraio 2018, Italy. (In Italian)

[16] EN 772-1 (2015) *Methods of test for masonry units - Part 1: Determination of compressive strength*, Brussels, Belgium: CEN.

[17] EN 1015-11 (2019) *Methods of test for mortar for masonry - Part 11: Determination of flexural and compressive strength of hardened mortar*, Brussels, Belgium: CEN.

[18] EN 1052-1 (2001) *Methods of test for masonry - Part 1: Determination of compressive strength*, Brussels, Belgium: CEN.

[19] ASTM E519-02 (2017) *Test Method for Diagonal Tension (Shear) in Masonry Assemblages*, ASTM International.

[20] EN 1052-3 (2001) *Methods of test for masonry – Part3: Determination of initial shear strength*, Brussels, Belgium: CEN

[21] EN 1052-2 (2016) *Methods of test for masonry - Part 2: Determination of flexural strength*, Brussels, Belgium: CEN.

[22] AC 156 (2010) *Acceptance criteria for seismic certification by shake-table testing of nonstructural components*, International Code Council. (n.d.).

[23] Milanesi, R. R., Morandi, P., Dacarro, F., Albanesi, L., Magenes, G. (2017) In-plane cyclic and out-of-plane dynamic testing procedures for infilled RC frames, *Proc. 7th International Conference on Advances in Experimental Structural Engineering*, Pavia, Italy.

[24] Hak, S., Morandi, P., Magenes, G., Sullivan. T.J. (2012) Damage control for clay masonry infills in the design of RC frame structures, *Journal of Earthquake Engineering*, **16**(1), pp. 1-35.

BEHAVIOUR OF MASONRY INFILLS WITH DOOR OPENINGS UNDER SEQUENTIAL IN-PLANE AND OUT-OF-PLANE LOADING

Aleksa Milijaš [1], Bogdan Šakić [2], Marko Marinković [3], Christoph Butenweg [4], Matija Gams [5], Sven Klinkel [6]

[1] *PhD Student, Chair of Structural Analysis and Dynamics, RWTH Aachen University, Aachen, Germany, e-mail address: milijas@lbb.rwth-aachen.de*

[2] *PhD Student, Chair of Structural Analysis and Dynamics, RWTH Aachen University, Aachen, Germany, e-mail address: sakic@lbb.rwth-aachen.de*

[3] *Assistant Professor, Chair of Engineering Mechanics and Theory of Structures, Faculty of Civil Engineering, University of Belgrade, Belgrade, Serbia, e-mail address: mmarinkovic@grf.bg.ac.rs*

[4] *Professor, Center of Wind and Earthquake Engineering, RWTH Aachen University, Aachen, Germany, e-mail address: butenweg@lbb.rwth-aachen.de*

[5] *Assistant Professor, Department of Structural and Earthquake Engineering, Faculty of Civil and Geodetic Engineering, University of Ljubljana, Ljubljana, Slovenia, e-mail address: matija.gams@fgg.uni-lj.si*

[6] *Professor, Chair of Structural Analysis and Dynamics, RWTH Aachen University, Aachen, Germany, e-mail address: klinkel@lbb.rwth-aachen.de*

Abstract

Reinforced concrete (RC) frame structures with masonry infills are common in seismic-prone regions. Masonry infills are activated in in-plane and out-of-plane directions under seismic loading and often damaged during earthquakes. Several recent investigations have shown that the combined effects of in-plane and out-of-plane loads are particularly dangerous for masonry infills. However, most of these studies focused on solid infills, and there is little information about the influence of openings on the seismic performance of infills, even though openings may alter the seismic performance of infilled frames significantly. This paper presents results of two experimental tests carried out on masonry infills with full-height door openings. One was tested under pure out-of-plane load, and the second one with sequential in-plane and out-of-plane loads. Thereafter, results of these two tests are compared with experimental findings obtained from two experimental tests with similar loading protocol conducted on solid masonry infills. Results of the study demonstrate the deteriorating effect of door openings, especially under combined in-plane and out-of-plane loads. The results also highlight a need for practical solutions for damage prevention in both infills with and without openings.

Keywords: *Seismic loading, In-plane load, Out-of-plane load, Interaction, Door opening*

1. Introduction

Masonry infills are non-load bearing masonry walls that are frequently installed as outer walls or inner partitions in RC frame buildings. As they are erected after the casting of the bounding frame (columns and upper and lower beams or slabs), they do not take part in the transfer of vertical loads. However, in the case of an earthquake event masonry infills are subjected to in-plane, out-of-plane and combined in-plane and out-of-plane seismic actions. Due to the rather complex seismic performance of infilled frames, most of the seismic codes consider masonry infills as non-structural elements, which is an unrealistic and non-conservative assumption.

Seismic performance of infilled frames has been investigated for more than seventy years. Results of some of the first experimental findings revealed that masonry infills significantly increase the in-plane stiffness and load capacity of RC frames [1,2]. This was followed by numerous experimental studies that focused on the in-plane performance of infilled frames [3-6]. Among various parameters investigated, openings were recognized to affect the in-plane behaviour of infilled RC frames most significantly because they can alter the stress field induced in the infill and thus change the infill failure mode [5,7]. In addition to this, in several experimental campaigns [8-10] the detrimental crack patterns on infills due to openings were observed, showing that openings had an adverse effect on the seismic safety.

In the pioneering studies on the out-of-plane behaviour of unreinforced masonry walls, McDowell et al. (1956a,b) [11,12] investigated experimentally the formation of the arching action within the wall, which has proven to be the load-resisting mechanism against out-of-plane seismic forces in masonry infills too. The findings on the out-of-plane behaviour of masonry infills were extended in [3,13,14]. Boundary conditions and slenderness ratio are recognized as the most influential parameters, while the effect of openings is still not clear, due to contradictory results from a limited number of studies [13,15,16].

However, particularly important for out-of-plane response of masonry infills are effects that can cause the reduction of out-of-plane capacity or even totally hinder the formation of arching action. Firstly, inappropriate execution of frame-infill mortar connections, especially the top connection, which is not the rare case in the practice, can be the reason for the worse out-of-plane behaviour of masonry infills, as reported in [15,17]. Furthermore, masonry infills at the lower and middle storeys can experience significant reduction of out-of-plane load capacity or even the complete out-of-plane failure due to the combined effects of in-plane and out-of-plane actions. This could be observed in recent earthquakes in L'Aquila, Italy (2009) and Albania (2019), where masonry infills obtained the life-threatening out-of-plane failures due to the in-plane and out-of-plane load interaction, as reported in [18-20].

One of the first studies on the effects of the prior in-plane damage on the out-of-plane behaviour of masonry infills were carried out by Angel et al. (1994) [3] and Flanagan and Bennett (1999) [21]. However, this topic has gained more attention recently and the number of experimental studies dealing with this topic increased. In experimental studies [22-26] mostly thin masonry infills used in the existing buildings in the Southern Europe were investigated. Reduction of out-of-plane capacity due to the prior in-plane damage was reported. Among these studies, interesting findings on the effect of the slenderness ratio [24] or aspect ratio [27] can be found. On the other side, less studies on the effect of the prior in-plane damage on the out-of-plane behaviour of modern strong masonry infill with larger thickness are available in the literature. Among them, Morandi et al. (2017) [28], Butenweg et al. (2019) [29] and da Porto et al. (2020) [30] observed the reduction of out-of-plane capacity due to the prior in-plane drifts too. Based on the available experimental database, some authors also proposed the reduction factors that could account for prior in-plane damage when estimating the out-of-plane capacity of masonry infills. Proposals for these reduction factors can be found in [23,31,32], for instance, but their correctness needs to be checked on the larger experimental database.

In addition to this, there is a clear gap in the experimental findings on the effect of the prior in-plane damage on out-of-plane behaviour of masonry infills with openings. This is somehow unjustified, as openings significantly affect the seismic performance of infilled RC frames. So far, da Porto et al. (2020) [30] carried out experimental tests on modern and thick masonry infills and Furtado et al. (2021) [16] investigated thin infills. Further experimental results on the topic are of the utmost importance for: a) the better understanding of the influence of the load interaction on masonry infills with different opening arrangements, b) validation of numerical results that can be used for extensive parametric studies and c) development of simple and practical approaches that could consider effects of the load interaction in seismic codes in the future.

In this paper the effects of prior in-plane damage on out-of-plane behaviour of masonry infills with full-height door opening are experimentally investigated. Out-of-plane behaviour of masonry infill with full-height door opening is first investigated in the pure out-of-plane test (T7). Afterwards, the behaviour of the same infill configuration is analysed in a sequential loading test (T8), in which masonry infill is first subjected to in-plane cyclic loads, which is followed by the out-of-plane load phase and the last in-plane load phase. Finally, in order to determine the effect of door opening, the experimental results obtained from these two tests are compared with experimental results of pure out-of-plane test (T1) and sequential loading test (T2) carried out on fully infilled RC frames [33]. The results of this study show that door openings further deteriorate the behaviour of infilled RC frames under interacting in-plane and out-of-plane loads.

2. Experimental campaign

2.1 Test specimens

The dimensions of the frame and masonry infill used in experimental tests are indicated in Fig. 1. The full-height door opening takes around 38 % of the wall surface. Masonry infill is built in line with the usual building practice. Thick hollow clay bricks with percentage of narrow vertical voids of around 56 % are used. Bed joints are filled with thin layer mortar, while head joints are executed as dry tongue and groove connections. The levelling layer and connections of masonry infill to the RC columns are made of mortar, while the gap between masonry infill and the top beam is filled with a thin layer mortar, which was inserted by a special hand pump. Due to this precise, but time-consuming execution, frame-infill connections at the top were exceptionally strong.
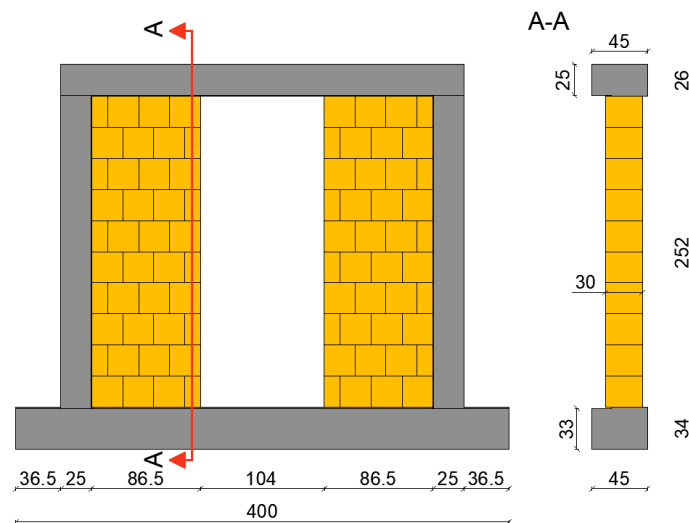
Figure 1. Test specimen
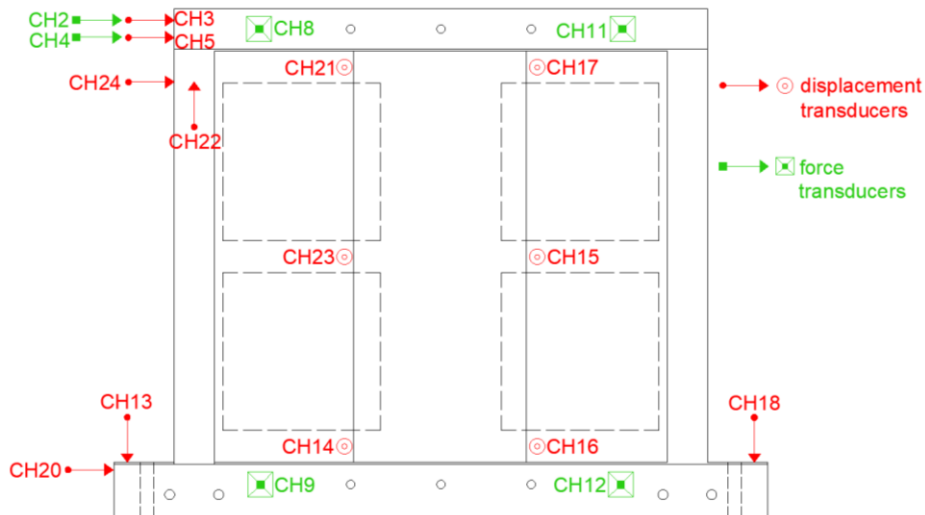
Figure 2. Position of measurement points and air bags on infilled frame with door opening

2.2 Test setup

Fig. 2 shows the specimen with position of force and displacement transducers. At the beginning of each test, vertical force of 200 kN per column is applied by one-way hydraulic actuators and it is kept constant throughout the test. In-plane loads are applied to the frame in a displacement-controlled manner by two servo-controlled hydraulic actuators, which are connected to a strong reaction wall on
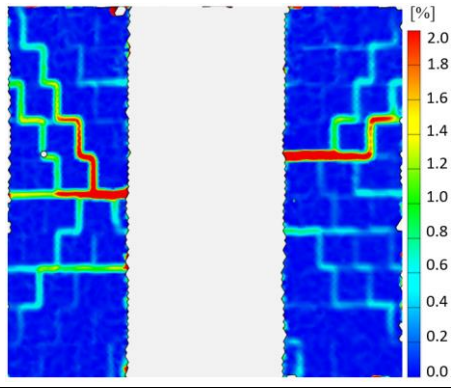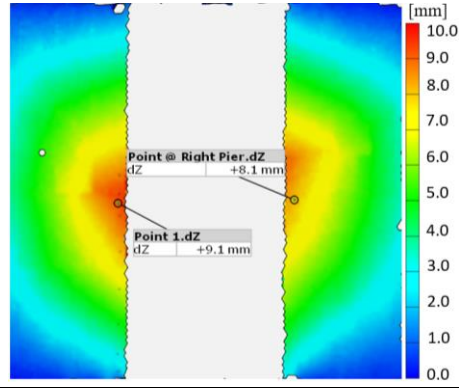
one side and to the top beam of the RC frame on the other side. Connection to the top beam is provided by a special harness with four steel tie rods that run along the top beam and that are connected to steel plate on the other side of the beam. These steel tie rods allow application of cyclic in-plane displacements (positive-push and negative-pull direction). Positions of two in-plane load actuators on the RC frame correspond to force transducers CH2 and CH4 on Fig. 2. Out-of-plane load is applied by inflating four air bags that are installed between the back side of the infill and the timber reaction wall. In Fig. 2 positions of air bags are presented with four dashed squares. Test setup is designed and constructed to allow the fast and simple application of in-plane and out-of-plane loads within the one test.

3. Experimental tests

3.1. Test T7 - Pure out-of-plane test

In test T7 out-of-plane load was imposed to the masonry infill with full-height door opening in six cycles. In Fig. 9a the load-displacement curve measured on the left infill pier is shown. Specimen responded linearly up to the out-of-plane force of around 60 kN in the second cycle, when the first light stepwise cracks appeared on the left pier. With the increase of out-of-plane load, more cracks through bed and head joints emerged leading to the further decrease of stiffness. In the last load cycle maximum out-of-plane force of 145.3 kN (33.6 kPa) was reached. The major strain propagation obtained by optical measurement system and measured out-of-plane displacements on both piers are shown in Table 1. They both depict the typical out-of-plane behaviour of masonry infill with strong connections to the frame along three sides. The load-resisting mechanism is strong vertical arching. In the last load cycle, due to the pronounced cracking and crushing of the bricks in the arc supports (Table 1, right), out-of-plane displacements increased significantly for the same level of out-of-plane force applied and the test was stopped due to the safety reasons. However, the reached out-of-plane force represents the high out-of-plane capacity for this masonry infill, which is explained by the low slenderness ratio of infill and its strong and stable connections to the surrounding frame.

Table 1. Selected experimental results at the maximum out-of-plane force of test T7

| Major strain at $F_{MAX,OOP}$ | OOP displacements at $F_{MAX,OOP}$ | Cracks in the bricks at $F_{MAX,OOP}$ |

3.2. Test T8 – Sequential in-plane and out-of-plane test

In test T8 masonry infilled RC frame with door opening was tested in three loading phases. In the first phase, cyclic in-plane displacements were applied to the specimen. Three load cycles were carried out for each level of in-plane displacement applied. After reaching 1.1 % of in-plane drift masonry infill experienced significant level of damage. Therefore, the specimen was unloaded and then loaded with seven cycles of out-of-plane loading in the second loading phase, in order to investigate the influence of the prior in-plane damage on the out-of-plane behaviour. This phase was terminated after reaching maximum out-of-plane force of 39.7 kN (9.2 kPa). In the third loading phase, cyclic in-plane displacements were applied again, up to the complete collapse of the infill at the 1.6 % of in-plane drift.
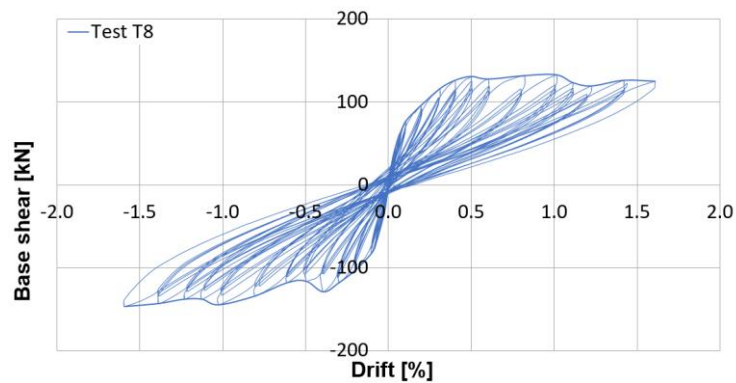
Figure 3. Hysteretic force-drift curve obtained from in-plane loading phases of test T8

The hysteretic curve obtained from in-plane loading phases is shown in Fig. 3. At the lower levels of in-plane drifts ($\Delta < 0.2$ %), the stepwise cracks already appeared in the bottom parts of both piers. At a drift of 0.5 % diagonal cracking through the middle parts of piers emerged and stepwise cracks through head and bed joints propagated in the upper part of piers too. In addition to this, the cracks due to the crushing of the corner bricks in the lowermost rows of bricks could be observed (Fig. 4). The maximum horizontal force in positive (push) direction was reached at 1.0 % of in-plane drift. With the increase of in-plane drifts, diagonal cracks widened (Fig. 5). In Fig. 6 triangular-like pieces of masonry defined by diagonal cracks that occurred due to the cyclically imposed in-plane displacements can be more clearly seen. These triangular-like pieces of the infill started to lose connection to the rest of the infill. Due to the significant damage at 1.1 % of in-plane drift, in-plane load was suspended.
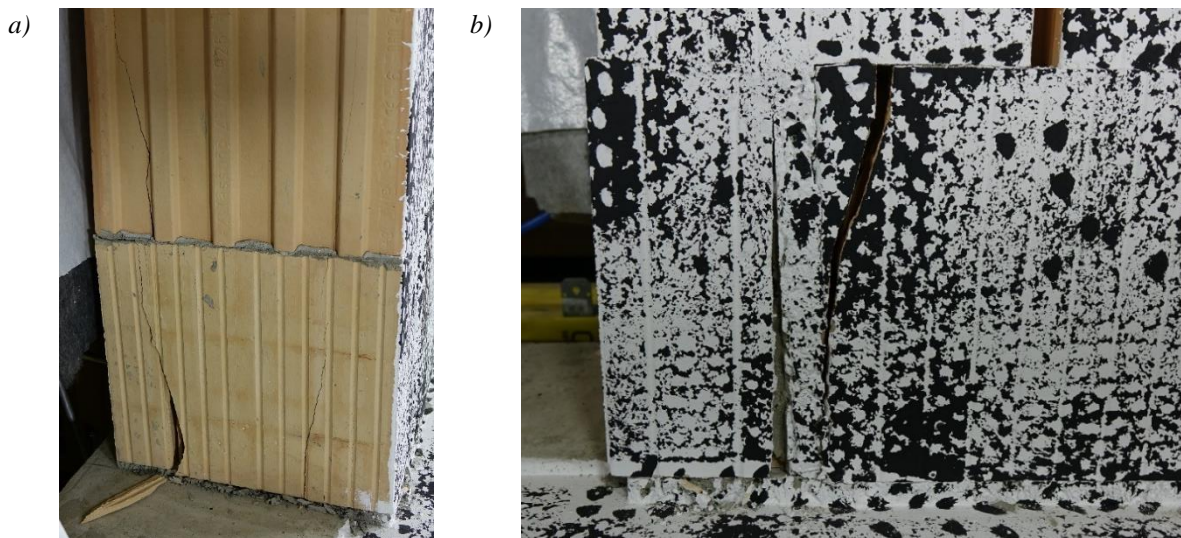
Figure 4. Cracks in the lowermost row of bricks ($\Delta = 0.5$ %): side view (a) and front view (b)

After the first in-plane loading phase, seven cycles of out-of-plane loading were applied. The out-of-plane load – displacement curve is shown in Fig. 9a. The maximum out-of-plane force of 39.7 kN was reached in the last cycle, which is only 27 % of the out-of-plane capacity of the masonry infill tested in test T7, which had no prior in-plane damage. In addition to this, the significant decrease of the out-of-plane stiffness can be noticed due to the prior in-plane damage. However, frame-infill connections remained in a quite good condition after the in-plane loading phase. Therefore, the boundary conditions for the vertical arching were provided. Table 2 shows selected experimental results at the maximum out-of-plane force of test T8. Due to the three-sided support and developed vertical arching in both piers, out-of-plane displacements were rather small with the largest values near the pier middle, at the pier edges. Larger out-of-plane displacements can be measured locally too, due to the detachment and initiation of the falling off of the brick outer shells, which already started under in-plane loads. Major strain propagation indicates that most of the cracks originate from the prior in-plane loading phase. Due

to increasing residual out-of-plane displacements and for safety reasons, out-of-plane loading phase was terminated.

Figure 5. Damage to masonry infill at 1.1 % of in-plane drift
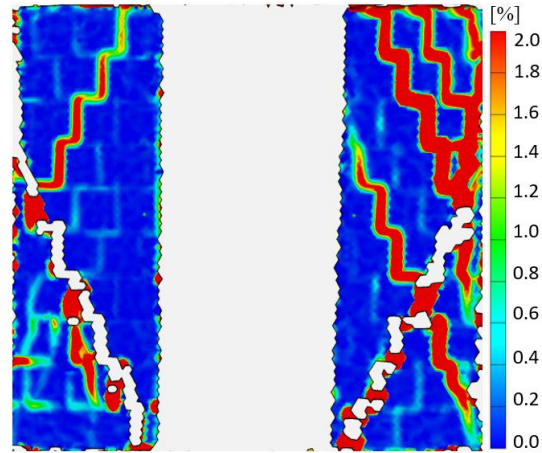
Figure 6. Major strain propagation at 1.1 % of in-plane drift

After the out-of-plane loading phase, one more in-plane loading phase was carried out to investigate the in-plane behaviour of the infilled frame with door opening. Already at 1.2 % of in-plane drift, diagonal cracks widened and more cracking through bricks could be observed. Furthermore, some brick outer shells fell off and the corner brick on the left infill pier was crushed (Fig. 7). The diagonal cracking propagated further with the increase of the applied in-plane displacements. Triangular-like masonry parts gradually lost their connection to the remaining parts of the infill, which resulted in a complete detachment and failure of the infill at 1.6 % of in-plane drift (Fig. 8). In addition to this, hysteresis curve obtained from in-plane loading phase shows that the in-plane force capacity remained almost constant in the second in-plane loading phase ($\Delta > 1.1$ %), due to the significant damage to masonry infill.

Table 2. Selected experimental results at the maximum out-of-plane force of test T8

OOP displacements at $F_{MAX,OOP}$	Major strain at $F_{MAX,OOP}$
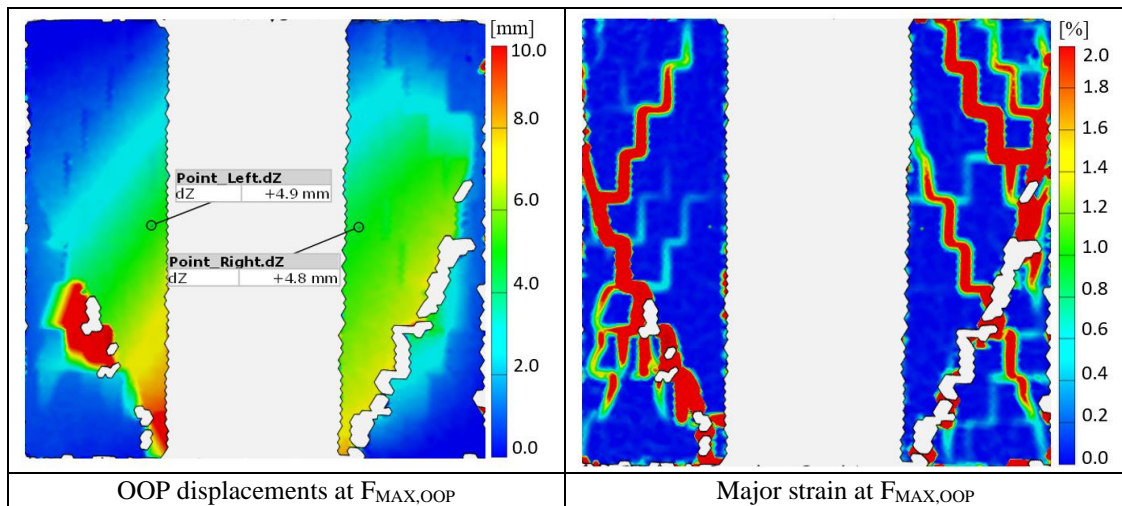
Figure 7. Damage to masonry infill at 1.2 % of in-plane drift

Figure 8. Collapse of masonry infill at 1.6 % of in-plane drift

4. Comparison of the test results

Fig. 9a shows load-displacement curves of out-of-plane test T7 and out-of-plane loading phase of test T8. In test T7 high out-of-plane capacity was reached due to the developed vertical arching action. Furthermore, in the first in-plane loading phase of test T8 frame-infill connections were not severely damaged and out-of-plane capacity was achieved due to the developed vertical arching too. However, due to the significant prior in-plane damage, out-of-plane capacity of masonry infill in test T8 is 3.7 times smaller than the out-of-plane capacity of masonry infill in test T7, which was tested under pure out-of-plane load only. In addition to this, effects of the prior in-plane damage can be seen in the significantly decreased out-of-plane stiffness of masonry infill in test T8.
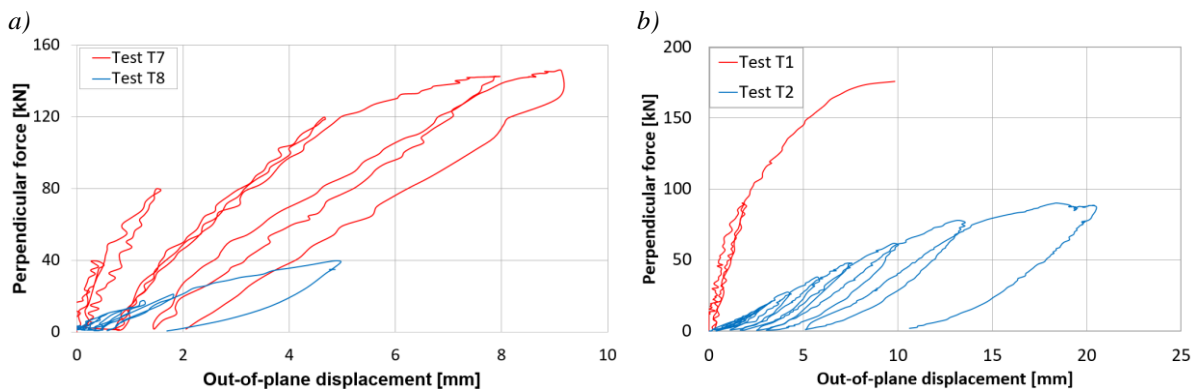
Figure 9. a) Load-displacement curves of test T7 and out-of-plane loading phase of test T8; b) Load-displacement curves of test T1 and out-of-plane loading phase of test T2 [33]

Tests with similar loading protocol were carried out on fully infilled RC frames within the same experimental campaign. Test T1 is a pure out-of-plane test, while in test T2 masonry infilled RC frame was firstly loaded in in-plane direction up to the 1.2 % of in-plane drift and then in out-of-plane direction. Further details can be found elsewhere [33]. Load-displacement curve obtained from test T1 and out-of-plane loading phase of test T2 are presented in Fig. 9b. In both tests high out-of-plane capacities were reached due to the developed two-way arching action in the wall, with dominant vertical arching. However, due to the prior in-plane damage in test T2, out-of-plane capacity was reduced around two times. Even larger reduction can be observed for the out-of-plane stiffness.

Furthermore, in Fig. 10 load-displacement curves obtained from out-of-plane loading phases of test T2 and test T8 are compared. It can be seen that masonry infill with door opening (test T8) reaches smaller out-of-plane load and displacement capacity than solid masonry infill (test T2). Moreover, the higher

reduction of out-of-plane capacity due to the in-plane damage is measured for masonry infill with door opening (test T8 - 3.7 times) than for solid masonry infill (test T2 - 2 times). The worse out-of-plane behaviour of masonry infill with door opening is attributed to the more pronounced in-plane damage in infill with door opening. Due to the centric full-height door opening, masonry infill in test T8 suffered more damage at 1.1 % of in-plane drift than solid masonry infill in test T2 at 1.2 % of in-plane drift. Furthermore, due to the door opening a specific crack pattern was formed in masonry infill, with triangular-like portions of masonry detaching from the rest of the infill. In masonry infill with door opening, diagonal cracking and crushing of edge bricks took part already at 0.5 % of in-plane drift, while solid masonry infill experienced more significant damage at around 1.0 % of in-plane drift.

In their extensive experimental campaign, da Porto et al. (2020) [30] investigated effects of the prior in-plane damage on out-of-plane behaviour of masonry infill with full-height door opening too. As in this study, the authors reported that masonry infill with full-height door opening obtained worse out-of-plane behaviour due to the more fragile crack patterns developed under prior in-plane loads. Moreover, more studies [8-10,34] showed that openings increase the seismic vulnerability of masonry infills, as unstable portions of masonry next to openings tend to fall out of wall plane in pure in-plane tests. In tests with sequential or simultaneous in-plane and out-of-plane loads, the worse performance and higher reductions of out-of-plane capacity could be expected. However, experimental campaigns on infills with openings with this loading protocol are still missing.
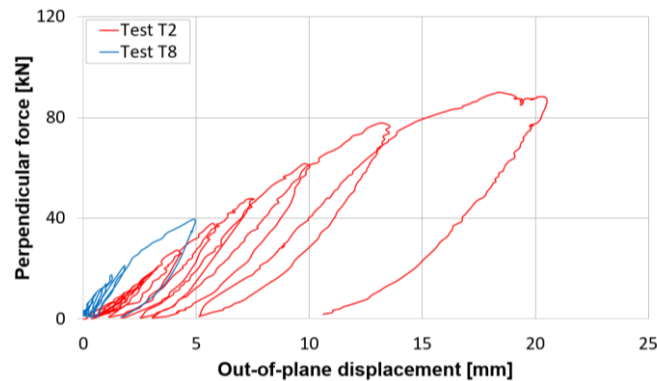
Figure 10. Load-displacement curves of out-of-plane loading phases of tests T2 and T8

5. Conclusions

Experimental tests conducted within the scope of the project named "Development of an innovative approach for decoupling infills and non-load-bearing masonry walls from the main structure" are presented in this paper. Experimental results show that full-height door opening has an adverse effect on seismic performance of infilled RC frames. Firstly, due to the presence of door opening damage to edge bricks occurs at already 0.5 % of in-plane drift, whereas solid masonry infill suffers more significant damage at 1.0 % of in-plane drift. Furthermore, with the increase of in-plane drifts, triangular-like portions of masonry formed around door opening gradually lose their connection to the rest of the infill along diagonal cracks and tend to fall out of wall plane. As a consequence of the more significant prior in-plane damage, out-of-plane capacity of masonry infill with door opening is reduced 3.7 times, while for solid infill out-of-plane capacity is reduced 2 times. However, it should be pointed out that vertical arching could be formed in all specimens in this experimental campaign. This was possible due to the strong boundary conditions provided by perfect execution of frame-infill connections, which is not common in practice. In more realistic cases even worse out-of-plane behaviour of masonry infills with and without door opening could be expected. Due to this, it seems reasonable to work on the development of the engineering solutions that could increase the seismic safety of masonry infilled RC frames. The decoupling system presented in the paper of [35] successfully prevented in-plane damage and at the same time provided a support for out-of-plane forces. However, the system was only tested on the fully infilled RC frame and it needs to be further validated on masonry infills with openings, which are definitely more prone to the seismic damage.

Acknowledgements

References

[1] Ockleston AJ (1955) Load tests on a three storey reinforced concrete building in Johannesburg. The Structural Engineer 33:304-322

[2] Read JB (1965) Testing to destruction of full-size portal frames. Cement and Concrete Association.

[3] Angel R, Abrams D, Shapiro D, Uzarski J, Webster M (1994) Behavior of reinforced concrete frames with masonry infills. Civil Engineering Studies, Structural Research Series No. 589, UILU-ENG-94-2005, Department of Civil Engineering, University of Illinois at Urbana Champaign

[4] Mehrabi AB, Shing PB, Schuller MP, Noland JL (1996) Experimental evaluation of masonry-infilled RC frames. J Struct Eng 122(3):228-237. https://doi.org/10.1061/(ASCE)0733-9445(1996)122:3(228)

[5] Kakaletsis DJ, Karayannis CG (2008) Influence of masonry strength and openings on infilled R/C frames under cycling loading. J Earthq Eng 12(2):197-221. https://doi.org/10.1080/13632460701299138

[6] Stylianidis KC (2012) Experimental investigation of masonry infilled RC frames. The Open Construction & Building Technology Journal 6(1):194-212. https://doi.org/10.2174/1874836801206010194

[7] Sigmund V, Penava D (2014) Influence of openings, with and without confinement, on cyclic response of infilled rc frames—an experimental study. J Earthq Eng 18(1):113-146. https://doi.org/10.1080/13632469.2013.817362

[8] Stavridis A (2009) Analytical and experimental study of seismic performance of reinforced concrete frames infilled with masonry walls. Ph.D. Thesis. University of California, San Diego

[9] Tasnimi AA, Mohebkhah A (2011) Investigation on the behavior of brick-infilled steel frames with openings, experimental and analytical approaches. Eng Struct 33(3):968-980. https://doi.org/10.1016/j.engstruct.2010.12.018

[10] Tu YH, Chao YF, Chiou TC (2016, November). Lateral load experiment and comparison with analytical model for in-filled masonry panels with openings in an RC frame. In *Proceedings of the 16th International Brick and Block Masonry Conference (IBMAC 2016)*.

[11] McDowell EL, McKee K, Sevin E (1956a) Arching action theory of masonry walls. J Struct Div 82(2):1-8

[12] McDowell EL, McKee KE, Sevin E (1956b) Discussion of Arching Action Theory of Masonry Walls. J Struct Div 82:27-40

[13] Dawe JL, Seah CK (1989) Out-of-plane resistance of concrete masonry infilled panels. Can J Civ Eng 16(6):854-864.

[14] Di Domenico M (2018) Out-of-plane seismic response and modelling of unreinforced masonry infill walls (Doctoral dissertation, PhD Dissertation. University of Naples Federico II).

[15] Akhoundi F, Vasconcelos G, Lourenço P (2018) Experimental out-of-plane behavior of brick masonry infilled frames. Int J Archit Herit 14(2):221-237. https://doi.org/10.1080/15583058.2018.1529207

[16] Furtado A, Arêde A, Rodrigues H, Varum H (2021) The role of the openings in the out-of-plane behaviour of masonry infill walls. Eng Struct 244:112793. https://doi.org/10.1016/j.engstruct.2021.112793

[17] Marinković, M., Brzev, S., Baballëku, M., Isufi, B., Blagojević, N., Milićević, I., Žugić, Ž., Bursać, P. (2021). Out-of-plane behaviour of loadbearing and non-structural masonry walls during recent earthquakes. In Conference proceedings from 1st Croatian Conference on Earthquake Engineering-1CroCEE, 22nd to 24th March 2021, Zagreb, 2021 (Vol. 64, pp. 213-207). University of Zagreb, Faculty of Civil Engineering.

[18] Braga F, Manfredi V, Masi A, Salvatori A, Vona M (2011) Performance of non-structural elements in RC buildings during the L'Aquila, 2009 earthquake. Bull Earthq Eng 9(1):307-324. https://doi.org//10.1007/s10518-010-9205-7

[19] Ricci P, De Luca F, Verderame GM (2011) 6th April 2009 L'Aquila earthquake, Italy: reinforced concrete building performance. Bull Earthq Eng 9(1):285-305. https://doi.org/10.1007/s10518-010-9204-8

[20] Marinković M, Baballëku M, Isufi B, Blagojević N, Milićević I, Brzev S (2022) Performance of RC cast-in-place buildings during the November 26, 2019 Albania earthquake. Bull Earthq Eng 1-54. https://doi.org/10.1007/s10518-022-01414-y

[21] Flanagan RD, Bennett RM (1999) Bidirectional behavior of structural clay tile infilled frames. J Struct Eng 125(3):236-244. https://doi.org/10.1061/(ASCE)0733-9445(1999)125:3(236)

[22] Calvi GM, Bolognini D (2001) Seismic response of reinforced concrete frames infilled with weakly reinforced masonry panels. J Earthq Eng 5:153-185. https://doi.org/10.1080/13632460109350390

[23] Ricci P, Di Domenico M, Verderame GM (2018a) Experimental assessment of the in-plane/out-of-plane interaction in unreinforced masonry infill walls. Eng Struct 173:960-978. https://doi.org/10.1016/j.engstruct.2018.07.033

[24] Ricci P, Di Domenico M, Verderame GM (2018b) Experimental investigation of the influence of slenderness ratio and of the in-plane/out-of-plane interaction on the out-of-plane strength of URM infill walls. Construction and Building Materials 191:507-522. https://doi.org/10.1016/j.conbuildmat.2018.10.011

[25] Furtado A, Rodrigues H, Arêde A, Varum H (2016) Experimental evaluation of out-of-plane capacity of masonry infill walls. Eng Struct 111:48-63. https://doi.org/10.1016/j.engstruct.2015.12.013

[26] Akhoundi F, Vasconcelos G, Lourenço P (2018) Experimental out-of-plane behavior of brick masonry infilled frames. Int J Archit Herit 14(2):221-237. https://doi.org/10.1080/15583058.2018.1529207

[27] De Risi MT, Di Domenico M, Ricci P, Verderame GM, Manfredi G (2019) Experimental investigation on the influence of the aspect ratio on the in-plane/out-of-plane interaction for masonry infills in RC frames. Eng Struct 189:523-540. https://doi.org/10.1016/j.engstruct.2019.03.111

[28] Morandi P, Hak S, Magenes G (2017) Experimental and numerical seismic performance of strong clay masonry infills. In appendix: guideline proposal for seismic design of masonry infills. Research Report 2017/02. EUCENTRE Foundation.

[29] Butenweg C, Marinković M, Salatić R (2019) Experimental results of reinforced concrete frames with masonry infills under combined quasi-static in-plane and out-of-plane seismic loading. Bull Earthq Eng 17(6):3397-3422. https://doi.org//10.1007/s10518-019-00602-7

[30] da Porto F, Donà M, Verlato N, Guidi G (2020) Experimental testing and numerical modeling of robust unreinforced and reinforced clay masonry infill walls, with and without openings. Front Built Environ 6:591985. https://doi.org/10.3389/fbuil.2020.591985

[31] Di Domenico M, De Risi MT, Ricci P, Verderame GM, Manfredi G (2021) Empirical prediction of the in-plane/out-of-plane interaction effects in clay brick unreinforced masonry infill walls. Eng Struct 227. https://doi.org/10.1016/j.engstruct.2020.111438

[32] Cavaleri L, Zizzo M, Asteris PG (2020) Residual out-of-plane capacity of infills damaged by in-plane cyclic loads, Eng Struct 209: 109957. https://doi.org/10.1016/j.engstruct.2019.109957

[33] Šakić B, Milijaš A, Marinković M, Butenweg C, Klinkel S (2021) Influence of prior in-plane damage on the out-of-plane response of non-load bearing unreinforced masonry walls under seismic load. In *COMPDYN 2021-8th ECCOMAS Thematic Conference on Computational Methods in Structural Dynamics and Earthquake Engineering*

[34] Mansouri A, Marefat MS, Khanmohammadi M. (2014) Experimental evaluation of seismic performance of low-shear strength masonry infills with openings in reinforced concrete frames with deficient seismic details. The Structural Design of Tall and Special Buildings 23(15):1190-1210. https://doi.org/10.1002/tal.1115

[35] Marinković M, Butenweg C (2019) Innovative decoupling system for the seismic protection of masonry infill walls in reinforced concrete frames. Eng Struct 197:109435. https://doi.org/10.1016/j.engstruct.2019.109435

DETERMINATION OF THE DYNAMIC BEHAVIOR OF A BRIDGE STRENGTHENED WITH SHOCK TRANSMISSION UNITS

Jurica Pajan[1], Ivan Duvnjak[2], Domagoj Damjanović[3], Tomislav Brozović[4], Suzana Ereiz[5]

[1] *Assistant, University of Zagreb Faculty of Civil Engineering, jurica.pajan@grad.unizg.hr*
[2] *Associate professor, University of Zagreb Faculty of Civil Engineering, ivan.duvnjak@grad.unizg.hr*
[3] *Full-time professor, University of Zagreb Faculty of Civil Engineering, domagoj.damjanovic@grad.unizg.hr*
[4] *Bridge Design Engineer, Institut IGH, tomislav.brozovic@igh.hr*
[5] *Assistant, University of Zagreb Faculty of Civil Engineering, suzana.ereiz@grad.unizg.hr*

Abstract

Shock Transmission Units (STU), also known as Temporary Connection Devices (TCD) or Lock-up Devices (LUD), are mechanical devices that provide a simple and economical way to improve the resistance of existing bridges. They are mainly used for retrofitting existing bridges to accommodate higher-intensity earthquakes and breaking loads defined by new design codes for which the existing bridges do not have sufficient load-bearing capacity. The basic idea of a shock transmission unit is to distribute seismic or other sudden impact loads only to different substructure elements of the bridge so that the bridge behaves as a rigidly connected structure. In the case of slowly acting loads such as temperature, creep, and shrinkage, the shock transmission units are not activated, so that the different parts of the bridge-bearing structure can move independently of each other. They behave like "seatbelts for bridges" because they restrain bridge movement for sudden dynamic loads but allow free movement under slowly acting static loads. To determine the real contribution of STU to the bridge stiffness and consequently, to the global dynamic behavior of the bridge in regular operating conditions, modal parameters such as natural frequency, mode shapes, and damping were determined on the pedestrian bridge, which had been strengthened with shock transmission units. The modal parameters were determined using operational modal analysis and the numerical model. This paper shows the difference between the experimental and numerical modal parameters and draws conclusions about the impact of the shock transmission units on global bridge stiffness. A proposal is also given for the numerical modeling of shock transmission units and their influence on the overall seismic action.

Keywords: shock transmission units, bridges, dynamic parameters, operational modal analysis

1. Introduction

The territory of the Republic of Croatia is in a seismically active area, and in 2020 the country was hit by two major earthquakes. Before that, earthquakes were quite rare, so citizens' awareness of seismic risk was relatively low [1]. Recent events have rapidly increased public interest in seismic risk, and the need to design earthquake-resistant buildings has finally become equally recognized among all participants in the building process. In particular, the need to rehabilitate and strengthen a large number of existing buildings and bridges to withstand the seismic loads prescribed by the existing technical standards (Eurocodes) presented new challenges to all. Such a task became a major challenge for existing bridges since many of them were built a long time ago and for some of them, seismic actions were not considered at all or with much smaller intensity [2–4]. Those bridges should remain in service after the earthquake to accommodate heavy traffic by emergency vehicles and to provide safe passage of lifeline supplies. The above requirements should be met as part of the technical solution during the reconstruction phase. This is hardly achievable with a traditional approach based on strengthening critical bridge parts. Therefore, more advanced methods and systems that can improve the seismic performance of the bridge need to be employed. Based on the functional characteristics of such systems and methods, they can be divided into three types [5], which are shown in Figure 1.
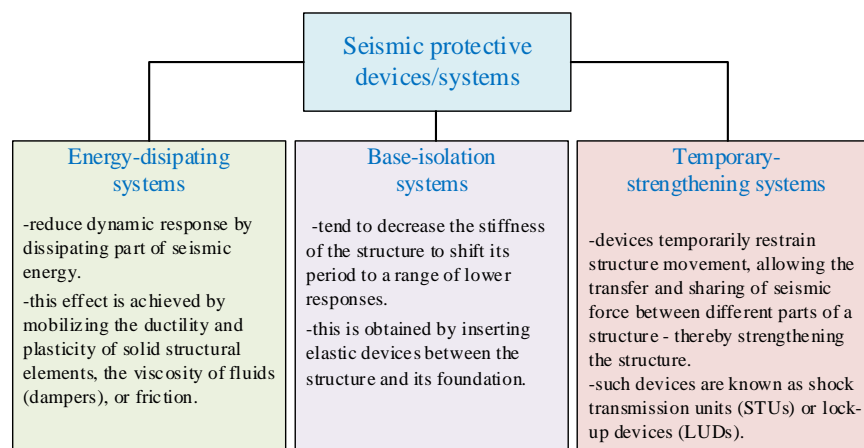
Figure 1. Seismic protective devices/systems

Base-isolation systems are not so suitable solution for existing bridges, since they require demanding and expensive construction procedures to install elastic devices beneath the foundation or other structural elements. On the other hand, the use of energy-dissipating systems and the energy-dissipation approach is quite limited since many of the existing bridges are built on masonry piers, and such substructures do not exhibit ductile behavior. Therefore, temporary strengthening systems also known as Shock Transmission Units (STU) occur as the most applicable ones to be used on existing bridges. They are easily installed and they don't require traffic closure which makes them ideal for investors. In addition, the basic principle of their contribution to overall seismic resistance is relatively easy to understand, making engineers more comfortable to use them in their designs.

The first known use of shock transmission units (STUs) in Europe was in the Netherlands in 1965 on the Oostehshelde Bridge [6]. They were used to transfer traction and braking forces across the central expansion joint. For seismic resistance, they were first used in Italy in 1974 [6]. To the authors' knowledge, shock transmission units are still rarely used in Croatia. A recent example of their use was on the Old Sava Pedestrian Bridge in Zagreb in 2019. Since it took almost fifty years for Croatian engineers to implement the use of shock transmission units in their design concept, the first aim of this article is to introduce the concept of strengthening existing bridges with STU based on the case study example of the Old Sava pedestrian Bridge in Zagreb. The second aim is to investigate the contribution of STUs on overall dynamic behavior through the use of a numerical model updated with experimental data collected through load testing and operational modal analysis.

2. Operational principle of STU

In this chapter, the basic concept of shock transmission units has been explained. To begin with, it is important to distinguish shock transmission units from dampers or energy absorbers. Although they look quite similar, their dynamic behavior and overall impact on the structure is different. STUs have negligible energy absorption capacity due to small piston movement and insignificant hysteresis loops [7]. From the designer's point of view, the STU behaves like an additional support or a rigid link between connected bridge elements, while dampers only increase the damping of an overall structure. In terms of energy handling, the dampers dissipate energy, while STUs distribute energy [8].
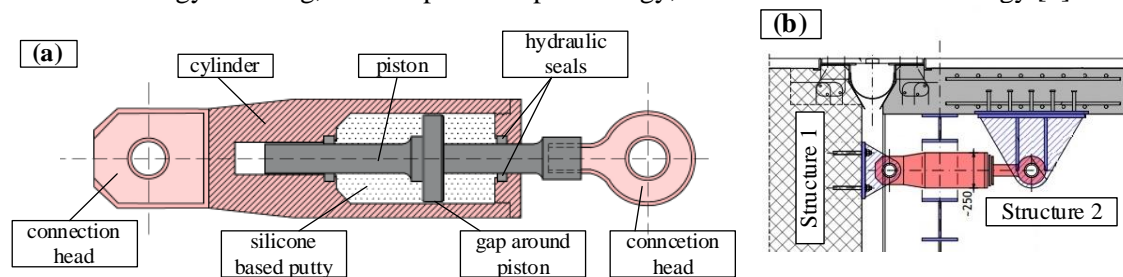
Figure 2. The operational principle of STU. (a) basic parts of the shock transmission unit, (b) the STU unit installed on the case study bridge

The operating principle of STU is based on the fact that rapid passage of viscous fluid through a narrow gap generates considerable resistance, while slow passage produces only minor resistance. As a result, STUs behave as a rigid link transmitting the forces between structural elements for dynamically applied forces such as seismic or braking forces. For slowly applied forces that are mainly caused by temperature, shrinkage, or creep the fluid has enough time to slowly pass the gap allowing free piston movement, therefore only a small amount of force is transmitted between connected elements.

In 1960, the USA Space Exploration Program developed a new material that has a particular thixotropic behavior that makes it optimal for use as a fluid in STU. It is commonly known as a silicone putty (a chemical compound of a boron-filled dimethyl siloxane) and it acts like a rigid body under impact loads, but under slowly applied loads, it deforms easily and without any delay [7]. This makes it ideal for use in shock transmission units as a filler material and it replaced oils and gases that were previously used. This resulted in significant cuts in STUs' need for maintenance which made them more suitable for use on real bridges and structures. Today, STUs are mainly used for (a) multi-span simply supported bridges, (b) multi-span continuous bridges, (c) bridges in seismic areas, and (d) for adjacent continuous viaducts. Although they are mainly used as a unidirectional device for temporarily restraining translational movements, a rotational STU is also produced and it was used on a military pontoon bridge [9].

3. Bridge studied

The Old Sava Bridge in Zagreb, also known as the "Blue Bridge" or "Sava Pedestrian Bridge", was designed by famous Croatian bridge engineer Milivoj Frković and was built in 1939. The new bridge superstructure consisted of steel and concrete bridge superstructure was built on an existing masonry substructure dating back to 1892. Previously, the existing superstructure had been constructed as a system of simply supported steel trusses with wooden deck elements. The design and construction technology of a new span structure was quite ahead of its time. According to the references [10–13], the main advancement was in design and welding technology. At the time, welding technology had difficulties when it came to welding thick steel elements together, but those obstacles have been mastered by the engineers (Fig. 2a) and the thick flanges (more than 90 mm) were successfully welded together, as the later welding tests revealed (Fig. 2b).
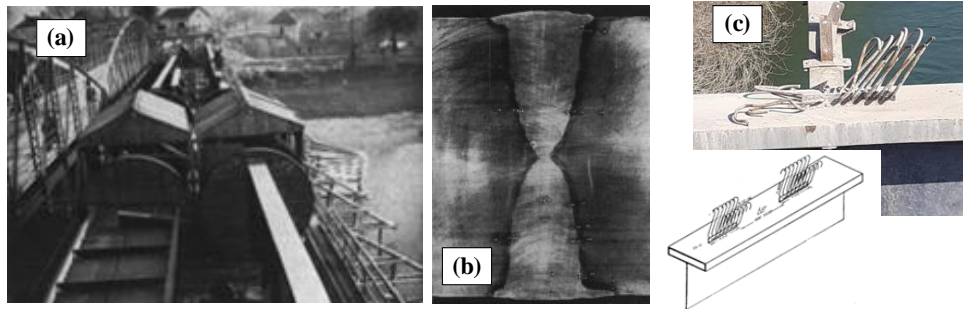
Figure 3. Details from the building process [11]. (a) welding technology, (b) weld quality control, (c) technical detail of the shear connector between the main girder and a concrete slab

Advancement in design is based on the designer's intention to use the reinforced concrete deck as a wind bracing. The installed shear connectors (Fig. 2c) contributed to the bond reaction between the main girders and the bridge deck. The favorable composite response of the superstructure was later demonstrated during the load tests. This encouraged Croatian engineers to further research the field of composite structures in bridge construction. All this led to the recognition of the importance of the bridge for the Croatian cultural heritage and the bridge was placed under strict monument protection. The protection guidelines and the poor condition of the bridge, caused by aging and poor maintenance, were a major challenge for the 2019 bridge reconstruction project. The complete concrete bridge deck had to be removed (fig. 3b) due to the existing damage, so the bridge structure needed to be reconstructed to meet all existing technical standards.
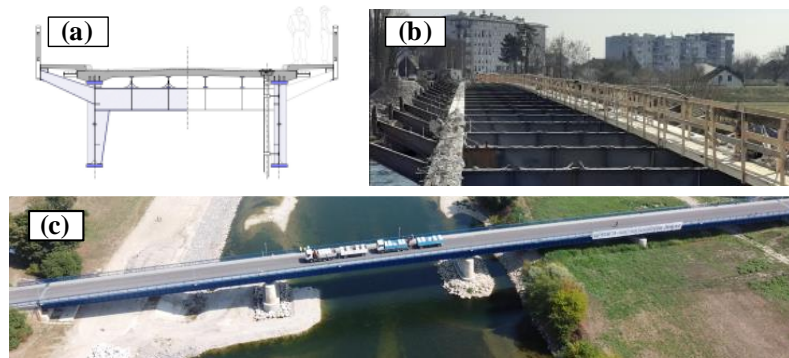
Figure 4. Bridge reconstruction phases. (a) bridge cross-section designed in 2019., (b) bridge superstructure without bridge deck, (c) bridge after reconstruction

The bridge was initially designed for car traffic and its new use was mainly as a pedestrian bridge. With an additional bearing capacity based on a composite behavior, the bridge was able to withstand all vertical loads without major interventions on the steel superstructure. The main problem was the masonry substructure and bearings, especially for seismic analysis. The bearing configuration of the bridge is shown in Figure 4.
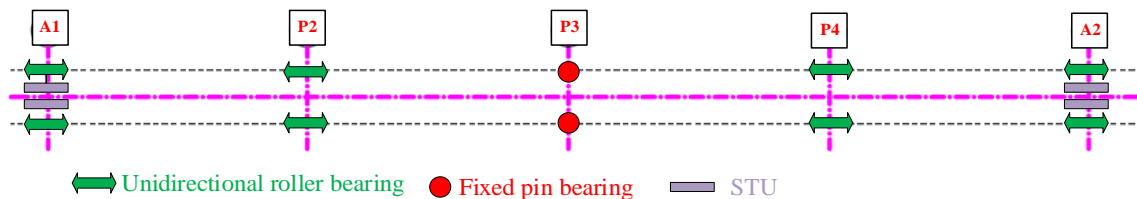
Figure 5. Bridge bearing and STU configuration

173

The seismic movement in the longitudinal direction is restrained only on the central masonry pier. The shock transmission units were used due to the low bearing capacity and small ductility of the central pier that couldn't resist seismic forces defined according to Eurocode standards. In this way, redistribution of the longitudinal seismic force component to the abutments was ensured, while the free movement was available for regular conditions (creep, shrinkage, and temperature).

3.1. Experimental analysis

According to the Croatian technical standard [14] and the project requirements, load tests had to be performed after the reconstruction of the bridge. The load testing of the bridge was divided into two parts. Static testing was performed according to the Croatian standard for bridge load testing [15]. In this part, the deflections caused by the known static loads have been determined. In the second part, dynamic tests were performed to determine dynamic parameters such as damping, natural frequencies, and mode shapes. The dynamic or modal parameters were determined by operational modal analysis (OMA) [16–19] after the bridge was completed and the STUs have been installed into the bridge. Since the complex mode shapes were expected to affect the limits of the equipment, two sets of measurements were made. First, to capture the horizontal mode shapes and second, to capture vertical ones. For each measurement, a separate experimental model was created using the computer program PULSE LAB SHOP developed by Bruel & Kjaer [20]. Piezoelectric accelerometers (sensitivity of 1000 mV/g) in combination with the Bruel & Kjaer 3560C analyzer have been used to record accelerations at different locations on the bridge and in different directions. For the first measurement setup, named Model_1_HOR, only the data recorded by the accelerometers in the horizontal direction were used for the analysis. Therefore, the mode shapes consisted only of the motions in the horizontal direction. The measurement setup named Model_2_ VERT was used with accelerometers oriented only in the vertical direction to obtain vertical and torsional mode shapes.
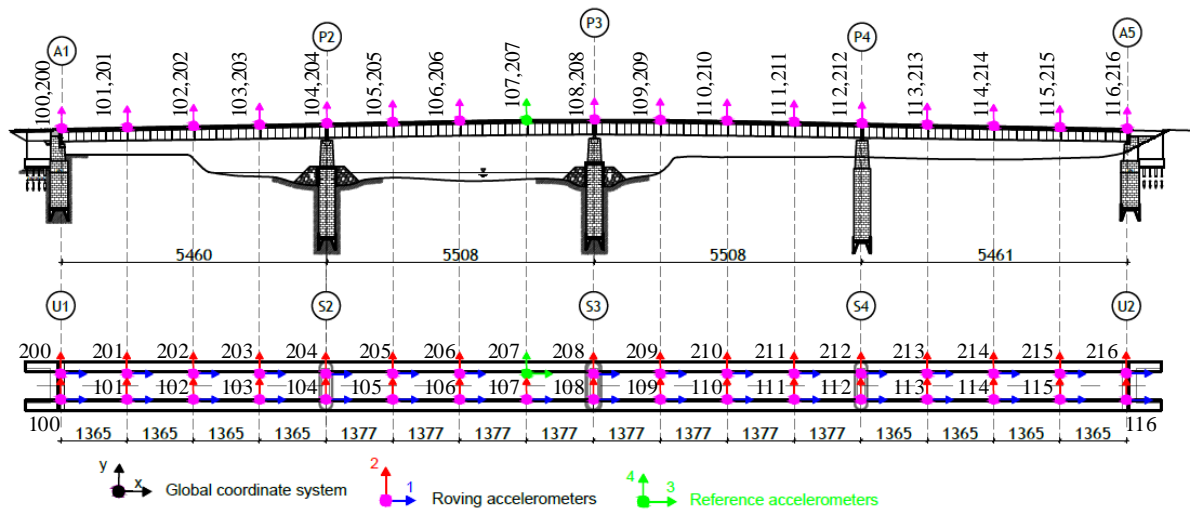
Figure 6. Location of measurement points on the bridge. Red and blue arrows represent the horizontal direction of accelerometers for the first set of measurements while magenta arrows represent the measured direction of accelerometers for the second measurement setup.

For data processing, the OMA techniques developed in the frequency domain, such as **FDD** (**F**requency **D**omain **D**ecomposition method [19]); EFDD (**E**nhanced **F**requency **D**omain **D**ecomposition method [21, 22]), CFDD (**C**urve-fitting **F**requency **D**omain **D**ecomposition method [23]) were used. The results from each used OMA technique are shown in Figure 7. and obtained results for the studied bridge are shown in Table 1.
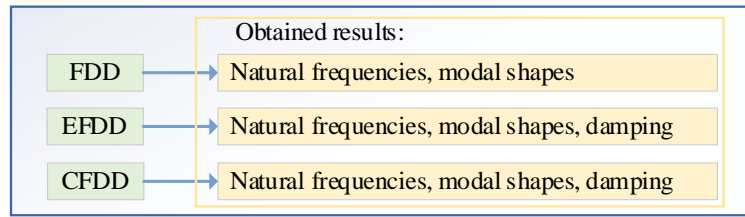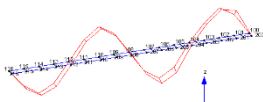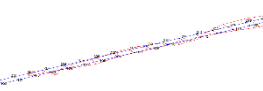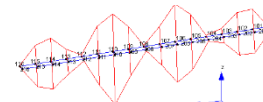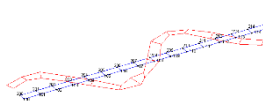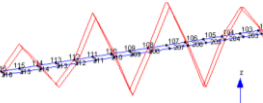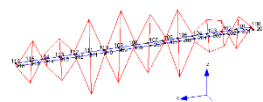
Figure 7. Used OMA data processing techniques and results

Table 1 – Obtained modal parameters

Modal shapes		Natural frequency [Hz]				Damping [%]	OMA model
NO.	Shape	FDD	EFDD	CFDD	Mean Value	EFDD	
1.		1,813	1,842	1,859	1,819	2,444	Model_2_VERT
		1,813	1,797	1,79		1,353	Model_1_HOR
2.		3,750	3,761	3,792	3,768	1,202	Model_2_VERT
3.		4,625	4,637	4,636	4,633	1,159	Model_1_HOR
4.		6,313	6,336	6,320	6,323	1,618	Model_2_VERT
5.		8,750	8,77	8,760	8,76	1,002	Model_2_VERT

3.2. Numerical analysis
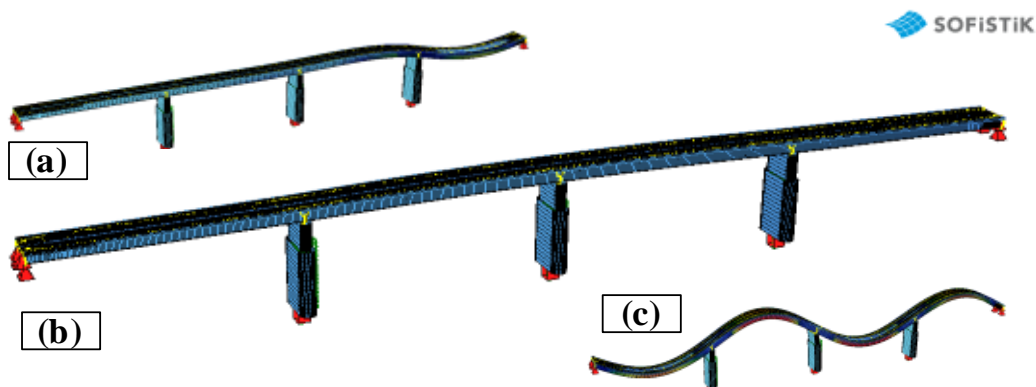
Figure 8. Numerical model of the bridge. (a) The deformed 3D model under the load test at the last span, (b) 3D FEM model, (c) First numerically obtained modal shape at the frequency of 1,798 Hz

175

Modal analysis and modal parameters are fundamental tools for understanding the dynamic behavior of the structure. In the previous chapter, the modal parameters such as natural frequencies and mode shapes were measured experimentally while the shock transmission units were installed in the bridge. Therefore, the contribution of the STUs could not be determined by experimental tests alone. So, an updated numerical model (Fig. 8) was used to determine the influence of the STUs on the structural dynamic parameters of the bridge.

The initial numerical model was developed in "SOFiSTiK", a commercial software specialized in structural analysis and engineering [24]. The main girders, cross girders, and secondary longitudinal beams were modeled as beam elements while the RC slab was modeled with area finite elements. Bridge piers were also included in the numerical model, along with STUs. STU was modeled as a beam element connecting the bridge RC deck with an additional pinned support at the abutment. The cross-section of this element is assumed to be equal to the cross-section of the STU's piston.

The defined numerical model was updated based on experimental data until a sufficient similarity between the results from the numerical model and those measured on the real structure was achieved. For the updating process, a direct method was used [25]. The method is based on the manual modification of structural parameters such as geometry, material parameters, and boundary conditions.

In Figures 9. and 10. difference between the numerically and experimentally obtained data from the static load test is shown.
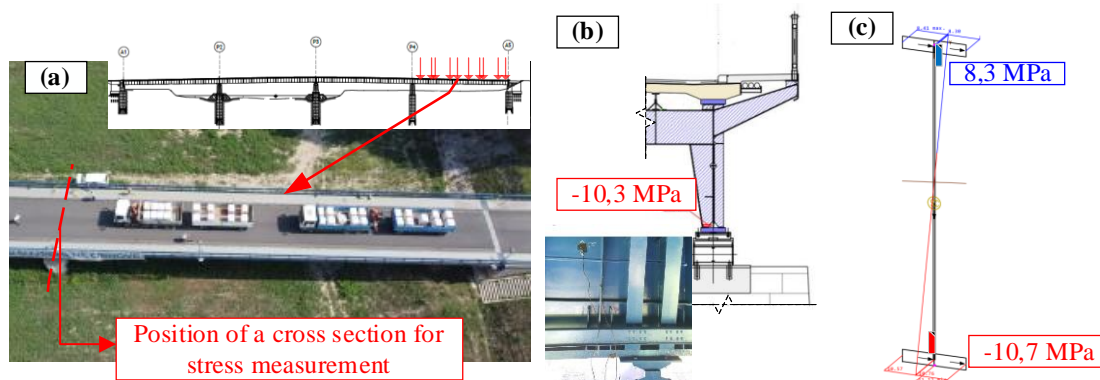
Figure 9. Test load in the last span. (a) Position of test load on the bridge (b) Measured stresses (c) Calculated stresses from an updated numerical model
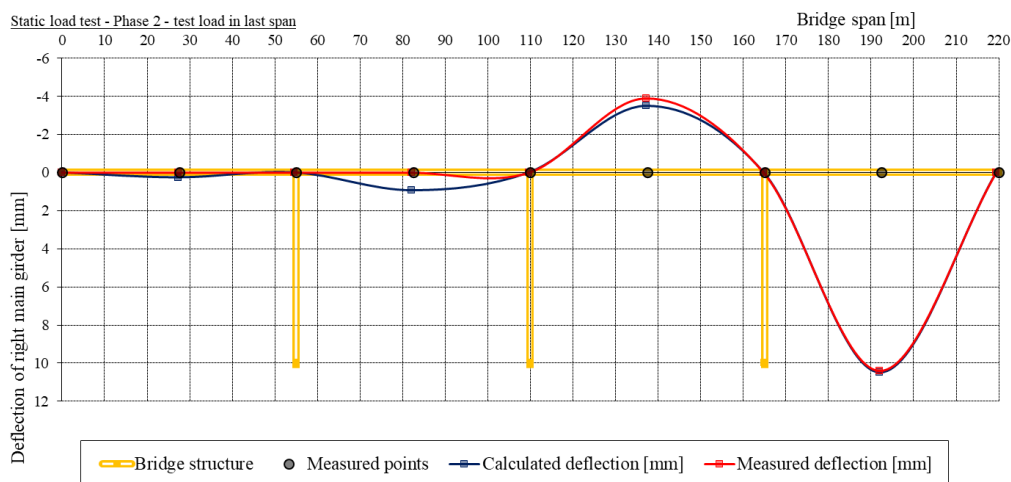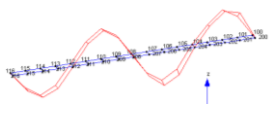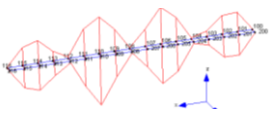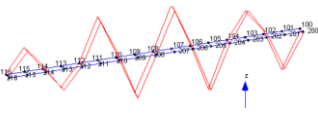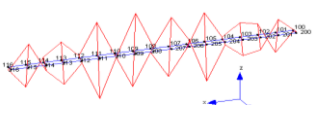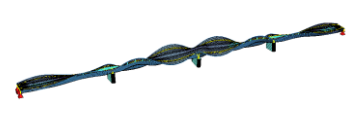
Figure 10. The difference in measured and calculated deflection of the right main girder under the test load in the last span.

The same updated model was then used to perform a modal analysis. In the modal analysis, the Lanczos method [26] was used to calculate the eigenvalues and eigenvectors. The primary load case, defined as a combination of permanent loads (self-weight of the structure and additional weight), was used to define the initial state for the modal analysis. In this way, the contribution of deflection and forces from permanent loads is considered.

Since a satisfactory match between experimental and calculated results for static and dynamic tests has been obtained, it was concluded that an approximation of a real structure with a numerical model was appropriate (at least the flexural stiffness of the superstructure). The modal shapes and frequencies from the operational modal analysis are used as the ground truth for determining the dynamic behavior of the bridge because they were obtained on the bridge with STUs installed while the bridge was in service. To determine the modal parameters of the bridge without STUs, the STUs were neglected in the calculation (they were removed from the model) in the second run of the modal analysis. The overall differences between the modal parameters (natural frequencies and mode shapes) determined by operational modal analysis and by updated numerical models simulating the bridge with and without STUs are shown in Table 2.

Table 2 – Modal shapes and frequencies obtained from experimental and numerical modal analysis

Experimental results	Numerical results	
Results from OMA	with STUs	without STUs
Horizontal (longitudinal) mode shapes		
		$f_0=1,175$ Hz
First vertical mode shapes		
$f_1^{exp}=1,819$ Hz	$f_1^{STU}=1,798$ Hz	$f_1=1,812$ Hz
First torsional mode shapes		
$f_2^{exp}=3,768$ Hz	$f_2^{STU}=3,795$ Hz	$f_2=3,795$ Hz
Second vertical mode shapes		
$f_3^{exp}=6,323$ Hz	$f_3^{STU}=5,913$ Hz	$f_3=5,909$ Hz
Second torsional mode shapes		
$f_4^{exp}=8,760$ Hz	$f_4^{STU}=8,615$ Hz	$f_4=8,619$ Hz

177

3.3. Discussion

Considering the updated numerical model, it can be concluded from the results presented in Table 2 that despite the installation of STUs, there is no significant increase or decrease in the natural frequencies of the bridge - the difference between the natural frequencies is less than 2%. The main difference can be seen in the mode shapes. The mode shape with the lowest frequency (1,175 Hz) was not detected in the case of the bridge straightened with STU. This mode shape involves a dominant displacement of the bridge superstructure in the longitudinal direction and thus has a significant influence on the dynamic forces acting on the central bearing and the pier (the longitudinal movement of the bridge deck is only restrained by the support in the middle bearings and by the low friction in other the bearings). This mode shape is critical to the design of the center bearing and pier. If we look at the mode shapes derived from the bridge structure with installed STUs (results of the OMA and the numerical model with STUs), the deflection shape at the frequency of 1,175 Hz is not dominant, and consequently, it is not recognized as a mode shape in the numerical model. This can also be seen in Figure 11, which shows the singular values of the spectral density matrices recorded in OMA Model_1_HOR setup. It can be seen that the first significant pick in frequencies is at 1,819 Hz. Therefore, the bridge with the STUs installed has no natural frequency at 1,175 Hz and the corresponding translational shape is avoided by installing the STUs.
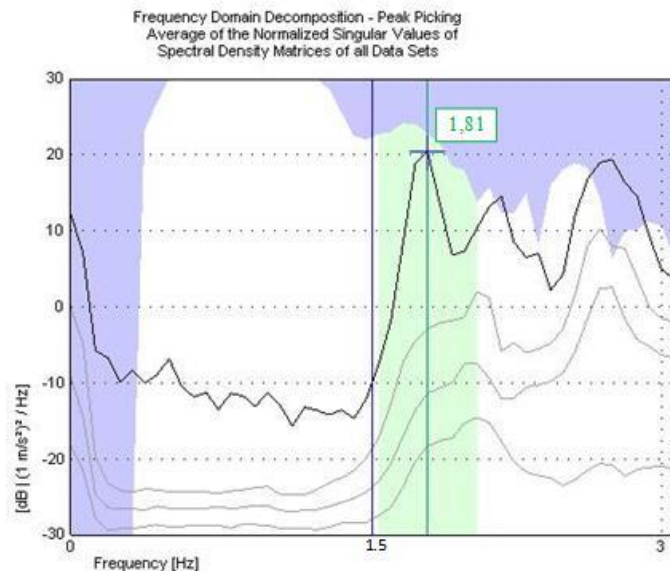
Figure 11. Singular values of spectral density matrices for OMA Model_1_HOR setup.

4. Conclusion

The primary aim of the presented study was to determine the effect of shock transmission units to bridge dynamic behavior. Their contribution was evaluated through modal parameters such as natural frequencies and mode shapes that were obtained from the updated numerical model. An updated numerical model, which performance under the known loads was quite similar to a real bridge, was used for modal analysis in which the contribution of installed STUs has been considered. It is important to note that in this study it was assumed that the STUs are fully activated since they are considered mainly for seismic analysis. The results have shown that the installation of STU makes the bridge stiffer in the directions in which STUs are installed, so the undesirable mode shape is avoided. By incorporating an STU, the first mode shape with a dominant displacement in the longitudinal direction has been avoided, resulting in a much more favorable response to dynamic load such as an earthquake.

While the study included experimental testing, numerical modeling, and updating of the numerical model, some additional conclusions could also be drawn.

The experimental tests and the operational modal analysis have shown that, despite equipment limits, it is possible to obtain horizontal and vertical modal shapes by dividing them into several separate measuring setups in which we combine different measurement directions. For example, as described in chapter 3.1, if we are measuring structures where we expect complex modal shapes (shapes where it is difficult to separate only one or two dominant directions), we can combine different directions to capture the most dominant modal shapes. For continuous bridges, such as the one presented in this study, the authors would recommend measuring the longitudinal direction in combination with the vertical direction in one setup and only the transverse direction for the second setup.

Since numerical modeling and updating a numerical model could be a story for themself, overall, it can be concluded that the data collected through load testing (which is still mandatory in Croatia) has a high value for further use in understanding the behavior of the real structure as it is built and not as it was designed in the project. In this way, a deeper and more reliable understanding of the structural performance of a built structure can be obtained. For this purpose, it is necessary to develop a more advanced and automated method for model updating, since the manual, direct approach is quite time-consuming.

For further studies, it would be interesting to experimentally investigate the process of activation of STUs, by simply conducting experimental modal analysis before and after the installation of STUs on a real structure. Since STUs transfer small amounts of force, even if it is slowly applied, it is important to see if the low-value excitation on which the operational modal analysis is based will activate shock transmission units.

Acknowledgements

References

[1]   Atalić, J., Šavor Novak, M., Uroš, M. (2019): Seismic risk for Croatia: overview of research activities and present assessments with guidelines for the future, *GRAĐEVINAR,* **71**(10), 923–947, doi: https://doi.org/10.14256/JCE.2732.2019

[2]   Hrelja Kovačević, G., Mandić Ivanković, A. (2019): Assessing seismic vulnerability of existing bridges using fragility curves, *In: 6th Symposium on Doctoral Studies in Civil Engineering*, 163–174, doi: http://master.grad.hr/phd-simpozij/2020/proceedings/13.html

[3]   Šavor, Z., Šavor Novak, M. (2015): Procedures for Reliability Assessment of Existing Bridges, *GRAĐEVINAR,* **67**(06), 557–572. doi: https://doi.org/10.14256/JCE.1190.2014

[4]   Mandić, A., Radić, J. (2003): Contribution to modernization of bridge load regulations, *GRAĐEVINAR* **56**(07), 409–422, doi: https://doi.org/624.21:69.009.182

[5]   Patel, D.J. (2013): *Seismic protection systems,. In: Shock Transmission Units in Construction.,* pp. 7–17, ICE Publishing, UK.

[6]   Patel, D.J. (2013): *Evolution of shock transmission units (STUs),. In: Shock Transmission Units in Construction,,* pp. 1–5, ICE Publishing, UK.

[7]   Pritchard, B.P. (1996): The use of shock transmission units in bridging, *Proceedings of the Institution of Civil Engineers - Structures and Buildings* **116**(1), 82–95, doi: https://doi.org/10.1680/istbu.1996.28156

[8]   Liang, J. (2013): Design and Testing of Shock Transmission Device for Bridge Protection, *Applied Mechanics and Materials,* **405,** 1517–1520, doi: https://doi.org/10.4028/www.scientific.net/AMM.405-408.1517

[9]   Patel, D.J. (2013): *Miscellaneous applications of STUs,. In: Shock Transmission Units in Construction.,* pp. 121–130, ICE Publishing, UK.

[10]   Marić, Z., Markulak, D., Varevac, D. (2009): The world's oldest major bridge with a composite deck

structure, *GRAĐEVINAR,* **61**(12), 1123–1128, doi: https://doi.org/10.14256/JCE.2732.2019

[11] Erega, J. (1940): Gradnja kolnog mosta preko Save kod Zagreba, *Građevinski vjesnik* **6**(7).

[12] Tonković, K. (1984): Kolni most na Savskoj cesti u Zagrebu, *Naši mostovi* **3,** 142–145.

[13] Radić, J. (2004): Arch Bridges made by Croatian Builder Milivoj Frkovic, *4ᵗʰ international arch bridges conference*, Barcelona, Spain, 8 pages.

[14] Technical standard for building structures (2017), *NN 17/2017*, Ministry of Physical Planning Republic of Croatia, Zagreb, Croatia.

[15] HRN U.M.1.046. (1984): Croatian tehnical standard for bridge load testing.

[16] Brincker, R., Ventura, C. (1995): *Introduction to operational modal analysis*. John Wiley&Sons, 2015 edition, UK.

[17] Brincker, R., Zhang, L., Andersen, P. (2001): Modal identification of output-only system using FDD, *Smart Materials and Structures,* **10,** 441–445.

[18] Zahid, F. Bin, Ong, Z.C., Khoo, S.Y. (2020): A review of operational modal analysis techniques for in-service modal identification, *Journal of the Brazilian Society of Mechanical Sciences and Engineering* **42** (8), 398, doi: https://doi.org/10.1007/s40430-020-02470-8

[19] Brincker, R., Zhang, L., Andersen, P. (2000): Modal Identification from Ambient Responses using Frequency Domain Decomposition, *Proceedings of the International Modal Analysis Conference (IMAC),* Texas, USA, 6 pages.

[20] Kjær, B.&: Brüel & Kjær Sound & Vibration Measurement, https://www.bksv.com/en/about, (accessed December 05, 2022).

[21] A. Hasan, M.D., Ahmad, Z.A.B., Salman Leong, M., Hee, L.M. (2018): Enhanced frequency domain decomposition algorithm: a review of a recent development for unbiased damping ratio estimates, *Journal of Vibroengineering*, **20** (5), 1919–1936, doi: https://doi.org/10.21595/jve.2018.19058

[22] Brincker, R., Ventura, C.E., Andersen, P. (2001): Damping estimation by frequency domain decomposition, *Proceedings of IMAC 19: A Conference on Structural Dynamic,* Florida, USA.

[23] Jacobsen, N.J., Andersen, P., Brincker, R. (2008): Applications of frequency domain curve-fitting in the EFDD technique, *Conference Proceedings of the Society for Experimental Mechanics Series.*

[24] Official SOFiSTiK web page, https://www.sofistik.com/, (accessed December 01, 2022).

[25] Ereiz, S., Duvnjak, I., Fernando Jiménez-Alonso, J. (2022): Review of finite element model updating methods for structural applications, *Structures* **41**, 684–723, doi: https://doi.org/10.1016/j.istruc.2022.05.041

[26] Wilkinson, J.H. (1958): The Calculation of Eigenvectors by the Method of Lanczos. *The Computer Journal,* **1**(3), 148–152.

ENVIRONMENTAL EFFECT ON THE DYNAMIC CHARACTERISTICS OF RC BRIDGES

Marija Vitanova[1], Igor Gjorgjiev[2], Nikola Naumovski[3], Viktor Hristovski[4]

[1] *Assoc. Prof. Dr., Ss. Cyril and Methodius University in Skopje, Republic of North Macedonia, Institute of Earthquake Engineering and Engineering Seismology, marijaj@iziis.ukim.edu.mk*

[2] *Prof. Dr., Ss. Cyril and Methodius University in Skopje, Republic of North Macedonia, Institute of Earthquake Engineering and Engineering Seismology, igorg@iziis.ukim.edu.mk*

[3] *Assist. Dr., Ss. Cyril and Methodius University in Skopje, Republic of North Macedonia, Institute of Earthquake Engineering and Engineering Seismology, nikolan@iziis.ukim.edu.mk*

[4] *Prof. Dr., Ss. Cyril and Methodius University in Skopje, Republic of North Macedonia, Institute of Earthquake Engineering and Engineering Seismology, viktor@iziis.ukim.edu.mk*

Abstract

Bridges represent key structural elements of transportation systems. They are exposed to different natural and environmental effects that may cause damage representing a potential threat mainly in disturbing the process of transportation of people and goods. The short- and long-term road closures might have a tremendous impact on regional economic and social development. Therefore, the definition of their dynamic characteristics as are natural frequencies by experimental measurements is very important for fast and early assessment of the current conditions. For that purpose, the method of experimental modal analysis is used. This method involves measurement of structural response under ambient conditions. Presented in this paper is investigation of environmental effects upon dynamic characteristics of RC frame bridges. The investigation was carried out on two overpasses with approximately the same geometry. Both structures have two spans each and are in straight direction, but are placed under a skew angle of 58° and 67.8°. The overpasses were constructed in 2016, but have still not been put into operation. They are situated along "Friendship" high-way in N. Macedonia and the distance between them is 3km. Three measurements were performed for each overpass, namely the first measurements were done in October 2017 when dynamic tests were performed, the second were done in March 2020 and the third were done in May 2022. Modal identification of the overpasses was effectively carried out using the enhanced frequency domain decomposition method in frequency domain and stochastic subspace identification method in time domain. The identified dynamic characteristics were compared with each other and with the environmental effects. The results from the analysis show that the identified natural frequencies effectively indicate change of dynamic characteristics of the overpasses due to environmental effects. Greater difference in identified natural frequencies is observed in longitudinal direction, while the least difference occurs in vertical direction.

Keywords: ambient vibration measurements, dynamic characteristics, reinforced concrete bridges, condition assessment

1. Introduction

Bridges, as a vital part of the transportation systems, are inevitably exposed on the daily, seasonal, and annual air temperature variations which affects on the characteristics of the structures. During their service life, local damage can be reflected by the changes in dynamic properties. Therefore, a successful damage assessment relies heavily on the prediction accuracy of the dynamic properties. The variations of modal parameters caused by environmental factors are very significant and often greater than those caused by structural damage [1] or normal loads [2]. The periodic (diurnal, seasonal, and yearly) and transient temperature variations always mask changes in dynamic properties due to actual damage. Recently, more research has focused on the effect of temperature on the dynamic properties of bridges [3].

In practice, the effect of temperature variations on structural dynamic properties have been attributed to the reasons outlined below. First, structural deformations occurred with variations in temperature-varying environments and were called large deformation effects [4]. Second, structural stiffness changed because of thermal stress in the well-known stress stiffening effect [5]. In addition, material

properties were temperature dependent; for example, the decrease in the elastic modulus of concrete and of steel led to a reduction in modal frequencies. Furthermore, and equally important, the elastic properties of support (especially for bridge structures) were more easily affected by thermal variations, and at low temperature, the boundary conditions also changed suddenly [6]. Accordingly, the factors that affected the dynamic properties of bridge structures were complex and led to some specific damage detection methods, such as technology that does not need estimations of the modal parameters [7]. In addition, a thermal performance study of bridges based on long-term monitoring data still piqued researcher interest [8]; however, the cost of the health monitoring system was high, despite increasingly more advanced structural health monitoring (SHM) technologies [9]. To remove the environmental impacts, regression-based analysis [10] and principal component analysis [11] were adopted, but these analyses were data-driven black box modeling techniques. Although Zhou and Song [12] proposed a physics-based environmental-effects-embedded model updating method to overcome these shortcomings, the selection of the updating parameters was also critical, and a large deflection effect was not taken in account.

In the present study, time-varying thermodynamic properties of 2 span girder bridges were analyzed and compared.

2. Review of the realization of the research and the achieved results

2.1 Applied procedure and description of measuring equipment

The dynamic characteristics have been determined by measurements of ambient vibrations. The equipment with an acquisition system that was used to take the measurements, is sensitive accelerometers that have recorded the acceleration at certain points on the bridge. In this case PCB Piezotronics devices, model 393B12, manufactured by National Instruments with a sensitivity of 10,000 mV and a range of up to 4.9 m/sec^2, with a size of 0.5g (Fig. 1 left) were used. Data acquisition was performed with the acquisition system - module NI cDAQ-9178 and 4 NI 9234 boards (Fig. 1, middle and Fig. 2). The recorded acceleration measurements are expressed in "Earth acceleration - g" (9.81 m/sec^2).

Fig. 1. Piesotronics PCB Accelerometer Model 393B12 (left), DAQ-9178 NI Data Acquisition System Module (middle) and NI 9234 Board (right)

Fig. 2. Field monitoring equipment (left), three-way accelerometer (right)

The measurements were carried out using a sampling rate of 2.048 Hz. In total, 15 accelerometers were used with various measurement locations and directions. The measurement system configuration is shown in Fig. 3.

Fig. 3. Acquisition System (left) and Accelerometer Configuration (right)

During the measurements, the sensors were placed in the different points of the bridge: in the middle of the bays and above the piers. During all measurements, one accelerometer was located in a reference point in order to enable the comparison of the amplitudes of the other sensors with the reference points for defining the tonal forms of vibration. These measurements cover a frequency range from 0 to 40 Hz, where the first resonant frequencies are found. The processing of the record was carried out by applying a fast Fourier transformation so that it was possible to define the frequency composition of the registered vibration from which the natural frequencies of the objects could be identified.

2.2 Bridge measurements

Withing the framework of this research, field measurements of two overpasses (OP2 and OP3) were carried out to determine their dynamic characteristics. The selected bridges are located over the "Friendship" highway, Demir Kapija - Gevgelija section, designed according to modern regulations that consider the seismic action.

The initial measurements of the structures were carried out in October 2017, during which the trial loading of the bridges with static and dynamic loads was performed. The load capacity and deformability of the built construction is compared with the results of the design project. The precision of the performance and the geometry of the elements were checked, and the quality of the incorporated materials and thus the usability of the construction was checked. At the beginning of March 2020, additional measurements were performed on the bridges with a duration of 10 min. The same measurements were repeated in May 2022. The two bridges were not put into use for all years during measurements. Therefore, only the environmental conditions are the external factors that may effect the dynamic properties of the bridges.
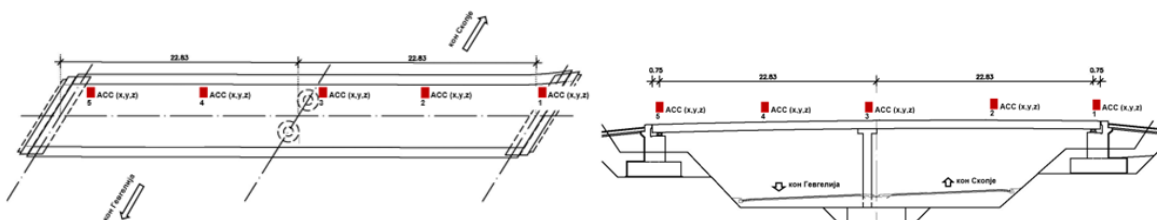
Fig. 4 Position of accelerometers on the measured bridge at base and cross-section for OP2
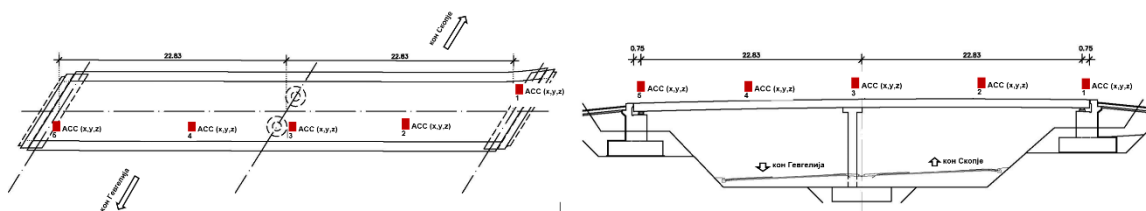
Fig. 5 Position of accelerometers on the measured bridge at base and cross-section for OP3

For performing the measurements, 15 accelerometers were used, in 5 places, 3 each in the longitudinal x direction, the transverse y direction and the vertical z direction, and they were placed on the edge of the upper structure, in the field and above the middle support (Fig. 4 and Fig. 5). During the first measurement, the accelerometers were placed on the part of the upper construction, in the direction of Skopje (Fig. 4), while during the second measurement, they were placed in the direction of Gevgelija, with the first accelerometer as a benchmark during both measurements being placed in the same place (Fig. 5).

2.2.1 Description of modal damping estimation methods

The methods available to perform identification of modal parameters (in this case modal damping, but it is the same for all modal parameters) of dynamic systems based on their response to ambient excitation are classified as frequency domain or time domain methods. The frequency domain methods start from the output spectrum of half- spectrum matrices estimated from the measured outputs. After obtaining the frequency response curves of the analysed system, modal damping can be measured using half-power bandwidth method and Enhanced Frequency Domain Decompositon (EFDD) method. The half-power bandwidth method consists of locating the resonant frequency and two nearby frequencies f1 and f2 located in the frequency spectrum by application of equation 1:

$$\xi = \frac{f_2 - f_1}{2f_r} \times 100\% \tag{1}$$

Enhanced Frequency Domain Decompositon was performed in order to calculate the damping (IRF) by using the impulse response of a single degree of freedom. Once a set of points with similar singular vectors is selected for a particular mode (Figure 6a), this segment of an auto-spectrum may be converted to a time domain (Figure 6b). An auto-correlation function with the contribution of a single mode is obtained. As the output correlation of a dynamic system excited by white noise is proportional to its impulse response, it is possible to estimate the modal damping coefficient. This can simply be performed by fitting an exponential function to the relative maxima of the correlation function and extracting the modal damping ratios from the parameters of the fitted expression taking into account the classical expression for the impulse response of a single degree of freedom.
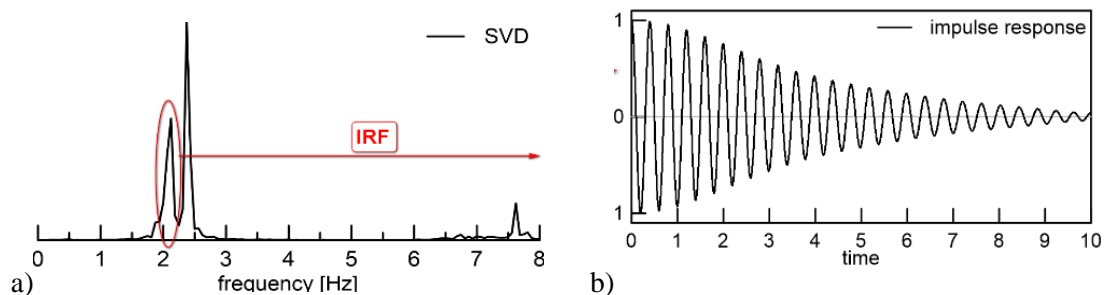
Fig. 6. FDD method, estimation of the modal damping ratio

2.2.2 Overpass OP2

Using the previously described procedure, most of the records were obtained at individual points of the investigated bridge. Based on these registrations and their singular value of spectral densities, a certain amount of data on the dynamic characteristics of the investigated structures were obtained. Below, on Fig.7 the curves of singular value of spectral densities for OP2 are presented.

Table 1 shows the frequencies obtained from all measurements, when the accelerometers were placed on the part of the upper construction in the direction of Skopje (measurement 1). From the obtained results, it can be concluded that almost all accelerometers that measured the acceleration in a certain direction show similar results, that is, for longitudinal direction, the frequency is 2.58Hz for 2017year, 3.58 for 2020year and 2.65Hz for 2022.

a)

b)

c)
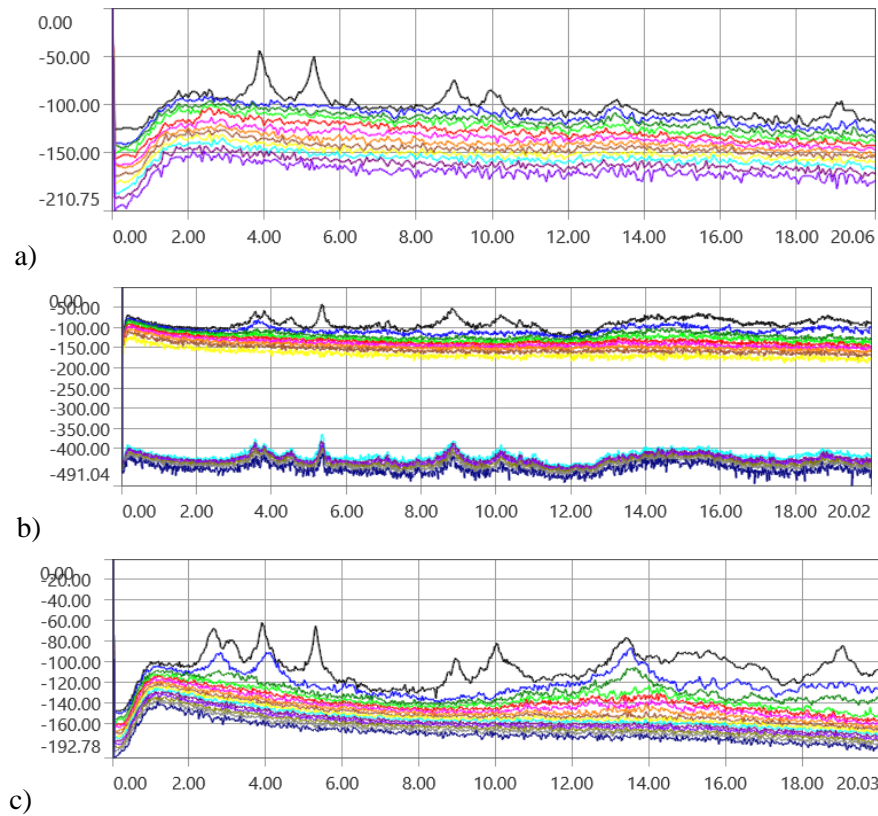
Fig.7 Singular value of spectral densities for OP2
a) 2017, b) 2020, c) 2022

It can be seen that the frequency has increased in 2020 and in 2022 came back. In the Transversal direction, the frequency of the structure is 2.97Hz for 2017year, 3.80 for 2020year and 3.12Hz for 2022. In the vertical direction, the frequency of the structure is 3.88Hz for 2017year, 3.81 for 2020year and 3.91Hz for 2022. In this direction, the frequency decreased in 2020 and then in 2022 increased to 3.91Hz.

Table 1 Natural frequencies of the structure for OP2

Mode	Direction	Frequency [Hz]		
		2017	2020	2022
1	Longitudinal	2.58	3.58	2.65
2	Transversal	2.97	3.80	3.12
3	Vertical	3.88	3.81	3.91
4	Vertical	5.31	5.36	5.32
5	Vertical	8.99	8.83	8.97
6	/	10.0	10.1	10.03

Table 2 shows the damping for each frequency by two methods: half power and IRF. In general, the damping calculated by the two methods corelates with each other. For the first frequency in the vertical direction, the damping is within the range of 0.88% for 2017, 0.73% for 2020 and 1.25% for 2022. For the first frequency in the Longitudinal direction, the damping is within the range of 0.71% for 2020 and 3.3% for 2022.

Table 2. Modal damping [%] for OP2

No.	2017			2020			2022		
	Freq.	Half Power	IRF	Freq.	Half Power	IRF	Freq.	Half Power	IRF
1 (Vertical)	3.88	0.80	0.88	3.81	0.37	0.73	3.91	0.73	1.25
2 (Vertical)	5.31	0.58	0.64	5.40	0.39	0.46	5.32	0.40	0.45
3 (Longitudinal)	2.58	n/a	n/a	3.58	0.54	0.71	2.65	2.43	3.3

2.2.3 Overpass OP3

Using the same procedure za OP2, all records were obtained at individual points of the investigated bridge. Based on these registrations and their singular value of spectral densities, a certain amount of data on the dynamic characteristics of the investigated structures were obtained. Below, on Fig.8 the curves of singular value of spectral densities for OP3 are presented.
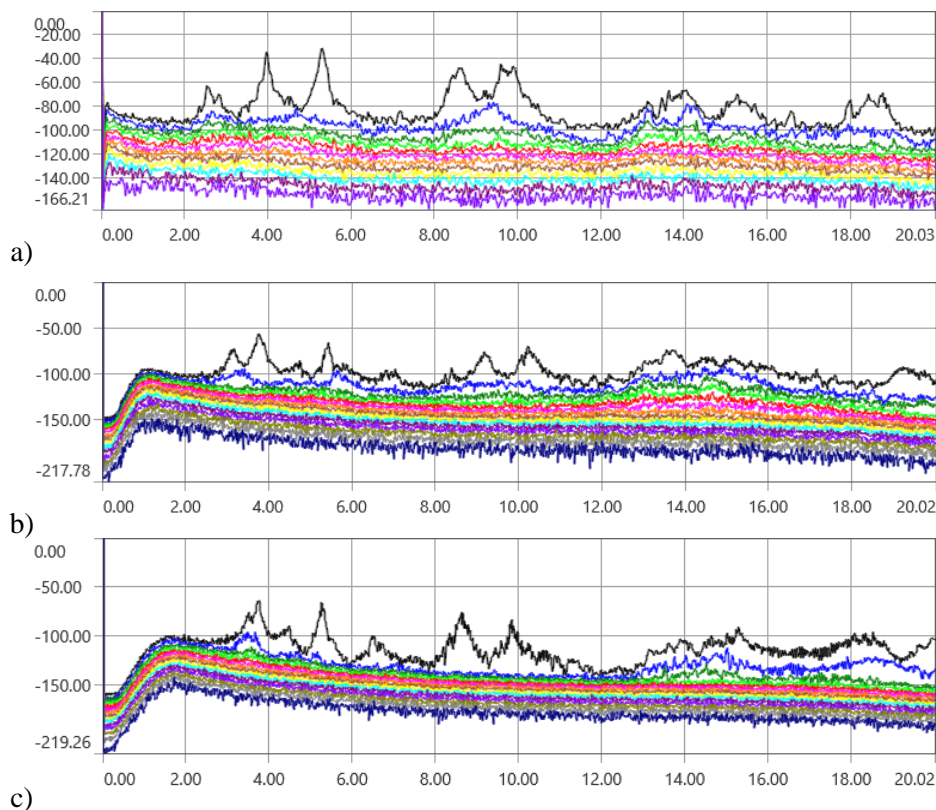
Fig. 8 Singular value of spectral densities for OP3
a) 2017 b) 2020 c) 2022

Table 3 shows the frequencies obtained from all measurements, when the accelerometers were placed on the part of the upper construction in the direction of Skopje (measurement 1) for bridge OP3. From the obtained results, it can be concluded that almost all accelerometers that measured the acceleration in a certain direction show small differences in natural frequencies. For longitudinal direction, the frequency is 2.53Hz for 2017year, 3.14 for 2020year and 3.50Hz for 2022. It can be seen that the frequency has continuously increased in 2020 and in 2022. In the Transversal direction, the frequency of the structure is 2.84Hz for 2017year, 3.49 for 2020year and 3.77Hz for 2022. In the vertical direction, the frequency of the structure is 3.98Hz for 2017year, 3.78 for 2020year and 3.78Hz for 2022. In this direction, the frequency decreased in 2020 and continued with same value till 2022.

Table 3. Natural frequencies of the structure for OP3

Mode	Direction	Frequency [Hz]		
		2017	2020	2022
1	Longitudinal	2.53	3.14	3.50
2	Transversal	2.84	3.49	3.77
3	Vertical	3.98	3.78	3.78
4	Vertical	5.28	5.35	5.27
5	Vertical	9.62	9.16	8.64

Table 4 shows the damping for each frequency by two methods: half power and IRF. In general, the damping calculated by the two methods corelates with each other. For the first frequency in the vertical direction, the damping is within the range of 0.78% for 2017, 1.44% for 2020 and 1.06% for 2022. For the first frequency in the Longitudinal direction, the damping is within the range of 0.82% for 2017 and 2.18% for 2020.

Table 4. Modal damping [%] for OP3

No.	2017			2020			2022		
	Freq.	Half Power	IRF	Freq.	Half Power	IRF	Freq.	Half Power	IRF
1 (Vertical)	3.98	0.59	0.78	3.78	1.15	1.44	3.78	1.06	1.06
2 (Vertical)	5.28	0.61	0.84	5.35	0.49	0.65	5.27	0.25	0.62
3 (Longitudinal)	2.58	0.69	0.82	3.14	2.02	2.18	3.50	n/a	n/a

3. Monitor the climate conditions

Engineering materials change their properties and are vulnerable to damage from the surrounding environment, whether they are concrete, steel, or wood. Some environmental factors are considered during structural design, primarily in terms of stress conditions. However, the changes in fundamental environmental conditions such as temperature and humidity can be challenging because they may influence structural dynamic properties. Environmental monitoring is therefore an essential component of this bridge measurement program. The monitoring program involves gathering information on temperature, humidity, and environmental data analysis. Because the object region has a limited number of monitoring sensors, a relatively good profile of the environmental conditions was constructed by collecting monitored data for at least 6 months before the bridge measurements. The weather monitoring was conducted for the years 2017, 2020 and 2022. The most essential information to consider in these records will be the extremes in averages of temperature and humidity.

3.1 Temperature

According to the monitored program, the regularly collected set of data was grouped into three monitoring periods. The first monitoring period was a period of one month before the bridge measurements, while the second monitoring period was a period of three months prior to the measurements. The last analyzed period was a period of six months before the structure's measurements. The determination of real temperature inside each structural part was not conducted because the measurements were only for ambient temperature. As a result, it was decided to evaluate how these conditions might affect the structural dynamic characteristics.

Tables 5 to 7 show the ambient temperatures for 2017, 2020 and 2022. The temperature was studied for three periods of 1, 3 and 6 months before the measurements. For a period of 6 months, the average mean temperature for 2017 is 19.2°, while for 2020 and 2022 it has dropped to around 7.5-9.2°. For a period of 3 months, the average mean temperature is different for each year, where for 2017 it is 20.5°, for

2020 it is 4.5° and for 2022 it is 10.1°. For a period of 1 month, the average mean temperature for 2017 and 2022 is around 15.5°, while for 2020 it has dropped to 6.5°.

Table 5 Temperature observation for period of 1 month before bridge measurements

Year	Avg Max [°]	Avg Mean [°]	Avg Min [°]	Max [°]	Min [°]
2017	23.7	15.7	8.3	37	-3
2020	13.3	6.5	0.3	25	-6
2022	23.1	15.2	7.5	34	-2

Table 6 Temperature observation for period of 3 months before bridge measurements

Year	Avg Max [°]	Avg Mean [°]	Avg Min [°]	Max [°]	Min [°]
2017	28.6	20.5	12.3	40	-3
2020	10	4.5	-0.4	25	-9
2022	17.2	10.1	3.3	34	-9

Table 7 Temperature observation for period of 6 month before bridge measurements

Year	Avg Max [°]	Avg Mean [°]	Avg Min [°]	Max [°]	Min [°]
2017	26.9	19.2	11.4	40	-3
2020	15.6	9.2	3.5	34	-9
2022	13.6	7.5	1.66	34	-10

Fig. 9 show the temperature observation over past six months before bridge measurements: maximum daily values, minimal daily values, and average daily data.
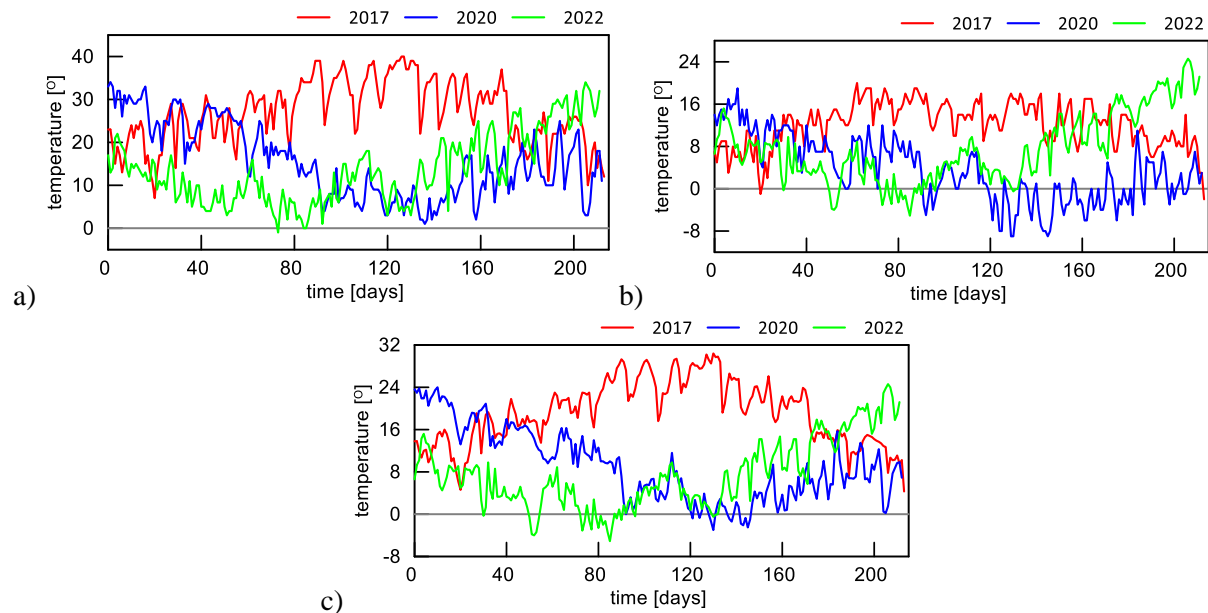
Fig. 9 Temperature observation over past six months before bridge measurements
a) Maximal daily values b) Minimal daily values c) Average daily data

Fig. 10 (left) shows the maximum, minimum and average temperatures (in °C) of the location in the period of the construction of the bridges to the end of the May, 2022, when the last measurements of the bridges were performed. Right figure (Fig. 10) presents the temperature the air needs to be cooled

to (at constant pressure) to achieve a relative humidity (RH) of 100% (source: www.wunderground.com).

a)   b)
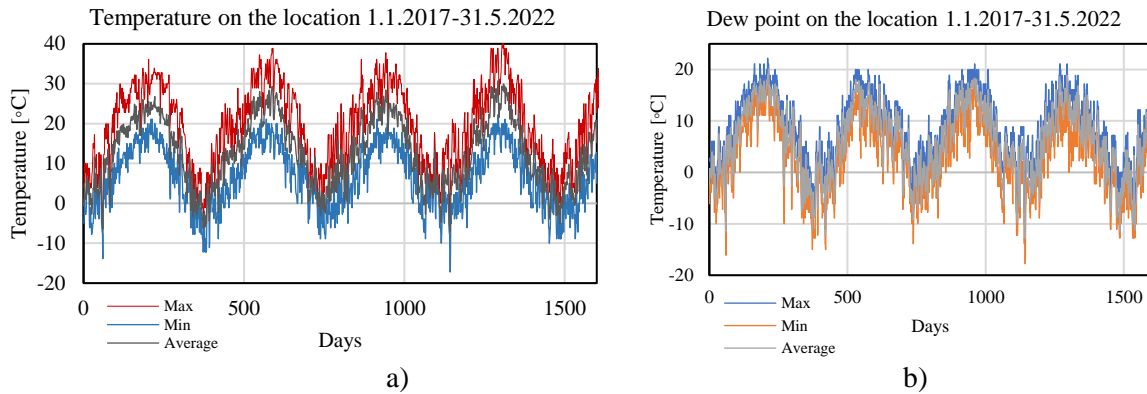
Fig. 10 a) Maximum, minimum and average temperatures on the location, b) dew point values for the period of existing the structures. *Source: www.wunderground.com*

3.2 Humidity

In addition to the analysis of the ambient temperature, an observation of humidity was also performed for a period of 1, 3 and 6 months before the measurement of the bridges. The results of this observation are shown in Table 8 through the average of daily maximum values. The average of daily maximum humidity for a period of 6 months is in range of 87.7%, 92.4% and 91.9%. In the case of a period of 1 month the average of daily maximum humidity is almost constant between 91.8% and 92.1%.

Table 8 Mean humidity of maximum daily values

Observation Period [months]	Average of daily maximum values [%]		
	2017	2020	2022
1	92.1	91.8	91.95
3	85.3	92.9	90.0
6	87.7	92.4	91.9

The maximum, minimum and average humidity on the location in the period of existing the structures, almost 5 years, (1.1.2017-31.5.2022) is presented on Fig. 11. This figure shows that the average humidity during the whole period is almost 70%.
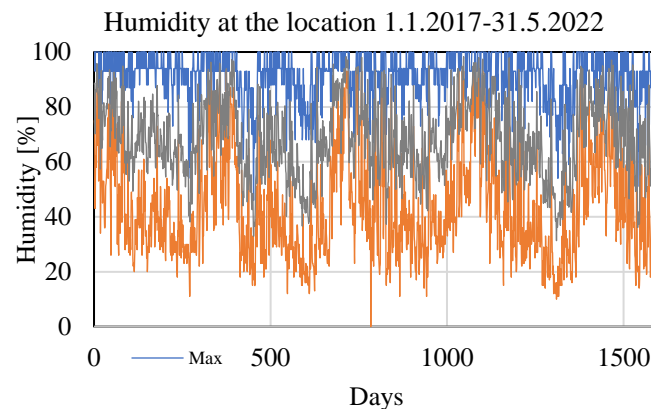
Fig. 11 a) Maximum, minimum and average humidity [%] on the location
Source: www.wunderground.com

3.3 Wind speed

Wind speed is a characteristic of air movement that can influence of the dynamic characteristics of bridge structures, especially of long span bridges. Minh et al. [13] concluded that the interaction of the structure with surrounding air currents can produce changes in structural dynamics as wind speeds change. In their investigation, they concluded that due to very low vibration frequencies, the gust response of a long-span bridge is very sensitive to turbulence properties, especially spatial coherence. Some of their effects on the gust response of long-span bridges have been pointed out.

Cheli et al. [14] showed that with increasing wind speed, the frequencies of the first vertical and torsional modes respectively rise and fall, and hence tend to converge. In addition, damping ratios generally increase significantly with wind speeds. These aero-elastic effects were confirmed in sectional model wind tunnel testing [15], but the range of wind speeds during the test have been not sufficient to confirm this behavior (being below 15m/sec and usually less than 10m/sec).

Since the measured bridges in this investigation do not have longe spans, the influence of the wind conditions of their dynamic characteristics have to be additionaly investigated. Herein, only maximum and average wind speed at the location is presented in the period of bridges existence (Fig. 12).
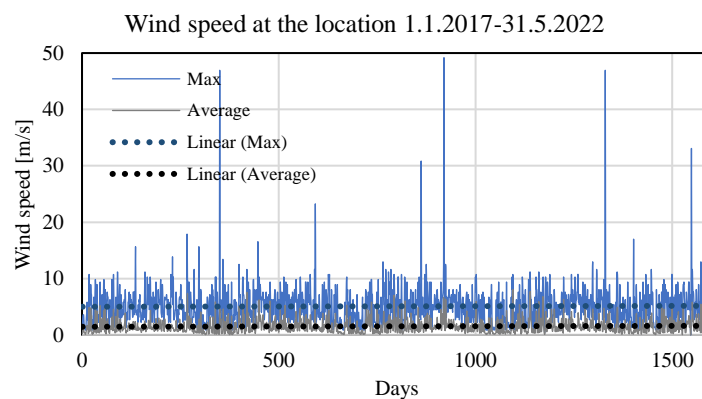
Fig. 12 Wind speed at the location of bridges
Source: www.wunderground.com

From the Fig. 12 it can be concluded that on the location of the bridges, the maximum wind speed is almost 50 m/s, but the average speed is 1.5m/s.

4. Conclusion

The objective of this study is to investigate the environmental effects on the dynamic characteristics of two base-isolated highway monolithically constructed frame overpasses. The dynamic characteristics of the structures are defined using large scale ambient vibration testing. To consider the difference in the dynamic characteristics of the structures, three measurements were performed to both bridges. The first measurements were realized after the construction of the structures, in 2017; second one 3 years later, in 2020; and the last one 2 years after the second measurements, in 2022. The ambient vibration tests were conducted under the environmental excitations in the bridges and the dynamic characteristics of structures were accurately extracted. Both overpasses were exposed on only environmental atmospheric conditions. They are still not in use, so they were no exposed-on service loads. From the obtained results and the environmental investigation, it can be stated that:

- There are differences in the results from the performed ambient vibration testing in three periods of the existing the structures. Since they are not in use and are no exposed to service loads, it can be concluded that the environmental conditions have influence of the dynamic characteristics of the structures.
- The natural frequencies of both structures are higher with the time. Especially in longitudinal and transversal directions. The difference in vertical direction is almost the same.

- The difference between the measured frequencies from first two measurements is bigger than the second and the third measurement, that means that the structure is getting stabilized.
- Temperature and humidity have influence of the dynamic characteristics of the structures.
- Wind speed do not have influence of the dynamic characteristics of the structures.

References

[1] Li, H., S. Li, J. Ou, and H. Li. 2010b. "Modal identification of bridges under varying environmental conditions: Temperature and wind effects." Struct. Control Health Monit. 17 (5): 495–512.

[2] Kulprapha, N., and P. Warnitchai. 2012. "Structural health monitoring of continuous prestressed concrete bridges using ambient thermal responses." Eng. Struct. 40 (Jul): 20–38.

[3] Zhou, G.-D., and T.-H. Yi. 2014. "A summary review of correlations between temperatures and vibration properties of long-span bridges." Math. Prob. Eng. 2014: 1–19. https://doi.org/10.1155/2014/638209.

[4] Lu, Z. R., and S. S. Law. 2006. "Identification of prestress force from measured structural responses." Mech. Syst. Sig. Process. 20 (8): 2186–2199.

[5] Cook, R. D., D. S. Malkus, M. E. Plesha, and R. J. Witt. 2001. Concepts and applications of finite element analysis. 4th ed. New York: John Wiley & Sons.

[6] Siddique, A. B., B. F. Sparling, and L. D. Wegner. 2007. "Assessment of vibration-based damage detection for an integral abutment bridge." Can. J. Civ. Eng. 34 (3): 438–452.

[7] Domaneschi, M., M. P. Limongelli, and L. Martinelli. 2013. "Vibration based damage localization using MEMS on a suspension bridge model." Smart Struct. Syst. 12 (6): 679–694.

[8] Xia, Q., J. Zhang, Y. Tian, and Y. Zhang. 2017. "Experimental study of thermal effects on a long-span suspension bridge." J. Bridge Eng. 22 (7): 04017034.

[9] Asadollahi, P., and J. Li. 2017. "Statistical analysis of modal properties of a cable-stayed bridge through long-term wireless structural health monitoring." J Bridge Eng. 22 (9): 04017051.

[10] Moser, P., and B. Moaveni. 2011. "Environmental effects on the identified natural frequencies of the Dowling Hall Footbridge." Mech. Syst. Sig. Process. 25 (7): 2336–2357.

[11] Giraldo, D. F., S. J. Dyke, and J. M. Caicedo. 2006. "Damage detection accommodating varying environmental conditions." Struct. Health Monit. 5 (2): 155–172.

[12] Zhou, S. L., and W. Song. 2017. "Environmental-effects-embedded model updating method considering environmental impacts." Struct. Control Health Monit. 25 (3): e2116.

[13] Minh, N. N., H. Yamada, T. Miyata, and H. Katsuchi. 2000. "Aeroelastic Complex Mode Analysis for Coupled Gust Response of the Akashi Kaikyo Bridge Model." Journal ofWind Engineering and Industrial Aerodynamics 88 (2–3): 307–324.

[14] Cheli, F., Collina, A., Diana, G., Zasso, A., Brownjohn, J. M. W., 1992. "Suspension bridge parameter identification in full-scale test". Journal of Wind Engineering and Industrial Aerodynamics 41, 165-176.

[15] Curami, A., Falco, M., Zasso, A., 1992. "Nonlinear effects in sectional model aeroelastic parameters identification". pp. 1321-1332.

COMBINED PROTECTION OF BRIDGES EXPOSED TO EARTHQUAKE AND FLOOD DISASTERS WITH NEW RB-UPGRADED ISOLATION SYSTEM

Jelena Ristic[(1)], Venera Hajdari[(2)], Labeat Misini[(3)], Danilo Ristic[(4)]

[(1)] *Assoc. Prof. Dr. Faculty of Engineering, Department of Civil Engineering, International Balkan University (IBU), Skopje, Republic of North Macedonia, e-mail: risticjelenaibu@gmail.com*

[(2)] *PhD student, Faculty of Civil Engineering, Ss. Cyril and Methodius University, Skopje, Republic of North Macedonia, e-mail: venerahajdari95@gmail.com*

[(3)] *PhD student, Institute of Earthquake Engineering and Engineering Seismology (IZIIS), Ss. Cyril and Methodius University, Skopje, Republic of North Macedonia, e-mail: labeat.misini@gmail.com*

[(4)] *Full Prof. Dr., Institute of Earthquake Engineering and Engineering Seismology (IZIIS), Ss. Cyril and Methodius University, Skopje, Republic of North Macedonia, e-mail: danilo.ristic@gmail.com*

Abstract

Combined and extensive experimental and analytical study devoted to development of an integrated earthquake and flood protection (EFP) bridge system was performed. It represents an extension of the integral research project led by the fourth author, conducted in the Institute of Earthquake Engineering and Engineering Seismology (IZIIS), Ss. Cyril and Methodius University (Skopje), during three and a half years, in the frames of the innovative NATO Science for Peace and Security Project "Seismic Upgrading of Bridges in South-East Europe by Innovative Technologies (SFP: 983828)", involving five European countries and led by the fourth author. The presently introduced EFP bridge system represents a specific, extended segment of the integral research. The upgraded, seismically isolated (USI) system with integrated space flange (SF) energy dissipation (ED) devices has been developed as a mechanical passive concept to provide harmonized response of bridge structures to earthquakes. It was formulated as an adaptive system, which follows the adopted concept of global optimization of seismic energy balance, through utilization of newly designed dissipation devices as a supplementary damping level to bridge isolation. The new EFP-bridge system is based on obligatory incorporation of the following four integrated complementary systems: (1) Seismic isolation (SI) system, (2) Seismic energy dissipation (ED) system, (3) Combined earthquake and flood displacement limiting (EFDL) system composed of new and experimentally tested RB devices and (4) Uplift protection system (UP). With the extensive experimental quasi-static cyclic tests conducted by simulated, gradually increased displacement amplitudes, there were confirmed very stable hysteretic responses of the created prototype models of rubber buffer (RB) devices applicable for efficient protection of common and isolated bridges exposed to either strong earthquakes or flood disasters. Following the upgrading of the seismically isolated (USI) bridge system with energy dissipation devices, the adopted original rubber buffer (RB) devices represent an important additional line of defense against abrupt loadings due to earthquake and flood disasters.

Keywords: bridge, model testing, earthquake, flood, rubber buffer, safety

1. Introduction

In the past, extensive studies in the field of seismic isolation of bridges were mostly performed in worldwide recognized research centers in Japan, USA, Italy, and New Zealand. However, in recent years, contributions from many other countries have been increased and have resulted in proposal of many new ideas and concepts. Intolerable severe impacts to modern bridge systems have been observed during strong recent earthquakes [1, 2]. This has given rise to strong arguments about further needs for development and practical implementation of seismic isolation systems for seismic protection of bridges, [3, 4, 5, 6, 7]. However, in addition to problems arising due to strong earthquakes, continuous functioning of highway bridges and highway networks can be seriously disrupted by various other existing types of hazards. Studies involving flood disaster prevention and preparedness against mobility disruption by floods have regularly been conducted, [9]. These have also included two-dimensional flood inundation modelling, [10] and development of seismically resilient hinges for bridge piers [11]. In recent years, various technical standards have been newly developed or upgraded [12-13]. Following

some specific observations published in prepared recent flood investigation reports [14], advanced concepts of protection of critical infrastructure systems located in a multi-hazard environment have been developed and proposed [15-19]. In this specific and wide research area, some fundamental studies have been realized. These have included determination of hydrodynamic forces on inundated bridge decks [20] and assessment of scour and other hydraulic actions on highway structures [21-22]. Recently, some integrated studies have been focused on development of practical measures assuring continuous functioning of entire road networks and providing assessment of road closure probabilities [23].

Presented in this paper is the developed new advanced earthquake and flood protection (EFP) bridge system, considering the results from the conducted combined and extensive experimental and analytical studies. Following the idea of upgrading of the developed, seismically resistant (USI) bridge system [5] involving seismic isolation and energy dissipation devices, the newly created specific rubber buffer (RB) devices have been added as an important additional line of defense against abrupt loadings due to earthquake and flood disasters. The resulting efficient bridge protection under possible bi-hazard effects was provided by means of the created new integrated earthquake and flood protection (EFP) system.

2. Concept of New EFP Bridge System

The presently introduced upgraded, seismically isolated (EFP) bridge system represents a newly created advanced technical concept developed as a specific segment of the integral research, Fig. 1. The previously developed upgraded seismically isolated (USI) system with integrated space flange (SF) energy dissipation (ED) devices, represented a passive mechanical technical concept providing safe harmonized response of bridge structures to earthquakes, [5]. It was formulated as an adaptive system, which follows the adopted concept of global optimization of seismic energy balance through utilization of newly designed, energy dissipation devices as a supplementary damping level to the bridge isolation.
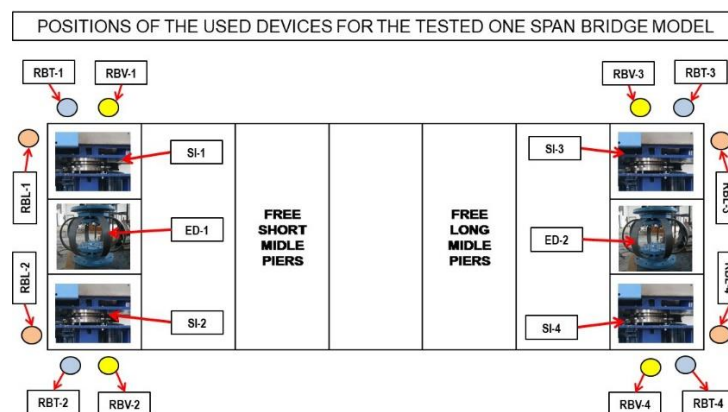
Fig. 1. Defined positions of the integrated devices in the tested EFP bridge model: Seismic isolation devices (SI), Energy dissipation devices (ED) and RB devices used in longitudinal, transversal and vertical direction.

The new EFP bridge system is based on obligatory incorporation of the following four integrated complementary systems: (1) Seismic isolation (SI) system, (2) Seismic energy dissipation (ED) system, (3) Combined earthquake and flood displacement limiting (EFDL) system composed of new and experimentally tested RB devices and (4) Uplift protection system (UP), Fig. 1. The developed SI and ED systems have been created and successfully implemented, [5]. However, with the conducted programmed quasi-static cyclic experimental tests under simulated, gradually increased displacement amplitudes, very stable hysteretic responses of the created new prototype models of rubber buffer (RB) devices have been confirmed. The created RB devices have been implemented very successfully in assembling a combined earthquake and flood displacement limiting (EFDL) system and an uplift protection system (UP). The created, integrally upgraded EFP bridge system represents a technically new applicable option for efficient protection of common and isolated bridges exposed to either strong earthquakes or severe flood disasters. Following the promoted further upgrading of the seismically isolated (USI) system with the adopted original rubber buffer (RB) devices in longitudinal-L,

transversal-T and vertical-V-direction, an important additional line of defense against possible bi-hazard abrupt loadings involving severe earthquake and flood disasters is provided.

3 Prototypes of Used Devices in EFP Bridge Model

3.1 Prototypes of tested DSSSB isolation devices

The implemented isolation system used for the experimental EFP bridge model was assembled by use of the developed models of double spherical sliding seismic bearing (DSSSB) devices with two large-radii of spherical surfaces, Fig. 2. The DSSSB devices were originally designed, constructed and used in a previous investigation carried out by Ristic, J., et al., 2016, [7]. The targets that were set prior to the design and construction of the device were fulfilled: (1) very small horizontal reaction and friction forces (reaching maximum 4.3% of the vertical load), and (2) stable hysteretic behavior along the entire range of large displacements. It was confirmed that the hysteretic behavior of the implemented DSSSB devices could be successfully simulated with the experimentally defined representative bilinear analytical model.
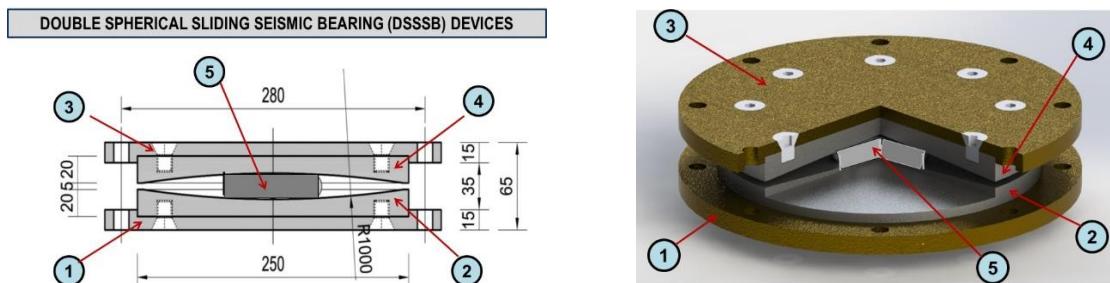
Figure 2. Basic elements of the constructed and used prototypes of DSSSB devices: (1) lower end metal plate; (2) lower spherical plate; (3) upper end metal plate; (4) upper spherical plate; (5) metallic slider;

Actually, the model was controlled by four parameters, DY=1.0 mm, FY=0.32 kN, DU=50.0 mm, FU=0.92 kN, defined experimentally under simulated vertical load and cyclic displacements with increasing amplitudes.

3.2 Prototypes of tested SF energy dissipation devices

The created seismic energy dissipation system installed in the tested EFP bridge prototype model was composed of the developed advanced steel space flange (SF) energy dissipation (ED) devices.

Table 1. Hysteretic behavior properties of SF-ED-M11 and SF-ED-M12 devices computed by using the formulated nonlinear FEM model and simulated cyclic displacements with increasing amplitudes

No.	SF-ED Device M11: SF-ED-8C-L1R-T1			SF-ED Device M12: SF-ED-4C-L1R-T1		
	Notation	FEM model	(%)	Notation	FEM model	(Δ%)
1	DY (mm)	5.0	100.0	DY (mm)	6.0	120.0
2	FY (kN)	21.0	100.0	FY (kN)	9.0	42.8
3	K0 (kN/mm)	4.0	100.0	K0 (kN/mm)	1.5	37.5
4	K1 (kN/mm)	0.18	100.0	K1 (kN/mm)	0.02	11.1
5	K1/K0	0.045	100.0	K1/K0	0.013	28.8

Up to date, SF-ED dissipation devices of the proposed type have been studied only by the first author and her collaborators involved in bridges, [7] and [25].

In this paper, the two basic types of SF-ED devices are presented in Table 1. The first SF device is composed of eight ED components, model M11, representing the SF-ED-8C-L1R-T1 device, Fig. 3. The second SF device consists of four ED components, model M12, representing the SF-ED-4C-L1R-T1 device, Fig. 4.
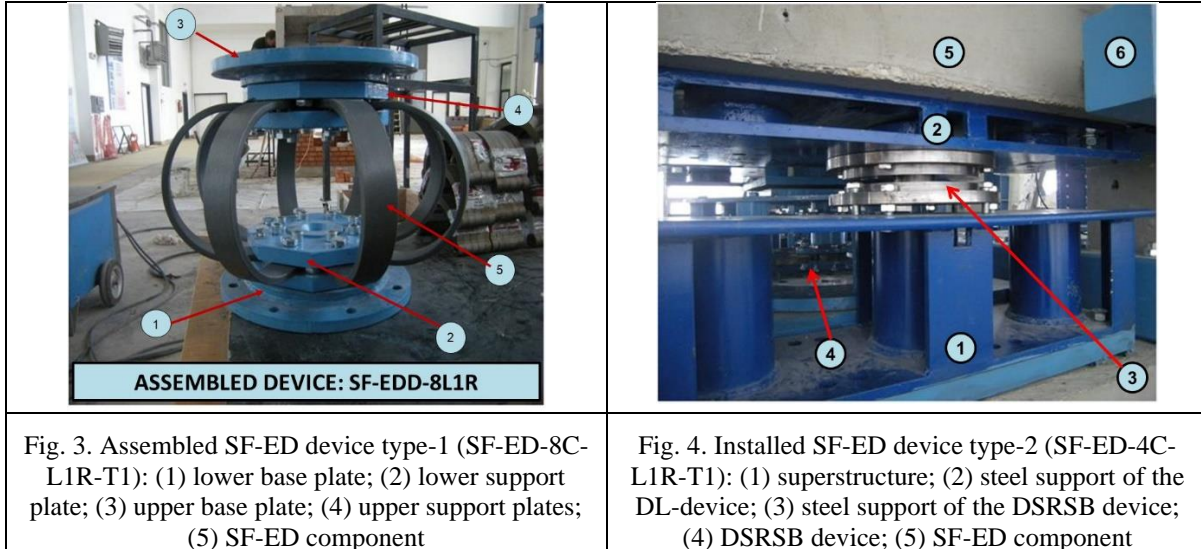
| Fig. 3. Assembled SF-ED device type-1 (SF-ED-8C-L1R-T1): (1) lower base plate; (2) lower support plate; (3) upper base plate; (4) upper support plates; (5) SF-ED component | Fig. 4. Installed SF-ED device type-2 (SF-ED-4C-L1R-T1): (1) superstructure; (2) steel support of the DL-device; (3) steel support of the DSRSB device; (4) DSRSB device; (5) SF-ED component |

Adopting the experimentally verified refined 3D nonlinear analytical model, the hysteretic responses of the assembled prototype devices exposed to cyclic loads were computed successfully. With the computed original results, it was confirmed that the adopted representative bilinear analytical model could be implemented to realistically model the full hysteretic behavior of the device. The defined parameters of the representative bilinear models are comparatively presented in Table 1.

3.3 Prototypes of tested displacement limiting RB devices

During strong earthquake vibrations, a limited number of very strong impulses may occur, followed by large displacement amplitudes, which are not controlled in a reliable engineering mode. Thus, the originally created advanced displacement limiting devices representing specific rubber buffer (RB) devices with provided wide geometrical and mechanical options, may be designed to reduce or eliminate earthquake damaging effects, Fig. 5.
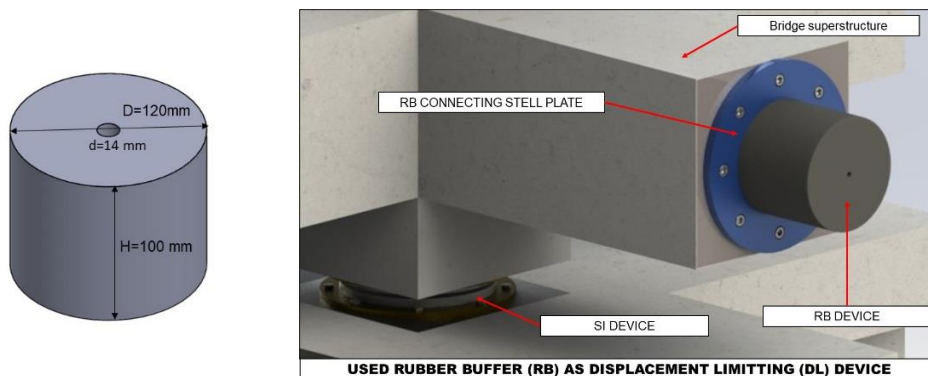
Figure 5. Geometry of the tested RB models used as displacement limiting devices.

However, if properly designed, the created RB devices can be also implemented to very efficiently protect large uncontrolled superstructure displacements in longitudinal (L), transversal (T) and vertical (V) direction, avoiding total collapse of bridge superstructure under generated, increasing or very strong damaging flood forces. If stiffness is properly designed, RB devices implemented in vertical (V)

direction can be used to efficiently protect against uncontrolled vertical uplifting displacements and total collapse of the bridge superstructure under generated strong vertical flood uplift forces. Actually, the developed RB devices can be integrated to act as a specific interactive displacement limiting system, protecting efficiently against uncontrolled failure of the bridge superstructure under generated, uncontrolled combined horizontal and vertical forces during extreme earthquakes and floods.

Table 2. Testing program & tests of elements (specimens) of prototype models of RB devices

Test No.	RB Model	RB Element	Test type	D (mm)	H (mm)
1	M1	M1-RB-40SH-E1	*Original*	120	100
2		M1-RB-40SH-E1	*Repeated*	120	100
3		M1-RB-40SH-E2	*Original*	120	100
4		M1-RB-40SH-E2	*Repeated*	120	100
5	M2	M2-RB-50SH-E1	*Original*	120	100
6		M2-RB-50SH-E1	*Repeated*	120	100
7		M2-RB-50SH-E2	*Original*	120	100
8		M2-RB-50SH-E2	*Repeated*	120	100
9	M3	M3-RB-60SH-E1	*Original*	120	100
10		M3-RB-60SH-E1	*Repeated*	120	100
11		M3-RB-60SH-E2	*Original*	120	100
12		M3-RB-60SH-E2	*Repeated*	120	100
13	M4	M4-RB-70SH-E1	*Original*	120	100
14		M4-RB-70SH-E1	*Repeated*	120	100
15		M4-RB-70SH-E2	*Original*	120	100
16		M4-RB-70SH-E2	*Repeated*	120	100

An extensive testing program was conducted [24]. It included realization of specifically programed cyclic tests of the constructed prototype models of RB devices. Presented in this paper are the representative results obtained from the realized extensive experimental tests of rubber buffer prototype models. The key functioning targets of the displacement limiting RB devices are: (1) enabling physical limitation of maximum relative displacements of seismic isolation devices; (2) achieving the predefined physical limitation of the relative displacements by properly avoiding the so called "hard" structural impact; and, (3) providing efficient protection of seismic isolation (SI) and energy dissipation (ED) devices by assured limitation of relative displacements.

Figure 6. Experimental test set-up used for testing of the model prototypes of RB displacement control devices under simulated cyclic loads with increasing displacement amplitudes.

To achieve all the stated goals, prototype models of RB devices were designed and manufactured in the form of cylindrical rubber (pads) buffers cast by use of rubber characterized by four different values of hardness measured in shores, H40, H50, H60 and H70. To obtain comparative experimental results, two experimental test specimens of each type of RB devices, amounting to a total of eight specimens, were constructed.

To investigate the effect of repeated loading, two tests (original and repeated) were performed on each test specimen. Therefore, the integral experimental program was extended to a total of completed 16 experimental quasi-static tests, Table 2. The presented experimental RB specimens were designed in the form of cylinders with a diameter of D=120 mm and height H=100 mm. In the middle of the cylinder, a central opening with a diameter d=14 mm was designed to be used for successful positioning of the experimental device prototype for its safe experimental testing, Fig. 6. Details of the produced original experimental models are shown in Table 2. More specifically, the table shows that, for each of the four RB models, two experimental elements (E1 & E2) were produced, meaning that the experimental program included testing of a total of eight different specimens. However, due to the need for getting an insight into the behavior of the innovative RB devices under repeated compressive loading effects, all 8 specimens were tested twice. The first (virgin) test was marked as original, while the second one was referred to as repeated, Table 2. Hence, the entire experimental program resulted in realization of a total of 16 cyclic experimental tests.
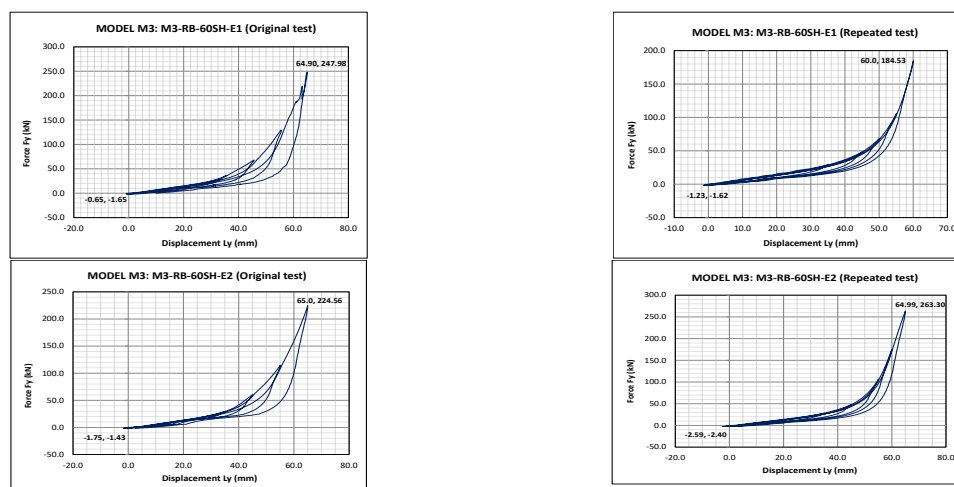
Figure 7. Recorded characteristic hysteretic response of model M3 during original and repeated tests of specimens M3-RB-60SH-E1 and M3-RB-60SH-E2 under simulated cyclic loads.

The role of the RB devices is to be effective only under generated compression forces during dynamic response of structures under strong earthquakes and floods. The experimental tests were realized by application of repeated compressive forces, which were increased in each successive cycle until reaching of the maximum "allowed" working level. Due to such defined specific experimental conditions, an adequate experimental frame was created, Figure 6. This frame enabled all the necessary conditions for the realization of the specified experimental tests. Testing was carried out by activation of an actuator in vertical direction in order to produce a compressive force upon the experimental element since it was fixed, on the upper side, to the constructed rigid steel frame. The experimental element (model) was completely made of rubber and, on the lower side, it was placed on a very rigid base that did not suffer any deformations, Figure 6. For "zero" point of deformation and "zero" point of force, there was selected a position indicating only a direct zero-contact between the actuator plate and the experimental rubber element, without transfer of any force (contact without force or zero contact). From that position, compressive forces were further simulated up to a certain initial level of deformation and then the deformation was returned to the zero point that represented a cycle. More concretely, a compression cycle was defined by loading up to a certain level of deformation and unloading down to zero deformation. The analogous cycles of loading and unloading were repeated a number of times, but in each successive cycle, the amplitude of deformation was increased. In that way, favorable conditions were created for identification of the real hysteretic behavior of all the tested experimental models up to the phase of deformations representing their optimal working level.

Fig. 6 (left) shows the experimental model with the defined zero level of deformations prior to the beginning of the realization of the experimental test, while Fig. 6 (right) shows the model with the realized considerable amount of total deformation (within the working deformation), being lower than the allowed working deformation, (D $_{allowed}$). In accordance with the provided conditions, it was clear that the realized experimental program provided original and highly valuable experimental results that enabled getting a realistic insight into the nonlinear-hysteretic behavior of the tested RB models and the respective elements. To demonstrate the evident suitability of the test results, Figure 7 shows four recorded hysteretic responses obtained from the conducted original and repeated tests of the specimens M3-RB-60SH-E1 and M3-RB-60SH-E2, under simulated cyclic loads.

4. Seismic Tests of EFP Bridge Model Under Simulated Earthquakes

Due to the size of the seismic shaking table (5.0 m x 5.0 m) and payload capacity, the originally designed EFP bridge prototype model had to be geometrically reduced in respect to the selected prototype. Adopted from these reasons was a geometrical scale factor of 1:9, which verified the referred constraints in this case, but with an adopted specific model design concept. As a consequence of the scale reduction, the relevant properties involved in the dynamic (seismic) tests were scaled according to the similitude law. Considering the main related factors, an adequate combined true replica-artificial mass simulation model was adopted. For simulation of the stiff RC superstructure, the stiff slab with added mass was adopted using the same material as that of the prototype structure. For simulation of the middle piers, steel material was used. The seismic DSSSB isolation devices and SF energy dissipation devices were designed and produced to a reduced scale. The similitude law implies adopted relations for different parameters, all given in terms of the geometrical scale factor (*lr*). Concrete material type C25/30 was used for construction of the RC segments of the bridge model, while for construction of the created SF devices, steel material type S355 was selected and applied.
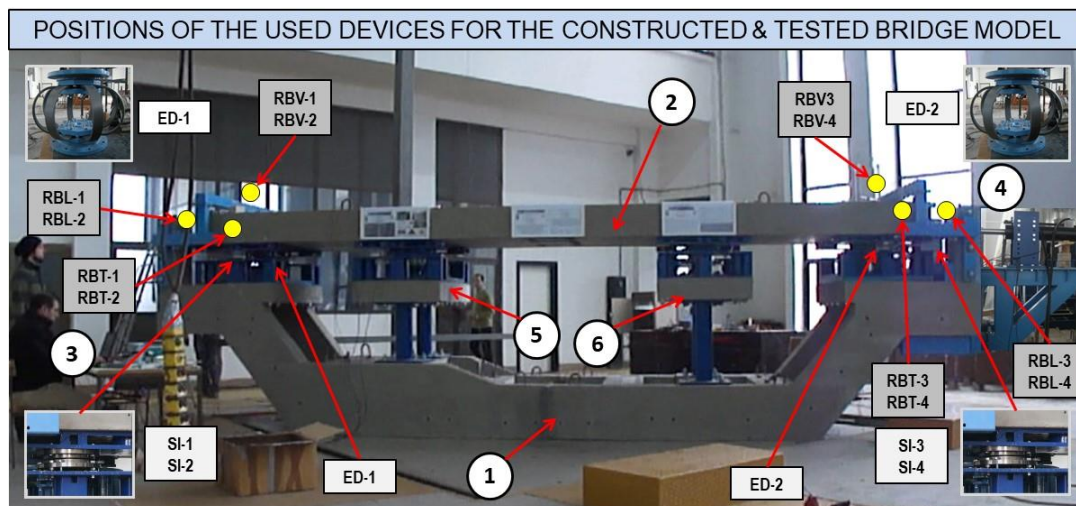
Fig. 8. Tested large-scale EFP bridge model composed of substructure (1), superstructure (2), left end support (3), right end support (4) and presently not-activated shorter (5) and longer (6) middle piers with indicated positions of the integrated devices: seismic isolation devices (SI), energy dissipation devices (ED) and rubber buffer (RB) devices used in longitudinal (RBL), transversal (RBT) and vertical (RBV) direction.

Regarding the proportions at the top level, the total length of the entire experimental bridge model was L=740.0 cm + 2 ∗ 20.0 cm + 2 ∗ 25.0 cm = 830.0 cm, Fig. 1 and Fig. 8. The RC deck was placed at a height distance of h_d = 40.0 cm from the highest RC substructure surfaces. This space (seismic gap) was used to install both the originally produced DSSSB devices and the new SF devices, Fig. 2 and Fig. 3.

Specially designed steel frame structures using steel profiles 100 mm x 120 mm were constructed and fixed to both ends of the tested EFP model. The shape of the frame structures was designed to provide favorable conditions for successful installation of the originally created and used rubber buffer devices in all three directions. The defined positions of the created and installed specific types of upgrading devices in the tested EFP bridge model are presented in Fig. 1 and Fig. 8.
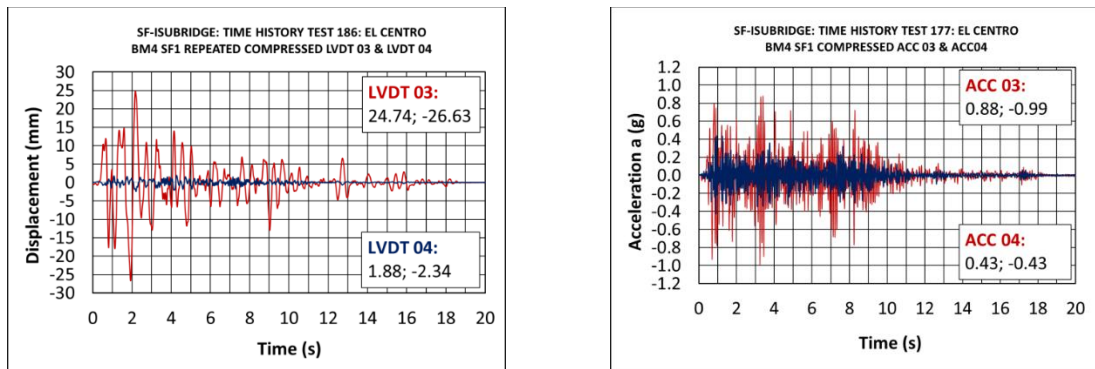
Figure 9. Relative superstructure displacement responses recorded by LVDT-03 & LVDT-04 (left) and acceleration responses recorded by ACC-03 & ACC-04 (right) during the EFP bridge model shaking table test conducted under simulated strong El-Centro earthquake.

Actually, in the tested EFP bridge model, there were integrated four constructed DSSSB seismic isolation devices (SI), then two originally created SF seismic energy dissipation devices (ED) and a respective number of displacement limiting devices, originally created, tested and used in the form of rubber buffer devices (RB). The positions of the rubber buffer devices were selected to be activated assuring limitation of displacements in longitudinal direction (RBL), transversal direction (RBT) and vertical direction (RBV), Fig. 1. After fabrication of all model segments and the specific SI, ED and RB devices and after preparing the other testing connections and instrumentation devices, the large-scale EFP bridge prototype model was assembled and tested in the Dynamic Testing Laboratory of the Institute of Earthquake Engineering and Engineering Seismology (IZIIS) in Skopje.
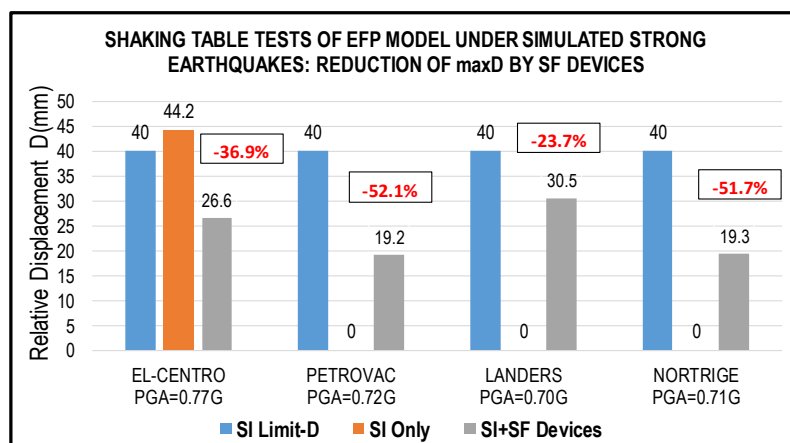
Figure 10. Advances of the EFP bridge system: Reduction of maximum relative displacements defined from the conducted seismic tests of the large-scale EFP model under simulated strong earthquakes.

With the adopted 20 active recording channels, approximately 5.000.000 numerical values were recorded in each single test. During the conducted four original and four repeated tests, a large experimental data volume containing about 40 million numerical values was obtained, integrally processed and analyzed.

As an example, Fig. 9 presents the time history responses of displacements and accelerations recorded during the seismic test under simulated real strong El-Centro earthquake scaled to PGA=0.77g. The conducted seismic shaking table tests showed that the seismically isolated bridge by using DSSSB devices and upgraded complementary SF energy dissipation devices and RB displacement limiting devices represented a highly efficient and practical engineering option for protection of bridges exposed to strong earthquakes. Actually, the new EFP system exhibited safe and very favorable behavior under strong earthquake excitations. Based on processing of the recorded original numerical data obtained from the realized extensive shaking table seismic tests by simulating strong earthquakes, the main qualitative advances of the innovative EFP system are summarized in Fig. 10. Very stable, reliable and safe seismic response was observed in all test cases due to the provided significant reduction of maximum relative displacements amounting to 36.9%, 52.1%, 23.7% and 51.7%, respectively, in the case of the simulated El Centro, Petrovac, Landers and Northridge earthquakes. All recorded peak values were lower than the defined allowable design displacement of Da=40.0 mm for the seismic isolators. The importance of upgrading the isolated bridge with the new SF devices was experimentally validated and confirmed with the conducted initial quantification test of the model with the installed seismic isolation only. Under the simulated strong El-Centro earthquake, the tested isolated system, without installed SF devices, showed an unsafe response. Large excessive relative displacement amounting to maxD=44.2 mm was recorded, Fig. 10.

5. Loading of EFP Bridge Model Under Simulated Flood Loading

The extensive stability studies of bridge structures exposed to the effects of severe flood disasters that have been carried out so far have mainly been focused on protection of substructure elements. The effect of water pressure on bridge piers, possible undermining and failure of foundation of middle piers, damage to bridge abutments, washing off or damage to river beds and alike have been the subjects of these investigations. However, quite few investigations have been dedicated to development of a modern technology for bridge protection against damage or complete failure of superstructure elements under the effect of potential large forces generated by severe floods. This problem has not been investigated to a sufficient depth up to date and combined systems capable of protecting bridge superstructures against severe earthquakes and floods have not been developed.

Figure 11. Typical loading of bridges under flood disasters: Collapse of the Guyandotte river bridge under flood, March 4, 2015 (left) and common water level of Guyandotte river in West Virginia, USA (right).

The observed severe destructions of bridge superstructures resulted from inappropriate protection measures in many cases, Fig. 11. The presented investigations were directed toward development of a new system to enable successful bridge protection against strong earthquakes and severe flood disasters. The presently created combined EFP system possesses an advanced capability for successful protection of bridges exposed to strong earthquakes. This was confirmed with the conducted original seismic tests of the constructed large-scale EFP bridge prototype model.

However, in the final research phase, detailed analytical study will be conducted to validate the capability of the same EFP system to successfully protect bridges subjected to expected severe flood loadings, including representative and critical load cases.

a) Safety analysis of the EFP system under symmetric transverse flood loading: To enable analysis of the bridge superstructure under symmetric transverse flood loading, the most important step to take is definition of the character and intensity of the flood loading. For design purposes, the symmetric transverse flood loading can be approximated by quasi-static loading. In that case, the distribution of the load would be uniform along the span length, while during the analysis, an increase of the load magnitude up to the defined limit would be enabled. However, according to their nature, loads generated during large floods are of dynamic character. In that case, the simulation of load forces requires definition of time functions of dynamic forces and expert analyses of structural response in time domain.

b) Safety analysis of the EFP system under non-symmetric transverse flood loading: Non-symmetric loading of the bridge superstructure could be more critical than symmetric loading in many cases. It is therefore very important to anticipate analysis of the stability of the bridge superstructure under generated large forces due to floods whose dominant effect is non-symmetric. As in the case of symmetric effects, in this case, one can also carry out quasi-static design analyses. However, more realistic and successful definition of the safety of the bridge superstructure can be achieved by expert analyses and simulation of dynamic effect of non-symmetric loads due to floods in transverse direction.

c) Safety analysis of the EFP system under combined transverse and uplift flood loading: The analyses of the stability of the bridge superstructure under combined transverse and uplift loading is very important since it can be the most critical option of loading. According to their nature, floods generate dynamic forces that can be spread in different directions. To confirm the real stability of the bridge structure, it is necessary to perform corresponding analyses under the effect of different combinations of potential loads due to severe flood disasters. Similarly, also in this case, loading can be treated as quasi-static for design purposes. However, during elaboration of final projects, it is necessary to define characteristic analysis combinations, considering all acting forces in the form of critical time functions, defined realistically by experts in hydrology and hydraulics. Realistic simulation of combined dynamic loads and detailed expert analyses in time domain may provide competent conclusions about the stability of the bridge superstructure under generated critical loads due to severe floods.

6. Conclusions

Based on the research results obtained from the conducted extensive experimental studies using the designed and constructed innovative EFP bridge model prototype, the following conclusions are drawn: (1) The novel DSSSB seismic isolation devices are very attractive and effective passive devices for seismic vibration isolation of bridges in arbitrary direction; (2) The new hysteretic multi-directional SF energy dissipation devices possess unique energy absorption features since they are capable of adapting their stable behavior to the arbitrary earthquake direction and to the actual level of seismic input energy. The used SF energy dissipation devices provided innovative, very stable and advanced 3D hysteretic response in the most critical cases of repeated strong earthquake effects in all directions; (3) The created displacement limiting devices in the form of rubber buffers (RB) represent very effective obligatory devices acting as the last line of defense against excessive displacements of the bridge superstructure. Actually, the rubber buffers (RB) represent an efficient passive system, whose activation provides bridge safety during the most critical loads generated by very strong earthquakes or severe floods; (4) The obtained results from the conducted experimental tests confirmed that the new EFP system represented an original high performance seismic isolation option for bridges. The system was created based on optimized seismic energy balance and represents an advanced technical innovation capable of integrating the advantages of seismic isolation, seismic energy dissipation and effective displacement limitation. (5) The new results obtained from recent experimental tests have shown that the created innovative RB displacement limiting devices possess preferable characteristics and can be used as the

last line of defense against extremely large lateral displacements; (6) Although only cyclic compressive loads were applied, occurrence of significant hysteresis and variable energy dissipation capacity was observed; (7) Although the tested RB specimens suffered very large total deformations and large distortions of their shape during the first experimental tests, they were able to regain their initial shape. Actually, the RB devices possess very specific, advanced and important shape-memory ability; (8) The difference in the restoring force is very large among rubbers of different hardness. This fact points out that selection of the rubber hardness is a very important step. Therefore, by adequate selection of rubbers of different hardness, it is possible to create different structural displacement limiting options in compliance with the specific requirements. (9) The created innovative EFP system represents a combined option for protection of bridge structures. The originally developed upgraded seismic isolation system was additionally upgraded with new advanced rubber buffer devices. The RB devices are optimally distributed in order to be activated in longitudinal, transversal and vertical direction. Actually, the created EFP system represents an advanced technical solution and can be regarded as efficient bi-hazard bridge protection technology and (10) During the next study phases, creative analytical study involving specific scenario modeling and refined simulations will be carried out, basically focused on validation of the EFP system response under simulated strong flood loadings and load combinations.

Acknowledgements

References

[1] Yuan, W., Feng, R., & Dang, X. (2018): Typical Earthquake Damage and Seismic Isolation Technology for Bridges Subjected to Near-Fault Ground Motions. *2018 International Conference on Engineering Simulation and Intelligent Control (ESAIC).* doi:10.1109/esaic.2018.00079.

[2] Kelly JM (1986): A Seismic Base Isolation: Review and Bibliography, *Soil Dyn. and Earthquake Eng.* 5(4): 202-216.

[3] Ristic D (1988): Nonlinear Behavior and Stress-Strain Based Modeling of Reinforced Concrete Structures under Earthquake Induced Bending and Varying Axial Loads, PhD Dissertation, School of Civil Engineering, Kyoto University, Kyoto, Japan.

[4] Ristic D, Ristic J (2012): *New Integrated 2G3 Response Modification Method for Seismic Upgrading of New and Existing Bridges,* In 15th World Conference on Earthquake Engineering, (WCEE), Lisbon, Portugal.

[5] Ristic J, Misini M, Ristic D, Guri Z, Pllana N (2018): Seismic Upgrading of Isolated Bridges with SF-ED Devices: Shaking Table Tests of Large-Scale Model, *Građevinar, 70* (6): 463-485. doi: https://doi.org/10.14256/JCE.2147.

[6] Ristic J (2011): *Comparative Seismic Analysis of RC Bridge Structure Applying Macedonian Seismic Design Regulations and Eurocodes.* MSc Thesis, Theory of Structures Department, "Ss. Cyril & Methodius" Univ., Skopje, Macedonia.

[7] Ristic J (2016): *Modern Technology for Seismic Protection of Bridge Structures Applying New System for Modification of Earthquake Response.* PhD Thesis, Institute of Earthquake Engineering and Engineering Seismology (IZIIS), "Ss. Cyril and Methodius" University, Skopje, Macedonia.

[8] Ristic D, Dorka U, Lako A, Zenunovic D, Folic R (2013): *Seismic Upgrading of Bridges in South-East Europe by Innovative Technologies,* NATO SfP Project 983828, Science for Peace and Security Programme, Final Report.

[9] Arrighi C., Pregnolato M., Dawson R., Castelli F., (2019): Preparedness Against Mobility Disruption by Floods, Science of the Total Env., 654: 1010-1022, https://doi.org/10.1016/j.scitotenv.2018.11.191, 2019

[10] Bates P.D., Horritt M.S. and Fewtrell T.J., (2010): A Simple Inertial Formulation of the Shallow Water Equations for Efficient Two-dimensional Flood Inundation Modelling, J. Hydrol. 387(1–2): 33-45. doi: 10.1016/j.jhydrol.2010.03.027, 2010

[11] Mitoulis et al. (2017) Seismic Performance of Novel Resilient Hinges for Columns and Application on Irregular Bridges. Journal of Bridge Engineering, 2017, 22(2), 04016114

[12] AASHTO: AASHTO LRFD, (2017): Bridge Design Specifications; 8th Edition, Washington, DC, 2017

[13] FEMA: HAZUS-MH MR1, (2003): Technical manual, Earthquake Model, Federal Emergency Management Agency, Washington, D.C., 2003

[14] EA: Carlisle Flood Investigation Report 2016. Environment Agency (EA), Cumbria County Council: https://www.cumbria.gov.uk/planning-environment/flooding/flood_investigation_reports_carlisle.asp, last access: 12 November 2020, 2016

[15] Argyroudis et al. (2020) Resilience Assessment Framework for Critical Infrastructure in a Multi-hazard Environment. Science of the Total Environment, 714, 136854. https://doi.org/10.1016/j.scitotenv.2020.136854

[16] Argyroudis, S.A., Mitoulis, S.A., Winter, M.G., Kaynia A.M., (2019): Fragility of Transport Assets Exposed to Multiple Hazards: State-of-the-Art Review toward Infrastructural Resilience, Reliability Engineering & System Safety 191, 106567, 2019, 421 https://doi.org/10.1016/j.ress.2019.106567

[17] Carey T.J., Mason H.B., Barbosa A.R., Michael H.S., (2019): Multi-hazard Earthquake and Tsunami Effects on Soil–Foundation–Bridge Systems, J. Bridge Eng., 24(4), 04019004, doi: https://doi.org/10.1061/(ASCE)BE.1943-5592.0001353, 2019

[18] Gidaris, I., Padgett, J. E., Barbosa, A. R., Chen, S., Cox, D. T., (2017): Webb, B. and Cerato, A.: Multiple-hazard Fragility and Restoration Models of Highway Bridges for Regional Risk and Resilience Assessment in the United States: State-of-the-art review, J. Struct. Eng. 143 (3), 04016188, https://doi.org/10.1061/(ASCE)ST.1943-541X.0001672, 2017

[19] Gehl, P. and D'Ayala, D., (2018): System Loss Assessment of Bridge Networks Accounting for Multi-hazard Interactions. Structure and Infrastructure Engineering, 14(10), 1355-1371, 2018

[20] Kerenyi, K., Sofu, T. and Guo: J., (2009): Hydrodynamic Forces on Inundated Bridge Decks, Federal Highway Administration, FHWA-HRT-09-028, 2009

[21] Highways England (HE), (2012): Design Manual for Roads and Bridges BD 97/12 The Assessment of Scour and other Hydraulic Actions at Highway Structures: http://www.standardsforhighways.co.uk/ha/standards/dmrb/ vol3/section4/bd9712.pdf, last access: 12 May 2020, 2012

[22] Arneson, L.A., Zevenbergen, L.W., Lagasse P.F., Clopper, P.E., (2012): Evaluating Scour at Bridges, 5th Edition, Publication no. FHWA-HIF-12-003, Hydraulic Engineering Circular No. 18. U.S. Department of Transportation, Federal Highway Administration, 2012

[23] Ertugay K., Argyroudis S. and Düzgün H.Ş., (2016): Accessibility Modeling in Earthquake Case Considering Road Closure Probabilities: a Case Study of Health and Shelter Service Accessibility in Thessaloniki, Greece, Int. j. of disaster risk reduction, 17, 49–66, doi: 10.1016/j.ijdrr.2016.03.005, 2016

[24] Ristic J., Hajdari V., Misini L., Ristic D., (2022) Testing of Rubber Buffer Models Protecting Bridges Under Earthquakes and Floods, 16. Congress of Association of Structural Engineers of Serbia.

[25] Misini, M., Ristic, J., Ristic, D., Guri, Z., Pllana, N. (2019). Seismic upgrading of isolated bridges with SF-ED devices: Analytical study validated by shaking table testing, *GRAĐEVINAR, 71* (4), 255-272, doi: https://doi.org/10.14256/JCE.2274.2017

EXPERIMENTAL AND NUMERICAL ANALYSIS OF DAMAGED MASONRY BUILDING

Ivan Duvnjak [(1)], Marina Frančić Smrkić [(2)], Domagoj Damjanović [(3)], Karla Grgić

[(1)] *Assoc. Prof. , University of Zagreb, Faculty of Civil Engineering, ivan.duvnjak@grad.unizg.hr*
[(2)] *Assist. Prof., University of Zagreb, Faculty of Civil Engineering, marina.francic.smrkic@grad.unizg.hr*
[(3)] *Prof., University of Zagreb, Faculty of Civil Engineering, domagoj.damjanovic@grad.unizg.hr*

Abstract

Recent seismic activity in Croatia has caused significant damage to a large number of old masonry buildings. Since the post-earthquake condition and mechanical properties are not known, on-site experimental testing is an important segment of the maintenance and repair of old masonry buildings. In this paper, the results of experimental determination of the mechanical properties and dynamic parameters on the damaged maisonette building of Sisak highschool are presented. In order to confirm and validate the experimental results, a numerical analysis of the building was performed. After making the initial FE model, the comparison between the natural frequencies obtained from the model and the experimental results revealed unsatisfactory outcomes. Therefore, the FE model was calibrated through a whole series of iterations: modification of the boundary conditions, modelling of partition walls, modelling of the damages and modification of the global stiffness of the structure. After a series of iterations, the global stiffness was significantly reduced by nearly 50% of the experimental results, ultimately leading to a satisfactory result. Apart from the reliability of the numerical model and the calibration of the numerical model analyzed here, by repeating the test after the future renovation (considering changes in building mass), the experimentally determined dynamic parameters of the structure can be used to verify the effects of the renovation of the building.

Keywords: masonry, numerical modeling, experimental testing, dynamic properties, mechanical properties

1 Introduction

Masonry buildings of traditional construction were mostly built at a time when there were no regulations for the construction of earthquake-resistant buildings. A large number of old masonry buildings have suffered significant damage from recent seismic activity. Due to the lack of knowledge about their condition and mechanical properties after the earthquake, experimental work is an important segment for future calculations of old masonry buildings [1]. The combination of experimental onsite testing and numerical analysis is often used in order to derive realistic information about the boundary conditions and the mechanical properties of the structure's constituent materials [2], [3]. These procedure typically consist in updating some parameters of the FE model in order to minimize the differences between numerical and experimentally obtained dynamic properties (natural frequencies and mode shapes) [4]. In this paper, the results of testing the mechanical properties and dynamic parameters on the damaged maisonette building of Sisak highschool are presented.

In order to validate the experimental results, a numerical analysis of the building was performed. The results of the natural frequencies of the numerical model compared to the experimentally obtained results were not satisfactory after first iteration of numerical model. Therefore, the model was updated through a whole series of iterations: modification of the boundary conditions, modelling of partition walls, modelling of the damage and modification of the global stiffness of the structure.

Highschool Sisak was built in 1935. The building has four floors: basement, ground floor and two floors, Figure 1. In the central part of the building there is a three-legged staircase with a landing. The foundations are constructed as a reinforced concrete slab. The load-bearing structure of the building consists of walls made of solid bricks, floor slabs and finely ribbed floor slabs made of reinforced concrete. At the entrance of the building on the first and second floors, there is a load-bearing part of the structure that rests on stone columns arranged in two rows.

2 Experimental analysis

During the investigation work, a visual inspection of the building was carried out and damage was observed on the load-bearing walls and partitions of the ground floor and the first floor. Some characteristic damage can be seen in Figure 2.

Figure 1. Sisak highschool building

Figure 2. Typical damage on the load-bearing wall

2.1 Experimental research of mechanical properties

Within the experimental investigation on highschool in Sisak, the following tests were conducted: *in situ* masonry shear strength, determination of existing compressive stress in masonry using *flat jacks*, determination of elasticity modulus.

Masonry shear strength testing is conducted using a small hydraulic jack by which a minimum damage is induced, Figure 3. After removing the plaster, a longitudinally oriented brick is selected. Before the test, head joint must be removed on one side of the brick and on the other side there should be enough space to install the hydraulic jack. The test involves determining shear strength f_V with the contribution of normal compressive stress σ_0. This is why it is important to accurately determine the test position, which enables the calculation of vertical load and the corresponding stress σ_0. Testing was performed on 15 measurement points, 5 on each floor. The mean value of the results on each floor are showed in Table 1.

Table 1. The results of shear strength f_V with the contribution of compressive stress

Position	Shear strength f_V with standard deviation (MPa)
Ground floor	$0,817 \pm 0,149$
First floor	$0,652 \pm 0,187$
Second floor	$0,515 \pm 0,048$
Average value	**$0,661 \pm 0,180$**

The determination of the existing compressive stress in the masonry is conducted using single *flat jacks*, Figure 4, [5]. The compressive stress in the masonry is partially relieved by removing the mortar from the bed joint. The stress is then compensated by inserting the flat jack into the opening until the initial state of stress and strain is established, which is controlled by measuring the displacement perpendicular to the opening. It should be noted that the stress obtained in this test is an average value of the stress in the part of the wall near the opening, i.e. it can be assumed that the stress is representative for the entire wall only if the wall is completely homogeneous and if the load is not eccentric. The test was conducted

at 3 measurement points, two on the ground floor and one on the first floor. The results are shown in Table 2.

Figure 3. Masonry shear strength testing

Figure 4. The determination of the existing compressive stress in the masonry

Two flat jacks connected to a single hydraulic pump must be used in order to determine the stress-strain dependence of masonry. The test is performed in the same location where the vertical compressive stress test was performed, creating another hole above the existing one (used to determine vertical pressure), Figure 5. Flat jacks are inserted into parallel horizontal openings in the masonry and the compressive stress is applied by locally applying pressure to the jacks. Devices for measuring strain are placed in between flat jacks, and the stress and strain values are measured simultaneously, which enables the determination of the modulus of elasticity, Table 2.

Table 2. The results of mechanical properties of masonry

Position	Measurement point	Compressive stress σ_0 (MPa)	Modulus of elasticity (MPa)	Shear strength without compressive stress f_{V0} (MPa)
Ground floor	FJ-PR-1	0,54	4020	0,171
Ground floor	FJ-PR-2	0,43	4122	0,825
First floor	FJ-1K-1	0,59	3407	0,134
		Average	**3850**	**0,377**

The shear strength of masonry without compressive stress f_{V0} was also determined experimentally using flat jacks at 3 measuring points, Table 2. In this method the compressive stress σ_0 in the masonry is checked during the shear test, Figure 6. During the test, the coefficient of friction μ is also determined. The shear strength of the masonry without compressive stress f_{V0} can be expressed as follows:

$$f_{V0} = f_V - \mu \cdot \sigma_0 \tag{1}$$

Figure 5. Elasticity modulus test

Figure 6. The shear strength of masonry without compressive stress
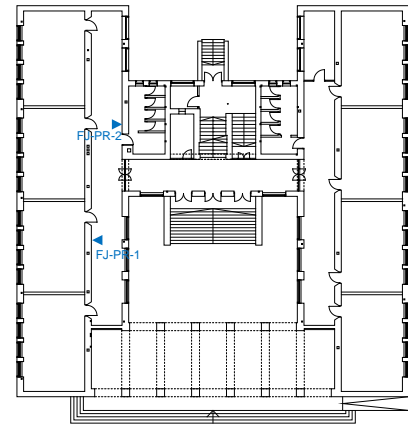
Figure 7. Measurement point locations on ground floor

2.2 Experimental research of dynamic properties

Within the experimental investigation of highschool in Sisak, operational modal analysis (OMA) was used to determine structural dynamic parameters. Unlike classical experimental modal analysis (EMA), the OMA method does not require known excitation. The experimental investigation was performed by using piezoelectric accelerometers (PCB Piezotronics, type 393B31 with nominal sensitivity of 10 V/g, PCB Piezotronics, Depew, NY, USA), an analyzer (Bruel and Kjaer, type 3560c, Bruel and Kjaer, Nærum, Denmark) and associated software. The measurement points were defined in 64 points, 32 in first floor and 32 in second floor, Figure 8. The measurement was performed at each of the measuring points in two perpendicular directions, x and y. Two reference accelerometers were placed in measuring point 213. Frequency domain decomposition (FDD) was used for the estimation of mode shapes. The values of experimentally obtained frequencies for the concerned mode shapes were read from the characteristc record, Figure 9. The results are shown in Table 3.
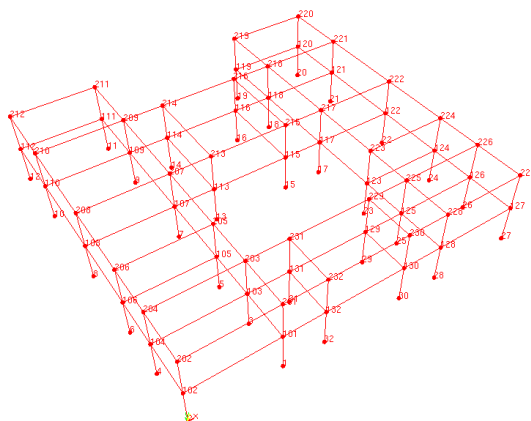
Figure 8. Dynamic properties measuring points in 3D
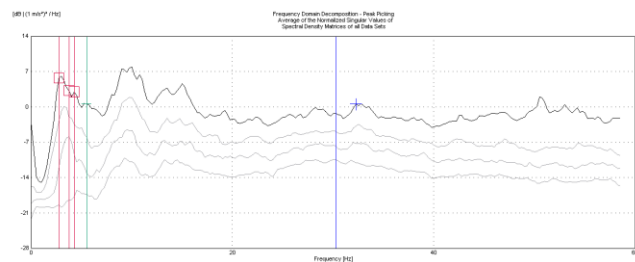
Figure 9. Characteristic record of frequency domian decomposition (FDD) for the determination of natural frequencies

Table 3. Values of first four experimentally obtained frequencies

Modal shape	Natural frequency [Hz]
1	2,98
2	3,96
3	4,45
4	5,92

3 Numerical analysis

The numerical model was developed in SCIA software. The material properties of the masonry used in the model are listed in Table 4. For data not obtained by experimental tests, the values according to EN 1996-1-1 [6] and EN 1998-1 [7] apply. For the modulus of elasticity, the average value of 3850 MPa obtained from three experimental tests, is used. The shear modulus G is calculated as follows:

$$G = 0.4 \cdot E \tag{2}$$

The characteristic compressive strength f_k can be calculated as

$$f_k = K \cdot f_b^{0,7} \cdot f_m^{0,3}, \tag{3}$$

where K is a constant assumed to be as $K = 0.55$ according to [6] , f_b is the compressive strength of the masonry unit, and f_m is the compressive strength of the masonry mortar. According to [8], f_b is assumed as 9.52 MPa, and according to [6], $f_m = 1.0$ MPa. Characteristic flexural strengths of masonry f_{xk1} and f_{xk2} are determined according to [6].

Table 4. Mechanical properties of masonry in numerical model

Density (kg/m³)	1800
Modulus of elasticity E (MPa)	3850
Shear modulus G (MPa)	1540
Charasteristic compressive strength f_k (MPa)	2.66
Charasteristic initial strength, under zero compressive stress f_{vk0} (MPa)	0.377
Charasteristic flexural strength of masonry having the plane of failure parallel to the bed joints f_{xk1} (MPa)	0.1
Charasteristic flexural strength of masonry having the plane of failure perpendicular to the bed joints f_{xk2} (MPa)	0.2

The numerical model was created based on the defined geometry and the material properties determined by experimental tests. Walls and solid slabs were modeled with standard plane elements, rib-reinforced slabs were modeled with coupled plane elements, and beam-reinforced slabs are a plane element connected by means of rigid rods to a beam or rod element. For the boundary conditions, pinned bearings under the load-bearing walls of the basement and fixed bearings on the columns were assumed. The numerical model of the building is shown in Figure 10. The roof of the building was not modeled as part of the building structure, so a submodel of the roof was created to calculate the load transfer, Figure 11. The reactions from the dead weight of the roof were calculated and applied to the model. The weight of the roof is necessary to define the self-weight of the structure and to determine the dynamic parameters of the structure. For the calculation of the dynamic parameters, it is necessary to convert the input load into mass.
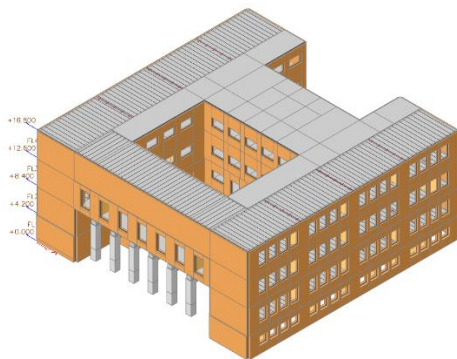
Figure 10. Numerical model of the building
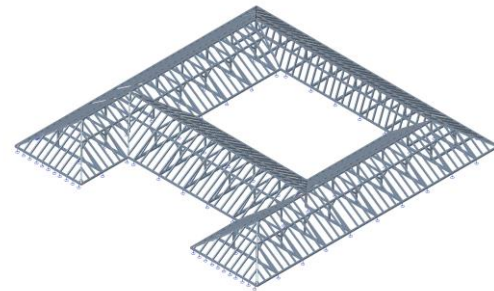
Figure 11. Submodel of the roof

The staircase was introduced into the model through the forces caused by the weight of the staircase at the point of support. For the calculation of the dynamic parameters it was necessary to convert the forces into mass, Figure 12. Partition walls are introduced into the model by the forces caused by the dead weight of the partition wall. In the numerical model, the forces are converted to mass to calculate the dynamic parameters. Since all partitions are damaged, they are defined as mass in the model, since it is assumed that they do not contribute to the stiffness, Figure 13.
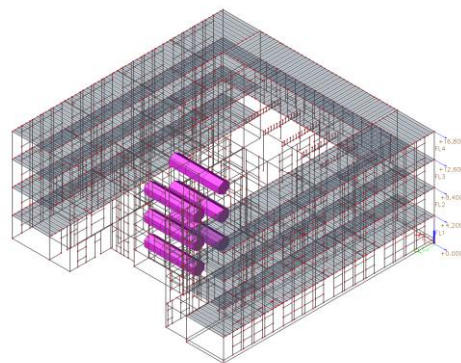
Figure 12. The mass of the staircase display
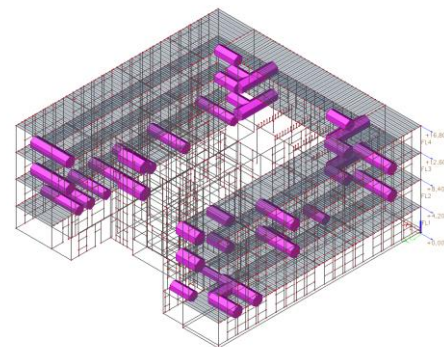
Figure 13. The mass of one part of the partition walls display

4 Model calibration

In the numerical model of the structure, the vertical compressive stress caused by the dead weight was read at the measurement points where the compressive stress determination test was performed, Figure 14. A comparison of the existing compressive stress of the walls was performed, Table 5. The numerically determined stress results for the ground floor roughly correspond to the experimental results, but the stress read at the 1st floor differs significantly from the experimental result.

Table 5 Comparison of numerical and experimental results of compressive stress

Position	Measurement point	Experimental compressive stress σ_0^{exp} (MPa)	Numerical compressive stress σ_0^{num} (MPa)
Ground floor	FJ-PR-1	0,54	0,55
Ground floor	FJ-PR-2	0,43	0,35
First floor	FJ-K-1	0,59	0,38
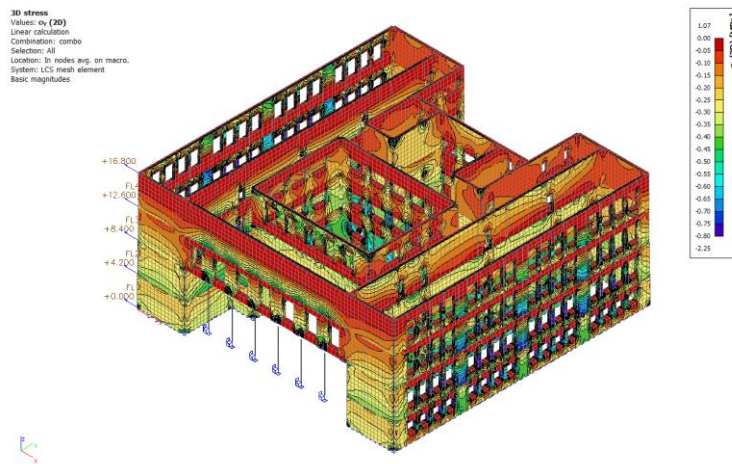
Figure 14. Compressive stress display in numerical model

The experimentally determined frequencies for the relevant mode shapes are compared with the numerically determined values. Although the numerically determined modal shapes agree with the experimental obtained shapes, a significant deviation of the frequency results can be seen in Table 6.

Table 6. Experimental and numerical frequencies comparison

Modal shape	f^{exp} (Hz)	f^{num} (Hz)	Deviation (%)
1	2,98	4,22	41,6
2	3,96	5,75	45,2
3	4,45	6,42	44,3
4	5,92	9,64	62,8

The results of the initial global numerical model agreed with the results of the local experimental tests, but the values of the frequencies of the numerical model compared with the experimental results were not satisfactory. Therefore, the improvement of the model in terms of the frequencies of the structure was approached through a whole series of iterations.

4.1 First iteration - boundary condition

A comparison of frequencies was made with respect to the change in boundary conditions. The numerical model retained the entered mass of the self-weight of the structure and the mechanical properties of the material. The results for fixed boundary conditions and pinned boundary conditions under the load-bearing walls of the structure are shown graphically, Figure 15. The applied boundary conditions showed no significant effect on the results of the structure's frequency. Therefore, a pinned boundary condition was used in the further analysis.

4.2 Second iteration - partitions

A comparison was also made of the frequency of numerical models in which the partitions were replaced with the appropriate mass, as described previously, and the model in which the partitions were modeled with a standard type of finite element of the wall surface, Figure 16. According to the standard [6], the characteristic flexural strengths of the masonry were entered. The modulus of elasticity, characteristic compressive strength and characteristic shear strength were taken from the tests described in section 2.1. In the numerical model, the mechanical properties of the solid brick wall material and the pinned boundary conditions were retained.

In the numerical model where the partitions were modeled as finite elements, the frequency of the structure increased compared to the numerical model where the partitions were input as mass. It can be concluded that the partitions contribute to the stiffness of the structure. However, in the following, the modeling of the partitions by mass in exchange for finite elements was retained in the numerical model because visual inspection revealed the damage of the partitions, then by inputting the seismic load to the numerical model, a significant excess of stress was found in the partitions, and insufficient thickness of each partition and excessive slenderness were found when the basic requirements were checked. Modeling of partitions using mass also contributes to a smaller number of finite elements.
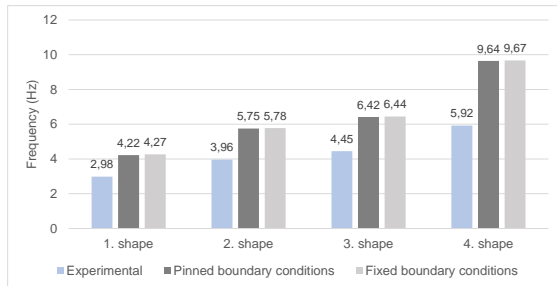
Figure 15. The frequencies for fixed boundary conditions and pinned boundary conditions
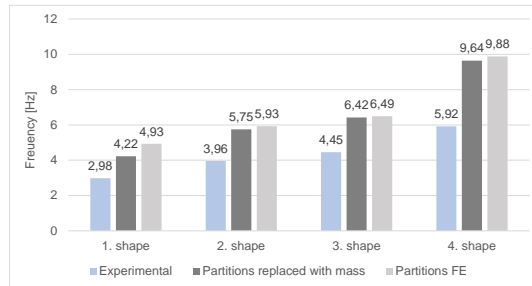
Figure 16. Frequency results depending on different partition modelling

4.3 Third iteration – damaged model

a) Reduction of the modulus of elasticity in damaged elements

The numerical analysis of the dynamic parameters is carried out by a linear analysis, which proves to be unsuitable for masonry because of its nonlinear behavior. Therefore, an attempt is made to describe the structure numerically, taking into account the existing damage. The damages are simulated on the numerical model by reducing the stiffness of the finite elements belonging to the damaged parts of the structure [4]. In order to reduce the difference between the experimentally and numerically determined dynamic parameters, a model is presented below in which an attempt is made to reduce the stiffness of the finite elements belonging to the damaged wall. The observed damage to the ground floor and the first floor structure is shown in Figure 17 and Figure 18. In the numerical model, the damaged parts of the structure are modeled with finite elements to which a material with modified properties, i.e. with reduced elastic modulus, is assigned. The reduction of the elastic modulus was performed in several steps, with the elastic modulus being reduced by 10% in each step. The numerical model retained the mechanical properties of the masonry, the pinned boundary conditions and the added masses of the non-structural elements. By reducing the elastic modulus, a reduction in the natural frequency of the damaged numerical model can be observed, Figure 19. Nevertheless, satisfactory results were not achieved by imitating the damaged parts of the structure using finite elements with a reduced elastic modulus.
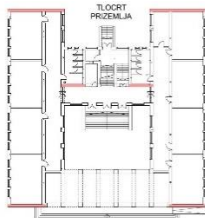
Figure 17. Damaged masonry in ground floor
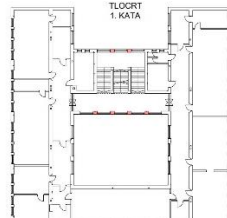
Figure 18. Damaged masonry in first floor
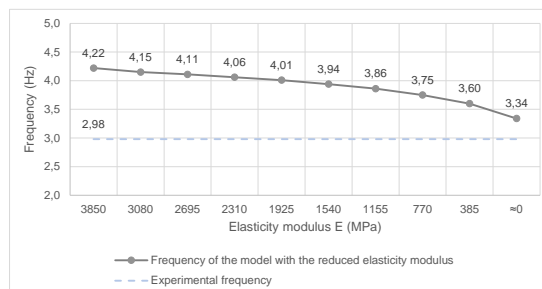
Figure 19. Frequency of the model with reduced elastic modulus of damaged elements, 1. modal shape

b) Reduction of elastic modulus at diagonal crack location

Since satisfactory results were not obtained for the model with reduced elastic modulus in damaged elements of the building, a new approach for modeling damaged parts of the structure was introduced. According to the recommendations of [4], the numerical simulation of the crack pattern was performed by defining finite elements with a reduced elastic modulus E≈0 MPa at the crack location, Figure 20. The elastic modulus is not zero, but was reduced to 100 MPa to avoid errors in the numerical calculation. The numerical model kept the mechanical properties of the masonry, set the pinned conditions and added the masses of the nonstructural elements. It can be seen that the frequency decreases with the introduction of the assumption of damaged finite elements. However, even with these models, the frequency is quite high compared to the experimental results, Table 7.
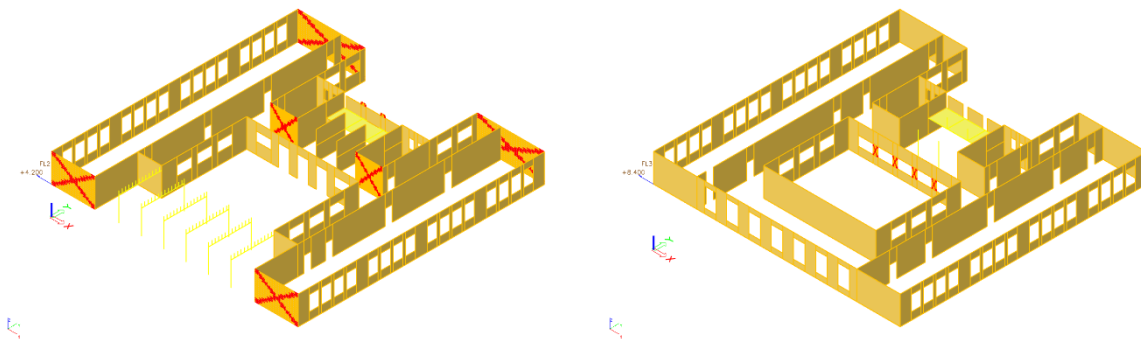
Figure 20. Numerical model with reduced elastic modulus at crack location in ground floor (left) and first floor (right)

Table 7. The comparison of experimental frequency and numerical frequency on model with diagonal damage

Modal shape	Frequency (Hz)		Difference (%)
	Experimental	Numerical	
1	2,98	3,78	26,8
2	3,96	5,29	33,6
3	4,45	6,29	41,3
4	5,92	9,43	59,3

4.4 Forth iteration - Reduction of the global elastic modulus

In the next iteration, the change in global elastic modulus was performed in increments of 500 MPa. Pinned boundary conditions were kept in the numerical model, the masses of non-structural elements were added, and the elastic modulus was reduced along the diagonal cracks of the damaged elements.

The obtained results of the frequency, depending on the reduction of the global elastic modulus, for the first modal shape are shown in the Figure 21. where the approaching of the results to the experimental values is visible. The modulus of elasticity at the level of 2000 MPa gives a very small deviation compared to the experimental result. The Table 8. shows a comparison of the experimental frequency and the frequency of the damaged numerical model with a global elastic modulus at the level of 2000 MPa. A small difference in natural frequency is observed for the first three modal shapes, while the frequency of the fourth modal shape has a larger deviation from the experimental result.
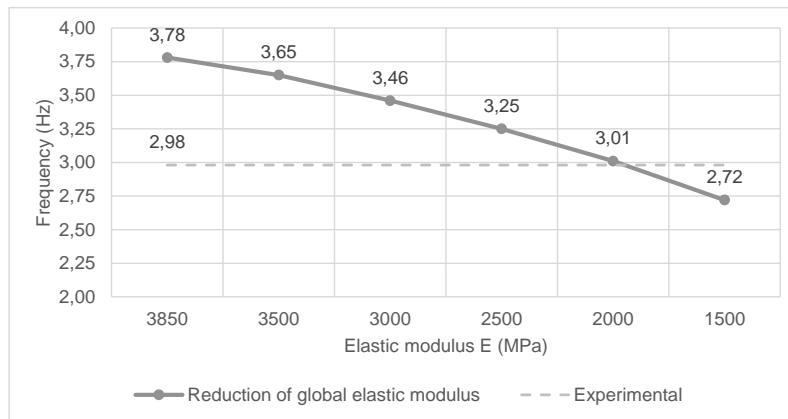
Figure 21. Results of the frequency, depending on the reduction of the global elastic modulus, for the 1. modal shape

Table 8. The comparison of experimental frequency and numerical frequency on model with a global elastic modulus reduced to 2000 MPa

Modal shape	Frequency (Hz)		Difference (%)
	Experimental	Numerical	
1	2,98	3,01	1,0
2	3,96	4,12	4,0
3	4,45	4,72	6,1
4	5,92	8,04	35,8

5 Discussion

The results of the natural frequencies of the initial numerical model compared to the experimental results were not satisfactory. Therefore, the model was updated through a whole series of iterations: modification of the boundary conditions, modelling of partition walls, modelling of the damage on structural elements and modification of the global stiffness of the structure, Figure 22. In relation to the initial numerical model, no significant differences in the frequencies of the structure were obtained by changing the boundary conditions of the numerical model. Then the comparison between the numerical model with the modelled partitions and the numerical model with the input mass of the partitions was started. The result was a higher frequency of the models with modelled partitions as the stiffness of the structure increased. In subsequent iterations, structural damage was added to the numerical model. The damage was first modelled by reducing the elastic modulus of the damaged parts of the building, but the results of the frequencies were not satisfactory. Then, damage modelling was started by reducing the elastic modulus of the finite elements along the cracks. In the end, the global stiffness was additionally reduced for this model by almost 50 % of the experimental values. Based on the mentioned assumptions introduced in the global numerical model, satisfactory results were obtained for the natural frequencies of the structure compared to the real behaviour of the structure.
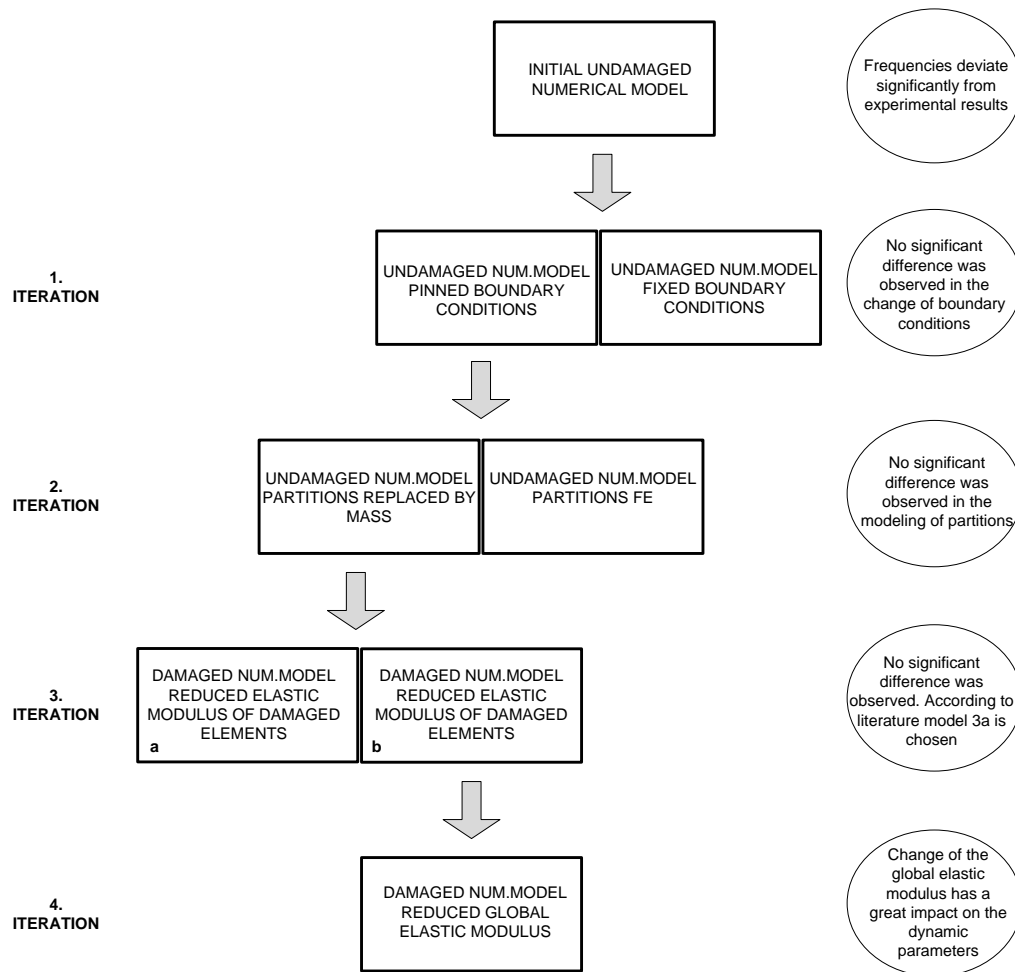
Figure 22. Flow chart of numerical model iteration

6 Conclusion

Experimental determination of mechanical properties of masonry and dynamic parameters of the structure can improve the accuracy of numerical models of structures. Determination of mechanical properties does not always give the correct results. In this case, the experimentally determined elastic modulus was reduced by almost 50% in the numerical model to obtain satisfactory results for the natural frequencies. The described uncertainty of the experimental results of the mechanical properties of the masonry can be eliminated by increasing the number of tests performed to obtain the global mechanical properties of the structure. However, such tests are time consuming and very expensive. Moreover, an attempt can be made to verify the assumptions of the performed tests of the mechanical properties of the masonry in order to make them more effective. Accordingly, the examination of the mechanical properties of the masonry could be directed to a more applicable and less expensive method, capable of determining the mechanical properties of the masonry at many more locations in the structure.

Apart from the reliability of the numerical model and the calibration of the numerical model analyzed here, by repeating the test after the future renovation under the condition of unchanged building mass, the experimentally determined dynamic parameters of the structure can be used to verify the effects of the future renovation of the building.

References

[1]   J. Krolo, D. Damjanović, I. Duvnjak, M. Frančić Smrkić, M. Bartolac, and J. Košćak, "Methods for determining mechanical properties of walls," *Gradjevinar*, vol. 73, no. 2, pp. 127–140, 2021, doi: 10.14256/JCE.3063.2020.

[2]   S. Ereiz, I. Duvnjak, D. Damjanović, and M. Bartolac, "Analysis of seismic action on the tie rod system in historic buildings using finite element model updating," *Buildings*, vol. 11, no. 10, 2021, doi: 10.3390/buildings11100453.

[3]   L. F. Ramos, L. Marques, P. B. Lourenço, G. De Roeck, A. Campos-Costa, and J. Roque, "Monitoring historical masonry structures with operational modal analysis: Two case studies," *Mech. Syst. Signal Process.*, vol. 24, no. 5, pp. 1291–1305, 2010, doi: 10.1016/j.ymssp.2010.01.011.

[4]   D. Pellegrini *et al.*, "Modal analysis of historical masonry structures: Linear perturbation and software benchmarking," *Constr. Build. Mater.*, vol. 189, pp. 1232–1250, 2018, doi: 10.1016/j.conbuildmat.2018.09.034.

[5]   Lulić, Luka; Stepinac, Mislav; Damjanović, Domagoj; Duvnjak, Ivan; Bartolac, Marko; Hafner, "The role of flat-jack testing after recent earthquakes," in *Proceedings of the 3rd European Conference on Earthquake Engineering & Seismology*, 2022, pp. 289–296.

[6]   *EN 1996-1-1 Eurocode 6 - Design of masonry structures - Part 1-1: General rules for reinforced and unreinforced masonry structures*. 2011.

[7]   *EN 1998 -1 Eurocode 8 - Design of structures for earthquake resistance - Part 1 : General rules, seismic actions and rules for buildings*. 2011.

[8]   M. Uroš, M. Todorić, M. Crnogorac, J. Atalić, M. Šavor Novak, and S. Lakušić, *Potresno inženjerstvo - Obnova zidanih zgrada*.

COMPARISON OF NON-DESTRUCTIVE AND SEMI-DESTRUCTIVE METHODS FOR THE POST-EARTHQUAKE ASSESSMENT OF EXISTING MASONRY

Luka Lulić [(1)], Mislav Stepinac [(2)], Karlo Ožić [(3)], Javier Ortega [(4)], Marieta Nunez Garcia [(5)], Savvas Saloustros [(6)]

[(1)] *PhD student, University of Zagreb Faculty of Civil Engineering, e-mail address: luka.lulic@grad.unizg.hr*
[(2)] *Assistant Professor, University of Zagreb Faculty of Civil Engineering, e-mail address: mislav.stepinac@grad.unizg.hr*
[(3)] *PhD student, University of Zagreb Faculty of Civil Engineering, e-mail address: karlo.ozic@grad.unizg.hr*
[(4), (5) and (6)] *FENEC-NDT and Specialized Structural Analysis for Built Heritage, Madrid, Spain, e-mail address: fenecforheritage@gmail.com*

Abstract

After a long period of inactivity, strong seismic events occurred in Croatia. Due to the extensive damage caused by the recent earthquakes, a significant phase of reconstruction and strengthening follows. Determining the actual seismic behavior of existing masonry structures is of great importance for future management and the economical and purposeful strengthening of the load-bearing structure. Modern software solutions and design methods are an essential part of the assessment, but they are only as useful as long as the input parameters are reliable. This is where in-situ test methods come into play, providing useful information about the mechanical properties of the structure. In the paper, the flat-jack method and sonic pulse velocity method are described in more detail and the results of certain tests are presented and compared.

Keywords: assessment, masonry, flat-jack, sonic pulse velocity, NDT, SDT

1. Introduction

After a long period of seismic inactivity, the recent 2020 seismic events in Croatia caused a lot of damage and suffering [1,2]. Despite the great effort made by scientists to raise awareness, the unpreparedness for such a situation was noticeable from several aspects. In response to this, many activities aimed at mitigating the consequences have been initiated. In addition to the rapid damage and usability assessments carried out immediately after the earthquake by volunteer engineers [3], a widespread process of more detailed assessment, restoration and reconstruction of the building stock began. The first inevitable step in this process is certainly the determination of mechanical properties.

Given that old unreinforced masonry (URM) structures that are occupied and mostly located in urban centres suffered the most, the examination of such structures is urgent and therefore most important. Existing URM structures are inherently vulnerable to violent ground motions. Due to its large mass and stiffness, as well as low ductility and poor ability to dissipate energy, it represents a danger to human life [4]. Moreover, the lack of connection between walls and floor structures can lead to the loss of global stability and the collapse of the structure as a whole.

For the assessment, various test methods are used, and one common and useful method is the flat-jack test. The method is semi-destructive, requires specialized equipment and the test itself is time-consuming [5]. With this in mind, comparisons between methods are undertaken with the aim of facilitating and speeding up the testing process. That is why this comprehensive investigative campaign is launched. The testing campaign is carried out following the devastating earthquakes of 2020. The research aimed to identify and compare the elastic properties of solid brick masonry on several case study buildings in Croatia using different testing methods. The experimental campaign was conducted in collaboration of the Faculty of civil engineering in Zagreb and the FENEC association. Most of the tested buildings are currently not operational due to damage caused by the earthquakes, so the investigative work is carried out without interruption. An integral part of this campaign are the case

216

studies shown in Figure 1. They are located in the capital Zagreb and its surroundings, and most of them are part of the cultural heritage.
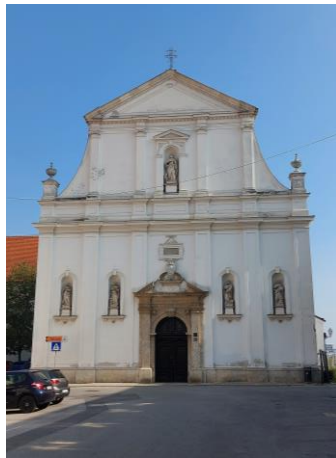
a) CS1

b) CS2

c) CS3

d) CS4

e) CS5

f) CS6

g) CS7

h) CS8

Figure 1. Case study buildings.

2. Assessment methods

Various non-destructive, semi-destructive and destructive methods are used for the assessment of existing URM structures. The emphasis in this paper is on the flat-jack method and sonic pulse velocity test or sonic test. The methods are explained in more detail in the following chapters. More information about other assessment methods can be found in [6,7].

2.1 Flat-jack method

The method is based on the principle of introducing stress into the masonry using metal flat-jacks of a semioval shape that are inflated like a balloon. This causes the masonry to deform, which is measured using a portable extensometer and a displacement sensor (LVDT). Using the flat-jack method, three useful masonry parameters can be determined, and therefore the test is performed in three phases. The first phase is about the state of vertical stress in the masonry, while the second and third phases provide information about the deformation and shear characteristics of the masonry. A more detailed description of the flat-jack method can be found in [8,9]. Before the aforementioned test phases, flat-jacks need to go through the calibration process due to certain pressure losses that occur as a result of the deformation of the flat-jack itself. The calibration process is carried out in an accredited laboratory and is repeated after every five in-situ tests. The next major concern is finding a favourable location in the structure that can be tested. It is important that the wall is load-bearing, without hidden openings, installations and similar obstacles. Next, all surface layers of the wall are removed until the brick is reached. The surface of the wall should be clean and dry. Wet basement walls are best avoided because of the degradation caused by moisture and the poor maturation of the adhesive, which is necessary for the test.

In the first stage, three pairs of vertically placed metal points are glued to the wall. An opening will be cut in the horizontal joint between the pairs of points with an eccentric ring saw. By measuring the spacing of the points before and after cutting, the deformation of the part of the wall due to the resulting discontinuity in the material is determined. By inserting a flat-jack into the newly created opening and gradually increasing the pressure, the deflection is reduced (Figure 2a). When the deflection is reduced to zero, i.e. when the wall returns to its initial position, the stress in the flat jack represents the state of vertical stress in the masonry. The obtained stress in the flat-jack is corrected with the coefficient obtained during the calibration process and with the ratio of the area of the flat-jack and the area of the opening in the wall.

In the second phase of the test, the flat-jack from the first phase is used, but another one is added above it (Figure 2b). In this way, a part of the wall is obtained that is in a uniform state of stress, and with the help of flat-jacks, this stress can be controlled. Three displacement sensors are placed between the flat-jacks, which measure the displacement of that part of the wall. The further procedure takes place so that the stress is gradually increased in small increments and the displacement is measured after each step. After a specific number of steps, a certain correlation between vertical stress and strain is obtained and based on this, the elastic property of masonry, i.e. the modulus of elasticity, is obtained.

The third phase (Figure 2c), which is also the last phase of the test, again uses two flat-jacks from the previous phase. Only now an additional third horizontal press is added which will push the selected brick to determine the coefficient of friction and initial shear strength values. The brick will be pushed parallel to the face of the wall and will be pushed along its longest side. To begin with, the level of vertical stress will be increased to a certain level. Then the brick will be pushed horizontally until failure, i.e. until it slips. The level of vertical stress is increased again and the brick is pushed horizontally until failure. This process is repeated several times. As a result, on the shear stress-vertical stress diagram, the best fitting line is obtained whose slope represents the friction coefficient and the intersection with the vertical axis represents the initial shear strength.

More detailed instructions on calibration, the test itself, as well as the processing of the results for determining the deformation properties of masonry, i.e. the modulus of elasticity, can be found in the form of the following guidelines [10,11].
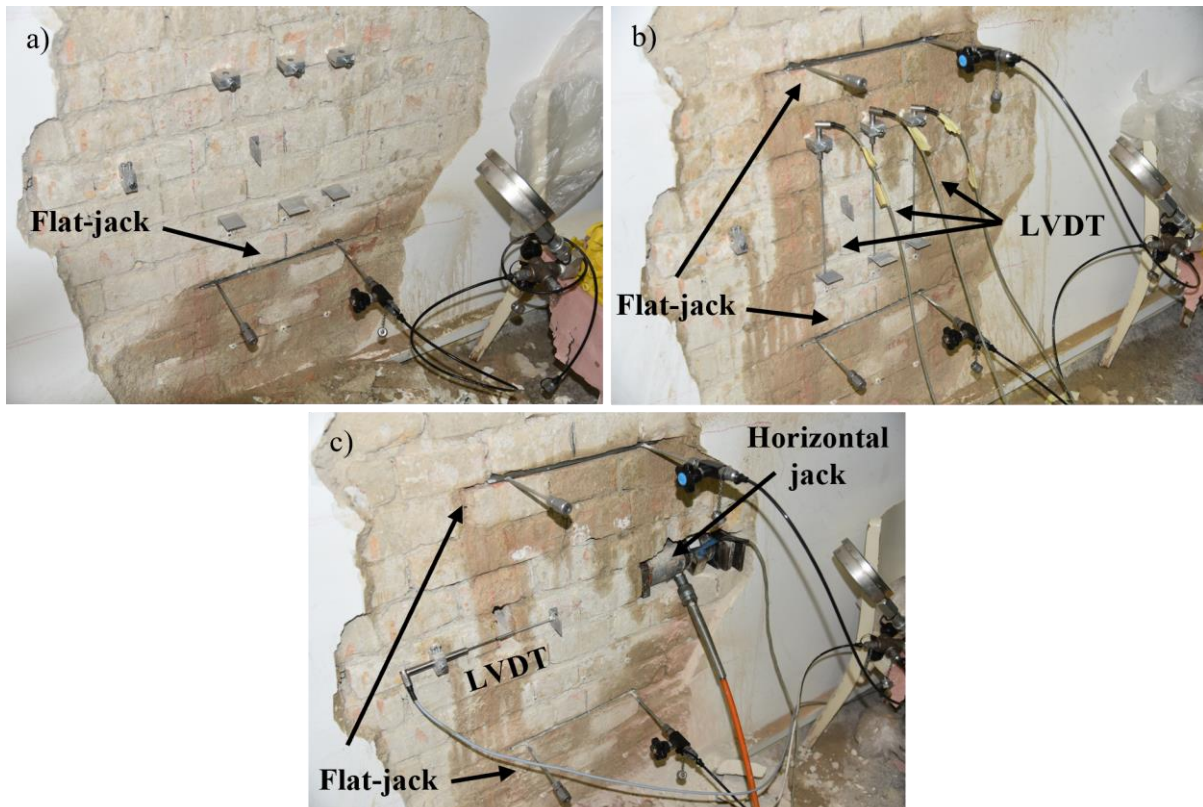
Figure 2. Flat-jack test phases: a) Vertical stress state; b) Elastic properties; c) Shear properties.

2.2 Sonic pulse velocity test

The sonic pulse velocity test method is a procedure used to estimate the elastic properties of masonry, i.e. the modulus of elasticity. The method aims to precisely measure the speed of propagation of an elastic longitudinal wave through the structure. The speed propagation can be then correlated with the dynamic elastic modulus, Poisson's ratio and material density. The wave propagation speed is obtained using the measured travel time of the elastic wave from the emitter to the receiver and assuming a linear distance between them. The receiver is an accelerometer with a sensitivity of 10 V/g and a frequency range from 0.15 Hz to 1000 Hz (measurement range ±0.5g) that is positioned by hand in a pre-marked place on the wall. The emitter is a specialized instrumented hammer that creates an initial signal by striking the wall. It has a specially shaped tip suitable for precise signal generation on the wall. The hammer and accelerometer are connected to a data processing system that is connected to a computer. In principle, the method is similar to the ultrasonic pulse velocity test, which is often used for the mechanical characterization of concrete. The main difference is the frequency (i.e. number of elastic waves emitted per second) of the transducers, which can be sonic or ultrasonic, e.g. frequency higher than 20 kHz is considered ultrasonic. Since there are no sonic test guidelines, the European and American guidelines for ultrasonic pulse velocity test given in [12,13] can serve as a reference.

In general, three different test configurations are possible depending on the position of the hammer and the accelerometer. The first is the direct configuration where the hammer and the accelerometer are placed in the same position but on opposite faces of the wall. The second is an indirect configuration where the hammer and the accelerometer are located on the same face of the wall. In the present research, an indirect configuration (Figure 3a) following a vertical direction was selected, aiming to estimate the vertical modulus of elasticity of the masonry. Tests are carried out at the wall side from where flat-jack tests are performed to take advantage of the surface preparation, which included render removal. The mentioned test procedure is shown in Figure 3b. Similar sonic investigations, but on regular and irregular stone masonry, are carried out in [14,15].

After testing, it is necessary to process the obtained data. The data display is shown in Figure 3c. The velocity (V_P) is calculated by measuring the travel time between the emission of the signal by the hammer and the reception of the signal by the accelerometer, divided by the distance between the transducers. The propagation velocity is then inserted into Eq. (1) from which the value of the dynamic modulus of elasticity (E_d) is obtained. Additional required data are the density (ρ) and Poisson's ratio (v) of the masonry. In this study, the values for density and Poisson's ratio are taken from the literature [16,17] for the corresponding masonry typology (solid brick masonry in lime mortar). The density is taken as 1800 kg/m^3 and the Poisson's ratio as 0.2.

$$V_p = \sqrt{\frac{E_d}{\rho} \frac{1-v}{(1+v)(1-2v)}} \tag{1}$$
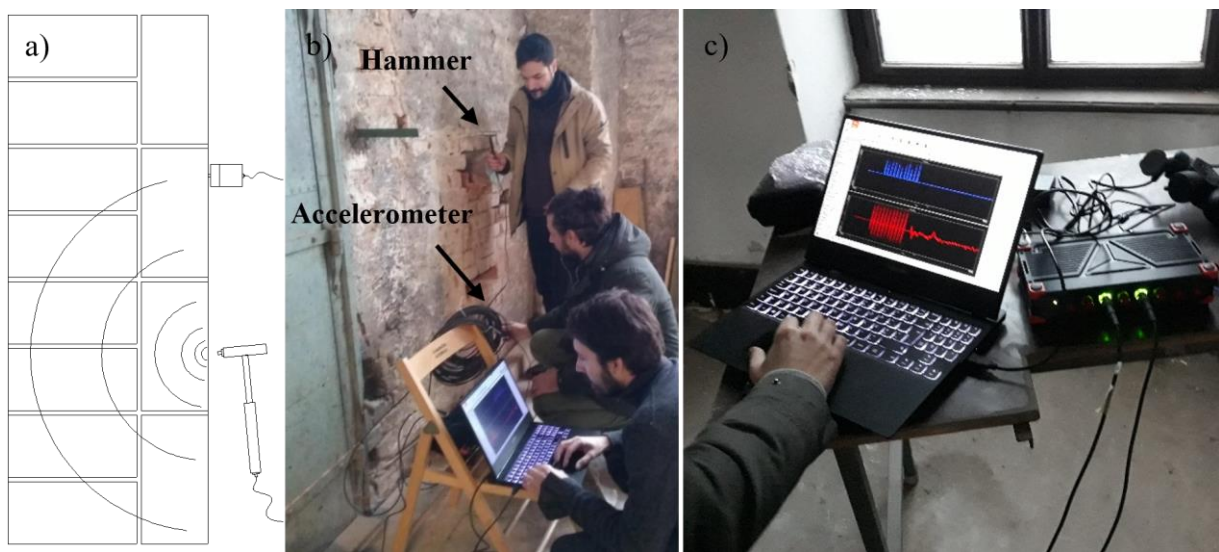
Figure 3. a) In-direct configuration; b) Test procedure; c) Data display.

3. Results

The results are obtained on eight different case study buildings at a total of 22 test locations. Several tests were carried out on each building. The results obtained on the same case study building are shown in the same colour for easier reference. The order of the results corresponds to the order of the case study buildings shown in Figure 1. The results of the flat-jack tests are presented in Figure 4, while Figure 5 presents the results of the sonic tests.

It should be emphasized that the values obtained by the flat-jack method represent the static modulus of elasticity, while the values obtained by the sonic method represent the dynamic modulus of elasticity. As a rule, the dynamic modulus of elasticity is 10-20% higher than the static modulus of elasticity [18]. The empirically observed inequality between static and dynamic modulus of elasticity of masonry and its components has been noted in several studies [19,20], which can be attributed to the different strain rate in the load application [21].
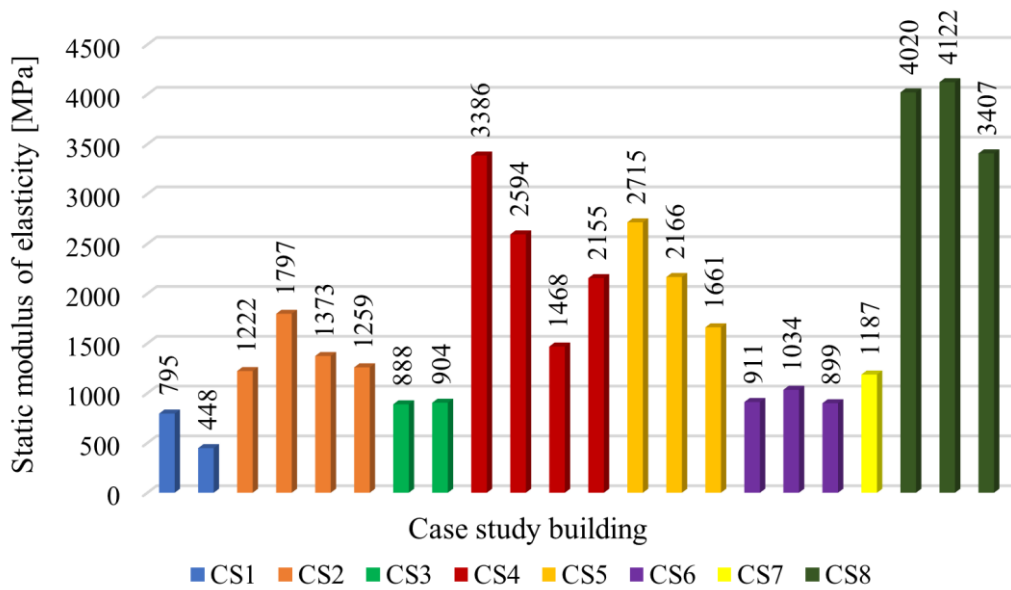
Figure 4. Flat-jack test results.
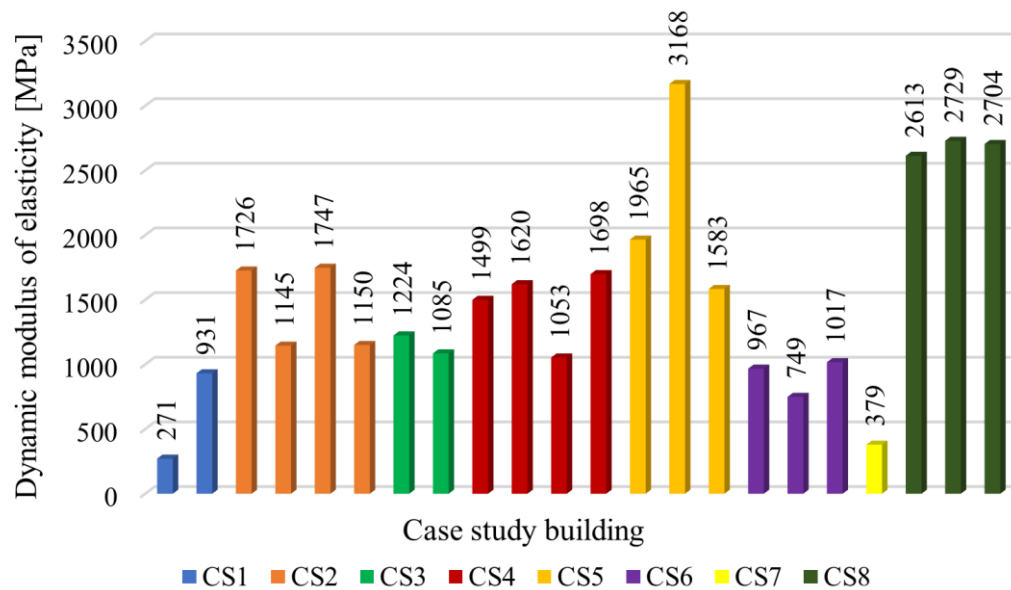
Figure 5. Sonic test results.

From Figure 4 and Figure 5 it can be seen that the results deviate not only from building to building but even, to a certain extent, within the same building. In existing masonry structures, scattering of results is expected and normal occurrence. This is not surprising considering that the mechanical properties are affected by numerous parameters such as material quality, construction quality, maintenance, degradation over time and similar effects. This is also why fast testing methods that allow an estimation of the variability of the masonry throughout the building are particularly important.

Figure 6 illustrates the mean values of the modulus of elasticity obtained by the sonic and flat-jack methods for each case study building. Flat-jack test results are shown in blue, while sonic test results are shown in orange. Below the graph, the exact values for each case study are shown in tabular form.
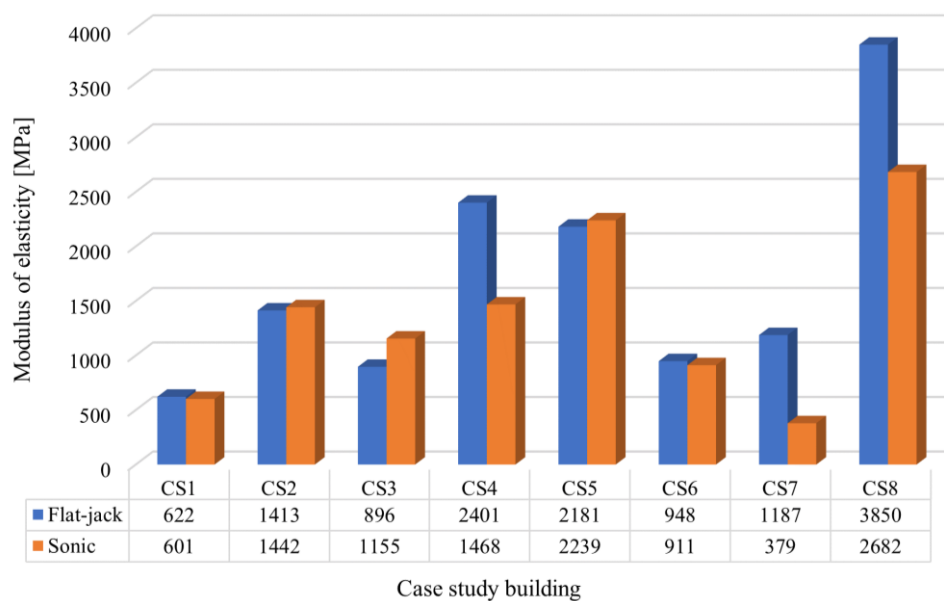
Figure 6. Comparison of results obtained by the sonic and flat-jack method.

Results of the flat-jack testing campaign will be published in more detail in [22] and more extensive insight into the comparison between flat-jack and sonic test results can be found in [23].

4. Discussion

Determining the actual seismic behavior of existing masonry structures is of great importance for future management and the economical and purposeful strengthening of the load-bearing structure [24]. Modern software solutions and design methods are an essential part of the assessment, but they are only as useful as long as the input parameters are reliable. This is where in-situ test methods come into play, providing useful information about the mechanical properties of the structure.

The sonic method is quite straightforward and the preparation as well as conducting of the test is relatively simple compared to the flat-jack method, not to mention the speed that is incomparable in favor of the sonic method, which allows measuring more locations within the same building and assess the variability of the masonry properties. The non-destructive nature of the test is also quite a big advantage, considering that it is only necessary to remove a layer of plaster in order to reach the masonry. But on the other hand, the flat-jack method also provides other useful parameters such as the vertical stress state as well as the shear properties of the masonry. Similar research combining NDT and SDT methods, but only at one test location, was carried out in [25].

The sonic method has been found to have the potential to be an indispensable part of the research arsenal when dealing with existing masonry. It was also shown that there is a certain correlation between the results obtained by the two methods. Incorporating the sonic method into a standard application during the assessment process can result in less destructive, more economical, but equally valuable investigative testing. In this way, the next phases such as design and strengthening will not be disturbed, and the entire reconstruction process will be more efficient. In addition to strengthening, it is of great importance to think about aspects of energy efficiency [26,27] and the preservation of cultural heritage [28,29] as well.

5. Conclusions

This research presents a comparison of the elastic properties of existing solid brick masonry obtained by different test methods. Sonic pulse velocity test and flat-jack test methods are used and presented. A comprehensive research campaign was undertaken on the continental part of Croatia on eight existing

unreinforced masonry structures. The tested structures are damaged in the recent earthquakes and are currently undergoing rehabilitation and strengthening. The presented work yielded new insights into the elastic properties of the existing unreinforced solid brick masonry buildings in Croatia.

The following list summarizes the main conclusions obtained from the research:

- The results deviate considerably in some cases, which is in the expected range considering that the existing masonry is tested, as well as the fact that these are different buildings with their inherited intrinsic differences and built in different times.
- The test results obtained by the mentioned two test methods have a positive correlation.
- The sonic method has the potential to be used in more locations given the faster procedure, which allows to assess the variability of the masonry elastic properties within a building.

Acknowledgements

References

[1] Stepinac, M., Lourenco, P.B., Atalić, J., Kišiček, T., Uroš, M., Baniček, M. et al. (2021): Damage classification of residential buildings in historical downtown after the ML5.5 earthquake in Zagreb, Croatia in 2020. doi: https://doi.org/10.1016/j.ijdrr.2021.102140

[2] Miranda, E., Brzev, S., Bijelic, N., Arbanas, Z., Bartolac, M., Jagodnik, V. et al. (2021): StEER-EERI: PETRINJA, CROATIA DECEMBER 29, 2020, Mw 6.4 EARTHQUAKE JOINT RECONNAISSANCE REPORT (JRR). doi: https://doi.org/10.17603/ds2-1w0y-5080

[3] Uroš, M., Šavor Novak, M., Atalić, J., Sigmund, Z., Baniček, M., Demšić, M. et al. (2020): Post-earthquake damage assessment of buildings – procedure for conducting building inspections. *Gradjevinar*, **72** (12), 1089–115, doi: https://doi.org/10.14256/JCE.2969.2020

[4] Kišiček, T., Stepinac, M., Renić, T., Hafner, I. and Lulić, L. (2020): Strengthening of masonry walls with FRP or TRM. Gradjevinar. Union of Croatian Civil Engineers and Technicians. p. 937–53, doi: https://doi.org/10.14256/JCE.2983.2020

[5] Lulić, L., Stepinac, M., Damjanović, D., Duvnjak, I., Bartolac, M. and Hafner, I. (2022): The role of flat-jack testing after recent earthquakes. *Proceedings of the 3rd European Conference on Earthquake Engineering & Seismology*, Bucharest, Romania. p. 8 pages,

[6] Stepinac, M., Kisicek, T., Renić, T., Hafner, I. and Bedon, C. (2020): Methods for the assessment of critical properties in existing masonry structures under seismic loads-the ARES project. Applied Sciences (Switzerland). MDPI AG., doi: https://doi.org/10.3390/app10051576

[7] Krolo, J., Damjanović, D., Duvnjak, I., Smrkić, M.F., Bartolac, M. and Košćak, J. (2021): Methods for determining mechanical properties of walls. *Gradjevinar*, Union of Croatian Civil Engineers and Technicians. **73** (2), 127–40, doi: https://doi.org/10.14256/JCE.3063.2020

[8] Gregorczyk, P. and Lourenco, P.B. (2000): A Review on Flat-Jack Testing.

[9] Lulić, L., Stepinac, M., Bartolac, M. and Lourenco, P.B. (2022): Review of the flat-jack method and lessons from extensive post-earthquake research campaign in Croatia (Under review).

[10] RILEM. (2005): RILEM Recommendation MDT. D. 5: In-situ stress - strain behaviour tests based on the flat jack. Mater Struct. p. 497–501,

[11] ASTM. (2014): ASTM C1197 - 14a: Standard Test Method for In Situ Measurement of Masonry Deformability Properties Using the Flatjack Method.

[12]   EN 12504. (2006): EN 12504-4. Testing Concrete - Part 4: Determination of ultrasonic pulse velocity. European Committee for Standardization (CEN), Brussels, Belgium.,

[13]   ASTM. (2016): ASTM C 597-16. Standard Test Method for Pulse Velocity Through Concrete. ASTM International. West Conshohocken.,

[14]   Miranda, L., Cantini, L., Guedes, J., Binda, L. and Costa, A. (2013): Applications of Sonic Tests to Masonry Elements: Influence of Joints on the Propagation Velocity of Elastic Waves. *Journal of Materials in Civil Engineering*, American Society of Civil Engineers. **25** (6), 667–82, doi: https://doi.org/10.1061/(ASCE)MT.1943-5533.0000547

[15]   Miranda, L., Cantini, L., Guedes, J. and Costa, A. (2016): Assessment of mechanical properties of full-scale masonry panels through sonic methods. Comparison with mechanical destructive tests. *Structural Control and Health Monitoring*, John Wiley & Sons, Ltd. **23** (3), 503–16, doi: https://doi.org/10.1002/stc.1783

[16]   EN 1998. (2005): EN 1998-3: Eurocode 8: Design of structures for earthquake resistance – Part 3: Assessment and retrofitting of buildings.

[17]   NTC. (2018): Italian Structural Code, D.M. 17/1/2018, Aggiornamento delle Norme tecniche per le costruzioni, 2018.

[18]   D'Ambrisi, A., Mariani, V. and Mezzi, M. (2012): Seismic assessment of a historical masonry tower with nonlinear static and dynamic analyses tuned on ambient vibration tests. *Engineering Structures*, **36** 210–9, doi: https://doi.org/https://doi.org/10.1016/j.engstruct.2011.12.009

[19]   Makoond, N., Pelà, L. and Molins, C. (2019): Dynamic elastic properties of brick masonry constituents. *Construction and Building Materials*, **199** 756–70, doi: https://doi.org/10.1016/j.conbuildmat.2018.12.071

[20]   Totoev, Y.Z. and Nichols, J. (1997): A Comparative Experimental Study of the Modulus of Elasticity of Bricks and Masonry. *11th International Brick/Block Masonry Conference*, doi: https://doi.org/10.13140/2.1.4411.4247

[21]   Mashinskii, E. (2003): Differences between static and dynamic elastic moduli of rocks: Physical causes. *Geologiya i Geofizika*, **44** (9), 953–9,

[22]   Stepinac, M., Lulić, L., Damjanović, D., Duvnjak, I., Bartolac, M. and Lourenco, P.B. (2022): Experimental evaluation of unreinforced brick masonry mechanical properties by the flat-jack method – An extensive campaign in Croatia (Under review).

[23]   Ortega, J., Stepinac, M., Lulić, L., Nunez Garcia, M., Saloustros, S., Aranha, C. et al. (2022): Correlation between sonic pulse velocity and flat-jack tests for the estimation of the elastic properties of unreinforced brick masonry (Under review).

[24]   Lulić, L., Ožić, K., Kišiček, T., Hafner, I. and Stepinac, M. (2021): Post-earthquake damage assessment-case study of the educational building after the Zagreb earthquake. *Sustainability (Switzerland)*, MDPI AG. **13** (11), doi: https://doi.org/10.3390/su13116353

[25]   Grazzini, A. (2019): Sonic and Impact Test for Structural Assessment of Historical Masonry. *Applied Sciences*, **9** 1–12, doi: https://doi.org/10.3390/app9235148

[26]   Sassu, M., Stochino, F. and Mistretta, F. (2017): Assessment Method for Combined Structural and Energy Retrofitting in Masonry Buildings. *Buildings*, **7** (3), doi: https://doi.org/10.3390/buildings7030071

[27]   Giresini, L., Casapulla, C. and Croce, P. (2021): Environmental and Economic Impact of Retrofitting Techniques to Prevent Out-of-Plane Failure Modes of Unreinforced Masonry Buildings. *Sustainability*, **13** (20), doi: https://doi.org/10.3390/su132011383

[28] Corradi, M., Mustafaraj, E. and Speranzini, E. (2021): Sustainability considerations in remediation, retrofit, and seismic upgrading of historic masonry structures. *Environmental Science and Pollution Research*, doi: https://doi.org/10.1007/s11356-021-17490-7

[29] Milić Mija, Stepinac Mislav, Lulić Luka, Ivanišević Nataša, Matorić Ivan, Čačić Šipoš Boja et al. (2021): Assessment and Rehabilitation of Culturally Protected Prince Rudolf Infantry Barracks in Zagreb after Major Earthquake. *Buildings*, **11** (11),

CRITICAL NEAR RESONANCE SHAKING TABLE TESTS OF CONSTRUCTED LARGE-SCALE UPGRADED ISOLATED USI-V-MG BRIDGE PROTOTYPE MODEL

Jelena Ristic[1], Ragip Behrami[2], Danilo Ristic[3]

[1] *Assist. Prof. Dr. Faculty of Engineering, Department of Civil Engineering, International Balkan University (IBU), Skopje, Republic of North Macedonia, e-mail: jelena.ristic.ibu@gmail.com*

[2] *PhD student, Institute of Earthquake Engineering and Engineering Seismology (IZIIS), Ss. Cyril and Methodius University, Skopje, Republic of North Macedonia, e-mail: rbehrami@gmail.com*

[3] *Prof. Dr., Institute of Earthquake Engineering and Engineering Seismology (IZIIS), Ss. Cyril and Methodius University, Skopje, Republic of North Macedonia, e-mail: danilo.ristic@gmail.com*

Abstract

Construction of modern, seismically safe bridge structures represents a permanent activity of the highest importance because bridge structures are important key elements responsible for providing continuous functioning of integral highway infrastructure systems. An extensive experimental and analytical research led by the third author was performed in the Institute of Earthquake Engineering and Engineering Seismology (IZIIS), Ss. Cyril and Methodius University in Skopje, lasting three and a half years, in the frames of the innovative NATO Science for Peace Project "Seismic Upgrading of Bridges in South-East Europe by Innovative Technologies (SFP: 983828)", involving five countries. The specific project part included development of the innovative upgraded seismically isolated system USI with vertical multi gap V-MG representing an advanced technology for seismic isolation and seismic protection of bridges. By integrating the new uniform, vertical multi-gap (V-MG) energy dissipation devices, qualitative advances of the USI-V-MG system were achieved. The original observations resulting from the conducted complex, unique and critical near resonance shaking table tests of the constructed large-scale bridge model are presented and discussed in this paper. The extensive experimental research program was realized on a bridge model constructed by using the seismically isolated system upgraded with uniform vertical multi-gap energy dissipation devices (USI-V-MG). The installed adaptive system for seismic protection of bridges utilizes originally produced double spherical rolling seismic bearings (DSRSB) as seismic isolators, while qualitative improvement of the seismic performances is achieved through the use of novel, uniform vertical multi-gap energy dissipation (V-MG-ED) devices.

Keywords: Shaking table, bridge model, seismic test, seismic isolation, energy dissipation

1. Introduction

In the past, extensive studies in the field of seismic isolation of bridges have been mostly performed in the world's renowned research centres in Japan, USA, Italy, and New Zealand. However, in the recent years, contributions from many other countries are increased and have resulted in proposing of many new ideas and concepts. The intolerable severe impacts to modern bridge systems during strong recent earthquakes [1, 2], have been observed. It has given rise to strong arguments about the further needs for development and practical implementation of seismic isolation systems in seismic protection of bridges, [3-7]. This paper shows the obtained important results from the realized creative research part of the innovative long-term study devoted to development of a new, experimentally verified, advanced USI-V-MG system that can provide qualitative seismic upgrading of isolated bridges by using of innovative V-MG-ED energy dissipation devices [8]. The conducted initial experimental part of the study included realization of original nonlinear quasi-static tests of the created individual energy dissipation components. Unique original experimental data have been obtained, enabling development of an advanced, experimentally validated, nonlinear micro-model for hysteretic behaviour study of the complete new vertical multi-gap energy dissipation (V-MG-ED) devices with possibility of optionally different arrangement of ED components. Following some recent author's developments [8], conditions for realization of the final original study were created, involving shaking table tests of the constructed

large-scale bridge prototype model with the applied new USI-V-MG system. The tested uniform upgrading system for seismic protection of bridges, USI-V-MG system, utilizes originally produced double spherical rolling seismic bearings (DSRSB) as seismic isolation system, while qualitative improvement of seismic performances is achieved through the use of novel uniform vertical multi-gap energy dissipation (V-MG-ED) devices.

2. Concept of New USI-V-MG Bridge System

The upgraded seismically isolated (USI) system with vertical multi gap (V-MG) energy dissipation (ED) devices represent newly created advanced technical concept providing harmonized modification and improvement of structural seismic response, Fig. 6. The USI-V-MG system is advanced alternative method for qualitative improvement of seismic protection of bridge structures through introduced concept of global optimization of seismic energy balance. The USI-V-MG system is created through obligatory incorporation of the following three complementary systems: *(1) Incorporation of seismic isolation (SI) system:* The applied system for seismic isolation of bridge superstructure should contain adequately selected seismic isolators that will provide very low stiffness in horizontal direction and will be capable of sustaining safely the total weight of the entire superstructure. In that way, it is enabled for an appropriately designed seismic isolation (SI) device to be installed at each supporting point of bridge superstructure whereas the total isolated weight will be directly transferred to the supporting middle piers and/or to the rigid supporting abutments of the bridge. Under such conditions, a wide range of possibilities of selecting the proper system for seismic isolation of bridge superstructure is given, including application of any newly developed advanced solutions for seismic isolation; *(2) Incorporation of seismic energy dissipation (ED) system:* Seismic isolators are characterized by insufficient damping for seismic energy dissipation, so additional seismic energy dissipaters have been introduced. For this reason, the ED devices should possess optimal stiffness, optimal bearing capacity and high ductility in relation to the seismic performances of implemented seismic isolators. Considered very large stiffness of the ED devices leads to undesired impact and impulsive transfer of inertial forces. To avoid such problem, it is favourable to reduce the initial stiffness of ED devices to an optimal level. In addition, if bearing capacity of ED devices is considered very high, large or critical forces will be transferred to the piers. To avoid related problem, bearing capacity of energy dissipation devices should be reduced to a design limit. Finally, the ductility capacity of ED devices should be sufficiently large. In the case of generated large inertial forces, relative displacements in full scale bridges can become quite large, of the order of 25-30 cm or larger. Therefore, the ED devices should possess the ability of sustaining large deformations without damage. Generally, it is necessary to introduce ED devices with greater capacity of seismic energy dissipation through nonlinear deformations and creation of pronounced hysteresis curves. In the frameworks of this study, very significant advances of the three above specified properties are achieved by formulation of the proposed advanced V-MG multi-directional energy dissipation devices, and *(3) Incorporation of displacement limiting (DL) system:* In the course of very strong earthquake large relative displacements may occur and sometimes they are not successfully controlled in a reliable engineering mode. By introducing specific displacement limiting devices (DLD), strong impact and negative effects will be reduced or avoided.

3. Creation and Testing of Prototypes of V-MG Energy Dissipation Devices

Within the frames of the conducted study, special attention has been paid to the formulation of integrated compact unit providing highly ductile response, as well as, structurally to represent innovative multi-gap (MG) and multi-directional (MD) energy dissipation (ED) device of a unique and large seismic energy dissipation capacity. Here, briefly are described the main creation steps, original structure and testing of prototypes of new V-MG-MD-ED energy dissipation devices:

1) Structure of multi-directional V-MG-ED devices: The structure of V-MG-ED device generally consists of: (1) base metal plate for fixation of the vertical cantilever components; (2) radial distributed in equidistance vertical energy dissipation components (EDC); and (3) upper metal plate with openings through which the energy dissipation components are activated based on gaps in different phases.

Characteristic activation modes include very frequent weak earthquakes, reduced number of moderately strong earthquakes and rare, but possible, very strong and destructive earthquakes. The prototype model of the proposed V-MG-MD-ED device, Figure 1, has been created considering several constituent parts that form a compact ED unit, including:

(a) Base plate: The base plate of the V-MG-MD-ED device is manufactured in the form of a base circular metal plate with thickness d = 25 mm and diameter of D = 450 mm. In the base metal plate, in each of the two concentric circles, eight regularly spaced equal openings with windings are made. The openings with windings are used to fix the vertical components by screwing. In the outer concentric circle with a diameter of d_1 = 340 mm, eight openings with windings are made for the fixation of the external eight vertical (V) energy dissipation components. In the internal concentric circle with a diameter of d_2 = 190 mm, spaced are other eight openings with windings for the fixation of the internal eight vertical (V) energy dissipation components.
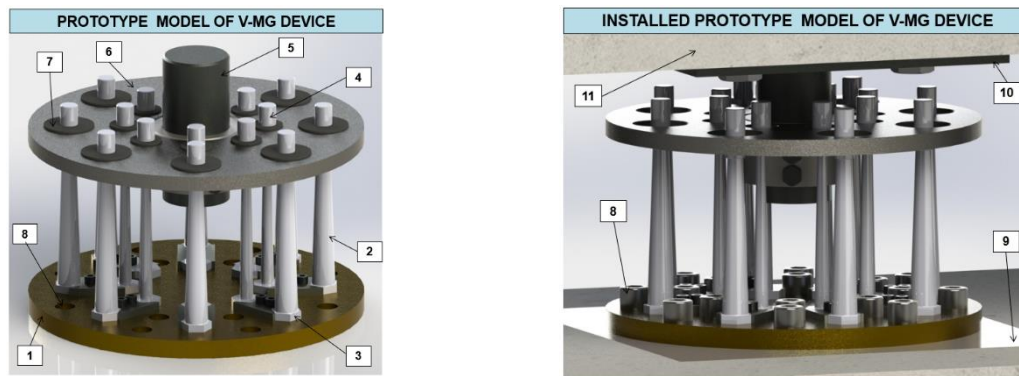
Figure 1. Prototype model of V-MG-ED device with installed V-MG-ED components: 1. Bottom fixing plate; 2. Outer V-MG components; 3. Bottom common fixing part; 4. Inner V-MG components; 5. Stiff central body; 6. Upper activating plate; 7. Gaps with distance protector; 8. Fixing bolts of base plate to substructure; 9. Substructure; 10. Upper plate fixed to superstructure; 11. Superstructure of prototype bridge.

(b) Vertical ED components: The vertical energy dissipation components are made of a ductile metal in the form of a moderately steep cut cone. According to the diameter of the cone base (Db), there have been adopted a total of four options from which there have arisen four prototype types of energy dissipation devices, Fig. 2. For each type of energy dissipation device, there have been designed vertical elements with two alternative variants of cones, regarding the considered different diameters of the top (Dt), whereat the diameter of the element at the base has been kept the same. In that way, four base-type prototypes of energy dissipation devices have been formed, each type with two variants of cones of vertical energy dissipation components as follows: *(1) Base type-1* with options: a) prototype model T11 with base and top diameters Db/Dt=32.0/25.6 mm and b) prototype model T12 with base and top diameters Db/Dt=32.0/19.2 mm; *(2) Base type-2* with options: a) prototype model T21 with base and top diameters Db/Dt=28.0/22.4 mm and b) prototype model T22 with base and top diameters Db/Dt=28.0/16.0 mm; *(3) Base type-3* with options: a) prototype model T31 with base and top diameters Db/Dt=24.0/19.2 mm and b) prototype model T32 with base and top diameters Db/Dt=24.0/14.4 mm; *(3) Base type-4* with options: a) prototype model T41 with base and top diameters Db/Dt=20.0/16.0 mm and b) prototype model T42 with base and top diameters Db/Dt=20.0/12.0 mm. All vertical components have the same height of the cone body of h1 = 190 mm and end with an identical cylinder with a diameter d = 24.0 mm with a constant height of h2 = 60.0 mm. With the adapted geometry of V-MG components, provided were equivalent conditions for fixation into the base plate, while the standard cylinder at the top provided equivalent gap-G1 and gap-G2 conditions for gap-based excitation (alternatively repeated contact and activation).

(c) Activating plate with holes: On the upper side of V-MG device, metal plate with thickness d=20.0 mm is constructed with openings with different diameters distributed along two concentric circles. The inner 8 openings are constructed with diameter d3=34.0 mm. Having standard top cylinders with

diameter of d=24.0 mm, a gap of G1=5.0 mm was provided in all directions. However, the external 8 openings are constructed with diameter d4=60.0 mm. Having top cylinders with diameter of do=24.0 mm, a gap of G2=18.0 mm was obtained in all directions. The upper metal plate is fixed to the central stiff body for which is assured strong connection to the superstructure of the large-scale bridge model. With presented original structure of V-MG device, activation of the inner ED components will start after relative displacement becomes larger than 5 mm in all directions. If relative displacement exceeds 18.0 mm, then activation of all ED components located on the external concentric circle takes place.

Figure 2. Cyclic testing of V-MG-ED devices (left) and Performance of EDC with simulated gap-G2 (right)

2) Testing of prototype models under cyclic loads: Within the frames of experimental testing of produced model prototypes of V-MG energy dissipation components, an experimental program has been carried out. Each individual V-MG component has been tested twice. First test-1, representing original test, was conducted to define hysteretic response of V-MG component under the initial conditions. Second test-2, representing repeated test was performed to get an insight into the hysteretic response of the model that has already been tested.

For testing of 8 prototypes of the V-MG components under cyclic loads, simulating gap-G1 in the first case and gap-G2 in the second case, a total of 16 components of type-V have been produced. With the anticipated realization of the original and the repeated tests of each component, a total of 32 nonlinear cyclic tests have been done, Fig. 2.

4. Refined Modelling of V-MG-ED Devices and Components

An important research part included refined modelling and hysteretic response simulation of V-MG-ED devices, Fig. 3. Nonlinear numerical analysis has been carried out using the formulated refined or micro-models of the created and tested model prototypes. Commonly, cyclic displacement of up to ±45mm in X direction has been simulated through the upper plate, with a step of 5mm increase in each cycle. The mathematical model represented refined 3D finite element mesh of installed EDD-s. Modelling and analysis of the hysteretic response and energy dissipation capacity of V-MG-ED devices has been done by the use of ABAQUS CAE software. With setting the real material characteristics, the element geometry, the contour and contact conditions, the imposed displacements and other required information, appropriate conditions were created to compute results as accurately as possible.
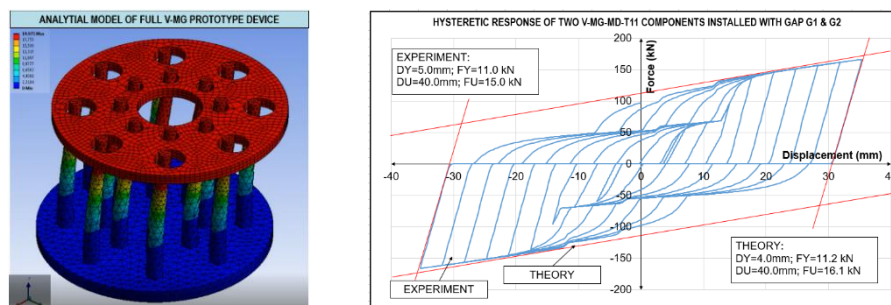
Figure 3. Formulated refined 3D ABAQUS model of full V-MG-MD-ED device (left) and computed hysteretic response of two V-MG-MD-T11 components installed with gaps G1 & G2 (right)

The calculations have been performed successfully, without shown any error during the step-by-step analysis process. Following the process of nonlinear micro-model formulation, considered and analysed was the specific example of partial device, assembled with two identical V-MG-MD-T11 components with different gaps G1 & G2. The resulting original and characteristic gap-based hysteretic response of the system was successfully computed, Fig. 3, right.

5. Prototype Testing of DSRSB Seismic Isolation Devices

The seismic isolation (SI) system used within the USI-V-MG bridge model was assembled by the use of prototype models of double spherical rolling seismic bearing (DSRSB) devices having two large-radius spherical surfaces (Fig. 4), which were originally designed for the purposes of the planned various experimental investigation phases [5].

Figure 4. Prototype of designed, constructed and tested DSRSB devices: (1) Cross-section with geometrical properties and (2) Device view with characteristic cross-section (*Commonly re-used prototype*)

The design of such device was conditioned by several requirements: to provide the sufficient bearing capacity for vertical loads; to provide the sufficient displacement capacity; to have radii of curvatures of the spherical surfaces adequate to achieve the targeted period of vibration; to have a sliding surface generating minimal friction and to have a central rolling part providing minimum reactive friction force. The resulting device is shown in Fig. 4. The lower (2) and upper (4) spherical plates were constructed of a hard inox polished to a mirror shine, providing durability and very low friction. Its diameter was 250mm, while the radii of the spherical surfaces were 1000mm. Both plates were fixed to the lower (1) and upper (3) steel end plates with diameter of 310mm. The inserted central rolling part (5) was constructed in the form of a ring of twelve balls with a diameter of 18mm, distributed uniformly along the circle around cylindrical slider and spaced with their opposite centres at 74mm. From the response, it is clear that the device has a sufficient capacity for horizontal deformation, amounting to over 45mm and that the shape of the hysteretic loops forms a skewed rectangle, which leads to its representation with bilinear model, Fig. 5.
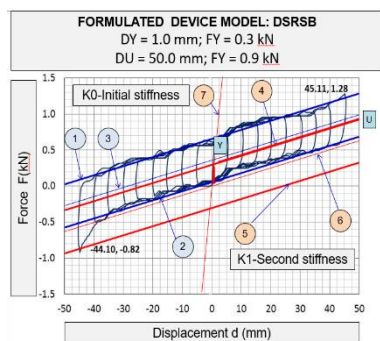
EXPERIMENTAL RECORDS:

(1) upper envelope curve (EC)

(2) lower EC

(3) symmetric line

(4) shifted upper EC

(5) shifted lower EC

(6) shifted symmetric line

(7) recorded initial stiffness

Quasi-static tests of isolation devices were carried out by the use of four DSRSB devices mounted at their original locations, two at each abutment. The RC slab, weighting 85kN, brought a vertical force of 21.25kN to each one. The representative hysteretic response for a single device is shown in Fig. 5.

Figure 5. Hysteretic response of tested DSRSB prototype [5]

6. Seismic Shaking Table Tests of Large-Scale USI-V-MG Bridge Model

Due to the size of the seismic shaking table (5.0mx5.0m) and payload capacity, the originally designed USI-V-MG bridge prototype model had to be geometrically reduced in respect to the selected prototype. From those reasons, adopted was geometrical scale factor of 1:9, which verified the referred constraints in this case, but with adopted specific model design concept. As a consequence of the scale reduction, the relevant properties involved in the dynamic (seismic) tests were scaled according to a similitude law. Considering the main related factors, an adequate combined true replica-artificial mass simulation model was adopted. For simulation of the stiff RC superstructure, the stiff slab with added mass was adopted using the same material as that of the prototype structure. For simulation of the middle piers, steel material was used.
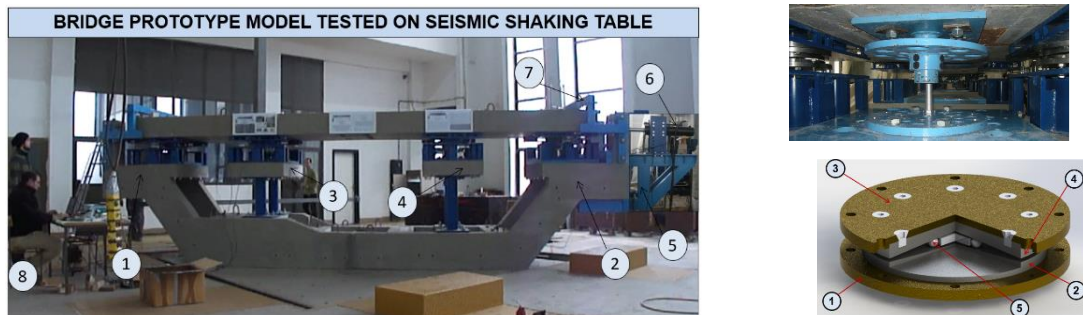
Figure 6. USI-V-MG (BM-V) bridge prototype model on IZIIS seismic shaking table: Left end support (1); right end support (2); support above shorter piers (3); support above longer piers (4); actuator supporting structure (5); actuator (6); DL devices (7); computer controlling cyclic tests (8), (Left); and Right: Disposition of DSRSB devices (superstructure supports) and partially between set new V-MG-ED device.

The seismic isolation and energy dissipation devices were designed and produced in reduced scale. The similitude law implies the adopted relations for the different parameters, all given in terms of the geometrical scale factor (*lr*). Concrete material type C25/30 has been used for construction of RC segments of bridge model, while for construction of steel V-MG devices, steel material type S355 was selected and applied. Considering final proportions at the top level, the total length of the entire experimental bridge model is L = 740.0 cm + 2 * 20.0 cm + 2 * 25.0 cm = 830.0 cm. The RC deck is placed at a height distance of h_d = 40.0 cm from the highest RC substructure surfaces. This space (seismic gap) is used to install both, originally produced DSRSB devices, as well as the new V-MG-MD-ED devices, Fig. 6 and Fig. 7. After fabrication of all model segments and specific SI, ED and DL devices, as well as, after preparing the other testing connections and instrumentation devices, the large-scale USI-V-MG bridge prototype model was assembled and tested in the Dynamic testing laboratory of the Institute of Earthquake Engineering and Engineering Seismology (IZIIS) in Skopje. With adopted 20 active recording channels, approximately 5.000.000 numerical values were recorded in each single test. Realizing four original and four repeated tests, large experimental data volume, containing about 40 million numerical values, have been recorded, integrally processed and analysed. In Fig. 7, as example, presented are time history responses of displacements and accelerations recorded during seismic test under simulated real strong El-Centro earthquake scaled to PGA=0.78g. The conducted seismic shaking table tests have shown that upgrading of seismically isolated bridges with vertical multi gap energy dissipation devices represent a highly efficient and practical engineering option.
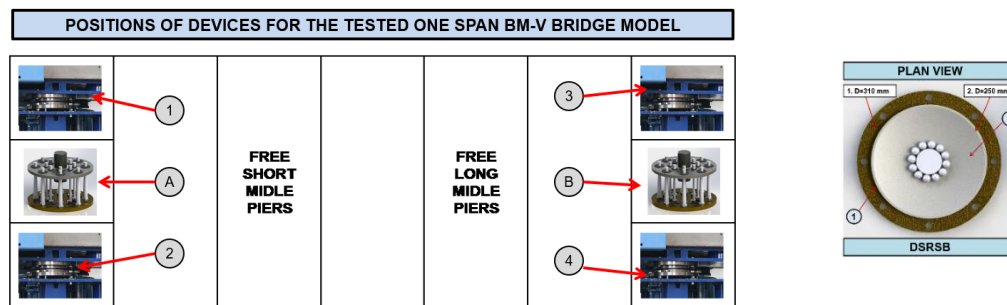
Figure 7. Defined positions of DSRSB devices (1 to 4, with details right) and V-MG-ED devices (A and B) of the tested one-span large-scale USI-V-MG (BM-V) bridge prototype model on seismic shaking table

7. Critical Seismic Shaking Table Tests near Resonance of USI-V-MG Model

The ultimate goal of the present research includes development of advanced technology for seismic protection of bridge structures under extreme seismic loading. To realize the planed unique and scientifically important and specific experimental analysis of actual seismic response characteristics of innovatively assembled large-scale bridge model, with DSRSB isolation and new V-MG energy dissipation devices, under simulated the most critical near-resonance earthquake excitations, extensive well-focused shaking table tests have been planned and realized in study phase-III. However, to provide highly valuable comparative experimental data and full evidence in differences in seismic responses of innovative bridge model tested with different test options, two additional series of shaking table tests have been planned and conducted.

The first test series included initial shaking table tests of assembled bridge model with seismic isolation only, item 7.1 (phase-I). Initial tests actually represent the first basic experimental study, devoted to experimental testing of seismic response of assembled isolated-bridge prototype model, without installed energy dissipation (ED) devices, under simulated strong earthquakes. The second test series included shaking table tests of innovatively-upgraded isolated bridge model, item 7.2 (phase-II). The conducted tests actually represent experimental study of real seismic response characteristics of constructed innovatively-upgraded isolated bridge prototype model, existing with seismic isolation (SI) and new energy dissipation (ED) devices, under simulated strong earthquakes. Finally, regarding the obtained large set of experimental results, the effects of critical near resonance (NR) earthquake input on innovatively-upgraded isolated bridge model was made possible, item 7.4 (phase-IV. Actually, the study phase-IV was devoted to processing and comparative presentation of extreme seismic responses of innovatively-upgraded isolated bridge model considering the obtained results from conducted shaking table test under simulated two series of seismic input: (1) seismic input representing critical near resonance (NR) earthquake excitations of Phase-III and (2) seismic input representing selected location representative (LR) strong earthquake excitations of Phase-II. As stated above, approximately 5 million numerical values were recorded in each single test. With newly realized four original tests of phase-I and four original tests of phase-IV, additional large experimental data volume, containing about 40 million numerical values, have been recorded, processed and analysed. Regarding the conducted very extensive experimental study program, including successfully realized full set of 16 original experimental tests, recorded were and processed about 80.000.000 numerical data values.

7.1. Phase-I: Initial shaking table tests of bridge model with isolation only

Study phase-I represent conducted initial experimental study devoted to experimental seismic response testing of constructed isolated bridge prototype model without ED devices under simulated strong earthquakes.

Table 1. Recorded difference in peak relative displacements during shaking table test of BM2-V1 model with ED devices [1c] and BM2 model without ED devices [1c*], under simulated *compressed* El-Centro earthquake

Tests	Test with ED devices [1c]	Test without ED devices [1c*]

[1c&1c*]	[1c] O-T1: C-El-Centro, PGA=0.78G			[1c*] O-T1: C-El-Centro, PGA=0.78G		
	Channel	MaxD [mm]	MaxD [%]	Channel	MaxD [mm]	MaxD [%]
diff.	LVDT-03	26.03	100.00	LVDT-03	40.77	**+56.62**

For the purposes of getting insight into contribution of the EDDs to the structural response, bridge model setup which involved only four DSRSB isolators (no SB dissipaters) has been tested on the shaking platform under compressed El Centro excitation scaled to PGA 0.78g. The relative displacements recorded by LVDT-03 for the system with and without SB energy dissipaters are shown in Table. 2. By comparing two responses, it may be noticed that use of dissipaters reduced maximum displacement from 40.77 mm to 26.03 mm, or 56.62%. Such favourable contribution of EDD, adequately designed in their mechanical properties, gain in importance for much stronger earthquakes.

7.2. Phase-II: Shaking table tests of innovatively-upgraded isolated bridge model

Study phase-II represent experimental study devoted to seismic response testing of constructed innovatively-upgraded isolated bridge prototype model with seismic isolation (SI) and energy dissipation (ED) devices under simulated strong earthquakes.

Regarding the stated objectives, conducted were extreme-loading experimental tests of innovatively-upgraded isolated bridge with new V-MG ED devices, simulating the following four representative and strong compressed earthquakes: [1c] El-Centro, PGA=0.78G, [2c] Petrovac, PGA=0.72G, [3c] Landers, PGA=0.76G, and [4c] Northridge, PGA=0.89G, earthquake Table 3. The peak relative displacements recorded by LVDT-03 of the system upgraded with SB energy dissipaters are well controlled in all cases. Regarding peak responses, it may be noticed that use of dissipaters reduced maximum displacements to 26.03mm, 26.61mm, 20.35mm and 31.61mm, respectively.

Table 2. Recorded peak relative displacements by LVDT sensors during conducted original shaking table tests of BM2-V1 model simulating *compressed:* [1] El-Centro, [2] Petrovac, [3] Landers and [4] Northridge eq.

Tests	[1c] O-T1: C-El-Centro, PGA=0.78G			[2c] O-T2: C-Petrovac, PGA=0.72G		
[1c&2c]	Channel	MaxD (-) [mm]	MaxD (+) [mm]	Channel	MaxD (-) [mm]	MaxD (+) [mm]
recorded	LVDT-03	-17.96	**26.03**	LVDT-03	**-26.61**	15.21
Tests	[3c] O-T1: C-Landers, PGA=0.76G			[4c] O-T2: C-Northridge, PGA=0.89G		
[3c&4c]	Channel	MaxD (-) [mm]	[1c&2c]	Channel	MaxD (-) [mm]	[1c&2c]
recorded	LVDT-03	**-20.35**	11.76	LVDT-03	-29.93	**31.61**

The observed favourable contribution of energy dissipation devices, provided reduction of maximum displacement bellow designed displacement limit of seismic isolators, amounting to 40.00mm. This reduction is gaining even higher importance for the case of bridge structures exposed to much stronger earthquakes.

7.3. Phase-III: Critical shaking table tests of innovatively-upgraded isolated bridge model

Study phase-III represent experimental study devoted to seismic response testing of constructed innovatively-upgraded isolated bridge prototype model with seismic isolation (SI) and ED devices under simulated critical near resonance (NR) earthquake input.

Realized model testing with compressed real earthquakes actually represent simulation of real seismic input regarding actual properties of designed and constructed scaled-model of bridge prototype, directly resulting from model similarity conditions. Frequency content of input records was accordingly changed. It is well demonstrated by presented acceleration response spectra for *compressed* Petrovac earthquake record with new frequency content used for testing, Figure 9. Dominant frequency domain includes periods less than 0.32s, while for periods T ≥ 0.32s, frequency domain is not significant.
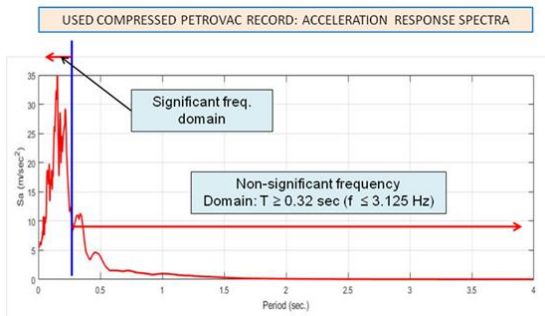
Figure 9. Acceleration response spectra of *compressed* Petrovac record with new frequency content used for testing
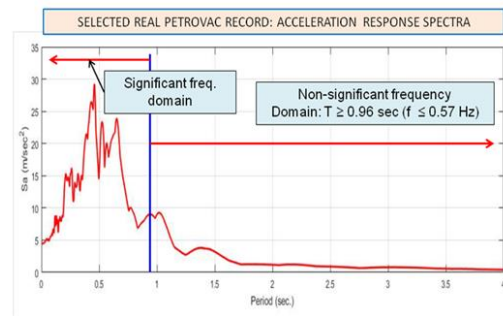
Figure 10. Acceleration response spectra of *real* (*not time compressed*) Petrovac record
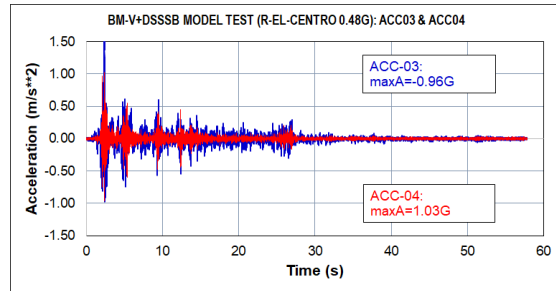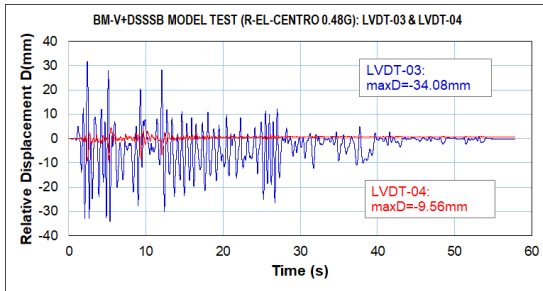
Figure 11. Relative superstructure displacement responses recorded by LVDT-03 & LVDT-04 (left) and acceleration responses recorded by ACC-03 & ACC-04 (right) during USI-V-MG (BM-V) shaking table bridge model test conducted with simulated *real* El-Centro earthquake.
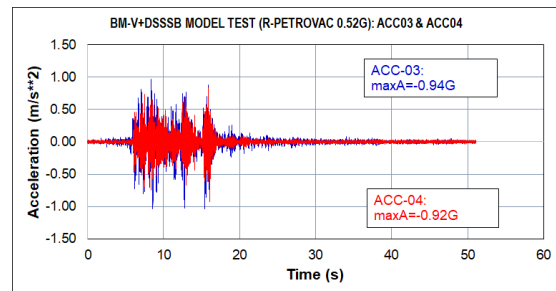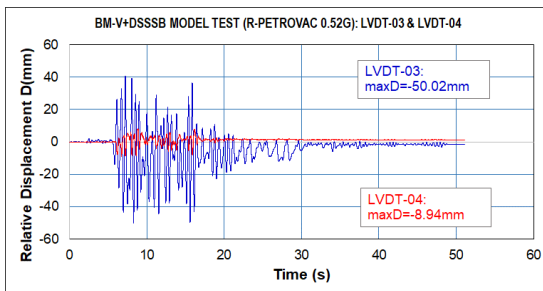
Figure 12. Relative superstructure displacement responses recorded by LVDT-03 & LVDT-04 (left) and acceleration responses recorded by ACC-03 & ACC-04 (right) during USI-V-MG (BM-V) shaking table bridge model test conducted with simulated *real* Petrovac earthquake.
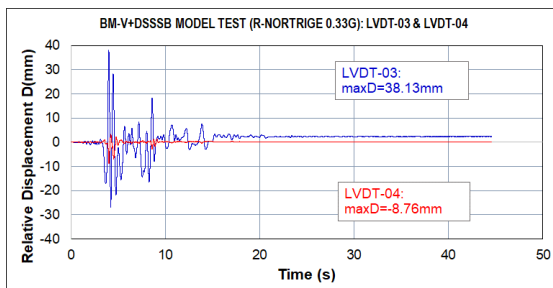
Figure 13. Relative displacement response recorded by LVDT-03 & LVDT-04 during shaking table bridge model test with simulated *real* Petrovac earthquake
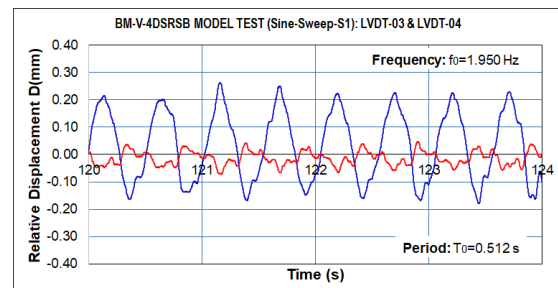
Figure 14. Vibration period of bridge model *with seismic isolation only* defined using recorded relative displacement during shaking table sine-sweep test

Figure 14 shows much larger initial vibration period of bridge model, T=0.512s, showing that dominant frequency content of seismic input was very well and significantly avoided. Initial vibration period was

defined based on recorded time history of relative displacement during conducted initial sine-sweep shaking table test. Due to very small vibration amplitudes and present initial gaps, the excited model vibration actually corresponds to initial state with activated seismic isolation only.

The final experimental study included specific near resonance (NR) testing of constructed innovatively-upgraded isolated bridge prototype model with seismic isolation (SI) and energy dissipation (ED) devices, characterized by initial vibration period T=0.512s. Selection of applicable critical near resonance (NR) input was made after analysing acceleration response spectra of used *real* (*not time compressed*) earthquakes. Regarding, for example, acceleration response spectra of real Petrovac record, Figure 10, dominant frequency content is mainly distributed near fundamental period of the system. Due to similar observations for other earthquakes, the same four real earthquake records were accepted to be actual critical near resonance (NR) seismic input for shaking table tests.

Table 3. Recorded peak relative displacements by LVDT sensors during conducted four original shaking table tests of BM2-V1 bridge prototype model simulating *real* [1] El-Centro, [2] Petrovac, [3] Landers and [4] Northridge earthquake

Tests	[1r] O-T1: **R**-El-Centro, **PGA=0.48G**			[2r] O-T2: **R**-Petrovac, **PGA=0.52G**		
[1c&2c]	Channel	MaxD (-) [mm]	MaxD (+) [mm]	Channel	MaxD (-) [mm]	MaxD (+) [mm]
recorded	LVDT-03	**-34.08**	31.92	LVDT-03	**-50.02**	40.69
Tests	[3r] O-T1: **R**-Landers, **PGA=0.76G**			[4r] O-T2: **R**-Northridge, **PGA=0.33G**		
[3c&4c]	Channel	MaxD (-) [mm]	[1c&2c]	Channel	MaxD (-) [mm]	[1c&2c]
recorded	LVDT-03	**-40.55**	40.11	LVDT-03	-26.90	**38.13**

Considering the stated critical test conditions, conducted were critical NR loading experimental tests of innovatively-upgraded isolated bridge with new V-MG energy dissipation (ED) devices, simulating the following four representative and strong real earthquakes: [1r] El-Centro, PGA=0.48G, [2r] Petrovac, PGA=0.52G, [3r] Landers, PGA=0.76G, and [4r] Northridge, PGA=0.33G, earthquake Table 4. The peak relative displacements recorded by LVDT-03 of the system upgraded with SB energy dissipaters are considerably larger in all cases due to NR earthquake input. Regarding peak responses, it may be noticed that with present dissipaters maximum displacements are 34.08mm, 50.02mm, 40.55mm and 38.13mm, respectively.

Fig. 11. and Fig. 12. present relative superstructure displacement responses recorded by LVDT-03 & LVDT-04 (left) and acceleration responses recorded by ACC-03 & ACC-04 (right) during USI-V-MG (BM-V) shaking table bridge model test conducted with simulated *real* El-Centro and Petrovac earthquake, respectively.

Fig. 13 presentsrelative displacement response recorded by LVDT-03 & LVDT-04 during shaking table bridge model test with simulated *real* Petrovac earthquake.

7.4. Phase-IV: Effects of critical near resonance (NR) earthquake input on innovatively-upgraded isolated bridge model

Study phase-IV was devoted to processing and comparative presentation of extreme seismic responses of innovatively-upgraded isolated bridge model considering the obtained results from conducted shaking table test under simulated two series of seismic input: (1) considered critical near resonance (NR) earthquake input of Phase-III and (2) selected location representative (LR) strong earthquakes of Phase-II.

Table 5. comparatively presents recorded peak relative displacements by LVDT sensors during conducted original shaking table tests of BM2-V1 bridge prototype model simulating both, *real and compressed* [1] El-Centro, [2] Petrovac, [3] Landers and [4] Northridge earthquake. To show actual

effects of frequency content of NR earthquake input, comparative values of peak relative displacements for the case of seismic tests with compressed earthquakes are shown for the same PGA levels.

In all four comparative test cases, much larger peak values of relative displacements were recorded during realized tests with simulated critical NR earthquake input. The recorded increase of peak response reached amounts of +112.86% for El-Centro, +160.38% for Petrovac, +99.26% for Landers and +225.34% for Northridge earthquake, Table. 5.

The presented results clearly pointed out the following highly important observations: (1) Seismic isolation only may be regarded as unsafe solution for bridges exposed to strong earthquakes; (2) The new V-MG energy dissipation device represent very efficient solution for seismic upgrading of isolated bridges exposed to very strong earthquakes and (3) The possible negative effects of critical NR seismic input should be avoided through application of effective design process of seismically upgraded isolated bridges with new V-MG-ED devices.

Table 4. Recorded peak relative displacements by LVDT sensors during conducted original shaking table tests of BM2-V1 bridge prototype model simulating ***real and compressed*** [1] El-Centro, [2] Petrovac, [3] Landers and [4] Northridge earthquake

No. 1	[1r] O-T1: **R**-El-Centro, **PGA=0.48G**			[1c] O-T1: **C**-El-Centro, **PGA=0.48G**		
[1r&1c]	Channel	MaxD [mm]	MaxD [%]	Channel	MaxD [mm]	MaxD [%]
diff.	LVDT-03	34.08	**+112.86**	LVDT-03	16.01	100.00
No. 2	[2r] O-T2: **R**-Petrovac, **PGA=0.52G**			[2c] O-T2: **C**-Petrovac, **PGA=0.52G**		
[2r&2c]	Channel	MaxD [mm]	MaxD [%]	Channel	MaxD [mm]	MaxD [%]
diff.	LVDT-03	50.02	**+160.38**	LVDT-03	19.21	100.00
No. 3	[3r] O-T3: **R**-Landers, **PGA=0.76G**			[3c] O-T3: **C**-Landers, **PGA=0.76G**		
[3r&3c]	Channel	MaxD [mm]	MaxD [%]	Channel	MaxD [mm]	MaxD [%]
diff.	LVDT-03	40.55	**+99.26**	LVDT-03	20.35	100.00
No. 4	[4r] O-T4: **R**-Northridge, **PGA=0.33G**			[4c] O-T4: **C**-Northridge, **PGA=0.33G**		
[4r&4c]	Channel	MaxD [mm]	MaxD [%]	Channel	MaxD [mm]	MaxD [%]
diff.	LVDT-03	38.13	**+225.34**	LVDT-03	11.72	100.00

8. Conclusions

Based on research results obtained from the conducted extensive experimental and theoretical studies using designed innovative USI-V-MG bridge model prototype, the following main conclusions are derived:

(1) The constructed and investigated novel DSRSB seismic isolation devices are very attractive and effective passive devices for seismic vibration isolation of bridges in arbitrary direction;

(2) The new vertical multi-gap multi-directional hysteretic V-MG energy dissipation devices possess unique energy absorption features since they are capable of adapting their stable behaviour to the arbitrary earthquake direction and to the actual level of seismic input energy. The new V-MG energy dissipation devices provided innovative, very stable and advanced 3D hysteretic response in the most critical cases of repeated strong earthquake effects in all directions;

(3) The displacement limiting devices, DLD, represent very effective obligatory measure in function of the last line of defence from excessive displacements of the bridge superstructure. DLD actually represent efficient passive system providing improvement of the bridge seismic safety with eventual activation only in critical cases of very strong earthquakes;

(4) With the results from the conducted experimental tests confirmed is that the new USI-V-MG system represents the upgraded high performance seismic isolation option for bridges. The system is created based on optimized seismic energy balance and represents effective technical innovation capable of integrating the advantages of seismic isolation, seismic energy dissipation

and effective displacement control. The developed and tested USI-V-MG system shows very high seismic response modification performances and could be used for efficient seismic protection of bridges in all directions under the effect of very strong repeated earthquakes; and

(5) During the further study phases, creative analytical research and simulation activities will be carried out, specifically directed to development of practical design rules of the developed new seismically safe USI-V-MG bridge system.

Acknowledgements

References

[1] Yuan, W., Feng, R., & Dang, X. (2018): Typical Earthquake Damage and Seismic Isolation Technology for Bridges Subjected to Near-Fault Ground Motions. *2018 International Conference on Engineering Simulation and Intelligent Control (ESAIC).* doi:10.1109/esaic.2018.00079.

[2] Kelly JM (1986): A Seismic Base Isolation: Review and Bibliography, *Soil Dyn. and Earthquake Eng.* 5(4): 202-216.

[3] Ristic D (1988): Nonlinear Behaviour and Stress-Strain Based Modelling of Reinforced Concrete Structures under Earthquake Induced Bending and Varying Axial Loads, PhD Dissertation, School of Civil Engineering, Kyoto University, Kyoto, Japan.

[4] Ristic D, Ristic J (2012): *New Integrated 2G3 Response Modification Method for Seismic Upgrading of New and Existing Bridges,* In 15th World Conference on Earthquake Engineering, (WCEE), Lisbon, Portugal.

[5] Ristic J, Misini M, Ristic D, Guri Z, Pllana N (2017): Seismic Upgrading of Isolated Bridges with SF-ED Devices: Shaking Table Tests of Large-Scale Model, Građevinar, 70 (6): 463-485. doi: https://doi.org/10.14256/JCE.2147.

[6] Ristik J (2011): Comparative Seismic Analysis of RC Bridge Structure Applying Macedonian Seismic Design Regulations and Eurocodes. MSc Thesis, Theory of Structures Department, "Ss. Cyril & Methodius" Univ., Skopje, Macedonia.

[7] Ristik J (2016): *Modern Technology for Seismic Protection of Bridge Structures Applying New System for Modification of Earthquake Response.* PhD Thesis, Institute of Earthquake Engineering and Engineering Seismology (IZIIS), "Ss. Cyril and Methodius" University, Skopje, Macedonia.

[8] Ristic D, Dorka U, Lako A, Zenunovic D, Folic R (2013): *Seismic Upgrading of Bridges in South-East Europe by Innovative Technologies,* NATO SfP Project 983828, Science for Peace and Security Programme, Final Report.

[9] Mitoulis et al. (2017) Seismic Performance of Novel Resilient Hinges for Columns and Application on Irregular Bridges. Journal of Bridge Engineering, 2017, 22(2), 04016114

[10] Argyroudis et al. (2020) Resilience assessment framework for critical infrastructure in a multi-hazard environment. Science of the Total Environment, 714, 136854. https://doi.org/10.1016/j.scitotenv.2020.136854

SEISMIC PROTECTION OF MASONRY AND INFILLED FRAME BUILDINGS USING UPGRADED SLIDING ISOLATION SYSTEM WITH SF DEVICES

Jelena Ristic[(1)], Valon Veseli[(2)], Labeat Misini[(3)], Danilo Ristic[(4)]

[(1)] *Assoc. Prof. Dr. Faculty of Engineering, Department of Civil Engineering, International Balkan University (IBU), Skopje, Republic of North Macedonia, e-mail: risticjelenaibu@gmail.com*

[(2)] *PhD student, Faculty of Civil Engineering, Ss. Cyril and Methodius University, Skopje, Republic of North Macedonia, e-mail: valon.veseli@uni-pr.edu*

[(3)] *PhD student, Institute of Earthquake Engineering and Engineering Seismology (IZIIS), Ss. Cyril and Methodius University, Skopje, Republic of North Macedonia, e-mail: labeat.misini@gmail.com*

[(4)] *Full Prof. Dr., Institute of Earthquake Engineering and Engineering Seismology (IZIIS), Ss. Cyril and Methodius University, Skopje, Republic of North Macedonia, e-mail: danilo.ristic@gmail.com*

Abstract

Presented in this paper is an innovative, uniform seismic protection system of masonry and infilled frame buildings created on the basis of a specifically upgraded sliding isolation system with new SF devices. The new building sliding-space flange protection system (BSSF system) represents a specific research segment of the integral research project, led by the fourth author, conducted in the Institute of Earthquake Engineering and Engineering Seismology (IZIIS), Ss. Cyril and Methodius University (Skopje), during three and a half years, in the frames of the innovative NATO Science for Peace and Security Project "Seismic Upgrading of Bridges in South-East Europe by Innovative Technologies (SFP: 983828)", involving five European countries. The upgraded, seismically isolated sliding system with integrated space flange (SF) energy dissipation (ED) devices has been developed as a mechanical passive concept to provide harmonized response of building structures to strong earthquakes. It is formulated as an adaptive system, which follows the adopted concept of global optimization of seismic energy balance, through utilization of newly designed dissipation devices as a supplementary damping level to the building isolation. The new BSSF protection system is based on obligatory incorporation of the following three integrated complementary systems: (1) Sliding seismic isolation (SSI) system, (2) SF seismic energy dissipation (ED) system and (3) Earthquake displacement limiting (EDL) system. The proposed seismically resistant BSSF building system represents a qualitatively new strategy for construction of modern masonry and framed masonry buildings by applying traditional and new construction materials and providing simultaneously: (1) Full seismic safety of protected buildings, (2) Reduction of construction time, and (3) Profitable construction in seismic areas achieved by the special system characteristics.

Keywords: building, masonry, framed masonry, seismic isolation, energy dissipation

1. Introduction

The need for more successful protection of specifically targeted buildings is becoming clearly evident considering the recorded heavy damages or total failure of these structures during the latest earthquakes that have occurred worldwide (Japan, Turkey, South Europe, China, the USA, Italy, Taiwan, Chile, New Zealand, etc.). The important initial studies in the field are fully documented in the published systematic review of seismic base isolation research [1]. For the last several decades, the most renowned research centers worldwide have been making continuous efforts toward reducing catastrophic earthquake consequences through improvement and advancement of the regulations for design and construction of structures in seismically active regions, [2-6]. To increase the energy dissipation performances of the system, specific U-shaped steel dampers have been studied and recommended for application in base-isolated structures, [7-9]. Also, various earthquake damaging phenomena have been experimentally studied to define possible solution options, [10-12]. Most of the latest research projects have been initiated based on published reports on recent post-earthquake investigations of earthquake

consequences related to existing various types of structures, [13-15]. Recently, extensive research involving costly shaking table tests on constructed large-scale models have been conducted by the first author and her collaborators, mainly targeted to seismic upgrading of isolated structures with specific energy dissipation devices, [16-18]. The needed basic concept of design and construction of reduced scale models for the considered complex shaking table tests carried out under simulated earthquakes, was successfully adopted considering the data available from a completed similar research, [19]. The applied response modification method for seismic upgrading of new and existing structures actually offers a very wide potential for practical application, particularly if refined nonlinear models and specific expert analysis procedures are consistently used, [20-21]. Presented in this paper is the developed innovative, multi-directional and uniform system applicable for advanced seismic protection of masonry and infilled frame masonry buildings. The new building-sliding space flange (BSSF) system was created based on adopted advanced upgrading of the initial sliding isolation system with the created new, efficient and experimentally proved SF energy dissipation devices.

2. The New BSSF Isolation System

A long-term experimental and analytical study was performed in the Institute of Earthquake Engineering and Engineering Seismology (IZIIS), Ss. Cyril and Methodius University (Skopje), as part of the NATO Science for Peace and Security Project "Seismic Upgrading of Bridges in South-East Europe by Innovative Technologies" (SFP: 983828), led by the fourth author. The developed BSSF system represents a specific product of the extended part of the integrated research.

The new uniform building-sliding space flange system (BSSF-system) has been developed based on the created compact passive SF energy dissipation device providing uniform multi-directional response and improved upgrading of buildings under very strong earthquakes. It has been formulated by implementation of the adopted concept of global optimization of the seismic energy balance. The designed SF energy dissipation devices used as supplementary damping represent a qualitative system improvement in respect to the building isolation only. The BSSF system is based on incorporation of three complementary systems: (1) Basic seismic isolation system (SI system) providing low stiffness in horizontal direction; (2) The new SF energy dissipation system to provide sufficient damping through dissipation of seismic energy, and, (3) Building displacement limiting (DL) devices to reduce or eliminate excessive displacements under strong impact effects.

3 Prototypes of SF Devices

The new seismic energy dissipation system installed in the tested BSSF building prototype model was composed of the developed advanced steel space flange (SF) energy dissipation (ED) devices. Up till now, SF-ED dissipation devices of the proposed type have been studied only by the first author and her collaborators for bridges, [16] and [22].

Table 1. Nonlinear model properties of SF-ED-M11 and SF-ED-M12 devices computed by using the formulated nonlinear FEM model and simulated cyclic displacements with increasing amplitudes

No.	SF-ED Device M11: SF-ED-8C-L1R-T1			SF-ED Device M12: SF-ED-4C-L1R-T1		
	Notation	FEM model	(%)	Notation	FEM model	(Δ%)
1	DY (mm)	5.0	100.0	DY (mm)	6.0	120.0
2	FY (kN)	21.0	100.0	FY (kN)	9.0	42.8
3	K0 (kN/mm)	4.0	100.0	K0 (kN/mm)	1.5	37.5
4	K1 (kN/mm)	0.18	100.0	K1 (kN/mm)	0.02	11.1
5	K1/K0	0.045	100.0	K1/K0	0.013	28.8

In this paper, the two basic types of SF-ED devices are presented (Table 1). The first SF device is composed of eight ED components, model M11, representing the SF-ED-8C-L1R-T1 device, Fig. 1.

The second SF device consists of four ED components, model M12, representing the SF-ED-4C-L1R-T1 device, Fig. 2. Adopting the experimentally verified refined 3D nonlinear analytical model, the hysteretic responses of the assembled prototype devices exposed to cyclic loads have been computed successfully, Fig. 3. With the computed original results, it was confirmed that the adopted representative bilinear analytical model could be implemented to realistically model the full hysteretic behavior of the device. The defined parameters of the representative bilinear models are comparatively presented in Table 1.
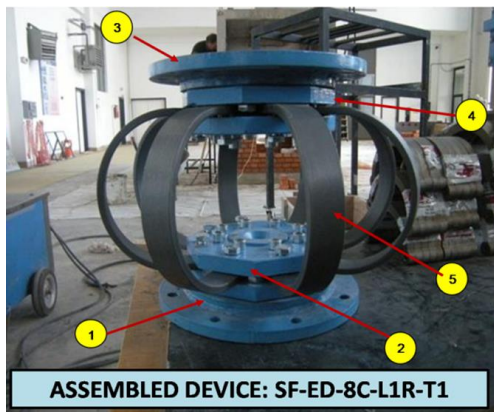
Fig. 1. Assembled SF-ED device type-1 (SF-ED-8C-L1R-T1): (1) lower base plate; (2) lower support plate; (3) upper base plate; (4) upper support plates; (5) SF-ED component
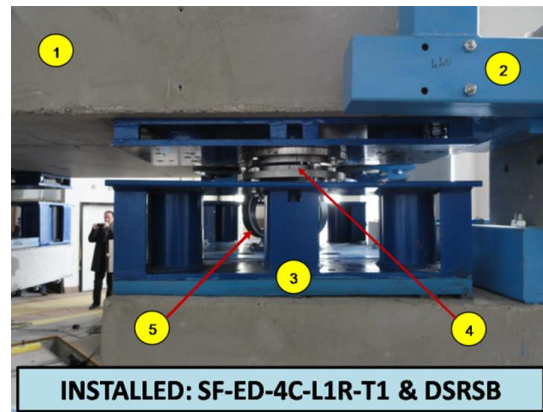
Fig. 2. Installed SF-ED device type-2 (SF-ED-4C-L1R-T1): (1) superstructure; (2) steel support of DL-device; (3) steel support of DSSSB device; (4) DSRSB device; (5) SF-ED component
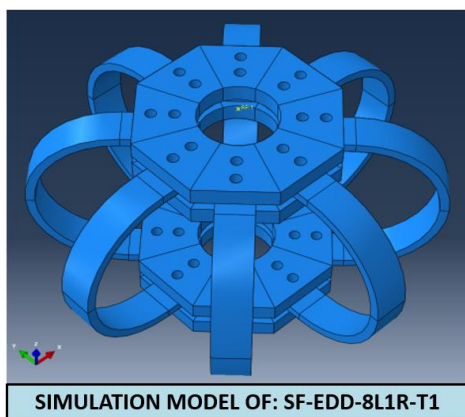
Figure 3 Modeling of the basic type-1 of the SF-ED prototype device composed of eight ED components representing the M11 prototype model.
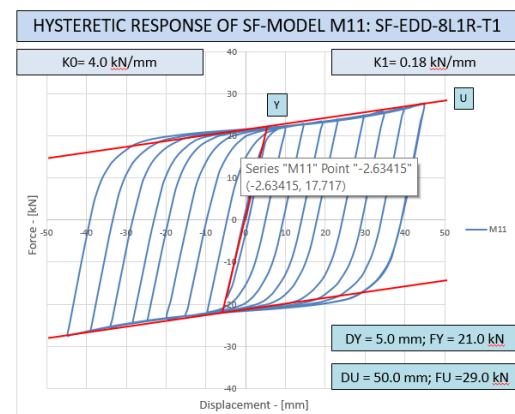
4 Prototypes of Isolation and Displacement Limiting Devices

4.1 Prototypes of DSSSB isolation devices

The present isolation system used for the experimental BSSF model was assembled by use of the developed models of double spherical sliding seismic bearing (DSSSB) devices with two large-radii of spherical surfaces (Fig. 4).

The DSSSB devices were originally designed, constructed and used in a previous investigation carried out by Ristic, J., et al., 2017, [16]. The targets that were set prior to the design and construction of the device were fulfilled: (1) very small horizontal reaction and friction forces (reaching maximum 4.3% of the vertical load), and (2) stable hysteretic behavior along the entire range of large displacements. It was confirmed that the hysteretic behavior of the implemented DSSSB devices could be successfully simulated with the experimentally defined representative bilinear analytical model.
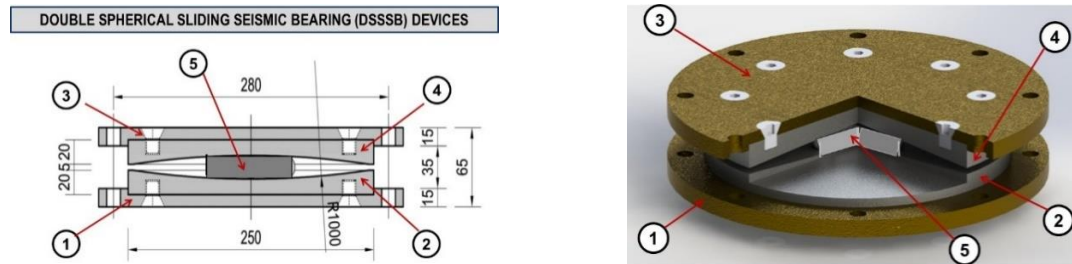
Figure 4. Basic elements of the constructed and used prototypes of DSSSB devices: (1) lower end metal plate; (2) lower spherical plate; (3) upper end metal plate; (4) upper spherical plate; (5) metallic slider;

Actually, the model was controlled by four parameters, DY=1.0 mm, FY=0.32 kN, DU=50.0 mm, FU=0.92 kN, defined experimentally under simulated vertical load and cyclic displacements with increasing amplitudes.

4.2 Displacement limiting devices

The DL system implemented in the tested BSSF model consisted of built-in four limiting devices marked by (6) in Fig. 7. The implemented DL devices were installed with a predefined gap. In practice, the new, specially designed and experimentally tested rubber buffers [18] can be an advanced solution.

5 Seismic Tests on Large-Scale BSSF Model

5.1 Construction of BSSF prototype model

The original design and construction of the test model of the innovative BSSF building prototype, Fig. 5 and Fig. 6, represented a complex and specific process, specifically focused on assuring conditions for realistic experimental simulation of pre-defined important testing objectives. The three basic data-sets, including (a) the main characteristics of the BSSF building model; (b) the available size of the seismic shaking table and (c) the implemented instrumentation system of the BSSF building model, were considered accordingly. Regarding the shaking table dimensions, its loading capacity and related characteristics, a geometric scale factor, l_r, of 1:4 was adopted. In order to preserve the model similarity, all the other characteristics related to the dynamic tests needed to be properly scaled. Considering the important factors addressed, the combined true replica-artificial mass simulation model was adopted as the most adequate. The scale factors for different physical quantities were defined as a function of the geometrical scale factor, according to the similitude law, [16] and [19]. The building prototype model, Fig. 5, Fig. 6 and Fig. 7, was constructed with dimensions of a=314.0 cm and b=174.0 cm at plan, while the considered total model height was h=231.0 cm. The frame system of the model consisted of RC columns (8) with section dimensions 12.0 cm x 12.0 cm, horizontal RC beams, in both directions, with section dimensions 12.0 cm x 12.0 cm and two integrating monolithic RC slabs with thickness of 8.0 cm, spaced between the RC beams. The masonry walls (9) having characteristic door and window openings (10), were constructed using plain brick with a width of 9.0 cm. The model-base isolated monolithic RC slab (7) was constructed with thickness of 15.0 cm. The upper part of the building model (the superstructure part) rested on four DSSSB devices (4) placed on constructed four special steel spacers (3). At both ends, between the DSSSB isolators, the two new SF devices for energy dissipation were installed (5), as indicated in Fig. 7.
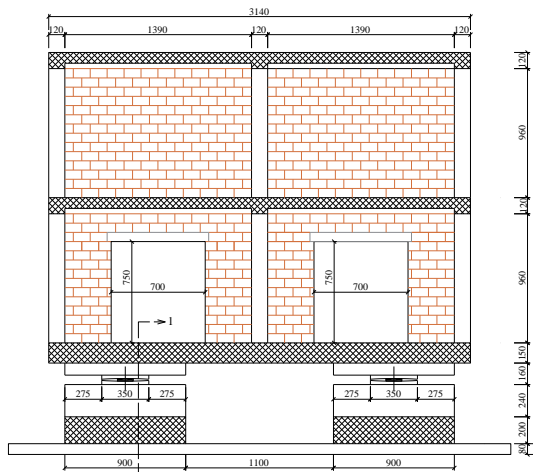
Figure 5. Side view of the designed and seismically tested BSSF large-scale prototype model.
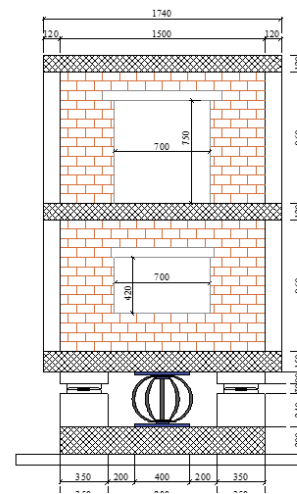
Figure 6. Front view of the designed and seismically tested BSSF large-scale prototype model.
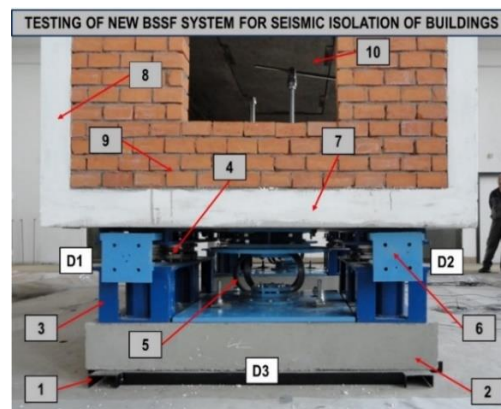
Figure 7. Isolation system of the BSSF model: Position of the installed four DSSSB devices (4), the new two assembled SF-ED devices (5) and the implemented four DL devices (6).

Similarly, at each model end, there were provided two DL devices in a cylindrical form that were tested before as special rubber buffers, (6). The integral BSSF system was supported by two RC slabs (2), proportioned 90 x 150x 20 cm, connected to the integrating base-metal frame (1), fixed to the seismic shaking table. Eight metal elements with bulk density of 400 kg each were installed on the three RC model slabs to appropriately increase the total mass of the model. Their distribution per story was 2+2+4. The DL devices were installed at 50mm gaps to prevent the destructive effects of possible excessive displacements. All steel parts were manufactured to a reduced scale by use of S355 steel material, while concrete C25/30 was used for construction of all RC parts of the constructed model. The existing laboratory seismic shaking-table was square-shaped (5.0 by 5.0 m). Seismic input could be applied in one horizontal and in vertical direction. To adapt the large-scale BSSF model for seismic testing, its longitudinal axis was positioned to coincide with the direction of motion of the shaking table (Fig. 8). In that way, generation of seismic forces was enabled in longitudinal direction of the BSSF model. The BSSF test model was integrally assembled on the shaking table and equipped with the defined instrumentation system. For seismic testing of the BSSF prototype model, the model superstructure (isolated building) rested on four DSSSB isolators spaced at the two model ends (using pairs of devices at each end), Fig. 7 and Fig. 8. The two SF energy dissipation devices were installed at the respective middle positions, between the seismic isolators, Fig. 7.

5.2 Instrumentation of BSSF prototype model

To ensure acquisition of all the required data during the conducted dynamic tests, a well-designed instrumentation system was installed. The BSSF large-scale prototype model assembled on the seismic shaking table was experimentally tested under compressed real strong earthquakes, according to the model scaling and similarity conditions. The selected strong earthquakes were simulated in the considered representative longitudinal direction of the constructed model. Actually, the designed instrumentation system of the model consisted of three different types of sensors, Fig. 8 and Fig. 7:

(a) Transducers of the type of LVDT, representing displacement sensors: Three displacement sensors were installed to measure relative displacements in longitudinal direction. The first two transducers of the type of LVDT, marked as D1 and D2, were used for recording time histories of relative displacements between the base-support of the isolation system and the bottom RC model slab located just above the seismic isolation devices. In addition, the third transducer of the type of LVDT, marked as D3, was used to measure possible relative displacements between the shaking table and the lowest fixed steel segment supporting the entire model structure;

(b) Transducers of the type of LP, representing linear potentiometers: Six sensors of the type of LP were used to measure the total displacements of the isolated building model in longitudinal direction. The first two transducers marked as L1 and L2 were located on the left and the right side of the bottom RC model slab, the next two transducers, L3 and L4, were installed on the left and the right side of the middle RC slab, and the last two transducers, L5 and L6, were spaced at respective locations on the top RC model slab. To assure conditions for such measurement, the second ends of the linear potentiometers were connected to the provided appropriate connection points. The required connection points were located in the constructed additional steel frame directly fixed to the existing, nonexcited, laboratory floor, spaced with a respective gap around the moving shaking table.
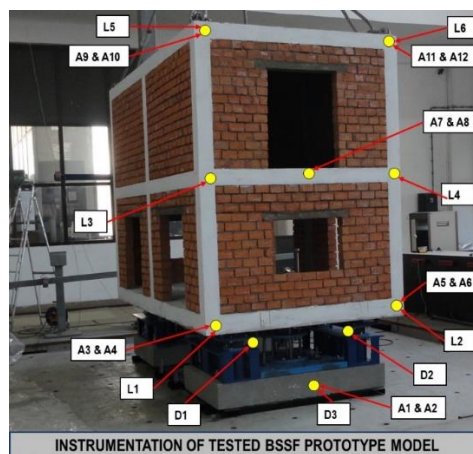
Figure 8. Acquisition points with sensors and recording channels for the BSSF large-scale prototype model tested on the seismic shaking table under simulated strong earthquakes.

(c) Transducers of the type of ACC, representing acceleration sensors: A total of twelve sensors of the type of ACC were installed, providing thus a pair of sensors at each of the selected six characteristic locations. The first and the second ACC sensor at each considered location were properly directed to measure acceleration time-histories in longitudinal (L) and transversal (T) direction, respectively. In the first (the lowest) ACC location, there were provided two measuring channels (A1 & A2), recording accelerations in longitudinal (L) and transversal (T) direction, respectively. Following the same instrumentation concept, at each of the next five ACC locations, two measuring channels were similarly provided. The first and the second channel (Ai & Aj) at each location were similarly used for recording accelerations in longitudinal (L) and transversal (T) direction, respectively.

5.3 Seismic shaking table tests of BSSF prototype model

(a) BSSF Model assembling: The innovative BSSF prototype model shown in Fig. 8 was appropriately assembled, incorporating four DSSSB isolation devices, two new SF energy dissipation devices and four displacement limiting (DL) devices, Fig. 7. The created SF energy dissipation devices were composed by installation of pre-defined four prototypes of energy dissipation components. Table. 1.

(b) Tests with sine-sweep: The dynamic tests carried out by simulated sine-sweep dynamic inputs, 0.02g and 0.04g, covering a range of frequencies from 1 to 35Hz and the use of the provided data sources, enabled definition of: (1) the initial fundamental period amounting to T_o=0.461s, corresponding to the case of the building model with installed DSSSB devices only. The new SF devices were not connected and not activated; and (2) Damping between 3.0 and 3.4%.

(c) Comparative testing: To assess the contribution of the SF devices to energy dissipation, the model was first tested with installed DSSSB isolators only, under simulated Petrovac earthquake scaled to PGA = 0.47 g. The comparative relative displacements recorded under equal test conditions for the system composed with and without SF devices are presented in Fig. 10. It was shown that the building model with installed SF devices represented a highly favorable upgrading option. For the system with seismic isolation only, an unacceptable relative displacement amounting to De = 42.6 mm was obtained. This excessive response actually represented the critical state, because the displacement limit of the used seismic isolators was 40.0 mm. However, regarding the BSSF system with the new SF devices, the relative displacement was reduced to a fully controlled value of Dc = 24.21 mm, representing an important reduction of -65.3%.

(d) Summary of testing conditions and selected results, including:

d1) Seismic input: Seismic testing of the new BSSF building model was carried out using four selected real earthquake records. Actually, to obtain representative experimental data, representative earthquake intensities were considered in all testing cases. The seismic input intensities were generated considering controlled high (possible) values of peak ground accelerations amounting to PGA=0.44g for the El Centro (1940) record, PGA=0.47g for the Petrovac (Montenegro, 1979) record, PGA=0.49g for the Landers record and PGA=0.27g for the Northridge record, respectively. Following the similitude law. the original earthquake records were time compressed for a time factor of 1/2, as a square root of lr.

Table 2. Maximum positive and negative relative displacements recorded by the installed LVDT sensors, during the conducted four original seismic tests of the new BSSF prototype model

No.	O-T1: C-El-Centro, PGA=0.44G			O-T2: C-Petrovac, PGA=0.47G		
	Channel	MaxD (-) (mm)	MaxD (+) (mm)	Channel	MaxD (-) (mm)	MaxD (+) (mm)
1	LVDT-01	-26.85	27.34	LVDT-01	-21.77	21.17
2	LVDT-02	-29.31	28.50	LVDT-02	-24.21	21.46
3	LVDT-03	-0.87	0.64	LVDT-03	-0.72	0.30

No.	O-T1: C-Landers, PGA=0.49G			O-T2: C-Northrige, PGA=0.27G		
	Channel	MaxD (-) (mm)	MaxD (+) (mm)	Channel	MaxD (-) (mm)	MaxD (+) (mm)
1	LVDT-01	-25.15	27.17	LVDT-01	-30.71	19.13
2	LVDT-02	-28.45	28.61	LVDT-02	-34.28	19.84
3	LVDT-03	-0.89	0.64	LVDT-03	-0.89	0.51

d2) Data acquisition: Extensive experimental data files were recorded from each acquisition channel. The integral data recording system included the full set of 21 channels instrumented with sensors according to the model instrumentation plan and additional extra sensors were used for full control of the shaking table.

Having such an extensive instrumentation system and refined data sampling rate from each seismic test, about 5 million numerical values were recorded. The testing process consisting of nine seismic tests, was completed very successfully and all sensors provided correct and complete experimental records continuously. The representative results showing the actual system response were selected, presented and discussed.
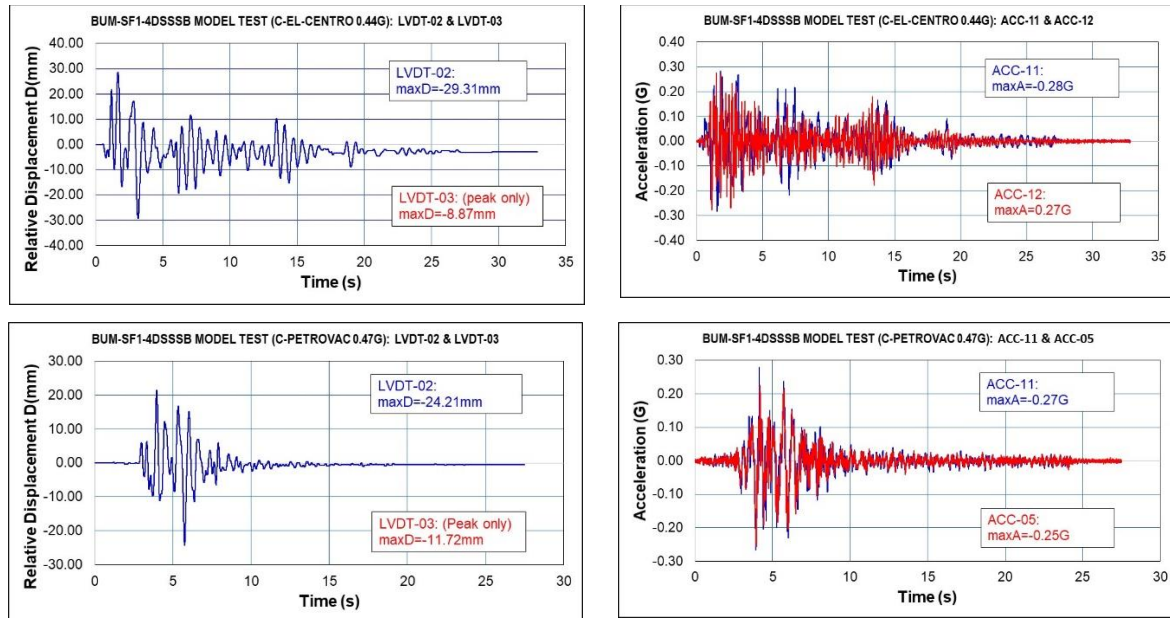
Figure 9. Relative displacements of the BSSF model-base (left) and recorded acceleration responses by ACC-11 & ACC-12 (right) during the tests carried out under simulated El-Centro and Petrovac earthquake.

Table 3. Maximum positive and negative displacements recorded by the installed LP sensors during the conducted four original seismic tests of the new BSSF prototype model

No.	O-T1: C-El-Centro, PGA=0.44G			O-T2: C-Petrovac, PGA=0.47G		
	Channel	MaxD (-) (mm)	MaxD (+) (mm)	Channel	MaxD (-) (mm)	MaxD (+) (mm)
1	LP-01	-44.04	36.98	LP-01	-21.38	16.64
2	LP-02	-44.69	37.26	LP-02	-22.41	15.74
3	LP-03	-45.62	37.65	LP-03	-22.50	17.48
4	LP-04	-44.55	40.19	LP-04	-23.30	16.55
5	LP-05	-46.45	38.31	LP-05	-23.27	17.96
6	LP-06	-46.88	36.91	LP-06	-24.00	16.93

No.	O-T1: C-Landers, PGA=0.49G			O-T2: C- Norhtrige, PGA=0.27G		
	Channel	MaxD (-) (mm)	MaxD (+) (mm)	Channel	MaxD (-) (mm)	MaxD (+) (mm)
1	LP-01	-15.44	21.60	LP-01	-51.97	39.77
2	LP-02	-16.91	20.28	LP-02	-53.58	39.89
3	LP-03	-16.74	22.90	LP-03	-53.32	40.76
4	LP-04	-17.83	21.59	LP-04	-54.46	41.10
5	LP-05	-17.53	23.62	LP-05	-54.17	41.63
6	LP-06	-18.57	22.08	LP-06	-55.73	40.31

Table 4. Maximum positive and negative accelerations recorded by the installed ACC sensors during the conducted four original seismic tests of the new BSSF prototype model

No.	O-T1: C-El-Centro, PGA=0.44G					O-T2: C-Petrovac, PGA=0.47G				
	Channel	MaxA G (-)	DAF	MaxA G (+)	DAF	Channel	MaxA G (-)	DAF	MaxA G (+)	DAF
1	ACC-01	-0.37	0.84	0.44	1.00	ACC-01	-0.48	1.02	0.39	0.82
2	ACC-02	-0.08	0.18	0.09	0.20	ACC-02	-0.06	0.12	0.08	0.17
3	ACC-03	-0.29	0.65	0.33	0.75	ACC-03	-0.28	0.59	0.21	0.44
4	ACC-04	-0.19	0.43	0.27	0.61	ACC-04	-0.23	0.48	0.29	0.61
5	ACC-05	-0.28	0.63	0.26	0.59	ACC-05	-0.25	0.53	0.22	0.46
6	ACC-06	-0.19	0.43	0.28	0.63	ACC-06	-0.22	0.46	0.30	0.63
7	ACC-07	-0.22	0.50	0.25	0.56	ACC-07	-0.20	0.42	0.19	0.40
8	ACC-08	-0.23	0.52	0.23	0.52	ACC-08	-0.29	0.61	0.23	0.48
9	ACC-09	-0.30	0.68	0.35	0.79	ACC-09	-0.25	0.53	0.28	0.59
10	ACC-10	-0.28	0.63	0.28	0.63	ACC-10	-0.38	0.80	0.32	0.68
11	ACC-11	-0.28	0.63	0.28	0.63	ACC-11	-0.26	0.55	0.27	0.57
12	ACC-12	-0.27	0.61	0.27	0.61	ACC-12	-0.37	0.78	0.33	0.70

No.	O-T1: C-Landers, PGA=0.49G					O-T2: C- Nortrige, PGA=0.27G				
	Channel	MaxA G (-)	DAF	MaxA G (+)	DAF	Channel	MaxA G (-)	DAF	MaxA G (+)	DAF
1	ACC-01	-0.50	1.02	0.44	0.89	ACC-01	-0.19	0.70	0.29	1.07
2	ACC-02	-0.07	0.14	0.08	0.16	ACC-02	-0.05	0.18	0.05	0.18
3	ACC-03	-0.32	0.65	0.29	0.59	ACC-03	-0.26	0.96	0.26	0.96
4	ACC-04	-0.25	0.51	0.26	0.53	ACC-04	-0.16	0.59	0.23	0.85
5	ACC-05	-0.26	0.53	0.32	0.65	ACC-05	-0.24	0.88	0.27	1.00
6	ACC-06	-0.26	0.53	0.26	0.53	ACC-06	-0.16	0.59	0.24	0.88
7	ACC-07	-0.22	0.44	0.23	0.46	ACC-07	-0.20	0.74	0.23	0.85
8	ACC-08	-0.24	0.48	0.23	0.46	ACC-08	-0.12	0.44	0.13	0.48
9	ACC-09	-0.32	0.65	0.35	0.71	ACC-09	-0.24	0.88	0.29	1.07
10	ACC-10	-0.37	0.75	0.35	0.71	ACC-10	-0.15	0.55	0.26	0.96
11	ACC-11	-0.34	0.69	0.31	0.63	ACC-11	-0.26	0.96	0.29	1.07
12	ACC-12	-0.37	0.75	0.35	0.71	ACC-12	-0.14	0.51	0.25	0.92

(d3) Relative displacements: The relative peak displacements, including positive and negative pulses, recorded during the seismic tests of the BSSF system under the simulated El-Centro, Petrovac, Landers and Northridge earthquake are presented in Table 2. Comparatively, Fig. 9 (left) shows the recorded time-histories of relative displacement responses in longitudinal (L) direction during the tests carried out by simulation of the El-Centro and Petrovac earthquake, respectively. Regarding the presented experimental results, the following important observations were made: (1) The recorded relative displacements in L direction (direction of earthquake excitation) were dominant; (2) It was confirmed that the test model was successfully fixed to the shaking table since the relative displacements in L direction recorded by LVDT-03 were very small in all test cases. (3) The absolute maximum recorded relative displacement amounting to Dmax = 34.28 mm was below the critical (allowable) relative displacement of the seismic isolators amounting to Da = 40.0 mm, and (4) Generally, the seismic response of the assembled BSSB system that was tested repeatedly appeared to be very similar twice. The results from the conducted original series of tests-1 are presented (O-Ti in Table 2). Consequently, the series of repeated seismic tests-2 (not presented) were realized using the same four earthquakes. Only small, negligible differences of maximum displacements were observed.

(d4) Accelerations: The representative time-histories of accelerations recorded by sensors ACC-11 and ACC-12, respectively in L and T-direction, during the seismic tests on the BSSF model conducted under the simulated El-Centro and Petrovac earthquakes are comparatively shown in Fig. 9 (right).

However, Table 4 shows the representative peak accelerations recorded by all sensors, namely, ACC-01 to ACC-12. At each measuring point, accelerations were recorded in L and in T-direction during the seismic tests on the BSSF model conducted under the simulated all four representative earthquakes. Considering the presented results, it was confirmed that: (1) The recorded accelerations at the superstructure, respectively in L and T-direction, were quite small (without amplification); and (2) Due to the present regular fluctuation, the recorded accelerations at the superstructure in L and T-direction were with similar peak values and in the expected range; (3) The new BSSF system showed sustainability since the response parameters recorded during the original (O) tests-1 and the repeated tests-2 were quite similar, and (4) Generally, the DAF (dynamic amplification factor) values presented in the same Table 4 were quite small (smaller than 1.0), demonstrating favorable and consistent response. It was confirmed that the obtained relations between the maximum response and the maximum input acceleration (DAF = Ar/PGA) were within the expected ranges in all cases.

(d5) Absolute displacements: The absolute displacement responses (in L -direction) recorded by the six LP sensors, Table 4, installed on the BSSF model, proved existence of small inter-story drifts and successful control of the shaking table in all realized testing cases.

(d6) System advances: Generally, the new BSSF system exhibited safe and very favorable behavior under strong earthquake excitations. Considering the processing of more than 50.000.000 recorded original numerical values obtained from the realized fifteen shaking table tests, the main qualitative advances of the innovative GHS system upgraded with SF energy dissipation devices, are summarized in Fig. 10. Stable, reliable and safe seismic response was observed in all test cases due to the provided significant reduction of maximum relative displacements amounting to 36.5%, 65.3%, 39.8% and 16.7%, respectively, in the case of the simulated El Centro, Petrovac, Landers and Northridge earthquakes. All recorded peak values were lower than the defined allowable design displacement of Da=40.0mm for the seismic isolators. The importance of upgrading the isolated masonry and infilled frame buildings with the new SF devices was experimentally validated and confirmed with the conducted initial quantification test of the model with the installed seismic isolation only. Under the simulated strong Petrovac earthquake, the tested system without SF devices showed an unsafe response to the recorded excessive relative displacement amounting to maxD=42.6 mm, Fig. 10.
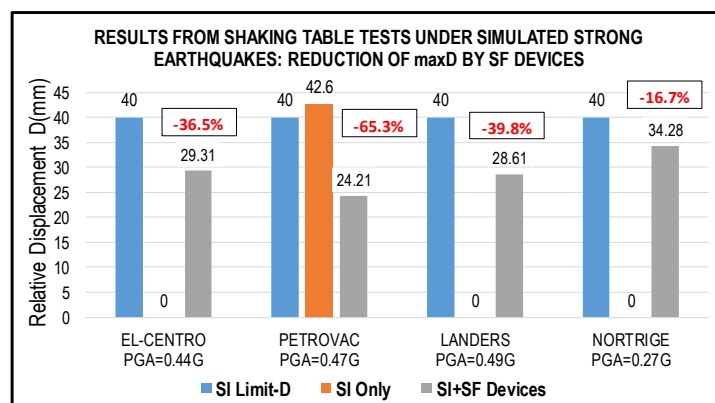
Figure 10. Advances of the BSSF system: Reduction of maximum relative displacements defined from the conducted seismic tests under simulated strong earthquakes.

6 Conclusions

Based on the results obtained from the conducted extensive experimental study, the following conclusions are drawn: (1) The new building-sliding space-flange (BSSF) system represents a favorable, efficient and experimentally proved option for seismic protection of masonry and framed masonry buildings.

The system shows a quite significant modification of the seismic response of the integral structure, resulting directly in efficient protection of buildings subjected to repeated and very strong earthquakes; (2) The originally designed, constructed and implemented double spherical sliding bearing (DSSSB) devices were confirmed as favorable types of isolation bearings for the new BSSF isolation system. However, the other developed and proved advanced types of isolation bearings may also be regarded as a potentially good application option; (3) The created new uniform space-flange energy dissipation devices (SF-ED) exhibited a very good and stable energy dissipation capacity. Their perfect capability to exhibit smooth and stable hysteretic response under arbitrary earthquake excitation was clearly confirmed. In addition, the new SF energy dissipation devices preserve their dissipation capability even in the cases of strong repeated cyclic earthquake loading; (4) The displacement limiting (DL) devices of the building should be considered as an obligatory constituent element of the created BSSF system serving as the last defense line against excessive displacements of the integral building. Their appropriate design is an important step toward providing their activation only in the critical cases of very strong and abrupt earthquakes; (5) The three-dimensional, hysteretic, uniform and multi-directional response of the new SF energy dissipation devices can be very successfully predicted by advanced application of the nonlinear micro-modeling concept with the adopted bilinear kinematic hardening steel material model; (6) The present study resulted in development of an experimentally proved basic concept required for successful elaboration of the advanced design procedure. The developed design concept can assure practical application of the new BSSF system providing a qualitatively upgraded seismic protection capability of masonry and framed masonry buildings located in seismic regions.

Acknowledgements

REFERENCES

[1]   Kelly, J. M. (1986): Aseismic Base Isolation: A Review and Bibliography, *Soil Dynamics and Earthquake Engineering* 5, 202-216. [DOI]

[2]   Robinson, W. H. (1982): Lead-Rubber Hysteretic Bearings Suitable for Protecting Structures During Earthquakes, *Earthquake Engineering and Structural Dynamics* 10, 593-604. [DOI]

[3]   Iemura, H., Taghikhany, T., Jain, S. K. (2007): Optimum Design of Resilient Sliding Isolation System for Seismic Protection of Equipment, *Bulletin of Earthquake Engineering* 5, 85–103. [DOI]

[4]   Zayas, V. A., Low, S. S., Mahin, S. A. (1990): A Simple Pendulum Technique for Achieving Seismic Isolation, *Earthquake Spectra* 6, 317-334. [DOI]

[5]   Mokha, A., Constantinou, M. C., Reinhorn, A. M. (1990): Teflon Bearings in Seismic Base Isolation I: Testing, *Journal of Structural Engineering* 116, 438-454. [DOI]

[6]   Skinner, R. I., Kelly, J. M., Heine, A. J. (1975): Hysteretic Dampers for Earthquake Resistant Structures, *Earthquake Engineering and Structural Dynamics* 3, 287-296. [DOI]

[7]   Ene, D., Yamada, S., Jiao, Y., Kishiki, S., Konishi. Y. (2017): Reliability of U-shaped Steel Dampers Used in Base-Isolated Structures Subjected to Biaxial Excitation, *Earthquake Engineering & Structural Dynamics* 46, 621–639. [DOI]

[8]   Oh, S., Song, S., Lee, S., Kim, H. (2013): Experimental Study of Seismic Performance of Base-Isolated Frames with U-shaped Hysteretic Energy-Dissipating Devices, *Engineering Structures* 56, 2014-2027. [DOI]

[9]   Jiao, Y., Kishiki, S., Yamada, S., Ene, D., Konishi, Y., Hoashi, Y., Terashima, M. (2014): Low Cyclic Fatigue and Hysteretic Behavior of U-shaped Steel Dampers for Seismically Isolated Buildings under Dynamic Cyclic Loadings, *Earthquake Engineering Structural Dynamics* 44(10): 1523–1538. [DOI]

[10] Jankowski, R., Seleemah, A., El-Khoribi, S., Elwardany, H. (2015): Experimental Study on Pounding between Structures During Damaging Earthquakes, *Key Engineering Materials* Vol. 627, 249-252. [DOI]

[11] Serino, G., Occhiuzzi, A. (2003): A Semi-Active Oleodynamic Damper for Earthquake Control: Part 1: Design, Manufacturing and Experimental Analysis of the Device. *Bulletin of Earthquake Engineering* 1: 269–301. [DOI]

[12] Tian, L., Fu, Z., Pan, H., Ma, R., Liu, Y. (2019): Experimental and Numerical Study on the Collapse Failure of Long-Span Transmission Tower-Line Systems Subjected to Extremely Severe Earthquakes, *Earthquakes and Structures* 16 No. 5. [DOI]

[13] UNCRD (1995): Comprehensive Study of the Great Hanshin Earthquake, UNCRD Research Report Series No. 12, United Nations Centre for Regional Development (UNCRD), Nagoya, Japan.

[14] Ghasemi, H., Cooper, J. D., Imbsen, R., Piskin, H., Inal, F., Tiras, A. (2000): The November 1999 Duzce Earthquake: Post- earthquake Investigation of the Structures on the TEM, Publication No. FHWA-RD-00-146, Federal Highway Administration Report.

[15] Erdik, M. (2001): Report on 1999 Kocaeli and Duzce (Turkey) Earthquakes, *Structural Control for Civil and Infrastructure Engineering*, pp. 149-186 (2001). [DOI]

[16] Ristic, J., Misini, M., Ristic, D., Guri, Z., Pllana, N. (2017): Seismic Upgrading of Isolated Bridges with SF-ED Devices: Shaking Table Tests of Large-Scale Model, *Gradjevinar*, 2147-2017. [DOI]

[17] Ristic, J., Brujic, Z., Ristic, D., Folic, R., Boskovic, M. (2021): Upgrading of Isolated Bridges with Space-Bar Energy-Dissipation Devices: Shaking Table Test, Advances in Structural Engineering, June 23, 2021; pp. 2948–2965.

[18] Ristic, J. (2016): Modern Technology for Seismic Protection of Bridge Structures Applying Advanced System for Modification of Earthquake Response, PhD Thesis, Institute of Earthquake Engineering and Engineering Seismology (IZIIS), "SS Cyril and Methodius" University, Skopje, Macedonia.

[19] Candeias, P., Costa, A. C., Coelho, E. (2004): Shaking Table Tests of 1:3 Reduced Scale Models of Four-Story Unreinforced Masonry Buildings, 13th World Conference on Earthquake Engineering, Vancouver, Paper: 2199.

[20] Ristic, D. (1988): Nonlinear Behavior and Stress-Strain Based Modeling of Reinforced Concrete Structures Under Earthquake Induced Bending and Varying Axial Loads, Doctoral Dissertation, School of Civil Engineering, Kyoto University, Japan.

[21] Ristic, D., Ristic J. (2012): Advanced Integrated 2G3 Response Modification Method for Seismic Upgrading of Advanced and Existing Bridges, 15th World Conf. on Earthquake Engineering, (WCEE), Lisbon.

[22] Misini, M., Ristic, J., Ristic, D., Guri, Z., Pllana, N. (2019). Seismic upgrading of isolated bridges with SF-ED devices: Analytical study validated by shaking table testing, *GRAĐEVINAR, 71* (4), 255-272, doi: https://doi.org/10.14256/JCE.2274.2017

TESTING OF MODELS OF ORIGINAL AND UPGRADED CONNECTION BETWEEN RC FLOOR-BEAM AND COLUMN USED IN MODERN PRECAST HALL SYSTEM

Labeat Misini[1], Jelena Ristic[2], Viktor Hristovski[3], Danilo Ristic[4]

[1] *PhD student, Institute of Earthquake Engineering and Engineering Seismology (IZIIS), Ss. Cyril and Methodius University, Skopje, Republic of North Macedonia, e-mail: labeat.misini@gmail.com*

[2] *Assoc. Prof. Dr. Faculty of Engineering, Department of Civil Engineering, International Balkan University (IBU), Skopje, Republic of North Macedonia, e-mail: risticjelenaibu@gmail.com*

[3] *Full Prof. Dr., Institute of Earthquake Engineering and Engineering Seismology (IZIIS), Ss. Cyril and Methodius University, Skopje, Republic of North Macedonia, e-mail: viktor@iziis.ukim.edu.mk*

[4] *Full Prof. Dr., Institute of Earthquake Engineering and Engineering Seismology (IZIIS), Ss. Cyril and Methodius University, Skopje, Republic of North Macedonia, e-mail: danilo.ristic@gmail.com*

Abstract

The design and construction of modern, globally upgraded and seismically safe industrial hall systems (SSIH Systems) is currently viewed as an activity of extraordinary importance since these structures most frequently house new advanced and robotically conceptualized industrial machines and equipment, whose value multiply exceeds the value of the integral structures. The SSIH systems are of vital importance because it is only by their practical application that efficient and continuous functioning of important production industrial systems and compounds is provided. The achieved safety margins, the actual seismic performances and the present limitations of the used pin-based floor-beam column connections of the existing precast N-system were integrally confirmed by the original results obtained from the conducted experimental tests of the constructed connection prototype models. The precast N-system is commonly used for intensive construction of large industrial structures in different regions and countries, including areas of Europe and wider characterized by high seismicity. The initial results obtained from the laboratory test of the constructed large-scale prototype model representing a common floor-beam column (CFBC) connection confirmed the actual bearing capacity of the connection, the damage propagation pattern and the specific total failure mode. To investigate possible upgrading of the connection safety, a specific supplementary test was performed using the created and constructed new experimental model, representing an upgraded floor-beam column (UFBC) connection by application of an improved concrete confinement and use of larger diameters of steel connection pins (dowels). The main conclusion regarding the safety increase was that such common upgrading concept of pin-based connections could not be considered as a basic adequate approach since it was able to provide only limited upgrading effects. The existing need for creation of a new, advanced, experimentally proved and effective innovative upgrading method was clearly pointed out.

Keywords: precast structures, connections, testing, damage propagation, seismic safety

1. Introduction

Although extensive research has been carried out during the recent period, [3-4], [6], [9-10], [12-17], [19-20], [22-24], heavy damages and total collapses of prefabricated industrial halls have been observed during past earthquakes widely in the world, [1-2], [5], [7-8], [11], [18], [21]. Creation, design and construction of a new, modern seismically safe precast system of industrial halls is presently of the highest importance since these structures most frequently house new, advanced and robotically conceptualized, industrial machines and equipment, whose value multiply exceeds the value of the integral structures. Today, such precast industrial hall structures are of vital importance. This is mainly the result of the real need for providing continuous production of important industrial products. This condition can be achieved only if high structural seismic safety level is provided in future practical applications. It is known that our region, the wider region of Europe and the World are characterized by pronounced to high seismicity. The high importance of these systems directly conditions the real need for application of an advanced, new and more successful technology for seismic protection.

Therefore, a specific research work has been conducted for the purpose of development of suitable systems for earthquake protection of large prefabricated industrial hall structures. The conducted extensive research work was focused on development of a new upgraded seismically safe system (USS-system) of prefabricated industrial halls. The development of the USS system of prefabricated industrial halls was based on the original experimental results from the extensive innovative experimental research project realized in the RESIN Laboratory (Skopje), led by Prof. Danilo Ristic. The project included realization of laboratory testing of constructed large-scale prototype models of critical connections up to failure (Ristic J. et al. 2017), [19-20]. The important part of the original experimental research work devoted to testing of large-scale prototype models of the original and upgraded connection between a precast RC floor-beam and an RC column used in a modern precast hall system are presented and discussed in this paper.

2. Experimental Testing of Model of Original Connection Between Precast RC Floor Beam and RC Column

2.1 Prototype and Experimental Model M3-A of Original Connection-OC3

The prototype of the original connection OC3, providing connection between a precast RC floor beam and an RC column, is of a great importance since the corbels provide conditions for support of longitudinal (floor) prefabricated RC beams.
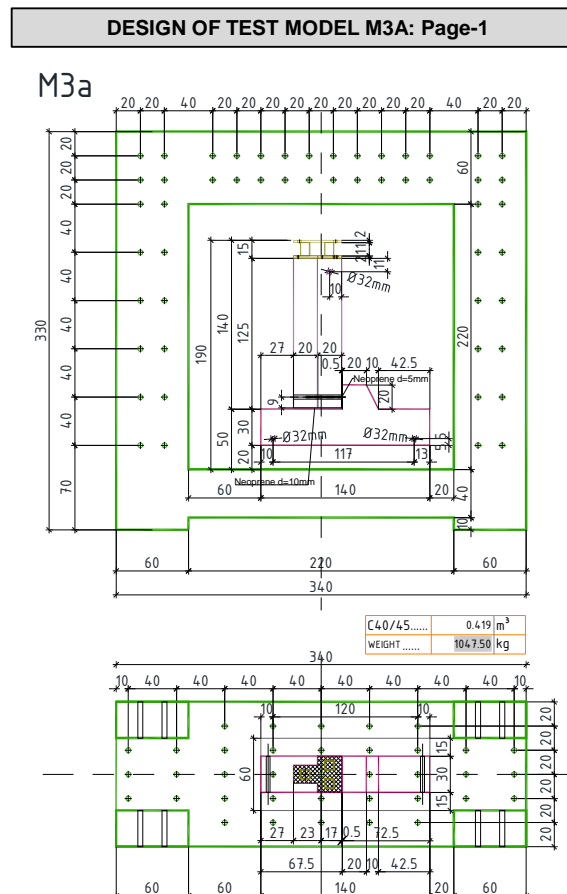
Fig. 1. Design of the prototype of model-M3A representing a connection between a precast RC floor beam and an RC column: Set-up of the test model.

At the same time, it is very important to execute a safe connection between RC corbels and RC columns. The connection between an RC corbel and an RC beam is realized by means of two anchors ϕ 25 mm that are concreted into the short cantilever, i.e., into the RC corbel. In the RC L-floor beam, two openings ϕ 70 mm are made because of the required clearance for assemblage. Prior to mounting of the L-floor beam, a neoprene bearing with hardness of 70 shores and thickness of d = 10 mm is placed on the short element. Following the placement of the floor beam, the openings are poured with non-shrink mortar of high strength. In 24 hours, such mortar achieves strength of 45 N/mm2, while after 28 days, its strength is 70kN/mm2 and ζp = 2,8 N/mm2. Isomat Megagrout 101 is used as mortar. The short RC cantilever and the RC beam are made of concrete class 50 (or C50), whereas the metal anchor is constructed of reinforcement steel B500B. For this structural connection, it is of importance to experimentally prove: (1) the vertical bearing capacity of the short RC element (corbel) and (2) the bearing capacity of the connection itself realized by application of a reinforcing anchor and pouring of mortar, which does not shrink during hardening, but is characterized by a high bearing capacity.
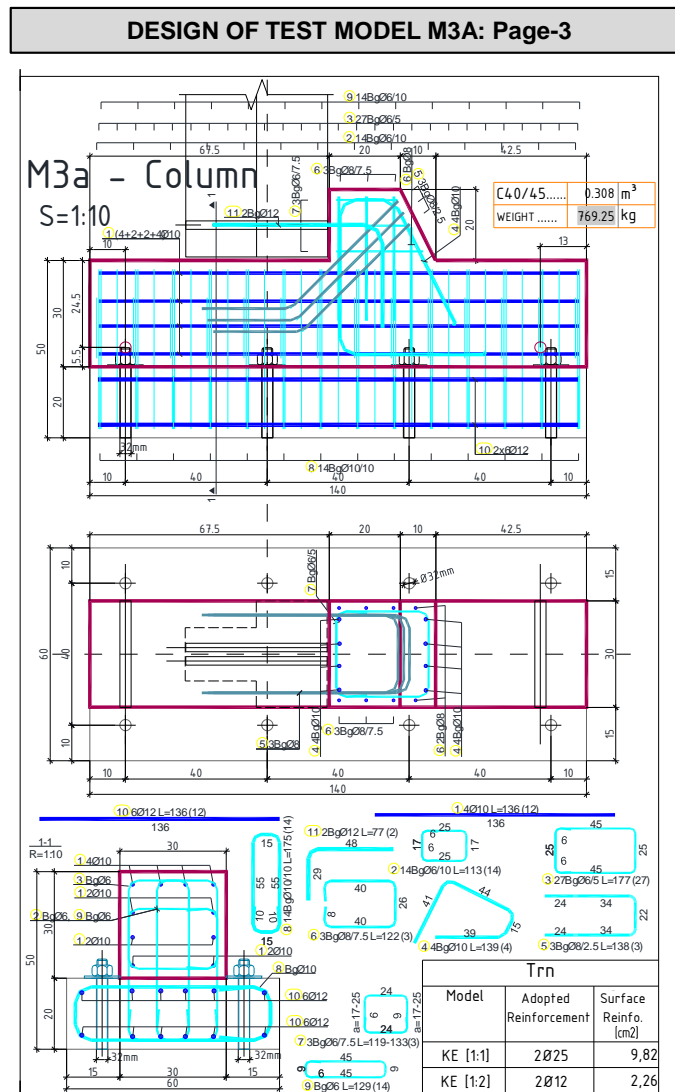
Fig. 2. Design of the prototype of model-M3A representing a connection between a precast RC floor beam and an RC column: Design of the RC column.

The actual design of the used prototype connection OC3, representing an original connection between a precast RC longitudinal floor beam and a column through an RC corbel (short RC cantilever) was studied comprehensively. Also, the original in situ construction during assemblage of the integral structure of the prefabricated hall was fully considered. For experimental testing of the connection, a large scale experimental model M3-A was designed and constructed, Fig. 1 and Fig. 2. The test was planned for the purpose of defining the bearing capacity of the used original (O) type of a commonly used connection. The experimental test model M3-A was constructed to a large scale (M=1:2) whereat the actual characteristics of the original prototype connection were applied. With the applied large scale of the experimental model, important advantages were achieved: (1) The concrete used for the construction of the experimental model remained with the same mechanical characteristics as the concrete used for the construction of the prototype connection; (2) The reinforcement of the model was also with the same mechanical characteristics as those of the structural connection prototype; (3) In accordance with the stated advantages, the design of the model of the connection was reduced only to geometrical scaling, and (4) The physical experimental model was successfully adapted to the laboratory conditions for its successful laboratory testing, Fig. 1 and Fig. 2. The project on construction of the experimental model M3-A was initially completed. The configuration of the experimental model M3-A was very successfully adapted for its installation into the experimental rigid frame, enabling successful testing under application of the predefined loading program.

Fig. 3. Construction of model-M3A: Segment of the precast RC floor beam.

Fig. 4. Construction of model-M3A: Segment of the precast RC column.

The construction of the experimental model M3-A was done completely in factory conditions and with identically high quality as that of the prototype. Fig. 3 shows a view of the constructed RC floor beam, whereas Fig. 4 provides a view of the concreted segment of the RC column with the RC corbel. From the presented figures, it could be concluded that the applied technology of construction of the experimental model M3-A was identical to the original technology that was applied in the construction of the prototype connection. Actually, the applied procedure provided all the needed prerequisites for obtaining experimental results of high quality and reliability for specific practical or research objectives.

2.3 Principal Results from OC-3 Connection Test

The laboratory test set-up of the connection model M3-A is shown in Fig. 5. The experimental test was realized by use of two hydraulic actuators. The horizontal hydraulic actuator was used for fixation of the vertical position of the RC floor beam segment. The vertical hydraulic actuator was used for application of a continuously increased vertical tensile force (upwards) up to total failure of the structural connection. In this way, an insight into all the characteristic phases of increase of damages to the connection was gained. The whole experiment was carried out through a predefined history of deformations.
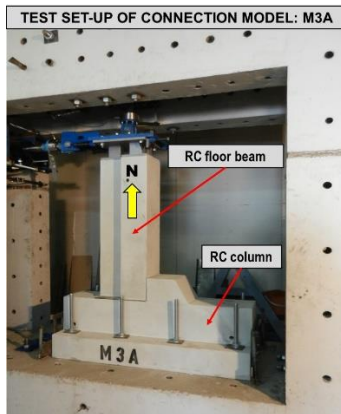
Fig. 5. Laboratory test set-up of the constructed model M3-A.
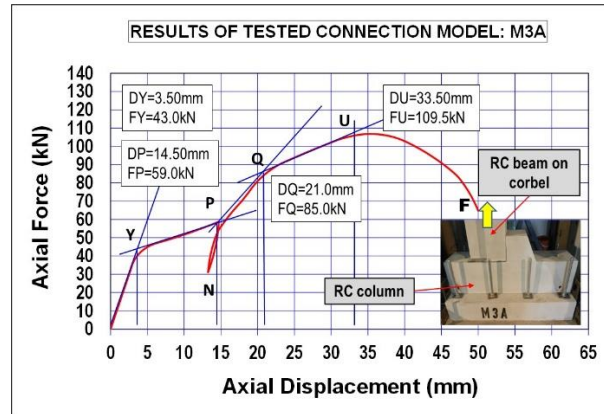
Fig. 6. Recorded nonlinear response of the constructed model M3-A.

The experimentally defined relationship between the applied vertical force and the vertical deformation is presented in Fig. 6. The recorded original force – deformation relationship was quite unusual and characteristic since it clearly reflected several phases of behavior. Phase 0-Y-P reflected the real bearing capacity of the connection. The next phase P-Q and the subsequent phase Q-U reflected the increase in force (with two inclinations of the envelope segments) due to stronger activation of the tensile anchors following larger cracks in concrete. After achievement of the maximum strength of the connection (point U), its strength decreased and total failure took place.

In the course of realization of the experimental testing of model M3-A, the development of the characteristic phases of damage to the structural connection was successfully monitored. For presentation of the damage degree, a scale for identification of the damage degree from 1 to 5 (DD = 1, 2, 3, 4, 5) was used. If there is no damage, the state is indicated by DD=1, while the state of failure is indicated by DD=5. States DD=2,3, 4 represent interim states characterized by consecutively increased damage degree. The states of occurred phases of damage are demonstrated in two characteristic figures, namely, Fig. 7 and Fig. 8 that show DD=1 and DD=5, respectively.

Fig. 7. Damage degree of model M3-A: Initial stage characterized by DD=1.
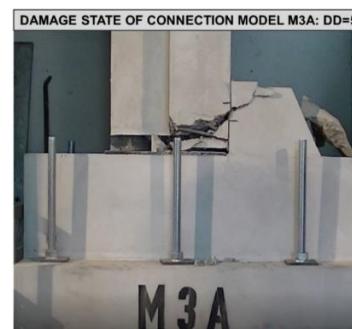
Fig. 8. Damage degree of model M3-A: Final stage characterized by DD=5.

2.4 Notes on Typical Response of OC-3 Connection

Following the obtained original results from the realized experimental testing of the behaviour of the respective structural connection using the constructed physical model M3-A, the following conclusions can be summarized: (1) The connection of this type formed with cast connecting anchors does not experience failure due to failure of the anchors themselves even in conditions of considerably increased deformations; (2) Progressive destruction of the connection accompanied by increase of damage generally takes place due to progressive cracking of concrete and propagation of concrete damage in

5

the zones of the occurred larger cracks; (3) In the next phases, crushing and falling of concrete from the most critical zones exposed to high stresses takes place; (4) The real bearing capacity of the connection is characterized only by the O-Y-P envelope that shows a bearing capacity that is quite lower than the recorded maximum; (5) The envelope part of the P-Q-U relationship shows an increased strength, but with presence of severe damage to concrete and increased deformations; (6) During design of structures in practice, behavior of the connection only in the linear domain, segment O-Y, can be accepted. However, for this segment, it is also necessary to define the corresponding safety factor for the purpose of avoiding damage to the connection under strong earthquake effects, and (7) Although the connection has proved to be considerably tough, it is recommended and it will also be of interest to introduce appropriate structural advancement of the connection. Therefore, the qualitatively improved option of the same connection was experimentally tested by means of the corresponding model M3-B.

3. Experimental Testing of Model of Upgraded Connection Between Precast RC Floor Beam and RC Column

3.1 Prototype and Experimental Model M3-B of Upgraded Connection-OC3

The new prototype connection UC3, representing an upgraded (improved) original connection between a precast RC longitudinal floor beam and a column through an RC corbel (short RC cantilever) was appropriately designed. For the connection itself, two improvements were made. Considered were steel anchors with increased diameter and provided was an improved reinforcement arrangement and concrete confinement in the region of the corbels. The procedure of the in situ construction during assemblage of the integral structure of the prefabricated hall remained the same in the case of the original (O) and the upgraded (U) connection. Experimental testing of the constructed experimental model M3-B was performed for the purpose of defining the bearing capacity of the upgraded (U) connection type, connecting also a prefabricated RC corbel (fixed to a column) with an RC longitudinal floor beam. The experimental test model M3-B was analogously constructed to a large scale (M=1 : 2) whereat the actual characteristics of the original prototype connection were applied. With the applied large scale of the experimental model, important advantages were also achieved. In accordance with the stated advantages, the design of the model of connection M3-B was simplified and reduced only to geometrical scaling. The physical experimental model M3-B was also successfully adapted to the laboratory conditions providing its successful laboratory testing.

3.2 Testing of Prototype Model M3-B of Upgraded Connection OC-3

The construction of the experimental model M3-B was done completely in factory conditions assuring its high quality identical to that of the constructed prototype. It should be pointed out that the applied technology of construction of the experimental model M3-B was also identical to the original technology that was applied in the construction of the prototype connection. By assuring this, there were provided the main important prerequisites for obtaining experimental results of high reliability.

3.3 Principal Results from UC-3 Connection Test

The laboratory test set-up of the connection model M3-B is given in Fig. 9. The experimental test was realized by use of two hydraulic actuators. The horizontal hydraulic actuator was used for fixation of the vertical position of the RC floor beam segment. The vertical hydraulic actuator was used for application of a continuously increased vertical tensile force (upwards) up to total failure of the structural connection. In this way, an insight into the present characteristic phases demonstrating increase of damages to the upgraded connection M3-B was gained. The whole experiment was carried out through simulated predefined history of vertical deformations. The experimentally defined relationship between the applied vertical force and the vertical deformation is presented in Fig. 10.

6

The recorded original force – deformation relationship was also quite unusual and characteristic compared with the M3-A model since it also clearly reflected several phases of behavior. Phase 0-Y-P reflected the actual initial bearing capacity of the connection.
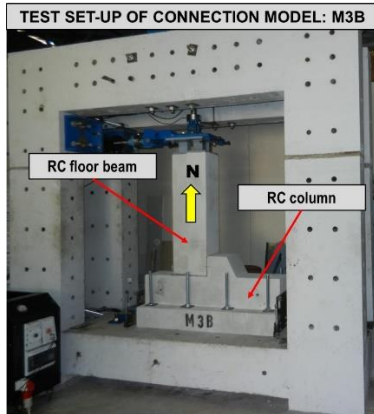
Fig. 9. Laboratory test set-up of the constructed model M3-B.
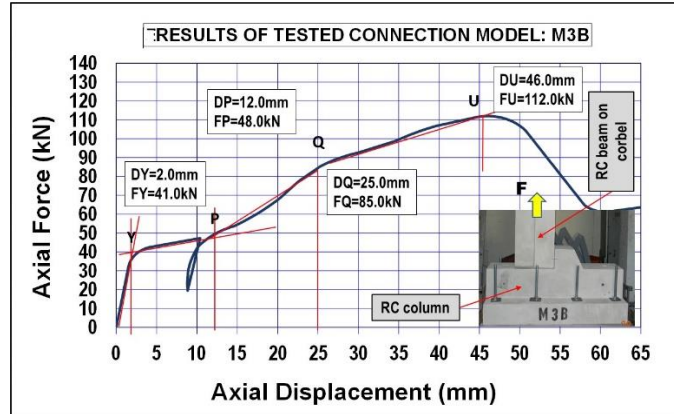
Fig. 10. Recorded nonlinear response of the constructed model M3-B.

The next phase P-Q and the subsequent phase Q-U reflected the increase in force (with two inclinations of the envelope segments) due to stronger activation of the tensile anchors following larger cracks in concrete. After achievement of the maximum strength of the connection (point U), its strength decreased and total failure took place.
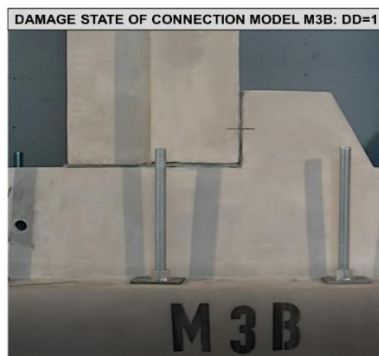
Fig. 11. Damage degree of model M3-B: Initial stage characterized by DD=1.

Fig. 12. Damage degree of model M3-B: Typical stage characterized by DD=2.
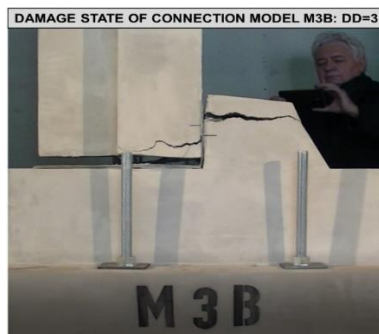
Fig. 13. Damage degree of model M3-B: Typical stage characterized by DD=3.

Fig. 14. Damage degree of model M3-B: Typical stage characterized by DD=4.

7

- In the course of realization of the experimental testing of model M3-B, the development of the characteristic phases of damage to the structural connection was successfully and continuously monitored. The states of occurred phases of damage are demonstrated in four characteristic figures, namely, Fig. 11, Fig. 12, Fig. 13 and Fig. 14 that show DD=1, DD=2, DD=3 and DD=4, respectively.

3.4 Notes on Typical Response of UC-3 Connection

Based on the obtained original results from the test of the respective structural connection using the constructed physical model M3-B, the following conclusions can be summarized:
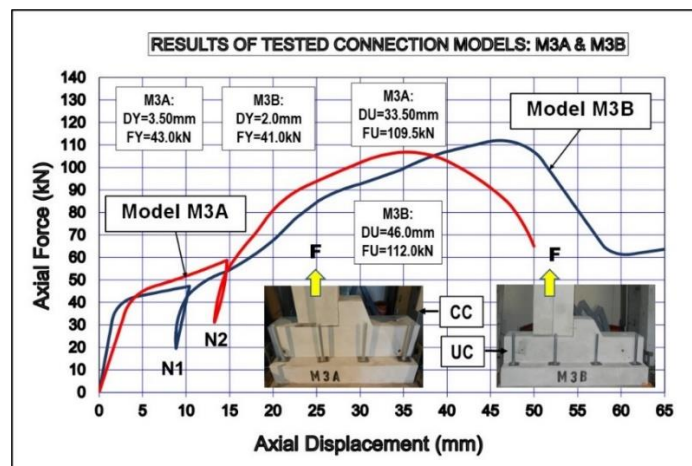
Fig. 15. Results for the experimentally tested model M3-A and M3-B representing the original and the upgraded connection between a precast RC floor beam and an RC column.

(1) The improved connection of this type formed by cast connecting anchors with increased diameter also does not experience failure due to failure of the anchors themselves even in conditions of considerably increased deformations; (2) Progressive destruction of connection M3-B accompanied by increase of damage generally takes place due to progressive cracking of concrete and propagation of concrete damage in the zones of occurred larger cracks, similar to model M3-A; (3) In the next phases, crushing and falling of concrete from the most critical zones exposed to high stresses takes place; (4) The real bearing capacity of the connection is characterized only by the O-Y-P envelope that shows bearing capacity that is quite lower than the recorded maximum; (5) The envelope part of the P-Q-U relationship shows an increased strength, but with presence of severe damage to concrete and increased deformations; (6) During design of structures in practice, behavior of the connection only in the linear domain, segment O-Y, can be accepted. However, for this segment, it is also necessary to define the corresponding safety factor for the purpose of avoiding damage to the connection under strong earthquake effects, and (7) Although the connection proves to be considerably tough, it is recommended and it will also be of interest to introduce appropriate innovative structural advancement of the connection.

5. Conclusions

Fig. 15 comparatively shows the actual nonlinear behavior characteristics of the tested original connection (OC3) and the upgraded connection (UC3) obtained from the realized experimental tests of model M3-A and M3-B, respectively. The two models represented alternative solutions for the same connection between an RC longitudinal floor beam and an RC column (using the anchors from the corbel). The following general observations can be made: (1) The original connection tested with the constructed model M3-A and the upgraded connection tested with the constructed model M3-B

showed quite similar force – deformation relationship and similar damage generation patterns; (2) Connection M3-B was, first of all, upgraded by increasing the diameter of the applied anchors and then, by adding some steel hoops to increase the concrete confinement. However, the experimental results showed that the upgraded connection did not enable considerable qualitative improvement of the connection response; (3) The upgraded connection showed only some increase of the deformation capacity. However, the remaining parameters characterizing the safety of the connection were not significantly improved; (4) The main reason for the occurrence of damage and failure of the connection was the crushing and failure of concrete. Therefore, the increase of the diameter of the anchors and the improved confinement of concrete did not provide a considerable upgrading effect; (5) From the general knowledge gained from the experimental investigations, it is concluded that the original connection used in practice represents the "optimal maximum" that can be achieved with this technological concept of a connection, and (6) Finally, the most important knowledge arising from the experimental results clearly demonstrates the fact that significant and qualitative improvement of the connection bearing capacity and seismic safety can only be achieved by the created new, original and innovative technological solution of a connection.

6. Acknowledgements

7. References

[1] Arslan MH, Korkmaz HH, Gulay DG (2006) *Damage and Failure Pattern of Prefabricated Structures after Major Earthquakes in Turkey and Shortfalls of the Turkish Earthquake Code.* Eng Fail Anal 13(4):537–557

[2] Belleri A, Brunesi E, Nascimbene R, Pagani M, Riva P (2015) *Seismic Performance of Precast Industrial Facilities Following Major Earthquakes in the Italian Territory.* J Perform Constr Facil 29(5):04014135. https ://doi.org/10.1061/(ASCE)CF.1943-5509.00006 17

[3] Bournas DA, Negro P, Molina FJ (2013) *Pseudodynamic Tests on a Full-Scale 3-Storey Precast Concrete Building: Behavior of the Mechanical Connections and Floor Diaphragms.* Eng Struct 57:609–627. https ://doi.org/10.1016/j.engst ruct.2013.05.046

[4] Bournas D, Negro P (2012) *Seismic Performance of Mechanical Connections in the SAFECAST Precast Building.* In: 15th World Conference on Earthquake Engineering (15 WCEE), Lisboa, p 10

[5] Bournas D, Negro P, Taucer FF (2013) *Performance of Industrial Buildings During the Emilia Earthquakes in Northern Italy and Recommendations for Their Strengthening.* Bull Earthq Eng 12(5):2383–2404. https ://doi.org/10.1007/s1051 8-013-9466-z

[6] Colombo A, Negro P, Toniolo G (2014) *The Influence of Claddings on the Seismic Response of Precast Structures: the Safecladding project.* In: Second European Conference on Earthquake Engineering and Seismology, pp 1–12

[7] EERI (1979) *Friuli, Italy Earthquakes of 1976.* Earthquake Engineering Research Institute, Oakland, California, USA

[8] Fajfar P, Banovec J, Saje F (1978) *Behaviour of Prefabricated Industrial Building in Breginj During the Friuli Earthquake.* In: 6th ECEE, Dubrovnik, vol 2. pp 493–500

[9] FIB (2003) *Seismic Design of Precast Concrete Building Structures,* Federation International du Beton, Lausanne, Bulletin 27

[10] Fischinger M, Zoubek B, Kramar M, Isakovic´ T (2012a) *Cyclic Response of Dowel Connections in Precast Structures.* In: 15th WCEE, Lisbon, 10 p

[11] Krausmann E (2014) *Report on Lessons Learned from Recent Catastrophic Events,* Zurich, Switzerland. https ://doi.org/10.2788/618

[12] Kramar M (2008) *Seismic Vulnerability of the Precast Reinforced Concrete Structures.* Ph.D. thesis (in Slovenian) University of Ljubljana, Ljubljana

[13] Kramar M, Isakovic´ T, Fischinger M (2010b) *Experimental Investigation of "Pinned" Beam-to-Column Connections in Precast Industrial Buildings.* In: 14th ECEE, Ohrid, 8 p

[14] Li Y, Geng F, Ding Y, Wang L (2020) *Experimental and Numerical Study of Low Damage Self-centering Precast Concrete Frame Connections with Replaceable Dampers Bournas.* Vol. 220, 1 October 2020, 111011.

[15] Magliulo G, Fabbrocino G, Manfredi G (2008) *Seismic Assessment of Existing Precast Industrial Buildings Using Static and Dynamic Nonlinear Analyses.* Eng Struct 30(9):2580–2588. https://doi.org/10.1016/j.engst ruct.2008.02.003

[16] Martinelli P, Mulas MG (2010) *An Innovative Passive Control Technique for Industrial Precast Frames.* Eng Struct 32(4):1123–1132. https ://doi.org/10.1016/j.engst ruct.2009.12.038

[17] Palanci M, Senel SM, Kalkan A (2017) *Assessment of One Story Existing Precast Industrial Buildings in Turkey Based on Fragility Curves.* Bull Earthq Eng 15(1):271–289. https ://doi.org/10.1007/s1051 8-016-9956-x

[18] Romão X, Costa AA, Paupério E, Rodrigues H, Vicente R, Varum H, Costa A (2013) *Field Observations and Interpretation of the Structural Performance of Constructions after the 11 May 2011 Lorca Earthquake.* Eng Fail Anal 34:670–692. https ://doi.org/10.1016/j.engfa ilana l.2013.01.040

[19] Ristic J., Pavlov S., Pavlov P., Misini L., Ristic D.: *Laboratory Testing of Constructed Prototype Models of Typical Connections Used in Prefabricated RC Construction System of Industrial Halls Implemented by PUT Inzenering,* Serbia: Experimental Laboratory Testing of Prototype Model-M5 Representing Original Connection between a Precast Roof RC Beam and an RC Column, RESIN Lab. of Industrial Sciences and Technology, Report: RESIN-015-2017.

[20] Ristic J., Pavlov S., Pavlov P., Misini L., Ristic D.: *Laboratory Testing of Constructed Prototype Models of Typical Connections Used in Prefabricated RC Construction System of Industrial Halls Implemented by PUT Inzenering,* Serbia: Experimental Laboratory Testing of Prototype Model-M6 Representing Upgraded Connection between a Precast Roof RC Beam and an RC Column, RESIN Lab. of Industrial Sciences and Technology, Report: RESIN-016-2017.

[21] Savoia M, Buratti N, Vincenzi L (2017) *Damage and Collapses in Industrial Precast Buildings after the 2012 Emilia Earthquake.* Eng Struct 137:162–180. https ://doi.org/10.1016/j.engstruct.2017.01.059

[22] Simeonov B, Park R. Building Construction under Seismic Conditions in the Balkan Region: Design and Construction of Prefabricated Reinforced Concrete Building Systems. UNDP/UNIDO project RER/79/015; 1985. p. 335.

[23] Zoubek B, Isakovic´ T, Fahjan Y, Fischinger M (2013b) *Cyclic Failure Analysis of the Beam-to-Column Dowel Connections in Precast Industrial Buildings.* Eng Struct 52:179–191

[24] Zoubek B, Fischinger M, Isakovic´ T (2014a) *Estimation of the Cyclic Capacity of Beam-to-Column Dowel Connections in Precast Industrial Buildings.* Submitted for publication in Bulletin of Earthquake Engineering, Springer, Netherlands

AMBIENT VIBRATION MEASUREMENT OF THE INSTITUTE FOR MATERIALS AND STRUCTURES BUILDING IN SARAJEVO

Enver Selimović [1], Hanka Hadžić [2], Goran Simonović [3], Sergey Churilov [4], Mustafa Hrasnica [5], Senad Medić [6]

[1] *Mag.ing.aedif., University of Sarajevo-Faculty of Civil Engineering, enver-selimovic@hotmail.com*
[2] *Univ.bacc.ing.aedif., University of Sarajevo-Faculty of Civil Engineering, hadzichanka94@gmail.com*
[3] *Associate professor, University of Sarajevo-Faculty of Civil Engineering, goransimonovic@yahoo.com*
[4] *Full professor, Ss. Cyril and Methodius University in Skopje-Faculty of Civil Engineering, curilov@gf.ukim.edu.mk*
[5] *Full professor, University of Sarajevo-Faculty of Civil Engineering, hrasnica@bih.net.ba*
[6] *Assistant professor, University of Sarajevo-Faculty of Civil Engineering, senad.medic@gf.unsa.ba*

Abstract

Determination of dynamic properties of structures is the first step in assessing seismic response, and they can be measured in several ways. Controlling or knowing the input excitation usually applied by impact hammer or vibration shaker, typical for experimental modal analysis (EMA) that has been around for the past few decades, is for majority of structures difficult or practically impossible. Ambient vibration testing (AVT) or operational modal analysis (OMA), on the other hand, is the output-only modal analysis. It does not require knowledge of the input excitation, which is practically induced by wind, traffic or similar random source. In this paper, an investigation of ambient vibrations and numerical modelling of the building of the Institute for Materials and Structures (IMK) of the Faculty of Civil Engineering in Sarajevo was carried out. The main goal was to determine the dynamic characteristics of the IMK building using the DIGITEX SENTRY system and Artemis modal software. In addition to testing the IMK building, testing of simpler systems such as a wooden simple beam and a steel cantilever was also conducted. For each experiment, a modal analysis was performed in the Tower 8 software package. The numerical model of the building was more flexible than measured in the experiments, and the results were only comparable after inclusion of partition walls in the analysis.

Keywords: operational modal analysis, ambient vibration testing, DIGITEX Sentry System

1. Introduction

Dynamic characteristics of buildings and other types of structures are essential ingredients in the analysis of the structural response under dynamic loads (e.g., earthquake shaking, strong winds, explosions etc.). Variation of dynamic properties in time (frequencies of vibration, damping ratios and mode shapes), closely related to the change of stiffness, can also be employed for identification of potential structural damage [1] and even assessment of soil-structure interaction [2]. They can be verified by conducting experiments on full-scale structures, usually by ambient and forced vibration [3,4,5]. Testing of small-scale models is conveniently executed in laboratories [6].

The use of experimental tests to gain knowledge about the dynamic response of civil structures is a well-established practice. In particular, the experimental identification of the modal parameters can be dated back to the middle of the twentieth century. Assuming that the dynamic behaviour of the structure can be expressed as a combination of modes, whose values depend on geometry, material properties, and boundary conditions, Experimental Modal Analysis (EMA) identifies those parameters from measurements of the applied force and the vibration response. EMA has been applied in different fields, such as automotive engineering, aerospace engineering, industrial machinery, and civil engineering. The identification of the modal parameters by EMA techniques becomes more challenging in the case of civil engineering structures because of their large size and low frequency range. The application of controlled and measurable excitation is often a complex task that requires expensive and heavy devices. For this reason, the community of civil engineers has more recently focused the attention on the opportunities provided by Operational Modal Analysis (OMA). OMA can be defined as the modal

testing procedure that allows the experimental estimation of the modal parameters of the structure from measurements of the vibration response only [7,8]. It is a so-called Output Only method, where it is assumed that the wind, traffic, and human activities can adequately excite a structure. Highly sensitive acceleration sensors are used to record, evaluate and interpret the vibration behaviour of a structure without forced excitation in all three directions in space. The main assumption of the Output-Only identification methods is that the ambient excitation input is a Gaussian white noise stochastic process in the frequency range of interest.

The eigenfrequencies are an essential parameter for the description of the vibration behaviour of a structure in the linear elastic field. A mode shape – i.e., a vibration form in which the structure oscillates with the respective eigenfrequency –belongs to every eigenfrequency. The actual oscillation of a real structure is composed of the respective shares of the individual mode shapes. The mathematical modal analysis supplies both the eigenfrequencies and the mode shapes of a structure. Both analyses have to be carried out for system identification. The actual static system is obtained by comparing the measuring results with the calculated values and adaptation of the calculation model to the measurements. To get a correct image of the actual load-bearing system, it is required to consider not only the first eigenfrequency and the respective modal form but also higher frequencies and the respective forms [9].

An important disadvantage of this measuring technique should be stressed. Since the amplitudes of vibrations are small, the ambient vibration tests describe only the linear behaviour of structures. They can be used also to describe the linear behaviour of damaged structures and of their components, and can guide researchers in developing time and amplitude dependent structural models and analysis algorithms, to be used in structural health monitoring and in structural control studies. The measured AVT data might not be representative of stronger earthquakes and should be adopted with care since amplitudes of displacements and accelerations are significantly larger. Cracking is expected for quasi-brittle concrete and masonry structures with low tensile strength and frequencies are generally lower than determined by AVT. Therefore, further development of experimental methods for in situ measurement of full-scale partially damaged structures is of great interest [2].

A process of implementing a damage detection and characterization strategy for engineering structures is often called Structural Health Monitoring (SHM). The SHM process involves the observation of a system over time using periodically sampled response measurements from an array of embedded sensors, extracting damage-sensitive features from these measurements, and performing statistical analysis of these features to determine the current state of system health. Over the long-term data analysis is used to assess the structure's ability to perform its intended function. After extreme events, such as earthquakes or blast loading, SHM is used for rapid condition screening and aims to provide reliable, real-time information regarding the integrity of the structure. SHM can be applied to fixed infrastructure, such as building and bridges, or mobile infrastructure, such as airplanes and trains [10]. In the case of civil engineering structures, the data provided by the sensors is usually transmitted to a remote data acquisition centre.

DIGITEX Innovative Systems has developed a framework for structural health monitoring using an intelligent and reliable monitoring system termed Sentry System – Digital Solution for Ambient Vibration Measurements [11]. A typical Sentry System architecture was employed for ambient vibration testing (AVT) of the building of the Institute for Materials and Structures (IMK) of the Faculty of Civil Engineering in Sarajevo. It was built more than 50 years ago and it houses laboratories for testing materials and structures, as well as the offices of all teachers from the Structural Department.

2. System Architecture

2.1 Sentry System

The Sentry System digital acquisition system is designed to be an IoT (Internet of Things) solution for structural health monitoring of civil engineering structures. It has a modular and dynamic architecture that allows seamless expansion of the number of channels at any time. The Sentry SHM system has

integrated several communication protocols that provide flexibility during the installation phase of the system depending on the complexity of the structure that is being monitored.

One of the main advantages of the Sentry SHM system is that it is a fully digital solution. This means that all AD conversion processes are done next to the sensor itself, thus avoiding to maximum, any inducted noise that is a common problem when using analog sensors and a remote acquisition station. Once the signal is digitized the system use variety of communication protocols (Ethernet, Serial, Wi-Fi) to transfer data to the centralized station for further processing and analysis.

All units of the Sentry System are using GPS timing source. This way multiple units distributed remotely around the world can be synchronized together. Together with the centralized processing part of the Sentry System that can run on any cloud service, the Sentry System can act as one virtual global SHM system with sensing units distributed anywhere.

The Sentry System family of products consist of several units that can be installed as standalone units or as a part of a general SHM system (Fig. 1), and the applied configuration is the following:

• Qty.1 xPlorer, central acquisition unit.
• Qty.5 xWave units - total of 15 channels of acceleration installed on different locations of the structure for monitoring vibration
• Qty.1 xSense units – total of 5 channels for measuring voltage-based sensors.
• Qty.2 xNet unit – total of 2 units for expanding the network coverage on the structure that is being measured.

Total number of channels that this system is acquiring is 15 for acceleration and 5 channels for measuring displacement. For comparison, HBM B12 acceleration sensors were also used for determination of natural frequencies [12].

Figure 1. Sentry System Architecture [11].

2.2 Software

Back in 1999, ARTeMIS software [13] was originally developed as a spin-off of research made Aalborg University, Department of Civil Engineering, and even the ARTeMIS name refer to its civil engineering roots as it is the abbreviation of Ambient Response Testing and Modal Identification Software.

ARTeMIS Modal includes up to eight methods for Operational Modal Analysis. From the user-friendly Frequency Domain Decomposition (FDD) methods to the powerful Crystal Clear Stochastic Subspace Identification (CC-SSI) methods. All versions also include Time and Frequency Domain Operating Deflection Shapes analysis (ODS). The modal estimation methods are designed to account for the

presence of deterministic signals (harmonics) in case of rotating structural parts or another sinusoidal excitation. ARTeMIS Modal Basic includes the Frequency Domain Decomposition (FDD) peak picking method. In this study, FDD was used for the approximate identification of natural frequencies and mode shapes. FDD is a modal analysis technique that estimates the modes of a system from the calculated spectral densities for a lightly damped structure in a condition of white noise input. ARTeMIS Modal Standard includes all features of the Basic version and adds the Enhanced Frequency Domain Decomposition (EFDD) and Curve-fit Frequency Domain Decomposition (CFDD) peak picking methods. ARTeMIS Modal Pro includes all available methods and adds support for Structural Health Monitoring (SHM) plugins used for long term monitoring of structures.

3. Ambient Vibration Tests

3.1 Simple tests

Two preliminary vibration tests were executed on a steel cantilever INP 120 beam and a simple 30/5 wooden beam (plank) to test the equipment and verify the results against analytical/numerical models (Fig. 2). To compare the natural frequencies, two tests were performed: a standard impact test and an ambient vibration test. Difference between the experimentally obtained results is negligible. Numerical analysis was performed using Radimpex Tower Software [14] employing densely discretized beam elements to better approach the analytical solution. Analytical expressions for vibration properties of simple structures with distributed mass for various boundary conditions can be found in literature [15]. A comparison of experimentally and numerically obtained frequencies for the steel beam are provided in Table 1.
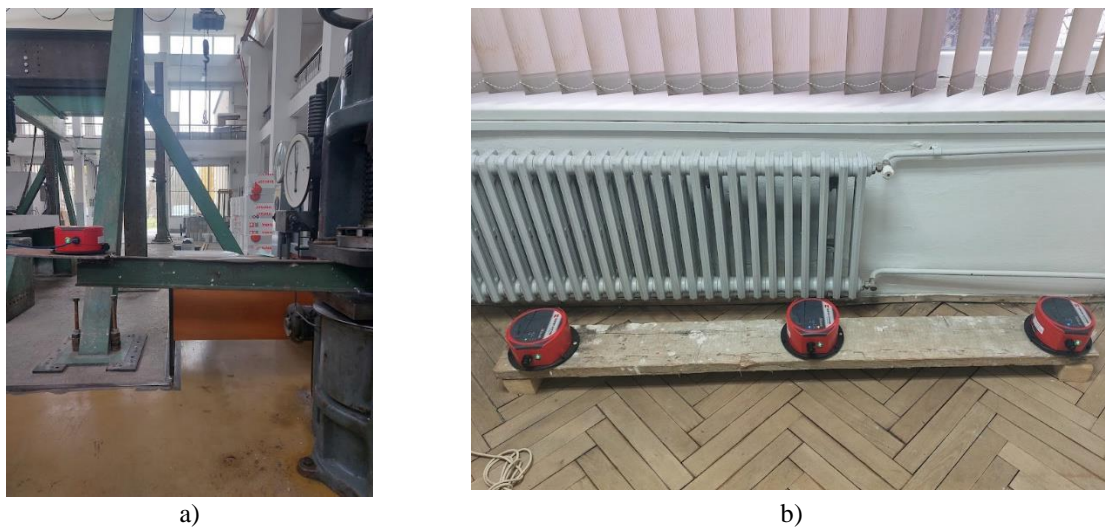
Figure 2. Simple tests: a) INP 120 cantilever steel beam; b) wooden plank 20/5 cm.

Table 1 – Experimentally and numerically obtained frequencies for the steel beam

Mode	Experimental f [Hz]	Numerical f [Hz]
1	11,03	11,87
2	30,76	36,61
3	67,87	59,35

3.2 IMK building

The building of the Institute for Materials and Structures is located within the Faculty of Civil Engineering in Sarajevo. The structure has three characteristic floors and a two-sided roof above the hall area where a 5t crane is in use. The first characteristic floor is a lower ground floor with a height

of 3.50 meters. Other characteristic floors are the upper ground floor, 4.0 meters high, and the first floor, 3.40 meters high. The building has basically an elongated rectangular shape with layout dimensions of 27.8x48.7 m, and a recess on the shorter left side of the building. Typical sections are shown in Fig. 3 and the layout is given in Fig. 4.

Reinforced concrete columns in the office area are 30/30 cm, while in the hall they are 30/60 cm. The floors have a monolithic fine ribbed structure, with narrow ribs at a distance of 33 to 60 cm and a thin topping slab. The foundation of the building is carried out on foundation strips under the walls and on spread footings below the columns. Individual footings are tied with foundation beams.

a)

b)
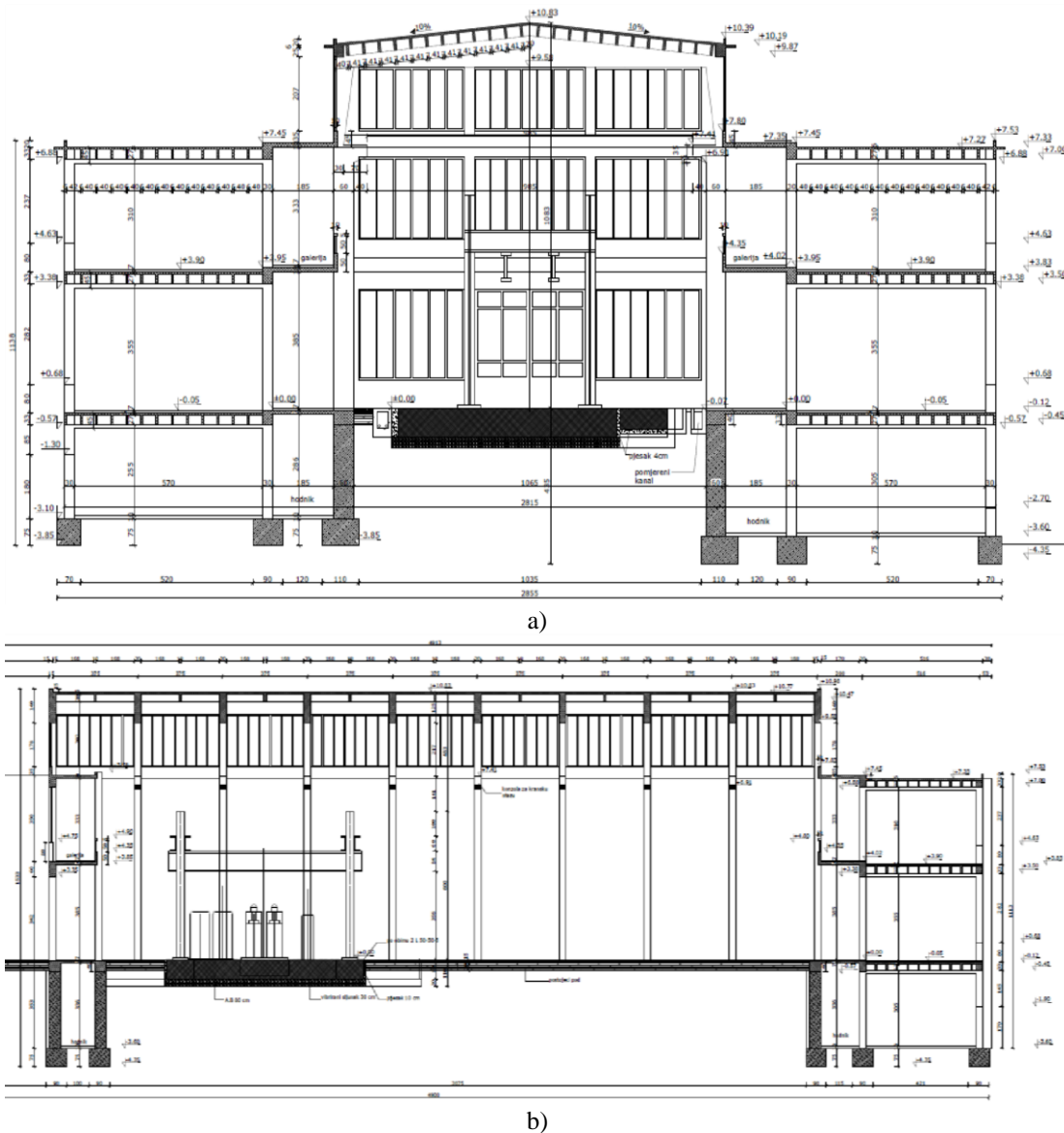
Figure 3. IMK building: a) cross-section; b) longitudinal section.

Digitex Sentry System was used for data acquisition. It consisted of an xPlorer central acquisition unit and 3 xWave triaxial digital accelerometers. The system is capable of providing realtime data acquisition for continuous structural health monitoring for several months. One stationary accelerometer was used as a reference, while the other two were placed in different locations (see Fig. 4). The sampling frequency was 200 Hz. In order to induce vibrations, the 5t crane was used (Fig.4b inset). Typical acceleration record is given in Fig.5 and a power spectrum for longitudinal direction is provided in Fig. 6.

a)

b)
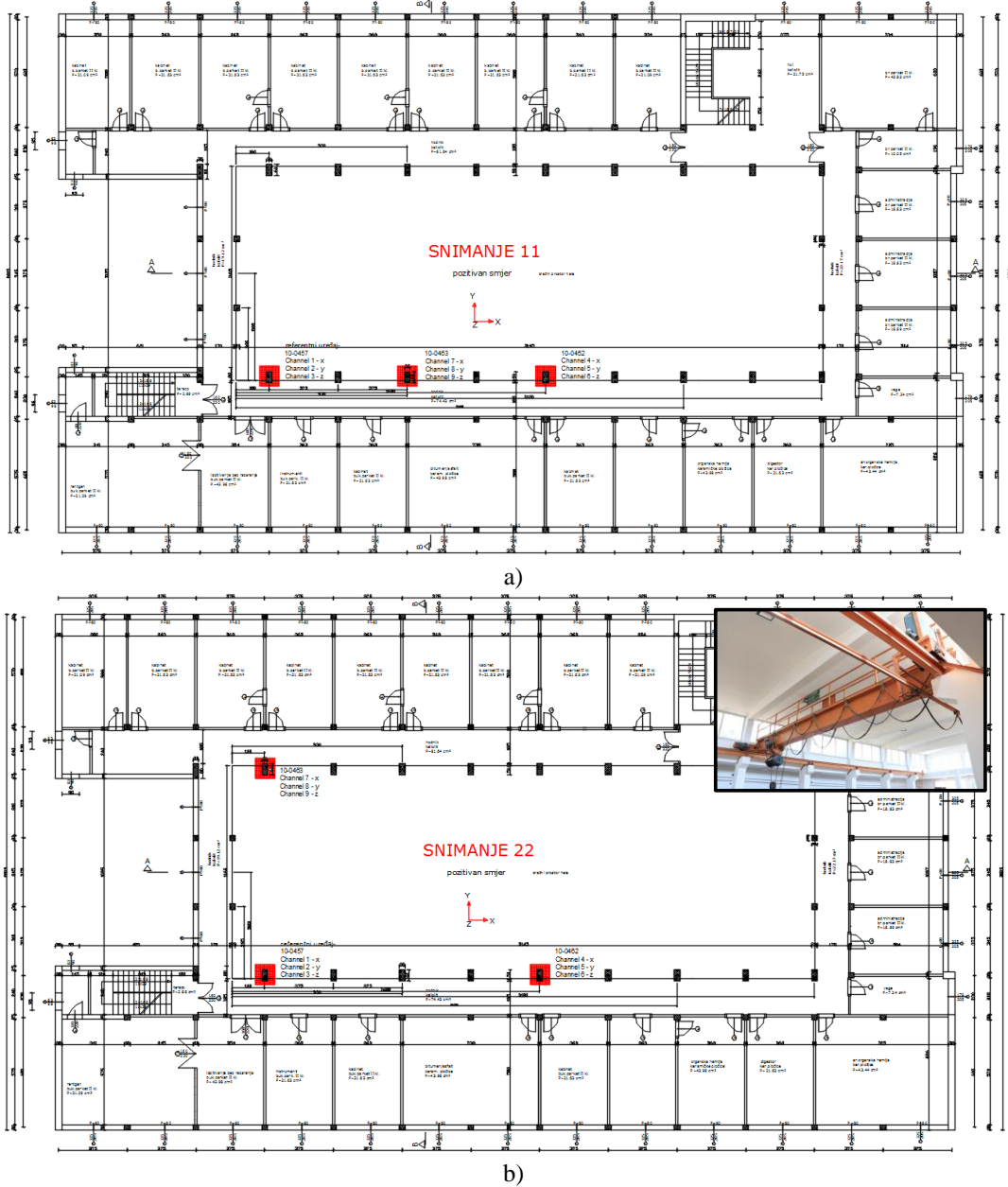
Figure 4. Different locations of sensors: a) record 11; b) record 22 (inset: IMK crane for vibration generation).
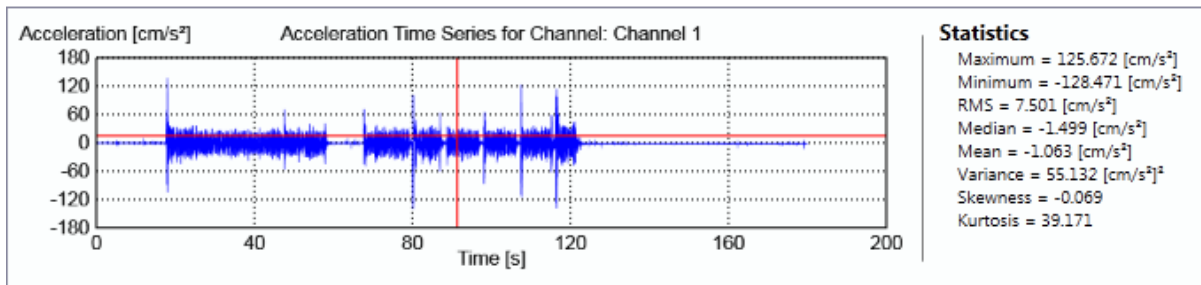
Figure 5. Typical acceleration record.
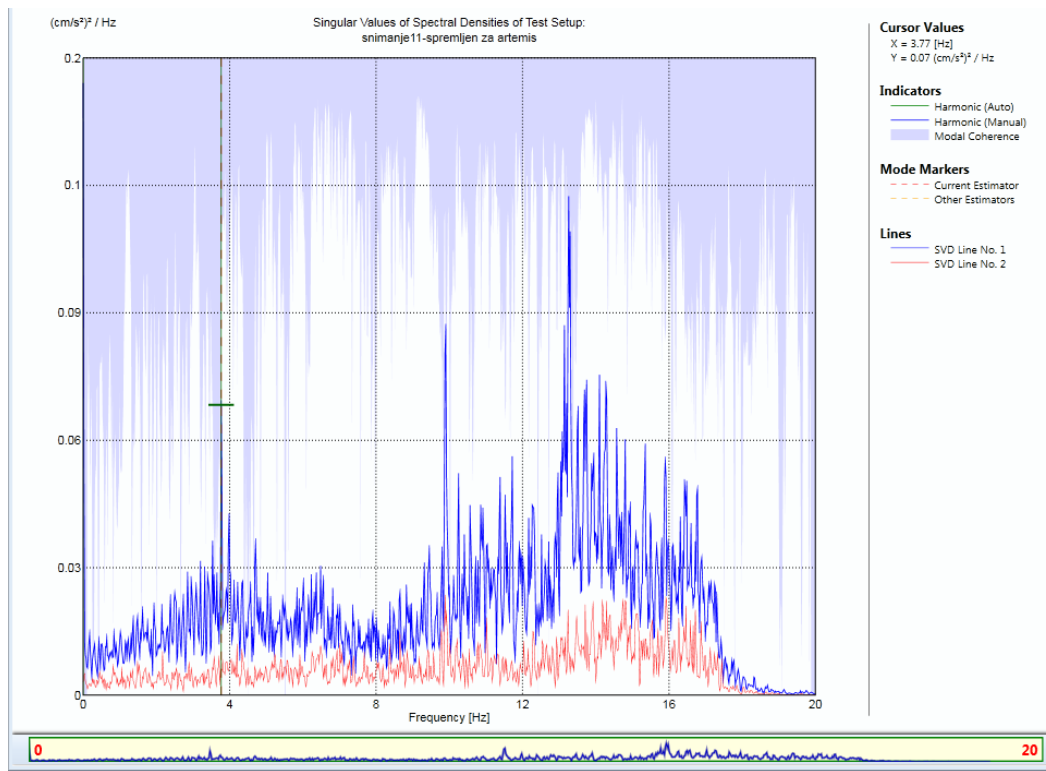
Figure 6. Power spectrum for longitudinal direction.

3D render of a numerical model is shown in Fig. 7a, and vibration modes are provided in Fig. 7b. The model includes all RC elements as well as masonry infill. Not including masonry resulted in large discrepancies between the measured and numerically obtained frequencies. The first mode refers to longitudinal translation (f_1 = 3,78 Hz); the lack of frames in longitudinal direction is obvious. A comparison of experimental and FEA frequencies is given in Table 2.

a)   b)
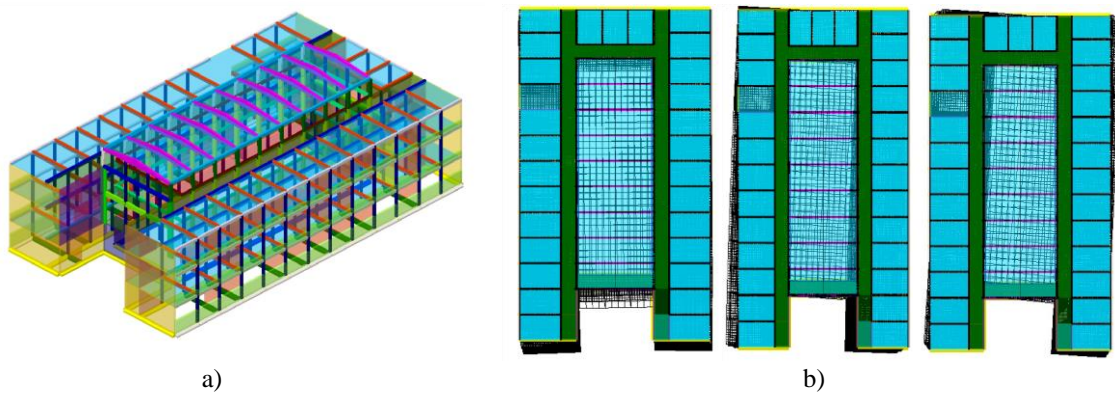
Figure 7. a) 3 D render of the building; b) the first three modes of vibration.

Table 2 – Experimentally and numerically obtained frequencies for the IMK building

Mode	Experimental f [Hz]	Numerical f [Hz]
1	3,77	3,78
2	3,93	3,99
3	4,33	4,55

266

4. Conclusion

Dynamic properties of two beams and the IMK building were determined using highly sensitive acceleration sensors and input from the ambient. The first natural frequency of the IMK building amounts to approx. 3.7 Hz and pertains to the longitudinal direction where RC frames do not exist. Frequencies and modal shapes from the finite element model and frequency domain decomposition of the measured signal fit well. Ambient vibration testing does not require knowledge of the input excitation practically induced by wind, traffic, or similar random source. It is practically very useful since the application of an impact hammer or vibration shaker for experimental modal analysis is for the majority of structures difficult or practically impossible.

Acknowledgements

References

[1] Rak, M., Bjelajac, N. (2001): Otkrivanje oštećenja konstrukcija mjerenjem dinamičkih karakteristika. *Građevinar*, *53*(10.), 631-639.

[2] Ivanović, S. S., Trifunac, M. D., Novikova, E. I., Gladkov, A. A., Todorovska, M. I. (2000): Ambient vibration tests of a seven-story reinforced concrete building in Van Nuys, California, damaged by the 1994 Northridge earthquake. *Soil Dynamics and Earthquake Engineering*, *19*(6), 391-411, doi: https://doi.org/10.1016/S0267-7261(00)00025-7

[3] Ivanovic, S. S., Trifunac, M. D., Todorovska, M. I. (2000): Ambient vibration tests of structures-a review. *ISET Journal of earthquake Technology*, *37*(4), 165-197.

[4] Churilov, S., Micevski, S., Dumova-Jovanoska, E. (2018): Ambient vibration testing of public unreinforced masonry buildings from the beginning of the 20th century. In *Proceedings of the 16th European Conference on Earthquake Engineering,* Thessaloniki, Greece.

[5] Baptista, M. A., Mendes, P., Oliveira, S. (2005): Use of ambient vibration tests for structural identification: 3 case studies. In *Proceedings of the 1st International Operational Modal Analysis Conference*.

[6] Franković, T., Paparić, K., Grandić, I. Š. (2019). Laboratorijsko određivanje dinamičkih parametara jednostavne grede OMA metodom. *Zbornik radova (Građevinski fakultet Sveučilišta u Rijeci)*, *22*(1), 43-57, doi: https://doi.org/10.32762/zr.22.1.3

[7] Rainieri, C., Fabbrocino, G. (2014): *Operational modal analysis of civil engineering structures.* Springer, New York.

[8] Brincker, R., Zhang, L., Andersen, P. (2001): Modal identification of output-only systems using frequency domain decomposition. *Smart materials and structures*, *10*(3), 441, doi: 10.1088/0964-1726/10/3/303

[9] Wenzel, H., Pichler, D. (2005): *Ambient vibration monitoring*. John Wiley & Sons.

[10] Sivasuriyan, A., Vijayan, D. S., Górski, W., Wodzyński, Ł., Vaverková, M. D., Koda, E. (2021): Practical implementation of structural health monitoring in multi-story buildings. *Buildings*, *11*(6), 263, doi: https://doi.org/10.3390/buildings11060263

[11] DIGITEX Innovative Systems (2020): General System Description – Sentry System. Digitex Systems. LLC, http://digitexx.website2.me

[12] Hottinger Brüel & Kjær (2023): https://www.hbm.com/de/

[13] Structural Vibration Solution (2023): https://svibs.com/

[14] Radimpex Software for Civil Engineers (2023): https://www.radimpex.rs/en

[15] Chopra, A.K. (2019): *Dynamics of structures*. Pearson Education, 5ᵗʰ edition, USA.

STUDY OF THERMAL PERFORMANCE OF PREFABRICATED LARGE PANEL BUILDINGS

Merita Guri[1], Flogerta Krosi [2], Klodjan Xhexhi [3],

[1] *Lecturer, POLIS University, merita_guri@universitetipolis.edu.al*
[2] *Assistant Lecturer, POLIS University, flogerta_krosi@universitetipolis.edu.al*
[3] *Lecturer, POLIS University, klodjan_xhexhi@universitetipolis.edu.al*

Abstract

Many countries in Eastern Europe, during the 1960–1970s, as well as Albania responded to the growing demand for new houses utilizing the emerging trends for industrialization of the construction process and mass construction of prefabricated residential buildings based on large-panel prefabricated RC elements. During the 1970s large-panel buildings spread throughout the country and became the main type of construction in the Albanian cities such as Shkodër, Tirana, Durrës, Elbasan, Berat, etc. Most of these buildings have five or six stories and comprise different modules, the number of which depended on the urban and architectonic projects.

The construction technology of these types of buildings included only the construction with prefabricated reinforced concrete material and did not take into account the energy performance of these structures. Since the moment of construction, only in the last year, several interventions have been made in different cities where a layer of polystyrene has been placed on the external walls of these buildings in order to enhance their termal insulation.

The aim of this paper is to improve the thermal performance of these buildings by introducing a comparison of their initial situation as they are today and how their performance would be if innovative technologies and materials will be applied. The study is going to analyse the thermal performance of the existing buildings, by means of thermal camera in the city of Kamez, located in Tirana, which has been chosen as a key study. Futhemore, the data obtained from MEEC application are gethered, in oder to compare the previvious, the existing situation and the proposed intervention. The results may be used by municipalities of different cities, not only in the Albanian contex, either where interventions have been made to improve their performance, or for municipalities where thermal regulation policies that have not been yet implemented to these types of buildings.

The existing situation of the buildings according to the calculations, showed a poor thermal performance, regardless of the fact that they are already equipped with thermal insulation building envelope. They have to be requalified in order to be categorized as a buildings with high thermal performance.

Keywords: prefabricated buildings, heat flow, building termal performance, materials of construction; thermal regulations

1. Introduction

Energy efficiency in buildings is one of the main strategic pillars in various EU strategic energy documents. The reason is pragmatic, based on the fact that 40% of total final energy consumption at EU level is consumed in buildings. In addition, traditional and conventional heating systems are mainly based on fossil fuels and thus contribute a large part of CO_2 emissions [1].

The thermal performance of different buildings in Albania has been studied by several different authors. The most studies have been done for different building typologies, especially for masonry buildings built around the 70-80s where their performance does not result in the right conditions as mention on a Marku's A. phd thesis [2].

Precast buildings are an assembly of different elements which are prefabricated in the fabric and connect with each other in the construction site by simple connection between them. The simplicity of the connection and the short time of prefabricating the panels and the assembly of the elements has made these types of structures quite popular in Albania, in the region and in the world.

Many other Eastern European countries, as well as Albania responded to the growing demand for new housing during the 1960s and 1970s by taking advantage of the emerging trends in the industrialization of construction processes and the mass construction of prefabricated dwellings. The buildings were built according to standardized formwork approved by the Albanian government authorities and thus represent standardized techniques widely used in Albania. In the 1970s, large-scale buildings spread across the country and became the main architectural style in Albanian in cities such as Shkoder, Tirana, Durrës, Lushnjë, Burrel, Elbasan, Berat, Pogradeci, Laç, Lezhë, Korçë, Tepelenë, Gjirokastër. The process was automatized and they were fabricated in a new plant near "Josif Pashko" which uses Chinese technology with 2000 apartaments per year capacity. These types of buildings with a residential function make up about 5% of the total residential apartments [3].

After World War II, the major problem was the housing of the population, as a result of the destruction of cities by the Second World War. The very first dwellings that were built were realized with voluntary contribution with blocks and temporary materials to solve the immediate needs. The neoclassical Russian school showed its character in this period with stable and mega buildings constructions. The architectural arguments were gigantism and ornament. However, in terms of appearance, these apartments were characterized by truncated and uncomfortable living space. Meanwhile from the urban and architectonic point of view, their placement in the plan created original squares in function of the community. The standardization of building elements were implemented by the development of the building materials industry. This strategy greatly facilitated the typification of dwellings by unifying the design elements. In the late 1960s and early 1970s, such schemes were strictly criticized for compositional solutions that promote antisocial behavior, for the social effects of expropriations, denying the city's construction tradition. During the late 1980s, the regime of that time managed to radically transform the vast majority of Albanian cities. During these years, large residential blocks were realized, at minimal cost (prefabricated residential blocks), as well as residential blocks with red clay bricks or silicate bricks. These dwelling can be spotted in the form of liner constructions as in the case of the city of Tirana [4].

The large panels, whether horizontal or vertical, are made of concrete, where some of the panels are filled with foam-concrete. The facades of the building are not a continuous element but consist of several small units. The connection of the panels is done using mortar in order to monolithic the structures and the joints between the pannels are considered weak structural points [5]. Most of these buildings have five or six floors and are composed of various modules. The number of the floors depended on the general local plan of the municipality of that time.

These types of buildings do not have a good energy performance because the main material of these buildings is concrete and it is known that concrete has high thermal conductivity and that causes significant heat loss. Many thermal bridges are present in the joint between the concrete panels, which often influence heat loss, and also turn into a problem for moisture infiltration into the building envelope. Because of amortization and lack of maintenance only in the city of Tirana, about 10% of the stock of prefabricated buildings have not had renovation interventions. Due to this situation the problems in these building have been amplified [6]. After their privatization in the early 90s, maintenance and care of the buildings has been the responsibility of the residents. In more than 15 years, the interventions that were made in these buildings were made by the owners, who only intervened in their properties. Only in the last 5 years, the government intervened in some of these types of buildings by thermal insulating them with the external coating system.

2. Evaluation methodology of thermal performance

The evaluation of thermal performance will be done by comparing three different models of the same building. The first model will be the prefabricated building as it was designed in its beginnings, without any kind of thermal intervention. Furthermore, the existing layers of the building envelope, specifically the terrace, ground floor, perimeter walls and windows are considered. In the second model, in addition to the existing construction layers, an external coating system with different layers was added exposing the current state of the building. In the third model, innovative materials will be introduced to increase the thermal performance of the building [7].

For each model, it is going to be analysed the heat flow from layer to layer and how the thermal insulation characteristics of different materials are affected. The total thermal performance of the building, due to the analized models will be given for each model. The study will not consider the intermadiate floors of the building and the coefficient U of the separation wall is considered to be U=0.4

2.1 Heat flow

Heat transfer means the transfer of kinetic energy. Heat is kinetic energy in transit. Heat transfer is always accompanied by a change in the temperature of an object.

Heat is transferred between two systems or bodies whenever there is a temperature difference between them. The greater the temperature difference between the two bodies, the greater will be the amount of heat that will flow through them. In this migration or transfer, according to the second law of thermodynamics, the natural direction of heat flow between two bodies is from the hotter body to the colder body and never in the opposite direction. The flow of heat from the warmer body to the colder body will continue as long as both objects have the same temperature. So until thermal equilibrium is reached between them. [8]

2.2 Methods of heat transfer

2.2.1 Solar Radiation

Albania belongs to the Mediterranean climate belt and it is caracterised with hot and dry summers and mild winters. The average annual precipitation over the country is about 1485 mm [9]. Albania is considered a country with an upper-average radiation potential, which varies between 1185 and 1700 kWh/(m2·year). The average annual number of sunny days is 240-260 days/year [10]. For Tirana, the average annual sunshine duration is about 2500 h/year and the average annual total solar radiation is 1500 kWh/(m2·year) [11].

Meanwhile, Podgorica is the capital and largest city of Montenegro. Under the Köppen climate classification, Podgorica is transitional between a humid subtropical climate (Cfa) and a hot-summer Mediterranean climate. The n annual rainfall is 1956 mm [12]. In Podgorica, the yearly sum of sunshine is estimated to be around 3065.99 hours. On average, this equates to a monthly figure of approximately 100.6 hours for each month [12].

The research have shown that there are small differences in terms of solar radiation between Tirana and Podgorica.

2.2.2 Temperatures

Calculations for heat transmission will be made with the MEEC application, which is a program used in Montenegro [13], [14]. Since Podgorica is the closest city to Albania, the calculations will be made with the mean temperatures of that city. According to a technical report made by Kamez Municipality [15], this area is included in the central plain Mediterranean climatic zone. The average annual temperature ranges from 15-16°C. The maximum temperature was recorded on 13.07.1973 with 43°C, while the minimum temperature was recorded on 15.01.1968 with - 14.4°C. The amplitude of the changes between day and night is significant and ranges from 6 to 12-14°C. For the city of Podgorica, the temperatures to be calculated are recorded directly in the program. In Podgorica, the average January temperature is 5.0° C, July 25.9° C, while the annual temperature is 15.3° C.

Meanwhile according to RETscreen expert (a Canadian application) the anual temperature in Tirana is also 15.3° and the avarage January temperature is 7° C, which means that the two cities have little differences in terms of climate parametres [8].

2.2.3 Thermal balance

Gain= Losses

The term "gain= Losses" refers to a situation where the heat gain in a system is equal to the heat losses. This means that the amount of heat entering the system is equal to the amount of heat leaving the system, and there is no net change in the temperature of the system.

$$q_s + q_m + q_{sol} + q_h + q_{vi} = q_{BE} + q_e + q_{ve} \tag{1}$$

Where:

q_s –Sensible gain, q_m -mechanical gain, q_{sol}-solar gain, q_h- supplementary heating, q_{vi} –ventilation inside, q_{BE} heat transfer building envelope, q_e -losses through evaporation, q_{ve} -ventilation outside

Using MEEC application the study will be focused just in building thermal performance and the simplifications and the calculation scheme will be as below:
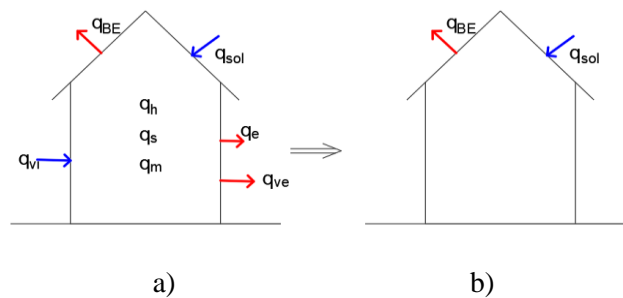
Figure 1. a) The real heat transfer proces b) the simplification of heat transfer; source: authors

So the expression (1) becomes:

$$q_{sol} = q_{BE} \tag{2}$$

Benefits as a result of solar radiation. SHGC (solar heat gain coefficient) is calculated in the window.
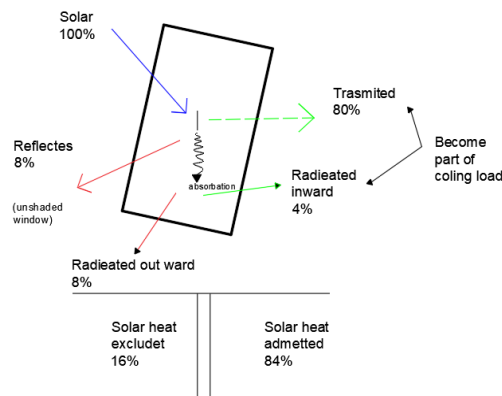
Figure 2. Solar radiation in window, source: authors

The calculation of heat transfer through a building element is

$$q_i = (G_i) * (SHGC) \tag{3}$$

Where

q_i Is the heat transfer through the element (in units of energy per unit time), (G_i) Incident irradiation, SHGC portion translated to heat gain

Fourier's law for thermal conduction in masonry

Fourier's law is used to describe the flow of heat in a solid material, such as masonry. It states that the rate of heat transfer through a material is proportional to the temperature gradient in the material and

the cross-sectional area perpendicular to the direction of heat flow, and is inversely proportional to the material's thermal conductivity. In other words, the equation for Fourier's law of heat conduction can be written as:

$$Q_{wall} = -kA\frac{\dot{T}_2 - T_1}{L} = -\frac{T_2 - T_1}{R_t} \qquad (4)$$

Where:

Q_{wall} is the rate of heat transfer (W), k is the thermal conductivity of the material (W/m.K), A is the cross-sectional area perpendicular to the direction of heat flow (m^2), L is the plane thickness (m), R_t Is thermal resistance , $T_2 - T_1$ Constant temperatures

In nature, heat transfer occurs in the following ways: by convection; by conduction; by radiation.

Heat transfer by conduction

Conduction is the process of heat transfer within a solid body (from one part to another) or between two bodies that are in direct contact with each other. In heat transfer by conduction, heat is transferred from one molecule to another neighboring molecule, which is in contact with it, through vibration, but without changing their position [16].

Different materials have different thermal conductivities (or conductivity) of energy. They can be compared with each other through the values of "U" as well as through the values of "R".

The value of "U" itself represents the coefficient of thermal conductance or transmittance and is also known differently as the heat transfer coefficient. The "U" value of a body indicates the heat transferred through one square meter of its surface, per unit of time, when the temperature difference between the external and internal environment is 1 °K (or 1ºC). The unit of measurement of the "U" value is: (W/m²K or W/m²°C). Usually solid bodies are better conductors than liquids, while liquids are better conductors than gases. The value of "U" is determined through the following relation:

$$U = \frac{1}{R} \qquad (5)$$

In those cases when a component of the building is composed of several layers of different materials, then the overall thermal transmittance value (or heat transmission coefficient) "UT" will be defined as the sum of the thermal transmittance of each material:

$$U_T = U_1 + U_2 + \cdots \ldots + U_N \qquad (6)$$

The value of "R" represents the thermal resistance of different materials, which means resistance to heat loss. The higher the "R" value, the more thermally insulating a material will be, and the higher the energy saving will be. In those cases when a building component is composed of several layers of different materials, then the general value of thermal resistance "RT" will be determined as the sum of the thermal resistances of any material:

$$R_T = R_1 + R_2 + \cdots \ldots + R_N \qquad (7)$$

2.3. Thermal camera

On 13.12.2022 at 13:30 some measurements were made with thermal cameras in the city of Kamza. During the measurements the air temperature was 13℃ and the humidity was 43%. This examination was carried out according to EN 13187 using a thermal imager TESTO 882. The results are shown in images with different colors that represent the temperature fluctuations. The lower temperatures are presented with black and dark blue colors. As the surface temperatures increases, the color changes from red, purple to yellow.

In the Figure 3 below are represented the results for one of the facade of the existing building.

a)

b)   c)
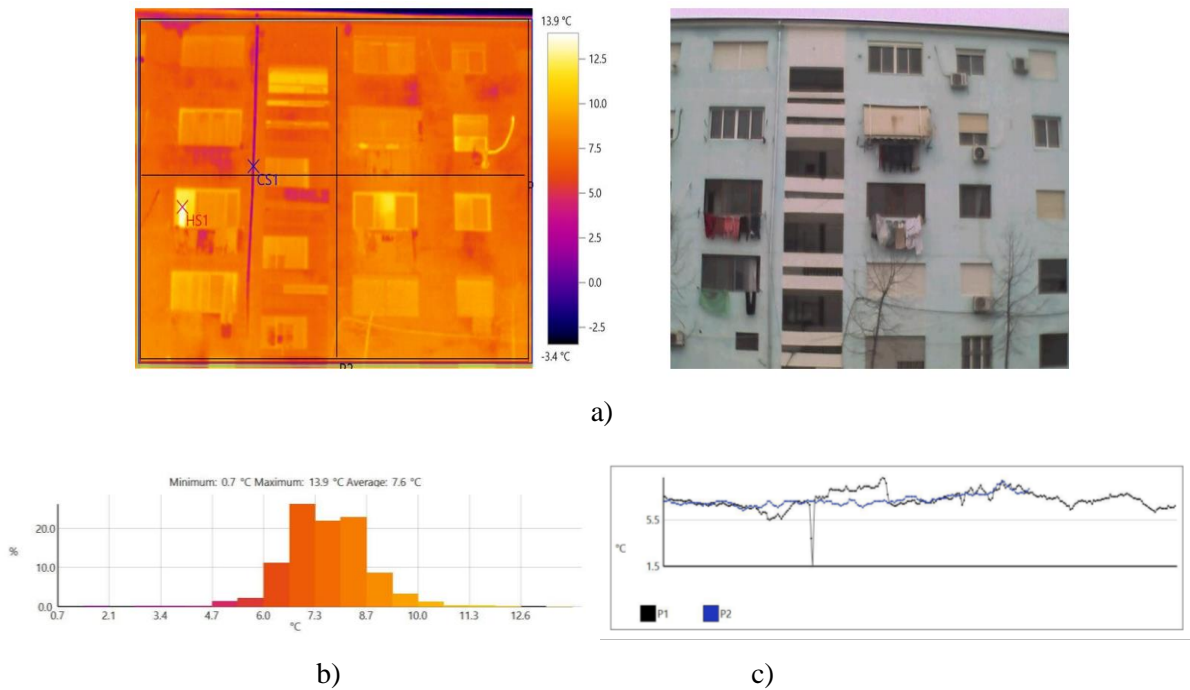
Figure 3. a) The facade temperatures, b) Histogram, c) Profile line; source: authors

In the facade as seen in Figure 3, two temperature profile lines are taken into consideration, one is horizontal and the other one is vertical. The graph presented above shows how the temperatures change along of the profile lines. The histogram shows the information about the maximum and minimum temperature as well as the average temperature on this facade. The point with the minimum temperature is marked with CS1 and the temperature is 0.7°C, which is called cold spot. According to the photo it is observed that this point is located on a metal exhaust pipe. Point HS1 is the point with the highest temperature of 13.9°C. Also, many purple spots are observed indicating the presence of moisture, which is accompanied by lower temperatures compared to the rest of the facade. According to figure 3, c, it is observed that in both the horizontal line P1 and vertical line P2 directions the temperature fluctuation is almost horizontal but the P1 at a certain point shows a drop of temperature because of the coldest point located in the thermal photo.

a)

b)   c)
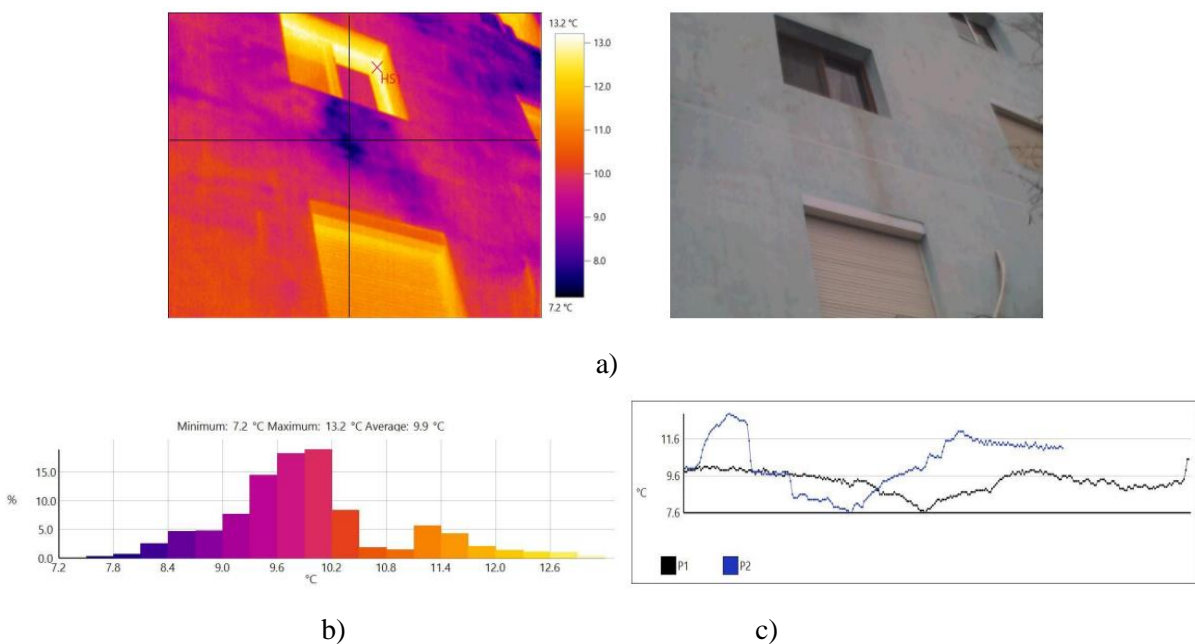
Figure 4. a) The window section, b) Histogram, c) Profile line

In the fragment of the facade as seen in figure 4, it is clearly observed the heat flow from the inside to the outside due to the poor connection of the window to the wall, where the hot point is found precisely in this connection. A little further down, near the window the hot spot can be observed, which is located in a plastic grille, that had a higher temperature than the facade. Plastic is a material with near zero water absorption in relation to the other part of the facade, which is saturated with water due to rainfall. In this fragment, the presence of moisture can be clearly distinguished, especially in the lower part of the window in figure 4. a, as a result of the lack of window drip detail. Furthermore, the presence of moisture is evident, and as a consequence lower temperaturas are observed. In the profile line fig. 4.c, it can be seen that both the horizontal and vertical directions have different temperature fluctuations.

a)

b)

c)
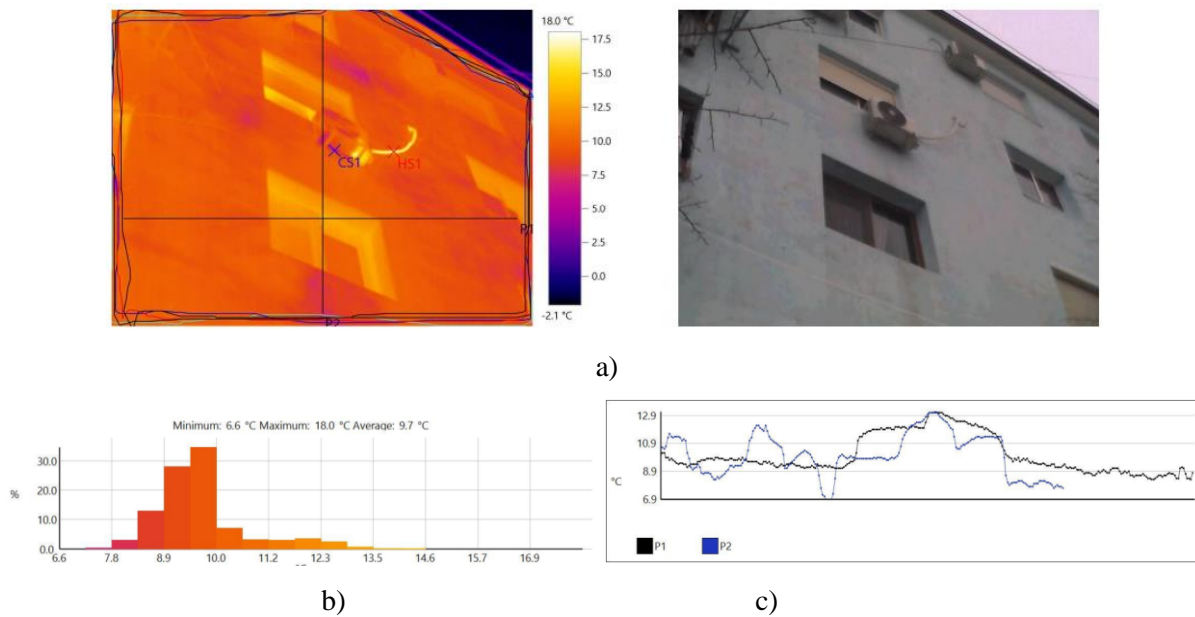
Figure 5. a) Air condition, b) Histogram, c) Profile line

Figure 5, shows two air conditioners, but with the help of the thermal camera, it is easy to observe that one of them is operating fig.5.a, and the other is not. The air conditioner pipe has a lighter yellow color, which indicates higher temperatures range. The hot spot appears precisely in the tube and the cold spot appears in the lower part of the air conditioner. In the profile line fig.5.c, it can be seen that both the horizontal and vertical directions have temperature fluctuations.

3. Case Study

The building under study is located in Manhatan Street in the city of Kamze. Kamza is a city northwest of the city of Tirana.

a)

b)

c)   d)
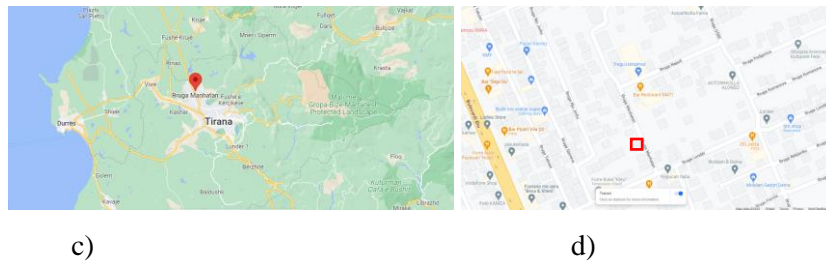
Figure 6. a) The building after the intervention; source authors b) the building without any intervention, source: authors c) location of te Manhatan Street, source: Google Earth d) A closer aerial look buildings, source: Google Earth

Only one block of section 2.1 was considered. The drawings are taken from AQTN [17].

a)   b)

c)   d)
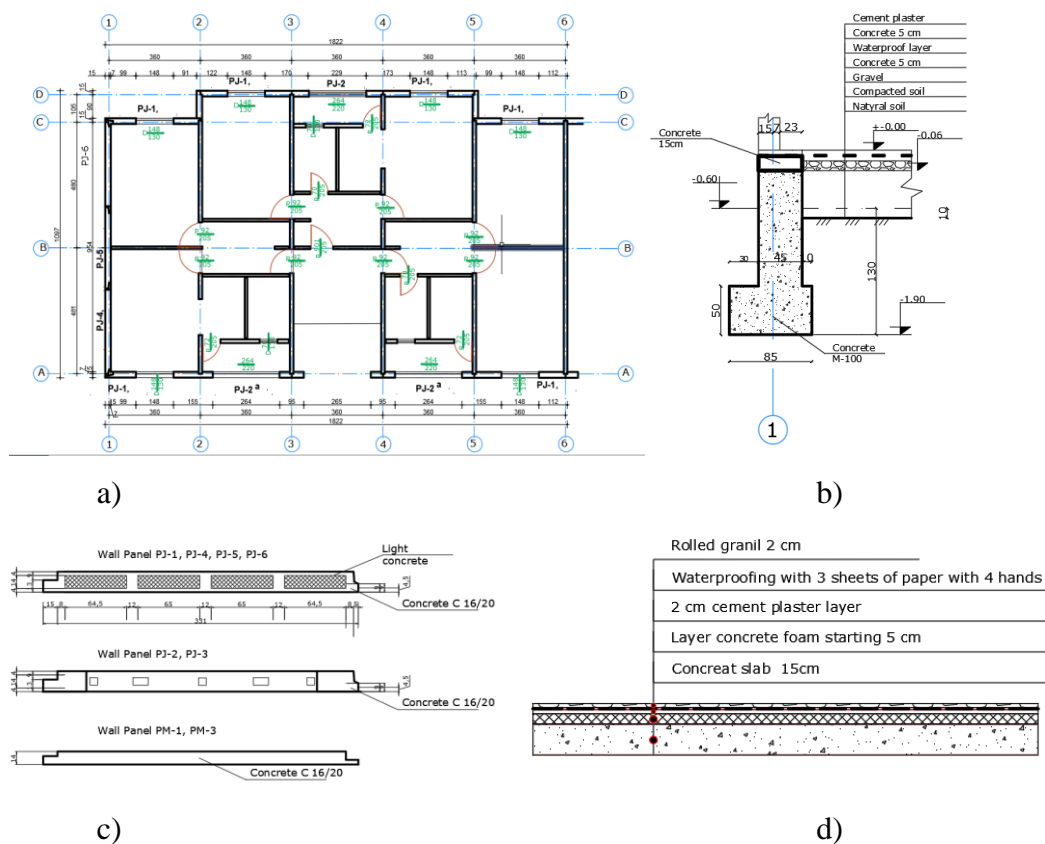
Figure 7. a) The plan of the building, b) foundation section c) wall cross sections d) slab section

Materials used for different elements, the characteristics of the materials are taken from technical design code [17] and the methodical guide for calculating the seismicity of building constructions [18].

For the vertical panels used as part of building envelope and partition walls. Large precast concrete panels are made from a mixture of cement, water, and aggregates, with the mix typically modified to improve the insulation properties of the panels, they can range in size from several meters in length, width, and height, with a typical thickness of 15 to 40 centimeters. Figure 7, c show the section Wall used in the key study and has the following features are used:

- Concrete class C16/20 unit weight $\gamma = 2400 kg/cm^2$.
- Foam concrete unit weight $\gamma = 500 kg/cm^2$.

For the basements, different layers are used as can be seen in Fig. 7. d, and each layer has the following characteristics

- Concrete C16/20 with an approximate weight $\gamma = 2400 kg/cm^2$
- The foam concrete unit weight $\gamma = 500 kg/cm^2$.
- Cement plaster with a unit weight $\gamma = 2000 kg/cm^2$
- Waterproofing with a unit weight $\gamma = 1200 kg/cm^2$

For the basements, different layers are used as can be seen in fig.7.b, and each layer has the following characteristics

- Concrete C16/20 with an approximate weight $\gamma = 2400 kg/cm^2$
- The foam concrete unit weight $\gamma = 500 kg/cm^2$.
- Cement plaster with a unit weight $\gamma = 2000 kg/cm^2$
- Waterproofing with a unit weight $\gamma = 1200 kg/cm^2$
- Gravel $\gamma = 1200 kg/cm^2$

The second calculated model is the building in the existing state as it is now. As mentioned above, in recent years, an intervention has been made in these buildings. A thermal insulation layer has been added to the external walls. The thermal insulation is made by an external coating system with layers, a 7 cm layer of polystyrene is applied and the other layer is adhesive in order to connect polystyrene with the wall. There are also implemented other layers such as plastic nets, basecoat adhesive primer and finishing coat.

The third model is the proposed interventions applied in the external walls, terrace, foundation and in the windows. The proposed windows have U=0.68 W/(m²K), the terrace U=0.27 W/(m²K), and the basement U=0.78 W/(m²K). The ground contact of the building will not be subject to further improvements, becuase the intervantion is rather difficult. The large prefabricated panels according to the calculation will have a U=0.26 W/(m²K) with light concrete and U=0.68 W/(m²K).

For calculation proposals the surfaces of the building envelope are calculated in Table 1 and 2.

Table 1-Wall and Window surface calculations

Orientation	Panel Type	Wall Area (m²)	Window Area (1,48*1,3) (m²)	Window Area (2,64*2,2) (m²)
North	PJ-4, PJ-5, PJ-6, PJ-B	155,952	0	0
South	PM-1, PM-3, PJ-B	140,495	0	0
West	PJ-2	51,264	0	29,04
	PJ-1,	205,056	38,48	0
East	PJ-1,	102,528	19,24	0
	PJ-2, PJ-3	121,848	0	58,08

Table 2-Slab surface

	Quantity	Slab Area (m2)	Openings	Net surface (m²)
Slab panel type 1 (S 1)	14	8,5383	0	119,5362
Slab panel type 2 (S-2)	3	13,3534		40,0602
Slab panel type 3 (S-3)	3	7,4464	0	22,3392
Total				181,9356

4. Results

MEEC application is used in order to observe the building thermal performace for the specific models.
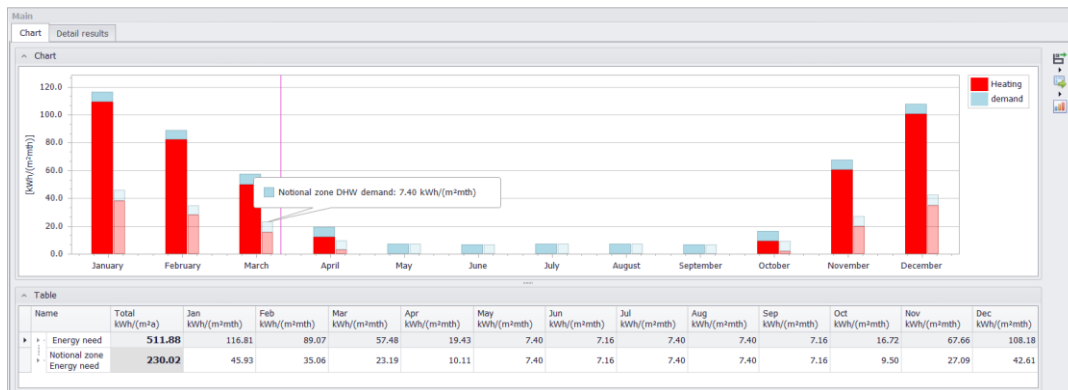
Figure 8. The results obtained for the model without thermal intervention
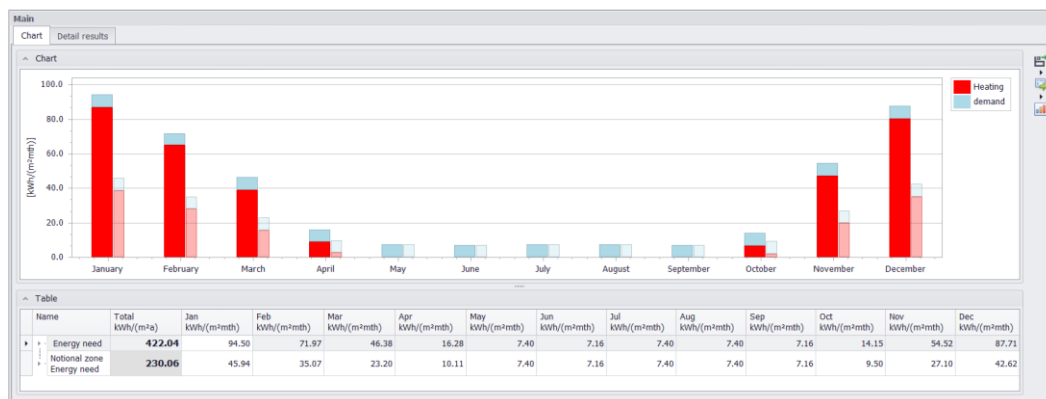
Figure 9. The results obtained for the model according to the existing intervention
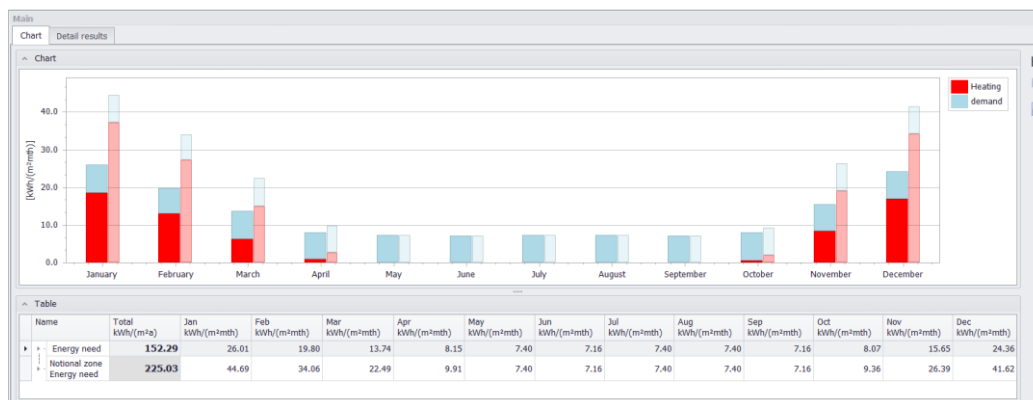
Figure 10. The results obtained for the model with proposed intervention

According to the obtained results extracted from the application, it can be observed how the required energy changes in the three cases. For the first model, in January, the required energy is 511.88 kwh/(m²a), while in the second model 422.04 kwh/(m²a) is required, which means a reduction of 17.55% in the energy required. For the third model, the required energy is 150.54 kwh/(m²a), which means a reduction of energy need of 70.59% in relation to the first model and 64.33% to the second model.

The introduction of foam concrete in the wall can decrease the U-value by 58.5%, reducing it from U = 3.57 W/(m2K) for the PJ-2 panel wich has foam concrete with a west orientation to U = 1.48 W/(m2K) for the PJ-1 panel which is the whole panel concrete C16/20, also facing the west.

5. Conclusions

It is observed in the existing situation that water absorption is relatively high, which negatively affects its thermal performance. The presence of water in the facade will increase the coefficient of thermal performance (U value) as a result of water absorption above the allowed rates.

Windows are one of the buildng elements with the highest heat flow, so it is necessary to intervene in these elements to significantly improve the thermal performance of buildings. The existing thermal performance of them is very poor.

In the case of old prefabricated buildings, it is recommended that before starting the application of the thermal insulation system, the foundation, exterior walls, terrace and windows must be requalified in terms of thermal performance. Insulation of all joints between prefabricated panels, surface treatment with concrete asar - contact concrete weberprim is needed.

The intervention only in the external walls brings a very small difference in the heat flow from the inside to the outside of the building so the terrace still needs thermal insulation. It is observed that the reduction of the U-value of the window can be of higher bennefits in terms of building thermal performance, moreover, their immediate improvement is strongly recommended.

References

[1] European Commission (2018), 'Assessment of the application of the EGTC regulation', Final report – 20.04.2018, written by Spatial Foresight, Project number 2017CE160AT116.

[2] Marku, A., (2022), SUSTAINABILITY - Low-cost strateg Low-cost strategies for renovation of Residential Building Stock of the 70s-80s in Albania. (Accessed December 1, 2022).
(https://issuu.com/polisuniversity/docs/phd_thesis_aguljeln_marku)

[3] Novikova, A., Z. Szalay, G. Simaku, T. Thimjo, B. Salamon, T. Plaku, and T. Csoknyai 2015. *The typology of theresidential building stock in Albania and the modelling of its low-carbon transformation.* Project SLED, RegionalEnvironmental Center for Central and Eastern Europe, Vienna. (Accessed December 7, 2022).

[4] K. Xhexhi (2021) "The impact of building materials in inhabitance lifestyle, case of Kruja, Albania" ISBN 9781639028627

[5] Guri, M., Brzev, S., Lluka, D., (2021), *Performance of Prefabricated Large PanelReinforced Concrete Buildings in the November2019 Albania Earthquake. Taylor&Fancis,* (3-6) *https://www.researchgate.net/deref/https%3A%2F%2Fdoi.org%2F10.1080%2F13632469.2021.1887010*

[6] GJERGJI, I., (2016). Përmirësimi i performancës energjetike në banesat me panele të parapërgatitura në Tiranë. [Improvement of energy performance in houses with prefabricated panels in Tirana].

[7] B. C. (17). Windows and glazed area technologies and materials in Europe. Building Envelope Technologies and Policies Workshop. Neuilly-sur-Seine.

[8] Xhexhi, K., (2023) Ecovillages and Ecocities. Bioclimatic applications from Tirana, Albania. ISBN 978-3-031-20958-1

[9] Albania's Second National Communication to the Conference of Parties under the United Nations Framework Convention on Climate Change. Tirana, 2009. Available at: http://unfccc.int/resource/docs/natc/albnc2.pdf

[10] Renewable energies in Albania-Solar energy, Table 1. Accessed on December 2022. Available at: http://www.akbn.gov.al/images/pdf/energji-terinovueshme/Energjia_Diellore.pdf.

[11] Tirana: Albania, Geographical names. Accessed on December 2022. Available at: http://www.geographic.org/geographic_names/name.ph p?uni=-168608&fid=283

[12] Podgorica climater, Accessed on December 2022. Available at: https://en.climate-data.org/europe/montenegro/podgorica/podgorica-1324/

[13]Budde, E., Erhorn, H., Koutsomarkos, K., Wössner, S., 2020, Technical Manual MEEC—Montenegrin Energy Efficiency Certification, Technical manual, Montenegro.

[14]Budde, E., Erhorn, H., Koutsomarkos, K., Wössner, S., 2020, Technical Manual MEEC—Montenegrin Energy Efficiency Certification, User manual, Montenegro.

[15] Bashkia Kamez. (n.d). Raport teknik. Market project. Retrieved December 13, 2022, from https://openprocurement.al/tenders/relacion/26890.pdf

[16]John H. Lienhard IV, Professor John H. Lienhard V, 2001, A Heat Transfer Textbook, Third Edition, Cambridge, Massachusetts, U.S.A. http://web.mit.edu/lienhard/www/ahtt.html

[17]AQTN, ARKIVI QËNDROR TEKNIK I NDËRTIMIT.[CENTRAL TECHNICAL BUILDING ARCHIVE].

[18] KTP-N.2-89. 1989. Kusht teknik projektimi per ndertimet antisizmike KTP-N.2-89 [Technical design code for earth-quake-resistant construction KTP-N.2-89]. Tirana, Albania: Akademia e Shkencave.

[19] AKADEMIA E SHKENCAVE & MINISTRIA E NDERTIMIT. (1990). Udhezues Metodik per llogaritjen ne sizmicitet te konstruksioneve ndërtimore.[Methodical guide for calculating the seismicity of building constructions].Tirane. 1990.

STRUCTURAL MONITORING TECHNOLOGY FOR OPERATIONAL/BUSINESS CONTINUITY AND RESILIENCE

Mauricio Ciudad-Real [(1)], Derek Skolnik [(2)], Khalid Saifullah [(3)]

[(1)] *VP Earthquake Engineering, Kinemetrics, Inc., mcr@kmi.com*
[(2)] *Senior Project Manager, Kinemetrics, Inc., das@kmi.com*
[(3)] *Project Engineer, Kinemetrics, Inc., mks@kmi.com*

Abstract

Large earthquakes are expected to cause structural damage even in modern buildings in full compliance with current design codes. While presumably safe, these and the much more frequent moderately sized earthquakes, can still negatively affect critical structures' function. For example, hospitals, by distressing staff and patients as well as supporting systems such as critical utilities, medical gases, and surrounding infrastructure (e.g. roads/bridges). Energy producing facilities, may overact shutting down plant functions or initiating evacuations which potentially costs millions of dollars in business interruption.

Today most earthquake instrumented structures focused their purpose on recording structural responses to damaging and potentially damaging earthquakes. This recorded data is then used to further understanding of actual building dynamic behavior, ultimately leading to advancements in research (e.g., damage detection) and building codes (e.g., improved empirical relations), Goel and Chopra [1]. Over time, owners, residents, and operators indirectly benefit from this work by owning, residing, operating safer structures. However, there is opportunity to benefit directly from structural monitoring technology. Advances in technology and client-based information-driven services have led to proven applications of structural monitoring in support of operational/business continuity ultimately contributing to resilience.

Although this concept of using earthquake recorded data to the benefit of building owners has been considered in the past, Celebi et.al. [2], there has only been a few implementation cases as a holistic, commercially viable solution for operational/business continuity, as a result of strategic industry partnerships (e.g., technology provider, engineering consultant, etc.), academia, and a growing knowledge and experience on the topic; mostly in the Middle East, Skolnik et.al. [3].

This paper will present commercially available technology platforms comprised of advanced sensing, performance-based engineering, centralized command console tied to mobile check-in, standard-based safety inspection tools, as well as training and certification. Implementation is illustrated with deployments at Hospitals and Energy producing facilities around the world.

Keywords: Structural Monitoring, Performance-Based Engineering, Earthquake Operational/Business Continuity, Resilience

1. Introduction

Critical and essential facilities such as hospitals, military installations, and financial institutions, cannot easily evacuate immediately after an earthquake or wait for a detailed safety assessment to reoccupy and resume operations. Post-disaster occupancy decisions are difficult, especially under such stressful conditions, and can have dire consequences if made hastily or too slowly (e.g. panic related injuries, losses due to unnecessary downtime, etc.) Examples of avoidable financial loss and injury ultimately due to uninformed decision-making are easily found across areas of low and high seismicity, Skolnik et.al. [3].

Hospitals and medical facilities, in particular, have a profound need to maintain building operational status and function in the aftermath of strong earthquakes to allow continued care for current patients and also to receive new patients injured by the disaster, Celebi et.al. [2], Wilson et.al. [4]. However, large earthquakes are expected to cause structural damage even in modern hospitals in full compliance

with current design codes. While presumably safe, these and the much more frequent moderately sized earthquakes, can still negatively affect a hospitals' function by distressing staff and patients as well as supporting systems such as critical utilities, medical gases, and surrounding infrastructure (e.g. roads/bridges). To ensure the shelter-in-place directive during earthquakes and continue to deliver on their mission, healthcare providers must confidently make rapid decisions often with little knowledge of the actual impact on their systems and resources.

On the other hand, at energy producing facilities such as nuclear plants, when an earthquake occurs, ground motion data recorded by the seismic instrumentation is used to make a rapid assessment of the degree of severity of the seismic event (required by regulators within 4 hours). This, combined with information from a plant walkdown (within 8 hours), is used to make the initial determination of whether the plant must be shutdown, if it has not already been shut down by operational issues resulting from the seismic event itself. If on the basis of these initial evaluations it is established that the plant shutdown criteria have not been exceeded, it is presumed that the plant will not be shut down or could restart following a post-trip review, if it tripped off-line because of the earthquake.

This assumes that seismic instrumentation is operable, otherwise determination of whether the plant must shutdown is solely based on the size and proximity to the earthquake, increasing the potential for millions of dollars in losses, due to business interruption. Similar requirements are imposed to LNG facilities.

Today, most instrumented buildings and facilities with seismic and structural health monitoring systems focused the purpose of this only on the recording structural responses to damaging and potentially damaging earthquakes, like is the case in California with the State of California Strong Motion Instrumentation Program and in the United States with the USGS National Strong Motion Project. However, there is opportunity to benefit directly from structural monitoring technology and that has been demonstrated with commercially available platforms such as Kinemetrics' OasisPlus, KMIDam, KMI-LNG, and KMIBridge. These platforms take advantage of advances in technology and client-based information-driven services leading to proven implementations of structural monitoring in support of operational/business continuity, which ultimately contribute to resilience.

In this paper we present such commercially available technology platforms comprised of advanced sensing, performance-based engineering, centralized command console tied to mobile check-in, standard-based safety inspection tools, as well as training and certification. Implementation of such platforms, is illustrated with deployments at Hospitals and Energy producing facilities around the world.

2. Background

Uninformed decision-making during an earthquake increases the potential for panic, injuries, and puts hospital patients at risk.

When an earthquake hits, disaster preparedness and response professionals have to move quickly. They are expected to make dozens of real-time decisions affecting patient safety, response procedures, and the continued operation of the hospital. Where should they send their resources first? Are the patients safe? What is the status of the critical services? These decisions have to be made quickly, and often without any real information.

Is the hospital safe to occupy? How do emergency managers know? What if it didn't have to be like this? What if they had the critical information needed at their fingertips? What if they had everything needed to make informed decisions, and respond quickly?

In the case of the energy producing facilities, such as LNG plants, decisions during an emergency are too important to make without the right information. Targeting response to the correct actions can be difficult, especially when time and accuracy are critical. In these situations, real-time information on potentially damaging ground motion is crucial to initiating the proper emergency response procedures.

At the same time, catastrophic losses could result from interrupted operations at LNG facilities during earthquakes if overreacted. Therefore, accurate assessment of structural impact, and informative alerts are critical to safe and efficient operation of these facilities during an emergency.

Decisions must be made quickly and responsibly to maintain operational continuity.

3. Solution: Oasisplus Platform

OasisPlus Earthquake Business Continuity, is a technology platform designed to provide the tools and information needed before, during, and after an earthquake to minimize impact and ensure an effective emergency response.

As a complete earthquake response platform for hospitals, OasisPlus delivers the tools and information needed to help ensure a coordinated, effective response to earthquakes to promote rapid safety assessments, help making informed decisions, and protect patient safety.

This allows for:

- Avoid Evacuations. Avoid unnecessary evacuations to protect patients and secure ongoing critical operations.
- Decision Making. Enable better-informed decision making to target emergency response to areas that need it most.
- Real-Time Monitoring. Understand the impact to the hospital building and know the condition of the patients in real time.
- Emergency Response. Leverage OasisPlus in hospital existing emergency response procedures, including Hospital Incident Command System (HICS).

OasisPlus delivers business continuity based on five key elements:

1. Advanced Sensing Technology. Implement advanced sensing technology to acquire essential data during shaking, and rapidly deliver actionable information to key decision makers, regardless of location.
2. SAFE Reports. SAFE Reports use the hospital structural monitoring instrumentation to deliver immediate information on the expected impact to everything important within the building immediately after an earthquake.
   - Structural Systems: the building itself
   - Non-structural Systems: architectural systems, mechanical, electrical, plumbing, & building contents
   - Occupants: patients, staff, and visitors
3. Command Console. Real-time information from sensors, injury & hazard reports, and occupant check-ins are presented via the console, enabling your response team to better manage the situation.
4. Mobile App. Your response team can check-in, report injuries or hazards, and receive instructions via the mobile app, simplifying communication to speed up decision-making and response.
5. Platform for Informed Decision-Making. OasisPlus delivers critical information you need to be confident in your decisions, provides situational awareness through real-time data, and promotes effective coordination of your emergency response in a manner compatible with your existing emergency response procedures.

This solution has been already implemented in various hospitals in the Western US and more recently deployed at a Children's Hospital in Seattle, Washington.

4. Case Study: Seattle Children's Hospital, Washington

In 2019, Kinemetrics, Inc. and Reid Middleton began work on the first OasisPlus implementation for a US Privately owned hospital, the Seattle Children's Hospital (SCH). The ever-expanding SCH campus,

located in Northeast Seattle, is composed of 15 seismically independent buildings ranging in elevation and height (up to 9 stories), and totalling over 1.2M square-feet. Several major expansions followed the initial 1951 building. In terms of occupancy and use, the hospital is based on four major areas with kid-friendly names (Forest, River, Mountain, and Ocean) each divided into wings (e.g., A, B, C) with uniform floor naming across all buildings. The complexity of the campus layout, coupled with structural systems ranging in type, size and vintage, posed unique challenges for instrumentation, engineering evaluation, and information dissemination. Figure 1 below illustrates our approach and Figure 2 shows the implemented Safe Report.
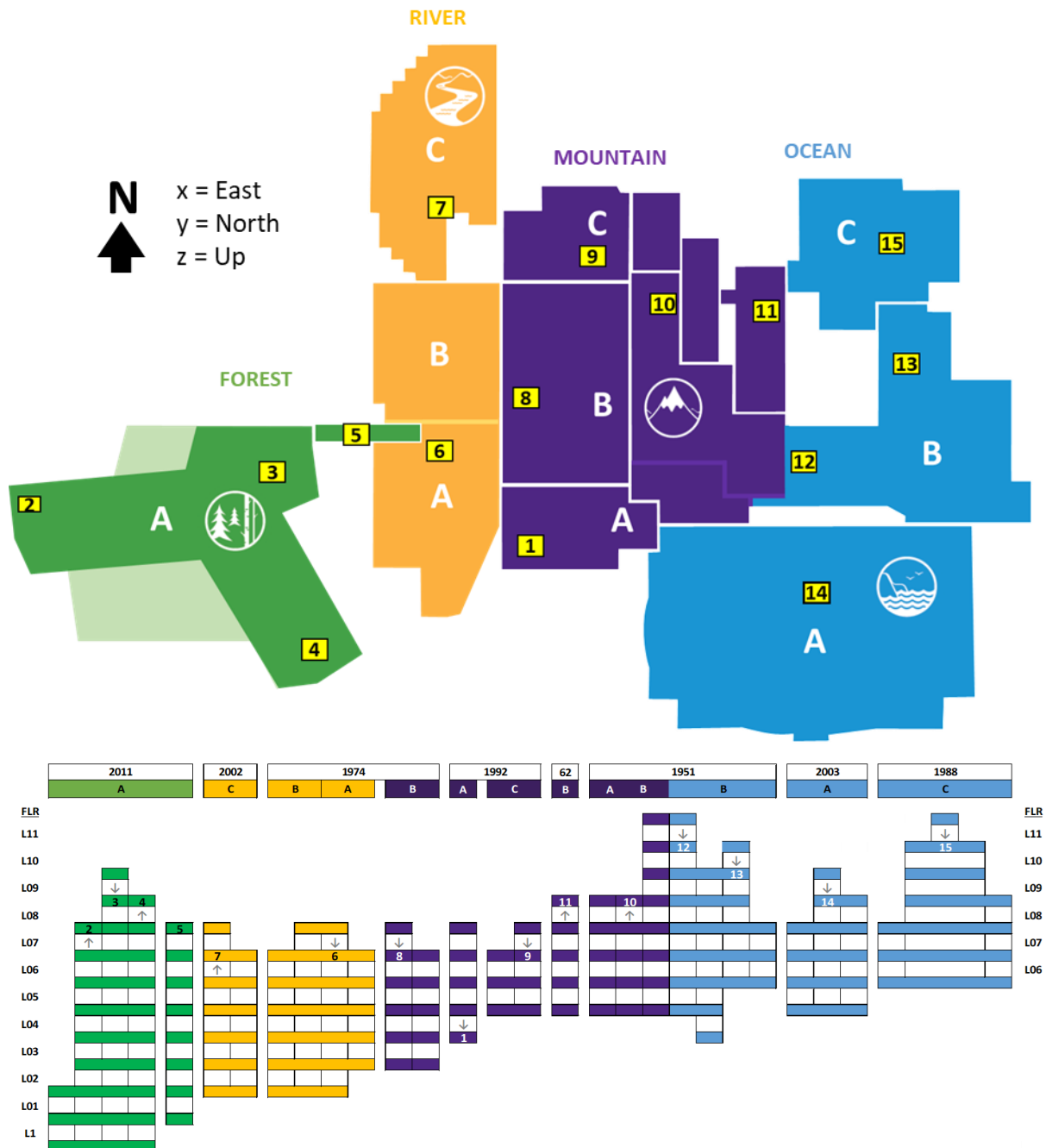
Figure 1. Seattle Children's Hospital OasisPlus Project Approach.

In terms of instrumentation, fifteen Etna2 Accelerographs were installed, one centrally located on the "base" and fourteen on the roof or upper levels.
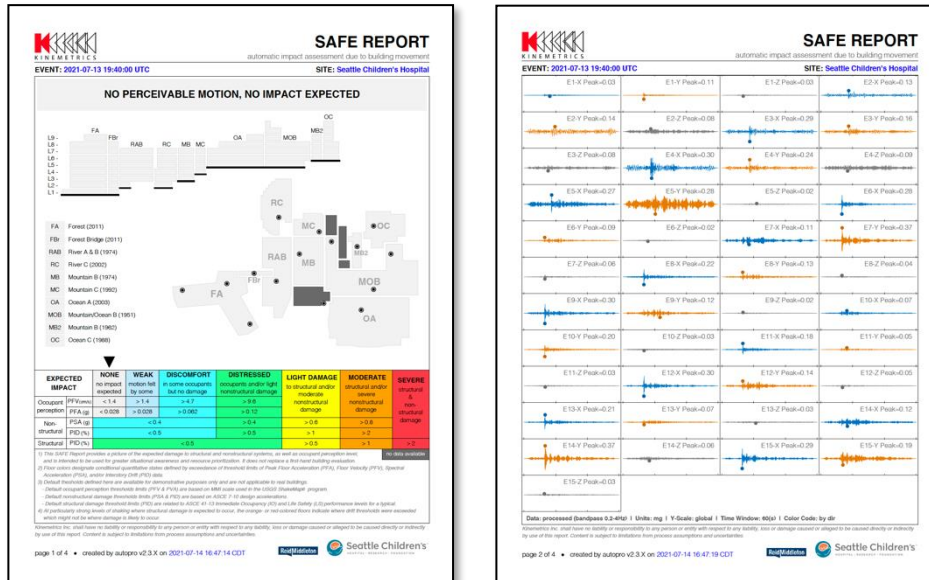
Figure 2. Seattle Children's Hospital OasisPlus' SAFE Report.

5. Solution: KMI-LNG Platform

KMI-LNG from Kinemetrics is a technology platform that enables operators to meet all their seismic-event related needs via one simple, standardized solution. Leveraging a combination of smart sensing, LNG-focused processing tools, and compliance with all industry and regulatory standards, KMI-LNG provides immediate feedback during events, to enable operators to make better decisions in driving their emergency procedures.

KMI-LNG is designed to meet the specific needs of LNG industry. It delivers seismic-event data recording, automatic retrieval, analysis and notification via hardware alarms, reports, and state-of-heath hardware monitoring with maximum effectiveness and ease of use from a single system.

Aimed at removing the guesswork from emergency response in LNG facilities, KMI-LNG quickly responds when a seismic event occurs delivering the information and tools required to enable LNG facility operators to make the most informed decisions possible.

Featuring comprehensive event-analysis and alarm-notification capabilities, this solution drastically reduces the time required for proper data analysis following a seismic event.

High reliability is ensured through redundancy of critical components, such as data storage, along with the confidence provided by the industry standard Rock+ family of recorders with phenomenal predicted MTBF values, over 1M hours.

KMI-LNG is delivered fully qualified to meet or exceed all applicable industry and regulatory standards with these key features.

- Automatic OBE/SSE & CAV analysis & alarm generation within minutes of seismic events.
- Hardware alarm notifications and easy integration with plant's DCS
- PDF file report generation.
- Easy maintenance – extensive built-in testability.

- Complete networking supports – could use plant's local area network to remotely control and monitor the system via TCP/IP protocol.
- Designed to meet all industry standards IEEE 344, CSA ATEX and IECEx, etc.

6   Case Study: Chevron Wheatstone LNG Project, Western Australia

Owned by Chevron and designed by Bechtel, the Wheatstone LNG Project is part of Western Australia's first natural gas hub and set to become one of the largest resource projects – providing greater security of supply in the Asia-Pacific region.

To ensure safe operations the project design included provisions for earthquakes and required seismic monitoring to assess plant condition after an earthquake and to determine if Operating Basis Earthquake (OBE) limits have been exceeded to continue operations safely or initiate emergency response procedures such as inspections or plant's safe shutdown if Safe Shutdown Earthquake (SSE) limits were exceeded.

The Kinemetrics KMI-LNG's CONDOR System deployed in 2015, monitors the free-field ground motions as well as the foundation and roof responses of one of the LNG tanks due to earthquakes and determines, in real-time, whether these have or have not exceeded the plant's OBE design requirements.

The system's Alarm Panel provides visual indication of the current state of the system with LED indicators and relay contacts are interfaced with the plant's Distributed Control System (DCS) for integration with other systems and functions at the plant.

Please refer to Figure 3 for a sample of a KMI-LNG's CONDOR SAFE Report.
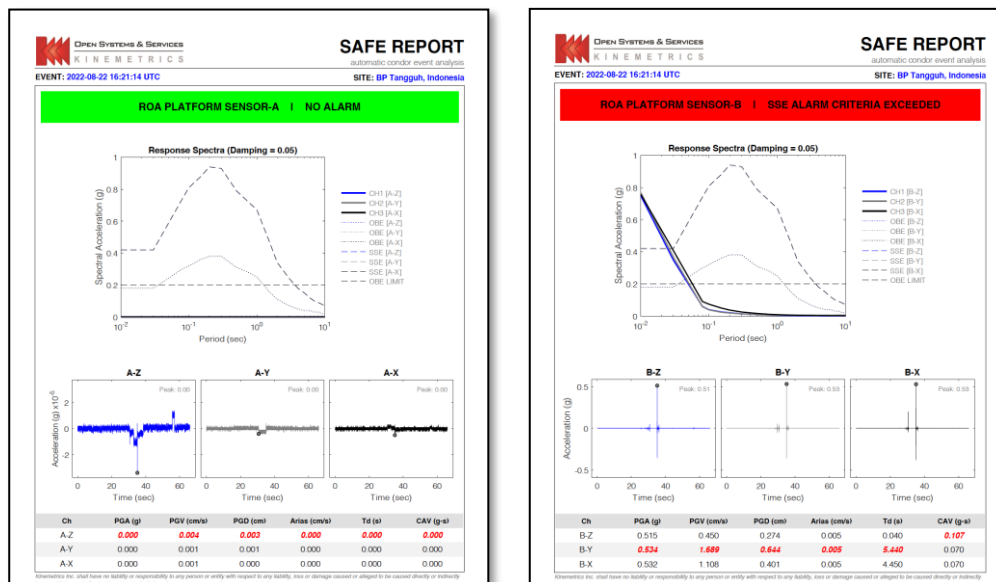
Figure 3. Sample KMI-LNG's CONDOR SAFE Report

7. Conclusions

Business/operational continuity comes from better-informed decision making and effective information dissemination. Commercially available technology platforms such as OasisPlus and KMI-LNG presented in this paper, are the solution to avoiding costly and potentially dangerous over-reaction by enabling better-prepared emergency response team members.

Such technology platforms are comprised of advanced sensing, performance-based engineering, command and control capabilities, tied to a mobile app, when applicable, or to a facility Distributed Control System (DCS), in the case of the energy producing sector, as well as standard-based safety inspection tools for a comprehensive and integrated monitoring.

Acknowledgements

References

[1] Goel, R.K., Chopra, A.K. (1997): Period Formulas for Moment-Resisting Frame Buildings, *Journal of Structural Engineering,* **123** (11), 1454-1461

[2] Celebi, M., Sanli, A., Sinclair, M., Gallant, S., Radulescu, D. (2004): Real-Time Seismic Monitoring Needs of a Building Owner-and the solution: A Cooperative Effort. *Earthquake Spectra,* **20** (2), 333-346

[3] Skolnik, D.A., Ciudad-Real, M., Swanson, D.B., Bishop, E. (2017), Improving Business Continuity for UAE Buildings Using SHM and PBEE-Based Rapid Evaluation, *16th World Conference on Earthquake Engineering*, Santiago, Chile

[4] Wilson, D.R., Kent, R.D., Stanek, S., Swanson, D.B. (2004) Rapid Evaluation and Assessment Checklist Program (REACH) – A Case Study at Naval Hospital Bremerton. *13th World Conference on Earthquake Engineering*, Vancouver, Canada

SEISMIC ANALYSIS OF ANCIENT MASONRY TOWERS

Ivan Balić [(1)], Nikolina Živaljić [(2)], Hrvoje Smoljanović [(3)], Ante Munjiza [(4)], Boris Trogrlić [(5)], Valentina Štefković [(6)], Ana Livaja [(7)]

[(1)] *Associate Professor, University of Split, Faculty of Civil Engineering, Architecture and Geodesy, ivan.balic@gradst.hr*
[(2)] *Associate Professor, University of Split, Faculty of Civil Engineering, Architecture and Geodesy, zivaljic@gradst.hr*
[(3)] *Associate Professor, University of Split, Faculty of Civil Engineering, Architecture and Geodesy, hsmoljanovic@gradst.hr*
[(4)] *Full professor (tenure), University of Split, Faculty of Civil Engineering, Architecture and Geodesy, amunjiza@gradst.hr*
[(5)] *Full Professor, University of Split, Faculty of Civil Engineering, Architecture and Geodesy, boris.trogrlic@gradst.hr*
[(6)] *M. Sc. CE. Student, University of Split, Faculty of Civil Engineering, Architecture and Geodesy, vstefkovic@gradst.hr*
[(7)] *M. Sc. CE. Student, University of Split, Faculty of Civil Engineering, Architecture and Geodesy, ana.livaja@gradst.hr*

Abstract

In this paper, numerical analysis of several historical masonry towers located in Italy was conducted. The towers differ in their geometric characteristics in terms of slenderness, thickness of the outer walls, the proportion of openings, while the material properties of all towers are similar.

The purpose of this paper was to analyse the influence of various geometries, soil properties and types of earthquakes on the seismic resistance of masonry structures. The geometries of the towers were taken from the available literature.

The analysis was carried out with the planar numerical model Y-2D, which is based on the finite-discrete element method (FDEM). The towers were discretized at the macro level using triangular three-node finite elements between which contact elements were implemented that take into account material nonlinearity.

The discretization of the towers was carried out at the macro level, taking into account the averaged properties of the mortar and blocks. This is modelled using triangular three-node finite elements between which contact elements are implemented to consider material nonlinearity. In this way, the phenomenon of the initiation and propagation of cracks in the tension and shear was modelled.

An incremental dynamic analysis was performed for three real earthquakes until the complete collapse of the structure. In each increment, the appearance of the first cracks, the propagation of the cracks, as well as the failure mode of the structure were monitored.

The performed numerical analyses highlight the suitability of the FDEM method in the analysis of the seismic resistance of masonry structures.

The conclusions reached in this paper can serve as guidelines for engineers in assessing the seismic resistance of existing masonry structures.

Keywords: historical structures, masonry tower, finite discrete element method, seismic resistance.

1. Introduction

Masonry towers represent an important portion of the built heritage. For that reason, their seismic resistance assessment against earthquakes appears to be of relevant importance for historical reasons. Two existing masonry towers, located in the north Italy are analysed in the presence of seismic excitation (Fig. 1). The geometry of towers is deduced from literature [1]. On the basis of such geometrical data 2D numerical models were built, where different thicknesses are assigned to adjoining elements. The analysis was carried out with the planar numerical model based on the finite-discrete element method (FDEM).

(a)   (b)
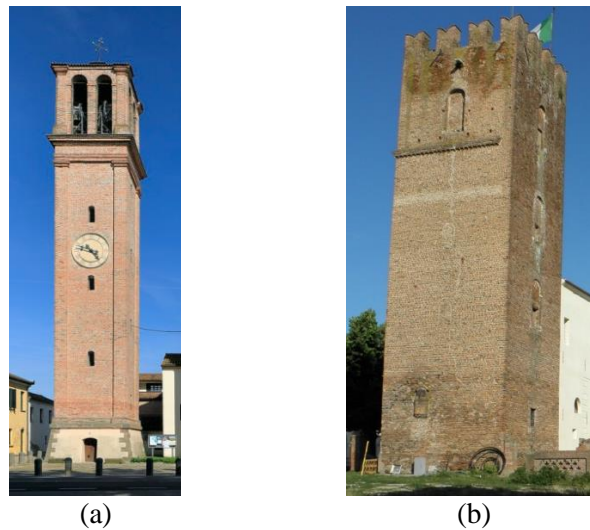
Figure 1. Towers: a) bell tower A located in Vescovana, b) military defence tower B located in Arquà Polesine.

2. Numerical analysis

2.1 Finite-Discrete Element method

Combined Finite-Discrete Element method is intended for the dynamic analysis of a large number of mutually interacting discrete elements, where the elements can fracture and fragment thus increasing the total number of discrete elements [2]. Within FDEM, each discrete element is discretised with its own finite element mesh thus enabling the deformability of discrete elements. Fracture and fragmentation processes are also implemented within the finite element mesh. The mass of discrete elements is lumped into the nodes of finite elements, while the time integration of the motion equation is applied node by node and degree-of-freedom by degree-of-freedom. This is performed in explicit form by using the central difference time integration scheme. The contact forces resulting from the interaction process between two discrete elements are determined by the numerical representation of contact impact, which is executed by employing contact detection and contact interaction procedures [2-4].

The model for fracture and fragmentation, adopted within FDEM is actually a combination of smeared and discrete crack approaches [5]. It was designed with the aim of modelling progressive fracture and failure including fragmentation and of creating a large number of rock fragments. For that purpose, the strain softening which appears in the material after reaching the tensile or shear strength is described in terms of displacement.

In all previous analyses [6-8], this method proved to be very suitable for numerical analyses of masonry structures exposed to dynamic loading. Therefore, it very well describes all the phenomena of the behaviour of the masonry structure exposed to seismic load, such as the formation and propagation of cracks, energy dissipation, the mode of failure, as well as the complete collapse of the structure.

2.2 Description of the numerical model

Historical masonry towers located in Italy presented in this paper (Fig. 1) were made of small clay bricks with low tensile strength [1]. In order to shorten the calculation time, the calculation was made at the macro level, which means that the discretization of each block and mortar was not performed separately, but the discretization of the structure was made by an irregular finite element network with average properties in terms of modulus of elasticity, tensile strength and shear to expect for this type of structure. For the purposes of numerical analysis, the tower A is discretized with 5073, while tower B with 5926 triangular finite elements [9,10].

The geometry of the models is shown in Fig. 2 (a) and (b), and the finite element mesh used in the numerical analyses in Fig. 2 (c) and (d). Contact elements have been implemented between the finite elements for the purpose of simulating the initiation and propagation of cracks in the structure.

The tensile strength of the contact elements taken was selected in the amount of 0.27 MPa, and the shear strength in the amount of 1.08 MPa. The coefficient of friction was adopted in the amount of 0.7. The modulus of elasticity of finite elements was chosen in the amount of 22500 MPa and the Poisson's ratio in the amount of 0.3. A simplified 2D discretization of the towers is adopted by assuming for the elements, whenever necessary, different thicknesses.
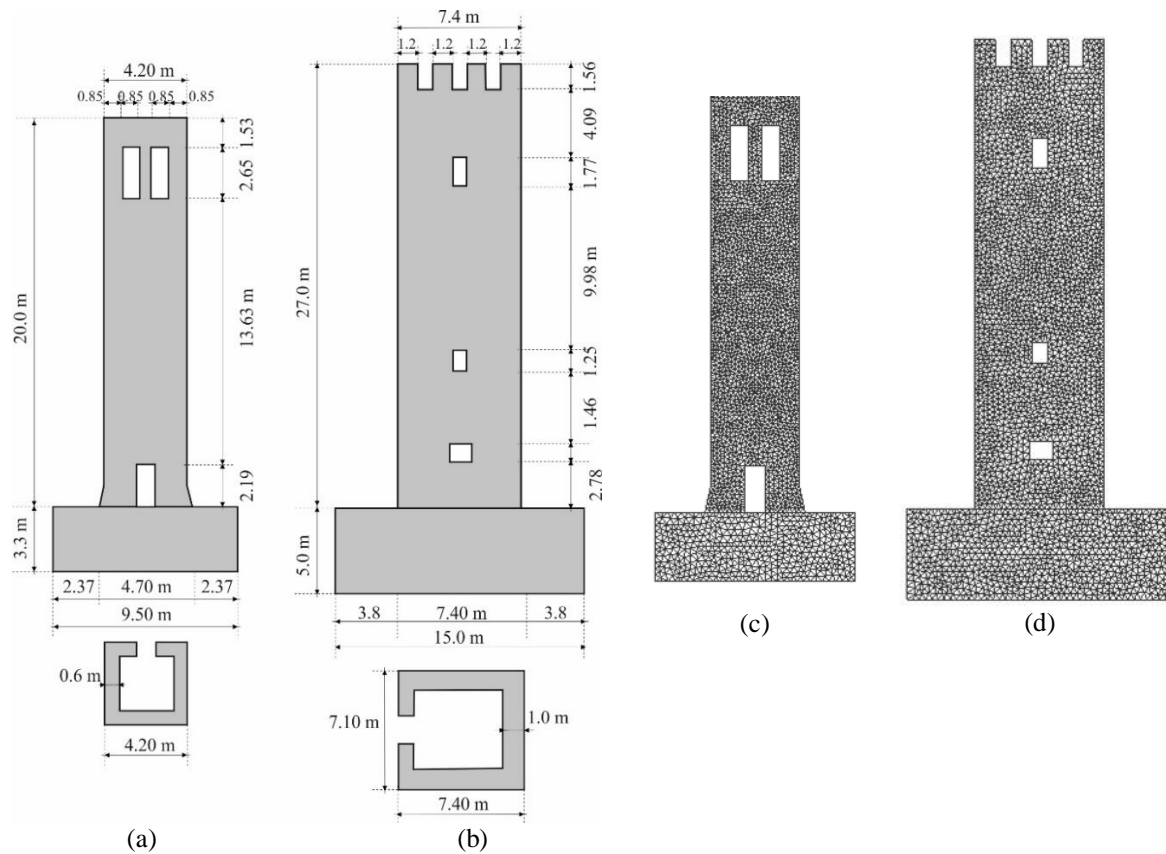
Figure 2. Geometry of tower: a) A; b) B; Discretization of tower: c) A; d) B.

In presented numerical analyses, the structures were exposed to horizontal and vertical ground acceleration (Fig. 3a and Fig. 3b) which was recorded on 15. April 1979. during an earthquake with the epicentre in Petrovac (Montenegro).
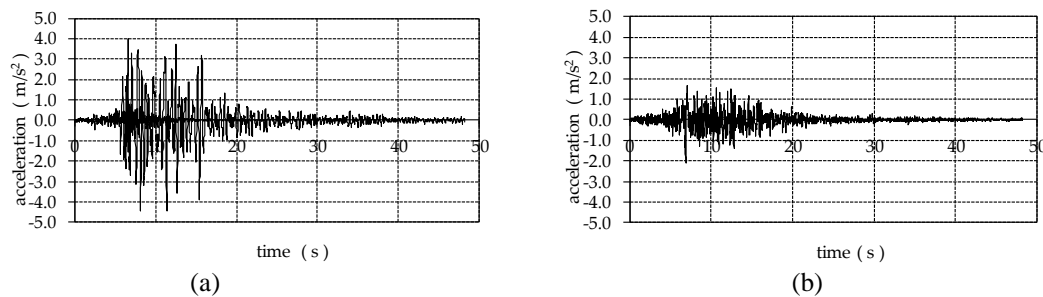
Figure 3. Accelerograms of the earthquake in Petrovac recorded on 15 April 1979.: (a) horizontal north-south direction; (b) vertical direction.

3. Results and conclusion

In this paper, an incremental dynamic analysis of masonry towers for two different support conditions, elastic and rigid base, was performed.

The displacement of the top of the tower A on elastic base under different peak ground accelerations are shown in Fig. 4, while the initiation and propagation of the cracks that appeared in this numerical model during the action of the given accelerogram (with the largest ordinate 0.7g) are shown in Fig. 5.
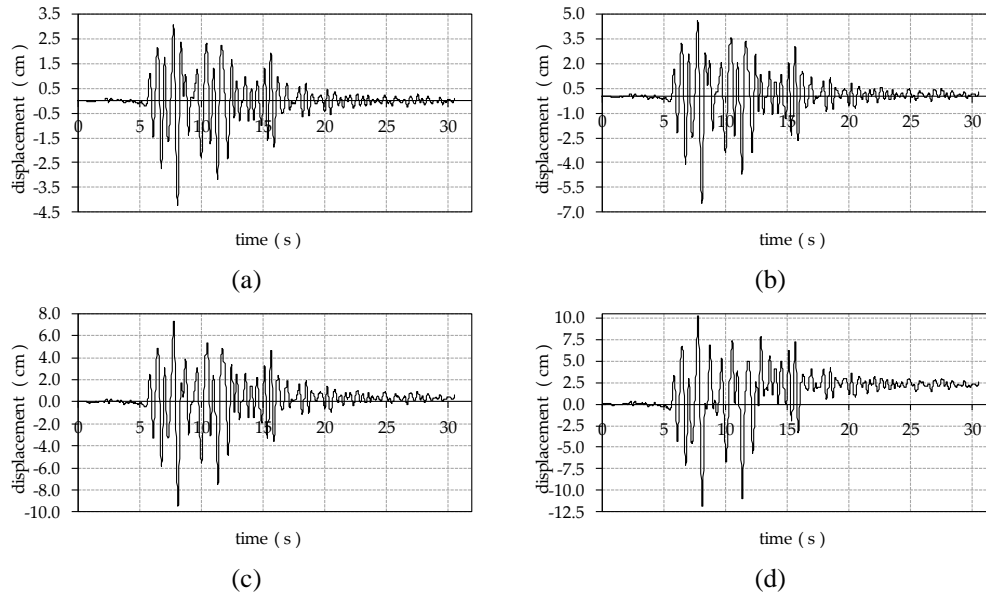
Figure 4. Displacement of the top of the tower A on elastic base under the peak ground acceleration of: (a) a_g=0.15 g; (b) a_g=0.30 g; (c) a_g=0.45 g; (d) a_g=0.60 g.
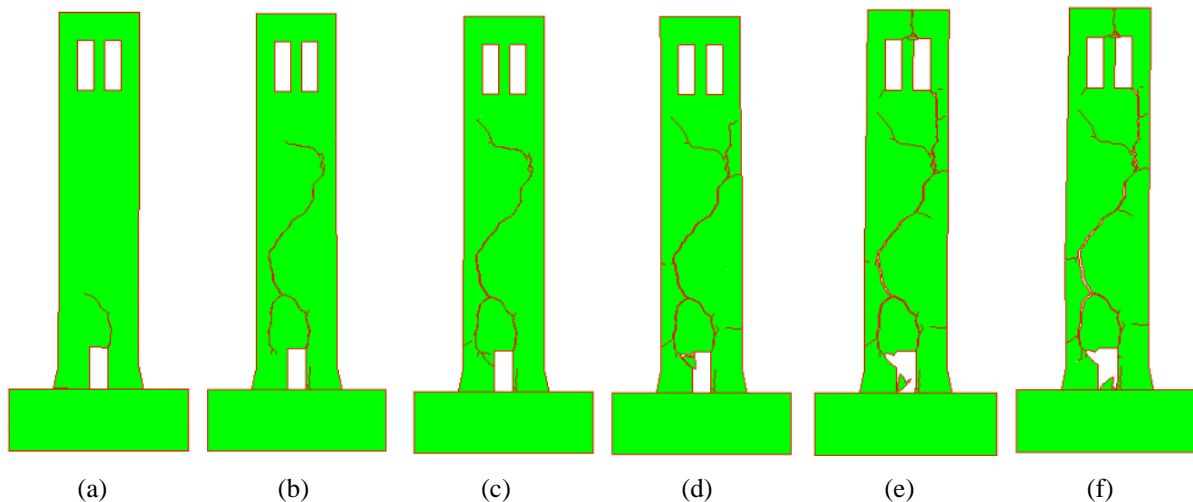
Figure 5. Crack pattern of the tower A on elastic base for acceleration ($a_{g.max.}$= 0.70 g) in time: (a) t = 7.9 s; (b) t = 8.5 s; (c) t = 9.5 s; (d) t = 14.5 s; (e) t = 32.0 s; (f) t = 48.2 s.

The displacement of the top of the tower A on rigid base under different peak ground accelerations are shown in Fig. 6, and the cracks of observed tower during the action of the given accelerogram (with the largest ordinate 0.5g) are shown in Fig. 7.
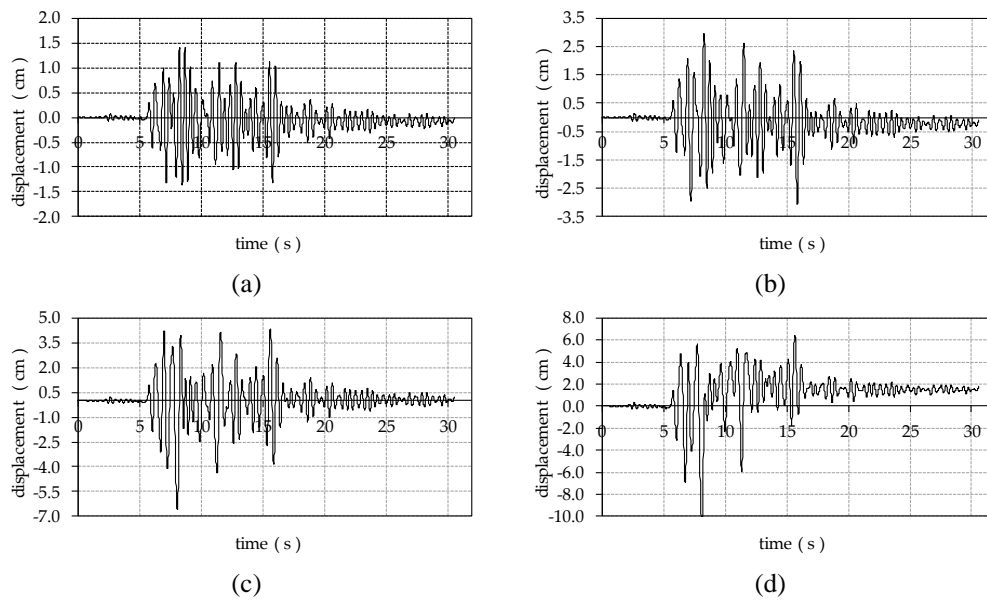
Figure 6. Displacement of the top of the tower A on rigid base under the peak ground acceleration of: (a) a_g=0.10 g; (b) a_g=0.20 g; (c) a_g=0.30 g; (d) a_g=0.45 g.
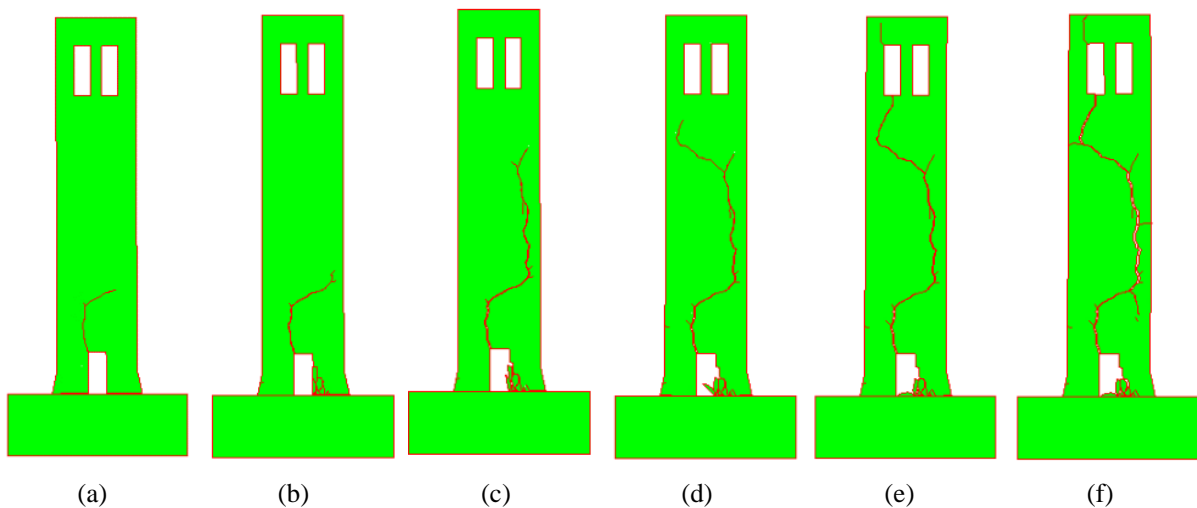
Figure 7. Crack pattern of the tower A on rigid base for acceleration ($a_{g.max.}$= 0.50 g) in time: (a) t = 8.0 s; (b) t = 8.3 s; (c) t = 8.5 s; (d) t = 9.5 s; (e) t = 9.8 s; (f) t = 48.2 s.

In Fig. 8, the displacement of the top of the tower B on elastic base under different peak ground acceleration are shown.
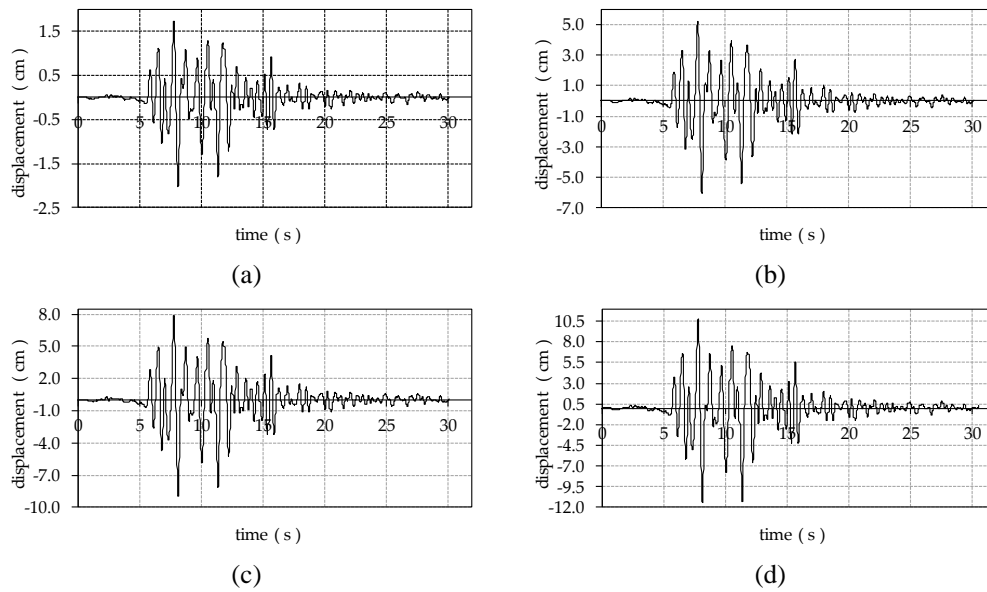
Figure 8. Displacement of the top of the tower B on elastic base under the peak ground acceleration of: (a) a_g=0.10 g; (b) a_g=0.30 g; (c) a_g=0.45 g; (d) a_g=0.60 g.

The initiation and propagation of the cracks that appeared in presented numerical model for tower B, during the action of the given accelerogram (with the largest ordinate 0.65g) is shown in Fig. 9.
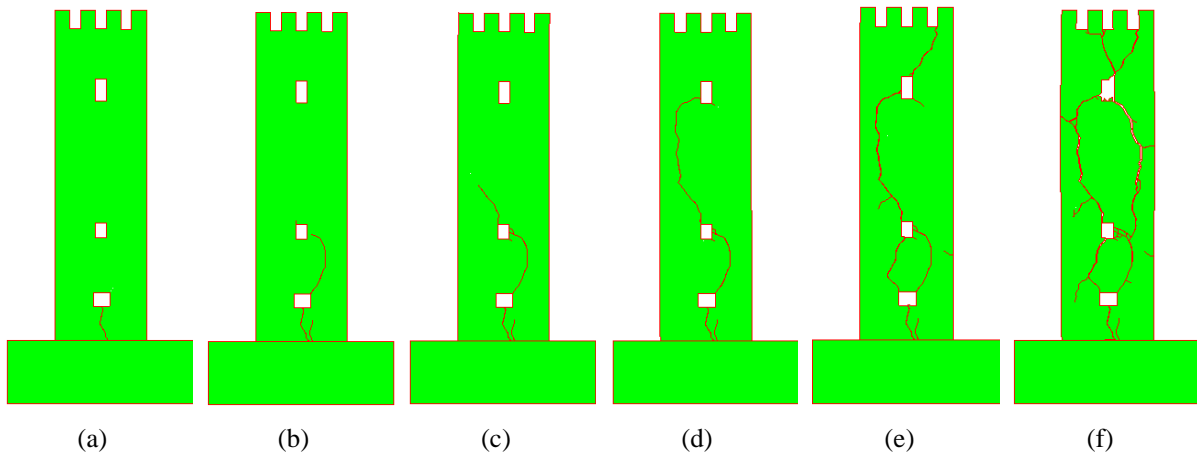
Figure 9. Crack pattern of the tower B on elastic base for acceleration ($a_{g.max.}$= 0.65 g) in time: (a) t = 9.0 s; (b) t = 11.8 s; (c) t = 12.0 s; (d) t = 12.3 s; (e) t = 13.0 s; (f) t = 17.0 s.

In Fig. 10, the displacement of the top of the tower B on rigid base under different peak ground acceleration are shown, while the cracks that appeared for the observed tower, during the action of the given accelerogram (with the largest ordinate 0.45g) is shown in Fig. 11.
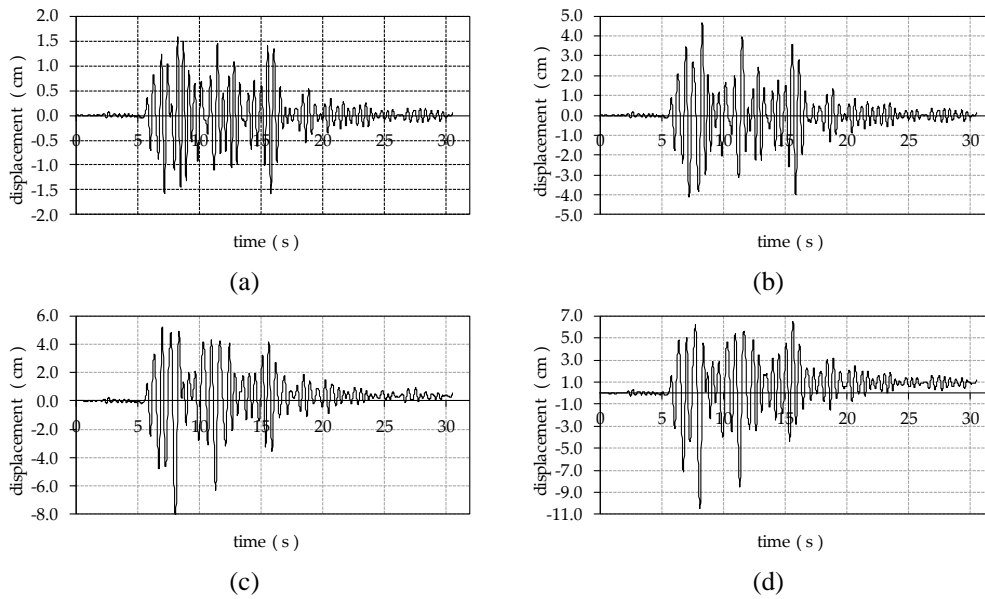
Figure 10. Displacement of the top of the tower B on rigid base under the peak ground acceleration of: (a) a_g=0.10 g; (b) a_g=0.25 g; (c) a_g=0.35 g; (d) a_g=0.44 g.
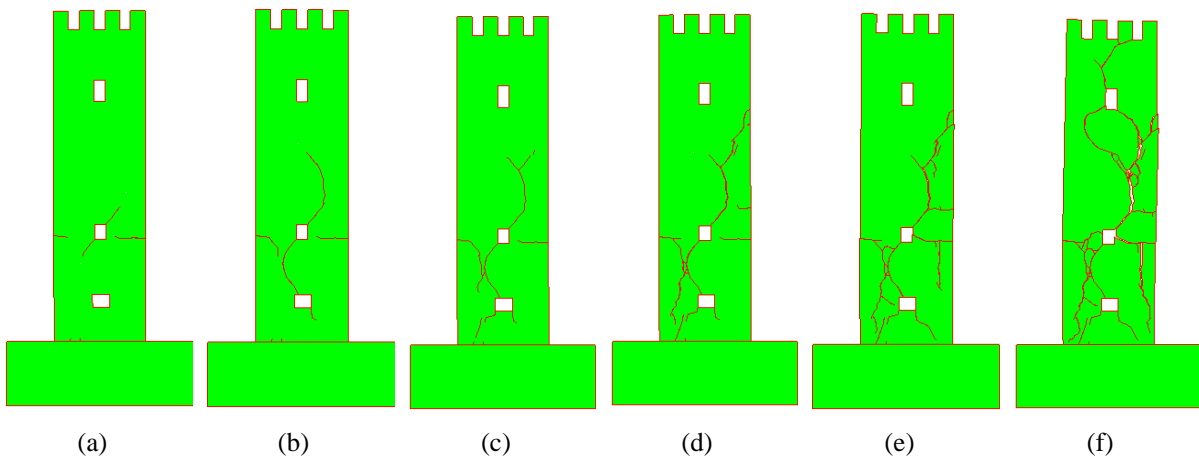
Figure 11. Crack pattern of the tower B on rigid base for acceleration ($a_{g.max.}$= 0.45 g) in time: (a) t = 8.3 s; (b) t = 8.5 s; (c) t = 10.2 s; (d) t = 11.5 s; (e) t = 12.0 s; (f) t = 17.0 s.

Figure 12 presents the comparison of the displacements for different peak ground acceleration on elastic and rigid base.
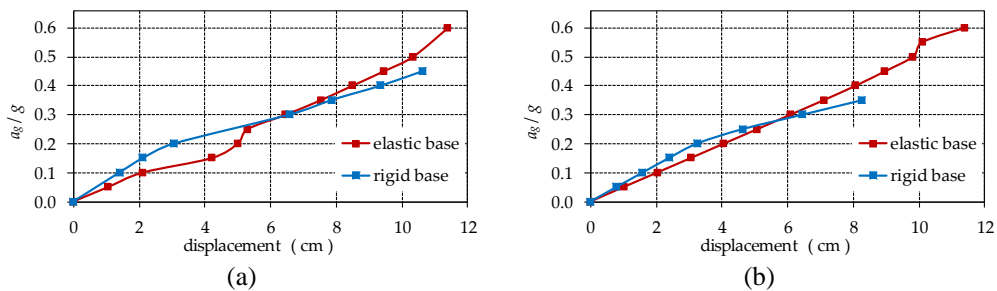
Figure 12. Displacement for different peak ground accelerations on rigid and elastic base for tower: (a) A; (b) B.

From the presented results, it can be seen that the tower on the elastic base has a higher seismic resistance in comparison to the tower on the rigid base. Also, the displacements achieved at the top of the tower are greater for the type of support on an elastic base.

Acknowledgements

References

[1] Casolo, S., Milani, G., Uva, G., Alessandri, C. (2013): Comparative seismic vulnerability analysis on ten masonry towers in the coastal Po Valley in Italy. *Engineering Structures*, **49**, 465-490, doi: https://doi.org/10.1016/j.engstruct.2012.11.033

[2] Munjiza, A. (2004): *The combined finite-discrete element method*. John Wiley & Sons, London. U.K.

[3] Munjiza, A., Andrews, K.R.F. (1998): NBS contact detection algorithm for bodies of similar size. *International Journal for Numerical Methods in Engineering*, **43** (1), 131-149, doi: https://doi.org/10.1002/(SICI)1097-0207(19980915)43:1%3C131::AID-NME447%3E3.0.CO;2-S

[4] Munjiza, A., Andrews, K.R.F. (2000): Penalty function method for combined finite-discrete element system comprising large number of separate bodies. *International Journal for Numerical Methods in Engineering*, **49** (11), 1377-1396, doi: https://doi.org/10.1002/1097-0207(20001220)49:11%3C1377::AID-NME6%3E3.0.CO;2-B

[5] Munjiza, A., Andrews, K.R.F., White, J.K. (1998): Combined single and smeared crack model in combined finite-discrete element method. *International Journal for Numerical Methods in Engineering*, **44** (1), 41-57, doi: https://doi.org/10.1002/(SICI)1097-0207(19990110)44:1%3C41::AID-NME487%3E3.0.CO;2-A

[6] Smoljanović, H., Nikolić, Ž., Živaljić, N. (2015): A combined finite-discrete numerical model for analysis of masonry structures. *Engineering Fracture Mechanics*, **136**, 1-14, doi: https://doi.org/10.1016/j.engfracmech.2015.02.006

[7] Smoljanović, H., Balić, I., Trogrlić, B. (2015): Stability of regular stone walls under in-plane seismic loading. *Acta Mechanica*, **226**, 1881-1896, doi: https://doi.org/10.1007/s00707-014-1282-2

[8] Balić, I., Živaljić, N., Smoljanović, H., Trogrlić, B. (2016): Seismic resistance of dry stone arches under in-plane seismic loading. *Structural Engineering Mechanics*, **58** (2), 243-257, doi: https://doi.org/10.12989/sem.2016.58.2.243

[9] Štefković, V. (2022): Seismic analysis of a defensive medieval masonry tower in Italy (in Croatian). *Graduation thesis*. University of Split, Faculty of Civil Engineering, Architecture and Geodesy, Croatia.

[10] Livaja, A. (2022): Seismic analysis tower in Italian province Rovigo by finite and discrete element method (in Croatian). *Graduation thesis*. University of Split, Faculty of Civil Engineering, Architecture and Geodesy, Croatia.

EXPERIENCE ON SEISMIC VULNERABILITY ASSESSMENT AND RETROFITTING OF SUPREME COURT BUILDING

Kirti Tiwari [1], NSET,et al.[2]

[1] *Structural Engineer, National Society for Earthquake Technology-Nepal, Nepal, ktiwari@nset.org.np[1]*

Abstract

The Supreme Court of Nepal is the highest court in Nepal. The Supreme Court of Nepal is an important building, built of brick in mud masonry structure and over 54 years of age which got moderate structural damage due to the recent Gorkha earthquake 2015. The need for safety of the building lying at high seismic zone in Nepal, the Seismic Vulnerability Assessment and Retrofit design was carried out to improve the building response in future earthquakes. The seismic vulnerability of the building was assessed after the following:(a) historical investigation about the building, (b) detailed geometrical investigation, (c) identification of materials by means of surveys and literature indications, (d) Detailed Intrusive Tests, (f) Detail linear static analysis of the building by means of a Finite Element (FE) model. After these steps, the FE model was used to assess the safety level of the building by means of linear static analyses and identifying a proper retrofitting strategy for this building. Both side wall jacketing and splint and bandage in some inner walls using the bar wire mesh was carried out for retrofitting this building.

Keywords: Historical Building, seismic vulnerability, FE modeling, Intrusive test, Retrofit

1. Introduction and Background

The Supreme Court of Nepal is the highest court in Nepal. The Supreme Court of Nepal is an important building, built of brick in mud masonry structure and over 54 years of age which got moderate structural damage due to the recent Gorkha earthquake 2015.
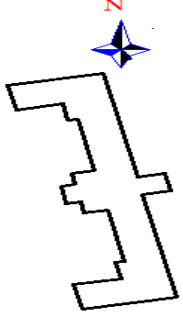
The detail seismic analysis was done based on the best engineering judgment arrived at from the site observation, destructive and non-destructive test carried out at site. Hilti PS 200 Ferroscan detector is used at few possible locations to identify the presence of lintel band on walls. All possible efforts have been made to provide an accurate and authoritative seismic vulnerability assessment and retrofit design of the building in the given circumstances of information provided by the client and limited number of field-tests. Therefore, the accuracy, completeness, or usefulness of the statements made is highly dependent on the accuracy of the information provided.

The detail seismic evaluation for retrofitting design, is carried out based on the first step evaluation of preliminary qualitative assessment of the building by the design team. If the qualitative approach identifies the seismic deficiencies in the building; and possible seismic performance is not up to the acceptable level/criteria, retrofitting design or demolition of the building is suggested. The second step involves the detail seismic evaluation followed by design for seismic strengthening measures as modifications to correct/ reduce seismic deficiencies identified during the evaluation procedure in first step. This is commonly known as seismic retrofitting of the building. Seismic retrofit becomes necessary if the building does not meet minimum requirements of the current Building Code and may suffer severe damage or even collapse during a seismic event [1].

2. Assessment of the Building

The Supreme Court Building is a four-storey brick in mud masonry building constructed on 2019 B.S. The building is almost of E shape, however in the east portion, small wing is projected in the middle. The floor of the building is rigid with reinforced concrete slab and the roof is flexible with CGI sheet covering as well as tile works. The building has many openings and there are very small piers in between openings. The summary of building is given below Table 1.

Table 1:Summary of Building Description

Building Name	The Supreme Court of Nepal	
Location	Ramshah Path, Kathmandu	
G.P. S	27° 41' 48.67" N, 85° 19' 18.65" E	
Terrain type	Plain Land	
Age of the building	Building was constructed in 2019 B.S.	
Type of structure	Brick in Mud Masonry Building	Figure 2.a) South view of the building
No of stories	Four Storied	
Plan configuration	Irregular (Nearly E-shaped in plan with slight projection at back side)	
Vertical configuration	Regular	
Position of the building block	Attached with other buildings with northeast corner and southeast corner	Figure 2.b) West View of the Building
Building dimension	Refer attached drawing	
Total Plinth Area	1610 sq. meters	
Storey height	3.5 m Ground floor and Second floor; 3.25 m first floor; and 3.1 m at the top floor on average	
Wall thickness	All peripheral and main load bearing walls are 530 mm thick however there are walls at few locations having thickness 250mm and 115mm.	
Building condition	Damaged and not occupied after 25th April 2015 Gorkha Earthquake	
Floor structure	Reinforced Concrete Slab with 150mm thick	
Roof Structure	CGI Sheet on steel truss, Clay tiles on steel truss and RC slab at some portion	
Local hazard	No possibilities of rock fall on the site. Not build on infill soil.	Figure 2.c) Building plan

2.1 Damage identification due to Gorkha Earthquake

The first site survey was done on 10th June 2015 and there have been frequent visits after that to prepare the as built drawings as well as to identify and locate cracks/damages in the building. It has been identified that the building has visible cracks in the periphery walls. Most of the peripheral walls have gone diagonal cracking due to in plane action of earthquake forces. Some of the walls have deep vertical and horizontal cracks as well. There are no visible problems of settlement, tilting and cracking in the foundation. There is also a markedly visible deep crack almost along the middle length to the full height of the building. This crack extends from one face to its opposite face (front face to back face). No falling hazard was seen in the site.

Internal walls have also suffered minor to moderate cracks at different locations. At few locations, there is very deep cracks in the slab which needs serious attention. Slab at these portions have gone cracking wider than 10 mm and reinforcements have buckled. The damage picture due to Gorkha Earthquake are shown below in Fig. 2.

Figure 2. a) Heavy vertical crack in the pier; b) Vertical crack in the pier; c) Deep crack in the first floor slab;d) Crack in the slab; e) Crack width of about 20 mm in the wall; f)Vertical crack in the Wall

2.2 Field Investigation

In Situ In-plane Shear Test

Reliable information on shear resistance is needed when performing retrofits and seismic upgrades of masonry buildings. The shear strength of a masonry wall is difficult to measure without resorting to large-scale testing. We cannot carryout destructive tests for evaluating the shear strength of the whole masonry wall of existing buildings. As an alternative, less destructive in-situ tests of single masonry units provide a comparative figure that can be correlated to full-scale wall behaviour. This less destructive alternative is more economical than large-scale testing and is desirable when a building's historic integrity must be maintained.

The in-situ shear test is also known as the push test. It provides a direct measurement of the shear resistance of mortar joints in masonry. The test is suitable for masonry that has relatively strong units and weak mortar so that shear cracks form in the typical stair step pattern along mortar joints and the units remain un-cracked. In this type of construction, the shear strength of the mortar joints limits the shear strength of the masonry wall. Five test locations were selected based on internal and external locations. The test was carried out at 3 locations on the ground floor and 2 locations at first floor which is shown in Fig.3a).

Figure 3 a) Conducting In-situ Shear Test on Wall

The test locations were prepared by removing the brick, including the mortar on one side of the brick to be tested. The head joint on the opposite side of the brick to be tested was also removed. This was done with caution that the mortar joint above or below the brick to be tested is not damaged. The hydraulic ram was inserted in the space where the brick was removed. A steel loading block was placed between the ram and the brick to be tested so that the ram will distribute its load over the end face of the brick. The dial gauge was inserted in the space. The brick was then loaded with the ram until the first indication of cracking or movement of the brick. The ram force and associated deflection on the dial gage were recorded. From the observation, final corrected shear strength of brick masonry is obtained as per ASTM standard and IITK- GSDMA Guideline and the corrected minimum shear strength obtained are 0.054 N/mm2 and 0.036 N/mm2 respectively. The difference in these values from two standards, ASTM[8] and IITK-GSDMA Guideline-EQ06[2], is due to the coefficient of friction between the brick and mortar is assumed as per the site conditions. Being on the conservative side, the value obtained from the GSDMA-EQ6 is used for checking the shear strength capacity.

Table 2 –Calculation of Shear Strength of Masonry Walls from Direct Shear Test

Shear test Number	Coeff.of friction	Overburden pressure	Shear Strength for Sample	Corrected Shear strength (N/mm2)	
	μ	p(N/mm2)		Va=Vte-μ*p	Va= 0.1Vte+0.15Pce/Ah
IP: ST1	0.8	0.1966	0.6437	0.486	0.093857308
IP: ST2	0.8	0.2091	0.4506	0.283	0.076428176
IP: ST3	0.8	0.1985	0.4828	0.324	0.078059031
IP: ST4	0.8	0.1339	0.1609	0.054	0.036172477
IP: ST5	0.8	0.1421	0.2897	0.176	0.050281099
Minimum Corrected Shear Strength				0.054	0.036

Brick Unit Test

Four brick samples were taken from the building wall and compressive strength and water absorption tests were carried out at Central Material Testing Laboratory (Pulchowk Campus), Institute of Engineering which is shown in Fig.3b). The average breaking strength of the three brick samples tested is was 42.51 kg/cm2 (4.17 Mpa) which indicates low strength brick. Water absorption of the three samples are 28.22%, 26.34% and 24.6%. As per the Nepal National Building Code (NBC 109), a first-class hand-made brick shall not absorb more water than 25% of its weight. The brick falls to lower category of second class [9].

Figure 3 b) Compressive Strength Test of Brick Unit performed at CMTL

Direct shear test of soil

Soil samples were taken from two locations, ground excavated for foundation exploration (at the premise of Supreme Court building) to determine the shear strength of soil which is shown in Fig.3c). The cohesion (c) and angle of friction (φ) of the soil below 1m from the existing ground level is found in the range of 0.1 to 0.13 kg/cm2 and 24.130 to 27.140.

Figure 3 c) Soil Sampling for direct shear test of soil

Foundation Inspection

To explore the foundation details of the building, excavation was carried out at three different locations; one at the North West wing (front face) of the building, another at the North-East (back face) and the other at the East (back face) of the building. The details of the foundations is shown in Figure 3 d) and e).The building has strip footings made of brick masonry. The depth of the foundation is same at all locations. Total, depth of strip footing is 4 feet and the width is around 40 inches. There is no plinth band in the walls.
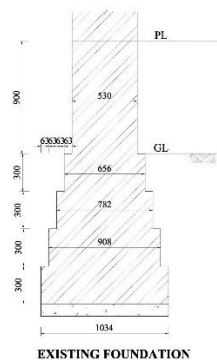
Figure 3 d) Foundation Section of Supreme Court building

Figure 3 e) Foundation Investigation

Investigation of the Brick Masonry Wall

Status of bricks, mortar and lay pattern is important parameter to determine the status of the building. For such purpose, opening of size 450mm x 450mm x450mm were created at two places and observations were recorded. The wall is constructed using burnt clay brick with mud mortar (mixed with bajra, chaku, mash, chun). Average thickness of mortar is 10 mm.All bricks are laid properly with offset along the length and breadth of the wall using an English bond. Brick Lay Pattern in Wall is shown in Fig 3 f)
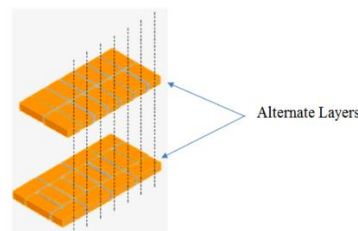
Figure 3 f) Brick Lay Pattern in Wall

2.2 Seismic intervention options for the building under study

The possible intervention options are selected based on the building typology and the expected performance of the building after retrofitting. The best applicable intervention options that are available are selected.

Following retrofitting strategy are adopted in this building:

- Some wing walls are added at strategic locations
- Both side wall jacketing and bandage in some inner walls of wall thickness 4" to provide integrity.
- Vulnerable half brick walls built out of main grid system are tied up.

3. Detailed structural analysis

Finite Element Modelling of the building of Supreme is done by using the structural analysis and design software program ETABS 2015. For the analysis of the system, whole building is modelled. Load bearing brick masonry walls and RC floor slabs are modelled as single layered shell elements. Since the roofing of the building is made of clay tiles in truss, tying element as beams are modelled.

Seismic coefficient method is used to analyse the building. Indian Seismic Code IS 1893:2002 is used for the lateral load calculations and the seismic coefficient value is also compared with the Nepal National Building Code NBC 105:1994. The building plan is shown is Figure 6 while 3D view of the analytical model is shown in Figure 4 a) and b).
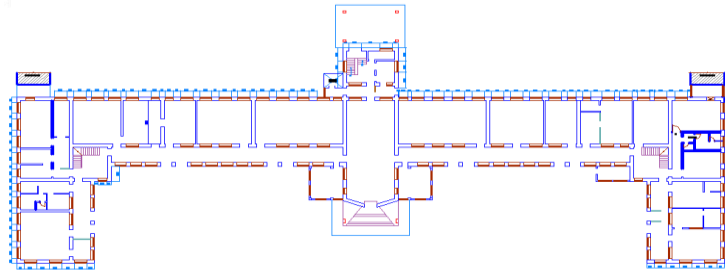
Figure 4 a) Plan of the Building
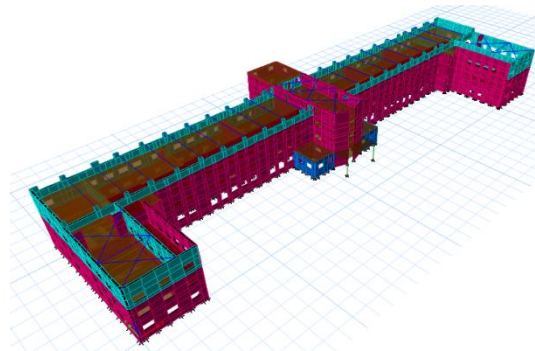
Figure 4 b) 3 D Analytical Model of the Supreme Court

2.2 Seismic analysis

The seismic analysis is a part of the detailed evaluation of an existing building. The steps involve in developing a computational model of the building include applying the external forces, calculating the internal forces in the members of the building, identifying deformations and capacity of the members and building, and finally interpreting the results. The structural analysis is carried out with the help of the available drawings and ETABS 2013, a structural analysis and design software. IS 1893:2002; criteria for earthquake resistant design of structures is used to determine the base shear in the building.

The modulus of elasticity is calculated using different formulas and codal provision from measuring the compressive strength of brick (fb') and weakest mortar suggested in NBC109. Many researchers (Deodhar 2000; Gumaste et al. 2006; Kaushik et al. 2007a; Kaushik et al. 2007b) have attempted to develop an empirical expression relating the brick unit, mortar and masonry compressive strengths as shown in Equation 1 (CEN 2005).

$$f'_m = K f'^{\alpha}_b \times f'^{\beta}_j \ \dots\dots\dots\dots\dots\dots\dots\dots\dots\dots \ (1)$$

Where:

f'_m is the characteristic compressive strength of masonry, in N/mm^2

K is a constant

$\alpha \ \beta$ are constant

f'_b is the normalized mean compressive strength of the units, in the direction of the applied action effect, in N/mm^2

f'_j is the compressive strength of the mortar, in N/mm^2

  Modulus of Elasticity(Em) =550f'_m …………….…………………(2)[From FEMA 306 (1999)-for existing masonry]

Table 5 –The modulus of elasticity is calculated using different formula and codal provision

Source	K	α	β	Compressive strength of Brick (f'b) form test(N/mm2)	f'_m	Modulus of Elasticity E(N/mm²)
Eurocode-6	0.5	0.65	0.25	4.17	1.064	585
Stress-Strain Characteristics of Clay Brick Masonry under Uniaxial Compression(Hemant B. Kaushik1; Durgesh C. Rai2; and Sudhir K. Jain, M.ASCE)	0.63	0.49	0.32	4.17	1.016	559

During the calculation from the empirical formulas, the mean compressive strength of unit is taken from the brick test result, 4.17 N/mm² and the weakest mortar suggested in NBC 109 having a compressive strength 0.5 N/mm². Value of compressive strength of masonry and modulus of elasticity of masonry obtained from the test results are used for the detailed evaluation of the building. The value of modulus of elasticity use during analysis is given below in Table 6.

Table 6-Element type and material properties used in the FE model

Structural Member	Etabs Element	Density (kg/m³)	Modulus of Elasticity E(N/mm²)	Poisson's Ratio
Wall	Shell	1900	585	0.1

In analysis we have taken Permissible Compressive Stress as 0.6 N/mm² considering the masonry wall confined by reinforced concrete elements on both sides.

2.3 Modelling output for existing building

Initially, the existing building is modeled and in-plane stresses along with out-of-plane moments are studied. The in-plane stress and moment diagrams obtained from analysis are shown in Fig.5 a),b) and c) below.

In plane Stress
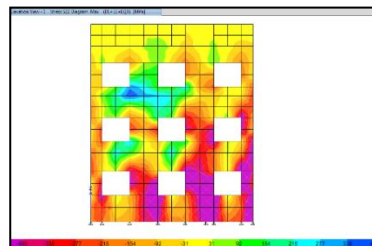
Figure 5 a) Compressive/Tensile stress (In plane stress (S22)) (X-direction: Grid 1-1: wall X1)
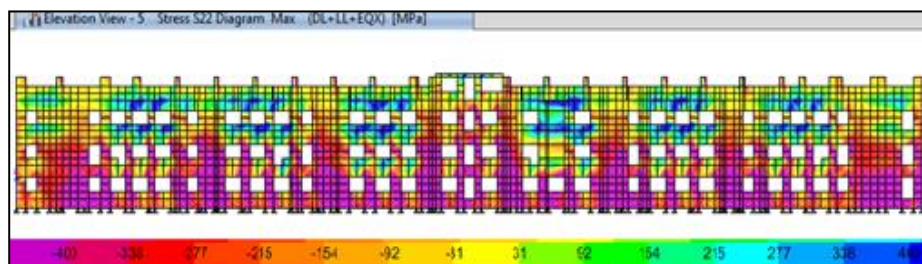
Figure 5 b) Compressive/Tensile stress (In plane stress (S22)) (X-direction: Grid 5-5: wall X5)
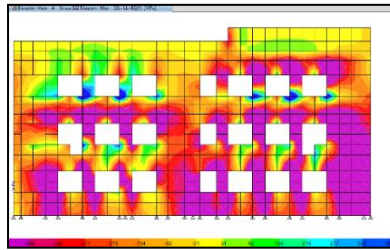
Figure 5 c) Compressive stress in wall (In plane stress (S22)) (Y-direction-A-A)

Table 7-Tensile and compressive stress in wall (In plane bending)
Walls along X/Y direction

Wall	Stress	Vertical Stress S22 (average)			
		0.7DL+EQx	0.7DL-EQx	DL+LL+EQx	DL+LL-EQx
		Stress	Stress	Stress	Stress
		N/mm²	N/mm²	N/mm²	N/mm²
X1	Tension	0.160	0.100	0.16	0.12
	Comp.	0.520	0.600	0.7	0.72
X4	Tension	0.170	0.190	0.28	0.27
	Comp.	0.610	0.640	0.91	0.86
X5	Tension	0.440	0.120	0.68	0.65
	Comp.	0.750	0.830	1.00	0.91
Wall	Stress	Vertical Stress S22 (average)			
		0.7DL+EQy	0.7DL-EQy	DL+LL+EQy	DL+LL-EQy
		Stress	Stress	Stress	Stress
		N/mm²	N/mm²	N/mm²	N/mm²
YA	Tension	0.480	0.480	0.68	0.65
	Comp.	0.690	0.650	0.94	0.86
YB	Tension	0.410	0.270	0.35	0.16
	Comp.	0.640	0.250	0.72	0.95
YE	Tension	0.350	0.130	0.53	0.49
	Comp.	0.860	0.680	0.85	1.01

Out of plane bending (horizontal bending):Show in Fig.5d),e)
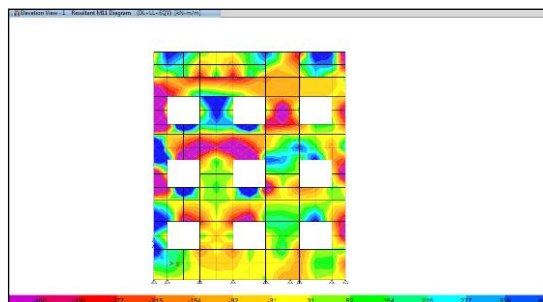
Figure 5 d) Moment Diagram (M11) for Grid 1-1
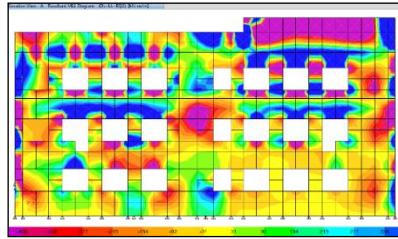
Figure 5 e) Moment Diagram M11 Obtained for Grid A-A

Table 8- Out of plane horizontal bending moment (M11)
Walls along X/Y direction

Walls	Moments M11 in kNm/m (average)				
	0.7 DL+ EQy	DL+ LL+ EQy	0.7 DL- EQy	DL+ LL- EQy	Max.
X1	0.835	1.506	1.573	2.478	2.478
X3	3.090	3.800	2.105	3.115	3.800
X4	1.270	1.579	0.916	0.981	1.579

Walls	Moments M11 in kNm/m (average)				
	0.7 DL+ EQx	DL+ LL+ EQx	0.7 DL- EQx	DL+ LL- EQx	Max.
YA	2.646	3.712	1.791	1.978	3.712
YE	6.815	7.415	4.598	5.947	7.415
YF	6.225	6.024	6.225	7.356	7.356

Out of plane bending (Vertical bending):Shown in Fig.5 f) and g)
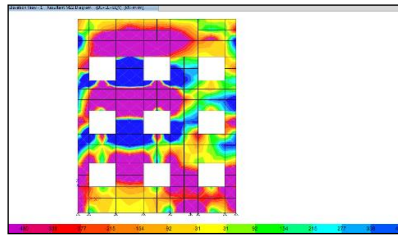
Figure 5 f) Moment Diagram (M22) for Grid 1-1
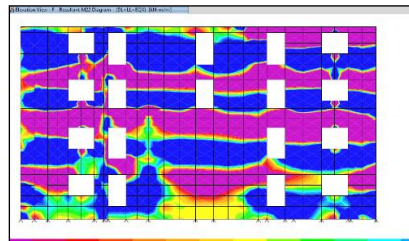
Figure 5 g) Moment Diagram (M22) for Grid F-F

Table 2: Out of plane Vertical bending moment (M22)
Wall along X/Y direction

Walls	Moments M22 in kNm/m (average)				
	0.7 DL+ EQy	DL+ LL+ EQy	0.7 DL- EQy	DL+ LL- EQy	Max.
	kNm/m	kNm/m	kNm/m	kNm/m	
X1	1.746	2.404	2.350	3.879	3.879
X3	8.255	9.800	13.295	14.804	14.804
X4	2.980	3.30	3.848	3.811	3.848
Walls	Moments M22 in kNm/m (average)				
	0.7 DL+ EQx	DL+ LL+ EQx	0.7 DL- EQx	DL+ LL- EQx	Max.
YA	6.229	7.209	4.654	3.674	7.209
YE	3.664	5.608	6.673	6.876	6.876
YF	6.635	8.468	3.434	6.528	8.468

Summary of retrofit design

Modifications	Addition of wing walls
	Closing of openings
	Tying of walls outside the main grid
Retrofitting of walls	a) Steel Jacketing with 4.75 mm Ø bar @ 250 mm c/c in horizontal direction.
	b) Steel Jacketing with 8 mm Ø bar @ 250 mm c/c in vertical direction
	c) Steel Jacketing with 8 mm Ø bar @ 200 mm c/c in vertical direction
Foundation	Addition of tie beam 300 mm x 450 mm along all main walls to connect with the bars of jacketing.
	Addition of a tying beam 300 mm x 450 mm inserted to a length of 300 mm at an interval of 1.5 m all around the peripheral tie beams.

3. Implementation of Retrofit options

Implementation of this building was carried out which above given options. Removal of plaster in required locations, dismantling of brick work, bar mesh splint and bandage on inner and bar mesh jacketing on outer walls, micro concreting, curing, plastering were done. Few photographs of accomplished retrofit work are presented in the Fig.6 below.

305

Figure 6 Implementation of Retrofit Option

Acknowledgements

References

[1] NSET [2015] A report on "Seismic Vulnerability Assessment and Retrofit Design of Kaiser Mahal Building"

[2] Dr. Rai, D.C. [2005] "IITK-GSDMA Guidelines for Seismic Evaluation and Strengthening of Buildings: Provisions with Commentary and Explanatory Examples", IIT, Kanpur

[3] Varum, H. et al. [2006] "Seismic Evaluation of Old Masonry Buildings: Performance and Strengthening", Paper 85, Proceeding of the Eighth International Conference on Computational Structures Technology, Civil-comp Press, Stirlingshire, Scotland.

[4] Romeu Vicente et al. [2011], Evaluation of strengthening Techniques of Traditional masonry buildings: Case Study of a Four Building Aggregate", Journal of Performance of constructed Facilities ASCE/May/June/2011

[5] Department of Archeology [1998] "An Assessment of the Structural Condition of 55 Windows Palace, Durbar Square, Bhaktapur" Investigation Team's Report Volume 1, Kathmandu.

[6] Ceroni Francesca et al. [2012] "Assessment of Seismic vulnerability of a historic masonry building", Buildings 2012, 2,332-358; doi:10.3390/buildings2030332

[7] Look W. David et al. [1997] "The seismic retrofit of historic buildings: Keeping preservation in the forefront", US Department of the Interior, National Park service cultural resources, heritage preservation services.

[8] ASTM C1197-04 [2013] "Standard Test Method for In Situ Deformability Properties Using Flat Jack Measurements", ASTM International, 100 Barr Harbor Drive, PO Box C700, West Conshohocken, US

[9] ASTM C1196-09 (2013) "Standard Test Method for In Situ Compressive Stress Within Unit Masonry Estimated Using Flat Jack Measurements", ASTM International, 100 Barr Harbor Drive, PO Box C700, West Conshohocken, US

[10] RILEM MDT.D.4 [2004] "In-situ Stress Tests based on the Flat Jack", RILEM TC 177-MDT: Masonry Durability and On-site Testing, Material and Structures, Vol. 37.

[11] RILEM MDT.D.5 [2004] "In-situ Stress-strain Behavior Tests Based on the Flat Jack", RILEM TC 177-MDT: Masonry Durability and On-site Testing, Material and Structures, Vol. 37.

RETROFITTING OF A BRIDGE FORM
HISTORICAL STATION USING SEISMIC ISOLATION

D. Kubin [(1)], J.Kubin[(2)], H. Sucuoglu [(3)], G. Feroglu [(4)], I.A.Ilis [(5)], U. Ozcamur [(6)], S. Yalcin [(7)],

[(1)] *Structural Engineer M. Sc., Prota Engineering Design and Consultancy Services Inc., dkubin@prota.com.tr*
[(2)] *Structural Engineer M. Sc., Prota Engineering Design and Consultancy Services Inc., jkubin@prota.com.tr*
[(3)] *Prof. Dr., Middle East Technical University, sucuoglu@metu.edu.tr*
[(4)] *Structural Engineer, Prota Engineering Design and Consultancy Services Inc., goksenin.feroglu@prota.com.tr*
[(5)] *Architecture M. Sc., Prota Engineering Design and Consultancy Services Inc., iailis@prota.com.tr*
[(6)] *Structural Engineer M. Sc, TIS Technological Isolator Systems, ugurcan.ozcamur@tis.com.tr*
[(7)] *Draftsman, Prota Engineering Design and Consultancy Services Inc., sinem.yalcin@prota.com.tr*

Abstract

Being the first railway station as bridge form above the train track, constructed in Istanbul in 1915, Göztepe Train Station is one of the most special structures conserved in terms of both structural and architectural features till today. In the scope of Marmaray CR3 project, this historical landmark has been renovated and actively used as a train station. The original structural system was composite masonry, including brick masonry walls, steel beams to support timber roof, stone masonry walls and a volta slab to elevate the station. Since the region is seismically active, requirement for seismic strengthening was mandatory in order to maintain the station. There were two main goals during this project: Modifying the main train station building with minimum intervention while achieving target seismic performance level and satisfying the increased demand requirements. Structural system of the historical structure underneath the main station required in order to increase the number of train tracks from two to three. Masonry walls on the sides of the rail tracks have been removed and replaced with reinforced concrete shear walls. While working underneath, the existing station building was suspended until the new structural system below the superstructure is constructed. A special methodology has been developed for this purpose. This method allowed keeping the entire station building intact and preventing any risk of damage to the adjacent structures. Since masonry structures are primarily vulnerable to lateral forces, the masonry structural system is converted to reinforced concrete without modifying the exterior shell of the station. This conversion is carried out by employing in-situ concrete members where special care has been taken to maintain the original facades. Additionally, a seismic isolation system composed of nine curved surface sliding devices has been installed in order to reduce the seismic actions transmitted to the upper structure. It should be noted that seismic isolation also facilitates reduction for modifications at the upper structure. Structural models have been developed based on the characteristics of the base isolation devices, and by considering the modifications on the substructure and the superstructure. As a consequence of the implemented retrofit methodology, the historical structure has been modified at the minimum level, earthquake performance is brought to the target seismic performance level, and the structure was made suitable for functioning of the increased number of tracks.

Keywords: Göztepe Station, Masonry Structure, Historical Building, Retrofit, Seismic Isolation.

1. Introduction

1.1 Brief History

When the Haydarpaşa-Pendik route was put into operation as a single-track line at the end of 1872, the old passenger building of Göztepe Station, which is currently used as a lodging building was also serving to the passengers. However, as time passes, the single-track line became inadequate and the railway was modified to be double-track line in 1912. During this revision it is estimated that the Haydarpaşa-Pendik alignment has also been modified. Additionally, the track line was lowered about 11 meters due to the fact that the trains were struggling because of steep gradient towards the Göztepe Station. As a result of this process, passenger building of Göztepe Station has lost its accessibility and the current passenger building which is the subject of this study has been constructed in the form of a bridge over the railway. (Figures 1 to 8).
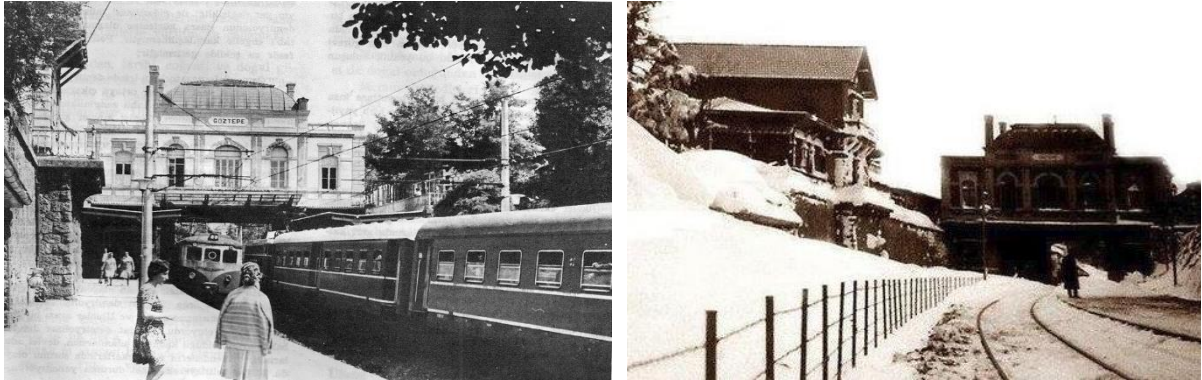
Figure 1 - 2. Views of the Göztepe Station from 1920's
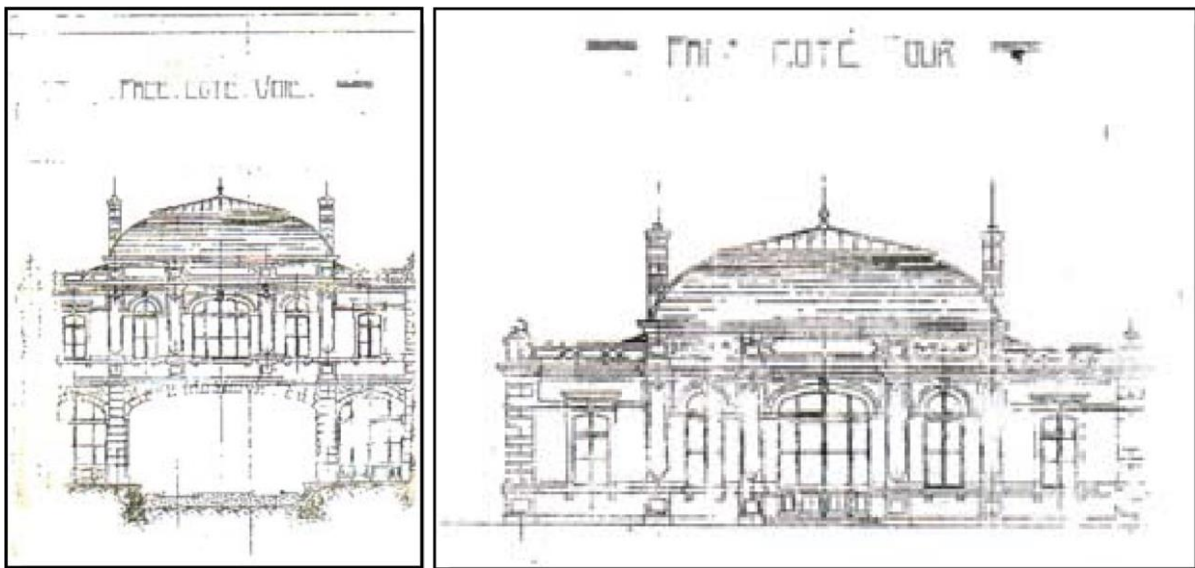
Figure 3 - 4. Historical Elevations from Southwest and Northeast
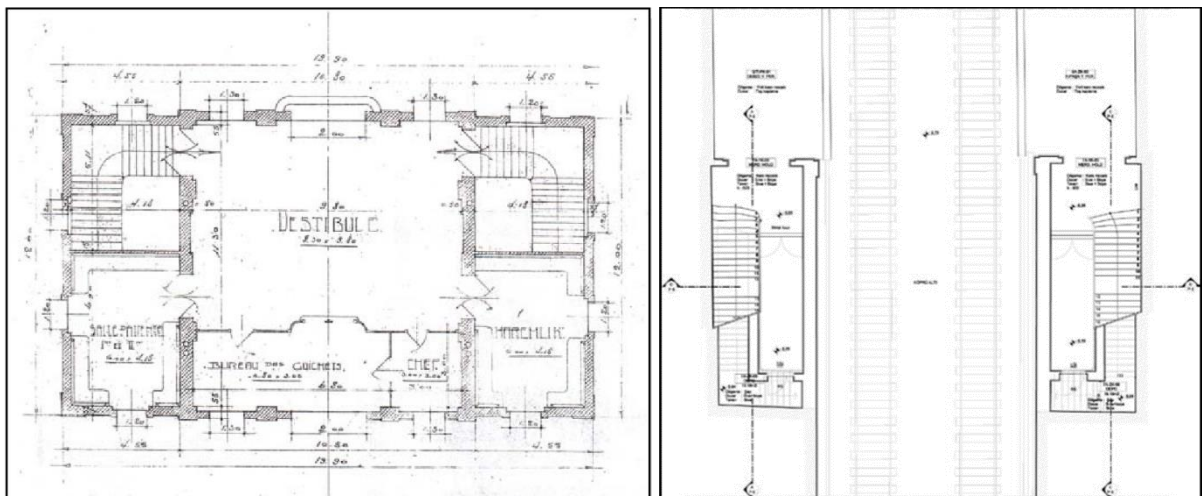
Figure 5 - 6. *Architectural Plans of the Station Building*
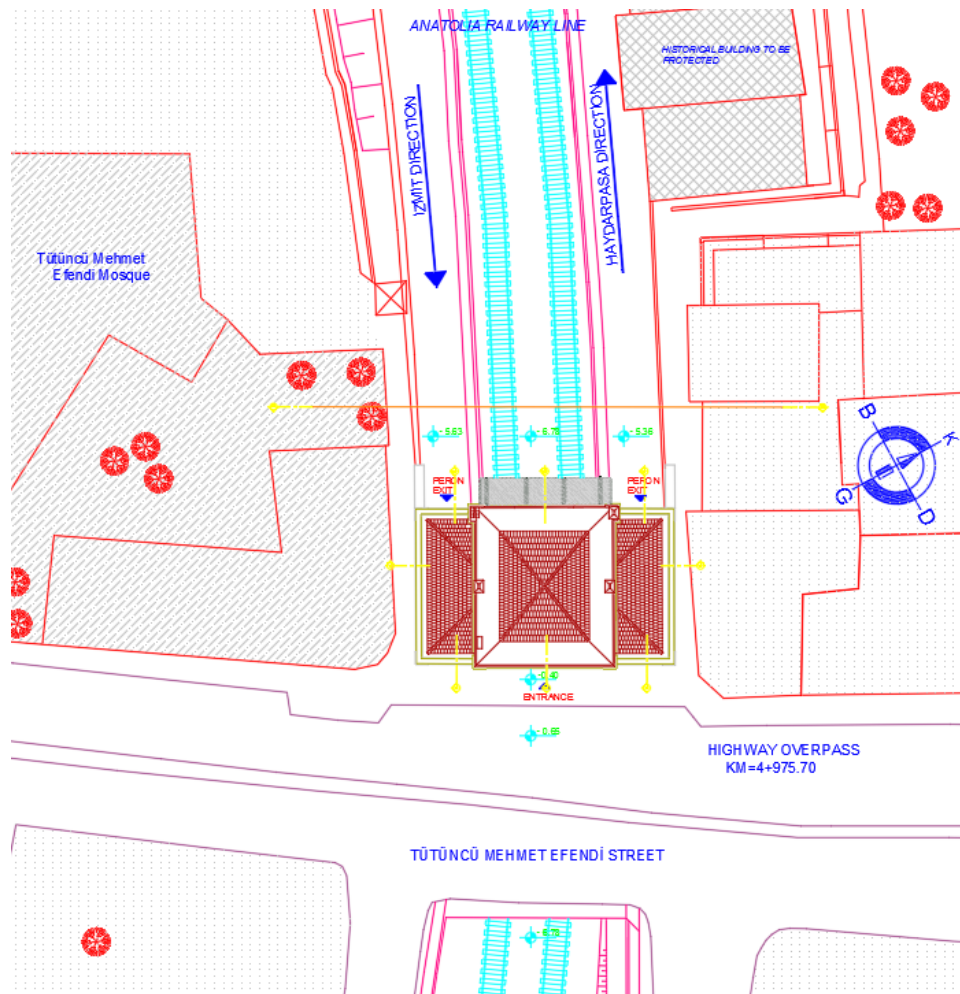
Figure 7. *Layout Plan of the Region*

1.2 Structural System and Materials of the Existing Structure

Göztepe railway station has been constructed as a 20 x 12 m rectangular block shaped bridge. Height of the building is approximately 15 m. The station consists of a platform level and a ground floor which is used as a ticket office and launch. The structural system of station is composite stone and brick masonry.

The primary load-bearing piers of the structure are the stone masonry stairs blocks leading to the platform at both sides of the building. Slab system of the building was constructed using one-way I-shape steel ribs with approximately 800 mm centres. Spaces between the steel ribs were filled using hollow bricks to create a slab system called Volta.

The ground level walls are brick masonry spanning from floor to the roof. All of the walls have been plastered. Walls thickness is around 700 mm at platform level and 400 mm at ground floor. All interior walls are also brick masonry with 300 mm thickness. These masonry walls carry the grey vault having a raised section at the middle of the structure. At both sides of the vault, gable roofs are constructed. During the assessment works conducted to determine the as built state of the building, no reinforced concrete elements were observed.

Observations revealed that some sections of the flooring system have experienced some revisions in time, since different timber cover sizes were measured in office areas. Original floor covers having thicknesses around 75 to 150 mm were used in these areas, whereas 200 x 200 mm square mosaic tiles were employed in the ground floor. It was also determined that the building did not experience any significant structural or architectural revision since it was constructed, with the exception of the canopies at the platform level that were added at a later date.

Figure 8. *Recent Photographs of the Station Before Strengthening*

1.3 Material Test Results of the Building

Several material tests were conducted by the Construction Materials Lab of Civil Engineering Department of Yildiz Technical University. The results using the samples taken at locations shown in Figure 9 are summarized below:

It has been determined that shear strength (τ) values between brick and mortar is around 0.26 to 0.44 MPa with the exception of KT1, which was significantly lower (τKT1 = 0.03 MPa).

Similarly, displacements measured under maximum loading were around 1.93-8.12 mm again with the exception of except KT1 location, which was 0.004 mm.

Based on the results of the uniaxial compressing test of bricks, it was determined that standardized compressive strength value varies between 3.7 – 4.4 MPa. Average compressive strength is accepted as 4.10 MPa. This value is slightly below the old 'National Classification for Bricks' code requirement which was 5 MPa.

According to the point loading test results which have been carried out to determine the mechanical properties of mortar samples, compressive strength was found to be as low as 0.2 to 0.4 MPa with conversion factor is taken as 11.

Physical properties of bricks, mortar and plaster samples reveal that they exhibit porous texture (p ~ 40%), having unit weight around 1.65 g/cm3 and specific gravity of 2.7 g/cm3. When open pores that indicate water absorption ratio by volume are examined, it is determined that approximately 75% are open pores.

Acid loss analysis of mortar material also indicate that this value, being 15%, is much lower compared to air-slaked lime mortars. When the low compressive strength of mortar (fc,h < 0,5 MPa) is considered, it is estimated that hydraulic lime have been used as binding material.

As a result of the sieve analysis, it has been determined that maximum aggregate size in mortars and plasters   were 5.6 and 4 mm, respectively.
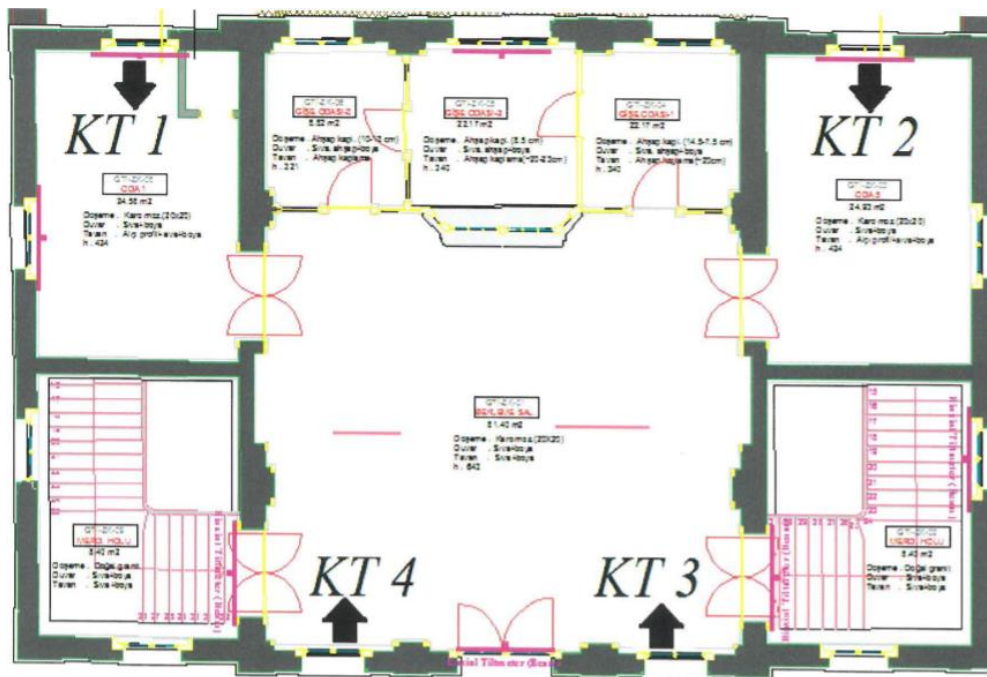
Figure 9. *Test Sample Locations [1]*

1.4 Assessment of the Existing Structural System

Based on the results obtained from the assessment analyses of the existing structural system, it has been determined that the building does not satisfy the "Life Safety" performance target under the design earthquake with 10% exceedance probability in 50 years (475 years return period earthquake). Moreover, the capacities of specific elements were determined to be significantly less than the seismic demands. Therefore, the decision was taken to replace the existing masonry bearing system with the composite system developed in this context.

Table 1 – Shear Demand and Capacity Checks of Masonry Walls

Shear Force Checks of Masonry Walls			
1st Floor			
Direction	Total Masonry Wall Area (m²)	Total Member Capacity (kN)	Total Seismic Demand (kN)
X	2.81	**982**	**36697**
Y	33.86	**11852**	**36697**
2nd Floor			
Direction	Total Masonry Wall Area (m²)	Total Member Capacity (kN)	Total Seismic Demand (kN)
X	13.12	**4593**	**16109**
Y	13.37	**4678**	**16109**

2. Assessment of Strengthening Needs and Methods

2.1 Determination of Retrofit Requirement

Historical Göztepe Station has been designed to meet the requirements of its era to serve with two tracks. Since the new Marmaray Project is designed with 3 tracks based on todays requirements, the station has to be revised to be a bridge structure allowing 3 tracks, as well as being strengthened to meet the seismic requirements of the current design codes.

The existing structural system of Historical Göztepe Station is masonry. In general, lateral design of low masonry structures are governed by shear stresses. Istanbul city is one of the highest seismic regions of the country (1st Earthquake Design Class according to the current seismic code). This fact increases the importance of shear capacity of the building, due to the fact that low strength and ductility materials used in the building that may yield to a brittle failure during even a moderate seismic activity. Consequently, retrofit decision became inevitable.

2.2 Determination of Construction Methodology

Factors taken into consideration in determination of strengthening approach:

- Expanding the historical bridge in order to allow the new design with 3-tracks,
- Increasing the seismic performance of the structure in order to satisfy the seismic performance target,
- Creating a solution that meets the principles of restoration with minimal interference to the original structure and unconditionally preserving its exterior appearance,
- Employing a construction methodology in order to preserve the historical texture of the building without creating any risk for neighbouring buildings during strengthening,
- Employing a method that is applicable and faster implementation.

2.3 Main Principles of Applied Methodology

The main principles of the applied strengthening approach are summarized below;

- Conventional cast-in-place reinforced concrete technique has been employed as strengthening method. It is found to be the most appropriate approach to be used to modify a brick/stone masonry structure. For this reason, contribution of the existing structural system (masonry structure and steel volta slab) was ignored and new system is established.
- It is noted that, it was not possible to provide sufficient lateral strength without excessive modification of the system. Therefore, seismic base isolation was utilized to reduce the effects transferred to the upper structure.
- All new structural elements employed for strengthening purposes are located at the interior of the structure in order to preserve the exterior facade.
- Existing load-bearing system has utilized in stages during until the completion of the construction. At each phase of construction, as the new system structural elements are created, the existing system gradually lost its functionality. For example; volta slab was actively supporting the floor until the new reinforced concrete slabs are constructed.

Figure 10 illustrates the final target of the strengthening process.
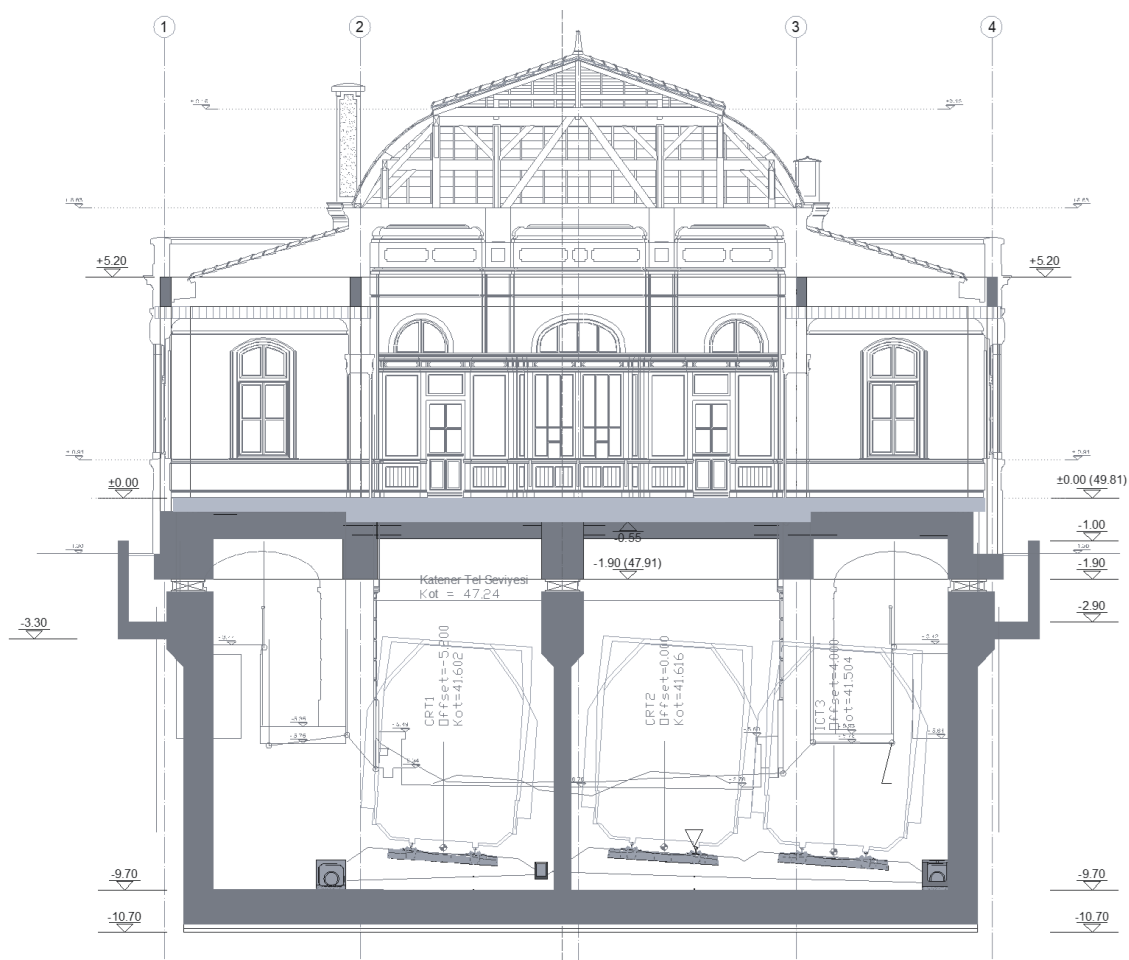
Figure 10. *The targeted state of the structure after strengthening (Elevation from Gebze direction).*

2. Assessment of Strengthening Needs and Methods

3.1 General Design Approach

The station is located in Kadıköy district of Istanbul, which is one of the highest seismicity regions of the city. As stated above, in order to reduce the seismic effects transferred to the building an isolation layer is considered just above the bridge piers.

Due to the fact that the function of the structure changed after strengthening, maximum architectural flexibility has been provided. Therefore, a system that consists of concrete beam, slab and column structure located at modular intervals has been designed. This system ensures the preservation of the historical essence of the structure by keeping the interference level at minimum. The architectural facade is preserved as is using design criteria that have been considered in conjunction with state-of-the-art construction techniques.

3.2 Earthquake Loading and Analyses

Structural design is based on the design earthquake that has 10% probability of exceedance in 50 years [2] (475 years return period Design Basis Earthquake). All structural members are designed considering this seismicity level in order to ensure "Life Safety" performance level[3]. In order to ensure that the displacement limits of the base isolator units under Maximum Credible Earthquake is not exceeded, isolators are designed to satisfy the displacements calculated using of 2% probability of exceedance in 50 years earthquake (2475 years return period) (Figure 11).
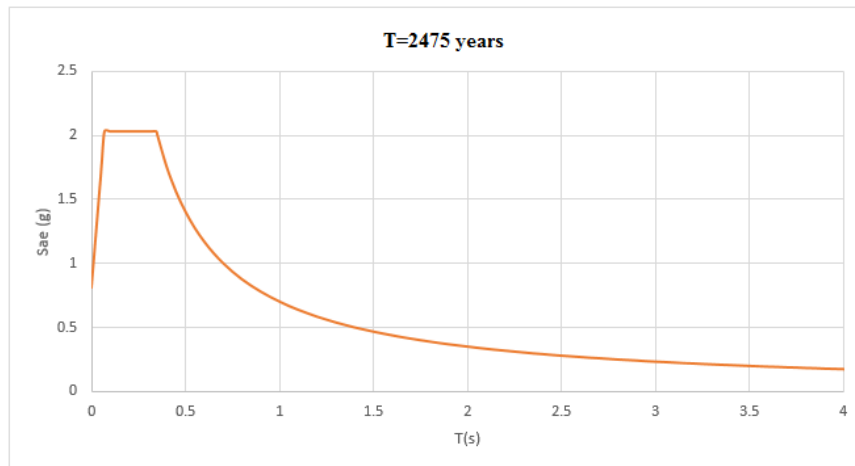
Figure 11. *Acceleration Design Spectrum of 2475 Years Earthquake Level*

3.3 Earthquake Performance of the Structure

Non-linear time history analyses were carried out using selected 11 earthquake acceleration records. These records are scaled using the 2475 year return period earthquake spectrum. Effective damping ratio is limited to 28% [4] in all analyses. The maximum horizontal displacement was calculated as 268 mm and with the application of 10% accidental torsion 294 mm is used for the determination of the seismic isolator unit dimensions. A similar analysis is also carried out for the design of the structural elements using the 475 year return period earthquake. The maximum base shear ratio has been determined as 8% (0.080W) [5]from this analysis. Consequently, 9 identical friction pendulum type isolators were used to support the building as illustrated in Figure 12 below.

Figure 13 illustrates the displacement history results [6] obtained for a selected column for all time history analyses. The surrounding circle illustrates the displacement limit of the base isolation units. Similarly, floor acceleration results are also plotted in Figures 14 and 15 for X and Y direction loading separately. In order to show the base shear time history, only one of the earthquake record (Duzce Earthquake) [7] is plotted for illustration purposes in Figure 16 below.
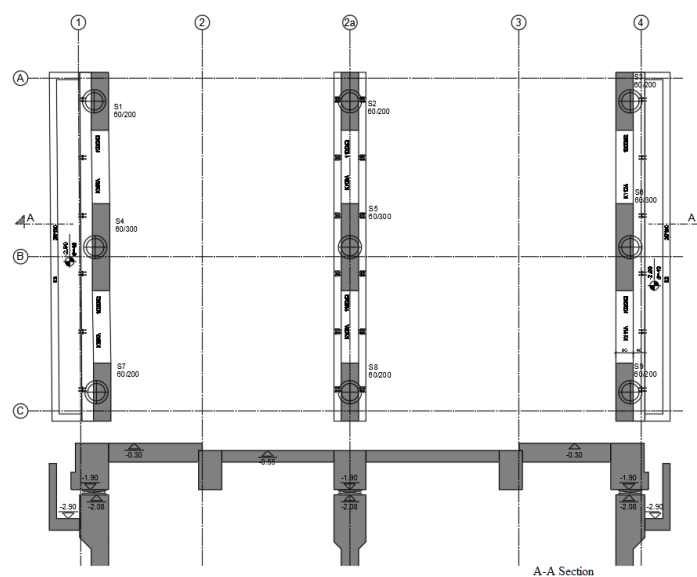
Figure 12. *Plan and section of isolator floor [8]*
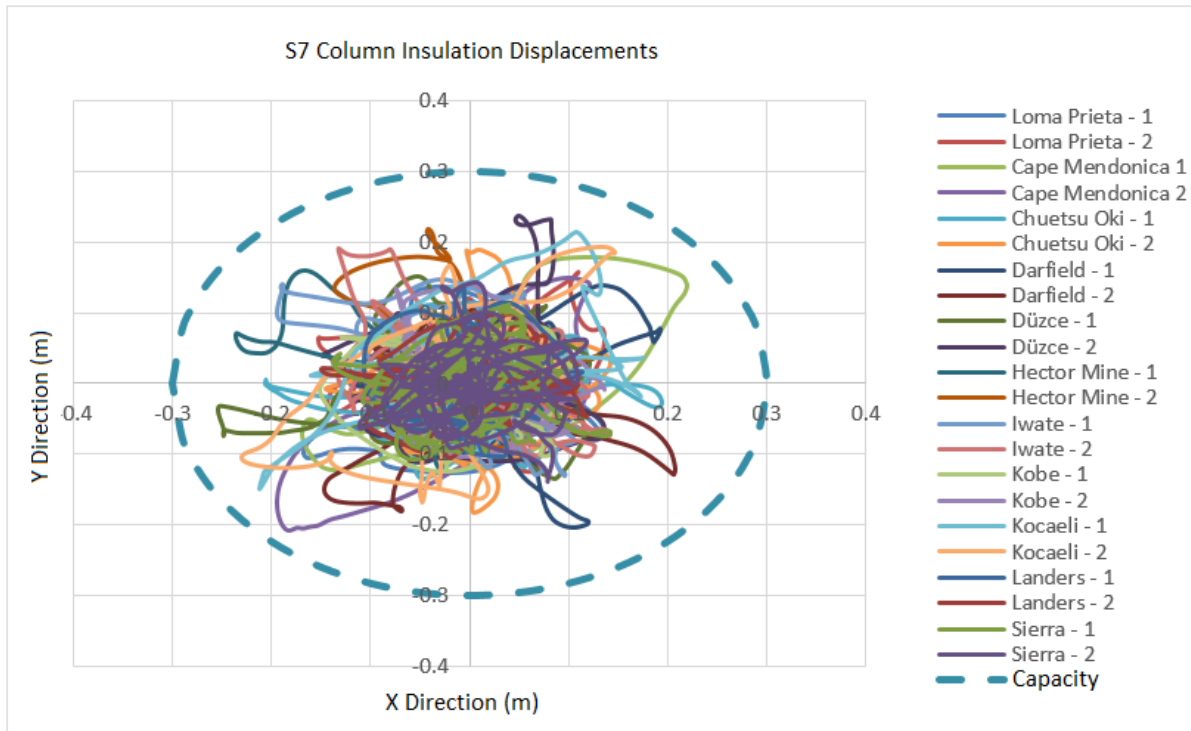
Figure 13. *Displacement History Result of Column S7*
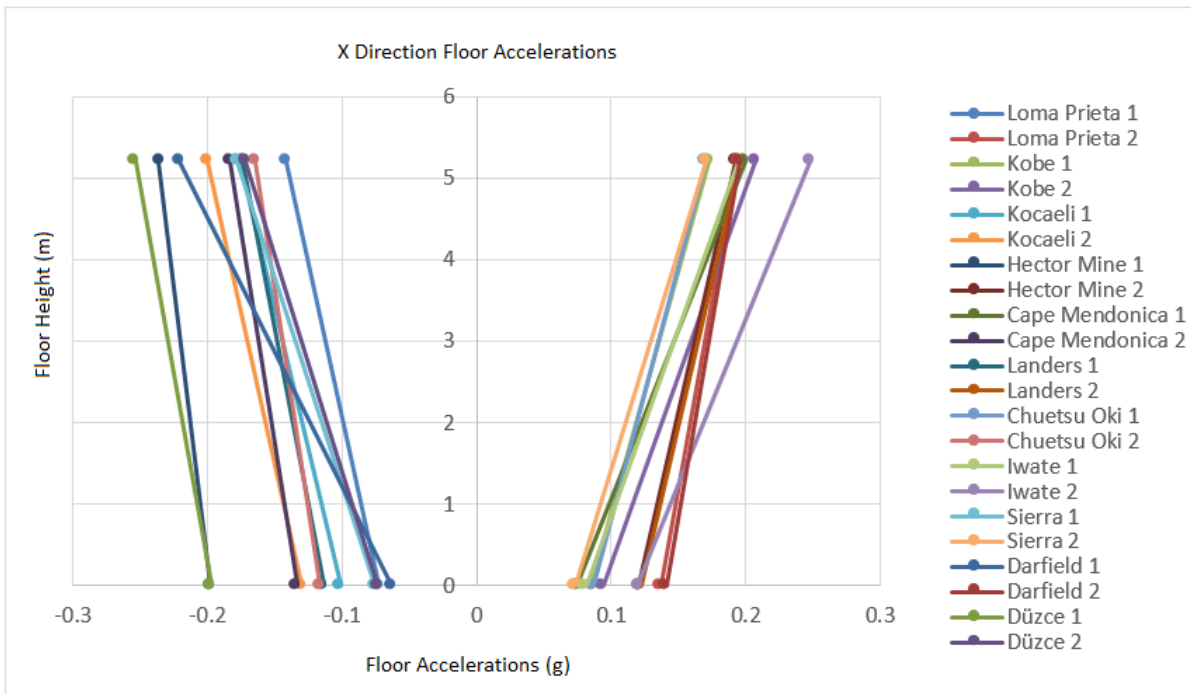
Figure 14. *X direction Floor Accelerations*
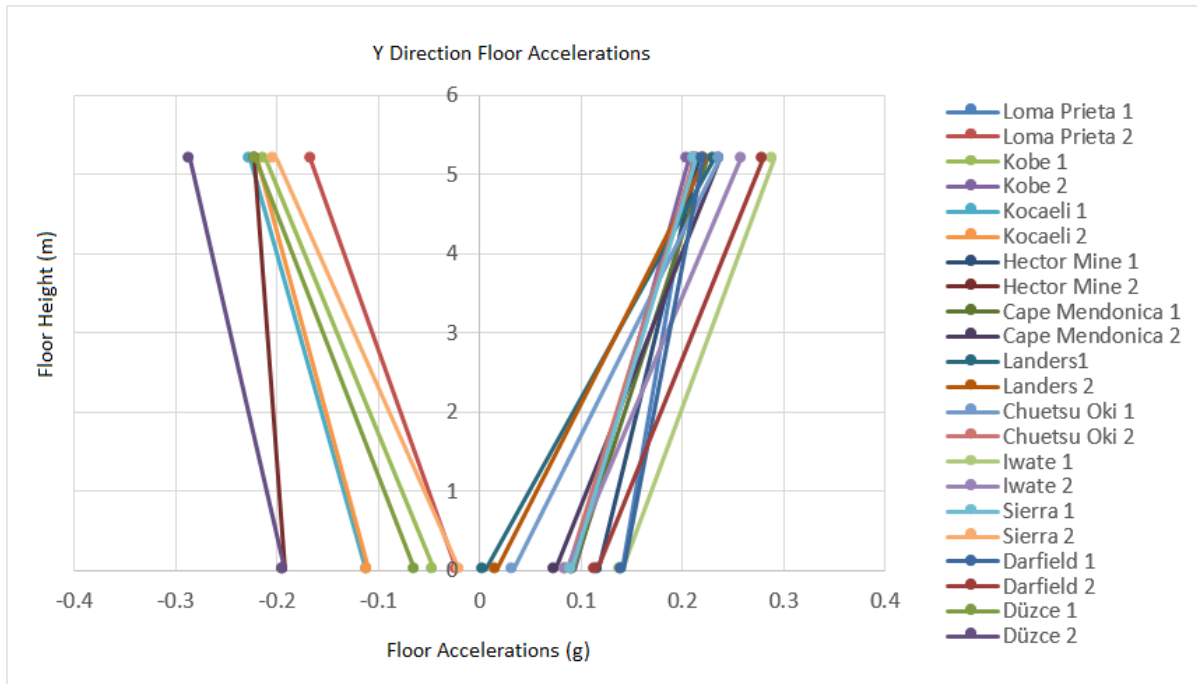
Figure 15. *Y direction Floor Accelerations*
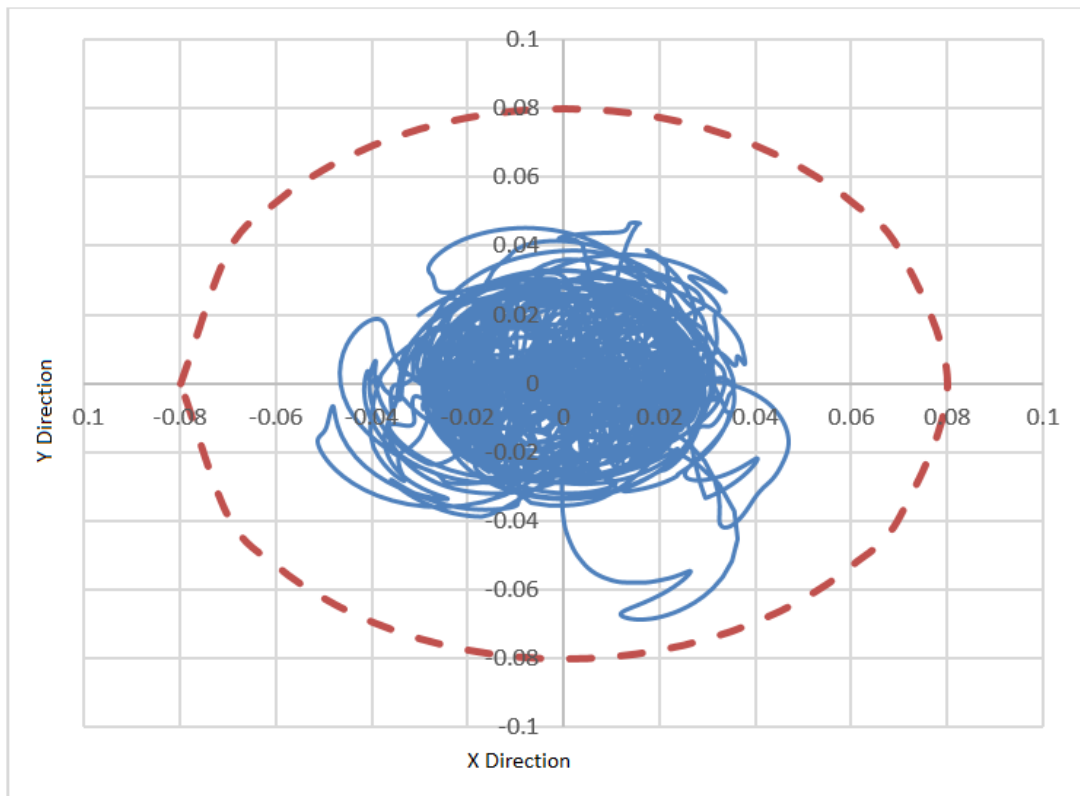
Figure 16. *Duzce Earthquake Base Shear Ratio*

4. Conclusions

The historical Göztepe Station, which was a composite masonry building was not satisfying the requirements of the current Turkish Earthquake Code 2007 and assessment analyses revealed that it should be retrofitted. Furthermore, as a bridge structure, it was not fulfilling the requirements of the 3-track rail system of the new Marmaray Project. As the consequence of this project developed for the protection of this important building:

Due to the historical importance of the building, the retrofit methodology was selected to have minimum interference to the existing facade and functionality. Most of the repair works and added elements were applied to the interior of the structure.

Most of the construction was carried out using conventional techniques.

Seismic performance of the structure was increased to satisfy the requirements of the current earthquake code. By the employment of the seismic isolators, most of the excitation was absorbed by the isolation layer.

The bridge was modified to fulfil the requirements of the new 3-track rail project.

5. Acknowledgement

References

[1] Nabi Yüzer (04.12.2017). Material Analysis Report of Historical Göztepe Station.

[2] Farzad Naeim, James M. Kelly (1999). Design of Seismic Isolated Structures, From Theory to Practice.

[3] Sinan Akkar, Bekir Özer Ay (2012), A procedure on ground motion selection and scaling for nonlinear response of simple structural systems. Published on Wiley Online Library.

[4] Turkish Standards for the Design of Buildings in Earthquake Regions, 2007.

[5] European Standards (CEN), Seismic Design of Buildings (Eurocode 8), EN 1998.

[6] Turkish Standards Institute (TSE). Requirements for the Design and Construction of the Reinforced Concrete Structures (TS500), 2000.

SEISMIC RETROFITTING OF SULTAN MURAT MOSQUE' CLOCK TOWER IN SKOPJE USING INNOVATIVE MATERIALS

Goran Jekic [1], Veronika Shendova [2], Aleksandar Zlateski[3]

[1] *Asst. Prof., Ss. Cyril and Methodius University in Skopje, Institute of Earthquake Engineering and Engineering Seismology (IZIIS), jekic@iziis.ukim.edu.mk*

[2] *Prof., Ss. Cyril and Methodius University in Skopje, Institute of Earthquake Engineering and Engineering Seismology (IZIIS), veronika@iziis.ukim.edu.mk*

[3] *Assistant., Ss. Cyril and Methodius University in Skopje, Institute of Earthquake Engineering and Engineering Seismology (IZIIS), azlate@iziis.ukim.edu.mk*

Abstract

The structure of the Clock Tower in Skopje is massive, constructed of stone masonry with a height of about 29 meters and brick masonry in the upper octagonal part. It was damaged during the Skopje Earthquake in 1963. A rehabilitation of the structure was carried out in 1964, but without a seismic strengthening. Recently, field investigations were carried out and a three-dimensional analysis of the structure in its actual state for gravitational and seismic forces was performed. It has been concluded that it is necessary to perform protective interventions to ensure longer-term protection, stability and further existence in the form of repair of existing structural damage, structural consolidation, repair of damaged timber elements and strengthening. To improve the behaviour and resistance to dynamic impacts, a technical solution for consolidation and retrofitting has been proposed. The basic concept consists of existing structural damage rehabilitation, structural consolidation with systemic injection, rehabilitation of load-bearing wooden beams and braces and strengthening the whole structure. Due to the specificity of the structure of the Clock Tower in terms of its shape, used material, structural system and the type of structural elements, as well as its importance as a cultural and historical heritage, which requires respect of certain conservation principles and rules, the options for rehabilitation and strengthening are strictly limited. It excludes inserting new structural elements that would provide sufficient ductility during maximum expected earthquakes. The rehabilitation and strengthening were carried out with innovative composite materials that were experimentally verified, but never applied before. The analysis results show that the retrofitted structure can withstand the maximum expected seismic loads according to the actual technical regulations.

Keywords: historic buildings, seismic retrofitting, innovative advanced composite materials, analytical investigation

1. Introduction

The Clock Tower building in Skopje is located in the Sultan Murat Mosque complex. According to information, it was constructed between 1566 and 1573 and was also the first clock tower on the territory of the Ottoman State [1]. It was built on the foundations of a former medieval defence tower. It was previously constructed as a wooden structure, but later it was completely constructed as a brick masonry. During the arson of the city of Skopje and the great fire from 1689, the tower suffered a great damage, but it remained in its original shape until 1904, when it was rearranged and got its present shape (Fig. 1).

During the 1963 Skopje Earthquake, the tower was damaged and the clock mechanism was lost. Later, the structure was repaired, but without its clock mechanism. The new clocks on the tower were added on May 26, 2008, as part of the Chair Municipality project for its reconstruction.

In the period after the earthquake, a report for structural strengthening was prepared. The strengthening was planned to be performed inserting reinforced concrete vertical and horizontal belt courses [2]. From the recent on-site inspection of the building, it was ascertained that the project was not implemented. Damage and cracks of the structural walls were still visible on the cleaned facade masonry as well as in the interior (Fig. 2).

Figure 1. The Sultan Murat Mosque Clock Tower (postcard from 1909) (left); Appearance in 2018 (right)
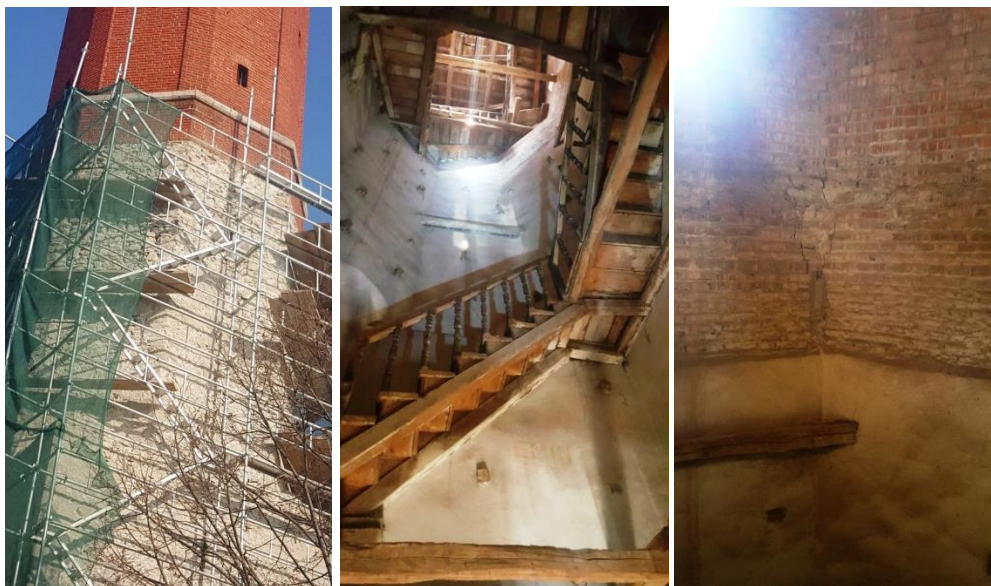
Figure 2. The condition of the structural masonry walls before rehabilitation

2. Structural concept and structural damages

From a structural point of view, the tower is constructed as massive stone masonry in lime mortar up to elevation +15.00 m, and from elevation +15.00 to the top (elevation 29.00 m) as brick masonry in lime mortar. In the lower part of the stone masonry (up to elevation +8.50), which is probably a remnant of the medieval defensive tower, the shape in plan is in the form of a square with a side length of 5.50 m and a wall thickness of 1.0 m, and then it turns into an octagonal shape. From elevation +8.50 m up to elevation +24.30 m the external dimensions are constant, and above this level to the top of the building there are two cascading reductions in size and in wall thickness to 80 cm and 60 cm. The connections between these various levels are constructively resolved by supporting load-bearing multi-layered wooden beams and with no direct contact between the lower and the upper masonry.

From the inspection of the building, it was generally concluded that the masonry was in good condition with some visible damages in the form of diagonal and vertical cracks on the facade stone

walls, on the inner side of the brick walls, damages from a deterioration of the wooden beams and the mortar due to aging, as well as damages due to an insufficiently regular maintenance.

For the structural analysis purposes, additional research was carried out to determine the foundation depth. The tower is founded on a sloping terrain, so the southern side is at an elevation of +0.00 m, while the elevation of the northern part is at an elevation of -2.00 m. From the investigation probe along the northeast corner of the building, the identification of the foundation was carried out (Fig. 3). The foundation is constructed of a solid stone masonry in lime mortar without extension up to elevation -4.00 m and it is a continuation of the stone masonry above the ground level.

Figure 3. An exploratory borehole along the northeast corner of the tower

3. Structural analysis of the tower's state before the seismic retrofitting

The structural analysis of the tower was carried out for gravitational and seismic forces, whereby the building is treated in accordance with the actual technical regulations for the appropriate category of the building according to its purpose. A three-dimensional static and seismic analysis was performed applying the finite element method using the SAP2000 software package. A medium-dense network of elements was adopted, covering the global geometric characteristics without considering the inhomogeneity of the built-in material (stone, brick and mortar). For the purposes of this analysis, a mathematical model for the structural system of the building was prepared (Fig. 4), where a three-dimensional finite element SOLID with eight nodes was used to model the load-bearing massive walls.

For the structure modelled in this way, a modal analysis was first performed, then an analysis with applied gravitational vertical loads and equivalent seismic forces, obtained according to the valid national regulations [3]. The following values, (typical for Ottoman monuments in N. Macedonia) are adopted for the input physical-mechanical parameters for stone masonry and brick masonry:

Weight of the stone masonry, $W_s = 20$ kN/m^3
Elasticity modulus of the stone masonry, $E_s = 1100$ MPa
Weight of the brick masonry, $W_b = 17$ kN/m^3
Elasticity modulus of the brick masonry, $E_b = 850$ MPa

According to the national regulations for high-rise buildings in seismically active regions [3], as well as considering that the tower is a cultural and historical heritage, the seismic analysis had been conducted as for a first category building, with the seismic force intensity equal to 30% of the total weight of the building.
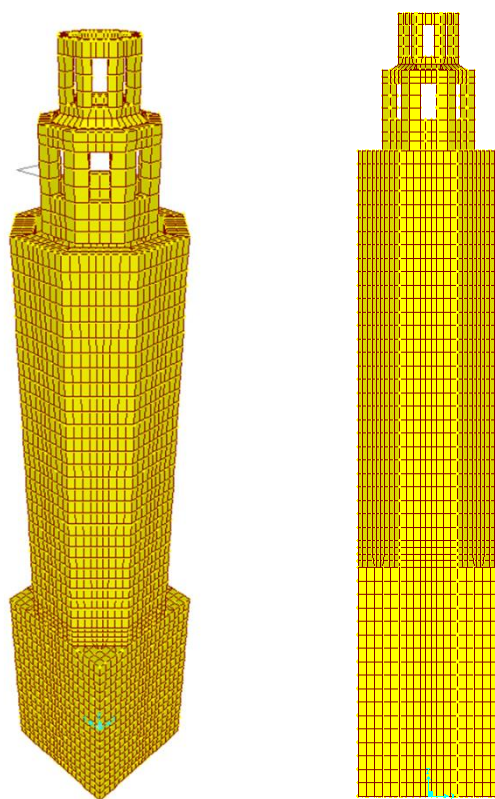
Figure 4. 3D solid finite element model of the tower

The total seismic coefficient was obtained by the Eq. 1:

$$K = K_0 * K_s * K_d * K_p \tag{1}$$

is K=0.3, where the values of each individual coefficients are given below:

Building category I coeff. (Ko = 1.5)
Site seismicity MCS IX coeff. (Ks =0.1)
Soil class I coeff. (Kd=1.0)
Ductility and damping coeff. for plane masonry (Kp= 2.0)

Since there is no direct connection of the masonry from elevation +24.30 above, further analyses were performed up to that level by considering the influence of the upper part of the building only as an additional weight. According to the numerical analysis the natural periods on both orthogonal directions have the same value ($T_{x-x} = T_{y-y} = 0.81s$), while the natural period in torsion is lower (T_{tor}=0.21s). These values are within the expected limits for natural period of clock towers, The total displacements from seismic force in the longitudinal and transverse directions are 11.2 cm in both directions (Fig. 5) and they are higher than the maximum allowed according to regulations (δ_{max}=H/600=2900/600=4.83cm).

The resulting stress-deformation state indicates a sufficient capacity of stability and reliability for gravitational loads since the maximum compressive stresses are lower than the expected ultimate compressive strength of stone masonry. However, considering the maximum expected seismic impacts, tensile stresses higher than the expected tensile strength of the masonry occur in local zones, which would result in structural damage due to the expected seismic action (Fig. 6). Thus, the need for structural consolidation and strengthening was determined in order the seismic protection level to be achieved.

321
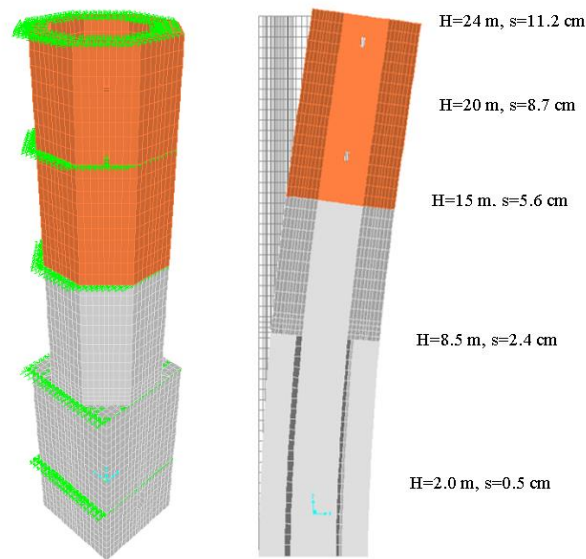
Figure 5. Unretrofitted state - elevations of applied seismic forces (left), displacements due to the design seismic actions (right)
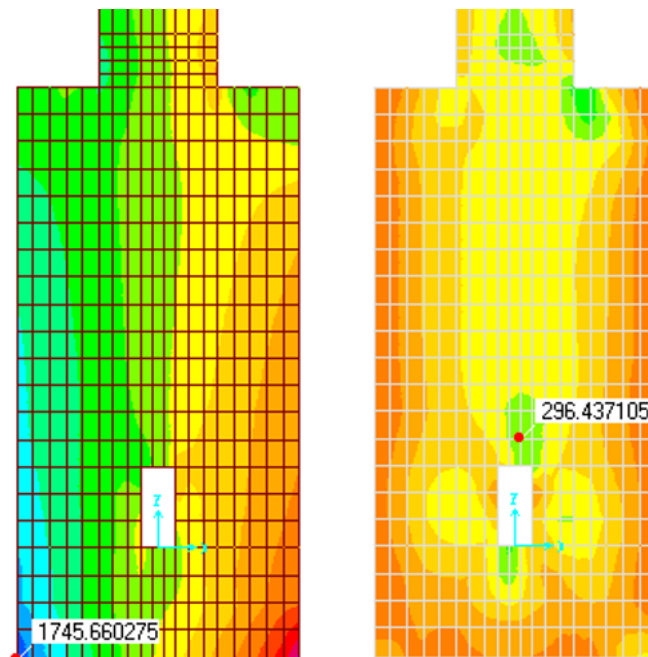
Figure 6. Unretrofitted state - stress in kPa under gravity loads and seismic actions in critical points – vertical tensile stress (left), shear stress (right)

An analysis of the overturning moments for the maximum expected seismic forces was also performed. The self-weight combined with the passive earth pressure provides a stabilizing moment of 26,807 kNm, while the seismic forces cause an overturning moment of 34,966 kNm. Therefore, it was concluded that it is necessary to strengthen (expand) the foundation to obtain a higher safety coefficient against overturning.

4. Technical solution for seismic retrofitting

The measures for improving the seismic reliability of culturally historical buildings, are defined with specific conditions that depend on the historical, architectural and cultural value of the building, on the seismic hazard level, but also on the possibility of applying an appropriate rehabilitation and strengthening measures. Buildings such as the Clock Tower in Skopje, due to their shape, built-in materials, structural system and especially the type of structural elements, as well as to respect certain conservation principles and rules, do not allow inserting enough new structural elements that would provide sufficient ductility during expected earthquakes.

To improve the behaviour and resistance to dynamic actions, the technical solution had been proposed [4], the basic concept consists of:

- Repair and rehabilitation of existing structural damage;
- Structural consolidation with systemic injection;
- Rehabilitation of load-bearing wooden beams and braces with modern composite materials;
- Strengthening the structure with advanced composite materials.

4.1 Rehabilitation, structural consolidation and strengthening

This measure included repair of visible cracks, as well as all existing cracks that were noticed after the surface mortar layer had been removed.

The process of repairing structural cracks started with cleaning the facade mortar and injection of mixtures based on lime mortar with additives, (crushed brick, pozzolan), fluidity improvement additives, improvement strength and adhesion with the substrate.

For structural consolidation and overall increase of the masonry compactness and thereby improving the load-bearing capacity and integrity of the masonry, a systemic injection had been performed. The process included cleaning the inner surface of the elements and removing the damaged and labile parts. The injection was carried out with similar mixtures with increased fluidity, under a pressure of 1-1.2 atmospheres with specialized equipment, along previously systemically laid pipes and in the direction from bottom to top.

Considering the significant role of the wooden beams at the level +24.30 and +27.00 as basic load-bearing elements for the masonry above them, as well as the role of the wooden braces as elements that receive the tension stresses that the masonry has no capacity to receive, the function of all wooden elements had been checked. All damaged or worn-out wooden elements were repaired or replaced with new ones. For effective rehabilitation and strengthening of load-bearing wooden beams, they were cover with polymer cloth or a belt reinforced with carbon fiber (CFRP Wrap, CFRP Laminate) after the preliminary cleaning and treatment of the surface layers.

The basic concept of the strengthening consisted of horizontal and vertical belts of modern polymer cloth, reinforced with fibers in a layer of lime mortar, which should ensure complete coverage of the tensile stress zones. Apart from absorbing the tension forces and preventing damage to the masonry, this system also enables greater integrity and increases the stiffness and ductility of the structure during dynamic loads.

For the implementation of the strengthening system, a modern, previously experimentally verified system (ROFIX SismaCalce [5]) has been adopted, which consists of three layers: (1) a primary layer of basic hydraulic lime mortar, (2) a layer of a mesh of polymer-coated aramid and glass fibers (Fig. 7) and (3) a layer of facade lime mortar of at least 2.0 cm.

| V – Verticale (principale) | H – Orizzontale | D – Diagonale |
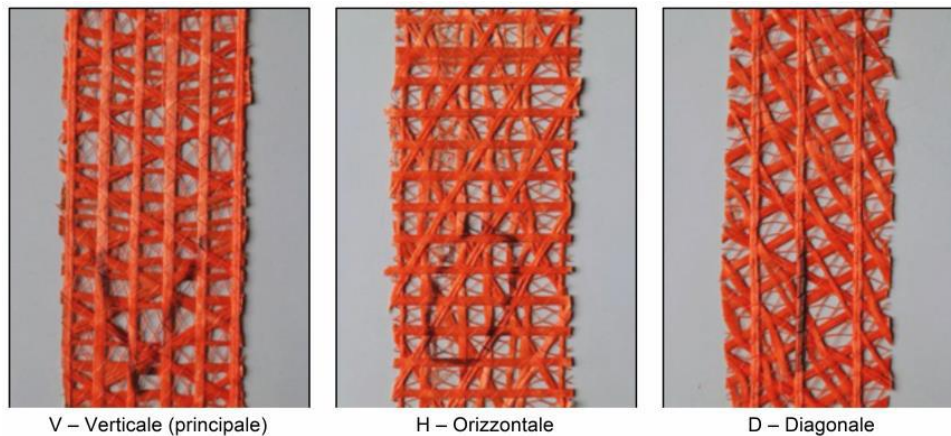
Figure 7. Used mesh of polymer-coated aramid and glass fibers

According to the conducted analyses and the possibilities for the application of the proposed system, the following strengthening elements were foreseen (Fig. 8):

- Vertical external elements VN1, VN2, VN3 and VN4 at the corners of the lower part of the stone masonry in the form of a square with a length of at least 320 cm and a height of at least 12.5 m (from elevation level -3.00 m to +8.50 m, plus overlapping length);
- Vertical external elements VN5, VN6, VN7 and VN8 on four of the eight sides of the octagonal part of stone masonry with a length of 220 cm and a height of 7.5 m (from elevation +8.50 m to +15.00, plus overlapping length);
- Vertical internal elements VV1, VV2, VV3 and VV4 on four of the eight sides of the brick masonry with a minimum length of 160 cm and a height of 10 m (from elevation +15.00 m to elevation +24.30 m, plus overlapping length). These elements were constructed on the inside of the walls due to the requirements for keeping the facade unchanged. In order to fully achieve the integrity effect, it is planned to connect these elements with composite bars (CFRP bars) placed next to the pilasters on the facade brick wall;
- Horizontal external elements HN1 and HN2 on the part of stone masonry in a square shape that go around the eternal facade on elevation +3.90 m and +8.00 m respectively, with a minimum width of 220 cm and 125 cm respectively and a length of 23 m;
- Horizontal external elements HN3 and HN4 on the section of stone masonry in an octagonal shape on elevation +10.50 m and +15.00 m respectively, with a width of at least 125 cm and a length of 18 m;
- Horizontal internal elements HV1, HV2 and HV3 on the section of brick masonry on elevation +16.90 m, +20.60 m and +23.70 m with widths of 3.20 m, 1.25 m and 1.25 m respectively, and a length of 13 m. The connection to the composite bars at the root of the pilasters described above applies to the connection to these elements as well. The connection should be achieved applying chromed steel stirrups inserted through the joints in the masonry on every 40 cm from elevation +16.40 m to elevation +23.40 m.

To consistently implement the strengthening below the ground level, based on the observation of the open probe, the knowledge obtained about the foundation and the calculations performed, a solution is provided for strengthening the foundation walls from elevation -4.00 m at least to elevation -2.00 m. It consists of a reinforced concrete wall, 25 cm thick with extra 80 cm of extension on the footing along the whole outer perimeter of the foundation walls after previous rehabilitation by injection and appropriate treatment of the surfaces. To achieve interaction with the existing foundation structure, chrome steel anchors with appropriate length were installed in previously drilled holes, filled with epoxy mortar. With such a solution, the reliability coefficient against overturning from maximum seismic forces have been significantly increased.
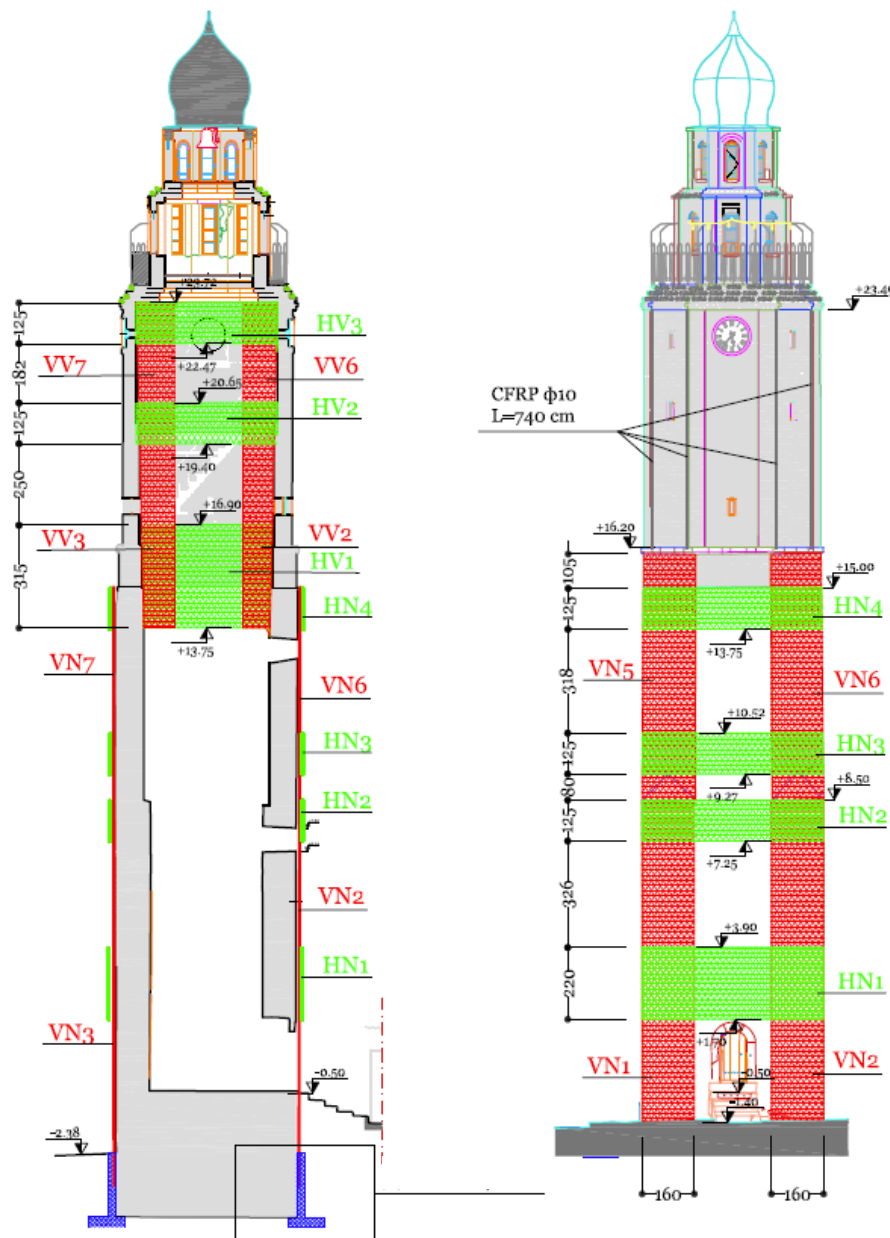
Figure 8. Strengthening elements – cross section (left), on the facade (right)

5. Structural analysis of the tower's state after the seismic retrofitting

For the strengthened state of the tower, a structural analysis for gravitational and seismic loads was carried out, whereby the structure is treated in accordance with the actual regulations and rules for the appropriate category of the building according to its meaning and purpose. For the purposes of this analysis, a mathematical model for the structural system was prepared (Fig. 9), where a two-dimensional finite element SHELL with four nodes was used to model the reinforcement elements.
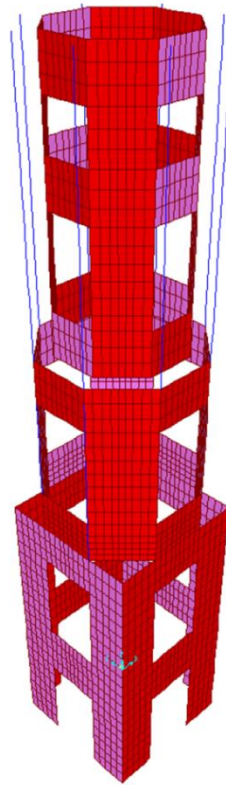
Figure 9. Numerical FEM model of the strengthening elements

For the strengthened structure modelled in this way, a modal analysis was performed, followed by an analysis from gravitational vertical loads as well as from equivalent seismic forces. According to the national regulations for high-rise buildings in seismically active regions [3], the seismic analysis had been conducted as for a first category building, with the seismic force intensity equal to 24% of the total weight of the building.

The mechanical parameters of the "ROFIX SismaCalce" system, were adopted according to the experimental verification results, obtained in IZIIS' laboratory [5]:

Weight W = 15.5 kN/m^3
Elasticity modulus (90^0) E^{90} = 51 000 MPa
Elasticity modulus (0^0) E^0 = 31 000 MPa

The total seismic coefficient was obtained using the Eq. 1 is K=0.24, where the values of each individual coefficients are given below:

Building category I coeff. (Ko = 1.5),
Site seismicity MCS IX coeff. (Ks =0.1),
Soil class I coeff. (Kd=1.0),
Ductility and damping coeff. for confined masonry (Kp= 1.6)

The natural periods of the retrofitted state T_{x-x} = T_{y-y} = 0.51s, T_{tor}=0.15s were obtained for the structure modelled in this way, which indicates a certain structural stiffening. The total displacements due to seismic force in the longitudinal and transverse direction are also reduced and within the allowed limits (δ_x=δ_y= 4.8 cm) (Fig. 10).
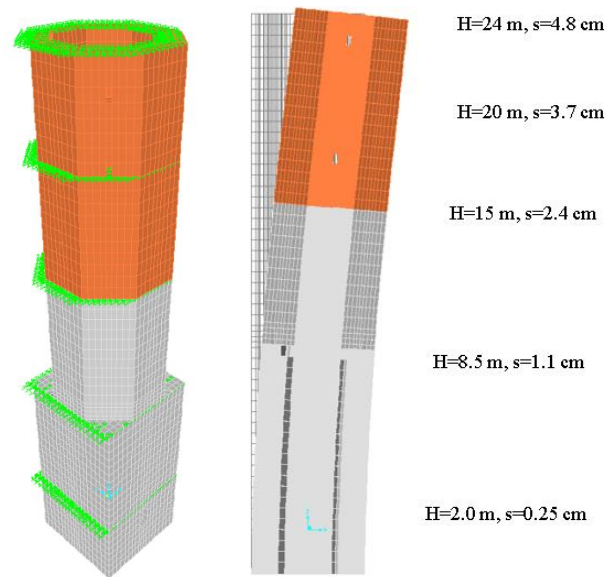
Figure 10. Retrofitted state - elevations of applied seismic forces (left), displacements due to the design seismic actions (right)

The resulting stress-deformation state of the retrofitted structure indicates that the maximum expected seismic impacts, tensile stresses is significantly reduced compared to the unretrofitted structure. Although remains higher than the expected tensile strength of the masonry in smaller local zones (Fig. 11), the global safety and stability of the structure to seismic events is significantly increased.
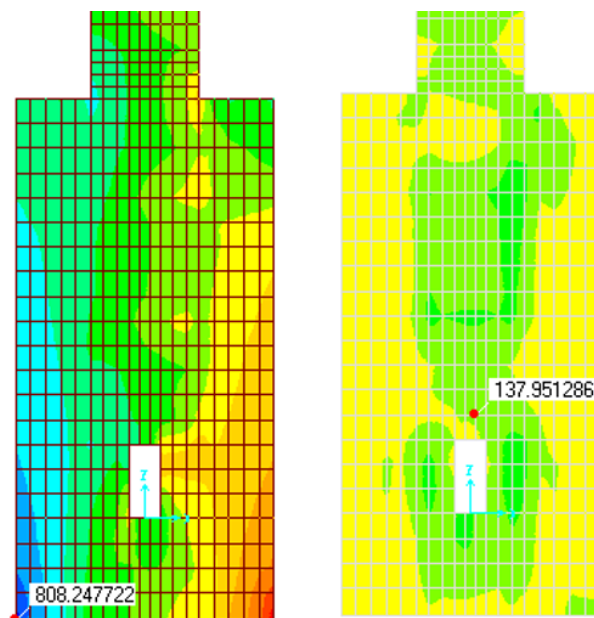
Figure 11. Retrofitted state - stress in kPa under gravity loads and seismic actions in critical points – vertical tensile stress (left), shear stress (right)

6. Conclusions

The paper presents seismic retrofitting of an important historic building – the Clock Tower in Skopje using the innovative Rofix SismaCalce System, that was previously experimentally verified. This system consists of a primary layer of basic hydraulic lime mortar, a layer of a mesh of polymer-coated aramid and glass fibers and a final layer of facade lime mortar. Comparison of the results from analytical investigation for both unretrofitted and retrofitted structure shows that the global safety and stability of the retrofitted structure to seismic events is significantly improved.

References

[1] Čolović D.M. (2010): Clock towers in the Republic of Macedonia. (in Macedonian), *Patrimonium III-Periodical for Cultural Heritage - Monuments, Restoration, Museums, N° 7-8,* (484-486), ISBN 978-9989-131-08-0.

[2] Nichota N. (1965): Design project for post-earthquake repair and strengthening of the Clock Tower. (in Macedonian), *Technical Report,* Republic Institute for protection of cultural heritage, N. Macedonia

[3] PIOVS (1981): Rulebook on technical regulations for construction of buildings in seismic regions, *OG SFRY No. 31/81*, Amendments 49/82, 29/83, 21/88 and 52/90.

[4] Shendova V., Jekic G. (2018): Design project for conservation, structural consolidation and retrofitting of the Clock Tower in the Sultan Murat Mosque complex. *Technical Report*, Republic Institute for protection of cultural heritage, N. Macedonia.

[5] Shendova V. (2013): IZIIS-RÖFIX scientific research project on experimental verification of inovative technique for seismic retrofitting of traditional masonry building. *Report IZIIS 2013-44*, N. Macedonia.

SEISMIC PERFORMANCE OF MASONRY POINTED VAULTS – CASE STUDY OF ST. ANTHONY CHURCH IN BARBAN, ISTRIA

Paulo Šćulac [(1)], Davor Grandić [(2)], Toni Šaina [(3)]

[(1)] *Assistant Professor, University of Rijeka, Faculty of Civil Engineering, Croatia, paulo.sculac@uniri.hr*
[(2)] *Professor, University of Rijeka, Faculty of Civil Engineering, Croatia, davor.grandic@uniri.hr*
[(3)] *Senior conservator-restorer, Croatian Conservation Institute, Department for Wall Paintings and Mosaics, tsaina@hrz.hr*

Abstract

More than 140 churches with medieval wall paintings have been preserved in Istria, which are an essential part of Istrian cultural identity, and classify Istria as the region with the greatest density of this type of cultural heritage. In the last 25 years considerable effort has been put into the preservation and conservation of the wall paintings, but also in the restoration of the churches from the structural point of view. The most significant adverse effects on the frescoes are capillary humidity and cracks that occur as a result of the ground settlement. In this paper we will focus on small single-nave churches with pointed barrel vaults, which are characteristic for the Gothic period. As a case study, the seismic capacity of the church of St. Anthony in Barban will be studied. The interior of the church was entirely painted in the early 15th century. The church has a simple architecture: a rectangular ground plan, roof covered with slate tiles and a bell gable present at the front façade. The walls are built of regular stone blocks in lime mortar. We present results of the numerical analysis of the pointed vault due to seismic actions. The admissible failure mechanisms related to formation of plastic hinges are examined.

Keywords: stone masonry, single-nave church, pointed barrel vault, medieval wall paintings, seismic capacity

1. Introduction

Due to a combination of favourable historical circumstances a large number of churches with wall paintings has been preserved in Istria. So far, more than 140 sites [1] with wall paintings dating from the 8th until the end of the 16th century have been investigated and documented [2, 3]. The most prominent researcher and connoisseur of Istrian wall paintings was academician Branko Fučić, who made a great contribution to their discovery, valorisation and popularization.

The standard procedure for preparation of the wall substrate for a wall painting consisted of two steps: first a thick layer of coarse lime plaster was applied, which was then followed by a final fine plaster, applied only on that wall area that could be painted during one day. This fine plaster was then painted with inorganic pigments. As a rule, the purpose of the wall paintings in the Middle Ages was to educate the illiterate population, therefore they were full of hidden messages, stories and warnings. Some of these messages were successfully interpreted while some of them still remained unrevealed due to the passage of time. An exceptional historic record is also hidden in the drawings and graffiti, written in Glagolitic or Latin, cut with a sharp object on the wall paintings [4].

In this work we explore the dynamic response of single-nave churches with pointed barrel vaults that contain these valuable wall paintings. In total, about 15 churches of such characteristics have been preserved [3]. Commonly, these are small churches whose ground plan dimensions do not exceed 10 m, built from local limestone shaped into more or less regular blocks. The vault, on the other hand, is usually made of smaller and less processed units and is significantly thinner than the load-bearing walls. Vaults were originally covered with slate tiles – in some cases they were replaced with clay tiles. The walls were mostly plastered on the outside (except in cases when large regular stone blocks were used). Nowadays, due to deterioration this plaster is often no longer present.

As a case study, the seismic performance of the pointed vault in St. Anthony church in Barban will be studied.

2. St. Anthony church in Barban

The church of St. Anthony in Barban is located in the immediate vicinity of the entrance gate and the walls of the former fortified castle (Fig. 1). It is a small single-nave Gothic building with rectangular ground plan (7,7 x 5,8 m) and a pointed barrel vault (Fig. 2), built at the turn of the 14th to the 15th century. Due to its preserved medieval frescoes the object is inscribed in the Croatian Register of Cultural Properties as a protected cultural heritage.

The walls are made of regular square stone blocks in lime mortar with very thin joints (not plastered on the outside). The thickness of the walls is 75-80 cm. On each façade a small narrow window is present; the front western façade also contains two square windows and a bell gable. Roof is covered with slate tiles (Fig. 1).

Figure 1. St. Anthony church in Barban: a) front view; b) Interior view.
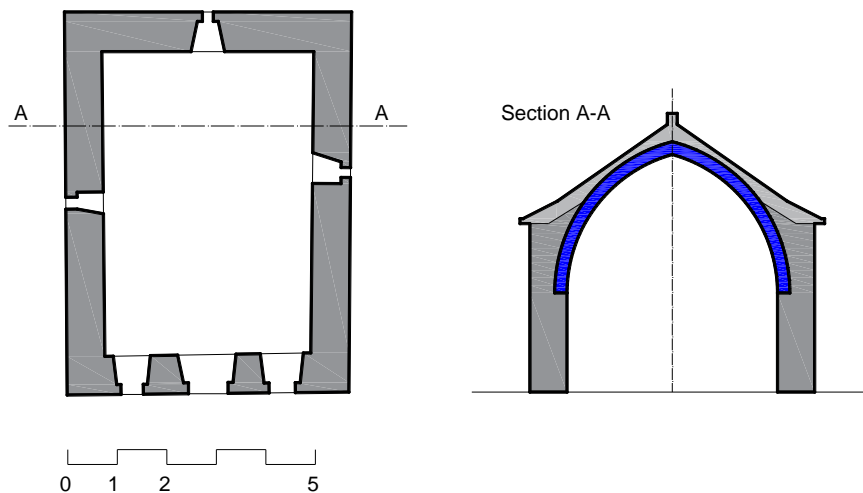
Figure 2. Ground plan and section A-A with marked pointed vault.

The area around the church has been raised afterwards by more than one meter thus making a basin around the church (Fig. 1). The walls of the church are separated from the surrounding elevated terrain by a narrow space; only in front of the western (entrance) façade there is a flat stone-paved area, reached by stairs. Due to the raised terrain, during heavy rains rainwater overflows from the nearby road and parking lot, which is retained in the area in front of the church. In this way, the walls of the church are filled with capillary moisture, which damages the structure of the wall, as well as the wall paintings inside the church.

At the beginning of the 15th century its interior was painted with 15 scenes from the legend of St. Anthony the Abbot, the patron saint of the church, shown in two opposite bands on the north and the south wall. The western and the eastern walls were also painted with depiction of the Virgin Mary with the Child and images of various saints important to the local community. On all surfaces of the preserved wall paintings we can find incised numerous Glagolitic graffiti, depictions of architecture (fortified towns, bell towers and churches), figural drawings, depictions of ships and stylized ornaments (Fig. 3). The time of painting can be determined by the oldest graffiti, dated before 1429 [4].

Figure 3. a) Drawing of a ship; b) Glagolitic graffiti.

By studying archival photos and conservation and restoration reports [5], it was detected that the church was repaired on several occasions. The last significant interventions were carried out in the 1960s: the works consisted of repairing the roof covering, some plastering in the interior and retouching of the paintings. From 2005 till 2013 the Croatian Conservation Institute carried out the necessary preventive works in the interior and a complete replacement of the roof covering (Fig. 4), since more than 80 slate tiles were damaged and with each heavy rain the roof and the vault leaked, so that some parts of the vault paintings were irretrievably lost [7].

3. Horizontal capacity of the pointed barrel vault

Pointed arches and vaults give smaller values of thrust than circular arches and can be made thinner than circular arches for large angles of embrace [8], which is why they were especially exploited during the Gothic period. Pointed arches can sustain greater support displacements as well [8]. When pointed arches supported on buttresses are subjected to horizontal accelerations, they have in most cases bigger horizontal capacity than their circular counterparts [9], but this should be confirmed on a case-by-case basis.

Following the Heyman's assumptions that sliding failure cannot occur and that masonry has no tensile strength but infinite compressive strength limit analysis may be applied to masonry structures [10]. This means that the collapse of the structure does not occur due to exceeding of the masonry strength but due to loss of stability. The collapse of the masonry vault will therefore occur due to formation of sufficient number of plastic hinges and transformation of the system into a mechanism. The analysis of masonry arch structures is thus based entirely on the arch geometry.

Figure 4. Extrados of the vault during the replacement of the roof tiles in 2008 [6].

Dynamic behaviour of pointed arches has been recently studied by Di Carlo et al. [11], Dimitri and Tornabene [9], Misseri and Rovero [12] and Zizi et al. [13]. Misseri et al. [14] performed an extensive experimental campaign on pointed arches under quasi-static horizontal loading, while Šćulac and Čeh [15] documented collapse mechanisms of a pointed arch tested on a shaking table.

Seismic capacity of buttressed masonry arches has been studied in detail in [16,17,18], although they focused only on semicircular or segmental arches (angle of embrace less than 180°). Seismic capacity of buttressed pointed arches is much less investigated. Two studies containing an extensive parametric investigation including various geometrical parameters were conducted by Dimitri and Tornabene [9] and Chisari et al. [19].

In this work the methodology proposed by Brandonisio et al. [17,18] for analysis of buttressed masonry arches under horizontal loads will be applied to the segmental pointed arch from St. Anthony church in Barban. The idealised geometry of the pointed arch supported by two walls (i.e. two buttresses) is shown in Fig. 5. A uniform arch thickness of 25 cm was assumed.
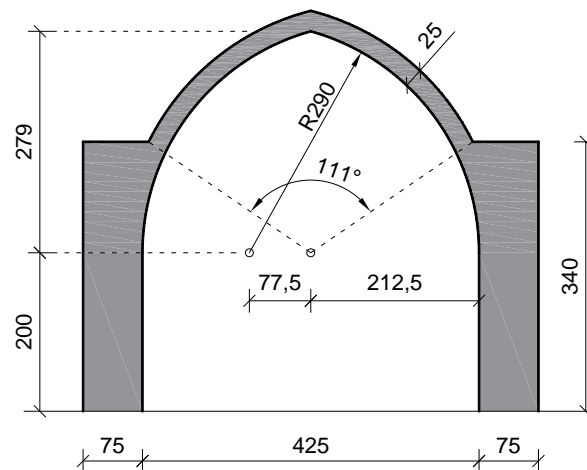
Figure 5. Idealised geometry of the pointed vault supported by two walls (buttresses).

Figure 6 shows three physically admissible hinging mechanisms of the buttressed pointed vault subjected to gravity loading and constant horizontal ground accelerations, that are usually evaluated [18]. The system is divided into rigid bodies connected by four hinges occurring alternately at the extrados and intrados of the system. In the local mechanism (Fig. 6a) the four-hinge mechanism develops only within the vault. This commonly happens in case when the vault is slender while the buttresses are squat [16]. In the semi-global mechanism (Fig. 6b) one wall (buttress) is included into the hinging mechanism and a hinge develops at the bottom of the wall. Finally in the global mechanism (Fig. 6c) two hinges open at the bottom of the walls and both walls are included into the hinging mechanism. In any case, the seismic capacity significantly depends on the geometry of the vault and the buttresses and the load values, and there is no exact rule which mechanism will be relevant.
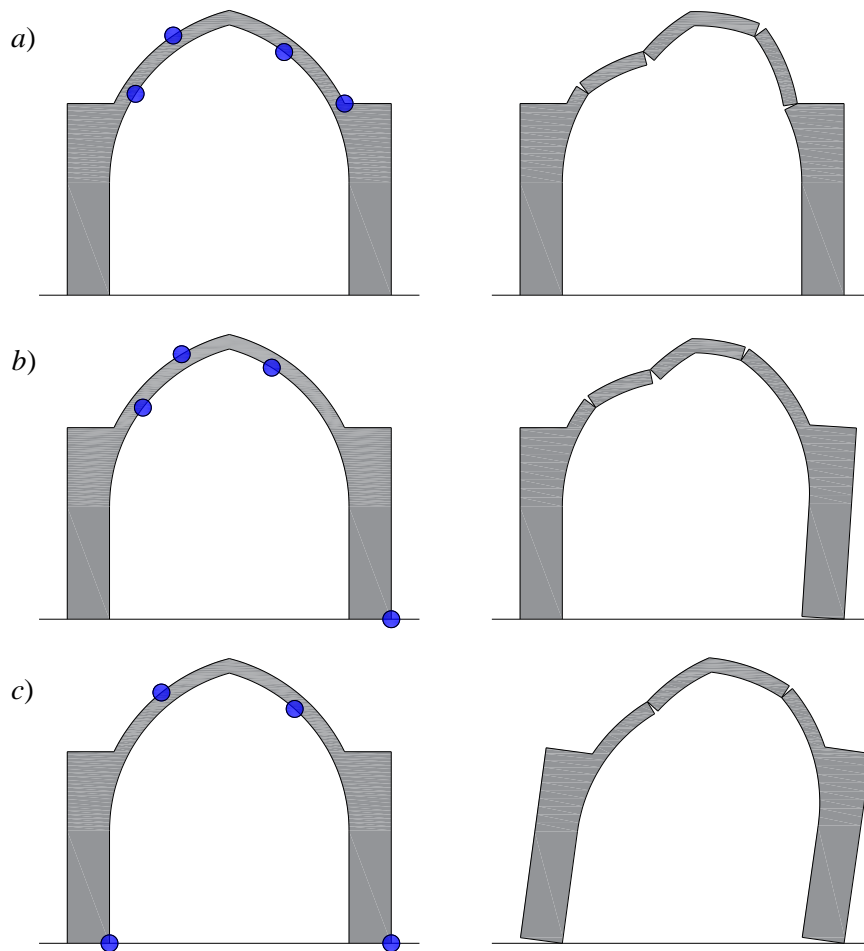
Figure 6. Collapse mechanisms: a) Local mechanism; b) Semi-global mechanism; c) Global mechanism.

Figure 7 presents the kinematics of the local mechanism (according to Fig. 6a) with the corresponding vertical and horizontal virtual displacements. The self-weight of the vault is applied as a vertical force W_i acting in the centre of mass of each rigid body i along with horizontal forces λW_i proportional to the self-weight of each rigid body i via horizontal load multiplier λ.

Applying the principle of virtual work and taking into account that the internal work is equal to zero (since we are dealing with rigid bodies) we obtain the following virtual work equation

$$\sum_{i=1}^{N} W_i \cdot \delta_{v,i} + \sum_{i=1}^{N} \lambda W_i \cdot \delta_{u,i} = 0 \qquad (1)$$

where N is the number of rigid bodies, while $\delta_{u,i}$ and $\delta_{v,i}$ are horizontal and vertical virtual displacements of the rigid body i, respectively.

The horizontal load multiplier λ may be obtained from (1) as

$$\lambda = -\frac{\sum_{i=1}^{N} W_i \cdot \delta_{v,i}}{\sum_{i=1}^{N} W_i \cdot \delta_{u,i}} \tag{2}$$

Solving the virtual work equation we obtain load multiplier λ equal to 0,39, i.e. ground acceleration equal to 0,39 g will cause the opening of four hinges in the vault and formation of the collapse mechanism.

The location of the hinges was found iterative in order to get the minimum value for λ. For acceleration acting to the right a hinge always forms at the extrados of the right springing (C_3). Note that the embrace angle is only 111°, so C_1 will also form at the left springing [9].
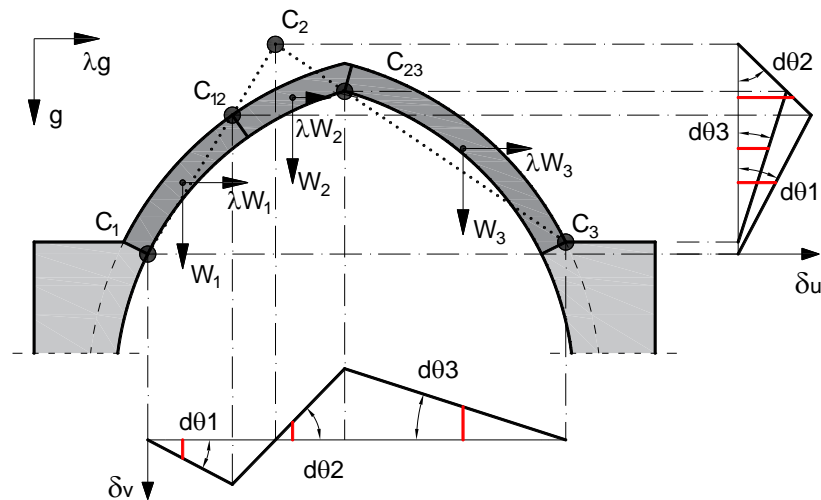
Figure 7. Formation of a local mechanism (hinges formed only in the vault)

Figure 8 presents the kinematics of the semi-global and global mechanism. Solving the virtual work equation we obtain load multiplier λ equal to 0,15 for semi-global and 0,19 for global mechanism.
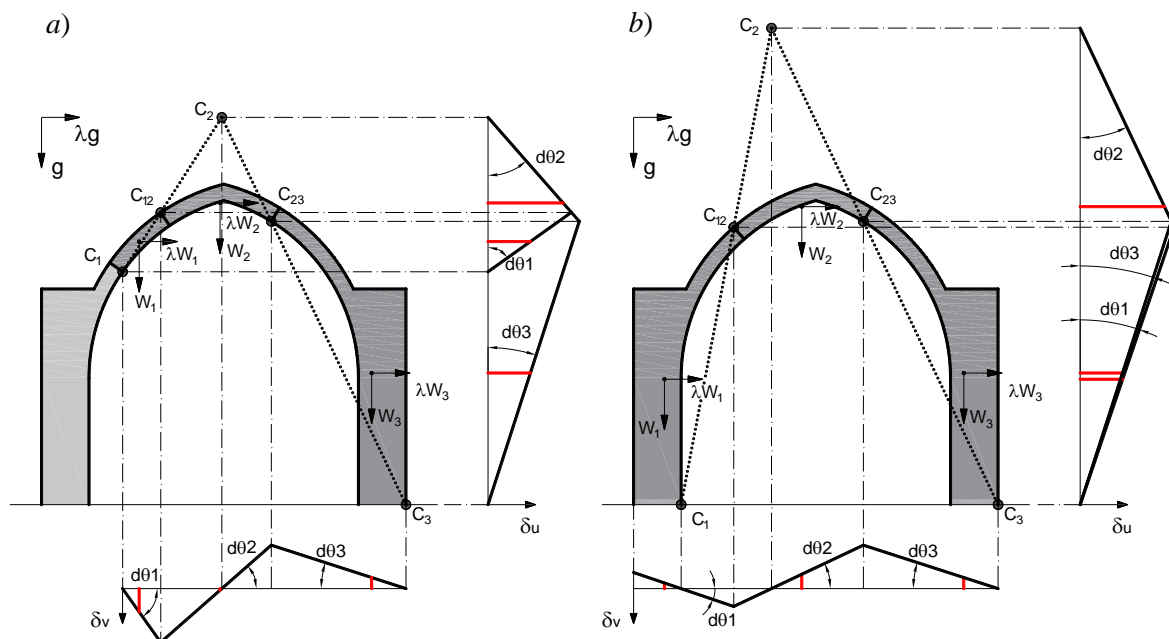
Figure 8. a) Semi-global mechanism; b) Global mechanism.

These mechanisms are originally proposed for buttressed arches i.e. when the arch is supported on piers. In the building under consideration the buttresses (walls) are supported by transversal walls at a small distance, thus achieving a spatial behaviour of the building. Due to the good quality of transversal walls, appropriate connection of walls and box-like behaviour the semi-global and global mechanism would not be activated. The relevant mechanism is thus the local mechanism with load multiplier λ equal to 0,39.

The reference peak ground acceleration on type A ground for the location considered equals to 0,134 g for a reference return period of 475 years [20]. In combination with the importance factor equal to 1,2 (due to social and economic consequences of collapse attributed to importance class III) the design ground acceleration equals to 0,16 g. This means that the considered pointed vault has satisfactory seismic resistance. In case the seismic capacity of the vault would not be satisfactory, the only appropriate vault strengthening would include reinforcement at the extrados, since the intrados of the vault contains wall paintings.

The peak ground acceleration demand 0,16 g refers to systems at the ground level. It is assumed that this value is the same at the level of the vault springing, since the height of the walls is small. In case of mid-rise and high-rise buildings the acceleration amplification effect resulting from the response of the global system on which the vault rests should be considered.

The effect of infill at the connection with the walls (see Fig. 4) was not taken into account in the analysis. Since the infill has a favourable effect on the behaviour of the vault [21], the seismic capacity would be even higher.

4. Conclusions

In this work we studied the dynamic response of St. Anthony church in Barban with pointed barrel vault, which contains valuable wall paintings. The physically admissible hinging mechanisms of the pointed arch subjected to gravity loading and constant horizontal ground accelerations have been analysed. The collapse of the buttressed vault will occur due to formation of four plastic hinges occurring alternately at extrados and intrados and transformation of the system into a mechanism.

Due to the good quality of transversal walls, appropriate connection of walls and box-like behaviour the semi-global and global mechanism would not be activated. The relevant mechanism is the local mechanism, i.e. the four-hinge mechanism would form only in the vault. The considered vault has satisfactory seismic resistance.

Acknowledgements

References

[1] Bistović, Ž. Wall paintings, https://istra.lzmk.hr/clanak.aspx?id=3092, (accessed September 21, 2022).

[2] Fučić, B. (1963): *Istrian frescoes (in Croatian)*. Zora, Zagreb.

[3] Bistrović, Ž. (2011): *Colourful trail of Istrian frescoes*. Istria County, Pula.

[4] Fučić, B. (1982): *Glagolitic Inscriptions (in Croatian)*. JAZU, Zagreb.

[5] Photo Archive of the Conservation Department in Rijeka, Ministry of Culture and Media - Republic of Croatia

[6] Author of photos: Serđo Tomišić, Kapitel d.o.o. (2008)

[7] Šaina, T. (2020): Restoration of frescoes in Barban churches, *The Parish Church of St. Nicholas in Barban*, Proceedings of the scientific conference in occasion of 310th anniversary of construction and consecration, Barban.

[8]   Romano, A., Ochsendorf, J.A. (2010): The mechanics of gothic masonry arches, *International Journal of Architectural Heritage*, **4** (1), 59-82, doi: https://doi.org/10.1080/15583050902914660

[9]   Dimitri, R., Tornabene, F. (2015): A parametric investigation of the seismic capacity for masonry arches and portals of different shapes, *Engineering Failure Analysis*, **52**, 1–34, doi: https://doi.org/10.1016/j.engfailanal.2015.02.021

[10] Heyman, J. (1982): *The masonry arch*, Ellis Horwood Limited.

[11] Di Carlo, F., Coccia, S., Piedigrossi M. (2017): Dynamics of masonry pointed arches under base motion, *International Journal of Masonry Research and Innovation*, **2** (4), 335-354, doi: https://doi.org/10.1504/IJMRI.2017.087447

[12] Misseri, G., Rovero, L. (2017): Parametric investigation on the dynamic behaviour of masonry pointed arches, *Archive of Applied Mechanics*, **87**, 385-404, doi: https://doi.org/10.1007/s00419-016-1199-4

[13] Zizi, M., Cacace, D., Rouhi, J., Lourenço, P.B., De Matteis, G. (2022): Automatic Procedures for the Safety Assessment of Stand-alone Masonry Arches, *International Journal of Architectural Heritage*, **16** (9), 1306-1324, doi: https://doi.org/10.1080/15583058.2021.1881655

[14] Misseri, G., DeJong, M.J., Rovero, L. (2018): Experimental and numerical investigation of the collapse of pointed masonry arches under quasi-static horizontal loading, *Engineering Structures*, **173**, 180-190, doi: https://doi.org/10.1016/j.engstruct.2018.06.009

[15] Šćulac, P., Čeh, N. (2023): Experimental test on a pointed arch model monitored by contactless optical system, *International Journal of Masonry Research and Innovation*, 1-16.

[16] Alexakis, H., Makris, N. (2017): Hinging Mechanisms of Masonry Single-Nave Barrel Vaults Subjected to Lateral and Gravity Loads, *Journal of Structural Engineering,* **143** (6), 04017026, doi: https://doi.org/10.1061/(ASCE)ST.1943-541X.0001762

[17] Brandonisio, G., Mele, E., De Luca, A. (2017): Limit analysis of masonry circular buttressed arches under horizontal loads, *Meccanica,* **52**, 2547-2565, doi: https://doi.org/10.1007/s11012-016-0609-6

[18] Brandonisio, G., Angelillo, M., De Luca, A. (2020): Seismic capacity of buttressed masonry arches, *Engineering Structures*, **215**, 110661, doi: https://doi.org/10.1016/j.engstruct.2020.110661

[19] Chisari, C., Cacace, D., De Matteis, G. (2021): Parametric investigation of the effectiveness of FRM-retrofitting in masonry buttressed arches, *Buildings*, 11, 406, doi: https://doi.org/10.3390/buildings11090406

[20] HRN EN 1998-1:2011/NA:2011 *Eurocode 8: Design of structures for earthquake resistance* - Part 1: General rules, seismic actions and rules for buildings -National Annex.

[21] Gago, A.S., Alfaiate, J., Lamas, A. (2011): The effect of the infill in arched structures: Analytical and numerical modelling, *Engineering Structures*, **33** (5), 1450–1458, doi: https://doi.org/10.1016/j.engstruct.2010.12.037

RETROFITTING OF SACRAL BUILDINGS AFTER THE RECENT EARTHQUAKES IN CROATIA

David Anđić [(1)], Maja Baniček [(2)], Tamara Horvat [(3)], Borna Doračić [(4)], Juraj Pojatina [(5)], Mislav Stepinac [(6)], Ana Baričević [(7)]

[(1)] *Structural Engineer, Studio Arhing ltd., david@studio-arhing.com*
[(2)] *Postdoctoral Researcher, University of Zagreb Faculty of Civil Engineering, maja.banicek@grad.unizg.hr*
[(3)] *Structural Engineer, Studio Arhing ltd, tamara@studio-arhing.com*
[(4)] *Structural Engineer, Studio Arhing ltd., borna@studio-arhing.com*
[(5)] *Structural Engineer, Studio Arhing ltd., juraj@studio-arhing.com*
[(6)] *Assistant Professor, University of Zagreb Faculty of Civil Engineering, mislav.stepinac@grad.unizg.hr*
[(7)] *Associate Professor, University of Zagreb Faculty of Civil Engineering, ana.baricevic@grad.unizg.hr*

Abstract

After the Petrinja earthquake in December 2020, 442 individual immovable cultural assets were damaged, including 124 cultural heritage buildings that suffered severe structural damage. The largest number of damaged cultural heritage assets concern sacral buildings, mainly churches and chapels. In this paper, a brief overview of the damage to several sacral buildings after the earthquakes in Croatia is presented. The failure mechanism and typical damages are presented graphically. In addition, special emphasis is placed on the complete retrofitting of a damaged church. The condition assessment, numerical modelling and full seismic retrofit of the selected church is shown.

Keywords: Retrofitting, Assessment, Heritage buildings, Church, Earthquake

1. Introduction

Following the Zagreb earthquake in March of 2020, a destructive 6.2 magnitude earthquake struck Croatia again in December of 2020. The Sisak-Moslavina county suffered the most severe consequences; many historical and cultural buildings were severely damaged [1]. According to the data collected by the Croatian Center for Earthquake Engineering (HCPI – in Croatian), more than 57 000 buildings were damaged [2]. The forms and features of the architectural heritage in the affected area are influenced by the attributes of a militarized frontier under the Habsburg monarchy [3]. The Sisak-Moslavina county is characterized by small historical settlements with prominent parish churches, chapels, and isolated aristocratic estates with palaces [4]. In Sisak-Moslavina county alone, 308 immovable cultural assets with 4,416 houses in cultural and historical areas were damaged. According to the data of the World Bank report [5] and HCPI [2], 206 religious buildings were damaged by the earthquake, 52 were severely damaged or demolished. Most churches suffered severe damage to the load-bearing walls, vaults, and bell tower walls, compromising the overall stability of the buildings. Several churches suffered collapse of parts of the building, usually the bell tower, the roof, the vaults, and parts of the perimeter walls. The degree and severity of the damage was classified according to EMS-98 [6]. In February 2021, the new Law on the Reconstruction of Earthquake-Damaged Buildings in the City of Zagreb, Krapina-Zagorje County, Zagreb County, Sisak-Moslavina County and Karlovac County was enacted [7]. The Law and Amendment to the Technical Regulation for Building Structures (Official Gazette 75/2020) [8] defines four different levels of reconstruction of earthquake-damaged structures in terms of achieved mechanical resistance and stability. In this paper, severely damaged churches (3 case studies) are presented. The focus of the study is on the condition assessment procedures and retrofitting methods following the holistic approach of the international council on monuments and sites (ICOMOS).

2. Condition assessment of selected churches

2.1 Historical background

The materials and geometry of the damaged churches coincide with the time and area of construction. The church of St Michael in Gračani (Zagreb) is a 17th century masonry structure with stone walls and brick arches and cross vaults. St. George's church and St. Mary's chapel are located in Mala Gorica, approximately 60 km from Zagreb (Figure 1). St. George's church is a masonry structure with stone walls, arches and cross vaults from the 18th century, while St. Mary's chapel is a 20th century structure with masonry walls and a wooden barrel vault, hanged onto the roof structure. Floor plans and sections are shown in Figures 2, 3 and 4.
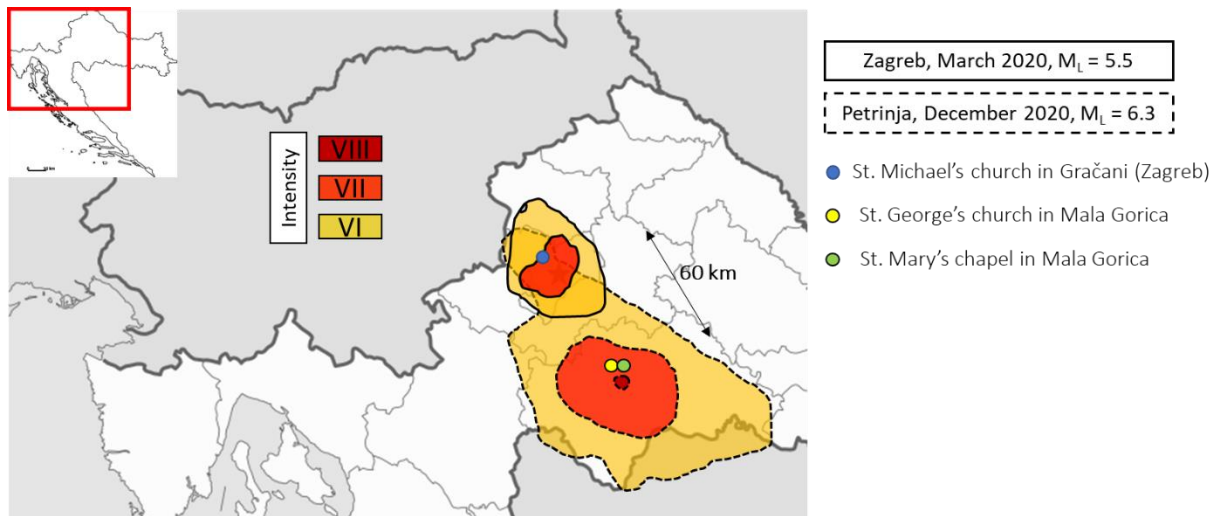
Figure 1. Map of church locations
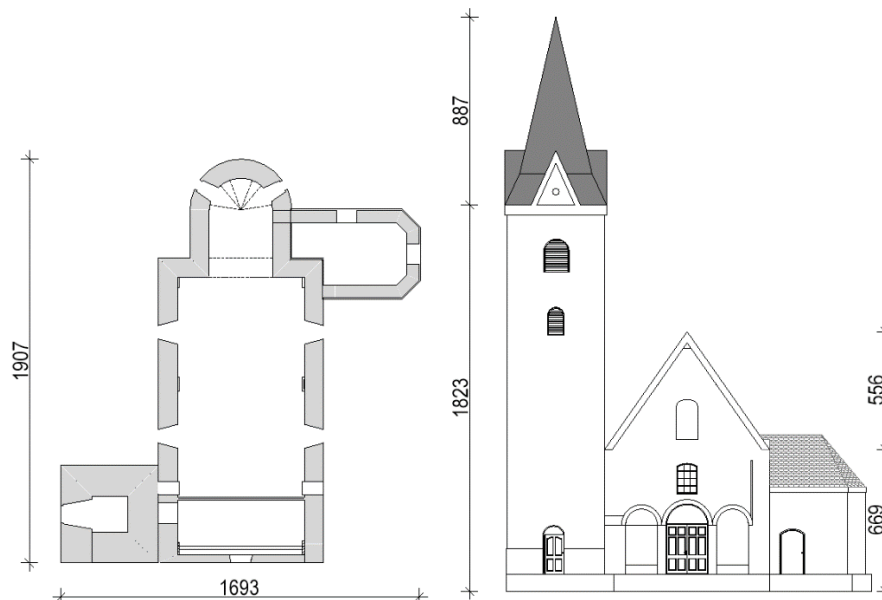
Figure 2. The Church of St. Michael in Gračani (architectural blueprint made in 2020.)
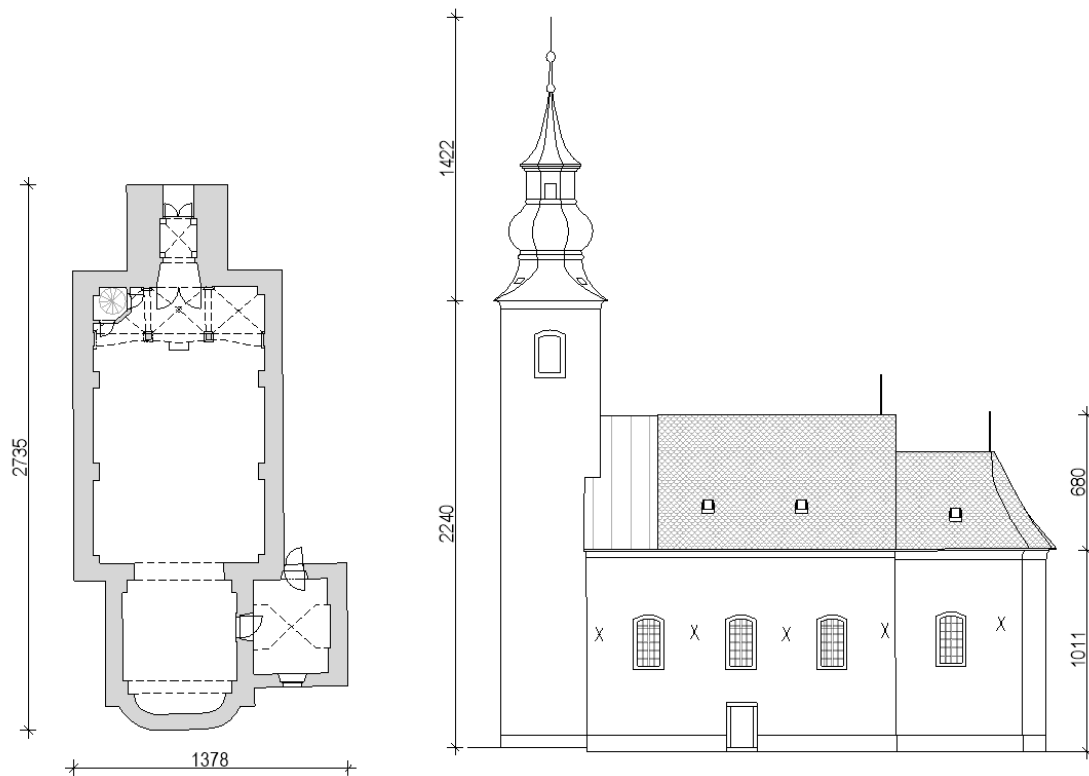
Figure 3. The Church of St. George in Mala Gorica (architectural blueprint made in 2021.)
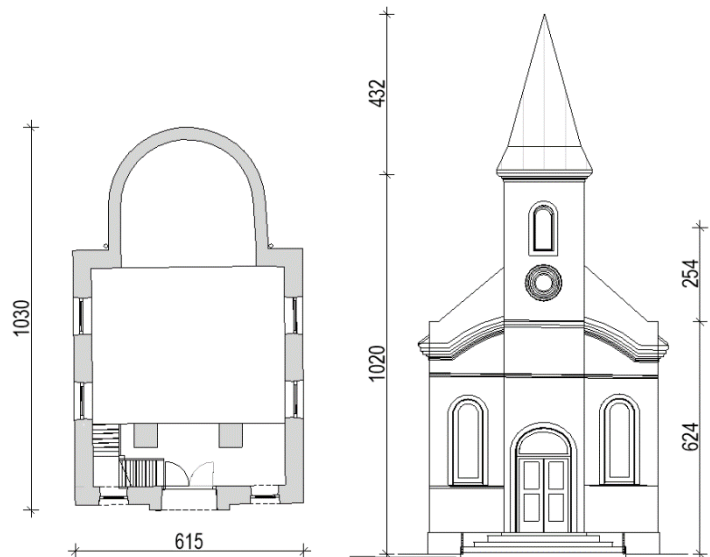
Figure 4. St. Mary's chapel in Mala Gorica (architectural blueprint made in 2022.)

As already mentioned, traditional materials were used. Multi-leaf stone or solid brick masonry with minimal lime mortar for the walls. Arches and vaults are made of stone, solid bricks or timber. Roof structures are mostly made of softwood.

2.2 Visual inspection

Visual inspection is the first step in condition assessment of an earthquake-damaged building. The result of the visual inspection is information about structural and/or mechanical damage to the structure (such as cracks, deformations and deflections), which are used to identify failure mechanisms.

2.2.1 The Church of Saint Michael, Gračani

The church of Saint Michael in Gračani (Zagreb) has suffered substantial damage to the tower. Diagonal cracks and local deviation from the verticality of the tower, Figure 5, clearly suggested the main failure mechanism, in-plane shear/tension failure of the tower walls. The damage was classified as level 3 in EMS-98.
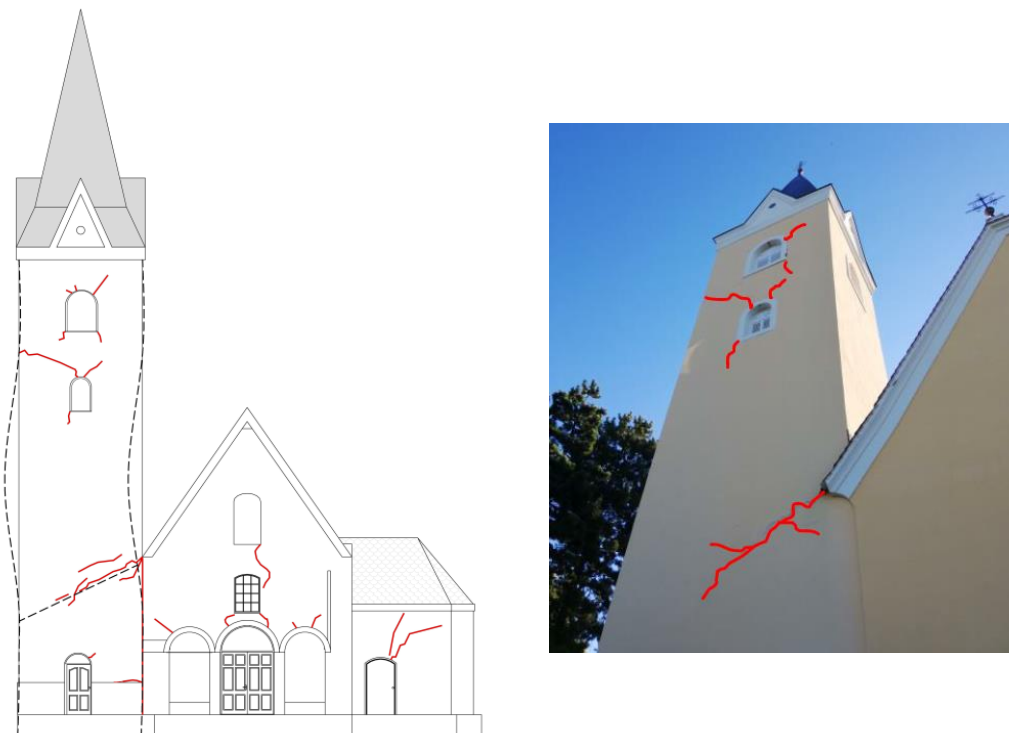
Figure 5. The main failure mechanism of the tower

Other main structural elements, such as walls and vaults, suffered damage characteristic of cyclic seismic excitation. Cracks on vaults occurred on the intrados when the tensile strength of masonry was reached, leading to the formation of plastic joints - hinges, while the walls were damaged mainly at the corners of the openings, i.e. at the points with the highest stress concentration. Timber roof structures were almost not damaged during the earthquake mostly due to their low mass.

2.2.2 St. Mary's chapel, Mala Gorica

St. Mary's chapel in Mala Gorica sustained very severe damage of the tower (level 4 in EMS-98). The combined shear and tension failure of the tower columns resulted in horizontal deflection of the tower in the range of 10 cm at the top, Figure 6. The triumphal arch was also severely damaged and exhibited wide cracks on the intrados and at the crown of the arch, characteristic for cyclic seismic excitation. Ground slab deflections were noted, indicating possible liquefaction of the soil.
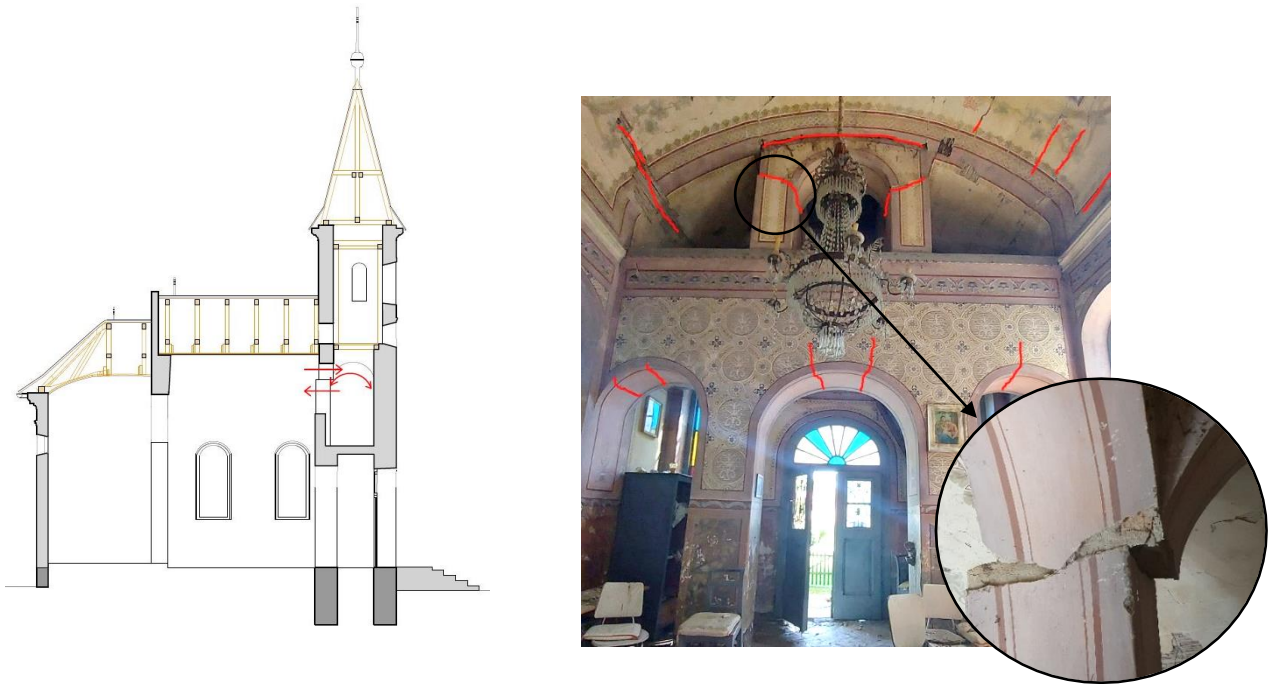
Figure 6. The main failure mechanism of the tower
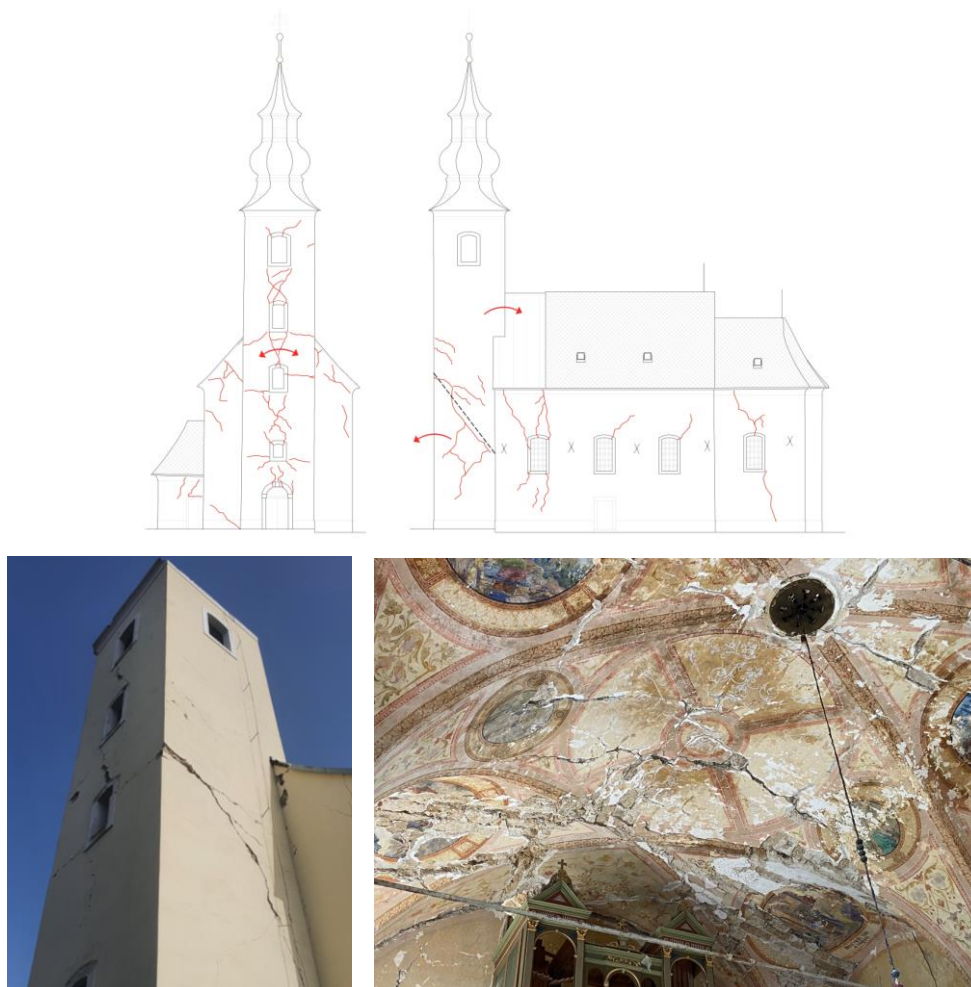
Figure 7. Main failure mechanism of the tower (left) and vaults (right)

341

Since the vault of the chapel is a timber barrel vault suspended from a timber roof structure, it was only slightly damaged in the earthquake – the transverse cracks, seen in figure 6, are merely surface cracks in the plaster.

2.2.3 St. George's church, Mala Gorica

On the northwestern façade of the tower, it is easy to distinguish two structural elements - vertical elements around the openings - piers connected with horizontal elements below/above the openings - spandrels. The damage pattern is shown in Figure 7. It refers to the extremely rigid spandrels that suffered shear failure. Diagonal cracks on the side walls form a clear sliding plane. Due to the very severe structural damage - level 4 on the EMS-98 scale - the upper half of the tower was dismantled as an urgent measure. The stone cross-vaults were significantly damaged by tensile failure on both the intrados and extrados. The walls, which were also of stone masonry, exhibited a number of cracks due to shear failure, out-of-plane bending failure (i.e. gable walls in the roof) and failure of the foundation soil. In this case, the timber roof structure was also affected by the earthquake – the failure of the gable walls caused mechanical damage to the timber columns and beams. In addition, the cyclic nature of an earthquake caused localized failure of timber connections, which is to be expected due to the low ductility of traditional carpentry connections.

2.3 Detailed investigation

Destructive, semi-destructive and/or non-destructive testing was performed. Destructive testing consisted of wall, floor and ceiling investigative probes and core drilling of walls. Semi-destructive testing was conducted on the timber structures of the building to determine density and moisture content. Non-destructive testing consisted of thermography and geotechnical investigative works. Thermography results were indicating elevated moisture content in the assessed structures, mainly in the Church of St. George in Mala Gorica. Increased moisture curing is proposed based on the assessment. One of the most important aspects of evaluating an existing structure is to gather all the necessary information crucial for the global stability of the structure. In the case of sacred structures, these include the geometry, wall thicknesses, wall structure in cross-section [9], foundation depth and soil type [10]. The existence and position of iron or steel ties, the condition of the roof structure is determined by visual inspection and are equally important for predicting the mechanical characteristics of the old masonry walls [11].

3. Structural Analysis of existing church in Gračani

The Church in Gračani is selected for further analysis and retrofit presenting as the only one where retrofitting works have already been executed. Numerical modelling and analysis were carried out in the Abaqus Standard software package [12] for academic purpose of writing this paper. The calculation is based on the finite element method and a dynamic nonlinear analysis of the structure was performed. The action of an earthquake was simulated with the acceleration of the ground at the location approximately corresponding to the earthquake that shook Zagreb on March 22, 2020. The frequency spectrum of the ground motion record corresponds to the currently valid regulation in the Republic of Croatia. The earthquake is defined by two horizontal and one vertical component. Due to the geometry and complexity of the model, volumetric finite elements were used. In addition, the Concrete Damage Plasticity (CDP) model was used to simulate the masonry wall behaviour. The CDP model of masonry assumes two types of failure mechanisms, namely tensile cracking and compression crushing of the material. In compression, the relationship between stress and strain is linear up to a certain point, followed by hardening to maximum stress and subsequent softening of the material with inelastic deformations. For tensile stresses, the model follows a linear relationship until a crack appears in the material. After that, softening occurs with the localised deformations in the element. The behaviour of masonry in the cracked state implies the definition of the post-critical stress as a function that depends on the crack tensile deformations. Due to the problem of excessive sensitivity of the mesh in materials with extremely unstable post-critical behaviour, the behaviour of the material in tension is described by the fracture energy criterion, which represents the energy required to open a unit area of the crack and

is a property of the material. In addition to the described behaviour in tension and compression, the function of the yield surface is additionally defined, which takes into account the triaxial stress state. The finite element mesh is formed by tetrahedrons and hexahedra of approximately equal size and regular shape and is coordinated with the behaviour of the material in the post-critical tensile region where the system is unstable and sensitive to mesh selection.
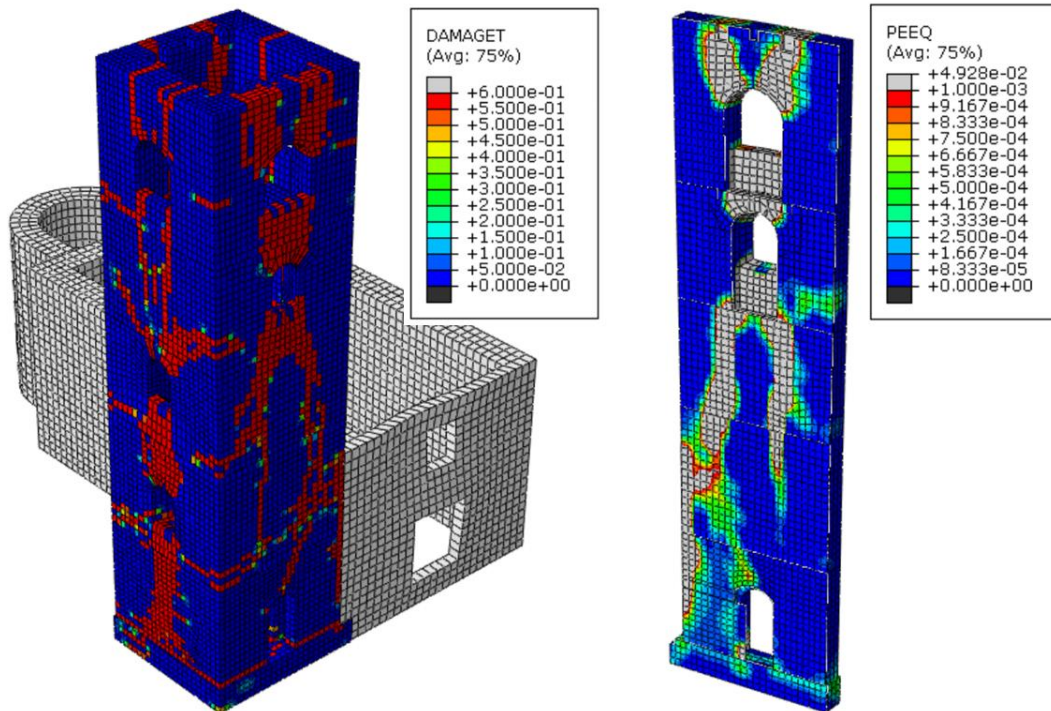
Figure 8. Bell tower damage distribution due to tensile stresses (a) and crack propagation area in the front wall (section through the front wall shown) (b) – existing condition

It can be seen that the numerical model complements relatively well with the cracks that appeared on the bell tower and the vault of the church, Figures 8, 9 & 10. It should be emphasized that a large part of the cracks in the structure is not visible due to the facade or because they are inside the wall. Areas of material damage (material crushing and tensile cracking) on the top of the church vault are more difficult to see visually because of the layers of the vault on the upper side. However, such damage is dangerous because it represents crack propagation sites even under dead load. Vaults are slender and very sensitive to any dynamic and horizontal influences.
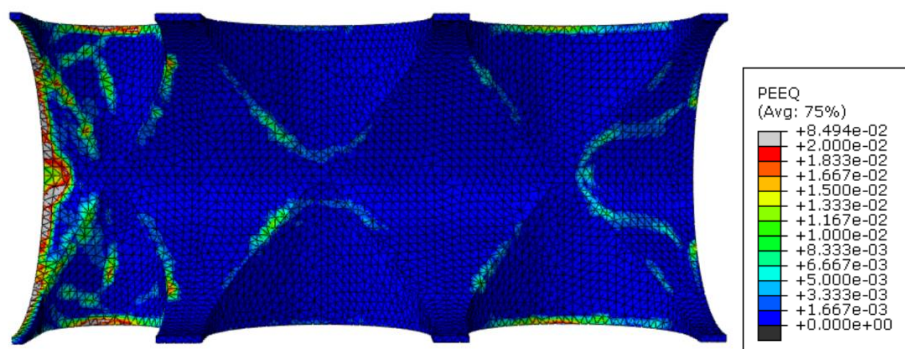
Figure 9. Area of propagation of cracks on the inside of the church vault shown through equivalent plastic deformations
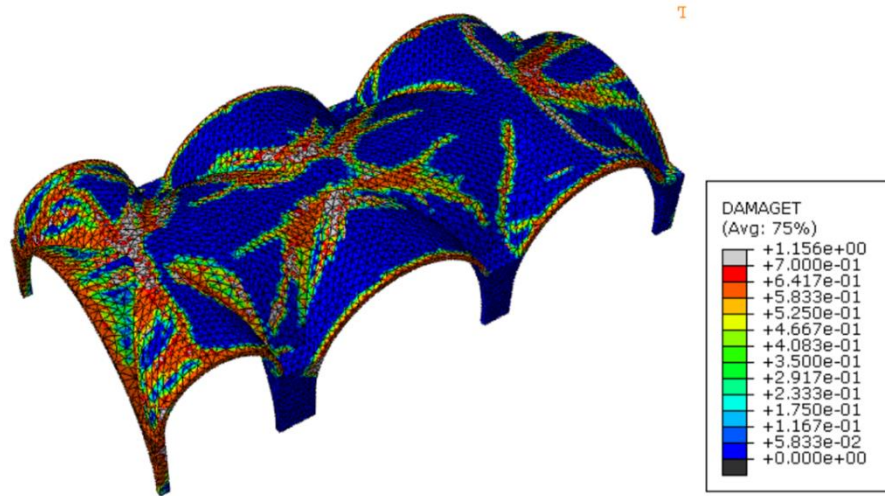
Figure 10. Propagation of material damage in the vault due to tensile stresses
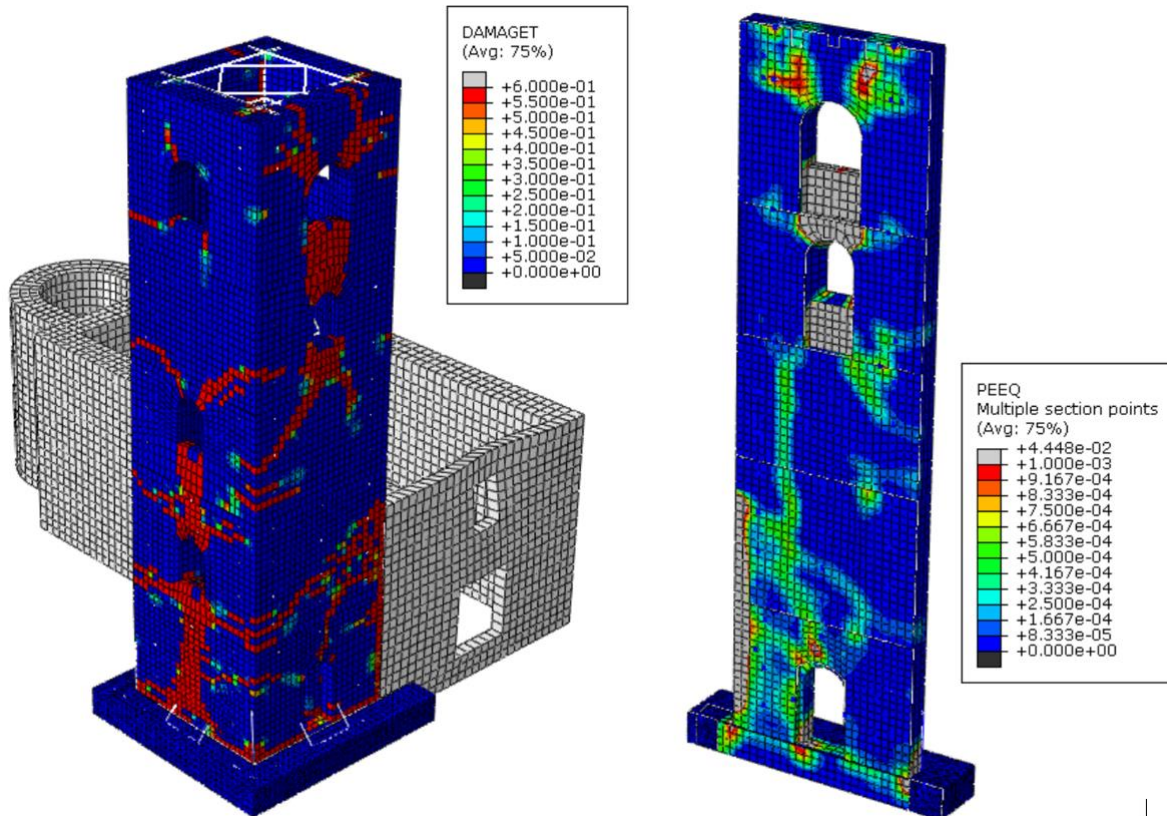
Figure 11. Bell tower damage distribution due to tensile stresses (a) and crack propagation area in the front wall
(section through the front wall shown) (b) – reinforced condition

The calculation was also performed for the retrofitted model of the structure. The result of plastic deformation and damage of the tower is shown in Figure 11. There are still areas where cracks occur and propagate. However, this area is clearly localized and confined. Based on the amplitude of the plastic deformations, it can also be seen that they are much smaller and narrower. The area of damage is similar even after the strengthening of the tower, affecting similar critical elements dominated by microcracks of limited width, since thanks to the reinforcing elements, the stress is redistributed within the material, preventing the collapse of the wall or the lintel. Critical elements are the parts between the

openings (arches and parapets), which are an integral part of the structure, but do not take over the dominant permanent load or the earthquake load. Therefore, it is important to preserve their integrity during an earthquake.

4. Retrofitting Techniques and Strengthening Materials

4.1 Bell tower

The strengthening of the bell tower due to a shear failure at the level of the church cornice is conceptually predicted by the interpolation of a new shear resistant structure along the inner side of the bell tower walls. Considering its importance for the global stability of the entire structure, the proposed concept can be implemented in two ways: with an interpolated steel grid discretely connected with anchors to the basic masonry structure or with a reinforced concrete insert in the form of unilaterally concreted wall adjacent to the inner wall at the critical height of the bell tower. The steel option is extremely complex to install, but it is a reversible design that does not significantly compromise the original stiffness of the historic structure, Figure 12. However, in conjunction with external horizontal clamps and stainless steel connection anchors, this steel structure upgrades the earthquake resistance capacity and prevents a whole range of premature local out-of-plane wall failures. The steel structure partially takes over the tensile component of the global bending resistance of the bell tower as a cantilever with steel tensile flanges at the corners of the bell tower. In principle, the reinforced concrete version is easier to implement than the steel version. However, this design has a significant effect on the global behaviour of the masonry tower, as new critical zones are created at the transitions between the reinforced and unreinforced segments. It is also important to note that this is an irreversible type of strengthening that irrevocably removes some of the historic value of the structure. Both options provide for strengthening of the foundation in the form of a grid of foundation strips, which are additionally anchored by vertical geotechnical anchors.

4.2 Vaults

Although the existing horizontal confinement concrete member along the perimeter of the church walls contributed significantly to the good behaviour of the structure during the earthquake, the cracks detected indicate the beginning of the opening of the damage mechanisms of the vault.
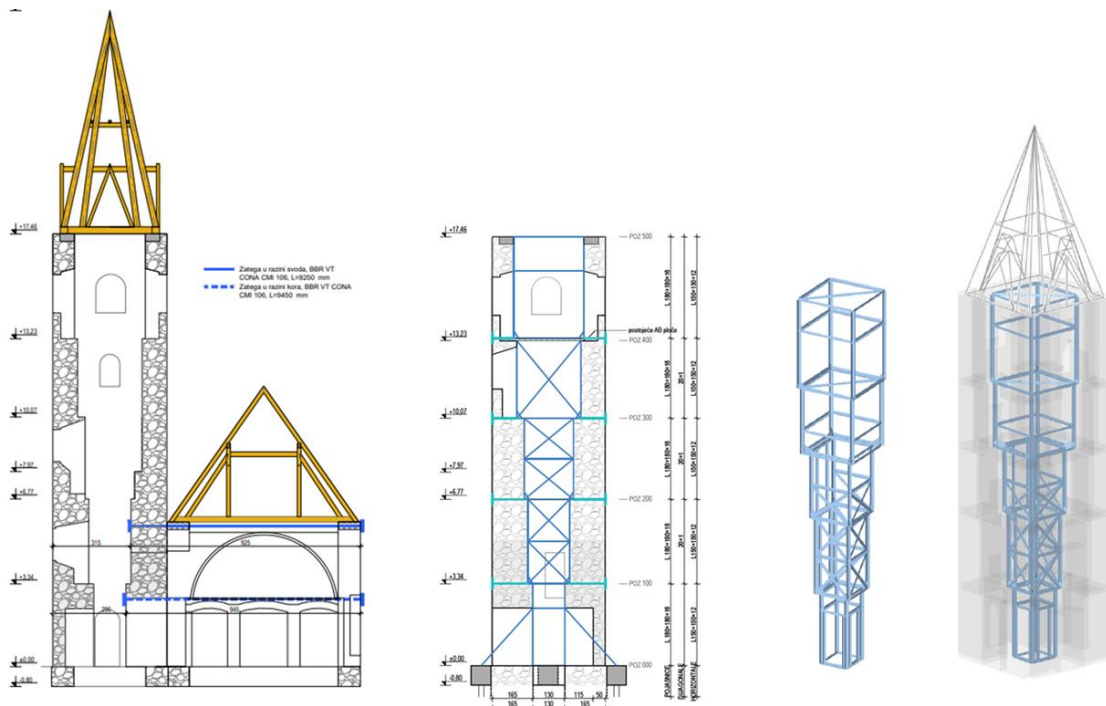
Figure 12. Chosen strengthening method for the tower

Slight separation of the longitudinal walls from the vault, leaves it in an unstable semi-restrained state, which can progressively result in partial collapse during stronger earthquakes. Therefore, both as a repair and strengthening measure, two groups of procedures are carried out, that would significantly increase the resistance of this masonry structure. As a stabilization measure, a system of orthogonal post-tensioned ties are installed in both main directions at the level of the top of the vaults. This reduces the possibility of detachment of the main support lines.
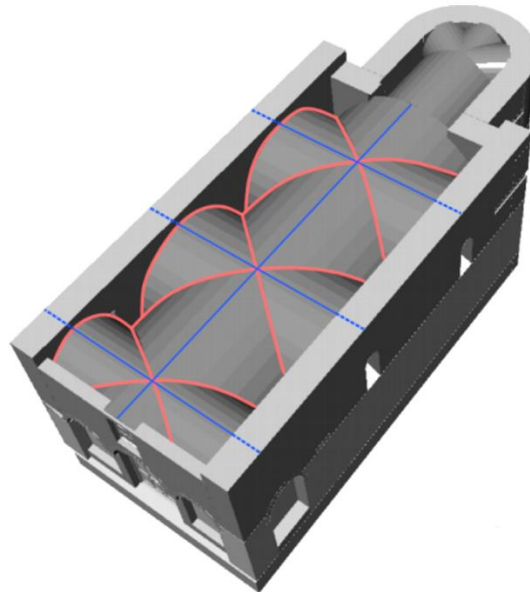
Figure 13. Strengthening of the masonry vaults (red line – uniaxial carbon fiber fabric, blue line – post tensioned steel ties)

The second strengthening method is linear strengthening of cross-sectional joists of cross vaults using carbon fiber fabric aligned in the direction of the joists, Figure 13. Both methods are reversible techniques that interfere minimally with the basic structure and can be performed effectively where monitoring and regular maintenance are performed.

4.3 Stone wall

Due to the poor stone structure of the masonry walls of the bell tower, as determined by investigative probes and endoscopic examinations of investigative boreholes through the body of the walls, measures are foreseen to connect the outer leaves of the walls with stainless steel rods. Grouting is also planned for the lower part of the tower walls with natural lime-based grout. Transverse connecting of two leaves of the walls is proposed via inox steel bars spaced in a 100 x 100 cm grid. It is important to not that inox steel bars must be installed and pretensioned before the grouting. Following the heritage guidelines (ICOMOS [13]), the retrofit techniques include materials that are sustainable and durable, such as Inox steel bars and hot-dip galvanized steel elements. All these materials are highly resistant to the atmosphere. The materials and products used improve the mechanical characteristics, ductility and durability of an existing structure.

5. Conclusion

Finally, safety requirements should also be mentioned, as they represent an inevitable challenge in the high-quality rehabilitation of historic structures. According to the regulations in force for the church of St. Michael, a complete renovation of the building is foreseen, with seismic action calculated for a return period of 225 years. At the same time, the rehabilitation project comply with the special conditions for the protection and preservation of cultural assets. Thus, according to the current

regulations, the designer must provide technical solutions that ensure the safety of people and preserve the authenticity of the architectural heritage, which is often a challenge. Often, the rehabilitation of the architectural heritage is seen as something permanent and regular maintenance, which is crucial for a longer service life of the structure, is often omitted. A holistic approach to architectural heritage rehabilitation is certainly the best guide for the future. Following the ICOMOS principles for analysis, preservation and retrofitting and using materials and products that are durable and reversible, the long-lasting and easily replaceable strengthening elements should be integrated into the existing structure in a way that ensures their preservation for future generations.

References

[1]   Stepinac, M.; Lourenço, P. B.; Atalić, J.; Kišiček, T.; Uroš, M.; Baniček, M.; Šavor Novak, M. Damage Classification of Residential Buildings in Historical Downtown after the ML5.5 Earthquake in Zagreb, Croatia in 2020. Int. J. Disaster Risk Reduct. 2021, 56, 102140. https://doi.org/https://doi.org/10.1016/j.ijdrr.2021.102140.

[2]   The Database of Usability Classification, Croatian Centre of Earthquake Engineering (HCPI - Hrvatski Centar Za Potresno Inženjerstvo), Faculty of Civil Engineering, University of Zagreb and The City of Zagreb, June 2020.

[3]   Salaman, A.; Stepinac, M.; Matorić, I.; Klasić, M. Post-Earthquake Condition Assessment and Seismic Upgrading Strategies for a Heritage-Protected School in Petrinja, Croatia. Build. 2022, Vol. 12, Page 2263 2022, 12 (12), 2263. https://doi.org/10.3390/BUILDINGS12122263.

[4]   Commission, U. S. S. All About Earthquakes: The Science Behind Earthquakes. All About Earthquakes: The Science Behind Earthquakes. Natural History, Museum of Utah, University of Utah: Salt Lake City 2010, p 1.

[5]   World Bank Report: Croatia December 2020 Earthquake – Rapid Damage And Needs Assessment, 2020, March 2021, Government of Croatia.

[6]   Comisión Sismológica Europea. Escala Macro Sísmica Europea EMS - 98; 1998; Vol. 15.

[7]   Law on Reconstruction of Earthquake-Damaged Buildings in the City of Zagreb, Krapina-Zagorje County, Zagreb County, Sisak-Moslavina County and Karlovac County (NN 102/2020, 10/21).

[8]   Tehnički Propis o Izmjeni i Dopunama Tehničkog Propisa Za Građevinske Konstrukcije [Internet]. [Cited 2021 Jun 29]. Available from: Https://Narodne-Novine.Nn.Hr/Clanci/Sluzbeni/2020_07_75_1448.Html.

[9]   Ortega, J.; Vasconcelos, G.; Rodrigues, H.; Correia, M. Seismic Vulnerability and Loss Assessment of Vila Real de Santo António, Portugal: Application of a Novel Method. Int. J. Archit. Herit. 2020. https://doi.org/10.1080/15583058.2019.1709915.

[10]   Cianchino, G.; Masciotta, M. G.; Verazzo, C.; Brando, G. An Overview of the Historical Retrofitting Interventions on Churches in Central Italy. Appl. Sci. 2023, 13 (1). https://doi.org/10.3390/APP13010040.

[11]   Borri, A.; Corradi, M.; Castori, G.; De Maria, A. A Method for the Analysis and Classification of Historic Masonry. Bull. Earthq. Eng. 2015, 13 (9), 2647–2665. https://doi.org/10.1007/s10518-015-9731-4.

[12]   https://www.3ds.com/products-services/simulia/products/abaqus/abaquscae/.

[13]   Lourenço, P. B. The ICOMOS Methodology for Conservation of Cultural Heritage Buildings: Concepts, Research and Application to Case Studies; 2014. https://doi.org/10.14575/gl/rehab2014/095.

LESSONS LEARNED FROM A PREDICTION AND POSTDICTION OF A SHAKE TABLE TEST ON AN UNREINFORCED MASONRY AGGREGATE

Igor Tomić [(1)], Katrin Beyer [(2)]

[(1)] *Postdoctoral Researcher, École Polytechnique Fédérale de Lausanne (EPFL), Lausanne, Switzerland, e-mail: igor.tomic@epfl.ch*

[(2)] *Associate Proffessor, École Polytechnique Fédérale de Lausanne (EPFL), Lausanne, e-mail:katrin.beyer@epfl.ch*

Abstract

Historical centers of Europe and Croatia are often formed by unreinforced masonry building aggregates that developed as the layout of the city or village was densified. In these aggregates, adjacent buildings can share structural walls with an older and a newer unit connected either by interlocking or just by a layer of mortar. Observations after for example the recent Central Italy and Croatia earthquakes showed that joints between the buildings were often damaged. This indicated a possible out-of-phase behaviour of units which can lead to the interaction which is demanding to capture with numerical models. The analysis of such building aggregates is difficult due to the lack of guidelines, as the advances were impeded by the scarce experimental data. The SERA project AIMS (Seismic Testing of Adjacent Interacting Masonry Structures) comprised a shake-table test of an aggregate of two buildings under two horizontal components of dynamic excitation, accompanied by the blind prediction competition. Each group was provided with a complete set of construction drawings, material properties, testing sequence and the list of measurements to be reported. After the results were reported, participants were able to compare the results, apply actual accelerations, and update their models within the postdiction phase. The prediction and postdiction of EPFL model were based on an equivalent frame model with a newly developed macroelement able to simulate both the in-plane and out-of-plane behaviour of unreinforced masonry piers, and a newly developed 3D material model allowing to simulate the interaction between the units. This paper deals with the prediction submitted by the EPFL team and discusses the results and possible pitfalls in modelling assumptions leading to unsatisfying prediction. Lessons learned are applied by updating the model for the postdiction analyses and discussing the updated results with the goal to improve the way we model unreinforced masonry aggregates using the equivalent frame approach.

Keywords: Historical centres, Masonry aggregates, Shake table test, Blind prediction, Equivalent frame model

1. Introduction

Historical centers around the Europe formed during long time spans, leading to the formation of masonry building aggregates. In aggregates, adjacent buildings can share structural walls, connected either by weakly interlocked stones or by a layer of mortar. The adjacent buildings can be constructed in different materials, with different distributions of openings and floor and roof heights. Post-earthquake observations show that the opening of the joint may lead to a complicated behaviour and interaction between the units [1,2] which is often ignored in numerical analyses. This is understandable due to a lack of experimental data, caused by a high cost and the complexity of performing tests on large-scale aggregates. These facts have inspired a joint research between École Polytechnique Fédérale de Lausanne (EPFL), Switzerland, University of Pavia, Italy, University of California, Berkeley, USA, RWTH Aachen University, Germany and National Laboratory for Civil Engineering, Portugal, named SERA AIMS – Adjacent Interacting Masonry Structures. As a part of this project, a shake table test was performed on a half-scale stone masonry aggregate at the LNEC laboratory in Lisbon, Portugal. Characterization tests on materials and components of the same typology were performed in parallel. As a part of the campaign, blind prediction competition was organized, with dozen of participants from both the research community and the industry. This paper presents in brief the experimental campaign,

and our own prediction and postdiction of the mentioned experimental campaign; for the detailed description and interpretation we would like to refer the readers to [3] for the experimental campaign and to [4,5] for the blind prediction competition.

2. Case study

The test specimen was a half-scale prototype of a masonry aggregate consisting of two units. Unit 2 had two storeys with height of 1.65 m and 1.5 m for the first and second storey, respectively. Unit 1 consisted of one storey with a height of 2.2 m. Unit 2 had a rectangular shape with four walls and the dimensions 2.5 x 2.5 m^2. Unit 1 had an u-shape with three walls and dimensions 2.5 x 2.45 m^2. The basic dimensions of the floor plan with beams, and facades are shown in Fig. 1. Unit 1 wall thickness was 30 cm and Unit 2 wall thickness was 35 cm and 25 cm of the first and the second floor, respectively. Spandrels under the openings had thickness decreased to 15 cm. Unit 2 was constructed first, replicating the sequence of construction from the historical centres. After the construction of a segment of Unit 2, the contact area was smoothed by mortar to ensure that there was no interlocking between the units. Different modal properties of two units, paired with this type of connection, led to the separation and out-of-phase behaviour during the test. Fig. 2 shows the constructed specimen before and after applying the plaster.
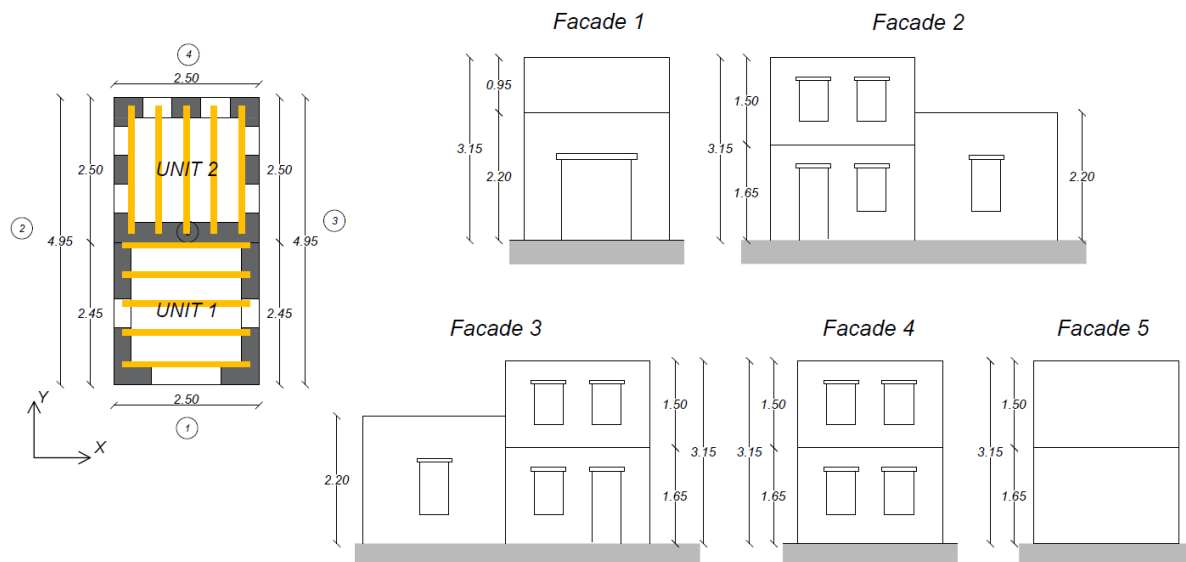
Figure 1 SERA AIMS test specimen floor plan with beam orientation and facade layout of the two units [3]
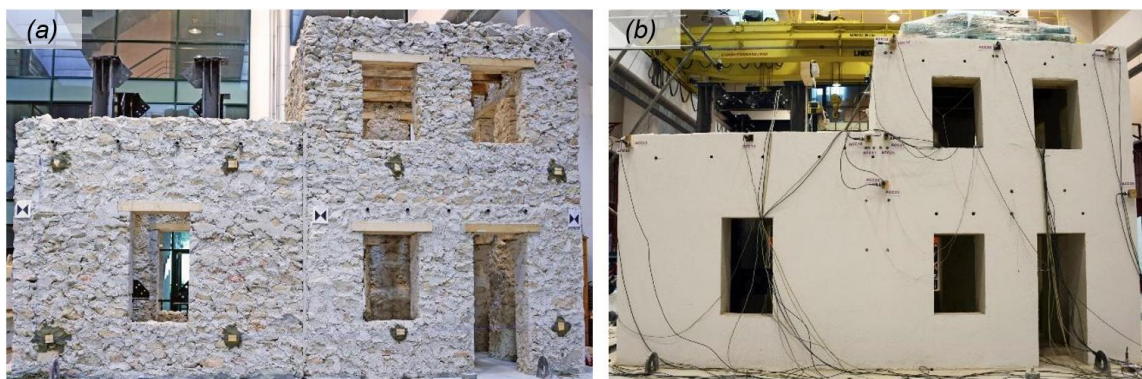
Figure 2 SERA AIMS specimen: a) before plastering; b) after plastering [3]

3. Modelling approach

An equivalent frame model approach using the OpenSEES framework [6] and the newly developed macroelement [7] was used to predict the behaviour of SERA AIMS unit. The macro-element is a three-node, three-dimensional element that can capture the in-plane and out-of-plane dynamic behaviour of masonry walls. Floors were modelled with elastic orthotropic membrane elements, a common practice in equivalent frame models. The orthotropic membrane provides only the membrane stiffness components, resulting in a zero-bending stiffness. Floor-to-wall connections were modelled with a frictional interface, limiting the shear force transmitted between floor and wall as a function of the vertical load acting on a floor node and the friction coefficient [8]. The material model can model the pounding of the beam when the slip is in the towards the wall [9]. Wall-to-wall connections were modelled with a one-dimensional non-linear interface, which provides linear elastic behaviour in compression, with no crushing, and a finite tensile strength paired with exponential softening law. The unit-to-unit connection within the aggregate was modelled with an n-dimensional zero-length element and a material model that captures linear elastic behaviour in the axial direction (perpendicular to the interface between the units) and a finite tensile strength paired with exponential softening law. In the perpendicular plane, the cohesive-frictional behaviour is based on the axial load, a friction coefficient, and an exponential damage law of cohesion [5].

4. Prediction and postdiction

After the test, the actual input acceleration, i.e., the recorded shake table acceleration was shared with all teams which participated in the blind prediction [4]. Now it was possible to rerun the analyses using the original prediction model, but with the effective seismic input, what we refer to as prediction in this paper. By doing so, it was possible to remove the ambiguity stemming from different input and obtain more meaningful comparison of results. The comparison of flexural drifts after the strongest longitudinal run (y-direction) [3] shown in Fig. 3 showed a satisfying match with the experimental crack maps, indicating that the model correctly captured the soft storey mechanism in the upper storey of Unit 2.
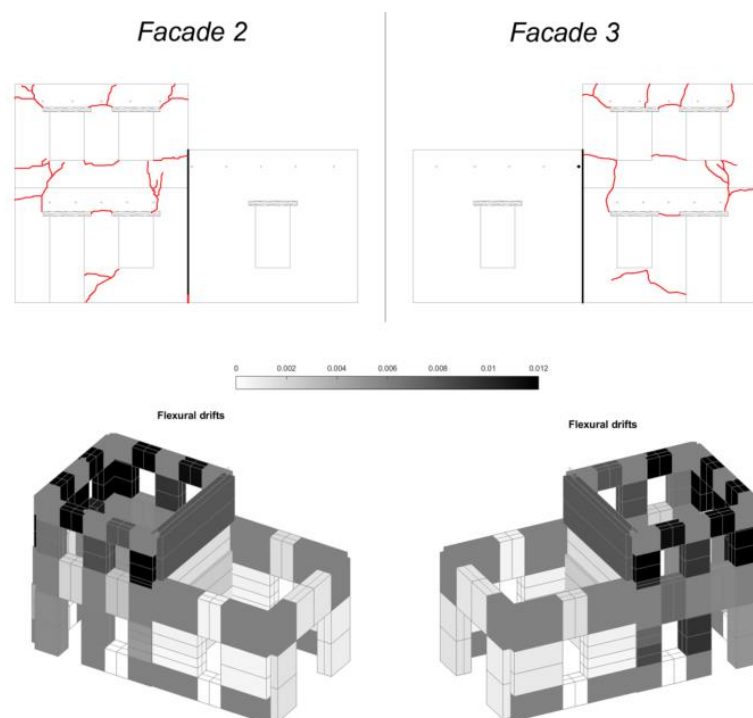
Figure 3 Comparison of the observed and predicted damage using the prediction model with 1% initial stiffness and mass proportional damping

At the same time, the comparison of recorded and predicted displacements using the prediction model with actual seismic input showed that the numerical model was too stiff and considerably underestimated the displacements. For example, Fig. 4 shows the comparison of the displacement at the corner of the upper storey of Unit 2 and opening of the interface in both directions.
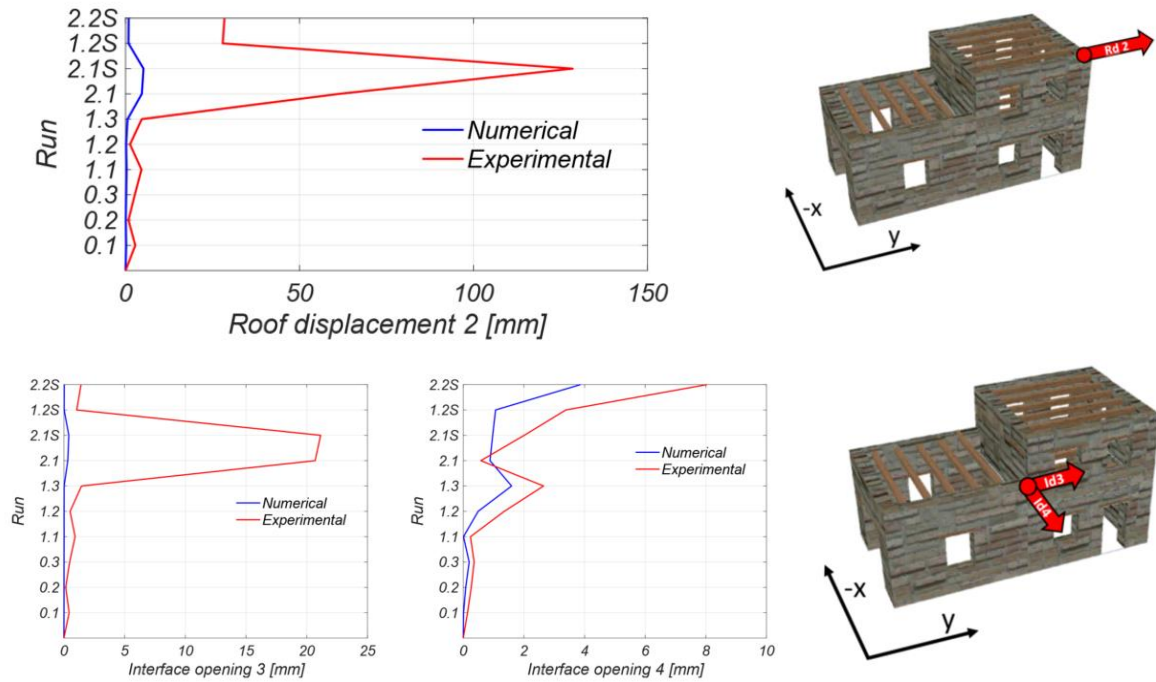
Figure 4 Comparing the response of the prediction model with 1% initial stiffness and mass proportional damping.

Initially the material parameters were taken from vertical compression and diagonal compression tests, but led to overestimating the stiffness [5]. Therefore, in the first phase of the postdiction, material parameters were recalibrated by fitting them against shear-compression tests on the masonry of the same typology, obtaining the values shown in Table 1. Normal and lognormal distributions were assigned to material parameters to account for uncertainties. Result were improved compared to the prediction, but the predicted response was still too stiff, as shown in Fig. 5.

Table 1 Recalibration of material parameters for postdiction [5]

Parameter (mean)	Prediction	Postdiction
E [MPa]	3462	**2030**
G [MPa]	1524	**609**
f_c [MPa]	1.30	**2.93**
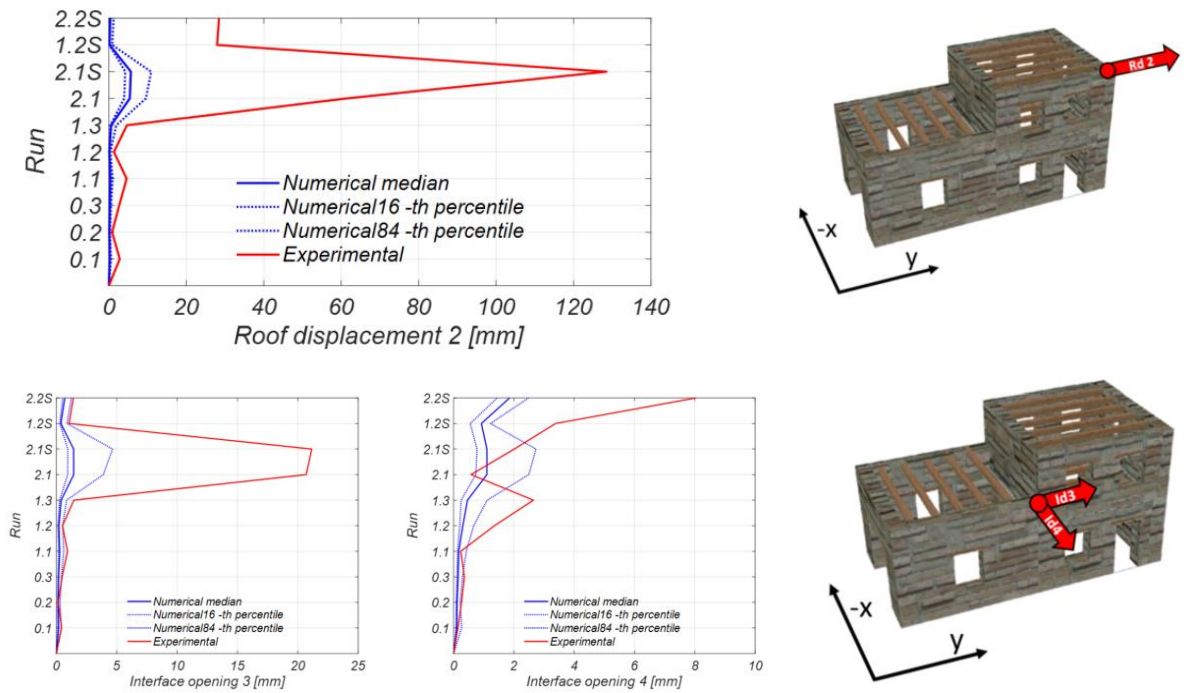
Figure 5 Comparing the stochastic response of postdiction models updated with material parameters calibrated according to shear-compression tests and 1% initial stiffness and mass proportional damping.

The prediction model and initial postdiction model were run with initial stiffness and mass proportional damping with 5% critical damping ratio. To further improve the postdiction, the damping model was updated to secant stiffness proportional damping model with 5% critical damping ratio, leading to the postdiction results shown in Fig. 6. The comparison with experimental results was better, especially considering the upper percentile, but still required further calibration presented in [5].
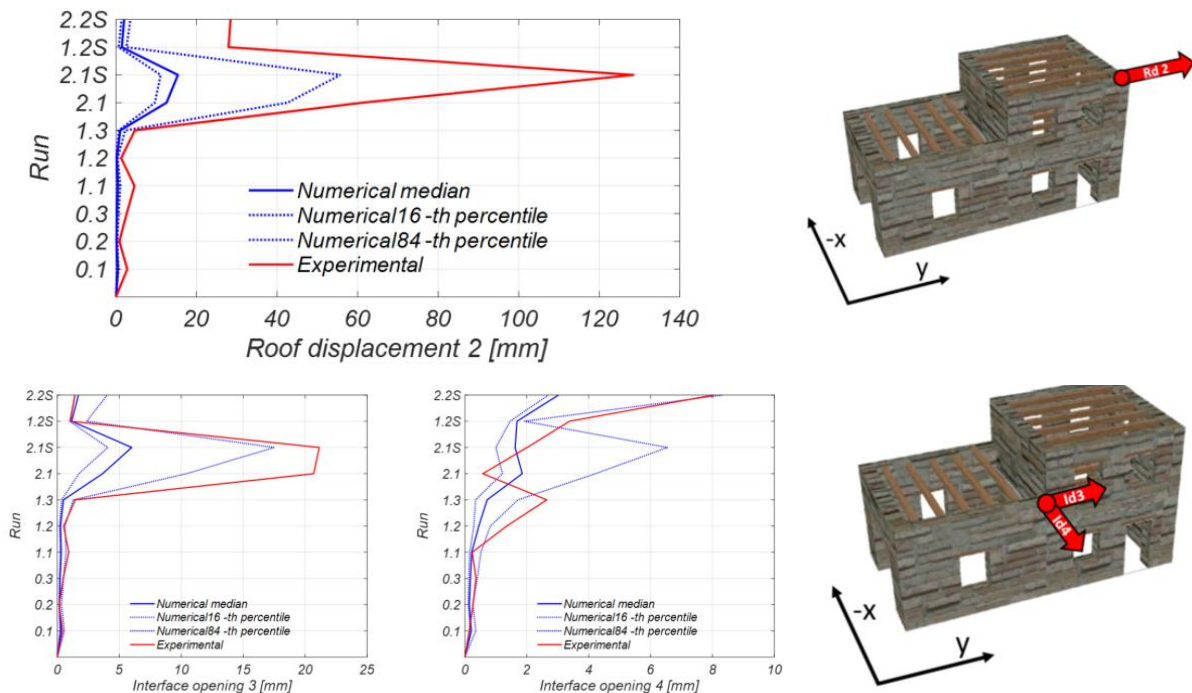
Figure 6 Comparing the stochastic response of postdiction models updated with material parameters calibrated according to shear-compression tests and 5% secant stiffness proportional damping.

5. Conclusions

This paper briefly presented the prediction and postdiction analyses performed for the SERA AIMS blind prediction competition. The equivalent frame model using newly developed macroelement captured the formation of the principal damage mechanisms. However, quantitative comparison with experimental data, even when including the actual seismic input in the analysis showed a too stiff response. First, the material parameters were updated by re-calibrating them against shear-compression tests instead of vertical and diagonal compression tests. This improved the prediction, but again resulted in a too stiff response. Therefore, damping model was updated from initial-stiffness and mass proportional damping to secant-stiffness proportional damping. This further improved the postdiction results. The first two lessons learned were the following:

- Calibration of material parameters based on shear-compression tests leads to a better prediction of building seismic behaviour than based on vertical compression and diagonal compression tests

- Simulating the building that develops out-of-plane mechanisms by nonlinear dynamic analyses in equivalent frame approach is more accurate using the secant stiffness proportional damping model that avoids overdamping the out-of-plane behaviour.

The future work relates to identifying other parameters and modelling decisions to reach even more accurate prediction of the aggregate seismic behaviour.

Acknowledgements

References

[1] Carocci, C. F. (2012). Small centres damaged by 2009 L'Aquila earthquake: on site analyses of historical masonry aggregates. Bulletin of earthquake engineering, 10(1), 45-71.

[2] Da Porto, F., Munari, M., Prota, A., & Modena, C. (2013). Analysis and repair of clustered buildings: Case study of a block in the historic city centre of L'Aquila (Central Italy). Construction and building materials, 38, 1221-1237.

[3] Tomić, I., Penna, A., DeJong, M., Butenweg, C., Correia, A.A., Candeias, P.X., Senaldi, I., Guerrini, G., Malomo, D., Beyer, K. .(2023). Shake table testing of a half-scale stone masonry building. Submitted to Bulletin of Earthquake Engineering

[4] Tomić, I., Penna, A., DeJong, M., Butenweg, C., Correia, A.A., Candeias, P.X., Senaldi, I., Guerrini, G., Malomo, D., Beyer, K. et al .(2023). Shake-table testing of a stone masonry building aggregate: Overview of blind prediction study. Submitted to Bulletin of Earthquake Engineering

[5] Tomić, I., Beyer, K., (2023) Shake table test on a historical masonry aggregate - prediction and postdiction using an equivalent frame model. Submitted to Bulletin of Earthquake Engineering

[6] McKenna, F., Fenves, G. L., Scott, M. H., & Jeremic, B. (2000). Open system for earthquake engineering simulation (OpenSees). Pacific Earthquake Engineering Research Center, University of California, Berkeley, CA.

[7] Vanin, F., Penna, A., & Beyer, K. (2020). A three‑dimensional macroelement for modelling the in-plane and out-of-plane response of masonry walls. Earthquake Engineering & Structural Dynamics, 49(14), 1365-1387.

[8] Almeida, J. P., Beyer, K., Brunner, R., & Wenk, T. (2020). Characterization of mortar–timber and timber–timber cyclic friction in timber floor connections of masonry buildings. Materials and Structures, 53(3), 1-14.

[9] Vanin, F., Penna, A., & Beyer, K. (2020). Equivalent-frame modeling of two shaking table tests of masonry buildings accounting for their out-of-plane response. Frontiers in Built Environment, 6, 42.

SEISMIC RETROFITTING OF BUILDING STRUCTURES AND MONUMENTS IN NORTH MACEDONIA – NECESSITY, SOLUTIONS AND CONSTRUCTION

Veronika Shendova [1], Roberta Apostolska [2], Goran Jekic [3], Aleksandar Zlateski [4], Aleksandar Zurovski [5] Elena Delova [6]

[1] *Prof. PhD, Institute of Earthquake Engineering and Engineering Seismology, IZIIS, Ss. Cyril and Methodius University, Skopje, North Macedonia, e-mail: veronika@iziis.ukim.edu.mk*

[2] *Prof. PhD, Institute of Earthquake Engineering and Engineering Seismology, IZIIS, Ss. Cyril and Methodius University, Skopje, North Macedonia, e-mail: beti@iziis.ukim.edu.mk*

[3] *Assoc. Prof. PhD, Institute of Earthquake Engineering and Engineering Seismology, IZIIS, Ss. Cyril and Methodius University, Skopje, North Macedonia, e-mail: jekic@iziis.ukim.edu.mk*

[3] *Assist. M,Sc, Institute of Earthquake Engineering and Engineering Seismology, IZIIS, Ss. Cyril and Methodius University, Skopje, North Macedonia, e-mail: azlate@iziis.ukim.edu.mk*

[4] *Assist. M,Sc, Institute of Earthquake Engineering and Engineering Seismology, IZIIS, Ss. Cyril and Methodius University, Skopje, North Macedonia, e-mail: azlate@iziis.ukim.edu.mk*

[5] *Assist. M,Sc, Institute of Earthquake Engineering and Engineering Seismology, IZIIS, Ss. Cyril and Methodius University, Skopje, North Macedonia, e-mail: zurovski@iziis.ukim.edu.mk*

[6] *Assist. M,Sc, Institute of Earthquake Engineering and Engineering Seismology, IZIIS, Ss. Cyril and Methodius University, Skopje, North Macedonia, e-mail: delova@iziis.ukim.edu.mk*

Abstract

The impact of present building code requirements for seismic design of new buildings can readily be acknowledged, however applying regulation to existing buildings is an area less well defined. Presently, there is a diverse list of existing code references which could be interpreted to require seismic upgrades of existing structures. Unfortunately, these references do not provide a clear path toward addressing the hazards, evaluation and retrofitting of existing buildings. And when it comes to existing old buildings and monuments, constructed with low or no seismic consideration, the topic becomes much more complex and challenging. The problem of earthquake protection of historic buildings and monuments is radically different from that of other existing structures, due to the priority given to preservation of aesthetic, architectonic and historic values instead of keeping the structure operational. In providing the protection of these structures in a manner that requires the least intervention and the greatest care to preserve authenticity, the experts are permanently challenged by the fast development and the improved performance of new materials and techniques. This paper presents the integrated multidisciplinary approach to seismic protection of important structures that has been developed by the Institute of Earthquake Engineering and Engineering Seismology, IZIIS, Skopje, and implemented in the process of seismic upgrading or reconstruction of historic buildings and monuments in the country and beyond.

Keywords: seismic retrofitting, historic buildings, monuments, multidisciplinary approach, analytical and experimental investigation

1. Introduction

Seismic retrofitting of historic structures is radically different from that of other structures, due to the priority given to preservation of aesthetic, architectonic and historic values instead of keeping the structure operational. The specific character of seismic protection of historical buildings and monuments resulting from the variety of structural systems, built-in materials, periods and techniques of construction, stability criteria and contemporary requirements incorporated in the modern principles of conservation and protection needs systematic and scientific approach to achieving a successful solution. Although there is a similarity between historical buildings and historical monuments, there also exist differences, for which each of these groups should be considered separately:

- A monument is a structure having an important "cultural value" so high that it is necessary to guarantee its preservation, generally with its architectural, typological and material characters;
- A historical building is a building of an urban area, which has a "cultural value" as a whole (historical urban area), while a single building is not a monument. This means that preservation concerns the general character of the construction techniques typical in the whole area.

Historic buildings usually present shear wall masonry structures that are basically non-ductile and insufficiently resistant to seismic effects. The problem of interaction between the "old" and the "new" materials and/or elements that arises in their strengthening requires experimental verification of all techniques that have so far been developed, (injection, grouting, jacketing, confining, base isolation). Since monuments are also masonry structures, same basic principles and requirements hold for them also, but are specific. The characteristic structural entity, the variability of the built-in materials, the complex history of successful modifications done in the past, as well as the degree of deterioration, makes each historic monument a case for itself. Therefore, the basic principle of minimum intervention – maximum protection and/or preservation of the monument's identity should be adopted.

Retrofitting of masonry structures as are the structures of historic buildings and monuments is an exceptionally large field of work elaborated in numerous books, publications, and individual reports. However, from the aspect of conservation and restoration of monuments, historic buildings, and sites - 1964 ICCOMOS' Venice Charter could be considered a basic document and a beginning of a systematic approach to general protection of these structures. The seismic protection of monuments, historic buildings and sites with all their structural and specific characteristics has intensively been developed throughout the last several decades within the frameworks of the scientific discipline of earthquake engineering - typically multi-disciplinary, including other related scientific spheres.

Materials for Retrofitting: The key for selecting materials and techniques is classification of retrofitting techniques into two main categories: reversible and irreversible. In selecting materials to be used in reversible interventions, there are usually only a few limitations. However, the materials used in irreversible interventions as are for example the unavoidable injection of cracks, do impose two additional limitations: compatibility of new with old materials and their durability. The best way of assuring compatibility and durability is usage of traditional materials, (stone, bricks, lime mortar and cement), which on the other hand, is not always possible. In selecting injection mixtures, advice should be asked from experts as to preventing separation of the old and new parts. Modern cement mixtures should carefully be applied particularly in the process of jacketing because of the irreversible modification of the surface of existing masonry. Steel, (as externally applied ties or as reinforcement incorporated into the existing masonry) is a very frequently applied material in the strengthening processes of both historic buildings and monuments.

Retrofitting Methods: The main problem imposed in masonry structures is to provide structural integrity at story level to avoid individual vibration of the elements after the occurrence of the first cracks. The most used procedure to achieve structural integrity is to incorporate horizontal steel ties into the existing masonry (at the top of the existing walls in order to be made invisible - churches and mosques), incorporate reinforced concrete belt courses or reinforced concrete slabs into structures where possible - structures in old towns. To improve the bearing characteristics of the walls and the columns as structural elements sustaining horizontal seismic forces, several techniques are used: injection of masonry, injection with jacketing, incorporation of vertical reinforced concrete columns, or even incorporation of new reinforced concrete walls (in the structures of the old towns). The injection technique, the material to be used, i.e., the pressure under which the prepared mixture will be injected are selected depending on the size, position and shape of the cracks. To increase the bearing and deformability capacity of the walls, jacketing of the walls with concrete on both their surfaces, i.e., incorporation of reinforced concrete belt courses is anticipated. Vertical reinforced concrete belt courses are used to increase the ductility of the considered element. The techniques of strengthening of the foundation structure mainly consist of extending the proportions of the foundation and their connection to the vertical elements, modifying the foundation structure and consolidating and improving of the characteristics of soil conditions.

2. Integrated Approach for Seismic Retrofitting of Historic Buildings and Monuments Developed by IZIIS

In providing the protection of these structures in a manner that requires the least intervention and the greatest care to preserve authenticity, the experts are permanently challenged by the fast development and the improved performance of new materials and techniques. However, the implementation of particular retrofitting methodology depends on the extent it has been investigated. The delicate problem of proving the effectiveness of the selected consolidation system can be successfully overcome by using the methodology of "*design assisted by testing*".

Within the frames of the research activities of the Institute of Earthquake Engineering and Engineering Seismology, IZIIS, in addition to seismic design of modern structures, particularly noteworthy is also the experience gathered in the field of protection of structures pertaining to the cultural historic heritage. During a period of more than forty years of activities in this field, the Institute has realized important scientific research projects involving analytical research, unique experimental shaking table test and field surveys of historic structures. These resulted in an integrated approach to seismic protection of extraordinarily important cultural historic structures that has been adopted by IZIIS and used in the process of reconstruction or seismic upgrading of important monuments. This approach should encompass the following:

- Definition of seismic potential of the site through detailed geophysical surveys for definition of geotechnical and geodynamic models of the site to consider the expected earthquake effect through a probabilistic approach, including also the local soil effects through nonlinear dynamic analysis of a representative geotechnical model;
- Determination of structural characteristics and bearing and deformation capacity of existing structure including investigation of the built-in materials, definition of structural dynamic characteristic through ambient vibration method, developing the corresponding mathematical model and determination of dynamic response for defined seismic parameters;
- Definition of criteria and selection of concept for seismic retrofitting respecting the country regulative as well as guidelines in the ICCOMOS and ISHARCH documents;
- Definition of structural methods, techniques, materials in accordance with defined criteria and positive national and international construction and conservation practice;
- Analysis of dynamic response of retrofitted structure and verification of their seismic stability;
- Definition and documentation of field works, and their execution by constant supervision by professionals from different fields.

The particularly important part of the IZIIS' experience in the field of earthquake protection of cultural heritage are the numerous shaking table testing of models for investigation of structural behaviour of historic building and monuments and methodologies for their repair and seismic strengthening, that have been carried out in the IZIIS' Dynamic Testing Laboratory, [1]. The most important seismic shaking table investigations of models of historical buildings and monuments are presented further, followed by their implementation in real structures, [2]. The considered structures have relatively low levels of axial stresses at the base which justifies the adoption of a model with neglected gravity forces, i.e. "gravity forces neglected" modelling principle, using the same materials as in the prototype structures.

3. Shaking Table Testing of Models of Historic Buildings and Monuments

3.1. Historic Buildings

Old towns along Mediterranean coast: The old towns of Budva, Kotor, Dubrovnik, etc. were severely damaged due to the April 1979 Montenegro earthquake. Considering the cultural value of most of the buildings in the old towns, extensive investigations for the purpose of searching for the optimum conditions and methods for reconstruction, repair and strengthening of structures were performed, thoroughly applying the methodology presented in chapter 2. Firstly, the buildings were classified into

structural units and then the methodology for structural retrofitting was determined based on detailed studies of structural characteristics, the damage level, the built-in materials, the foundation conditions as well as local seismicity. Since the injection was the most frequently applied method, for its testing and verification a 1:2 scaled model of a typical single-story building was constructed of the same original stones and mortar and tested on the IZIIS' seismic shaking table applying the 1979 Petrovac earthquake. After testing and occurring of diagonal cracks, the model was repaired by injection and tested again, in which case the model suffered less damage, (Fig. 1). Using the acquired knowledge on the technique application, the consumption of material and the effect of applied injection, more than three hundred buildings within the old towns along Mediterranean coast have been repaired at the same time, including structural repair, repair of facade walls and the interior of each individual building, [3].

Figure 1. Original and repaired model of a typical masonry building in Budva

Adobe Structures in California: Since 1990, the Getty Conservation Institute (GCI) carried out a multi-year, multi-disciplinary project, the *Getty Seismic Adobe Project*, (GSAP), including a survey of existing historic adobe buildings in California, dynamic testing of small-scale model buildings (scale 1:10) at the Stanford University, and the preparation of an Engineering Guide for designing seismic retrofit measures. As an extension of GSAP, tests were conducted on two large-scale models (scale 1:2) on the seismic shaking table in IZIIS, [4].

The first model was a control model while second was retrofitted with a combination of horizontal and vertical straps, center cores, and partial plywood diaphragms. The applied retrofitting proved very effective in improving stability and preventing collapse, (Fig. 2). Based on all the results and the GCI' Engineering Guidelines a number of historic adobes structures in south California were seismically upgraded applying this experimentally verified methodology, [5].

Unretrofitted Adobe Model -UAB   Retrofitted Adobe Model – RAB
Figure 2. The gable end wall after testing of the UAB and RAB model
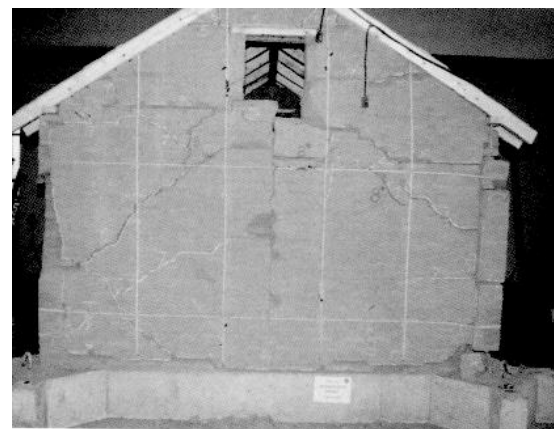
3.2. Monuments

*Byzantine Churches in Macedonia***:** Within the long-term research project entitled *"Study for Seismic Strengthening, Conservation and Restoration of Churches Dating from the Byzantine period (9th-14th century) in the Republic Macedonia"* realized jointly by IZIIS, Skopje, National Conservation Center of R.N. Macedonia and GCI, Los Angeles, [6, 7], ample experimental and analytical investigations were performed to verify an original methodology that was developed for the repair and seismic retrofitting of Byzantine churches. For the first time in the world provided was shaking table testing of a model of St. Nikita to a scale of 1 : 2.75, simulating the existing and the strengthened state, (Fig. 3) to investigate its behavior in elastic, nonlinear and heavily damaged state (close to failure). The applied methodology for repair and retrofitting, consisting of incorporation of horizontal and vertical belt courses, significantly increases the bearing capacity and deformability of the structure. The tests approved that applied methodology increases the bearing capacity and deformability of the structure up to the level of the designed protection.
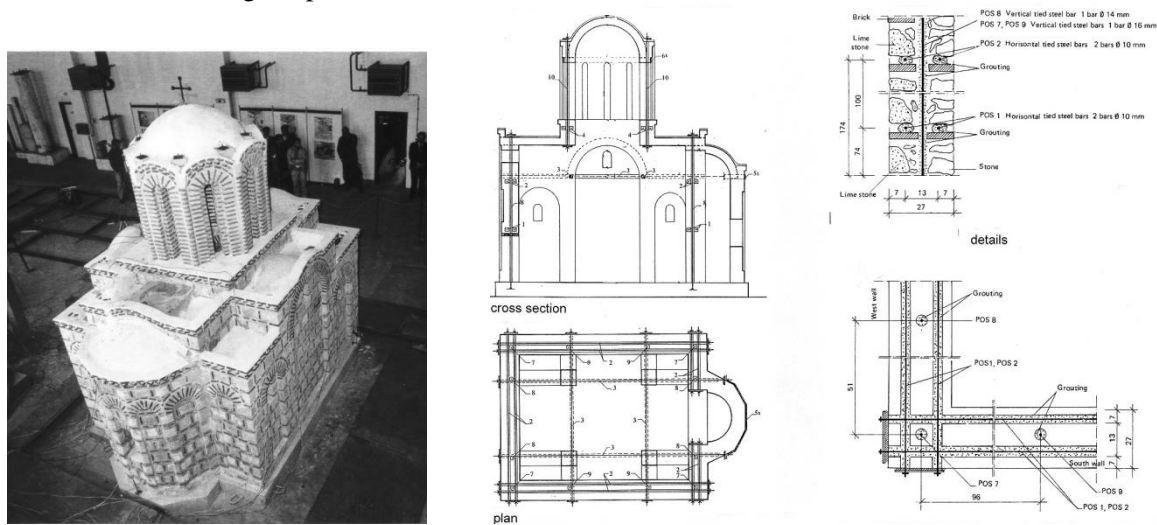
Figure 3. The 1:2.75 scaled church model (left) and the applied strengthening method (right)

Mustafa Pasha mosque in Skopje: Within the frames of FP6 PROHITECH project *"Earthquake Protection of Historical Buildings by Reversible Mixed Technologies"*, experimental shaking table tests on the models of three important historical monuments, mosque, cathedral and church, were carried out in IZIIS. Mustafa Pasha's Mosque, one of the biggest and the best-preserved monuments of the Ottoman sacral architecture in Skopje and the Balkan, was selected as representative mosque for shaking table testing, (Fig. 4).

Figure 4. Mustafa Pasha Mosque: prototype (left), 1:6 scaled model (middle), phase 3 – damages (right)

Experimental investigation was performed in three main phases: (1) testing of the original model under low intensity level, with the aim of provoking damage to the minaret only; (2) testing of the model with strengthened minaret, with the aim of provoking its collapse and damage to the mosque, and (3) testing of the strengthened mosque model until reaching heavy damage. The applied strengthening solution, consisting of formation of a horizontal belt course around the bearing walls by CFRP rods as well as around the tambour and at the base of the dome by CFRP wrap, has significantly improved the seismic resistance of the monument, [8].

4. Implementation of the Developed Retrofitting Methodologies in North Macedonia

After the realization of these projects and gained unique and incomparable knowledge, IZIIS became a partner of the Republic Institute for Protection of Cultural Historic Monuments of R.N. Macedonia, which enabled direct application of the gained knowledge in actual conditions and for specific historic monuments. Presented further are the most characteristic examples of application of the developed methodologies for seismic upgrading of monuments and historic building.

4.1. Reconstruction of St. Pantelymon Church in Plaoshnik, Ohrid

In the process of conservation and rebuilding of the St. Panteleymon Church in Ohrid, having in mind the importance and specific nature of the structure representing a historic monument classified in the first category, it was necessary to design a building structure that will satisfy the stability conditions in the process of application of the conservation principles regarding shape, system, and materials, [9]. The principal structural system of the church consists of massive stone and brick masonry in lime mortar. Seismic strengthening was provided in accordance with the previously developed and verified methodology for Byzantine churches, (chapter 3.2). i.e. the horizontal and vertical steel ties were proportioned and a solution for consolidation of the foundation was given. The church was reconstructed in the course of 2001, (Fig. 5).

Figure 5. St. Panteleymon church: during reconstruction, (left, middle), rebuilt church (right)

4.2. Reconstruction of St. Athanasius Church in Leshok

On August 21, 2001, during the armed conflict in R. Macedonia, the monastic church of St. Athanasius in Leshok experienced strong detonation, which resulted in its almost complete demolition, (Fig.6). Based on previous knowledge, there have been two approaches taken in the reconstruction of the church: (i) repair and strengthening of the existing damaged part and (ii) complete reconstruction of ruined part with strengthening elements, [10].

The solution for repair and structural strengthening of damaged existing part of the structure anticipates injection of all the cracks and incorporation of horizontal and vertical RC strengthening elements on certain levels. For the demolished part of the structure, a concept of complete reconstruction by maximum possible use of selected material has been adopted, whereat elements for structural strengthening for providing the designed level of seismic safety have also been anticipated: (i) RC belt course below the floor level, in the existing foundation walls, for anchoring the vertical strengthening elements, (ii) vertical strengthening steel elements at the ends of the massive walls and around openings, (iii) vertical strengthening steel elements into the tambour columns, (iv) horizontal steel elements along

the walls, in the base of the tambour and the dome. Due to the different treatment of the structural units constituting the integral structure, an expansion joint between them is anticipated to be constructed.

Figure 6. St. Athanasius church: after detonation, (left) during reconstruction, (middle), rebuilt church (right)

The church was reconstructed according to the designed methodology during 2005-2007. The results from the analysis show that both structural units constituting the integral structure possess a sufficient bearing and deformability capacity up to the designed level of seismic protection.

4.3 Repair and Seismic Retrofitting of Mustafa Pasha Mosque in Skopje

Respecting the modern requirements in the field of protection of historical monuments, as is the application of new technologies and materials, reversibility and invisibility of the applied technique, concept of repair and strengthening involving the use of composite materials was used for seismic upgrading of Mustafa Pasha Mosque in Skopje, [11]. It has been selected based on investigations of the: characteristics of the built-in materials, main dynamic characteristics, shaking table testing of the mosque model, (chapter 3.2); investigations of the soil conditions as well as detailed geophysical surveys for definition of geotechnical and geodynamic models of the site.

The accepted solution of structural strengthening, (Fig. 7), consists of incorporation of CFRP wrap in a layer of epoxy glue along the perimeter of the dome base, placement of CFRP bars in an epoxy mortar layer in horizontal joints of bearing walls, and construction of RC wall along the perimeter of the foundation walls, below the terrain level. Strengthening of the mosque structure in accordance with the designed system started in the fall of 2008.
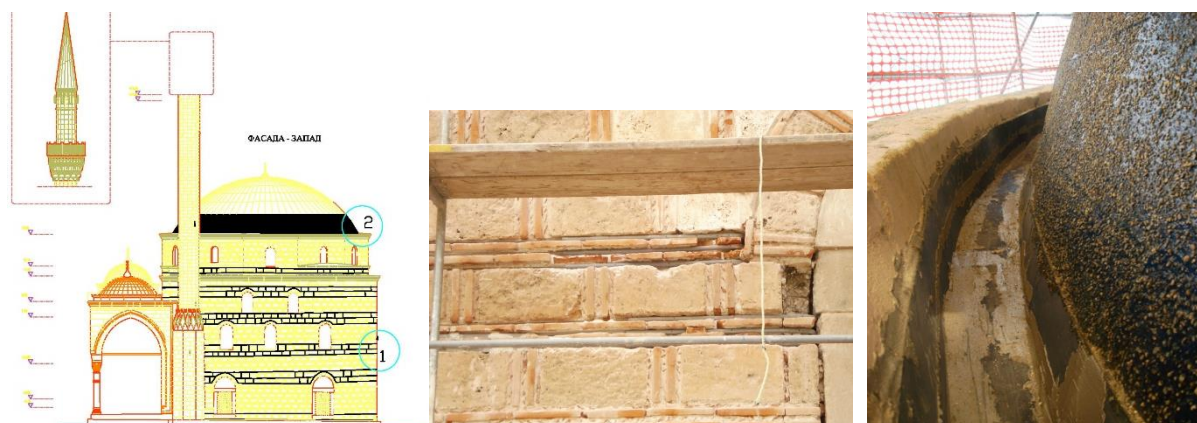
Figure 7. Mustafa Pasha Mosque: proposed retrofitting, (left), CFRP bars in the walls, (middle), CFRP wrap around the dome (right)

Following the successful seismic upgrading of Mustafa Pasha Mosque, the same or slightly modified retrofitting methodology by using CFRP has been so far implemented in several other mosques on the territory of North Macedonia and Kosovo, all of them from the Ottoman period: Isaki and Gazi Hajdar Kadi Mosques in Bitola, Ali Pasha Mosque in Ohrid, Yashar Pasha and Fatih Mosques in Pristina, as well Sinan Pasha Mosque in Prizren, while for Orta Mosque in Strumica the process of construction is currently under way.

4.4. The Parliament building in Skopje

The Parliament Building of the Republic of North Macedonia was more than 70 years old, (Fig. 8). As a historic building, it is protected by the Law on Protection of Cultural Heritage. Throughout its existence, a lot of changes, enlargements, adaptations, damaging during 1963 Skopje earthquake as well as post-earthquake repair and strengthening of this building have been done. Within the project on *Enlargement, Building of Another Storey and Adaptation of the Building*, the necessity for increasing the seismic safety of main structural system has been defined, [12].

Figure 8. Parliament of Republic of North Macedonia (north facade – left, aerial view – right)

Starting with the essential difference between "plain" and "confined" masonry, the most important phase was in-situ technical investigations performed to identify the principal structural system of the pentagonal outline, evaluated as the oldest and most critical part for the planned building of another storey. The analysis of the bearing and deformation capacity of the structure shows that the shear base coefficient for the seven structural units is in the range of 6-18%, much smaller than that required one by the regulations for plain masonry, (30%), while the relative storey displacements do not satisfy the requirements for earthquakes that may occur in this area. Thus, the need for strengthening of the structure becomes even more topical and economically justified.
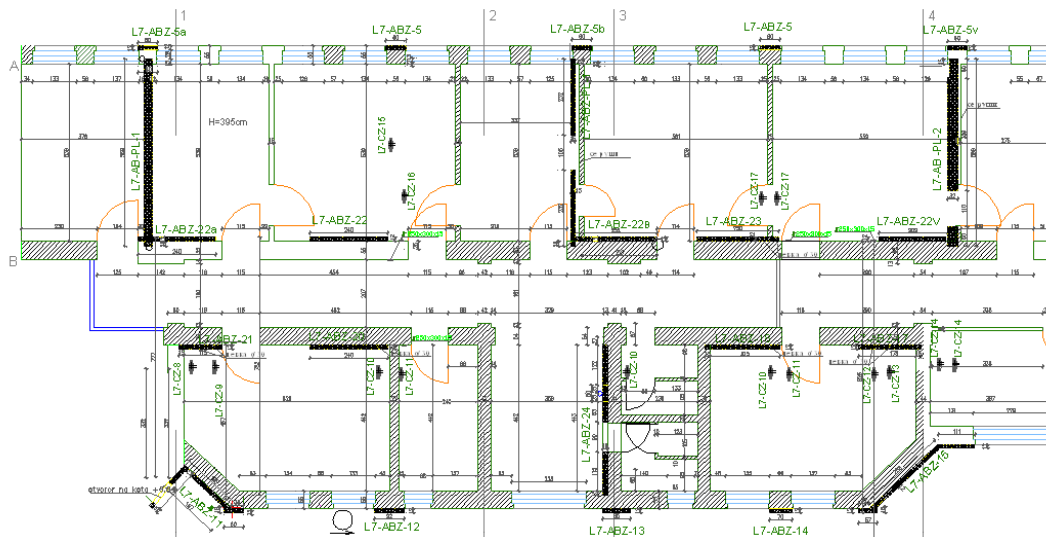
Figure 9. Strengthening of representative unit – L7

Based on the required strength and deformation characteristics of the elements and the system as a whole on one hand, and the possibilities for adding new elements in the structure, on the other hand, the most appropriate (from the aspect of stability and economy) technical solution for strengthening has been selected. During the selection, particular attention has been paid to the possibility of achieving optimal strength, stiffness and deformability by minimal interventions. It has also been endeavoured to

avoid structural intervention in the functionally necessary premises and premises with interior of particular value and importance. With the solution of strengthening of the principal structural system, classical methods and strengthening elements have been anticipated for the purpose of use of materials with characteristics like the existing ones. Fig. 9 shows the strengthening solution for the representative unit, L7. Generally, by selected strengthening the existing structural system was converted form plain to confined masonry.

Subsequent final analysis of strength and deformability of the elements and the system as a whole has been made up to ultimate states of strength and deformability for each unit taken separately. Comparative force-displacement storey relationships for the three analysed conditions (existing, existing with additional storey, and strengthened structure) for selected unit gives a very clear insight into the effect of the selected strengthening solution, (Fig. 10), pointing to a considerable increase of both the bearing and deformation capacity of the system.

--- existing state, ⎯⎯ with additional storey, ▬▬ strengthened structure
Figure 10. Comparative Q-d diagrams for characteristic units
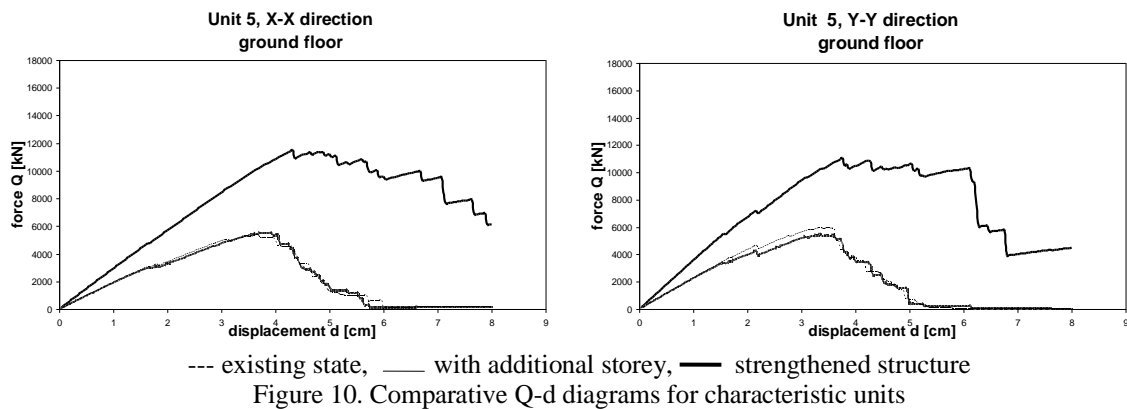
Figure 11. Strengthening of a characteristic column with a plastic hinge, unit L3

Figure 12. The Parliament building after seismic retrofitting, adaptation and building of another storey

The process of strengthening while continuously functioning of the Parliament, was carried out quite successfully despite number of limitations in the period 2010-2014, (Fig. 11, 12).

5. Conclusion

The paper presents successful implementation of previously developed and experimentally verified retrofitting methodologies in seismic upgrading or reconstruction of important buildings in the country and beyond, which followed the modern principles for seismic protection of historical buildings and monuments. The delicate problem of proving the effectiveness of the selected retrofitting has been successfully overcome by using the "*design assisted by testing*" methodology. This methodology, which has been recently codified in all Eurocodes, represents a very powerful tool especially in the case of a complex structures, which are difficult, and therefore unsafe, to analyse using traditional methods. The knowledge gained through shaking table testing is unique and incomparable and hence necessary for design of seismic strengthening of individual important cultural-historic structures where it is important to have an insight into the effect of the interventions upon the authenticity of the monument.

Acknowledgements

References

[1] Shendova V., Rakicevic Z., Krstevska L., Tashkov Lj, Gavrilovc P. (2011): Shaking Table Testing of Models of Historic Buildings and Monuments - IZIIS' Experience. *FP7 SERIES Workshop on the Role of Seismic Testing Facilities in Performance-Based Earthquake Engineering*, © Springer International Publishing, Switzerland 2011, ISBN 978-94-00701976-7, pp:221-245

[2] Shendova V., Rakicevic Z., Garevski M., Apostolska R., Bozinovski Z. (2014): Implementation of experimental developed methodology for seismic strengthening and repair in historic monuments. *Seismic Evaluation and Rehabilitation of Structures, Geotechnical, Geological and Earthquake Engineering 26*, © Springer International Publishing, Switzerland, DOI 10.1007/978-3-319-00458-7_8

[3] Stankovic V. (1984). Vulnerability of urban assets of old towns and cultural-historic buildings. *Doctoral Dissertation*, IZIIS, Skopje

[4] Gavrilovic P, Sendova V, Tashkov Lj, Krstevska L, Ginell W, Tolles L. (1996): Shaking Table Tests of Adobe Structures, *Report IZIIS 96-36*

[5] Tolles L., Kimbro E., Webster F., Ginell W. (2000): Seismic Stabilization of Historic Adobe Structures. *Final Report of the Getty Seismic Adobe Project*, The Getty Conservation Institute, Los Angeles

[6] Gavrilovic P., Shendova V., Ginell W. (1999): Seismic Strengthening and Repair of Byzantine Churches. *Journal of Earthquake Engineering 3, Imperial College*, London, pp: 199-235

[7] Gavrilovic P, Ginell W, Shendova V., Sumanov L. (2004): Conservation and seismic strengthening of Byzantine churches in Macedonia. The Getty Conservation Institute, *GCI Scientific Program Reports*, ISBN 0-89236-777-6, J. Paul Getty Trust, LA, USA

[8] Mazzolani F M, Krstevska L, Tashkov Lj, Gramatikov K, Landolfo R. (2007): Shaking Table Testing of Mustafa Pasha Mosque Model. *FP6-PROHITECH Final Report,* IZIIS Skopje

[9] Necevska-Cvetanovska G, Apostolska R (2008): Consolidation, Rebuilding and Strengthening of St. Pantelymon Church, Plaoshnik, Ohrid. *Engineering Structures 30*, pp:2185-2193

[10] Shendova V, Stojanoski B. (2004): Main Project on Repair, Strengthening and Reconstruction of St. Athanasius Church in Leshok. *IZIIS Report 2004-15*

[11] Shendova V, Stojanoski B, Gavrilovic P. (2007): Main Project on Repair and Strengthening of the Mustafa Pasha Mosque in Skopje. *IZIIS Report 2007-41*

[12] Bozinovski Z., Shendova V., Cvetanovska G., Garevski M., Apostolska R. (2008): Analysis of Seismic Stability with Technical Solution for Repair and Seismic Strengthening of the Structure of the Parliament of Republic of Macedonia. *Report IZIIS 2008-53*

APPLICATION OF WOOD-BASED SEISMIC RETROFITTING TECHNIQUES ON EXISTING TIMBER AND MASONRY STRUCTURES: DESIGN STRATEGIES, MODELLING APPROACHES AND PRACTICAL BENEFITS FOR TWO CASE-STUDY BUILDINGS

Michele Mirra [(1)], Andrea Gerardini [(2)], Geert Ravenshorst [(3)], Jan-Willem van de Kuilen [(4)]

[(1)] *Postdoctoral researcher, Delft University of Technology, m.mirra@tudelft.nl*
[(2)] *Professional engineer, Gerardini Ingegneria Sismica, gerardini.a@gmail.com*
[(3)] *Assistant professor, Delft University of Technology, g.j.p.ravenshorst@tudelft.nl*
[(4)] *Full professor, Delft University of Technology & Technical University of Munich, j.w.g.vandekuilen@tudelft.nl*

Abstract

Reversible retrofitting techniques for protecting architectural heritage against seismic events have found increasing application in existing or historical buildings. In this framework, the use of wood-based strengthening solutions for both timber and masonry structures has shown promising results, as proved by several recent research studies. Starting from these outcomes, the present work aims at highlighting the potential of such timber-based retrofitting methods from both the academic and the professional perspective, considering two case-study buildings: a stone-masonry church from 18th century with a timber roof, and a Venetian sawmill composed of masonry and timber structural portions. In the first case-study building, the church of St. Andrew in Ceto (province of Brescia, Italy), the lack of joints among the roof timber members and the masonry walls, as well as the in-plane flexibility of the roof structure itself, made the church vulnerable to seismic actions and prone to local out-of-plane masonry collapses. The second case-study building, the sawmill of Vallaro (province of Brescia, Italy), was composed of two building units, one featuring mainly timber structural elements, the other consisting of masonry walls and a wooden roof. This second intervention was very complex, because of the different materials involved, their conservation state, and the need to transform part of the building in a museum, with increased design static and seismic loads. For both case studies, timber-based seismic retrofitting interventions were applied, consisting of the addition of new wooden members, and the use of plywood panels and cross-laminated timber elements. This work presents and discusses the adopted design and modelling strategies, as well as the practical benefits of the applied solutions. The present study can thus contribute to the promotion of timber-based techniques in the combined structural, seismic, and conservation upgrading of existing buildings belonging to the architectural heritage of seismic-prone countries.

Keywords: seismic retrofitting, timber, masonry, architectural conservation, wood-based strengthening.

1. Introduction

Existing or historical buildings that are part of the architectural heritage of several countries, often feature masonry walls as vertical loadbearing structural components, and timber floors or roofs as horizontal elements. With reference to the Italian context, these building typologies are very frequent, and have highlighted significant vulnerabilities from the seismic point of view, as proved by several local or global collapses observed after recent earthquakes [1–3]. The poor characteristics of masonry walls, the lack of adequate connections among vertical and horizontal structural components, as well as the flexibility and insufficient capability of timber floors to transfer and redistribute seismic loads, can be identified as the main causes of such collapses. Hence, the improvement of these characteristics is essential for preserving monumental constructions and the architectural heritage in general, by limiting as much as possible the structural damage induced by earthquakes.

However, when designing seismic retrofitting methods for such buildings, their historical value has to be taken into account as well. The selected interventions have thus to be reversible, not invasive, and enable the architectural conservation of these structures. In this context, timber-based techniques

constitute a promising, effective opportunity for reversible seismic strengthening and restoration of existing buildings [4–7]. With reference to the improvement of the response of timber floors to earthquakes, research studies on wood-based retrofitting techniques such as the overlay of cross-laminated timber (CLT) [8], oriented strand board (OSB) [9], or plywood panels [10–14], demonstrated the excellent performance and high potential of these strengthening methods. In particular, an overlay of plywood panels fastened around their perimeter to the existing sheathing can greatly increase not only the in-plane strength and stiffness of a wooden floor, but also its energy dissipation, providing additional benefits for the whole masonry building [15–18].

In this work, the application of this strengthening technique to two existing masonry buildings is discussed, highlighting the advantages of a seismic wood-based retrofitting, also from the professional and practical point of view. The case-study buildings consist of the Church of St. Andrews in Ceto and the Venetian sawmill of Vallaro (both located in the mountain area of the Province of Brescia, Italy), and are shown in Fig. 1. After describing the buildings and their vulnerabilities in detail (Section 2), the applied reversible, wood-based retrofitting interventions are discussed (Section 3). The contribution of these strengthening solutions to the seismic improvement of the buildings are analysed, in agreement with the Italian Building Code [19], by means of numerical models, presented in Section 4, where also the specific modelling strategies are discussed. The results from the analyses are presented in Section 5, followed by a detailed overview of the benefits of applying wood-based retrofitting techniques to the two case-study buildings (Section 6), and by the conclusions of this work.

2. Analysed case-study buildings

2.1 St. Andrew's church

The Church of Ceto (Fig. 2), built 1708–26, is a stone masonry building consisting of a single nave measuring 21×14 m, with an average height of 14.5 m, and covered with a barrel vault. The apse has dimensions of 8.2×8.2 m, with an average height of 13 m, and is covered with a cross vault. The building rests on sloping rocky ground and is located on top of a retaining wall. With regard to the main structural components of the church, all walls are composed of stone masonry, reaching an average thickness of about 220 cm in the location of the buttresses, which also feature existing metal ties at the vault height. Elsewhere, the thickness of the walls varies from 70 cm to 100 cm. The roof entirely consists of wooden structural elements (spruce and larch), shown in Figs. 2-3.

Overall, the case-study church did not present issues from the static structural point of view. Several cracks and detachments of material could be observed from the first inspection, but these only involved the finishing layer, and had been caused by the chemical and thermo-hygrometric incompatibility between stone masonry and cement plaster, here improperly applied in past restoration works. The existing metal ties were in good state and well restrained to the walls, and the masonry structural elements appeared to be well dimensioned and constructed.
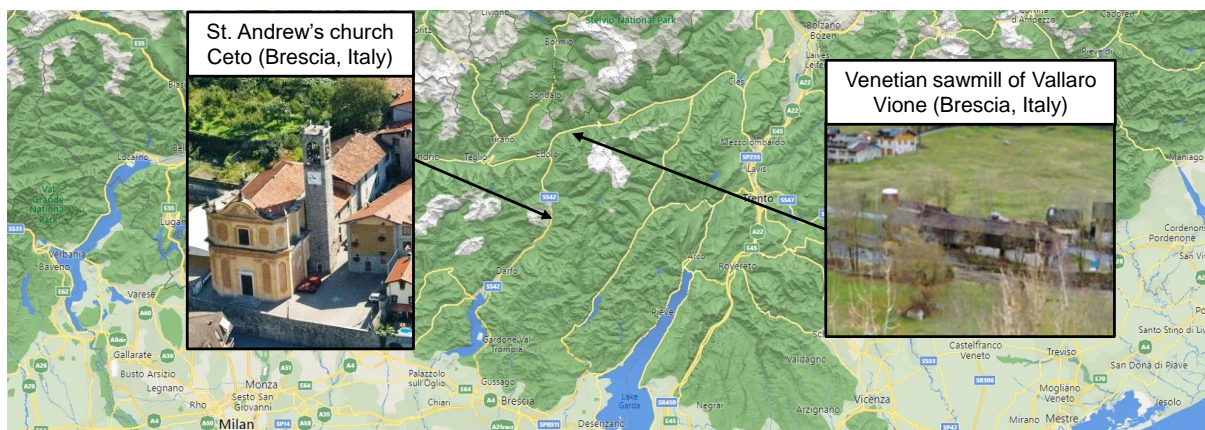
Figure 1. Location and view of the two analysed case-study buildings in the Province of Brescia, Italy.
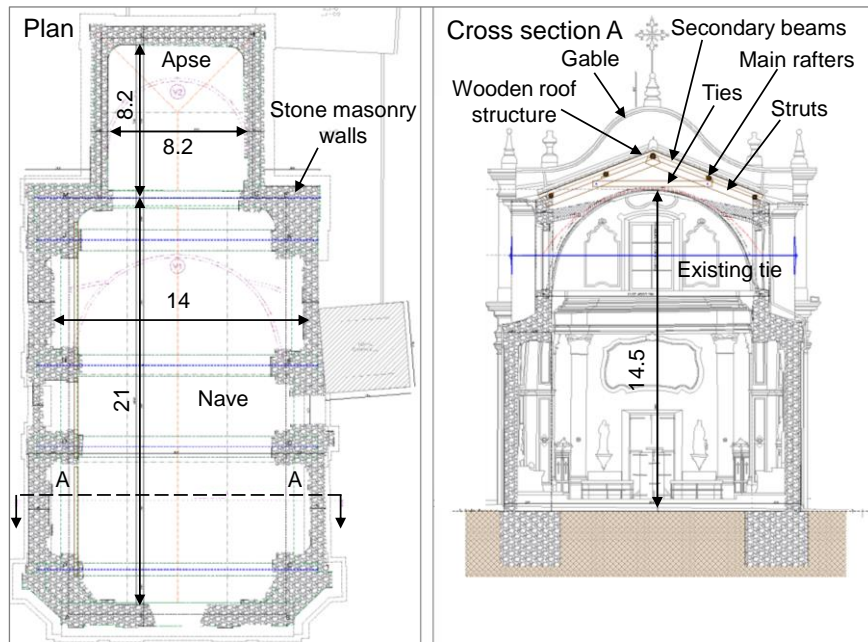
Figure 2. Plan and cross section of the case-study church; dimensions in m.

The wooden roof structure was found in fair state of conservation, but was very difficult to inspect, as the attic of the nave and the apse is narrow and normally not accessible. Most of the roof joists were found in good conditions, only a small number (≈ 15%) were locally affected by biological degradation, mainly due to slight water infiltrations. However, the ridge beam (Fig. 3c) appeared to be very undersized, also considering the spans involved, up to 8 m: large deflections could be observed, which had been compensated over time by additional wooden blocks, to keep the support for the secondary beams as horizontal as possible. The main wooden struts and ties were in a good state, and had adequate dimensions for their structural purpose. Yet, the existing connections with metal pins (Fig. 3b) did not appear to be very effective, and the ties could not fully absorb the thrusts induced by the struts, which seemed thus to be partly taken by the buttresses.

The latter mechanism could be particularly critical in the event of an earthquake, also considering the absence of effective joints among the structural elements of the roof. In other words, the roof would not be able to act as a diaphragm, absorbing the seismic actions and redistributing them to the masonry walls. Besides, effective connections between the timber roof structure and the walls or buttresses were also absent, thus the shear forces induced by an earthquake could not be transferred properly. In light of these findings from the performed inspections, reversible, timber-based seismic retrofitting interventions were designed and applied to the roof, as presented in section 3.

(a)　　　　　　　　　(b)　　　　　　　　　(c)
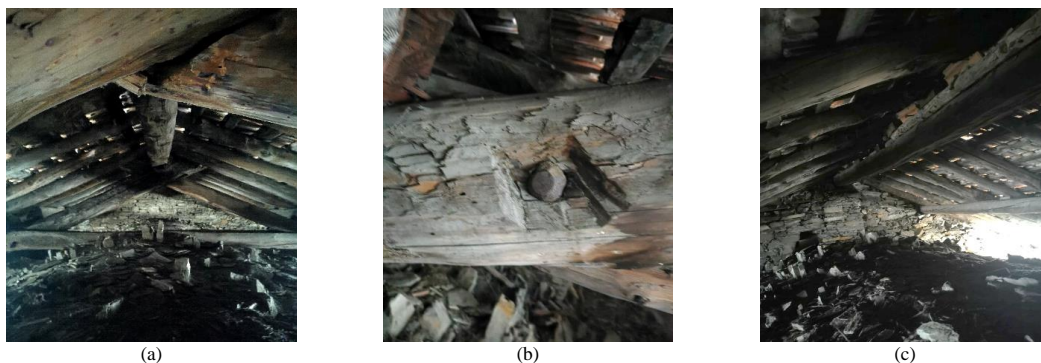
Figure 3. (a) Existing wooden roof structure; (b) existing metal pin between timber struts and ties; (c) ridge beam undergoing excessive deflection.

2.2 Venetian sawmill of Vallaro

The Venetian sawmill of Vallaro (Fig. 4), in the municipality of Vione, was built at the end of the 19th century, and has been selected for a full restoration plan in order to transform it in a museum. The building can be subdivided in three independent portions A, B, and C.

- Portion A (280 m², Fig. 5a-c) consists of a single-storey timber structure and a stone masonry basement, featuring 50-60 cm thick walls. The ground timber floor is composed of spruce joists and planks, but part of it was strengthened in the past with an incompatible 20-mm-thick concrete slab. The whole wooden roof structure is also made of spruce, and rests on timber columns. The timber members were found in a bad state of conservation.
- Portion B (50 m², Fig. 5d) is a two-story stone masonry structure (wall thickness 50-60 cm) with timber floors and roof.
- Portion C (80 m²) consist of a prolongation of the roof structure of portion A, and was found in bad state of conservation as well.

The existing structure is the result of a series of interventions carried out over time, causing overlapping between original members and elements added later, often incompatible or of low quality. This is the main reason for the poor conditions of the building from the point of view of conservation, with extended degradation phenomena caused by water infiltrations from the roof.
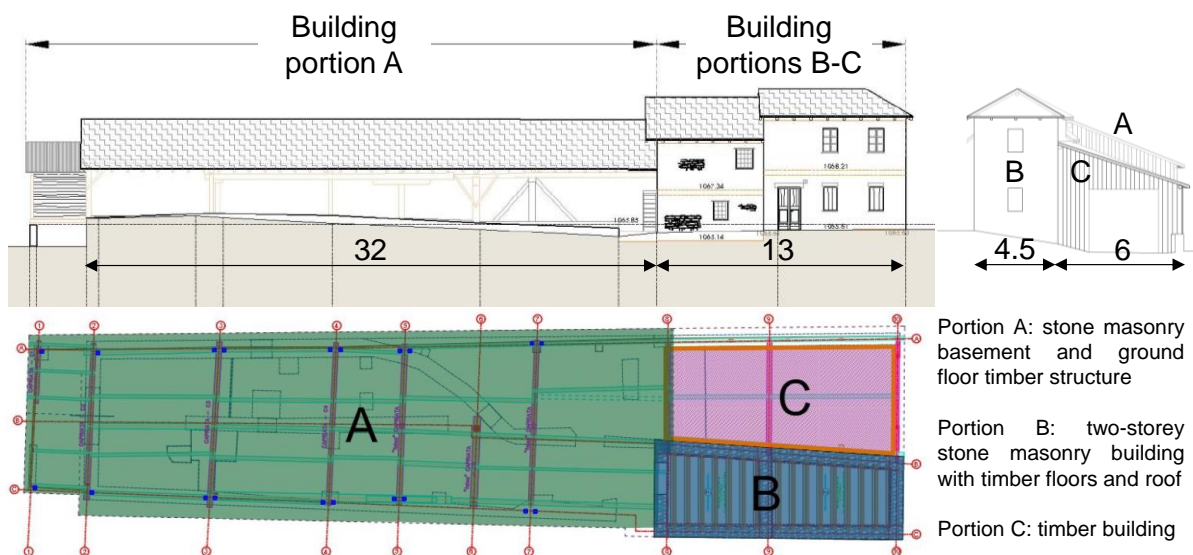
Figure 4. Plan and side views of the case-study sawmill; dimensions in m.

(a) (b) (c) (d)

Figure 5. Front (a), side (b), and interior (c) views of portion A of the sawmill; view of portion B (d).

The main vulnerabilities that were found, were also related to the poor state of the building. Firstly, the whole portion A presented insufficient load-carrying capacity of the wooden columns, with the existing structure able to sustain static actions only because of provisional strengthening members. All wooden floors and roofs were not in good state, and also very undersized for the future increased design loads (snow, wind and crowd). Furthermore, local cracks were detected in the masonry walls of building portions A and B. Finally, all horizontal structural elements were not able to create an effective diaphragmatic and dissipative action against seismic loads, and joints between floors and walls were absent. Therefore, similarly to the church of Ceto, wood-based retrofitting systems were applied for this building as well.

3. Applied timber-based techniques

3.1 General

The retrofitting interventions on the two buildings were subjected to several strict requirements imposed by the Italian Superintendence for Architectural Heritage, especially in terms of reversibility and compatibility with the existing structures. Thus, the use of mostly wood-based solutions was found to be appropriate and effective to strengthen both case-study buildings from the static and seismic point of view.

More specifically, besides the necessary improvement of the static behaviour of the roof in the church of Ceto and of all floors in the sawmill of Vallaro, the applied retrofitting methods were designed in the framework of the seismic upgrading interventions, pursuant to § 8.4.2 of the Italian Building Code [19]. According to the standard, a quantity ζ_E is defined, representing the ratio between the seismic action that can be withstood by the existing structure, and the seismic action that would be considered in the design of a new building in the same site. In terms of peak ground acceleration (PGA), this quantity can be defined as $PGA_{capacity}/PGA_{demand}$. After having evaluated $\zeta_{E,1}$ for the as-built state and $\zeta_{E,2}$ for the building after retrofitting, the requirement of seismic improvement is met when the designed strengthening solutions ensure that $\zeta_{E,2} - \zeta_{E,1} \geq 0.1$ [19].

3.2 St. Andrew's church

In the church of Ceto, adequate connections between timber roof and masonry walls were absent, therefore the construction would very likely develop local overturning mechanisms in the event of an earthquake, and without retrieving its global resistance. Hence, the main retrofitting intervention consisted of transforming the existing roof in a diaphragm. To this end, an overlay of 30-mm-thick plywood panels fastened to the existing sheathing with 4×60 mm Anker nails at 80 mm spacing, was realized (Fig. 6). This solution enables the adequate transfer of seismic forces and the development of the box behaviour of the construction, but without significantly changing the stiffness of the entire building [7]. Besides, this type of diaphragm can also potentially act as dissipative element, absorbing part of the energy imparted by the earthquake by means of the yielding of the fasteners connecting planks and plywood panels [7]. The retrofitted roof could provide a strength of 275 kN per pitch, reached at a maximum deflection of 35 mm, and an initial stiffness of 44 kN/mm, following the design procedures reported in [7, 18]. As an extra safety measure, in addition to the plywood panels overlay, a light bracing system consisting of 5×80 mm S275 steel plates was designed to promptly prevent local overturning mechanisms of the gable, by directly transferring the pertaining shear forces to the buttresses (Fig. 6). On the perimeter of the walls, the steel plates were adequately connected to the existing masonry through M20 anchor bars, enabling the transfer of shear and tensile stresses.

Some of the members of the existing roof structure were also subjected to local wood-based interventions. The few joists and planks damaged by water infiltrations were integrated with newly supplied joists, laid alongside the existing ones, and featuring their same geometry and wood species. For the undersized existing main beams, flexural reinforcements were created, by placing additional wooden beams clamped to the main ones by means of steel plates and screws. These newly supplied beams had again the same geometrical characteristics and wood species as the existing ones.
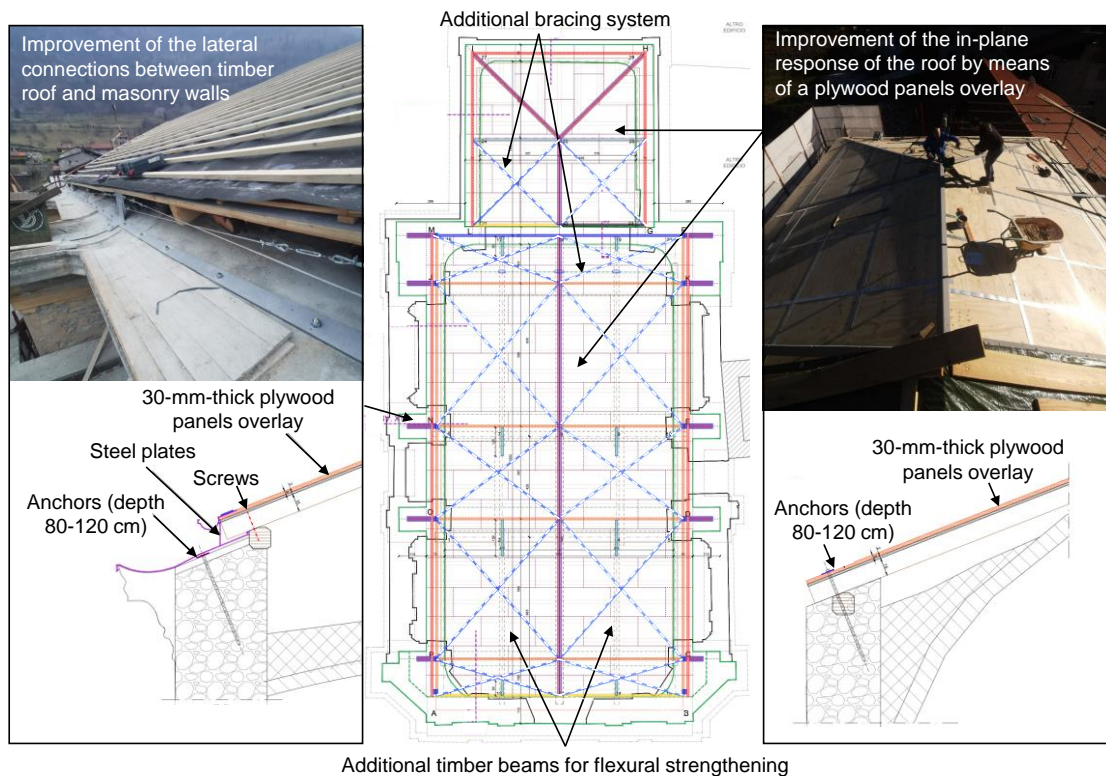
Figure 6. Main strengthening solutions applied to the church of Ceto.

Additionally, screwed joints were created between all secondary joists and the main loadbearing beams, to avoid the possible loss of support due to the vertical seismic component. Likewise, connections between main beams and wooden struts, as well as between the struts themselves and the timber ties, were realized. In this way, besides improving the structural in- and out-of-plane response of the whole roof, it was possible to create an adequate contrast to the aforementioned thrusts induced by the struts, thus beneficially removing this out-of-plane action on the masonry walls.

3.3 Venetian sawmill of Vallaro

The sawmill of Vallaro required several strengthening interventions, not only because of the overall poor conditions of the building, but also in light of the future increased design loads (crowd, snow and wind). Thus, besides the target seismic upgrading, also measures to radically improve the static behaviour of the sawmill were designed. An overview of these interventions is shown in Fig. 7, for all building portions.

For portion A (Fig. 7a), given the low residual load-carrying capacity of the decayed timber columns, newly integrated slender steel elements were designed, along with a new steel frame connected to the strengthened foundations. This allows not only to improve the structural response under vertical loads, but also provides sufficient strength to horizontal actions. In this specific case, in consultation with the local Superintendence, a wood-based solution was not adopted, because it would have required very massive structural elements, which could partly hide the original appearance of the existing building. A timber-based strengthening was, on the contrary, designed to preserve the wooden roof and enhance its structural response. Thus, 12-cm-thick C24 cross laminated timber (CLT) plates, along with additional steel strands were used to improve the static behaviour of the roof, and enable its diaphragmatic action, while contemporarily preserving the existing wooden trusses. Besides, also the ground timber floor was strengthened with 30-mm-thick plywood panels and additional wooden elements. For all realized diaphragms, effective joints with the masonry walls were realized, mostly through S275 or S355 steel angles and M14 or M20 threaded bars. All incompatible past interventions (concrete slabs and elements) were demolished and integrated with new wooden or steel members.
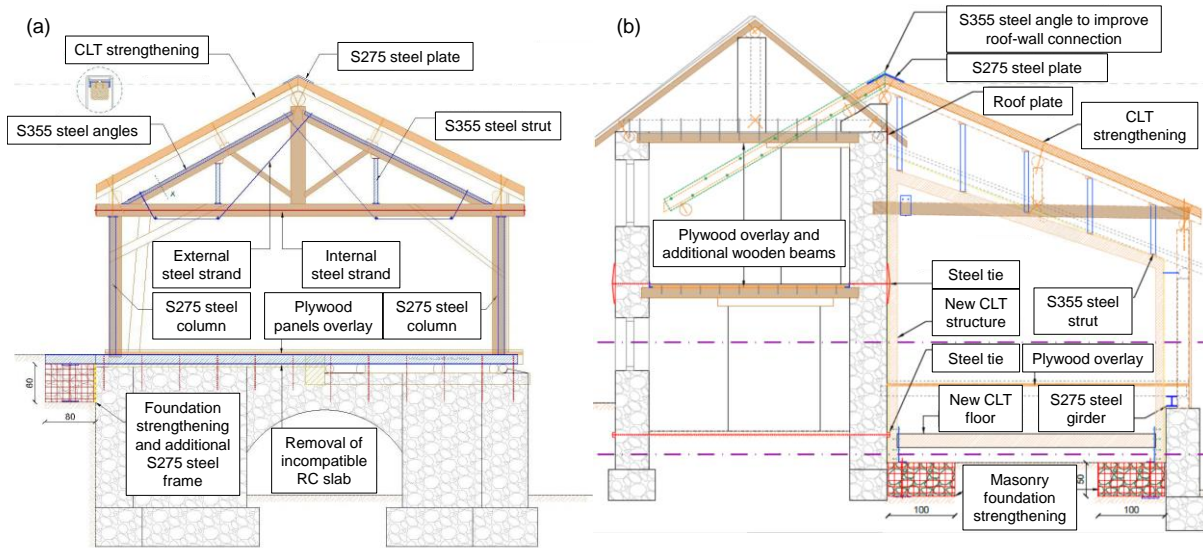
Figure 7. Main strengthening solutions applied to the sawmill of Vallaro: portion A (a) and portions B-C (b).

For portion B (Fig. 7b), flexural strengthening of the timber floors and roofs was necessary. This was realized by means of new wooden beams and a 20-mm-thick plywood panels overlay fastened on them with 6×120 mm screws at 300 mm spacing. Besides, effective connections between horizontal and vertical structural elements were designed, including also new steel ties for an improved confinement of the stone masonry. In portion C (Fig. 7b), these measures were integrated with the realization of an entirely new prefabricated CLT structure, able to support the existing wooden elements, which showed severe decay and excessive lack of load-carrying capacity. These solutions allowed to preserve as much as possible the original appearance and features of the sawmill, despite its bad conditions.

4. Numerical models of the case-study buildings

4.1 St. Andrew's church

For the church of Ceto, a first numerical model was created in the commercial finite element software Aedes.PCM (Fig. 8a). For all walls, the properties for stone masonry suggested by the Italian Building Code [19] were adopted, thus a Young modulus of 870 MPa, a shear modulus of 290 MPa, a compressive strength of 1 MPa, and a tensile/shear strength of 0.018 MPa. Given the overall good state of timber structural members, a C24 strength class was assumed for them. The seismic action for the location of Ceto was prescribed, corresponding to a peak ground acceleration (PGA) of 0.08g.

Figure 8. Models of the church in Aedes.PCM (a) and DIANA FEA (b), including cyclic response of roof (c).

After having specified these properties, the as-built configuration of the church was firstly analysed, evaluating its vulnerability in terms of local collapse mechanisms, as prescribed by the Italian guidelines for seismic assessment of churches [20]. From these investigations, the aforementioned ratio $\zeta_{E,1}$ was determined.

For the retrofitted configuration, with a roof well connected to the walls and able to act as a stiff diaphragm, local mechanisms can be prevented, also given the compactness of the church. Thus, after a modal analysis, a series of 16 pushover analyses were conducted on the whole building in both plan directions, and from the governing curve, the aforementioned ratio $\zeta_{E,2}$ was derived. For these pushover analyses, the control node was taken as the centre of mass of the building, on top of the vault, and the masonry was simulated with an equivalent frame modelling strategy. In order to conservatively not overestimate the displacement capacity of the building, each analysis was stopped as soon as the first pier experienced a drop in in-plane capacity larger than 20% of its strength.

Besides, to validate the use of equivalent frame modelling adopted by Aedes.PCM, a more advanced model was also constructed in DIANA FEA, considering a configuration where the roof was modelled as rigid, similarly to Aedes.PCM (Fig. 8b), and one that also simulated, through a macro-element modelling strategy [7, 17, 18], the full nonlinear, cyclic, dissipative response of the retrofitted roof (Fig. 8c). For all walls, eight-node shell elements featuring the Engineering Masonry Model of DIANA FEA were adopted [21], with the same properties used in Aedes.PCM. Nonlinear incremental dynamic analyses were performed, adopting accelerograms compatible with the design response spectrum for the location of Ceto.

4.2 Venetian sawmill of Vallaro

Two numerical models were realized for the case-study sawmill: portion A was simulated in PRO_SAP software (Fig. 9a), while portion B was once more modelled in Aedes.PCM (Fig. 9b). The first model could be considered as a simulation of an almost entirely new construction, since an adequate response to static and dynamic loads is only provided by newly installed structural elements (CLT and plywood panels, steel members), given the bad conditions of the existing ones. For this case, a modal analysis with response spectrum was performed, considering a behaviour factor of 1.5.

In the second model, instead, an approach similar to St. Andrew's church was adopted, firstly assessing the seismic response of the as-built state through local collapse mechanisms, and then evaluating the improvement in performance after retrofitting, by means of pushover analyses. The modelling assumptions and the properties of masonry and timber were identical to those reported for the church of Ceto. In both cases, the reference PGA for the site was 0.09g, and the floors were assumed as rigid. Portion C was not modelled, because it was a prefabricated structure, directly designed by the supplier.

5. Results

5.1 St. Andrew's church

From the kinematic analysis of the as-built configuration (Fig. 10a), the front façade showed a strong vulnerability, leading to $\zeta_{E,1} = 0.23$ only (PGA at collapse of $\approx 0.02g$). It should be noticed that this value can be considered as very conservative, since from the conducted inspections the façade appeared to be well connected to the rest of the structure. Yet, without a roof acting as diaphragm and proper joints, able to redistribute seismic actions among other structural components, similar failure mechanisms could still take place in the event of an earthquake.

With regard to the retrofitted configuration, the modal analyses highlighted a regular dynamic response and close results among the different models: the first fundamental period of the church was 0.47 s in the Aedes.PCM model, 0.47 s and 0.50 s in the DIANA models featuring a rigid and a dissipative roof, respectively. This is coherent with the regularity and symmetry of the church, as well as the proper distribution and arrangement of all masonry piers and buttresses, allowing also the equivalent frame modelling strategy of Aedes.PCM to provide reliable results.
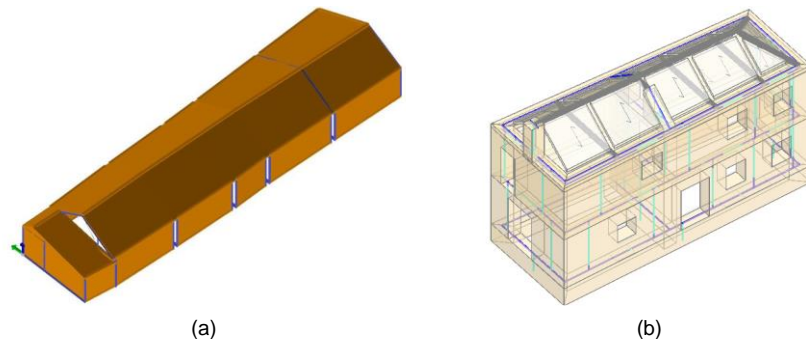
Figure 9. Models of portions A (a, PRO_SAP), and B (b, Aedes.PCM) of the Venetian sawmill of Vallaro.
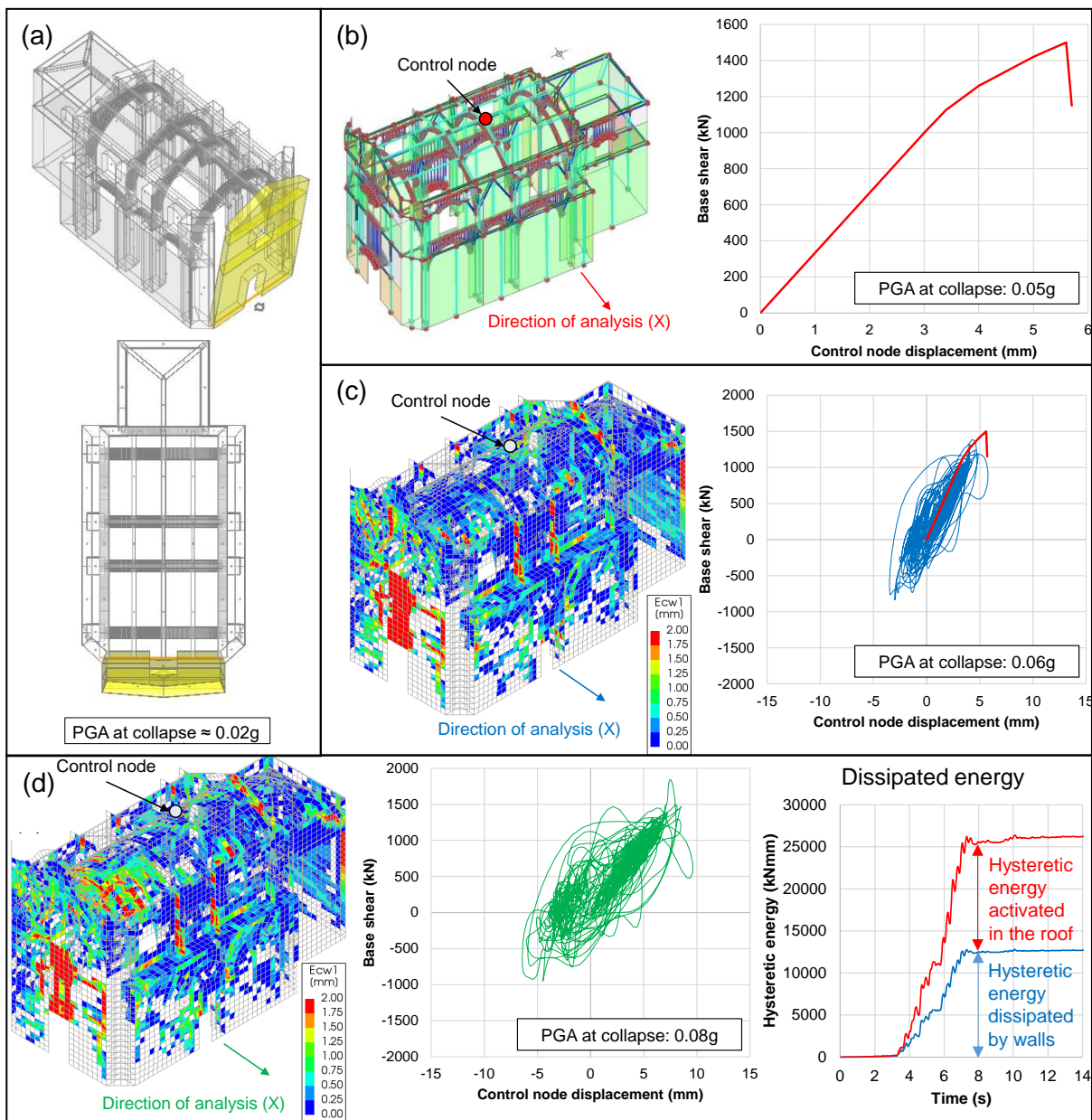
Figure 10. (a) Governing kinematic mechanism of as-built church; (b) governing pushover curve in PCM.Aedes model; (c) crack pattern and base shear-displacement graph from DIANA FEA model with rigid roof, including comparison with pushover curve; (d) crack pattern, base shear-displacement graph and dissipated energy from the model in DIANA FEA featuring the full simulation of the roof retrofitted with plywood panels.

From the conducted pushover analyses in Aedes.PCM, the governing curve is shown in Fig. 10b, and corresponded to a ratio $\zeta_{E,2} = 0.61$ (PGA at collapse of ≈ 0.05g). It should be noticed that this value represents a lower bound for the seismic performance of the church after retrofitting, because of the conservative assumptions behind the conducted analyses (see Section 4.1). Yet, the requirement of seismic upgrading according to [19] is already met, since $\zeta_{E,2} - \zeta_{E,1} = 0.38 >> 0.1$. Thus, the applied interventions allow to greatly improve the structural behaviour of the building, from both static and seismic perspective.

Similar results (PGA at collapse ≈ 0.06g) were obtained from the time-history analyses in the DIANA model with rigid roof (Fig. 10c), confirming once more that for this case-study also the simplified approach of PCM.Aedes could be sufficient for a correct assessment of the influence of the retrofitting. However, both models cannot capture the beneficial energy dissipation provided by the plywood panels overlay, as highlighted by Fig. 10d, showing the DIANA model where the full cyclic response of the roof was included. When this is also taken into account, the church could potentially survive the on-site design earthquake, and the energy dissipated in the roof could be associated to an equivalent damping ratio of 0.12-0.13 for this case, beneficially reducing the actions that are transferred to masonry walls.

5.2 Venetian sawmill of Vallaro

The retrofitting solutions applied to portion A allowed the new structure to efficiently withstand the expected future design static and seismic loads, for both the additional steel elements and the existing and additional timber members, with unity checks up to 0.95 and a first fundamental period of 0.20 s. Thus, the choice of slender elements allowed portion A to perform as a fully new construction, while keeping as much as possible its original appearance.

More interesting is the case of portion B (Fig. 11), which in the as-built state would be able to withstand less than half of the design PGA ($\zeta_{E,1} = 0.45$) due to out-of-plane walls overturning. After retrofitting, the building could fully withstand the future static actions, while providing an enhanced box behaviour (first fundamental period of 0.13 s). Yet, the retrofitted structure did not show significant ductility, because of the choice of terminating the analysis once in a single masonry elements the shear capacity decreased more than 20% of the peak strength. This allowed not to overestimate the displacement capacity, given the overall bad conservation state of the building. Nevertheless, the requirement of seismic upgrading according to [19] was still met, since $\zeta_{E,2} - \zeta_{E,1} = 0.63 - 0.45 = 0.18 > 0.1$. It should be noticed that, considering the conservative assumptions at the basis of the model, and the additional energy dissipation that is provided by the retrofitted timber diaphragms, the actual expected improvement could be much larger. Yet, given the initial poor conditions of the existing structure, the designed interventions could still lead to a safer, renovated environment for hosting a museum.

6. Practical benefits of the applied wood-based seismic retrofitting techniques

The timber-based retrofitting solutions applied to the case-study buildings are all reversible interventions, and compatible with the existing structural members, which could be effectively strengthened and protected: thus, the adopted retrofitting methods also enable the conservation of the two buildings. Besides, all floors and roofs can now act as diaphragms and prevent local (out-of-plane) collapses of masonry walls, allowing the buildings to develop a box behaviour against seismic actions. The additional plywood panels overlay fastened to the existing sheathings constitutes a reversible, not invasive intervention, which does not excessively increase mass and stiffness of the floors, and potentially enables additional ductility and energy dissipation, as proved in the conducted numerical analyses.

The applied retrofitting methods are not only convenient in terms of seismic improvement, but also from a more practical point of view. The designed solutions were particularly appreciated by both the Curia of Brescia and the Superintendence for Architectural Heritage, as the historical and architectural value of the buildings was preserved. The reasonably low impact on the constructions, linked to a large improvement in their structural properties, is surely a first point of strength of the use of wood-based techniques in these case-study buildings.
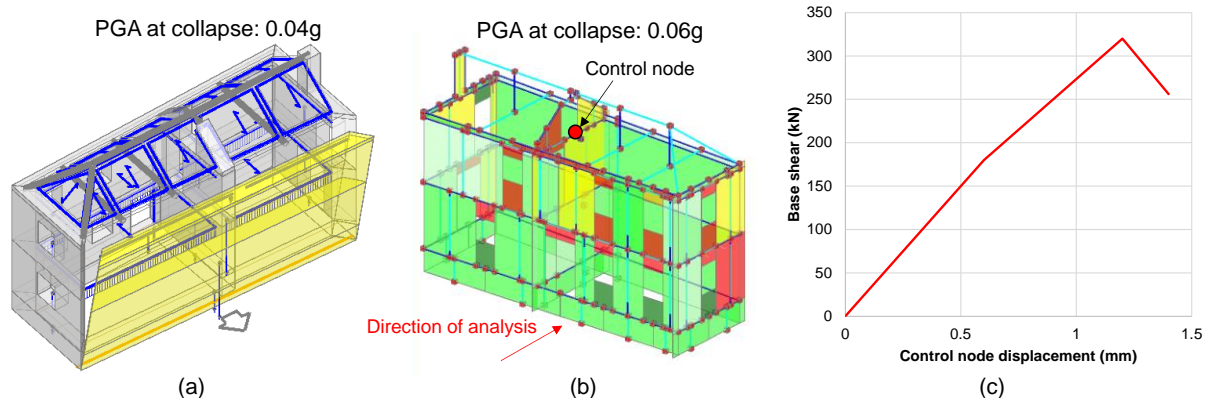
Figure 11. Governing kinematic mechanism of as-built configuration of portion B (a); results from governing pushover analysis in terms of damage on piers and spandrels (b), and load-displacement curve (c).

Besides, from the perspective of professional engineers, these interventions can be efficiently designed and are particularly affordable. The overlay of plywood panels is a very cost-effective measure, and could be realized within the limited budgets available. This result was possible not only because of lower material costs compared to other solutions, but also due to the fast and manageable application of the intervention. For instance, for the church of Ceto, the whole plywood panels overlay was fastened to the existing roof by a local building enterprise composed of only three employees within a single working day.

7. Summary and conclusions

This work has presented the application of several wood-based seismic strengthening techniques on two case-study buildings, St. Andrew's church in Ceto and the venetian sawmill of Vallaro, both located in the Province of Brescia, Italy. The design choices, modelling approaches, and practical benefits of these retrofitting solutions were discussed throughout the paper.

For both structures, local out-of-plane collapses of masonry walls were very likely in the as-built state for already very low seismic actions. Hence, wooden floors and roofs were strengthened with a plywood panels overlay (or CLT for the sawmill of Vallaro, which was in poorer conditions and also needed a static strengthening); the new diaphragms were also well connected to the walls, in order to prevent local failure mechanisms and ensure the development of a proper box behaviour.

The benefits of wood-based solutions have been highlighted from both the seismic and the practical perspective, focusing on their reversibility, lightness, as well as cost- and execution effectiveness. In particular, after retrofitting, a great increase in seismic performance of the buildings can be obtained: the outcomes from the conducted numerical analyses show that the strengthened structures could potentially be able to almost or fully withstand the expected seismic actions on their site, because of the improved box behaviour and additional energy dissipation provided by the strengthened floors.

The results obtained within the analysis of these case-study buildings can contribute to further highlight the benefits of timber-based retrofitting techniques, and to support the research framework promoting their use for the preservation of architectural heritage in seismic-prone countries.

Acknowledgements

References

[1] Lagomarsino, S. (2012): Damage assessment of churches after L'Aquila earthquake. *Bulletin of Earthquake Engineering*, 10, 73–92.

[2] Indirli, M., Marghella, G., Marzo, A. (2012): Damage and collapse mechanisms in churches during the Pianura Padana Emiliana earthquake. *Energia, Ambiente e Innovazione*, 4-5, 69–94.

[3] Penna, A., Calderini, C., Sorrentino, L., Carocci, C.F., Cescatti, E., Sisti, R., Borri, A., Modena, C., Prota, A. (2019): Damage to churches in the 2016 central Italy earthquakes. *Bulletin of Earthquake Engineering*, 17.

[4] Gubana, A. (2015): State-of-the-Art Report on high reversible timber to timber strengthening interventions on wooden floors. *Construction and Building Materials*, 97, 25–33.

[5] Pozza, L., Marchi, L., Trutalli, D., Scotta, R. (2021). In-plane strengthening of masonry buildings with timber panels. *Proceedings of the Institution of Civil Engineers – Structures and Buildings*, **174** (5), 345–358.

[6] Mirra, M., Ravenshorst, G., van de Kuilen, J.-W. (2021): Comparing in-plane equivalent shear stiffness of timber diaphragms retrofitted with light and reversible wood-based techniques. *Practice Periodical on Structural Design and Construction*, **26** (4).

[7] Mirra, M., Ravenshorst, G. (2021): Optimizing Seismic Capacity of Existing Masonry Buildings by Retrofitting Timber Floors: Wood-Based Solutions as a Dissipative Alternative to Rigid Concrete Diaphragms. *Buildings*, **11** (12), 604.

[8] Branco, J. M., Kekeliak, M., Lourenço, P.B. (2015): In-Plane Stiffness of Timber Floors Strengthened with CLT. *European Journal of Wood and Wood Products*, 73, 313-323.

[9] Gubana, A., Melotto, M. (2018): Experimental tests on wood-based in-plane strengthening solutions for the seismic retrofit of traditional timber floors. *Construction and Building Materials*, 191, 290–299.

[10] Peralta, D.F., Bracci, M.J., Hueste, M.B.D. (2004): Seismic Behavior of Wood Diaphragms in Pre-1950s Unreinforced Masonry Buildings. *Journal of Structural Engineering*, **130** (12).

[11] Brignola, A., Pampanin, S., Podestà, S. (2012): Experimental Evaluation of the In-Plane Stiffness of Timber Diaphragms. *Earthquake Spectra*, **28** (4), 1–23.

[12] Giongo, I., Dizhur, D., Tomasi, R., Ingham, J.M. (2013): In-plane assessment of existing timber diaphragms in URM buildings via quasi-static and dynamic in-situ tests. *Advanced Materials Research*, 778, 495–502.

[13] Wilson, A., Quenneville, P.J.H., Ingham, J.M. (2014): In-plane orthotropic behavior of timber floor diaphragms in unreinforced masonry buildings. *Journal of Structural Engineering*, **140** (1).

[14] Mirra, M., Ravenshorst, G., van de Kuilen, J.-W. (2020): Experimental and analytical evaluation of the in-plane behaviour of as-built and strengthened traditional wooden floors. *Engineering Structures*, 211, 110432.

[15] Mirra, M., Ravenshorst, G., van de Kuilen, J.-W. (2021): An analytical model describing the in-plane behaviour of timber diaphragms strengthened with plywood panels. *Engineering Structures*, 235, 112128.

[16] Mirra, M., Ravenshorst, G., van de Kuilen, J.-W. (2021): Dissipative properties of timber diaphragms strengthened with plywood panels. *World Conference on Timber Engineering*, Santiago, Chile, 8 pages.

[17] Mirra, M., Sousamli, M., Longo, M., Ravenshorst, G. (2021): Analytical and numerical modelling of the in-plane response of timber diaphragms retrofitted with plywood panels. *8th International Conference on Computational Methods in Structural Dynamics and Earthquake Engineering*, Athens, Greece, 27 pages.

[18] Mirra, M., Ravenshorst, G. (2022): A seismic retrofitting design approach for activating dissipative behavior of timber diaphragms in existing unreinforced masonry buildings. *Eighth International Conference on Structural Engineering, Mechanics and Computation*, Cape Town, South Africa, 6 pages.

[19] NTC 2018. Norme tecniche per le costruzioni (Italian Building Code). Ministry for Infrastructures and Transports (in Italian).

[20] DPCM 09-02-2011. Valutazione e riduzione del rischio sismico del patrimonio culturale con riferimento alle norme tecniche per le costruzioni di cui al decreto ministeriale 14 gennaio 2008 (in Italian).

[21] Schreppers, G.M.A., Garofano, A., Messali, F., Rots, J.G. (2017): DIANA validation report for masonry modelling. DIANA FEA BV and Delft University of Technology, Delft, The Netherlands.

THE CASE STUDY OF PRINCE RUDOLF INFANTRY BARRACKS - ASSESSMENT, MODELLING AND RECONSTRUCTION

Boja Čačić Šipoš [(1)], Nataša Ivanišević [(2)], Mija Klasić [(3)], Luka Lulić [(4)], Ivan Matorić [(5)], Mislav Stepinac [(6)]

[(1)] *Civil engineer, Peoples Associates Structural Engineers, e-mail address: boja.cacic.sipos@pase.com*
[(2)] *Architect, A&A Architects, e-mail address: natasa@aa-architects.net*
[(3)] *Civil engineer, Peoples Associates Structural Engineers, e-mail address: mija.milic@pase.com*
[(4)] *PhD student, University of Zagreb Faculty of Civil Engineering, e-mail address: luka.lulic@grad.unizg.hr*
[(5)] *Civil engineer, Peoples Associates Structural Engineers, e-mail address: ivan.matoric@pase.com*
[(6)] *Assistant Professor, University of Zagreb Faculty of Civil Engineering, e-mail address: mislav.stepinac@grad.unizg.hr*

Abstract

The procedure of a detailed condition assessment of the building under heritage protection in Zagreb is presented. A detailed historical background of the case study building is shown, and observed damage and conducted in situ tests are discussed. The nonlinear static seismic analysis performed in the 3Muri software is extensively elaborated. Four different levels of reconstruction according to new Croatian law are briefly presented. Additionally, several strengthening scenarios are proposed with various strengthening techniques. The renovation of the case study building is presented through extensive photo documentation. The problems in renovations of culturally protected buildings in a specific case study are raised.

Keywords: assessment, masonry, renovation, NDT, case study, 3Muri

1. Introduction

Unreinforced masonry (URM) structures are primarily located in European urban centres and are highly vulnerable to earthquake excitations. After the Zagreb earthquake in 2020, they suffered significant damage and should be upgraded, renovated, or demolished [1]–[3]. This paper presents the procedure for a detailed condition inspection, modelling, and reconstruction of a building under cultural heritage protection. The case study building was damaged in the earthquake and needs to be renovated according to the new Croatian laws to ensure the safe and functional future use of the building. The case study building is located within the historic complex of buildings in the western part of the Zagreb 'Lower Town", the so-called Infantry Barracks of Prince Rudolf. The entire complex of the Rudolf Barracks is protected as an immovable individual cultural property and is registered in the Register of Cultural Heritage of the Republic of Croatia. The protection of the complex refers to the main building and the entire area of the former pedestrian barracks with the existing high-quality green areas, undeveloped areas, and peripheral buildings of high environmental value. The Rudolf Barracks complex is located in Protection Zone A of the historical and urban unit of the City of Zagreb, which is protected as a cultural asset and entered in the Register of Cultural Heritage of the Republic of Croatia - List of Protected Cultural Heritage.

The infantry barracks complex was built in the period from 1887 to 1889, according to the project of Viennese architects Franz Gruber and Carl Voelckner. The complex consisted of 13 buildings, most of which were two-story buildings, and was named after the son of Emperor Franz Joseph I and Empress Sisi, Prince Rudolf [4],[5]. The entire complex was built within 15 months after Prince Rudolf laid the foundation stone. The construction of the complex was triggered by tensions related to the Austro-Hungarian occupation of Bosnia and Herzegovina and the need to accommodate the army.

Figure 1. Case study building

The case study building is a public-purpose building with a rectangular floor plan of 25.18 m × 11.42 m and a height of approximately 15.50 m. The building has five floors, and all are used as office space. The building has undergone minor changes in the original geometry and space over time and has been properly maintained. More information about the building can be found in the paper by Milić et al. [6].

2. Condition assessment and modelling of the case study building

Various non-destructive, semi-destructive, and destructive methods are used to assess existing URM structures. More information about assessment methods can be found in [7],[8].

The particular case study was inspected after the earthquake on 22 March, 2020. It was assigned the usability mark PN2. The mark PN2 refers to buildings with moderate damage without the risk of collapse, but the usability is questionable due to the potential risk of collapse of some elements [9],[10]. The building did not experience severe damage, but several parts of the structure should be repaired. The more significant damage was observed at the connection of partition and load-bearing walls, as well as at the connection of walls and ceilings. The damage observed is not surprising since at the connections of partition and load-bearing walls, as well as walls and ceilings, there is a discontinuity of materials and contact of different materials with different behavior, thus causing different displacements that cause cracks (Figure 2). This inspection established a conservation guideline for repairing load-bearing and partition walls, staircases, and floor structures [6].
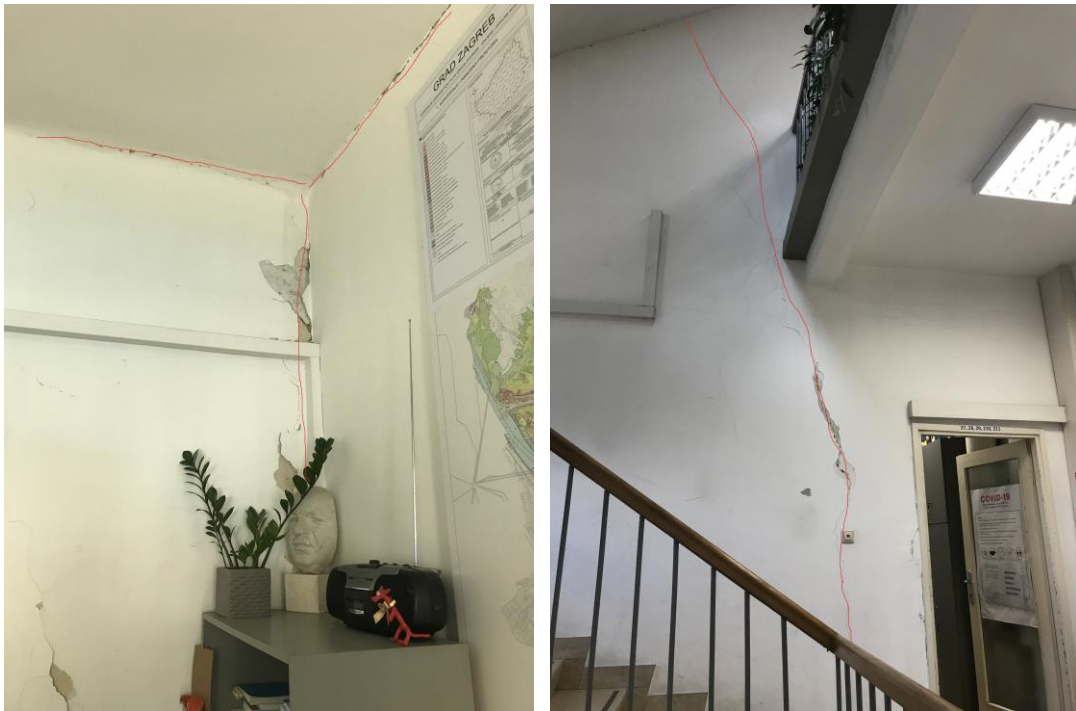
Figure 2. Observed damage

2.1 Flat-jack method for obtaining mechanical properties of masonry

The method is based on the principle of introducing stress into the masonry using metal flat-jacks of a semioval shape that is inflated like a balloon. A more detailed description of the flat-jack method can be found in [11],[12]. According to the tests (Figure 10), the following values were obtained: compressive stress state in masonry at test location $\sigma_0 = 0.46$ N/mm^2 (used for model calibration regarding weight distribution), modulus of elasticity E = 1469.5 N/mm^2 (used for wall stiffness definition), initial shear strength f_{v0} = 0.323 N/mm^2 (used for wall shear resistance definition) and coefficient of friction μ = 0.447. The whole procedure is shown in Milić et al. [6].

2.2 Numerical modelling

The modelling was done with the software 3Muri [13]. Modelling of the building in 3Muri software is done by inserting walls, columns, and beams, which are then discretized into macro elements. There are two types of macro elements, and these are the piers and parapets, where all the damage is concentrated. Parts of the wall, which are often undamaged, are defined as rigid nodes connecting the former two [34]. The mathematical concept underlying the use of macroelements makes it possible to determine the mechanism of collapse, i.e., the mechanism of damage. The damage may be due to shear in the central part of the macroelements or to combined compressive and bending stress in the peripheral parts of the macroelements [14].

Horizontal diaphragms are modelled using floor elements connected by three-dimensional nodes. The loads on the horizontal diaphragms (used only for mass calculation and distribution) are perpendicular to the floor level, and the seismic action is in the direction of the floor level. For this reason, the horizontal diaphragms can be modelled as axially stiff or flexible but without bending stiffness. Such shaping of the horizontal diaphragms is permissible because their main function is to absorb the horizontal actions from the seismic action and transmit them to the vertical load-bearing elements [15]. 3Muri assumes good wall-to-wall and wall-to-floor connections, i.e., box behavior, which is desirable but often unrealistic in existing structures. Therefore, the modelling assumes that the damaged masonry has been restored to its original, undamaged condition by methods such as grouting and that the necessary measures have been taken to ensure the box behavior of the observed structure. In addition,

3Muri allows for out-of-plane failure analysis of local mechanisms in a separate module. This is extremely useful since the box behavior can only account for in-plane masonry failure. More about the analysis of local mechanisms in 3Muri can be found in [16].

Figure 3 shows a 3D model of the building in 3Muri. More about modelling can be found in the paper by Milić et al. [6]. Three-dimensional model with damage for the near-collapse limit state: (a) x-direction; (b) y-direction can be seen in Figure 4.
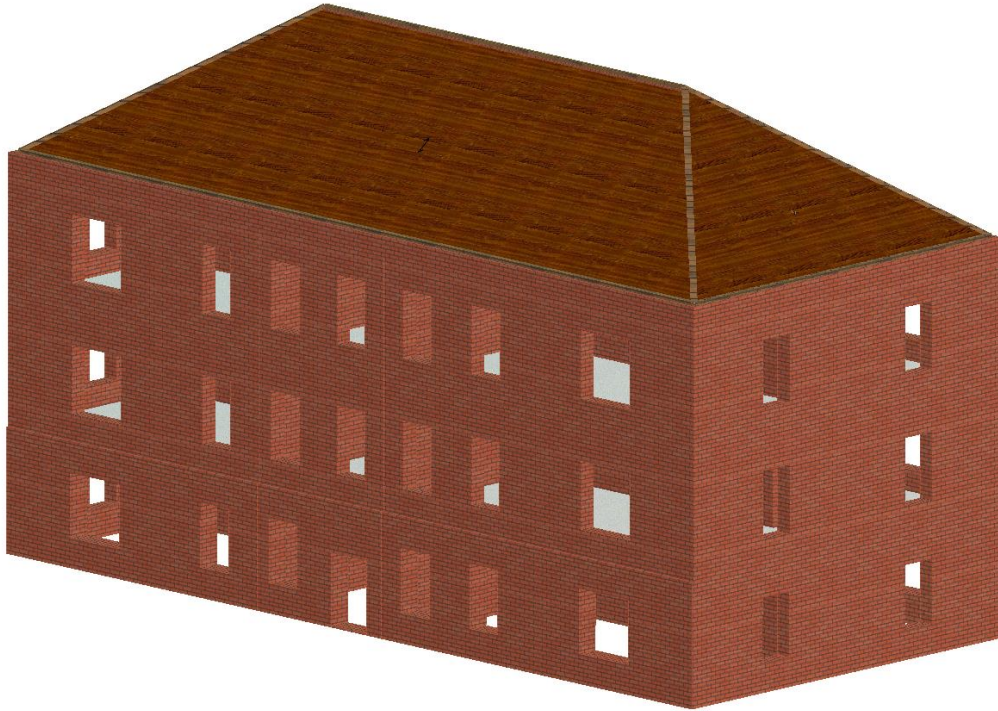
Figure 3. 3Muri model of observed building

a)   b)
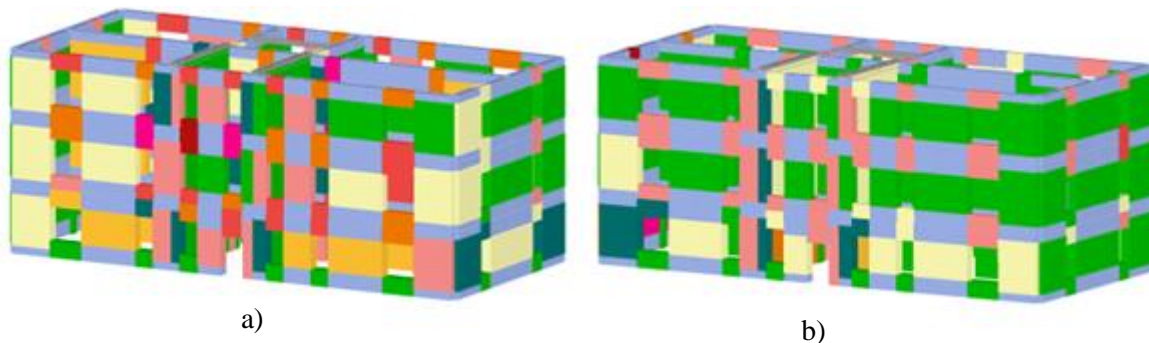
Figure 4. 3Muri model – observed damage in the model

3. Renovation strategies

For the successful renovation of buildings damaged by the earthquake, appropriate measures must be taken to repair and strengthen the building without compromising the mechanical properties of the material and the properties of the structure, which contribute to the durability of the building. Following the obtained results, a proposal of measures for the repair and reinforcement of buildings is given. Measures should follow the seismic design and be in line with the conservation and restoration rules [17],[18].

As a measure of repair and reinforcement of the walls of the building, it is recommended to reinforce load-bearing walls by, e.g., FRCM system or concrete jacketing. Figure 5 shows a proposal for reinforcing load-bearing walls. To obtain good resistance in the transverse direction (y-direction), it is proposed to add new load-bearing walls with a minimum thickness of 38 cm. In addition, it is proposed to remove the brick partition walls and replace them with a drywall system. Figure 6 shows a proposal for the position of the new load-bearing walls and a proposal for the removal and replacement of partition walls. In addition to the above methods, it is necessary to strengthen the ceiling structure. Therefore, to repair and reinforce the wooden ceiling structure, a thin reinforced concrete compression slab is proposed to increase the load-bearing capacity and stiffen the structure (rigid). All vaulted elements and vaults in the basement are to be maintained in their original form, with the possibility of reinforcing them with carbon fiber and maintaining the original proportions of the vaults to preserve the building's original construction and design features. Figure 7 shows the strengthening of the timber roof structure.
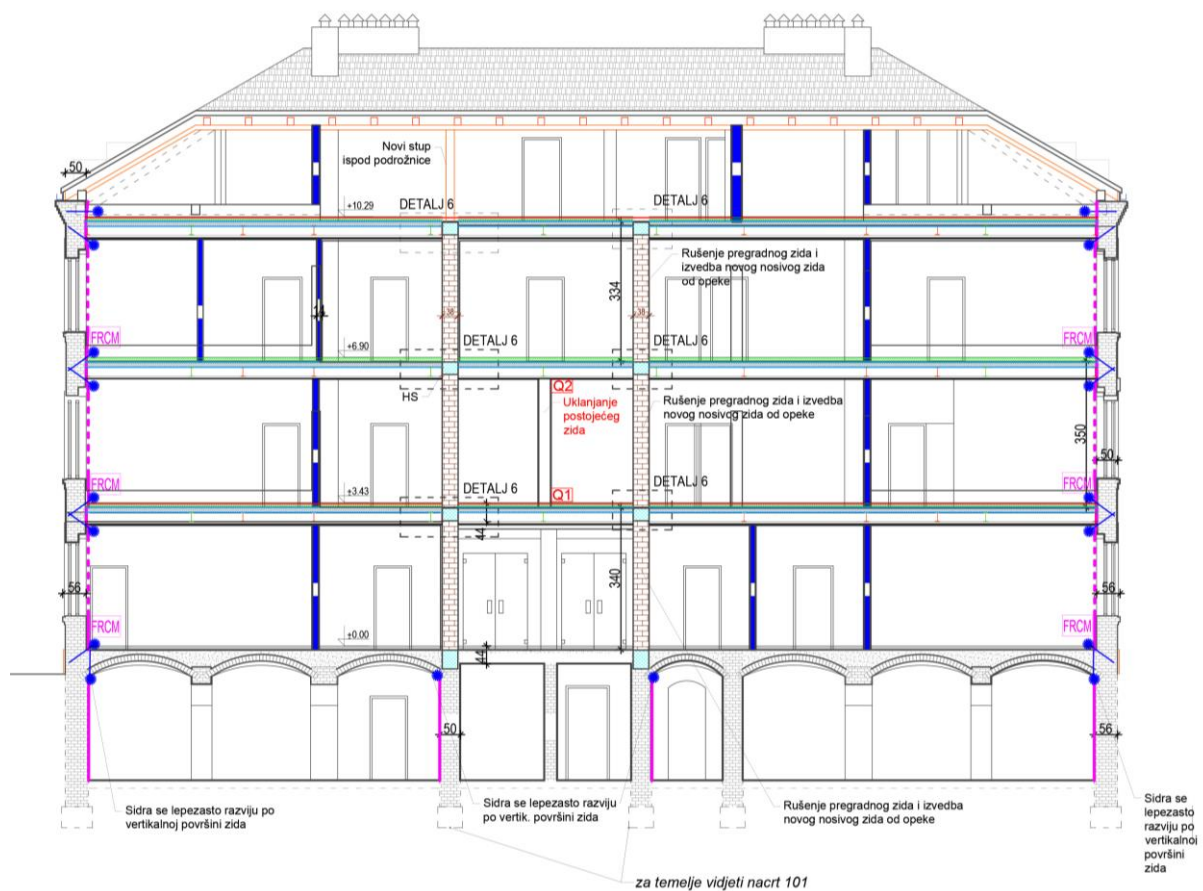
Figure 5. Strengthening proposal
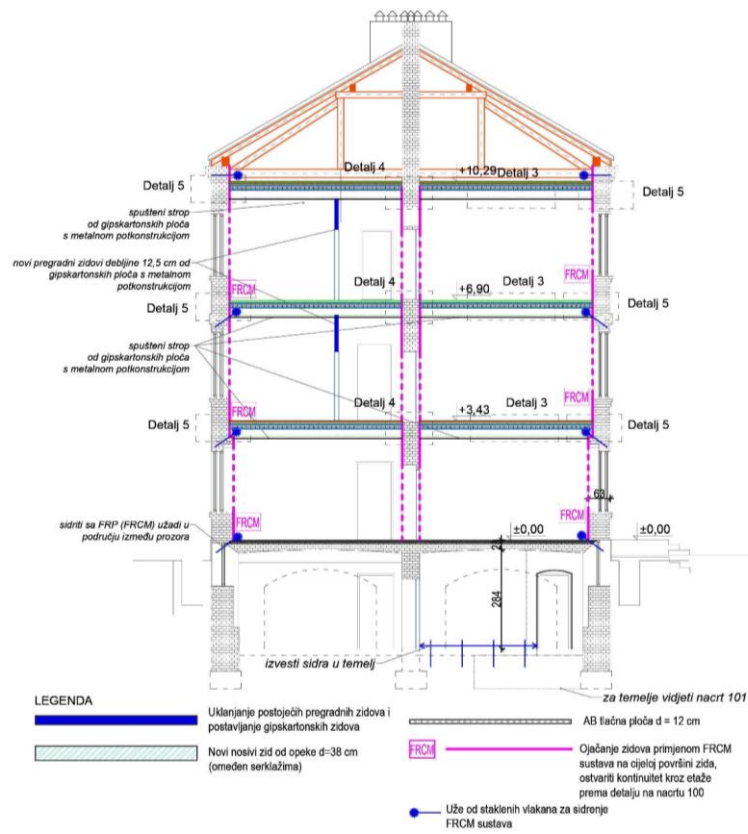
Figure 6. Proposal for the position of the new load-bearing walls and proposal for the removal and replacement of partition walls
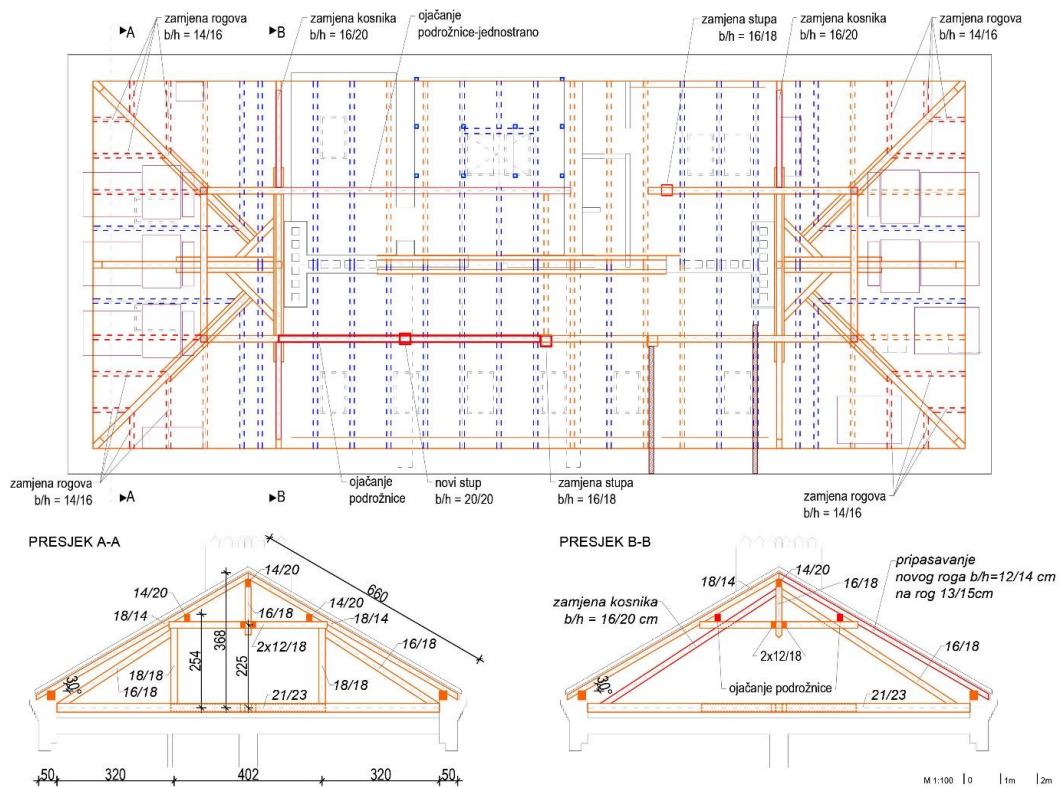
Figure 7. Strengthening of the roof structure

The renovation of the building started in June 2022. The plaster was removed from all the elements (Figure 8), and the masonry joints were cleaned. A new stiff diaphragm is placed (Figure 8).

Figure 8. Plaster removal and preparations for strengthening

Currently, seismic retrofit with FRCM system is underway. The procedure includes the removal of all existing plaster coats from the walls with complete repointing of the walls [19]. Also, the removal of all partition walls made of unreinforced masonry and replacement with drywall systems is underway.

New confined masonry walls as lateral force-resisting systems have been added to provide a continuous and competent load path from the top of the structure to the foundation. A new existing staircase that doesn't meet the actual technical requirements is planned to be replaced with a new steel stairway that will be completely independent of the rest of the building structure.

New rigid diaphragms have replaced existing flexible diaphragms as steel-concrete composite structures, which have been proven with high resistance to seismic and cyclic loading [20] and to secure evenly distribution story shear and torsional moment (Figure 9). On top of the concrete architectural floor, layers are planned to be installed: topping slab with sound insulation, PE foil, cement screed, and finishing skin. During the construction work, it was revealed that some of the elements were not in the right place or not built in a predicted manner, so it was essential to have construction administration included all the time. For example, it was noted that existing steel members were not where they were supposed to be, nor did the number of steel members match the previous design, so it was crucial to have designers involved in the construction so the site would not be paused.

Figure 9. New stiff diaphragm

New bracing elements in longitudinal directions are included to improve the roof structure's lateral system. Some decay effects due to dry and wet rot on the roof elements are noted, which caused some rafters to be changed completely [21]. This retrofit was planned to change thermal insulation entirely and use a warm roof system to improve envelope performance.

During the design process, technical solutions were driven by the idea to use as many as possible or, to say, barre minimum of invasive methods for this historical building and to preserve the layout as much as possible not to interfere with its functionality. This project envisioned appropriate materials for the structural retrofit of a historical building to enable the preservation and presentation of the original construction characteristics in the interior of the building.

For this building, besides the seismic retrofit, the plan is to complete a renovation with a new heating and cooling system. Also, a new ventilation system is planned to be implemented as a centralized system installed in the Attic of the building with new dormers for air intake and exhaust on the north and south sides of the roof. New AC wall units are planned to be installed in the basement and attic, while on all other floors, they are planned to be ceiling units.

Complete new electrical installations are planned to be installed, a new hydrant network, new fire suppression and detection system, and new plumbing and drainage systems are planned. After retrofitting and renovation, the building will be ''upgraded'' to new regulatory requirements that each new building needs to meet.

4. Discussion and conclusions

Determining the actual seismic behavior of existing masonry structures is of great importance for future management and the economic and purposeful strengthening of the load-bearing structure [22]. Modern software solutions and design methods are an essential part of the assessment, but they are only as useful as the input parameters are reliable [23]. In addition to strengthening, it is of great importance to consider aspects of energy efficiency [24] and the preservation of cultural heritage.

This research presents a simple case study of a whole procedure of seismic updating of an existing masonry building. The results obtained with the 3Muri software and the simplified method show that the case study building does not meet the conditions of limited damage, significant damage, and near collapse with return periods of 95 years, 225 years, and 475 years, respectively. Therefore, in addition to the structure's condition assessment and seismic design, a proposal for measures to repair and strengthen the structure per current legislation and new regulations was prepared.

When designing an engineering solution for the renovation and strengthening of the seismic safety of the protected heritage building, strengthening methods that are least invasive to the historic structure

should be used, applying appropriate materials and methods to allow the preservation and presentation of the original exterior and interior building features.

Retrofits must consider and improve the energy efficiency of the building and preserve the architectural and historical values of the protected heritage while ensuring the safe and functional use of the building. Earthquake-related measures, visible or not, should respect and visually harmonize with the character and integrity of the heritage site. The seismic system should be reversible to the extent possible so that more advanced seismic measures can replace it in the future.

Acknowledgements

References

[1] Stepinac, M.; Lourenço, P. B.; Atalić, J.; Kišiček, T.; Uroš, M.; Baniček, M.; Šavor Novak, M. Damage Classification of Residential Buildings in Historical Downtown after the ML5.5 Earthquake in Zagreb, Croatia in 2020. Int. J. Disaster Risk Reduct. 2021, 56, 102140. https://doi.org/https://doi.org/10.1016/j.ijdrr.2021.102140.

[2] Moretić, A.; Stepinac, M.; Lourenço, P. B. Seismic Upgrading of Cultural Heritage – A Case Study Using an Educational Building in Croatia from the Historicism Style. Case Stud. Constr. Mater. 2022, 17, e01183. https://doi.org/10.1016/J.CSCM.2022.E01183.

[3] Novak, M. Š.; Uroš, M.; Atalić, J.; Herak, M.; Demšić, M.; Baniček, M.; Lazarević, D.; Bijelić, N.; Crnogorac, M.; Todorić, M. Zagreb Earthquake of 22 March 2020 – Preliminary Report on Seismologic Aspects and Damage to Buildings. Gradjevinar 2020. https://doi.org/10.14256/JCE.2966.2020.

[4] Knežević, S.: Povijest Područja Bivše Rudolfove Vojarne i Trga Francuske Republike u Zagrebu; Godišnjak Zaštite Spomenika Kulture Hrvatske, 22-23 (1996-1997), 57-72, Institut Za Povijest Umjetnosti, Zagreb, 1997.

[5] Knežević, S.: Zagrebačke Planirane Vojarne Iz Doba Habsburške Monarhije; Institut Za Povijest Umjetnosti, Zagreb, 2007.

[6] Milić, M.; Stepinac, M.; Lulic, L.; Ivanisevic, N.; Matoric, I.; Cacic Sipos, B. Assessment and Rehabilitation of Culturally Protected Prince Rudolf Infantry Barracks in Zagreb after Major Earthquake. Buildings 2021.

[7] Krolo, J.; Damjanović, D.; Duvnjak, I.; Frančić Smrkić, M.; Bartolac, M.; Koščak, J. Metode Određivanja Mehaničkih Svojstava Ziđa. Građevinar 2021, 73 (2), 127–140. https://doi.org/https://doi.org/10.14256/JCE.3063.2020.

[8] Stepinac, M.; Kisicek, T.; Renić, T.; Hafner, I.; Bedon, C. Methods for the Assessment of Critical Properties in Existing Masonry Structures under Seismic Loads-the ARES Project. Appl. Sci. 2020, 10 (5). https://doi.org/10.3390/app10051576.

[9] Uroš, M.; Šavor Novak, M.; Atalić, J.; Sigmund, Z.; Baniček, M.; Demšić, M.; Hak, S. Procjena Oštećenja Građevina Nakon Potresa - Postupak Provođenja Pregleda Zgrada. Građevinar 2020, 72 (12), 1089–1115.

[10] Hafner, I.; Lazarević, D.; Kišiček, T.; Stepinac, M. Post-Earthquake Assessment of a Historical Masonry Building after the Zagreb Earthquake–Case Study. Buildings 2022, 12 (3). https://doi.org/10.3390/buildings12030323.

[11] Gregorczyk, P.; Lourenço, P. B. A Review on Flat-Jack Testing A Review on Flat-Jack Testing. 2019, No. January 2000.

[12] Lulić, L.; Ožić, K.; Kišiček, T.; Hafner, I.; Stepinac, M. Post-Earthquake Damage Assessment-Case Study of the Educational Building after the Zagreb Earthquake. Sustain. 2021. https://doi.org/10.3390/su13116353.

[13] S.T.A. DATA, 3Muri Program, Release XXX. Www.Stadata.Com.

[14] Lagomarsino, S.; Penna, A.; Galasco, A.; Cattari, S. TREMURI Program: An Equivalent Frame Model for the Nonlinear Seismic Analysis of Masonry Buildings. Engineering Structures. 2013, pp 1787–1799. https://doi.org/10.1016/j.engstruct.2013.08.002.

[15] Mirra, M.; Ravenshorst, G.; van de Kuilen, J.-W. Comparing In-Plane Equivalent Shear Stiffness of Timber Diaphragms Retrofitted with Light and Reversible Wood-Based Techniques. Pract. Period. Struct. Des. Constr. 2021. https://doi.org/10.1061/(asce)sc.1943-5576.0000602.

[16] Salaman, A.; Stepinac, M.; Matorić, I.; Klasić, M. Post-Earthquake Condition Assessment and Seismic Upgrading Strategies for a Heritage-Protected School in Petrinja, Croatia. Build. 2022, Vol. 12, Page 2263 2022, 12 (12), 2263. https://doi.org/10.3390/BUILDINGS12122263.

[17] Funari, M. F.; Mehrotra, A.; Lourenço, P. B. A Tool for the Rapid Seismic Assessment of Historic Masonry Structures Based on Limit Analysis Optimisation and Rocking Dynamics. Appl. Sci. 2021, 11 (3). https://doi.org/10.3390/app11030942.

[18] Funari, M. F.; Silva, L. C.; Mousavian, E.; Lourenço, P. B. Real-Time Structural Stability of Domes through Limit Analysis: Application to St. Peter's Dome. Int. J. Archit. Herit. 2021, 1–23. https://doi.org/10.1080/15583058.2021.1992539.

[19] Kišiček, T.; Stepinac, M.; Renić, T.; Hafner, I.; Lulić, L. Strengthening of Masonry Walls with FRP or TRM. Gradjevinar 2020, 72 (10), 937–953. https://doi.org/https://doi.org/10.14256/JCE.2983.2020.

[20] Stepinac, M.; Rajčić, V.; Barbalić, J. Influence of Long Term Load on Timber-Concrete Composite Systems. Gradjevinar 2015, 67 (3). https://doi.org/10.14256/JCE.1170.2014.

[21] Stepinac, M.; Rajčić, V.; Barbalić, J. Pregled i Ocjena Stanja Postojećih Drvenih Konstrukcija. Gradjevinar 2017, 69 (9), 861–873. https://doi.org/10.14256/JCE.1994.2017.

[22] Stepinac, M.; Skokandić, D.; Ožić, K.; Zidar, M.; Vajdić, M. Condition Assessment and Seismic Upgrading Strategy of RC Structures—A Case Study of a Public Institution in Croatia. Buildings 2022, 12 (9), 1489. https://doi.org/10.3390/buildings12091489.

[23] Colombo, C.; Savalle, N.; Mehrotra, A.; Funari, M. F.; Lourenço, P. B. Experimental, Numerical and Analytical Investigations of Masonry Corners: Influence of the Horizontal Pseudo-Static Load Orientation. Constr. Build. Mater. 2022, 344, 127969. https://doi.org/10.1016/j.conbuildmat.2022.127969.

[24] Milovanovic, B.; Bagaric, M.; Gaši, M.; Stepinac, M. Energy Renovation of the Multi-Residential Historic Building after the Zagreb Earthquake - Case Study. Case Stud. Therm. Eng. 2022, 38 (July). https://doi.org/10.1016/j.csite.2022.102300.

PRELIMINARY EARTHQUAKE SURVEY OF BUILDINGS – CASE STUDY OF SENJ

Josipa Mihaljević [(1)], Davor Grandić [(2)], Paulo Šćulac [(3)]

[(1)] *Research assistant, Faculty of Civil Engineering, University of Rijeka, josipa.mihaljevic@uniri.hr*
[(2)] *Professor, Faculty of Civil Engineering, University of Rijeka, dgrandic@gradri.uniri.hr*
[(3)] *Assistant Professor, Faculty of Civil Engineering, University of Rijeka, paulo.sculac@uniri.hr*

Abstract

Senj is a medieval town located on the eastern coast of Kvarner. In addition to the destruction caused by World War II, Senj has been hit by strong earthquakes throughout history. The appearance of significant earthquakes in this area is not surprising because, according to the seismic area classification of the Republic of Croatia, Senj is located in an area where the horizontal peak ground acceleration equals 0,24g. Within the historic city center of Senj, some stone masonry buildings date back to the 12th century. Those two facts present a good reason for selecting Senj as a representative research area. In order to evaluate the overall behavior and seismic resistance of existing buildings, it is first necessary to visually establish the characteristics of stone masonry buildings (typology of buildings). The connection of timber floors with stone masonry walls needs to be addressed as well. It needs to be investigated if the timber floor forms a diaphragm or whether it is flexible in its plane because it significantly affects the behavior of masonry buildings during an earthquake. Visual inspection of buildings indicated that most of the buildings were built with mixed materials (which is a result of fast renovation after great destruction in World War II), which implies the use of stone elements, brick parts, and mortar. In almost all stone masonry buildings, a tie system is present as a kind of reinforcement that ensures the integrity of the buildings.

Keywords: preliminary assessment, heritage buildings, stone masonry. seismic resistance, Senj

1. Introduction

Senj (Roman Senia) is a medieval town characterized by spontaneous development throughout history. The rapid development of the city took place in the 15th century in different directions, with trade being especially emphasized because Senj was an important port center at that time [1]. Numerous historical representations of the city have been preserved in the form of vedutes and cartographic representations. However, most of them did not faithfully depict the state of the city at that time. The oldest urban plan of the city from 1749 is shown in Figure 1. a), while Figure 1. b) shows the historic city center of Senj before the Second World War. The Second World War left the city of Senj with great damage caused by numerous aerial bombardments. In terms of urbanism, it is one of the most significant historical events for Senj. Various authors [1, 2, 3] state that 80% of the historic city center was destroyed, and this is confirmed by some of the remaining archive documents.

Another important influence should not be ignored: a stream flowed through the historic city center, which usually turned into a torrent during the melting of snow and heavy rainfall, and on one occasion demolished 50 houses [1]. The aforementioned torrent is thought to have brought the drift of gravel and sand that formed part of the coast. Over time, the stream was regulated outside the city walls. With the sudden development of Rijeka in the 16th century, Senj lost its importance. Senj's trade revived in the 18th century, resulting in the construction of new buildings and the refurbishment of old ones to accommodate the need for storage space. According to the administrative division, Senj is one of four towns located in Lika-Senj County. It is surrounded by the slopes of Velebit and Kapela and occupies most of the eastern coast of Kvarner.
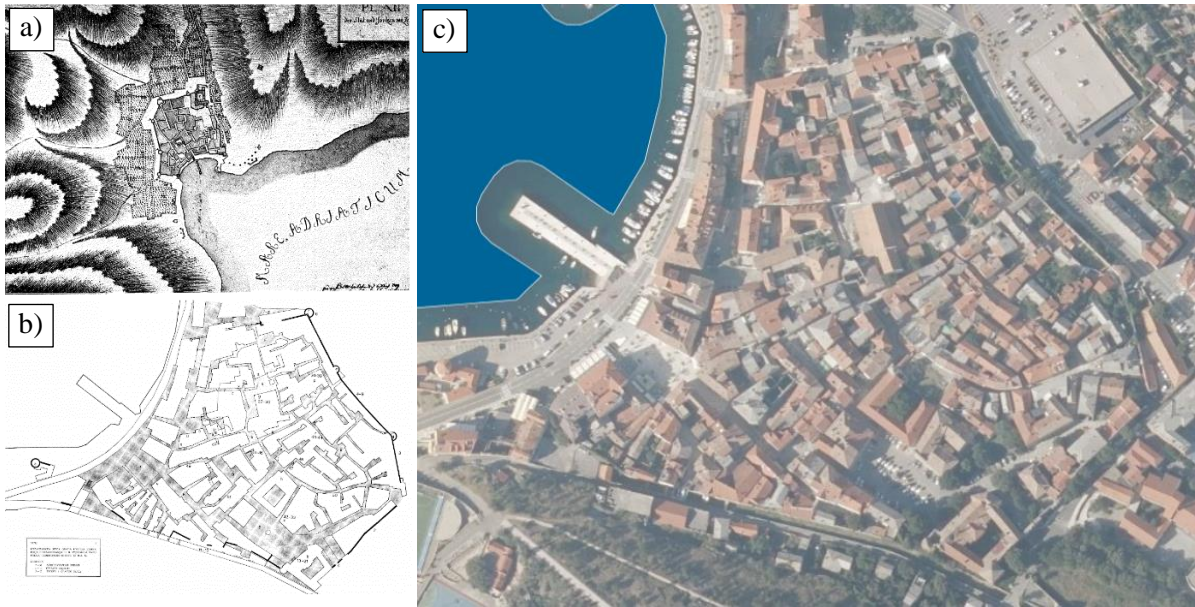
Figure 1. Old town center of Senj: a) the oldest urban plan of the city from 1749 [1]; b) the historic city center of Senj before the Second World War [1]; c) ortophoto view of the historic city center of Senj 2019/20[6]

In addition to war destruction, floods and fires, Senj has been hit by earthquakes of great magnitude throughout history. Božičević talks about Senj as a seismically active area in his work Earthquakes in Senj [4]. The paper describes the first classification of the territory into six earthquake zones with regard to the expected strength of the earthquake, which are also graphically shown on the map. Significant earthquakes that hit Senj and its surroundings have been documented, and are presented here in Table 1. The seismic area classification of the Republic of Croatia for the return period of 475 years is shown in Figure 2 [5], which shows that the area of the city of Senj is in the red area, i.e., that the horizontal peak ground acceleration is 0,24g.
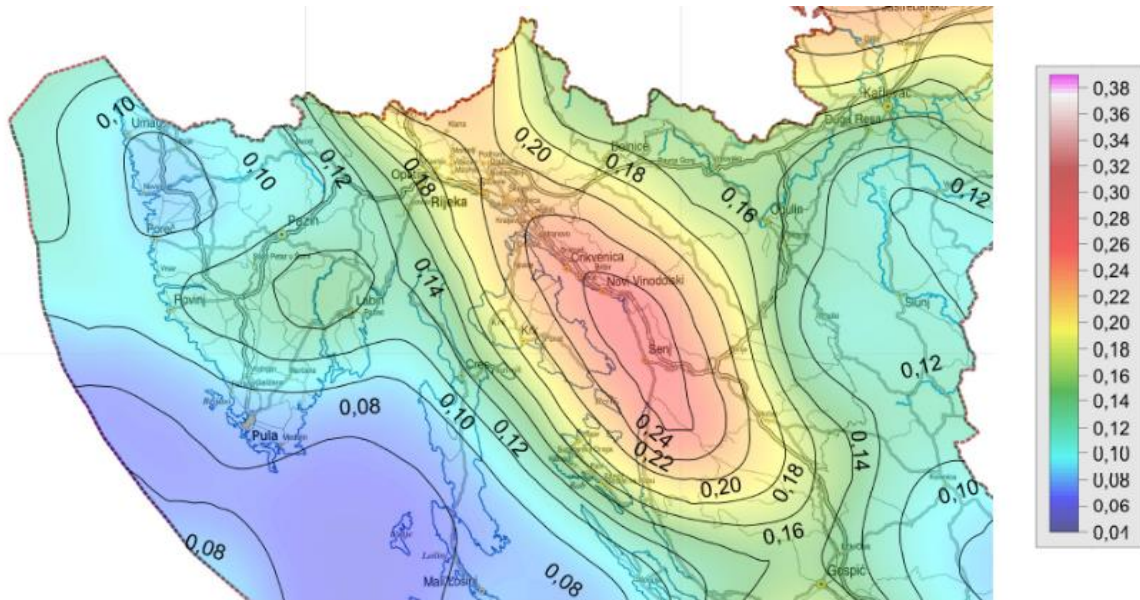
Figure 2. The seismic area classification of the Republic of Croatia for the return period of 475 years [5]

Table 1. Chronicle of strong earthquakes in the vicinity of Senj (according to data from [4])

Chronicle of strong earthquakes in the vicinity of Senj (Earthquakes of the sixth degree and higher according to MCS)	
1639 Senj	18. I. 1902 Novi Vinodolski
1648 Senj	1. II. 1905 Novi Vinodolski
24. IV. 1776 Bakar	4. III. 1906 Brinje, Senj
26. XII. 1857 Kraljevica	4. IX. 1908 Novi Vinodolski
5. XII. 1868 Senj	12. III. 1916 Grižane, Bribir
30. III. 1869 Senj	14. VII. 1916 Brinje, Senj
3. I. 1870 Senj	14. X, 1916 Crikvenica
19. IV. 1873 Senj	30. VII. 1920 Baška, otok Krk
30. III. 1877 Senj	5. IX. 1925 Grižane, Bribir
23. IX. 1878 Senj	11. IX. 1925 Grižane, Bribir
3. V. 1885 Senj	1. I. 1926 Crikvenica
18. VII. 1890 Novi Vinodolski	21. X. 1926 Senj
30. VII. 1890 Novi Vinodolski	5. II. 1939 Omišalj, otok Krk
13. IX. 1890 Novi Vinodolski	6. II. 1939 Omišalj, otok Krk
3. V. 1891 Novi Vinodolski	18. II. 1939 Omišalj, otok Krk
12. VI. 1893 Grižane, Bribir	30. VI. 1949 Baška, otok Krk
9. VIII. 1895 Brinje, Senj	20. I. 1949 Baška, otok Krk

2. Visual inspection of buildings

A visual inspection of buildings gives an insight into the existing condition of the buildings in the observed area. It is the first step in determining the parameters for assessment, i.e., the behavior and seismic resistance of existing buildings. The first step of the visual inspection would be to determine the typology of the buildings, while the second step is related to the masonry typology.

2.1 Building typology

The building typology includes the layout and number of storeys. Due to the lack of design documentation, the floor layout of the buildings can be determined through the orthophoto map of the historic city center of Senj (Figure 1.c)). The historic city center of Senj occupies an area of about 0,07 km² and is surrounded by city walls for which there is no exact information on when they were actually built. Certain documents mention how the walls changed their position over time, which would mean that the historic city center expanded. From a series of historical documents related to the 13th and 14th centuries, it can be noticed that the space inside the city walls was not as densely built as is the case today [1]. The densely built/populated area within the city walls forms a network of narrow and winding streets, so it can be assumed that Senj has retained the medieval character of the city. The construction of individual buildings developed horizontally, while the majority of buildings are characterized by one-storey construction [1].

According to the orthophoto map (Figure 1. c)), it can be seen that the buildings mostly have a regular floor plan (rectangular or square). However, some objects fall out of the scope of "regular." The majority of them are objects that had special significance in Senj's past. First of all, there is Frankopan's castle. In addition to these building, which stands out for its size, there is also a building that previously served as a Franciscan monastery and a cathedral. Due to the extremely dense typology, the buildings lean against each other (perhaps some of them are connected in a certain way?). Within the city center of Senj, buildings with two to three stories prevail. The buildings located close to the coast are up to 4 stories high, but it should be mentioned that they are more recent buildings built on the place of demolished, badly damaged salt warehouses after World War II.

It is interesting to note that there were 14 sacred buildings within the historic city center, in a relatively small area, 12 of which were churches and two of which were monasteries. Most of the churches have lost their sacred significance and have been converted into residential and commercial

buildings. Also, numerous buildings of profane architecture have been repurposed over time and, for this purpose, often extended and rebuilt either for residential or business purposes [1]. Vaulted streets (passages) are one of the architectural features characteristic for the historical city center of Senj. Observing individual buildings, cracks formed around the window openings at the level of the first and second floors which can be seen in the Figure 3 (middle photo).

Figure 3. The facades of buildings within the historic city center of Senj

2.2 Masonry typology

The next step would be to determine the masonry typology, which implies the type and structure of the stone masonry walls. It also covers the recognition of the used materials. Material is meant for the use of stone blocks, part of bricks, and mortar. Stone masonry walls can be made of roughly shaped and processed stone elements. Stone masonry buildings built of roughly shaped are divided into several types: a wall built of rubble stone, a wall built of boulder stones, a cyclopean stone masonry , and a wall built of slab stone. Processed stone elements are divided depending on the method of processing, so the brickwork can be made of roughly processed stone, finely processed stone, or by stonemasons [6].

Figure 4. Masonry typology

For example, in the case of mortar, one can see what kind of sand was used (fine or coarse), which affects the strength of the mortar itself. It is difficult to discuss about the type of masonry when "open" access to the wall does not exist. Since there are several ruins within the historic city center, it was possible to see that the buildings were built as single leaf masonry, up to 50 cm thick (Figure 4). It is assumed that the other buildings were built according to the same or a similar principle. There are few buildings built with finely processed stone elements, while in most buildings mixed materials are used (Figure 4). Mixed material means the use of stone elements, brick parts, and mortar. Here, the regularity of the alternation of tone and brick layers cannot be precisely identified. Brick fragments were added to a thick layer of mortar. Apart from brick fragments, pebbles can be seen in the mortar. Some written sources [3] emphasize the use of stone elements made of white-gray limestone, tufa (quarried in the Gacka bed), and gray hard limestone. Figure 4 (below, left) shows part of the wall of one observed building where empty joints are clearly visible, which is the result of a weak bond between the mortar and the stone elements. Precisely in such places, it was observed that mortar with fine aggregate (sand) was used and that it crumbles under the fingers, which indicates low mortar strength.

Figure 5. Timber floor construction

According to photo documentation [8] and by observing the badly damaged buildings in some parts of the historic city center, it can be concluded that the floor structures were formed by single timber beams placed at equal spans and supported on load-bearing facade walls (Figure 5). The floor consists of planks laid on joists, on which additional floor layers are placed. The underlay of the floor structure is formed by the formwork (slats) on which the reeds are placed and the final layer of plaster. However, to be able to say with certainty which is the predominant type of timber floor construction, it

is necessary to further research this area. The connection between the timber floor structure and the stone masonry wall is of great importance considering the behavior of the structure during earthquakes. One of the structural details that are characteristic of almost every old stone masonry building are the tie rods, which are shown in Figure 6. The ties were made of wrought iron.

Figure 6. Tie rods visible on the facade of the building (left) and inside the section of the Wall (right)

3. Conclusion

Certain buildings within the city center date back to the 15th century, while several of them date from the 12th century. Senj was chosen as a representative research area due to the large number of historic stone masonry buildings in the historic city center and the area with high horizontal peak ground acceleration. First of all, it should be pointed out that such old buildings were not designed according to standards that take into account seismic effects. The visual inspection aims to collect as much data as possible about the condition of existing buildings, which will be used for further analysis of the buildings in order to evaluate their seismic resistance. A visual inspection revealed that the buildings mostly have a regular floor layout and were built mostly with mixed materials. The stone elements are mostly broken or roughly shaped, but in some places, buildings built with regular shaped stone elements have been observed. It is assumed that brick fragments and pebbles were used to fill wide joints between stone elements, i.e., to reduce the thickness of the mortar layer. Observing the walls, it is not possible to clearly determine the regularity in the sequence of alternating layers of stone elements and bricks in buildings built with mixed materials. On some buildings, we observed "empty" joints between the stone elements, which is an indication of the mortar's deterioration. Due to the great damage caused during the Second World War, there was a need for quick action - reconstruction and repair of buildings, which is partly considered the cause of the mixed structure of the masonry. When it comes to floor structures, according to what has been observed, we can assume that the other buildings have the same type of timber floor construction. A characteristic of masonry buildings in general, and also of those in Senj, is the use of tie rods, which are mostly visible on the facades of the buildings. The lack of design documentation and limited access to the interior of the structure requires an additional inspection of the timber floor structures in order to accurately identify the typology characteristic of this area. This preliminary assessment will serve as the basis for future research on the seismic resistance of masonry stone buildings in a representative area.

Acknowledgements

References

[1] Viličić, M. (1971): Proceedings 360 (in Croatian). JAZU, Zagreb

[2] Sobolevski, M. (2003): Bombardment of Senj by airplanes in the Second World War (in Croatian). Senj's proceedings, 30, 363-376, doi: https://doi.org/10.31953/sz

[3] Glavičić, A. (1995): Stone facades of medieval houses in Senj (in Croatian). Senj's proceedings, 22, 111-138, doi: https://doi.org/10.31953/sz

[4] Božičević, S. (1968): Eartquakes in Senj (in Croatian). Senj's proceedings, 3, 256-261, doi: https://doi.org/10.31953/sz

[5] HRN EN 1998-1:2011/NA:2011 Eurocode 8: Design of structures for earthquake resistance -- Part 1: General rules, seismic actions and rules for buildings -- National Annex, Croatian Standards Institute

[6] https://oss.uredjenazemlja.hr/map (accessed January 27, 2023)

[7] Crnković. B, Šarić, Lj. (2003): Building with natural stone (in Croatian), 2nd edition, Zagreb

[8] Photo archive of the Ministry of Culture and Media, Republic of Croatia, Conservation Department in Rijeka

EARTHQUAKE PERFORMANCE OF A CULTURAL HERITAGE BUILDING: THE JESUIT COLLEGE IN DUBROVNIK, CROATIA

Aanis Uzair [1], Lars Abrahamczyk [2], Dagoberto Gómez [3], Kinda Elias [4], Ante Vrban [5], Davorin Penava [6], Snježana Markušić [7]

[1] *Research Assistant, Chair of Advanced Structures, Faculty of Civil Engineering, Bauhaus-University Weimar,*
aanis.uzair@uni-weimar.de

[2] *Professor, Chair of Advanced Structures, Faculty of Civil Engineering, Bauhaus-University Weimar,*
lars.abrahamczyk@uni-weimar.de

[3] *Graduate Student, Chair of Advanced Structures, Faculty of Civil Engineering, Bauhaus-University Weimar,*
dagogomez08@gmail.com

[4] *Graduate Student, Chair of Advanced Structures, Faculty of Civil Engineering, Bauhaus-University Weimar,*
kinda.elias@outlook.com

[5] *PhD Student, Faculty of Civil Engineering and Architecture Osijek, Josip Juraj Strossmayer University of Osijek,*
ante.vrban@gfos.hr

[6] *Professor, Faculty of Civil Engineering and Architecture Osijek, Josip Juraj Strossmayer University of Osijek,*
ante.vrban@gfos.hr

[7] *Professor, Department of Geophysics, Faculty of Science, University of Zagreb, markusic@gfz.hr*

Abstract

Cultural heritage buildings generally refer to the ancient structures having high cultural and historical significance. These buildings are constructed using obsolete practices and require special considerations with respect to the lateral resistance, especially in moderate and high seismic regions. This study focuses on the earthquake performance assessment of the Episcopal Seminary Building and Classical Gymnasium (Jesuit College) located in the Old City of Dubrovnik, Croatia (UNESCO World Heritage Site). The construction dates back to 1662 and was developed in different stages until 1765. During this period, Jesuit College suffered damages from two major earthquakes i.e., M7.6 Dubrovnik in 1667 and M6.9 Montenegro in 1979. The material composition, structural drawings, and fundamental frequencies of the building were previously obtained in the framework of the research project "Seismic Risk Assessment of Cultural Heritage in Croatia – SeisRICHerCRO". The material is predominantly composed of irregular stone blocks laid in lime mortar. The structural details such as floor vaults, arches, flexible diaphragms, and spatially irregular openings are numerically modelled using the finite element method. The analytical model is calibrated by performing eigenvalue analysis to compute the material parameters i.e., elastic modulus and density (supported by extensive literature review) that allows the modal frequencies to match with the values obtained from the ambient vibration testing. The seismic performance is then evaluated using the linear analysis procedure in accordance with the current guidelines of the Eurocode 8 and the corresponding Croatian National Annex. For the design earthquake, critical damage zones are identified and recommendations for retrofitting measures are proposed.

Keywords: unreinforced masonry, cultural heritage, finite element model updating, earthquake performance assessment

1. Introduction

Cultural heritage buildings symbolize our history by providing insight into the evolution of our culture and society over a long period of time. These buildings are predominantly built with traditional materials such as masonry and timber and are often exposed to the lack of maintenance, water induced deterioration, foundation settlement, fluctuating environmental loads, floods, and earthquakes [1]. The seismic performance of built cultural heritage is particularly difficult to access and requires detailed knowledge of the material composition, geometrical characteristics, nonlinear effects, connections between different structural elements, stiffness of the horizontal diaphragms, and the building condition [2,3].

In the case of historical structures, the availability of input data is often limited either by the incompleteness of the archived documents or because of the impracticality to conduct in-situ experiments while preserving the architectural features. In this context, vibration-based techniques to evaluate the structural dynamic response appears particularly attractive [4–6]. In recent years, many studies demonstrate the successful application of Ambient Vibration Tests (AVT) in combination with Finite Element (FE) model updating, for the performance assessment of cultural heritage buildings [7–10]. The model updating process calibrates the unknown structural parameters to minimize the error between experimental and analytical dynamic response i.e., modal frequencies and mode shapes. This process is often accomplished manually through trial and error and becomes cumbersome for complex buildings, causing uncertainty in the estimation of the unknown structural parameters [11].

This paper presents the earthquake performance assessment of the Episcopal Seminary Building and Classical Gymnasium (Jesuit College) using AVT in combination with FE model updating. The Jesuit College was built from 1662 to 1725 and lies in the UNESCO's World Heritage List Old City of Dubrovnik, Croatia. The building is primarily used as an educational institute. The historical seismicity of Dubrovnik shows a considerable seismic potential with the 1667 earthquake considered to be the strongest documented earthquake in the coastal region of Croatia [12]. By its seismic and tectonic potential, it is also the most striking area in Croatia with estimated maximum possible magnitude of 7.5. Historic data note about ten earthquakes in the region with intensity of VIII or more °MCS out of which the most significant one is the 1667 earthquake of X °MCS [13].

2. Material and Methods

2.1 Episcopal Seminary Building and Classical Gymnasium

The Episcopal Seminary Building and Classical Gymnasium is one of the city's oldest educational institutes (shown in Fig. 1). The construction dates back to 1662 and was further developed over the years until 1725. The internal walls are predominantly composed of irregular stone masonry laid in lime-mortar. The deterioration of exterior walls exposes the variability in the material composition mainly attributed to the different construction stages and maintenance over the years, as shown in Fig. 2. The geometry, structural details, and damage conditions were assessed previously through a qualitative site inspection in part of the research project SeisRICHerCRO [14]. The roof structure is predominantly made of wood with no precise information available regarding the material properties. Wooden beams supporting the flexible floor system are supported on top of masonry corbels without embedment into the adjacent walls. The most important structural and architectural feature of this building is the different type of vaults supporting the floor slab. Fig. 3 shows the location of the cross and barrel vaults laid in stone masonry. In addition, the top floor also features tensile tie rods, providing additional lateral support to the parallel walls in the out-of-plane direction.

Figure 1. Episcopal Seminary Building and Classical Gymnasium, Dubrovnik, Croatia [15].

Figure 2. Materials characteristics of the external walls (composite clay bricks and stone masonry of variable sizes).

Figure 3. Location and types of different vault systems in the Jesuit College.

2.2 Ambient Vibration Testing

The fundamental frequencies in North-South (NS) and East-West (EW) directions were previously determined using AVS in part of the research project SeisRICHerCRO [14]. Three sensors located on the first floor recorded continuous data with a sampling rate of 128Hz for three consecutive days. Fourier Amplitude Spectra (FAS) for the two horizontal components and the Horizontal to Vertical Spectral Ratio (HVSR) is used to obtain the fundamental frequencies in the NS and EW direction as shown in Table 1. It is important to note that for this study, only the fundamental frequencies were obtained without the identification of structural mode shapes.

Table 1 – Fundamental frequencies [Hz] in the NS and EW direction obtained from the ambient vibration testing [16].

Frequency	Lower Bound	Average	Upper Bound
$f_{NS,ref}$	6.34	7.88	8.28
$f_{EW,ref}$	4.72	5.38	6.01

3. Finite Element Model Updating

The building is analysed utilizing the macro modelling approach, where the walls and vaults are modelled using solid elements and a linear masonry material property. The interaction among building sections built in different years is neglected and the basement is excluded from the structural model since its contribution to the fundamental period is negligible. Timber floors and the roof structure are modelled as equivalent flat shell elements allowing the transfer of bending effects due to the gravitational loads and in plane stresses, simulating the level of rigidity associated with a flexible diaphragm. The in-plane stiffness of the wooden structure and its components is represented by an equivalent Young's Modulus. The spiral staircase is neglected from the modelling since the surrounding walls are considerable rigid. The iron tie-rods are included in the model as regular truss elements carrying a pre-stressing axial force and allowing deformations only along the element axis. The mesh consists of hexahedral and quadrilateral elements for the solids and flat shells respectively. The basic mesh element size is 0.5m with a 65% transition smoothness for the edges and corners shaped by the vaults as shown in Fig. 4. The final mesh has a total of 119'306 nodes from which 2'659 are the restricted nodes at the base and, 184'821 elements distributed as 173'628 solids, 11'176 shells and 17 trusses.
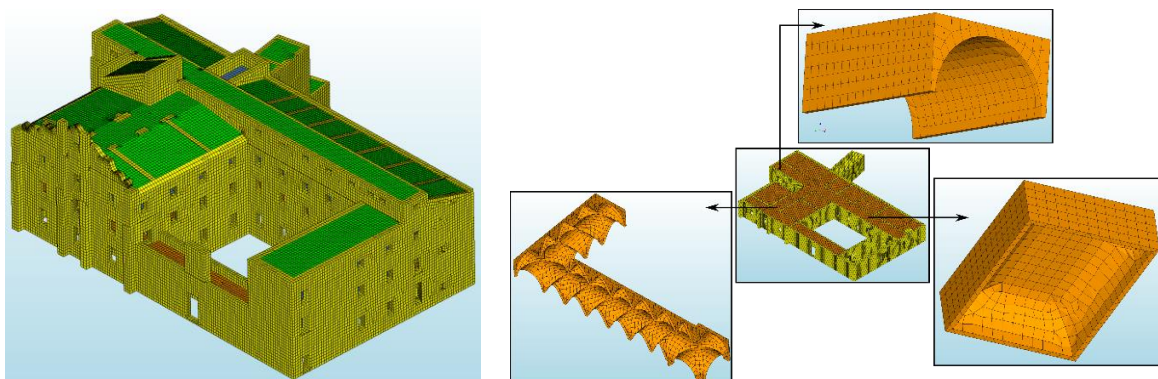
Figure 4. FEM mesh with hexahedral and quadrilateral elements with an approximate size of 0.5m.

The initial material properties used for the FE model updating are collected from the literature in conjunction with the observations made during the qualitative site inspection in part of the research project SeisRICHerCRO [14]. Starting with a reference set of material properties not only provides a physical sense to the calibrated values but also optimizes the time required for convergence in case of

manual updating. The possible range of values considered for the material properties are summarized in Table 2. Since the model updating is performed manually, the unknown material parameters are restricted to the elastic modulus (E_{ref}), unit weight (p_{ref}) and poison ratio (v_{ref}), reducing uncertainty in the calibrated parameters. Free vibration Eigen Value Analysis is performed for a total of 21 parameter combinations to minimize the error between numerical and experimental dynamic response. The error obtained at the end of each model updating run is shown in Fig. 5.

Table 2 – Range of material properties considered for the FE model updating [17].

Parameter	Lower Bound	Average	Upper Bound
$E_{,ref}$ [MPa]	2000	2650	3300
$p_{,ref}$ [kg/m^3]	2000	2350	2700
$v_{,ref}$	0.10	0.20	0.30
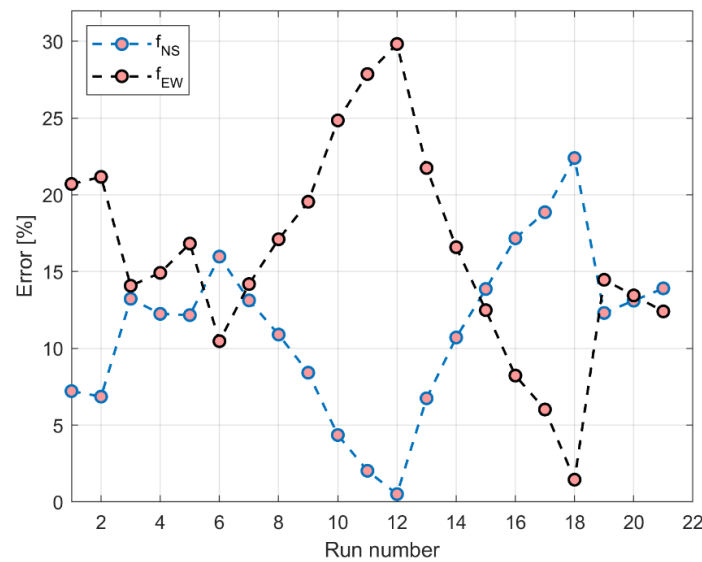
Figure 5. Error obtained in the NS and EW frequencies for each run of the FE model updating process.

The analytical frequencies with the least error are 6.05Hz corresponding to the NS (mode 2) and 6.79Hz corresponding to the EW (mode 5) direction respectively, as shown in Table 3. The most relevant mode shapes are shown in Fig. 6. Mode shape 1 has the lowest frequency representing the local vibration mode of the cantilever clock wall, anticipating tensile stresses concentration at the base of the wall. Mode shape 2 and 5 represents the translational modes in NS and EW directions respectively.

Table 3 – Modal frequencies obtained for the calibrated material properties.

Mode	Period [s]	Frequency [Hz]	Mass Participation [%]		Mode	Period [s]	Frequency [Hz]	Mass Participation [%]	
			EW	NS				EW	NS
1	0.193	5.18	0.0037	3.3227	6	0.145	6.88	11.8290	0.0037
2	0.165	6.05	0.0521	61.2830	7	0.129	7.78	2.5400	4.6558
3	0.155	6.47	0.0016	0.0055	8	0.121	8.24	1.7574	0.0859
4	0.154	6.49	0.0209	0.0043	9	0.119	8.42	0.0083	0.0054
5	0.147	6.79	56.1830	0.0101	10	0.112	8.94	0.0137	0.7164

(a)   *(b)*   *(c)*
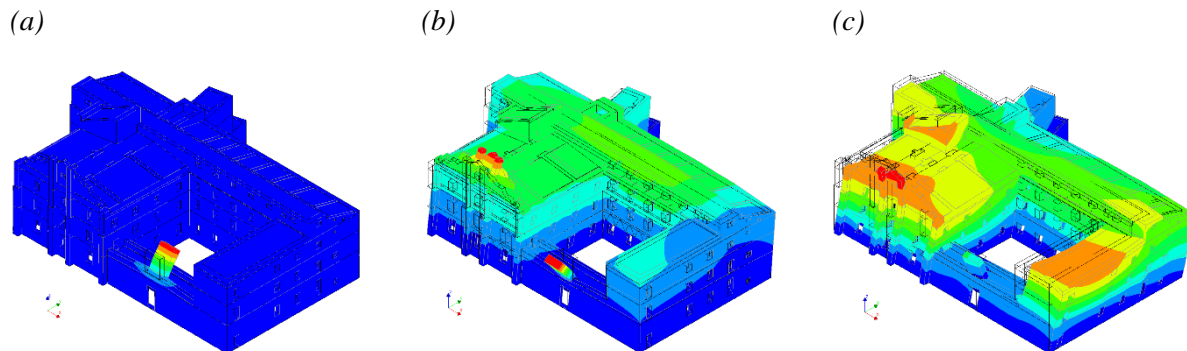
Figure 6. Relevant mode shapes obtained using the calibrated finite element model. a) Mode shape 1 (local mode, f = 5.18 Hz); b) Mode shape 2 (global mode, f = 6.05 Hz); c) Mode shape 5 (global mode, f = 6.79 Hz).

4. Earthquake Performance Assessment

4.1 Seismic Hazard Definition

The seismic hazard is defined according to the Eurocode 8 guidelines for assessment and retrofitting of buildings using the nationally defined reference peak ground acceleration (a_{gR}) for the no-collapse requirement, corresponding to a return period T_{NcR} of 475 years [18,19]. Recent studies describe the site conditions of Dubrovnik as cretaceous dolomitic limestone and quaternary clay, with sand sediments of up to 5m thick, classifying the site as soil type A with an a_{gR} of 0.30g [20,21].

4.2 In-Plane Assessment

The in-plane lateral capacity is evaluated using permanent, imposed, seismic and snow loads. The load combination (LC1) acting mainly in the X-direction, additionally includes the factored Y-direction component as well. The opposite occurs in the case of LC2 acting mainly in the Y-direction. Both the load combinations include the accidental torsional effects according to the Eurocode 8. The tensile ($f_{t,CF}$ = 0.30MPa) and compressive ($f_{t,CF}$ = 0.30MPa) elastic stress limits of the masonry material are reduced using a confidence factor (CF) equal to 1.35 corresponding to the knowledge level KL_1 according to Eurocode 8. The tensile and compressive elastic stress limits are given by Eq. (1) and (2).

$$f_{t,CF} = \frac{f_t}{CF} = \frac{0.39}{1.35} = 0.30 \, MPa \tag{1}$$

$$f_{c,CF} = \frac{f_t}{CF} = \frac{6.90}{1.35} = 5.0 \, MPa \tag{2}$$

The principal tensile and compressive stresses due to the two load combinations i.e., LC1 and LC2 are shown in Fig. 7. The color scale is bounded such that the red color represents the regions where maximum tensile stress is higher than $f_{t,CF}$ and cracking is expected to occur. High stress is observed around the corners of the opening and at the piers between adjacent openings. Comparable high stresses are obtained in the wall segments having fewer openings, representing concentrated shear stresses. The perpendicular walls show considerable tensile stresses due to Out-of-Plane (OoP) deformations especially in the upper portions of the walls where the cantilever motion is not restricted. The principal compressive stresses from Fig. 7b shows high stresses in the columns of the north facade at the east wing because of the overturning moment caused by the direction of the seismic forces. Moreover, the upper part of the columns resist the compression generated by the OoP bending of the cantilever wall in the north facade, indicated by stresses in the light green color. High compressive stresses are also located at the base of the clock wall, since this wall is identified as critical zone due to the OoP bending; previously identified from the local vibration mode shown in Fig. 6a.
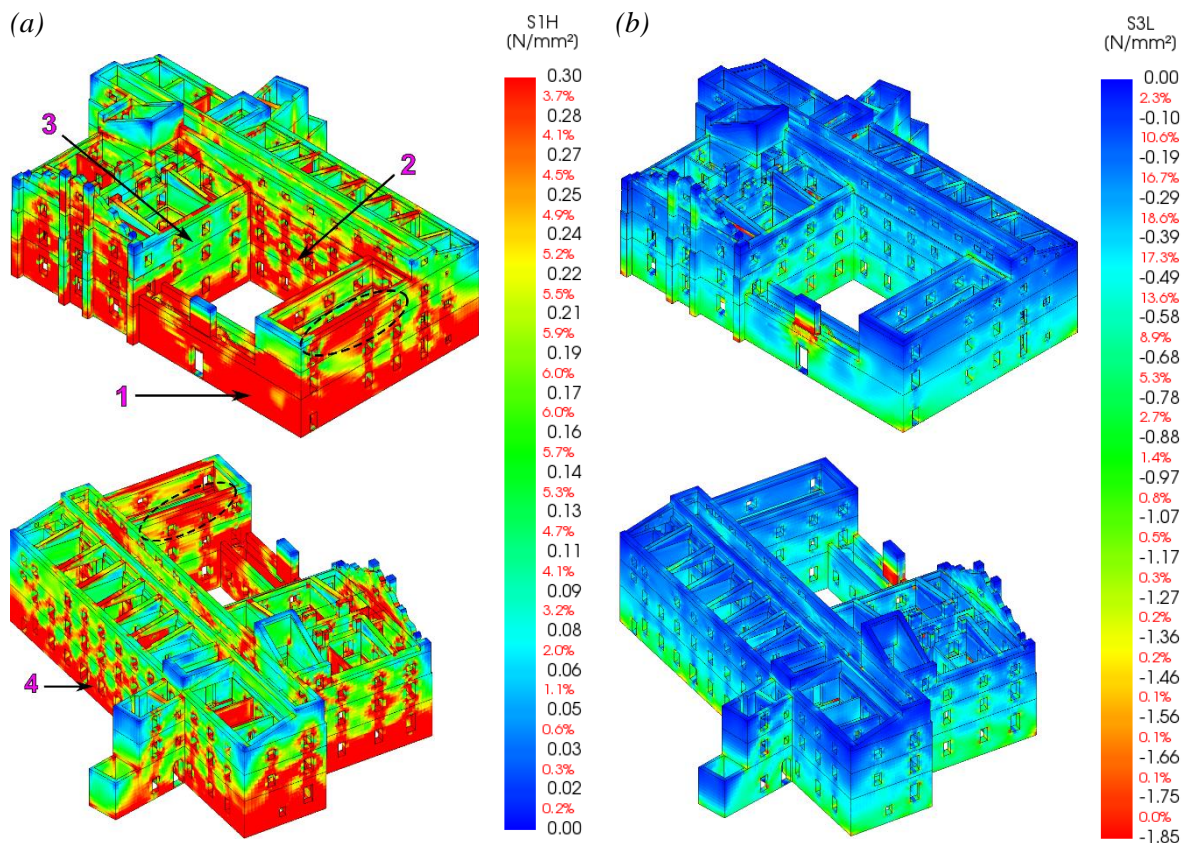
Figure 7. Resulting principal tensile and compressive stresses. a) Principal tensile stress (S1H) resulting from LC1; b) Principal compressive stress (S3L) resulting from LC2.

The shear stress concentration for the two load combinations is shown in Fig. 8. The XZ plane show high shear stresses (SZXH) between the openings of the north facade with visible diagonal concentration at the corners of the north wing walls. The north and south facades of the south wing also indicate shear stresses with diagonal trajectory located at the piers between the openings. Similar results are obtained for the stresses in the YZ plane (SYZH), with the particularity that the stresses are higher on the walls at the east wing because of the high mass resulting in higher seismic forces. Additionally, high shear stresses are obtained at the base of the clock wall in the YZ plane due to the OoP deformation.

Fig. 9 shows the tensile stresses in the masonry vaults in both X and Y directions. For the stresses in the X direction (SXX), the higher tensile stresses are developed near the wall connection and along the longitudinal direction of the vault in the east wing hallway. It is analogous in Fig. 9b for the stresses in Y direction (SYY) where, the development of stresses goes along the cross vault of the hallway in the south wing. The response is repeated at the entrance in the north wing, and additionally in some regions along the vault, preventing the lateral walls to bend separately out of the plane. The stresses are generated when the vault is oriented perpendicular to the direction of the seismic forces. Tensile stresses SXX also develop in the vault of the north wing, at the regions near the connections with the east and west wings. The latter is due to the pulling force generated by the east and west wings when the earthquake occurs in the X direction.

The numerical model is further evaluated for increasing values of a_{gR} corresponding to different seismic zones in Croatia. Fig. 10 shows a gradual increase of tensile stresses (S1H) where, the limit $f_{t,cF}$ of 0.30MPa is exceeded. For low seismic hazard level (a_{gR} = 0.10g) the stresses are below the limit in practically all areas. The limit is exceeded for a_{gR} = 0.20g in localized regions such as openings and critical corners.
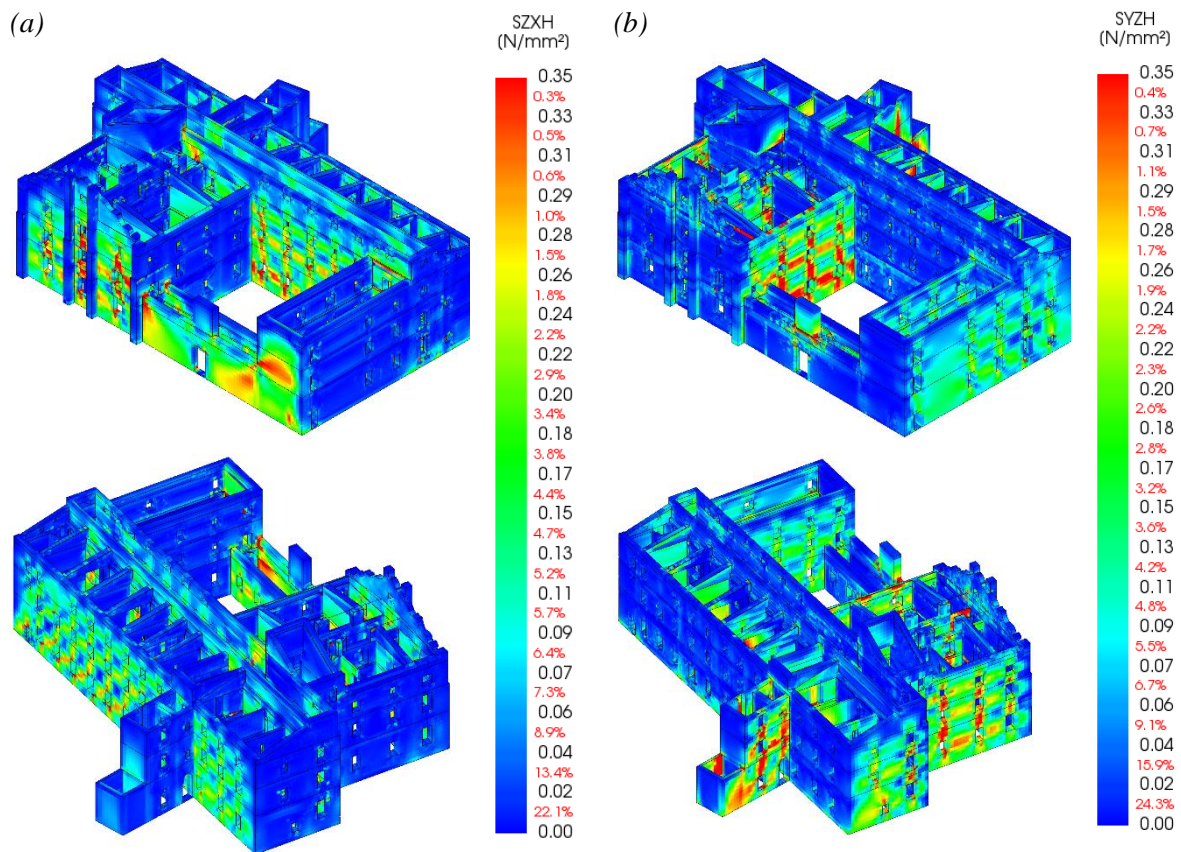
Figure 8. Resulting shear stresses in the global XZ and YZ directions. a) Shear stress in XZ plane (SZXH) resulting from LC1; b) Shear stress in YZ plane (SYZH) resulting from LC2.
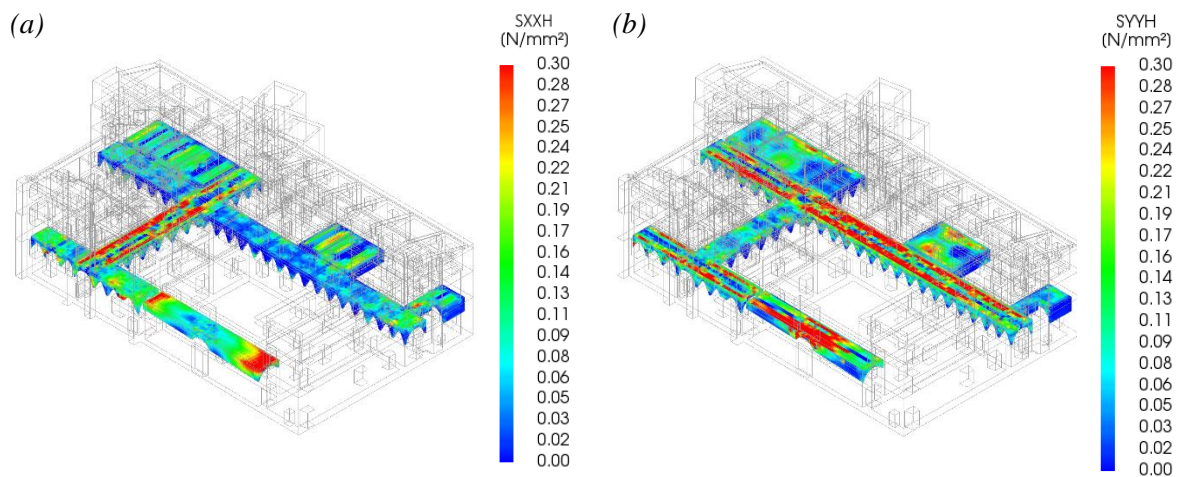
Figure 9. Resulting tensile stresses in the vaults. a) Tensile stress in global X direction (SXXH) resulting from LC1; b) Tensile stress in global Y direction (SYYH) resulting from LC2. The minimum and maximum values on the colour scale are bounded for stress comparison in the two orthogonal directions.
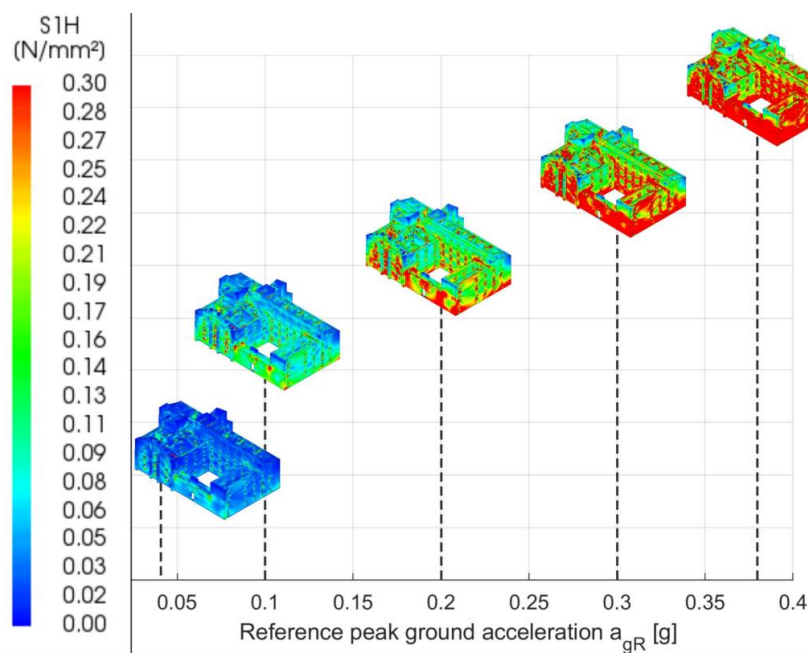
Figure 10. Progression of principal tensile stresses S1H obtained using LC1 by considering different peak ground acceleration values corresponding to the seismic zones in Croatia.

4.2 Out-of-Plane Assessment

The out-of-plane (OoP) assessment of masonry structures is highly dependent on the choice of deformation mechanism whose boundary conditions are usually unknown. In this study, the OoP failure mechanism is assumed based solely on the FEM model results i.e., no observation of cracking is recorded at the site. The assumed mechanism to be activated is dependent on the tensile stress distributions within the localized vulnerable areas. As a result, two mechanisms for two different walls are studied. The acceleration activating the mechanism is estimated based on a linear kinematic analysis using NTC 2018 [22]. The analysis with linear kinematic approach (or linear kinematics) requires the calculation of only the activation multiplier of the mechanism (α_0) and can be used to perform both the verification at the Damage Limit State (activation of the local mechanism) and the Ultimate Limit State. Moreover, the OoP failure is investigated for different levels of a_{gR} by calculating the compliance factor α_{eff} such that, the spectral acceleration required for the activation of local mechanism is smaller than the demand spectral acceleration.

Fig. 11 shows the two probable local failure mechanisms i.e., LM1 and LM2 for the clock and gable walls. The local mechanism (LM1) is the overturning of the whole wall assuming no connection to the orthogonal walls. The local mechanism (LM2) indicates the overturning of the upper part of the clock wall. Fig. 12 illustrates the change in compliance factor for different levels of seismic demand. For the clock wall, the relatively smaller value of α_{eff} in case of LM1 shows that only 0.053g is needed to activate the mechanism, making the clock wall very vulnerable to OoP damages. In the gable wall, LM1 is activated at an a_{gR} of 0.144g. The Croatian NA to Eurocode 8 requires the verification of significant damage (SD) and damage limitation (DL) limit states with peak ground accelerations 0.301g and 0.156g respectively [18]. The small values of compliance factor for both limit states indicate the high vulnerability of the clock and gable wall.

(a)
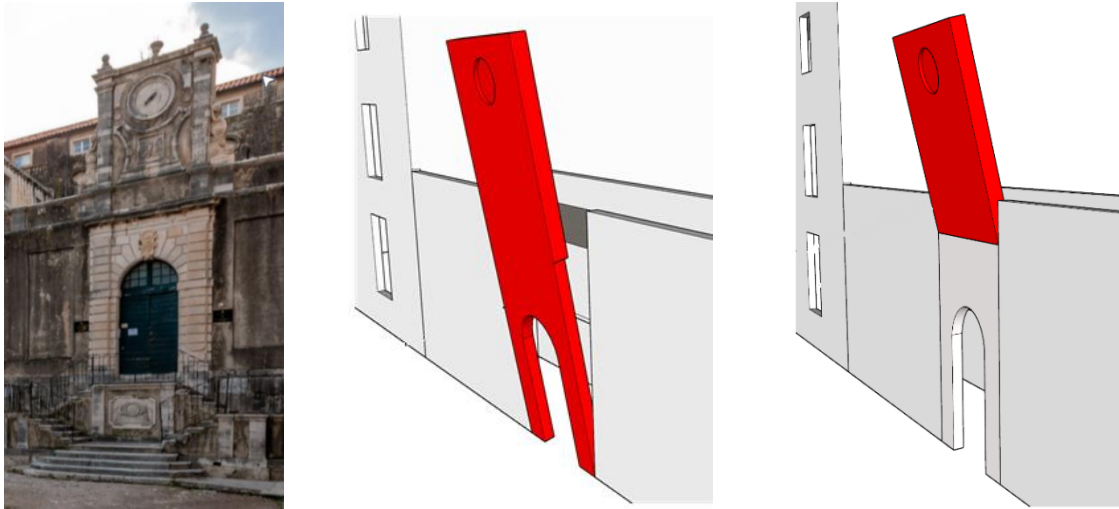
(b)

Figure 11. Description of the assumed local mechanisms LM1 and LM2. a) Clock wall; b) Gable Wall.
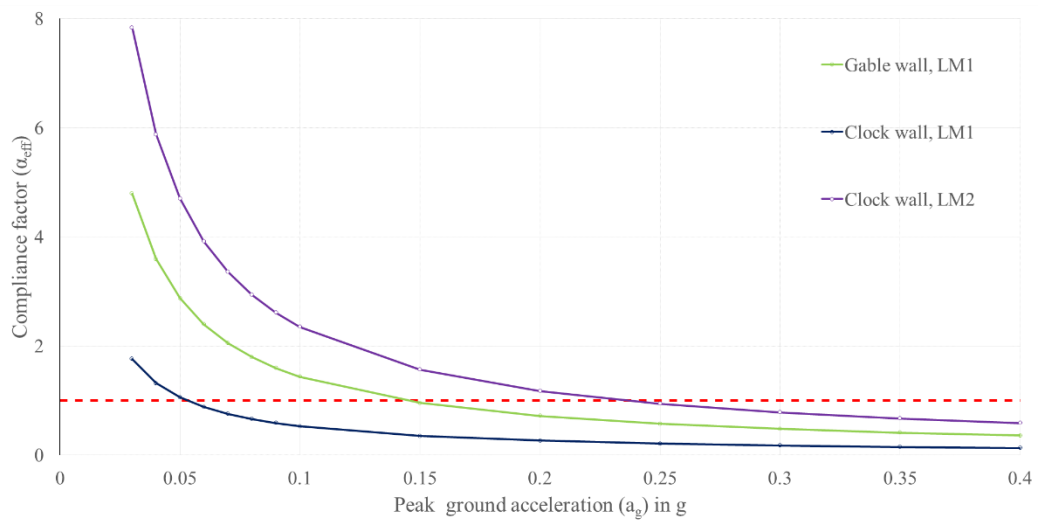
Figure 12. Compliance factor calculated for different demand acceleration levels for clock and gable walls.

Conclusions

This study presents the earthquake performance assessment of the Jesuit College in Dubrovnik, Croatia using Ambient Vibration Measurements and Finite Element Modelling. The Ambient Vibration Measurements identifies structural frequencies that are excited by low amplitude vibrations required to validate the finite element model. A total of 250 Eigen frequencies are required to accumulate 90% mass participation due to the complexity and size of the numerical model. The free vibration eigenvalue analysis shows the existence of both global and local mode shapes. The mode shapes that excites the major percentage of mass participation in X and Y directions are selected as global modes for the model calibration. Mode shape 1 represents a local bending vibration of the clock wall. Mode shape 2 shows translation in the Y direction. There is no pure translational mode in the X direction; instead, translation in the X direction is accompanied by torsional effects due to the irregularity and the floor plan of the building. In general, several modes describe OoP local vibration of walls.

Several sections of the walls experience stresses that are higher than the material elastic limit. This indicates the presence of cracking that might occur either at the wall surface or internally. From the analysis it is possible to identify zones with high compressive stresses and critical zones of tensile stresses due to the OoP bending of the walls. Compressive stresses are far from the material's elastic limit. The OoP occurs at the west and south wing walls due to the absence of intermediate walls and rigid diaphragms, as well as torsional effects caused by eccentricity. Shear stresses are concentrated in wall sections between adjacent openings i.e., short piers that carry high shear loads in unreinforced masonry structures. The regions with higher shear stresses shows a diagonal trajectory at the piers, and high shear stresses at the bottom of the clock wall due to out-of-plane deformations.

The vaults mainly function as rigid diaphragms, distributing lateral loads and torsional effects to the adjacent walls as shear forces. Therefore, the vaults develop principal tensile stresses as well, which are higher than the material tensile stress limit in some parts of the structure. High tensile stresses are developed in the hallway cross vaults oriented perpendicularly to the main direction of the seismic action between the vault and the lateral walls. The highest stresses are caused by the rigid diaphragm action that the vaults provide as they join portions of long walls that lack of transverse resistance to prevent out-of-plane movement.

Critical zones are identified in order to provide recommendations for strengthening and retrofitting. These are mainly located at the corners of the north wing where the walls intersect with east and west wings, the locations at the north facade of south wing where there is intersection with east and west wings, the walls of the hallway in south wing, the south wing facade, the facade walls of the west wing, and the base of the clock wall and, at the piers between wall openings.

Retrofitting by FRP can be applied to the piers to provide high strength and ductility to minor deformations. Grouting or epoxy injection solution is a low-cost solution that can restore the initial strength state of the wall requiring minimal intervention. The strengthening of wooden diaphragms would enhance the overall seismic response of the building by redistributing the lateral seismic forces along the walls, while dissipate energy through the diaphragm at the same time, reducing the occurrence of out-of-plane bending of the walls. Bracing and tying can provide high resistance against lateral loads, especially in the case of cantilevered walls such as the clock and gable walls. The iron tie-rods installed in the building contributes to the building's resistance to lateral forces by counteracting the out-of-plane bending of the walls. Future retrofitting works involving the tie rods should include experimental determination of the actual tensile forces in the tie-rods.

Acknowledgements

References

[1] Lourenço PB. Conservation of cultural heritage buildings: Methodology and application to case studies. 1 2013;3(2):98–110. https://doi.org/10.21041/ra.v3i2.46.

[2] Lourenco P, Karanikoloudis G. Seismic behavior and assessment of masonry heritage structures. Needs in engineering judgement and education. RILEM Tech Lett 2018;3:114–20. https://doi.org/10.21809/rilemtechlett.2018.76.

[3] D'Ayala D, Lagomarsino S. Performance-based assessment of cultural heritage assets: outcomes of the European FP7 PERPETUATE project. Bull Earthquake Eng 2015;13(1):5–12. https://doi.org/10.1007/s10518-014-9710-1.

[4] Alban K, Nicola C, Gabriele C, Filippo U. Dynamic testing and monitoring of historic towers for seismic damage detection. In: ; 2017, p. 2564–2577.

[5] Lorenzoni F, Casarin F, Caldon M, Islami K, Modena C. Uncertainty quantification in structural health monitoring: Applications on cultural heritage buildings. Mechanical Systems and Signal Processing 2016;66-67:268–81. https://doi.org/10.1016/j.ymssp.2015.04.032.

[6] Ramos LF, Marques L, Lourenço PB, Roeck G de, Campos-Costa A, Roque J. Monitoring historical masonry structures with operational modal analysis: Two case studies. Mechanical Systems and Signal Processing 2010;24(5):1291–305. https://doi.org/10.1016/j.ymssp.2010.01.011.

[7] Galić J, Vukić H, Andrić D. Structural Assessment of Dubrovnik Cathedral, Croatia. Structural Studies, Repairs and Maintenance of Heritage Architecture XVI 2019;191:467.

[8] Radnić J, Matešan D, Abaza A. Restoration and Strengthening of Historical Buildings: The Example of Minceta Fortress in Dubrovnik. Advances in Civil Engineering 2020;2020:1–17. https://doi.org/10.1155/2020/8854397.

[9] Torres W, Almazán JL, Sandoval C, Boroschek R. Operational modal analysis and FE model updating of the Metropolitan Cathedral of Santiago, Chile. Engineering Structures 2017;143:169–88. https://doi.org/10.1016/j.engstruct.2017.04.008.

[10] Ramos LF, Alaboz M, Aguilar R, Lourenço PB. Dynamic Identification and FE Updating of S. Torcato Church, Portugal. In: Dynamics of Civil Structures, Volume 4. Springer, New York, NY; 2011, p. 71–80.

[11] Standoli G, Salachoris GP, Masciotta MG, Clementi F. Modal-based FE model updating via genetic algorithms: Exploiting artificial intelligence to build realistic numerical models of historical structures. Construction and Building Materials 2021;303:124393. https://doi.org/10.1016/j.conbuildmat.2021.124393.

[12] Markušić S, Ivančić I, Sović I. The 1667 Dubrovnik earthquake–some new insights. Stud Geophys Geod 2017;61(3):587–600. https://doi.org/10.1007/s11200-016-1065-4.

[13] Jemo I, Brigović N. The Restoration of Dubrovnik. The Catalogue of Works in the Historic Centre of Dubrovnik from 1979 till 2009.

[14] SeisRICHerCRO. Seismic Risk Assessment of Cultural Heritage Buildings In Croatia. [January 14, 2023]; Available from: https://seisrichercro.wordpress.com/.

[15] Penava D, Vrban A, Uglešić J, Stanko D, Markušić S. Episcopal seminary building and classical gymnasium (Jesuit college) in Dubrovnik construction 1662-1765 in terms of contemporary earthquake resistant design supported by measurements // Proceedings of the 10th International Congress of Croatian Society of Mechanics / Skozrit, Ivica ; Tonković, Zdenko ; Sorić, Jurica (ur.). Pula: Croatian Society of Mechanics, 2022. str. 39-40.

[16] Horvat LK, Haničar BI, Vareško G. The building of the Episcopal Seminary and Classical Gymnasium Jesuit College in Dubrovnik. Conservation study with guidelines for restoration (in Croatian: Zgrada biskupskog sjemeništa i klasične gimnazije (Isusovački kolegij) u Dubrovniku. Konzervatorska studija sa smjernicama za obnovu). Zagreb, Croatia; 2022.

[17] Morić D. Floor Structures and Seismic Resistance of Cultural Heritage Stone Masonry Buildings; 2003.

[18] Eurokod 8: Projektiranje potresne otpornosti konstrukcija -- 1. dio: Opća pravila, potresna djelovanja i pravila za zgrade (EN 1998-1:2004+AC:2009).

[19] Eurokod 8: Projektiranje potresne otpornosti konstrukcija -- 3. dio: Ocjenjivanje i obnova zgrada (EN 1998-3:2005+AC:2010).

[20] Ivančić I, Herak D, Herak M, Allegretti I, Fiket T, Kuk K et al. Seismicity of Croatia in the period 2006-2015. geofizika 2018;35(1):69–98. https://doi.org/10.15233/gfz.2018.35.2.

[21] Markušić S, Stanko D, Korbar T, Sović I. Estimation of near-surface attenuation in the tectonically complex contact area of the northwestern External Dinarides and the Adriatic foreland. Nat. Hazards Earth Syst. Sci. 2019;19(12):2701–14. https://doi.org/10.5194/nhess-19-2701-2019.

[22] NTC 2018 – Nuove norme sismiche per il calcolo strutturale.

ANALYTICAL SEISMIC FRAGILITY CURVES FOR ANCIENT MASONRY BUILDINGS IN PORTUGAL

Vasco Bernardo [(1)], Alfredo C. Costa [(2)], Paulo Candeias [(3)], Aníbal Costa [(4)], Paulo B. Lourenço [(5)]

[(1)] *Postdoctoral researcher, University of Minho (Department of Civil Engineering), vbernardo@civil.uminho.pt*
[(2)] *Senior Researcher, National Laboratory for Civil Engineering (Structures Department), alf@lnec.pt*
[(3)] *Invited Assistant Researcher, National Laboratory for Civil Engineering (Structures Department), pcandeias@lnec.pt*
[(4)] *Full Professor, University of Aveiro (Department of Civil Engineering), agc@ua.pt*
[(5)] *Full Professor, University of Minho (Department of Civil Engineering), pbl@civil.uminho.pt*

Abstract

The seismic performance of buildings has received special attention due to the interest in the built heritage conservation and protection of human life. The historic urban centers are dominated by old unreinforced masonry (URM) buildings, which techniques and construction materials have evolved during centuries. Given the presence of these buildings in areas of significant seismicity, extensive research is needed to assess the seismic risk and define mitigation policies. This kind of studies is often supported by empirical methods and based on expert judgment due to the high variability of the building stock and lack of information. The main purpose of this work is to provide analytical fragility curves for representative masonry buildings in Portugal, built before the introduction of the first design code for building safety against earthquakes (RSSCS) in 1958. Thus, the fragility curves derived can characterize the capacity of the Portuguese building stock considering the randomness in the material properties and the variability in the geometry.

Keywords: pre-code masonry buildings; seismic probabilistic approach; seismic safety; seismic fragility analysis

1. Introduction

Over the years, masonry structures have shown evidence of good behavior under vertical static loads. However, its characteristics, such as the high specific mass, low tensile and shear strength, make the use of this heterogeneous material unsuitable in earthquake prone areas, e.g., Andradiva – Greece (2008), L'Aquila – Italy (2009), Emilia-Romagna – Italy (2012), Umbria – Italy (2016), Abruzzo – Italy (2017). Although Portugal has not been the target of high magnitude earthquakes in recent years, it remains susceptible, due to this geographical location, as it occurred in the past [1]: the 1755 Lisbon earthquake ($M_w = 8.5$), 1909 Benavente earthquake ($M_w = 6.3$), the 1969 Algarve earthquake ($M_w = 7.8$), Azores 1980 ($M_w = 7.2$) and 1998 ($M_w = 5.8$). These events caused significant damage in the affected regions, and particularly on masonry constructions [2].

The Portuguese building stock in historic urban centers is predominantly constituted by old unreinforced masonry (URM) residential buildings [3]. Their characteristics are the result of different periods of construction and construction practice due to the available materials, existing techniques, and society needs.

In the last decades, the performance of buildings under seismic action has received special attention due to the interest in the conservation of heritage and protection of human life. The seismic risk at a national scale was evaluated by [4] and [5], and by other authors at urban scale, e.g.: Coimbra [6], Faro [7], Seixal [8]. Most of these studies employed statistical data and expert opinion combined with empirical methods to derive fragility and vulnerability functions to characterize the building stock.

In order to support similar studies related to vulnerability and seismic risk assessment, this work aims to provide analytical fragility curves for the population of old (pre-code) URM buildings in Portugal with rigid and flexible floor diaphragms. Although the analyses carried out in the present work have been derived to account only for the in-plane mechanisms to be compliant with the current version of

EC8-3, which assumes these as being prevented from occurring, several works regarding out-of-plane fragility functions for masonry buildings can be found in literature, emphasizing the importance of such mechanisms, namely in buildings with flexible floor diaphragms [9]–[15].

In the framework of the present study, the development of the fragility curves involves the following steps: (i) generation of a synthetic database of 18.000 masonry buildings up to 5 stories high, including different archetypes based on statistical information previously collected and different material properties to cover the variability found in the literature; (ii) estimate the in-plane seismic behavior of the entire database through displacement-based nonlinear static methods; (iii) derivation of fragility functions for the capacity expressed by the maximum interstorey drift. The fragility curves proposed are only related to the deformation capacity of the buildings in order to be applied in seismic risk studies or safety assessment.

2. Old masonry buildings description

Four typologies of masonry buildings are typically identified in the urban centers of Portugal (Figure. **1**.): *"Pre-Pombalino"* (before 1755), *"Pombalino"* (1755 to 1870), *"Gaioleiro"* (1870 to 1930) and *"Placa"* (1930 to 1960). The "Pre Pombalino" buildings, constructed before the 1755 earthquake, are recognized by their irregular geometry, reduced dimensions, narrow facades, high density of walls and few openings to the exterior. They usually are four stories high and are constituted by poor-quality masonry walls supporting the timber floors. The "Pombalino" buildings emerged after the Lisbon earthquake and are particularly known by the improvements in the anti-seismic conception in that period. They usually have up to five stories high and regular geometry. This typology was standard in the building construction practice for more than one century. On the other hand, the "Gaioleiro" buildings represent a downgrade when compared to the previous typology, with the adoption of more simplified construction techniques and the use of low-quality materials which was promoted by the rapid expansion of the urban centers and the housing demand. This typology is significantly more vulnerable, from a seismic point of view, compared with the previous one. Finally, *"Placa"* buildings emerged before the enforcement of the first seismic-code in 1958 and introduced the use of lightly reinforced concrete slabs at the floors level. The high mass of the RC slabs and the low strength capacity of the load bearing walls to horizontal forces results in an unsatisfactory structural seismic performance. The main characteristics of these typologies are briefly described in Figure. **1**.

Figure. 1 Main features of old masonry buildings

3. Geometry of representative masonry buildings

3.1 Geometry characterization and definition of archetypes

The geometry characterization comprises the information gathered through detailed drawings from the original projects and collected from municipal archives, for a population of 100 old (pre-code) masonry buildings. This data represents the geometry for the most typical masonry buildings built before the decade of 1960 and described in the previous section. The geometric parameters obtained, such as plan dimensions, height of the stories, openings ratio, interior walls density, walls thickness and type/thickness of floors, were statistically characterized and described in Bernardo *et al*. 2021.

Based on this information, 9 archetypes – A1, A2, A3, B1, B2, B3, C1, C2 and C3 – with different configurations and up to 5 stories high, were generated for the subsequent analyses. Figure. 2 presents the layout of these archetypes. Table 1 summarizes the statistical information for the geometry and the parameters adopted (underlined) to represent the archetypes.

The archetype B2 (Figure. 2) represents the mean size configuration (12.6x12.1m). The plan dimensions for the remaining were derived from the mean archetype, considering a dispersion equals to one standard deviation: $L_x = 12.6 \pm 5.0$m and $L_y = 12.1 \pm 4.1$m. The total area ranges approximately between 60.0m^2 to 285.0m^2. The layout for the arrangement of the partitions/interior walls follows, in a reasonable manner, the typical size of the compartments for theses typologies (3x3m up to 4x5m), representing a mean value for the interior walls' density equal to 0.054.

Regarding the walls thickness, considering the enormous variability in the type of material, arrangement and absence of information in the documentation gathered, were considered the mean thickness for the facades and side walls. For the interior/partition walls the most common value (mode) were adopted, which are representative for more than 60% of the buildings collected [20]. The intrinsic variability in the wall's characteristics (type of masonry, morphology and arrangement) was computed in the material mechanical properties uncertainty, carried out in section 3.2. For the remaining variables, the mean values adopted are mentioned in Table 1.

Table 1 Statistical properties for the geometric parameters [20]

Statistical properties	L_x [m]	L_y [m]	IWD [-]	H_0 [m]	H_n [m]	OR_F [-]	OR_B [-]	Th_1 [m]	Th_2 [m]	Th_3 [m]	Th_4 [m]	AWTR [-]
Mean μ	12.6	12.1	0.054	3.23	3.01	0.23	0.21	0.47	0.34	0.21	0.14	0.11
Std. deviation σ	5.00	4.1	0.01	0.42	0.24	0.08	0.08	0.14	0.11	0.05	0.02	0.06
mode	-	-	-	-	-	-	-	-	-	0.25	0.15	0.10

L_x and L_y – size; H_0 and H_n – ground and upper floor stories high; OR – openings ratio: front (OR_F) and back (OR_B) facade; IWD – interior walls density; Th – walls thickness: facades (1), lateral side (2), interior (3), partition (4); AWR – average walls thickness reduction on the facade
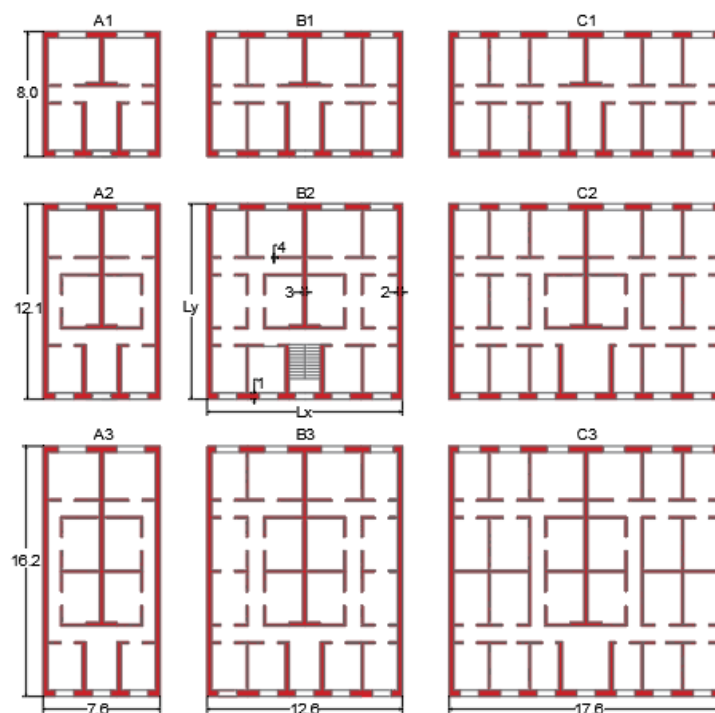
Figure. 2 Archetypes adopted to represent the population of old masonry buildings in Portugal

3.2 Material properties selection

The definition of material mechanical properties was based on literature review, which includes the masonry properties that can be identified in the Portuguese building stock and the suggested properties by the latest version of EC8-3 (see Candeias *et al.* 2020).

Taking into account the wide range of masonry mechanical properties, the uncertainty was propagated through *Monte Carlo* simulations [22]. For that purpose, two groups of buildings were considered with different material properties (see Table 2): *Type I* – typologies with good quality masonry (e.g., regular and squared masonry, brick masonry with cement lime mortar) and *Type II* – typologies with poor quality masonry (e.g., ruble stone masonry, brick masonry with lime mortar). Given the differences of the interior/partition walls (e.g., *tabique*[1], *frontal* walls[2], perforated brick masonry) when compared with the exterior walls (e.g., solid masonry bricks, stone masonry or concrete blocks), two sub categories were defined: *Type I-1* and *Type II-1*, to represent the properties of exterior walls, and *Type I-2* and *Type II-2* for the interior/partition walls. A set of 100 samples for each typology – Type I and Type II – were generated to describe the material variability, attaining an error of around 5% (95% confidence interval) for the material population generated.

Table 2 Mean values and dispersion adopted for the material mechanical properties

Random variable	Distribution	COV	Mean value			
			Type I-1	Type I-2	Type II-1	Type II-2
Compressive strength f_c [MPa]	**LogNormal**	**0.40**	**5.00**	**2.00**	**2.50**	**1.25**
Factor K * [-]	**Truncated Normal**	**0.25**	**800 (250 - 1100)**			
Young's modulus E [MPa]	**-**	**-**	**4000**	**1600**	**2000**	**1000**
Shear modulus G [MPa]	**LogNormal**	**0.40**	**1700**	**650**	**850**	**450**
Density ρ [kg/m³]	**Normal**	**0.10**	**1800**	**1200**	**1800**	**1200**
Cohesion τ_0 [MPa]	**LogNormal**	**0.40**	**0.15**	**0.15**	**0.07**	**0.07**
Friction coefficient μ** [-]	**LogNormal**	**0.40**	**0.40**	**0.40**	**0.40**	**0.40**
* Factor k correlates the Young's modulus and compressive strength: $E = K \cdot f_c$ ** According to EC8-3						

4. Numerical modelling assumptions

4.1 Modelling strategy and general assumptions

Considering the previous geometric statistical information, tridimensional multi degree of freedom models (MDOF) were developed to simulate the nonlinear response of the buildings. For this purpose, an equivalent frame modeling strategy available in the research version (2.1.104) of *TREMURI* software [23] was used. Some of the features of the model include the accurate representation of the principal in-plane failure mechanism, including the stiffness and strength degradation, such as bending rocking, diagonal shear and sliding.

The software was originally developed for frame-type analysis of the entire URM buildings whereby the response is governed by the in-plane behavior of the walls. On the other hand, the current version of EC8-3 also does not include the out-of-plane mechanisms or assumes these as being prevented from occurring. Hence, the behavior of the buildings analyzed is only restricted to in-plane mechanisms.

4.2 Macroelement model validation

The macroelement model is defined by a set of mechanical parameters at macroscopic scale that should be representative of an average of the masonry panel properties: Young's modulus – *E*, shear modulus

---

[1] set of vertical long boards connected by horizontal small wood stripes, normally filed with pieces of bricks and lime mortar
[2] set of plane wood trusses very common in "Pombalino" typology

– G, density – ρ, compressive strength – f_c, cohesion – τ_0, friction coefficient – μ, and by two phenomenological parameters related to the shape of nonlinear shear constitutive model – c_t that expresses the shear deformability in the inelastic range, wherein the amplitude in the inelastic displacement is proportional to the product G_{Ct}; and β_s that controls the slope of the softening branch in the post-peak region [23].

The validation of the macroelement model was performed using the results of an in-plane quasistatic experimental test carried out on a full-scale masonry panel, with aspect ratio of 1.325:1 (2.65x2.00x0.25m – height, length and thickness), made of solid clay bricks, extracted from an old masonry building. Further details can be found in [24].

4.3 Floor diaphragms modelling

Floor diaphragms were modelled as a two-dimensional orthotropic membrane element, defined by four nodes with two displacement degrees of freedom each, and characterized by the equivalent mechanical properties: equivalent thickness – t_{eq}, modulus of elasticity of the diaphragm in the principal direction – E_1 – and perpendicular direction – E_2, shear modulus – G, that influence the horizontal force distribution between walls, and Poisson ratio – v.

Two types of floor diaphragms, rigid and flexible, were considered. Rigid diaphragms were modelled by RC slabs and assuming a load distribution in the walls proportional to the influence area. In this case, it was assumed a good connection between the walls to ensure equal planar displacements at floor level, simulated through rigid links beams. A typical timber floor was adopted for flexible diaphragms, constituted by timber sheathing and timber joists perpendicular to the facades. In this case, the load was distributed by the main timber joists and the connections between walls were modelled through equivalent elastic link beams at the floor level to simulate medium to weak connections, according to [25]. Table 3 and Table 4 summarize the mechanical properties for the membrane elements (rigid and flexible) and for the connection between walls, respectively.

Table 3 Mechanical properties adopted for the floor diaphragms

Type of floor	Equivalent thickness t_{eq} [m]	Elastic modulus E_1 [GPa]	Elastic modulus E_2 [GPa]	Shear Modulus G [GPa]	Poisson coefficient v [-]
Rigid	0.20	30.0	30.0	13.0	0.20
Flexible [25]	0.022	29.0	12.0	0.011	-

Table 4 Parameters adopted to simulate the connections between walls [25]

Type of connections	Area A [m²]	Inertia I [m⁴]	Elastic modulus E [GPa]
Good (rigid)	10.0	5.0	30.0
Medium to weak (flexible)	0.0004	0.0002	

4.4 Representative buildings models

Considering the assumptions related to geometry layout and discussed in previous sections, 45 archetypes of buildings were modelled (A1, A2, A3, B1, B2, B3, C1, C2 and C3), up to 5 stories high, as shown in Figure. **3**. Attending to materials variability and different type of floor diaphragms (rigid and flexible), a population of 18000 buildings was generated, based on the modelling assumptions previously described. With regard to gravity loads applied, the prescriptions of Eurocode 8 [26] are followed, combining the nominal values of permanent loads G with the quasi-permanent live loading $\Psi_E Q$. The permanent loads are defined by the self-weight of the masonry, timber floors (1.10 kN/m²) and timber roof (1.30 kN/m²). The live loads depend on the building category, which is assumed for domestic and residential purpose (category A).
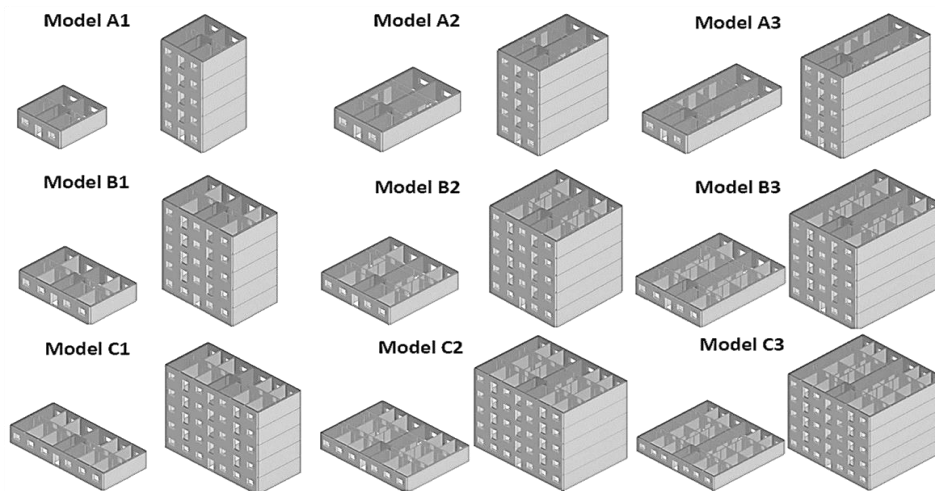
Figure. 3 Archetypes of masonry old buildings modelled in TREMURI

5. Numerical analysis and seismic behavior

5.1 Methodology for seismic assessment

In order to develop the fragility curves compatible with the current version of EC8-3, the methodology to evaluate the seismic behavior of the buildings follow the recommendations of the standards for the in-plane global safety verification using nonlinear methods.

The general methodology of EC8-3 uses a performance- and displacement-based approach to assess the safety level of a given structure. Regarding the required performance levels for Portugal, implicitly related to the seismic hazard, three limit states (LS) are defined to assess the structural performance of an existing building, depending on its importance class: Damage Limitation (DL), Significant Damage (SD) and Near Collapse (NC). The return periods (RP) prescribed by EC8-3 for these LS are defined in accordance with levels of protection, having values of 73, 308 and 975 years for the DL, SD and NC limit states, respectively, corresponding to probabilities of exceedance of 50%, 15% and 5% in 50 years. For residential buildings (importance class II) the safety verification is only mandatory for the SD limit state.

5.2 Nonlinear static analysis

The buildings' capacity was predicted from nonlinear numerical static analysis (pushover), through monotonic horizontal forces, which requires particular attention on the choice of load pattern. In general, design codes propose to assume two load patterns (e.g., uniform and triangular) to simulate the distribution of inertial forces during the seismic loading on the deformed shape of the buildings. However, the deformed shape depends on the damage on the building and may change during the loading scenario. To overcome this limitation, [29] propose an adaptive pushover algorithm for masonry buildings, wherein the load pattern is proportional to the displacement shape in the previous step. This approach revealed to be more suitable for masonry buildings with rigid floors, comparing with time-history analysis. However, for flexible floors, given the local mechanisms and the mass participation of each single wall in the vibration mode, that approach does not provide significant improvements. In that case, the pseudo-triangular load pattern is better suited to assure that all mass is mobilized [30]. For the present study, adaptive pushover analyses with inverse triangular first ratio pattern were adopted for buildings with rigid floors and an inverted pseudo-triangular for flexible floors. The control node was selected at the top level and the shear was measured on the base up to reaching 20% decay of the maximum shear strength (NC limit state), as recommend by the EC8-3 for a global safety verification. Figure. **4** presents the capacity curves normalized for spectral acceleration S_a and spectral displacement S_d for the archetypes A1, B2, and C3, with 3 to 5 stories high. The red and blue dots correspond to the

maximum shear strength and the ultimate displacement for the NC limit state, respectively. The results are presented for the seismic action in the longitudinal direction (parallel to the facade walls), which revealed to be more critical for the geometry layout defined by exterior lateral walls without openings.
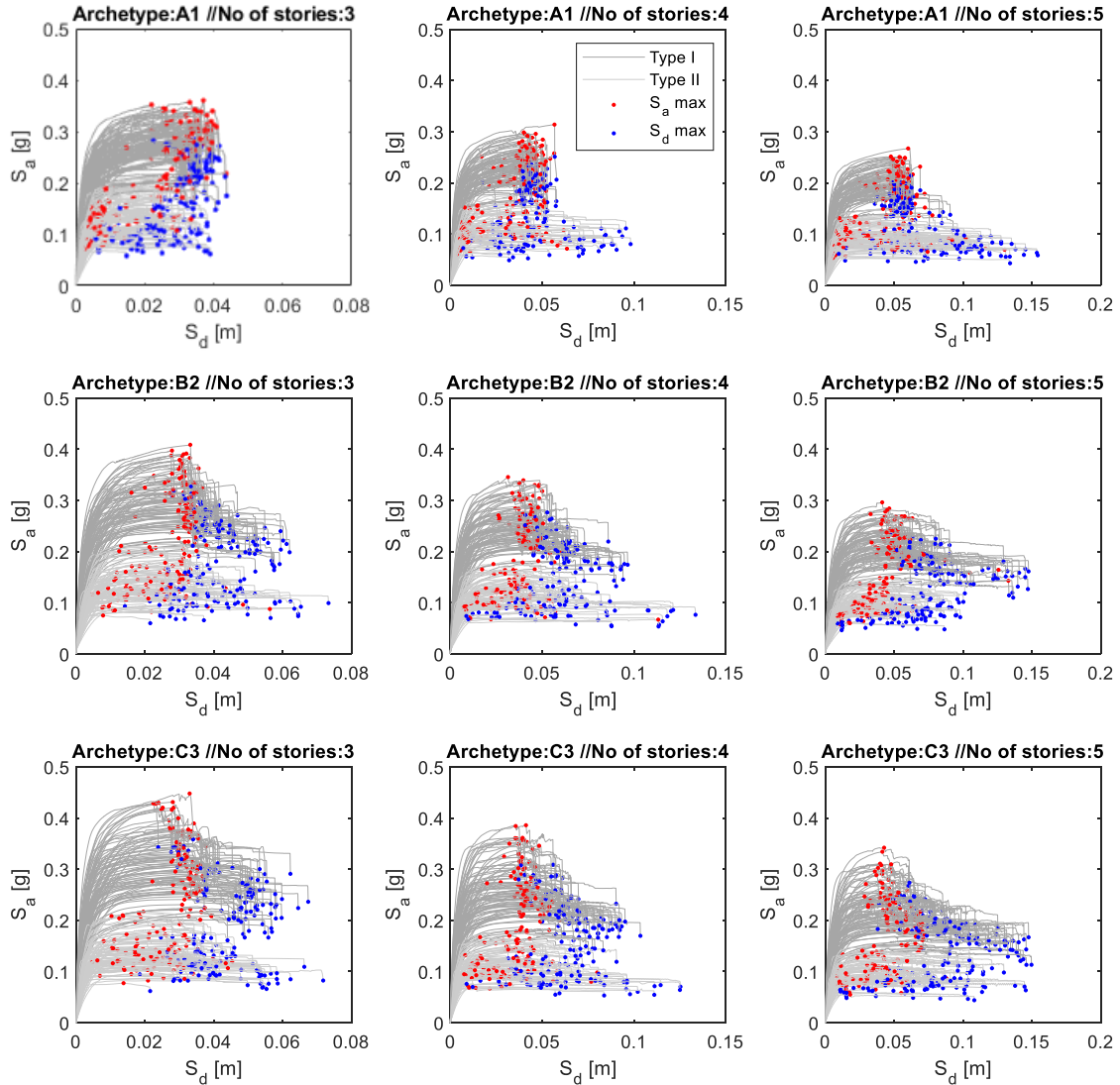
Figure. 4 Capacity curves for archetypes A1, B2 and C3, with 3, 4 and 5 stories heigh and rigid floors

5.3 Seismic performance-based assessment

In this study, the seismic performance was evaluated for each building, adopting the response spectrum for the seismic action offshore (seismic action type 1) and inland (seismic action type 2) defined in EC8-1 for Portugal, an equivalent viscous damping equal to 5%, soil amplification factor corresponding to a soil type A, B and C, and a wide range of return periods (*RP*) up to 5000 years. Taking the 475-years *RP* as the reference period RP_{ref}, the acceleration on the ground a_g can be scaled to other *RP* as suggested in the comments to the Portuguese version of EC8-1: $a_g = a_{gr}(RP_{ref}/RP)^{-1/k}$, where a_{gr} is the acceleration for the RP_{ref} and k take the values of 1.5 and 2.5 for seismic action in mainland offshore and onshore, respectively, and 3.6 for Azores. These coefficients assume the mean values obtained in the counties and a first-order power law approximation for the seismic hazard.

6. Seismic fragility analysis

In the present work, the limit state (LS) thresholds follow the global scale criterion as a percentage of maximum shear (F_{max}) defined in the capacity curves, which are in line with the LS proposed by the EC8-3. Therefore, the LS are expressed in terms of spectral displacement (S_d) as a function of the base shear measured, according to criteria indicated in Table 5. The LS1 was defined at the yielding point of the idealized capacity curve and LS2 and LS3 correspond to the peak of maximum shear and post-peak range, respectively.

Table 5 Damage state definition for unreinforced masonry buildings

Limit state	Performance Level	Description	Criteria
LS1 – DL	Immediate Occupancy: Damage Limitation	Minor structural damage; moderate non-structural damage	S_{dy}
LS2 – SD	Life Safety: Significant Damage	Significant structural damage; extensive non-structural damage.	$S_d (F_{max})$
LS3 – NC	Collapse Prevention: Near Collapse	Near collapse; repairing the building is not feasible	$S_d (0.80F_{max})$

The fragility curves proposed in this section were derived from empirical cumulative distribution functions (CDF) for the data analyzed, directly obtained from the nonlinear response of the buildings, considering the limit states indicated in Table 5. Therefore, the fragility curves presented are independent of the seismic action, or spectrum format, and represent the capacity exceedance probability conditioned on a value of demand for the three limit states adopted.

For this purpose, the archetypes were grouped and analyzed by number of stories, typology (Type I and Type II) and type of floor diaphragm rigid (RD) or flexible (FD). The best cumulative analytical function was fitted to the data based on Kolmogorov-Smirnov tests, and follow, in a reasonable manner, a LogNormal (LN) and Weibull (W) distribution for typologies Type I and Type II, respectively. Figure. **6** presents the proposed fragility curves, expressed as a function of interstorey drift θ_C, by number of floors, typology and type of floor diaphragm. Table 6 summarizes the median values of θ_C and dispersion β_D for the analytical fragility functions proposed for the buildings' capacity. Note that, the values of dispersion achieved in this section include the randomness in material properties defined for each typology and the variability in the geometry layout of the archetypes, allowing to account both variables in the capacity of the buildings for seismic risk studies or seismic assessment.

Bar chart of Figure. **5** presents a comparison of the moments proposed for the different typologies, type of floor diaphragm and number of stories, to support the discussion of results. For the mean values θ_C (%) computed, the main differences are observed between typologies and type of floor diaphragm: Type I/RD 0.09 to 0.12 (DL), 0.37 to 0.47 (SD), 0.45 to 0.70 (NC); Type II/RD 0.07 to 0.09 (DL), 0.22 to 0.31 (SD), 0.38 to 0.70 (NC); Type I/FD 0.21 to 0.40 (DL), 0.65 to 0.91 (SD), 0.70 to 1.09 (NC); Type II/FD 0.23 to 0.33 (DL), 0.51 to 0.75 (SD), 0.70 to 0.91 (NC). As can be noticed, high values of θ_C are attained for structures with FD and mostly for type I typology. In contrast, the type II-rigid presents minor drifts, followed by the type I-rigid. In general, buildings with good quality masonry (Type I) present higher values of θ_C, except for one storey height with FD.

Regarding the dispersion β_D, the range of values vary from: Type I/RD ¬ 0.30 to 0.33 (DL), 0.12 to 0.26 (SD), 0.15 to 0.32 (NC); Type II/RD ¬ 0.41 to 0.51 (DL), 0.50 to 0.58 (SD), 0.20 to 0.50 (NC); Type I/FD ¬ 0.20 to 0.40 (DL), 0.19 to 0.30 (SD), 0.22 to 0.33 (NC); Type II/FD ¬ 0.27 to 0.62 (DL), 0.34 to 0.60 (SD), 0.30 to 0.50 (NC). Thus, in general, the values of dispersion attained are higher for typology Type II. For the same typology, minor differences between the number of floors are noticed, except for buildings with one story. For the SD limit state, the dispersion has a slight range between the number of floors, comparing to the other limit states, excluding the Type II-flexible typology with relatively similar dispersion. Finally, for the DL seems to be some trend for lower dispersion in low-rise buildings, in contrast to the higher dispersion computed in taller buildings for the NC limit state.
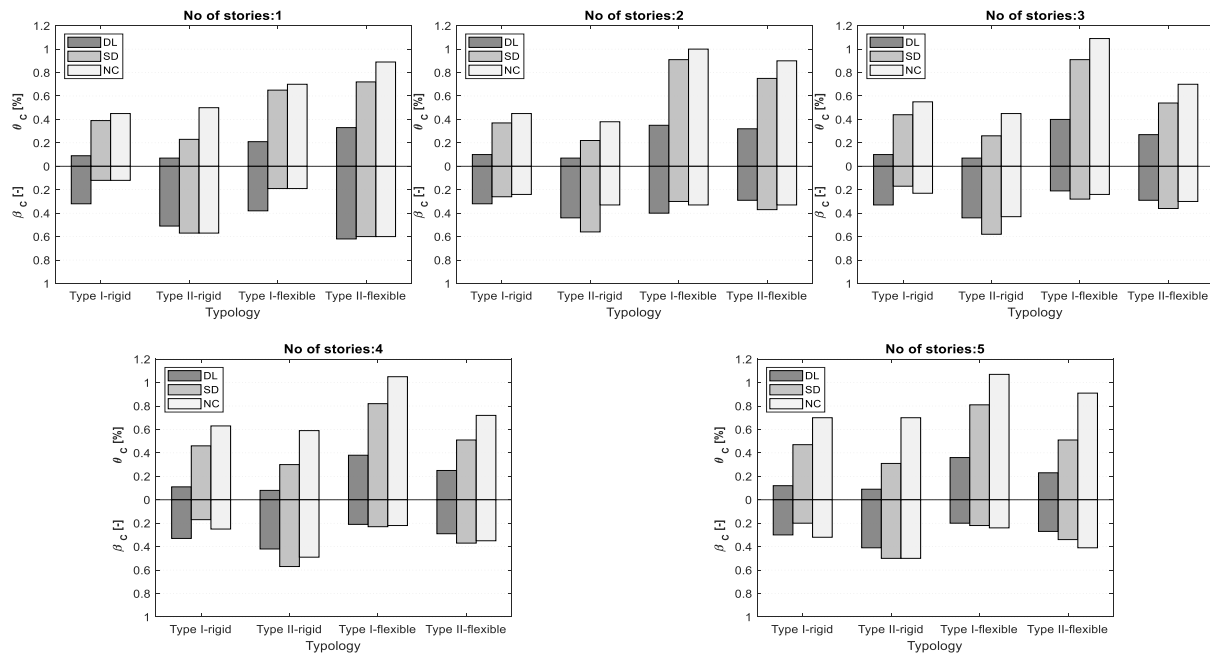
Figure. 5 Analytical fragility curves proposed for the buildings' capacity: comparison of the median θ_C and dispersion β_C values by number of stories, typology and type of floor diaphragm.

Table 6 Moments of the analytical fragility curves proposed for the buildings' capacity.

No of stories	Typology	Function	LS1 – DL				LS2 – SD				LS3 – NC			
			θ_C [%]	β_C [-]	a	b	θ_C [%]	β_C [-]	a	b	θ_C [%]	β_C [-]	a	b
1	Rigid-Type I	LogN	0.09	0.32	-	-	0.39	0.12	-	-	0.45	0.15	-	-
	Rigid-Type II	Weibull	0.07	0.51	0.08	2.05	0.23	0.57	0.26	1.83	0.50	0.20	0.54	5.80
	Flexible-Type I	LogN	0.21	0.38	-	-	0.65	0.19	-	-	0.70	0.22	-	-
	Flexible-Type II	Weibull	0.33	0.62	0.43	1.75	0.72	0.60	0.87	2.63	0.89	0.50	1.04	2.91
2	Rigid-Type I	LogN	0.10	0.32	-	-	0.37	0.26	-	-	0.45	0.24	-	-
	Rigid-Type II	Weibull	0.07	0.44	0.07	2.41	0.22	0.56	0.25	1.85	0.38	0.33	0.42	3.33
	Flexible-Type I	LogN	0.35	0.40	-	-	0.91	0.30	-	-	1.00	0.33	-	-
	Flexible-Type II	Weibull	0.32	0.29	0.36	3.92	0.75	0.37	0.82	3.07	0.90	0.33	1.03	3.60
3	Rigid-Type I	LogN	0.10	0.33	-	-	0.44	0.17	-	-	0.55	0.23	-	-
	Rigid-Type II	Weibull	0.07	0.44	0.08	2.42	0.26	0.58	0.29	1.79	0.45	0.43	0.50	2.47
	Flexible-Type I	LogN	0.40	0.21	-	-	0.91	0.28	-	-	1.09	0.24	-	-
	Flexible-Type II	Weibull	0.27	0.29	0.30	3.84	0.54	0.36	0.59	2.79	0.70	0.30	0.80	3.80
4	Rigid-Type I	LogN	0.11	0.33	-	-	0.46	0.17	-	-	0.63	0.25	-	-
	Rigid-Type II	Weibull	0.08	0.42	0.09	2.56	0.30	0.57	0.34	1.83	0.59	0.49	0.67	2.17
	Flexible-Type I	LogN	0.38	0.21	-	-	0.82	0.23	-	-	1.05	0.22	-	-
	Flexible-Type II	Weibull	0.25	0.29	0.27	3.84	0.51	0.37	0.55	2.71	0.72	0.35	0.82	3.36
5	Rigid-Type I	LogN	0.12	0.30	-	-	0.47	0.20	-	-	0.70	0.32	-	-
	Rigid-Type II	Weibull	0.09	0.41	0.10	2.61	0.31	0.50	0.34	2.09	0.70	0.50	0.79	2.12
	Flexible-Type I	LogN	0.36	0.20	-	-	0.81	0.22	-	-	1.07	0.24	-	-
	Flexible-Type II	Weibull	0.23	0.27	0.25	4.28	0.51	0.34	0.53	3.55	0.91	0.41	0.90	2.84
a, b are, respectively, the scale and shape parameter for the Weibull distribution														
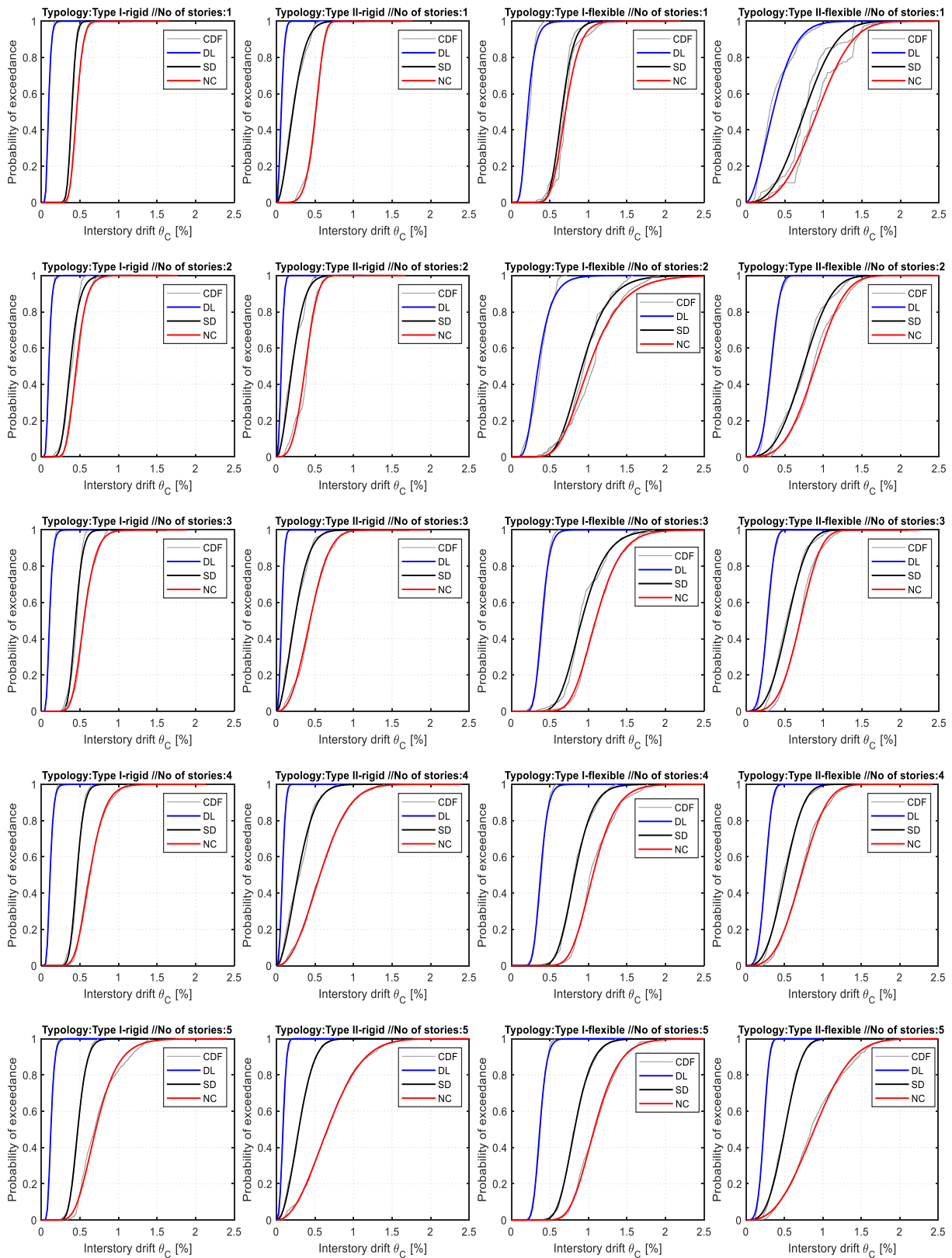
Figure. 6 Analytical fragility proposed curves for the buildings' capacity expressed by $\boldsymbol{\theta_C}$.

7. Final comments and conclusions

Seismic risk studies are of extreme importance in regions with moderate to high seismicity, such as Portugal, to estimate losses and establish policies for risk mitigation. This kind of studies requires knowledge about the building stock, which is often characterized by empirical methods and expert opinion when performed at large scale. The main purpose of the present paper was to derive analytical fragility curves that can be used to conduct more detailed seismic risk studies or employed for seismic assessment of pre-code masonry buildings.

The development of the proposed fragility curves considered a synthetic database of 18.000 masonry buildings, based on statistical information previously collected about the geometry, allowing to define nine archetypes (A1, A2, A3, B1, B2, B3, C1, C2, C3), which were further combined with a wide range of material properties (Type I – good quality and Type II – poor quality) and type of floor diaphragm (rigid and flexible).

Based on the previous analyses, analytical fragility curves for the buildings' capacity were derived for both typologies and type of floor diaphragm. Among the results gathered, the following stand out: i) buildings with good quality materials and flexile diaphragm (Type I FD) reach higher drift values (up to 0.41%DL, 0.91% SD and 1.09% NC). In contrast, smaller drifts (up to 0.09%DL, 0.31% SD and 0.70% NC) are attained for structures with poor quality masonry and rigid diaphragm (Type II RD); ii) the dispersion achieved is higher in Type II FD buildings (up to 0.62 DL, 0.60 SD and 0.50 NC) and smaller in Type I RD buildings (up to 0.33 DL, 0.26 SD and 0.32 NC); iii) in general, drift values and respective dispersion seems to be higher with the increase in number of floors.

The proposed fragility curves are not linked to a ground motion intensity, or spectrum format, and can be applied in a more general context to characterize the capacity of the building stock considering the randomness in the material properties and the variability in the geometry.

Acknowledgements

References

[1]   C. S. Oliveira, "A sismicidade historica e a revisao do catalogo sismico. National Laboratory for Civil Engineering. Report 36/11/7368." National Laboratory for Civil Engineering, Lisbon, Portugal [in Portuguese], 1986.

[2]   M. R. Correia, P. B. Lourenço, and H. Varum, *Seismic retrofitting: Learning from vernacular architecture. Taylor & Francis. 1st edition. ISBN 9781138028920*. 2015.

[3]   INE, "Censos 2011 Resultados Definitivos. Report," Lisbon, Portugal [in Portuguese], 2012.

[4]   M. L. Sousa, "Seismic risk in Mainland Portugal," Technical University of Lisbon, Lisbon, Portugal [in Portuguese], 2006.

[5]   V. Silva, H. Crowley, H. Varum, and R. Pinho, "Seismic risk assessment for mainland Portugal," *Bulletin of Earthquake Engineering*, 2014.

[6]   R. Vicente, S. Parodi, S. Lagomarsino, H. Varum, and J. Silva, "Seismic vulnerability and risk assessment: Case study of the historic city centre of Coimbra, Portugal," *Bulletin of Earthquake Engineering*, 2011.

[7]   R. Vicente, T. Ferreira, and R. Maio, "Seismic Risk at the Urban Scale: Assessment, Mapping and Planning," *Procedia Economics and Finance*, 2014.

[8]   T. M. Ferreira, R. Vicente, J. A. R. Mendes da Silva, H. Varum, and A. Costa, "Seismic vulnerability assessment of historical urban centres: Case study of the old city centre in Seixal, Portugal," *Bulletin of Earthquake Engineering*, vol. 11, no. 5, pp. 1753–1773, Oct. 2013.

[9]   G. Sumerente, H. Lovon, N. Tarque, and C. Chácara, "Assessment of combined in-plane and out-of-plane fragility functions for adobe masonry buildings in the peruvian andes," *Frontiers in Built Environment*, 2020.

[10]   N. Giordano, F. De Luca, and A. Sextos, "Analytical fragility curves for masonry school building

portfolios in Nepal," *Bulletin of Earthquake Engineering*, 2021.

[11]   H. B. Ceran and M. A. Erberik, "Effect of out-of-plane behavior on seismic fragility of masonry buildings in Turkey," *Bulletin of Earthquake Engineering*, 2013.

[12]   A. G. Simões, R. Bento, S. Lagomarsino, S. Cattari, and P. B. Lourenço, "Seismic assessment of nineteenth and twentieth centuries URM buildings in Lisbon: structural features and derivation of fragility curves," *Bulletin of Earthquake Engineering*, 2020.

[13]   M. A. Jaimes, M. M. Chávez, F. Peña, and A. D. García-Soto, "Out-of-plane mechanism in the seismic risk of masonry façades," *Bulletin of Earthquake Engineering*, 2021.

[14]   A. A. Costa, "Seismic assessment of the out-of-plane performance of traditional stone masonry walls (PhD Thesis). Faculty of Engineering, University of Porto," FEUP, Porto, 2012.

[15]   T. M. Ferreira, A. A. Costa, R. Vicente, and H. Varum, "A simplified four-branch model for the analytical study of the out-of-plane performance of regular stone URM walls," *Engineering Structures*, 2015.

[16]   S. Lagomarsino and S. Cattari, "Fragility Functions of Masonry Buildings," *Geotechnical, Geological and Earthquake Engineering*, 2014.

[17]   M. Rota, A. Penna, and G. Magenes, "A methodology for deriving analytical fragility curves for masonry buildings based on stochastic nonlinear analyses," *Engineering Structures*, 2010.

[18]   J. Milosevic, S. Cattari, and R. Bento, "Definition of fragility curves through nonlinear static analyses: procedure and application to a mixed masonry-RC building stock," *Bulletin of Earthquake Engineering*, 2020.

[19]   S. Lagomarsino, S. Cattari, and D. Ottonelli, "The heuristic vulnerability model: fragility curves for masonry buildings," *Bulletin of Earthquake Engineering*, 2021.

[20]   V. Bernardo, R. Sousa, P. Candeias, A. Costa, and A. Campos Costa, "Historic Appraisal Review and Geometric Characterization of Old Masonry Buildings in Lisbon for Seismic Risk Assessment," *International Journal of Architectural Heritage*, 2021.

[21]   P. Candeias *et al.*, "General aspects of the application in Portugal of Eurocode 8 – Part 3 – Annex C (Informative) – Masonry Buildings [in Portuguese]," *Revista Portuguesa de Engenharia de Estruturas*. RPEE série III , nº 12, Lisbon, Portugal [in Portuguese], 2020.

[22]   M. J. Fryer and R. Y. Rubinstein, "Simulation and the Monte Carlo Method.," *Journal of the Royal Statistical Society. Series A (General)*, 1983.

[23]   S. Lagomarsino, A. Penna, A. Galasco, and S. Cattari, "TREMURI program: An equivalent frame model for the nonlinear seismic analysis of masonry buildings," *Engineering Structures*, 2013.

[24]   V. Bernardo, A. Campos Costa, P. Candeias, and A. Costa, "Seismic Vulnerability Assessment and Fragility Analysis of Pre-code Masonry Buildings in Portugal (under review - BEEE-D-21-00264R2)," *Bulletin of Earthquake Engineering*, 2021.

[25]   A. G. Simões, R. Bento, S. Lagomarsino, S. Cattari, and P. B. Louren o, "The seismic assessment of masonry buildings between the 19th and 20th centuries in lisbon-evaluation of uncertainties," in *Proceedings of the International Masonry Society Conferences*, 2018.

[26]   CEN, *Eurocode 8: Design of structures for earthquake resistance - Part 1: General rules, seismic actions and rules for buildings*. Brussels, Belgium: Comite Europeen de Normalisation, 2004.

[27]   A. G. G. Simões, "Evaluation of the seismic vulnerability of the unreinforced masonry buildings constructed in the transition between the 19th and 20th centuries in Lisbon (PhD Thesis). Technical University of Lisbon, Lisbon, Portugal [in Portuguese], 2019.," 2018.

[28]   J. Milosevic, "Seismic vulnerability assessment of mixed masonry-reinforced concrete buildings in Lisbon (PhD Thesis)," Technical University of Lisbon, Lisbon, Portugal [in Portuguese], 2019.

[29]   A. Galasco, S. Lagomarsino, and A. Penna, "On the use of pushover analysis for existing masonry buildings," *First European Conference on Earthquake Engineering and Seismology*, no. September, pp. 3–8, 2006.

[30]   S. Lagomarsino and S. Cattari, "Seismic performance of historical masonry structures through pushover and nonlinear dynamic analyses," *Geotechnical, Geological and Earthquake Engineering*, 2015.

Keynote Lecture

COUPLING OF HIGHRISE BUILDING EARTHQUAKE RETROFIT AND BUILDING INFORMATION MANAGEMENT (BIM) SYSTEM

Do-Soo Moon [1], Amr S. Elnashai [2]

[1] *Assistant Professor, University of Hawaii at Manoa, dsmoon@hawaii.edu*
[2] *Vice President for Research and Technology Transfer, University of Houston, elnashai@uh.edu*

Abstract

Highrise buildings that have structural irregularities are in general more susceptible to damage from earthquakes. Such damage is primarily due to the coupling of torsional and translational vibrational response whereby the building twists even though it is being excited in translational modes only. For optimal earthquake design and retrofit of such structures, several cycles of iterations of structural analysis followed by design change are often needed. To provide efficiency and accuracy of iterative assessment-adjustment cycles in the design process, this study proposes an integrated seismic design and assessment framework. The 'Revit Structure' platform from Autodesk, a prominent member of the Building Informational Modeling software family, and ZEUS-NL from Mid-America Earthquake Center, one of the most advanced earthquake simulation programs, are utilized for seismic design and analysis tools, respectively. An advanced bi-directional linkage interface is developed so that two distinct and complex computer codes can exchange essential structural or non-structural member data in both directions without any loss of information. This coupled approach also provides improved earthquake analysis and design guidelines which can address damaging torsional effects. The feasibility of the proposed framework and its components are successfully evaluated and verified through an application example. It is observed and verified that more reliable and better seismic design for irregular buildings can be achieved using the proposed framework.

Keywords: Building Information Modeling (BIM), Seismic Design, Earthquake Damage, Irregular Structures

1. Introduction

In highrise buildings with structural irregularities, seismic deformation demand can be considerably increased due to the additional torsional moment caused by non-coincident centers of mass and rigidity, resulting in significant earthquake damage. In fact, this type of seismic damage to structures has been commonly observed during numerous past earthquakes [1,.2, 3, 4, 5]. As the dynamic response of highrise irregular buildings is complicated owing to the nonlinear lateral-torsional coupling effect, their earthquake retrofit designs usually require more iterative seismic performance assessments and structural design adjustments.

In earthquake design and retrofit development, structural engineers often generate multiple analytical models from the architectural design, and adjust the structural design based on the results from a series of earthquake simulations. It is critical to keep in sync all analytical models resulting from different design stages because any structural analysis using inconsistent analytical models would not be valid. To overcome the consistency concern in different analytical models throughout the earthquake design process, this study proposes an integrated seismic assessment and design framework that ensures a closed loop of structural adjustment and assessment. The proposed platform enables the pursuit of more reliable and optimal seismic design and retrofit, especially for highrise buildings having structural irregularities requiring many design and analysis iterations.

2. Integrated Seismic Assessment and Design Framework

To ensure fine-tuning of earthquake design, a seamless interaction should be guaranteed between the structural analysis and design software packages. This can be done by developing a bi-directional link interface that can transfer required data from one program to the other flawlessly. The Building

Informational Modeling software program, Revit Structure [5], was chosen as the design tool while one of the most advanced earthquake simulation analysis programs, ZEUS-NL [7] from Mid-America Earthquake Center, was utilized as the structural analysis tool. Then, this study developed an advanced bi-directional linking module which can communicate between two different programs using the Revit Structure API (Application Programming Interface) [8]. This linking tool can export and update both structural and non-structural components in each software. Thus, any structural members as well as non-structural members that may affect the overall structural behavior can be included in the analysis. The export function accesses the structural model data in Revit Structure, mines it, and writes a ZEUS-NL input file. With this export feature, various analytical models can be easily created from the physical model in the design software. The update function works in the opposite way. It interprets the data in ZEUS-NL, converts it into the format that can be accessed by Revit API, and then updates structural or non-structural components in Revit Structure. The affected components are highlighted in Revit Structures so that designers can visually check which members are modified. The update tool can not only modify/update the data in Revit Structure, but also create/store structural analysis results in its database. This could be very beneficial for structural engineers as the stored analysis data can be re-utilized for subsequent structural analysis. This advanced linking interface also has added functionality for irregular structures; it can show how severe torsional response would be, and it guides how to achieve better seismic performance by providing suggested seismic assessment and design guidelines. Fig. 1 shows the integrated seismic assessment and design platform introduced in this study. Iterative seismic performance assessment and structural design modification procedure under the proposed framework is described in Fig. 2. The developed framework offers several advantages including easy analytical model generation, elimination of model inconsistency in the design process, and better visualization capability to check structural analysis results. It is expected that more reliable and optimal seismic design and retrofit can be achieved under the proposed platform.
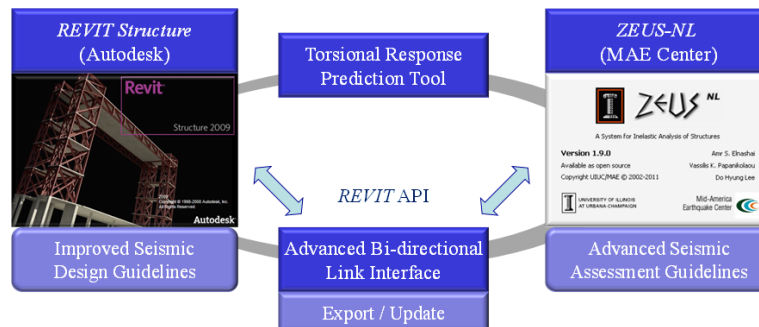
Figure 1. Proposed integrated seismic assessment and design framework.
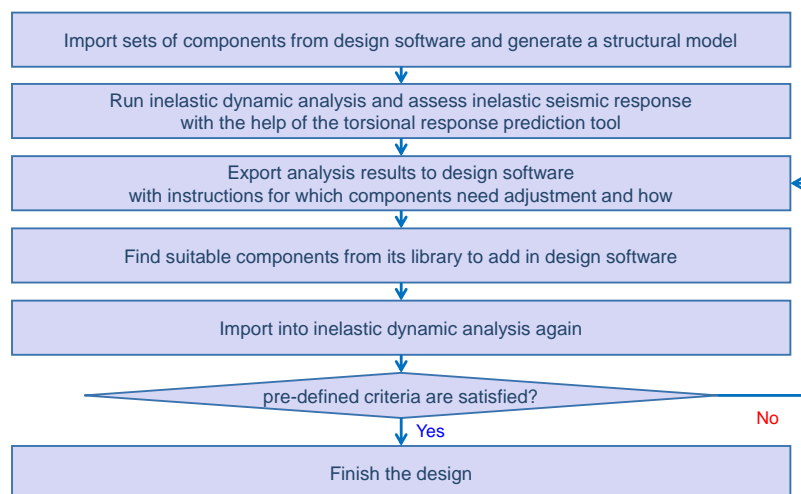
Figure 2. Seismic design process under the proposed framework.

3. Framework Verification

In order to verify the proposed integrated framework and its components, a three-story, two-bay by one-bay, reinforced concrete moment resisting building is utilized. The bay length and story height are 4 m and 3 m, respectively, and each story is assumed to have five percent mass eccentricity in its initial design. The studied structure is first created in Revit Structure, and its analytical model for earthquake simulations is automatically generated in ZEUS-NL via the advanced bi-directional link interface developed in this study. As the link tool provides various exporting options, users can create various numerical models depending on their analysis needs. For example, two different analytical models can be developed with and without non-structural components such as infills. Fig 3 depicts the initial design of the target structure in Revit Structure and its corresponding analytical model created in ZEUS-NL.
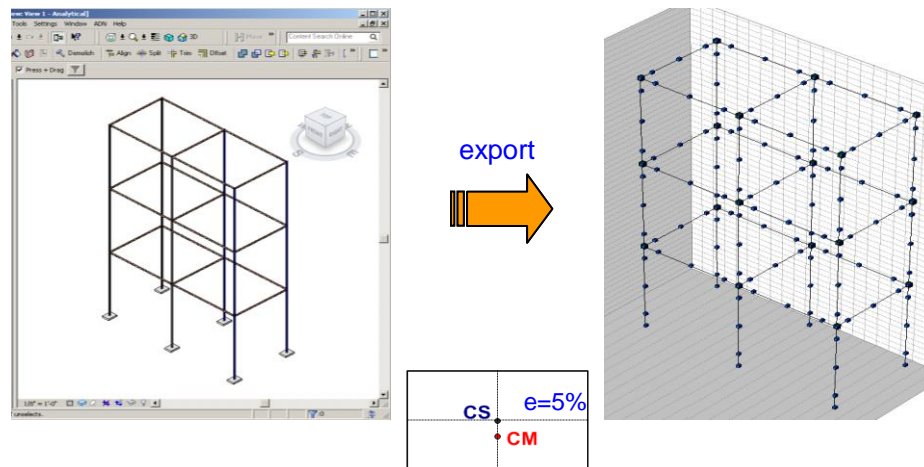
Figure 3. Analytical model generation from initial design in Revit Structure.

Inelastic dynamic response-history analysis (RHA) with the generated analytical model is conducted to evaluate its seismic performance. The concrete material was represented by a uniaxial model that follows the constitutive relationship proposed by Mander et al. [9] and the cyclic rules proposed by Martinez-Rueda and Elnashai [10]. The confinement effect provided by the transverse reinforcement is incorporated while constant confining pressure is assumed. For reinforcing steel, a bilinear elasto-plastic model with a kinematic hardening rule is employed [11,12]. The concrete compressive strength and steel yield strength were 18.7 MPa and 383 MPa, respectively. The contribution of the slab to the beam stiffness and strength was considered by using the effective flange width of the T-shape beam and diagonal diaphragm; lumped masses corresponding to the seismic weights were placed only at beam-column connections to reduce mass matrix size. Ten simulated ground motion records were utilized to represent the design uniform earthquake hazard spectra, and more detailed descriptions about ground motion records can be found in Mid-America Earthquake (MAE) Center report by Wu and Wen [13]. The selected input motions were scaled to have peak ground accelerations of 0.1g, 0.3g and 0.5g. Additionally, equivalent lateral force (ELF) analysis is conducted; ELF is the static analysis procedure allowed in IBC (International Building Code) [14] and code-adopted design eccentricities were utilized in the analysis.

The analysis results with the original design model are reported in Table 1; they are maximum ductility demand values of lateral-resisting members in the first story obtained from the dynamic RHA and static ELF procedure. The ductility demands in flexible and stiff-side members are not the same as the studied structure experiences added torsional vibration originated from its mass irregularity. It is observed that the static analysis increasingly underestimates the ductility demands for both flexible- and stiff-side members as the earthquake intensity increases; it is expected that the structure designed based on static analysis would not well perform under strong earthquake shaking.

Table 1 – Maximum ductility demand of initial design

PGA	Flexible-side		Stiff-side	
	RHA	ELF	RHA	ELF
0.1g	1.78	1.92	1.34	1.51
0.3g	3.35	2.73	2.07	1.73
0.5g	4.51	3.17	3.85	2.31

The developed platform recommended that the rigidity center needs to move toward the mass center for better seismic performance; it suggested to increase flexural rigidity of the lateral load-resisting members on the flexible side by changing their cross-sectional dimensions. Then, the linking module found suitable structural components from the Revit library, and it updated the corresponding structural members and highlighted them. Fig. 4 shows the new Revit design model and its analytical model exported to ZEUS-NL for another structural performance evaluation. Note that analysis results as well as dynamic characteristics such as structure periods and mode shapes were stored in the Revit database with the update tool. The dynamic RHA and static ELF results with the new design are shown in Table 2. It is proved that the new structure performs better than the old one when comparing the results from the new and original designs.
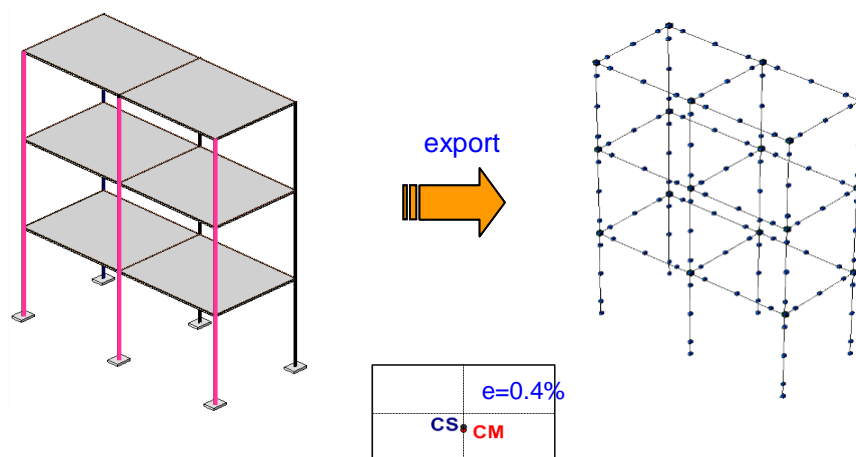
Figure 4. Analytical model generation from new design in Revit Structure.

Table 2 – Maximum ductility demand of new design

PGA	Flexible-side		Stiff-side	
	RHA	ELF	RHA	ELF
0.1g	1.44	1.63	1.38	1.52
0.3g	2.36	2.26	2.18	2.01
0.5g	3.45	2.81	3.29	2.89

4. Conclusion

An integrated environment for seismic assessment and design of highrise irregular structures is introduced in this study to address the iterative process of effecting design changes to reduce torsional effects arising from non-coincidence of centers of mass and stiffness. The proposed framework and its components are described and verified through realistic design and assessment scenarios. To establish the integrated computational platform, structural analysis and design tools are determined, and an advanced bi-directional linkage interface is developed. The Building Informational Modeling software

'Revit Structure' and the structural analysis program ZEUS-NL are employed for seismic design and analysis, respectively. To achieve a seamless interaction between the two selected programs, a robust bi-directional linkage interface is developed. This interface has functionality of exporting and updating structural components as well as non-structural ones and of providing guidance for seismic assessment that addresses the damaging effects of torsional coupling in high-rise buildings. An application example confirms the feasibility and effectiveness of the proposed framework and its components are successfully evaluated and verified.

References

[1] Ellingwood, B.R. (1980): An Investigation of the Miyagi-ken-oki, Japan Earthquake of June 12, 1978. *U.S. Department of Commerce/National Bureau of Standards*, NBS Special Publication, 592.

[2] Rosenblueth, E., and Meli, R. (1986): The 1985 Earthquake: Causes and Effects in Mexico City. *Concrete International,* 8(5), 23-34.

[3] Wyllie, L.A., Abrahamson N., Bolt, B., Castro, G., Durkin, M.E., Escalante, L., Gates, H.J., Luft, R., McCormick, D., Olson, R.S., Smith, P.D. and Vallenas, J. (1986): The Chile Earthquake of March 3, 1985, *Earthquake Spectra*, 2(2), 293-371.

[4] Anderson, R.W. (1987): The San Salvador earthquake of October 10, 1986 – review of building damage, *Earthquake Spectra*, 3(3), 497-541.

[5] Elnashai, A.S., Gencturk, B., Kwon, O.S., Al-Qadi, I.L., Hashash, Y., Roesler, J.R., Kim, S.J., Jeong, S.H., Dukes, J., and Valdivia, A. (2010): The Maule (Chile) Earthquake of February 27, 2010: Consequence Assessment and Case Studies, *Technical Report, CD-Release 10-04*, Mid-America Earthquake (MAE) Center Urbana, IL, USA.

[6] Autodesk, Inc. (2008): *Revit Structure 2009 User's Guide*, User's Manual, Autodesk, Inc.

[7] Elnashai, A.S., Papanikolaou, V.K. and Lee, D.H. (2010): *ZeusNL – A System for Inelastic Analysis of Structures*, User's Manual, Mid-America Earthquake (MAE) Center, Urbana, IL, USA.

[8] Moon, D.S. (2012): *Integrated Seismic Assessment and Design of Plan-Irregular Structures*, Ph.D. Dissertation, University of Illinois at Urbana-Champaign, Urbana, IL, USA.

[9] Mander, J.B., Priestley, M.J.N. and Park, R. (1988): Theoretical stress-strain model for confined concrete, *Journal of Structural Engineering,* 114(8), 1804-1826.

[10] Martinez-Rueda, J.E. and Elnashai, A.S. (1997): Confined concrete model under cyclic load, *Materials and Structures,* 30(3), 139-147.

[11] Elnashai, A.S. and Elghazouli, A.Y. (1993): Performance of composite steel/concrete members under earthquake loading, Part I: Analytical model, *Earthquake Engineering & Structural Dynamics,* 22(4), 315-345.

[12] Elnashai, A.S. and Izzuddin, B.A. (1993): Modeling of material non-linearities in steel structures subjected to transient dynamic loading, *Earthquake Engineering & Structural Dynamics,* 22(6), 509-532.

[13] Wen, Y.K. and Wu, C.L. (2001): Uniform Hazard Ground Motions for Mid-America Cities, *Earthquake Spectra,* 17(2), 359-384.

[14] ICC. (2009): *International Building Code (IBC)*, International Code Council, Washington, D.C., USA.

POWER RESPONSES OF A BUILDING UNDER THE EXCITATION OF PULSE-LIKE GROUND MOTIONS

Jui-Liang Lin [(1)]

[(1)] Research Fellow, National Center for Research on Earthquake Engineering, Taipei, Taiwan, jllin@narlabs.org.tw

Abstract

In comparison with far-field (FF) ground motions, near-fault (NF) ground motions with forward directivity or fling-step effect are characterized by large pulses. These pulse-like (PL) ground motions have pronounced coherent pulses in velocity and displacement histories. Even though these prominent pulses generally have very few cycles in a PL ground motion, the destruction they cause to structures is severe and distinctive compared with non-pulse-like (NPL) ground motions. The present study suggests power demand as an alternative engineering demand parameter for reflecting the severity of the risk posed by PL ground motions. The proposed parameter is simply a product of story shears and inter-story velocities. Through an investigation using a three-story building subjected to ensembles of PL and NPL ground motions, this study confirms that power demand satisfactorily elucidates the destructive potential of PL ground motions. In contrast, force demand, which is the cornerstone laid in building seismic design codes, cannot adequately reflect the destructive potential of PL ground motions. In addition to power, power density and normalized power density were introduced to obtain a sense of the magnitude of power demand relative to the degree of structural damage.

From the energy response histories of a three-story building, extraordinary increments of kinetic energy under a PL ground motion are closely followed by significant increments of strain energy, indicating large structural deformations. It was found that damping energy is not effectively built up at the first significant increment of strain energy. This implies that inherent or supplemental damping hardly protects building structures against the first crucial strike of PL ground motions, which usually cause the most damage to structures.

Keywords: near-fault ground motion, power response, seismic response, velocity pulse, vertically irregular building

1. Introduction

In comparison with far-field (FF) ground motions, near-fault (NF) ground motions with forward directivity or fling-step effect are characterized by large pulses [1-4]. These pulse-like (PL) ground motions have pronounced coherent pulses in velocity and displacement histories. Even though these prominent pulses generally have very few cycles in a PL ground motion, the destruction they cause to structures is severe and distinctive compared with non-pulse-like (NPL) ground motions.

Kalkan and Kunnath [4] demonstrated that the velocity pulse of an NF ground motion causes structures to dissipate considerable input energy in relatively few large deformation cycles. They questioned the validity of the process of amplifying elastic design spectra with NF factors to reflect NF effects, which is commonly stipulated in design codes [5]. They also pointed out that the maximum inter-story drift ratio is a function of the ratio of pulse period to fundamental structural period. The study concluded that acceleration and velocity response spectra should be collectively examined to rationally assess the damage potential of NF ground motions [4]. Through conducting incremental dynamic analyses (IDA), Sehhati et al. [6] showed that neither the PGA nor the spectral acceleration corresponding to the first-mode period are an ideal intensity measure (IM) for capturing structural responses to PL ground motions. They found that the PGV seems to be the only IM valid for both NF and FF ground motions. Enderami et al. [7] showed that the hysteretic energy caused by FF ground motions increases gradually, whereas in NF ground motions most hysteretic energy occurs in the first two yield excursions. This was believed to be the main difference between the effects of FF and NF ground motions on structures. Accordingly, they proposed an energy-based pushover analysis approach to estimate the NF ground

motion-induced seismic demands of structures [7]. Recognizing that structural seismic damage is associated with input energy and the ability of structural components to dissipate energy, Kalkan and Kunnath [8] proposed an energy measure to correlate with peak seismic demands. That energy measure is defined as the energy demand imposed on a structure over an effective duration, namely the time between two zero-crossings of the effective velocity pulse.

Because many densely populated cities of Taiwan are near active faults, the seismic responses of a three-story reinforced concrete (RC) building (Fig. 1) to NF ground motions were investigated through a shaking table test [9]. The three-story building was vertically irregular, with a soft bottom story due to an elevated first story and additional RC walls only on the two exterior sides of the third story. The three-story building purposely mimicked many existing buildings, where the first stories are elevated and used for stores or parking lots; the other stories with many partition walls are used for residences. The numerical model of the three-story building was satisfactorily calibrated and verified with experimental results [9]. By performing IDA on the numerical model, it was found that when the building is collapsed, the total input energy from an amplified NF ground motion record was approximately half of that from an amplified FF ground motion record. This finding demonstrated that the amount of input energy is not a measure that appropriately reflects the potential damage caused by NF ground motions. Moreover, a notable two-sided spike with almost equal positive and negative displacement magnitudes was observed when the amplified NF ground motion collapsed the building. Meanwhile, the kinetic energy of the building, which reflects structural velocity, drastically increased [9]. This observation suggests that outstanding structural velocity accompanying a prominent structural displacement (i.e., a large restoring force) is one of the characteristics of buildings responding to NF ground motions, compared with FF ground motions. It is thus reasonable to infer that great power demands are imposed on buildings under NF ground motions.

A useful analogy is that the work done by an adult carrying a 30 kg object up three stories in ten minutes is the same as that done in ten seconds, whereas the power demand in the latter case is 60 times the power demand of the former case. It is reasonable to presume that the former case is achievable, or even simple, for an ordinary adult, but most adults would be hard pressed or unable to achieve the second effort. Another analogy is to consider two identical steel boxes, one containing coals, the other bombs. Assuming that the energy dissipated by burning the coals and exploding the bombs are equal, the degree of damage is expected to be substantially different because of the discrepancy between the power, rather than the energy imposed on the two boxes. Accordingly, it seems intuitive and desirable to distinguish the threats of PL and NPL ground motions to buildings by examining their respective induced power demands. The present study therefore examines the power responses of the validated numerical model of the abovementioned three-story building to PL and NPL ground motions. The results are expected to provide a window into the understanding of the distinctive threat to buildings under PL ground motions.
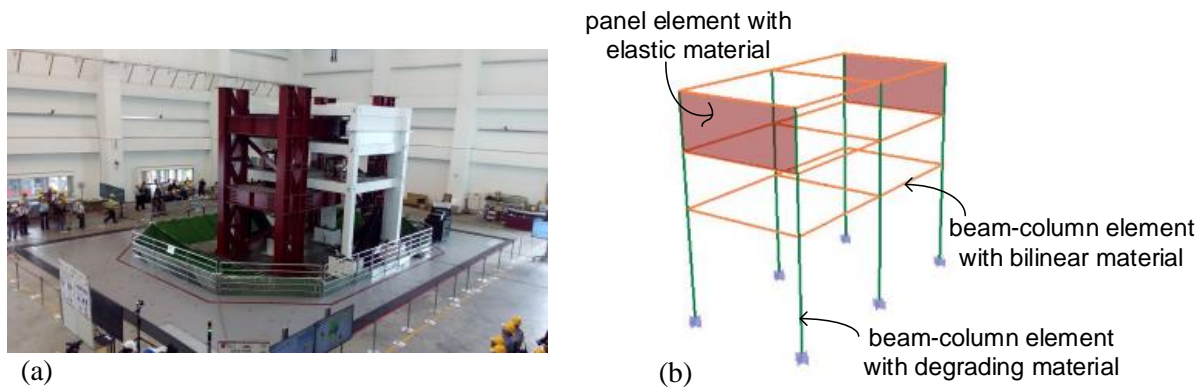
Figure 1. a) The three-story RC building (the white part) on an 8 m × 8 m shaking table; b) the numerical model.

2. Power responses of a three-story building

Power response, denoted by $P(t)$, of an N-story building is defined as:

$$P(t) = \sum_{i=1}^{N} P_i(t) = \sum_{i=1}^{N} h_i \theta_i'(t) V_i(t) \tag{1}$$

where $P_i(t)$, h_i, and $V_i(t)$ are the power, story height, and story shear of the ith story, respectively. Parameter $\theta_i'(t)$ is the time derivative of the ith inter-story drift ratio $\theta_i(t)$. Thus, $h_i\theta_i'(t)$ represents the inter-story velocity of the ith story. Under a ground motion excitation, both $V_i(t)$ and $\theta_i'(t)$, of an elastic building structure vary linearly as the ground motion intensity (e.g., PGA) varies. Consequently, the power response is a quadratic function in terms of the ground motion intensity (Eq. 1).

2.1 Numerical model

To maintain the integrity of the present paper but avoid duplications, the details of the three-story building [9] are supplied in Appendix A. In addition to the elastic panel elements for simulating the RC walls, the numerical model of the three-story building consists of beam-column elements for simulating the beams and columns. A degrading material capable of reflecting strength degradation, stiffness degradation, and pinching is used for the columns. A bilinear material is adopted for the beams, and all the floor slabs are assumed to be rigid diaphragms. The calibration and verification of the numerical model have been conducted through shaking table tests, in which the three-story building went into a significant inelastic excursion with a peak inter-story drift of 2.49% rad [9]. The shaking table tests also confirmed that the building had a first-mode vibration period (T_1) of 0.395 s in the short direction (i.e., x-direction). The effective modal participation mass ratio of the first vibration mode is 98.63%. The first vibration mode thus overwhelmingly dominates the seismic vibrations of the building, whose deformation is concentrated in the soft bottom story. Moreover, Rayleigh damping, with the damping ratios of the first two x-directional vibration modes equal 3%, is used to represent the inherent damping of the building [9].

2.2 Selected ground motion records

The present numerical study considers an ensemble of 19 PL ground motion records and an ensemble of 19 NPL ground motion records. All the selected records were from seismic events in Taiwan. Ten records in each ensemble are from the 1999 Chi-Chi earthquake, which created an abundance of PL ground motion records. Table 1 shows the details of the selected PL and NPL records. The identification of ground motions with PL velocities is based on the wavelet approach proposed by Shahi and Baker [10]. The ground motion is classified as PL when the proposed pulse indicator is positive and the pulses arrive early in the time history. Moreover, the period associated with the maximum Fourier amplitude of the extracted wavelet, also known as the pseudoperiod of the wavelet, is estimated as the pulse period T_p [10]. Figure 2a–2f illustrates the 5%-damped displacement response spectra (S_d), pseudo-velocity response spectra (PS_v), and pseudo-acceleration response spectra (PS_a) of the two ground motion record ensembles. Figure 2a–2f clearly shows that PL records generally have greater spectral values at medium and long periods compared with NPL records. Figure 2g–2i plots the PL and NPL medians of S_d, PS_v, and PS_a to facilitate comparison. It should also be noted that four PL records (No. 2, 5, 6, and 7 in Figure 2a and 2b) possess outstanding S_d and PS_v values at medium and long periods. With all the selected ground motion records applied in the x-direction of the building, the IDA [11] were carried out. The pseudo-spectral acceleration at the first-mode period, denoted by $S_a(T_1)$, was used as the IM, and was scaled from 0.15 g to 3.0 g with increments of 0.15 g. With the IDA results, it was found that No. 9 of the PL records and No. 6 of the NPL records (CHY080_EW listed in Table 1a and TCU076_NS listed in Table 1b) resulted in the most significant seismic demands, which will be addressed in the following section. Besides the PL and NPL medians, the spectra of PL No. 9 and NPL No. 6 are also illustrated in Figure 2g–2i. Figure 2g–2i clearly indicates that all the PL medians of S_d, PS_v, and PS_a at the first-mode period (T_1 = 0.395 s) are lower than their NPL counterparts. The PS_v and PS_a of PL No. 9 at the first-mode period are also lower than their counterparts of NPL No. 6, whereas their S_d values are

essentially equal. Moreover, the median PL PS_a has a substantial and wider plateau, compared with the NPL median. The median PL PS_v has an outstanding ridge at a period of one-second, whereas the median NPL PS_v is not obviously ridge-shaped.

Table 1 – Ensembles of selected (a) PL and (b) NPL ground motion records.

(a)

GM No.	EQ Event	Magnitude (M_w)	Station	Component	R_{rup} (kM)	V_{s30} (m/s)	Duration (s)	T_p (s)
1	1999_ChiChi	7.65	CHY006	EW	9.158	422.68	100	2.57
2	1999_ChiChi	7.65	CHY101	NS	9.150	252.37	90	5.34
3	1999_ChiChi	7.65	TCU045	NS	26.060	706.96	90	9.33
4	1999_ChiChi	7.65	TCU047	EW	35.095	522.97	90	12.31
5	1999_ChiChi	7.65	TCU052	EW	1.040	589.22	90	12.29
6	1999_ChiChi	7.65	TCU065	EW	0.176	290.11	90	5.74
7	1999_ChiChi	7.65	TCU068	EW	0.429	490.00	90	12.29
8	1999_ChiChi	7.65	TCU095	EW	45.076	454.10	90	8.69
9	1999_ChiChi	6.3	CHY080	EW	22.398	499.17	90	1.38
10	1999_ChiChi	6.19	TCU084	EW	15.919	733.78	34	1.44
11	1999_Chiayi	5.86	CHY073	EW	7.549	201.48	90	1.13
12	2006_Taitung	6.17	TTN027	EW	9.104	318.22	71	1.27
13	2010_Jiaxian	6.29	CHY063	EW	4.806	287.66	103	1.16
14	2013_Nantou	6.01	TCU143	EW	23.626	465.91	75	1.27
15	2013_Nantou	6.3	TCU167	EW	14.518	363.85	83	1.19
16	2016_Meinong	6.4	CHY062	EW	21.519	597.85	80	0.90
17	2016_Meinong	6.4	CHY063	EW	16.829	287.66	106	1.44
18	2016_Meinong	6.4	CHY089	NS	19.013	396.20	120	2.58
19	2018_Hualien	6.4	HWA028	NS	0.900	404.91	120	4.17

GM = ground motion, EQ = earthquake; R_{rup} is the distance from the station to the ruptured fault; V_{S30} is the average shear-wave velocity at depths between 0 and 30 m.

(b)

GM No.	EQ Event	Magnitude (M_w)	Station	Component	R_{rup} (kM)	V_{s30} (m/s)	Duration (s)
1	1994_Nanao	6.35	ILA031	EW	13.758	657.39	90
2	1999_ChiChi	7.65	CHY028	NS	2.049	546.91	90
3	1999_ChiChi	7.65	CHY041	NS	19.411	488.12	90
4	1999_ChiChi	7.65	TCU071	NS	5.793	614.75	90
5	1999_ChiChi	7.65	TCU072	EW	6.731	471.88	90
6	1999_ChiChi	7.65	TCU076	NS	1.945	573.23	90
7	1999_ChiChi	7.65	TCU078	EW	8.664	444.54	90
8	1999_ChiChi	7.65	TCU079	EW	11.401	353.94	90
9	1999_ChiChi	7.65	TCU084	NS	11.714	733.78	90
10	1999_ChiChi	7.65	TCU129	EW	0.990	506.46	90
11	1999_ChiChi	6.3	TCU078	EW	7.768	444.54	105
12	1999_Chiayi	5.86	CHY035	EW	17.814	554.22	68
13	1999_Chiayi	5.57	CHY106	EW	17.092	227.63	94
14	2003_Taitung	6.83	TTN041	EW	24.718	431.59	186
15	2003_Taitung	6.83	TTN042	NS	14.340	824.52	186
16	2003_Taitung	6.83	TTN046	EW	15.200	529.10	183
17	2010_Jiaxian	6.29	CHY047	EW	45.941	183.52	80
18	2016_Meinong	6.4	CHY061	EW	19.917	499.94	82
19	2018_Hualien	6.4	HWA051	NS	—	449.74	104
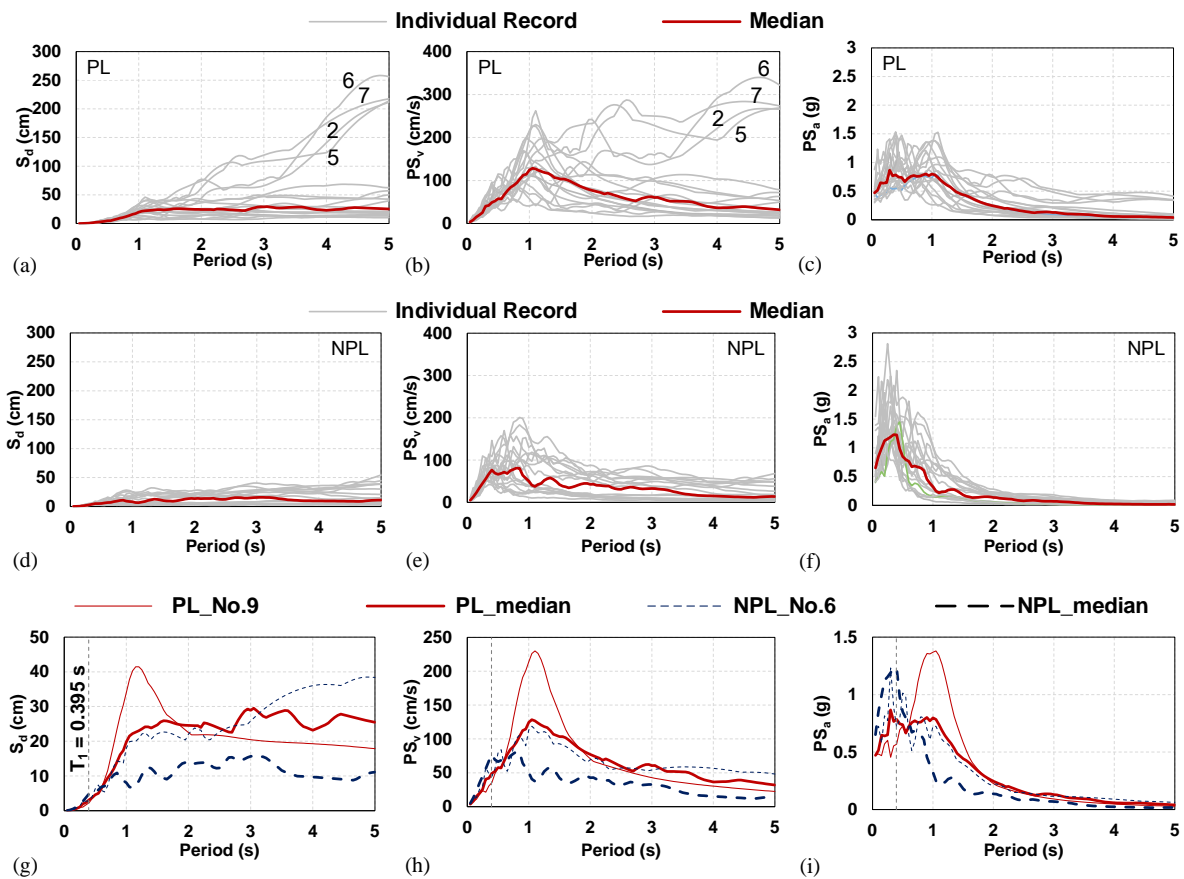
Figure 2. (a) S_d, (b) PS_v, and (c) PS_a PL response spectra; (d) S_d, (e) PS_v, and (f) PS_a NPL response spectra; (g) S_d, (h) PS_v, and (i) PS_a response spectra of PL No. 9, NPL No. 6, PL median, and NPL median.

3. Seismic responses to ensembles of ground motion records

Fig. 3a–3d illustrates the peak values of the inter-story drift, inter-story velocity, story shear, and story power of the first story (denoted by $\theta_{1,\text{peak}}$, $h_1\theta'_{1,\text{peak}}$, $V_{1,\text{peak}}$, and $P_{1,\text{peak}}$, respectively) when the three-story building is subjected to the PL ground motions (No. 1 to 19 in Table 1a). The value of h_1 is 300 cm (Fig. A1). Fig. 3e–3h represents the counterparts when the building is subjected to the NPL ground motions (No. 1 to 19 in Table 1b). In each plot of Fig. 3, there are twenty lines or layers, each of which is the structural response corresponding to a certain value of $S_a(T_1)$, which varies from 0.15 g to 3.0 g with increments of 0.15 g. The value of $S_a(T_1)$ essentially increases from the bottom line to the top line. In fact, Fig. 3 shows few crossings between different lines. This phenomenon reflects "structural resurrection", which means that a greater IM ($S_a(T_1)$) results in less structural response [11]. Comparing the ordinates of Fig. 3a–3d with Fig. 3e–3h indicates that, except for $V_{1,\text{peak}}$, the seismic responses ($\theta_{1,\text{peak}}$, $h_1\theta'_{1,\text{peak}}$, and $P_{1,\text{peak}}$) resulting from the PL records are noticeably greater than those resulting from the NPL records when $S_a(T_1)$ approaches 3.0 g. This indicates that force demand is not an appropriate measure for distinguishing the seismic risks posed by PL and NPL ground motions. In other words, structural damage caused by PL ground motions is more likely to be due to power demand or velocity demand. Further, compared with inter-story velocity demand, power demand seems to be a physical quantity that is more straightforward and explicit for representing destructive potential of PL ground motions.

Because of structural softening, Fig. 3a clearly shows that the spacing between layers with greater values of $S_a(T_1)$ is generally and noticeably larger than that for lower values of $S_a(T_1)$. In contrast, because of the gradually saturated story shear, Fig. 3c shows that the spacing between the layers with greater values of $S_a(T_1)$ is generally less than that compared with smaller values of $S_a(T_1)$. As $S_a(T_1)$

increases, curves in Fig. 3a, 3b, and 3d are strikingly alike, whereas those in Fig. 3e, 3f, and 3h are not as alike as their PL counterparts. Speaking in detail, there are four outstanding peaks in each of Fig. 3a, 3b, and 3d, which correspond to the No. 5/6, 9/10, 12/13, and 17 PL ground motions, and which are not necessarily the same as the four ground motion records with outstanding S_d and PS_v values shown in Fig. 2a and b (No. 2, 5, 6, and 7). Furthermore, the magnitude sequence from large to small of the four peaks in Fig. 3a, 3b, and 3d are identical (No. 9/10, 5/6, 17, and 12/13). As for the NPL records, there are seven outstanding peaks in Fig. 3e, 3f, and 3h. The seven peaks correspond to No. 2, 4, 6, 8, 11, 13, and 18 NPL ground motions. Nevertheless, the magnitude sequence of the seven peaks is rather inconsistent. These observations again confirm that power demand is an effective measure that reflects the damage potential of PL ground motions. However, the effectiveness decreases when power demand is used as a measure for reflecting the damage potential of NPL ground motions. In other words, power demand plays a critical role in the seismic damage to buildings under PL ground motions, which usually only exhibit two or three extraordinarily large excursions in the corresponding hysteretic loops. In contrast, in the seismic damage to buildings under NPL ground motions, where gradually increasing hysteretic loops (i.e., cumulative damage) are more common, power demand is not as crucial.
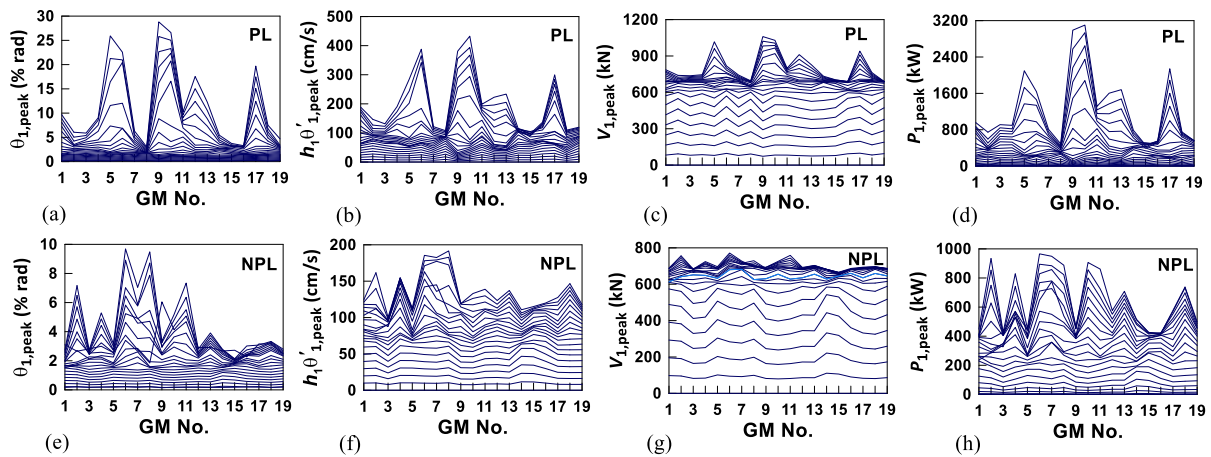
Figure 3. (a) $\theta_{1,\text{peak}}$, (b) $h_1\theta'_{1,\text{peak}}$, (c) $V_{1,\text{peak}}$, and (d) $P_{1,\text{peak}}$ of the three-story building subjected to the PL ground motions scaled from $S_a(T_1) = 0.15$ g to 3.0 g; (e)–(h) are the counterparts of (a)–(d) subjected to the NPL ground motions.

Fig. 4a–4d shows the IDA curves of $\theta_{1,\text{peak}}$, $h_1\theta'_{1,\text{peak}}$, $V_{1,\text{peak}}$, and $P_{1,\text{peak}}$ for the three-story building under the PL excitations. The 16%, 50% (median), and 84% percentiles of the IDA curves are shown together. Fig. 4e–4h shows the counterparts under the NPL excitations. Comparison of these graphs indicates that the PL ground motions impose greater seismic threats to the building than the NPL ground motions. In addition, the variation in seismic demand among the PL ground motions is more significant than among the NPL ground motions. For clarity, Fig. 4i–4l compares the medians of the $\theta_{1,\text{peak}}$, $h_1\theta'_{1,\text{peak}}$, $V_{1,\text{peak}}$, and $P_{1,\text{peak}}$ IDA curves resulting from the two ground motion record ensembles. Fig. 4i and 4k indicates that the building is essentially elastic when $S_a(T_1)$ is less than 1.0 g. Note that the first vibration mode of the building overwhelmingly dominates the seismic vibrations [9]. Therefore, as long as the ground motion records are scaled to an identical pseudo-spectral acceleration $S_a(T_1)$, i.e., $(2\pi/T_1)^2 S_d(T_1)$, the elastic drift response $\theta_{1,\text{peak}}$ (Fig. 4a, 4e, and 4i) of the building is mostly unvaried from ground motion to ground motion. On the other hand, the values of $h_1\theta'_{1,\text{peak}}$, $V_{1,\text{peak}}$, and $P_{1,\text{peak}}$ are much more diverse from ground motion to ground motion even when the building is elastic (Fig. 4b–4d and 4f–4h). This phenomenon possibly results from varying spectral values of $h_1\theta'_{1,\text{peak}}$, $V_{1,\text{peak}}$, and $P_{1,\text{peak}}$ among ground motion records, although all the ground motion records are scaled to an identical $S_a(T_1)$. In addition, higher-mode effects may be more substantial in these three types of seismic responses ($h_1\theta'_{1,\text{peak}}$, $V_{1,\text{peak}}$, and $P_{1,\text{peak}}$) compared with $\theta_{1,\text{peak}}$.

When the building is elastic ($S_a(T_1) \leqq 1.0$ g), the quadratic variation of $P_{1,peak}$ (Fig. 4l) appears unique in comparison with the linear variations of $\theta_{1,peak}$, $h_1\theta'_{1,peak}$, and $V_{1,peak}$ (Fig. 4i–4k). Moreover, the $h_1\theta'_{1,peak}$ and $P_{1,peak}$ of the building responding to the PL ground motions are initially lower but eventually much greater than their NPL counterparts (Fig. 4j and 4l). As the seismic intensity of the PL ground motion increases, the rapidly increased $P_{1,peak}$ poses a severe threat to the building (Fig. 4l). This threat is clearly reflected in the median $\theta_{1,peak}$ of the building in response to the PL ground motions, which remarkably surpasses its NPL counterpart as the $S_a(T_1)$ gradually approaches 3.0 g (Fig. 4i). In contrast, the discrepancy between the maximum base shears, i.e., the peak first story shears ($V_{1,peak}$), resulting from the PL and NPL ground motions (Fig. 4k) is not so significant in comparison with the discrepancy between the corresponding $\theta_{1,peak}$ medians (Fig. 4i) when $S_a(T_1) = 3.0$ g. This phenomenon indicates that force demand is not adequate for differentiating the seismic risks posed by PL and NPL ground motions.
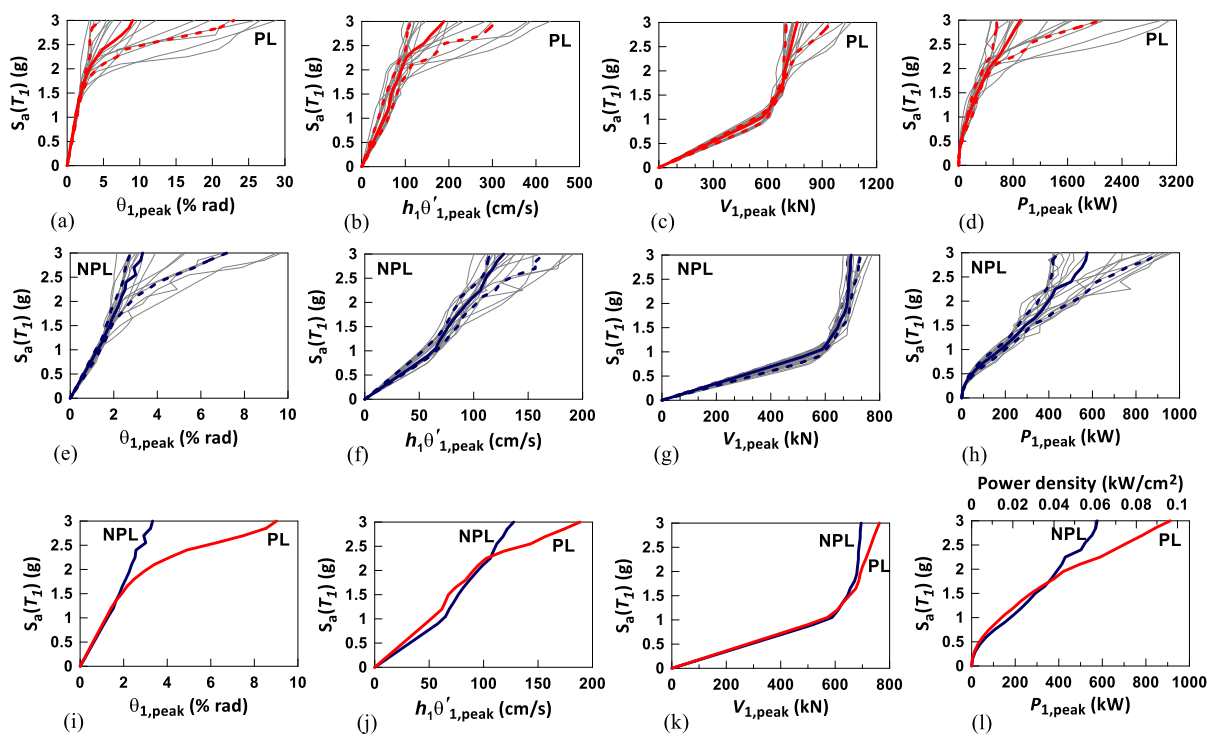
Figure 4. (a) $\theta_{1,peak}$, (b) $h_1\theta'_{1,peak}$, (c) $V_{1,peak}$, and (d) $P_{1,peak}$ IDA curves for the three-story building subjected to the PL ground motions. (e)–(h) are the counterparts of (a)–(d) subjected to the NPL ground motions. The medians of the (i) $\theta_{1,peak}$, (j) $h_1\theta'_{1,peak}$, (k) $V_{1,peak}$, and (l) $P_{1,peak}$ IDA curves for the three-story building subjected to the PL and NPL ground motions.

Conclusions

Pulse-like (PL) ground motions with prominent velocity pulses usually pose a severe risk to building structures. The present study suggests power demand as an alternative engineering demand parameter for reflecting the severity of the risk posed by PL ground motions. The proposed parameter is simply a product of story shears and inter-story velocities. Through an investigation using a three-story building subjected to ensembles of PL and non-pulse-like (NPL) ground motions, this study confirms that power demand satisfactorily elucidates the destructive potential of PL ground motions. In contrast, force demand, which is the cornerstone laid in building seismic design codes, cannot adequately reflect the destructive potential of PL ground motions.

Acknowledgements

Appendix A

Fig. A1a–A1c shows the top view, front elevation, and side elevation of the three-story building. There is one bay in the x-direction and two bays in the y-direction of the building. The span of each bay is 350 cm. The walls are infilled only on the two exterior sides of the third story along the x-direction (Fig. A1c). The first story height, measured from the top of the pedestals (footings) to the top of the first floor slab, is 300 cm. The other story heights, measured from slab top to slab top, are 150 cm (Fig. A1b and A1c). The size of all beams is 25 cm × 40 cm. The size of the three columns in column line A, denoted by C2, is 75 cm × 30 cm, and the size of the three columns in column line B, denoted by C1, is 30 cm × 30 cm (Fig. A1a). Fig. A1d and A1e shows the details of the reinforcements for beams and columns. The materials used for the #3 (10ϕ) and #6 (19ϕ) reinforcements are SD280W and SD420W, respectively, and the nominal yielding strengths of these reinforcements are 280 MPa and 420 MPa, respectively. The 28-day compression strength of the concrete, denoted by f_c', is 21 MPa. According to the material tests on the reinforcements and concrete cylinders, the actual yielding strengths of the #3 and #6 reinforcements are 355 MPa and 454 MPa, respectively. In addition, the average 28-day compression strength is 21.96 MPa. The thickness of the slabs and walls are 10 cm and 15 cm, respectively. The details of the reinforcements for walls and slabs are #3@15 cm on two sides and in two directions. The size of each concrete pedestal is 75 cm (length) × 115 cm (width) × 70 cm (height). The pedestal is connected to a steel base plate with shear studs. The base plates are fixed to the shaking table by bolts (Fig. A1f). Two additional concrete mass blocks, each of which is 110 cm (length) × 110 cm (width) × 50 cm (height), are embedded in the second and third story slabs (Fig. A1a). Because the 50 cm height of the mass blocks is greater than the thickness of the slab (10 cm), the 30 cm and 10 cm heights of the mass blocks protrude from the bottom and top surfaces of the slabs, respectively. This three-story building was modularly constructed, using a combination of modules A, B, and C connected via steel connection plates (Fig. A1g). The vertical bars of the columns and walls were welded to steel connection plates. Consecutive modules were connected by having their respective steel plates bolted together (Fig. A1g). The resultant weight of the three-story building is 505 kN, which consists of 183.8 kN, 168.9 kN, and 152.3 kN for the first, second, and third stories, respectively.
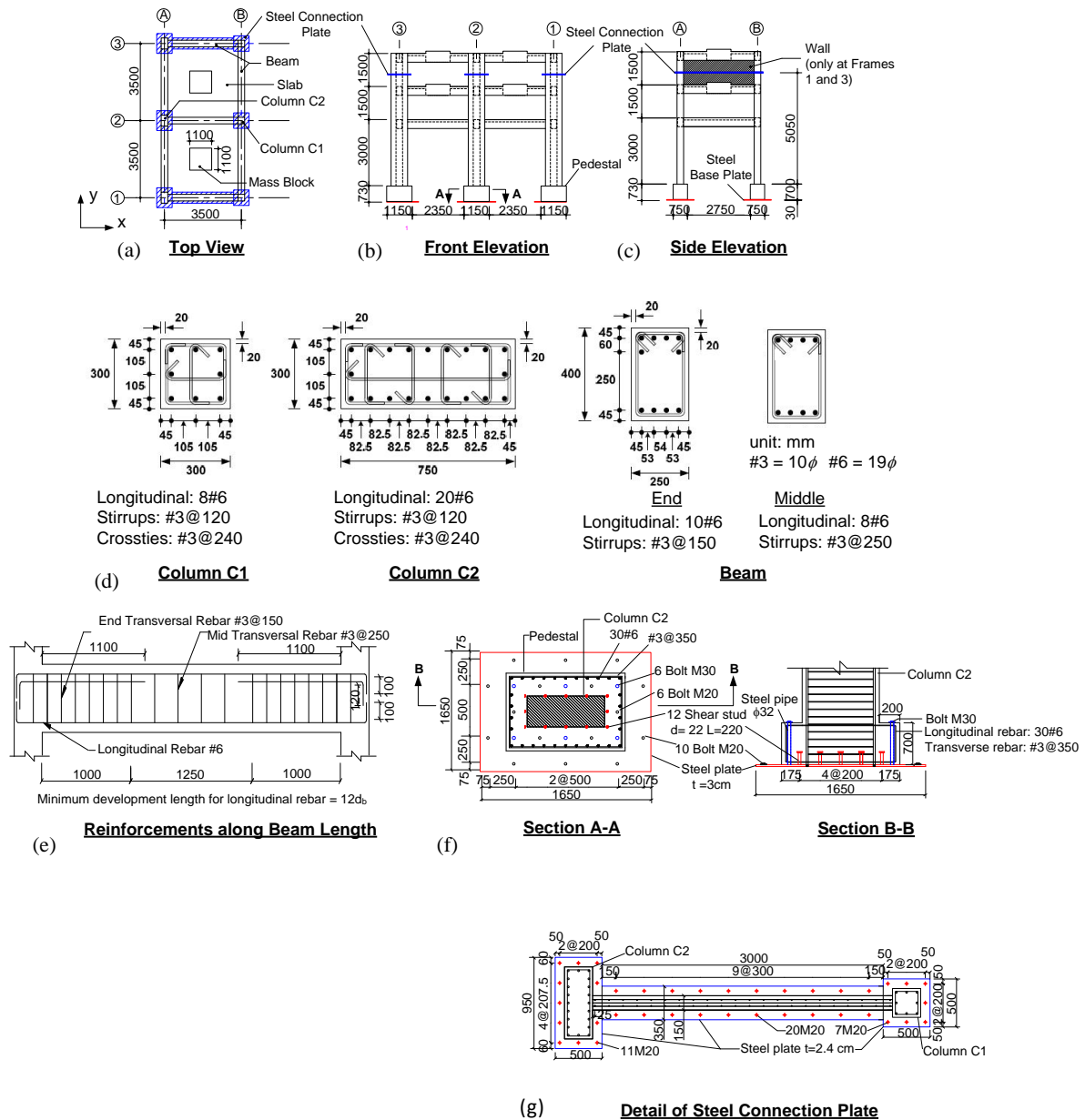
Figure A1. (a) Top view, (b) front elevation, and (c) side elevation of the three-story building; (d) cross sections of beams and columns; (e) reinforcements along beam length; (f) detail of the pedestal; and (g) detail of a steel connection plate.

References

[1] Bolt, B.A., Abrahamson, N.A. (2003): Estimation of strong seismic ground motions. *International Handbook of Earthquake and Engineering Seismology*, 81B, 983–1001.

[2] Mavroeidis, G.P., Papageorgiou, A.S. (2003): A mathematical representation of near-fault ground motions. *Bulletin of the Seismological Society of America*, **93**(3), 1099–1131.

[3] Bray, J.D., Rodriguez-Marek, A. (2004): Characterization of forward-directivity ground motions in the near-fault region. *Soil Dynamics and Earthquake Engineering*, **24**, 815–828.

[4] Kalkan, E., Kunnath, S.K. (2006): Effects of Fling Step and Forward Directivity on Seismic Response of Buildings. *Earthquake Spectra*, **22**(2), 367–390.

[5] International Conference of Building Officials (ICBO). *International Building Code*, Whittier, CA; 2000.

[6] Sehhati, R., Rodriguez-Marek, A., ElGawady, M., Cofer, W.F. (2011): Effects of near-fault ground motions and equivalent pulses on multi-story structures. *Engineering Structures*, **33**, 767–779.

[7] Enderami, S.A., Beheshti-Aval, S.B., Saadeghvaziri, M.A. (2014): New energy based approach to predict seismic demands of steel moment resisting frames subjected to near-fault ground motions. *Engineering Structures*, **72**: 182–192.

[8] Kalkan, E., Kunnath, S.K. (2007): Effective cyclic energy as a measure of seismic demand. *Journal of Earthquake Engineering*, **11**(5), 725–751.

[9] Lin, J.L., Chen, W.H., Hsiao, F.P., Weng, Y.T., Shen, W.C., Weng, P.W., Li, Y.A., Chao, S.H. (2020): Simulation and analysis of a vertically irregular building subjected to near-fault ground motions. *Earthquake Spectra*, **36**(3), 1485–1516.

[10] Shahi, S.K., Baker, J.W. (2014): An efficient algorithm to identify strong-velocity pulse in multicomponent ground motions. *Bulletin of the Seismological Society of America*, **104**(5), 2456–2466.

[11] Vamvatisikos, D., Cornell, C.A. (2002): Incremental dynamic analysis. *Earthquake Engineering and Structural Dynamics*, **31**, 491–514.

ENGINEERING MODEL FOR ANALYIS OF MASONRY STRUCTURES

Goran Simonović [1], Mustafa Hrasnica [2], Senad Medić [3]

[1] *Associate professor, University of Sarajevo – Faculty of Civil Engineering, goransimonovic@yahoo.com*
[2] *Full professor, University of Sarajevo – Faculty of Civil Engineering, hrasnica@bih.net.ba*
[3] *Assistant professor, University of Sarajevo – Faculty of Civil Engineering, senad_medic@yahoo.com*

Abstract

This paper presents the methodology for seismic analysis of masonry structures that can be employed in commercial software packages such as SAP2000. The concept of elementary block which combines non-linear spring and linear shell elements is used for discretization of masonry walls. The proposed modelling technique with localized nonlinearity can successfully simulate in-plane wall failure modes induced by compressive or tensile axial force and transverse force. It can also be used to investigate out-of-plane collapse which makes it a good candidate for 3D static and dynamic analysis of buildings. The modelling approach is tested on two examples where pushover analysis was performed: a single slender cantilever masonry wall and a family house. The response was verified against the results delivered by 3MURI and MINEA, and reasonable agreement was obtained. It is demonstrated that the transverse walls have significant contribution to the load bearing capacity of buildings.

Keywords: masonry structures, elementary block, nonlinear spring elements, SAP 2000.

1. Introduction

There are at least two motives for the research presented in this paper. First, during the two previous decades it has become a common practice to upgrade the existing multi-story masonry buildings for one or two new floors. One example is showed on figure 1, presented the former existing masonry building and the upgraded one, situated in the vicinity of the Faculty of Civil Engineering in Sarajevo. Second, a large number of masonry buildings in our country were built before the introduction of the first seismic codes. These buildings don't fulfill most of design requirements set by modern seismic regulations. However, the experiences gained during past earthquakes in the region of the South-East Europe showed us that the existing masonry buildings possess higher resistance than one might conclude from the everyday engineering analysis. It is obvious that the masonry structure should be modelled as a whole.

Figure 1. Masonry building before reconstruction (left), after reconstruction (right).

This paper presents the concept of seismic analysis based on macro-element named "elementary block" and non-linear link elements. Such model is then implemented in software SAP2000 [4]. Numerical analysis of the building is based on a 3D model with transversal walls that carry a seismic load in their plane and to some extent out-of-plane. Model comprises the interaction of reinforced concrete slab with masonry walls as well as torsional effects. Verification of suggested concept is performed comparing the results of the analysis with results obtained from finite element programs 3MURI [1] and MINEA [3]. Comparing the results, it is shown that masonry building behavior can be successfully described through numerical models, composed of the proposed elementary blocks and nonlinear link elements. The proposed procedure could be implemented into other finite element software, which provides the masonry wall models composed of elementary blocks and nonlinear connection elements [7].

2. Elementary block

It is known from the theory of structures that the most stressed places in structure due to the ordinary loads are in the joints of the structure, such as beam-column connections, wall and slab connections, foots of the walls and columns etc. It is therefore possible to predict the locations in structures where nonlinear deformations would appear. Less stressed structural parts are modelled as linear elastic, while nonlinear behavior is restricted to the most stressed parts. This is the approach applied in this work, where we investigate the behavior of masonry structures under seismic loading. However, in everyday engineering practice non-linear behavior of the structure is assumed only in the case of moderate or stronger earthquake loadings. The structure exposed to gravity loads alone, including combination with usual wind loads, should remain elastic.

The simple engineering model that can simulate the participation of all elements in the structure in taking over the seismic load is presented. Assumed that we know the stress state in a wall (Fig. 2 left). We divide the wall cross-section into segments. The normal force in each of those segments is the product of the mean value of the stress and the cross-sectional area of that segment. The total normal force in the wall is the sum of the normal forces in the segments, and the total moment in a cross-section of the wall is the sum of the product of the distance of an individual force and the intensity of that force.
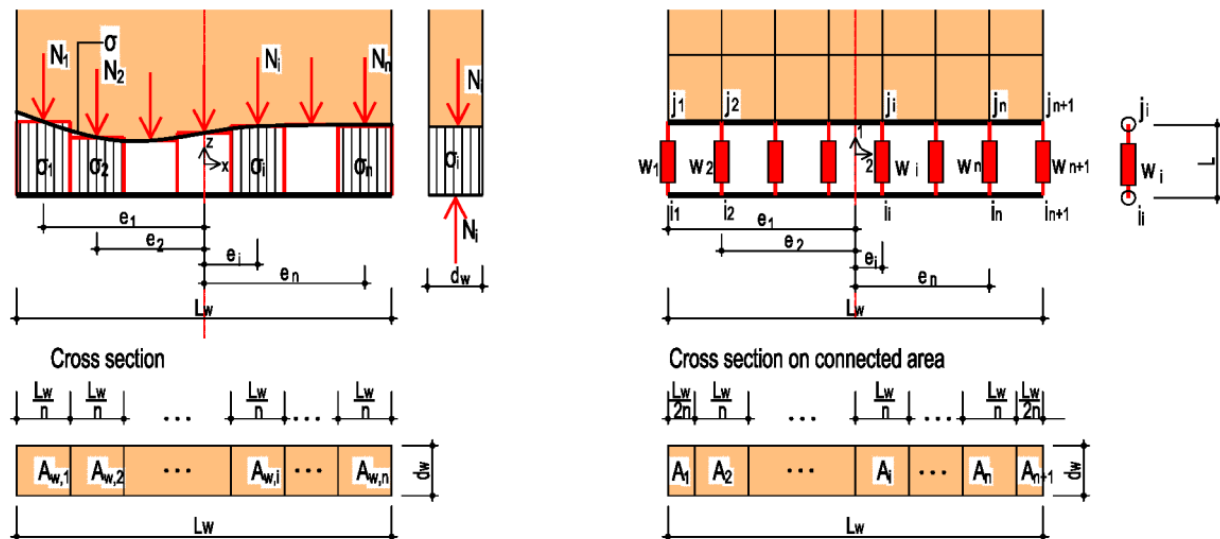
Figure 2. Distribution of normal stresses (left) and finite element discretization (right).

The division of the wall into the segments corresponds with the mesh of finite elements. The position of each finite element in the wall is known (Fig. 2 right). Between the wall and the close surroundings (could be another wall or wall segment), an element with zero-length ($L \rightarrow 0$) is introduced. Each node of the finite element network above the joint (ji) can be connected to the other part of the structure by nonlinear spring in the nodes (ji). The geometric properties of the spring correspond to the surface of

the connecting wall, and the material properties of the spring correspond to the material properties of the wall. The calculated load capacities of individual connecting elements N_i, R_d are determined as the product of the area of the wall segment A_i connected by these link elements and the calculated strength of the wall f_d. There are two types of adopted axial connecting elements (Figure 3). Type A (E) is a connecting element on the edge of the coupling. Types of connecting elements B (C, D) are located inside the coupling. Specific role of the connecting element (C, D, E) will be clarified later. For the adopted types of connecting elements, the calculated axial load capacity is:

$$N_{A,Rd} = N_{E,Rd} = \frac{L_w \cdot d_w}{2 \cdot n} \cdot f_d \tag{1}$$

$$N_{B,Rd} = N_{C,Rd} = N_{D,Rd} = \frac{L_w \cdot d_w}{n} \cdot f_d \tag{2}$$

Axial forces in individual connecting elements are a function of the stiffness and displacement of the nodes of the finite elements used to model the wall:

$$N_i = f(k, u) \le N_{i,Rd} \tag{3}$$

With the gradual increase of the design load, which can be set by the software, the design forces in the connecting elements also increase, that is, the stresses σ_i increase in the part of the wall where the connecting elements are introduced. Upon reaching the given computational strength of each link element, the nonlinear behavior of the model begins. Upon reaching the calculated bearing capacity of all connecting elements in the coupling, the model will yield. The total calculated bearing capacity of the wall under the action of the normal force N_{Rd} represents the sum of the calculated bearing capacities of all connecting elements of the joint:

$$N_{Rd} = \sum_{i=1}^{n+1} N_{i,Rd} = 2 \cdot N_{A,Rd} + (n-2) \cdot N_{B,Rd} + N_{C,Rd} = A \cdot f_d \tag{4}$$

The number of finite elements n along the length of the wall depends on the geometry of the wall and cannot be determined in advance. Therefore, it is not possible to determine the number of connecting elements in the coupling. Two connecting elements of type A and one connecting element of type C represents basic connection model. The number of connecting elements of type B depends on the ratio of height and length of the wall. The minimum number of finite elements per connector is n=4, and the number of connecting elements is n+1.

The model can also simulate the behavior of a wall exposed to normal pressure force with eccentricity. The calculated bearing capacity of the wall under the action of the bending moment in the plane of the wall, expressed through the axial forces in the connecting elements and the position of the connecting elements in the wall, is:

$$M_{Rd} = \sum_{i=1}^{n+1} N_i \cdot e_i \tag{4}$$

The connection element C is used to simulate the behavior of the wall exposed to the transverse loads in the plane of the wall. In the direction of the axis 1 of the n-link element, this connecting (link) element has properties like connection element B. However, in the direction of axis 2, it describes the in-plane shear capacity of the wall. Connecting elements A and B are pure axial elements. Depending on the height the wall could be modelled as an elementary block with connecting elements at the bottom and top of the wall, In the case of relatively higher masonry walls, a few elementary blocks and connection levels could be modelled along the height of the wall. In that case, on possibility is to introduce connecting elements E and D, which are transversely rigid, and axially behave like elements A and B.
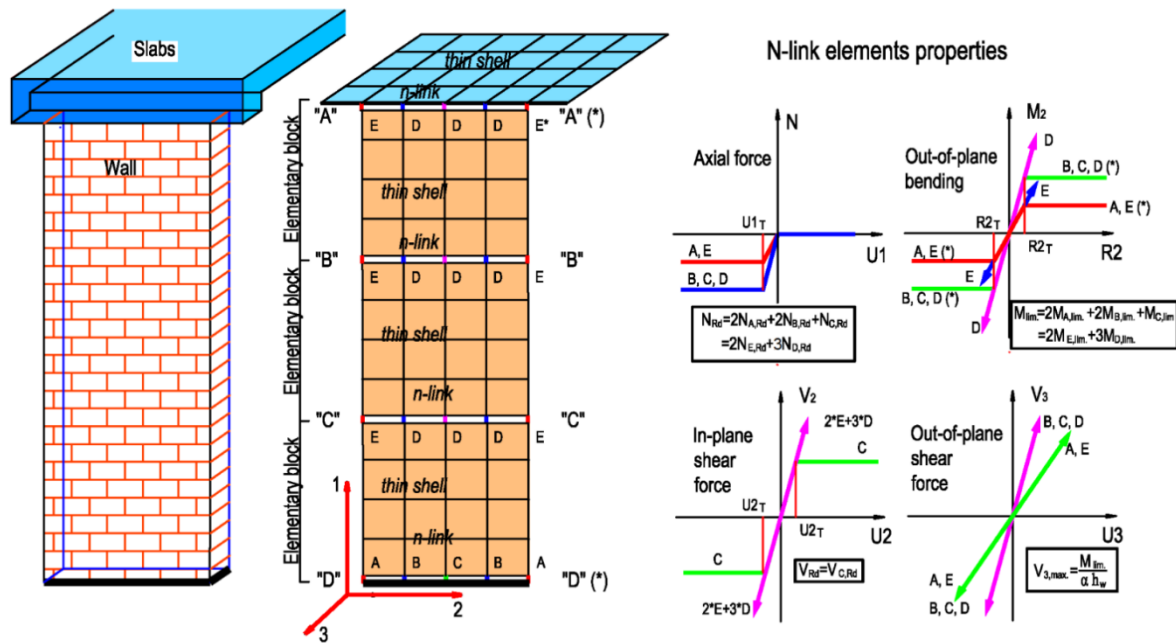
Figure 3. Concept of elementary block.

Simulation of out of plane behavior is possible by coupling elements "A" and "D". For a known normal force in the wall, the components of M2 can be calculated and limited, so that, for example, the normal force remains in the core of the section. Couplings "A", "B", "C" and "D" are axially non-linear. They simulate the collapse of a wall under the action of a centric or eccentric normal force in wall plane. Couplings "A", "B", and "C" assume a linear transverse force, while nonlinearity to transverse forces is introduced in coupling "D" with link C. For the case of analysis in and out of plane of the wall, couplings "A" and "D" are rotationally limited in their plane.

One such composition of finite elements and connecting (links) elements is called an elementary block. Finite elements within the elementary block provide linear behavior of the wall, while connecting elements in the joints (connection) provide nonlinear behavior. That means, non-linear behavior is limited to the connection elements.

3. Verification of the modelling approach

3.1 Behavior of the model

The following figure shows the collapse situation of the wall in the plane according to FEMA[5]. The different behavior of the model, on the example of a cantilever wall, each of these responses are illustrated is also shown on the right side of the Figure 4. At the top floors of the building, where the normal and transverse forces in the wall are relatively smaller, we have the behavior of the wall as a rigid body, due to the bending, opening of the joints for tension without crushing at the edges. Similar behavior is also on the floor below, but with crushing at the edge in pressure. If the transverse forces are dominant, then the collapse occurs due to sliding. Diagonal cracks that are typical damages of the masonry wall, appears when the principal stresses reach the tensile strength of the wall cannot be directly simulated by the proposed model because the joints of elementary blocks are introduced horizontally. Nevertheless, indirectly, through the limitation of the transverse force for the known normal force, this fracture can also be simulated, and in the model it manifests itself as sliding.
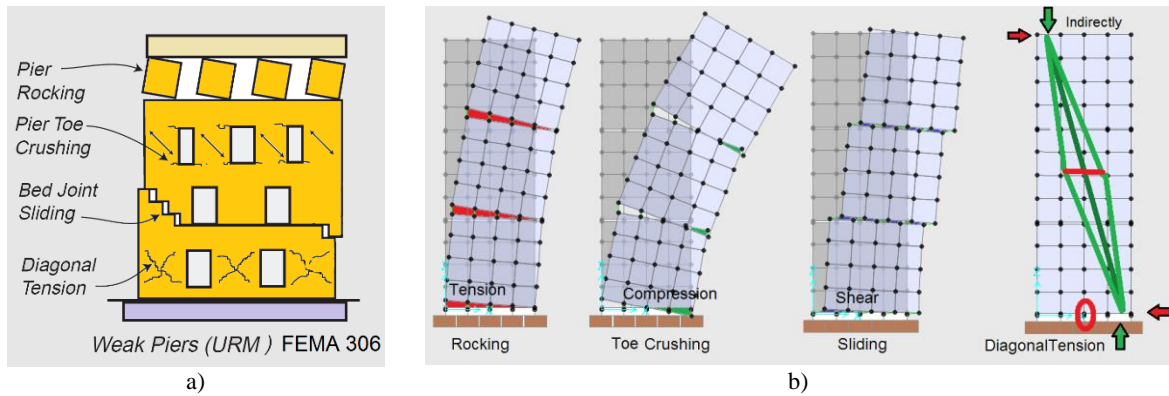
Figure 4. a) Failure modes according to FEMA, b) response capacity of the model.

3.2 Analysis of a family house

This example analyses a typical German family house which has a system of bearing walls in two orthogonal directions (x and y). The whole urban settlements are formed by the rows of these simple buildings. Building lies side by side; separated by joints, so each building represent structurally independent unit. At the building lay-out the walls are marked as W1, W2...and W9 and their cross-sections are constant from the ground to the roof of the building (Figure 5). Other walls are partition walls and do not have vertical continuity as well. Seismic load in x direction is resisted mainly by walls W2, W3, W5, W6, W7 and W8. According to building tradition at similar buildings, slabs are monolithic casted in situ and without beams. It is obvious that the building is more vulnerable in a shorter (transverse) direction, view in the plane of the building.

Capacity curves obtained by software 3MURI are a function of effective plate area. Due to the absence of the usual beams, the space frames are modelled with the effective width of the reinforced concrete plate. Capacity curve obtained by software SAP2000 presents the result of the analysis where the walls are modelled in plane with elementary blocks. Limited out-of-plane behavior is included in curve SAP-b. Good matching of results obtained by different analysis is obvious. Capacity curve obtained from software MINEA has almost the same capacity as curve obtained from software SAP2000, but quite different form, because the capacity determined by MINEA software is based on experimental data on different masonry wall's bearing capacity, incorporated in software. Comparing with experimental results of the tests conducted in research project ESECMASE [3], it can be concluded that the proposed model shows significant advantages over traditional modelling of masonry structures in commercial software.
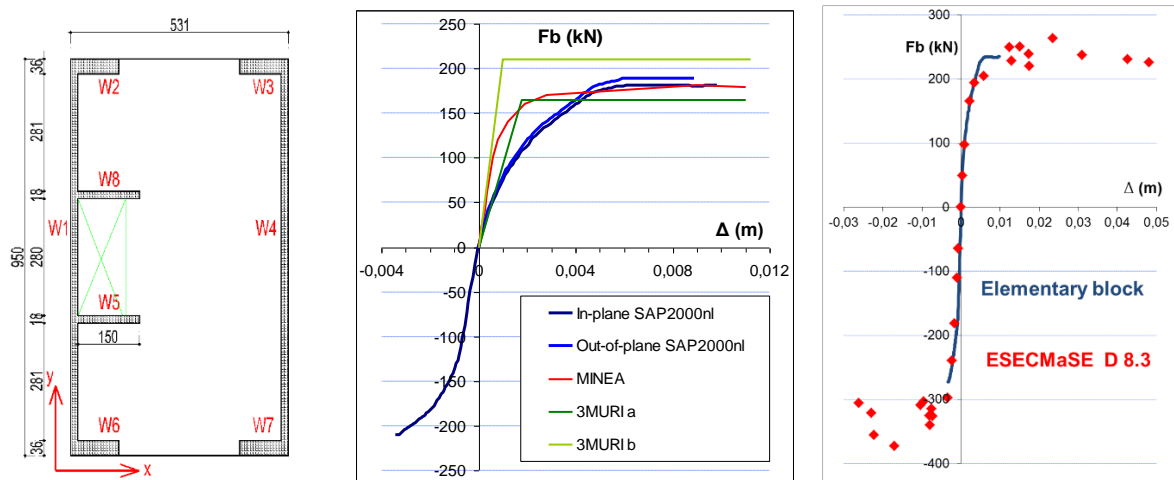
Figure 5. a) Lay-out of the building b) Capacity curve obtained by different analysis c) Comparison with experiment

3.3 Some specifics of the model

Implementing the proposed modeling procedure different performances of masonry walls can be included. On the left side of the Figure 6 the rocking of the masonry wall pier is presented. The uplifting is prevented by floor structure. Due to the restraint an additional normal force could be imposed on the wall structure. The effect can be covered by proposed modelling strategies using commercial software. On the right side of the Figure 6 the shear behavior of the wall is dominant, characterized by typical diagonal cracks mostly through mortar joints. The former effect of uplifting and increased axial force is missing.
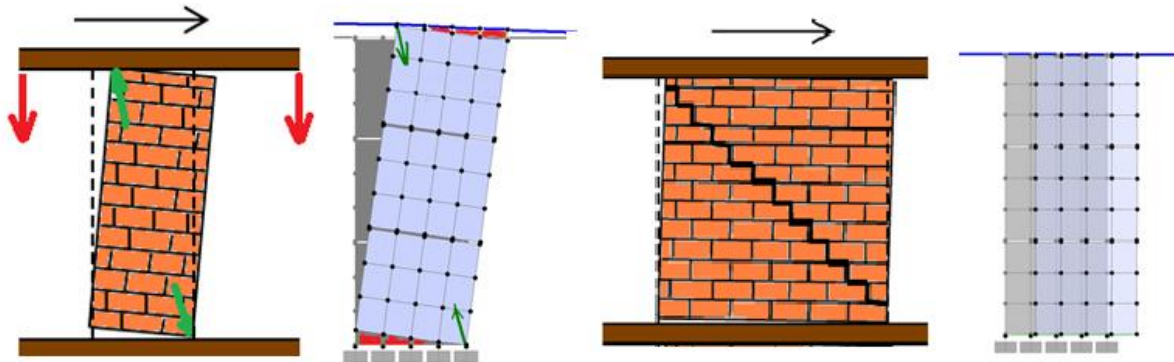
Figure 6. Rocking with increase in normal force (left) and sliding (right).

The response of the walls in the direction of the earthquake can also lead to the collapse of the connecting perpendicular walls due to tension and uplifting. In the Figure 7 below, for the positive direction of the push in wall W1, there is a decrease in the normal (vertical) force, opening of joints in wall W1, strong rocking behavior that detaches the floor structure from wall W2, which results in a tensile fracture of wall W2. For the opposite direction of pushing, in wall W1 there is an increase in the normal force, which results in its higher bearing capacity for the transverse forces. These affects can be successfully modelled by presenting procedure and it is shown on the right side of the Figure 7 through the deformation of the elements mesh.
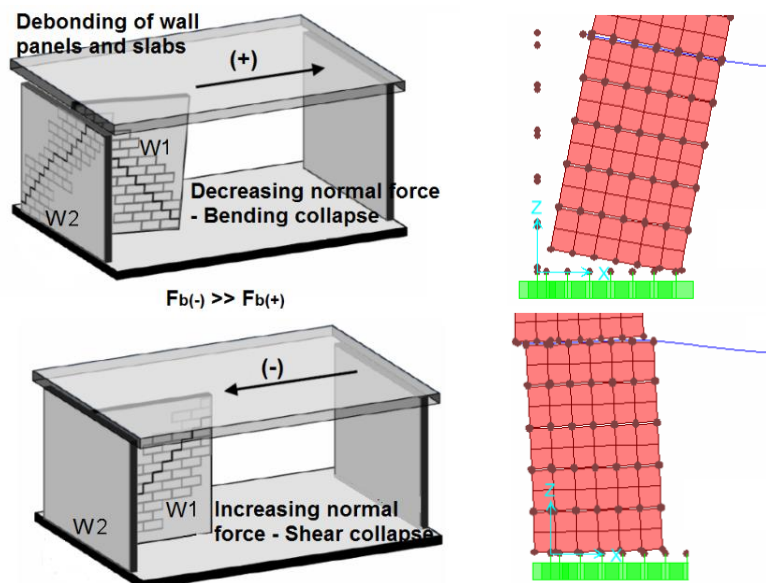
Figure 7. Interaction of longitudinal and transversal wall [6].

It should be emphasized that the model take in account torsional effects for structures where the center of mass does not coincide with the center of stiffness.

4. Conclusion

With this relatively simple engineering approach, it is possible to successfully simulate the behavior of buildings up to the point of failure implementing finite element software that contains connecting or link element capable to describe non-linear behavior. If the incremental dynamic analysis is included, the history of stresses and crack formations could be followed step by step. The proposed procedure is suitable for every day engineering praxis and more user friendly comparing to highly specialized software. This is even more true if one wants to build three-dimensional model of the masonry structure and wants to include the major effects produced in a masonry building exposed to the stronger earthquake motion. The concept of elementary blocks and reduction of non-linear behavior to the known critical areas facilitates the review and analysis of the usually very extensive results of three-dimensional structural analysis, especially if the non-linear behavior of the structure is included. And, the inclusion of the whole building structure (3-D analysis) gives us better insight into the seismic response and the capacity of the building, if it's exposed to moderate or stronger earthquake.

References

[1] S.T.A. DATA (2009): *3muri - manuale d'uso*, S.T.A. DATA srl - C.so Raffaello, Torino.

[2] SDA-engineering GmbH MINEA (2017): *Programm für den Nachweis von Mauerwerksbauten nach DIN4149*, https://www.sda-engineering.de/startseite

[3] ESECMaSE (2009): Enhanced Safety and Efficient Construction of Masonry Structures in Europe, http://www.esecmase.org

[4] CSI Computers & Structures Inc. (2002): *SAP2000 - Analysis reference manual*, Berkley.

[5] FEMA 306 (1998): *Evaluation of earthquake damaged concrete and masonry wall buildings – Basic Procedures Manual*, Applied Technology Council (ATC), Publication No. 306, Federal Emergency Management Agency, Washington D.C.

[6] Butenweg, C., Gellert, C. (2008): Displacement based design of masonry structures under earthquake loading. In *14th International Brick and Block Masonry Conference, Sydney, Australia*.

[7] Simonović, V., Simonović, G. (2018): Numerical Investigation of Possible Strengthening of Masonry Walls, *International Symposium on Innovative and Interdisciplinary Applications of Advanced Technologies*, page 175-181, Jahorina, doi: https://doi.org/10.1007/978-3-030-02577-9_17

SEISMIC PERFORMANCE OF RUBBERIZED CONCRETE IN STRUCTURAL APPLICATIONS

Tanja Kalman Šipoš [(1)], Kristina Jeleč [(2)], Ivana Miličević [(3)],

[(1)] *Associate professor, Faculty of Civil Engineering and Architecture Osijek, Croatia, tkalman@gfos.hr*
[(2)] *Research assistant, Faculty of Civil Engineering and Architecture Osijek, Croatia, kstrukar@gfos.hr*
[(3)] *Associate professor, Faculty of Civil Engineering and Architecture Osijek, Croatia, ivana.milicevic@gfos.hr*

Abstract

Rubberized concrete is a promising material for the structural elements, created by replacing sand with rubber particles in order to significantly reduce environmental impacts from large tyre waste with improved behaviour under earthquake loads.

Experimental studies on nine columns and three frames were carried out in order to determine the capacity of different structural elements in regard to conventional concrete. The specimens were subjected to a cyclic loading following loading protocol used for the seismic performance assessment of structural and non-structural components, as it allows all damage states to be quantified to develop the corresponding fragility models. The results indicated that rubberized concrete columns and frames made of rubberized concrete can delay and reduce the amount of damage occurring under seismic loading. This is attributed to the higher deformability of rubberized concrete compared to conventional.

With these contributions, an increased use of rubberized concrete in global construction can promise a reduction of the significant environmental impacts caused both from waste tyres and the exploitation of natural resources with promotion of environmentally friendly alternative to conventional concrete in structural applications in earthquake prone areas.

Keywords: rubberized concrete, seismic performance, cyclic testing, structural applications

1. Introduction

Tire waste is a significant global concern for a number of reasons, including its propensity to spontaneously combust, the non-biodegradable nature, and the difficulties associated with landfilling it. The construction industry was identified as having a possible application for waste tyres. Since concrete is the material that is utilised the most in this sector, one of the research directions that has been taken recently is the use of recycled tyre waste to produce rubberized concrete [1]. This may be done as a partial substitute for natural aggregate and/or cement.

Concrete has a low ductility and a high brittleness, both of which lead this material to fracture without major deformations. The behaviour of concrete structures can be particularly unreliable under certain stresses, most notably seismic loads, because of these properties. On construction sites, this fact, however, does not make concrete any less appealing due to the many other advantages it offers. Reviewing previous studies [2] on rubberized concrete, which included both normal and self-consolidating concrete, showed that the addition of recycled rubber particles caused decreased density, increased hardness and ductility, improved dynamic properties, and resistance to crack propagation [3–8]. This has been observed after the recycled rubber particles were mixed into the normal and self-consolidating concrete. According to the advantages of rubberized concrete, it is possible to reach the conclusion that recycled rubber particle have a great potential in the production of light-aggregate concrete in structural elements. This is the case despite the fact that a decrease in compressive strength and the modulus of elasticity was also observed [9–12]. Especially those that are likely to be exposed to the effects of earthquakes, and the objective is to lower the probability of spalling on the concrete surface as well as the concrete cover [13, 14].

In order to ensure that a structure can resist a certain amount of ground shaking, it is highly necessary to know how reinforced concrete structures react to earthquakes. Regarding the seismic behaviour of

reinforced rubberized concrete columns, there have only been a few experimental investigations conducted. Youssf et al. [13], [15], Hassanli et al. [16], [17], Li and Li [18] and Elghazouli et al. [19] investigated the behaviour of rubberized concrete columns when subjected to cyclic activity. Their findings suggested that by partially replacing the mineral aggregate with recycled rubber particles, the hysteretic damping ratio and energy dissipation were enhanced. This was the case even though the total amount of mineral aggregate remained the same. Additionally, it was discovered that both the flexural and compressive toughness of the material had greatly improved, as had its hysteretic curve and its ductility. First shake-table tests on two large size cantilever reinforced concrete columns were carried out by Moustafa et al. [14]. Columns were tested by going through a series of ground motions that were calibrated to a certain design spectrum. It was shown that the capacity for lateral drift and the amount of energy lost in a column made of rubberized concrete were both enhanced. Because of the greater energy dissipation, the fracture of the rebar was delayed. Higher values were observed for both hysteresis and viscous damping. Study [2] provided a collection that is more extensive and goes into further depth regarding these experimental results.

This study's major objective was to present general results from an experimental evaluation of reinforced concrete columns and frames made using partially replaced aggregate and recycled rubber particles with a cyclic loading used to evaluate their seismic response.

2. Experimental program

A total of three different self-compacting concrete mixes were used to cast a total of nine column specimens and three frames. The target compressive strength for all specimens was 30 MPa; however, the first mixture was made from conventional self-compacting concrete (SCC-0CR), while the other mixtures, 10% and 15% (with 5% of silica fume) of the fine aggregate volume was replaced by rubber particles (RP).

2.1 Material properties

The production of concrete mixes required a number of different components, including Portland cement 42.5 R, which was manufactured in accordance with HRN EN 197-1:2005, mineral and recycled aggregates, dolomite powder, water, and admixtures as it is presented in Table 1. The mineral aggregates comprised fine aggregates (FA) with a particle size range of 0–2 mm and 2–4 mm, as well as coarse aggregates (CA), which included gravel with a particle size range of 4–8 mm and 8–16 mm. In place of a 10% volume ratio of fine mineral aggregate, recycled aggregate crumb rubber (CR) with particles ranging in size from 0.5 to 4 millimetres and with a density of 1050 kilogrammes per cubic metre was utilised as a replacement in concrete mixtures. In addition, dolomite powder was included in the mixture of concrete in order to cover any pores that were present.

Table 1 – Concrete mixture proportions

Mixture ID	w/b	Cement 42.5R [kg/m³]	VMA [kg/m³]	DP [kg/m³]	CR 0-4mm [kg/m³]	FA 0-2mm [kg/m³]	FA 2-4mm [kg/m³]	CA 4-8mm [kg/m³]	CA 8-16mm [kg/m³]
SCC-0CR-0SLF	0,4	450	1,35	80	0	324,45	614,00	362,18	452,72
SCC-10CR-0SLF	0,4	450	1,13	80	66	324,45	438,42	362,05	452,56
SCC-15CR-5SLF	0,4	427,5	1,07	80	98,75	323,51	349,84	361,13	451,41

Table 2 contains the results of tests conducted to determine compressive strength, modulus of elasticity, and flexural strength. These data include mean values (μ), as well as the coefficient of variation (CoV). It is clear from this that the addition of up to 15% rubber particles can result in a reduction of compressive strength and modulus of elasticity of up to 29.34% and 27.2%, respectively, when compared to the original value (RP). When it comes to compressive strength, it can be observed that the difference between SCRC mixes M2 and M3 is extremely modest. The reason for this is most likely due to the addition of silica fume to the M3 mixture, which enhances compressive strength. The modulus of elasticity, on the other hand, does not seem to have changed noticeably as a result of this improvement. The results concerning flexural strength revealed a beneficial affect

by adding RP and raising it up to 7.47%, which is in contrast to the fact that the addition of RP had a detrimental effect on the qualities of the prior concrete.

Table 2 - Hardened concrete's properties

Mixture ID	Compressive Strength f_{ck} [MPa]		CoV	Modulus of Elasticity E_c [MPa]		CoV	Flexural Strength f_{ct} [MPa]		CoV
	μ			μ			μ		
SCC-0CR-0SLF (REF)	43.70	REF	0.058	38576.62	REF	0.077	4.95	REF	0.065
SCC-10CR-0SLF (R10)	31.25	-28.5%	0.092	35256.04	-8.61%	0.036	5.15	+4.04%	0.020
SCC-15CR-5SLF (R15)	30.88	-29.3%	0.067	28061.61	-27.26%	0.120	5.32	+7.47%	0.045

It was selected to use ribbed reinforcement B500B for the longitudinal column reinforcement, with a diameter of 12 millimetres, and 8 millimetres for the transverse column reinforcement. Reinforcing steel has a nominal yield strength of 500 MPa, and its elongation under ultimate strength is equivalent to 15%. The fym value represents the nominal yield strength. It is anticipated that the ultimate strength will be 600 MPa, and the ultimate elongation will be 20%.

2.2 Specimen's geometry

When measured from the end that is fixed to the location where the transverse force is applied, the length of the column is equal to two hundred centimetres. The square cross-section of the column measures 30 centimetres by 30 centimetres, giving the column a slenderness of 23, which is the consequence of this measurement. The element has a critical length of 35 centimetres when measured from the end of the column that is fixed, which suggests that the formation of the plastic hinge is most likely to occur at that location. The longitudinal reinforcement of the column is comprised of eight bars, each of which has a diameter of twelve millimetres. These bars take up exactly one percent of the column's gross cross-section.
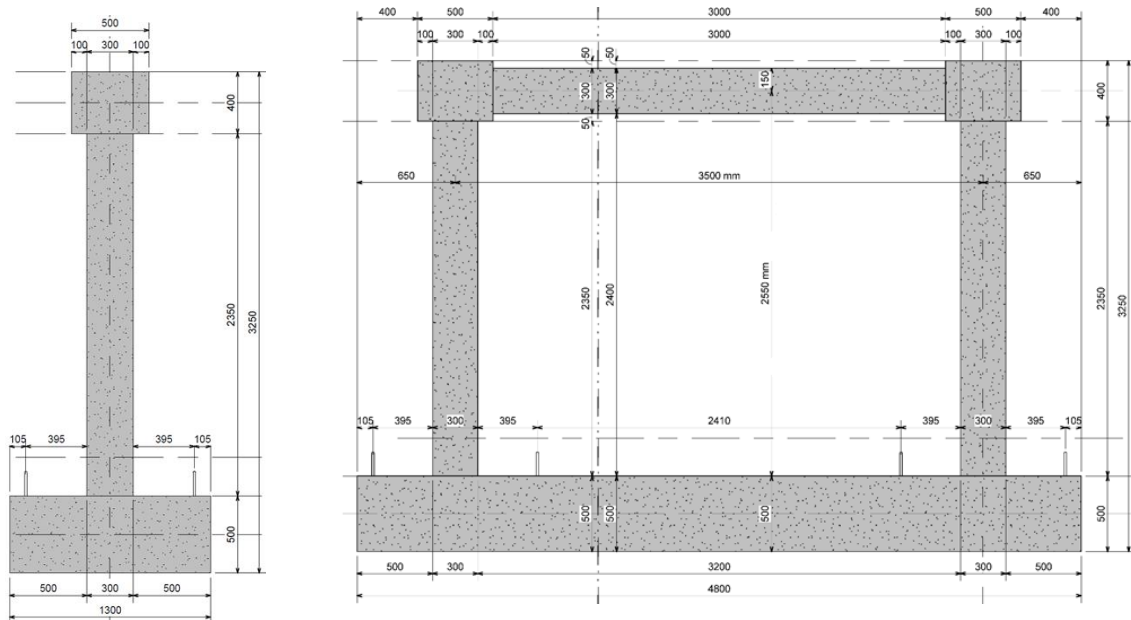
Figure 1. a) Column specimen geometry; b) Frame specimen geometry

The transverse reinforcement, on the other hand, is made up of square and diamond hoops with a diameter of eight millimetres at a distance of seventy-five millimetres inside the critical zone and one hundred fifty millimetres beyond the critical zone.

The axial dimensions of the frames are 3.5 metres by 2.55 metres; the cross-sections of the columns are 30 centimetres by 30 centimetres; and the cross-sections of the beams are 20 centimetres by 30 centimetres. All of these measurements are in centimetres. When you include the foundation beam in the measurement, the entire width and height of the frame comes out to 4.8 metres on each side and 3.25 metres in height. Because the column-beam nodes are wider than the columns, they offer an upper surface that is 40 centimetres by 50 centimetres in size for the application of vertical forces. The total weight of a single frame was 5 tonnes.

2.3 Testing protocol

All specimens went through a cyclic loading method (Fig. 2). This was done in accordance with the loading approach that was recommended by FEMA 461. (2007). Because it enables the quantification of all damage states, this procedure is frequently used for the seismic performance evaluation of structural and non-structural components and equipment. This is necessary for the development of the related fragility models, and it is one of the reasons why it is frequently used. The loading procedure involves a large number of repetitions of cycles, each of which has an amplitude that steadily increases by 1.4 times at each stage. At each amplitude level, two cycles of loading are carried out in order to load the system. The process needs to be carried out a minimum of six times before there is any evidence that an injury has occurred. As a consequence of this, a total of fourteen distinct amplitude levels were selected, and the procedure resulted in a final lateral displacement of 6%, which is equivalent to 120 millimetres. The load application rate is initially set at 0.05 mm/s for the first few cycles of the test, and then it gradually increases to 0.5 mm/s for the final few cycles. This brings the overall amount of time for the testing procedure per specimen up to ninety minutes.
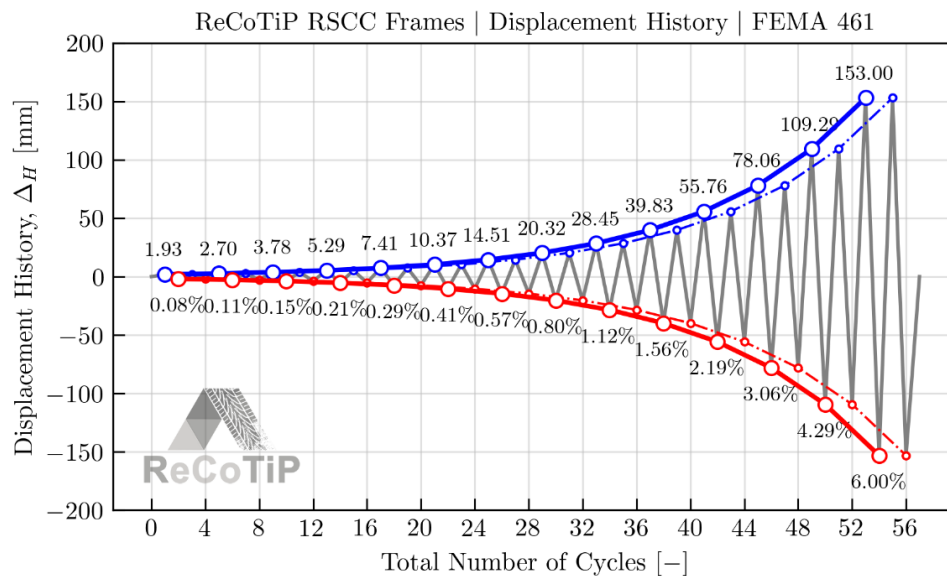
Figure 2. Loading protocol for columns and frames

Instead of being tested in the vertical orientation that was initially planned, the columns were tested in the horizontal orientation at Laboratory in Faculty of Civil Engineering and Architecture Osijek. The availability of a Shimadzu device for universal compressive-tensile testing in the vertical direction is the impetus for this move. The apparatus for compressive-tensile testing that has the potential for accurate computer control permits uncompromising control of the application of force and control of displacement to the test sample, which for this type of testing must be positioned horizontally. As a result, the test specimens are fastened into place with the column foundation beam positioned on the vertical reactive wall and the column body arranged in a horizontal orientation as it is presented in Fig. 3.
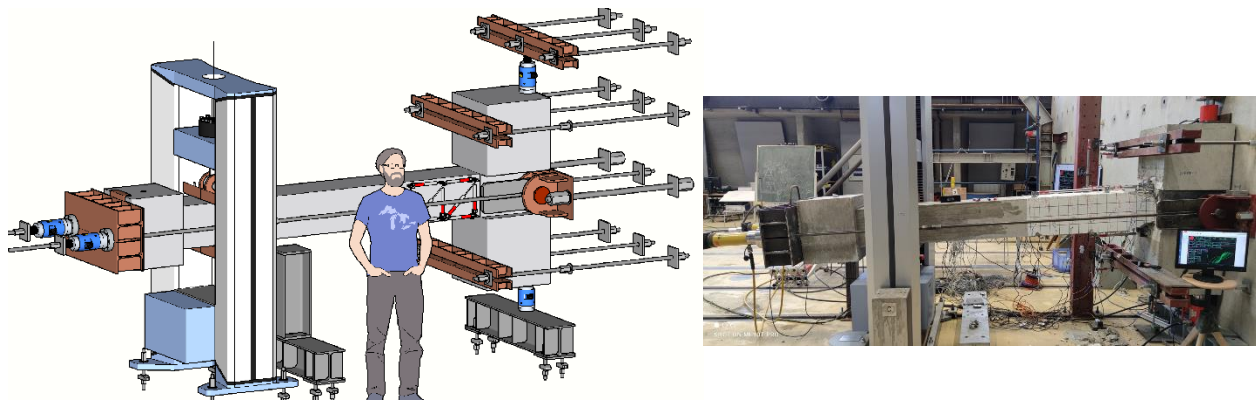
Figure 3. a) Scheme for column testing; b) Testing of columns

Figure 4. a) Scheme for frame testing; b) testing of frames

The testing setup was prepared in Laboratory in ZAG Ljubljana for cycle tests on reinforced concrete frames consisted of a rigid testing floor with a modular system of steel structural parts and a 6 x 7 m huge reaction wall, both of which have a load-carrying capability of 1000 kN/m2 and were spaced apart by a distance of 7 metres. The specimen was fastened to the testing floor using a structure of steel beams and rods that were positioned at both the beginning and the end of the foundation block for the frame. The vertical load of 300 kN on each concrete column was applied by a system consisting of two vertical rods M42, a short beam, and a hydraulic servo-controlled actuator with a capacity of 600 kN. There was a distance of 3.6 metres between the centre lines of the two vertical systems.

Horizontal load (compression and tension) was delivered by a hydraulic servo-controlled actuator with a capacity of 1000 kN and a stroke extension of +/-500 mm, which was part of the horizontal loading system. Yoke is used to make the connection between a specimen and an actuator, which is positioned on the reaction wall. Yoke was constructed using two steel plates and two M42 rods as the component parts. The displacement serves as the controller for the hydraulic actuator.

The system of supports that prevents the specimen from rotating around the vertical axis consisted of two steel frames with four steel modular consoles that block the concrete frame's ability to spin around the vertical axis.

3. Results

By comparing columns in terms of global capacity (Fig. 5) REF specimens reached a maximum shear force of 56 kN at a drift of 3,1% before it reached an ultimate drift of 6% with the force of 48kN.
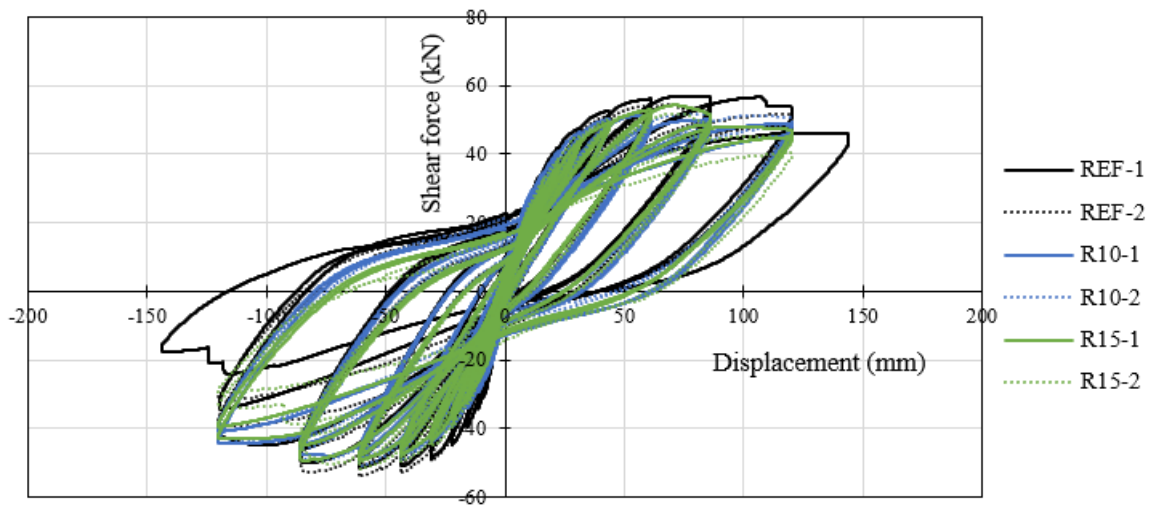
Figure 5. Global hysteresis for columns
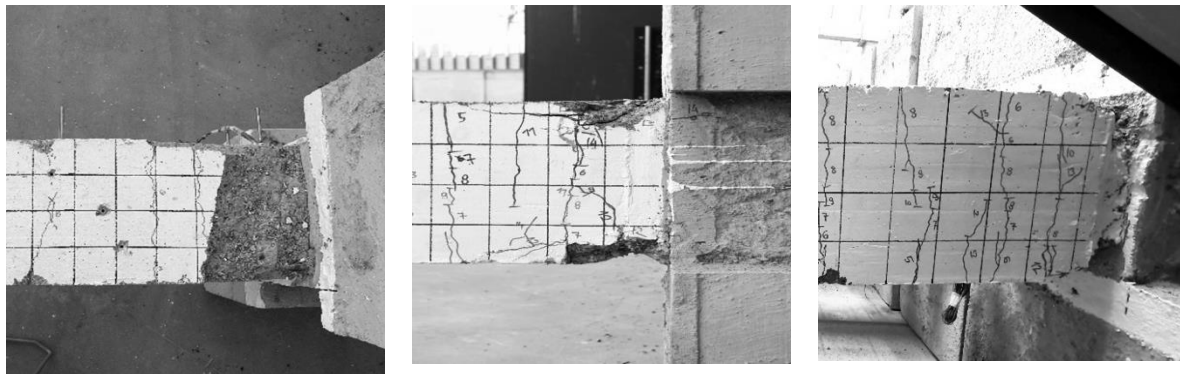
Figure 6. Crack propagation in columns: a) REF column; b) R10-1 column; c) R15-2 column

The R10 and R15 column specimens, attained a maximum force of 51 kN at a drift of 3% with the same ultimate force. As a result, the use of the rubber in the concrete may decrease the maximum force while maintaining the ultimate. The REF specimen had an average fc of 43,7 MPa in comparison to fc of 31,25 MPa for the R10 specimen, indicating that the rubberized column would have higher deformability.

Concrete cover spalling in columns began at a drift of 2,2% in the bottom-most 200 mm of the column above the footing and progressed to 250 mm height above the footing at the end of the test (6% drift). According to the Figure 6 it is visible that plastic hinge area is much smaller and crack are much more cracks are much narrower compared to columns made of conventional concrete.

The results of the frame's tests (Fig. 7) reveal that all three frames have a fairly similar global behaviour. Frame REF, which is made of traditional concrete without additions of rubber aggregates, had the highest load capacity, but the difference between the two is insignificant in comparison to the difference in the compressive strength of the material. When compared to frame REF, frames R10 and R15 (with silica fume), had a load capacity that was only 3% lower than frame REF. What is distinctive about frame REF is that the reinforcement cracked, although in the other frames, there was no such behaviour. In spite of the material's reduced compressive strength, it is feasible to deduce, based on the hysteresis curves, that concretes containing rubber can fully take up the entire load just as well as conventional concretes can.
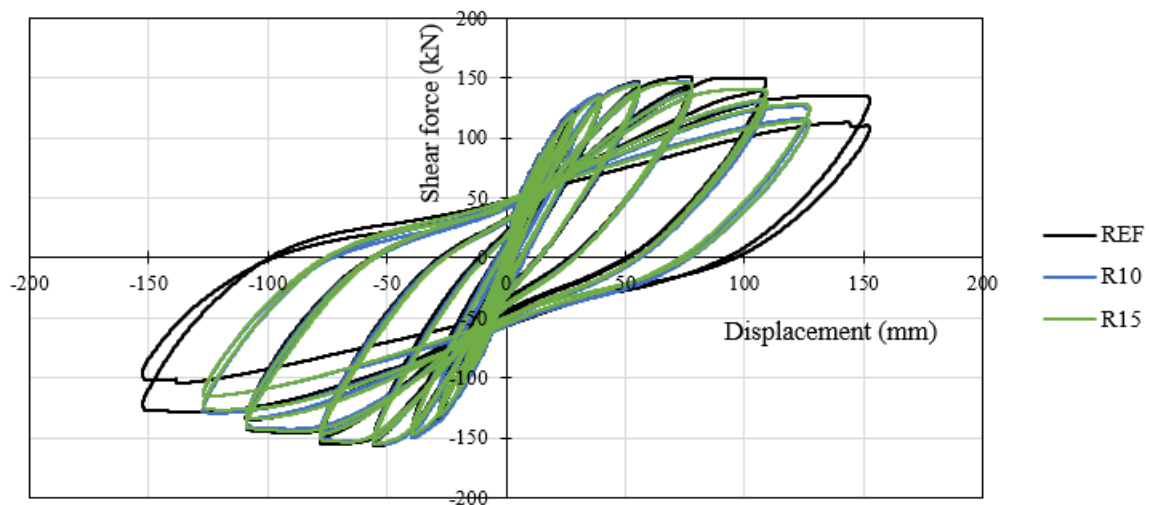
Figure 7. Global hysteresis for frames

Figure 8. Crack propagation and damage in frames

When the frames were inspected after tests have been finished (Fig. 8), the discrepancies become considerably more apparent. That was done by characterising the damage in terms of the location and size of the plastic joints, as well as the position and width of any cracks that have been formed. When compared to frame REF, frames R10 and R15 had less damage (a smaller region of the plastic joint), less falling off of the protective layer, and in the end, there was no breakdown of the reinforcement in the case of the frames with the rubber particles.

Therefore, it is necessary to conclude that there are no restrictions on the use of rubber aggregates as a replacement for one part of the total volume of aggregates (up to 20%) in load-bearing structures at any level. This includes the control of bending, load-bearing capacity, stiffness, while undergoing cyclic loading, and behaviour that corresponds to the action of an earthquake.

In regions that are prone to seismic loads, constructions made of concrete with the addition of rubber can be fully utilised for load-bearing elements and all parts of load-bearing structures. This is especially true in regions where there is a greater risk of damage to structures on a local level from earthquakes, as compared to the case with conventional concrete.

4. Conclusions

The objective of this study is to determine whether or not the incorporation of crumb rubber concrete into reinforced concrete structures, which serves as a material that has the potential to increase the structure's ability to disperse energy, would be beneficial. During the course of the testing procedure,

each of the three frames and each of the six reinforced concrete columns were put through axial compression in addition to being subjected to reversed cyclic loads.

In spite of the fact that the compressive strength of rubberized elements was 28% lower than that of conventional concrete components, the system as a whole was able to withstand a lateral load that was approximately 92% of what traditional concrete elements were capable of managing. This was the case even though the rubberized elements had the ability to withstand a load. This demonstrated that rubber can be used in concrete columns despite having a lower axial compressive strength without having a detrimental impact on the final lateral strength or deformability of the columns. This was demonstrated by the fact that there was no change in either of these characteristics as a result of using rubber. This came to light as a consequence of the investigation that was outlined up top. In addition, the use of rubberized concrete might delay the commencement of the damage caused by an earthquake, which in turn can help to serve to decrease the degree of the damage. The concrete cover spalling was delayed due to the increased flexibility of rubberized concrete in comparison to conventional concrete, and the amount of concrete cracking that occurred was reduced to a minimum. Both of these benefits can be attributed to the fact that rubberized concrete is more elastic than conventional concrete. Because of this, the column cross-section was able to keep its integrity for a greater portion of the test than would have been conceivable in the event that it had not been subjected to this modification. Rubberized concrete is an alternative better for the environment than regular concrete and has the potential to be used in structural sections that are susceptible to the impacts of seismic loading.

Acknowledgements

References

[1] Oikonomou, N., & Mavridou, S. (2009). The use of waste tyre rubber in civil engineering works. *Sustainability of Construction Materials*, 213-238. doi: https://doi.org/10.1533/9781845695842.213

[2] Strukar, K., Kalman Šipoš, T., Miličević, I., & Bušić, R. (2019). Potential use of rubber as aggregate in structural reinforced concrete element – A review. *Engineering Structures*, **188**, 452-468. doi: https://doi.org/10.1016/j.engstruct.2019.03.031

[3] Bompa, D., Elghazouli, A., Xu, B., Stafford, P., & Ruiz-Teran, A. (2017). Experimental assessment and constitutive modelling of rubberised concrete materials. *Construction and Building Materials*, **137**, 246-260. doi: https://doi.org/10.1016/j.conbuildmat.2017.01.086

[4] Khaloo, A. R., Dehestani, M., & Rahmatabadi, P. (2008). Mechanical properties of concrete containing a high volume of tire–rubber particles. *Waste Management*, **28**(12), 2472-2482. doi: https://doi.org/10.1016/j.wasman.2008.01.015

[5] Li, D., Zhuge, Y., Gravina, R., & Mills, J. E. (2018). Compressive stress strain behavior of crumb rubber concrete (CRC) and application in reinforced CRC slab. *Construction and Building Materials*, **166**, 745-759. doi: https://doi.org/10.1016/j.conbuildmat.2018.01.142

[6] Zheng, L., Sharon Huo, X., & Yuan, Y. (2008). Experimental investigation on dynamic properties of rubberized concrete. *Construction and Building Materials*, **22(5)**, 939-947. doi: https://doi.org/10.1016/j.conbuildmat.2007.03.005

[7] Hernández-Olivares, F., Barluenga, G., Bollati, M., & Witoszek, B. (2002). Static and dynamic behaviour of recycled tyre rubber-filled concrete. *Cement and Concrete Research*, **32(10)**, 1587-1596. doi: https://doi.org/10.1016/S0008-8846(02)00833-5

[8] Strukar, K.; Kalman Šipoš, T.; Dokšanović, T.; Rodrigues, H. (2018) Experimental Study of Rubberized Concrete Stress-Strain Behavior for Improving Constitutive Models. *Materials*, *11*, 2245. doi: https://doi.org/10.3390/ma11112245

[9] Gupta, T., Chaudhary, S., & Sharma, R. K. (2014). Assessment of mechanical and durability properties of concrete containing waste rubber tire as fine aggregate. *Construction and Building Materials*, **73,** 562-574. doi: https://doi.org/10.1016/j.conbuildmat.2014.09.102

[10] Ganesan, N., Raj, B., Shashikala, A. P. and Nair, N. S. (2017) Effect of steel fibres on the strength and behaviour of Self Compacting Rubberised Concrete, Int. J. Civ. Eng. Technol.

[11] Ismail, M.K., Grazia, M.T., & Hassan, A.A. (2015): Mechanical Properties of Self-Consolidating Rubberized Concrete with Different Supplementary Cementing Materials. Int. Conf. Transp. Civ. Eng., pp. 68–74, doi: http://dx.doi.org/10.17758/UR.U0315331.

[12] AbdelAleem, B. H., & Hassan, A. A. (2018): Development of self-consolidating rubberized concrete incorporating silica fume. *Construction and Building Materials*, **161**, 389-397. doi: https://doi.org/10.1016/j.conbuildmat.2017.11.146

[13] Youssf, O., ElGawady, M. A., & Mills, J. E. (2015): Experimental Investigation of Crumb Rubber Concrete Columns under Seismic Loading. *Structures*, **3**, 13-27. doi: https://doi.org/10.1016/j.istruc.2015.02.005

[14] Moustafa, A., Gheni, A., and ElGawady, M.A. (2017): Shaking-Table Testing of High Energy–Dissipating Rubberized Concrete Columns, J. Bridg. Eng., 22 (8), doi: 10.1061/(ASCE)BE.1943-5592.0001077.

[15] Youssf, O., ElGawady, M. A., & Mills, J. E. (2016): Static cyclic behaviour of FRP-confined crumb rubber concrete columns. *Engineering Structures*, **113**, 371-387. doi: https://doi.org/10.1016/j.engstruct.2016.01.033

[16] Hassanli, R., Youssf, O., Mills, J. E. (2017): Seismic Performance of Precast Posttensioned Segmental FRP-Confined and Unconfined Crumb Rubber Concrete Columns, *J. Compos. Constr.*, 21(4), p. doi: 10.1061/(ASCE)CC.1943-5614.0000789.

[17] Karim, R., & Vincent, T. (2018): Performance of segmental self-centering rubberized concrete columns under different loading directions. *Journal of Building Engineering*, **20**, 285-302, doi: https://doi.org/10.1016/j.jobe.2018.08.003

[18] Li, Y., & Li, Y. (2017): Experimental study on performance of rubber particle and steel fiber composite toughening concrete. *Construction and Building Materials*, **146**, 267-275. doi: https://doi.org/10.1016/j.conbuildmat.2017.04.100

[19] Elghzaouli, A. Y., Bompa, D., Xu, B., Ruiz-Teran, A. and Stafford, P. (2018): Performance of rubberised RC members under cyclic loading, *16th European Conference on Earthquake Engineering* (16ECEE), Thessaloníki, Greece, 12 pages.

BEHAVIOR OF WELDED BOLT SHEAR CONNECTORS SUBJECTED TO REVERSED CYCLIC LOADING

Marines Perez [1], Carlos Alberto Bermudez [2], Tiziano Perea [3]

[1] *Ph.D. Candidate, Universidad Nacional de Colombia, Manizales, Colombia, mperezr@unal.edu.co*
[2] *Professor, Universidad Nacional de Colombia, Manizales, Colombia, cabermudezm@unal.edu.co*
[3] *Professor, Universidad Autonoma Metropolitana, Ciudad de Mexico, Mexico, tperea@azc.uam.mx*

Abstract

Conventional bolts fillet-welded to steel and embedded in concrete have been a common method of force transfer between steel and concrete materials in composite construction in some Latin American countries. Welded bolt shear connectors have been used in both low-rise and mid-rise constructions replacing headed steel stud shear connectors. Whereas the installation of headed studs requires the use of a special high voltage equipment, welded bolts can be welded with fillet welds using shielded metal arc welding process more economically.

Welded bolt shear connectors are also used in lateral load resisting composite systems. Natural cyclic loads from earthquakes cause connectors to be subjected to alternating shear forces. For this reason, the cyclic behavior of shear connectors is particularly important in these systems.

In this study, a series of experimental tests on composite push-out specimens with welded bolt shear connectors were performed to investigate the behavior of shear connectors subjected to fully reversed cyclic loading. Of specific interest was the behavior under low-cycle fatigue. Results show up to 57 % reduction in connector shear capacity under reversed cyclic loading compared to static capacity.

Keywords: shear connectors, welded bolts, low-cycle fatigue, composite structures, push-out tests.

1. Introduction

Composite steel-concrete structural systems are commonly used worldwide to resist both gravity loads and seismic forces due to the high strength and stiffness these systems provide. In both cases, it is essential that shear connectors can transfer the shear forces between the steel and concrete. In composite beams, for example, shear connectors must transfer the longitudinal shear forces between the steel beam and the concrete slab to provide higher strength and stiffness, thus reducing the mid-span deflection with a higher span-to-depth ratio compared to the bare steel or the concrete counterparts [1]. In collector elements of a seismic resistance system, the shear connectors must transmit diaphragm shear forces, even when the overall structure is designed without composite action [2]. In seismic resistance systems, such as in the system called steel frame with reinforced concrete infill wall and semirigid joints (SRCW), with headed studs as shear connectors in all around the infill wall perimeter, the composite interactions are achieved by the headed studs that transfer the shear forces between the steel frames and infill walls. According to [3], the headed studs are responsible for transferring most of lateral load (80-100 %), while the steel frames transfer around 10-20%, and the diagonal struts transfer around 10-15%.

The inertial forces induced in buildings during seismic events are cyclical with similar magnitudes in both directions. This is a significant difference from the cyclic loading expected on highway bridges where, even when loading is reverse, one direction loading is dominant. Furthermore, the number of cycles in a seismic event is much lower than those examined in fatigue studies. Low-cycle fatigue generally refers to loads that approach or exceed the yield capacity of a section, with failure occurring prior to 1000 load cycles [2]. In this research, the behavior of low-cycle fatigue of headed studs was studied from modified push-out tests and its results showed that there is a significant reduction in shear stud capacity when subjected to reverse cyclic loading. This reduction in capacity is due to a combination of strength degradation in the stud combined with concrete crushing, which causes the stress distribution to migrate up the shank of the stud. This increased bending stresses in the stud causing

earlier failures. Strength degradation occurred at less than 5 mm, so the authors recommended applying a reduction factor of 0.6 or less to the ultimate strength of the corresponding static push-out tests.

In [1], the cyclic behavior of bolted shear connectors in steel-concrete composite beams was experimentally studied from push-out tests. One conclusion of this research was that the load capacity of the bolted shear connectors in the monotonic specimens are much higher than that in the cyclic specimens at the same level of slip.

This paper focusses on the low-cycle fatigue behavior of welded bolts from push-out tests since, in some low-rise and mid-rise constructions in some Latin American countries (e.g., Colombia and Mexico), standard steel headed stud anchors are replaced by conventional steel bolts that are manually welded (SMAW) to the steel beam with fillet weld around the shank. Steel headed studs are replaced due to logistical issues in the installation process, particularly for the need of special high voltage equipment, and consequently, construction costs with welded bolts are expected to be less than with steel headed studs.

2. Materials and methods

Push-out tests with welded bolt shear connectors was performed at the Structures Laboratory of the Department of Civil Engineering at the National University of Colombia, campus Manizales. Bolts were fillet welded to the beam flange using shielded metal arc welding with E7018 electrode. The variables considered were diameter of bolt and the type of load (i.e., static, and cyclic). Three bolt diameters were considered: 12.7 mm (1/2 in), 15.9 mm (5/8 in) and 19.1 mm (3/4 in). Each specimen was tested with monotonic static loading and with reverse cyclic loading. A total of 18 specimens were tested.

2.1. Specimens

The specimens in this research are fabricated and tested in accordance with the modified tests of Annex B of Eurocode 4 [4]. They consist of two reinforced concrete slabs and an IPE200 steel beam with SAE grade 2 headed hexagonal bolts (F_u = 510 MPa = 74 ksi) welded by manual procedure (SMAW) according to the AWS D1.1. [5]. All concrete slabs have a strength of 27.6 MPa (4000 psi), reinforced by two electro-welded mesh with 6 mm bars spaced 150 mm apart, and dimensions of 120×500×600 mm. Figure 1 and Table 1 shows details of the specimens. The effective height-to-diameter ratio (h_{ef}/d) of the bolt was at least 4.0 (where h_{ef} is measured to the bottom of the bolt head), so failure is expected to occur in the bolt connector.
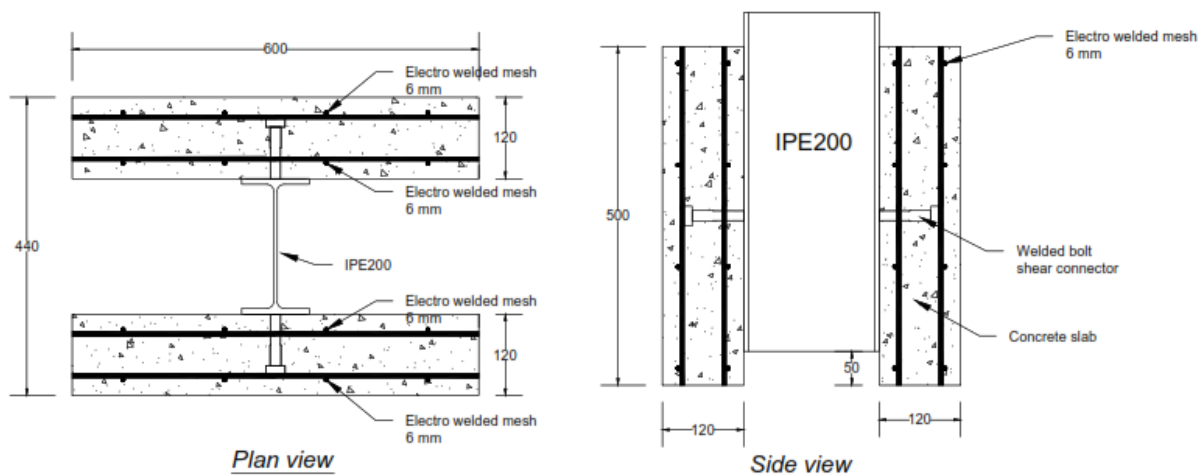
Figure 1. Specimen details (units: mm)

Table 1 – Tested specimens

Specimen	No of connectors per slab	Diameter (mm – in)	Effective height (h_{ef}) (mm – in)	h_{ef}/d	Dimensions of concrete slabs (mm)
PT1	1	12.7 – 1/2	72.6 – 3.0	6.0	120×500×600
PT2	1	15.9 – 5/8	72.6 – 3.0	4.8	120×500×600
PT3	1	19.1 – 3/4	72.6 – 3.0	4.0	120×500×600
PT1-RC	1	12.7 – 1/2	72.6 – 3.0	6.0	120×500×600
PT2-RC	1	15.9 – 5/8	72.6 – 3.0	4.8	120×500×600
PT3-RC	1	19.1 – 3/4	72.6 – 3.0	4.0	120×500×600

2.2. Experimental setup

The vertical force was applied in displacement control by the hydraulic jack having the capacity of 500 kN. In the first series of tests, the load was applied continually until failure. In the seconds series of tests, the specimens were loaded with cyclic loading according to the test method B of ASTM E2126 standard [6]. Displacement controlled loading procedure involves displacement cycles grouped in phases at incrementally increasing displacement levels. Loading schedule consists of two displacement patterns. The first displacement pattern consists of five single fully reversed cycles at displacements of 1.25%, 2.5%, 5%, 7.5%, and 10% of the ultimate displacement Δ_m. The second displacement pattern consists of phases, each containing three fully reversed cycles of equal amplitude, at displacements of 20%, 40%, 60%, 80%, 100%, and 120% of the ultimate displacement Δ_m. The sequence of amplitudes is a function of the mean value of the ultimate displacement (Δ_m) obtained from specimens in the monotonic tests.

In monotonic tests, compressive load was applied through contact between plate of loading and the beam of the specimen as shown in Figure 2a. In reversal cyclic tests, with the aim to avoid any vertical displacement of the concrete slabs when tension load is applied, two steel beams were placed on the top of the concrete slabs and eight steel rods were used to connect these steel beams to the base steel beam as shown in Figure 2b.

a)   b)
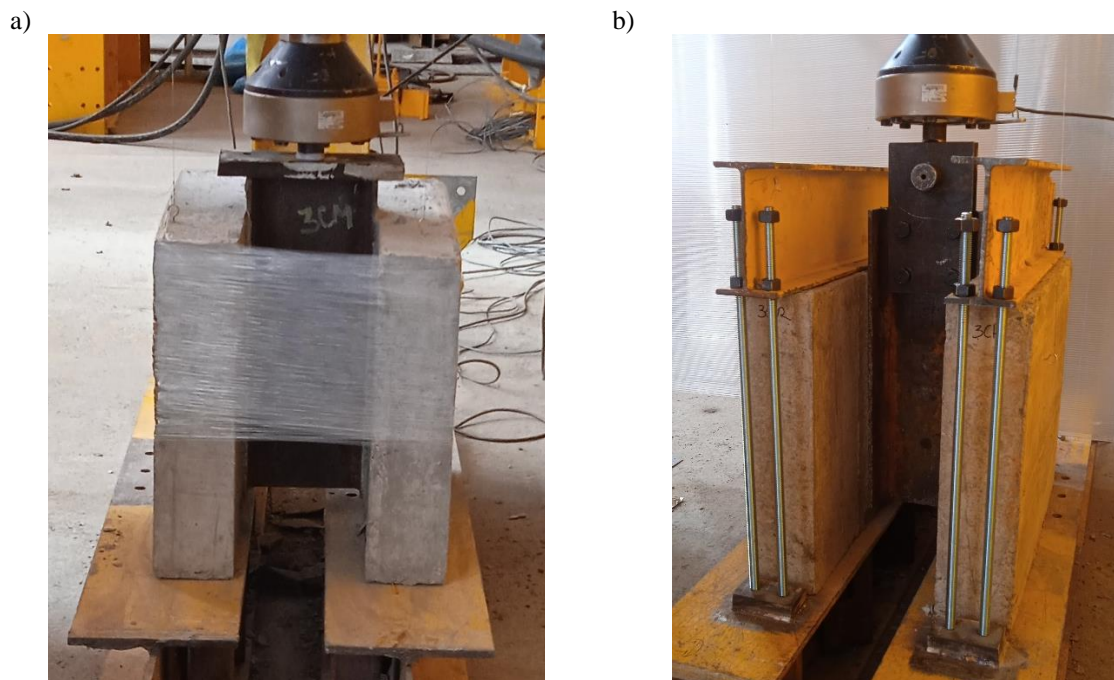
Figure 2. Experimental setup: a) monotonic test b) cyclic test

3. Results and discussion

The results were analyzed just in terms of load because the slip at the interface of both materials couldn't be measure. The displacement measured was the displacement of all system. Table 2 shows the maximum load results of the experimental monotonic tests. Figure 3 presents the load-displacement curves from monotonic push-out tests. We can see increases in capacity with the increase in diameter.

Table 2 – Load results of experimental monotonic tests

Specimen	Maximum load (kN)	Maximum load per connector (kN)	Failure mode
PT1-1	101.2	50.6	Shank failure
PT1-2	116.8	58.4	Shank failure
PT1-3	112.5	56.3	Shank failure
Mean	**110.2**	**55.1**	
PT2-1	153.2	76.6	Shank failure
PT2-2	151.0	75.5	Shank failure
PT2-3	164.7	82.4	Shank failure
Mean	**156.3**	**78.2**	
PT3-1	213.4	106.7	Shank failure
PT3-2	223.3	111.7	Shank failure
PT3-3	214.2	107.1	Shank failure
Mean	**217.0**	**108.5**	

Table 3 – Main results of experimental cyclic tests

Specimen	Maximum compression load (+) (kN)	Maximum tension load (−) (kN)	Failure load (kN)	Failure cycle	Δ_m (mm)	Failure mode
PT1-RC-1	75.8	-72.8	-48.4	Phase 80% Δ_m 2nd cycle tension		Shank failure
PT1-RC-2	78.1	-81.6	-81.6	Phase 80% Δ_m 1st cycle tension		Shank failure
PT1-RC-3	72.3	-71.1	-54.5	Phase 80% Δ_m 1st cycle tension		Shank failure
Mean	**75.4**	**-75.2**			**11.0**	
PT2-RC-1	157.8	-134.5	-109.8	Phase 100% Δ_m 2nd cycle tension		Shank failure
PT2-RC-2	124.3	-109.3	-105.4	Phase 100% Δ_m 1st cycle tension		Welding failure
PT2-RC-3	120.6	-101.1	-67.3	Phase 100% Δ_m 1st cycle tension		Welding failure
Mean	**134.2**	**-115.0**			**12.8**	
PT3-RC-1	203.8	-128.6	173	Phase 100% Δ_m 1st cycle compression		Shank failure
PT3-RC-2	178.9	-128.2	-96.5	Phase 100% Δ_m 1st cycle tension		Shank failure
PT3-RC-3	152.7	-160.7	152.7	Phase 100% Δ_m 1st cycle compression		Shank failure
Mean	**178.5**	**-139.2**			**16.0**	
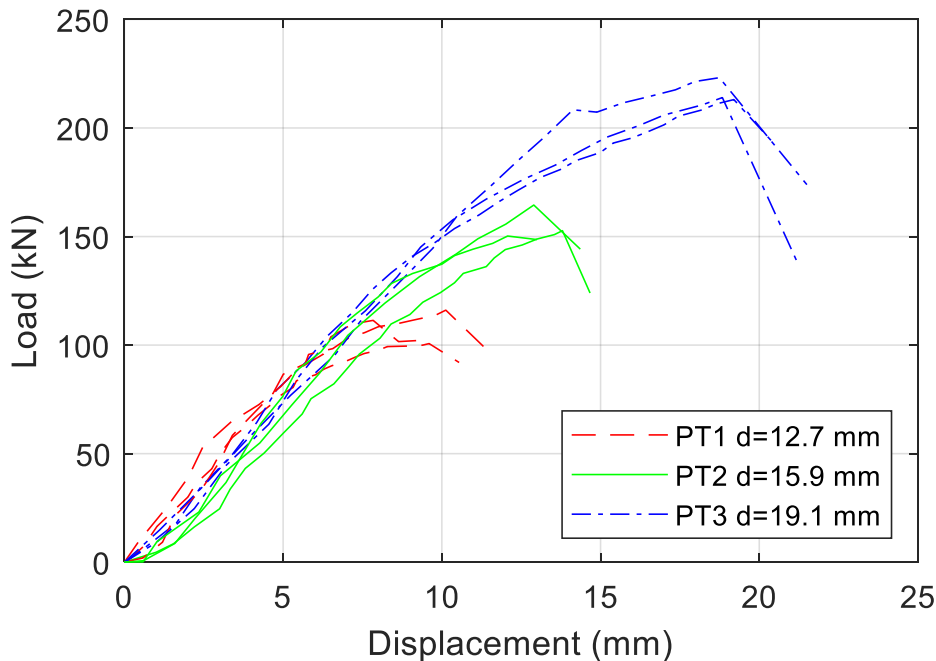
Figure 3. Load-displacement curves for monotonic tests

Table 3 summarizes the results of the experimental cyclic tests. This table contains the maximum load reached in both compression and tension, the value of the failure load, and the cycle in which failure occurs. Figure 4 shows the behavior from cyclic push-out tests compared to maximum monotonic mean load (Figure 4a-4c). Most of the specimens subjected to reversal cyclic loading did not reach the maximum monotonic loading as seen in these figures. The failure occurred before reaching the maximum monotonic capacity in 8 of the 9 cyclic tests. Figure 4d shows typical behavior for cyclic loading. A decrease in load for each cycle can be clearly seen. This decrease starts at the first phase, i.e., at displacements of ±20% of the ultimate displacement Δ_m. As seen in Figure 4d, the specimen PT1-RC-1 reached a displacement of ±80% Δ_m (±8.8 mm) in the first cycle and fails in the second cycle in tension load (-48.4 kN) as indicated in the "failure cycle" column in Table 3. In the first cycle of 80% Δ_m, the specimen reached 75.8 kN in compression and 72.8 kN in tension. At the second cycle of 80% Δ_m, the specimen reached 59.8 kN in compression and failed with 48.4 kN in tension.

Figure 5 shows the comparison between the envelope curves of the cyclic tests with the monotonic curves. As general trend, cyclic specimens have shown a reduction in strength capacity. Figure 6 shows the percentage reduction due to the cyclic loading effect. The reduction of the compression load with respect to the monotonic loading reaches 34% for the PT1 specimens (d = 12.7 mm), 23% for the PT2 specimens (d = 15.9 mm), and 30% for the PT3 specimens (d = 19.1 mm), while the tension load reaches 35% for the PT1 and PT2 specimens, and 41% for the PT3 specimens. The reduction in failure load was even greater, reaching 56% for the PT1 and PT3 specimens, and 57% for the PT2 specimens. In 6 of 9 cyclic tests, the failure load was below the maximum load achieved in early cycles of the series due to low-cycle fatigue in the steel or degradation in the concrete.

a) Diameter 12.7 mm
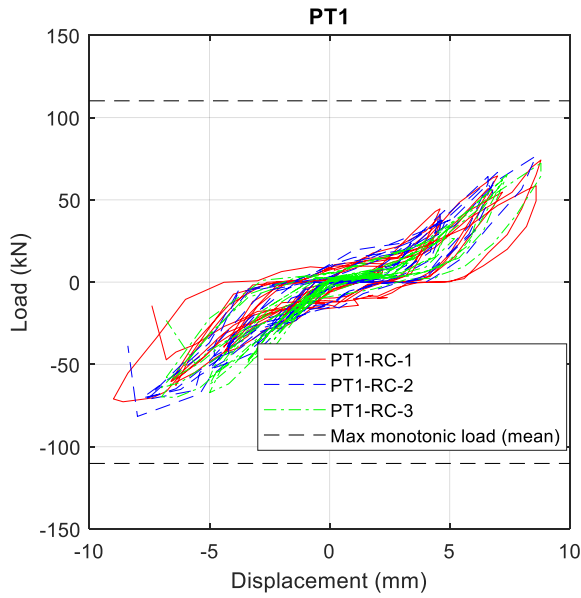
b) Diameter 15.9 mm
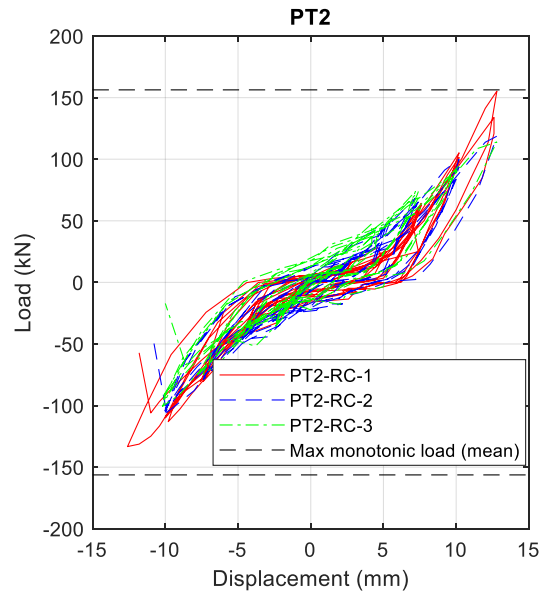
c) Diameter 19.1 mm
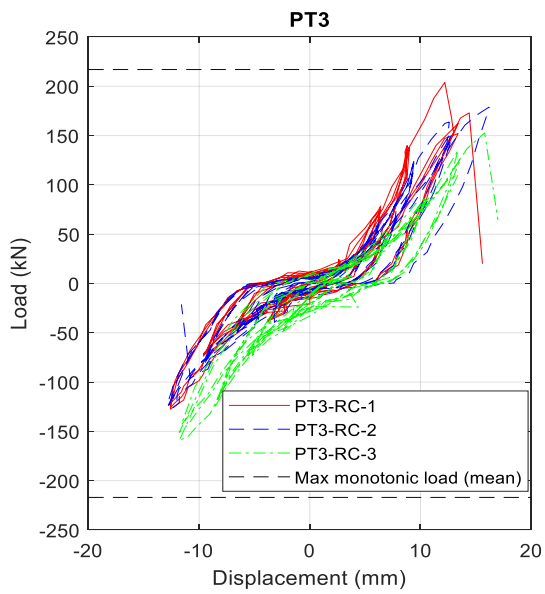
d) Typical cyclic load-displacement curves
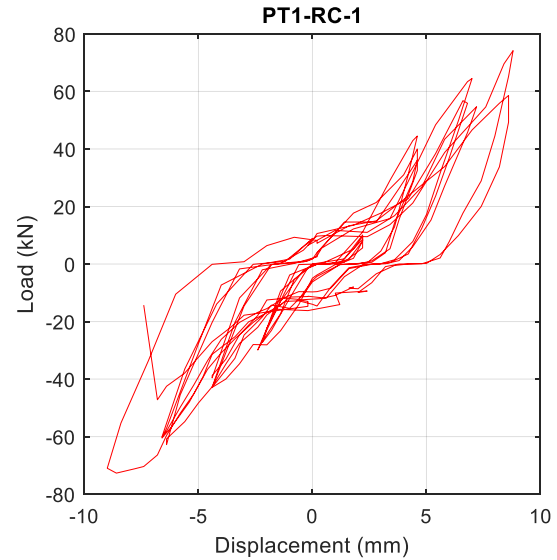
Figure 4. Load-displacement curves for cyclic tests
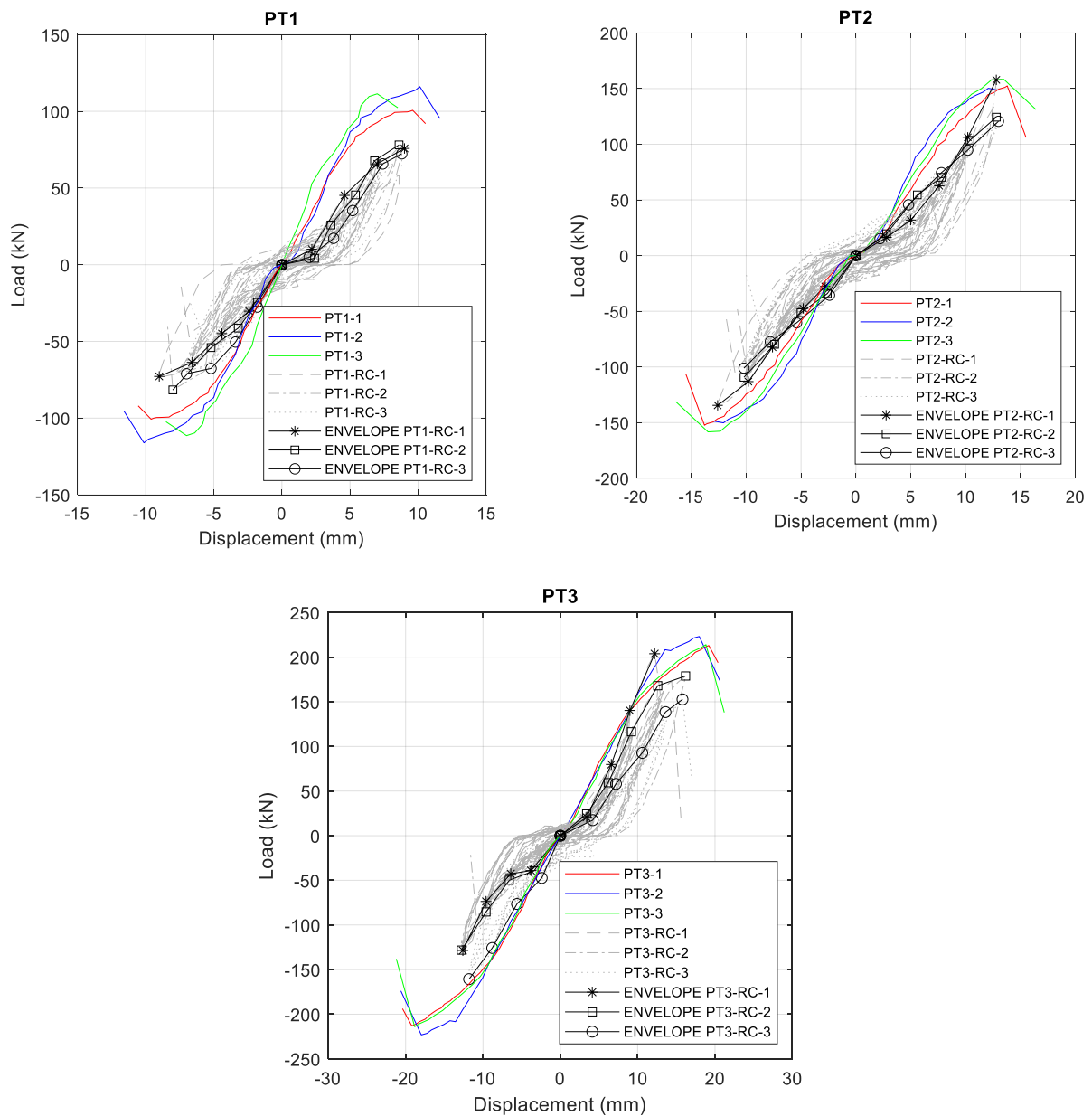
Figure 5. Comparison between envelopes of the cyclic test with the monotonic curves

Figure 7 shows the typical failure modes for the three diameters with both monotonic and cyclic loading. As seen in this figure, two failures modes occurred, where one mode of failure was shear rupture between the threads at the bolt shank at the top of the welding, and the other mode was welding failure. Except for the PT2-RC-2 and PT2-RC-3 specimens, all series of tests have the same shear failure at the bolt shank (see Table 2 and Table 3). There is no evidence of concrete crushing, except for the concrete located at the base of the bolt. Inspection after the tests revealed that the maximum bolt slip in monotonic loading was around 4 mm for the PT1 specimens, around 5 mm for the PT2 specimens, and around 6 mm for the PT3 specimens. An evident reduction of slip capacity of bolt due to cyclic loading for all diameters can be observed in Figure 7. Inspection after the tests revealed that the slip achieved in cyclic loading was around 2 mm for all the specimens.
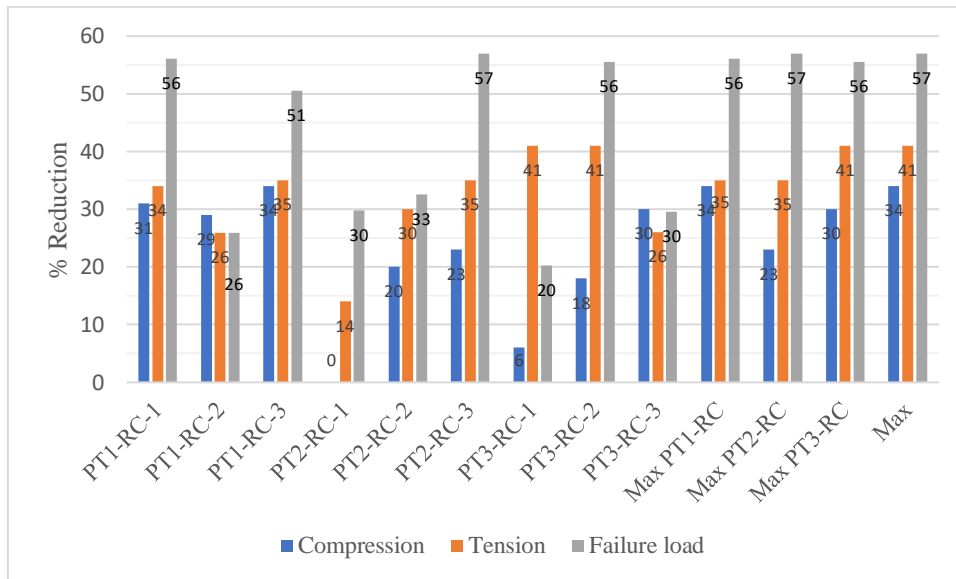
Figure 6. Percentage reduction in capacity due to cyclic loading
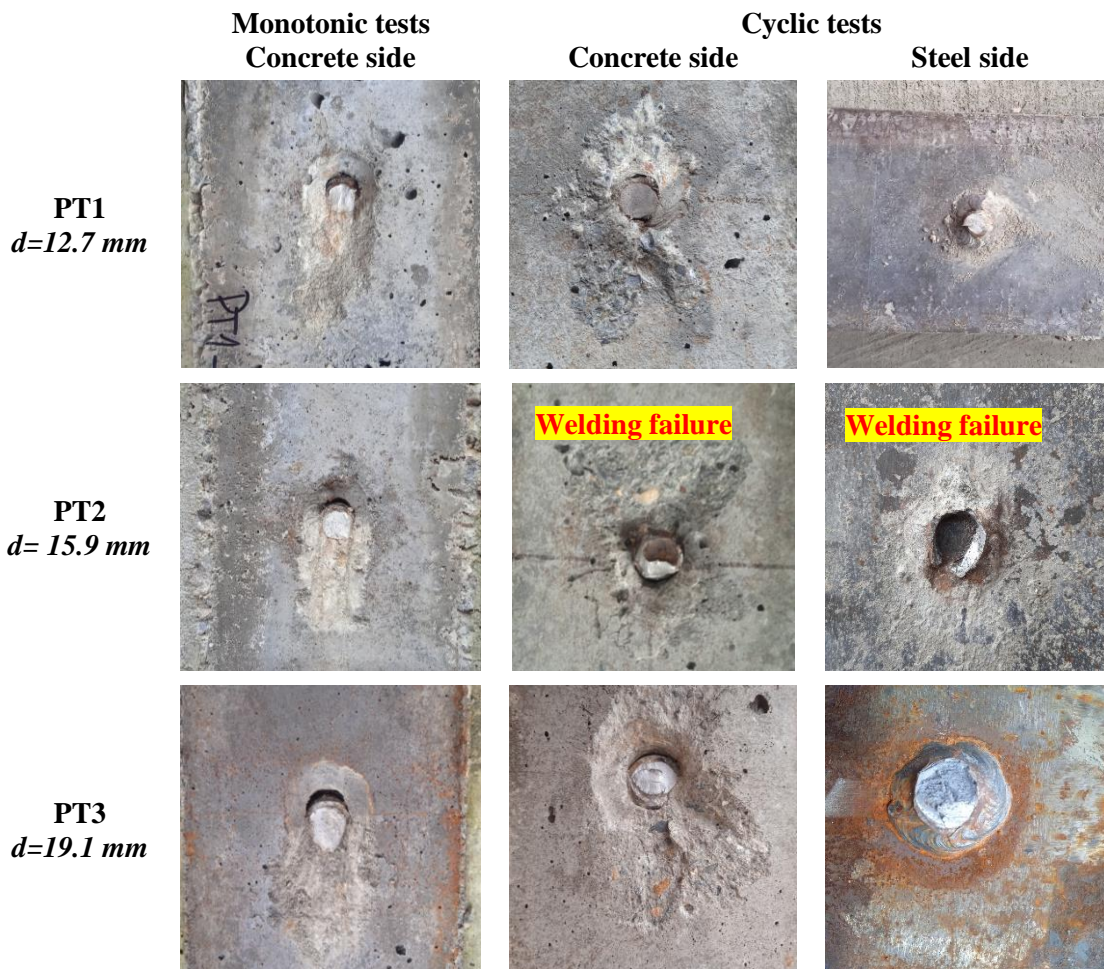
Figure 7. Typical failure modes

4. Conclusions

A series of experimental tests on push-out specimens with variable bolt diameter were performed to investigate the behavior of welded bolts shear connectors subjected to fully reversed cyclic loading. The obtained results showed that the diameter is a significant variable to increase the shear capacity of welded bolts in both monotonic and cyclic loading. The load capacity and slip capacity increased with the increased of diameter. When welded bolts were subjected to fully reversal cyclic loading, a significant reduction in shear capacity was observed. This reduction was up to 57% of the failure load. Therefore, it is recommended that a reduction factor less than or equal to 0.43 be applied to the monotonic shear capacity of welded bolts when considering low-cycle fatigue. This factor may need to be reviewed when applied to prediction models of capacity.

Acknowledgements

References

[1] Ataei, A., Zeynalian, M., Yazdi, Y. (2019): Cyclic behaviour of bolted shear connectors in steel-concrete composite beams. *Engineering Structures.* 198, 109455, doi: https://doi.org/10.1016/j.engstruct.2019.109455.

[2] Civjan S.A., Singh P. (2003): Behavior of shear studs subjected to fully reversed cyclic loading. *Journal of Structural Engineering ASCE.* **129** (11), 1466–74, doi: https://doi.org/10.1061/(ASCE)0733-9445(2003)129:11(1466)

[3] Xiaotong, P., Qiang, G., Chen, L. (2008): Experimental study on the composite steel frame-RC infill wall structure, *14WCEE* Fourteenth World Conference on Earthquake Engineering, Beijing, China, 8 pages.

[4] Eurocode-4 (2011): Design of composite steel and concrete structures — Part 1.1: General rules and rules for buildings, European Standard.

[5] American Welding Society (AWS) (2000): Structural welding code – Steel AWSD1.1:2000. American Welding Society, Miami.

[6] ASTM E2126-11 (2011): Standard Test Methods for Cyclic (Reversed) Load Test for Shear Resistance of Vertical Elements of the Lateral Force Resisting Systems for Buildings, American Society for Testing and Materials, West Conshohocken PA.

PUSHOVER ANALYSIS OF A 12-STOREY CROSS-LAMINATED TIMBER BUILDING

Luka Naumovski [1], Matija Gams [2], Tomaž Pazlar [3], Boris Azinović [4]

[1] *Research Assistant, Slovenian National Building and Civil Engineering Institute, luka.naumovski@zag.si*
[2] *Assist. Prof., University of Ljubljana, Faculty of Civil and Geodetic Engineering, matija.gams@fgg.uni-lj.si*
[3] *Head of Section for Timber Structures, Slovenian National Building and Civil Engineering Institute, tomaz.pazlar@zag.si*
[4] *PostDoc Researcher, Slovenian National Building and Civil Engineering Institute, boris.azinovic@zag.si*

Abstract

Due to recent developments in net-zero policy, cross-laminated timber (CLT) structures, with their low carbon footprint and potential competitiveness with steel and concrete structures, have gained popularity and are also considered in earthquake-prone regions. The present study analyses whether a seismically inadequate 12-storey residential building from the 1960s can be replaced with a 12-storey platform-type CLT building. The structural model is developed in two steps. In the first step, a nonlinear model of a single shear wall is calibrated against experiments and data from the literature. The CLT shear walls are modelled as elastic orthotropic shell elements and the various connections (wall-to-foundation and wall-to-floor) as nonlinear spring-link elements. The model is expanded in the second step to the entire structure and analysed using the basic and extended N2 method and displacement-based design (DBD). Response and seismic behaviour are assessed by analysing global and local limit states. The critical results of the analyses reveal large lateral displacements and local failures of connections. Based on the nonlinear analysis and the assumptions used in the model, it is demonstrated that a multi-story CLT platform-type building could be considered also for regions with moderate seismic risk, such as Ljubljana.

Keywords: *CLT, timber engineering, multi-storey timber buildings, earthquake engineering, displacement-based seismic design, pushover analysis, seismic design, N2 method.*

1. Introduction

The potential of Cross laminated timber (CLT) can play a vital role in meeting the challenges of the 21st century construction industry. As a result, it is increasingly being used for mid-rise multi-story buildings such as condominiums, commercial buildings, offices and public buildings. Nevertheless, seismic design of taller timber buildings has only been a topic of mostly isolated research for less than 20 years, with the current state of knowledge still lagging behind that of concrete or steel and currently not included in the EN 1998-1:2004 [1].

The most extensive experimental studies of full-scale single and multi-story CLT structures have been conducted as part of the SOFIE project (e.g. [2]–[4]). Experimental shake table tests were carried out on one, three and seven-story platform-type buildings. All investigated structures were erected with narrow or segmented CLT panels with typical hold-downs (HD) and angle brackets (AB). Other test programmes included full-scale CLT buildings and CLT as a seismic force resisting system (e.g., [5]–[7]), monotonic and cyclic loading tests of CLT walls (e.g., [8]–[10]), cyclic behaviour of HD and AB, and presence of shear-axial interaction (e.g., [11]–[15]). Nevertheless, the overall performance of CLT based structural systems is not fully understood and tested in real earthquake scenarios. Therefore, further experimental and numerical investigations of CLT structures, substructures, and connections are necessary to fully identify the potential undesirable behaviour.

Considering that CLT panels are relatively rigid and delivered prefabricated or in modules on the construction site, connections play a critical role in the assembly and behaviour of the structure. In addition, the properties of the connections (e.g., stiffness, slip modulus, orientation) affect the final stiffness of the system and thus the vibration period and mode shapes of the structure, which indirectly affects the seismic forces. Thus, it cannot be argued that the behaviour of CLT structures and the ability to dissipate energy are directly affected and modified by all types of connections. Several studies and manuals have introduced linear and nonlinear modelling techniques for the design. The mechanical connections have been modelled by elastic and nonlinear springs, links, trusses, and frame elements, however friction has not been directly considered (e.g., [10], [16]–[20]).

The new generation of Eurocodes, Chapter 8 within Eurocode 8, will address many topics and areas of the design process that are not present in the current version, including CLT-based structural systems with definitions of dissipative and non-dissipative zones, and q - behaviour factors recommendations based on different dynamic analyses for different ductility classes, see e.g. [21], [22]. Such an approach will lead to an optimisation of the design process, since the current practice, for linear analysis assumes parameters based on engineering judgement, which in most cases, for a more accurate investigation, requires implementation of the nonlinear analysis. Finally, a new procedure for the application of nonlinear static or pushover analysis will be defined [23].

This paper aims to provide basic information on the mechanical performance of CLT platform type structures consisting of CLT panels for high-rise buildings subjected to seismic loads. The response of individual walls and ductile connections was simulated based on literature data and previously conducted experiments on the cyclic shear resistance of individual walls and connection elements. A nonlinear computational shear wall model with material orthotropy and the nonlinear behaviour of the connection elements was developed and further validated. The modelling principle was later on utilised in a three-dimensional nonlinear model used for the nonlinear analysis of the case study high-rise building. The structure consisted of large monolithic walls with low to moderate energy dissipation capacity. Three types of traditional connection systems were implemented: hold-downs (HDs), angle brackets (ABs) and screwed or nailed panel-to-panel vertical joints. The spectral displacements obtained by the N2 method were compared with the predefined limit states for the global and local limit states. Finally, the extended N2 and the calculated correction factors were used to estimate torsional effects.

2. Model description and assumptions

In this study, the nonlinearities that occur in a CLT building during a seismic action are represented by nonlinear springs and link elements combined with rigid frame elements. In the proposed model for numerical simulations, which adopts a combination of approaches by Yasumura et al. [9] and Follesa et al. [16], they are represented by spring or link elements with negligible length between two nodes. Depending on the options provided by the software used - *RFEM* 5.24 or *ETABS 19* – spring or link elements were selected. *RFEM* was chosen for the design as it is more commonly used by practising engineers in the design of CLT structures, however, for the pushover analysis of the case study building, the used version lacked an appropriate force lead - displacement controlled solver. Therefore, *ETABS* was implemented as a substitute for the nonlinear pushover analysis.

As shown in Fig. 1 with a pair of CLT wall panels and connections at the base of the building and connections with the walls of the upper floor, five types of FE elements are used for a 3D model:

- 4-noded, 24 DOFs, shell elements with membrane and bending capabilities for the CLT wall panels with a typical mesh of 0.5 x 0.5 m and appropriate material properties,
- nonlinear tension-only link or spring elements as a ductile HD connection,
- nonlinear shear-only link or spring elements as a ductile AB connection,
- nonlinear compression and friction elements as parallel to grain compression and friction,
- linear link or spring elements with suitable stiffness as self-tapping screws (STS).
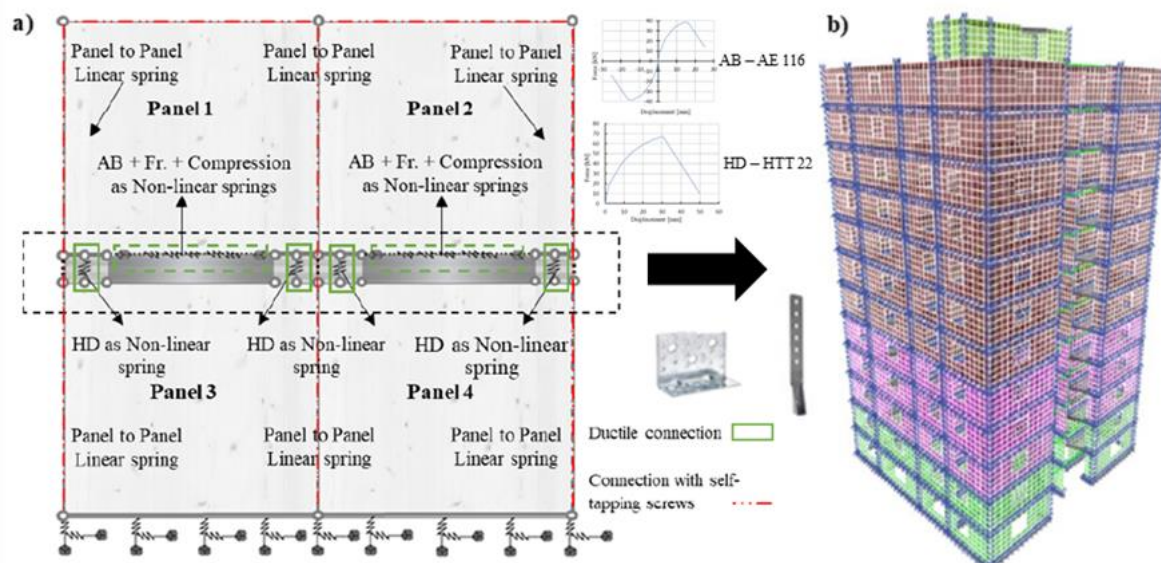
Figure 1. a) Proposed modelling principle and input parameters used for the shear-only and tension-only connection elements; b) Model application – a 12-storey case study building.

The model is based on some simplified assumptions:

- connections between perpendicular walls are assumed to be rigid,
- connections between floors and supporting walls are assumed to be rigid,
- perpendicular and parallel to grain compression properties of timber are not considered,
- the simultaneous presence of shear-axial interaction in the HDs and ABs is not addressed,
- the friction model is based on constant friction coefficient values from experimental data [24],
- the obtained vertical load from the top reactions of every wall panel, based on the linear analysis for vertical loads, is applied directly on wall panels,
- masses are concentrated at mass centres of floors,
- floors are considered as in-plane rigid diaphragms.

For more detailed information on the model principles and assumptions please refer to [25].

The hysteretic and monotonic behaviour of six different configurations of tested CLT wall panels in the OPTIMBERQUAKE project was used to validate the proposed model, as listed in Table 1 and shown in Fig. 2. Please refer to [9] and [13] for further reading and additional data.

Table 1. List of the wall setups for model validation [9].

Test series	Test	Anchoring	Support	Vertical load	Protocol
I + II	W-CLT-1.1	2 HD, 3 AB	rigid (steel)	10 kN/m	monotonic
	W-CLT-1.2	2 HD, 3 AB	rigid (steel)	10 kN/m	ISO
	W-CLT-2.1	2 HD, 3 AB	rigid (steel)	50 kN/m	monotonic
	W-CLT-2.2	2 HD, 3 AB	rigid (steel)	50 kN/m	ISO
IV	W-CLT-4.3	2 HD, 3 AB	rigid (steel)	100 kN/m	ISO

For the sake of comparison, the numerical models reproduced the geometry, mechanical properties, loading, and boundary conditions of the tested specimens and were analysed using a multi-step nonlinear static analysis. The numerical model in *RFEM* was used for the purpose of investigating the influence of friction and contribution to overall top displacement, while the suitably adapted *ETABS* model was used further for analysing the case study building. The models were validated by comparing the shear load-displacement curve and contribution to the average total top displacement, as shown in Table 2. As expected, the deformations from the numerical simulations showed that if friction is considered, the resistance to shear and slip is higher. Moreover, a lower bearing capacity and a decrease in deformation capacity were also observed in models without friction, although the difference on a global scale was insignificant. The maximum deviation from the average test value of each contributor was ≈ 10 %. However, in the last test series, the observed strong nonlinear behaviour on both comparison levels is slightly different, indicating that the model is more suitable for low to midrange vertical loads since it does not include irreversible (plastic) deformation of CLT. Nevertheless, the observed numerical results were sufficiently accurate for using on a CLT building modelling scale, since as mentioned the margin of error between comparable values from experiments and numerical analysis was in the range of 10%.
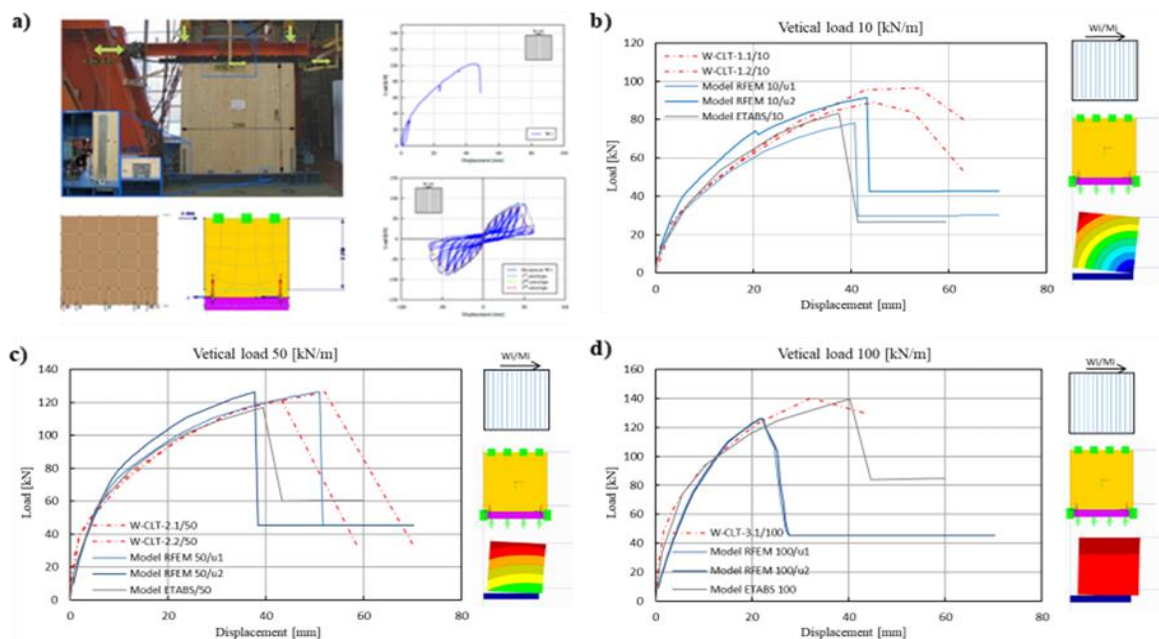
Figure 2. a) Example of a wall panel test setup [9] and nonlinear FE models [25]; Experimental and numerical shear load-displacement curves for series I, II & IV with vertical load: b) 10 kN/m, c) 50 kN/m & d) 100 kN/m.

Table 2. Comparison of average numerical and experimental results for the overall deflection - rocking, slip and CLT deformation as a percentage of the total shear displacement at the top.

Test	Experimental value			Models 10/50/100 u1			Models 10/50/100 u2		
	Slip:	Rocking:	CLT:	Slip:	Rocking:	CLT:	Slip:	Rocking:	CLT:
W-CLT-1.1	26%	69.5%	4.5%	18 %	66 %	16 %	23 %	60 %	17 %
W-CLT-1.2									
W-CLT-2.1	42%	47.5%	10.5%	37 %	44 %	19 %	45 %	33 %	22 %
W-CLT-2.2									
W-CLT-4.3	43 %	44 %	13 %	64 %	9 %	27 %	66 %	7 %	27 %

models u1 - friction coefficient = 0.5   *models u2 - without friction*

Based on the validated results, the proposed model and input data for the link and spring properties were used as a suitable approximation for the modelling and numerical simulations of the case study CLT building, which was considered as a replacement possibility of seismically inadequate unreinforced concrete and masonry multi-story apartment buildings built in the 1960s in Ljubljana, when suitable earthquake codes did not exist. The case study corresponds to the gross dimensions of the old building, with a typical floor plan in a rectangular shape of 21.7 m x 19.6 m used in all floors and a maximum height of 39.6 m with a storey height of 3.0 m. The CLT building was proposed due to its fast erection time and improved sustainability aspects when compared to other alternatives.

The main load-bearing structure of the proposed platform type building consists of massive CLT wall and floor panels with various thicknesses and lamellae layout (CLT cross-section reduces with storey level), and steel beams along the edges or the cantilever balconies for larger spans, as illustrated in Fig. 3. The vertical means of communication, elevators and stairs, are located in the CLT core, which consists of panels subdivided according to the maximum available production length and width. Transport logistics are also taken into account. Thus, the core is divided into three vertical segments, two segments of 16.0 m and 7.0 m, with different widths between 2.4 – 3.5 m and a total height of 39 m. This warrants a rigid box-like behaviour of the core. The perimeter of the building consists of panels with openings, while the other CLT panels are massive - without any openings. The complete design process of the cross-sections was carried out in three separate phases: initial selection with preliminary design tables, *RFEM* FE analysis for vertical loads, and final 2D check and utilisation of CLT panels performed in *Calculatis* [26]. In addition, the structure is assumed to be placed on a rigid reinforced concrete platform on soil type A. Finally, a conservative behaviour factor of 2.0 (as for monolithic shear walls) was assumed for the analysis.
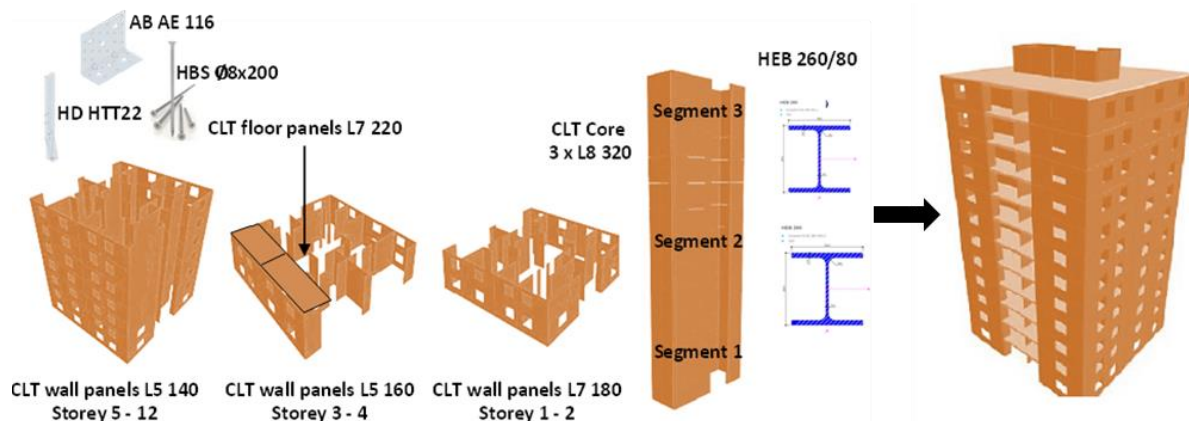
Figure 3. Final sizes of structural elements, CLT wall and floor panels type, CLT core segments and connection types considered for the design & seismic analysis of the case study building.

3. Results

3.1 Linear analysis

The behaviour of the structure was studied with the numerical models in *RFEM 5.24.* and *ETABS 19*. Initially, only the vertical load model was created, followed by the modified seismic model that takes into account the stiffness parameters of the connections, the seismic joint masses and the mass moments of inertia. All CLT panels were modelled as 2D shell elements with respect to their principal bearing direction. The core was modelled as a continuous element along the length of one segment, connections between adjacent core panels were completely hinged. The steel members were modelled as 1D frame elements with moment end releases, while the connections between adjacent panels were modelled by releasing the corresponding rotational DOFs for moment transfer by implementing line-hinges. AB and HD stiffness parameters were assigned within the line hinges or line releases as linear springs. The rigid, box-like behaviour of the core was replicated with a nodal constraint inserted as a diaphragm at each floor level of the CLT core. All of the supports were hinged line supports. The automatic FE mesh size was set to 0.5 x 0.5 m.

The seismic design for the assumed location in Ljubljana, corresponding to a seismic action of 0.25g, was performed in three phases, as shown in Fig. 4. First, the lateral force method provided the required number of shear connectors calculated from the distributed base shear per story. This was followed by optimisation using the response spectrum method, which provided the final arrangement of AB connections: storey 1 – 5 at ≈ 0.5 m, storey 6 – 10 at ≈ 0.5 - 1.0 m, and storey 11 – 12 at ≈ 1.0 - 1.5 m with a shear stiffness of 5000 kN/m per AB connection. HD connections were placed only at panels edges with an axial stiffness of 10000 kN/m per connection. Finally, vertical step joints between wall panels with a stiffness of 1500 kN/m per spring or 10500 kN/m per wall-to-wall connection were introduced as Self-tapping screws (STS) connections.
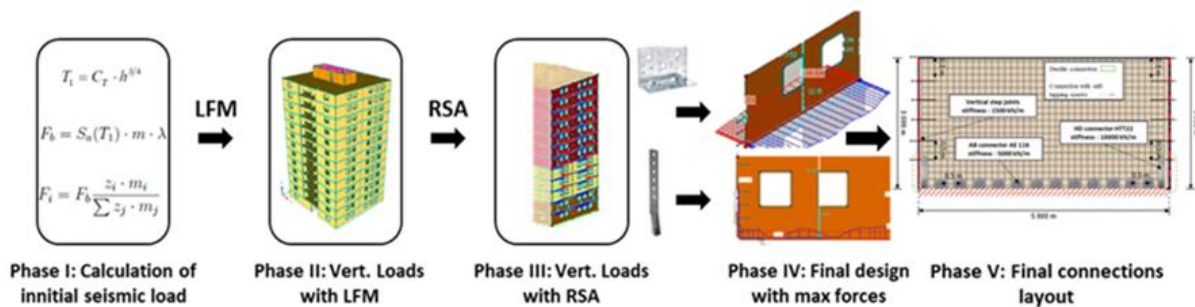
Figure 4. Phases of the seismic design procedure, with LFM as lateral force method and RSA as response spectrum analysis.
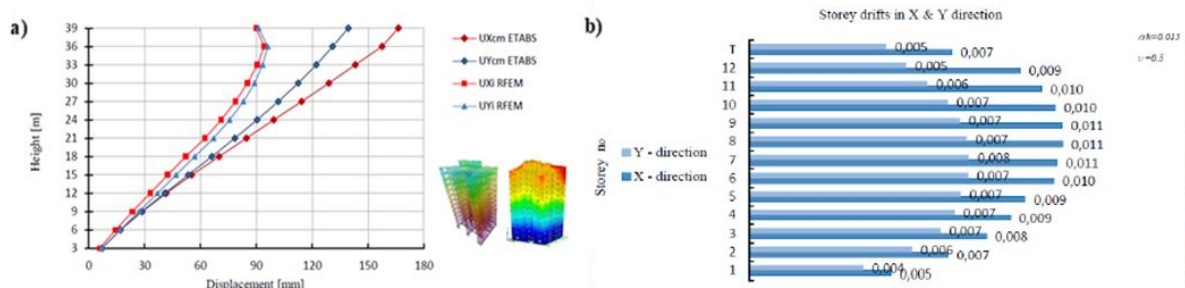
Figure 5. a) Displacements (U) of mass centres (cm/i) in X and Y direction for the ETABS and RFEM model – elastic response spectrum analysis; b) Limitation of interstorey drift check for damage limitation requirement as specified in EN 1998-1:2004 in X and Y direction for the ETABS model.

The obtained results from the linear analysis, as shown in Fig. 5, as expected indicate that the model in *RFEM* which incorporates line-hinges as linear springs is stiffer than the one made in *ETABS* with individual joint links. The difference is even more evident in higher stories, where the distance between individual elements becomes larger. Furthermore, the modal mass participation factor of the *RFEM* model is lower for the first two periods of vibration than in the *ETABS* model, which could also lead to an overall decrease of top storey displacements. Finally, the intersotey drift check as defined in EN 1998-1:2004 satisfied the selected design criteria.

3.2 Pushover analysis

The input parameters of the nonlinear ductile connection elements of the nonlinear model in *ETABS* were assumed to be the same as in the validated nonlinear modelling proposal. In addition, the typical wall scheme of the proposed model, as shown in Fig. 1, was extended to the entire structure. The first step of the pushover analysis was to apply gravity loads, followed by the lateral loads, which were displacement controlled at every storey centre of mass for X and Y direction separately and were monotonically increased in proportion to the predefined load pattern, uniform or modal, as specified in Chapter 4.3.3.4.2.2 of EN 1998-1:2004. The reference point, which was selected as the specified displacement control node for automatic termination of the analysis, was located at the roof slab. The pushover curve was created using the base shear, which was calculated as the sum of all reaction forces in the direction of lateral load application, and the top displacement at the reference point, which was recorded at each incremental step during the analysis, see Fig. 6.
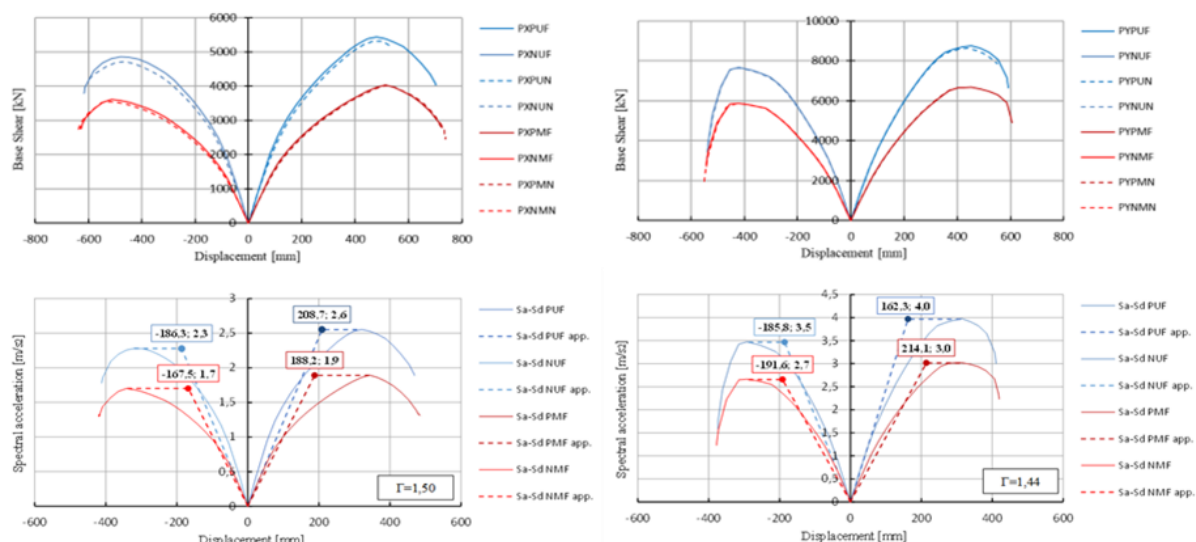
Figure 6. (above) Capacity curves from nonlinear pushover analysis in the positive (P) and negative (N) X (left) & Y (right) -direction for modal (M) and uniform (U) load pattern, model with friction (F) and without (N); (below) Bilinear approximation of transformed SDOF capacity spectrum curves (Sa – Sd) in positive (P) and negative (N) X (left) & Y (right) -direction for modal (M) and uniform (U) load pattern with friction (F) and without (N).

An important step before determining the performance points, as the intersection between the demand spectrum and the capacity spectrum, is to convert the capacity curves into a capacity spectrum type curves, i.e., *Sa - Sd* diagram. The method is based on the idea that an MDOF system of a multi-story building can be transformed into an equivalent SDOF system [27]. This is necessary because it allows the response spectra to represent the seismic action and the building capacity curve to be compared with the demand. In addition, to determine the performance points using the N2 method based on the inelastic spectrum and the $R_\mu - \mu - T$ relationship given in EC8, a bilinear idealisation that applies the equal energy principle is required.

The performance evaluation of the reference building was performed using limit states predefined at two levels: (*i*) locally on individual elements and (*ii*) globally as structure occupancy levels. The local

levels were defined as specified in FEMA 356 (IO – Immediate Occupancy, LS – Life Safety and NC – Near Collapse) and are based on the achieved deformation of the implemented nonlinear ductile connections, AB and HD units, respectively. On the other hand, the global occupancy levels are associated with the predefined local levels, where: IO - the first element reaches the LS acceptance limit; LS – the first element reaches the NC acceptance limit; NC – more than 10 elements reach NC acceptance limit.

Based on the obtained results, listed in Table 3, it is noticeable that the performance points are mostly in a range where the period is higher than the upper limit of the period of the constant spectral acceleration branch – T_C. At the same time, performance points for the modal load pattern in the X-direction were mainly found near the branch with constant spectral displacement.

Table 3. Calculated spectral displacement values of performance points for different demand spectra, direction and load pattern – uniform (E) and modal (M) for an equivalent SDOF system – N2 method.

Demand a_g max [g]	Spectral displacement of the performance point [mm]							
	XM+	XM-	YM+	YM-	XE+	XE-	YE+	YE-
0.250	122.7	122.5	104.0	105.0	111.7	108.1	80.3	93.8
0.325	159.9	159.3	135.3	136.5	145.0	140.5	102.7	121.9
0.350	172.7	171.9	145.7	146.8	159.2	151.3	110.8	131.5

The capacity curves shown in Fig. 7 and Fig. 8 with the indicated global limit states and the calculated spectral displacements for different demand spectra – performance points, and the total base shear for different demand spectra, are used to show the behaviour of the building on a global level. The results confirm that both loading patterns – uniform and modal should be considered for design, as both could be critical for undesirable structural behaviour at both global and local level. The patterns implicitly account for the different deformations considered in the simplified model – bending, rocking, shear, and sliding – inherent for CLT structures. Nevertheless, the spectral displacement from the N2 method is significantly higher for the modal load pattern. As we can see from the obtained capacity curves in both perpendicular directions, the analysis in positive and negative direction is mandatory since the curves differ significantly.
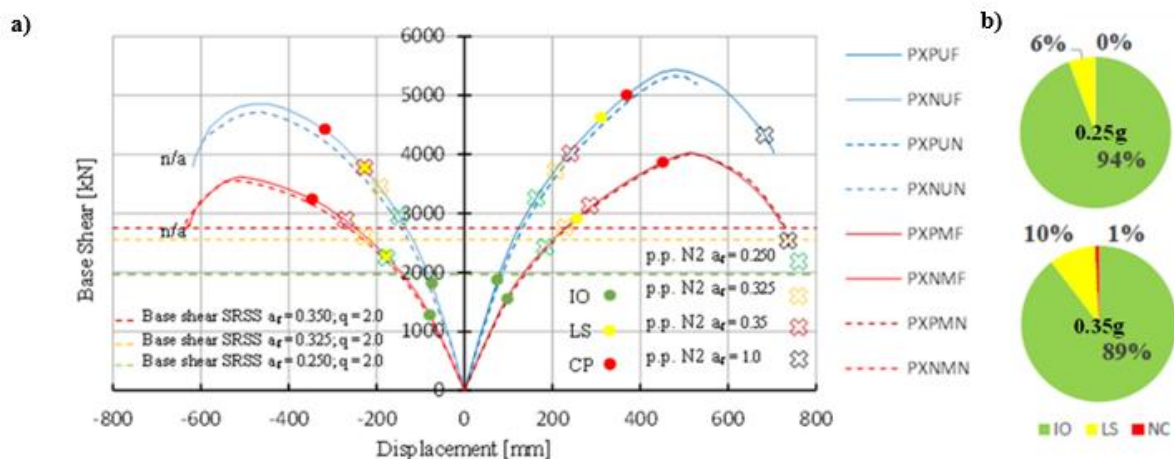
*g - acceleration of gravity (9.81 m/s²); SRSS - Square Root of the Sum of the Squares; p.p – perfomance point N2 method.

Figure 7. a) Capacity curves in positive (P) & negative (N) X-direction for uniform (U) and modal (M) load pattern with friction (F) and without (N), indicated global limit states, N2 p.p., and total base shear obtained based on different design spectrum; b) Yielding of connection elements with reference to local limit states for p.p. N2 a_g 0.25 g & 0.35 g and pushover analysis in positive X – direction with a modal load pattern.
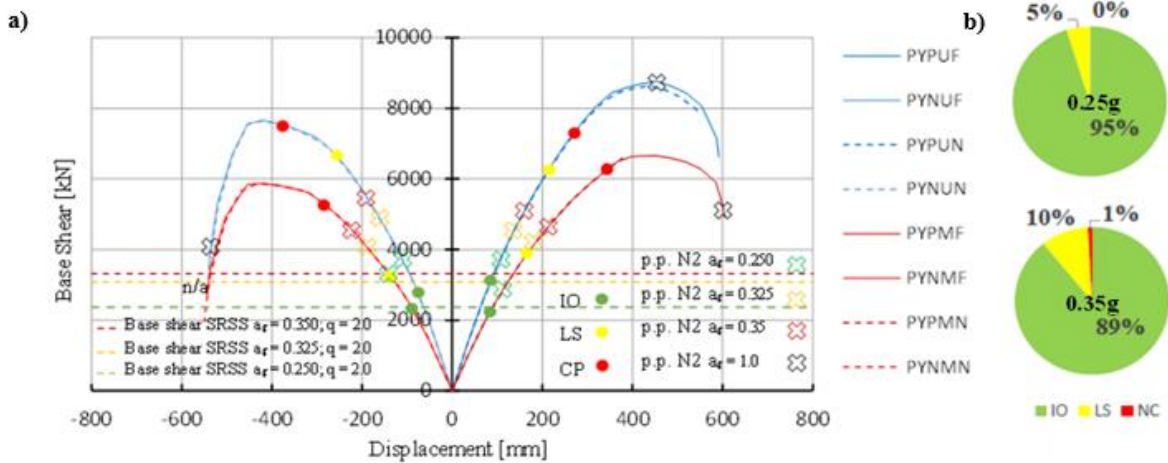
*g - acceleration of gravity (9.81 m/s²); SRSS - Square Root of the Sum of the Squares; p.p – perfomance point N2 method.

Figure 8. a) Capacity curves in positive (P) & negative (N) Y-direction for uniform (U) and modal (M) load pattern with friction (F) and without (N), indicated global limit states, N2 p.p., and total base shear obtained based on different design spectrum; b) Yielding of connection elements with reference to local limit states for p.p. N2 a_g 0.25 g & 0.35 g and pushover analysis in positive Y – direction with modal load pattern.

As further confirmation of the overall obtained results, the calculated values for the high peak ground accelerations were in agreement with the shake table tests conducted as part of the SOFIE project, where the unscaled Kobe (1995) earthquake - 0.91g resulted in horizontal displacements of the uppermost floors of about 1.0 % to 1.6 %. In comparison, the simplified numerical model and the spectral displacement determined by the N2 method were between 1.5 % and 1.7 %, and this for a much higher and heavier building. The analysis with reference to the local limit states of connections revealed that for both directions, on average, the highest degree of damage - above the IO state - of the connecting elements occurred on the outer walls with openings. As expected, the core segments were more subjected to rocking behaviour, resulting in an increased damage to the HD units, particularly those on the ground floor. In contrast to the core wall segments, pure shear behaviour was observed in the section with the highest number of shear walls, resulting in a greater number of damaged AB units. The earlier discussed performance evaluation with reference to the local limit states and the level of reached limit state of connection elements for selected axis and the least favourable load scenarios for 0.35g peak ground acceleration are illustrated in Fig. 9. However, as already discussed, the simplified model does not account for the shear-axial interaction, especially the uplift load capacity of the ABs, which partially increases the load bearing capacity and changes the overall behaviour.
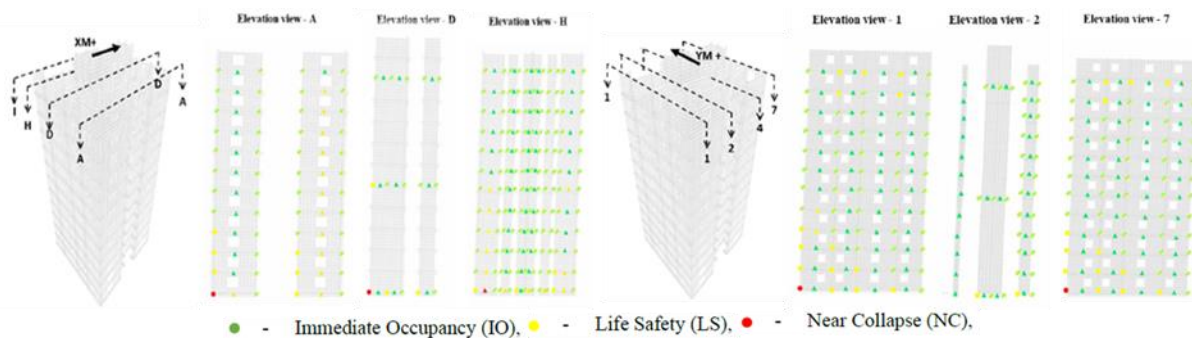
Figure 9. Yielding of connection elements for selected axes, AB and HD, with reference to local limit states for p.p. N2 a_g=0.35g and pushover analysis in positive X and Y – direction with modal load pattern.

Although the effects of irregularities can have a significant impact on the behaviour of the structure, they are not well known for CLT structures. Here, the extended N2 estimates the possible unfavourable effect of irregularities in the geometry. The calculated correction factors differed depending on the subsets of the load pattern considered and the load direction. For both directions and patterns, the factors corresponded to values between 1.0 and 1.4, with the less stiff X - direction leading to higher values, as shown in Fig. 10. Since the extended method provides adequately conservative results for structures that are not too torsionally flexible, the estimations of the increase of the absolute displacements seem probable.
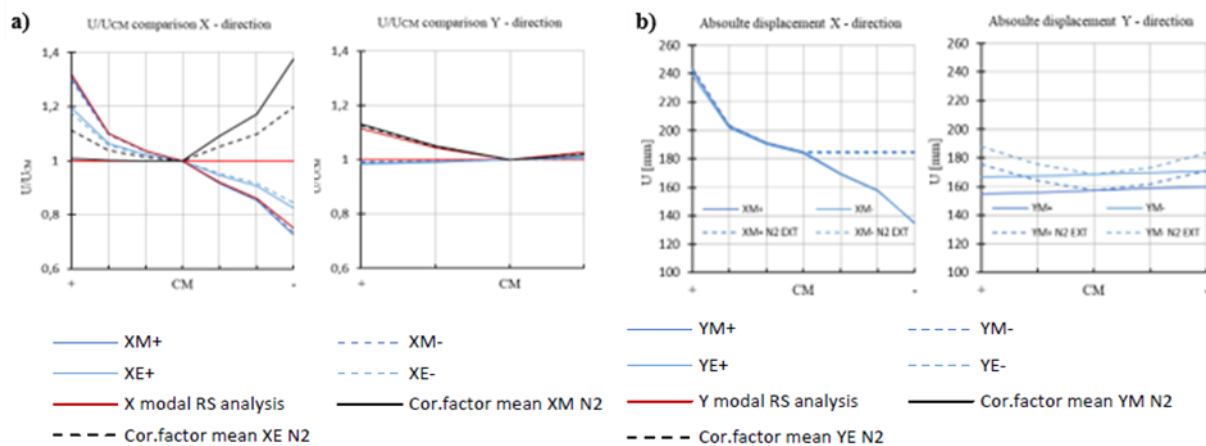
Figure 10. a) Torsional effects in terms of normalised top displacements obtained by elastic modal analysis, by pushover analysis for modal (M) and uniform (E) load pattern for the positive (+) and negative (-) direction and the corresponding correction factors for the extended N2 method – X (left) and Y (right); b) Torsional effects in terms of absolute top displacements - 0.25 g, obtained by the normal and the extended N2 method for modal load pattern for the positive (+) and negative (-) direction with the associated correction factor – X (left) and Y (right).

For further reading and more information regarding the modelling procedure and additional input data used for the case study building, as well as detailed representation of reached damage levels of connection elements with reference to local limit states please refer to [25].

4. Conclusion and future work

As architectural design proposals for tall timber buildings are becoming increasingly more present in earthquake-prone areas, seismic design is becoming increasingly important. Since multi-storey CLT-based structures are a relatively new structural system, there is still a lack of experience, uncertainty about modelling assumptions, and insufficient references, thus it is a challenge to develop an accurate nonlinear model for the design. As a result, this study investigated the seismic performance of CLT structures by developing a nonlinear computational shear-wall model of a 12-storey platform-type building. The results presented met the predefined performance design objectives for a maximum considered earthquake on both levels. At local level, the connections damage level above the IO – state ranged between 5% and 11%. In addition, a satisfactory global behaviour with yielding of connection elements distributed throughout the whole structure was also observed. The extended N2 lead to an increase of all relevant quantities on both edges in both directions, especially X. However, it was shown that the torsional effects are not significant and do not cause global failure of the analysed structure, even in cases where the global level limit states are decided upon rather conservative criteria (effects on non-structural secondary elements were not considered).

Although the results of the nonlinear static analysis and the N2 method (for $a_g = 0.25 - 0.35$ g), did not expose a significantly damaged CLT structure or an undesirable global failure mechanism, it should be noted that such structures in seismically active areas should be designed with caution.

Based on the findings, we assume that the building would have likely sustained the 2020 Petrinja earthquake, which in the epicentral area resulted in PGA bedrock values from 0.29 to 0.44 g [28], with mild to moderate damage levels. In this context, PGA is not a completely reliable indicator of the damaging capacity of the earthquake, as it does include its frequency. Nevertheless, a holistic design approach considering all accidental load situations might require contradictory solutions for high rise CLT buildings, such as for example an increase of mass at top stories in order to improve wind serviceability issues. Moreover, a direct comparison between the available test results acquired from simplified numerical models and real earthquake scenarios where the increase of the building height leads to complex material and geometric nonlinearities, is not always possible. Future experimental and numerical research should therefore aim at full-scale CLT structures testing campaigns, such as the ongoing NHERI Tall Wood Project of a 10-story timber building shake table test [29] and nonlinear time-history analyses with hysteric behaviour of the ductile connections implemented into the actual model, estimation of IDA curves, and calculation of fragility curves. Finally, a resilient-based seismic design methodology for future tall timber buildings should be developed.

Acknowledgements

References

[1] EN 1998-1: Eurocode 8: Design of structures for earthquake resistance – Part 1: General rules, seismic actions and rules for buildings, 2004.

[2] Ceccotti, A. and Follesa, M. (2006): Seismic behaviour of multi-storey XLam buildings, *In COST E29 International Workshop on Earthquake Engineering on Timber Structures* (pp. 81-95).

[3] Ceccotti, A., Sandhaas, C., Okabe, M., Yasumura, M., Minowa, C. and Kawai, N. (2013): SOFIE project– 3D shaking table test on a seven-storey full-scale cross-laminated timber building. *Earthquake Engineering & Structural Dynamics*, 42(13), pp.2003-2021, doi: https://doi.org/10.1002/eqe.2309

[4] Lauriola, M.P. and Sandhaas, C. (2006): Quasi-static and pseudo-dynamic tests on XLAM walls and buildings, *In Cost E29 international workshop on earthquake engineering on timber structures* (pp. 119-133).

[5] Flatscher, G. and Schickhofer, G. (2015): Shaking-table test of a cross-laminated timber structure. Proceedings of the Institution of Civil Engineers-Structures and Buildings, 168(11), pp.878-888, doi: https://doi.org/10.1680/stbu.13.00086

[6] Popovski, M. and Gavric, I. (2016): Performance of a 2-story CLT house subjected to lateral loads. *Journal of Structural Engineering*, 142(4), p.E4015006, doi: https://doi.org/10.1061/(ASCE)ST.1943-541X.0001315

[7] van de Lindt, J.W., Furley, J., Amini, M.O., Pei, S., Tamagnone, G., Barbosa, A.R., Rammer, D., Line, P., Fragiacomo, M. and Popovski, M. (2019): Experimental seismic behavior of a two-story CLT platform building. *Engineering Structures*, 183, pp.408-422, doi: https://doi.org/10.1016/j.engstruct.2018.12.079

[8] Dujic, B., Aicher, S. and Zarnic, R. (2006): Racking behaviour of light prefabricated cross-laminated massive timber wall diaphragms subjected to horizontal actions. *Otto Graf Journal*, 17, pp.125-142.

[9] Seim, W. and Hummel, J. (2013): Deliverable 2D CLT-wall elements-monotone and cyclic testing.

[10] Yasumura, M., Kobayashi, K., Okabe, M., Miyake, T. and Matsumoto, K. (2016): Full-scale tests and numerical analysis of low-rise CLT structures under lateral loading. *Journal of Structural Engineering*, 142(4), p.E4015007, doi: https://doi.org/10.1061/(ASCE)ST.1943-541X.0001348

[11] Gavric, I., Fragiacomo, M. and Ceccotti, A. (2015): Cyclic behaviour of typical metal connectors for cross-laminated (CLT) structures. *Materials and structures*, 48(6), pp.1841-1857, doi: https://doi.org/10.1617/s11527-014-0278-7

[12] Flatscher, G., Bratulic, K. and Schickhofer, G. (2015): Experimental tests on cross-laminated timber joints and walls. *Proceedings of the Institution of Civil Engineers-Structures and Buildings*, 168(11), pp.868-877, doi: https://doi.org/10.1680/stbu.13.00085

[13] Seim, W., Hummel, J. and Vogt, T. (2013): Deliverable 2C Anchoring units-monotone and cyclic testing.

[14] Masroor, M., Doudak, G. and Casagrande, D. (2020): The effect of bi-axial behaviour of mechanical anchors on the lateral response of multi-panel CLT shearwalls. *Engineering Structures*, 224, p.111202, doi: https://doi.org/10.1016/j.engstruct.2020.111202

[15] Pozza, L., Ferracuti, B., Massari, M. and Savoia, M. (2018): Axial–Shear interaction on CLT hold-down connections–Experimental investigation. *Engineering Structures*, 160, pp.95-110, doi: https://doi.org/10.1016/j.engstruct.2018.01.021

[16] Rinaldin, G., Amadio, C. and Fragiacomo, M. (2013): A component approach for the hysteretic behaviour of connections in cross-laminated wooden structures. *Earthquake engineering & structural dynamics*, 42(13), pp.2023-2042, doi: https://doi.org/10.1002/eqe.2310

[17] Follesa, M., Christovasilis, I.P., Vassallo, D., Fragiacomo, M. and Ceccotti, A. (2013): Seismic design of multi-storey cross laminated timber buildings according to Eurocode 8. *Ingegneria Sismica*, 4.

[18] Sandoli, A., D'Ambra, C., Ceraldi, C., Calderoni, B. and Prota, A. (2021). Role of perpendicular to grain compression properties on the seismic behaviour of CLT walls. *Journal of Building Engineering*, 34, p.101889, doi: https://doi.org/10.1016/j.jobe.2020.101889

[19] Andrea, P. and Luca, P. (2016). Proposal for a standardized design and modeling procedure of tall CLT buildings. *International Journal for Quality Research*, 10(3), p.607.

[20] Z. Chen, D. Tung, and E. Karacabeyli. (2022): *Modelling Guide for Timber Structures.* FPInnovations, First Edition, Canada.

[21] Pozza, L., Trutalli, D., Polastri, A. and Ceccotti, A. (2013): Seismic design of CLT Buildings: Definition of the suitable q-factor by numerical and experimental procedures. *In Proceedings of the second international conference ICSA*, Guimaraes, Portugal, structures and architecture (Vol. 9, pp. 90-97).

[22] Pozza, L. and Trutalli, D. (2017): An analytical formulation of q-factor for mid-rise CLT buildings based on parametric numerical analyses. *Bulletin of Earthquake Engineering*, 15(5), pp.2015-2033, doi: https://doi.org/10.1007/s10518-016-0047-9

[23] Follesa, M., Fragiacomo, M., Casagrande, D., Tomasi, R., Piazza, M., Vassallo, D., Canetti, D. and Rossi, S. (2018): The new provisions for the seismic design of timber buildings in Europe. *Engineering structures*, 168, pp.736-747, doi: https://doi.org/10.1016/j.engstruct.2018.04.090

[24] Azinović, B., Pazlar, T. and Kržan, M. (2021): The influence of flexible sound insulation layers on the seismic performance of cross laminated timber walls. *Journal of Building Engineering*, 43, p.103183, doi: https://doi.org/10.1016/j.jobe.2021.103183

[25] Naumovski, L. (2022): Nelinearna statična analiza večetažne stavbe iz križno lepljenega lesa. Magistrsko delo. Ljubljana: Univerza v Ljubljani. Dostopno: https://repozitorij.uni-lj.si/IzpisGradiva.php?lang=slv&id=142314

[26] Calculatis, Calculatis by Stora Enso - Version 4.07.1 (n.d). URL https://www.storaenso.com/en/products/wood-products/calculatis (accessed 21.11.22).

[27] Fajfar, P. (1999): Capacity spectrum method based on inelastic demand spectra. Earthquake Engineering & Structural Dynamics, 28(9), pp.979-993, doi: https://doi.org/10.1002/(SICI)1096-9845(199909)28:9<979::AID-EQE850>3.0.CO;2-1

[28] Markušić S, Stanko D, Penava D, Ivančić I, Bjelotomić Oršulić O, Korbar T, Sarhosis V. (2021): Destructive M6.2 Petrinja Earthquake (Croatia) in 2020—Preliminary Multidisciplinary Research. Remote Sensing, 13(6):1095., doi: https://doi.org/10.3390/rs13061095

[29] The big shake: Designing tall timber buildings that are resilient to earthquakes (n.d.). ULR http://nheritallwood (accessed 21.11.22).

FRAGILITY AND VULNERABILITY ANALYSIS OF RC BUILDINGS WITH DIFFERENT SHAPES IN THE BASE

Radomir Folić [(1)], Miloš Čokić [(2)], Boris Folić [(3)]

[(1)] *Professor emeritus, University of Novi Sad, FTS Civil engineering and Geodesy, Novi Sad, Serbia, folic@uns.ac.rs*
[(2)] *Structural Engineer, Belgrade, Serbia, cokicmilos@gmail.com*
[(3)] *Scientific researcher, University of Belgrade, Innovation center, Faculty of Mechanical Engineering, Kraljice Marije 16. Belgrade, Serbia, boris.r.folic@gmail.com*

Abstract

In this paper, the seismic response of a three 5 story reinforced concrete (RC) frame system buildings is analysed through the fragility and vulnerability analyses. The constructions are designed in accordance with the structural Eurocodes. All three buildings have the same area, but different shape in the base. For the analysis of the response of structural system to the earthquake actions, the method of nonlinear static (NSA) analysis was applied and based on the obtained results, fragility probability density functions and vulnerability curves were constructed using statistical methods. Structural damage state threshold parameters are determined based on the methodologies described in RISK-UE project. Comparative analysis of the structural damage probability for the three analysed RC buildings is applied in both main directions and as the whole as well. Based on the analysis results, final remarks and conclusions were formulated.

Keywords: RC building, seismic nonlinear pushover analyses, fragility, vulnerability, RISK-UE

1. Introduction

The behavior of any building depends on the arrangement of structural elements present in it. The important aspects on which the structural configuration depends are geometry, shape and size of the building. Under seismic actions, inertial forces concentrated at the center of mass of the structure, and the vertical bearing element (columns and shear walls) resist the horizontal inertia forces which concentrated at a point called center of stiffness [1].

During an earthquake, failure of structure starts at points of weakness. This weakness arises due to discontinuity in mass, stiffness and geometry of structure. The structures having these discontinuities are termed as irregular structures. Many results of seismic behaviour reinforced concrete (RC) buildings indicate that regularity of their structures considerably affects the structural response with respect to the regular configuration. Regular buildings perform better in earthquakes than do irregular buildings. Irregularities bring down the structural response under seismic loads. However incorporation of some irregularity in structures, during structural design, is inevitable.

Location and size of structural elements have significant effect on torsional coupling which results in damage of structures. Regular structures have no significant discontinuities in plan or in vertical configurations. Structures shall be designed with a clearly defined load path, or paths, to transfer the inertial forces generated in an earthquake to the supporting ground. The building shall be designed to meet the requirements of this subsection and of the design standards referenced in Section 4.2. [2].

Basic principles shall be taken into account in the early stages of the conceptual design of a building and provide structural simplicity, uniformity, symmetry, torsional resistance and stiffness et other. Structural simplicity, characterised by the existence of clear and direct paths for the transmission of the seismic forces. [2]
Uniformity in plan is characterised by an even distribution of the structural elements which allows short and direct transmission of the inertia forces created in the distributed masses of the building. A close relationship between the distribution of masses and the distribution of resistance and stiffness eliminates large eccentricities between mass and stiffness. [2]

A comparative analysis of the behavior of regular and irregular building structures is presented in [3]. Seismic analysis of plan irregular RC building frames is subject of paper [4]. In analysis multimode pushover procedure for the approximate estimation of the seismic response of asymmetric in plan buildings under biaxial seismic excitation described in [5].

This is why analysis of fragility and vulnerability analysis of an RC building is important wich is subject paper [6]. In doing so, extensive literature was cited and an overview of the situation was presented. The analysis of numerical analyzes in this paper refers to regular structures of buildings so this paper analyses the constructions of buildings with irregular structures of buildings.

In this paper, the seismic response of a three 5 story RC frame system buildings is analysed through the fragility and vulnerability analyses. The constructions are designed in accordance with the structural Eurocodes: EN1990 [7]; EN1991 [8]; EN1992 [9]; EN1998 [2,10,11], as a ductility class high (DCH) system. All three buildings have the same area, but different shape in the base. For the analysis of the response of structural system to the earthquake actions, the method of nonlinear static (NSA) analysis was applied and based on the obtained results; fragility and vulnerability curves were constructed using statistical methods. Structural damage state threshold parameters are determined based on the methodologies described in RISK-UE project [12]. Comparative analysis of the structural damage probability for the three analysed RC buildings is applied in both main directions and as the whole as well. Based on the analysis results, final remarks and conclusions were formulated.

2. Methodology of the analysis and structural modelling

2.1 Geometric and material properties of the structure

The subject of the analysis are three office-residential building (Fig. 1, 2 and 3) with 5 levels (ground floor+4 stories). The structural systems exhibits the properties of a frame structural system [2]. The plan view and the 3D model of the structures are shown in Fig. 1, 2 and 3.
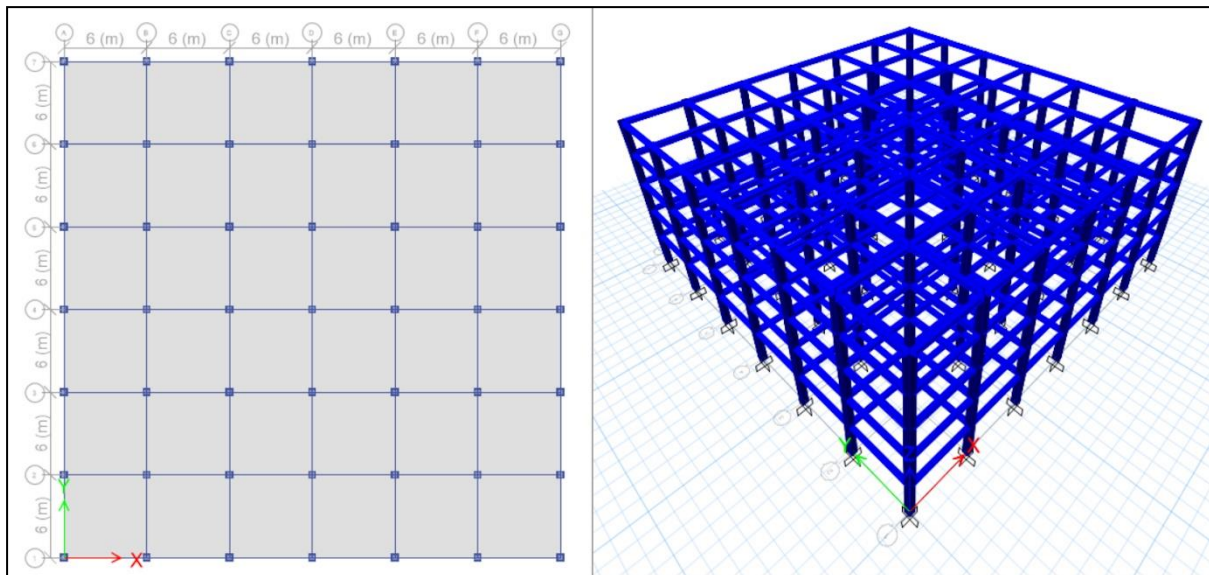
Figure 1. M1: a) Building plan; b) Numerical model [13]
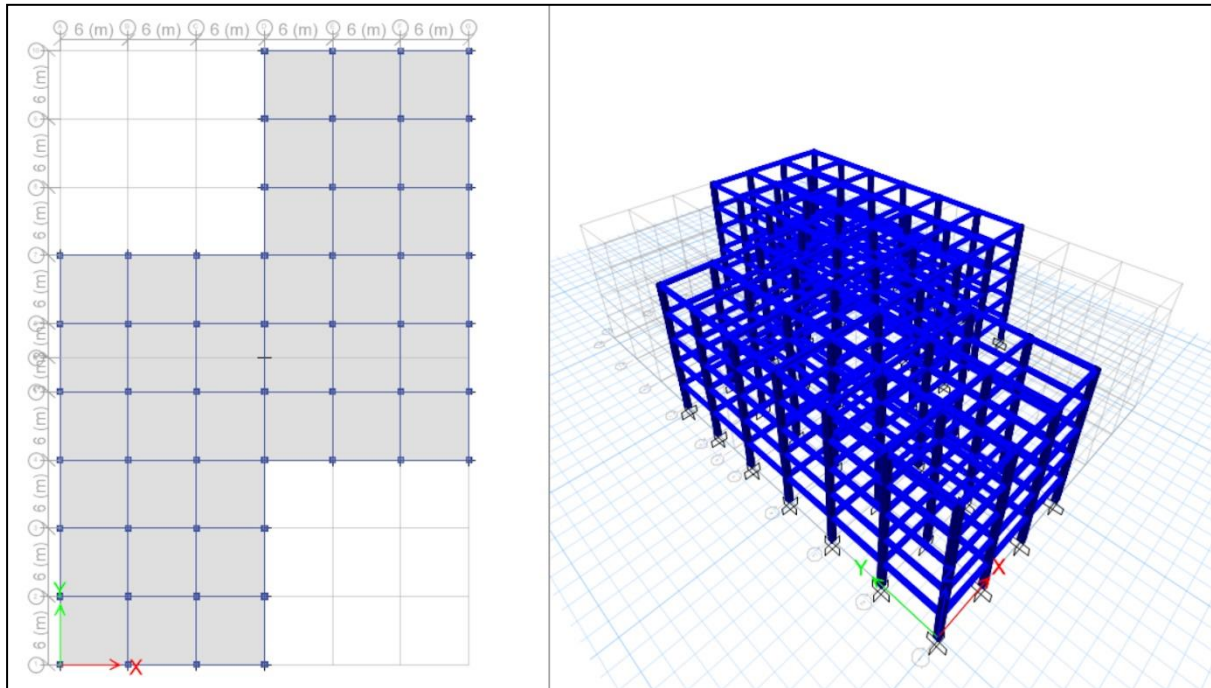
Figure 2. M2: a) Building plan; b) Numerical model [13]
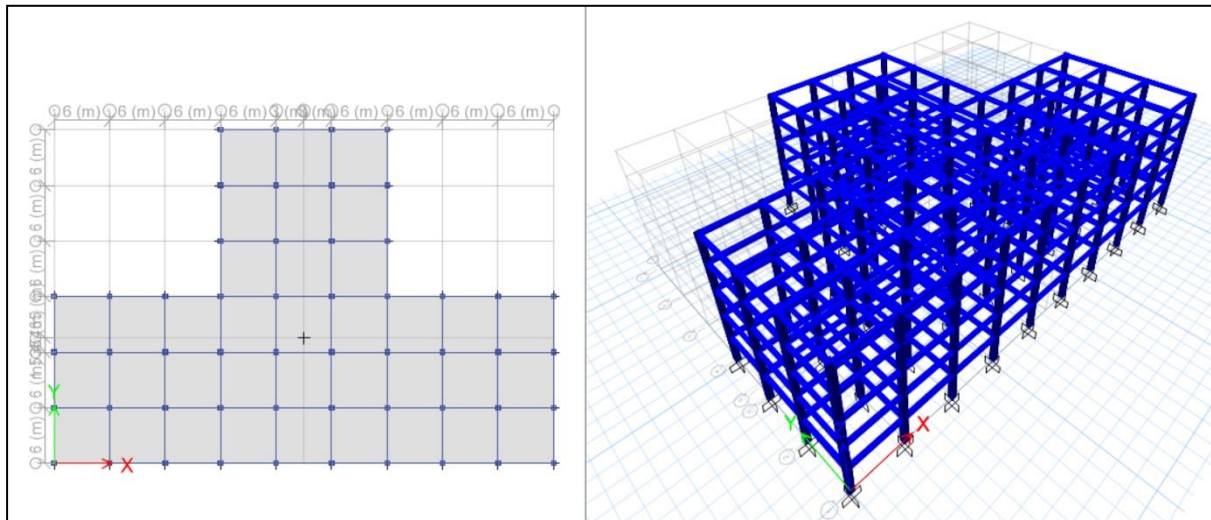
Figure 3. M3: a) Building plan; b) Numerical model [13]

The length of one span in both directions is 6.0 m. The height of the first story is 3.6 m and the height of the other stories is 3.2 m which makes the total height of the building 16.4 m. In order to simplify the modelling and calculation process, all vertical elements are fixed at the bottom level of the structure, i.e. soil-structure interaction is not included in the calculation and design. Characteristics of the structural elements are given in the Table 1.

Table 1 – Geometric characteristics of structural elements

Model	Column b_c / d_c [cm]	Beam b_b / d_b [cm]	Plate d_{pl} [cm]
M1	50 / 50	30 / 40	16
M2	50 / 50	30 / 40	16
M3	50 / 50	30 / 40	16
Long. reinf.	Column $Ø_{bL}$ [bar nr. - mm]	Beam $Ø_{bL}$ [bar nr. - mm]	Plate $Ø_{bL}$ [mm / cm]
M1	16 Ø14	3 Ø22 3 Ø20	Ø12/15
M2	16 Ø14	3 Ø25 3 Ø22	Ø12/15
M3	16 Ø14	3 Ø25 3 Ø22	Ø12/15
Stirrups	Column $Ø_{sw}$ [bar nr. – mm / cm]	Beam $Ø_{sw}$	Plate /
M1	3 Ø10/10	2 Ø10/10	/
M2	3 Ø10/10	2 Ø10/10	/
M3	3 Ø10/10	2 Ø10/10	/

3. Methodology of the analysis and structural modelling

3.1 Geometric and material properties of the structure

Tables For calculation and design of the structure in [13], a spatial (3D) model was used. The following parameters, assumptions and simplifications were adopted:

- The calculation includes the effects of second order logic (*P-Δ*);

- Occurrence of cracks in structural elements was included in the calculation with the stiffness reduction of the elements according to [2].

- The elastic bending stiffness and shear stiffness of columns and beams was reduced to 50%;

- Torsion stiffness of columns and beams was reduced to 10% of their elastic stiffness;

- The elastic stiffness of the RC plate was reduced to 50%.

3.2 Model for nonlinear analysis

In models for post-elastic analysis of structural response to the removal of individual vertical elements, the following assumptions and simplifications were used:

- The calculation includes the effects of second order logic (*P-Δ*);

- To describe the nonlinear behaviour of the material, the nonlinear properties of the material were used to describe the behaviour of concrete (Fig. 4, left) and reinforcement steel (Fig. 4, right) [2], [10], [14];

- Columns and beams were modelled as confined RC elements with a protective layer of concrete (Fig. 4, left) [10]. [14];

- RC plates are modelled as rigid diaphragms in seismic analysis.
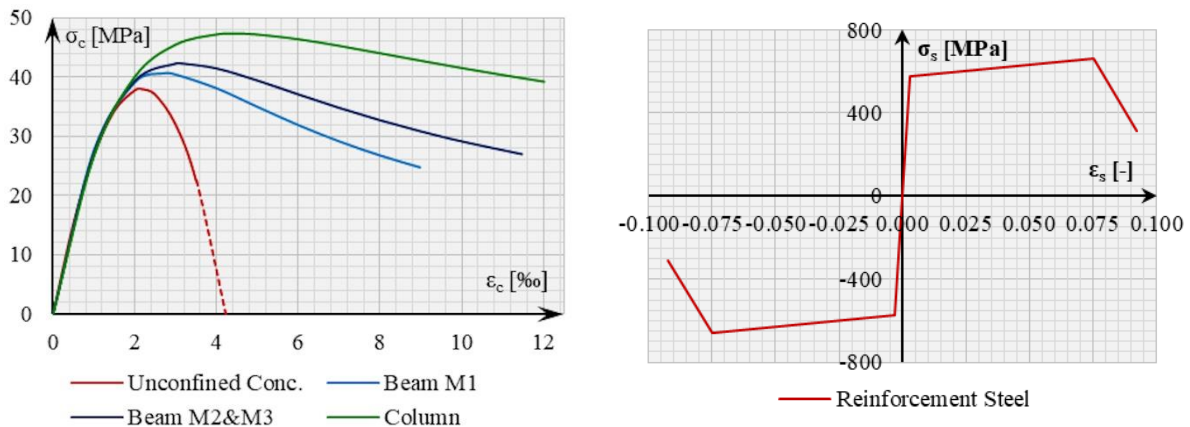
Figure 4. Material properties of concrete (left) and rebar (right)

3.3 Properties of plastic hinges

Plastic hinges are modelled as fiber cross sections. They are modelled by automatic selection of fiber division in the cross section of elements [13] for seismic analysis. The lengths of plastic hinges, are equal to the relative lengths of columns and beams of $0.2L$, where L is the length of the element. Therefore, the locations of the hinges are assigned as $0.1L$ and $0.9L$ to columns and beams.

4. Non-linear analysis results and calculation of fragility curves

4.1 Nonlinear static pushover analysis

The results of NSA for modal (MOD) load distribution are shown in Fig. 5. Modal pushover curve was chosen as a referent curve for the calculation of fragility curves, according to [12].
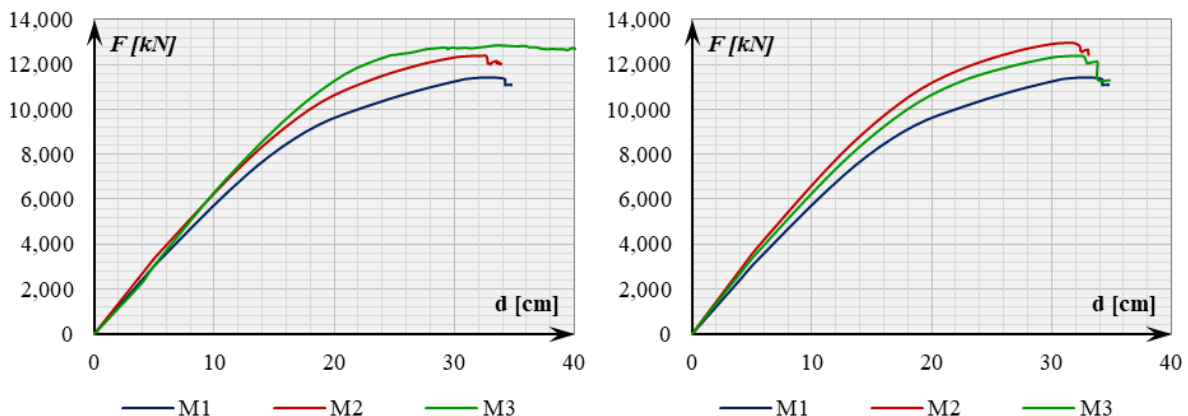
Figure 5. Pushover curves for X (left) and Y direction (right)

The results of pushover analysis for MDOF systems show different responses in both main directions. In the X direction, the structural response of M3 will be somewhat stronger than M2 and in the end M1, while in the Y direction, the response of M2 is better than M3 and then M1.

To calculate damage state (DS) threshold values, it was necessary to do a bilinear approximation of NSA pushover curve, using Equivalent Energy Elastic-Plastic (EEEP) method and determine yielding (Sd_Y, Sa_Y) and ultimate capacity (Sd_U, Sa_U) points on capacity (spectral displacement – spectral acceleration) curve of SDOF system for M1, M2 and M3 (Fig. 6).
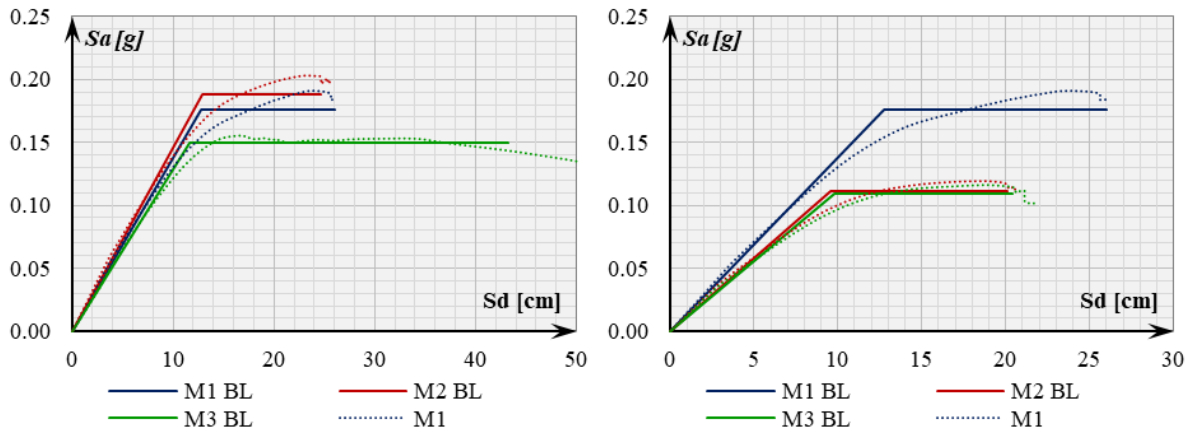
Figure 6. Capacity curves and their bilinear approximation for X (left) and Y direction (right)

The capacity curve comparison results for SDOF systems show different responses in both main directions. In the X direction, the structural response of M2 will be somewhat stronger than M1 and in the end M3, but M3 will give the most ductile response, while in the Y direction, the response of M1 is better and more ductile than M2 and then M3, which are very similar.

The results of NSA are shown in Figure 7. for target displacement (d_t) and target spectral displacement (Sd_t), for the design PGA = 0.2g. The displacement and spectral displacement values for the three models for the design PGA can be described through the relations: $d_{t,X}^{M3} > d_{t,X}^{M1} > d_{t,X}^{M2}$ in X and $d_{t,Y}^{M3} > d_{t,Y}^{M2} > d_{t,Y}^{M1}$ in Y direction for MDOF and $Sd_{t,X}^{M3} > Sd_{t,X}^{M1} > Sd_{t,X}^{M2}$ in X and $Sd_{t,Y}^{M3} > Sd_{t,Y}^{M2} > Sd_{t,Y}^{M1}$ in Y direction for MDOF.
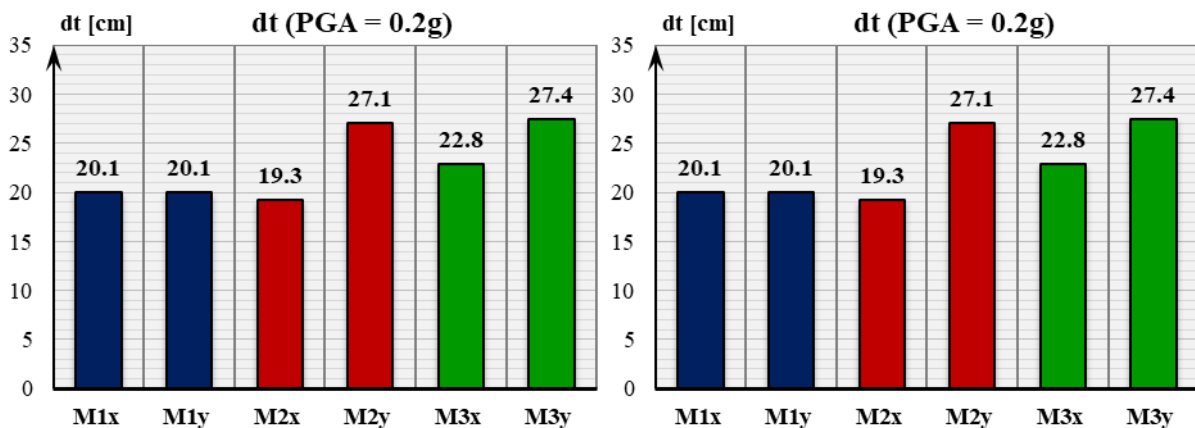
Figure 7. Target displacement and spectral target displacement points

4.2 Damage state performance points

Damage of a structural system may be quantified through threshold performance points (small damage – SD; moderate damage – MD; extensive damage – ED; complete damage – CD), which are determined according to [12] for seismic fragility analysis (Table 1).

Table 1 – Seismic structural DS threshold values, according to [12]

DS	SD [M1 / M2 / M3]			MD [M1 / M2 / M3]			RD [M1 / M2 / M3]			CD [M1 / M2 / M3]		
μ_{DS}	$0.7 \cdot Sd_Y$			Sd_Y			$Sd_Y + 0.25 \cdot (Sd_U - Sd_Y)$			Sd_U		
$\sigma_{LN,DS}$	$0.25 + 0.07 \cdot ln(\mu_U)$			$0.2 + 0.18 \cdot ln(\mu_U)$			$0.1 + 0.4 \cdot ln(\mu_U)$			$0.15 + 0.5 \cdot ln(\mu_U)$		
	X direction											
μ_{DS}^{Sd} [cm]	8.92	9.00	8.10	12.75	12.85	11.58	16.06	15.80	19.48	25.99	24.64	43.20
μ_{DS}^{PGA} [g]	0.122	0.128	0.107	0.172	0.179	0.150	0.213	0.216	0.249	0.331	0.329	0.590
$\sigma_{LN,DS}$ [g]	0.300	0.296	0.342	0.328	0.317	0.437	0.385	0.360	0.627	0.506	0.475	0.808
	Y direction											
μ_{DS}^{Sd} [cm]	8.92	6.69	6.84	12.75	9.56	9.77	16.06	12.20	12.43	25.99	20.10	20.40
μ_{DS}^{PGA} [g]	0.122	0.085	0.085	0.172	0.118	0.119	0.213	0.148	0.148	0.331	0.239	0.239
$\sigma_{LN,DS}$ [g]	0.300	0.302	0.302	0.328	0.334	0.333	0.385	0.395	0.394	0.506	0.521	0.518

4.3 Statistical analysis of the results

It is generally assumed that fragility curve is a lognormal distribution function, which means that "If a variable is log-normally distributed, its natural logarithm is normally distributed. Which means it must take on a positive real value, and the probability of it being zero or negative is zero." [15] For seismic fragility analysis, lognormal distribution is adopted [12].

4.4 Calculation of fragility curves

In case of the calculation of fragility curves, using spectral displacement (*Sd*) as a referent IM value for the DS threshold [12], the fragility functions are calculated as analytical cumulative distribution functions (CDF) for lognormal (LN) distribution:

$$P_{DS_i|IM}\left(IM_j, \mu_{LN|DS_i}^{IM}, \sigma_{LN|DS_i}^{IM}\right) = \Phi\left[\frac{1}{\sigma_{LN|DS_i}^{IM}} \cdot \ln\left(\frac{IM}{\mu_{LN|DS_i}^{IM}}\right)\right] = \Phi\left(\frac{\ln IM - \mu_{LN|DS_i}^{IM}}{\sigma_{LN|DS_i}^{IM}}\right) \quad (1)$$

where Φ is the cumulative distribution function of the standard normal distribution, $\mu_{LN|DS_i}^{IM}$ and $\sigma_{LN|DS_i}^{IM}$ are the mean and standard deviation of LN distribution values shown in Table 2. However, because it is possible to determine the relation between *Sd* and PGA, it is possible to present the fragility curves with the PGA as the IM.

Probability density function values for the exceedance of different states of damage for the design PGA = 0.2*g* (Fig. 10, 13 and 16) are calculated using the equations [15], [16]:

$$P_{DS_0} = 1 - P_{DS_1}\left[IM_j, \mu_{LN|DS_1}, \sigma_{LN|DS_1}\right]$$
$$P_{DS_i} = P_{DS_i}\left[IM_j, \mu_{LN|DS_i}, \sigma_{LN|DS_i}\right] - P_{DS_{i+1}}\left[IM_j, \mu_{LN|DS_{i+1}}, \sigma_{LN|DS_{i+1}}\right] \quad (2)$$
$$P_{DS_n} = P_{DS_n}\left[IM_j, \mu_{LN|DS_n}, \sigma_{LN|DS_n}\right]$$

where P_{DS_0} is a probability of no damage to occur and $i = 1, \dots, n$ and $IM_j = (0.1g - 1.0g]$. i is an index of a particular DS, and j is an index of a particular IM (PGA). n is a total number of damage states. Probability density functions for damage state exceedance in both main X and Y directions are shown in Figures 8 - 12. As a result, the values of probability for the exceedance of each damage state for all three models in both main directions are given in Figures 13 and 14, for the design PGA = 0.2*g*.
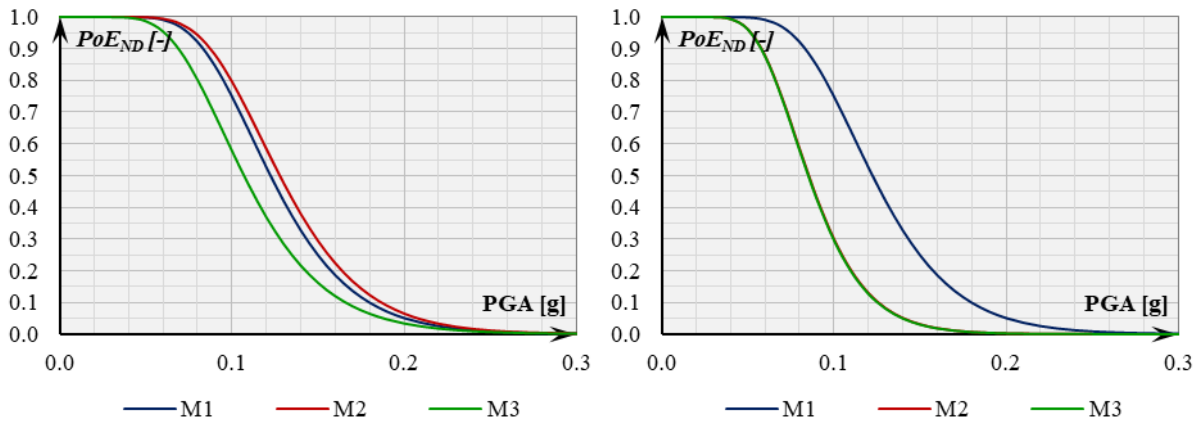
Figure 8. Probability density functions for damage state exceedance probability for ND in X (left) and Y direction (right)
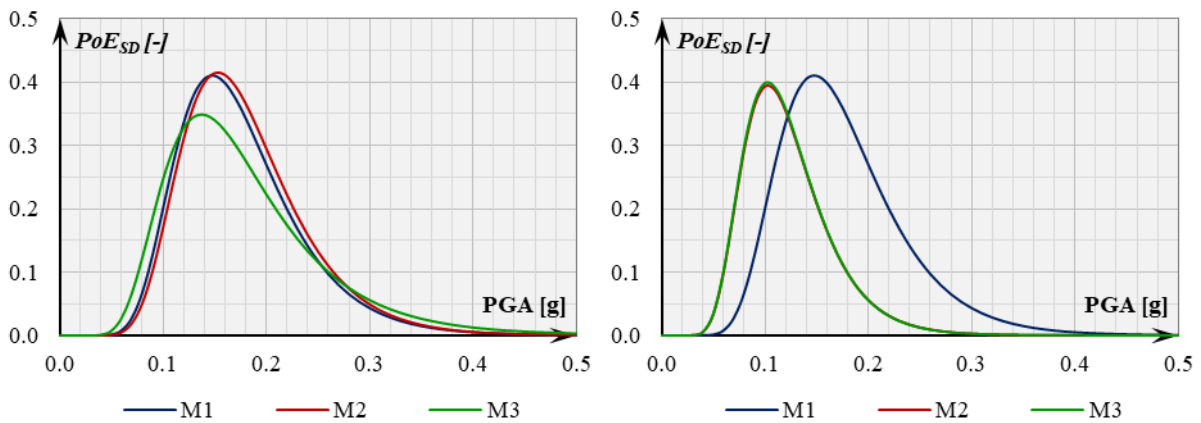
Figure 9. Probability density functions for damage state exceedance probability for SD in X (left) and Y direction (right)
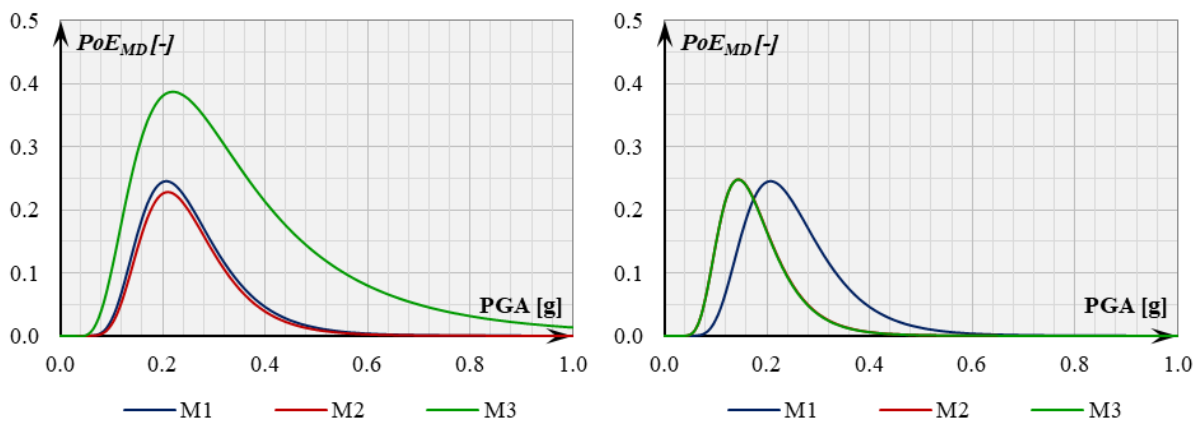
Figure 10. Probability density functions for damage state exceedance probability for MD in X (left) and Y direction (right)
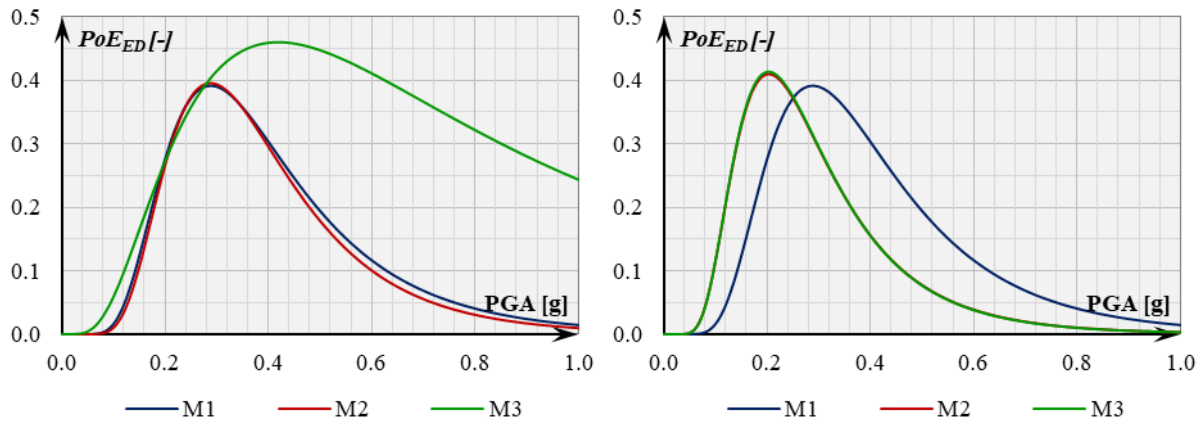
Figure 11. Probability density functions for damage state exceedance probability for ED in X (left) and Y direction (right)
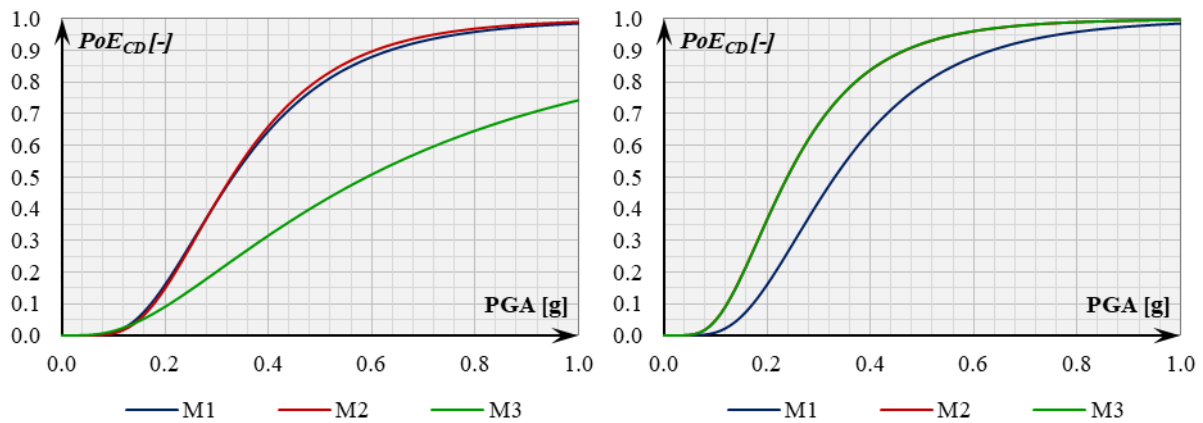
Figure 12. Probability density functions for damage state exceedance probability for CD in X (left) and Y direction (right)

Damage state exceedance probability values in X direction for the design PGA = 0.2g are shown in Figure 13. From the aspect of damage states, it can be noticed that M1 and M2 show the similar response for the seismic action in X direction for the design PGA intensity. However, M1 is a bit more prone than M2 to ED (3.4%) and to CD (8.1%). M3 shows much better response than M1 and M2 for the seismic action in X direction for the design PGA intensity. While it is much more prone to exceed the level of MD than M1 (56.1%) and M2 (68.6%), it has much lower probability to exceed CD than M1 (-43.8%) and M2 (-39.2%).
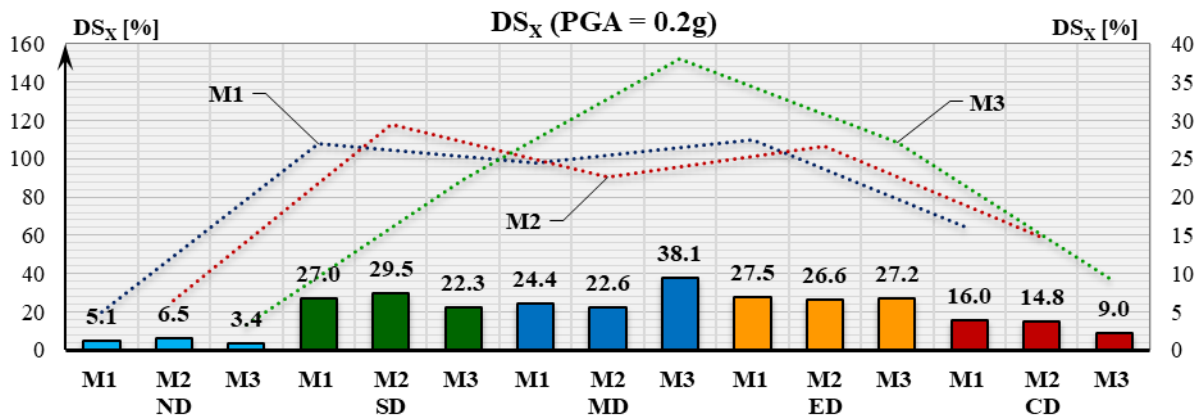
Figure 13. Damage state exceedance probability in X direction for the design PGA

Damage state exceedance probability values in Y direction for the design PGA = 0.2*g* are shown in Figure 14. From the aspect of damage states, it can be noticed that M2 and M3 show very similar or almost the same response for the seismic action in Y direction for the design PGA intensity. The difference between the response of M2 and M3 varies from 0.1% - 0.3% in probability. M1 shows much better response than M2 and M3 for the seismic action in Y direction for the design PGA intensity. While it is much more prone to exceed the level of SD and MD than M2 (-79.3% and -32.0%) and M3 (-79.6% and -32.8%), it has much lower probability to exceed ED and CD than M2 (-32.9% and -56.3%) and M3 (-33.4% and -56.0%).

Figure 14. Damage state exceedance probability in Y direction for the design PGA

Damage state exceedance probability values in Y direction for the design PGA = 0.2*g* are shown in Figure 14. From the aspect of damage states, it can be noticed that M2 and M3 show very similar or almost the same response for the seismic action in Y direction for the design PGA intensity. The difference between the response of M2 and M3 varies from 0.1% - 0.3% in probability. M1 shows much better response than M2 and M3 for the seismic action in Y direction for the design PGA intensity. While it is much more prone to exceed the level of SD and MD than M2 (-79.3% and -32.0%) and M3 (-79.6% and -32.8%), it has much lower probability to exceed ED and CD than M2 (-32.9% and -56.3%) and M3 (-33.4% and -56.0%).

In order to calculate the seismic response of each model for both directions, the values of probability of damage state exceedance and vulnerability mean damage values (MDF) are calculated using geometric mean equation:

$$\left(\prod_{i=1}^{n} x_i\right)^{\frac{1}{n}} = \sqrt[n]{x_1 \cdot x_2 \cdot \ldots x_n} \tag{3}$$
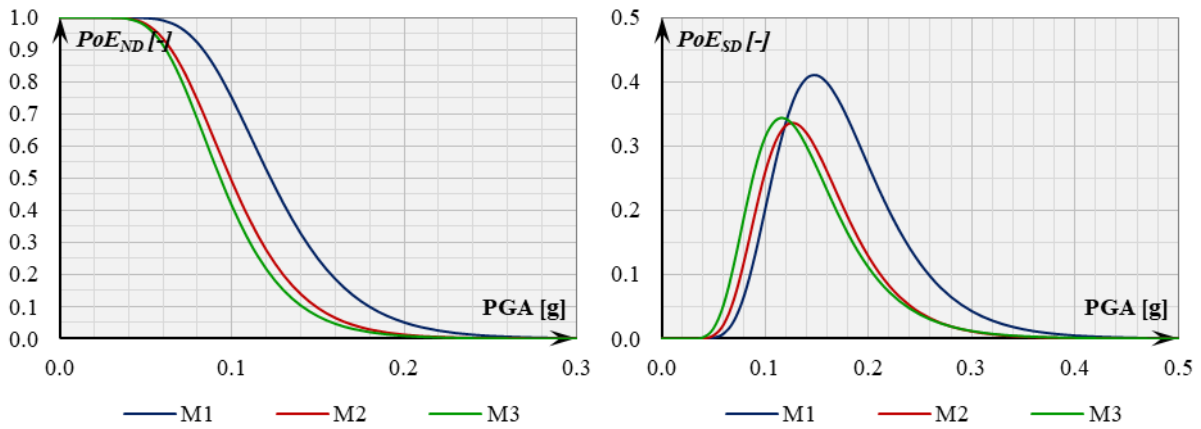
Figure 15. Probability density functions for damage state exceedance probability for ND (left) and SD (right), geometric mean for both directions
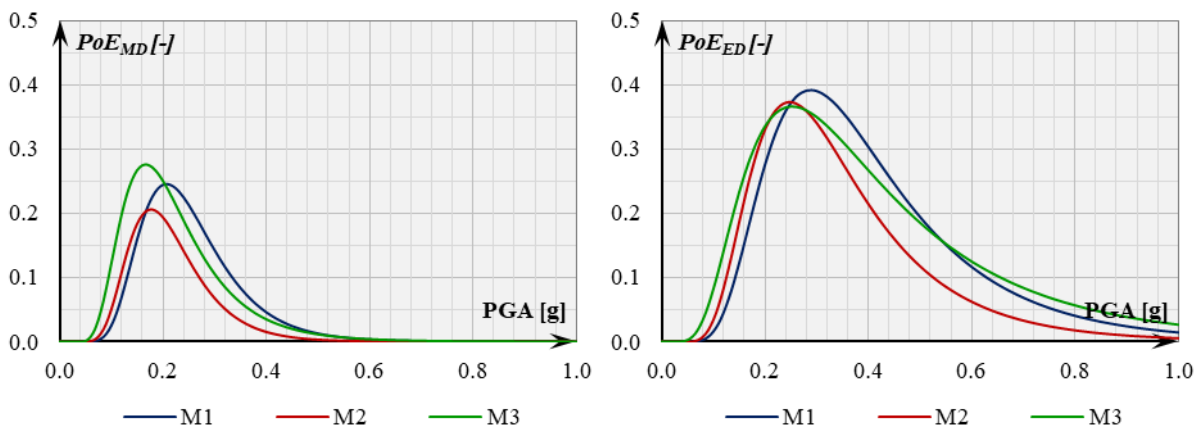
Figure 16. Probability density functions for damage state exceedance probability for MD (left) and ED (right), geometric mean for both directions
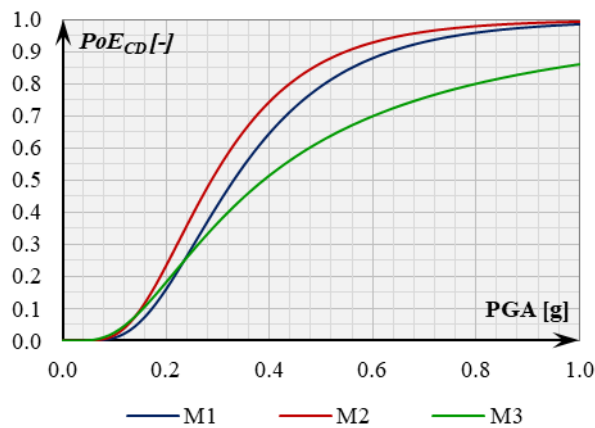
Figure 17. Probability density functions for damage state exceedance probability for CD, geometric mean for both directions

Damage state exceedance probability geometric mean values for both directions for the design PGA = 0.2g are shown in Figure 18. From the aspect of damage states, it can be noticed that in general, M1 has better response than M3, which has a similar, but slight better response than M2. The percentual comparison of values of M2 and M3 to M1 as a referent model is given in Table 3.
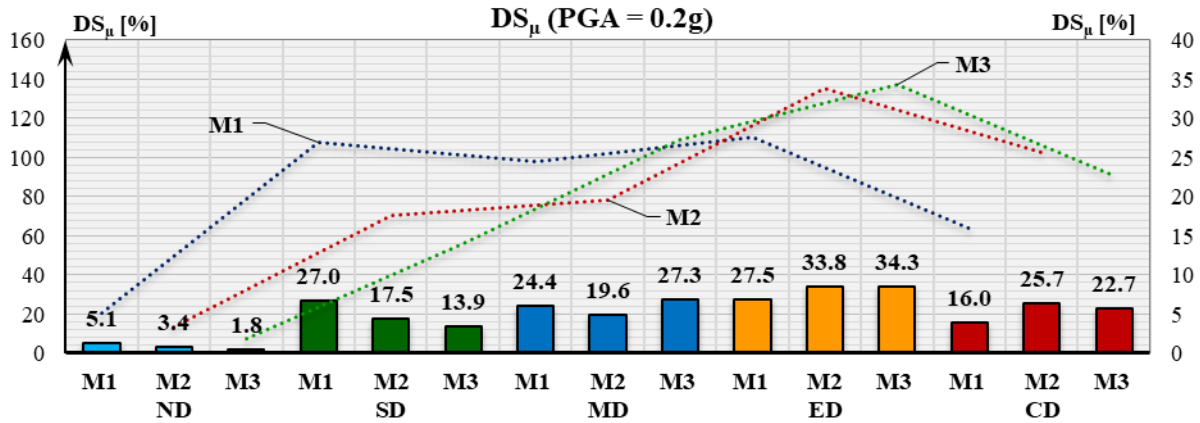
Figure 18. Damage state exceedance probability for the design PGA, geometric mean for both directions

Table 3 – Comparison of PoE values of M2 and M3 to M1

DS [%]	NDμ	SDμ	MDμ	EDμ	CDμ
M1	0.00	0.00	0.00	0.00	0.00
M2	-33.75	-34.93	-19.83	22.67	60.88
M3	-64.47	-48.39	11.58	24.47	42.24

4.5 Vulnerability analysis

Calculation process of vulnerability curves was performed according to the method described in [17]. Calculation of the vulnerability curves, based on the fragility results was done according to the equation and process described in paper [17]:

$$E(C|IM) = \sum_{i=0}^{n} E(C|DS_i) \cdot P(DS_i|IM) \qquad (3)$$

where *n* is the number of considered DS (DS_i), $P(DS_i|IM)$ is the damage probability; $E(C|DS_i)$ and $E(C|IM)$ are the cumulative distribution of cost (or loss) according to [17]. The values of $E(C|DS_i)$ are adopted from [17]. The results are compared and displayed in Figures 19 and 20.

Table 4 – Damage factor functions of building typology according to [17]

Damage Scale	$E(C|DS_i)$			
Damage State	**Slight (SD)**	**Moderate (MD)**	**Extensive (ED)**	**Complete (CD)**
	2%	10%	50%	100%

Vulnerability MDF values in X and Y direction for the design PGA = 0.2g are shown in Figure 20. It can be noticed that M1 and M2 have very similar or almost the same response for the seismic action in X direction (Figure 19, left and Figure 21, left) for the design PGA intensity and that M3 have much better response than both M1 and M2. In Y direction (Figure 19, right and Figure 21, left), M1 has

better response than both M2 and M3, which both have almost the same response for the seismic action. Regarding the comparison of the models in both directions from the aspect of geometric mean values (Figure 20 and Figure 21, right), M1 has the best response, after which is M3 and then M2. However, for the value of PGA > 0.3*g* (Figure 20). the response of M3 is better than M1 and M2
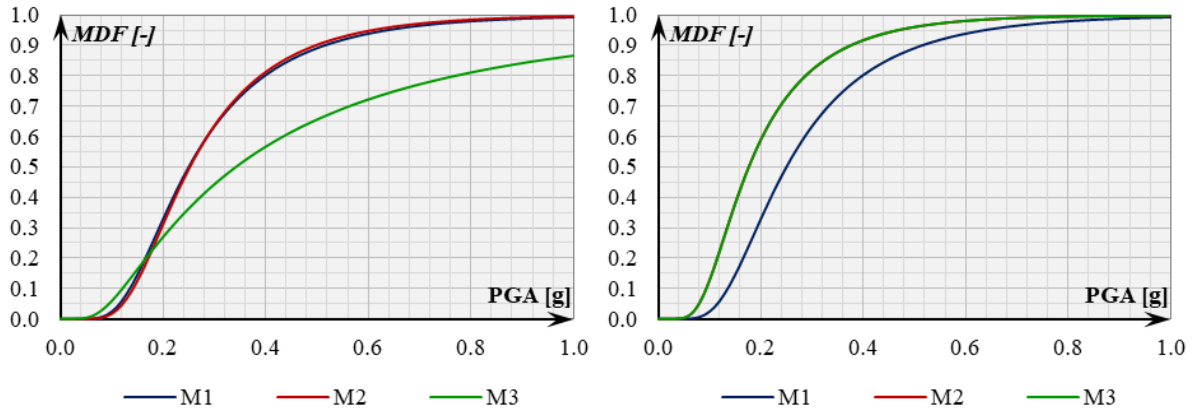
Figure 19. Vulnerability curves for X (left) and Y direction (right)
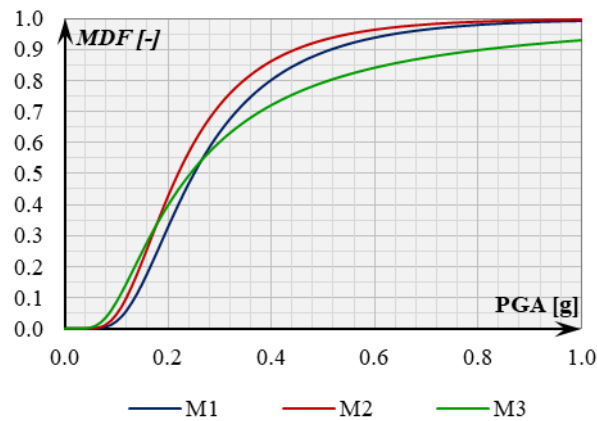
Figure 20. Vulnerability curves geometric mean values for both directions
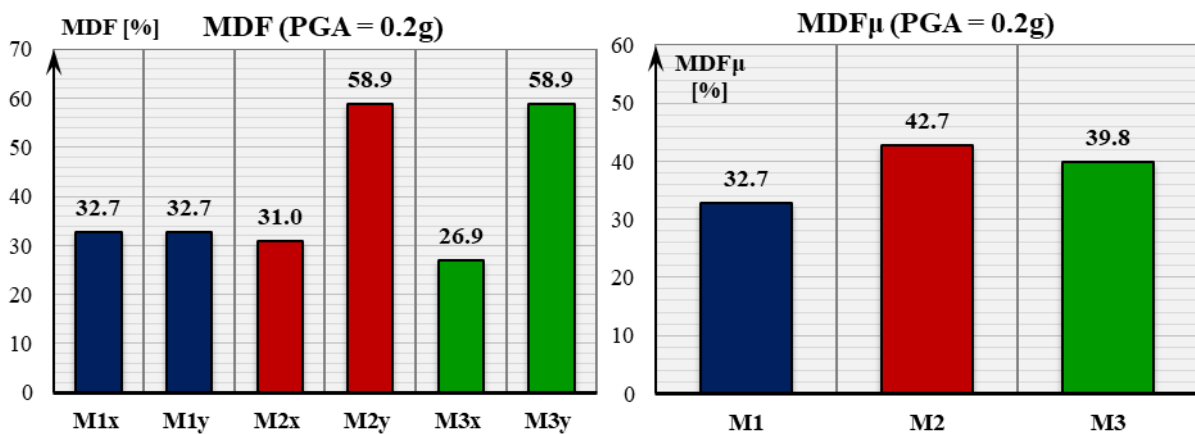
Figure 21. MDF for both directions (left) and MDF values mean for both directions (right) for design PGA

5. Conclusions

In this paper, the fragility and vulnerability of a three 5 story RC frame system buildings exposed to seismic action is analysed through their nonlinear response. The constructions are designed in accordance with the structural Eurocodes, as DCH systems. The common characteristic of all three buildings are: the same area and the same number of stories, but different shape in the base. For the analysis of the response of structural system to the earthquake actions, the method of nonlinear static (NSA) analysis was applied and based on the obtained results; fragility functions, probability density functions for damage state exceedance probability and vulnerability curves were calculated using statistical methods. Comparative analysis of the structural damage probability for the three analysed RC buildings is applied in both main directions and as the whole as well, using the geometric mean values. Based on the analysis results, some conclusions may be formulated:

- In the main X direction, M2 shows a bit better characteristics than M1, which can be explained by the arrangement of the elements in the structure and the distribution of mass and inertial forces induced by seismic action. M3 has much better performance in the X direction than both M1 and M2, because it's resisting to seismic action with a longer, stiffer frames in the part of the structure.
- In the main Y direction, M1 shows much better response than both M2 and M3, which can be explained by the arrangement of the elements in the structure and the distribution of mass and inertial forces induced by the seismic action. However, it is noticable that both M2 and M3 have almost the same response in the Y direction.
- As expected, the building which is regular in plan (M1) will in general have better response than the other two models (M2 and M3), which can be seen through the geometric mean fragility and vulnerability results.

Acknowledgements

References

[1] S. E Naveen, N. M. Abraham, A. S. Kumari, Analysis of Irregular Structures under Earthquake Loads, 2nd International Conference on Structural Integrity and Exhibition 2018, Procedia Structural Integrity 14, 2019, pp. 806–819.

[2] EN1998—Part 1, Eurocode 8: Design of Structures for Earthquake Resistance—Part 1: General Rules, Seismic Actions and Rules for Buildings; European Committee for Standardization (CEN): Brussels, Belgium, 2004.

[3] P. Dewangan, T. Saxena, Seismic Analysis of Regular & Irregular Structures and its Comparison, Int. Research Journal of Engineering and Technology (IRJET) Volume: 05 Issue: 09, Sep 2018.

[4] P A. Krishnan, N. Thasleen, Seismic analysis of plan irregular RC building frames, IOP Conf. Ser.: Earth Environ. 2020, Sci. 491, 012021.

[5] G. E. Manoukas Evaluation of a multimode pushover procedure for asymmetric in plan and non-regular in elevation R/C buildings, Elsevier, Soil Dynamics and Earthquake Engineering 115, 2018, pp. 742-775.

[6] R. Folić, M. Čokić, Fragility and Vulnerability Analysis of an RC Building with the Application of Nonlinear Analysis. Buildings 2021, 11, 390. https://doi.org/10.3390/buildings11090390

[7] EN 1990. ICS 91.010.30, Basis of Structural Design; European Committee for Standardization (CEN): Brussels, Belgium, 2005.

[8] EN1991, Eurocode 1: Actions on Structures—Part 1-1: General Actions—Densities, Self-weight, Imposed Loads for Buildings; European Committee for Standardization (CEN): Brussels, 2002.

[9] EN1992—Part 1, Eurocode 2: Design of Concrete Structures—Part 1-1: General Rules and Rules for Buildings; CEN: Brussels, Belgium, 2004.

[10] EN1998—Part 2, Eurocode 8: Design of Structures for Earthquake Resistance—Part 2: Bridges; European Committee for Standardization (CEN), Brussels, Belgium, 2005.

[11] EN1998—Part 3, Eurocode 8: Design of Structures for Earthquake Resistance—Part 3: Assessment and Retrofitting of Buildings; European Committee for Standardization (CEN): Brussels, 2004.

[12] Z.V. Milutinović, G.S. Trendafiloski, RISK-UE, An advanced approach to earthquake risk scenarios with applications to different European towns. In Contract: EVK4-CT-2000-00014, WP4 Vulnerability of Current Buildings; 2003; 110p. Available online: http://www.civil.ist.utl.pt/~mlopes/conteudos/DamageStates/Risk%20UE%20WP04_Vulnerability.pdf (accessed on 1st January 2021)

[13] ETABS, version 17, Computers and Structures, Inc., Berkeley, California, USA, 2018.

[14] J. Mander, M. Priestley, R. Park, Theoretical Stress-Strain Model for Confined Concrete. J. Struct. Eng. 1988, 114, 1804–1825.

[15] K. A. Porter, Beginner's Guide to Fragility, Vulnerability, and Risk; University of Colorado Boulder: Boulder, CO, USA, 2015; doi:10.1007/978-3-642-35344-4_256.

[16] J.W. Baker, Efficient analytical fragility function fitting using dynamic structural analysis. Earthq. Spectra 2015, 31, 579–599.

[17] D. D'Ayala, A. Meslem, D. Vamvatsikos, K. Porter, T. Rossetto, V. Silva, Guidelines for Analytical Vulnerability Assessment of Low/Mid-Rise Buildings. GEM Technical Report 2015-08 V1.0.0. GEM Foundation: Pavia, Italy, 2014, doi:10.13117/GEM.VULN-MOD.TR2014.12.

CUSTOMIZED SEISMIC SCREENING TOWARD SUSTAINABLE PUBLIC BUILDINGS ENERGY EFFICIENCY

Veronika Shendova [1], Roberta Apostolska [2], Vlatko Sesov [3]

[1] *Prof. Ph.D., Institute of Earthquake Engineering and Engineering Seismology, IZIIS, Ss. Cyril and Methodius University, Skopje, North Macedonia, e-mail: veronika@iziis.ukim.edu.mk*

[2] *Prof. Ph.D., Institute of Earthquake Engineering and Engineering Seismology, IZIIS, Ss. Cyril and Methodius University, Skopje, North Macedonia, e-mail: beti@iziis.ukim.edu.mk*

[3] *Prof. Ph.D., Institute of Earthquake Engineering and Engineering Seismology, IZIIS, Ss. Cyril and Methodius University, Skopje, North Macedonia, e-mail: vlatko@iziis.ukim.edu.mk*

Abstract

Increasing energy efficiency of final energy consumption is a very actual and important topic, in parallel with activities and measures worldwide targeting an increased share of renewable energy sources. Despite recent expansion in building construction, old buildings characterized by high energy consumption still represent a great majority of both residential and public building stock in many countries in the Balkan region. Located in seismic-prone countries, such as the Republic of North Macedonia, these old buildings are also characterized by the high risk of partial or complete destruction during earthquakes. This imposes the need for mandatory screening at the outset of an energy efficiency program, which will categorize buildings according to seismic risk and thus determine which buildings are suitable for energy efficiency investments. This paper presents how the methodology for high-level seismic screening, originally proposed in the World Bank's Country Report (North Macedonia), is extended and customized by the Institute of Earthquake Engineering and Engineering Seismology, IZIIS, Skopje to correspond to the country specificities, i.e., to be based on overall knowledge on aseismic design and construction practice in the country, detailed on-site inspection of each particular building, and to be carried out by structural engineers with appropriate knowledge and experience in earthquake engineering. The high-level seismic screening was performed in the Republic of North Macedonia, applying this extended and customized methodology, for a total number of 27 medical facilities, dominantly healthcare centers, and 50 municipality buildings (schools, kindergartens, and municipal buildings).

Keywords: seismic performance of existing structures, knowledge level, aseismic design practice, construction practice, nondestructive testing, public buildings

1. Introduction

Situated in the southern part of the Balkan Peninsula, the territory of the Republic of North Macedonia belongs to the Mediterranean seismic belt. It is characterized by extensive neotectonics and recent destructive processes resulting in several regions' intensive seismic activity. According to the earthquake catalog, several hundreds of earthquakes have occurred on the territory of Macedonia over the last century, most of them with destructive nature and some even with catastrophic consequences. However, the studies related to seismic design, vulnerability and exposure modeling, and enactment of seismic code generally started after the Skopje earthquake in 1963, following the need for damage assessment, reconstruction, and recovery of the city of Skopje.

As there is no regular inventory of buildings in the country, official data can be obtained from the population and dwellings censuses (the last one was carried out in 2021 but is still without official data on dwellings). Summarizing cross-analysis of the statistical data from the last censuses (1991, 2002.) and the available data from the State Statistical Office, it can be concluded that in 2002 the percentage of buildings built before 1970, out of the total number of the particular type of facilities, is 35% for residential, 82% for school, 81% for tourist and 39% for health facilities [1, 2]. Based on the trend of newly built residential buildings in the last two decades, it can be estimated that the percentage of residential buildings built before 1970 is undoubtedly reduced, but the percentage of school and

health facilities is still high. Thus, for a significant percentage of the construction stock in the country, the level of seismic protection is unknown. Besides their high seismic risk, these old buildings are also characterized by high energy consumption.

As a signatory of the EU and International Energy Charters as well as the Protocol for Energy Efficiency and Relevant Environmental Protection Aspects, North Macedonia is funding several energy efficiency programs through available financial instruments to reduce the energy consumption of public buildings. Since the vast majority of target buildings are characterized by high energy consumption and seismic risk, integration of seismic risk considerations into energy efficiency programs should be mandatory. This can be achieved by providing the high-level seismic screening process at the outset of an energy efficiency program, which will categorize buildings according to seismic risk based on knowledge of aseismic design and practice in the country, thus determining which buildings are suitable for energy efficiency investments.

2. Aseismic Design and Construction Practices in North Macedonia

The existing building stock in North Macedonia reflects the history of urban development, which, until 1990, is typical for the whole territory of former Yugoslavia. The prevailing building types differ from the building function to different regions where they have been built according to local traditional practices. Standard legislation defines the procedures and the demands for seismic protection and dominantly refers to problems of acceptable risk for buildings [3]. Briefly, there were three significant threshold changes in seismic standards during the Yugoslav (pre-1991) period.

- The first standards addressing the seismic requirements were the "Temporary Technical Provisions for Loading of Buildings" (PTP-2), adopted in 1948, that prescribed structural analysis by additional horizontal forces (representing effects of wind) taken as 2% of the total building weight. However, it was required only for higher buildings, and no specific reinforcement detailing was defined.

- Prompted by the devastating Skopje earthquake of July 26, 1963, the first seismic design code, "Temporary Technical Provisions for Building in Seismic Regions," was adopted in 1964, which improved methods for determining design loads on buildings and introduced quality requirements for materials and construction. Significant progress in structural design, construction practice, and scientific development in the field of earthquake engineering took place in the entire region in the 1970s, led by the Institute of Earthquake Engineering and Engineering Seismology (IZIIS) established in 1965 upon UN recommendation for the recovery of Skopje and conducting research, education, training, development, and improvement of technical regulations in the field of earthquake-resistant structures.

- In the 1981 "Rulebook on Technical Regulations for Construction of Buildings in Seismic Regions," a significant update was made to the seismic design, partly in response to the 1979 Montenegro earthquake, and it was mandatory for any type of building. Along with the amendments from 1982, 1983, 1988, and 1990, it is still an official and valid regulation in the country. Macro-seismic maps for several characteristic return periods were incorporated to comply with the seismic hazard levels. The seismic shear base coefficient was introduced and calculated according to building importance, structural system, local soil conditions, and region seismicity. Limits on permissible heights of masonry construction, introduced in 1964, were further revised based on the construction method. Importantly for reinforced concrete moment frame systems, detailing requirements in the heavily loaded zones at the end of beams and columns were introduced. Also, the regulations that were adopted in the designated period and are still in power are the "Code for Repair and Strengthening of Earthquake Damaged Buildings" (1985) and the "Rulebook on Concrete and Reinforced Concrete" (1987).

The period from 1964 to 1991 is considered a period of exceptionally high-quality structural design and control that resulted in safe buildings with a seismic risk equal to or lower than the maximum acceptable. However, the period from 1991 to 2005, after the country gained independence, was a transition period in which many individual initiatives for the design and construction of residential and

business areas were taken. Although seismic design regulations existed, Macedonian society struggled with the strict implementation of technical standards that regulated the construction of building structures. Material and construction quality control was not mandatory by any regulations. As a result, there is no clear picture of the building quality during this period.

This period ended in 2005 with the enactment of the Law of Construction. This law established the Technical Chamber of Architects and Engineering to control professional competencies by enforcing the certification requirements for structural design, project revision, construction execution, and supervision. There are no laws mandating seismic assessment of existing structures unless they are undergoing structural modification, nor specific licensing process or qualification for demonstrating competency in the seismic assessment of existing buildings. Structural engineers with appropriate knowledge and experience must carry out seismic assessments and strengthening designs. Many structural engineers who are highly experienced and skilled in designing new buildings may not have experience in assessing old buildings or the field of seismic assessment. The effective implementation of seismic assessment and design of strengthening requires a range of specialist skills characteristic of the discipline of earthquake engineering.

In 2013, an Annex to the Law on Construction of Building Structures was adopted, further improving the construction regulation process mandating the expert review of the scientific institution with respectful experience (IZIIS, http://www.iziis.ukim.edu.mk/en/) to obtain a construction permit for all buildings and usage permit for buildings above 300 m² area.

In 2020, Eurocodes were adopted in the Republic of North Macedonia as parallel legislation to the currently valid Codes, after which the building design and construction practice is expected to be more harmonized with the European practice.

Taking the above into account, the roughest general building categorization could be done according to the main structural system and year of construction, meaning three basic types:

- *Non-Earthquake Resistant* Masonry Buildings (pre-Code) involving unreinforced, plain masonry buildings with several sub-categories that were implemented dominantly in urban and rural areas up to 1964 when the first seismic code was enforced
- *Moderate Earthquake Resistant* Confined Masonry Buildings (Low-Code) involving plain masonry structures strengthened by vertical and horizontal reinforced concrete belts or by jacketing of the bearing walls, frequently implemented after the Skopje earthquake for seismic upgrading of existing buildings as well as the construction of new houses, dwellings, and low-rise public buildings
- *Earthquake Resistant* Reinforced Concrete Buildings (High-Code) involving low, mid, and high-rise public and residential buildings, residential complexes in urban areas, with extensive usage after 1970 until nowadays

3. High-level Seismic Screening Methodologies

3.1. High-Level Screening – Level 1 according to the World Bank's Country report

Within the Public Sector Energy Efficiency Project (REP No: MK-MOF-001-2021-CS-SC), financed by the International Bank for Reconstruction and Development (IBRD) with the Ministry of Finance of the Republic North Macedonia as the implementing agency, IZIIS has been assigned to provide technical assistance for seismic screening of public facilities in the country, following the methodology described in the Country Report (North Macedonia) on Integrating Seismic Risk Consideration into Energy Efficiency Investments World Bank #1265632, applying Level 1 seismic screening and using the template data record Level_1_Data_Record_form [3].

This screening process, according to the given methodology, includes two types of information that should be filled in the Form: (1) General information that anyone could gather and does not require specialist expertise (construction date, location, input information from hazard maps and a number of storeys) and (2) Specific information that requires engineering judgment (general structural type,

structural irregularities, evidence of strengthening, and other structural issues). Several methods are proposed that could be used to collect data depending on the quality of existing records:

- Desk study and remote data collecting (if there is good coverage of Google Street-view or Google 3D buildings in the region being studied)
- Building manager questionnaire
- A rapid visual survey by a structural engineer (if data and photo records are incomplete).

According to the Country Report, two different seismic hazard information are required in the screening form to obtain a hazard comparison rating of A, B, C, or D, irrespective of the knowledge of local seismicity (Table 1):

- The seismic hazard at the building location is defined using the current earthquake hazard map produced for the country's Eurocode National Annex.
- The seismic hazard value that was applicable at the time of the building's construction. This value can be obtained from the historic hazard maps published in 1964, 1982, and 1990.

Table 1 - Hazard comparison rating (according to Country Report)

		Eurocode peak ground acceleration agR								
		0.05	0.10	0.12	0.15	0.20	0.25	0.30	0.35	0.40
	Band	0.04-0.08	0.09-0.11	0.12-0.13	0.14-0.18	0.19-0.23	0.24-0.28	0.29-0.33	0.34-0.38	0.39+
MSK Intensity from 1964, 1982 or 1987 Map	pre1964	A	C	C	C	D	D	D	D	D
	VI	A	C	C	C	D	D	D	D	D
	VII	A	B	B	C	D	D	D	D	D
	VIII	A	A	B	B	C	C	C	D	D
	IX	A	A	A	B	B	B	C	C	C

Table 2 - Seismic risk rating (according to Country Report)

🟩 Green	**Green: The building is suitable for the EE programme without further seismic assessment.** This is either because it has acceptable document records to indicate that the building meets current building standards or because the building is in a region of low earthquake hazard and is judged likely to have good earthquake resilience, although document records are not available to formally validate this status.
🟨 Yellow	**Yellow: The building could progress in the EE programme, but compliance with modern standards is not guaranteed.** A further assessment is likely to conclude that the building has reasonable seismic performance. However, there are some uncertainties. A deficiency-based or detailed assessment is needed to confirm seismic risk status and identify recommended strengthening interventions. The building may require localized earthquake-strengthening work to achieve acceptable seismic performance, and these may be achievable for a cost within 10% of the building value.
🟧 Orange	**Orange: The building could progress in the EE programme, but building performance is likely below modern standards.** A further assessment will likely conclude that the building has moderate seismic performance. However, there are some uncertainties, and the building may contain critical weaknesses that are not detectable in the high-level screening. A deficiency-based or detailed assessment is needed to confirm seismic risk status and identify recommended strengthening interventions. The building may require strengthening to reach acceptable seismic performance. Bringing the building closer to modern standards is likely to require moderate costs in the range of 10 to 50% of the building value.
🟥 Red	**Red: A detailed assessment is likely to conclude that this building has a high vulnerability which may include a critical structural weakness**. Strengthening the building to meet a reasonable benchmark performance level would likely require significant investment exceeding 50% of the building value.

Building structural systems should be classified, and eventual structural irregularities or evidence on structural strengthening should be noted following the given guidance. Then, using the rating schedule, preliminary color classification (red, orange, yellow, green) should be chosen by selecting the row matching the characteristics of the building. If there are unknowns in the building data, the rating corresponding to the most conservative (highest vulnerability) assumption has to be used. A preliminary color classification might be revised in relation to the seismic risk rating descriptions for each color (Table 2), thus leading to the final color status.

3.2. IZIIS' Approach for customized seismic screening

Data requirements for the screening process according to the given methodology in the Country report have been established to balance the effort required to collect the data with the benefit in terms of reliability of seismic assessment. This will undoubtedly lead to more conservative decisions if the screening takes place rapidly, based on a desk study and remote data collection, and especially without trying to increase the knowledge level for the particular structure, thus minimizing the uncertainties. Despite precise general building classification, for reliable seismic safety assessment, the method of detailed site inspection of the building is indispensable and irreplaceable.

To achieve a more reliable seismic risk rating, IZIIS proposed and carried out the extended and upgraded technical approach for customizing the high-level seismic screening to correspond to the specifies of medical facilities in the country, represented by the following steps, [4]:

STEP 1: Desk study, remote data collecting, putting efforts in providing the technical design documentation and reviewing it;

STEP 2: On-site screening inspection by survey teams involving the following activities:

- conducting the interview with the facility representatives who has sufficient knowledge of the facility since its commissioning,
- outdoor/indoor visual inspection with control measurements of building geometry,
- indoor visual inspection for identification of overall integrity of the structural system, irregularities, structural and non-structural changes during exploitation, damages to the bearing elements, evidence of strengthening, other operating and maintenance problems, and control measurements of structural elements geometry,
- nondestructive measurements (NDT tests) of selected structural members (were available) applying the following testing equipment:
  - SCLEROMETER Digi Schmidt, a mechanical device designed to define the compressive strength of a material (primarily concrete)
  - PROFOMETER, a rebar detection system for identifying the presence of the columns hidden in the walls and obtaining data on the built-in reinforcement
  - TROMINO portable ultra-mobile seismometers for a definition of structural fundamental dynamic characteristics (natural frequencies);
- filling the Level 1_Data_Record_Form during the survey with the preliminary seismic color rating (green, yellow, orange, red) for each structural unit within the medical facility.

(STEP 3): Post-screening desk study involving:

- Reconsidering the information obtained during the survey,
- Definition of the final color status in accordance with complete findings and observations on existing seismic structural stability.+

(STEP 4): Repeated on-site screening involving more detailed (destructive) control investigation of the quality and quantity of built-in materials (concrete grade, reinforcement type) in case this additional information was needed to justify the final color rating.

To realize the activities mentioned above, IZIIS engaged the following teams:

- One supervising team, consisting of four key experts in the field, who set up the criteria for seismic screening, coordinated all the activities, revised and harmonized the survey data, and confirmed the screening rating of each building assigned by the survey teams,

- Five survey teams, consisting of two to three structural engineers (one expert as team leader and collaborators), who interviewed the representatives of each of the selected medical facilities to obtain the necessary information and better organize the on-site visual survey, reviewed the technical documentation, provided the on-site visual survey along with NDT tests and filled-in the Level_1_Data_Record_Form.

Structural analysis of the surveyed structures was not carried out, so the seismic assessment was qualitative and based on the IZIIS' knowledge and expertise in addition to the conducted interviews, project and drawing reviews, visual observations, nondestructive measurements, and limited control investigations (destructive testing).

4. Comparative Presentation of the Seismic Screening Results

4.1. Results for 27 medical facilities

The high-level seismic screening was performed for a total number of 27 medical facilities with different functions, selected by the Ministry of the health of North Macedonia, including dominantly healthcare centers, but also infirmaries and pharmacies [5]. The vast majority of the selected healthcare centers represent complexes with several separate structural units, thus, the total of 65 structural units with a total floor area of 54005 m² was surveyed. Among them, 47 are reinforced concrete structures, 14 are masonry structures, three are reinforced concrete ground floor upgraded with additional steel structures, and one is wooden.

According to the relevant standard when the structures were designed (Table 3), which according to the methodology is one of the deciding factors for the color rating, the facilities have been dominantly designed according to the first seismic code in the country, while only small part of them have been designed according to current standards. However, there is not an insignificant number of facilities older than 60 years, which have not been designed as earthquake-resistant structures, and, according to Table 1, are automatically excluded from the energy efficiency program, irrespectively the existing state of their structural systems.

Table 3 - Distribution according to the relevant standard when the medical facilities were designed

year of issuing the relevant standard	number of facilities	number of structural units	total floor area in m²
1948	7	14	8119
1964	16	43	40298
1981	4	8	5588

An on-site visual inspection of the medical facilities was carried out in August –September 2021. During the visual survey and inspection (step 1 and part of step 2), the Level_1_Data_Record_Forms for all the buildings were filled in by adopting the color rating status in accordance with the methodology given in the Country Report (North Macedonia). Results for color rating presented in Fig.1 show that none of the structural units is categorized as green, meaning that no one is suitable for progression in the EE program without further seismic assessment. 22 (yellow) units with about 35% of the total floor area could enter the EE program if further assessment satisfies the criteria. For the 32 (orange) units, with 54% of the total floor area, it is not cost-effective to enter the EE program since it will require structural strengthening, while the rest 11 (red) units, with about 10% of total floor area are automatically excluded from the EE program.
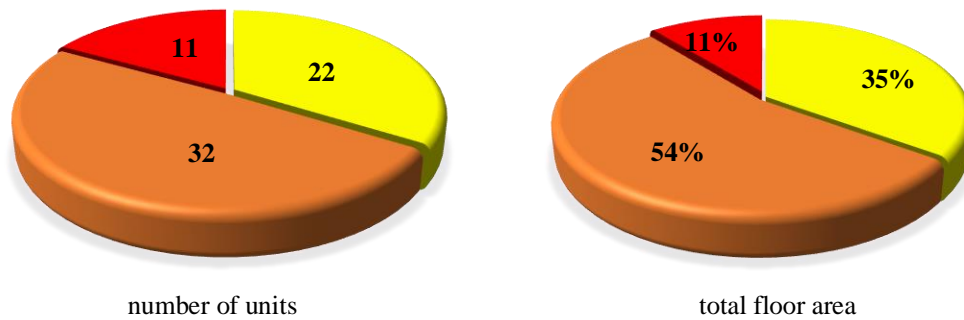
Figure 1. Distribution of medical facilities according to Country report' methodology
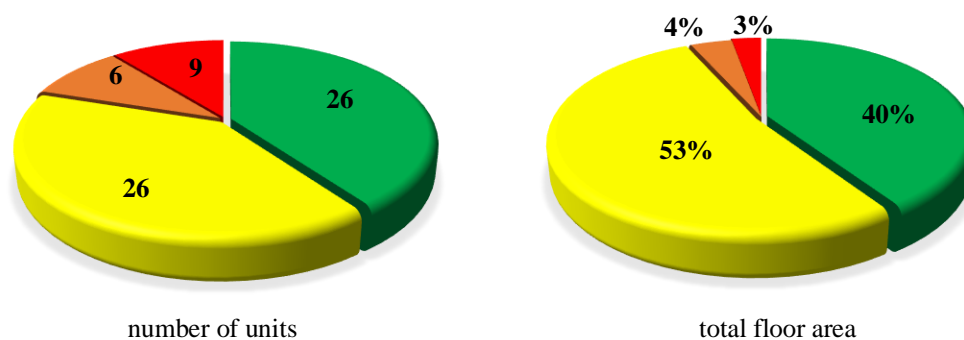
Figure 2. Distribution of medical facilities according to IZIIS' methodology

However, implementing IZIIS' extended and upgraded methodology, (steps 2, 3 4) which gives the possibility to take into account and reconsider the in-situ situation of each of the structural unit, confirmed with the site inspection and nondestructive measurement, as well as the elaborated acceptable level of risk from the deficiencies to meet the current seismic code, results in significantly different building categorization, (Fig. 2). Due to these reconsideration, vast majority of the structural units are categorized with lower seismic risk by at least one level, although there is one structural unit which turned in "red" from "orange" since it was seriously damaged.

4.2. Results for 50 municipal buildings

The high-level seismic screening was also performed for a total number of 50 municipal buildings selected by 14 Municipalities in the Republic of North Macedonia (Mogila, Kavadarci, Ohrid, Dojran, Valandovo, Gostivar, Resen, Kichevo, Skopje Centar, City of Skopje, Pehchevo, Struga, Rankovce and Kisela Voda), including dominantly elementary or high schools, but also kindergartens, administrative municipality buildings, fire stations, libraries, and cultural centers, [6]. Most of the selected municipal buildings represent complexes with several separate structural units or enlargements. Thus, 115 structural units with a floor area of 123339 m^2 were surveyed. Among them, 85 are reinforced concrete structures, 19 are masonry structures, 7 are steel structures, 2 are wooden structures, and 2 are mixed structures with masonry and RC parts.

According to the relevant standard when the structures were designed (Table 4), the structural units within the municipal building complexes have been dominantly designed according to the first seismic code in the country, while only a tiny part has been designed according to current standards. However, a significant number of facilities older than 60 years have not been designed as earthquake-resistant structures and, according to Table 1, are automatically excluded from the energy efficiency program, irrespectively the existing state of the structural system. Typical for many primary schools and kindergartens are enlargements, which were usually built in different periods compared to main buildings and often with different structural systems and according to different standards.

Table 4 - Distribution according to the relevant standard when the municipal buildings were designed

year of issuing the relevant standard	number of structural units	total floor area in m²
1948	16	13437
1964	75	85601
1981	24	24302

An on-site visual inspection of the municipal buildings was carried out in March –April 2022. During the visual survey and inspection (step 1 and part of step 2), the Level_1_Data_Record_Forms for all the buildings and units were filled in by adopting the color rating status in accordance with the methodology given in the Country Report (North Macedonia). Results for color rating presented in Fig.3 show that none of the structural units is categorized as green, meaning that no one is suitable for progression in the EE program without further seismic assessment. 55 (yellow) units with about 52% of the total floor area could enter the EE program if further assessment satisfies the criteria. For the 42 (orange) units, with 34% of the total floor area, it is not cost-effective to enter the EE program since it will require structural strengthening, while the rest 18 (red) units, with about 14% of the total floor area are automatically excluded from the EE program.

number of units   total floor area
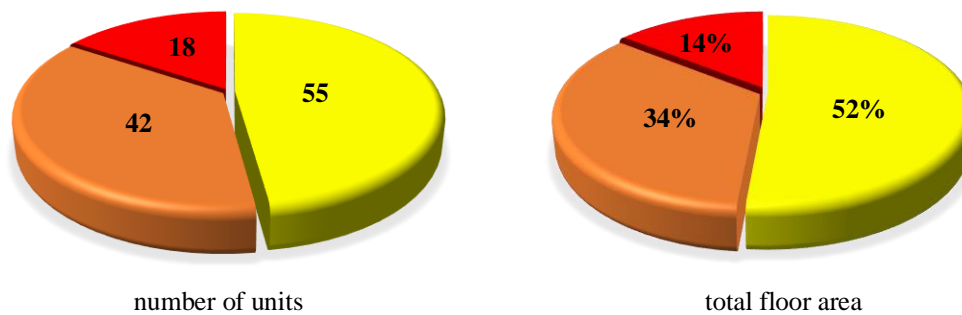
Figure 3. Distribution of municipal buildings according to Country report' methodology

number of units   total floor area
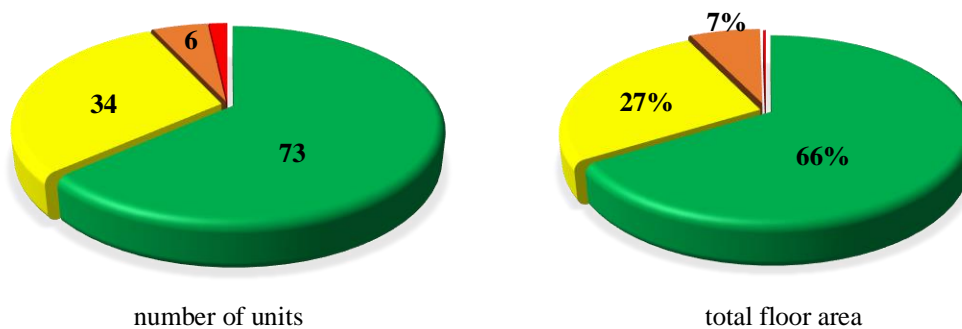
Figure 4. Distribution of municipal buildings according to IZIIS' methodology

However, implementing IZIIS' extended and upgraded methodology, (steps 2, 3 4) which gives the possibility to take into account and reconsider the in-situ situation of each of the structural unit, confirmed with the site inspection and nondestructive measurement, as well as the elaborated acceptable level of risk from the deficiencies to meet the current seismic code, results in significantly different building categorization, (Fig. 4). Due to this reconsideration, almost all of the structural units are categorized with lower seismic risk by at least one level, resulting in 73 (green) units with 66% of total floor area suitable for progression in the EE programme without further seismic assessment, and another 34 (yellow) units with 27% of total floor area if the further assessment satisfies the criteria, i.e. only 8 (6 orange and 2 red) units with 7% of total floor area were excluded from the EE programme.

It has to be noted that, besides the Ministry of Finance of North Macedonia, this approach resulted in the categorization of more than 90% of both the medical facilities and municipal buildings with the lowest seismic risk (green and yellow final color status) was accepted and approved by the World Bank too, which provide the financial support for overall energy efficiency program.

5. Conclusion

Improving existing buildings' energy efficiency is a very important and "hot" topic worldwide. For the seismic-prone regions, it is recommended to perform seismic screening before deciding whether the structure is suitable for energy efficiency investment. However, the seismic screening must be based on overall knowledge on aseismic design and construction practice in the country, detailed on-site inspection of each building, and to be carried out by structural engineers with appropriate knowledge and experience in earthquake engineering. Applying seismic screening, which is developed without considering the country specificities and allows only desk study and remote data collection, often leads to conservative and nonrelevant decisions.

Acknowledgments

References

[1] Shendova, V., (2011): Building Inventory Data for Republic of Macedonia, NERA. European Building Inventory Workshop, EU FP7-infrastructures ID 262330, May 2011, Pavia, Italy

[2] Shendova, V., Apostolska, R., Vitanova M., (2019): Structural Classification of Building and Bridge Assets in R. N. Macedonia. SERA Balkans Seismic Risk Workshop, EU Horizon 2020, ID 730900, June 2019, Belgrade, Serbia

[3] Sesov, V., Apostolska, R., Shendova, V., Salic, R., Zhurovski, A., Poposka, M., (2020): Integrating Seismic Risk Considerations into Energy Efficiency Investments in the Western Balkans. Activity 1_Baseline Definition, Technical Proposal Selection #1265632, *IZIIS Report 2020-33*

[4] Apostolska, R, Necevska-Cvetanovska, G, Shendova, V, Bojadzieva, J., (2018): Seismic performance assessment of "hybrid" structures using two-level multy-group GIS oriented approach: case studies. Bull Earthquake Eng https://doi.org/10.1007/s10518-018-0366-0

[5] Sesov, V., Apostolska, R., Shendova, V., Bozhinovski, Z., Gjorgjiev, I., Bojadjieva, J., Vitanova, M., Jekic, G., Stojanoski, B., Zlateski, A., Zhurovski, A., Kitanovski, T., Zafirov, T., Delova E., (2021): High-level Seismic Screening of the Structures of Medical Facilities in North Macedonia. Summary Report, *IZIIS Report 2021-58*

[6] Sesov, V., Apostolska, R., Shendova, V., Gjorgjiev, I., Micov V., Bojadjieva, J., Vitanova, M., Jekic, G., Zlateski, A., Zhurovski, A., Kitanovski, T., Zafirov, T., Delova E., Chapragoski G., Poposka M., Shoklaroski A., Ivanovski D., Tomic D., (2022): High-level Seismic Screening of the Structures of Municipal Buildings in North Macedonia. Summary Report, *IZIIS Report 2022-35.*

STATISTICAL SEISMIC PERFORMANCE ASSESSMENT OF VISCOUS DAMPER IN BENCHMARK BUILDINGS UNDER FAR-FAULT AND NEAR-FAULT EARTHQUAKES

M. Fahimi Farzam [(1)], T. Dehghan Kalajahi [(2)]

[(1)] *Department of Civil Engineering, Faculty of Engineering, University of Maragheh, m.farzam@maragheh.ac.ir*
[(2)] *Department of Civil Engineering, Faculty of Engineering, University of Maragheh, Taherehdehghankalajahi@yahoo.com*

Abstract

The viscous damper produces a force proportional to the velocity by moving the fluid inside their cylinder and, causes energy dissipation due to the dynamic vibrations by converting mechanical energy into heat. Viscose dampers with their three special features as powerful passive control devices have been widely studied in recent decades. The ability to improve the seismic performance of the structures with significant energy loss, production of out-of-phase damping force relative to displacement, and the increase of the structural damping without making major changes in the stiffness characteristics of the structure are its distinguishing features in comparison with other passive control methods. In this study, the seismic performance of viscous dampers is investigated to control the vibration of three benchmark steel buildings (i.e. 3-, 9-, and 20-story buildings designed for the SAC project) under two sets of recorded near-fault (NF) ground motions possessing forward-directivity (FD) or fling-step (FS) features and compared with the building responses under a suite of far-fault (FF) accelerograms. The results indicate the superior performance of viscous dampers in low-rise buildings and under FF earthquakes, i.e. 59% and 53% reduction in the mean of the maximum roof displacement and velocity, respectively. However, to control the mean of the maximum roof acceleration, the best performance was obtained in the high-rise buildings and under FF earthquakes, showing a maximum of 84% reduction. In general, it can be concluded that the damper has the highest reduction in acceleration response under the FF records, and under the NF records with FD has the least decrease in the velocity response.

Keywords: Passive Control, Viscous Dampers, SAC Benchmark Buildings, Near-Fault Ground Motions, Far-Fault Ground Motions.

1. Introduction

Conventional seismic design establishes the desired performance levels based on a combination of resistance and ductility for the structural elements. In this approach, structural engineers determine the resistance capacity and ductility of the structures to provide the life safety performance of the designed buildings under earthquakes [1]. In parallel and in a different approach, the seismic performance of the structure can be improved by using control strategies under lateral dynamic loads. According to Lu et al. [2], the idea of control was first proposed more than 130 years ago by John Milne, whose idea was to use a seismic isolator as a passive control device to reduce the vibration of structures under earthquake loads.

Viscous fluid dampers are one of the well-developed passive control devices invented to dissipate energy caused by vibration or impact for the first time in military and aerospace sciences [3]. In the last few decades, these dampers have been widely studied and applied to improve the seismic performance of the structures. As a well-recognized design advantage, viscous dampers do not alert the inherent stiffness of the host structure compared to other passive control devices (such as viscoelastic dampers, tuned mass dampers, and seismic isolators) [4], which eliminates the need for an iterative design method based on trial and error. In addition, the ability to dissipate significant energy and improve the seismic performance of the structure, out-of-phase damping force compared to the displacement and elastic force, easy installation, low sensitivity to a wide band of excitation

frequencies and temperature changes, as well as the need for limited space compared to the amount of displacement and obtainable force are the main advantages of this passive control system [5].

In recent years, investigating the statistical and probabilistic performance of the viscous damper under FF and NF records has received more attention [6]. In 2020, the performance of the viscous damper in a single-degree of freedom system and three shear buildings of 4, 8, and 12 floors has been investigated under a set of NF records with FS features. The results showed the proper performance of the damper in reducing the acceleration of the high-rise building compared to its displacement [7].

About half a century ago and due to the Bolt's opinion, earthquakes were categorized into FF and NF according to the distance from the building site to the active fault, and after the occurrence of destructive NF earthquakes such as Loma Prieta (1989), Northridge (1994), Kobe (1995) and Chi Chi (1999), identifying the areas near the fault became important [8, 9]. Based on the interest of structural engineers, the NF earthquakes can be divided into three categories of records with FD, FS and without pulse characteristics [10].

In this study, the statistical performance assessment of viscous damper on two-dimensional steel frames of 3-, 9- and 20-story benchmark buildings has been investigated under the FF and NF earthquakes. Therefore, three suites of 7 records of FF and NF with FD or FS features have been applied to the benchmark buildings investigating the seismic performance of the controlled buildings with viscous dampers subjected to NF and FF earthquakes. The viscous damping at the height of the building was distributed using inter-story drift proportional distribution determined on the basis of the first mode deformations. In the following, the results of the analysis of the buildings with and without dampers are studied statistically under all types of earthquakes. Finally, the ability of the viscous damper has been investigated to reduce the response of buildings with different heights and under the FF and NF records with different characteristics.

The difference of this article from the previous studies in this field are: (1) in this study, three benchmark buildings with different heights have been modeled to investigate the seismic performance of viscous damper in steel buildings. (2) Six different performance criteria have been compared including the maximum and norm of different responses (i.e., absolute acceleration, velocity, and displacement) which respectively represent the best performance and the mean performance of the damper in the entire length of the record. (3) Statistical seismic performance of the viscous damper has been evaluated under the effect of a suitable number of benchmark natural ground motions (21 records with different characteristics) with reporting not only the mean of responses but also their standard deviation.

2. Viscous Fluid Dampers

Viscous fluid dampers consist of a cylinder and a stainless steel piston with a bronze cap. When the piston rod moves inside the cylinder, the liquid is forced through the orifices built into the cap (piston head), and mechanical energy is consumed by converting it into Heat [11]. As the fluid passes through the orifices, the pressure difference created on the both sides of the damper creates the damper force [12]. Viscous fluid dampers are velocity-dependent devices that dissipate energy by changing the shape of a viscous fluid [13]. The shape, size, configuration, and arrangement of these orifices are the most important factors in the design of viscous dampers, which are the result of experimental tests. Various components of a viscous damper are presented in Fig. 1.
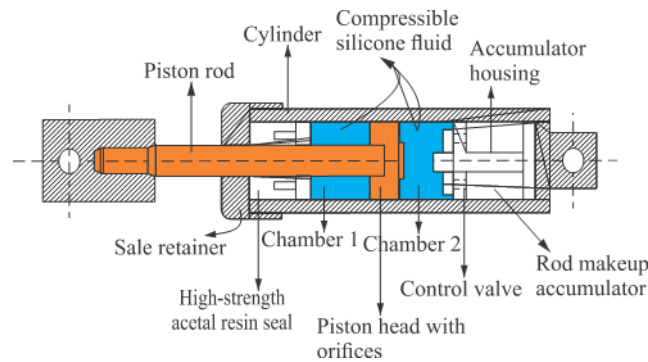
Figure 1. Various components of a viscous damper

3. Verification and numerical study

In this section, first, the verification of modeling and analysis results has been discussed to ensure the accuracy of the obtained results. Then, the benchmark natural ground motions has been presented. Finally, the applied design strategy of the viscous dampers has briefly been reviewed based on the acknowledged literature.

3.1 Verification of benchmark buildings

The benchmark buildings are modeled according to the study of Ohtori et al. [14]. Then a comparison has been made between the frequencies of the buildings based on Ohtori et al.'s article and the frequencies calculated in Table 1. Then, the comparison between the responses under the effect of 50% of the Hachinohe (1968) earthquake is reported in Table 2.

Table 1- Comparing the natural frequencies of the SAC buildings with Ohtori et al. [14]

	frequency (Hz)			
Struc.	Erorr (%)	calculated	Ohtori et al	No.mode
	1.010	0.980	0.990	1
3	0.230	3.050	3.060	2
	4.340	5.577	5.830	3
	0.452	0.442	0.440	1
9	0.508	1.186	1.180	2
	0.880	2.032	2.050	3
	2.700	0.253	0.260	1
20	4.000	0.720	0.750	2
	4.610	1.240	1.300	3

Table 2- Comparing the roof response of the SAC buildings with Ohtori et al. [14]

	Parameter			
Struc.	Erorr (%)	calculated	Ohtori et al	Roof Response
	1.420	0.091	0.090	Disp. (m)
3	0.370	0.535	0.537	Vel. (m/s)

	1.850	4.004	3.930	Acc. (m/s^2)
	1.060	0.188	0.186	Disp. (m)
9	4.420	0.627	0.656	Vel. (m/s)
	5.800	2.750	2.590	Acc. (m/s^2)
	4.700	0.166	0.174	Disp. (m)
20	6.700	0.424	0.451	Vel. (m/s)
	0.110	1.832	1.830	Acc. (m/s^2)

3.2 Benchmark natural ground motions

The response history analysis of the benchmark buildings has been performed under 21 benchmark earthquake records composed of 3 suites of 7 records with various characteristics. This category includes records of NF with FS or FD effect and FF records. The specifications of these records are presented in Table 3. Numbers 1 to 7 are the NF with FS, numbers 8 to 14 are NF records with FD, and numbers 15 to 21 are FF records.

Table 3- Benchmark ground motions

No.	year	Eq.	Station	PGA (g)	No.	year	Eq.	Station	PGA (g)
1	1999	Kocaeli	Yarimca(YPT)	0.23	12	1984	Morgan Hill	Anderson Dam	0.29
2	1999	Chi-Chi	TCU052	0.44	13	1987	Superstition Hills	Parachute Test Site	0.45
3	1999	Chi-Chi	TCU068	0.50	14	1979	Imperial-Valley	Brawley Airport	0.16
4	1999	Chi-Chi	TCU074	0.59	15	1952	Kern County	Taft	0.18
5	1999	Chi-Chi	TCU084	0.98	16	1979	Imperial Valley	Calexico	0.27
6	1999	Chi-Chi	TCU102	0.29	17	1989	Loma Perieta	Presidio	0.10
7	1999	Chi-Chi	TCU128	0.14	18	1994	Northridge	Century CCC	0.26
8	1992	Cape Mendocino	Petrolia	0.66	19	1994	Northridge	Moorpark	0.29
9	1994	Northridge	Olive View	0.84	20	1994	Northridge	Montebello	0.18
10	1992	Erzincan	Erzincan	0.50	21	1971	San Fernando	Castaic	0.27
11	2004	Park field	Fault Zone 1	0.50					

Records are scaled due to the ASCE7-10 regulations. In this method, first, all records are scaled to their maximum value, so that the maximum acceleration of all records reaches the g value. Then, by plotting the response spectrum of 5% damping of the records, the average spectrum for all the records is obtained in such a way that it is not lower than the spectrum of the design for type D soil in the period range of 0.2 to 1.5 T [4]. Notably, in the SAC project, soil type D has been selected [15]. For example, the response spectrum of the records and their average spectrum along with the spectrum of the regulation plan for a 3-story building are presented in Fig. 2.
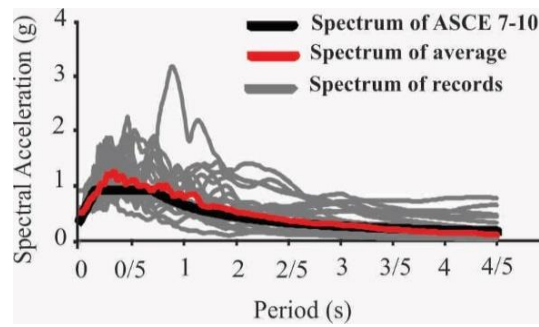
Figure 2. Response spectrum of scaled records for a 3-story building

3.3 Design of viscous dampers

The overall damping required for each building is calculated by Eq. (1) [16]. Then, the calculated total damping should be distributed at the height of the building using a well-approved method. In this study, the first mode shape method [17] has been preferred for the damping distribution through the height of buildings.

$$C = \frac{(\zeta_e - \zeta) \times T_o \times K}{\pi} \tag{1}$$

In Eq. (1), C, ξ_e, and ξ are the damping coefficient of the damper, the target damping ratio and the inherent damping ratio of the structure, respectively. T_o and K are equal to the period of the first mode and the stiffness of the structure, respectively. Inherent damping of SAC project buildings is 2% and target damping for dampers is adopted 20%. The stiffness of the buildings is obtained by the stiffness calibration method. In this method, first, the building is subjected to a lateral load with a triangular distribution, then, the shear and deformation of the floors are calculated, and the stiffness of each floor is extracted from the ratio of the shear of the floors to the relative deformation of the floors, and the stiffness of the whole building is derived from the sum of the stiffness of the floors.

The schematic arrangement of dampers at the height of the examined frame is presented in Figure (3). For information on the complete sections of the buildings, refer to the article by Ohtori et al. [14].
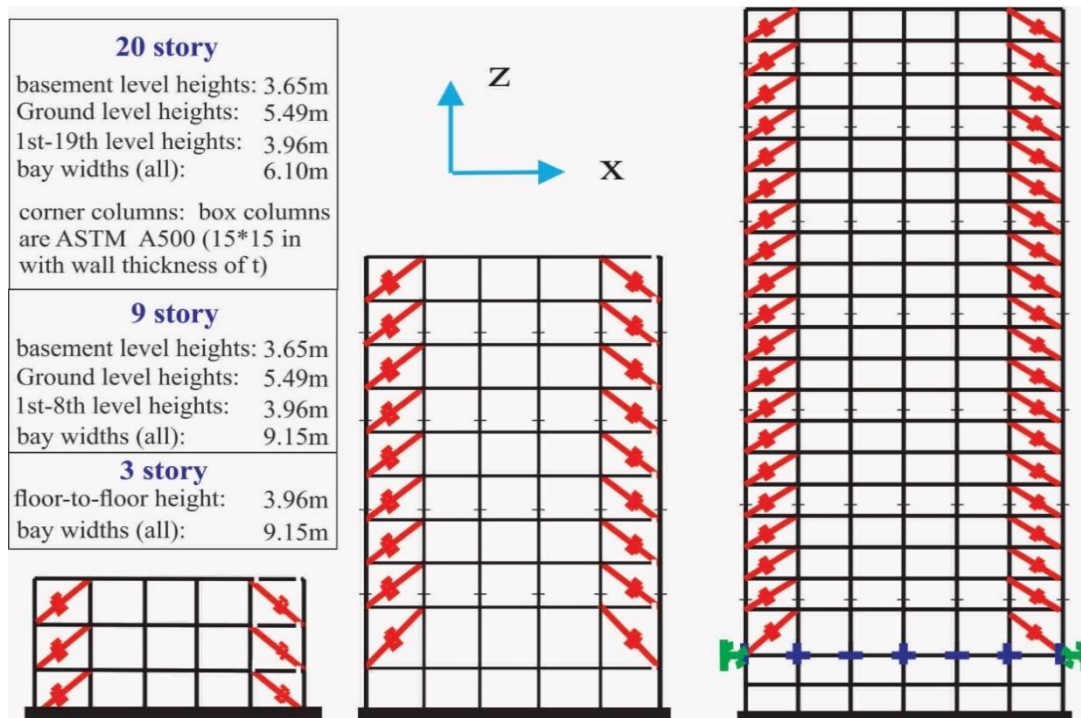
Figure 3. Viscose damper configurations in 3-, 9- and 20-story buildings

In the following, the distribution of viscous dampers at the height of the buildings based on the first mode shape method is briefly described in a simple flowchart in Fig. 4.

Structural modeling	step 1
Structural spectral analysis	step 2
Selecting the Target Damping	step 3
Determine the stiffness of stories	step 4
Determine the total damping of relation 1	step 5
Total damping distribution in height based on the first mode [29]	step 6
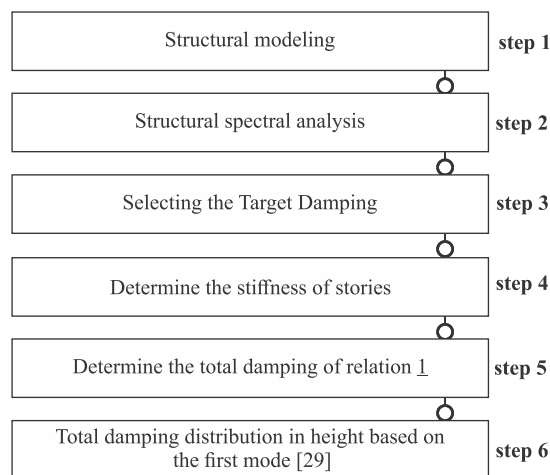
Figure 4. Viscous damper design flowchart

4. Seismic performance assessment and comparison

In this section, the response history results of the uncontrolled and controlled buildings are obtained under the benchmark earthquakes and compared based on the maximum and norm of responses. As an example, the 40 seconds of the response history of all three benchmark buildings is presented in Fig. 5

under one of the records. Notably, after 25 seconds from the start of the excitation time, the displacement response has decreased by 50, 60, and 75%, for 3-, 9- and 20-story buildings, respectively.
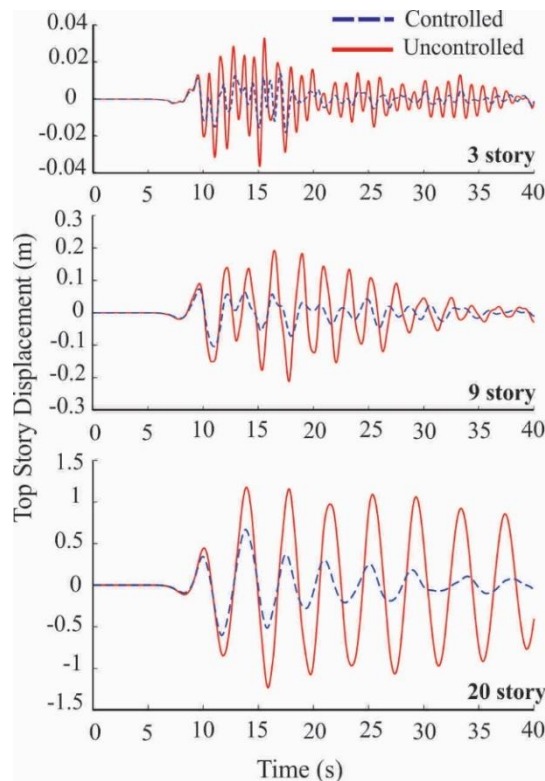
Figure 5. Response history of the roof displacement in 3-, 9- and 20-story buildings under record number 1

4.1 Comparing maximum and norm of responses

In the previous section, the performance of the viscous damper was shown under a specific record and qualitatively during the excitation time. In this section, the maximum and norm of different responses of the building, including displacement, velocity, and absolute acceleration of the building roof are calculated and compared for both uncontrolled and controlled buildings under 3 categories of records. The results for 3-, 9-, and 20-story buildings are presented in Figs. 6-8, respectively. In all figures, the responses of the controlled buildings are normalized to the responses of the uncontrolled ones. The maximum and norm of displacement, velocity, and acceleration responses of the buildings are plotted in the subplot of a-c for each figure, respectively under all records (3 suites of 7 records). The red, green, and blue colors show the responses under NF records with FS, FD, and FF records, respectively. Also, in the subplot of d-e of the figures, the mean and standard deviation of each response under 7 records are presented in column diagrams and the value of these criteria is reported over each column.

In Fig. 6 (d-f), results show that for the 3-story building, the mean of maximum reduction for roof displacement, velocity and acceleration is 59%, 53% and 63%, respectively under FF records. Also, the minimum reduction in the mean of maximum response for displacement, velocity, and acceleration responses was obtained by 48%, 50%, and 52%, respectively under NF records with FD. Therefore, the effect of viscous damper in reducing the acceleration response was the highest under the FF records in reducing the velocity response was the least under NF records with FD.
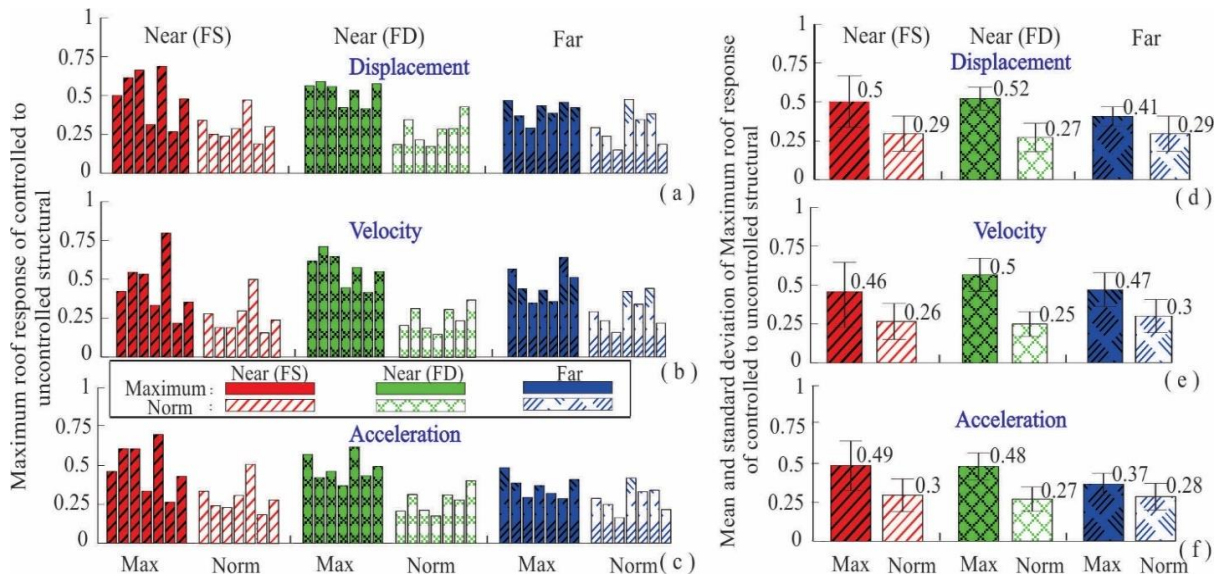
Figure 6. The maximum and the norm of response for 3-story building under 21 benchmark records

In Fig. 7, the performance of the viscous damper is presented in the control of the 9-story building. Vividly, the effect of the damper in reducing the acceleration response is obvious compared to reducing the displacement and velocity responses. According to Fig. 7 (d-f), the maximum reduction of the mean response for the roof displacement, velocity, and acceleration were 52%, 53%, and 75%, respectively under the FF records. Additionally, the minimum reduction in the mean response for displacement, velocity and acceleration responses was obtained by 46%, 44%, and 64% under the NF records with FD.

Remarkably, in the 9-story building, there is a slight difference between the performance of the building under FF and NF records in the reduction of the displacement and velocity responses. However, a noticeable reduction could be obtained in the reduction of the acceleration response, especially under the FF records.
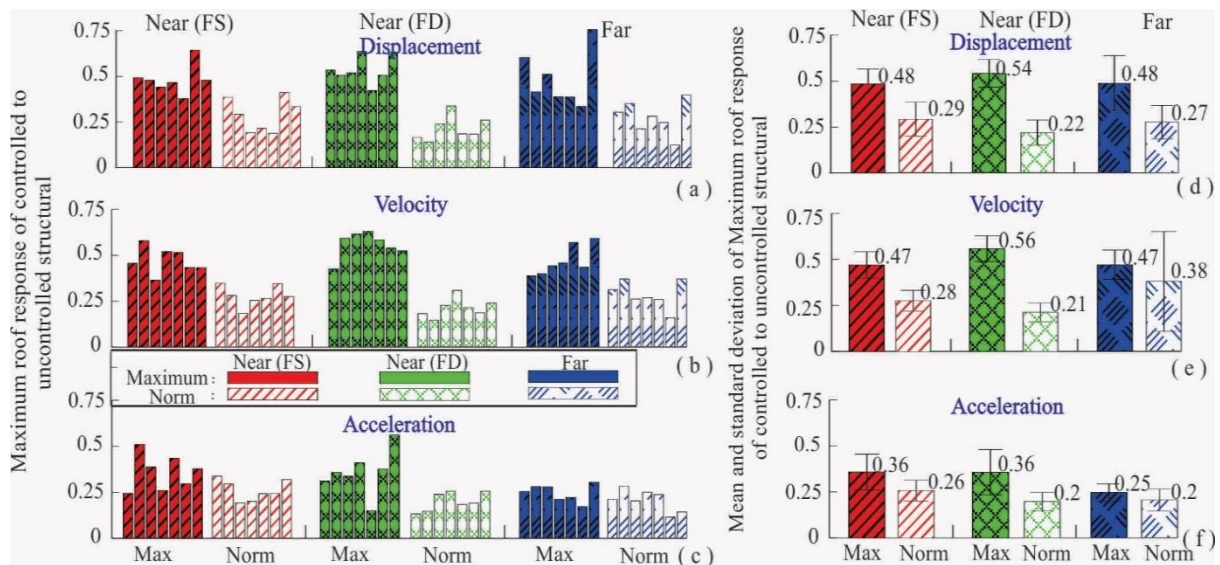
Figure 7. The maximum and the norm of response for 9-story building under 21 benchmark records

In Fig. 8, for the 20-story building as well as the 9-story building, due to the reduction of 46%, 44%, and 84% respectively for the response of displacement, velocity, and acceleration under the FF records, it can be attributed to the role of improved control in reducing the acceleration response of the building. He pointed to two other answers. Also, the minimum reduction in the mean of maximum response has been obtained for the roof displacement, velocity, and acceleration to the amount of 35%, 42%, and 65%, respectively under the NF records with FS.
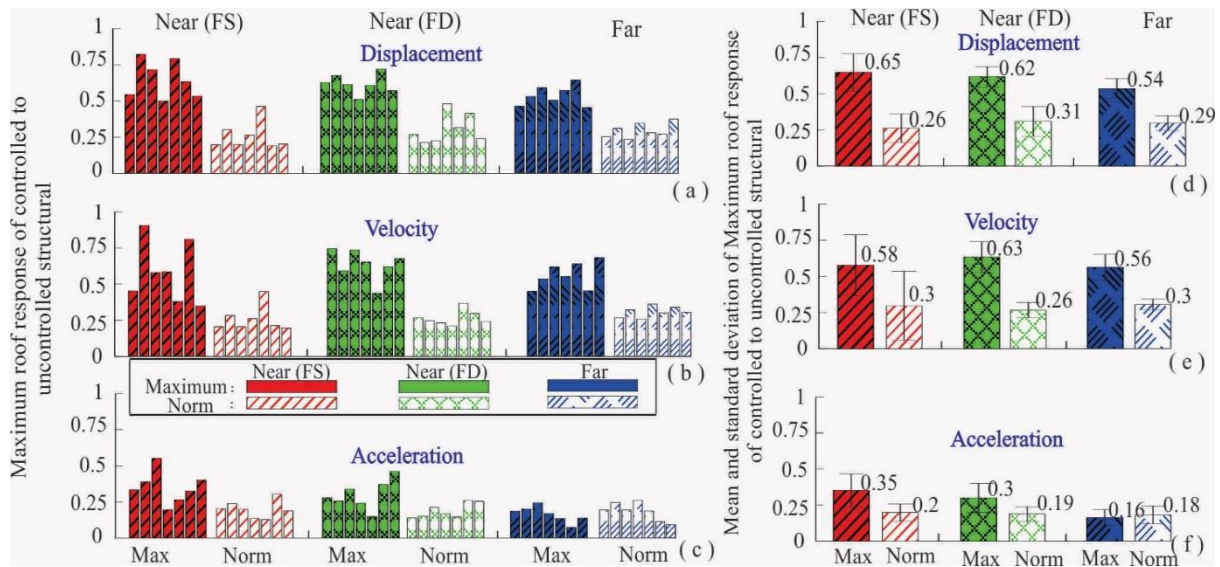
Figure 8. The maximum and the norm of response for 20-story building under 21 benchmark records

In general, regarding the mean of maximum response reduction, the viscous damper has the greatest effect in reducing acceleration under the FF records, and the least effect is almost in reducing the velocity response under NF records with FD.

In Table 3, the mean and standard deviation of the maximum and norm of different responses are presented for all three benchmark buildings under 3 suites of ground motions with different characteristics. In general, all responses have decreased between 30% and 85%, where absolute acceleration experienced the greatest reduction while displacement and velocity experience the least and almost similar reduction. Notably, the maximum and minimum reduction is obtained in the 20-story building related to the mean of the maximum of the roof acceleration and displacement, respectively. Additionally, the damper almost showed the predominant performance under the FF records, while the inferior performance has almost been obtained under the NF records with negligible difference between records with FD or FS.

Table 3- The mean and standard deviation of the maximum and norm of responses for 3-, 9- and 20-story buildings

		Performance Ceriteria											
		Displacement				Velocity				Acceleration			
$\zeta = \%2$		Max		Norm		Max		Norm		Max		Norm	
Strct.	Eq. Ch.	Mean	S.d	Mean	S.d	Mean	S.d	Mean	S.d	Mean	S.d	Mean	S.d
	FS	0.50	0.17	0.29	0.09	0.46	0.19	0.26	0.11	0.49	0.16	0.30	0.10
3	FD	0.52	0.07	0.27	0.09	0.50	0.11	0.25	0.08	0.48	0.09	0.27	0.08
	Far	0.41	0.06	0.29	0.11	0.47	0.11	0.30	0.11	0.37	0.07	0.28	0.09

	FS	0.48	0.08	0.29	0.09	0.47	0.07	0.28	0.06	0.36	0.12	0.26	0.06
9	FD	0.54	0.07	0.22	0.07	0.56	0.08	0.21	0.05	0.36	0.12	0.20	0.05
	Far	0.48	0.15	0.27	0.09	0.47	0.07	0.38	0.27	0.25	0.11	0.20	0.06
	FS	0.65	0.13	0.26	0.10	0.58	0.21	0.30	0.24	0.35	0.11	0.20	0.06
20	FD	0.62	0.07	0.31	0.10	0.63	0.10	0.26	0.05	0.30	0.10	0.19	0.05
	Far	0.54	0.07	0.29	0.05	0.56	0.09	0.30	0.04	0.16	0.05	0.18	0.06

5. Conclusion

In this study, the performance of viscous dampers to control the seismic vibration of steel benchmark buildings i.e., short-, mid-, and high-rise buildings were investigated under natural ground motions with different characteristics. Generally, the mean of the norm of responses experienced more reduction than the mean of the maximum of responses. Remarkably, in terms of the mean of the norm of responses (through the whole earthquake time), the maximum reduction is related to the acceleration response, and its values for the 3-, 9-, and 20-story buildings are 73%, 80%, and 82%, respectively, and under FF earthquakes. Also, in terms of the mean of the maximum of responses, the minimum percentage of reduction is related to the velocity response, which values are 50%, 44%, and 37%, respectively, and under NF earthquakes with FD. However, in terms of the mean of norm responses, it is possible to see a maximum decrease in the velocity response to 75% in a 3-story building and under NF earthquakes with FD, and in 9 and 20-story buildings to a maximum decrease in the acceleration response to values of 80% and 82% under the FF earthquakes. Therefore, the viscous damper has a commendable performance in all buildings and under all earthquake records. However, the performance of the viscous damper in reducing the velocity or displacement responses in short-rise buildings and under FF records outperforms the mid-rise buildings, and in mid-rise buildings, it is far better than high-rise buildings. In contrast, in reducing the acceleration responses, the viscous damper has a profound effect on high-rise buildings.

References

[1] Symans, M.D.and Constantinou, M.C. (1999): Semi-active control systems for seismic protection of structures: A state-of-the-art review. *Engineering Structures*, Vol. 21(6), 469-487. DOI: 10.1016/S0141-0296(97)00225-3.

[2] Lu, Z.,Wang, Z.,Zhou, Y.and Lu, X. (2018): Nonlinear dissipative devices in structural vibration control: A review. *Journal of Sound and Vibration*, Vol. 423, 18-49. DOI: 10.1016/j.jsv.2018.02.052.

[3] Ras, A.and Boumechra, N. (2016): Seismic energy dissipation study of linear fluid viscous dampers in steel structure design. *Alexandria Engineering Journal*, Vol. 55(3), 2821-2832. DOI: https://doi.org/10.1016/j.aej.2016.07.012.

[4] Haseli, S.and poursha, M. (2018): Investigation of seismic responses of isolated isolated buildings under earthquakes near the fault zone. *Journal of Civil Engineering Amirkabir*, Vol. 50(3), 579-596. DOI: 10.22060/ceej.2017.11973.5159.

[5] De Domenico, D.,Ricciardi, G.and Takewaki, I. (2019): Design strategies of viscous dampers for seismic protection of building structures: A review. *Soil Dynamics and Earthquake Engineering*, Vol. 118, 144-165. DOI: 10.1016/j.soildyn.2018.12.024.

[6] Wu, X.,Guo, W.,Hu, P.,Bu, D.,Xie, X.and Hu, Y. (2020): Seismic performance evaluation of building-damper system under near-fault earthquake. *Shock and Vibration*, Vol. 2020.

[7] Hu, G.,Wang, Y.,Huang, W.,Li, B.and Luo, B. (2020): Seismic mitigation performance of structures with viscous dampers under near-fault pulse-type earthquakes. *Engineering Structures*, Vol. 203, 109878.

[8] Lu, L.Y.,Lin, C.C.and Lin, G.L. (2013): Experimental evaluation of supplemental viscous damping for a sliding isolation system under pulse-like base excitations. *Journal of Sound and Vibration*, Vol. 332(8), 1982-1999. DOI: 10.1016/j.jsv.2012.12.008.

[9] Bolt, B.A. (2004): Seismic input motions for nonlinear structural analysis. *ISET journal of earthquake technology*, Vol. 41(2), 223-232.

[10] Bhagat, S.,Wijeyewickrema, A.C.and Subedi, N. (2018): Influence of Near-Fault Ground Motions with Fling-Step and Forward-Directivity Characteristics on Seismic Response of Base-Isolated Buildings. *Journal of Earthquake Engineering*, 1-20.

[11] Qian, F.,Ding, S.,Song, J.and Chen, C.-C. *Testing of fluid viscous damper*. in *15th World Conference on Earthquake Engineering*. 2012.

[12] mousavi, s.and ziyaeefar, m. (2017): Behavioral model for a Contractable Viscous Dashpot. *Modares Civil Engineering journal*, Vol. 17(1), 234-253.

[13] Marshall, J.D.and Charney, F.A. (2012): Seismic response of steel frame structures with hybrid passive control systems. *Earthquake Engineering & Structural Dynamics*, Vol. 41(4), 715-733. DOI: 10.1002/eqe.1153.

[14] Ohtori, Y.,Christenson, R.,Spencer Jr, B.and Dyke, S. (2004): Benchmark control problems for seismically excited nonlinear buildings. *Journal of Engineering Mechanics*, Vol. 130(4), 366-385.

[15] 2000 State of the art report on systems performance of steel moment frames subject to earthquake ground shaking,*Federal Emergency Management Agency Washington, DC, USA*

[16] Cimellaro, G.P.and Retamales, R. (2007): Optimal softening and damping design for buildings. *Structural Control and Health Monitoring: The Official Journal of the International Association for Structural Control and Monitoring and of the European Association for the Control of Structures*, Vol. 14(6), 831-857.

[17] Landi, L.,Conti, F.and Diotallevi, P.P. (2015): Effectiveness of different distributions of viscous damping coefficients for the seismic retrofit of regular and irregular RC frames. *Engineering Structures*, Vol. 100, 79-93. DOI: https://doi.org/10.1016/j.engstruct.2015.05.031.

NUMERICAL STUDY ON MECHANICAL PARAMETERS OF NOVEL DRILLED PLATE METALLIC DAMPER (DPMD)

Peyman Shadman Heidari [(1)]

[(1)] Department of Civil Engineering, East Tehran Branch, Islamic Azad University, Tehran, Iran,
peyman_shademan@yahoo.com

Abstract

The purpose of this study is to investigate the seismic performance of a new type of yield metal dampers. Drilled plates are used in these metal dampers. These plates use holes with different diameters. Various drilling arrangement have also used to evaluate and improve the seismic performance of these types of dampers. For this study used a reference sample and 15 proposed models. The overall numerical results show that the proposed metal dampers have similar hysteretic curves. According to the hysteresis curves of drilled plate metallic damper (DPMD) under in-plane seismic loading; obtained mechanical parameters such as ductility ratio, initial stiffness, effective stiffness, total dissipated energy, dissipated energy in the last cycle, elastic strain energy, equivalent viscous damping (EVD) and equivalent plastic strain (EPS). Also, a formula is proposed to estimate the EVD value based on the ductility ratio of the proposed samples. The analytical results showed that the amount of stiffness, ductility ratio and equivalent viscous damping depends on the location and diameter of the holes. Also, the concentration of plastic strain between the holes increases the ductility ratio and EVD value of these types of dampers.

Keywords: Drilled Plate Metallic Damper (DPMD), Mechanical parameters, Ductility ratio, Equivalent viscous damping

1. Introduction

The occurrence of devastating earthquakes can cause life and financial losses. Especially the devastating earthquakes that have occurred in recent years around the world emphasize require of a suitable and reliable solution to this natural phenomenon. The performance of metallic dampers based on nonlinear behavior of metals is one of the most effective mechanisms of damping and absorption of input energy to structures during earthquakes. Kelly et al [1] used the idea of metallic dampers to absorb earthquakes energy in the structure. They introduced several hysteretic energy absorption mechanisms in structures. Skinner et al [2, 3] proposed several yielding metal dampers, including torsion beam dampers, bending beam dampers, and U-shaped dampers. Kasai and Popov [4] presented yielding damper using steel plate and stiffener. They tested it and introduced the hysteresis curve. Bergman and Goel [5] proposed flexural yielding metallic dampers. They tested added damping and stiffness (ADAS) and Triangular-ADAS (TADAS) systems. In ADAS and TADAS dampers are used parallel X and V shaped steel plates, respectively. Whittaker et al [6] tested X-shaped metallic dampers as ADAS under cyclic load. Tsai et al [7], in order to fix the defects of the XADAS dampers, studied TADAS triangular steel plate dampers. Also, they developed a simple mathematical model for force-displacement, which was reasonably accurate compared to laboratory work. Dargush and Soong [8] conducted a more detailed study of the phenomenon of fatigue in low cycles based on the behavioral theories of TADAS dampers and developed their analytical models. Gang Li and Hongnan Li [9] presented a new idea for designing metallic damper. They tested dual functions metallic damper (DFMD) with quasi-static loading. Soni and Sanghvi [10] described a technique to find out combined stiffness of model equipped with ADAS damper. They proposed a mathematical model. Teruna et al [11] investigated four steel damper specimens with specific geometry. They obtained energy absorption capabilities, hysteresis loop and stiffness in specimens. Sahoo et al [12] investigated passive energy dissipation of steel plates in both flexure and shear yielding under cyclic loading.

Their specimens consist of two flexure (end) plates of X-shape and a shear (web) plate of rectangular shape. Garivani et al [13] introduced a new type of flexural yielding metallic damper and they called comb-teeth damper (CTD). Their damper included number of teeth steel plates that absorb energy through in-plane flexural yielding. Ghaedi et al [14] introduced a new hysteretic metallic bar damper that they named bar damper (BD). BD included three simple steel plates and a number of solid bars which dissipate input energy due to vibration loads through flexural yielding.

This research aims to introduce a new type of shear yielding metallic damper. In this type of dampers are used the shear plate with hole. Forasmuch as in this idea it is easy to construct and perform samples in the structure, various dampers can be produced by changing the location and diameter of the holes. Based on the hysteresis curves of DPMD sample under in-plane cyclic load; mechanical parameters such as ductility ratio, initial stiffness, effective stiffness, total dissipated energy, dissipated energy in the last cycle, elastic strain energy, equivalent viscous damping (EVD) and equivalent plastic strain (EPS) are determined.

2. Drilled Plate Metallic Damper

2.1. Geometry of DPMD

ADAS dampers are usually used in steel bracing frames, as shown in Figure 1. The DPMD consists of a series of drilled steel plates. In this new type of damper can produce a variety of DPMD with changing location and diameter of the holes.

(a)   (b)
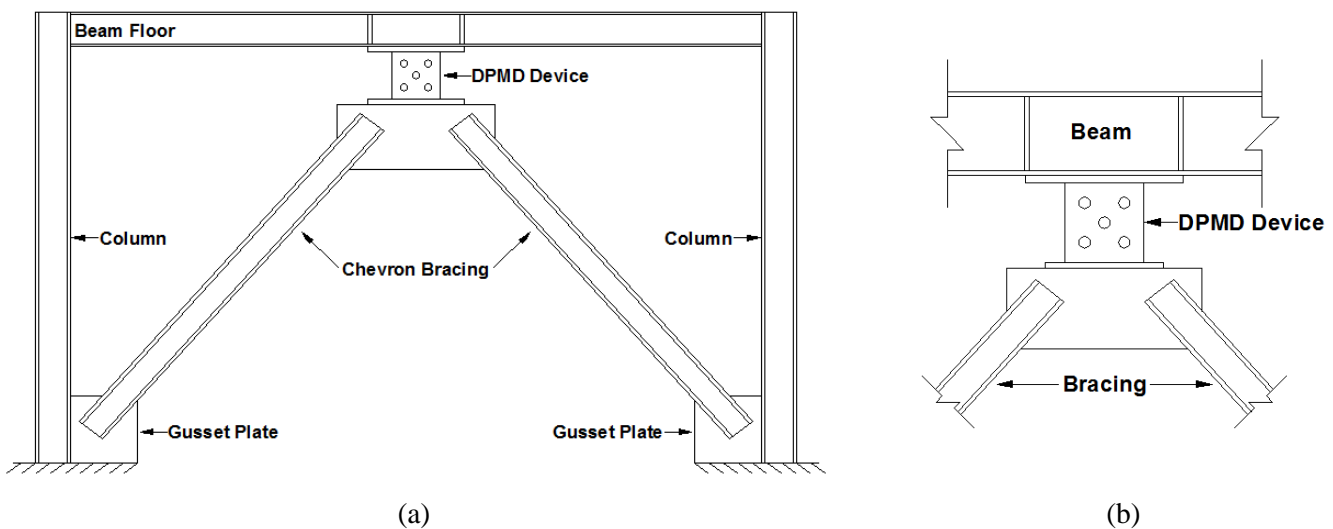
Figure 1. a) Frame system and DPMD position, b) Connection of DPMD to beam and bracing

The 15 different models were proposed based on the various arrangements and diameter of the holes. All of samples have the same width, height and thickness 210, 300, 20 millimeters, respectively. Also thickness of end plate assumed 50 mm. In samples used diameter of holes 31.5, 42 and 52.5 mm which are equivalent to 30%, 40% and 50% reduction of cross sectional areas in plate, respectively. Figure 2 shows the drilling arrangement and the hole diameters of the samples.
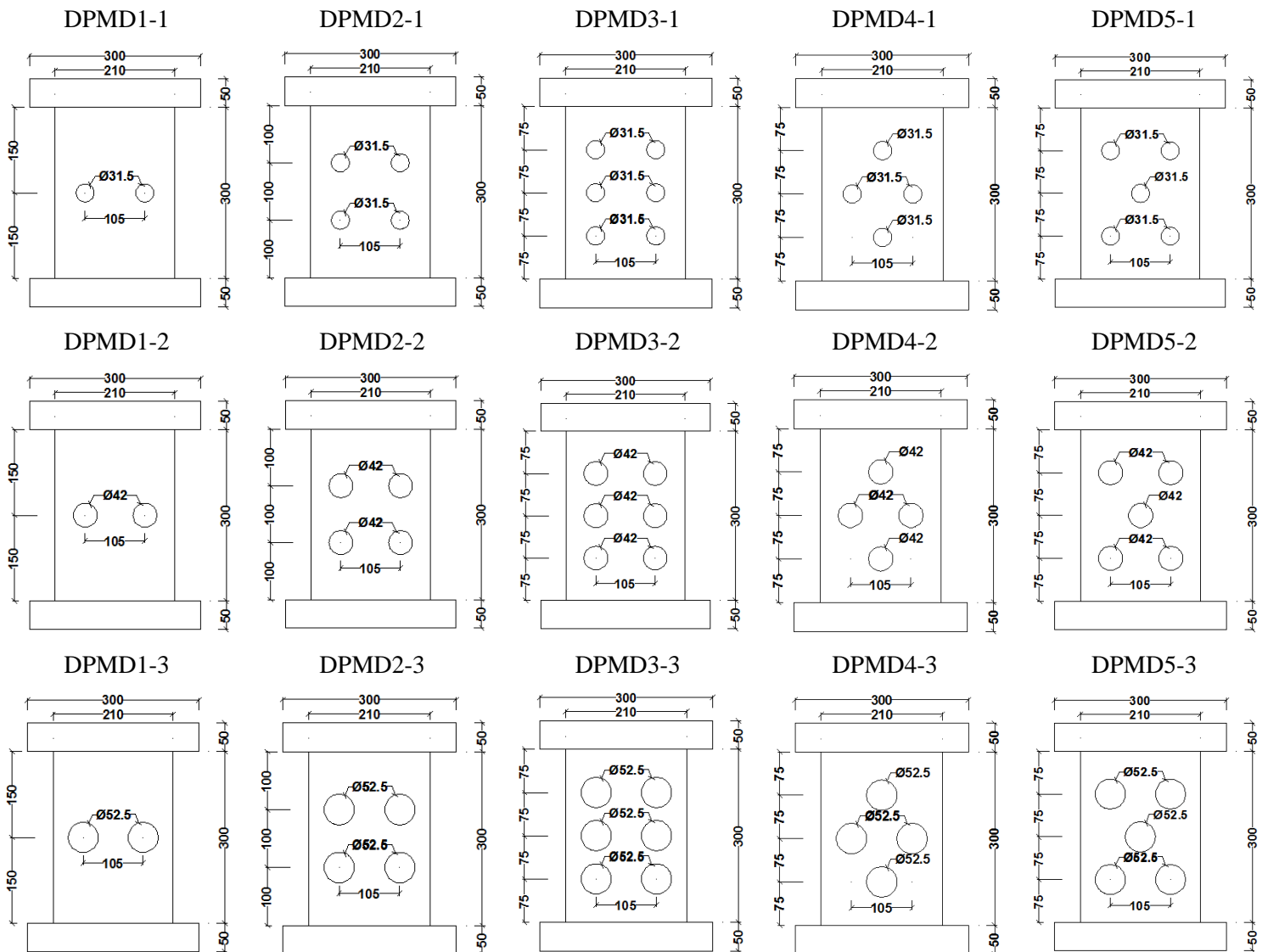
Figure 2. Details of samples

2.2. Loading pattern and material properties

In order to evaluate the performance of drilled plate metallic dampers; quasi-static cyclic loading pattern was used. Cyclic loading pattern specified by ATC 24 [15] was used for the cyclic loading of the analytical in this research. The loading pattern, magnitude of displacement and number of cycles are illustrated in Figure 3-a. There are seven steps with three cycles and other steps with two cycles. Displacement amplitude is from 1 to 84 mm. This general loading protocol is common for metallic damper. In this research mild steel plate was used with specifications that conform to JIS-SS400 [11]. The amount of yield stress, tensile strength and modulus of elasticity are 292, 456 and 2.06×10^5 MPa respectively. Also, the measured yield strain and elongation are 1.42×10^{-3} and 16% respectively. Figure 3-b shows material strength curve [11].

(a)	(b)
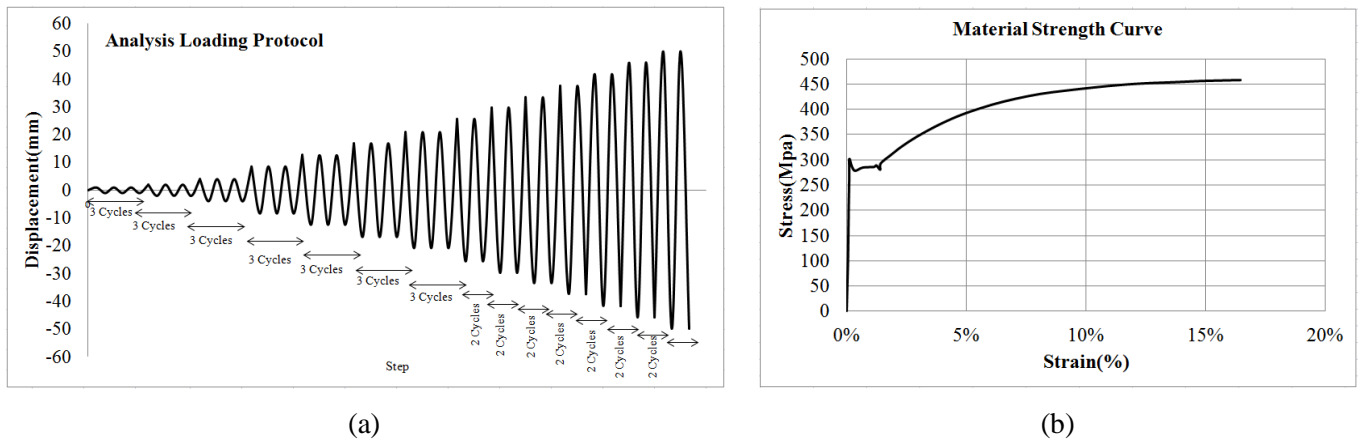
Figure 3. a) The applied cyclic displacement loading protocol based on ATC-24[15], b) Stress-strain curve obtained from a coupon test [11]

3. Finite Element Modeling procedure

3.1. FEMs of DPMD

To study the mechanical parameters of the drilled plate metallic damper, nonlinear finite element (FE) analyses were carried out using ANSYS R16 FEM [16] software. Fifteen FEMs with different configurations and diameters were modeled. Steel plate elements were modeled using a 3D solid element. SOLID 185 (brick 8 node 185) element was used for modeling of proposed samples. Multi linear kinematic hardening plastic model [16] was used to model the plasticity and cyclic inelastic behavior of steel material, respectively. In order to prevent out of plane buckling of the end plate, the transitional degree of freedom in the Z and Y directions are closed. Mesh sensitivity analysis was performed to find proper element sizes in the FEMs. Mesh size was used 10x10 mm, and they are the same in all FEMs. Figure 4 shows the FEMs of the DPMD1-1, DPMD2-1, DPMD3-1, DPMD4-1 and DPMD5-1 used in this study.

| DPMD1-1 | DPMD2-1 | DPMD3-1 | DPMD4-1 | DPMD5-1 |
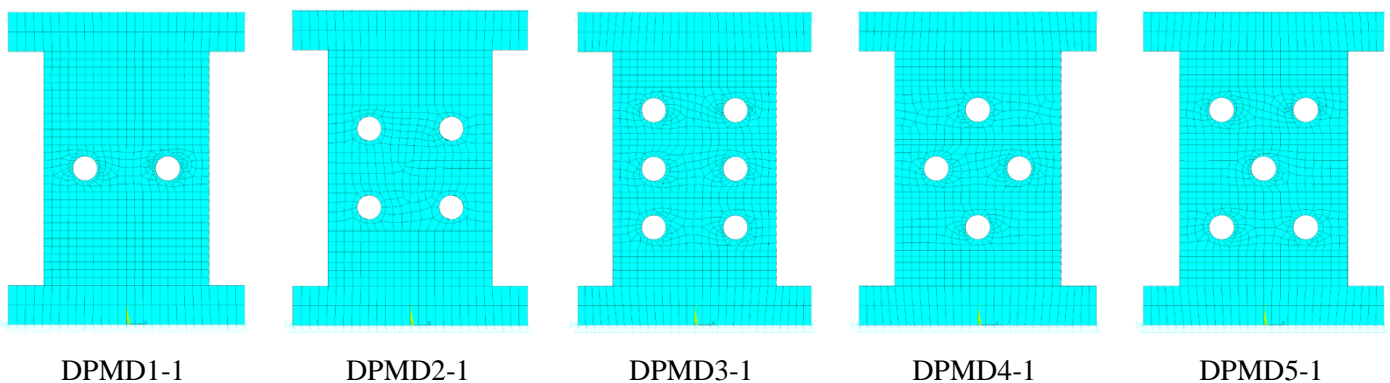
Figure 4. Finite element models of DPMD samples

3.2. FEM of DHSD-1 experimental specimen

In order to validate the FEMs, the experimental specimen (DHSD-1[11]) was modeled in ANSYS R16 FEM [16] software. Maximum displacement applied at top sample is 50.1 mm. Figure 5 illustrates details of test specimen, specimen shape and FEM in ANSYS software.

| (a): Details of test specimen [11] | (b): Specimen shape [11] | (c): FEM |
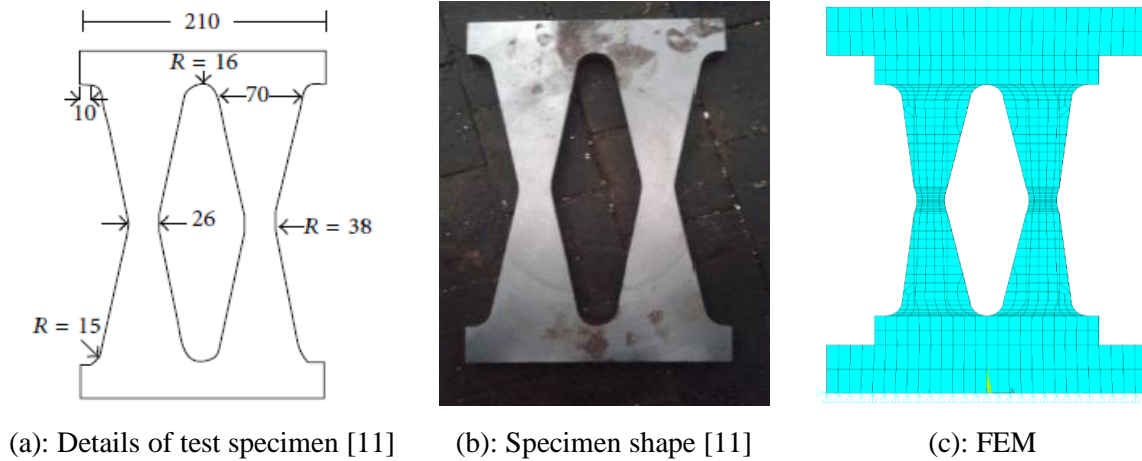
Figure 5. Experimental and Finite element models [11]

The results of analytical and experimental analysis were compared. According to Figure 6, there is an acceptable agreement between the results of analytical and experimental studies.

| (a): Failure of specimen [11] | (b): Total mechanical strain | (c): Hysteresis curve of experimental and FEM of DHSD-1[11] |
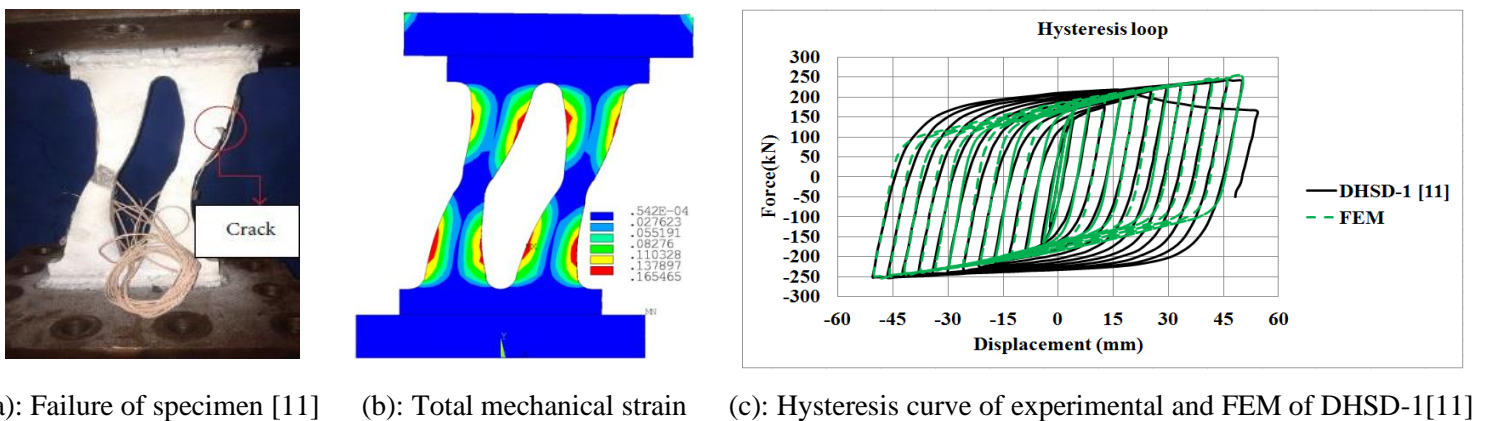
Figure 6. Failure of specimen, distribution of Total mechanical strain at maximum displacement and Comparison of hysteresis curves

3.3. Hysteresis behavior of DPMDs

Hysteresis curves are needed to determine the mechanical parameters of the DPMD proposed damper. In the force-displacement hysteresis curve such as yield force, yield displacement, ultimate force, and ultimate displacement can be obtained parameters. For this purpose, force-displacement hysteresis curves of analytical samples were determined. Figure 7 shows the force-displacement hysteresis curves of the DPMD dampers.
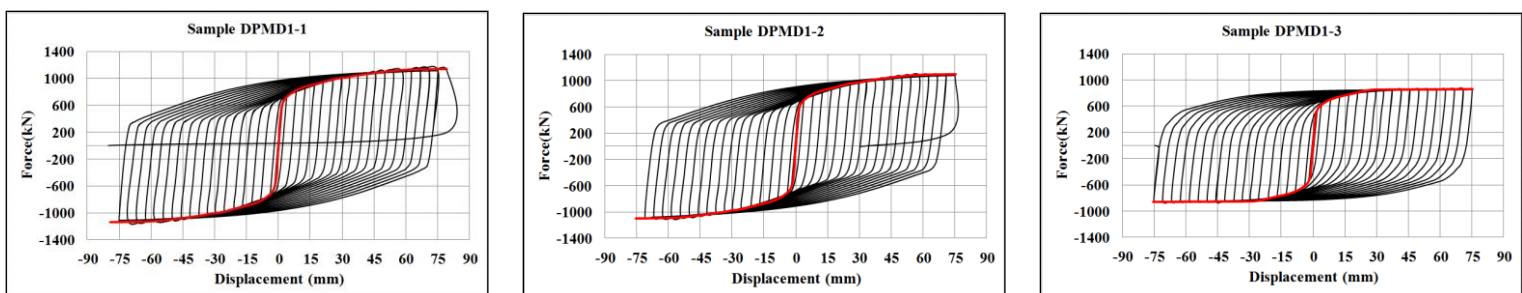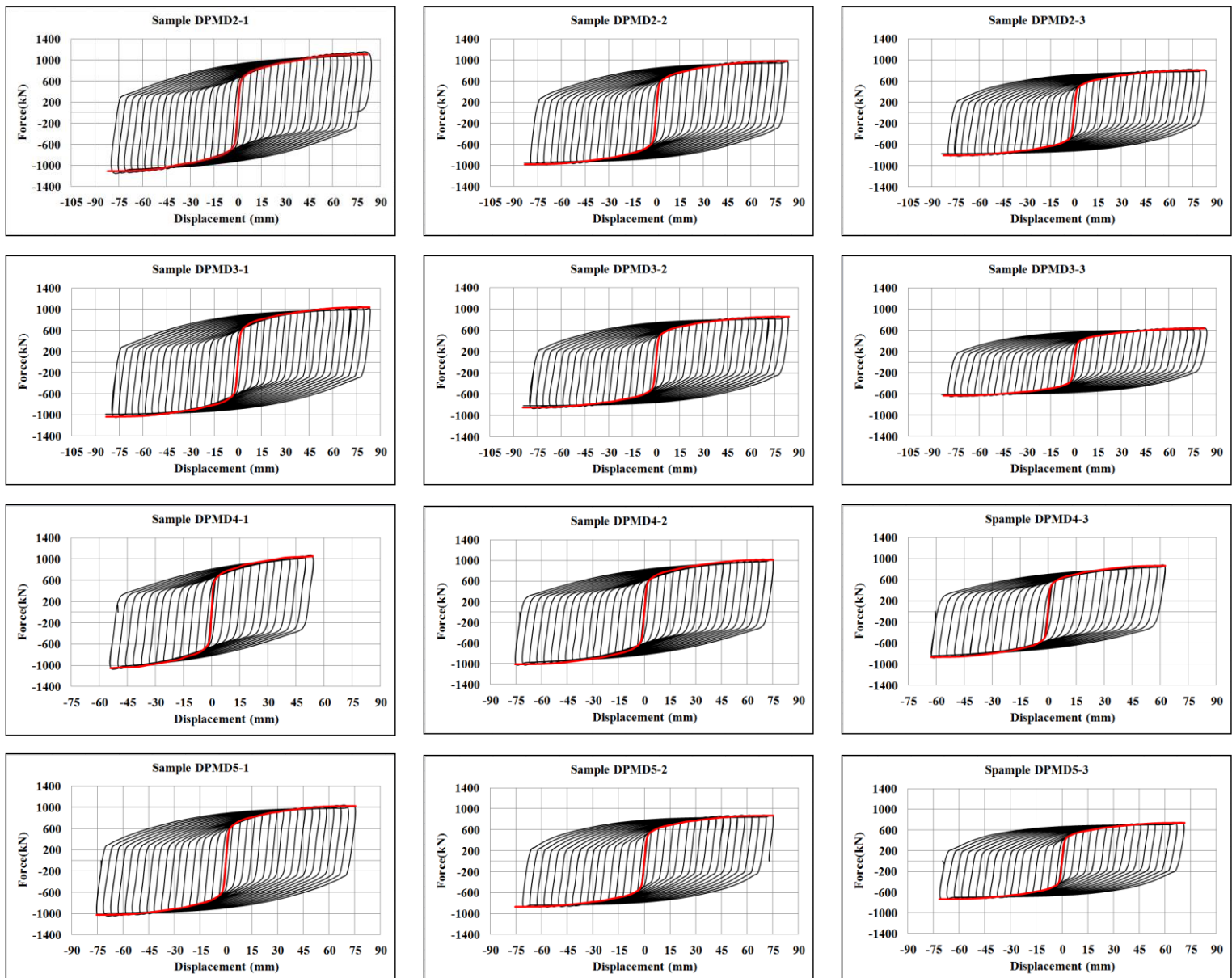
Figure 7. Force-displacement hysteresis loops of the DPMD and backbone curves

4. Mechanical parameters of DPMD dampers

4.1. Ductility ratio, effective and initial stiffness, total dissipated energy and equivalent viscous damping

Ductility ratio can be defined as the ratio of maximum deformation capacity to the deformation level corresponding to a yield deformation. The value of ductility ratio is given by:

$$\mu = \frac{\Delta_{max}}{\Delta_y} \tag{1}$$

Where Δ_{max} and Δ_y are ultimate displacement and yield displacement, respectively. In each loop of the force-deformation hysteresis curve the secant or effective stiffness can be defined. The effective stiffness for maximum displacement was obtained as the average from minimum and maximum force

over the average from minimum and maximum displacement, respectively. According to Figure 8, effective stiffness equation is obtained as follows:

$$K_{eff} = \frac{\dfrac{|P_{max}| + |P_{min}|}{2}}{\dfrac{|\Delta_{max}| + |\Delta_{min}|}{2}} = \frac{P_{ave}}{\Delta_{ave}} \tag{2}$$

Where Δ_{max}, Δ_{min}, Δ_{ave}, P_{max}, P_{min} and P_{ave} are ultimate displacement, minimum displacement, average displacement, ultimate force, minimum force, average force in each loop, respectively. In this research, effective stiffness was calculated for maximum displacement and last loop of the force-displacement hysteresis curves of the DPMD samples. Also, initial stiffness is calculated as follows:

$$K_{initial} = \frac{P_y}{\Delta_y} \tag{3}$$

Where Δ_y and P_y are yield displacement and yield force, respectively. In this paper, initial stiffness was calculated for first loop of the force-displacement hysteresis curves of the DPMD samples. Effective stiffness represents the damping force in response to the desired displacement. The ultimate displacement and yield displacement values were obtained from the force-displacement hysteresis curve. Table 1 illustrates the ductility ratio, effective stiffness and initial stiffness for the DPMD samples.

The rate of damage in structures under seismic load depends on transfer seismic energy. By using passive dampers a large amount of seismic energy can be absorbed. Therefore, the amount of seismic energy absorbed by the principal structural members is reduced, and structure elements have elastic behavior. The amount of energy absorption per cycle is the area under the force-displacement hysteresis curve for one loop. Figure 8 shows amount of energy dissipated in last cycle and elastic strain energy. The amount of total dissipated energy in each force-displacement hysteresis curve includes the sum of the areas under the curve of all cycles. In this study, E_T, E_D and E_S are total dissipated energy, dissipated energy in the last cycle and elastic strain energy, respectively. According to the description given and existing hysteresis curves, it is possible to calculate total dissipated energy, dissipated energy in the last cycle and elastic strain energy. The E_T, E_D and E_S values are shown in Table 2.
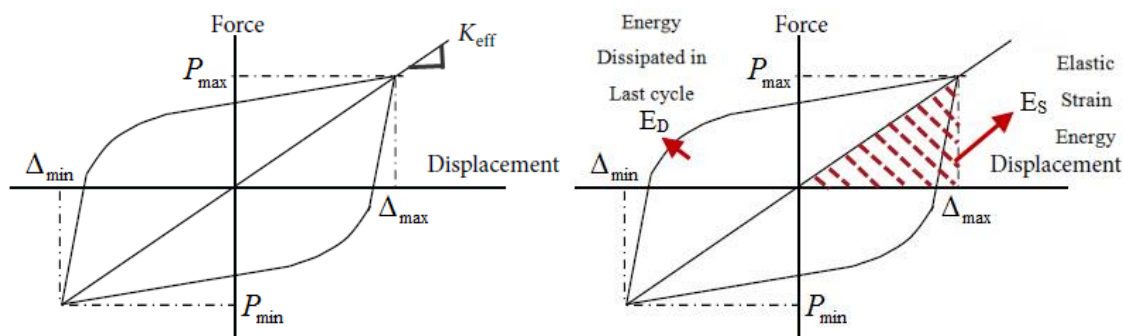
Figure 8. Definition of effective stiffness and energy dissipated in the last cycle and elastic strain energy

Table 1 – Ductility ratio, effective stiffness and initial stiffness of DPMD samples

Series	FEMs Pattern	Δ_y (mm)	Δ_{max} (mm)	Δ_{min} (mm)	Δ_{ave} (mm)	P_y (kN)	P_{max} (kN)	P_{min} (kN)	P_{ave} (kN)	μ	$K_{initial}$ (kN/mm)	K_{eff} (kN/mm)
DPMD1	DPMD1-1	1.75	75.1	-74.4	74.8	603	1112	-1113	1113	42.91	344.6	14.883
	DPMD1-2	1.67	70.9	-70.9	70.9	585	1077	-1078	1078	42.46	350.3	15.197
	DPMD1-3	1.66	75.2	-75.2	75.2	513	850	-850	850	45.30	309.0	11.303
DPMD2	DPMD2-1	1.84	79.2	-79.3	79.3	579	1087	-1087	1087	43.04	314.7	13.716
	DPMD2-2	1.82	83.6	-79.4	81.5	519	939	-938	939	45.93	285.2	11.515
	DPMD2-3	1.81	83.6	-79.4	81.5	428	774	-774	774	46.19	236.5	9.497
DPMD3	DPMD3-1	1.86	83.5	-79.3	81.4	549	988	-987	988	44.89	295.2	12.131
	DPMD3-2	1.84	83.6	-79.4	81.5	452	813	-812	813	45.43	245.7	9.969
	DPMD3-3	1.83	83.7	-79.5	81.6	338	608	-607	608	45.74	184.7	7.445
DPMD4	DPMD4-1	1.19	54.1	-54.1	54.1	543	1028	-1028	1028	45.46	456.3	19.002
	DPMD4-2	1.65	75.1	-75.1	75.1	537	984	-984	984	45.52	325.5	13.103
	DPMD4-3	1.38	62.6	-62.6	62.6	458	839	-839	839	45.36	331.9	13.403
DPMD5	DPMD5-1	1.68	75.1	-75.1	75.1	543	987	-987	987	44.70	323.2	13.142
	DPMD5-2	1.64	71.0	-71.0	71.0	464	841	-841	841	43.29	282.9	11.845
	DPMD5-3	1.58	71.1	-71.1	71.1	392	699	-699	699	45.00	248.1	9.831

The highest and lowest ductility values are for DPMD2-3 and DPMD1-2 samples, respectively. As can be seen, the proposed samples have high ductility values. Due to the high ductility of the proposed samples, it is possible to tolerate non-elastic deformations without significant degradation of strength and stiffness in the structures.

The equivalent viscous damping (EVD) or effective damping is effective index in evaluating the seismic performance of passive energy dissipation systems. The EVD has defined the combined effects of elastic and hysteretic damping. The EVD concept was first proposed by Jacobsen [17, 18]. The value of EVD based on Jacobsen's approach can be calculated with equation 4. The ξ_{hyst} represents the dissipation energy due to the hysteretic behavior.

$$\xi_{hyst} = \frac{E_D}{4\pi E_S} = \frac{E_D}{2\pi K_{eff}\delta_{ave}^2} \tag{4}$$

Table 2 presents equivalent viscous damping for the fifteen samples of DPMD. It is calculated at the maximum displacement. The EVD of DPMPs can be calculated using the proposed formula below.

$$\xi_{equ} = 0.055\mu^{0.58} \tag{5}$$

The calculated error values can also be computed as follows:

$$\%e = \frac{\xi_{equ} - \xi_{hyst}}{\xi_{hyst}} \times 100 \tag{6}$$

Also, Table 2 shows the values of ξ_{equ} and error values of proposed formula with Jacobsen's approach.

Table 2 – Total dissipated energy, dissipated energy in the last cycle, elastic strain energy and EVD of DPMD samples and proposed formula

Series	FEMs Pattern	E_T (N.m)	E_D (N.m)	E_S (N.m)	$\frac{E_D}{E_T}$	$\frac{E_S}{E_T}$	EVD ξ_{hyst} (%)	Proposed formula ξ_{equ} (%)	%e
DPMD1	DPMD1-1	4546533.1	300509.2	41579.7	6.6%	0.9%	57.5	48.67	-15.4
	DPMD1-2	3895810.1	228666.5	38197.4	5.9%	1.0%	47.6	48.37	1.5
	DPMD1-3	3938765.4	222333.9	31960.0	5.6%	0.8%	55.4	50.22	-9.3
DPMD2	DPMD2-1	4840810.6	258172.2	43072.4	5.3%	0.9%	47.7	48.76	2.2
	DPMD2-2	4508396.9	241985.7	38243.9	5.4%	0.8%	50.4	50.63	0.5
	DPMD2-3	3838292.5	210534.2	31540.5	5.5%	0.8%	53.1	50.79	-4.4
DPMD3	DPMD3-1	4662833.4	259236.2	40191.3	5.6%	0.9%	51.3	49.96	-2.7
	DPMD3-2	3957426.1	219552.2	33109.4	5.5%	0.8%	52.8	50.31	-4.7
	DPMD3-3	3029986.1	164074.1	24786.0	5.4%	0.8%	52.7	50.50	-4.1
DPMD4	DPMD4-1	2104193.4	160074.9	27807.4	7.6%	1.3%	45.8	50.33	9.9
	DPMD4-2	3835282.4	219018.9	36949.2	5.7%	1.0%	47.2	50.36	6.8
	DPMD4-3	2360628.2	156908.4	26260.7	6.6%	1.1%	47.5	50.26	5.7
DPMD5	DPMD5-1	4047102.7	233607.3	37061.9	5.8%	0.9%	50.2	49.84	-0.6
	DPMD5-2	3309210.9	194731.8	29855.5	5.9%	0.9%	51.9	48.92	-5.8
	DPMD5-3	2706086.6	163682.2	24849.5	6.0%	0.9%	52.4	50.03	-4.6

Due to the maximum displacement value of 79.3 mm and maximum force value of 1087 kN, the most total energy absorption occurred in DPMD2-1 sample. On the other hand, the total energy absorption of the samples decreases by increasing the amount of cross-sectional area reduction from 30% to 50% in the series samples. Also, elastic strain energy decreases by increasing the cross-section reduction in the series samples. The almost in all series increased the EVD amount with increasing cross-sectional area reduction. DPMD1-1 sample have most of equivalent viscous damping. Increasing the amount of damping ratio ξ increases the damping in the structural system. On the other hand, increasing damping in structure causes decreases response spectra under severe seismic load.

4.2. Equivalent plastic strain

The equivalent plastic strain (EPS) is calculated from the component plastic strain. The equivalent plastic strain is a scalar parameter that ANSYS output label is EPEQ. The EPS describes the degree of

work hardening in a material. Increasing the equivalent plastic strain increases the fracture potential. Reduction of equivalent plastic strain indicates a decrease in strain as well as an increase in the ductility of the material. The EPS inappropriate distribution causes stress concentration and rapid crack growth. The equivalent plastic strain can be defined as follows:

$$EPS = \varepsilon_{eqv}^{pl} = \sqrt{\frac{2}{3}\varepsilon_{ij}^{pl}\varepsilon_{ji}^{pl}} \tag{7}$$

Where ε_{ij}^{pl} and ε_{ji}^{pl} are components of plastic strain. Figure 9 illustrates distribution of equivalent plastic strain in maximum displacement of DPMD samples. Also, in figure 10 comparison of the maximum equivalent plastic strain of DPMD samples is shown.
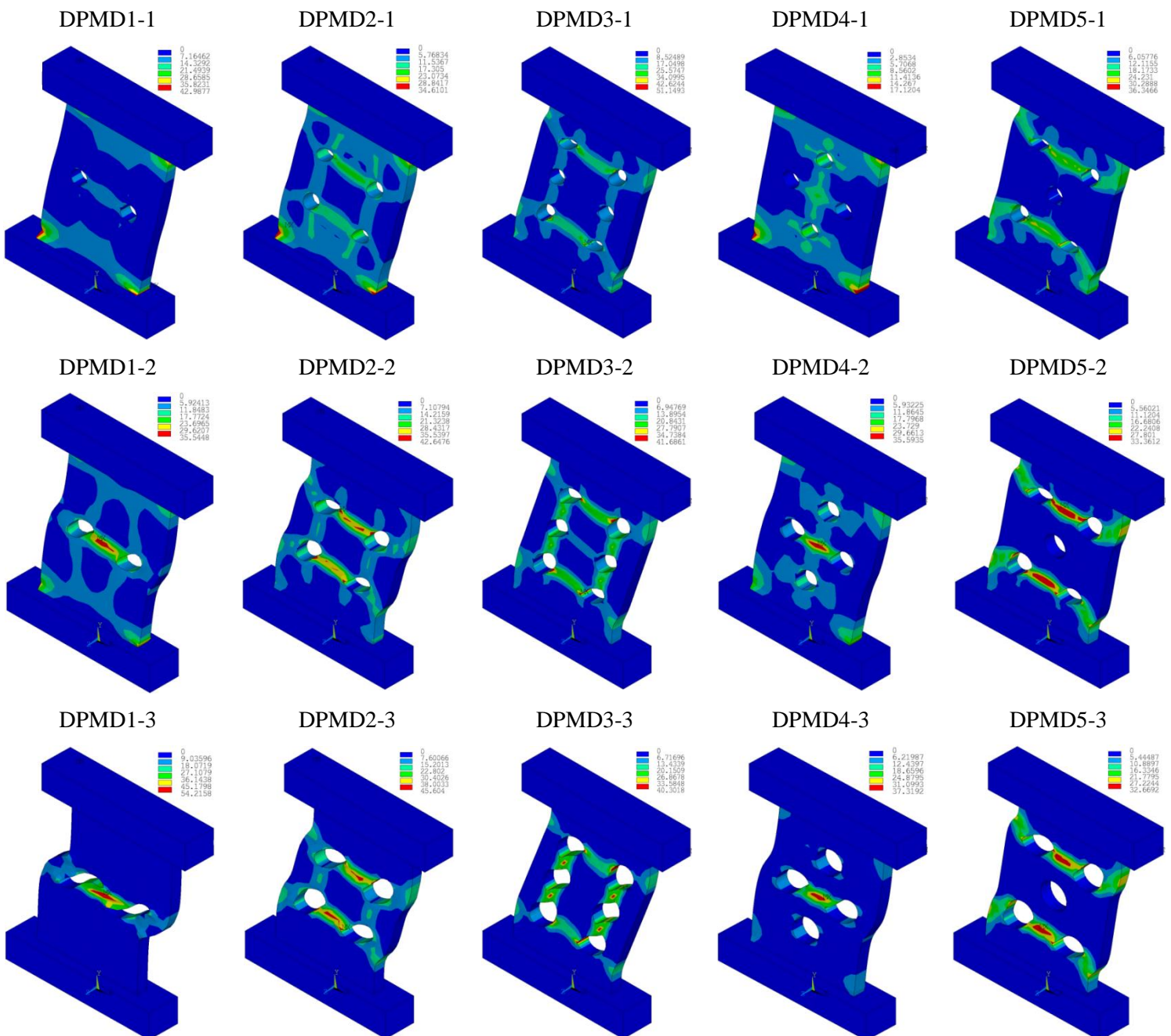
Figure 9. Distribution of equivalent plastic strain in maximum displacement of DPMD samples
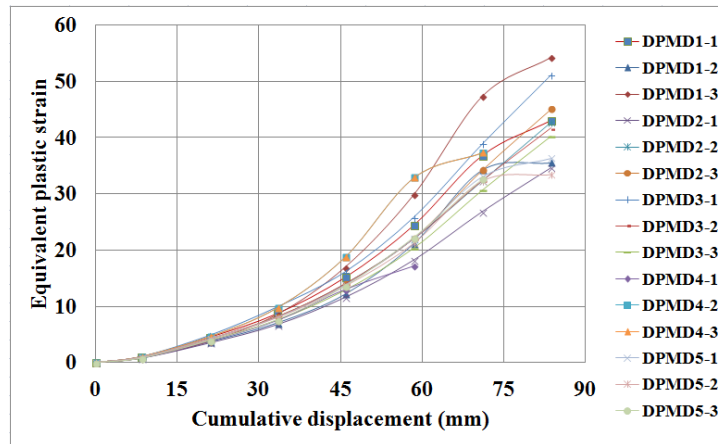
Figure 10. Comparison of the maximum equivalent plastic strain of DPMD samples in each displacement

$$MEPS(\Delta) = -0.104\Delta^4 + 1.529\Delta^3 - 6.639\Delta^2 + 14.307\Delta - 8.3 \tag{8}$$

Where $MEPS(\Delta)$ and Δ are the maximum equivalent plastic strain and applied displacement top of sample, respectively. In all the proposed samples, with changing the location of the holes changes the distribution of equivalent strain. The contour plots show that the plastic strain and failures started to grow from corners of shear plate and beside the holes. In each series of samples proposed, with increasing cross section reduction changes the location of occurrence of the maximum equivalent plastic strain. The location of the maximum equivalent plastic strain changes from the corners of the shear plate to the intermediate between the holes. The lowest amount of EPS occurs in the DPMD2-1 sample.

5. Conclusions

In this study, a new shear yielding metallic damper is introduced. The advantage of this type of damper is simple implementation procedure using the drilling of the plate. Changing the drilling arrangement and the diameter of the holes are effective on the mechanical parameters of the dampers. By studying the finite element analysis of the proposed samples, it is observed that the ductility ratio and EVD can be increased by increasing the diameter of the holes. Total dissipated energy, dissipated energy in the last cycle, elastic strain energy, initial stiffness and effective stiffness decrease as the increasing diameter of the holes. The DPMD2-3 sample has a ductility ratio of 46.19 which is the maximum amount among the other samples. Also, the maximum EVD occurs in DPMD1-1 sample. The maximum error between the values of EVD based on Jacobsen's approach and the values of EVD based on proposed formula is less than 15.4%. In most cases the EVD of proposed formula values have good accuracy. The location and increasing the diameter of the holes can be effective in changing the location of the start rupture from the corner of the shear plate to beside of the holes. Given the amount of maximum EPS and contour plot, the start location and growth of crack in samples with high EVD than others begins near the holes.

6. Acknowledgment

7. References

[1] Kelly J.M., Skinner R.1., Heine A.J., (1972): Mechanisms of Energy Absorption in Special Devices for Use in Earthquake Resistant Structures. *Bulletin of N. Z. Society of Earthquake Engineering,* Vol. 5 No. 3.

[2] Skinner R.1., Kelly J.M., Heine A.J., (1975): Hysteretic Dampers for Earthquake Resistant Structures. *Earthquake Engineering and Structural Dynamics*, 287- 296.

[3] Skinner R.1., Tyler R.G., Heine A.J. and Robinson W.H., (1980): Hysteretic Dampers for the Protection of Structures from Earthquakes. *Bulletin of N. Z. Society of Earthquake Engineering,* Vol 13. No 1.

[4] Kasai K., Popov E.P., (1986): General behavior of WF steel shear link beams. *J. Struc. Eng.*, 112(2), 362-382.

[5] Bergman D. M., Goel S.C., (1987): Evaluation of cyclic testing of steel plate device for added damping and stiffness. *Report No. UMCE 87-10, the University of Michigan, Ann Arbor, MI.*

[6] Whittaker A.S., Bertero V.V., Thompson C. L., Alonso L.J., (1991): Seismic Testing of Steel Plate Energy Dissipation Devices. *Earthquake Spectr,* Vol. 7, No. 4, pp. 563-604.

[7] Tsai K.C., Chen H.W., Hong C.P., Su Y.F., (1993): Design of steel triangular plate energy absorbers for seismic-resistance construction. *Earthquake Spectra,* 9(3), pp. 505-528.

[8] Dargush G.F., Soong T.T., (1995): Behavior of Metallic Plate Dampers in Seismic Passive Energy Dissipation Systems. *Earthquake Spectra*, 11(4), 545-568.

[9] Gang Li, Hongnan Li, (2008): Earthquake resistant design of RC frame with dual functions metallic damper. *The 14th World Conference on Earthquake Engineering*. Beijing, China.

[10] Soni A.H., Sanghvi C.S., (2012): Mathematical modeling of ADAS damper element and nonlinear time history analysis of SDOF steel structure using ETABS. *Journal of Engineering Research and Studies.*

[11] Teruna D.R., Majid T.A., Budiono B.,(2015): Experimental Study of Hysteretic Steel Damper for Energy Dissipation Capacity. *Advances in Civil Engineering,* Article ID 631726, 12 pages.

[12] Sahoo D.R, Singhal T., Taraithia S.S, Saini A., (2015): Cyclic behavior of shear-and-flexural yielding metallic dampers. *Journal of Constructional Steel Research*, 114 (2015) 247–257.

[13] Garivani S., Aghakouchak A.A., Shahbeyk S., (2016): Numerical and Experimental Study of Comb-Teeth Metallic Yielding Dampers. *International Journal of Steel Structures,* 16(1), 177-196.

[14] Ghaedi K., Ibrahim Z., javanmardi A., (2018): A new metallic bar damper device for seismic energy dissipation of civil structures. *14th International Conference on Concrete Engineering and Technology.*

[15] ATC 24., (1992): Guidelines for cyclic seismic testing of components of steel structures. *Applied Technology Council.*

[16] ANSYS Meshing User's Guide, (2016), Release 16.0. ANSYS, Inc.

[17] Jacobsen L.S., (1930): Steady forced vibration as influenced by damping. *Transactions of ASME,* 52, 169–181.

[18] Jacobsen L.S., (1960): Damping in composite structures, *Proceedings of the Second World Conference on Earthquake Engineering*, Vol 2, pp. 1029–1044.

THE INFLUENCE OF SECTION SIDES RATIO OF RECTANGULAR COLUMN ON SEISMIC RESPONSE OF RC BUILDING

Igor Gjorgjiev [1], Aleksandar Zhurovski [2], Borjan Petreski [3]

[1] *Prof., Ss. Cyril and Methodius University in Skopje, Institute of Earthquake Engineering and Engineering Seismology, Skopje, Republic of North Macedonia, igorg@iziis.ukim.edu.mk*

[2] *PhD Student, Ss. Cyril and Methodius University in Skopje, Institute of Earthquake Engineering and Engineering Seismology, Skopje, Republic of North Macedonia, zurovski@iziis.ukim.edu.mk*

[2] *PhD Student, Ss. Cyril and Methodius University in Skopje, Institute of Earthquake Engineering and Engineering Seismology, Skopje, Republic of North Macedonia, borjan@iziis.ukim.edu.mk*

Abstract

The response of structures exposed to earthquakes is mainly defined by the stiffness, capacity and ductility of the structural elements which is governed by their dimensions and the material properties. The buildings' seismic performance is essential for their earthquake resilience especially beyond safety point defined by the building code. The main philosophy of modern codes is to increase the earthquake resiliency of the buildings. Unfortunately, Macedonia is one of the last European countries where designing the structures according to outdated codes is allowed. The older national seismic codes have not been modified in view of the implementation of the most recent knowledge. In this sense, there are no strict limits to prevent the design of rectangular columns with an unsuitable ratio of the section sides. Mainly, due to the need for greater open space and flat interior walls, the columns are designed as rectangular where the lower section side is oriented along a larger span. This results in decrease of the global structural capacity in that direction affecting its response under earthquake excitation. In order to investigate the influence of the ratio of section sides of a rectangular column on seismic performance of building structures, an existing RC frame structure was chosen for analysis. The results of the performed seismic assessment of the selected structure by nonlinear static analysis, emphasize the importance of choosing square shaped columns or rectangular columns with appropriate arrangement in plan even for low-rise buildings. Based on the analysis' results, we conclude that designers need to pay more attention when choosing columns' cross section dimensions and orientation to achieve an acceptable building resilience against earthquakes.

Keywords: nonlinear static analysis; RC buildings; column cross-section; global response; element behavior

1. Introduction

The whole territory of N. Macedonia is in a seismically prone region where earthquakes with intensity between VII and IX according to European intensity scale can occur. Since Macedonia is located in the central Balkan Peninsula, a region often in the history exposed by the devastating nature of strong earthquakes [1], there have been several earthquakes in recent history that have resulted in considerable economic damage and social disruption. The building stock in the country is generally characterized by two types of existing buildings. The first type includes the buildings constructed prior to 1969 which do not meet the current seismic design standards. The second type covers newly build structures which are designed according to different seismic design standards and have different seismic capacity.

Because the buildings' seismic performance is essential for their earthquake resilience, especially beyond safety point defined by the building code, it is crucial to make a proper arrangement of the columns during building design. The response of structures exposed to earthquakes is mainly defined by the stiffness, strength, and ductility of the structural elements, resulting in varying seismic capacity. Therefore, the seismic capacity of characteristic existing buildings should be evaluated.

Unfortunately, N. Macedonia is one of the last European countries where the design of structures according to outdated codes is allowed. The national seismic codes have not been modified yet, in view of the implementation of the most recent advancements in the earthquake engineering field. In this

sense, there are no strict limits for design of beam-columns joints for satisfying the moment capacity and achieving an acceptable level of ductility through 'strong column/weak beam' principle. Nowadays, due to the architectural demand for more open space, the columns are designed as rectangular where the shorter cross-section side is oriented along a larger span. This results in decrease of the column capacity in that direction, which affects the global response of the structure under earthquake excitation. In order to investigate the influence of the ratio of section sides of a rectangular column on the seismic performance of building structures, an existing RC frame structure designed according to the Macedonian seismic codes of practice was chosen for analysis. The analyzed structure is a three-story residential building which is regular in plan and elevation.

The analysis of the structure involves applying nonlinear static analysis to the designed structure and evaluating the performance through a pushover curve. In order to demonstrate the differences between the design of the structure following Macedonian codes of practice and more sophisticated capacity-based design procedure, pushover curves comparison is performed. Initially, the structure is analyzed as designed, with the existing column arrangement and direction – Model 3. Then, three models (Model 1, 2 and 4) based on the designed structure, but with different column arrangements are developed. Subsequently, pushover curves are calculated for each model and the comparison of the results is performed.

2. Analysis Procedure

Recently, there has been an increase in the use of nonlinear static analyses, in contrast to the ductility-modified spectra analyses. The nonlinear static analysis, also called pushover analysis, perfectly defines the deformation curve of a structure and shows its capacity through a pushover curve. This method is considered a step forward from the use of linear analysis and ductility-modified response spectra because it is based on a more accurate estimate of the distributed yielding within a structure, rather than an assumed, uniform ductility [2]. According to the NEHRP classification [3], the nonlinear response analysis is performed for many reasons including the designing of new buildings and assessing the performance of new and existing buildings. Additionally, a number of codes and guidelines have indicated it as a preferred assessment procedure [4].

For the evaluation of the performance of the investigated structural configurations, static pushover analyses were performed. A predefined set of lateral forces was applied to the structures stepwise, as a function of their masses and first mode shape vectors. At each step of the analyses, the yielding of beams or columns was accounted for by updating their stiffness matrices. The pushover analyses were performed until the structures reached collapse.

Considering the outdated Macedonian seismic design code, the performance levels for the assessment of the structures were obtained from more advanced contemporary codes of practice. For example, the Italian National Code defines 4 limit states: Operational, Damage Control, Life Safety and Collapse Prevention [5]. Based on FEMA 273 recommendations [6] for concrete frames, drift limit indicators are provided following the structure's response to different performance levels. FEMA 273 categorizes the drift limitations in three classes: 1) immediate occupancy, represented with 1% transient and negligible residual drift, 2) life-safety, exhibiting maximum of 2% transient and 1% residual drifts, and 3) collapse prevention, limited with 4% of transient and residual drifts. Therefore, in this study, a combination of the codes of practice can be observed as the FEMA 273 performance assessment limits are used for concrete frames designed following the Macedonian code of practice.

3. Case Study

3.1 Structural description of the building

The residential building that is the subject of this research is an RC frame structure. Due to the need for greater open space and flat interior walls, the columns were designed as rectangular, with shorter section side oriented along a larger span. The shape of the building in the plan is rectangular, and can be classified as regular. There are three floors with a story height of 2.9m. The spans in x-direction are 6.4

and 5.65m, while the spans in y-direction are 3.4 and 4.5m. The beams are rectangular with dimensions 25/40cm and 25/45cm, while all columns are with dimension 25/45cm. This structural configuration is in accordance with the analytical model 3.
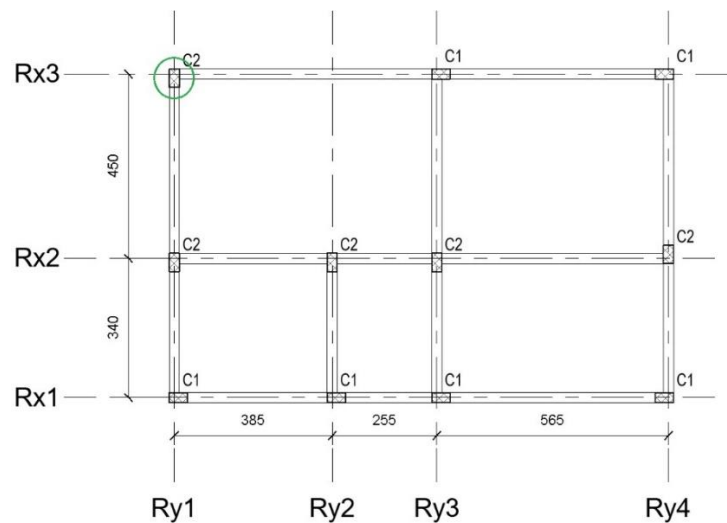
Figure 1. Layout of the building (Model 3).

Four structural analytical models were used to study the effect of column cross-section orientation on structural seismic capacity. The need for the layout given in Figure 1 is due to an architectural demand. Some columns are oriented with shorter section side along the longer span. In Model 1, the shorter section side of all columns is oriented along direction Y (C1 - 45/25 cm), while in Model 2, the shorter section side of all columns is oriented along direction X (C2 - 25/45 cm). The third analytical model represents a mixed arrangement of columns C1 and C2 (Figure 1) as it was designed. The last model - Model 4, is a structure where the cross-section of all columns is square (C4 - 35x35cm).

3.2 Numerical modeling

Perform3D software for nonlinear analysis and design was used to model and analyze the structure [7]. It offers several different types of elements for use, depending on the modeling requirements. Each element consists of numerous basic components that are used to simulate the nonlinear behavior of all types of structural elements. For this case study, the basic components used for the modelling are as follows:

- Inelastic non-buckling steel material was defined for the reinforcement according to the provisions given in the national standard. The stress-strain relationship of the reinforcement was modelled as trilinear, with strength loss (at point L), without cyclic stiffness degradation. The model curve is shown in Figure 2 (left).
- A macro model with Mander stress-strain relationship is most frequently used to describe the working condition of confined concrete in uniaxial compression [8], which is related to section shape and the configuration condition of the stirrup. By the program, the model is transferred in the standard force-deformation (F-D) relationship. Hence, for the design quality of concrete, a concrete model curve was computed according to the Mander model, mean value of concrete's strength and elastic modulus (Figure 2 - right).

The steel material properties are characterized with yield strength of f_y=400MPa, yield strain of ε_y=2‰, ultimate strength of f_u=500MPa and the ultimate strain of ε_u =25‰. The concrete material properties are obtained from the Mander stress-strain model for confined concrete. Therefore, the characteristic values are f_{co}'=30MPa, f_{cc}'=35MPa, ε_{co}=2‰, ε_{co}=3.5‰ and ε_{cu}=17.5‰ (the ultimate compressive strain ε_{cu} is obtained at first hoop fracture).
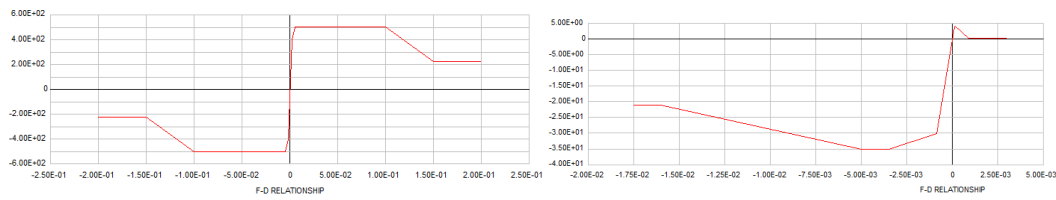
Figure 2. Material models for reinforcement (left) and confined concrete (right).

The columns were modelled using inelastic fiber sections that were assigned at the corresponding lengths of the elements to simulate the plastic hinge region, with the rest of the element remaining elastic. Concentrated (lumped) plasticity approach was used for the beams using inelastic moment hinges, rotation type. Beam-column joints were considered as rigid elements.

The deformation capacities for the components or the so-called performance acceptance criteria corresponding to different building performance levels are generally defined in terms of plastic rotation capacities. In the present study, plastic rotation capacities for Immediate Occupancy (IO), Life Safety (LS) and Collapse Prevention (CP) levels given in ASCE-41[9] were used for the column and beam elements (Table 1). In the analysis, only one criterium was used for performance-based evaluation. Namely, the performance of the structure was evaluated based on the flexural behavior of the columns only. It was assumed that the flexural behavior of the columns governs the structure's behavior, and the columns define the structure's failure mechanism. For the analysis, the rotation capacities in columns were used as referent. The damaged state of the structure corresponded to reaching the specified level of rotation in columns.

Table 1 – Rotation capacities for the structural elements used in the analysis

Level	Column Rotation Capacities (rad)	Beam Rotation Capacities (rad)	Color
IO	0,005	0,005	
LS	0,025	0,025	
CP	0,035	0,05	

3.3 Evaluation of the seismic performance

The moment-curvature relationships of a column section are highly important to assess the ductility of the element, the amount of the possible redistribution of stresses and its resistance against dynamic loading. The tool developed by Bentz and Collins [10] is used to calculate the moment-curvature relationship of the three implemented column cross sections. Moment-curvature relationships of the column cross-sections were calculated along the local x-axis for columns C1(45x25cm), C2(25x45cm) and C4(35x35cm) for predefined axial force from the gravity loads (Figure 3).
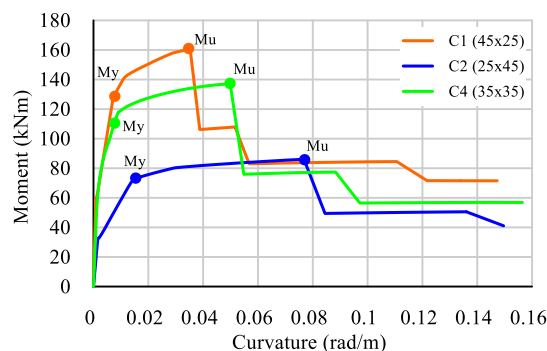
Figure 3. Moment-curvature relationships of the column cross-sections for axial force from gravity loads.

520

As seen from Figure 3, the column C1 has the largest moment capacity, whereas the column C2 has the lowest moment capacity. The yield moment M_y for column C1 is 134kNm for C2 is 76kNm and for C4 is 112kNm. The ultimate moment M_u for column C1 is 167kNm for C2 is 92kNm and for C4 is 141kNm.

The calculated curvatures at yield and ultimate moments of the columns for three different levels of axial force are given in Table 2. The curvature ductility of all concrete columns is calculated accordingly. It is defined as the ratio of ultimate curvature to yield curvature and it presents a metric for warning of failure. The ductility for design gravity axial load for C1 is 5.05, while for C2 and C3 it is 6.73. The columns C2 and C4 have larger ductility than column C1. Therefore, the square column C4 shows balanced behavior regarding the ductility and moment capacity along both axes compared to the rectangular columns investigated. Table 2 consists of two additional axial load levels that show the variations in axial load in the column due to the pushover analysis.

Table 2 – Rotation capacities for the structural elements used in the analysis

Column	N = 380kN			N = 300kN			N = 550kN		
	φ_y [rad/m]	φ_u [rad/m]	μ_φ	φ_y [rad/m]	φ_u [rad/m]	μ_φ	φ_y [rad/m]	φ_u [rad/m]	μ_φ
C1 (45x25cm)	0.00767	0.03878	5.05	0.00767	0.03525	4.59	0.00844	0.03878	4.59
C2 (25x45cm)	0.01141	0.07678	6.73	0.01141	0.07678	6.73	0.01256	0.07678	6.12
C4 (35x35cm)	0.00741	0.04986	6.73	0.00741	0.04986	6.73	0.00815	0.04986	6.12

The results obtained from the nonlinear static analysis in terms of Pushover curves (Base shear vs. Top Drift) for the four models in both x and y orthogonal directions are shown in Figure 4. On the diagrams, several top drift levels arranged in regions (cyan, orange, red) are marked. The lines that lie in these regions were set by following the response of the structure under the increasing displacement in the analysis and the nonlinear response of the columns, as they are governing the stability of the building structure. The acceptance criteria directly follow the rotation capacities given in table 1. Top drift when the structure reaches IO, LS and CP damage states (acceptance criteria) is marked.
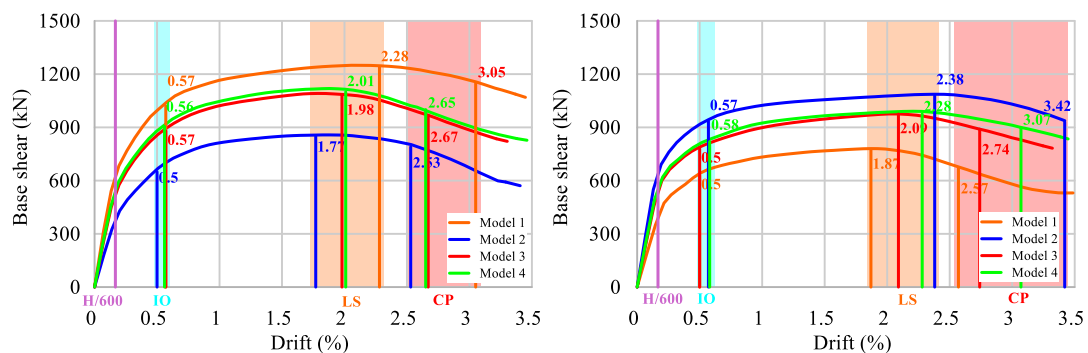
Figure 4. Pushover curves for Models 1, 2, 3 and 4 in x-direction (left) and y-direction (right).

It is observed from Figure 4 that the base shear capacity is highly dependent on the column cross-section orientation in plan. Therefore, Model 1 shows highest base shear capacity in x-direction (the direction of the longer column cross-section side), while Model 2 shows highest base shear capacity in y-direction. It is noted that Models' 3 and 4 base shear capacity is similar and demonstrates uniform capacity in both directions. This is a demonstration of balanced choice of column cross-section orientation for Model 3 and accordingly good choice of rectangular column cross-sections for Model 4. On the other hand, Models' 1 and 2 base shear capacity in both orthogonal directions shows differences of more than 30%.

Regarding the Macedonian code of practice and its total horizontal deflection limitations (H/600, where H is the total height of the structure), it is observed that the IO performance criteria are reached at greater drift level for every model. This demonstrates the stringency of the Macedonian seismic code of practice since the total drift limitation is at 1/3 of the earliest plastic rotation capacity of a column as per the IO performance criterium.

Another parameter investigated is the design base shear according to the Macedonian seismic code. The structures are designed with a total base shear load of 350kN, for which the previously mentioned total drift limitation is assessed. This study demonstrates that the drift of the lowest capacity models in each direction is closest to the H/600 limitation, while Models 3 and 4 exhibit lower drifts for the same base shear load.

The performance criteria levels also show varying response of the models. For instance, the IO performance level region is quite narrow, showing similar results for each model with the highest difference being 16%. The LS and CP regions, on the other hand, demonstrate greater variation in the models' behaviour. They show wider drift regions associated with the plastic rotation capacities of the columns for LS and CP performance levels. The width of the LS and CP regions along with the narrowness of the IO performance level region indicate varying global structural ductility of the models investigated.

Figure 5 contains the damage state of the structure and the performance of the columns when the IO damage state is reached. It should be noted that the color when a column reaches certain rotation capacity limit is given in table 1 and it corresponds to the colors given in the diagrams and figures.
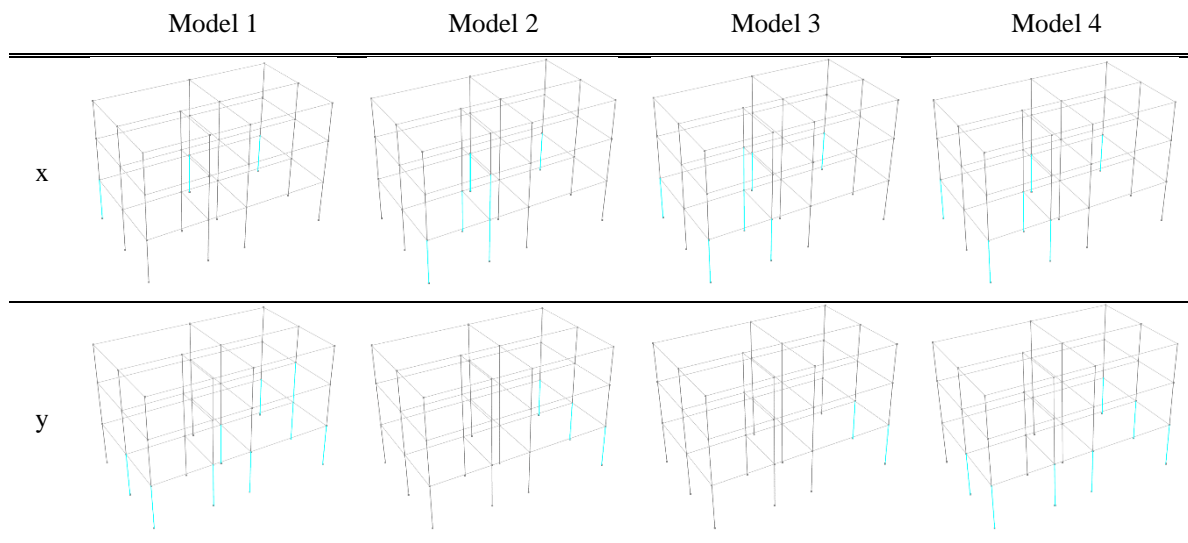
Figure 5. IO damage states in x and y direction for Models 1, 2, 3 and 4.

Figure 5 demonstrates some similarities between the investigated models. Previously, it was established that for IO performance level, the response of the four models is showing similar results. Thus, figure 5 additionally shows that IO is reached only for the ground floor columns for every model. However, the pattern for each model is different and governed by the column cross-section orientation and span length. The three-dimensional analysis additionally allows for different redistribution of loads for each model and affects the varying plastic rotation demand pattern.

After the evaluation of the global response of the four models, the study focuses on the response of a selected column (green circled in Figure 1). The response of the selected column is investigated in order to discuss the influence of the choice of different type of column on its response under the pushover loading. Figure 6 presents two graphs depicting the relationship between the ground floor interstorey drift and bending moment of the selected column for each direction. The graphs contain four curves that correspond to the four models and the appropriate regions of yielding moment for the selected

column. The yielding moment regions are defined by the boundary values of calculated yielding moment for different levels of axial force. The graphs also contain two limit states defined in the national regulations, namely h/150=0.667% (allowable interstorey drift for design earthquake i.e. moderate nonlinear deformation in the structure), and h/350=0.2857% (allowable interstorey drift for linear behavior of the structure).
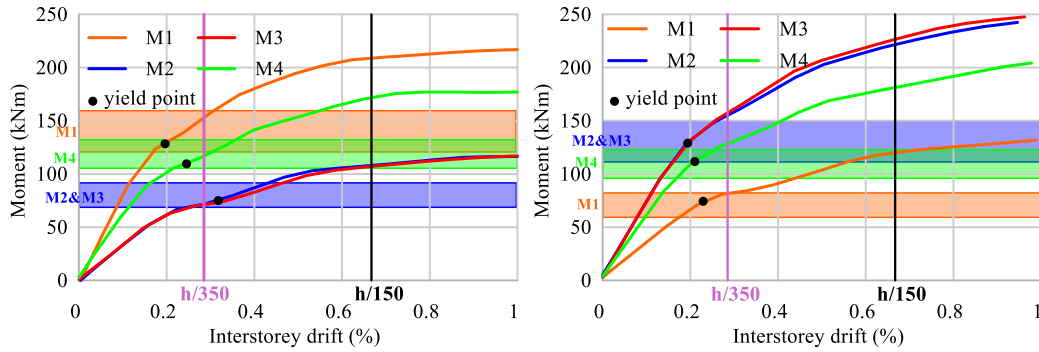
Figure 6. Moment in column vs. Interstorey drift in x–direction (left) and y–direction (right).

Generally, the results from Figure 6 demonstrate that when the ground level reaches the linear allowable interstorey drift limit, the selected column is already yielding. The column in Models 2 and 3 in x-direction reaches the yielding moment after reaching the allowed interstorey drift, which can be considered as favorable response. It is also important to note that the model with a square shaped column (M4) gives certain level of balanced behavior. The column reaches yielding in both orthogonal directions before the ground floor reaches linear interstorey drift limit. The hatched regions represent the yielding moment boundaries for varying axial force levels in the column caused by horizontal loading. The yielding moment associated with greater axial force in x-direction for all four models occurs after the code's linear interstorey drift limit. In the case for y-direction, all models experience yielding before linear interstorey drift limit (H/350).

Figure 7 contains two graphs showing the relationship between total base shear and bending moment in selected column (7 - left - pushover in X direction, 7 - right - pushover in Y direction). Four curves (M1, M2, M3 & M4) corresponding to the four models and the yielding moment regions of the column are shown. The yielding moment regions for each model (Model 1, 2, 3 & 4) are defined by the boundary values of calculated yielding moment for different levels of axial force, same as above (Figure 6). The results in x-direction showed that the yielding moment for M2 occurs at the lowest base shear, while for the other models, the yielding moment occurs at similar base shear. Considering y-direction, the yielding moment for M1 occurs at the lowest base shear. For the other models, there is a slight difference in base shear at which the yielding moment occurs. The yielding moment for M3 and M4 occurs at a similar base shear force in the x and y directions, indicating that both structural configurations behave similarly. Also, it can be noticed that the yielding moment for M3 is lower than the yielding moment for M4 for the same base shear force.
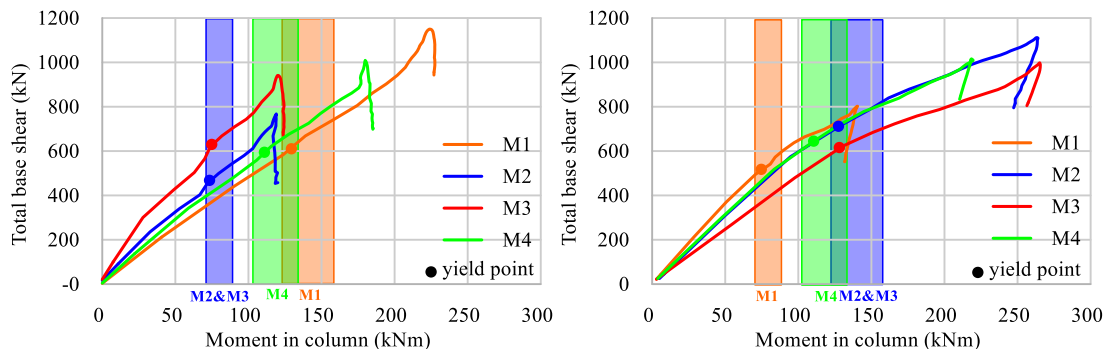
Figure 7. Moment in column vs. Base shear in x–direction (left) and y–direction (right).

The results of the performed seismic assessment of four structural configurations by nonlinear static analysis, emphasize the importance of choosing the appropriate column arrangement in plan even for low-rise buildings. Therefore, the designers need to pay more attention when choosing columns' cross section dimensions and their orientation to achieve acceptable building resilience against earthquakes. The investigated influence of the column section orientation on seismic performance of building structures showed that the model with squared column cross-section demonstrated the most balanced behavior in both directions.

4. Conclusions

A comparison arising from an ongoing problem in the structural engineering field was portrayed in this study. Using a more sophisticated nonlinear static analysis for the assessment of the structural response of low rise reinforced concrete residential buildings, several cases were examined.

The results of the performed seismic assessment of the selected structures by nonlinear static analysis, emphasize the importance of choosing square shape columns or rectangular columns with appropriate arrangement even for low-rise buildings. When choosing rectangular shaped columns with relatively small dimension of a single cross-section side, greater attention should be paid to the layout and distribution of columns in plan, in order to provide sufficient bearing capacity and deformability of the structure in both orthogonal directions. Although the structure's global behavior can be optimized with these measures, it remains questionable if the rectangular shaped columns provide sufficient resilience against earthquakes. In any case, the square shaped columns also demonstrated more optimal balanced element behavior. Based on the analysis results, we conclude that designers need to pay more attention when choosing columns' cross section dimensions in order to achieve acceptable building resilience against earthquakes. This also points out that although the national codes do not explicitly describe the behavior at a local level, following these regulations leads to good design.

References

[1] INFRANAT (2019): Increased Resilience of Critical Infrastructure under Natural and Human- induced Hazards (INFRA-NAT), Deliverable D1.1, INFRANAT Project, Italy.

[2] Elghazouli, A. (Ed). (2009): *Seismic Design of Buildings to Eurocode 8 (1st ed.)*. CRC Press. https://doi.org/10.1201/9781482266177

[3] Haselton, C., Whittaker, A., Hortacsu, A., Baker, J., Bray, J. & Grant, D. (2012): Selecting and scaling earthquake ground motions for performing response-history analyses, *Proceedings of the 15th World Conference on Earthquake Engineering*, Lisbon, Portugal, 10 pages.

[4] Sullivan, T.J., Saborio-Romano, D., O'Reilly, G.J., Welch D.P., Landi L. (2018): Simplified Pushover Analysis of Moment Resisting Frame Structures, *Journal of Earthquake Engineering*, 25 (4), 621-648, doi: https://doi.org/10.1080/13632469.2018.1528911

[5] O'Reilly, G.J., Sullivan, T.J. (2018): Quantification of modelling uncertainty in existing Italian RC frames, *Earthquake Engng Struct Dyn*., 47, 1054-1074, doi: https://doi.org/10.1002/eqe.3005

[6] FEMA (1997): NEHRP Guidelines for the Seismic Rehabilitation of Buildings. Report No. 273, Federal Emergency Management Agency, Washington DC.

[7] Computers and Structures, Inc. (2018): CSI PEFRORM-3D- Components and Elements. Version 7.

[8] Mander, J.B., Priestley, M.J.N., Park, R. (1984): Theoretical stress-strain model for confined concrete, *Journal of structural engineering*, **114** (8), 1804-1826, doi: https://doi.org/10.1061/(ASCE)0733-9445(1988)114:8(1804)

[9] ASCE (2014): ASCE/SEI standard 41-13, Seismic evaluation and retrofit of existing buildings. American Society of Civil Engineers.

[10] Bentz, E.C., Collins, M.P. (2000): "Response 2000." Software program for load-deformation response of reinforced concrete section.

2CroCEE
22 - 24 March 2023

ASSESSMENT OF FUNDAMENTAL PERIODS OF VIBRATION THROUGH ANALYTICAL AND EXPERIMENTAL IN-SITU MEASUREMENTS

Marija Vitanova [(1)], Radmila Salic Makreska[(2)], Daniel Tomic [(3)], Aleksandra Bogdanovic [(4)], Julijana Bojadjieva [(5)] and Kemal Edip [(6)]

[(1)] *Assoc. Prof., Institute of Earthquake Engineering and Engineering Seismology, Skopje, N.Macedonia, marijaj@iziis.ukim.edu.mk*

[(2)] *Assoc. Prof., Institute of Earthquake Engineering and Engineering Seismology, Skopje, N.Macedonia, r_salic@iziis.ukim.edu.mk*

[(3)] *Assist., Institute of Earthquake Engineering and Engineering Seismology, Skopje, N.Macedonia, danielt@iziis.ukim.edu.mk*

[(4)] *Assoc. Prof., Institute of Earthquake Engineering and Engineering Seismology, Skopje, N.Macedonia, saska@iziis.ukim.edu.mk*

[(5)] *Assoc. Prof., Institute of Earthquake Engineering and Engineering Seismology, Skopje, N.Macedonia,, jule@iziis.ukim.edu.mk*

[(6)] *Assoc. Prof., Institute of Earthquake Engineering and Engineering Seismology, Skopje, N.Macedonia,, kemal@iziis.ukim.edu.mk*

Abstract

The structural response due to the seismic load depends on the dynamic structural properties and incoming ground motion. Although for low amplitude ground motions the material behaviour is assumed to be linear, as the amplitude increases the dynamic properties of the structures are changed so that the nonlinear effects should be considered. In determining the nonlinear characteristics of structures, the vibrational periods are important step to be followed. On the other hand, the local site effects have impact on earthquake motion alteration which in most cases contribute to the dynamic amplification of the ground motions. The definition of natural periods of existing buildings including the foundation structure of the whole system can be done by in-situ experimental methods. These experimental methods being cost-effective are constituted by various techniques relating the measurement of structural natural vibrations. This work sums up the experience of UKIM-IZIIS in measuring the in-situ dynamic characteristics of different types of buildings in N. Macedonia. The measurements are based on ambient vibration using the newest technological methods. The established database apart from the vibrational periods includes the geometrical and structural properties of the measured structures which are shown in this paper. The results have shown that apart from geometry the material characteristics play important roles in definition of dynamic characteristics of the structures. The inclusion of brick masonry infills in the final establishment of the dynamic properties plays important role and should be considered in the analysis of the structural analysis. Last but not least is the definition of representative hazard which indirectly influences the dynamics of the structures.

Keywords: Ambient vibration measurements; Period of vibration, RC Buildings, N. Macedonia

1. Introduction

Overall behaviour of structures is directly affected by their dynamic characteristics, for instance eigenvalues, eigenvectors, and damping. In this sense, non-destructive techniques appear as useful tools to provide information about the structural behaviour of the building. In particular, dynamic properties provided by ambient vibration techniques have proved to be quite well-suited to validate and update numerical models. In the last years this technique has attracted the interest of many researchers [1, 2], because no excitation equipment is needed, involving minimum interference with the normal use of the structure. The experimental "in situ" testing method has very wide application especially in structures from where identity card of the structure can be obtained accounting for all dynamic characteristics [3, 4]. The advantages of this method are the light equipment easy for transportation and management and the non-destructive procedure without altering the normal operation of structures. So, using this non-

destructive method fundamental dynamic characteristics for the structure can be obtained, such as natural frequencies and corresponding mode shapes, as well as damping in each mode, without altering their normal operation [5-9]. Having this data as a valuable parameter, leads in the correlation of experimental and analytical results as a confirmation for accurate mathematical model formulation. In the beginning of this century, significant improvement of sensors and data acquisition system technologies was evident. The analogue recording and acquisition of data were replaced by digital systems providing the large analytical possibilities. Also, the software's for data processing were adequately upgraded. Considering "in situ" experimental testing, ambient vibration testing methods prevailed, being applicable for all types of structures, components, and materials in practice as a reason for getting more realistic evaluation of dynamic properties of structures. This method is based on recording and processing of structural response to wind and other ambient excitations, like traffic noise, some other microtremor and impulsive forces like wave loading or periodical rotational forces of some automatic machines. The experimental and theoretical procedure is based on the assumption that the exciting force is a stationary stochastic process with a relatively flat amplitude spectrum. In such conditions, the structures will vibrate and their response will contain all their normal modes. The Institute of Earthquake Engineering and Engineering Seismology (UKIM-IZIIS) from Skopje has an extensive experience in the field of ambient vibration testing starting from 1978 with more than 500 tests performed during this period [10-14]. The subject of this paper is to present the summary of natural vibration period measurements from ambient vibration signal records for 169 representative buildings with different structural characteristics. The influence of height of the building and infill wall effects are evaluated and commented further.

2. In-situ ambient vibration measurements

UKIM-IZIIS in the last decade has been performed several hundreds of in-situ measurements of ambient vibrations on buildings for different investigations and research purposes. For the need of this paper, 169 representative measurements have been selected and analysed. It must be pointed out that those measurements were performed for the purpose of rapid screening with one three-component measurement mostly on the highest assessable level of the related buildings. Dominantly, the recording instrument was placed in a central position with respect to the layout, where applicable.

The measurements were performed with a portable TROMINO® velocimeter (https://moho.world/en/tromino/) from the first generation (Fig. 1) with measurement duration of 10 minutes and certain pre-defined parameters as given in Tab. 1.

Fig. 1. Some photos from the performed measurements with TROMINO instrument

TROMINO® instruments, originally conceived for the dynamic characterization of subsoils, has been increasingly used for the operational modal analysis of structures to such an extent that this has become its primary application over the years. TROMINO® has been extensively used worldwide for ambient vibration measurements, not only on regular structures but also on some of the most iconic structures

worldwide, such as the Eiffel tower, the Golden Gate Bridge in San Francisco, the Shanghai tower, the leaning tower of Pisa, the landmark skyscrapers in Abu Dhabi and many more.

Table 1 - Standard Site Measurement and Processing Parameters

Site Measurement Parameters		Processing Parameters	
Record (trace) length	10 min	Window length	20 sec
Sampling frequency	128 Hz	No. of windows	60
Nyquist frequency	64Hz	Tapering	Bartlett window (20 sec, 2561 points)
Frequency range of interest	0.1 - 32 Hz	Smoothing function	Konno – Omachi, b=20, or Triangular window (5% smoothing)

Amplitude spectra of the different components (channels N-S, E-W, Z) of the recorded ambient vibration motion are computed by MOHO's software package GRILLA™ (http://www.tromino.it/soft-database.htm). The results derived in terms of average velocity amplitude spectra, have been studied in all details for defining the building modal parameters. They are relevant for linear (elastic) behaviour of studied structural system, only. The ambient vibration measurements have been performed on a fully constructed structure, thus incorporating not only the fundamental modal characteristics of the structural system itself, but also the influence of internal and external walls and other non-structural elements.

The results are summarized in the direction for which the vibration periods are obtained. For the analysed buildings, a correlation analysis was performed with the dynamic characteristics, i.e., the basic periods of vibration extracted from the design documentation. The created database was composed in tabular format in which, in addition to the dynamic characteristics of the buildings, the type of structure, total area of the building and the number of stories were included as well. For a certain number of buildings, two types of vibration periods from the project documentation were presented i.e., on a fixed and on an elastic base.

3. Analysed and inspected structures

The database established in UKIM-IZIIS for this study allows detailed classification of the structures. The types of structures considered are mainly reinforced concrete (RC) buildings built in the last decade while the biggest part of the buildings are located in the Skopje area. The reinforced concrete structures are predominantly frame structures with and without shear walls. All the buildings in the established database are build and constructed according to the latest design regulations. In the last years, efforts have been made to improve detailing and increase inelastic capacity of the building to resist potential earthquake ground motions. Although not very common but in some cases the buildings have been built over soft soil deposits in which the dynamic characteristics of the structures are influenced by the presence of soil stiffness characteristics making the soil structure interaction phenomenon important to be considered. Moreover, the ground floor in some of the structures is used for commercial purposes, thus increasing the height and decreasing the stiffness of the ground floor, creating the conditions for appearance of soft-story effect. The height of the analyzed buildings varies from one to 14 floors.

The majority of analyzed buildings are of frame type structures in which the column-beam connections have been given special importance in order to resist the seismic forces, thus preventing the columns of collapse assuring life safety design criteria. The principal structural system for buildings with 1-3 levels is reinforced concrete frame with beams and columns, and the structures with more than 4 storeys are reinforced concrete frame with shear walls in both directions. The dynamic characteristics of these domestic RC buildings show periods in relation of 0.1 times the number of the floors which is a rule of thumb and is a widely accepted worldwide practice.

All investigated structures are designed according to the Code of Technical Regulations for the Design and Construction of Buildings in Seismic Regions (OGoSFRY No. 31/81 of June 5, 1981 with

Amendments 49/82, 29/83, 21/88 and 52/90), where the total horizontal seismic force acting on a building is given with the equation (1)

$$S = K \cdot G \tag{1}$$

where:

K = the total seismic coefficient for the horizontal direction

G = the total weight of the building and its equipment

The seismic coefficient for the horizontal direction K depends directly by the coefficient of building category, coefficient of seismic intensity, coefficient of dynamic response, and coefficient of ductility and damping. The coefficient of ductility and damping, depends on the type of structure under consideration (modem reinforced-concrete structures, steel structures, reinforced masonry, and for braced steel structures masonry structures, strengthened by means of vertical reinforced-concrete tie-beams' for reinforced-concrete shear-wall structures etc).

4. Investigations results

A total number of 169 newly built reinforced concrete structures are considered in this study. All the structures were measured using ambient vibration testing method. Ambient vibration collected data have been used to extract dynamic characteristics of the structures. As an addition, numerical analyses were performed for all examined structures.

(a)   (b)   (c)   (d)

Fig. 2. Selected measured structures in Skopje (a) Bitola (b), Veles (c) and Ohrid (d)
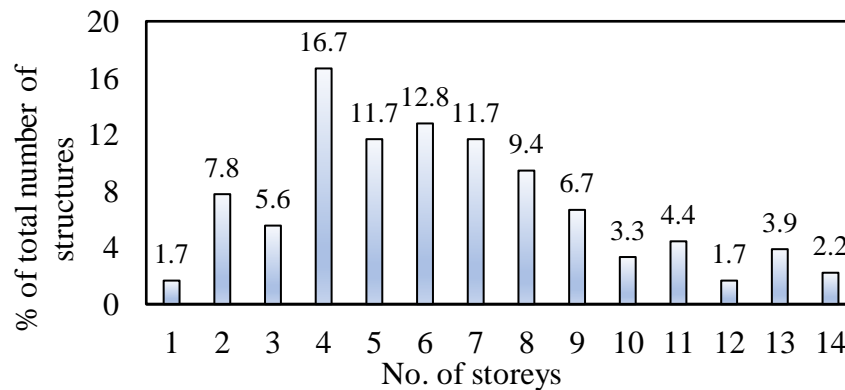
Fig. 3 Percentage of structures with different no. of stories

The buildings are with 1 to 14 storeys. The principal structural system for buildings with 1-3 levels is reinforced concrete frame with beams and columns, and the structures with more than 4 storeys are reinforced concrete frame with shear walls in both directions.

Some photos of the measured buildings are shown on Fig. 2. Regarding the number of stories, most of the buildings have between 2-9 levels. Larger number of them are with 4 (16.7%) and 6 stories (12.8%) (Fig. 3).

Ambient vibration spectrum graphs of some selected sample buildings are shown in Fig. 4.
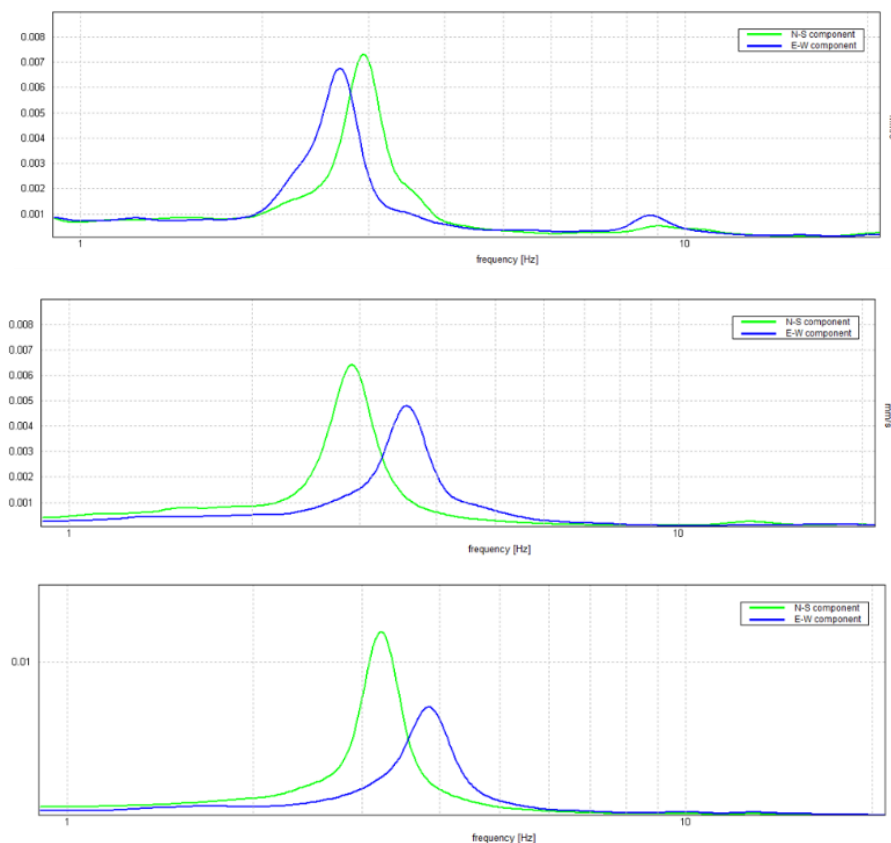
Fig. 4 Two-component ambient vibration spectra's of selected buildings in from database (N-E: north-east, E-W: east-west)

The vibration periods obtained from ambient vibration measurements were compared with the periods obtained by analytical models. The buildings were modeled with infill walls as dead loads in 3-D models. Aerated concrete blocks are used in the buildings as infill wall elements. All other infill walls with openings that prevent diagonal strut formation were considered as dead loads. Other dead loads such as slab weight were also considered as a distributed load.

Concrete compressive strength, steel properties, and size of structural members were taken from construction drawings. Most of the buildings higher than 3 levels were reinforced concrete frame-type structures with shear walls. Structures with lower heights are without shear walls.

A database with all measurement results and results from the numerical analyses which contains the fundamental characteristics of those structures and their most important geometric and structural properties with the aim of setting correlations between structural typologies and fundamental periods or frequencies has been created. The distribution of natural vibration periods obtained for all structures with respect to the building's height is shown in Fig.5. These results are related to building structures with infill walls. As expected, building periods increase with respect to height. Fig.5 shows that the measured fundamental periods are higher than the analyzed (numerically obtained), what is expected due to level of the construction of the infill walls.
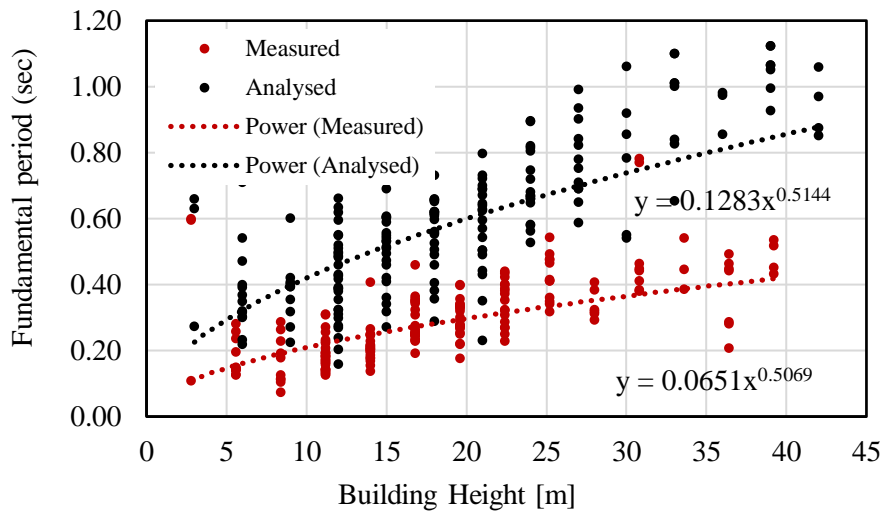
Fig.5. Fundamental period of measured and analyzed structures as a function of building height (m)

The height-period curve parameters are defined in many design regulations as well as in Eurocode 8 [15]. Ambient vibration signal measurements were compared to evaluate the consistency of obtained data with other results available in the literature (Fig. 6). Empirical equation derived by Eurocode 8 is given in equation (2). *T* defines the building period and *H* defines the building height in the following equation

$$T = 0.075H^{0.75} \tag{2}$$

Gallipoli et al. [16] derived equation (3) by using ambient vibration signal records taken from 244 buildings located in various regions in Europe:

$$T = 0.016H \tag{3}$$

Based on the measurements in this study, we propose an empirical equation (4) with respect to height-period parameters given in the following form

$$T = 0.0651H^{0.5069} \tag{4}$$
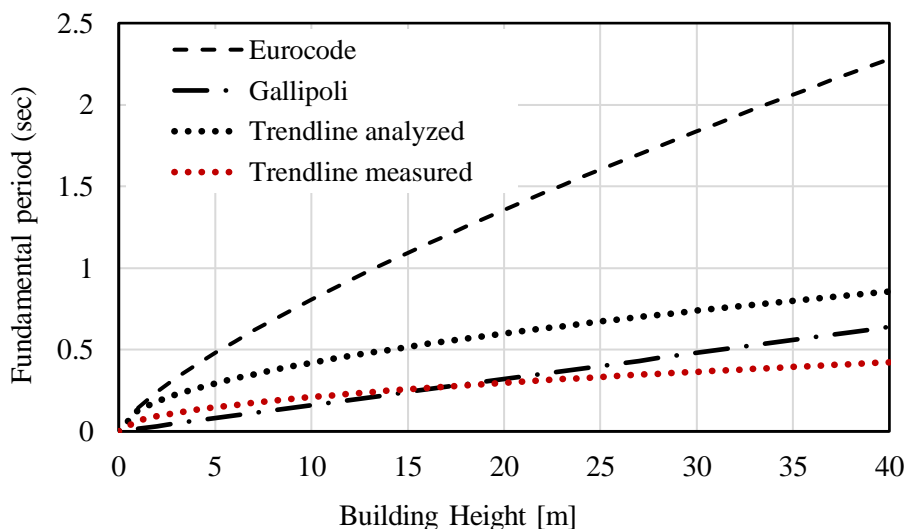
Fig. 6 Distribution of fundamental periods with respect to building height

When results are compared, it is observed that the data obtained from these measurements have a similar tendency to the equation proposed by Gallipoli et al. [16]. The Eurocode 8 code height-period curve resulted in estimations much higher than expected for all ranges due to omitting the stiffness contribution of infill walls. Another significant point is that buildings used in this study are residential buildings of similar characteristics. These buildings have reinforced concrete frame structures, are constructed in accordance with current design codes and do not have great differences. For buildings with a higher amount of shear walls, lack of such a high-level relationship between height and period can be expected depending on the amount of shear walls [17].
The period/height ratio of the measured and analytically obtained results are given in Tab. 2.

Table 2 - Period/height ratio

Period/height ratio	Analytical	Measured
max	0.118	0.065
min	0.001	0.006

The strength of infill walls is influenced by many parameters such as material and mortar properties and production quality. Therefore, it is reasonable that under large displacements, building periods even in elastic regions can be higher than the period values determined based on ambient vibration records.

5. Notes and conclusions

The ambient vibration measurements from the 169 new buildings have been evaluated. More than, half of the residential buildings that have been tested were measured after the construction of infill walls. All the obtained results and the authors experience during many years of work in this field with in-situ measurements of structures under the most varied conditions (in construction, full occupancy, using various sources of excitation, etc.) and numerical modelling for typical structures, has led to the following conclusions:

- The measured fundamental periods of all structures are lower than the analytically obtained, which is expected due to the influence of general stiffness contribution of infill walls.
- There is a close correlation between natural vibration periods and building height in RC frame buildings with and without constructed infill walls.
- Based on the measurements in this study, an empirical equation with respect to height-period parameters is derived as eq. (4).
- The obtained results revealed a similar distribution with height-period equations in the selected literature by using ambient vibration signal records, especially to the Gallipoli et al. [16]. The relationship used in Eurocode 8 (1) revealed higher natural vibration period estimates than the measured periods.
- The highest period/height ratio from analytical results was found to be 0.096 and the value for minimum ratio is 0.008. The measured minimum and maximum values are 0.005 and 0.060 respectively. The uppermost values are so low, that are appropriate for newly building structures.
- It is relatively easy to identify the two basic modes using a single instrument for the structures which are regular to a certain extent, the first two modes in each horizontal direction.
- The effect of infill brick walls in RC structures, is larger for more flexible structures.
- Analytical modelling can reach results remarkably close to the measured ones if infills and stairways are modelled.

References

[1] Foti, D., Diaferio, M., Giannoccaro, N. I., Mongelli, M. (2012): Ambient vibration testing, dynamic identification and model updating of a historic tower. *NDT & E International*, **47**, 88–95. DOI: 10.1016/j.ndteint.2011.11.009

[2] Hashim H, Ibrahim Z, Razak H.A. (2013): Dynamic characteristics and model updating of damaged slab from ambient vibration measurements. *Measurement* 2013; 46: 1371–1378. DOI: 10.1016/j.measurement.2012.11.043.

[3] Hudson, D. E. (1972): Dynamic properties of full-scale structures determined from natural excitations. In: Herrmann, G., Perrone, N. (eds.), *Dynamic response of structures*, pp. 28–29. Pergamon Press, NY.

[4] Salawu, O. S., Williams, C. (1995): Bridge assessment using forced-vibration testing. *Journal of Structural Engineering*, 121(2), 161–173. DOI 10.1061/(ASCE)0733-9445(1995)121:2(161).

[5] Jaishi, B., Ren,W. X. (2005): Structural finite element model updating using ambient vibration test results. *Journal of Structural Engineering*, 131(4), 617–628. DOI 10.1061/(ASCE)0733-9445(2005)131:4(617).

[6] 10.1016/j.ndteint.2011.11.009.

[7] Bassoli, E., Vincenzi, L., D'Altri, A. M., de Miranda, S., Forghieri, M. et al. (2018): Ambient vibration-based finite element model updating of an earthquake-damaged masonry tower. *Structural Control and Health Monitoring*, 25(5), e2150. DOI 10.1002/stc.2150.

[8] Bartoli, G., Betti, M.,Marra, A. M., Monchetti, S. (2020). On the role played by the openings on the first frequency of historic masonry towers. *Bulletin of Earthquake Engineering*, 18(2), 427–451. DOI 10.1007/s10518-019-00662-9.

[9] Russo, S., Spoldi, E. (2020): Damage assessment of Nepal heritage through ambient vibration analysis and visual inspection. *Structural Control and Health Monitoring*, **27** (5), S1. DOI 10.1002/stc.2493.

[10] Bogdanovic, A., Rakicevic, Z., Poposka, A. et al. (2016): Definition of Dynamic Characteristics of the Structure of the Italian Embassy in Skopje by Experimental Ambient Vibration Method, *Technical Report No.46 2016*, Institute of Earthquake Engineering and Engineering Seismology – IZIIS, Skopje, R. Macedonia

[11] Krstevska, L, Taskov, Lj, (2006): Ambient vibration measurements of Beylerbeyi Palace in Istanbul, *Technical Report IZIIS 2006-030* (FP6 Research Project PROHITECH).

[12] Rakicevic, Z., Bogdanovic, A., Poposka, A. et al.(2017): Ambient Vibration Testing of the hypothetical model of Antenna System for Control and Monitoring of Radiofrequencies in the Territory of R. Macedonia, *Technical Report No.1 2017*, Institute of Earthquake Engineering and Engineering Seismology – IZIIS, Skopje, R. Macedonia

[13] Rakicevic, Z., Bogdanovic, A., and Markovski, I. (2012): Ambient Vibration Measurements and Determination of Dynamic Properties of a three storey masonry building in Sofia, Bulgaria, *Technical Report No.19 2012*, Institute of Earthquake Engineering and Engineering Seismology – IZIIS, Skopje, R. Macedonia

[14] Taskov, Lj., Krstevska, L. (2006): Evaluation of seismic safety of the historical masonry monuments, Joint reserah project: YILDIZ Technical University, Istanbul & IZIIS, *Technical Final Report, IZIIS 2006-37*, Skopje, R. Macedonia.

[15] EN 1998-1, 2004. Eurocode 8: Design of Structures for Earthquake Resistance, Part 1: General Rules, Seismic Actions and Rules for Buildings, European Committee for Standardization, Brussels, Belgium.

[16] Gallipoli, M.R., Mucciarelli, M., Šket-Motnikar, B. et al. (2010): Empirical estimates of dynamic parameters on a large set of European buildings. *Bull Earthquake Eng* **8**, 593–607 https://doi.org/10.1007/s10518-009-9133-6.

[17] Inel, M., Bilgin, H., Ozmen, H.B. (2008): Seismic capacity evaluation of school buildings in Turkey, *Proceedings of the Institution of Civil Engineers—Structures and Buildings*, vol. 161, no. 3, pp. 147–159.

NUMERICAL MODELING OF THE IN-PLANE BEHAVIOR OF EXPERIMENTALLY TESTED SOLID BRICK MASONRY WALLS

Senad Medić [1], Mustafa Hrasnica [2]

[1] *Assistant professor, University of Sarajevo-Faculty of Civil Engineering, senad.medic@gf.unsa.ba*
[2] *Full professor, University of Sarajevo-Faculty of Civil Engineering, hrasnica@bih.net.ba*

Abstract

Unreinforced unconfined solid brick masonry walls were experimentally tested in full scale (233x241x25cm) and reduced scale (100x100x25cm) at the laboratory of the Institute for materials and structures, Faculty of Civil Engineering in Sarajevo. Cantilever walls were loaded in cyclic shear or pushed monotonically. In order to study the nonlinear behavior in a detailed and global manner, finite element meso- and macro-models of the tested walls were created using the finite element software Diana FEA. Brick units are discretized by continuum elements in a meso-model and discontinuity in displacement field is introduced by interface elements between units. In order to account for brick cracking, an additional interface element was added in the unit middle. Continuum macro-models approximate heterogeneous masonry wall by a single material and discretization is independent of brick layout, i.e., bricks, mortar and unit-mortar interface are smeared out in the continuum. The recently developed engineering masonry model is an orthotropic total-strain continuum model with smeared cracking and it was used with shell elements. Numerical results are verified against the data obtained from the experimental research program. The walls exhibit rocking failure mode in low precompression, while diagonal cracking occurs for higher vertical stresses. The results show good matching with the experimentally obtained curves regarding the ultimate load and ductility.

Keywords: masonry walls, finite elements, meso- and macro-models, experimental testing.

1. Introduction

Bosnia-Herzegovina is situated in a seismically active region of South-East Europe, and it is divided into seismic zones with peak ground acceleration (PGA) ranging from 0.1-0.2g for 475 years return period in most parts of the country up to a PGA of 0.30-0.35g in some regions. The majority of multi-story residential buildings erected in the years following World War II were unreinforced unconfined masonry buildings with 4-6 floors. Concerning seismic vulnerability classification (EMS), masonry structures belong to classes B and C, which means that heavy and hefty damages, including partial collapse, could occur in the case of stronger earthquake motions. Unfortunately, this was proven during several regional earthquakes, Skopje 1963, Banjaluka 1969, and Montenegro Coast 1979 [1].

According to EC 8 compared to the old national standard, increased seismic demand poses new challenges in verifying existing buildings' load-bearing capacity. Faculty of Civil Engineering in Sarajevo initiated a specific research program with experimental testing and computational modeling to assess masonry behavior and risk [2]. Masonry is a composite material consisting of units and joints usually filled with mortar, and it is a complex material with a 3D internal arrangement (bond). Not only varying material characteristics but also building technology can significantly influence masonry response, making modeling a demanding task for structural engineers. The low tensile strength of masonry imposes nonlinear constitutive laws in assessment of existing structures and seismic analysis of new buildings [3].

Experimental testing of masonry is essential in understanding structural behavior; however, numerical modeling can complement experimental research and provide new insights. Masonry structures are usually analyzed by finite elements (FEM), and based on the level of detail, computational strategies are traditionally divided into the following categories: micro-, meso- or macro-modeling techniques. One modeling strategy cannot be preferred since different application fields exist for each model type.

Linear elastic methods like the lateral force method or response spectrum analysis do not seem adequate to describe the quite nonlinear response of masonry and estimate global ductility.

This paper focuses on the nonlinear quasi-static cyclic analysis of individual masonry walls using smeared continuum models discretized by shell elements. Additionally, several meso-models were created, where nonlinear behavior was lumped into traction-displacement relation in interface elements at joints. The numerical models were verified against experimental data obtained from the tests performed at the Institute for materials and structures laboratory in Sarajevo. Unreinforced unconfined masonry walls were built in full scale (233x241x25cm) and reduced scale ca. 1:2 (100x100x25cm). The walls were loaded in cyclic shear under constant vertical pressure or pushed monotonically. Mechanical properties of masonry components (brick, mortar, and interface) and homogenized masonry (compressive strength and elastic modulus) were determined using appropriate specimens [4]. Dispersion of material properties that can be found in literature is considerable [5-8]

Nonlinear static pushover analysis of an old masonry building carried out under constant gravitational load and monotonous horizontal loads in the form of displacement increments is also presented. The building was heavily damaged during the war in Sarajevo, and the floors were destroyed. Pushover analysis verifies the nonlinear behavior of newly-designed structures and the existing ones. Two numerical macro-models were created. The first model represents the existing damaged structure. In the second model, which represents the rehabilitated structure, R.C. floors, and internal walls were added to the building in order to increase the load-bearing capacity.

2. Experimental tests of wallets and walls

In the first step, a testing program was designed to identify the mechanical properties of masonry and its components. Compressive and tensile strength, elastic modules of brick and mortar, and the properties of their mutual contact were investigated separately. The compressive strength and the modulus of elasticity of the solid brick masonry were determined on the reduced wall samples – wallets. In the next step, physical models of plain (unconfined unstrengthened) masonry walls were constructed in the full scale (233x241x25cm) (Fig. 1) and the reduced scale (100x100x25cm) [2, 4].
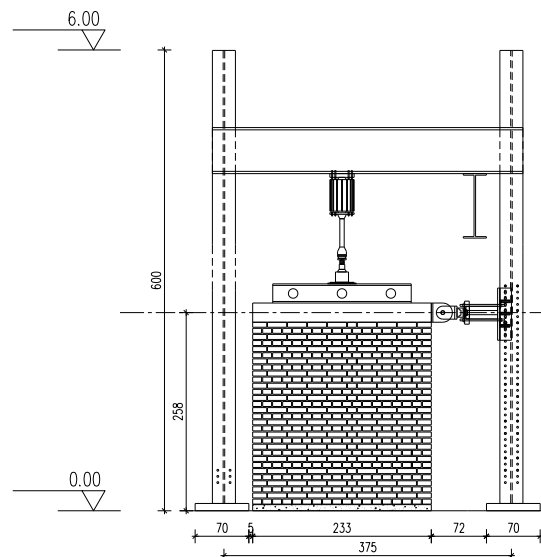
Figure 1. Test set-up.

The chosen wall geometry introduces a complex response to seismic action because the walls cannot be classified as slender or squat. Two plain walls statically modeled as cantilevers were tested for the horizontal static cyclic in-plane load under a vertical pressure of 0.4 N/mm². A vertical load was applied to the wall centerline via a steel loading beam, and then displacements were incrementally and cyclically imposed at the RC top tie beam. The walls failed at almost equal horizontal load levels with the

appearance of the characteristic diagonal crack pattern (Fig. 2). The measured force at failure agrees well with the ultimate load obtained using the expression from EC 6. Unexpectedly, plain masonry walls have considerably greater ductility than recommended in seismic codes using behavior factors.

Reduced model walls were exposed to a cyclic loading program under variable values of vertical pressure. For compressive stress of 0.4 N/mm^2, the wall rotates in a rigid body mode without cracking. On the other hand, under 0.6 N/mm^2 pressure, the wall rotates, but with the occurrence of cracks that develop on the compressed toe and extend diagonally through the wall. For a stress level of 1.0 N/mm^2, a crack appears in the middle of the wall, which is characteristic of shear failure.

a)   b)
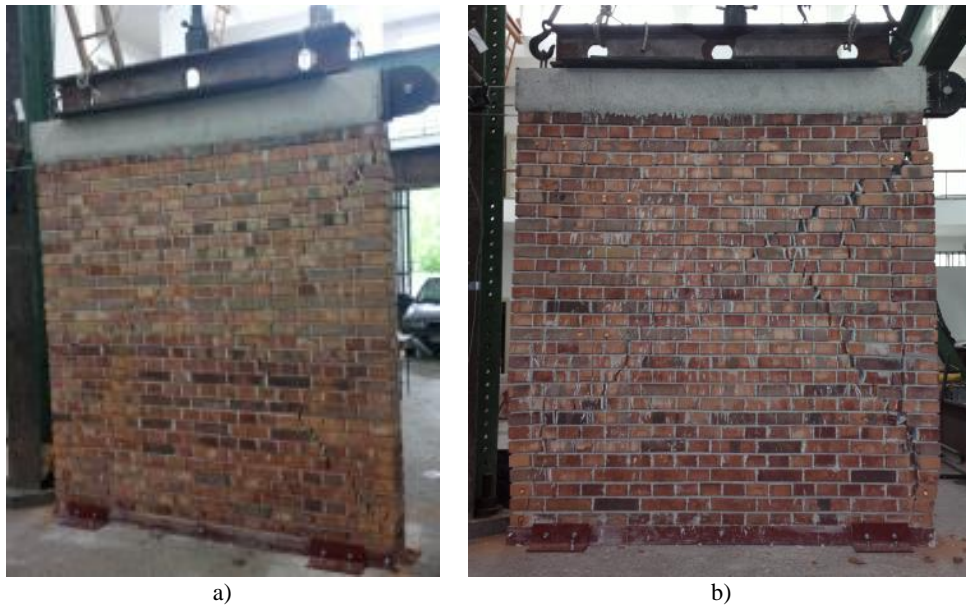
Figure 2. Diagonal failure pattern of the tested walls: a) W1, b) W2.

3. Nonlinear finite element modeling and results

3.1 Macro-model of the tested wall

Masonry is homogenized in a macro-model employing the recently developed Engineering Masonry model [9]. The Engineering Masonry model is an orthotropic total–strain continuum model with smeared cracking, and it can be used with membrane or shell elements. The model can simulate compression, tensile and shear failure modes and crack in bed joints, head joints, and diagonally. The crushing, shear, and tensile behavior of the Engineering Masonry constitutive model is illustrated in Fig. 3 [10]. Parameters of the constitutive model for the wall analysis are given in Table 1. All nodes on the upper edge were rigidly connected to have the same horizontal displacement and free rotation. The walls were discretized using 2D plane stress elements with eight nodes of an average size of 0.1 m. A quasi-static implicit nonlinear analysis was performed with the Newton-Raphson iterative scheme involving both material and geometric nonlinearity. The loading program is shown in Fig. 4, and each cycle consists of three runs. The model was run until the model ceased to converge or the maximum displacement of the actual experimental test was attained.

A comparison of hysteretic curves of the macro-model and the results of the previously described experiment are shown in Fig. 5 where one can notice a pretty good matching. Wall displacement patterns and accumulated shear strains that pertain to the major cracks are shown in Fig. 6. The damage pattern is diagonal, which complies with the experimental observations.
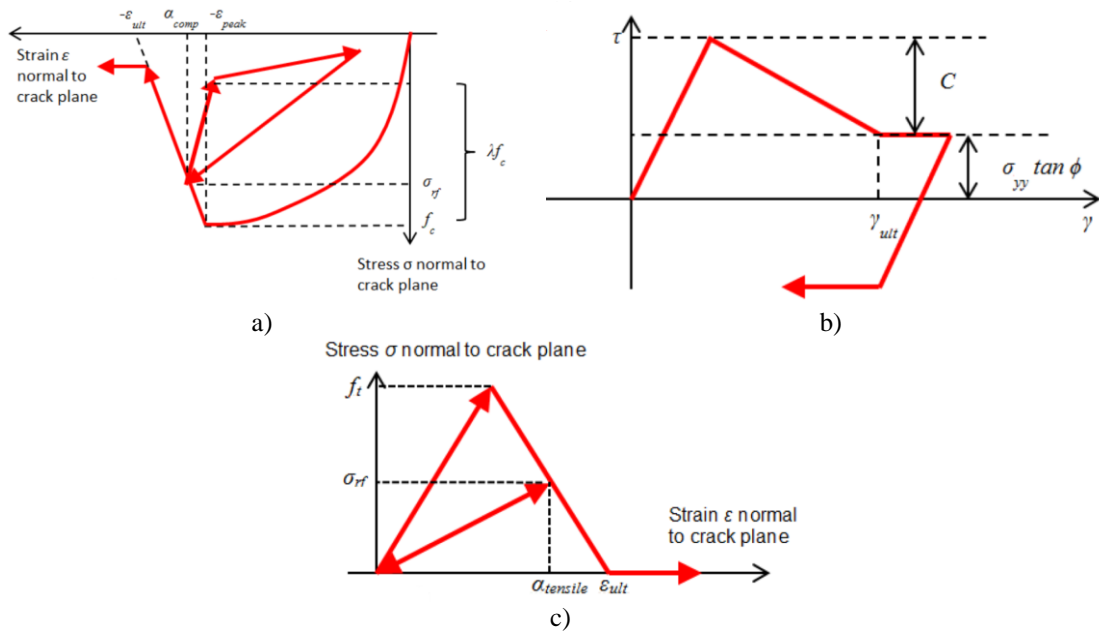
Figure 3. Engineering masonry model: a) crushing behavior, b) shear behavior, c) cracking behavior.

Table 1 – Parameters of engineering masonry model used for the wall analysis

Parameter	Value	Parameter	Value	Parameter	Value
E_x	4e+09 N/m²	G_{ft}	10 N/m	G_{fs}	20 N/m
E_y	4e+09 N/m²	HEADTP	NO	f_c	6.48e+06 N/m²
G_{xy}	1.6e+09 N/m²	h	Rots	n	4
ρ	1850 kg/m³	c	90000 N/m²	G_c	40000 N/m
f_{tx}	90000 N/m²	φ	0.78 rad	λ	1
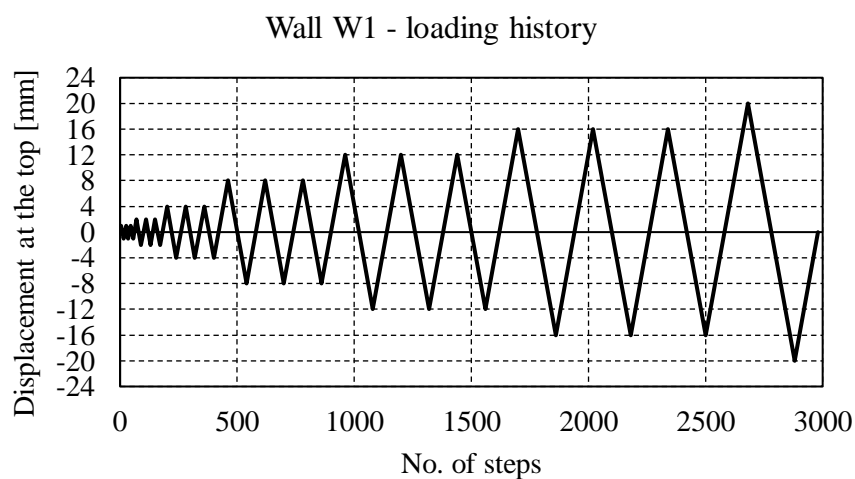
Figure 4. Loading program for wall W1.

Hysteretic curves - wall W1
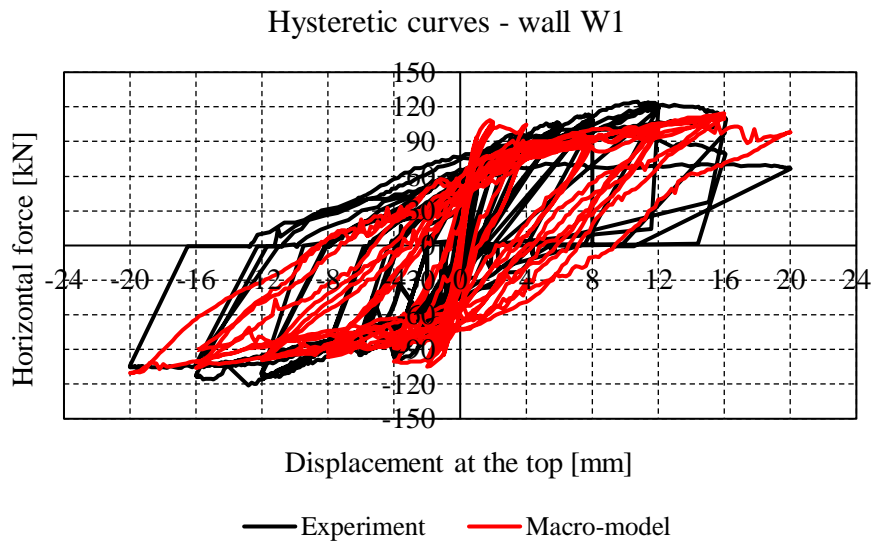
Figure 5. Comparison of hysteretic curves of the macro-model and the experiment for W1.
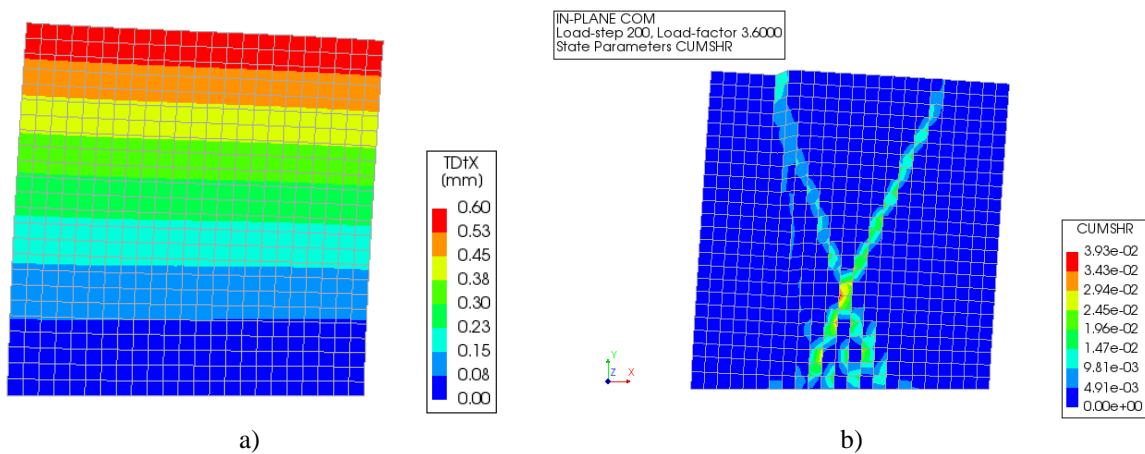
Figure 6. Results of the numerical analysis: a) wall displacements, b) accumulated shear strains.

In the case of low precompression, rocking failure mode was detected on reduced-scale walls. Since the wall behaves as a rigid body, masonry was modeled as a linear elastic material in this case. Nonlinearity is concentrated in the interface element at the contact between the wall and the foundation, with the properties listed in Table 2. An opening mode (gap) was set for the interface. Wall displacements and comparison of experimentally obtained hysteresis and numerical pushover curve are given in Fig. 7.

Table 2 – Parameters of Mohr-Coulomb interface for rocking failure mode

Parameter	Value
k_n	1e+06 N/mm^3
k_s	1e+06 N/mm^3
c	0 N/mm^2
ϕ	0.38 rad
f_t	0 N/mm^2
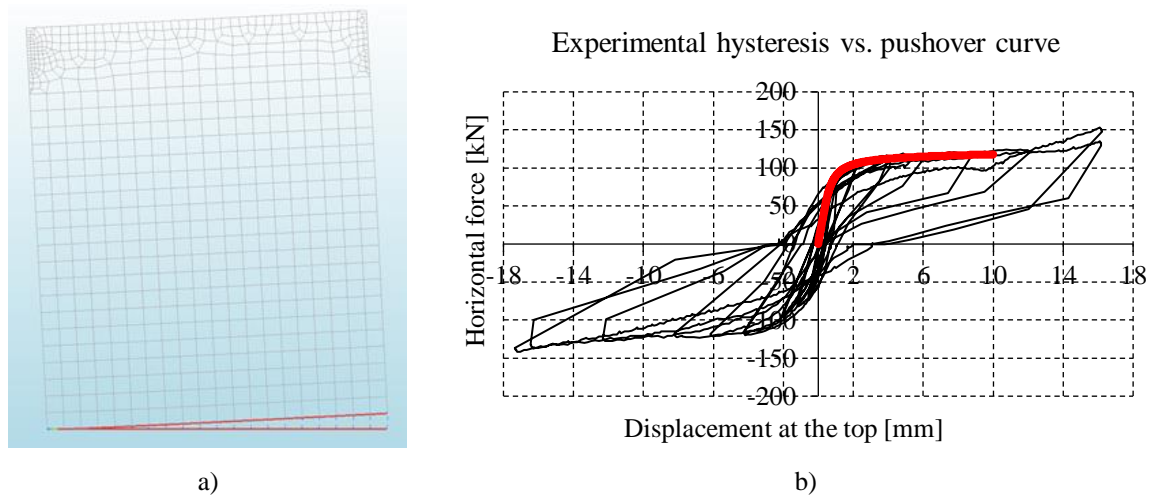
Figure 7. Results of the numerical analysis in case of rocking: a) wall displacements, b) comparison of experimentally obtained hysteresis and numerical pushover curve.

3.2 Meso-model of the tested reduced scale wall

The contact material model, also known as the "Composite Interface model," is appropriate for the simulation of fracture, frictional slip, and crushing along material interfaces, for instance, at joints in masonry. Usually, the brick units are modeled as linear elastic continua, while the mortar joints are modeled with interface elements, which obey the nonlinear behavior described by this combined cracking-shearing-crushing model (acronym CCSC). Fig. 8a shows the elements of a meso-model, with an additional interface element in the unit middle [9]. This interface was modeled in order to enable the cracking of bricks which was experimentally observed. A plane stress interface model was formulated by Lourenço [11]. It is based on multi-surface plasticity, comprising a Coulomb friction model combined with a tension cut-off and an elliptical compression cap (Fig. 8b). Softening acts in all three modes, and it is preceded by hardening in the case of the cap mode.
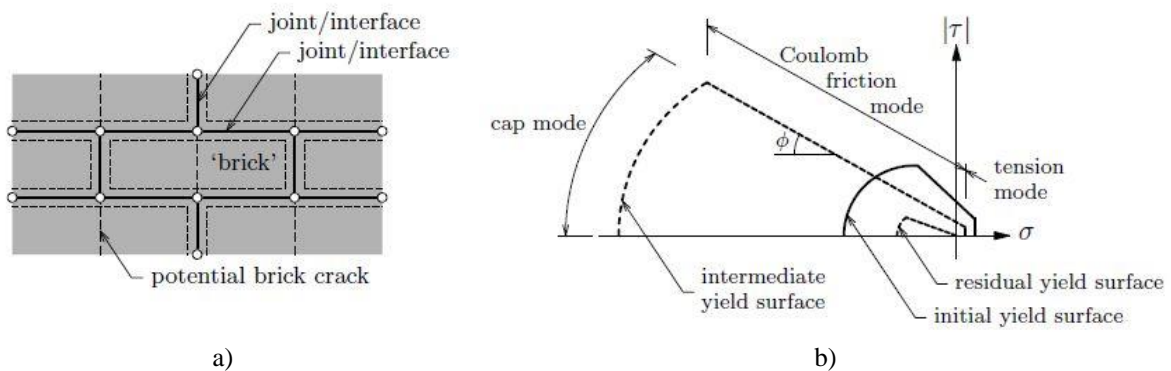
Figure 8. Meso-model of masonry: a) locations of interfaces, b) multi-surface plasticity for CCSC model.

Parameters of CCSC interface (horizontal and vertical joints) and Coulomb interface with zero-tension gapping mode (brick contact) are listed in Table 3. The brick behavior was assumed linear elastic with Young's modulus equal to 20 000 N/mm2 and Poisson ratio of 0.15. The input parameters were based on measured material properties [2] or previous numerical and experimental studies [11, 12]. Mesh, loading, and boundary conditions for the meso-model of the reduced-scale wall are shown in Fig. 9a. The resulting normal interface tractions are given in Fig. 9b. It can be noticed that the mortar joint opens at the tension side and that rocking governs the failure mechanism. The comparison of experimentally and numerically obtained pushover curves is given in Fig. 10, and it can be concluded that the curves match pretty well.

Table 3 – Parameters of CCSC interface (joints) and Coulomb interface (brick contact)

CCSC	Value	CCSC	Value	Coulomb	Value
k_n	50 N/mm³	σ_u	- 0.75N/mm²	k_n	1000 N/mm³
k_s	10 N/mm³	δ	1.8	k_s	500 N/mm³
f_t	0.1 N/mm²	a	- 0.8	f_t	3.6 N/mm²
G_t	0.003 N/mm	b	0.05	G_t	0 N/mm
c	0.09 N/mm²	f_c	6.5 N/mm²	c	1.2 N/mm²
ϕ	0.785 rad	C_s	9	ϕ	0 rad
Ψ	0.540 rad	G_c	10 N/mm	Ψ	0
ϕ_r	0.785 rad	κ_p	0.015	ϕ_r	0
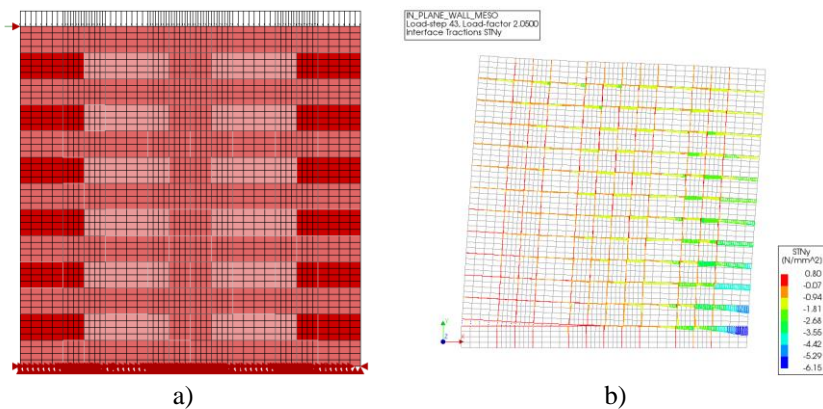
Figure 9. Meso-model of reduced-scale masonry wall: a) mesh, loading, and boundary conditions, b) normal interface tractions.
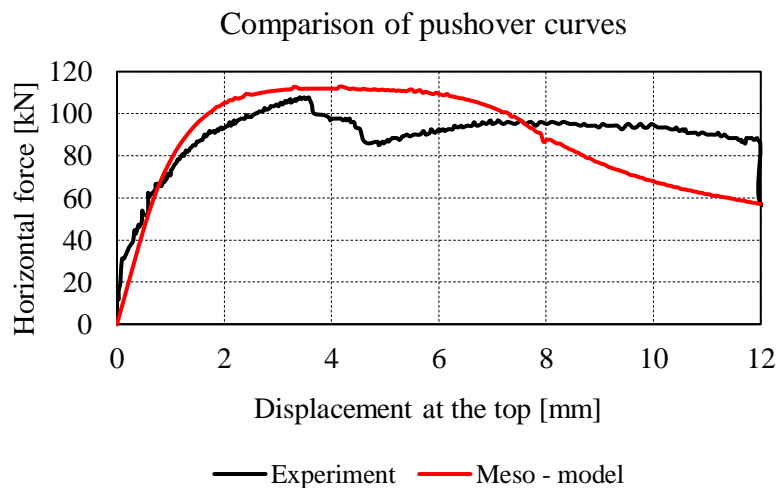
Figure 10. Comparison of pushover curves obtained experimentally and numerically.

4. Conclusion

Different classes of numerical models are presented in the paper. Two modeling approaches were used to simulate the tested walls: the macro-model, where the structure is a homogeneous continuum, whose behavior is described with the engineering masonry model, and the meso-model where the structure is discretized using the continuum elements (bricks) and contact elements (joints, cracks). In the discrete model, the bricks are linear elastic, and nonlinear behavior is possible on the contact elements where the composite CCSC (combined cracking-shearing-crushing) model is employed for the joints and Mohr-Coulomb for cracks in the bricks. The models are planar so that the 3D character of the masonry structure is neglected (longitudinal and transverse layout of brick elements).

The advantage of the macro-model lies in the simplicity of the finite element mesh and the construction of the model, so the requirements for computer time are much lower than in the meso-model. It is possible to apply the complete loading program without divergence at large displacements, resulting in a failure mode with cross-diagonal cracks. On the other hand, the macro-crack is most often diagonally localized, while the models' cracks are smeared along a specific width or the cracking pattern is diffuse. When using macro models, it is tacitly assumed that the structure, load, and boundary conditions are such that the mortar and the brick do not have to be separately discretized, which is also the lack of a macro-model. The element and the joint are no longer distinguished, so it is impossible to determine the degree of stress of the brick or mortar.

Generally, different failure modes can be obtained using macro-models. In case of low precompression, rocking, and local crushing occurs. Shear failure with a diagonal cracking pattern develops for higher precompression levels. Depending on the loading program, the force-displacement relationship shows a pushover or a hysteretic curve. Linear force increase with displacement increment is typical for the initial phase of the obtained pushover curves. The other part of the curve is almost horizontal, implying stiffness degradation and yielding. However, in the case of rocking, yielding is not caused by material degradation but by reducing the compressed zone as imposed displacement increases. Hysteretic curves are full and significant energy is dissipated when shear governs failure. The slope of the hysteretic curve decreases when unloading, which means that, aside from plastic deformations typical for joint failure, bricks fail in tension, and damage occurs. The numerically obtained hysteretic curve agrees reasonably well with the one determined by the experimental program. The initial elastic stiffness, ultimate resistance, failure mode, and cracking pattern were predicted quite well by the nonlinear finite element analysis. However, further numerical investigations related to mesh sensitivity and variability of material properties are necessary.

The bending failure mode of reduced-scale masonry walls loaded with horizontal force and low vertical precompression can be modeled with meso-model quite well. When tensile strength is reached, the joint opens, and the wall rotates around the compressed toe. Generally, this failure pattern is obtained regardless of the changes in model parameters, and the reason is that the wall geometry and the boundary conditions between the bricks are correctly modeled, so the weak spots can easily be identified. The level of detail of a discrete model cannot be achieved by using a homogenized continuum, such as in the case of separating individual bricks from the rest of the structure. Also, the stress state in bricks and contacts is well described. Regardless of the many advantages of the discrete model, there are several significant shortcomings. It is necessary to invest considerably more time in modeling geometry and analyzing the results than with the continuum model. The analysis is more demanding ("expensive") due to additional contact elements.

References

[1] Hrasnica, M., Medic, S. (2012): Structural challenges of historical stone masonry in Bosnia Herzegovina. In: Ibrahimbegovic A, Hrasnica M, Zlatar M, Dolarevic S, Madzarevic M (eds) *IASS-IACM 7th International Conference on Computational Mechanics for Spatial Structures*. Faculty of Civil Engineering, University of Sarajevo, pp. 144-147.

[2] Medić, S., Hrasnica, M. (2021): In-Plane Seismic Response of Unreinforced and Jacketed Masonry Walls. *Buildings*, 11(10), 472, doi: https://doi.org/10.3390/buildings11100472

[3] Lourenço, P.B. (2008): Structural masonry analysis: Recent developments and prospects, *Proceedings of the 14th international brick and block masonry conference,* 13-20 February, Sydney, Australia.

[4] Hrasnica, M., Biberkic, F., Medic, S. (2017): In-plane behavior of plain and strengthened solid brick masonry walls. *Key Engineering Materials* 747, 694-701. https://doi.org/10.4028/www.scientific.net/kem.747.694

[5] Berto, L., Saetta, A., Scotta, R., Vitaliani, R. (2004): Shear behaviour of masonry panel: parametric FE analyses. *International journal of solids and structures*, *41*(16-17), 4383-4405. doi: https://doi.org/10.1016/j.ijsolstr.2004.02.046

[6] Magenes, G., Calvi, G. M. (1997): In-plane seismic response of brick masonry walls. *Earthquake engineering & structural dynamics*, *26*(11), 1091-1112. doi: https://doi.org/10.1002/(SICI)1096-9845(199711)26:11<1091::AID-EQE693>3.0.CO;2-6

[7] Chaimoon, K., Attard, M. M. (2007): Modeling of unreinforced masonry walls under shear and compression. *Engineering structures*, *29*(9), 2056-2068. doi: https://doi.org/10.1016/j.engstruct.2006.10.019

[8] Burnett, S., Gilbert, M., Molyneaux, T., Beattie, G., Hobbs, B. (2007): The performance of unreinforced masonry walls subjected to low-velocity impacts: Finite element analysis. *International Journal of Impact Engineering*, *34*(8), 1433-1450. doi: https://doi.org/10.1016/j.ijimpeng.2006.08.004

[9] DIANA FEA (2016): *DIANA - User´s Manual, Material library*, Delft, The Netherlands.

[10] Schreppers, G.J., Garofano, A., Messali, F., Rots, J.G. (2016): *DIANA Validation report for Masonry modelling*, DIANA FEA BV and TU Delft, Delft, The Netherlands.

[11] Lourenço, P.B. (1996): Computational Strategies for Masonry Structures, *Ph.D. Thesis,* Faculty of Civil Engineering and Geosciences, Delft University of Technology, The Netherlands.

[12] Allen, C., Masia, M., Page, A., Griffith, M., Ingham, J. (2017): Nonlinear finite element modelling of unreinforced masonry walls with openings subjected to in-plane shear, *13th Canadian Masonry Symposium*, 4-7 June 2017, Halifax, Canada.

RELIABILITY ANALYSIS OF REINFORCED CONCRETE FRAME BY FINITE ELEMENT METHOD

Marin Grubišić[(1)], Jelena Ivošević[(2)], Ante Grubišić[(3)]

[(1)] *Assist. Professor, Faculty of Civil Engineering and Architecture Osijek, University of Osijek, marin.grubisic@gfos.hr*
[(2)] *MEng, SIRRAH Projekt Ltd, Osijek, jelenaivosevic9@gmail.com*
[(3)] *MEng, TRINAS Ltd, Osijek, ante.grubisic@trinas.hr*

Abstract

Since the prediction of the seismic response of structures is highly uncertain, the need for the probabilistic approach is clear, especially for the estimation of critical seismic response parameters. Considering the uncertainties present in the material and geometric form of reinforced concrete (RC) structures, reliability analyses using the Finite Element Method (FEM) were performed in the context of Performance-Based Earthquake Engineering (PBEE). This study presented and compared the possibilities of nonlinear modelling of the reinforced concrete (RC) planar frame and its reliability analysis using different numerical methods, Mean-Value First-Order Second-Moment (MVFOSM), First-Order Reliability Method (FORM), Second-Order Reliability Method (SORM) and Monte Carlo simulation (MCS). The calibrated numerical models used were based on the previous experimental test of a planar RC frame subjected to cyclic horizontal load. Numerical models were upgraded by random variable (RV) parameters for reliability analysis purposes, and, using implicit limit state function (LSF), pushover analyses were performed by controlling the horizontal inter-storey drift ratio (IDR). Reliability results were found to be sensitive to the reliability analysis method. The results of reliability analysis reveal that, in a nonlinear region, after exceeding the yield strength of the longitudinal reinforcement, the cross-sectional geometry parameters were of greater importance compared to the parameters of the material characteristics. The results also show that epistemic (knowledge-based) uncertainties significantly affected dispersion and the median estimate parameter response. The MCS sampling method is recommended, but the First-Order Reliability Method (FORM) applied to a response model can be used with good accuracy. Reliability analysis using the FEM proved suitable for directly implementing geometric and material nonlinearities to cover epistemic (knowledge-based) uncertainties.

Keywords: *reinforced concrete (RC) frame; cyclic response; reliability analysis; MVFOSM/FORM/SORM; Monte Carlo; OpenSees*

1. Introduction

The structural design aims to achieve structures that satisfy safety criteria, serviceability, and durability under specified service conditions. Since uncertainty is an inherent characteristic that cannot be avoided in engineering design, incorporating uncertainties in engineering design is required [1]. Reliability analysis offers a well-established theoretical framework for considering uncertainties in the engineering decision scheme. We can define reliability as the probability that a structure or system can perform a required function (or limit state function, LSF) under specified service conditions during a given period and stated conditions [2]. Conversely, the failure probability, pf (or probability of failure) is the probability that a structure does not perform satisfactorily within a given period and stated adverse conditions [3]. In the context of seismic risk analysis, the probability of exceeding the given LSF, obtained from the reliability analysis, is integrated with the seismic risk of the locality. The related term used in conjunction with seismic reliability analysis and structural risk is fragility analysis. The fragility analysis is aimed at finding the probability of a particular structural failure for different levels of intensity measures (IM) such as PGA (peak ground acceleration) or $S_A(T_1, 5\%)$ (5%-damped elastic first-period spectral acceleration), and analysis is closer to the actual estimation of structural seismic risk. Despite these fine distinctions, seismic risk, reliability, safety, and structural fragility analysis are used in various ways to denote the seismic probability of structural failure, so that the failure is defined by different structural limit state conditions [4].

The most important aspect of the structural reliability analysis is the consideration of uncertainties that make a structure vulnerable to failure for a pre-defined limit state condition. The accuracy of the reliability analysis depends on how exactly all the uncertainties are considered during the analysis. First, the challenge is identifying all the sources of uncertainties; therefore, crucial uncertainties must be identified. Second, the techniques of explicit or implicit modelling are difficult to implement, therefore a certain degree of uncertainty is associated with the modelling method, with some necessary simplifications. Finally, the analytical formulation of the limit state equations and integration of the probability density function (PDF) in this domain is complex and results in various approximations. Consequently, there are different degrees of simplification in the reliability analysis leading to various reliability analysis methods, as explained below [5,6].

Considering the foregoing, the bearing capacity of the structure or element can be obtained in many ways, being the most simple and direct to use an explicit design equation, when the LSF $g(x)$ can be expressed as an explicit form or simple analytical form in terms of the basic variables x, which characterise the structural behaviour, relating the many variables, defined by probabilistic distributions. If an explicit function capable of defining the behaviour of the structure is not available, it is possible to use the FEM with implicit LSF to compute the behaviour of the structure. Such implicit LSF are encountered when the structural systems are complex and numerical analysis such as FEM must be adopted for the structural response prediction.

We can simplify the safety assessment procedure with implicit functions, by getting an explicit alternative LSF that allows a significant decrease in the response calculation time. We can obtain this function through the Response Surface Method (RSM) by fitting a surface to various realisations, for a set of variables, based on an MCS using an implicit LSF provided by the FEM [7,8]. In addition to all the well-established postulates of individual reliability methods, one of the hypotheses of this study is that even when using the FEM, the least numerical model settings can have a relatively significant impact on the reliability analysis results. These settings relate to the type of element, the plastic hinge length, the number of integration points along the element, numerical integration options for the force-based beam–column element, geometric transformation type, etc.

The described procedures in this study are compatible with the implementation of the model in the PEER PBEE framework (Pacific Earthquake Engineering Research Performance-Based Earthquake Engineering) [9,10], which besides structural responses considers the consequent functions and interaction with the Performance Assessment Calculation Tool (PACT P-58) [11]. A flexible feature of this approach is two-way communication with Python and MATLAB, which is important for applying sophisticated sampling techniques.

This paper presents the numerical calibration of the experimental RC frame model, which was later upgraded for reliability analysis. The methods of reliability analysis of MVFOSM, FORM, SORM and MCS were used, after which the basic results and conclusions were presented. All numerical analyses presented in this paper were carried out by combining OpenSees and MATLAB with customisable algorithms.

2. Experimental Model

In accordance with the prototype of a typical mid-rise building, the central bay RC frame from the ground floor was chosen and constructed at a scale of 1:2.5, which makes an aspect ratio of 1.4 [4,12,13]. Geometry, cross sections, and the amount of main longitudinal and transverse reinforcement are shown in Figure 1. The prototype of a typical building [14], from which the central frame on the scale was separated, was designed in accordance with the relevant codes [15,16], for ductility class DCM, which required concrete grade C30/37 and reinforcement B500B. The actual mechanical properties, modulus of elasticity, yielding strength, and ultimate strengths were determined in accordance with the applicable norms. After the frames were made and concrete samples were tested, the average compressive strength of the concrete cubes was 50 MPa, while the yielding and ultimate tensile strength, and the modulus of elasticity of the reinforcement were 550, 650 and 210000 MPa respectively. All these parameters of material characteristics were determined by standardised

compressive and tensile tests, whose values were rounded off from a series of nine repeated tests. The model was cyclically tested in a horizontal direction, with a constant total vertical force in columns of 730 kN, i.e., 365 kN per column, to ensure an axial load ratio of 18% in each column, as defined by design (9 MPa of the axial stress relative to the gross cross-section of the column). During testing, the horizontal force was controlled, i.e., beam level displacement up to 1.0% of inter-storey drift ratio (IDR) or 14 mm, by repeating each cycle twice, resulting in damage to the ends of the columns and the beam by crushing the concrete and reaching the yield strength of individual longitudinal reinforcement.
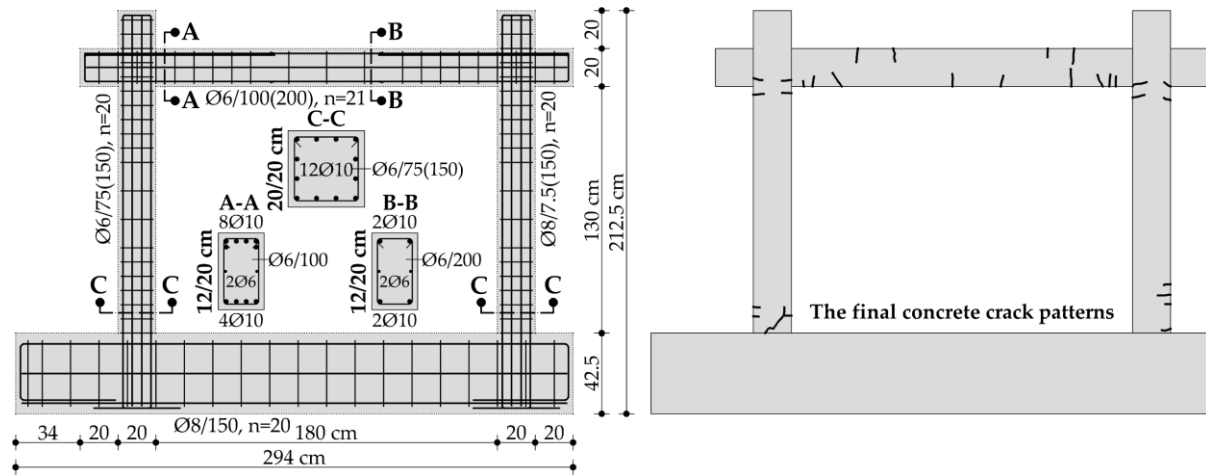
Figure 1. Schematic representation of geometry, cross sections, and the amount of reinforcement (left) and crack development during the cyclic test (right).

Figure 2 shows the hysteresis curve as a basic view of the system's behaviour, with insight into the secant stiffness (K), bearing capacity and ductility of the system and the trend of component stiffness degradation. When describing the behaviour of such models, it is necessary to evaluate the stiffness, strength, and deformation properties of individual components to numerically model the same effects and expand the analysis, such as sensitivity or reliability analysis. The specimen was not tested until the collapse but up to the targeted drift of 1.0% to preserve the specimen for further testing. The distribution and the type of cracks showed a clear flexural behaviour, with no shear failures.

The definition of the trilinear backbone curve (i.e., bearing capacity curve), which represents the three different areas of behaviour, is based on the mean value of the bearing capacity of the positive and negative horizontal direction, as shown in Figure 3.
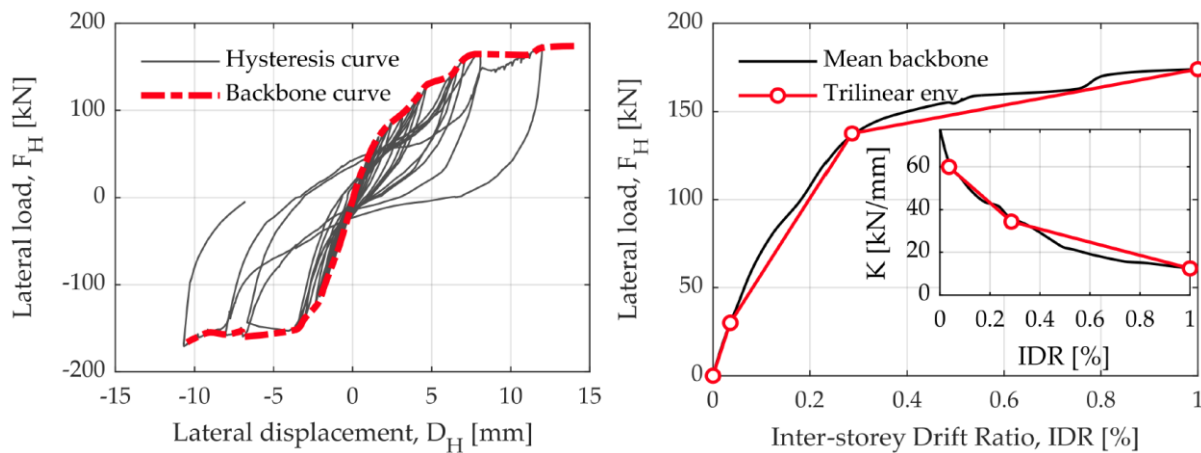
Figure 2. The hysteresis curve (left) and the average of two backbone curves as well as the secant stiffness curve, K (right).

When defining the trilinear backbone curve, the formation moment of the first significant crack was considered (1), as well as the continuation of cracks development up to the level of the global model

yielding, i.e., temporary lack of bearing capacity (2) and the targeted drift (3). The characteristic points of the trilinear backbone curve and the stiffness curve were: IDR = [0.0, 0.036, 0.286, 1.0]%, FH = [0.0, 30, 137.5, 174] kN, and K = [60, 34.375, 12.428] kN/mm.

3. Numerical Model

The numerical model is constructed in two ways by the OpenSees (Figure 4) to construct as simpler a model as possible to describe the frame behaviour in relation to experimental testing. In the first part of modelling hysteresis response, a well-known approach to the theoretical semi-empirical model of concentrated plasticity (CP) was used, with hysteresis rules for RC elements according to Takeda [17], for easier and robust control of hysteresis behaviour. It should be noted that both concentrated plasticity (CP) and distributed plasticity (DP) numerical models are, by definition, suitable for reliability analysis. For this study, the DP model was chosen only because of engineering comprehension and the easier understanding of RVs and their associated coefficients of variation (COV). The nonlinearities in the CP model are defined based on the moment–rotation relationship (M–θ), which may be less understandable for practitioners, especially due to the lack of knowledge about the dispersion of these parameters at the yielding limit and ultimate bearing capacity. The nonlinearities in the DP model are defined by fibre sections, which have implemented uniaxial material behaviour parameters, based on which RVs are defined. All variables in the DP model are engineer understandable, and the dispersion of these parameters is well documented in the literature.

BeamWithHinges element was used for modelling columns and beams, which considers force-based distributed plasticity over specified plastic hinge lengths near the element ends. Two-point Gauss–Lobatto integration rule was used over the hinge regions, where the bending moments were largest, which gave the desired level of element integration accuracy [23,24]. The basic uniaxial material models were attributed to fibre cross sections to keep the model as simple as possible, but also due to certain limitations in the OpenSees program's sensitivity module at the time of the study. These uniaxial materials are Concrete01 (Kent–Scott–Park) for concrete and Steel01 (Bi-linear) for reinforcing steel. It should be emphasised that the initial modulus of elasticity of concrete directly depends on the peak strength and the associated deformation, expressed as $E_c = 2 \cdot f_{c1C}/\varepsilon_{c1C}$. Fracture energy in compression for the Kent–Scott–Park concrete model can be expressed as $G_f^c/L_p = 0.6 \cdot f_{c1C} (\varepsilon_{20,C1C} - \varepsilon_{c1C} + (0.8 \cdot f_{c1C})/E_c)$. Additional introduced model parameters for the Kent–Scott–Park concrete model are elastic modulus, E_c, strain corresponding to 20% of the compressive strength, $\varepsilon_{20,C1C}$. The parameter G_f^c is the concrete fracture energy in compression (plain concrete crushing energy), which often serves for material regularisation and L_p is the plastic hinge length, which acts as the characteristic length for the purpose of providing an objective response.
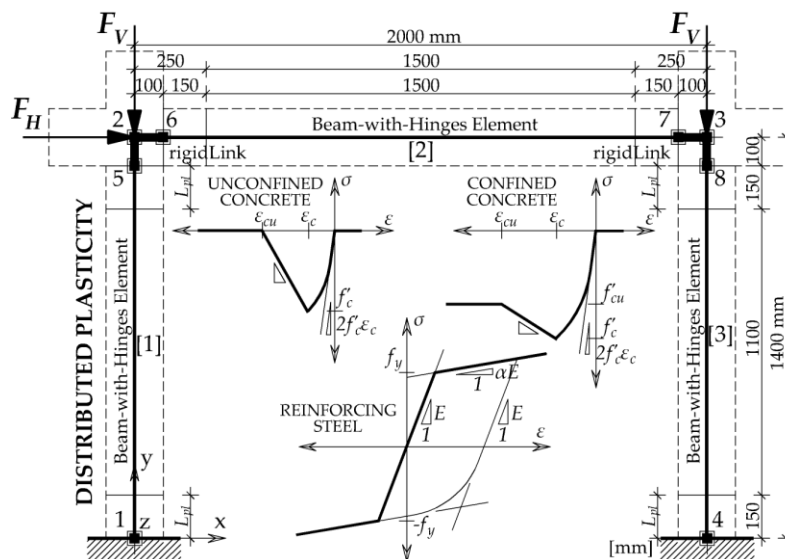
Figure 3. Distributed plasticity numerical model configuration scheme for reliability analysis

The plastic hinge length was specified using an empirically validated relationship, such as the [18] equation for reinforced concrete members $L_p = 0.08 \cdot L + 0.022 \cdot f_y \cdot d_b$ [kN, mm], where L is the length of the member and f_y and d_b are yield strength and diameter, respectively, of the longitudinal reinforcing bars. The advantage of this approach is that the plastic hinge length includes the effect of strain softening and localisation as determined by experiments. Finally, the plastic hinge length was adopted as 150 mm for columns and beam. Since the parameters E_c and G_f^c are directly related to f_{c1C} and ε_{c1C}, they are not further considered RVs, as defined below. The confinement factor for columns and beams was adopted as a rounded value of 1.15, for a given cross-sectional configuration and transverse reinforcement spacing (which is closed at 135 degrees). The corotational geometric transformation was also applied in the DP model to consider the second-order effects [19–22]. The beam–column joints were considered rigid, as well as the base of the columns with a foundation. Detailed information on the parameters and settings for reliability analysis are given below.
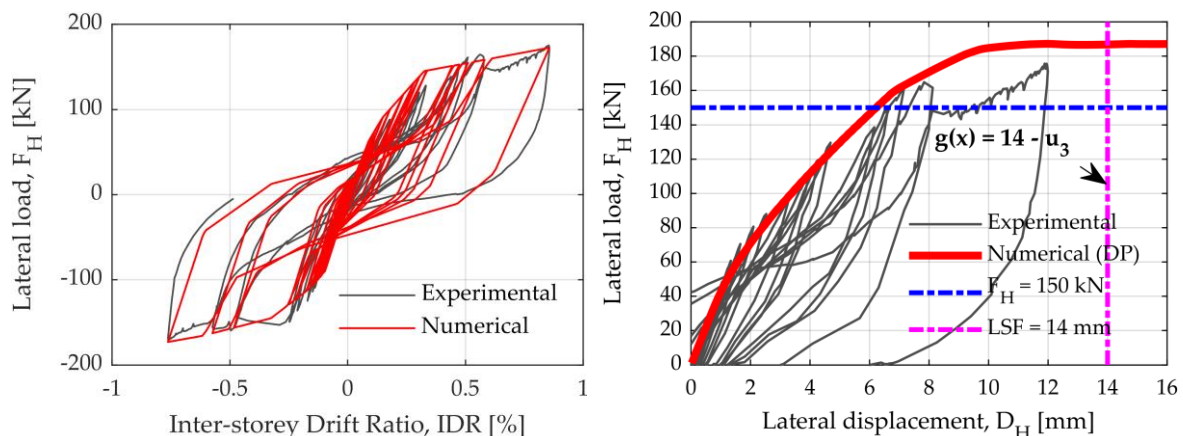
Figure 4. Comparison of hysteresis curve with pushover curve for distributed plasticity model (DP), with corresponding drift limit and horizontal load level at reinforcement yielding.

4. Reliability Analysis Results

The calibrated numerical model shown was upgraded with defined RVs of normal (N) and log-normal (LN) distributions and defined parameters associated with RVs. It should be emphasised that the numerical model was adapted to the extent that its elements or sections were defined as fibre sections, therefore not defined by springs, whose characteristics were also derived from the fibre cross-sectional analysis. This was an easier understanding of RVs and their associated parameters. As RVs, we wanted to define the parameters of material characteristics, cross-sectional geometry, depth of the concrete cover, etc. compared to the parameters of the concentrated plasticity or the pair of the moment–rotations (which is not a limit, but an intuitive approach has been adopted). The definition of RVs primarily refers to parameters of material properties of concrete and reinforcing steel and then the geometrical characteristics of the cross-section and the width and height of the RC frame. The mean values of all RVs were obtained from the experiments and calibrations, while their coefficients of variation (COV) were obtained partly from experimental material testing by comparing available literature (Table 1).

To present the possibilities of reliability analysis by FEM, a correlation between individual parameters or RVs was introduced. For example, a correlation was introduced between the yielding strength and the modulus of elasticity of reinforcing steel as 60% correlation, as obtained from the literature [25,29,30]. A complete correlation was found between the peak compressive strength of concrete for the concrete cover and core (i.e., unconfined and confined concrete section) and for the associated deformation, as 100% [25]. Thus, the importance of some RVs for the LSF could be ranked according to two parameters: $\boldsymbol{\alpha}$ and $\boldsymbol{\gamma}$ (Importance vectors). Thus, the importance vector $\boldsymbol{\alpha}$ does not consider the correlation between RVs, while the importance vector $\boldsymbol{\gamma}$ considers the defined correlation. In Table 1, the symbols of the parameters show the reinforcing steel yield strength (f_y), the elasticity modulus of the reinforcing steel (E_s), the compressive strength of the confined concrete core with corresponding

deformation (f_{c1C}, ε_{c1C}), the compressive strength of the unconfined concrete with corresponding deformation (f_{c1U}, ε_{c1U}), the confined concrete crushing strength with corresponding deformation (f_{c2C}, ε_{c2C}), the unconfined concrete crushing strength with corresponding deformation (f_{c2U}, ε_{c2U}), the vertical load per column (F_v), the length of the columns and beam (L_{column}, L_{beam}), the depth of the concrete cover for both columns and beams (c_{cover}), the cross section depth of the columns and beam (H_{column}, H_{beam}) and plastic hinge length for both columns and beam (L_p).

Table 1. Summary of RVs with their mean values (μ_i), standard deviations (σ_i) and coefficients of variation (COV).

RV_i	Param.	Mean, μ_i	St. Dev., σ_i	COV	Units	Distr.	References for COV
101	f_y	550	44	0.08	[MPa]	LN	Exp. + [9–11]
102	E_s	210 000	12 600	0.06	[MPa]	LN	Exp. + [8,9,12]
103	f_{c1C}	−57.5	−8.63	0.15	[MPa]	N	Exp. + [9,13–16]
104	ε_{c1C}	−0.005	−0.0008	0.15	[–]	N	Exp. + [9,13–17]
105	f_{c1U}	−50	−7.5	0.15	[MPa]	N	Exp. + [9,12,15,16]
106	ε_{c1U}	−0.002	−0.0003	0.15	[–]	N	Exp. + [9,13,17]
107	f_{c2C}	−11.5	−2.3	0.20	[MPa]	N	Exp. + [9,13–16]
108	ε_{c2C}	−0.0085	−0.0017	0.20	[–]	N	Exp. + [9,13–17]
109	f_{c2U}	−10	−2	0.20	[MPa]	N	Exp. + [9,13,15,16]
110	ε_{c2U}	−0.0035	−0.0007	0.20	[–]	N	Exp. + [9,13,17]
111	F_v	365	36.5	0.10	[kN]	N	Exp. + [11,14]
112	L_{column}	1400	–	0.01	[mm]	N	[9,14,18]
113	c_{cover}	15	–	0.25	[mm]	N	[9,14,18]
114	H_{column}	200	–	0.05	[mm]	N	[9,14,18]
115	H_{beam}	200	–	0.05	[mm]	N	[9,14,18]
116	L_{beam}	2000	–	0.01	[mm]	N	[9,14,18]
117	L_p	15	–	0.10	[mm]	N	[9,14,18]

Material and geometric nonlinear parameters, formulation of boundary conditions, static indeterminacy, and several DOF are already defined within the numerical model, so the evaluation of RVs and the implicit LSF for the calculation of structural responses is more straightforward regarding defining explicit LSF. Figure 4 (right) shows the pushover curve of a fibre-based numeric model regarding the cyclic response of the experiment. In the exact figure, the IDR limit is defined for the ultimate LSF. In addition, the constant horizontal load value of 150 kN was adopted, which for this deterministic model is the amount of horizontal load at which the yielding strength is exceeded of reinforcing steel, after which the RC frame progressively loses its horizontal load bearing capacity. Thus, the limit state of the displacement is limited to 14 mm or 1.0% IDR.

The aim of all reliability analyses is to verify their comparability and applicability; thus, for Monte Carlo simulation (MCS), we expect the probability of p_f for a reasonable number of simulations ($N_{MCS} \geq 10^5$) close to FORM and SORM analyses. The SORM method improves the assessment given by FORM by including information about the curvature, approximating the nonlinear LSF (related to the second-order derivatives of the LSF with respect to the basic variables), while FORM approach approximates the LSF with a linear function.

4.1. MVFOSM, FORM, and SORM Analyses

Table 2 shows the difference in the order of importance vectors with and without a defined correlation. The values of X_i^* show the values of individual parameters for the same horizontal load of 150 kN reaching exactly the Design Point response, defined by the LSF and in this case was 14 mm or 1.0% of IDR. The pushover curves with the mean values of all parameters, and the design point values, are shown below for all MCS. The values of X_i^* can also optimise the system in such a way that the iterative procedure monitors the mean value difference μ_i regarding design point values X_i^*, thereby rationalising

specific cross-section dimensions, frame geometry or mechanical properties of the material (reliability-based design optimisation). It is important to emphasise that the list of parameters of RV, ranked by the importance vectors, is certainly sensitive to specific implicit LSF, i.e., the order of importance vectors does not apply to any other pre-defined LSF, which is visible from the Tornado Diagram Analysis (TDA). In addition, most design solutions will remain in the linear range of behaviour throughout their lifetime, where the optimisation of such linear systems would be even more straightforward, and there would be no significant between individual LSFs regarding the importance of some RVs if the structure behaves linearly. Correlation affects not only the parameters it relates but also all the parameters with which they interact within a numerical model.

Table 2. The rank of RVs and parameters by importance vectors, obtained from the FORM analysis, according to the γ_i vector, i.e., *considering* the correlation between the defined RVs for the LSF $g(x) = 14.0 - u_3$.

RV_i	Param.	Units	Mean, μ_i	Design Point, X_i^*	Importance, γ_i	Importance, α_i
103	f_{c1C}	[MPa]	$-5.750 \cdot 10^1$	$-3.789 \cdot 10^1$	0.460179	-0.714091
114	H_{column}	[mm]	$2.500 \cdot 10^2$	$2.322 \cdot 10^2$	-0.449068	-0.374476
104	f_{c1U}	[MPa]	$-5.000 \cdot 10^1$	$-3.296 \cdot 10^1$	0.400155	-0.047072
116	L_{beam}	[mm]	$2.000 \cdot 10^3$	$2.023 \cdot 10^3$	0.346749	0.289152
101	f_y	[MPa]	$5.500 \cdot 10^2$	$5.092 \cdot 10^2$	-0.336795	-0.324799
113	c_{cover}	[mm]	$1.500 \cdot 10^1$	$1.733 \cdot 10^1$	0.245127	0.204410
115	H_{beam}	[mm]	$2.000 \cdot 10^2$	$1.922 \cdot 10^2$	-0.220742	-0.184076
109	ε_{c2C}	[–]	$-8.500 \cdot 10^{-3}$	$-8.500 \cdot 10^{-3}$	0.214387	-0.251653
111	F_v	[mm]	$-3.650 \cdot 10^5$	$-3.420 \cdot 10^5$	0.116115	-0.096828
112	L_{column}	[mm]	$1.400 \cdot 10^3$	$1.405 \cdot 10^3$	0.092027	0.076741
110	ε_{c2U}	[–]	$-3.500 \cdot 10^{-3}$	$-3.500 \cdot 10^{-3}$	0.088277	-0.010384
102	E_s	[MPa]	$2.100 \cdot 10^5$	$1.992 \cdot 10^5$	-0.087742	-0.058500
107	f_{c2C}	[MPa]	$-1.150 \cdot 10^1$	$-1.150 \cdot 10^1$	0.015339	-0.023803
108	f_{c2U}	[MPa]	$-1.000 \cdot 10^1$	$-1.000 \cdot 10^1$	0.013338	-0.001569
105	ε_{c1C}	[–]	$-3.500 \cdot 10^{-3}$	$-4.001 \cdot 10^{-3}$	0.008499	-0.011096
117	L_p	[mm]	$1.500 \cdot 10^2$	$1.507 \cdot 10^2$	0.007419	0.006187
106	ε_{c1U}	[–]	$-2.000 \cdot 10^{-3}$	$-2.286 \cdot 10^{-3}$	0.004856	-0.000571

At the cross-sectional level, maximum compressive strength of the confined and unconfined concrete, f_{c1C} and f_{c1U}, the total height of the beam and columns cross-section, H_{column} and H_{beam}, the depth of the concrete cover for both columns and beams affecting the effective height of the cross sections, c_{cover} and yield strength of reinforcing steel, f_y were the most sensitive parameters for the main LSF, considering the correlation between the parameters. Since the characteristics of reinforcing steel affect the behaviour of the confined concrete, the parameter f_{c1C} became the most important parameter for the LSF $g(x) = 1.0\% \cdot L_{column} - u_3$.

SORM analysis was also performed in two ways: by adopting the First Principal Curvature, SORM-FP, and by applying Curvature Fitting by combining 10 curvatures for a better approximation of the SORM-CF reliability index. The difference in the reliability index of β_{FORM} and $\beta_{SORM-CF}$ was only 0.13%, thus, the probability of the limit state exceeds $p_{f,FORM} = 0.079\%$ or $p_{f,SORM-CF} = 0.078\%$.

In Table 3, the reliability indexes for MVFOSM, FORM, SORM-FP and SORM-CF were compared for the 14 mm, 10 mm, and 6 mm horizontal displacements as LSF. During these analyses, it was concluded that the ranks of important parameters based on α_i and γ_i vectors were not the same for all three LSF, which is common for nonlinear systems since not all parameters equally affect the predominantly linear and nonlinear part of the model response. Based on these conclusions, a tornado diagram is constructed [32,41–43], by applying displacement control as deterministic sensitivity.

It is worth mentioning that the values of the reliability index, β in Table 4 for FORM and SORM analysis, are less than the guidelines for Eurocode 0 for residential and office buildings.

Table 3. Comparison of the reliability indexes (and their probabilities) for MVFOSM, FORM, SORM-FP and SORM-CF analysis for three different LSFs.

Analiza	Indeks pouzdanosti, β	LSF #1, $D_H = 14$ mm	LSF #2, $D_H = 10$ mm	LSF #3, $D_H = 6$ mm
MVFOSM	β_{MVFOSM} ($p_{f,MVFOSM}$)	4.816 ($7.338 \cdot 10^{-4}$)	2.511 ($6.028 \cdot 10^{-3}$)	0.205 ($4.186 \cdot 10^{-1}$)
FORM	β_{FORM} ($p_{f,FORM}$)	3.161 ($7.868 \cdot 10^{-4}$)	2.304 ($1.062 \cdot 10^{-2}$)	0.318 ($3.751 \cdot 10^{-1}$)
SORM–FP	$\beta_{SORM-FP}$ ($p_{f,SORM-FP}$)	3.161 ($7.868 \cdot 10^{-4}$)	2.304 ($1.062 \cdot 10^{-2}$)	0.318 ($3.751 \cdot 10^{-1}$)
SORM–CF	$\beta_{SORM-CF}$ ($p_{f,SORM-CF}$)	3.165 ($7.752 \cdot 10^{-4}$)	2.310 ($1.045 \cdot 10^{-2}$)	0.321 ($3.741 \cdot 10^{-1}$)

According to Eurocode 0 [44], the recommended minimum value for the reliability index, β (ultimate limit states) for Consequences Class 2 (CC2), that is Reliability Class 2 (RC2) and 50 years reference period is $\beta_{EC0,RC2} = 3.8$ or $p_f \approx 7.2 \cdot 10^{-5}$.

4.2. Monte Carlo Simulations

The results of the Monte Carlo analysis (conventional brute-force Monte Carlo) for the 10,000 simulations are presented below, carrying out a nonlinear analysis with Load Control (LC) of 150 kN in 40 steps per 5 kN (Figure 7). Figure 7 shows values of log-normal (LN) mean (β_{LN}) and standard deviations (θ_{LN}), and the diagrams are normalised based on horizontal force. The difference between the red and blue pushover curves should be noted. The red pushover curve was derived using the arithmetic mean values of all RV parameters.

Table 4. Comparison of the number of Monte Carlo Simulation (MCS-LC), together with the FORM analysis, on the exceedance probability of an LSF.

Total MCS, N_{MCS}	LSF #1, $D_H = 14$ mm, $p_{f,MCS}$	LSF #2, $D_H = 10$ mm, $p_{f,MCS}$	LSF #3, $D_H = 6$ mm, $p_{f,MCS}$	Running Time MCS (h:m:s)
1 000 (10^3)	0.0008	0.0048	0.3288	0:00:04
10 000 (10^4)	0.0006	0.0064	0.3077	0:00:39
100 000 (10^5)	0.0008	0.0068	0.3058	0:06:23
500 000	0.0008	0.0072	0.3024	0:35:20
$p_{f,MVFOSM}$	0.0000	0.0060	0.4186	0:00:01
$p_{f,FORM}$	0.0008	0.0106	0.3751	0:00:03
$p_{f,SORM-FP}$	0.0008	0.0106	0.3751	0:00:06
$p_{f,SORM-CF}$	0.0008	0.0105	0.3741	0:00:19
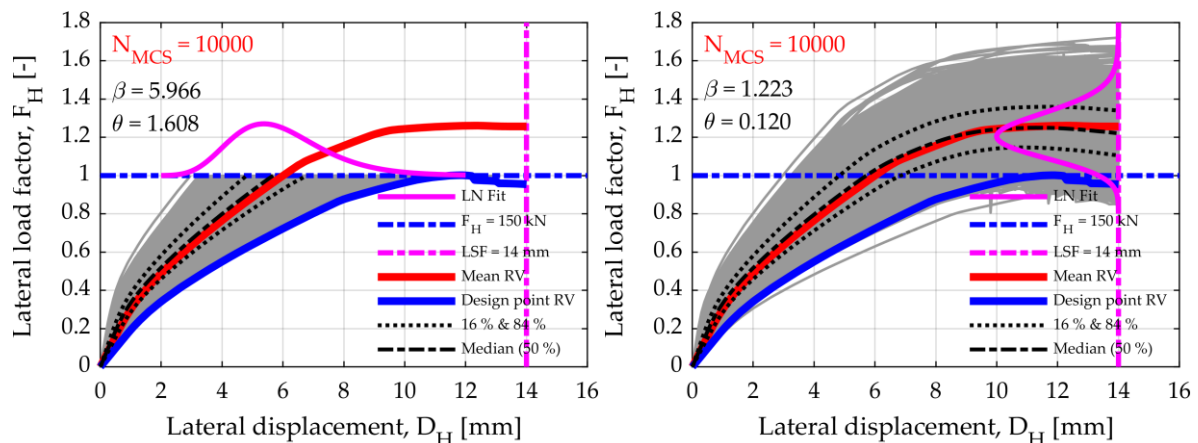
Figure 5. Illustration of MCS, for $N_{MCS} = 10^4$ simulations, load control MCS-LC (**left**) and displacement control MCS-DC (**right**)

The blue pushover curve was based on the RV parameters obtained by FORM analysis (X_i^* values based on the Design Point) regarding the default LSF $g(x) = 1.0\% \cdot L_{column} - u_3$. As a by-product, FORM analysis provided importance measures (α_i and γ_i vectors in Tables 2 and 3) to rank the uncertain parameters according to their relative influence on the structural reliability index, β. Based on these importance vectors, FORM optimised the values of all RVs (X_i^* values), in which combination exactly reached the Design Point (DP) or Most Probable Point (MPP). Thus, the difference between red and blue pushover curves is necessary and presents a useful product of the FORM analysis.

The tornado diagrams (Figure 6) were also constructed by applying the displacement control (DC) pushover analysis for deterministic sensitivity, which has become commonplace in reliability analysis of the field of earthquake engineering [31,32,41–43,47,48]. The TDA is a first-order sensitivity analysis. It comprises a set of horizontal bars, one for each input RV, whose lengths represent the variation of the EDP due to each considered input RV. The diagram is intuitive to read, and it helps the analyst identify which parameters to focus on. Each input variable is set to its median value (50th percentile), and the output is measured, establishing in this way a baseline output. One by one, each input parameter is fixed to both high and low extreme values of their probability distributions (generally corresponding to the 16th and 84th percentile, especially if the input distributions are different). The input parameters are ranked according to their absolute response difference (also called "swing") so that the larger swing belongs to the variable producing the most significant uncertainty [43]. Repeated analyses observe the difference in the model response; in this case, the horizontal bearing capacity was represented in the percentage of response difference regarding the median pushover curve.
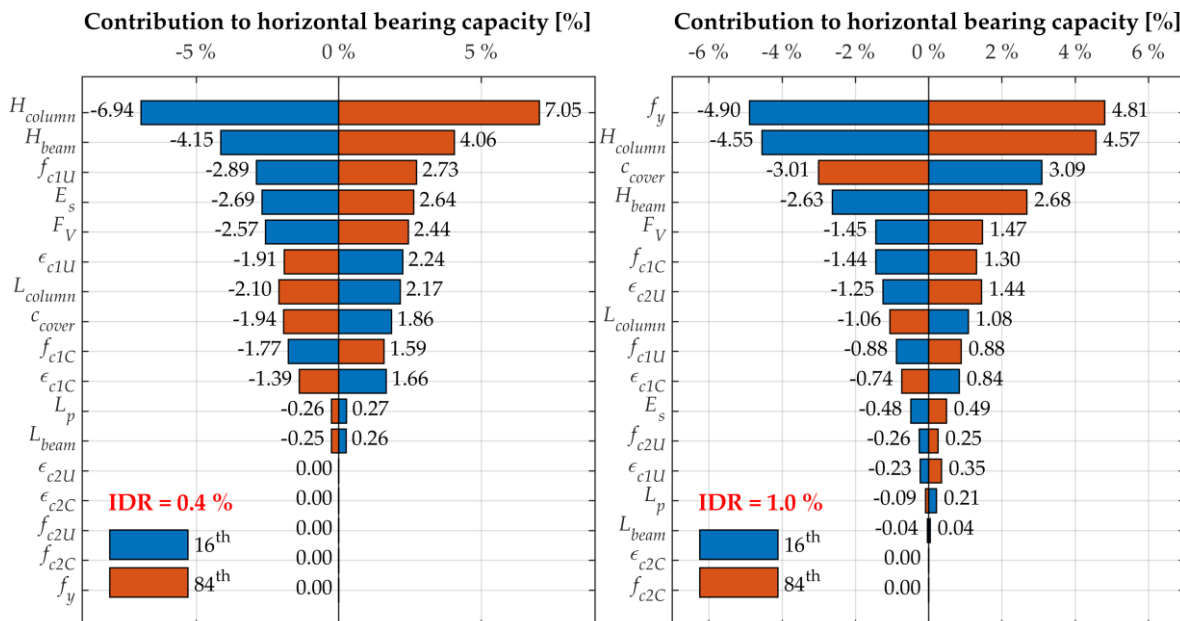
Figure 6. Tornado diagrams for three LSFs, showing the contribution of individual variables to horizontal bearing capacity, for IDR = 0.4% (**left**) and IDR = 1.0% (**right**)

Figure 7 shows the sensitivity of individual RV in the form of a standard deviation relative to the horizontal displacement, D_H. It is interesting to see when specific parameters were activated with their contribution to the system's bearing capacity. Notice the parameter f_y at a horizontal displacement of 6 mm (0.43% IDR). Almost the same trend had the crushing concrete parameters f_{c2C}, f_{c2U}, ε_{c2C}, ε_{c2U}. It is interesting that almost none of the parameters related to the properties of concrete had a linear median curve due to significant softening effects. The following limits are also shown in Figure 7: the maximum reached compressive strength limit of the unconfined concrete, f_{c1U} and ε_{c1U}, the reinforcement yield strength limit, f_y, and the limit as the beginning of concrete crushing, f_{c2C}, f_{c2U}, ε_{c2C} and ε_{c2U}.
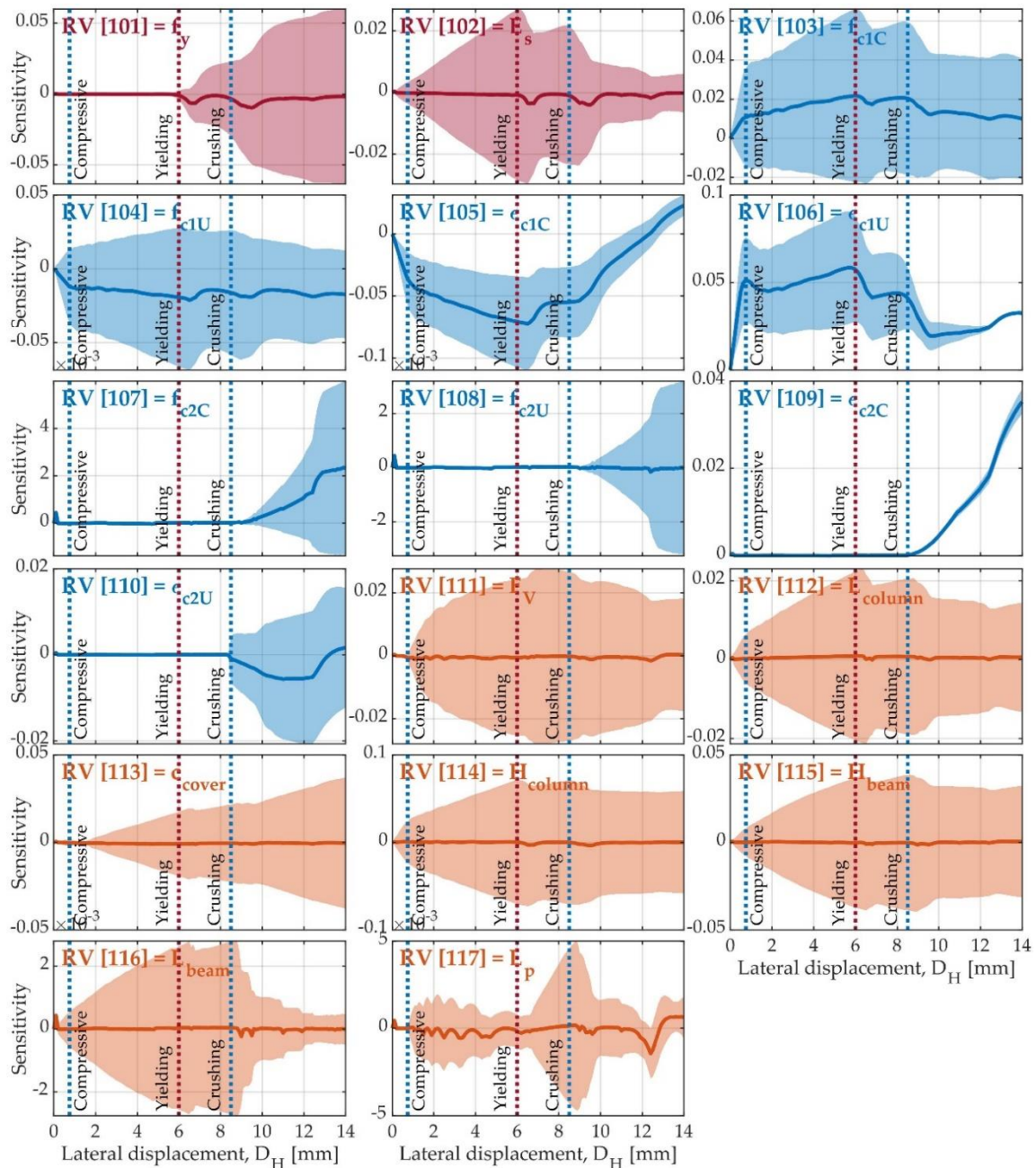
Figure 7. Overview of the sensitivity of individual RV on the nonlinear response of the RC frame (MCS-DC)

In the predominant linear range of system behaviour (0.4% IDR), the effect of significant parameters responsible for influencing the initial stiffness of the system, such as H_{column}, H_{beam}, f_{c1U}, ε_{c1U}, E_s, F_V, L_{column} and c_{cover} is visible. Parameters of crushed confined concrete did not contribute to any of the LSFs shown. For 0.4% IDR, the parameter f_y did not affect the system's bearing capacity, as expected, while for 1% IDR it was the main significant parameter affecting the system's capacity. In the linear range, it is evident that the geometrical characteristics of the cross sections were the main contributors to the system's bearing capacity (H_{column} and H_{beam}) and the stiffness of constituent materials expressed as elastic modulus (E_s and E_c defined as $E_c = 2 \cdot f_{c1C/U}/\varepsilon_{c1C/U}$).

5. Conclusions

This paper describes the reliability analyses of the RC frame by the FEM. The numerical model was based on and calibrated based on experimental testing of the single-bay single-storey planar RC frame at a scale of 1:2.5. The numerical model is shown in two variants, the nonlinear elements of which are defined by rotational springs (concentrated plasticity), and by the uniaxial fibre cross sections (distributed plasticity). The calibration of the numerical model was based on the cyclic hysteretic response of the frame, while the reliability analyses were based only on the pushover bearing curve obtained by pushing the frame monotonously and unilaterally.

The ability to apply reliability analysis on a completely nonlinear numerical model using FEM and the comparability of MVFOSM, FORM, SORM-FP and SORM-CF methods with MCS is what makes this study innovative. The MVFOSM analysis overestimated the reliability index β_{MVFOSM} by up to 52% compared to the FORM and SORM analyses that have proven comparable to the MCS. The FORM analysis gives insight into the importance of some parameters through the importance vectors without considering correlation (α_i) and considering correlation (γ_i). The SORM analysis with respect to the FORM analysis gave a smaller difference in the reliability index of the individual LSF, and that order was 0.13%, which is negligible. MCS gave accurate exceedance probabilities (p_f) of LSF for the number of simulations greater than $N_{MCS} \geq 10^5$, whereas this required number of simulations is expected to be significantly reduced by using sophisticated sampling techniques such as LHS. Significant parameters for the main LSF that is $g(x) = 1.0\% - u_3$ (horizontal statistics), based on the importance vectors γ_i, are: f_{c1C} peak compression strength of the confined concrete (core), H_{column} total depth of the column cross-section, f_{c1U} peak compression strength of the unconfined concrete (cover), L_{beam} beam length, f_y tensile yield strength of reinforcing steel, and c_{cover} depth of the concrete cover directly affecting the effective cross-sectional depth.

As shown in Table 2, it is interesting that the beam length, L_{beam}, and thus the frame span, was the fourth most significant parameter, showing the importance of imperfections in the frame's geometry, even with the low COV of 1%. In addition, parameters H_{column}, H_{beam} and c_{cover} were the main and leading geometric parameters that control the frame response to the targeted design point. These results indicate the high influence of geometrical imperfections on the reliability of the RC structure. It was also noted that the depth of the concrete cover ranked high in importance, which is not surprising since its COV was 25% due to uncertainty in the construction of such structures. This finding may justify further investigation of the dispersion in the amount of cover in RC structures. The importance ranking of geometrical imperfections relative to other structural parameters indicated a significant influence of uncertain geometrical parameters on reliability assessments, even when the dispersion in the probability distribution is small.

These analyses can be used to minimise the total volume or the total expected cost of the structure subject to structural reliability constraints, to maximise the structural security subject to a given structural cost or simply to achieve a target structural reliability. This approach is particularly suitable for the possible implementation of geometric and material nonlinearities, the implementation of static and dynamic analysis, the simple coverage of aleatory (data-based) variability and epistemic (knowledge-based) uncertainty in terms of material and geometric characteristics, and earthquake time history records in the case of dynamic analysis. It is also possible to optimise significant Design Point-based parameters and define multiple LSFs during the same analysis, which can be based on local or global system responses, following internal forces and displacements or deformations. As a guideline for future researchers, for similar construction systems, it is enough to conduct FORM analysis, where importance vectors are available, while, for greater flexibility and especially parametric studies in earthquake engineering, we prefer the use of MCS. MVFOSM proved to be very proximate and as such incorrect for the nonlinear model response, while the two SORM variants did not contribute much to the accuracy of the reliability index.

References

[1] Huang, C.; El Hami, A.; Radi, B. Overview of Structural Reliability Analysis Methods—Part I: Local Reliability Methods. Incert. Fiabil. Syst. Multiphys. 2017, 17, 1–10.

[2] Scott, M.H.; Fenves, G.L.; McKenna, F.; Filippou, F.C. Software Patterns for Nonlinear Beam-Column Models. J. Struct. Eng. 2008, 134, 562–571.

[3] Yaw, L.L. Co-Rotational Meshfree Formulation for Large Deformation Inelastic Analysis of Two-Dimensional Structural Systems. Ph.D. Thesis, University of California Davis, Davis, CA, USA, 2008.

[4] Denavit, M.D.; Hajjar, J.F. Description of Geometric Nonlinearity for Beam-Column Analysis in OpenSees; Technical report; Northeastern University: Boston, MA, USA, 2013.

[5] Rinchen; Hancock, G.J.; Rasmussen, K.J. Formulation and Implementation of General Thin-Walled Open-Section Beam-Column Elements in OpenSees; Technical Report 961; School of Civil Engineering, The University of Sydney: Sydney, Australia, 2016.

[6] Deng, J.; Gu, D.; Li, X.; Yue, Z.Q. Structural reliability analysis for implicit performance functions using artificial neural network. Struct. Saf. 2005, 27, 25–48.

[7] Haukaas, T.; Scott, M.H. Shape sensitivities in the reliability analysis of nonlinear frame structures. Comput. Struct. 2006, 84, 964–977.

[8] Hess, P.E.; Bruchman, D.; Assakkaf, I.A.; Ayyub, B.M. Uncertainties in Material and Geometric Strength and Load Variables. Nav. Eng. J. 2002, 114, 139–166.

[9] Buonopane, S.G. Strength and Reliability of Steel Frames with Random Properties. J. Struct. Eng. 2008, 134, 337–344.

[10] JCSS. Probabilistic Model Code Part III; Technical report; Technical University of Denmark, Joint Committee on Structural Safety (JCSS): Kongens Lyngby, Denmark, 2000.

[11] Celarec, D.; Ricci, P.; Dolšek, M. The sensitivity of seismic response parameters to the uncertain modelling variables of masonry-infilled reinforced concrete frames. Eng. Struct. 2012, 35, 165–177.

[12] Scott, M.H.; Haukaas, T. Software Framework for Parameter Updating and Finite-Element Response Sensitivity Analysis. J. Comput. Civ. Eng. 2008, 22, 281–291.

[13] Ellingwood, B.; Galambos, T.; MacGregor, J.; Cornell, C.A. Development of a Probability—Based Load Criterion for American National Standard A58; Technical Report; National Bureau of Standards: Washington, DC,USA, 1980.

[14] El-Reedy, M.A. Reinforced Concrete Structural Reliability; CRC Press, Taylor & Francis Group: Boca Raston, FL, USA, 2013; p. 369.

[15] Robertson, L.E.; Naka, T. Tall Building Criteria and Loading; American Society of Civil Engineers: New York, NY, USA, 1980; p. 900.

[16] Mishra, D.K. Compressive Strength Variation of Concrete in a Large Inclined RC Beam by Non-Destructive Testing; Technical report; Associated Cement Companies Ltd.: Mumbai, India, 1990.

[17] Obla, K. Variation in Concrete Strength Due to Cement—Part III of Concrete Quality Series. Improv. Concr. Qual. 2014, 9, 7–16.

[18] Sundararajan, C. Probabilistic Structural Mechanics Handbook: Theory and Industrial Applications; Springer: New York, NY, USA, 1995; p. 745.

[19] Bartlett, F.M.; MacGregor, J.G. Assessment of Concrete Strength in Existing Structures; Technical Report; Department of Civil Engineering, University of Alberta: Edmonton, AB, Canada, 1994.

[20] Haukaas, T.; Kiureghian, A.D. Finite Element Reliability and Sensitivity Methods for Performance—Based Earthquake Engineering; Technical report, Pacific Earthquake PEER Report 2003/14; Engineering Research Centre, PEER, University of California: Berkeley, CA, USA, 2004.

[21] EN 1990-1:2002. Eurocode 0—Basis of Structural Design; European Committee for Standardization, CEN: Brussels, Belgium, 2002.

[22] Porter, K.A.; Beck, J.L.; Shaikhutdinov, R.V. Sensitivity of Building Loss Estimates to Major Uncertain Variables. Earthq. Spectra 2002, 18, 719–743.

[23] Celarec, D.; Dolšek, M. The impact of modelling uncertainties on the seismic performance assessment of reinforced concrete frame buildings. Eng. Struct. 2013, 52, 340–354.

[24] Porter, K. A Beginner's Guide to Fragility, Vulnerability, and Risk; Technical report; University of Colorado Boulder; SPA Risk LLC: Denver, CO, USA, 2019.

[25] Lee, T.H.; Mosalam, K.M. Probabilistic Seismic Evaluation of Reinforced Concrete Structural Components and Systems; Technical report, PEER Report 2006/04; Pacific Earthquake Engineering Research Centre, College of Engineering, PEER, University of California: Berkeley, CA, USA, 2006.

[26] Huang, Y.; Whittaker, A.S.; Luco, N. Performance Assessment of Conventional and Base-Isolated Nuclear Power Plants for Earthquake and Blast Loadings; Technical Report MCEER-08-0019; University of Buffalo: Buffalo, NY, USA, 2008.

NONLINEAR SEISMIC ASSESSMENT OF COUPLED WALLS DESIGNED IN ACCORDANCE WITH EUROCODE 8

Ivan Mrdak [(1)], Marina Rakočević[(2)]

[(1)] *Msc.in civ.eng Civil Engineering Faculty, Podgorica, Montenegro, ivanm@ucg.ac.me*
[(2)] *PhD in civ.eng, Full proffesor, Civil Engineering Faculty, Podgorica, Montenegro, , marinara@ucg.ac.me*

Abstract

Experience from previous earthquakes have shown that wall structural systems experience less damage during earthquake compared to frame systems. Wall systems for functional and architectural reasons frequently have openings (windows, doors, elevators, esc.). Wall systems with regularly distributed openings represent efficient system for resisting earthquake loads. Coupling beams connecting the walls, if designed and detailed properly, increase seismic resistance of the building by distribution of inelastic deformations both vertically and in plan. Eurocode 8 introduced set of rules for design and detailing of coupled walls and coupling beams.

In order to access performance of coupled walls and beams designed in accordance with EC8, linear and nonlinear analysis of 11 story building was performed. Linear elastic modelling was done using software for linear analysis. The walls and coupling beams were designed and detailed in accordance with the provisions of Eurocode 8, part 1. Nonlinear model and assessment of inelastic response was conducted using Perform 3d CSI software for nonlinear analysis. For the modelling of coupled walls, wall section with fibers is used. The confined constitutive relationship is used for concrete edge elements, and unconfined relationship for concrete for the rest part. The reinforcement constitutive model was defined with bi-linear curve. Coupling beams are modelled using frame elements with shear hinge elements. Deformation capacities of elements was defined in accordance with EC8 provisions. Considering that EC8 doesn't provide provisions for deformation capacities of diagonally reinforced coupling beams, deformation capacities for these elements is defined in accordance with the provisions of ASCE 41-06 standard. Static nonlinear analysis is performed in accordance with EC8 provisions and deformation capacities of wall elements and coupling beams checked in accordance with the provisions EC8 part 1 and part 3, where applicable. Characteristic results are presented on the end of paper, with conclusions and recommendations.

Keywords: coupler walls, coupling beams, diagonal reinforcement, pushover analysis, shear hinge

1. Introduction

Coupled walls are shear walls intermittently connected with beams (coupling beams) along the height. Shear walls are designed to allow dissipative inelastic behaviour at the base of the walls. By connecting shear walls with beams, dissipative behaviour can also be enabled in the locations of coupling beams along the height of structure. The proportions of walls and stiffness of coupling beams determine the response of the coupled walls.

The difference in behaviour of shear and coupled walls can be explained by comparing the shear forces in base of the walls (Fig. 1). It can be noted that in addition to bending moments, additional axial forces are registered in coupled walls which are result of shear forces in the coupling beams. For the same external loads the forces at the base of coupled walls must be in equilibrium with the moment in equivalent shear wall as shown in equation below.

$$M = M1 + M2 + T \cdot L \tag{1}$$

The ratio between moment T·L of the coupled wall and moment M for the wall without openings, indicates the impact of the coupling beams on the coupling wall response. The contribution of strong

coupling beams to the seismic response of coupled wall is significant because the above mentioned ratio is larger.
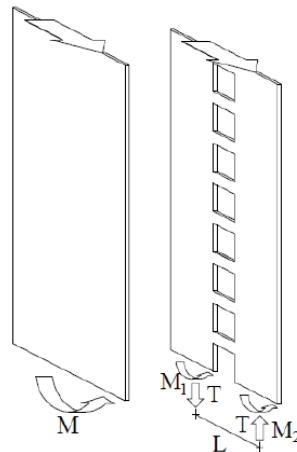
Figure 1. Comparison of internal forces at the base of different type of walls

2. Definition and provisions for coupled walls in accordance with EC8

In accordance with EC8 [1], coupled wall is structural element composed of two or more single walls, connected in a regular pattern by adequately ductile beams ("coupling beams"), able to reduce by at least 25% the sum of the base bending moments of the individual walls if working separately.

EC 8 prescribes capacity design provisions for the design of coupling walls and beams. The coupling beams can be designed with the same provisions as conventional beams when cracking in both directions in unlikely to happen (verified by formula 5.48 in EC8 [1]), and prevailing flexural mode of failure is ensured with the acceptable application rule is:

$$l/h \geq 3 \tag{2}$$

If neither of the conditions are met, the resistance to seismic actions should be provided by reinforcement ensured along both diagonals of the beam. When this type of detailing is applied the inelastic behaviour of beam is expected along the entire length of the beam and whole beam is plastic region for dissipation of energy. Considering that beams is subjected on large shear forces, diagonally reinforced beams behave like a truss, no protection from shear failure is needed. Redistribution of seismic effects between coupling beams of different floors up to 20% is allowed, provided that the seismic axial force at the base of each individual wall (the resultant of the shear forces in the coupling beams) is not affected. Formula for calculating the required amount of reinforcement in diagonal columns according to EC8 [1] is given in following expression:

$$A_{sj} \geq \frac{v_{Ed}}{2 \cdot f_{yd} \cdot \sin\alpha} \tag{3}$$

v_{Ed} is the design shear force in the coupling element ($v_{Ed} = 2 \cdot M_{Ed} / l$);

A_{sj} is the total area of steel bars in each diagonal direction;

α is the angle between the diagonal bars and the axis of the beam.

3. Modelling and building data for linear analysis

Analysis of coupled walls system was performed on the example building with 11 storeys. The layout of building is rectangular with dimensions 30x30 m. Ground floor height is 4.0 m, and for other storeys is 3.2m. The structure has reinforced concrete slab with thickness d = 16 cm. The beams are with dimensions b/d = 30/60 cm, columns have square cross section dimensions b/d = 60/60 cm and coupling beams are with dimensions b/d = 30/100 cm. All shear walls and have the same thickness of d=30cm. Characteristic layout of structure and characteristic frame are given on Fig. 2 and Fig. 3.
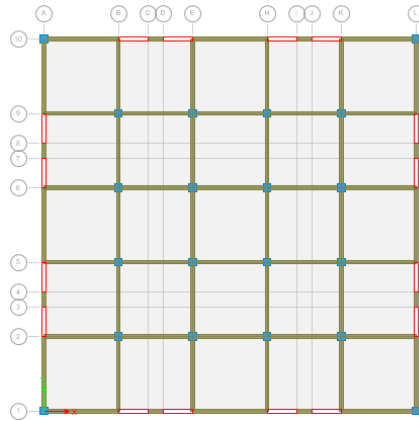
Figure 2. Characteristic layout of structure
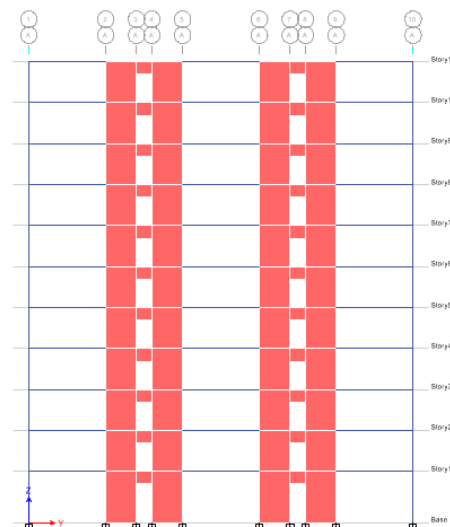
Figure 3. Characteristic cross section in axes A

Linear model was prepared in software for linear analysis. Geometric characteristics of elements and material properties are adopted in accordance with European regulations. Columns and beams are modelled as prismatic 3D beam elements and shear walls as shell elements. Stiffness properties are taken as one-half of the corresponding stiffness of the un-cracked elements including the coupling beams. It is noted that most of modern regulations give particular formulas for stiffness properties of coupling beams considering that the level of stiffness degradation of coupling beams is higher than on other elements [2]. For the adopted return period for the reference earthquake of 475 years, the peak ground acceleration $a_{gR} = 0.36g$. The ground type at the structure location is A. The structure is designed for high ductility class DCM. The structure is classified as coupled walls structure with behaviour factor $q = 3.6$.

Lateral force analysis was performed in accordance with EC8 [1]. Total mass of structure was obtained from software with value 9597,92 ton and total seismic force $Fbx = Fby = 6779,2\ kN$.

2.1 Dimensioning of coupled walls

The dimension of considered coupled wall is given in the Fig. 4.
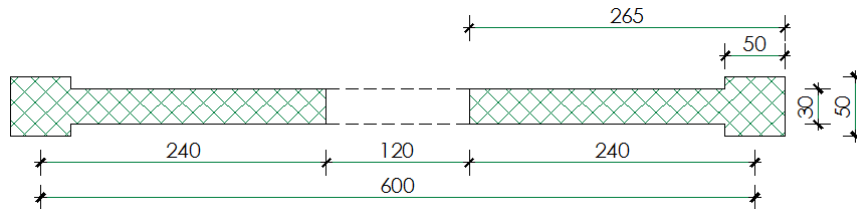
Figure 4. Characteristic cross section of coupled wall

In accordance with EC8 [1], the control was performed if coupling beams reduce by at least 25% the sum of the base bending moments of the individual walls if working separately.

Total base moments obtained with lateral force method for coupled walls and uncoupled walls are given below:

Coupled walls: $Mp = 2 \cdot 2651 = 5302\ \text{kNm}$

Un-coupled walls: $Mp = 2 \cdot 4827 = 9654\ \text{kNm}$

The difference is 45%, which satisfies criterion for the walls to be treated as coupled.

During the action of strong earthquakes in (selected) critical regions, significant non-linear deformations should be allowed to occur (in the case of shear walls, this is zone in the base of the wall. It is possible, even desirable, for the cross-sectional forces-moments and shear force to be redistribute between the walls in order to obtain better utilization and more uniform stressing of the elements. It is also possible to perform redistribution of forces in coupled walls including axial forces that are result of seismic loads. In wall no.1 there is an axial tensile force that reduces the bending capacity of the wall and increases edge longitudinal reinforcement, while in wall 2 there is an axial compressive force with the opposite effect. For this reason, it makes sense to redistribute part of the moment M_1 and entrust it to wall no.2, which will result in equalizing the load capacity and amount of reinforcement in both walls.

It is recommended that the percentage of redistribution does not exceed 30% according to EC8 [1], so that crack openings and damage during the impact of earthquakes of minor and medium intensity remain within acceptable limits. EC8 [1] (5.4.2.4 (2)) provides a procedure for redistribution the effects is walls, with condition that the total required bearing capacity is not reduced. The shear forces are redistributed together with the bending moments, in such a way that it does not have a significant impact on the relationship between bending moments and transverse forces in individual walls. In walls subjected to large fluctuations of axial force, as e.g. in coupled walls, moments and shears should be redistributed from the wall(s) which are under low compression or under net tension, to those which are under high axial compression. Due to this effect, often confinement of whole section of wall has to be performed because of high axial forces in critical regions of the coupled walls.

The adopted reinforcement for the critical region of coupled wall is given on Fig. 5. It is noted that the reinforcement is not symmetric on both sides and this is result of axial forces in the walls.

Figure 5. Reinforcement of coupled wall in the critical region

2.2 Dimensioning of coupling beams

In EC8, there are rules for reinforcing coupling beams as primary structural elements. Coupling beams act as high beams with shear forces as dominant load. According to EC8 [1], coupling beams are usually reinforced with diagonal reinforcement in the form of elements that resemble pillars. Classic reinforcement of connecting beams is done only if the shear forces are small. Experiments have shown that diagonally reinforced coupling beams have significantly better inelastic behaviour than classically reinforced.

Assessment of criterions given in formula 5.48 in EC8 [1] is done and it is noted that coupling beams are supposed to be reinforced with diagonal reinforcement.

Redistribution of seismic effects between coupling beams for different floors up to 20% is performed and the results are shown in the table 1. The difference is exceeded only on the last four floors. This can be ignored because the coupling beams on the last four floors can be classically reinforced. Also, the calculation of seismic forces performed by lateral force method, which doesn't take effect of higher mode effects on seismic response. Considering this redistribution and diagonal reinforcement is justified also on higher floors.

Table 1 – Redistribution of effects in coupling beams

Storey	VED (kN)	Required reinforcement	Adopted bars	Reinforcement cm2	Actual force	Difference (%)
11	144	3,12	4ø12	4,52	208,31	-44%
10	54	1,17	4ø12	4,52	208,31	-285%
9	131	2,84	4ø12	4,52	208,31	-59%
8	291	6,31	4ø12	4,52	208,31	29%
7	439	9,52	4ø18	10,18	469,17	-7%
6	574	12,45	4ø18	10,18	469,17	18%
5	701	15,21	6ø18	15,27	703,75	0%
4	820	17,79	6ø18	15,27	703,75	14%
3	933	20,24	6ø22	22,81	1051,24	-13%
2	1036	22,48	6ø22	22,81	1051,24	-1%
1	1078	23,39	6ø22	22,81	1051,24	3%
	Σ=6201				Σ=6332,8	2,1%

The adopted reinforcement in the coupling beams, for the first three floors, is given on Fig. 6.

Figure 6. Reinforcement of coupling beam on lower storeys

4. Nonlinear analysis

Planar model of coupled wall is created in PERFORM 3d software package [3] (Fig. 7). The floor diaphragms were modelled as rigid with the masses lumped at the corresponding centre of gravity. The mass is modelled in accordance with the results of linear analysis for combination of dead load and 30% of live load.

4.1 Modelling for nonlinear analysis

The modelling of coupled walls is performed by modelling wall section with fibers. The confined constitutive relationship is used for concrete edge elements, and unconfined relationship for concrete for the rest part. The reinforcement constitutive model was defined with bi-linear curve.

The coupling beams are modelled using frame elements with shear hinge.
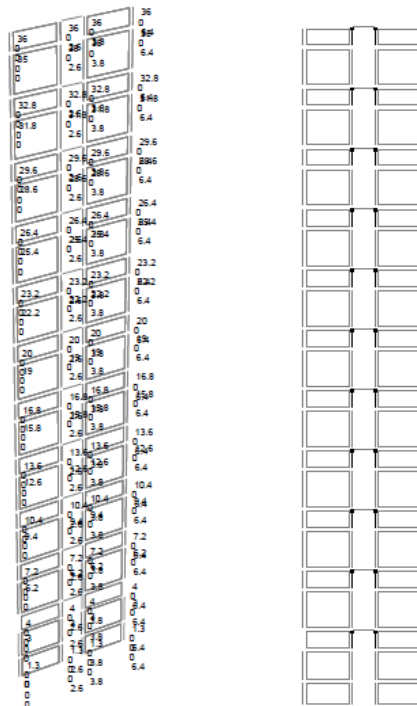
Figure 7. Reinforcement of coupling beam on lower storeys

Main location for dissipation of seismic energy is in the base of the wall. Nonlinear behaviour in the base of the wall is gained by yielding of vertical reinforcement on the edges of the walls. Modelling of wall elements is done with Shear Wall elements consisting of number of fiber elements (reinforcement, confined and unconfined concrete). For analysed coupled wall, 10 characteristic cross sections were defined in accordance with adopted reinforcement from linear analysis. Fiber section of wall is consisted from two components. First component includes concrete (confined and unconfined) and reinforcement of edge elements. Second component includes shear reinforcement. Length of plastic hinge is defined in accordance with the provisions of EC8, part 3 [4]. The rotation is controlled with Rotation Gage elements.

4.2 Modelling of coupling beams

In PERFORM [3], coupling beams for shear walls can be modelled using Frame elements or Wall elements in accordance with the guidelines from CSI [5]. Considering dimensions of coupling beams b/d=30/100 and the length of 120cm, the coupling beams can be considered moderately deep. In accordance with model with frame elements was adopted.
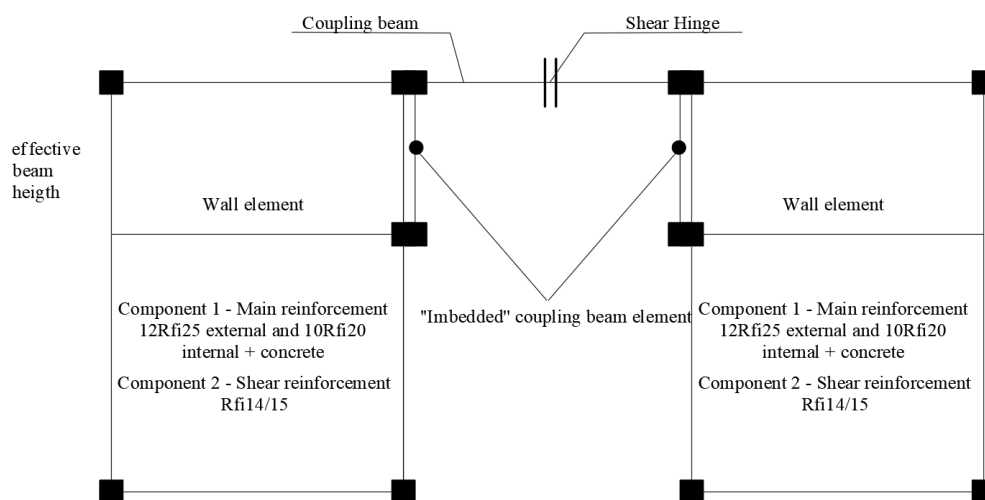
Figure 8. Schematic representation of nonlinear model of coupling wall on first floor

Moderately deep coupling beams were modelled using Frame elements, as shown in Fig. 8. The coupling beam was modelled with shear hinges because the shear behaviour governs and the coupling beams are diagonally reinforced. The coupling beam compound component consists of two elastic beam segments and a rigid-plastic shear hinge. The coupling beam element must be connected to the piers by "imbedded" beam elements. If this is not done, the coupling beam will be effectively pin-connected to the wall. These beams should be stiff enough in bending to provide a stiff connection to the piers and have negligible axial stiffness to avoid stiffening the piers. Bending in the coupling beam is transferred to the piers by these vertical beams (as a tension-compression couple).

4.3 Deformation capacities and limit states

Length of plastic hinge and rotation capacity is calculated in accordance with EC8 part 3 provisions.

The calculated length of plastic hinge is $l_p = 130cm$, and the rotation capacity is 0.09 rad.

In EC8, the deformation capacity of coupling beams is not defined, so the deformation capacities were taken from the American regulations, ASCE 41 [5], for diagonally reinforced coupling beams. For Collapse Prevention, the level of object damage plastic shear rotation (shear dilation) is 0.03 radians. For the beam span of 120cm displacement across the shear hinge is 3.6cm.

Following deformation limit states are defined:

- o Bending rotation in shear walls was checked with rotation gages for the location within plastic hinge and outside – Check was performed in accordance with no-collapse requirement defined in EC8-part 1;
- o Coupling beam shear deformation. This covers the shear hinges in all coupling beam elements in accordance with no-collapse requirement defined in EC8-part 1 ;
- o Tension strain, hinge region, 1%. This covers tension strain in all strain gages in the hinge regions. The D/C ratio for any gage is the tension strain in percent. This is mainly for interest, but also checks that the steel strains are not excessive.
- o Compression strain, hinge, crushing. This covers compression strain in walls hinge regions. This checks that there is no significant concrete crushing in the hinge regions.
- o Tension strain-This covers tension strain in all strain gages above the bottom story. This checks that there is no significant hinging outside the hinge regions;
- o Compression strain, upper stories, crushing. This covers compression strain in all strain gages above the bottom story. This checks that there is no significant concrete crushing outside the hinge regions.

Following strength limit states are defined:

- o Shear force capacity for walls in accordance with the no-collapse requirement defined in EC8-part 1 (2004) corresponding to NC. The shear capacity of walls is checked whether the elements remain in the elastic range regarding shear during the seismic action;

4.3 Nonlinear static (PUSHOVER) analysis

Pushover analysis is a nonlinear static analysis carried out under conditions of constant gravity loads and monotonically increasing horizontal loads in accordance with N2 method [6] from EC8.
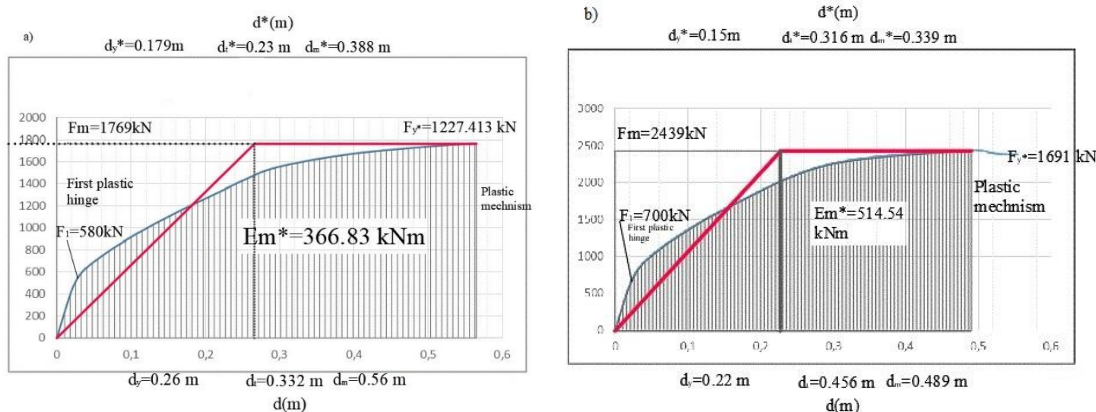
Figure 9. Total base shear force F with a) modal pattern; b) uniform pattern of forces.

According to EC8 at least two vertical distributions of the lateral loads should be applied. After obtaining the results, the most unfavourable results obtained by these two analyses are used in the design. For this case study, vertical distribution was done with "modal" and uniform pattern. The relation between base shear force and the control displacement (the "capacity curve") was determined for values of the control displacement ranging between zero and the value corresponding to 150 % of the target displacement and presented on the Fig. 9a and Fig. 9b.

5. Results

In the Fig. 10a and Fig. 10b presents plastic deformations at the target displacement and displacement when plastic mechanism is formed for the modal load distribution. From the figure it can be seen that preferred mechanism of plastic deformations was formed. At lower intensities of horizontal forces, plastic deformations occurred in the coupling beams, and with the increase of forces, plastic mechanisms are additionally formed at the base of the walls.
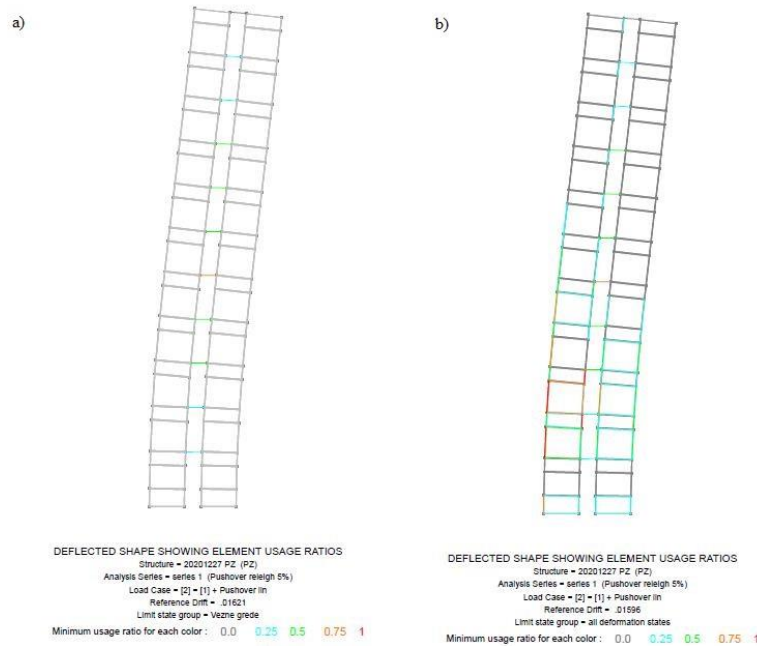
Figure 10. Plastic deformation at the a) target displacement; b) displacement when plastic mechanism is formed for the modal load distribution.

In the Fig. 11a and 11b presents plastic deformations at the target displacement and displacement when plastic mechanism is formed for the uniform load distribution. From the figure it can be seen that plastic deformations occurred simultaneously in the coupling beams and at the base of the walls.

From the Fig. 10 and Fig. 11 it can be seen that with the uniform distribution of forces along the height of the structure, plastic deformations appear earlier at base of the walls. The subject distribution of forces along the building height serves to present the possibility of the appearance of a "weak storey" in the structure. From the analysis of this structure it can be concluded that the deformation capacity of the coupling beam will be exhausted before deformation capacity plastic hinge at the base of wall is exhausted.

With pushover analysis, it is also possible to check the value of the ratio α_u/α_1 given in EC8, which directly affects the value of the behaviour factor q. Analogous to the definition given in EC8, Article 5.2.2.2(4), the values α_u and α_1 multiplier of horizontal seismic design action at formation of global plastic mechanism and at formation of first plastic hinge in the system, respectively. Equation below provides value of ratio.

$$a_u/a_1 = F_m/F_1 = 2432/2000 = 1.216 \qquad (4)$$

It can be concluded that the recommended value corresponds to the recommended value in EC8 for DCM which is 1.2. The value of the ratio for the structure with non-coupled walls is 1.0, so this increase is the ratio is product of additional locations for energy dissipation within the shear plastic hinges in coupling beams.
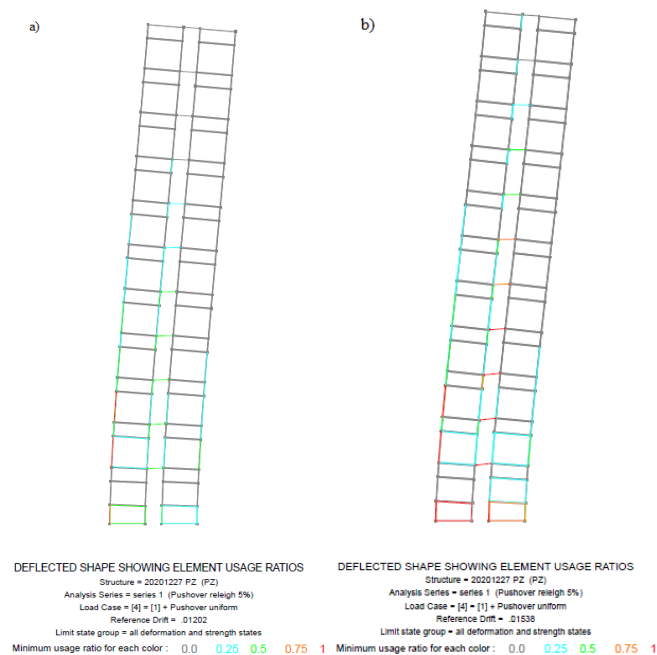
Figure 11. Plastic deformation at the a) target displacement; b) displacement when plastic mechanism is formed for the uniform load distribution.

In accordance with the "no collapse" requirement, load bearing capacity of brittle elements and deformation capacity dissipative zones (e.g. rotation of plastic joints) should be checked. Brittle failure of elements is shear failure of walls. Deformation capacity of plastic hinge rotation at the base of the walls and capacity of shear hinge in coupling beams was checked. Results are given in table 2.

Table 2 – Maximum D/C values for Redistribution of effects in coupling beams

	D/C ration for shear in wall	D/C ration for plastic hinge at the base of the wall	D/C ration for shear hinge in coupling beam
Pushover - uniform pattern	0.65	0.64	0.6
Pushover - modal pattern	0.57	0.62	0.58

6. Conclusions

Following conclusions and recommendations are obtained from results:

- Eurocode 8 recognizes coupled walls as a special type of structural elements that, with proper calculation and reinforcement details, have excellent ductility capacity. Connected walls enable the distribution of inelastic deformations at the base and in height;
- Dimensioning of coupled walls is done according capacity design method EC8, part 1. Redistribution of seismic effects between coupling beams of different floors up to 20% is allowed in order to obtain a more uniform reinforcement on the floors. It is possible, even desirable, for the cross-sectional forces-moments and shear force to be redistribute between the walls in order to obtain better utilization and more uniform stressing of the elements;

  According to EC8, connecting beams are usually reinforced with diagonal reinforcement in the form of elements that resemble columns. Classic reinforcement of connecting beams is applied only if the shear forces are with lower intensity;

563

- It is noted that most of modern regulations give particular formulas for stiffness properties of coupling beams, which is not the case with EC8. Considering that the level of stiffness degradation of coupling beams is higher than on other elements this should be defined in next version of EC8.

- There are limited guidelines in EC8 for nonlinear analysis of coupled walls. There are no information related to selection of model for coupling beams with diagonal reinforcement and connections of coupling beams with coupled walls so the guidelines from ASCE 41 and CSI knowledge base were used. Also, EC8 part 3 guidelines for determination of plastic hinge length are the same as for uncoupled wall which should be investigated. Considering the extensive use of coupled walls the guidelines for nonlinear modelling of coupling beams should be provided in next versions of EC8.

- Results of nonlinear static (pushover) analysis show generally very good behaviour of coupled wall designed in accordance with "no collapse" requirement given in EC8. The brittle elements remained in elastic region of deformation and elements for dissipation have shown that D/C ration is below 1. The critical region at the base of the wall is two storey in accordance with the EC8 and it is noted that for subject structure plastic deformations have been noted also on the third storey so further investigation is necessary in order to check if critical regions should be extended for coupled walls in higher buildings.

- Value of the ratio α_u/α_1 was checked and it can be concluded that the recommended value corresponds to the recommended value in EC8 for DCM which is 1.2. The value of the ratio for the structure with non-coupled walls is 1.0, so this increase is the ratio is product of additional locations for energy dissipation within the shear plastic hinges in coupling beams.

References

[1] Strujic K., Mrdak I., Rakocevic M. (2020): Analysis of different models for structural system with coupled walls according to national regulations and eurocodes, *7th International conference "CIVIL ENGINEERING - SCIENCE AND PRACTICE*, Kolasin, Montenegro, 9 pages.

[2] EN 1998-1, 2004. Eurocode 8: Design of Structures for Earthquake Resistance. 1st ed. Brussels, Belgium.

[3] Perform3D, Nonlinear analysis and design product focused on displacement-based and capacity design of buildings CSI, Computers & Structures, INC. California, USA

[4] EN 1998-3, 2005. Eurocode 8: Design of structures for earthquake resistance Part 3: Assessment and retrofitting of buildings. 1st ed. Brussels, Belgium

[5] ASCE/SEI 41-13, Seismic Evaluation and Retrofit of Existing Buildings, American Society of Civil Engineers, ISBN 978-0-7844-7791-5, Reston, Virginia.

[6] Fajfar P., Gašperšič P. (1996): The n2 method for the seismic damage analysis of rc buildings, *Earthquake Engineering & Structural Dynamics*, doi:10.1002/(SICI)1096-9845(199601)25

SEISMIC PERFORMANCE EVALUATION OF EXISTING RC HIGH-RISE BUILDING IN MONTENEGRO

Nikola Popović [(1)], Jelena Pejović [(2)]

[(1)] *MSc, University of Montenegro – Faculty of Civil Engineering, nikolapopovicjnk@gmail.com*
[(2)] *Assistant professor, University of Montenegro – Faculty of Civil Engineering, jelenapej@ucg.ac.me*

Abstract

Seismic performance evaluation of buildings represents a basis for seismic vulnerability and risk assessment. Considering the importance of seismic risk assessment nowadays, as one of the most actual topics in earthquake engineering, in this paper, a seismic performance evaluation of an existing RC high-rise building with walls on the Montenegrin coast, an area with high seismic risk, is conducted. The aim of the paper is to evaluate the performance of this type of buildings built on the Montenegrin coast and thus contribute to their vulnerability assessment. Two EN 1998-1 fundamental requirements are examined for seismic performance evaluation: non-collapse and damage limitation requirements.

A non-linear 3D building model is defined in the PERFORM 3D software. Modelling is performed by taking into account realistic characteristics of used materials, constructed geometry of structural elements and realistic loads. Non-linear time history analyses are performed using 112 ground motion records, from which 56 are used for evaluation of non-collapse requirement and the other 56 for evaluation of damage limitation requirement. Ground motion records were selected and scaled according to EN 1998-1. Peak horizontal ground acceleration of 0.34g for ground motions with a return period of 475 years for checking non-collapse requirement is adopted, and 0.15g for ground motions with a return period of 95 years for checking damage limitation requirement. Inter-storey drift, wall rotations, dilatations in structural elements and shear capacity are the main parameters that are analysed to obtain conclusions on acceptable seismic performance.

Useful conclusions related to the seismic performance of existing RC high-rise buildings of structural systems with ductile walls built on the Montenegrin coast are pointed out.

Keywords: non-linear time history analyses, non-collapse requirement, damage limitation requirement, seismic performance, damage state, EN 1998-1

1. Introduction

Montenegrin coastline is a seismically active area, with the highest earthquake potential of IX degrees on the Mercalli scale. The rapid development of coastal tourism caused the construction of many multi-storey residential buildings and hotels, which now represent the characteristic urban scenery of that part of the country. A very dense built-up urban environment warns of significant seismic risk and consequences of seismic hazard. For that reason, it is imperative to assess the seismic performance and safety of existing high-rise buildings on the Montenegrin coast, improve vulnerability assessment, and reduce seismic risk.

EN 1998-1 [1] defines two fundamental requirements prescribing acceptable seismic performance of the buildings: non-collapse requirement and damage limitation requirement. Performance assessment and fulfilment of EN 1998-1 [1] basic requirements can be reliably assessed using non-linear time history analysis (NTHA). Applying NTHA gives insight into the intensity of damage and damage locations, which creates the possibility for qualitative and quantitative damage assessment. In the existing literature, there is a large number of papers where NTHA has been used to evaluate building's vulnerability. Luco, Bazzuro and Cornell [2] implemented NTHA on case study building to assess the damage state and remaining lateral capacity. Aghagholizadeh and Massumi [3] examined the behaviour of RC frames using NTHA, where they evaluated damage grade and period elongation. Reuland, Lestuzzi and Smith [4] examined the vulnerability of

constructions after the main shock for buildings with limited data on previous damages. Orlacchio, Baltzopoulos and Iervolino [5] examined the possibility of creating an SDOF model to evaluate residual displacements. Trevlopoulos et al. [6] analysed the damage state after the main shock, where they simulated the impact of several aftershocks after the damage made by the main shock.

In this paper, the existing high-rise RC building (Fig. 1a) built in Budva, part of the Montenegrin coastline with high seismic risk, is selected as a case study. Construction of the building took place in the 2010-2015 period, and the design was done according to EN 1992-1-1 [7] and EN 1998-1 [1] provisions.

Performance assessment of case study building and fulfilment of the basic requirements prescribed in EN 1998-1 [1] was obtained using NTHA on 3D non-linear building model. CSI PERFORM 3D software was used for non-linear modelling. One hundred twelve ground motion time histories were used for NTHA, 56 for the evaluation of non-collapse requirement and the other 56 for the damage limitation requirement. Ground motion time histories have been scaled according to EN 1998-1, to peak horizontal acceleration of 0.34g for earthquakes with a return period of 475 years and 0.15g for earthquakes with a return period of 95 years, appropriate for the Budva's location. Inter-storey drifts, dilatations in structural elements, wall rotations and shear strength have been the main parameters for seismic performance evaluation.

2. Basic information on case-study building

The building consists of 19 storeys, i.e., two underground garage storeys, a basement, ground level, a mezzanine, thirteen residential floors and a roof. MEST EN 1998-1 [8] provides that in the location of Budva, earthquakes with a return period of 475 years have a peak horizontal acceleration of 0.34g, while earthquakes with a return period of 95 years have a peak horizontal acceleration of 0.15g. The height of the building is 55.9m, out of which 13.4m is below ground level. Non-structural walls are made out of bricks and gypsum boards. Plans of the characteristic floor below and above ground level are shown in Fig. 1b and Fig. 1c. The thicknesses of the designed walls are 20cm, 25cm, 30cm and 40cm. Structural elements are founded in the foundation slab, which thickness is 120cm. Frames have negligible stiffness compared to walls, which makes the structural system of the building a system with ductile walls. The ductility class is medium (DCM). All slabs have a thickness of 15cm. Walls ZP1, ZP2, ZP3 and ZP4, are passing all floors consistently from garage walls up to the roof, while ZP5 and ZP6 are passing all floors from the foundation slab up to the roof.

The used concrete class is C30/37, and the rebar reinforcement class is B500B. Concrete class C30/37 has Young's modulus E=3300 $kN/cm2$, with characteristic unconfined strength f_{ck}=3.00 kN/cm^2. The designed yield stress of B500B is f_{yd}=50.00 kN/cm^2 and Young's modulus E=20500 kN/cm^2. Reinforcement yield dilatation is 0.000234, while maximum dilatation is 0.05. Structural elements have been designed on dead, live and seismic loads. Seismic analysis has been conducted using multimodal spectral analysis according to EN 1998-1 [1], where masses of dead loads and 30% live loads with an eccentricity of 5% have been used.

Figure 1. a) existing RC high-rise building; b) floor plan for floors above ground level; c) floor plan for floors below ground level.

3. Non-linear model of existing RC high-rise building

Modelling of the building is conducted in CSI PERFORM 3D [9] software. Modelled structural elements are walls, floor slabs and foundation slab. The foundation slab is modelled with restraints in the base. Slabs are modelled as rigid diaphragms, with accompanying mass of dead loads and 30% of live loads. According to Powell's recommendations [10], walls are modelled as fibre elements, except garage walls, which are modelled as elastic elements. The walls are modelled using two components which are acting in parallel. The first component contains vertical reinforcement fibres and concrete fibre with negligible strength and Young's modulus, in order not to interfere with the behaviour of the concrete fibres from the second component. The second component contains bending reinforcement and concrete fibres. Concrete of the boundary elements is modelled with confined concrete characteristics, while web concrete is modelled with unconfined concrete characteristics. The area and coordinates of each reinforcement or concrete fibre are separately defined. Shear behaviour is considered elastic, where the shear D/C ratio is examined. Out of plane behaviour of the walls is modelled as elastic without considering P-Δ effects. Columns and beams are not modelled since frames stiffness compared to walls are negligible. Fibres of both reinforcement and concrete are modelled with bilinear stress-strain relationships.

In order to evaluate the non-collapse requirement and damage limitation requirement, a few limit states have been defined and analysed: the strength limit state, the limit state of inter-storey drifts and limit

567

states for deformations. The strength limit state is analysed for shear loads. Shear strength has been assigned as the elastic strength of concrete. Inter-storey drifts have been analysed for both planar directions. Capacity for inter-storey drifts has been assigned according to EN 1998-1 [1] from the damage limitation requirement for the non-structural brittle elements. Deformation limit states have been examined in two ways. The first way is the evaluation of the dilatations in the fibres of boundary elements on tension and compression. The examination is conducted using axial strain gauge elements in the software. These elements measure dilatations on node spans where they have been assigned. It has been examined if there was concrete cracking in the wall, i.e., was there any yielding of the reinforcement. The second way of evaluation is the examination of the rotations in the walls. On facade walls, plastic hinges have been modelled on the ground floor and above garage walls, while on the inside walls, plastic hinges have been modelled on the base and ground levels. The plastic hinge's height has been assigned according to recommendations of FEMA 356 [11], i.e., depending on the planar length, they have been assigned as one-half of the length. In cases when the plastic hinge length has been greater than the floor height, then the floor height has been assigned as plastic hinge length. Rotations have been checked using rotation gauge elements from software. Rotation capacities have been assigned according to FEMA 356 [11].

4. Analysis of non-collapse requirement

EN 1998-1 [1] prescribes that „Construction has to be designed and constructed, so that resists to seismic loads without local or global collapse, i.e., to hold its capacity, construction integrity and remaining lateral capacity after seismic events ". In order to define precise criteria based on which would be evaluated acceptable seismic behaviour, damage locations and damage states have been analysed. Following this provision, D/C of rotations, dilatations and shear strength have been evaluated. For non-collapse requirement, 56 NTHA analyses have been performed, 7 for each planar direction, and soil types A, B, C and D. 7 ground motions by the group for each direction and soil type have been chosen because it is the minimum number of analyses prescribed in EN 1998-1 [1] for using mean values. REXEL v 3.5 software [12] has been used for scaling ground motions to the referent peak horizontal acceleration of 0.34g. In Figs. 2-9, the D/C ratios of all deformations are shown. White represents the D/C ratio from 0 to 40%, blue from 40% to 60%, green from 60% to 80%, yellow from 80% to 100%, and red is the state when the ratio goes beyond 100%. D/C ratios have been examined through the following parameters: $R_M/R_{C,M}$, which represents the D/C ratio for rotations, $D_{CO}/D_{C,CO}$, which represents the D/C ratio for compression dilatations, $D_T/D_{C,T}$ which represents the D/C ratio for tension dilatations and $V_S/V_{C,S}$ which represent shear capacity D/C ratio. In Table 1, results for deformations D/C ratios are presented. Maximum wall rotations are defined for LS damage state according to FEMA 356 [11], in the amount of 0.006 radiations.
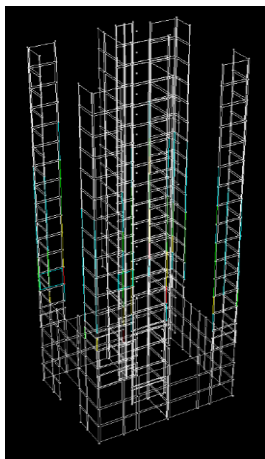
Figure 2. D/C deformation ratio for soil
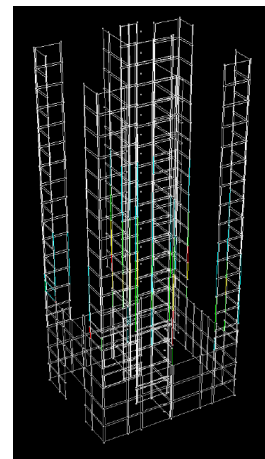
Figure 3. D/C deformation ratio for soil

type A in the X direction.

type A in the Y direction.
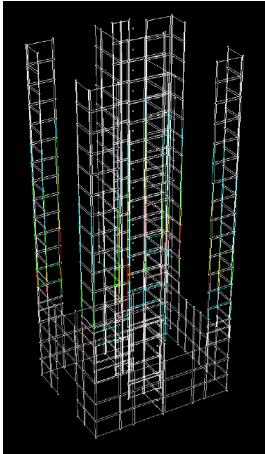
Figure 4. D/C deformation ratio on soil type B in the X direction.
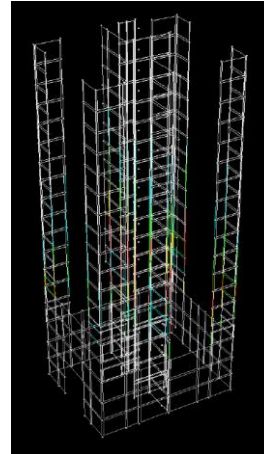
Figure 5. D/C deformation ratio on soil type B in the Y direction.

Figure 6. D/C deformation ratio on soil type C in the X direction.
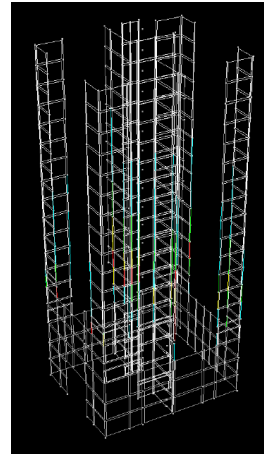
Figure 7. D/C deformation ratio on soil type C in the Y direction.

Figure 8. D/C deformation ratio on soil type D in X direction.
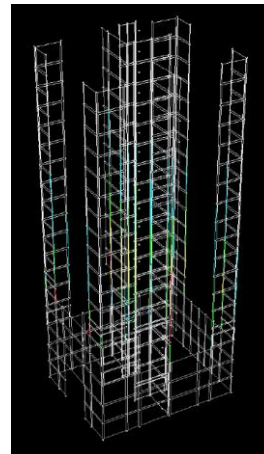
Figure 9. D/C deformation ratio on soil type D in the Y direction.

Table 1 – Demand capacity ratios of deformations for non-collapse requirement analysis

D/C ratios for soil type A in the X direction				D/C ratios for soil type A in the Y direction			
Ground motion	$D_T/D_{C,T}$	$D_{CO}/D_{C,CO}$	$R_M/R_{C,M}$	Ground motion	$D_T/D_{C,T}$	$D_{CO}/D_{C,CO}$	$R_M/R_{C,M}$
Montenegro	1,56	0,39	0,50	South Iceland 2	0,94	0,25	0,28
Vrancea	0,48	0,17	0,16	Campano Lucano	1,57	0,32	0,43
South Iceland	1,89	0,43	0,54	Montenegro	1,5	0,31	0,41
Tabas	0,55	0,16	0,16	Vrancea	1,89	0,33	0,51
South Iceland 2	1,58	0,43	0,47	South Iceland	1,07	0,25	0,28
South Iceland 1	2,87	0,59	0,85	Tabas	0,76	0,23	0,23
Campano Lucano	0,89	0,28	0,30	South Iceland 1	2,88	0,39	0,77
D/C ratios for soil type B in X direction				D/C ratios for soil type B in Y direction			
Ground motion	$D_T/D_{C,T}$	$D_{CO}/D_{C,CO}$	$R_M/R_{C,M}$	Ground motion	$D_T/D_{C,T}$	$D_{CO}/D_{C,CO}$	$R_M/R_{C,M}$
Tabas	1,89	0,46	0,56	Montenegro	1,4	0,3	0,38
Montenegro	0,77	0,2	0,24	Campano Lucano	0,88	0,19	0,24
Campano Lucano	1,08	0,31	0,30	Biga	3,4	0,46	0,91
Biga	5,06	1,39	1,49	Racha aftershock	0,92	0,26	0,31
Racha aftershock	0,79	0,27	0,27	Strofades aftershock	0,79	0,2	0,25
Strofades aftershock	1,04	0,31	0,35	Aigion	5,35	0,9	1,30
Aigion	4,82	1,16	1,39	Tabas	6,22	1,02	1,50
D/C ratios for soil type C in X direction				D/C ratios for soil type C in Y direction			
Ground motion	$D_T/D_{C,T}$	$D_{CO}/D_{C,CO}$	$R_M/R_{C,M}$	Ground motion	$D_T/D_{C,T}$	$D_{CO}/D_{C,CO}$	$R_M/R_{C,M}$
Azores	3,45	0,68	1,04	Kefallinia aftershock	0,7	0,19	0,20
Kefallinia aftershock	0,83	0,26	0,25	Umbria Marche 1	0,86	0,22	0,26
Umbria Marche 1	1,04	0,31	0,37	Umbria Marche 2	0,45	0,12	0,13
Umbria Marche 2	1,09	0,28	0,33	Dinar	3,24	0,54	0,86
Dinar	1,74	0,35	0,50	Izmit	4,31	0,74	1,04
Izmit	3,34	0,88	1,04	Strofades aftershock	1,13	0,31	0,39
Strofades aftershock	0,79	0,25	0,26	Azores	0,91	0,22	0,25
D/C ratios for soil type D in X direction				D/C ratios for soil type D in Y direction			
Ground motion	$D_T/D_{C,T}$	$D_{CO}/D_{C,CO}$	$R_M/R_{C,M}$	Ground motion	$D_T/D_{C,T}$	$D_{CO}/D_{C,CO}$	$R_M/R_{C,M}$
Umbria Marche	1,31	0,35	0,42	Umbria Marche	1,38	0,31	0,38
Izmit aftershock 1 x	0,92	0,28	0,31	Izmit aftershock 1 x	1,29	0,23	0,35
Izmit aftershock 1 y	0,86	0,26	0,24	Izmit aftershock 1 y	1,36	0,26	0,37
Izmit aftershock 2	4,11	0,8	1,24	Izmit aftershock 2	1,83	0,37	0,49
Izmit aftershock 3	1,05	0,28	0,35	Izmit aftershock 3	1,11	0,28	0,31
Duzce aftershock	1,48	0,4	0,43	Duzce aftershock	2,28	0,37	0,61
Duzce aftershock	1,15	0,32	0,39	Duzce aftershock	1,76	0,31	0,47

From D/C rotation ratios can be seen that on 9 from 56 ground motions, the D/C ratio has exceeded value 1, i.e. that the probability of overcoming LS state is 9/56=16.7%. However, considering mean values for each group then can be concluded that obtained rotation haven't exceeded the LS damage state. Considering that rotation capacities have been assigned according to FEMA 356 [11], in Table 2 are shown rotation capacities prescribed with EN 1998-3 [13]. Moment and shear forces for calculating rotation values have been taken from a linear model made in the software CSI ETABS [14], based on seismic forces for referent horizontal peak acceleration 0.34g and elastic response spectrum. Rotation capacities have been calculated for the most vulnerable cross sections from Figs. 2-9. θ_{SD} represents rotation capacity for significant damage limit state, which is the counterpart for LS damage state rotation according to FEMA 356 [11].

Table 2 – Rotation capacity for limit state significant damage

Rotation capacity	Z2x	Z3x	Z4x	Z5x	Z6x	Z1y	Z2y	Z3y	Z4y	Z5y	Z6y
θ_{SD}	0,0072	0,0079	0,0072	0,0088	0,0109	0,009	0,0076	0,0065	0,0067	0,0058	0,0082

From Table 2, rotations obtained according to EN 1998-3 [13] are somewhat greater than those obtained by FEMA 356 [11], which means that D/C ratios for rotations are acceptable by EN 1998-3 [13].

Compression dilatations have exceeded limit values for certain load cases, but according to mean values for each group, compression dilatations are below limit values.

For most load cases, mean tension dilatations have exceeded the yield point. That kind of behaviour is desirable and expectable because it represents the ductile non-linear behaviour of structural walls. The desirable non-linear behaviour of the structural system with ductile walls, which is the case here, is when energy dissipation occurs in the plastic hinges zone above the foundations. From Figs. 2-9 can be observed that reinforcement yielding mainly occurred on higher floors.

Mean values for shear D/C ratios are presented in Table 3 for each wall and planar direction. It can be seen that all D/C ratios are below 1, except on wall 4 where it is 1.00. Since shear capacity is defined in software as concrete shear capacity and that horizontal reinforcement also takes a certain percentage of shear loads, the non-collapse requirement is also fulfilled in this wall.

Table 3 – Demand capacity ratios of shear forces for non-collapse analysis

Shear mean value	Wall 1	Wall 2	Wall 3	Wall 4	Wall 5	Wall 6	Ground motion	Wall 1	Wall 2	Wall 3	Wall 4	Wall 5	Wall 6
D/C ratios for soil type A in X direction							D/C ratios for soil type A in Y direction						
V_{mean}	0,32	0,71	0,82	0,90	0,85	0,47	V_{mean}	0,39	0,4	0,48	0,42	0,61	0,55
D/C ratios for soil type B in X direction							D/C ratios for soil type B in Y direction						
V_{mean}	0,38	0,8	0,95	1	0,93	0,56	V_{mean}	0,42	0,43	0,62	0,56	0,8	0,25
D/C ratios for soil type C in X direction							D/C ratios for soil type C in Y direction						
V_{mean}	0,34	0,76	0,88	0,93	0,91	0,52	V_{mean}	0,37	0,34	0,48	0,44	0,67	0,54
D/C ratios for soil type D in X direction							D/C ratios for soil type D in Y direction						
V_{mean}	0,39	0,73	0,83	0,90	0,88	0,49	V_{mean}	0,23	0,24	0,31	0,33	0,30	0,22

5. Analysis of damage limitation requirement

For damage limitation requirement, EN 1998-1 [1] prescribes that "construction shall be designed and constructed to withstand a seismic action having the larger probability of occurrence than the design seismic action, without the occurrence of damage and the associated limitations of use, the costs of which would be disproportionately high in comparison with the costs of the structure itself". The return period of considered earthquakes to examine damage limitation requirement is 95 years. Therefore, D/C ratios have been examined through the following ratios: $R_M/R_{C,M}$, which represents the D/C ratio for rotations, $D_{CO}/D_{C,CO}$, which represents the D/C ratio for compression dilatations $D_T/D_{C,T}$ which represents the D/C ratio for tension dilatations and $D_R/D_{C,R}$ which represents D/C ratio for inters-storey drifts (Table 4, Figs. 10-17).

Capacity rotations for the walls have been taken for the state IO according to FEMA 356 [11], in the amount of 0.003 rad. Damage limitation requirement evaluation for dilatations implies that no reinforcement yielding should be present in the wall, nor the concrete cracking.
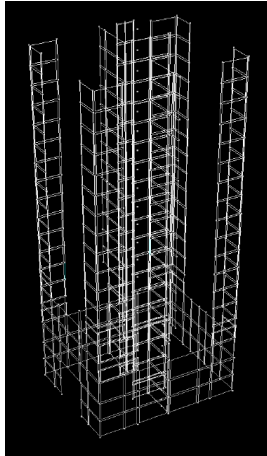
Figure 10. D/C deformation ratio on soil type A in X direction.
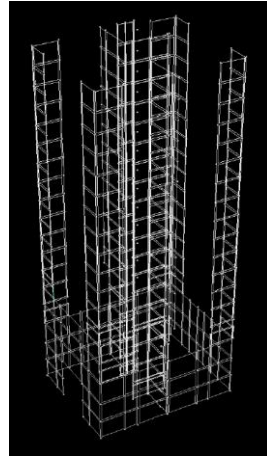
Figure 11. D/C deformation ratio on soil type A in Y direction.
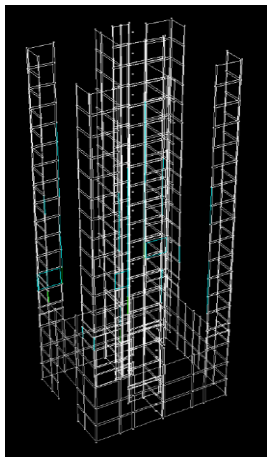
Figure 12. D/C deformation ratio on soil type B in X direction.
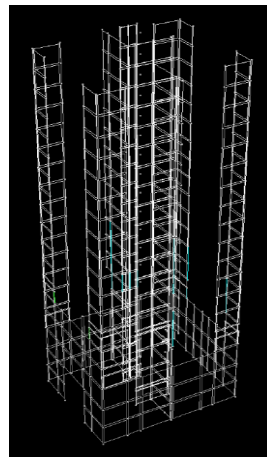
Figure 13. D/C deformation ratio on soil type B in Y direction.
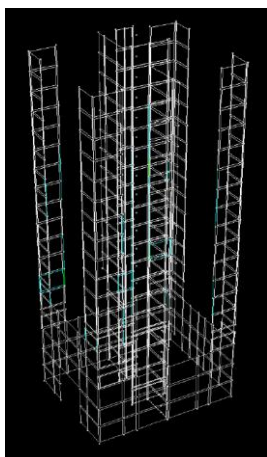
Figure 14. D/C deformation ratio on soil type C in X direction.
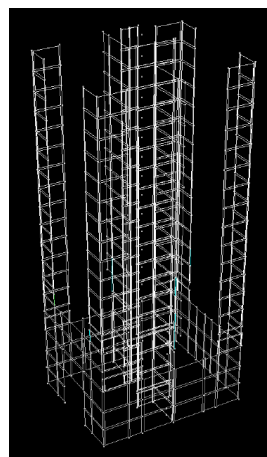
Figure 15. D/C deformation ratio on soil type C in Y direction.
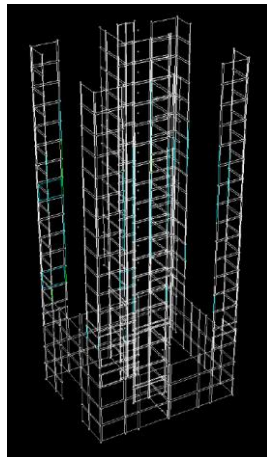
Figure 16. D/C deformation ratio on soil

type D in X direction.
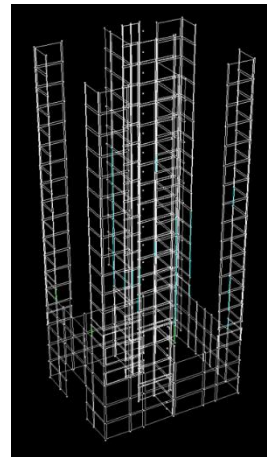
Figure 17. D/C deformation ratio on soil

type D in Y direction.

The limit state for inter-storey drift has been adopted in value 0.05 from design criteria for damage limitation when non-structural elements on the building are brittle.

Table 4 – Demand capacity ratios of deformations for damage limitation requirement analysis

	D/C ratios on soil type A in X direction				D/C ratios on soil type A in Y direction			
Ground motion	$D_T/D_{C,T}$	$D_{CO}/D_{C,CO}$	$R_M/R_{C,M}$	$D_R/D_{C,R}$	$D_T/D_{C,T}$	$D_{CO}/D_{C,CO}$	$R_M/R_{C,M}$	$D_R/D_{C,R}$
Campano Lucano 1	0,54	0,17	0,32	0,55	0,66	0,14	0,36	0,75
Campano Lucano 2	0,48	0,17	0,32	0,41	0,59	0,16	0,33	0,65
Izmit	0,46	0,16	0,34	0,50	0,59	0,14	0,33	0,50
South Iceland 1	0,74	0,23	0,5	0,95	0,48	0,09	0,26	0,45
Mt. Vatnafjoll	0,39	0,13	0,29	0,4	0,46	0,12	0,25	0,60
Kalamata	0,42	0,13	0,25	0,35	0,47	0,10	0,26	0,75
South Iceland 2	0,49	0,18	0,35	0,55	0,55	0,14	0,30	0,65
	D/C ratios on soil type B in X direction				D/C ratios on soil type B in Y direction			
Ground motion	$D_T/D_{C,T}$	$D_{CO}/D_{C,CO}$	$R_M/R_{C,M}$	$D_R/D_{C,R}$	$D_T/D_{C,T}$	$D_{CO}/D_{C,CO}$	$R_M/R_{C,M}$	$D_R/D_{C,R}$
Friuli	0,49	0,16	0,29	0,55	0,48	0,14	0,31	0,8
Montenegro	0,41	0,14	0,30	0,45	0,41	0,12	0,25	0,75
Campano Lucano	0,56	0,16	0,40	0,60	0,50	0,11	0,27	0,70
Izmir	0,57	0,18	0,38	0,65	0,43	0,11	0,24	0,70
Biga	0,36	0,11	0,25	0,3	1,13	0,25	0,62	0,65
Aigion 1	1,44	0,37	0,85	1,25	1,43	0,30	0,78	1,05
Aigion 2	2,04	0,50	1,19	2,05	0,68	0,20	0,45	1,55
	D/C ratios on soil type C in X direction				D/C ratios on soil type C in Y direction			
Ground motion	$D_T/D_{C,T}$	$D_{CO}/D_{C,CO}$	$R_M/R_{C,M}$	$D_R/D_{C,R}$	$D_T/D_{C,T}$	$D_{CO}/D_{C,CO}$	$R_M/R_{C,M}$	$D_R/D_{C,R}$
Friuli aftershock	0,45	0,16	0,31	0,55	0,40	0,11	0,21	0,55
Azores	0,76	0,21	0,52	0,85	0,44	0,11	0,24	0,50
Kefallinia aftershock	0,73	0,22	0,42	0,55	0,45	0,10	0,25	0,90
Umbria Marche	0,39	0,14	0,23	0,35	0,45	0,10	0,25	1,30

Dinar	0,62	0,18	0,41	0,60	0,89	0,23	0,51	0,55
Izmit	1,49	0,42	0,94	1,85	1,57	0,27	0,85	0,60
Griva	0,78	0,24	0,54	1,00	0,59	0,16	0,33	0,55
	D/C ratios on soil type D in X direction				D/C ratios on soil type D in Y direction			
Ground motion	$D_T/D_{C,T}$	$D_{co}/D_{c,co}$	$R_M/R_{C,M}$	$D_R/D_{C,R}$	$D_T/D_{C,T}$	$D_{co}/D_{c,co}$	$R_M/R_{C,M}$	$D_R/D_{C,R}$
Izmit aftershock 1	0,49	0,15	0,30	0,50	0,43	0,11	0,25	0,90
Izmit aftershock 2	0,51	0,17	0,30	0,65	0,47	0,13	0,28	0,70
Izmit aftershock 3	0,55	0,15	0,30	0,50	0,44	0,14	0,30	1,40
Izmit aftershock 4	1,37	0,40	0,83	1,50	1,65	0,33	0,90	1,00
Izmit aftershock 5	1,11	0,28	0,2	1,00	0,96	0,18	0,48	0,60
Izmit aftershock 6	0,61	0,17	0,35	0,50	0,54	0,14	0,30	1,25
Duzce aftershock	0,87	0,25	0,52	1,00	0,94	0,20	0,51	0,70

The mean values of inter-storey D/C ratios are below 1.00 for each group, which means that the damage limitation requirement is fulfilled from this point of view.

Considering the tension dilatations D/C ratios, it can be seen that for each load case, those values are below 1, except on 5 load cases. That means that the probability of reinforcement yielding is 5/56=8.9%. On the other hand, considering the mean values for each group, yielding did not occur.

Limit values haven't exceeded state IO. In Figs. 10-17, several cross-section rotations are between 40%-60% (cross-sections marked with blue colour). For those cross-sections, rotation capacities have been calculated according to EN 1998-3 [13], as in chapter 4, for damage state damage limitation θ_y. Results are presented in Table 5. Based on the ratio $\theta_y/\theta(IO)$ and the exact value of rotations, rotation capacity according to EN 1998-3 [13] is not exceeded.

Table 5 - Rotation D/C ratios according to EN 1998-3 [14]

Cross-section	$\theta(IO)$	θ_y	$\theta_y/\theta(IO)$
Z2x	0,003	0,0017	56,7%
Z4x	0,003	0,0017	56,7%
Z6x	0,003	0,0021	70%

6. Conclusion

Based on the conducted analysis, it can be concluded following:

- The case study building has shown satisfactory performance for seismic loads with a return period of 475 years. Mean values of rotations did not exceed capacities for significant damage limit state. In addition, compression dilations did not exceed the capacity of concrete deformations, and shear capacity was not exceeded. Therefore, the non-collapse requirement is fulfilled.
- Yielding of the reinforcement in the higher floors occurred for seismic loads with a return period of 475 years, which did not represent desirable building performance.
- The damage limitation requirement is fulfilled since construction damage did not occur for seismic loads with a return period of 95 years.

References

[1] EN 1998-1 (2005): Eurocode 8: Design of structures for earthquake resistance – Part 1: General rules, seismic actions and rules for buildings, European Committee for Standardization.

[2] Luco, N., Bazzuro, P. and Cornell, A. (2004): Dynamic versus static computation of the residual capacity of a mainshock-damaged building to withstand an aftershock, *13th World Conference on Earthquake Engineering*, Vancouver, B.C., Canada, August 1-6, Paper No. 2405.

[3] Aghagholizadeh, M. and Massumi, A. (2016): *A new method to assess damage to RCMRFs from period elongation and Park-Ang damage index using IDA*. Int J Adv Struct Eng **8**, 243-252, doi: https://doi.org/10.1007/s40091-016-0127-8

[4] Reuland, Y., Lestuzzi, P. and Smith I.F.C. (2019): *A model-based data-interpretation framework for post-earthquake building assessment with scarce measurement data*. Soil Dynamics and Earthquake Engineering **116**, 253-263, doi: https://doi.org/10.1016/j.soildyn.2018.10.008

[5] Orlacchio, M., Baltzopoulos, G. and Iervolino, I. (2019): Constant-ductility residual displacement ratios, *7th ECCOMAS Thematic Conference on Computational Methods in Structural Dynamics and Earthquake Engineering*, Crete, Greece, 24-26 June.

[6] Trevlopoulos, K., Gueguen, P., Helmstetter, A. and Cotton F. (2020): *Earthquake risk in reinforce concrete buildings during aftershock sequences based on period elongation and operational earthquake forecasting*. Structural Safety **84**, 2020, 101922, doi: https://doi.org/10.1016/j.strusafe.2020.101922

[7] EN 1992-1-1 (2004): Eurocode 2: Design of concrete structures – Part 1-1: General rules and rules for buildings, European Committee for Standardization.

[8] MEST EN 1998-1 (2005): Eurocode 8: Design of structures for earthquake resistance – Part 1: General rules, seismic actions and rules for buildings – National annex, Institute for standardization of Montenegro.

[9] CSI (2005-2018): PERFORM 3D Nonlinear analysis and performance assessment of 3D structures, Computers and Structures Inc, Berkeley.

[10] CSI (2007): PERFORM 3D detailed example of a tall shear wall building by Dr. Graham H. Powell, Nonlinear modelling, analysis and performance assessment for earthquake loads, Computers and Structures Inc, Berkeley.

[11] FEMA (2000): Prestandard and commentary for the seismic rehabilitation of buildings, Federal Emergency Management Agency, Washington D.C.

[12] Iervolino, I., Galasso, C. and Cosenza, E. (2010): *REXEL: computer aided record selection for code-based seismic structural analysis*. Bulletin of earthquake engineering, **8**, 339-362, doi: https://doi.org/10.1007/s10518-009-9146-1

[13] EN 1998-3 (2005): Eurocode 8: Design of structures for earthquake resistance – Part 3: Assessment and retrofitting of buildings, European Committee for Standardization.

[14] CSI (2019): ETABS 19 Building analysis and design, Computers and Structures Inc, Berkeley.

SELECTION AND REPLACEMENT OF BRIDGE EXPANSION JOINTS IN SEISMIC PRONE AREAS

Klara Krišto [(1)], Mladen Srbić [(2)], Ana Mandić Ivanković [(3)]

[(1)] *Junior Civil Engineer, Krilić Inženjering d.o.o., klarakristo9@gmail.com*
[(2)] *PhD, Faculty of Civil Engineering, Department of Structural Engineering, mladen.srbic@grad.unizg.hr*
[(3)] *Prof. PhD, Faculty of Civil Engineering, Department of Structural Engineering, ana.mandic.ivankovic@grad.unizg.hr*

Abstract

Expansion joints on bridges are devices that enable relative displacements of the superstructure spans from the effects of temperature, traffic load and long-term effects. They are placed at the ends of the bridge, where they bridge the space between the superstructure and the abutment, while on very long bridges they are installed at all places where the superstructure breaks between individual sections of the bridge, in order to enable safe and unhindered traffic. They are the "weak points" of the bridge, as their "leakage" can seriously threaten the function of the bridge. In the seismic prone areas, encompassing seismic action in their design and selection is inevitable.

This paper will overview the types of expansion joints, design approach in their selection for new bridges and problems that may arise during their replacement in the rehabilitation process of existing bridges. Movements due to traffic load, seismic movements, movements due to long term effects of the deck (creep and shrinkage) and thermal movements will be considered. Based on practical examples, design for either no damage due to seismic action or partially damaged expansion joints for seismic action, will be contemplated.

Keywords: bridge, expansion joint, bearing, movements, earthquake, creep, shrinkage, temperature, traffic

1. Requirements, types and causes of defects of expansion joints

Expansion joints on bridges must sustain the loads and accommodate movements without causing failure to itself or other section of the structure. They must assure water does not enter the structure and accumulate in the joint, and they must be compatible with the waterproofing system of the roadway. They should allow smooth traffic flow while remaining safe for all categories of road users. Noise generated when crossing the joint should be kept to a minimum, especially if the bridge is located in a populated area. They should be easily accessible for inspection and maintenance [1] and regularly inspected and maintained to ensure that they continue to operate in accordance with all the requirements.

Guideline for European technical approval of expansion joints for road bridges specifies numerous requirements on expansion joint such are mechanical resistance, resistance to fatigue, seismic behaviour, movement capacity, cleanability, resistance to wear, watertightness, safety in case of fire, release of dangerous substances, safety in use, protection against noise, energy economy and heat retention, aspects of durability, serviceability and identification of products [2]. In this paper movement capacity and seismic behaviour will be overviewed and discussed.

According to typical movement ranges, expansion joints may be categorised as (i) joints for minimum movements of up to 20 mm (±10); (ii) joints for small movements of up to 40 mm (±20); (iii) devices for medium movements of up to 150 mm (±75); (iv) devices for large movements of up to 300 mm (±150) and (v) devices for very large movements over 300 mm (≥ ±150) [1, 3]. The new approach [2, 4] specifies families of expansion joints according to their principle of operating as described in columns left and middle of the Table 1. The right column of the Table 1 specifies equivalent joint types.

Table 1 – Families and types of expansion joints according to [2 & 4]

Joint family	Short description	Joint type
Buried expansion joints	This expansion joint is formed in place with components such as waterproofing membranes or an elastomeric pad to distribute the deformations over a wider width and support the pavement that runs continuously across the deck joint gap. The components of the expansion joint are located under the pavement.	Buried joint under continuous surfacing
Flexible plug expansion joints	An in-situ poured joint consisting of a band of specially formulated flexible material (binder and aggregate) that also forms the pavement and is held in place over the joint gap of the pavement by thin metal plates or other suitable components. The joint material is flush with the pavement surface.	Asphaltic plug joint
Nosing expansion joints	The gap between the edges prepared with concrete, resin mortar or elastomer is filled by a flexible profile, which is not traffic load carrying.	Nosing joint with poured sealant / Nosing with preformed compression seal
Mat expansion joints	The expansion joint uses the elastic properties of a prefabricated elastomeric strip or pad to allow for the expected movements of the structure. The strip is attached to the structure with bolts. The subcomponent of the joint is flush with the running surface.	Reinforced Elastomeric
Cantilever expansion joints	The expansion joint consists of cantilevered symmetrical and asymmetrical subcomponents (such as comb or sawtooth panels) anchored to one side of the deck joint gap and interpenetrating to bridge the deck joint gap. The subcomponents are flush with the running surface.	Cantilever comb or tooth joint
Supported expansion joints	The expansion joint consists of one subcomponent flushed with the running surface, secured on one side by hinges and on the other (by a second element) by sliding supports, spanning the deck joint gap. The expected movement of the structure is enabled by sliding on the unattached side of the hinged substructure member, i.e., on the support element anchored to the substructure.	Not covered
Modular expansion joints	The expansion joint consists of a sequence of watertight subcomponents (in the direction of travel) consisting of motion-controlled metal girders supported by movable substructures that bridge the structural gap (i.e., cross girders, cantilevers, and current collectors). The metal girders are flush with the pavement surface.	Elastomeric in metal runners

Example of joint for small movements of up to ±20 mm is asphaltic plug expansion joint made of flexible bituminous material (thorma joint, Figure 1a). Nosing expansion joints permit a movement range of up to ±6 mm with poured sealant and up to ±20 mm with a performed compression seal (Figure 1b). Example of device for medium movements (although there are various sizes giving movement range of up to ±165 mm) is reinforced elastomeric expansion joints (Figure 1c). Movement range of elastomeric in metal runners expansion joints is up to ±40 mm for single element joint consists of a profiled elastomeric seal fitted between two metal runners, one fixed to each side of the deck joint gap. Multi element modular joints (Figure 1d) can accommodate much larger movements of up to ±480 mm. Cantilever comb or tooth joints (Figure 1e) have a movement range of up to ±300 mm which puts them, together with multi element modular joints, into to category of devices for very large movements.

If a regular expansion joint closes more than the design allows during an earthquake, severe damage to the joint and the bridge could result. This could be avoided by using fusible links (fusible box, Figure 1f), which act as a predominant predetermined breaking point and allow for a controlled failure.

Depending on the design of the fusible link, the link moves either vertically upward or horizontally in a specific, defined space. During seismic opening movements, the extended support bars protect the expansion joint from falling into the construction gap. After the earthquake, a quick and easy repair of the predetermined breaking points within the fuse box and its roadway surface is easily and quickly possible [5].
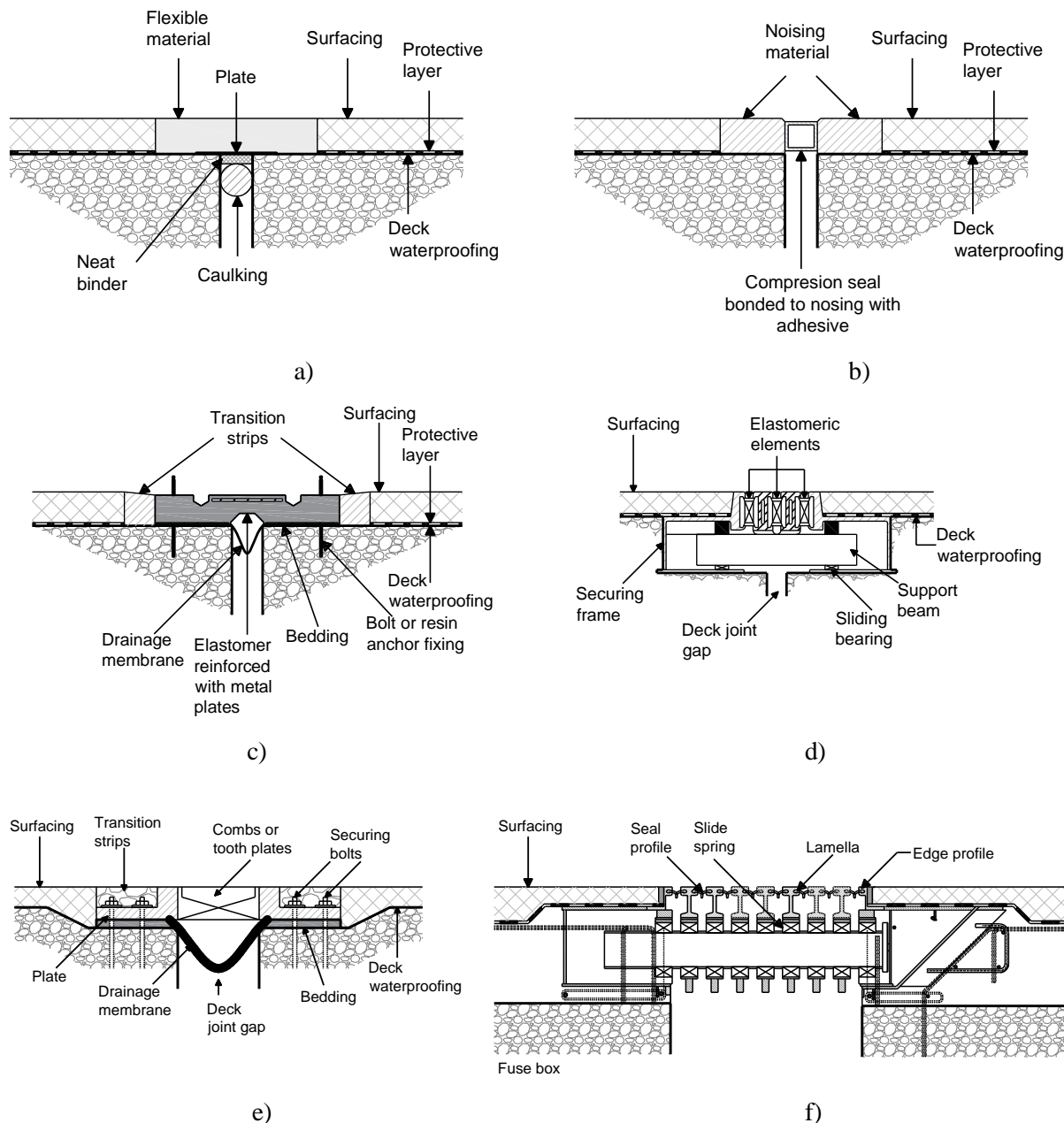
Figure 1. Examples of expansion joints: a) bituminous, b) nosing, c) reinforced elastomeric d) elastomeric in metal runners, e) cantilever comb or tooth expansion joint, f) fuse box; reproduced based on [2 & 5]

During the use of the bridge, the expansion joints are exposed to various defects. Defects can be the result of eight main causes systematised in [6]: (i) *inadequate design*, i.e., in relation to the movements of the structure; (ii) *defects in the technical specifications*, such as insufficient adaptation to the service conditions or lack of connection between the joint and the rigid element; (iii) *defects in the production*, i.e., inadequate anti-corrosion treatment or incorrect geometry; (iv) *errors during installation*, such is for example incorrect definition of the neutral point of the joint or inadequate anchoring; (v) *lack of*

proper maintenance resulting in accumulation of debris or moisture from vegetation on the deck and water leaks; (vi) *changes from the intended conditions of use*, such as a deck with a different long-term behaviour than predicted, settlement of abutments or foundations, a higher traffic load than expected; (vii) *environmental effects* such as higher or lower temperatures (which may already occur during device installation), freeze-thaw cycles; and finally (viii) *random impacts* due to natural events or human influences.

The studies summarised in the above-mentioned study [6] conclude that a large part of the costs in bridge management (up to 20% in some cases) is related to the repair and replacement of expansion joints. In addition, rehabilitation measures that result in disruption, slowing, or detour of traffic flow can cause inconvenience to users and significant indirect costs.

2. Design approach in seismic prone areas

In bridge design, thus in displacement calculation, it is necessary to assimilate temporary procedures of Eurocodes. For the total design displacement under seismic conditions in accordance with EN 1998-2, an adequate structural gap is required to protect critical or major structural elements from damage. The total value of the design displacement under seismic conditions d_{Ed} [7] is determined as follows:

$$d_{Ed} = d_E + d_G + \psi_2 d_T$$

where:

d_E is the design seismic displacement; d_G is the displacement due to the permanent and quasi-permanent actions measured over the long term (e.g. post-tensioning, shrinkage and creep for concrete decks); d_T is the displacement due to thermal movements; ψ_2 is the reduction factor for the quasi-permanent value of thermal action to be taken as 0,5.

In order to receive expansion joints without damages due to seismic action, they need to be select to undertake full design seismic displacement as described above. But this is reasonable only when seismic displacements are not very high. Namely, expansion joints are non-critical structural elements expected to be damaged due to other actions besides seismic action and changed few times in the design work life of bridge. Therefore, Eurocode gives correction of full seismic displacement with the recommended value of factor 0,4 d_E which means that local damage of the expansion joint will be admissible and damages under frequent earthquakes are still avoided. But damages due to seismic action should be predictable, without the need for immediate repair and with no influence to the emergency traffic safety.

Design requirements for expansion joints under seismic conditions consider the importance of the bridge and the expansion joint. A declaration of seismic performance is not required for buried and flexible plug expansion joints, while two main approaches with several subdivisions are provided for all other families of joints.

Movement capacity design is to be applied for bridges with small seismic displacements (i.e. $d_{Ed} \leq 200$ mm) allowing expansion joints with movement capacity (possibility to allow the displacement of the parts of the main structure) under serviceability conditions even during the earthquake for the total displacement d_{Ed}. When the design includes provisions limiting movements of the bridge, thus preventing the joint from being affected by seismic effects, no combination for seismic design situations exists (approach A1). The seismic design combination for approach A2 is selected for seismic actions with a high probability of occurrence or with smaller values for A_{Ed} [2].

For larger seismic displacements, $d_{Ed} > 200$ mm, former design according becomes uneconomic, so *restricted movement and load capacity design* is to be applied, accepting controlled damage for severe earthquakes (with a low probability of occurrence). Still, the damage under frequent earthquakes is to be avoided by providing structural gaps for long term creep and shrinkage effects plus appropriate fractions of the design seismic displacement (40%) and thermal movements (50%) [2].

Table 2 – Design requirements during and after design earthquake according to [2]

Design approa	Requirements posed at the expansion joints	Actions to be considered during design earthquake	Load bearing capacity and serviceability after design earthquake	Expected repair work
A	*Movement capacity design*			
A1	Movement capacity exists under serviceability condition even during the earthquake.	The expansion joint is not affected by seismic actions. Fundamental combination is used as per EN 1990.	The expansion joint is assumed to be resistant to any kind of effects after the design earthquake. Load bearing capacity and serviceability are as before the earthquake.	No repair work has to be applied.
A2	The seismic movement capacity of the joint exists for total displacement d_{Ed}	The resistance to static actions during the earthquake shall be checked for the frequent combination of actions: $C_{ULS-SEISMIC} = G_k \text{ "+" } F_{ik} \text{ "+" } \psi_{1k} [Q_{1k} \text{ "+" } Q_{lk1} \text{ "+" } Q_{tk1}] \text{ "+" } A_{Ed}$ where $\psi_{1k} = 0{,}4$ is a combination factor for frequent value of a variable action; $A_{Ed} = d_E \text{ "+" } d_G \text{ "+" } \psi_3 d_{Tk}$ is design seismic situation (imposed displacements for the derivation of internal forces); $\psi_3 = 0{,}5$ is the reduction factor for the quasi-permanent value of thermal action		
B	*Restricted movement and load capacity design*			
B1	No damage with reduced load bearing capacity and increased gap width during earthquake.	The resistance of load carrying structural elements shall be checked for the seismic design situation: $C_{ULS-SEISMIC} = G_k \text{ "+" } F_{ik} \text{ "+" } \psi_{2k} [Q_{1k} \text{ "+" } Q_{lk1} \text{ "+" } Q_{tk1}] \text{ "+" } A_{Ed}$ where ψ_{2k} is a combination factor for quasi-permanent value of a variable action: $\psi_{2k} = \psi_3 = 0{,}3$ for B1 $\psi_{2k} = \psi_3 = 0{,}1$ for B2 $\psi_{2k} = \psi_3 = 0{,}1$ for B3 $\psi_{2k} = \psi_3 = 0{,}0$ for B4 After earthquake → $\psi_{2k} = \psi_3 = 0{,}2$ for B3 $\psi_{2k} = \psi_3 = 0{,}2$ for B4 on the joint $\psi_{2k} = \psi_3 = 0{,}0$ for B4 on the fuses G_k = self weight; F_{ik} = internal force – expansion joints may show internal forces from imposed displacements, rotations and/or prestress caused by e.g. compression or elongation, and/or relative movements; Q_{1k} = vertical traffic in lane 1, axle 300 kN; Q_{1k1} horizontal traffic direction, axle 120kN; Q_{tk1} horizontal perpendicular to traffic direction, axle 60kN	Load bearing capacity and serviceability are as before the earthquake.	No repair work has to be applied.
B2	Minor damages to secondary elements are allowed. Load carrying elements are allowed to have a reduced load bearing capacity and increased gap width during earthquake.		Load bearing capacity as before the earthquake.	Secondary elements shall be replaceable or repairable after the earthquake.
B3	Minor damage to structural elements or fusible devices due to a combination of reduced traffic load bearing capacity and increased gap width during earthquake.		The expansion joint is assumed to be resistant to frequent traffic loads according to EN 1990 after the earthquake and to fulfil all the ULS and SLS requirements after small repairs.	Small repairs on structural elements and fusible devices.
B4	Major damage to fusible devices and minor damage on the joint. Fusible devices should avoid or minimize damage on the structural elements of the bridge reducing at the mean time the required size of the expansion joint.		No remaining load bearing capacity and increased gap width. In the case of emergency traffic, the expansion joint shall comply with approach B3 load and the width of possible gaps shall be as a max 300 mm.	The possibility of permanent repair shall be described.

3. Performance of expansion joints of the existing bridge

The bridge we consider below, with 17 spans of 24.5 m, an end span of 18.92 m and a total length of 435.42 m, was built half a century ago and was the subject of the student master's thesis [1]. The bridge deck is 3x3.5=10.50 m wide with 2.55 m wide corridors on the west side and 0.90 m on the east side. The total width of the bridge is 13.95 m. The span is a grill type girder concrete structure consisting of transversely prestressed reinforced concrete deck slab, post-tensioned main longitudinal T-section girders and transverse reinforced concrete beams. The grill type girders are connected to each other in continuous systems over three spans. In total, there are six continuous superstructure sections on the bridge, separated by expansion joints.

During examinations of the structure and laboratory tests of samples of the structure, numerous damages were found, especially to the protective layer of the reinforcement. In 2007, a project was launched to rehabilitate the bridge. First, the entire upper structure and then the lower structure of the bridge were repaired. A major part of the rehabilitation involved the restoration of the protective reinforcement layer. Using hydro demolition, the crumbling surface concrete was removed, the corroded reinforcement was cleaned, repair mortar was applied, and all concrete surfaces were coated with a protective layer of polymer cement coating, which prevented carbonation of the concrete and corrosion of the reinforcement.

The most demanding measure was the rehabilitation of the bridge deck. This involved the process of deepening the concrete by 2 cm, and then installing new reinforcement and concreting. Altogether 4 cm of new concrete was poured, 2 cm of concrete below the installed reinforcement, and 2 cm above it. The entire renovation process of the slab was carried out using the counterweight method, the most demanding renovation method in terms of time and technology.

After the completion of the repair work on the bridge deck, the installation of waterproofing and asphalt, expansion joints were installed. It should be noted that in the original rehabilitation project of 2007 reinforced elastomeric expansion joint with a total movement of 50 mm were foreseen (Figure 2a). The connection with the reinforced concrete structure was to be made with bolts, and the connection of the corridor with the pavement was to be welded.

However, in practice, these devices did not prove to be of high quality because they allowed water to penetrate the structure, so during the rehabilitation in 2012, it was decided to install flexible seamless expansion joints (asphaltic plug joints) with a total movement of 40 mm, made of highly polymerized asphalt, reinforced with anchor elements (Figure 2b). The advantage over other devices of the same type is the simplicity and speed of installation. And what was considered very important for rehabilitation, this device can be installed halfway, that is, one lane can always remain free for traffic. Selected expansion joint consists of polymer-modified bitumen, structural reinforcement with a neoprene insert that allows the operation of the device (the length of the element is 1.5 m) and anchors Φ13 mm, a base coat (primer), bitumen tape for reinforcement, bitumen adhesive tape and foam rubber sealant insert.

The width of such an expansion joint is 400 mm and the depth is 80 mm with a possible displacement of 40 mm (+-20 mm), and it was considered suitable for new concrete bridges, viaducts and overpasses with a span of up to 40 metres. For old concrete bridges, where the rheology of the concrete is complete, the work of the span structure is 0.4 mm/1m (three times less than for new bridges). For this bridge, the work is 70 m x 0.4 mm/m = 24 mm, and it was assumed that a device that allows displacement of 40 mm is suitable.

But this solution turned out to be extremely bad after implementation. Because the contractor was late in procuring the equipment from Japan, the equipment was installed in December at a temperature of about 0ºC, in high humidity, and on a wet concrete slab, and subsequently the expansion joint leaked in almost all seven places where it was installed. This is because elastic expansion devices, which are made of bituminous mixes, require higher temperatures to bond aggregates and binders during installation.

Asphalt mixture is installed only when weather conditions are favourable. Paving asphalt in the rain and on a wet surface is not allowed. During the production of the wearing layer, the temperature of the substrate and the air must be higher than 10ºC, and during the installation of the bonding and bearing layer higher than +5ºC. At higher temperatures, asphalt mixtures are prone to plastic deformation, including the appearance of rutting, which can cause considerable counter-impact forces at low temperatures, but also limit their use in areas with a moderate climate. In practice, asphalt expansion joints often fail at the joints to the pavement. This can lead to the formation of cracks and leakage of liquids, which is due to the extremely high hardness of the material at low temperatures.

The design of the bridge in accordance with modern European guidelines for the assessment of suitable expansion joints was carried out as a student master's thesis [1]. Design included bridge self-weight, additional dead load, traffic load, temperature effects, wind and seismic action and their relevant combinations. A grill model of the bridge consisting of beam elements in longitudinal and transverse direction, and spring elements for the bearings (elastomeric bearings without steel restraints which freely deform horizontally in all directions depending on the values of the horizontal and vertical reaction and enter the model via the defined stiffness of the springs) and KF connections for points with the same boundary conditions (the node at the upper end of the support has the same displacements and rotations as the node at the lower end of the support).

Effects of temperature are considered through: uniform temperature load: maximum temperature difference of the bridge (highest temperature – construction temperature $44-15=29°C$); uniform temperature load: minimum temperature difference of the bridge (construction temperature – minimum temperature $15-(-15)=30°C$); uniform temperature load for the selection of expansion joints and bearings (with an addition of $\pm$ 20°C which increased the maximum/minimum temperature difference of the bridge $30 + 20 = 50°C$ and $29 + 20 = 49°C$); non-uniform temperature load along the height of the concrete superstructure: the upper edge is warmer (negative value); non-uniform temperature load along the height of the concrete superstructure: lower edge warmer (positive value); with the simultaneous effect of uniform and non-uniform temperature components through eight combinations.

Seismic loading is determined by the response spectra for ground acceleration for the return period $T = 475$ years $a_g = 0.23$ g, elastic non-ductile behaviour of columns without the possibility of developing plastic joints with the behaviour factor $q = 1.0$, structure importance factor 1.0 and soil category C. Multimodal analysis, combining eigenfrequencies and design spectra for the three directions of earthquake action, was applied.

The displacements for the selection of expansion joints were determined in a combination of 40% seismic and 50% temperature action according to the EC8 guidelines, which allow damage to the expansion devices under severe earthquakes, while damage under frequent values can still be avoided, as explained in the previous chapter of this paper. Full temperature load displacements and full wind load displacements were calculated separately as well.

Based on the calculations, the largest horizontal displacements of about 56 mm in the longitudinal direction of the bridge were determined for the seismic combination. Based on the determined displacements, the type of expansion joint was proposed that would allow displacements of at least $\pm$ 60 mm in the longitudinal direction. Large transverse displacements, exceeding 40 mm at the first pier dilatations from both sides, should be covered with the appropriate expansion joint capability in the transverse direction (see proposed example in Figure 2c) or transverse restraint in the form of earthquake-resistant blocks would be required. Of course, it is necessary to assess and confirm the installation possibility of the selected device.

Bearings are selected for the relevant combination of vertical reaction and displacement at a particular bearing location. On the abutments and columns under the expansion devices, except for the central column, bearings are selected for the largest displacements of 75 mm, along the central spans of the entire bridge for spans between 50 and 65 mm, and in the edge spans for the smallest displacements of up to 25 mm.

This example shows how important and demanding the choice of expansion joints is in bridge rehabilitation. It should be based on knowledge of modern load requirements for bridge structures and of the expansion joint devices themselves and the current knowledge of how they work and perform during the use of bridge. But, replacing the expansion joint on the existing bridge also depends on moving capacity existing bridge poses and the space allowable for installation of the expansion joint.

Apart from the extremely important correct installation under appropriate climatic conditions, which was not suitable during the installation of the transition device foreseen in the rehabilitation project of the above bridge, the calculation in accordance with the modern earthquake design guidelines showed that these devices would not provide sufficient movement capacity during earthquake of frequent occurrence without damages and especially during serious earthquakes of low probability of occurrence.

a)

b)

c)

d)
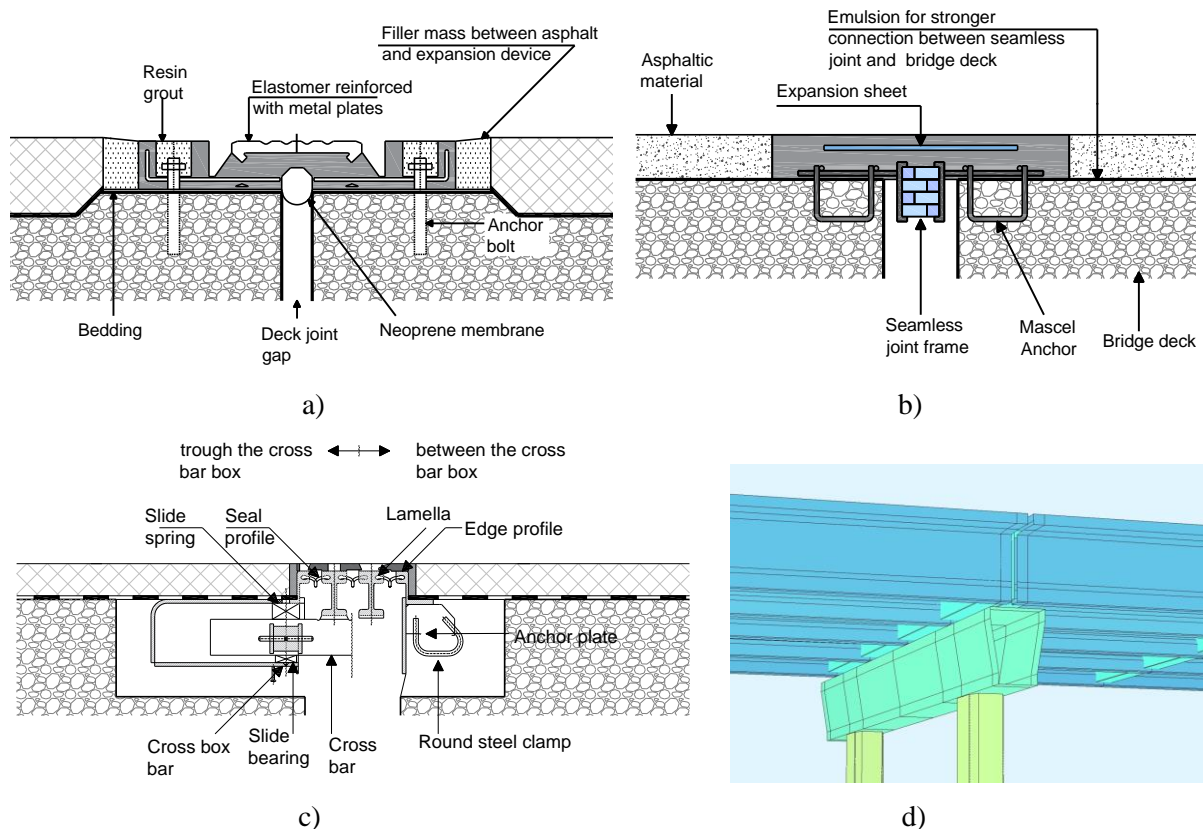
Figure 2. Expansion joints for existing bridge: a) reinforced elastomeric expansion joint 50 mm selected by the original rehabilitation project, b) asphaltic plug joints 40 mm installed during actual rehabilitation process and c) elastomeric in metal runners girder grid expansion joint proposed by the valid contemporary seismic design of the bridge in the master's thesis, figures reproduced based on [8, 9 & 10]; d) section of the bridge model in the area of transversal beam at the supports

4. Expansion joint selection in the design of the new bridges

The following section considers the selection of expansion devices in the construction of two semi-precast prestressed concrete grillage type bridges. Both bridges span four spans 26+31+31+26 m, one of which is designed as a system of simply supported girders and the other as a continuous superstructure.

Models of the bridge consisting of beam elements in longitudinal and transverse directions and spring elements with a defined stiffness for the bearings and KF fixed connections for points with the same boundary conditions.
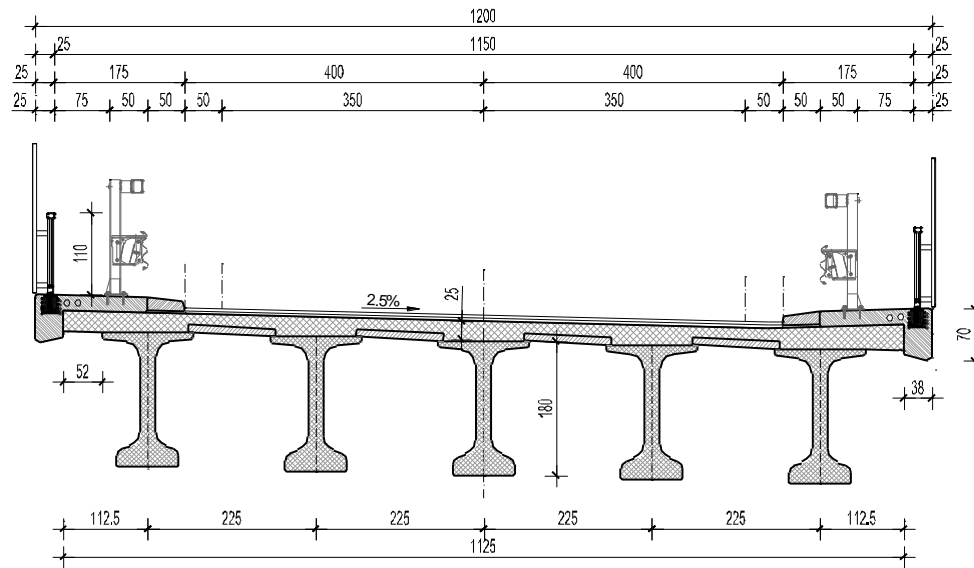
Figure 3. Cross section of case study bridges

The difference between the model of the bridge consisting of a series of girders and the bridge with a continuous superstructure is visible in the Figure 4. The simply supported girders have two cross beams above the piers, one for connecting left span main girders and one for the right span. The continuous superstructure consists of a common cross member at each pier. The first variant is easier to build, while the second is a more durable and robust construction. Expansion joints in both cases are provided above the abutments.
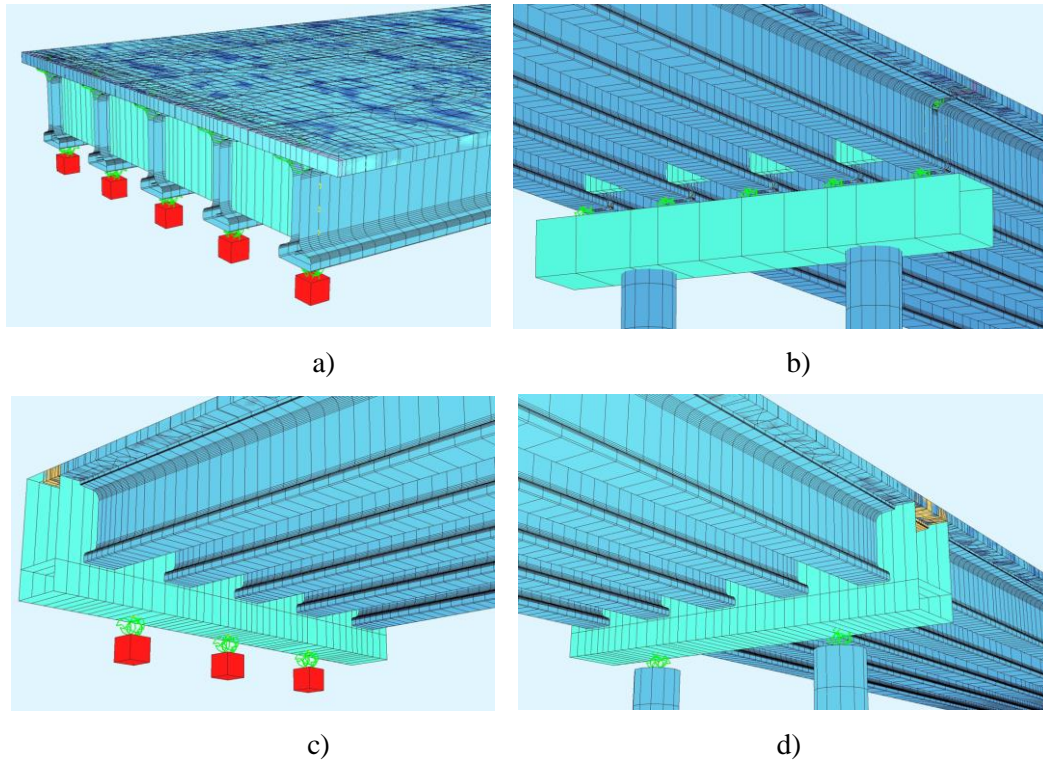
Figure 4. Extract from the bridge models in the software: a) set of simply supported girders supported at the abutment, b) set of simply supported girders supported at the pier, c) continuous superstructures supported at the abutment, d) continuous superstructure supported at the pier

The design according to the Eurocodes includes the self-weight of the bridge, additional dead loads, long-term effects (creep and shrinkage), traffic loads, temperature effects, earthquake effects and their relevant combinations.

Creep and shrinkage were observed at all stages of bridge construction. The calculation of displacement due to these long-term effects was performed for a relative humidity of 80% and a temperature of 20 °C, with the end of the bridge's service life set at 50 years.

Traffic load is represented with the Model 1 from EN 1991-2 as a vertical load comprising both continuous and concentrated load and adequate braking and accelerating forces as a horizontal traffic load.

Uniform temperature load is considered as maximum temperature difference of the bridge (highest temperature – construction temperature $42-10=32°C$) and minimum temperature difference of the bridge (construction temperature – minimum temperature $10-(-18)=28°C$). Uniform temperature load for the selection of expansion joints and bearings increases the maximum/minimum temperature difference of the bridge by ± 20°C: $32 + 20 = 52°C$ and $28 + 20 = 48°C$).

For the multimodal analysis, combining eigenfrequencies and design spectra for the three directions of earthquake action, seismic loading is determined by the response spectra for ground acceleration for the return period $T= 475$ years $a_g = 0.241$ g, elastic non-ductile behaviour of columns with the behaviour factor $q = 1.0$, structure importance factor 1.0 and soil category B.

For the calculation of the vertical, horizontal longitudinal and horizontal transverse reactions as well as the displacements in longitudinal and transverse direction, all relevant combinations of the above loads are considered. The displacements for the selection of expansion joints were determined in a combination of 40% seismic, 50% temperature action and 100 % long-term effects of creep and shrinkage according to the EC8 guidelines, which allow damage to the expansion joints under severe earthquakes, while damage under frequent values can still be avoided, as explained in the previous chapter of this paper.

The table 3 gives an overview of the results in terms of reactions and displacements for the selection of bearings and expansion joints.

For bridge composed of simply supported girders in each span, five reinforced elastomeric bearings are provided at each abutment (Figure 4a) and altogether ten bearings at the pier, five for the left and five for the right part of the superstructure (Figure 4b). In the longitudinal direction, displacements due to seismic loading are equal, within acceptable limits for these types of bearings and it could be considered that the bridge will "float" during an earthquake. In transversal direction displacements are of course the smallest at the abutments and the largest at the middle pier due to the expected vibration in the transverse direction of the bridge. For the selected bearings layout, expansion joints are to be selected to provide both longitudinal and transversal displacements during an earthquake.

Note that the horizontal stiffness of the bearings for the model is calculated based on the shear modulus, the area of the bearing surface, and the total thickness of the elastomer layers, while the vertical stiffness is calculated based on the elastic modulus, the area of the bearing surface, and the total thickness of the elastomer layers for selected bearing types.

In the case of the continuous bridge, where only two bearings movable in all directions are used at the abutment and on the piers (Figure 4d), the large response due to seismic loading in transversal direction (2135 kN) at the abutment required an additional middle bearing designed as a seismic transverse bearing (see Figure 4c). This bearing limited the movement in the transverse direction, so that the selection of the expansion joints was based only on the longitudinal movements.

This example shows that the final choice of expansion joint is highly dependent on the intended behaviour of the bridge system, which includes the arrangement of the selected bearings.

Table 3 – Selection of bearings and expansion joints in design of new bridges

Simply supported girders						
position	U1 EX. J	U1 B	S2 B	S3 B	S4 B	U4 B	U4 EX. J
V_{max}		2295	3010	2750	3010	2295	
$H_{x,max}$		405	358	333	358	405	
$H_{y,max}$		235	335	430	335	235	
$d_{x,max}$	+ 63, -25	72	72	72	72	72	+ 63, -25
$d_{y,max}$	19	46	66	85	66	46	19
possible selection	D160* with 2 sealing elements	5x EB 400x500 (3000/74)	10x EB 450x600 (4210/74)	10x EB 450x600 (4210/85)	10x EB 450x600 (4210/74)	5x EB 400x500 (3000/74)	D160* with 2 sealing elements

*D160 stands for expansion joint for movement component rectangular to the gap axis of 130 mm according to [10].

**EB 400x500 (3000/74) stands for elastomeric bearing for the maximum load of 3000 kN and displacement of 74 mm according to [11]

Continuous Superstructure Bridge						
position	U1 EX. J	U1 B	S2 B	S3 B	S4 B	U4 B	U4 EX. J
V_{max}		4315	8460	8605	8460	4315	
$H_{x,max}$		778	813	780	813	778	
$H_{y,max}$		(2135)	485	800	485	(2135)	
$d_{x,max}$	+ 87, -59	145	145	145	145	145	± 87
$d_{y,max}$	0	0	90	140	90	0	0
possible selection	D240* with 3 sealing elements	2x V2S5800 (74/158) ** + transverse restraint seismic bearing	2x V2S8500 (63/180)	2x V2S9500 (63/180)	2x V2S8500 (63/180)	2x V2S5800 (74/158) + transverse restraint seismic bearing	D240 with 3 sealing elements

*D240 stands for expansion joint for movement component rectangular to the gap axis of 195 mm according to [10] as the first lower D160 allows only 130 mm.

**V2S5800 (74/158) stands for seismic isolator/elastomeric bearing for the maximum load of 5800 kN, service displacement of 74 mm and seismic displacement of 158 mm according to [12]

5. Conclusion

After carrying out the overall design of the bridge in accordance with Eurocode standards, including seismic design in earthquake prone areas and calculation of displacement for relevant combinations of actions, the final choice of expansion joint should be the optimal solution in terms of performance, the cost of the equipment itself and its maintenance, additionally using an appropriate choice of design approach for the expansion joints.

For the bridges analysed in this paper and the selected expansion joints, this is the A1 approach for the transverse direction, where the movements of the bridge should be limited with anti-seismic blocks or seismic restraint devices, and the A2 approach for the longitudinal or transversal direction, which allows the seismic movement capacity of the joint for the total displacement d_{Ed} calculated for earthquakes with frequent values, that is, for seismic actions with a high probability of occurrence.

If the design of longer bridges under severe earthquakes will result in larger seismic displacements (i.e. $d_{Ed} > 200mm$, see example bridge in [13]), then restricted movement and load capacity design B1-B4 approaches of expansion joints could be investigated. These approaches could also be beneficial for old bridges designed without seismic activity, when installing a new expansion joint for adequate seismic movement according to current seismic demands will not be possible.

References

[1] Krišto, K. (2022): Izvanredna sanacija mosta. *Diplomski rad.* Građevinski fakultet Sveučilište u Zagrebu

[2] EOTA (2013): *Guideline for European technical approval of expansion joints for road bridges*, ETAG 032, Brussels

[3] Radić, J., Mandić, A., Puž, G. (2005.) Konstruiranje mostova. Hrvatska sveučilišna naklada, Građevinski fakultet – Sveučilište u Zagrebu, Jadring. Zagreb.

[4] Highway Structures and Bridges (2019): *Bridge expansion joints.* CD 357. Highways England.

[5] Maurer SE (2020): Maurer Expansion Joints State of the art of sustainable solutions, https://www.maurer.eu/fileadmin/mediapool/01_products/Dehnfugen/Broschueren_TechnischeInfo/MAU_Expansion_Joints_GB_Online.pdf (assessed December 2nd 2022)

[6] Marques Lima, J., de Brito, J. (2010) Management system for expansion joints of road bridges, Structure and Infrastructure Engineering, 6:6, 703-714, DOI: 10.1080/15732470802087823

[7] EN 1998-2:2005+A2 (2011) Design of structures for earthquake resistance - Part 2: Bridges

[8] Polirol (2014): Katalog prijelaznih naprava http://www.polirol.com/images/katalog/POLIROL_KATALOG_2014_HR_Polidil.pdf (assessed December 5th 2022)

[9] Heat Rock Kohgyo: Seamless Joint, https://www.tokyo-belt.com/wp-cntpnl/wp-content/uploads/2020/12/SJ-Method-Brochure.pdf (assessed December 5th 2022)

[10] Maurer Sohne (2007): Girder grid joints technical approval, https://www.maurer.eu/fileadmin/mediapool/01_products/Dehnfugen/Zulassungen/Technical_Approval_for_MAURER_Girder_Grid_Joints.pdf (assessed December 5th 2022)

[11] Gumba GmbH catalog: Bridge bearings – Bearings for Bridges and Civil Engineering Structures, Reinforced Elastomeric Bearings according to DIN 4141, part 14

[12] Maurer Sohne (2004): Maurer Seismic Protection Systems, https://www.addbeton.com/documentation/EQUIPEMENTS%20D'OUVRAGES/MAURER/Equipements%20sismiques%20et%20controle%20de%20vibration/Brochure%20Seismic%20Protection%20Systems.pdf (assessed January 12 2023)

[13] Mandić, A., Šavor, Z., Gukov, I., Kindij, A. (2004) Selection of bridge expansion joints. In Proceedings of International Symposium Durability and maintenance of concrete structures. Croatian society of structural engineers and Austrian society for concrete and construction technology. Pg. 337-344

PUSHOVER ANALYSIS OF CONFINED MASONRY WALLS USING EQUIVALENT DIAGONAL STRUT MODELS

Nemanja Krtinić [(1)], Matija Gams [(2)], Marko Marinković [(3)]

[(1)] *Young researcher, Faculty of Civil and Geodetic Engineering, University of Ljubljana, nkrtinic@fgg.uni-lj.si*
[(2)] *Assistant professor, Faculty of Civil and Geodetic Engineering, University of Ljubljana, mgams@fgg.uni-lj.si*
[(3)] *Assistant professor, Faculty of Civil Engineering, University of Belgrade, mmarinkovic@grf.bg.ac.rs*

Abstract

Masonry structures are commonly used for building residential buildings throughout the Balkans and worldwide, in urban and rural areas and areas with seismic risk. For masonry construction in regions with seismic risk, confined masonry (CM) construction offers an appealing alternative to unreinforced masonry (URM) due to its better seismic performance. The numerical simulation of CM is often based on the Equivalent Strut Model (ESM). Such a model provides a very reasonable compromise between accuracy and efficiency and is simple enough for use in design. The purpose of this paper is to compare the results of an experimental shear compression test on a modern CM wall with different ESM models. Five ESM models proposed by various authors are compared. The numerical pushover analyses were performed in the SAP2000 software, and the reference points of the model that gave the best alignment with experimental results were estimated using regression analyses. The results show that the simple modelling of CM walls with an equivalent diagonal strut, which carries load only in compression, can accurately simulate the global seismic response and is suitable for practical applications.

Keywords: Confined masonry, Equivalent strut model (ESM), Numerical modelling, Pushover analysis, SAP2000.

1. Introduction

Masonry structures are traditionally used for low- to mid-rise buildings, particularly in regions characterised by high seismic hazard. Although unreinforced masonry structures did not perform well during the past earthquakes in Italy, the Balkans (Croatia, Slovenia, Serbia and Albania), Latin America (Chile, Peru and Mexico), the Middle East and South Asia, masonry is still one of the most commonly used building materials in earthquake-prone areas. Field observations after major earthquakes showed that earthquakes could cause significant damage to structures or even total collapse. Therefore, many researchers are working to prevent or reduce the consequences of earthquakes with alternative construction technologies with improved seismic performance.

One such technology is confined masonry, consisting of masonry walls and reinforced concrete (RC) confining elements. The confining tie-columns and tie-beams fully enclose the walls in vertical and horizontal directions [1]. These RC ties effectively improve the integrity and stability of masonry walls to in-plane and out-of-plane earthquake effects [2]. In the past decades, CM buildings have withstood major earthquakes, such as the 2010 Chile earthquake, which caused substantial damage to URM masonry and RC buildings without collapse [3]. It should also be noted that properly constructed confined masonry buildings performed very well and substantially better than URM buildings in the recent Petrinja, Croatia M 6.4 earthquake [4].

Confined masonry technology presents a viable alternative for unreinforced masonry (URM) and reinforced concrete (RC) frames with masonry infills because it does not require advanced construction skills and equipment. The increasing use of confined masonry requires reliable methods for structural response analysis, not only for the design of new construction but also for evaluating existing buildings [5].

Most research on CM is based on experimental testing of walls subjected to in-plane lateral loading [6, 7]. In contrast, there appears to be less research on the numerical modelling of CM walls. However, it is essential both for research and design to supplement and extend experimental results and to derive

appropriate computational models. Marques et al. [8] discussed several numerical models currently available for the seismic analysis of CM structures. Confined masonry walls exhibit complex and highly inelastic behaviour during seismic loading. Therefore, their proper consideration requires sophisticated computational techniques, which are usually not practical for designers. The finite element method-based approaches differ in degrees of refinement and accuracy. They can generally be divided into three groups: detailed micro model, simplified micro model and macro model. An appropriate approach is chosen depending on the analysis's purpose and the required detail level.

The numerical simulation of CM is often based on a macro-modelling approach, i.e. Equivalent Strut Model (ESM). This most straightforward type of modelling requires less computational effort and is suitable for routine design, wherein a compromise between accuracy and efficiency is needed [9]. The aim of this paper is to compare five nonlinear ESM models proposed by different authors with the experimentally obtained response of modern CM walls. The experimental tests were in-plane cyclic shear compression tests.

The following section presents the Equivalent Strut Models used in the analyses, with an additional theoretical explanation. The experimental investigation of two modern CM walls, as well as the results of the experiment, are briefly described in section 3. The numerical model was built in the SAP 2000 software [19]. Model calibrations and a comparison between experimental and numerical results are presented in section 4, followed by conclusions.

2. The Equivalent Strut Models (ESMs)

The Equivalent Strut Model (ESM) is one of the most known macro models, which was first proposed in the 1960s to model masonry infills in RC frames with diagonal struts. The diagonal strut model arose from the observation that during horizontal in-plane loading of an RC frame with masonry infill, the compression field in the masonry infill develops mainly along its diagonal (see Fig. 1b). Several researchers have later proposed using the ESM to model CM structures [10]. The present work was guided by the assumption that failure modes in CM walls and RC frames with infills are similar.

In case the ESM model is used in a linear analysis for, e.g. design, the only required parameters are the modulus of elasticity and the strut dimensions. For nonlinear analysis, on the other hand, the whole axial force-displacement curve is needed [11]. In the past decades, many researchers [12-16] have proposed approaches to model the lateral force-displacement relationship. These can represent the masonry wall's monotonic or cyclic behaviour, both of which are calculated based on the mechanical and geometrical characteristics explained below.

A multilinear relationship usually describes the constitutive law of an equivalent strut. Various models [13, 16, 17] have been proposed that take into account multiple failure modes and, based on the expected failure mode, calculate the lateral strength of the panel. However, other proposed models [12, 14, 15] seem to be easier to apply because they only require knowledge of the mechanical properties of the wall, even if they do not predict failure modes. It should be noted that in the proposed models, the initial stiffness and strength refer to the horizontal direction and have to be transformed to the diagonal (strut) direction. The models used in this study and corresponding equations to determine the envelope of the force-displacement curve for the lateral strength F or the strut axial strength N are shown in Table 1.

If the strut axial strength N is determined first, the lateral strength of the wall F is obtained using the following equation:

$$F = N \cos \varphi \tag{12}$$

The model by Panagiotakos and Fardis [12] used a four-linear lateral force-displacement curve that describes the cracking force, peak strength and residual strength after the failure of the masonry infill, as shown in Fig. 2a. The maximum lateral strength (F_m in Fig. 2a) is assumed equal to 1.3 times the cracking strength, while the lateral residual strength (F_u in Fig. 2a) is taken as 10% of the peak strength. The ultimate strength of the wall is a function of the masonry shear strength determined from the diagonal compression test τ_{cr} (Eq. (1)).

Table 1 – Equations for the strut axial strength or lateral strength

Reference	Lateral strength F / Strut axial strength N	
Panagiotakos and Fardis [12]	$F_{max} = 1.3 f_{ms} l_m t_m$	(1)
Decanini et al. [13]	$N_{dt} = \left(0.6 \tau_{m0} + 0.3 \sigma_0\right) t_w d$	(2)
	$N_s = \left(\left(1.2 \sin\theta + 0.45\cos\theta\right)\tau_0 + 0.3\sigma_0\right) t_w d$	(3)
	$N_{cc} = \dfrac{1.12\sin\theta\cos\theta}{K_1\left(\lambda_h\right)^{-0.12} + K_2\left(\lambda_h\right)^{0.88}}\sigma_{m0} t_w d$	(4)
	$N_{dc} = \dfrac{1.16\sigma_{m0}\tan\theta}{K_1 + K_2\lambda_h} t_w d$	(5)
Dolšek and Fajfar [14]	$F_m = 0.818\dfrac{L_{in} t_w f_{tp}}{C_I}\left(1+\sqrt{C_I^{\,2}+1}\right)$	(6)
Teni et al. [15]	$F_{max} = 1.3\tau_{cr} l_w t_w$	(7)
Liberatore et al. [16]	$N_s = \left(\left(1.2\sin\varphi + 0.45\cos\varphi\right)\tau_0 + 0.3\sigma_y\right) td$	(8)
	$N_{dt} = \left(0.6\tau_{m0} + 0.3\sigma_y\right) t l_m$	(9)
	$N_{dc} = 1.16\tan\varphi\, f_m \lambda_h^{-1}$	(10)
	$N_{cc} = 1.12\sin\varphi\cos\varphi\, f_m \lambda_h^{-0.88}$	(11)

F_{max} - maximum strength of masonry wall; N_{dt} - strength in the diagonal tension failure mode; N_s - strength in the bed-joint sliding failure mode; N_{cc} - strength in the corner compression failure mode; N_{dc} - strength in the diagonal compression failure mode; $l_w, d, L_{in}, l_m, \theta, \varphi$ - geometrical characteristics (see Fig. 1); t_w, t_m, t – wall thickness; $\tau_{cr}, \tau_{m0}, f_{ms}$ - shear strength evaluated through diagonal compression tests; τ_0 - shear strength of bed joints; f_{tp} - referential tensile strength of masonry; f_m, σ_{m0} - compression strength of masonry; σ_0, σ_y - vertical stress of the applied load; C_I - coefficient of interaction between the wall and the surrounding frame; λ_h - non-dimensional parameter (Eq. (18)); K_1, K_2 - empirical coefficients (see Table 2).
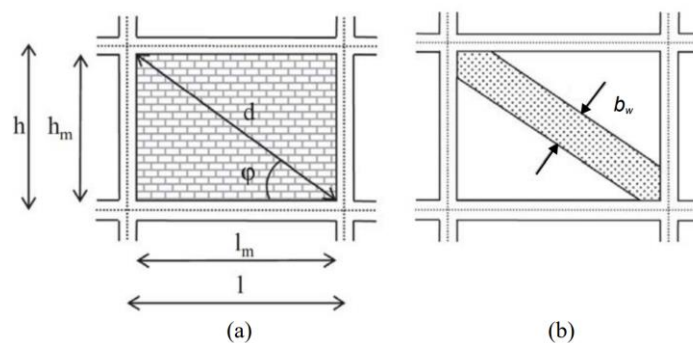
Figure 1. Equivalent strut model: (a) in-plane geometrical characteristics and (b) equivalent diagonal strut [16].

The most physically sound approach considers all possible failure mechanisms in masonry. Therefore, it is necessary to calculate the strength associated with each mechanism and then adopt the lowest value, which is the most likely failure mode that can occur when the wall is loaded. That value is then the assumed strength of the equivalent diagonal strut. The model by Decanini et al. [13] adopted a four-branched backbone curve that describes: (a) the linear elastic uncracked phase H_{mf}; (b) the post-cracking stage until reaching the maximum strength H_{mfc}; (c) the descending branch until H_{mr} and (d) the residual strength characterised by a horizontal line as shown in Fig. 2b. Decanini et al. [13] consider four

different possible failure mechanisms shown in Table 1 (Eqs. (2) – (5)). The strength values related to diagonal tension, N_{dt}, and to sliding shear failure, N_s, depend on the masonry shear strength and the vertical stress acting on the infill. The resistance associated with corner compression, N_{cc}, and diagonal compression, N_{dc}, are a function of the masonry compressive strength.

(a) (b) (c)

(d) (e)
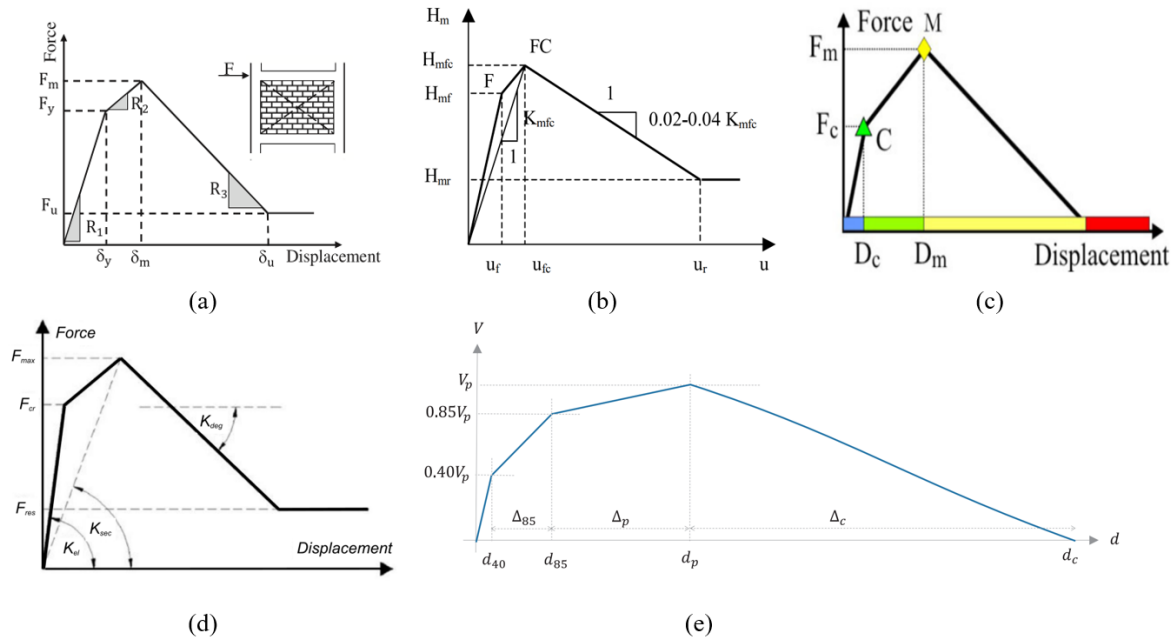
Figure 2. The multilinear force-displacement curve of (a) model by Panagiotakos and Fardis [12]; (b) model by Decanini et al. [13]; (c) model by Dolšek and Fajfar [14]; (d) model by Teni et al. [15] and (e) model by Liberatore et al. [16].

The envelope of the force-displacement curve adopted in the model of Dolšek and Fajfar [14] is presented by three branches (see Fig. 2c). To calculate the maximum strength of the wall F_{max} (Eq. (6)), the expression proposed by Žarnić and Gostič [18] was used. The cracking force F_c is obtained assuming the ratio of F_c/F_{max} of 0.6.

Teni et al. [15] proposed the model shown in Fig. 2d. The behaviour of the diagonal strut is defined with an envelope of horizontal force and displacement, which is adopted from Panagiotakos and Fardis [12]. The difference is that the residual strength (F_{res} in Fig. 2d)) is taken as 30% of F_{max}.

Finally, Liberatore et al. [16] proposed a model that considers uncertainties in its "backbone" curve. The proposed force-displacement curve is defined by four characteristic points (Fig. 2e) with different shear values: 40% of V_p, 85% of V_p, V_p and zero, where V_p is the peak load. The corresponding displacements are d_{40}, d_{85}, d_p and d_c, respectively. For the estimation of the peak load, V_p, Liberatore et al. [16] consider four failure mechanisms (Eqs. (8) – (11)), the same as in the model of Decanini et al. [13]. The strut axial strength, N, is the minimum value among the different failure mechanisms. In addition to the mechanical characteristics of the masonry, this advanced model also takes into account various characteristics, such as the presence of vertical or horizontal holes in the units, the type of test (monotonic or cyclic), etc.

The axial stiffness of the diagonal strut, K_s, is generally calculated as a function of the strut width, b_w, according to the following equation:

$$K_s = \frac{E_m t_w b_w}{d} \tag{13}$$

591

where E_m is Young's modulus, t_w is the thickness of the masonry wall, and d is the length of the strut. The secant stiffness associated with the load capacity of the wall (K_{sec} in Fig. 2d), determined from the axial stiffness of the equivalent strut, is given by the following equation:

$$K_{sec} = \frac{E_m t_w b_w}{d} \cos^2 \theta \tag{14}$$

The equations used to determine the equivalent strut width that the authors used in their models are shown in Table 2.

Table 2 – Equivalent strut width predictive equations

Reference	Equivalent strut width b_w		
Panagiotakos and Fardis [12]	$b_w = 0.175 \left(\lambda_h \right)^{-0.4} d$		(15)
Decanini et al. [13]	$b_w = \left(\dfrac{K_1}{\lambda_h} + K_2 \right) d$	for $\lambda_h < 3.14$ $K_1 = 3, K_2 = -0.178$ for $3.14 < \lambda_h < 7.85$ $K_1 = 0.707, K_2 = 0.01$ for $\lambda_h > 7.85$ $K_1 = 0.47, K_2 = 0.04$	(16)
Teni et al. [15]	$b_w = 0.175 \left(\lambda h_c \right)^{-0.4} d$		(17)

b_w - the width of the strut; h_c - the column height; d - the length of the compressive diagonal; λ_h – see below

The formula used to calculate the equivalent strut width (Eq. (15)) in the study by Panagiotakos and Fardis [12] is straightforward. The strut width b_w from Eq. (16) is calculated from the non-dimension parameter λ_h and two constants, K_1 and K_2, calibrated from experimental tests [13]. To calculate the strut width b_w, Teni et al. [15] use a slightly modified formula (15), as shown in Table 2 (Eq. (17)).

The width of the strut is based on the dimensionless parameter λ_h, which takes into account the material and geometric characteristics of the frame-infill system

$$\lambda_h = \sqrt[4]{\frac{E_m t_w \sin 2\theta}{4 E_c I_c h_m}} h \tag{18}$$

Where E_c is the elastic modulus of concrete, I_c is the moment of inertia of columns, h_m is the height of the masonry panel, and θ is the slope of the strut relative to the horizontal axis.

Teni et al. [15] use the parameter λ according to a modified equation that has the following form:

$$\lambda = \sqrt[4]{\frac{E_m t_w \sin 2\theta}{4 E_c I_c h_m}} \tag{19}$$

The formulas listed in Table 1 require knowledge of the mechanical and geometric parameters of the masonry wall. Among others, the parameters needed to determine the maximum lateral strength of the wall are the compressive strength of masonry, f_m, the shear strength evaluated through diagonal compression tests, τ_{m0}, and the shear strength of bed joints, τ_0. When parameters τ_{m0} and τ_0 are not available, Liberatore et al. [16] in their study propose the following equations for determining these parameters:
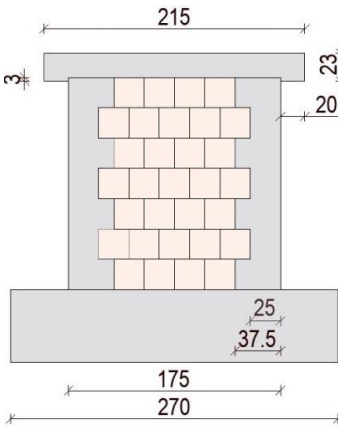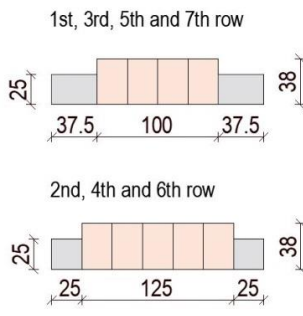
$$\tau_{m0} = 0.285 \sqrt{f_m} \ \text{(MPa)} \tag{20}$$

$$\tau_0 = \frac{2}{3} \tau_{m0} = 0.211 \sqrt{f_m} \ \text{(MPa)} \tag{21}$$

3. Experimental cyclic shear test

The seismic response of modern CM walls was tested in a cyclic shear compression test on two samples (W7 and W8, see Table 3). In the test, the compressive stress state due to the weight above is modelled by additional vertical forces applied before the lateral load. The seismic load is imposed on the wall in the form of prescribed displacements, which act cyclically in positive and negative directions (three times) and with increasing amplitude until collapse. Finally, the boundary conditions in the test were the so-called fixed-fixed boundary conditions (no rotation at the top with constant vertical force).

Table 3 – Confined masonry walls for cyclic shear tests (dimensions in cm)

Label	
W7, W8	
Dimensions	
Height [cm]	175
Length [cm]	175
Thickness [cm]	38
Tie-columns	
yes	
No. of samples	
2	

The walls were constructed from modern large chamber blocks (nominal dimensions of the unit are 250 x 249 x 380 mm) with insulation material in the chambers and polyurethane (PU) glue instead of mortar. They were built on RC foundations for transport and later fixing to the laboratory floor. There was first a 1–2 cm thick layer of general-purpose mortar on the foundation to provide a level surface for constructing the wall. Wall above was built using PU glue, which was applied to bed joints in four strips. The units were laid into the PU glue, and the final thickness of the bed joint was less than 1 mm. Head joints were unfilled and interlocked with the feather and groove type of contact. Perfect overlapping of units was used (overlap equal to half the length of the unit). RC bond beams were constructed on top of the walls to distribute vertical and horizontal loads during testing. The dimensions of the tested CM walls are shown in Table 3.

3.1 Material properties

Material properties were measured using dedicated tests. Some of the parameters were determined by calculation. Because the diagonal compression test was not performed in the experimental cyclic shear tests of CM walls, the shear cracking strength of masonry τ_{cr} was calculated as 0.285 times the square root of compressive strength of masonry f_m (see Eq. (20)). The shear strength of bed joints, τ_0, was also calculated using Eq. (21). The reference tensile strength of masonry (f_{tp}) can be derived from the diagonal tension test, which was also not performed in this experiment. Žarnić and Gostič [18] predict that this value is usually in the range between 4 % and 8 % of the compressive strength of the wall. In this study, it is assumed that this value was 8 % of f_m.

All relevant parameters are shown in Table 4.

Table 4 – Material property values used for concrete, masonry and reinforcement steel.

Concrete	Value	Source
Elastic modulus of concrete E_c [MPa]	33000	Standard EC2
Masonry		
Elastic modulus of masonry E_m [MPa]	2200	Experiment
Shear strength of masonry τ_{m0} [MPa]	0.556	Calculated
Referential tensile strength of masonry f_{tp} [MPa]	0.304	Calculated
Compressive strength of masonry f_m [MPa]	3.8	Experiment
Basic shear strength of bed joints τ_0 [MPa]	0.411	Calculated
Vertical stress of the applied load σ_0 [MPa]	0.63	Experiment
Reinforcement steel		
Elastic modulus of reinforcement steel E_s [MPa]	200 000	Experiment
Yield tensile strength f_y [MPa]	551	Experiment
Ultimate tensile strength f_u [MPa]	658	Experiment

3.2 Experimental results

The comparison between the numerical pushover analysis and experimental tests is performed on the envelope curves of the response. Fig. 3 shows the envelope curves for both tested walls (W7 and W8) and the average pushover curve used to compare with the results from the numerical simulations.
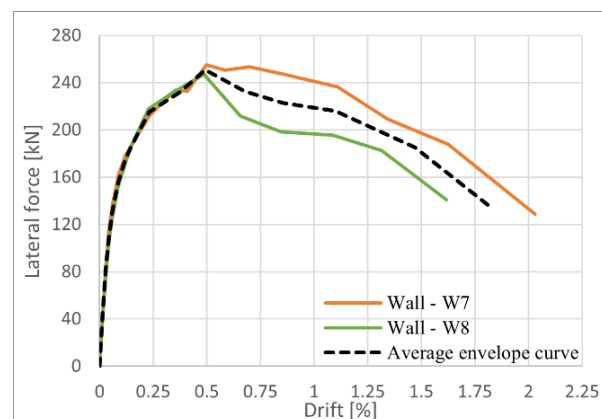
Figure 3. Experimental envelope curves of the tested confined walls.

4. Numerical simulations

4.1 Description of the numerical model

As mentioned in chapter 2, the Equivalent Strut model was used to model the CM wall. The model consists of a frame, which can develop plastic hinges at the corners (Fig. 4a) and a diagonal strut to model the effect of masonry (Fig. 4b). For the frame, interacting P-M2-M3 hinges were used in the tie-columns, and moment M3 hinges were used for the bond beam. Plastic hinges were defined at relative distances of 0.05 and 0.95, as seen in Fig. 4a. The strut is modelled using the "link" elements in SAP2000 [19]. This type of element is used because it can connect two joints (RC ties and wall) and behaves non-linearly. The link element consists of six springs for each of the six degrees of freedom, and different linear or nonlinear properties can be assigned to each spring [19].

The nonlinear characteristics of hinges in the frame were calculated based on the characteristics of the materials taken from experimental tests. Mander's model [20] was used for concrete when defining the

stress-strain curve, which was automatically defined by the program. A stress-strain curve was specified for the rebars based on the mechanical characteristics of the steel (see Table 4).
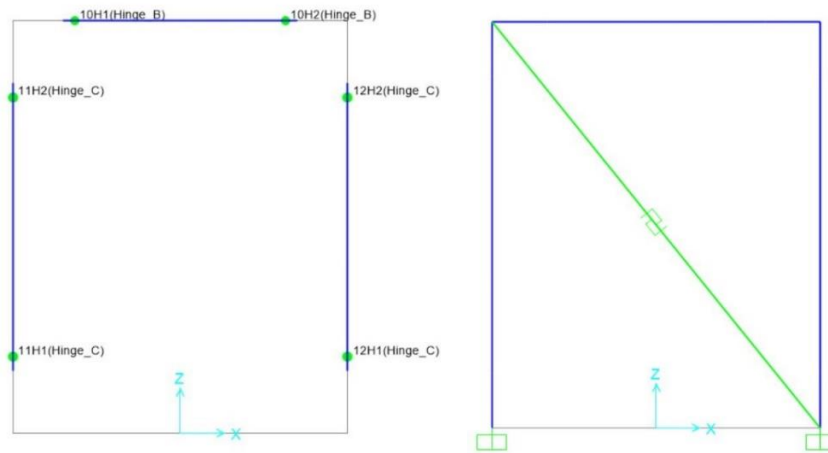
Figure 4. a) Hinge locations in the numerical model [19]; b) Numerical model with diagonal strut [19].

The multilinear plastic "link" element connects two diagonally opposite corners and has defined only the properties in the U_1 direction because the equivalent diagonal strut "works" only in compression. The force-displacement multilinear curve is the nonlinear property assigned to the "link" element. The parameters and formulas that define the force-displacement curves and corresponding constitutive models are shown below.

Fig. 5 shows the final axial force-axial displacement curves for strut proposed by different authors, which serve as input data in numerical analyses.
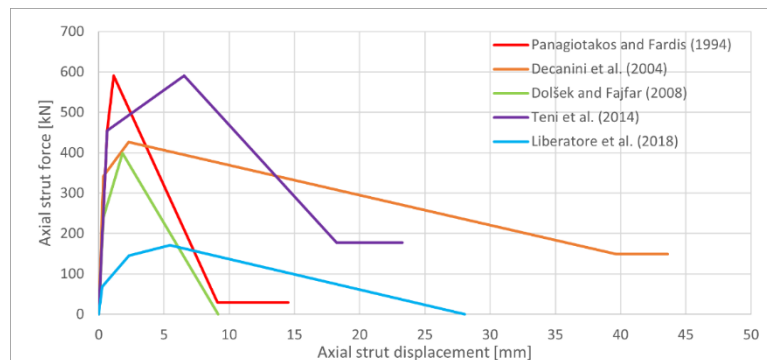
Figure 5. Final axial force-axial displacement curves for strut proposed by various authors.

4.2 Comparison of the results

The results from the numerical pushover analyses were compared to the envelope curve of the test in Fig. 6. The Panagiotakos and Fardis (red) model significantly overestimates peak strength (the relative percentage error e_r=148%). Based on the softening branch of the numerical curve, it can be concluded that these authors' model is more suitable for walls with extremely brittle failure. A similar observation can be made for the Dolšek and Fajfar model (green curve). However, the overestimation of peak strength is smaller, at about 82%.
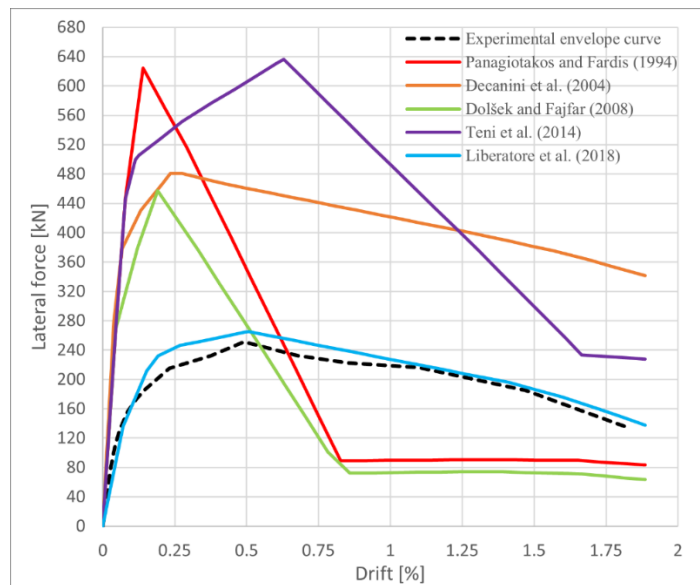
Figure 6. Comparison of the results between the numerical and experimental curves.

The model by Decanini et al. (orange) similarly overestimates peak strength by about 90% and underestimates drift at peak strength. The softening stiffness after reaching peak force is much better estimated, as it aligns with the experiment quite well.

Teni et al. (purple) model significantly overestimates peak strength (153%). However, this model is the only one that overestimates drift at peak resistance (0.63% in the model and 0.49% in the experiment). The model predicts a more brittle response than what was observed in the test.

Finally, the model proposed by Liberatore et al. shows a remarkable resemblance between the numerical model (light blue) and the experimental one (black dashed), as seen in Fig. 6. After the elastic phase, the numerical model curve's peak is reached around 8.9 mm (drift 0.51%). The experimental one peaked at 8.6 mm (drift 0.49%). Moreover, the numerical results match the initial stiffness, peak load capacity and stiffness degradation quite well. Therefore, it can be said that the model proposed by Liberatore et al. [16] is suitable for confined masonry walls of this type.

Relatively bad alignment of models [12-15] with the experiment indicates they should be calibrated to give better results.

4.3 Calibration of models and results

This subsection presents the improved numerical curves of calibrated models [12-15]. The results of the calibrated strut envelopes are shown in Fig. 7.
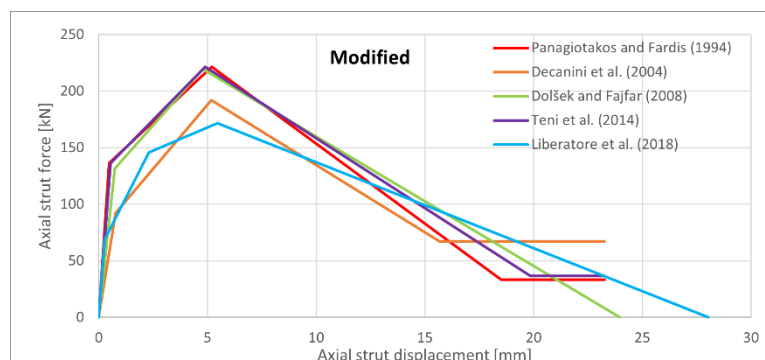
Figure 7. Modified axial force-axial displacement curves for equivalent diagonal strut.

Analysis of experimental values from cracking-to-peak strength (F_{peak}) suggests that such a ratio can be fixed and equal to 0.6 in the models [12] and [15], while the peak strength of the wall is equal to 0.5 τ_{cr} A_w. The residual strength F_{res} is calculated as 15% of the peak strength. The secant stiffness K_{sec} is corrected by factors of 0.2 and 0.5 for models [12] and [15], respectively. Secant-to-cracking stiffness K_{el} and softening stiffness K_{deg} are finally presented as a fraction of K_{sec}. The elastic stiffness was obtained as 3.0 K_{sec} and 2.7 K_{sec} for models [12] and [15], respectively, while the degrading stiffness for both models was adopted as 0.15 K_{sec}.

To better match the experimental results with the numerical results, the model of Dolšek and Fajfar [14] also had to be calibrated. The maximum force F_{max} (see Eq. (6)) was corrected by a factor of 0.55. The cracking force F_c was calculated assuming a ratio between the cracking force and the maximum force of 0.35. Secant stiffness K_{sec} was corrected by a factor of 0.2, while the elastic stiffness K_1 was obtained as 2.0 K_{sec}. It was also concluded that using a modified force-displacement curve for the strut model, the numerical (green) and experimental curves (black dashed) show good similarity, except that the numerical model gives an overestimation of peak strength as in models [12] and [15].

In the calibrated model by Decanini et al. [13], the minimum lateral strength H_{mfc} was considered to be only 45% of the lateral strength previously calculated via the most probable failure mode of the CM wall. The linear elastic uncracked strength H_{mf} is assumed as 50% of lateral strength, while the residual strength H_{mr} takes 35% of H_{mfc}. The stiffness of the wall at the stage of complete cracking K_{mfc} was corrected by a factor of 0.15, which directly affected the uncracked stiffness K_0. A modification for the uncracked stiffness K_0 is also proposed, considering 60% of the calculated elastic stiffness.

Finally, the calibrated model by Decanini et al. shows slightly better results than the previous models in terms of overestimating peak strength (about 12%). The model by Liberatore et al. [16] was not modified because it considered all the uncertainties in its "backbone" curve that the previous four models did not consider.

As in the previous subchapter, all five numerical pushover curves are shown in Fig. 8, and compared with the experimental envelope curve.
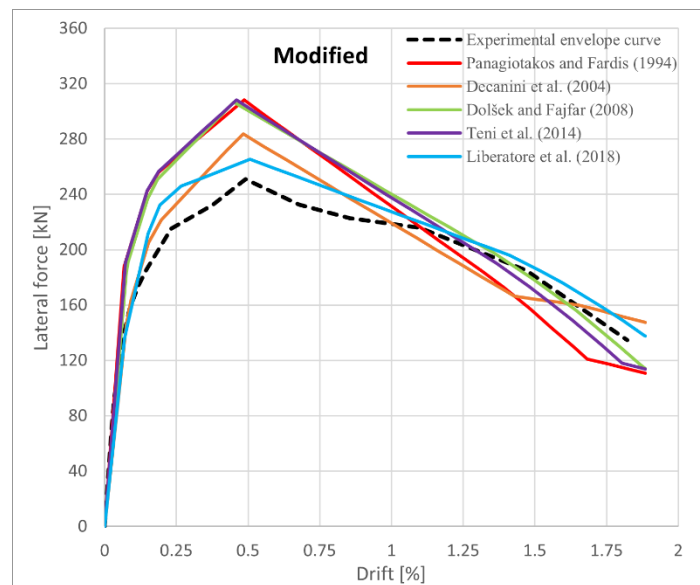
Figure 8. Comparison of the calibrated numerical and experimental curves.

5. Conclusions

Confined masonry (CM) is a construction technology that has the potential for seismically resilient masonry construction. However, the broader application of this technology for the design of new construction and evaluation of existing buildings requires improving relevant codes and developing simple and reliable numerical models for seismic analysis.

The Equivalent Strut Model (ESM) proposed in this study can be used for nonlinear static analysis of CM structures as one of the most straightforward macro-modelling approaches. In this approach, the RC confining elements are modelled as horizontal (beam) and vertical (column) elements, while the masonry wall is modelled as a diagonal strut.

The numerical analyses were performed in the SAP2000 software using five models of force-displacement curves for the confined masonry wall proposed by the various authors. Straightforward use of the models showed significant discrepancies with the experiments, except in the case of Liberatore et al. model. In the next step, the models were calibrated, and the alignment with the experiments was much better. The following conclusions have been drawn based on this study:

- Simple modelling with an equivalent diagonal strut, which carries load only in compression, can simulate the global seismic response of the CM walls and is suitable for practical applications. Unfortunately, this kind of model does not identify local effects or low ductility zones.

- By comparing the experimental results and the results of the numerical pushover analyses, it was concluded that the strength and stiffness of the wall in the force-displacement curve models proposed by different authors must be calibrated. The calibrated models showed reasonably good agreement with the experimental results. The recommended models should be verified by additional experiments, which will be the subject of future work.

- Good compatibility between the numerical and experimental curves was obtained by the Decanini et al. model, with a slight overestimation in the peak strength of 12%. On the other hand, the best alignment with the experimental results was obtained by the force-displacement curve model proposed by Liberatore et al. with a practically negligible overestimation of the ultimate strength (less than 5%). The reference points of the model were estimated using regression analyses in which the presence of holes in the units, the type of test (monotonic or cyclic), and the type of masonry material were taken into account. None of the remaining four models makes such considerations.

- The considered modern confined masonry appears to have a very good seismic response and a large capacity for energy dissipation.

6. Acknowledgements

7. References

[1] Ghaisas, V.K., Basu, D., Brzev, S., Pérez Gavilán, J.J. (2017): Strut-and-Tie Model for seismic design of confined masonry buildings. *Construction and Building Materials*, **147**, 677–700, doi: https://doi.org/10.1016/j.conbuildmat.2017.04.200

[2] Brzev, S., Hart, T. (2017): Confined masonry network: an overview of guidelines and initiatives, *Proceedings of the 16th World Conference on Earthquake Engineering 16WCEE*, 09-13 January, Santiago, Chile.

[3] Astroza, M., Moroni, O., Brzev, S., Tanner, J. (2012): Seismic Performance of Engineered Masonry Buildings in the 2010 Maule Earthquake. *Special Issue on the 2010 Chile Earthquake. Earthquake Spectra*, **28** (S1), S385-S406.

[4] Miranda, E., Brzev, S., Bijelić, N., Arbanas, Ž., Bartolac, M., Jagodnik, V., Lazarević, D. et al. (2021): StEER-EERI: Petrinja, Croatia December 29, 2020, Mw 6.4 Earthquake Joint Reconnaissance Report (JRR). The Structural Extreme Events Reconnaissance (StEER) Network, United States.

[5] Lang, A.F., Crisafulli, F.J., Torrisi, G.S. (2014): Overview and assessment of analysis techniques for confined masonry buildings, *Proceedings of the 10th National Conference in Earthquake Engineering*, 21-25 July, Anchorage, Alaska.

[6] Singhal, V., Rai, D.C. (2016): In-plane and out-of-plane behavior of confined masonry walls for various toothing and openings details and prediction of their strength and stiffness. *Earthq. Eng. Struct. Dyn*, **45** (15): 2551-2569, doi: https://doi.org/10.1002/eqe.2783

[7] Pérez-Gavilán, J.J., Flores, L.E., Alcocer, S.M. (2015): An experimental study of confined masonry walls with varying aspect ratios. *Earthquake Spectra*, **31** (2): 945–968, doi: https://doi.org/10.1193/090712EQS284M

[8] Marques, R., Pereira, J.M., Lourenço, P.B. (2020): Lateral in-plane seismic response of confined masonry walls: from numerical to backbone models. *Engineering Structures*, **221**, 111098. doi: https://doi.org/10.1016/j.engstruct.2020.111098

[9] Nguyen, L. (2014): Confined Masonry: Theoretical Fundamentals, Experimental Test, Finite Element Models, and Future Uses, PhD Thesis, University of Colorado, Boulder, USA.

[10] Rankawat, N., Brzev, S., Jain, S.K., Pérez Gavilán, J.J. (2021): Nonlinear seismic evaluation of confined masonry structures using equivalent truss model. *Engineering Structures*, **248**, 113114, doi: https://doi.org/10.1016/j.engstruct.2021.113114

[11] Crisafulli, F.J. (1997): Seismic behaviour of reinforced concrete structures with masonry infills, PhD Thesis, University of Canterbury, Christchurch, New Zealand.

[12] Panagiotakos, T.B., Fardis, M.N. (1994): Proposed Nonlinear Strut Models for Infill Panels, 1st year Progress Report of HCM-PREC8 Project, University of Patras.

[13] Decanini, L., Mollaioli, F., Mura, A., Saragoni, R. (2004): Seismic performance of masonry infilled R/C frames, *Proceedings of the 13th World Conference on Earthquake Engineering 13WCEE*, 01-06 August, Vancouver, B.C., Canada.

[14] Dolšek, M., Fajfar, P. (2008): The effect of masonry infills on the seismic response of a four-storey reinforced concrete frame-a deterministic assessment. *Engineering Structures*, **30** (7), 1991-2001, doi: https://doi.org/10.1016/j.engstruct.2008.01.001

[15] Teni, M., Grubišić, M., Guljaš, I. (2014): Simplified Approaches for Modeling Infilled Frames. Electronic *Journal of the Faculty of Civil Engineering Osijek, e-GFOS*, **5** (9), 70-88, doi: http://dx.doi.org/10.13167/2014.9.8

[16] Liberatore, L., Noto, F., Mollaioli, F., Franchin, P. (2018): In-plane response of masonry infill walls: Comprehensive experimentally-based equivalent strut model for deterministic and probabilistic analysis. *Engineering Structures*, **167**, 533-548, doi: https://doi.org/10.1016/j.engstruct.2018.04.057

[17] Saneinejad, A., Hobbs B. (1995): Inelastic design of infilled frames. *Journal of structural engineering*, **121** (4), 634-650, doi: 10.1061/(ASCE)0733-9445(1995)121:4(634)

[18] Žarnić, R., Gostič, S. (1997): Masonry infilled frames as an effective structural sub-assemblage. In: Fajfar, Krawinkler, editors. Seismic Design Methodologies for the Next Generation of Codes. Rotterdam: Balkema, pp. 335-46.

[19] Computers & Structures, Inc. (2016): CSI Analysis Reference Manual for SAP2000, ETABS, SAFE and CSIBridge, Berkeley, California, USA.

[20] Mander, J. B., Priestley, M. J., Park, R. (1988): Theoretical stress-strain model for confined concrete. *Journal of structural engineering*, **114** (8), 1804-1826.

STUDY OF SIMULTANEOUS INTER-STOREY DRIFT IP AND OOP LOADS ON RC FRAMES WITH AND WITHOUT INFILL WALLS AND OPENINGS BY A VARIATING ANGLE

Filip Anić[(1)], Davorin Penava[(2)], Vasilis Sarhosis[(3)], Lars Abrahamczyk[(4)]

[(1)] *Postdoctoral researcher, Josip Juraj Strossmayer University of Osijek, Faculty of Civil Engineering and Architecture Osijek, filip.anic@gfos.hr*

[(2)] *Associate professor, Josip Juraj Strossmayer University of Osijek, Faculty of Civil Engineering and Architecture Osijek, davorin.penava@gfos.hr*

[(3)] *Associate professor, University of Leeds, Faculty of Engineering and Physical Sciences, School of Civil Engineering, v.sarhosis@leeds.ac.uk*

[(4)] *Associate professor, Bauhaus-Universität Weimar, Faculty of Civil Engineering, lars.abrahamczyk@uni-weimar.de*

Abstract

Within the literature, no examples of equations were found that account for out-of-plane inter-storey drift force resistance, nor any that tested RC frames under them. Moreover, no studies were even done that combined in-plane forces. Consequently, this paper presents an equation development for estimating the resistance of RC frames containing infill walls with and without openings subjected to simultaneous IP and OoP loading. The equations were derived from data obtained from 3D high fidelity finite-element micromodels calibrated against a series of small- and large-scale experimental tests. An estimation of resistance is done by obtaining a coefficient based on the opening area and the angle of the resultant in-plane and out-of-plane load and multiplying it with the in-plane load-bearing capacity of a bare frame. The derived equation showed a good correlation with the computational data.

Keywords: in-plane, out-of-plane, simultaneous load, RC frame, infill wall, openings, resistance estimation

Abbreviations and notations

Latin based

IP	In-Plane
OoP	Out-of-Plane
V_R	Shear resistance – resultant force
$V_{R,IP,BF}$	IP Shear resistance of a BF model
k_o	Coefficient used for calculating the shear resistance of an RC frame with an infill wall and an opening
k_i	Coefficient used for calculating the shear resistance of an RC frame with an infill wall (no opening)
A_o	Area of opening
A_i	Area of infill wall

Greek-based

α	The angle of the resultant force V_R
β	The ratio of opening to infill wall area (A_o/A_i)

1. Introduction

Many modern, high-rise structures in Croatia and the rest of Europe are made of reinforced concrete (RC) frames with masonry infill walls. During an earthquake event, such structures are excited in Out-of-plane (OoP) and In-plane (IP) directions. Simply by the geometry of frame structures, its IP behaviour is always governed by inter-storey drift forces. On the other hand, the OoP ones are governed by both the inter-storey drift and inertial forces. Inertial forces are carried out by the accelerated masses of the infill wall and the inter-storey drift ones -by the movement of the rigid slab *i.e.,* the frames.

The effects of the earthquake action on frame structures were investigated in IP and OoP directions separately and in combination. The combined IP and OoP loads were considered in three ways. Firstly,

previous IP damage followed by OoP load. This combination is the most prevalent in the literature. Secondly, previous OoP damage followed by IP load and thirdly simultaneous IP and OoP load. Namely, most of the research that combined the loads was done using inertial OoP load and IP load. Besides the contribution of the authors of this paper, only two were found that investigated the OoP inter-storey drift forces on the structural steel frames with masonry infill walls [1,2].

Furthermore, no equations are avaliable to consider OoP inter-storey drift forces or their combination with IP loads. All the equations within the literature are either *flexural* or *arching-action* based *i.e.,* grounded on research that used inertial force approaches [3–5].

Consequently, this paper presents a computational study and analytical model development based on the simultaneous inter-storey drift OoP and IP loads on RC frames with unreinforced masonry infill walls with and without openings.

2. Methodology

Prior to computational studies and their calibrations, a series of experimental tests were undertaken. Small-scale experiment tests were undertaken to obtain the mechanical properties of the materials involved (concrete, rebar, masonry units, mortar). Also, experimental tests were undertaken on scaled specimens of frames with and without masonry infill walls and openings. In these cases, masonry walls (shear, compression, bending) were subjected to IP [6] and OoP [7] drift-driven cyclic, quasi-static tests (Fig. Figure 1). The tested specimens included a bare frame (BF), fully infilled frame (FI), frame with centric door (CD), centric window (CW), eccentric door (ED) and eccentric window (EW) openings within the infill wall.

The frame was designed using EN1998 provisions [8] following medium ductility class specifications. The masonry infill units were locally sourced and classified as Group 2 using the EN1996 provision [9], and by the same provision, a cementitious mortar was used and classified as M5 [9].

Figure 1. Experimental tests. a) OoP bend test on masonry infill wall [10]. b) IP cyclic, quasi-static test on frames with and without masonry infill walls and openings [11]. c) IP cyclic, quasi-static test on frames with and without masonry infill walls and openings [7]

Based on the OoP wall bend experiments that were done with the load parallel and perpendicular to the bedjoints (Fig. Figure 1a) and by the IP (Fig. Figure 1b) and OoP (Fig. Figure 1c) cyclic, quasi-static tests, computational models were developed and calibrated against them [12]. The computational models were developed using a FEM 3D micromodel approach via Atena Engineering 3D [13] software with manually edited *input* files.

The micromodels used the 3D solid elements to simulate concrete and masonry, 2D elements for contacts (hed- and bedjoints) and 1D truss elements for rebar (Fig. Figure 2). Nonlinear cementitious material model was used for both concrete and masonry; interface – gap elements for head- and bedjoints, and cyclic reinforcement model for rebars.
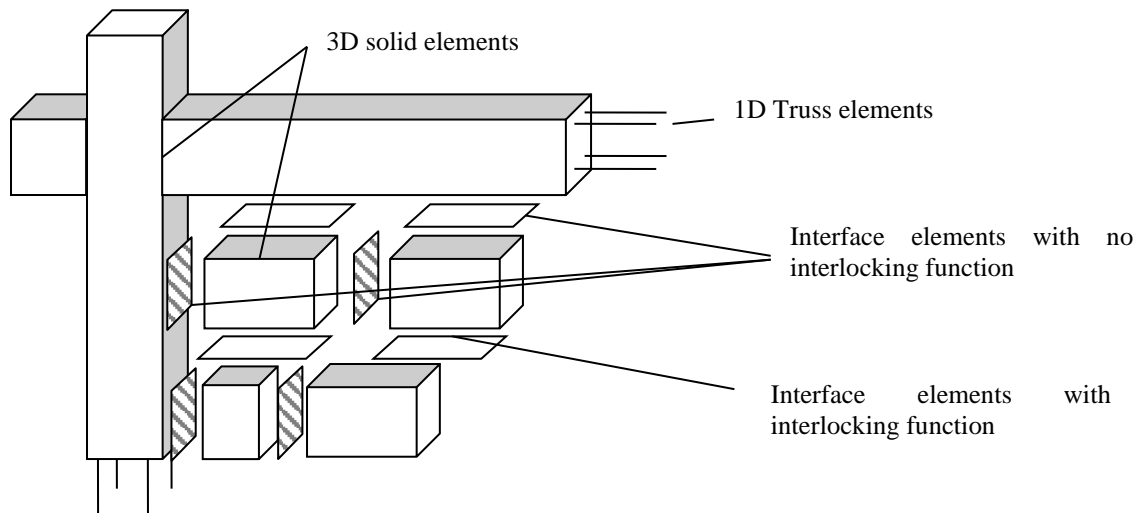
Figure 2. Parts of the 3D micromodel

The calibration process started with IP tests, followed by the OoP bend tests and finally, OoP cyclic, quasi-static tests. If there were any corrections during the process, it would be reverted to the simulation of the earlier calibrated models. Furthermore, the calibration process yielded the governing factors of each experiment.

With the calibrated models, further simulations were carried out *i.e.*, extrapolated to include simultaneous IP, OoP and gravitational load along with variating door and window opening sizes and positions.

Based on the data available in the literature, a limit of opening to infill wall area ratio was found to be $A_o/A_i \in [0.1, 0.3]$. If the ratio is below 0.1, the opening has no influence [9]; whereas if it is above 0.3, the infill wall does not [14]. Therefore, the ratios that were included in the simulations were approximately the minimum, mean, and maximum of the limits ($A_o/A_i \in \approx \{0.1, 0.2, 0.3\}$), an example of such variating size is visible in Figure 3 on a CW model. The dimensions of openings were chosen based on *architectural standards* that present common practices [15].

$A_o/A_i = 12.31\ \%$　　　　$A_o/A_i = 21.54\ \%$　　　　$A_o/A_i = 30.15\ \%$
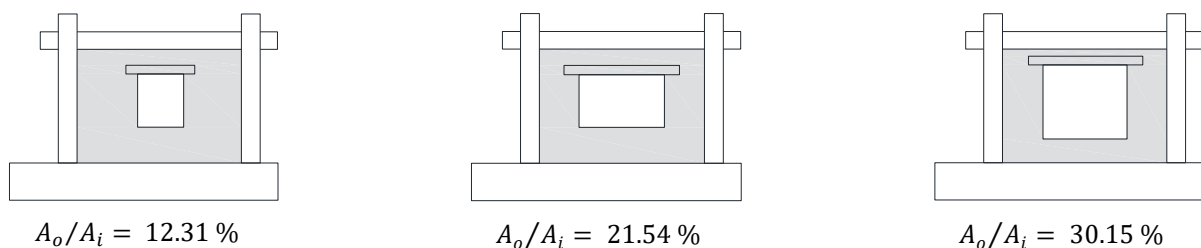
Figure 3. Example of opening size variation on CW model

Unlike the calibrated models, the load was monotonic, *i.e.*, the pushover method. This was done since the computational time was immense, especially considering that there were more than 250 models to compute.

The simultaneous load was defined by varying the angle $\alpha \in \{0, 15, 30, 45, 60, 75, 80, 85, 90\}°$ where $0°$ is pure IP and $90°$ pure OoP load. The resultant shear load V_R is calculated by the sum of squares of IP and OoP load-bearing resistance.

So, the models were further abbreviated as: $model(A_o/A_i)\{l, r\}$. Where the *model* is one of the BF, EW, etc.; *l,r* load direction in case of an eccentric opening.

3. Results and discussions

Since this paper aimed to present the equation development, only the primary outcomes of computations are presented. An example of load-bearing capacities is presented in Figure 4 in the form of a *polar plot*. The polar plot shows the values of load-bearing capacities within the polar coordinate system, where the angle of the system is also the angle of the resultant force α and the distance from the null point is the load-bearing capacity. The load-bearing capacity is expressed with its value (vertical axis) and normalised to a BF model's pure IP load-bearing capacity. The blue-filled curve is the FI's, yellow-filled BF's and cyan-filled of the referent model with openings.

The other polar plots follow the same patterns as those in Figure 4. Namely, the load-bearing capacity starts as a maximum at pure IP load ($\alpha = 0°$), and drop with the increase of α whistl finally reaching the OoP load-bearing capacity of a BF. The decline in load-bearing capacity is gradual up to 45°, while afterwards, the decline is more rapid. The reason behind it is that up to 45°, the mechanical system is frame-dominated; afterwards, it is beam-dominated. Also, with the tension introduced by bending the wall caused by OoP drift-driven load, the beneficial IP-compression strut loses its effectiveness.
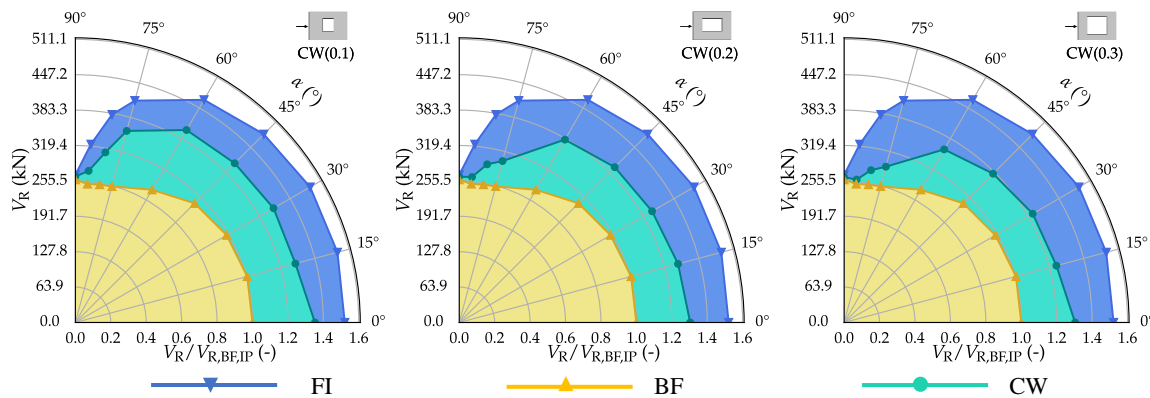
Figure 4. Example of the load-bearing capacity of CW model with different area ratios

Interaction curves were set up for one referent model *e.g.,* CW and plotted against normalized load-bearing capacity k_o, angle of the resultant force α, and the ratio of opening to infill wall area in *surface* and *contour plots* (topographical view of the surface) as visible in examples in Figure 5. Other models had similar plots, showing a mathematical pattern governing the curves.

Hence, such a mathematical pattern could be exploited to create an equation that could estimate the load-bearing capacity of an RC frame with a masonry infill wall with or without openings. The equation (Eq. 1) was arranged in a way so that the IP load-bearing capacity of a bare frame ($V_{R,BF,IP}$) is multiplied by a coefficient (k) that considers the sizes of the openings and the angle of the resultant force. Since the FI models do not have an opening, the coefficient was then divided into that those that take openings into account (k_o) and those that do not (k_i). The IP load-bearing capacity of a bare frame was chosen as a bare frame is an elementary example and IP being more researched. Such a capacity could be obtained through calculations, numerical computations or experiments.

$$V_{R,\alpha} = V_{R,BF,IP} \cdot k, \qquad k \in \{k_o, k_i\} \tag{1}$$

From the interaction curves in Figure 5, it is clear that the relation of α and normalized force is of an exponential kind, while the area ratio $\beta = A_o/A_i$ is linear. So, in order to formulate the coefficient k, first it was related to angle α forming $k(\alpha)$. Multiple equations were tested to fit the data, namely in the sphere of growth modelling (economic, natural, *etc.*). A *Monomolecular,* also known as *Brody* or *Mitscherlich* function, was implemented (Eq. 2).

$$k = c_1 - \frac{c_2}{c_3}(1 - e^{-c_3 x}) \tag{2}$$
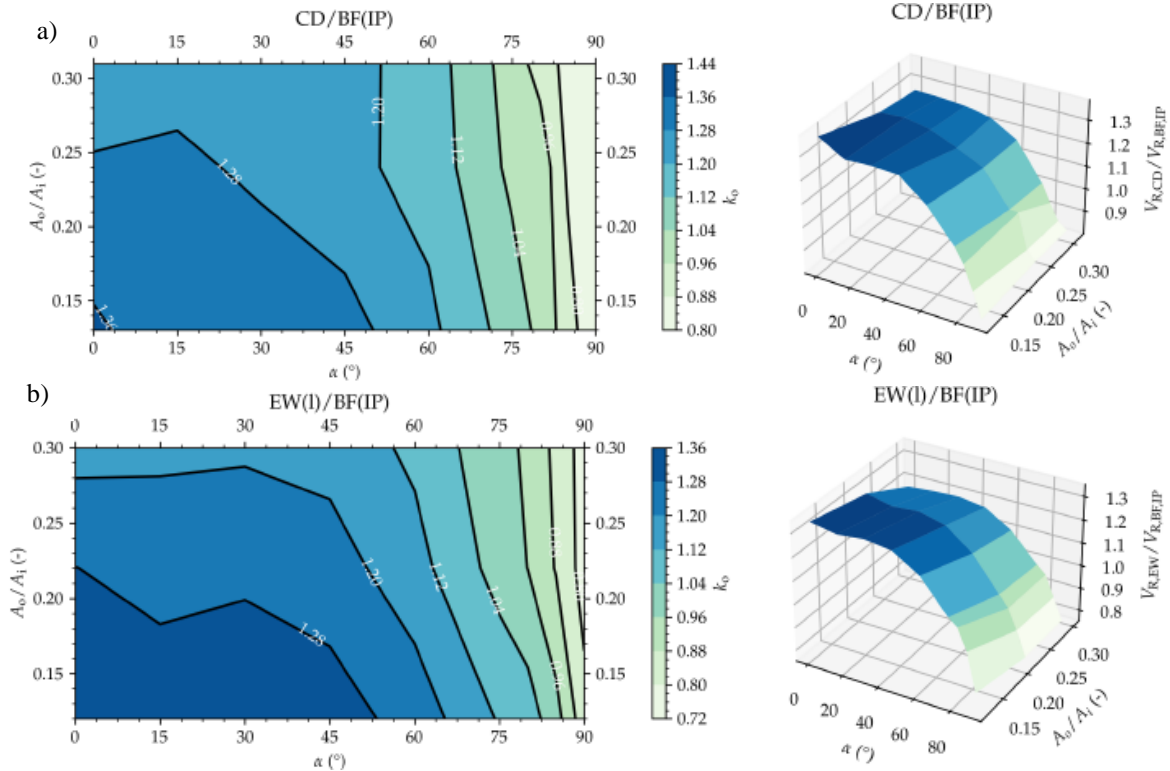
Figure 5. Example of interaction curves. a) CD model. b) EW model.

Again, the equation was then correlated to $\alpha \rightarrow k(\alpha)$ for each model of the same group by different area ratios β (*e.g.*, CW(0.1), CW(0.2), and CW(0.3)). Using a *SciPy curve fit* tool [16], the coefficients were optimised to produce the best fit with the data. So, the coefficients c_1, c_2, and c_3 were β dependable. Knowing that the β to normalized force has a linear relation, a line equation was used to calculate their governing function. Finally, with some optimisations and simplifications, the coefficient for opening (Eq. 3) and without it (Eq. 4) were formed. For the coefficient k_o That considers the openings, parameters a and b can be extracted from Table 1.

$$k_o = a + b\beta\left(1 - e^{-0.05\alpha(\beta-1)}\right) \tag{3}$$

$$k_i = 1.53 + 0.003(1 - e^{-0.085\alpha}) \tag{4}$$

$$\forall\ \alpha \in [0, 90],\ \beta \in [0.1, 0.3]$$

Table 1. Coefficients needed for Equation (3)

Type	Opening Position	Load direction		a	b
Door	Centric	/		1.29	0.071
Window	Centric	/		1.30	0.075
Door	Eccentric	Left		1.30	0.065
Door	Eccentric	Right		1.24	0.070
Window	Eccentric	Left		1.27	0.070
Window	Eccentric	Right		1.23	0.070

The equations show a good correlation with the simulation data, as visible in the examples in Figure 6. In Figure 6, the *surface* is the normalized force calculated using Equations (3,4) with the domain that

covers $\alpha \in [0, 90]$ (°) and $\beta \in [0.1, 0.3]$; while the red spheres are the datapoints from micromodel computations.
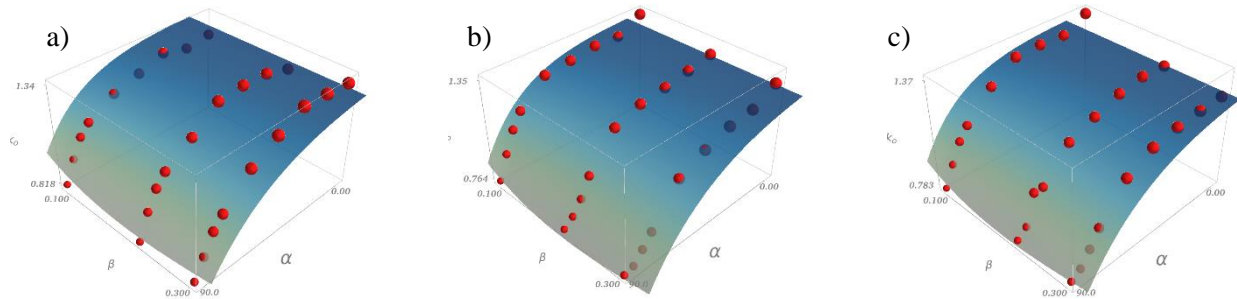
Figure 6. Data fitting results. a) CD model. b) CW model. c) ED(l) model

4. A worked example for determining the load-bearing capacity

An example of determining load-bearing capacity is described here.

Problem: Determine the load-bearing capacity of a frame with a URM infill wall and centric door opening under the angle of loading $\alpha = 45°$ (equal IP and OoP load). The IP load-bearing capacity of the frame was calculated as $V_{R,IP.BF} = 400$ kN, and the ratio of the opening and infill wall is $A_o/A_i = \beta = 0.24$.

Solution with equations: Using Equation (3), one can obtain a more refined answer when compared to the interaction curves. Firstly, one should obtain coefficients from Table 2: $a = 1.29$ and $b = 0.071$. Then use Equation 8 with the data from the problem and Table 1.

$$
\begin{aligned}
k_o &= a + b\beta\left(1 - e^{-0.05\alpha(\beta-1)}\right) \\
&= 1.29 + 0.071 \cdot 0.24\left(1 - e^{-0.05\cdot45(0.24-1)}\right) \\
&\approx 1.213
\end{aligned}
$$

Finally, multiply the BF's IP capacity with ko, thus obtaining the requested capacity:

$$
\begin{aligned}
V_{R,CD,\alpha=45} &= k_o V_{R,BF,IP} \\
&= 1.213 \cdot 400 \\
&= 485.20 \text{ kN}
\end{aligned}
$$

Solution with interaction curves (graphical): The process is described in Figure 7. The first one should find the appropriate interaction curve. In this case, the CD one. Then find the A_o/A_i and draw a horizontal line, in this case, red. Next, find the angle and draw the vertical line, in this case, green–coloured. The intersection of the red and green lines is the requested coefficient. A more conservative approach would read it as 1.2, more detailed would estimate it as 1.23. Finally, multiply the BF's IP capacity with the coefficient, and follow the solutions below.

Detailed approach:

$$
\begin{aligned}
V_{R,CD,\alpha=45} &= k_o V_{R,BF,IP} \\
&= 1.23 \cdot 400 \\
&= 492 \text{ kN}
\end{aligned}
$$

Conservative approach:

$$= \quad 1.2 \cdot 400$$

$$= \quad 480 \text{ kN}$$
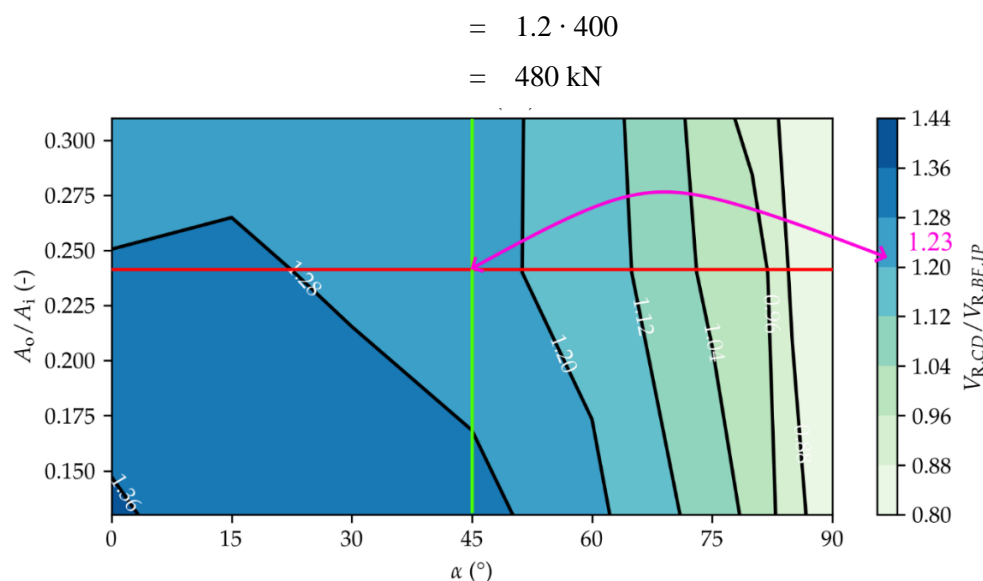
Figure 7. Determination of coefficients for the example

5. Conclusions

Using the calibrated 3D FEM micromodels, a computational campaign was conducted that included applying simultaneous IP and OoP drift-force on RC frames with and without infill walls and openings. An angle defines the simultaneous load that the resultant of IP and OoP resistance closes with the IP resistance. It was found that the greatest load-bearing capacity is with pure IP load that drops with the angle change until it reaches pure OoP load. With pure OoP load, there is no difference between the BF or other models with infill walls or openings. The decline in the capacity is gradual up to 45° when afterwards it is more rapid. Such a decline is due to a shift from the frame- to a beam-based mechanical system, and by beneficial IP compression strut losing its effectiveness caused by tension from OoP loads.

It was found that all models had similar angle-openings size-resistance interaction curves, i.e., the same mathematical pattern that accounts for the ratio of opening to infill wall area and the angle of the resultant force. Those patterns were used to derive an equation i.e., coefficients to calculate the load-bearing capacity of an RC frame with a masonry infill wall with or without openings loaded under the desired angle. The derived equation revealed a good correlation with the computational micromodel data; yet, it could not be validated against others since there is no like research with OoP drift-force approaches.

References

[1]   Flanagan RD. Behavior of structural clay tile infilled frames. Tennessee, USA: 1994.
[2]   Henderson R, Jones W, Burdette E, Porter M. The effect of prior out-of-plane damage on the in-plane behavior of unreinforced masonry infilled frames. Fourth DOE Nat. Phenom. Hazards Mitig. Conf., 1993, p. 18.
[3]   Anić F, Penava D, Abrahamczyk L, Sarhosis V. A review of experimental and analytical studies on the out-of-plane behaviour of masonry infilled frames. Bull Earthq Eng 2020;18:2191–246. doi:10.1007/s10518-019-00771-5.
[4]   Asteris PG, Antoniou ST, Sophianopoulos DS, Chrysostomou CZ. Mathematical macromodeling of infilled frames: state of the art. J Struct Eng 2011;137:1508–17. doi:10.1061/(ASCE)ST.1943-541X.0000384.
[5]   Pasca M, Liberatorea L, Masiani R. Reliability of analytical models for the prediction of out-of-plane capacity of masonry infills. Struct Eng Mech n.d.;64:765–81. doi:https://doi.org/10.12989/sem.2017.64.6.765.
[6]   Sigmund V, Penava D. Influence of openings, with and without confinement, on cyclic response of infilled

r-c frames — an experimental study. J Earthq Eng 2014;18:113–46. doi:10.1080/13632469.2013.817362.

[7] Anić F, Penava D, Guljaš I, Sarhosis V, Abrahamczyk L. Out-of-plane cyclic response of masonry infilled RC frames: An experimental study. Eng Struct 2021;238:112258. doi:10.1016/j.engstruct.2021.112258.

[8] CEN. Eurocode 8: Design of Structures for Earthquake Resistance - Part 1: General Rules, Seismic Actions and Rules for Buildings (EN 1998-1:2004). Brussels: European Committee for Standardization; 2004.

[9] CEN. Eurocode 6: Design of masonry structures - Part 1-1: General rules for reinforced and unreinforced masonry structures (EN 1996-1-1:2005). Brussels: European Committee for Standardization; 2005.

[10] Anić F, Penava D, Varevac D, Sarhosis V. Influence of Clay Block Masonry Properties on the Out-of-Plane Behaviour of Infilled RC Frames. Teh Vjesn 2018.

[11] Penava D. Influence of openings on seismic response of masonry infilled reinforced concrete frames. 2012.

[12] Anić F, Penava D, Sarhosis V, Abrahamczyk L. Development and Calibration of a 3D Micromodel for Evaluation of Masonry Infilled RC Frame Structural Vulnerability to Earthquakes. Geosciences 2021;11:468. doi:10.3390/geosciences11110468.

[13] Cervenka Consulting. ATENA for Non-Linear Finite Element Analysis of Reinforced Concrete Structures 2015.

[14] Penava D, Sarhosis V, Kožar I, Guljaš I. Contribution of RC columns and masonry wall to the shear resistance of masonry infilled RC frames containing different in size window and door openings. Eng Struct 2018;172:105–30. doi:10.1016/j.engstruct.2018.06.007.

[15] Neufert E, Neufert P. Architects' data. 4th ed. Wiley-Blackwell; 2012.

[16] Jones E, Oliphant T, Peterson P, Others. SciPy: Open Source Scientific Tools for Python, 2001 (http://www.scipy.org/). Http://WwwScipyOrg/ 2015.

COMPARISON OF DUCTILITY CLASS REQUIREMENTS FOR SEISMIC DESIGN OF REINFORCED CONCRETE WALLS IN A TALL BUILDING

Luka Čičak [(1)], Anđelko Vlašić [(2)], Dominik Skokandić [(3)]

[(1)] *Mag.Ing.Aedif., Studio Arhing l.t.d., luka@studio-arhing.com*
[(2)] *Assoc. Professor, University of Zagreb Faculty of Civil Engineering, andjelko.vlasic@grad.unizg.hr*
[(3)] *Post Ph.D. Assistant, University of Zagreb Faculty of Civil Engineering, dominik.skokandic@grad.unizg.hr*

Abstract

The seismic design of reinforced concrete walls is greatly influenced by the selected ductility class. The ductility class directly determines the reduction of seismic loading by reducing the response spectrum using an appropriate behaviour factor. A higher ductility class can only be achieved by following more stringent design rules related to the type, amount, and detailing of reinforcement. In this paper, an overview of the differences in the design criteria required to achieve a medium (DCM) and high (DCH) ductility class is presented. The difference in behaviour factor between these two ductility classes is 50%. Three buildings of different heights (40 m, 50 m, and 60 m) in which reinforced concrete walls are arranged around a central core are analysed. The dimensions of the core and the thickness of the walls were chosen primarily to achieve the required stiffness of the building and to meet the conditions for total and inter-story displacements. Seismic loads for ductility classes DCM and DCH were calculated for all buildings, and a seismic response spectrum analysis was performed. Finally, a seismic design of selected walls was performed for each ductility class according to EN 1998-1-1. The results show a difference in the required amount of reinforcement, and its placement, depending on the reinforcement type (B500B or B500C). The main difference in design was found to be the resistance to sliding shear failure, which requires additional angled reinforcement for DCH ductility class. Examples of reinforcement detailing are shown graphically for each ductility class. A conclusion is drawn regarding the advantages of choosing the highest ductility class, taking into account the cost of reinforcement.

Keywords: tall building, shear walls, reinforced concrete, seismic analysis, ductility

1. Introduction

Given the resurgence of seismic activity in Croatia in recent years, there is increasing interest in researching various earthquake-related topics. In Croatian practise, the modelling and design of structures is usually done according to the DCM rules, which place the structure in the medium ductility class. The high ductility class DCH is not a common requirement for structures, and for this reason there are very few case studies on its benefits and related design challenges.

The structural system with the reinforced concrete core and surrounding frames is one of the most widely used in high-rise building construction. The use of shear walls is equally represented in both high and low buildings. They are important parts of the structure that contribute significantly to lateral stiffness. They can be compared in their behaviour to vertical consoles, i.e., it can be said that these are "high consoles" fixed to the foundation. Together with the columns, they contribute to the transfer of vertical loads, and thus have a significant normal force. In some structures, coupled shear walls may be required, where the beams and the floor system connect the two or more walls together as a coupled system to provide greater stiffness. In tall buildings, shear walls are usually located in the centre of the building and typically form a central core that houses the vertical communication system such as stairwells and elevators. As such, they are a very common form of lateral load support system in tall buildings [1].

The response of high-rise buildings in earthquake areas is an essential criterion for seismic design. If the structure is "too stiff", greater internal forces will occur, and if it is "too soft", excessive displacements will occur. By properly selecting the type, quantity, position, and dimensions of

structural elements, we can achieve a balance between these two limitations. According to research [2] carried out on more than 2500 high-rise buildings in China, a diagram of typical relationships between building heights and fundamental vibration periods was given. Using this diagram, we can estimate how the building will react based on its stiffness.
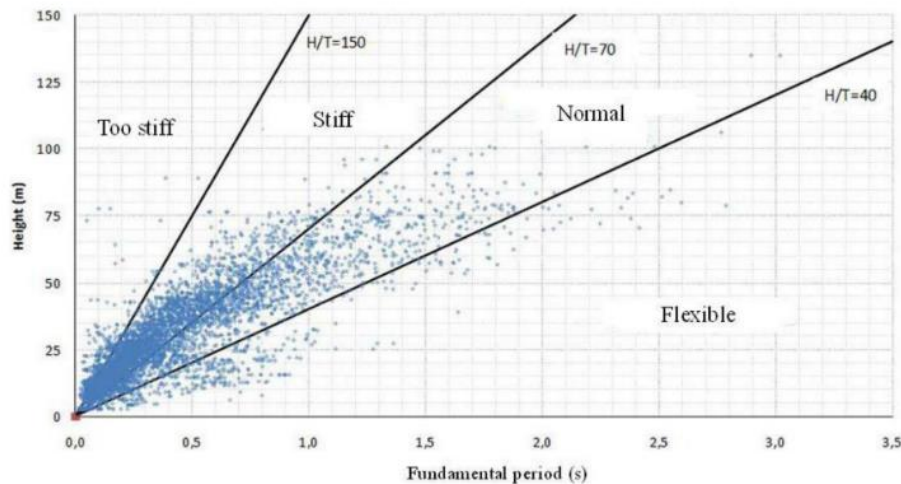
Figure 1. Relationship between fundamental periods and structural heights [2]

2. Ductility classes DCM and DCH

The ductility of the structure reflects its ability to maintain load-bearing capacity high in the plastic range, exhibiting high deformations before failure. Ductile structures are particularly important in seismic areas due to their energy dissipation properties, reflected by high enclosed area of the load-displacement hysteresis loops. Ductile behaviour in reinforced concrete structures can be achieved by special reinforcement design and detailing which results in adequate longitudinal reinforcement, stirrups for confinement of the compressed sections, and transverse or inclined reinforcement to prevent shear failure. The goal is to achieve ductile wall failure mode by yielding of the tensile reinforcement and wide cracks in the tension zone, rather than brittle compressive failure with crushing of the concrete and buckling of the reinforcement. In addition, shear failure modes such as diagonal tension and diagonal compression, as well as sliding shear in the region of the plastic joint, must be prevented. Sliding shear is attributed to the relatively low allowable compression, which is limited to only 40% of the concrete compressive strength for DCH according to the provisions of the Eurocode. By applying the rules for design and detailing of a selected ductility class, the desired behaviour of the structure can be achieved. As far as ductility class is concerned, HRN EN 1998-1 [3] makes the biggest difference in the design for shear, where DCH has much stricter rules compared to DCM. The multiplication factor for the design seismic shear force derived from the analysis is 1.5 for DCM, while for DCH it is calculated according to the expression (Table 1) and is limited to a value less than or equal to the behaviour factor. According to EN 1998 [3], the resistance to sliding shear failure must be checked for ductility class DCH. This resistance is composed of three parts: the resistance of the vertical bars, the resistance of the inclined bars and the frictional resistance. According to these design rules, the design was carried out for two case study walls and the results are presented in the continuation.

Table 1 (part 1) – EN 1998 rules for the detailing and dimensioning of ductile walls [4]

	DCH	DCM	DCL
Web thickness, $b_{w0} \geq$	max(150mm, $h_{storey}/20$)		-
critical region length, h_{cr}	$\geq$ max(l_w, $H_w/6$) $\leq$ min($2l_w$, h_{storey}) if wall $\leq$ 6 storeys $\leq$ min($2l_w$, $2h_{storey}$) if wall > 6 storeys		-

Table 1 (part 2) – EN 1998 rules for the detailing and dimensioning of ductile walls [4]

	DCH	DCM	DCL
Boundary elements:			
a) in critical region:			
- length l_c from edge $\geq$	0.15lw, 1.5bw, length over which $\varepsilon_c>0,0035$		-
- thickness b_w over o $l_c \geq$	0.2m; $h_{st}/15$ if $l_c\leq max(2b_w,l_w/5)$, $h_{st}/10$ if $l_c>max(2b_w, l_w/5)$		
- vertical reinforcement:			
ρ_{min} over $A_c=l_cb_w$	0,5%		0,2%
ρ_{max} over A_c	4%		
- confining hoops (w):			
$d_{bw} \geq$	6mm, $0.4(f_{yd}/f_{ywd})^{1/2}d_{bL}$	6mm	in the part of the section where $\rho_L>2$: as over the rest of the wall (case b, below)
spacing $s_w \leq$	$6d_{bL}$, $b_0/3$, 125mm	$8d_{bL}$, $b_0/2$, 175mm	
$\omega_{wd} \geq$	0,12	0,08	
$\alpha\omega_{wd} \geq$	$30\mu_\phi(\nu_d+\omega_v)\varepsilon_{sy,d}b_w/b_0-0,035$		
b) over the rest of the wall height:	In parts of the section where $\varepsilon_c>0,2$%: $\rho_{v,min}=0,5$%; elsewhere 0,2% In parts of the section where $\rho_L >2$%: distance of unrestrained bar in compression zone from nearest restrained bar $\leq$150mm; hoops with $d_{bw}\geq max(6mm, d_{bL}/4)$ & spacing $s_w\leq min(12d_{bL}, 0.6b_{w0}, 240mm)$ up to a distance of $4b_w$ above or below floor beams or slabs, or $s_w\leq min(20d_{bL}, b_{w0}, 400mm)$) beyond that distance		
Web:			
- vertical bars (v):			
$\rho_{v,min}$	Wherever in the section $\varepsilon_c>0,2$%: 0,5%; elsewhere 0,2%		0,2%
$\rho_{v,max}$	4%		
$d_{bv}\geq$	8mm	-	
$d_{bv}\leq$	$b_{w0}/8$	-	
spacing $s_v\leq$	min($25d_{bv}$, 250mm)	min($3b_{w0}$, 400mm)	
- horizontal bars:			
$\rho_{h,min}$	0,2%	max(0.1%, $0.25\rho_v$)	
$d_{bh}\geq$	8mm	-	
$d_{bh}\leq$	$b_{w0}/8$	-	
spacing $s_h\leq$	min($25d_{bh}$, 250mm)	400mm	
axial load ratio $\nu_d=N_{Ed}/A_cf_{cd}$	$\leq$0,35	$\leq$0,4	-
Design moments M_{Ed}:	If $H_w/l_w\geq2$, design moments from linear envelope of maximum moments M_{Ed} from analysis for the "seismic design situation", shifted up by the "tension shift" a_I		from analysis for design seismic action & gravity

Table 1 (part 3) – EN 1998 rules for the detailing and dimensioning of ductile walls [4]

	DCH	DCM	DCL
Shear design:			
Design shear force V_{Ed} = shear force V'_{Ed} from the analysis for the design seismic action, times factor ε	if $H_w/l_w \leq 2$: $\quad$ $\varepsilon = 1.2 M_{Rd0}/M_{Ed0} \leq q$ if $H_w/l_w > 2$: $\varepsilon = \sqrt{\left(1.2 \dfrac{M_{Rd0}}{M_{Ed0}}\right)^2 + 0.1\left(q\dfrac{S_e(T_C)}{S_e(T_{C1})}\right)^2} \leq q$	ε=1.5	ε=1.0
$V_{Rd,max}$ outside critical region	As in EC2: $V_{Rd,max} = 0{,}3(1 - f_{ck}(MPa)/250)b_{w0}(0{,}8l_w)f_{cd}sin2\delta,\ 1 \leq cot\delta \leq 2{,}5$		
$V_{Rd,max}$ in critical region	40% of EC2 value	As in EC2	
$V_{Rd,s}$ in critical region; web reinforcement ratios: ρ_h, ρ_v			
(i) if $\alpha_s = M_{Ed}/V_{Ed}l_w \geq 2$: $\rho_v = \rho_{v,min}$, ρ_h from $V_{Rd,s}$:	$V_{Rd,s} = b_{w0}(0{,}8l_w)\rho_h f_{ywd}$	As in EC2: $V_{Rd,s} = b_{w0}(0{,}8l_w)\rho_h f_{ywd}cot\delta,$ $1 \leq cot\delta \leq 2{,}5$	
(ii) if $\alpha_s < 2$: ρ_h from $V_{Rd,s}$	$V_{Rd,s} = V_{Rd,c} + b_{w0}\alpha_s(0{,}75l_w)\rho_h f_{yhd}$	As in EC2: $V_{Rd,s} = b_{w0}(0{,}8l_w)\rho_h f_{ywd}cot\delta,$ $1 \leq cot\delta \leq 2{,}5$	
ρ_v from:	$\rho_v f_{yvd} = \rho_h f_{yhd} - N_{Ed}/(0{,}8l_w b_{w0})$		
Resistance to sliding shear: via bars with total area A_{si} at angle α to the horizontal	$V_{Rd,s} = A_{si}f_{yd}cos\alpha +$ $A_{sv}\min\left(0{,}25f_{yd}, 1{,}3\sqrt{(f_{yd}f_{cd})}\right) +$ $0{,}3(1 - f_{ck}(MPa)/250)b_{w0}f_{cd}$		

3. Worked examples

3.1 Buildings for comparison – layout and height

A comparison of the analysis and design is given for buildings with three different heights, all of which have the same fixed arrangement of elements in the floor plan. The heights vary between 40 m, 50 m and 60 m. Fig. 2 shows the arrangement of the elements in the floor plan of each building. The floor plan is symmetrical in both directions, with a central reinforced concrete core and frames arranged around it. The reinforced concrete core is the primary horizontal load-bearing element and consists of a closed walled section 8.0 x 8.0 m in size. Access to the core, which houses all vertical communications is provided through two openings in opposing walls, thus creating a coupled wall system. The openings in the walls of the core are 2.0 x 2.1 m in size. The height of the floor ranges from 2.95 m to 3.1 m, depending on the height of the building. Since the focus of the design is on the walls, their thickness varies depending on the height of the model and the position of the walls along the height of the building. For the 40-meter-high building, the walls of the first five floors are 40 cm thick, and the walls of the next eight floors have a thickness of 30 cm. In the 50-meter building model, the first seven floors have a wall thickness of 50 cm, and the remaining ten floors have a wall thickness of 40 cm. In the last model, the tallest building, the first eight floors have a wall thickness of 60 cm, and the remaining eleven floors have a wall thickness of 50 cm. These wall thicknesses were chosen according to the dynamic analysis to calibrate the behaviour of the building to the expected periods of the modal shapes and to limit the amount of compressive stress in the wall according to the ductility class requirements. Inter storey drift and displacements at the top of the buildings were also checked and limited to H/500 restriction. All columns have the same constant cross-section, 50 x 50 cm, throughout the entire height of the building in all models. The dimensions of the beams are 50 x 50 cm and are the same throughout the height of

the building. The horizontal diaphragms (slabs) are 16 cm thick. All vertical elements are fixed at the bottom to simulate a rigid underground foundation level, which was not modelled (Fig. 3). The material used was concrete of class C50/60.
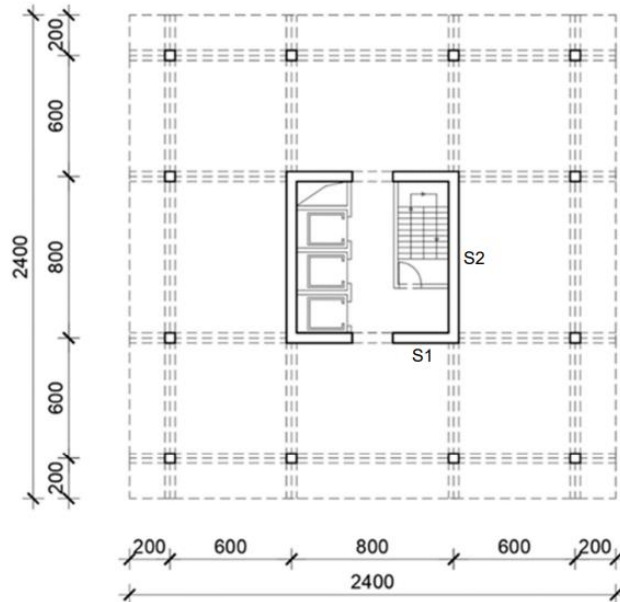
Figure 2. Characteristic floor plan of the building considered in the design
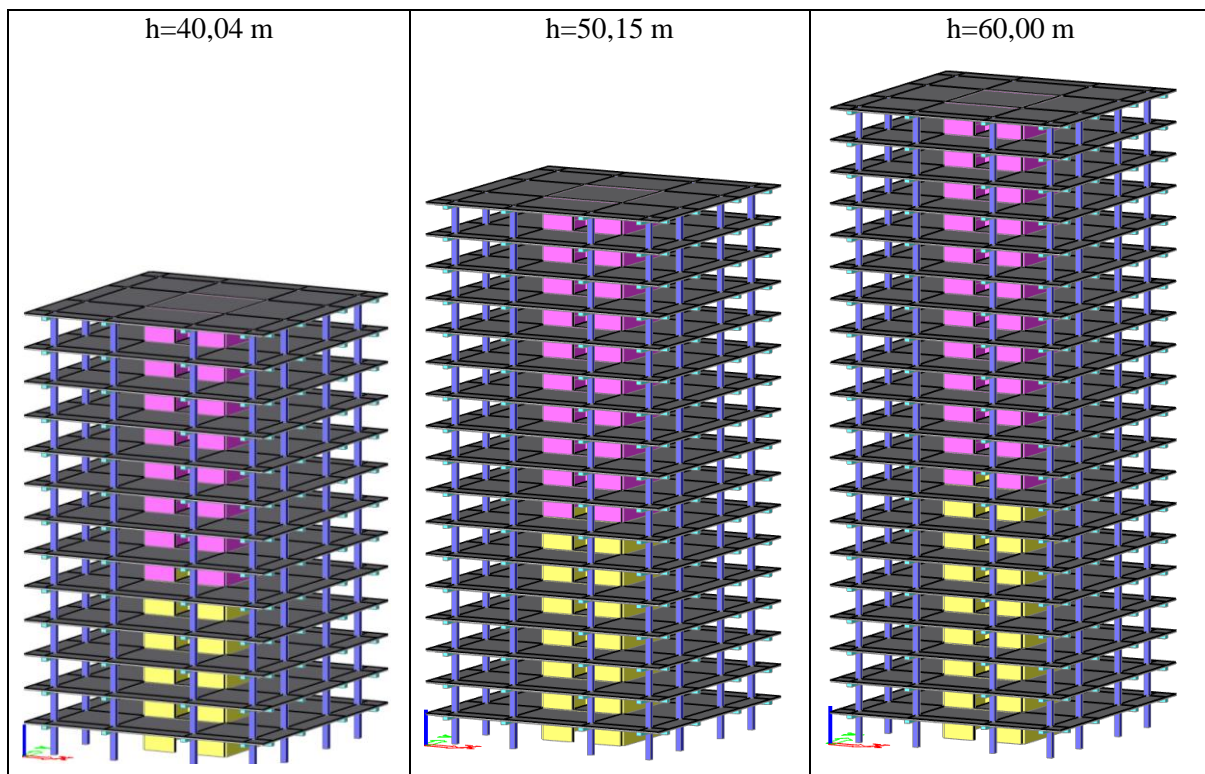
Figure 3. 3D view of three models

3.2 Modal analysis and behaviour

The behaviour factor q was determined according to the instructions given in EN 1998-1-1 and is calculated as 3.6 for DCM, and 5.4 for DCH. Based on these values, two spectres were defined, and a modal analysis was performed in the software. The 3D numerical model was developed using finite element method (FEM) in software for static analysis. All load bearing elements are defined in the model, while the non-bearing ones are taken into account with additional dead load. Walls and slabs are defined using shell elements, with the mesh size of 25x25 cm, while the 1D beam elements were defined with corresponding cross sections. All vertical elements are placed on rigid supports (in node for 1D and on bottom edge for 2D elements) on the bottom of the ground floor. The modulus of elasticity of the horizontal diaphragms, the slabs, is 37300 MPa. According to HRN EN 1998-1-4.3.1(7), the modulus of elasticity of all other concrete elements is to be taken as half the value, 18650 MPa, due to the assumption of the cracked concrete sections. Modal spectral analysis is performed, with 20 eigenvalues for each of the three models, to be in accordance with the minimum number of modes, equal to the $3\sqrt{n}$, where the n is the number of floors. Tables 2-4 show the results of the modal analysis, and Fig. 4 shows the design spectra with plotted corresponding values of buildings first periods.

Table 2 – Modal analysis results for building h = 40 m

Mode	Omega [rad/s]	Period [s]	Freq. [Hz]	W_{xi}/W_{xtot}	W_{yi}/W_{ytot}	W_{zi}/W_{ztot}	W_{xi_R}/W_{xtot_R}	W_{yi_R}/W_{ytot_R}	W_{zi_R}/W_{ztot_R}
1	6,87508	0,91	1,09	0,6911	0	0	0	0,2565	0,0001
2	7,4443	0,84	1,18	0	0,6507	0	0,2921	0	0,0005
3	8,22718	0,76	1,31	0,0001	0,0004	0	0,0002	0	0,7817
4	23,5615	0,27	3,75	0,1727	0	0	0	0,3901	0,0001
5	24,2208	0,26	3,85	0,0002	0	0	0,0001	0,0005	0,1198
6	28,1011	0,22	4,47	0	0,0921	0,001	0,3625	0	0
7	28,7503	0,22	4,58	0,0002	0,0003	0,6738	0,0005	0,0015	0
8	29,76	0,21	4,74	0,0081	0,0001	0,0152	0,0001	0,0496	0
9	32,158	0,2	5,12	0	0,1181	0,0001	0,0281	0	0
10	40,3878	0,16	6,43	0	0	0	0	0	0,0421
11	46,4411	0,14	7,39	0,0512	0	0	0	0,0939	0
12	55,93	0,11	8,9	0	0	0	0	0	0,0201
13	60,6207	0,1	9,65	0	0	0,0642	0	0,0005	0
14	60,8107	0,1	9,68	0	0,0258	0	0,0962	0	0
15	61,6163	0,1	9,81	0,0002	0	0,0026	0	0,0127	0
16	64,2709	0,1	10,23	0	0,0389	0	0,0286	0	0
17	68,8677	0,09	10,96	0,0226	0	0	0	0,0558	0,0001
18	69,1251	0,09	11	0,0001	0	0	0	0,0002	0,0128
19	69,8406	0,09	11,12	0,0001	0	0,0202	0	0,0001	0
20	71,5292	0,09	11,38	0	0	0	0	0	0
				0,9466	0,9263	0,7773	0,8084	0,8616	0,9772

Table 3 – Modal analysis results for building h = 50 m

Mode	Omega [rad/s]	Period [s]	Freq. [Hz]	W_{xi}/W_{xtot}	W_{yi}/W_{ytot}	W_{zi}/W_{ztot}	W_{xi_R}/W_{xtot_R}	W_{yi_R}/W_{ytot_R}	W_{zi_R}/W_{ztot_R}
1	5,16589	1,22	0,82	0,6806	0,0001	0	0	0,2878	0
2	5,5102	1,14	0,88	0,0001	0,6409	0	0,3242	0	0,0001
3	6,87628	0,91	1,09	0	0,0001	0	0,0001	0	0,7782
4	18,3599	0,34	2,92	0,1794	0	0	0	0,3623	0
5	20,501	0,31	3,26	0	0,0001	0	0,0002	0,0001	0,1158
6	22,8246	0,28	3,63	0	0,155	0	0,3286	0	0,0001
7	24,3841	0,26	3,88	0,0001	0,0001	0,6635	0	0,0006	0
8	25,4948	0,25	4,06	0,0048	0	0,0094	0	0,026	0
9	26,7396	0,23	4,26	0	0,052	0,0003	0,0023	0	0
10	34,9582	0,18	5,56	0	0	0	0	0	0,0423
11	37,2832	0,17	5,93	0,0506	0	0	0	0,0995	0
12	49,163	0,13	7,82	0	0	0	0	0	0,0218
13	51,6847	0,12	8,23	0	0,06	0	0,1335	0	0
14	54,1018	0,12	8,61	0,0002	0	0,0478	0	0,0018	0
15	54,5276	0,12	8,68	0,0007	0	0,0215	0	0,003	0
16	55,4021	0,11	8,82	0	0,0087	0,0001	0,0004	0	0
17	56,5972	0,11	9,01	0,0256	0	0	0	0,0657	0
18	61,5051	0,1	9,79	0	0	0	0	0	0,0129
19	66,9404	0,09	10,65	0	0	0,0216	0	0	0
20	69,0877	0,09	11	0,0001	0	0	0	0,0023	0
				0,9422	0,9169	0,7643	0,7894	0,8492	0,9712

Table 4 – Modal analysis results for building h = 60 m

Mode	Omega [rad/s]	Period [s]	Freq. [Hz]	W_{xi}/W_{xtot}	W_{yi}/W_{ytot}	W_{zi}/W_{ztot}	W_{xi_R}/W_{xtot_R}	W_{yi_R}/W_{ytot_R}	W_{zi_R}/W_{ztot_R}
1	4,19184	1,5	0,67	0,6663	0,0002	0	0,0001	0,3126	0
2	4,31474	1,46	0,69	0,0002	0,6339	0	0,3422	0,0001	0
3	6,35601	0,99	1,01	0	0	0	0	0	0,7822
4	15,7529	0,4	2,51	0,1894	0	0	0	0,3382	0
5	18,9387	0,33	3,01	0	0,0206	0	0,0322	0	0,0981
6	19,0886	0,33	3,04	0	0,165	0	0,261	0	0,0124
7	21,9378	0,29	3,49	0	0	0,6545	0	0,0002	0
8	23,1493	0,27	3,68	0,0041	0	0,0059	0	0,0115	0
9	23,8354	0,26	3,79	0	0,0189	0,0003	0,0004	0	0
10	32,2195	0,2	5,13	0,0001	0	0	0	0,0003	0,041
11	32,7902	0,19	5,22	0,0525	0	0	0	0,1068	0,0001
12	44,318	0,14	7,05	0	0,0682	0	0,1349	0	0
13	45,5048	0,14	7,24	0	0	0	0	0	0,0216
14	48,943	0,13	7,79	0,0012	0	0,0193	0	0,0008	0
15	49,3369	0,13	7,85	0,001	0	0,0491	0	0	0
16	49,6946	0,13	7,91	0	0,0022	0,0004	0,0008	0	0
17	50,3042	0,12	8,01	0,0241	0	0,0003	0	0,0673	0
18	57,3445	0,11	9,13	0	0	0	0	0	0,013
19	63,8374	0,1	10,16	0	0	0,0215	0	0	0
20	65,1029	0,1	10,36	0,0002	0	0,0003	0	0,001	0
				0,9393	0,9092	0,7517	0,7715	0,8387	0,9684
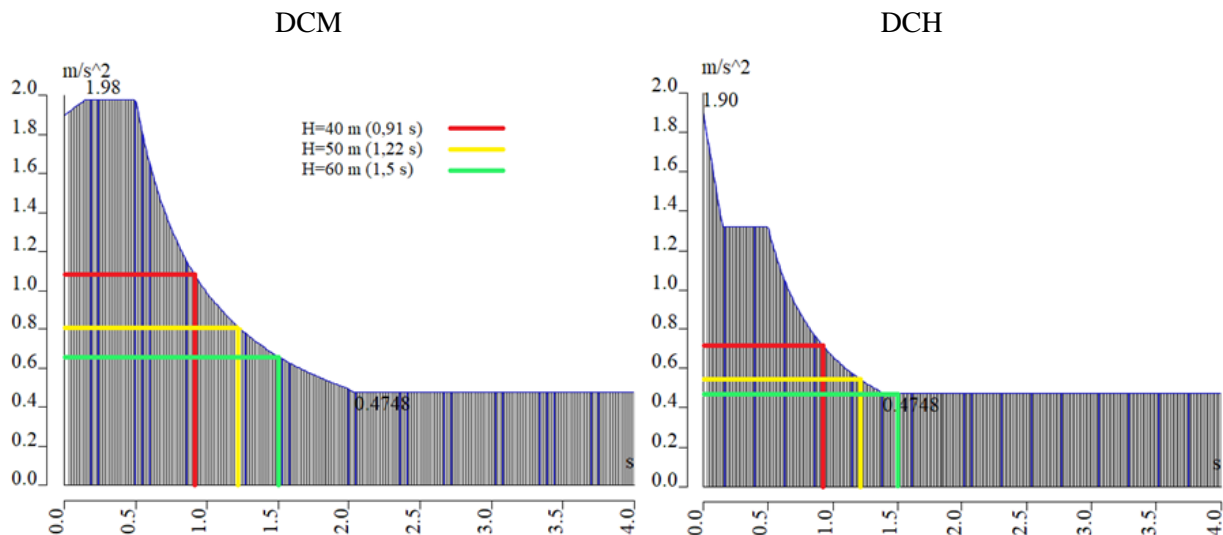
Figure 4. The relationship between the period and the response for each height of the building and ductility class

4. Reinforcement comparison for different ductility classes

Design and comparison of the results was done for two intersecting walls on the ground floor of each model - S1 shorter wall and S2 longer wall (Fig. 2). Reinforcement design results and comparison can be observed in Table 5. The main difference in the reinforcement concerning the ductility class is in the stirrups spacing. The curvature ductility factor μ_φ varies greatly depending on the final ductility of the structure we want to achieve, and it will affect the stirrups spacing. For DCM either B500B or B500C reinforcement can be used, while for DCH only B500C reinforcement is allowed. If B500B reinforcement steel is used, curvature ductility factor μ_φ must be taken 50% higher which places it close to curvature ductility factor μ_φ according to DCH design (Table 6). Thus, there is only a small difference in the stirrup spacing between DCM and DCH when B500B is used in DCM design compared to the case when B500C is used for both DCM and DCH design. Furthermore, to achieve a high ductility class (DCH) it is necessary to meet shear resistance requirements which are much demanding in relation to the requirements for the medium class of ductility (DCM). Conditions for both ductility classes are shown in Table 1 (part 3). Fig. 5 shows reinforcement for DCM design of a 50 m high building.

Table 5 – Comparison of design reinforcement for DCM and DCH ductility class design

Model/Wall	Web		Boundary elements		
	Vertical bars	Horizontal bars	Vertical bars	Stirrups	Inclined bars
H40/S1 (DCM)	±Ø12/10 cm	±Ø12/10 cm	14Ø16	Ø12/12 cm	-
H40/S1 (DCH)	±Ø12/10 cm	±Ø12/10 cm	12Ø16	Ø12/8 cm	±7Ø32
H50/S1 (DCM)	±Ø12/10 cm	±Ø12/10 cm	16Ø16	Ø12/12 cm	-
H50/S1 (DCH)	±Ø12/10 cm	±Ø12/10 cm	16Ø16	Ø12/9 cm	±9Ø32
H60/S1 (DCM)	±Ø12/9 cm	±Ø12/9 cm	18Ø16	Ø12/12 cm	-
H60/S1 (DCH)	±Ø12/10 cm	±Ø12/10 cm	18Ø16	Ø12/9 cm	±8Ø32
H40/S2 (DCM)	±Ø12/10 cm	±Ø12/10 cm	28Ø16	Ø12/18 cm	-
H40/S2 (DCH)	±Ø12/10 cm	±Ø12/10 cm	28Ø16	Ø12/9 cm	±16Ø28
H50/S2 (DCM)	±Ø12/10 cm	±Ø12/10 cm	24Ø20	Ø12/18 cm	-
H50/S2 (DCH)	±Ø12/10 cm	±Ø12/10 cm	24Ø20	Ø12/10 cm	±17Ø28
H60/S2 (DCM)	±Ø12/9 cm	±Ø12/9 cm	28Ø20	Ø12/20 cm	-
H60/S2 (DCH)	±Ø12/10 cm	±Ø12/10 cm	28Ø20	Ø12/12 cm	±15Ø28

Table 6 – The curvature ductility factor and stirrups spacing for each ductility class and reinforcement type

Model	DCM/DCH (B500B/B500C)	Wall	Curvature ductility factor μ_φ	Stirrups
H40	DCM (B500B)	S1	9,3	Ø12/8 cm
		S2	9,3	Ø12/10 cm
	DCM (B500C)	S1	6,2	Ø12/12 cm
		S2	6,2	Ø12/18 cm
	DCH (B500C)	S1	9,8	Ø12/8 cm
		S2	9,8	Ø12/9 cm
H50	DCM (B500B)	S1	9,3	Ø12/9 cm
		S2	9,3	Ø12/10 cm
	DCM (B500C)	S1	6,2	Ø12/12 cm
		S2	6,2	Ø12/18 cm
	DCH (B500C)	S1	9,8	Ø12/8 cm
		S2	9,8	Ø12/10 cm
H60	DCM (B500B)	S1	9,3	Ø12/9 cm
		S2	9,3	Ø12/12 cm
	DCM (B500C)	S1	6,2	Ø12/12 cm
		S2	6,2	Ø12/20 cm
	DCH (B500C)	S1	9,8	Ø12/9 cm
		S2	9,8	Ø12/12 cm

Sliding shear resistance is particularly important in this comparison because this proof is needed only in DCH design. Sliding shear can occur only in the region of a plastic hinge and particularly at the position of a construction joint (Fig. 6) [5]. The design shear force is to be multiplied with a factor ε which is 1.5 for DCM, while the expression for DCM yields a much larger factor equal to DCH behaviour factor of 5.4. To achieve a high sliding shear resistance needed for such a large design shear force, it is necessary to use an angled "X" shaped reinforcement in the region of the plastic hinge (Fig. 6). Without this reinforcement it is impossible to meet the sliding shear design requirements for DCH ductility class. Fig. 7 shows DCH reinforcement with bidiagonal bars for a 50 m high building.
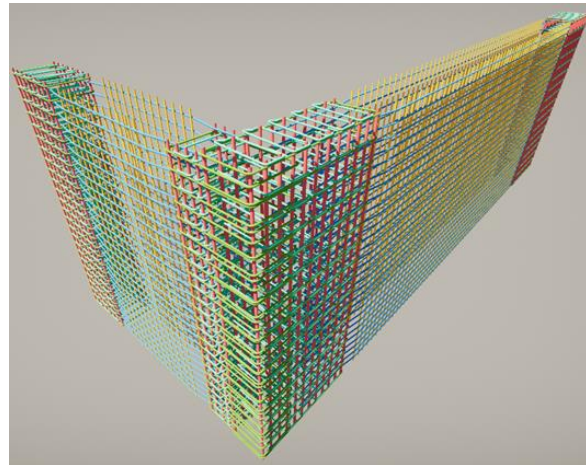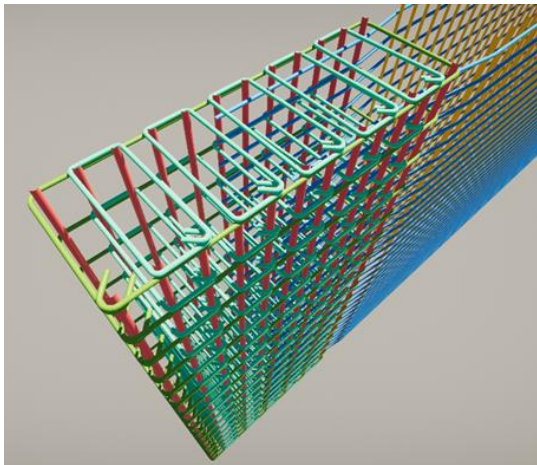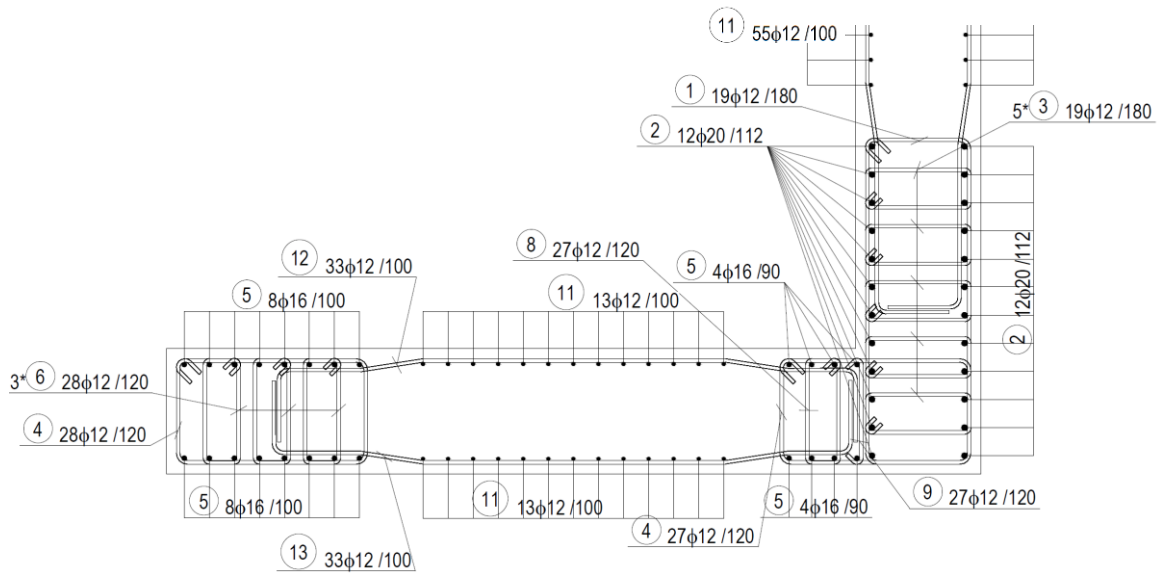
Figure 5. Reinforcement: boundary element and the crossing of two walls (DCM design, building height 50 m)
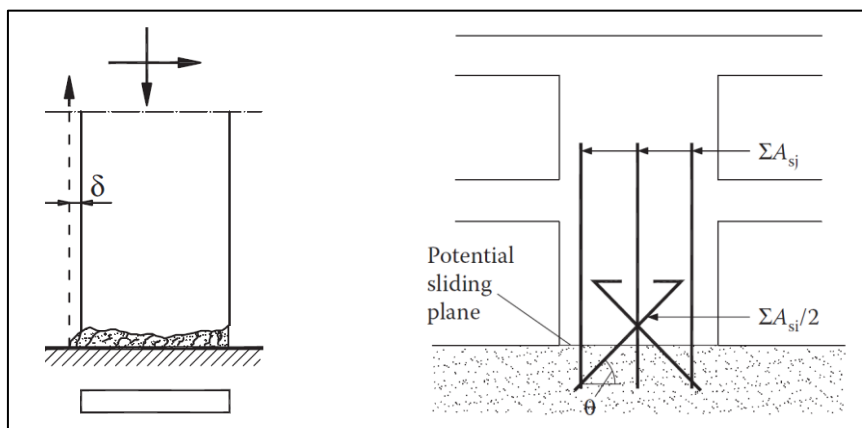
Figure 6. Sliding shear failure and bidiagonal X shaped reinforcement for added resistance [5]
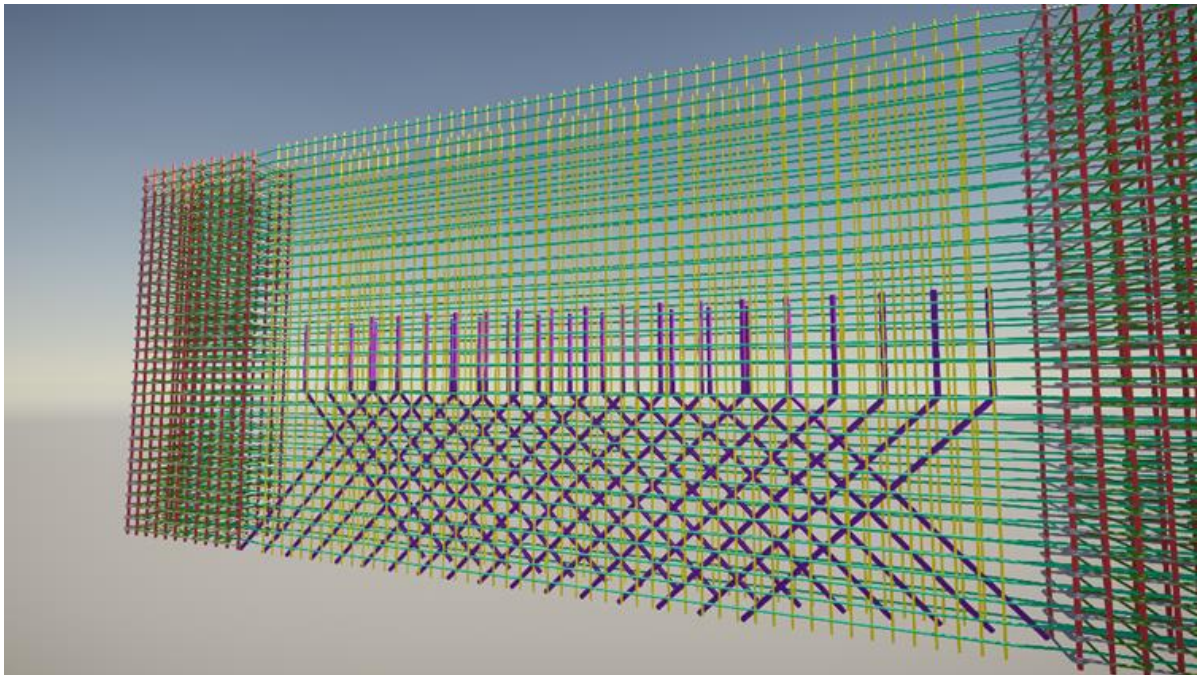
Figure 7. Bidiagonal X shaped reinforcement for sliding shear (DCH design)

5. Conclusion

Worked examples show that when the element is designed according to the DCM rules with the use of B500B reinforcing steel compared to the design of the same element according to the DCH rules with B500C reinforcing steel, the only major difference is the need for inclined reinforcement to prevent sliding shear failure. The DCM design, such verification is not required, so no inclined reinforcement is needed. When reinforcement steel class B500C is used for both designs, the possible stirrup spacing in the boundary element is significantly larger when designing according to the DCM rules. The reason for this is the required ductility, which is higher for the DCH design than for the DCM design when B500C class reinforcing steel is used. The required ductility depends on the behaviour factor and the first period. Since the behaviour factor for DCM and DCH is not the same, the required ductility is also not the same. Using B500B steel in the DCM design according to HRN EN 1998-1 [3] increases the required ductility by 50%, which brings it significantly closer to the ductility calculated for DCH. This ultimately leads to equal spacing of stirrups in the boundary element.

As mentioned earlier, one of the main differences in the design between DCM and DCH is the design for shear. The DCH requires a much more stringent constraint on shear resistance compared to the DCM method. Under the DCH design, shear resistance must satisfy three checks: diagonal compression failure of the web due to shear, diagonal tension failure of the web due to shear, and sliding shear failure. The DCM method also provides checks for diagonal compression and diagonal tension failure of the web due to shear, but the major difference is in the factorization of the shear force. In DCM, the factor by which the design shear force from the seismic analysis is multiplied is 1.5, while in DCH it is much higher and is limited only to the maximum value of q (Table 1).

At the time of writing, the price difference between B500B and B500C reinforcing steel is about 15%, with B500C being more expensive. If we add the necessary inclined reinforcement, the placement of which significantly complicates the execution and concreting, thus increasing the construction costs, the economic viability of such a design and construction for the seismic zone as analysed in this work, is questionable.

References

[1]   F. Fu, Design and Analysis of Tall and Complex Structures, Butterworth-Heinemann Elsevier, Cambridge, Massachusetts, 2018.

[2]   P. Xu, C. Xiao, J. Li, International Journal of High-Rise Buildings 3 (2014) 49–64.

[3]   HRN EN 1998-1 Eurocode 8: Design of Structures for Earthquake Resistance – Part 1: General Rules, Seismic Actions and Rules for Buildings (EN 1998-1:2004+AC:2009), Croatian Standards Institute, Zagreb, 2011.

[4]   P. Bisch, E. Carvalho, H. Degee, P. Fajfar, M. Fardis, P. Franchin, M. Kreslin, A. Pecker, P. Pinto, A. Plumier, H. Somja, G. Tsionis, Eurocode 8: Seismic Design of Buildings Worked Examples, Luxembourg, 2012.

[5]   G.G. Penelis, G.G. Penelis, Concrete Buildings in Seismic Regions, CRC Press, Taylor & Francis Group, Boca Raton, Florida, 2014.

THE BUILDING CODE SIA 269/8 FOR A RISK-BASED SEISMIC SAFETY ASSESSMENT AND RETROFIT OF STRUCTURES IN SWITZERLAND

Blaise Duvernay [(1)],

[(1)] *Head of Earthquake Risk Mitigation, Swiss Federal Office for the Environment, blaise.duvernay@bafu.admin.ch*

Abstract

This contribution presents the central concepts of the swiss building code SIA 269/8 [1] for the verification of the seismic safety of existing structures.

The first central concept of SIA 269/8 is the compliance factor. It indicates the degree of compliance of an existing structure in comparison with the requirements for new structures. The second central concept is the recommendation of measures based on the value of the compliance factor. If the seismic safety of an existing structure lies below a minimum threshold value of the compliance factor, retrofitting is mandatory to reach this minimum threshold whatever the costs. If the compliance factor is smaller than 1.0 and higher or equal to the minimum compliance factor, only efficient measures, with a risk reduction greater than the costs, have to be implemented.

The third central concept of SIA 269/8 is the evaluation of the commensurability of measures through the explicit computation of their efficiency. The risk reduction is computed using a set of standardized curves linking the compliance factor with different risk unit values. The efficiency is computed as the ratio between the risk reduction in Swiss francs (CHF) per year and the annualized cost of measures. For the computation of the risk reduction for human life, a value of statistical life of 10 million Swiss francs is used.

This elegant and relatively simple framework allows to focus retrofit measures for constructions with an unacceptable risk level as well as for constructions for which commensurate retrofit measures can be found. It has been widely applied in Switzerland since 2004 and is well accepted in practice.

Keywords: building code, existing structures, seismic safety, retrofit, risk-based

1. Introduction

The prestandard SIA 2018 [2] for the seismic safety verification and retrofit of existing buildings in Switzerland was published in 2004 and updated as the SIA 269/8 building code [1] in December 2017. SIA 269/8 extends the application domain to other construction types than buildings and extends the available standardized methodologies to compute the risk reduction through seismic retrofit measures to other risks than the risk to human life.

The risk-based concepts of SIA 2018 and SIA 269/8 have been applied since 2004 . They show an adequate balance between a consistent probabilistic risk-based framework and the necessary ease of use for a broad application in practice. A large number of seismic verifications and retrofits of existing buildings and bridges have been performed in Switzerland using these standards, such as documented in [3]. They usually happen in the framework of global retrofit or transformation projects.

2. Compliance factor and recommendation of measures

The first central concept of SIA 269/8 is the **compliance factor α_{eff},** which indicates the degree of compliance of an existing structure with the requirements for new structures in the building code SIA 261 [4].

For constructions of importance class I (ordinary constructions, such as habitation and commercial buildings) and II (constructions with a higher human occupancy and content value), the **minimum compliance factor α_{min}** is 0,25. Below this minimum compliance factor, the safety of individuals is

deemed unacceptable with an expected annual probability of death exceeding 10^{-5} (see also Fig. 2a). For constructions of importance class III (vital infrastructure function), II-s (school buildings) and II-i (important infrastructure function), the minimum compliance factor α_{min} is 0,40.

The second central concept of SIA 269/8 is the **recommendation of measures,** which is derived from the level of the compliance factor after a seismic safety verification (α_{eff}) such as depicted in Fig. 1.
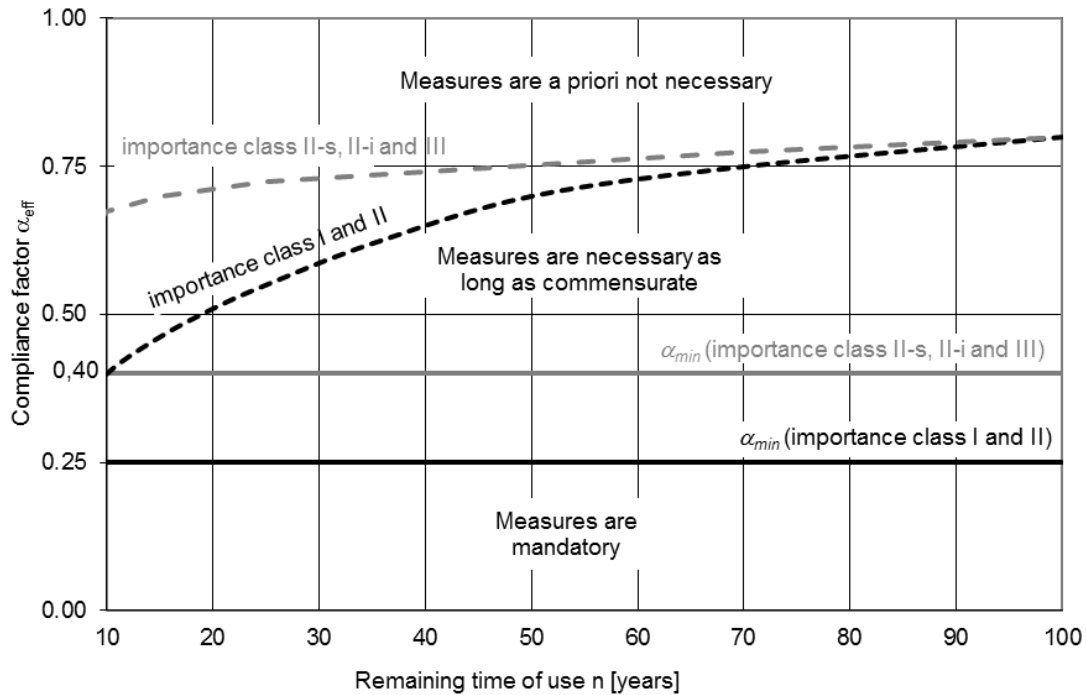
Fig. 1 - Recommendations of measures according to the new SIA building code 269/8.

Three cases are distinguished:

1. If the compliance factor α_{eff} is lower than α_{min}, retrofit measures are mandatory in order to reach a compliance factor after intervention (α_{int}) at least equal to α_{min}. The efficiency of possible further retrofit measures to achieve a higher compliance factor than α_{min} must be evaluated according to case 2.

2. If the compliance factor α_{eff} is between α_{min} and the dashed curve , then concepts for retrofit measures must be developed and implemented if they are *commensurate*. The objective is to reach a compliance factor of 1,0. If this is not possible, measures must be implemented until the limit of commensurability is reached. If no commensurate measures can be found then the level of seismic safety can be accepted as is.

3. If the compliance factor α_{eff} is above the dashed line in Figure 1, commensurate measures are probably impossible to find and the level of seismic safety can be accepted as is.

3. Computation of the commensurability of measures

In SIA 269/8 commensurate measures are defined as measures with an efficiency $EF_M \geq 1$. The efficiency of measures EF_M is defined as the ratio between the annualized risk reduction ΔR_M in Swiss francs per year and the annualized cost of measures SC_M (Eq. 1).

$$EF_M = \Delta R_M / SC_M \qquad (1)$$

3.1 Computation of risk reduction

To compute the different components of the yearly risk reduction ΔR_M, SIA 269/8 provides standardized curves that link the compliance factor with different risk units (Fig 2.) or the willingness to pay to protect the infrastructure function (Fig. 3). The curves in Fig. 2 were derived from probabilistic risk studies such as in [5] and [6]. The curves in Fig. 3 were set based on the empirical observation of the willingness to pay for seismic retrofit measures by constructions with an important or vital infrastructure function. The risk curves in Fig. 2 are only used for the domain of compliance factors $\geq \alpha_{min}$, to compute the commensurability of measures.

<center>(a)</center> <center>(b)</center>
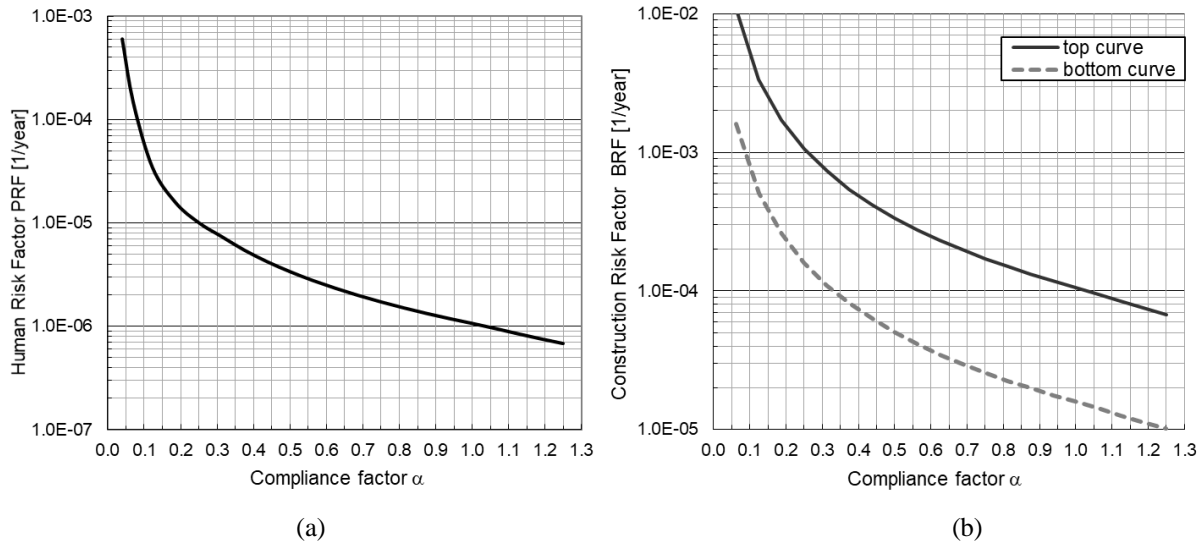
<center>Fig. 2 – Human risk factor curve (a) and construction risk factor curve (b).</center>
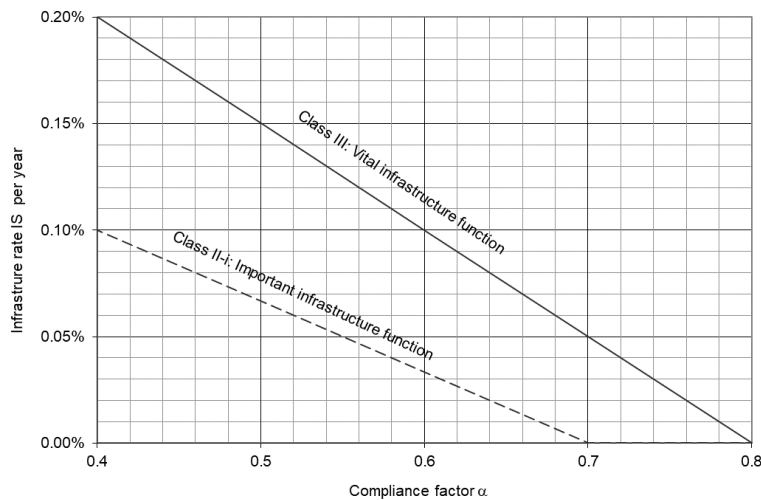
<center>Fig. 3 – Infrastructure rate curves to compute the willingness to pay to protect the infrastructure function</center>

Fig. 2a is a risk curve linking the compliance factor with the human risk factor *PRF*. *PRF* is the probability of death per year per unit of average human occupancy in the construction. The risk reduction related to human casualties ΔRP_M is computed according to Eq. (2) as the difference between the human risk factor ΔPRF_M before and after retrofit, multiplied by the average human occupancy in the construction *PB* and a value of statistical life *GRK* set as CHF 10 million.

$$\Delta RP_M = \Delta PRF_M \cdot PB \cdot GRK \tag{2}$$

Fig. 2b has two risk curves linking the compliance factor with a construction risk factor *BRF*. *BRF* is the probability of loss per year per unit of the replacement value of the construction. The risk reduction related to the direct damage to the construction ΔRB_M is computed according to Eq. 3 as the difference between the construction risk factor ΔBRF_M before and after retrofit, multiplied by replacement value of the construction *BW*. For constructions with a high proportion of secondary elements, such as buildings, the upper curve in Fig. 2b is used. For constructions with a low proportion of secondary elements, such as bridges or retaining walls, the lower curve in Fig. 2b is used.

$$\Delta RB_M = \Delta BRF_M \cdot BW \tag{3}$$

SIA 269/8 also provides methods to estimate the risk reduction for the content value ΔRS_M as well as the business interruption ΔRU_M. The computation of ΔRS_M and ΔRU_M is based on ΔBRF_M according to Fig. 2b. ΔRS_M is computed according to Eq. (4) as ΔBRF_M multiplied by the replacement value of the content *SW* that can be damaged by the construction collapse and a calibration factor *SRF*. Depending on the situation *SRF* take on value of 0.05 or 0.2. ΔRU_M is computed according to Eq. (5) as ΔBRF_M multiplied by the cost of business interruption *UK* over the estimated interruption time and a calibration factor *URF* of 0.5. For ordinary buildings, ΔRS_M and ΔRU_M are usually negligible.

$$\Delta RS_M = SRF \cdot \Delta BRF_M \cdot SW \tag{4}$$

$$\Delta RU_M = URF \cdot \Delta BRF_M \cdot UK \tag{5}$$

For constructions of importance class III (vital infrastructure function) and II-i (important infrastructure function), the efficiency of measures is computed using the concept of willingness to pay to protect the infrastructure function ΔZI_M. ΔZI_M is computed using Fig. 3, which relates a so-called infrastructure rate *IS* with the compliance factor. ΔZI_M is computed according to Eq. (6) as the difference in infrastructure rate ΔIS_M before and after retrofit multiplied by the replacement value of the construction and the directly impacted goods *BSW* (usually the value of the construction and its content).

$$\Delta ZI_M = \Delta IS_M \cdot BSW \tag{6}$$

The total risk reduction ΔR_M for constructions of importance classes COI, COII and COII-s is the sum of the risk reduction contributions such as given by Eq. (7). The total risk reduction ΔR_M for constructions of importance classes COII-i and COIII is given by Eq. (8).

$$\Delta R_M = \Delta RP_M + \Delta RB_M + \Delta RS_M + \Delta RU_M \tag{7}$$

$$\Delta R_M = \Delta RP_M + \Delta ZI_M \tag{8}$$

According to SIA 269/8, it is mandatory to consider the risk reduction for human casualties ΔRP_M and the willingness to pay to protect the infrastructure function ΔZI_M for the computation of the efficiency of measures. It is only recommended to consider other risk reductions such as ΔRB_M, ΔRS_M, ΔRU_M.

3.2 Computation of the yearly cost of measures

The yearly cost of measures SC_M is computed according to Eq. (9) as the cost of retrofit measures SIC_M multiplied by a discounting factor *DF*. *DF* is determined according to Eq. (10) using the remaining time of use of the construction *dr* in years and a discounting rate *i* of 2 % per year.

$$SC_M = SIC_M \cdot DF \tag{9}$$

$$DF = i \cdot (1 + i)^{dr} / [(1 + i)^{dr} - 1] \tag{10}$$

3.3 Computation of limit costs for commensurable measures

Using the equations presented in 3.1 and 3.2, it is possible to compute the limit costs of retrofit measures so that $EF_M = 1.0$ for a known initial situation and a target compliance factor after retrofit. The general formulation for these limit costs SIC_{Mlim} is given in Eq. (11), with ΔR_M being the risk reduction that is obtained with the target compliance factor. SIC_{Mlim} is useful to assess the approximate maximum budget that could be justified for commensurate retrofit measures.

$$SIC_{Mlim} = \Delta R_M / DF \tag{9}$$

4. Examples

4.1 Office building

The initial compliance factor for the office building is 0.3 (above the minimum required compliance factor of 0.25). For this example, the risk reduction for human life (mandatory) as well as the risk reduction for the direct damage to the building (owner's decision) are considered in the evaluation of the efficiency of possible retrofit measures. The values of the relevant parameters are given in Table 1.

Table 1 – Example of an office building

Parameter	Value	Description / Comment
Importance class	I	Office building
dr	50 years	Remaining life time of the building
PB	21 persons	Average human occupancy 100 employees, 8 hours a day, 5 days a week, 47 weeks a year : $PB = 100 \cdot 8/24 \cdot 5/7 \cdot 47/52 \sim 21$
BW	CHF 8 million	Building replacement value.
α_{eff}	0.3	Compliance factor after seismic verification.
α_{int}	0.8	Compliance factor after the considered retrofit measures.
SIC_M	CHF 150'000	Cost of the retrofit measures.
SC_M	CHF 4'800 / year	Yearly cost of the retrofit measures according to Eq. (9) with a discounting factor DF = 0.032 according to Eq. (10).
ΔRP_M	CHF 1'260 / year	Risk reduction for human life. Eq. (2) with $\Delta PRF \sim 6 \cdot 10^{-6}$ per year according to Fig 2a.
ΔRB_M	CHF 4'800 / year	Risk reduction for direct damage to the building. Eq. (3) with $\Delta BRF \sim 6 \cdot 10^{-4}$ / year according to Fig 2b, upper curve.
ΔR_M	CHF 6'620 / year	$\Delta RP_M + \Delta RB_M$
EF_M	1.3	EFM ≥ 1.0. Measures must be implemented.
SIC_{Mlim}	CHF 207'000	Limit costs for commensurable measures $\Delta R_M / DF$

The proposed retrofit measures have an efficiency $EF_M = 1.3$ (> 1.0) and must be implemented. If only the risk reduction to human life had been considered (owner's decision), the efficiency of the proposed measure would be $EF_M = 0.3$ (<< 1.0).

4.2 School building

The initial compliance factor is below the required minimum compliance factor of 0.4. A seismic retrofit to reach the minimum compliance factor of 0.4 is mandatory. In this example the efficiency of additional retrofit measures to try to reach a compliance factor of 1.0 is evaluated. As in example 1, the risk reduction to human life (mandatory) as well as the risk reduction for direct damage to the building (owner's decision) are considered. The values of the relevant parameters are given in Table 2.

Table 2 – Example of a school building

Parameter	Value	Description / Comment
Importance class	II-i	School building
dr	50 years	Remaining life time of the building
PB	55 persons	Average human occupancy
BW	CHF 4 million	Building replacement value.
α_{eff}	0.4	Compliance factor after initial mandatory retrofit.
α_{int}	1.0	Compliance factor after the considered additional retrofit measures.
SIC_M	CHF 60'000	Cost of the retrofit measures.
SC_M	CHF 1'920 / year	Yearly cost of the retrofit measures according to Eq. (9) with a discounting factor DF = 0.032 according to Eq. (10).
ΔRP_M	CHF 2'200 / year	Risk reduction for human life. Eq. (2) with $\Delta PRF \sim 4 \cdot 10^{-6}$ per year according to Fig 2a.
ΔRB_M	CHF 1'600 / year	Risk reduction for direct damage to the building. Eq. (3) with $\Delta BRF \sim 4 \cdot 10^{-4}$ per year according to Fig 2b, upper curve.
ΔR_M	CHF 3'800 / year	$\Delta RP_M + \Delta RB_M$
EF_M	1.7	EFM ≥ 1.0. Measures must be implemented.
SIC_{Mlim}	CHF 127'000	Limit costs for commensurable measures $\Delta R_M / DF$

In this case, the proposed additional retrofit measures have an efficiency $EF_M = 1.7$ (> 1.0) and must be implemented. If only the risk reduction to human life had been considered, the efficiency of the proposed measure would be $EF_M = 1.1$ (> 1.0), still justifying the additional retrofit measures to achieve a compliance factor of 1.0.

4.3   Hospital building

The initial compliance factor for the hospital building is 0.5 (above the minimum required compliance factor of 0.4). For this example, the risk reduction to human life (mandatory) as well as the willingness to pay to protect the infrastructure function (mandatory) are considered in the evaluation of the efficiency of possible retrofit measures. The values of the relevant parameters are given in Table 3.

Table 3 – Example of a hospital building

Parameter	Value	Description / Comment
Importance class	III	Hospital building with emergency and intensive care unit
dr	50 years	Remaining life time of the building
PB	110 persons	Average human occupancy
BW	CHF 135 million	Building replacement value.
SW	CHF 55 million	Content's value
α_{eff}	0.4	Compliance factor in the initial condition $\alpha_{eff} \geq \alpha_{min} = 0.4$.
α_{int}	1.0	Compliance factor after the considered retrofit measures.
SIC_M	CHF 2 million	Cost of the retrofit measures.
SC_M	CHF 64'000 / yr	Yearly cost of the retrofit measures according to Eq. (9) with a discounting factor DF = 0.032 according to Eq. (10).
ΔRP_M	CHF 4'400 / year	Risk reduction for human life. Eq. (2) with $\Delta PRF \sim 4 \cdot 10^{-6}$ per year according to Fig 2a.
ΔZI_M	CHF 380'000 / yr	Willingness to pay to protect the infrastructure function. Eq. (6) with $\Delta IS_M = 0.2\%$ per year according to Fig 3, upper curve and BSW = BW + SW..
ΔR_M	CHF 384'400 / yr	$\Delta RP_M + \Delta ZI_M$
EF_M	6.0	EFM ≥ 1.0. Measures must be implemented.
SIC_{Mlim}	CHF 12 million	Limit costs for commensurable measures $\Delta R_M / DF$

The proposed retrofit measures have an efficiency $EF_M = 6.0$ (> 1.0) and must be implemented. The willingness to pay for the protection of the infrastructure function largely dominates the risk reduction in the computation of the efficiency of measures. The computation of limit costs for commensurable measures SIC_{Mlim} amounts to CHF 12 million. This represents 6.3% of the building and content value. Only taking into account the risk reduction to people would reduce SIC_{Mlim} to only CHF 137'000 (only around 0.1 % of the building replacement value).

4.4 Highway bridge

The initial compliance factor for the bridge is 0.4 (equal to the minimum required compliance factor of 0.4). For this example, the risk reduction to human life (mandatory) as well as the willingness to pay to protect the infrastructure function (mandatory) are considered in the evaluation of the efficiency of possible retrofit measures. The values of the relevant parameters are given in Table 4.

The proposed retrofit measures have an efficiency $EF_M = 2.0$ (> 1.0) and must be implemented. The willingness to pay for the protection of the infrastructure function largely dominates the risk reduction in the computation of the efficiency of measures. The computation of limit costs for commensurable measures SIC_{Mlim} amounts to CHF 800'000. This represents 4.0% of the bridge replacement value.

Table 4 – Example of a highway bridge

Parameter	Value	Description / Comment
Importance class	II-i	Highway bridge with an important infrastructure function
dr	80 years	Remaining life time of the building
PB	1 person	Average human occupancy is negligible
BW	CHF 20 million	Building replacement value.
SW	CHF 0.1 million	Content's value is negligible
α_{eff}	0.4	Compliance factor in the initial condition $\alpha_{eff} \geq \alpha_{min} = 0.4$.
α_{int}	1.0	Compliance factor that can be reached with the considered additional retrofit measures.
SIC_M	CHF 400'000	Cost of the retrofit measures.
SC_M	CHF 10'000 / year	Yearly cost of the retrofit measures according to Eq. (9) with a discounting factor DF = 0.025 according to Eq. (10).
ΔRP_M	CHF 0 / year	Risk reduction for human life. Eq. (2) with $\Delta PRF \sim 4 \cdot 10^{-6}$ per year according to Fig 2a.
ΔZI_M	CHF 20'000 / year	Willingness to pay to protect the infrastructure function. Eq. (6) with $\Delta IS_M = 0.1\%$ per year according to Fig 3, lower curve and BSW = BW + SW.
ΔR_M	CHF 20'000 / year	$\Delta RP_M + \Delta ZI_M$
EF_M	2.0	EFM ≥ 1.0. Measures must be implemented.
SIC_{Mlim}	CHF 800'000	Limit costs for commensurable measures $\Delta R_M / DF$

5. Concluding remarks

The building code SIA 269/8 was published in 2017 on the basis of the prestandard SIA 2018 from 2004. Many buildings and other constructions have been verified and retrofitted using these standards in Switzerland.

The minimum compliance factor ensures that constructions with a very insufficient seismic safety have to be retrofitted up to a minimum standard. For situations where the minimum compliance factor is reached, the computation of the efficiency of measures helps to discriminate situations for which a seismic retrofit is justifiable from situations where it is not.

It should be stressed that the computation of the efficiency of measures is not the only criteria to decide a seismic retrofit. The ratio between the cost of a construction project (cost of global retrofit or transformation) and the cost of the seismic retrofit measures is also an important parameter to consider. If the cost of a seismic retrofit becomes negligible in relation to the cost of the whole construction project, the measures should be implemented regardless of the value of EF_M.

Further detailed information is available in French and German in a downloadable documentation of the Swiss Society for Earthquake Engineering and Structural Dynamics (www.sgeb.ch)

References

[1] Swiss Society of Engineers and Architects SIA (2017). Erhaltung von Tragwerken - Erdbeben (maintenance of structures - earthquakes), *building code SIA 269/8*, Zurich.

[2] Swiss Society of Engineers and Architects SIA (2004). Überprüfung bestehender Gebäude bezüglich Erdbeben (Verification of the seismic safety of existing buildings), *Pre-Standard SIA 2018*, Zurich.

[3] Wenk T. 2008: Seismic retrofitting of structures. Strategies and collection of examples in Switzerland. Environmental studies No. 0832. Federal Office for the Environment, Bern. 84 pp. Available at www.bafu.admin.ch.

[4] Swiss Society of Engineers and Architects SIA (2020). Actions on Structures, *building code SIA 261*, Zurich.

[5] Jamali, N., Kölz, E., Duvernay B. (2012), Seismic Risk Assessment for Typical Swiss Buildings Based on Mechanical and Empirical Approaches, Proceedings of the 15th World Conference on Earthquake engineering, Lisbon, Portugal.

[6] Duvernay, B., Kölz, E., Jamali, N., Michel, C., Is the residual risk related to the Swiss seismic code provisions acceptable?, Proceedings of the 16th European Conference on Earthquake engineering, Thessaloniki, Greece.

NONLINEAR STATIC AND DYNAMIC ANALYSIS OF A TYPICAL MASONRY BUILDING IN PALMOTIĆEVA STREET IN ZAGREB

Vanesa Jusufbašić [(1)], Senad Medić [(2)], Mario Uroš[(3)]

[(1)] *Mag.ing.aedif., IPSA Institute, vanesa.jusufbasic10@gmail.com*
[(2)] *Assistant professor, University of Sarajevo – Faculty of Civil Engineering, senad_medic@yahoo.com*
[(3)] *Associate professor, University of Zagreb – Faculty of Civil Engineering, mario.uros@grad.unizg.hr*

Abstract

In this study, nonlinear static pushover and dynamic time-history analyses of a typical masonry building situated on Palmotićeva street in downtown Zagreb were performed. The building was erected in 1922 before any seismic codes were introduced in practice. It has a basement, four stories, an attic (total height equal to ca. 23m), and an asymmetric plan consisting of two connected parts: a street part (24.4x12 m) and a courtyard part (10.6x12 m). The floor structure consists mainly of wooden beams except above the basement, where the RC slab was installed. The solid brick masonry walls with variable thicknesses (15-90 cm) are evenly distributed in both directions. Two numerical macro-models were created employing Diana 10.4. Engineering masonry constitutive law was used to describe the highly nonlinear behavior of masonry walls which can crush, crack or fail in shear. Three numerical models were created describing the current damaged state and the possible strengthening with rigid floor diaphragms. The response of the building was assessed in terms of capacity curves, inter-story drifts, and cracking patterns.

Keywords: damaged building, engineering masonry model, nonlinear analysis, seismic capacity

1. Introduction

Unreinforced masonry (URM) structures are made of brick units connected by mortar joints. The behavior of a masonry structure strongly depends on the type of brick, mortar composition, brick dimensions, and the way bricks are assembled [1]. In general, brick and mortar perform well under compression, but their tensile capacity is considerably lower. Three different in-plane failure mechanisms can occur in URM walls: diagonal cracking, shear sliding, and rocking [2,3]. Diagonal cracking and sliding are failure modes caused by shear, and rocking is a consequence of flexural behavior. The occurrence of different failure modes depends on the geometry of the pier, boundary conditions, axial load, mechanical properties of masonry, and geometrical characteristics of masonry. Several experimental tests have been performed to find the relation between different failure modes and the mentioned parameters. Generally, it has been concluded that rocking tends to occur in slender piers with lower precompression, shear sliding in squat piers, and diagonal cracking in moderately slender piers [4, 5].

The Republic of Croatia is among the most earthquake-prone countries in Europe, yet the current activities related to assessing potential earthquake risk and its reduction can be characterized as individual and insufficient [6]. The city of Zagreb has a moderate seismic hazard, but it is highly exposed (densely populated), and the built environment is quite vulnerable, meaning the seismic risk is high. A severe earthquake hit Zagreb on March 22, 2020 (magnitude ML = 5.5, with an epicenter 7 km north of the city center). The event occurred during the COVID-19 lockdown and caused significant damage to the built environment and enormous disruption in everyday life [7].

Since the old URM typologies were not designed to withstand seismic loads, they were heavily affected by the earthquake. In addition to the design characteristics, their age and often inadequate maintenance contributed to the poor performance of these buildings. Aggravating factors are the subsequent renovations, upgrades, and changes in function. The original up to 60 cm thick solid brick load-bearing walls, composed of two to three rows of molded clay bricks, are often reduced in thickness or partially

628

or even entirely removed at the ground level to install street store windows. Steel lintels are frequently installed to span new or extended openings. In certain cases, the upper floors' partitions and interior bearing walls are entirely disregarded as part of the structure and removed to gain space. Such interventions result in unsupported walls, initially continuous in the vertical direction, or out-of-plane critical walls, significantly weakening the structural system. These interventions are seldom documented, and the current condition of the building differs significantly from the original documentation [8, 9, 10].

Accurate assessment of masonry buildings is a challenge due to the nonlinear behavior of masonry and the dynamic nature of a seismic load. A Nonlinear Time History (NLTH) analysis considers both factors, but the computer resources and huge amount of time limit its everyday use. Another widely used method is the Modal Response Spectrum method, where the nonlinear material response is considered indirectly via a behavior factor. The results of the Response Spectrum method are considered too conservative [11]. A third method is the Nonlinear Pushover (NLPO) method. It considers nonlinear material behavior, and compared to NLTH, NLPO is computationally more efficient. An equivalent lateral load pattern is applied in a quasi-static fashion producing a capacity curve that is subsequently compared to demand in terms of an acceleration-displacement response spectrum. Pushover analysis is a practical alternative because it gives good insight into the seismic response.

The structure's performance is studied by looking into the force-displacement response, displacement profile, and damage pattern. Another aspect that requires attention is the different modeling strategies used to execute an analysis [12,13]. This paper employed the continuum finite element approach by assuming shell elements in DIANA [14].

The goal of the case study is to numerically describe the response of a typical unreinforced masonry building located at 64a Palmotićeva Street in Downtown Zagreb. All results pertain to the N-S direction of the ground motion (X-axis of the building).

2. Building Description

The building was built in 1922 and has a basement, ground floor, three floors, and an attic (Fig. 1). The plan dimensions of the building are 24.40x12 m (street part) and 10.6x12 m (courtyard part), and the floor area is about 407 m². The total gross floor plan area of the building is 2440 m², while its total height is 22.70 m (6x3.5+2.9), i.e., the building extends from -1.2 to 22.70 m. The street and courtyard sections of the building are connected and form one unit, but this is also the cause of asymmetry. The building meets the criterion of regularity in elevation, while the criterion of regularity in the plan is not met. A heterogeneous horizontal load-bearing structure does not act as a rigid floor diaphragm. Hence, an unfavorable and irregular structural response, where parts of the building behave independently, is expected during an earthquake. The structure consists of connected solid brick walls extending continuously from the foundation to the roof.

The walls are evenly spaced in both directions. Load-bearing walls are made of the old format brick (290x140x65mm) and have a variable thickness (90, 65, 45, or 15 cm). Partition walls are made of solid brick with 7- and 15-cm thicknesses. The walls are tied by lintels, parapets, and beams, the composition and quality of which are not fully known. The parapets and lintels on the facade openings are thinner than the connecting walls and are usually 30 cm. The horizontal structure above the street part of the basement is an RC slab with a system of RC beams. Above the ground floor and upper floors, the structure consists of wooden beams with planks and loose filling inside the deck structure. On the south side of the building above the ground floor and the third floor, during subsequent reconstructions, RC slabs with a thickness of 8 cm were constructed and coupled to wooden beams. The roof structure is wooden and gabled, and the attic was converted into a living space over time. The building has an internal U-shaped staircase made of prefabricated RC elements supported on the walls and steel profiles with RC landings.

Faculty of Civil Engineering in Zagreb conducted the experimental investigation of mechanical properties of masonry and ambient vibration tests, the results of which were used as input parameters and calibration of numerical models [10].
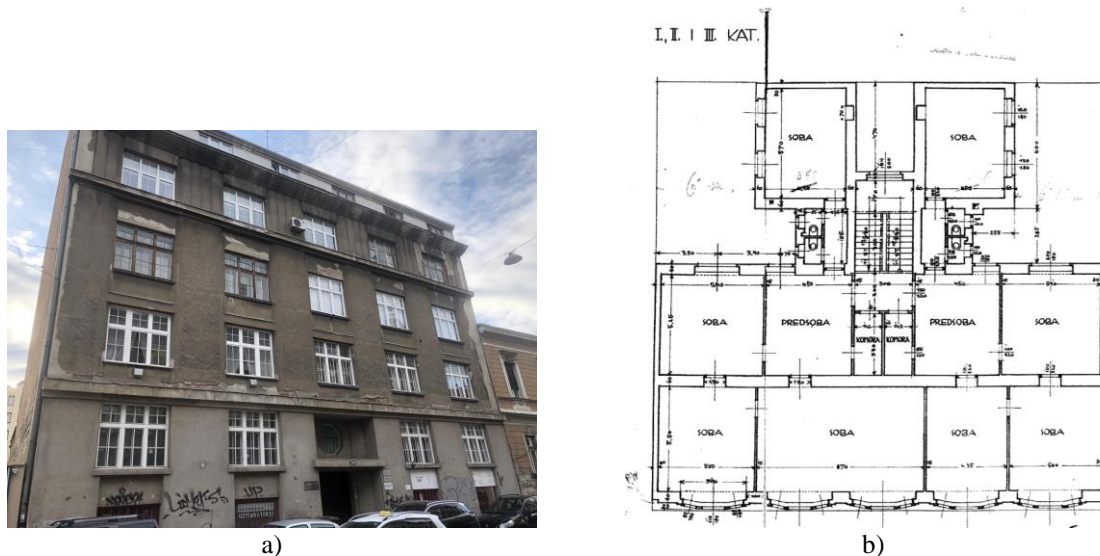
Figure 1. a) View of the building; b) Layout of the typical story (Courtesy of Zagreb City Archives).

3. Numerical Modeling

3.1 Engineering masonry material model

Creating powerful micro-models, in which each constituent of composite masonry is described separately (brick, mortar, interface), is often not feasible in practice. Besides difficulties related to individual material properties, the considerable computational time is required even for small-scale models. The approach based on averaged constitutive equations seems suitable for large-scale finite element analyses by collating experimental data at an average level (macro-modeling) or from homogenization techniques [15]. A popular model for the simulation of quasi-brittle materials such as concrete and masonry where cracking is smeared over the finite element is the Total Strain Crack model [16]. However, two shortcomings when masonry is cyclically loaded were noted in the literature [17]. The model was derived for isotropic materials, and the secant reloading curves underestimate the energy dissipation under cyclic conditions.

A type of masonry model that avoids the limitations of the Total Strain Crack model is the Engineering Masonry model (ENGMAS) [17]. This model has been proposed by DIANA FEA and the Technical University of Delft to evaluate the building masonry stock after a series of earthquakes caused by gas extraction in the Groningen area [18]. The Engineering Masonry model describes the unloading behavior more realistically than the Total Strain Crack model. It assumes a substantial stress decay with the initial linear stiffness. Anisotropy is included by considering different stiffness in the direction of the bed and head joints. Stresses in both directions are defined by their respective strain components and the maximum value of the strain that has been reached in the lifetime of an element.

3.2 Model properties

Three models with respect to the horizontal load-bearing structure were created: model 1 – rigid floor diaphragms, model 2 – wooden beams, and model 3 – modified RC floors coupled with wooden beams above the ground floor and the third floor (reconstruction). The gravity load is assumed to be 2.5 kN/m2, and the live load equals 1.5 kN/m^2. Walls and slabs are discretized with curved shell finite elements CQ40S and CT30S with a high integration scheme [14]. The floor structure is elastic, while masonry is described with the ENGMAS material model. The properties of masonry are listed in Table 1.

Table 1 – Parameters of engineering masonry model for the analyzed building

Parameter	Value	Parameter	Value	Parameter	Value
E_x	1500 MPa	G_{ft}	10 N/m	G_{fs}	20 N/m
E_y	1500 MPa	HEADTP	NO	f_c	3,4 MPa
G_{xy}	500 MPa	h	Rots	n	4
ρ	1800 kg/m³	c	0,16 MPa	G_c	16000 N/m
f_{tx}	0,114 MPa	ϕ	32 °	λ	1

The presented modeling strategy was validated by comparing analytical, numerical, and experimental results obtained from cyclic static tests of URM cantilever walls under constant vertical precompression [19, 20]. Vibration modes for model I are shown in Fig. 2. Eigenfrequencies for the three models in the initial (no damage) state are listed in Table 2. The reduction of frequencies for model II with wooden floor beams is as expected, while the eigenmodes basically retain the same shape for all models.

a)   b)   c)
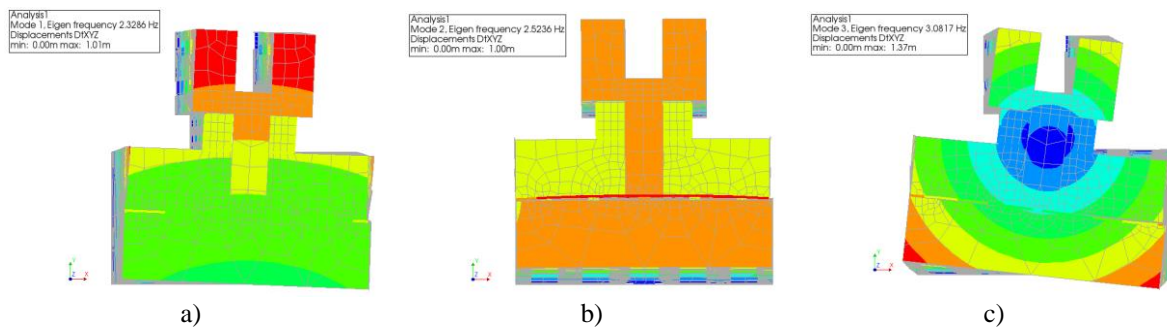
Figure 2. Eigen modes for model I: a) mode I, f_1 = 2,32 Hz; b) mode II, f_2 = 2,52 Hz; c) mode III, f_3 = 3,08 Hz.

Table 2 – Eigen frequencies of the three models

Model	f_1 [Hz]	f_2 [Hz]	f_3 [Hz]
I	2,32	2,52	3,08
II	2,08	2,39	2,71
III	2,13	2,43	2,80

3.3 Nonlinear time history analysis

In NLTH, the seismic load is considered by applying a ground motion signal to the soil or directly to a structure. Several earthquake signals should be applied to scrutinize the substantial spread an earthquake scatter could have at a single location. Both material and geometric nonlinearity are considered. The analysis was executed for 38-sec duration of the Zagreb earthquake by applying the signal recorded at the Office of emergency management of the City of Zagreb. The PGA of the N-S component was 0.22 g, whereas the peak ground acceleration of the E-W component amounted to 0.179g (Fig. 3). The model is shown in Fig. 4a, and the crack status for model II is provided in Fig. 4b.
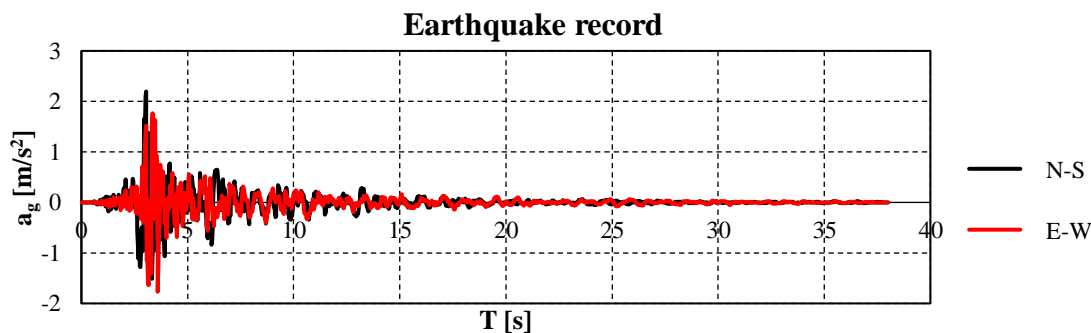
Figure 3. Zagreb earthquake record (March 22, 2020).
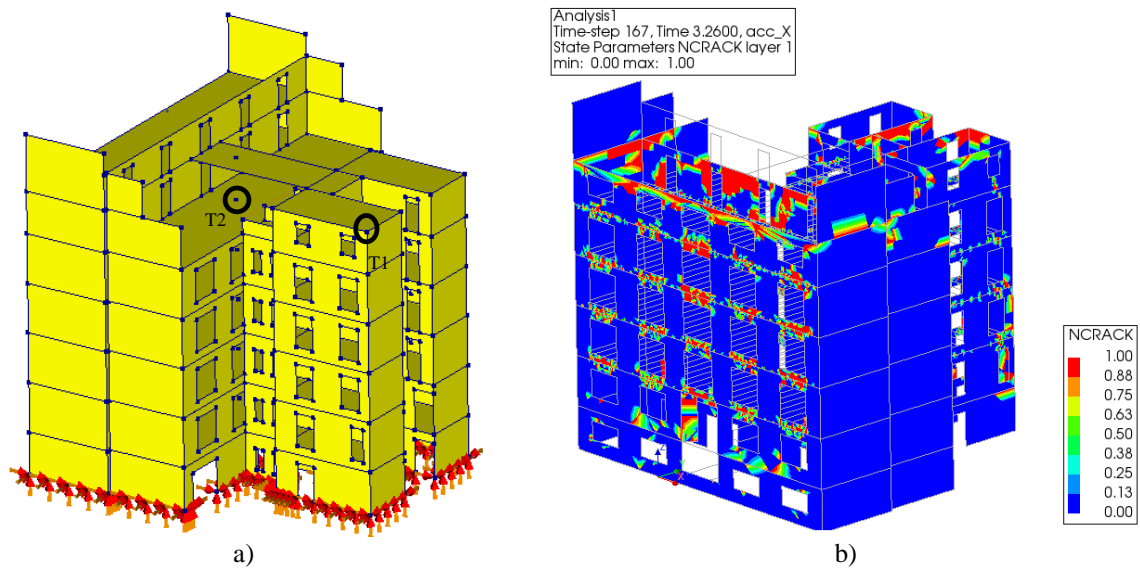
Figure 4. a) Model of the building with control points; b) Crack status for model II.

Crack distribution should serve as an indication of potential damage or weak spots (e.g., lintels in Fig. 4b). The displacement history of the center of mass (point T2 of model II) for the first 7 seconds of earthquake duration is given in Fig. 5. Maximum displacements of the control point T2 at h = 20m for all three models are listed in Table 3. The maximum attained displacement is approximately 4 cm. Maximum relative displacements (d/h), e.g., inter-story drifts, are shown in Fig. 6.
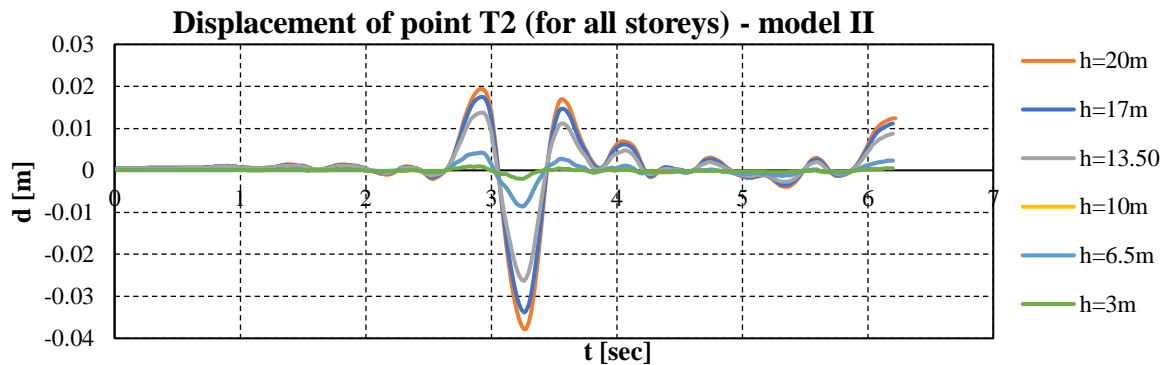
Figure 5. Displacement history of point T2 (center of mass) for model II (d_{max} = 3.8 cm).

Table 3 – Maximum displacements of the three models

Model	d [cm] – T1	d [cm] – T2
I	3,88	3,12
II	3,88	3,78
III	4,09	3,94

632
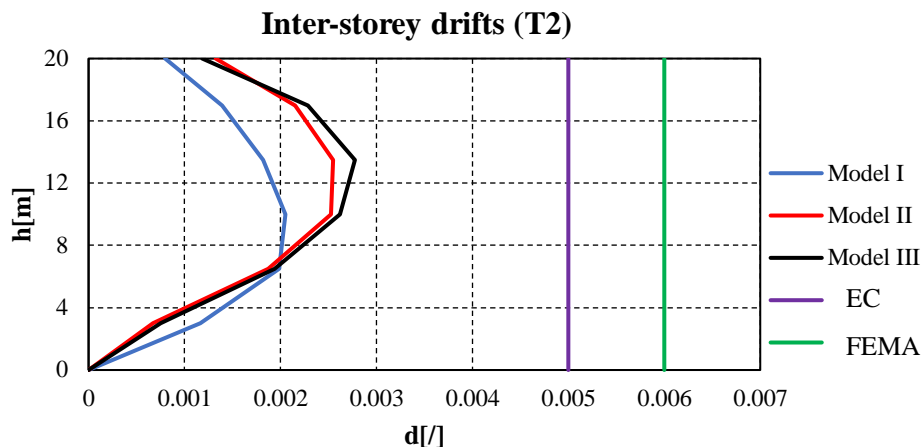
Figure 6. Maximum inter-story drifts.

Fig. 7 shows the western courtyard wall that was most damaged in the earthquake. It also compares the actual state and the results of numerical modeling. It has long diagonal cracks that run along the entire wall and end at the side window openings. The width of the cracks is up to 15mm - which means that the wall has failed and represents a great danger for the building and the tenants in case of subsequent earthquakes. The causes of the degradation of the walls are related to the following:

a) The floor structure is not anchored to the perimeter walls; the beams are parallel to the western walls. There is a thin concrete slab, but the connection with the perimeter and western walls is missing. Additionally, the western wall is connected to perpendicular walls, which are weakened by large openings.

b) The western wall is exposed to the highest seismic demand being far from the stiffness center.

a)

b)
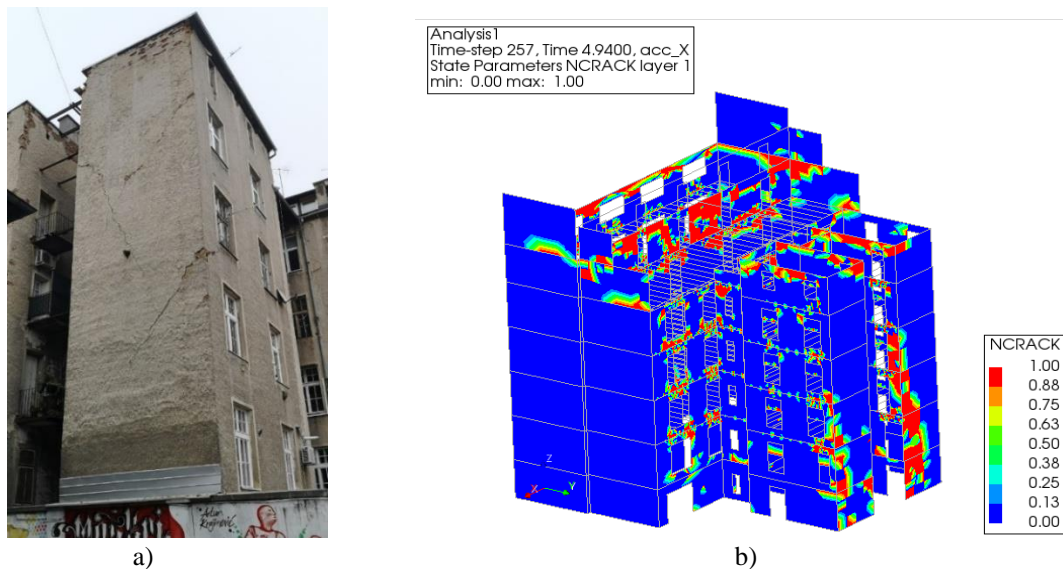
Figure 7. Degradation of the building: a) Actual state after Zagreb earthquake; b) Cracking pattern.

3.4 Pushover method

The pushover analysis is a nonlinear static procedure in which the magnitude of the lateral load excited in a structure increases monotonically until failure, while the load distribution remains constant. The lateral load is applied in a predefined load pattern that follows the fundamental mode from the elastic analysis. The relation between the control node displacement (usually the center of mass of the roof of the building) and base shear is plotted subsequently in a so-called capacity curve (pushover curve).

Pushover curves for three different models are provided in Fig. 8 (base shear vs. displacement of the center of mass CM/T2). As expected, the model I with rigid diaphragms representative of possible strengthening has the largest stiffness and load-bearing capacity.
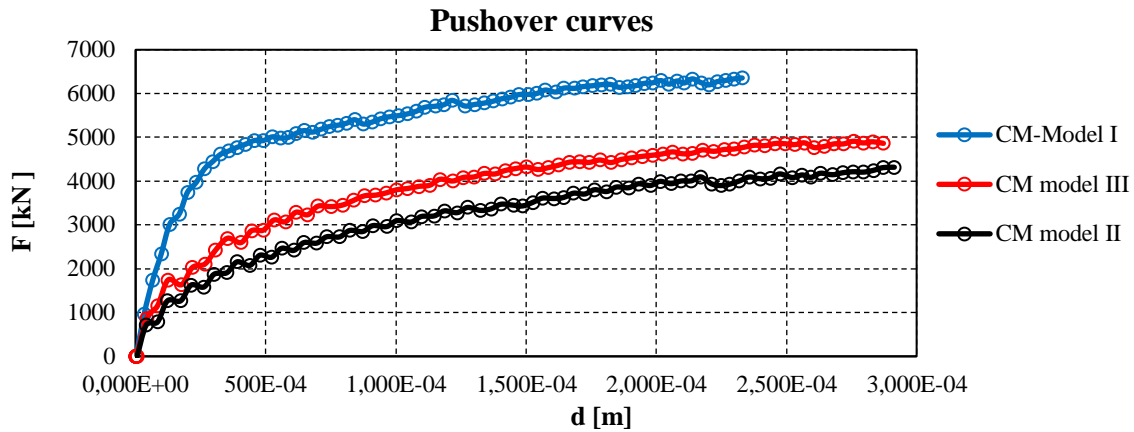
Figure 8. Pushover curves for three different models.

This capacity curve is used to determine the seismic capacity of a structure. The earthquake demand is represented by the smoothed elastic response spectrum, which is formed considering the peak acceleration of the soil and the soil category. The design spectrum can be formed by introducing the behavior factor q=1.5 (most common for masonry structures), and thus reduce the earthquake requirement by considering the expected plastic deformations. The pushover curve and the response spectrum need to be transformed into the capacity spectrum using the structure's originally elastic dynamic properties (participation factor and modal mass) to compare the capacity with demand. This capacity spectrum is represented in the Acceleration Displacement Response Spectrum format (ADRS), using spectral displacements ($S_d = S_a/\omega^2$) and spectral accelerations (S_a) (Fig. 9). The intersection of the capacity curve with the spectral curve is called the performance point.
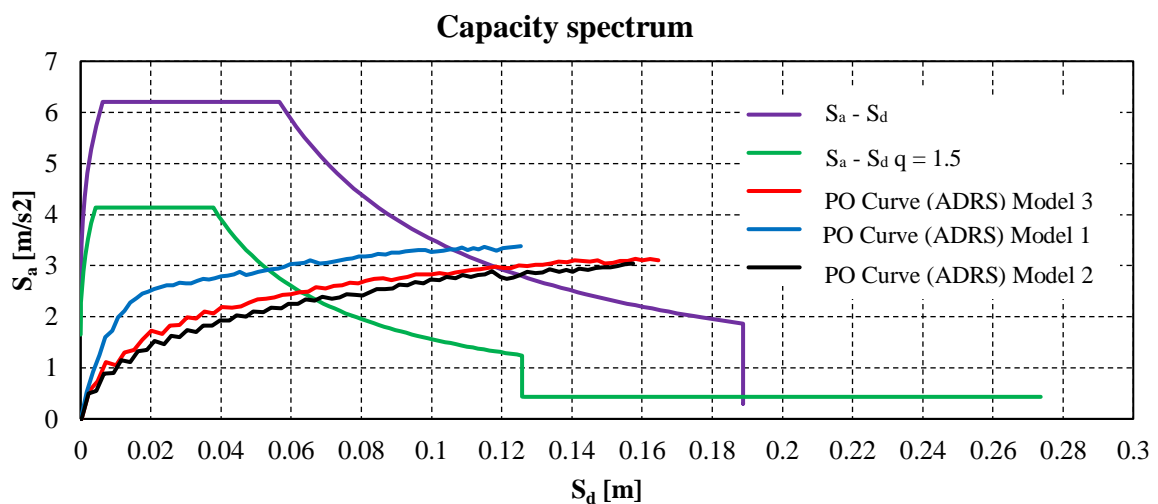
Figure 9. ADRS format.

3.5 Influence of element type

The influence of the finite element type is investigated by choosing linear and quadratic interpolation functions while keeping the average element area the same. In addition to previously shown results related to quadratic polynomials, triangular T15SH and rectangular Q20SH finite elements with linear shape functions are employed for pushover and NLTH analysis. The results show that linear elements

are generally stiffer and yield a larger load-bearing capacity. The difference in pushover curves for the two models is provided in Fig. 10. The same is valid regarding the NLTH and inter-story drifts. On the other hand, due to the reduced number of degrees of freedom for linear elements, the computational time is shorter and convergence faster.
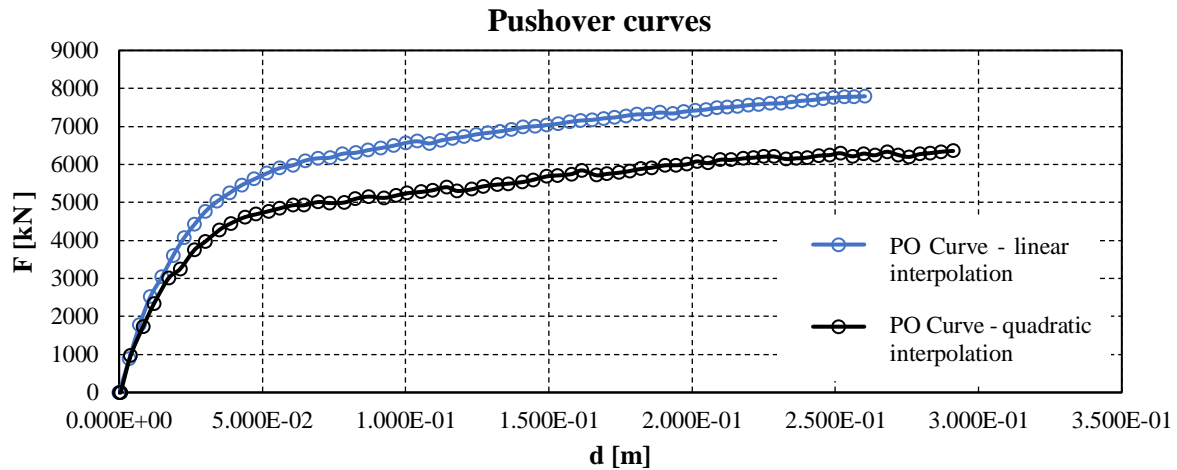
Figure 10. Pushover curves for linear and quadratic interpolation functions.

4. Conclusion

This paper employed DIANA FEA to conduct a nonlinear static and dynamic analysis of the existing residential masonry building in Zagreb Lower Town. The geometry of the building was adopted after drawings were made available by the Zagreb City Archives. Material properties and essential dynamic characteristics were taken from experimental investigations conducted by the Faculty of Civil Engineering in Zagreb. Recently developed Engineering Masonry Model was used to describe walls in a continuum macro model. Three models with respect to the horizontal load-bearing structure were created: model 1 – rigid floor diaphragms, model 2 – wooden beams, and model 3 – modified RC floors coupled with wooden beams above the ground floor and the third floor (reconstruction).

Nonlinear dynamic analysis implies the application of ground acceleration records at the base level. This method requires more input parameters, memory, and computer speed. Therefore, it is limited for everyday engineering applications. On the other hand, true dynamic behavior can be examined at any time instance. The calculations for a limited earthquake duration (1/5 of the total record) lasted three days. Pushover analysis was proven helpful in monitoring the formation and distribution of cracks in load increments and controlling the global structural response. Limitation to buildings of a regular shape without particular eccentricities is the disadvantage of this method. The dynamic calculation should be taken with a grain of salt due to the incomplete input data required for such a calculation, but also the possibility that the ground motion records used did not sufficiently shake the building, leaving the possibility that another earthquake with the same peak ground acceleration could have a more devastating effect. As expected, the analysis showed that the model with RC slabs is the stiffest compared to the other two.

The cracks occur in areas where the initial shear strength is reduced and the low tensile strength is exceeded (corners around the openings, joints of the walls, lintels, and junction of the main and the central/courtyard section). Damage is evident, especially on the courtyard wall. In the model with beams, cracks are visible at the contact of floors and walls. A rigid or partially rigid diaphragm is essential for favorable earthquake response. Damage is mainly concentrated on the higher floors due to the smaller thickness of the walls and lower compressive stress.

Determining the stiffness of walls and lintels is a problem even for vertical loads, especially for cyclic seismic loads. The change in stiffness occurs in larger areas or locally due to cracking, crushing, or

sliding. Modal analysis was executed after NLTH, and the obtained fundamental frequency matches the experimental determined by ambient vibration tests after the earthquake.

The influence of finite element type was investigated by choosing linear and quadratic interpolation functions while keeping the average element area the same. The results show that linear elements are generally stiffer and yield a larger load-bearing capacity. On the other hand, due to the reduced number of degrees of freedom for linear elements, the computational time is shorter and convergence faster.

Acknowledgements

References

[1] Mosalam, K., Glascoe, L., Bernier, J. (2009): *Mechanical Properties of Unreinforced Brick Masonry, Section1* (No. LLNL-TR-417646). Lawrence Livermore National Lab. (LLNL), Livermore, CA (United States).

[2] Petrovčič, S., Kilar, V. (2013): Seismic failure mode interaction for the equivalent frame modeling of unreinforced masonry structures. *Engineering structures*, *54*, 9-22, doi: http://dx.doi.org/10.1016/j.engstruct.2013.03.050

[3] Mistler, M. (2006): *Verformungsbasiertes seismisches Bemessungskonzept für Mauerwerksbauten* . Mainz.

[4] Magenes, G., Calvi, G. M. (1992): Cyclic behaviour of brick masonry walls. In *Proceedings of the 10th world conference on earthquake engineering* (pp. 3517-3522).

[5] Tomazevic, M. (1999): *Earthquake-resistant design of masonry buildings* (Vol. 1). World Scientific.

[6] Atalić, J., Šavor Novak, M., Uroš, M. (2019): Seismic risk for Croatia: Overview of research activities and present assessments with guidelines for the future. *Građevinar*, 71(10.), 923-947, doi: https://doi.org/10.14256/JCE.2732.2019

[7] Stepinac, M., Lourenço, P. B., Atalić, J., Kišiček, T., Uroš, M., Baniček, M., Novak, M. Š. (2021): Damage classification of residential buildings in historical downtown after the ML5. 5 earthquake in Zagreb, Croatia in 2020. *International journal of disaster risk reduction,* 56, 102140, doi: https://doi.org/10.1016/j.ijdrr.2021.102140

[8] Atalić, J., Uroš, M., Šavor Novak, M., Demšić, M., Nastev, M. (2021): The Mw5. 4 Zagreb (Croatia) earthquake of March 22, 2020: impacts and response. *Bulletin of Earthquake Engineering,* 19(9), 3461-3489, doi: https://doi.org/10.1007/s10518-021-01117-w

[9] Novak, M. S., Uros, M., Atalic, J., Herak, M., Demsic, M., Banicek, M., Lazarevic, D., Bijelic, N., Crnogorac, M., Todoric, M. (2020): Zagreb earthquake of March 22 2020-preliminary report on seismologic aspects and damage to buildings. *Gradevinar*, 72, 843-867, doi: https://doi.org/10.14256/JCE.2966.2020

[10] Uroš, M., Todorić, M., Crnogorac, M., Atalić, J., Šavor Novak, M., Lakušić, S. (2021): *Potresno inženjerstvo-Obnova zidanih zgrada.* Građevinski Fakultet, Sveučilišta u Zagrebu: Zagreb, Croatia.

[11] Wilson, E.L. (2013): *Educational Priorities of an Old Professor on Seismic Analysis of Structures.* http://www.edwilson.org/History/Educational%20Priorities%20of%20an%20Old%20Professor.pdf

[12] D'Altri, A. M., Sarhosis, V., Milani, G., Rots, J., Cattari, S., Lagomarsino, S., Sacco, E., Tralli, A., Castellazzi, G., de Miranda, S. (2020). Modeling strategies for the computational analysis of unreinforced masonry structures: review and classification. *Archives of computational methods in engineering*, *27*, 1153-1185, doi: https://doi.org/10.1007/s11831-019-09351-x

[13] Medić, S., Hrasnica, M. (2018): Modeling strategies for masonry structures. *In Advanced Technologies, Systems, and Applications II: Proceedings of the International Symposium on Innovative and Interdisciplinary Applications of Advanced Technologies (IAT)* (pp. 633-644). Springer International Publishing, doi: https://doi.org/10.1007/978-3-319-71321-2_55

[14] DIANA FEA (2016): *DIANA - User's Manual, Material library*, Delft, The Netherlands.

[15] Lourenço, P. B. (2015). Masonry modeling. *Encyclopedia of Earthquake Engineering*, 1-13, doi: https://doi.org/10.1007/978-3-642-36197-5_153-1

[16] Rots, J. G., Blaauwendraad, J. (1989): Crack models for concrete, discrete or smeared? Fixed, multidirectional or rotating?. *HERON, 34 (1), 1989.*

[17] Schreppers, G.J., Garofano, A., Messali, F., Rots, J.G. (2016): *DIANA Validation report for Masonry modelling*, DIANA FEA BV and TU Delft, Delft, The Netherlands.

[18] Noortman, F. (2019): *Applicability of the Pushover Method for the Seismic Assessment of URM Structures in Groningen: A Case Study of a Low-Rise Apartment Building*, TU Delft, Delft, The Netherlands.

[19] Jusufbašić, V. (2021): *Nelinearna statička i dinamička analiza stambene zgrade u Palmotićevoj ulici*, Master thesis (in Bosnian). University of Sarajevo – Faculty of Civil Engineering, Sarajevo, Bosnia Herzegovina.

[20] Medić, S., Hrasnica, M. (2021): In-Plane Seismic Response of Unreinforced and Jacketed Masonry Walls. *Buildings*, 11(10), 472, doi: https://doi.org/10.3390/buildings11100472

NUMERICAL INVESTIGATION OF THE SEISMIC RESPONSE OF AN UNREINFORCED MASONRY RESIDENTIAL BUILDING HIT BY ZAGREB EARTHQUAKE IN 2020

Silvia Pinasco [(1)], Marija Demšić [(2)], Marta Savor Novak [(2)], Mario Uroš [(2)], Serena Cattari [(1)], Sergio Lagomarsino [(1)]

[(1)] *Department of Civil, Environmental, and Chemical Engineering, University of Genoa, 16145 Genova, Italy*
[(2)] *University of Zagreb, Faculty of Civil Engineering, Department of Engineering Mechanics*

Abstract

Despite the moderate intensity, the series of earthquakes in Zagreb (2020) caused significant social and economic impacts and damage to the built environment. The city of Zagreb has a moderate seismic hazard, but it is highly exposed (densely populated) and the built environment is quite vulnerable (age of structures, low maintenance, illegal construction, and numerous reconstructions). The greatest damage was sustained by unreinforced masonry (URM) buildings for residential use in the historic downtown of Zagreb built in the late 19th and early 20th centuries. In addition to material deterioration, the transformations suffered by these buildings – often without being driven by anti-seismic standards - may increase their seismic vulnerability. Within this context, the main goal of the paper is to analyse the seismic response of an unreinforced masonry residential building selected to be representative of the existing historical masonry heritage in Zagreb downtown, built in the early twentieth century. The URM building has a rectangular floor plan and a 4-story elevation. Numerical investigations are carried out by using the equivalent frame method implemented in Tremuri software and by performing both nonlinear static and dynamic analyses. Since it is part of a typical residential block in the centre of Zagreb, the case study was analysed in two configurations: considering it isolated from the rest of the aggregate and sandwiched between two adjacent structural units. The results reported in this paper must be intended as a preliminary step for addressing future developments oriented to deepen the effects of interaction with adjacent buildings varying the position of the structure into the aggregate as well as those due to possible transformations and strengthening interventions.

Keywords: unreinforced masonry structures, equivalent frame model, nonlinear static and dynamic analyses, seismic vulnerability

1. Introduction

On 22 March 2020, at 6.24 a.m., the Zagreb city area was hit by an earthquake of magnitude 5.5 (ML) and intensity VII according to the EMS-98 scale (Figure 1). The epicentre was approximately 7 km north-east of the centre of Zagreb, in Podsljeme district, at a depth of 10 km. This seismic event caused significant damage to existing structures in the city of Zagreb, in fact approximately 25,000 buildings were damaged [1]. The city centre, known as Lower Town, is mainly composed of traditional masonry structures arranged in aggregate conditions. The potential high seismic vulnerability of masonry structures to both in-plane and out-of-plane actions has been already proved by many seismic events [2]–[4]. Moreover, when they are included in a building aggregate, the vulnerability factors may potentially increase because the structural units that compose it date back to different periods, present different construction techniques, different degrees of maintenance and different structural systems. All these factors contribute to a great structural variability that makes very difficult the behavioural analysis of this structural typology as well as to define at priori if the "aggregate effect" (meant as the effect played by the boundary conditions provided by adjacent structural unit with respect to the same structure analyses as "isolated") may be beneficial or detrimental. Following the earthquake that struck the city

of Zagreb on 22 March 2020, numerous inspections were conducted to assess the damage. The assessment was carried out regarding the usability criteria to ensure the safety of the residents and to prevent further human casualties. Non structural damage in the form of local separation and decay of the plaster was registered very often. In plane mechanisms for bearing walls rarely appeared, mostly it was just for partition walls. On the other hand, out of plane mechanisms appeared most often due to the disconnection between the structures and the wooden beam floors. The damage in Zagreb is described in [5] and [6]. The database about buildings was obtained by collecting documentation from archives, performing visual inspections and gaining access to post-earthquake assessments.

In this paper, we chose to analyse a building in Zagreb's Lower Town, belonging to a building aggregate, of which we have information on mechanical and geometric parameters, but also information on post-earthquake damage. The examined building was modelled both by considering it isolated from the rest of the building aggregate and by modelling the two buildings adjacent to it. Two events were considered in order to conduct the non-linear dynamic analyses and thus obtain the damage level of the building: the Zagreb earthquake (22 March 2020), measured at a distance of 10 km from the case study, and the earthquake that struck the city of Petrinja (29 December 2020), 50 km from the city of Zagreb where the building is located (Figure 2). Numerical investigations are carried out by using the equivalent frame method implemented in Tremuri software and by performing both nonlinear static and dynamic analyses. Only the in-plane response is considered at this stage of the research, consistently also with the actual response of the examined building. Since the structure is part of a typical residential block, it was considered both as isolated and in aggregate through two adjacent structural units; however, in this paper, only a possible position within the aggregate has been considered and by assuming only one of possible interlocking conditions among adjacent units. In fact, the purpose of this study is preparatory research for a wider parametric evaluation of the seismic response of typical buildings in the city of Zagreb constructed in the late 19th and early 20th centuries.
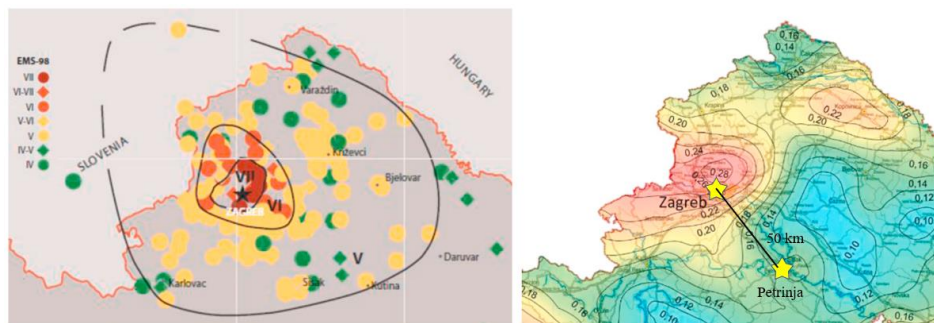
Figure 1. Preliminary Earthquake Intensity Map (left) from the 22nd of March 2020, at 6:24 (CET) compared with expected peak ground accelerations (right) for a return period of 475 years [7]
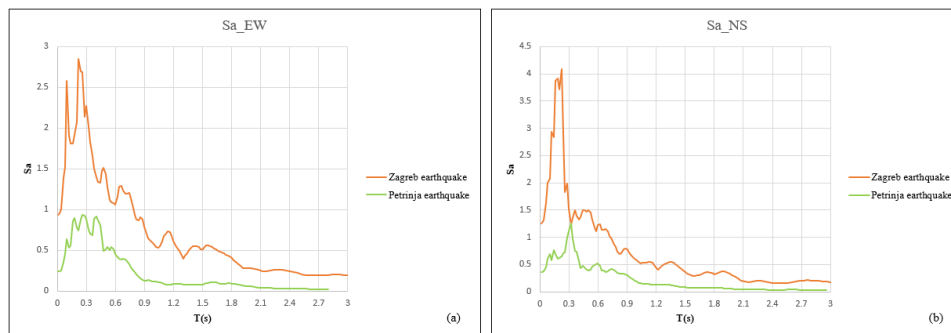
Figure 2. Response spectra of the Zagreb earthquake (22 March 2020) and the Petrinja earthquake (29 December 2020) in EW direction (a) and NS direction (b)

2. Features of the building stock in Zagreb and selected case study

The case study presented here is a typical residential building in the city of Zagreb belonging to a building aggregate with a very recurring shape in the centre of Zagreb - Lower Town.

In the Zagreb Lower Town, most of the buildings are constructed in aggregates, built after the 1880 earthquake. These buildings of unreinforced masonry are built in relatively large aggregates or 'row aggregates' and were built until about 1920. There are at least 5 buildings on each side of the aggregate, and the side length of the aggregates ranges from 50 meters to as much as 150 meters. Although they do not have a common wall, they are built side by side without gaps or seismic dilation. It should be noted that the horizontal structures are mostly made of the timber joists with a rubble filling and rest on the longitudinal walls parallel to the street. Other horizontal structures used are shallow masonry vaults with steel beams or solid concrete slabs, usually used above the basement. The longitudinal direction is generally the stronger bearing direction for horizontal actions, while the weaker direction is the transverse direction, which usually includes only the staircase walls and perimeter transverse walls that are not adequately connected to the floor structures [8].

The case study building shown in Figure 3 was built in 1908 and is one of the representative examples of a building typology built in long row aggregates in the Lower Town in the centre of Zagreb. It has a basement, ground floor, 3 floors and an attic. The floor plan dimensions are 19.20 x 12.35 m, the height of the basement is 3 m, ground and upper floors are 3.85 m and the attic is 4.2 m, while the total height of the building is 22.70 m. The load- bearing walls are made of solid bricks with a thickness of 30, 45, 60 and 75 cm without any confinement RC elements. The thickness of the walls decreases with the height of the building. The basement floor structures are shallow vaults with steel beams and the upper floors are timber joists between planks with rubble material between the beams. The joist is oriented transversely and rest on the facade and the central longitudinal walls.

The building was modelled both in the configuration in which it is isolated from the rest of the aggregate and in the case in which the two adjacent buildings are also present Figure 3. For simplicity's sake, as we did not have detailed information, we chose to model the neighbouring buildings with the same footprint, geometric and mechanical characteristics as the building under study. The mechanical characteristics assumed in both models are as follows: $E = 1400$ Mpa, shear modulus $G = 462$ Mpa, compressive strength $f_m = 2.89$ Mpa, tensile strength $\tau_0 = 0.09$ Mpa and density of 18 kN/m^3.
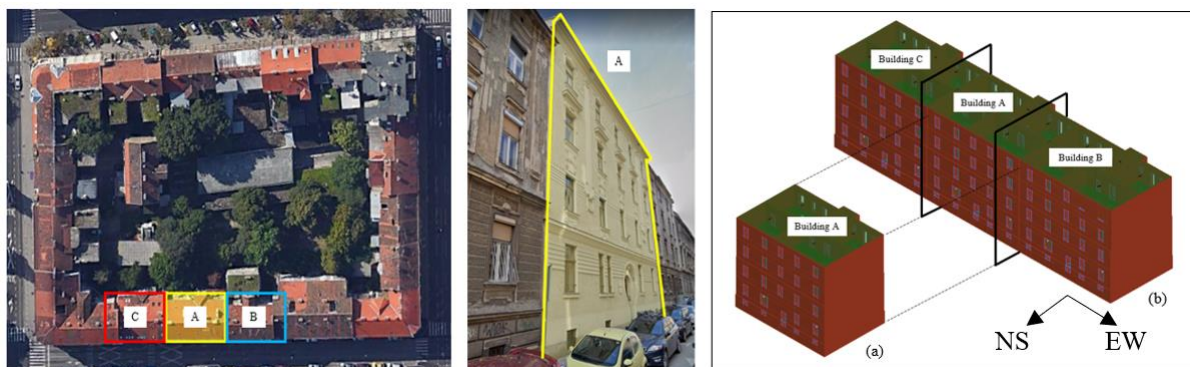
Figure 3. On the left - typical aggregate of the Lower Town of Zagreb to which the case study belongs; in the centre - elevation of the structural unit under study; a on the right - 3Muri model of the case study building in both isolated and aggregate configuration

In this paper, reference will be made to the east-west (EW) direction, i.e., the direction of development of the aggregate under consideration, and the north-south (NS) direction perpendicular to it.

3. Modelling criteria

The structural model of both configurations was performed according to the equivalent frame (EF) modelling strategy implemented in Tremuri software [9], which considers masonry walls as a combination of piers (vertical elements) and spandrels (horizontal elements), connected by rigid areas (nodes).

The model of the isolated building and the model of the building connected to adjacent structures are shown in Figure 3. In the models, the non-linear response of the panels is described by a constitutive law based on a phenomenological approach and a piecewise-linear beam model (i.e. NLBEAM) proposed in Figure 4 [10]. The NLBEAM is characterised by a constitutive law describing the non-linear response up to very severe damage levels (DL, from 1 to 5) through the definition of a relationship between the drift value $\delta_{E,i}$ and the corresponding fraction of the residual shear strength $\beta_{E,i}$ upon reaching the i-th DL differentiated for piers, spandrels, bending and shear behaviour Table 1. Please refer to [11] and [12] for further details on the formulation of NLBEAM and its potential in executing NDA. Diaphragms are modelled as orthotropic membrane elements. The moduli of elasticity describe the connection degree between diaphragms and vertical wall parallel to its reference direction, whereas the shear modulus represents the shear stiffness of the floor and the horizontal force transfer among the walls.

Table 1. Main parameters adopted in the non linear analyses

	SHEAR								
	dirft Θ [%]			*residual strength β [%]*		*hysteretic response*			
	DL3	DL4	DL5	DL3	DL4	c1	c2	c3	
PIERS	0.47	0.73	0.94	0.6	0.2	0.8	0.8	0	
SPANDRELS	0	1	1.5	0.6	0.6	0.2	0	0.3	
	FLEXURAL								
	dirft Θ [%]			*residual strength β [%]*		*hysteretic response*			
	DL3	DL4	DL5	DL3	DL4	c1	c2	c3	c4
PIERS	0.6	0.9	1.2	1	0.85	0.9	0.8	0.6	0.5
SPANDRELS	0.6	1	1.5	1	0.6	0.2	0	0.3	0.8
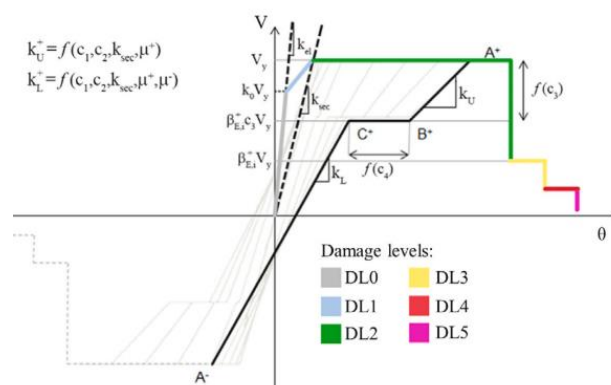
Figure 4. Piecewise-linear constitutive law and hysteretic response of the model

To explicitly account for the interaction effect between adjacent units, in the aggregate configuration, the procedure proposed in [12] has been implemented. Thus, the units were modelled separately to each other by introducing a finite-length gap represents the semi-length of the shared wall and, then, connected by elastic truss elements (sectional area of 0.00164 m2 and elastic modulus E of 210,000 MPa with null tensile behaviour) as well as orthotropic membranes (thickness of 0.05 m, E = 39,420 MPa, G = 13,112 MPa) to simulate possible transversal sliding between structural units (*Figure 5*).

Struts, on the other hand, allow for the modelling of the ability of structural units to spread apart while avoiding the interpenetration of elements.
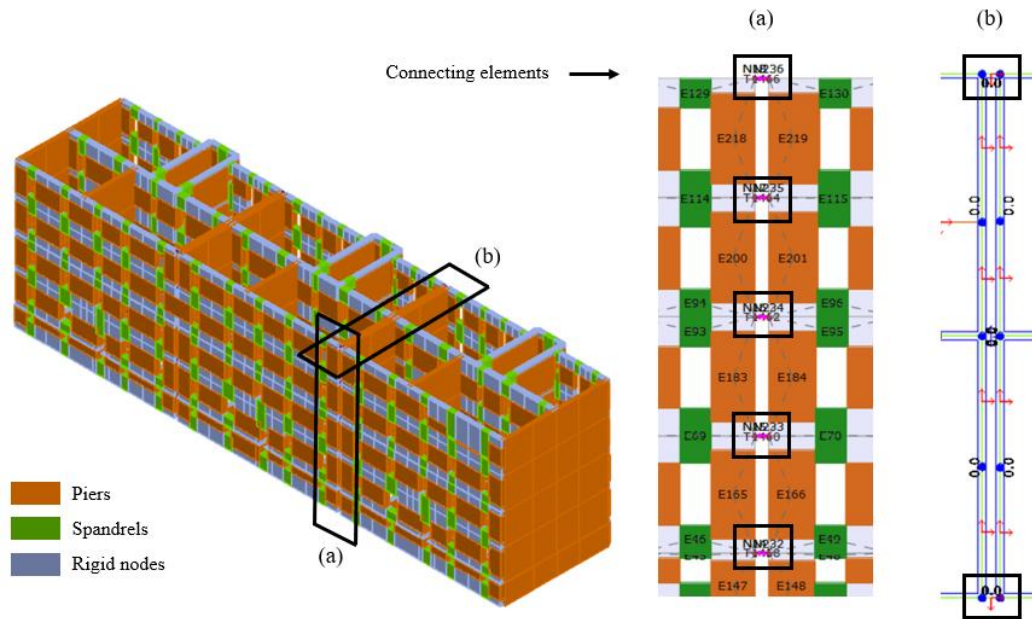
Figure 5. (a) Tremuri model of the aggregate configuration - (b) detail of the model elevation at the connection between two adjacent structural units and detail of the elastc truss elements with null tensile behavior and of the fictious floor connecting two adjacent units.

4. Main outcomes of numerical analyses

Modal analyses were conducted on the 3D equivalent frame model in order to obtain the dynamic behaviour of the building in the two configurations by identifying the main vibration modes, the corresponding periods and the participating mass.

Based on the results of the modal analysis for the isolated case (IB) and those for the aggregate case (AGG), it is possible to estimate the damping coefficients of the Rayleigh model needed for the NDAs [13]. These coefficients were found to be α = 0.364243 s^{-1} and β = 0.002196 s^{-1} for the isolated configuration (IS) case and α = 0.377368 s^{-1} e β = 0.00212 s^{-1} for the configuration in aggregate (AGG) case.

Table 2. Period, participant mass in x-direction (EW) and y-direction (NS) for both the isolated and aggregate case

Mode	*Isolated configuration*			*Aggregate configuration*		
	Period (T)	M$_x$ [%]	M$_y$ [%]	Period (T)	M$_x$ [%]	M$_y$ [%]
1	0.345	0.003	68.269	0.333	0.001	70.417
2	0.295	24.353	0.167	0.321	0.728	0.483
3	0.242	43.072	0.076	0.275	0.012	0.003
4	0.17	0.085	0.170	0.259	57.902	0.018
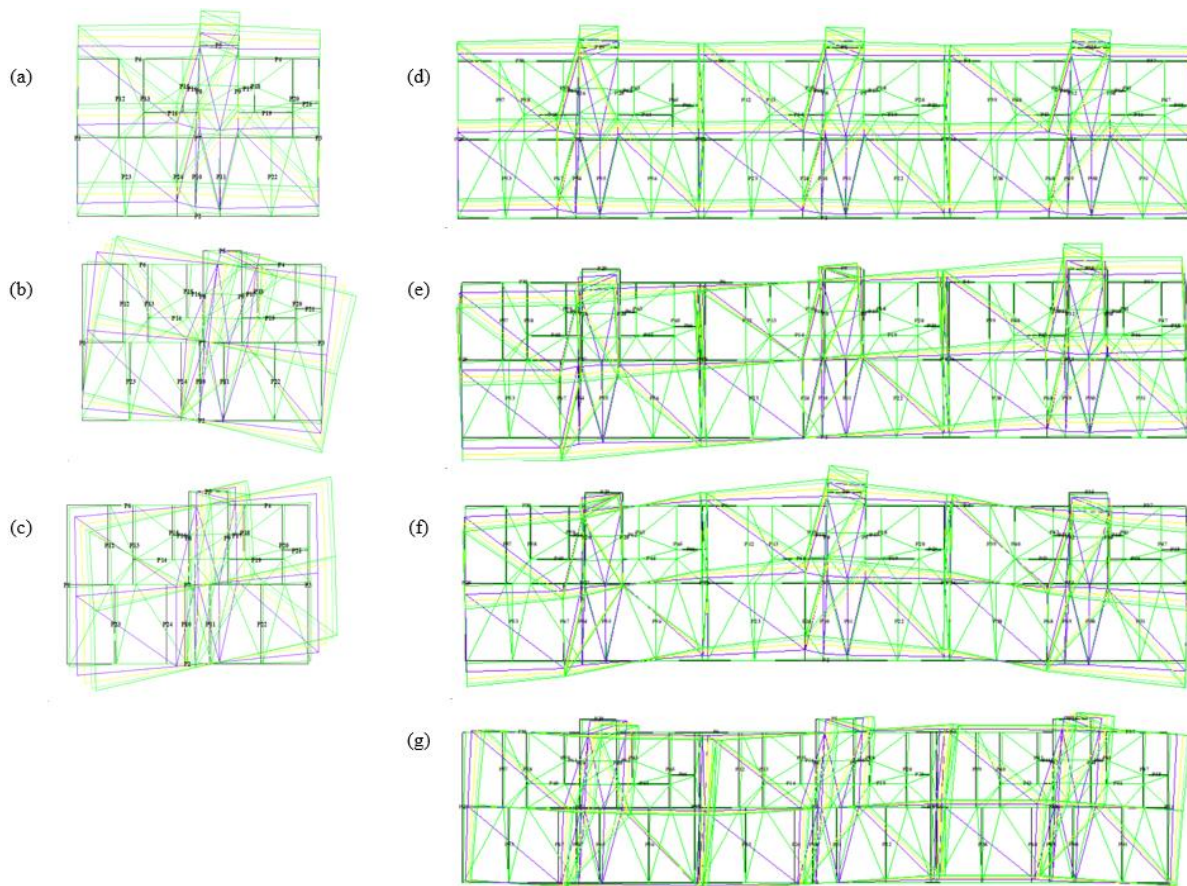
Figure 6. Modal forms. (a, b, c) first, second and third modal forms of the isolated configuration. (d, e, f, g) first, second, third and fourth modal forms of the configuration in aggregate.

Figure 7 and Figure 8 show the comparison between the pushover curves of the two configurations in terms of base shear-average last plane displacement (V-d). NSAs were performed for X and Y direction, both in the positive and negative directions, considering uniform load distributions proportional to the masses. NSAs were performed to estimate the capacity in terms of displacement in order to compare the results obtained from the NDAs. The NDAs were obtained by simultaneously applying the two components of the accelerogram along the X and Y direction. The Petrinja earthquake signal was reprocessed to take into account the variation of macroseismic intensity with distance from the epicentre [14]. The vertical component of the accelerograms was not considered.
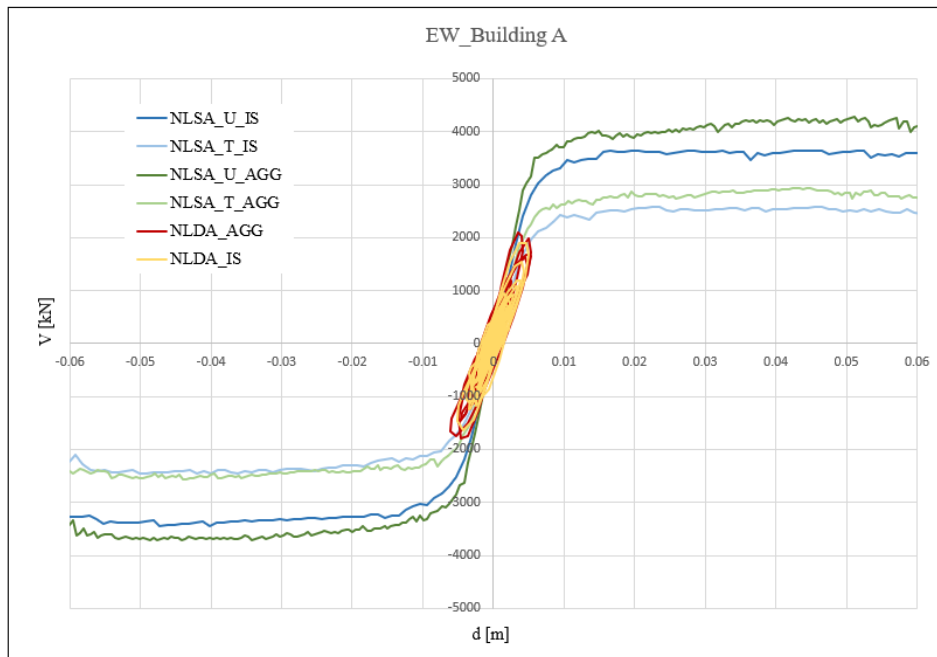
Figure 7. Overlapping of the non-linear static analyses (NLSAs) and non-linear dynamic analyses (NLDAs) of building A in both the isolated and aggregate case for the EW direction, i.e. that of the development of the aggregate.
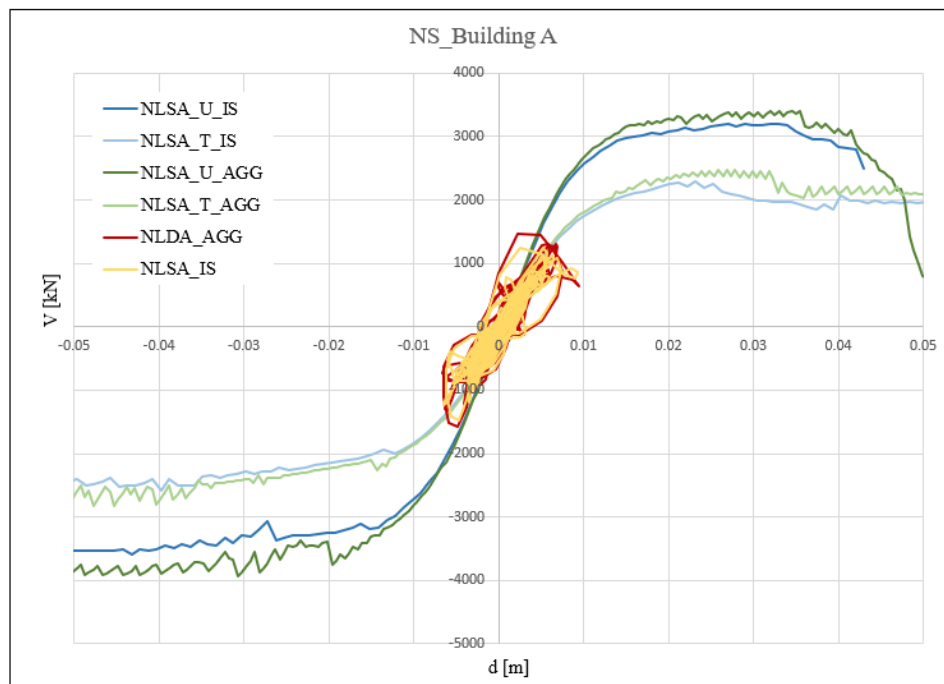
Figure 8. Overlapping of the non-linear static analyses (NLSAs) and non-linear dynamic analyses (NLDAs) of building A in both the isolated and aggregate case for the NS direction, i.e. the direction perpendicular to the development of the aggregate.

In order to synthetically interpret the data from the NLDAs, the multiscale approach originally proposed in [15], and then further developed in [16] and in [17] was adopted to assign a specitfic damage level to the building compatible with the EMS98 scale (i.e. from DL1 ti DL5) [18]. In particular, the adopted multiscale approach is associated to the wall scale. It is based on the extension of the "minimum DL"

that occurred to piers ($DL_{min,P}$), weighted on their shear stress contribution. The concept of the "minimum DL" was originally proposed in [19] to replace the adoption of the interstorey drift thresholds at the wall scale, as previously adopted in [15]; in particular, such a proposal assigns a damage level to the wall based on the minimum damage level attained by all the elements of a certain floor [18].

Table 3. Average damage level of walls in both directions

	Event	Isolated configuration		Aggregate configuration	
		Dir X	Dir Y	Dir X	Dir Y
Level Damage	Zagreb earthquake	0	1	0	1
	Petrinja earthquake	0	0	0	0
Cum DL wall DL1	Zagreb earthquake	16.79	52.51	7.26	51.73
	Petrinja earthquake	2.71	1.56	7.26	5.81
Cum DL wall DL2	Zagreb earthquake	4.76	28.72	4.47	5.82
	Petrinja earthquake	0	0	0	5.81

As Table 2 shows, the Y component of the earthquake does not lead to changes in modal behaviour between the isolated and the aggregate configuration. In that direction, the participating mass remains more or less the same. What does vary is what happens in the X direction. The second mode is a mode in X with a participating mass of 24.35% in the isolated configuration and which is reduced to 1.73% in the aggregate configuration, so the earthquake does not excite this torsional mode in the aggregate configuration. In the isolated configuration the torsions are instead activated by the second and third modes of vibration. In the aggregate configuration, on the other hand, only the first and fourth modes do not torsionally operate. This explains what is shown in the table, i.e. the fact that in the Y direction, in the isolated configuration, the walls are damaged more than in the aggregate configuration, since they are more stressed by the torsional component.
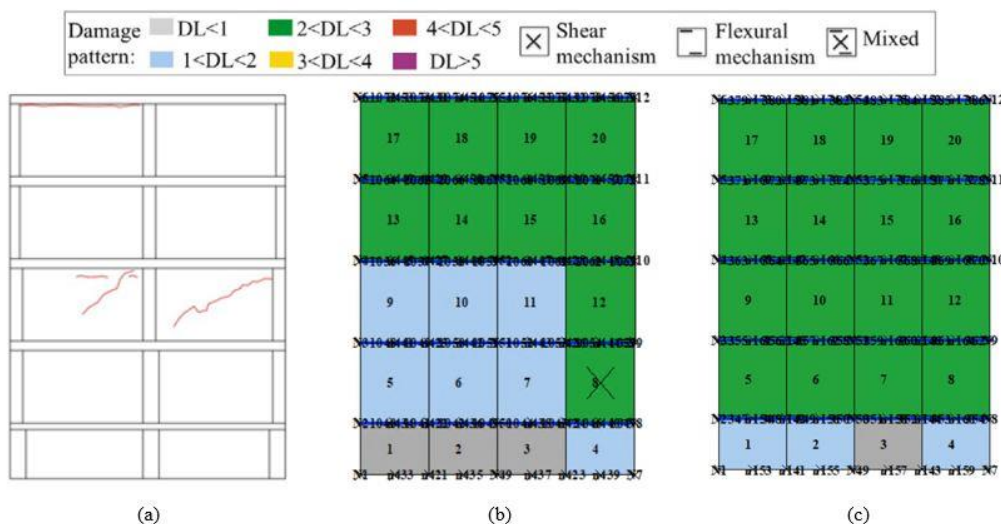
Figure 9. Wall in NS direction of building A. (a) Schematisation of actual damage - (b) damage obtained with the NLDA considering the aggregate configuration - (c) damage obtained with the NLDA considering the isolated configuration
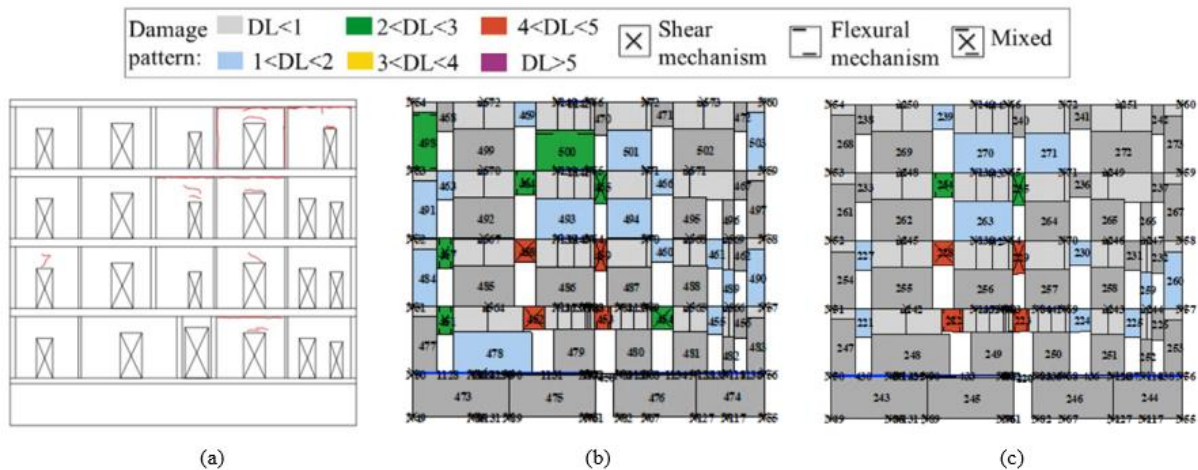
Figure 10. Wall in EW direction of building A. (a) Schematisation of actual damage - (b) damage obtained with the NLDA considering the aggregate configuration - (c) damage obtained with the NLDA considering the isolated configuration

The simulated damage in X direction appears more consistent with the actual one in the case of AGG configuration. Moreover, the overall damage level is substantially in agreement with that observed.

3. Conclusions

The study presented here proposes an evaluation of the seismic behaviour of an unreinforced masonry building located in an aggregate with a typical configuration in the historic centre of Zagreb Lower Town. The building in question was analysed both in the case in which it is considered isolated from the rest of the aggregate, and in the case in which it is included in the aggregate by considering the influence of the two buildings adjacent to it. The aggregate model showed a lower level than that of isolated building and generally gives a better description of the actual damage to the building.

This work is intended as a preparatory study for a broader analysis of the behaviour of the entire structural aggregate and the effect of different position of the structural units within it. In fact, it should be noted that buildings in a row aggregate during the Zagreb earthquake proved to be more resistant, as minor to moderate damage was found on these buildings. Buildings that are taller than the adjacent buildings proved to be more vulnerable, with significant damage occurring on the 'freestanding' floors above the adjacent buildings. On the other hand, it is common for a row unit to be interrupted for some reason (demolition of an adjacent building, opening of parking lots and access roads, etc.). Such buildings, which do not have an adjacent building on one side, sustained severe damage in some cases. Clearly, further research is needed on the properties of the connection between the buildings, as well as on the position within the aggregate and on the relative geometric and material properties of the adjacent buildings, to allow better calibration of the numerical models and realistic damage assessment. In fact, in the analysis presented here, the presence of orthotropic membranes of far from negligible stiffness has been assumed between the units. This assumption may not be always representative of reality, thus a future development will consist in carrying out sensitivity analyses on the various types of connections between adjacent units and also, if possible, performing in-situ dynamic identification investigations to validate assumptions made in numerical models.

Acknowledgements

References

[1] M. Stepinac *et al.*, "Damage classification of residential buildings in historical downtown after the ML5.5 earthquake in Zagreb, Croatia in 2020," *Int. J. Disaster Risk Reduct.*, vol. 56, no. February, 2021, doi: 10.1016/j.ijdrr.2021.102140.

[2] D. F. D'Ayala and S. Paganoni, "Assessment and analysis of damage in L'Aquila historic city centre after 6th April 2009," *Bull. Earthq. Eng.*, vol. 9, no. 1, pp. 81–104, 2011, doi: 10.1007/s10518-010-9224-4.

[3] M. G. Penna A, Morandi P, Rota M, Manzini CF, da Porto F, "Performance of masonry buildings during the Emilia 2012 earthquake," *Bull Earthq Eng 122255–2273*.

[4] L. Sorrentino, S. Cattari, F. da Porto, G. Magenes, and A. Penna, "Seismic behaviour of ordinary masonry buildings during the 2016 central Italy earthquakes," *Bull. Earthq. Eng.*, vol. 17, no. 10, pp. 5583–5607, Oct. 2019, doi: 10.1007/S10518-018-0370-4.

[5] J. Atalić, M. Uroš, M. Šavor Novak, M. Demšić, and M. Nastev, "The Mw5.4 Zagreb (Croatia) earthquake of March 22, 2020: impacts and response," *Bull. Earthq. Eng.*, vol. 19, no. 9, pp. 3461–3489, Jul. 2021, doi: 10.1007/S10518-021-01117-W.

[6] M. Š. Novak *et al.*, "Zagreb earthquake of 22 March 2020 – Preliminary report on seismologic aspects and damage to buildings," *Gradjevinar*, vol. 72, no. 10, pp. 843–867, 2020, doi: 10.14256/JCE.2966.2020.

[7] A. Moretić, N. Chieffo, M. Stepinac, and P. B. Lourenço, "Vulnerability assessment of historical building aggregates in Zagreb: implementation of a macroseismic approach," *Bull. Earthq. Eng.*, no. 0123456789, 2022, doi: 10.1007/s10518-022-01596-5.

[8] "Uroš, M., Todorić, M., Crnogorac, M., Atalić, J., Šavor Novak, M., Lakušić, S., (Eds.) Earthquake Engineering—Retrofitting of Masonry Buildings; University of Zagreb, Faculty of Civil Engineering: Zagreb, Croatia, 2021.".

[9] S. Lagomarsino, A. Penna, A. Galasco, and S. Cattari, "TREMURI program: An equivalent frame model for the nonlinear seismic analysis of masonry buildings," *Eng. Struct.*, vol. 56, pp. 1787–1799, 2013, doi: 10.1016/j.engstruct.2013.08.002.

[10] "Cattari S, Lagomarsino S. Masonry structures, pp. 151-200. In: Sullivan T, Calvi GM, editors. Developments in the field of displacement based seismic assessment. IUSS Press (PV) and EUCENTRE, pp. 524, 2013a. ISBN:978-88-6198-090-7. ."

[11] S. Cattari, D. Camilletti, S. Lagomarsino, S. Bracchi, M. Rota, and A. Penna, "Masonry Italian Code-Conforming Buildings. Part 2: Nonlinear Modelling and Time-History Analysis," *J. Earthq. Eng.*, vol. 22, no. sup2, pp. 2010–2040, 2018, doi: 10.1080/13632469.2018.1541030.

[12] M. Angiolilli, S. Lagomarsino, S. Cattari, and S. Degli Abbati, "Seismic fragility assessment of existing masonry buildings in aggregate," *Eng. Struct.*, vol. 247, p. 113218, Nov. 2021, doi: 10.1016/J.ENGSTRUCT.2021.113218.

[13] M. Liu and D. G. Gorman, "Formulation of Rayleigh damping and its extensions," *Comput. Struct.*, vol. 57, no. 2, pp. 277–285, 1995, doi: 10.1016/0045-7949(94)00611-6.

[14] F. Sabetta and A. Pugliese, "Estimation of response spectra and simulation of nonstationary earthquake ground motions," *Bull. Seismol. Soc. Am.*, vol. 86, no. 2, pp. 337–352, 1996.

[15] S. Lagomarsino and S. Cattari, "PERPETUATE guidelines for seismic performance-based assessment of cultural heritage masonry structures," *Bull. Earthq. Eng.*, vol. 13, no. 1, pp. 13–47, 2015, doi: 10.1007/s10518-014-9674-1.

[16] D. Sivori, S. Cattari, and M. Lepidi, *A methodological framework to relate the earthquake-induced frequency reduction to structural damage in masonry buildings*, vol. 20, no. 9. Springer Netherlands, 2022. doi: 10.1007/s10518-022-01345-8.

[17] A. Brunelli, F. de Silva, and S. Cattari, "Site effects and soil-foundation-structure interaction: derivation of fragility curves and comparison with Codes-conforming approaches for a masonry school," *Soil Dyn. Earthq. Eng.*, vol. 154, no. June 2021, p. 107125, 2022, doi: 10.1016/j.soildyn.2021.107125.

[18] M. Angiolilli, A. Brunelli, and S. Cattari, "Fragility curves of masonry buildings in aggregate accounting for local mechanisms and site effects," *Bull. Earthq. Eng.*, pp. 1–43, Feb. 2023, doi: 10.1007/S10518-023-01635-9/FIGURES/19.

[19] S. Marino, S. Cattari, and S. Lagomarsino, "Are the nonlinear static procedures feasible for the seismic assessment of irregular existing masonry buildings?," *Eng. Struct.*, vol. 200, no. September, p. 109700, 2019, doi: 10.1016/j.engstruct.2019.109700.

2CroCEE
22 - 24 March 2023

SEISMIC STRENGTHENING OF THE HISTORIC BUILDING OF "SOKOLANA" IN KUMANOVO

Elena Delova [(1)], Aleksandar Zlateski [(2)], Veronika Shendova [(3)], Zivko Bozinovski [(4)]

[(1)] *Young Research Assistant, Ss Cyril and Methodius University in Skopje, Institute of Earthquake Engineering and Engineering Seismology (IZIIS), Skopje, North Macedonia, e-mail: delova@iziis.ukim.edu.mk*

[(2)] *Research Assistant, Ss Cyril and Methodius University in Skopje, Institute of Earthquake Engineering and Engineering Seismology (IZIIS), Skopje, North Macedonia, e-mail: azlate@iziis.ukim.edu.mk*

[(3)] *Professor, Ss Cyril and Methodius University in Skopje, Institute of Earthquake Engineering and Engineering Seismology (IZIIS), Skopje, North Macedonia, e-mail: veronika@iziis.ukim.edu.mk*

[(4)] *Professor, Ss Cyril and Methodius University in Skopje, Institute of Earthquake Engineering and Engineering Seismology (IZIIS), Skopje, North Macedonia, e-mail: zhivko_bozinovski747@yahoo.com*

Abstract

The historic building of "Sokolski dom" in Kumanovo belongs to the plain masonry type of buildings. Built in the thirties of the last century for the needs of the "Sokolski Society", this building was once the main impetus for enrichment of cultural, entertainment and sports life, enabling the proper development of many generations. Due to its significance it was put under the protection as cultural-historic heritage in the country.

The subject of this paper is a detailed analysis of the stability of existing structure, which proved the need for its repair and seismic upgrading. With detailed analysis of the bearing and deformation capacity it was determined that the existing structure does not meet the requirements according to the national regulations. Therefore, the need for repair and strengthening was imposed, with the main goal of ensuring seismic stability of the building. Considering the possibilities and certain limitation for structural interventions from one hand, and the required bearing and deformation characteristics of the elements and the structure as whole from other hand, a traditional solution for strengthening was adopted, by reinforced concrete jackets and horizontal belt course. This technical solution provides increase of the structural bearing and deformation capacity of the system, as well as its ductility capacity, which is especially important for this type of buildings in case of seismic excitations. By increasing the deformation capacity, the input energy in the system would be consumed, which would greatly increase the seismic safety and security of the building.

Keywords: Repair, Strengthening, Masonry Structures, Capacity Analysis.

1. Introduction

Masonry structures, as a traditional type of construction, are especially present in the Balkan region. With cross-analysis of the statistical data from the last censuses from 1991 and 2002 and the available data from the State Statistical Office, it can be summarized that one third of the buildings in the Republic of North Macedonia belong to this type of constructions. Most of them were built in the second half of the XX century, before enactment of first seismic code in the country, and constructed on the basis of experiential knowledge. The most important and undeniable fact is that these buildings are still operating as buildings of vital importance for the society (schools, hospitals, cultural-historical monuments, etc.), Shendova et al. (2019).

The building of "Sokolana" in Kumanovo (Fig. 1), belongs to this type of buildings. Built in the thirties of the last century for the needs of the "Sokolski Society" from Kumanovo, this building was once the main impetus for enrichment of cultural, entertainment and sports life, enabling the proper psycho-physical development of many generations.

This paper presents a detailed analysis of the stability of the existing structural system of the "Sokolana" building, the need for repair and strengthening of the "Sokolana" building, the selection of the most adequate solution for repair and strengthening, as well as an analysis of the stability of the strengthened structural system of the building. For that purpose, the multidisciplinary approach was applied,

developed in the Institute of Earthquake Engineering and Engineering Seismology in Skopje (UKIM-IZIIS) based on gathered experience in the field of earthquake protection. This approach includes detailed technical and experimental investigations of the facility, in order to determine the actual input parameters for the analysis, and then analysis for the load-bearing elements in order to determine the limit state of strength, deformability and ability of load-bearing elements and the system as a whole to dissipate seismic energy, Bozinovski et al. (2019).

Figure 1. Front view of the building "Sokolski dom" in Kumanovo

2. Analysis of the existing building

2.1 Description of the structural system of the existing building

For the purposes of the analysis visual inspection of the building was carried out, with outdoor visual inspection, control measurements of building dimensions and structural elements, indoor visual inspection for identification/verification of the structural system.

The building consists of a central part (sports hall), with a maximum height on the load-bearing walls up to level + 9.60m, and total floor area of 525m2. In one part, above the main entrance there is a gallery (level + 3.86m). The building also has three additional ground floor structures of lower height that were built through the years of exploitation, with a total area of approximately 440m2. (Fig. 2, 3).
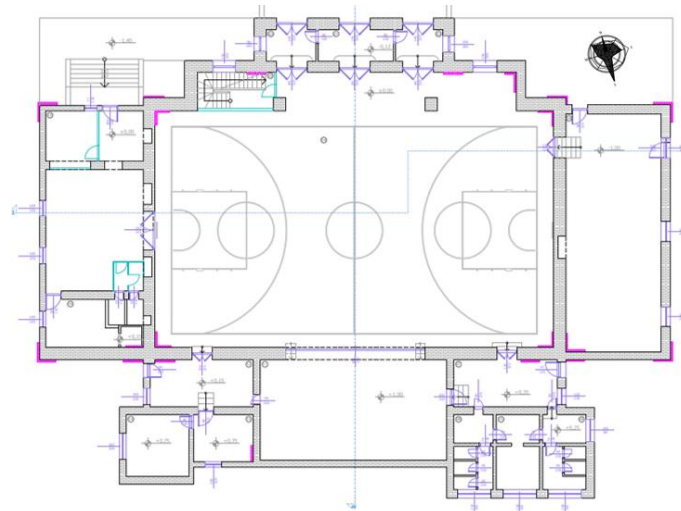
Figure 2. Ground floor of the building
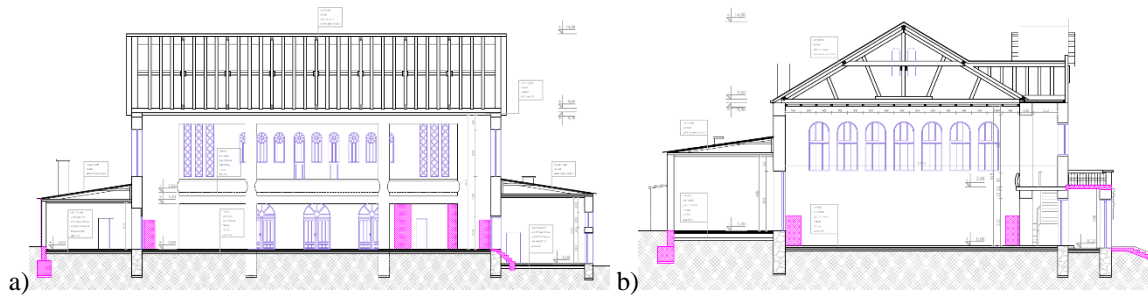
Figure 3. a) Longitudinal cross section of the building, c) Transverse cross section of the building

The principal structural system consists of bearing walls made of brick, in both orthogonal directions. The wall thickness varies from 75cm, for the main hall, and 35-60cm for the annex ground floor structures. The foundations are made of stone. For the gallery, there is a wooden floor structure. The main entrance is covered with a reinforced concrete slab. The roof for both the hall and the accompanying ground floor parts is made as a wooden structure, only on small part there is a ribbed reinforced slab. Many years ago an attempt for strengthening intervention was made, with reinforced concrete jackets. This process was stopped, so for the new solution as a starting point was reviewing and analysing the existing construction interventions.

During the inspection, significant damage was observed on the load-bearing wall elements, manifested with large cracks on the walls. Heavy damage was observed also in the roof - wooden structure and ribbed reinforced slab, in the annex ground floor structures. (Fig. 4) After the visual inspection it was concluded that, in order to bring the building in functional condition, it is necessary to make a repair and strengthening.

Figure 4. a), b), c), d) Severe cracks on the load-bearing wall elements

The input values for quality of the masonry of the load-bearing walls of the building, expressed through the modulus of elasticity, compressive and tensile strength, were assumed based on the experiences of examined elements of similar quality and construction time, and were confirmed by experimental

651

testing. Therefore, the following input parameters are adopted: modulus of elasticity E = 680MPa, shear modulus G = 170MPa, compressive strength f_c = 12MPa, tensile strength f_t = 0,12MPa.

2.2 Analysis of bearing and deformation structural capacity

Based on the defined geometry of the structural systems of the building, the physical-mechanical characteristics of the embedded materials and the load of the elements, an analysis was performed to determine the load-bearing capacity and deformability of the building, with the main purpose of defining its behaviour under seismic action.

To determine the real strength and deformation characteristics depending on the quantity and quality of the embedded materials, the computer program developed in UKIM-IZIIS was used. The program determines the displacement and the lateral force at yielding point (Δy and $Q y$), the ultimate displacement and lateral force ($Q u$ and Δu), for each individual element of the storey, i.e., the initial stiffness and the stiffness at yielding point. In this way, the force-displacement relationship is obtained for each element of each storey separately, whereby, the load-bearing and deformation capacity of each storey is defined. The deformation capacity also defines the displacement ductility capacity for each floor as $\mu = \Delta u / \Delta y$. The load-bearing and deformation capacity are determined for both orthogonal directions. The strength capacity is shown in the form of the ultimate storey shear force, which compared to the equivalent seismic force gives the safety factor.
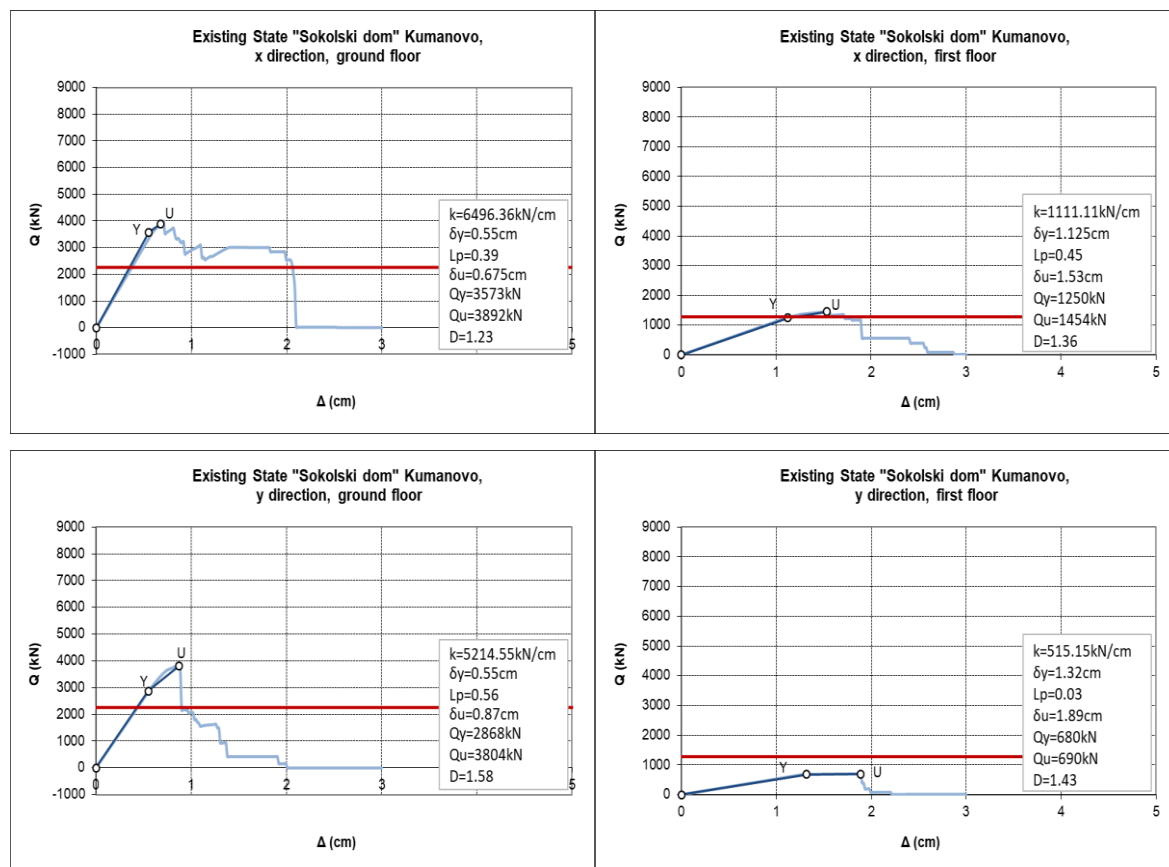
Figure 5. Storey Q-Δ relationship (existing state) for both orthogonal directions

The results of the analysis, in the form of summary storey Q - Δ diagrams for the two orthogonal directions respectively, are shown in Fig.5. The bilinear diagrams with the characteristic yield points "Y" and the ultimate point "U" are shown in blue, while the required load capacity of each floor is marked in red. Table 1 summarizes the obtained and required load-bearing capacities of the structure for each storey.

Table 1 – Structural bearing capacity for the existing structure

Existing state, x-direction					
Level	Qy [kN]	Qu [kN]	Qs [kN]	Qy/Qs	Qu/Qs
1st floor	1250	1454	1280	0.97	1.13
GF	3573	3892	2259	1.58	1.72

Existing state, y-direction					
Level	Qy [kN]	Qu [kN]	Qs [kN]	Qy/Qs	Qu/Qs
1st floor	680	690	1293	0.52	0.53
GF	2868	3804	2259	1.26	1.68

Based on the performed analysis of the existing structure and the obtained results, it was concluded that the strength capacity of the building for the ground floor for x-direction and y-direction is higher than the required according to the regulations, but for the first storey in both directions, it does not meet the requirements according to the regulations, PIOVS (1981). The ductility capacity for both directions in height is relatively small. The structure does not have sufficient strength for the ground floor for both directions, also the bearing capacity and deformability is relatively small for both directions, Bozinovski, Shendova et al. (2021). Given that structural interventions are going to be made, it is necessary to provide adequate strength and sufficient deformability, providing structural elements with greater ductility and increasing the integrity of the structure in both directions. From the above, the need for repair and strengthening is justified and necessary to improve the strength and deformation requirements and to achieve the desired dynamic response during future earthquakes.

3. Repair, strengthening and analysis of the structural system

3.1 Description of the technical solution for strengthening of the existing structure

Based on the required strength and deformation characteristics of the elements and the whole structural system, several variant solutions for strengthening of the structure were considered. During the selection of the repair and strengthening solution a few aspects were considered including the possibilities for interventions in the building and the economic aspect. Also, for each variant solution a preliminary analysis was obtained (for the structure stability for the two orthogonal directions). Comparison was made of the strength and deformability characteristics obtained with the required by the regulations.

From several variant solutions, a traditional solution for strengthening has been selected, the most appropriate from the economic aspect and from the aspect of assuring the strength and deformation requirements, according to the current technical regulations.

The solution for strengthening of the structural system includes the following, Bozinovski, Shendova et al. (2021): (i) strengthening of load-bearing walls with reinforced concrete jacketing in longitudinal and transverse direction along with the new foundations (shown with red color in figures 6, 7, 8); (ii) connecting the RC jacketings with horizontal reinforced concrete belt courses (shown with blue color in figures 7, 8) or rectangular steel profiles (shown with green color in Figures 7, 8), in transverse and longitudinal direction; (iii) strengthening of wooden joists from the roof truss with steel profiles (shown in figures 7,8 with green color) in order to form ties for connecting the elements in the transverse direction; (iv) local repair of the cracks manifested in the bearing walls; (v) local remove and replacement of the damaged wooden roof structure; (vi) local remove and replacement of the damaged ribbed reinforced slab above the ground floor. Figures 6, 7 and 8 show the formwork plans and characteristic cross-sections of the proposed technical solution for strengthening the "Sokolana" Structure.

The new reinforced concrete elements are intended to be of quality MB30 concrete (E_c = 31500Mpa, f_c = 21.5MPa) and reinforcement of the type RA400 / 500-2 (E_a = 210000MPa, f_{ta} = 400Mpa). Reinforced concrete elements of the structure are proportioned according to the theory of limit loads, i.e., according to PBAB (1987).
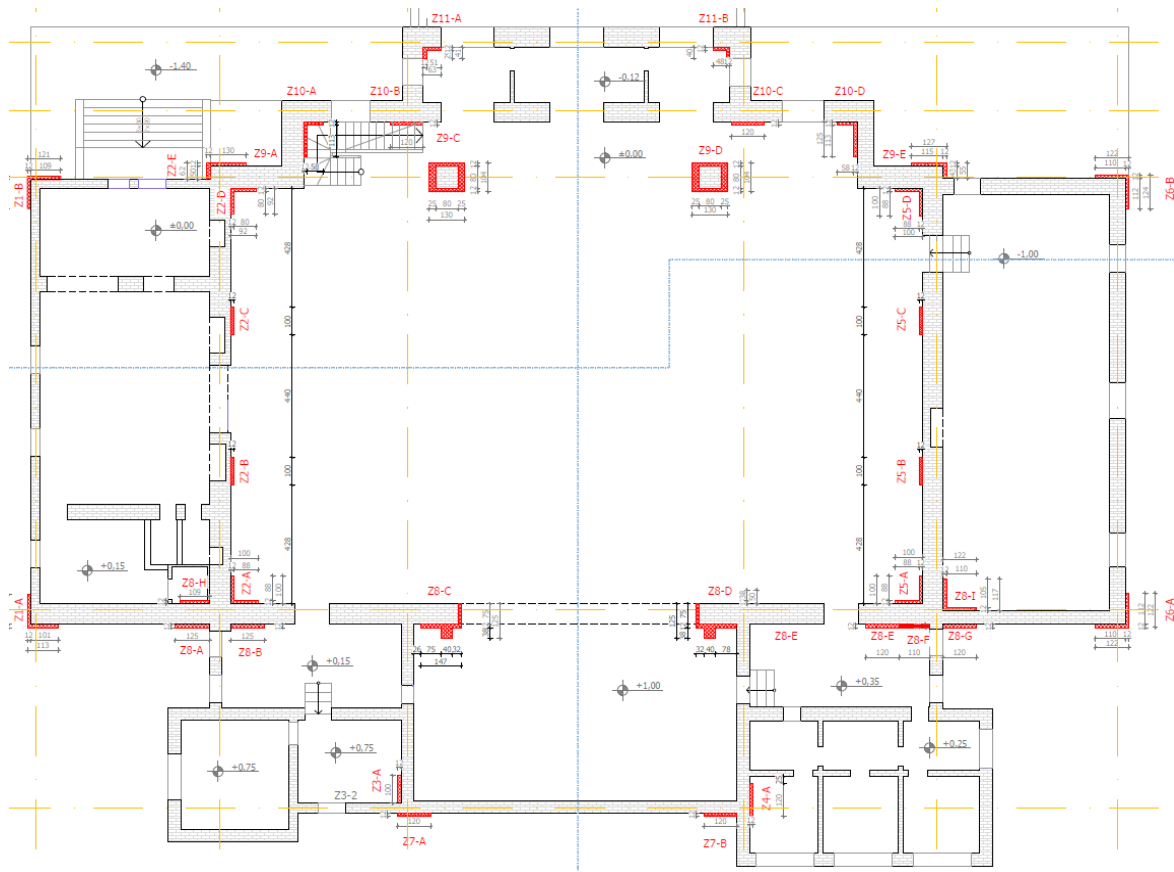
Figure 6. Formwork plan of the ground floor for the proposed strengthening solution
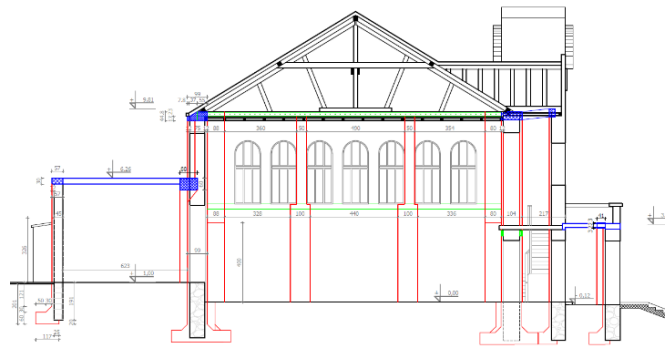
Figure 7. Characteristic cross sections for the proposed strengthening solution: transverse cross section
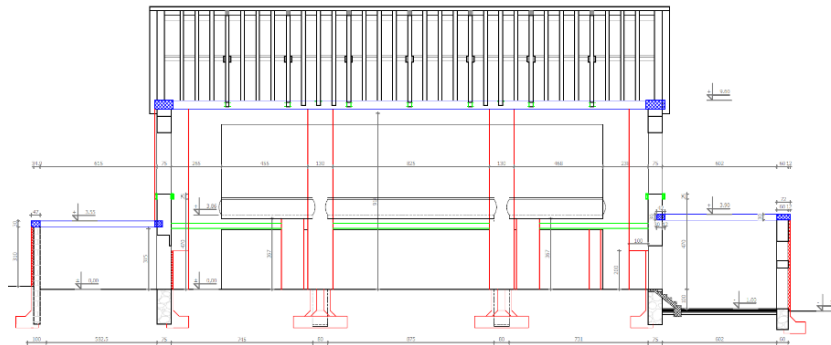
Figure 8. Characteristic cross section for the proposed strengthening solution: longitudinal cross section

654

3.2. Analysis of bearing and deformation capacity for the strengthened structural system

For verification of the proposed technical solution for repair and strengthening of the building, the procedure shown in Chapter 2.2 was applied again, through which the load-bearing and deformation capacities are defined, but this time of the strengthened structure. The computer program recalculates the displacement and shear force at yielding point (Qy and Δy), as well as at the ultimate point (Qu and Δu) for each individual element of each storey, but for the integrated structural system of masonry and reinforced concrete elements, with the corresponding characteristics of the built-in material. The results are presented in the form of summary storey Q - Δ diagrams for the two orthogonal directions respectively.
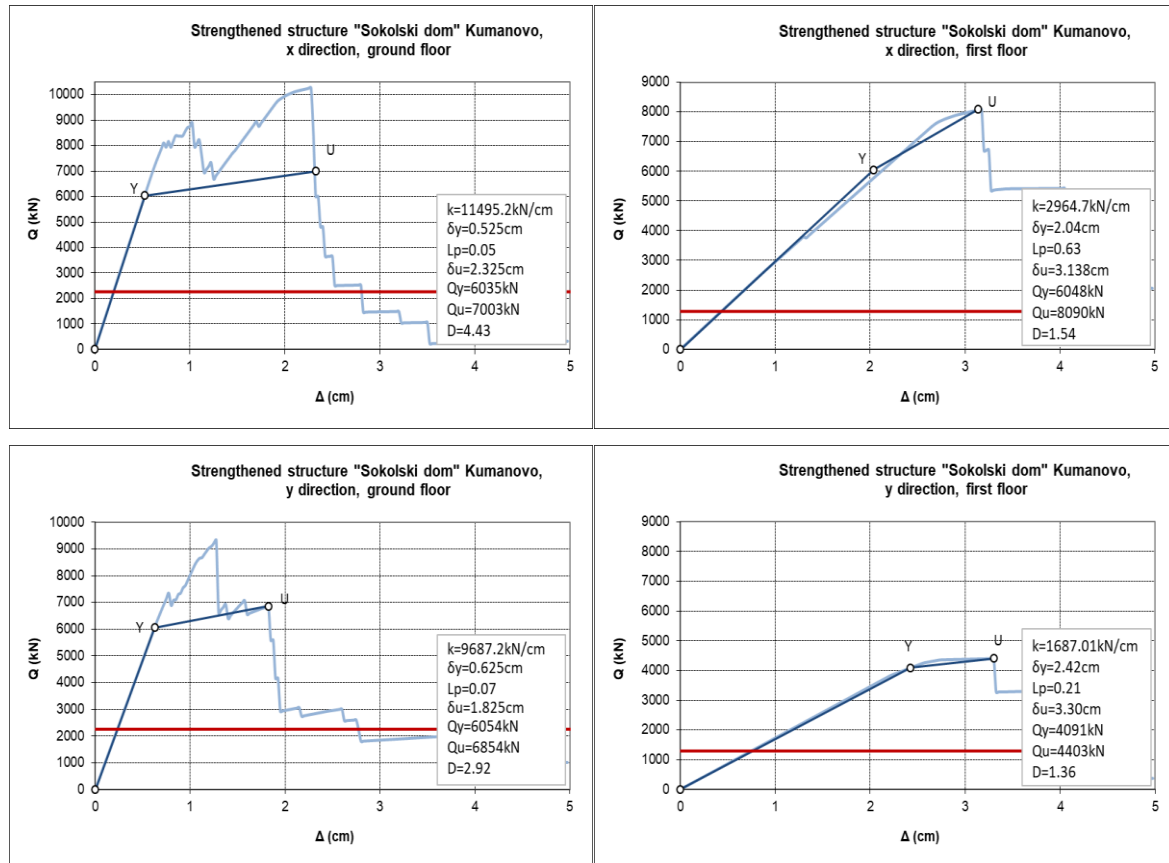
Fig. 9 - Storey Q-Δ relationship (strengthened structure) for both orthogonal directions

The bilinear diagrams with the characteristic yield points "Y" and the ultimate point "U" are shown in blue, while the required load capacity of each floor is marked in red (Fig. 9). Table 2 summarizes the obtained and required load-bearing capacities of the building by storey and directions, showing the new calculated safety factor.

Table 2 – Structural bearing capacity for the strengthened structural system

Strengthened structure, x-direction					
Level	Qy [kN]	Qu [kN]	Qs [kN]	Qy/Qs	Qu/Qs
1 floor	6048	8090	1280	4,725	6,32
GF	6035	7003	2259	2,67	3,10

Strengthened structure, y-direction					
Level	Qy [kN]	Qu [kN]	Qs [kN]	Qy/Qs	Qu/Qs
1 floor	4091	4403	1293	3,16	3,40
GF	6054	6854	2259	2,67	3,03

From the results of the analysis of the repaired and strengthened structure, it is noted that the capacity of the strength in both orthogonal directions of the building is significantly greater than the required limit capacity according to the regulations, PIOVS (1981). The bilinear diagrams show an increase in the deformation capacity of each of the storeys in both directions respectively, with an increase in the ductility capacities. This leads to the conclusion that the strengthening will increase the ability of the system for greater dissipation of energy, Bozinovski, Shendova et al. (2021). This is especially important for this type of buildings in case of seismic excitations. By increasing the deformation capacity, the input energy in the system would be consumed, which would greatly increase the seismic safety and security of the building, Bozinovski et al (2021).

4. Conclusions

The building of "Sokolana" in Kumanovo is a historic building built in the thirties of the last century. During the visual inspection, significant damage was observed on the load-bearing walls, due to the negligence of the building, manifested with large cracks on the walls. Heavy damage was observed also in the roof-wooden structures, and ribbed reinforced slab in the annex ground floor structures.

Based on the results form performed analysis of the existing structure it was concluded that the strength capacity of the building for the ground floor is higher than the required one according to the regulations, but for the first storey it does not meet the requirements for both directions. The ductility capacity for both directions is relatively small. The structure does not have sufficient strength, also the deformation capacity are relatively small, for both directions. Given the results of the existing structure, the need for repair and strengthening is justified and necessary in order to improve the strength and deformation capacity and achieve the desired dynamic response during future earthquakes.

From several analysed variants, a traditional solution for strengthening has been selected, the most appropriate from the economic aspect, satisfying the strength and deformation requirements according to the current technical regulations. The analysis of the repaired and strengthened structure of the "Sokolana" building, clearly shows that the strengthened system has significantly increased strength (load-bearing capacity) in both orthogonal directions and satisfies the required limit load capacity in accordance with current regulations. At the same time the results of the strengthened structure show an increase in the deformation capacity of each of the storeys in both directions respectively, i.e. an increase in the ductility. This leads to the conclusion that the proposed strengthening will increase the ability of the system to greater dissipation of energy, which is especially important for this type of buildings in case of seismic excitations.

References

[1] Bozhinovski Z., Shendova V., Zlateski A., Delova E. (2021). Analysis of Seismic Stability with Technical Solution for Strengthening for "Sokolana" in Kumanovo, Report IZIIS 2021-48, August 2021

[2] Bozinovski Z., Necevska-Cvetanovska G., Delova E., Zlateski A. (2021). IZIIS Methodology for Design, Repair and Strengthening of Earthquake Resisting Masonry and Reinforced Concrete Structures, 1st Croatian Conference on Earthquake Engineering 22nd - 24th March 2021, Zagreb, (Croatia).

[3] Bozinovski Lj. Z., Dojcinovski D., Delova E., Poposka M. (2019). Identification, Repairing, Strengthening and Revitalization of Existing Masonry and RC Buildings Structures in Seismic Prone Areas, Workshop on Earthquake Disaster Prevention and Mitigation in the "Road & Belt" countries, September 3-14, 2019, Dalian (China).

[4] Shendova, V., Apostolska, R., Vitanova M., (2019). Structural Classification of Building and Bridge Assets in R. N. Macedonia, SERA Balkans Seismic Risk Workshop, EU Horizon 2020, ID 730900, June 2019, Belgrade, Serbia

[5] PIOVS (1981): Rulebook on Technical Regulations for Construction of Buildings in Seismic Regions, (OG SFRY No. 31/81, Amendments 49/82, 29/83, 21/88 and 52/90)

[6] PBAB (1987): Rulebook on Technical Regulations for Concrete and Reinforced Concrete, (OG SFRY No. 11/87)

REPAIR AND STRENGTHENING OF OLD FIRST CATEGORY BUILDING IN SKOPJE, N. MACEDONIA IN ACCORDANCE WITH IZIIS METHODOLOGY

Aleksandra Bogdanovic[1], Vlatko Sheshov[2], Zivko Bozhinovski[2], Kemal Edip[1], Julijana Bojadjieva[1], Elena Delova[4], Aleksandar Zurovski[3], Antonio Shoklarovski[4]

[1] *Assoc. Prof. PhD, Ss. Cyril and Methodius University in Skopje, Institute of Earthquake Engineering and Engineering Seismology-IZIIS, N. Macedonia, saska@iziis.ukim.edu.mk; kemal@iziis.ukim.edu.mk; jule@iziis.ukim.edu.mk;*

[2] *Prof. PhD, Ss. Cyril and Methodius University in Skopje, Institute of Earthquake Engineering and Engineering Seismology-IZIIS, N. Macedonia, vlatko@iziis.ukim.edu.mk; zivko@iziis.ukim.edu.mk;*

[3] *Res. Assist.,MSc, Ss. Cyril and Methodius University in Skopje, Institute of Earthquake Engineering and Engineering Seismology-IZIIS, N. Macedonia, zurovski@iziis.ukim.edu.mk;*

[4] *Ext. Professional Associate, MSc, Ss. Cyril and Methodius University in Skopje, Institute of Earthquake Engineering and Engineering Seismology-IZIIS, N. Macedonia, delova@iziis.ukim.edu.mk; antonio@iziis.ukim.edu.mk;*

Abstract

The potentially high vulnerability and poor performance of the existing buildings, after past seismic events, including exploitation period has raised awareness of the need to improve their seismic performance. Repair and strengthening gives new life to existing or ageing structures that might otherwise be demolished and replaced.

This paper will address the issues related to repair and strengthening techniques for the first category building in Skopje, N Macedonia dated from 1924. Structural and nonstructural damages were observed due to the inappropriate foundation and maintenance of the building, which have increased during exploitation period and seismic actions. In order to define the stability of the building, non-destructive tests were applied for definition the material characteristics, further used in numerical analysis. Based on the performance assessment, retrofit schemes were proposed to address the main structural deficiencies and to meet national code requirements in N. Macedonia.

The results of the overall investigations and analyzes for the capacity of the building are presented in this paper. Also summarized are the necessary structural interventions to ensure the necessary stability and reliability of the building for gravitational and seismic actions in accordance with the existing legislation in the Republic of North Macedonia. Since it is a first category, the dynamic response of the structure to real seismic actions, expected at site, is also considered according to the valid legislature which defines the assessment of seismic force considering local soil conditions.

The outcomes from this project indicate the efficiency of the retrofit options utilized in reducing both the economic losses and collapse vulnerability of the building.

Keywords: repair, strengthening, non-destructive tests, structural and non-structural damages, dynamic analysis

1. Introduction

This paper is part of a project that was realized for the needs of the army of the Republic of North Macedonia.[1] In this paper a detailed analysis of the stability of the existing structural system has been presented, the necessity for repair and strengthening of the building has been proven, and an analysis of the stability of the repaired and strengthened structural system of the building has been performed. In the following, the results of the overall investigations and analyzes for the capacity of the building are presented. Also summarized are the necessary structural interventions to ensure the necessary stability and reliability of the building for gravitational and seismic actions in accordance with the existing legislation in the Republic of North Macedonia. The building is analysed as first-category building according to the current technical regulation, including the dynamic response of the structure to real seismic actions expected at the site.

2. Existing structural system

The building consists of ground floor, first floor and an attic with a relatively low height. The principal structural system represents brick masonry in lime mortar load-bearing perimeter walls, in combination with reinforced concrete frames in the interior of the building. Reinforced concrete slabs are constructed above the ground and first floor, which are supported on longitudinal and transverse beams. The foundation structure of the perimeter walls consists of strip foundations made of brick masonry in lime mortar without extensions, which represents an unusual foundation for this type of building. The columns located in the middle longitudinal line of the building are constructed on individual reinforced concrete footings. Façade of the building and building interior is shown in Fig. 1.

Figure 1. Façade of the building and building interior

Structural and non-structural damages were observed due to the inappropriate foundation and maintenance of the building, which have increased during the exploitation period and seismic actions (Fig. 2, Fig. 3).

Figure 2. Horizontal and diagonal cracks

Figure 3. Cracks in masonry walls

In order to define the stability of the building, non-destructive tests (Fig. 4) were applied[1] for definition the material characteristics, further used in numerical analysis.

Figure 4. Non-destructive tests

3. Analysis of the existing structure

An analysis of the existing structure was performed, due to the gravitational and equivalent seismic forces in accordance with the existing legislation in the Republic of North Macedonia. Seismic forces are defined based on the characteristics of the building and its purpose, as well as the characteristics of the location where the building is placed.

The analysis up to strength and deformability limit states was performed, with aim of defining the actual capacity of the structure and comparing it with the requirements in accordance with the existing legislation. Since it is a first-category building, the dynamic response of the structure to real seismic actions, expected at site, is also considered.

3.1 Quality and characteristics of the embedded materials

For the purposes of the analysis, a visual inspection of the structure was performed. The inspection defined the type and condition of the embedded material for the masonry walls, the quality of the materials, its strength and deformation characteristics. The quality of the masonry, for the structural walls, expressed through the limit bearing capacity of pressure (σ_c) and tension (σ_t) is evaluated based on the experiences of tested elements of similar quality and construction time. From the experimental tests carried out by the Institute of Earthquake Engineering and Engineering Seismology (IZIIS) on other buildings, the following characteristics of the existing masonry were determined: $\sigma_t = 100 - 300$ kPa; $\sigma_c = 1000 - 3000$ kPa.

For the existing condition, when we have clean masonry with vertical horizontal and diagonal cracks, as in the case, the analysis used $\sigma_t = 100$ kPa and $\sigma_c = 1000$ kPa, which according to the condition of the masonry and the degree of damage, are real.

With the strengthening, the masonry gets horizontal and vertical cerclages, reinforced concrete foundations and jackets, which significantly improves the strength and deformable characteristics of the structural elements, so in the analysis for the strengthened state, slightly higher characteristics were used, namely: $\sigma_t = 150$ kPa and $\sigma_c = 1500$ kPa.

The quality of the concrete and the embedded reinforcement is defined through non-destructive tests (Fig. 4). From the results, it was determined that the strength of the embedded concrete in the columns ranges from 22-25MPa, while in the beams from 19-22MPa. Reinforcement bars in the columns with a diameter of 16Φ, 18Φ, 20Φ, longitudinal, as well as 10Φ, 12Φ, 14Φ transverse, were found, and it was determined that smooth reinforcement GA240/360 was used.

3.2 Analysis of the strength-deformation characteristics of the existing structural system

The existing structural system presents a combined system of load-bearing walls made of solid brick in lime mortar, combined with reinforced concrete frames inside the building. The results of the analysis are given in the form of floor diagrams Q-Δ, separately for the two orthogonal directions (Fig. 5).
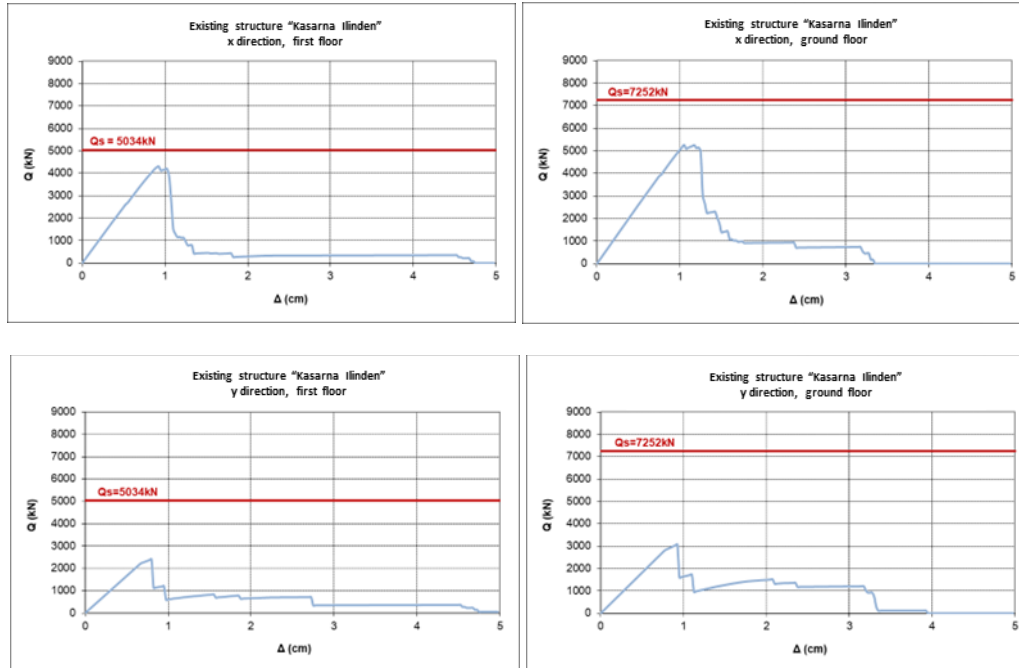
Figure 5. Floor Q-Δ diagrams for x and y direction

The summary strength and deformation characteristics are given in Table 1 and Table 2.

Table 1. Strength and deformation characteristics

Mass and seismic forces of the building by floors - existing structure						
level	Hi	m	Sx	QSx	Sy	Qsy
	[m]	[kN]	[kN]	[kN]	[kN]	[kN]
1st F	3,72	12530	5034	5034	5034	5034
GF	3,72	11643	2218	7252	2218	7252
Existing structure (x-direction)						
level	K	δY	L.P.	δU	D_cap	Qy	Qu
	[kN/cm]	[cm]		[cm]		[kN]	[kN]
1st F	4286	0,70	0,817	1,00	1,43	3000	4050
GF	5000	0,80	0,440	1,30	1,63	4000	5100
Existing structure (y-direction)						
level	K	δY	L.P.	δU	D_cap	Qy	Qu
	[kN/cm]	[cm]		[cm]		[kN]	[kN]
1st F	3333	0,60	0,450	0,80	1,33	2000	2300
GF	3636	0,55	0,963	0,85	1,55	2000	3050

3.3 Analysis results and conclusions on the necessity for strengthening

Based on the performed analysis of the existing structure and the obtained results, it was concluded:

Table 2. Strength and deformation characteristics

Existing structure (x-direction)					
level	Qy	Qu	Qs	Qy/Qs	Qu/Qs
	[kN]	[kN]	[kN]		
1stF	3000	4050	5034	0,525	0,551
GF	4000	5100	7252	0,804	0,703

Existing structure (y-direction)					
level	Qy	Qu	Qs	Qy/Qs	Qu/Qs
	[kN]	[kN]	[kN]		
1stF	2000	2300	5034	0,397	0,275
GF	2000	3050	7252	0,457	0,421

The structure's strength capacity for both directions is lower than required by the regulations, PIOVS 81, which is 16.5% for the X-X direction and 8.27% for the Y-Y direction of the total weight of the building. The required capacity according to regulations is 30%. Consequently, the structure does not have sufficient strength for the longitudinal direction and significantly insufficient strength for the transverse direction. The deformability capacity is relatively small for both directions. In addition to the requirements for seismic stability of the building, which have not been met, the building also has severe structural damage due to settlements of the foundation structure. The above mentioned demonstrates the necessity of improving the strength and deformation characteristics, in order to satisfy the basic requirements according to the existing technical regulation.

4. Selection of the Most Adequate Repair and Strengthening Solution for the Principal Structural System

Out of a number of variant solutions, the most appropriate solution has been selected from both low-cost aspect and the aspect of satisfying the strength and deformation requirements in compliance with the valid technical regulations. The solution for strengthening of the principal structural system mainly anticipates strengthening of the structural bearing elements, walls, columns and beams, creating lines of defence against external seismic effects in both orthogonal directions (Fig. 7, Fig. 8). Repair of cracks in bearing walls and reinforced concrete elements as well as partial repair of the floor structure is done additionally. More specifically, this involves the following:

- Strengthening of the foundation structure and recommendations for drainage of atmospheric waters from the structure;
- Strengthening of the bearing walls by reinforced concrete jackets in longitudinal and transverse direction;
- Strengthening of reinforced concrete columns mainly along strengthening lines of external walls;
- Strengthening of transverse beams along the strengthening line of walls and columns;
- Foundation of reinforced concrete jackets into own footings. The same also holds for the strengthened reinforced concrete columns;
- Inter-connection of jackets by horizontal reinforced concrete belt courses mainly along the perimeter of the structure and at the level of the floor structure over the ground floor and over the storey;
- Local repair of cracks manifested in bearing walls and reinforced concrete elements;
- Local repair of the deformed floor structure at the ground floor.
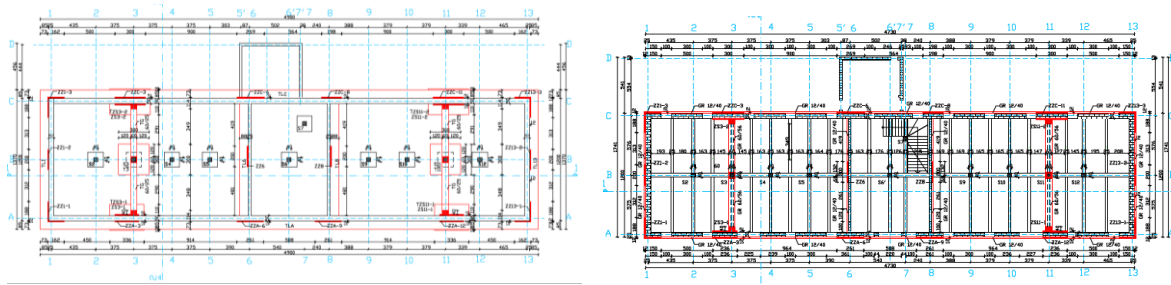
Figure 6. Strengthened and existing state at plan of foundations (left), ground floor and storey (right)
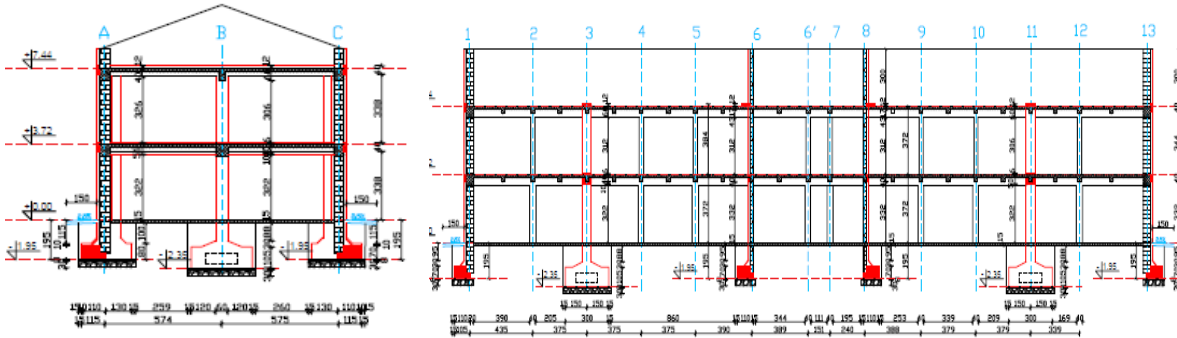
Figure 7. Cross-section of the strengthened and existing structure.

5. Analysis of the repaired and strengthened structural system

For the strengthened structural system, analysis of strength and deformability to strength and deformability limit states was performed, for the structural elements and the global structural system, for its dynamic response under real expected seismic actions.

On the basis of the performed analysis of the strengthened structural system the following condition was established.

5.1 Storey diagrams Q-Δ

On the basis of the defined diagrams base shear-displacement and moment-curvature for every element and their transformation in diagrams force-displacement, the following floor diagrams force-deformation were defined (Fig. 8).
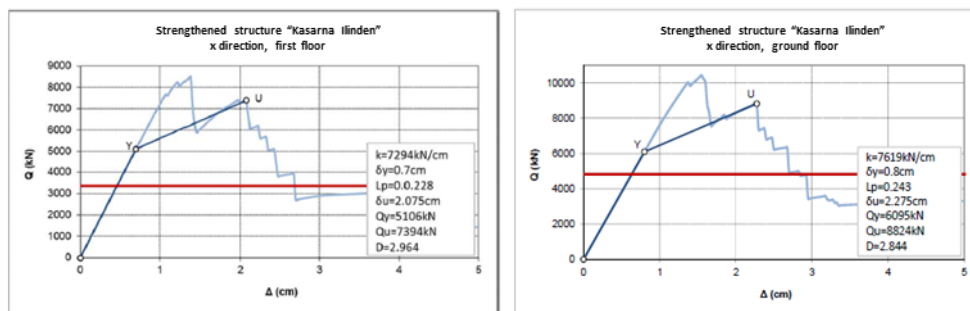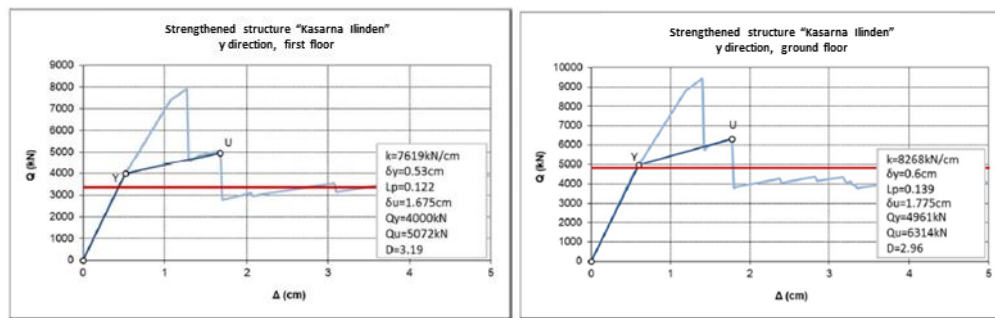
Figure 8. Floor diagrams force- deformation in X and Y direction (strengthened structure)

The total strength and deformability characteristics are given in the Table 3 and Table 4:

Table 3. Total strength and deformability characteristics

Strengthened structure Direction X-X

	Qy [kN]	dy [cm]	Qu [kN]	du [cm]	K1 [kN/cm]	K2 [kN/cm]	L. P.	Ductility
1st F	5106	0.7	7394	2.075	7294	1664	0.228	2.964
GF	6095	0.8	8824	2.275	7619	1850	0.243	2.844

Strengthened structure Direction Y-Y

	Qy [kN]	dy [cm]	Qu [kN]	du [cm]	K1 [kN/cm]	K2 [kN/cm]	L. P.	Ductility
1st F	4000	0.525	5072	1.675	7619	932	0.122	3.190
GF	4961	0.6	6314	1.775	8268	1151	0.139	2.958

Table 4. Total strength and deformability characteristics

Strengthened structure Direction X-X

level	Qy	Qu	Qs	Qy/Qs	Qu/Qs
	[kN]	[kN]	[kN]		
1st F	5106	7394	3362	1,52	2,20
GF	6095	8824	4825	1,26	1,82

Strengthened structure Direction Y-Y

level	Qy	Qu	Qs	Qy/Qs	Qu/Qs
	[kN]	[kN]	[kN]		
1st F	4000	5072	3362	1,18	1,51
GF	4961	6314	4825	1,03	1,31

The analysis of strength and deformability characteristics of the structure show that the capacity of strength at the base of the stracture totals 36.5% of the total weight of the structure for X-X direction and 26.12% of the total weight of the structure in Y-Y direction. The demand capacity from the codes is 19.5% because of the change in the coefficient of ductility and damping for strengthened masonry. These data are from manually schematized diagrams force-displacement. From the diagrams, it is clear that the capacity of strength and deformability are larger, as well as the capacity for dissipation of seismic energy. The capacity of the strength of the structure in both directions is larger than the demand according to technical regulations.

5.2 Dynamic response for real seismic actions

For the location of the structure, a maximal acceleration of 0.25g was defined, together with recommended accelerograms (time- history records):

- Ulcinj (Albatros) N-S;

- El Centro;
- Ulcinj (Olimpik) N-S;
- Bar (municipality parliament) N-S;
- Robic- excitation with wide frequency range;

The results are shown as diagrams floor- displacement and floor- ductility (Fig. 9).
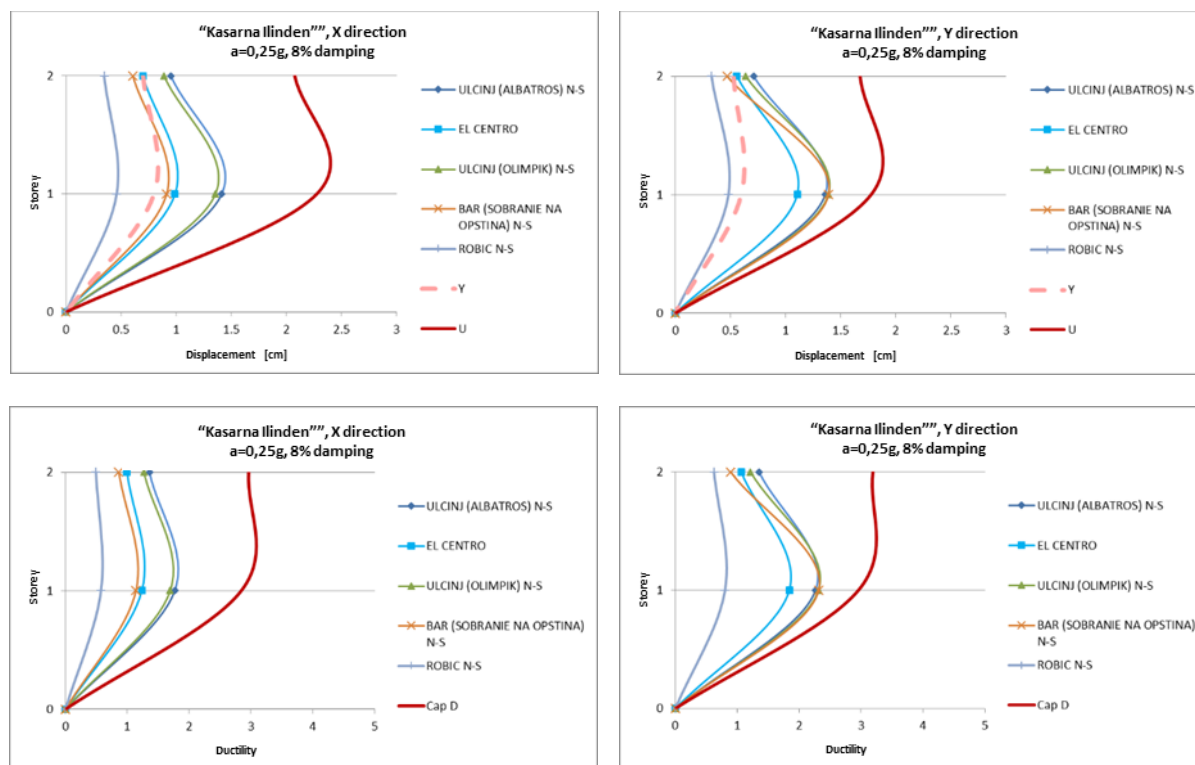
Figure 9. Diagrams floor- displacement and floor – ductility for X and Y direction

With the repair and strengthening of the structural system, a significant increase in ductility capacity and dissipation of seismic energy capability of the elements and the structural system as a whole can be noted. The dynamic response for real expected seismic actions for the location confirms that too.

5.3 Dynamic response for real seismic actions

Proportioning of new RC elements according to the theory of limit states i.e. current technical regulations in the country was performed. For part of the elements, reinforcement is placed gradually from 0.6% to reach the necessary strength and deformability.

6. Technology of Construction

The strengthening effect depends on the consistency of the performance of the construction works. The preparation works are not carried out simultaneously for the jackets, the foundation of the external walls and the foundation of the central column. The foundation of the external wall beyond the jacket is performed in parts of 2 – 3 m. Prepared and constructed simultaneously is a jacket on the left front wall, a jacket on the rear external wall, one column and 4 parts of the foundation of the external walls according to the construction plan approved by the Engineer following the excavation for the first jacket and assessment of the rockfall hazard and possibility for performance of simultaneous activities in a long run. One of the reasons for controlled construction is also a possible earthquake that may affect the weakened structural system. Parallel to the preparation works, injection of cracks in the solid brick walls is performed. The crack is cleaned and widened upon the surface of the cracked and damaged

bricks and is injected with repaired concrete or strong cement mortar. Local strengthening is done irrespective of strengthening because global strengthening of the structure prevents further opening of cracks.

Preparation works consist of: chase cutting of mortar on the walls made of solid bricks in lime mortar at places of their strengthening with reinforced concrete jackets. Then, half bricks are taken from the wall at distance of 40 cm along horizontal and vertical line, in a chess shape, in order to provide a better connection between the masonry and the concrete part.

As an example, the figure below shows a detail of a jacket with minimal reinforcement and way of efficient connection with a solid brick wall. In addition to dowels, the wall is additionally connected to the jacket by a reinforcing wire and a metal plate on the opposite side. The next step is excavation for the foundation of the jacket. The excavation is done beside the wall, at depth down to the lower edge of the existing foundation plus 30 cm for the tooth, 8 cm for the lean concrete and 30 cm for the gravel layer. Details of the technology of performance of repair are shown on Fig. 10.

Figure 10. Details of the technology of performance of repair.

Following the excavation, compaction of the base is done by means of a light rammer (the so called frog rammer). Consolidation is done by light compaction. Upon the base, a layer of lean concrete is poured. With this, conditions are created for the construction of the jacket. The wall and the foundation are prepared for the placement of the anticipated reinforcement. Following placement, connection and checking of the reinforcement, shuttering of the jacket and the foundation into the planned shape is done. Concreting is done per phases, the first phase - upper edge of the foundation, i.e., down to the lower edge of the connecting foundation beam, second phase – connecting foundation beam, third phase – down to the lower edge of the transverse beam and longitudinal belt course. In the fourth phase, concreting of belt courses and transverse beams is done. The fifth phase involves the jackets over the storey and the last one includes the end belt courses over the storey. After concreting of the foundation, the earth is returned over the foundation and conditions are created for the construction of the footways. Simultaneously with these activities, preparations for the connection of the transverse beam and the external jackets are made, leaving sufficient space for embeddment of reinforcement and the jacket–transverse beam concrete connection. Details of repair of end column and central column are shown on Fig.11.
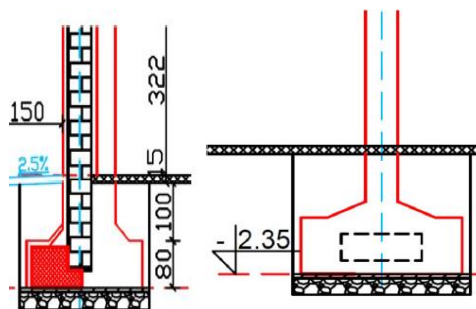
Figure 11. Details of repair of end column and central column

A similar procedure is applied in strengthening of a central column. Chase cutting of the mortar from the column and roughening of the external surface are done in order to create a better connection between the old column and the jacket. Excavation for the foundation follows. The base is compacted, the gravel layer and the lean concrete are placed. Further on, reinforcement, shuttering and concreting are done in a number of phases. The transverse beam is constructed as entirely continuous. The same holds also for the external horizontal belt courses.

7. Conclusions

With its strength and deformability characteristics, the existing structural system does not satisfy the requirements pertaining to the Regulations and recent knowledge on behaviour of masonry structures exposed to gravity and seismic effects.

A number of variant solutions have been proposed and analyzed for repair and strengthening of the principal structural system.

Selected out of a number of variant solutions has been the most appropriate one from low-cost aspect and from the aspect of satisfying the strength and deformability requirements of the valid technical regulations.

The repair and strengthening of the bearing structural system have been done in such a way as to satisfy the requirements of valid technical regulations and enable a favourable dynamic response to the realistic seismic effects defined for the considered location.

Strengthening practically enables greater stiffness, strength and deformability by optimizing these three characteristics, obtaining thus optimal quantities and providing the required seismic safety.

A greater percentage of the strengthening activities refers to strengthening due to inappropriate foundation resulting in diagonal cracks in bearing walls made of solid bricks in lime mortar, whereas strengthening against seismic effects is done to a relatively lesser extent.

This report contains the minimal necessary elements for repair and strengthening of the principal structural system, by means of dimensions and reinforcement.

Out of own reasons, the Contractor may adopt, according to the possibilities for performance or available equipment and material, different dimensions of elements or different reinforcement provided that the dimensions and the reinforcement are not lesser than those defined in this report. Each change should be reported to us in order that we can check whether the change affects the level of seismic protection and stability of the structure.

The analysis of the strength and deformability capacity of the repaired and strengthened structure has proved that it satisfies the strength and deformability requirements of the valid regulations and the most recent knowledge on behaviour of masonry structures exposed to static-gravity and dynamic-seismic loads.

References

[1] Sheshov, V., Bozhinovski, Z., Bogdanovikj, A., Edip, K., Delova, E., Zhurovski, A., Shoklarovski, A. (2020). Analysis of Seismic Stability with Technical Solution for Strengthening for "Objekt 48" in Military Barracks Ilinden in Skopje, Report IZIIS 2020-71, December 2020

[2] Sheshov, V., Bozhinovski, Z., Bogdanovikj, A., Edip, K. (2020). Inspection Report on the Condition of the Building Facility – Military Barracks Ilinden, Skopje with a Proposed Solution for Strengthening – IZIIS 08-1624/1

[3] Delova, E., Zlateski, A., Shendova, V., Bozhinovski, Z., Mijalkova, L. (2022). Analysis of the Seismic Stability with Technical Solution for Strengthening of an Existing Building, 3rd European Conference of Earthquake Engineering and Seismology, September 4-9, 2022, Bucharest, Romania.

[4] Bozhinovski, Z., Necevska-Cvetanovska, G., Delova, E., Zlateski, A. (2021). IZIIS Methodology for Design, Repair and Strengthening of Earthquake Resisting Masonry and Reinforced Concrete Structures, 1st Croatian Conference on Earthquake Engineering, March 22nd - 24th, 2021, Zagreb, Croatia (Online conference)

[5] Zlateski, A., Delova, E., Poposka, A., Bozhinovski, Z., Gjorgjievska, E. (2019). Analysis of the Seismic Stability with Technical Solution for Strengthening for the Prison Building in Bitola, 18th International Symposium of Macedonian Association of Structural Engineers (MASE 2019), October 02-05, 2019, Ohrid, North Macedonia

[6] Bozhinovski, Z., Shendova, V., Stojanoski, B., Nechevska-Cvetanovska, G., Apostolska, R., Gjorgjievska, E., Jekic, G. (2011). Strengthening of the Principal Structural System of the Parliament Building of Republic of Macedonia – Technical Solution and Construction, 14th International Symposium of Macedonian Association of Structural Engineers (MASE 2011), Struga, North Macedonia

SEISMIC PERFORMANCE ASSESSMENT OF RC INDUSTRIAL BUILDING AFTER RETROFITTING BEAMS AND COLUMNS

Niharika Peddaprolu [1], Pradeep Ramancharla [2], Aishwarya Gupta [3],

[1] *PhD student, IIIT Hyderabad, niharika.peddaprolu@research.iiit.ac.in*
[2] *Professor, IIIT Hyderabad, ramancharla@.iiit.ac.in*
[3] *M. Tech, IIIT Hyderabad, aishwarya.gupta727@gmail.com*

Abstract

A numerical study is done to determine the seismic performance of G+1 industrial RC building after retrofitting beams and columns. Deterioration of building has occurred due to excess chemical spillage over structural elements. Distressed beams and columns were retrofitted using jacketing techniques. The building is located in Indian Seismic Zone IV, so there is a need to understand the global seismic behaviour of the building after retrofitting. Nonlinear static pushover analysis is carried out to and the results indicate a decrease in the storey shear values.

Keywords: Compressive Strength, Seismic Retrofitting, Push-over Analysis, Base Shear, Displacement, Jacketing

1. Introduction

The G + 1 building was constructed 15 years ago. It is an industrial production plant where due to chemical spillage, the deterioration of beams and columns has occurred. A visual inspection is done along with Non-destructive testing. The results indicated that the compressive strength decreased to 10MPa and longitudinal reinforcement corroded up to 25 percentage. The structure is located in Indian Seismic Zone IV. Since the building was industrial plant with hazardous materials, there is a need for checking the seismic safety of the structure concerning the safety of the occupants.

In the detailed report after Non-destructive Testing, it was mentioned that the distress in beams was majorly due to chemical spillage. In columns due to penetration of chemicals into the concrete substrate, large cracks were formed which lead to the corrosion of longitudinal reinforcement.

To bring the structural elements to original strength, concrete jacketing of 100mm thickness on all sides for columns and 75mm thickness on three sides were suggested. The additional longitudinal and transverse reinforcement is added in the jacketed beams and columns. A total of 6 columns and 5 beams were retrofitted. Figure 1a and 1b represent the jacketed columns and beams respectively.
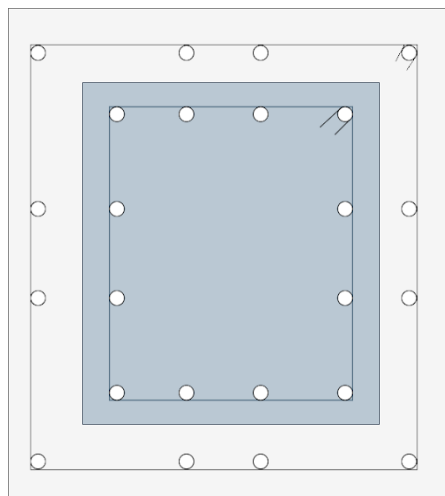
Figure 1a: Column with 100mm concrete jacket
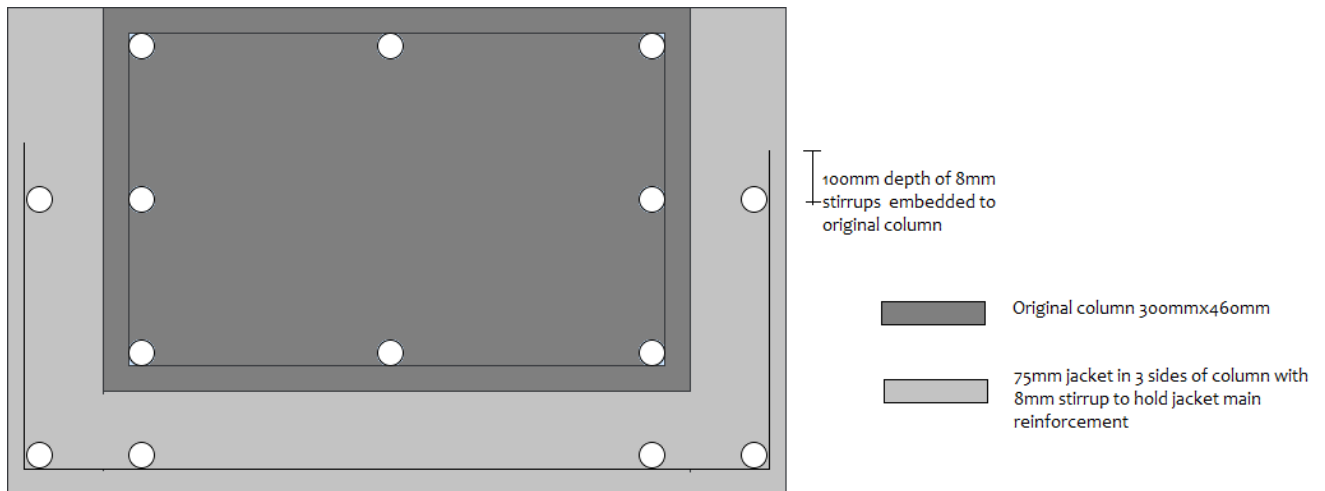
Figure 2b: Beam jacketed with 75mm on three sides

The Nonlinear static pushover (NSP) analysis predicts the seismic forces and deformation demands of the structure. For this purpose, NSP analysis is performed and the seismic safety of the industrial structure was done to check the reliability of the strengthening design of distressed structural elements.

The results indicated that after strengthening the columns and beams, the elements are able to withstand the demand.

By encasing the distressed beams and columns, the seismic stability of the structure increased which can be observed from the decrease of storey shear and deformation values after strengthening.

2. Details of existing structure

The building plan and elevation is mentioned in the below figures.
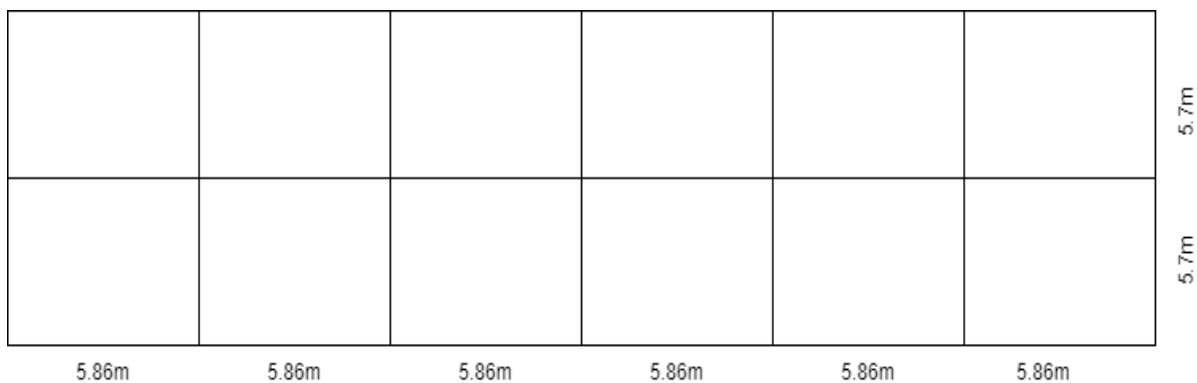
Figure 2 : Plan of the Building
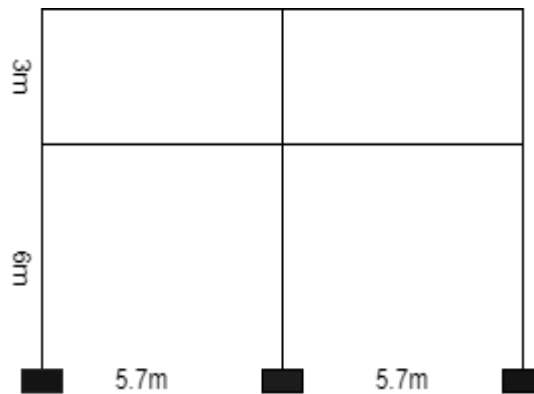
Figure 3: Elevation of Building

The existing condition of the structure is shown in the below figure 4. The results of the Non-destructive testing using rebound hammer, ultra-sonic pulse velocity and Core cutting are presented in Table1 of appendix for reference.

Figure 4: Existing condition of Columns and Beams

The height of ground floor is 6m and first floor is 3m. Plan area is 34.8 x 11.4 square meters. Live load is considered as 5 kN/m. The slab thickness is 150mm, the beams dimension is 300mmx360mm and column dimension is 400mmx480mm. The reinforcement details of beams and columns are tabulated in table of Appendix. The grade of concrete for beams is M20 and for column is M30.

3. Analysis procedure:

As the first step of analysis, Equivalent static analysis is performed. The lateral force distribution at various floors levels is represented in figure 5. To determine the lateral forces at each floor the design seismic base shear value V_b must be calculated. The total seismic weight of the building is 13745 kN. The importance factor is taken as 1.5, since the building is industrial building.

The fundamental Natural Period is 0.133 seconds. The design acceleration coefficient (Sa/g) for medium stiff soil is 2.5. The design base shear is calculated as 1237 kN.

In the below table 1 given, W_i is the seismic weight of the building. W_i is calculated by considering full dead load and part live load acting on the structure. Since the structure is industrial type, load of the machinery is included as well along with the floor finishing load. As per the IS: 1893(Part1):2016, percentage of imposed load is calculated using Clause 7.3.1.

Table 1 – Vertical Base Shear Details

Floor	W_i	h_i	$W_i h_i^2$	$W_i h_i^2 / \Sigma W_i h_i^2$	V_b	Q_i
1	13745	9	1240486	0.715	1237	884
2	13745	6	494820	0.285	1237	353

Lateral force distribution at each floor is shown in figure 5.
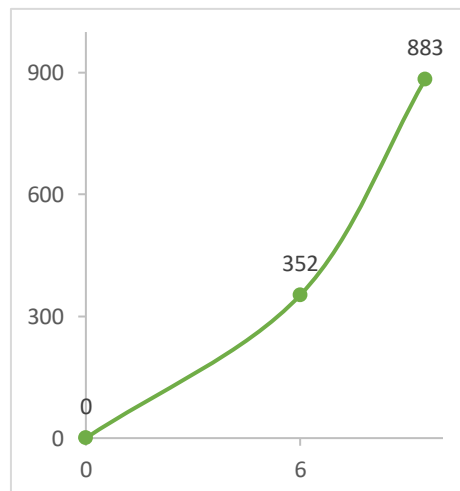
Figure 5: Loading Diagram

Non linear static pushover analysis is carried out for the structure after strengthening beams and columns. The displacements of the each floor is plotted with the storey height for strengthened building and original existing structure. The results indicate that the máximum storey displacement has decreased for retrofitted building.
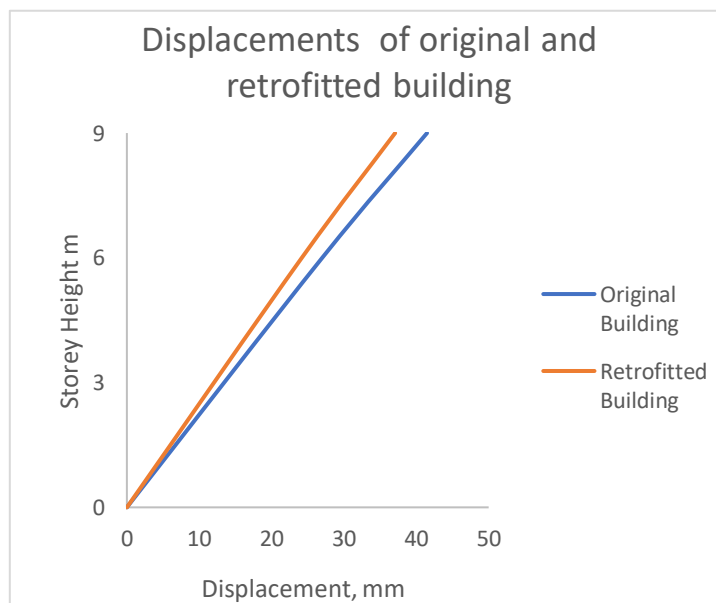
Figure 6: Storey displacements Vs Storey Height for existing building and retrofitted building.

671

The drift values are plotted for Push X direction and Push Y direction. The drift value of retrofitted building is less than original building in both X and Y directions.

This proves that after strengthening columns and beams, the global displacement of retrofitted structure reduced improving the seismic capacity of structure. The drift values in X and Y directions for retrofitted structure are 4mm and 10mm respectively which are less than the maximum allowable drift value of 0.4 percent of storey height i.e., 36mm.
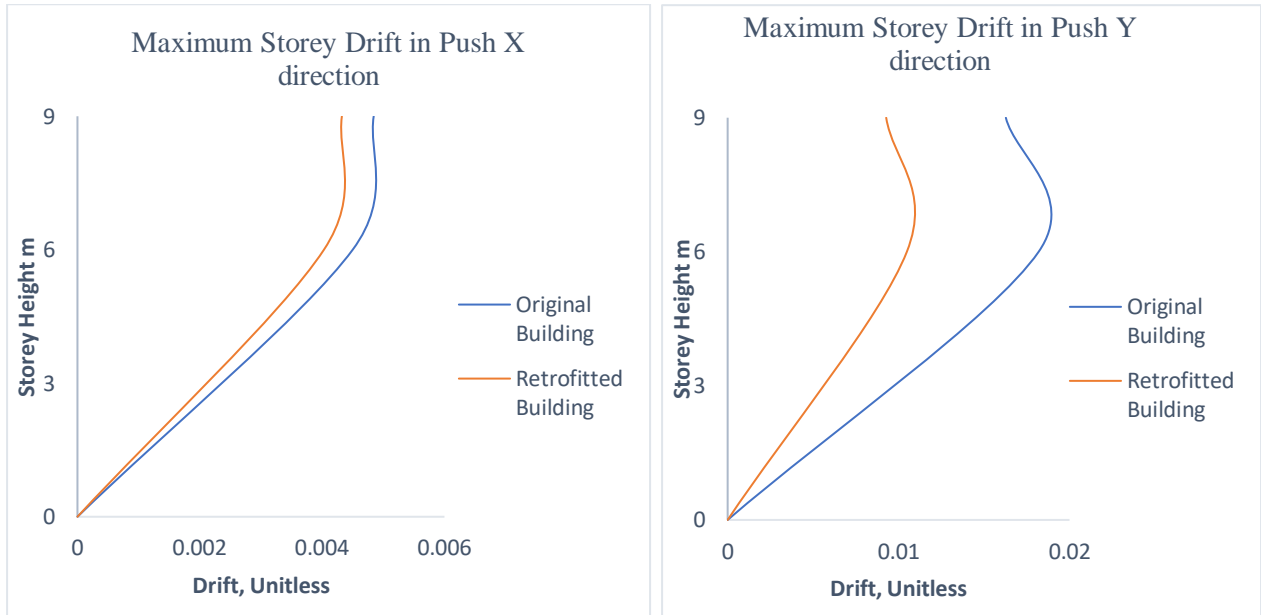
Figure 7. Maximum Storey Drift

The Base shear and roof displacement are plotted for original and retrofitted structure for X direction.
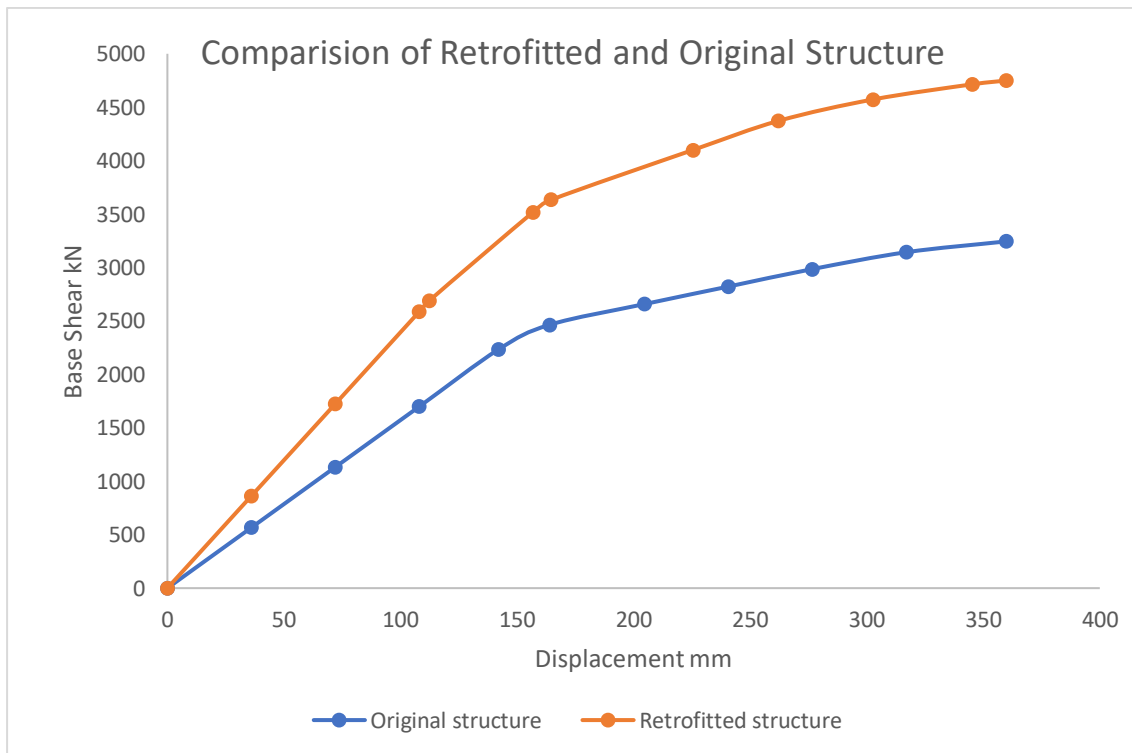
Figure 8: Pushover analysis in X direction for retrofitted and original structure.

4. Conclusion

The distressed elements are treated using concrete jacketing for beams and columns. For beams due to accessibility three sides 100mm concrete jacket is applied and for columns 100mm concrete jacket on four sides is encased with additional longitudinal and transverse reinforcement. For economical design, concrete jacketing is used as strengthening technique. The jacketed elements are modelled in ETabs19 and Nonlinear static pushover analysis is performed. From the pushover analysis the results indicated that the after strengthening the roof displacement of retrofitted structure is reduced in X and Y direction. The pushover analysis results in X direction indicate that the base shear value is increased by 1500kN improving the seismic capacity. The drift values in Y direction are more when compared to X direction and less than the maximum allowable drift value. The overall global seismic performance of structure is affected by strengthening.

5. Appendix

Table 1 – NDT Results

S. No.	Identifications	Rebound Value (NDT)	Ultrasonic Pulse Velocity Value	Concrete Quality	Approx. Compressive Strength (N//mm2)
1	Column A1	34.5	3.78	Good	30
2	Column A2	35	3.9	Good	31
3	Column A3	25	3.1	Doubtful	16
4	Column C2	24.5	3.45	Doubtful	15.25
5	Column C3	26	3.3	Doubtful	17.5
6	Column D2	28	3.15	Doubtful	20
7	Column D3	26	3.2	Doubtful	17.5
8	Column E2	27	3.55	Doubtful	19.5
9	Column E3	35	3.96	Good	31
10	Column F2	31.25	3.83	Good	32
11	Column F3	27.5	3.5	Doubtful	19.75
12	Beam A2-A3	31.5	4	Good	25
13	Beam C1-C2	25.5	3.23	Doubtful	16.75
14	Beam C2-C3	25	3.6	Doubtful	16
15	Beam D1-D2	24	3.3	Doubtful	14.5
16	Beam D2-D3	26	3.35	Doubtful	17.5
17	Beam E1-E2	34	4.1	Good	29
18	Beam E2-E3	34	4.2	Good	29
19	Beam C2-D2	26	3.61	Doubtful	17.5
20	Beam D2-E2	23	3.14	Doubtful	13
21	Beam E2-F2	24.5	3.42	Doubtful	15.25
22	Beam E2-E3	23.5	3.5	Doubtful	13.75
23	Beam F2-G2	31.5	4.3	Good	25
24	Beam F2-F3	22	3.6	Doubtful	12

Beam Dimensions and Reinforcement Details:

Table 2 – Beam Details

S. No.	Details	
1	Width	300 mm
2	Depth	460 mm
3	Diameter of main bar	16 mm
4	Number of bars	8
5	Concrete Cover	25 mm
6	Spacing of Ties	200 mm
7	Diameter of Ties	8 mm

Column Dimensions and Reinforcement Details:

Table 3 – Column Details

S. No.	Details	
1	Width	400 mm
2	Depth	480 mm
3	Diameter of main bar	16 mm
4	Number of bars	12
5	Concrete Cover	40 mm
6	Spacing of Ties	200 mm
7	Diameter of Ties	8 mm

Concrete Jacketing Details:

Table 4 – Column Jacketing Details

S. No.	Details	
1	Grade of Concrete	30 MPa
2	Diameter of main bar	20 mm
3	Number of bars	10
4	Spacing of Ties	200 mm c/c
5	Diameter of Ties	10 mm
6	Spacing of Shear Keys	200 mm c/c
7	Diameter of Shear Keys	10 mm

Beam Jacketing Details:

Table 5 – Beam Jacketing Details

S. No.	Details	
1	Grade of Concrete	30 MPa
2	Diameter of main bar	16 mm
3	Number of bars	5
4	Spacing of Ties	200 mm c/c
5	Diameter of Ties	8 mm
6	Spacing of Shear Keys	200 mm c/c
7	Diameter of Shear Keys	8 mm

References

[1] Murthy, C.V.R. (2012): *Earthquake Behaviour of Buildings*. Gujarat State Disaster Management Authority, Government of Gujarat

[2] IS Code 1893: 2016 (Part1), *Earthquake Resistant Design of Structure*

[3] Paulay, T., Priestley, M.J.N. (19920: *Seismic Design of Reinforced Concrete and Masonry Buildings*. John Wiley and Sons, Inc.

[4] Sonawane, M.B., Dubey, S.K., Deodhar, S.V., (2013): *An Analytical Approach To Demand Capacity Method*, International Journal of Advanced Technology in Civil Engineering

[5] Hashmi K., Arshad (2015*): Preliminary seismic evaluation aid for reinforced concrete frame structures based on IS 15988 (2013) guidelines*, The Indian Concrete Journal, Vol 89

[6] Arya, Anand S., *Seismic Evaluation and Strengthening of Existing Reinforced Concrete Building*, prepared under GOI-UNDP Disaster Risk Management Programme.

[7] Julio, E.S. (2003):, Structural Rehabilitation of Columns with Reinforced Concrete Jacketing, John Wiley and Sons, Inc.

EXTENSION OF SYSTEMS FOR SEISMIC SECURING OF HEAVY FAÇADES THROUGH REFURBISHMENT, STRENGTHENING AND RETROFITTING

Samuel Hine [(1)], Matthias Roik [(2)]

[(1)] *Research & Development, Leviat LTD, sam.hine@leviat.com*
[(2)] *Research & Development, Leviat GmbH, matthias.roik@leviat.com*

Abstract

Recent earthquakes have shown that existing older buildings are not sufficiently safe against seismic loads. This applies to both structural and non-structural elements of buildings. Damage to so-called 'heavy' façade structures is of particular concern, as falling components can cause personal injury and block important traffic and escape routes.

Heavy facades made of masonry, natural stone cladding or concrete panels with dead loads exceeding 100 kg/m² are usually anchored to the supporting structure by steel anchors that transfer the loads from the cladding panels. Although new façades are very secure against earthquakes, the field of seismic strengthening of heavy façades is largely unproven, although several product systems are available on the market that enable repair and strengthening.

These systems will be investigated to see if they are suitable to take the additional loads caused by earthquakes. Ongoing trials are expanding the range of fastening systems suitable for heavy façade retrofitting as well as repair. This will utilise the experience already presented at the last 1CroCEE conference. An independent test series will allow the knowledge already gained to be reflected in a range of products for repair.

This paper presents a method for repairing existing facades. This method can be used to preserve the fabric of historic buildings but can also be used to strengthen façade structures with the aim of meeting seismic design requirements, such as protecting human life after an earthquake or enabling rescue operations. As an alternative to large-scale shake table tests, so-called mesoscale tests for checking load-bearing capacity are described. The technical background is explained, and the test results are presented.

Keywords: seismic retrofitting, seismic repair, façade systems; testing methods, non-structural elements

1. Introduction

The façade of a building not only defines the building's appearance by harmonising it with other buildings or making it stand out, but also serves a number of other purposes, such as protecting the internal structure and occupants from the effects of weather, including rain and wind. For example, cavities can improve ventilation and thermal performance can be improved by adding a layer of insulation.

Facade fixings are an integral part of this structure and must safely transfer dead loads (of the facade itself) and loads (wind, earthquake, etc.) to the structure, while at the same time maintaining the distance between the support layer and the facade layer. 'Heavy' façades, such as brickwork, natural stone and concrete, with dead loads in excess of 100 kg/m² which place high demands on the façade fixings. Not only do fixings need to carry high point loads back to the structure, but the nature of the structure means that the distance the fixings have to span between the inner and outer layers can be significant (up to 300 mm or even more).

BS EN 1998-1 [2013] classifies façades and façade fixings as non-load-bearing components, i.e. lumps without inherent stiffness attached to load-bearing structures. Such items can be designed against seismic loads by using static equivalent horizontal loads acting in the most unfavourable direction.

In the following, as a first step, only masonry facades will be considered, as the range of these repair products has been examined. However, the lessons learned can also be applied to other façade materials, such as natural stone and concrete.

Hairline cracks and other minor damage can occur to masonry facades as a result of earthquakes. Although the aesthetics of the building will be compromised, such damage does not usually pose an imminent hazard. However, major damage, such as the partial or total collapse of a façade, creates greater risks and hazards for occupants attempting to escape and for emergency services trying to access a building. As well as the imminent danger from falling masonry, important access routes in and around the building may be blocked. Damage to facades and falling stones is evident in post-earthquake photographs from Christchurch (2011) and Zagreb (2020), see Figure 1.

Figure 1. Masonry façade damage – Zagreb 2020 (Photo credit REUTERS/Antonio Bronic).

Damage to the façade may indicate that the structure itself has been weakened, reducing its potential seismic performance during aftershocks and subsequent earthquakes. In order to restore the seismic integrity of the building and the façade, damage (including to the structure and façade itself and associated fixings) should be assessed quickly to identify where repairs are required.

Once damaged, the seismic performance of a building can be restored through repairs, but retrofitting existing facades with new components can improve their seismic performance and reduce the likelihood of damage occurring in the first place. This reduces the human risk in the event of an earthquake and reduces the time and cost of repairs.

Seismic retrofitting is particularly applied to older historic facades that were built before modern standards were introduced and usually do not include any seismic fixings. Retrofit methods can be carried out with minimal or no visual impact, which can improve seismic performance while preserving the aesthetics of the façade.

Rather than assessing façade fixings in isolation, the interaction of fixings with other components such as the structural frame and façade should be considered. Analysing fixings in this way allows load-bearing capacity and ductility to be assessed. In addition, different scale tests can be carried out to assess the load-bearing capacity of the system in different scenarios. Macroscale testing offers the opportunity to accurately replicate field conditions, but requires large, expensive test facilities and can be very time-

consuming. On the other hand, small-scale testing, such as mesoscale and microscale testing, provides a viable alternative where representative results can be obtained at a lower cost.

This paper discusses methods for seismic repair and retrofitting of existing masonry facades. Different approaches for testing façade fixings are presented and evaluated.

2. Brickwork Façades

Modern buildings with brick facades usually rely on several layers to achieve the necessary weather resistance, thermal performance and ventilation. The external-facing façade layer is generally separated from the insulation layer by a clear air gap or cavity, with the structural frame located behind the insulation layer. Shelf angles or brick support brackets (Fig. 2) are used to support the dead loads on brick façades, and these must span between the layers and be firmly fixed to the frame through the insulation. They are usually designed as cantilever or tension members with spacers and are fixed using suitable anchor bolts or channels.

Loads acting perpendicular to the façade, such as wind loads, are separately accommodated by horizontal restraints. These members transfer tensile and compressive loads between the masonry facade and the structure and limit movement between them. The anchorage method shown in Figure 2 is not designed to transfer loads parallel to the façade layers. If seismic loads are anticipated, load-bearing members must be added. This is important not only for new buildings, but also for repairs and refurbishments.
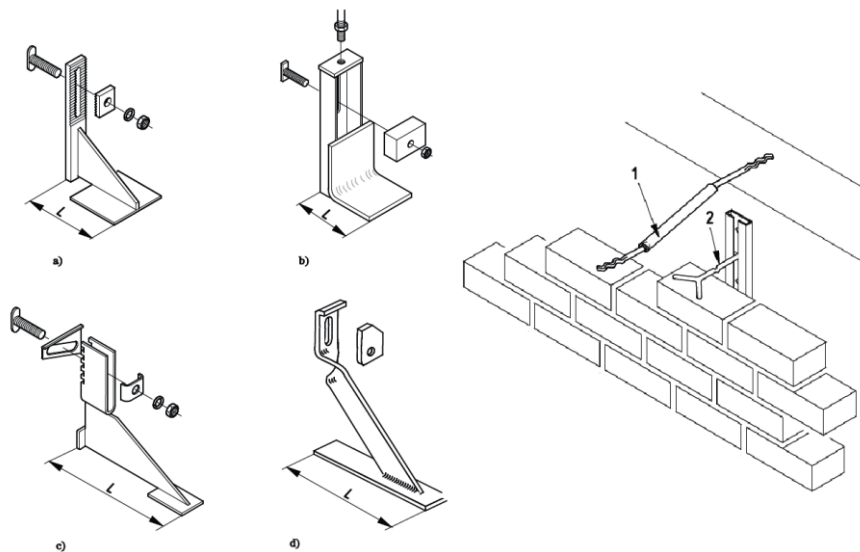
Figure 2. Examples of brickwork support brackets and movement-tolerant wall ties [xxx].

3. Seismic strengthening Methods

Strengthening methods fall into two main categories: repair and retrofit; BS EN 1990 [2005] defines repair as *'activities undertaken to maintain or restore the function of a structure that fall outside the definition of maintenance'*. Whereas repairs are carried out in response to damage to a building, retrofitting is a more proactive approach and is carried out in anticipation of the occurrence of an event, such as an earthquake. The ultimate aim is to reduce or completely eliminate damage. This has the dual benefit of lower risk to health during an event and reducing the amount and cost of repairs required after the event. A variety of retrofit strategies exist, ranging from simple single components to more

complex connected systems. Many methods can be installed sympathetically and with minimum disruption to the existing façade – this can be of great importance when working with older buildings of historic significance. A number of such methods are presented below and assessed for their ability to secure masonry façades against seismic loads..

3.1 repair methods for masonry façades

Repair methods are important to restore the structural integrity of stone facades after damage has occurred. If building damage is left unchecked, the facade's seismic integrity will be compromised in the event of a subsequent earthquake, increasing the likelihood of damage and loss of life. It is therefore important to repair cracked, damaged or collapsed masonry as soon as possible.

One method of repairing cracked masonry is to insert long twisted (helical) stainless steel bars into horizontal mortar joints and grout them in place (see Figure 3). The helical bars and thixotropic cementitious grout bond tightly to the existing masonry, redistributing the tensile load down the length of the panel and minimising the occurrence of cracks. With careful consideration of the mortar to be used in the grouting process, façades can be repaired technique in a very aesthetically sympathetic manner.

Figure 3. Thixotropic cementitious grout applied to a horizontal slot in preparation for insertion of helical bar.

Another use of helical stainless steel bar for façade repair is the creation of deep masonry beams. In a similar way to crack stitching, bars are grouted in place in horizontal slots cut in the mortar joints. By using pairs of bars installed a number of courses apart, structural integrity and load-bearing capacity of the façade can be restored.

Masonry façades which are bowing out of plane can be repaired by using threaded or helical stainless steel bars to reinstate the connection between the façade and the structural frame – see Figure 4. By driving the bars through the façade and into the internal timber joists (either into the ends or the sides), the masonry can be stabilised and further movement prevented. As external spreader plates are not required, this method is again easily concealed and presents a quick, permanent repair solution.

For masonry façades which have suffered more significant damage or have high load applications, a more robust system of threaded stainless steel bar, heavy duty mesh fabric sleeves and cementitious

grout may be required. The bars and sleeves are inserted into the walls through drilled holes, grout is then pumped into the sleeves which expand and form a strong chemical/ mechanical bond with the existing masonry ad internal structure – see Figure 4. Again, with good detailing and workmanship to fill the drilled cores this solution is fully concealed and can leave the façade looking virtually un-touched.
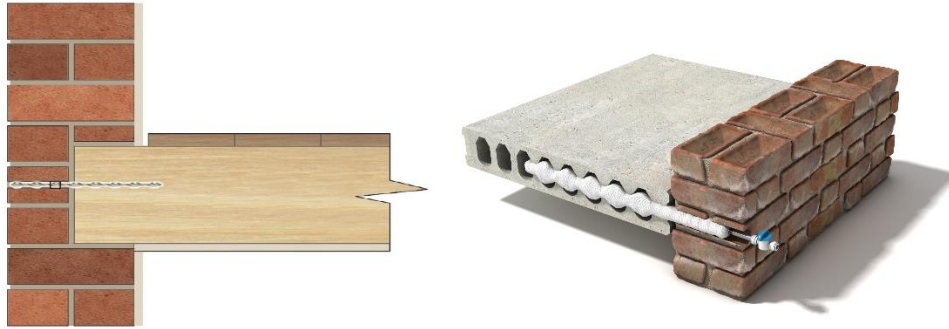
Figure 4. Brickwork façade restrained from bowing out of plane and heavy duty repair to masonry façade.

If complete masonry collapse has occurred and the façade is to be re-built, cavity wall ties can be employed to join the leaves of masonry together. This improves the wall stability by tying the layers together and allowing them to act as one homogenous unit. Many different wall tie profiles and end types are available to suit different applications – ties can be bedded in mortar at both ends, mechanically fixed using screws or bolts, or resin-bonded directly to the masonry. Typically wall ties are made from stainless steel but pultruded basalt fibre ties are also available when even lower thermal conductivity is required.

3.2 retrofit methods for masonry façades

When retrofitting stone facades to improve their seismic performance, a different philosophy is utilised. Instead of waiting for damage to occur and then repairing it, retrofitting is a proactive approach that spends time and money up front, with a view to reducing future expenditure.

On brick facades, a similar effect to crack stitching can be achieved by installing stainless steel helical bars at mortar joints. These long bars can be connected via stainless steel components to short helical ties driven vertically through the façade and into the internal structure (see Figure 5). By connecting the bars and ties in this way, long repair masonry can be installed to improve the in-plane and out-of-plane performance of the façade with minimal increase in seismic strength. If required, the anchorage strength can be verified in situ by a simple tensile test.

Stainless steel helical ties may also be used to mechanically (or chemically) fix brick facades, render and masonry to the structural frame. Ties are driven into small pre-drilled holes inside the bricks to hold the brick layers together and prevent the masonry from collapsing due to earthquakes (see Figure 5). Depending on the application, cementitious grout or fabric sleeves can also be used with ties. The technology can be used on both cavity walls and solid walls and is suitable for fixing to brick, block, concrete and timber.

Tests have shown that retrofitting stainless steel helical ties can effectively improve the out-of-plane performance of masonry walls [EQ Struc. 2013], and Newcastle Innovation [2010] found that the Australian Standard AS/NZ2699.1 medium load for earthquake It has also been shown that the requirements for ties can be met in this way.
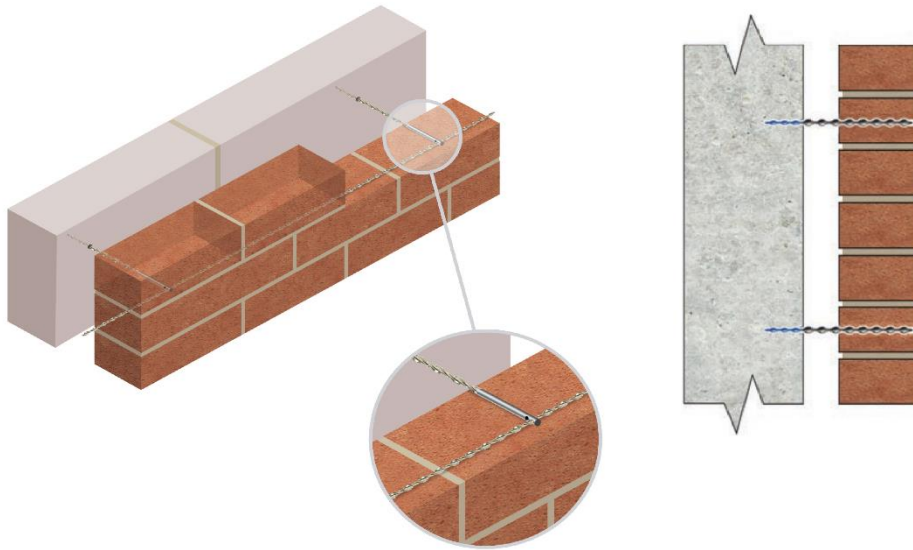
Figure 5. Long helical bars connected to perpendicular helical ties and a mechanically pinned masonry façade.

Seismic performance can be further improved by the use of 'rigid' and 'ductile' anchors. Typically these require more invasive installation procedures; individual masonry support brackets ('rigid' anchors) can be installed to carry horizontal seismic loads whilst angled wall ties ('ductile' anchors) can transfer both transverse and longitudinal loads back to the structure. This has been shown to be an effective method of limiting damage to heavy façades during shake-table testing [Roik and Piesker, 2017].

4. Testing of Repair & Retrofit for Masonry Façades

4.1 Introduction

Roik and Piesker [2019] describe the different test scales that are suitable for heavy façade fixings; macro, meso and micro. Each scale has various advantages and disadvantages but, generally, the larger the scale, the greater the expense and time required. For this reason, meso-scale testing presents a good compromise where the full representative façade system and inter-linked components can be evaluated without requiring large-scale testing facilities.

4.2 Meso-scale Testing

Mesoscale tests are much easier to carry out than large-scale shake table tests, as they utilise an area of approximately 1 m2 representative of the façade. Importantly, even with an area of 1 m2, all components of the façade anchorage system can be assessed together, so that important interactions between elements are not lost. The low cost makes it more practical to carry out project-specific tests with relevant predefined static equivalent loads.

As there are no specific regulations on test methods for façade systems subjected to seismic loads, the regulations in Annex E [2013] of ETAG 001 are proposed. The only exception is that the calculated horizontal equivalent loads (taken from the relevant seismic design standards) are used as the maximum load N max in tension and compression and V max in shear.

Figure 6 shows an example of a mesoscale test where a 1 m2 masonry façade section was supported on brickwork support brackets and fixed back to a concrete frame. Vertical wall ties were placed as the bricks were stacked and the mortar was left to cure. Once the design strength was reached, two helical bars were driven diagonally from the bricks into the concrete frame and resin-fixed with 'ductile' anchors to accurately represent the retrofit scenario. Horizontal loads were applied in the plane of the wall, in accordance with ETAG 001, Annex E [2013], at a continuous loading rate, with load increments. Horizontal displacements of the facade were measured using displacement transducers.

Straight wall ties

Seismic-Helifix anchor
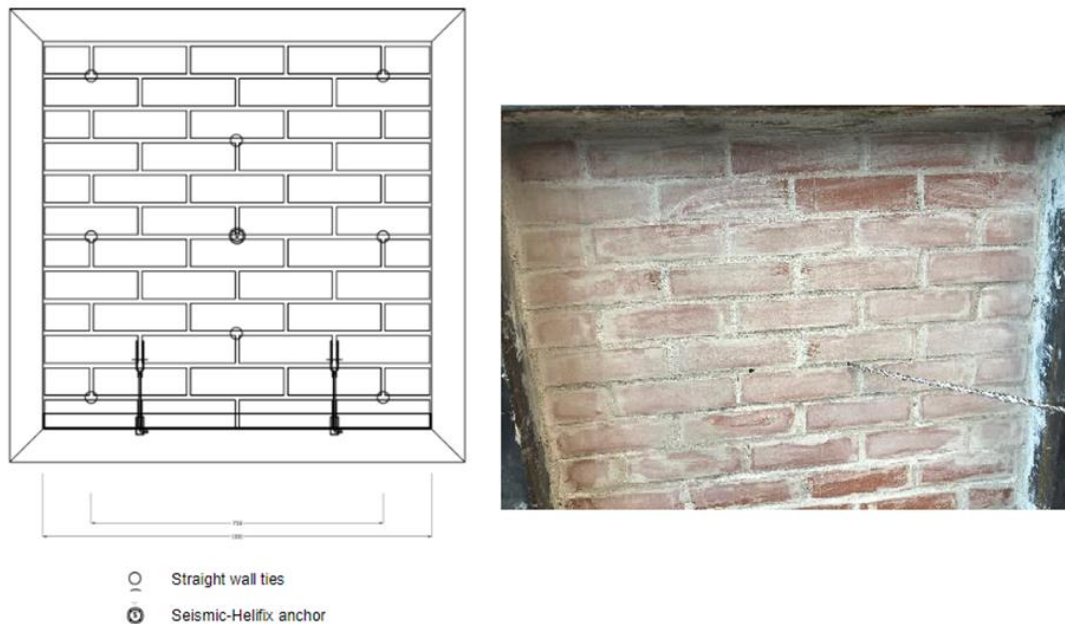
Figure 6. Meso-scale test concept and installation of helical bar through brickwork.

The test results show minimal horizontal displacement (less than 1mm) is exhibited with load application Vmax = ±2.0kN (equivalent to 1 x G). Plastic deformation starts to become apparent around Vmax = ±4.0kN (2 x G) with horizontal displacement of ±9mm. With further load increases the displacement grows strongly up to around 50mm (applied loading in the region of 4 x G). However, even at 'failure' when the wall ties have buckled and bent the masonry is still held together and does not collapse – suggesting that in the event of an earthquake such a design would reduce the risk of falling masonry.

4.3 Macro- & Micro-scale Testing

Macroscale tests are usually carried out on a one-to-one scale using a shake table, allowing the entire façade and anchorage system to be tested in as-built conditions. The behaviour under load can be accurately investigated, giving a very good representation of the building's performance in the 'real world'. However, due to the large scale of the tests, it is very costly and time-consuming to repeat them in new scenarios.

Microscale testing, on the other hand, focuses on a single component only and analyses its behaviour and performance individually. Microscale testing can be easily carried out in the laboratory or on site, is quick and inexpensive, and can test many different scenarios. However, the results do not take into account interactions with other building components and should therefore be considered carefully.

4. Conclusion

The latest seismic design standards classify façades and façade fixings as non-structural members. Static equivalent horizontal loads acting in the most adverse direction are used in the design of these members.

Damage to façades caused by earthquakes can range from small hairline cracks to more dangerous partial or total collapse. It is crucial to prevent major damage in order to reduce the risk of injury to people in the vicinity of the building and to aid rescue efforts in the immediate aftermath. Following an earthquake, any damage sustained by the stone façade must be assessed and repaired as soon as possible. Even if the damage is apparently not aesthetically displeasing, the building's seismic resistance may have been compromised and must be addressed as soon as possible. The longer a building remains in a damaged state, the greater the risk of future earthquakes, including danger to human life and increased repair costs. Depending on the use of the masonry, different repair methods are available.

Seismic strengthening of existing buildings can reduce the risk to human life by taking action before damage occurs, or at least reduce repair work after an earthquake. By combining components such as stainless steel helical bars, resin, grout and sleeves, a suitable seismic reinforcement system can be constructed and installed quickly and with minimal disruption.

When assessing the seismic performance of façade fixings, the interaction of all components in the system should be considered. Elements such as the façade fixings, the façade itself and the structural frame must all be included in the assessment to ensure that the load-bearing capacity and ductility meet the requirements. Physical testing is a valuable way of determining the actual performance of an element or system, whereas theoretical calculations can only give a partial picture. Tests can be carried out to local standards if required, and specifications can be modified to suit specific project conditions.

Testing can be carried out at different scales, depending on the space, time and cost limitations applied; macroscale testing, carried out at 1:1, can give a very accurate representation of overall load-bearing performance, but is very time-consuming and costly. Microscale tests tend to be much easier and cheaper to carry out, but focus only on isolated components and may miss important system interactions. Mesoscale testing is a compromise between the two. A facade test area of approximately 1 m2 is used to keep costs low, but it is still possible to analyse the interactions between different elements.

Tests carried out at the meso-scale have been used to show the success of retrofitted façade fixings in limiting deflection of brickwork when subjected to cyclical horizontal loading. Even when taken to 'failure' with large plastic deformations, the façade fixings were able to provide sufficient integrity to the test wall to prevent any collapse of the masonry.

References

[1] BS EN 845-1 (2016) Specification for ancillary components for masonry - Part 1: Wall ties, tension straps, hangers and brackets, British Standards Institution, UK.

[2] BS EN 1990 (2005) Eurocode: Basis of structural design, British Standards Institution, UK.

[3] BS EN 1998-1 (2013) Eurocode 8: Design of structures for earthquake resistance - Part 1: General rules, seismic actions and rules for buildings, British Standards Institution, UK.

[4] "Seismic performance of twisted steel bars used as wall ties and as remedial wall stitching: 2010/2011 Canterbury Earthquakes", Commissioned report, New Zealand.

[5] ETAG 001, Annex E (2013) Metal Anchors for Use in Concrete, Annex E: Assessment of Metal Anchors under Seismic Action, European Organization for Technical Approvals, Belgium.

[6] Roik, M., Piesker, C. (2017) "A concept for fixing "heavy" façades in seismic zones", Proceedings of 16th World Conference on Earthquake Engineering, Santiago de Chile, Chile.

[7] Roik, M., Piesker, C. (2019) "Streamlining the Test Methods for Seismic Verification of Façade Anchors", Fourth International Workshop on the Seismic Performance of Non-structrual Elements (SPONSE), Pavia, Italy.

[8] Simundic, G. (2011) "Helifix wall ties testing", Individual Study, University of Newcastle, NSW, Australia.

IMPROVEMENT OF BUILDING'S WALLS BEARING CAPACITY AFTER AN EARTHQUAKE

Alush Shala [(1)], Jelena Bleiziffer [(2)]

[(1)] *PhD Candidate, Faculty of Civil Engineering Zagreb, alushshala@albarchitect.com*
[(2)] *Assistant Professor, University of Zagreb, Faculty of Civil Engineering, jelena.bleiziffer@grad.unizg.hr*

Abstract

Strengthening and increasing the capacity of load-bearing walls of buildings after an earthquake is a challenge that requires special study. A viable option is strengthening using standard cement-based materials.

This paper will first present and discuss the buildings with load-bearing walls that have shown earthquake survival ability, as well as some methods to improve their performance.

The example that is used for discussion is a building that has suffered significant damage from the 2019 earthquake in Albania. The paper will present the calculation of the performance and load-carrying capacity of this building with the load-bearing walls made of clay and silicate bricks after an earthquake of magnitude M=6.2 Richter. The building comprises load-bearing walls and was built in the 1960s-70s. The materials characteristics used in calculations are derived from laboratory tests and on-site non-destructive testing. The results obtained from the calculation of the building before and after the earthquake and after the reinforcing of the building will be compared. The strengthening of walls is made using cement-based materials. The calculations are performed using SAP2000 and ETABS software and include static and dynamic performance.

The results of the calculations will be analyzed to conclude the effectiveness of the rehabilitation of the buildings. The environmental and socio-economic impacts on society from the strengthening of buildings damaged by earthquakes will also be presented.

Keywords: earthquake, buildings, damage, strengthening, materials, impact.

1. Introduction

Early constructions in most cases are made of load-bearing walls with clay, silicate or stone bricks. Masonry is one of the oldest types of construction. The building material brick was easy to produce [1]. Taking into account structural-physical properties and the quite easy construction process, this construction system is used until today. This paper will present the results obtained from the software calculations of the building that survived the M=6.3 earthquake in Albania in 2019. Earthquakes are often accompanied by aftershocks which may cause additional damage to an already damaged structure or lead to failure [1]. The reason to analyse the building which suffered damage – vertical and diagonal cracks in the walls, is to identify the possibility of its survival and use after the earthquake. During the treatments, samples were taken and the walls were tested with destructive methods. The paper presents dimensions, the static system and linear and non-linear analysis of the building. During the analysis, the reduction of mass is taken into account by eliminating heavy layers, heavy non-constructive walls and replacing them with lighter material. Reductions in mass result in direct reductions in both the forces and deformations produced by earthquakes and therefore can be used in lieu of structural strengthening and stiffening [2]. From the obtained results, the dynamic characteristics of the building and the bearing capacity were calculated. The building was built from load-bearing walls in the years 1960-70. All the findings are presented in tabular form. Pre-earthquake performance was analyzed using the laboratory results, while the post-earthquake performance analysis took into account reducing the bearing capacity of the cracked walls based on the codes and technical norms for this type of objects such as FEMA 273, EC6 & EC8. The analysis was also made for the case of rehabilitation and improvement of building performance. Its rehabilitation is made with ordinary cement-based material. The strengthening is executed in two layers of 25 mm on each side of the wall. Then the performance

and bearing capacity of the building was calculated using the linear and nonlinear calculations of the ETABS and SAP2000 software. During the calculations, the dynamic and static parameters were taken as a basis spectrum data for the area of Tirana where the facility is built. The results obtained in the three cases are analyzed and important conclusions are drawn. From the performance calculations, a great stiffness of the building can be seen. With the addition of mesh reinforcement, the ductility of the building increases. In such cases, the results can be of great benefit for executing rehabilitation at an optimal cost. Rehabilitation and reinforcement from standard materials also has a socio-economic impact. The investment will be returned in a shorter time than the cost of expensive modern materials. The purpose of the reinforcement is sufficiently achieved and the building will survive the challenges in the future and meet the demands of the community. It also has an important impact on the environment. The renovation preserves the green space and the pollution from the demolition of the entire building. A total demolition would have a high cost and environmental pollution from waste. Such treatment would emit a significant amount of carbon dioxide.

2. Geometric and mechanical characteristics of the building

The geometric and mechanical characteristics of the building members and materials are presented in the following sections. This includes a description of the old and new design and the materials that have been used and have an impact on the structure and its behaviour to seismic impacts.

2.1 Geometric characteristics

The building was built in 1966 and serves as a hospital in Tirana. The foundations are made of stone and are unreinforced with different dimensions for balancing the stresses and the depth of the foundation is hf=1.30m. The soil has a good bearing capacity σ=0.25 MPa. The walls can be classified as primary, secondary and dividing or tertiary walls: primary walls are the bearing walls which also carry external loads and are longitudinal with thicknesses t_1=50 cm, t_2=40 cm, t_3=30 cm, secondary walls are most of the transverse walls that have a thickness of t_1=30 cm and t_2=25 cm, while the dividing walls, that have the purpose of dividing spaces only and can be removed and replaced with lighter walls, are t_1=20 and t_2=12 cm. The floor structure or floor slab system is made of clay elements filled with concrete in a patterned shape every 20 cm and ribs t=8 cm, plate thickness d=4 cm. There are beams on the walls from a C-16/20 concrete grade along the building's perimeter and the columns inside the building, in the elevator and installation space, dimensions w/h = 40/40 cm, w/h=40/25 cm and w/h =25/25 cm. The loads from the floor layers and internal walls are g=3.70 kN/m^2 on the floors and g=3.50 kN/m^2 on the roof.

2.1.1 Design of old existing building

The plan view of the old existing building is shown in Fig. 1, while Figs. 2 and 3 show some photos of damage after the earthquake, prior to and after the mortar layer was removed. Before removing the mortar, vertical cracks, tending diagonally, can be seen, and they were temporarily closed until the building was completely repaired. After the mortar was removed, diagonal cracks can be seen.

2.1.2 Renovation design of the building

During the renovation, it was taken as a basis that the materials that will be used in the floor and the tertiary or dividing walls should have a lighter specific weight. Partition walls are taken from Knauf walls, and now we have a floor load reduction of g=2.80 kN/m^2 on floors and of g=1.50 kN/m^2 on the roof. The other walls were not damaged, they were only reinforced with two layers of compressed or cast plaster with a thickness of t=25 mm, class C-25/30. Fig. 4 shows the renovation design plans with the walls' changes. Fig. 5 illustrates the renovation execution of the building which is the subject of the analysis.

a)

b)

Figure 1. Design of the old building: a) Basement story, ground story; b) First story, second story.

Figure 2. Cracks in the wall from the earthquake in 2019 Tirana, Albania.

Figure 3. Wall after demolishing mortar.

a)

b)
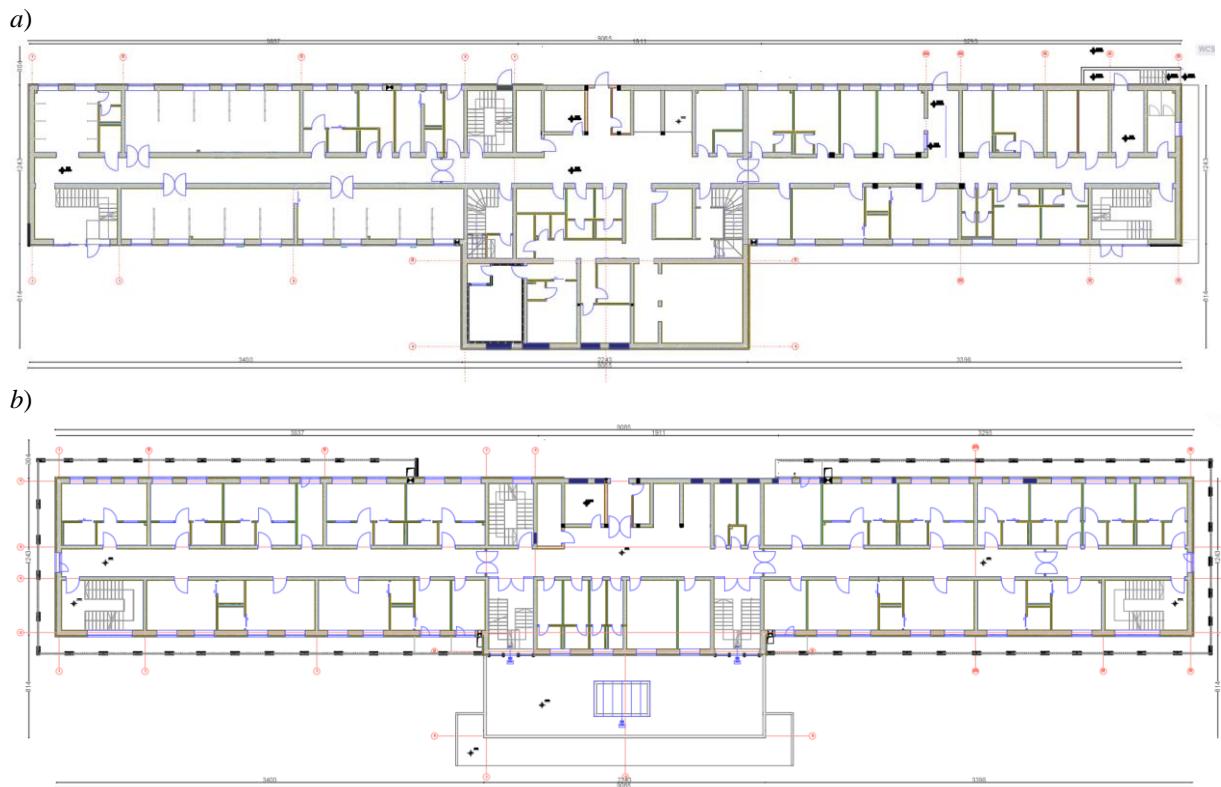
Figure 4. Design of renovated building: a) Basement story, ground story; b) First story, second story.

Figure 5. Renovated building.

2.2 Mechanical characteristics

The mechanical characteristics of materials used in the existing building are given in Table 1. These characteristics are derived from testing results. Concrete tested by destructive methods and taking samples on-site turns out to be class C-20/25, and the steel used is class S 240/360. The samples were taken and the results were obtained for the silicate and clay bricks, the paste for plastering, and the type of the wall masonry and its mechanical characteristics according to the technical norms (e.g. EN 772)

were also obtained. The characteristics of materials composing the structure are input data for structural analysis. Namely, the compressive-tensile strength of the materials, their modulus of elasticity and their Poisson ratio are of primary importance [3].

Table 1 – Mechanical characteristics of materials in MPa

Materials	f_{ck} (MPa)	f_b (MPa)	f_m (MPa)	f_k (MPa)	f_{yk} (MPa)	E (MPa)	G (MPa)
C-20/25	20					30 000	12 000
S-240/360					240	200 000	80 000
Silicate Brick		20.6				20 600	8 240
Clay Brick		13.67				13 670	5 468
Mortar			7			7 000	2 800
Masonry clay				6.15		6 150	2 460
Masonry silicate				8.37		8 370	3 348
C-25/30-Cement mortar	25					31 000	12 400
S-400/500-steel mesh					400	200 000	80 000

The calculation of the characteristic value of the masonry using the characteristic values for brick and mortar is taken from EC6, the characteristic compressive strength of masonry should be determined from [4]:

$$f_k = K f_b^\alpha \, f_m^\beta \qquad (1)$$

f_k – characteristic compression strength of masonry

K – is constant from tab.3.3 page 37, EC 6-1-1 2006 [3]

α, β – are constants

f_b – normalised mean compressive strength of units

f_m – is the compressive strength of mortar.

3. Results of Case Analysis

To calculate the performance and bearing capacity of the building, linear and non-linear analyses were used. In the analysis, the permanent live loads were applied. The modal and seismic analysis was based on the seismic conditions of Tirana, from the data extracted after the 2019 earthquake. The acceleration was obtained a_g=0.29g, the object of importance γ_I=1.40, while the soil is of category C and the behaviour factor is q=2.50 for buildings with unreinforced retaining walls according to EC8 [5]. Table 2 presents the loads before and after renovation.

Table 2 – Comparison of loads on the building

	Building before renovation	Building after renovation	Comparison (%)
Dead Load of Layer in floor	3.70 kN/m2	2.80 kN/m2	-24.30
Live Load in Floor	5.0 kN/m2	5.0 kN/m2	0.00
Dead Load of Layer in roof	3.50 kN/m2	1.50 kN/m2	-57.14
Seismic acceleration a_g	0.24 g	0.29 g	20.83

3.1 Linear analysis

The linear analysis of the building was carried out based on the data extracted and presented in Tables 1 and 2. Table 3 summarizes the dynamic data of the building and the participation of the mass in vibration modes. Four cases were analyzed by changing the construction and loading conditions in this analysis. Practically most of the structural and non-structural damage sustained in such buildings is produced by lateral displacements [7]. Therefore, the focus of calculations and design of the buildings is to eliminate as much as possible lateral displacements. Table 3 shows the results for the first three periods for each case.

Table 3 – Periods and mass participation

Building	Modes	Periods (s)	Mx	My	MRz
Old Building before the earthquake	1	0.214	0	0.721	0.007
	2	0.172	0.001	0.005	0.741
	3	0.083	0.736	0	0.741
Old Building after the earthquake	1	0.237	0	0.651	0.025
	2	0.21	0.02	0.02	0.68
	3	0.108	0.664	0	0.68
Renovated Building with cement mortar	1	0.208	0	0.677	0.01
	2	0.171	0	0.008	0.7
	3	0.086	0.71	0	0.7
Renovated Building with cement mortar and reinforced mesh	1	0.215	0	0.687	0.009
	2	0.174	0	0.007	0.71
	3	0.088	0.719	0	0.71

In Fig. 6, the cases after the earthquake are presented as follows: the type of cracks encountered; the form of repair with cement mortar t=25 mm with casting; and repair using the grid Ø 3/100/100 mm reinforcement, each with connecting anchors (5 pieces in m^2 of cement mortar t=25 mm).
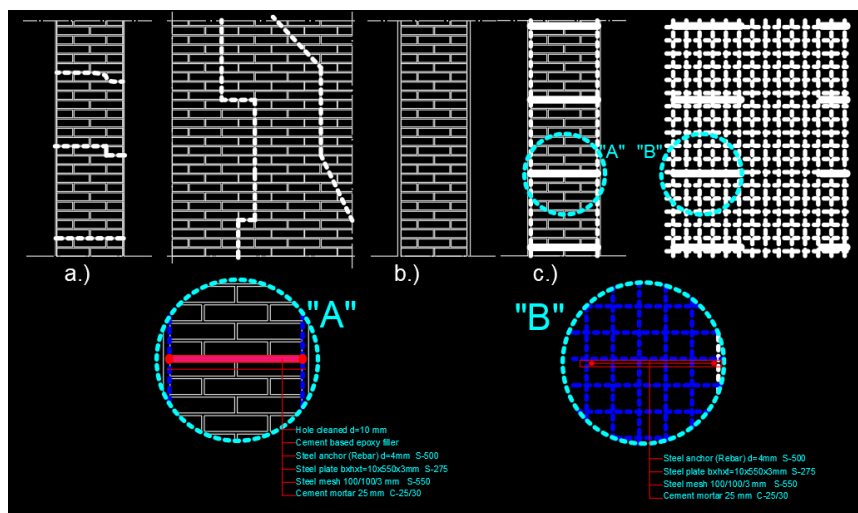
Figure 6. a) Cracked wall after the earthquake; b) Repaired wall; c) Proposed reinforced wall.

Center of mass and centre of rigidity were calculated using ETABS 19 software. Their values are listed in Table 4 along with the eccentricity in both orthogonal directions x and y for each story.

Table 4 – Centre of rigidity and centre of mass for each story, and each of the cases considered – before the earthquake, after the earthquake, renovated with mortar only, and renovated with added reinforcement (XCCM, YCCM, XCR, YCR and ex, ey)

	Story	XCCM (m)	YCCM (m)	XCR (m)	YCR (m)	ex (m)	ey (m)
Building before earthquake	1	44.971	13.330	47.135	13.048	2.164	0.282
	2	45.109	13.488	46.307	12.663	1.198	0.825
	3	45.128	14.027	46.163	13.021	1.035	1.006
	4	45.064	14.046	46.172	13.258	1.108	0.788
Building after earthquake	1	44.011	13.293	47.370	12.820	3.3591	0.473
	2	45.028	13.552	46.377	12.453	1.3492	1.099
	3	45.042	14.327	46.162	12.877	1.1192	1.450
	4	44.976	14.156	46.118	13.171	1.1413	0.985
Renovated building with cement mortar 25 mm	1	44.288	13.351	46.523	13.577	2.235	0.226
	2	45.312	13.442	46.143	13.430	0.832	0.012
	3	45.284	14.224	46.326	13.576	1.042	0.648
	4	45.073	14.063	46.463	13.666	1.390	0.397
Renovated building with cement mortar 25 mm and steel mesh	1	44.327	13.362	46.581	13.580	2.254	0.219
	2	45.306	13.451	46.186	13.428	0.880	0.023
	3	45.270	14.225	46.346	13.577	1.076	0.648
	4	45.063	14.069	46.477	13.662	1.414	0.408

Repairing walls using layers of cement plaster and metal mesh as reinforcing elements also changes the performance of the wall out of its plane. This type of wall cross-section works like composite elements. The mesh on the surface absorbs the tensile stress caused by the seismic impacts on the wall.

3.2 Nonlinear analysis

Non-linear analysis was also done for all cases. By adopting pushover analysis as a nonlinear analysis tool, the behaviour of damaged buildings may be simulated with suitable modification of plastic hinges for damaged elements. Such modification is based on stiffness, strength, and displacement reduction factors accounting for the achieved damage states for the structural elements, as could be detected by visual inspection of post-earthquake damage [8]. Therefore, the results show that we are dealing with a heavy object. The failure mechanism did not depend on the materials of construction but depended on structural configuration [6]. The configuration of the static system and the design of the bearing walls of the buildings have a major role in the collapse of buildings from the action of seismic loads. The representation of the displacement of the building in the direction of the y-axis by the action of the force is shown in Fig. 7, indicating performance for each of the cases.
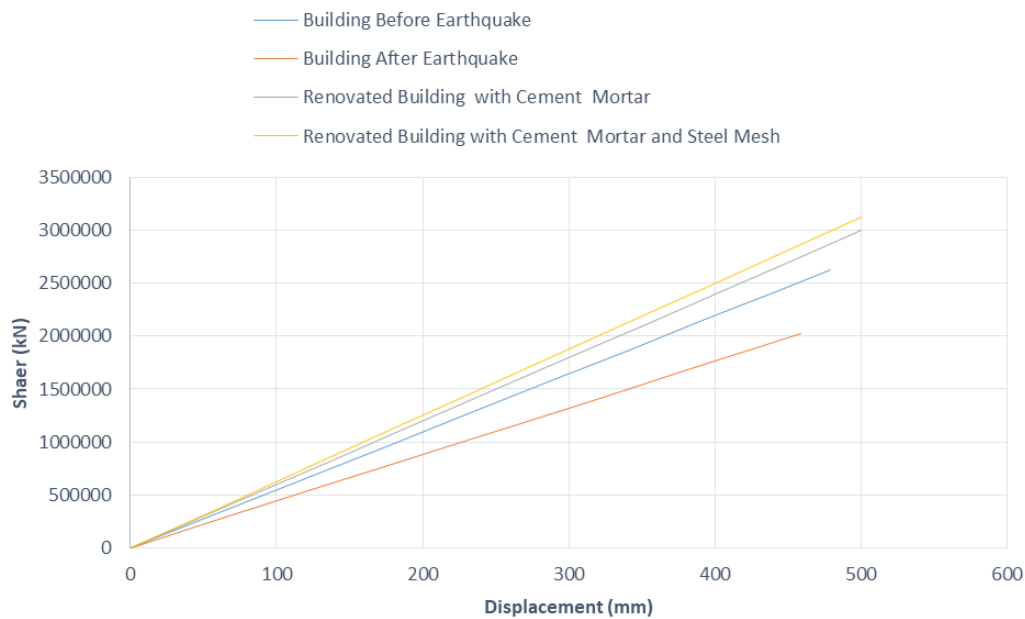
Figure 7. Pushover Curve – Base Shear vs Displacement for all cases.

Table 5 shows the comparison of the force for a base displacement by turning it into a percentage for each analysed case. From EC8 the designed displacement is:

$$d_g = 0.025 \cdot a_g \cdot S \cdot T_C \cdot T_D \tag{2}$$

$$a_g = \gamma_I \cdot a_{gR} \tag{3}$$

Therefore, the comparison is made for the following value of the designed displacement:

$$d_g = 0.025 \cdot 0{,}354 \cdot g \cdot 1{,}15 \cdot 0{,}6 \cdot 2{,}0 = 119{,}81 \text{ mm}$$

Table 5 – Comparison of results in percentage

Cases	d_g (mm)	Shear Force (kN)	Comparison with the building before the earthquake (%)	Comparison with the building after the earthquake (%)
Building before the earthquake	119.81	656 436.14	0	24.276
Building after the earthquake	119.81	528 210.152	-19.534	0
Renovated building with cement mortar 25 mm	119.81	718 618.65	9.473	36.048
Renovated building with cement mortar 25 mm and steel mesh	119.81	749 484.071	14.175	41.891

Pushover capacity curves in y direction, from ETABS and according to EC8, are shown in Fig. 8 for four considered cases. Y-direction is presented because stiffness is lower in that direction than in x direction, and most major damage during the earthquake in Tirana, Albania came from the earthquake action in y direction. Comparison of capacity in percentage at the target displacement in y direction is provided in Table 6. Target displacement is read from ETABS 19, and is according to EC8 2004. Shear forces and performance percentages are calculated for the target displacement.
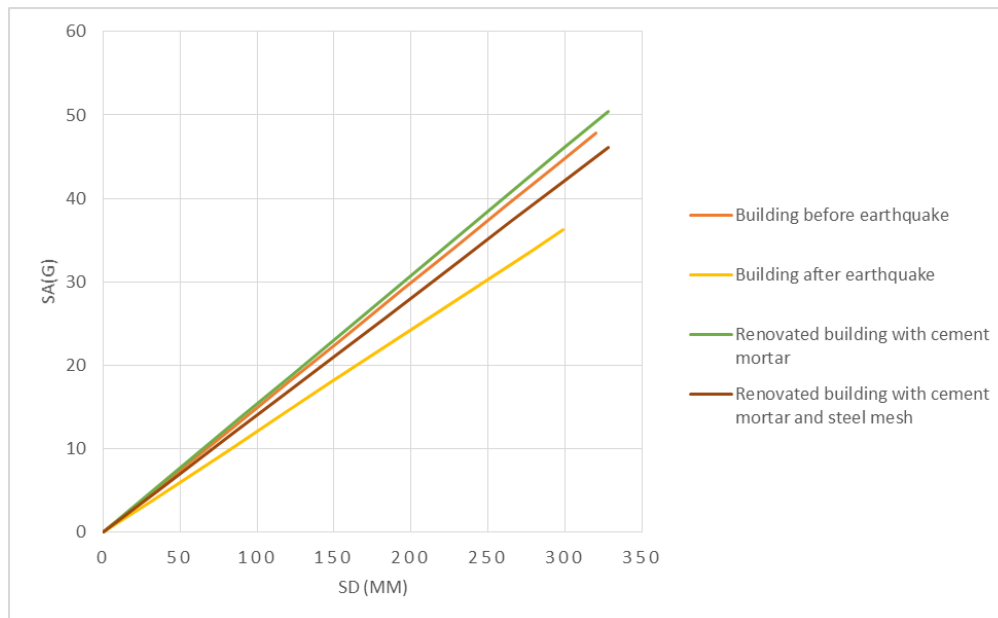
Figure 8. Pushover capacity curve SD-spectral displacement vs SA-spectral acceleration as EC8 2004.

Table 6 – Comparison of case capacities in percentage according to EC8 2004, d_t – target displacement

Cases	d_t (mm)	Shear Force (kN)	Comparison (%)
Old building before the Earthquake	3.826	20 979.225	0
Old building after the Earthquake	4.989	22 017.828	-25.447
Renovated building with cement mortar 25 mm	3.772	22 638.734	9.322
Renovated building with cement mortar 25 mm and steel mesh	4.189	26 216.363	15.476

4. Discussion of the results

The results from the linear and non-linear approaches are discussed in this chapter. The loads that were used in the renovated building are lighter than those that were in the building before the earthquake. Comparatively, for the floors (as presented in Table 2), it can be seen that there is a 24.30% decrease, while for the roof the load is 57.14% lighter. The seismic load for calculation for the return period of 10% in 475 years has increased from 0.24g to 0.29g, after the 2019 earthquake in Durres, Albania, which is an increase of 20.83%. The calculations were carried using these values. The results show an impressively positive effect of interventions considered – every variant leads to better performance than the one before the earthquake. The building has high stiffness, which is also demonstrated by the periods obtained from the linear analysis. There is a large eccentricity in the direction of the x-axis, which in the results is reflected by twisting in the direction of the translatory oscillations x and y. Because of this, the second period appears as the angular period. The periods and the centre of mass and stiffness are presented in Tables 3 and 4. The results from the non-linear analysis using pushover analysis were

shown in Tables 5 and 6. Fig. 7 presents the comparison of the displacement curves and the shear force of the building. It can be seen from those results that the building has the best performance in the case of renovation which is made with two layers of plaster with cement mortar and metal mesh 3/100/100 mm. For comparison, the displacement of a point d_g=119.81 mm was calculated according to EC8 (Table 5). To achieve this displacement, the necessary force was calculated, and performance was compared to that of the building before the earthquake. After the earthquake, the building loses in load-carrying capacity and stability by about 19.534%, while after renovation using the standard material plaster with 25 mm cement mortar, the building shows a better performance than the building before the earthquake by 9.473%. If the plastering of the walls is done with cement mortar, but we also add the metal mesh 3/100/100 mm and anchor with 5 anchors per square meter according to Fig. 6. c, then the performance in bearing capacity of the building increases compared to that before the earthquake by 14.175%. These comparisons were made using the method of displacement and shear force in pushover in the direction of the y-axis because, in the direction of the x-axis, we have great inertia and the displacements are negligible. Fig. 8 shows the diagrams of the four cases using the diagrams of the capacity curves according to EC8 2004 using the displacement and the shear force and setting the target displacement. Table 6 presents the results for the target displacement, which force it can withstand and the capacity is extracted in percentage, again in comparison to the building before the earthquake. From the results presented, the building after the earthquake loses capacity by about 25.447%, while after interventions with the plastering of the walls with 25 mm thick cement varnish on both sides of the walls, the capacity increased by 9.322%. If the steel mesh 3/100/100 mm is also used in the building, then the capacity of the building compared to the building before the earthquake increases by 15.476%.

It can be seen that the intervention results are impressive and it is possible to achieve a lot in the socio-economic aspect and in the preservation of the environment and the emission of carbon dioxide, as discussed earlier.

5. Conclusion

From the obtained and analyzed results, we conclude that by reducing the specific weight of the layers of materials used, they positively affect the response of the building by reducing the impact force from the earthquake. Lightening the weight of the materials and reducing the impact force from the earthquake enables smaller-scale damage to buildings. From the results obtained with the use of plaster reinforcement with a cement base and mesh reinforcement, good performance of the building may be observed, especially when it is known that the acceleration a_g has also increased.

The results show that the buildings that were repaired with cement mortar on both sides of the wall with 25 mm increased the performance (1.1-9.3) % from the performance of the building before the earthquake, depending on which method is evaluated.

The results obtained for the walls repaired with 25 mm cement mortar and reinforced with 3/100/100 mm steel mesh anchored on both sides of the wall increase the performance of the building (3.8-15.4)% from the building before the earthquake.

With the restructuring of the internal tertiary walls, which were made of clay bricks and their replacement with modern light walls such as canvas, also affect the reduction of eccentricity and improve the behaviour of the building against the earthquake, which reduces the rotational strength of the building and reduces the damage.

The use of steel mesh increases the ductility of the walls and eliminates cracks from earthquakes on the surface of the walls and increases the stability of the wall outside its plane.

After an earthquake, quick intervention is always required, and the use of standard materials is an ideal solution. Whereby using the plastering of the walls with cement plaster cast to create great compactness, not only the sturdiness and the initial capacity of the building obtained but also the absorption capacity of the earthquake is increased. But one of the benefits is how quickly remediation can be made and the building put into use, reducing the financial costs of remediation and rent for residents who need to be sheltered after the earthquake. The impact on the environment is evident

because the pollution from the collapse of the building is eliminated, the cost of waste treatment is eliminated, and with it the emission of carbon dioxide and gases that affect global warming.

Acknowledgements

References

[1] Moustafa, A. (2012): *Earthquake-Resistant Structures – Design, Assessment and Rehabilitation*. InTech. doi: 10.5772/2460.

[2] Zeller, E. et al. (1997): NEHRP Guidelines for the Seismic Rehabilitation of Buildings (FEMA Publication 273), *Building Seismic Safety Council (A council of the National Institute of Building Sciences) Seismic Rehabilitation Project*, Washington D.C., USA.

[3] Giannopoulos, I. P., Asteris, P .G. (2011): Earthquake Resistant Design of Masonry Structural Systems, *3rd International Conference on Computational Methods in Structural Dynamics and Earthquake Engineering COMPDYN 2011,* Corfu, Greece.

[4] European Committee for Standardization CEN (2005): EN 1996-1-1, Eurocode 6: Design of masonry structures - Part 1-1: General rules for reinforced and unreinforced masonry structures, Brussels.

[5] European Committee for Standardization CEN (2004): EN 1998-1, Eurocode 8: Design of structures for earthquake resistance – Part 1: General rules, seismic actions and rules for buildings, Brussels.

[6] Tomaževič, M., Weiss, P. (2010): Displacement capacity of masonry buildings as a basis for the assessment of behaviour factor: an experimental study, *Bulletin of Earthquake Engineering*, 8, 1267–1294, doi: https://doi.org/10.1007/s10518-010-9181-y

[7] Dicleli, M., Durucan, C. (2013): Evaluation of displacement coefficient method for seismically retrofitted buildings with various ductility capacities, *Earthquake Engineering & Structural Dynamics*, 43, 1285-1306, doi: https://doi.org/10.1002/eqe.2397

[8] Polese, M., Di Ludovico, M., Prota, A, Manfredi, G. (2012): Damage-dependent vulnerability curves for existing buildings, *Earthquake Engineering & Structural Dynamics*, 42, 853-870. doi: https://doi.org/10.1002/eqe.2249

EXPERIMENTAL AND NUMERICAL IN-PLANE SEISMIC BEHAVIOUR OF AN INNOVATIVE STEEL REINFORCEMENT SYSTEM FOR URM WALLS

Luca Albanesi [(1)], Nicolò Damiani [(2)], Carlo Filippo Manzini [(3)], Paolo Morandi [(4)]

[(1)] *Department of Construction and Infrastructure - EUCENTRE Foundation, Pavia, Italy, luca.albanesi@eucentre.it*
[(2)] *UME Graduate School, IUSS Pavia, Pavia, Italy, nicolo.damiani@iusspavia.it*
[(3)] *Department of Construction and Infrastructure - EUCENTRE Foundation, Pavia, Italy, carlo.manzini@eucentre.it*
[(4)] *Department of Construction and Infrastructure - EUCENTRE Foundation, Pavia, Italy, paolo.morandi@eucentre.it*

Abstract

An experimental campaign, followed by a numerical research, aimed at evaluating the in-plane seismic behaviour of an innovative steel modular system (named "Resisto 5.9", designed by Progetto Sisma s.r.l.) for the reinforcement of load-bearing masonry walls, has been performed at the EUCENTRE Foundation in Pavia. Different masonry typologies, selected among the most common solutions in Italian existing buildings, were considered in this study. In this paper, the results related to a solid clay bricks masonry, assembled using lime mortar in "header bond" pattern, are reported. A complete mechanical characterization of units, mortars, masonry typologies and of the strengthening system components (*i.e.* steel elements and anchors) has been carried out. In-plane cyclic pseudo-static tests were then performed on full-scale specimens to investigate the influence of the proposed reinforcement system on the lateral in-plane response of the walls, compared to their unreinforced conditions. The main parameters which characterized the cyclic behaviour of the masonry piers, *i.e.* elastic stiffness, lateral strength and displacement capacity, were analysed in relation to the achieved damage mechanism. The numerical study of the research consisted of a series of parametric non-linear analyses on advanced discontinuous models based on the Distinct Element Method (DEM). Different wall dimensions, vertical load levels and boundary conditions, in addition to those tested experimentally, were considered. Moreover, the numerical campaign was also extended varying the bond pattern and the mechanical properties with respect to the experimentally tested solutions. In this paper, the results of the experimental tests on solid brick masonry together with the calibration of the related numerical DEM models were reported.

Keywords: unreinforced masonry walls, masonry seismic strengthening, experimental tests, in-plane cyclic response, non-linear analyses, Distinct Element Method

1. Introduction

The increased interest in improving the energy efficiency of buildings and the seismic performance of structures have recently led to the development of innovative combined reinforcement systems for existing masonry buildings (for example, see [1] and [2]). In this context, Progetto Sisma s.r.l. designed "Resisto 5.9", an external steel modular reinforcement system integrated with a thermal coating made up by insulation panels (*e.g.*, polystyrene, see Fig. 1b). The reinforcement system, reported in Fig. 1a, consists of steel frames, made up of cold formed L-shaped sections and plate elements (obtained from galvanized steel thin sheets), connected to each other by means of steel bolts and to the masonry through chemical anchoring with threaded bars. The modules should be positioned on the external surface of the wall and connected to each other and to the masonry with regular pitch, in order to guarantee the continuity of the reinforcing elements in all directions, as shown in Fig. 1c. More details on the reinforcement system can be found in [3]. Focusing on the structural aspects, the proposed system aims to guarantee an improvement in the connection between orthogonal walls and among walls and horizontal elements, a better redistribution of the seismic actions among the different structural elements, a limitation of the out-of-plane overturning of strengthened walls and an improvement of their in-plane performance.
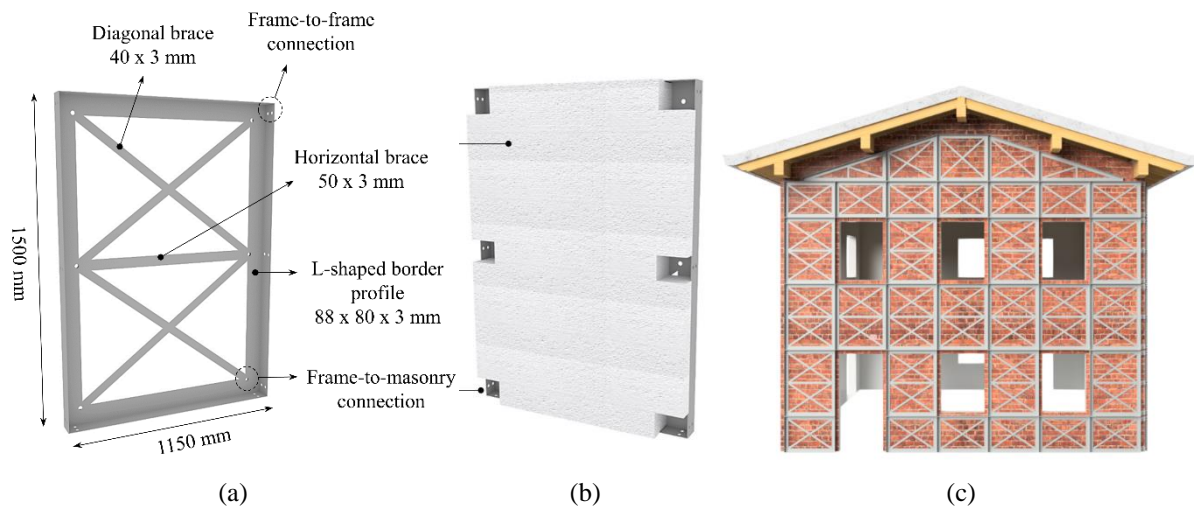
Figure 1. "Resisto 5.9" system: a) retrofit module details; b) insulation panel; c) example of retrofitted facade.

The study of the in-plane seismic behaviour of the "Resisto 5.9" reinforcement system is the main objective of the experimental and numerical research currently underway at the EUCENTRE Foundation in Pavia. Two different masonry typologies, representing common solutions in Italian existing buildings, have been considered so far in the campaign. This paper focused on a typology made up by solid clay bricks and lime mortar, assembled in "header bond" pattern.

The experimental campaign comprised firstly the complete mechanical characterization of units, mortars, masonry and of the reinforcement system components (*i.e.* steel sections and chemical anchors). Subsequently, the lateral performance of existing masonry piers has been evaluated through cyclic in-plane pseudo-static tests on different sets of full-scale specimens, comparing unreinforced walls with strengthened ones, in order to investigate the effects of the proposed reinforcement system. The cyclic behaviour of the masonry walls was analysed in terms of elastic stiffness, lateral strength, displacement capacity and energy dissipation, associated to the different failure modes.

The experimental results were then supported and extended through an extensive numerical study, which consisted in the development of advanced discontinuum models based on the Distinct Element Method (DEM). Past works in the literature have demonstrated that such models are able to satisfactorily predict the response of unreinforced masonry structures (*e.g.*, [4], [5], [6], [7] and [8]), but the inclusion in DEM framework of possible retrofit solutions represents a topic that has not yet been fully explored. In this study, a numerical procedure to explicitly consider in the models the proposed retrofit system is outlined, and experimental and numerical results are then compared to validate the proposed modelling strategy.

2. Experimental campaign

2.1 Performed tests

The cyclic in-plane pseudo-static shear-compression tests on full-scale masonry specimens were performed at EUCENTRE Foundation, whose experimental laboratory provides a three-dimensional configuration for these type of tests, composed of a strong floor and two orthogonal strong walls. The set-up, reported in Fig. 2a, includes a horizontal actuator, fixed to the strong wall perpendicular to the specimen, that applied the horizontal force, and two vertical actuators, reacting on a steel frame fixed on the strong wall parallel to the specimen, which controlled the applied vertical load and the different boundary conditions. The specimens are built on reinforced concrete (RC) footings, clamped to the strong floor by means of post-tensioned steel bars, while the connection with the actuators is realized through a steel spreader beam connected with the RC beam at the top of the wall. The forces are

measured by load cells in the different actuators, while the horizontal displacement (δ) of the RC beam at the top of the wall is controlled by an external linear potentiometer. Additional displacement transducers were installed on each wall, in order to evaluate the internal deformations of the masonry pier and, in the case of the strengthened specimens, of the reinforcement system and the relative displacements between them.

The applied testing protocol includes, for all the tests, an initial force-controlled phase followed by displacement-controlled cycles, in which programmed displacements of increasing amplitudes are imposed in both directions, up to the attainment of ultimate conditions of the specimens. At each level of force/displacement amplitude, three cycles were performed, as usually done in similar experimental tests in the past (see [9]). More information about the test set-up, the instrumentation and the testing protocol are reported in [3].

As already stated in the previous section, only solid brick masonry specimens, among the tested ones, are considered in this paper. Specifically, two squat specimens, one unreinforced (Fig. 2b) and the other strengthened (Fig. 2c), with the same mechanical and geometrical properties, were tested. Double-fixed boundary conditions were imposed, along with a realistic value of vertical stress (on this topic, see [10]), in order to achieve a shear failure, according to predictions evaluated with the relevant codified formulations (more information on this issue can be found in [11]). The nominal dimensions and the applied vertical stress level for the considered walls are summarized in Table 1, as well as the already mentioned boundary conditions and failure mode.

Table 1 – Considered masonry specimens subjected to cyclic in-plane tests.

Specimen	Masonry typology	Reinforcement	l (mm)	t (mm)	h (mm)	σ_v (MPa)	σ_v/fc_m (%)	Boundary conditions	Failure mode
UBPS01	Brick	No	2330	250	2435	0.50	7.1	Double fixed	Shear
RBPS01	Brick	Yes	2330	250	2435	0.50	7.1	Double fixed	Shear
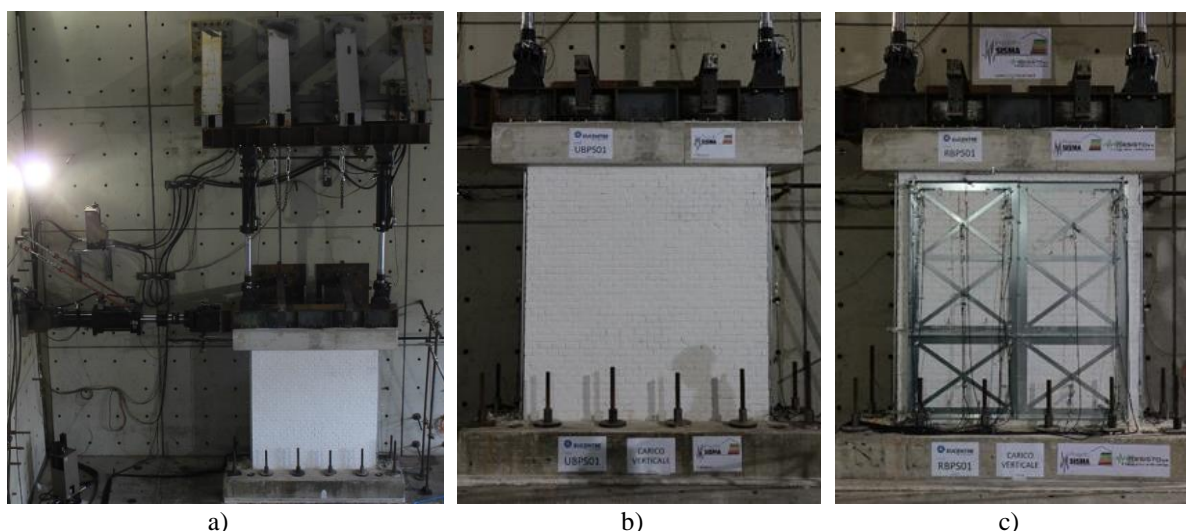
Figure 2. Experimental in-plane tests: a) set-up; b) unreinforced specimen UBPS01; c) retrofitted specimen RBPS01.

2.2 Experimental results

The experimental results, in terms of hysteretic curves and related global force-displacement envelopes for the considered tests, are reported in Fig. 3.

As correctly estimated, both specimens, UBPS01 and RBPS01, displayed pure shear failures, with a typical crack pattern characterized by bi-diagonal cracks spreading from corner to corner of the pier. In both cases, cracks were concentrated mostly in the mortar bed- and head-joints with a limited amount in the clay bricks. The shear cracking started developing from a drift ratio ($\theta = \delta/h$) of 0.10% in specimen UBPS01 and 0.15% in the case of specimen RBPS01. Cracks grew in number and width with the increase of the lateral displacement amplitude, progressively reducing the lateral strength and stiffness of the specimens up to their ultimate conditions. Test UBPS01 was stopped at $\theta = 0.25\%$, while RBPS01 at $\theta = 1.00\%$, in both cases to prevent the collapse. Hence, the retrofit system allowed to increase the ultimate displacement capacity of the specimen by about four times, as evident comparing the curves in Fig. 3. The comparison of the results also demonstrates that the initial stiffness was not affected by the presence of the retrofit, as well as the maximum base shear V_{max}, which resulted to be around 240 kN for both specimens. It is evident that, once shear cracks formed, the retrofit contributed in holding the masonry together, significantly reducing and delaying the damage, and thus exploiting the compressive strength of masonry.
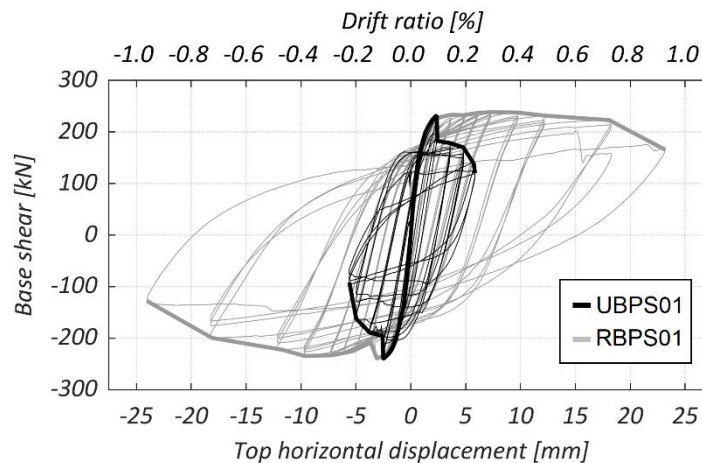
Figure 3. Experimental results, force-displacement curves.

3. Numerical simulation

A simplified micro-modelling strategy, based on DEM, was employed to simulate numerically the in-plane lateral response of the tested specimens. In this type of simplified micro-models, masonry units are expanded up to the half-thickness of the mortar joints (both horizontal and vertical). Bricks are then modelled as continuum blocks, while mortar joints as zero-thickness interface springs. For the complete description of the chosen modelling approach and comprehensive definitions of all the considered parameters it is possible to make reference to [12].

Note that the boundary RC elements, *i.e.* the fully-fixed foundation and the top beam, were modelled as an assembly of linear elastic FD regions (with $E = 40000$ MPa). Equivalent densities were assigned to the top beam to reproduce the compressive load actually imposed to the specimens.

All the presented numerical models have been implemented within the software 3DEC [13].

3.1 Modelling of the masonry

In this work, masonry units are modelled as deformable blocks, divided into multiple finite-difference (FD) regions, each of them consisting in constant-strain tetrahedral elements. When two blocks are

detected to be in contact, subcontacts are generated along their interface and zero-thickness springs, characterized by both normal and shear contact stiffnesses (named respectively k_n and k_s) are assigned to these subcontacts. Contact stresses are then calculated in the normal (σ) and shear (τ) directions depending on the related contact stiffnesses. In Fig. 4a a schematic outline of the adopted modelling strategy is reported.

A Coulomb-slip model is employed to represent the contact spring shear behaviour, whereas in the normal direction only a tensile failure is admitted, while no compressive failure is allowed for the joint. In this study, a contact model recently proposed by Pulatsu et al. [7] is employed. This constitutive model allows to account for softening regimes in tension and shear through the definition of fracture energies. Actually, shear (G_s) and tensile ($G_{t,j}$) fracture energy values can be specified to control the contact post-peak behaviour, as shown in Fig. 4c.

The masonry compressive behavior has to be accounted for in the constitutive model defined for masonry units since, as stated previously, no failure in compression is allowed at the interface springs. Therefore, a Mohr-Coulomb plasticity model (MPM) was assigned to the blocks to account for both masonry crushing and unit flexural-splitting failure, as reported in Fig. 4b. It is worth to underline that the proposed strategy combines a discrete modeling approach with masonry units modelled independently, constitutive laws describing their mutual interaction, and a smeared modeling approach to account specifically for masonry crushing and unit failure.
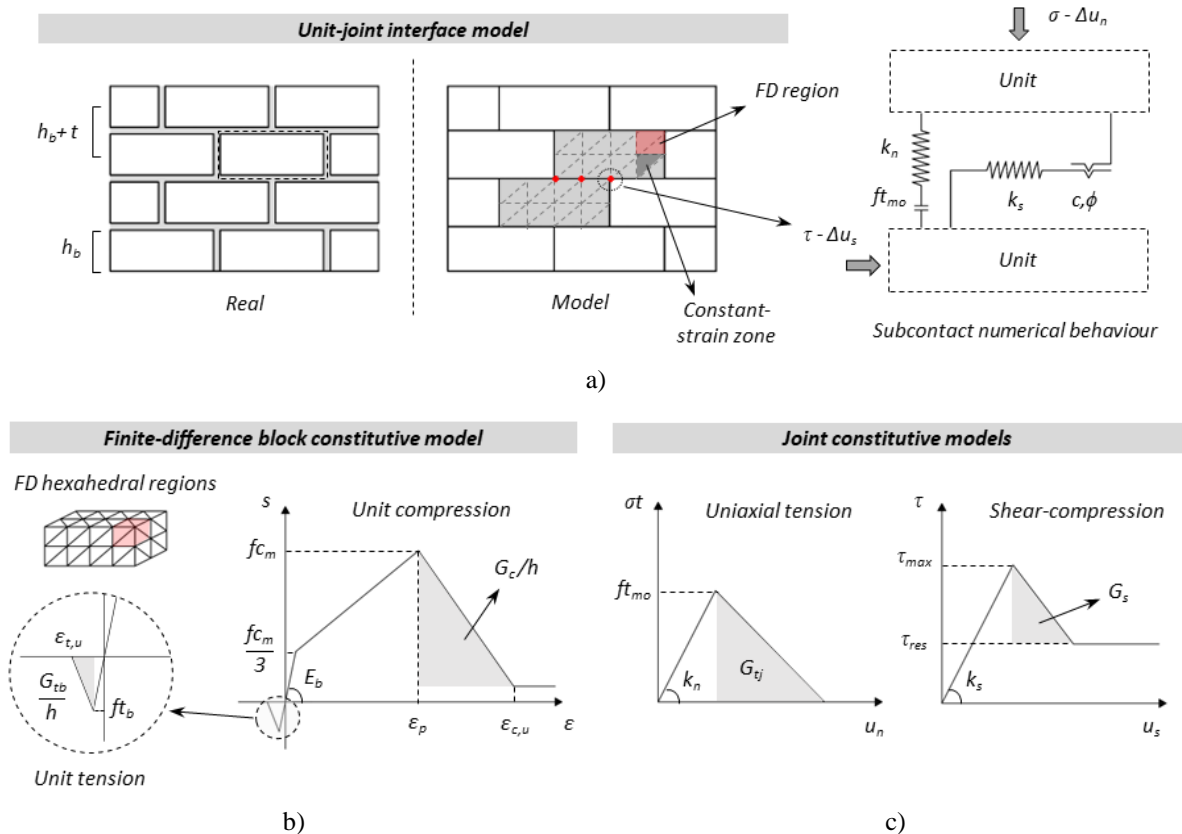
Figure 4. Distinct element modelling of masonry: a) unit-joint interface model; b) block constitutive model; c) joint constitutive model.

Before modelling the response of the tested full-scale specimens, the proposed modelling strategy was validated against the characterization tests performed on small-scale assemblages. Specifically, uniaxial compression tests on wallets and shear tests on triplets were reproduced numerically to calibrate the

required properties, as shown in Fig. 5a,b. Table 2 summarizes all the experimental and inferred properties assigned in the models to blocks and interface springs.

Table 2 – Experimental and inferred material properties employed in the DEM models.

Masonry & Units	E_m [MPa]	G_m [MPa]	fc_m [MPa]	ρ_m [kg/m³]	fc_b [MPa]	E_b [MPa]	c_b [MPa]	ϕ_b [°]	ft_b [MPa]
	4265[a,b]	1706[a]	7.03[a]	1300[a]	19.22[a]	7207	3.51	0	1.79
Joints	k_n [GPa/m]	k_s [GPa/m]	c [MPa]	ϕ [°]	ft_{mo} [MPa]	G_c [N/m]	G_{tb} [N/m]	G_s [N/m]	G_{tj} [N/m]
	126	50	0.15[a]	31.38[a]	0.05[a]	11248	60	50	10

[a] Value determined through material characterization tests

[b] Evaluated in the direction perpendicular to bed joints as secant value between 10% and 33% of fc_m
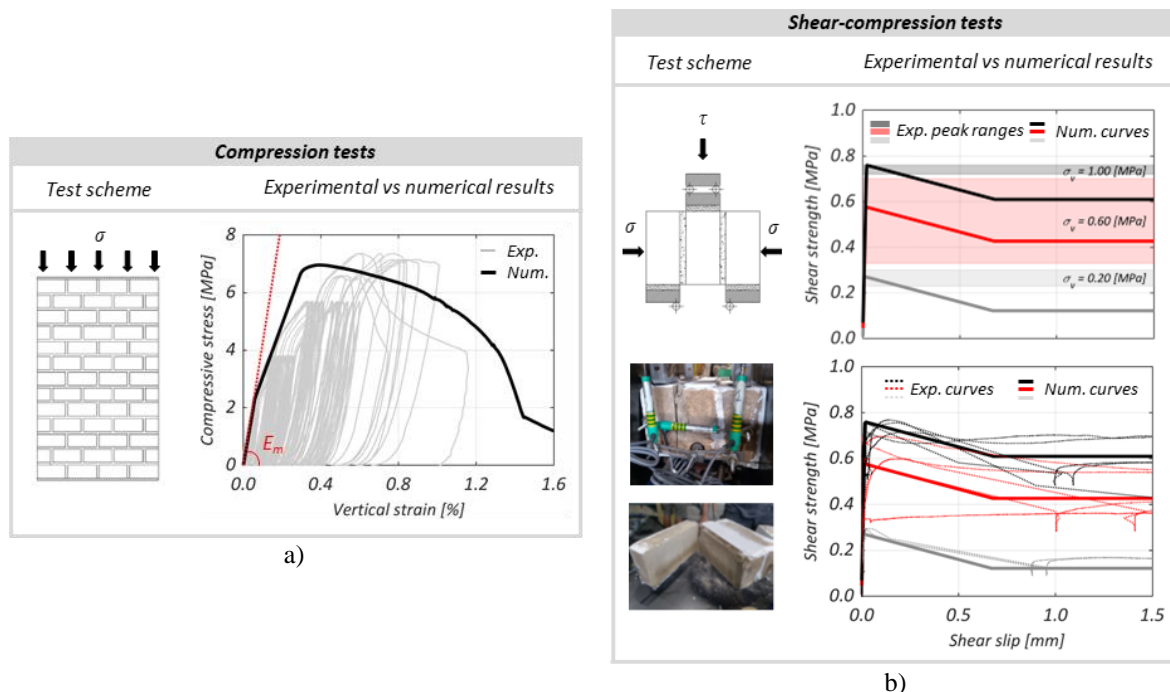
Figure 5. Verification of the modeling strategy with characterization tests on small masonry assemblages: a) vertical compression test; b) shear tests.

3.2 Modelling of the retrofit system

The modular steel frames were numerically reproduced by explicitly modelling each component as a one-dimensional beam finite element (FE) with an isotropic elastic behaviour, with no failure limit. Although this represents a simplified modeling assumption, it was deemed reasonable since experimental evidences demonstrated that the retrofit behaviour was mainly controlled by the failure of the retrofit-to-masonry anchors rather than the attainment of the axial or flexural strength of the steel components (for a complete description, see [14]). FE beams were defined according to the experimental retrofit scheme, connecting the actual positions of the retrofit-to-masonry anchors, as sketched in Fig. 6a. Cross-sectional areas and moments of inertia were then properly assigned, reproducing the actual stiffnesses of the steel members. Moreover, rigid links were inserted in the model in the actual positions to simulate the steel bolts connecting adjacent modular frames (Fig. 6a).

It is important to point out that the thin plate elements employed for the diagonal and horizontal braces (*i.e.* 40x3 and 50x3 mm sections, respectively) experimentally evidenced buckling phenomena that can

significantly limit their effective compressive strength. For this purpose, an out-of-plane initial deformation was assigned in the numerical models at the mid-length of each diagonal and horizontal brace to account for buckling effects in their compressive behaviour.

As anticipated above, the retrofit system effectiveness was mainly affected by the behaviour of retrofit-to-masonry anchors. Therefore, to simulate correctly the retrofit influence on the pier lateral response, an accurate modelling strategy was required to characterize the connections between the FE beams and the masonry block assembly. In detail, deformable links were defined in correspondence of the actual position of anchors, as shown in Fig. 6a. A shear-yield constitutive model was assigned to each link for the translational in-plane degrees of freedom (directions x and z, Fig. 6b), while a normal-yield model was assigned for the translational out-of-plane degree of freedom (direction y): rotational degrees of freedom were considered as free. The structural link behaviour was calibrated against the results of characterization tests (both shear and pull-out tests) performed on retrofit-to-masonry anchors during the same experimental campaign [3]. A comparison between the experimental shear force-displacement behaviour of anchors and the in-plane numerical model assigned to the structural links is reported in Fig. 6c. Similarly, referring to the experimental results of pull-out tests, a simplified bilinear force-displacement rule was assigned to the out-of-pane translation degree of freedom of the links.
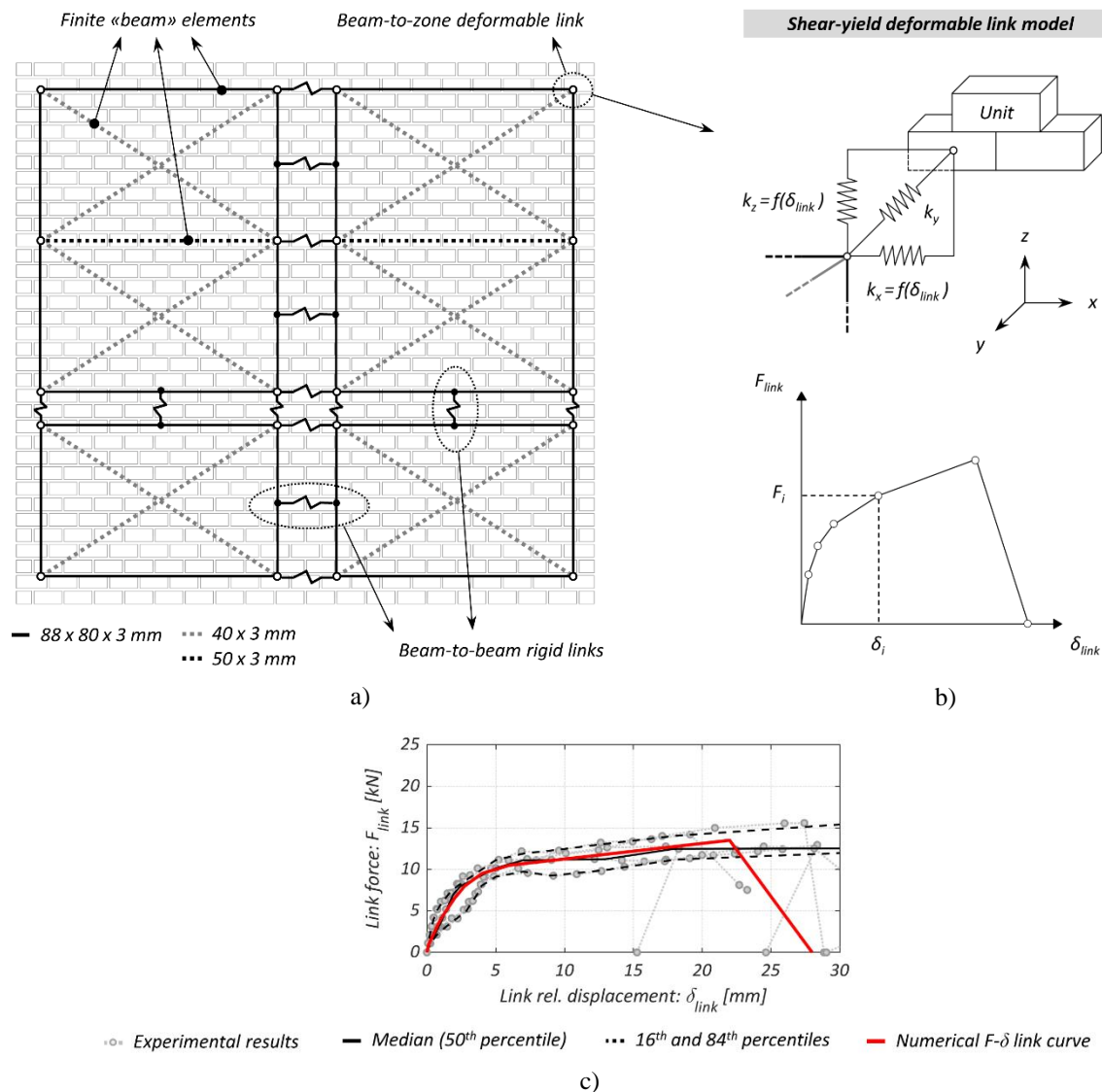
Figure 6. Modelling of the retrofit system: a) retrofit numerical layout; b) retrofit-to-masonry anchors model; c) experimental and numerical anchors shear behaviour along x and z directions.

3.3 Numerical results

The computational procedure of 3DEC is based on a dynamic time-integration algorithm that solves the equations of motion by an explicit finite difference method. Quasi-static phenomena can be solved with the same algorithm adopting an approach conceptually similar to dynamic relaxation [15]. Specifically, the equations of motion are damped to quickly reach a force equilibrium state through a numerical servo-mechanism, named adaptive global damping [16]. Size, density and time-scaling techniques were also employed according to [6] to obtain an acceptable compromise between the accuracy of results and the computational effort.

The capability of the numerical models to replicate the experimental response was assessed through cyclic and monotonic (*i.e.* pushover) in-plane analyses. It is important to point out that only one cycle for each target displacement has been implemented in cyclic analyses, instead of the three performed in the experimental tests, in order to reduce the computational expense.

The comparison between the numerical and experimental responses of the unreinforced pier (UBPS01) is reported in Fig. 7. Although the numerical model underestimated the initial peak force in both cyclic and monotonic analyses (due to the current inability to capture the tension component of the lateral response of this masonry typology), satisfactory results were obtained in terms of initial stiffness, post-peak response and progressive stiffness and strength degradation (Fig. 7a,b). This latter aspect is particularly relevant, considering that the investigated retrofit solution allowed the wall to reach higher drifts without substantially increasing its lateral strength [14]. Moreover, a good agreement was found between the numerically predicted and the experimental in-plane failure mechanisms, with bi-diagonal stair-stepped cracks adequately simulated by the DEM model crack pattern, as shown in Fig. 7c.

Figure 7. UBPS01 results: a) experimental and numerical hysteresis; b) experimental envelope and numerical pushover; c) experimental and numerical (cyclic and pushover) failure mechanisms.

The addition of the retrofit frames in the models and the larger target displacements reached in the experimental test of the retrofitted specimen, significantly increased the computational effort resulting in a prohibitive analysis time required for the simulation of the entire experimental cyclic tests. Since the results presented in Fig. 7 demonstrated that monotonic pushover analysis satisfactorily captured the in-plane behaviour of the unreinforced wall, also the numerical performance of the retrofitted one was investigated through this type of analysis. However, the experimental cyclic test was also numerically simulated, but only up to the drift ratio corresponding to the ultimate conditions of the unreinforced specimen (*i.e.* 0.25%).

Fig. 8a compares the numerical and experimental in-plane cyclic responses of the retrofitted pier, simulated, as explained above, only up to the ultimate conditions of the unreinforced specimens, whereas in Fig. 8b, the numerical pushover curve for the retrofitted pier is compared with the experimental envelope. Although the model was not able to capture the specimen maximum lateral strength, as consistently observed for the unreinforced model the numerical response matched satisfactorily the experimental one and reproduced the overall behaviour change caused by the retrofit system. In fact, the comparison between the numerical pushover curves of unreinforced and retrofitted specimens, reported in Fig. 8b, demonstrates that the retrofit system is able to increase the pier ultimate displacement capacity, postponing the strength degradation observed in the unreinforced models, without significantly affecting the pier initial stiffness and strength, as observed experimentally. The ultimate drift of piers subjected to increasing monotonic loads was identified on the pushover curves at a strength reduction of 20% of the maximum base shear. This resulted in an ultimate drift ratio of 0.41% for UBPS01 and of 1.40% for RBPS01.

The retrofit performance can be also appreciated in Fig. 8c (for cyclic analysis) and Fig. 8d (for pushover), with the comparison of the numerical damage patterns at the same level of drift corresponding to the ultimate conditions of URM pier. The damage patterns of the retrofitted wall presented only few diagonal shear cracks with a decreased number of failures in the masonry units, if compared to the unreinforced ones. In Fig. 8c, the cyclic numerical crack pattern of the retrofitted wall is also compared with the corresponding experimental one: the DEM prediction of the effects of the retrofit system on the in-plane behaviour of the specimen closely simulated the reduction of the damage observed in the experimental test. Fig. 8d reports also the damage pattern of the retrofitted piers at its ultimate conditions; the presence of the reinforcement did not alter the diagonal shear failure mechanism exhibited by the unreinforced specimen but, once the mechanism formed, the steel frames restrained the relative displacement of the masonry portions created by the diagonal cracks, reducing the joint opening and spreading the damage over the masonry pier surface.

In Table 3, a comparison between the experimental and numerical values of some of the most relevant parameters of the in-plane lateral response of the investigated specimens is reported, as well as the ratio between retrofitted and unreinforced results. In detail, the maximum absolute base shear (V_{max}), the associated drift ratio (θ_{Vmax}), and the ultimate drift ratio ($\theta_{20\%}$), evaluated at a strength reduction equal to 20% of V_{max}, are considered. Although the numerical ultimate conditions of the retrofitted pier were studied using a monotonic analysis rather than a cyclic one, the experimental response improvement was satisfactorily simulated by the numerical models, especially in terms of displacement capacities, thus confirming the effectiveness of the proposed modelling approach.

Table 3 – Comparison of experimental and numerical retrofit performance.

Specimen	Experimental (Cyclic)			Numerical (Pushover)		
	V_{max} [kN]	θ_{Vmax} [%]	$\theta_{20\%}$ [%]	V_{max} [kN]	θ_{Vmax} [%]	$\theta_{20\%}$ [%]
UBPS01	239.4	0.08	0.14	184.1	0.06	0.41
RBPS01	238.9	0.10	0.57	200.5	0.20	1.40
R/U ratio [-]	1.00	1.25	4.07	1.09	3.33	3.50

a)

b)

R (θ = 0.25%)   U (θ = 0.25%)

— Joint relative displacements   — Unit failure

c)

R (θ = 1.40%)   R (θ = 0.41%)   U (θ = 0.41%)

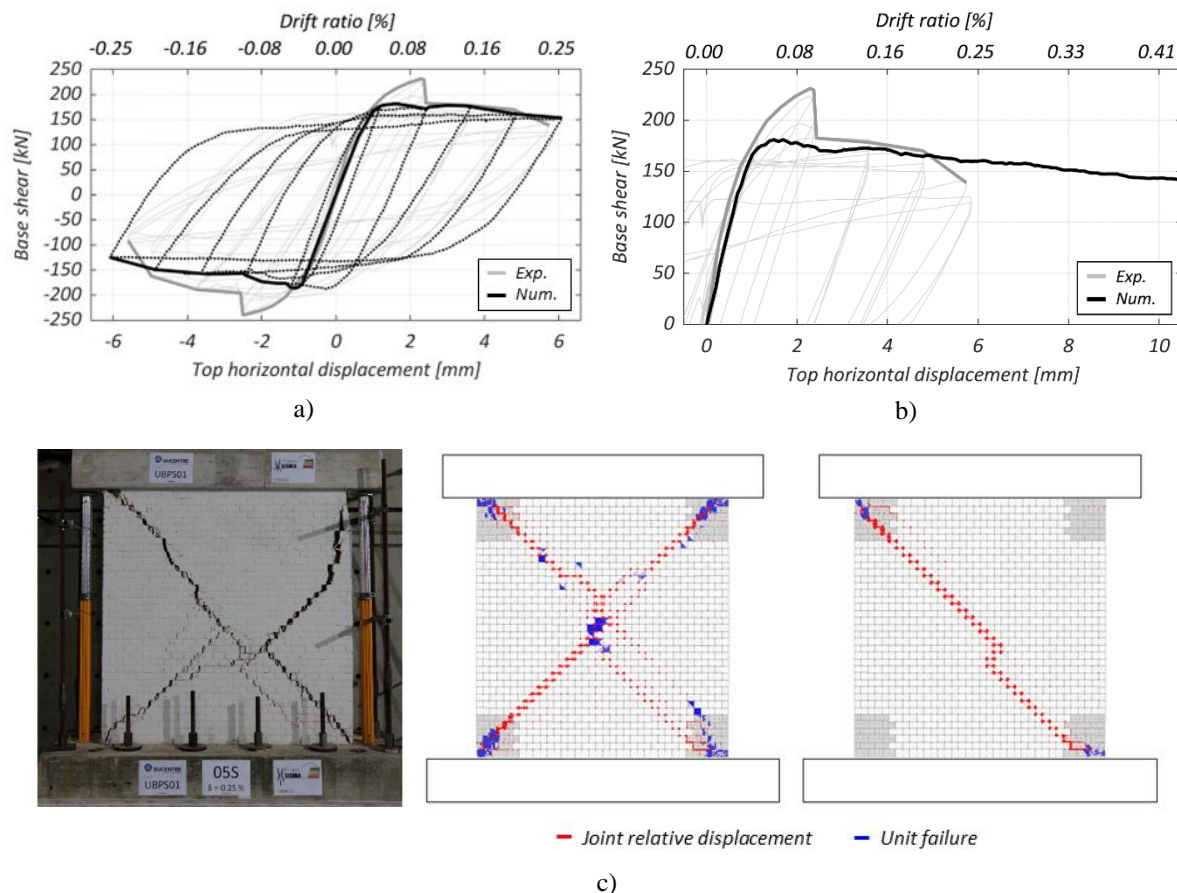— Joint relative displacements   — Unit failure

d)
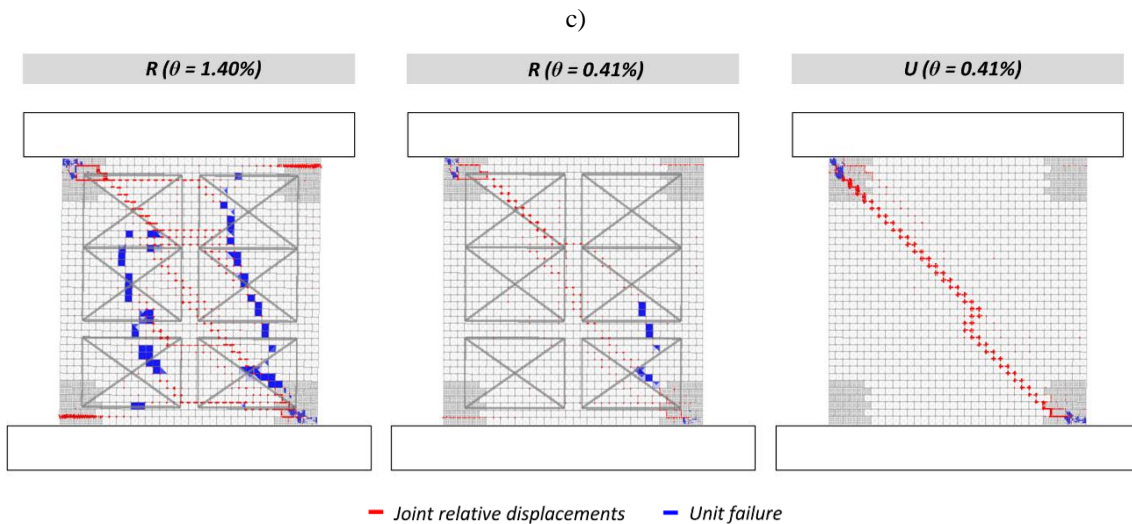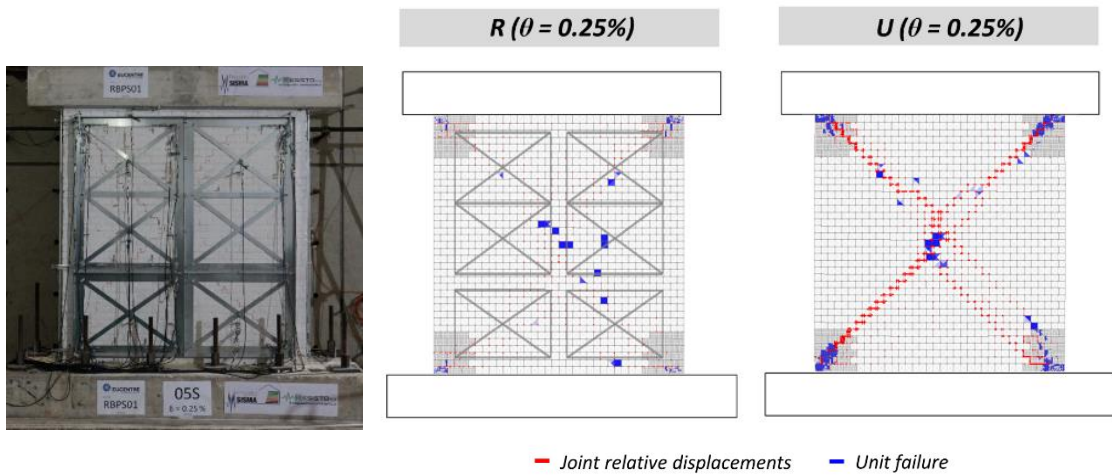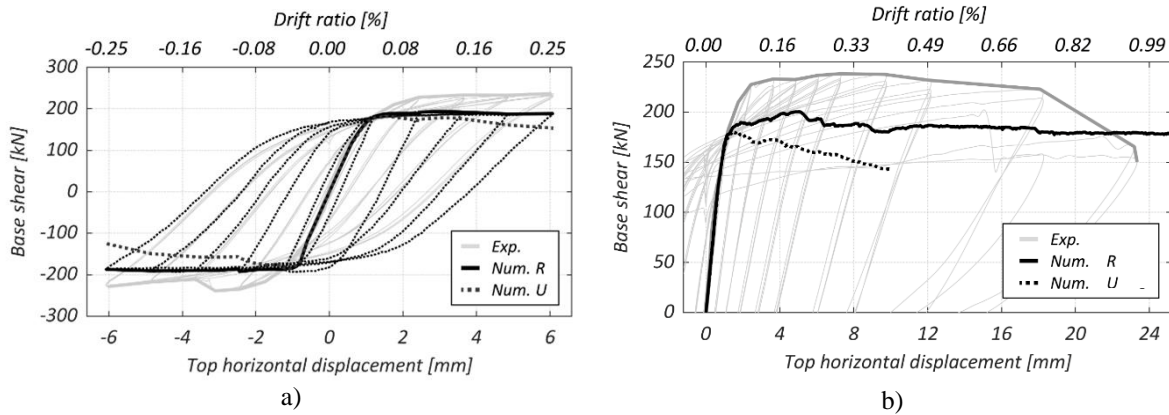
Figure 8. RBPS01 results and comparison with UBPS01: a) experimental and numerical hysteresis; b) experimental envelope and numerical pushover; c) experimental and numerical (cyclic) failure mechanisms; d) numerical (pushover) failure mechanism.

4. Conclusions

In this paper, an innovative steel strengthening system for the seismic retrofit of unreinforced masonry piers is discussed. The proposed system consists of modular steel frames connected to each other with steel bolts and to the masonry panels through chemical anchors, and aims at enhancing the in-plane and out-plane response of masonry piers. In the experimental campaign, the retrofit was applied to a masonry made of clay bricks arranged in a header bond pattern. Pseudo-static in-plane cyclic tests were performed on both unreinforced and strengthened piers. The tested retrofit solution allowed to increase the displacement capacity of the specimen by approximately four times, while no significant improvement was observed in terms of stiffness and strength.

Advanced discontinuum models based on the Distinct Element Method (DEM) were developed to assess the behaviour of the tested unreinforced and retrofitted piers. A strategy to model unreinforced masonry, simulating all the possible failure mechanisms of masonry components (*i.e.* mortar joint tensile and shear failure, unit flexural and splitting failure, unit crushing) was developed and validated against experimental tests.

A specific modelling strategy to explicitly include the contribution of the investigated steel retrofit solution in DEM framework was then defined. In particular, the retrofit system was modelled as finite-element frames which were connected to the masonry by means of three-dimensional structural links. Despite some differences in terms of maximum lateral strength, the developed model for the strengthening system was able to satisfactorily capture the experimental improvement of the lateral response. Numerical cyclic and pushover analyses demonstrated the capability of the implemented retrofit in delaying the strength degradation and enhancing the pier displacement capacity, without modifying the unreinforced masonry initial failure mechanism, in accordance with the experimental evidences.

In order to generalize the experimental results and to further investigate the effectiveness of the retrofit system, the proposed DEM modelling strategy will be employed to perform a series of parametric analyses aimed at assessing the benefits of the investigated retrofit solution for different pier aspect ratios, vertical loads, boundary conditions, bond patterns, and masonry typologies, as well as retrofit system details.

Acknowledgements

References

[1] Guerrini, G., Damiani, N., Miglietta, M., Graziotti, F. (2021): Cyclic response of masonry piers retrofitted with timber frames and boards, *Proceedings of the Institution of Civil Engineers - Structures and Buildings*, 174(5), 372-388, DOI:10.1680/jstbu.19.00134.

[2] Miglietta, M., Damiani, N., Guerrini, G., Graziotti, F. (2021): Full-scale shake-table tests on two unreinforced masonry cavity-wall buildings: effect of an innovative timber retrofit, *Bulletin of Earthquake Engineering*, 19, 2561-2596, DOI:10.1007/s10518-021-01057-5.

[3] Manzini, C., Albanesi, L., Morandi, P. (2022): Studio del comportamento sismico di murature portanti con rivestimento esterno modulare in acciaio - Rapporto Sperimentale, *EUCENTRE Report*. https://www.progettosisma.it/wp-content/uploads/2022/05/2%C2%B0_Sperimentazione_EUCENTRE.pdf

[4] Lemos, J.V. (2007): Discrete element modeling of masonry structures, *International Journal of Architectural Heritage*, 1(2), 190-213. DOI:10.1080/15583050601176868.

[5] Lemos, J.V. (2019): Discrete element modeling of the seismic behavior of masonry construction, *Buildings*, 9(2), 43. DOI:10.3390/buildings9020043.

[6] Malomo, D., DeJong, M.J., Penna, A. (2019): Distinct element modelling of the in-plane cyclic response of URM walls subjected to shear-compression, *Earthquake Engineering & Structural Dynamics*, 48(12), 1322-1344. DOI: 10.1002/eqe.3178.

[7] Pulatsu, B., Erdogmus, E., Lourenço, P.B., Lemos, J.V., Tuncay, K. (2020): Simulation of the in-plane structural behavior of unreinforced masonry walls and buildings using DEM, *Structures*, 27, 2274-2287. DOI:10.1016/j.istruc.2020.08.026.

[8] Malomo, D., DeJong, M.J. (2021): A Macro-Distinct Element Model (M-DEM) for simulating the in-plane cyclic behavior of URM structures, *Engineering Structures*, 227, 111428. DOI:10.1016/j.engstruct.2020.111428.

[9] Morandi, P., Albanesi, L., Graziotti, F., Li Piani, T., Penna, A., Magenes, G. (2018): Development of a dataset on the in-plane experimental response of URM piers with bricks and blocks, *Construction and Building Materials*, 190, 593-611. DOI:10.1016/j.conbuildmat.2018.09.070.

[10] Morandi, P., Albanesi, L., Magenes, G. (2021): In-plane cyclic response of new URM systems with thin web and shell clay units, *Journal of Earthquake Engineering*, 25(8), 1533-1564. DOI:10.1080/13632469.2019.1586801.

[11] Albanesi, L., Morandi, P. (2021): Lateral resistance of brick masonry walls: a rational application of different strength criteria based on in-plane test results, *International Journal of Architectural Heritage*. DOI:10.1080/15583058.2021.1992533.

[12] Damiani, N., DeJong, M., Albanesi, L., Morandi, P., Penna, A.: Distinct Element Modelling of the in-plane response of a steel-framed retrofit solution for URM structures, *Earthquake Engineering and Structural Dynamics*.

[13] Itasca (2019): 3 Dimensional Distinct Element Code (3DEC): Theory and Background, 7ᵗʰ edition, Itasca Consulting Group, Minneapolis, USA.

[14] Albanesi, L., Manzini, C.F., Morandi, P.: In-plane experimental performance of URM walls strengthened with steel modular framing system integrated with thermal coating, *Engineering Structures*.

[15] Otter, J.R.H. (1966): Dynamic relaxation compared with other iterative finite difference methods, *Nuclear Engineering Design*, 3(1), 183-185. DOI: 10.1016/0029-5493(66)90157-9.

[16] Cundall, P.A. (1982): Adaptive density-scaling for time-explicit calculations, *Proceedings of the 4ᵗʰ International Conference on Numerical Methods in Geomechanics*, Edmonton, Canada, 23-26.

SEISMIC AND ENERGY UPGRADING OF EXISTING RC BUILDING

Margareta Zidar [(1)], Dominik Skokandić [(2)], Matija Vajdić [(3)], Karlo Ožić [(4)], Mislav Stepinac [(5)]

[(1)] *Researcher, Energy Institute Hrvoje Požar, e-mail address: mzidar@eihp.hr*
[(2)] *Postdoctoral researcher, University of Zagreb Faculty of Civil Engineering, e-mail address: dskokandic@grad.hr*
[(3)] *Researcher, Energy Institute Hrvoje Požar, e-mail address:* mvajdic@eihp.hr
[(4)] *PhD student, University of Zagreb Faculty of Civil Engineering, e-mail address:* karlo.ozic@grad.unizg.hr
[(5)] *Assistant Professor, University of Zagreb Faculty of Civil Engineering, e-mail address:* mislav.stepinac@grad.unizg.hr

Abstract

This paper presents the preliminary results of the project called Establishment of the national training centre for nearly Zero Energy Buildings (nZEB). The project is funded by EEA Grants (Energy and Climate Change Programme). Seismic condition assessment and upgrading of existing RC structures are presented with a case study building in Zagreb. New technologies were applied and followed by numerical modeling and verifications. A strategy for energy retrofitting will be presented. As the integrated approach should be respected in the renovation of existing buildings, this case study can represent an example of good practice in seismic and energy retrofitting.

Keywords: assessment, RC, renovation, case study, energy

1. Introduction

Devastating earthquakes recently struck Southern Europe, and the same problems regarding the vulnerability of the building stock appeared in Italy [1], Albania [2], Greece [3], Turkey [4], and Croatia [5]–[10]. Most damaged objects are older masonry buildings built according to older codes without proper consideration of seismic loads. However, in all the countries, there was also slight damage to RC buildings [11]–[17]. In Croatia's scenario, these buildings were built in1960s, with plain bar reinforcement and lightly reinforced shear walls.

The poor energy efficiency of public buildings in Croatia has been addressed in the main energy policy documents, the National Energy and Climate Plan (NECP) for the period 2021-2030 (adopted at the end of 2019) [18] and the Long-Term Strategy for Energy Retrofit of the National Building Stock by 2050 (adopted at the end of 2020). The latter document introduced the concept of comprehensive renovation, which includes not only energy renovation measures but also optimal measures to improve the overall regulatory requirements for the building. Instructions were published on assessing the existing condition and what measures should be considered to increase fire safety, ensure a healthy indoor environment, and improve the mechanical resistance and stability of the building, especially to reduce the operational seismic risk. This analysis was introduced as a mandatory document to be submitted when applying for public grants. It is up to the building owner to decide on the scope of the retrofit and the savings target. A higher savings target and a larger scope of improvements allow for a higher percentage of capital cost funding. This leads to one of the problems hindering nZEB renovation potential in Croatia today, namely how to efficiently communicate the relevant regulations and recently developed methodologies related to nZEB standards to all key stakeholders involved in the renovation of the existing building stock. nZEB projects lead to complex partnerships where there is not only one investor, but the active participation of the local government and the neighborhood is required.

In 2021, a comprehensive pilot project to renovate a public office building was initiated to apply the nZEB standard [19]. The entire process of developing the design documentation, as well as the steps of the regulatory approval process and construction work, is thoroughly documented and monitored by the expert group and has the role of a living laboratory for all stakeholders. The project's overall objective is to improve the knowledge of professionals dealing with buildings and to raise the awareness

of other stakeholders on all aspects of building renovation by introducing innovative technical solutions that meet nZEB requirements. This will be achieved by establishing a national training center for nZEB.

2. PDP-nZEB project

The project is financed from the „Energy and Climate Change" Fund, part of the Financial Mechanisms 2014 – 2021 in Croatia, courtesy of the European Economic Area (EEA). The PDP aims to raise awareness and increase the relevant stakeholders' capacities in the field of the energy performance of buildings to implement innovative technical solutions of the nearly zero energy standards. The goal will, inter alia, be achieved by establishing a national training center targeting experts' education tied to the nearly Zero Energy Buildings (nZEB).

Addressing the poor energy performance of public buildings is at the core of Croatian energy strategies and action plans. The newly implemented building standard – nearly zero energy building (nZEB)- has been adopted; however, the actual implementation is still lagging behind. One of the growing issues in Croatia today is how to transfer the respective regulations efficiently and recently developed methodologies regarding nZEB standards to all the key stakeholders. This project will therefore support the key stakeholders in realizing all the benefits of nZEB standard. The project will prove that nZEB approach, although innovative, is the optimal and cost-effective solution for the renovation of public buildings. The project also aims to capitalize on the results of the key Norwegian initiatives developed by the well-known research institution SINTEF, regarding nZEB and zero-emission neighbourhoods (Figure 1).

This objective will be explicitly achieved by the following main activities:

- Development of all the required documentation needed for achieving nZEB standard while retrofitting the existing public building
- Deep retrofit of the existing public building with state-of-the-art technologies which will be thoroughly documented and monitored by the group of nZEB experts
- Design of the training programme and project development assistance for nZEB projects for the neighborhood with the action plan on how to achieve the zero-emission neighborhood
- Established cooperation with Norwegian scientific institutions and other nZEB initiatives.

In this manuscript, just the idea of seismic upgrading will be presented. The energy evaluation of the real case study is still ongoing. It pertains to the advantages of seismic retrofitting of existing building stock according to the "full Eurocode 8" [20], as well as the discussion of evaluation methods of RC structures and the implementation of new technologies in the evaluation process. The processes are demonstrated through a specific case study and a detailed plan of activities for the specific case study.
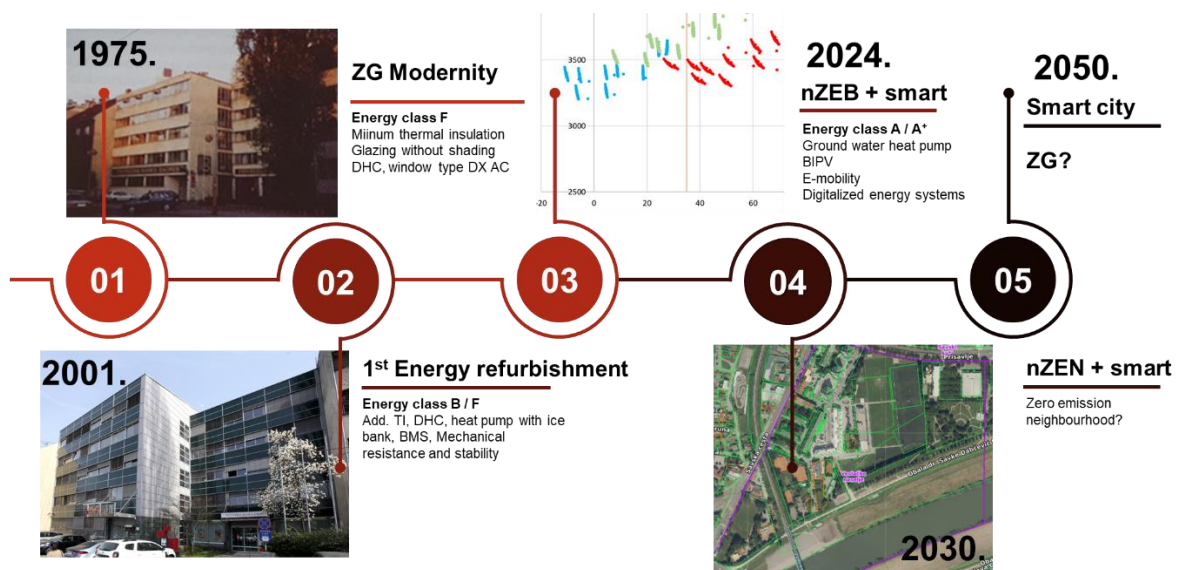
Figure 1. nZEB vision

3. Case study building

For the successful renovation of buildings damaged by the earthquake, appropriate measures must be taken to repair and strengthen the building without compromising the mechanical properties of the material and the properties of the structure, which contribute to the durability of the building. Following the obtained results, a proposal of measures for repair and reinforcement of buildings is given. Measures should follow the seismic design and be in line with the conservation and restoration rules [21],[22] but also be in line with energy demands [18],[23].

The office building was built in 1975 and was refurbished for the first time in 2001. Energy consumption, energy costs, and associated CO_2 emissions for the existing facilities were analyzed. The specific annual electricity consumption is 90.51 kWh/m^2, district heating consumption is 65 kWh/m^2, and CO_2 emissions are 90 tCO_2. The total annual energy cost is 30,775 EUR or 14.93 EUR/m^2. All energy efficiency indicators show a high potential for energy and cost savings. A detailed energy study to determine the energy retrofit concept has been conducted. This includes modelling of the building's energy demand, assessment of energy performance, and identification and analysis of cost-effective and technically feasible energy efficiency measures combined with the integration of on-site available renewable energy sources suitable to meet the nZEB target. The maximum savings potential estimated can achieve energy consumption and CO_2 emissions reduction by ten times and energy consumption reduction by five times. There were 720 combinations of energy efficiency measures tested for specific technical systems (including subsystems) such as heating, ventilation, and air conditioning (HVAC), lighting system, and building envelope improvement [11]. Next, a multicriteria analysis provided insight into specific criteria such as primary energy, global cost, CO_2 emission, and operational costs to define the optimal nZEB solution. Along with the energy demand and CO_2 emission reduction, further building system digitalization and energy storage systems are planned.

Existing building

Data on building systems, use, energy consumption, weather data

$Q_{H,nd}$ 38.06 (B)

E_{prim} 156.14 kWh/m^2 (F)

Definition of energy efficiency measures

Building envelope

HVAC system

Lighting system

Dynamic simulations

Energy demand

720 Combination of EE measures

Multicriteria analysis

Primary energy

Global cost

CO_2 emission

Operational costs

Optimal nZEB solution

$Q_{H,nd}$ 12,86 kWh/m^{2}a (A+)

E_{prim} -29,09 kWh/m^{2}a (A+)

Figure 2 Methodology for selection of optimal nZEB solution

The case study building is divided into three structural sections, labeled as sections A to C. The structural system of sections A and C is a combination of uncoupled shear walls and frames, while section B is comprised only of shear walls. Reinforced concrete walls are 20 cm thick (except in the basement, where the walls are 30 cm thick), and the columns have a cross-section of 30 × 40 cm on which the beams with a height of 40 cm are supported. Floor structures are RC slabs with a thickness of 14 cm. There are six stories, including the basement and attic, with a total height of 18.53 m. The foundations are constructed as pad foundations for the columns and foundation beams for the shear walls. In the following figures, the building is shown (Figure 2), followed by the laser scanning procedure with Leica Bulk 360 (Figure 3) and BIM model (Figure 4).

Figure 3. Front view of the case study building

711
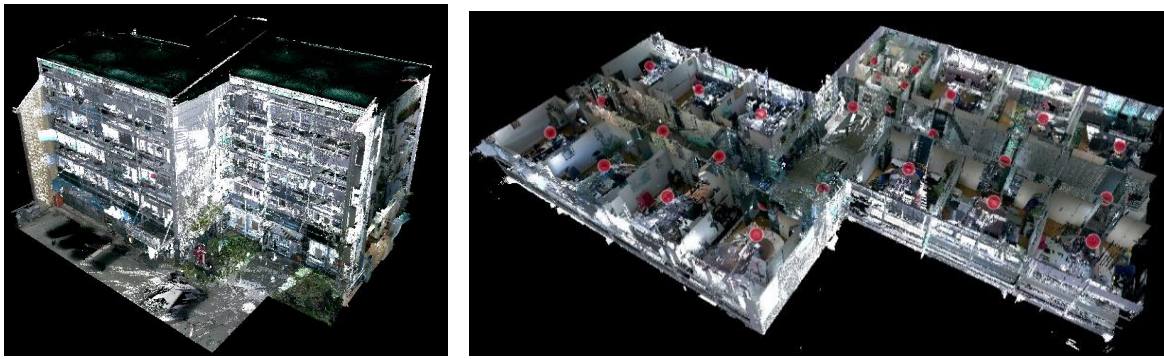
Figure 4. Laser scanning procedure: case study building (a) and scanning locations for one floor (b)

Figure 5. BIM model

In order to determine the material mechanical properties of the constructive elements, a detailed visual inspection, and non-destructive and semi-destructive investigative works, were required.

The compressive strength of concrete was determined with the standard test method for obtaining and testing drilled cylindrical specimens. The numerical model for the case study building was developed in the SCIA software for static analysis using the finite element method (FEM). All load-bearing elements were defined in the model, including RC shear walls, columns, beams, slabs, and the steel structure of the roof.
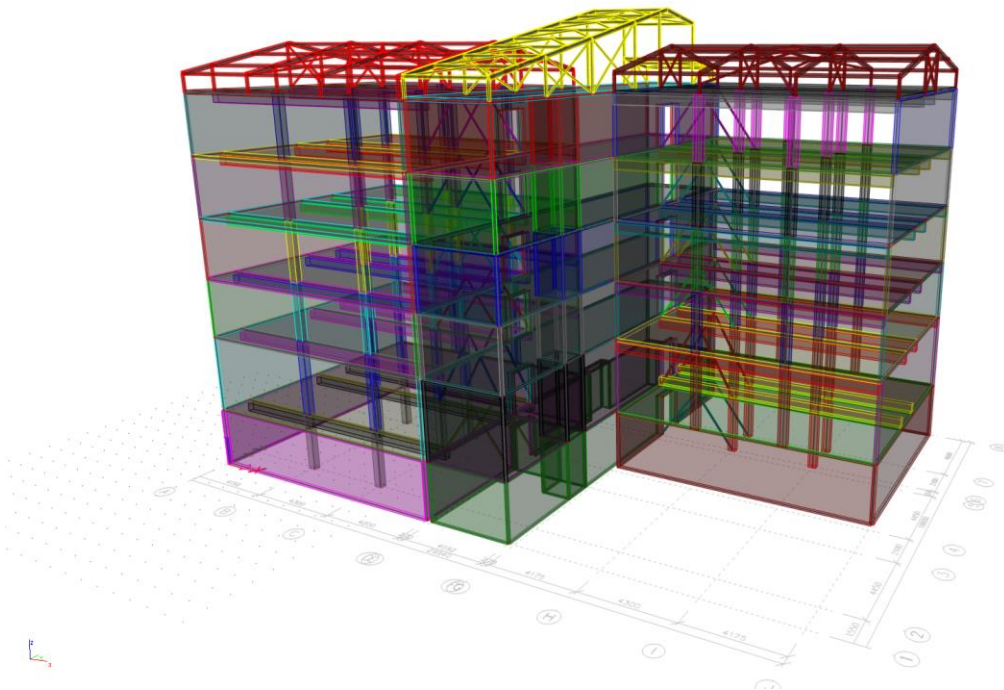
Figure 6. FEM model

In situ testing showed that the shear walls are reinforced with rectangular meshes on each side of the wall, consisting of Ø8 bars spaced 15 cm in the vertical and 25 cm in the horizontal direction. The whole FEM procedure with the results is shown by Stepinac et al. [11]. The summary of the results showed that the shear failure of walls (basement and ground floor), and the shear failure of columns are the main issues that need to be addressed with the strengthening project. Additionally, global modal analysis proved that all three sections lack lateral stiffness in direction X. In accordance with the results, several preliminary solutions for strengthening are given and presented in Figures 7-9.
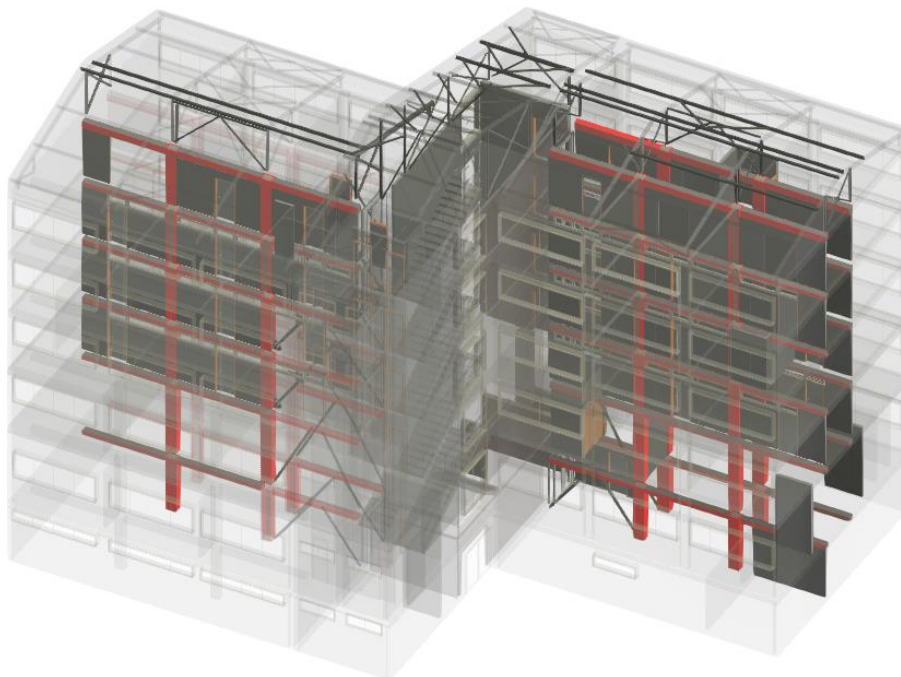
Figure 7. Strengthening solution no.1 (Elements in red require FRP jacketing)
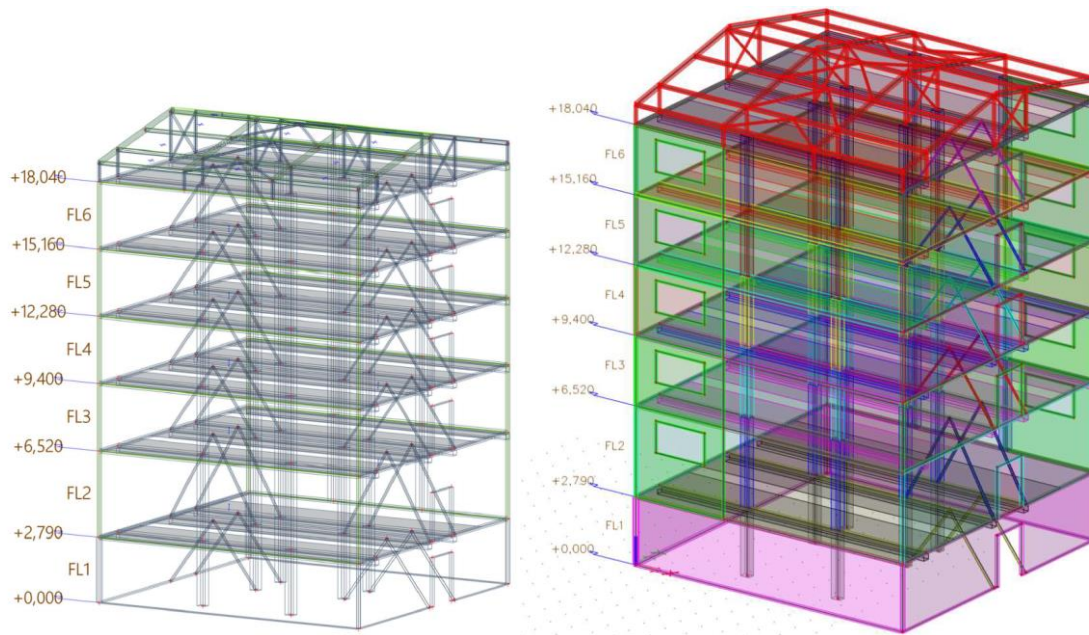
Figure 8. Strengthening solution no.2 – additional steel bracing,
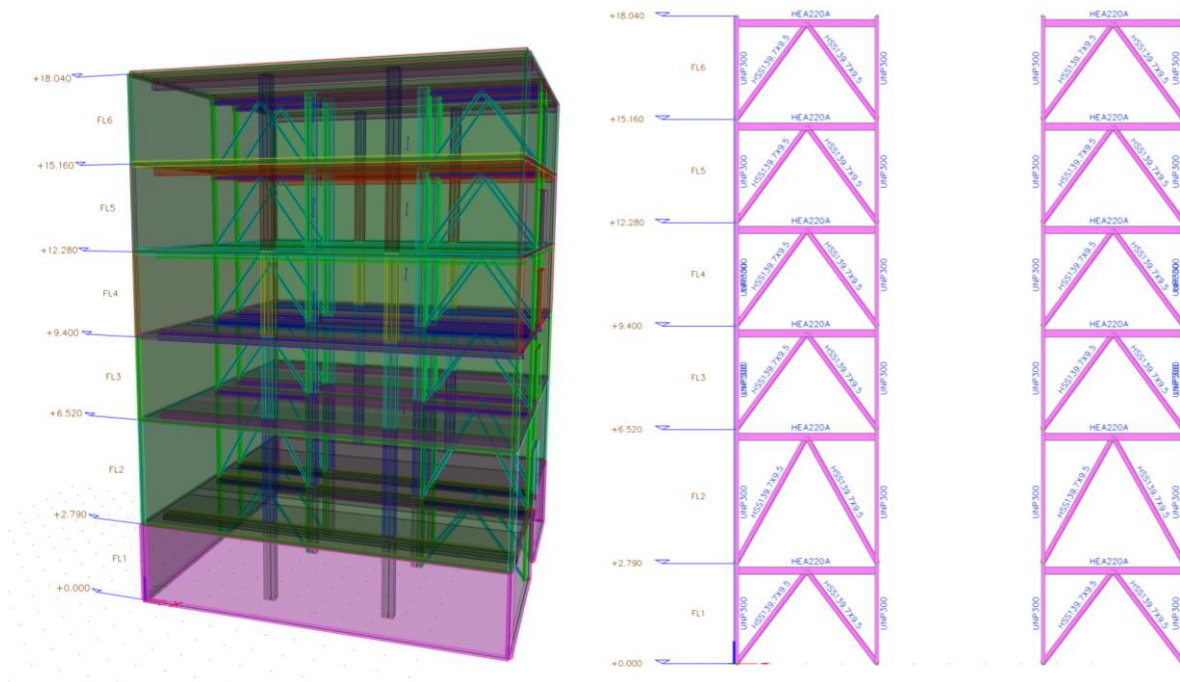
Figure 9. Strengthening solution no.4 – additional steel frames

4. Discussion and conclusions

Determining the actual seismic behavior of existing structures is of great importance for future management and the economic and purposeful strengthening of the load-bearing structure [11]. Modern software solutions and design methods are an essential part of the assessment, but they are only as useful as the input parameters are reliable [24]. So, precise information is crucial from condition assessment to FEM modelling and seismic and energy upgrading. Assessing existing buildings is always connected to many epistemic and aleatory uncertainties, and reducing them often requires extensive on-site testing. The critical aspect is knowing if gathering additional information is worthwhile. A Value of Information

(VoI) analysis is introduced to answer this question, as seen in [25]. It quantifies the expected utility or benefit increase due to additional or predicted information. It allows decision-makers to know each assessment's benefits before deciding while maximizing the utility.

The integrated nZEB refurbishment approach is based on improving the building elements and systems performance. The airtight building envelope is a major requirement for the nZEB standard and is investigated by relevant measurements. When refurbishing existing buildings, a detailed investigation of the existing structure helps define the best air-tightness and heat retention systems. Building systems should be based on on-site renewable energy generation to reduce operational costs and CO_2 emissions.

It remains to be determined if the optimal nZEB solution can be implemented, as the administrative barriers have hindered the permitting procedure. The groundwater wells are located on publicly owned property, and the consent of the City of Zagreb is required to perform the investigation works for the groundwater use and later on for implementation of infrastructure works. It took many stakeholders' careful and lengthy discussions to determine the competent City Office to issue the consent. If administrative barriers remain unresolved, a less effective nZEB solution will need to be implemented, not using available on-site renewable energy to its fullest potential.

In this short overview of one case study building, the authors wanted to show the whole procedure and the complexity of the processes.

In addition to seismic upgrading, energy updating is significant, and these two approaches must be presented as integrated procedures. PDP-nZEB project is trying to show it primarily to the Croatian audience. The first part of the seismic assessment procedure is presented in this paper, together with numerical modeling based on laser scanning and the implementation of BIM. Subsequently, more complex analyzes, including the nonlinear pushover method, are performed, and the reinforcement proposals are updated accordingly. The project team has been selected, and design documentation for the specific building systems is being prepared. The design process has been documented for training designers for nZEB retrofits. The goal of this project is also to promote the nZEB standards to local governments so that the strategic value and environmental benefits of such projects are recognized, and local governments can take ownership as initiators and participants in improving the built environment.

Acknowledgments

References

[1] Mazzoni, S.; Castori, G.; Galasso, C.; Calvi, P.; Dreyer, R.; Fischer, E.; Fulco, A.; Sorrentino, L.; Wilson, J.; Penna, A. et al. 2016–2017 Central Italy Earthquake Sequence: Seismic Retrofit Policy and Effectiveness. Earthq. Spectra 2018, 34 (4), 1671–1691. https://doi.org/https://doi.org/10.1193/100717EQS197M.

[2] Bilgin, H.; Shkodrani, N.; Hysenlliu, M.; Baytan Ozmen, H.; Isik, E.; Harirchian, E. Damage and Performance Evaluation of Masonry Buildings Constructed in 1970s during the 2019 Albania Earthquakes. Eng. Fail. Anal. 2022, 131, 105824. https://doi.org/10.1016/J.ENGFAILANAL.2021.105824.

[3] Sarhosis, V.; Giarlelis, C.; Karakostas, C.; Smyrou, E.; Bal, I. E.; Valkaniotis, S.; Ganas, A. Observations from the March 2021 Thessaly Earthquakes: An Earthquake Engineering Perspective for Masonry Structures. Bull. Earthq. Eng. 2022, 20 (10), 5483–5515. https://doi.org/10.1007/S10518-022-01416-W/FIGURES/29.

[4] Papadimitriou, P.; Kapetanidis, V.; Karakonstantis, A.; Spingos, I.; Kassaras, I.; Sakkas, V.; Kouskouna, V.; Karatzetzou, A.; Pavlou, K.; Kaviris, G.; et al. First Results on the Mw=6.9 Samos Earthquake of 30 October 2020. Bull. Geol. Soc. Greece 2020. https://doi.org/10.12681/bgsg.25359.

[5] Stepinac, M.; Lourenço, P. B.; Atalić, J.; Kišiček, T.; Uroš, M.; Baniček, M.; Šavor Novak, M. Damage Classification of Residential Buildings in Historical Downtown after the ML5.5 Earthquake in Zagreb, Croatia in 2020. Int. J. Disaster Risk Reduct. 2021, 56, 102140. https://doi.org/https://doi.org/10.1016/j.ijdrr.2021.102140.

[6] Novak, M. Š.; Uroš, M.; Atalić, J.; Herak, M.; Demšić, M.; Baniček, M.; Lazarević, D.; Bijelić, N.; Crnogorac, M.; Todorić, M. Zagreb Earthquake of 22 March 2020 – Preliminary Report on Seismologic Aspects and Damage to Buildings. Gradjevinar 2020. https://doi.org/10.14256/JCE.2966.2020.

[7] Kišiček, T.; Stepinac, M.; Renić, T.; Hafner, I.; Lulić, L. Strengthening of Masonry Walls with FRP or TRM. Gradjevinar 2020, 72 (10), 937–953. https://doi.org/10.14256/JCE.2983.2020.

[8] Pojatina, J.; Barić, D.; Anđić, D.; Bjegović, D. Structural Renovation of Residential Building in Zagreb after the 22 March 2020 Earthquake. Gradjevinar 2021, 73 (6), 633–648. https://doi.org/10.14256/JCE.3195.2021.

[9] Salaman, A.; Stepinac, M.; Matorić, I.; Klasić, M. Post-Earthquake Condition Assessment and Seismic Upgrading Strategies for a Heritage-Protected School in Petrinja, Croatia. Build. 2022, Vol. 12, Page 2263 2022, 12 (12), 2263. https://doi.org/10.3390/BUILDINGS12122263.

[10] Atalić, J., Krolo, J., Damjanović, D., Uroš, M., Sigmund, Z., Šavor Novak, M., Hak, S., Korlaet, L., Košćak, J., Duvnjak, I., Bartolac, M., Serdar, M., Dokoza, I., Prekupec, F., Oreb, J., Mušterić, B.: Studija Za Saniranje Posljedica Potresa, I-VII F.

[11] Stepinac, M.; Skokandić, D.; Ožić, K.; Zidar, M.; Vajdić, M. Condition Assessment and Seismic Upgrading Strategy of RC Structures—A Case Study of a Public Institution in Croatia. Buildings 2022, 12 (9), 1489. https://doi.org/10.3390/buildings12091489.

[12] Šavor Novak, M.; Uroš, M.; Atalić, J.; Herak, M.; Demšić, M.; Baniček, M.; Lazarević, D.; Bijelić, N.; Crnogorac, M.; Todorić, M. Potres u Zagrebu 22 . Ožujka 2020 . - Preliminarni Izvještaj o Seizmološkim Istraživanjima i Oštećenjima Zgrada. 2020, 72, 843–867.

[13] Uroš, M.; Atalić, J.; Demšić, M.; Šavor Novak, Marta Baniček, M.; Pilipović, A.; Jevtić Rundek, R. Damage to Masonry Buildings after Petrinja Mw 6.4 Earthquake in 2020. In Proceedings of the 3rd european conference on Earthquake engineering and seismology; Bucharest, 2022; pp 273–282.

[14] Uroš, M.; Šavor Novak, M.; Atalić, J.; Sigmund, Z.; Baniček, M.; Demšić, M.; Hak, S. Procjena Oštećenja Građevina Nakon Potresa - Postupak Provođenja Pregleda Zgrada. Građevinar 2020, 72 (12), 1089–1115.

[15] Uroš, M.; Demšić, M.; Baniček, M.; Pilipović, A. Seismic Retrofitting of Dual Structural Systems—A Case Study of an Educational Building in Croatia. Buildings 2023, 13 (2), 292. https://doi.org/10.3390/buildings13020292.

[16] Predari, G.; Stefanini, L.; Marinković, M.; Stepinac, M.; Brzev, S. Adriseismic Methodology for Expeditious Seismic Assessment of Unreinforced Masonry Buildings. Buildings 2023, 13 (2), 344. https://doi.org/10.3390/buildings13020344.

[17] Vlašić, A.; Srbić, M.; Skokandić, D.; Mandić Ivanković, A. Post-Earthquake Rapid Damage Assessment of Road Bridges in Glina County. Buildings 2022, 12 (1), 42. https://doi.org/10.3390/buildings12010042.

[18] Milovanovic, B.; Bagaric, M.; Gaši, M.; Stepinac, M. Energy Renovation of the Multi-Residential Historic Building after the Zagreb Earthquake - Case Study. Case Stud. Therm. Eng. 2022, 38 (July). https://doi.org/10.1016/j.csite.2022.102300.

[19] EEA Project, Https://Www.Nzebcentar.Hr/Nzeb-Trening-Centar/.

[20] EN 1998-1. Eurocode 8: Design of Structures for Earthquake Resistance—Part 1: General Rules, Seismic Actions and Rules for Buildings. Eur. Comm. Norm. Brussels 2004. https://doi.org/[Authority: The European Union per Regulation 305/2011, Directive 98/34/EC, Directive 2004/18/EC].

[21] Funari, M. F.; Mehrotra, A.; Lourenço, P. B. A Tool for the Rapid Seismic Assessment of Historic Masonry Structures Based on Limit Analysis Optimisation and Rocking Dynamics. Appl. Sci. 2021, 11 (3). https://doi.org/10.3390/app11030942.

[22] Funari, M. F.; Silva, L. C.; Mousavian, E.; Lourenço, P. B. Real-Time Structural Stability of Domes through Limit Analysis: Application to St. Peter's Dome. Int. J. Archit. Herit. 2021, 1–23. https://doi.org/10.1080/15583058.2021.1992539.

[23] Stepinac, M.; Kisicek, T.; Renić, T.; Hafner, I.; Bedon, C. Methods for the Assessment of Critical Properties in Existing Masonry Structures under Seismic Loads-the ARES Project. Appl. Sci. 2020, 10 (5). https://doi.org/10.3390/app10051576.

[24] Colombo, C.; Savalle, N.; Mehrotra, A.; Funari, M. F.; Lourenço, P. B. Experimental, Numerical and Analytical Investigations of Masonry Corners: Influence of the Horizontal Pseudo-Static Load Orientation. Constr. Build. Mater. 2022, 344, 127969. https://doi.org/10.1016/j.conbuildmat.2022.127969.

[25] Ožić, K.; Skejić, D.; Lukačević, I.; Stepinac, M. Value of Information Analysis for the Post-Earthquake Assessment of Existing Masonry Structures—Case Studies. Buildings 2023, 13 (1), 144. https://doi.org/10.3390/buildings13010144.

POSSIBLITIES OF USING UHPC AS A REPAIR MATERIAL

Antonija Ocelić [(1)], Ana Baričević [(2)], Marina Frančić Smrkić[(3)]

[(1)] *PhD student, University of Zagreb, Faculty of Civil Engineering, antonija.ocelic@grad.unizg.hr*
[(2)] *Associate Professor, University of Zagreb, Faculty of Civil Engineering, ana.baricevic@grad.unizg.hr*
[(3)] *Assistant Professor, University of Zagreb, Faculty of Civil Engineering, marina.francic.smrkic@grad.unizg.hr*

Abstract

More and more buildings need to be repaired and strengthened, both for durability and for the effects of natural disasters such as earthquakes. The repair material should ensure compatibility with the substructure materials and contribute to their improvement. The continuous development of materials has led to their excellent properties and application possibilities. In addition, the new generation of materials offers more environmentally friendly solutions, which is certainly in line with repair as part of sustainable development. In an effort to meet all these requirements, the use of mortars with exceptional properties and environmental efficiency can be the key to solving repair works.

Materials such as ultra-high performance concrete (UHPC) are characterised by exceptional mechanical and durability properties. In its usual composition, it contains large amounts of cement, which can be reduced by using waste materials to improve its environmental performance. One of the properties of UHPC worth highlighting is its toughness, which is achieved through the use of fibres that ensure a cement composite with ductile behaviour. Therefore, this paper presents a general overview of UHPC and the possibility of its application as a repair material. The evaluation of UHPC as a repair material is based on the studies carried out. These are divided into tests of interfacial properties, which include bond strength, microstructure, and permeability. The influence of additional cementitious materials on the interfacial microstructure is presented. Finally, the importance of fibres and the potential self-healing effect of UHPC in repair are highlighted and opportunities for new studies are identified.

Keywords: repair, ultra-high performance concrete, waste materials, fibres, self-healing, interface microstructure

1. Introduction

There is an increasing need for the repair of concrete structures built in the 20th century, as well as newly constructed structures that are deteriorating rapidly due to adverse effects of weathering and mechanical loads [1]. These negative influences include freeze-thaw cycles, de-icing salts, marine influences, and increased live loads, all of which cause serious deterioration of concrete structures [2]. This raises the question for civil engineers of how to rehabilitate, retrofit, and maintain these structures in an efficient and cost-effective manner [2]. Although many repair materials have been developed, such as high flow concrete, resin-based repair mortar and concrete, polymer-modified mortar and concrete, etc., and many different repair techniques, such as patching, overlaying, spraying, and pressure grouting, it is devastating that nearly half of all concrete repair systems fail in use [3]. However, to ensure a successful repair, two factors must be considered: a suitable repair material and good adhesion of the repair interface [4]. The weakest zone in the repair system is the interface between the repair material and the concrete substrate [1], [4], [5]. It is important to mention that this bond, i.e. the bond between the substrate and the repair material, depends on some factors that can be divided into the surface condition of the substrate, the curing process, the compaction method, the use of binders, the age of the chemical bonds and the mechanical properties of the material [6].

As mentioned earlier, the challenge in repair systems is to find a durable and efficient repair material. One possible solution to this challenge lies in ultra-high performance concrete (UHPC). With its excellent mechanical and durability properties, UHPC offers many advantages in the rehabilitation of

concrete structures. These advantages include shorter rehabilitation times and longer service life and durability of the structures, so that sustainable construction can be achieved with a minimum of intervention and maintenance [7]. On the other hand, there are also some challenges in using UHPC as a rehabilitation material, such as interfacial adhesion and interaction with the subgrade [8]. Therefore, most of the studies [1]–[4], [6], [8]–[24] on the use of UHPC in repair works are concerned with the interfacial properties and adhesion.

In this paper, the possibilities of using UHPC are presented based on a brief general overview of UHPC and the studies found evaluating UHPC as a repair material in cementitious composites.

2. UHPC in general

UHPC represents a new generation of cementitious materials with improved strength, ductility, and durability [25], with compressive strength greater than 100 MPa and tensile strength greater than 15 MPa [26]. Due to its durability, it is resistant to acids and alkalis [27]. As for the name, it is important to point out that it is not concrete but mortar, since it does not contain large aggregates and the name concrete is due to the presence of steel fibres in the usual composition [25]. The main principles for the production of ultra-high performance concrete are to reduce porosity, improve microstructure, improve homogeneity, and increase toughness [28]. Thus, the reduction of porosity is the reason for the high durable properties of UHPC [29] and is achieved by compacted composition and reduction of water-cement ratio (0,15-0,25) [30] using superplasticizers [28], [31]. Reducing the size of the aggregate leads to a homogeneous microstructure, i.e. a reduction in the size of the cracks and a more similar zone of the interface and the cement matrix [28], [31], [32]. To improve the toughness properties, fibres are added, which also increase the impact strength [28], [32]. Since the usual composition of UHPC contains large amounts of cement (800-1000 kg/m^3), the unfavorable environmental impact of UHPC production is highlighted, as the estimated CO_2 emissions from cement account for 7% of global CO_2 emissions [33]. Therefore, the use of supplementary cementitous materials, i.e. industrial by-products, is emphasised [33], [34]. UHPC can be used in structural and non-structural applications. In the structural field it allows the production of smaller, lighter and thinner elements, while the non-structural application is in the field of repairs, improving the properties of the repaired parts with less maintenance [25].

3. Evaluation of UHPC as a repair material

3.1 Application of UHPC in repair

With its excellent properties mentioned above, UHPC is particularly suitable for the rehabilitation or repair of concrete structures in the form of an overlay [19], [24] and offers the possibility of thinner surface layers, which reduce the self-weight of the structure and improve structural efficiency [16], [17]. Due to its resistance to weathering, chemical treatment and mechanical loads typical for bridge decks, it is a particularly suitable material for bridge decks [13], [17], but also for the lateral and lower bridge elements [13]. In addition to rehabilitation, the application of a UHPC overlay to existing or new structures represents a potential for modification [2]. In the study [35], UHPC was used as a repair material for repairing lock walls because they need frequent repair due to their exposure to ship impact and UHPC is a material that can dissipate more energy during impact loads compared to normal strength concrete (NSC) [29].

To ensure monolithic behavior of the repaired system, a strong and durable bond is required [19]. Although there is a major modulus mismatch between UHPC and NSC that can cause local stress concentrations at the interface, leading to a reduction in strength, the bond properties also depend on the microstructure of the interface, creep and shrinkage of the repair materials, etc [4]. The

incompatibility of two materials, i.e., non-uniform expansion and shrinkage, cause stress concentrations at the interface and thus delamination of the interface (Figure 1) [5]. Therefore, UHPC has a denser microstructure at the interface between UHPC and substrate and lower creep and drying shrinkage, which makes it a promising material for improving bond strength [4].
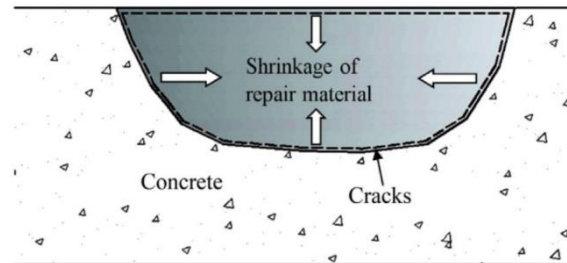
Figure 1 Schematic representation of the shrinkage of repair materials in patch repair [5]

3.2 Testing interface properties

Various test methods are available to evaluate the bond strength between two concrete materials, which can be divided into three categories depending on the stress state: Tension (splitting, direct tension, pull-off), shear (L-shaped shear, direct shear, bi-surface shear), combined shear and compression (slant shear) [4]. Of the test methods listed, only the pull-off test is the standard test for evaluating adhesion strength [8]. Adhesive bond evaluation is also the main study in the found papers/articles on UHPC for rehabilitation works, as shown in Table 1, where the substrate material was normal strength concrete (NSC). It can be seen that the most commonly performed tests are pull-off, splitting tensile and slant shear tests. The reason for the pull-off test, apart from being the only standard test, is that it can be done in situ [20]. However, some studies [8], [22] have highlighted the unsuitability of these test methods for evaluating the bond strength of interface. In [22], a new test method has been developed, namely the debonding test, which ensures debonding failure at the interface and has been shown to be a suitable solution to the problems of other test methods, such as user influences and sensitivity to eccentricity. On the other hand, [8] has pointed out that the slant-shear test is the most suitable of all test methods to evaluate bond performance, since complex loading conditions occur in the actual overlay application of UHPC material.

Table 1 Studies on the bond propertis of UHPC as a repair material

Studied interface properties			Bond parameters
Mechanical	Durability	Microstructure	
Pull-off [8], [12], [15], [20]–[22] Spiltting tensile [2]–[4], [8], [10], [12], [17], [19]–[21] Slant-shear [2]–[4], [6], [8], [10], [12], [17], [19], [21] Indirect tensile [22] Direct tensile [19] Push-off [16] Modified pull-off [22] Third-point flexure [6] Direct shear [6] Bi-surface shear [8], [13] Double-sided shear [11] Single-side shear [24]	Gas permeability [3] Rapid chloride permeability [2], [3] Water permeability [3]	SEM-EDS [15], [20] SEM [2], [3] BSE-EDX [4] BSE [24]	Surface roughness [8], [10]–[13], [16]–[21] Moisture degree [11], [12], [19] UHPC age [11], [19] Curing conditions [11], [19] Substrate strength [4], [11], [19] Bonding agent [13], [19] Expansive agent [11], [19] Age of composite [12] Stress state of the interface [11] Interface shear reinforcement [16] Mechanical connector [13] Formwork influence [15]

As shown in Table 1, some studies have also investigated durability properties and interface microstructure, and some have included bonding parameters to evaluate all of these bonding properties. Testing permeability properties is especially important for repaired concretes, as the presence of degraded chemicals through the adhesive joints can cause irreversible damage to the structure [1]. The bond parameters considered in most studies are substrate properties: surface roughness, moisture degree, and strength. This was to be expected, since surface preparation is the key to effective adhesion [9] and the properties of the repair are highly dependent on the nature of the substrate surface [17]. Also in [19], the test results have shown that the surface roughness, the degree of moisture and the strength of the substrate are the most important factors affecting the interfacial adhesion, with higher strength, suitable roughness preparation and complete moisture of the substrate ensuring reliable bond performance. This was also confirmed in [22], where the test results showed excellent adhesion between UHPC and substrate with proper surface preparation and no binder. On the other hand, UHPC has shown good bond with old concrete in [20], regardless of surface roughness. This can be partially confirmed in [12], where the importance of adequate wetting of the substrate is emphasized, since then the roughness of the surface of the substrate is not decisive in ensuring a good bond. The influence of the saturated surface of the substrate on the improvement of bond strength described in [12] can be explained by the fact that UHPC is a material with a low w/c ratio, containing a large amount of non-hydrated particles that can be hydrated by the substrate and generate hydration products in the transition zone, creating cohesion between the two materials during the curing time. The addition of binders has been shown to increase adhesion on smooth substrate surfaces, while weakening it on rough substrate surfaces [13], [19]. It is worth noting that these bond parameters, such as surface roughness, depend on the test methods used, i.e. it has no influence in the case of the pull-off test, while in other test methods, such as the split tensile and shear tests, surface preparation plays a role [21]. In the case of the pull-off test , the insensitivity of the test to the surface preparation parameters can be explained by the effect of a stronger chemical bond than the effect of the mechanical bond on interfacial adhesion [21].

The adequate bond performance of UHPC for a wide range of surface conditions was demonstrated by test results in [17], while also in [3], [10] UHPC overlays showed excellent bond quality in split tensile test, with most of the failure modes caused by the NSC substrate, indicating a higher bond strength between UHPC and NSC substrate than the strength of NSC. Concrete repaired with UHPC is stronger by a factor of two compared to concrete substrate repaired with NSC [13]. The slant shear test results also showed a strong bond between UHPC and NSC substrate, as the failure of the interface occurred after the substrate was damaged [3]. In terms of permeability properties, UHPC shows high resistance to degradation processes such as the penetration of carbon dioxide, chloride, sulfate, etc., which was also confirmed when UHPC was used as an overlay in [23]. The durability tests (capillary absorption, air/gas permeability, freeze-thaw resistance, chloride penetration) have shown that the quality of the interfacial composite can withstand severe environmental conditions [23]. This was also proved in [2], where the results of the rapid chloride test confirmed the low permeability of UHPC, resulting in higher chloride resistance of the composite, so the better mechanical bond between UHPC and NSC substrate could improve the chloride resistance of the composite, resulting in longer service life of the repaired structures (Figure 2). As for the interface microstructure, the SEM /EDS results showed that UHPC improves the microstructure by forming a C-S-H gel that fills the voids, resulting in a dense, strong and uniform composite bond [20].
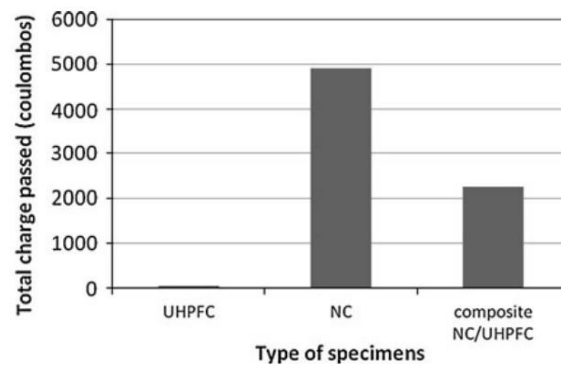
Figure 2 Comparison of the rapid chloride permeability [2]

3.2 Economic aspects

In addition to bond strength, service life and economic aspects are also decisive in assessing the suitability of repair systems for concrete rehabilitation. For example, in [36], the service life of concrete structures in chloride-stressed environments repaired with UHPC was calculated. The results show that the service life increases by 7 to 9 times when a UHPC layer is applied [36]. In another study [14], the effect of UHPC as a repair material on the service life of the repaired system was investigated based on the time required for chloride ions to reach the surface of the reinforcement. In this case, the service life was also extended, by 5 to 10 times, depending on the environment (Table 2).

Table 2 Comparison of the protective layer of UHPC and NSC based on service life [14]

Chloride Concentration (C_0) (kg/m³)	Protective Layer Material	Protective Layer Thickness (cm)	$t_{critical}$ (years)
10	UHPC	2	31
		5	140
	NSC	2	6
		5	19
20	UHPC	2	21
		5	95
	NSC	2	4
		5	13
30	UHPC	2	17
		5	80
	NSC	2	3
		5	11

3.3 Fibre influence

Steel fibres have been shown to increase the bond strength of the repaired system through a "dowel effect" [5], [24]. On the other hand, repair materials with steel fibres ensure the toughness properties of the repaired system compared to ordinary cement-based repair materials. However, other types of fibres, such as polypropylene fibres, have been shown to improve the bond strength and contribute to the anti-cracking effect [5]. Another study [35], in which a lock wall was repaired with UHPC and the behaviour of the repaired system after one year showed that UHPC was firmly bonded to the structure due to the

anchoring effect of the fibres (Figure 3). In this case, the fibres were metal fibres with a diameter of 0.2 mm and a length of 13 mm.
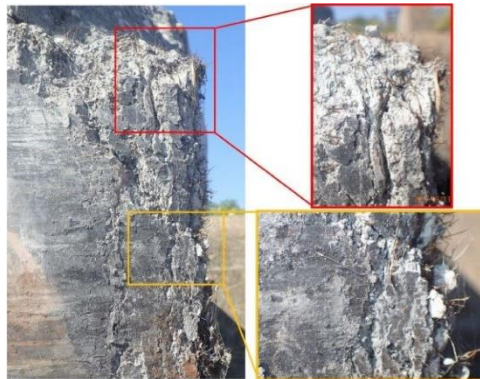
Figure 3 UHPC repair layer after one year [35]

In general, fibre-reinforced cementitious composites meet all the requirements demanded of a repair material, i.e. impermeability to aggressive liquids and gases, adequate bonding to the substrate and ensuring structural integrity, durability and resistance to severe environmental conditions, and compatibility with the substrate concrete [37]. Apart from these few studies, the exact influence of fibres on the properties of the repair interface when using UHPC repair material has not yet been found, so this is a potential that needs to be investigated.

3.4 Cementitous materials influence

As mentioned earlier, it is not only the mechanical properties that affect the bonding between two materials, but also the chemical properties. Therefore, some studies [2]–[4], [15], [20], [24] have investigated the microstructure of the UHPC/substrate interface. The usual composition of UHPC contains silica fume, which refines the pore system of the transition zone, making it dense and uniform. It alsoprovides stronger bonding through the reaction of the contained silica (SiO_2) with the $Ca(OH)_2$ of the substrate, forming a C-S-H gel [21]. This was confirmed by SEM-EDS test results showing the influence of silica fume from UHPC in generating C-S-H gel products at the interface reacting with $Ca(OH)_2$, but also the possibility of a secondary reaction with the $Ca(OH)_2$ to further improve the microstructure of the transition zone and thus increase the bond strength [4]. The reaction of silica fume in UHPC with the $Ca(OH)_2$ in the substrate in the formation of C-S-H gel was also confirmed in [24], due to the lower Ca/Si ratio of the UHPC-NSC interface, as shown in the results of EDS. SEM Images of UHPC-NSC interface have shown very good interlocking of UHPC with NSC, leading to strong bonding and consequently efficient repair [2], [3]. Since UHPC contains a large amount of unhydrated particles, exposure to freeze-thaw cycles could favour the hydration of these particles at the interface and in this way also improve cohesion [12]. When using UHPC, there is always the possibility of creating an eco-UHPC that is also suitable for use as a repair material. This was done in the study [15], where 50% limestone filler was used for UHPC repair material. In this way, the use of supplementary cementitious materials in repair UHPC materials reduces CO_2 emissions and production costs. However, with the exception of [15], no studies on UHPC with waste materials, i.e. cementitious materials, were found. This opens new possibilities in the study of UHPC in repair works.

3.5 Self-healing effect

In the study [15], another important property of UHPC materials was briefly investigated. This is autogenous self-healing, which is defined as the process that occurs when materials recover themselves after damage [38], [39]. In the case of UHPCs, which contain a significant amount of unhydrated cementitious materials, self-healing is expected to be an efficient process for autogenous self-healing when continued hydration is considered [38]. In [15], among other tests conducted to test UHPC as a

repair material, self-healing effectiveness was also investigated, which showed limited healing, with only cracks smaller than 50 µm being completely healed. However, the potential for self-healing was highlighted due to the high content of unhydrated cement and limestone particles, which could be further improved by a more efficient curing process [15].
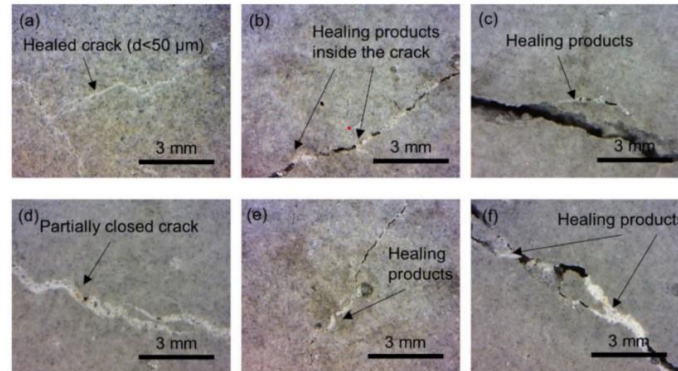
Figure 4 Self-healing of surface cracks on the UHPC layer: a) completely healed cracks; b)-f) partially healed cracks [15]

In this way, self-healing is a valuable property of UHPC that should also be investigated in the case of UHPC repair material, as it could further reduce the costs and improve durability and service life along with supplementary cementitious materials and fibres.

4. Conclusion

UHPC has demonstrated its potential as a material for future repair work due to its mechanical properties and permeability. In this paper, a brief overview of the most important of these properties that are and could be important for rehabilitation works is presented. Most studies investigated the bond strength when using UHPC as a repair material for NSC substrates, and the results showed very good or excellent interfacial adhesion in most cases. For better adhesion, different adhesion parameters were investigated, and different test methods were used depending on the stress of the repaired system, of which the pull-off test is a standard method. Since most failure modes occur in the substrate material, this emphasises a strong mechanical and chemical bond between UHPC and substrate. From the studies found, there is a lack of further studies to understand this chemical bond, i.e., the microstructure of the interface and the potential that the materials in UHPC offer in creating this bond. In this sense, there is also the possibility to investigate the use of other supplementary cementitious materials in the composition of UHPC repair materials. On the other hand, few studies have investigated the effect of fibres on interfacial adhesion, which also opens new opportunities for using other types of fibres and improving the microstructure of the interface, as well as providing mechanical bonds as an anchoring effect. Finally, abundant cement and supplementary cementitious materials in the composition of UHPC always provide the possibility of a self-healing effect, for which there is a lack of studies on repair materials.

Acknowledgements

References

[1]   W. L. Baloch, H. Siad, M. Lachemi, and M. Sahmaran, "A review on the durability of concrete-to-concrete

bond in recent rehabilitated structures," *J. Build. Eng.*, vol. 44, no. September, p. 103315, 2021, doi: 10.1016/j.jobe.2021.103315.

[2]   B. A. Tayeh, B. H. Abu Bakar, and M. A. Megat Johari, "Characterization of the interfacial bond between old concrete substrate and ultra high performance fiber concrete repair composite," *Mater. Struct. Constr.*, vol. 46, no. 5, pp. 743–753, 2013, doi: 10.1617/s11527-012-9931-1.

[3]   B. A. Tayeh, B. H. Abu Bakar, M. A. Megat Johari, and Y. L. Voo, "Mechanical and permeability properties of the interface between normal concrete substrate and ultra high performance fiber concrete overlay," *Constr. Build. Mater.*, vol. 36, pp. 538–548, 2012, doi: 10.1016/j.conbuildmat.2012.06.013.

[4]   S. Feng, H. Xiao, and H. Li, "Comparative studies of the effect of ultrahigh-performance concrete and normal concrete as repair materials on interfacial bond properties and microstructure," *Eng. Struct.*, vol. 222, no. January, p. 111122, 2020, doi: 10.1016/j.engstruct.2020.111122.

[5]   X. Song *et al.*, "Cement-Based Repair Materials and the Interface with Concrete Substrates: Characterization, Evaluation and Improvement," *Polymers (Basel).*, vol. 14, no. 7, 2022, doi: 10.3390/polym14071485.

[6]   M. Farzad, M. Shafieifar, and A. Azizinamini, "Experimental and numerical study on bond strength between conventional concrete and Ultra High-Performance Concrete (UHPC)," *Eng. Struct.*, vol. 186, no. December 2018, pp. 297–305, 2019, doi: 10.1016/j.engstruct.2019.02.030.

[7]   B. A. Tayeh, B. H. Abu Bakar, M. A. Megat Johari, and Y. L. Voo, "Utilization of ultra-high performance fibre concrete (UHPFC) for rehabilitation a review," *Procedia Eng.*, vol. 54, no. April 2014, pp. 525–538, 2013, doi: 10.1016/j.proeng.2013.03.048.

[8]   D. K. Harris, M. A. Carbonell Muñoz, A. Gheitasi, T. M. Ahlborn, and S. V. Rush, "The challenges related to interface bond characterization of ultra-high-performance concrete with implications for bridge rehabilitation practices," *Adv. Civ. Eng. Mater.*, vol. 4, no. 2, pp. 75–101, 2015, doi: 10.1520/ACEM20140034.

[9]   A. Ibrahim, B. Farouk, and S. I. Haruna, "Evaluation of Bond Strength between Ultra-High-Performance Concrete and Normal Strength Concrete: An Overview," *J. Kejuruter.*, vol. 32, no. 3, pp. 397–407, 2020, doi: 10.17576/jkukm-2020-32(3)-04.

[10]   B. A. Tayeh, B. H. Abu Bakar, M. A. Megat Johari, and Y. L. Voo, "Evaluation of bond strength between normal concrete substrate and ultra high performance fiber concrete as a repair material," *Procedia Eng.*, vol. 54, no. Farhat 2010, pp. 554–563, 2013, doi: 10.1016/j.proeng.2013.03.050.

[11]   Y. Zhang, C. Zhang, Y. Zhu, J. Cao, and X. Shao, "An experimental study: various influence factors affecting interfacial shear performance of UHPC-NSC," *Constr. Build. Mater.*, vol. 236, p. 117480, 2020, doi: 10.1016/j.conbuildmat.2019.117480.

[12]   M. A. Carbonell Muñoz, D. K. Harris, T. M. Ahlborn, and D. C. Froster, "Bond Performance between Ultrahigh-Performance Concrete and Normal-Strength Concrete," *J. Mater. Civ. Eng.*, vol. 26, no. 8, pp. 1–10, 2014, doi: 10.1061/(asce)mt.1943-5533.0000890.

[13]   A. Valikhani, A. J. Jahromi, I. M. Mantawy, and A. Azizinamini, "Experimental evaluation of concrete-to-UHPC bond strength with correlation to surface roughness for repair application," *Constr. Build. Mater.*, vol. 238, p. 117753, 2020, doi: 10.1016/j.conbuildmat.2019.117753.

[14]   M. Farzad, A. Sadeghnejad, S. Rastkar, A. Moshkforoush, and A. Azizinamini, "A theoretical analysis of mechanical and durability enhancement of circular reinforced concrete columns repaired with UHPC," *Eng. Struct.*, vol. 209, no. June, p. 109928, 2020, doi: 10.1016/j.engstruct.2019.109928.

[15]   A. Kothari, M. Rajczakowska, T. Buasiri, K. Habermehl-Cwirzen, and A. Cwirzen, "Eco-uhpc as repair material—bond strength, interfacial transition zone and effects of formwork type," *Materials (Basel).*, vol. 13, no. 24, pp. 1–19, 2020, doi: 10.3390/ma13245778.

[16]   S. Sharma, V. S. Ronanki, S. Aaleti, and P. Okumus, "Experimental Investigation of Surface Preparation on Normal and Ultrahigh-Performance Concrete Interface Behavior," *J. Bridg. Eng.*, vol. 26, no. 4, pp. 1–13, 2021, doi: 10.1061/(asce)be.1943-5592.0001697.

[17]   D. K. Harris, J. Sarkar, and T. T. M. Ahlborn, "Characterization of interface bond of ultra-high-performance concrete bridge deck overlays," *Transp. Res. Rec.*, no. 2240, pp. 40–49, 2011, doi:

10.3141/2240-07.

[18]   A. Valikhani, A. J. Jahromi, I. M. Mantawy, and A. Azizinamini, "Numerical modelling of concrete-to-UHPC bond strength," *Materials (Basel).*, vol. 13, no. 6, pp. 26–29, 2020, doi: 10.3390/ma13061379.

[19]   Y. Zhang, P. Zhu, Z. Liao, and L. Wang, "Interfacial bond properties between normal strength concrete substrate and ultra-high performance concrete as a repair material," *Constr. Build. Mater.*, vol. 235, p. 117431, 2020, doi: 10.1016/j.conbuildmat.2019.117431.

[20]   B. A. Tayeh, B. H. Abu Bakar, M. A. Megat Johari, and A. M. Zeyad, "Microstructural analysis of the adhesion mechanism between old concrete substrate and UHPFC," *J. Adhes. Sci. Technol.*, vol. 28, no. 18, pp. 1846–1864, 2014, doi: 10.1080/01694243.2014.925386.

[21]   B. A. Tayeh, B. H. A. Bakar, M. A. M. Johari, and M. M. Ratnam, "The relationship between substrate roughness parameters and bond strength of ultra high-performance fiber concrete," *J. Adhes. Sci. Technol.*, vol. 27, no. 16, pp. 1790–1810, 2013, doi: 10.1080/01694243.2012.761543.

[22]   M. Valipour and K. H. Khayat, "Debonding test method to evaluate bond strength between UHPC and concrete substrate," *Mater. Struct. Constr.*, vol. 53, no. 1, pp. 1–10, 2020, doi: 10.1617/s11527-020-1446-6.

[23]   Y. Huang, S. Grünewald, E. Schlangen, and M. Luković, "Strengthening of concrete structures with ultra high performance fiber reinforced concrete (UHPFRC): A critical review," *Constr. Build. Mater.*, vol. 336, no. September 2021, 2022, doi: 10.1016/j.conbuildmat.2022.127398.

[24]   S. Feng, H. Xiao, R. Liu, and M. Liu, "Single-Side Shear Bond Strength and OTZ Microstructure of UHPC Repair Materials with Concrete Substrate," *J. Mater. Civ. Eng.*, vol. 34, no. 9, pp. 1–15, 2022, doi: 10.1061/(asce)mt.1943-5533.0004360.

[25]   N. M. Azmee and N. Shafiq, "Ultra-high performance concrete: From fundamental to applications," *Case Stud. Constr. Mater.*, vol. 9, 2018, doi: 10.1016/j.cscm.2018.e00197.

[26]   R. Pernicova, D. Dobias, and T. Mandlík, "Mechanical properties of UHPC with different kinds of glass fibres," *Proc. Int. Conf. FIBRE Concr.*, vol. 2015-Janua, pp. 353–359, 2015.

[27]   S. R. Rosseli *et al.*, "Ultra High-Performance Concrete as Alternative Repair Method: A Review," *J. Fail. Anal. Prev.*, vol. 21, no. 6, pp. 2072–2080, 2021, doi: 10.1007/s11668-021-01296-3.

[28]   C. Shi, Z. Wu, J. Xiao, D. Wang, Z. Huang, and Z. Fang, "A review on ultra high performance concrete: Part I. Raw materials and mixture design," *Constr. Build. Mater.*, vol. 101, pp. 741–751, 2015, doi: 10.1016/j.conbuildmat.2015.10.088.

[29]   S. Abbas, M. L. Nehdi, and M. A. Saleem, "Ultra-High Performance Concrete: Mechanical Performance, Durability, Sustainability and Implementation Challenges," *Int. J. Concr. Struct. Mater.*, vol. 10, no. 3, pp. 271–295, 2016, doi: 10.1007/s40069-016-0157-4.

[30]   J. Du *et al.*, "New development of ultra-high-performance concrete (UHPC)," *Compos. Part B Eng.*, vol. 224, no. August, p. 109220, 2021, doi: 10.1016/j.compositesb.2021.109220.

[31]   O. Mishra and S. P. Singh, "An overview of microstructural and material properties of ultra-high-performance concrete," *J. Sustain. Cem. Mater.*, vol. 8, no. 2, pp. 97–143, 2019, doi: 10.1080/21650373.2018.1564398.

[32]   Shweta Mishra, "Reviewing Some Properties of Ultra High Performance Concrete," *Int. J. Eng. Res.*, vol. V9, no. 06, pp. 108–121, 2020, doi: 10.17577/ijertv9is060156.

[33]   M. A. Hamad *et al.*, "Production of ultra-high-performance concrete with low energy consumption and carbon footprint using supplementary cementitious materials instead of silica fume: A review," *Energies*, vol. 14, no. 24, pp. 1–26, 2021, doi: 10.3390/en14248291.

[34]   R. Yu, Q. Song, X. Wang, Z. Zhang, Z. Shui, and H. J. H. Brouwers, "Sustainable development of Ultra-High Performance Fibre Reinforced Concrete (UHPFRC): Towards to an optimized concrete matrix and efficient fibre application," *J. Clean. Prod.*, vol. 162, pp. 220–233, 2017, doi: 10.1016/j.jclepro.2017.06.017.

[35]   A. Maltais, N. Petrov, M. Thibault, and B. Bissonnette, "UHPFRC for concrete repair," *MATEC Web Conf.*, vol. 199, pp. 1–8, 2018, doi: 10.1051/matecconf/201819907007.

[36] C. P. Gu, W. Sun, L. P. Guo, and Q. N. Wang, "Ultrahigh performance concrete: A potential material for sustainable marine construction in view of the service life," *Appl. Mech. Mater.*, vol. 438–439, no. October, pp. 108–112, 2013, doi: 10.4028/www.scientific.net/AMM.438-439.108.

[37] N. Banthia, C. Zanotti, and M. Sappakittipakorn, "Sustainable fiber reinforced concrete for repair applications," *Constr. Build. Mater.*, vol. 67, no. PART C, pp. 405–412, 2014, doi: 10.1016/j.conbuildmat.2013.12.073.

[38] M. Rajczakowska, L. Nilsson, K. Habermehl-Cwirzen, H. Hedlund, and A. Cwirzen, "Does a high amount of unhydrated Portland cement ensure an effective autogenous self-healing of mortar?," *Materials (Basel).*, vol. 12, no. 20, 2019, doi: 10.3390/ma12203298.

[39] E. Cuenca and L. Ferrara, "Self-healing capacity of fiber reinforced cementitious composites. State of the art and perspectives," *KSCE J. Civ. Eng.*, vol. 21, no. 7, pp. 2777–2789, 2017, doi: 10.1007/s12205-017-0939-5.

RETROFIT OF MASONRY BUILDINGS WITH CRM - *COMPOSITE REINFORCED MORTAR* - SYSTEM: PRACTICAL DESIGN CONSIDERATIONS ABOUT SEISMIC CAPACITY

Mr Allen Dudine [1], Ms Alessia Bez [1], Mr Mihel Bosankić [2], Mr Pierpaolo Turri [1]

[1] *Fibre Net S.p.a., Via Jacopo Stellini, 3 - Z.I.U., 33050 Pavia di Udine (UD), Italy*
[2] *Röfix d.o.o., Ulica Lusci br. 3, HR-10294 Pojatno, Croatia*

Abstract

Ancient masonry buildings are characterized often by a high seismic vulnerability: innovative intervention strategies for strengthening, based on the use of FRP composite materials are gradually spreading. In particular, the coupling of FRP preformed elements (meshes, angles and connectors) with mortar layers (*Composite Reinforced Mortar* techniques - CRM) evidenced a good physical, chemical and mechanical compatibility with the historical masonry and experimental campaigns proved to be effective for the enhancement of both in-plane and out-of-plane performances of masonry, contrasting the opening of cracks and improving both resistance and ductility. The resistant mechanisms that are created in CRM reinforced masonry walls subjected to in-plane horizontal actions are analyzed in the paper and a practical design approach to evaluate their performances is illustrated, evidencing the dominant collapse mode at the varying of the masonry characteristics. Some masonry walls are analyzed numerically and analytically, as "case study".

Keywords: CRM Reinforcement, existing masonry structures, full-scale experimental test, Composite structures, Glass fibre reinforcement.

1. Introduction

Masonry is one of the most widespread structural systems in Europe for ancient buildings. This principally due to an easy constructions process and due to the availability of materials involved. Since many of these buildings have been realized in the past century, seismic actions have not been considered in the design and, for this reason, structures are dangerously inadequate to resist seismic events. Typical structural weaknesses that can be observed in existing structures are poor lime mortar in masonry joints, irregular or multi-leaf masonry, lack of keying between perpendicular walls or between walls and ceilings and the absence of story diaphragms. The current design challenge is to find a way to make existing structure seismically safer and reduce these deficiencies.

An innovative strengthening technique is the application of the CRM System, namely *Composite Reinforced Mortar*. This system consists of a coupling of FRP preformed elements and a mortar layer. As a first important benefit, the application of this reinforcement allows to reach very high levels of resistance and ductility, often with a negligible impact on the structure stiffness. Furthermore, the system can be effective even when applied on one side only, and for this reason the intervention does not require occupant to move out of their buildings and can represent an effective solution for the ancient structures with architectural or monumental restrictions. To investigate the behaviour of this technology, several studies have been carried out on the CRM System. Gattesco N., Boem I. (2017): Characterization tests of GFRM coating as a strengthening technique for masonry buildings. *Composite Structures*, vol. **165**, 39-52, doi: 10.1016/j.compositesb.2017.07.006.) [1] have carried out several test on CRM elements, to understand the behaviour of the system individually. Moreover, shear compression tests, diagonal compression tests and bending tests on reinforced masonry elements have been developed experimentally and then studied numerically in Gattesco N., Boem I. (2017): Out-of-plane behavior of reinforced masonry walls: Experimental and numerical study. *Composites Part B*, vol. **128**, 209-222, doi: 10.1016/j.compstruct.2017.01.043. [2] and Boem I., Gattesco N. (2021): Rehabilitation of Masonry Buildings with Fibre Reinforced Mortar: Practical Design Considerations

Concerning Seismic Resistance. *Key Engineering Materials*, vol. **898**, 1-7, doi: 10.4028/www.scientific.net/KEM.898.1. [3]. Among all studies, an experimental and numerical analysis on a full-scale masonry building test is missing.

In the present paper, the recent findings about experimental tests on masonry elements (Gattesco N., Rizzi E., Bez A., Dudine A. (2022). Out-of-plane behavior of reinforced masonry walls: Experimental and numerical study, *XIX ANIDIS Conference, Seismic Engineering in Italy*, Turin, Italy. [4]) and on a full-scale test on a masonry building (Gattesco N., Rizzi E., Facconi L., Minelli F., Dudine A. (2022). Investigating the effectiveness of a CRM system: full scale reverse cyclic tests on a two-storey rubblestone masonry building, *XIX ANIDIS Conference, Seismic Engineering in Italy*, Turin, Italy. [5]) are reported. Moreover, several considerations on design approach and an overview of the case studies will be reported.

2. CRM System

The Composite Reinforced Mortar system is a modern reinforcement technology. Modern means that FRP technologies and reinforced mortars replaced the traditional materials like steel and concrete. The modern technologies have the aim to provide the same or better performance with cleaner and faster realization (and lower environmental impact). This system is particularly compatible with masonry.

The reinforcement system consists of a GFRP mesh embedded in a mortar layer. The GFRP (Glass Fiber Reinforced Polimer) mesh is a pre-formed grid composed by horizontal parallel fibers and vertical twisted fibers wires (Fig. 1a), spaced 33 mm, 66 mm or 99 mm. The mortar layer is normally 30-50 mm thick, and it is constituted by a hydraulic lime-based mortar (with a tensile strength determined based on the existing masonry strength). The mortar coating is made effective with a mixed mechanism, by means of adhesiveness and the presence of GFRP connectors.
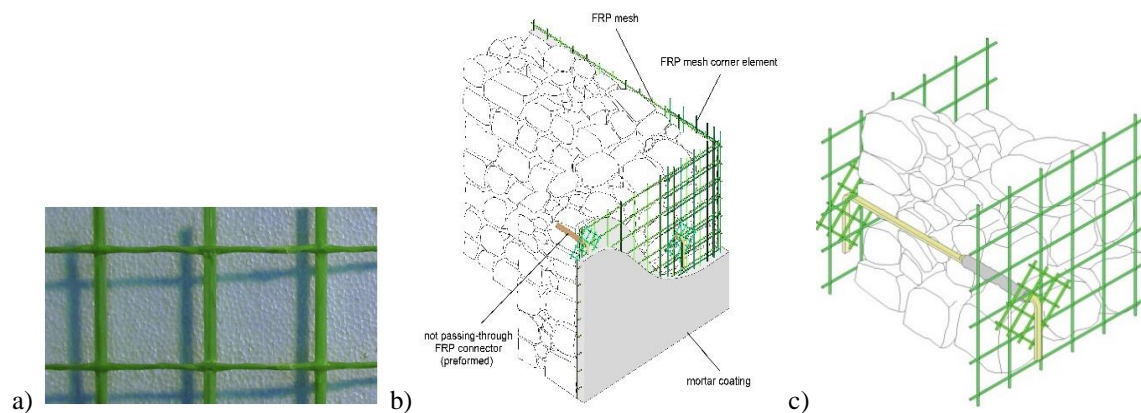
Figure 1. a) GFRP mesh detail (weft wires in vertical direction and warp wires in horizontal direction); b) Fibre Net system application on one side and c) on two sides.

The phases of the system application are briefly reported:

1. Preliminary study of the masonry in its existing conditions (geometry and materials);
2. Removal of eventual existing plasters and scarification of the surface, with high-pressure cleaner;
3. Wetting the masonry surface;
4. Initial stretch coat laying. Under certain conditions, the coat layer is scratched (depending on the conditions of the wall support and mortar characteristics);
5. Prepare the holes for the connectors. The holes, from the diameter of approx. 12 mm, must cross the entire thickness of the masonry so that the two connectors are inserted: a long connector and a short connector. The connectors must overlap inside the hole;
6. Placement of the mesh and insertion of the connectors. In correspondence of the connectors, a stress distributor device must be placed. The stress distributors consist in a GFRP mesh sheet.

7. Placement of the mesh on the other side of the wall, resin injection in the enlarged zone of the hole. Placement of the other stress distributor device and the connector;
8. Application of the mortar coating after the complete hardening of the injected resin, in one or more subsequent layers. The mesh must be placed in the middle of the thickness;
9. Placement of finishing layer and, after the maturing, the paintings and final coverings.

The CRM application allows to achieve higher resistance, because of the mesh which provides tensile strength (otherwise quite low in the unreinforced masonry). Moreover, the system guarantees higher ductility. In fact, the mesh has the capability to confine the cracks and limit their opening.

3. Experimental Campaign

Within the CONSTRAIN project, several experimental tests have been carried out to learn more about the CRM system. As a first step, several tests have been carried out on masonry specimens, on the mortar used for strengthening, on the GFRP mesh in order to investigate on single materials.

3.1 Materials

The stone masonry specimens were realized with rubble limestone blocks. Simple Compression tests carried out on some samples provided average values for the Young's modulus and the compressive strength equal to $E_{masonry}$ = 1074 MPa and $f_{c,masonry}$ = 2.48 MPa, respectively. The experimental tests provided an average compressive strength of the mortar equal to $f_{c,mortar}$ = 0.93 MPa and an average tensile strength of $f_{t,mortar}$ = 0.17 MPa. The brick masonry tests provided $E_{masonry}$ = 2183 MPa and $f_{c,masonry}$ = 6.43 MPa for the double leaves specimens, $E_{masonry}$ = 2341 MPa and $f_{c,masonry}$ = 6.70 MPa for the single leaf specimens.

For the reinforcement, a regular 66x66 mm^2 pattern of the square shape GFRP mesh has been installed. The single parallel wire has a cross section of 11.6 mm^2 and the twisted wire has a cross section of 8.9 mm^2. The GFRP mesh has an average Young's modulus $E_{bar} \geq 25$ GPa, an ultimate characteristic tensile resistance $F_{ub,bar}$ = 4.3 kN and an ultimate tensile strain $\varepsilon_{u,bar}$ = 1.45%. The 30 mm thick mortar coating is based on natural hydraulic lime and has an elastic modulus $E_{mortar} \leq 10$ GPa and a compressive strength at 28 days ageing ≥ 15 MPa. Six L-shaped GFRP elements connectors per m^2 have been placed. Their average ultimate tensile resistance $F_{ub,conn}$ = 21 kN and an average Young's modulus E_{conn} = 21.4 GPa. The distribution GFRP mesh sheets (150x150 mm^2 with mesh dimension 33x33mm^2) have been placed in correspondence of the connectors. Diatons have been also placed, by drilling a 50mm diameter hole and by positioning a steel threaded bar M16, injected with high strength thixotropic mortar.

3.2 Test on Masonry Specimen

Several tests have been made on masonry elements, piers and spandrels, to characterize the behaviour of the entire system. An overview of all the tests carried out is reported below.

Table 1 – Experimental tests overview

Test	Specimen dimension	Masonry type	Reinforcement
Shear compression test on piers	B = 1.50 m H = 1.96 m T = 0.35 m	Double leaves stone masonry - DLSM	NO CRM on one side CRM on two sides
	B = 1.50 m H = 1.96 m T = 0.25 m	Double leaves brick masonry - DLBM	NO CRM on one side CRM on two sides
		Single leaf brick masonry - SLBM	NO CRM on one side
Out-of-plane bending tests on piers	B = 1.03 m H = 2.48 m T = 0.35 m	Single leaf brick masonry	CRM on one side
	B = 1.03 m	Double leaves brick masonry	CRM on one side

| H = 2.48 m T = 0.25 m | Double leaves stone masonry | CRM on one side |

3.2.1 Shear Compression Test

Each specimen was laid over a reinforced concrete element, which is rigidly bounded to the floor. A second reinforced concrete element was placed on the top of the masonry specimens and connected to the steel beam, able to apply both vertical and horizontal forces to the masonry walls. During the tests the out-of-plane displacements were avoided by proper restrain. Firstly, a vertical compression was applied, in order to simulate the loads from the floors (and after that maintained constant during the test). Then, the horizontal force at the top of the specimens was applied to obtain a quasi-static response. The force was varied cyclically in a displacement-controlled test protocol.

Comparing top displacement - applied force trend for the different specimens can give a useful evaluation of the upgrade in resistance provided by the *CRM System*. The trends obtained for the different masonry specimen are reported in Fig. 3.
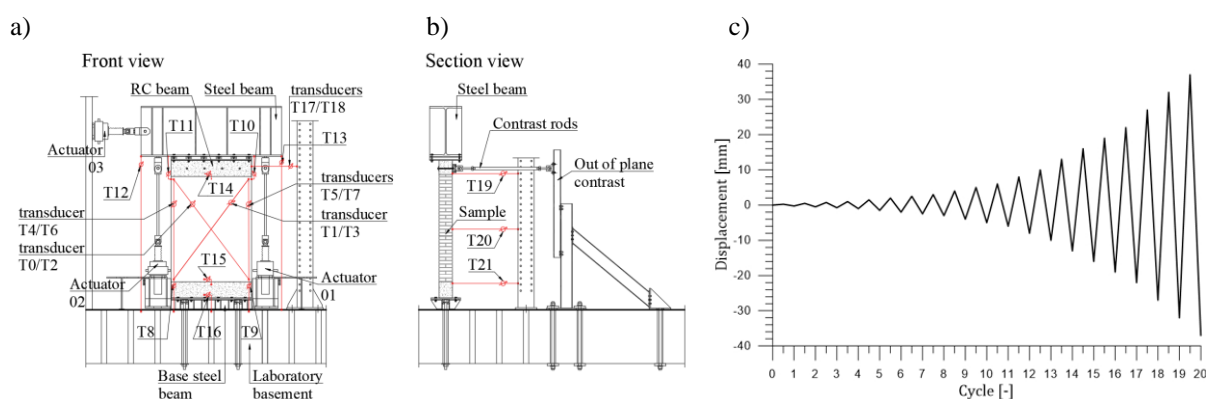
Figure 2. a) Front view of the test setup; b) section view and c) example of a loading time history.
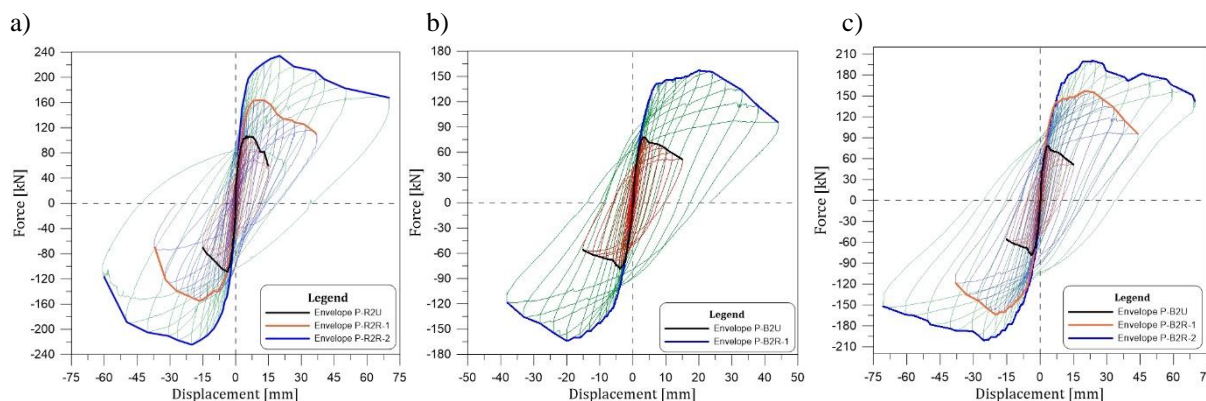
Figure 3. a) Force-displacement trends for DLSM; b) for SLBM; c) for DLBM

Table 2 - Experimental test main results for the shear compression test

Sample	Peak resistance [kN]	Drift at peak resistance [%]	Ultimate Drift [%]
Rubblestone - Unreinforced	107.8	0.24	0.75
Rubblestone – Reinforced on one side	159.5	0.66	1.76
Rubblestone - Reinforced on two sides	229.4	0.99	3.01
Single leaf Brick - Unreinforced	101.9	0.32	0.91
Single leaf Brick – Reinforced on one side	166.4	0.7	1.558
Double leaves Brick - Unreinforced	78.3	0.19	15.03
Double leaves Brick – Reinforced on one side	160.5	1.04	41.12

Sample	Peak resistance [kN]	Drift at peak resistance [%]	Ultimate Drift [%]
Double leaves Brick – Reinforced on two sides	201.1	1.24	70.21

a)   b)   c)   d)   e)
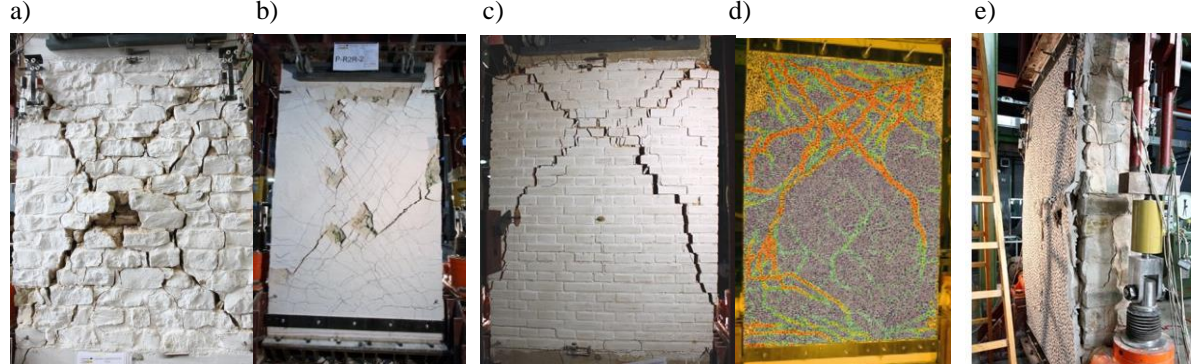
Figure 4. Stone masonry specimen at the end of the shear compression test on unreinforced (a) and reinforced (b) side; brick masonry specimen on the unreinforced (c) and reinforced side (d); detachment of the coating (e)

3.2.2 Out of plane Bending Test

Once again in these tests, the specimens were laid over a reinforced concrete element, which was rigidly bounded to the floor both in vertical and in horizontal directions. A second reinforced concrete element was placed on the top of the masonry specimens and connected to the steel structure of the setup structure. Three-point bending tests were carried out by applying a horizontal force at the mid-height section of the specimen and by varying it cyclically in a displacement-controlled test protocol, until a certain damage was reached in the unreinforced side of the wall. The test was then pursued monotonically until failure of the reinforced side. The test setup is reported in Fig.5.

a)   b)   c)
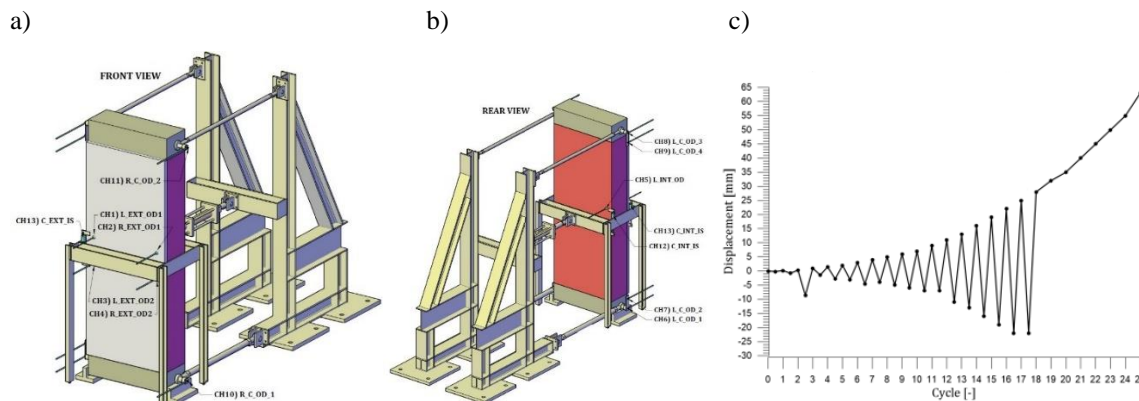
Figure 5. a) Front view of the test setup; b) rear view and c) example of a loading time history.

Comparing top displacement - applied force trend for the unreinforced and reinforced specimens can give a useful evaluation of the upgrade in resistance provided by the *CRM System*. The trends obtained in the different cases are reported in Fig. 5.

Table 3 - Experimental test main results for the three-point bending test

Sample	P_{cr} [kN]	$P_{u(R)}$ [kN]	M_{cr} [kNm]	M_u [kNm]	M_u/M_{cr} [-]	d_{cr} [mm]	d_u [mm]	d_u/d_{cr}
Rubblestone – Double leaves	6.5	52.0	4.4	35.5	8.01	2.81	63.0	22.41
Brick – Single leaf	3.4	35.1	2.3	24.0	10.36	4.31	58.6	13.59
Brick – Double leaves	3.4	29.0	2.3	19.8	8.50	3.13	44.5	14.23

a)   b)   c)
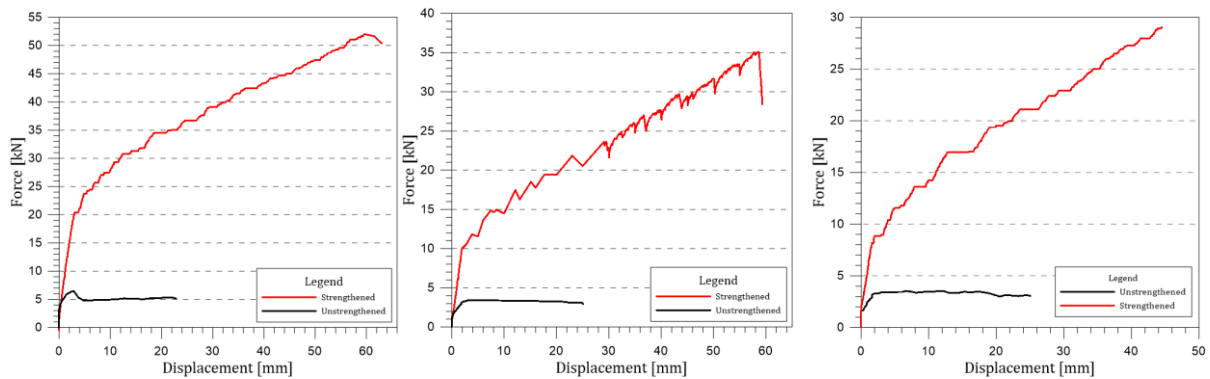
Figure 5. a) Force-displacement trends for rubblestone masonry specimen (unreinforced, reinforced on one side and on two sides); b) Force-displacement trends for single leaf brick masonry specimen (unreinforced, and reinforced on one side); c) Force-displacement trends for double leaves brick masonry specimen (unreinforced, reinforced on one side and on two sides)
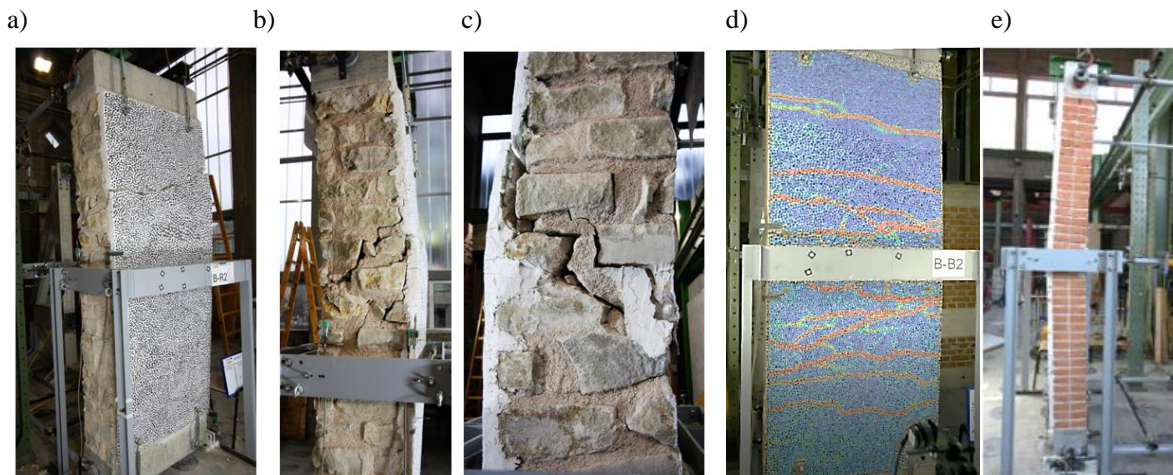
Figure 6. Stone masonry specimen at the end of the bending test on reinforced side (a); detail of the cracks on the specimen (b), (c); brick masonry specimen on the reinforced side (d) and lateral side (e)

3.3 Test on Pilot Building

To conclude the campaign, two experimental tests have been carried on a full-scale building. The structure consists of two-story stone masonry building, composed of four walls (referred to as North, West, South, and East wall), a wooden floor and an ordinary wooden gabled roof. The in-plane dimensions are 5.75 m x 4.35 m, the total height is 6.733 m. The positioning of the openings was design to have different piers aspect ratio, in order to have both shear and flexural collapse mechanisms. During the construction the materials involved were tested and characterized. As can be noted from Fig.7, the loading was applied in the plane of West and East walls (North-South direction) at the first and second story levels, through a vertical stiff steel device connected to the actuator. Load was applied proportionally to the floor mass of every floor level. Vertical loads were applied at floor levels through concrete blocks (first floor) and clay bricks (roof). The structure was strengthened with the *CRM System* on the external side. The reinforcement system was composed by: GFRP mesh with 66x66 mm^2 grid dimension; 30÷40 mm thick mortar coating, L-shaped connectors (4/m^2), 16 mm diameter steel bar which represents the artificial diatons (fixed with thixotropic cement-based mortar and set in the number of 2/m^2); 8 mm steel bars with a fixed spacing had the aim to connect the coating to the concrete foundation.

The behaviors in terms of Base Shear - 2nd story av. lateral displacement are reported below.

733

a)   b)
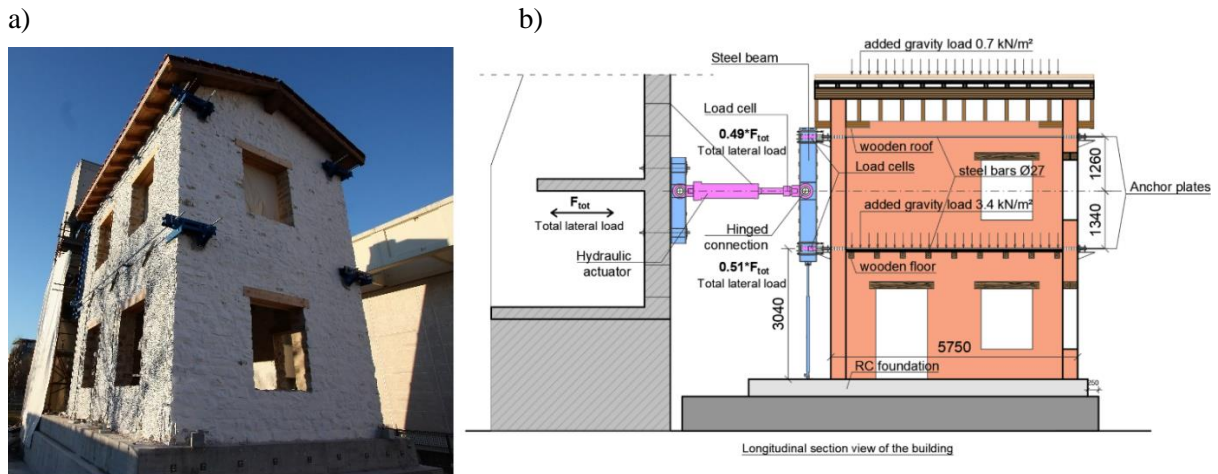
Figure 7. North-East view of the Pilot Building (a); Test setup (b)

The experimental tests give the following results. The crack pattern at the end of the two tests on the East Walls are reported in Fig.9.
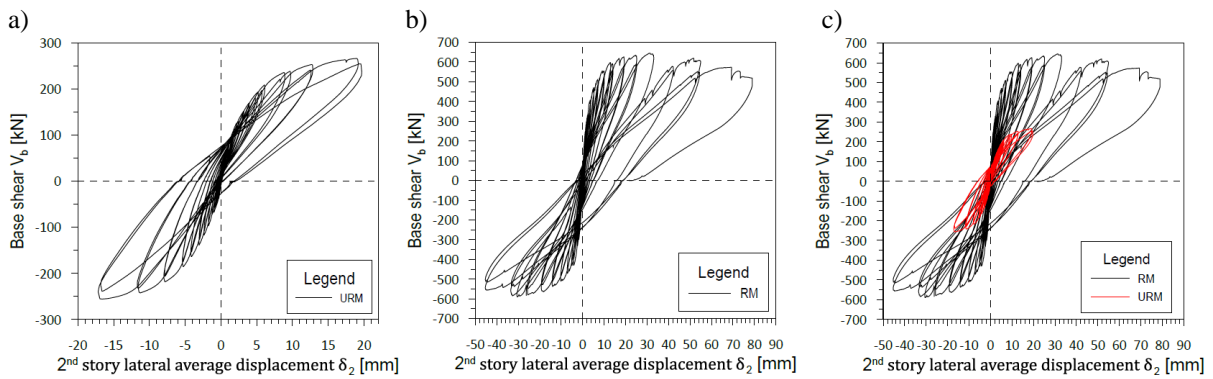
Figure 8. Base Shear – 2nd story displacement curves for the unreinforced building (a), reinforced building (b) and comparison between reinforced and unreinforced behaviors (c)

Table 4 - Experimental test main results for the three-point bending test

Sample	Load direction	$V_{b,max}$ [kN]	$\delta_{2,max}$ [mm]	$\gamma_{2,max}$ [%]
Unreinforced Building	Positive	267	19.68	0.35%
	Negative	256	17.17	0.30%
Reinforced Building	Positive	645	78.95	1.55%
	Negative	590	45.35	0.89%

a)   b)
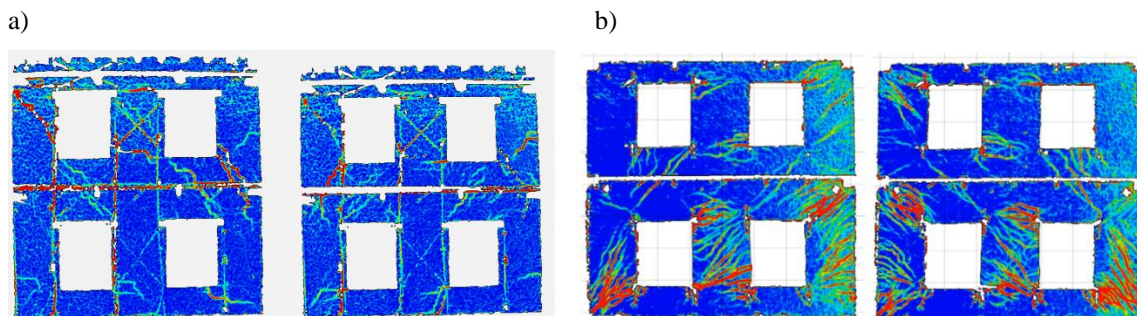
Figure 9. Crack pattern on the East wall loaded in negative and positive direction for the unreinforced building (a) and reinforced building (b)

4. Design Formulas

In order to evaluate the improvement provided by the reinforcement system in the practical design, a correct formulation to be used can be the one contained in the CNR DT 215/18 [6]. The relations can be related to the ones valid for the reinforced concrete or the reinforced masonry.
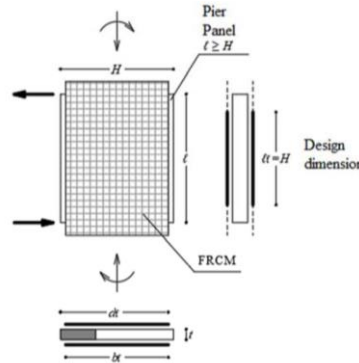
Figure 10. Scheme of a reinforced pier according to [6].

Three cases are considered for the bending resistance of the piers: i) compressive crushing on the compressive edge ($\varepsilon_m = \varepsilon_{mu}$), ii) tensile fracture of mesh ($\varepsilon_f = \varepsilon_{fd}$) and non-linear stress distribution in compression ($\bar{\varepsilon}_m \leq \varepsilon_m \leq \varepsilon_{mu}$), and iii) tensile fracture of mesh ($\varepsilon_f = \varepsilon_{fd}$) and linear stress distribution in compression ($\varepsilon_m \leq \overline{\varepsilon_m}$). The solution is the lowest of the three cases.

For the case i), failure due to compressive crushing of masonry, the equations are:

$$M_{Rd}(N_{Sd}) = f_{md} \cdot \frac{t \cdot y_n}{2} \cdot \left[H \cdot (1-k) - y_n \cdot (1-k)^2 + k \cdot \left(\frac{H}{2} - y_n + \frac{2}{3} \cdot k \cdot y_n \right) \right] + \frac{\varepsilon_{mu}}{y_n} \cdot E_f \cdot t_{2f} \frac{(d_f - y_n)^2}{12} \cdot (2 \cdot y_n + 4 \cdot d_f - 3 \cdot H)$$

(1)

$$k = \frac{\bar{\varepsilon}_m}{\varepsilon_{mu}}$$

(2)

$$y_n = \frac{N_{Sd} - E_f \cdot t_{2f} \cdot d_f \cdot \varepsilon_{mu} + \sqrt{N_{Sd}^2 + E_f \cdot t_{2f} \cdot d_f \cdot \varepsilon_{mu} [(2-k)t \cdot d_f \cdot f_{md} - 2N_{Sd}]}}{t \cdot f_{md}(2-k) - E_f \cdot t_{2f} \cdot \varepsilon_{mu}}$$

(3)

For case ii), failure due to tensile fracture of mesh ($\varepsilon_f = \varepsilon_{fd}$) and non-linear stress distribution in compression ($\bar{\varepsilon}_m \leq \varepsilon_m \leq \varepsilon_{mu}$) the equations are:

$$M_{Rd}(N_{Sd}) = f_{md} \cdot \frac{t}{12} \cdot \left[2 \cdot d_f \cdot y_n \cdot \xi \cdot (2 \cdot \xi + 3) + 3 \cdot H \cdot [y_n \cdot (2+\xi) - \xi \cdot d_f] - 2 \cdot y_n^2 \cdot (\xi^2 + 3 + 3 \cdot \xi) - 3 \cdot \xi^2 \cdot d_f^2 \right] + \varepsilon_{fd} \cdot E_f \cdot t_{2f} \frac{d_f - y_n}{12} (2 \cdot y_n + 4 \cdot d_f - 3H)$$

(4)

$$\xi = \bar{\varepsilon}_m / \varepsilon_{fd}$$

(5)

$$y_n = \frac{2 \cdot N_{Sd} + t \cdot \xi \cdot f_{md} \cdot d_f + E_f \cdot t_{2f} \cdot d_f \cdot \varepsilon_{fd}}{t \cdot f_{md}(2+\xi) + E_f \cdot t_{2f} \cdot \varepsilon_{fd}}$$

(6)

Finally, for case iii), tensile fracture of mesh ($\varepsilon_f = \varepsilon_{fd}$) and linear stress distribution in compression ($\varepsilon_m \leq \overline{\varepsilon_m}$) the equations are:

$$M_{Rd}(N_{Sd}) = \frac{t \cdot E_m \cdot \varepsilon_{fd}}{12} \cdot \frac{y_n^2}{d_f - y_n} (3 \cdot H - 2 \cdot y_n) + \varepsilon_{fd} \cdot E_f \cdot t_{2f} \frac{d_f - y_n}{12} (2 \cdot y_n + 4 \cdot d_f - 3 \cdot H)$$

(7)

$$y_n = \frac{N_{Sd} + E_f \cdot t_{2f} \cdot d_f \cdot \varepsilon_{fd} - \sqrt{N_{Sd}^2 + E_m \cdot \varepsilon_{fd} \cdot d_f \cdot t \cdot (E_f \cdot t_{2f} \cdot d_f \cdot \varepsilon_{fd} + 2N_{Sd})}}{\varepsilon_{fd} \cdot (E_f \cdot t_{2f} - t \cdot E_m)}$$

(8)

For the definition of quantities, it can be useful to refer to the standard. For the shear resistance, the standard refers to the Turnšek - Čačovič formulation as follows:

$$V_{Rd(CRM)} = \frac{1.5 \cdot \tau_{0(R)} \cdot b \cdot t}{\alpha} \cdot \sqrt{\left(1 + \frac{\sigma_0}{1.5 \cdot \tau_{0(R)}}\right)} \tag{9}$$

where $\tau_{0(R)}$ is the equivalent resistance value that takes into account also the reinforced coating:

$$\tau_{0(R)} = \beta \cdot \left(\tau_{0(U)} + m \cdot \frac{t_c}{t} \cdot \frac{f_{t,c}}{1.5}\right) \tag{10}$$

The last part of the project will concern the validation of the analytical formulas proposed by CNR DT 215/2018 [1] with the results obtained in the ongoing experimental tests.

5. Conclusions

The present paper had the principal aim to give an overview of the experimental tests carried out during the project CONSTRAIN, to better understand the role of the CRM System in existing masonry structures. The reinforcement guarantees very good performance, increasing both resistance and ductility. As a practical design advice, the relations to be used are reported in the paper, these relations provided consistent results with the experimental findings. All these considerations can be very useful to further improve the CRM System.

Acknowledgements

References

[1] Gattesco N., Boem I. (2017): Characterization tests of GFRM coating as a strengthening technique for masonry buildings. *Composite Structures*, vol. **165**, 39-52, doi: 10.1016/j.compositesb.2017.07.006.

[2] Gattesco N., Boem I. (2017): Out-of-plane behavior of reinforced masonry walls: Experimental and numerical study. *Composites Part B*, vol. **128**, 209-222, doi: 10.1016/j.compstruct.2017.01.043.

[3] Boem I., Gattesco N. (2021): Rehabilitation of Masonry Buildings with Fibre Reinforced Mortar: Practical Design Considerations Concerning Seismic Resistance. *Key Engineering Materials*, vol. **898**, 1-7, doi: 10.4028/www.scientific.net/KEM.898.1.

[4] Gattesco N., Rizzi E., Bez A., Dudine A. (2022). Out-of-plane behavior of reinforced masonry walls: Experimental and numerical study, *XIX ANIDIS Conference, Seismic Engineering in Italy*, Turin, Italy.

[5] Gattesco N., Rizzi E., Facconi L., Minelli F., Dudine A. (2022). Investigating the effectiveness of a CRM system: full scale reverse cyclic tests on a two-storey rubblestone masonry building, *XIX ANIDIS Conference, Seismic Engineering in Italy*, Turin, Italy.

[6] CNR DT 215/2018 (2020) 'Guide for the Design and Construction of Externally Bonded Fibre Reinforced Inorganic Matrix Systems for Strengthening Existing Structures'. National research Council, Rome, Italy.

SEISMIC RETROFITTING OF POST-WWII MID-RISE UNREINFORCED MASONRY RESIDENTIAL BUILDINGS IN THE BALKANS

Svetlana Brzev [(1)], Predrag Blagojević[(2)], and Radovan Cvetković [(3)]

[(1)] *Adjunct Professor, Department of Civil Engineering, University of British Columbia, Canada, sbrzev@mail.ubc.ca*
[(2)] *Faculty of Civil Engineering and Architecture, University of Niš, Serbia, predrag.blagojevic@gaf.ni.ac.rs*
[(3)] *Assistant Professor, Faculty of Civil Engineering and Architecture, University of Niš, Serbia, radovan@gaf.ni.ac.rs*

Abstract

There is a significant building stock of the existing low- and mid-rise unreinforced masonry (URM) buildings constructed after World War II in Serbia and neighbouring countries. Numerous buildings of this typology collapsed in the devastating 1963 Skopje, North Macedonia earthquake, causing fatalities, injuries, and property losses, and experienced damage in a few recent earthquakes in the region, including the 2010 Kraljevo, Serbia earthquake and the 2020 Petrinja, Croatia earthquake. These buildings are 3- to 5-storey high, have URM walls and rigid reinforced concrete (RC) or semi-prefabricated concrete and masonry floor slabs, usually with a RC ring beam at each floor level. The paper will provide an overview of seismic retrofitting approaches for these buildings, starting from provisions of design codes which were previously followed in Serbia and former Yugoslavia as well as Eurocode 8 (Part 3). Conventional seismic retrofitting technologies based on RC wall overlays which were applied in past earthquakes, including the 2010 Kraljevo earthquake, will be presented and their advantages and disadvantages will be discussed. Finally, a case study of a building in Kraljevo which was damaged in the 2010 earthquake and subsequently retrofitted, will be presented, including the results of seismic analysis and design solution. The paper should be of interest to engineers and academics interested in seismic retrofitting of masonry buildings.

Keywords: unreinforced masonry buildings; earthquake damage; seismic retrofitting; residential buildings.

1. Introduction

Masonry construction technology has been traditionally used for residential construction in European countries, including Serbia and the Balkan region [1,2]. Since the second half of 19th century construction of residential and public buildings in Serbia and the region has been performed using clay brick masonry. Reinforced concrete (RC) has been a technology of choice for construction of mid- and high-rise buildings since 1950s, however masonry has been widely used for low- to mid-rise residential construction in the region. According to the 2011 Census of Serbia [3], low-rise single family buildings constitute 95% of the national residential building stock, corresponding to 65.9% of all housing units. Multi-family housing accounts for only 2.6% of the housing stock in terms of the number of buildings, but the proportion is significantly higher (33%) in terms of the number of housing units. According to the Census, 72% of all residential buildings in Serbia were constructed between 1946 and 1990, when Serbia was a part of the Socialist Federal Republic of Yugoslavia (SFRY), also known as "former Yugoslavia". According to the Census, 72% of all residential buildings in Serbia were constructed between 1946 (after WWII) and 1990, when Serbia was a part of the Socialist Federal Republic of Yugoslavia (SFRY), referred to as "former Yugoslavia" in this paper (note that Croatia, Slovenia, North Macedonia, Montenegro, and Bosnia and Herzegovina were also a part of the former Yugoslavia). The majority of pre-1960 multi-family residential buildings were unreinforced masonry (URM) buildings, with load-bearing masonry walls as a structural system for resisting both gravity and lateral loads. Most of URM multi-family residential buildings of post-WWII vintage have semi-prefabricated RC floor systems. Buildings of this type constitute a significant fraction of the building stock in urban areas of Serbia and neighbouring countries and are the focus of this study. Examples of urban URM multi-family residential building from Serbia are shown in Fig. 1.

<div align="center">a)   b)</div>
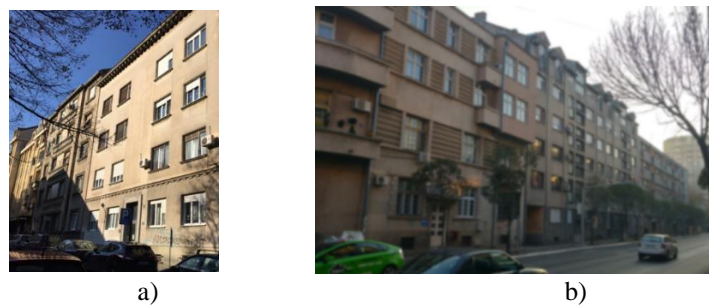
Figure 1. Examples of URM multi-family residential buildings in urban areas of Serbia: a) Belgrade and b) Niš.

Buildings of this typology were exposed to several damaging earthquakes in the region, including the 1963 Skopje, North Macedonia earthquake (M 6.0) (Fig. 2a), the 2010 Kraljevo, Serbia earthquake (M_W 5.5), and the 2020 Petrinja, Croatia earthquake (M 6.4) (Fig. 2b) [4, 5]. The buildings of this type which performed poorly in the 1963 Skopje earthquake were designed according to standardized designs, with load-bearing walls provided only in one horizontal direction (longitudinal or transverse) [6].

<div align="center">a)   b)</div>

Figure 2. Performance of URM multi-family residential buildings in past earthquakes in the region: a) a collapsed building due to the 1963 Skopje earthquake (credit: Z. Milutinović) and b) a damaged building due to the 2020 Petrinja earthquake (credit: SUZI-SAEE).

Urban areas of Serbia were not affected by major damaging earthquakes in the last 100 years, with the exception of the 2010 Kraljevo earthquake. A few other damaging earthquakes tool place in Serbia during the same period, namely the 1980 Kopaonik earthquake (M 5.8) and the 1998 Mionica earthquake (M 5.7), but they affected mostly rural areas. Consequently, design and construction experience in Serbia related to repair and seismic retrofitting of buildings in post-earthquake situations has been rather limited. The 2010 Kraljevo earthquake prompted a need for the repair and retrofitting of a significant number of damaged URM residential buildings. The main objective of the post-earthquake recovery was to restore damaged building infrastructure to its original pre-earthquake condition within a relatively short time frame and with limited financial resources. An additional constraint was to minimize the impact of construction activities on building occupants. As a result, the design and execution of seismic rehabilitation projects related to residential buildings used simple retrofitting techniques which were suitable for easy on-site implementation on a large scale. RC jacketing was selected because it was a well-established technique used for the structural strengthening of URM buildings in Serbia before the 2010 earthquake.

After the devastating 1963 Skopje earthquake, the first comprehensive seismic design code in the SFRY was published in 1964 [7]. A subsequent edition of the same code, PTN-S [8], issued in 1981, was the governing design code in Serbia until 2019. It was reported that the PTN-S code was at a similar level of advancement like other international seismic design codes at the time [9]. In 1982, deterministic seismic hazard maps for SFRY were issued as a companion to the PTN-S code, and were updated in 1987. The territory of Serbia was divided into zones VI to IX based on the MCS-64 seismic macrointensity scale. According to that map, majority of sites in Serbia, including Kraljevo, were assigned seismic zone VIII.

Eurocodes were adopted as official codes for the design, construction, and maintenance of building structures in Serbia in 2019 [10]. As a result, Eurocode 8 – Part 1 [11] (also referred to as EC8-1 in this paper) is currently applied for seismic design of new buildings (SRPS EN 1998-1/NA:2018) [12]. An official seismic hazard map for Serbia was developed for design according to Eurocode 8 [13]. According to the map, the Peak Ground Acceleration (PGA) for a rock site (a_g) for design level earthquake with 10% probability of exceedance in 50 years is largest for Southern and Central Serbia (0.25g and 0.20g respectively), while other sites in Serbia were assigned lower PGA values. For example, Kraljevo was was assigned a_g value of 0.2g. Seismic design requirements for masonry buildings for Serbian codes and a comparison with the corresponding Eurocode 8 provisions were presented elsewhere [1], [2].

The first Yugoslav design code for repair, rehabilitation, and retrofitting of existing buildings was issued in 1985 (PTN-R) [14] based on the experience gained after the 1979 Montenegro earthquake, and it had been followed in Serbia until 2019. The code addressed seismic retrofitting of masonry and RC buildings and the foundations. Eurocode 8, Part 3 [15] (also referred to as EC8-3 in this paper) has been followed for seismic assessment and retrofitting of existing buildings in Serbia since 2019 (SRPS EN 1998-3/NA:2018, 2018) [16]. Annex C of EC8-3 contains specific provisions related to masonry buildings. In addition to the PTN-R code, which was the governing code for seismic retrofitting of buildings in Serbia until 2019, all masonry structures had to be designed or evaluated according to the PTN-Z code which was issued in 1991 [17]. Similarly, Eurocode 6 (EN 1996-1-1:2004) [18], which is currently used in Serbia [19], contains design provisions for masonry buildings.

In this paper, the authors have shared lessons related to seismic retrofitting of URM buildings damaged in the 2010 Kraljevo, Serbia earthquake. Various seismic retrofitting techniques for URM buildings have been discussed, but the focus is on of RC jacketing, a common seismic retrofitting technique for URM buildings which has been used in Serbia and other countries. The authors have presented selected results of seismic analysis and retrofitting design for a typical URM building in Kraljevo, which was damaged due to the 2010 earthquake and subsequently retrofitted. A comparison of the capacity/demand ratios has been performed for the original and retrofitted building, according to both the Yugoslav seismic design and retrofit codes and Eurocode 8. The results of the study showed that the implemented retrofit solution satisfied the Yugoslav seismic code requirements, but it is not adequate according to the Eurocode 8 requirements. Findings of the paper may be particularly of interest to engineers in the Balkan countries, which recently adopted Eurocode 8 as the governing code for seismic design of new buildings and evaluation/retrofitting of existing buildings.

2. Seismic retrofitting techniques for URM buildings

2.1 Seismic retrofitting objectives and goals

Seismic retrofitting solutions should be effective in enhancing the performance of existing structures to achieve predetermined performance objectives. Performance ob-jective(s) for a specific structure are either set by a seismic design code or project-specific criteria. In some countries, technical codes/standards for existing buildings may permit relaxed seismic performance objectives for the evaluation and retrofitting of existing buildings relative to the design of new structures, e.g. ASCE/SEI 41-17 code in the USA [20]. In the context of a specific project, these performance objectives are either prescribed by the seismic codes, or they are defined by project-specific criteria. According to the PTN-R code, similar to other older seismic codes, the main performance objective for rehabilitated or strengthened buildings was same as for new structures: structural damage due to a major damaging earthquake was acceptable, but the collapse had to be avoided. On the other hand, EC8-3 contains elements of modern approaches such as Performance-Based Earthquake Engineering (PBEE), hence performance objectives have been specified by the code. For example, capacity models for assessment of existing buildings considered for the limit states "near collapse", "significant damage", and "damage limitation", as outlined in Eurocode 8.

One of the key design aspects of a seismic retrofitting project is to identify retro-fitting goal(s). After the seismic evaluation of a building is performed and the defi-ciencies have been identified, a designer should be able to determine the retrofitting goal(s). Is the main goal of the retrofitting to enhance the lateral load-resisting capacity and/or stiffness and/or ductility of the existing structure - or perhaps a combination of those structural characteristics? An appropriate seismic retrofitting solution may be selected after the goals have been established.

Retrofitting may be able to enhance lateral load-resisting capacity and/or stiffness and/or ductility of the existing structure, as shown in Fig. 3 [21]. In many cases, the primary goal of retrofitting is to enhance the ductility of the existing structure, which may be feasible for retrofitting of older RC structures (Fig. 3a). Alternatively, stiffness and capacity enhancement (Fig. 3b) may be feasible for retrofitting of an existing non-ductile structure. Stiffness, capacity, and ductility enhancement (illustrated in Fig. 3c) may be feasible for existing buildings with high seismic demand, which prompts a need for increased lateral load-resisting capacity. In the context of URM structures, it is important to note that it is unlikely for a retrofitting solution to achieve a significant increase in ductility due to the brittle nature of masonry. It is expected that a typical global retrofitting solution for a URM structure should primarily be effective in increasing its lateral load-resisting capacity. Several researchers have studied different seismic retrofitting techniques for masonry buildings and compared their effectiveness [22-25].
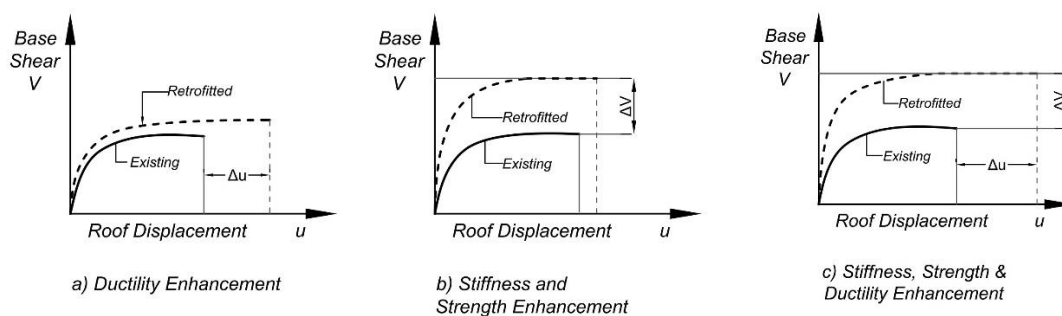
Figure 3. Seismic retrofitting goals [22].

2.2 An overview of seismic retrofitting techniques for masonry buildings

Seismic retrofitting projects in the Balkan region were initiated after the 1979 Montenegro earthquake (M 6.9), which caused damage and collapse of buildings in coastal areas of Montenegro and Croatia. Engineers and academics from all parts of the former Yugoslavia participated in the planning, design, and construction supervision of post-earthquake recovery. The earthquake also prompted a few relevant regional projects, which engaged experts from neighboring countries, such as the UNIDO-sponsored project "Building Construction Under Seismic Conditions in the Balkan Region". A series of comprehensive technical resources were produced as a result of the project, including the guidelines for seismic retrofitting of existing RC and masonry buildings [26]. Notable experimental research studies and field applications of seismic retrofitting on existing masonry buildings were performed by Prof. Miha Tomaževič and his colleagues at ZAG, Slovenia [25, 27]. Comprehensive technical guidelines have recently been developed for repair and retrofitting of masonry buildings affected by the March 2020 Zagreb, Croatia earthquake [28]. A valuable resource is available in Serbia for engineers engaged in structural and seismic rehabilitation of buildings [29].

The most common retrofitting approaches for URM structures include: i) retrofitting of existing masonry walls by means of thin overlays, ii) construction of new RC walls attached to the existing masonry walls, iii) retrofitting of intersecting wall connections, and iv) retrofitting of the existing floor and/or roof structures and the wall-to-floor connections. In some cases, retrofitting of existing foundations may also be required (when shear and/or flexural capacity of the retrofitted wall have increased as a result of the retrofit). It should be noted that approaches i) and ii) are related to enhancing lateral load-resisting capacity of individual masonry walls, while approaches iii) and iv) are related to enhancing the integrity of entire building. Since the focus of this study are URM buildings constructed

with clay brick masonry walls and rigid floor systems, it can be expected that in most cases only approaches i) and ii) need to be implemented. Approach iii) may need to be implemented in case of low-strength masonry (e.g. stone masonry structures), or when bond between the intersecting walls is inadequate (which is often the case in building expansions). Finally, approach iv) may be required in case of flexible (timber) diaphragms, or prefabricated hollow-core RC slabs. Therefore, this section is focused mostly on approaches i) and ii), with the main focus on RC jacketing as a widely used seismic retrofitting technique in the region, as well as in other parts of the world.

2.3 Common retrofitting techniques for the existing URM walls

Seismic retrofitting of URM walls is performed to enhance their in-plane and/or out-of-plane seismic capacity/resistance. As discussed in the previous section, common retrofitting techniques involve application of new coatings/overlays, which are attached/bonded to an existing masonry wall. These overlays can be classified based on their thickness into thin and thick. Thin overlays (also known as surface coatings) consist of cement-based coating reinforced with steel mesh reinforcement, which is also known as RC jacketing or reinforced plaster; alternatively, a thin coating may consist of Fiber Reinforced Polymer (FRP) strips or fabrics which are bonded to an existing wall by means of epoxy resin (or alternative). Thick overlays are in the form of new RC walls which are attached to an existing masonry wall by means of steel anchors embedded into the wall. There is no hard rule regarding the maximum thickness for thin cement-based coatings, but the thickness usually ranges from 3-8 cm, while the thickness of thick RC overlays may range from 10-30 cm.

RC jacketing technique (Fig. 4) consists of constructing one- or two-sided RC jackets attached to exterior and/or interior wall surfaces [22, 27]. A jacket consists of a 3 to 8 cm thick concrete overlay with reinforcement in the form of steel mesh (usually small-sized bars, 4 to 10 mm diameter). RC jackets are usually attached to an existing masonry wall via steel anchors inserted in pre-drilled holes, which are subsequently filled with cement- or epoxy-based grout. The required size and spacing of anchors depends on seismic demand (shear force) that needs to be transferred from the jackets to the original masonry wall. Either cast-in-place concrete or sprayed concrete (shotcrete) can be used for construction of RC jackets.
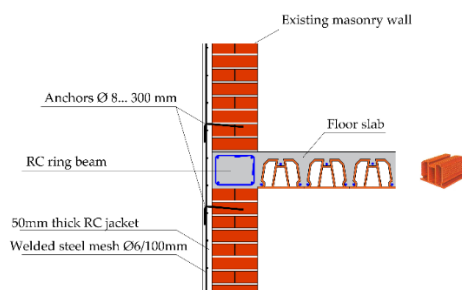
a)   b)

Figure 4. RC jacketing: a) vertical section of a retrofitted wall in Kraljevo, Serbia and b) shotcrete application in a retrofitted school building in Kyrgyzstan [22].

Several experimental research studies on masonry wall specimens subjected to monotonic and/or reversed cyclic lateral loading have shown a significant increase in the shear capacity and stiffness of URM walls retrofitted using RC jacketing [31-36]. The results confirmed that RC jacketing was able to increase lateral capacity of the specimens by a factor of 2.0 to 3.0. Specimens with two-sided jacketing showed higher ductility and energy dissipation capacity compared to one-sided jacketing. The results of extensive experimental research studies on masonry walls with RC jacketing by Prof. Miha Tomaževič in Slovenia showed an increase in shear strength by 1.3 to 3.6 for retrofitted walls [27]. A research study involving shaking table testing of a four-storey masonry building model retrofitted with RC jacketing was performed at IZIIS, Skopje [37].

Seismic retrofitting of masonry walls can also be achieved by applying thin Fiber Reinforced Polymer (FRP) overlays or strips on wall surfaces that were previously saturated by epoxy resin (or alternative) [22, 38]. A FRP overlay is typically made of glass or carbon fibers in an adhesive matrix. FRP overlays may cover the entire wall surface, or applied in the form of strips aligned in horizontal, vertical, or diagonal directions (Fig. 5). FRP overlays and strips can be used either as one-sided or two-sided applications. These overlays are very thin and light-weight (overall thickness on the order of few milimeters). To ensure an adequate anchorage, these FRP overlays/strips can either be wrapped (extended) at the wall ends, or custom-designed fiber anchors can be installed along the wall perimeter. Polymer fibers act as tension reinforcement for the wall and should be aligned in the direction of tensile stresses. The required effective area of fibers per unit width and the FRP contribution to shear capacity of a retrofitted wall are governed by bond and anchorage strength at the FRP-to-wall interface. Design procedures for FRP-based retrofitting of masonry structures are well established [39]. Experience related to the application of FRP technology in Serbia and the region is limited, however this technology has been recently used for retrofitting of masonry buildings after the 2020 Zagreb, Croatia earthquake [40].

When an existing URM wall has a deficient gravity and lateral load-resisting capacity, it can be retrofitted by constructing a thick RC overlay (new RC shear wall) which is attached to the existing masonry wall [41]. The concept is essentially similar to RC jacketing. Addition of a new RC wall results in a significant increase in lateral stiffness, shear and flexural capacity of the existing wall. A new RC wall is attached to the existing masonry wall in the same manner as previously explained for RC jacketing, except that the amount of wall reinforcement and anchors may be different. Retrofitting of wall foundations is usually required due to a significant increase in the shear and flexural capacity of a retrofitted wall.
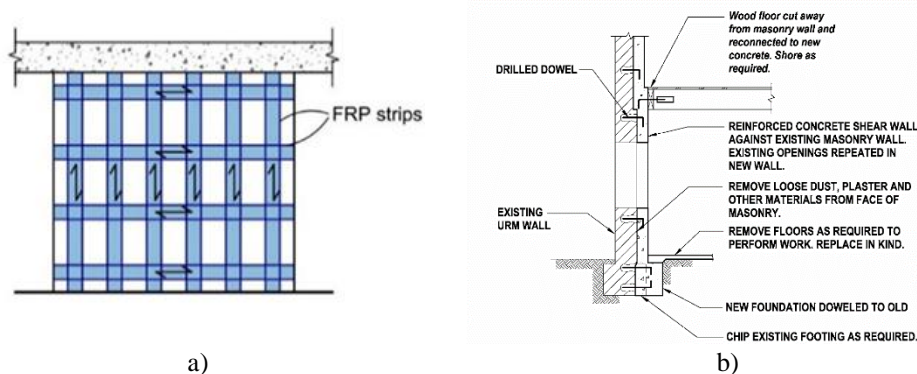
Figure 5. Techniques for seismic retrofitting of masonry walls: a) thin overlays – FRP strips [22] and b) thick overlay (new RC shear wall) [38].

Design of a masonry wall retrofitted by overlays is performed by considering stiffness of the retrofitted wall as the sum of the stiffnesses of the original masonry wall and the overlays. An example of a retrofitted URM wall with two-sided RC jacketing is presented in Fig. 6. Internal shear force in an RC jacket (Q_B) is obtained when the total force Q is multiplied by a ratio of the jacket stiffness (K_B) relative to the total wall stiffness ($K_Z + 2 K_B$). Note that the stiffness of an RC jacket is influenced by its thickness and the mechanical properties of concrete (modulus of elasticity E_c and modulus of rigidity G_c) – stiffness of reinforcement does not need to be considered.

Verification of lateral load-resisting capacity of a retrofitted wall with RC jackets needs to be performed by verifying the capacity of a composite section. For example, capacity of a masonry wall needs to be determined based on the applicable code equations and subsequently compared with the corresponding demand (shear force Q_Z and the corresponding axial force and bending moment). On the other hand, shear capacity of an RC jacket needs to be determined based on the shear contribution of steel mesh, while the concrete contribution may be ignored. The corresponding shear demand for an RC jacket is Q_B (as explained earlier in this section). It should be noted that PTN-R code prescribed a simplified procedure for determining shear capacity of an URM wall with RC jackets, which considered a

retrofitted wall as an equivalent masonry section, with the thickness equal to the sum of thicknesses of masonry wall (t_Z), plus thickness of each RC jacket (t_B).
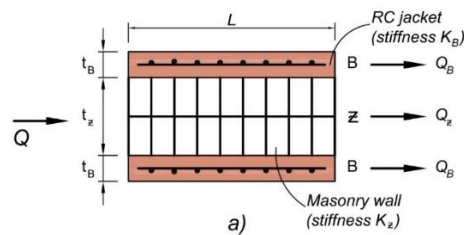
Figure 6. Internal force distribution in a retrofitted URM wall with RC jackets [23].

3. Seismic retrofitting of damaged URM buildings after the 2010 Kraljevo earthquake

3.1 Performance of mid-rise URM buildings in the earthquake

Several multi-family URM buildings (3- to 5-storey high) constructed after WWII (1945-1963) were damaged in the earthquake and required repair and retrofit [41, 42]. Masonry walls were typically constructed using solid clay bricks and their thickness ranged from 25 cm (interior walls) to 38 cm (exterior walls). The floors were ribbed RC slabs, and RC tie-beams (ring beams) were provided at each floor level. In most cases the walls experienced moderate damage in the form of cracks due to in-plane or out-of-plane seismic loads. The damage patterns observed in these buildings after the earthquake were discussed in a few publications [4, 41]. Some of the damaged buildings had vertical extensions (additional floors). It was reported that the extensions which were not compliant with the technical regulations were damaged in many cases [43].

This section discusses a typical URM building in Kraljevo which was damaged in the 2010 earthquake and was subsequently retrofitted by applying RC jacketing, in compliance with the PTN-R code that was used in Serbia and former Yugoslavia since 1985. The building is located in the Njegoševa Street No. 2 in Kraljevo, and was constructed around 1950 as a 3-storey residential building with a basement and a half-floor at the top, and a typical storey height of 2.8 m, see Fig. 7. Walls at the lower 3 floors were constructed using 25 cm solid clay bricks in 1:3:9 cement:lime:sand mortar, while non-structural walls at the top floor were constructed using 120 mm thick modular (multi-perforated) clay blocks. In the absence of material testing data M25 class bricks (2.5 MPa compressive strength) were assumed for the original building and M100 class modular blocks (10 MPa compressive strength) for the extended top floor.

Floors and roof were constructed using semi-prefabricated composite masonry and concrete system (see Fig. 4a), and were considered to act as rigid diaphragms. RC tie-beams were provided at each floor level. Since the building was constructed around 1950, seismic actions were likely not considered in the original design. The building was damaged in the 2010 earthquake. Structural damage in lower portion of the building was mostly in the form of inclined cracks due to in-plane seismic effects. Refer to [2] for more details related to seismic performance of the building in the 2010 Kraljevo earthquake and a detailed seismic evaluation of the damaged structure according to the PTN-S code and Eurocode 8.

The building was retrofitted according to the PTN-R code. The main goal of seismic retrofitting was to enhance the overall structural integrity, by constructing vertical RC jackets along the façade, embellished in blue colour on the floor plan in Fig. 8. The main reason for performing exterior retrofitting (at the façade) was to minimize disruption to the building occupants. Many earthquake-damaged URM buildings in Kraljevo were retrofitted using the same approach. Refer to [44] for more details related to the seismic evaluation and retrofitting design for this building.

a) b) c)
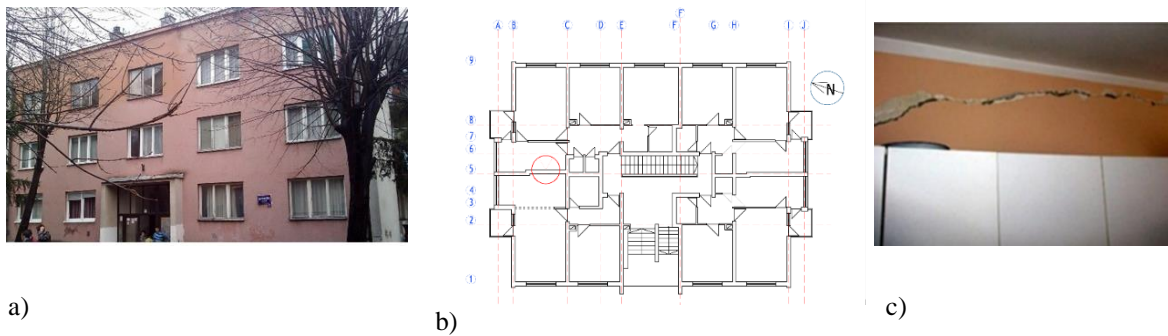
Figure 7. URM building located in the Njegoseva Street No.2, Kraljevo: a) west façade; b) typical floor plan, and c) severe cracking in a longitudinal wall at the 2nd floor level (gridline 5).
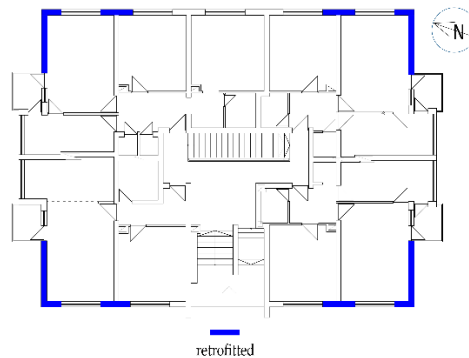
Figure 8. Typical floor plans showing locations of RC jackets.

3.3 Seismic analysis of the original and the retrofitted building

Seismic evaluation and retrofit design of earthquake-damaged buildings in Kraljevo was performed in line with the technical regulations which were enforced in Serbia at the time of the 2010 earthquake, that is, PTN-S and PTN-R. These codes prescribed linear elastic analysis for both the original and retrofitted structures. The effect of nonlinear seismic response of cracked URM walls was considered in line with the EC8-3 provisions for masonry buildings (by reducing the wall stiffness), but nonlinear seismic analysis was not performed.
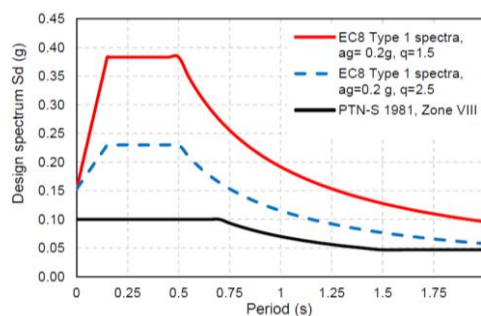
Figure 9. Design response spectra for Kraljevo, Serbia according to Eurocode 8 and PTN-S code.

Equivalent static seismic analysis according to the PTN-S code was performed using the following parameters: seismic intensity coefficient Ks of 0.05 (seismic intensity zone VIII), building category coefficient K_o of 1.0 corresponding to Category I, dynamic response coefficient K_d of 1.0, and the ductility and damping coefficient K_p of 2.0 (corresponding to URM building). The soil was classified as Category II according to the PTN-S code. It should be noted that seismic hazard parameters for Kraljevo were revised after the earthquake, hence the building site is currently located in seismic intensity zone IX. Multi-modal seismic analysis was performed for both the original and retrofitted

structure according to EC8-1. The design ground acceleration for soil type A was 0.2g, while ground type B was considered for the site. Spectral accelerations for the elastic design spectrum Sd(T) according to Eurocode 8 were divided by the behaviour factor q of 1.5 for URM structures designed without seismic provisions (for original structure) and q= 2.5 (for retrofitted structure). Type 1 spectrum was deemed appropriate, given the seismic hazard setting for the building site. Design response spectra for Kraljevo, Serbia, based on the PTN-S code and Eurocode 8 are presented in Fig. 9.

A 3-D numerical model of the building was created using the Tower software package by considering the walls as shell finite elements and slabs as plate elements. Floor and roof structures were treated as rigid diaphragms, which the foundations were simulated as fixed-base restraints. A cantilever numerical model, which considered only wall piers (no spandrels) was developed for the original structure because it resulted in a more conservative seismic force demand compared to an alternative Equivalent Frame Model. Modulus of elasticity for masonry was taken as 2410 MPa. Dynamic properties of the numerical model were obtained as a result of modal analysis. The seismic masses were calculated according to the PTN-S code. Fundamental period for the longitudinal (N-S) and transverse (E-W) directions were 0.267 sec and 0.20 sec respectively.

According to the PTN-R code, a retrofitted masonry wall with an RC jacket was modelled as an equivalent masonry wall with the thickness equal to thickness of the original wall plus additional thickness (equal to 4 times the thickness of an RC jacket). According to the EC8-3 code, the designer is expected to simulate the effect of an RC jacket by modelling it as a separate shell layer, or a part of a composite equivalent column section, where masonry and concrete materials would be simulated using appropriate mechanical and geometric properties. Numerical models for the original and retrofitted structure are shown on Fig. 10.

The following three models were considered to account for the effect of cracking on the original and retrofitted structure: a) Model 1, which considered uncracked (gross) properties of the original structure in line with PTN-S code (referred to as Original 1 and Retrofitted 1); b) Model 2, which considered the effect of moderate cracking (20% stiffness reduction), which is referred to as Original 2 and Retrofitted 2, and c) Model 3, which considers 50% stiffness reduction in line with EC8-3 (Original 3 and Retrofitted 3).

(a)   (b)
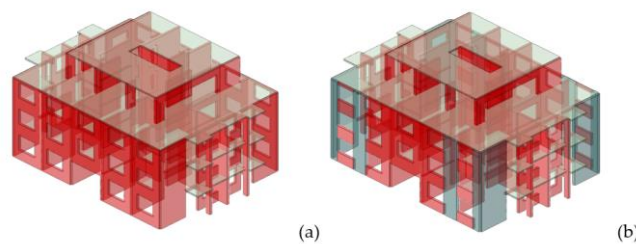
Figure 10. Numerical models: a) original structure and b) retrofitted structure.

To illustrate the effectiveness of retrofitting, seismic base shear force V_{Ed} (kN) (seismic demand) was compared with the shear capacity at the ground floor level V_{Rd} (kN), which was taken equal to the sum of capacities for all walls aligned in the same direction (N-S or E-W). The results for longitudinal (N-S) direction are illustrated in Fig. 11. It can be seen from the chart that the capacity of the building was satisfactory according to the PTN-S, since the capacity (C) versus demand (D) ratio, C/D, is larger than 1.0 both for the Original 1 (uncracked) model (in line with the PTN-S) and the Original 2 model (cracked, 20% stiffness reduction), but it is not satisfactory for the Original 3 model (cracked, 50% stiffness reduction – in line with EC8-3). The results also indicate that, according to the PTN-S code, the retrofit has resulted in an increased C/D ratio for the building to 1.52, 1.22, and 0.76 for Models 1, 2, and 3, respectively. The results indicate that the Retrofitted 3 model (which considers 50% stiffness reduction) is not satisfactory, since the corresponding C/D value is less than 1.0. The analysis performed according to the EC8 requirements showed that the capacity of the structure is not satisfactory even after the retrofit for Model 3, which is in line with the EC8-3 (C/D < 1.0); however,

the retrofit solution seems to be effective for Model 1 (in line with the PTN-S code), since the corresponding C/D ratio is 1.03.
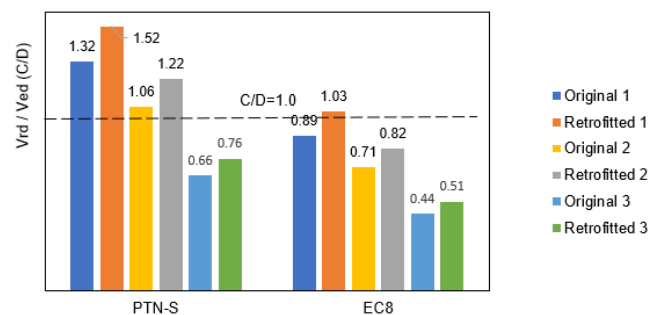
Figure 11. Seismic capacity versus demand (C/D) ratio for the ground floor of the building in N-S direction (for the original and retrofitted building).

4. Conclusions

The paper presents a study on seismic retrofitting of URM mid-rise residential buildings of post-WWII vintage, which are typical for the Balkans, in particular Serbia and neighbouring countries. An overview of common seismic retrofitting solutions for URM walls has been presented, and a typical building damaged in the 2010 Kraljevo earthquake and subsequently retrofitted using RC jacketing technique was analysed. A comparison of the results for seismic analyses performed according to the Yugoslav seismic codes and Eurocode 8 has shown that the seismic demand according to Eurocode 8 is significantly higher compared to the Yugoslav seismic codes PTN-S and PTN-R, which were used for seismic evaluation and retrofitting design. The key finding is that the retrofitting design solution performed according to the Yugoslav seismic codes for a URM building in Kraljevo does not meet the seismic safety requirements of Eurocode 8. In order to satisfy the seismic demand requirements according to Eurocode 8, a more extensive retrofitting would be required, most likely applied to interior walls - in addition to exterior walls which were retrofitted according to the original solution.

Acknowledgements

References

[1] Blagojević, P., Brzev, S., Cvetković, R. (2021): Simplified Seismic Assessment of Unreinforced Masonry Residential Buildings in the Balkans: The Case of Serbia. *Buildings*, **11**(9), 392-414, doi:https://doi.org/10.3390/buildings11090392.

[2] Brzev, S., Blagojević, P., Cvetković, R. (2021): Wall Index Requirements for Seismic Design and Assessment of Masonry Buildings. *Proceedings of 1st Croatian Conference on Earthquake Engineering*, Zagreb, Croatia, 8 pages.

[3] Statistical Office of the Republic of Serbia (SORS). Number and the floor space of housing units and dwellings according to the occupancy status, by settlements. The Census of Population, Households and Dwellings. Statistical Office of the Republic of Serbia, Serbia, 2011. https://www.stat.gov.rs/sr-latn/oblasti/popis/popis-2011/popisni-podaci-eksel-tabele/ (accessed on 10th July 2021).

[4] Manić, M. and Bulajić, B. (2013): Ponašanje zidanih zgrada u kraljevačkom zemljotresu od 03. novembra 2010. godine–iskustva i pouke (Behaviour of masonry buildings during the November 03, 2010 Kraljevo earthquake). *Izgradnja*, 67 (5-6), 235-246 (in Serbian).

[5] Miranda, E., Brzev, S., Bijelić, N. (2021): Petrinja, Croatia December 29, 2020, Mw 6.4 Earthquake. StEER-EERI Joint Reconnaissance. *Report*. Available online: https://www.designsafe-ci.org/data/browser/public/designsafe.storage.published/PRJ-2959 (accessed on 15th December 2022).

[6] Berg, G. V.; (1964): The Skopje, Yugoslavia Earthquake July 26, 1963. American Iron & Steel Institute: USA.

[7] PTP-12 (1964): Privremeni tehnički propisi za građenje u seizmičkim područjima (Provisional Technical Regulations for Construction in Seismic Regions). Yugoslav Institute for Standardization, Official Gazette of SFRY No. 39/64, Yugoslavia. (in Serbian).

[8] PTN-S. (1981): Pravilnik o tehničkim normativima za izgradnju objekata visokogradnje u seizmičkim područjima (Technical Regulations for the Design and Construction of Buildings in Seismic Regions). Yugoslav Institute for Standardization, Official Gazette of SFRY No. 31/81 (Amendments 49/82, 29/83, 21/88, 52/90). Yugoslavia. (in Serbian, partial English version available at https://iisee.kenken.go.jp/worldlist/64_Serbia/64_Serbia_Code.pdf) (accessed on 10th July 2021).

[9] Fajfar, P. (2018): Analysis in seismic provisions for buildings: past, present and future. The fifth Prof. Nicholas Ambraseys lecture. *Bull Earthq Eng*, 16, 2567–2608.

[10] PGK (2019): Pravilnik za građevinske konstrukcije (Building regulations). Institute for Standardization of Serbia, Official Gazette of Republic of Serbia No. 89/2019, 52/2020, 122/2020, Serbia, (in Serbian).

[11] CEN (2005): Eurocode 8 - Design of structures for earthquake resistance-Part 1: General rules, seismic actions and rules for buildings, EN 1998-1:2005. European Committee for Standardization, Belgium.

[12] SRPS EN 1998-1/NA:2018 (2018): Evrokod 8-Projektovanje seizmički otpornih konstrukcija Deo 1: Opsta pravila, seizmicka dejstva i pravila za zgrade. Institute for Standardization of Serbia, Serbia, (in Serbian).

[13] Seismological Survey of Serbia (SSS) (2018): Seismic hazard maps for Serbia. Seismological Survey of Serbia, Belgrade, Serbia. http://www.seismo.gov.rs/Seizmicnost/Karte_hazarda_e.htm (accessed on 10th July 2021).

[14] PTN-R (1985): Pravilnik o tehničkim normativima za sanaciju, ojačanje i rekonstrukciju objekata visokogradnje oštećenih zemljotresom i za rekonstrukciju i revitalizaciju objekata visokogradnje (Technical regulations for repair, strengthening and reconstruction of building structures damaged by earthquakes and for reconstruction and rehabilitation of buildings). Službeni list SFRJ No. 52/85, Yugoslavia (in Serbian).

[15] CEN (2005): Eurocode 8 - Design of structures for earthquake resistance-Part 3: Assessment and retrofitting of buildings, EN 1998-3:2005. European Committee for Standardization, Belgium.

[16] SRPS EN 1998-3/NA:2018 (2018): Evrokod 8-Projektovanje seizmički otpornih konstrukcija Deo 3: evaluacija i ojačanje konstrukcija. Institute for Standardization of Serbia, Serbia (in Serbian).

[17] PTN-Z (1991): Pravilnik o tehničkim normativima za zidane zidove (Technical norms regulation for masonry walls). Yugoslav Institute for Standardization, Official Gazette of SFRY No. 87/91, Yugoslavia, (in Serbian).

[18] CEN (2004): Eurocode 6-Design of Masonry Structures. Part 1-1: General rules for reinforced and unreinforced masonry structures. EN 1996-1-1:2004. European Committee for Standardization, Belgium.

[19] SRPS EN 1996-1-1:2016 (2016): Evrokod 6-Projektovanje zidanih konstrukcija Deo 1-1: Opšta pravila za armirane i nearmirane zidane konstrukcije. Serbian Institute for Standardization, Serbia, (in Serbian).

[20] ASCE/SEI (2017): Seismic Evaluation and Retrofit of Existing Buildings, Standard (ASCE/SEI 41-17), American Society of Civil Engineers/Structural Engineering Institute, USA.

[21] Thermou, G.E., Pantazopoulou, S.J., and Elnashai, A.S. (2004): Upgrading of RC Structures for a Target Response Shape, *Proceedings of the 13th World Conference on Earthquake Engineering*, Vancouver, BC, Canada, Paper No. 1412.

[22] Brzev, S. and Begaliev, U. (2018): Practical seismic design and construction manual for retrofitting schools in the Kyrgyz Republic, World Bank, USA.

[23] Ademović, N.; Oliveira, D. V.; Lourenço, P. B. (2019): Seismic Evaluation and Strengthening of an Existing Masonry Building in Sarajevo, B&H. *Buildings*, 9, 30.

[24] Salaman, A., Stepinac, M., Matorić, I., Klasić, M. (2022): Post-Earthquake Condition Assessment and Seismic Upgrading Strategies for a Heritage-Protected School in Petrinja, Croatia. *Buildings*, 12, 2263. https://doi.org/10.3390/buildings12122263.

[25] Triller, P., Tomaževič, M., Lutman, M., and Gams, M. (2017): Seismic behavior of strengthened URM masonry–an overview of research at ZAG. International Conference on Analytical Models and New Concepts in Concrete and Masonry Structures AMCM'2017, Procedia Engineering, 193: 66–73.

[26] UNIDO (1983): Building Construction Under Seismic Conditions in the Balkan Region: Repair and Strengthening of Reinforced Concrete, Stone and Brick Masonry Buildings, Vol. 5, First Edition, United Nations Industrial Development Programme, Vienna.

[27] Tomaževič, M. (1999): *Earthquake-Resistant Design of Masonry Buildings*, Imperial College Press, London, U.K.

[28] Uroš, M., Todorić, M., Crnogorac, M., Atalić, J., Šavor Novak, M., Lakušić, S. (Eds.) (2021): *Potresno inženjerstvo-Obnova zidanih zgrada.* Građevinski fakultet, Sveučilišta u Zagrebu: Zagreb, Croatia, ISBN 978-953-8163-43-7.

[29] Muravljov, M., Stevanović, B., Ostojić, D. (2022): *Sanacije građevinskih konstrukcija i objekata*, 1st ed.; Faculty of Civil Engineering, University of Belgrade, Serbia, (in Serbian).

[30] Sheppard, P. and Terčelj, S. (1980): The Effect of Repair and Strengthening Methods for Masonry Walls. *Proceedings of the 7th World Conference on Earthquake Engineering*, Istanbul, Turkey.

[31] Churilov, S. and Dumova-Jovanoska, E. (2012): Analysis of Masonry Walls Strengthened with RC Jackets, *Proceedings of the 15th World Conference on Earthquake Engineering*, Lisbon, Portugal.

[32] Medić, S., Hrasnica, M. (2021): In-Plane Seismic Response of Unreinforced and Jacketed Masonry Walls. *Buildings,* 11, 472. https://doi.org/10.3390/buildings11100472

[33] El Gawady, M, Lestuzzi, P. and Badoux, M. (2006): Retrofitting of Masonry Walls Using Shotcrete. *Proceedings of the 2006 NZSEE Conference*, Napier, New Zealand.

[34] Proença, J. M. et al. (2012): Strengthening of Masonry Wall Load Bearing Structures with Reinforced Plastering Mortar Solution. *Proceedings of the 15th World Conference on Earthquake Engineering*, Lisbon, Portugal.

[35] Kadam, S.B., Singh, Y., and Li, B. (2014): Strengthening of Unreinforced Masonry Using Welded Wire Mesh and Micro-Concrete–Behaviour Under In-Plane Action. *Construction and Building Materials*, 54: 247–257.

[36] Lin, Y., Biggs, D., Wotherspoon, L., and Ingham, J.M. (2014): In-Plane Strengthening of Unreinforced Concrete Masonry Wallettes Using ECC Shotcrete. *Journal of Structural Engineering*, Vol. 140, Issue 1. https://doi.org/10.1061/(ASCE)ST.1943-541X.0001004

[37] Jurukovski, D., Krstevska, L., Alessi, R., Diotallevi, P.P., Merli, M., and Zarri, F. (1992): Shaking Table Tests of Three Four-Storey Brick Masonry Models: Original and Strengthened by RC Core and RC Jackets. *Proceedings of the 10th World Conference on Earthquake Engineering*, Madrid, Spain.

[38] FEMA 547 (2006): Techniques for the Seismic Rehabilitation of Existing Buildings (FEMA 547). Washington D.C., USA.

[39] INRC (2014): Guide for the Design and Construction of Externally Bonded FRP Systems for Strengthening Existing Structures: Materials, RC and PC structures, Masonry Structures, Italian National Research Council, Advisory Committee on Technical Recommendations for Construction, CNR-DT 200 R1/2013, Rome, Italy.

[40] Kišiček, T., Stepinac, M., Renić, T., Hafner, I., and Lulić, L. (2020): Strengthening of masonry walls with FRP or TRM. *Građevinar*, Vol. 72, No 10, 937-953.

[41] Ostojić, D., Stevanović, B., Muravljov, M., and Glišović, I. (2012): Sanacija i ojačanje zidanih objekata oštećenih zemljotresom u Kraljevu. *Proceedings of the 4th International Conference: Civil Engineering–Science and Practice*, Žabljak, Montenegro (in Serbian).

[42] Ostojić, D., Muravljov, M. and Stevanović, B. (2011): Primeri sanacije višespratnih stambenih zidanih zgrada oštećenih zemljotresom u Kraljevu. *Izgradnja*, 5-6, 315-325 (in Serbian).

[43] Manić, M. and Bulajić, B. (2012): Zašto procena šteta na građevinskim objektima u kraljevačkom regionu nije izvršena ni godinu dana nakon zemljotresa od 03.11.2010. godine?, *Izgradnja*, 66(5-6), 269-308 (in Serbian).

[44] Blagojević, P., Brzev, S., Cvetković, R. (2023): Seismic Retrofitting of Mid-Rise Unreinforced Masonry Residential Buildings after the 2010 Kraljevo, Serbia Earthquake: A Case Study. *Buildings*, 11(9).

EQIVALENT FRAME MODELS FOR FRP-STRENGTHENED MASONRY BUILDINGS

Ivana Božulić [(1)], Francesco Vanin [(2)], Katrin Beyer [(1)]

[(1)] *Earthquake Engineering and Structural Dynamics Laboratory (EESD), EPFL, Lausanne, Switzerland, e-mail: (ivana.bozulic@epfl.ch, katrin.beyer@epfl.ch)*

[(2)] *Résonance Ingénieurs-Conseils SA, 1227 Carouge, Switzerland, e-mail: (francesco.vanin@resonance.ch)*

Abstract

Fibre-reinforced polymers (FRP) strengthening can be applied to decrease the seismic vulnerability of existing masonry buildings, both with regard to in-plane and out-of-plane failure mechanisms. Experimentally, the impact of strengthening solutions has been thoroughly studied. There are, however, few efficient and reliable numerical modeling approaches that can accurately capture the effect of such strengthening on the seismic response of the masonry building. Therefore, we herein develop and validate a modeling approach to capture the effect of FRP strengthening on the behaviour of masonry walls. To model this effect, we use a recently developed macro-element, which can capture both in-plane and out-of-plane failure modes. In the macro-element, the intervention is modelled by adding fibres representing the longitudinal FRP strips to the section model. These fibres were modelled as linear elastic in tension up to the failure with a zero compressive strength. Transversal FRP strips effect the shear strength, and in the macro-element, this is accounted for by increasing the cohesion in the equation for the shear strength. To validate the model, we also compare the numerical simulations with existing experimental results obtained from the literature. Overall, the proposed modeling approach accurately predicts the in-plane and out-of-plane response, implying that equivalent frame models can predict the response of masonry buildings with FRP-strengthened walls. To conclude, the models described in this paper can be used for a time-efficient assessment. Moreover, it can help in selecting the optimal strengthening approach for future retrofitting. This aspect is especially important for the cultural heritage structures, where excessive retrofitting should be avoided.

Keywords: fibre-reinforced polymer, equivalent frame models, in-plane capacity, shear reinforcement, masonry, building strengthening

1. Introduction

Equivalent frame models (EFMs) are extensively used for modeling the nonlinear seismic response of entire unreinforced masonry buildings (URM) because they provide a good balance of accuracy and computational cost [1, 2, 3, 4]. Various strengthening techniques of URM buildings have been tested experimentally; a recent review can be found in [5]. Since strengthening one element can induce the failure of another, it is important to assess the entire system response through a numerical model of the entire building.

The goal of this article is to develop and validate a method for modeling FRP-strengthened URM buildings using EFMs. We illustrate how a novel macro-element developed by [4] may be used to investigate the impacts of FRP strengthening on the in-plane and out-of-plane capacity of masonry walls, as well as on the overall behavior of a building.

2. Numerical approach

The three-dimensional macro-element by [4], which has been implemented in OpenSees [6] is the basis for our EFM approach for retrofitted masonry walls. This macro-element has been built on the in-plane response developed by [2] and enhanced to capture the out-of-plane response of the masonry panel. When modelling the FRP strengthening, we separately address the increase in shear and flexural capacity.

2.1. Increase in shear capacity

The increase in shear capacity, obtained from applied FRPs, is calculated using engineering models that anticipate the shear resistance of FRP retrofitted masonry walls. Several guidelines and design standards are available in the literature, [7] and [8] provide a review of existing models. Shear strength of FRP-strengthened masonry panel is calculated as the sum of the shear strength of the uncracked masonry wall and the shear strength provided by the FRP reinforcement. We differ the increase due to grid and diagonal FRP layout. Following the macro-element formulation, this increase in shear capacity is taken into account through the value of cohesion.

2.2. Increase in flexural capacity

The flexural behaviour of the macro-element can be characterized by using fibre sections, where the cross-section of a wall is discretized in fibres and a specific material law can be assigned to it. We used the approach by [9] to model the increase in flexural strength due to FRP reinforcement by adding FRP fibres to the section. The macro-element developed by [4] comprises three fibre sections that can contain three nonlinear sections at the element ends and at midlength. This option can be useful for representing the difference between FRPs that are anchored or not to the slabs. The material model that is assigned to masonry fibres has zero tensile strength, limited compressive strength, a damage behaviour in compression and no strength degradation [4]. The FRP reinforcement was formulated as linear elastic in tension up to failure and with a zero compressive strength.

3. Validation of numerical approach

3.1. Masonry walls

Monotonic, quasi-static cyclic, dynamic, and four-point bending (out-of-plane) experimental campaigns were chosen to validate our approach [10].

For the in-plane response validation, we choose the experimental campaign done by [11] on brick half-scale hollow clay block masonry walls retrofitted on only one side with quasi-static shear compression test setup. Figure 1 presents the force-displacement response of a masonry wall retrofitted with glass fibres. Experimental data is presented in black, while red shows the response we obtained numerically using herein proposed approach. It can provide accurate estimates of the initial stiffness and maximum force capacity.
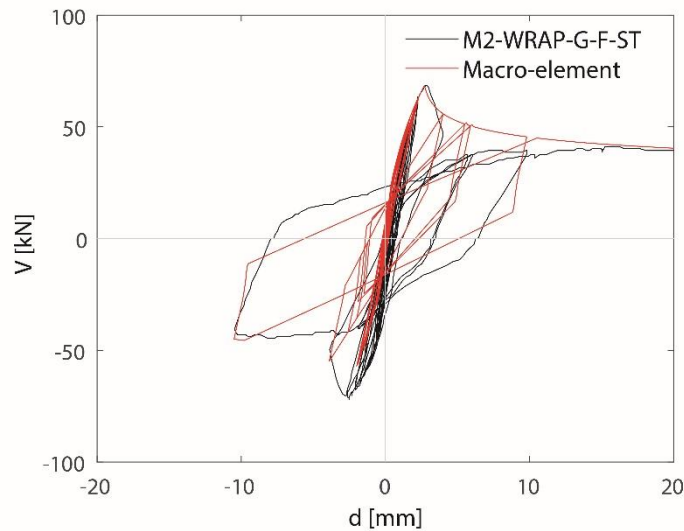
Figure 1 - Resulting output from our model for the simulation of the quasi static cyclic tests carried out by [11] specimen retrofitted with GFRP M2-WRAP1-G-F-ST

3.1. Masonry building

We examine hypothetical retrofit solutions of a structure that was dynamically tested in its unretrofitted configuration [12] to demonstrate how our approach for FRP-strengthened masonry walls may be used to evaluate potential retrofit solutions at the building level. The CoMa-WallS building, which is a modern mixed reinforced concrete - unreinforced masonry structure, tested by [12] was chosen for this purpose. In [13] the building was modelled in its unretrofitted state. When tested on uni-axial shake table, it experienced out-of-plane failure in the top storey and in-plane failures in the first and second storey.
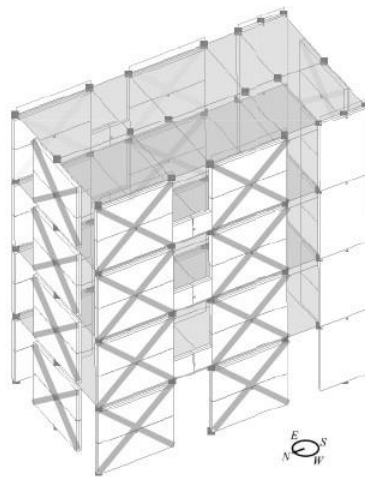
Figure 2 - Equivalent frame model of the building tested by [12] modelled in unstrengthened configuration in [13] with applied CFRPs

The numerical models included a hypothetical configuration with carbon fibres applied in a diagonal arrangement on both sides of the wall; it was assumed that the fibres were not anchored in the slab (Figure 2).

When the out-of-plane displacement of the middle section of the top storey wall of the unretrofitted configuration (i.e. the configuration that was tested experimentally) is compared to that of the proposed strengthened configuration, we can see that the FRP-strengthened model demonstrates the efficiency of FRPs in preventing excessive out-of-plane displacements (Figure 3). As a result, local failures might be avoided by using composites, assuring the global response of a building.

The effect of the retrofitting solutions was also visible when the deformation demands in terms of shear and flexural deformation at failure were examined. Furthermore, the failure mode changed, the shear failure was developed instead of flexural. The maximum displacement is significantly reduced after applying CFRP, even if the CFRP is not anchored in the slabs. The PGA that the retrofitted structure can resist is therefore greater than when no strengthening is applied.
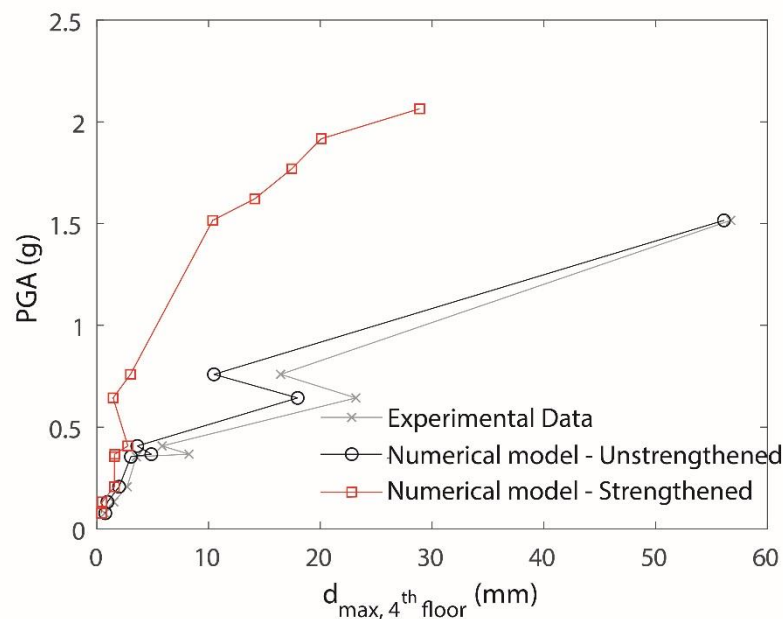
Figure 3 - Resulting output from our numerical model (strengthened configuration) for the simulation of the shake table tests by [12] modelled in unstrengthened configuration in [13]. Comparison of the global response in terms of maximum displacements.

4. Conclusions

In this paper, we propose a numerical approach for modelling FRP-strengthening applied on masonry structural elements. Our main objective is to develop and validate a tool that can be used for reliable and time-efficient assessment of FRP-retrofitted masonry buildings. We can obtain a simulation of probable failure mechanisms and damage patterns for different types of FRP materials and retrofitting configurations in this way. Finally, the models presented here can assist in determining the optimal strengthening strategy for future retrofitting. This is especially relevant when it comes to cultural heritage structures, where excessive retrofitting should be avoided. Future work based on this paper could include the application of textile-reinforced mortars (TRM) instead of FRPs.

Acknowledgements

References

[1]   Lagomarsino, S., Penna, A., Galasco, A., & Cattari, S. (2013). TREMURI program: An equivalent frame model for the nonlinear seismic analysis of masonry buildings. *Engineering Structures*, *56*, 1787–1799. https://doi.org/10.1016/j.engstruct.2013.08.002

[2]   Penna, A., Lagomarsino, S., & Galasco, A. (2014). A nonlinear macroelement model for the seismic analysis of masonry. *Earthquake Engineering and Structural Dynamics*. https://doi.org/10.1002/eqe

[3]   Quagliarini, E., Maracchini, G., & Clementi, F. (2017). Uses and limits of the Equivalent Frame Model on existing unreinforced masonry buildings for assessing their seismic risk: A review. *Journal of Building Engineering*, *10*(March), 166–182. https://doi.org/10.1016/j.jobe.2017.03.004

[4]   Vanin, F., Penna, A., & Beyer, K. (2020a). A three-dimensional macroelement for modelling the in-plane and out-of-plane response of masonry walls. *Earthquake Engineering and Structural Dynamics*, *March 2019*, 1–23. https://doi.org/10.1002/eqe.3277

[5]   Wang, C., Sarhosis, V., & Nikitas, N. (2018). Strengthening/Retrofitting Techniques on Unreinforced Masonry Structure/Element Subjected to Seismic Loads: A Literature Review. *The Open Construction and Building Technology Journal*, *12*(1), 251–268. https://doi.org/10.2174/1874836801812010251

[6]   McKenna, F., Fenves, G. L., & Scott., M. H. (2000). *"Open system for earthquake engineering simulation."* University of California, Berkeley, CA .

[7]   Zhuge, Y. (2010). FRP-retrofitted URM walls under in-plane shear: Review and assessment of available models. *Journal of Composites for Construction*, *14*(6), 743–753. https://doi.org/10.1061/(ASCE)CC.1943-5614.0000135

[8]   Kišiček, T., Stepinac, M., Renić, T., Hafner, I., Lulić, L. (2020). Strengthening of masonry walls with FRP or TRM, *GRAĐEVINAR, 72* (10), 937-953, https://doi.org/10.14256/JCE.2983.2020

[9]   Grande, E., Imbimbo, M., & Sacco, E. (2011). A beam finite element for nonlinear analysis of masonry elements with or without fiber-reinforced plastic (FRP) reinforcements. *International Journal of Architectural Heritage*, *5*(6), 693–716. https://doi.org/10.1080/15583058.2010.490616

[10] Bozulic, I., Vanin, F., Beyer, K. (2023). Modelling of FRP-Strengthened Masonry Buildings with Equivalent Frame Models - Manuscript submitted for publication.

[11] ElGawady, M., Lestuzzi, P. & Badoux, M.. (2007). Static Cyclic Response of Masonry Walls Retrofitted with Fiber-Reinforced Polymers. *Journal of Composites for Construction - J COMPOS CONSTR*. 11. 10.1061/(ASCE)1090-0268(2007)11:1(50).

[12] Beyer, K., Tondelli, M., Petry, S., & Peloso, S. (2015). Dynamic testing of a four-storey building with reinforced concrete and unreinforced masonry walls : Prediction , test results and data set. *Bulletin of Earthquake Engineering*, *April*. https://doi.org/10.1007/s10518-015-9752-z

[13] Vanin, F., Penna, A., & Beyer, K. (2020b). Equivalent-Frame Modeling of Two Shaking Table Tests of Masonry Buildings Accounting for Their Out-Of-Plane Response. *Frontiers in Built Environment*, *6*(April), 1–18. https://doi.org/10.3389/fbuil.2020.00042

PERFORMANCE EVALUATION OF CHEVRON BRACED FRAME AND TADAS DAMPER ON SEISMIC RESPONSE OF STEEL MRFs

Marin Grubišić[(1)], Benjamin Pervan[(2)], Ivica Guljaš[(3)]

[(1)] *Assist. Professor, Faculty of Civil Engineering and Architecture Osijek, University of Osijek, marin.grubisic@gfos.hr*
[(2)] *MEng, IGH Ltd, Zagreb, benjaminpervan@gmail.com*
[(3)] *Full Professor, Faculty of Civil Engineering and Architecture Osijek, University of Osijek, iguljas@gfos.hr*

Abstract

The aim of this study is to evaluate the feasibility of seismically strengthening existing steel frames. Through computational analysis of the existing bare frame, two methods of seismic strengthening are proposed. The expected behaviour of each of the three tested steel frames was determined through an initial iterative calculation using numerical models. The dimensions for the two types of strengthening were established based on numerical analysis of the bare frame: one utilizing a specialized inverted V-bracing (Chevron) system, and the other utilizing a dissipative TADAS connection. Following the design of the strengthening, three frames were subjected to static reversed cyclic displacement control tests up to failure, according to FEMA 461. The experimental testing of the bare frame (BF) and TADAS frame (TF) was halted due to the emergence of significant global out-of-plane instability, and testing of the Chevron frame (CF) was discontinued following a brace tensile failure. The ductility of the Chevron frame (CF) is found to be 0.6 times lower, while that of the TADAS frame (TF) is 1.4 times higher in comparison to the bare frame (BF). The initial stiffness of the system is 5 times higher in the CF and 2 times higher in the TF than that of the BF. The cyclic responses of the specimens exhibit a symmetrical behaviour. The TADAS frame dissipates 4 times more energy at the point of failure (brace fracture vs out-of-plane instability) than the CF. Careful design of the braces and plates of the TADAS element is necessary to maintain the plasticization hierarchy.

Keywords: steel frames, seismic strengthening, moment-resisting frame (MRF), TADAS dissipative element, cyclic tests

1. Introduction

The primary objectives of earthquake-resistant design for structures include preventing collapse or severe damage during infrequent but destructive earthquakes, minimizing damage to the supporting structure, and reducing structural damage during occasional moderate earthquakes, and protecting non-structural elements during frequent weak earthquakes. Thus, the acceptable level of damage and the cost of repairs are crucial performance criteria for evaluating the seismic resistance of structures. However, designing structures that meet these objectives while also balancing structural capacity and seismic requirements can be challenging.

Steel is an ideal material for seismic design due to its high strength, ductility, and ability to dissipate energy through yielding and large plastic deformations. It also has a low specific weight and relatively high fracture toughness. To take full advantage of the benefits that steel offers in seismic design, certain conditions must be met:

- The structural system must be designed to ensure inelastic behaviour throughout the system, not just in individual elements, to prevent buckling under cyclic loading.

- Adequate lateral restraints must be provided to prevent lateral buckling.

- Elements with a compact cross-section must be used to prevent local buckling.

Overall, steel's combination of strength, ductility, and low specific weight make it an ideal material for seismic design, but the system must be designed to take full advantage of steel's properties. Two methods for seismically reinforcing steel structures are: a) enhancing the load-carrying capacity while preserving ductility, b) reducing the cross-sectional dimensions of the elements.

2. Relevant strengthening methods

The seismic safety of steel structures can be improved through the identification and strengthening of the structure's vulnerable points. The presence of substantial constant gravity loads can significantly increase the seismic demands placed on the structure. Thus, it is advisable to reduce the existing constant load and subsequently reinforce the structure's horizontal load-bearing system using appropriate techniques. The use of steel for seismic strengthening is cost-effective and efficient due to the following factors:

- Steel structures are particularly well-suited for performance-based design (PBD)

- Steel elements exhibit ductile behaviour even after reaching the yield point, thus effectively dissipating a significant amount of energy before failure.

- Steel elements have a high strength-to-weight ratio, which results in lower seismic forces acting on the structure.

Concentrically braced frames (CBF) demonstrate superior resistance to horizontal forces and displacement, primarily through the utilization of the longitudinal strength and stiffness of the braces. These frames are engineered such that the centroidal axes of the columns, beams, and braces align, thereby minimizing bending effects. CBFs are designed to exhibit low levels of inelastic deformation and to withstand larger seismic forces to compensate for their lack of ductility. They are well-suited for use in smaller structures as the design calculations are relatively simple compared to other types of braced frames. Additionally, CBFs are more cost-effective than moment-resisting frames (MRF) due to their lower material requirements. However, they may be less suitable for larger structures and structures subject to high seismic demands [1].

Special concentrically braced frames (SCBF) have distinct requirements in comparison to conventional frames, which concentrates the inelastic behaviour of the structure on the braces and enhances the ductility of the braces and their connections. These requirements enable greater energy dissipation and ductility, resulting in the ability to design these frames for lower loads than regular braced frames. The increased energy dissipation capacity and ductility make them particularly suitable for use in areas with higher seismic demands. Figure 1 illustrates typical configurations of concentrically braced steel frames.

Other frequent strengthening techniques include eccentrically braced frames and buckling-restrained braced frames (BRBF), which are not the focus of this research.
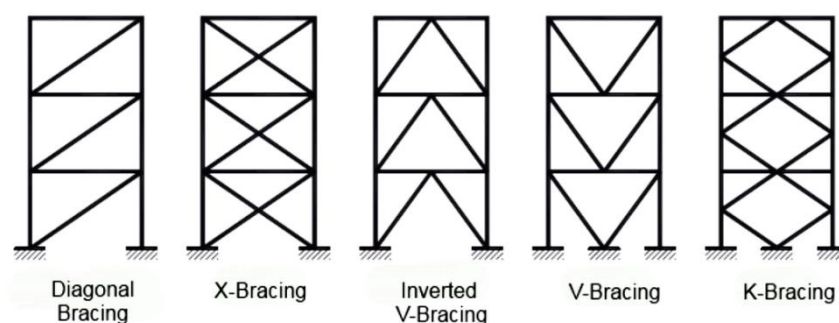
Fig. 1 – Typical configurations of centric steel braced frames [2]

Numerous studies have been conducted to enhance the seismic performance of Chevron braced frames (Inverted V-Bracing). Researchers have specifically examined the use of novel technologies such as dampers, and each system has its own advantages and disadvantages. The idea of using dampers in bracing systems was first proposed by [3] who developed the ADAS (Added Damping and Stiffness) system and [4] who created TADAS (Triangular Plate Added Damping and Stiffness), conducted experimental tests and theoretical studies.

The ADAS and TADAS steel plate devices (Figure 2) are a series of steel plates intended for use in frame structures. They are activated during relative story displacement, causing the top of the plate to move horizontally relative to the bottom of the plate. The yielding of the steel plates enables the ADAS/TADAS device to dissipate a significant amount of energy during an earthquake. The energy dissipation through yielding ADAS/TADAS devices has several benefits:

- the energy dissipation is concentrated in designated areas,
- the energy dissipation demands of other structural elements are reduced,
- the yielding of the ADAS/TADAS device does not compromise the capacity of the vertical load-bearing system supporting the gravity loads, as the device is a component of the horizontal stiffness system and does not significantly affect the vertical stiffness.
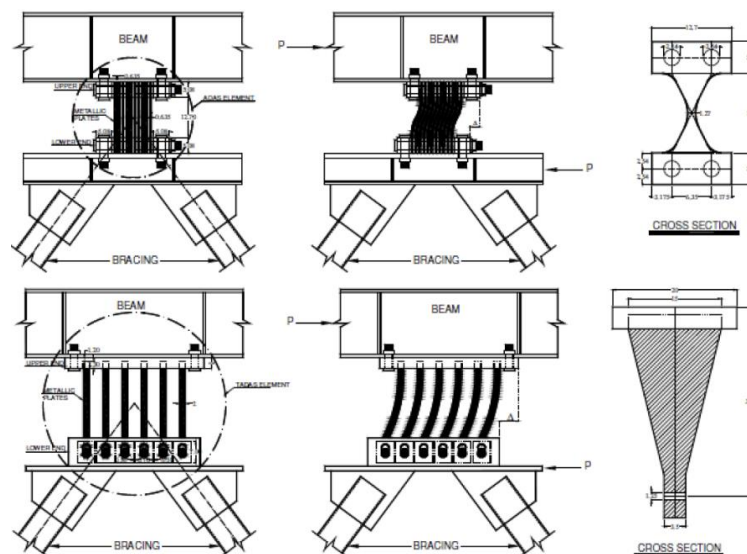
Fig. 2 – The behaviour of ADAS (upper) and TADAS (lower) dampers during an earthquake [3, 4]

3. Geometric and material properties of the frame specimens

The steel frame specimens used in this study consist of HEA 120 columns connected at the top to HEA 120 beam. The beam is equipped with face plates, which serve to increase the contact area over which shear loads are applied. The columns are connected at the bottom by a beam with HEB 220 cross-section (Figure 3). The yield strength and tensile strength are obtained from [5], with an average yield strength of 337 MPa and an average tensile strength of 483 MPa. The modulus of elasticity is 210 GPa. It is worth noting that the frames utilized in this research have already been tested by [5] and as such have minimal imperfections stemming from residual deformation, as the frame specimens barely reached their yield strength. A bare frame is depicted in Figure 3a. The rotational stiffness of the joint was determined numerically to be 2 MNm/rad, which is essential for future numerical analyses.

It was determined to use the Special Concentric Braced Frame (SCBF) in conjunction with the dissipative TADAS device. All steel used for the strengthening is of grade S235. The Chevron-shaped Special Concentric Braced Frame (CSCBF) allows for in-plane or out-of-plane buckling of the diagonal elements. For architectural and safety reasons, a design was chosen in which the diagonals buckle in-plane. The diagonal buckling is ensured by a knife plate with a clear width of $3 \cdot t_p$, where t_p is a knife plate thickness of 8 mm. The design of all details was carried out iteratively [1, 6]. Figures 3b and 4 illustrates the adopted dimensions, which ensure over 85% utilization of the element and the compliant hierarchy of diagonal brace elements (HSS 50×50×3.2 mm). The same brace cross-section is employed when the bare frame is strengthened with a TADAS dissipation device. In this instance, the utilization of the diagonal braces is slightly lower as the buckling length is smaller. The calculation was performed according to [4], and the dimensions can be seen in Figures 3c and 6.
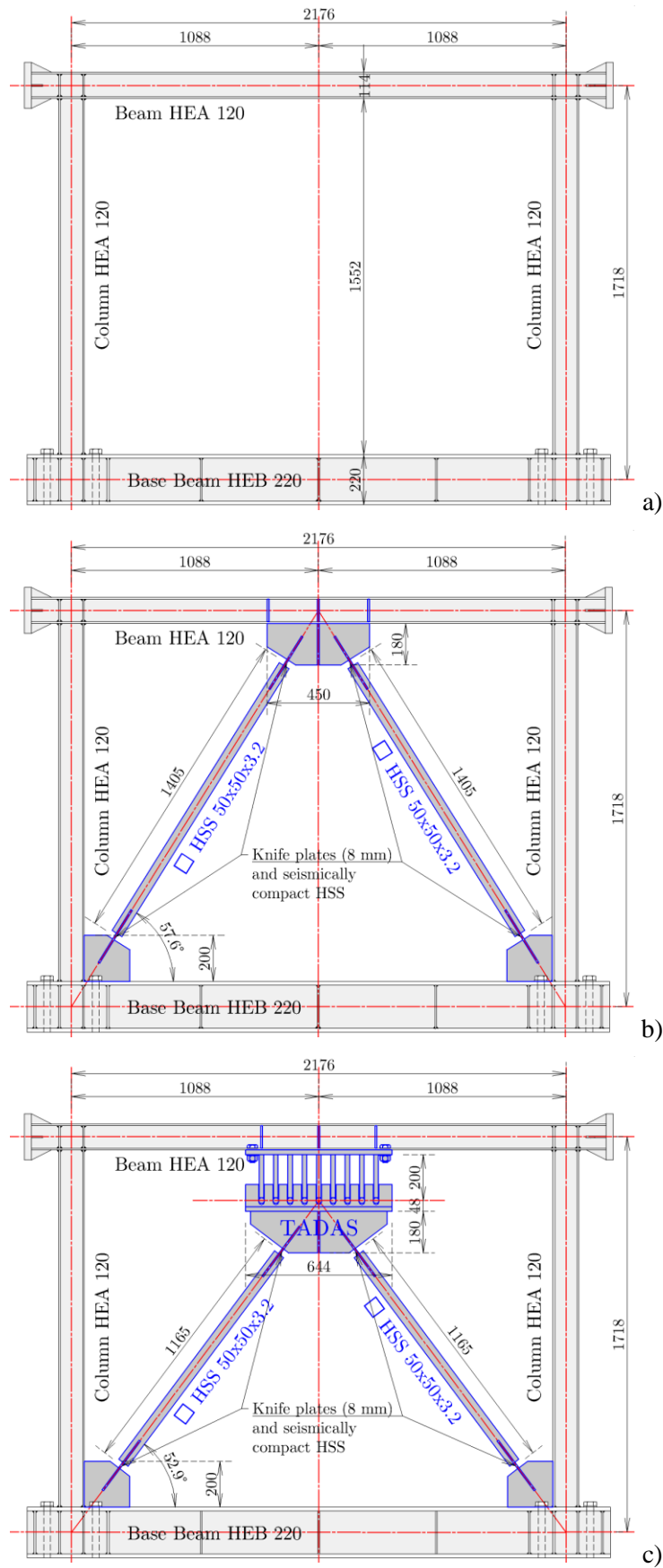
Fig. 3 - Geometries of test steel frames: a) Bare frame, b) Inverted V-braced/Chevron frame, c) TADAS frame
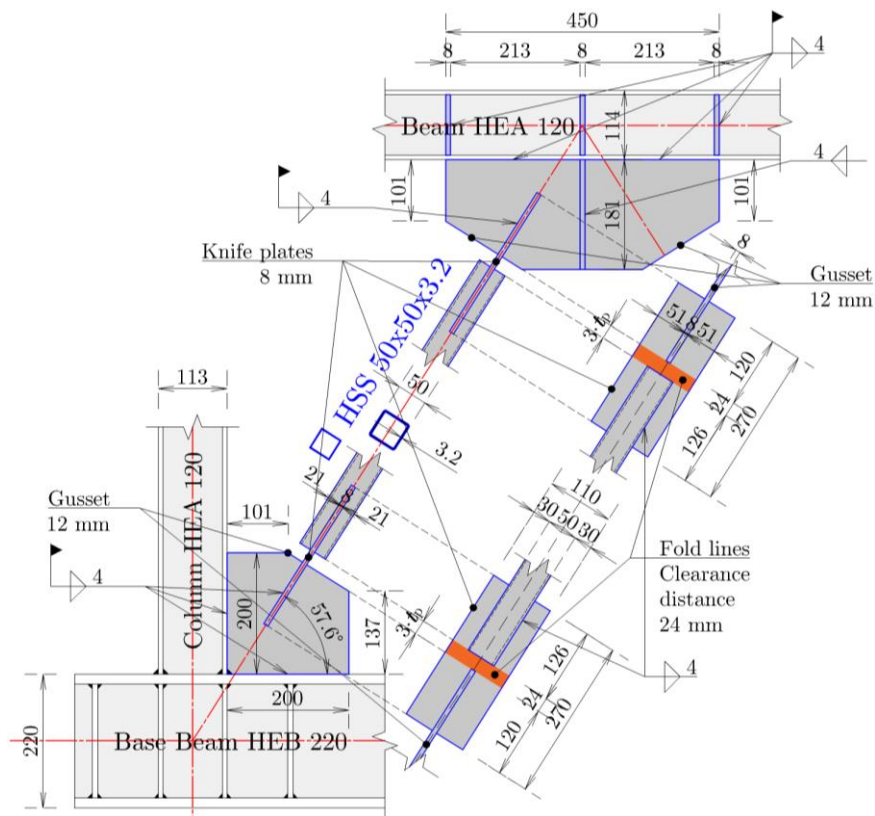
Fig. 4 - Details of diagonal element connections, gusset plates, knife plates, clearance distances and welds
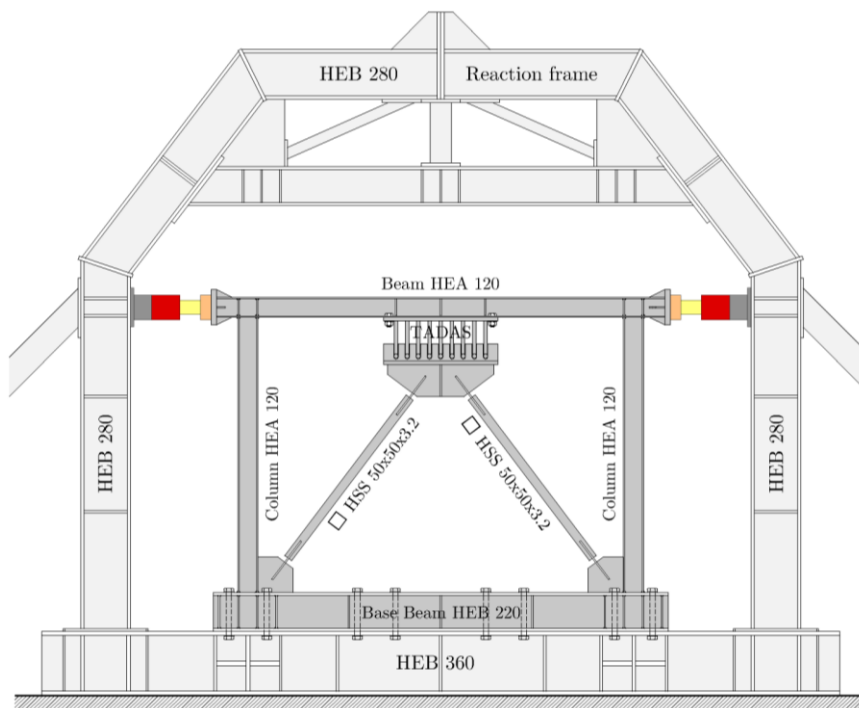
Fig. 5 – Steel frames within reaction frame for cyclic testing

TADAS was designed and ultimately consisted of 9 plates of class S235, a height of 200 mm, a base width of 80 mm and a thickness of 20 mm (Figure 6). Before the static cyclic tests, the first three natural frequencies were determined and summarized in Table 1.
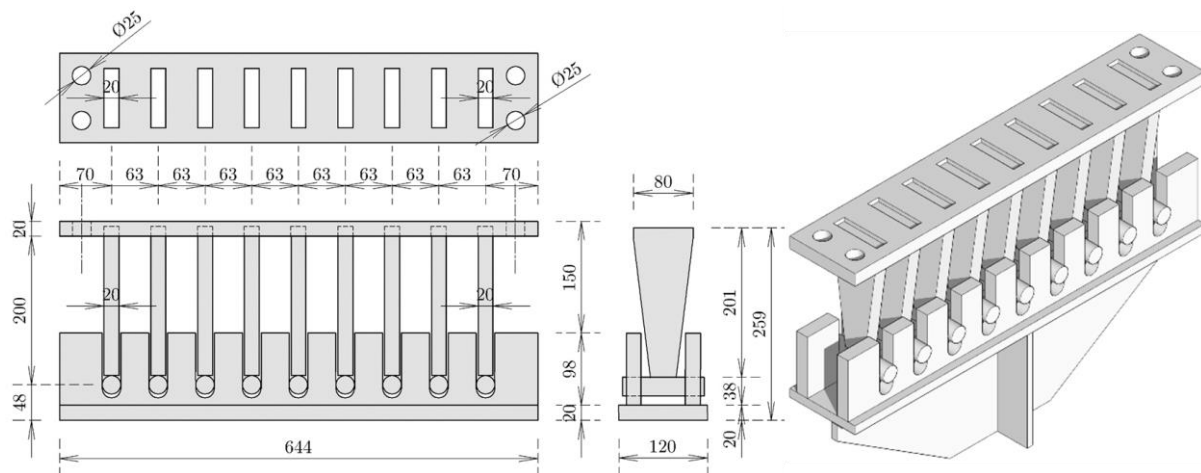
Fig. 6 – Geometric details of the TADAS dissipative element

Table 1. Natural frequency values for all tested frames

Eigenmode shape	Natural frequencies [Hz]		
	Bare frame	Chevron (Inverted V-braced) frame	TADAS frame
#1 / Out-of-plane	8.36	9.40	7.20
#2 / Torsion	10.80	12.45	12.51
#3 / In-plane	30.09	86.30	46.88

4. Global response of steel frames

The static cyclic tests were conducted in accordance with the protocol of FEMA 461 [7], using a total of 13 cycles to target displacement. The frames were loaded in the horizontal direction only, without any constant gravity loading. The maximum lateral load capacity for the Chevron frame was twice as high (up to 200 kN) and three times as high for the TADAS frame (up to 300 kN) compared to the bare moment-resisting steel frame (up to 100 kN) as illustrated in Figure 8. Testing was interrupted for the bare and TADAS frames after substantial out-of-plane instability occurred, and for the Chevron frame after a diagonal tensile failure (Figure 7). In the case of the TADAS frame, buckling of the compression diagonals did not occur, which would have been anticipated with larger displacements. This is because the dissipative TADAS element, consisting of 9 plates, hardens during the test, resulting in an emphasized isotropic hardening.

a)   b)
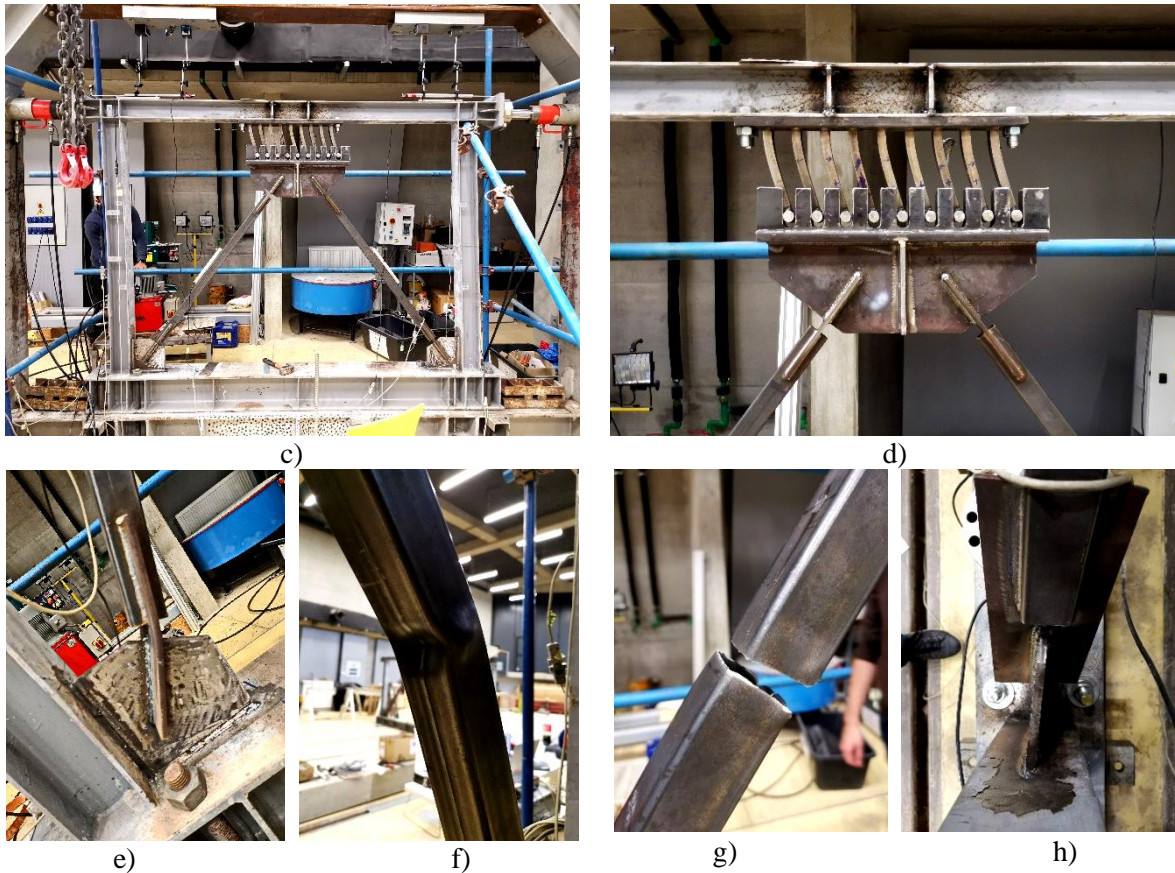
Fig. 7 - Photos of steel frame specimens during static tests, a) Bare frame, b) Chevron frame (Inverted V-braced frame), c) & d) TADAS frame, e) rotation of knife plate on Chevron frame due to buckling of compression diagonals, f) & g) before and after fracture of tension diagonals in Chevron frame, h) out-of-plane instability of frame (torsion), whereupon tests on TADAS frame were stopped.

Figure 9 presents the hysteresis envelopes in conjunction with the corresponding secant stiffnesses of individual specimens. The envelopes are generated as an average of the positive and negative load directions to consider imperfections in the test specimens and boundary conditions.
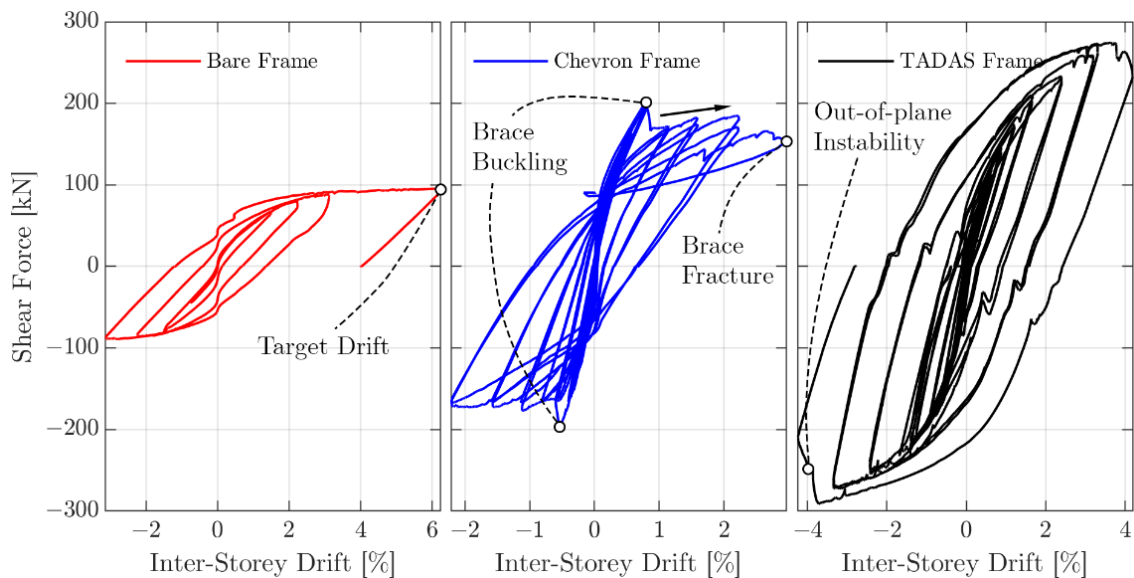
Fig. 8 - Global hysteresis responses of all steel frames
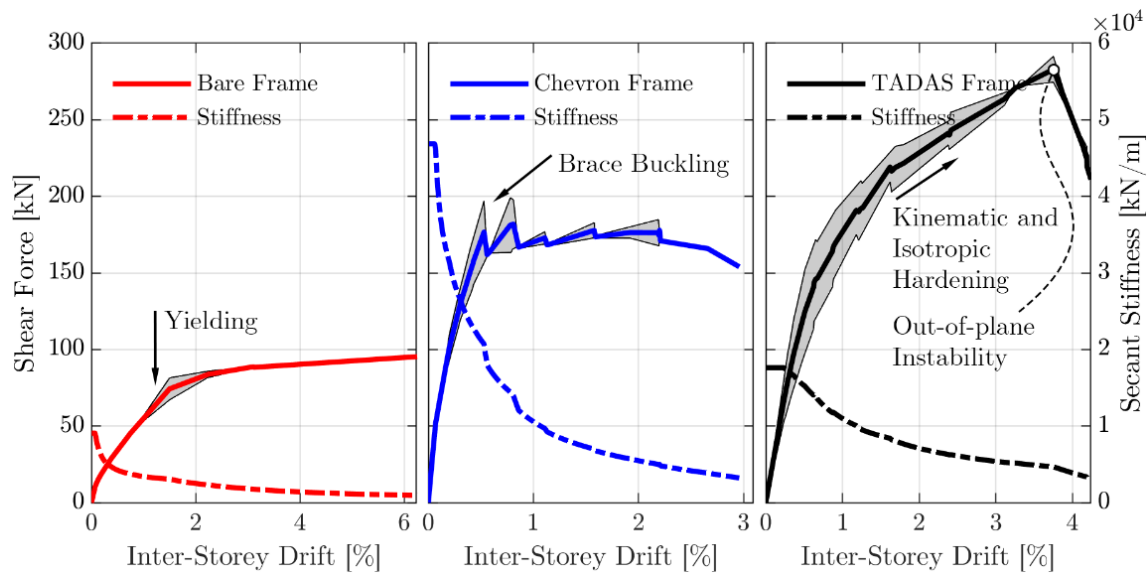
Fig. 9 - Hysteresis envelopes and associated secant stiffnesses for all steel frames

The experimental testing of the bare frame (BF) and TADAS frame (TF) was prematurely terminated because of significant global out-of-plane instability. Similarly, testing of the Chevron frame (CF) was discontinued due to a brace tensile failure. No buckling of the compression diagonals was observed in the TF. The TF exhibited a greater emphasis on isotropic hardening. The ductility of the CF was found to be 0.6 times lower, while that of the TF was 1.4 times higher in comparison to the BF. The initial stiffness of the system was determined to be 5 times higher in the CF and 2 times higher in the TF, in comparison to the BF. The cyclic responses of the specimens displayed symmetrical behaviour. The cumulative energies are illustrated in Figure 11, up to the largest common cumulative displacement.
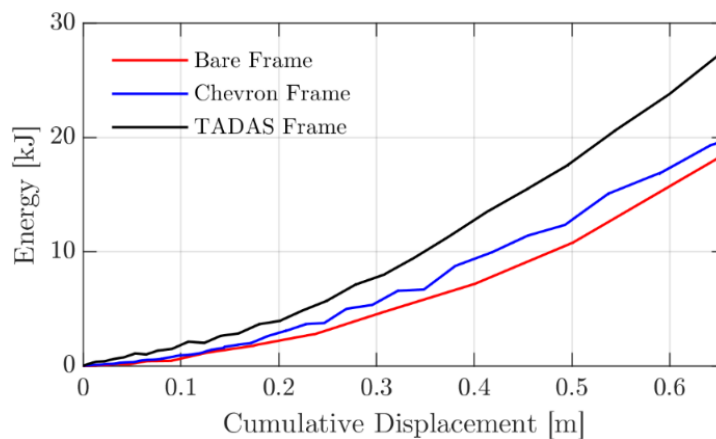
Fig. 11 – Cumulative hysteretic energies up to the largest common cumulative displacement

4. Conclusions

The utilization of strengthening techniques can significantly contribute to an improved response of steel frame structures in seismic design scenarios. The strengthening measures can be applied during the design stage of the structure or after it has been constructed. During design, the incorporation of strengthening measures can decrease the dimensions of the column cross-section, resulting in a more efficient design. By strengthening an existing structure, an increase in horizontal stiffness can be achieved.

Both types of strengthening resulted in higher load-bearing capacity compared to the un-reinforced frame. The diagonally braced frame (Chevron frame) achieved twice the lateral load-bearing capacity

compared to the bare frame, while the TADAS frame achieved almost three times the load-bearing capacity compared to the un-reinforced frame. A frame with concentric bracing could only achieve just under half the displacement compared to a bare frame. The frame with the dissipative TADAS connection achieved 32% greater displacement than the frame stiffened with concentric bracing. The TADAS frame is more ductile than the Chevron frame and has a higher load-bearing capacity, which is a desirable behaviour. The behaviour of a bare frame can be predicted well. Damage occurs at the expected locations, namely at the base of the columns. It is assumed that the bare frame would have made larger displacements if there had not been a loss of out-of-plane stability.

It was expected that the TADAS frame would withstand a greater load than a Chevron frame, which was the case. The advantage of this type of strengthening is that it has retained the best behavioural characteristics of the other two types of strengthening, i.e., the advantage of higher load-bearing capacity with sufficient ductility.

Experimental testing of the bare frame (BF) and TADAS frame (TF) was prematurely terminated due to the emergence of significant global out-of-plane instability. Testing of the Chevron frame (CF) was similarly discontinued as a result of brace tensile failure. Analysis revealed that the ductility of the CF was found to be 0.6 times lower, while that of the TF was 1.4 times higher, in comparison to the BF. The initial stiffness of the system was determined to be 5 times higher in the CF and 2 times higher in the TF, in comparison to the BF. The cyclic responses of the specimens displayed symmetrical behaviour. The TF was observed to dissipate 4 times more energy at the point of failure (brace fracture vs out-of-plane instability) than the CF. It is thus important to carefully design the braces and plates of the TADAS element in order to maintain the plasticization hierarchy.

References

[1] AISC, American Institute of Steel Construction (2018) Seismic Design Manual, Third Edition, ISBN: 978-1-56424-035-4.

[2] Ülker, M., Işik, E., Ülker, M. (2017) The Effect of Centric Steel Braced Frames with High Ductility Level on the Performance of Steel Structures, *In proceedings: International Conference on Advances and Innovations in Engineering* (ICAIE)

[3] Whittakar, A., Bertero, V., Alonso, J., Thompson, C. (1989) Earthquake Simulator Testing of Steel Plate Added Damping and Stiffness Elements. *Report No. UCB/EERC-89/02*. Earthquake Eng. Res. Center Univ. California, Berkely, URL: https://nehrpsearch.nist.gov/static/files/NSF/PB92192988.pdf

[4] Tsai, K., Chen, H., Hong, C., Su, Y. (1993) Design of Steel Triangular Plate Energy Absorbers for Seismic-Resistant Construction. *Earthq. Spectra*; 9(3): 505-28., DOI: https://doi.org/10.1193/1.1585727

[5] Radić, I. (2012) Ponašanje čeličnih okvirnih građevina sa zidanim ispunom pri djelovanju potresa, PhD Thesis, University of Osijek, Croatia, URL: https://www.bib.irb.hr/608906

[6] Landolfo, R., Mazzolani, F., Dubina, D., Simões da Silva, L., D'Aniello, M. (2017). Design of Steel Structures for Buildings in Seismic Areas: Eurocode 8: Design of structures for earthquake resistance. Part 1-1 – General rules, seismic actions and rules for buildings, Print ISBN: 9783433030103, Online ISBN: 9783433609194, DOI: https://doi.org/10.1002/9783433609194

[7] FEMA 461 (2007), Interim Testing Protocols for Determining the Seismic Performance Characteristics of Structural and Nonstructural Components, Applied Technology Council, Prepared for Federal Emergency Management Agency, URL: https://www.atcouncil.org/pdfs/FEMA461.pdf

SEISMIC BEHAVIOUR OF BEAM-COLUMN JOINT IN R/C FRAMES AND STRENGTHENING WITH FRP

Naser Kabashi [(1)], Enes Krasniqi [(2)], Milot Muhaxheri [(3)], Florentinë Latifi [(4)], Ylli Murati [(5)]

[(1)] *Professor, Faculty of Civil Engineering, naser.kabashi@uni-pr.edu*
[(2)] *PhD cand. Assistant , Faculty of Civil Engineering, enes.krasniqi@uni-pr.edu*
[(3)] *Prof. ass, Faculty of Civil Engineering, milot.muhaxheri@uni-pr.edu*
[(4)] *Msc.,Faculty of Civil Engineering, florentinelatifi.ce@gmail.com*
[(5)] *Msc.,Faculty of Civil Engineering, yllimurati.bm@gmail.com*

Abstract

Multi-story reinforced concrete structures in previous periods, in general, do not meet current seismic design code requirements, including the poor materials and execution of civil engineering works. In the scope of this, is analyzed the behavior of the structures during the Earthquake of November 2019, in Albania, specifically in different building stocks.

Typical structural deficiencies observed in reinforced concrete (R/C) frame buildings affected by the 2019 earthquake reveal that many collapses occurred could be attributed to the poor quality of construction and use of non-ductile detailing and during the assessment that deficiency beam–column joints can jeopardize the integrity of structures. In general, it is accepted that beam-column joints are critical elements of reinforced concrete buildings subjected to lateral loads and that they may require specific design. Assessment reports have often indicated that beam-column joints, which are one of the most vulnerable and critical structural elements, often suffer shear and/or bond (anchorage) failures leading to a partial or total collapse of the structure.

This paper will present some of the destructive and non-destructive tests specifically to the beam-column joints and techniques using fiber-reinforced polymers (FRP) for strengthening. Strengthening of beam-column joints by FRP materials nowadays is treated with various analytical approaches integrated in different software. Various analyses have been conducted and a practical proposal for retrofitting is presented in cohesion with the study case and the implementation.

Keywords: beam-column joint, moment-resisting frame, seismic behavior, strengthening, FEM analysis

1   Introduction

An earthquake generates multiple seismic loads of varying intensities that can damage a building, necessitating the design of all components to withstand such loads. The reinforced concrete (R/C) frame joints are crucial in providing a continuous load path to transfer applied loads between beams and columns. These joints experience significant forces during an earthquake and can reach their maximum capacity before the building stops swaying. Inadequate design and detailing of the joints can lead to premature failure, causing the structure to collapse. Therefore, proper detailing and design of R/C frame joints are critical for ensuring the building's stability and safety during seismic events[1]. At the beam-column joint, transversal reinforcement is used to enhance the ductility of the element and, therefore, the structure. The amount of seismic energy absorbed by joints depends on how much the column and beam deform without reaching their ultimate capacity[2]. Fig. 1 illustrates the behavior of an element under bending, from the initial cracks to ultimate deformations. Under both permanent and transient design situations, the structure is calculated with linear-elastic approaches and has linear elastic behavior. However, under seismic loads, the elements enter the plastic phase of non-elastic behavior. As shown in Figure 1, the plastic zone is from point A to point D. Point D' is reached through retrofitting. The figure also demonstrates how the use of additional exterior reinforcement with FRP extends the plastic zone. This kind of improvement provides a significant increase in the strength of the joint, which is essential for horizontal loads. The purpose of this paper is to investigate the feasibility of retrofitting the joints in RC frames, specifically in older buildings[3]. The case studies used in this research were

chosen to represent the in-situ conditions of collapsed buildings in Albania. Whether it's inadequate material quality or reinforcement ratio, the examples show the clear difference in behavior between an unreinforced joint and one reinforced with FRP.

a) Unstrengthened   b) FRP strengthened
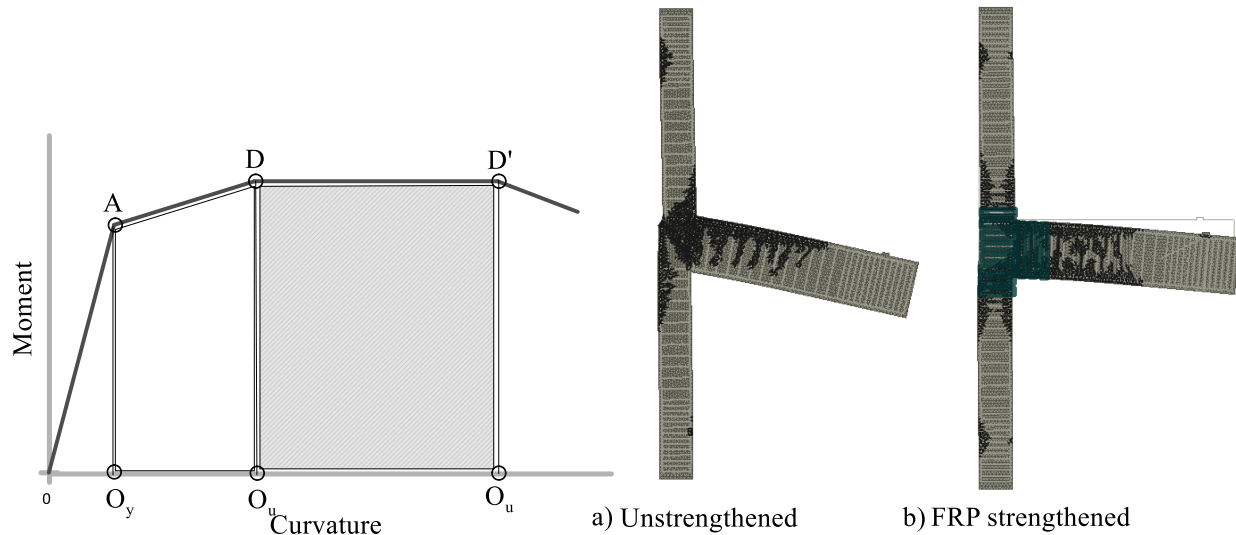
Fig. 1. Beam/column plastic zone enhancement.

2   Joints in resisting frames structures

Reinforced concrete is a popular construction material due to its strength, durability, and low maintenance cost. However, concrete beams and columns without reinforcing bars lack ductility and are brittle. Although steel reinforcement adds ductility to the structure, it alone does not guarantee the desired behaviour of the beam-column joint. Comprehensive and adequate joint detailing is critical to ensure its performance and ability to withstand anticipated loads. Building codes prescribe detailed requirements for joint detailing, including member sizes, reinforcement ratios, anchorage lengths, and flexural strength. Compliance with these codes ensures the desired performance of the structure under various loading conditions, ensuring safety and structural integrity[4]. A nonlinear analysis is necessary to understand the behaviour of a reinforced concrete (R/C) frame during seismic events. The collapse of an R/C frame is due to the formation of a plastic hinge mechanism caused by the cycling load on frame components that develops a hysteric loop in the beam/column. During high seismic forces, failure occurs in the joint due to the failure of the diagonal compression strut and the development of large shear cracks, resulting in spalling of the concrete core, buckling of rebars, beam failure, and, ultimately, column failure.

Tests have been conducted to investigate the effects of different joint configurations on the seismic performance of R/C frames. Results suggest that joint performance improves when the hooks' ends are bent into the joint core. Additionally, 14 experiments examined the impact of axial column force and reinforcement on joint behaviour. These experiments provide valuable insights into the behaviour of R/C frames under seismic loading, which can inform the development of more robust and reliable structures[5]. It is noticeable that specimens with higher axial load had delayed shear cracking. Shear reinforcement within the joint gave higher capacities and gradual strength degradation. Depending on the joint's reinforcement detailing, damage mechanisms are also different. As for the system, early cracks in joints reduce the rigidity of the system and cause an uncontrolled redistribution of the stresses. Some of those cracks are shown in the figures below[6].
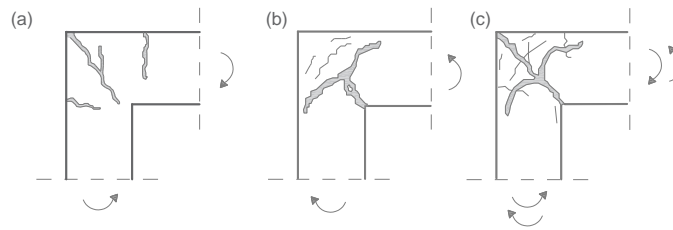
Fig. 2. (a) Compression of the inner fibers; (b) tension of the inner fibers and; (c) alternative moment.
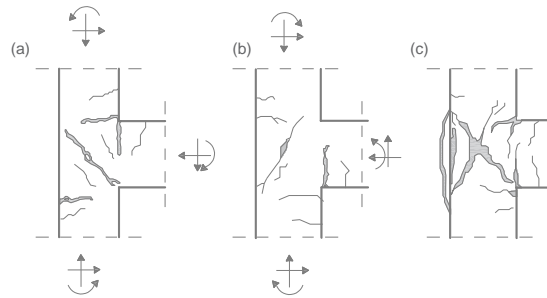
Fig. 3.(a) Compression of the lower fibers; (b) tension of the lower fibers and; (c) alternative moment.
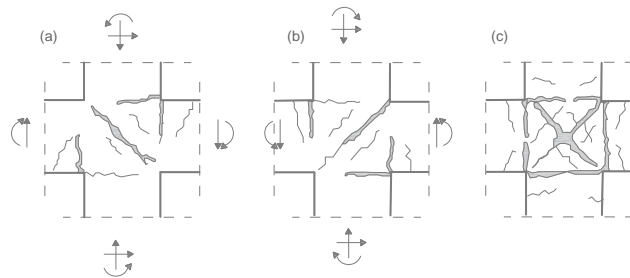
Fig. 4. Interior joint: (a)Horizontal load from the right side; (b) Horizontal load from the left side and (c) alternative horizontal load.

3   Assessments in Albania

The recent earthquake in Albania highlights the critical significance of proper detailing, dimensioning, appropriate construction materials, and foundation design. The failure of many buildings during the earthquake was attributed to the removal of masonry walls on the first floor, creating soft stories and discontinuity in the rigidity of the structural system, resulting in the structure's collapse at the early stages the earthquake. Various factors, such as concrete quality discontinuity, low concrete strength, construction errors, artistry, and steel bar corrosion, can adversely impact the lateral stiffness of the structural system[7]. The in-situ testing proves the latter statement. The quality of concrete was assessed using both non-destructive and destructive methods which are shown below[8]. For a more detailed analysis, we used in-situ testing methods for evaluating concrete strength with Hammer Schmidt and the damaged parts
to evaluate the concrete by taking and preparing samples with dimensions 60x60x60mm for laboratory investigations as described in Table 1.

Table 1. – Test results – Nondestructive (Non damaged part) and Destructive (Damaged part) [8]

Pos	X_{min}	X_{avg}	f_{cki} (N/mm^2)
Circular	30	37.6	38.8

Column			
Rectangular Column	33	38.3	40.0
Rectangular Column (laboratory test)	N/A	N/A	8.58

Fig. 5. Plastic hinge at the columns of multi stories building, inadequate materials and other deficiencies.

3.1 Retrofitting strategy

FRP exhibits elastic behaviour, characterized by the absence of a distinct yield plateau. Its tensile strength significantly exceeds that of steel, making it an ideal choice for external reinforcement layers, which enhance joint resistance. The present study involves column jacketing and single-sided joint cover retrofitting, utilizing the Mapewrap system fabrics. The approach adopted for quantifying the contribution of FRP reinforcement is based on the guidelines outlined in the recent FIB Bulletin 90, which addresses the use of FRP for reinforcing existing structures[9]. A two-dimensional sectional analysis program for beams and columns is used to calculate the strength and ductility of a R/C cross-section subjected to shear, moment, and axial load, thus extracting the moment-curvature and moment-max cracks joint curves[10]. The calculations are based on the following approaches: Shear tensile stress of FRP (expression (2)); shear tensile stress in the joint (expression (3)) and shear tensile capacity of the joint (expression (4)).

$$V_{jh.d.max} = V_{jh.d} = \frac{M_{Ed.sx}}{0.9(h_{b.sx} - c)} + \frac{M_{Ed.dx}}{0.9(h_{b.dx} - c)} - V_{Ed} \qquad (1)$$

$M_{ed,sx}$ – Bending moment on the left beam

$M_{ed,dx}$ – Bending moment on the right beam

c – Cleare concrete cover

$h_{b.dx}$ – Height of the right beam

$h_{b.sx}$ – Height of the left beam

V_{Ed} – Shear force acting on the base of the upper column

$$\sigma_{jt,FRP} = \varepsilon_{f.d} \, E_f \, A_f / \left(\frac{b_c \, h_c}{sin\theta} \right) \qquad (2)$$

$$\sigma_{jt} = \left| N/2A_j - \sqrt{(N/2A_j)^2 + (V_j/A_j)^2} \right| \leq 0.3 \sqrt{f_c} \qquad (3)$$

In accordance with what is prescribed in the guideline, the resistant capacity of the node panel is fixed at the drawing of a main traction stress equal to 0.3√fc. The question comes calculated as a function of the knot shear, Vj, and the normal force acting at the base of the primary column.

$$\sigma_{jt} \leq 0.3 \sqrt{f_c} + \sigma_{jt,FRP} \qquad (4)$$

4 Study case

A representative model is developed referencing common structures in Albania, and the internal forces taken into consideration here are from the joints of the first floor. The following examples are presented here; 3D geometry of study case where interstory height is 2.7m; bay dimensions are 4mx4m, the number of stories is 6 and referent modes are $T_1=0.95s$; $T_2=0.93s$; $T_3=0.77s$. The observed damage to buildings caused by earthquakes is various, and for analysis, three main study cases have been considered: study case 1- Inadequate detailing, good material properties, study case 2- Inadequate material properties, moderate detailing and study case 3- Moderate detailing and material qualities.
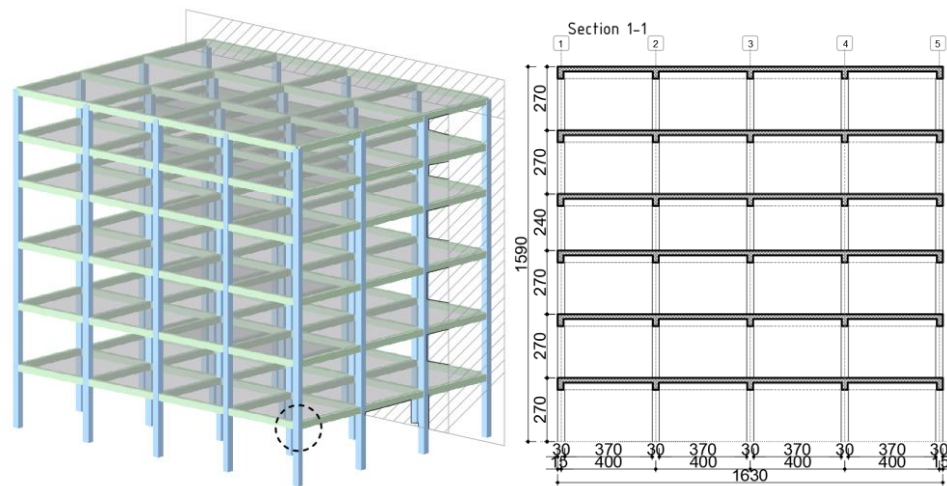
Fig. 6. 3D geometry of the reference structure and referent plane section.

ATENA in combination with GiD is used to conduct FEM analysis because it provides the possibility to model the strengthening of different structures[11]. ATENA-GiD is a finite element-based software system specifically developed for the nonlinear analysis of reinforced concrete structures. The reference experimental investigation uses light FRP strengthening solutions that are applied to the joint panel completely from the exterior of a building[12]. The investigated FRP-strengthening layouts are designed according to minimize the level of disruption caused by their application. Material model for 1D reinforcement is the most suitable for FRP lamellas where lamellas are more line strengthening elements than planar, they are modelled as 1D reinforcement elements[13].
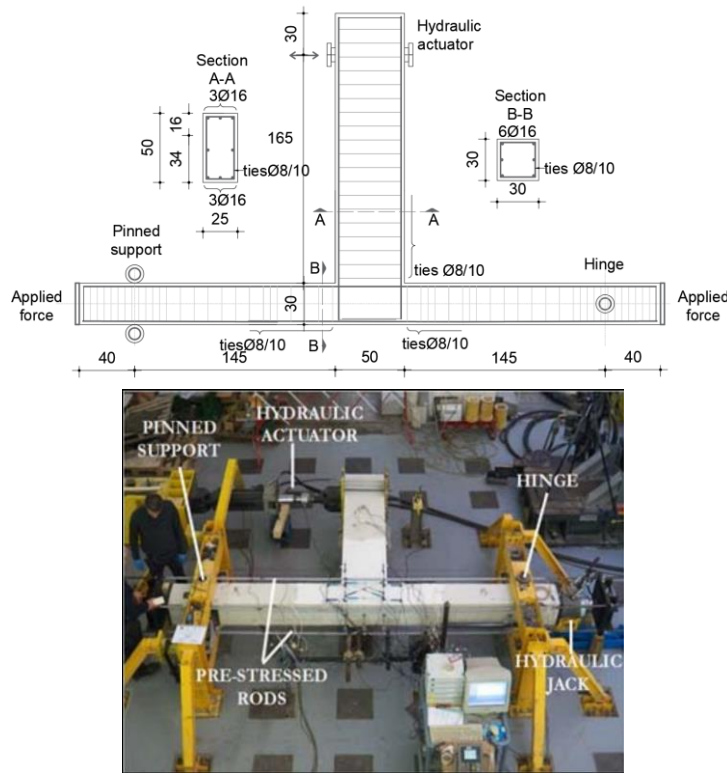
Fig. 7. (a)Description of geometry and reinforcement; (b) Instrumentation and test setup.
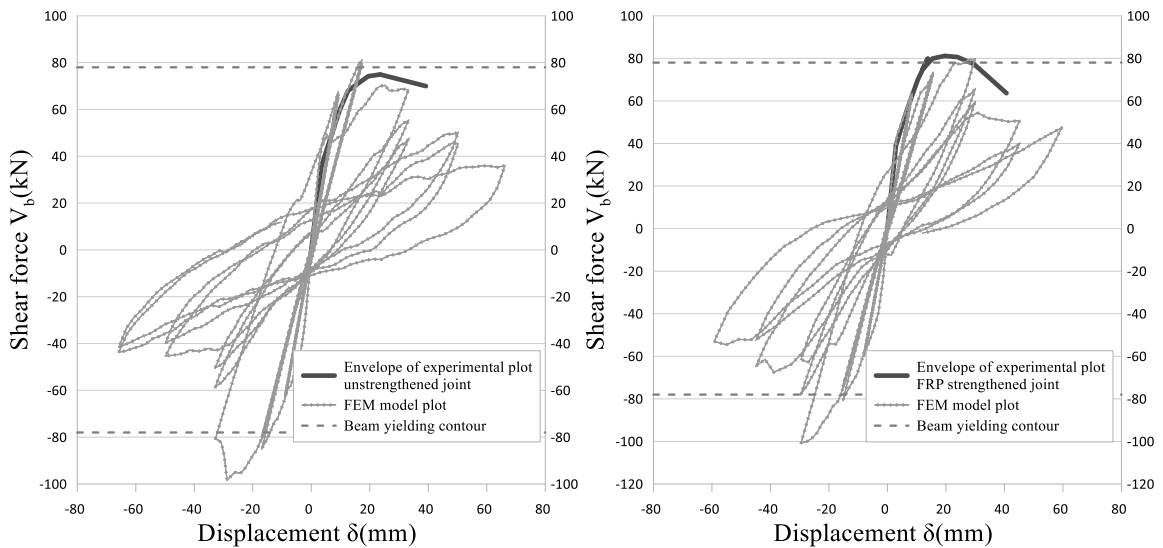
Fig. 8. Shear-drift response of tested joints: (a) envelope of unstrengthened joint vs FEM model plot; (b) first cycle envelope of FRP strengthened joint vs FEM model.

FE analysis of joints under cyclic incremental loading is conducted in reference to the control joint. Material constitutive laws and bond slip parameters of FRP are determined through an iterative process. Iteratively the procedure for obtaining a new bond slip function of FRP is progressively repeated until an acceptable adjustment of the load-displacement diagram is achieved where the percentage of error is achieved.

4.1 Study Case 1

The primary factors that characterize Study Case 1 are inadequate detailing and material properties, as indicated by the data presented in table 4. The moment-curvature diagram, which illustrates the capacity of the column and beam, further supports this assessment. Additionally, data pertaining to the FRP strengthening system, as presented in [14], further highlights the deficiencies in the structural system. These examples demonstrate the significance of proper detailing and quality material properties in ensuring the structural integrity of a building.

Table 2. Geometry of the joint for all study cases

	Top col.	Bottom col.		Left beam	Right beam
h_c [mm]	300	300	h_b [mm]	500	0
h_c [mm]	300	300	h_b [mm]	250	0
				Left	Right
Bay length [mm]				4000	0
				Top	Bottom
Interstory height				2700	2700

Table 3. FRP "MapeWrap C BI-AX 300 - E 256" mechanical properties for all study cases

σ_k	ε_{fk}	E_f	t_f	Fibers	f_{fd}
4830 MPa	0.021%	230000MPa	0.164mm	Carbon	3421.25MPa

Table 4. Column beam detailing data for study case 1

Concrete	D_{max}	$C_{o.nom}$	Rebars f_y
C20/25	31.5mm	2.0cm	240MPa
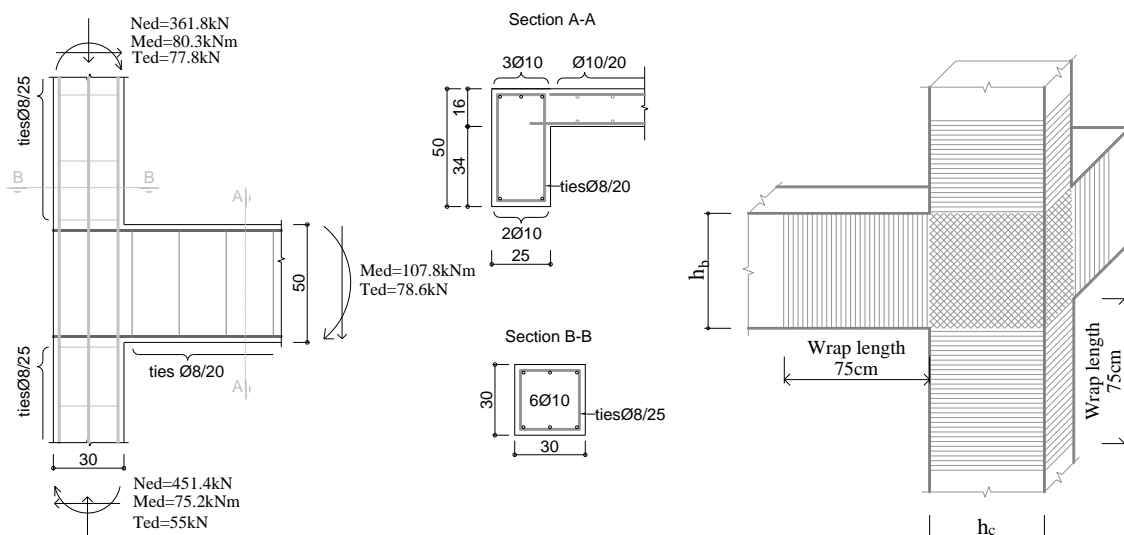
Fig. 7. Reinforcement detailing of the joint and the layout of the strengthening scheme.

The U-wrap end anchorages typically involve the utilization of uniaxial fabric that is extended by approximately 750 millimeters at the terminus of the beams and columns that frame the joint.

The moment-curvature diagram depicts the correlation between the bending moment (M) and curvature (Φ) of the beam/column, with a characteristic shape observed in all study cases. This diagram serves as a tool to evaluate the stiffness of the beam/column, its ultimate strength, load-deflection behaviour, and design considerations. The vertical axis represents the bending moment, while the horizontal axis indicates the curvature (mrad/m). Additionally, the moment-max crack width diagram represents the element's behaviour, where the inertia moment, stiffness, and other parameters decrease as the crack width increases.
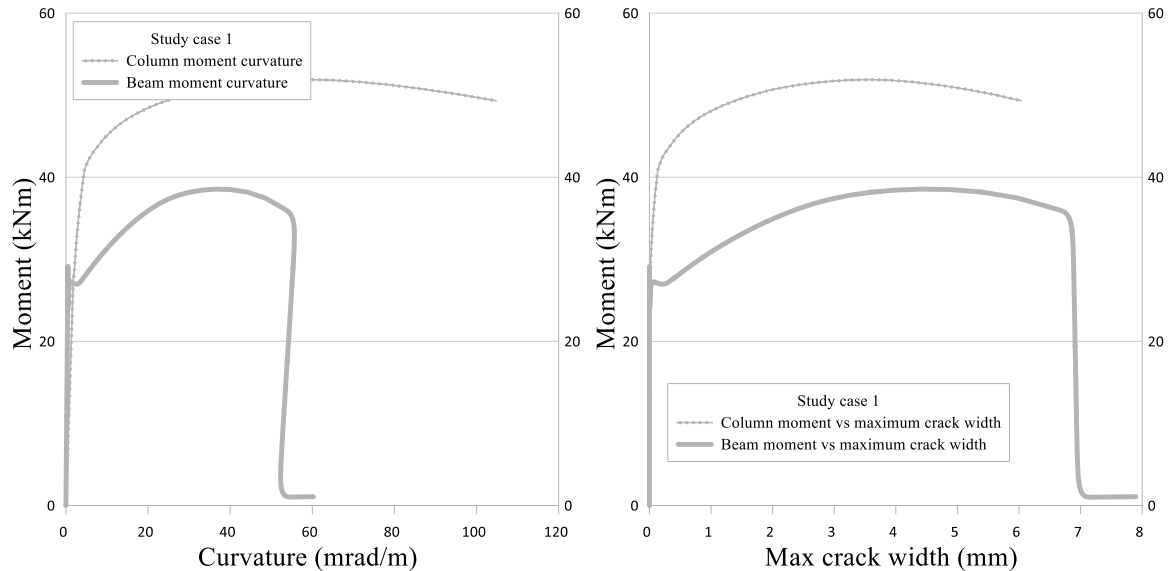
Fig. 8. (a)Beam and column moment-curvature diagram; and (b)Moment-max crack width diagram.

In the first study case, the column moment yield point exceeds the maximum moment resistance of the beam, meeting the criteria for satisfaction as per the Eurocode 8 standards. A comparison of the diagrams from all study cases allows us to infer that favorable material properties significantly impact the behaviour of the beam/column system. At the same time, the reinforcing measures exert a more significant influence on the joint's response.

4.2 Study Case 2

The analysis of Study Case 2 reveals moderate detailing and inadequate material properties, as evidenced by the data presented in 5. Moderate detailing and inadequate material properties of R/C joints can reduce the capacity to resist lateral forces from earthquakes, resulting in premature failure. Inadequate material properties can lower strength and ductility, while moderate detailing can result in insufficient reinforcement and anchorage. These factors increase the risk of joint failure, causing significant damage to the structure and jeopardizing the safety of occupants. Properly detailing and using high-quality materials are essential for optimal joint performance during seismic events.

Table 5. Column beam detailing data.

Concrete	D_{max}	$C_{o.nom}$	Rebars f_y
C12/15	31.5mm	2.0cm	400MPa
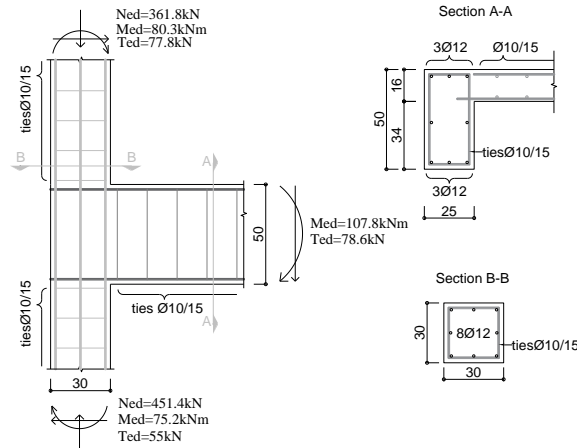
Fig.9. Reinforcement detailing of the joint.
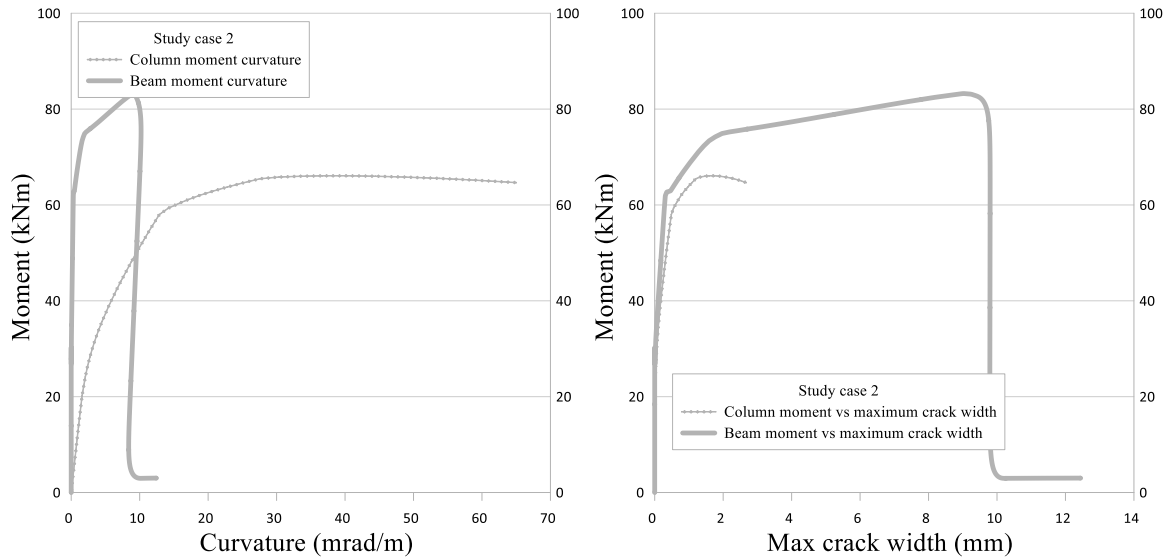
Fig. 10. (a)Beam and column moment-curvature diagram; and (b)Moment-max crack width diagram.

The diagram above demonstrates that the column moment yield point is significantly lower than the maximum moment resistance of the beam. Despite the joint possessing moderate detailing, its response is unsatisfactory.

4.3 Study case 3

The examination of Study Case 3 elucidates a state of moderate detailing and material characteristics substantiated by the data presented in Tables 12 and 13. The moment-curvature and moment crack width diagrams, derived from the aforementioned tables, provide additional evidence to support this classification. This instance exemplifies the interdependence between the quality of detailing and material attributes in determining the structural soundness of a building.

Table 5. Column beam detailing data

Concrete	D_{max}	$C_{o.nom}$	Rebars f_y
C20/25	31.5mm	2.0cm	400MPa
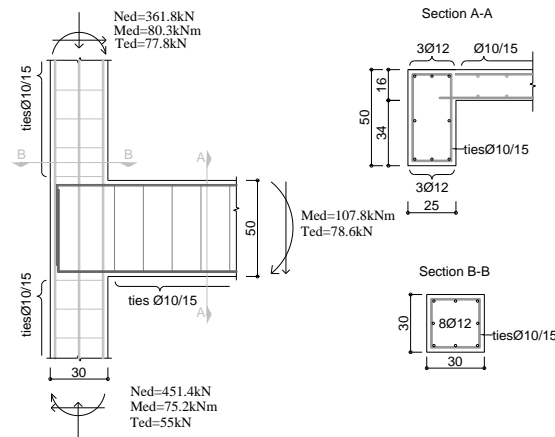
Fig. 11. Reinforcement detailing of the joint
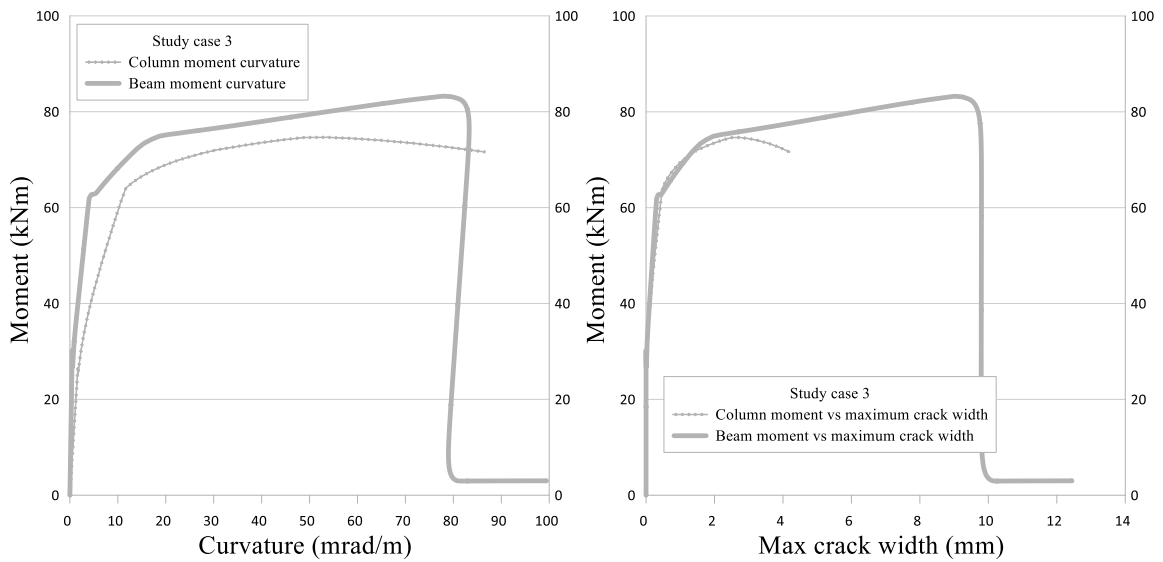
Fig. 12. (a)Beam and column moment-curvature diagram; and (b)Moment-max crack width diagram

In the above diagrame the beam and column have a similar response to the load applied. All three study cases give the capacity of the joint, which, when compared is below the demand.

Table 6 Results of joint capacity and demand values for all study cases.

		Study case 1	Study case 2	Study case 3
Capacity	$0.3\sqrt{f_{cd}}$	0.4	0.34	0.4
Demand	σ_{jt}	1.05	1.05	1.05
Result	$0.3\sqrt{f_{cd}} \geq \sigma_{jt}$	Failure	Failure	Failure

Table 7 Joint safety check after strenghtening. The following results have those inputdata on n_s=1; n_s=1; n_l=1; η_a=0.85; Υ_f=1.1 and the data in **Error! Reference source not found.**

		Study case 1	Study case 2	Study case 3
Capacity	$0.3\sqrt{f_{cd}} + \sigma_{jt.FRP}$	1.26	1.09	1.26
Rezult	$0.3\sqrt{f_{cd}} + \sigma_{jt.FRP} \geq \sigma_{jt}$	Satisfied	Satisfied	Satisfied
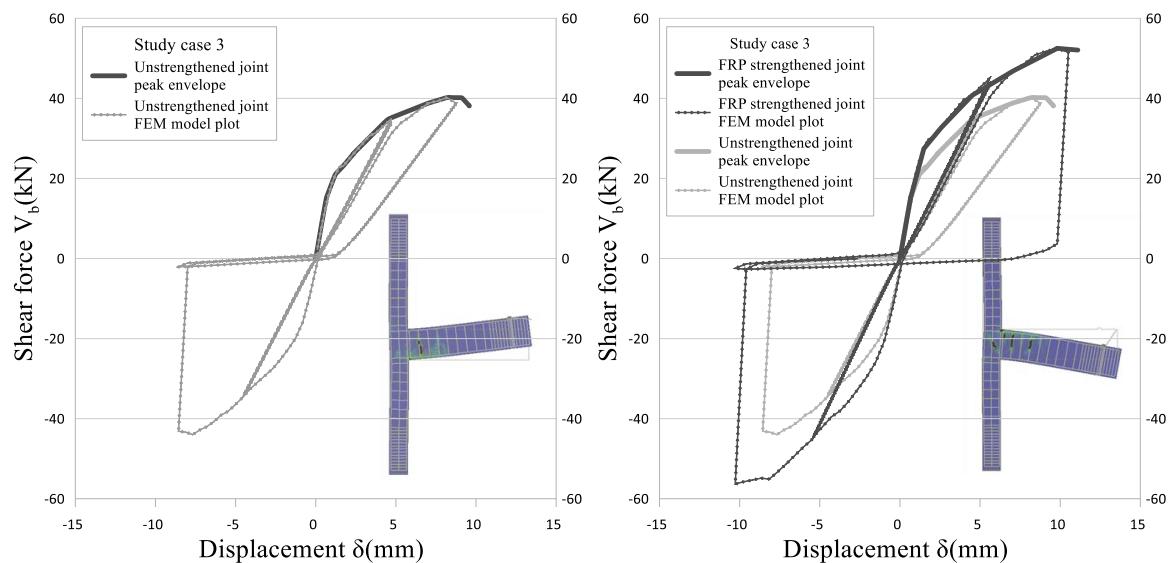
Fig. 13. Joint shear-drift response of analyzed joints: (a) FEM model plot and peak to peak envelope of unstrengthened joint; and (b) FRP strengthened vs unstrengthened joint

5 Conclusions

In seismic design scenarios, the behaviour of reinforced concrete (R/C) frame joints plays a pivotal role in determining the failure mechanism of the structure. Typically, the tensile shear capacity dominates the failure mode, while the compression strut exhibits adequate capacity.

The use of FRP as a strengthening material in exterior or corner joints can increase the shear tensile capacity. Notably, up to three layers of FRP can result in a substantial improvement in capacity, beyond which further layering is not recommended due to diminished retrofitting efficacy.

The layout scheme should incorporate mechanical anchors to prevent FRP failure resulting from low bond strength between FRP and concrete. Examples of such anchors include a U-wrap at the end of the beams or FRP spike anchors.Under seismic design situations the deformation of R/C frame joints determine the collapsing mechanism of the structure.

References

[1] Penelis, G. and Penelis, G. (2014) "Concrete buildings in seismic regions." Available at: https://doi.org/10.1201/b16399.

[2] Ingle, P.G. and Bhusare, V.P. (2018) "Performance based seismic design of reinforced concrete building by non-linear static analysis," *Journal of Advances and Scholarly Researches in Allied Education*, 15(2), pp. 340–344. Available at: https://doi.org/10.29070/15/56843.

[3] Fardis, M.N. (2009) "Seismic Assessment and retrofitting of existing concrete buildings," *Geotechnical, Geological, and Earthquake Engineering*, pp. 595–693. Available at: https://doi.org/10.1007/978-1-4020-9842-0_6.

[4] Elghazouli, A.Y. (2017) *Seismic design of buildings to eurocode 8*. Boca Raton, FL: CRC Press, Taylor & Francis Group.

[5] Beres, A. *et al.* (1996) "Implications of experiments on the seismic behavior of gravity load designed RC beam-to-column connections," *Earthquake Spectra*, 12(2), pp. 185–198. Available at: https://doi.org/10.1193/1.1585876.

[6] Penelis, G.G. and Penelis, G.G. (2018) *Concrete buildings in seismic regions, second edition*. Milton: Chapman and Hall/CRC.

[7] JOINT FRP v.2.0/ Software for the design of beam-column FRP. Developed and realized in the context of the research activities conducted in the DPC-ReLUIS Project 2019-2021. 2-nd release February 2022. Ciro Del Vecchio, Marco Di Ludovico, Alberto Balsamo, Andrea Prota

[8] Kabashi, N., Krasniqi, E. and Muhaxheri, M. (2021) "A typical column failure in 2019 Albania earthquake and retrofitting strategy." 1st Croatian Conference on Earthquake Engineering 22nd - 24th March 2021, Zagreb, Croatia

[9] Matthys, S. (2019) "General," *fib Bulletin 90. Externally applied FRP reinforcement for concrete structures*, pp. 1–5. Available at: https://doi.org/10.35789/fib.bull.0090.ch01.

[10] Bentz, E. C. (2000). Sectional analysis of reinforced concrete members [PhD Thesis]. *Toronto: University of Toronto*.

[11] Cervenka Consulting s.r.o. *ATENA for Non-Linear Finite Element Analysis of Reinforced Concrete Structures*. Prague: Červenka Consulting s.r.o.; 2015.

[12] De Risi, M.T. *et al.* (2020) "Light FRP strengthening of poorly detailed reinforced concrete exterior beam–column joints," *Journal of Composites for Construction*, 24(3). Available at: https://doi.org/10.1061/(asce)cc.1943-5614.0001022.

[13] Pryl D, Cervenka J. *ATENA program documentation, part 1 of 1, troubleshooting manual*. Prague: Cervenka Consulting Ltd.; 2013.

[14] Mapei, MapeWrap11 and MapeWrap11- In compliance with European standard EN-1504-4:2009-Provides specifications for structural bonding.

Keynote Lecture

DAMAGE, LOSSES, RECONSTRUCTION POLICIES, AND RETROFIT INTERVENTIONS ON RESIDENTIAL BUILDINGS IN HISTORICAL CENTERS AFTER RECENT ITALIAN EARTHQUAKES

Marco Di Ludovico [1]

[1] *Associate Professor, Department of Structures for Engineering and Architecture University of Naples Federico II*
Via Claudio, 21 - 80125 Naples - Italy, diludovi@unina.it

Keywords: post-earthquake reconstruction, historical centers, aggregate, empirical damage, losses.

1. Abstract

The reconstruction process of residential buildings damaged by L'Aquila 2009 earthquake initially involved buildings outside historical centres and then, starting from August 2012, residential buildings in historical centres. The reconstruction model related to buildings in historical centres was developed by two special offices, involved in the reconstruction process of L'Aquila municipality and other municipalities, respectively. Both special offices introduced new procedures to manage the reconstruction based on a parametric model to define the maximum public grant to repair and strengthen the damaged buildings in historical centres. The new model was necessary to deal with the reconstruction of historical centres mainly characterized by old masonry building aggregates with a cultural and architectural heritage value. The data collected in the management process of reconstruction outside and inside historical centers, allowed obtaining precious and unique information on buildings and aggregates characteristics, damage and usability ratings as well as repair and retrofitting cost data obtained by funding requests. Furthermore, these data are the basis to carry out a comparison between the repair and retrofit cost data and peculiarities of residential buildings outside and inside historical centers.

2. Reconstruction process of residential buildings inside and outside historical centers

Two different phases can be clearly distinguished in the reconstruction process after the L'Aquila earthquake. A first phase involved the reconstruction of residential buildings outside historical centres (OHC); the reconstruction policy was regulated by Law 77/2009 and several Ordinances of the President of the Council of Ministers (OPCM). At this stage the financial strategy of the Italian government was to fully cover the repair work costs to restore the usability of damaged buildings; furthermore, different thresholds were defined for strengthening interventions as a function of the usability rating of each building. The usability rating was determined by proper post earthquake field inspections carried out by team of surveyors; the AeDES survey form (Baggio et al. 2007) was adopted as a tool for the seismic damage and usability assessment. According to the AeDES survey form, the buildings can be classified into the following categories: A. Usable buildings (slightly damaged, can keep on housing the functions to which it was dedicated); B. Building usable only after short term countermeasures (buildings with limited or no structural damage but with severe non-structural damage); C. Partially usable building (build-ings with limited or no structural damage but with severe non-structural damage located in a part of the building); D. Building to be re-inspected (due to atypical damage scenario a specific, but still visual, investigation is required); E. Unusable building (high structural or non-structural risk, high external or geotechnical risk); F. Unusable building for external risk only.

For each building the repair and strengthening works and relevant costs were determined by practitioners engaged by owners. A proper team, called "Filiera" was set up to oversee these projects from the administrative, technical and economic angle and to deal with the numerous applications for

funding. At the end of this reconstruction phase, funding applications related to 5,775 residential buildings outside the historical centre of L'Aquila and other municipalities were examined and approved by the Filiera. The total amount allocated residential buildings outside the historical centre of L'Aquila municipality allocated until September 2013 was about 2,1 billion and the total amount due to the activity of the Filiera can be estimated of the order of 2.6 billion euros. Details about this first phase of the reconstruction process can be found in Di Ludovico et al. 2016a,b.

The second phase of the reconstruction process involved buildings inside historical centres (IHC) of L'Aquila and other municipalities; the reconstruction policy was regulated by Law 134/2012, which introduces a parametric model to determine the maximum public grant eligible to restore the usability of damaged buildings. The financial strategy of the Italian government was to fully cover not only the repair and strengthening costs to restore the usability of damaged buildings but also to establish some extra public funds to preserve the cultural and architectural heritage value of these buildings.

A new reconstruction model defined on the basis of new procedures was necessary in order to deal with the reconstruction of old masonry building aggregates (i.e. groups of masonry buildings to form complex building agglomerates) with a cultural and architectural heritage value. In this case, the reconstruction model refers to: a) Building Aggregates (namely BA); b) a portion of the BA with homogeneous characteristics, Aggregate Minimum Unit (namely AMU), see Figure 1 (e.g. the aggregate depicted in such figure is analysed by means of two applications related to AMU).The application for funding related to BA or AMU contains data related to one or more buildings (B) which consist of one or more dwellings.

Historical masonry buildings incorporate structural elements, such as arches, domes, vaults and irregular shaped-columns, with earthquake-response, which is difficult to simulate and predict in numerical analyses; furthermore, the seismic retrofitting measures in these cases are not straightforward because they should encompass efficiency and safety, compatibility with existing materials, non-invasive scheme and reversibility, as well as durability of the intervention. The built heritage conservation requires to apply minimally invasive techniques, but capable to ensure a significant increase of seismic safety. Operating on such a context involves a high level of un-certainty to define the state of preservation of structural and non-structural elements. It is particularly difficult to predict the exact amount of works to be performed during the design phase, therefore implementing a procedure capable of guaranteeing work in progress variants with an agile tool becomes essential, also ensuring expenditure control in the meantime.

Figure 1. Building Aggregate and sub-units.

Given the complex spatial and morphological structure of the territory, special rules for reconstruction have been issued for historical centres. The management of such stage of the reconstruction process was assigned to two special offices: the Special Reconstruction Office of L'Aquila - USRA - for the

reconstruction process of buildings in historical centres of L'Aquila, and the Special Reconstruction Office of the Crater Municipalities - USRC - for the reconstruction process of buildings in historical centres of other municipalities (56 municipalities in the area hit by the earthquake, the so called "crater").

To date the reconstruction process of IHC residential buildings is still ongoing. Details about this phase of the reconstruction process can be found in a "white book", published within the framework of the PE2019–2021 joint program DPC-ReLUIS, WP7: "Post-earthquake data analysis", consisting of seven chapters dealing with different aspects (Di Ludovico at al. 2022): *i)* Reconstruction procedures for residential buildings damaged by L'Aquila 2009 earthquake; *ii)* The reconstruction process inside the historical centers; iii) Characteristicts of building stock in the historical centers; iv) Damage on buildings in the historical centers; v) Repair and retrofit interventions; vi) Cost analysis; vii) Comparative analysis between repair costs for the reconstruction inside and outside the historical centers. The book reports data related to funding requests for repair and strengthening interventions on 1,421 BAs, 1,595 AMUs and 6,198 Bs. They corresponds to total amount of about 3,0 billion euros.

Details about number of buildings per AMU and their total gross surface as well number of storey and total gross surface of Bs are reported in Figure 2; it clearly appears that in most cases (56%) AMU consists of three of less buildings and have an average surface of 1,343 m^2 while buildings are commonly made by two or three storeys with an average surface of about 294 m^2
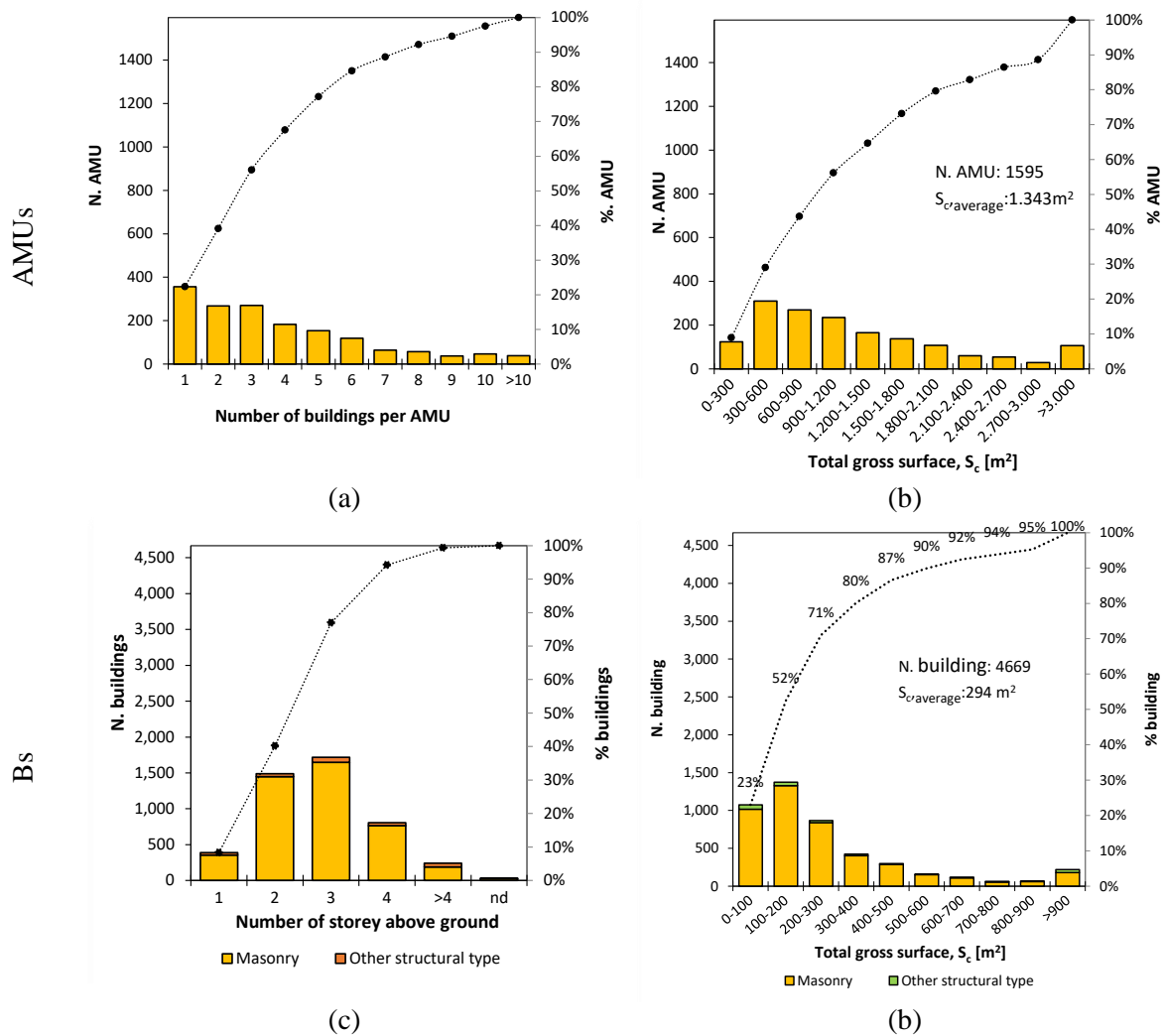
Figure 2. AMUs and Bs characteristics.

The data reported in the study shows that damage suffered by the buildings located in the historical centers may significantly differ from that detected on isolated buildings outside the historical centers;

furthermore, for building aggregates, edge and corner buildings are more vulnerable than the internal ones. The cost analysis carried out on both OHC and IHC building stock, showed that significant extra costs need to be accounted in the reconstruction process to preserve, restore and mitigate the seismic risk of historic-architectural valuable elements, buildings with landscape interest or buildings of cultural interest

The data collected by the Government Institutions involved in the 2009 post-earthquake reconstruction, both for OHC and IHC reconstruction process, provides an important database for future analyses and promote the definition of a unique code defining basic principles and rules for reconstruction. Furthermore, they are a precious for the calibration and refinement of models aiming at the evaluation of the seismic risk at large scale (Dolce et al. 2020, Di Ludovico et al .2022).

Acknowledgements

References

[1]   Law June 24, 2009 n. 77, in Official Journal of the Italian Republic, June 27, 2009, n. 147.

[2]   Baggio C, Bernardini A, Colozza R, Di Pasquale G, Dolce M, Goretti A, Martinelli A, Orsini G, Papa F, Zuccaro G, Pinto AV and Taucer F, Field Manual for post-earthquake damage and safety assessment and short term countermeasures (AeDES). EUR 22868 EN, Joint Research Centre, ISPRA, Italy, 2007.

[3]   Law August 07, 2012 n. 134, in Official Journal of the Italian Republic, August 11, 2012, n. 187.

[4]   O.P.C.M. August 15, 2009, n. 3803 - "Ulteriori interventi urgenti diretti a fronteggiare gli eventi sismici verificatisi nella regione Abruzzo il giorno 6 aprile 2009 e altre disposizioni di protezione civile".

[5]   Decree of the head of the USRC February 06, 2014 n. 1 "Disposizioni per riconoscimento del contributo per gli interventi sull'edilizia privata nei centri storici dei Comuni del Cratere".

[6]   D.G.R. 615/2010 Resolution of the Abruzzo Regional Executive committee, August 09, 2010, n. 615 "Limiti massimi di costo per gli interventi di edilizia sovvenzionata ed agevolata da realizzarsi sul territorio regionale".

[7]   Di Ludovico M, Prota A, Moroni C, Manfredi G, Dolce M (2017a) Reconstruction process of damaged residential buildings outside the historical centres after L'Aquila earthquake - part I: "light damage" reconstruction. Bull Earthq Eng 15:667–692

[8]   Di Ludovico M, Prota A, Moroni C, Manfredi G, Dolce M (2017b) Reconstruction process of damaged residential buildings outside the historical centres after L'Aquila earthquake - part II:"heavy damage" reconstruction. Bull Earthq Eng 15:693–729

[9]   Di Ludovico M., Dolce M., Prota A., "Libro bianco sulla ricostruzione privata dei centri storici nei comuni colpiti dal sisma dell'Abruzzo del 6 aprile 2009" - Doppiavoce – 2022, https://www.reluis.it/doc/pdf/pubblicazioni/Libro_bianco2.pdf.

[10] Dolce M, Prota A, Borzi B, da Porto F, Lagomarsino S, Magenes G, Moroni C, Penna A, Polese M, Speranza E, Verderame GM, Zuccaro G (2020) Seismic risk assessment of residential buildings in Italy. Bull Earthq Eng. https:// doi. org/ 10. 1007/ s10518- 020- 01009-5.

[11] Di Ludovico M, De Martino G, Prota A, Manfredi G., Dolce M.,(2022) Relationships between empirical damage and direct/indirect costs for the assessment of seismic loss scenarios. Bull Earthq Eng 20:229–254. https://doi.org/10.1007/s10518-021-01235-5.

BEHAVIOUR OF SEISMIC ISOLATED BUILDING DURING CENTRAL ITALY 2016 – 2017 EARTHQUAKES

Antonello Salvatori [(1)]

[(1)] *Professor of Seismic Engineering, University of L'Aquila, antonello.salvatori@univaq.it*

Abstract

The seismic sequence during years 2016 and 2017 involved a great area In Central Italy, involving four regions and more than 100.000 buildings. Many main shock events occurred, namely Amatrice earthquake (Mw 6.0 on August 24th, 2016), Valnerina earthquakes (Mw 5.9 and 5.4 on October 26th, 2016), Norcia earthquake (Mw 6.5 on October 30th 2016), and Montereale – Capitignano earthquakes (Mw 5.0, 5.5 on January 18th 2017) About 80.000 buildings were damaged in the seismic events. In particular, some areas were involved also in the 2009 seismic events (L'Aquila earthquake).

After L'Aquila earthquake, during reconstruction period, many buildings with base isolation (both existing and new ones) have been realized in the city area.

Furthermore, collapsed buildings, or heavily damaged buildings, were demolished and reconstructed with base isolation (both in foundation and above first elevation columns). The isolation systems were generally composed by both rubber high damping isolators, and plane friction isolators (sliding).

Some buildings, which reported less structural damage during 2009 L'Aquila earthquake, were retrofitted with isolation systems, both with rubber high damping isolators, and plane friction isolators.

All these isolated buildings were completed before year 2016, that is before the new strong seismic events in Central Italy.

Several different dynamic and seismic behaviour were observed in those buildings, depending upon isolation system (noticeable differences have been observed between curved sliding isolators and rubber high damping isolators) and upon soil – structure interaction. Significant displacement has been observed caused by soft soil, and inverse velocity seismic soil profile. Also, frequency response influenced isolated building behaviour.

In the work several buildings are examined, analysing the seismic behaviour both in the 2009 earthquake (with no isolation system) and during 2016 – 2017 seismic events (with isolation system).

Keywords: Seismic isolation, earthquake, structure monitoring.

1. Introduction

According to the available data, more than 20,000 structures in the world have been protected by passive anti-seismic (AS) techniques such as seismic isolation (SI) or energy dissipation (ED) systems, shape memory alloy devices (SMADs), or shock transmitter units (STUs) [1-5]. They are located in more than 30 countries (Fig. 1) and concern both new constructions and retrofits of existing structures of all kinds: bridges & viaducts, civil and industrial buildings, cultural heritage and industrial components and installations, including some high risk nuclear and chemical plants and components.

The use of SI became particularly rapid especially after the Abruzzo earthquake of April 6, 2009, as a consequence of the large damage caused by this event to the conventionally founded structures and cultural heritage [8-9]. The use of the traditional High Damping Rubber Isolators (HDRBs), in conjunction with some sliding devices (SDs), is also going on, in both L'Aquila and other Italian sites, for several new constructions and retrofits [6, 7, 10, 11]. The application of new retrofit techniques using SI, has also been applied for both reconstructing L'Aquila and for enhancing the seismic protection in a very earthquake-prone area.
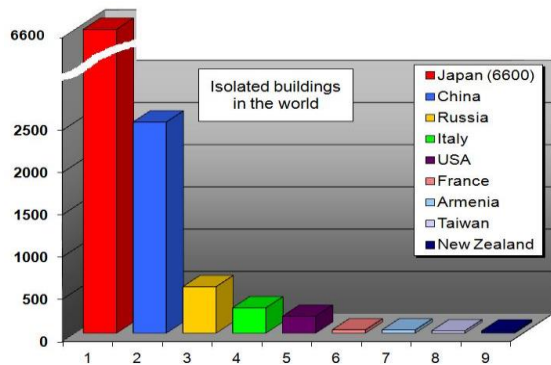
Figure 1. a) Isolated Buildings in the World;   b) Buildings with Seismic Isolation in Italy.
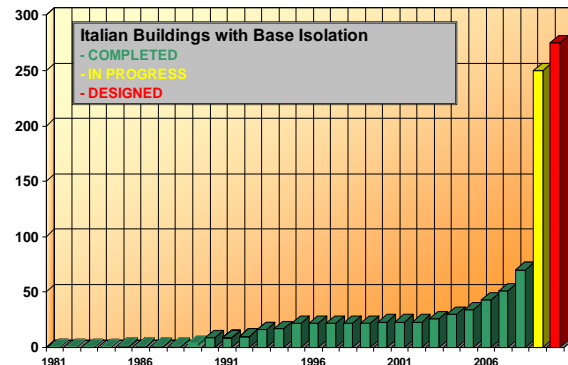
2. Buildings retrofitted with seismic isolation after L'Aquila earthquake

L'Aquila city was struck down by a 6.3 M_w and seismic moment $M0 = 3.7 \times 1018$ N m (according to INGV) earthquake in 2009 April 6th. Its historical centre and all the surrounding suburbs were severely damaged, causing 309 casualties, and more than 1500 people injured. L'Aquila has been the first Italian important city directly destroyed by a near fault earthquake since Messina earthquake (1908). Many buildings collapsed completely, both in masonry structure and in reinforced concrete ones. Many buildings suffered heavy structural damages, like shear cracks in the pillars, shear cracks in the concrete walls, nodal ruptures, and even total or partial collapses. Some more recent buildings evidenced noticeable structural damage, mainly due to design errors and constructive inadequacy.

Registered data showed response spectra very different due to the local amplification effects.as shown in Fig. 2.

In particular, response spectra evidenced a local strong amplification in correspondence of the high frequencies (0 – 3 Hz) in the suburbs (Mount Pettino west area, in correspondence with an active local fault), where several reinforced concrete buildings were heavily damaged also in structural elements.

The damage can be associated to dynamic resonance in correspondence of the highest values in the response spectra, due to the reinforced concrete building characteristics (main frequency often in the range 2.0 – 10.0 Hz). Some differences, due to soil amplification effect, were found in the centre of the city, as shown in fig. 3. The local site effect reveals itself noticeable in relationship with the dynamic behaviour of seismic isolated buildings.
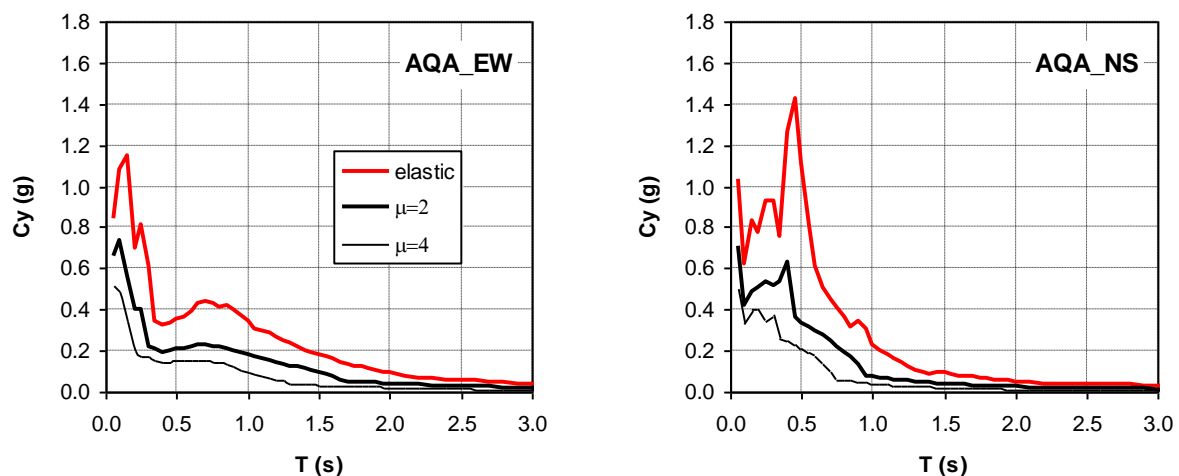
Figure 2. Response spectra in L'Aquila west area (near fault), amplification effect at 10.0 – 2.0 Hz.
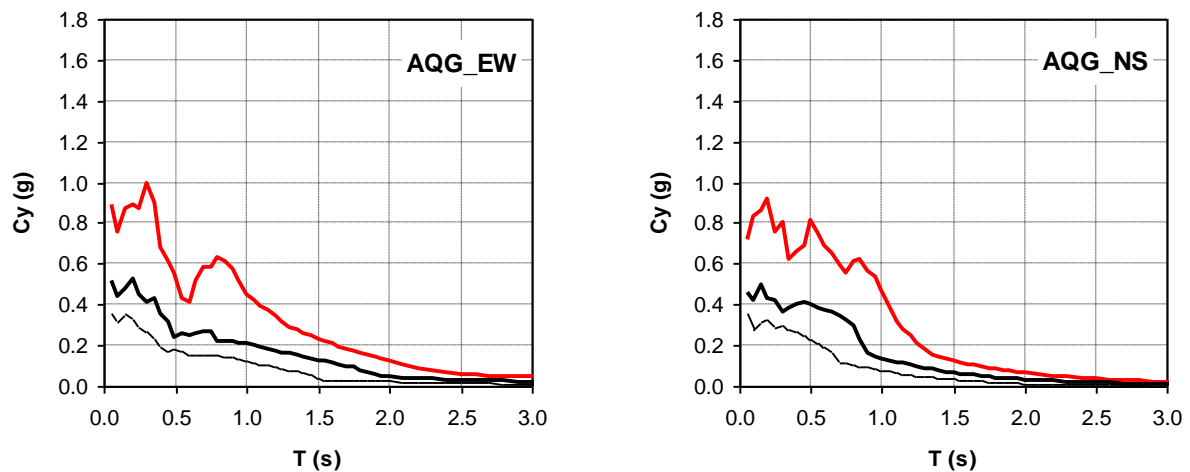
Figure 3. Response spectra in L'Aquila central area, with secondary amplification effect at 0.6 – 0.7 Hz

After the main seismic event, many buildings were retrofitted by the application of an isolation system.

The base isolation seismic protection is a technique increasingly widespread in Central Italy, which is strategic for repair and strengthening both damaged and retrofitted buildings and new ones. In particular, when in the presence of structures with considerable structural irregularities, both elevations that planimetric, with structural elements with poor energy dissipating capacity of the seismic input energy, and construction details not satisfying due to the seismicity of the area, the base seismic isolation is the only constructive solution to the problem of making these structures seismic-resistant under conditions compatible even with a complex architectural appearance of the buildings themselves.

The use of the anti-seismic systems and devices in the city context already includes not only the strategic structures (civil defence centres, hospitals) and the public ones (schools, churches, commercial centres, hotels), but also, and mainly, residential buildings and even many small and light private houses.

A noticeable number of existing (and also reconstructed) buildings were seismically improved by application of seismic isolators, in particular High Damping Rubber Isolators (HDRB) and Sliding Devices (SD). In the following some of them will be examined in their main features.

2.1 Building #1 (near west area)

The first building under examination is located in the west area of the city, were no secondary amplification effect are detected. The building was heavily damaged during L'Aquila earthquake and was retrofitted by an isolation system. The damage concerned mainly brittle fracture in some pillars at low levels, and significant damage to the external infill panels, internal brick masonry panels and secondary non-structural elements. The type of non-structural elements damage is strongly variable but it is mainly related to wrong construction techniques, and, in second order, to wrong design.

In most of these collapses, the presence of non-structural columns would prevent the rotation and failure.

The high deformability of reinforced concrete structures has carried out to high levels of the compression and shear forces. Storey drifts have reached high values, not compatible with the stiffness and relevant flexibility of masonry infills. After 2009 earthquake, which caused the noticeable damage in structural and non-structural elements, the only way to prevent further damage and increased collapse risk probability has been the seismic behaviour enhancement by applying anti seismic devices (isolators) with a retrofitting technique. Furthermore, the high planimetric non regularity of the building (T-shaped) can be regularized only by the application of an isolation system.

| Figure 4. a) Building # 1 (seven storeys) | b) Brittle fracture in a pillar |

By cutting pillar top edge, after reinforcing foundation and pillar lower part, 32 elastomeric isolators and sliders have been positioned. The HDRBs are 9 FIP SI-S 700/200 and 10 SI-S 800/200, and the sliding devices area 13 FIP VM 250/700/100. In fig. 5 the insertion of an isolator in the top of the pillar is shown.
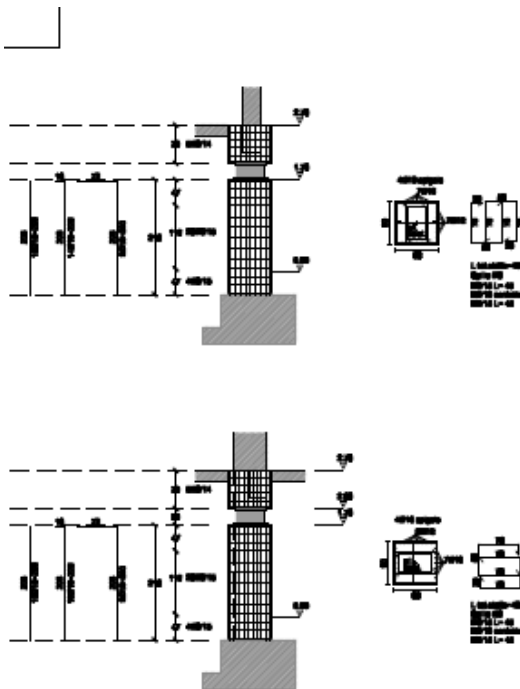
| Figure 5. a) Enhancement of the lower part of pillars | b) Insertion of a HDRB isolators at the top of the pillar |

| Figure 5. a) Strengthening of a pillar | b) Cutting a pillar for isolator insertion |
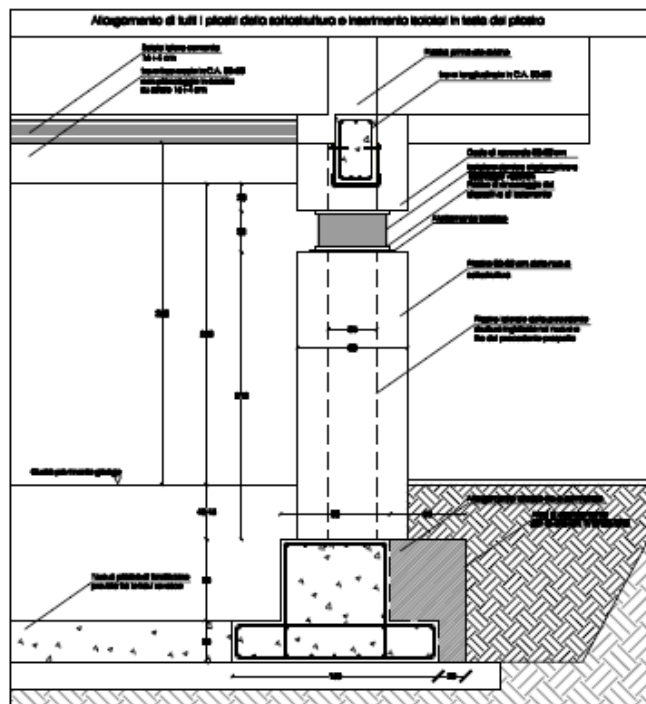
Figure 5. a) Strengthening and cutting the top of a pillar

b) Control of the cutting of a pillar

Figure 6. a) Insertion of an elastomeric HDRB SI-S 800

b) Insertion of a slider Vm 250/700/700

Figure 6. a, b) Level 0 with all isolators at the top of strengthened pillars

b)

The retrofitted structure has reached a level of vulnerability, by applying anti-seismic isolation, equal to the 80% of the corresponding new structure, according Italian seismic code. The same level of seismic vulnerability, before the application of the isolation system, was equal to only the 15%, value which is confirmed by the damage in the 2009 earthquake. This building was hit again by nine strong earthquakes almost in the same area (Central Italy, epicentral distance from 30 to 50 km), in 2016 and 2017, (Mw 6.0 on August 24th, 2016), Valnerina 3 earthquakes (Mw 5.9 and 5.4 on October 26th, 2016), Norcia earthquake (Mw 6.5 on October 30th 2016), and Montereale – Capitignano 4 earthquakes (Mw 5.0, 5.5 on January 18th 2017) with no damage at all.

2.2 Building #2 (west area)

The second building under examination is located in the west area of the city too, were no secondary amplification soil effect are detected. Also this building was heavily damaged during L'Aquila earthquake, and was retrofitted by an isolation system. The damage concerned mainly brittle fracture in almost all pillars at ground level, and heavy damage to the external infill panels, internal brick masonry

panels and secondary non-structural elements. The type of non-structural elements damage has been caused by the low stiffness of the vertical structure, with expulsion of the infills at the first and second storey.

The high deformability of reinforced concrete structures has carried out to high levels of the compression and shear forces. Storey drifts have reached high values, not compatible with the stiffness and relevant flexibility of masonry infills. After 2009 earthquake, which caused the noticeable damage in structural and non-structural elements, the only possibility to prevent further damage and increased collapse risk, also for this building, has been evaluated by enhancing the seismic behaviour with the application of anti seismic devices (isolators) with a retrofitting technique. Instead of realizing great plinth above the pillars, in this building the uplift of the structure was performed by inserting high strength steel bars, sustaining all the structure weight during isolators insertion in the top of the pillars.
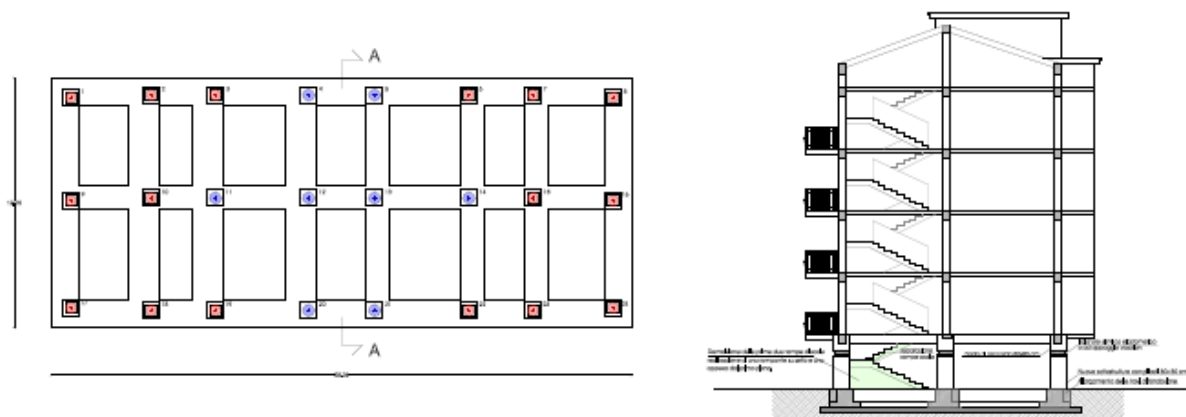
Figure 7. a) Position of isolators: red rubber isolator SI/N 450/126, blue sliders VM 250/250; b) section.

Figure 8. a) Building # 2 (six storeys)   b) damage end demolition of the infills

The damage caused by the 2009 earthquake in the building infills determined the need to completely demolish all the infills at the first two levels, and partially at superior levels (Fig. 8).

The particular (and regular) shape in plan ed in elevation permitted to easily insert an isolation system, directly in the zero level, at the top of pillars, without any interference with secondary elements (infills, garage doors, lift) and with no compromission of the utilization of the rooms at that level.

In order to strengthen the structure, an enlarged concrete section with new reinforcement bars were set up in all the pillars (Fig. 9 b).

Figure 9. a) Brittle fracture in the top of a pillar   b) Increase of section and reinforcement bar in a pillar

Depending on the structural characteristics (stiffness, residual capacity, deformability and interaction with infills), the isolation system has been designed in order to full satisfy the seismic demand in terms of displacement at the isolation level. It's worth noticing that this building is located near an important fault (which caused destructive earthquake in the pas centuries), were near faults effects have to be taken into account in order to avoid inappropriate dynamical behaviour (vertical and horizontal resonances, soil – isolation system – structure interaction)

Figure 10. a) HDRB and sliding devices at top of pillar   b) Sliding device at top of a pillar

Figure 11. a) HDRB rubber isolator SI/N 450/126   b) Sliding device in correspondence of the staircase

The building has been retrofitted with sixteen SI-N 450/126 high damping rubber isolators and eight sliding devices VM 250/250. It's worth noticing the position of sliding devices in correspondence of the staircase, (Fig. 11b) where they have been placed at a different height with respect the isolation level. The area of this retrofitted building is quite different from the preceding one, and is located near an active fault which caused several strong earthquakes in the past. The area has some resonances caused by the fault proximity. Also, this structure has been completely designed according to Italian code for new structures.

2.2 Building #3 (central area)

The third building under examination is located in the central area of the city, were an important secondary amplification soil effect is detected. Also this building was heavily damaged during L'Aquila earthquake, and after demolition has been rebuilt with isolation system.

Figure 12. Isolated building in the centre of the city of L'Aquila,

where secondary amplification effects occur at low frequencies.

The maximum seismic performance for this building has been gained by seismic isolation, but, according to the shown amplification effect (fig. 3), an accurately seismic design has been performed to take into account the probable high displacement during earthquakes in this area.

Isolators were positioned underground, in correspondence of the new pillars, following the scheme in fig. 13a, with HDRB isolators FIP SI-S 800/160, and sliding devices FIP VM 300/600/600.
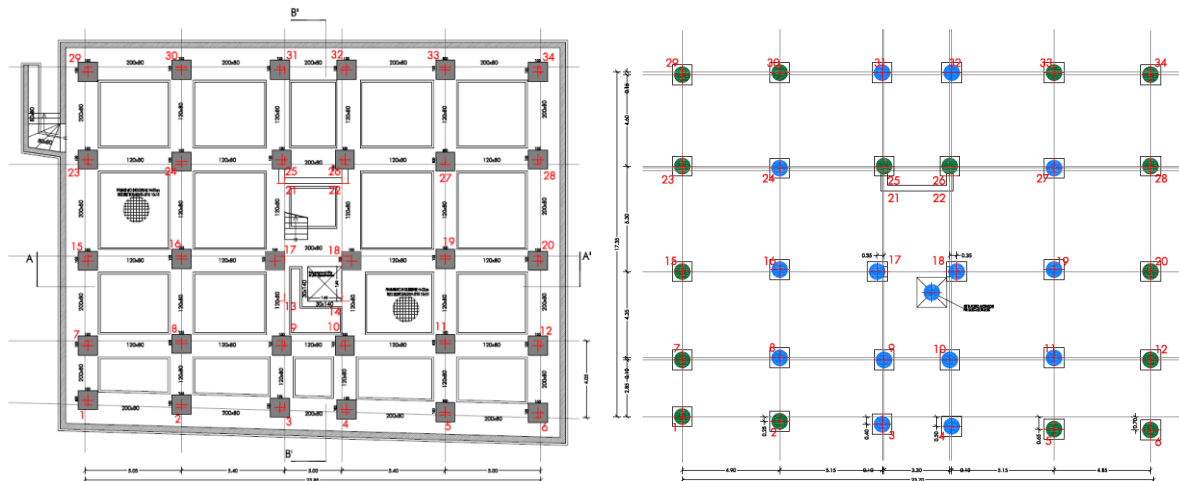
Figure 13. a) Undestructure of the isolation system   b) HDRB isolator SI-S 800/160, sliders VM 300/600/600

The isolation system has been designed in order to take into account not only the structure typology, but also the soil – structure interaction, in particular the secondary resonance at low frequencies which area typical of the centre of the city (Fig. 3). In particular (Figs. 14, 15), seismic movement joints have been designed to permit large displacement of the superstructure.

787

Figure 14. a) HDRB isolator SI-S 800/160

b) sliding device VM 300/600/600

Figure 15. a) HDRB isolator with external seismic joint

b) Horizontal joint with superstructure

The 2016 – 2017 seismic events and the behaviour of the isolated buildings
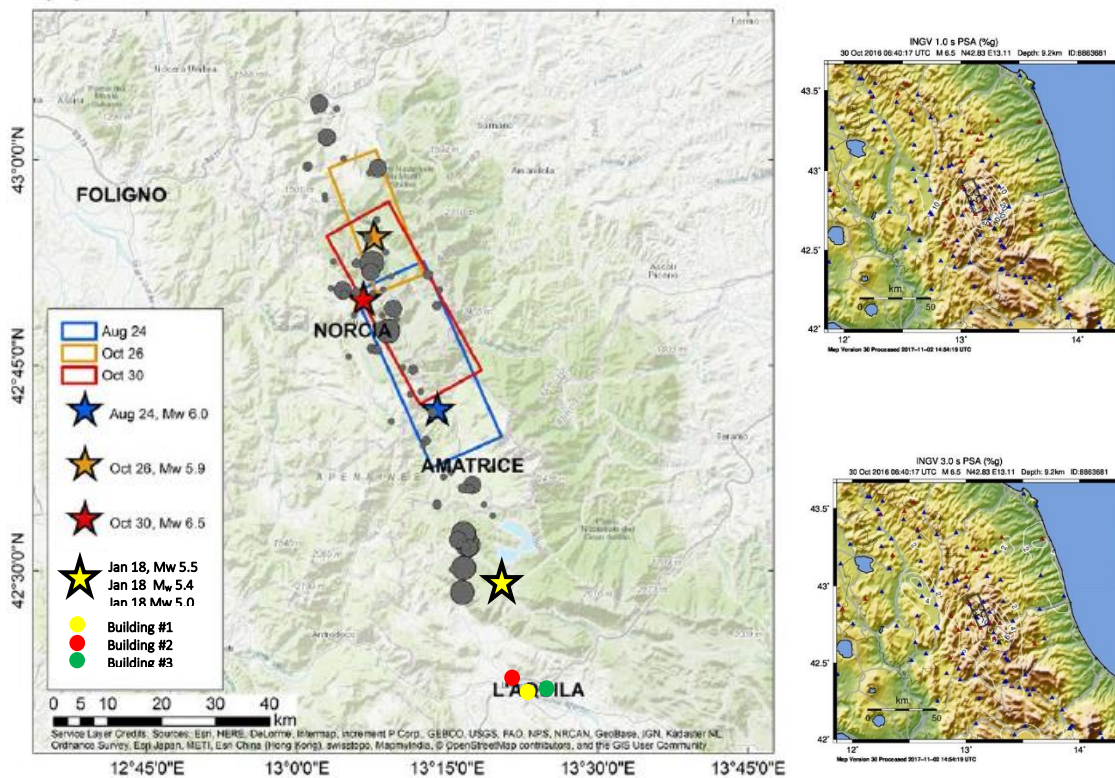
Figure 16 a)– 2016 – 2017 seismic events and position of the isolated buildings b) spectral data (INGV)

The above mentioned earthquakes, with a continued sequence of nine mainshocks, occurred in the same area of L'Aquila and 2009 earthquake. In particular, the buildings under examination have a short distance from the epicentres (about 35 km from Amatrice, 55 km from Norcia, and 20 km from the 2017 sequence). The overall main events are reported in the following table.

Table 1 – main seismic 2016 events in the area

SOURCE Time [Utc]	Latit.	Longit.	Depth [km]	Magnitude	Source	Name Record
24/08/2016 01:36:32	**42,698**	**13,234**	**8.1**	**6.0-Mw**	**BULLETIN**	**TN015**
24/08/2016 01:56:01	42,601	13,276	7.7	4.3-Mw	BULLETIN	TN018
24/08/2016 02:33:29	42,792	13,151	8.0	5.4-Mw	BULLETIN	TN032
24/08/2016 03:40:11	42,614	13,244	10.7	4.1-Mw	BULLETIN	TN045
24/08/2016 04:06:51	42,771	13,124	6.2	4.4-Mw	BULLETIN	TN047
24/08/2016 11:50:31	42.82	13.16	9.8	4.5-Mw	BULLETIN	TN066
24/08/2016 17:46:09	42,659	13,215	10.3	4.2-Mw	BULLETIN	TN074
24/08/2016 23:22:06	42,654	13.21	11.8	4.0-Mw	BULLETIN	TN078
25/08/2016 03:17:17	42,745	13,193	9.0	4.3-Mw	BULLETIN	TN080
25/08/2016 12:36:05	42.6	13,282	7.5	4.4-Mw	BULLETIN	TN083
26/08/2016 04:28:26	42,605	13,292	8.7	4.8-Mw	BULLETIN	TN086
27/08/2016 02:50:59	42,843	13,238	7.8	4.0-Mw	BULLETIN	TN093
28/08/2016 15:55:35	42,823	13,232	8.7	4.2-Mw	BULLETIN	TN102
03/09/2016 01:34:12	42.77	13,132	8.9	4.2-Mw	BULLETIN	TO015
03/09/2016 10:18:51	42,861	13,217	8.3	4.3-Mw	BULLETIN	TO017
16/10/2016 09:32:35	42,748	13,176	9.2	4.0-Mw	BULLETIN	TP016
26/10/2016 17:10:36	**42.88**	**13,128**	**8.7**	**5.4-Mw**	**BULLETIN**	**TP021**
26/10/2016 19:18:06	**42,909**	**13,129**	**7.5**	**5.9-Mw**	**BULLETIN**	**TP026**
26/10/2016 21:42:02	42,863	13,121	9.9	4.5-Mw	BULLETIN	TP053
27/10/2016 03:19:27	42,843	13,143	9.2	4.0-Mw	BULLETIN	TP071
27/10/2016 03:50:24	42,984	13.12	8.7	4.1-Mw	BULLETIN	TP073
27/10/2016 08:21:46	42,873	13,097	9.4	4.3-Mw	BULLETIN	TP086
27/10/2016 17:22:23	42,839	13,099	9.0	4.2-Mw	BULLETIN	TP103
29/10/2016 16:24:33	42,811	13,095	10.9	4.1-Mw	BULLETIN	TP144
30/10/2016 06:40:17	**42,832**	**13,111**	**9.2**	**6.5-Mw**	**BULLETIN**	**TP151**
30/10/2016 07:34:48	42,922	13,129	9.9	4.0--ML	Survey	TP170
30/10/2016 11:58:17	42.84	13,056	10.2	4.0-Mw	Survey	TP235
30/10/2016 12:07:00	42,845	13,078	9.7	4.5-Mw	Survey	TP237
30/10/2016 13:34:54	42,803	13,165	9.2	4.1-Mw	Survey	TP251
30/10/2016 18:21:09	42.79	13,152	9.6	4.0-Mw	Survey	TP275
31/10/2016 03:27:40	42,766	13,085	10.6	4.0-Mw	Survey	TP310
31/10/2016 07:05:45	42,841	13,129	10.0	4.0-Mw	Survey	TP322
01/11/2016 07:56:40	43	13,158	9.9	4.8-Mw	Survey	TP354
03/11/2016 00:35:01	43,029	13,049	8.4	4.7-Mw	Survey	N.R.
12/11/2016 14:43:34	42,723	13,209	10.1	4.1-Mw	Survey	TQ077
14/11/2016 01:33:44	42.86	13,158	11.0	4.0--ML	Survey	TQ092
29/11/2016 16:14:03	42,529	13.28	11.1	4.4-Mw	BULLETIN	TQ171

Many buildings in the area are under monitoring. The three examined buildings reported an ideal behaviour in heavy seismic conditions.

Spectral data, recorded at the site of L'Aquila, evidenced some differences between central area and the western area of the city, due to well known soil resonances in the central area.

The 2016 Norcia earthquake, in particular, caused a damaged building collapse in the central area.

The isolated building had an optimal behaviour during the earthquake. They reported absolute absence of any kind of damage, structural and non-structural. Also, isolators (both HDRB and SD) had no damage and no residual displacement.

The control of the displacement of the isolated structures, in the examined buildings, put into evidence some differences.

In particular, maximum displacement was measured for each superstructure and insolation system in each building, as follows:

Building #1 – maximum displacement 25 mm

Building #2 – maximum displacement 30 mm

Building #1 – maximum displacement 100 mm

The difference of displacement depends on the soil – structure interaction and the relevant differences between the considered areas.

It's worth noticing that each system has been designed according to the parameters reported in table 2.

Table 2 – design parameter and maximum displacement for the buildings

Building #	HDRB	SD	K_{esi} [KN/mm]	$\acute{\xi}$	Isolation Period	Design displacement	Maximum displacement
1	9 FIP SI-S 700/200 10 FIP SI-S 800/200	13 FIP VM 250/700/100	17.03	15%	2.64 s	300 mm	25 mm
2	16 FIP SI-N 450/126	8 FIP VM 250/250	16.16	10%	2.28 s	250 mm	30 mm
3	16 FIP SI-S 800/160	15 FIP VM 300/600/600	20.16	10%	2.43 s	300 mm	100 mm

Conclusion

The behaviour of the isolated buildings retrofitted or rebuilt after L'Aquila earthquake, subjected to new strong earthquakes in the same area, has been clear evidence of the excellent performance obtained by seismic isolation. After the 2009 earthquake, in the city of L'Aquila some hundred buildings have been seismically isolated. None of them reported any damage in consequence of the seismic events of 2016 – 2017, in the neighbourhoods of L'Aquila. In particular, three isolated buildings have been monitored and controlled, and the results show that each building, without damage, had an optimal performance, permitting the use of the buildings itself with no interruption. Also the isolation system didn't reported any damage and any residual displacement and deformation.

Seismically isolating the structure represents the best tool in order to maintains seismic security, resilience, total absence of damage (both structural and non-structural) and immediate usage of buildings and infrastructures even during very strong earthquakes.

References

[1] Buffarini, G., Clemente, P., De Flaviis, A., Ormando, C., Salvatori, A., (2023), Seismic Retrofit of r.c. Buildings with Base Isolation. In: *Cimellaro, G.P. (eds) Seismic Isolation, Energy Dissipation and Active Vibration Control of Structures. WCSI 2022. Lecture Notes in Civil Engineering*, vol 309, Springer, Cham. https://doi.org/10.1007/978-3-031-21187-4_85 , ISBN 978-3-031-21186-7, Online ISBN 978-3-031-21187-4

[2] Antonello Salvatori, Giovanni Bongiovanni, Paolo Clemente, Chiara Ormando, Fernando Saitta, Federico Scafati. (2022). Observed seismic behavior of a HDRB and SD isolation system under far fault earthquakes. *Infrastructure,* Vol 7 N. 2, 13, DOI: https://doi.org/10.3390/infrastructures7020013

[3] Paolo Clemente, Antonio Di Cicco, Fernando Saitta, Antonello Salvatori. (2021). Seismic behaviour of the base isolated Civil Protection Operative Centre at Foligno, Italy. *ASCE Journal of Performance of Constructed Facilities,* Vol 35 (4); 04021027, Article ID CFENG-3346R2, pages 04021027-1 – 04021027-12, DOI: 10.1061/(ASCE)CF.1943-5509.0001589, ISSN (print): 0887-3828 | ISSN (online): 1943-5509

[4] Fernando Saitta, Paolo Clemente, Giacomo Buffarini, Giovanni Bongiovanni, Antonello Salvatori and Cristian Grossi. (2018). Base Isolation of Buildings with Curved Surface Sliders: Basic Design Criteria and Critical Issues. *Advances in Civil Engineering,* vol. 2018, Article ID 1569683, 14 pages, ISSN: 1687-8094, DOI 10.1155/7074, https://doi.org/10.1155/2018/1569683

[5] A.Martelli, P. Clemente, A. De Stefano, M.Forni and A.Salvatori. (2014). Recent development and application of seismic isolation and energy dissipation and conditions for their correct use. *In Geotechnical, Geological and Earthquake Engineering*, vol. **34**, pages 449-488, ISSN 1573-6059, ISSN 1872-4671 (electronic), ISBN 978-3-319-07117-6, ISBN 978-3-319-07118-3 (eBook)**,** DOI 10.1007/978-3-319-07118-3_14, Kluwer Academic Publisher, Springer Cham Heidelberg New York Dordrecht London, Library of Congress Control Number: 2014946618

[6] Salvatori A., Di Cicco A., Clemente P.. (2021). Monitoring of base isolated building subjected to far fault earthquake. In: *Rainieri C., Fabbrocino G., Caterino N., Ceroni F., Notarangelo M.A. (eds) Civil Structural Health Monitoring. CSHM 2021. Lecture Notes in Civil Engineering*, vol 156. Springer, Cham. DOI https://doi.org/10.1007/978-3-030-74258-4_21 , pages 311 - 338, ISSN 23662557; Print ISBN 978-3-030-74257-7, Online ISBN 978-3-030-74258-4

[7] A. Salvatori, A. Di Cicco e P.Clemente. (2019) Seismic Monitoring Of Buildings With Base Isolation. In "*7th ECCOMAS Thematic Conference on Computational Methods in Structural Dynamics and Earthquake Engineering", COMPDYN 19*, M. Papadrakakis, M. Fragiadakis (eds.), ISBN 978-618-82844-5-6, id SCOPUS 2-s2.0-85079091857, DOI: 10.7712/120119, DOI URL: https://doi.org/10.7712/120119.7301.19221 , pagg. 5254 - 5275 , ISSN:2623-3347

[8] Bongiovanni, G., Buffarini, G., Clemente, P., Saitta, F., Salvatori, A., Scafati, F. (2019). Experimental seismic behaviour of base isolation systems in Italy during the 2016-2017 seismic sequence in central Italy., In Proceedings of XVIII Convegno Nazionale ANIDIS L'Ingegneria Sismica in Italia, SS01-125 – SSS01-133, Ascoli Piceno, Italy, ISBN 978-88- 3339-256-1, ISSN 2532-120X

[9] Buffarini, G., Clemente, P., Serafini, S., De Stefan,o A., Olivieri, R, Salvatori, A. (2012). Experimental dynamic analysis and seismic rehabilitation of Palazzo Margherita in L'Aquila. EAI Knowledge, Diagnostics and Preservation of Cultural Heritage, spec. II, ISBN E185775

[10] Clemente, P., Bongiovanni, G., Benzoni, G. (2017). Monitoring of seismic isolated buildings: state of the art and results under high and low energy inputs. Proc. New Zealand Society for Earthquake Annual Conf. and 15th World Conf. on Seismic Isolation, Energy Dissipation and Active Vibration Control of Structures, NZSEE2017 and 15WCSI, Wellington, 27-29).

[11] A. Salvatori. (2018). Seismic base isolation: retrofitting application in structures damaged by earthquake. In "16th European Conference on Earthquake Engineering", 18-21/06/2018, Thessaloniki, Greece.

LARGE SCALE SEISMIC ISOLATION FOR A POST-EARTHQUAKE RECONSTRUCTION PRESERVING IDENTITY OF SITES

Marco, Mezzi[1] , Alessandro, Fulco[2], Stefano, Nodessi[3], Gianluca, Fagotti[4], Nicola, Alemanno[5], Maurizio, Rotondi[6]

[1] *Professor, University e-Campus, marco.mezzi@uniecampus.it*
[2] *Tutor, University e-Campus, alessandro.fulco@uniecampus.it*
[3] *Director, USR Regione Umbria, snodessi@regione.umbria.it*
[4] *Head Private Rebuilding Office, USR Regione Umbria, gfagotti@regione.umbria.it*
[5] *Mayor, Comune di Norcia, segreteria.sindaco@comune.norcia.pg.it*
[6] *Head Private Rebuilding Office, Comune di Norcia, maurizio.rotondi@comune.norcia.pg.it*

Abstract

The effects of seismic attacks in oldest parts of hit towns mostly depend on the quality of materials and construction technique even for low and medium intensity earthquakes. The negative consequences of traditional construction approaches appeared in all their evidence in many areas of Central Italy affected by recent seismic sequences of medium intensity (M5-M6) in 2016-17 where entire villages were destroyed. The reconstruction should solve the problem to rebuild with safety but preserving the historical aspect of buildings and landscape. This paper presents a particular application of the known technique of seismic isolation for the reconstruction with integral seismic protection of the worldwide known village of Castelluccio di Norcia in Umbria (Central Italy). The adoption of a seismic isolation system at city scale involves the construction of a large floating platform, having the dimensions of the entire compartment, supported by seismic isolators. In the considered case the platform is stepped due to the site orography, and, above it buildings are built with the aesthetic and constructive characteristics of the collapsed original ones. The solution allows a correct interpretation of the objective to rebuild "as it was, where it was", safeguarding the landscape, prolonging the lifetime, saving the expected cost.

Keywords: seismic isolation, artificial ground, large scale isolation.

1. Introduction

The main events of the seismic sequence of the 2016-17 Central Italy earthquake resulted in the total destruction of some small towns like Arquata del Tronto, Pescara del Tronto, Castelluccio di Norcia, as well as of the large historic center of Amatrice [1]. The buildings that form these agglomerations, generally being spontaneous buildings, are characterized by a high seismic vulnerability [2] due to well-known multiple causes: low quality of the materials and construction methods; lack or absence of earthquake-resistant details; decay of materials and damage associated with the age of the buildings and the attacks suffered over the lifetime; absence or inadequacy or harmfulness of maintenance works.

For the management of the post-earthquake rebuilding, the Legislative Decree 189/2016 provided for an Extraordinary Commissioner carrying out his duties also by means of ordinances. To cope with difficulties that emerged during the first rebuilding phase, the Legislative Decree 76/2020 introduced a significant strengthening of the commissioner powers in derogation from the current legislation. The Extraordinary Commissioner has therefore, among others, the task of identifying urgent and particularly critical interventions and works, also in relation to the rebuilding of historical centers of the hardest hit municipalities, in order to arrange the acceleration measures necessary to ensure their fastest and most effective implementation. In order to achieve an immediate implementation of the interventions and ensure a rapid recovery of the territories damaged by the earthquake, both in terms of relaunching the normal living conditions of the population, and to support the restoration and restart of the economic activities present therein, the ordinances provided for derogating provisions of the regulations in force, with particular regard to the rules of the code of public contracts, taking into account that the

rebuilding's needs are of such complexity that they cannot be effectively addressed with ordinary procedures.

In particular, the Special Ordinance no. 18/2021 entrusts the rebuilding of the entire village of Castelluccio di Norcia, almost entirely destroyed by the seismic crisis of 2016, to the public management, within a single recovery program that integrates the construction of primary services and the restoration of both public and private buildings, in order to allow the complete rebuilding of the *forma urbis* by restoring the morphology of the soil and the configuration of public and private spaces. The Rebuilding Special Office (USR) of Umbria Region is identified as the implementing body for the execution of the interventions which procedural simplifications have been envisaged. The Ordinance defines the actions and activities that have to be implemented to start the overall rebuilding of Castelluccio's historical center, identifying the works whose rebuilding or restoration takes on a particularly urgent and critical nature in relation to both intrinsic functions and characteristics, and to purposes the rebuilding of the social and economic fabric.

This paper presents the results of a feasibility study [3] [4] that was the base for the reconstruction of the entire town of Castelluccio on a single seismically isolated platform, evaluating the main aspects of technical-economic feasibility: earthquake-resistant performance; construction technologies; compatibility of the urban fabric; cost/benefit analysis.

2. The village of Castelluccio di Norcia

Castelluccio, 1452 m a.s.l., is a fraction of Norcia's Municipality, located between Monte Vettore (2470 m) and Monte Patino (1885 m). Below the town extends the Conca di Castelluccio, a great depression at an altitude between 1250 and 1350 meters, surrounded by particularly high hillsides, which make the area unique and a source of tourist attraction. The area (greater than 17 km^2) includes the so-called "Piani di Castelluccio": Pian Perduto, Pian Grande and Piano Piccolo. The city center, due to its position on the hill overlooking the plateaus on the border between Umbria and the Marches, has a conspicuous symbolic, identity and cultural value for the entire region and, thanks to the flowering's phenomenon of the Pian Grande (Figure 1a), of international fame and recognition.

The history of Castelluccio date back to some centuries prior to 1200, the date of the first mention in the archive and is also linked to the tectonic and seismogenic characteristics of its territory. For seismic events of the past there are certain sources starting from 1703; in more recent times, we recall the several damages resulted from the Valnerina earthquake of September 9, 1979; from the seismic events of 1997; up to the earthquakes of 2016. Currently Castelluccio is almost entirely destroyed (Figure 1b): the seismic shock of 2016 caused the collapse of many buildings and the instability on the portions of the surviving buildings that led to their mandatory demolition and prohibition access to the area. The characteristic and typological image of the area is seriously compromised and altered due to the extensive damage and therefore requires an immediate and accurate rebuilding and restoration.
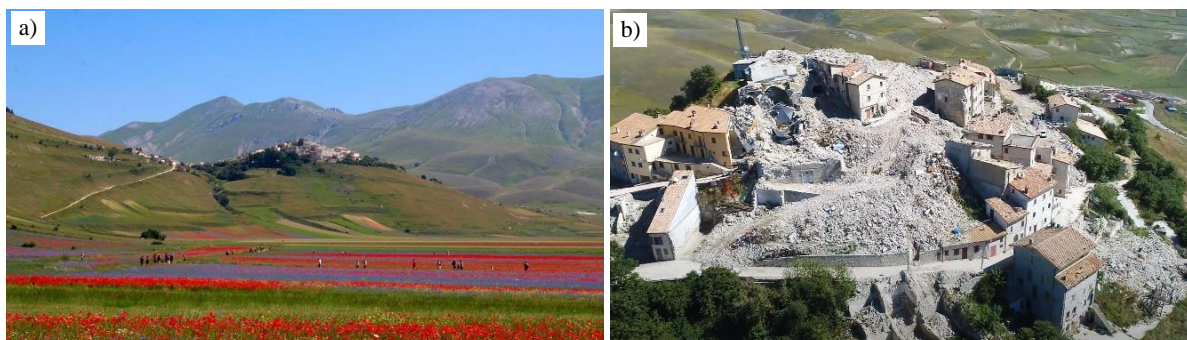
Figure 1. Castelluccio di Norcia: a) flowering phenomenon of Pian Grande; b) post-earthquake conditions.

3. Target of the rebuilding

The reconstruction works aims not only to provide the community with the ability to cope with a future calamitous event, but most of all to create a resilient village capable of transforming a critical issue into an opportunity for territorial development and progress research. It is evident that in the recovery's context of small historic villages a more resilient system is, and must be in general, an urban system of higher quality (landscape, environmental, social, construction) which aims at respecting and enhancing local identities, with the regeneration of the affected areas through new unitary revitalization visions, territorial's reactivation and anthropic balances, as well as the rebuilding not only of the buildings, but of the communities, reducing the risk of isolation of these places.

The rebuilding of Castelluccio's center has the ambition to constitute an important design model not only for the safety of the inhabitants and of the many tourists who visit every year the site, but also for the research and innovation sector from an anti-seismic perspective, through the creation of a system of spaces and paths that will make the infrastructure accessible and open to insiders and the entire scientific community interested in advanced processes and methods for post-seismic rebuilding [5].

The examination of places and works has highlighted a strong mutual interference between the buildings undergoing rebuilding and the public spaces, both for the direct sharing of containment structures of the foundational land and for the proximity of the location, which makes it strictly necessary to coordinate the construction site, imposing a specific implementation sequence.

Based on the objectives contained in the board resolution of 24/05/2021 and the general principles laid down in Art.1 of the Special Ordinance no.18/2021, confirmed with the approval of the Implementation Plan (Resolution of the Municipal Council of Norcia no.1 of 03/14/2022), the public priority and preparatory interventions have been identified for public and private rebuilding, essential to fulfil the urban planning and primary services for the overall rebuilding of Castelluccio village and to provide it with the necessary functional autonomy. These works, calibrated on the basis of the site characteristics and the area conditions of the built center, are designed to prepare and offer the essential elements for the reconstruction of living conditions for individual citizens and the community. It is important to highlight the complexity of the rebuilding action aimed at restoring functionality, in addition to preserving and restoring the identity of the places, through the safeguarding and rebuilding of the peculiar and representative elements of the architectural-landscape heritage, as well as of the cultural symbolic values.

The priority public works, included in Annex n.1 of the Special Ordinance no.18/2021, relevant and urgent for the correct organization of territory protection and urban context, consist of: restoration of the main and secondary roads of the inhabited nucleus; terracing of the inhabited nucleus necessary for the consolidation and restoration of the morphology, as well as for the foundations themselves of the aggregates and religious buildings; underground utilities of the inhabited nucleus; construction of public areas; construction of underground parking lots, pedestrian and safety paths. To complete the implementation of the priority public interventions, necessary for the recovery of village livability and its socio-cultural values, it was also considered essential to regenerate, or rebuild, the entire building heritage due to its structural peculiarities of setting the buildings one above the other and in direct correlation with the roads and containment works, in order to coordinate and convey a quick and organized rebuilding with the full regeneration of this territory's iconographic symbol.

Along with the public interventions priority, therefore, the repair and rebuilding of the aggregates, private buildings and places of worship will have to be carried out, through a single recovery program that includes the restoration of public buildings and private residential fabric, simultaneously with the restoration of related infrastructures and underground services. The need to recover Castelluccio di Norcia village as soon as possible with a single program obviously cannot ignore the coordination and the organized action of the total rebuilding of the built complex and its public services, which, due to the center characteristics and to their complexity and identity value, must necessarily be carried out jointly to obtain a quick and synergistic implementation with the restoration of the *forma urbis*.

The Implementation Plan identified the urban core to be rebuilt in the pre-existing volumetric and architectural configuration, according to the provisions of Ordinance no. 110/2020 and the Special Ordinance no. 18/2021. The goals that the Commissioner action intends to pursue in the rebuilding of the inhabited centers damaged or destroyed by the seismic events are the city rebirth, understood as the social and economic fabric underlying the urban's agglomeration life, and the rebuilding speed, understood as effectiveness and efficiency of physical rebuilding processes of buildings and urban spaces. In order to ensure compliance with these principles, the rebuilding of the *forma urbis* configuration with a unitary intervention, through the public rebuilding of public and private buildings coordinated with morphology's restoration of the soil and the configuration of both public and private spaces, represents an innovative solution.

The portion of Castelluccio that will be treated with the "artificial ground" solution is the one represented by the historic center; this, in fact, is also the only possible isolation solution due to the excessive buildings' proximity: the construction of a single terraced platform including the entire historic portion of Castelluccio avoids possible lengthening of the construction times deriving from working with independent construction sites relating to individual aggregates, furthermore avoids the criticalities and further interferences connected with the construction of support works and terracing.

4. Artificial ground for seismic isolation

The term "artificial ground" defines a solution that provides for the seismic isolation of large platforms above which different constructions are built [6] [7]. Referring to the post-seismic reconstruction proposals based on the application of "artificial ground" previously formulated [5] [8] and to the realizations referred to in the aforementioned works, a collaboration activity was started between the Department of Civil and Environmental Engineering of University of Perugia, the USR of Umbria Region, and the Municipality of Norcia aimed at defining a seismic isolation system on a large platform for the reconstruction of Castelluccio.

The use of artificial ground for post-earthquake reconstruction can only be planned in cases in which the destruction of a portion or an entire inhabited center is complete, and therefore a total reconstruction of the entire village or neighborhood should be provided. Within the historic center of Castelluccio, an area of approximately 6000 m^2 was identified to be rebuilt on an isolated platform. The area (Figure 2a) has an irregular in-plan shape with overall dimensions of 90 x 80 m and is characterized by average slopes equal to 25% in the NS direction and 15% in the EW direction. Before the seismic events of 2016, the area included 18 masonry aggregates of 1, 2 and 3 stories, which covered about 4150 m^2 of ground area, with 59 residential units with a total floor area of about 12880 m^2 and a volume of about 38650 m^3. Among the buildings there are the Oratory Church of the Sacramento, completely destroyed, and the Church of Santa Maria dell'Assunta, of which only a portion of the apse remains.
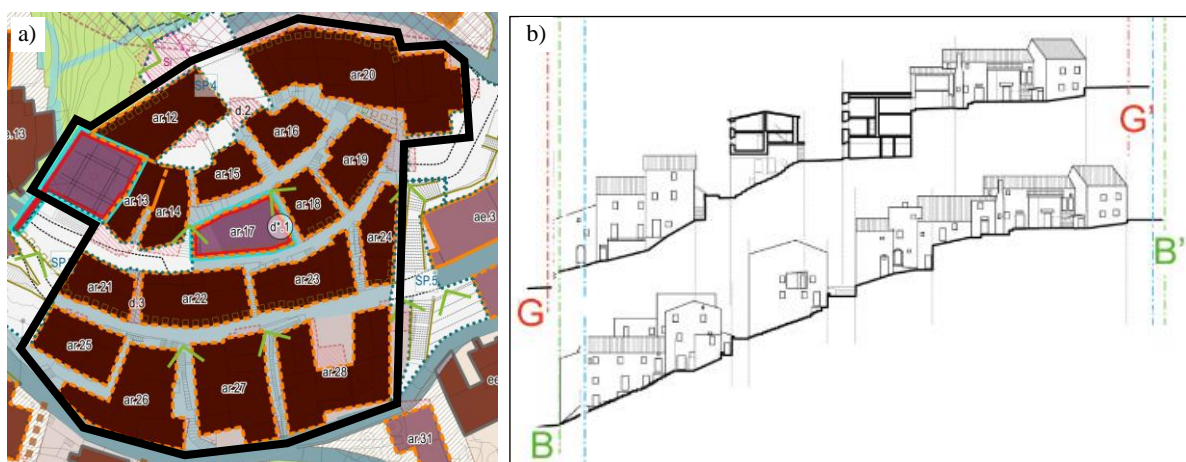
Figure 2. a) Implementation Plan for reconstruction (cultural heritage building in red color) and perimeter of the seismically isolated area (black color); b) typical development of buildings along the streets.

The total mass of the buildings involved in the project is equal to approximately 17300 t (assuming a unit mass of 1.3 t/m^2 for masonry buildings). Since the building land area is 4150 m^2, the unit mass of buildings to be isolated is 4.10 t/m^2. To this contribution must be added the mass related to the "remaining" area, required for the restoration of the urban aspect, that is estimated equal to 11500 t: the unit mass of the "remaining" area to be insulated, equal to 2120 m^2, is equal to 5,40 t/m^2.

The fundamental aspects that are the subject of the evaluation of the technical feasibility of the project are the following [5] [8] [9]: (1) definition of the heights of buildings and plates; (2) optimization of excavations; (3) consolidations and terracing; (4) foundation and substructure; (5) isolation system; (6) isolated plate; (7) basements for elevation compensation; (8) plants and sub-services; (9) restoration of the urban fabric.

5. Isolated stepped platforms

The trend of the altitudes, with very significant slopes, represents one of the most problematic and characterizing aspects of the project. Figure 2b shows, as an example, the development of the elevations along one of the transversal streets of the village. In order to achieve a reconstruction spatially equivalent to the pre-earthquake situation, the aspect of the elevations must be considered as a priority. The base quotas and the elevation development of the buildings must be maintained or restored, both for the principle of restitution "where it was" and for avoiding incompatibility in the solutions of continuity between the isolated portion and the fixed base boundary. The isolated plate, which acts as the foundation of the buildings, is stepped and organized on a limited number of staggered elevations defined in order to satisfy two criteria: (i) to envelop the base quotas of buildings with a lowering from 0.70 m (minimum) to 4.00 m (maximum); (ii) to limit the elevation differences of the steps below 6.00 m. The resulting stepped plate has 11 reference elevations (Figure 3a) which cover the maximum difference in height of 25 m between the lowest and the highest area.

Below the plate, the isolation interface and the foundation structure are provided. Figure 3b shows a constructive section of the solution. The base quotas of the excavation follow the same trend of the plate but are deepened by 1.50 m to cover the height of the isolation system and foundation structures. Similarly, the vertical retaining walls are set back by about 0.80 m with respect to the vertical faces of the stepped isolated plate. Ultimately, there is an increase in excavation volume of approximately 8000 m^3 compared to that of a conventional fixed-base solutions.

A total number of 301 devices is provided for the seismic isolation of the plate. Their positioning derives from: (i) the arrangement at a distance of about 5-6 m, compatible with the vertical bearing capacity of the isolated plate, (ii) the modulation on the shapes of the horizontal shelves, (iii) the optimization of the dynamic response. The isolated plate has a height of 0.70 m which derives from a pre-dimensioning based on the assumption of a permanent load of 40 kN/m^2 and an accidental load of 8 kN/m^2, derived from the estimates of the provided superstructure (buildings and fillings). In order to satisfy the strength check, a total reinforcement percentage equal to 0.8% is assumed.
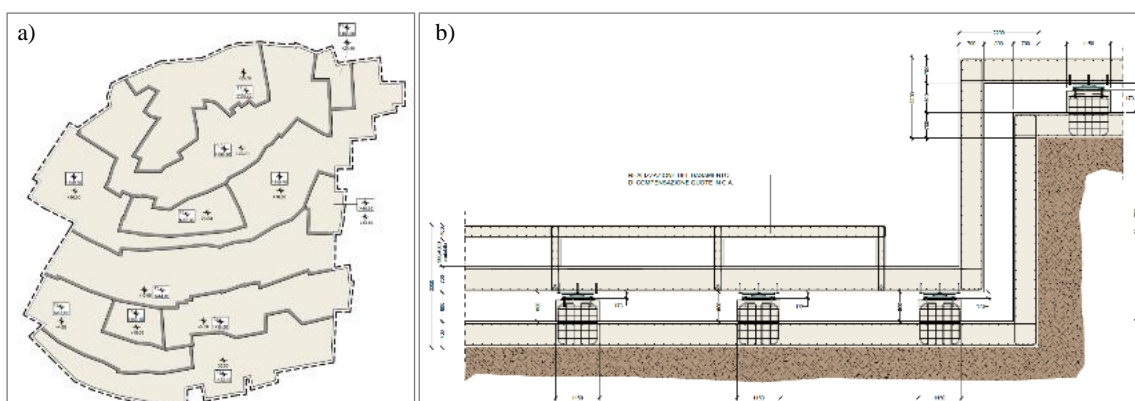
Figure 3. a) elevations of the stepped isolated plate; b) section of the isolated plate and sub-structures.

The isolators are arranged on pedestals having a section of 1.15×1.15 m set on a foundation consisting of a grid of 0.70 m thick r.c. beams. The space between the lower edge of the isolated plate and the upper edge of the foundation is limited to a height of 0.80 m, allowing for inspection operations also using self-moving automated systems.

The equipment serving the buildings are installed in the space between the foundation and the isolated plate and are collected in the tunnels created in correspondence with the roads. The plants network include: water supply, sewer, electricity, optical fiber and telephone, gas. As regards the water (white/black) leaving the houses, pipes for the collection of the down pipes coming from each house are provided to converge to the lowest point of the plate where there will be flexible pipes descending towards the "fixed" ground below the isolated compartment.

The urban fabric is reconstituted in a way that substantially corresponds to that pre-existing at the 2016 seismic event (Figure 4a) according to the concept "where it was, how it was", except for minor variations provided by the urban Recovery Plan.

Above the isolated plate, both the road network and the buildings will be reconstituted. The correct positioning in elevation is got through rigid r.c. boxed bases (Figure 3b), located under the buildings and roads, which ensure the compensation of the differences between the quotas of the isolated plate and those of roads and buildings. These volumes do not have a functional definition but could be used as basements or for public use. The achievement of the design road quotas can be locally obtained through the filling of landfill material.

Another important element, not related to the structural aspects and seismic protection, is given by the infrastructural nature and the urban dimension of the work, and is represented by the possibility of making a part of it visible and open to visitors with the creation of a multifunctional space accessible from the outside (Figure 4b) designed by prof. arch. Paolo Verducci. Accessibility to the infrastructure is guaranteed by an annular path (also designed for maintenance and monitoring) and through the creation of multi-purpose vaulted hypogeal spaces. On a strictly functional level, it is envisaged a museum use aimed at illustrating the main characteristics of the seismic isolation intervention and telling the millennial history of the territories of the plateau of Castelluccio di Norcia. The architectural form of the rooms is characterized by a double arch structural system resting on a reticular mesh of seismic isolators. The area, to be checked in the subsequent design phases, is approximately 650 m².
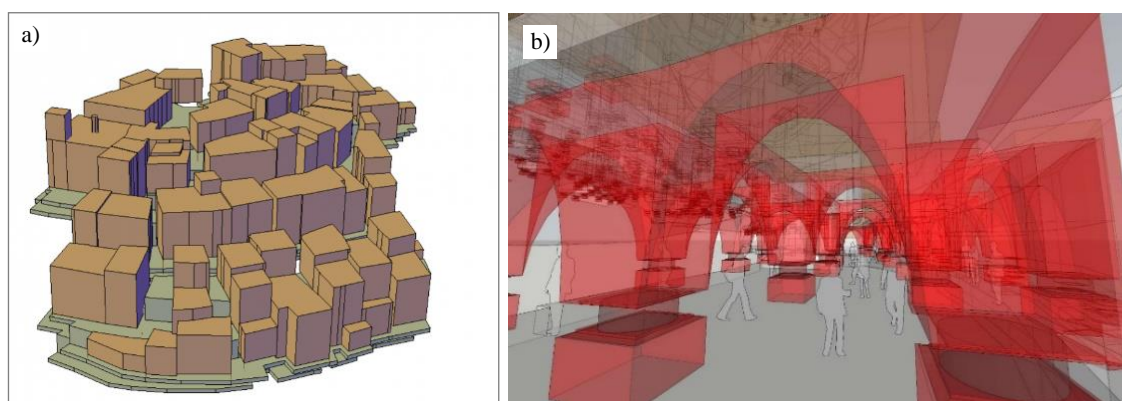
Figure 4. a) 3D simulation of rebuilt compartment; b) representations of the polyfunctional underground space.

6. Characteristics and design of isolation system

Given the importance of the project, the design has been carried out ensuring to the isolated system a performance level higher than the standard one, considering that this can be achieved without significant cost increases. It has been considered a reference period V_r = 200 years. The corresponding design seismic action is identified by a return period T_r = 2475 years.

On the basis of the available information, the subsoil category is B (semi-rigid soil) and the topographical condition is T3 (slope >15%). Ultimately, the elastic acceleration spectrum for the collapse limit state (SLC) is characterized by the following values of the seismic parameters:

• bedrock acceleration $a_g = 0.441$ g;
• amplification coefficient $F_O = 2.45$;
• characteristic period $T_C* = 0.497$ s;
• soil amplification coefficient $S = 1.20$;
• horizontal ground acceleration PGA = 0.529 g.

The total isolated seismic mass given by platform shelves and walls, buildings, volumes of non-built areas, is approximately equal to $M_{iso}=45000$ t. The average load acting on the isolated plate is $Q=70$ kN/m^2.

The use of curved surface sliding devices with a coefficient of friction μ equal to 2.5% is assumed. This type of device is characterized by a bi-linear force-displacement behavior. The effective stiffness is equal to the sum of two contributions

$$K = N(1/R + \mu/d) \qquad (1)$$

where
N is the axial load,
R is the radius of curvature,
μ is the coefficient of friction,
d is the maximum displacement.

Since the stiffness is proportional to the axial load and therefore to the mass that determines it, the isolation system is characterized by a substantial coincidence of the centers of mass and stiffness and therefore by the absence of significant torsional effects. Actually, this condition is not fully attained because also the friction coefficient is dependent on the axial load. The eccentricity between the centers of mass and the stiffness is anyhow reduced to values lower than 0.2% of the platform dimensions.

From the preliminary assessments carried out with the aim of an oscillation period of the isolated system in the interval 2.50 - 3.50 s, the adoption of market devices with the following characteristics appears appropriate:

$D_g = 880$ mm, diameter;
$H = 173$ mm, total height;
$N_{Ed} = 6000$ kN, maximum vertical load in the presence of horizontal displacements;
$K_d = 591$ kN / m, effective lateral stiffness for mean axial force;
$K_v = 10000000$ kN / m, vertical stiffness;
$d_E = 350$ mm, maximum displacement (collapse limit state).

In order to optimize the response of the isolated compartment by mitigating the torsion effects, the possible additional installation of dissipating devices, strategically located and working in parallel and synergistically with the isolator system, has been hypothesized. The adoption of magneto-rheological (MR) dissipating devices is hypothesized which, through an intelligent system for regulating their stiffness, allow to control the response with instantaneous re-centering.

For the purposes of evaluating the seismic response of the system, a numerical model was built in which the stepped plate is reproduced with two-dimensional elements and the devices with linear elements. The superstructure (constructions and infrastructures) was considered in terms of loads acting on the plate with the values previously reported. Linear dynamic analyses were carried out to determine the response of the isolated platform and to carry out checks on the isolators.

The two main translational modes have oscillation period values equal 3.16 s with nearly unitary participation mass rates. The maximum values of displacement and axial force on the isolators at the collapse limit state (SLC) are equal to 335 mm and 4201 kN, respectively, both compatible with the performance of the hypothesized devices. The maximum horizontal force value is 360 kN. None of the isolators exhibit tensile axial force. The 1.15×1.15 m section pillars of the substructure meet the SLV checks with reinforcement percentages less than 1.00%.

As regards the other categories of loads, in the examined situation the effects of the wind are not relevant [10], while the deformations associated with thermal variations are evaluated in the order of 10 mm in consideration of the thermally insulated conditions of the substructure. The effects of temperature and shrinkage under construction can be mitigated and compensated by means of suitable technological and constructive solutions.

7. Response to earthquakes recorded at site

In order to analyze the actual seismic response of the isolated compartment, nonlinear dynamic analyses were carried out using as input the accelerograms recorded in the destructive seismic event of October 30, 2016. The values of the peak accelerations for the three components corresponding to the X (EW), Y (NS) and Z (VERT) directions of the model are equal to 0.420 g, 0.634 g, and 0.801 g, respectively. The elastic acceleration response spectra of the two horizontal components of the event are greater than the SLV site spectrum provided by code. In the field of the fundamental periods of ordinary masonry and r/c structures (between 0.1 s and 0.5 s), the values of the spectral accelerations double those of the SLC site spectrum, reaching values of 2.00 g. On the contrary, in the range of oscillation periods typical of seismically isolated systems (> 3.00 s), the spectral accelerations of the records are lower than those predicted by the standard spectrum, with values of around 0.10-0.15 g. Therefore, considering the event of October 30, 2016, the reduction in the response spectral accelerations of the isolated base systems compared to the fixed base ones is about 15 times.

The nonlinear behavior of the isolators was reproduced in the nonlinear numerical model by means of an elastic-plastic law characterized by the following parameters:
K_1 = 60 MN / m, stiffness of the initial elastic branch;
F_1 = 60 kN, force at the elastic limit;
d_1 = 1 mm, displacement at the elastic limit;
K_2 = 386 kN / m, stiffness of the plastic branch, considering the average axial load.
The values derive from the geometric and physical characteristics of the hypothesized devices:
R = 3700 mm, radius of curvature;
μ = 4%, coefficient of friction (taking into account actual vertical loads).

To evaluate the seismic response of the superstructures, the numerical model was integrated with linear elements constrained to the plate and characterized by periods of oscillation typical of the real buildings (0.10 - 0.40 s). The response was calculated for both the isolated and fixed base condition by applying the recorded accelerograms of October 30, 2016. The maximum displacement of the isolators is 274 mm, lower than those resulting from linear analyses with site spectra. The maximum accelerations evaluated on building above the isolated plate vary from 0.15 g and 0.20 g, that is the seismic isolation determines a reduction in acceleration at the base of the buildings varying between 2.4 and 3.6 times that of the fixed base condition.

Figure 5 shows, for the elements simulating superstructures with different number of floors, the following parameters; the fundamental period of oscillation, T_{FB}; the maximum values of the two components of the top displacements with respect to the base, in the two conditions of base isolation, $\delta_{x,BI}$ and $\delta_{y,BI}$, and fixed base, $\delta_{x,FB}$ and $\delta_{y,FB}$. The isolated solution determines a reduction in displacements, compared to the fixed base solution, varying from 3 to 13 times (8 times on average), with an average interstory drift approximately equal to 0.1%. The displacement values calculated for the fixed base condition exceed the limits of the linear behavior of the structures, but also those of the plastic range, with a ductility demand overwhelming that available for the typical constructions: they therefore identify conditions of severe collapse of the superstructures, like those actually occurred on the occasion of the actual event.
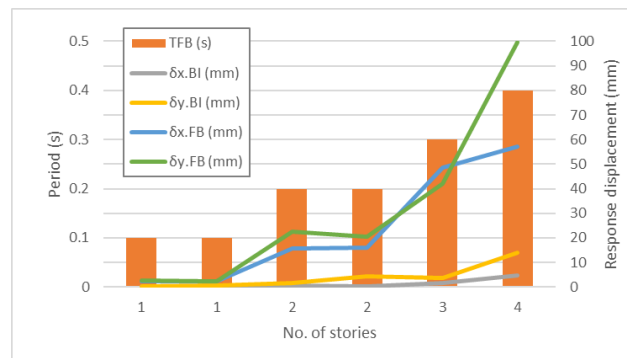
Figure 5. Lateral displacement of buildings in BI and FB scenarios.

Figure 6 shows, for the fixed base and isolated configurations, respectively, the acceleration diagrams at the base and at the top of the element reproducing a superstructure characterized by an oscillation period equal to 0.20 s, in the most significant time window. In the case of isolated plate, the amplifications of the accelerations from the base to the top are very low, going from values equal to about 0.10 g at the base up to values of about 0.20 g at the top. On the other hand, in case of fixed base systems acceleration values go from about 0.5 g at the base to 2.0 g at the top. The isolated solution therefore determines a reduction of floor accelerations by about 10 times. The resulting displacement and acceleration values of the buildings in the isolated solution are even below the limits corresponding to the operational limit state of the constructions.
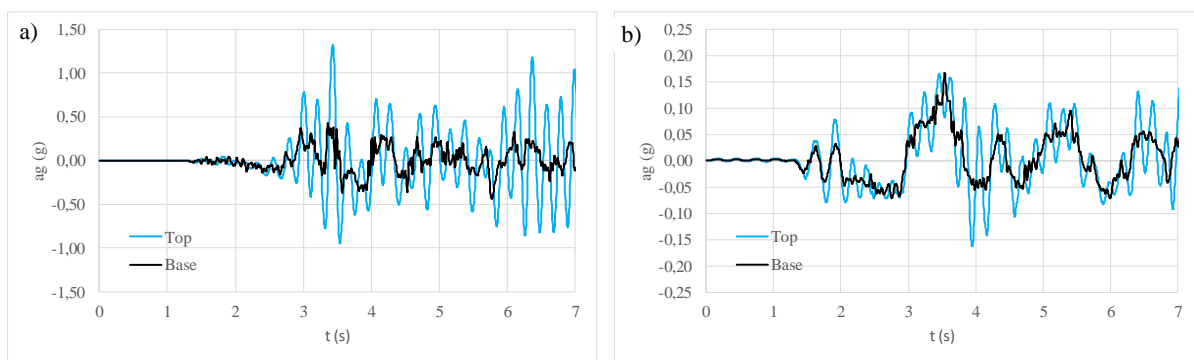
Figure 6. Accelerations at the base and at the top of buildings: a) FB solution; b) BI solution.

8. Cost and benefits of the isolated solution

Aiming at performing economic comparisons, the direct and indirect costs related to the reconstruction of the superstructures as well as the additional costs associated with the adoption of the isolated solution have been analyzed, evaluating the expected consequences over time horizons of 10, 50 and 100 years have been carried out.

First of all, the cost necessary for the restoration of the considered sector has been assessed, concerning both the reconstruction (direct costs) and the emergency and post-event management (indirect costs). The former were assessed in accordance with the ordinances of the Commissioner for reconstruction, considering a unit cost, including the various envisaged increases, of 1740 €/m^2 for a total area of approximately 13000 m^2. Adding the costs related to non-residential reconstruction (public, cultural, social infrastructures), estimated by the Commissioner at 14 M€, it results an estimate of direct costs of 37 M€. To validate the assumed costs, the funding provided by the government for the entire Umbria region and equal to 3.7 G€ were taken into consideration. It was therefore estimated, proportionally, that resources of 80-120 M€ (including indirect costs) are allocated to the area affected by the intervention in question.

To integrate the sector with a "artificial ground" system, a total cost, additional to that already foreseen for the superstructures, equal to 5 M€ was estimated on the basis of a prompt calculation of the works and related costs: 0.50 M€ for excavation; 0.60 M€ for substructure and foundation; 0.70 M€ for the devices; 2.70 M€ for the stepped isolated plate; 0.20 M€ for the basements; 0.20 M€ for the repost. Therefore, the economic impact of the sector isolation system is equal to about 14% of the direct costs and 5-6% of the total costs.

It is also necessary to consider that an extreme seismic event entails further costs connected to the social, cultural and organizational consequences, such as the depopulation, the critical issues of resettlement and social reintegration, the deficit in production activities, the compensation of investments, the state debt. Moreover, last but not least, the direct consequences on human beings (dead and injured) must be taken into consideration. All these aspects are not evaluated in this work but assume a decisive importance in the choices and strategies for managing extreme events.

To define the convenience criteria in the context of an optimal reconstruction strategy, it is appropriate and necessary to move from economic estimates to performance evaluations [11] [12]. The conventional reconstruction project strategy, in line with current codes, would provide for the achievement of the life safety limit state for a seismic intensity with an exceeding probability of 10% in 50 years. Exceeding this limit state would result in costs substantially of the same order as those of the event that occurred and for which the reconstruction is carried out, but lower damage is to be expected even for events of lesser intensity.

Once L levels of consequences have been defined, it is possible to estimate the expected cost in N years, C_{EXP}, as

$$C_{EXP}^{(N)} = \left[\sum_{l=1}^{L-1} C_{EG,l} \cdot \left(P_l^{(N)} - P_{l+1}^{(N)} \right) + C_{EG,L} \cdot P_L^{(N)} \right] \qquad (2)$$

with

$$P_l^{(N)} = 1 - e^{N/T_{R,l}} \cong 1 - \left(1 - \frac{1}{T_{R,l}} \right)^N \qquad (3)$$

equal to the probability of occurrence, in N years, of an event of seismic intensity for which l-th level consequences are reached, where
L is the number of considered scenarios;
$T_{R,l}$ is the return period of the seismic intensity corresponding to the l-th scenario;
$C_{EG,l}$ = total costs corresponding to the l-th level of consequences.

The economic consequences must include both the direct costs associated with repairing the damage and the indirect costs. As regards indirect costs, the following aspects must be considered: (a) displacement of the inhabitants; (b) interruption of activities; (c) emergency management. At this stage, an amount of indirect costs has been assumed, expeditiously and precautionary, approximately double that of direct costs. A preliminary estimate of the expected consequences was carried out, with reference to the damage levels provided for by the Commissioner's ordinances (Ord. 19 and subsequent) for private and public reconstruction, i.e. L0, L1, L2, L3-L4. The parametric direct cost of reconstruction, $C_{U,DIR}$, was attributed to each of the four levels in accordance with the aforementioned ordinances and therefore the overall direct costs C_{DIR} results. The direct costs of the public works, $C_{DIR,OP}$, were estimated with the same proportions for all the levels, being known the amount allocated for public works corresponding to the L3-L4 state observed in Castelluccio di Norcia. The total direct cost, $C_{DIR,tot}$, is then given by the sum of the quantities provided for private and public works. Also the total equivalent parametric cost $C_{U,DIR,tot}$ can be computed. Indirect costs, C_{IND}, were estimated with the previous proportions for all the levels, considering for level L3-L4 an amount approximately double that of direct costs. This assumption is congruent with the actual allocations foreseen by the reconstruction plan defined by the Commissioner. Finally, it is possible to obtain the overall C_{EG} costs potentially achievable for each level of damage

$$C_{EG} = C_{DIR,tot} + C_{IND} \quad C_{EG} = C_{DIR,tot} + C_{IND} \qquad (4)$$

The following Table 1 reports the values of the parameter described above considering the reconstruction area equal to 13000 m^2.

Table 1. Direct, indirect, and total costs for the four considered damage levels.

Damage level		L0	L1	L2	L3-L4
$C_{U,DIR}$	($€/m^2$)	300	1,000	1,375	1,800
C_{DIR}	($M€$)	3,900	13,000	17,875	23,400
$C_{DIR,OP}$	($M€$)	2,333	7,778	10,694	14,000
$C_{DIR,tot}$	($M€$)	6,233	20,778	28,569	37,400
$C_{U,DIR,tot}$	($€/m^2$)	479	1,598	2,197	2,876
C_{IND}	($M€$)	390	6,500	26,813	46,800
C_{EG}	($M€$)	6,623	27,277	55,381	84,200

The four damage levels have been associated with the performance levels (limit state) provided by the Italian code for the design of buildings, therefore the operational (SLO), damage (SLD), life-safety (SLV) and collapse (SLC) limit states have been considered respectively corresponding to the damage level L0, L1, L2, L3-L4. The return periods $T_{R,l}$ of the seismic intensity corresponding to the limit states for a conventional reference life of 50 years, can be then attributed to each of the damage levels and the exceeding probabilities of the damage level $P_l(10)$, $P_l(30)$, $P_l(100)$ for three significant time horizons of 10, 30, 100 can be computed (Figure 7).
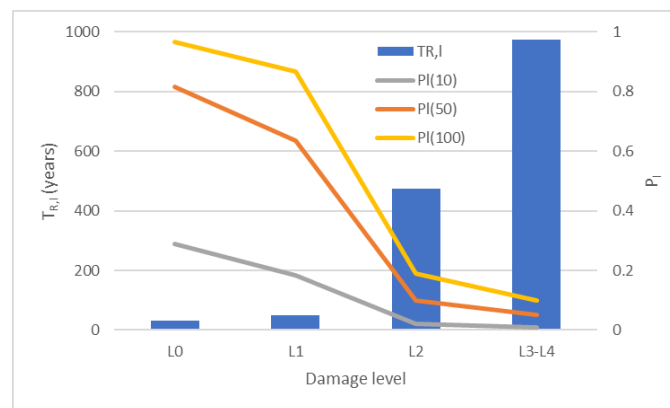
Figure 7. Exceeding probabilities of the damage levels for three significant time horizons of 10, 30, 100 years.

The expected costs probabilistically obtained through the Eq. (1) for the three time horizons considered of 10, 50 and 100 years are equal to 6,563 M€, 22,792 M€ and 32,466 M€, respectively. It is therefore obtained that the expected consequences over the next 50 years for the urban sector in question conventionally rebuilt, are equal to approximately 23 M€. This cost is about 5 times higher than the immediate cost increase associated with seismic isolation and does not take into account the consequences on people. Considering instead a time horizon of 100 years, the total cost associated with the expected consequences would be more than 6 times higher than that associated with seismic isolation.

The expected cost for the sector equipped with "ground isolation" is instead practically absent, in fact, as illustrated in this work, even an extreme seismic event, of an intensity corresponding to or greater than that of SLC, such as the one recorded in 2016, would not produce significant damage on the sector that would remain below the operational limit state. Moreover, in addition to mitigating (canceling) the economic consequences, there would be an almost total reduction of the socio-cultural consequences that are not strictly economically assessable and above all of the consequences on people.

9. Conclusions

The paper illustrates the study concerning the application of the seismic isolation on a single platform according to the technology defined "ground seismic isolation" or "artificial ground" to the town of Castelluccio di Norcia, practically destroyed in the earthquake of 30 October 2016, for which the reconstruction project is currently being carried out under the guidelines established by the Commissioner for the reconstruction. Due to the dramatic reduction of the seismic response allowed by the isolation technology, the objective of rebuilding "how it was, where it was" can be fully implemented, even applying techniques that can be traced back to traditional ones and by building constructions with "almost zero" expected damage, even for extreme expected earthquakes characterized by return periods of 1000-2000 years. The economic evaluations of the expected costs show that the extra costs associated with the use of the ground isolation technique are 3-6 times lower than the expected costs over the reference life for buildings rebuilt according to conventional criteria. Moreover, there are the enormous benefits associated with the absence of direct consequences on people and social, cultural, organizational consequences, all components whose values cannot be, and are not, evaluated economically.

References

[1] Mazzoni, S. Fulco, A., Castori, G., Galasso, C., Calvi, P., Dreyer, R., Fisher, E., Sorrentino, L., Wilson, J., Penna, A., Magenes, G., (2018): 2016–17 Central Italy Earthquake Sequence: Seismic Retrofit Policy and Effectiveness. *Earthquake Spectra*, 34(4).

[2] Valluzzi, M.R., Munari, M., Modena, C., Cardani, G.,Binda, L., (2007): Analisi di vulnerabilità sismica degli aggregati storici: il caso di Castelluccio di Norcia, *Convegno ANIDIS*. Pisa.

[3] Mezzi, M., Fulco, A. (2022): Isolated Artificial Ground for the Seismic Safety in the Urban Reconstruction of Castelluccio di Norcia, *Seismic Isolation, Energy Dissipation and Active Vibration Control of Structures - 17th World Conference on Seismic Isolation (17WCSI)*. Torino.

[4] Fagotti, G., Nodessi Proietti, S., Soccodato, F., Alemanno, N., Rotondi, M., Mezzi, M., Verducci, P., Bavicchi, M., Ciavaglia, C., Cincini, L., Finotto, M., Gabbarelli, E., Morosia, F., Di Carlo, S. (2022): The integrated project for the post-earthquake reconstruction of Castelluccio di Norcia: procedures, techniques, implementation, *XIX ANIDIS*. Torino.

[5] Mezzi, M. (2019): Meta-isolation of entire urban sectors for a resilient post-earthquake reconstruction preserving the pre-existing landscapes, *44th Conf. on Our World in Concrete & Structures,* Singapore

[6] Martelli, A., Forni, M., Bettinali, F., Bonacina, G., Bergamo, G., Castellano, M.G., Medeot, R., Marioni, A., Sanò, T., Pugliese, A., (1999): New Activities Performed in Italy on Innovative Anti-Seismic Techniques for Civil and Industrial Structures. *Proc. ASME-PVP Conf.*, Boston, USA, PVP-Vol. 387 pp. 311-326.

[7] Zhou, F. L., Yang, Z., Liu, W.G., Tan, P., (2004): New seismic isolation system for irregular structure with the largest isolation building area in the world, *13th World Conference on Earthquake Engineering*, Vancouver, Canada. August 2004.

[8] Fulco, A., Comodini, F., Mezzi, M., (2019): Isolamento sismico a grande scala per la salvaguardia del tessuto urbano nella ricostruzione post-sisma, *Convegno ANIDIS*, Ascoli Piceno (IT).

[9] Mezzi, M. and Fulco, A. (2020): Seismic isolation of whole city quarters for an effective and preservative reconstruction. *Procs. EURO-MED-SEC-3 - ISEC - Holistic Overview of Structural Design and Construction*, Limassol, Cyprus.

[10] Ubertini, F., Comodini, F., Fulco, A., Mezzi, M., (2017): A Simplified Parametric Study on Occupant Comfort Conditions in Base Isolated Buildings under Wind Loading, *Advances in Civil Engineering, Hindawi Publishing Corporation*, Article ID 3524975, 13 pages.

[11] Comodini, F., Fulco, A., Mezzi, M., Petrella, P. (2017): Fast risk assessment of losses in r/c buildings, *Procs. 16WCEE*, Santiago. Chile.

[12] Fulco, A., Mezzi, M., Comodini, F. (2020): Practical procedure to assess the expected consequences of earthquakes on buildings, *Procs. 17thWCEE*, Sendai. Japan.

SEISMIC RETROFIT OF R.C. BUILDINGS IN USE THROUGH SEISMIC ISOLATION. THREE CASE STUDIES IN L'AQUILA, ITALY.

Maria Gabriella Castellano [(1)], Riccardo Vetturini [(2)]

[(1)] *Academy Unit, FIP MEC srl, Italy, maria.gabriella.castellano@fipmec.it*
[(2)] *Ingenium srl, Italy, ing.vetturini@gmail.com*

Abstract

Seismic isolation (SI) advantages for new buildings are well known: not only it allows to avoid damage of both structural and non structural elements under strong earthquake, but it mantains building functionality as well. This is possible thanks to strong reduction of accelerations and interstorey drift in the superstructure, i.e. the part of structure above the isolation layer.

SI offers additional advantages for seismic retrofit of existing buildings. The main advantage is that the works can be limited at one floor (usually the basement, plus the foundation), without any strenghtening on the superstructure. Consequently, the building can be used during the retrofit works.

The safety of the retrofitted building increases significantly. Reaching exactly the same safety level of a new building in the same site would be possible, but it would need some strenghtening in the superstructure, and thus is usually avoided in order to keep the building in function during the works. It is worth noting that for the seismic isolation system, the safety is the same than for a new building.

The paper presents in detail three case studies of framed r.c. buildings built in the 1980s and now under retrofit with seismic isolation, that could be representative of many other buildings. During 2009 L'Aquila earthquake, those residential buildings were only slightly damaged, and immediately repaired but without any improvement of their seismic performance. Now the retrofit design is carried out for an earthquake stronger than the 2009 earthquake. Despite the buildings are in the same area (a_g=0.261g for the Life Safety Limit State earthquake; a_g=0.334g for the Collapse Limit State earthquake, used to design the seismic isolation system), the design spectrum is different because of different type of soil. The isolators are inserted in the basement or in the ground floor that host the garages, thus without affecting the apartments. The safety level reached in the three buildings was higher than 70% of that of new buildings in the same site, while before retrofit it was lower than 16%.

Keywords: seismic isolation, seismic retrofit, building

1. Introduction

Seismic isolation (SI) advantages for new buildings are well known: not only it allows to avoid damage of both structural and non structural elements, thanks to strong reduction of accelerations and interstorey drift in the superstructure, i.e. the part of structure above the isolation layer, but it allows to mantain building functionality as well, even under strong earthquake. That is why its use in strategic buildings - e.g. hospitals - is increasing everywhere in the world, including developing countries. In Turkey, seismic isolation is mandatory for large hospitals in high seismic areas. In Italy, seismic isolation of buildings is not anymore limited to strategic or public buildings; it is continuously increasing for residential buildings as well, in particular in areas with high seismicity, in which the additional cost of seismic isolation is compensated by the savings in the superstructure, and thus the global cost could be the same or lower of that of a conventional structure, but with much higher performance. Amongst a total of about 900 seismically isolated buildings in Italy until summer 2022, almost one half are residential buildings [1].

The strong reduction of acceleration provided by SI is of course beneficial to existing buildings as well; consequently, seismic retrofit of buildings with SI is carried out all over the world since the 1980s [2]. In Italy, seismic retrofit of buildings with SI became relatively common after the 2009 L'Aquila earthquake, initially on buildings strongly damaged by the earthquake. Recently, retrofit with SI is continuosly increasing, even in areas not recently affected by earthquakes. One additional

advantage of retrofit with SI, in comparison with other conventional approaches, is that the works can be limited at one - two levels (usually the basement and the foundation level in r.c. buildings), without any strenghtening intervention on the superstructure. Consequently, the building can be mantained in use during the retrofit intervention. Moreover, the cost of intervention is reduced, in particular the cost portion not related directly to the structural intervention, but to demolition and refurbishment of non-structural parts. Mezzi and Petrella [3] report a cost comparison of alternative seismic retrofit strategies for two RC buildings damaged by the L'Aquila earthquake, showing that the strategy with seismic isolation allowed a saving higher than 30%. Now the Italian buildings retrofitted with SI are about 1/3 of the total number of seismically isolated buildings [1].

The safety of a building retrofitted with seismic isolation can become almost equal to that of a new building in the same site, i.e. with a Capacity/Demand (C/D) ratio equal to 1 or very close to 1. Reaching the same safety level (C/D=1) would be technically possible, but it would make necessary some intervention in the superstructure, and thus is usually avoided in order to keep the building in function during the works. However, it is worth noting that in Italy, for the seismic isolation system, the safety shall be the same than for a new building, even though the C/D of the superstructure is lower than 1. Furthermore, a specific Limit State (Collapse Limit State) is introduced by the Italian Code, i.e. the earthquake used for the design of seismic isolation system has an higher return period than the earthquake used for the design of the building. This approach substitutes in Italy the reliability factor required by Eurocode 8 on the displacement of the isolation system (1.2 recommended value for buildings).

2. Seismic retrofit through seismic isolation: case studies in L'Aquila

The paper describes 3 case studies of seismic retrofit of r.c. buildings with SI. The buildings, built in the 1980s, are residential buildings located in L'Aquila, that were only slightly damaged by the 2009 L'Aquila earthquake, and immediately repaired but without any improvement of their seismic performance. Taking the opportunity of the tax reduction offered by the Italian state in 2020, the owners decided to improve the seismic performance of the buildings, but requiring to keep the apartments in use during the works. Seismic isolation was thus selected as intervention strategy in all these buildings, with works at the garage level (basement or ground level) and foundation. The position selected for the isolation system is different in the 3 buildings, that thus become representative of many other buildings. It is important to note that a very short work time was imposed by the tax reduction law, and that energy redevelopment was carried out together with seismic retrofit: the fact that the structural works are located at one story only (ground story or basement, and foundation) has allowed to reduce a lot the total working time, because the seismic retrofit was carried out at the same time that the external thermal insulation.

The types of seismic isolators mostly used in buildings in Italy are elastomeric isolators (with high damping rubber) and curved surface sliding isolators (pendulum isolators). In retrofit of existing buildings, pendulum isolators are more frequently used, because they allow to reach high value of isolated period for any kind of structure. However, in these case studies the seismic isolation system comprises high damping rubber bearings (HDRB) and free sliding bearings. The latter are often used in Italy combined with HDRB, for two main reasons: they allow to increase the fundamental period even in low-rise buildings, and they make easier the reduction of eccentricity between center of mass of the superstructure and center of stiffness of the isolation system in very irregular structures. The equivalent viscous damping offered by HDRB is 15%. Linear analyses is admitted with this isolation system by both European and Italian standards. According to the standards, the damping is taken into account reducing the design spectrum for periods higher than 80 % of the fundamental period of the isolated building. The design spectra for the seismic isolation system of the 3 case studies are reported in Figure 1. Despite the buildings are in the same area, the design spectrum is different because of different type of soils. For Case Study 1, the soil is better than for the other two buildings. The difference between the spectra of case study 2 and 3 is only due to the different fundamental period of the isolated building selected in the design phase.
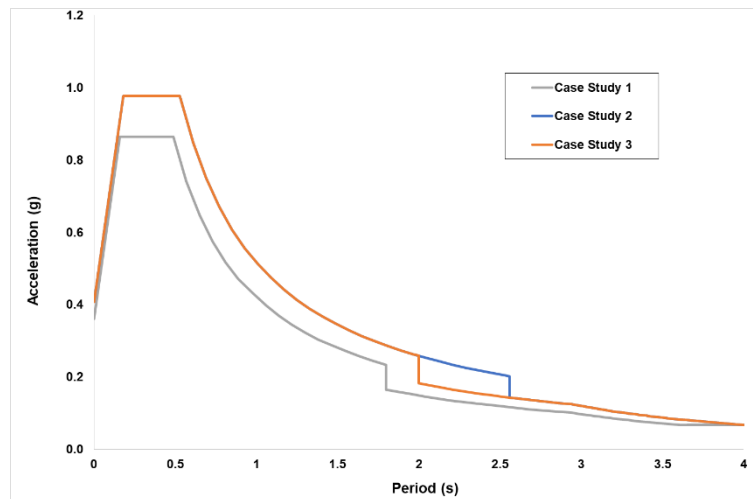
Figure 1. Design spectra for the three seismic isolation systems (at Collapse Limit State).

3. Case study 1: Crefel building

The building includes three units, built at the end of the 1980s with structure in reinforced concrete. Unit A and B are identical, with 6 floors, an height of 14 m and plan size 28.5 m x 12.5 m. Unit C has one floor only, and connects units A and B (Fig. 2 and Fig. 3). The r.c. structure is framed but includes shear walls as well (around the elevators). The foundations are ground beams. Both the infill and partition walls are masonry walls.

Units A and B have been seismically isolated, while Unit C strengthening has been conventional. In order to allow the big horizontal displacement associated with seismic isolation, a proper gap has been realized around the building, and of course Unit C has been disconnected from Units A and B. New steel columns have been inserted to sustain the floor of Unit C where the new seismic gap has been created, and the sidewalks were modified to cover the gap and allow the displacements at the same time.

Figure 2. CREFEL Building

The isolators have been installed on top of the columns of the underground floor, where the garages are located (Fig. 3). As it is well known, for a proper functioning of seismic isolation in a building, a stiff floor below and above the seismic isolation layer shall be guaranteed. In this case, the existing ground floor, immediately above the isolation layer, is stiff enough. Below the isolators, the needed stiffness is guaranteed by the foundation and the columns properly stiffened through an increase

of their section. The steps followed for the installation of the isolators in each column are shown in Fig. 4 and described here below:

- enlargement of the column in the portion below the isolator, leaving proper recesses to be used for the lower anchorage of the isolator with dowels;
- core drilling of the upper part of the column, and insertion of ferrules to connect to the column the steel brackets that will serve to transfer the vertical load to hydraulic jacks;
- placing of hydraulic jacks to unload the portion of column to be removed; the load is transferred to foundation through provisional steel columns;
- diamond wire cutting and removal of the segment of the column where the isolator will be installed;
- levelling of the lower surface, and installing the upper anchorage of the isolator; this is a steel structure that embraces the column, to trasfer to it the shear force transmitted from the isolator;
- fixing the isolator to its upper anchorage, then grouting of the upper anchorage with antishrinkage cement or epoxy resin mortar;
- placing of non-returnable flat jack to load the isolator;
- final grouting of the bottom anchorage, including the non-returnable flat jack;
- removal of external hydraulic jacks.
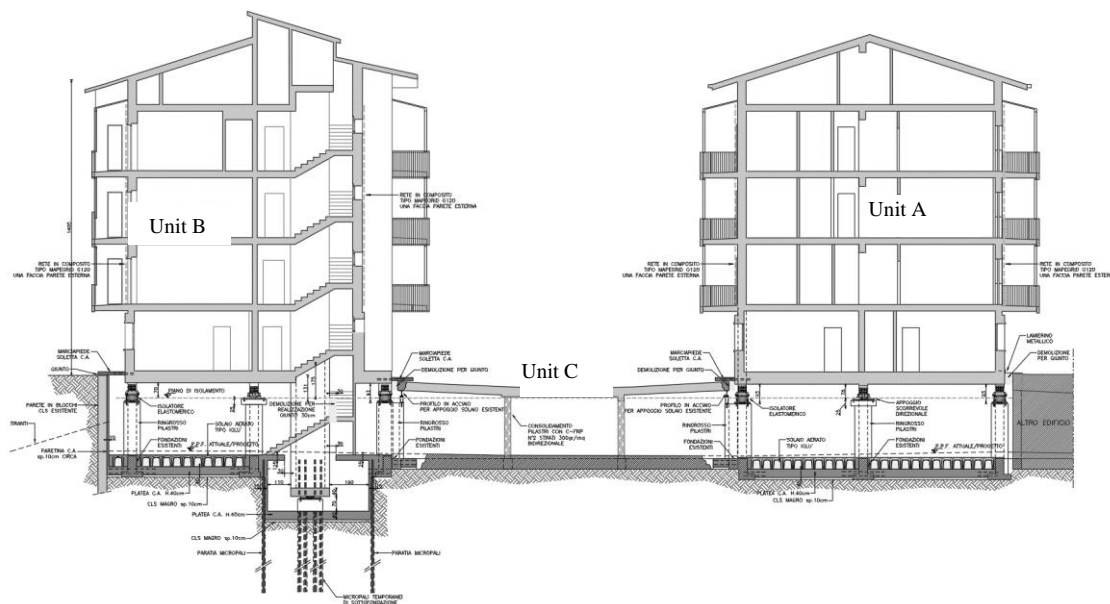
Figure 3. Cross section of Crefel Building.

The seismic isolation system includes 28 elastomeric isolators, type SI-N 450/98, and 10 free sliding pot bearings (Fig. 6), with displacement capacity of ± 200 mm. The pot bearing are installed in the central columns of each unit, and below each elevator; the elastomeric isolators in the perimetral columns, in order to guarantee a proper torsional stiffness of the isolation system. Of course the position of elastomeric isolators and sliders is selected with special attention at reducing the eccentricity between center of mass of the superstructure and center of stiffness of the isolation system. Said seismic isolation system allows to increase the fundamental period from the original value of 0.80s to 2.47s, and consequently to significantly improve the building's seismic response. Said "improvement" has been quantified in about 65% (C/D changed from 0.09 to 0.76). In terms of seismic risk classification [4], the seismic risk class changes from F for the original building to B for the seismically isolated building.

1) the column before retrofit;

2) column enlargement;

3) fixing of steel brackets;

4) placing of hydraulic jacks;

5) cutting and removal of column segment;

6) insertion of upper anchorage structure;

7) isolator fixed to upper anchorage structure;

8) grouting of upper anchorage structure;

9) insertion of non-returnable flat jack;

10) final grouting of the isolator.
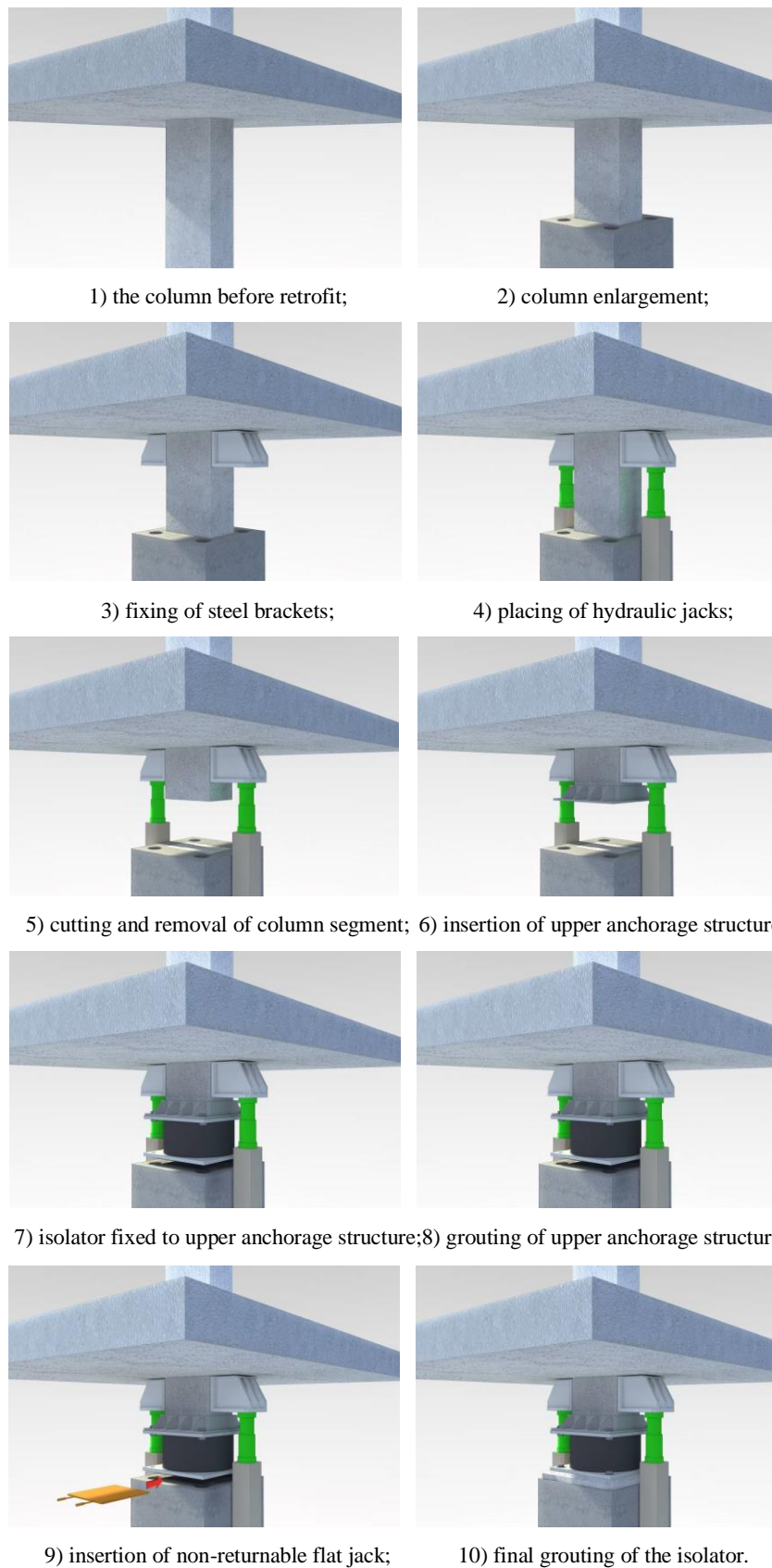
Figure 4. Steps for isolators installation in Crefel Building.

Figure 5. Crefel Building: two phases of the installation of the isolators.
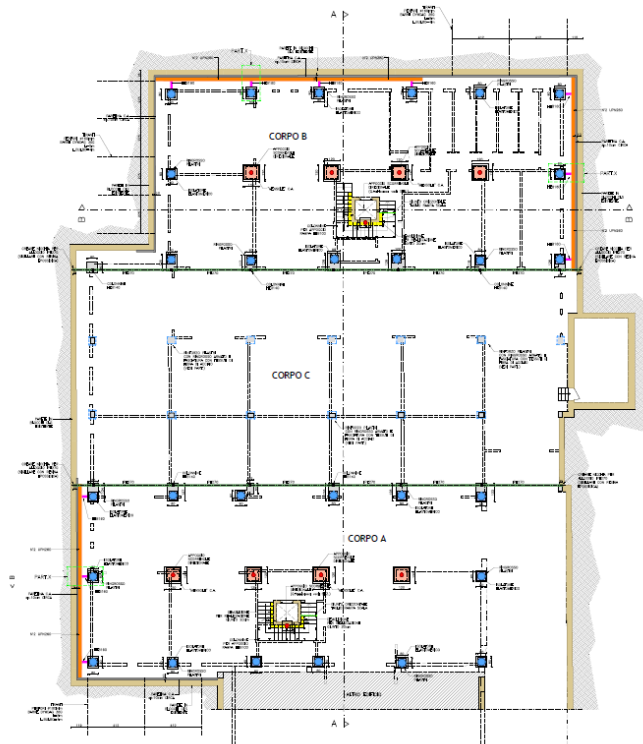
Figure 6. Plan of the isolation system for Crefel Building.
Elastomeric isolators are in blu, free sliding pot bearings in red.

4. Case study 2: building in via Di Vincenzo 23

The building has 5 floors, with garages at the ground floor (Fig. 7). It has total plan size 56 m x 16 m, is built in the first 1980s with r.c. frame. It includes two units, separated by a structural joint of about 20 cm. For this building it was not possible to insert the isolators at top of the columns of the garages, as in previous case, mainly because the height of ground floor was not enough to have the isolation level above the garage doors. Consequently, the isolators have been inserted at the foundation level, and a new floor was built above the isolators, acting as new ground floor (Fig. 8).

The isolators have been inserted at the base of the columns, modifying the existing foundations. Fig. 9 shows all the steps executed for the modification of the foundation system and the installation of the isolators. At the base of each column, part of the foundation has been cutted in order to create the space needed to insert the isolator. Furthermore, new micropales are inserted, new plinths are created under each column, to serve as basis for each isolator, and a new foundation slab is made to connect the plinths. Of course all these activities shall be carried out with care, to allow the transfer of load from

old to new foundations, through the isolators. The columns are reinforced as well, at the ground level, in order to increase their strength; this is important in particular to resist local actions during works.

The joint between the two built units was left as it is in the superstructure, but it was eliminated at the floor immediately above the isolation layer, to guarantee that the two units will move together during earthquake. This is usually done in seismic isolation of existing buildings, because the existing gap would not be enough to accomodate the horizontal displacement of each seismic isolated building unit, that of course is much larger than in the fixed base building. Furthermore, even in new seismically isolated buildings, it is quite common to eliminate completely the internal seismic joints amongst different built units, or keep them just as thermal joints in the superstructure, in order to avoid the difficulties and costs of large seismic joints.

New perimetral retaining walls and special sidewalks to allow the horizontal displacement of the building complex were built.

Figure 7. The building in via Di Vincenzo 23.
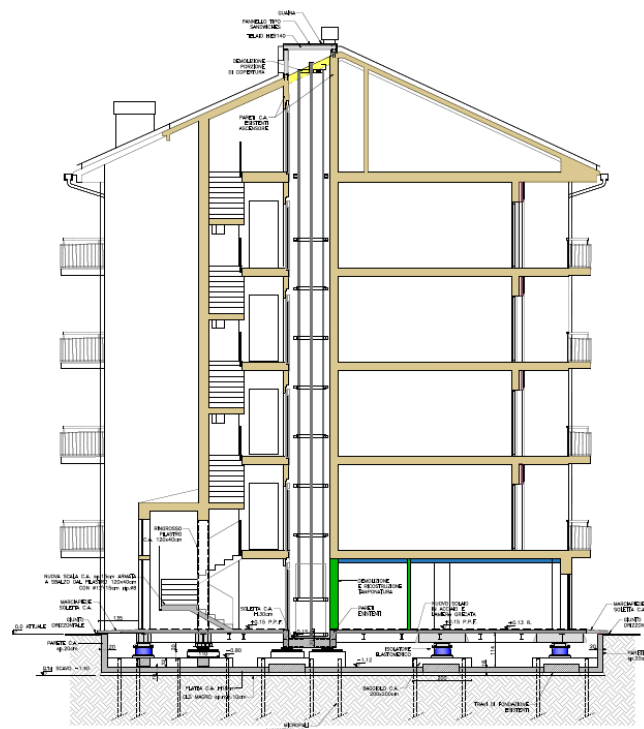
Figure 8. Cross section of the building in via Di Vincenzo 23.
Elastomeric isolators are in blue, free sliding bearings in black.

1) before intervention;
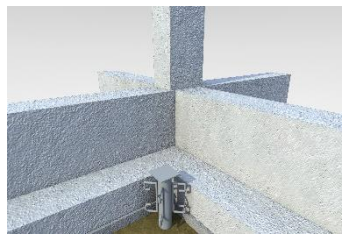
2) insertion of micropiles;
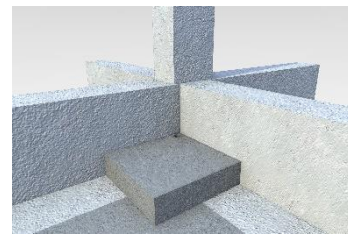
3) new plinth between the column and the micropiles;
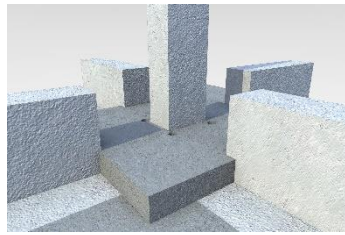
4) cutting of part of foundation around the column;

5) insertion of steel structure for upper anchorage of the isolator;

6) insertion of hydraulic jacks, transfer of loads, and cutting of column;

7) insertion of the isolator;

8) loading of non-returnable flat jack & grouting of the isolator's bottom ancorage;

9) removal of hydraulic jacks, installation of beams for the new ground floor;

10) completion of new ground floor.

Figure 9. Steps for isolators installation in Building in via Di Vincenzo 23 (Case Study 2).

The seismic isolation system includes 35 elastomeric isolators, type SI-S 600/200 and 35 free sliding bearings, type VM 200/700/700 (Fig. 10). Both isolator types have maximum displacement capacity of +/- 350 mm. The displacement capacity required is much higher than in Case Study 1, mainly because the soil type is worse. The fundamental period changes from the original value of 1.05s to 3.2 s. The seismic risk class [4] changes from F for the original building to B for the seismically isolated building. And the C/D ratio changes from 0.03 to 0.75.
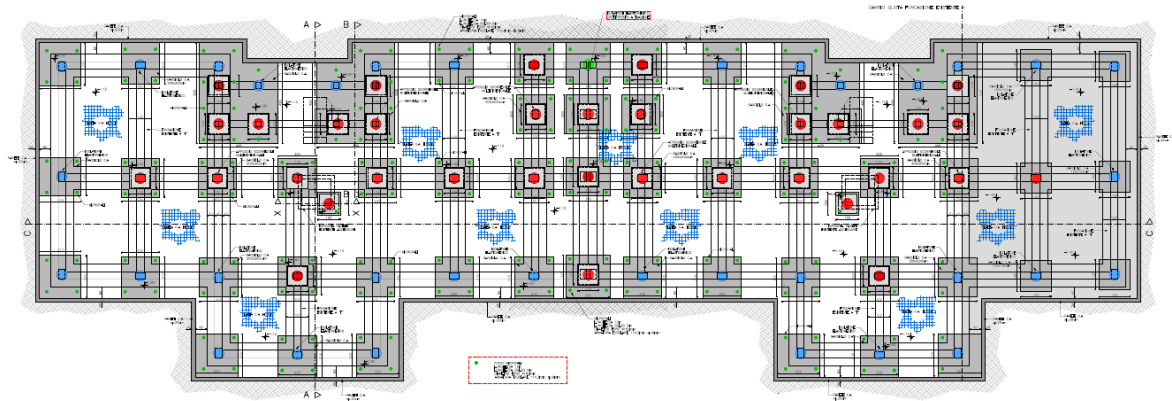
Figure 10. Plan of the isolation system for the building in via Di Vincenzo 23.
Elastomeric isolators are in blu, free sliding pot bearings in red.

5. Case study 3: building in via Di Vincenzo 23 A

The building complex includes two units, with r.c. framed structure, separated by a joint (Fig. 11). The foundation is on piles connected by beams in both directions. Each built unit has a plan of 29.55m x 13.3m, and an height of 16.5 m. In this case the existing joint is not large enough to allow displacement under earthquake, not just for isolated buildings, but for fixed base buildings as well.

Figure 11. View of the building complex in via Di Vincenzo 23 A (at the right, image from Google Maps).

The solutions selected for the insertion of the isolators in previous two case studies were not feasible in this building, due to its geometry, in particular the height of the basement used as garage. Thus, a third solution has been studied, i.e. the insertion of the isolators immediately below the existing foundation beams, on top of the piles (Fig. 12 and Fig. 13). This solution made necessary an excavation below the existing foundation for a depth of about 3.3 m (of course after the construction of a new retaining wall), and the construction of a new foundation slab properly connected to the existing piles. Around each pile, two r.c. plinths are built, above and below the volume where the isolator shall be installed. Then, hydraulic jacks are inserted between said two new plinths, and loaded, so that the vertical load is transmitted through the jacks to the bottom plinth, and the top portion of pile can be cutted. The isolators are then inserted and loaded through non-returnable flat jacks, as in previous two cases. The installation is then completed with proper grouting of the isolators and with the construction of a new floor above the isolators, stiff enough in its plan to guarantee a rigid body motion of the isolated buildings. Said new floor connect the two building units, as the new foundation slab does; the existing joint between the two built units keep its function as thermal joint only, while under earthquake the isolated building behave as one unit. Fig. 14 shows all the steps described above for the installation of the isolators.
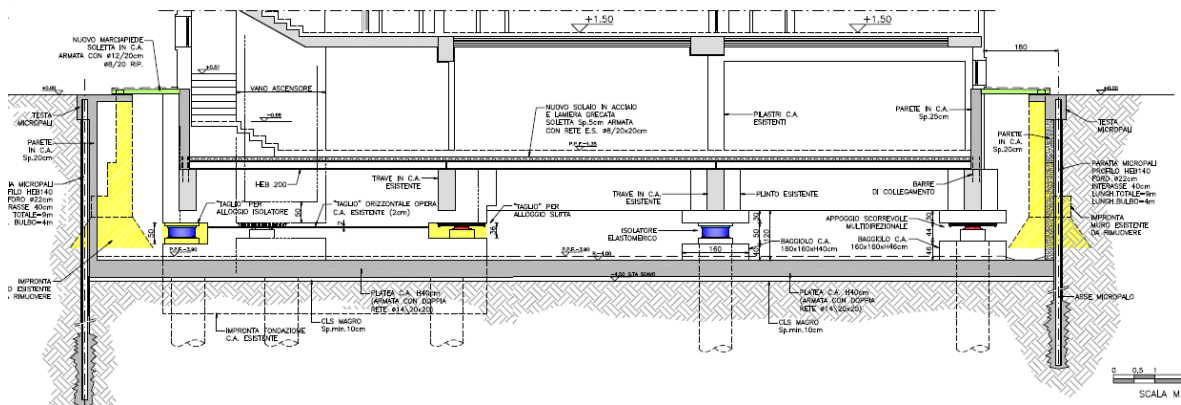
Figure 12. Cross section of the building in via Di Vincenzo 23 A at the basement/foundation level.
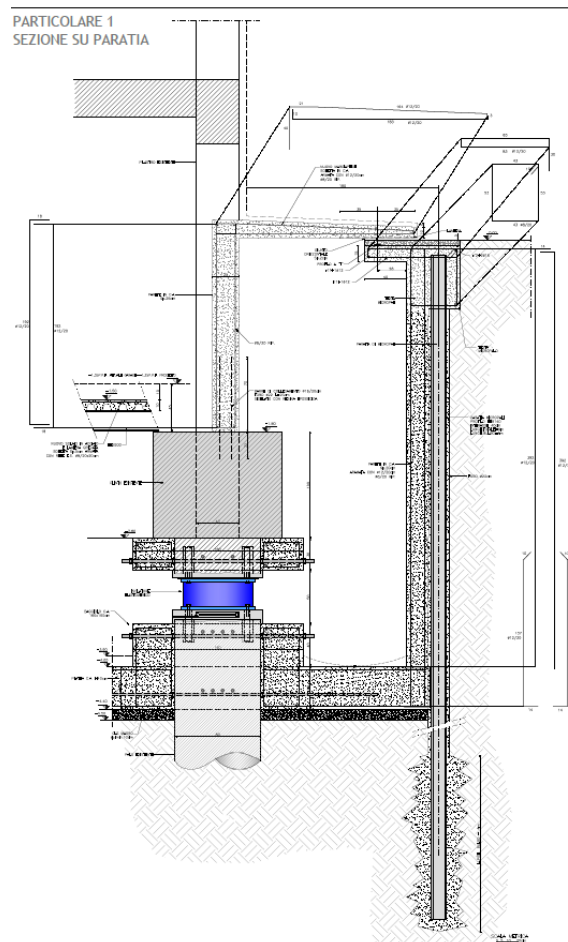
Figure 13. Cross section of the building in via Di Vincenzo 23 A:
detail of the perimetral retaining wall and of an isolator installed on the perimeter of the building.

The seismic isolation system includes 23 elastomeric isolators, type SI-N 650/162, and 24 free sliding bearings, type VM 350/700/700 (Fig. 15). The maximum displacement capacity is ±350 mm. Thanks to seismic isolation, the fundamental period increases from the original value of 0.85s to 2.57s. The consequent reduction of earthquake input energy transmitted to the superstructure allows that the seismic risk class [4] changes from E for the original building to B for the seismically isolated building. The C/D ratio changes from 0.16 to 0.71.

1) excavation below the existing foundation beams;

2) placing reinforcement for the new structure (plinths and foundation slab);
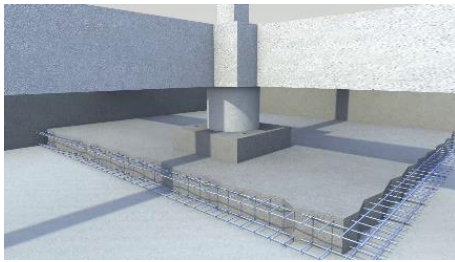
3) the new foundation slab and the bottom plinth;
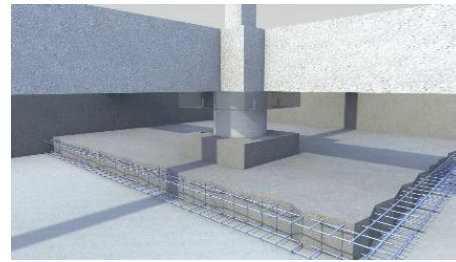
4) the top plinth including dowels for the mechanical connection of the isolator;

5) placing of hydraulic jacks and displacement transducers;

6) cutting the top of the pile with diamond wire;

7) the isolator during installation: non-returnable flat jack has been already injected, while bottom anchorage grouting is not yet carried out.

Figure 14. Steps for isolators installation in Building in via Di Vincenzo 23 A.
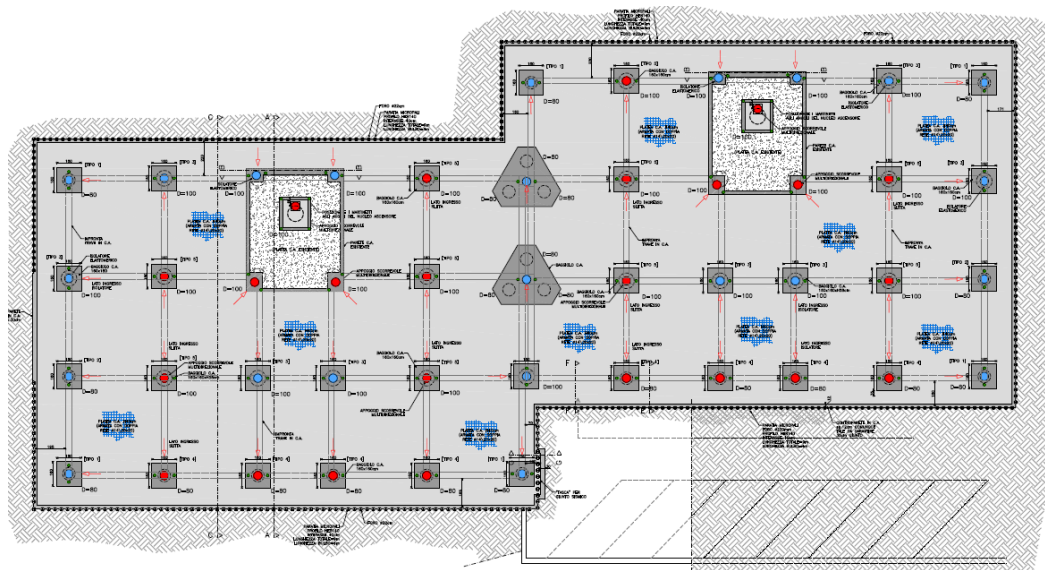
Figure 15. Isolation system of the building in via Di Vincenzo 23 A:
Elastomeric isolators are in blu, free sliding pot bearings in red.

5. Conclusions

The three case studies described above show the feasibility and advantages of seismic isolation of buildings in use. The apartments use was never interrupted during the works, only the garages were temporarily not available. The different positions of the seismic isolation layer where selected on the basis of the peculiar geometry of each building. The solution used in case study 1 is the simplest and the cheapest. However, in all the 3 cases the costs were fully within the limits of conventional retrofit works, defined by the Italian state within the tax reduction law used for such works.

The improvement in seismic behaviour is impressive. The original C/D ratio was originally not higher than 0.16, and after seismic isolation becomes higher than 0.7, and this goal was reached without any intervention in the superstructure. The seismic isolation system is designed for C/D ratio equal to 1, and for an earthquake stronger than the design earthquake for the building, corresponding to the Collapse Limit State, according to the Italian Seismic Standard.

Acknowledgements

References

[1] Clemente P. (2023): Applications and recent studies on seismic isolation in Italy. In: Cimellaro G.P. (ed) *Seismic Isolation, Energy Dissipation and Active Vibration Control of Structures. WCSI 2022*. Lecture Notes in Civil Engineering, Vol. 309, 3-16. Springer, Cham. Invited lecture, https://doi.org/10.1007/978-3-031-21187-4_1

[2] Bayley, J., Allen, E., (1989): Seismic isolation retrofitting of the Salt Lake City and County building, *Post-SMIRT 8 Seminar,* paper 14.

[3] Mezzi, M., Petrella, P. (2015): Base isolation in seismic retrofitting of buildings damaged by 2009 L'Aquila earthquake, *14ᵗʰ World Conference on Seismic Isolation, Energy Dissipation and Active Vibration Control of Structures*, San Diego, USA.

[4] Cosenza, E., Del Vecchio, C., Di Ludovico, M. et al. (2018): The Italian guidelines for seismic risk classification of constructions: technical principles and validation. *Bull Earthquake Eng,* **16**, 5905–5935. doi: https://doi.org/10.1007/s10518-018-0431-8

SEISMIC ISOLATION ON EXISTING RC BUILDINGS: OVERVIEW OF SOME ISSUES AND APPLICATIONS TO CASE STUDIES

Gino Di Trocchio [(1)], Marco Zaccari [(1)], Michele D'Amato [(2)], Rosario Gigliotti [(3)]

[(1)] *Structural Engineering, EI srl - Engineering Innovation, via Martin Luther King 39, Potenza (Italy), ei.amministrazione@engineeringinnovation.it*
[(2)] *Assistant Professor, Department of European and Mediterranean Cultures (Architecture, Environment and Cultural Heritage), University of Basilicata, Via Lanera, 75100 Matera, Italy, michele.damato@unibas.it*
[(3)] *Associate Professor, Department of Structural and Geotechnical Engineering, Sapienza University of Rome, Via Eudossiana 18, 00184 Rome, Italy, rosario.gigliotti@uniroma1.it*

Abstract

The paper presents an overview of some common issues related to the seismic isolation technique applied to existing RC buildings. At first, the issues considered are briefly described. Then, solutions on how to solve them are illustrated with reference to case studies on which the seismic isolation is applied. The interventions are to date only designed or in progress of being realized. All case studies considered are existing RC structures designed only for vertical loads with a non-ductile behaviour and located in Potenza, a city in the South of Italy in a high seismic hazard area.

Keywords: rubber device. friction pendulum, seismic isolation, seismic devices, retrofit, existing RC building

1. Seismic isolation principles

Nowadays, seismic isolation is a technique largely applied for protecting buildings against earthquakes, applied both in designing new buildings, and in seismically retrofitting the existing ones. It is aimed to reduce the lateral accelerations demand and, consequently, to reduce elements internal forces through the superstructure natural period elongation. This is obtained introducing, typically above the foundation, a disconnection consisting of seismic devices having a low horizontal stiffness. In this way a decoupling between the superstructure and substructure is obtained, with an increment of lateral displacement demand (Figure *1*).
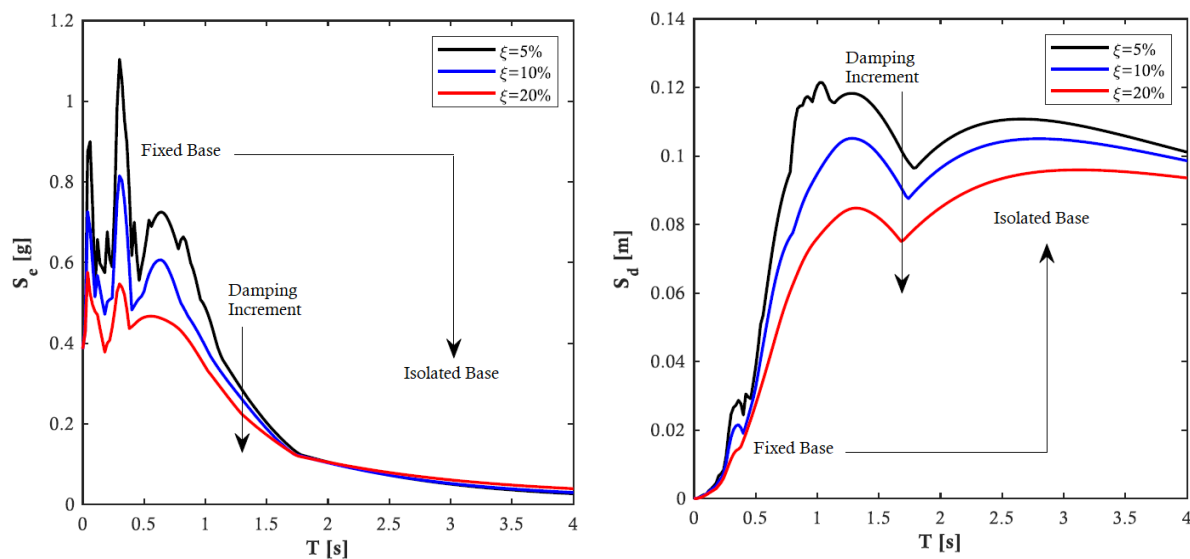
Figure 1: Acceleration and Displacement Response Spectra for different damping factor

Very often the seismic isolation technique represents a very versatile solution in the case of Reinforced Concrete (RC) existing buildings, mainly designed only for vertical loads without any specific regulation for lateral loads, because of:

- it increases the safety building level since the seismic load acting on the superstructure may be significantly reduced due to natural period lengthening;
- it permits a more regular dynamic behaviour, reducing the eccentricity between the center of mass and stiffness;
- it ensures limited damages of non-structural elements and equipments for all the limit states, thanks to the drastic reduction of the interstory drifts and floor shear;
- it is minimally invasive since requires spaces of small dimensions to be realized, by acting on a limited portion of the structure, and in many cases it does not even require the occupants evacuation.

Starting from these premises, in this work some issues related to the seismic isolation strategy applied to existing RC buildings are examined. The issues considered play a central role during the seismic isolation design, since if not properly considered, they may lead to in an incorrect evaluation of the devices displacement demand and, in general, to a different behaviour of the isolated structure with respect to the predicted one. In detail, in this study particular attention is paid to:

- column cap and external jacketing, in order to guarantee a correct rebar anchorage length embedded in the concrete of substructures columns;
- torsional effects on the isolation system, to correctly evaluate the displacement demand;
- second-order effects, to consider the effective loads on the superstructure and substructure;
- superstructure stiffness evaluation, to properly design seismic isolation system.

At the first, the above-mentioned issues are discussed from a design perspective. Then, they are commented in detail with particular reference to some case studies briefly illustrated in this work.

2. Design Criteria

In this section, the issues previously listed are briefly introduced and commented from a design perspective. Afterwards, they are contextualized with reference to some case studies chosen in this work, where the interventions are yet in progress or, else, already realized.

2.1 Column cap and jacketing

A fundamental issue linked for installing seismic devices in the case of existing buildings, is represented by the cutting of existing RC columns involving, of course, as well the cutting of longitudinal steel rebars. For instance, Figure 2 refers to the case of seismic isolation realized at the top of the ground floor RC columns. In this new configuration, if no additional construction detail is adopted, the longitudinal bars at the superstructure columns base would have an inadequate anchorage length that, consequently, conspicuously reduces the columns flexural strength resulting hinged at the base. A possible solution is represented by realizing an appropriate column cap below the superstructure floor, in which longitudinal bars may be anchored. Whereas, in the case of seismic isolators installed above the foundation (seismic isolation at the base), an improvement of the column flexural strength may be obtained with an external additional column jacketing. Figure 3 depicts the solution proposed, where the floor at the base of the super-structure is realized through a concrete slab.

2.2 Torsional effects on isolated buildings

In designing the seismic isolation bi-directional earthquake loadings should be considered including the torsional effects in order to properly evaluate maximum displacement demand. This aspect becomes very important when seismic devices non-linear behaviour is modelled by means of visco-elastic equivalent schemes. As far as the torsional effects are concerned, caused by the structure geometry and the bi-directional earthquake loadings, recent studies on existing RC buildings showed that the

displacement demand on devices may result greatly increased with respect to the simplified mono-directional analysis [1], resulting greater up to 1.8 times because of also the torsional effects produced by accidental eccentricity [2].
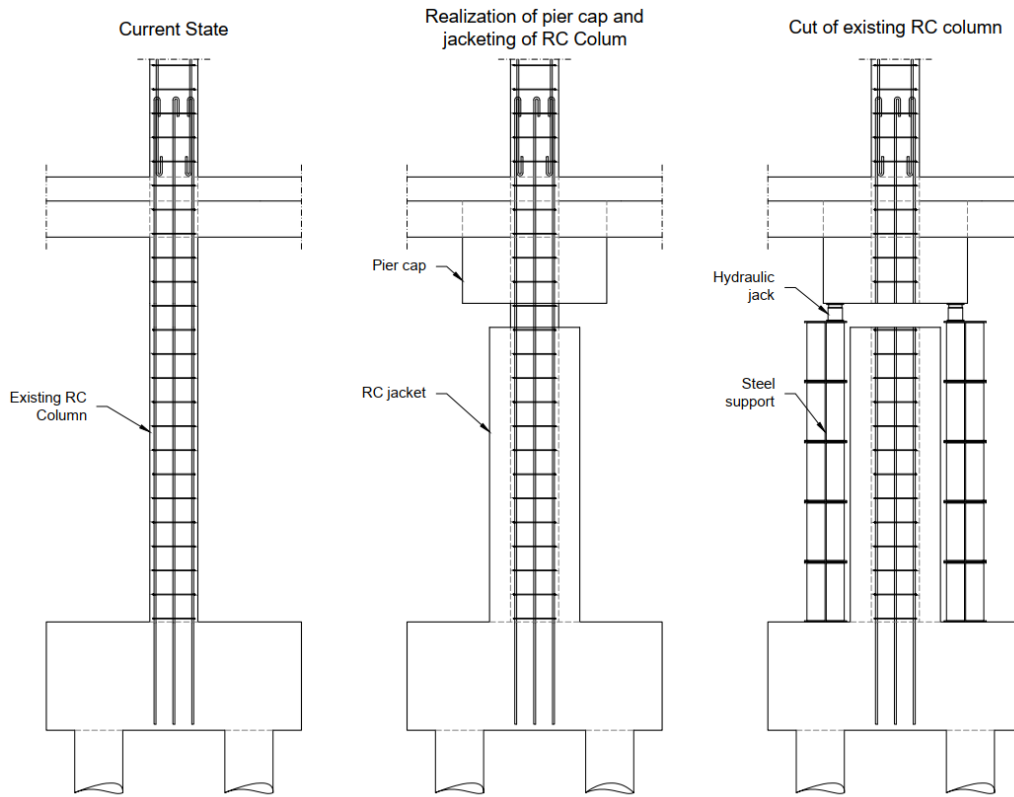
Figure 2: RC column cutting for seismic device installation
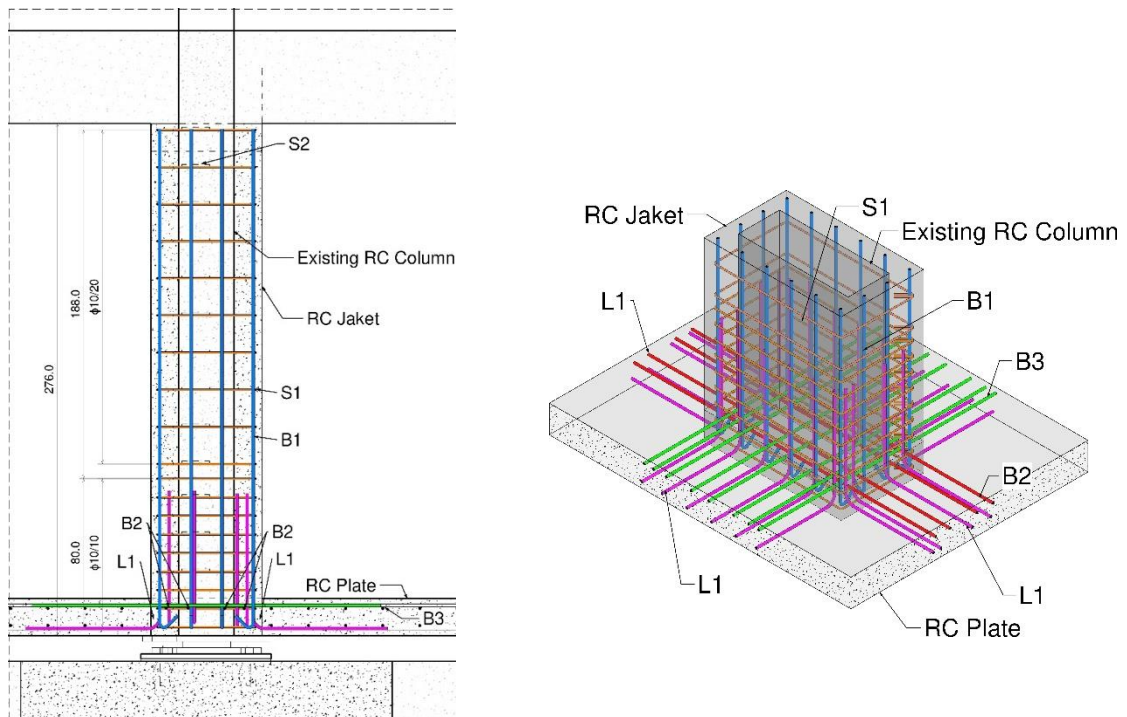
Figure 3: Example of RC columns jacketing with a concrete slab

2.3 Second-order effects

The installation of seismic devices within structures involves an in-depth analysis related to second-order effects due to load eccentricity acting during the earthquake motion. When the device is shifted, the vertical load does not act vertically and an additional moment is generated given, in the case of friction pendulum or HDRB device, by the axial load into half maximum displacement of the seismic device. This additional moment is acting on both superstructure and substructure with, of course, the same intensity. Whereas, in the case of sliding isolators, the axial load eccentricity provokes an additional moment depending on how the seismic device is mounted (Figure 4): if the plate is placed at the top of the substructure column (slider at the bottom of the superstructure), the additional moment acts on the substructure; conversely, the additional moment acts on the superstructure (the moment intensity in both the configuration discussed results of course the same).
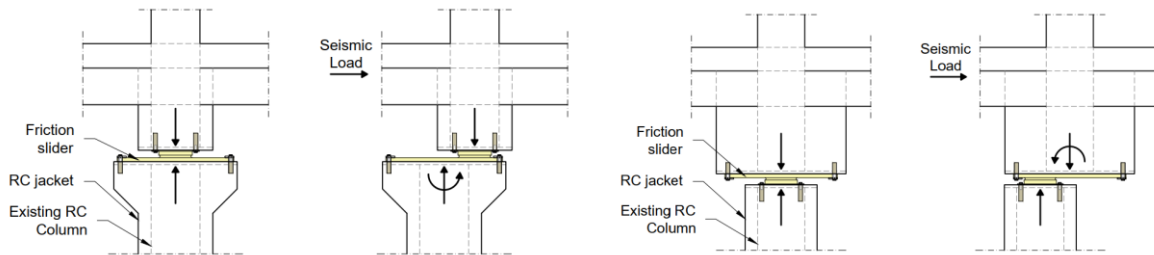
Figure 4: Sliding isolator: second-order moment due to the vertical load eccentricity

Therefore, the solution chosen may vary case-by-case, and it must be accompanied by a careful assessment of the second-order effects, including the local intervention needed. If the slider is applied on the superstructure or at the substructure e bottom column, the additional moment has to be supported by the superstructure beams converging at the upper column base where the plate is placed, requiring a local verification. Moreover, in order to reduce the internal forces acting on the column cap, the seismic device should be placed as low as possible for reducing the tensile forces acting along the horizontal tie according to the strut and tie model.

2.4 Superstructure stiffness

Superstructures stiffness plays a central role in the dynamic response of a seismically isolated building. Investigations carried out on existing RC buildings mainly designed only for vertical loads and seismically isolated highlight the importance to increase the superstructure stiffness with respect to the horizontal actions in order to reduce the effects of higher vibrational modes [3].
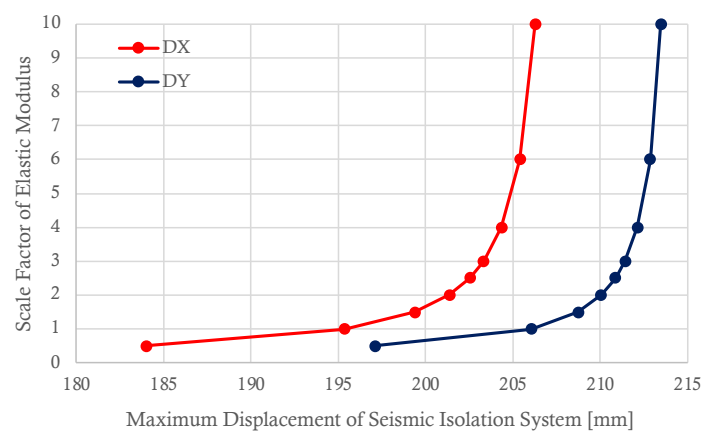
Figure 5: Displacement of seismic isolation system as a function of superstructure stiffness

Investigations conducted, linked to the FEM analysis, showed how the high buildings stiffness to the lateral actions is given by masonry infills (perimetral and internal), mostly interacting dynamically with

the RC frame [4,5]. This important interaction is beneficial for seismic isolation because it increases the superstructure isolation degree (that should reflect a rigid-body behaviour), making the dynamic behaviour more regular, and strictly depending on the dynamic characteristics of seismic isolation system. The superstructure stiffening definitively implies an increment of the displacement demand on the seismic devices. As proof of this Figure 5 reports, by referring to a case study analysed, the isolation system displacement along the two directions without eccentricity by varying the scale factor of the superstructure elasticity modulus. As one may note, the higher the scale factor the higher the system displacement, with an asymptotic trend of the displacements as a function of elastic modulus.

2.5 Fragility curves

Thanks to the isolation strategy the seismic damage of superstructure elements may be nullified due to a drastic reduction of interstory drifts and floor accelerations that are Engineering Demand Parameters (EDPs) strictly correlated to the elements' internal forces. Consequently, the internal actions of superstructures elements are mainly due to the vertical loads, that are the reference loads when existing structures were designed.

Benefits of seismic isolation may be proved through the fragility curves, expressing the probability to be equal or greater of a certain damage D_i for a given *Intensity Measure (IM)* representing the ground motion. In particular, one of the most largely applied functions to describe a fragility curve is the lognormal cumulative distribution function, expressed as follows [6]:

$$F_{D_j}(IM) = P\left(D \geq D_j | IM\right) = \Phi\left[\frac{\ln(IM) - \mu}{\sigma}\right] \quad j = 0, 1, \dots, 5, \quad (1)$$

where Φ is the standard normal cumulative distribution function of $ln(IM)$ (i.e., gaussian function), where μ and σ are the natural logarithmic mean and natural logarithmic standard deviation defining the lognormal distribution, respectively. In this study, μ and σ of the *IM* considered are calculated using the maximum likelihood estimation method [7]. As example, fragility curves for existing RC buildings designed only for vertical loads are reported in Figure 6, by considering three different *IMs*, which are Peak Ground Acceleration (*PGA*), Intensity of Arias (*I_A*), and horizontal spectral acceleration [$S_e(T_f)$] [8].
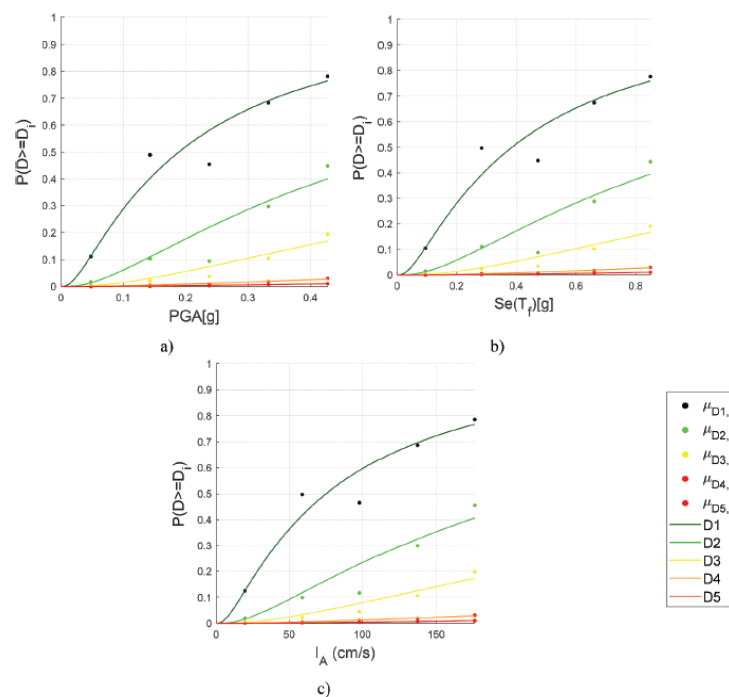
Figure 6: Fragility curves of RC buildings by assuming IM: (a) PGA, (b) Se(T$_f$), and (c) I$_A$ [8]

3. Case Studies

The issues previously introduced are discussed in this section with reference to some Italian case studies. The interventions illustrated are designed or already in progress to be realized.

3.1 "Palazzo Gaeta" building

The building named "Palazzo Gaeta" was designed in 1962 only for vertical loads and then built in 1969. The RC structures consist of n. 12 floors: n. 8 levels above ground, including the roof, with a total height of about 24.60 m; and n. 4 underground floors, down to a depth of 14.30 m. In elevation the building has three distinct structures (hereinafter indicated as Fab. A, Fab. B and Fab. C) separated by structural joints. The total floor area is of about 1280.0 m^2. The structure is located on a slope with a difference along the height of about 14 m, where the Fab. A if located downhill. In the following some views of the FEM model implemented are shown (Figure 7).
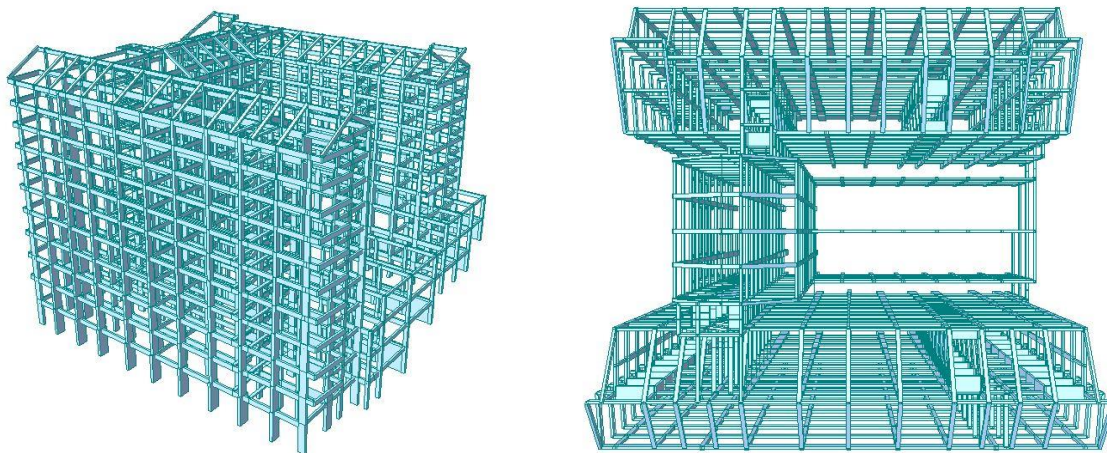
Figure 7: 3D views of the FEM model implemented

In this case an aspect that deserved particular attention in designing the seismic isolation system was the influence of the current lateral stiffness of the structures. In fact, the flexibility due to the height may involve, if not properly assessed, a not controlled isolation system response because of an inadequate seismic isolation degree. Therefore, in order to estimate the foundational periods of the structure, a dynamic identification was conducted starting from the results of a modal analysis carried out on the three frame structures (Fab. A, Fab. B and Fab, C). A comparison among the fundamental periods obtained along the two principal directions are reported in the Table 1. The periods estimated through the dynamic identification are indicated as T_{ID}, whereas the ones resulting from the modal analysis are indicated as T_{FEM}.

Table 1 – Fundamental periods comparison

Structure	$T_{X,FEM}$ (s)	$T_{Y,FEM}$ (s)	$T_{X,ID}$ (s)	$T_{X,ID}$ (s)
Fab. A	1.6	2.8	0.5	0.6
Fab. B	1.8	1.6	0.6	0.5
Fab. C	1.2	1.9	0.4	0.5

As one may easily note, the fundamental periods obtained with the dynamic identification are significantly lower than the numerical ones computed with the numerical model, implying that the structures, in reality, are significantly stiffer with respect to the later loads than the ones implemented in the FEM model.

A plan of the hybrid isolation system adopted in this case is reported in Figure 8a, while Figure 8b reports its force-displacement relationship. Figure 9 shows a section of the building indicating that the isolation system is placed at three different heights.
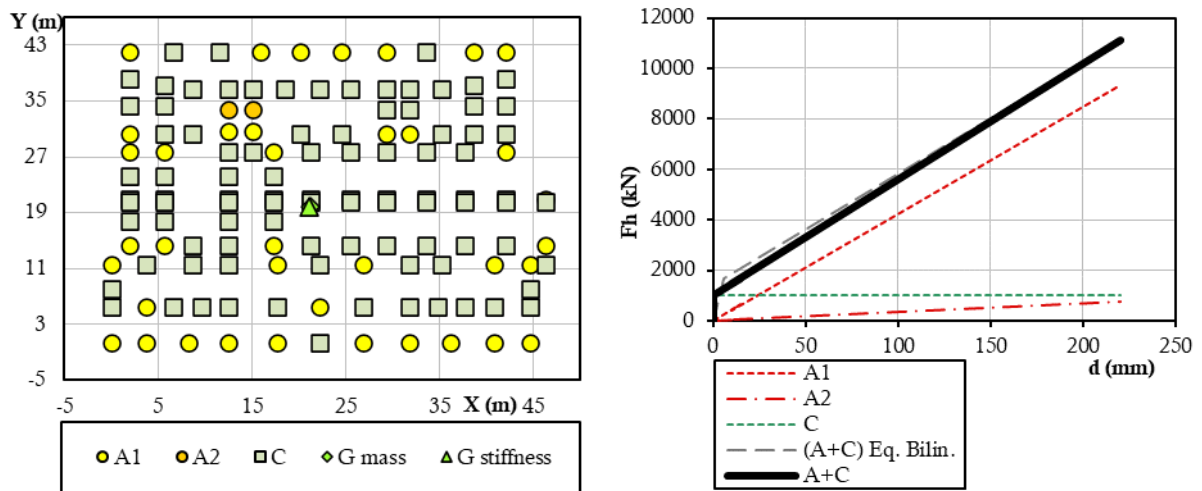
Figure 8: a) Plan and b) force-displacement relationship of seismic isolation system

In detail, the isolation system adopted has an equivalent viscous damping equal to 14.9% and consists of: n. 38 HDRB type A1 (28% of the total devices); n. 2 HDRB type A2 (1% of devices); and n. 94 friction sliders type C (70% of devices). The maximum displacement demand is of: 219.9 mm, calculated if only a SDOF system is assumed; 250.7 mm, including also the system eccentricity; 351.04 mm including both system eccentricity and torsional effects. As one may note a simplified approach considering as simple SDOF the superstructure would lead to a conspicuous underestimation of the displacement demand on seismic devices.
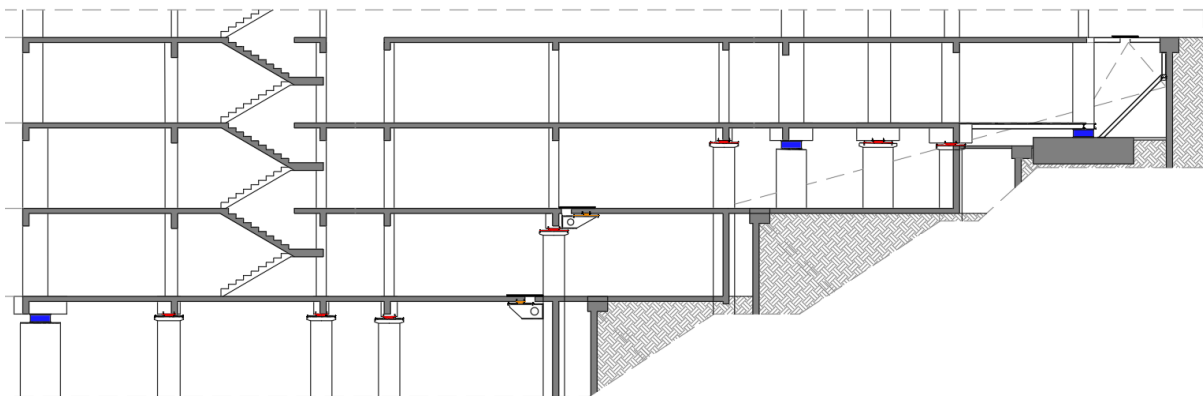
Figure 9: Palazzo Gaeta section illustrating the isolation system levels

3.2 "Zara 4" building

The building named "Zara 4" is a RC frame structure built in the '60s. It consists of n. 7 floors, including the roof, for the highest part of the building, of n. 5 floors for the lowest part, with a total height of about 21.40 m. In plan, the building may be schematized into n. 3 blocks, with a floor type of about 435.0 m^2.

Figure 10a reports the isolation system plan placed at the top of the ground floor columns, except for a small number of columns placed instead above the foundation. It is composed in total by n. 29 friction-pendulum devices, obtaining the force-displacement relationship indicated in Figure 10b. The maximum displacement demand is of: 163.1 mm, calculated if only a SDOF system is assumed; 197.0 mm, including also the system eccentricity; 275.86 mm including both system eccentricity and torsional

effects. Again, a rough simplification as SDOF system would lead a significant underestimation of the devices displacement. For completeness, drift ratios evaluated for Life Satefy Limit State are reported in Figure 11. The ratios refer to: the As-Built configuration (i.e. fixed base building) and with the Isolation System. Moreover, in the same graph the limits for Damage Limit State in the case of fixed based building (dashed red line) and isolated building (dashed blue line) are reported according to the Italian Design Code [9]. As it is easy to observe the isolation system drastically reduces the drift ratios on the superstructure ensuring that RC elements and infills are not damaged with respect to the lateral seismic design action.

Figure 12 reports a detail of the columns jacketing designed for increasing the flexural strength and the cut elements rebars anchorage length. Whereas, Figure 13 shows a detail of connecting beams realized for resisting to the additional moments acting on the sub-structure due to vertical-load eccentricity occurs during the earthquake motion (second-order effects).
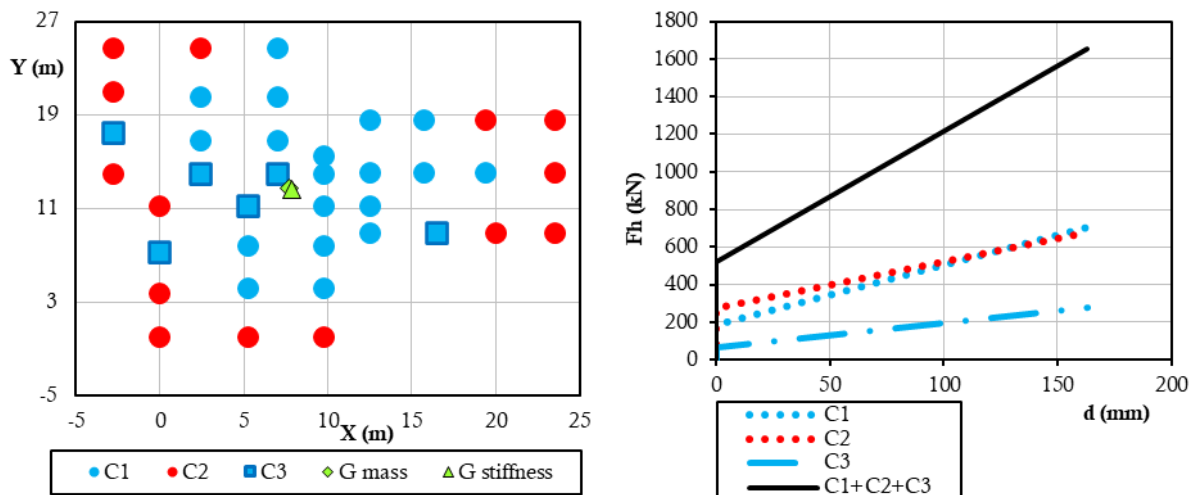
Figure 10: a) Plan and b) force-displacement relationship of seismic isolation system
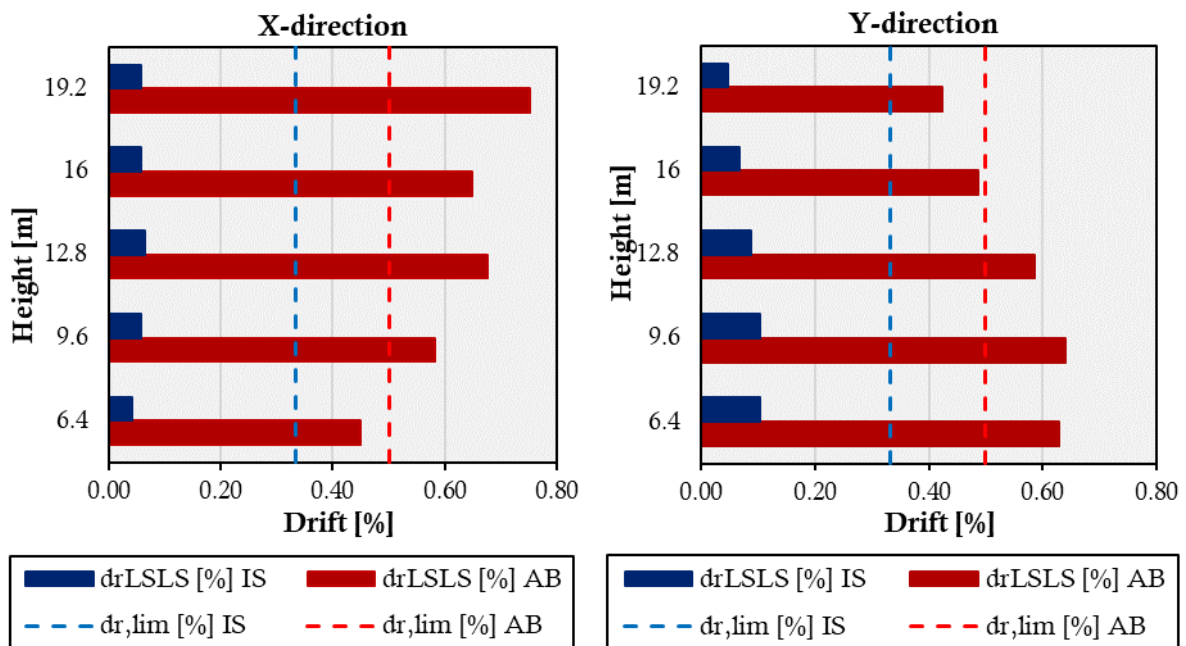
Figure 11: Drift ratios along the height: AB, As-Built configuration; and with the IS Isolation system
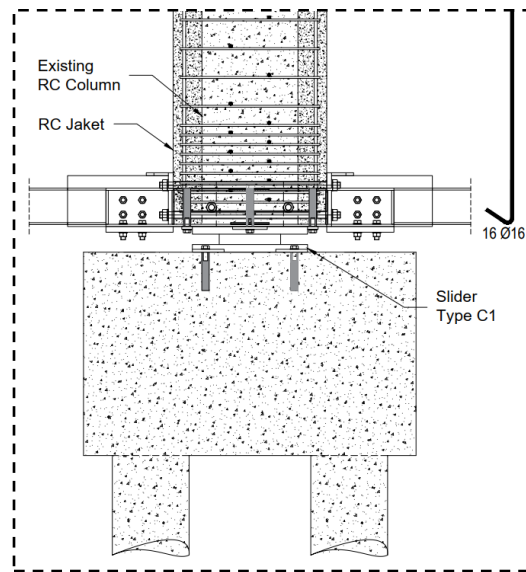
Figure 12: Detail of the external jacketing applied to the columns
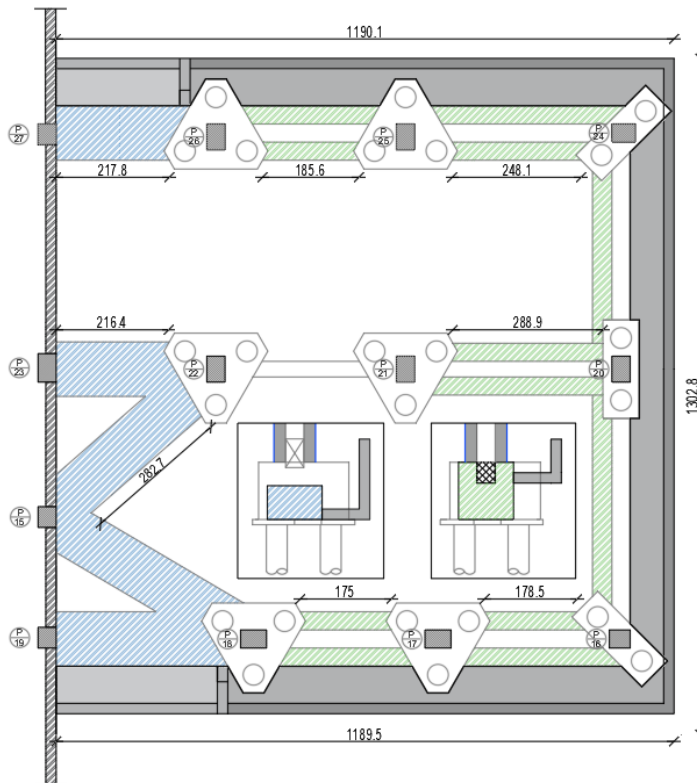
Figure 13: Detail of connecting beams realized among the foundation

3.3 "Zara 11" building

The building named "Zara 11" has a RC frame structure and it was built in 1969. It has n. 6 floors, with a total height of about 19.20 m. In plan the building may be schematically divided into three blocks with a floor plan of about 480.0 m². The hybrid isolation system is placed at the top of the ground floor columns, except for the ones below elevator and stairs that are at the base, above the foundation. The isolation system has 14.0% equivalent viscous damping and is composed by: n. 20 HDRB (type A), and n. 41 friction sliders (type C). The maximum displacement demand is of: 187.4 mm, calculated if only

a SDOF system is assumed; 210.8 mm, including also the system eccentricity; 295.16 mm including both system eccentricity and torsional effects.
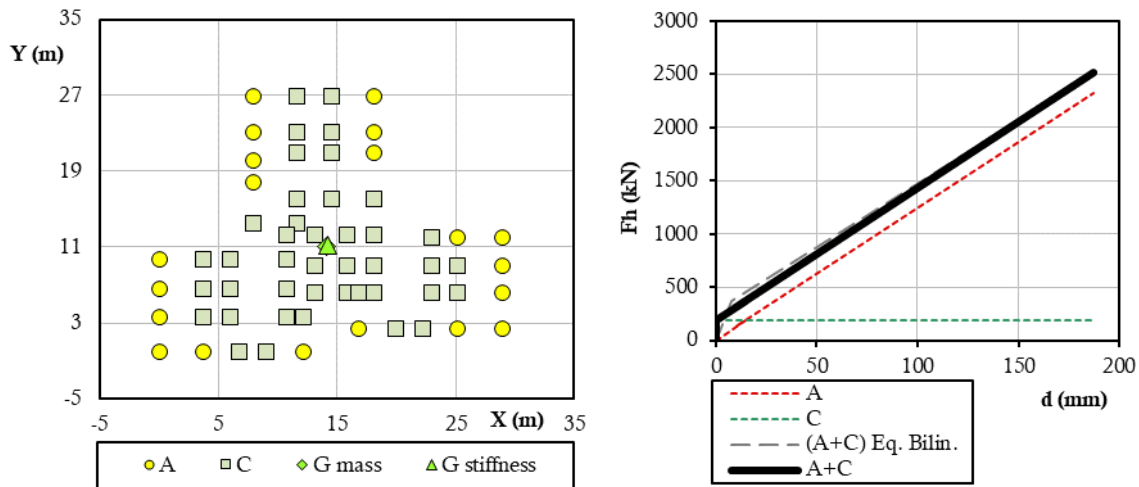
Figure 14: a) Plan and b) force-displacement relationship of seismic isolation system
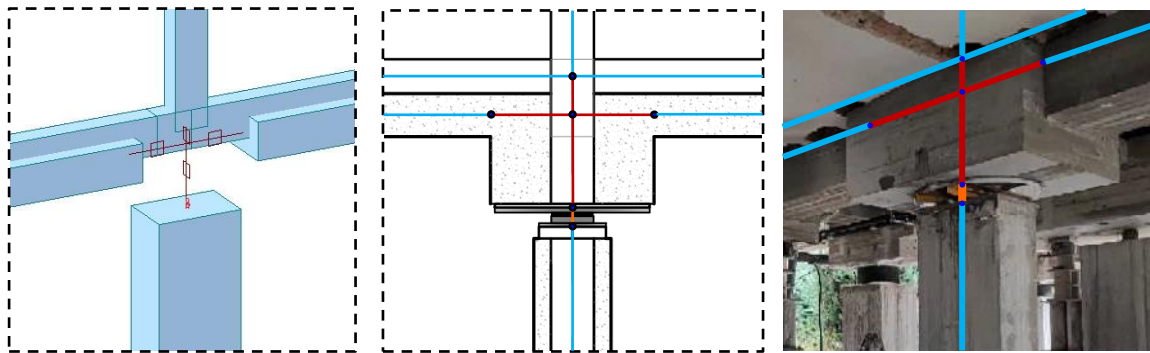
Figure 15: a) Plan and b) force-displacement relationship of seismic isolation system
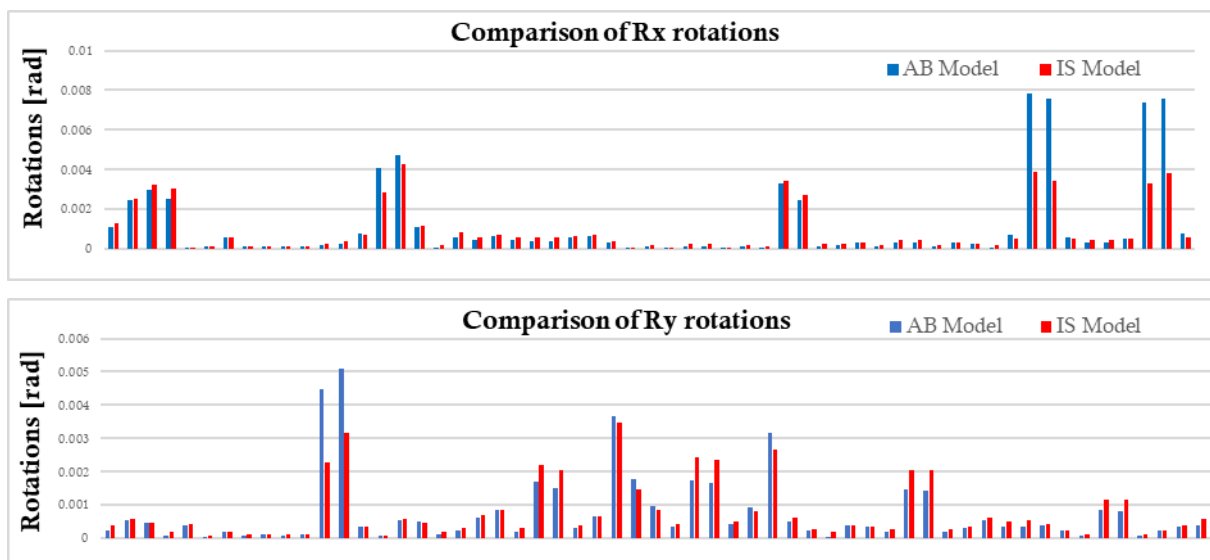
Figure 16: Rotation at the columns base without and with the grid floor along the two direction at the Life Safety Limit State

In order to reduce the additional superstructure internal forces (second-order effects) because of the HDRB and the slider devices shifted position, a floor grid has been designed at the isolation floor

composed by new RC beams, jacketing of existing beams, and new steel beams, the latter inserted between the unconnected columns. The new steel beams may not be too high because of the installations, that are very close to the floor intrados. In order to quantify these additional internal forces numerical simulations have been conducted, reproducing the structural joints geometry including beams, columns and caps (Figure 15). Figure 16 compares the columns base rotations without and with the grid floor along the two directions at the Life Safety Limit State. It is easy to note that the grid added reduces the rotations of some columns and, consequently, the internal action born due to the second-order effects. Finally, Figure 17 reports some pictures of the intervention realized for installing the isolation system.

Figure 17: Details of the interventions realized

4. Conclusions

Seismic isolation is nowadays a largely applied strategy in designing new buildings or, else, in retrofitting the existing ones. However, its application requires the resolution of some specific aspects that may conspicuously condition the designing of the isolation devices and local details.

In this paper some issues related to the seismic isolation strategy applied to existing RC buildings have been discussed. The issues considered play a central role during the seismic isolation design because of, if not adequately considered, the may lead to an incorrect evaluation of the devices displacement demand and of the internal forces of the superstructure and substructure elements. Numerical simulations validate the importance of the issues investigated that very often are not negligible, and that may be properly taken into account for reaching the desired structure isolation degree, without any premature failure of seismic devices or structural elements.

References

[1] Laguardia, R., Morrone, C., Faggella, M., Gigliotti, R. (2019): A simplified method to predict torsional effects on asymmetric seismic isolated buildings under bi-directional earthquake components. *Bulletin of Earthquake Engineering*, 17, 6331–6356, doi: https://doi.org/10.1007/s10518-019-00686-1

[2] Wolff, E.D., Ipek, C., Constantinou, M.C., Morillas, L. (2014): Torsional response of seismically isolated structures revisited. *Engineering Structures*, 59, 462–468, doi: https://doi.org/10.1016/j.engstruct.2013.11.017

[3] D'Amato, M., Laguardia, R., Gigliotti, R. (2020): Seismic Retrofit of an Existing RC Building With Isolation Devices Applied at Base. *Frontiers in Built Environment*, 6, doi: https://doi.org/10.3389/fbuil.2020.00082

[4] Braga, F., Laterza M., Gigliotti, R. (2001): Comportamento Sperimentale del Sistema di Isolamento Scivolatori - Richiamatori Elastomerici applicato all'Edificio per Civile Abitazione Costruito nel Comune di Rapolla. *10° Convegno Nazionale "L'Ingegneria Sismica in Italia"*, Potenza-Matera, Italy, 12 pages

[5] Porter, K. A., J. L. Beck, and R. Shaikhutdinov. 2004. Simplified estimation of economic seismic risk for buildings. Earthquake Spectra 20 (4): 1239–63. doi: 10.1193/1.1809129.

[6] Braga, F., Laterza, M., Gigliotti, R., Nigro, D. (2001): Prove di Rilascio di un Edificio per Civile Abitazione Costruito nel Comune di Rapolla: SISTEMA DI ISOLAMENTO ISOLATORI ELASTOMERICI. *10° Convegno Nazionale "L'Ingegneria Sismica in Italia"*, Potenza-Matera, Italy, 12 pages

[7] Baker, J. W. (2015): Efficient analytical fragility function fitting using dynamic structural analysis. *Earthquake Spectra*, **31** (1), 579–99, doi: https://doi.org/10.1193/021113EQS025M

[8] Laguardia, R., D'Amato, M., Coltellacci, M., Di Trocchio, G., Gigliotti, R. (2022): Fragility Curves and Economic Loss Assessment of RC Buildings after L'Aquila 2009 Earthquake. *Journal of Earthquake Engineering*, doi: https://doi.org/10.1080/13632469.2022.2038726

[9] Norme tecniche per le costruzioni (NTC 2018) D. Min. Infrastrutture e Trasporti 17 gennaio 2018. In Italian

[10] Romano, F., Faggella, M., Gigliotti, R., Zucconi, M., Ferracuti, B. (2018): Comparative seismic loss analysis of an existing non-ductile RC building T based on element fragility functions proposals. *Engineering Structures*, 177, 707–723, doi: https://doi.org/10.1016/j.engstruct.2018.08.005

SEISMIC RETROFIT OF STRATEGIC MASONRY STRUCTURES WITH BASE ISOLATION TECHNIQUE: THE CASE STUDY OF "GIACOMO MATTEOTTI" SCHOOL BUILDING IN GUBBIO, ITALY

Stefano Barone [(1)], Riccardo Vetturini [(2)]

[(1)] *Design & Sales Engineer, Freyssinet, stefano.barone@freyssinet.com*
[(2)] *Technical Director, Ingenium Design Company, ing.vetturini@gmail.com*

Abstract

Seismic retrofit of existing structures is an extremely important topic in the field of earthquake engineering. For strategic structures such as school and military buildings, bridges and infrastructures in general, the expected performance level is further raised compared to conventional structures to guarantee two fundamental targets: to resist the ultimate design seismic action corresponding to the life safety limit state and to guarantee immediate occupancy after an earthquake event. This means no damage to the structural elements as well as protection of internal equipment from excessive accelerations. Structure functionality is therefore the minimum acceptable level of retrofit for strategic structures.

In case of masonry buildings located in medium-high seismicity zones, conventional retrofit (i.e. wall-to-roof and wall-to-floor anchorage, out-of-plane wall bracing, diaphragm strengthening) does not allow to fully achieve the above objectives. Furthermore, the application of these techniques causes an important and invasive impact on the structure, distorting the building on both architectural and functional level.

Base isolation is a technical solution that allows to drastically reduce the seismic demand on the structure using special anti-seismic devices characterized by high horizontal flexibility.

This paper describes the application of seismic isolation technique to protect the "Giacomo Matteotti" school building, located in the city of Gubbio, Italy. The building was built in the 1940s, and it is made of cast stone and bricks and reinforced concrete-hollow tiles mixed floors. The building has three floors, a total area of 6.000 m^2, an inter-storey height of 4 m and a total volume of about 23.750 m^3.

The City of Gubbio (Umbria region, Italy), is located in an area where strong earthquakes can occur, with expected peak ground acceleration on rock soil equal to 0.29g for 475 years return period (i.e., 10% exceedance probability in 50 years).

For the base isolation system, Freyssinet has supplied 94 anti-seismic rubber isolators ISOSISM® type HDRB-H 550x155 and 93 flat sliders with confined elastomeric disc TETRON® type CD GL 3000.600.600 in order to reduce the eccentricity between centre of mass and centre of stiffness of the isolation system and consequently the torsional effects on the superstructure.

This paper describes the performance characteristics of the isolators with particular attention to the experimental dynamic response. A special focus is given to all the construction phases and details necessary to isolate a masonry structure.

Keywords: masonry structure, seismic isolation, energy dissipation, anti-seismic rubber isolators, retrofit procedure.

1. Introduction

Seismic retrofit of existing structures is a very topical issue in the field of seismic engineering. Moreover, strategic structures such as school and military buildings, bridges and infrastructures in general, must not only be protected against earthquakes but must ensure immediate occupancy and full functionality after a seismic event. In case of masonry buildings located in medium to high seismicity areas and designed for static loads only, conventional retrofit (e.g. wall-roof and wall-floor anchoring, out-of-plane bracing, diaphragm reinforcement) does not allow to protect the structure from the design

seismic action (i.e. damage of structural elements is allowed without collapse), therefore not being able to guarantee immediate occupancy after a seismic event. Furthermore, the application of these techniques alters the building from an architectural and functional point of view. Therefore, seismic isolation is often the best strategy for the seismic protection of structures.

Nowadays, seismic protection through base isolation represents a consolidated technique of protection against earthquakes. This strategy is extensively applied on existing structures, due to the fact that it does not require any interruption of the building use and occupants' dislocation. Essentially, it consists in decoupling the superstructure motion from the ground one by installing anti-seismic devices characterized by low horizontal stiffness. The fundamental natural period of the superstructure is therefore lengthened, thus reducing the lateral acceleration demand, with a consequent increase of lateral displacement at the isolation level.

The dynamic response of an isolated building strictly depends on the characteristics of the isolation devices and having the combined function of building re-centering after an earthquake event and dissipating the seismic kinetic energy. Different typologies of anti-seismic devices may be applied and combined among them such as elastomeric isolators, curved surface sliders, elasto-plastic dissipators. General studies and applications with these devices for isolation buildings may be found in [1, 2, 3, 4] and specific applications on existing buildings having also historic value may be found in [5, 6, 7, 8].

This paper describes the application of seismic isolation to protect the "Giacomo Matteotti" school institute, an existing masonry building located in the city of Gubbio, Umbria region, Italy. The building was designed for vertical loads only since at the time of construction (1940), the Italian standard (Regio Decreto n. 193 del 18 Aprile 1909) for structures did not include anti-seismic design procedures.

The isolation system at the base of the building consists of 94 High Damping Rubber Bearings ISOSISM® type HDRB-H 550x155 and 93 flat sliders with confined elastomeric disc TETRON® type CD GL 3000.600.600 supplied by Freyssinet, a world reference in specialist civil engineering.

This paper reports the performance characteristics of the isolators with attention to the experimental response. A special focus is given to all the construction phases and details necessary to isolate a masonry structure.

2. Case study description

2.1 Seismic vulnerability of "Giacomo Matteotti" school building

The chosen case study is the "Giacomo Matteotti" masonry school building located in Gubbio, a medieval city belonging to the Province of Perugia, Italy.

Figure 1. Identification of the building.

The construction of the building dates back to the late 1930s, with construction beginning in 1937 and inauguration in 1940, after only three years.
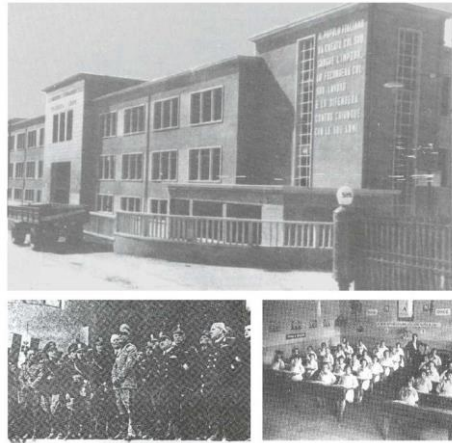
Figure 2. Historical photos of the opening day.

The building is made of cast stone and bricks and reinforced concrete-hollow tiles mixed floors. The building has three floors, a total area of 6.000 m^2, an inter-storey height of 4 m and a total volume of about 23.750 m^3.

The structure is characterized by a high seismic vulnerability determined by the following factors:

• low number of structural masonry walls in relation to the global surface of the building;

• large rooms;

• inter-storey heights of 4 m or more;

• four levels above the ground;

• geometric irregularity both in plan (the building has a large E shape extremely disadvantageous in seismic conditions) and elevation;

• large corridors along the longitudinal side without transversal walls clamped to the facade perimeter walls;

• absence/low number of transverse resisting masonry.

Therefore, it is clearly perceived that the building has a simple and effective static concept. The foundations are continuous and always made of masonry which rests on loose soils. The seismic vulnerability of the building is clearly related to the high seismic hazard of the construction site. Indeed, the City of Gubbio is characterized by medium-strong earthquakes, with expected peak ground acceleration on rock soil equal to 0.29g for 475 years return period (i.e. 10% exceedance probability in 50 years). The building is very stiff, with a fundamental period of vibration of about 0.27 sec which corresponds to a design horizontal acceleration equal to 1.20g. It has been estimated that the building is able to resist only 25% of the design earthquake. Fig. 3 shows the design elastic acceleration spectra for the collapse limit state (1950 years return period, as per Italian Standard NTC 2018).
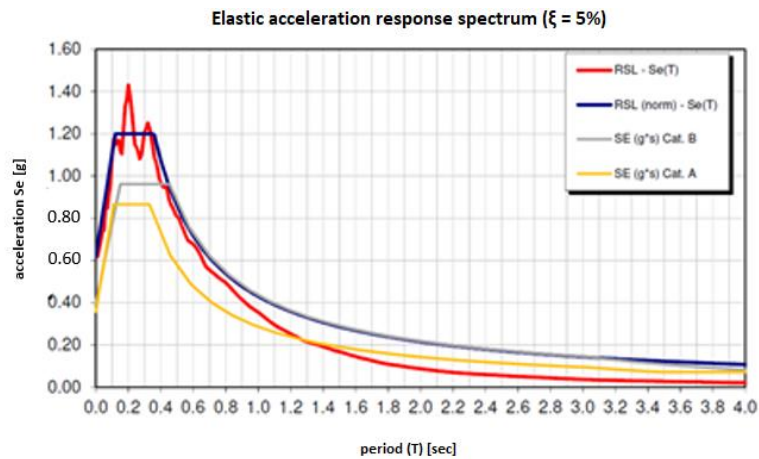
Figure 3. Design elastic acceleration spectra for 1950 yrs return period (SE = design elastic spectrum, RSL = site response spectrum)

The school building has a strong monumental value, therefore the retrofit strategy must increase the seismic safety level by at least 3-4 times without having a major and invasive impact on the building itself. In fact, conventional retrofit procedures such as construction of new structural walls, metal hoops and/or strengthening with fibre reinforced polymers allow to reduce the seismic vulnerability of the building, but they are in contrast with the reasons for architectural protection and conservation. Finally, a traditional retrofit strategy would not guarantee the absence of damage (both structural and non-structural) and therefore the functionality of the structure after a seismic event.

2.2 Retrofit strategy with seismic isolation

As already described in the introductory chapter, seismic isolation is actually a design strategy largely applied all over the world either for designing new buildings or for retrofitting existing ones. Thanks to the decoupling of the superstructure motion from the ground one by installing anti-seismic devices with low horizontal stiffness, the fundamental period of the structure is strongly lengthened, thus allowing to significantly reduce the seismic accelerations on the superstructure. In this way the superstructure elements damage may be nullified thanks to the drastic reduction of the interstorey drifts and floor shear. Fig. 4 shows the comparison between the response of the original structure (fixed base) and that with seismic isolation at the base.
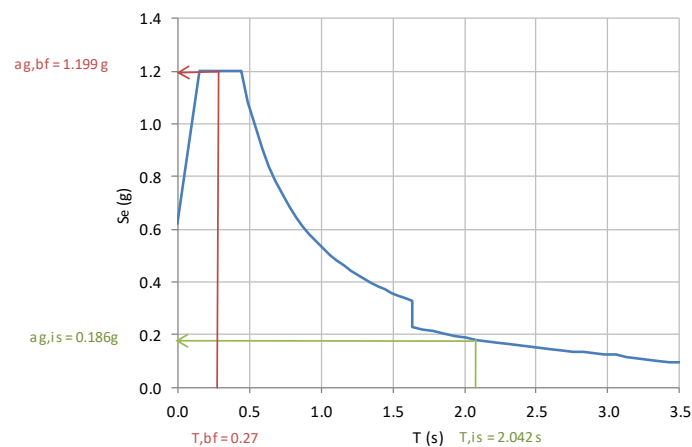
Figure 4. Spectral acceleration comparison between fixed base building (red line) and isolated one (green line).

Analysing Fig. 4 it is possible to quantify the main benefits obtained from seismic isolation:

• drastic reduction (up to 6 times) of seismic acceleration transmitted to the superstructure;

• system damping increase up to 16% with further reduction of acceleration transmitted to the building and of displacements at the isolation level;

• very high decoupling of superstructure motion from the ground one (isolation ratio $T_{,bf}/T_{,is} = 7.6$).

For the isolation system of the building, Freyssinet has supplied 94 high damping rubber bearings ISOSISM® type HDRB-H 550x155 and 93 flat sliders with confined elastomeric disc TETRON® type CD GL 3000.600.600. Fig. 5 shows a rendering of the isolation system implemented at the base of the structure.
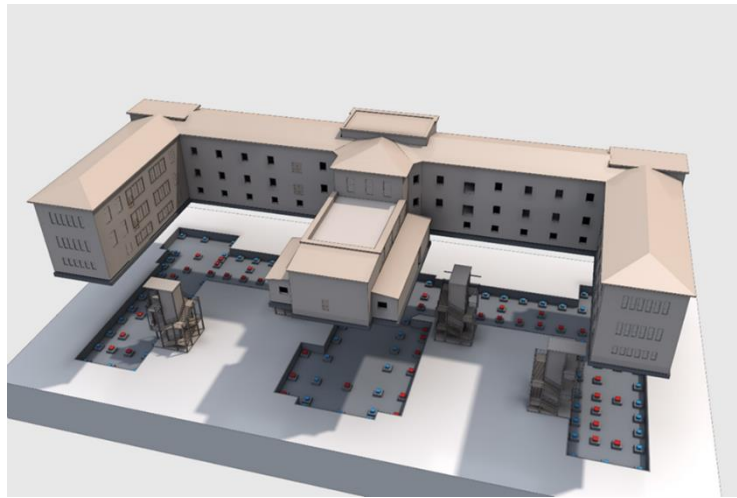
Figure 5. Rendering of the isolation system at the base of the building.

Isolators and flat sliders are positioned to achieve excellent centering between centre of mass and stiffness, thus reducing torsional effects during a seismic event. The layout of the devices is shown in Fig. 6.
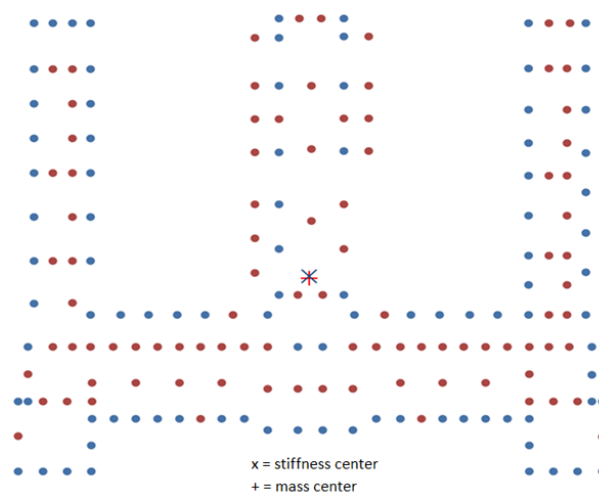
Figure 6. Plan arrangement of isolators (blue circles) and sliders (red circles).

Finally, Fig.7 shows a global view of the finite element model of the building while Fig. 8 the first two vibration modes from which it is possible to appreciate that the total mass of the building is mobilized through purely translational behaviour.
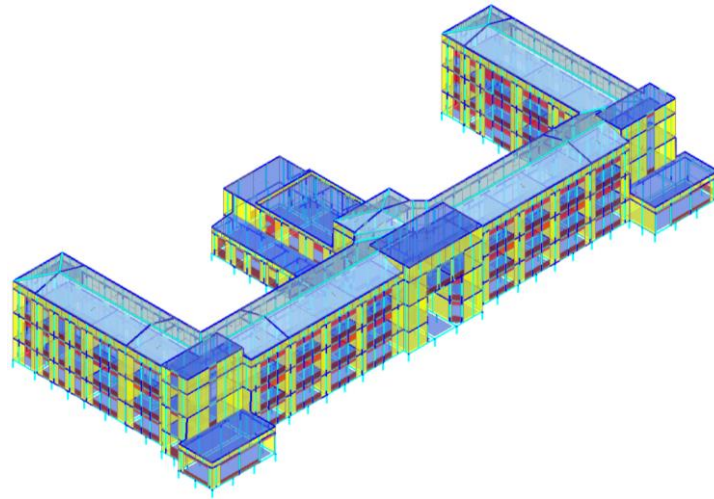
Figure 7. Finite element model of the building.
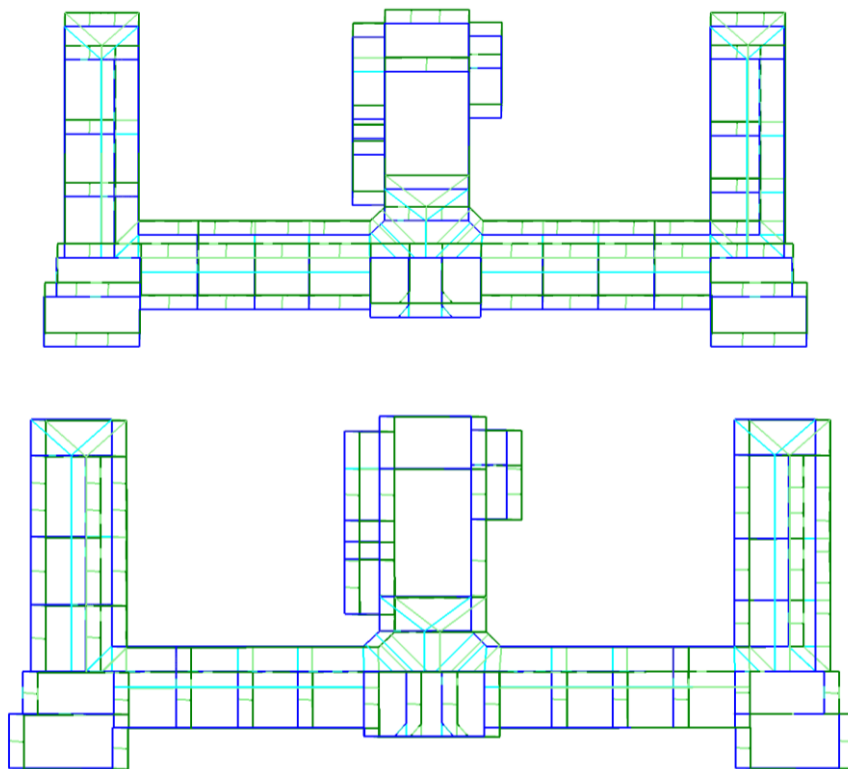
Figure 8. Top: 1st mode (T = 2.036 sec and M_y = 99.8%); bottom: 2nd mode (T = 2.035 sec and M_x = 99.7%).

3. Freyssinet anti-seismic devices

To achieve the seismic isolation objectives (acceleration reduction, damping increase, decoupling), Freyssinet has designed and supplied a total of 187 devices, half of which are rubber isolators and half are flat sliders.

3.1 ISOSISM® HDRB and TETRON® CD: design parameters

The elastomeric isolators ISOSISM® type HDRB are reinforced rubber bearings made up of alternating layers of hot vulcanized rubber and steel laminates. These devices are characterized by high vertical stiffness, low horizontal stiffness and a suitable damping capacity. These features allow, respectively, to resist to vertical loads without appreciable setting, to lengthen the fundamental period of vibration of the structure, and to limit the horizontal displacements of the isolation system itself.

For the seismic isolation of the school building, 94 ISOSISM® type HDRB were supplied, with a rubber compound characterized by high stiffness and damping capacity. Fig. 9 shows the 3D exploded view of the isolator while Table 1 reports the main design parameters.
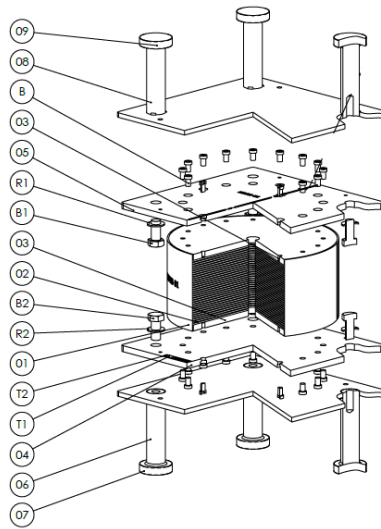
Figure 9. 3D exploded view of ISOSISM® HDRB-H 550x155.

Table 1 – Technical properties of ISOSISM® HDRB-H 550x155

Parameter	Unit	Value
Rubber diameter, D_r	mm	550
Rubber height, T_r	mm	155
Total height, H	mm	295
Side length of outer steel plates, B	mm	600
Weight, W	kg	488
Maximum static vertical load, $N_{ULS,max}$	kN	3000
Maximum seismic vertical load, $N_{Ed,max}$	kN	2500
Design displacement, d_{bd}	mm	±153
Displacement capacity, d_c	mm	±300
Effective horizontal stiffness, $K_{eff}(d_{bd})$	kN/mm	1.76
Vertical stiffness, K_v	kN/mm	$\geq 800 \cdot K_{eff}(d_{bd})$
Equivalent viscous damping, $\xi_{eq}(d_{bd})$	-	16%

The isolators are then combined with flat sliders TETRON® type CD GL 3000.600.600 to minimize the eccentricity between centre of mass and stiffness. The confined elastomeric disc allows to increase the vertical stiffness of the slider. Fig. 10 shows the 3D exploded view of the slider while Table 2 reports the design parameters.
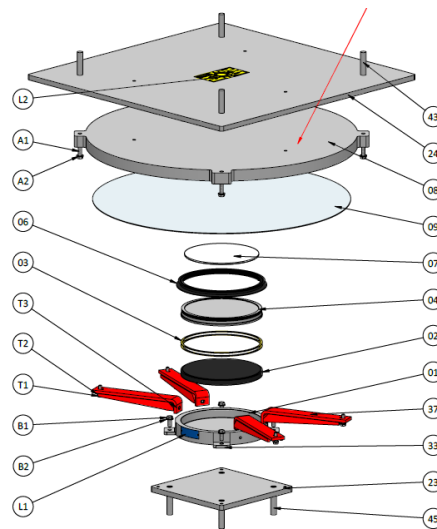
Figure 10. 3D exploded view of TETRON® CD GL 3000.600.600.

Table 2 – Technical properties of TETRON® CD GL 3000.600.600

Parameter	Unit	Value
Pot diameter, D_p	mm	330
Sliding plate diameter, D_s	mm	970
Total height, H	mm	106
Weight, W	kg	446
Maximum vertical load, $N_{ULS,max}$	kN	3000
Horizontal load, F_H	kN	-
Displacement capacity, d_c	mm	±300

All the devices are equipped with upper and lower masonry plates for easy installation and replacement in the future, if required.

3.2 ISOSISM® HDRB: experimental response

The isolators were tested full-scale to check their performances. According to European Standard EN 15129:2009 and Italian Standard "Norme Tecniche per le Costruzioni 2018", 20% of the production was subjected to vertical compression and horizontal dynamic tests to fully characterize the response of the devices and compare it with the theoretical behaviour. All tests were carried out by Politecnico di Milano (in charge of execution and certification) at ISOLAB laboratory (Montebello della Battaglia, Italy), the testing facility of Freyssinet. Table 3 illustrates the test protocol of the devices. Fig. 11 shows one device under testing and its experimental response.

Table 3 – Factory Production Control Test protocol for ISOSISM® HDRB-H 550x155

test name	main dof [-]	max displ [mm]	max vel [mm/s]	load shape [-]	vertical load [kN]	cycles [-]
Compression stiffness	vert	-	5.0	ramp	3000	1
Horizontal characteristics under cyclic deformation	hor	±155 mm	200	sine	1425	3
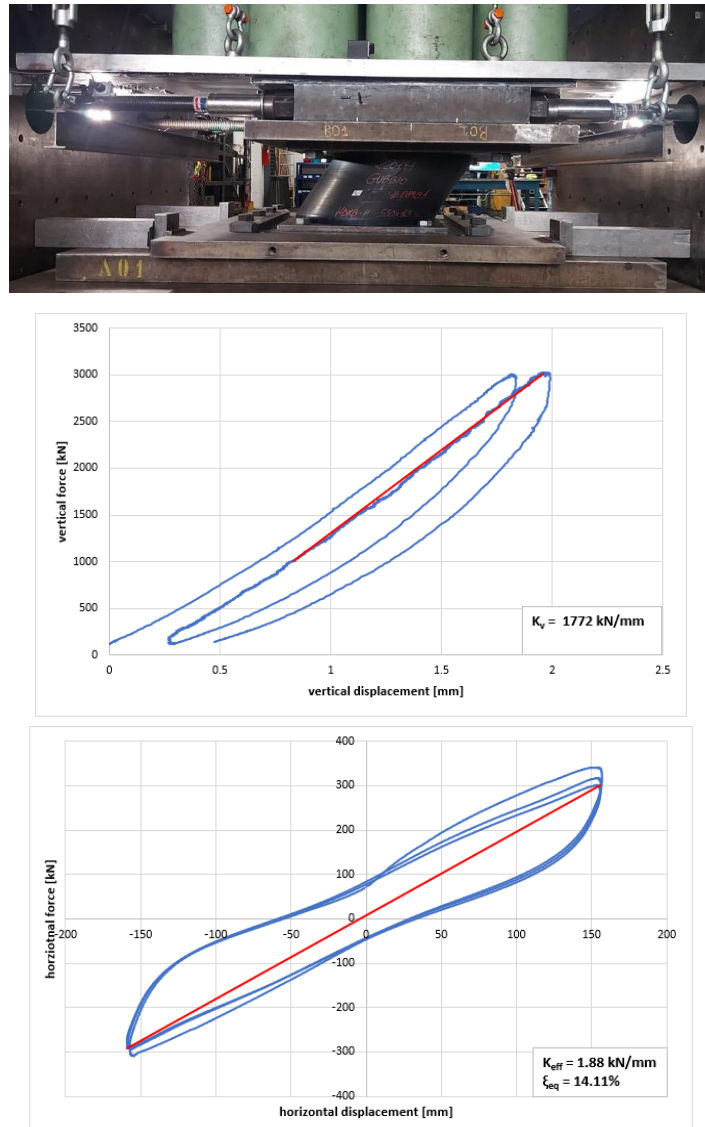
Figure 11. ISOSISM® HDRB-H 500x155 under testing (top), vertical (middle) and horizontal (bottom) response.

After testing, all devices were shipped for on-site installation.

4. Implementation of the isolation system: construction phases

The construction of the seismic isolation level at the base of a masonry building requires complex site activities that have to be planned in time.

First of all, the execution phases foresee the repair of the weaker masonry walls, through local reconstructions. Subsequently the soil is dug and removed inside the rooms of the building, for about two meters below the basement. Then parts of the foundations and soil under the walls are removed.

Through the use of props and jacks, two new reinforced concrete foundations are created: the first at the base (foundation slab), resting on the ground and the second, at the base of the masonry walls (curb beams). Devices are then installed between the two new foundations, thus realizing the seismic isolation of the building. Finally, at the location of the devices, the foundation slab will have short concrete

columns (cap) to support the devices. Fig. 12 shows a rendering of the new elements at the base of the isolated building.
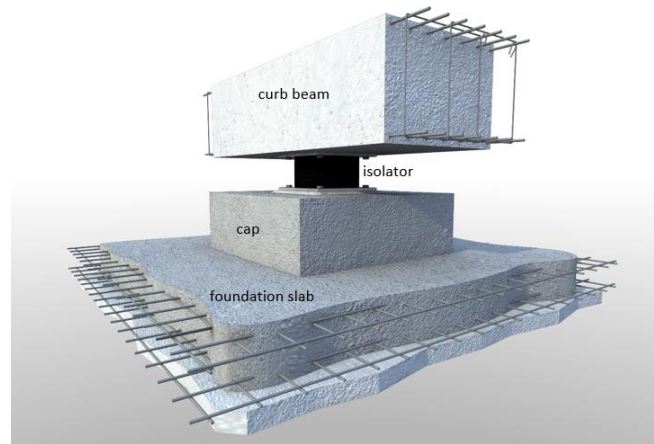
Figure 12. New elements at the base of the isolated building: foundation slab, cap, isolators, curb beams.

Flat jacks are installed underneath the devices. By injecting epoxy resin inside the jacks, part of the upper structure's load is transferred to the devices and the new foundation (cap and foundation slab) is also compressed. This procedure allows to eliminate differential settlements in the foundation due to a step-by-step construction.

By implementing seismic isolation at the base, the building needs to move with respect to the surrounding ground during a seismic event. This makes it necessary to have a perimeter cavity, which allows free relative movement between the ground and the building during an earthquake. This gap is covered by the perimeter sidewalk which completely hides the seismic joint. In fact, the sidewalk is a sort of overhang that allows relative movement between the surrounding ground and the isolated building. Fig. 13 shows typical construction details provided at the isolation level.
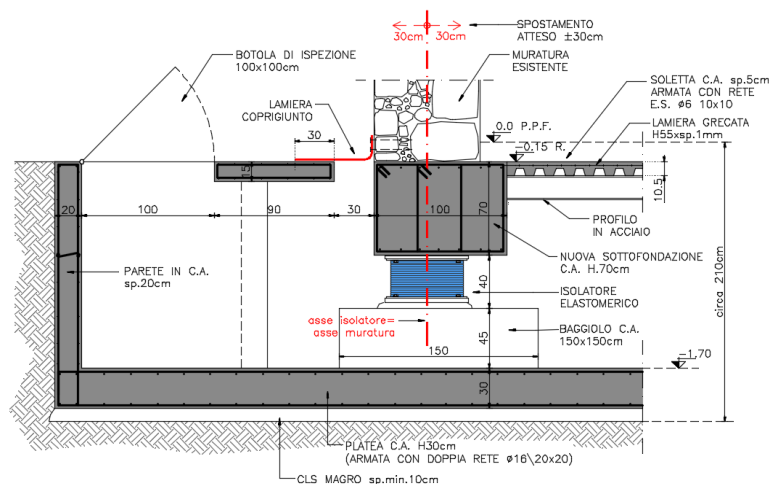
Figure 13. Construction details of the isolation level.

Fig. 14 groups together the main construction phases described above.

a) Demolition of existing foundation, new foundation reinforcement and support of masonry wall with props

b) Formwork for concrete casting of upper curb beams

c) Installation of flat jack

d) Installation of isolator

Figure 14. Base isolation construction phases.

The last operation is the construction of the new base floor below which there will be the technical compartment for maintenance and inspection of the devices.

It is important to underline that this executive method allows the school to be fully operational, even if with a reduced usable surface. This type of construction framework allows to work in macro areas of the building that are temporarily unused and then re-occupied after installing the devices. Only the ground floor immediately above the isolation level cannot be used for the entire duration of the construction site.

Conclusions

An application of seismic isolation at the base of an existing masonry building has been presented in this paper. The "Giacomo Matteotti" school building has been designed for vertical loads only, since at the time of the construction, no seismic design was required by law.

The building is characterized by high seismic vulnerability due its static structural conception and due to the high seismic hazard of the site. The structure, in addition to being strategic, has a strong historical value. For these reasons, seismic isolation retrofit technique was adopted as an alternative to conventional strategy. In fact, this technique allows to protect the building from earthquakes and to be fully operational and it does not have an invasive impact on the building's architecture.

Seismic isolation therefore enable to drastically reduce (up to 6 times) the accelerations transmitted to the superstructure, to increase the system damping (up to 16%) and to strongly decouple the superstructure motion from the ground one ($T_{,bf}/T_{,is} = 7.6$).

The isolation system of the building consists of 94 anti-seismic rubber devices ISOSISM® type HDRB-H 550x155 and 93 flat sliders TETRON® type CD GL 3000.600.600 supplied by Freyssinet, a world reference in specialist civil engineering. 20% of the isolators were tested in accordance with EN 15129:2009 and NTC 2018 Standards, complying with relevant acceptance criteria.

The construction of the isolation system at the base of the masonry building required numerous and complex construction site activities, including the demolition of the existing foundation and the consequent construction of two new concrete foundations: a base slab resting on the ground and curb beams below the masonry walls. The devices were then installed between the two new concrete elements.

The building retrofit procedure was implemented progressively working in macro areas. This allowed keeping the school in operation during all phases of the construction site.

References

[1] Braga, F., Faggella, M., Gigliotti, R., Laterza, M. (2005): Nonlinear dynamic response of HDRB and hybrid HDRB-friction sliders base isolation systems. *Bulletin Earthquake Eng.*, **3**, 333–353, doi: 10.1007/s10518-005-1242-2.

[2] Constantinou, M., Mokha, A., Reinhorn, A. (1990): Teflon bearings in base isolation II: modeling. *J. Struct. Eng.*, **116**, 455–474, doi: 10.1061/(ASCE)0733-9445(1990)116:2(455).

[3] Martelli, A., Forni, M. (1998): Seismic isolation of civil buildings in Europe. *Progress Struct. Eng. Mater.*, **1**, 286–294, doi: 10.1002/pse.2260010310.

[4] Kawamura, S., Sugisaki, R., Ogura, K., Maezawa, S., Tanaka, S. (2000): Seismic isolation retrofit in Japan, *12th World Conference of Earthquake Engineering*, Auckland.

[5] De Luca, A., De Mele, E., Molina, J., Verzeletti, G., Pinto, A.V. (2001): Base isolation for retrofitting historic buildings: evaluation of seismic performance through experimental investigation. *Earthquake Eng. Struct. Dynam.*, **30**, 1125–1145, doi: 10.1002/eqe.54.

[6] Tomazevic, M., Klemenc, I., Weiss, P. (2009): Seismic upgrading of old masonry buildings by seismic isolation and CFRP laminates: a shaking-table study. *Bulletin Earthquake Eng.*, **7**, 293–321, doi: 10.1007/s10518-008-9086-1.

[7] Castellano, A., Foti, P., Fraddosio, A., Marzano, S., Mininno, G., Piccioni, M.D. (2014): Seismic response of a historic masonry costruction isolated by stable unbonded fiber-reinforced elastomeric isolators (SUFREI). Key Eng. Mater., **628**, 160-167, doi: 10.4028/www.scientific.net/KEM.628.160.

[8] Petrovčič, S., Kilar, V. (2017): Seismic retrofitting of historic masonry structures with the use of base isolation – modeling and analysis aspects, *Int. J. Archit. Heritage*, **11**, 229-246, doi: 10.1080/15583058.2016.1190881.

IMPACT OF MODERATE SIZE EARTHQUAKES THROUGH SKOPJE 2016 AND ZAGREB 2020 CASE STUDIES

Radmila Salic Makreska [(1)], Katerina Drogreska [(2)], Cvetan Sinadinovski [(3)], Zabedin Neziri [(4)], Ljubco Jovanov [(5)], Zoran Milutinovic [(6)], Lazo Pekevski [(7)], Jasmina Najdovska [(8)], Dragana Chernih Atanasovska [(9)], and Daniel Tomic [(10)]

[(1)] *Assoc. Prof. Dr., Ss. Cyril and Methodius University in Skopje, Institute of Earthquake Engineering and Engineering Seismology (IZIIS) – Skopje, Republic of North Macedonia, r_salic@iziis.ukim.edu.mk*

[(2)] *Assist. Prof. Dr., Ss. Cyril and Methodius University in Skopje, Faculty of Natural Sciences and Mathematics, Seismological Observatory – Skopje, Republic of North Macedonia, katerinadrogreska@yahoo.com*

[(3)] *Dr., Global SeismiCS - Canberra, Australia, cvetansin@hotmail.com*

[(4)] *Ph.D. Student, M.Sc., Ss. Cyril and Methodius University in Skopje, Institute of Earthquake Engineering and Engineering Seismology (IZIIS) – Skopje, Republic of North Macedonia, zabedin@iziis.ukim.edu.mk*

[(5)] *Eng., Ss. Cyril and Methodius University in Skopje, Faculty of Natural Sciences and Mathematics, Seismological Observatory – Skopje, Republic of North Macedonia, ljubco.jovanov@hotmail.com*

[(6)] *Prof. Dr., Retired, Ss. Cyril and Methodius University in Skopje, Institute of Earthquake Engineering and Engineering Seismology (IZIIS) – Skopje, Republic of North Macedonia,milutin.zvm@gmail.com*

[(8)] *Prof. Dr., Retired, Ss. Cyril and Methodius University in Skopje, Faculty of Natural Sciences and Mathematics, Seismological Observatory – Skopje, Republic of North Macedonia, lazo9pekevski@gmail.com*

[(7)] *Assist. Prof. Dr., Ss. Cyril and Methodius University in Skopje, Faculty of Natural Sciences and Mathematics, Seismological Observatory – Skopje, Republic of North Macedonia, najdovskaj@yahoo.com*

[(9)] *Prof. Dr., Ss. Cyril and Methodius University in Skopje, Faculty of Natural Sciences and Mathematics, Seismological Observatory – Skopje, Republic of North Macedonia, dcernih@gmail.com*

[(10)] *Ph.D. Student, M.Sc., Ss. Cyril and Methodius University in Skopje, Institute of Earthquake Engineering and Engineering Seismology (IZIIS) – Skopje, Republic of North Macedonia, danielt@iziis.ukim.edu.mk*

Abstract

Even today, moderate earthquakes can cause considerable damage and social disturbance, especially in areas populated with old and masonry buildings. Two recent moderate earthquakes that hit the Balkan peninsula in 2016 and 2020 affected the capital cities of Skopje and Zagreb, respectively. Both have shown the high vulnerability pattern of a current masonry building stock and emphasised the necessity for improvement of existing response, preparedness, and protection measures.

The manuscript analyses, summarizes, and presents the crucial seismo-tectonic aspects and seismological data of both affected cities, then defines P-nodal planes for both strongest earthquake events affecting Skopje 2016 (M_L=5.3) and Zagreb 2020 (M_L=5.5). We analysed and compared macroseismic data, and strong motion records in respect to their amplitude and frequency characteristics and showed the building damage and usability statistics.

The observed differences and similarities that have resulted from this comparative study are to be used further to increase the awareness of the impact of moderate earthquakes, identify gaps and inconsistencies in the coping capacity domain and propose systematic measures to decrease vulnerability of the existing masonry building portfolio.

Keywords: Moderate earthquake, Response measures, Building damage, Skopje, Zagreb

1. Introduction

Earthquakes, especially moderate ones, are frequently experienced natural hazards in the Balkan Peninsula. Non-structural damage patterns characteristic of this type of earthquakes creates enormous panic among residents and building owners/managers. The uncertainty regarding structural stability and building safety becomes an issue related to public (hospitals, schools, kindergartens, etc.), commercial and industrial buildings since the earthquake impact phase dominantly results in disrupted function and evacuation of these buildings. Management of the created panic and safety assurance of the population

for the purpose of building re-occupation requires rapid building damage and usability assessments (Milutinovic et al., 2018).

The authors were challenged to compare the two recent moderate size earthquakes that hit the Balkan peninsula in 2016 and 2020 and affected the capital cities of Skopje and Zagreb. Both earthquakes have resulted in high vulnerability pattern of a current masonry building stock and emphasised the necessity for improvement of existing response, preparedness, and protection measures. This study provides a general overview comparing the exposure, seismo-tectonic aspects, seismological observations, response measures and procedures as well as discusses in general terms building damage and usability statistics.

2. Exposure

The capital cities of N. Macedonia and Croatia, Skopje and Zagreb, both the largest cities in the country, are representing administrative-political, economic, educational-scientific and cultural centers. Skopje is located in the northern part of the country, in the Skopje valley, along the Vardar River, while Zagreb is placed in the northwestern part of Croatia, along the Sava River and the southern slopes of Medvednica mountain.

The capital cities of Skopje and Zagreb, although recently affected by similar magnitude size earthquakes of $M_L5.3$ (2016) and $M_L5.5$ (2020) (https://www.emsc-csem.org/), are also comparable in terms of urban area size (https://en.wikipedia.org/) and number of inhabitants (https://worldpopulationreview.com/) (Figure 1). Moreover, the two cities in the period 1945-1991 were part of the same country (SFR Yugoslavia) in which over those years similar construction typologies were built, the same design standards and construction practices were applied. These similarities widely open the door for a comparative study of the impact of recent moderate size earthquakes on the built environment and population, as well as the implementation of earthquake protection, preparedness and mitigation measures.

City:	Skopje	Zagreb
Urban area (km²):	571.5	641.0
Altitude (m):	240	158
Population (Nº):	567.800 (2016)	684.900 (2020)
Last Earthquake (M_L):	5.3 (11.09.16)	5.5 (22.03.20)
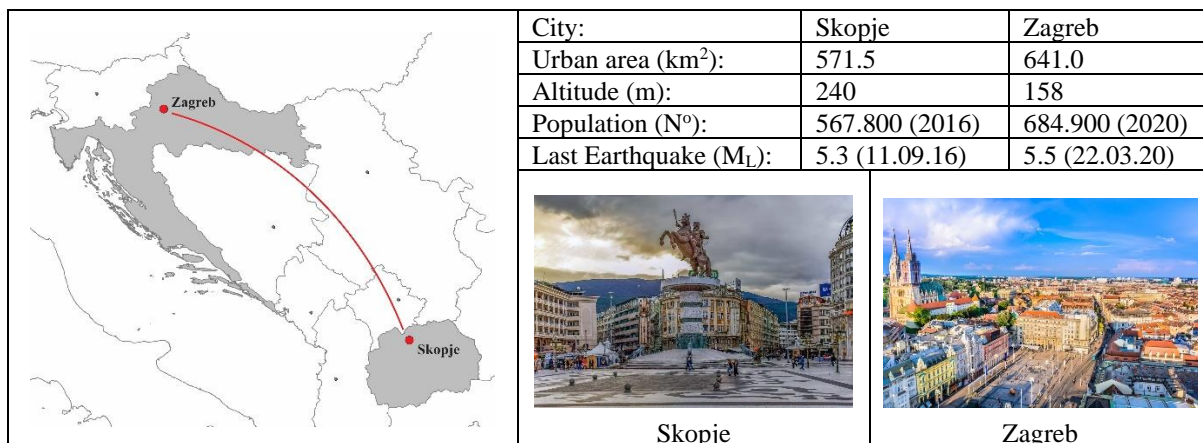
Figure. 1. General facts about Skopje and Zagreb Cities

Exposure as one of basic components of seismic risk, according to the UNDRR[1] Terminology (2017) is defined as situation of people, infrastructure, housing, production capacities and other tangible human assets located in hazard-prone areas. Accordingly, the most important part of the exposure is the inventory of existing buildings, which overwhelmingly contributes to the social and economic risk (Spence et al., 2012). Systematic collection of exposure data usually is performed in the frame of the official censuses, although the collected attributes most often are very general and not quite reliable for regional risk assessment. Typically, a building inventory usually consists of the following major

---

[1] UNDRR: United Nations Office for Disaster Risk Reduction

attributes: location, year of construction, dimensions (height, number of stories, footprint), structural type, dominant construction material (wood, steel, concrete, masonry), lateral force resisting system (bearing wall, shear wall, frame, etc.), occupancy (residential, industrial, critical infrastructure, etc.), number of residents, replacement cost (basis for calculation of economic losses). Once those attributes are collected, a given building is assigned appropriate description code (taxonomy) within a standard classification scheme able to capture average properties among the different building types so that an unambiguous classification is made (Atalić et al., 2019).

According to the summary presented in NERA[2] EC FP7 Project, in relation to the state of knowledge on building inventory data in Europe in the national databases, limited data are available for Skopje and very few about Zagreb (Table 1). Although presented, it must be noted that for N. Macedonia, data related to the lateral load resisting system and exterior walls doesn't exists in the national census database. Also, for N. Macedonia all census 2021 data and statistics related to building inventory are not officially published yet and posted on MAKSTAT database. As of moment, only census 2002 data related to building inventory are available for presentation and analysis. It can generally be concluded that building inventory in both cities is a very poorly defined, and not suitable for reliable risk assessment study.

Table 1. Summary of attributes in national building/dwelling databases, extract (NERA, D.7.2)

Country	Structural System		Building Information			Exterior Attributes				Roof/Floor System		
	Material of Lateral Load Resisting System	Lateral Load Resisting System	Number of Stories	Date of Construction	Occupancy	Building Position within a block	Shape of building plan	Structural Irregularity	Exterior Walls	Roof	Floor	Foundation System
MKD	X	X	X	X	X	-	-	-	X	-	-	-
CRO	-	-	-	X	X	-	-	-	-	-	-	-

For general idea, information related to current building stock that has been affected in the recent earthquakes, presented in uniform manner, can be found in the latest published ESRM20[3] exposure model (Crowley et al., 2021) for residential, commercial, and industrial buildings. For the purpose of this study, building inventory has been extracted related to the wider cities area on NUTS[4]3 level i.e., Skopje region that comprises of 17 both urban and rural municipalities (Aerodrom, Butel, Gazi Baba, Gjorche Petrov, Karposh, Kisela Voda, Saraj, Centar, Chair, Shuto Orizari, Arachinovo, Zelenikovo, Ilinden, Petrovets, Sopishte, Studenichani and Chucher – Sandevo) and Zagreb that comprises of City of Zagreb and Zagreb County (Table 2). What can be observed is that in both cities and surrounding area around 80% of the building stock (Skopje 82.73% and Zagreb 80.10%) belongs dominantly to 3 building typologies (marked with yellow in the table) i.e., (1) Concrete frame with infill panels, low rise, low/moderate code, (2) Confined or reinforced masonry, low rise and (3) Unreinforced masonry, low rise; according GEM[5] Building Taxonomy v3.1 (Silva et al., 2021). Also, it is notable that, the masonry building typologies in total dominates over others (Skopje 54% and Zagreb 71%), out of which for the Zagreb case it is obvious prevalence of the unreinforced masonry low rise typology with approximately 38% of total stock.

---

[2] NERA: Network of European Research Infrastructures for Earthquake Risk Assessment and Mitigation
[3] ESRM20: European Seismic Risk Model
[4] NUTS: Nomenclature of territorial units for statistics - Eurostat
[5] GEM: Global Earthquake Model

Table 2. ESRM20 Exposure model, extract (Crowley et al., 2021)

MACRO__ TAXONOMY	SKOPJE REGION					GRAD ZAGREB & ZAGREB COUNTY				
	RES	COM	IND	Total	%	RES	COM	IND	Total	%
Concrete frame with infill panels, low rise, low/moderate code	36695	2574	0	39269	**29.86**	50346	784	408	51538	**13.83**
Concrete frame with infill panels, low rise, pre code	8017	1215	614	9846	**7.49**	0	135	0	135	**0.04**
Concrete frame with infill panels, midrise, low/moderate code	1469	594	154	2217	**1.69**	43895	730	0	44625	**11.98**
Concrete frame with infill panels, midrise, pre code	948	491	0	1439	**1.09**	2516	870	0	3386	**0.91**
Concrete frame, low rise	0	0	307	307	**0.23**	0	0	2925	2925	**0.79**
Concrete frame, low rise, low/moderate code	0	0	338	338	**0.26**	0	0	476	476	**0.13**
Concrete frame, low rise, pre code	0	0	338	338	**0.26**	0	0	0	0	**0.00**
Concrete frame, mid rise	0	0	61	61	**0.05**	0	0	0	0	**0.00**
Concrete frame, midrise, low/moderate code	0	0	61	61	**0.05**	0	0	0	0	**0.00**
Concrete wall, low rise	0	985	0	985	**0.75**	0	0	0	0	**0.00**
Concrete wall, low rise, low/moderate code	0	673	0	673	**0.51**	0	0	952	952	**0.26**
Concrete wall, low rise, pre code	0	312	0	312	**0.24**	0	0	0	0	**0.00**
Concrete wall, midrise, low/moderate code	833	698	0	1531	**1.16**	448	113	0	561	**0.15**
Concrete wall, midrise, pre code	0	328	0	328	**0.25**	0	0	0	0	**0.00**
Confined or reinforced masonry, low rise	34898	3988	399	39285	**29.87**	102160	758	272	103190	**27.70**
Confined or reinforced masonry, mid rise	807	888	0	1695	**1.29**	11468	154	0	11622	**3.12**
Steel, low rise	0	1649	614	2263	**1.72**	0	0	1088	1088	**0.29**
Steel, mid rise	0	0	123	123	**0.09**	0	0	612	612	**0.16**
Unreinforced masonry, low rise	30179	0	61	30240	**23.00**	142070	1542	68	143680	**38.57**
Unreinforced masonry, mid rise	188	0	0	188	**0.14**	7675	96	0	7771	**2.09**
Total:	114034	14395	3070	**131499**	100.00	360578	5182	6801	**372561**	100.00

3. Seismo-tectonic aspects

3.1. Geology and seismotectonics

The territory of the Balkan Peninsula (Figure 2) is characterized by active geodynamics, controlled by the active tectonic processes in the Eastern Mediterranean. Nowadays, the Balkan Peninsula is in a collision zone between three major plates: Eurasian, African, and Arabian. The active tectonic processes in the Eastern Mediterranean are most influenced by the: (1) subduction of the Adriatic microplate under the Dinarides; (2) subduction of the Ionian and Levant micro plains under the Hellenic trench; and (3) the collision between the Eurasian and the Arabian plates, related to the North Anatolian fault zone (NAFZ). (Dumurdzanov et al. 2005; Burchfiel et al., 2006). Due to this complex tectonic setting, the

Balkan Peninsula is one of the most seismically active regions in the Eastern Mediterranean, where strong and damaging earthquakes are quite frequent.
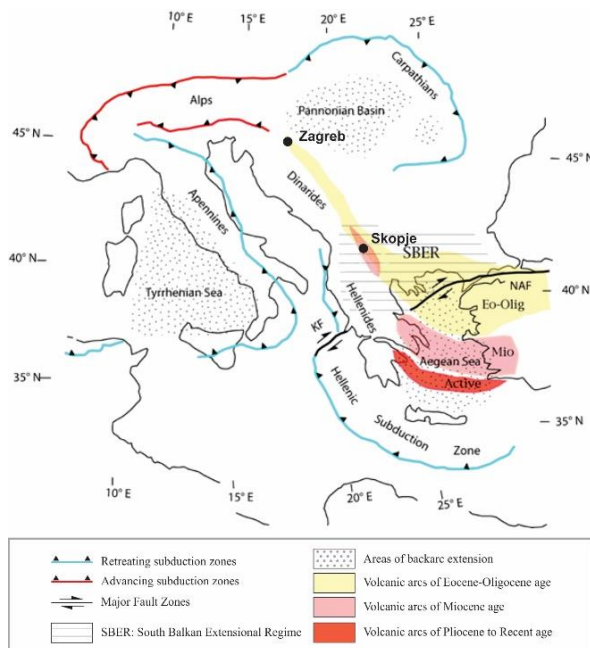
Figure 2. Simplified tectonic map of Eastern Mediterranean region (Dumurdzanov et al., 2005)

The capital of N. Macedonia, Skopje is located in the Skopje valley closely related to the contemporary tectonic activity of the valley, a young tectonic depression, intersected by many neotectonic faults. On the other side, Zagreb is located in a contact zone of the Alps, the Dinarides and the Western regions of the Pannonian Basin, with complex tectonic and structural relationships (Markušić, 2008), as a result of the interaction of the upper crustal tectonic blocks formed during the Mesozoic to Cenozoic evolution of the area (Van Gelder et al., 2015). Seismicity of both epicentral areas where the capitals are located, is due to different tectonic processes, with frequent occurrence of weak to strong earthquakes. In Skopje epicentral area, the subduction of the Skopje valley and the differential vertical and horizontal displacements of the surrounding mountains, are expressed in the regional tectonic compression with the activation of the mostly active Skopje – Kjustendil and Skopje – Crna Gora faults (Fig. 3a).

The Zagreb area belongs to the epicenter area Medvednica Mountains. This is a part of the contact area of three major regional tectonic units: the Alps in the northwest, the Pannonian Basin in the east and the Dinarides in the south. The causes of earthquakes are tectonic movements that occur in the upper crust because of interactions between the underlying lithospheric plates: the European plate and the Adriatic microplate. As a result of the compression and/or subduction of the plates, the upper crustal faults become seismic sources of earthquakes. The earthquakes in the area are the result of the interface between crustal fragments bordered by active faults (Markušić at al., 2020), (Fig. 3b).
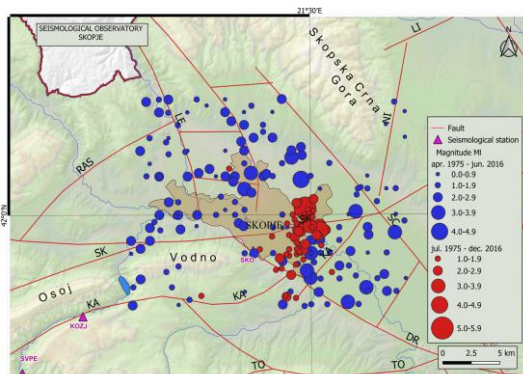
Figure 3a. Seismotectonic map of the Skopje area (SO-PMF[6], Skopje)
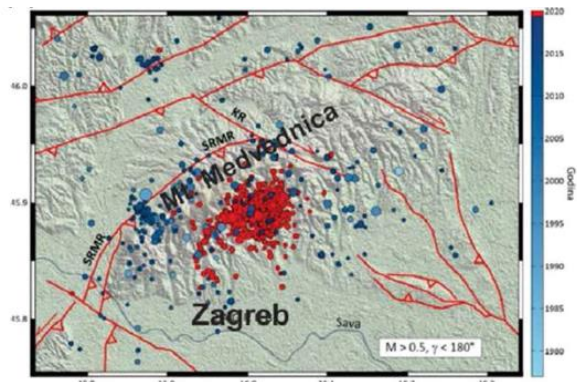
Figure 3b. Seismotectonic map of the Zagreb area (Atalić et al., 2021)

Figure 3. Seismotectonic maps of Skopje and Zagreb wider area

---

[6] SO-PMF: Seismological Observatory, Faculty of Natural Sciences and Mathematics, Ss. Cyril and Methodius University in Skopje

3.2. Seismicity

Both considered regions are characterized by pronounced seismic activity. The historic evidence shows that Skopje epicentral area has been destroyed by strong earthquakes in 518, 1555 and 1963 (Jordanovski et al., 1998; Milutinovic et al., 1998), while the Medvednica Mountains epicentral area experienced strong earthquakes in 1830, 1838 and 1880, the great Zagreb earthquake (Kozák and Čermák, 2010). Besides from local earthquakes, those areas have suffered several times from earthquakes that occurred in the wider area like the impact of Gnjilane earthquake (1921) (Jancevski, 1987) in South Serbia on Skopje, Ljubljana earthquake in 1978 (Kozák and Čermák, 2010) and Petrinja earthquake in 2020 on Zagreb (Markusic et al,. 2021). As the evidence shows, both areas have a rich seismic history which continues even today, as a result of the constant activity of the normal strike-slip Skopje – Kjustendil fault (SK, Fig.3a) (striking approximately E-W, dipping NNE) and Skopje – Crna Gora fault (SC, Fig.3a) (striking approximately N-S, dipping WSW) for the Skopje epicentral area (Jordanovski et al., 1998; Milutinovic et al., 1998), and the reverse northern edge of Medvednica fault (striking approximately NE-SW, dipping SE) (SRMR on Fig.3b) and nearly perpendicular normal strike-slip Kasina fault (KR on Fig.3b) (Van Gelder et al., 2015) for the Medvednica Mountains epicentral area (Tomljenovic, 2002). The predominant hypocentral depth of the located earthquakes in the Skopje area is ranging between 0.1 and 10 km (Sinadinovski et al., 2021) and pretty similar, for the Medvednica Mountain area ranges between 3 and 10 km (Markušić, 2008), which makes the granite layer of the crust active, while the lower part of the crust is almost aseismic.

3.3. Seismic hazard

Estimation of probabilistic seismic hazard for both Skopje and Zagreb cities in relation to referent EC8[7] return periods (95 and 475 years) are comparable. The latest national (EC8 maps; Milutinovic et al., 2016, Herak et al., 2011), regional (BSHAP; Gulerce et al., 2017), and European studies (ESHM20; Danciu et al., 2021) have shown that the values are ranging between 0.20-0.25g for Skopje and 0.20-0.26g for Zagreb for RP475 and 0.07-0.10g for Skopje and 0.08-0.13g for Zagreb in relation to RP95 (Table 3). Seismic hazard values used as referent in the design practice (EC8) are also very similar (Table 3, Figure 4) which implies a design of regular buildings with similar strength characteristics.

Table 3. Seismic hazard values for EC8 referent return periods (Soil type A)

	RP95		RP475	
	SK	ZG	SK	ZG
BSHAP2	0.10	0.08	0.20	0.20
ESHM20	0.07	0.09	0.20	0.24
NA/EC8	0.10	0.13 *(0.12-0.14)*	0.25	0.25 *(0.24-0.26)*

Figure 4a. N. Macedonia, extract (MKC EN 1998-1/NA:2020)
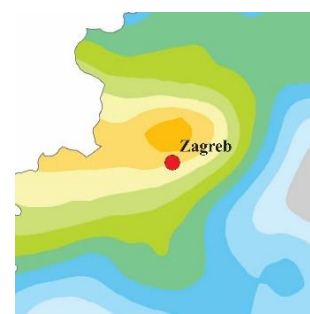
Figure 4b. Croatia, extract (HRN EN 1998-1/NA:2011)

Figure 4. Seismic hazard maps for RP475 related to EC8 National Annexes

4. Seismological observations

4.1. Comparison of M_L5.3 2016 Skopje and M_L5.5 Zagreb 2020 earthquake's parameters

On 11 September 2016 at 13:10 UTC a moderate size earthquake M_L5.3, with a focal depth of approximately 10km occurred near the N. Macedonian capital, Skopje. Using the data from the Macedonian Seismological Network (MA), the epicentre was located at 42.008°N and 21.488°E,

---

[7] EC8: Eurocode 8

approximately 5km from the downtown area. The mainshock caused significant macroseismic effects and was felt in the city area with a maximum intensity of VII degrees EMS-98 scale (Fig 5a), making it the strongest earthquake that hit Skopje in the last 59 years.

An earthquake with a similar magnitude of $M_L 5.5$ with a focal depth of 10km was registered on 22 March 2020 at 05:24 UTC in Zagreb. Using the data from the Croatian national seismological network (CR), the epicentre was located at 45.907°N and 15.970°E about 7 km north of the downtown area, in the Markuševec and Chučerje neighbourhoods. The mainshock caused significant macroseismic effects and was felt in the city area with a maximum intensity of also about VII degrees EMS-98 scale (Fig 6a) (Markušić et al., 2020). This is the strongest earthquake recorded in the last 140 years in the area of Zagreb.
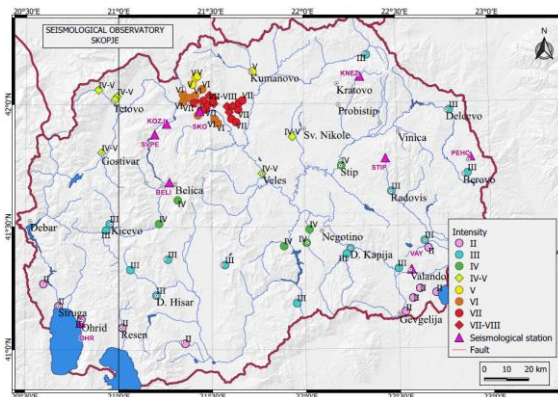
Figure 5a. Intensity map of the 11 September 2016 $M_L 5.3$ Skopje earthquake (SO-Skopje)
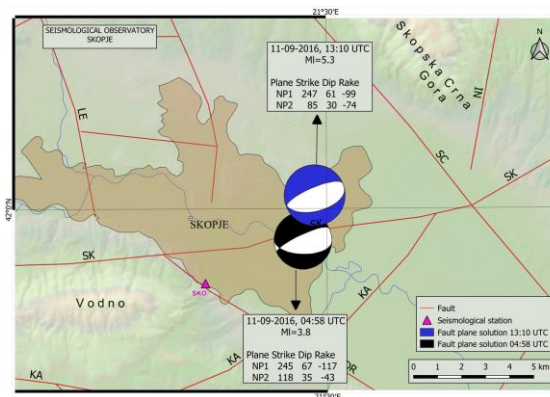
Figure 5b. Fault plane solution of the 11 September 2016 Skopje earthquake, blue for the main shock, black for the foreshock (SO-Skopje)

Figure 5. Skopje earthquake, intensity and FPS maps
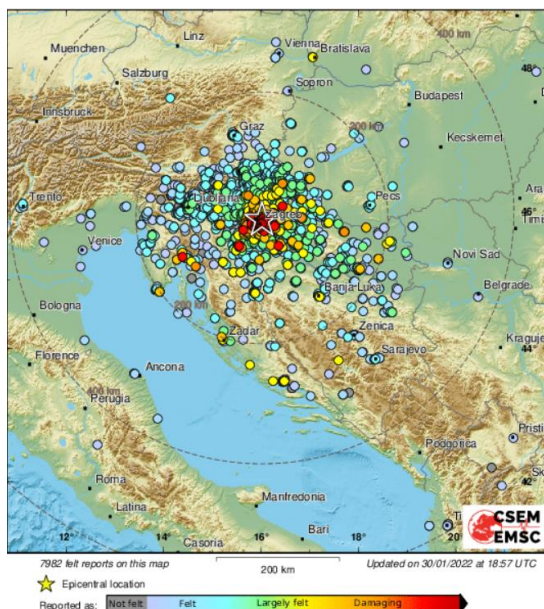
Figure 6a. Intensity map for Zagreb earthquake (EMSC)
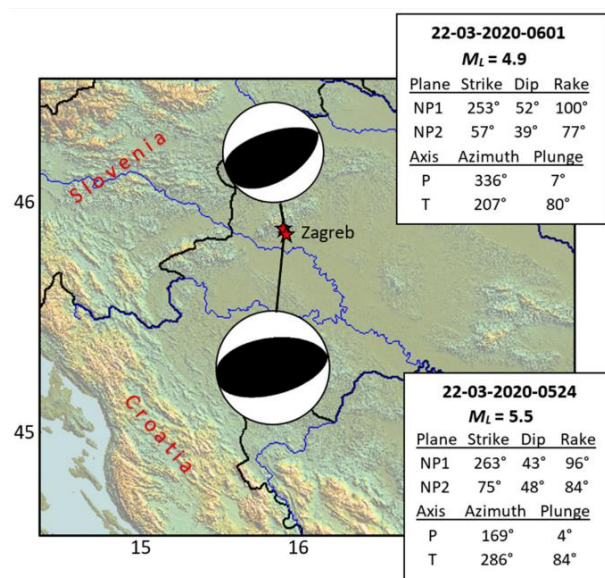
Figure 6b. Fault plane solution for the Zagreb 2020 main earthquake and the strongest aftershock (Markušić et al., 2020)

Figure 6. Zagreb earthquake, intensity and FPS maps

Both events were followed by an aftershock sequence, while the Skopje earthquake had one significant foreshock earlier the same day. The source mechanisms for the main shocks (11.9.2016, 13:10 UTC, $M_L5.3$ – Skopje; 22.3.2020, 05:24 UTC, $M_L5.5$ – Zagreb), the strongest foreshock (11.9.2016, 04:58 UTC, $M_L3.8$ – Skopje) and the strongest aftershock (22.03.2020, 06:01 UTC, $M_L4.9$ – Zagreb) of the earthquake sequences were calculated using the most prominent method using the polarities of the first P seismic motions (Fig. 5b and 6b). The source mechanism's parameters confirm that Skopje's mainshock is a normal right lateral faulting, striking toward WSW, dipping toward NNW, corresponding to a block of regional Skopje – Kjustendil fault - contact between the uplifting Skopje-Crna Gora and Vodno blocks and the Skopje depression. The source mechanisms for Zagreb's sequence define both events as reverse right lateral faulting, striking toward WSW, dipping toward NNW. According to the mechanism parameters, these faultings are associated with the Medvednica fault (Markušić et al., 2020).

4.2. Strong motion and spectral analysis

Two representative strong motion records from both Skopje and Zagreb earthquakes are selected for comparative purposes only, presented in detail in Sinadinovski et al. (2022).

The records from the station in N. Macedonia coded as SKO (Skopje, Seismological Observatory) equipped with EpiSensor Kinemetrics instrument, a maximum acceleration for the Skopje mainshock was detected on the Z-component with a measured zero-to-peak value of 555,000 counts or peak ground acceleration (PGA) of 0.140 g (Fig. 7a). Similarly, the records from the station in Croatia coded as QUHS equipped with Güralp T5GD1 instrument with a general set of response curves to convert the measurements from counts into units of acceleration, a maximum acceleration for the Zagreb mainshock shows the vertical Z component with a value of 0.225g (Fig. 7b), even though the horizontal components carried most of the energy in their respective S-waves (Sinadinovski et al., 2022).
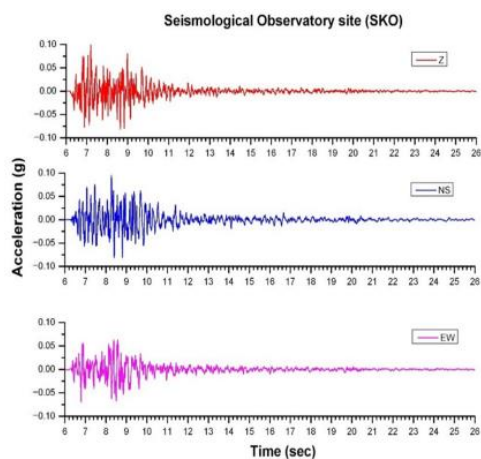
Figure 7a. Skopje Earthquake $M_L5.3$, Station SKO
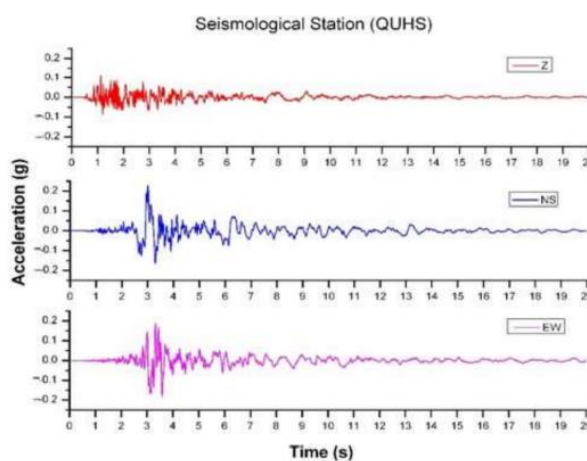
Figure 7b. Zagreb Earthquake $M_L5.5$, Station QUHS

Figure 7. Acceleration records (Sinadinovski et al., 2022)

A response spectra analysis for the selected earthquakes were performed on the whole record length in raw format over various natural periods. Although the range of main interest for structural engineers is between 0 to 4 s, a response acceleration spectrum (in g) for 5% damping, with a period up to 10s was performed to order to detect any anomalies due to resonance effects, polarization, or surface waves reflection of the sub-layers (Fig 8) (Sinadinovski et al., 2022).

The maximum spectral peaks for the SKO records were at 0.2 s on all of the three components, while secondary peaks were concentrated between 0.06 and 0.1 s, equivalent to a frequency of 5–16 Hz. The dominant frequencies of 5 Hz or 0.2 s found on the SKO record of the instrument installed on bedrock (ground type A, according to Eurocode 8), and the top layers velocities using the Balkan model (Jancevski, 1987), lead an estimated value of 0.9 V_S velocity which is a general rate for rupture propagation on faults. The spectral peaks for the QUHS station are mainly between 0.1 and 0.2 s, equivalent to a frequency of 5–10 Hz, with the horizontal components having an additional peak at around 0.5 s or 2 Hz. According to geological maps, QUHS station is located in an area with alluvial deposits (ground type C, according to Eurocode 8). In Table 4, represented are observed and computed parameters for the selected events (Sinadinovski et al., 2022).
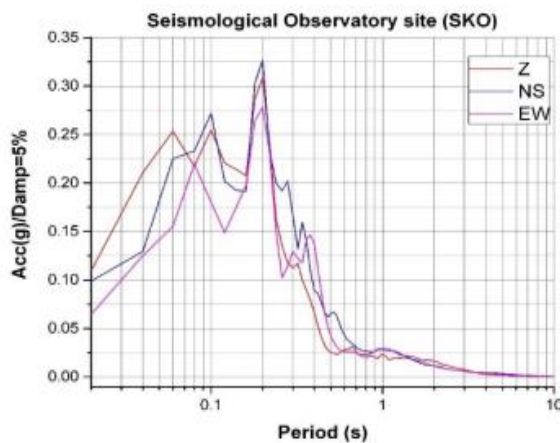
Figure 8a. Skopje 2016 M_L5.3 earthquake at the seismological station SKO
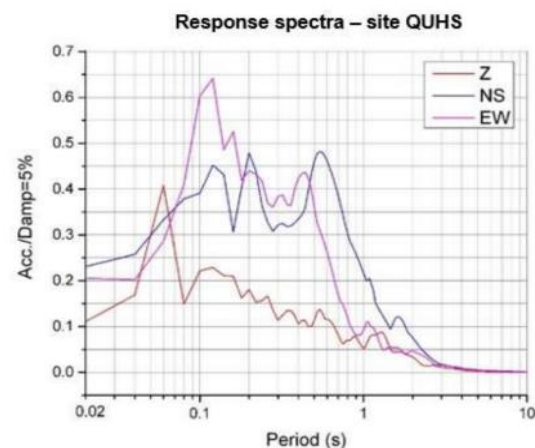
Figure 8b. Zagreb 2020 M_L5.5 earthquake at the seismological station QUHS

Figure 8. Three component response spectra (Sinadinovski et al., 2022)

Table 4. Observed and computed parameters for the selected events

	Hypocentral Distance (km)	PGA (g)	PGV (cm/s)	Sa (5%) (g)	Period Range
Skopje 2016	12.3	0.140	4.3	0.325	0.2
Zagreb 2020	12.5	0.225	7.2	0.4-0.65	0.1-0.2

5. Response measures and procedures

Being hit by an earthquake, although moderate size, both capitals and mandated institutions were challenged to enforce rapid response measures with an aim to help the eventually injured residents, manage panic and fear as well as rapidly screen the damage situation.

5.1. Immediate response measures

Right after the occurrence of the main shock in the afternoon hours on Sunday, September 11, 2016, the Managing Committee of the Crisis Management Centre (CMC) in Skopje, called an urgent meeting with the representatives of all institutions mandated by crisis management i.e. representatives of the Ministries for: internal affairs, external affairs, health, economy, environment and spatial planning, then representatives of the Republic President Office, Seismological Observatory (SO-PMF/UKIM), Institute of Earthquake Engineering and Engineering Seismology (UKIM-IZIIS), Health Centre – Skopje and University Clinics in Skopje. On the first Committee session, since there were no reported victims or injured, was decided that of the primary importance is performing fast safety and usability assessment of the buildings, with priority on buildings that are of public and special interest (hospitals,

schools, kindergartens etc.) for which the users reported certain mode of damage. This fast assessment was agreed to be performed by the expert teams form UKIM-IZIIS. For the purpose of declaring damages, the CMC dedicated a special telephone line and e-mail (Milutinovic et al., 2018). Quite enormous panic among the residents and occupants was created due to the main shock. Despite the negligible earthquake effects on the built environment, the created panic was also result of the remaining memory of the devastating Skopje Earthquake from July 1963. Panic was successfully managed with frequent media statements as well as frequent on-site visits and interactions with the local residents from various experts and representatives from mandated institutions.

The March 2020 Zagreb earthquake occurred in the specific conditions of beginning of Covid-19 pandemic. It was a period when the pandemic measures, likewise in most of the European countries, were extremely strict. A number of employees were advised to take annual leave and left Zagreb just before the earthquake happened. Zagreb was much deserted on that early Sunday morning, a fortunate circumstance given the aftermath of the earthquake. Immediately after the main shock, the Civil protection services were activated for emergency action. The members of the Zagreb EMO, the Directorate of Civil Protection of the Ministry of the Interior and of the Zagreb Faculty of Civil Engineering convened establishing the Crisis headquarters for operational management at the EMO. Fire and communal services together with units of the Croatian army were called upon to maintain order and start clearing the city center and surrounding streets. made Fortunately, the earthquake did not cause any major collapse of buildings or transportation facilities that would fully occupy the emergency services. The focus was therefore put on the assessment of damage and safety of affected buildings and infrastructure. Since there was no previously established inspection plan at city level, the technical experts self-organized using their experience and previous collaborations and under the guidance of experts from the Faculty of Civil Engineering (Atalić et al., 2021). As the scale of the destruction was unknown in the first hours all engineers who had undergone exercises and training for post-earthquake inspection of buildings were called upon by private calls. One of the first actions was to send them to lead the inspection of hospital buildings in the historic downtown, already identified as critical for post-earthquake recovery (Šavor Novak et al. 2019). A public call line was made available for all the civil engineers, on the first day after the main shock, to help and assist in the preliminary assessment of damaged buildings, by contacting first the Directorate. The total number of volunteer engineers was about 500 (Stepinac et al., 2021).

5.2. Earthquake damage and usability assessment procedures

Yugoslavia has a long experience in administratively institutionalized damage assessment. The first Guidelines on the "Unique methodology for estimation of losses from elementary disasters", based on Federal agreement for evaluation and assessment of losses from elementary disasters (OGoSFRY No. 24/78 of 5 May 1978) was enforced in 1979 (OGoSFRY No. 17/79 of 21 April 1979), being revised in 1987 (OGoSFRY No. 27/87 of 10 April 1987) and in Macedonia again in 2001 (OGoRM No. 75/01 of 19 September 2001) and 2021 (OGoRNM No. 181/21 of 5 August 2021).

5.2.1. Assessment procedure used after 2016 Skopje earthquake

The inspection of the building stock after 2016 Skopje earthquake does not include standard damage assessment procedure defined by Unique Methodology (OGoRM No. 75/01 of 19 September 2001) but fast (rapid) assessment of building stability and usability, since it was estimated that the effect of the earthquake on the build environment is negligible. Damage and usability classification was done according to the UKIM-IZIIS methodology which classifies buildings into three (3) damage states, five (5) damage degrees and three (3) usability categories. All received requests for inspection through CMC concerning buildings from public and special interest were send to the managing body in UKIM-IZIIS, and all the others (dominantly residential buildings) were sent to the managing bodies in the appropriate Skopje City Municipalities. The buildings that were inspected by Municipality teams and diagnosed as

buildings with possible stability issues were sent to UKIM-IZIIS for second assessment (Milutinovic et al., 2018) (Figure 9).
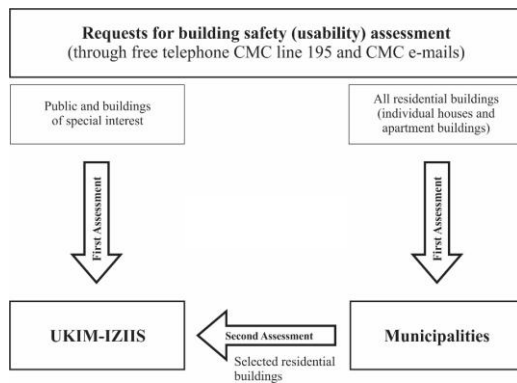
Figure 9. Requests for usability and safety assessment process flow chart

The overall assessment was performed in the period September 11 – October 31, 2016. The inspection of the majority of the building stock (84.8%) was realized during the month of September 2016.

It has to be stated also that, the teams of UKIM-IZIIS inspect the bridges located on the main roads in Skopje and its vicinity for any potential damage. Further on, some industrial buildings were also checked on the demand of their management.

5.2.2. Assessment procedure used after 2020 Zagreb earthquake

Immediately after Zagreb earthquake, at the EMO headquarters was initiated the fine adjustment of the initial safety and usability assessment methodology. Promptly, a general call was sent for mobilization of all engineers with expertise in the (1991–1995) post-war reconstruction or with knowledge related to traditional masonry structures. Programming of a mobile application (Collector for ArcGIS) for acquisition of field observations was initiated at the end of the first day; it was then tested the next day and put into operation a day later. The form was created according to the Italian (Baggio et al. 2007) and Greek (Anagnostopoulos et al. 2004) experience taking into account local building features and observed characteristic damage to gable walls, roofs and chimneys. The form is firstly considered for the assessment of masonry and reinforced concrete buildings, but it can be also used for other building types (Uros et al., 2020). All data was stored in a GIS based database for efficient information flow in both directions. (Atalić et al., 2021). Used methodology classifies buildings into three (3) usability categories and six (6) usability subcategories.

The work on post-earthquake damage inspection and assessment was coordinated by the Ministry of Construction and Physical Planning in cooperation with numerous partners from the government and the industry. The inspection of residential buildings was conducted visually and was more detailed in case of older masonry buildings and buildings that suffered apparent structural damage. Decisions on the short-term usability were made in discussion between the team members based on the current damage state and considering potential behaviour of the structure in case a stronger shaking should have occurred during the still ongoing aftershock sequence. Decisions on usability of critical infrastructure (e.g., bridges) and of essential facilities (e.g., hospitals, schools) were made in agreement with the headquarters and people responsible for the institution. In both cases, the engineering experience and intuition were decisive for the evaluation of the safety and accessibility (Atalić et al., 2021).

The post-earthquake field inspections of damage incurred to buildings were carried out until June 30th, 2020, when the inspections were officially finished.

6. Building damage and usability statistics

After 2016 Skopje earthquake, through CMC channels were obtained in total 2,885 requests for usability and safety assessment, out of which 625 (Figure 9) were assessed by UKIM-IZIIS. The biggest concentration of all inspected buildings was related to four (4) Municipalities: Chair, Centre, Gazi Baba and Kisela Voda as it was expected since those Municipalities contains considerable number of

masonry, pre 1963 and sub-standard buildings. Also, those Municipalities were found to be very near to the epicentre of the main shock. According to Usability Classification (UC), 94.19% of the inspected buildings are classified as usable i.e., with slight non-structural damage, very isolated or negligible structural damage, 5.61% as temporary unusable i.e., with extensive non-structural damage, considerable structural damage but yet repairable structural system and 0.20% unusable i.e., destroyed, partially or totally collapsed structural system (Milutinovic et al., 2018) (Figure 10a).

In parallel after 2020 Zagreb earthquake, in total, more than 25,500 building inspections were performed or about 19.6% of the approximately 130,000 buildings within the city limits. Overall, about 75% of all inspected buildings were green tagged (U1 and U2), 20% temporarily unusable (PN1 and PN2) and 5% unusable (N1 and N2). It may be observed that the highest concentration of inspected buildings and at the same time of the unusable buildings is located in the central city area and in districts close to the epicentre (Atalić et al., 2021; Stepinac et al., 2021) (Figure 10b).

UC	I	II	III
% INS IZIIS	73.17	25.91	0.91
% INS TOT	94.19	5.61	0.20
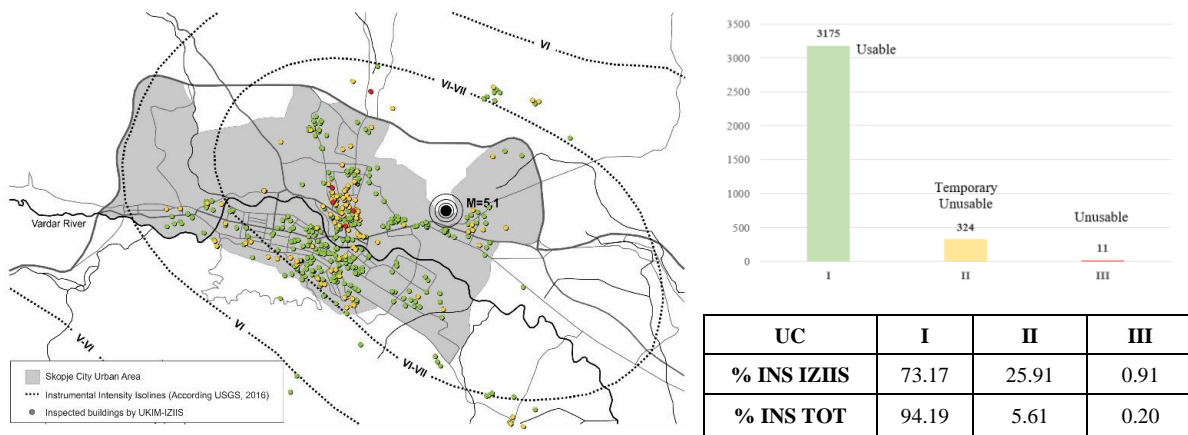
a) Disposition of inspected buildings in Skopje (according to Milutinovic et al., 2018)

UC	I	II	III
% INS	75.16	19.58	5.26
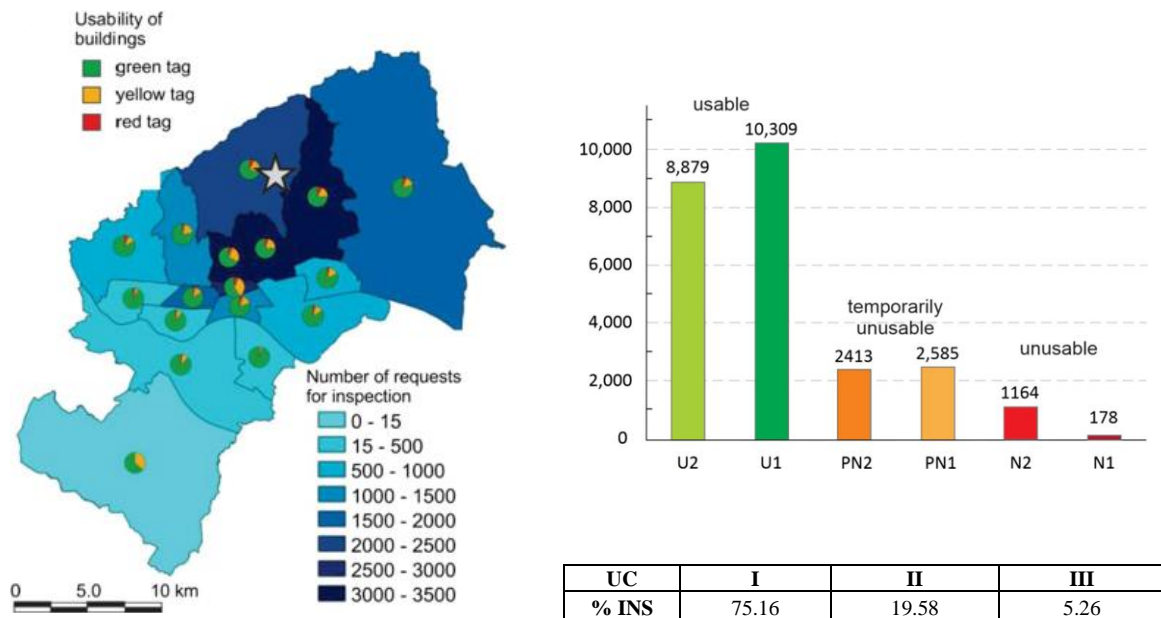
b) Disposition of inspected buildings in Zagreb (according to Atalić et. al., 2021)

Figure 11. Disposition of the inspected buildings by Usability Category (UC)
(● Usable [I]   ● Temporary Unusable [II]   ● Unusable [III])

In relation to 2016 Skopje earthquake, Milutinovic et al. (2018) stated that the concentration of the reported damages was found to be in the masonry type structures, buildings constructed before 1964, dominantly residential buildings and low to medium rise story buildings. Similarly, inspection results after 2020 Zagreb earthquake according to Atalić et al. (2021) suggest that nearly all of the damage occurred in older masonry housing units and heritage buildings not designed to resist lateral dynamic loads. About one third of all buildings in Zagreb were built before 1964, when the first Seismic Construction Code was introduced. The vast majority of buildings built afterwards did not suffer any apparent impacts during the earthquake.

If compared the number of inspected buildings classified under the usability category II (Temporary Unusable) together with III (Unusable) in relation to the total number of buildings in the city affected region, can be concluded that very negligible number of buildings in Skopje were affected (0.12%) and much larger number in Zagreb (1.70% if considered ESRM20 data or 4.87% if considered building stock count in Atalić et al., 2021) (Table 5). Taking aside the other parameters, most probably the obvious difference in damage degree distribution (Figure 11) is due to the fact that Zagreb building stock contains larger amount of masonry structures compared to Skopje, which is also evident from ESRM20 exposure model (Table 2), especially in the group of unreinforced masonry, low rise buildings.

Table 5. Usability of inspected buildings in relation to the current exposure

	Buildings/No		Usable		Temporary Unusable		Unusable	
			D1	D2	D3	D4	D5	-
Skopje	Inspected	2,885	2445	273	133	28	6	-
			84.74%	9.45%	4.62%	0.99%	0.20%	-
			94.19%		5.61%		0.20%	
	ESRM20	131,499	1.86%	0.21%	0.10%	0.02%	0.00%	-
			2.07%		0.12%		0.00%	

	Buildings/No		Usable		Temporary Unusable		Unusable	
			U2	U1	PN2	PN1	N2	N1
Zagreb	Inspected	25,528	8879	10309	2413	2585	1164	178
			34.78%	40.38%	9.45%	10.13%	4.56%	0.70%
			75.16%		19.58%		5.26%	
	ESRM20	372,561	2.38%	2.77%	0.65%	0.69%	0.31%	0.05%
			5.15%		1.34%		0.36%	
	Atalić et al., 2021	130,000	6.83%	7.93%	1.86%	1.99%	0.90%	0.14%
			14.76%		3.84%		1.03%	
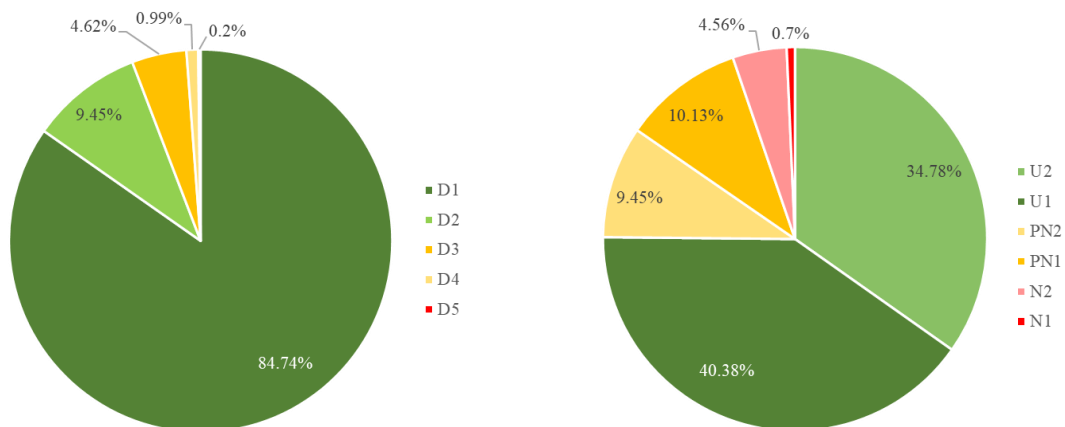
a) Skopje   b) Zagreb

Figure 11. Damage and usability degree in respect to inspected buildings

7. Conclusions

Moderate size earthquakes are quite a frequent hazard in the Balkan Peninsula. Even today they can cause significant material losses and disruption to basic and vital services, due to the fact that in the Balkan countries still prevails masonry type buildings, dominantly built before 1964. This fact was confirmed by the impact of the last two moderate size earthquakes that hit Skopje and Zagreb in 2016 and 2020.

The latest developed exposure model for Europe (Crowley et al., 2021) accounting for residential, commercial, and industrial buildings, shows that masonry building typologies in total dominates over others for Skopje 54% and Zagreb 71%, out of which for the Zagreb case it is obvious prevalence of the unreinforced masonry low rise typology with approximately 38% of total stock.

The complex geotectonic setting of both Skopje and Zagreb cities conditions relatively high seismic hazard values ranging between 0.20-0.25g for Skopje and 0.20-0.26g for Zagreb (RP475) and 0.07-0.10g for Skopje and 0.08-0.13g for Zagreb (RP95), according the latest national, regional and European studies (Milutinovic et al., 2016; Herak et al., 2011; BSHAP - Gulerce et al., 2017; ESHM20 - Danciu et al., 2021). Those values are also in line with the historical seismicity data, according to which Skopje and Zagreb in the past has also experienced moderate to strong damaging earthquakes.

Although similar in magnitude size, hypocentral depth and macroseismic intensity, the focal mechanisms of 2016 Skopje and 2020 Zagreb earthquakes significantly differs, i.e., normal right lateral faulting in Skopje and reverse right lateral faulting in Zagreb.

Two strong motion records were selected for comparison purposes, obtained from SKO (Skopje, Soil type A) and QUHS (Zagreb, Soil Type C) stations, on relatively equal distances from the epicenter. The maximum spectral peaks for the SKO records were at 0.2 s on all of the three components, while secondary peaks were concentrated between 0.06 and 0.1 s, equivalent to a frequency of 5–16 Hz. The spectral peaks for QUHS station are mainly between 0.1 and 0.2 s, equivalent to a frequency of 5–10 Hz, with the horizontal components having an auxiliary peak at around 0.5 s or 2 Hz. SKO station has recorder maxPGA of 0.14g and QUHS station 0.22g (Sinadinovski et al., 2022).

Despite Yugoslavian long experience in administratively institutionalized damage assessment, the last 2 earthquakes were "surprise" to the relevant authorities in both countries, which clearly shows the need of urgent system preparedness measures and improvement of current procedures and legislations, as well as implementation of the latest smart technologies and GIS developments.

Effective and very fast damage assessment comes out as a necessity in both cases. Rapid procedures were used, for Skopje modified UKIM-IZIIS methodology, and for Zagreb methodology adopted from Baggio et al. (2007) and Anagnostopoulos et al. (2004), modified to account for the local building features and observed characteristic damage to gable walls, roofs and chimneys. Both methodologies used have classified the buildings in three usability categories: usable, temporary unusable and unusable.

After Skopje earthquake inspected were 2,885 buildings for the period of app 50 days, and 25,528 for the period of app 100 days after Zagreb earthquake. In relation to both earthquakes, the concentration of the reported damages was found to be in the masonry type structures, buildings constructed before 1964, dominantly residential and heritage buildings and low to medium rise story buildings. Comparing to current building exposure (ESRM20), out of function (temporary unusable and unusable) buildings for Skopje were reported 0.12% and much larger number in Zagreb (1.70% if considered ESRM20 data or 4.87% if considered Atalić et al., 2021 data). The larger percentage of affected buildings in Zagreb, in mostly due to the fact that Zagreb building portfolio contains larger amount of masonry and historical buildings, especially from the group of unreinforced masonry (ESRM20). It must be mentioned that the

last damaging earthquake in Skopje in 1963 has "cleared" considerable amount of masonry building stock in the city, and also afterwards with the city new urban reconstruction. Moreover, considerable amount of pre 1964 masonry structures in Skopje that exists today were strengthened to comply with the strength characteristics of the that time new 1964 code.

The similarities, impacts and lessons learned from those two earthquakes opens a wide space for further research with aim to build more effective system for response, creation of adequate preparedness measures and increase the resilience of urban systems.

References

[1] Anagnostopoulos, SA., Moretti, M., Panoutsopoulou, M., Panagiotopoulou, D., Thoma, T. (2004): Post earthquake damage and usability assessment of buildings: further development and applications, Final report, European Commission-D.G. Environment, and Civil Protection EPPO, Patras, Greece.

[2] Atalić, J., Šavor Novak, M., Uroš, M. (2019): Seismic risk in Croatia: an overview of the current research and existing assessments with suggestions for future activities, Građev J Croatian Assoc Civil Eng 71(10):923–947.

[3] Atalić, J., Uroš, M., Šavor Novak, M., Demšić, M., Nastev, M., (2021): The Mw5.4 Zagreb (Croatia) earthquake of March 22, 2020: impacts and response, Bull Earthquake Eng 19, 3461–3489 (2021). https://doi.org/10.1007/s10518-021-01117-w.

[4] Baggio, C., Bernardini, A., Colozza, R., Corazza, L., Della Bella, M., Di Pasquale, G., Dolce, M., Goretti, A., Martinelli, A., Orsini, G., Papa, F., Zuccaro, G. (2007). Field Manual for post-earthquake damage and safety assessment and short-term Countermeasures (AeDES), Eur Commission Joint Res Centre 22868:89.

[5] Burchfiel, B.C., Todosov, A., King, R. W., Kotzev, V., Dumurdjanov, N., Serafimovski, T., Nurce, B. (2006). GPS Results for Macedonia and Its Importance for the Tectonics of the Southern Balkan Extensional Regime: Tectonophysics 413, 239–248.

[6] Crowley, H., Dabbeek, J., Despotaki, V., Rodrigues, D., Martins, L., Silva, V., Romão, X., Pereira, N., Weatherill, G., Danciu, L. (2021): European Seismic Risk Model (ESRM20), EFEHR Technical Report 002 V1.0.0, https://doi.org/10.7414/EUC-EFEHR-TR002-ESRM20.

[7] Danciu, L., Nandan, S., Reyes, C., Basili, R., Weatherill, G., Beauval, C., Rovida, A., Vilanova, S., Sesetyan, K., Bard, P-Y., Cotton, F., Wiemer, S., Giardini, D. (2021): The 2020 update of the European Seismic Hazard Model: Model Overview, EFEHR Technical Report 001, v1.0.0, https://doi.org/10.12686/a15.

[8] Dumurdzanov, N., Serafimovski, T., Burchfiel, B. C. (2005): Cenozoic tectonics of Macedonia and its relation to the South Balkan extensional regime: Geosphere 2005, 1, 1–22, Doi: 10.1130/GES00006.1.Gulerce et al., 2017.

[9] Herak, M., Allegretti, I., Herak, D., Ivančić, I., Kuk, V., Marić, K., Markušić, S., Sović, I. (2011): Republic of Croatia, Seismic hazard map. http://seizkarta.gfz.hr.

[10] Janchevski, J. (1987). Classification of fault structures by genesis, age and morphology with reference to their seismicity in the territory of Macedonia. Doctoral dissertation. Faculty of Mining and Geology, Stip (in Macedonian)

[11] Jordanovski, Lj., Pekevski, L., Cejkovska, V., Chernih, D., Hristovski, B., Vasilevski, N. (1998): Basic characteristics of the seismicity of the territory of the Republic of Macedonia, Seismological Observatory, Faculty of Natural Sciences and Mathematics, Ss. Cyril and Methodius University in Skopje, Report 98/01.

[12] Kozák, J., Čermák, V. (2010): A Review of "The Illustrated History of Natural Disasters", Heidelberg, Germany: Springer, 2010, ISBN 9789042133246.

[13] Markušić, S., Stanko, D., Penava, D., Ivančić, I., Bjelotomić Oršulić, O., Korbar, T., Sarhosis, V. (2021). Destructive M6.2 Petrinja Earthquake (Croatia) in 2020 - Preliminary Multidisciplinary Research. Remote Sens. 2021, 13, 1095. https://doi.org/10.3390/rs13061095

[14] Markušić, S., Stanko, D., Tvrtko, K., Belić, N., Penava, D., Kordić, B. (2020): The Zagreb Croatia M5.5 earthquake on 22. Geosciences. https:// doi.org/10. 3390/ geosciences1007 0252.

[15] Markušić, S. (2008). Seismicity of Croatia. In: Husebye, E.S. (eds) Earthquake Monitoring and Seismic Hazard Mitigation in Balkan Countries. NATO Science Series: IV: Earth and Environmental Sciences, vol 81. Springer, Dordrecht. https://doi.org/10.1007/978-1-4020-6815-7_5.

[16] Milutinovic, Z., Mihailov, V., Talaganov, K., Trendafiloski, G., Olumceva, T., Sesov, V. (1998). Spatial Plan of Republic of Macedonia, Conditions for occurrence and protection from seismic disasters, IZIIS Report 98-29 (In Macedonian).

[17] Milutinovic, Z., Salic, R., Dumurdzanov, N., Cejkovska, V., Pekevski, L., Tomic, D. (2016): Seismic Zoning Maps for Republic of Macedonia according to the Requirements of MKS-EN 1998-1:2004 - Eurocode 8, IZIIS Report, 2016-26, August 2016 (in Macedonian).

[18] Milutinovic, Z., Salic, R., Micajkov, S., Tomic, D., Ristovska, H. (2018): Managerial Aspects of September 11, 2016, 5.1 Skopje Earthquake, 16th European Conference on Earthquake Engineering, 18-21 June 2018, Thessaloniki, Greece.

[19] NERA, D.7.2: State of the Knowledge of Building Inventory Data in Europe, FP7, EC project number: 262330.

[20] Šavor Novak, M., Atalić, J., Uroš, M., Prevolnik, S., Nastev, M. (2019): Seismic risk reduction in Croatia: mitigating the challenges and grasping the opportunities, Future Trends in Civil Engineering, University of Zagreb, Faculty of Civil Engineering, Croatia, (pp 71–109).

[21] Sinadinovski, C., Markušić, S., Stanko, D., McCue, K.F., Pekevski, L. (2022): Seismic Analysis of Moderate Size Earthquakes Recorded on Stations at Close Epicentral Distances, Appl. Sci. 2022, 12, 470. https://doi.org/10.3390/app12010470.

[22] Sinadinovski, C., Pekevski, L., Chernih, D., Drogreshka, K., Najdovska, J. (2021): Seismicity Detection in Skopje Region Using Tomographic Methods and 3-D Modelling, DOI: 10.5194/egusphere-egu21-6950, 2021

[23] Spence, R., Foulser-Piggott, R., Pomonis, A., Crowley, H., Masi, A., Chiauzzi, L., Zuccaro, G., Cacace, F., Zulfikar, C., Markus, M., Schaefer, D., Sousa, M.L., Kappos, A. (2012): The European Building Stock Inventory: Creating and Validating a Uniform Database for Earthquake Risk Modelling, Proceedings of the 15th World Conference of Earthquake Engineering, Lisbon, 2012.

[24] Stepinac, M., Lourenço, P. B., Atalić, J., Kišiček, T., Uroš, M., Baniček, M., & Šavor Novak, M. (2021). Damage classification of residential buildings in historical downtown after the ML5.5 earthquake in Zagreb, Croatia in 2020. International Journal of Disaster Risk Reduction, 56, 102140. doi:10.1016/j.ijdrr.2021.102140

[25] Uroš, M., Šavor Novak, M., Atalić, J., Sigmund, Z., Baniček, M., Demšić, M., Hak, S. (2020). Post-earthquake damage assessment of buildings – procedure for conducting building inspections, GRAĐEVINAR, 72 (12), 1089-1115, doi: https://doi.org/10.14256/JCE.2969.2020

[26] Van Gelder, I.E., Matenco, L., Willingshofer, E., Tomljenović, B., Andriessen, P.A.M., Ducea, M.N., Beniest, A., Gruić, A. (2015): The tectonic evolution of a critical segment of the Dinarides-Alps connection: Kinematic and geochronological inferences from the Medvednica Mountains, NE Croatia, Tectonics 2015, 34, 1952–1978; doi:10.1002/2015TC003937.

ARCHITECTURAL DESIGN AND EARTHQUAKE CONSEQUENCES IN BUILDINGS

Marsida Tuxhari [(1)], Markel Baballëku [(2)], Merlin Asllani [(3)]

[(1)] *Lecturer, Department of Restoration and Architecture Technology, Faculty of Architecture and Urbanism, PUT, Albania*
marsida.tuxhari@fau.edu.al
[(2)] *Lecturer, Structural Mechanics Department, Faculty of Civil Engineering, PUT, Albania*
markel.baballëku@fin.edu.al; markel77@gmail.com
[(3)] *UTS-01 Design Studio. Tirana, Albania*
merlin.asllani18@gmail.com

Abstract

This paper focuses on earthquake consequences in buildings, analyzed in terms of architectural design choices. The Durrës earthquake of 11.26.2019 showed lot of damages of non-structural nature, in buildings of various ages, structural systems, and volumetric shapes.

The object of the article is precisely the treatment of the variety of these "types of damages", which require to be carefully analyzed in order to understand the causes of which some of the consequences came from. The behavior of the building during the earthquake showed that the reasons for the damages were also related to the architect's choices and the corresponding conditions in the technical design codes. For example: the shape of the building, the regularity of the structure, seismic joints, cantilever volumes, parapets, stairs, doors etc. So, the purpose of the article is to highlight the damages that come as a result of those design factors, which directly involve the architect. The article does not undertake to limit the functional and aesthetic choices on buildings but emphasizes the importance of the early collaboration of the architect and structural engineer in seismic-prone areas, taking into account that construction works should be built at optimal cost, with the aim of minimizing such damages in the future.

Keywords: nonstructural damages, irregularities, seismic joint, architectural design.

1. Introduction

The earthquake of November 26th, 2019 in Durrës, which was preceded by another earthquake, approximately of the same magnitute on September 21th, 2019 with almost the same epicenter, caused significant damages on buildings which was followed by strong debates even among the engineers themselves. The earthquake caused a lot of non-structural but still significant damages, in more buildings than those that were structurally demaged.

These damages cannot only be addressed to a specific construction discipline. They have come for various reasons which can be summarized in these 4 main groups:

1. Damages related to the design of the buildings;
2. Damages coming from the lack of knowledge and non-implementation of technical design conditions;
3. Damages related to construction details in the project;
4. Damages related to the construction process and necessary construction details.

A critical look at earthquake damage to buildings, shows that the architectural configuration, which (according to Arnold) is defined as: the building's size, three-dimensional shape, two-dimensional shape and location of structural elements, as well as the nature and location of non-structural components that can affect the seismic performance, aesthetic choices and technical details implemented in many cases, although not the only factors, have contributed to serious structural and non-structural damage to buildings. [1]

All of the four groups above require full attention of the civil engineer, but for some of them, the role of the architect is a major influencing factor and should not be avoided. Engineers often say that the configuration given by the architects for the building makes their job more difficult, increases construction costs and decreases the safety of the building. So the architectural design of the building is also decisive for its structural configuration, and both of these factors are responsible for the seismic behavior of the entire building.

Many experienced earthquake engineers say that the architect plays a key role in ensuring the satisfactory seismic performance of a building. [1]

So designing for seismic safety should not always be seen as a task only for the structural engineer. In fact, this paper does not aim to limit architects in their functional and aesthetic choices for buildings, but through some case studys, to emphasize the importance of knowing the technical guidelines for architectural design decisions in seismic-prone zones and the importance of cooperation with the structural engineer from the early stages project idea. This way, past mistakes can be avoided and future construction works can be built at optimal cost, because cost and safety issues are top priorities.

Seismic Design Code (KPT-N.2-89) is the official design document in Albania, which gives principles, design rules and recommendations about seismic design of buildings, and other construction works. [3]

Eurocode 8 (EN 1998-1) is also being adapted in Albania, but not yet approved by the relevant State authorities. Due to this, it's unofficial and not mandatory to be followed and implemented by engineers. However, it is used by all as a guide in the design of engineering projects. [4]

2. Earthquake consequences (case studys of damaged buildings)

According to Albania Post-Disaster Needs Assessment Document (Government of Albania; European Union; United Nations agencies; World Bank, February 2020) (CEN, 2005) 18% of housing units in Albania are overall affected by the earthquake.

In their multitude, this paper focuses on the damages caused to multi-story buildings in Durrës and Tirana regions in Albania, which indirectly or directly involve the architect.

The inspection and analysis of earthquake-damaged buildings plays an important role in understanding the causes of damage and justify the importance and effectiveness of seismic design and construction. There have been damage models, related only to the configuration characteristics of particular buildings, which have resulted in structural damage consequently the destruction of buildings. There were damage models related to the configuration and simultaneously to technical aspects of the construction details. As there have been models of non-structural damage, due to technical details far from anti-seismic design conditions.

Through an architetct's lens, confronting: cause-and-effect of the actual models and patterns of earthquake damage in buildings can be interpreted related to 3 elements of the building, such as:

1. The volume configuration of the building;
2. The facade of the building;
3. The inside of the building.

The volumetric configuration is related to the both architectural and structural features of the overall building (geometry in plan and elevation), cantilever volumes, height of the building and changes in floor heights, transparency and the height of the ground floor, regularity of the structure in plan and elevation, dimensioning of the seismic joints and taking them into consideration during architectural design.

The facade of the building is related to: the envelope of the building in its opaque and transparent parts, facade cladding and parapets. The interior of the building is related to: stairs and common space of movement, partitions between diferent residential units and those inside the same unit and main apartment door clearance.

Some of the features mentioned above may be associated with more than one building element, e.g. transparent coatings are related to both the volumetric configuration and the facade; seismic joints are related to the volumetric configuration and in some cases to the interior of the building.

2.1 Residential buildings with irregular configuration

In the multitude of damaged buildings due to irregular volumetric configuration, the following case is singled out, in which there are damages caused by the effects of the interaction of the neighboring buildings with each other, the irregular configuration in the plan and the increased volume on the upper floors.The buildings are located at the entrance to the city of Durrës and were built one after the other in the period 2006-2012, the first with 9 floors above ground (on the right) while the second with 12 floors above ground + attic (on the left). Fig. 2. During the construction of the second building, an additional volume has been proposed in the form of a "connecting bridge" with the first existing building, which is attached with 3 floors and there are 3 more floors above the "bridge".

This volume added to the form of the bridge is partly supported on two columns attached to the facade of the first building but not connected to it and not far from it (on the right) and partly emerges as a cantilevered volume on the last three floors of of it, on the terrace of the existing building.

Due to the irregular configuration in plan, the added mass on the upper floors of the second building and the irregular and large-amplitude seismic waves, two effects were produced: the buildings collided with each other in the joint area and the cantilever volume has increased the height of the center of mass of the second building and has had the effect of increasing its behavior as an inverted pendulum. As a result, parts of walls have fallen from the facade. Fig. 1.

Figure 1. Collapse of the facade walls in the "connecting bridge" area
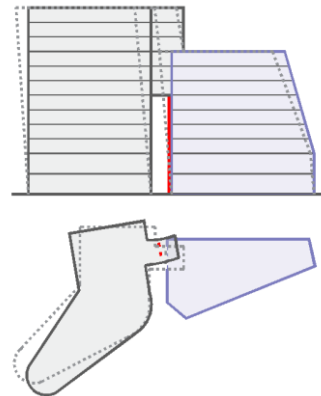
Figure 2. Behavior of buildings during the seismic event

Most of the buildings after the 1990s in Albania are cases of irregular volumetric configuration, dictated by the geometry of the property, the use of the building for several functions and the demand of investors or the architects themselves, who are always looking for the most accurate volumetric form. nice, they wanted to achieve something "unusual", but in this way the project creates a conflict with the seismic design codes and rules. Skilled engineers have taken these projects as a professional challenge to execute them, but experience has shown that the construction of these types of constructions can cost on average about 20% more than the construction of a building with conventional configuration. And yet their behavior during the earthquake has again caused increased damage to the non-structural elements of many buildings and therefore increased cost which is difficult to calculate. On the other hand, in seismic areas, "unusual" buildings cannot provide the same safety as those with a regular configuration.

The main responsibility of the geometric configuration of the building lies with the architect from the first stages of conception. If architectural design geometry and structural design geometry are determined independently of seismic considerations, it is not possible to simultaneously achieve a

building with appropriate architectural design, desirable seismic behavior, and optimal construction cost. [10]

In these cases, there is a deviation from the code instructions for regular volumetric configuration in plan and height of the building. Both documents, as KTP-N.2-1989, in chapter 1, part 1.4, as well as EN 1998-1, in chapter 4, in general terms recommend the conception of buildings with regularity in plan and height in terms of compactness and volumetric symmetry, looking for: non-pronounced breaks in plan and in height.

According to EN 1998-1, (part 4) uniformity in the development of the structure along the height of the building is important, because it tends to eliminate the occurrence of sensitive zones, where stress concentrations or high ductility requirements can cause significant damage or structurally irreversible.

2.2 Irregular distribution of non-structural components of the building (infill walls and partitions)

The building in Figure 3, with 6 floors and a reinforced concrete supporting structure, built during 2008-2010, is one of many buildings with the same irregularities in their configuration. The building's volatility has been high, among other issues, due to the following factors: low stiffness on the first two floors; low stiffness in twisting and irregular distribution of strucutural elements in the added mass of upper floors and non-uniform distribution of non-structural elements, with added mass on upper floors.

Damage observed in this building after the November earthquake is concentrated on the first floor. The reason why the "soft story" mechanism was developed on the first floor and not on the ground floor is related to the largest shifts that took place on this floor. The best design of the ground floor (the size of the columns and their reinforcement) may have also influenced. On the other side, the lack of non-structural walls in these two floors has contributed to the structural damages, taking into consideration the shape of the damage, it can be estimated that the low rigidity in the torsion and the increased mass of the upper floors (console volumes on both sides) also had their impact. Figure 4

| Figure 3. Non-uniform distribution of non-structural components | Figure 4. Damage due to "soft story" and torsional effect | Figure 5. "soft story" mechanism was developed |
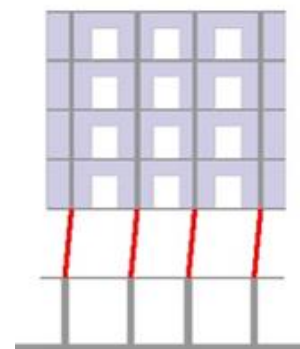
This damage mechanism has been observed in many other buildings with similar geometric configuration and structural features of which are probably design factors.

Irregular distribution of non-structural elements in height, e.g. in cases where the resistance of the infill walls on one floor is very small compared to the other floors... the result of all this is the creation of a soft floor. This happens, especially in the case of open ground floors with infill walls on one or both sides or without infill walls. [4]

According to Ambrose and Vergun (1985) state that reduction of the soft story effect can be possible. The remedies for soft story are:
- to brace some of the openings;

- to keep the building plan periphery open, while providing a rigidly braced interior;
- to increase the number or the stiffness of the ground floor column;
- to use tapered or arched forms for the ground floor;
- to develop a rigid ground story as an upward extension of heavy foundation structure;
- to equalize the rigidity of the stories by separating the non-structural elements from the structural ones or using light and less rigid non-structural elements for infill walls and exterior claddings. [14]

All of the above guidelines relate to design issues, most of which structural engineering is responsible for. The architect must be cooperative and prepared to accept structural forms (such as increased size and number of columns and beams).

2.3 Cantilever volumes

From a seismic point of view, cantilever volumes present at least two complications in the dynamic behavior of the building: First, they affect the overall structural irregularity, a problem that requires careful handling in the distribution of primary seismic structural elements. Second, it requires attention to the self-sustainability of construction elements in the area of the cantilever volume. The impact on the overall behavior of the building requires proper structural treatment and is not the scope of this paper.

Due to the simultaneous oscillation in the vertical and horizontal direction, the cantilever volumes are in a delicate situation of balance. In the cases shown in Fig. 6 and Fig. 7, this state of the cantilever volumes is also accompanied by the lack of implementation of technical details to properly connect the walls at the ends of the cantilevers. As a result, the walls of the facade on several floors of the cantilevered volume have collapsed, exactly at the outer corners of the cantilevers.

The main cause of this damage model is the deviation from the anti-seismic design conditions, due to the irregular volume configuration with the cantilevers and the added weight of the walls in them, because the architect has chosen to treat the cantilever as a volume attached to the rest of the facade.

Figure 6. Walls collapse in the cantilever volumes
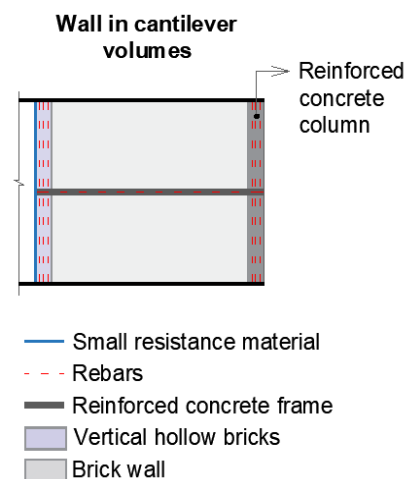
Figure 7. Wall above cantilever reinforcement model

Sandwich walls, which are designed for heat insulation, are also to be tied to each other with cramps in order to prevent overturning due to seismic forces. [9]

Due to their behavior during seismic events, cantilever volumes on facades are recommended to be avoided. If cantilever volumes are a must, technical measures with special construction details must be taken to avoid damage to this model in buildings. These types of damages are the result of simultaneous combinations of some of the 4 groups of causes as outlined in the introduction of this article.

Many architects believe that seismic design is totally controlled by the engineers in their team and they should not be involved in the conception or coordination of seismic design. But successful seismic design begins and ends with the architect. It is true that engineers can control the details of many components within the building, but it is the architect who must understand the interrelationship between the various systems within the building for successful performance during and after an earthquake. [6]

2.4 Sizing and inclusion of anti-seismic joints in architectural design

Generally, buildings that are separated by an anti-seismic joint have suffered damage in the joint area, generally due to the collision of the buildings during the seismic action. In all these cases, it is understood that their cause is the incorrect dimensioning of the joint. The case of Fig. 8, shows the breaking of the wall up to its separation (also due to the inertial forces caused by the collision of the supporting structures of the buildings). Another consequence of this cause is the damage to the neighboring buildings on the upper floors due to the collision with the greater displacement of the top floors and their uneven swaying.

Also, both documents, [3] and [4], respectively in chapters 1 and 4, recommend the use of anti-seismic joints in cases where the building and structure deviate from the regular configuration on the plan. Anti-seismic joints should turn the building into two or more dynamically independent units, although the parts may function as a single building. The size of the joint must be designed to ensure that its parts do not collide during seismic shaking. During the design process, it is the structural engineer who decides on the position and dimension of the anti-seismic joint. In cases where parts of the building serve as a single functional unit, it is important that the architect respects the position of the seismic joint and its geometry, possibly by revising the project.

Figure 8. Damage caused during the collision in the joint position

A visit to the damaged buildings was neccessary after the earthquake of November 26, 2019, in order to point out the phenomenon of organizing the same functional space of the apartment over the anti-seismic joint. The photos in Fig. 9, were made in the same apartment in a multi-storey residential building built before 2000 in the center of the Albanian capital. Proving whether this choice was design avoidance during implementation was not possible, but the fact shows that the housing unit falls on the seismic joint. This either shows unfair solutions of the architect, for the above mentioned, or shows a complete lack of cooperation and coordination of the design work between the architect and the structural engineer. This must be a widespread phenomenon because the same situation of the extension of the same residential apartment over the seismic joint of 2 neighboring buildings was also found in a building in the city of Durrës. Fig. 10.

Everyone could imagine the experience of residents in an apartment in two dynamically separated buildings during the seismic event, when the floor and the ceiling of the same space in their apartment experienced double shaking.

| a) interior of a room | b) Interior of a sanitary unit |

Figure 9. Interior view from an apartment in Tirana. Source: Marin Zaimi

| a) interior of the corridor | b) Interior of the sanitary unit |

Figure 10. Interior view from an apartment in Durrës city. Source: Entela Kapllani

2.5 Balconies and terraces parapets

During the earthquake of November 26, 2019, there were cases of terrace parapets falling for various reasons. In Fig. 11, the case of a building whose parapet collapsed due to non-implementation of the technical detail of the brick parapet reinforcement and the thickness of the terrace layers. During the seismic event, a 20 years old girl lost her life, struck in the head by a piece of parapet going out of the building, although the building itself did not sustain significant damage.

Gable walls and the parapets of balconies and terraces, which tend to overturn in an earthquake, should not be built out of masonry construction. They are to be made of reinforced concrete in order not to be separated from the structure. The damage of gable wall may be prevented by placing it between the frames. [13] A solution to the reinforcement of the brick parapet is given in Fig. 12.

Figure 11. Collapsed brick parapet. 1970s construction building
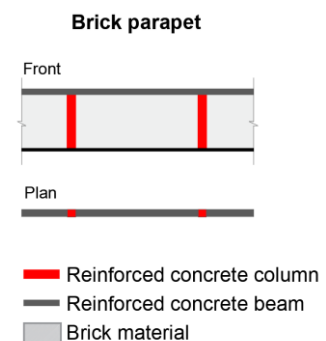
Figure 12. Brick parapet reinforcement model

862

2.6 Facade cladding

The pictures below show 2 different buildings with concrete construction to which coatings of different materials have been applied but with the same technique. In the building in Fig. 13, natural stone slabs were applied with glue adhesion on one of the facades, during the implementation and outside the forecast of the project, while in the building in Fig. 14, ceramic tiles are applied by gluing.

In the first case, not only the detachment of the stone slabs from the facade occurred, but also the structural damage of the columns in the facade covered with stones, because during the seismic event they could not withstand the increased stress as a result of the unforeseen weight of the natural stones on the facade. The destruction of the building was identified as a consequence of the deviation from the design during implementation and the loading of the structure with a weight outside of the design. In other cases of cladding facades with natural stone tiles with mortar adhesion, their detachment from the facade has also occurred.

In the second case, the ceramic tiles were detached from the facade due to their gluing assembly with mortar on the exterior facade. However, the adherence, breaking and tensile strength of the mortar are restrictive. The consecutive drift movement due to earthquake forces between stories makes the mortar exceed its strength and makes the finishes separate from the walls due to properties of mortar in between. [13]

Hence, chemical connections, such as mortar, are inconvenient, which are also prohibited in western countries prone to earthquakes. Instead of chemical connections, mechanical connections such as cramp anchorage with proper details and intervals are appropriate to be used. [9]

Figure 13. Cladding with natural stone

Figure 14. Cladding with ceramic tiles

According to KTP-N.2-1989, Chapter 3, Point 3.4.2, the plates used for covering external walls with a surface area greater than 0.1 m^2 ... are anchored to the walls with the help of metal ties.

Selection for the wall and its finishes must be realized taking into considerations whether the main structure is flexible or rigid. For rigid structures, finishes such as stone facing can be utilized, if precautions are taken in the method of attachment. In flexible structures, wall finishes, which can adapt themselves to deflections of the main structure, can be used. [11]

The types of damage so that cases of damage to non-structural elements on the facades are not repeated, the implementation project must be completed with technical details of the realization of the connections of the component elements of the facade with each other and with the supporting structure of the building at the same time to avoid the detachment of the tiles due to "fatigue of the material", from the cyclic change of air temperatures.

2.7 Common stairwell space

Stairs and corridors provide exits from the building. In many cases of high-rise buildings in the Durrës area, the damage to the stairs itself, accompanied by the fall of parts from the damaged surrounding walls of the stairwells, which have occupied the bases and landings of the stairs, making it even more

difficult to move residents during and after the seismic event. As the panic grew during the descent to quickly leave the building, many people fell and suffered physical injuries. Fig. 15, shows cases of inerts falling down stairs.

One of the solutions is to design fixed bearing from one corner of the staircase to the frame and unrestrained bearings from the other corners. Another solution is to separate the staircase as a separate building block with seismic joints. Hence, the staircases and the corridors of them should be surrounded by shear walls in order to form cores. [9]

Figure 15. Damaged stair ramps

Figure 16. Inerts fallen down stairs.

2.8 Masonry opening for exterior apartament doors

Also, due to the deformation of the walls, the door frames have suffered deformations, especially those of the outer doors of the apartments, which have blocked the opening. As a result, residents experience increased panic due to the inability to immediately leave the building during and after the seismic event and also to enter the apartment after the seismic event in the case that they went to the apartment after the earthquake. In Fig. 17, shows door with damaged lock to enable opening.

When the walls surrounding the doors and windows are subject to their deformation or blocking, then the solution is: appropriate framing of the cracks in the walls with reinforced concrete and the plastering of the walls is accompanied by galvanized steel mesh, as shown in Fig. 18, and Fig. 19.

Figure 17. Exterior door with damaged lock
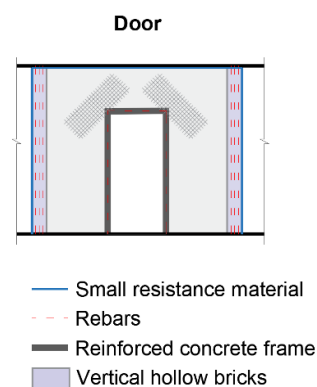
Figure 18. Exterior door reinforcement model
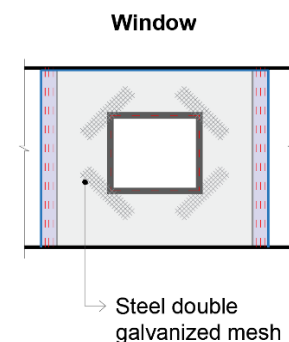
Figure 19. Exterior window reinforcement model

2.9 Partition walls, suspended ceilings.

In Albania, in most buildings, the dividing walls are made of brick masonry. In many residential buildings, complete parts of the walls were detached from their initial position, similar to the case

given in Fig. 20. Usually, rigid partitions need to be anchored top and bottom to provide lateral support or stability, against toppling. To avoid stiffening the structure, upper anchors must accommodate both in-plane and vertical movement. [16]

Light partition walls is recommended when they do not conflict with the requirements for acoustic insulation and fire resistance.

Figure 20. Collapse of the partition wall

Figure 21. Collapse of suspended ceiling and light fixtures during the earthquake of September 21th, 2019. Faculty of Geology and Mining. PUT. Tirana. Sourse: http://redaktori.net/?p=17147

Since suspended ceiling often falls during earthquake, Figure 21, connections with the suspended members must be properly designed. As the suspended ceiling is subjected to horizontal movement due to seismic forces, a gap should be made at the perimeter of it in order to prevent the ceiling pounding to the walls. The suspension system for the ceiling should also minimize vertical motion in relation to the structure. [10]

The types of damage mentioned in the last three cases so that cases of damage to internal non-structural elements are not repeated, because their fall has the potential to injure users, the implementation project must be completed with technical details of the implementation of the elements as appropriate and take into consideration the lessons learned from previous earthquakes.

3. Findings (Lessons to be learned)

The findings are based on post-earthquake damage observation and assessments performed for this purpose, both in the examples presented in this paper and in other similar examples investigated during and after the earthquake. The following findings refer to those damages that are directly or indirectly caused by the interweaving of structural and architectural choices and solutions. Summarized in groups these are:

1. The earthquake showed that the seismic action in some areas was higher than predicted by the seismic code; in these cases many non-structural elements suffered significant damage in both old and new buildings: parapets, cladding, partition walls and anti-seismic joints between buildings;

2. In earthquake-damaged areas, there are lot of cases where the functional solution and architectural design do not fully take into account the guidelines of the seismic design code. They are related to: the regularity of the building in plan and height, anti-seismic joints, flat slabs, changing the transparency of the facade in height, non-structural construction details related to the facade and the interior of the building;

3. Functional solutions for medium- and/or high-rise buildings, especially when they combine different functions of use, have helped to create the conditions for earthquakes that cause significant damage and increased panic to users: masonry built and interwoven with the

elements of others (doors, windows, etc.) inappropriately; the high number of apartments on the floor and the solution of the main staircase, also helped by the stability of the doors, has created panic and injuries when leaving the building.

4. Conclusions

Because configuration is important, and since the architect creates and controls the configuration, it follows that he is a key participant during the seismic design process. The configuration problem is a universal concern, affecting all types of buildings and constructions. To the extent that the architect is influencing seismic performance through his choice of configuration, he should be better informed about the consequences of his actions. [2]

The challenge for architects, engineers and builders is to ask why so much damage occurs and what can be done to prevent the problem. [5]

Architects and engineers learn from detailed investigations of damage from past earthquakes and can document important issues and lessons about particular problems. Some problems occur due to improper design or construction or irregular volume configuration. Some because the building or structure cannot uniformly distribute the seismic energy, and some because of excessive loads caused by dynamic resonance between the ground shaking and the building.

Geometrical concepts of the correct volumetric and structural configuration of buildings should be given to architects from school grades. The architect at any time of his professional development can be familiar with the irregular volumetric models or the irregularity of the configurations of structural systems, etc., given schematically according to (SEAOC) and Arnold. [1]

At the same time, the architect can become familiar with the seismic behavior of irregularly shaped buildings, understand where their weakest point is and the danger they may present during an earthquake. Even engineers may seek to convince architects to use conventional, regular and preferably symmetrical forms in seismic locations. If reference is made to history, there is evidence of buildings of antiquity and those of several hundred years which have resisted many earthquakes and this is thanks to their shape.

Seismic design is utilitarian and should be considered more important than aesthetic design. To resolve the conflict, it is required to increase the level of collaboration between the architect and the engineer in the building's conception stages. For this process to be successful, the architect and the engineer must have mutual knowledge of the fundamental principles of their disciplines. Therefore, it is always necessary for the architect to familiarize himself with the newest codes of seismic design, to which he can look for recommendations and principles of design of volumetric forms, configuration and constructive systems of buildings. On the other hand, the engineer must understand and respect the functional and aesthetic context within which the architect works.

It is necessary that the legislation and technical construction regulations, especially those of urban and architectural design, include as best as possible the general principles and criteria of seismic design and be in line with the seismic design code;

The damage in the areas affected by the earthquake highlighted a series of weaknesses of the buildings that are also related to the architecture, both in conception and construction details, such as regularity, seismic joints, facades, stairs, interior, etc. These damages and the technical solutions for them should serve both for the repair and reinforcement of damaged buildings as well as for the design of new buildings, in areas affected by the earthquake and in areas with high seismicity;

Special recommendations:

1. The rregularity of the building should be part of an exhaustive discussion from the conception of the design. In cases where this rregularity can be avoided, should be taken all the necessary measures;

2. It is advised to avoid cantilever volumes in regions with high seismicity. If unavoidable, their impact on the overall seismic behavior of the building, as well as design construction details with a focus on the stability of the cantilever elements themselves must be taken into account;

3. During the design and implementation, it is recommended that for elements inside the building, such as partition walls, windows, doors, stairs and their vertical outline, etc., should take into account the rules of seismic design that limit damage to non-structural elements of the building;

4. Seismic joints need to have adequate dimensions; to be provided in well thought out areas (not inside the dwellings) in advance; to be disguised, "furnished" in a distinctive way so that during future seismic events the dividing line appearing should not misinterpreted as serious damage;

5. Parapets, especially in existing buildings, should be checked and where they result with insufficient ability to withstand seismic action or where they are damaged, they should be reinforced.

References

[1] ARNOLD, C. (2006): *Seismic issues in architectural design in designing for earthquakes. A manual for architect*s, FEMA, Oakland, California, USA.

[2] ARNOLD, C. (1984): *Building configuration: The architecture of seismic design*, Vol. 17, No. 2. New Zealand.

[3] Akademia e Shkencave, Ministria e Ndërtimit (1989): *Kusht teknik projektimi për ndërtimet antisizmike. KTP-N.2-89,* Instituti Hidrometeorologjik, Tiranë, Albania.

[4] EN 1998-1 (2004): Eurocode 8: Design of structures for earthquake resistance – Part 1: General rules, seismic actions and rules for buildings*, The European Union Per Regulation 305/2011, Directive 98/34/EC, Directive 2004/18/EC*, CEN.

[5] ELSESSER, E. (2006): *Seismic design-past, present and future in Designing for Earthquakes-A manual for Architects*, FEMA, Oakland, California, USA.

[6] McGAVIN, G. (2006): *Nonstructural design philosophy in designing for earthquakes. A manual for Architects*, FEMA, Oakland, California, USA.

[7] Real time information and earthquakenotification services: https://www.emsc-csem.org/Earthquake

[8] The USGS and its partners monitor and report earthquakes, assess earthquake impacts and hazards, and perform research into the causes and effects of earthquakes: https://earthquake.usgs.gov/earthquakes

[9] Erman, E. (2002): *Earthquake Knowledge and Earthquake Safe Architectural Design*, Middle East Technical University Faculty of Architecture Printing Office, Ankara, Turkey.

[10] Noorifard A. PhD, Mehdizadeh Saraj F. PhD (Spring 2018) : Role of Architects in the Seismic Performance of conventional medium-rise buildings by using the experiences of past earthquakes, Naqshejahan, University of Tehran, Tehran, Iran, 17 pages.

[11] Dowrick, D. J. (1987): *Earthquake resistant design*, Second Edition, Wiley, Chichester, UK.

[12] Architectural Institute of Japan (1970): *Design Essentials in Earthquake Resistant Buildings*, Tokyo, Japan.

[13] Bayülke, N. (2001): *Earthquake Resistant Reinforced Concrete and Masonry Structure Desig*n, Extended 3rd Edition, Chamber of Civil Engineers İzmir Branch Publication No: 39, İzmir, Turkey.

[14] Zacek, M., (Translation: Akbulut, M. T.)(2002): *Earthquake Resistant Structure Design Preliminary Project Phase*, Yıldız Technical University Press and Publication Center, Istanbul, Turkey.

[15] Ambrose, J., Vergun, D. (1985): *Seismic Design of Buildings*, John Wiley & Sons. Inc., New York, USA.

[16] Charleson, A., (2007): *Architectural Design for Earthquake,* 2nd edition, School of Architecture, Victoria University of Wellington, New Zealand.

MOST AFFECTED TYPOLOGIES FROM THE 26 NOVEMBER 2019 EARTHQUAKE

Markel Baballëku [(1)], Rikard Luka [(2)], Klajdi Shaholli [(3)]

[(1)]*Civil Engineering Faculty, Polytechnic University of Tirana, Albania; e-mail: markel.baballeku@fin.edu.al*
[(2)]*Civil Engineering Faculty, Polytechnic University of Tirana, Albania; e-mail: rikard.luka@fin.edu.al*
[(3)]*Civil Engineering Faculty, Polytechnic University of Tirana, Albania; E-mail: klajdi.shaholli@fin.edu.al*

Abstract

Assessing and finding the causes of damages in buildings belonging to construction typologies severely damaged as a result of the 26 November 2019 earthquake is of significant importance. Not only to better understand the causes of severe damage and the measures that should be taken specifically for these buildings, but also for planning the necessary interventions in these typified buildings typologies not only in the damaged areas but also in non-affected areas. This paper aims to carefully analyse some of the most severely damaged buildings by the earthquake, which have been associated with human casualties. Three construction typologies are considered in this paper, where two of them are design and build before the '90s as a typified buildings implemented in different cities, and the third one is a modification of typified RC building, constructed mainly after the '90s. One of the buildings build before the 90s is a masonry structure, while the others are reinforced concrete structure. Through damage and collapse mechanism assessment as well as using results of non-linear analysis, the paper attempts to highlight the primary causes of severe damage, compliance with building codes and the necessary measures that are recommended to reduce the vulnerability of these buildings

Keywords: construction typology, brittle failure, soft story, shear resistance, nonlinear analysis, vulnerability

1 Introduction

According to IGJEO on November 26, 2019, 03:54 local time, a Mw 6.4 earthquake occurred 16 km north of Durrës and about 35km from Tirana, in the western region of Albania, at a depth of 38 km. The event was preceded by an Mw 5.6 earthquake with approximately same epicentre which occurred on September 21, 2019, causing considerable damage, mainly non-structural, and affected roughly the same area as the November 2019 earthquake (26Nov ADE); (RPI-Nov.26, 2020).

The 2019 earthquakes were recorded by several IGJEO stations and the data are provided online (IGEO, 2019). Unfortunately, the Durrës station (most important one close to the epicentre), recorded only the first 15 seconds of the main shock due to a technical issue (Duni L, Theodoulidis N, 2019). Some of the elastic response spectra, from Sept. 21 and Nov. 26, 2019 earthquakes records are presented in Fig. 1. The recorded PGA values were 0.114g and 0.194g in the Durrës station for the Sep.21 and Nov.26, 2019 earthquakes, respectively. In contrary, Sep.21, 2019 Earthquake produced higher PGA value in Tirana (0.183g) than Durrës (0.116g). The Nov.26, 2019 earthquake induced high seismic demands in flexible buildings in Durrës and Sep.21, 2019 earthquake induced high seismic demands in stiff buildings in Tirana. It should be noted that the Durrës station is located in very weak soil conditions (IGEO reported $v_{s,30}$ = 202 m/s). Very close to that station (50m away), the measurements shows $v_{s,30}$ less than 170 m/s and shear wave velocity decrease with depth Fig. 2, so, soil category can be classified as S1 according to the EN 1998-1:2004.

The seismic event caused 51 fatalities, more than 913 injuries and up to 17,000 people were displaced. The total effect of the disaster in the three regions Durrës, Tirana and Lezha amounts to 985.1 million EUR, of which 70% belongs to housing sector. It was estimated that 18% of all housing units in the affected area required either reconstruction or rehabilitation (PDNA-A, 2020).

Fatalities have been concentrated in two municipalities, Durrës and Thumana (an administrative unit of Kruja). In addition to the earthquake magnitude, the vicinity to the epicentre and the soil conditions, the fatalities happened in these areas are also closely related to the typified buildings that have suffered heavy damages and collapse from the seismic event.
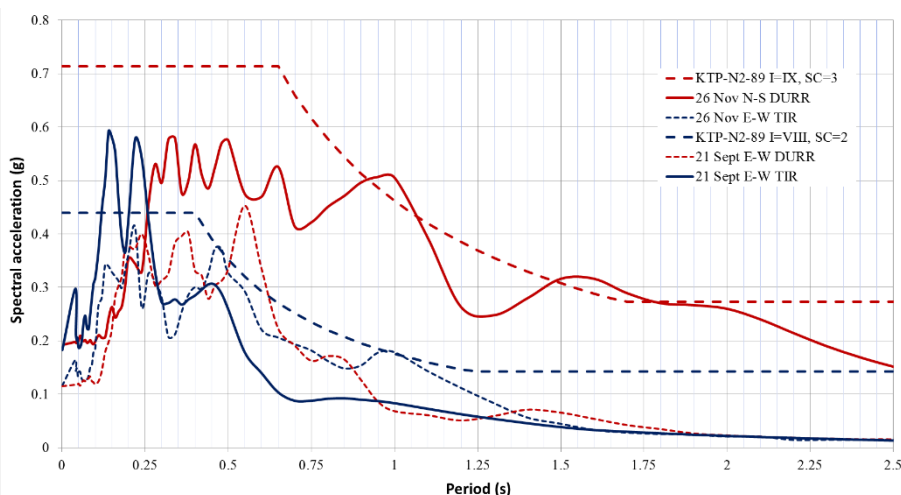
Fig. 1. Elastic response spectra of the ground motion records for Sep. and Nov. 2019 earthquakes at Tirana and Durrës (5% damping ratio) and national seismic design code (KTP-N2-89) elastic response spectra.
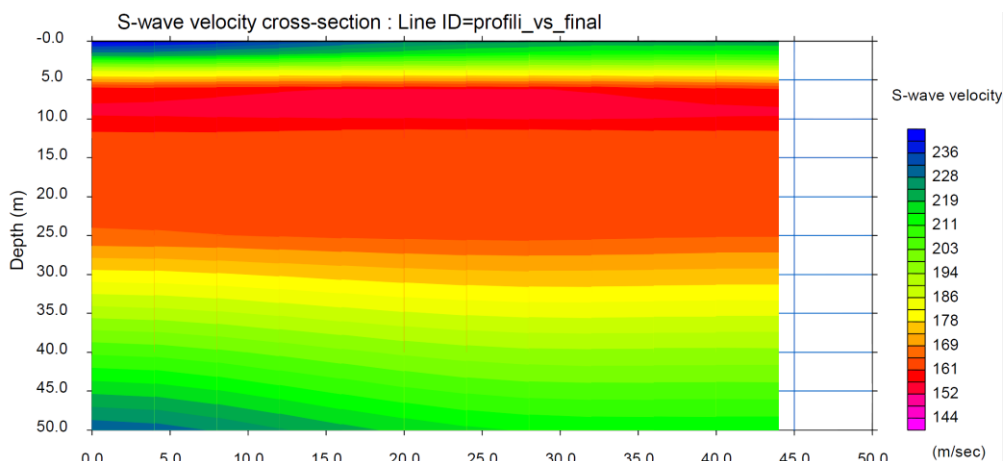
Fig. 2.Shear wave velocity, very near to the Durrës station (A. G. Consulting, UTS-01, 2022)

In Table 1 are presented the building places, their typology and collapse mechanism as well as number of fatalities for each of them [see also (EEFIT Report, 2020)]. From the 51 fatalities, 3 persons that lose their life in other circumstances, rather than related to the building collapse are not presented in this table. If some associations to the total number of fatalities presented in Table 1 can be done, 33 fatalities occurred in typified buildings having a construction permit and build previous or around '90 and 13 fatalities in buildings without construction permit of with a violated permit in the period 1990-2005.

Table 1 – Fatalities and their connection with location and building model and typology

No.	Municipality	Admin Unit	Coordinate	Typology	Model	Floors	Fatalities	Comments
1	Kruja	Thumana	41.5499; 19.6791	URM	Model 77/5	5	**17**	Partially collapsed
2	Kruja	Thumana	41.5495; 19.6797	URM	Model 77/5	5	**7**	Partially collapsed
3	Durrës	Lagje 18, Durrës	41.3275; 19.4529	RC	Model 82/2	6	**7**	Total collapse
4	Durrës	Këneta, Durrës	41.3281; 19.4591	RC	Informal	4	**8**	Total collapse
5	Durrës	Lagje 6, Durrës	41.3214; 19.4468	RC	Model 82/2	6	**2**	Soft story
6	Durrës	Plazh, Durrës	41.3092; 19.4871	RC	Informal	6	**2**	Total collapse
7	Durrës	Plazh, Durrës	41.3131; 19.4777	RC	Informal	5	**2**	Total collapse
8	Durrës	Plazh, Durrës	41.2728; 19.5169	RC	Informal	8	**1**	Total collapse
8	Durrës	Plazh, Durrës	41.2728; 19.5169	RC	Not typified	5	**1**	Soft story
9	Tirana	Kombinat, NJA 6	41.3129; 19.7701	URM	Not typified	5	**1**	Parapet felt down
		Total fatalities due to building collapse =					**48**	

This paper will be focused analysing the performance of the typified buildings with fatalities, highlighting the primary cause for their heavy damages/collapse and giving recommendations to reduce the vulnerability of these typified buildings.

2   Description of the typologies considered

In the following chapters three main typified buildings, causing most of fatalities during November 26, 2019 earthquake will be analysed in more details. The analysis will be focused on:

1. Typified URM building, Model 77/5 – Two buildings caused 24 fatalities;
2. Typified RC building, Model 82/2, original and modified – Two buildings caused 9 fatalities;

Table 2 summarizes important structural characteristics of selected buildings, related to general geometry and dimensions as well as material properties and structural details. Structural analysis and respective results are based on these data.

2.1   Typified URM building - Model 77/5

The Typified URM 77/5 Model was designed and started to construct in 1972 (the 72/5 Model). Later, in 1977 it was introduced with some architectural and functional improvements and was presented as Model 77/5. Only few changes can be found between these models, and the most important, its structural regularity – it is increased. Although the Seismic Code KT-63 (Goverment of Albania, 1963), Point 25, doesn't allow such layouts without dividing them into simple shapes by seismic joints for areas with seismic intensity 7 or higher, this model is found in many areas which suffer higher intensity due to September 21, and November 26, 2019 Earthquakes.

The general data of the URM model 77/5 are given in Table 2. The masonry wall are constructed with thickness 38cm in the first three floors and 25cm in remaining two. Masonry wall are composed with brick strength 7.5 Mpa (clay or silicate bricks) and mortar strength 1.5Mpa. Foundation are stone masonry embedded not less than 1.3m. Slabs are composed with prefabricated panels, placed in one direction, supported directly to masonry walls and without any additional concrete layer on top.

Table 2 – Main characteristics of the case study buildings

No	Item	5-Story building, 77/5 URM Model	RC and M-RC 82/2 Model, Durrës
1	Seismic design code	KT-1963	Improved KTP-N.2-78
2	Year of construction	1977-1982	1982-1996
3	Interventions	Openings in ground floor walls (not confirmed)	Added one floor
4	Soil category	III (KTP-N.2-89), D (Eurocode 8)	III (Improved KTP-N.2-78 and KTP-N.2-89), D (Eurocode 8)
5	Structural system	Unreiforced Masonry	RC moment frame
6	Structural regularity	Irregular in plan and regular in elevation	Regular in plan and irregular in elevation
7	Building height	5x2.8=14.0m	RC 4.06+4x3.06=15.3m or M-RC (3.8+5x2.8=17.8m)
8	Storey height	All floors 2.8m	Ground floor 4.06/3.8m, others 3.06/2.8m
9	Plan dimensions and area	18.8x14.21m (same layout); Area=225m2	RC = 10.0x20.7m, Area=220m2; M-RC = 13.7x20.7m, Area=279m2
10	Building mass (ton)	URM = 2000 ton	RC = 1100 ton; M-RC = 1600 ton
11	Foundations	Continues T shape stone masonry foundations, 0.7x1.5m+1.0x0.5m thick, depth at least 1.5m	Footings 2.5(2.8)x2.5(2.8)x1.0m connected with tie beam bxh=0.3x0.4m only outside (inner foots dim, PL2); depth at least 1.5m
12	Basement available	No (exists only in some specific cases)	No (exists only in some specific cases)
13	Slabs and Beams	One-way prefabricated ribbed slabs with brick infill 15cm or RC hollow pannels, 11cm thick. No tie beams on top of the wall	One-way prefabricated RC hollow pannels, 11cm thick. Beams bxh: transversal 30x40cm, longitudinal 40x30cm* (* differ in some M-RC buildings)
14	Materials (based on design and tests)	Design: Mortar 1.5Mpa, Bricks 7.5Mpa, Tests: Mortar 1.6Mpa, Bricks 8.6Mpa	Design: Concrete C16/20, Steel yield strength 210 MPa; Tests: Concrete cubic strength 20-23Mpa; Steel yield strength 320 MPa (plain rebar)
15	Column/Wall spacing	Max walls spacing: Transversal direction 10.7m*, Longitudinal direction 4.35m	Transversal direction 3.6m, Longitudinal direction 4.2-5.4m
16	Column/Wall cross-sectional dimensions	Walls: Three floors - 38cm thick and two other floors 25cm thick.	bxh = 30x40cm
17	Column reinforcement	NA	K1 GF: 2.4%; Other floors: 1.4%; K2 GF: 2.9%; Other floors: 1.9%; Single hoops: Ø8 at 10/20/10cm spacing
18	Beam reinforcement	NA	Long. rebar ratio approx. 1.8%, with 80cm critical regions and stirrups Ø8 at 10/20/10cm spacing (spacing differ in some M-RC buildings)

The April 15, 1979 earthquake provided valuable information on: used materials (mortar and weak bound between silicate bricks and mortar) and the building layout (Stermasi F, Premti K, Meka K, 1980) (Pistoli, 1980). In year 1982, in accordance the 77/5 model was reviewed and improved Fig. 3 for use

in seismic areas with intensity VII and VIII by adding columns (K1) to the corners of the building; by increasing the mortar strength from 1.5Mpa to 2.5Mpa for walls with clay bricks and 5.0Mpa for walls with silicate bricks; by adding RC horizontal tie beam 15x38(25)cm on the top of the masonry wall at each floor. Slight improvements are done also for out-of-plane behaviour (AQTN).
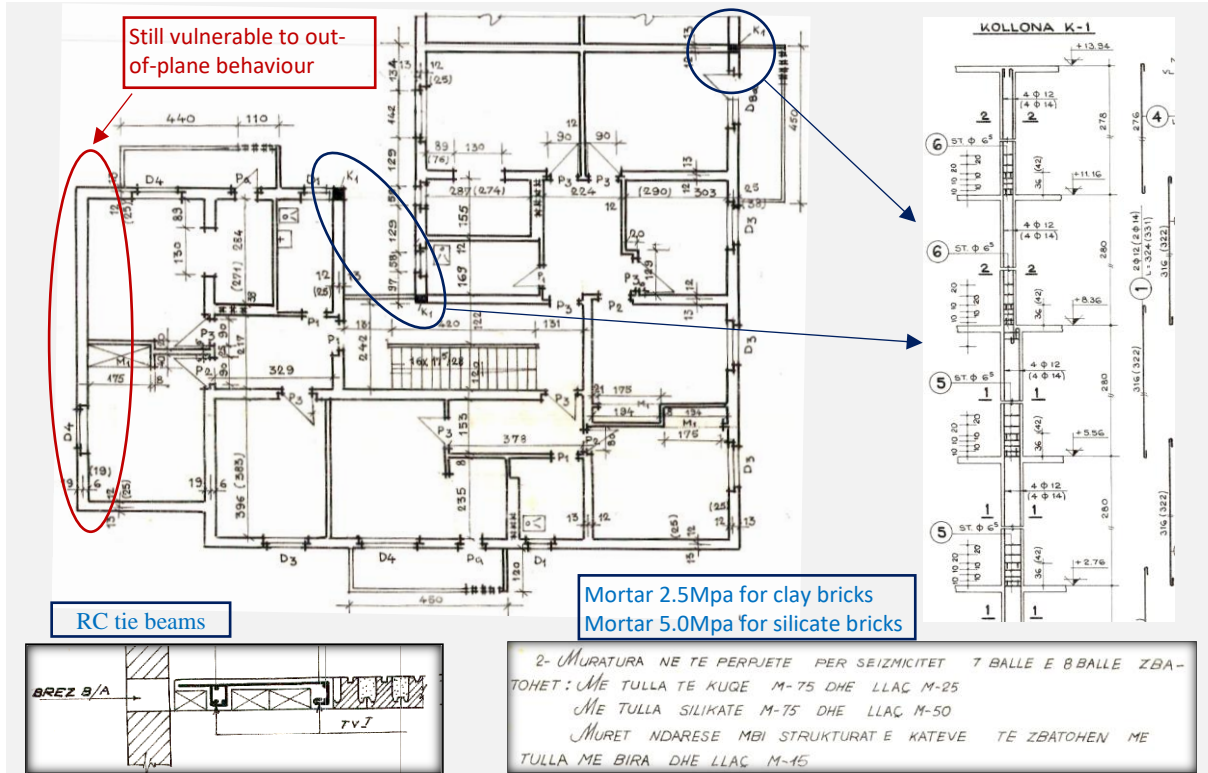
Fig. 3. Improved 77/5 Model, by adding at least 3 RC columns at the corners; improving the mortar strength; reinforced concrete tie beams were also added at the floor levels

Fig. 4. Location of URM Model 77/5 in Thumana and their damage degree

Unfortunately, many buildings with URM 77/5 models has been constructed since its release and the improved 77/5 model in 1982 wasn't use to retrofit the existing building stock. During the 2019 Earthquakes many buildings belonging to this model suffer moderate-heavy damages. Four partially

collapsed buildings in Thumana belonged to this model as well and 24 people lost their lives in two of them Fig. 4.

From the structural point of view, URM 77/5 Model can be considered composed of two "separate" structural units having a weak "connection unit" Fig. 5, comprising: low percentage of transversal walls and high potential of out-of-plane failure of longitudinal walls; stairs; longitudinal walls weakened by the presence of doors and windows. The prefabricated slab panels, placed in one direction and without tie beam connecting to the wall also affect the joint work of the units A and B.
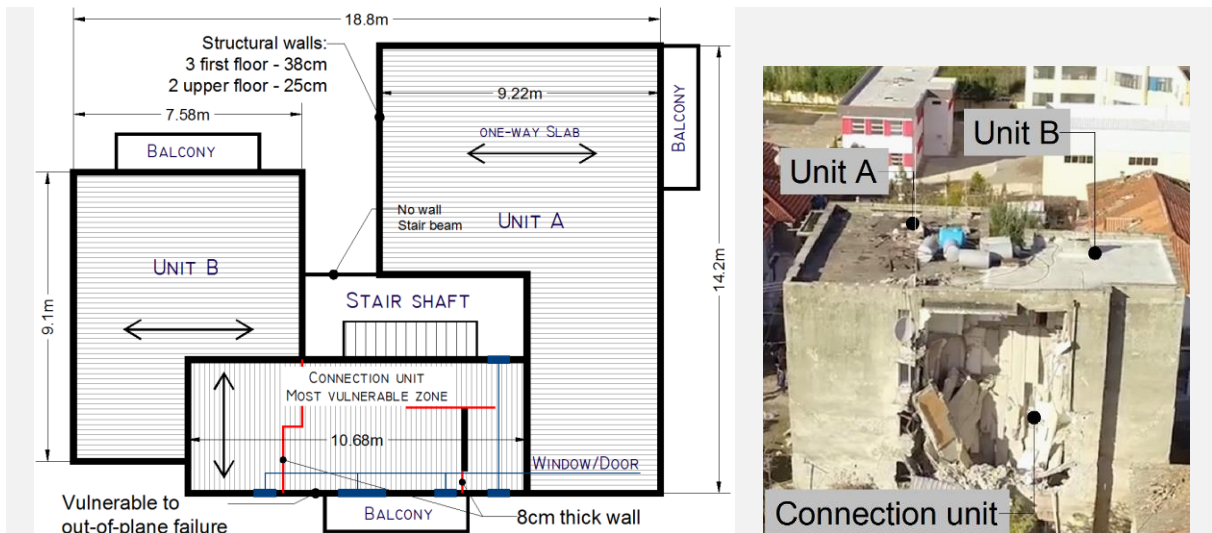
Fig. 5. Structural unit composition of 77/5 URM Model

Due to the layout geometry, the weak "connection unit" and the distribution of the masonry walls and their openings, the torsion and the interaction of the structural units A and B increase the seismic effect to each other. The interaction may have contributed to the heavy damages and falling parts of the "connection unit" as well as to the collapse of the small unit B in two cases, during 26 November earthquake. The photos of the heavily damaged buildings clearly show the collapse of small units in two buildings and damage to the connecting area in the two others.

The damage pattern appear in this building typology are: 1-) diagonal cracks in masonry walls, especially in the weak pears and spandrels; 2-) disconnection of the slab panels from the masonry walls due to lacking of the tie beams and inadequate or missing connection between slab panels; 3-) moderate to heavy damages at the masonry walls in the upper floors due to low normal stresses; 4-) Out-of-plane failure; 5-) parapet failure in many cases, especially when masonry buildings are situated in areas without or with low seismicity and the parapets are not strengthened. In the "Kombinat" area near Tirana, as a result of their vulnerability, a lot of parapets felt down and one of them caused a fatality, a girl loss her life. Summarising, the factors increasing the damageability of the 77/5 URM model are:

- The mortar quality and the bound connection between silicate bricks and the mortar;
- In-plane irregularities with an added vulnerable member "connection unit" between two main structural units;
- Some masonry wall are vulnerable to out-of-plane failure – max wall length 10.68m;
- The absence of tie beams on the top of the masonry wall at each floor as well as one direction prefabricated slabs without any additional RC top layer;
- Workmanship quality and competence – many buildings previous to '90 have been constructed by voluntary workers;
- Environmental factors, especially humidity, which has deteriorated the quality of mortar as well as the lack of building maintenance;
- Possible interventions to these buildings, without verifying the existing capacity. The intervention can be both in openings in the ground floor and adding floor or lateral areas.

Based on the structural assessment carried out through pushover analysis, using two-dimensional masonry elements (Baballëku, 2014), obtaining mortar properties directly from laboratory tests (Mortar strength = 1.6 Mpa and Bricks strength = 8.6 Mpa) and comparing the structural capacity of the building with the seismic demand, the following main conclusions are drown and highlighted:

1-) Using as demand, the fitting response spectrum of all 2019 earthquakes recorded at Tirana station (Fig. 6-a), the URM 77/5 model suffer significant damages, but no collapse (Fig. 6-b). The buildings with URM 77/5 model situated in "Kombinat" area, periphery of Tirana have suffer moderate-heavy damages and fit quite well with analysis results;

2-) Other factors i.e.: damages from previous earthquakes (July 2018 Mw=5.2 and 21 September 2019 Mw=5.6), lower mortar quality, out-of-plane failure or unknown interventions, may have increase the damages, leading to the building collapse in Thumana.

Fig. 6. Target displacement in ADRS format: a-) demand spectra fitting all 2019 earthquakes records in Tirana station (Type2, SC B and ag=0.15g); b-) target displacement (performance point) of the URM model 77/5

Another analysis - using as demand the Eurocode design response spectrum with seismic characteristics: Type1 Spectra, Soil Category C and ag = 0.248g (SZMA-ASH, 2010) – shows that the URM 77/5 model collapse. The fitting demand spectrum (Fig. 6-a) gives another important hint: Stiff structures (including URM 77/5 and other similar models) may have suffer more during Sep.21 than Nov.26, 2019 Earthquake.

2.2 Model 82/2 – Cast in place RC Model

From an architectural perspective, the RC 82/2 model was used even before 1982, but in most of cases with masonry structure. In 1982, this model was introduced initially as prefabricated RC moment frame, to be used for areas with seismic intensity 9 and in accordance with improved KTP-N2-78 code (ktp-n2-78-r, Janar 1982). The main building properties can be found in Table 2 and in the Fig. 7 is given the structural layout of original RC 82/2 Model (prefabricated or cast-in-place).
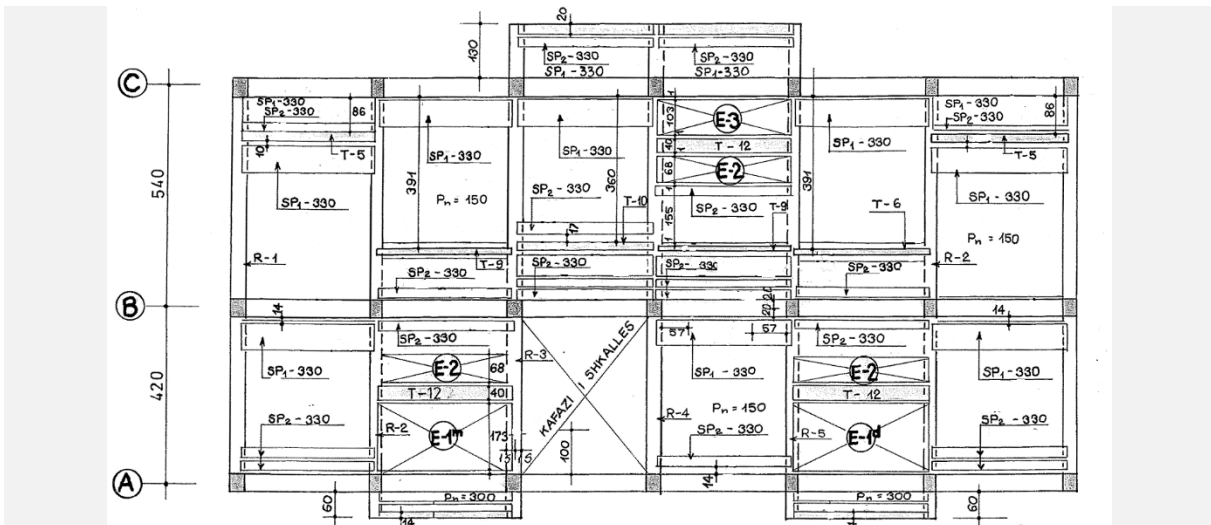
Fig. 7. Structural layout of original RC 82/2 Model (AQTN)

From local technical office this model was proposed to be constructed as cast-in-place RC 82/2 Model in Durrës area, initially without any change in layout, number of storeys and element dimensions. The main change was related to concrete strength and the reinforcement percentage, Fig. 8. This model is regular in plan but with irregularities in elevation due to: a-) ground floor at least 1m higher than the other floors (masonry wall under +0.00 and tie beam at top of it is not uniform and doesn't have adequate stiffness); b-) immediately reduction of columns rebar percentage (Fig. 8-b.), and, c-) often infill walls exists only partially in the ground floor – often this floor is used for services. Moreover, in some cases infill walls distributed asymmetrically in ground floor affect also the plan regularity.
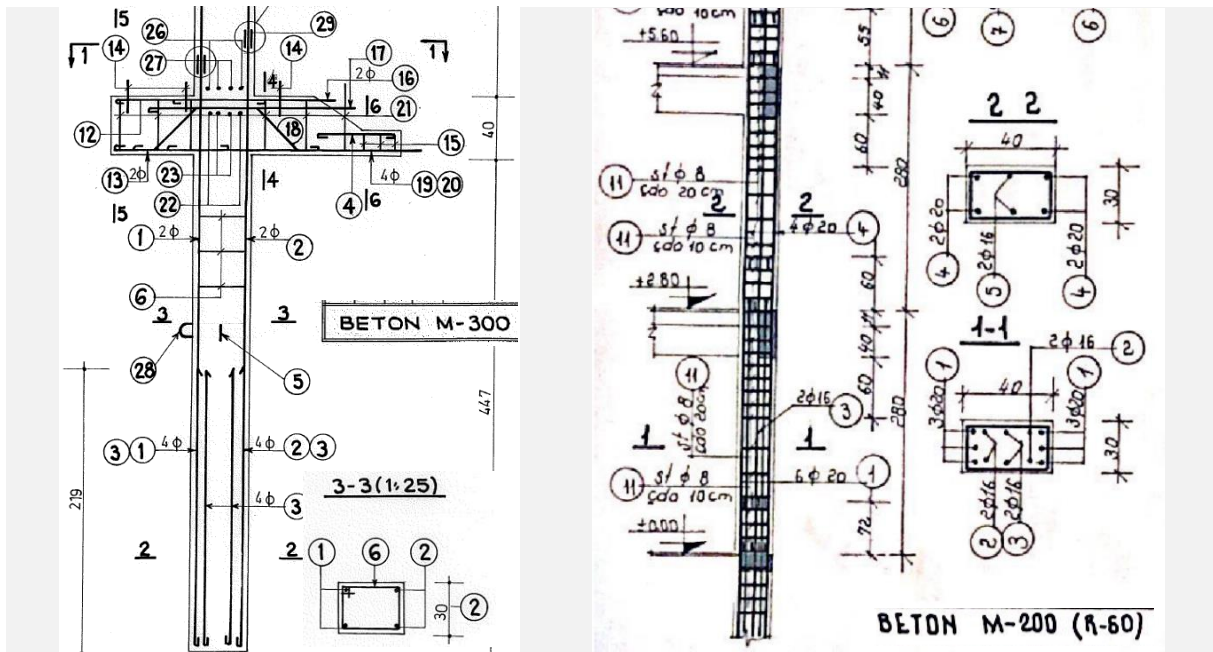
Fig. 8. Column material and details: a-) Prefabricated RC Model 82/2: Concrete C25/30; Rebar 4Ø18 (less than 1%); Single hoop Ø6.5/20cm; b-) Cast-in-place RC Model 82/2: Concrete C16/20; Rebar 6Ø20+4 Ø16 (2.2%); Single hoop Ø8/10/20cm

In different periods, previous and after '90, designs with several changes (in layout and/or number of stories) of cast-in-place RC Model 82/2 are proposed and constructed until year 2000. Hereunder, these modified cast-in-place models will be named M-RC 82/2 Model.
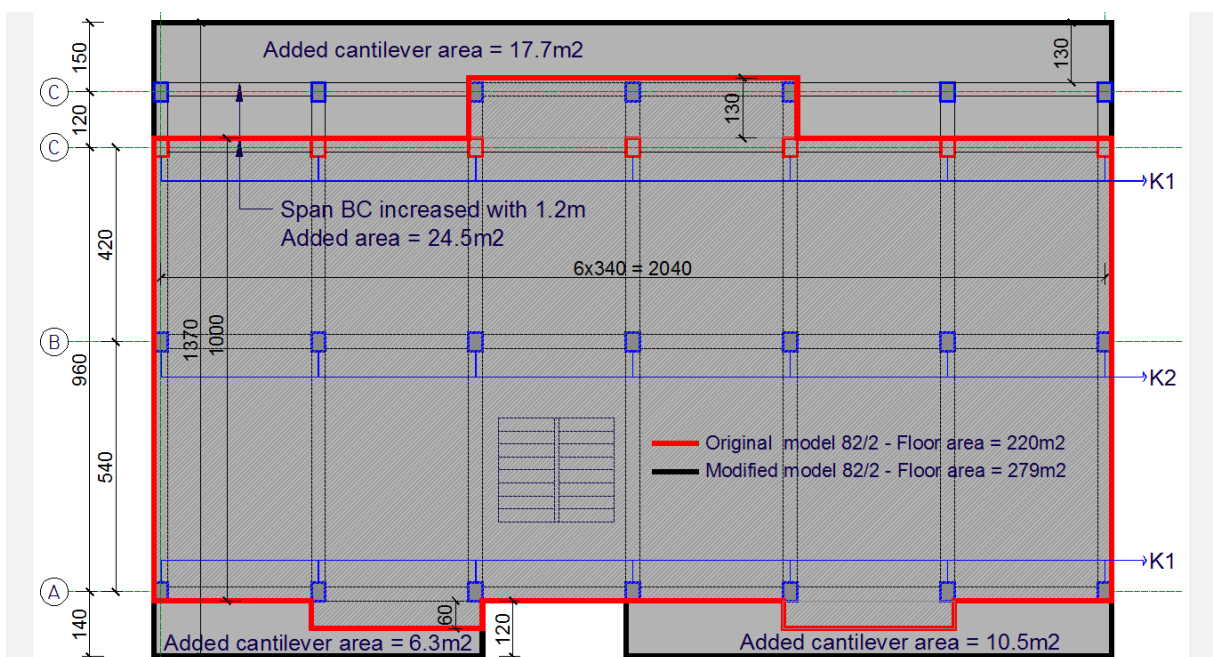
Fig. 9. Structural layout of RC Model 82/2: a-) Original model; b-) Modified model

874

In Fig. 9 are given layouts of two cast-in place models: Original RC 82/2 and M-RC 82/2 with the extensive changes in layout, by increasing plan area with 26.8% and in elevation by adding generally one floor. In some cases these adding volumes are followed by increasing rebar percentage (generally in beams), but in most of them the columns reinforcement remain unchanged towards original cast-in-place RC Model 82/2.

In Durrës, two buildings with the M-RC 82/2 Model collapsed, both with "soft story" mechanism. One of them subsequently develop also pancake collapse. Heavy damages suffer most of cast-in-place RC Models 82/2, original and modified ones in Durrës area.

Fig. 10. Two cast-in-place M-RC 82/2 Model collapsed buildings: a-) pancake mechanism; b-) "soft story" mechanism

The damage patterns appears in cast-in-place 82/2 model are mainly concentrated on the ground floor: 1-) joint crush at the top of the ground floor; 2-) shear crack in columns and beams; 3-) columns buckling; 4-) failure due to high normal forces; 5-) diagonal cracks in the filling walls.

Damages and collapses on RC and M-RC 82/2 Model are connected with different issues:

1-) Cast-in-place RC Buildings for residential purposes just started massively in the beginning of '80 and the experience regarding their seismic behaviour have not been comprehensive. Most of damaged buildings during the earthquake of April 15, 1979 have been with masonry structure;

2-) KTP-N2-78 (1978) gives only few criteria for seismic details. Moreover, the cast-in-place concrete quality and the RC elements detail accuracy didn't results as required in design. Even in those cases when the design has foreseen seismic details beyond the KTP-N2-78 (or in accordance with KTP-N2-89) requirements, they have not been implemented;

3-) Both stiffness and resistance in longitudinal direction results smaller than in the transverse direction and "soft story" mechanisms are dominant in the longitudinal direction. This is also confirmed by calculations.

Summarising, the factors that have caused or increased the damages in the cast-in-place RC and M-RC 88/2 Model are:

- Poor concrete quality and inappropriate detailing's: a-) low concrete strength; insufficient dimensions for primary structural element; b-) low percentage of the longitudinal reinforcement

and low volume ratio of the transversal reinforcement; c-) inappropriate reinforcement details: absence/deficiency of hoops in critical regions, deficiency in bar anchorage and lap-splicing, hoops bent not more than 90° and insufficient anchorage length into the concrete core; d-) inadequate stirrup/hoops amount and detailing in beam-column joints; e-) plain rebars;

- The severe reduction of the columns resistance above the ground floor – abrupt change in rebar percentage above ground floor;
- Insufficient stiffness and resistance in the longitudinal direction of the building;
- Prefabricated slab panels placed in one direction and without cast-in-place any top RC layer – no rigid diaphragm behaviour;
- Added floors and/or increased floor area without making appropriate structural verifications and design adaptions;
- Environmental factors deteriorating the qualities of the materials - is evident in the columns base. Lack of maintenance and possible interventions during the design working life.
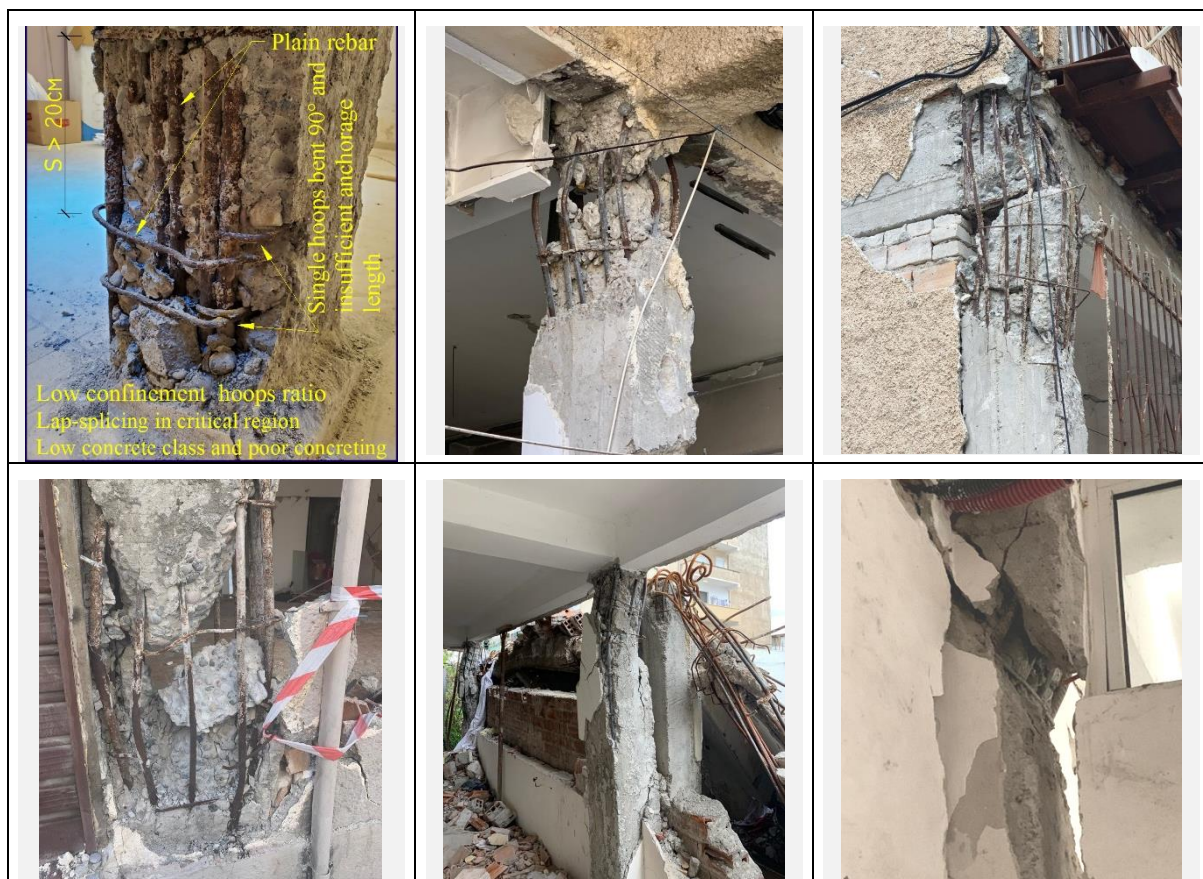
Fig. 11. Columns damaged in six different cast in place RC and M-RC 82/2 Model

Based on the structural assessment carried out through pushover analysis, using material properties based on tests (checking also with those given in design) and comparing the structural capacity of the building with the seismic demand, the following main conclusions are noted and highlighted:

1-) Using as demand, the fitting demand spectrum comprising the 2019 earthquakes recorded at the Durrës station (Fig. 12-a), the RC 82/2 model suffer near-collapse (Fig. 12-b). The failure mechanism result soft story.

2-) The same demand is used also for the M-RC 82/2 model and the structure collapsed (Fig. 12-c). The failure mechanism is still soft story.

In both analysis the soft story mechanism is developed in longitudinal direction. Exist high possibility that the "soft story" mechanism to be developed in the first floor rather than ground floor, in those cases

were columns rebar amount is immediately reduced above ground floor. In fact, one of the two collapsed RC Model 82/2 has developed soft story in first floor.
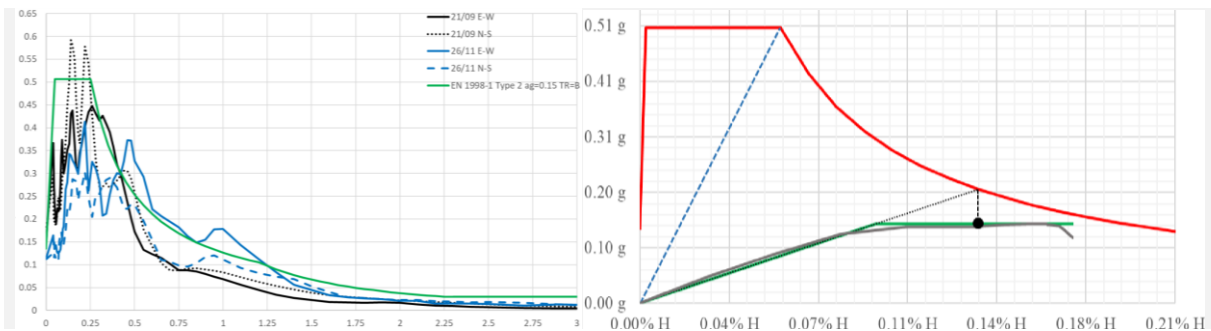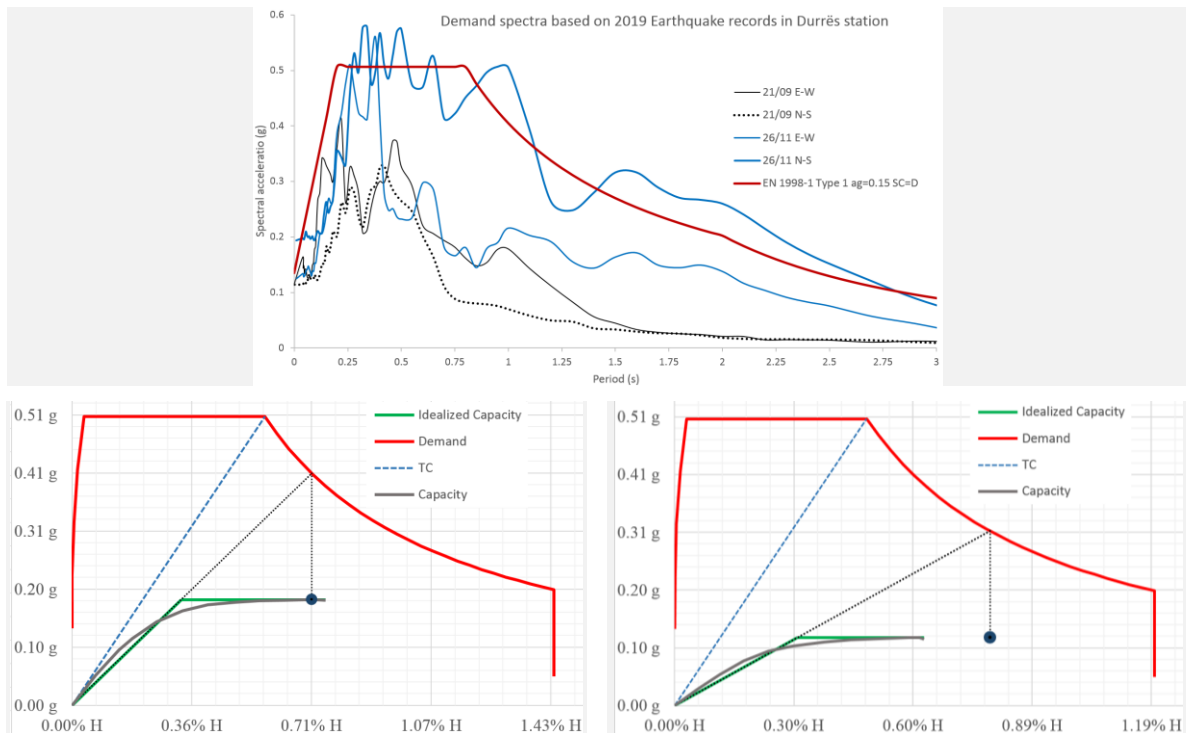

Fig. 12. Target displacement in ADRS format: a-) demand spectra fitting all 2019 earthquakes records in Durrës station (Type1, SC D and ag=0.15g); b-) target displacement RC 82/2 Model; c-) target displacement M-RC 82/2 Model

3 Findings and recommendations

The following findings and recommendations are based on the observation of damages after the 2019 earthquakes and on the assessment carried out, analysing each building as well as other similars.

3.1 Findings

Buildings heavily damaged and/or near-collapsed by November 26, 2019 Earthquake are the result of one or more of the following factors:

1-) Are located in areas where the seismic action has been higher than that foreseen in the seismic code. There are buildings in Tirana, Thumana and other areas which have been designed and constructed with low seismic action or without (areas with seismic intensity VII or lower previous to 1979) than what results from the 2019 earthquakes;

2-) Although significant previous earthquakes (especially those of April 15, 1979 and January 8, 1988) have taught valuable lessons, producing instantly recommendations for new design and construction processes, there are no clear evidences demonstrating that these findings have been used for retrofitting of the existing building stock;

3-) Due to their fundamental vibration period, URMs were moderately damaged during the September 21, 2019 Earthquake. Further, during the 26 November 2019 earthquake, their damages increased and in some cases these buildings collapsed;

4-) Different typologies of the building stock, URM or RC, show limited seismic capacity as a result of the combination of the following factors:

- Structural irregularity in plan and/or height;
- Low materials quality (concrete for RC and mortar for URM);

- Unsuitable construction details for buildings situated in areas resulting with moderate to high seismicity: for URM – weak pears and spandrels, one direction slabs panels and lack of connecting ties beams; for RC - inadequate element dimensions and critical regions confinement and inadequate shear resistance for columns, beams and beam-column joints;

5-) Building interventions performed without taking the necessary structural verifications (and eventual retrofitting). The most common interventions: a-) adding floors; b-) lateral extensions and opening in structural masonry walls, especially in the ground floor in case of URM buildings;

6-) An essential factor have been also the workmanship and their competence during the execution process, since many buildings are constructed based on voluntary work. Adequate execution of details affect directly the seismic building capacity.

3.2 Recommendations

Based on three building typologies analysed above and findings, some recommendations are summarized and listed following:

1-) Typified building (models URM 77/5 and RC 82/2 or M-RC 82/2) – located in the earthquake-affected areas and in other areas with high seismic risk – need to be fully assessed and after a unified retrofitting strategy is necessary to prepare for each model. The retrofitting interventions should be comprehensive: unified solution for typified buildings and special instructions for those cases where buildings are constructed with some differences from "prototype" and where quality of materials, maintenance, environmental or soil conditions, etc. induced extra effects;

2-) An improved typified design has been drafted for the model 77/5 after the April 15, 1979 Earthquake. The performance of buildings with improved model 77/5 during the 2019 Earthquakes should be assessed carefully in order to check the effectiveness of the improvements and to considered them during retrofitting strategy for buildings with unimproved model;

3-) The following vulnerable elements should be remember for retrofitting of the 77/5 model: the low quality of the mortar (when documented); connection unit with high damage potential; low resistance of piers and spandrels; the missing diaphragm behaviour of the slabs and their connections to the masonry walls; large spacing and lack of uniformity of some transversal walls;

4-) For the assessment of the RC 82/2 models it is recommended to follow also these steps: a-) Verify the compatibility of the in-situ building with the typified model, since in many cases are present additional area, cantilever in each floor or added storey on the top of the building; b-) checking material strength and the condition of RC elements, especially the concrete deterioration and rebar corrosion; c-) assessing the existing capacity, paying special attention to: the longitudinal direction capacity, shear capacity, soft story mechanisms in ground and first floor, infill walls and one direction panel slabs.

4 Bibliography

[1] A. G. Consulting, UTS-01. (2022). Geophysics field investigation using ERT amd MASW 2D seismic methods / Studim Gjeofizik me metoden e ERT dhe metoden sizmike aktive MASW 2D. Geophysics study in the site of new residential building on street "Dalip Peza", Durrës (41.319, 19.457).

[2] Alam M, Alberto Y, Aranha C, … Hakhamaneshi M. (2019). Virtual Earthquake Reconnaissance Team: Phase 1 Response to M6.4 Albania Earthquake November 26, 2019.

[3] Aliaj Sh, Koçiu S, Muço B, Sulstarova E. (2010). Sizmiciteti, sizmoteknika dhe vlerësimi i rrezikut sizmik në Shqipëri 2010. Tirana, Albania: Academy of Sciences of Albania.

[4] Andonov A, Andreev S, Freddi F, Greco F, Gentile R, Novelli V, Veliu E, Zhuleku E. (2020). EEFIT Report On Albania Mw 6.4 2019. EEFIT. doi:10.13140/RG.2.2.34488.57601

[5] AQTN. (n.d.). Design documents for typified buildings and their improvements.

[6] Baballëku, M. (2006). Fragility of Typified Educational System Facilities in Albania, INTERNATIONAL POST GRADUATE STUDY PROGRAM EARTHQUAKE ENGINEERING IZIIS-TEMPUS MASTER COURSE. Skopje: IZIIS. doi:10.13140/RG.2.2.17061.45282

[7] Baballëku, M. (2014). Vlerësimi i dëmtimeve strukturore në ndërtesat tip të sistemit arsimor - Structural damages assessment of typified educational facility buildings. Polytechnic University of Tirana, Tirana, Albania. doi:http://dx.doi.org/10.13140/RG.2.2.19785.36962/1

[8] Bossu R, Fallou L, Landès M, Roussel F, Julien-Laferrière S, Roch J, Steed R. (2020, August 4). Rapid Public Information and Situational Awareness After the November 26, 2019, Albania Earthquake: Lessons Learned From the LastQuake System. Frontiers in Earth Science, 8. doi:https://doi.org/10.3389/feart.2020.00235

[9] Duni L, Theodoulidis N. (2019). Short note on the November 26, 2019, Durres (Albania) M6.4 earthquake: strong ground motion with emphasis in Durres city.

[10] Freddi F, Novelli V, Gentile R, Veliu E, Andreev S, Andonov A, Greco F, Zhuleku E. (2021, March). Observations from the 26th November 2019 Albania earthquake: the earthquake engineering field investigation team (EEFIT) mission. Bulletin of Earthquake Engineering 19(5):1-32. doi:10.1007/s10518-021-01062-8

[11] Goverment of Albania. (1963). Rregullore mbi kushtet teknike për ndërtimet antisizmike dhe ngritjen e shërbimit sizmollogjik në vendin tonë - Technical provisions for seismic resistance buildings and establishing seismological institute. Tirana, Albania: VKM Nr. 206 dt. 04-06-1963.

[12] Goverment of Albania. (1978). Kushte teknike të projektimit / Technical Design Code - KTP 78 N1-N24. Tirana, Albania: VKM Nr. 38 datë 03.V.1978.

[13] Goverment of Albania. (1978). Kushtet teknike të projektimit për ndërtimet në zona sizmike - KTP-2-78. Tirana, Albania: VKM Nr. 38 datë 03.V.1978.

[14] Government of Albania; European Union; United Nations agencies; World Bank. (2020). AlbaniaPost-Disaster Needs Assessment - Volume A. Tirana: Government of Albania.

[15] Government of Albania; European Union; United Nations agencies; World Bank. (February 2020). AlbaniaPost-Disaster Needs Assessment - Volume B. Tirana: Government of Albania.

[16] IGEO. (2019). Strong motion records - Durresi Earthquake 26 November 2019. Accessed September 23, 2021. Tirana: IGEO. Retrieved from https://www.geo.edu.al/newweb/Durresi_earthquake_26_November2019.rar

[17] Këshilli i Ministrave. (1963). "Rregullore mbi kushtet teknike për ndërtimet antisizmike dhe ngritjen e shërbimit sizmollogjik në vendin tonë", Vendim i Këshillit të Ministrave Nr. 206 dt. 04-06-1963. Tirana, Albania: Këshilli i Ministrave.

[18] Marinković M, Baballëku M, Isufi B, Blagojević N, Milićević I, Brzev S. (2022). Performance of RC cast-in-place buildings during the November 26, 2019 Albania earthquake. Bulletin of Earthquake Engineering 20:5427–5480. doi:10.1007/s10518-022-01414-y

[19] Ministria e Ndërtimit, Akademia e Shkencave, Qendra Sizmologjike. (1989). Kusht Teknik Projektimi për ndërtimet antisizmike / Seismic design Code KTP-N.2-89. Tiranë: Ministria e Ndërtimit.

[20] Ministria e Ndërtimit, K. t.-s. (Janar 1982). Plotësime dhe Korrigjime në Kushtet teknike të projektimit për ndërtimet në zona sizmike - KTP-2-78. Tirana, Albania: Vendim nr.20 datë 25.12.1981.

[21] Papadopoulos GA, Agalos A, Carydis P, Lekkas E, Mavroulis S, Triantafyllou I. (n.d.). The 26 November 2019 Mw 6.4 Albania Destructive Earthquake. Seismological Research Letters. doi:https://doi.org/10.1785/0220200207

[22] Pistoli, V. (1980). Behaviour of brick-masonry buildings during the April 15, 1979 earthquake and calculation of resistance to seismic forces. Reports and papers of the symposium of Shkodra, April 4-5, 1980 - The earthquake of April 15, 1979 and the elimination of its consequences. Shkodra: Academy of Science of Albania.

[23] Stermasi F, Premti K, Meka K. (1980). Technical analysis of the damage caused to buildings and conclusions regarding anti-seismic design as a result of the experience obtained from the earthquake of April 15, 1979. Reports and papers of the symposium of Shkodra, April 4-5, 1980 "The earthquake of April 15, 1979 and the elimination of its consequences". Shkodra: Academy of Science of Albania.

LESSONS OF THE LUGOVSKY EARTHQUAKE IN THE REPUBLIC OF KAZAKHSTAN

Yeraly Shokbarov [(1)], Begman Kulbaev [(2)], Gani Temiraliuly [(3)]

[1)] *Managing Director of Production of "Kazakh Scientific-Research Institute of Construction and Architecture", www.kazniisa.kz, Eshokbarov@kazniisa.kz.*
[(2)] *General manager of "Kazakh Scientific-Research Institute of Construction and Architecture", bkulbaev@kazniisa.kz.*
[(3)] *Master of construction Leading engineer "Kazakh Scientific-Research Institute of Construction and Architecture", gtemiraliuly@kazniisa.kz.*

Abstract

The introductory part of this work gives a brief description of the recent earthquakes that have occurred in recent years in the Republic of Kazakhstan. The following is more detailed information about the consequences of an earthquake: the scale of destruction, the procedure for dealing with the consequences of an earthquake, methods of strengthening buildings.

Keywords: earthquake, magnitude of earthquake, intensity of earthquake manifestation, epicenter, ground vibrations, surveys, building reinforcement.

Introduction

The territory of the south and south-east of Kazakhstan is one of the most seismic of the Central Asian seismically active east of the Kazakhstan. Over the past three, 120 strong earthquakes have occurred here: Vernenskoye – 7.3 with a magnitude of 1887, Chilikskoye – with a magnitude of 8.3 since 1889, and Keminskoye – with a magnitude of 8.2 since 1911, and the weaker number (5-7 points) is estimated in dozens.

Seismic regions of Kazakhstan occupy about 43% of the total area of the territory of the republic. More than 6 million live here. a person or about 40% of the total Kazakh population of the city. At the same time, the population of the city, in 9 living-2.0 million, is a ball zone. a person (V. G.) in the core. Almaty – 1.85 million people); in the 8-ball zone-1.1 million people; in the 7-ball zone – 2.0 million and 6-ball zone – 1.2 million people.

The earthquake of May 12, 2003 at 01:23 a.m. occurred Destructive local time (on May 12 at 18: 22 GMT) Of the Republic of Kazakhstan in the part west of the territory of the southern (350 km) city of Almaty, east (100 km) of the city. Taraz, point coordinates VS: 42o 52' s.sh., 72o 53' v.d. at the epicenter station of Lugovoye village. According to the data of the engineering seismometric station "Almaty" to the Lugovsky magnet, the earthquakes are M = 5.4 on the Richter scale, the focal depth (different estimates) is from 4 to 8 kom. According to the intensity of the MSK scale of the earthquake at the epicenter of 7-8, the score is 64. For almost 3 to 3 repeated Aftershocks with a ball intensity every day for months.

1. Parameters of The Lugovsky earthquake shock

The Lugovsky earthquake occurred on May 23, 2003 at 01:12 local time (May 22 at 18:12 GMT) in the area named after T.Rysukulov, Zhambyl region, in the southern part of the territory of the Republic of Kazakhstan, west (350 km) of Almaty, east (100 km) of Taraz.

According to the Almaty Seismic Observatory, the earthquake was located at a depth of about 14 km near the Lugovaya railway station. The coordinates of the epicenter of the main shock are 42o 52☐ north latitude, 72o 53☐ east longitude, with a magnitude, M = 5.4 [1].

The epicenter of the earthquake is located on the territory of the Lugovaya station and does not coincide with the position of the epicenter determined by instrumental data. Approximately the epicenter, determined by instrumental data, is located at a distance of 7 km in the direction to the northwest from

the center of Lugovaya station. In the epicenter zone, no seismic dislocations were detected on the ground surface during the survey.

According to the network of stations of the Institute of Seismology of the Ministry of Education and Science of the Republic of Kazakhstan, the magnitude of the earthquake was 5.4 with a depth of the hearth (according to various estimates) from 4 to 8 km.

Based on the studies, a preliminary scheme of the isoseist of the Lugovsky earthquake was compiled (see Fig. 1).
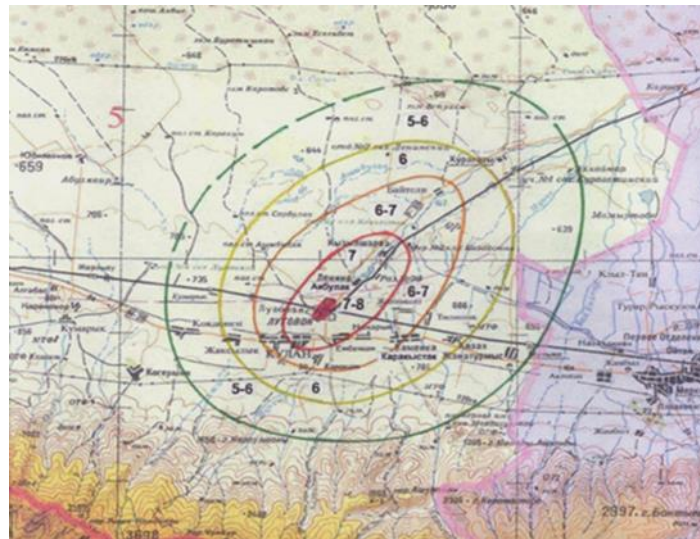
Fig. 1. Earthquake isoseist.

Instrumental data on ground fluctuations in the epicentral zone were not obtained, therefore, the intensity of the earthquake manifestation was estimated based on the descriptive part of the MSK-64 seismic scale.

The intensity of the earthquake manifestation in the macroseismic epicenter varies from 7 to 8 points (the assessment was made according to the macroseismic part of the MSK-64 scale) [1].

A preliminary analysis of digital recordings obtained at the station showed that in the first 7 hours after the earthquake, 75 aftershocks occurred in the intensity range of 2-4 points, three of which were noticeable.

The main results of the macroseismic survey are given in Table 1.

Table 1

№	Name of the locality	Earthquake intensity in points
1	Lugovaya station	7-8
2	Enbekshi village	7
3	village Kyzylsharva	7
4	villageillage Kulan	6-7
5	the village of Karakystak	6-7
6	village Akbulak	6-7
7	Zhalpak saz	6-7
8	village Kazakh village Tasholak	6
9	village	6
10	Military camp	6

11	village Zhaksylyk	6
12	the village of Kokdonen	5-6
13	the village of Koragaty	5-6
14	village Karakat	5-6
15	the village of Zhanaturmys	5-6
Note. *The table shows data on localities where the earthquake occurred with an intensity of at least 5 points.*		

By May 26, the number of aftershocks decreased to 27 per day. The strongest was recorded with an intensity of 4 points on May 26, 2003.

1.2. Comparative assessment of earthquake intensity

According to the results of research by the US Geological Survey, in the XX century, the annual purity of earthquakes with $M \geq 8$ (I= 11-12 points) averaged 1 case; $M \geq$ 7-7.9 (I=9-10 points) about 20; $M \geq$ 6-6.9 (I=7-9 points) – 120; $M \geq$ 5-5.9 (I=6-7 points) - 800; $M \geq$ 3-4.9 (I=4-6 points) – with more than 50 thousand cases.

Thus, the Lugovsky earthquake with $M = 5.4$ on a global scale does not belong to the category of rare events. On average, there are 2-3 such earthquakes on earth per day [2].

1.3. The number of dead and injured people

The population of the T.Ryskulov district as of January 1, 2003 was 61.5 thousand. Human. The affected area is dominated by a rural population with a low density of 6.8 inhabitants per 1 m2. The district center named after T.Ryskulov is the village of Kulan. On the territory of the district there was 1 settlement district, 13 rural districts, 44 settlements.

As a result of the Lugovsky earthquake, 29 people were injured, including 3 were killed, 10 were hospitalized with injuries of varying severity, 16 received medical assistance on the spot. 20,900 people were left homeless. 18 settlements with a population of 38 thousand people were in the zone of severe destruction [2].

Fig. 2. One of the families affected by the Lugovsky earthquake

1.4. Direct and indirect material damage

The economic damage caused by the earthquake exceeded $ 120 million, of which $ 95 million (78%) - the cost of demolition and new construction and $ 27 million (22%) – the cost of strengthening buildings and repair and restoration work. The elimination of the consequences of the earthquake was carried out by the own forces of the Republic of Kazakhstan.

The demolition of such houses and the construction of earthquake-resistant ones will lead to large material costs. It is more expedient to strengthen the houses of this design, as can be seen from the example of the Lugovsky earthquake. Economic analysis shows that the construction of a new house that meets the requirements of the norms costs about $ 20,000, strengthening the affected house – $ 5,000. In addition, the reinforcement of houses significantly reduces the time of housing commissioning [2].

2. The causes of the devastating consequences of the Lugovsky earthquake

The territory of the south and south-east of Kazakhstan is one of the most seismically active areas in Central Asia. Three strong earthquakes have occurred here over the past 120 years: Vernenskoye – in 1887 with a magnitude of 7.3, Chilikskoye – in 1889 with a magnitude of 8.3, and Keminskoye – in 1911 with a magnitude of 8.2, and the number of weaker ones (5-7 points) is in the tens. Seismic regions of Kazakhstan occupy about 18% of the total area of the republic. More than 7 million people live here, or about 42% of the total population of Kazakhstan. At the same time, the population living in the 9-ball zone is 2.0 million people (including 1.85 million people in Almaty); in the 8–ball zone - 1.1 million people; in the 7–ball zone - 2.0 million people and the 6–ball zone - 1.2 million people [3].

The first information about strong and destructive earthquakes in this area dates back to ancient times. The collection and systematization of macroseismic data on tangible earthquakes in the Northern Tien Shan began only in the second half of the XIX century, and instrumental observations - since 1927. The depth of the foci of these earthquakes varies from 15 to 40 km. On the modern Map of the general seismic zoning of the territory of Kazakhstan, the 8-point zone extends in a wide band from the village of Merke in the west to the east and northeast. The presence of this zone is historically due to the pleistoseist zone of the Belovodsk earthquake of 1885 (the epicenter of this earthquake was located on the territory of the modern Kyrgyz Republic, east of the village of Kara-Balta). Zhambyl region of Kazakhstan is located in the earthquake hazard zone (Fig. 3). The zone of active seismic impact with an intensity of 7-8 points occupies 21.6% of the total area of the region, where 75% of settlements are located, including the regional center - the city of Taraz with a population of more than 300 thousand people (2003). Seismicity of the territory in the south of the district them. T.Ryskulova of the Zhambyl region, where the Lugovsky earthquake occurred, has been accepted as equal to 8 points on the MSK-64 scale since 1951. After the Zhambyl earthquake of May 10, 1971, which had a local character (M = 5.5), there was no information about noticeable damage to buildings and structures on the territory of the modern T. Ryskulov district [3]. After this earthquake, the seismicity for the territory of Taraz (Dzhambul) in 1971 was changed to 8 points. These changes practically did not affect the territory of the T. Ryskulov district. The southern part of the territory of the district named after T. Ryskulova experienced noticeable concussions in 1992 during the Suusamyr earthquake on the territory of the Kyrgyz Republic (M= 7.7). The intensity of the manifestation of this earthquake on the territory of the T. Ryskulov district did not exceed 8 points and corresponded to the seismicity of the area adopted according to the current Map of the general seismic zoning of the Republic of Kazakhstan [3].

Thus, one of the main reasons for the devastating consequences of the Lugovsky earthquake is the natural realization of the natural potential seismicity of the region into a random event within the maximum previously predicted levels of seismicity and probability.
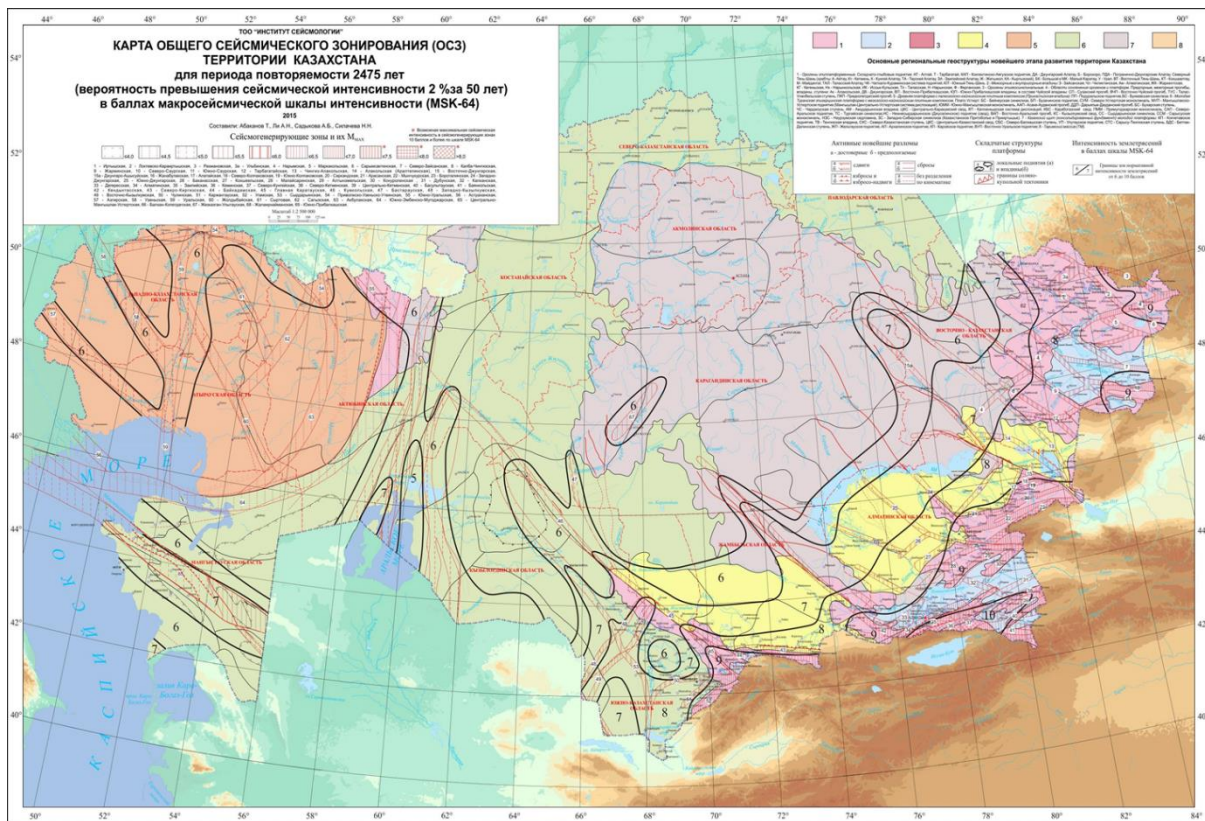
Fig. 3. Map of the general seismic zoning of the Republic of Kazakhstan

3. Residential buildings in the earthquake zone

Single-storey residential buildings with load-bearing walls made of adobe masonry predominate in the settlements, the total number of individual residential buildings in the earthquake zone is 8878 buildings, of which 62% are adobe; 26% are brick; 3% are wooden; 2% are made of reinforced concrete structures.

Residential buildings at the Lugovaya station had the greatest degree of damage, where the intensity of the earthquake manifestation on the international scale MSK-64 ranged from 7 to 8 points. On the territory with an earthquake intensity of 7 points (part of the Lugovaya station, the villages of Enbekshi, Kokaryk, Kzylsharua), residential buildings were damaged from 2 to 3 degrees. With an earthquake intensity of 6 to 7 points (the villages of Zhalpaksaz, Kulan, Karakystak, Akbulak), residential buildings were damaged from 2 to 3 degrees. With an earthquake intensity of 6 points (the villages of Kazakh, Tasholak, Zhaksylyk), residential buildings received mainly damage of 2 degrees. With an earthquake intensity of 5 to 6 points (the villages of Kokdonen, Karakat, Zhanaturmys), residential buildings received mainly damage from 1 to 2 degrees.

With an earthquake intensity of 5-6 points, there was serious damage. Almost all houses with adobe masonry walls were damaged at least 2 degrees during the earthquake. Approximately 50% of these houses were damaged from 2 to 3 degrees, and some - 4 and 5 degrees (complete collapse). Damage to adobe houses (see Fig. 4).

Fig. 4. Destruction of adobe houses as a result of the earthquake on May 23, 2003

Such serious damage to residential buildings with an earthquake intensity of 5-7 points is explained by the low strength of adobe blocks used in construction. The average compressive strength of adobe samples was 3 kg/cm2.

A small group is represented by one, two and three-storey houses with load-bearing external and internal walls made of brickwork and wooden or precast reinforced concrete floors, as well as with walls made of wooden sleepers

The most severe damage was caused to low-rise buildings at Lugovaya station with the maximum intensity of the earthquake manifestation on the MSK-64 scale from 7 to 8 points. At the same time, in buildings with wooden floors, the degree of damage was higher than in buildings with reinforced concrete floors [4].

Houses with wooden floors located in an area with an earthquake intensity on the MSK-64 scale from 7 to 8 points were damaged from 2 to 3 degrees and recommended for strengthening with the transfer to complex structures. These houses were recommended for demolition.

Large-panel houses are made with one, two and four floors. The structural scheme of the houses is adopted with load-bearing transverse and longitudinal walls made of reinforced concrete panels. The ceilings of four-storey houses are made of panels with a support along the contour.

As a result of the earthquake, all the supporting structures of buildings in this group received minor damage in the form of small cracks in the seams between the floor panels, crumbling in some areas of whitewash and plaster. In general, the load-bearing structures of large-panel buildings have satisfactorily endured earthquakes, and does not require reinforcement. The partitions were damaged up to 2 degrees on the MSK-64 scale and recommended for strengthening.

3.1 Recommendations for strengthening residential buildings

In the process of eliminating the consequences of the earthquake, the construction organizations of the Republic of Kazakhstan strengthened and repaired 4,756 residential buildings and built 2,563 new houses.

In a two-week period, the KazNIISA Institute developed ways to strengthen buildings. For the first time in our practice, a massive reinforcement of adobe houses was carried out [5].

To obtain complex structures, it was recommended to strengthen all bearing walls of buildings with double-sided vertical layers of high-strength reinforced plaster on a cement-sand mortar grade of at least 150 or shotcrete and a thickness of at least 40 mm along reinforcing wire mesh with a diameter of at least 5 mm of class Bp-I (see Fig. 5).

To prevent wall breaks in at the floor level, flat reinforcement frames were installed on both sides of the walls, replacing antiseismic belts.

The flat frames were made of two longitudinal reinforcing rods Ø12 mm of class A-III and transverse rods Æ6 mm of class AI with a step of 300 mm. For anchoring in the antiseismic belt, the floor beams were connected to flat frames with clamps made of reinforcement rods of A6 mm class AI.
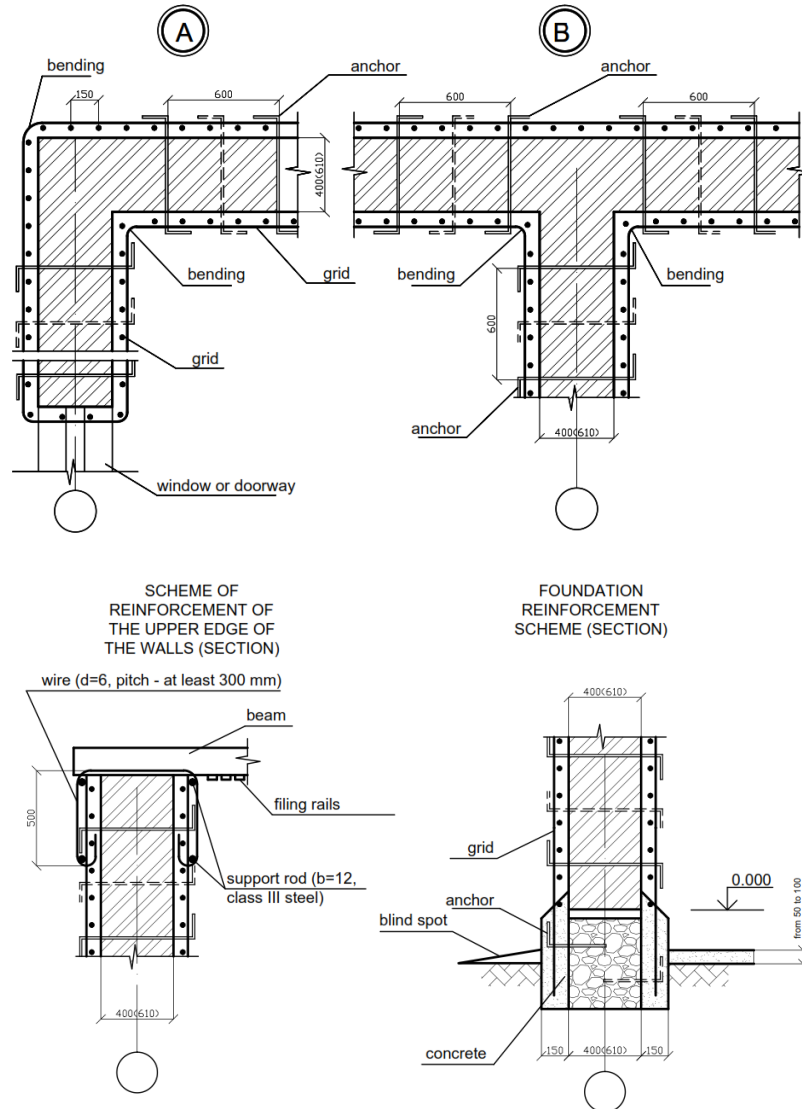
Fig. 5. Reinforcement of adobe walls and foundations with reinforcing grids in a layer of high-strength mortar.

The rubble stone foundations were also reinforced on both sides with reinforcing grids in a layer of fine-grained concrete of class at least B12.5 and with a thickness of at least 100 mm. The grids were made of reinforcement rods Ø8 mm of class A-III with cell sizes 200x200 mm [5].

With the proposed method of reinforcement, a rigid spatial system was obtained, consisting of reinforced external and internal walls reinforced with double-sided vertical layers of high-strength reinforced plaster. In order to evaluate the effectiveness of the proposed reinforcement method, instrumental studies of the dynamic characteristics (periods and forms of natural oscillations, logarithmic decrements) of houses with adobe walls, brickwork before and after reinforcement and the

actual strength of cement-sand plaster reinforcement were carried out. Dynamic tests showed that the periods of natural oscillations of adobe houses with damage of 3 degrees before amplification were equal, about 0.16 seconds. The periods of natural oscillations of adobe houses after amplification were equal to 0.04 seconds. The rigidity of adobe houses after reinforcement increased by an average of 16 times compared to the rigidity of non-reinforced houses (Fig.6.).
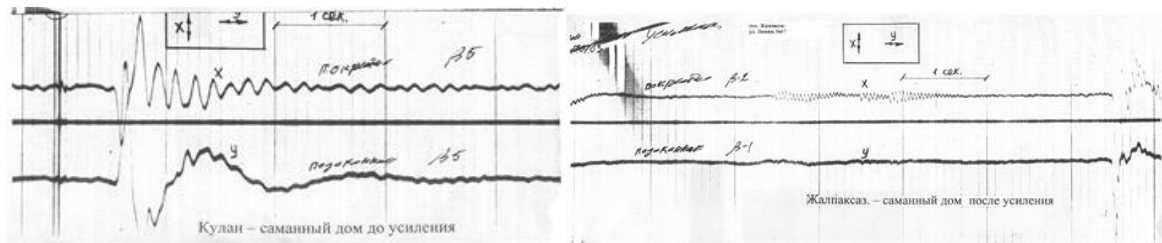
Fig.6. Periods of natural oscillations of adobe houses before and after strengthening

4. School buildings

There are 15 schools located on the territory of the earthquake-affected area.

Seven schools are made with load-bearing brick walls. The ceilings in five of them are made of precast reinforced concrete multi-hollow slabs. In two schools, the ceilings are made of wooden structures.

Five schools are made with load-bearing brick walls of complex construction (see Fig.7).

Fig. 7. General view of schools with load-bearing brick walls of complex construction

Three schools are made with a reinforced concrete frame.

One school is made with load-bearing wooden walls and one school is made with load-bearing walls of adobe masonry.

School buildings, which were subjected to seismic impacts of intensity 6-8 points, also received serious damage. Of the fifteen buildings of secondary schools:

Three that did not have antiseismic measures had to be demolished; 3 new schools were erected instead by the first of September.

Twelve, despite the presence of some antiseismic measures in them, had to be strengthened. All these schools were put into operation by the beginning of the school year.

The main causes of damage to school buildings were associated not so much with the intensity of the seismic impacts that took place, as with the poor quality of construction and deviations from design decisions.

During the examination by the KazNIISSA Institute, the strength of the masonry adhesion was checked in all schools with load-bearing walls made of brickwork. In all academic buildings of schools, the values of the temporary resistance of brickwork Rr varies from 0.3 to 0.7 kg / cm2, which is significantly lower than those established in the norms (at least 1.2 cm2).

4.1 Hospital and polyclinic buildings

Hospitals and polyclinics - a total of 18, of which 1 is with load-bearing wooden walls; 1 is with load-bearing adobe walls masonry; 16-with load-bearing brick walls. As well as a large group of administrative buildings, social and cultural facilities, communication companies and hotels.

Within two weeks after the earthquake, the KazNIISSA Institute conducted a detailed survey and developed project documentation to strengthen 15 school buildings. The survey showed that buildings with load-bearing brick walls received severe damage during an earthquake with an intensity of 7 points (see Figure 8). Buildings damaged from 3 to 4 degrees are recommended for demolition. Buildings that have received damage from 2 to 3 degrees are recommended for strengthening.

Fig. 8. Damage to schools with load-bearing brick walls.

The school building in the village of Zhaksylyk with monolithic reinforced concrete frames with external brick walls. The structures of the monolithic reinforced concrete frame were severely damaged at an earthquake intensity of 6 points due to the extremely poor quality of construction (see Fig. 9.

Fig. 9. Damage to the reinforced concrete crossbar in the School building

4.2 Recommendations for strengthening public buildings

To ensure the seismic safety of school buildings, the following measures are recommended to strengthen:

- transfer load-bearing walls from non-reinforced brickwork to the category of complex structures. To do this, double-sided reinforcement of all walls with reinforcing grids should be carried out in a layer of high-strength plaster made of cement-sand mortar [5].

- to reduce the distances between the transverse walls in the compartments of the building, it is necessary to introduce additional (replacing transverse walls) into the existing structural scheme steel reinforcement frames associated with ceilings and wall structures (see Fig.10).

In order to make the proposed reinforcement method effective, instrumental studies of the dynamic characteristics (periods and forms of natural oscillations, logarithmic decrements) of school buildings before and after reinforcement were carried out.

The periods of natural oscillations of buildings with brick walls before amplification were equal, about 0.45 seconds, after amplification decreased, to 0.24 seconds. Accordingly, the rigidity of buildings after reinforcement increased 3 times.

Fig. 10. Reinforcement of brick walls with reinforcement grids

Brick walls and partitions received serious damage, which absorbed the bulk of the seismic load, which saved the building from collapse. It is recommended to strengthen the buildings: a) strengthen the columns of the transverse frames of the frame with clips made of steel corners; b) strengthen the crossbars of the frames by increasing the compressed zones of the crossbar, with the device in the upper zone of additional reinforcing rods and grids (see Fig. 11).

Fig. 11. Reinforcement of columns and beams with steel clips

Dynamic tests showed that the periods of natural oscillations of frame buildings before amplification were about 0.34 seconds, and after amplification about 0.2 seconds. The rigidity of the building after reinforcement increased by an average of 3 times compared to the rigidity before reinforcement [5].

In the process of eliminating the consequences of the earthquake, 12 schools were strengthened and repaired by construction organizations. 1 district hospital was demolished, 1 new hospital was built, 17 hospitals were strengthened. And all administrative buildings were subject to strengthening.

All schools were completed by the first of September.

The general management of survey and design work was carried out by the head research Institute of the Republic of Kazakhstan in the field of earthquake-resistant construction "KazNIISSA".

In the process of construction by the KazNIISSA Institute, in newly erected houses and in newly built 3 schools with load-bearing walls of brickwork, the strength of the clutch of the masonry was checked for separation along unbound seams in accordance with GOST 24992-81, sustained for at least 7 days.

The tests showed the following results of 0.1 kg/cm2 to 0.4 kg/cm2. The low adhesion strength of the masonry is explained by the violation of the technology of work. The brick was laid without soaking in water, was not cleaned of dust. After testing the masonry for separation, the quality of construction improved for the better. The clutch strength of the masonry for separation was 1.2 kg/cm2 to 2.4 kg/cm2.

The construction of new residential buildings and the reinforcement of existing residential buildings was completed by the end of 2003.

Conclusion

In the process of eliminating the consequences of the earthquake, the technical and economic efficiency of the work on strengthening mass buildings in comparison with new construction has been proven.

In the studied area for a long time, the construction of residential buildings was carried out without any projects and without proper control of the architectural and construction inspection.

The damage from the Lugovsky earthquake could have been significantly less, provided that the basic requirements of the building regulations governing construction in seismic areas were met.

The effectiveness of work on strengthening buildings (especially with load-bearing walls made of adobe masonry) was confirmed experimentally by dynamic tests performed by KazNIISSA for a number of buildings before and after their reinforcement.

References

[1] "Scale for assessing the intensity of earthquakes MSK-64 (K). -Almaty, 2004.

[2] Lessons of the Lugovsky earthquake on May 23, 2003 in Kazakhstan. United Nations Development Program in Kazakhstan, Almaty 2004.

[3] Seismic zoning of the territory of the USSR. Edited by V.I. Bune, G.P. Gorshkov. M., Nauka, 1980, 307 p.

[4] SNiP RK 2.03-30-2006 'Construction in seismic areas". Almaty, 2006

[5] Ashimbayev M.U., Tuleev T.D., Aldakhov S.D., Taubaev A.S., Shokbarov E.M. "Recommendations for the design, construction and reinforcement of residential buildings made of local building materials (adobe, slag blocks) in the seismic regions of Kazakhstan" Almaty, 2008.

THE CRISIS PLATFORM: A CROSS-BORDER PLATFORM FOR RISK ASSESSMENT AND MANAGEMENT

Antonella Di Meo [1], Barbara Borzi[2], Davide Quaroni[3], Antonino Famà[4], Vlatko Sheshov[5], Roberta Apostolska[6], Kemal Edip[7], Marija Vitanova[8], Julijana Bojadjieva[9], Aleksandra Bogdanovic[10], Goran Jekic[11], Markel Baballëku[12], Neritan Shkodrani[13], Genti Qirjazi[14] Stavroula Fotopoulou[15], Christos Pedritis[16], Evi Riga[17], Dimitris Pitilakis[18]

[1] *Research Engineer at the Risk Scenarios Department, EUCENTRE, Italy, antonella.dimeo@eucentre.it*
[2] *Head of the Risk Scenarios Department, EUCENTRE, Italy, barbara.borzi@eucentre.it*
[3] *Developer Engineer at the Risk Scenarios Department, EUCENTRE, Italy, davide.quaroni@eucentre.it*
[4] *Research Engineer at the Risk Scenarios Department, EUCENTRE, Italy, antonino.fama@eucentre.it*
[5] *Professor, Ss. Cyril and Methodius University in Skopje, Institute of Earthquake Engineering and Engineering Seismology, N. Macedonia, vlatko@iziis.ukim.edu.mk*
[6] *Professor, Ss. Cyril and Methodius University in Skopje, Institute of Earthquake Engineering and Engineering Seismology, N. Macedonia, beti@iziis.ukim.edu.mk*
[7] *Assoc. Professor, Ss. Cyril and Methodius University in Skopje, Institute of Earthquake Engineering and Engineering Seismology, N. Macedonia, kemal@iziis.ukim.edu.mk*
[8] *Assoc. Professor, Ss. Cyril and Methodius University in Skopje, Institute of Earthquake Engineering and Engineering Seismology, N. Macedonia, marijaj@iziis.ukim.edu.mk*
[9] *Assoc. Professor, Ss. Cyril and Methodius University in Skopje, Institute of Earthquake Engineering and Engineering Seismology, N. Macedonia, jule@iziis.ukim.edu.mk*
[10] *Assoc. Professor, Ss. Cyril and Methodius University in Skopje, Institute of Earthquake Engineering and Engineering Seismology, N. Macedonia, saska@iziis.ukim.edu.mk*
[11] *Assoc. Professor, Ss. Cyril and Methodius University in Skopje, Institute of Earthquake Engineering and Engineering Seismology, N. Macedonia, jekic@iziis.ukim.edu.mk*
[12] *Post-Doc Researcher, Polytechnic University of Tirana, Faculty of Civil Engineering, Albania, markel.baballeku@fin.edu.al*
[13] *Assoc. Professor, Polytechnic University of Tirana, Faculty of Civil Engineering, Albania, neritan.shkodrani@fin.edu.al*
[14] *Post-Doc Researcher, Polytechnic University of Tirana, Faculty of Civil Engineering, Albania, genti.qiriazi@fin.edu.al*
[15] *Researcher, Aristotle University of Thessaloniki, Greece, sfotopou@civil.auth.gr*
[16] *Post-Doc Researcher, Aristotle University of Thessaloniki, Greece, cpetridi@civil.auth.gr*
[17] *Researcher, Aristotle University of Thessaloniki, Greece, eviriga@civil.auth.gr*
[18] *Associate Professor, Aristotle University of Thessaloniki, Greece, dpitilakis@civil.auth.gr*

Abstract

This paper aims to describe the CRISIS web-based platform (WBP) in all its parts and functionalities. The platform is the main result of the two-year EU-funded project CRISIS (Comprehensive RISk assessment of basic services and transport InfraStructure). It has been developed by EUCENTRE (European Centre for Training and Research in Earthquake Engineering) using the most up-to-date web programming frameworks and technologies. The CRISIS WBP is a user-friendly tool intended to support disaster and emergency management authorities in case of earthquakes and/or seismo-induced landslides in the cross-border region of Albania, North Macedonia, and Greece. It has been designed to collect, organise, and visualise for the project target area: i) the exposure data of educational facilities, health facilities, and bridges; ii) the seismic and landslide hazard data; iii) the earthquake damage scenarios (calculated both for selected historical events and in real-time); and iv) the landslide risk scenarios related to the considered exposure dataset. The tool also allows the identification of alternative routes to the nearest available safe facilities, if the main one cannot be used due to damage to the transport infrastructure following a seismic event. This feature can be particularly useful for rescuers who have to intervene promptly after damaging earthquakes. In addition to supporting emergency management, the CRISIS platform can also be used to identify the most vulnerable assets and prioritise actions to increase the resilience of the project target area. As a case study, two earthquakes that affected the cities of Ohrid and Valandovo in 1911 and 1931, respectively, have been simulated. The results of these simulations, also in terms of emergency management (e.g., how to get to the nearest hospitals in the cross-border areas), are presented in detail hereinafter.

Keywords: Earthquakes, Landslides, Risk Assessment, Emergency Management.

1. Introduction

Disasters know no national borders and often emergency conditions require rescue action even from neighbouring countries. It is therefore important to minimise as far as possible all disruptions, even temporary ones, that could significantly alter cross-border flows. This was the primary goal of the CRISIS (Comprehensive RISk assessment of basic services and transport InfraStructure) project, which aimed to increase the resilience of critical infrastructure in emergencies after catastrophic events through preventive measures, effective resource management, and risk assessment of basic services, i.e., health and educational facilities (hospitals and schools) as well as transport infrastructure (bridges and viaducts).

CRISIS was a two-year EU-funded project that started in November 2020 and focused on the cross-border region (henceforth CBR) of North Macedonia, Albania, and Greece. This target area, consisting of eighteen municipalities in North Macedonia, eleven districts in Albania, and twelve municipalities in Greece, has been affected by destructive earthquakes in the past (Mw≥6). Moreover, this region is also susceptible to landslides, mainly due to its topography, lithology, vegetation cover distribution, and weather conditions. Hence the need to develop cross-border harmonised hazard models and a common platform for sharing risk data/information. This paper focuses on the second objective, i.e., to describe the CRISIS web platform (henceforth WBP), developed by EUCENTRE (European Centre for Training and Research in Earthquake Engineering) within the framework of the project.

The CRISIS WBP is a georeferenced tool that provides rapid risk for educational and health facilities and transport infrastructure in case of potential earthquakes or landslides. It aims to collect, organise, and visualise: i) the exposure data on cross-border basic services and transport infrastructure; ii) the cross-border hazard data; iii) the earthquake damage scenarios, and iv) the landslide risk scenarios. Once an earthquake damage scenario has been calculated, the tool also allows the identification of possible alternative routes to the nearest available safe facilities (i.e., *routing*). As designed and developed, the CRISIS WBP is a user-friendly tool intended to support disaster and emergency management authorities in the event of an earthquake or landslide emergency.

2. Cross-border exposure and vulnerability model for basic services and transport infrastructure

The CRISIS project aimed to improve disaster and emergency management by creating a harmonised and efficient system for risk assessment of basic services and transport infrastructure in the target CBR. For the project purposes, only facilities located in largely populated areas, connected to border crossings and serving a significant number of users have been considered. This is because they can ensure greater cross-border cooperation and coordination in disaster risk management. For these facilities, a harmonised risk exposure model has been created.

For schools and hospitals, it has been used the *Global Earthquake Model (GEM) - Direct Observation Tool* [1]. Afterwards, buildings in the database have been grouped into taxonomies based on the criteria adopted by the *GEM Building Taxonomy* [2]. In particular, the latter classifies buildings according to thirteen attributes, ranging from their intended use (i.e., occupancy) to the building's construction and structural characteristics, which allow their seismic behaviour to be assessed.

For bridges in the CBR network, each neighbouring country has gathered all possible and useful data for a seismic assessment of their structural behaviour, following a common data collection method established beforehand. Afterwards, bridges have been grouped into taxonomies based on construction material, static scheme (e.g., arch bridges, continuous girder bridges, simply-supported bridges), and geometric characteristics (e.g., span length).

Table 1 reports the final exposure model defined for the CRISIS project, divided by the number of educational and health facilities as well as road infrastructure in each of the three neighbouring countries of the target CBR. This exposure model has been implemented in the CRISIS WBP, which allows it to be visualised by activating dedicated layers in the "Exposure layers" tab (see Figure 1). Once one or more layers have been activated and a specific item has been selected, the corresponding information collected in the exposure database can be viewed through a pop-up window, as shown in Figure 1.

Table 1 – Educational facilities, health facilities, and road infrastructure in the harmonised CBR exposure database

Country	Educational facilities	Health facilities	Road infrastructure
North Macedonia	57	15	166
Albania	49	12	190
Greece	19	7	16
Total	**125**	**34**	**372**
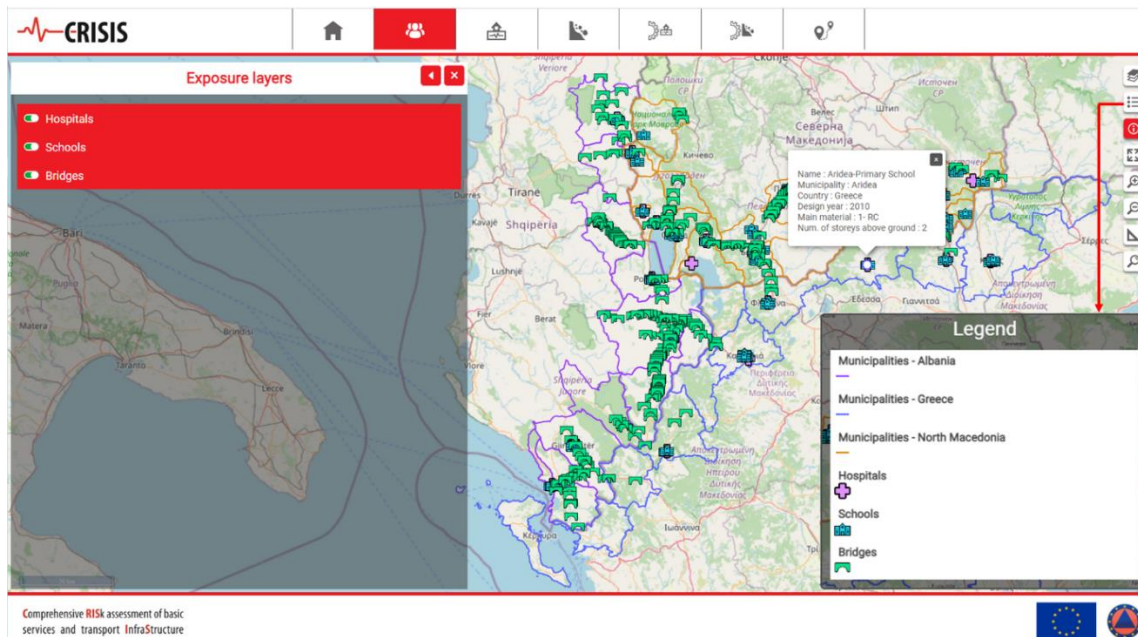
Figure 1. "Exposure layers" tab: visualisation of the harmonised CBR exposure database and corresponding legend

In addition to the exposure model, the calculation of seismic damage scenarios (see section 4.1) requires the earthquake behaviour of each structure and infrastructure in the database to be defined. This was done by associating appropriate fragility curves with each taxonomy of educational and health facilities and road infrastructure. In particular, for educational and health facilities, each neighbouring country of the project CBR proposed sets of fragility curves from the literature that best describe the seismic behaviour of its buildings, also according to their construction characteristics. Each of these sets is composed of five fragility curves, one for each damage level (DLi) as defined by the European Macroseismic Scale 98 (EMS98; [3]). For road infrastructure, instead, the fragility curves defined by EUCENTRE have been associated with reinforced concrete and masonry bridges with continuous and supported decks ([4], [5]) as well as with masonry and slightly reinforced arch bridges ([6], [7]). Fragility curves in [8] have been used for frame bridges. Finally, unlike structures, only two damage levels have been considered for road infrastructure, i.e., slight damage and collapse.

3. Cross-border multi-hazard assessment

3.1 Seismic hazard cross-border harmonization and mapping

The target area of the CRISIS project has been selected because of its high seismicity. In the past, several earthquakes occurred in this region, causing considerable damage as well as numerous deaths and injuries (see Figure 2). To estimate in this area the probability of a certain earthquake occurring in a given time interval, a review of the different seismic hazard models available in the literature has been carried out for each country and/or region involved in the project CBR, as well as for various European projects. In the end, the ESHM13 (2013 European Seismic Hazard Model, [9]) hazard model has been selected because it has resulted in the most up-to-date and the only one to consider all three countries

of the project area. The hazard maps in Peak Ground Acceleration (PGA) referring to the ESHM13 [9] mean hazard model have thus been implemented in the CRISIS platform for three return periods (RTs), i.e., 102 years (39% probability of exceedance in 50 years), 475 years (10% probability of exceedance in 50 years), and 975 years (5% probability of exceedance in 50 years). These maps are available in the "Seismic Hazard" tab together with the Vs30 (the time-averaged shear-wave velocity to 30 m depth) map proposed by the United States Geological Survey (USGS, earthquake.usgs.gov/data/vs30). The latter was implemented in the platform to take site effects into account in the calculation of real-time damage scenarios (see section 4.1).
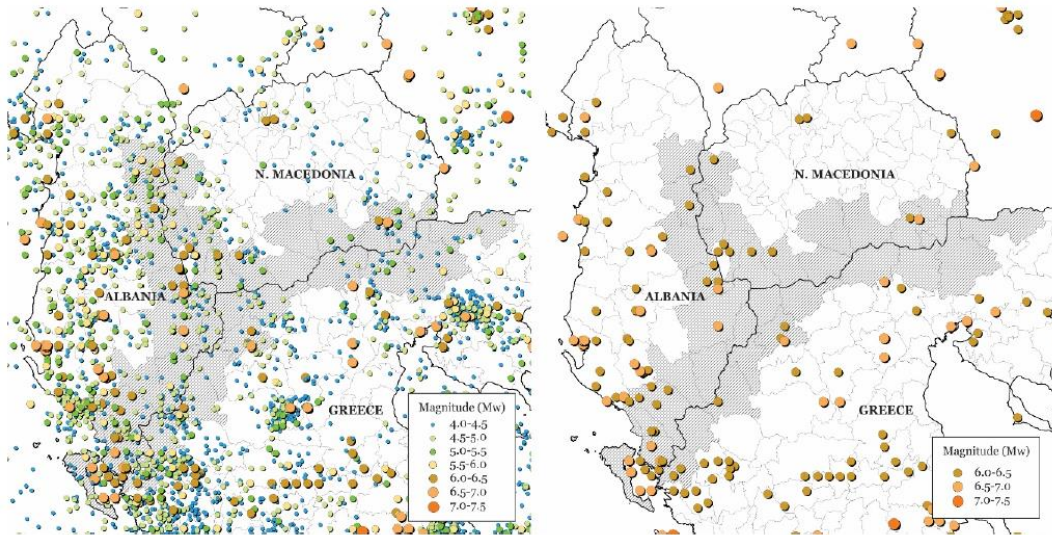
Figure 2. Seismicity data for the target CBR related to the period 1000 A.D.-2006 A.D. from the SHARE European Earthquake Catalogue (SHEEC; [9], [11], [12])

Figure 3 shows the activation of the seismic hazard map for an RT equal to 475 years (mean hazard model and to rock site conditions) with the relative legend in the CRISIS platform. Figure 3 highlights the high seismicity of the project CBR, where PGA estimates can range from 0.20g to 0.45g. In particular, the area with the highest seismic hazard is in the southwestern part of the CBR where PGA is reaching values of 0.45g (dashed red box in Figure 3), followed by the one at the border between Albania and North Macedonia where the PGA values can reach 0.40g (dashed orange box in Figure 3).
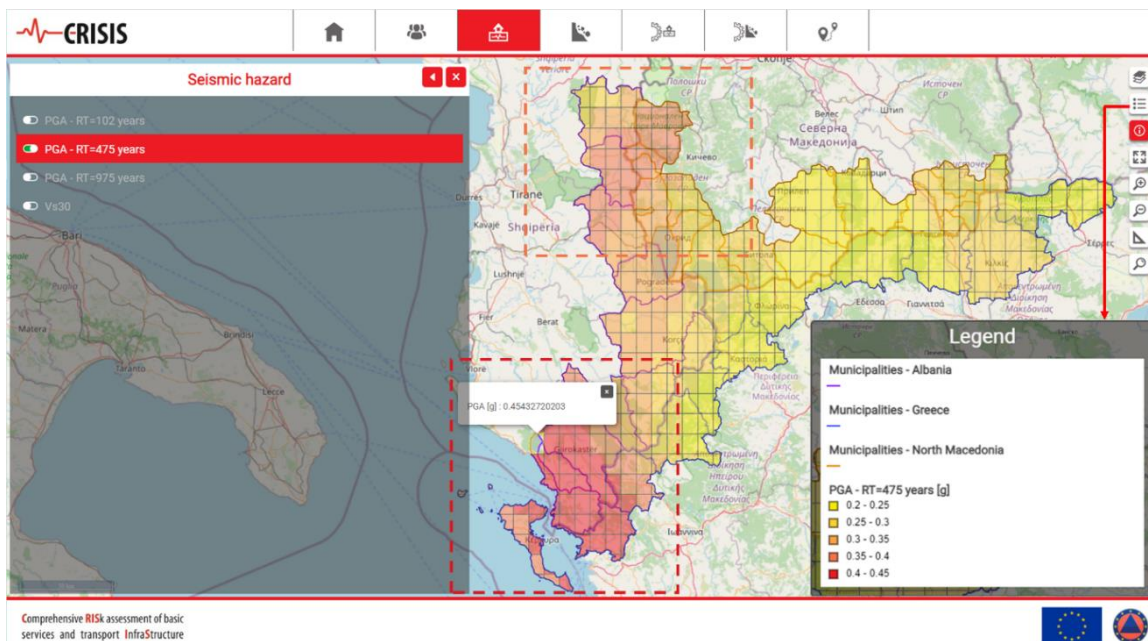
Figure 3. "Seismic hazard" tab: seismic hazard map for RT=475 years and corresponding legend

3.2 Landslide hazard cross-border harmonization and mapping

The project CBR is prone to a high landslide hazard due to its topography, lithology, vegetation cover distribution, and meteorological conditions. As with the seismic hazard, all available data and studies on landslides in each of the three CBR countries have been reviewed to produce landslide hazard maps for the project target area. This review has also been extended to European projects from which the European Landslide Susceptibility Map version 2 (ELSUS v2, [13]) approach has been selected. Indeed, the latter has turned out to be the most suitable methodology for the harmonised assessment of landslide susceptibility and hazard in the project CBR.

As reported in section 3.1, this region is highly earthquake-prone. So, it is not possible to decouple seismic phenomena from landslides. Seismically induced landslides are triggered when the critical acceleration a_c causes the factor of safety to fall below 1. A_c is commonly determined from pseudo-static analyses of slope stability and/or empirically from observations of slope behaviour during past earthquakes. In the CRISIS project, a_c values have been deduced from ELSUS v2 [13] and engineering judgements. The hazard maps for seismically induced landslides have instead been derived in terms of permanent ground displacements (PGD) triggered by earthquake scenarios with RTs of 475 years and 975 years according to the following relationship [14]:

$$Ln(PGD)=-2.965+20217 \times ln(PGA) -6.583 \times k_y +0.535 \times M \pm \varepsilon \times 0.72 \tag{1}$$

where: (i) PGA is the peak ground acceleration at the ground surface in g for RT=475 years and RT=975 years derived from the ESHM13 hazard maps [9] and amplifications due to site effects according to USGS Vs30 map; (ii) k_y is the yield coefficient, commonly used to represent the overall resistance of the slope in displacement-based approaches; (iii) M is the earthquake magnitude, i.e., M=6 (RT=475 years) and M=7 (RT=975 years); and (iv) ε is the standard normal variant with zero mean and unit standard deviation. More details on the harmonised approach for mapping the earthquake-induced landslide hazard in the project CBR can be found in [15].

The hazard maps in PGD are available in the CRISIS WBP in the "Landslide Hazard" tab together with all those maps defined for the CBR in the project for the landslide phenomenon (see Figure 4). Figure 4 shows the PGD map for RT equal to 475 years. This map identifies the southern part of the Albanian-Greek border region as having the highest seismically induced landslide risk, with PGD values ranging from approximately 14.5 cm to 18 cm. These values can reach up to 60 cm in the case of seismic events with an RT of 975 years.
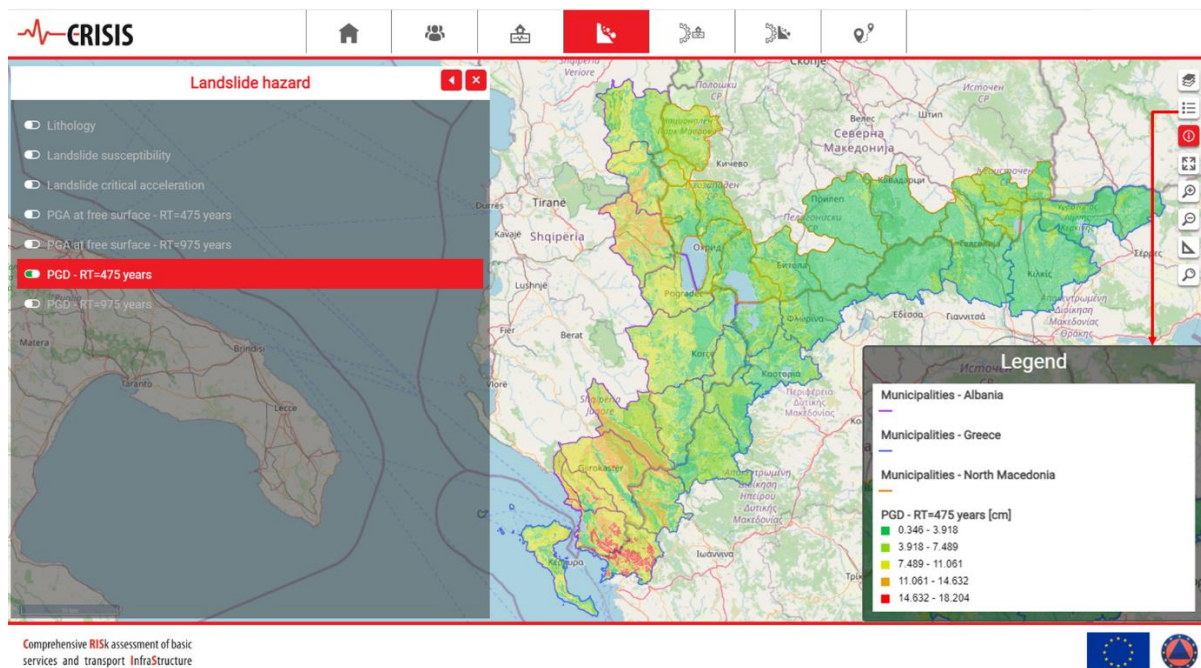
Figure 4. "Landslide hazard" tab: PGD map for RT=475 years and corresponding legend

4. Cross-border risk assessment

4.1 Earthquake damage scenario

Due to its peculiarity of calculating seismic damage scenarios, the CRISIS WBP represents a valuable support tool for both emergency management and policymakers. Indeed, the former can use the tool in the immediate aftermath of an earthquake to assess which structures/infrastructure are usable, while the latter can use it to plan seismic interventions on the most vulnerable structures in peacetime.

Under the "Earthquake scenario" tab, the CRISIS WBP allows viewing damage scenarios calculated for selected historical events. These scenarios are important for estimating the impact in terms of damage (and thus economic losses) that would be incurred in the territory if an event of the same or similar characteristics were to occur again. In particular, eleven significant historical events affecting the project CBR have been considered. These events with their respective characteristics (magnitude, epicentre depth/longitude/latitude, fault type, and date) are listed in Table 2. Figure 5 shows the damage scenario calculated for the historical earthquake event E06 and DL5. In particular, the legend associated with the scenario for DL5 in Figure 5 reveals that bridges around the epicentre might reach the considered DL with a probability of about 30%. The probability might increase by 10% in the case of schools.

Table 2 – Selected earthquake scenarios from the SHARE European Earthquake catalogue (SHEEC; [9], [11], [12]) and corresponding characteristics

Events	Mw	Depth	Longitude	Latitude	Fault type	Date
E1	7.0	-	20.30	39.20	Reverse	05.02.1786
E2	6.6	-	20.00	39.50	Reverse	01.01.1674
E3	6.7	-	20.00	40.30	Normal	04.12.1866
E4	6.3	10	20.70	40.10	Right Lateral Strike-Slip Fault	22.12.1919
E5	6.7	-	20.10	41.10	Right Lateral Strike-Slip Fault	--.--.1380
E6	6.8	21	20.70	40.85	Normal	18.02.1911
E7	6.5	-	21.30	40.50	Normal	29.05.1812
E8	6.1	15	20.66	41.72	Normal	07.12.1922
E9	6.0	12	21.19	41.10	Normal	01.09.1994
E10	6.7	-	22.20	40.90	Normal	--.10.1395
E11	6.7	-	22.51	41.32	Normal	08.03.1931
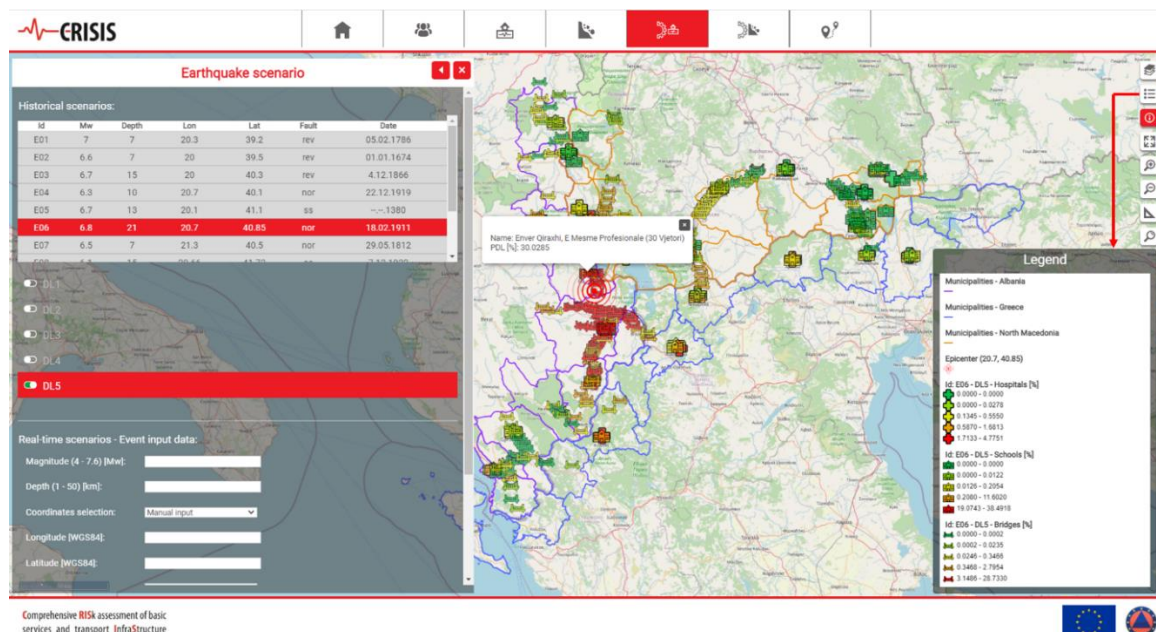
Figure 5. "Earthquake scenario" tab: scenario for the historical seismic event E6 and DL5 and corresponding legend

In addition to damage scenarios of historical events, in the same tab real-time damage scenarios can be calculated by providing the following information in the "Real-time scenarios - Event input data" section:

- Magnitude (Mw). The damage scenario calculation works for 4≤Mw≤7.6.
- Depth of the epicentre (D). The damage scenario calculation works for 1 km≤D≤50 km.
- Coordinates of the epicentre. The epicentre can be located by entering its longitude and latitude according to the WGS84 (World Geodetic System) or by positioning it directly on the map. In the latter case, the longitude and latitude fields will be filled in automatically.
- Fault type. The fault type can be defined in a drop-down menu, by choosing among *Normal*, *Reverse*, and *Lateral Strike-Slip*.

After clicking on the "Calculate" button, the calculation of the scenario is launched. Simultaneously, the launched scenario is loaded into the "Calculated real-time scenarios" table (see Figure 6), where it is also possible to check the status of the calculation. Once completed, the performed scenario can be selected to be viewed for each of the five DLs. Figure 6 shows the real-time damage scenario for DL1 calculated by considering an Mw6 earthquake with epicentre at the border between North Macedonia and Greece (i.e., Lon.=21.72422 and Lat.=40.9176) and a normal type of fault. Figure 6 shows that for the considered event a large number of bridges in all three neighbouring countries might reach the DL1 with a probability of about 30 %, thus causing problems for the network of possible rescue aid. This probability might even increase to 40% for schools and hospitals and only decrease moving away from the epicentre.
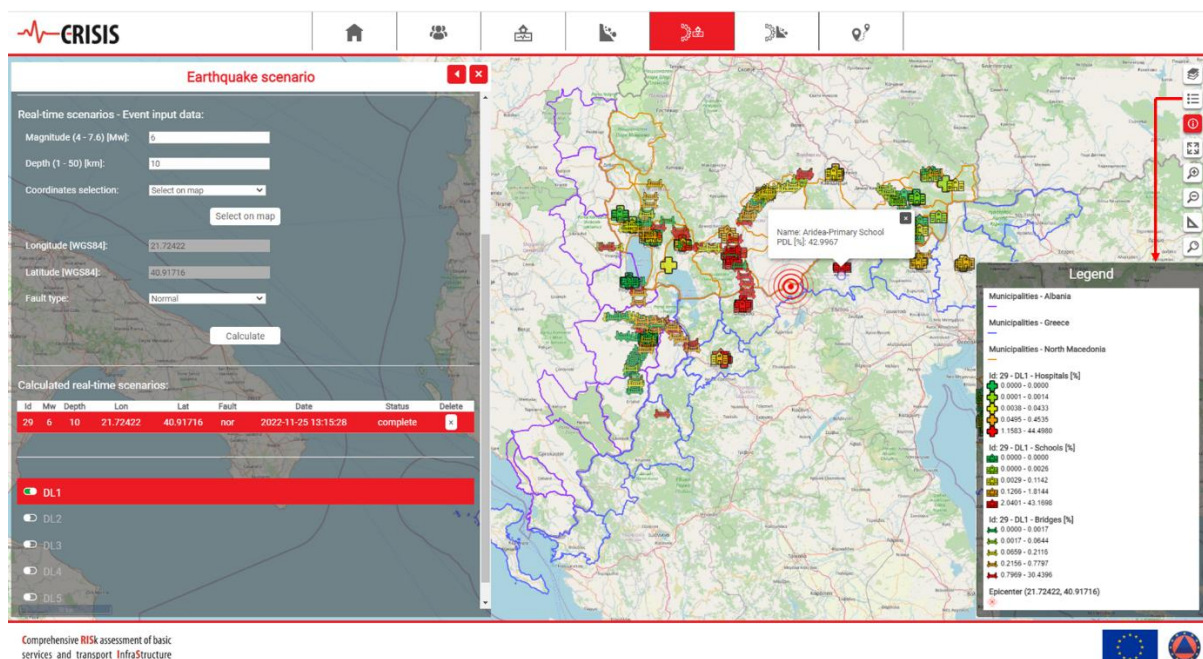
Figure 6. "Earthquake scenario" tab: real-time damage scenario for DL1 and corresponding legend

As can be seen from Figure 5 and Figure 6, all items considered in the calculated scenarios take on a different colouring, depending on the probability of reaching the selected damage level reported in the "Legend" tab. Also, the platform allows checking the probability of reaching the activated DL for a specific element by clicking on it and reading the required information in a label on the screen. As already specified in section 2, five DLs have been accounted for school and hospital buildings according to the EMS98 scale [3] while slight damage and collapse have only been considered for bridges. Consequently, bridges are only included in the calculation of the historical and real-time damage scenarios for DL1 and DL5.

The damage scenarios for historical events and those calculated in real-time have inherent differences that make them not comparable. The first concerns the used calculation engine. In fact, the damage scenarios of the historical events have been calculated using the *Scenario Damage Calculator of the OpenQuake Engine* [16], while those in real-time are determined with an ad hoc tool developed by EUCENTRE. This leads to a second difference, i.e., the adopted ground motion prediction equation (GMPE) and how site effects are accounted for. In particular, damage scenarios for historical events have been calculated according to what [17] and [18] define for the GMPE and site amplification effects, respectively. Instead, the GMPE in [19] and the Vs30 map proposed by USGS have been used in the real-time damage scenario tool.

Finally, contrary to the damage scenarios of historical events, the real-time damage scenarios only include in the calculation those elements of the exposure database for which the PGA assumes a value greater than 1%g.

4.2 Landslide risk scenario

In addition to seismic damage scenarios, the CRISIS WBP enables the visualisation of landslide risk maps calculated for schools, hospitals, and bridges. In particular, the landslide risk for educational and health facilities has been defined according to a semi-quantitative procedure fully implemented in a GIS environment based on [20]. Instead, the landslide risk for bridges has been defined using the fragility curves due to ground failure proposed by HAZUS [21] and considering seismic events triggering landslides with RTs equal to 475 and 975 years, respectively. The landslide risk has not been calculated for all bridges in the exposure database but for a part of them, selected based on their position and importance in terms of cross-border connection.

Figure 7 shows the landslide risk scenario for schools, hospitals, and bridges. For the latter, the landslide risk scenario refers to slight damage and a seismic event with an RT of 475 years triggering the landslide.
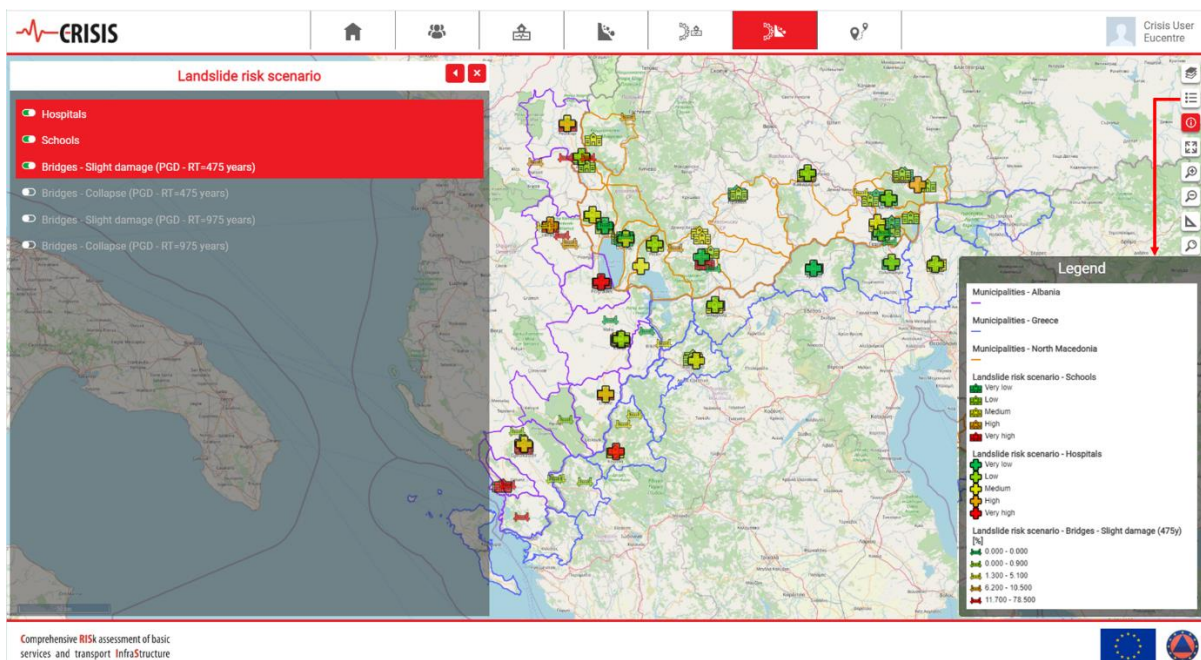
Figure 7. "Landslide risk scenario" tab: landslide risk scenario for schools, hospitals, and bridges. For bridges, the activated layer refers to slight damage and an earthquake with an RT of 475 years triggering the event

5. The routing: a cross-border disaster management

The CRISIS WBP features a tool that provides information on possible routes to follow in an emergency to avoid potentially unusable bridges due to a seismic event. The tool is available under the "Routing"

tab and is important for cross-border disaster management. In fact, disasters know no national borders and the affected areas often require immediate rescue interventions even from neighbouring countries. As shown in Figure 8, the route needs to be identified by start and end points on the map through the "Add start point" and "Add destination point" buttons, respectively. To check whether the route has damaged infrastructure due to a seismic event, a scenario previously calculated in the "Earthquake Scenario" tab has to be loaded in the "Scenario ID" field. Then, the "Create route" button needs to be clicked. If there are no damaged bridges in the defined route, the platform will return the fastest route for rescue teams to follow. Otherwise, it will provide the shortest alternative route, as in Figure 8.
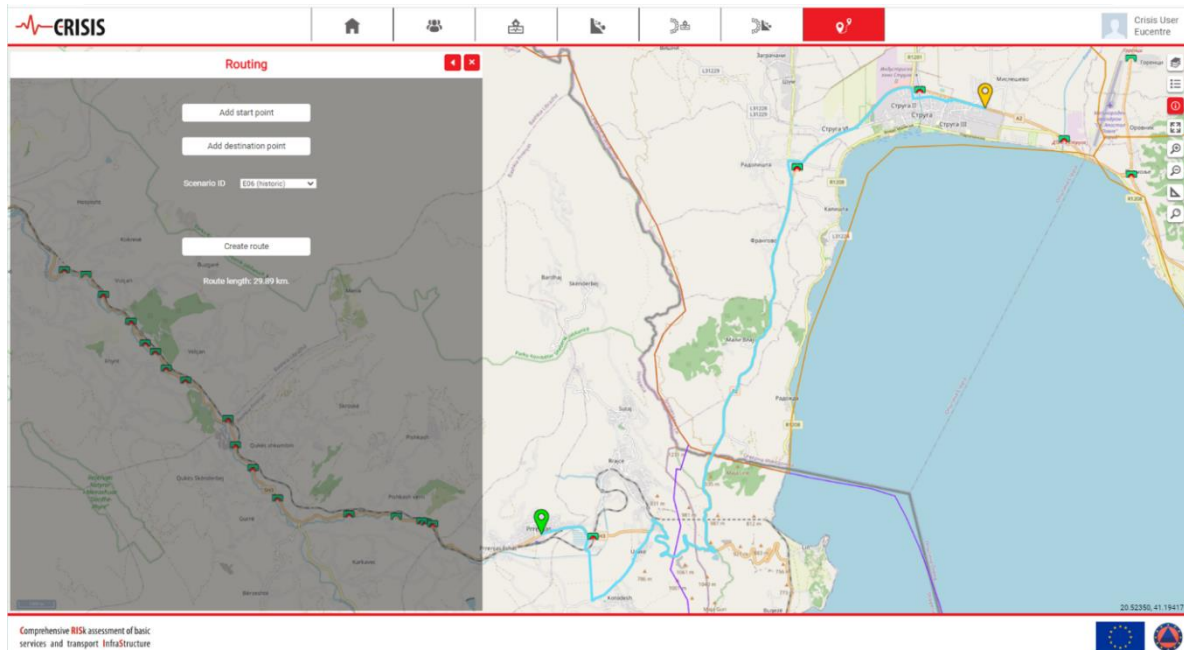
Figure 8. "Routing" tab: alternative route to the main one to bypass bridges damaged by the considered event

To demonstrate the usefulness of the routing tool, two earthquakes that occurred in the regions of Ohrid (M_W=6.4, May 1960) and Valandovo (M_W =6.7, May 1931) are considered as case studies (see Figure 9).

Figure 9. Locations of the earthquakes in the Ohrid and Valandovo regions considered as case studies

For citizens living in these seismically active regions, it is very important to have access to the nearest hospital facilities in case an earthquake occurs. As shown in Figure 10, the hospital facility chosen for the earthquake simulation in the Ohrid region is located in the city of Librazhd (Albania) and is a 4-storey building capable of accommodating a large number of patients. The route calculated under non-emergency conditions is 68.9 km and consists of a large number of bridges. To understand whether this route is usable even after an earthquake like the one in the Ohrid region (Mw6.4), it is necessary to calculate the corresponding damage scenario with the real-time damage scenario tool in the "Seismic

scenario" tab and load it into the routing tool. Figure 11 shows that most of the bridges along the route might be damaged by the event. Therefore, the tool suggests an alternative route that, although longer, allows bypassing the damaged bridges.
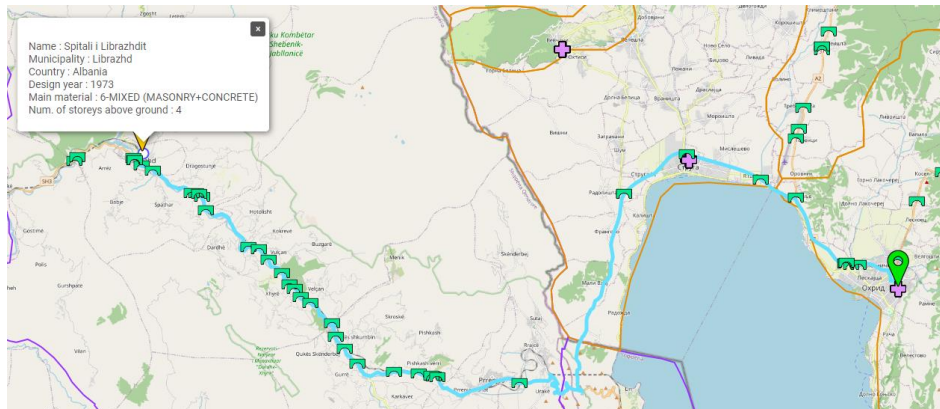
Figure 10. Route to the hospital in Librazhd (Albania) from the Ohrid region under non-emergency conditions
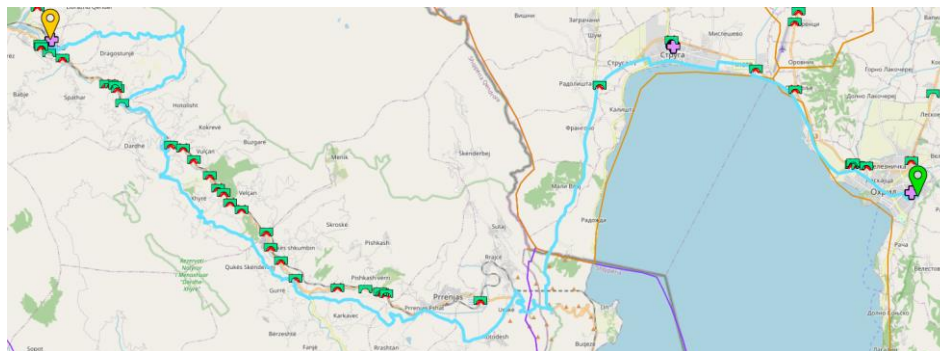
Figure 11. Alternative route to the hospital in Librazhd (Albania) from the Ohrid region to bypass damaged bridges on the main road due to an earthquake like the one in the Ohrid region (Mw6.4)

The situation is much different if we simulate an earthquake such as the one that occurred in the Valandovo region (Mw6.7). In fact, as shown in Figure 12, the connection between the region and neighbouring Greece appears to suffer no damage to the infrastructure along the considered route linking four hospitals. This is because the infrastructure in the region has undergone significant structural renovation and seismic retrofitting in the past.

Both simulations carried out with the "Routing" tool highlight that areas considered in the case studies appear to be functional even in the case of damaging earthquakes since viable routes are guaranteed to quickly transport patients to the nearest hospitals.
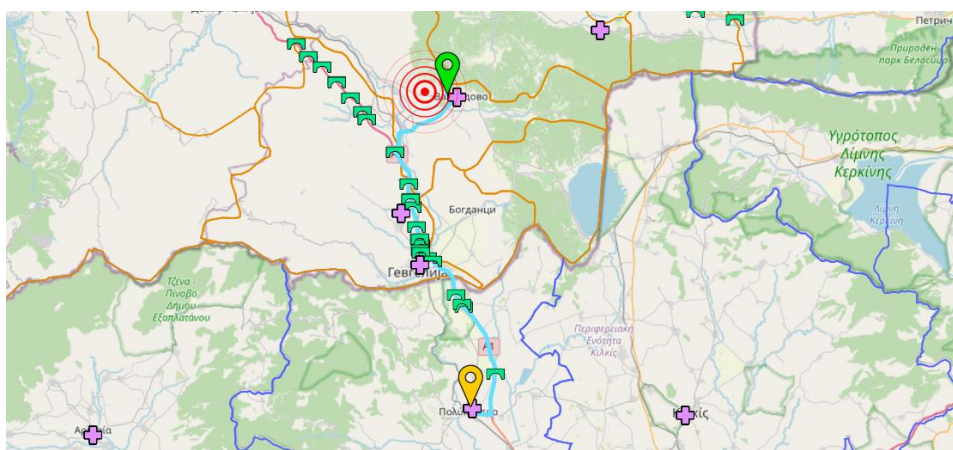
Figure 12. Route to reach a hospital in Greece after an earthquake like the one in the Valandovo region (Mw6.7)

6. Conclusion

This article describes the geo-referenced WBP developed within the CRISIS project to support policymakers as well as disaster and emergency management in the CBR of North Macedonia, Albania, and Greece. The CRISIS WBP contains, organises, and enables the visualisation of all cross-border health and educational facilities (i.e., hospitals and schools) and transport infrastructure (i.e., bridges) data collected within the project. In addition to the exposure database, the tool displays the harmonised seismic and landslide hazard models defined for the target CBR. Rapid information is also available on the level of damage that hospitals, schools, and bridges in the reference area could suffer in the event of an earthquake. Specifically, the platform allows displaying damage scenarios calculated for selected historical events that occurred in the project CBR but also to calculate real-time scenarios using a proper tool implemented in it. Furthermore, it is possible to identify which areas of the CBR are most susceptible to landslides and consequently which assets are most at risk in the event of seismic-induced landslides. No less important is the routing tool, which is useful in the emergency conditions caused by earthquakes to identify alternative routes to be followed by the rescue teams if the main ones are unusable due to damaged road infrastructure.

Acknowledgements

References

[1] Jordan, C.J., Adlam, K., Lawrie, K., Shelley, W., Bevington, J. (2014): User guide: Windows tool for field data collection and management. *Technical Report 2014-04*, Global Earthquake Model Foundation, Pavia, Italy, doi: https://doi.org/10.13117/GEM.DATA-CAPTURE.TR2014.04.

[2] Brzev, S., Scawthorn, C., Charleson, A. W., Allen, L., Greene, M., Jaiswal, K., & Silva, V. (2013): GEM building taxonomy version 2.0. *Technical Report 2013-02*, Global Earthquake Model Foundation, Pavia, Italy, doi: https://doi.org/10.13117/GEM.EXP-MOD.TR2013.02.

[3] Grüntal, G. (1998): European Macroseismic Scale. *Technical Report*, Conseil de L'Europe, Cahiers du Centre Européen de Géodynamique et de Séismologie, Luxembourg.

[4] Bellotti, D., Famà, A., Di Meo, A., Borzi, B. (2019): Large-scale vulnerability analysis of girder railway bridges. In *Risk-based Bridge Engineering*, 239-251. CRC Press.

[5] Bellotti, D., Famà, A., Di Meo, A., Borzi, B. (2019): Fragility curves for large-scale assessment of RC railway bridges, *7th ECCOMAS Thematic Conference on Computational Methods in Structural Dynamics and Earthquake Engineering COMPDYN2019*, Crete, Greece, 13 pages.

[6] Morandi, P., Manzini, C. F., Borzi, B., Mauro, A., Vecchi, A., Tisalvi, M., & Iacobini, F. (2019): Simplified seismic vulnerability assessment of railway masonry arch bridges, *Proceedings of the 10th New York City Bridge Conference*, New York City, USA.

[7] Manzini, C. F., Morandi, P., Borzi, B., Iodice, F., Mauro, A., Vecchi, A., & Iacobini, F. (2021): Derivation of fragility curves for the seismic vulnerability assessment of railway masonry arch, *1st Conference of the European Association on Quality Control of Bridges and Structures EUROSTRUCT 2021,* Padua, Italy, 10 pages.

[8] Nguyen, D.D., Park, D., Shamsher, S., Nguyen, V.Q., Lee, T.H. (2019): Seismic vulnerability assessment of rectangular cut-and-cover subway tunnels. *Tunnelling and Underground Space Technology* **86**, 247–261, doi: https://doi.org/10.1016/j.tust.2019.01.021.

[9] Woessner, J., Danciu, L., Giardini, D., and the SHARE consortium (2015): The 2013 European Seismic Hazard Model: key components and results. *Bulletin of Earthquake Engineering*, **13**(12), 3553-3596, doi: https://doi.org/10.1007/s10518-015-9795-1.

[10] Stucchi et al. (2013): The SHARE European Earthquake Catalogue (SHEEC) 1000–1899. *Journal of Seismology*, **17**(2), 523-544, doi: https://doi.org/10.1007/s10950-012-9335-2.

[11] Grünthal, G., Wahlström, R. (2012): The European‑Mediterranean Earthquake Catalogue (EMEC) for the last millennium. *Journal of Seismology*, **16**(3), 535-570, doi: https://doi.org/10.1007/s10950-012-9302-y.

[12] Grünthal, G., Wahlström, R., Stromeyer, D. (2013): The SHARE European Earthquake Catalogue (SHEEC) for the time period 1900‑2006 and its comparison to the European‑Mediterranean Earthquake Catalogue (EMEC). *Journal of Seismology*, **17**(4): 1339-1344, doi: https://doi.org/10.1007/s10950-013-9379-y.

[13] Wilde, M., Günther, A., Reichenbach, P., Malet, J. P., & Hervás, J. (2018): Pan-European landslide susceptibility mapping: ELSUS Version 2. *Journal of maps*, **14**(2), 97-104, doi: https://doi.org/10.1080/17445647.2018.1432511.

[14] Fotopoulou, S. D., Pitilakis, K. D. (2015): Predictive relationships for seismically induced slope displacements using numerical analysis results. *Bulletin of Earthquake Engineering*, **13**(11), 3207-3238, doi: https://doi.org/10.1007/s10518-015-9768-4.

[15] Bojadjieva, J., Sheshov, V., Edip, K., Shalic, R., Stojmanovska, M., Apostolska, R., Fotopoulou, S., Pitilakis, D., Shkodrani, N., Babaleku, M., Bozzoni, F., Di Meo, A. (2022): Harmonized approach for mapping the earthquake-induced landslide hazard at the cross-border region between North Macedonia, Greece and Albania. *5th Regional Symposium on Landslides in the Adriatic-Balkan Region Landslide Modelling & Application* ReSyLAB, Rijeka, Croatia.

[16] Silva, V., Crowley, H., Pagani, M., Monelli, D., Pinho, R. (2014): Development of the OpenQuake engine, the Global Earthquake Model's open-source software for seismic risk assessment. *Natural Hazards*, **72**(3), 1409–1427, doi: https://doi.org/10.1007/s11069-013-0618-x.

[17] Kotha, S. R., Weatherill, G., Bindi, D., Cotton, F. (2020): A regionally-adaptable ground-motion model for shallow crustal earthquakes in Europe. *Bulletin of Earthquake Engineering*, **18**(9), 4091–4125, doi: https://doi.org/10.1007/s10518-020-00869-1.

[18] Weatherill, G., Kotha, S. R., Cotton, F. (2020): Re-thinking site amplification in regional seismic risk assessment. *Earthquake Spectra*, **36**(1), 274–297, doi: https://doi.org/10.1177/8755293019899956

[19] Akkar, S., Sandıkkaya, M.A. & Bommer, J.J. (2014): Empirical ground-motion models for point- and extended-source crustal earthquake scenarios in Europe and the Middle East. *Bulletin of Earthquake Engineering*, **12**(1): 4681–4717, doi: https://doi.org/10.1007/s10518-013-9461-4.

[20] Arnaouti, S., Fotopoulou, S., Pitilakis, K., Chatzigogos, Th., Puissant, A., Malet, J.P. (2013): Indicator kriging for locating risk zones: an application to buildings at risk in the Barcelonnette Basin. *4th International Symposium on Geotechnical Safety and Risk*, Hong Kong, China.

[21] National Institute of Building Sciences (NIBS) (2004): Earthquake Loss Estimation Methodology HAZUS 2004. *Technical Manual*, FEMA, Washington DC, USA.

HARMONIZED REGIONAL RISK EXPOSURE MODEL OF BASIC SERVICES AND TRANSPORT INFRASTRUCTURE OF CBR BETWEEN N.MACEDONIA, GREECE AND ALBANIA

Vlatko Sheshov[1], Roberta Apostolska[2], Marija Vitanova[3], Goran Jekic[4], Aleksandar Zlateski[5], Radmila Salic[6], Stevko Stefanoski[7], Markel Baballëku[8], Neritan Shkodrani[9], Dimitris Pitilakis[10], Christos Pedritis[11]

[1] *Prof. Dr., Ss. Cyril and Methodius University in Skopje, Republic of North Macedonia, Institute of Earthquake Engineering and Engineering Seismology, vlatko@iziis.ukim.edu.mk*

[2] *Prof. Dr., Ss. Cyril and Methodius University in Skopje, Republic of North Macedonia, Institute of Earthquake Engineering and Engineering Seismology, beti@iziis.ukim.edu.mk*

[3] *Assoc. Prof. Dr., Ss. Cyril and Methodius University in Skopje, Republic of North Macedonia, Institute of Earthquake Engineering and Engineering Seismology, marijaj@iziis.ukim.edu.mk*

[4] *Assit.Prof. Dr., Ss. Cyril and Methodius University in Skopje, Republic of North Macedonia, Institute of Earthquake Engineering and Engineering Seismology, jekic@iziis.ukim.edu.mk*

[5] *Assist. MSc., Ss. Cyril and Methodius University in Skopje, Republic of North Macedonia, Institute of Earthquake Engineering and Engineering Seismology, azlate@iziis.ukim.edu.mk*

[6] *Assoc. Prof. Dr., Ss. Cyril and Methodius University in Skopje, Republic of North Macedonia, Institute of Earthquake Engineering and Engineering Seismology, r_salic@iziis.ukim.edu.mk*

[7] *Dr., Crisis Management Center of N.Macedonia, stevko.stefanoski@cuk.gov.mk*

[8] *Prof. Dr., Faculty of Civil Engineering in Tirana, Albania, markel.baballeku@fin.edu.al*

[9] *Prof. Dr., Faculty of Civil Engineering in Tirana, Albania, neritan.shkodrani@fin.edu.al*

[10] *Assoc. Prof. Dr., Aristotle University of Thessaloniki (AUTH), Greece, dpitilakis@civil.auth.gr*

[11] *Dr., Aristotle University of Thessaloniki (AUTH), Greece, cpetridi@civil.auth.gr*

Abstract

In recent years, the improvement of disaster and emergency management through building a harmonized and efficient system for risk assessment of structures in the cross-border region (CBR) has become increasingly popular. Harmonization of the risk exposure model for cross border regions is first and most important step for assessment of risk in the region. Different countries, even neighboring ones, have different frameworks in which buildings for basic services and transport infrastructures are designed, built and maintained. Hence, they involve different institutions and employ different ways of gathering information on existing structures within their networks. Each of them may use different methods and systems for keeping records on their assets. Therefore, there is no readily available inventory which covers the entire stock of bridges and buildings for basic services in any of the CRISIS adjacent partner countries. The harmonized regional risk exposure model is result of the activities carried out within one of the working packages of two-year EU-funded project CRISIS (Comprehensive RISk assessment of basic services and transport InfraStructure). In this paper harmonized regional risk exposure model for the basic services (schools and hospitals) and transport infrastructure (bridges) is shown. Herein presented are the realized activities that enabled developing a harmonized cross-border regional risk exposure model, which encompasses all relevant assets related to the basic services and transport infrastructure. A regional exposure database has been created based on contemporary practice and research compatible with the GEM Exposure Database (https://storage.globalquakemodel.org/what/physical-integrated-risk/exposure-database/). This database is specific enough to conduct numerical analysis and develop or select proper vulnerability functions.

Keywords: harmonized exposure model, basic services, transport infrastructure, risk assessment, bridges

1. Introduction

In recent years, the improvement of disaster and emergency management through building a harmonized and efficient system for risk assessment of structures in the cross-border region has become increasingly popular. This research specifically focuses on enhancing the cross-border cooperation and coordination in disaster risk management based on developed models and tools and raising public awareness and preparedness for disasters.

The main objective of this paper is to present the harmonized regional risk exposure model for the basic services and transport infrastructure. The realized activities enable creation of a harmonized cross-border regional risk exposure model, which encompasses all relevant assets related to the basic services and transport infrastructure. A regional exposure database has been created based on contemporary practice and research compatible with the GEM Exposure Database (https://storage.globalquakemodel.org/what/physical-integrated-risk/exposure-database/). This database is specific enough to conduct numerical analysis and develop or select proper vulnerability functions. A vital phase of this work is basis for the vulnerability assessment of the representative structural typology concerning the identified levels of seismic and landslide hazards.

2. Methodology

Different countries, even neighboring ones, have different frameworks in which buildings for basic services and transport infrastructures as well as bridges are designed, built and maintained. Hence, they involve different institutions and employ different ways of gathering information on existing structures within their networks. Each of them may use different methods and systems for keeping records on their assets. Therefore, there is no readily available inventory which covers the entire stock of bridges and buildings for basic services in any of the CRISIS adjacent partner countries.

2.1 Buildings for basic services

To provide a set of tools and models for risk analysis, the Global Earthquake Model (GEM) has been used. The purpose of the GEM Building Taxonomy is to describe and classify buildings in systematic and uniform manner. It is a key step towards assessing the seismic risk pertaining to buildings.
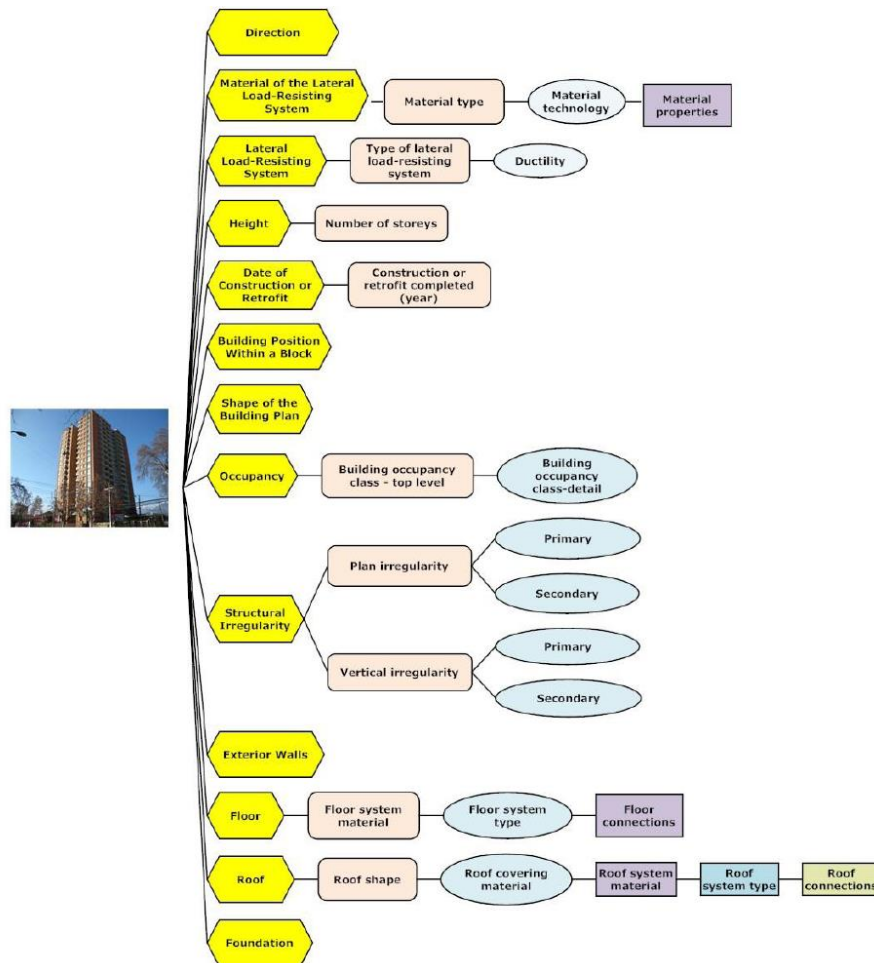
Figure 1. GEM Building Taxonomy v2.0: attributes and associated levels of detail [1]

The Building Taxonomy data model is highly flexible and has the ability to represent building typologies using a shorthand form. This taxonomy was independently evaluated and tested by the Earthquake Engineering Research Institute (EERI), which received 217 TaxTreports from 49 countries, representing a wide range of building typologies, including single and multi-story buildings, reinforced and unreinforced masonry, confined masonry, concrete, steel, wood, and earthen buildings used for residential, commercial, industrial and educational occupancy [1]. Attributes and associated details included in the GEM Building Taxonomy are presented in Fig. 1.

The GEM Building Taxonomy describes a building or a building typology through 13 attributes which are associated with specific building characteristics that can potentially affect seismic performance:

1. **Direction** - this attribute is used to describe the orientation of building(s) with different lateral load resisting systems in two principal horizontal directions of the building plan which are perpendicular to one another.

2. **Material of the lateral load-resisting system** - e.g. "masonry" or "wood".

3. **Lateral load-resisting system** - the structural system that provides resistance against horizontal earthquake forces through vertical and horizontal structural components, e.g. "wall", "moment frame", etc.

4. **Height** - building height above ground in terms of number of storeys (e.g. a building is 3-storeys high); this attribute also includes information on number of basements (if present) and ground slope.

5. **Date of construction or retrofit** - identifies the year when the building construction was completed.

6. **Occupancy** - the type of activity (function) within the building; it is possible to describe a diverse range of occupancies - for example, residential occupancies include informal housing (slums) as well as high-rise apartment buildings.

7. **Building position within a block** - the position of a building within a block of buildings (e.g. "detached building" is not attached to any other building).

8. **Shape of the building plan** - e.g. L-shape, rectangular shape, etc.

9. **Structural irregularity** - a feature of a building's structural arrangement, such as one story significantly higher than other stories, an irregular building shape, or change of structural system or material that produces a known vulnerability during an earthquake. Examples: re-entrant corner, soft storey, etc. Recognizing the fact that a building can have more than one irregularity, the user is able to identify primary and secondary irregularity.

10. **Exterior walls** - material of exterior walls (building enclosure), e.g. "masonry", "glass", etc.

11. **Roof** - this attribute describes the roof shape, material of the roof covering, structural system supporting the roof covering, and roof-wall connection. For example, roof shape may be "pitched with gable ends", roof covering could be "tile", and roof system may be "wooden roof structure with light infill or covering".

12. **Floor** - describes floor material, floor system type, and floor-wall connection. For example, floor material may be "concrete", and the floor system may be "cast in-place beamless reinforced concrete slab".

13. **Foundation system** - that part of construction where the base of the building meets the ground. The foundation transmits loads from the building to the underlying soil. For example, a shallow foundation supports walls and columns in a building for hard soil conditions, and a deep foundation needs to be provided for buildings located in soft soil areas.

Each attribute has been described by one or more levels Level 1, 2, 3, etc. [1].

To collect data for the basic services structures: schools and hospitals in the CRISIS project, GEM – Direct Observation Tool has been used [2]. This tool, which contains all these attribute levels leads to creation of a regional exposure model. This dataset contains specifically information related to structural characteristics and population data related to general basic services in different spatial

resolutions. This geospatial exposure database will facilitate global earthquake risk and loss estimation through the GEM's OpenQuake platform.

2.2 Bridge structures

Within this project activities, a system for data collection has been determined to gather as much information as possible about the bridge network in each country and to gain enough insight into the bridge inventory and permit further modelling and risk assessment, as foreseen by the project.

In this case, two categorizations of different type of data have been performed. The first categorization includes basic information on the structures - information on existence, location and overall length of the bridge. The second set of data includes information on the structural system and material of the bridge, as well as incomplete geometrical characteristics of the structural elements. This information has been used to classify the assets according to the taxonomy scheme. In this project, the taxonomy used in the Infra-NAT project has been applied [3].

3. Regional risk exposure model

Presented further is a cross-border harmonized regional risk exposure model related to the targeted cross-border region between the three partner countries: N. Macedonia, Greece and Albania. A regional exposure database that has been created is based on contemporary practice and research [4]. In this study, schools, hospitals and bridges are taken into account. For the purposes of this project, only structures in larger populated areas related to border crossings and serving a larger number of users have been considered. It is assumed that this type of structures will be the most beneficial in the period after any natural or human-induced hazard. Taking these structures into account, each neigbouring country in the region will be able to provide enhanced cross-border cooperation and coordination in disaster risk management. Integrated cross-border region municipality map is presented in Fig. 2.
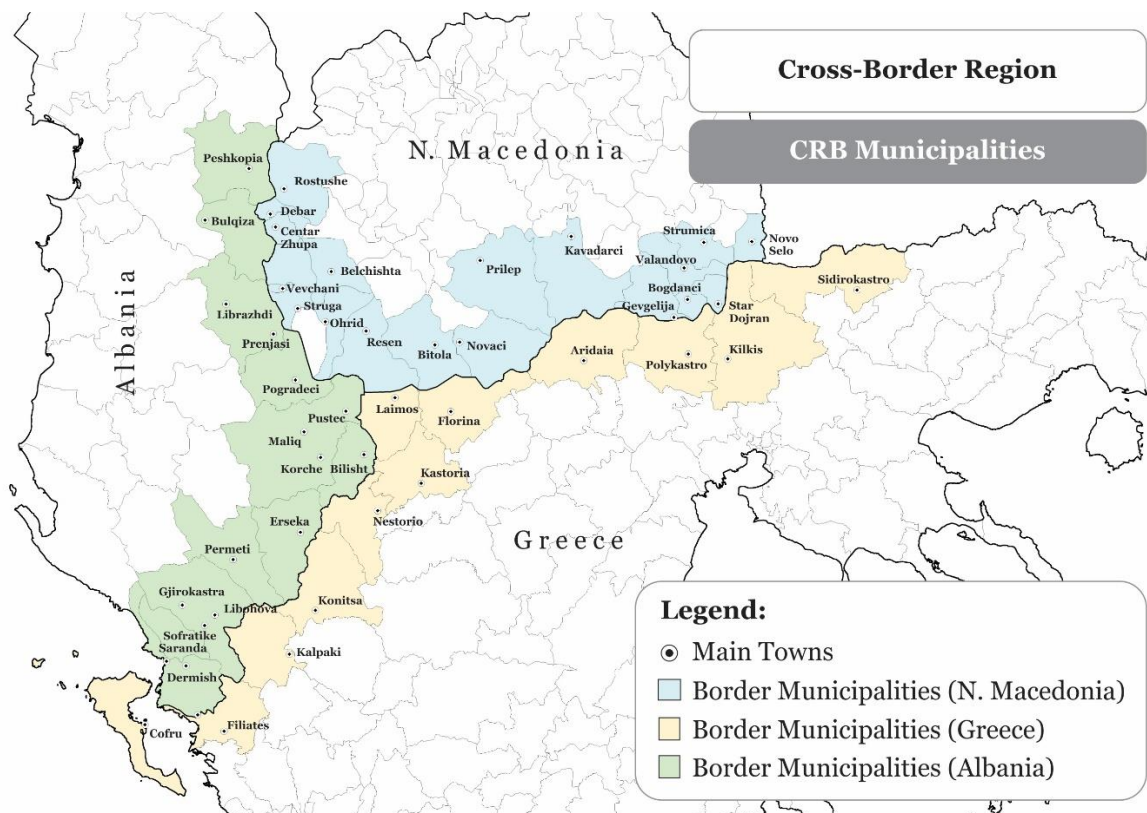
Figure 2. Integrated cross-border region; Main cities

The cross-border region that belongs to N. Macedonia (CBR-MKD), consists of 18 municipalities, the Greek cross-border region (CBR-GR), consists of 12 municipalities and the Albanian cross-border region near N. Macedonia and Greece consists of 17 municipalities. This region covers almost all the south-east and east part of Albania [4]. The region with the largest population is N. Macedonian.

3.1 Buildings for basic services

3.1.1 Schools

To collect data regarding basic services of structures, for the needs of the project, a special form containing all data necessary to fill out the GEM Tool was prepared. These data shall further serve to create the risk and emergency management platform. The initial idea was to distribute this form through the regional centres of the Crisis Management Centre (CMC) in the cross border municipalities and people working in these centres to appoint persons who work in corresponding institutions (schools and hospitals) to provide data and fill out the forms, in which way, the collected data were to be transferred to the GEM tool. To explain data to be collected through the form, instructions were prepared additionally to present all questions and possible answers through pictures and examples.

Since the Crisis Management Centre is partner institution in this project, and given that the objective of this project is improvement of the crisis management system for the purpose of more efficient response of the authorities managing emergency situations and catastrophes, a team from the Crisis Management Centre was engaged in upgrading their already existing module (http>//procena.cuk.gov.mk/) with data that are necessary in this project phase for regional risk exposure model harmonization.

The process of data acquisition was carried out in the already adopted way, through engagement of persons from the regional crisis management centres. In this way, the Crisis Management Centre acquired an improved system for evaluation of the endangerment

According to the State Statistical Office of the Republic of N. Macedonia [5], the total number of primary and secondary schools in the cross-border municipalities including all schools in the main towns and all schools in the remaining towns and smaller villages is 322. From a total number of schools in the considered region, 281 are primary schools and 41 are secondary schools.

According to the Hellenic School Network (https://www.sch.gr/), the total number of buildings used exclusively as schools in the cross-border region is 1174, while there are additional 88 buildings with mixed use, including that of schools.

In the Albanian cross-border municipalities, there are 138 primary schools, 275 mixed primary and secondary schools, 343 secondary schools and 83 high schools, allocated in the seventeen considered municipalities.

Considered in CRISIS project have been only structures located in larger populated areas related to border crossings for which corresponding data have been provided. The number of considered schools located in larger populated areas related to border crossings on the territory of N. Macedonia is 57 (40 primary and 17 secondary), on the territory of Greece 19, and in Albania 115 (total 191). According to the material technology, most of the considered schools in all three countries are constructed of cast-in-place concrete (CIP) while others are constructed of fired clay solid bricks (CLBRS). A quite minor part of them are constructed by use of another masonry unit technology (MO), whereas the remaining ones are constructed by use of an unknown technology involving stone (ST99), masonry (MUN99) and concrete (CT99). All structures constructed by use of the cast-in-place technology are constructed of reinforced concrete (CR). Most of the structures constructed by use of the masonry technology are constructed of confined masonry (MCF) and unreinforced masonry (MUR). A quite smaller part are constructed of reinforced masonry. According to the number of storeys of the schools, most of them have two and three storeys above ground and have either one or none level below ground. Most of the school structures that have been considered in this database are built between 1960-1990.

3.1.2 Hospitals

The buildings for basic services considered in this project have been health care buildings representing: general hospitals, clinics, special hospitals and health care centres, i.e., those health care structures that can provide corresponding care and hospitalization of the injured. The number of considered hospitals located in larger populated areas related to border crossings on the territory of N. Macedonia is 16, on the terotory of Greece 17, and in Albania 13 (total 46).

Most of the health care structures in the cross-border region for which data have been provided are constructed by use of reinforced concrete (CR). A minor part of them are constructed of masonry with unknown reinforcement (M99), unreinforced cement masonry (MUR), reinforced masonry (MR) and concrete with unknown reinforcement (C99). According to number of storeys above and below ground, more than half of the health care structures have 2 levels above ground and 1 level below ground. According to data available on these structures, most of them are regular from structural aspect.

3.1.3 Bridges

A database on bridges situated along the main roads within the cross-border region with Albania and Greece has been created. A total of 372 bridges have been considered (165 in N.Macedonia, 16 in Greece and 191 in Albania).
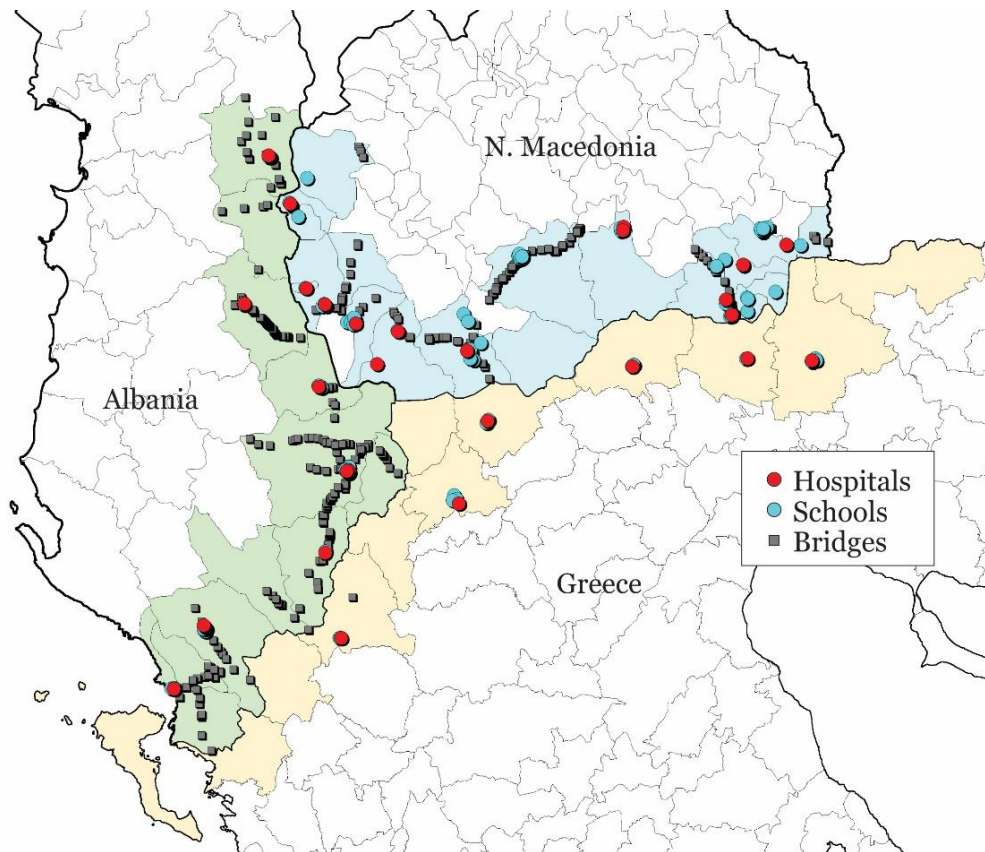
Figure 3. Cross-border region, location of the considered hospitals, schools and bridges

For some of these bridges, complete data have been available, while for some of them, there have been only basic data. Most of the bridges are situated along roads running to the border crossings on these two countries. For most of these bridges, there are basic data on the material of which they are constructed, total length, number of spans and structural system. According to type of structural system, the most frequently found bridge types in this region are bridges with frame structural system, then bridges with a girder system (with beam and slab main girders), while arch bridges account for the least

number of bridges. As to the number of spans of structures for which there are data, more than half of them have 1 span, less than 1/3 have 3 spans, while the greatest number of spans in this region is 6.

The location of the considered hospitals, schools and bridges is presented on Figure 3.

4. Summary

The following points can be made to summarise the harmonized risk exposure model of basic services and transport infrastructures:

- For the cross-border region among the countries – participants in this project, a harmonization of the exposure model has been made for educational structures, health care structures and bridges as part of the transport infrastructure by use of the GEM taxonomy.

- In this project, only structures in larger cities related to cross-border areas and serving a larger number of users have been considered. This holds for all countries –partners in the project.

- From the cross-border region, in the territory of N. Macedonia, a total of 57 schools out of which 40 primary and 17 secondary schools have been included.

- A total of 16 health care structures from the cross-border region of the territory of N. Macedonia have been analyzed.

- For the purposes of this project, a database on bridges situated along main roads within the frames of the cross-border region has been created. From the territory of N. Macedonia, a total of 165 bridges along main roads leading to border crossings on the neighbouring countries Albania and Greece have been considered.

- For Greece, a total number of 19 schools, 17 healt-care facilities and 16 bridges were assessed.

- A database on bridges situated along main roads within the frames of the cross-border region has been created. From the territory of Albania, a total of 191 bridges along main roads leading to border crossings on the neighbouring countries N. Macedonia and Greece have been considered.

- For the considered cross border region between N.Macedonia, Greece and Albania, total number of 191 school buildings, 46 health care structures, and 372 bridges are observed.

References

[1] Brzev S., C. Scawthorn, A.W. Charleson, L. Allen, M. Greene, K. Jaiswal, and V. Silva (2013), GEM Building Taxonomy Version 2.0, GEM Technical Report 2013-02 V1.0.0, 188 pp., GEM Foundation, Pavia, Italy, doi:10.13117/GEM.EXP-MOD.TR2013.02.

[2] Jordan, C.J., K. Adlam, K. Lawrie, W. Shelley, J. Bevington (2014), User guide: Windows tool for field data collection and management, GEM Technical Report 2014-04 V1.0.0,60 pp., GEM Foundation, Pavia, Italy, doi: 10.13117/GEM.DATA-CAPTURE.TR2014.04.

[3] Deliverable D3.2, Portfolio of bridge typology numerical models and fragility functions, Increased Resilience of Critical Infrastructure under Naturaland Human- induced Hazards (INFRA-NAT), https://drive.google.com/file/d/1csLv3z9tpdK52hOCvDVe_7ELH_icN1DC/view

[4] D2.1, Cross-Border Multi Hazard Assessment, Identification of all relevant natural and human-induced hazards in the crossborder region, Comprehensive Risk Assessment of Basic Services and Transport Infrastructure, 101004830 - CRISIS - UCPM-2020-PP-AG, http://www.crisis-project.org/

[5] Statistical review, State statistical office of the Republic of Macedonia, ISSN 0580-454X. Population and social statistics, ISSN 1409-8997; 2.4.18.04 (895), 2017/2018

SIMULATION SYSTEMS IN SUPPORT OF THE ORGANIZATION AND IMPLEMENTATION OF CRISIS MANAGEMENT EXERCISES

Marko Šimić [(1)], Zvonko Sigmund [(2)]

[(1)] *Lieutenant colonel, Croatian Defence Academy doc. Franjo Tuđman, marko.simic2@gmail.com*
[(2)] *Assistant professor, University of Zagreb Faculty of Civil Engineering, zvonko.sigmund@grad.unizg.hr*

Abstract

Simulations and simulation systems are effective tools for training, verification and analysis. They protect the environment, and they do not have many restrictions. They enable exercises to be carried out in irrelevant of the location of the trainee, they save resources, and they enable training in an international environment with the aim of achieving compatibility and joint interoperability and allied cooperation. The aim of this paper is to explain the possibilities offered by modelling and simulation systems in the process of supporting the organization and implementation of exercises, as well as the way of planning and organizing computer-aided exercises, the ultimate goal of which is to train training groups in solving problems caused by various crisis situations.

Keywords: simulation systems, crisis management, examples, education of crisis management teams.

1. Introduction

Timely and complete information is defined as one of the key factors for the successful resolution of problems arising from various crisis situations. The complexity of the interplay between key information, human resources, and techniques for effective crisis management has always been a challenge for crisis management; therefore, training processes in crisis management situations are critical to their effective management.

Training processes must be as challenging and realistic as possible so that the training group can experience being in a real situation. The use of simulation systems that replicate the actual situation in the field is one of the most effective and economically viable ways to train personnel involved in crisis management. The increasing power of IT systems and the faster turnover of information are elevating the capabilities of simulation systems to previously unimaginable heights, but simulation systems have their limitations and will never be able to fully replace training activities at specialized training sites or training ranges.

The main purpose of simulations is to prepare training groups to implement training content on the training site. When the training group has reached a satisfactory level of training, which is tested by the simulation system, the trained group is ready to conduct the main event. This is conducted on specialized training areas and polygons. The Armed Forces of the Republic of Croatia (OSRH) have been using simulations and simulators in training for decades.

Recently, the number of crisis situations and events on the territory of the Republic of Croatia has increased, which has led to an increase in the intensity and challenges of training personnel in the field of crisis management. Simulation systems are a logical, economically justified and cost-effective solution. OSHR are also one of the key factors of the crisis management system, so the connection of all stakeholders involved in this process is extremely important for its effectiveness. The connection and interaction of all stakeholders in the crisis management system are a guarantee of success. Tactics, techniques, and procedures in the decision-making process are targeted through training with simulation systems. OSRH, with its simulation systems and infrastructure, as well as its vast experience and knowledge in organizing and preparing simulation exercises, supports civilian institutions that are an integral part of the homeland security system and are aimed at management in crisis situations. This type of cooperation is extremely useful for the Armed Forces, as in this way the members of the Armed

Forces become part of the training group and gain new knowledge and experience. Such exercises are organized with the aim that all elements and actors of the crisis management system are trained together, making the whole system interoperable and decisions in the crisis management process easier, faster and more efficient. In addition, it is important that all actors receive information on how parts of the system work, what their capabilities are, and what their role is in the crisis management system so that the resources of specific segments of the system can be used efficiently. In addition to training at the national level, simulation systems, because of their linkage capabilities, also allow for the training of larger international coalitions to achieve compatibility and joint interoperability with other nations. In this way, they create better international relationships and sometimes alliances with other countries. This type of international cooperation in conducting joint training as part of the crisis management system has become a necessity, as has training at the national level, because crises know nations and international borders, so international cooperation in this regard is extremely important. During the pandemic COVID 19 it has been shown that only cooperation and coordination at the international level can bring effective results in managing crisis situations on an unimaginable scale

2. Simulations

2.1 Virtual space

The virtual space in which certain activities take place is a digital simulation, generally created by inserting various factors, events, or situations into a digital environment using various mathematical functions that define relationships in space and time - a so-called model.

To set the scene, the term "war games" is explained: The war game is briefly defined by the arrangement of two foe enemy forces on the field. The goal of the "games" is to make a decision on the engagement of forces through a version of action. The process of making military decisions is defined by certain steps, and the war game is only one of the steps. This kind of decision-making process is not necessarily reserved only for war operations, with minor changes and adaptations to the user, it is applicable in almost all areas when it is necessary to manage people and resources with defined goals. To make the implementation of the "war game" understandable to the users and to visualize the distribution of forces as easily as possible to the user, in 1958 Charles Roberts invented the first war game on the board and a set of models that were used throughout the American military schools, academies and colleges. Such didactic aids proved to be extremely effective and useful in the development of the war games and therefore had a positive effect in the process of making a military decision.

The accelerated development of computer equipment and communications systems initiated the development of commercial computer games, which contributed greatly to the development of military simulations, and military simulations in turn influenced the development of military-themed computer games. This symbiosis led to the development of tiered games - arcade games. The development of computers in terms of hardware and software and the possibility of connecting several people to one system (game) led to the development of new generations that grew up playing computer games. This was one of the ways to connect young people in the virtual world with the help of computers. Thus, the so-called digital natives were born. One of the games that pioneered the playing of computer games in a networked system is called Battlezone, whose theme was military in nature, more specifically the training and deployment of armed forces.

As we noted in the text above, training activities must be as realistic as possible, and simulations are the tools used in training. Depending on the type and level of training, there are three main types of simulations: live, virtual, and constructive, so the type of simulation used is determined by the level of training being conducted. The aforementioned types of simulation can be networked, i.e. connected, and used individually or simultaneously, depending on the type and scenario of the training event.

Virtual simulations are a type of in which living actors control the simulation system, i.e., the simulator. Simulators are replicas of a specific real device used to simulate the most real conditions using computers and mechanical systems. They put the user at the center of the training, training psychomotor skills, communication in a team and independently, quick reaction and decision-making skills. The use

of virtual simulations reduces operating costs and provides more latitude for risk-taking. Simulations are more environmentally friendly compared to real training, as users can cross rivers, destroy buildings, put out fires, rescue victims, and generally act in situations that would be too dangerous in live simulations.

Live simulations are operated by real people with real systems such as tanks or infantry weapons equipped with laser devices that simulate the effects of weapons in combat. Such systems vividly convey the difficult conditions of combat and the demanding way of life and work on the front line. Organizing and conducting training content using live simulations is logistically and organizationally very demanding.

When people, with their actions and decisions, initiate a certain situation that, within the simulation system, changes a certain sequence of events, we call such simulations constructive simulations. Constructive simulations, known as war games, got their name from the fact that the operational actions on the battlefield would not be conducted by a single tank or aircraft, but rather an array of different weapons or equipment that different units are composed of.

Virtual and live simulations are used to train people who supervise leaders, who see the battle in a more abstract form at the command post, or who perform various more complex tasks during protection and rescue in crisis situations, while constructive simulations allow commanders or other personnel in the role of leaders to analyse the current situation, its analysis and decision-making under time pressure, certain human and material resources, and any other issues that may arise in the given situation. Constructive simulations can put commanders and leaders in unpredictable situations and require them to solve complex problems.

The goal of simulation system is to create an artificial environment that allows unlimited integration of all three types of simulations that are interoperable, and such systems can be interconnected by simulation type, but also by user (alliances, international cooperation, etc.).

At the centre of each simulation is a machine or engine that "generates" different situations. It contains a model of the terrain, the weather, the workforce and the equipment. It changes the situation according to the reactions of the trained group to a particular event, so that mathematical algorithms execute commands, creating situational events and their consequences.

2.2 Technical organization of simulation exercises

For the simulation engine to work, data must be processed and manipulated. We call this type of data manipulation a "scenario". The team that creates the scenarios is responsible for defining this data in a form that can be used by the simulation engine.

At the end of the exercise or an exercise phase, a post-exercise analysis (RND) must be conducted to provide information about the consequences of the trained group's response to a particular event or incident. The analysis can be done in several ways, either through a simulation system only or through a discussion between a trained group and a supervisor or supervisee (controller). RND allows understanding what happened and adjusting the course of the exercise so that the trained group learns as much as possible from it, i.e., trains for the task.

Controllers are experts in their field who start and stop the simulation, control execution times, and steer the training group with the goal of making the right decision. They record and evaluate the key reactions of the training group. During RND, controllers explain to the training group how to react to a specific event or incident, and give them advice and suggestions on how to better solve the tasks they are given.

2.3 Exercise support in the form of models and simulations

Exercise support in the form of models and simulations is more than just setting up and implementing a constructive simulation system. Models and simulations and their tools should be included in all stages of the exercise process to automate processes, avoid duplication of effort, improve the exercise environment and ensure that the exercise process is focused on achieving the objectives.

2.4 Developing a database for simulation exercises

In computer-based exercises, a computer simulation model is used to systematically represent physical activity in terms of time and space. Physical aspects related to movement, resource use and perception are represented in the simulation model. However, the definition and properties of the body are not part of the simulation model. The collected data about the environment, the bodies and the resource characteristics have to be defined as data for the simulation model. The data collected in this way is called the simulation database. To define the database, a common approach is required. Bodies must be defined, their descriptive data must be collected and verified, and their behaviour must be confirmed through simulation. The Database Management Team (DMT) is responsible for carrying out this task.

Simulation data for the computer-assisted exercise (CAX) can be obtained from a number of sources, including other electronic files. The data includes terrain information, group and unit descriptions, modelling parameters, target descriptions, logistical parameters, prototype descriptions, force command and logistics structures and threat data. Terrain is represented in different formats in the various simulation systems. Terrain data includes data on terrain constants, hexagonal conversion constants, terrain features (open terrain, city, mountain, sea, etc.), obstacle features (dry riverbed, river, thin pavement, etc.), terrain permeability, obstacle permeability and obstacle permeability capacity.

The information on groups, units and facilities includes the names of the systems they operate, their characteristics (losses, weight, speed, supply category, etc.) and probability of effectiveness tables. Modelling parameters are represented by weapon, tool and system effect times and response assessment times. Target information includes repair time, target category, name, location and size. Logistical data consists of the number of supply categories, convoy speed, various lethality probabilities and damage categories.

The database management team collects data that is identified as high value data. Low-value data is usually collected in advance and stored in a database. However, some low-value data may need to be modified, such as the creation and modification of basic tactical unit characteristics, the creation of weather fronts, the modification of terrain data and the creation or specification of a type of technique or system.

2.5 Organization and implementation of simulation exercises

The simulation exercise consists of five parts: Programming, Planning, Implementation, Evaluation, and Reporting. To get the most accurate picture of the complexity of organizing and conducting simulation exercises, we need to emphasize that the preparation and execution time of an average joint international simulation exercise is rarely shorter than two years, with the planning part taking eighteen months.

Once we have clearly defined the objectives of the future exercise, we begin programming. Programming runs through the entire process of planning, preparing, and conducting the exercise. Planning an exercise involves determining the objective, participants, host, and resources of the exercise, as well as the area of interest.

Planning an exercise is the process of developing exercise specifications that define the objectives of the training group and, when done well, result in a successful exercise. The planning process is accomplished through the work of planning bodies, namely the exercise schedule and content team, the exercise execution team, the exercise organization team, and finally the planning conferences and workshops.

Well-planned and executed planning conferences are the foundation for the success of the exercise. Planning conferences are conducted in a specific order based on their content. The first is the preparatory planning conference. Here, the elements of interoperability between participants and organizers are agreed upon (time for conducting subsequent planning conferences, financial and other necessary support, distribution of roles). This is followed by the initial planning conference, where participants are identified and the scenarios of the exercise are additionally defined and reviewed. And

the final planning conference, which serves primarily to fine-tune the documentation and the presentation of the exercise to the media and the public.

Usually, the work of the various working groups takes place in the context of planning conferences, but sometimes they are convened independently when necessary. Especially when the composition of the team, e.g. for the preparation of a scenario or MEL / MIL (Main Event List/Main Incident List) teams, consists of different units, institutions and bodies, or in the case of international exercises and participants from different countries. Workshops are usually organized in the following areas: Management, Deployment, Technical, Evaluation and Support.

The success of the exercise is directly related to the exercise planning process and the success of the planning conferences. Larger and more complex exercises typically last five to ten days in their execution part, and activities are usually conducted around the clock, which has significant organizational and work implications. Recently, many exercises are organized in such a way that some of the forces or personnel being trained are dislocated; they are usually located in special exercise areas for the activities for which they are being trained. Such exercises are extremely demanding from an organizational and technical point of view, as additional efforts have to be made to provide the training group with timely information and data, which of course increases the cost of the exercise itself and places an additional burden on all logistical capacities.

After-action analysis (RND) or analysis is a process conducted for the purpose of evaluating the training of exercise participants and gathering data that will provide a clearer picture of what needs to be done to address identified deficiencies, whether they arose during the preparation phase or the execution phase of the exercises. The end result of the RND or the analysis of the organization and execution of the exercise are the lessons learned that will be used as input material for the next such or similar exercise in the future. It is important that the objectives of the exercise are clearly defined in a timely manner so that the control and monitoring apparatus can be staffed with professional and competent personnel.

The event and incident list development team workshop (MEL /MIL) is used to define event and incident development scenarios to initiate the training group and its response. The personnel involved in the work of the MEL /MIL workshop must have a high professional and technical level, because if the events and incidents are not prepared logically and in accordance with the training objectives, they can take the exercise in an undesirable direction and lead to the failure of months of effort in the process of preparing and planning the exercise.

3. Simulations as used in the Armed Forces of the Republic of Croatia

The simulation models currently used by OSRH are JTLS - Joint Theater Level Simulation (joint simulations at the global level) and JCATS - Joint Combat and Tactical Simulation, and these simulation models are currently used in modern helicopters around the world. The aforementioned models are of U.S. production and have become the most widely used simulation models deployed in large and small defense systems due to their universality and adaptability. The OSRH is equipped with the above systems, donated by the Americans and fully integrated into the training system.

JTLS is a simulation model for training forces operating on a global scale. However, as potential threats and hazards change, and with them the doctrines for responding to potential threats, such a global system allows specific forces to be deployed on an almost individual level. According to simulation system and model users, JCATS is currently the most advanced and versatile simulation model that can train forces from the individual to the joint operational level. Both systems are "alive," constantly evolving and improving, and providing more and more opportunities for training and force demonstration.

4. Examples of simulation exercises

The following exercises were organized mainly by OSRH, members of the Ministry of Interior and Civil Protection, firefighters, representatives of the Ministry of Health, and other organizations and institutions involved in the system for protection and rescue and crisis management.

Conducting national and international simulation exercises is an irreplaceable tool for training multinational coalition forces, institutions, and personnel in the protection and rescue system, and any other way is almost irrational, as it requires significant resources and usually only serves to convey clear political messages (large live exercises of multinational forces). Exercises that are not organized exclusively for a specific task are aimed at gaining experience in working in an international environment, convergence and harmonization of procedures and standards, mutual understanding, and interoperability. Large international simulation exercises require a great deal of effort from both the host and the organizer and are not often held, but when they are organized they serve as a promoter of one's goals and achievements.

4.1 SEESIM initiative (South Eastern Europe Simulation Network)

The most important exercises on crisis situation management and protection and rescue in which the Republic of Croatia actively participated were SESIM 02, 04 and 06, which in many ways represent progress for the OSRH and the protection and rescue system in the Republic of Croatia and the entire region. In the recent past, the Republic of Croatia was affected by a series of catastrophic events such as floods, fires and earthquakes, so the training with using simulation exercises proved to be a necessity.

Disasters and threats in peacetime in the modern world, which are increasing exponentially, and in the last decade the number of disasters and the number of victims and even more the material damage, require from every organized state the establishment of an active integrated protection and rescue system. Experience shows that it is necessary to link countries to create a network of national structures with the task of carrying out joint planning, actions and procedures in disaster management, joint education and training of rescue teams, the establishment of international teams for operations, the development of material and technical resources and the establishment of a joint IT network to support national disaster planning, mitigation and reconstruction. By joining the SEDM (Forum of Defense Ministers of Southeast Europe - Albania, Bulgaria, Greece, Italy, Macedonia, Romania, Slovenia, Turkey and Ukraine), the Republic of Croatia has gained the opportunity for better cooperation in the field of defense and protection, but has also committed itself to actively participate in SEDM initiatives.

SEESIM, one of the main SEDM initiatives, stands for the creation of a network of national simulation centers with the aim of conducting computer simulation exercises.

The exercise was organized as a computer simulation based on the JTLS model with the support of a commercial communications system and focused on international protection and rescue operations. extraordinary) situations. The general scenario included major flooding, landslides, and terrorist threats to the countries of SEVEN due to the use of SEEBRIG in Operation NATO ISAF in Afghanistan. The scenario resulted in thousands of casualties, and the disaster severely damaged the transportation network, leading to further complications at all levels of defense. Observations of exercise participants during the analysis pointed to deficiencies in the overall preparedness and defense system, as a result of which the amendment of legal regulations in the system of protection and rescue and crisis management was initiated with the aim of creating a law that precisely defines the roles of all participants in the above system.

4.2 BAKLJA 2013

Exercise "Baklja 2013" was held in May 2013 for the Armed Forces of the Republic of Croatia and the Republic of Croatia. The exercise was conducted entirely using the JCATS simulation system. The exercise was hosted by the Directorate of Civil Protection of the Ministry of the Interior (MUP RCZ), and the representatives of OSRH - SIMS were involved in conducting and supporting the exercise. The objective of the exercise was to prepare participants to conduct complex activities to be carried out in

the field in cooperation with other civilian structures. The primary exercise group consisted of regional fire chiefs, while the secondary exercise group consisted of county fire chiefs. The exercise scenario was set up in the Ravni Kotar area in such a way that two fires broke out in the Ravni Kotar area. The county headquarters in Zadar and the fire department commands "Sjenokos" and "Bubnjari" were formed. The fire was extinguished by fire brigades on the ground (16 DVDs (volunteer fire department) and JVP (public fire department)) with the possibility of using air forces.

4. Conclusions

To effectively and vigorously meet today's security challenges in developing and procuring modern equipment and systems, training and education are the foundations of success, and simulations and simulation systems in particular are the simplest, least expensive, and most effective tool for achieving training and education goals. To achieve such standards, it is necessary to invest in the development of new knowledge and skills among personnel in the security system, as well as in society at large. Clearly, keeping up with the evolution of global technology and knowledge is difficult and costly, but falling behind in knowledge, equipment, and training in crisis situations will ultimately be much more costly. The price of ignorance during disasters is paid in human lives and material damage. Continued investment in training, education, and equipping with new systems at a given time will pay for itself many times over, and using and developing new simulation systems and models is just one of the ways to create an efficient and energised safety system.

References

[1] Alluisi, E. A. (1991). The Development of Technology for Collective Training: SIMNET, a Case History. Human Factors, 33(3), 343–362. https://doi.org/10.1177/001872089103300308

[2] Ernest H. Page, Bradford S. Canova, and John A. Tufarolo. 1997. A case study of verification, validation, and accreditation for advanced distributed simulation. ACM Trans. Model. Comput. Simul. 7, 3 (July 1997), 393–424. https://doi.org/10.1145/259207.259375

[3] Smith RD. Analytical computer simulation of a complete battlefield environment. SIMULATION. 1992;58(1):7-16. doi:10.1177/003754979205800103

[4] Judith S. Dahmann, Richard M. Fujimoto, and Richard M. Weatherly. 1997. The Department of Defense High Level Architecture. In Proceedings of the 29th conference on Winter simulation (WSC '97). IEEE Computer Society, USA, 142–149. https://doi.org/10.1145/268437.268465

[5] MacDougall, M. H. 1987. Simulating Computer Systems: Techniques and Tools, Massachusetts: The MIT Press.

[6] Farid Mamaghani. 1998. Creation and use of synthetic environments in realtime networked interactive simulation. Digital illusion: entertaining the future with high technology. ACM Press/Addison-Wesley Publishing Co., USA, 99–114.

[7] NATO Handbook – NATO Office of Information and Press, 2001.Brussels, Belgium

[8] Uputa o vojnim vježbama u OS RH, GS OS RH, Zagreb, 2002.

THE ROLE OF DISASTER RISK GOVERNANCE IN POST-DISASTER RECOVERY

Zvonko Sigmund [(1)], Marko Šimić [(2)]

[(1)] *Assistant professor, University of Zagreb Faculty of Civil Engineering, zvonko.sigmund@grad.unizg.hr*
[(2)] *Lieutenant colonel, Croatian Defence Academy doc. Franjo Tuđman, marko.simic2@gmail.com*

Abstract

This paper emphasizes the role of decision-making and disaster risk governance in post-disaster recovery on the example of the post-disaster recovery of Croatia after a series of strong seismic events in mainland Croatia. The analysis is based on a thorough review of the national documents of Croatia that overlapped with the national journals reporting on the situation from the affected areas.

Keywords: Disaster risk governance; disaster risk management; Sendai framework; Croatia; case study.

1. Introduction

Natural disasters, alongside climate change cause, ever-increasing losses with a 3 x increase in losses only in the last 20 years [1]. In order to improve the rate of implementation of scientific advances effectively in disaster risk reduction it is important to understand what the major barriers to effective disaster risk management are.

Disaster risk governance has traditionally been fragmented between local, state, and national entities and between sectors, and compartmentalized in highly variable bureaucratic structures [2], which is the case in Croatia as well. Risk governance is mostly viewed through the lens of disaster or emergency management departments, agencies, or organizations, which often have little interaction with other governmental, civil society, or corporate entities. Visible in times of crises, risk governance is rarely seen as part of everyday public or private functions such as planning, social welfare, investments, or fiscal responsibilities [2], [3].

The statement that disaster risk needs to be taken care of in a more holistic way whereby also DRM capacity is built is a widely supported thesis [4], [5]. This includes moving beyond a focus in DRM on preparedness and emergency management to building capacity in disaster prevention, mitigation, and long-term recovery [6]. This need, to advance the DRM becomes a necessity as soon as a disaster happens, as did in Croatia in the year 2020.

This paper aims to emphasize the importance of decision-making on a higher, governmental level, but also the role of disaster risk governance in the implementation of disaster risk recovery in the example of Croatia. Hereby, the authors are only concentrating on the construction industry. Disaster risk governance principles as were defined and planned through regulatory framework as well as the changes that were introduced after the earthquake series that struck mainland Croatia during the year 2020 are reviewed in this paper.

For the need of this paper, the UNDRR terminology glossary [7] is used. Disaster risk governance is defined as "The system of institutions, mechanisms, policy and legal frameworks and other arrangements to guide, coordinate and oversee disaster risk reduction and related areas of policy", and disaster risk management is "the application of disaster risk reduction policies and strategies to prevent new disaster risk, reduce existing disaster risk and manage residual risk, contributing to the strengthening of resilience and reduction of disaster losses" [7].

Croatia was struck with two major earthquakes: the Zagreb earthquake that struck on March 2020 (M5.0), just after the Croatian government issued a complete lockdown due to the COVID pandemic; and the Petrinja (about 50 km from Zagreb) earthquake (M6.4) on December 2020.

On 22 March 2020, Zagreb was struck by an M5.5 [8]. A pronounced issue that arose is the damaging of many historical buildings which were in many cases used for public purposes: hospitals, schools, theatres, local or state administration, etc. The earthquake was followed by 10 aftershocks of M3+ during the time of the next 4 months[9]. 1 person succumbed to injuries caused by the earthquake, and about 24.000 buildings were reported to have been damaged, of which about 5.000 buildings were heavily damaged [10]. Total damages and losses according to the rapid damage and needs assessment were 11.3 billion Euros [11].

Petrinja earthquake began with an earthquake of M5.0 followed by M4.5 and M3.8 on the same day on December 28th, 2020, [12]. The behavior was considered to be a sign of calming down, this, however, was not the case. On December 29th the main shock struck Petrinja with M6.4 [13], [14]. In the aftermath of the Petrinja earthquake [12]: 7 persons were confirmed dead, and about 45.000 buildings were reported to have been damaged, of which about 11.000 buildings were assessed by engineers to be unusable due to the damages [15]. Total damages and losses according to the rapid damage and needs assessment were assessed at 4.8 billion Euros [16].

2. Seismic disaster risk management -case of Croatia

Croatia has just recently (within the last few years) started switching its focus from disaster risk preparedness to disaster risk management with the introduction of the Homeland Security System Act [17].

While mainly oriented toward disaster response, in general, the Croatian disaster risk management system (regulatory framework) recognizes only two areas of disaster risk management: prevention and response. Therefore, the Croatian disaster risk management system can hardly be fully valorized through the objectives of the Sendai framework for disaster risk reduction.

2.1 Croatian disaster recovery framework after the earthquake series in the year 2020

Prior to the earthquake, the only law to regulate recovery is the Law on mitigation and elimination of the consequences of natural disasters. This law regulates governmental financial responsibility towards all affected by disasters and the operationalization of the activities of the Ministry of Finance in cases of disasters. The responsibility is instrumentalized through financial support but includes an assessment of the effects of disastrous events and the allocation of partial financial relief to affected areas [18]. Other institutionalized measures for disaster recovery were so far regulated only after the occurrence of the disaster, as was the case of the area destructed by flooding in 2014 [19].

As soon as the first earthquake struck Zagreb, on the governmental level, it was clear that the Croatian legal framework cannot be kept as was. The new legislation would need to come in place to enable recovery and reconstruction works. Nevertheless, even though the legislator had a clear vision of the regulatory framework that needed to be defined, the disaster recovery and reconstruction regulatory framework that was initially prescribed needed to be adapted in accordance with needs identified during the practical use of the legislation:

On March 21, 2020. Croatian Government introduced a "stay at home" order for the whole country due to the COVID-19 pandemic, and the very next day a magnitude 5.5 quake shook the capital - city of Zagreb [19]. The regulatory framework for disaster recovery was structured in a series of different measures: suspension of COVID-19 restricting measures in the affected areas, financial relief and support, disaster emergency housing, emergency repair support in terms of financial and workforce organization, and finally the framework supporting the recovery and repair of damaged infrastructure and the built environment.

The main goal of the regulatory framework, after the earthquake series, was to assist the owners or co-owners of damaged and destroyed real estate to set up their estates as quickly and with less effort in comparison to the previously available legal framework. The first recovery and reconstruction law was created to aid the affected areas of the first earthquake: Law on the reconstruction of buildings damaged by earthquakes in the City of Zagreb, Krapina-Zagorje County, and Zagreb County [20]. The main goals of the Law were to reduce and simplify the documentation needed for the approval of the reconstruction, and:

- To establish the "Reconstruction fund" - the main governmental executive body for organization, implementation, and monitoring of the implementation of reconstruction activities of earthquake-damaged buildings [21].
- To define the process of building reconstruction in case the building was only damaged, construction of replacement housing in case a house was destroyed or damaged in a way that repair is not possible or financially inefficient.
- To prescribe financial support for temporary repair works, building reconstruction and repair works

In addition to the law, in October 2020 the First program of measures for the reconstruction of earthquake-damaged buildings in the City of Zagreb, Krapina-Zagorje County, and Zagreb County was prescribed. This program of measures would define the levels and scopes of repair and/or reconstruction that can be financed from the reconstruction fund. Further on it would define the organizational structure of the governmental bodies responsible for activities in the reconstruction, criteria for project parties' selection, reconstruction priorities, etc. [22]. As the title of the law shows, the law regulates the recovery measures only in the affected areas and cannot be implemented outside of the mentioned counties.

By October 2020, 7 months from the earthquake have passed. By that date mainly the emergency repair works were done, besides these only a few reconstruction projects were started among which the City of Zagreb was the main investor. By that time, even though there is no official data, the number of reconstruction activities in the affected region is at a minimum.

With the occurrence of the second earthquake series in the area of Petrinja (Sisak-Moslavina county) amendment to the already existing law on reconstruction was made with the Law amendments from the February of 2021 [23] (just two months after the December earthquake series). As the new situation required a new approach, the amendment of the law was not only used to broaden the area of use to the newly affected areas, but also to accommodate new needs. Except for the historic city centers in the affected areas of Sisak-Moslavina County and the other affected areas, these areas are more rural type areas with occasional historic buildings and the occasional industrial facilities, which have now sustained major damages, as opposed to the earthquakes of Zagreb, where most damages were sustained in the historical buildings which were not designed to withstand seismic activities of any kind.

By the time of the Law amendment publication, the Reconstruction fund began to function as intended resulting in the first 231 finished reconstruction investments with the investment sum of about 1.1 mil EUR [24]. As the earthquake from December 2020 had more serious consequences than the one from Zagreb County (March 2020) the main changes in legislation were oriented toward creating emergency housing capacities for people whose homes were destroyed or severely damaged. Herefore, a part of the responsibilities and powers that were the main activities of the Reconstruction fund was transferred to the Central State Office for Reconstruction and Housing to divide the intensity and the activity scope of the Reconstruction fund [23].

During the reconstruction process, several main issues were encountered that were slowing down the reconstruction process:

- The owners (potential investors) were not allowed to start the reconstruction on their own, but to be entitled to governmental funding, the reconstruction process had to start via the governmental administration [25], which process was rather sluggish
- Co-financing measures are limited to 80% of the cost of structural renovation of a building which in the whole process of reconstruction would cover no more than 30% of the whole

reconstruction investment causing many potential investors to give up on the potential reconstruction investment [26]

- There is a problem of unresolved ownership relations for which the process of renewal is entirely disabled even for cases when real ownership is not in question, but it is not legally implemented, or the legal trace of ownership is difficult to prove (problem expressed in rural parts of Croatia) [27]
- Construction works prices have risen uncontrollably on the global market, which is more pronounced in Croatia due to a sped-up increase in demand for construction and reconstruction works and the COVID-19 sanitary crisis. Hereby the owners' ability to invest is severely diminished [28]
- The affected area is widely marked by cultural heritage buildings, which also make up a significant share of the damaged buildings. The necessary activities of the relevant administration for cultural heritage are poorly defined even by basic laws, which is even more evident in crisis situations [29]
- The reconstruction process indicated some administrative deficiencies in the process [29]among which is for instance the Demolition of heavily damaged buildings that potentially threaten the environment requires a series of administrative approvals

Still, even with the flaws of the law, the rate of investments in reconstruction rose to 792 reconstruction investments in total and approximately 5,6 mil EUR [24]. In relation, the investments rose from form 33 cases per month and approximately 160.000 Eur/month to 99 cases / months and 700.000 EUR/month. Still, these numbers cannot be taken as the absolute measure of the success of the Laws, but still, they can be taken as an indicator that the reconstruction measures are giving positive results.

These mentioned issues were to be resolved by the latest amendment of the Law on reconstruction [30] with next measures:

- Main and most important change is the reorganization and improved definition of the tasks of governmental bodies included in the process of reconstruction. The improvements also include the definition of the maximum allowed time for decision-making in the process of project approval or the definition of requested conditions that must be obeyed (e.g., preservation measures for cultural heritage buildings).
- The governmental financial support for reconstruction increased from 80 to 100% of the construction reconstruction cost with the possibility to receive the governmental subsidies in advance (only in the case where the building has a legal and official representative). This reduces the initial cost of reconstruction and repairs at the start of the investment process.
- For the cases where family house owners are willing to invest in the recovery of their real estate, they are now allowed to finance the works by themselves with the possibility to request a full refund of the applicable reconstruction costs (only for the construction reconstruction)
- To improve the implementation rate of the Law, the state can buy off the ownership of a building or a part of the ownership to improve the implementation of the Law on reconstruction
- The demolition of heavily damaged buildings is financed completely by the government, and in case a building is endangering the surroundings or persons, the building can be demolished by a shortened administrative procedure (duration of up to 5 days); where the owners of a demolished real estate have the possibility to receive financial reimbursement for their real estate or they can request a replacement house (only for real estate where owners were living in at the time of the earthquake)

Hereafter until the day of writing this paper (02.03.2023.) further 911 reconstruction investments and approximately 9,5 mil EUR [24] were approved. In relation to the previous regulatory framework, the investment number fell from 99 cases per month and almost 700.000 EUR/month to 53 cases per month and 560.000 EUR/month.

Interestingly enough, in the current state, the Croatian government introduced a new Law on reconstruction with new by-laws. Still, as the innovation in the regulatory framework is completely new the effects cannot be seen yet. The new Law on reconstruction [31]:

- emphasizes self-renovation as the government will give more financial support even before the reconstruction process starts
- ownership issues are regulated in cases where the data from the land register does not match the actual situation or the land register does not exist.
- reduces the number of participants in the renovation process hoping to boost the reconstruction and recovery
- reconstruction of buildings cultural heritage buildings is made more easy by regulating the involvement of cultural heritage protection experts in the renovation process
- introduces the provision of financial aid to citizens for the removal of all destroyed buildings, as well as financial aid for project development costs.
- it is now possible to build a replacement family house when it is determined that the repair of the structure is not justified due to landslides and other geological changes that caused a change in the basic characteristics of the soil.

3. Conclusions

The Croatian case study emphasizes the role of disaster risk governance showcasing the adaptation process for the post-disaster recovery process to start. Here the process could have evidently been shortened had the post-disaster recovery regulatory framework been ready and waiting in case of an emergency. That the disaster risk recovery governance was weakly developed was already identified by the National disaster risk assessment. This emphasizes the importance of the second Sendai framework priority, which also highlights the importance of the necessary political will and the positive and enabling surrounding for effective disaster risk reduction measures. Without either the political will or the enabling surrounding the disaster risk management is next to impossible.

The National risk assessment clearly states that the government had been strongly and intensively investing in preparedness, and these activities played an important role in the short-term post-disaster process. It can be safely assumed that the disaster risk management disabling surrounding and the nonexistent political will made it tough and de-motivating to invest in preventive disaster risk-reducing measures, at least when it comes to retrofitting the built environment to resist the expected seismic events. Hereby the number of investments aimed at reducing the risk of damage to the built environment was severely reduced, making another strong statement that national governance makes a strong impact on enabling disaster risk management. One can argue that both issues can be attributed to a weak understanding of the risk at hand, here for however it is unclear which awareness-raising processes could have achieved the wanted result.

Analysis shows that disaster risk reduction measures need time to be adopted in a culture, and Croatian risk-raising campaigns have started only a decade ago, still, it is unclear if a longer or more aggressive risk-raising campaign would have had a wanted impact and would have enabled the creation of the so much needed disaster risk reduction governance.

Whether known or unknown disaster risk sources are numerous, and their direct impacts are very well-known, and these are ever-increasing. However, as currently we are living in a globalized world real unwanted impacts of a particular disaster can only be discovered once the disaster happens. These can have a much more spread-out impact than obvious at the first sight. At the time of writing this article, the Covid-19 pandemic has made this global risk landscape more evident than ever. Due to the current global crisis, States must undertake immediate action at community, national, and international levels to reduce the risks.

References

[1]   Statista research department, "Cost of natural disaster losses worldwide from 2000 to 2020, by type of loss," Natural disaster losses cost worldwide 2000-2020, 2021. https://www.statista.com/statistics/612561/natural-disaster-losses-cost-worldwide-by-type-of-loss/ (accessed Oct. 17, 2021).

[2]   A. Altshuler et al., "Socioeconomic and data challenges: disaster risk reduction in Europe," 2019.

[3]   M. Gall and S. L. Cutter, "Governance in Disaster Risk Management Social Sensing and Big Data Computing for Disaster Management View project SoVI Brazil View project," 2014, doi: 10.13140/2.1.2130.2568.

[4]   T. Bryant, "Mapping Vulnerability: Disasters, Development and People," Geographical Research, vol. 44, no. 3, pp. 328–329, 2006, doi: https://doi.org/10.1111/j.1745-5871.2006.00395.x.

[5]   C. Wisner and D. Nivaran, "At Risk: natural hazards, people's vulnerability and disasters," 2003.

[6]   R. Few, Z. Scott, K. Wooster, M. F. Avila, M. Tarazona, and A. Thomson, "Strategic Research into National and Local Capacity Building for DRM Synthesis Report," Geneva, 2015. [Online]. Available: www.ifrc.orgSavinglives,changingminds.

[7]   UNDRR, "Terminology - Online glossary," 2017. https://www.undrr.org/terminology (accessed Oct. 17, 2021).

[8]   S. Markušić, D. Stanko, T. Korbar, N. Belić, D. Penava, and B. Kordić, "The Zagreb (Croatia) M5.5 earthquake on 22 March 2020," Geosciences (Switzerland), vol. 10, no. 7, pp. 1–21, 2020, doi: 10.3390/geosciences10070252.

[9]   "Analiza naknadnih potresa." https://www.pmf.unizg.hr/geof/seizmoloska_sluzba/o_zagrebackom_potresu_2020/pola_godine_od_potresa/analiza_naknadnih_potresa (accessed Oct. 13, 2021).

[10]   HCPI, "Rezultati procjena oštećenja građevina nakon potresa u Zagrebu 2020," 2020. https://www.hcpi.hr/rezultati-procjena-ostecenja-gradevina-nakon-potresa-31 (accessed Oct. 13, 2021).

[11]   Government of Croatia and World Bank, "CROATIA EARTHQUAKE Rapid Damage and Needs Assessment," Zagreb, 2020.

[12]   S. Markušić et al., "Destructive m6.2 petrinja earthquake (croatia) in 2020—preliminary multidisciplinary research," Remote Sens (Basel), vol. 13, no. 6, Mar. 2021, doi: 10.3390/rs13061095.

[13]   USGS, "Earthquake near Petrinja, Croatia," 2020. https://earthquake.usgs.gov/earthquakes/eventpage/us6000d3zh/map (accessed Oct. 17, 2021).

[14]   EMSC, "M 6.4 - CROATIA - 2020-12-29 11:19:54 UTC," 2020. https://www.emsc.eu/Earthquake/earthquake.php?id=933701#providers (accessed Oct. 17, 2021).

[15]   HCPI, "Hrvatski Centar za Potresno Inženjerstvo," 2021. https://www.hcpi.hr/ (accessed Dec. 28, 2021).

[16]   Government of Croatia and World Bank, "Croatia December 2020 Earthquake - Rapid Damage and Needs Assessment," Zagreb, 2021.

[17]   Parliament of Croatia, "Homeland Security System Act (NN108/17)," Zagreb, 2017. Accessed: Oct. 13, 2021. [Online]. Available: https://narodne-novine.nn.hr/clanci/sluzbeni/2017_11_108_2489.html

[18]   Pairlament of Croatia, Law on mitigation and elimination of the consequences of natural disasters. Croatia: Official Gazette, 2019.

[19]   Z. Sgmund, M. Uroš, and J. Atalić, "The Earthquake in Zagreb amid the COVID-19 Pandemic: OPINION," 2020. Accessed: Dec. 28, 2021. [Online]. Available: https://www.undrr.org/news/earthquake-zagreb-amid-covid-19-pandemic-opinion

[20]   Pairlament of Croatia, NN 102/20 - Law on Reconstruction of Earthquake Buildings on the Territory of the City of Zagreb, Krapina-Zagorje County and Zagreb County. Croatia: Official Gazette, 2020. Accessed: Nov. 01, 2021. [Online]. Available: https://narodne-novine.nn.hr/clanci/sluzbeni/2020_09_102_1915.html

[21]   C. and S. P. Ministry of Physical Planning, "Fond za obnovu," 2020. https://mpgi.gov.hr/o-ministarstvu/djelokrug/graditeljstvo-98/obnova-zgrada-ostecenih-potresom-na-podrucju-grada-zagreba-i-krapinsko-zagorske-zupanije/fond-za-obnovu/11220 (accessed Nov. 06, 2021).

[22]   Pairlament of Croatia, NN 119/20 - First Program of Measures For Reconstruction of Earthquake Damaged Buildings in the City of Zagreb, Krapina-Zagorje County And Zagreb County. Croatia: Official Gazette, 2020. Accessed: Nov. 01, 2021. [Online]. Available: https://narodne-novine.nn.hr/clanci/sluzbeni/2020_10_119_2309.html

[23]   Pairlament of Croatia, NN 10/21 - Amendments to the Law on Reconstruction of Earthquake Damaged Buildings on the Territory of the City of Zagreb, Krapina-Zagorje County and Zagreb County. Croatia: Official Gazette, 2021. Accessed: Nov. 01, 2021. [Online]. Available: https://narodne-novine.nn.hr/clanci/sluzbeni/2021_02_10_191.html

[24]   Reconstruction fund, "Reconstruction fund - overview of payments and costs," 2021. https://www.arcgis.com/apps/dashboards/fd7f27fcda014e97a8ef1238729f837e (accessed Nov. 23, 2021).

[25]   Ministry of Physical Planing Construction and State Assets, "Expert reconstruction advice meeting - 03.02.2021.," Feb. 03, 2021. https://mpgi.gov.hr/vijesti/izmjenama-programa-mjera-dodatno-ce-se-pojednostaviti-procedure-u-obnovi-i-smanjiti-potrebna-dokumentacija/11497 (accessed Nov. 23, 2021).

[26]   A. Latinović, "GDJE JE ZAPELO? Obnova nakon potresa u Italiji najbolji je putokaz za Hrvatsku, trebamo međunarodnu pomoć, ali i onu iz dijaspore...," 2021. Accessed: Nov. 23, 2021. [Online]. Available: https://direktno.hr/direkt/gdje-je-zapelo-obnova-nakon-potresa-u-italiji-najbolji-je-putokaz-za-hrvatsku-trebamo-medunarodnu-pomoc-ali-i-onu-iz-dijaspore-247986/

[27]   M. Pušić, "Prizori s Banije prije i poslije: Novi krovovi niču, ali postoji jedan veliki problem," 2021. Accessed: Nov. 23, 2021. [Online]. Available: https://www.jutarnji.hr/vijesti/hrvatska/prizori-s-banije-prije-i-poslije-novi-krovovi-nicu-ali-postoji-jedan-veliki-problem-15107101

[28]   E. Felić, "GRAĐEVNI MATERIJAL - Cijene poludjele, a rast će i dalje," 2021. Accessed: Nov. 23, 2021. [Online]. Available: https://lider.media/poslovna-scena/hrvatska/gradevni-materijal-cijene-poludjele-a-rast-ce-i-dalje-135844

[29]   Ministry of Physical Planing Construction and State Assets, "Expert reconstruction advice meeting - 27.10.2020.," Oct. 27, 2020. https://mpgi.gov.hr/vijesti-8/pocetak-obnova-manjih-zgrada-trebao-bi-krenuti-do-proljeca/11155 (accessed Nov. 23, 2021).

[30]   Pairlament of Croatia, NN 117/21 - Amendments to the Law on Reconstruction of Earthquake Damaged Buildings on the Territory of the City of Zagreb, Krapina-Zagorje County and Zagreb County. Croatia: Official Gazette, 2021.

[31]   Pairlament of Croatia, Law on Reconstruction of Earthquake Damaged Buildings on the Territory of the City of Zagreb, Krapina-Zagorje County and Zagreb County. 2023.

SEISMIC RESILIENCE OF THE SCHOOLS IN BANJA LUKA - some constructional and preparedness aspects

Vesna Šipka [(1)], Velibor Lalić [(2)], Slavica Radovanović[(3)], Cvjetko Sandić[(4]

[(1)] *DRR and planning expert, Department for Civil Protection, City of Banja Luka, BiH, vesna_sipka@hotmail.com*
[(2)] *Associate Professor, Faculty of Security Studies, University of Banja Luka, BiH, velibor.lalic@fbn.unibl.org*
[(3)] *Director, Seismo SR d.o.o., Beograd, Serbia, seismobeo@yahoo.com*
[4)] *Deputy Director, Geological Survey of the Republic of Srpska, Zvornik, BiH, cvelesandic@hotmail.com*

Abstract

Banja Luka is a city which, in October 1969, experienced the strongest earthquake in the territory of Bosnia and Herzegovina. On that occasion 2/3 of the school buildings were severely damaged or destroyed. Banja Luka students were forced to attend that school year throughout the former Yugoslavia. Seismic risk management for schools on the territory of Banja Luka is significant from the aspect of protecting students as a vulnerable category of society. It is also important observing the fact that school facilities are used as facilities for temporary mass accommodation of the affected population during emergencies. Examining the level of earthquake protection, i.e. seismic resilience of the schools in Banja Luka, as a city with a high seismic hazard, implies the resistance of school buildings (material resilience) but also the preparedness of school communities (administration, students and teachers) to react properly in the event of an earthquake (non-material resilience). The results of the research indicate weaknesses in both the material and non-material resilience of schools. The structural aspects of school resilience include the seismic hazard of the area, the soil at school locations in terms of the expected seismic effect, the age and poor maintenance of the buildings, and the undefined ownership of school buildings. Regarding non-structural resistance, a low level of carrying out preventive activities such as education, training and practical exercises for dealing with earthquakes was identified as well as inadequate planning documentation.

Keywords: earthquake, schools, seismic resilience, preparedness

1. Introduction

The devastaded eartqhuake occured in Banja Luka October 27, 1969. This EQ with 6.6 Richter scale units magnitude is the strongest in history of the Banja Luka region and entire Bosnia and Herzegovina. The entire city was destroyed and the consequences were severe for educational institutions since Banja Luka was an educational and cultural center. Severe or moderate damage was recorded in 23 elementary school buildings, 9 high school buildings, 3 high school buildings, and two facilities for students accomodation. The extent of the destruction is also shown by the fact that in only 8 out of 346 classrooms in primary and secondary schools education could be continued after the earthquake without any reparations.

During 2016, research and analysis of existing school buildings in the territory of the city of Banja Luka was carried out relating to material resistance to earthquakes, i.e. seismic vulnerability [2]. In the meantime, new researchs have not been conducted. The need for research into the non-material and material resistance of school facilities in the territory of the city of Banja Luka comes from the both facts confirmed seismic hazard and the age of the school facilities. Even though Banja Luka is regional educational center, only one new school building has been built in the last 30 years. According to paper [2], about 35,000 students attend primary and secondary schools in the city.

The resilience of the schools to earthquake effects, as objects of mass gathering of people, should be considered from a material and non-material aspect. The material resistance of schools means the resistance of the school building to the effects of earthquakes, while the non-material resistance

refers to the preparedness of users of school buildings for adequate behavior before, during and after an earthquake. The resilience of a school building on eartquake depends on a number of factors such as age, construction, materials used and maintenance of the buildings, as well as the soil type where the buildings were located. Since amplification seismic signal caused by soil is important it is clear that the composition and quality of the soil affects the vulnerability of buildings in case on earthquakes. Importance of the soil types in seismology is shown by the more detailed classification of the soil as part of the modern building codes. The complete risk assessment should include beside parameters of seismic hazard, the seismic vulnerability of buildings, impact of the local soil also assessment of non-material resistance - that is, the preparedness of the school community

The aim of this paper is to highlight some problems related to the material and non-material resilience of the schools in the city of Banja Luka.

2. Constructional resilience of the schools in Banja Luka

Objects of mass residence of people, especially schools, are important for Disaster risk reduction (DRR) plans as well as for the local community's DRR plan in case of earthquake. School facilities are treated as critical infrastructure in these documents and those buildings are planned for temporary mass accommodation of the affected population in the case of earthquake.

Data collected for the 71 school buildings enabled an overview of the basic architectural and structural characteristics of the schools in Banja Luka. The most important data for the assessment of expected structural and non-structural elements damage and the assessment of the usability of the buildings after earthquake are shown in Figure 1.

The largest number of school buildings were built before the catastrophic earthquake in 1969; they are symmetrical in shape and consist of a ground floor and an upper floor. Branch schools are mostly smaller one-storey buildings. The number of students in urban schools ranges from 500-1000 students, in suburbs up to 200, as well as in rural schools up to 50 students. Regarding construction types, the most of the schools are brick buildings of typical construction at the end of the 20th century, mostly of brick and less of stone [2].
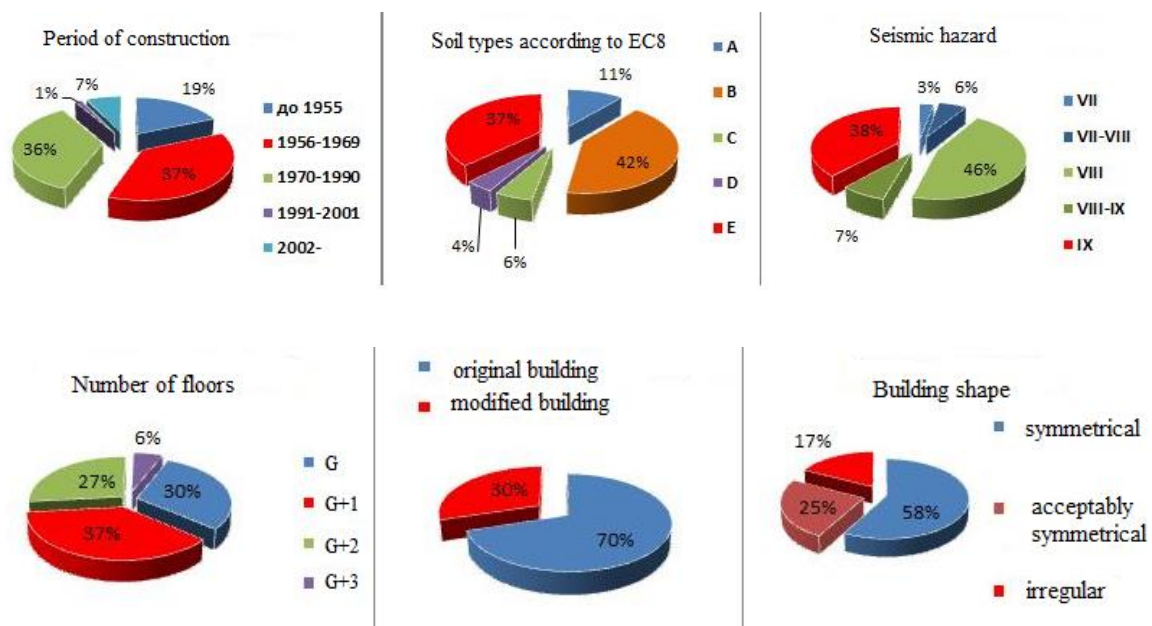
Figure 1. The characteristics of the school buildings [2]

Analysis of the vulnerability of school buildings was carried out on the basis of data related to building construction method, applied materials and knowledge about construction characteristics in specific areas as well as descriptions of individual classes of vulnerability given in the EMS-98 scale, [3]. Vulnerability classes were determined by expert assessment based on the above criteria.
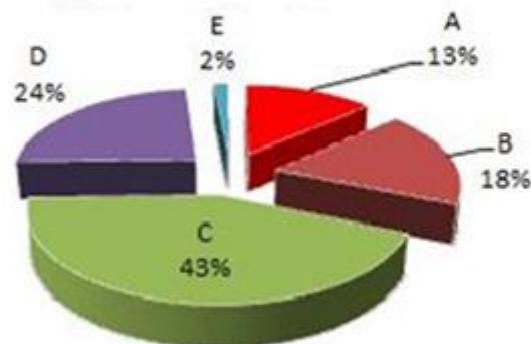
Figure 2. Vulnerability classes according to EMS-98 criteria [2]

Considering that vulnerability classes A, B and C represent buildings where seismic measures have not been applied, we conclude that 74% of existing school buildings are not built under seismic codes which clearly shows that the structural resilience of the schools in Banja Luka is not satisfactory.

Due to the reconstruction after the earthquake in Banja Luka in 1969, the most of the schools buildings belong to vulnerability class C type. According to assessment seismic risk 7% vulnerability class C building are in significant risk to collapse in case of IX earthquake intensity EMS-98 while 17% of buildings of this type can suffer structural damage[4].

Modern science on the design of seismically resistant buildings has recognized the type of soil as extremely important, so Eurocode 8 defines 5 basic soil categories A, B, C, D and E, and two special ones S1 and S2 for which special research is necessary. A map of the local soil of the municipality Banja Luka was created for school risk assessment purposes. Based on the local soil map according to EC8 for the territory of the city of and the geospatial distribution of school facilities, the type of local soil was determined for each school facility. The results of the soil analysis [2] showed that 37% of school buildings are located on type E soil, which is the lowest quality type of soil according to the Eurocode 8 classification.
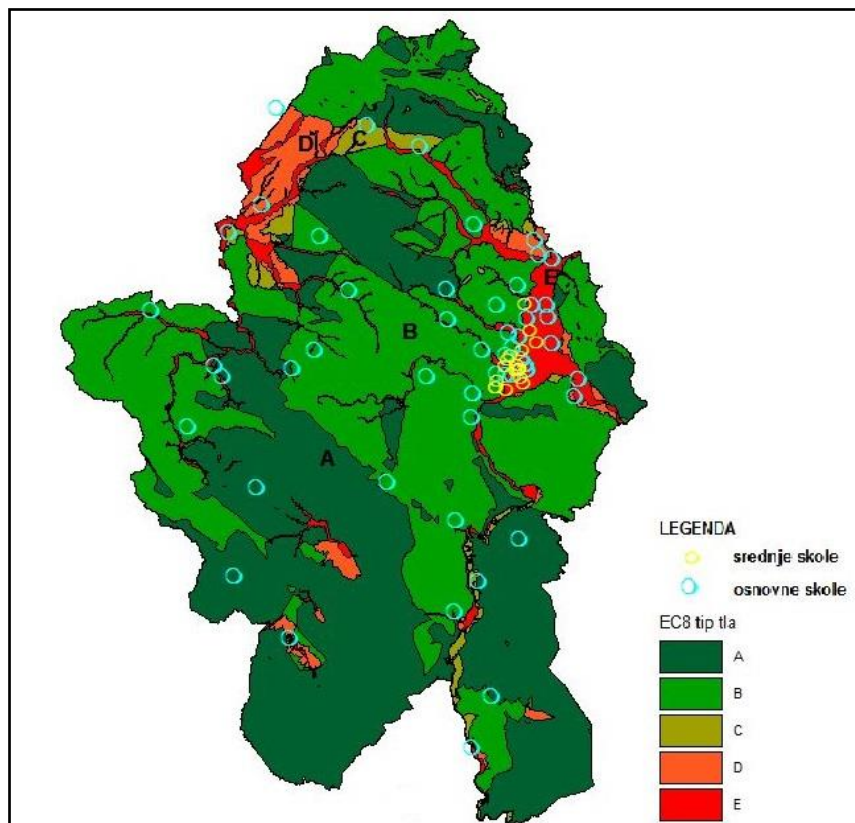
Figure 2. The school building positions on the local soil map [2]

The results of research [2, 4] on the construction characteristics of school buildings showed that their structural resistance is unsatisfactory. The results of the research [5] indicate numerous problems. The official attitude of the Ministry of Education as well as the local community is that complete organization of school life is obligation of the school management. School principals are expected to provide funds for maintaining school facilities, as well as to perform all other duties independently and without any support. The schools itself, according to the principal's statements, barely manage to meet the needs necessary for the basic functioning of the school including conducting teaching process, children stay, providing energy supply, as well as hygienic and office materials, etc. The schools receive funding for material costs monthly, but the school's investment needs are defined by the school's annual working program, which are submitted to the Ministry of Education and the City Banja Luka.

Regarding to structural resilience of secondary schools in Banja Luka, there is a strong attitude by principals and employees that position of secondary schools is poor. Functioning of secondary schools, i.e. the budget for secondary schools is provided by the municipality i.e. all expenses except salaries, which are financed by the Ministry of Education. All respondents in the survey confirmed that the municipality Banja Luka has become more involved in financing both secondary and primary schools in recent years.

City departments do not have funds to carry out this type of maintenance regularly. The department which is in charge for cooperation with educational institutions receives requests from schools and allocates the available funds to selected schools after submitting requests and cost estimates. Those funds are not planned (scheduled) for major investments, but to help schools to resolve specific difficulties. There is no clear criteria for rating requests, assessing priorities or for allocating funds. The supervision of reconstruction and restauration works has not been defined by any department.

The Department for inspection affairs plans funds for emergency interventions on buildings in case of damage. Urban planning and civil engineer inspectors after receiving request do field inspection and record damage on schools building according to their authority but not assess damage. For the

evaluation of the degree and type damage of the building, a civil engineering expert witness should be hired, whose competence is to evaluate the condition of the building.

The owner of the remaining school buildings in the territory of the City of Banja Luka is not known at the moment as well as the status of the school buildings where the ownership transfer process has started but not completed. There are cases elementary schools with several building that for instance one building is now in ownership of the City of Banja Luka but another is not (for instance schools with central urban building and suburb or rural buildings). Knowing that the central, usually urban school, building with the other school building (suburb, rural) is one legal entity, it is clear how complicated is maintaining buildings and even determining the responsibilities for it.

The problem of using non-purpose facilities as school facilities was recorded in two secondary schools as well as the absence of regular and planned monitoring of the state of school facilities on the territory of the Banja Luka. The department in charge of reconstruction acts upon receiving requests and establishing priorities from the department in charge of educational institutions. None of the departments has obligation to carry out regular and detailed monitoring of the construction characteristics of school buildings, although this would be a useful practice, considering the age and insufficient maintenance of school buildings. When earthquake occurs and some damages, even slight, on school building were recorded it is difficult to determine the origin of damage when their previous conditions was not known.

3. Earthquake preparedness of the schools in Banja Luka

Regarding non-material resilience, it is necessary to observe and determine the level of school communities' preparedness and capability for adequately responding if earthquake happens. The adequate reaction means reaction according to the DRR plan and training of school community should be carried out according to regulation [8]. The existence, content, quality and application of planning documentation in schools is one of the key elements of resilience. Another important element of resilience is preparedness, which is achieved through the practical implementation of the DRR plan, by practicing all planned activities as well as other preventive activities such as training and education, which is defined [8]. However, the different authorities started dealing with this issue after the catastrophic floods, which affected in 2014 entire West Balkan countries, including Bosnia and Herzegovina as well as Banja Luka region.

The Mayor of Banja Luka, in accordance with his authority, defined with a decision important subjects of for the protection and rescue system in the City. All primary and secondary schools, according to that document have been declared as subjects of special interest for the protection and rescue system. According to the regulation [9], they have the obligation to prepare planning documents, and to harmonize them with the DRR plan of the City of Banja Luka.

The research of the mentioned resilience elements of school communities [5] following weaknesses were identified. DRR plan exists in most schools, but the schools did not develop it themselves than hired agencies and other entities did it for schools. This is a consequence by lack of supervision related to application of regulations [10] that defines the area, development and implementation of planning documents.

DRR plan is not applied in most schools and the employees are not familiar with its contents. The intention of adopting the DRR plan for the most schools, was formal compliance with the law and nothing else. According to the research results after the DRR plan have been adopted by the School Board and the proof about adoption delivered, according to the Law [9] to the Civil protection department, they do not use the DRR plan at all. In a some schools, the DRR plan is available to employees on the notice board but only few of them organize introduction and discussion about the DRR plan at session of the teachers' council. Further application of the DRR plan, especially the Evacuation plan is the most important for schools, were part or even completely absent.

- Education of students related to seismic hazard and protection measures topics practically does not exist in schools. Teachers and principals confirmed there is no seismic hazard or protection

measures as teaching subjects in the regular curriculum. The regulation [10] defines that students get knowledge about natural disaster and protection against it through the class community program. The curriculum for the classwork prepared by the Republic Educational and Pedagogical Institute contains 4 areas: Culture of Living, Children's Rights and Responsibilities, Healthy Lifestyles and Free topics. Since there is no DRR topics it remains to believe that they teach it in the Free topics section.

- Training of employees on the seismic hazard and protection measures topic is not carried out in schools. The research [5] confirmed that training of teachers, professional associates and other employees in schools is one of the activities that is not carried out, although it is defined by the regulation [10]. There is neither an agreement about the way it should be implemented, nor any subordination of authority departments, coordination as well as cooperation on this issue. The representatives of the school management and the teaching staff believe that the initiative for this training should come from the civil protection department of the City of Banja Luka and that they, as "professionals, also carry out this training", without considering the real human capacities or financial resources of this department. The other side opinion from civil protection department is that the initiative, including proposals training topics and modality, should come from the schools.

- Lack of coordination and subordination between the authorities and institutions: Republic Administration of Civil Protection (RUCZ), Civil protection department of the City of Banja Luka, schools, Ministry of Education as well as inspectorates. The key weaknesses is the lack of control and supervision over the development and implementation of DRR plans as well as conducting of the preventive educational and training activities defined by regulation [8]. The RUCZ is in charge of administrative supervision including revision the methodological compliance of the schools DRR plans with the regulation defined this area [10] such as content and methodology as well as compliance with the local community's DRR plan. However, this kind of revision or supervision has never been carried out in schools.

- The Inspectorate of the Republic of Srpska respectively the educational inspection, supervises the schools legal acts as well as checking the legality of citizens 'complaints and requests regarding the activities carried out in schools. Regarding schools protection and rescue activities the jurisdiction of the inspectorate includes checking existence and content of the school DRR plans as well as its compliance with the legal regulations. All respondents from school principals confirmed that there was no any supervision related to implementation of DRR plans or carrying out preventive activities according to regulations [8].

4. Conclusion

The weaknesses related to the structural resilience of the schools are the characteristics of the school facilities, i.e. age, undefined ownership and inadequate monitoring and maintenance. More than 50% of school buildings were built before the earthquake in 1969, when there were almost no earthquake resistance design (ERD) codes. Knowing that vulnerability classes A, B and C are facilities without ERD measures, we conclude that the 74% out of total number of school buildings are without ERD measures according to the descriptions for the EMS -98 classification [3]. The maintaining of the school facilities depends not only of financial resources, than from the legally determined obligation that is related to the determination of ownership. Department in charge of inspections affairs neither do perform regular monitoring of school facilities, nor assess their needs for reparation. In addition, none of the departments does not plan funds for regular investments of the school buildings. The regular procedure is approval of funds after submitting the requests of schools on a case-by-case basis. Schools are according to the law [9] declared as important institutions for protection and rescue

system, and they are obliged to develop DRR plan and to update it once a year. The school's DRR are not updated regularly, and especially not every year. The school management and employees do not prepare DRR plans independently in cooperation with the Department for Civil Protection, which was the intention of the legislator since the process of planning lead to finding DRR solutions and vice versa. Instead of this, school's DRR plans were prepared by third parties/agencies usually with licenses in the field of occupational safety and fire protection. The extremely low level of awareness of the seismic hazard was observed as well as lack of the preventive activities which schools carry out, primarily education and training of students and teachers. The level of the non-structural resilience of the schools in Banja Luke regarding preparedness for adequate response in case of earthquake is very low. Schools in the territory of the City of Banja Luka should be given more attention by the local community, the Ministry of Education as well as other authorities and institutions.

References

[1] Kuzmanović, R. (1986). *Banjalučko školstvo u zemljotresu*. Banja Luka. Glas

[2] Šipka, V., Radovanović, S., Jarić D., Kukrić, L.&Sandić C.(2016). Upravljanje seizmičkim rizikom za škola u Banjoj Luci, *5. Naučno stručno međunarodno savetovanje "Zemljotresno inženjerstvo i inženjerska seizmologija* ", Sremski Karlovci

[3] European Macroseismic Scale 1998,EMS-98,(1998).Editor G. Grünthal, European Seismological Commission, Luxembourg

[4] Šipka, V.&Radovanović, S. (2014) Procjena seizmičkog rizika-Banja Luka, *4. Naučno stručno međunarodno savetovanje "Zemljotresno inženjerstvo i inženjerska seizmologija* ", Bor

[5] Šipka, V.(2022), Upravljanje seizmičkim rizikom osnovnih i srednjih škola na području Grada Banja Luka, Master teza,Univerzitet u Banjoj Luci, Fakultet bezbjednosnih nauka

[6] Zakon o utvrđivanju i prenosu prava raspolaganja imovinom na jedinice lokalne samouprave, "Službeni glasnik Republike Srpske ", 70/06

[7] Zakon o stvarnim pravima, "Službeni glasnik Republike Srpske "124/08, 58/09, 95/11, 60/15 i 107/19),

[8] Pravilnik o obučavanju lica u okviru osnovnog i srednjeg obrazovanja o opasnostima i zaštiti od elementarne nepogode i druge nesreće , "Službeni glasnik Republike Srpske" 74/14

[9] Zakon o zaštiti i spasavanju u vanrednim situacijama "Službeni glasnik Republike Srpske" 121/12, 47/17 и 111/21

[10] Uredba o sadržaju i načinu izrade plana zaštite i spasavanja od elementarne nepogode i druge nesreće, "Službeni glasnik Republike Srpske " 68/13.

Invited Lecture

CLASSIFICATION OF RESIDENTIAL BUILDING STOCK IN SERBIA

Svetlana Brzev [(1)], Jovana Borozan [(2)], Marko Marinković [(3)], Marijana Hadzima-Nyarko [(4)], Nikola Blagojević [(5)], Milica Petrović [(6)], Veljko Koković [(7)], Borko Bulajić [(8)], and Božidar Stojadinović [(9)]

[(1)] *Department of Civil Engineering, University of British Columbia, Canada, sbrzev@mail.ubc.ca*

[(2)] *Nanometrics Inc., Kanata, Ontario, Canada, jovanaborozan@nanometrics.ca*

[(3)] *Department of Engineering Mechanics and Theory of Structures, Faculty of Civil Engineering, University of Belgrade, Serbia, mmarinkovic@grf.bg.ac.rs*

[(4)] *Faculty of Civil Engineering and Architecture, University of Osijek, Croatia, mhadzima@gfos.hr*

[(5)] *Department of Civil, Environmental and Geomatic Engineering, ETH Zurich, Switzerland, blagojevic@ibk.baug.ethz.ch*

[(6)] *Department of Architectural Technology, Faculty of Architecture, University of Belgrade, Serbia, milica.petrovic@arh.bg.ac.rs*

[(7)] *Department of Materials and Structures, Faculty of Civil Engineering, University of Belgrade, Serbia, veljko@imk.grf.bg.ac.rs*

[(8)] *Department of Civil Engineering and Geodesy, Faculty of Technical Sciences, University of Novi Sad, Serbia, borkobulajic@uns.ac.rs*

[(9)] *Department of Civil, Environmental and Geomatic Engineering, ETH Zurich, Switzerland, stojadinovic@ibk.baug.ethz.ch*

Abstract

Developing a classification system (taxonomy) for buildings is a critical step for seismic risk assessment studies. Such a system can be used to characterize a building portfolio within urban/rural settlements or building stock for the entire country. Serbia is located in a region characterized by a moderate seismic hazard. In the last century, 10 earthquakes of magnitude 5.0 and higher occurred in Serbia, the strongest (M 6.0) in 1922. The strongest earthquake in the 21st century (M_w 5.5), with an epicenter close to Kraljevo, occurred in November 2010 and caused significant damage to residential buildings. In 2019, members of the Serbian Association for Earthquake Engineering (SUZI-SAEE) contributed to the SERA project and its goal to develop a seismic risk model for Europe. A taxonomy of residential buildings in Serbia was developed based on previous national and regional building stock studies. The proposed taxonomy includes the Lateral Load-Resisting System (LLRS) (e.g., wall, frame, dual wall-frame system) and material of the LLRS (e.g., masonry, concrete, wood) as the main attributes. The type of floor diaphragm (rigid or flexible) has been specified only for masonry typologies with unreinforced masonry walls, while building height and date of construction have been implicitly considered. According to the proposed taxonomy, there are 9 residential building typologies in Serbia; out of those, 5 typologies are related to masonry structures, 3 are related to RC structures, and one is related to wood structures. This paper describes the proposed taxonomy and outlines the characteristic features of different building typologies and their relevance for estimating seismic vulnerability and risk. A comparison of the proposed taxonomy for Serbia and published taxonomies for Croatia is also presented.

Keywords: residential buildings, building taxonomy, seismic risk assessment, exposure model

1. Introduction

Seismic risk assessment studies can be performed at different scales (municipal, regional, national, etc.) to estimate potential earthquake-induced losses and identify highly vulnerable assets (e.g., buildings) that may need to be retrofitted as a part of a disaster mitigation initiative. It is well established that seismic risk for a specific building or a building portfolio depends on the corresponding seismic hazard, vulnerability, and exposure. Seismic hazard can be quantified based on a probabilistic estimate of the expected earthquake intensity for a specific location or region, while vulnerability is related to chances of damage and losses for assets exposed to specific hazard levels. Finally, exposure is related to the number, type, and value of assets that are the scope of a specific risk

assessment study. One of the most comprehensive initiatives focused on developing a seismic risk model for Europe, undertaken under the HORIZON2020 SERA project, used the seismic risk assessment framework originally developed under the Global Earthquake Model (GEM). Serbia participated in the SERA project by sharing information related to the exposure model [1]. This project motivated the members of the Serbian Association for Earthquake Engineering (SUZI-SAEE) to initiate a seismic risk assessment study focused on the Serbian building stock.

The first step towards developing an exposure model consists of developing a building classification system, also known as a building taxonomy. Buildings can be classified in different ways, but in most cases, the selected building characteristics (also known as attributes or facets) which are used to develop a taxonomy are similar, including the material of Lateral Load Resisting System (LLRS) (e.g., masonry, reinforced concrete - RC), type of LLRS (e.g., moment frame, wall system, etc.), and a few other attributes.

A few taxonomies were developed for applications on a global scale. PAGER-STR is a global building taxonomy that classifies buildings into 101 classes and has been organized hierarchically. The main attributes include the material of LLRS, type of LLRS, building height, and type of diaphragm [2]. The most comprehensive global building taxonomy is the GEM Building Taxonomy V2.0 [3, 4], which was developed for seismic risk assessment purposes in the Global Earthquake Model (GEM) framework. The taxonomy is multi-faceted and characterizes buildings through 13 attributes, which could be thought of as a building's genome (DNA), see Fig.1. While some of the GEM Building Taxonomy attributes are the same or similar to those in other taxonomies (e.g., PAGER-STR), it also includes a few unique attributes (e.g., building irregularities, type of occupancy, the position of building within a block, etc.). The taxonomy enables the user to explain each attribute in detail. For example, attribute Material of LLRS (e.g. masonry) can be characterized through "details", such as Material technology (e.g. unreinforced masonry, confined masonry), and Material properties. According to the GEM taxonomy, a building class can be described as a "taxonomy string", which combines the information related to each attribute and the associated detail. A slash sign (/) is used to separate attributes, while a plus sign (+) includes an additional level of detail for a specific attribute. Each attribute and detail have a unique ID. For example, the ID for unreinforced masonry is MUR, the ID for Wall (a type of LLRS) is LWAL, and the ID for building height (number of storeys) is HEX. Therefore, a taxonomy string for a 3-storey loadbearing URM building is /MUR/LWAL/HEX:3/ (the other 10 attributes can be omitted if no information is available). The taxonomy is flexible and enables the user to describe a building class at different granularity (level of detail) as needed. The taxonomy has been widely used for natural hazard and risk assessment via the Open Quake platform [5] and has been expanded into the GED4ALL Building Taxonomy, which includes additional attributes and details required for multi-hazard risk assessment studies [4]. The European seismic risk model developed in the framework of SERA project [6, 7, 8] also used the GEM taxonomy V2.0 to classify European building stock.
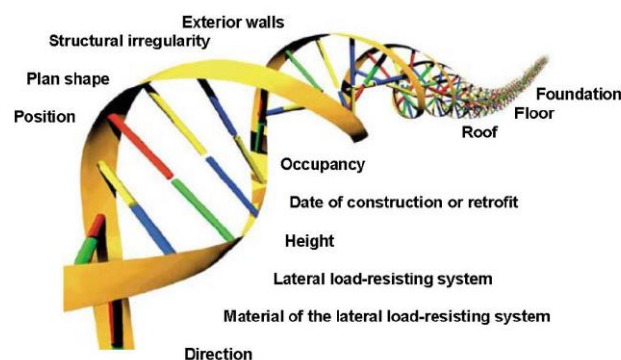

Figure 1. DNA for a building: attributes of the GEM building taxonomy V2.0 [3].

The EMS-98 Macroseismic Scale [9] also contains a well-known building taxonomy specifically developed for classifying European building stock. According to the EMS-98, buildings have been classified into 15 classes, including 6 RC classes, 7 masonry classes, steel and timber building classes. Each building class has been assigned an expected seismic vulnerability rating, which was empirically determined, but is a valuable reference for seismic vulnerability studies. According to the building taxonomy developed in the framework of the RISK-UE project, buildings were classified into 23 classes depending on the LLRS, construction material, building height, and building design code level [10]. The Syner-G taxonomy was also developed to classify the European building stock. It includes 15 main attributes/facets and can be used to classify buildings in a flexible (non-hierarchical) manner [11].

This paper presents a proposed building taxonomy for Serbia, developed as a part of the SUZI-SAEE study, and compares key features (attributes) for relevant building taxonomies. The paper may be of interest to earthquake engineers and other professionals interested in seismic risk assessment, with a particular focus on the Balkan region.

2. Regional building taxonomies

The authors have also reviewed building taxonomies developed in the region, particularly in the neighbouring countries which were a part of former Yugoslavia. One of the early regional taxonomies was developed in the 1980s as a part of the UNIDO project "Building Construction under Seismic Conditions in the Balkan Region" [12]. The classification was based on the material of LLRS (e.g., masonry, RC), construction technology (e.g., cast-in-situ or prefabricated concrete), and the LLRS (e.g., wall, frame, frame-wall system, etc.). The rapid assessment form developed in this project was used for the damage assessment of buildings affected by the 1990 Gevgelija earthquake in North Macedonia [13]. Classification of buildings in North Macedonia was performed based on a comprehensive building database compiled by IZIIS, Skopje, from 2013-2019 [14]. Masonry buildings were classified into MB (non-earthquake resistant, pre-1964 vintage) and CMB (moderate earthquake-resistant confined masonry buildings, post-1964 vintage). RC buildings (earthquake-resistant, post-1970 vintage) included different LLRSs, e.g. moment frame, dual frame-wall system, RC shear walls, and flat slab systems. A recent seismic loss assessment study for Skopje was based on the inventory of 59,950 buildings classified according to the RISK-UE building taxonomy [15].

Several seismic risk-related projects in Croatia required the development of building taxonomies for major urban centres, such as the capital Zagreb [16]. An initial building taxonomy comprised 14 building classes and was developed for a national seismic risk assessment study [17]. The taxonomy was used for surveying the building inventory in Zagreb. Further studies indicated a need for a more granular classification to reflect the building characteristics better. Hence a more detailed taxonomy, which included 42 building types, was created [18]. The following 4 construction periods were considered: i) PC before 1964 (pre-code), ii) LC from 1964-1981 (low-code), iii) MC from 1981-2005 (medium code), and iv) HC after 2005 (high code, after Eurocode 8 was adopted). A separate project was focused on Osijek, the fourth largest city in Croatia, resulting in a custom building taxonomy for exposure model development purposes. This taxonomy included 15 prevailing building types and was used for a field survey of 1100 local buildings [19].

A few seismic risk assessment studies in Bosnia and Herzegovina required the classification of building portfolios. A seismic risk assessment study was performed in Tuzla, the third-largest city in the country [20]. In total, 203 RC and masonry buildings were surveyed. RISK-UE building taxonomy was used for structural and typological characterization of the buildings. An ongoing research study in Sarajevo, the country's capital, focuses on developing a database of 700 structures in two selected municipalities as the starting point for developing a national building taxonomy [21].

A recent scenario-based risk assessment study in Slovenia [22] used building data contained in the Real Estate Register, which contains information related to building units, including the year of construction, occupancy, built-up floor area, the material of the LLRS, building value based on the appraisal, number of storeys, and building height.

A summary of relevant international building taxonomies and national/local taxonomies for the neighbouring countries has been presented in Table 1. The table identifies key building attributes, which are intended to differentiate between seismic vulnerabilities associated with different building typologies for seismic risk assessment purposes.

Table 1 – International and national building taxonomies: a summary of attributes

	Attributes	International taxonomies			National taxonomies			
		GEM V2.0	RISK-UE	EMS-98	Croatia-Zagreb	Croatia-Osijek	North Macedonia	Slovenia
		[3]	[10]	[9]	[18]	[19]	[14, 15]	[22]
1	Material of the LLRS	✓	✓	✓	✓	✓	✓	✓
2	Type of LLRS	✓	✓	✓	✓	✓	✓	✓
3	Building height	✓	✓		✓	✓	✓	✓
4	Date of construction	✓			✓	✓		✓
5	Seismic code level	E[1]		E[2]	E	I	I	I
6	Occupancy (function)	✓				✓		
7	Structural irregularity	✓	✓		✓	✓		
8	Material of exterior walls	✓				✓		
9	Roof type	✓						
10	Floor type	✓			✓	✓		
	Other attributes	Direction; building position within a block; shape of the building plan; foundation		Material technology (masonry);	Material technology (masonry); wall layout; hybrid LLRS	Building condition; building size; floor area; built-up area; soil type		
	Total number of typologies	Very large	23	13	42	12	7	14

Notes: 1-included only in the GED4ALL taxonomy; 2-only for RC structures; E- explicitly stated in the classification; I- implicit (can be deducted based on the period of construction)

It can be seen from Table 1 that all taxonomies have at least two attributes: the material of the LLRS and the type of LLRS. The most detailed international taxonomy is GEM V2.0, since it can characterize many building typologies due to a large number of attributes and details (secondary attributes). Among the national typologies developed in the neighbouring countries, the most detailed ones are from Croatia. The taxonomy developed for the Zagreb study [18] describes building features characteristic of local construction practices.

3. Proposed classification of residential buildings in Serbia

3.1 Background

Previous research studies on the Serbian building stock were mainly based on the review of the building stock of various European countries. The most relevant project for the current study is the

TABULA project (2009-2012), a European project co-founded by Intelligent Energy Europe [23]. In the framework of the TABULA project, a detailed analysis of residential building typologies was performed based on the construction period, façade systems, and energy consumption. Two taxonomies were developed for each country participating in the project: a taxonomy in the predetermined TABULA form and a national one. Both taxonomies classified residential buildings based on the year of construction and the building type. The TABULA taxonomy divided buildings into single-family houses, terraced houses, multifamily houses, and apartment blocks. The national building taxonomy for Serbia is more complex, categorizing the buildings into six types. Single-family housing was classified into freestanding houses and houses in a row, while multifamily housing was categorized into freestanding buildings, lamella (housing block), buildings in a row, and high-rise buildings. Each typology was described in detail on an example (building archetype) and included a description of the structural system and horizontal and vertical structural elements. The TABULA project also offered an insight into the built-up area and the number of residential buildings for various typologies in Serbia, based on the 2011 Census data, as well as a detailed survey of 10,000 buildings. It was shown that most buildings in Serbia are freestanding single-family houses (57.0% based on the built-up area and 92.1% based on the estimated number of buildings). Also, it was concluded that most freestanding single-family houses were built from 1971 to 1980. The TABULA project deliverables prepared by the Serbian team [23-25] were important resources for the present study. The only previous study related to Serbian building classification for seismic risk assessment purposes was reported by Radovanović and Petronijević [26]. The authors applied the EMS-98 scale to identify common building typologies in Serbia and concluded that seven EMS-98 typologies (5 masonry typologies and two RC typologies) are sufficient for characterizing building stock in Serbia.

A review of previous studies on the residential building stock revealed a need to develop a novel classification of residential buildings in Serbia, which is presented in Table 2. The presented building classification comprises 9 building typologies, including 5 masonry typologies (M), 3 reinforced concrete (RC) typologies, and a wood typology (W). Each building typology is described using an alphanumeric ID, name, and primary and secondary taxonomy attributes, as shown in the table. The primary attributes which are used to describe building types include Lateral Load-Resisting System (LLRS), e.g., wall, frame, dual wall-frame system; material of the LLRS (e.g., masonry, concrete, wood), and floor diaphragm type (rigid or flexible). Unreinforced masonry (URM) buildings with flexible diaphragms (building types M1, M2) are more vulnerable to earthquake shaking when compared to URM buildings with rigid diaphragms, as demonstrated by numerous surveys and studies. Flexible diaphragms may cause large lateral displacements and the out-of-plane toppling of the walls in the weak direction (normal to the earthquake action), which reduces the building integrity and prevents the walls from acting together as a box (box action). Building height is also an important attribute to consider for M3 building type (URM buildings with rigid diaphragms). Based on the number of floors, this typology was further subdivided into single- and multifamily building types (M3-S and M3-M). The secondary attributes include building height and period of construction. Building height is related to the dynamic characteristics of a structure, whereas the year of construction can be related to the seismic code level to which the building was designed.

A detailed description of masonry and RC building typologies is presented in the following sections. Since wooden buildings represent only a tiny fraction of Serbia's residential building stock, they have been omitted from this paper.

Table 2 – Proposed classification of residential buildings in Serbia

ID	Building typology	Primary attributes			Secondary attributes
		Material	LLRS	Type of roof/floor diaphragm	
(1)	(2)	(3)	(4)	(5)	(6)
M1	Unreinforced earthen or stone masonry walls with flexible diaphragms	Masonry	**LLRS:** Wall (constructed using stone masonry, rammed earth, or load-bearing adobe brick masonry)	Flexible (wooden structure)	**Height:** 1-2 floors **Date of construction:** before 1945
M2	Unreinforced masonry walls with flexible diaphragms	Masonry	**LLRS:** Wall (constructed using solid clay bricks in low-strength mortar)	Floor: flexible (wooden structure or Prussian vault) Roof: flexible (sloped wooden structure)	**Height:** 1-4 floors **Date of construction:** before 1960
M3	Unreinforced masonry walls with rigid diaphragms	Masonry	**M3-S (single-family) LLRS:** Wall (constructed using modular clay blocks in cement mortar)	Floor: rigid (semi-prefabricated concrete and clay floor system) Roof: flexible (sloped wooden structure)	**Height:** 1-2 floors **Date of construction:** 1960-present
	Unreinforced masonry walls with rigid diaphragms	Masonry	**M3-M (multifamily) LLRS:** Wall (constructed using solid clay bricks in cement mortar)	Floor: rigid (semi-prefabricated ribbed RC floor or composite RC&clay floor) Roof: rigid (flat RC slab) or flexible (sloped wooden structure)	**Height:** 3-6 floors **Date of construction:** 1920-1970
M4	Confined masonry buildings	Masonry	**LLRS:** Wall (constructed using modular clay blocks in cement mortar)	Rigid (semi-prefabricated RC or composite concrete and clay system)	**Height:** 1-5 floors **Date of construction:** 1970-present
RC1	RC frames (cast in-situ) with masonry infills	Reinforced concrete (RC)	**LLRS:** RC frame with masonry infills built using solid clay bricks or modular clay blocks	Rigid (semi-prefabricated RC or composite concrete and clay floor system)	**Height:** 4-10 floors **Date of construction:** 1960-present
RC2	RC walls (cast in-situ) or dual frame-wall system	Reinforced concrete (RC)	**LLRS:** Wall (although a frame may resist a small fraction of seismic load)	Rigid (solid RC slab)	**Height:** 5-15 floors **Date of construction:** 1960-present
RC3	Prefabricated RC buildings	Reinforced concrete (RC)	**LLRS:** Wall (large panel buildings), or dual frame-wall system	Rigid (prefabricated RC slab)	**Height:** 6-15 floors **Date of construction:** 1960-1990

3.2 Masonry building typologies

The proposed classification includes 4 basic masonry typologies (M1 to M4). Typology M3 is subdivided into two subtypes (M3-S and M3-M), see Table 2. Masonry typologies denoted by M1, M2, and M3 characterize older, unreinforced masonry (URM) buildings, whereas typology M4 characterizes confined masonry buildings of more recent construction.

Buildings classified as M1 and M2 typologies have wooden floors which act as flexible diaphragms, and they were predominantly used in Serbia until the end of WWI. Floor systems in buildings classified as M3 or M4 typologies can be treated as rigid diaphragms, but there are a few types, depending on the construction period. The application of ribbed RC floors started at the beginning of the 20th century. A semi-prefabricated ribbed RC floor system (Herbst), consisting of 25 cm deep prefabricated RC ribs and a cast-in-situ concrete layer, was practiced until the end of WWII. Avramenko is another semi-prefabricated floor system that has been used since the 1930s. A shift towards semi-prefabricated concrete and clay floor system happened during the mid-1960s. For example, LMT (light prefabricated floor) is a semi-prefabricated floor system consisting of cast-in-situ RC joists placed between masonry elements. Since mid-20th century, solid RC slabs have been used in multi-story masonry and RC buildings. Examples of masonry building typologies are presented in Fig. 2, and a brief description of each typology is presented in this section.

a) b) c) d)

Figure 2. Examples of masonry building typologies from Serbia: a) M1- a single-family building in Irig (Vojvodina); b) M2 – an early 20th century URM building in Zemun; c) M3-M – an apartment building in Belgrade; d) M4- a single-family house under construction, Zlatibor.

M1: Unreinforced earthen or stone masonry walls with flexible diaphragms

Earthen construction and adobe masonry were common for residential buildings of M1 building type, whereas stone masonry was primarily used for public buildings, fortresses, churches, etc. Houses of earthen construction were common in Vojvodina from the 18th century until the first half of the 20th century, mainly in the form of low-rise (one-story) single-family houses with walls constructed using rammed earth technology (called *naboj* in Serbia). These buildings are characterized by rectangular or L-shaped plans, and the wall thickness is 50 cm or higher. Adobe masonry, characterized by walls constructed using unburnt clay bricks in mud mortar, was more common in urban construction. These buildings had wooden floors and roofs and usually had two-floor levels. Historic urban centres in Vojvodina have many examples of such buildings, some of which were recognized as heritage structures in the city of Novi Sad.

Stone masonry was rarely used in the construction of single-family residential buildings in Serbia; however, large residential buildings with foundations, basement walls, and/or load-bearing walls made of stone masonry were constructed in Belgrade in the 1870s. Several tower-like dwellings dating from the 19th century were also constructed using stone masonry in rural areas near Dečani Monastery in Kosovo and Metohija. Such buildings feature wooden floors, a square plan shape, and thick walls with a few windows.

M2: Unreinforced masonry walls with flexible diaphragms

This building typology was common in urban regions of Serbia during the 19th century and the first half of the 20th century. These buildings usually have 1 to 4 floors and were used as single-family or multi–family residential buildings (depending on the building height and economic status of the owners). The key feature of these buildings is the use of fired (burnt) solid clay bricks for the first time in Serbia. The first brick manufacturing facilities in Serbia were established in the second half of the 19th century, which enabled wider use of brick masonry construction. The 1896 building Act for the Town of Belgrade restricted the use of timber and dictated standard dimensions for clay bricks as a common material for wall construction [27]. The prescribed wall thickness reduced over time, ranging from 45 - 60 cm before 1933 to 25-51 cm after 1933. Lime mortar was used for masonry construction until the end of WWII. Wooden floors with 14 cm x 20 cm beams at 80 cm spacing and 2.5 cm thick wooden planks were typically used on upper floors, while suspended floors above the basement and ground floor levels were usually constructed as a jack arch system (Prussian vault), consisting of shallow brick vaults spanning between the iron beams. These buildings have sloped wooden roofs with clay tiles.

M3: Unreinforced masonry walls with rigid diaphragms

This building typology has been widely used both in urban and rural regions of Serbia. They are characterized by rigid floor diaphragms. This typology can be subdivided into M3-S and M3-M typologies based on the building height and masonry technology. Typology M3-S is related to low-rise single-family residential houses with load-bearing walls constructed of modular (multi-perforated) clay blocks or solid clay bricks bonded by cement:lime:sand mortar. Wall thickness is influenced by building height and type of masonry element (solid brick or modular block), and it usually ranges from 19 cm to 38 cm. These buildings have sloped wooden roofs and clay tiles. Construction of these buildings started in the 1960s and continues to date, mostly in the parts of the country where construction of confined masonry (M4-type) is not mandatory.

M3-M typology is related to multifamily apartment buildings with load-bearing masonry walls constructed of solid clay bricks and cement:lime:sand mortar. These are mid-rise buildings (with 3-6 floors) and have regular plans and elevations with symmetrical wall layouts. The thickness of interior walls ranges from 25 cm to 30 cm, whereas exterior walls are usually 38-51 cm thick. This type of construction was practiced from the end of WWII until the beginning of the 1970s. The buildings constructed in the period 1950-1970 have horizontal RC ring beams at floor/roof levels, but they do not have vertical RC confining elements, which are present in confined masonry construction. These buildings usually have flat roofs (the same construction as floors). A detailed description of typical M3-M buildings from Serbia and their seismic performance can be found elsewhere [28].

M4: Confined masonry buildings

The first Yugoslav seismic design code, issued in 1964, contained provisions on horizontal and vertical RC confining elements in masonry buildings, which are characteristic of modern confined masonry construction currently practiced in Serbia. The code prescribed building height limits depending on the seismic hazard level and other criteria, as summarized in [29]. These are low-rise residential buildings, typically 1-4 floors high. Masonry walls in these buildings are constructed using modular (multi-perforated) clay blocks, which superseded the use of solid clay bricks in the 1970s [30]. Due to the use of modular blocks, wall thickness has been reduced to 19-25 cm. These buildings have rigid floor diaphragms, usually with semi-prefabricated floor systems. Flat RC and sloped wooden roofs are typical for multifamily and single-family buildings.

Although confined masonry technology is widely used in Serbia, it is not always easy to distinguish buildings of M4 typology from RC frames with masonry infills (RC1) in field surveys of existing buildings. Similarly, identifying vertical RC confining elements in existing buildings is often challenging. Hence it is possible to wrongly classify buildings that could be potentially classified either as M3 or M4 buildings. The use of thermal imaging has proven to be helpful in identifying RC elements in field surveys of RC and masonry buildings [31].

3.3 Reinforced concrete building typologies

RC buildings were classified into three typologies. Two out of three RC typologies are associated with cast-in-situ concrete construction technology (RC1 and RC2), while the third is associated with prefabricated RC construction (RC3). Construction of RC residential buildings in Serbia started after WWII, and is limited primarily to multifamily residential buildings. Initially, RC1 building typology was popular, but since the 1960s, most RC buildings have at least a central (elevator) core and additional structural walls (RC2 systems). Prefabricated RC technology (RC3 typology) was widespread in urban areas of former Yugoslavia, including Serbia, from the late 1950s until the early 1990s. Prefabricated RC systems were not used after the dissolution of Yugoslavia; hence dual wall-frame system (RC2 typology) remains the only RC system used in multifamily residential building construction. Recent RC construction features RC walls and flat slab frames acting as a gravity load-resisting system. Examples of RC building typologies are presented in Fig. 3, and a brief description of each typology is presented in this section.
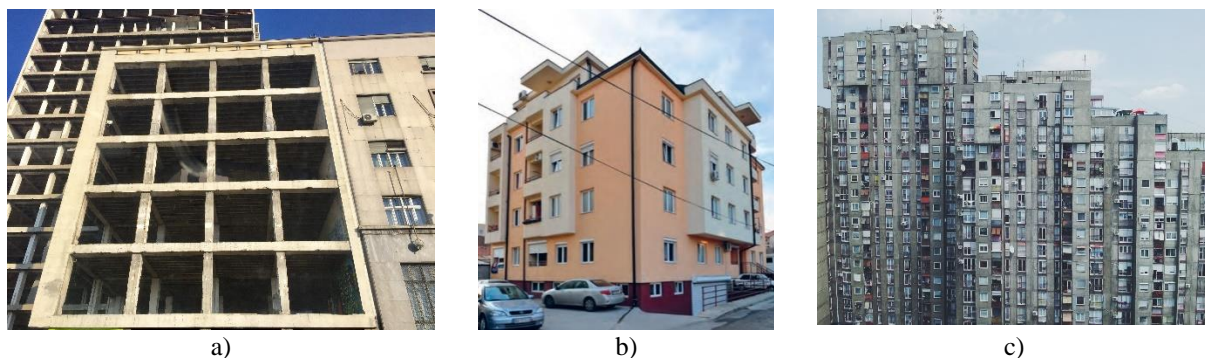

a)   b)   c)

Figure 3. Examples of RC building typologies from Belgrade, Serbia: a) RC1 - original office of "Energoprojekt" consulting firm; b) RC2 – a multifamily residential building [25] and c) RC3 – high-rise prefabricated large panel RC buildings, New Belgrade

RC1: RC frames (cast in-situ) with masonry infills

Construction of the first cast-in-situ RC frame buildings dates back to the late 1930s; however, construction of such buildings for residential purposes was more common after the end of WWII, due to the migration of the population to urban regions and post-war rebuilding efforts [25]. These were mid-rise buildings (up to 10 floors high) and usually had a regular plan shape; however, there was often an open space on the ground floor used for commercial purposes. Until the 1970s, stiff infills (solid clay brick masonry walls) were used, but they later changed to modular clay blocks and, in some cases, precast concrete panels for exterior infills. In the initial period, cast-in-situ ribbed RC floor system was used, but it was later replaced by cast-in-situ RC flat slabs. The typical foundation system for RC buildings was strip footings, whereas mat foundations were used in buildings with underground floors. Growing market needs and the introduction of the first seismic design codes in 1964 led to the construction of buildings with dual RC frame-wall systems (RC2) and prefabricated RC buildings (RC3), which entirely replaced the RC1 typology.

RC2: RC walls (cast in-situ) or dual frame-wall system

RC wall system was introduced after WWII, consisting of structural RC walls that resist lateral and gravity walls in RC buildings. This system became more common in the late 1950s with the

application of the slip-form construction method for high-rise buildings (more than 10 floors high). During the same period, the tunnel-form method was used to construct high-rise buildings with elongated plan shapes. These buildings have a central core and regularly spaced structural walls with the same thickness along the building height. The dual wall-frame system, in which lateral loads are resisted both by the structural walls and the frames, was more widely used after 1964, when the first seismic design code was issued.

RC3: Prefabricated RC buildings

Construction of prefabricated RC buildings started in the 1950s in former Yugoslavia, Eastern European countries, and the Soviet Union. More than 15 prefabricated construction technologies were developed in the former Yugoslavia, including the IMS Building System, Trudbenik, Yugomont YU-61, etc. [32]. Large panel systems, consisting of RC wall and floor panels, were particularly popular. These elements were prefabricated, transported, and joined together at the construction sites. After erecting in the final position, structural elements were connected via welded steel connections and/or cast-in-situ grouted concrete. French large panel system Balency was modified by the Belgrade-based engineering firm "Rad" into the "Rad-Balency" system, which was used for the construction of high-rise buildings (6-15 floors), many of which exist in Belgrade and other urban regions [33]. The IMS Building System, developed by Prof. Branko Žeželj at the Institute IMS in Belgrade and used in other parts of former Yugoslavia, consisted of prefabricated RC columns, waffle slabs, and edge girders. Columns and slabs were joined together at each floor level by post-tensioning in two orthogonal horizontal directions. It was a dual frame-wall system that included cast-in-situ RC shear walls. The system was used to construct mid- and high-rise buildings (6-20 floors) [34].

4. Conclusions

The paper presents a classification (taxonomy) of residential buildings in Serbia, which has been proposed by the authors. According to the taxonomy, there are 9 prevalent building typologies, including 5 typologies related to masonry buildings, 3 typologies related to RC buildings, and a typology related to wooden buildings. This initial taxonomy is based on reviewing previous studies related to the building stock in Serbia and a survey of experts, which resulted in developing seismic fragility curves for typical buildings [35]. A comparison with the building taxonomies from neighbouring countries with similar construction practices and design codes points to numerous similarities in the attributes and the main building typologies. It is expected that the taxonomy will be further developed with a higher level of granularity after future field surveys of typical buildings. The proposed taxonomy will be used to develop an exposure model for Serbia and future seismic risk assessment studies.

Acknowledgments

References

[1] Borozan, J. (2019). Exposure model for Serbia. Presentation at the SERA Balkans Seismic Risk Workshop, Belgrade, Serbia.

[2] Jaiswal, K., Wald, D. (2008). Creating a global building inventory for earthquake loss assessment and risk management. U.S. Geological Survey Open-File Report 2008-1160, Washington, DC.

[3] Brzev, S., Scawthorn, C., Charleson, A. W., Allen, L., Greene, M., Jaiswal, K., Silva, V. (2013). GEM Building Taxonomy Version 2.0. Pavia, Italy: GEM Foundation. doi:10.13117/GEM.EXP-MOD.TR2013.02

[4] Silva, V., Brzev, S., Scawthorn, C., Yepes, C., Dabbeek, J., Crowley, H. (2022). A Building Classification System for Multi-hazard Risk Assessment. International Journal of Disaster Risk Science, 13, 161–177.doi:https://doi.org/10.1007/s13753-022-00400-x

[5] Silva, V., Crowley, H., Monelli, D., Pinho, R. (2014). Development of the OpenQuake engine, the Global Earthquake Model's open-source software for seismic risk assessment. Natural Hazards, 72, 1409–1427.doi:https://doi.org/10.1007/s11069-013-0618-x

[6] Crowley, H., V. Silva, P. Kalakonas, L. Martins, G. Weatherill, K. Pitilakis, E. Riga, B. Borzi, M. Faravelli. (2020). Verification of the European seismic risk model (ESRM20). In Proceedings of the 17th World Conference on Earthquake Engineering, 13–18 September 2020, Sendai, Japan.

[7] Crowley, H., V. Despotaki, D. Rodrigues, V. Silva, D. Toma-Danila, E. Riga, A. Karatzetzou, Z. Zugic, et al. (2020). Exposure model for European seismic risk assessment. Earthquake Spectra 36(1). https://doi.org/10.1177/8755293020919429.

[8] Crowley, H., Dabbeek, J., Despotaki, V., Rodrigues, D., Martins, L., Silva, V., . . . Danciu, L. (2021). European Seismic Risk Model (ESRM20). EFEHR Technical Report 002, V1.0.1. doi:https://doi.org/10.7414/EUC-EFEHR-TR002-ESRM20

[9] Grünthal, G. (1998). European Macroseismic Scale 1998 (EMS-98). Luxembourg: Centre Europèn de Géodynamique et de Séismologie.

[10] Milutinović, Z., Trendafiloski, G. (2003). WP4: Vulnerability of current buildings. European Commission. Retrieved from http://www.civil.ist.utl.pt/~mlopes/conteudos/DamageStates/Risk%20UE%20WP04_Vulnerability.pdf

[11] Pitilakis, K., Crowley, H., Kaynia, A. M. (Eds.). (2014). SYNER-G: Typology Definition and Fragility Functions for Physical Elements at Seismic Risk. Springer.

[12] UNIDO. (1985). Post-Earthquake Damage Evaluation and Strength Assessment of Buildings under Seismic Conditions. Building Construction Under Seismic Conditions in the Balkan Region. Volume 4. Vienna: UNDP/UNIDO Project RER/79/015.

[13] IZIIS. (1991). Catalog of standardized projects for repair and strengthening of structures damaged by the December 21, 1990 earthquake on the territory of the municipality of Gevgelija. Skopje, North Macedonia: IZIIS - Institute for earthquake engineering and engineering seismology.

[14] Šendova, V., Apostolska, R., Vitanova, M. (2019). Structural classification of building and bridge assets in Republic North Macedonia. SERA Balkans Seismic Risk workshop, Belgrade, Serbia.

[15] Mircevska, V., Abo-El-Ezz, A., Gjorgjeska, I., Smirnoff, A. (2022). First-Order Seismic Loss Assessment at Urban Scale: A Case Study of Skopje, North Macedonia. Journar of Earthquake Engineering, 26, 70-88. doi:10.1080/13632469.2019.1662342

[16] Šavor Novak, M., Atalić, J., Uroš, M., Prevolnik, S., Nastev, M. (2019). Seismic risk reduction in Croatia: mitigating the challenges and grasping the opportunities. Proceedings, Scientific Symposium Future Trends in Civil Engineering, Zagreb, Croatia,

[17] Atalić, J., Šavor Novak, M., Uroš, M. (2018). Updated risk assessment of natural disasters in Republic of Croatia – seismic risk assessment (in Croatian), Faculty of Civil Engineering in collaboration with Ministry of Construction and Physical Planning and National Protection and Rescue Directorate, 2018.

[18] Atalić, J., Krolo, J., Damjanović, D., Uroš, M., Sigmund, Z., Šavor Novak, M., Hak, S., Korlaet, L., Košćak, J., Duvnjak, I., Bartolac, M., Serdar, M., Dokoza, I., Prekupec, F., Oreb, J., Mušterić, B.: Study on earthquake risk reduction in the City of Zagreb, Phase 1–6 (in Croatian), Faculty of Civil Engineering, Department of Engineering Mechanics, 2013-2018.

[19] Pavić, G., Hadzima-Nyarko, M., Bulajić, B. (2020). A Contribution to a UHS-Based Seismic Risk Assessment in Croatia—A Case Study for the City of Osijek. Sustainability, 12(5), 1796.doi:https://doi.org/10.3390/su12051796

[20] Ademović, N., Hadzima-Nyarko, M., Zagora, N. (2022). Influence of site effects on the seismic vulnerability of masonry and reinforced concrete buildings in Tuzla (Bosnia and Herzegovina). Bulletin of Earthquake Engineering, 20, 2643-2681. doi:10.1007/s10518-022-01321-2

[21] Piljug, A., Medanović, Ć., Ademović, N., Hadzima-Nyarko, M., Zagora, N. (2022). Quick visual seismic assessment of existing buildings in Sarajevo (BiH). 3rd European Conference on Earthquake Engineering & Seismology, (p. (in press)). Bucharest, Romania.

[22] Babič, A., Dolšek, M., Žižmond, J. (2021). Simulating Historical Earthquakes in Existing Cities for Fostering Design of Resilient and Sustainable Communities: The Ljubljana Case. Sustainability, 13(14), 7624-7645. doi:https://doi.org/10.3390/su13147624

[23] Jovanović Popović, M., Ignjatović, D., Radivojević, A., Rajičić, A., Đukanović, L., Ćuković Ignjatović, N., Nedić, M. (2013). National Typology of Residential Buildings in Serbia. Belgrade: Faculty of Architecture University of Belgrade, GIZ - Deutsche Gesellschaft für Internationale Zusammenarbeit.

[24] Jovanović Popović, M., Ignjatović, D., Radivojević, A., Rajčić, A., Đukanović, L., Ćuković Ignjatović, N., Nedić, M. (2013). Atlas of Family Housing in Serbia. Belgrade: Faculty of Architecture, University of Belgrade, GTZ Deutsche Gesellschaft für Technische Zusammenarbeit.

[25] Jovanović Popović, M., Ignjatović, D., Radivojević, A., Rajčić, A., Đukanović, L., Ćuković Ignjatović, N., Nedić, M. (2013). Atlas of Multifamily housing in Serbia. Belgrade: Faculty of Architecture, University of Belgrade, GTZ Deutsche Gesellschaft für Technische Zusammenarbeit.

[26] Radovanović, S., Petronijević, M. (2009). Building types and vulnerability to ground shaking in Serbia. Proceedings of the International conference on earthquake engineering on the occasion of the 40 anniversary of Banja Luka Earthquake. Banja Luka.

[27] Radivojević, A., Đukanović, L., Roter-Blagojević, M. (2016). From tradition to modernization - building techniques in Serbia during 19th and early 20th century. Structural Analysis of Historical Constructions: Anamnesis, Diagnosis, Therapy, Controls Proceedings of the 10th International Conference on Structural Analysis of Historical Constructions. London: CRC Press.

[28] Blagojević, P., Brzev, S., Cvetković, R. (2021): Simplified Seismic Assessment of Unreinforced Masonry Residential Buildings in the Balkans: The Case of Serbia. *Buildings*, **11**(9), 392-414, doi:https://doi.org/10.3390/buildings11090392.

[29] Brzev, S., Blagojević, P., Cvetković, R. (2021): Wall Index Requirements for Seismic Design and Assessment of Masonry Buildings. *Proceedings of 1st Croatian Conference on Earthquake Engineering*, Zagreb, Croatia, 8 pages.

[30] Đukanović, L. (2021). Komfor u beogradskim stambenim zgradama (Comfort in residential buildings in Belgrade). Belgrade: Faculty of Architecture University of Belgrade.

[31] Jovanović Popović, M., Ignjatović, D. (2011). Seeing Energy (Videti energiju). Belgrade: Faculty of Architecture, University of Belgrade GTZ Deutsche Gesellschaft für Technische Zusammenarbeit.

[32] Vuković, S. (2007). Stanje i pravci razvoja industrijalizacije građenja (State and development directions of the building industrialization). Izgradnja, 61, 557-567.

[33] Velkov, M., Ivkovich, M., Perishich, Z. (1984). Experimental and analytical investigation of prefabricated large panel systems to be constructed in seismic regions. Proceedings of the Eighth World Conference on Earthquake Engineering (pp. 773-780). San Francisco, CA: IAEE - International Association of Earthquake Engineering.

[34] Dimitrijević, R., Gavrilović, B. (2000). Precast prestressed concrete skeleton in contemporary buildings - IMS System. Belgrade: IMS - Institute for testing materials. Retrieved from https://www.institutims.rs/publikacije/ABOUT%20IMS%20SYSTEM.pdf

[35] Blagojević, N., Brzev, S., Petrović, M., Borozan, J., Bulajić, B., Marinković, M., Hadzima-Nyarko, M., Koković, V., Stojadinović, B. (2023). Residential building stock in Serbia: classification and vulnerability for seismic risk studies. Bull. Earthq. Eng. 2023 (accepted for publication).

DISASTER RISK REDUCTION IN THE MUNICIPALITY OF LEZHË. SEISMIC RISK AS PART OF A MULTI-RISK ANALYSIS

Merita Guri [(1)], Endri Duro [(2)]

[(1)] *Lecturer, POLIS University, merita_guri@universitetipolis.edu.al*
[(2)] *Assistant Lecturer, POLIS University, endri_duro@universitetipolis.edu.al*

Abstract

Disaster Risk Reduction (DRR) and community resilience is considered as a global priority. For several decades the focus has been on changing the approach from emergency response towards prevention strategies. Within this approach local authorities have a fundamental role in reducing such disasters as they represent the link between the community and other stakeholders; from central authorities to engineers, planners and disaster specialists. As such the quality, efficiency and the way the risk information is provided to such authorities is of the utmost importance.

Albania is located in one of the most active areas from the seismic point of view and therefore is an earthquake-prone country. The latest seismic event was the 6.4 Magnitude earthquake of November 2019 in Durrës which caused several fatalities and a considerable amount of economic damage, whose impact is still evident nowadays, three years after the event, with the recovery phase still ongoing. Such consequences clearly reflect the low levels of resilience and preparedness urban and non-urban systems in Albania unfortunately have. The aim of this paper, is the evaluation of seismic risk in semi-quantitative terms based on indices, within a wider multi-risk analysis including also flooding, fire, wind, snow etc. for one of the most strategic municipalities of Albania, Lezhë. The analysis is done by taking into consideration several aspects of vulnerability; physical, social, economic, environmental and cultural. The results of such analysis are aimed to be used for several decision-making processes by the local authorities as part of improving the strategies for Disaster Risk Reduction (DRR) and Disaster Risk Management (DRM).

Keywords: decision-making, disaster, earthquake, seismic risk, vulnerability,

1. Introduction

Due to a combination of several external and internal factors, Albania is a country prone to natural disasters including mainly flooding and seismic events. The Mw 6.4 earthquake of November 26, 2019 that struck the city of Durrës, at the Adriatic coast clearly showed several issues amongst which the lack of proper coordination and disaster management. This event brought to the attention of local and central authorities the need for preparedness and special attention to civil protection and disaster risk reduction [1].

Disaster Risk Reduction (DRR) and community resilience is a global priority. It is expected that local authorities play a central role in developing strategies and policies to achieve resilience. The importance of local authorities is clearly emphasized in the SENDAI Framework, in which the need for a focused action in understanding disaster risk, the strengthening disaster governance, the investment in DRR for resilience and the enhancement disaster preparedness are all developed around not only on a national but specifically on a local level [2].

The Lezhë municipality, located in the western part of Albania, consists of 10 administrative units with 2 urban areas (Lezhë and Shëngjin) and a total of 65 rural areas with the total area of approximately 508.9km². Due to its location, Lezhë is considered as one of the most strategic municipalities in Albania, having great potential mainly in tourism. Lezhë is a hazard prone area due to its geographic location, natural and anthropogenic features. Floods are the main hazard for this municipality due to the flow from the two main rivers Mat and Drin river, flash floods and also coastal flooding. Such events are

often due to the climate change. Seismic events are also a constant hazard since the entire country is located near several faults and many historical events were registered in the 20th century. In addition to floods and earthquakes, other hazards like landslides, rock fall, wildfires and snow are also present [3].

Taking into consideration the diversity of hazards a research study was developed to conduct a multi-risk analysis and improve the risk information and perception and help the municipality to improve policies in terms of decision-making and DRR. Such methodology is also aimed to serve as a model for other municipalities in Albania. From the methodological point of view, the research applies an integrated and participatory approach, since participatory planning is considered as an optimal method that helps in the identification of the problem and also aims at training not only the local authorities, but also the community. The focus of this paper is on the analysis of seismic risk as part of a broader multi-risk assessment study.

2. Multi-risk analysis and methodological approach

According to the terminology related to Disaster Risk Reduction, risk represents a "...*combination of the probability of an event and its negative consequences*" [4]. Mathematically the risk (R) can be expressed as a product of three components:

$$R = H \times V \times E \tag{1}$$

The first component is hazard (H), which is based on historical and instrumented data of previous earthquakes in order to determine the severity of such an event. Seismic hazard is characterized mainly in terms of return period, magnitude, intensity, probability of exceedance etc.

Vulnerability (V) and Exposure (E) are components of the risk which determine the level of impact which a hazardous event might have in a built environment. The former represents

"The characteristics and circumstances of a community, system or asset that make it susceptible to the damaging effects of a hazard." [4]

while the latter represent

"People, property, systems, or other elements present in hazard zones that are thereby subject to potential losses." [4]
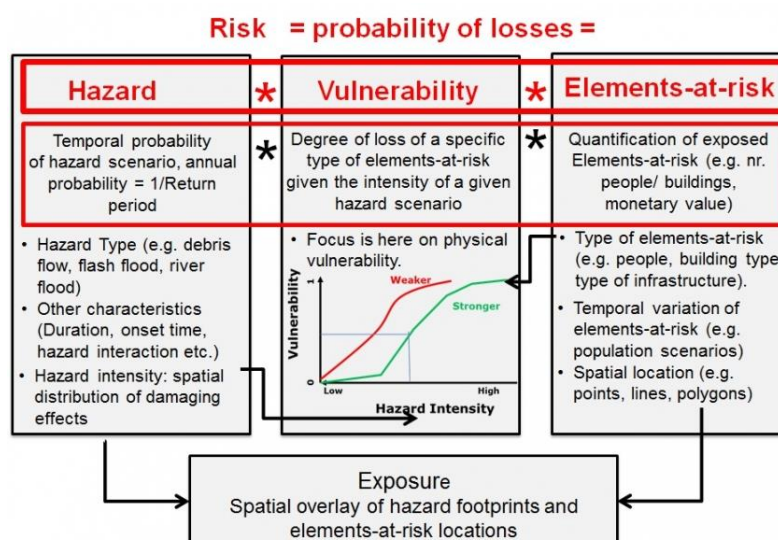

Figure 1. Schematic representation of risk [4]

From the methodological point of view, the approach for assessing seismic risk, includes the following activities:

1. Site visits
2. Interviews with stakeholders e.g. local community, experts, organizations etc.
3. Participatory hazard maps
4. Focus on thematic groups based on the hazard (in this case earthquakes), and
5. Presenting risk assessment results using the GIS platform

2.1 Indicator- Based Approach (IBA)

A literature review revealed previous studies provide a variety of approaches and methodologies that can be used for risk assessment ranging from qualitative deterministic methodologies to more advanced probabilistic approaches. For the research purposes, the proposed methodology corresponds to a semi-quantitative approach. According to the approach, the overall risk is divided into several components, and for each component a number of indicators are selected, and subsequently standardized within a specific range based on the provided data (qualitative or quantitative) using various analysis methods and then weighted to determine the relative importance of each parameter.
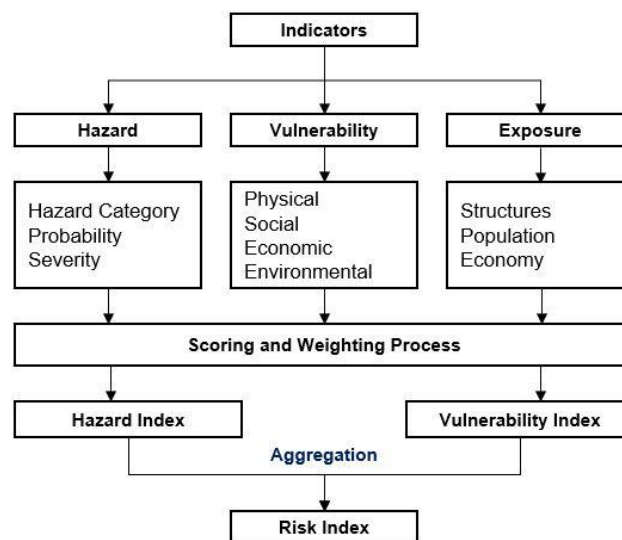

Figure 2. An overview of the Risk Indicator Based Approach (IBA)

Although this method is not purely quantitative it has several advantages. Firstly, it allows for risk to be evaluated in large areas, or in areas that have restricted or limited data. Secondly, the method gives a possibility to perform a holistic risk assessment by combining components of different nature (physical, social, economic, environmental etc). A considerable number of research studies and applied projects [5], [6], [7], [8] have shown that the indices can be easily combined with Spatial Multi-Criteria Evaluation (SMCE) to map the information. In mapping the information from the risk point of view the use of a risk matrix in addition to IBA can be helpful to combine and categorize the levels of risk based on its components.

2.2 Selected Indicators

For the multi-risk analysis, a total of 29 indicators were selected and analysed. Out of these, 6 indicators characterize the hazard, 12 indicators characterize the exposure and 11 indicators are used to

characterize vulnerability. Based on the analysis, following the aforementioned methodological approach each of the indicators is standardized and for the purpose of this research the range of standardized values is from 0 to 4, where 0 represents the minimum (best) value based on the risk component and 4 the maximum (worst) value of the risk and its components. As part of a multi-risk analysis some indicators may be relevant for a specific hazard, and might be not applicable (n/a) for other hazards.

Table 1 – Summary of the indicators

HAZARD	EXPOSURE	VULNERABILITY
Normal Frequency	Number of Objects	The dependency on social help
Fatality Frequency	Infrastructure	Lonely elderly people
Duration of the Event	Service Objects	Age of population
Probability of Occurrence	Industrial Area in the Hazard Area	People with disabilities
Spatial Distribution (Hazard Area)	Population	Mean distance from municipality
Hazard Exposure	Natural Monuments	Mean distance from administrative unit
	Protected Areas	Services
	Forest Area	Percentage of hiring in service
	Agricultural Area	Distance to work outside residential unit
	Educational Institutions	Percentage of youngsters
	Cultural Monuments	Lack of sanitary systems in the family
	Buildings with cultural Relevance (ex. religious, museums etc.)	Working on agricultural systems

3. Seismic Risk Analysis

3.1 Seismic Hazard

The seismic hazard for Lezhë municipality is based on previous research studies [9] and is focused on the determination of peak ground acceleration on base rock for a return period of 475 years with a probability of exceedance 10% in 50 years. [9] gives the spatial distribution of PGA for the entire country (as seen in Fig. 3) and an analysis is done for all administrative units of Lezhë municipality with values of peak ground acceleration given in Table 2. The values of PGA show that Lezhë is characterized by a high level of hazard with values of PGA varying from 0.208g up to 0.373g which can potentially amplify due to soft soil deposits.
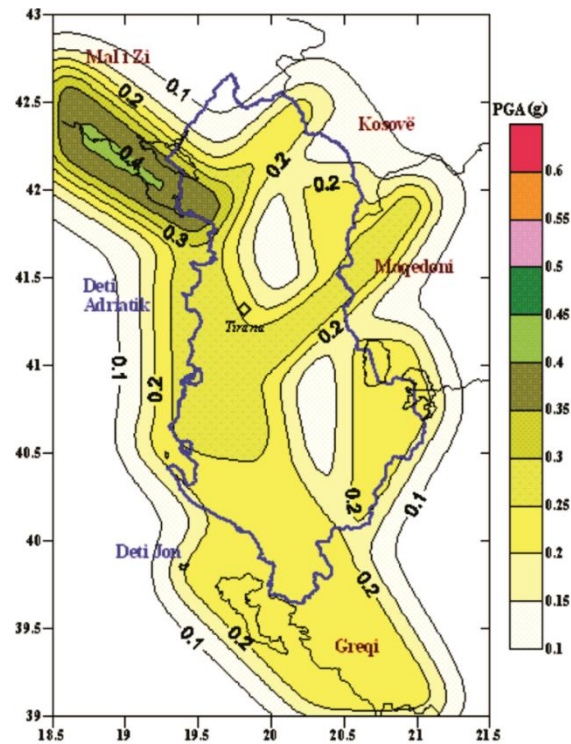
Figure 3. PGA map for Albania. RP= 475 years with probability of exceedance 10% in 50years [9]

Table 1 – Values of PGA for the administrative units in Lezhë Municipality

Administrative Units	PGA RP=475years 10%/50 years
Lezha	0.338
Shëngjin	0.338
Zejmen	0.238
Shënkoll	0.285
Balldren	0.338
Kallmet	0.274
Blinisht	0.373
Dajç	0.373
Ungrej	0.208
Kolsh	0.274

3.2 Aspects of Vulnerability and Exposure

The analysis of the vulnerability was done in a holistic way. The following four aspects of vulnerability were taken into consideration in this study:

1. Physical Vulnerability- physical aspects of buildings, such as age, structural typology, determination of buildings in liquefaction areas, informal settlement, critical infrastructure,
2. Social Vulnerability- Administrative Units having a high percentage of senior people (age 65 or above) percentage of people with disabilities and the part of community having the need of social support

3. <u>Economic Vulnerability</u>- businesses located in buildings older than 30 years, businesses located in informal settlements and areas prone to liquefaction, tourism facilities were recorded,
4. <u>Environmental Vulnerability</u>- was not applied for the case of seismic risk
5. <u>Cultural Vulnerability</u>- Monuments located in areas prone to liquefaction were recorded and classified based on the soil type and the values of PGA in these areas

For the determination of the physical vulnerability in Lezhë municipality a thorough analysis of building typologies was done based on the building age and structural typology:

In terms of the building age the buildings constructed from 1945 up to 1960 were mostly low-rise masonry buildings, with only few buildings using concrete or steel.

Figure 4. Examples of buildings built in the 1945-1960 period

From 1960 up to 1979 some changes were made due to some important seismic events. The quality of materials improved, some additional structural elements were added to the masonry buildings. Prefabricated buildings were added as a new typology to be used for residential and industrial use.

Figure 5. Examples of buildings built in the 1960-1979 period

The 1979-1990 period was characterized by additional improvement in materials and construction technologies which resulted in improved building response to seismic actions. Vertical and horizontal confining elements were added in masonry buildings.

Figure 6. Examples of buildings built in the 1979-1990 period

During the period, from 1990-2000 a considerable number of high-rise buildings were built and reinforced concrete technology was more widely used than masonry construction.

Figure 7. Examples of buildings built in the 1990-2000 period

From 2000 up to present important developments were made in construction technologies and the way buildings were designed taking into account the need for the implementation of Eurocodes. RC frame systems, shear walls and dual systems were widely used to construct high-rise buildings.

Figure 8. Examples of buildings built after 2000

The buildings in Lezhë municipality can be classified into four main typologies:

1. Unreinforced masonry structures located mainly in "Besëlidhja" and "Grumbullimi" areas of the city, and also along Mother Teresa Boulevard in Shëngjin,
2. Reinforced masonry buildings with horizontal and vertical elements located mainly in the same areas as the unreinforced masonry structures,
3. Prefabricated concrete buildings located mainly along the Frang Bardhi street, and
4. Reinforced concrete buildings (frame, shear walls, dual systems, inverted pendulum) located along Franz Josef Strauss Street in "Besëlidhja" area, and also between "Qendër Plazh" and "Qendër Shëngjin".

A map of Lezhë municipality in terms of vulnerability and exposure for seismic action is shown in Figure 9.
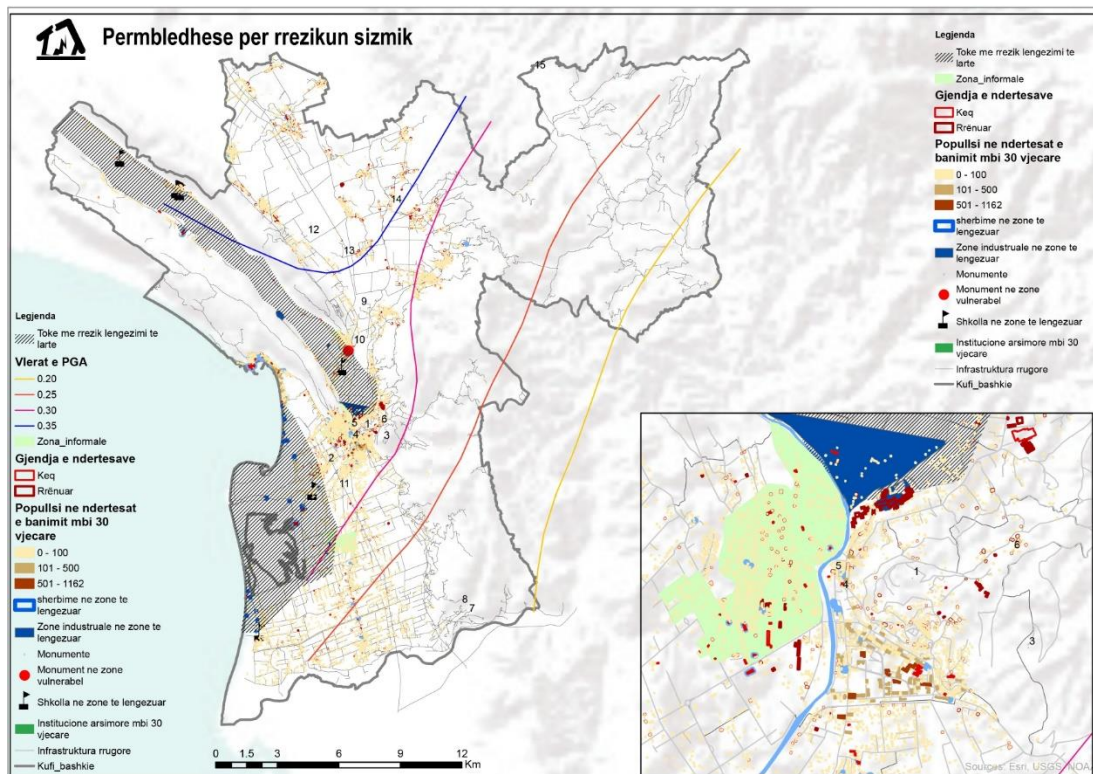

Figure 9. The vulnerability and exposure map for the Lezhë municipality [10]

3.3 Seismic Risk Index Evaluation

Based on the aforementioned risk indicators an indexing process was performed for the multi-risk approach. The results are summarized in Tables 2 to 4 in terms of seismic hazard, exposure and vulnerability. The analysis was performed considering buildings older than 30 years, soil liquefaction, and buildings in informal settlements. The final representative value of each risk element identified in Section 2 was generated as a mean value for all corresponding indicators.

Table 2 – Hazard Index for Seismic Event (adapted from Co-Plan, 2020)

	SEISMIC HAZARD (probability/ frequency)						
	Normal Frequency	Fatality Frequency	Duration	Probability of Occurrence	Spatial Distribution	Hazard Exposure	
	1.00	3.00	3.00	1.00	1.00	3.00	
Damage of buildings > 30 years	1.00	3.00	3.00	1.00	1.00	3.00	2.00
Liquefaction	1.00	3.00	3.00	1.00	1.00	3.00	
Damages in informal settlements	1.00	3.00	3.00	1.00	1.00	3.00	

Table 3 – Vulnerability Index for Seismic Event (adapted from)

	SEISMIC VULNERABILITY												
	The dependency on social help	Lonely elderly people	Age of population	Persons with disabilities	Mean distance from municipality	Mean distance from administrative unit	Services	Employment rate	Distance to work outside residential unit	Percentage of youth population	Lack of sanitary systems in housed apartment	Agricultural workers	
	1.00	1.00	1.67	1.33	1.67	1.00							
Damage of buildings > 30 years	1.00	1.00	2.00	1.00	2.00	1.00	n/a	n/a	n/a	n/a	n/a	n/a	1.28
Liquefaction	1.00	1.00	1.00	2.00	2.00	1.00	n/a	n/a	n/a	n/a	n/a	n/a	
Damages in informal settlements	1.00	1.00	2.00	1.00	1.00	1.00	n/a	n/a	n/a	n/a	n/a	n/a	

Table 4 – Exposure Index for Seismic Event (adapted from [10])

THE HAZARD	EXPOSURE												
	Number of Objects	Infrastructure	Service Objects	Industrial Area in the Hazard Area	Population	Natural Monuments	Protected Areas	Forest Area	Agricultural Area	Educational Institutions	Cultural Monuments	Building with cultural relevance	
SEISMIC	1.67	0.33	1.67	1.00	1.67	-	0.33	-	0.67	1.67	1.67	2.00	
Damage of buildings > 30 years	2.00	-	2.00	1.00	2.00	-	-	-	-	3.00	3.00	2.00	1.06
Liquefaction	2.00	1.00	2.00	-	2.00	-	1.00	-	2.00	1.00	1.00	2.00	
Damages in informal areas	1.00	-	1.00	2.00	1.00	-	-	-	-	1.00	1.00	1.00	

The final risk index was generated by multiplying the results of each risk element as shown in Equation (1) and for the case of Lezhë corresponds to a value of **2.7** which corresponds to moderate levels of risk. Table 5 presents a summary of the indices for each element of risk and, for each type of hazard, to illustrate how seismic risk is positioned among other hazards.

Table 5 – Risk Index for different Hazards (adapted from [10])

Event	Hazard	Exposure	Vulnerability	Risk
Flooding	1.50	1.28	1.79	3.43
Geo-Hazards	1.67	0.79	1.83	2.42
Earthquake	2.00	1.06	1.28	2.7
Meteorological	2.17	0.92	2.06	4.08
Wildfire	2.17	2.33	1.83	4.63
Pandemic	2.60	0.58	1.90	2.88
Climate Change	1.92	1.17	1.51	3.37

4. Conclusions

The seismic risk of Lezhë municipality was assessed as a part of multi-risk assessment study for decision-making purposes showed that the municipality has moderate level of risk due to a combination of moderate hazard levels with low to moderate exposure and vulnerability. Compared to other hazardous events, seismic risk index has the second lowest value, while more frequent events like wildfires and flooding have almost a double value compared to risk. A risk analysis presented in this study could serve as a starting point for detailed risk assessment which would take into consideration several factors like construction technology, building design codes, informal settlements, and other planning aspects. The results might reveal higher levels of seismic risk that require major mitigation measures.

Acknowledgements

References

[1] Toto, R., 2020. Building Resilience for Local Governments in Albania: Legal and Institutional Challenges. MetroPOLIS, Co-PLAN Resilience Series, Policy Paper, 1(1).

[2] UNISDR. (2015). Sendai Framework for Disaster Risk Reduction 2015-2030. *Document*. Geneva: United Nations Office for Disaster Risk Reduction.

[3] Bashkia Lezhë, 2018. Plani i Emergjencave Civile, Lezhë: Bashkia Lezhë.

[4] UNISDR. (2009). 2009 UNISDR Terminology on Disaster Risk Reduction. Geneva: United Nations.

[5] Eastman, J. R. (2005). Multi-criteria evaluation and GIS.

[6] Abella, E., & Van Westen, C. (2007). Generation of a landslide risk index map for Cuba using spatial multi-criteria evaluation. Landslides, 311-325. doi:https://doi.org/10.1007/s10346-007-0087-y

[7] Sinha, N., Priyanka, N., & Joshi, P. K. (2016). Using Spatial Multi-Criteria Analysis and Ranking Tool (SMART) in earthquake risk assessment: a case study of Delhi region, India. Geomatics, Natural Hazards and Risk, 7(2), 680-701. doi:https://doi.org/10.1080/19475705.2014.945100

[8] Patel, M. R., Vashi, M. P., & Bhatt, B. V. (2017). SMART- Multi-criteria decision-making technique for use in planning activities. New Horizons in Civil Engineering (NHCE-2017).

[9] Aliaj, S., Muço, B., Koçiu, S., & Sulstarova, E. (2010). Sizmiciteti, sizmotektonika dhe vlerësimi i rrezikut sizmik në Shqipëri. Tiranë: Akademia e Shkencave e Shqipërisë.

[10] Co-Plan (2020). *Raport i analizës së rrezikut dhe vlerësimit të riskut të fatkeqësive natyrore për bashkinë Lezhë.* Tiranë, Albania

SEISMIC RISK IN THE DISTRICT/MUNICIPALITY OF DURRËS

Markel Baballëku [1], Klajdi Shaholli [2], Rikard Luka [3], Genti Qirjazi [4], Renti Haziraj [5]

[1] *Faculty of Civil Engineering, Polytechnic University of Tirana, Albania, E-mail: markel.baballeku@fin.edu.al*
[2] *Faculty of Civil Engineering, Polytechnic University of Tirana, Albania, E-mail: klajdi.shaholli@fin.edu.al*
[3] *Faculty of Civil Engineering, Polytechnic University of Tirana, Albania, E-mail: rikard.luka@fin.edu.al*
[4] *Faculty of Civil Engineering, Polytechnic University of Tirana, Albania, E-mail: genti.qirjazi@fin.edu.all*
[5] *Urban and Transport Structures ltd, Tirana, Albania, E-mail: rentihaziraj@gmail.com*

Abstract

After the seismic events of 2019, one of the first difficulties encountered was finding and focusing attention on the most damaged areas. It is understood that the aid of the affected population was forthcoming, but the impact of the panic and the overall chaotic circumstances left little opportunity to focus proper attention on the areas with greater damage. A document with analysis, findings and conclusions that showed in advance the areas with the highest risk and their treatment in the territory was missing. By trying to evaluate every clarifying and helpful element in damage assessment even in disaster situations, the consequences that occurred, their analysis and interpretation take on significant importance in risk assessment. This paper is focused at two main topics:

1-) Through the assessment of the seismic risk and all its affecting factors (hazard, exposure and vulnerability) to compare the results of the assessment with the results obtained based on the preliminary assessments carried out after the earthquake of 26 November and presented in the PDNA document;

2-) To establish a procedure which can be used for risk assessment on a similar scale for other municipalities/districts of the country.

This paper will not only highlight the strong and weak points for the territory of Durrës, but will give useful instructions in using the proposed methodology in other territories, without waiting for the next seismic event with possible damaging consequences.

Keywords: seismic risk, 26 November Earthquake, PDNA document, RA methodology

1. Introduction

According to the Albanian Institute of Geosciences [1], on 26th November 2019 at 03:54 local time, a devastating earthquake, with a magnitude of 6.3 on the Richter scale at a depth of 38 km, hit the country. The epicentre was about 16km from Durrës and about 35km from Tirana. As a result of the disaster, a total of 202,291 people were affected in the country, 47,263 directly, and 155,029 indirectly. The earthquake caused 51 fatalities and injured at least 913 people. Moreover, up to 17,000 people were displaced due to the loss of their homes. Overall, first responders rescued 48 people from collapsed houses. [2]. The earthquake caused extensive damage in 11 municipalities, including the two most populous, urbanized and developed municipalities (Tirana and Durrës). The worst affected municipalities were: Durrës, Tirana, Shijak, Kruja, Kamza, Kavaja, Kurbin and Lezha. Based on the PDNA report, the total effect of the disaster in the 11 municipalities amounts to 985.1 million EUR (121.21 billion ALL), of which 843.9 million EUR (103.84 billion ALL) represents the value of destroyed physical assets and 141.2 million EUR (17.37 billion ALL) refer to losses.

A similar earthquake has happened in Durrës in December 1926 [3], with a magnitude of 6.2. This shock destroyed and damaged heavily many buildings in Durrës, Kavaja and Shijak towns and surrounding villages. Many good buildings of the town suffered heavy damage; concrete buildings suffered only slight damage. In Kavaja all houses were damaged and all minarets of mosques were cut off. Based on [3] earthquakes with a magnitude of M=6.5 have a return period of 93.9 years, which is confirmed by the earthquake of 26 November 2019.

Directly after the earthquake, a process of rapid assessment started from different team of experts, who filled out a form with a brief description of the building, its damages and the damage scale of the building (DS1÷DS5). After this process, a process of detailed assessment and retrofitting started for buildings classified with a damage scale DS4 and DS5, while for the other buildings with damage scale DS1÷DS3 the government compensated the inhabitants with a specific value based on the damage scale of the building.

This paper will be focused on risk assessment from the 26 November Earthquake, using the Event Based Method from the OpenQuake engine, and establishing a procedure which can be used for risk assessment in the future.

2. Risk Drivers

Three main risk drivers must be defined to conduct risk assessment: Hazard model (for event-based method – earthquake rapture file); Exposure model; Vulnerability model.

2.1 Hazard

The earthquake rapture file is taken from EFEHR [4]. The data on the earthquake scenario considered are given hereinafter.
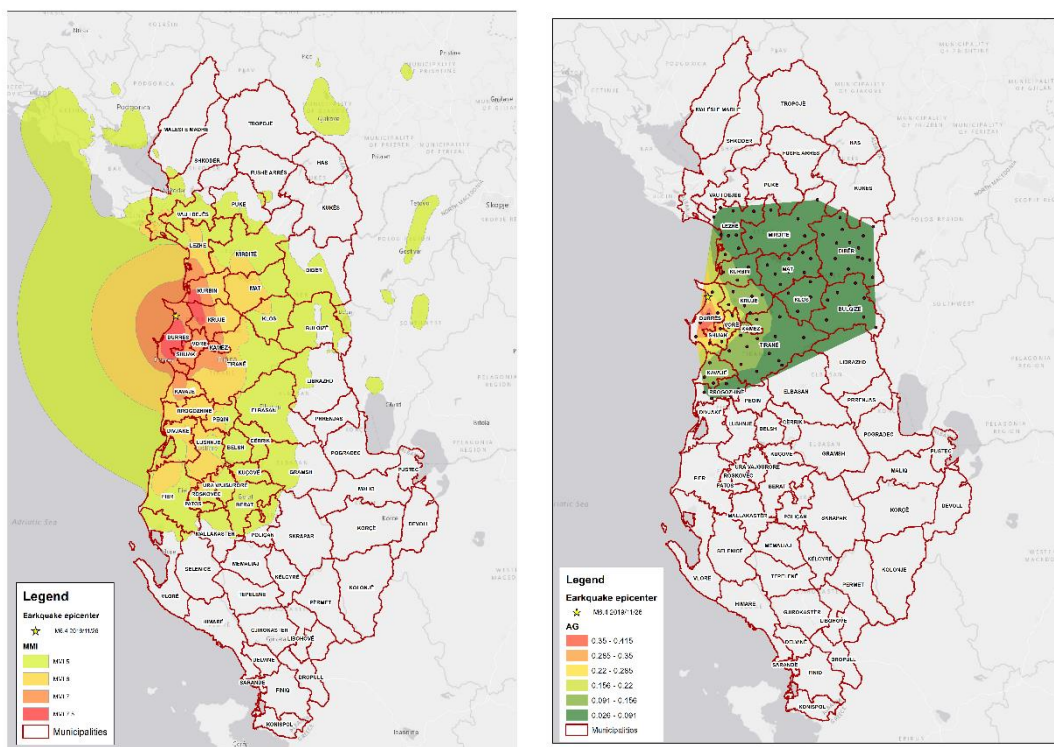
Figure 1: 26 November Earthquake ShakeMap (USGS) (left)[20]; 26 November Earthquake ground motion field (right)[21]

2.2 Exposure

The exposure model is based on the data available on the building stock taken from INSTAT [5]. The exposure model taken into account: the taxonomy model and the asset value (economic cost). The taxonomy model is based on GEM taxonomy [6] and the following main criteria have been used:

Construction period - The construction period has served as a criterion to take into account the design code, construction typology of the time and developments in the country. Three main periods have been used: a-) Before the '60s, Between the' 60s and '90s, After the years '90.

Building height (number of stories) - Three main categories have been distinguished: a-) low-rise buildings 1÷2 floors, medium-rise buildings 3÷5 floors, high-rise buildings over 6 floors.

Main construction material - Two main categories have been distinguished: a-) masonry buildings; b-) reinforced concrete buildings.

A total of 12 taxonomies are used, which are shown in the table below.

Table 1: Taxonomy model

ID	Taxonomy	Description
TAX1	MUR_HBET:2,1_YPRE:19960	Low-rise masonry building build before 1960
TAX2	MUR_HBET:5,3_YPRE:19960	Mid-rise masonry buildings build before 1960
TAX3	CR_HBET:2,1_YBET:1960÷1990	Low-rise RC building build between 1960÷1990
TAX4	CR_HBET:2,1_YPOST:1990	Low-rise RC building build after 1990
TAX5	CR_HBET:5,3_YBET:1960÷1990	Mid-rise RC building build between 1960÷1990
TAX6	CR_HBET:5,3_YPOST:1990	Mid-rise RC building build after 1990
TAX7	CR_H:>5_YBET:1960÷1990	High-rise RC building build between 1960÷1990
TAX8	CR_H:>5_YPOST:1990	High-rise RC building build after 1990
TAX9	MUR_HBET:2,1_YBET:1960÷1990	Low-rise masonry building build between 1960÷1990
TAX10	MUR_HBET:2,1_YPOST:1990	Low-rise masonry building build after 1990
TAX11	MUR_HBET:5,3_YBET:1960÷1990	Mid-rise masonry building build between 1960÷1990
TAX12	MUR_HBET:5,3_YPOST:1990	Mid-rise masonry building build after 1990

The economic cost for each taxonomy is divided into three components: structural cost, nonstructural cost, and contents cost. The economic cost for each component is calculated based on the construction area and the value for unit of area. The value for unit area is taken from [7].

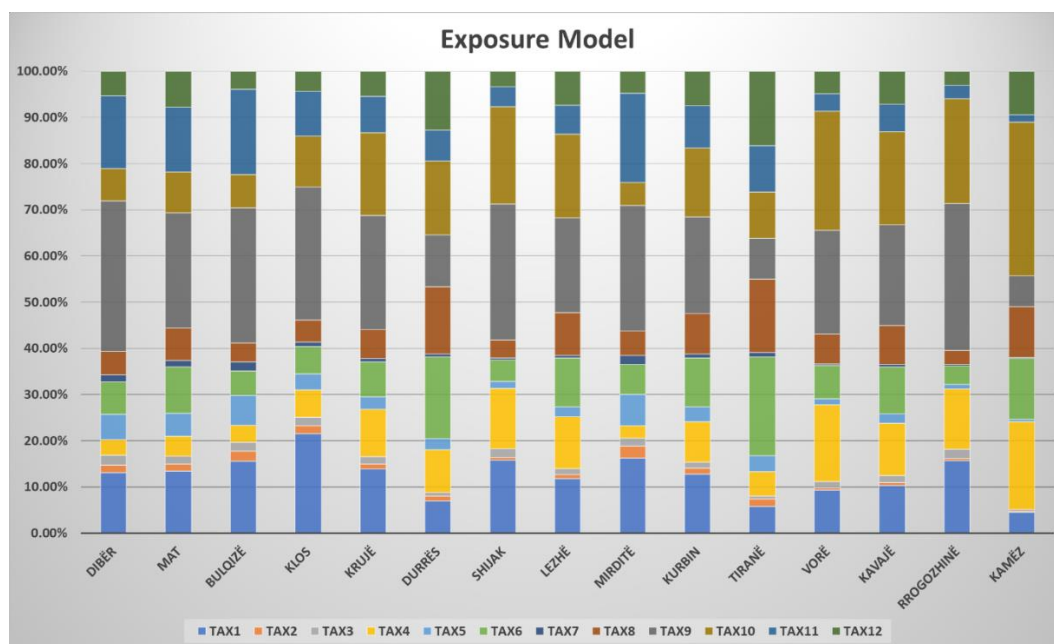The exposure model is given hereinafter.

Figure 2: Exposure model

2.3 Vulnerability

The vulnerability model is build based on fragility curves for each taxonomy and loss functions. The fragility functions are based on the knowledge of the building stock, design and construction codes [8], [9], [10], [11], [12], variety and categorization of works, references to well-known publications in neighbouring and international countries [13], [14], references to studies on specific construction typologies in our country [16], [17], data from specialized institutions and their analysis, and the PDNA reports after the 2019 earthquake.

Hazard related: 1-) National seismic hazard zoning maps, used in the design of buildings in different time periods; 2-) Seismic hazard micro-zoning maps, designed mainly for urban areas with high residential density; 3-) Maps of geological hazard and ground type; areas with significant alternation of use (lagoons, swamps, etc.).
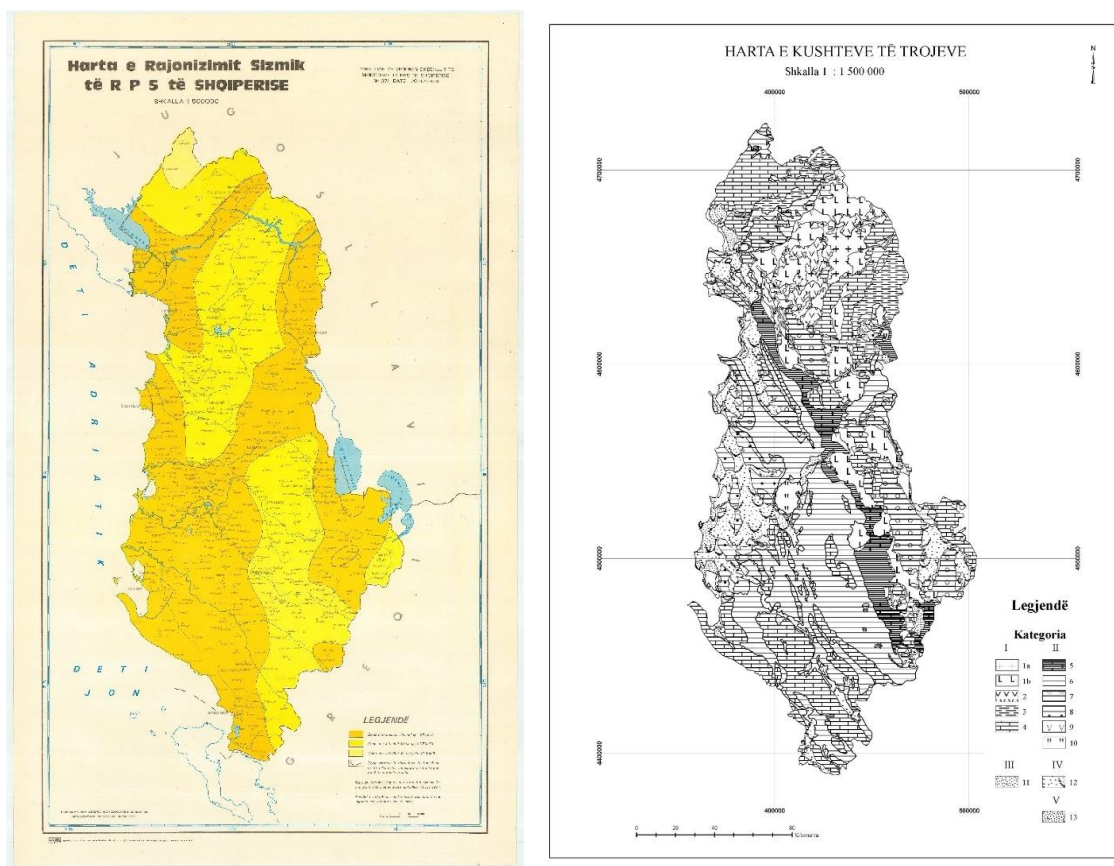
Figure 3: Official seismic intensity map (left)[20]; Soil category map (right)[21]
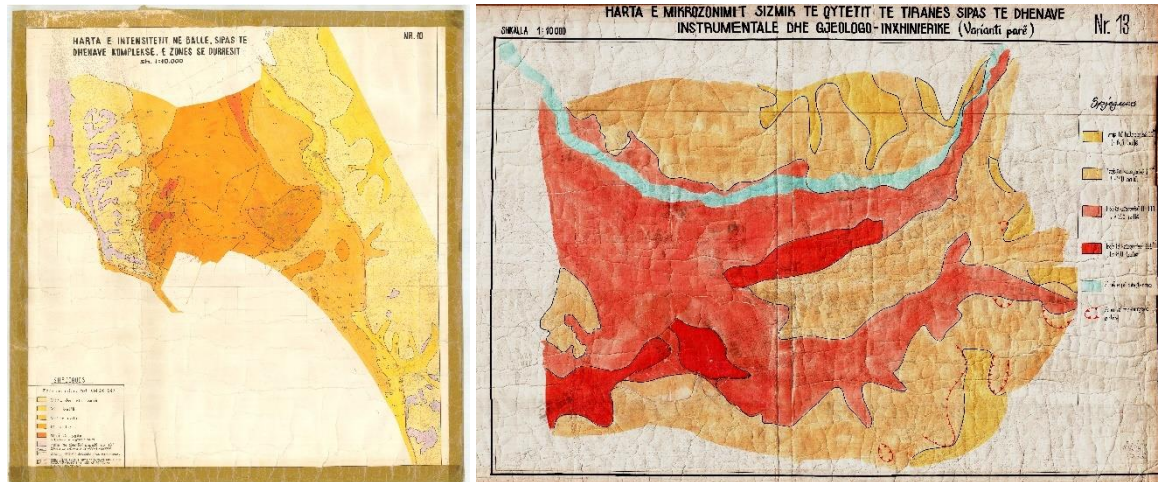
Figure 4: Seismic hazard micro-zoning maps, Durrës (left)[22], Tirana (right)[23]

Related to the exposure: 1-) The importance of the works, their function and the respective categorizations; 2-) Construction intensity and density of use; 3-) Categorization based on the construction period, height / extent of the buildings and construction typology;

Related to vulnerability: In addition to the factors listed above (related to hazard and exposure), other factors directly or indirectly related to vulnerability are: 1-) Design codes; 2-) Workmanship and tradition of implementation; 3-) Norms and experience in structural assessment and retrofitting; 4-) Typified construction models; 5-) Statistics of damages and losses after dangerous previous events; 6-) The spread of severely damaged buildings in the territory and the distinction of the most affected areas.

The fragility functions used for risk assessment are given hereinafter.

Table 2: Fragility functions

Taxonomy	DS1		DS2		DS3		DS4		DS5	
	μ	σ	μ	σ	μ	σ	μ	σ	μ	σ
TAX1	0.124	0.247	0.177	0.247	0.231	0.247	0.295	0.247	0.393	0.247
TAX2	0.152	0.369	0.217	0.369	0.284	0.369	0.362	0.369	0.483	0.369
TAX3	0.191	0.267	0.273	0.267	0.432	0.267	0.682	0.267	0.909	0.267
TAX4	0.140	0.228	0.200	0.228	0.317	0.228	0.501	0.317	0.668	0.317
TAX5	0.143	0.295	0.205	0.295	0.324	0.295	0.511	0.295	0.682	0.295
TAX6	0.169	0.305	0.242	0.305	0.383	0.305	0.605	0.383	0.807	0.383
TAX7	0.148	0.284	0.211	0.284	0.335	0.284	0.529	0.284	0.705	0.284
TAX8	0.193	0.277	0.276	0.277	0.437	0.277	0.690	0.277	0.920	0.277
TAX9	0.130	0.224	0.186	0.224	0.243	0.224	0.310	0.224	0.414	0.224
TAX10	0.143	0.229	0.205	0.229	0.268	0.229	0.342	0.229	0.456	0.229
TAX11	0.160	0.336	0.229	0.336	0.299	0.336	0.381	0.336	0.508	0.336
TAX12	0.176	0.279	0.252	0.279	0.329	0.279	0.420	0.279	0.560	0.279

The loss functions for structural, non-structural and contents losses are taken from [18] and are given hereinafter.

Table 3: Loss functions

Damage State	Structural	Nonstructural	Contents
DS1	2%	2%	1%
DS2	10%	10%	5%
DS3	50%	50%	25%
DS4	75%	75%	37.5%
DS5	100%	100%	50%

2.4 Scenario Building

All the data given above are used as input in the OpenQuake [19] engine for the calculation of the risk assessment.

3. Risk assessment

The economic cost is calculated using the OpenQuake engine and the results obtained are compared with the economic cost given in PDNA report. The economic cost for each municipality is given hereinafter.

Table 4: Economic cost

Municipality	PDNA report	Risk Assessment
Bulqizë	€ -	€ 834,327
Dibër	€ -	€ 1,014,573
Mat	€ -	€ 2,629,347
Klos	€ -	€ 1,305,829
Durrës	€ 220,780,000	€ 336,252,343
Shijak	€ 52,910,000	€ 56,171,318
Krujë	€ 73,010,000	€ 39,039,273
Kurbin	€ 25,390,000	€ 15,750,854
Lezhë	€ 22,180,000	€ 11,112,220
Mirditë	€ 4,420,000	€ 1,252,069
Kavajë	€ 28,620,000	€ 19,034,778
Rrogozhinë	€ -	€ 5,824,497
Kamëz	€ 14,490,000	€ 55,091,351
Tiranë	€ 214,330,000	€ 153,967,205
Vorë	€ 40,160,000	€ 33,172,853
Total	€ 696,290,000	€ 732,452,837

As it can be seen from the table above, the results taken from the risk assessment analysis are comparable with the values given in the PDNA report.
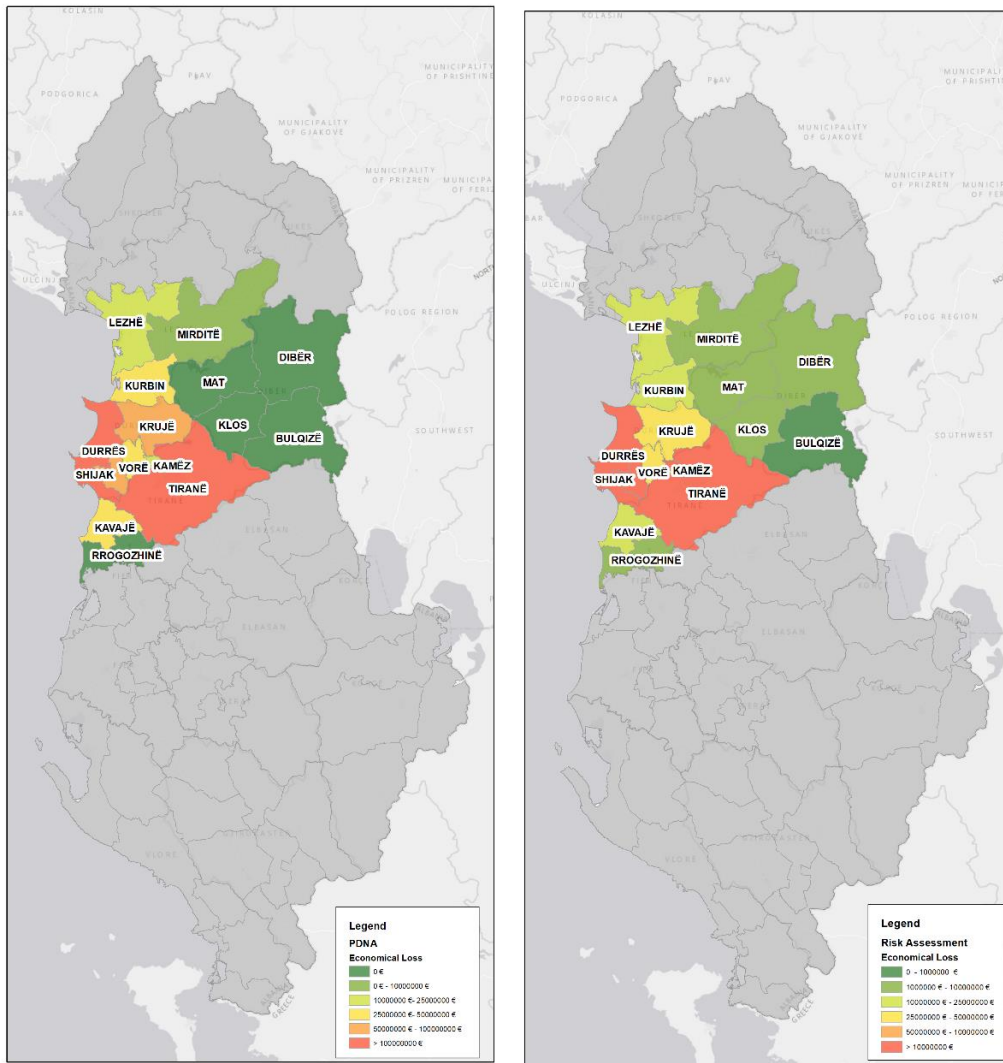
Figure 5: Economic cost PDNA report (left), Risk Assessment (right)

The economic cost for each taxonomy is given hereinafter.
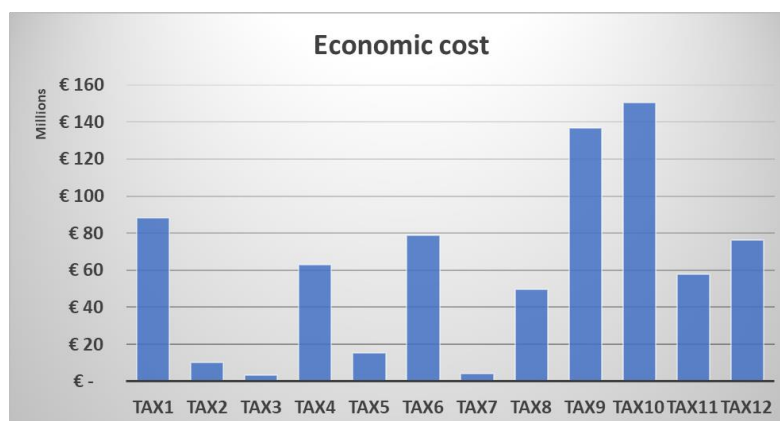
Figure 6: Economic cost for each taxonomy

Based on the chart above, the most damaged building typologies are the low-rise masonry buildings build in each of the considered construction periods, and midrise reinforce concrete buildings build after 1990.

Referring to the distribution of damages in buildings according to the damage scale (DS), it is observed that the simulation of the scenario and the data collected in the field in some cases coincide. For administrative unit of Durrës (city), the comparative results are satisfactory, while for Shijak and Krujë administrative units, the results differ significantly. The distribution of damages for each case are given hereinafter.
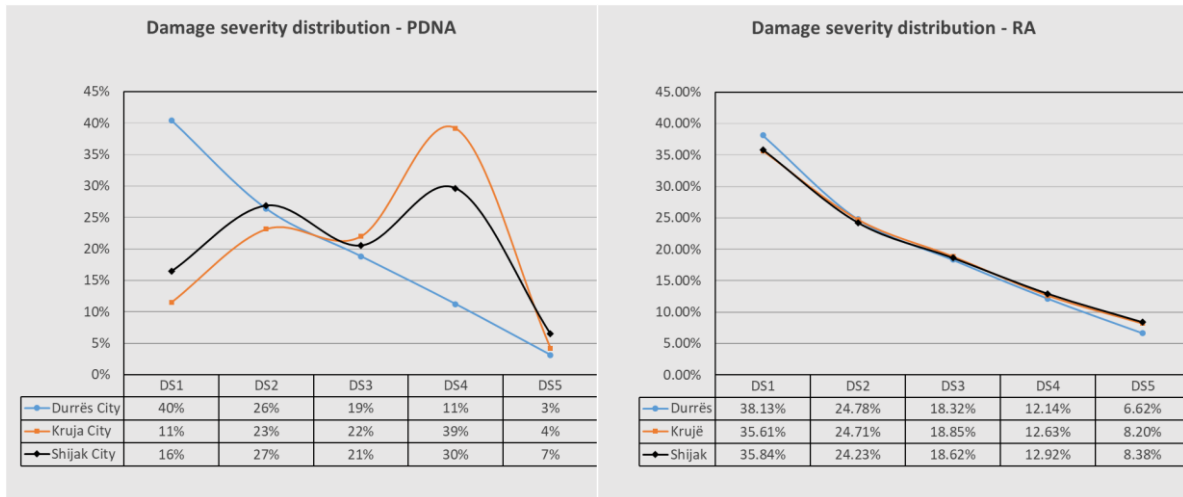
Figure 7: Damage distribution (PDNA report left, Risk Assessment right)

As it can be seen above according to Risk Assessment the damage distribution is similar in all three administrative units, while according to PDNA report, the damage distribution for the administrative unit of Durrës is similar to the damage distribution of the Risk Assessment, while for the administrative units of Kruja and Shijak, the damage distribution differs significantly, having the number of buildings with damage scale DS4 higher that the number of lower damage scales (DS1÷DS3).

4. Recommendations for future risk assessment

The earthquake of November 26, today's studies on seismic risk and the findings of this risk analysis show that the "design earthquake" is higher than the one predicted in the current seismic map.

In areas with dense construction and in areas with weak soil properties, the data on soil conditions needs to be prepared/updated on a smaller scale with focus on the seismic amplification factor.

We advise that either the next census take into account the completion of a series of technical data for buildings or a special project starts for completing the database of buildings with technical data, suitable for the construction of the taxonomy;

Academic institutions, the national civil defense agency and experts in the field need to be involved and undertake research projects to build fragility and vulnerability models for building stock and critical infrastructure. The accuracy of these models directly affects the accuracy of seismic risk calculations;

The typologies that are the most damaged by the earthquake, reported and found by the risk analysis in this paper, require increased attention for their evaluation and rehabilitation.

5. Conclusions

Seismic hazard: The November 26 earthquake added data to seismic models and reinforced previous studies (betim muco ref) that similar seismic events occur with 100-year return periods. As a result, the earthquake that occurred can be considered a "service earthquake" according to the provisions of the Eurocode and meanwhile coincides with the maximum seismic action provided in ktp-n2-89.

Due to the extremely poor ground conditions in some areas of Durrës, their impact on the seismic risk assessment is significant and must therefore be kept in mind.

Exposure: The exposure model - prepared with data available from census2001, census2011 and other data collected in local institutions and in the field - is not comprehensive and needs further improvement by enriching it by structuring it according to known taxonomies for building stock, critical infrastructure and cultural heritage.

Vulnerability: for fragility and vulnerability models, there are few studies conducted at the territorial scale. Their drafting is based on: Durrës earthquake data, design codes and recent studies. The fragility and vulnerability model are of key importance in the preparation of seismic risk analysis, and it needs to be prioritized by experts in the field and state bodies.

Seismic risk: The comparison between the seismic risk scenario presented in this paper with the data obtained from the rapid assessments in the field (presented in PDNA) shows that the results on a macro scale are comparable. Meanwhile, some of the specific findings obtained from this risk analysis are presented below:

1-) The administrative unit with the most losses is the administrative unit of …

2-) The most damaged buildings are buildings with 1-2 storeys

3-) The taxonomies with the most losses are low rise masonry buildings build in each considered construction period

4-) Referring to the distribution of damages in buildings according to the degree of damage (DS), it is observed that the simulation of the scenario and the data collected in the field in few cases coincide. For administrative unit of Durrës (city), the comparative results are satisfactory, while for Shijak and Kruje administrative units, the results differ significantly.

References

[1] IGEO, "Institute of Geosciences," 2021. [Online]. Available: https://geo.edu.al/site/.

[2] Government of Albania, European Union, United Nations agencies, World Bank, "Albania Post-Disaster Needs Assessment, Volume A and B Report," Tirana, 2020.

[3] Aliaj Sh, Koçiu S, Muço B, Sulstarova E, "Sizmiciteti, sizmoteknika dhe vlerësimi i rrezikut sizmik në Shqipëri 2010", Academy of Sciences of Albania

[4] H. Crowley, J. Dabbeek, L. Danciu, P. Kalakonas, E. Riga, V. Silva, E. Veliu, & G. Weatherill. (2021). Earthquake Scenario Loss Testing Repository (v1.0) [Data set]. Zenodo. https://doi.org/10.5281/zenodo.5774113

[5] INSTAT, "INSTAT," Annual Books [1990-2021], Census 2001, Census 2011, [Online]. Available: http://www.instat.gov.al/al/temat/censet/censusi-i-popullsis%C3%AB-dhe-banesave/#tab2.

[6] C. S. A. C. L. A. M. G. K. J. a. V. S. Brzev S., "GEM Building Taxonomy Version 2.0," Pavia, Italy, 2013.

[7] Udhëzim Nr.3, date 28.12.2016 për "Miratimin e kostos mesatare të ndërtimit të banesave nga enti kombëtar i banesave, për vitin 2016".

[8] Këshilli i Ministrave, "Vendim nr. 817 datë 27/12/1952 mbi aprovim dispozitash për ndërtimet antisizmike," Këshilli i Ministrave, Tirana, Albania, 1952.

[9] Këshilli i Ministrave, ""Rregullore mbi kushtet teknike për ndërtimet antisizmike dhe ngritjen e shërbimit sizmollogjik në vendin tonë", Vendim i Këshillit të Ministrave Nr. 206 dt. 04-06-1963," Këshilli i Ministrave, Tirana, Albania, 1963.

[10] Ministria e Ndërtimit, "Kushte teknike të projektimit, KTP-1-78 deri në KTP-24-78," Ministria e Ndërtimit, Tirana, Albania, 1978.

[11] Ministria e Ndërtimit, "Kushtet teknike të projektimit për ndërtimet në zona sizmike - KTP-2-78 (Kapitulli 1) Për ndërtesa qytetare, industriale dhe ekonomike (plotësime dhe korrigjime), Tiranë, janar 1982. Miratuar me Vendim nr.20 datë 25.12.1981 të këshillit tekniko-shkencor t," Ministria e Ndërtimit, Tirana, Albania, 1982.

[12] Qendra Sizmologjike, Akademia e Shkencave, "Kusht Teknik Projektimi për ndërtimet antisizmike - KTP-N.2-89. Miratuar me Vendim nr.40 datë 10.01.1989 të këshillit shkencor të Ministrisë së Ndërtimit," Qendra Sizmologjike, Akademia e Shkencave, Tirana, Albania, 1989.

[13] R. M. P. A. Rosti A, "Empirical fragility curves for Italian URM buildings," Bull Earthq Eng, 2020

[14] P. A. D. G. C. R. P. D. L. M. V. G. R. M. Rosti A., "Empirical fragility curves for Italian residential RC buildings," 2020

[15] UNDP, Ministry of Local Government and Decentralization, "Executive Summary "Risk Assessment - Albania, within the "Disaster management and emergency preparedness" Project," 2003.

[16] M. Baballëku, "Vlerësimi i dëmtimeve strukturore në ndërtesat tip të sistemit arsimor - Structural damages assessment of typified educational facility buildings," Tirana, Albania, 2014.

[17] M. Baballëku, "Fragility of Typified Educational System Facilities in Albania, INTERNATIONAL POST GRADUATE STUDY PROGRAM EARTHQUAKE ENGINEERING IZIIS-TEMPUS MASTER COURSE", 2006

[18] C. A. e. Kircher, "Estimation of earthquake losses to buildings. Earthquake Spectra. s.l.," *Earthquake Engineering Research Institute (EERI),* 1997.

[19] GEM (2022). The OpenQuake-engine User Manual. Global Earthquake Model (GEM) OpenQuake Manual for Engine version 3.15.0. doi: 10.13117/GEM.OPENQUAKE.MAN.ENGINE. 3.15.0

[20] Këshilli i Ministrave, "Harta e rajonizimit të RPSSH (miratuar me VKM 371, dt. 20.12.1979)," Këshilli i Ministrave, Tirana, Albania, 1979.

[21] Sulstarova E., Koçiaj S., Aliaj Sh., "Rajonizimi sizmik i Republikës Popullore Socialiste të Shqipërisë," Qendra Sizmologjike, Akademia e Shkencave, Tirana, Albania, 1980.

[22] S. Koçiaj, E. Sulstarova, S. Aliaj, L. Duni, V. Peçi, N. Konomi, H. Dakoli, I. Fuga, K. Goga, A. Zeqo, L. Kapllani, S. Kozmaj and M. Lika, "Mikrozonimi sizmik i qytetit të Durrësit," Tirana, Albania, 1985.

[23] Koçiaj S., et al., "Mikrozonimi sizmik i qytetit të Tiranës "Seismic microzonation of Tirana City"," AQS - Seismological Institute archive, Tirana, 1988.

APPLICATION OF ANALYTIC HIERARCHY PROCESS (AHP) IN EARTHQUAKE RISK ASSESSMENT

Anita Cerić [(1)], Ivona Ivić [(2)]

[(1)] *University of Zagreb, Faculty of Civil Engineering, Department for Organization, Technology and Management in Construction, anita@grad.hr*

[(2)] *University of Zagreb, Faculty of Civil Engineering, Department for Organization, Technology and Management in Construction, iivic@grad.hr*

Abstract

Different types of disasters, including earthquakes, are causing social, health, economic, and environmental damage worldwide. In this regard, the need for comprehensive and effective disaster and risk management becomes even more recognised, especially from public institutions. Risk management includes careful identification, analysis, and development of risk mitigation strategies, which implies planning and a certain degree of prediction of future events and their consequences. However, all risk components of earthquakes are not measurable or have a very high degree of uncertainty. Therefore, earthquake risk management activities are challenging throughout entire earthquake risk management activities. In this paper, the Analytic hierarchy process (AHP) for effective earthquake risk assessment is presented. AHP belongs to the group of multi-criteria analysis that combines quantitative and qualitative data with the aim of making decisions in defining the priorities of alternative solutions to a given problem. It is particularly suitable in cases where there is a lack of statistical data to conduct the analysis. The use of AHP is explored in the context of producing earthquake risk priority lists for a certain geographical region. A hierarchical model for risk assessment of five different counties was developed. The three main criteria that have influence on the earthquake risk are used: hazard, exposure, and vulnerability of the built environment. AHP was used to determine the priority list of counties according to these three criteria. The resulting priority list of counties can be used to produce earthquake risk maps, thus provide a useful tool for allocation of available mitigation resources.

Keywords: analytical hierarchy process (AHP), decision making, earthquake risk assessment, risk management

1. Introduction

Due to the large consequences on human lives, health, finances, and environment, natural disasters such as earthquakes have been attracting more and more attention from scientific community. Moreover, public institutions with the aim of mitigating natural disasters and governments across the world acknowledge the importance of building resilience of nations and communities to disasters. In that regard, the new UN's *Sendai Framework for Disaster Risk Reduction 2015-2030* [1] emphasises the importance of management of disaster risks, instead of disaster management. The main objective of the Sendai Framework and similar initiatives is to prevent new and reduce the existing risk of disasters through the implementation of integrated and inclusive economic, structural, legal, social, health, cultural, educational, environmental, technological, political, and institutional measures. In Europe, similar initiative is set by JRC's *Recommendations for National Risk Assessment for Disaster Risk Management in EU* [2]. In these guidelines, disaster risks are approached from the point of view of the ISO 31000 standard [3], and the emphasis is given to four steps of risk management: identification; analysis; evaluation; and response to disaster risks.

Earthquake risk or seismic risk describes the negative consequences caused by an earthquake (victims, number of damaged and collapsed buildings, financial losses, etc.) and the probability of their occurrence for a certain level of seismic activity. Earthquake risk is usually calculated using a set of variables or elements of earthquake risk: earthquake hazard (or seismic hazard), exposure and vulnerability. These elements represent the input data for earthquake risk assessment, but in many cases

are not measurable or have a very high degree of uncertainty. In recent years, several big projects with the aim of collecting more input data for earthquake risk management have been implemented across the world (see for example GEM [4] and SERA [5]). Nevertheless, the lack of correct input data remains the major challenge in earthquake risk assessment.

In the case when there is not a large enough number of input data, the analytical hierarchy process (AHP) method has proven to be very accurate and suitable for risk assessment. AHP is a multi-criteria analysis that combines quantitative and qualitative data with the aim of making decisions in defining the priorities of alternative solutions to a given problem. It is particularly suitable in cases where we do not have a sufficient number of statistical data, when almost all risk components are not measurable or have a very high degree of uncertainty. In the case of earthquake risk, the input data have the same uncertain characteristics, and therefore AHP is a suitable and widely applicable method for its assessment. The application of the AHP method in earthquake risks can be found in many scientific papers and case studies of practical examples. AHP is used to assess earthquake risk independently or in combination with other methods in the scientific studies by Fariza et al. [6], Nyimbili et al. [7], Jena et al. [8], Jena and Pradhan [9], Özkazanç et al. [10], Shadmaan and Islam [11].

In this paper, AHP is described in more detail and an example of its application for earthquake risk assessment of certain geographical areas is given.

2. An overview of Analytic hierarchy process (AHP)

AHP was developed by Thomas L. Saaty as a decision aid [12-14] that results in the priorities of different alternative options compared according to complex or multiple criteria. By simple comparisons of pairs of model elements, AHP obtains the weight value of each alternative option. AHP can best be used for multi-criteria problems in which it is not possible to precisely quantify how alternatives impact decision making. Values for comparison can be obtained by actual or relative measurements, or subjective assessments by experts with extensive experience.

The method is applied to numerous concrete examples of various types of decision making. Subjective assessments and objective facts are incorporated into a logical hierarchical AHP framework to provide decision makers with an intuitive and common-sense approach in quantifying the importance of each decision element through a comparison process. This process enables decision makers to reduce a complex problem to a hierarchical form with several levels, with a minimum of three: the goal of analysis, criteria, and alternatives [15].

The first step in implementing the model is dividing the decision problem into hierarchical levels [15-17]. This means that at least three levels of decision making should be defined: goal, criteria, and alternatives.

Each model has a hierarchical structure and consists of several levels. The highest level on the hierarchical scale is the goal. Then follow the criteria, possibly sub-criteria, and alternatives. The hierarchical structure of the decision making model is shown schematically in Fig. 1.

The second step is forming comparative matrices for all hierarchical levels [17, 18]. This step is the most important and sensitive step. It is also the only subjective step (in case we do not have quantified input parameters) and depends on professional knowledge, experience and personal priorities defined by the decision maker. For each level, it is necessary to compare and evaluate the elements of that level in relation to each element of a higher level. For the previously defined three levels, this means that at level 1, a comparison of all set criteria will be performed in relation to the given goal, while at level 2, all alternatives will be compared with each other, i.e. evaluated in relation to the given criteria. The process starts by determining the relative importance of particular alternatives with respect to the criteria and the sub-criteria [16]. Then the criteria are compared with respect to the goal. Finally, the results of these two analyses are synthesised by calculating the relative importance of the alternatives with respect to achieving the goal. The process of comparison is represented by forming a comparative matrix [12]. If the analyst has at his disposal n alternatives, or criteria that form the comparative matrix, then he

must make $n(n-1)/2$ evaluations [17]. In order to quantify the comparative evaluation, it is necessary to perform standardization. The proposal of one such standardization is presented in Table 1.
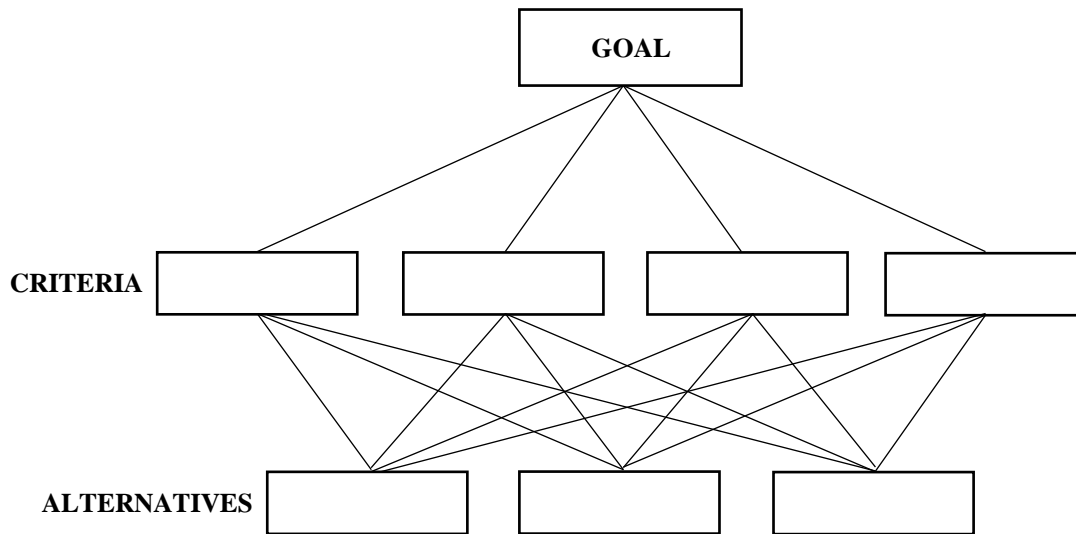

Figure 1. Hierarchical structure of the AHP model.

Table 1 – The scale for pairwise comparisons [13, 19]

Intensity of importance on an absolute scale	Definition	Explanation
1	Equal importance	Two elements contribute equally to the objective
3	Moderate importance of one over another	Experience and judgment slightly favour one element over another
5	Essential or strong importance	Experience and judgment strongly favour one element over another
7	Very strong importance	An element is strongly favoured and its dominance demonstrated in practice
9	Extreme importance	The evidence favouring one element over another is of the highest possible order of affirmation
2,4,6,8	Intermediate values between the two adjacent judgments	When compromise is needed
Reciprocals	If activity i has one of the above numbers assigned to it when compared with activity j, then j has the reciprocal value when compared with i	

Examples of using Table 1:

- If the decision maker estimates that criterion 1 is extremely more important than criterion 2 with regard to the set goal, then the matrix element gets the value 9.
- If the decision maker estimates that alternative 1 is moderately more important than alternative 2 with regard to criterion 2, then the matrix element gets the value 3.

Furthermore, Table 2 shows that criterion 1 is moderately (3) more important than criterion 2, considering the goal of decision making. Table 3 shows that alternative 2 is moderately to strongly (4) more important than alternative 5, with regard to criterion 2.

Table 2 – Example of a comparative matrix with regard to level 1 of the hierarchy

With regard to Goal	Criterion 1	Criterion 2	Criterion 3
Criterion 1	1	3	5
Criterion 2	1/3	1	4
Criterion 3	1/5	1/4	1

Table 3 – Example of a comparative matrix with regard to level 2 of the hierarchy

With regard to Criterion 2	Alternative 1	Alternative 2	Alternative 3	Alternative 4	Alternative 5
Alternative 1	1	1/3	½	1/4	2
Alternative 2	3	1	2	1/2	4
Alternative 3	2	1/2	1	1/3	3
Alternative 4	4	2	3	1	5
Alternative 5	1/2	1/4	1/3	1/5	1

The third step is calculating regional eigenvectors and eigenvalues for the comparative matrices for all hierarchical levels. The normalized eigenvector of each comparative matrix is the priority list, while the maximum eigenvalue gives the measure of consistency in making the assessment or comparison. On the level of criteria the regional eigenvector defines the priority, with respect to weight, of the individual criteria for achieving the goal, while on the level of alternatives the regional eigenvector defines the priority of the alternatives with respect to the given criterion. The synthesised eigenvector is the global sequence of the alternatives with respect to achieving the goal. A global consistency ratio smaller than 0.10 is acceptable, otherwise the assessments must be revised.

The eigenvector and the maximum eigenvalue of the comparative matrix are determined by solving the general problem of eigenvalues:

$$AW = \lambda_{max}W \qquad (1)$$

where

A – comparative matrix,

$W = (W_1, W_2, W_3, W_4, W_5)^T$ – eigenvector, and

λ_{max} – maximum eigenvalue.

The fourth step is calculating the consistency ratio for each comparative matrix on all levels, and this is determined from the eigenvalue of the comparative matrix. AHP calculates a consistency ratio comparing the consistency index of the matrix versus the consistency index of a random matrix. A random matrix is a matrix where the judgments have been entered randomly. Therefore, it is expected to be highly inconsistent. If the consistency ratio exceeds 0.10 then inconsistent assessments were made in forming the comparative matrices on particular hierarchical levels and such matrices must be formed anew. If the consistency ratio is smaller than 0.10 then it is possible to move on to the next step.

Consistency index (CI) is calculated according to the expression:

$$CI = (\lambda_{max} - n) / (n-1) \qquad (2)$$

where

λ_{max} – maximum eigenvalue of the comparison matrix,

n - dimension of the comparison matrix.

Consistency ratio (CR) is calculated according to the expression:

$$CR = CI \, / \, RI \tag{3}$$

where random consistency index (RI) is given in Table 4.

Table 4 – Random consistency index (RI) values

n	1	2	3	4	5	6	7	8	9	10
RI	0.00	0.00	0.58	0.90	1.12	1.24	1.32	1.41	1.45	1.49

The fifth step is synthesising the calculation results from all levels and weighting each alternative in relation to achieving the goal. The global eigenvector and the global consistency ratio are calculated. If the global consistency ratio exceeds 0.10 then inconsistent judgments still exist and the comparative matrices must be redefined. If the consistency ratio is smaller than 0.10 then the process of defining the weight and interdependency of the alternatives with respect to the given goal has been concluded.

3. Application of AHP in earthquake risk assessment

The application of AHP is shown on the example of earthquake risk assessment for individual geographic areas. With the help of the AHP, it is possible to determine a list of priorities of individual districts, cities, counties, countries, etc., according to the severity of the earthquake risk. In this way, it is possible to create and display comprehensive risk maps of an area, which include all elements of earthquake risk (hazard, exposure, vulnerability, but also cost, social and other aspects of earthquakes).

The *Super Decisions* software for decision support [20] based on the AHP method is used as an auxiliary tool in this analysis.

3.1 Hierarchical levels

The problem of prioritizing certain geographical areas is divided into three hierarchical levels: goal, criteria, and alternatives.

Level 1 always represents the set goal to be achieved by the analysis, and in this case it refers to the earthquake risk assessment. It is the highest hierarchical level whose priority is quantified by the priority index for each individual alternative, that is, the geographical area we are observing. In the given example, the goal is to determine the earthquake risk of the counties.

Level 2 contains criteria that are assumed to be important attributes with regard to meeting the goal at level 1. Setting these criteria is a very important step, because they must cover all important elements of earthquake risk. In this example, the criteria are:

- **Exposure** – the extent of human activity (for example, the presence of buildings) in areas exposed to seismic hazard. The most important part of the exposure data refers to the list of existing buildings (fund) which significantly contributes to social and economic risk.
- **Hazard** – potentially devastating effects of an earthquake (for example, ground shaking, liquefaction, landslides, tsunamis, etc.) at the observed location.
- **Vulnerability** – susceptibility of exposed buildings to the effects of earthquakes (damages) described with structural features of the building fund.

Level 3 provides alternatives that are compared with respect to the criteria at level 2, all in function of the goal set at level 1. At the national level, the alternatives could be counties or cities and municipalities. In this example, several arbitrary counties will be displayed, for the purpose of presenting the method:

- County 1,
- County 2,
- County 3,
- County 4,
- County 5.

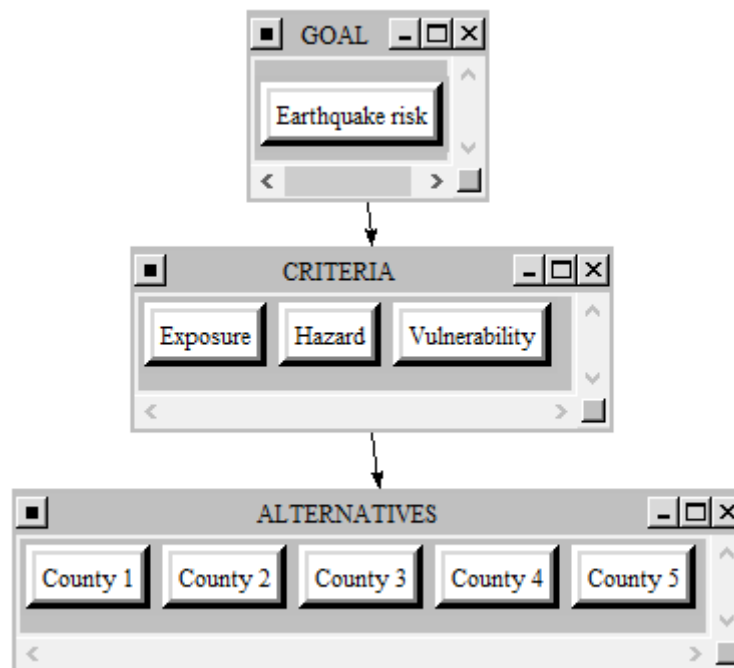The model described in this way is defined in the *Super Decisions* software (Fig. 2).

Figure 2. Decision making model in the *Super Decisions*.

3.2 Comparative matrices

After defining a model with a minimum of three hierarchical levels, it is possible to format the comparative matrices. In this example, there are four comparison matrices: one in relation to level 1 (goal level) and three in relation to level 2 (criteria level). The number of comparisons that need to be made within each matrix is $n(n-1)/2$, if n is the number of defined criteria or alternatives. In this example, the evaluation was carried out based on the standardization from Table 1.

Table 5 shows a comparative matrix with regard to level 1, in which the defined criteria are compared. The importance of individual criteria in relation to the defined goal is determined by the decision maker. Such decisions are subjective, but based on the knowledge available to the decision maker at the time of analysis.

Table 5 – Comparison matrix with respect to goal

Wrt Earthquake risk	Exposure	Hazard	Vulnerability
Exposure	1	1/2	2
Hazard	2	1	3
Vulnerability	1/2	1/3	1

As shown in Table 5, hazard is rated as equally to slightly (2) more important than exposure in terms of determining earthquake risk. This applies only for our example of specific counties, and does not provide a general conclusion on the importance of earthquake elements. Fig. 3 shows a screenshot from the *Super Decisions*, where the value of the eigenvector W_c and the consistency ratio CR_c for level 1 are calculated as:

$$W_c = (W_1, W_2, W_3)^T = (\textbf{0.297, 0.540, 0.163})^T$$

$$CR_c = \textbf{0.009} < 0.10$$
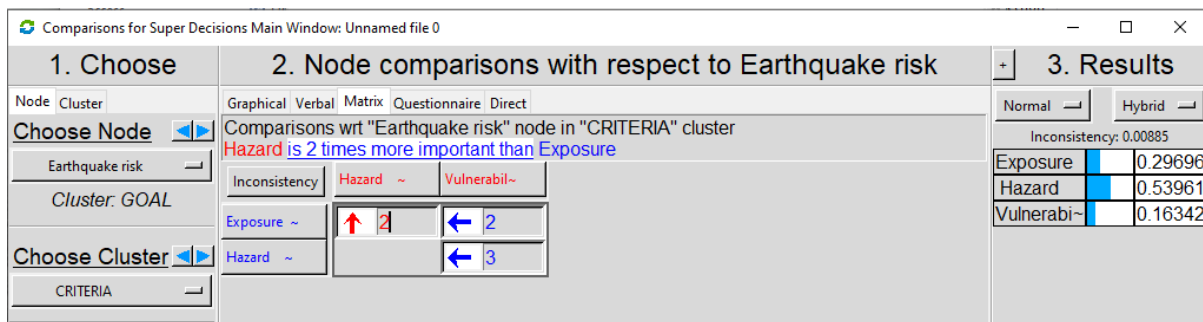
Figure 3. Comparison of criteria in relation to the goal – *Super Decisions*.

Table 6 shows a comparative matrix with regard to level 2, in which the defined alternatives are compared with each other with regard to the criterion of exposure of the built environment. The importance of individual alternatives in relation to the exposure criterion can be determined on the basis of input data on exposure in the territory of each county. When comparing alternatives, the county in whose territory the exposure of the built environment is higher, that is, the losses due to earthquakes are higher, receives higher marks.

Table 6 – Comparison matrix with respect to level 2 – criterion: exposure

Wrt Exposure	County 1	County 2	County 3	County 4	County 5
County 1	1	3	9	2	3
County 2	1/3	1	6	1/2	1
County 3	1/9	1/6	1	1/6	1/5
County 4	1/2	2	6	1	2
County 5	1/3	1	5	1/2	1

As shown in Table 6, in County 1 the exposure of buildings is extremely higher (9) than in County 3. Fig. 4 shows a screenshot from the *Super Decisions*, where the value of the eigenvector W_{a1} and consistency ratio CR_{a1} for level 2 are calculated as:

$$W_{a1} = (W_1, W_2, W_3, W_4, W_5)^T = (\textbf{0.419, 0.152, 0.035, 0.249, 0.145})^T$$
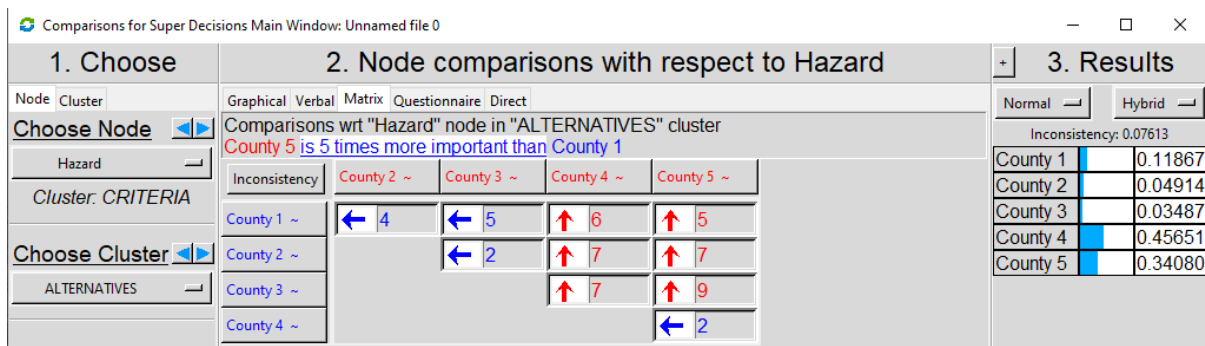
$$CR_{a1} = \textbf{0.016} < 0.10$$
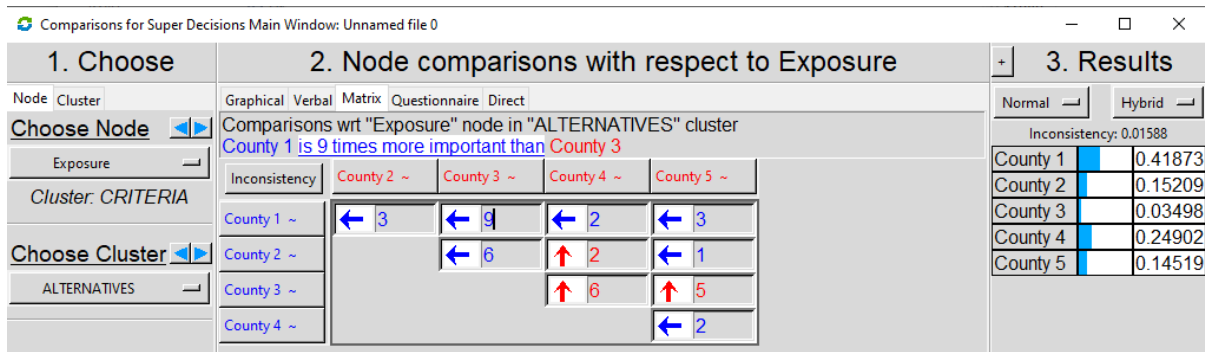
Figure 4. Comparison of alternatives in relation to the exposure criterion – *Super Decisions*.

Table 7 shows a comparative matrix with regard to level 2, in which the defined alternatives are compared with each other with regard to the earthquake hazard criterion. The importance of individual alternatives in relation to the hazard criterion can be determined based on the input data on the earthquake hazard in the territory of each county. When comparing the alternatives, the county in which the hazard is higher, i.e. the potential devastating effects of an earthquake (for example, ground shaking, liquefaction, landslides, tsunami, etc.) are more serious in the observed location, receives higher marks.

Table 7 – Comparison matrix with respect to level 2 – criterion: hazard

Wrt Hazard	County 1	County 2	County 3	County 4	County 5
County 1	1	4	5	1/6	1/5
County 2	1/4	1	2	1/7	1/7
County 3	1/5	1/2	1	1/7	1/9
County 4	6	7	7	1	2
County 5	5	7	9	1/2	1

As shown in Table 7, in County 5 the earthquake hazard is strongly higher (5) than in County 1. Fig. 5 shows a screenshot from the *Super Decisions*, where the value of the eigenvector W_{a2} and consistency ratio CR_{a2} for level 2 are calculated as:

$$W_{a2} = (W_1, W_2, W_3, W_4, W_5)^T = (\mathbf{0.119, 0.049, 0.035, 0.457, 0.341})^T$$

$$CR_{a2} = \mathbf{0.076} < 0.10$$

Figure 5. Comparison of alternatives in relation to the hazard criterion – *Super Decisions*.

971

Table 8 shows a comparative matrix with regard to level 2, in which the defined alternatives are compared with each other with regard to the vulnerability criterion. The importance of individual alternatives in relation to the criterion of vulnerability can be determined based on input data on the vulnerability of the built stock of buildings in the territory of each county. When comparing alternatives, the county in whose area the vulnerability of the built environment is higher, i.e. the structural features of the exposed buildings are such that they are more susceptible to the effects of earthquakes (damages), receives higher marks.

Table 8 – Comparison matrix with respect to level 2 – criterion: vulnerability

Wrt Vulnerability	County 1	County 2	County 3	County 4	County 5
County 1	1	2	2	5	7
County 2	1/2	1	1	2	4
County 3	1/2	1	1	2	4
County 4	1/5	1/2	1/2	1	3
County 5	1/7	1/4	1/4	1/3	1

As shown in Table 8, in County 2 the vulnerability of buildings is the same as in County 3. Fig. 6 shows a screenshot from the *Super Decisions*, where the value of the eigenvector W_{a3} and consistency ratio CR_{a3} for level 2 are calculated as:

$$W_{a3} = (W_1, W_2, W_3, W_4, W_5)^T = (0.426, 0.207, 0.207, 0.109, 0.050)^T$$

$$CR_{a3} = 0.009 < 0.10$$
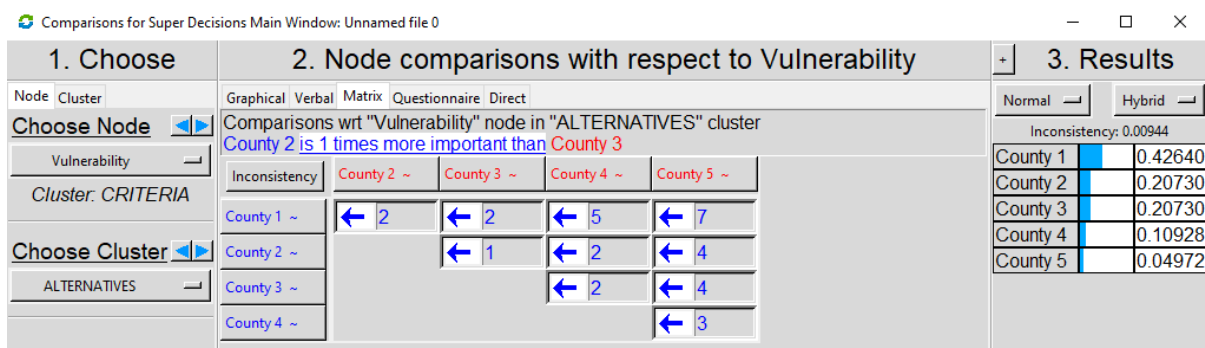
Figure 6. Comparison of alternatives in relation to the vulnerability criterion – *Super Decisions*.

3.3 Synthesis of results

After all comparison matrices are defined, a global eigenvector is calculated, which indicates the weight in prioritizing the alternatives.

Global eigenvector calculation is a simple weighted averaging technique. Eigenvectors of level 1 multiplied by eigenvectors of level 2, and summed for each alternative, give the global eigenvector. The AHP results are shown in Fig. 7, with the global eigenvector shown in the middle column.
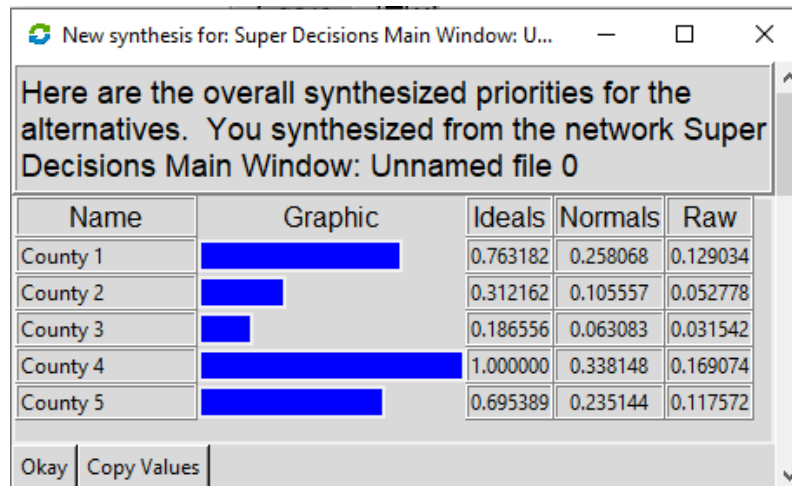
Figure 7. Results of AHP for earthquake risk of counties.

According to the AHP results, the relative weights of each alternative (W), i.e. their earthquake risk indices, are:

W (County 1) = 0.258

W (County 2) = 0.106

W (County 3) = 0.063

W (County 4) = 0.338

W (County 5) = 0.235

Such results can also be interpreted linguistically, if individual weight values of the alternatives are assigned meanings such as: very low, low, medium, high, very high risk. Therefore, County 4 has a high seismic risk, Counties 1 and 5 have a medium seismic risk, County 2 has a low seismic risk, and County 3 has a very low seismic risk. The same can be interpreted with colours or in any other similar way. The earthquake risk of individual counties can be shown very clearly on the map, which takes into account all elements of earthquake risk.

4. Conclusion

This study presents an example of using the analytical hierarchical process for the assessment of earthquake risk. AHP has proven to be very accurate and suitable for risk assessment, especially in the case when there is not a large enough number of input data, which is the case when dealing with earthquake risk.

The study shows how different elements of earthquake risk, namely hazard, exposure and vulnerability, can be combined by using AHP. By simple comparisons of pairs of model elements, AHP model in this study obtained the weight value of each county (alternative option). The same can be applied at the global, country, city, and municipality level.

The resulting priority list of counties (or other geographical areas) can further be used to produce earthquake risk maps. The information obtained from AHP analysis can also be used by governments or public institutions dealing with disaster management as a useful tool for allocation of mitigation resources and effort.

References

[1] UN (2015): *Sendai Framework for Disaster Risk Reduction 2015 – 2030*. United Nations, Sendai, Japan.

[2] JRC (2021): *Recommendations for National Risk Assessment for Disaster Risk Management in EU*, *Science for Policy report*. European Commission Joint Research Centre (JRC), Ispra, Italy.

[3] ISO (2018): *ISO 31000:2018 Risk management — Principles and guidelines*. International Organization for Standardization (ISO), 2nd ed.

[4] GEM: *Global earthquake maps*, www.globalquakemodel.org/gem (accessed April 12, 2022).

[5] SERA: *Seismology and Earthquake Engineering Research Infrastructure Alliance for Europe*, http://www.sera-eu.org (accessed February 7, 2022).

[6] Fariza, A., Abhimata, N.P., Hasim, J.A.N. (2016): Earthquake Disaster Risk Map in East Java, Indonesia, using Analytical Hierarchy Process – Natural Break Classification, *2016 International Conference on Knowledge Creation and Intelligent Computing (KCIC)*, 15-17 November, Manado, Indonesia. IEEE.

[7] Nyimbili, P.H., Erden, T., Karaman, H. (2018): Integration of GIS, AHP and TOPSIS for earthquake hazard analysis, *Natural Hazards,* 92, 1523–1546.

[8] Jena, R., Pradhan, B., Beydoun, G., Nizamuddin, Ardiansyah, Sofyan, H., Affan, M. (2020): Integrated model for earthquake risk assessment using neural network and analytic hierarchy process: Aceh province, Indonesia, *Geoscience Frontiers*, 11, 613-634.

[9] Jena, R., Pradhan, B. (2020): Earthquake Risk Assessment Using Integrated Influence Diagram–AHP Approach, *IOP Conf. Series: Earth and Environmental Science*, 540, 012078.

[10] Özkazanç, S., Sıddıquı, S.D., Güngör, M. (2020): Sensitivity Analysis of Earthquake Using the Analytic Hierarchy Process (AHP) Method: Sample of Adana, *Idealkent Dergisi (Journal of Urban Studies)*, 11 (30), 570-591.

[11] Shadmaan, S., Islam, A.I. (2021): Estimation of earthquake vulnerability by using analytical hierarchy process, *Natural Hazards Research*, 1, 153–160.

[12] Saaty, T.L. (1992): *Multicriteria Decision Making - The Analytic Hierarchy Process*. RWS Publications, Pittsburgh, Vol. I, AHP Series.

[13] Saaty, T.L. (1994): *Fundamentals of Decision Making and Priority Theory with the Analytic Hierarchy Process*. RWS Publications, Pittsburgh, Vol. VI, AHP Series.

[14] Saaty, T.L., Alexander, J.M. (1989): *Conflict Resolution - The Analytic Hierarchy Process*. Praeger, NY.

[15] Saaty, T.L., Forman, E. (1993): *The Hierarchon*. RWS Publications, Pittsburgh, Vol. V, AHP Series.

[16] Saaty, T.L., Kearns, K. (1991): *Analytical Planning*. RWS Publications, Pittsburgh, Vol. IV, AHP Series.

[17] Saaty, T.L., Vargas, L. G. (1991): *Prediction, Projection and Forecasting*. Kluwer Academic Publishers, Boston, Mass.

[18] Forman, E.H. (1990): Random Indices for Incomplete Pairwise Comparison Matrices, *European Journal of Operations Research,* 48 (1), 153-155.

[19] Shen, Q., Lo, K.-K., Wang, Q. (1998): Priority Setting in Maintenance Management of Public Building - A Modified Multi-Attribute Approach Using AHP, *Construction Management and Economics*, 16, 693-702.

[20] Super Decisions: *Super Decisions CDF*, https://www.superdecisions.com (accessed December 1, 2022).

ON THE INFLUENCE OF ROAD AND RAIL TRAFFIC ON SEISMIC VULNERABILITY OF HISTORIC MASONRY BUILDINGS

Ivo Haladin [(1)], Krešimir Burnać [(2)], Katarina Vranešić [(3)]

[(1)] *Associate professor, Department of Transportation Engineering, Faculty of Civil Engineering, University of Zagreb,*
  ivo.haladin@grad.unizg.hr
[(2)] *Research assistant, Department of Transportation Engineering, Faculty of Civil Engineering, University of Zagreb,*
  kresimir.burnac@grad.unizg.hr
[(3)] *Postdoctoral researcher, Department of Transportation Engineering, Faculty of Civil Engineering, University of Zagreb,*
  katarina.vranesic@grad.unizg.hr

Abstract

In the event of the earthquake that struck the city of Zagreb on the 22nd of March 2020. many of the buildings in the old city centre suffered from various types of damage. Most of the masonry buildings in the old city of Zagreb are over 100 years old, and so is the tramway infrastructure running alongside the buildings. The long operational period of tramway traffic can be an important factor when we talk about the influence of traffic-induced vibrations on the seismic vulnerability of the buildings. Long-term exposure to high levels of traffic-induced vibrations can lead to mortar deterioration and detachment of masonry units. To analyse the influence of vibrations induced by tramway traffic, historic data on tram operations and earthquake damage have been investigated. Segmentation of rail tracks was made taking into consideration the distance between the track and surrounding buildings as well as the assessment of damage on the buildings after a recent 2020 earthquake. Furthermore, to inspect the influence of various types of traffic on the surrounding buildings, eight different locations in Zagreb's urban core have been chosen for statistical analysis (six streets in the north-south direction and two intersections).

Keywords: earthquake, masonry buildings, vibrations, rail traffic, road traffic, vulnerability

1. Introduction

In the city of Zagreb, a vast number of structures are built before the first seismic code was implemented (in 1964) and a high percentage of them are in the old city centre. Those buildings were built as unreinforced masonry buildings with timber or reinforced concrete floor structures with very high seismic vulnerability [1]. Because of the modern need of making the transportation system more efficient, new, special requirements are taken upon the road and rail infrastructure to take into consideration the influence that traffic could have on the surrounding buildings. Noise and vibrations coming from the traffic can be potentially dangerous for the surrounding buildings, and installations and can annoy the residents. Ground-borne vibrations and their propagation from the source to the recipient is a complex problem that could not be unambiguously defined. It is of great importance to take the problem seriously and take the vibration matter into account from the early stages of the planning process [2].

One of the main factors contributing to the historic masonry buildings' aesthetic degradation is the vibrations caused by traffic in older city centres. Even though the phenomenon is well-known and has already been debated by the scientific community, a framework to evaluate the limited vibration levels does not exist. Single events that lead to higher vibration amplitudes are synchronized bus passages as well as the irregularities of the road pavements [3]. In addition to that, an inspection of the behaviour of the building cyclic loads of road and rail traffic can be challenging because it is hard to define how many cycles could be dangerous for the historically significant buildings due to their masonry structure and lack of documentation on how and from what materials were they built [4]. Numerous factors can have an influence on the extent of traffic vibrations such as the quality of the pavement, maximum vehicle weight, duration of vibrations, average distance from the axis, and many others [5], the average distance from the axis of the road (potential damage increases with the reduction of the distance) and

975

duration of vibrations being detected as one of the most important ones [2–4]. When we talk about possible negative effects on structural and non-structural elements of old, masonry buildings, traffic could be a possible cause of damage initiation and propagation. Normally, the influence that traffic-induced vibrations have on the surrounding is negligible, but in the event of some sort of individual event that could cause a natural frequency of vibration with the frequency of the excitation, additional damage can occur. In [6] long-term effect of vibrations is inspected, on the series of stone-masonry walls that have been constructed in the laboratory and possible changes in mechanical properties have been investigated. It was concluded that traffic vibrations caused the propagation of existing cracks on the previously damaged walls and that vibration amplitudes and duration represent significant parameters when we talk about the vulnerability of the structures. According to [7] structures that exhibit the problem of settlement, either at the level of their foundations or of the entire structure, and that has been subjected to earthquake vibrations are extremely vulnerable when they are subsequently subjected to traffic-induced vibrations as well.

An orthogonal grid of transportation infrastructure (road and tramway) is integrated in Zagreb historic lower town, figure 1. Both tramway and road vibrations influence the surrounding masonry buildings. Rail induced vibrations have generally higher excitation due to less damping of vibrations at the contact surface between wheel and the rail than is present in road vehicles with pneumatics. Tramway infrastructure is situated close to surrounding masonry structures. Rail irregularities such as bad or broken welds, corrugation, surface discontinuity in switches and crossings can induce high level of vibrations. Influence of tram induced vibrations in such conditions recorded on the surrounding buildings can exceed limits given by DIN 4150-3 and be considered harmful for the structure[8]. Due to these recent research findings, this paper aims to analyse whether the percentage of damaged buildings is higher in streets and intersections with tram traffic opposed to ones with road traffic only. For this purpose, a statistical analysis was carried out at several locations, which is described in the following chapter.

2. Analysis of tram-induced vibrations on a building damaged by an earthquake

2.1. Methodology

After the M5.5 magnitude earthquake that struck the city of Zagreb in 2020, more than 6500 buildings were reported damaged, of which about one-third were classified as unusable or temporarily unusable [9]. An on-site assessment of the buildings was performed, and the buildings were assigned to the following colours depending on the level of damage: green (can be used without limitations - U1, or can be used with recommendation for short-term countermeasure - U2), yellow (temporarily unusable, detailed inspection needed - PN1, or building can become usable after performing urgent interventions - PN2), and red (unusable due to external risks - N1, or unstable due to damage - N2) [10]. The most damaged buildings are historical buildings in the city centre, where tram traffic also runs in their close vicinity (less than 7 meters) [11]. These buildings have been exposed to tram-induced vibrations at some level for more than 70 years (and in some locations for more than 100 years). According to [6] and [12] tram induced vibrations cause crack widening and macroscopic crumbling of the plaster and subsequent softening and disintegration of the walls. For that reason, it is necessary to analyse and monitor the influence of vibrations caused by the operation of tram vehicles on earthquake-damaged buildings.

Buildings located less than 7 m from the street or intersection that were marked green (U1 and U2) or yellow (PN1 and PN2) during the inspection are included in this analysis. Since the buildings marked in red have suffered great structural deterioration due to their long service life, inadequate maintenance, etc., the vibrations caused by the operation of tram vehicles to which these buildings were subjected will have no effect on their degradation after the earthquake, so they were excluded from this analysis.

2.2. Measuring locations

To determine if vibrations from the tram traffic have an impact on building damage, a statistical analysis was performed in this paper to determine the percentage of buildings marked yellow or green in the vicinity of the tram traffic streets and intersections. The analysis was performed for 6 streets with road traffic only and 3 streets with mixed tram/road traffic (Figure 1).
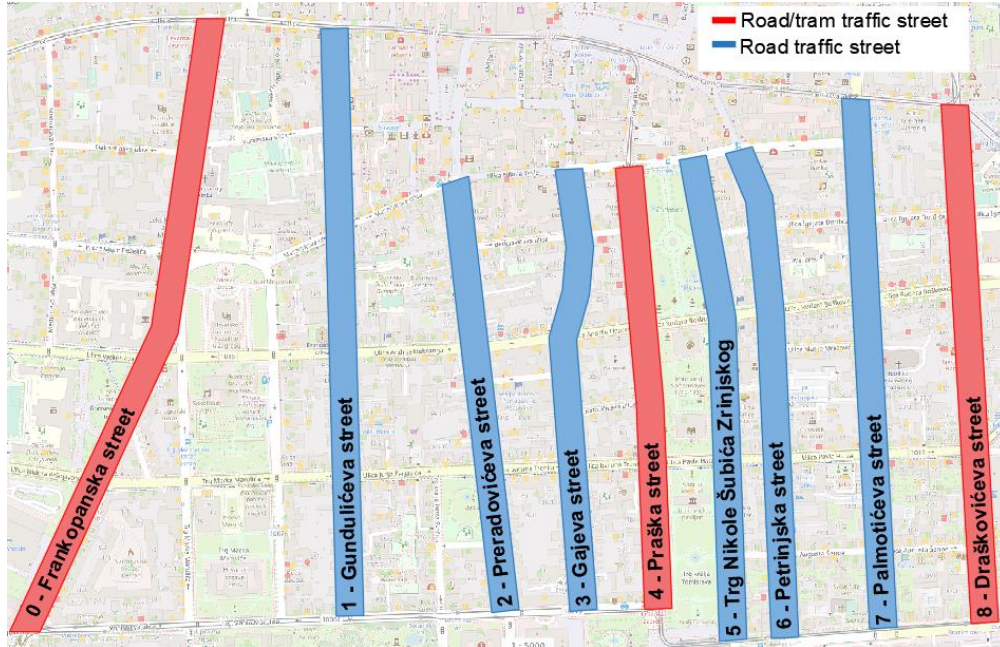

Figure 1. Display of nine streets that served as locations for statistical analysis in the north-south direction
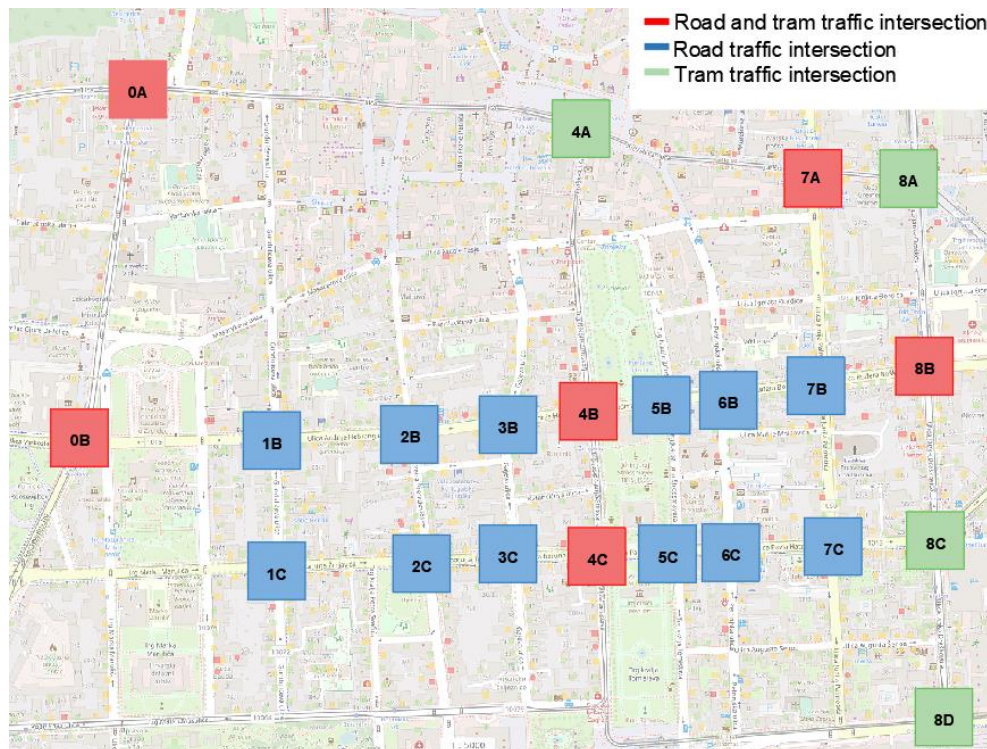
Figure 2. Display of 22 intersections in total (road-road traffic, road-tram traffic and tram-tram traffic) that were analyzed as a part of this paper

In addition to streets, different types of intersections were studied: intersections for road traffic, intersections for tram traffic, and intersections for road and tram traffic. All analysed locations are shown in Figure 2 and described in Table 1. Different types of analyzed intersections with their location .

Table 1. Different types of analyzed intersections with their location descriptions

Road traffic intersection		Tram traffic intersection	
ID	**Description**	**ID**	**Description**
1B	Gundulićeva – A. Hebranga	0A	Frankopanska – Ilica
1C	Gundulićeva - Jurja Žerjavića	4A	Praška – Trg bana J. Jelačića
2B	Preradovićeva – A. Hebranga	4D	Praška – Mihanovićeva
2C	Preradovićeva -Petra Svačića	8A	Draškovićeva – Trg hrvatskih velikana
3B	Gajeva – A. Hebranga	8C	Draškovićeva – Pavla Hatza
3C	Gajeva – Baruna Trenka	8D	Draškovićeva – Branimirova
5B	Trg N.Š. Zrinjskog – Boškovićeva	**Road and tram traffic intersection**	
5C	Trg N. Šubića Zrinjskog – Pavla Hatza	**ID**	**Description**
6B	Petrinjska – Boškovićeva	0B	Frankopanska – A. Hebranga
6C	Petrinjska – Pavla Hatza	4B	Praška – Zrinjevac
7B	Palmotićeva – Boškovićeva	4C	Praška – Baruna Trenka
7C	Palmotićeva - Pavla Hatza	7A	Palmotićeva – Jurišićeva
		8B	Draškovićeva - Boškovićeva

2.3. Data analysis

Data were analysed according to the on-site assessment of the condition of the building (PN1, PN2, U1, and U2). Two different analyses were conducted, the first one for the surrounding buildings located in the vicinity of the streets (the corridor stretches 7 meters to the west and 7 meters to the east from the street axis). The second analysis was conducted for buildings 7 meters from the centre of each intersection in every direction, with different types of traffic that operates on them.

2.3.1. Streets

In streets with road traffic only the total number of buildings that are 7 m or less from the street is 320. A total of 30 buildings were red tagged in the damage assessment conducted after the earthquake, and these buildings were excluded from this analysis. Of the remaining 290 buildings, 134 (46%) were damaged during the earthquake and are marked yellow. 156 (54%) had no building damage and were labelled green. In streets that have mixed tram and road traffic, of the 87 buildings surveyed, 54 (62%) were damaged and were marked yellow. The results are shown in Table 2.

Table 2. Statistical analysis of buildings marked in yellow or red, located in road/tram traffic or tram traffic street

Type of street	**PN1 & PN2**	**U1 & U2**
Road traffic street	46%	54%
Tram/road traffic street	62%	38%

Since a larger number of damaged buildings (marked yellow) were found in the tram/road traffic street, an analysis of the tram traffic load in each tram/road traffic street was performed. The results are shown

in Table 3. In addition to the traffic load, the percentage of damaged buildings was also analysed for each location separately concerning the total number of yellow and green buildings in the observed location. From the table, it can be seen that a higher traffic load does not necessarily result in a larger number of buildings damaged during an earthquake.

Table 3. Analysis of tram traffic load and percentage of damaged buildings in the tram/road traffic street

Tram/road traffic street		
ID	Tram traffic load [Mtpa]	Buildings marked PN1 and PN2 [%]
0	14.86	77
4	5.68	75
8	6.19	49
Mtpa- Million Tonnes per Annum		

2.3.2. Intersections

The total number of buildings near the road and tram traffic intersection is 22. Only 1 building is marked in red and is excluded from this analysis. Of the remaining 21 buildings, 16 (76%) are marked yellow, indicating that they are temporarily unusable and require a detailed inspection or urgent intervention. The total number of buildings at road traffic intersections that are 7 or fewer meters from the observed intersection is 68, of which 8 buildings were marked red in the damage assessment and are excluded from this analysis. Of the remaining 60 buildings, 32 (53%) were marked yellow and 28 (47%) were marked green. At the tram traffic intersection, 18 buildings were recorded, 3 of which were marked red in the damage assessment and are excluded from this analysis. Of the remaining 15 buildings, 3 (20%) were marked yellow and the remaining 12 (80%) were marked green. The results are presented in

Table 4.

Table 4. Statistical analysis of the yellow or red-marked buildings at the different types of intersections

Type of intersection	PN1 & PN2	U1 & U2
Road and tram traffic intersection	**76%**	**24%**
Road traffic intersection	**53%**	**47%**
Tram traffic intersection	**20%**	**80%**

As can be seen from the results, a high percentage of the buildings marked yellow are located near road/tram traffic intersections. The tram traffic load and the percentage of damaged buildings near road traffic and road/tram traffic intersections were analysed (Table 5). The percentage of damaged buildings for each location is calculated concerning the total number of yellow and green buildings at the observed location. It can be concluded that a high tram traffic load does not result in a higher number of damaged buildings near these intersections.

Table 5. Analysis of tram traffic load and percentage of damaged buildings in the tram/road traffic street

Road and tram traffic intersection			Tram traffic intersection		
ID	Tram traffic load [Mtpa]	Buildings marked yellow [%]	ID	Tram traffic load [Mtpa]	Buildings marked yellow [%]
0A	25,46	67	4A	25,46	-
0B	14,83	50	8A	25,97	11
4B	5,68	0	8C	9,31	67
4C	5,68	100	8D	17,13	50
7A	19,78	100	*Mtpa- Million Tonnes per Annum*		
8B	6,19	75			

3. Conclusion

Although the vibration amplitudes generated by traffic are generally low, they can be harmful to historic masonry buildings because of the numerous cyclic loads. Since masonry buildings are not resistant to tensile, these vibrations cause damage to the plaster and detachment of masonry elements, which can gradually lead to reduced resistance of the entire structure. Structures that exhibit the problem of settlement, either at the level of their foundations or of the entire structure, and that have been subjected to earthquake vibrations are extremely vulnerable when they are subsequently subjected to traffic-induced vibrations as well.

Based on performed analysis it can be seen that there is larger number of damaged buildings in streets and intersections that include tram traffic. Based on traffic load analysis, however, it cannot be concluded that higher traffic load leads to greater building vulnerability. From this preliminary analysis therefore it cannot be claimed that the frequent exposure to vibrations caused by tram traffic caused major difference in vulnerability of buildings after the earthquake in Zagreb in March 2020. To obtain more accurate results, the analysis needs to be performed on a larger sample with more data - e.g. the exact condition of the buildings based on detailed inspection after earthquake, the year they were built and renovated, the type of buildings, traffic load, etc. Also further analysis should include wall and mortar testing such as shear tests and flat jack tests [13] in characteristic buildings under considerable traffic load.

This preliminary study and literature indicate that the vibrations caused by traffic will lead to the propagation of cracks in historic buildings damaged by earthquakes and will certainly cause inconvenience to the residents who live and work in such buildings. Therefore, especially in the historic urban areas where tram traffic runs in the immediate vicinity of buildings, as in the city of Zagreb, it is of great importance to continuously monitor vibration levels. In this way, changes and increases in the vibration level can be detected in time and appropriate measures can be taken to ensure that the vibration level remains within the permissible values specified in the standards.

References

[1] Stepinac M, Lourenço PB, Atalić J, Kišiček T, Uroš M, Baniček M, et al. Damage classification of residential buildings in historical downtown after the ML5.5 earthquake in Zagreb, Croatia in 2020. International Journal of Disaster Risk Reduction 2021;56. https://doi.org/10.1016/j.ijdrr.2021.102140.

[2] Massarsch K. R. Investigation of ground vibrations and their mitigation. 2004.

[3] Zini G, Betti M, Bartoli G. Experimental analysis of the traffic-induced-vibration on an ancient lodge. Struct Control Health Monit 2022;29. https://doi.org/10.1002/stc.2900.

[4]   Bongiovanni G, Clemente P, Rinaldis D, Saitta F. Traffic-induced vibrations in historical buildings. Proceedings of the 8th International Conference on Structural Dynamics, Leuven, Belgium: EURODYN 2011; 2011.

[5]   Jakubczyk-Galczynska A, Jankowski R. Traffic-induced vibrations. The impact on buildings and people. 9th International Conference on Environmental Engineering, ICEE 2014, Dept. of Mathematical Modelling; 2014. https://doi.org/10.3846/enviro.2014.028.

[6]   Tomaževič M, Žnidarič A, Klemenc I, Lavrič I. The influence of traffic induced vibrations on historic stone masonry buildings. In Proceedings of the 12th European Conference on Earthquake Engineering, London, UK, 9–13 September 2002., Stationery Office; 2002, p. 631.

[7]   Erkal A. Transmission of Traffic-induced Vibrations on and around the Minaret of Little Hagia Sophia. International Journal of Architectural Heritage 2017;11:349–62. https://doi.org/10.1080/15583058.2016.1230657.

[8]   Haladin I, Lakusic S, Bogut M. Analysis of tram traffic vibrations in respect to tram track structure and exploitation period. In: Crocker MJ, Pawelczyk M, Paosawatyanyong B, editors. 20th International Congress on Sound and Vibration 2013, ICSV 2013, vol. 4, Bangkok, Thailand: International Institute of Acoustics and Vibration; 2013, p. 7–11.

[9]   Stepinac M, Lourenço PB, Atalić J, Kišiček T, Uroš M, Baniček M, et al. Damage classification of residential buildings in historical downtown after the ML5.5 earthquake in Zagreb, Croatia in 2020. International Journal of Disaster Risk Reduction 2021;56. https://doi.org/10.1016/j.ijdrr.2021.102140.

[10]   Novak MŠ, Uroš M, Atalić J, Herak M, Demšić M, Baniček M, et al. Zagreb earthquake of 22 March 2020 – Preliminary report on seismologic aspects and damage to buildings. Gradjevinar 2020;72:843–67. https://doi.org/10.14256/JCE.2966.2020.

[11]   Connolly GP, Florentin D, Conti J, Verlinden C. Building vibrations induced by railways: An analysis of commonly used evaluation standards. 2014.

[12]   Lakušić S, Haladin I, Vranešić K. Railway infrastructure in earthquake affected areas. Gradjevinar 2020;72:905–21. https://doi.org/10.14256/JCE.2967.2020.

[13]   Krolo J, Damjanović D, Duvnjak I, Smrkić MF, Bartolac M, Košćak J. Methods for determining mechanical properties of walls. Journal of the Croatian Association of Civil Engineers 2021;73:127–40. https://doi.org/10.14256/JCE.3063.2020.

THE EFFECT OF COLUMN WEB STIFFENERS ON MOMENT RESISTANCE AND DUCTILITY OF EXTENDED END-PLATE BOLTED CONNECTION

Anita Gjukaj [1], Petar Cvetanovski [2], Ferit Gashi [3]

[1] *Teaching Assistance, Faculty of Civil Engineering University of Prishtina "Hasan Prishtina", Albanian,*
anita.gjukaj@uni-pr.edu

[2] *Prof. PhD, Faculty of Civil Engineering, University "Ss. Cyril and Methodius", Skopje, Republic of North Macedonia,*
cvetanovski@gf.ukim.edu.mk

[3] Department of Structural and Geotechnical Engineering, Sapienza University of Rome, Italy,
Gashi.1670547@studenti.uniroma1.it

Abstract

Extended end-plate bolted connections as moment-resistant connections between beam and column usually fall in the semi-rigid partial strength category. Simplicity, duplication, and economy made this joint widely used in steel frame structures. This type of joint is prevalent nowadays which requires knowledge of the entire nonlinear moment-rotation behaviour of the joints. Using ABAQUS FE software in this paper, a three-dimensional finite element model (FEM) is developed to identify the effect of different geometrical parameters on the behaviour of extended end-plate bolted connection with four bolts per horizontal row as a semi-rigid beam-to-column joint. The component method which, is adopted in Eurocode 3, parts 1-8, provides detailed application rules for the design of bolted end-plate connections when most of them are limited to configurations with two bolts only in each horizontal row, without column web stiffeners.

By using the finite element model, a parametric study is conducted to study the influence of column web stiffeners (compression and tension stiffeners, K stiffeners, and double web stiffeners) on three main properties of extended end-plate bolted connection, moment capacity ($M_{j,Rd}$), initial rotational stiffness ($S_{j.in}$) and rotation capacity (Φ_{cd}) under monotonic loading, using finit element (FE) analyses.

The analytical research work, done here gives specific attention to the characterization of joint ductility, which is one of the critical behaviours of semi-rigid connections compared with rigid or pinned ones based on finite element analyses.

Keywords: Beam-to-column connection, analytical modelling, moment-resisting joints, column stiffeners, ductility, four bolt per horizontal row, finite element method.

1. Introduction

In the designing and analyzing of the steel frames, there are three essential components which have an impact on the structural behaviour of a construction building. There are beams, columns and the elements connecting them, so beam-to-column connection. Columns and beams must be designed in that way to fulfil the requirements regarding strength, stiffness and serviceability. The moment-resisting joints must show stiffness characteristics to allow the connected component and the entire structure to remain within allowable deflection limits and still have sufficient ductility to keep permanent damage at a minimum of the structure during serve loading. For all the cases analyzed in this paper, the resistance of the joint can be calculated through the component method, EN 1993-1-8, [1,2,3,4]. For simplicity, any joint can be subdivided into three zones: compression, tension and shear. Each of these zones is composed of components that contribute to the overall response of the joint. For the computation of the design properties of the joint, the active joint components for this configuration, according to Eurocode 3, are (1) column web in shear, (2) column web in compression, (3) beam flange in compression, (4) column web in tension, (5) column flange in bending, (6) bolt row in tension, (7) end plate in bending. These individual components are assembled into a mechanical model to evaluate the M-Φ response of the whole joint represented in Fig.1. Components of the joint may be strengthened by providing additional stiffeners, which are elaborated on below. In particular, this paper emphasizes analytical analyses of an extended end-plate bolted connection with four bolts per horizontal row and a different strengthening type of column web to increase the mechanical properties of the joint. The purpose is to increase the resistance and rotational stiffeners of the column panel in shear, compression and tension ensuring, also the appropriate rotation capacity.

a./   b./
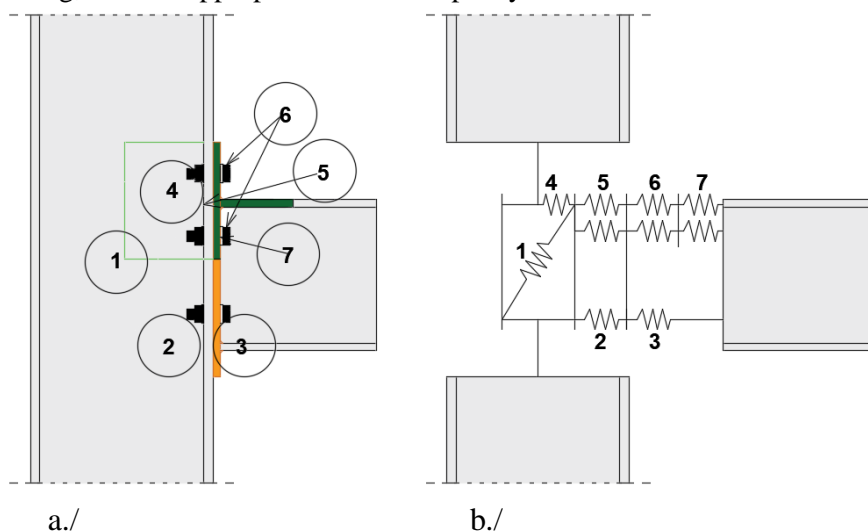
Figure 1. extended end-plate Steel joint a./Bolted beam-to-column connection and b./ component method

2. Applied strengthening of column web

The design philosophy of the semi-rigid/partial strength joints usually leads to simple solutions and more economical ones. During the designing of the joint, the proper selection of the strengthening of the joint will lead to a more cost-efficient structure. There exist several ways of strengthening each zone of the column web: compression stiffeners are generally required in portal frame joint, and their effect is by increasing the resistance to compression of the column web. A tension stiffener is used to increase the bending resistance of the column flange and the tension resistance of the column web. When the resistance of the column web does not fulfil the requirement, supplementary web plates, diagonal stiffener, and K stiffener should be used to increase the capacity of the web. Each of these stiffeners can contribute to enhancing the capacity of the connection. Stiffeners as a method of strengthening are unavoidable in a connection which are defined in Fig 2.

3. FE numerical model

In order to investigate the contribution of the column web stiffeners, finite element (FE) analyses have been used. In general, are analysed four types of extended end-plate bolted connections, with four bolts per horizontal row; when the variable here is the way of strengthening the column web, the FE models were run using the general static analysis modelled in Abaqus [5]. The column and beam lengths were set to 2000mm and 1500 mm respectively. The Young's modulus and the Poisson's ratio were taken equal to 21000MPa and 0.3, receptively. While the other mechanical properties of the steel and bolts are taken from [7].

Table 1- Connections geometry data.
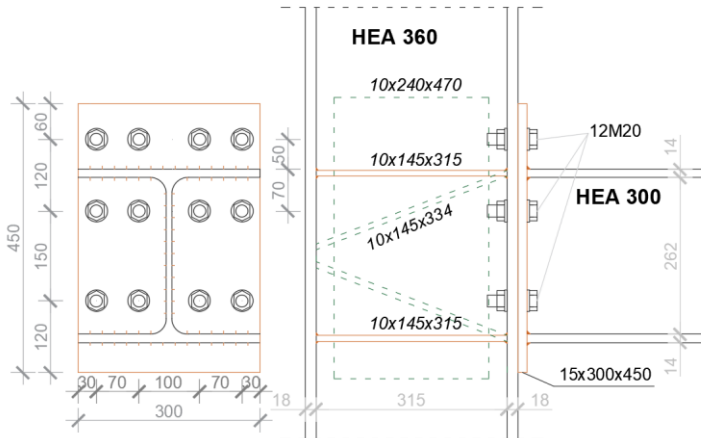
	Type 1	Type 2	Type 3	Type 4
Stiffeners	Non (mm)	Tension Compresion 10x145x315 (mm)	K- Stiffeners 10x145x334 (mm)	Web double - plate 10x240x470 (mm)
Column	360	360	360	360
Beam	300	300	300	300
End-plate	15	15	15	15
Bolts	d-20, 8.8	d-20, 8.8	d-20, 8.8	d-20, 8.8
Steel	235	235	235	235
Stiffnes class	Semi	Semi	Semi	Semi
Strength Class	Partial	Partial	Partial	Partial

Figure 2. Typology of connections

The overall mesh sizes for the column and the beam were set as 20mm and 25, respectively, and the much finer mesh was prescribed in the region of connection, end-plate, column flange and bolts. The three-dimensional FE model of a typical beam-to-exterior column joint is shown in Fig 3. While regarding the boundary conditions in FE models, all DOF at each end of the column were restrained, except for the rotation about the strong axis of the column. Similarly, the degrees of freedom of the beam ends were restrained except for the vertical displacement. Meanwhile, the bolt pretension forces were defined by using the bolt load command, which was taken according to Eq. (1). In general, four contact pairs between the end-plate and column flange, the bolt head and column flange, the bolt nut and end-plate, and the bolt shank and corresponding bolt hole were defined. The property of the contact pairs was defined as finite-sliding and surface-to-surface with a friction formulation using the penalty method for tangential response with friction coefficient 0.15 of all contact surfaces, while the default hard contact model was used for the normal behaviour.

$$F_{pre} = \frac{0.7 \cdot f_{ub} \cdot A_s}{\gamma_{M7}} \tag{1}$$
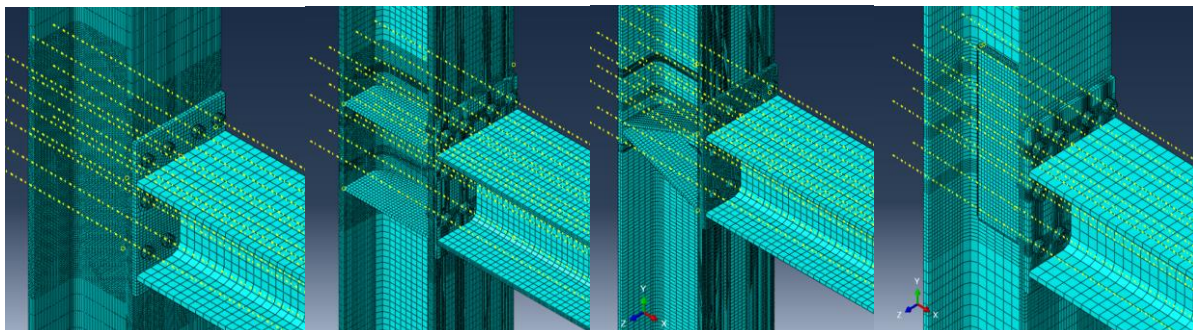
Figure 3. FE model for beam-to-column extended end-plate joint

The failure modes include bending deformation of the end-plate and column flange, buckling of the compression beam flange, bolt rapture, and failure of the fillet welds between the end-plate and beam flange. The end plate in bending and the column web panel in shear are the main dissipative components

involved in the connections, displaying apparent ductile features. The results are shown in Figures 4 and 5. When it is displayed and can be concluded that in Type 1 failure is governed by the failure of filled welds and column web panel in shear, Type 2 and Type 3 respond in the elastic range displaying a failure mode one by forming a plastic hinge in the beam flange and bolt rapture. Type 4 exhibits a failure mode due to bolt fracture and buckling of the end plate.
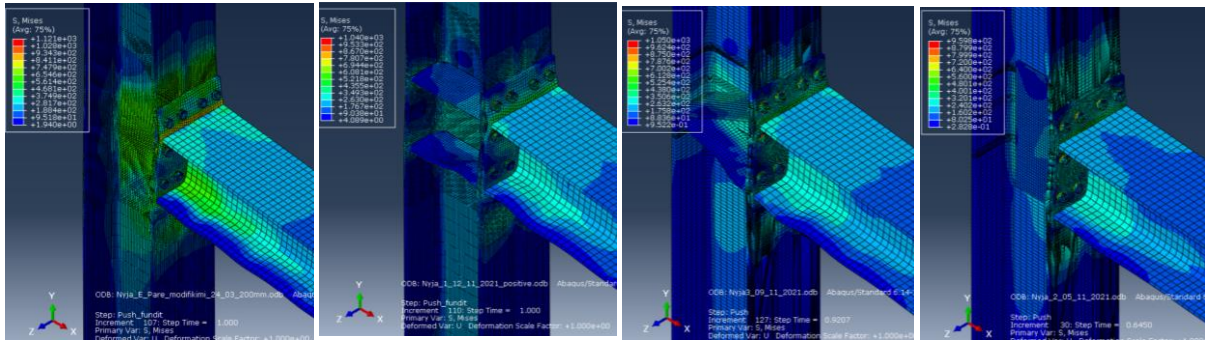
Figure 4. Von Mises stress representation and ultimate failure modes.
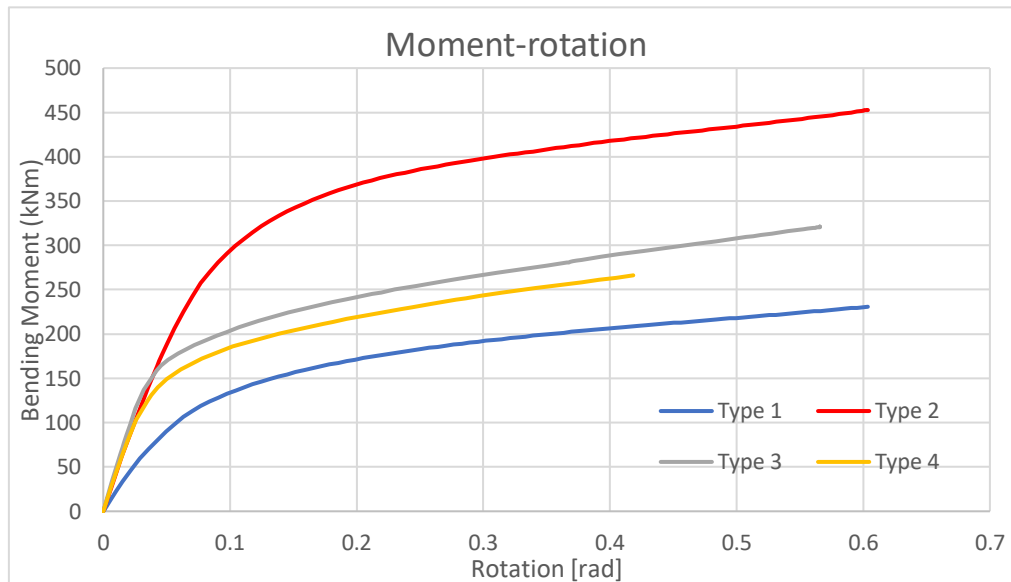
Figure 5. Monotonic results for moment and rotation capacity of the connections.

4. Conclusion

The results herein focused on developing a finite element model developed in ABAQUS, capable of representing the monotonic behaviour of the extended end plate connections with the partial strength and stiffeners classification according to [1] by using different column web stiffeners. The finite element method for the monotonic analyses allowed concluding that the numerical behaviour is in good agreement with the procedures described in [1.2,3,4] for the estimation of connection response and can provide valuable results for the mechanical behaviour of connections. The column web stiffeners described in this paper increase the moment resistance and the rotation capacity Figure 5, especially at Type 2 when the plastic strain concentration is close to welds between the beam flange and the end plate. Using each of these stiffeners can minimise the deformation of the panel zone of the connection. Designing the end-plate bolted connection without column web stiffeners can lead to column web buckling. According to [1], the connection design process is very time-consuming, so creating tables for designing end-plate bolted connections with or without column web stiffeners would be an excellent solution, also future investigations should provide information on FE model calibration according to the experimental results.

References

[1] British Standards Institution (2005) BS EN 1993-1-8:2005, Eurocode **3:** *Design of steel structures Part 1.8 Design of joints*, London, BSI.

[2] Pisarek Z., Kozłowski A (2006).: End plate steel joint with four bolts in the row, *In: Progress in Steel, Composite and Aluminum Structures*, Ed.: Giżejowski, Kozłowski, Ślęczka & Ziółko, Taylor & Francis Group, London.

[3] Demonceau J.-F.,Weynand.K, Jaspart J.-P., Muller C.(2010) : Application of Eurocode 3 to Steel connections with four bolts per horizontal row, *SDSS'Rio 2010, Stability and Ductility of steel structures,* Brazil.

[4] Kozłowski A., Pisarek Z.: Resistance and stiffness of T-stub with four bolts, Archives of Civil Engineering, Vol. 54, No.1, 2008, pp. 167-191.

[5] Abaqus (2014). Abaqus analysis user's manual, version 16.4

[6] Beg, D., Zupančič, E., Vayas, I. (2004). On the rotation capacity of moment connections, *Journal of Constructional Steel Research, 60: 601-620,* www.elsevier.com/locate/jcsr

[7] Gashi Ferit, F.Bontempi,F.Petrini (2021).Experimental study on steel slit and shear panel for seismic Resistance , https://onlinelibrary.wiley.com/doi/full/10.1002/cepa.1519

[8] Gashi Ferit, F.Bontempi,F.Petrini (2021).Component test,fracture simulation,and Experimental study on steel damper ofr passive energy dissipation, https://crocee.grad.unizg.hr/event/1/contributions/70/

[9] Girão Coelho, A.M. (2004). *Characterization of the ductility of bolted end plate beam-to-column steel connections*. PhD Thesis, University of Coimbra.

[10] Zoetemeijer P, Munter H. (1983) Proposal for the standardization of extended end plate connections based on test results – *Test and analysis. Stevin Laboratory Report 6-83-23.* Faculty of Civil Engineering, Delft University of Technology.

[11] Zoetemeijer, P, (1974) "A design method for the tension side of statically loaded bolted beam-to column connections", Heron, Delft University, Vol. 20, n° 1.

[12] Ghobarah A, Korol RM, Osman A (*1992).* Cyclic behaviour of extended endplate joints. *J Struct Eng ASCE;118(5):1333–53.*

[13] Deniziak P., Galewska E.U., (2014): The influence of applying supplementary web plates on structural joint moment resistance and rotational stiffness, https://www.researchgate.net/publication/318701788

[14] Augusto, H., Castro, M.J., Rebelo, C., Silva, S.L., (2013): Numerical simulation of partial-strength steel beam-to-column connections under monotonic and cyclic loading: *Congreso de Metodos Numericos en Ingenieria*, Bilbao, Espana, 121 pages.

COMPILATION OF AVAILABLE SEISMOTECTONIC DATA FOR NORTH MACEDONIA AS AN INPUT FOR PSHA

Zabedin Neziri [(1)], Radmila Salic Makreska [(2)]

[(1)] *Ph.D. Student, M.Sc., Ss. Cyril and Methodius University in Skopje, Institute of Earthquake Engineering and Engineering Seismology (IZIIS) – Skopje, Republic of North Macedonia, zabedin@iziis.ukim.edu.mk*
[(2)] *Assoc. Prof. Dr., Ss. Cyril and Methodius University in Skopje, Institute of Earthquake Engineering and Engineering Seismology (IZIIS) – Skopje, Republic of North Macedonia, r_salic@iziis.ukim.edu.mk*

North Macedonia is a country characterized by moderate seismic activity. As a consequence of its special tectonic regime, and occurrence of damaging earthquakes (12 earthquakes $M_L \geq 6$ after 1900; [1]), necessity for reliable seismic hazard and risk assessments are of outmost importance. Initial and one of the most important steps in PSHA is the seismic source characterization. Reliable seismological and tectonic data are one of the key pillars of the reliable seismic hazard assessment. For the purpose of this study a compilation, comparison, and analysis of available national and regional seismotectonic data for North Macedonia ([2]; [3]; [4]; [5]; [6]; [7]; [8]) have been performed. In relation to seismological data, three earthquake catalogues that can be used with reliability are selected and comparatively analyzed: the national catalogue from the seismological observatory (SO-PMF)[1] [9], the BSHAP-2[2] catalogue [10] and the ESHM20[3] catalogue [8].

Detailed analysis of the available national fault databases shows that none of them comprises of all relevant state-of-the-art seismicity parameters, needed for reliable seismic hazard definition. The most comprehensive national database as of now is the one given by [4]. The databases presented in the [2], [3] and [5] although containing valuable geological and tectonic information, does not offer a consistent and harmonized set of seismic fault parameters. The latest national research presented in [7] should be considered as valuable in the domain of fault classification and slip rate determination. Regarding the latest European research, the 2020 update of the European Seismic Hazard Model – ESHM20, although comprehensive by its structure and content, this database is created with larger regional resolution and contains information only for seismogenic faults that may be capable of generating earthquakes with magnitude ≥ 5.5, which limits the overall fault modelling excluding the faults that are capable of generating earthquakes with magnitude 4.0 – 5.5.

Analyzed earthquake events from the three chosen catalogues refer to the region defined by the boundaries 40.6°N≤φ≤42.4°N and 20.3°E≤λ≤23.2°E (Republic of North Macedonia and surrounding areas) and the 100 km belt around the zone (39.8°N≤ φ≤43.3°N, 19.3°E≤λ≤24.2°E). To compare the catalogues, two main criteria were taken: time period 1900-2012 and moment magnitude of earthquakes ≥ 4.0. For the selected earthquake catalogues, a detailed analysis has been performed including comparison of the completeness magnitude (Mc), histogram analysis, time domain analysis for the selected parameters of interest, comparison of completeness intervals and comparison of spatial distribution of seismic hazard parameters (λ, b и Mmax) [11]. Also, earthquakes with moment magnitude ≥ 6.0 are spatially analyzed and their magnitude and epicentral deviation in relation to the ESHM20 catalogue have been calculated. Significant differences have been observed between the

---

[1] SO-PMF: Seismological Observatory, Faculty of Natural Sciences and Mathematics, Ss. Cyril and Methodius University in Skopje, N. Macedonia.
[2] BSHAP-2: NATO SpS-984374 project, Improvements of the Harmonized Seismic Hazard Maps for the Western Balkan Countries
[3] ESHM20: European Seismic Hazard Model 2020

analyzed earthquake catalogues generally resulting from the difference in the number of events and the related parameters, which ultimately affect the estimation of the seismic hazard parameters.

References

[1] Salic, R., Neziri, Z., Dimitrovski, M., Milutinovic, Z., Trajchevski, J., Tomic, D. (2020). Need for advanced Seismogenic Fault characterisation Study as a Basis for Reliable Seismic Hazard, 17th World Conference on Earthquake Engineering (17ECEE), Sendai, Japan, 1a-006, 13-18 September 2020.

[2] A set of basic geological maps for the territory of North Macedonia (1: 100,000), parts of the Basic Geological Map of Yugoslavia, issued by the Federal Geological Institute - Belgrade (1967-1984).

[3] Arsovski M., Petkovski R. (1975). Neotectonic of SR Macedonia, Publication IZIIS-49, Institute of Earthquake Engineering and Engineering Seismology in Skopje, 1975 (in Macedonian).

[4] Janchevski, J. (1987). Classification of fault structures by genesis, age and morphology with reference to their seismicity in the territory of Macedonia. Doctoral dissertation. Faculty of Mining and Geology, Stip (in Macedonian).

[5] Arsovski, M. (1997). Tectonics of Macedonia, Faculty of Mining and Geology Stip (in Macedonian).

[6] Dumurdzanov, N., Serafimovski, T. and Burchfiel B. C. (2005). Cenozoic tectonics of Macedonia and its relation to the South Balkan extensional regime: Geosphere 2005, 1, 1–22, Doi: 10.1130/GES00006.1

[7] Drogeska, K (2018). Application of dislocation theory in defining epicentre areas and tectonic conditions for territory of the Republic of Macedonia, University "Ss. Cyril and Methodius", Faculty of Natural Sciences and Mathematics, Institute of Physics. Doctoral dissertation, Skopje.

[8] Danciu L., Nandan S., Reyes C., Basili R., Weatherill G., Beauval C., Rovida A., Vilanova S., Sesetyan K., Bard P-Y., Cotton F., Wiemer S., Giardini D. (2021) - The 2020 update of the European Seismic Hazard Model: Model Overview. EFEHR Technical Report 001, v1.0.0, https://doi.org/10.12686/a15

[9] Cejkovska, V., L. Pekevski, K. Drogeska, J. Najdovska (2016). Report per the Project of the Standardization Institute of the Republic of Macedonia entitled National Annexes for Eurocodes, Faculty of Natural Sciences and Mathematics, Seismological Observatory, Ss. Cyril and Methodius University, Skopje, February 2016 (in Macedonian).Milutinovic, Z., V. Mihailov, K. Talaganov, G. Trendafiloski, T. Olumceva, V. Sesov (1998). Spatial Plan of Republic of Macedonia, Conditions for occurrence and protection from seismic disasters, IZIIS Report 98-29 (in Macedonian).

[10] Markusic, S., Z. Gulerce, N. Kuka, L. Duni, I. Ivancic, S. Radovanovic, B. Glavatovic, Z. Milutinovic, s. Akkar, S. Kovacevic, J. Mihaljevic and R. Salic (2016). An Updated and Unified Earthquake Catalogue for the Western Balkan Region, Bulletin of Earthquake Engineering, February 2016, Volume 14, No.2, DOI 10.1007/s10518-015-9833-z, pg.321–343.Stamatovska, S.G. & I. Z. Paskaleva-Koytcheva (2013). Seismic Hazard Assessment for Life-Line Systems Passing through Macedonian-Bulgarian Border, 50SE-EEE, Skopje, Republic of Macedonia, 2013.

[11] Kijko (2011). CODE: HS_CLAIRE_generic, v (1.02),

CRONOS PROJECT: MAIN FEATURES OF SEISMICITY ANALYSIS FOR THE CENTRAL AND SOUTHERN CROATIAN COASTAL AREA

Iva Lončar [(1)], Snježana Markušić [(2)], Ines Ivančić [(3)]

[(1)] *Project associate - seismologist, Andrija Mohorovičić Geophysical Institute, Department of Geophysics, Faculty of Science, University of Zagreb, iva.loncar@gfz.hr*

[(2)] *Associate Professor, Andrija Mohorovičić Geophysical Institute, Department of Geophysics, Faculty of Science, University of Zagreb, snjezana.markusic@gfz.hr*

[(3)] *Seismologist, Croatian Seismological Survey, Department of Geophysics, Faculty of Science, University of Zagreb, ines.ivancic@gfz.hr*

Keywords: CRONOS project, seismicity, earthquake catalogue, catalogue completeness

1. About CRONOS project

The overall objective of the project "Investigation of seismically vulnerable areas in Croatia and seismic ground motion assessment" – CRONOS – is to make Croatian society more resilient to the impact of destructive earthquakes. The aim of the CRONOS project, funded by Norwegian Financial Mechanism, is to facilitate this through the development and modernization of seismic hazard assessment in Croatia and stimulate the development of seismic risk reduction policies through scientific infrastructure and capacity building, knowledge transfer, and international research cooperation.

2. Seismicity analysis of the central and southern Croatian coastal area

Croatia is characterized by a moderate-to-high seismicity in its coastal and moderate seismicity with the rare occurrence of strong earthquakes in its continental parts. More than 145.000 earthquakes from the period before Christ till the end of 2020 are contained in the Croatian Earthquake Catalogue (CEC) – an updated and continuously supplemented version first described in [1]. There were more than 100 stronger earthquakes, whose computed or estimated magnitudes were more than 5. Most of the earthquakes on Croatian territory are the result of the strain accumulation caused by the rotation of the Adria microplate towards the Eurasian tectonic plate [2]. Central Croatia is in a contact zone of three big geological units: The Alps, the Dinarides (or The Dinaric Alps), and the Pannonian Basin.

2.1 General observations and statistical analysis

The main area of focus of this research is central and southern Croatian coastal areas – the targeted region of the CRONOS project. The first step towards the presented goal is to analyse and understand the past seismicity of the given area. Therefore, for the chosen area (42.5 – 44.5 °N, 14.75 – 17.75 °E) an earthquake catalogue CEC-Cronos has been prepared. The given revised catalogue contains 44049 earthquakes which occurred between the years 306 and 2020 (Fig. 1). Those earthquakes, magnitudes up to 6.7 and intensities in the epicentre up to IX °MSK, have been statistically processed and will be further presented.

Within 44049 earthquakes contained in CEC-Cronos, making the area of interest significantly seismically dense, around 400 of them are of magnitude M4+. Most of these earthquakes occurred at depths between 10 and 15 km. Although the most significant seismicity noted in the catalogue occurred before instrumental recording began, the last century was seismically turbulent as well. It is worth mentioning Imotski (29 Dec 1942) M6.2 and Makarska (11 Jan 1962) M6.1 (preceded by the M5.9 foreshock four days before) earthquakes, all causing great human casualties and severe damage.

The completeness of the declustered CEC-Cronos has been tested for three different years representing the milestones in the technology development, and therefore the quality of the seismic

recordings, over the years. Along with magnitudes of completeness for given years, Table 1 shows the corresponding Gutenberg-Richter coefficients from the given year until 2020.

Analysis of the seismicity of an area, spatial and statistical, and the characterization of the same, is a necessary preliminary work and prerequisite for the seismic hazard assessment. Proper understanding of the seismicity of the area is crucial for further seismic hazard assessment and therefore the preparedness for future stronger events for which it is not a question of if but when they will happen. Moreover, significant historical events have drawn attention to the importance of the proper single-event critical reanalysis which is the next step for thorough seismicity research of the given area.
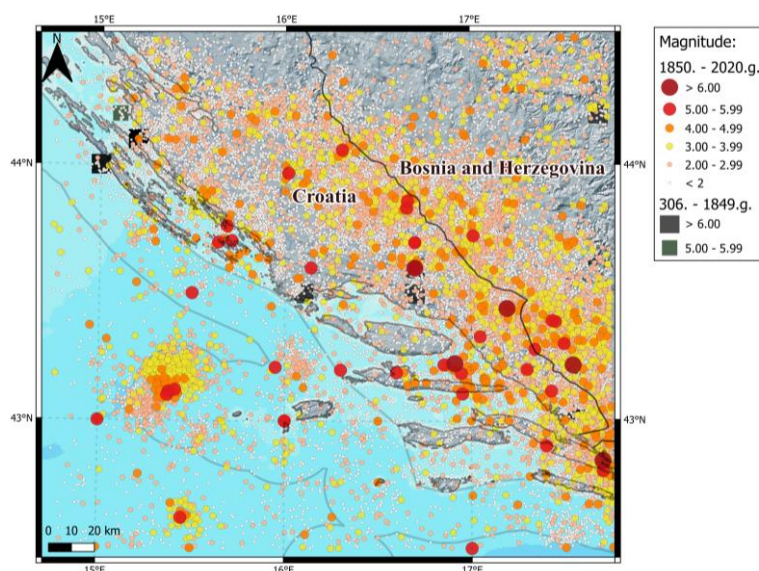
Figure1. Spatial distribution of earthquakes contained in CEC-Cronos.

Table 1 – CEC-Cronos magnitudes of completeness

t_0	M_c	a	b
1908.	3.9	4.23	0.98
1982.	3.1	4.43	1.02
2000.	2.9	4.38	1.01

Acknowledgements

References

[1] Herak, M., Herak, D., Markušić, S. (1996): Revision of the earthquake catalogue and seismicity of Croatia, 1908–1992. *Terra Nova*, 8, 86–94, doi: https://doi.org/10.1111/j.1365-3121.1996.tb00728.x

[2] Weber, J., Vrabec, M., Pavlovčič-Prešeren, P., Dixon, T., Jiang, Y., Stopar, B. (2010): GPS-derived motion of the Adriatic microplate from Istria Peninsula and Po Plain sites, and geodynamic implications. *Tectonophysics*, 483 (3-4), 214-222, doi: https://doi.org/10.1016/j.tecto.2009.09.001

SEISMIC INTERFEROMETRY FOR DAMAGE IDENTIFICATION OF LARGE SCALE MODEL OF RC SHEAR WALL STRUCTURE

Aleksandar Zhurovski [(1)], Igor Gjorgjiev [(2)]

[(1)] *Research assistant- PhD student, Institute of Earthquake Engineering and Engineering Seismology, Skopje, North Macedonia, zurovski@iziis.ukim.edu.mk*

[(2)] *Professor, Institute of Earthquake Engineering and Engineering Seismology, Skopje, North Macedonia, igorg@iziis.ukim.edu.mk*

Keywords: seismic interferometry, wave method, damage identification, shaking- table model

1. Introduction

The wave method for structural health monitoring (SHM) aims at detecting changes in stiffness of a structure, possibly caused by damage during extreme event, by monitoring changes in the velocity of waves propagating trough the structure [1]. The data used in this study are for a shaking table model of 3 storey reinforced- concrete (RC) shear wall building, which had been tested on the shaking table in the dynamic testing laboratory in IZIIS in Skopje in the frames of SERA project (fig 1). The model was shaken by eleven earthquakes (EQ) with increasing amplitude that progressively damaged it- table 1.
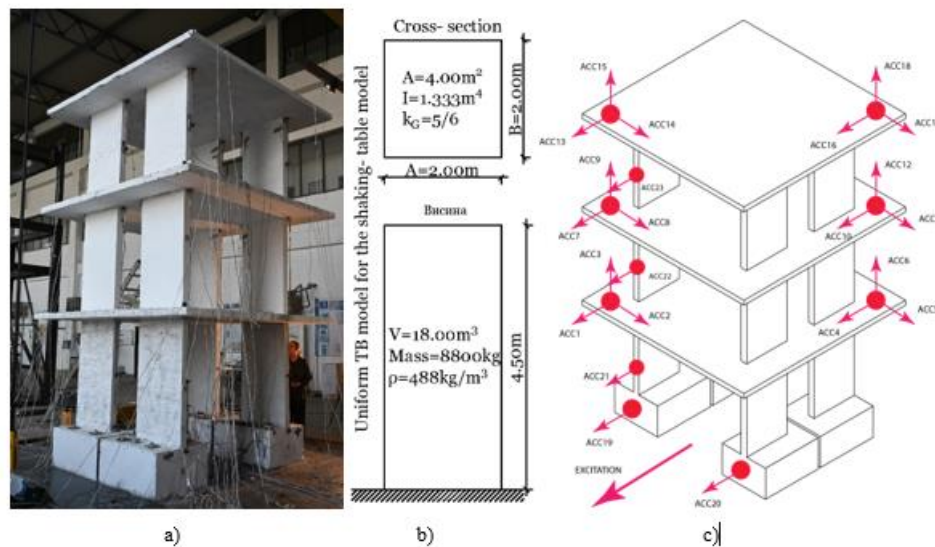
Figure 1. a) Shaking- table model; c) Uniform TB of the model d) Distribution of accelerometers.

2. Methodology

The shaking table model is numerically modelled as uniform Timoshenko beam (TB), of height H=4.5m, stress free at the top, cantilevered at the base (restrained translation and rotation) and excited by base motion- fig 1.b [1]. The material is characterized by mass density, ρ=488kg/m^3, Young's modulus E and shear modulus G, which implies longitudinal and shear wave velocities in the material $c_L=\sqrt{E/\rho}$ and $c_s=\sqrt{G/\rho}$. The beam cross section is with dimensions 2.0mx2.0m, cross- sectional area of A=4.0m^2, second moment of inertia with respect to (w.r.t) axis of excitation of I=1.333m^4 and shear factor of k_G=5/6. The horizontal displacement of the neutral axis of the beam u(z,t) e.g. the solution of the TB under base excitation satisfies the differential equation:

$$c_L^2 c_S^2 k_G \left(1 + \mu \frac{\partial}{\partial t}\right)\frac{\partial^4 u}{\partial z^4} - (c_L^2 + k_G c_S^2)\left(1 + \mu \frac{\partial}{\partial t}\right)\frac{\partial^4 u}{\partial z^2 \partial t^2} + \frac{k_G c_S^2}{rg^2}\left(1 + \mu \frac{\partial}{\partial t}\right)\frac{\partial^2 u}{\partial t^2} + \frac{\partial^4 u}{\partial t^4} = 0 \qquad (1)$$

The equation is solved in the frequency domain and the solution is consequently used to compute the beam transfer- function (2) and impulse response functions (3) as:

$$\hat{h}(z, z_{ref}, \omega) = \frac{\hat{u}(z,\omega)}{\hat{u}(z_{ref},\omega)} = \frac{U(z)}{U(z_{ref})} \quad (2), \quad h(z, z_{ref}, t) = FT^{-1}\{\hat{h}(z, z_{ref}, \omega)\} \quad (3)$$

The structure is then identified by matching the model and observed impulse response functions, representing physically the propagation of virtual pulse through the structure (fig 2). The impulse responses and transfer functions were calculated from accelerograms of accelerometers 13 (roof) and 19 (foundations)- fig 1.c. for all tests (fig 2). Two unknown parameters of the TB are c_L and c_S which were calculated by fitting the model and observed impulse responses and transfer functions in specified frequency band 0-11Hz (that included only the first mode) and time band. In this case, the structure is very stiff in shear and deforms predominantly in bending meaning that varying the value of c_S does not introduce error in the fitted functions. Therefore, only the value of c_L was fitted.
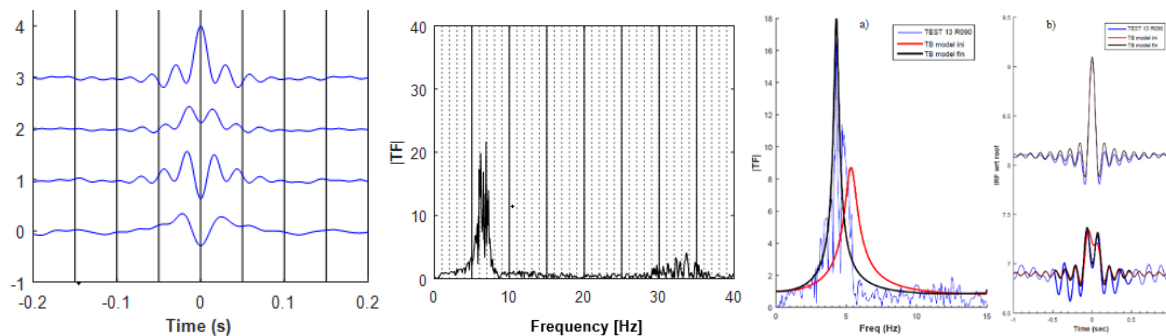
Figure 2. a) IRF for R030; b) TF of roof with respect to foundation for R030 c) Fitting TB for R090

3. Results and discussion

The results from fitting are sublimated in table 1, and one characteristic result is presented in figure 2.c (for R090). Similar results are obtained by fitting for all excitation levels. Table 1 also contains information regarding characteristic observed damage of the model after the tests [2].

Table 1 – Tests, fitted values of c_L and damage description of the model

Test	Fitted value of c_L [m/s]	Change of c_L w.r.t test R010 [%]	Damage description
R010	490	/	
R020	477	2.65	
R030	435	11.22	First crack at contact with foundation- SE pier
R050	390	20.41	
R060(1)	321	34.49	
R060(2)	313	36.12	Crack in all piers- all length of foundation
R080	303	38.16	Horizontal cracks along whole height of all piers in the ground floor
R090	281	42.65	Visible rocking of the model
R120	236	51.84	Cracks in all contacts of piers with slabs- all levels
R150(1)	226	53.88	Concrete crushing in corners of piers
R150(2)	209	57.35	Collapse state

The results from the fitting indicate that it is possible to detect damage in structures using the wave method. C_L as a parameter describing the material of the TB was sensitive to the damage of the test structure, and changes proportional to the level of damage were detected. The reduction of c_L relative to the undamaged state when first cracking in the piers were observed, was about 11%. Reduction of about 38% was detected in the state where horizontal cracks along whole height of all pies in the ground floor were observed. Finally, reduction of more than 50-55% was detected when crushing of concrete and collapse of the structure was observed and stated.

References

[1] Ebrahimian M., Todorovska I. M., Falborski T., (2017): Wave method for Structural Health Monitoring: Testing Using Full- Scale Shake Table Experiment Data. *Journal of Structural Engineering*, 143(4): 04016217. DOI 10.1061/(ASCE)ST.1943-541X,0001712

[2] Rakicevic Z., Bogdanovic A., Krstevska L., Apostolska R., Jekic G., Isakovic T., Fishinger M., Gams M., Wallace J., Kolozvari K. (2021) Influence of the floor- to piers interaction on the seismic response of coupled wall systems, final report, SERA project, N.Macedonia, DOI: 10.7471/SERA-TA.DYNLAB.Project13

PHYSICAL AND VIRTUAL EXPERIMENTAL INVESTIGATION OF SELF-CENTRING CONCENTRICALLY BRACED FRAMES

Borjan Petreski [(1)], Igor Gjorgjiev [(2)]

[(1)] *Assistant MSc, Ss. Cyril and Methodius University in Skopje, Institute of Earthquake Engineering and Engineering Seismology, borjan@iziis.ukim.edu.mk*

[(2)] *Professor PhD, Ss. Cyril and Methodius University in Skopje, Institute of Earthquake Engineering and Engineering Seismology, igorg@iziis.ukim.edu.mk*

Keywords: innovative, self-centring concentrically braced frames, experimental calibration, model error

1. Introduction

One of the main structural typologies of steel frames considered by the codes of practice for resisting the lateral forces, are the concentrically braced frames (CBFs). They are characterized by the dissipative performance of the diagonal braces that simulate truss behaviour due to the axial forces that develop during horizontal loading. The seismic response of the CBFs is represented through the cyclic compressive buckling and tensile yielding of the diagonals which induce the development of plastic hinges within the element. Due to the existence of diagonal braces, their lateral stiffness is well above that of the moment resisting frames (MRFs) and are very effective in maintaining the lateral drifts in the design range. Additionally, they represent the most economical structural form for providing lateral seismic resistance [1]. The global performance of the CBFs during high intensity earthquake loading is generally assessed by the frame drifts. After reaching inelastic residual deformations, the braces are unable to provide the initial lateral resistance to the system and the frame experiences residual displacements. To tackle the residual displacements of the frames, innovative damage control procedures have been suggested, such as buckling-restrained braces [2] and self-centring systems [3]. This study presents the experimental findings on the latter method in which post-tensioning (PT) arrangements are used to return the structure to its original position following inelastic deformation demands. The basis for the experimental research is a novel self-centring CBF (SC-CBF) system that has been developed and examined through push-over physical laboratory tests and nonlinear time-history analysis of numerical model [4]. This structural type's main characteristic is the re-centring of the frame following the earthquake loading in the initial vertical position, thus reducing the post-earthquake cost and time for retrofitting. It also reduces the material used for repair since the only elements needing retrofitting remain the diagonal braces that undergo many cyclic loadings and plastic deformations under the earthquake excitation.

2. Experimental studies

Previously, experimental studies have been performed to characterise the behaviour of the individual elements of SC-CBF by investigating several parameters. Shake table tests carried out on bracing members with slenderness values exceeding the limits imposed by seismic codes demonstrated generally satisfactory performance [5]. However, in order to test the overall behaviour of the SC-CBF under horizontal loading and to verify its self-centring behaviour, a more complex testing procedure is required. Therefore, the novel self-centring system that eliminates the residual deformations in the structure by using a post-tensioning arrangement, rocking connections and inelastic behaviour of tubular steel bracing members was tested under quasi-static cyclic tests [6].

The testing proved the self-centring behaviour of the SC-CBF after many cycles of inelastic deformation. It validated the rocking behaviour of the beam-column connection demonstrated by bilinear elastic performance. Also, great structural lateral capacity was observed when combining the

rocking behaviour with the diagonal bracing members. The complete improvement of the CBF structures' performance was observed after the increase of post-tensioning force in the cables when the gap opening in the rocking connection occurred.

To support the development and validation of the SC-CBF, shake table tests were performed in the framework of the SERA project [7]. The test setup was similar to the one used for quasi-static testing of the structure and comprised a single storey steel frame with a central SC-CBF containing the brace specimens and self-centring system and two external non-braced gravity frames with very low lateral resistance. During the experimental testing procedure, varying observations were indicated related to the structural brace configuration and the ground motion applied. However, some general observations contained negligible residual drifts, excellent functioning of the PT strands, energy dissipation through the braces and rocking connection behaviour between beams and columns, as verified by scratches at the connections.

In order to describe the need for a virtual experimental framework for the investigation of SC-CBF structures, the issues arising from the calibration of the simulated and reference model must be stated. If a calibration model is needed to provide optimal parameters for simulation, it has to focus on the component behaviour that is important from the perspective on the global structural behaviour. However, performing a sufficiently large number of full-scale dynamic experiments for calibration purposes is expensive [8]. The calibration of the physical and numerical model of the SC-CBF would normally consist of: global structural investigation under seismic loading, local brace investigation under seismic loading, brace investigation under virtual quasi-static loading and comparison of errors from dynamic simulation and calibration procedures to evaluate the efficiencies of the calibration methods and quantify uncertainties.

3. Conclusions

This study presents the types of experimental research needed for validation of the structural system and calibration of the numerical models for simulation of the structural behaviour. The various types of experimental procedures are then combined in order to form a complete methodology for estimation of the main characteristics of the novel system and proceeding to a code conforming evaluation procedure.

References

[1] Elghazouli, A. (2003): Seismic design procedures for concentrically braced frames, *Structures and Buildings*, **156** (4): 381-394, https://doi.org/10.1680/stbu.2003.156.4.381

[2] Fahnestock, L., Ricles, J., Sause, R. (2007): Experimental evaluation of a large-scale buckling-restrained braced frame, *Journal of structural engineering*, **133** (9): 1205-1214, https://doi.org/10.1061/(ASCE)0733-9445(2007)133:9(1205)

[3] Christopoulos, C., Filiatrault, A., Folz, B. (2002): Seismic response of self-centring hysteretic SDOF systems, *Earthquake engineering & structural dynamics*, **31** (5): 1131-1150, https://doi.org/10.1002/eqe.152

[4] O'Reilly, G., Goggins, J., Mahin, S. (2012): Behaviour and design of a self-centering concentrically braced steel frame system, *Proceedings of 15th World Conference on Earthquake Engineering*, Lisbon, Portugal.

[5] Elghazouli, A., Broderick, B., Goggins, J., Mouzakis, H., Carydis, P., Bouwkamp, J., Plumier, A. (2005): Shake table testing of tubular steel bracing members, *Structures and Buildings*, **158** (4): 229-241, https://doi.org/10.1680/stbu.2005.158.4.229

[6] O'Reilly, G., Goggins, J. (2021): Experimental testing of a self-centring concentrically braced steel frame, *Engineering Structures*, 238, 111521, https://doi.org/10.1016/j.engstruct.2020.111521

[7] SERA (2020): Investigation of Seismic Deformation Demand, Capacity and Control in a Novel Self-Centring Steel Braced Frame (SC-CBF), *Deliverable 10.1,* SERA Project, EU.

[8] Zsarnóczay, A., Baker J. (2019): Using model error in response history analysis to evaluate component calibration methods, *Earthquake Engineering & Structural Dynamics*, **49** (2): 175-193, https://doi.org/10.1002/eqe.3234

INVESTIGATION OF OUT-OF-PLANE SEISMIC BEHAVIOUR OF EXISTING MASONRY INFILLS

Maithree Kurukulasuriya [1], Riccardo Milanesi [2], Paolo Morandi [2], Guido Magenes [3]

[1] *PhD student, IUSS Pavia, University of Advanced Studies of Pavia, maithree.kurukulasuriya@iusspavia.it*
[2] *Researcher, European Centre for Training and Research in Earthquake Engineering, {riccardo.milanesi, paolo.morandi}@eucentre.it*
[3] *Professor, University of Pavia, guido.magenes@unipv.it*

Keywords: Masonry infills, Existing infills, Shaking table tests, In-plane, Out-of-plane, Seismic behaviour

The importance of accurate seismic assessment of masonry infills has been recognized after their high seismic vulnerability led to severe damages during past earthquakes. In this study, the out-of-plane behaviour of an existing masonry infill typology is characterized through experimental and numerical investigations with the aim of proposing improved formulations to assess its out-of-plane capacity and seismic demand parameters. The experimental program consisted of pseudo static in-plane cyclic tests and out-of-plane dynamic shake table tests on full scale single storey single bay infill specimens. Based on the experimental results, a numerical model is developed and validated to conduct parametric studies.

1. Introduction

The seismic behaviour of masonry infills has been extensively studied in the last decades [1, 2] to improve their detrimental response observed during many past earthquakes. The out-of-plane failure of infills is critical regarding life safety, especially when the out-of-plane capacity is impaired by in-plane damage. The out-of-plane capacity of infills is attributed to the arching action [3] owing to the presence of the surrounding frame, influenced by many factors such as infill properties, boundary conditions, slenderness ratio, and the stiffness of frame elements. In the current seismic codes, infills are assessed as non-structural elements and their safety is verified without giving special consideration to infill typology or structural configuration. Therefore, a better understanding of the out-of-plane behaviour of masonry infills is crucial to develop improved guidelines to minimize damage and prevent out-of-plane collapse. In this context, an experimental campaign was implemented to investigate the seismic behaviour of an existing masonry infill typology which was used in the 1960s-1980s in Italy as enclosures and partitions in reinforced concrete frame structures. The first phase of the experimental campaign involved five infill panels constructed surrounded by steel/concrete composite frames. Four specimens were fully adhered to the frame, and subjected to in-plane, out-of-plane, and successive in-plane and out-of-plane loading. The remaining specimen had free vertical edges and was tested in the out-of-plane direction. From experimental results, the influence of the boundary conditions and the level of in-plane damage on the out-of-plane behaviour was substantiated. Following the experiment, numerical simulations will be carried out to further investigate the influence of parameters such as infill properties, different geometries, frame properties and openings, on the out-of-plane behaviour of infills.

2. Experiment

Five infill specimens (T1-T5) were constructed with 12 cm thick 25x25 cm horizontally perforated clay units and 10 mm thick mortar joints. The panels were 3.5 m in length, 2.75 m in height and 13 cm in thickness including a 10 mm plaster layer on one side, built within steel/concrete composite frames. Four specimens (T1-T4) were fully bonded to the frame with a mortar layer. The remaining specimen T5 was connected to the frame at the top and bottom edges only. In-plane pseudo static cyclic tests on specimens T1, T2 and T3 were performed in displacement control and out-of-plane dynamic tests were conducted on specimens T2, T3, T4 and T5 on a shaking table. Specimens T2 and T3 were first

subjected to in-plane nominal drifts of 0.3 and 0.65%, respectively, and then to out-of-plane motion until failure.
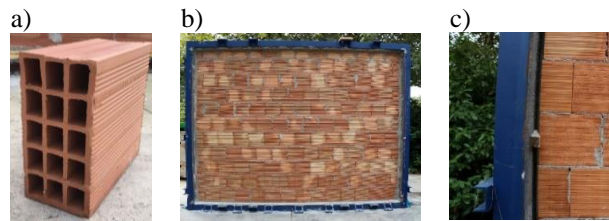

Figure 1. a) Units; b) Specimen with full adherence; c) Specimen with vertical gap

3. Preliminary results

From the pure-in-plane tests on T1, the in-plane drift capacity was found as 0.9%. In combined tests, the collapse was reached for specimens T2 and T3 at 2.5g and 1.5g nominal peak floor acceleration (PFA), respectively. In pure out-of-plane tests, the fully connected T4 did not show any significant damage or reach failure at PFA of 1.8g where the test was stopped. Specimen T5 exhibited vertical arching mechanism with horizontal cracks at boundaries and around mid-height, and the capacity was reached at a nominal PFA of 0.6g. The reduction of the out-of-plane capacity of the panel T3 with respect to T2 was 42% in terms of maximum acceleration at the centre of the panel. The out-of-plane response of specimen T5 completely differed to that of T4 with a higher flexibility and a lower capacity. Furthermore, the acceleration profiles observed in the infills were triangular between two supported opposite edges (for fully supported infills, along length and height, for T5 along height) inferring that the applied out-of-plane load on the panel is not uniform but close to triangular.

4. Conclusions and future work

1. An undamaged infill possesses considerable out-of-plane capacity, which drastically reduces with the presence of previous damage due to in-plane loading.

2. The boundary conditions of the panel significantly influence the out-of-plane response. The vertically spanning infill had a lower stiffness and capacity compared to the fully supported undamaged infill.

3. Effectuating the next phases of the experiment involving specimens with a gap on the top and specimens with openings, implementing numerical analyses, and finally proposing capacity and demand evaluation formulations are envisaged as future work.

Acknowledgements

References

[1] Abrams, D.P., Angel,R., Uzarski, J. (1996): Out-of-Plane Strength of Unreinforced Masonry Infill Panels, *Earthquake Spectra*, **12**(4), 825–844.

[2] Morandi, P., Hak, S., Milanesi, R.R., Magenes, G. (2022): In‑plane/out‑of‑plane interaction of strong masonry infills: From cyclic tests to out‑of‑plane verifications, *Earthquake Engineering Structural Dynamics*, **51**(3), 648‑672.

[3] McDowell, E. L., McKee, K.E., and Sevin, E. (1956): Arching action theory of masonry walls, *ASCE Journal of the Structural Division*, **82**(ST2): 915.1-915.18.

EXTRACTION AND PROCESSING OF ABAQUS OUTPUT DATA FOR USE IN SEISMIC ANALYSIS

Romano Jevtić Rundek[1], Ante Pilipović [2], Marija Demšić [3] Mario Uroš [4]

[1] Assistant, Faculty of civil engineering in Zagreb, romano.jevtic.rundek@grad.unizg.hr
[2] Assistant, Faculty of civil engineering in Zagreb, ante.pilipovic@grad.unizg.hr
[3] Associate professor, Faculty of civil engineering in Zagreb, marija.demsic@grad.unizg.hr
[4] Associate professor, Faculty of civil engineering in Zagreb, mario.uros@grad.unizg.hr

1. Introduction

Abaqus [1] is a quality engineering simulation software that offers FEM, DEM, MEM and other simulation methods to the user. In seismic analysis of structures, it is a valuable tool for performing time-history analyses as it provides complex simulation of material behaviour under dynamic excitation, geometric nonlinearities, and has a efficient solver. While Abaqus is powerful and can perform a wide range of general-purpose engineering simulations, it also comes at a cost of inefficient workflows for some specific tasks required in seismic analysis of buildings. In calculating the response of masonry walls and buildings to seismic action using Abaqus time-history analysis, the main problem is the interpretation of the results, as a large number of elements need to provide output data for each time step. That is, a large number of walls, consisting of a large number of 3D elements. It is impractical to do this in the native Abaqus GUI, so Python [2] scripts are developed to automate this workflow.

2. Structure of the scripts, workflow and output description

The scripts are in essence a sequence of commands that extracts processes and stores data. They can be run in different python environments. In this paper models consisting of 3D volumetric elements are considered. The main function of the scripts is identifying cross sections of PIER, SPANDREL or other elements in a model and outputting relevant forces and displacements. To obtain forces on cross section level, nodal forces are integrated across the cross sections. Cross section displacements are obtained by defining a regression plane for the field of deformed cross section nodes (example of such field output on Fig 1a)). Scripts will also monitor displacements of stories to provide story drift data.

Once analysis is complete, a script extracts field output data from the model (example used in this paper on Fig 1c)), process it into cross section based data and saves it in a database as forces, moments, displacements and deflection angles of cross sections. Then a postprocessing script is used to extract relevant data for PIER or SPANDREL elements, story drift data, etc. This processed data is exported in a text file that is suited for importing into excel, which allows easy further data visualisation. In terms of modifying the model for this scripted output and processing there are 2 options. One is defining each cross section as a set of surfaces before running the analysis. The other is identifying the finite element nodes of each cross section, if definition of sections prior to running the analysis wasn't possible. The second way requires some knowledge of coding in Python.

The scripts for data extraction are run inside Abaqus GUI, while further postprocessing is done using standard python code that can be run by a interface like IDLE. Output data can be customised when running the postprocessing script. It is possible to export specific components of forces of displacements, or select specific postprocessing like only PIER elements or only story drifts etc. Example of processed output data is shown on Fig 1b) and Fig 1d). Displayed are hysteresis of one PIER element in a building, analysed in the Dubrovnik B-17 study [3], for 3 different earthquake loads (analysis) on Fig 1b). On Fig 1d) are extremes of the drift, force and moment of the same PIER.
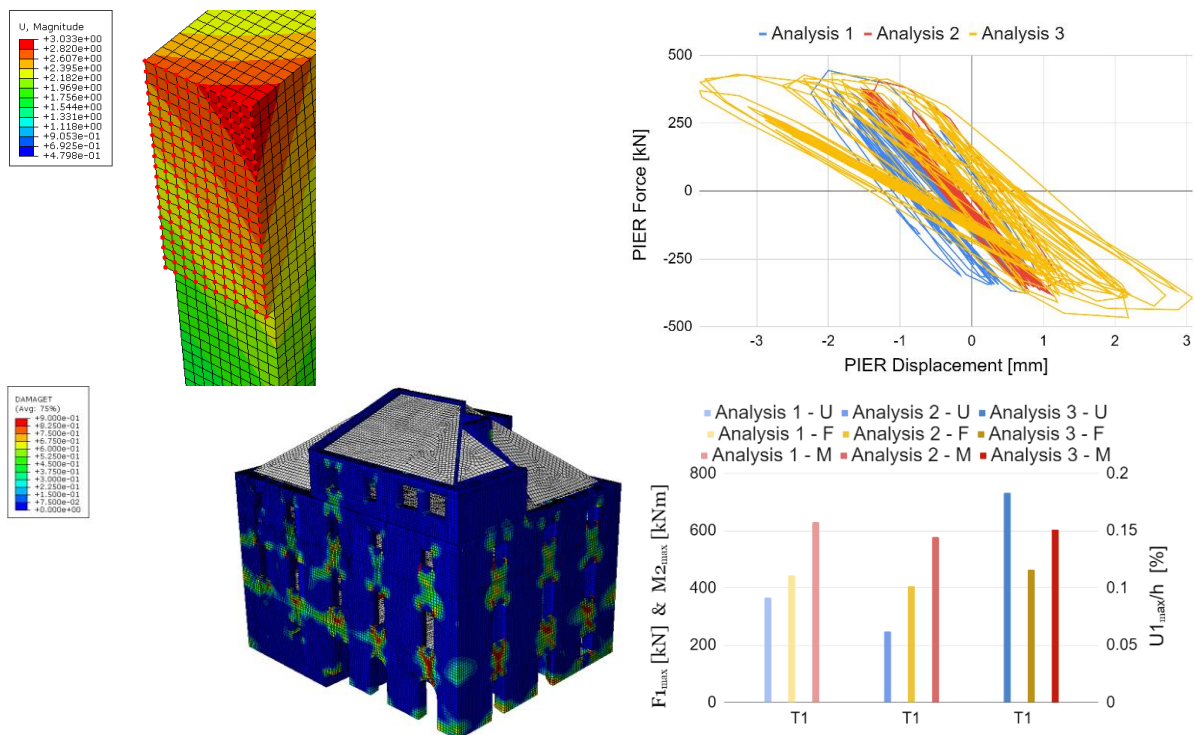
Figure 1. a)[top left] Displacement field on a cross section; b) [top right] Hysteresis of a PIER section in 3 different analysis; c)[bottom-left] FEM model [3]; d)[bottom-right] Maximum values of Force, Moment and drift of a PIER element for 3 different analysis

3. Conclusion

Abaqus data postprocessing presents a better insight into vast quantities of data and enables interpretation of more complex analysis or larger numbers of analysis. Good compiling of data for interpretation cannot be overstated as it is crucial for more extensive application of complex models to real world buildings. While the scripts in their current form offer good insight, there is still a significant issue with interpreting the results. Challenges presented here include estimating cross section based values from fields of values, shown on Fig 1a), identifying damage states of structural elements from time history data show on Fig 1b) and identifying structures health (for use as engineering demand parameter) from data shown in Fig 1d). Estimating cross section based values from a field output is currently done by a regression plane, with the assumption that cross sections are mostly flat enough after deformation. Identification of damage states of elements needs to be automated if multiple analysis on larger models are to be conducted. Once individual element damage states can be identified it is beneficial to able and interpret the whole structures health, since failure of 1 element doesn't always mean collapse of a structure. These challenges will be addressed in the future.

Acknowledgements

References

[1] Abaqus manual, software version: Abaqus 2021; http://130.149.89.49:2080/v6.14/

[2] Python manual, software version: Python 3.10.0; https://docs.python.org/3/

[3] Uroš, M., Demšić, M., Atalić, J., Gidak, P., Šavor Novak, M., Duvnjak, I., Baniček, M., Jevtić Rundek, R., Pilipović, A., Oreb, J.(2022): Procjena otpornosti bloka B-17 u gradskog jezgri u Dubrovniku i utjecaj ojačanja kamenih zidova na njegovo ponašanje pri djelovanju potresa. Faculty of civil engineering in Zagreb, Croatia

RISK-BASED SEISMIC PERFORMANCE ASSESSMENT OF A TYPICAL MASONRY BUILDING IN THE URBAN AREA OF ZAGREB

Ante Pilipović [(1)], Mario Uroš [(2)], Marta Šavor Novak [(3)], Snježan Prevolnik [(4)]

[(1)] *PhD Student, Faculty of Civil Engineering, University of Zagreb, ante.pilipovic@grad.unizg.hr*
[(2)] *Associate Professor, Faculty of Civil Engineering, University of Zagreb, mario.uros@grad.unizg.hr*
[(3)] *Associate Professor, Faculty of Civil Engineering, University of Zagreb, marta.savor.novak@grad.unizg.hr*
[(4)] *Seismologist, Faculty of Science, Department of Geophysics, University of Zagreb, snjezan.prevolnik@gfz.hr*

Keywords: seismic risk assessment, masonry buildings, building damage assessment, incremental dynamic analysis, seismic hazard, performance-based earthquake engineering

1. Introduction: Seismic risk assessment in post-earthquake Zagreb

The Zagreb 2020 earthquake has damaged many historical buildings within the old city centre despite its medium intensity. Damaged buildings were mostly typical masonry buildings in aggregates built in the first half of the 20ᵗʰ century when seismic codes were not developed. Simultaneously, seismic risk assessment has been carried out for the city of Zagreb indicating these typical masonry buildings as high-risk in case of an earthquake. Since then, efforts have multiplied to improve risk inputs and performance assessments of buildings in Zagreb. The present study is a case study of a typical masonry building in the urban area of Zagreb and a risk-based assessment of its seismic performance.

2. Case study: Typical masonry building in the urban area of Zagreb

2.1 Model definition

Several similar typical unreinforced masonry buildings (URM) from the Zagreb historical centre area have been analyzed and joined into a simplified model of a four-storey building without basement using ETABS, as shown in Fig 1. Material nonlinearity has been introduced as plastic in-plane shear hinges in the center of shear walls using parameters from detailed studies of similar buildings [1].
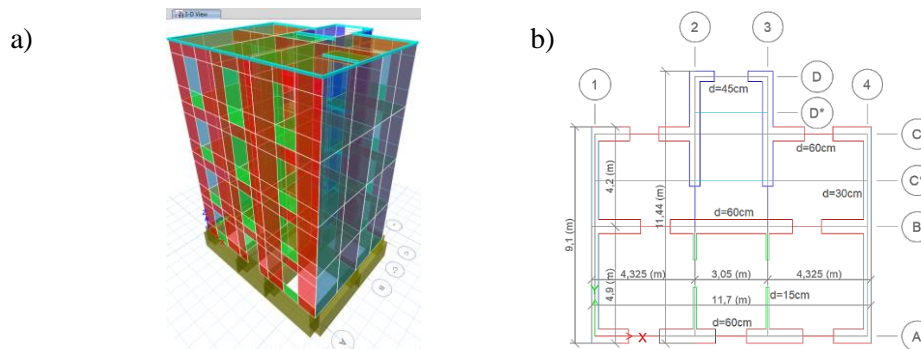
Figure 1. a) 3D numerical model in ETABS; b) Building plan

2.2 Incremental dynamic analysis (IDA) results

Performance assessment has been carried out using 13 ground motion records selected according to local seismotectonic conditions (active shallow crustal earthquakes, reverse thrust and strike-slip faulting) linearly scaled to 7-9 intensity levels of PGA in range 0.1g-0.3g in X direction (scale factor of X direction used for scaling in Y direction) and applying time-history analyses with both horizontal components simultaneously on the 3D model for each record thus generating 13 IDA curves up to collapse and 96 performance points in total. Average maximum inter-storey drift is used as engineering demand parameter (EDP) and average spectral acceleration in range of periods 0.5s-0.8s as the optimal

intensity measure (IM) for this type of buildings [2]. Each IDA run has been assigned a damage state by direct visual inspection of the 3D model state after each run based on EMS-98 damage classification using nonlinear hinge states as main criteria for the assessment of wall damage states and damage spread [3]. The performance points and their inspected damage states are shown in Fig. 2. a).
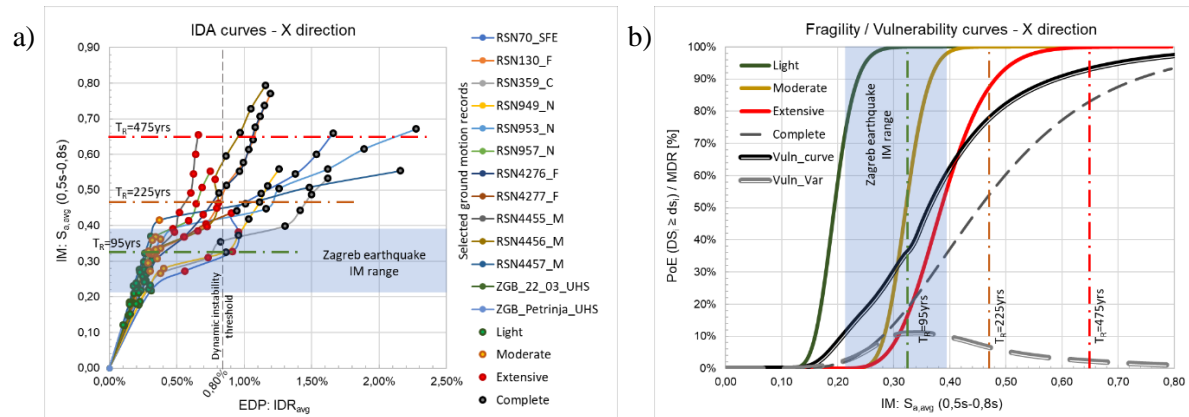
Figure 2. a) IDA curves and performance points for X direction; b) Fragility and vulnerability curves for X direction; Zagreb 2020 earthquake IM range is marked along with IM values for return periods T_R=95, 225 and 475 years (elastic EC8 spectrum, type 1, soil type C, $a_{g,ref}$ value from Croatian national seismic hazard map)

2.3 Risk-based seismic performance assessment

Fragility curves have been derived for slight, moderate, extensive and complete damage states using IM-based approach, but instead of EDP thresholds, visual inspection results have been used for each IDA curve. The only exception is complete damage threshold which has been set to EDP value 0.8% according to IDA results (limit that keeps lognormal distribution of EDP results). Vulnerability curves have been developed using MDR (mean damage ratio) values of 10%, 30%, 60% and 100% for slight, moderate, extensive and complete damage states respectively [4] for URM buildings. Fig. 2. b) shows the fragility and vulnerability curves with marked IM values corresponding to Zagreb 2020 earthquake components and code-based return periods. Results show that the building reaches slight damage state for T_R=95 years. For T_R=225 years moderate damage levels are already exceeded and for T_R=475 years extensive and complete damage can be expected. Zagreb 2020 earthquake IMs already fall into the peak derivative of the vulnerability curve although the earthquake is only of medium intensity according to hazard and losses up to 60% can be expected, indicating extensive damage. This building type is therefore very vulnerable according to code-based hazard and should be retrofitted in order to increase its seismic performance.

Acknowledgements

References

[1] Uroš, M., Todorić, M., Crnogorac, M., Atalić, J., Šavor Novak, M., Lakušić, S. (Ed). (2021): *Earthquake Engineering: Retrofitting of masonry buildings*, University of Zagreb, Faculty of Civil Engineering, 1st edition, Croatia

[2] Pilipović, A., Uroš, M. (2022): Selection of optimal intensity measure for a typical masonry building in the urban area of Zagreb, *8. Doctoral Symposium in Civil Engineering*, Zagreb, Croatia, 14 pages

[3] Grünthal, G. (Ed) (1998): *European Macroseismic Scale 1998 (EMS-98)*, European Seismological Commission, Cahiers du Centre Européen de Géodynamique et de Séismologie, Vol. 15, Luxembourg

[4] Presidency of the Council of Ministers, Italian Civil Protection Department (PCM ICPD) (2018): National risk assessment. Overview of the potential major disasters in Italy: seismic, volcanic, tsunami, hydro-geological/hydraulic and extreme weather, droughts and forest fire risks, Italy.

ADVERTISEMENTS

Hrvatska komora
inženjera građevinarstva

Hrvatska komora
inženjera građevinarstva

Hrvatska komora inženjera građevinarstva (HKIG) osnovana je na temelju *Zakona o arhitektonskim i inženjerskim poslovima i djelatnostima u prostornom uređenju i gradnji*, kao pravna sljednica Hrvatske komore arhitekata i inženjera u graditeljstvu. Započela je s radom 22. svibnja 2009. godine.

HKIG je samostalna i neovisna strukovna organizacija ovlaštenih inženjera građevinarstva, inženjera gradilišta građevinske struke i voditelja radova građevinske struke, te stranih osoba građevinske struke s poslovnim nastanom u RH, koji obavljaju poslove regulirane profesije građevinske struke u svojstvu odgovorne osobe, u skladu s posebnim propisima koji uređuju obavljanje djelatnosti u području prostornog uređenja i gradnje, i posebnim zakonom kojim se uređuje priznavanje inozemnih stručnih kvalifikacija.

Hrvatska komora inženjera građevinarstva je danas, sa skoro 8.200 članova, najveća i najsnažnija inženjerska komora u državi. Ima veliku, aktivnu ulogu u reguliranju profesije i u zastupanju interesa struke koja je važan faktor gospodarskog rasta. Komora kontinuirano radi na unaprjeđenju uvjeta u graditeljstvu, zaštiti interesa inženjera građevinarstva i pozicioniranju HKIG-a kao jednog od ključnih dionika u kreiranju uvjeta razvoja i napretka građevinarstva.

www.hkig.hr

Zračna luka Zagreb
Izvor: Institut IGH d.d.

Most Čiovo
Izvor: Institut IGH d.d.

Most Pelješac
Izvor: Institut IGH d.d.
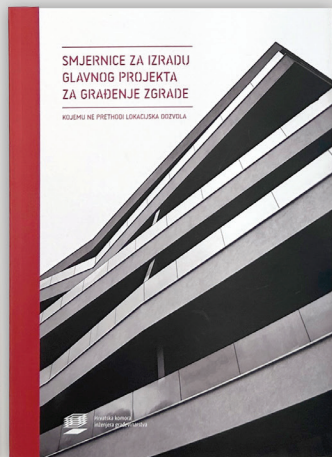
RECENTNA STRUČNA IZDANJA HRVATSKE KOMORE INŽENJERA GRAĐEVINE

Zbornik KOLOS 2011.–2021.

Hrvatska komora inženjera građevinarstva izdala je **Zbornik dobitnika nagrade Kolos 2011-2021**.
Nagrada Kolos najznačajnija je nagrada u građevinarstvu, a Komora je dodjeljuje još od 2011. godine. **Nagrada KOLOS** dodjeljuje se za osobit doprinos graditeljskoj struci, razvoj građevinske djelatnosti i doprinos Komori njezinoj promidžbi u zemlji i inozemstvu. Simbolika Kolosa je neupitna. Radi se o nagradi za izvrsnost u graditeljstvu, koja se dodjeljuje u više različitih kategorija: za iznimne rezultate trajne vrijednosti na unapređivanju i razvoju struke, za javnu prepoznatljivost i priznatost te razvoj tehničkog stvaralaštva u Republici Hrvatskoj i u svijetu, za izuzetna inženjerska dostignuća primijenjena u izgradnji objekata konstrukcije te za poticanje investicija i doprinos razvoju i unapređenju graditeljske djelatnosti. Ono što je zajedničko svim dobitnicima Kolosa je da se radi o nagradi koja je potvrda za stečena znanja, ali i poticaj za daljnji napredak i razvitak.
Nagrada ima iznimno značenje za građevinsku struku. To je nagrada koja dolazi kao kruna na sav trud, rad, znanje i profesionalnost koju inženjeri građevinarstva ulažu u svaki projekt na kojem rade.

Smjernice za BIM pristup u infrastrukturnim projektima

Hrvatska komora inženjera građevinarstva, potaknuta tehnološkim trendom kretanja projekata na tržištu i planiranim brojnim infrastrukturnim investicijama na državnoj razini, izradila je **nove specijalizirane smjernice** - Smjernice za BIM pristup u infrastrukturnim projektima. Smjernice razmatraju cjelovitu primjenu BIM pristupa u infrastrukturnim projektima i mogu se koristiti kao alat koji omogućuje integraciju rezultata inženjerskih zadaća kako bi se smanjila mogućnost neusklađenih tehničkih rješenja i skratilo vrijeme potrebno za eventualne promjene u projektu. Izrada ovih smjernica jasna je i jednoznačna poruka kako hrvatske tvrtke u svojemu radu trebaju primjenjivati BIM pristup radi povećanja konkurentnosti na domaćemu i stranome tržištu. Na taj način može se podići razina kvalitete projektiranja i građenja te se u konačnici mogu smanjiti troškovi izgradnje i održavanja građevina.

Monografija HKIG 2018.–2022.

Hrvatska komora inženjera građevinarstva izdala je 2022. godine Monografiju - **pregled rada Komore u razdoblju 2018.-2022.**, u kojoj je, uz povijesni razvoj HKIG-a, prikazan i sažet rad i aktivnosti Komore tijekom proteklog četverogodišnjeg razdoblja. To je razdoblje obilježio mandat prve žene predsjednice Hrvatske komore inženjera građevinarstva, Nine Dražin Lovrec, dipl. ing. građ. Principi kojima se vodstvo komore rukovodi u radu vrlo su jasni i konzistentni: struka i stručnost prije svega, proaktivna obrana interesa inženjerske struke uz istovremenu zaštitu interesa društva kao cjeline, javnost i otvorenost rada Komore, partnerski odnos s državnim i javnim institucijama u okruženju i odmak od bilo kakve politike i političkih interesa.
Monografija prikazuje sve relevantne informacije, ulogu, strateške ciljeve, viziju i misiju te i strukturu Komore. Rad predsjednice Dražin Lovrec kako u prvom mandatu tako i danas fokusiran je na snažno i čvrsto javno zagovaranje i zastupanje interesa inženjera građevinarstva i svih članova Komore. U proteklom četverogodišnjem razdoblju primarni cilj vodstva Komore bio je postizanje što većeg i uspješnijeg utjecaja Komore i struke na kreiranje zakonodavnog okvira inženjerske djelatnosti koji je podloga za kvalitetno obavljanje posla i napredak struke.
"Naš utjecaj gradili smo na aktivnom doprinosu naših članova, stručnosti i argumentiranosti naših prijedloga, aktivnoj prisutnosti vodstva Komore u medijima i javnosti. Sve to doprinijelo je osnaživanju pozicije naše struke u društvu kao i jačanju reputacije struke i Komore", istaknula je Dražin Lovrec. Inženjerke i inženjeri građevinarstva, kao i graditeljstvo u cjelini, sve više postaju prepoznati kao pokretači i nositelji razvoja gospodarstva i društva. Stoga s ponosom možemo reći da je Hrvatska komora inženjera građevinarstva postala lider u zastupanju njihovih interesa i interesa građevinskog sektora.

SPEGRA

SPECIJALNI GRAĐEVINSKI RADOVI

www.spegra.hr

PARTNER OF MODERN REHABILITATION
SINCE 1989

spegra

SPEGRA d.o.o. osnovana je 1989. godine u Splitu, a u svojoj **34-godišnjoj tradiciji** usko se specijalizirala isključivo za izvođenje **spe**cijalnih **gra**đevinskih radova, počevši od izvođenja sanacijskih radova zaštite kulturne baštine do vrlo složenih inženjerskih sanacija. Tvrtka je nastala spontano i igrom slučaja, kao što često svaka velika priča o uspjehu nastane, a pogotovo u svijetu poduzetništva. SPEGRA je osnovana iz praktične potrebe, kada je direktor Berislav Borovina, na samom početku uspješne karijere, pri radu na jednom projektu, uvidio da ne postoji tvrtka koja bi mogla izvesti potrebne radove na sanaciji. Odlučio je odgovoriti na potrebe građevinskog tržišta i osnovati upravo tvrtku kakvu je tražio.

Od nabavke prvog stroja, Hamelmannove visokotlačne pumpe i od svega par zaposlenika, tvrtka je u tri desetljeća narasla do oko **250 zaposlenika** te postala sinonim za radove sanacije građevinskih objekata te nacionalni, ali i internacionalni lider u izvođenju ove vrste radova s najmodernijom opremom i strojevima kakve koriste najbolje svjetske tvrtke iz branše.

Od samog početka, što zbog težnje ka izvrsnosti, a što zbog specifične djelatnosti, SPEGRA d.o.o. prati suvremene, globalne građevinske trendove i materijale. Početkom 90-ih, u vrijeme kada se i na svjetskoj razini počelo ozbiljnije pristupati sanaciji objekata, posebno onih starih s kulturnom i povijesnom vrijednošću, tada je i SPEGRA s jednakom ambicijom krenula u taj posao u Hrvatskoj i do danas postala **mjerilo za kvalitetu i inovaciju**. Upravo su ta dva kriterija ono što krasi svaki projekt izveden od Spegre i zbog čega je SPEGRA angažirana na izvođenju mnogih, velikih i značajnih projekata sanacije.

Izvođenje sanacijskih radova spada u najzahtjevnije i najizazovnije radove na polju građevinarstva. Zahtijeva prvenstveno znanje i izvrsne ljudske kapacitete, a tvrtka SPEGRA tijekom godina postala je upravo baza ovih specifičnih znanja koje je nastalo iz konstantnog učenja i iz ogromnog iskustva uspješno odrađenih projekata.

Svoje projekte SPEGRA je radila uspješno surađujući sa brojnim stručnim autoritetima, od visokoobrazovnih institucija (Fakulteta građevinarstva i arhitekture), konzervatorskih odjela, Ministarstva kulture..., a praktična i teoretska znanja je razmijenjivala i s europskim stručnjacima što dokazuje da razina stručnosti SPEGRA-inih djelatnika ne zaostaje za najboljim stranim stručnjacima. Nerijetko, SPEGRA-ini inženjeri drže predavanja na stručnim skupovima i konferencijama za kolege iz struke.

Za svoj rad SPEGRA je nagrađivana desetke puta, a posljednje, ujedno i najvrjednije postignuće je **nagrada Europske komisije - Europa Nostra**, najprestižnije europsko priznanje u području baštine koje je u kategoriji konzervacije dodijeljeno Hvarskom Arsenalu, a zahtjevan projekt obnove i ojačanja nosive konstrukcije izvela je upravo SPEGRA. Ovo priznanje svrstalo je SPEGRA-u uz bok najboljim europskim tvrtkama koje se bave obnovom spomeničke baštine.

Osim Hvarskog Arsenala, u SPEGRA-inom potrfelju posebno se ističu projekti sanacije na objektima kao što je **Knežev dvor i brojne palače i crkve u Dubrovniku**, Krstionica Sv. Ivana (Jupiterov hram) u Splitu, Biskupova palača u Stonu, dvorac Veliki Tabor... SPEGRA je radila i obnovu Starog mosta u Mostaru, obnovu mostova od Ploča i Pila u Dubrovniku, ali i Krčkog i Paškog mosta.

SPEGRA je u svojoj 31-godišnjoj tradiciji radila i brojne sanacije na hidroelektranama, kao što su HE "Peruča", HE "Zakučac", HE "Prančevići", HE "Orlovac", HE "Gojak", a obnavljala je i brojne građevine oštećene u Domovinskom ratu.

Najrecentniji SPEGRA-in projekt je obnova Zagrebačke katedrale koja je značajno oštećena potresima. **Zagrebačka katedrala** predstavlja najveću hrvatsku sakralnu građevinu i jedan od najvrjednijih spomenika hrvatske kulturne baštine.

Mnogi SPEGRA-ini projekti tako ostaju trajan biljeg u prostoru, nadograđujući i uljepšavajući vizure.

Mnoge mlade tvrtke u Hrvatskoj danas su konkurentne na svjetskoj razini i među najboljima su u svojim industrijama, počevši od IT-a, automobilske industrije, farmacije... Spegra je jedan od prvih hrvatskih primjera kako se uz volju, ambiciju i inovativnost i u Hrvatskoj može napraviti svjetska tvrtka, lider u znanju i izvrsnosti.

PARTNER OF MODERN REHABILITATION
SINCE 1989

Graditi po sistemu

RÖFIX je članica krovne organizacije/koncerna pod nazivom FIXIT GRUPPE i sinonim za proizvođača građevinskih sustava. Od 1994. godine RÖFIX je prisutan i u Hrvatskoj.

Tijekom više od 20 godina postojanja na hrvatskom tržištu razvili se u jednu od vodećih tvrtki za proizvodnju i veleprodaju građevinskog materijala. RÖFIX materijal na skladišta i police trgovina građevinskim materijalom, diljem Hrvatske, ali i Europe, stiže iz tri proizvodna pogona smještenih u Pojatnom, Zaprešiću i Siveriću. Osim na kvalitetu i učinkovitost, proizvodna politika tvrtke RÖFIX u velikoj mjeri usmjerena je na kreiranje i proizvodnju dugoročno održivih i ekološki prihvatljivih sustavnih rješenja usklađenih s potrebama i željama krajnjih kupaca. Inovativnim građevinskim rješenjima omogućava jednostavnu primjenu u praksi, a stručnim savjetovanjem osigurava podršku u svakoj fazi gradnje. U centru za istraživanje i razvoj kontinuirano razvija suvremene i moderne proizvode, te sustave izvrsne kvalitete. Suradnja građevinskih tehnologa, mineraloga i kemičara čini snažnu sinergiju koja jamči trajno visokokvalitetne proizvode. Zajedno s kupcima i partnerima kontinuirano radi na poboljšanju proizvoda. Uz jednostavnu ugradnju materijala na gradilištu i integraciju proizvoda u razne sustave, RÖFIX neprestano razvija različita rješenja koja u konačnici stvaraju dodatnu vrijednost za sve, od izvođača radova do krajnjeg korisnika.

Graditi po sistemu

STRONGER THAN EVER

FIBRE NET GROUP i RÖFIX Hrvatsku povezuje zajednička uspješna dugogodišnja suradnja na području konstrukcijskih ojačanja. Zajedno nudimo sustavna rješenja koja se sastoje od kompozitnih materijala tvrtke FIBRE NET GROUP i konsolidacijskih mortova/žbuka tvrtke RÖFIX. Pružamo podršku od faze projektiranja pa sve do faze izvođenja radova na gradilištu.

FIBRE NET GROUP razvija certificirane sustave od kompozitnih materijala ojačanih vlaknima koji se upotrebljavaju u obnovi konstrukcija, seizmičkom poboljšanju i sanaciji postojeće građevinske i infrastrukturne baštine. Istraživanje i razvoj temelji se na stalnoj suradnji s domaćim i stranim sveučilištima, istraživačkim institutima i neovisnim tijelima.

FIBRE NET GROUP razvija certificirane sustave od kompozitnih materijala ojačanih vlaknima koji se upotrebljavaju u obnovi konstrukcija, seizmičkom poboljšanju i sanaciji postojeće građevinske i infrastrukturne baštine. Istraživanje i razvoj temelji se na stalnoj suradnji s domaćim i stranim sveučilištima, istraživačkim institutima i neovisnim tijelima.

Povijest FIBRE NETA započela je 2001. s vizijom: razviti potpuno novi proizvod, GFRP (Glass Fiber Reinforced Polimer) mrežicu. Danas, nakon više od dvadeset godina, više ne govorimo o poduzeću, već o FIBRE NET GRUPI, dinamičnoj tvrtki u stalnoj potrazi za izvrsnošću. Stalna ulaganja u istraživanje i razvoj, visoka razina konkurentnosti i stalni rast u smislu znanja i produktivnosti omogućuju grupi razvoj tehnološki naprednih rješenja, proizvoda i sustava koji se široko koriste u više od 30 zemalja diljem svijeta.

FIBRE NET pruža tehničku podršku od projektiranja preko ugovaranja do izvedbe na licu mjesta: analiza izvedivosti, konstrukcijski dizajn, kontrola kvalitete, ispitivanje na licu mjesta, praćenje vremena i troškova. Temeljne vrijednosti FIBRE NET GROUP temelje se na pažnji prema kvaliteti i usmjerenosti prema kupcima. Predanost informiranju i stalnom usavršavanju usmjerena je na aktivnosti namijenjene osoblju tvrtke, kao i izvođačima i projektantima.

RI-STRUTTURA Sustav ojačane žbuke CRM

RI-STRUTTURA upotrebljava tehniku ojačane žbuke nove generacije CRM - Composite Reinforced Mortar – kroz upotrebu mreža, kutnika i spojnih elemenata od predgotovljenog kompozitnog materijala od AR staklenih vlakana i termostabilnih smola. Naposljetku se nanosi mort za žbukanje na bazi prirodnog hidrauličnog vapna (NHL) ili cementa.

- Konstrukcijski zahvati na stambenim i industrijskim zgradama nakon potresa
- Seizmičko poboljšanje povijesnih i zaštićenih zgrada
- Konsolidacija degradiranih konstrukcijskih elemenata
- Poboljšanje i prilagodba nakon promjene namjene

RI-STRUTTURA predstavlja rješenje za jednostavnu upotrebu, posebno na povijesnim zidanim zgradama gdje je potrebna učinkovita konsolidacija i konstrukcijsko poboljšanje neinvazivnim i kompatibilnim metodama, često u složenim radnim i logističkim uvjetima.
Lagani materijali i mreže dostupne u rolama do 100 m2 olakšavaju rukovanje i omogućuju brzo polaganje koje se izvodi ručnim ili strojnim nanošenjem morta u samo jednom sloju i bez potrebe nanošenja „mokro na mokro". Rezultat je ušteda vremena i troškova polaganja i bolja organizacija gradilišta.
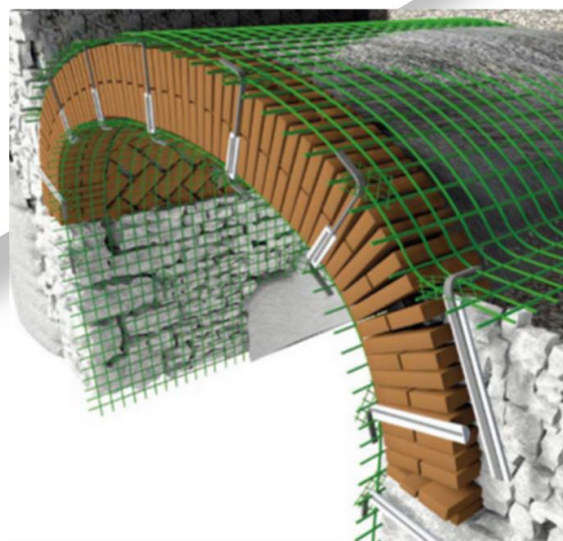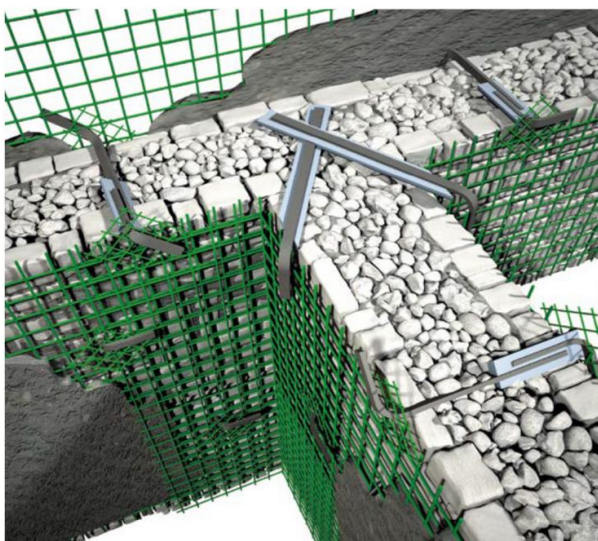
BE SURE.
BUILD SURE.

Svaki ugrađeni proizvod može biti od presudne važnosti i kritično utjecati na cijelu konstrukciju ili njezinu sanaciju. Odabir pogrešnih rješenja ili njihova pogrešna primjena može dovesti do oštećenja elemenata i konstrukcija, a u ekstremnim slučajevima čak i do ugrožavanja života. Stoga projektanti, inženjeri i izvođači snose značajnu odgovornost. Pouzdanim tehničkim savjetima i proizvodnim rješenjima - ulažemo napore, brigu i pažnju osiguravajući da svaki projekt koji izvedu naši kupci bude sigurno izveden. Dio bivanja MC-om doista znači prihvaćanje odgovornosti za živote i reputaciju. Gradnju shvaćamo ozbiljno.

Zahvaljujući stečenom znanju i iskustvu, kupcima pružamo proizvode kojima će biti zadovoljni i iznova se vraćati. Predani smo razvoju naprednih rješenja za obradu betona te zaštitu i popravak građevina i struktura. Kontinuirani rad doveo nas je do toga da se danas ubrajamo u vodeće svjetske proizvođače građevinskih kemikalija i novih tehnologija u građevinarstvu.

Proizvodi i usluge koje pokrivamo se protežu od sanacije betona, zaštite površina i tehnologija injektiranja do podnih obloga i brtvljenja. Također, nudimo i jedinstvene proizvodne sisteme, a sve u cilju zaštite građevinskih struktura od svih vrsta mehaničkih utjecaja, procesa starenja i agresivnih utjecaja sredine.

Porotherm Profi grinded bricks in the infill masonry system

www.wienerberger.hr

Wienerberger

Samoborka®
www.samoborka.hr

SANACIJE I OJAČANJA
U PROTUPOTRESNOJ OBNOVI

- Ojačanje zidanih konstrukcija FRCM sustavom
- Ojačanje zidanih konstrukcija CRM sustavom
- Ojačanje zidova torkretiranjem
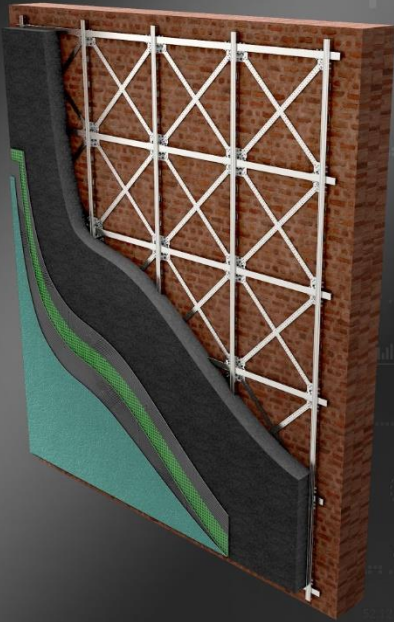
Hrvatska akademija znanosti i umjetnosti, u skladu sa svojom dugogodišnjom zakladnom tradicijom, na svojoj Skupštini od 29. lipnja 1993. utemeljila je Zakladu, kojoj je cilj unapređivanje kulture, umjetnosti, znanosti i odgoja, kao bitnih čimbenika duhovnoga, gospodarskoga, političkoga i sveopćega napretka Hrvatske.

Sredstva Akademijine Zaklade služe potpomaganju izdavačke djelatnosti, organiziranju znanstvenih skupova, uspostavljanju posebnih znanstvenih središta, otkupu umjetnina, unapređivanju kulture, umjetnosti i znanosti davanjem stipendija i nagrada za posebna dostignuća.

Proceedings of the
2nd Croatian Conference on Earthquake Engineering
2CroCEE
22-24 March 2023, Zagreb, Croatia

Engineering Seismology

Geotechnical Earthquake Engineering

Experimental Techniques
for Characterization of Materials and Structures

Historical Structures

Seismic Performance of Structures

Repair and Strengthening of Structures

Post-Earthquake Reconstruction Process

Lessons Learnt from Earthquake Disasters

Preparedness and Emergency Management

Seismic Loss and Risk Analysis

PhD Special Session